Mol Imaging Biol (2016) 18 (Suppl 1):S1–S1553
DOI: 10.1007/s11307-016-0969-2

Found 978 Records

CONTROL ID: 2218021
TITLE: Spectroscopic Photoacoustic Molecular Imaging of Breast Cancer Using an Antibody-Dye Contrast Agent
PRESENTER: Katheryne Wilson
ABSTRACT BODY:
Abstract Body: Introduction: Spectroscopic photoacoustic (sPA) imaging allows for identification of individual optical absorbers within biological tissues, endogenously limited to hemoglobin, melanin, and lipids. Molecularly specific contrast agents are needed to investigate other tissue markers, but few agents are considered readily clinically translatable. Our objective was to explore the potentially clinically translatable combination of antibodies (Ab) and the FDA-approved near-infrared, fluorescent dye indocyanine green (ICG) for sPA imaging of CD276, a molecular marker differentially expressed in breast cancer[1], which may improve accuracy of ultrasound imaging for breast cancer detection.
Methods: Succinimidyl ester modified ICG was conjugated to monoclonal Ab specific to the CD276 marker. Ab-dye binding ratios were determined using spectrophotometric analysis and protein concentration was determined with a standard BCA assay. A transgenic mouse model for breast cancer development (FVB/N Tg(MMTV/PyMT634Mul) was used to assess the ability of sPA imaging to detect the accumulation of CD276-ICG contrast agent in breast cancer. Mice with invasive breast adenocarcinoma (10-12 weeks of age) were injected intravenously with 33 μg of CD276-ICG or control agents, including isotype Ab conjugated with ICG (Iso-ICG), ICG dye alone, or CD276-ICG in tumor negative mice. Fluorescence, multi-wavelength (680-950 nm, 10 nm increments) sPA, and B-mode ultrasound imaging were performed before and 24h, 48h, and 72h after i.v. administration using the VisualSonics LAZR and the Xenogen IVIS Spectrum. Anatomical B-mode images were used to guide ROI selection for sPA data analysis. Using an in-house sPA data analysis algorithm, the average molecular CD276 signal in the tumor ROI was determined by monitoring absorbance shifts of ICG. CD276-ICG uptake and clearance were monitored with fluorescence imaging. Immunohistochemical (IHC) staining was used to quantify CD276 expression in breast cancer and normal mammary gland tissue.
Results: In total, 80 tumors were imaged over the five day period with another 110 monitored with various control agents (Iso-ICG (n= 30), CD276-ICG in normal mammary glands (n = 60), and ICG only (n=20). Tumors showed a 3.15±0.42 fold increase in molecular CD276 signal compared to pre-injection values with sPA (range 0.30–20.0 fold increase, $p<0.001$) and a 1.37±0.15 fold increase in CD276 signal with fluorescence imaging (range 0.75–2.02 fold increase, $p<0.001$). Control agent values showed no significant increase in signal compared to background values. Murine breast cancer tissue, both epithelial and endothelial cells, stained positive for CD276, while normal tissue did not express CD276.
Conclusions: Spectroscopic photoacoustic imaging is able to detect clinically translatable antibody-dye contrast agents in a transgenic mouse model of breast cancer. CD276-targeted molecular sPA signals were detected as early as 24 hours and for at least 96 hours after injection. Molecular sPA imaging may become a complementary parameter to ultrasound imaging for more accurate earlier detection of breast cancer.
1. Seaman S., et. al. *Cancer Cell*. 2007;11(6):539-554
AUTHORS (LAST NAME, FIRST NAME): Wilson, Katheryne[1]; Bachawal, Sunitha[1]; Willmann, Juergen K.[1]
INSTITUTIONS (ALL):
1. Radiology, Stanford University, Stanford, CA, United States.
(No Image Selected)

CONTROL ID: 2232731

TITLE: Radiosensitization of HER2-overexpressing cancer cells upon treatment with targeted functionalized silica nanoparticles

PRESENTER: Haruka Yamaguchi

ABSTRACT BODY:

Abstract Body: 【Purpose】We investigated the effect of targeted functionalized silica nanoparticles on cancer cell radiosensitization. Previous studies from our lab have shown that targeted functionalized silica nanoparticles become specifically internalized by the targeted cancer cells. Despite the fact that high concentrations of silica nanoparticles cause toxicity, the first clinical trial investigating modified fluorescent core-shell silica nanoparticles is in progress. Better control of the local concentration of silica nanoparticles may allow their use as an adjuvant in conjunction with ionizing radiation to target cancer cells while avoiding damage to normal cells . To assess the ability of silica nanoparticles as radiosensitizers, we used HER2-targeted polyamidoamine-coated PAMAM silica nanoparticles (PCSNs) in cell culture experiments.

【Materials and Methods】 Hyperbranched PAMAM (generation 3) was grafted onto the surface of Aerosil 200 synthetic amorphous silica nanoparticles to functionalize the particles for multimodal imaging. The processed nanoparticles (PCSNs) were suspended in 50% ethanol diluted in distilled-deionized water and then centrifuged (11,000 rpm for 5 minutes) using spin columns for purification. PCSNs were conjugated with fluorescent dyes (Alexa Fluor® 488, carboxylic acid, succinimidyl ester or ICG-sulfo-OSu). Anti-HER2 antibodies (HER2/ErbB2 (D8F12) XP Rabbit mAb) were covalently attached to the labeled PCSNs after which the PCSNs were labeled with ^{99m}Tc. To remove the ethanol, PCSN probes were washed twice with PBS. The HER2-overexpressing breast carcinoma cell line SK-BR3 and the low HER2-expressing breast carcinoma cell line MDA-MB231 were incubated in medium containing the PCSN probes for 24 hours. After incubation, the cells were exposed to X-ray radiation (2-4 Gy). All samples were counted using the Cell Counting Kit-8 and a hemocytometer. Apoptotic cells were detected using the terminal deoxynucleotidyl transferase dUTP nick-end labeling (TUNEL) assay. To take fluorescence images, we used a fluorescence microscope and a Pearl Imager. To take phosphor images, we used an imaging plate and an FLA-2000 fluorescent laser scanning imager.

【Results】

The results of the cell survival studies showed that the combination of the targeted PCSNs and radiation decreased the survival rate of SK-BR3 cells to a greater extent than when either PCSNs or radiation was used alone. The TUNEL assay showed an increase in apoptosis in the SK-BR3 cells that and those cells were internalized. SK-BR3 cells were more sensitive to radiation treatment than MDA-MB231 cells. ^{99m}Tc-tagged targeted PCSNs also showed increased radioactivity in SK-BR3 cells.

【Conclusions】The results of this study demonstrated that targeted PCSNs can act as specific radiosensitizing agents in SK-BR3 cells. This approach could be used to image specific cells and could be used as a targeted therapy to decrease the side effects of radiotherapy in cancer patients.

AUTHORS (LAST NAME, FIRST NAME): Yamaguchi, Haruka[5, 1]; Hayama, Kazuhide[2]; Kameta, Ayako[2]; Yasuo, Okada[3]; Sasagawa, Ichiro[4]; Yoshie, Sumio[6]; Kawase, Tomoyuki[7, 4]; Tsubokawa, Norio[8, 4]; Tsuchimochi, Makoto[2, 4]

INSTITUTIONS (ALL):

1. Department of Life Science Dentistry, Nippon Dental University, Niigata , Japan.
2. Department of Oral and Maxillofacial Radiology, Nippon Dental University, Niigata, Japan.
3. Department of Pathology, Nippon Dental University, NIigata, Japan.
4. Advanced Research Center, Nippon Dental University, Niigata, Japan.
5. Quantitative Diagnostic Imaging Program, Nippon Dental University Graduate School of Life Dentistry at Niigata, Niigata, Japan.
6. Department of Histology, Nippon Dental University, Niigata, Japan.
7. Division of Oral Bioengineering, Institute of Medicine and Dentistry, Niigata University, Niigata, Japan.
8. Faculty of Engineering, Niigata University, Niigata, Japan.

(No Image Selected)

CONTROL ID: 2230381

TITLE: Activated Platelet Targeted Theranostic Microbubbles for Concurrent Diagnosis and Treatment of Thrombosis via ultrasound

PRESENTER: Xiaowei Wang

ABSTRACT BODY:

Abstract Body: Background – Most acute cases of myocardial infraction and stroke are caused by atherothrombosis, when platelet adhesion, activation and aggregation, lead to thrombus formation and vessel occlusion. Glycoprotein (GP) IIb/IIIa complex, is the most abundant receptor expressed on the platelet surface, responsible for adhesion and aggregation. We have developed conformation-specific single-chain antibodies (scFv) that bind specifically to ligand-induced binding sites on activated GPIIb/IIIa. In addition, current drug therapy of atherothrombosis is hampered by side effects such as bleeding complications and neurotoxicity. We hypothesized that thrombolytic drugs loaded microbubbles (MBs), which are selectively targeted to activated platelets, will allow high-resolution, real-time imaging of thrombosis, and at the same time offer potent thrombolytic efficacy without bleeding complications, and enable the immediate monitoring of success or failure of thrombolysis.

Methods and Results – Our targeted theranostic microbubbles (TT-MB) comprise of three components. 1. Ultrasound contrast agents, microbubbles, for visualization by ultrasonography; 2. Activated-platelet-specific scFv for targeting of thrombi; and 3. Fibrinolytic drug urokinase for breaking down of blood clots. In the ferric-chloride induced carotid artery thrombosis mouse model, we observed that treatment with TT-MB significantly reduced thrombus size after 45 min, while no significant difference was observed in the MB that were targeted but without urokinase (37 ± 6 vs. 97 ± 4, mean % change ± SEM, normalized to baseline thrombus size, $p<0.001$). The same degree of efficient thrombolysis was only achievable using a high dose of urokinase (NS). We also show that the targeting and thus clot-enrichment effect of TT-MBs results in a highly potent fibrinolysis that could only be matched using high doses of non-targeted urokinase. However, the latter is associated with a highly prolonged bleeding time (79 ± 7 vs. 1079 ± 261, sec ± SEM, $p<0.001$). In contrast, TT-MB does not prolong bleeding time (NS).

Conclusions – We are able to demonstrated that activated platelet targeted microbubbles conjugated with recombinant urokinase represent a novel and unique theranostic approach to simultaneously diagnose and treat thrombosis as well as to immediately monitor success or failure of thrombolysis. This unique, non-invasive and cost effective technology holds promise for major progress towards rapid diagnosis and bleeding-free, potent therapy of the vast number of patients suffering from thrombotic diseases.

AUTHORS (LAST NAME, FIRST NAME): Wang, Xiaowei[1]; Gkanatsas, Yannik[1]; Palasubramaniam, Jathushan[1]; Hohmann, Jan David[1]; Hagemeyer, Christoph E.[1]; Peter, Karlheinz[1]

INSTITUTIONS (ALL):

1. Atherothrombosis and Vascular Biology, Baker IDI Heart andDiabetes Institute, Melbourne, VIC, Australia.

(No Image Selected)

CONTROL ID: 2219457

TITLE: Intraoperative micro-hepatocellular carcinoma detection using surgical navigation system with fluorescence molecular imaging technology

PRESENTER: Chongwei Chi

ABSTRACT BODY:

Abstract Body: Introduction: For liver cancer surgery, how to find the micro-hepatocellular carcinoma (MHCC) is a challenge to surgeons. Radiology approaches such as X-rays, computed tomography (CT), ultrasound (US), magnetic resonance imaging (MRI) and positron emission tomography (PET) have been considered for diagnosis and postoperative evaluations. However, these medical imaging methods were not applicable for intraoperative MHCC surgery. In order to assist the surgeons to precisely locate MHCC during surgery, we developed a novel surgical navigation system for real-time fluorescence molecular imaging. To prove its feasibility, the experiments on patients for detecting the MHCC in liver cancer with indocyanin green (ICG) were executed.

Methods: We used a CCD camera (MVC1500MF-M00, Microview, China) to collect near-infrared (NIR) fluorescence images. The fluorescence filter (wavelength 810nm-870nm) was fixed in front of CCD camera and C-mount lens (12.5mm, f/1.4, Pentax) was chosen. We used laser (MW-GX-785, Feimiao Technology Co., Ltd. China) to provide NIR light source. About 72 hours prior to surgery, according to liver monitoring usage of 0.5mg/kg, indocyanine green (ICG, Yichuang Pharmaceutical Co., Ltd., China), which was diluted to 5mg/ml, were intravenously injected and during surgery real-time fluorescent video images were acquired.

Results: 30 patients were included in this study. 2-5mm MHCCs were only diagnosed by our system in 4 of all patients. Furthermore, the surgeons can dissect liver tumor margins according to the guidance of our system. Compared to the current methods, one patient was diagnosed positive tumor margin by our system after the enlarge dissection and confirmed by intraoperative pathology verification. No allergic reactions were reported after the injection of ICG.

Conclusions: This study demonstrates our system can achieve the precision detection of MHCC during surgery.

AUTHORS (LAST NAME, FIRST NAME): Chi, Chongwei[1]; Liu, Bing[2]; Fang, Cheng[3]; Yang, Xin[1]; Fang, Chihua[3]; Dong, Jiahong[2]; Tian, Jie[1]

INSTITUTIONS (ALL):

1. Institute of Automation, Chinese Academy of Sciences, Beijing, China.
2. Hospital and Institute of Hepatobiliary Surgery, Chinese PLA General Hospital, Beijing, China.
3. Department of Hepatobiliary Surgery, Zhujiang Hospital, Southern Medical University, Beijing, China.

In 30 liver cancer cases, there were 4 cases, whose small tumor lesions only detected by our system.

From Zhujiang hospital

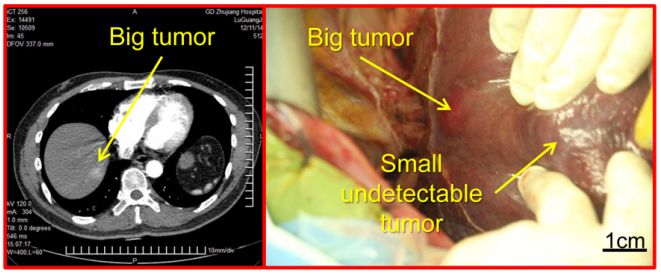

CT cannot find small tumor

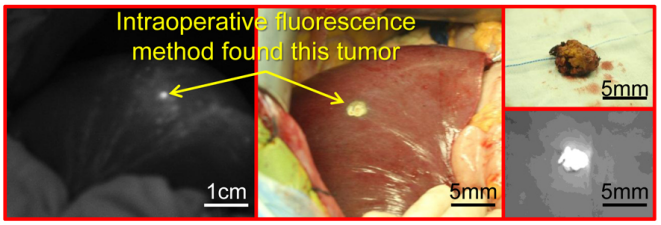

Molecular specific method found small tumor

CONTROL ID: 2244674

TITLE: Disease Screening Pill: *In Vivo* Demonstration of an Orally Available Near-Infrared Molecular Imaging Agent for Early Diagnosis of Cancer Using Mouse Xenografts

PRESENTER: Greg Thurber

ABSTRACT BODY:

Abstract Body: The high cost and associated risks of molecular imaging techniques such as MRI, PET, and SPECT preclude their use in screening large populations for early detection of diseases such as cancer and rheumatoid arthritis. However, early detection can improve patient outcomes through increased survival and reduction in irreversible damage. In this work, **we present the first ever reported orally available molecular imaging agent for completely non-invasive screening of cancer and other inflammatory diseases.** The probe is delivered orally, absorbed into the systemic circulation, and targets diseased tissue. Near-infrared (NIR) light is shined through the skin and detected at the surface resulting in an overall method that is less invasive than a blood test. A successful disease screening pill requires an optimal balance between three competing factors: high oral bioavailability, efficient *in vivo* targeting, and ideal optical properties for non-invasive imaging. Unfortunately, there are direct trade-offs between these properties. High bioavailability typically requires high lipophilicity and low molecular weight, while high targeting efficiency often benefits from low lipophilicity (to reduce non-specific sticking) and higher molecular weight (to increase the binding interface/affinity). We generated a series of fluorescently labeled targeting compounds with varying physiochemical properties that ranged in their oral absorption, targeting efficiency (concentration in tumor versus concentration in other organs), and optical properties (wavelength, extinction coefficient, and quantum yield). Many of these compounds failed for one or more reasons. For example, a DDAO fluorophore conjugate had high bioavailability and good targeting efficiency, but the optical properties did not allow whole animal imaging. A sulfo-Cy7 conjugate had excellent targeting efficiency and great optical properties, but the oral bioavailability was less than 1%. Fortuitously, the compound with the highest bioavailability was the second most efficient targeting agent, and the excitation and emission wavelengths are at the ideal far end of the NIR spectra (750-850 nm). This agent has 70% bioavailability in mice and results in raw target to background ratios in tumor xenograft models averaging greater than 4 (and as high as 8) after oral gavage with relatively low doses (less than or equal to 1 mg/kg). Biodistribution data show the tumor has the highest %ID/g of all organs, indicating efficient targeting and renal clearance of the agent following oral absorption. This never-before-published strategy has great potential for completely non-invasive screening for early disease detection, and we believe the lessons learned in developing this agent will be beneficial for designing novel orally available molecular imaging agents against other targets and diseases.

AUTHORS (LAST NAME, FIRST NAME): Bhatnagar, Sumit[2]; Dhingra, Kirti[2]; Liao, Jianshan[2]; Thurber, Greg M.[1]

INSTITUTIONS (ALL):

1. Chemical Engineering and Biomedical Engineering, University of Michigan, Ann Arbor, MI, United States.
2. Chemical Engineering, University of Michigan, Ann Arbor, MI, United States.

Lead Compound - Oral Delivery

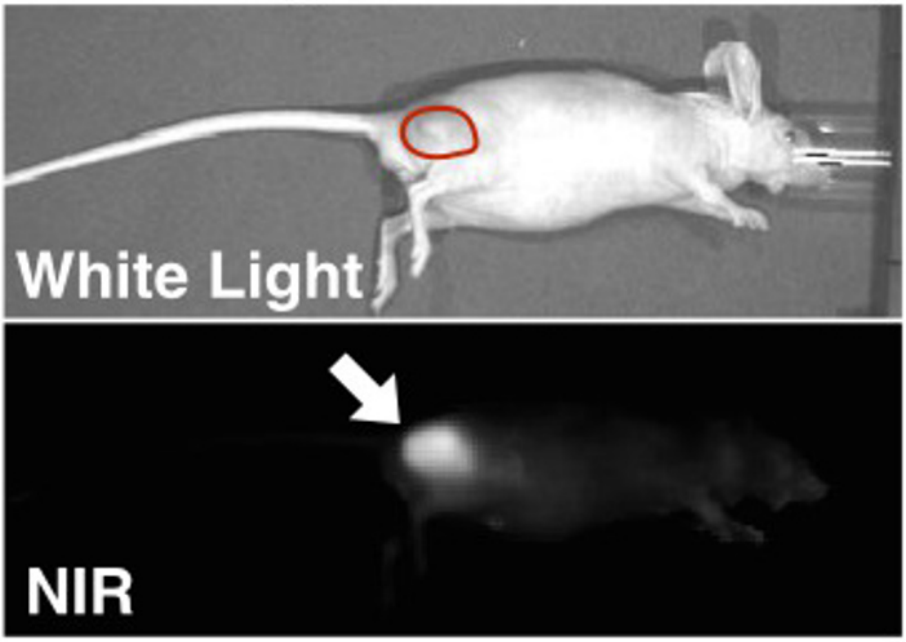

Fig. 1 - **Orally Available Near Infrared Fluorescence Molecular Imaging Agent for Disease Screening:** The lead compound has high oral bioavailability, excellent tumor targeting following oral garage (raw TBR >= 4), and optical properties in the ideal 750-850 nm window. The white light image has the tumor circled in red (top), while the NIR fluorescence image (bottom) shows the high tumor uptake (arrow) after 24 hrs.

CONTROL ID: 2206396

TITLE: Not all DTC patients with N positive disease deserve the attribution “high risk”. Contribution of the MSDS trial

PRESENTER: Alexis Vrachimis

ABSTRACT BODY:

Abstract Body: Background and Objectives: To investigate if patients having N1a disease are at the same risk with N1b using the collective of the well-defined European prospective Multicentre Study Differentiated Thyroid Cancer (MSDS).

Methods: Overall (OS) and event free survival (EFS) were calculated. Cox multivariable regression analysis was performed in order to calculate Hazard ratios (HR).

Results: EFS was significantly decreased only in patients with N1b metastasis as compared to N0 patients and became worse when N1a was concomitantly affected. A superior survival in favor of N1a patients as compared to N1b patients with regard to EFS was also observed. The patients having N1a disease showed no differences in the EFS as compared to N0. OS did not differ significantly in any of the groups. There was an increased HR for events with regards to histology, T-stage, tumor size, UICC stage, recurrent laryngeal nerve palsy and cervical lymph node metastasis. Tumor size showed a significantly increased risk for OS.

Conclusions: Patients with pT3b and pT4a tumors with N1b are of higher risk for relapse, albeit not affecting overall survival. Patients with N1a are of no higher risk. The risk stratification of these patients may be adapted accordingly.

AUTHORS (LAST NAME, FIRST NAME): Vrachimis, Alexis[1]; Wenning, Christian[1]; Riemann, Burkhard[1]

INSTITUTIONS (ALL):

1. Nuclear medicine, University Hospital of Muenster, Muenster, Germany.

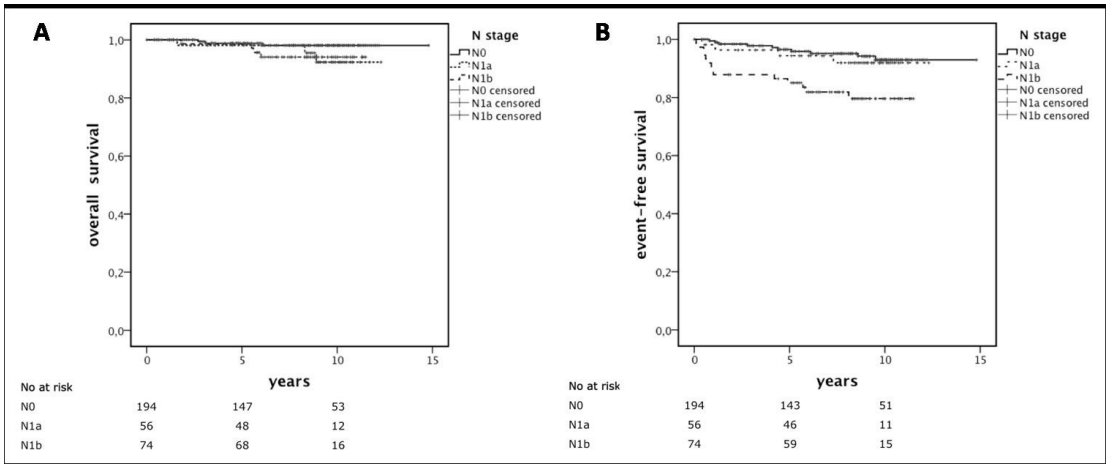
A
overall survival
1,0
0,8
0,6
0,4
0,2
0,0
0
5
10
15
years
N stage
N0
N1a
N1b
N0 censored
N1a censored
N1b censored
No at risk
N0 194 147 53
N1a 56 48 12
N1b 74 68 16
B
event-free survival
1,0
0,8
0,6
0,4
0,2
0,0
0
5
10
15
years
N stage
N0
N1a
N1b
N0 censored
N1a censored
N1b censored
No at risk
N0 194 143 51
N1a 56 46 11
N1b 74 59 15

CONTROL ID: 2206423

TITLE: The survival-paradox of patients with differentiated thyroid cancer

PRESENTER: Alexis Vrachimis

ABSTRACT BODY:

Abstract Body: The aim of this study was to compare the overall survival of a large single center cohort of patients with differentiated thyroid cancer (DTC) to that of a matched general population.

Methods: We have analyzed 2428 consecutive patients with DTC, who underwent treatment from 1965 to 2013 at the Department of Nuclear Medicine of the University Hospital of Münster (Germany) according to international standards. Patients were classified using the current 7^{th} edition of the AJCC/UICC classification system. The overall survival of the patients was compared to the expected survival of the general population based on age and sex as provided by the Federal Statistical Office of Germany.

Results: Compared to the expected survival, stage I patients paradoxically have a significantly better overall survival ($p < 0.001$). Furthermore, the results of previous studies showing a worse survival rate for patients ≥ 45 years with distant metastasis, yet no worse survival rates in all other patients, were confirmed.

Conclusion: Using one of the largest single center DTC-databases known, we were able to confirm the excellent overall survival rates of patients with DTC, with the exception of the patients ≥45 years diagnosed with distant metastases. Additionally we could demonstrate for the first time that stage I patients have a longer life expectancy than the general population in Germany.

AUTHORS (LAST NAME, FIRST NAME): Vrachimis, Alexis[1]; Wenning, Christian[2]; Schäfers, Michael[1]; Riemann, Burkhard[3]

INSTITUTIONS (ALL):

1. Nuclear medicine, University Hospital of Muenster, Muenster, Germany.
2. Nuclear Medicine, University Hospital Münster, Muenster, Germany.
3. Nuclear Medicine, University Hospital Münster, Münster, Germany.

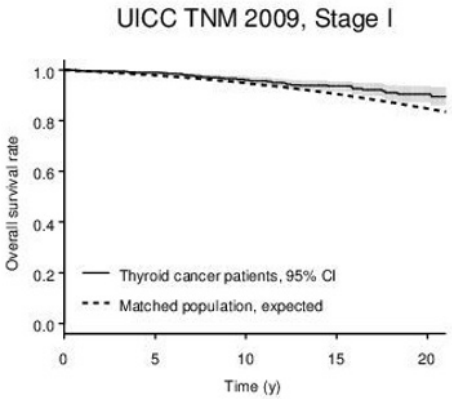
UICC TNM 2009, Stage I
Overall survival rate
1.0
0.8
0.6
0.4
0.2
0.0
0
5
10
15
20
Time (y)
Thyroid cancer patients, 95% CI
Matched population, expected

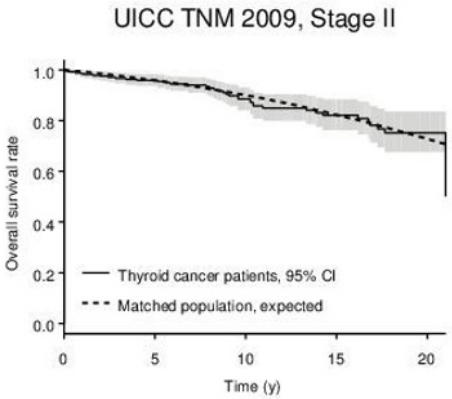
UICC TNM 2009, Stage II
Overall survival rate
1.0
0.8
0.6
0.4
0.2
0.0
0
5
10
15
20
Time (y)
Thyroid cancer patients, 95% CI
Matched population, expected

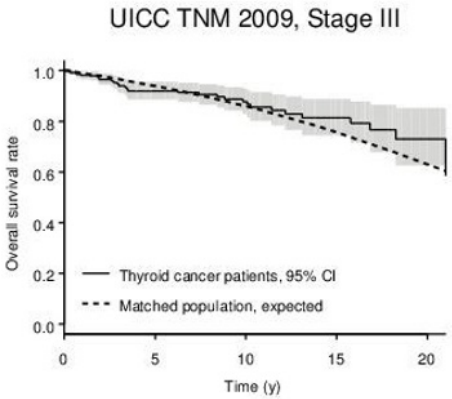
UICC TNM 2009, Stage III
Overall survival rate
1.0
0.8
0.6
0.4
0.2
0.0
0
5
10
15
20
Time (y)
Thyroid cancer patients, 95% CI
Matched population, expected

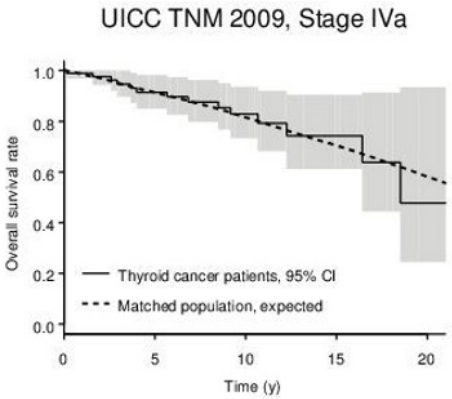
UICC TNM 2009, Stage IVa
Overall survival rate
1.0
0.8
0.6
0.4
0.2
0.0
0
5
10
15
20
Time (y)
Thyroid cancer patients, 95% CI
Matched population, expected

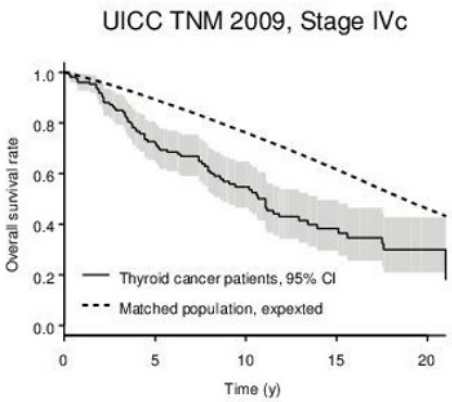
UICC TNM 2009, Stage IVc
Overall survival rate
1.0
0.8
0.6
0.4
0.2
0.0
0
5
10
15
20
Time (y)
Thyroid cancer patients, 95% CI
Matched population, expexted

CONTROL ID: 2232360

TITLE: Investigation of Cancer Vaccine Formulations Using MRI and PET/CT

PRESENTER: Christa Davis

ABSTRACT BODY:

Abstract Body: **Introduction:** Understanding the mechanism of action of cancer immunotherapies is crucial to their development and clinical application, particularly since traditional metrics for evaluating treatment success (i.e. tumor regression) may not apply. Previously, we evaluated the biodistribution of vaccine components in a novel immunotherapy, DepoVax^{TM}, using superparamagnetic iron oxide (SPIO) and MRI. This work uses MRI to evaluate the effect of vaccine formulation on tumor response and antigen distribution, and employs PET/CT to evaluate metabolic responses at the vaccine site.

Materials & Methods: Female C57BL/6 mice (4-6 weeks old) were implanted with $5x10^5$ C3 cells subcutaneously (s.c.) into the left flank. 5 days post-implantation, mice were vaccinated with 5ug of SPIO-R9F antigen in 100µl of one of three formulations (n=18): group 1 received DepoVax (DPX), group 2 received a squalene oil-in-water emulsion (SQUAL) and group 3 received a saponin/liposome adjuvant (SAP/LIP). Mice were imaged once prior to implantation, then weekly for four weeks. A b-SSFP sequence on a 3T preclinical MRI was used to image tumors, the site of injection (SOI), and both inguinal lymph nodes simultaneously. Two mice from each group also received weekly ^{18}FDG PET/CT scans, centered on the same FOV as MRI.

Results: The SAP/LIP group had the highest average post-study tumor volume, and DPX mice consistently had lower tumor volumes, but they were not significantly different. In the SAP/LIP group, two mice had ulcerations at the SOI one week post-vaccination, requiring immediate termination, while two others had visible swelling. No other mice had SOI reactions.

MRI: Hypointensity was visible at the SOI in all mice throughout the study. DPX and SQUAL mice showed sustained antigen clearance from the SOI over 4 weeks. For SAP/LIP mice, a strong hyperintensity surrounded the antigen, likely edema from an overstimulatory immune response (correlating with physical observation). This reaction decreased over time, disappearing by week 4. Antigen (in the form of hypointense spots) was visible in the right draining inguinal lymph node (RLN) for DPX and SQUAL mice, but not in SAP/LIP mice, which had regions of hyperintensity in the RLN for two weeks post-vaccination. MR volumetry revealed moderate swelling of the RLN in DPX mice that may be correlated with treatment success, but no swelling in the RLN for group 2 mice. For SAP/LIP, the RLN underwent extreme growth, peaking at >800% at 10 days post-injection and remaining enlarged through week 4

PET-CT: Persistent FDG activation was seen at the vaccine site in at least one of 2 DPX mice throughout the study, but was only visible in the SQUAL mice at 10 days post-injection. SAP/LIP mice had strong FDG activity for up to 10 days post-injection, but disappeared by week 4.

Conclusions: MRI and PET-CT indicated biological differences between vaccine formulations which may be linked to their immunostimulatory response and mechanism of action. This improved understanding of immunotherapies may aid in their future development and has important implications on the safety and immunological activity of the various adjuvant formulations.

AUTHORS (LAST NAME, FIRST NAME): Davis, Christa B.[1, 4]; Stanley, Olivia[1]; Stanford, Marianne M.[3]; Weir, Genevieve[3]; Mansour, Marc[3]; Bowen, Chris[1, 4]; Brewer, Kim[1, 2]

INSTITUTIONS (ALL):

1. Biomedical Translational Imaging Centre, Halifax, NS, Canada.
2. QEII Health Sciences Centre, Halifax, NS, Canada.
3. Immunovaccine Inc, Halifax, NS, Canada.
4. IWK Health Centre, Halifax, NS, Canada.

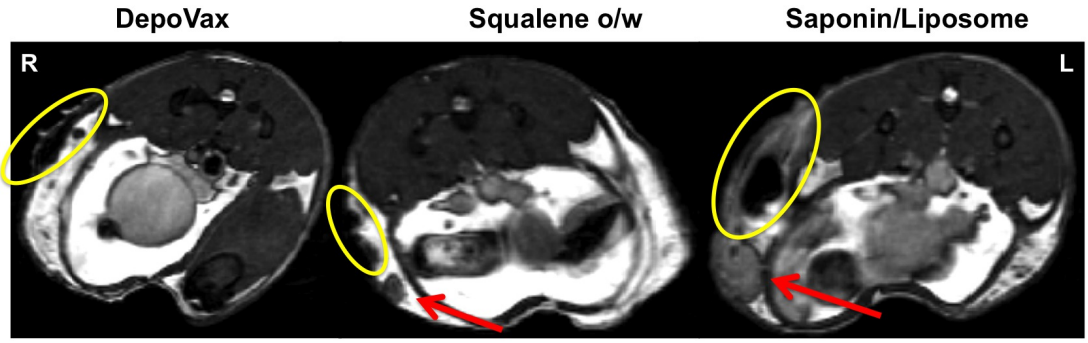

Figure 1 – MR Images of vaccine sites for a representative mouse from each group ~10 days post-injection. Yellow circles indicate vaccine site, red arrow indicates draining inguinal lymph node (RLN).

CONTROL ID: 2233505

TITLE: Bone formation is induced in mouse calvarial defects after transplanting mesenchymal stem cells with CMKLR1 knockdown

PRESENTER: Kim Brewer

ABSTRACT BODY:

Abstract Body: Bone is a dynamic tissue that undergoes continual remodeling through resorption of old bone by osteoclasts and subsequent formation of new bone by osteoblasts. Chemerin is an adipocyte-derived signaling protein that activates chemokine-like receptor 1 (CMKLR1), a G protein-coupled receptor expressed by various cell types within the bone including adipocytes, osteoblasts, osteoclasts, mesenchymal and hematopoetic stem cells. Previously, we identified chemerin/CMKLR1 signaling as a regulator of osteoblast and osteoclast differentiation. Specifically, knockdown of CMKLR1 expression induced osteoblast differentiation accompanied with loss of adipocyte differentiation in mouse bone marrow mesenchymal stem cells (MSCs). Herein we examined the clinical relevance of modulating CMKLR1 expression in MSCs as a therapeutic approach to repair defective bones in mice. We used short hairpin RNA (shRNA) delivered by adenoviral vectors to knockdown CMKLR1 in MSCs (CMK^{kd}MSCs). MSC with LacZ knockdown ($LacZ^{kd}$MSCs) were used as a control. We designed mouse bone defect models with either critical size defects by surgical methods or progressive bone erosions by injecting lipopolysaccharide (LPS) at weekly intervals. The surgically created large bone defects were filled with either $LacZ^{kd}$MSCs or CMK^{kd}MSCs seeded collagen scaffolds. The mice were anaesthetised and examined for bone regeneration on the calvarial defects by m-CT analysis at 0, 2, 4 and 6 weeks following the surgical procedure. In the calvarial bone erosion model, LPS (10 mg/kg, s.c.) was injected over the calvarial region at weekly intervals and $LacZ^{kd}$MSCs or CMK^{kd}MSCs ($1x10^6$ cells in 0.2 ml PBS/mouse) were injected intravenously through the tail vein on day 8 following the first injection of LPS. The mice were examined for the severity of erosive bone phenotype by m-CT analysis at weeks 0, 2, 3 and 4 following the first injection of LPS. We found that the CMK^{kd}MSCs improved bone regeneration within the calvarial defects and reduced lipopolysaccharide (LPS)-induced bone erosions on calvariae as indicated by improved bone volume, calvarial thickness and bone mineral density. Taken together, these findings indicate that loss of CMKLR1 expression in MSCs could provide a novel approach to the treatment of disorders of bone loss such as osteoporosis.

AUTHORS (LAST NAME, FIRST NAME): Muruganandan, Shanmugam[2]; Davis, Christa B.[1, 3]; Bowen, Chris[1, 3]; Brewer, Kim[1]; Sinal, Christopher[2]

INSTITUTIONS (ALL):

1. Biomedical Translational Imaging Centre, Halifax, NS, Canada.
2. Pharmacology, Dalhousie University, Halifax, NS, Canada.
3. IWK Health Centre, Halifax, NS, Canada.

Systemic Administration of CMKLR1 Knockdown MSCs Reduces Bone Erosion in Local Bone Resorption Model.

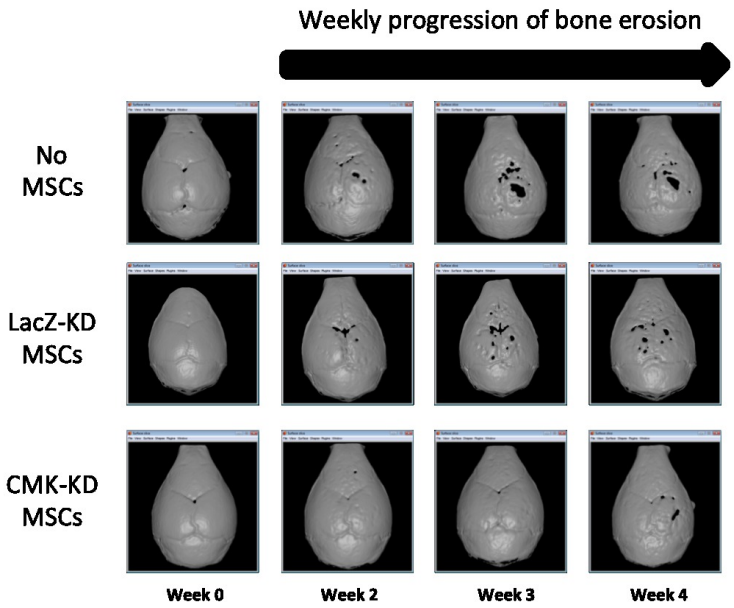

CONTROL ID: 2227837

TITLE: Spatially Resolved Quantification of Gd (III)-based Magnetic Resonance Agents in Tissue by MALDI Imaging Mass Spectrometry after in vivo MRI

PRESENTER: Moritz Wildgruber

ABSTRACT BODY:

Abstract Body: Purpose: To evaluate MALDI Imaging for spatially resolved ex-vivo quantification of a gadolinium-based Magnetic Resonance Agent in correlation to in-vivo Magnetic Resonance Imaging.

Materials and Methods: In-vivo deposition of Gadofluorine M was investigated in a mouse model of myocardial infarction. Mice were investigated by in-vivo MRI at 7T at 6h, 24h and 48h after injection of 0.2mmol/kg Gadofluorine M. Delayed enhancement was detected in the infarct scar using a conventional FLASH technique and quantified by calculating signal- and contrast-to-noise ratios. Additionally T1 mapping studies were performed using a snapshot technique. Animals were sacrificed after each time point and hearts were prepared for quantitative assessment by MALDI Imaging.

Results: Delayed enhancement imaging revealed signal enhancement in the myocardial scar beginning at 6h after Gadofluorine M injection with peak enhancement at 24h hours and residual enhancement at 48h post injection. Contrast-to-noise ratios were highest at 24h post injection due to high agent accumulation in the infarct and low signal from the blood. R1 values in the infarct were highest at 6h and steadily decreased at 24h and 48h post injection. MALDI Imaging was able to corroborate the in-vivo imaging results and enabled in-situ quantification of the in-vivo applied Gadolfuorine M with high spatial resolution.

Conclusion:
MALDI Imaging is able to provide a mass-spectrometry based quantification of gadolinium containing contrast agents in tissue with high spatial resolution. MALDI determined gadolinium concentration correlate with SNR and r1 values of in-vivo MRI. For the first time quantitative ex-vivo validation of in-vivo contrast agent distribution is possible.

AUTHORS (LAST NAME, FIRST NAME): Wildgruber, Moritz[1]; Aichler, Michaela[2]; Huber, Katharina[3]; Schilling, Franz[4]; Kosanke, Katja[5]; Lohoefer, Fabian[6]; Meier, Reinhard[7]; Rummeny, Ernst J.[8]; Walch, Axel K.[9]

INSTITUTIONS (ALL):

1. Department of Radiology, TU München, München, Germany.
2. Research Unit Analytical Pathology, Helmholtz Zentrum Muchen, Oberscheissheim, Germany.
3. Helmholtz Zentrum Muchen, Oberscheissheim, Germany.
4. Nuclear Medicine, TU Munchen, München, Germany.
5. TU Munchen, München, Germany.
6. Radiology, TU Munchen, München, Germany.
7. Radiology, University of Ulm, München, Germany.
8. Radiology, TU Munchen, München, Germany.
9. Research Unit Analytical Pathology, Helmholtz Zentrum München , Oberscheissheim, Germany.

MALDI Imaging of Gadofluorine

Chemical structure of Gadofluorin M

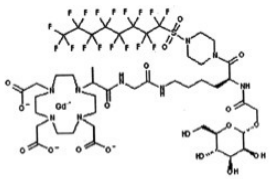

Mass spectrum of a Gadofluorin M analysis

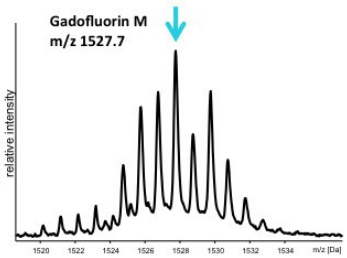

Magneic Resonance Imaging of Gadofluorine M in infarcted myocardium

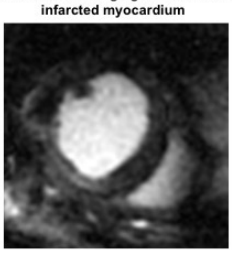

Post-portem spatially resolved quantification of contrast agent

MALDI Imaging mass spectrometry of Gadofluorin M

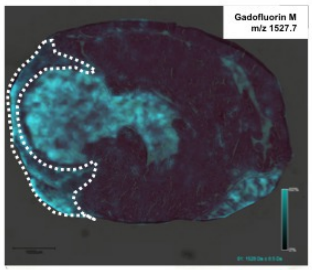

Ex-vivo validation of in-vivo imaging

CONTROL ID: 2227817

TITLE: Intravital visualization and quantification of thrombotic processes based on non-linear microscope

PRESENTER: Satoshi Nishimura

ABSTRACT BODY:

Abstract Body: The cellular mechanisms associated with cardiovascular events remains unclear, largely because of an inability to directly visualize and evaluate thrombus formation in living body. Thus, we developed in vivo imaging technique based on multi-photon microscopy and light-manipulation technique to reveal the multicellular processes during thrombus development.

We visualized the cell dynamics in single platelet levels, and assessed thrombus formation processes using three animal models.

First, we induced rapidly developing thrombi composed of discoid platelets, which was triggered by ROS stimulation by photo-chemical reactions. In this model, thrombus development was mainly dependent on P-selectin and GPIIbIIIa activations, and we also elucidated the contribution of Lnk (adapter protein) for the stabilization of developing thrombus. The functional properties including activation, aggregation, and fibrinogen binding were different between ‘newer’ and ‘aged’ platelets in developing thrombus. We quantified three-dimensional thrombus volume changes and leukocyte recruitment steps by custom software for objective evaluation with high reproducibilities.

In the second model, thrombus formation was induced by endothelical cell disruption by laser irradiations. With the rapid recruitment of inflammatory leukocytes into damaged area, fibrin net formation and tissue regenerative changes were also observed. TLR4 signaling contributed to these steps, and pretreatmet of LPS markedly enhanced inflammatory reactions.

In last model, spontaneous platelet aggregations were induced by transient ischemia and reperfusions. Ly6G+ Ly6C+ CD11b+ cells recruited from bone marrows to ischemic areas.

AUTHORS (LAST NAME, FIRST NAME): Nishimura, Satoshi[1]

INSTITUTIONS (ALL):

1. the Univ of Tokyo, Jichi Med Univ, Tokyo, Japan.

1st mode: ROS induced platelet aggreations

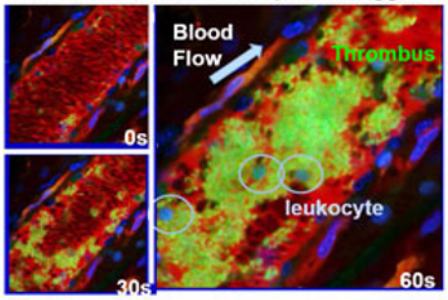

2nd model: laser endothelium injury

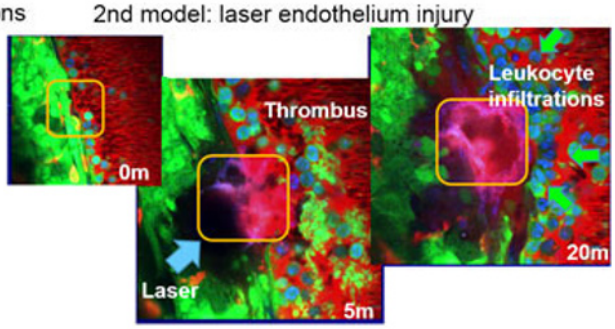

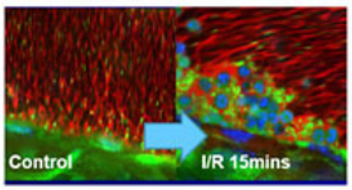

3rd model:

Ischemia and reperfusion

green:CAG-eGFP:platelet
blue:Hoechst:leukocyte
red:dextran:blood flow

CONTROL ID: 2227823

TITLE: The novel and acute rupture-like thrombopoiesis processes from bone marrow megakaryocyte is regulated by IL-1alpha

PRESENTER: Satoshi Nishimura

ABSTRACT BODY:

Abstract Body: Blood platelets are generated in the bone marrow (BM) from their precursors, megakaryocytes (MK). Although we know that MKs produce platelets throughout life, precisely how platelets are produced in vivo remains uncertain, largely because of the rarity of MKs in the BM and the lack an adequate visualization technique. To clearly understand the nature of thrombopoiesis in BM MKs, we optimized an in vivo imaging technique based on two-photon microscopy that enabled us to visualize living BM in CAG-, CD41-, and/or PF4- enhanced green fluorescent protein (eGFP) mice. By visualizing living bone marrow in vivo, we observed that a second thrombopoietic process, 'rupture'-like MK fragmentation, can be ongoing simultaneously with previously identified 'proplatelet formation' in the same mouse BM. Short proplatelets predominated in the steady state, but highly elongated proplatelets were apparent when thrombopoietin (TPO) levels were high (e.g., after BM transplantation). Conversely, following blood loss, 5-FU administration, antibody-based platelet depletion or acute inflammation, there was accelerated release of larger platelets from mature MKs mediated via the interleukin-1 (IL-1)alpha-type1 IL-1 receptor axis and ERK-dependent MK apoptosis. Moreover, microtubule assembly contributed to proplatelets in TPO-stimulated MKs but did not in IL-1alpha-stimulated MKs due to uncoordinated expression of alpha- and beta-tubulin. We also evaluated the functional instability of plasma membrane after IL-1alpha treatment in MKs using atomic-force microscopy and FRAP analysis. These findings support the idea that IL-1alpha acts acutely as a platelet releasing factor, coordinating with TPO to dynamically modulate the cellular programming of MKs that regulates platelet counts.

AUTHORS (LAST NAME, FIRST NAME): Nishimura, Satoshi[1]

INSTITUTIONS (ALL):

1. the Univ of Tokyo, Jichi Med Univ, Tokyo, Japan.

(No Image Selected)

CONTROL ID: 2227812

TITLE: Smart DCM-Based Fluorescence Probes for Cerebral β-Amyloid Plaques

PRESENTER: Yan Cheng

ABSTRACT BODY:

Abstract Body: In vivo detection of cerebral β-amyloid (Aβ) plaques may facilitate the monitoring of β-amyloidosis in the brain and effectiveness of anti-amyloid therapies. In the study, a series of DCM-based fluorophores with push-pull electronic structure were synthesized and evaluated as novel fluorescence probes for optical imaging of cerebral Aβ plaques. These fluorophores were proved to have high affinity to Aβ plaques in fluorescent staining of brain sections from an APP/PS1 transgenic mouse, as well as in fluorescence binding assay using $Aβ_{1-42}$ aggregates. Upon mixing with $Aβ_{1-42}$ aggregates, these fluorophores displayed a turn-on effect, showing significant enhancement in fluorescence. These fluorophores penetrated the blood-brain barrier of normal brain efficiently with high initial brain uptake and rapid washout after intravenous injection. In vivo imaging with these fluorophores showed higher fluorescence signals in the brain area of APP/PS1 transgenic mice than that of the age-matched controls. Ex vivo study confirmed substantial labeling of Aβ plaques in brain tissue from APP/PS1 transgenic mice but not in the age-matched controls. Thus, these smart DCM-based fluorophores could be potentially selected for the detection of Aβ plaques both in vitro and in vivo.

AUTHORS (LAST NAME, FIRST NAME): Cheng, Yan[1]; Zhang, Zhirong[1]

INSTITUTIONS (ALL):

1. Sichuan University, Chengdu, China.

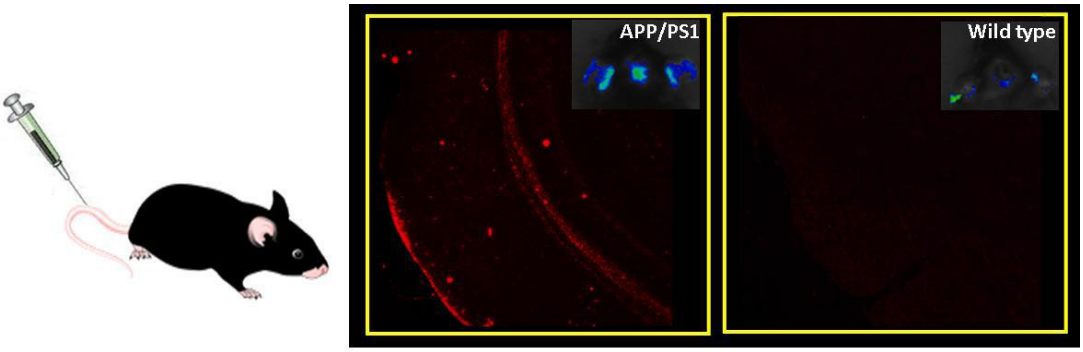
APP/PS1
Wild type

CONTROL ID: 2229182

TITLE: Altered $GABA_A$ receptor function by the administration of tiagabine in the rat brain: [^{18}F]Flumazenil PET study using a bolus plus constant infusion protocol

PRESENTER: Wook Kim

ABSTRACT BODY:

Abstract Body: Enhanced synaptic GABA concentration by the administration of selective GABA transporter reuptake inhibitor resulted in increased binding affinity of the $GABA_A$ receptor antagonist (termed 'GABA shift'). We assessed GABA shift by a $GABA_A$-targeting drug, tiagabine, using [^{18}F]Flumazenil (FMZ) PET with bolus plus constant infusion (B/I) protocol in an attempt to develop a single session imaging technique for GABA-targeting drug development.

The determination of K_{bol} was preceded before the PET studies with B/I protocol. In the 90 min B/I scan session, tiagabine (10 mg/kg) was intravenously injected after the baseline scan. [^{18}F]FMZ binding potential (BP_{ND}) before and after the tiagabine injection were calculated using a model-independent method, then regional brain BP_{ND} change (%) was calculated. The single bolus [^{18}F]FMZ PET studies were followed with pretreatment of tiagabine to validate the feasibility of the B/I protocol.

[^{18}F]FMZ distribution in the target (frontal cortex) and reference tissue (pons) reached rapidly equilibrium by K_{bol} = 20 min. The greatest $\%BP_{ND}$ change was shown in the thalamus (16.8%), which was followed by the frontal cortex (9.2%), striatum (9.2%), hippocampus (8.8%) and superior colliculus (5.5%) after tiagabine administration. Brain regional BP_{ND} and $\%BP_{ND}$ changes were comparable across the injection protocols.

Data demonstrated that [^{18}F]FMZ PET study with B/I of K_{bol} = 20 min is reliable to assess altered $GABA_A$ receptor function induced by tiagabine administration in the rat brain. These results may help to improve the efficiency of the development of new GABA-targeting drugs in the preclinical stage using [^{18}F]FMZ PET.

AUTHORS (LAST NAME, FIRST NAME): Kim, Wook[2]; Park, Hyun Soo[2]; Jung, In Soon[1]; Moon, Byung Seok[1]; Lee, Byung Chul[1]; Kim, Sang Eun[1]

INSTITUTIONS (ALL):

1. Department of Nuclear Medicine, Seoul National University Bundang Hospital, Seoul National University College of Medicine, Seoul, Korea (the Republic of).

2. Department of Transdisciplinary Studies, Graduate School of Convergence Science and Technology, Soul National Unversity, Soul, Korea (the Republic of).

(No Image Selected)

CONTROL ID: 2227805

TITLE: AS1411 aptamer guided QD655 labeled DNA Origami working as a novel nanoprobe for fluorescence molecular imaging in breast tumor mouse model

PRESENTER: Yang Du

ABSTRACT BODY:

Abstract Body: Aims: DNA-based nanostructures have been widely utilized in various applications due to their structural diversity, programmability and uniform structures, and their intrinsic biocompatibility and biodegradability further motivates the investigation of DNA-based nanostructures as delivery vehicles. DNA origami nanostructures exhibited great potential application in molecular imaging, targeted payload delivery and controlled drug release. AS1411 is a DNA aptamer that specifically binds to the nucleolin, a protein highly expressed in the plasma membrane of cancer cells and has been successfully exploited as a targeting ligand for tracking tumor cells. The aim of this study is to create a novel fluorescence imaging probe by assembling QD655 onto the surface of AS1411 aptamer conjugated DNA origami delivery system, which may facilitate a more efficient and specific accumulation of probes at the tumor sites in vivo with improved fluorescence imaging of tumors.

Methods: Human MDA-MB-231 breast tumor bearing nude mice were used, and AS1411-QD655-DNA Origmai probes were injected intravenously. Small animal optical molecular imaging system (IVIS Imaging System, Caliper, USA) was used for animal fluorescence imaging acquisition. Imaging was performed before injection and 1 h, 4 h, 6 h, 12 h and 24 h after probe injection.

Results: The result showed that there was no fluorescence signal in the control group, and the QD655 signal was distributed allover the mouse body without specific accumulation at the tumor site in the free QD655 treated group during the whole 24 h obesrvation. In the QD655 labeled DNA origami (QD655/DO) treated tumor bearing mouse, the strong fluorescence can be detected both in the liver and tumor sites 1-6 h after injection, and then the signal gradually decreased at both sites thereafter. While in the AS1411 aptamer guided QD655 labeled DNA origami (QD655/DO-AS1411) treated mice, we found that the signal can be detected both in the liver and tumor sites 1 h after injection, and then stronger and more specific signal can be detected at the tumor site and decreased signal in the liver tissues 4-24 h postinjection. Moreover, the strong fluorescence signal of tumors can be maintained till 24 h. It suggested that through specific binding to the nucleolin expressed in the cytoplasm of cancer cells, AS1411 aptamer can promote the diffusion of QD655 labeled DNA origami nanoparticles to the tumorous mass and facilitated targeted molecular imaging of tumors in vivo.

Conclusion: Incorporating AS1411 aptamers into DNA origami leads to enhanced intracellular uptake by cancer cells, achieved the improved targeted imaging of tumors in vivo. Furthermore, fluorescence labeled and aptamer-displaying DNA origami can further work as imaging guided nanoparticle for tumor therapy. These findings reinforce the potential of DNA-based nanostructures for theranostic applications.

AUTHORS (LAST NAME, FIRST NAME): Du, Yang[1]; Zhang, Qian[1]; Tian, Jie[1]

INSTITUTIONS (ALL):

1. Chinese Academy of Sciences, Institute of Automation, Beijing, China.

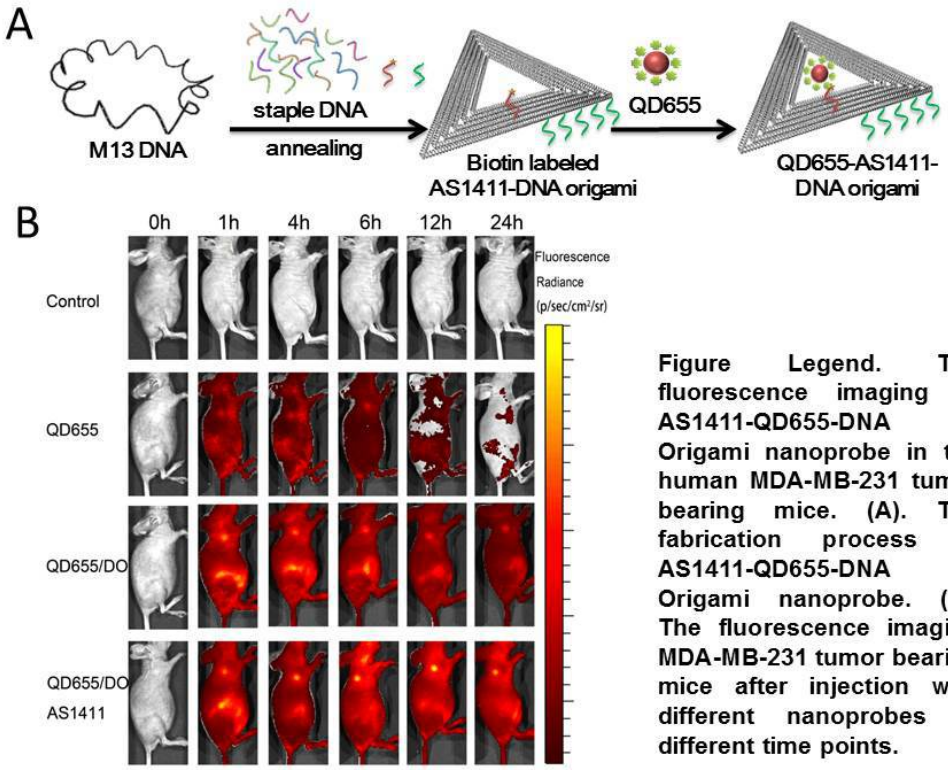

Figure Legend. The fluorescence imaging of AS1411-QD655-DNA Origami nanoprobe in the human MDA-MB-231 tumor bearing mice. (A). The fabrication process of AS1411-QD655-DNA Origami nanoprobe. (B). The fluorescence imaging MDA-MB-231 tumor bearing mice after injection with different nanoprobes at different time points.

CONTROL ID: 2195829

TITLE: **^{18}F-Albumin PET imaging detects efficacy of the targeted angiogenesis inhibitor, sunitinib (RTK) in human glioblastoma (U87-MG) tumors**

PRESENTER: Elaine Jagoda

ABSTRACT BODY:

Abstract Body: Objectives: ^{18}F Albumin (FALB) may have clinical utility as an imaging agent for measuring tumor angiogenesis and monitoring responses to targeted anti-angiogenic therapies by quantitation of the tumor's distribution volume (tDV). FALB has exhibited appropriate in vivo blood retention and stability in rats allowing for quantitation of normal tissue blood volumes and thus may have potential for quantifying cancerous lesions (Basuli F, *Nucl Med Biol* 42, 2015). In initial studies FALB was evaluated in various human derived tumor mouse xenograft models and found to have tDVs consistent with histological determined levels of vascularization suggesting that FALB may offer real time readouts of the angiogenic status of tumors as well as changes due to treatment. In these studies the capability of FALB to detect tumor angiogenic inhibition resulting from sunitinib treatment was evaluated in a U87-MG (U87) mouse xenograft model. RTK treated (TX) and controls (Co) xenografts were imaged weekly for changes in FALB tDVs and tumor physical volumes (tPV) were determined. **Methods:** FALB was synthesized via coupling of ^{18}F-2, 3, 5, 6-tetrafluorphenyl 6-fluornicotinate to rat albumin. U87 xenografts treated with the RTK (TX), or Co were imaged (BioPET, 60 min post FALB injection, IV) before treatment (Day 0) and then at Day (D) 7, 14, and 21 post treatment. Tumor DVs were calculated: NAU_{tumor}/ NAU_{blood} (Normalized Activity Units = **[**ROIs (µCi, whole tumor or blood (heart left ventricle)) x body weight]/[ROI volume (cm^3) x injected dose (µCi)**]**. At the same time as imaging tumor PVs were determined by caliper and used to calculate % tPV increases from baseline for each time (**[**tPV_{day}- $tPV_{baseline}$**]** / [$tPV_{baseline}$]). At D21 after FALB imaging biodistributions were done with TX and Co groups from which tumor DVs were calculated ($\%ID/g_{tissue}$/ $\%ID/g_{blood}$). TX and Co tumors were then sectioned to determine blood vessel counts by CD31 IHC.

Results: PET images of U87 xenografts exhibited high FALB retention in the blood allowing for visualization of the left ventricle of the heart from which the FALB blood concentrations (NAU_{blood}) were determined; tumors were discernible and ROIs included the FALB content for the entire tumor (NAU_{tumor}) which was then used for determining the tDV (Figure 1). Significant decreases of 39%, 56%, and 43% in mean FALB tDVs were observed in the TX vs Co groups at D7 and D14 and D21, respectively (Table 1). Tumor volumes (% tPV from baseline) were significantly decreased 29% and 33% at D14 and 21, respectively in TX vs Co but not at D7 (39%)(Table 1). D21 biodistribution FALB tDVs were significantly decreased (44%) in TX vs Co comparing favorably with the imaging results. Vessel counts (IHC) from the D21 tumor sections were decreased in TX vs Co confirming the imaging results. **Conclusions**: FALB was able to detect efficacy of an anti-angiogenic inhibitor as early as 7 days after treatment in U87 tumors whereas significant changes in tumor volumes were observed later at 14 days. These data suggest that FALB imaging may better detect early changes in tumor angiogenesis, thereby providing a more sensitive readout of therapeutic responses.

AUTHORS (LAST NAME, FIRST NAME): Jagoda, Elaine[1]; Kuo, Frank[1]; Basuli, Falguni[2]; Williams, Mark[1]; Wong, Karen J.[1]; Green, Michael[1]; Seidel, Jurgen[1]; Adler, Stephen[1]; Xu, Biying[2]; Choyke, Peter L.[1]

INSTITUTIONS (ALL):

1. Molecular Imaging Program, NCI, Bethesda, MD, United States.
2. Imaging Probe Development Center, NHLBI, Bethesda, MD, United States.

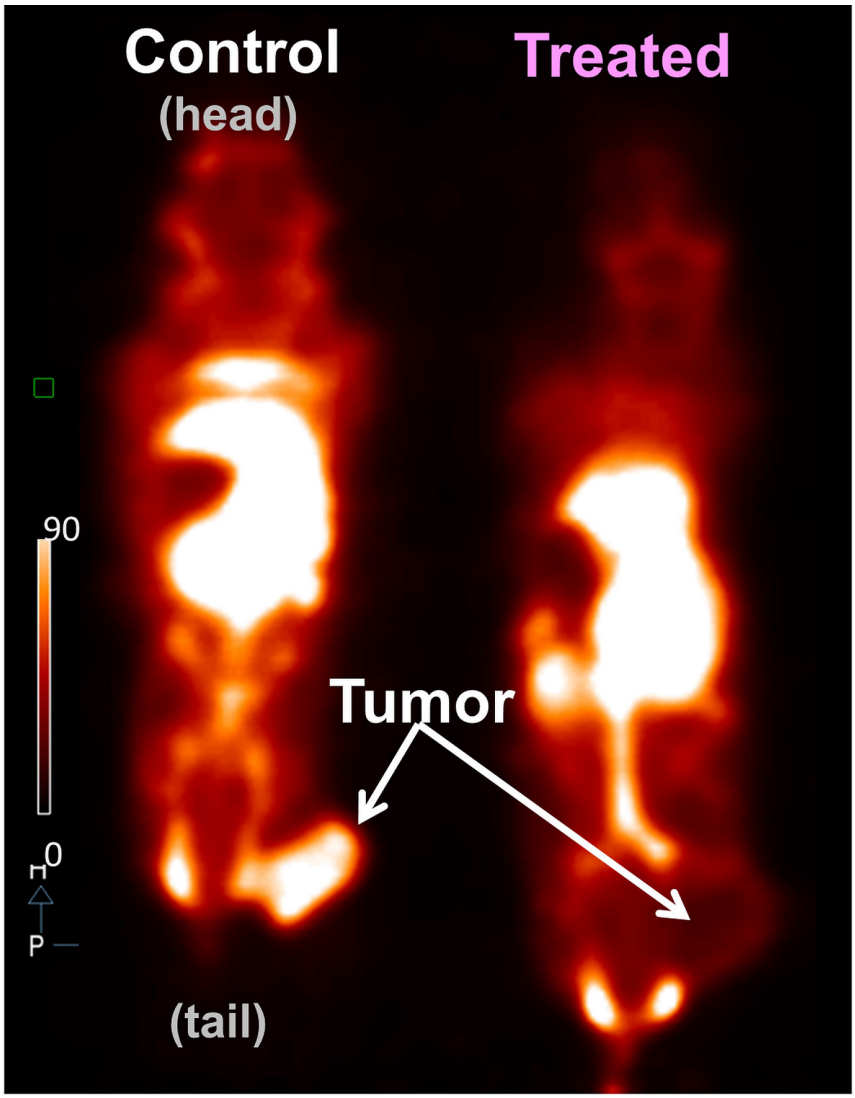

Fig.1. Representative coronal images of a control and sunitinib treated mouse with U87-MG tumors (right thigh) at 7 days post treatment; images were obtained 60 min after injection of ^{18}F-Albumin (~ 300 µCi, IV).

CONTROL ID: 2229263

TITLE: Integrin $\alpha_2\beta_1$ targeting PET imaging as a prognostic biomarker of malignant non-small Lung cancer in vivo: comparison with ^{18}F-FDG

PRESENTER: Shih-Ting Hsu

ABSTRACT BODY:

Abstract Body: Introduction

Lung cancer is by far the most common and leading cause of cancer-related death among both men and women worldwide. The ectopic overexpression of integrin $\alpha_2\beta_1$ has been implicated in giving untransformed lung cancer cells both tumorigenic and metastatic potential.[1] Therefore, the development of integrin $\alpha_2\beta_1$ targeted agent may significantly increase the delivery efficacy and detection specificity towards various lung cancer types increased with their malignancy level.

Methods

To prospectively verify the prognostic value of integrin $\alpha_2\beta_1$, the *in vitro* western blot was performed to validate the integrin expression level of human non-small lung cancer cells (CL1-0, CL1-5 and A549). Then, both ^{18}F-FDG and ^{68}Ga labeled integrin $\alpha_2\beta_1$ (^{68}Ga-A2B1) PET imaging studies of A549 non-small lung cancer xenograft mice (n=3) were performed at either 45min (^{18}F-FDG) or 15min (^{68}Ga-A2B1) post-injection after injection of 7-8MBq tracers. The non-tumor ROIs was determined in the contralateral tumor region manually. The biodistribution of tracers was also determined at 60 min post-injection in tumor-bearing athymic mice. The average radioactivities of regions-of interest (ROIs) were determined by multiple regions of interest volumes manually using 50% of maximum minus minimum %ID/g value within a tumor or an organ. The average radioactivity accumulation within a tumor or an organ was further analyzed in accordance with the pathologic data.

Results

Extremely high expression level of integrin $\alpha_2\beta_1$ correlated with tumorigenic potential among selected lung cancer cells (A549 > CL1-5 > CL1-0) in western blot results justifies its role as a potential prognostic marker. Although, the ^{68}Ga-A2B1 tracer uptake in malignancies (A549) was 0.44 SUVmax (n=3), the ratios of tumor/muscle (T/M) was 2.01 making the tumor is clear visible; in contrast, the accumulation of 18F-FDG can reach 0.61 SUVmax (n=3) but due to the high background uptake the T/M value is only 1.17 and almost invisible under the PET imaging analysis; These results suggest that there are significant differences in ^{68}Ga-A2B1 accumulation when comparing with the clinical usage 18F-FDG PET tracer, and these differences might offer a critical diagnostic imaging criterion in the identification of aggress phenotype of lung cancer. Thus, the non-invasive detection of integrin $\alpha_2\beta_1$ activity in vivo may serve as a valuable biomarker for overcoming the confusing false positive (negative) of FDG-PET scan by bring in the more specific tracer uptake.

Conclusion

Compared with 18F-FDG tumor uptake, the integrin $\alpha_2\beta_1$ tracer ^{68}Ga-A2B1 is more subjectively adequate in evaluation of the integrin profiling in staging of non-small lung cancer, which represents a highly sensitive and useful PET imaging agent for evaluation of disease course and therapeutic efficacy at the earliest stages of treatment.

Reference:

Gogali A et. al, Integrin receptors in primary lung cancer. Exp Oncol. 2004 Jun;26(2):106-10. Review.

AUTHORS (LAST NAME, FIRST NAME): Hsu, Shih-Ting[2]; Hsieh, Wen-Chuan[2]; Chung, Yi-Hsiu[2]; Chiu, Han[2]; Chang, Wen-Chi[2]; Yen, Tzu C.[1, 2]; Huang, Chiun-Wei[2]; Huang, Feng-Ting[3]

INSTITUTIONS (ALL):

1. Department of Nuclear Medicine, Chang Gung Memorial Hospital, Taoyuan, Kueishan, Taiwan.
2. Center for Advanced Molecular Imaging and Translation, Tao-yuan, Taiwan.
3. Biochemical Science and Technology, National Taiwan University, Taipei, Taiwan.

(No Image Selected)

CONTROL ID: 2232542

TITLE: Prognostic evaluation of PET/MR imaging with [68Ga]-DOTA-A2B1 in gliomas

PRESENTER: Chiun-Wei Huang

ABSTRACT BODY:

Abstract Body: Introduction

Despite recent advances in diagnostic and therapeutic techniques, prognosis of patients with many brain tumors, and particularly malignant gliomas, remains dismal. This reflects in part the diagnostic uncertainty in identifying infiltrative tumor growth of malignant gliomas which in turn affects subsequent treatment strategies. Besides, the difficulty in delineating brain tumor margins during the surgery is a major obstacle in the path toward better outcomes for patients with brain tumors. Hence, the early detection of glioma tumor and its phenotype change might possess prognostic value for better arrangement of patients.

Methods

Positron emission tomography (PET) imaging can noninvasively monitor molecular function in vivo using suitable radiolabeled tracers. Despite targets' high specific uptake, the nuclear imaging only reveals low anatomical details. To overcome this, a quantitative technique to image both structure and function by combining PET and magnetic resonance (MR) imaging might open a window to verify tumor morphology and stage more precisely. Herein, the PET/MR hybrid brain tumor imaging were performed with novel integrin α2β1 targeting PET tracer ([68Ga]-DOTA-A2B1)[1] in orthotopic U-87MG glioma xenograft mice (n=5; integrin α2β1-positive) and the tumor regions of interest (ROIs) was determined by manually 50% of maximum minus minimum tumor activity. The non-tumor ROIs was determined in the contralateral tumor region manually. The tumor volume was calculated by length*width*height*π/6 inT2-weighted MR images. The combined PET/MR imaging data were analyzed to provide unique diagnostic parameter such as aggressive potential, which may reflect histological changes during the tumor growth.

Results

The [68Ga]-DOTA-A2B1 PET tracer longitudinally demonstrated prominent tumor uptake in orthotopic U-87MG xenografts along with the steady growth of tumor size monitoring with MR imaging. The tracer uptake in malignancies were 0.30+/-0.05, 0.34+/-0.05 and 0.58+/-0.11 (%ID/g) at day 7, day 14 and day 21, respectively. Furthermore, due to the low normal brain uptake background, the tumor contrast ratio of tumor/contralateral region increased significantly from 2.22 (day 7) to 2.80 (day 14) and 3.11 (day 21), which can achieve precise whole brain tumor localization for preoperative planning and delineate the tumor margins with high sensitive and high spatial resolution from con-registeered PET/MR imaging data.

Conclusion

These results suggest that there is significant uptake in [68Ga]-DOTA-A2B1 accumulation along with the tumor growth monitoring by MR imaging. The specific uptake might offer a critical diagnostic imaging criterion in the identification of aggress phenotype of gliomas. Thus, the non-invasive detection of integrin α2β1activity in vivo may permit a more precise definition of the roles of integrin α2β1 in tumor progression stages and yield insight regarding novel therapeutic strategies in molecular level.

Reference:

1. Chung YH et. al., "Evaluation of Prognostic Integrin α2β1 PET Tracer and Concurrent Targeting Delivery Using Focused Ultrasound for Brain Glioma Detection ",2014 Nov, 3;11(11):3904-14 Mol Pharm.

AUTHORS (LAST NAME, FIRST NAME): Chiu, Han[1]; Hsieh, Wen-Chuan[1]; Hsu, Po-Hung[3]; Chung, Yi-Hsiu[1]; Chang, Wen-Chi[1]; Hsu, Shih-Ting[1]; Huang, Feng-Ting[4]; Yen, Tzu C.[2]; Huang, Chiun-Wei[1]

INSTITUTIONS (ALL):

1. Center for Advanced Molecular Imaging and Translation, Chang Gung Memorial Hospital, Taoyuan, Taiwan.
2. Department of Nuclear Medicine, Chang Gung Memorial Hospital, Taoyuan, Kueishan, Taiwan.
3. Electrical Engineering, Chang Gung University, Tao-Yuan, Taiwan.
4. Biochemical Science and Technology, National Taiwan University, Taipei, Taiwan.

(No Image Selected)

CONTROL ID: 2205054

TITLE: Development of a PET/OMRI combined system for simultaneous imaging of positron and free radical probes in small animals

PRESENTER: Seiichi Yamamoto

ABSTRACT BODY:

Abstract Body:

Positron emission tomography (PET) has high sensitivity for imaging the radioactive tracer distribution in subjects. However it is not possible to image the free radical distribution in subjects by PET. The Overhauser enhanced MRI (OMRI) is so far an only method to image the free radical distribution in vivo. Combining PET and OMRI will become possible to simultaneously image the radioactive tracer and free radical distributions in subjects. For this purpose, we developed a PET/OMRI combined system for small animals.

PET/OMRI combined system consists of an optical fiber based small animal PET system combined with a permanent magnet based OMRI system. The optical fiber based PET system used flexible optical fiber bundle. In the input surface, LGSO scintillators of 0.025 mol% (decay time:~31ns: 0.9mm x 1.3mm x 5mm) and 0.75 mol% (decay time:~46ns: 0.9mm x 1.3mm x 6mm) were optically coupled in depth direction to form depth-of-interaction (DOI) detector, arranged in 11 x 13 matrix and optically coupled to the fiber bundle and coupled to a Hamamatsu 1-inch square position sensitive photomultiplier tube (PSPMT). Eight optical fiber based block detectors (16 LGSO blocks) were arranged in a 56mm diameter ring to form a PET system. The LGSO blocks were located inside the field-of-view (FOV) of OMRI and the PSPMTs were positioned outside the OMRI to minimize the interference between PET and OMRI.

The OMRI system used 0.0165T permanent magnet with resonance frequency of 0.7 MHz for nuclear magnetic resonance (NMR) and 670MHz for electron spin resonance (ESR). The system has an ESR coil to enhance the MRI signal by the use of Overhause effect to image the free radical in the field-of-view of the PET/OMRI system. For measuring the OMRI image, ESR RF pulses are irradiated just before the MRI sequences to the subject. The ESR coil has a 20mm diameter single ring surface coil located inside the MRI receiver coil. These coils were set inside the optical fiber PET system for simultaneous imaging of PET and OMRI.

Spatial resolution and sensitivity of the optical fiber based PET system were 1.2mmFWHM and 1.2% at the central FOV, respectively. The OMRI system could image the distribution of nitroxyl radical solution. Simultaneous imaging of positron radiotracer (Na-22) and nitroxyl radical solution was possible with the developed PET/OMRI system.

We could successfully develop a PET/OMRI combined system. The system has a potential to provide interesting results with the simultaneous imaging of positron tracers and free radical distribution in small animals.

AUTHORS (LAST NAME, FIRST NAME): Yamamoto, Seiichi[1]; Watabe, Tadashi[2]; Ikeda, Hayato [2]; Kanai, Yasukazu [2]; Ichikawa, Kazuhiro[3]; Nakao, Motonao [4]; Kato, Yoshinori[1]; Hatazawa, Jun[2]

INSTITUTIONS (ALL):

1. Nagoya University Graduate School of Medicine, Nagoya, Japan.
2. Osaka University, Suita, Osaka, Japan.
3. Kyushu University, Fukuoka, Japan.
4. Japan REDOX, Fukuoka, Japan.

(No Image Selected)

CONTROL ID: 2230236

TITLE: Intestinal fatty acid uptake is not enhanced in diabetic and hypercholesterolemic animals; validation study with positron emission tomography

PRESENTER: Henri Honka

ABSTRACT BODY:

Abstract Body: *Background and aims* Intestine, its endogenous metabolism and gut microflora have gathered considerable interest in the regulation of intermediary metabolism (1-3). The aims of the present study was to validate the feasibility of palmitate analogue 14(R,S)-[^{18}F]fluoro-6-thia-heptadecanoic acid ([^{18}F]FTHA) and positron emission tomography (PET) for the measurement of intestinal fatty acid fluxes, and to determine the physiological distribution of fatty acids in the gut wall in a rodent model.

Materials and methods Four healthy (strain C57BL/6N) and four obese diabetic and hypercholesterolemic (strain IGF-II/LDLR$^{-/-}$ApoB$^{100/100}$) mice aged six months were studied during fasting state. Four mice (two controls, two obese) were orally administered with 15MBq of [^{18}F]FTHA mixed with 20% Intralipid solution, and four mice (two controls, two obese) received a 15MBq bolus of [^{18}F]FTHA in saline intravenously. After 155±41 and 31±1.0 minutes (for p.o. and i.v., respectively), mice were sacrificed and abdominal cavity was accessed. Small intestine, liver, and skeletal muscle *ex vivo* tissue radioactivity concentration in %ID g^{-1} was measured using γ-counter and normalized to plasma level of free fatty acids (expressed as mM %ID g^{-1}). Tracer distribution within the gut wall was visualized and quantified by means of autoradiography and photostimulated luminescence per area (PSL/mm^2). To explore dynamics of fatty acid uptake within the intestine, one obese mouse was anesthetized after oral tracer administration and whole-body PET acquisition was performed for three hours (frames 36 × 5 minutes) using a combined PET/CT scanner.

Results During PET-scan, intestinal radioactivity was rapidly increased and reached a plateau at 150 minutes post-administration. After oral administration, small intestinal fatty acid uptake was highest in the duodenum (16.1±8.4 mM %ID g^{-1}), and decreased in anterograde fashion in jejunum and ileum (4.7±3.5 and 4.0±5.1 mM %ID g^{-1}, respectively; both $P < 0.05$ *vs.* duodenum). Whereas hepatic and skeletal muscle fatty acid uptake differed between oral/intravenous routes of administration (26.8±11.5 *vs.* 3.2±1.1 mM %ID g^{-1} and 1.5±0.5 *vs.* 0.3±0.2 mM %ID g^{-1}, respectively; both $P < 0.01$), no difference was seen in duodenum, jejunum and ileum (all $P > 0.05$). Small intestinal fatty acid uptake was similar in obese and healthy mice. In both routes of administration, autoradiography analysis showed preferential uptake of [^{18}F]FTHA in the mucosal layer with mucosa:non-mucosa PSL-ratios ranging between 1.9 and 3.3 (all $P < 0.01$).

Conclusions Our results revealed that PET coupled with intravenous [^{18}F]FTHA administration is a feasible method to investigate small intestinal fatty acid metabolism *in vivo*, offering a valuable tool for the investigation of obesity-related metabolic diseases, and the effects of bariatric surgery (4). Enterocyte layer accounts for a majority of gut wall fatty acid fluxes during fasting and postprandial state.

References 1. Lin & Sun, J Endocrinol 2010, 2. Delzenne et al., Nat Rev Endocrinol 2011, 3. Holst et al., Mol Cell Endocrinol 2009, 4. Saeidi et al., Science 2013.

AUTHORS (LAST NAME, FIRST NAME): Honka, Henri[1]; Ståhle, Mia[1]; Liljenbäck, Heidi[1]; Jauhiainen, Matti[2]; Sarja, Nina[1]; Ylä-Herttuala, Seppo[3]; Nuutila, Pirjo[1, 4]; Roivainen, Anne[1, 5]

INSTITUTIONS (ALL):

1. Turku PET Centre, University of Turku, Turku, Finland.
2. Public Health Genomics Unit, National Institute for Health and Welfare, Helsinki, Finland.
3. A.I. Virtanen Institute for Molecular Sciences, University of Eastern Finland, Kuopio, Finland.
4. Department of Endocrinology, Turku University Hospital, Turku, Finland.
5. Turku Center for Disease Modeling, University of Turku, Turku, Finland.

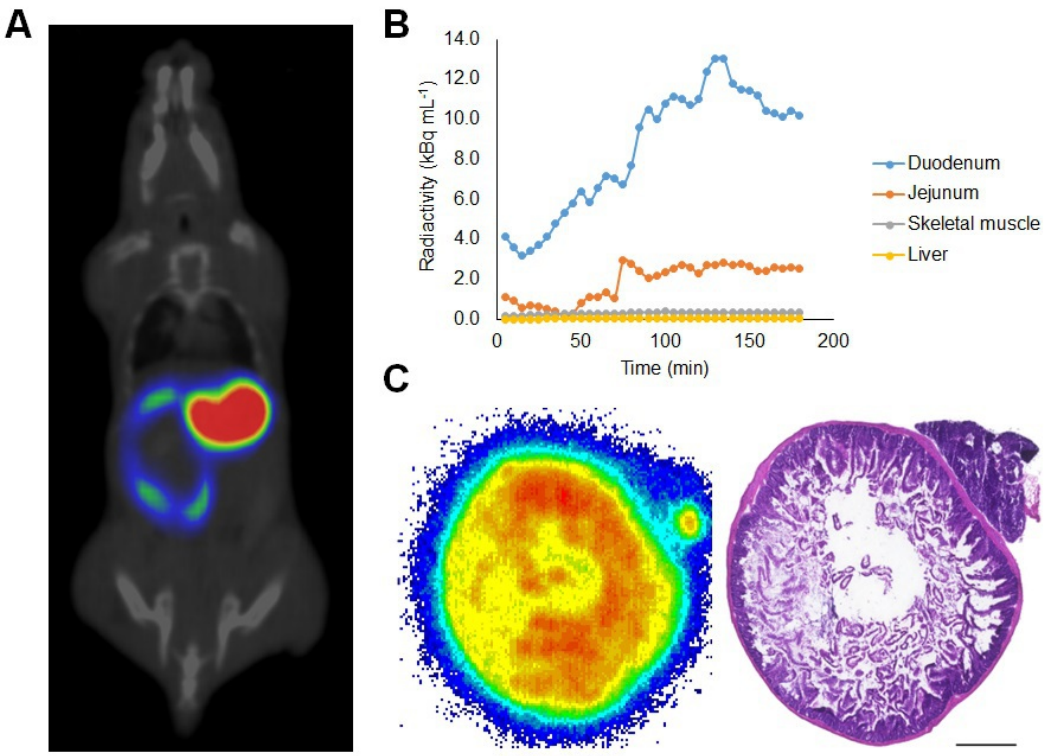

Figure 1. Kinetics of orally administered [^{18}F]FTHA in a rodent model. To ascertain adequate time of sacrifice, a whole-body PET/CT acquisition was performed for one mouse (A). Intestinal radioactivity progressively increased, and reached a plateau at 100-150 minutes post-administration, whereas hepatic and skeletal muscle remained nearly inactive for the whole imaging period (B). In the autoradiography analysis enterocyte layer accounted for 74-94% of gut wall [^{18}F]FTHA derived radioactivity highlighting it's importance in the regulation of intestinal fatty acid fluxes (Scalebar 500 µm; ^{18}F-ARG and hematoxylin-eosin stained sample of duodenum) (C).

CONTROL ID: 2233716

TITLE: Engineering of a multi-functional nucleolin-targeted nucleic acid delivery system

PRESENTER: Surong Zhang

ABSTRACT BODY:

Abstract Body: New therapeutics that target gene expression such as nucleic acid (NA) -based constructs continue to attract great interest due to their promise for attenuating the expression of “non-druggable” disease-associated targets. However, the implementation of these new therapies is complicated due to the inefficient delivery of engineered NAs to the target tissues and cells mainly due to the inability to pass across the plasma membrane. Here we report the design and synthesis of a novel delivery system based on chemically modified gold nanoparticles (GNPs) for delivery of a NA-based compound (signal transducer and activator of transcription 3 decoy oligonucleotide (STAT3d)) that has previously shown effectiveness in the treatment of head and neck squamous cell carcinoma (HNSCC).

We engineered three stable GNP-based NA systems by forming Au-S bond between ODN and GNP. The three GNP constructs are: 1) nucleolin aptamer (NUAP) and control aptamer (CTAP) with GNP; 2). STAT3-bearing GNP (STAT-GNP) and control STAT3 decoy-bearing GNP (COTR-GNP); 3). GNPs containing both NA and STAT3 decoy (NUAP-GNP-STAT, CTAP-GNP-STAT). To ensure that obtained GNP-based systems can be tracked in vitro while the fluorescence of NA/STAT-GNP is minimally affected by the surface of GNP we conjugated fluorescent dyes AF488, Cy5.5 or 800CW to the 5’-end of ODNs.

The NA/STAT3-GNP constructs were characterized by UV/VIS and photon correlation spectroscopies as well as transmission electron microscopy (TEM). The diameters of engineered ODN-GNP constructs varied from 18.21nm to 71.43nm. Zeta potential of ODN-GNP constructs were a little more negative than original GNP citrate. The integrity of ODNs linked to GNPs was demonstrated by using gel electrophoresis (Fig. 1). The total amount of bound ODN on GNP was determined using the difference between added ODN and free ODN after sedimenting the obtained GNPs. The shorter ODN (18 bases) (STAT-GNP 46.07%, COTR-GNP 27.75%) was binding to GNPs more efficiently than the longer one (32 bases) (NUAP-GNP 2.5%, CTAP-GNP 10.3%). NUAP-GNP showed low stability against aggregation. However, when NUAP and STAT were added together to GNPs, the yield was increased and the number of NUAP (49) ODNs exceeded the number of STAT(17). The average total number of ODNs linked to GNP was approximately 100.

Cytotoxicity study showed no toxicity of aptamers, decoy duplexes and GNP constructs in all cell lines tested (A431, OVCAR3, MCF-10A and FaDu). The HNSCC cell line FaDu was confirmed to have nucleolin on its cell surface by immunofluorescence and Western blotting.

We expected to observe NUAP aptamer binding to cell-surface expressed nucleolin in vitro. The cell-binding study revealed that NUAP had much higher uptake by the cells than control aptamer CTAP. NUAP-GNP has almost the same strong binding at 4-times lower concentration of ODN than that of NUAP alone. The further study will focus on the efficacy of STAT3 decoy duplex and the NA-GNP-STAT3d system in attenuating STAT3d-mediated gene expression in HNSCC cell lines and testing the combined effect of STAT3d and GNP-mediated radiosensitization on the viability of HNSCCs in culture.

AUTHORS (LAST NAME, FIRST NAME): Zhang, Surong[1]; Gupta, Suresh[1]; Bogdanov, Alexei A.[1]

INSTITUTIONS (ALL):

1. UMASS Medical School, Worcester, MA, United States.

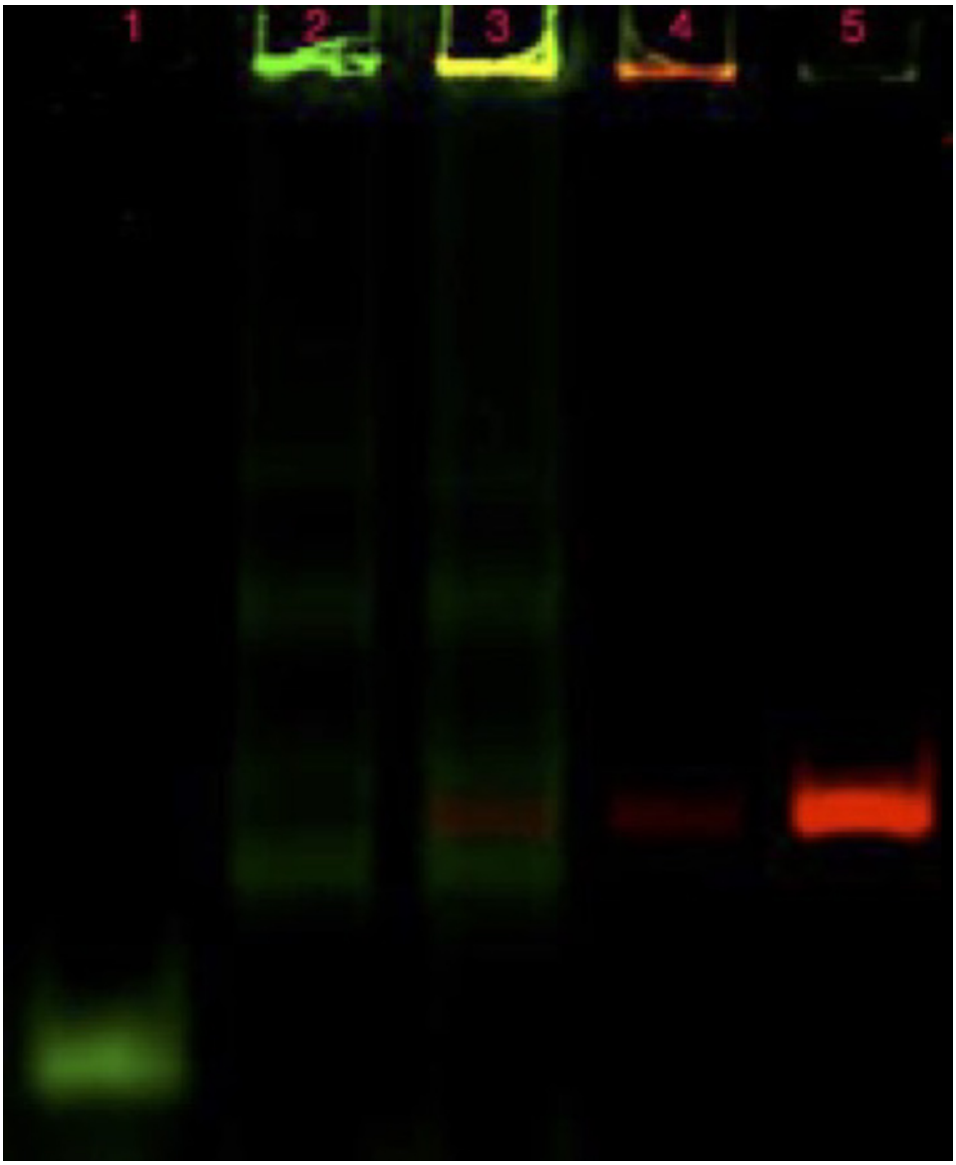

ODN/GNP constructs gel electrophoresis (10% TBE gel). From left to right, lane 1: STAT-800CW; 2: STAT (800CW)-GNP; 3: CTAP(Cy5.5)-GNP-STAT(800CW); 4: CTAP (Cy5.5)-GNP; 5: CTAP-Cy5.5.

CONTROL ID: 2231326

TITLE: Cherenkov-excited luminescence scanned imaging (CELSI) for high-resolution, deep-tissue, *in vivo* optical molecular imaging

PRESENTER: Rongxiao Zhang

ABSTRACT BODY:

Abstract Body: Cherenkov emission (Cherenkov, 1938) during radiation therapy can be utilized to excite optical molecules (Demers, et al. 2013; Zhang, et al. 2013; Zhang, et al. 2012). In this study, a new imaging modality is introduced, based upon Cherenkov-excited luminescence scanned imaging (CELSI) which was demonstrated by using a 5 mm thick line-excitation megavoltage X-ray beam (6 MV) collimated by the multi-leaf collimator (MLC) of a linear accelerator (LINAC) and was scanned in 3 orthogonal directions. The spatial resolution of the imaging approach is dictated by the step size of the radiation beam, not the diffuse emission of the fluorescence, allowing high resolution imaging through thick animal tissues. The scan in this demonstration was through a rat abdomen. When the lymph node had been injected with an oxygen-sensitive phosphor (Oxyphor PtG4) (Esipova, et al. 2011), which has strong luminescence lifetime which is sensitive to the local oxygen concentration. During the scanning, Cherenkov-excited luminescence was continuously integrated by an intensified charge-coupled device (ICCD) synchronized to radiation pulses (Andreozzi, et al. 2015; Glaser, et al. 2012), and the position of the total signal was back-projected to the position of the scanning beam.

Typical reconstruction of diffusive optical signals emitted from turbid medium is generally an ill-posed problem. But unlike optical photons, x-rays do not experience dominant scattering, and so the luminescence that was excited locally by Cherenkov had originated exclusively along the pathway of the radiation beam. By measuring total luminescence signal and utilizing the prior spatial information of scanning beam location, the distribution of optical signal along the direction of scanning can be recovered. The intensified CCD camera simply worked as a single point detector to measure the intensities of interested signals. Therefore, the distribution of optical probes could be resolved with high spatial resolution and accuracy by CELSI without complex reconstruction models or algorithms.

The additional data file shows that, based on back projections of Cherenkov excited luminescence profiles acquired from scans in three orthogonal dimensions, the lymph node was located in the axillary region. By measuring the lifetime of the excited luminescence from the located lymph node, which is correlated to the local oxygen partial pressure, deoxygenation was observed after euthanasia of the rat. Phantom studies validated that an inclusion with a size below 1 mm can be reconstructed through a layer of 20 mm thick tissue equivalent phantom material. Concentrations of PtG4 down to 100 nM were detectable and capillary tubes containing the probe with diameters down to 200 μm could be resolved by CELSI at 5 mm depth in tissue equivalent phantoms.

In conclusion, CELSI is reported here for the first time, as an innovative optical molecular imaging technique by utilizing the LINAC as an optical scanning and excitation device. Potential applications of CELSI include reconstructions of interested optical probes and recoveries of local physiological information with relatively high spatial resolution.

AUTHORS (LAST NAME, FIRST NAME): Zhang, Rongxiao[1]; DSouza, Alisha V.[4]; Gunn, Jason R.[3]; Esipova, Tatiana V.[2]; Vinogradov, Sergei A.[2]; Glaser, Adam[4]; Jarvis, Lesley A.[3]; Gladstone, David J.[3]; Pogue, Brian W.[4, 1]

INSTITUTIONS (ALL):

1. Physics and Astronomy, Dartmouth College, Hanover, NH, United States.
2. Perelman School of Medicine, University of Pennsylvania, Philadelphia, PA, United States.
3. Dartmouth-Hitchcock Medical Center, Dartmouth College, Hanover, NH, United States.
4. Thayer School of Engineering, Dartmouth College, Hanover, NH, United States.

(No Image Selected)

CONTROL ID: 2227781

TITLE: High Contrast T2 MRI Nanoprobes with Minimal Complement Activation and Immune Recognition in Mice

PRESENTER: Dmitri Simberg

ABSTRACT BODY:

Abstract Body: There is an unmet need in efficient and safe contrast agents for molecular magnetic resonance imaging of various pathologies. Dextran iron oxide nanoparticles are efficient contrast agents, but their use is associated with significant immune reactions and propensity for clearance by liver and spleen (1). Complement is the system of 30+ serum proteins that represents the first immune barrier to invading pathogens (2). The hypothesis is that complement activation could be responsible for some of the immune effects of iron oxide nanoparticles. Superparamagnetic iron oxide (SPIO) nano-worms were synthesized from ferrous and ferric chlorides and 20kDa dextran using a modified Molday method (3). The nanoparticles exhibited high molar transverse relaxivity (r2) of ~400 mM-1 s-1 but activated complement in serum as evidenced by deposition of C3b fragment (200-500 copies per nanoparticle). The nanoparticles exhibited complement dependent uptake by macrophages, neutrophils and monocytes. The mechanisms of complement activation were studied using mouse sera deficient for main complement factors. There was no C3b deposition in mannose binding lectin (MBL)-deficient sera, suggesting that nano-worms triggered complement predominantly via the lectin pathway due to the presence of dextran coating. In order to block complement activation, the dextran shell of nano-worms was further modified by a novel procedure using crosslinking-hydrogelating agent epichlorohydrin (4). The treatment resulted in complete blockade of dextran immunogenicity as measured by recognition of anti-dextran antibody. As a result, there was a 95% decrease of binding and activation of lectin complement pathway, and 90% decrease in C3b opsonization. The resulting nano-worms showed minimal recognition by peritoneal macrophages in vitro, and liver macrophages and leukocytes in vivo. Moreover, the circulation half-life of nano-worms in mice was increased 60-fold. Due to the high T2 contrast, long circulating properties and minimal immune recognition, the reported contrast agents have a potential for development as selective and specific molecular MRI probes. Moreover, this study demonstrates that understanding the mechanism of immune recognition and complement can be very useful for rational design of improved imaging agents.

References

1. Gupta, A. K.; Gupta, M. Synthesis and surface engineering of iron oxide nanoparticles for biomedical applications. Biomaterials 2005, 26, (18), 3995-4021.
2. Ricklin, D.; Hajishengallis, G.; Yang, K.; Lambris, J. D. Complement: a key system for immune surveillance and homeostasis. Nat Immunol 2010, 11, (9), 785-97.
3. Molday, R. S.; MacKenzie, D. Immunospecific ferromagnetic iron-dextran reagents for the labeling and magnetic separation of cells. Journal of immunological methods 1982, 52, (3), 353-67.
4. Holmberg, L.; Lindberg, B.; Lindqvist, B. The reaction between epichlorohydrin and polysaccharides: Part 1. Syntheses of some model substances with non-cyclic substituents. Carbohydr Res 1994, 262, (2), 213-21.

AUTHORS (LAST NAME, FIRST NAME): Wang, Guankui[4]; Moghimi, Seyed Moein[3]; Serkova, Natalie J.[2]; Simberg, Dmitri[1]

INSTITUTIONS (ALL):
1. Pharmaceutical Sciences, University of Colorado, Aurora, CO, United States.
2. Anesthesiology, University of Colorado Anschutz, Aurora, CO, United States.
3. Pharmacy, University of Copenhagen, Copenhagen, Denmark.
4. Pharmaceutical Sciences, University of Colorado, Aurora, CO, United States.

(No Image Selected)

CONTROL ID: 2227801

TITLE: Choosing the right carrier for siRNA-based therapy – a new reporter system which acts by induction of an endogenous intracellular fluorescence

PRESENTER: Wolfgang Kemmner

ABSTRACT BODY:

Abstract Body: A new detection mechanism for the control of successful siRNA delivery to cells or tissue is introduced using a siRNA-based probe that is capable of inducing a specific intracellular fluorescence emission. The last step of heme synthesis is incorporation of iron into the heme-precursor Protoporphyrin-IX (PpIX) that takes place in the mitochondria catalyzed by the enzyme ferrochelatase (FECH). Experimentally induced knock down of FECH expression in cells by RNA-interference leads to a dramatic accumulation of fluorescent PpIX (Kemmner W et al.,FASEB J, 2008). Meanwhile, we were able to demonstrate that PpIX-fluorescence within tumor tissue can be induced by FECH-siRNA carried by folate-coupled liposomes or dendritic polyglycerolamine nanoparticles (Wan K et al., Nanomedicine:NBM, 2012). PpIX-based fluorescence is excited only if the siRNA hits its target, FECH mRNA, within the cytosol. Hence, this method allows an evaluation of siRNA delivery by the detection of the newly formed PpIX-based fluorescence e.g. by flow cytometry. Due to the omnipresence of the heme synthesis pathway, targeted application of FECH-siRNA may provide a general means for cellular imaging and determination of the successful delivery of siRNA. This approach exhibits no relevant toxicity, because siRNA-silencing of FECH leads to an endogenous and non-toxic fluorescence by affecting the cellular metabolism. Specific advantages of this reporter system are the positive readout of siRNA delivery, no need for transfection of a reporter gene and no need for long and complex procedures involving transcription, translation, and posttranslational modifications of the reporter molecule itself. Carriers that are able to transport FECH-siRNA in a highly efficient manner may also be suitable for other siRNA-based probes. Thus, this novel reporter system enables selection and optimization of carriers for siRNA transport and transfection of the target tissue.

AUTHORS (LAST NAME, FIRST NAME): Kemmner, Wolfgang[1]

INSTITUTIONS (ALL):

1. ECRC at the Max Delbrueck Center, Berlin, Germany.

(No Image Selected)

CONTROL ID: 2216086

TITLE: Clinically translatable cathepsin imaging agents that exploit a latent lysosomotropic effect

PRESENTER: Matthew Bogyo

ABSTRACT BODY:

Abstract Body: Cysteine cathepsins are highly up-regulated in a wide variety of cancers, both in tumor cells and in the tumor-supporting cells of the surrounding stroma. Therefore tools that can be used to dynamically monitor their activity *in vivo* could be used as imaging contrast agents for intraoperative fluorescence imaged guided surgery (FGS). Here we describe a series of near infrared fluorogenic substrate probes for the lysosomal cathepsins and their application as contrast agent in FGS. We found that by tuning the structural and physicochemical properties of these probes and by exploitation of a latent cationic lysosomotropic effect (LLE), we could generate substrates with tumor specific activation and retention, fast activation kinetics, and rapid systemic clearance. These probes were suitable for detection of diverse cancer types including breast, colon and lung tumors. Most importantly, the agents were compatible with the existing da Vinci® surgical system for fluorescence guided tumor resection. Therefore, our data confirm that, once approved for human use, the probes reported here can be used with existing clinical instrumentation to detect tumors and potentially other types of inflammatory lesions to guide surgical decision making in real time.

AUTHORS (LAST NAME, FIRST NAME): Bogyo, Matthew[1]; Ofori, Leslie O.[1]; Withana, Nimali P.[1]; Sorger, Jonathan[2]

INSTITUTIONS (ALL):

1. Pathology, Stanford University, Stanford, CA, United States.
2. Intuitive Surgical Inc., Sunnyvale, CA, United States.

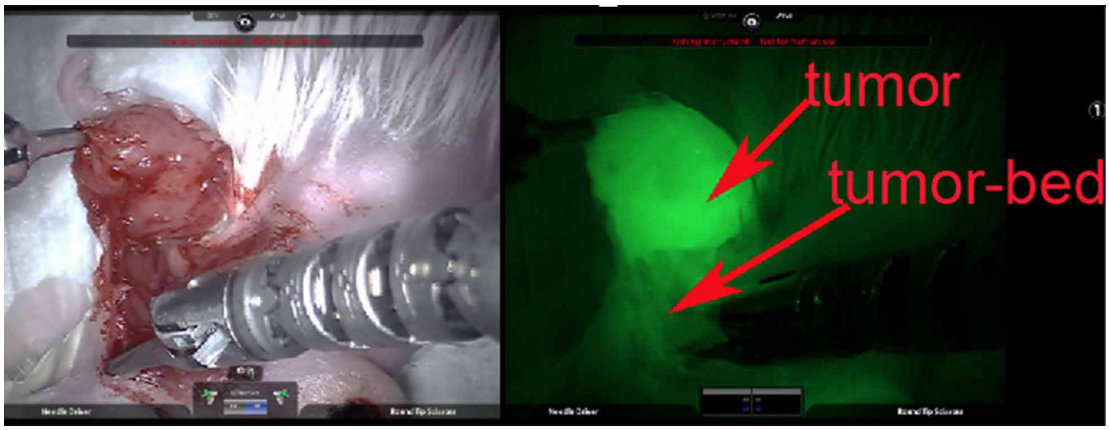

Breast tumor imaging with the da Vinci Surgical System

CONTROL ID: 2227791

TITLE: Clinically translatable cathepsin imaging agents that exploit a latent lysosomotropic effect

PRESENTER: Matthew Bogyo

ABSTRACT BODY:

Abstract Body: Cysteine cathepsins are highly up-regulated in a wide variety of cancers, both in tumor cells and in the tumor-supporting cells of the surrounding stroma. Therefore tools that can be used to dynamically monitor their activity in vivo could be used as imaging contrast agents for intraoperative fluorescence imaged guided surgery (FGS). Here we describe a series of near infrared fluorogenic substrate probes for the lysosomal cathepsins and their application as contrast agent in FGS. We found that by tuning the structural and physicochemical properties of these probes and by exploitation of a latent cationic lysosomotropic effect (LLE), we could generate substrates with tumor specific activation and retention, fast activation kinetics, and rapid systemic clearance. These probes were suitable for detection of diverse cancer types including breast, colon and lung tumors. Most importantly, the agents were compatible with the existing da Vinci® surgical system for fluorescence guided tumor resection. Therefore, our data confirm that, once approved for human use, the probes reported here can be used with existing clinical instrumentation to detect tumors and potentially other types of inflammatory lesions to guide surgical decision making in real time.

AUTHORS (LAST NAME, FIRST NAME): Bogyo, Matthew[1]; Ofori, Leslie O.[1]; Withana, Nimali P.[2]; Sorger, Jonathan[3]

INSTITUTIONS (ALL):

1. Pathology, Stanford University, Stanford, CA, United States.
2. Pathology, Stanford University, Stanford, CA, United States.
3. Intuitive Surgical, Inc., Sunnyvale, CA, United States.

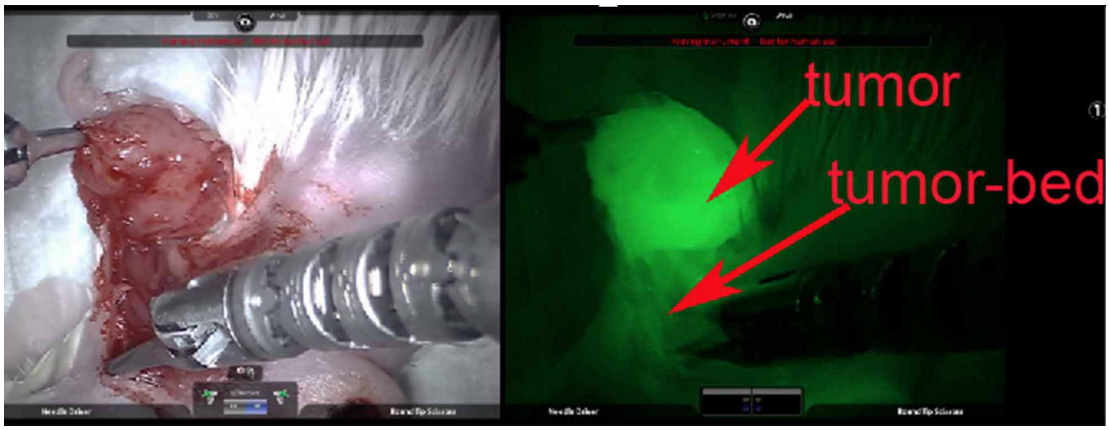
tumor
tumor-bed

CONTROL ID: 2215994

TITLE: Enhancing Cerenkov luminescence via radionuclide attachment to High Refractive Index Nanoparticles

PRESENTER: Travis Shaffer

ABSTRACT BODY:

Abstract Body: Introduction: Cerenkov luminescence (CL) is produced when a charged particle has a greater velocity than light in that particular medium. The threshold energy necessary for CL is mostly dependent on the refractive index (RI) of the medium, as expressed by the Frank-Tamm equation (**Equation 1**). As the RI of a solution or material increases, the threshold energy needed for CL is lowered, resulting in a greater percentage of emitted particles reaching this threshold. This results in an increase in CL, as shown in numerous experiments involving solutions and bulk materials. The clinical utility of CL has recently been shown using various medical radioisotopes for applications for imaging and therapy. However, the very low levels of CL is a continual challenge for in vivo use, and increasing CL output through attachment to nanoparticles with a higher RI could result in improvements in imaging and therapy that utilize CL.

Methods and Results: We recently published a general method to radiolabel silica nanoparticles (SNPs) with various medical radioisotopes without the need for a chelator[1]. The SNPs were tested in vivo via positron emission tomography (PET) imaging, which showed the stability and utility of the particles for PET imaging. Here we show SNPs, aluminum oxide nanoparticles, and titanium dioxide nanoparticles radiolabeled with yttrium-90 using our published method. These nanoparticles were chosen due to their high refractive index (1.5-2.5). Following radiolabeling, the nanoparticle solutions were imaged on a pre-clinical IVIS instrument (**Figure 1),** with regions of interest (ROIs) drawn over each well. Quantification of the total Cerenkov luminescence showed greater CL (50-150% depending on the nanoparticle) than the radioisotope in buffer, with a tissue model also showing increased CL over control solutions. This increased CL was seen both with an open filter and with emission 500-840nm(**Figure 2)**. As each of the nanoparticle constructs have a higher RI (1.5-2.5) compared to buffer (1.33), the Frank-Tamm equation predicts this increase in CL via radionuclide attachment to nanoparticles.

Conclusions: As interest in CL for medical applications increases, the strategy of radioisotope attachment to nanoparticles with high RI may become an important strategy for Cerenkov work. Additionally, the routine use of SIO_2 as a nanoparticle coating means that this method for enhancing CL can be used for an array of nanoparticles such as quantum dots. With the theoretical background established by this work, nanoparticle systems for an array of applications including photodynamic therapy, imaging, and light-activated drug release may benefit.

1. Shaffer TM, Wall MA, Harmsen S, Longo VA, Drain CM, Kircher MF*, et al.* Silica Nanoparticles as Substrates for Chelator-free Labeling of Oxophilic Radioisotopes. *Nano letters* 2015, **15**(2)**:** 864-868.

AUTHORS (LAST NAME, FIRST NAME): Shaffer, Travis[1, 2]; Pratt, Edwin C.[3]; Drain, Charles M.[2]; Grimm, Jan[1]

INSTITUTIONS (ALL):

1. Radiology, Memorial Sloan Kettering Cancer Center, New York, NY, United States.
2. Chemistry, Hunter College and the Graduate Center, City University of New York, New York, NY, United States.
3. Pharmacology and Chemistry, Weill Cornell Graduate Program, New York, NY, United States.

(No Image Selected)

CONTROL ID: 2225042

TITLE: A novel small-molecule CXCR4 PET radioligand as companion diagnostics for anti-CXCR4 therapy

PRESENTER: Yoon Hyeun Oum

ABSTRACT BODY:

Abstract Body: Objectives: CXCR4 is associated with various cancers, where it facilitates metastasis, angiogenesis, and tumor growth through the interaction with SDF-1.[1-2] Several CXCR4 antagonists have been developed to inhibit CXCR4/SDF-1 interactions and are currently under different stages of development.[3-5] In an effort to develop companion diagnostics[6] for anti-CXCR4 therapy, we designed and synthesized a novel CXCR4-targeting PET radioligand.

Methods: We have designed a novel CXCR4-PET agent (DS-219) as a companion diagnostic by combining our sulfonamide pharmacophore[7-8] with a prosthetic labeling component by virtue of click chemistry. We evaluated the binding affinity of the new compound by molecular docking and competition-binding assays using the potent peptidic antagonist (TN14003[9]). ^{18}F-labeled compound was synthesized by combining the precursor derivative with K^{18}F in the presence of K_{222}.

Results: In vitro competition studies demonstrates that DS-219 bound to CXCR4-expressing cells with low nanomolar affinity (IC_{50} = 6.9 nM) blocks TN14003 binding to CXCR4 expressing cells. Further, the Matrigel invasion assay[10] shows DS-219 bound to CXCR4 can interfere with CXCR4 function >50% at low nanomolar concentration. To determine the specificity of ^{18}F-labeled DS-219 toward CXCR4, we used competition assays against the corresponding ^{19}F derivative and CXCL12 at various concentrations. MicroPET images of [^{18}F]DS-219 in a head and neck cancer orthotopic primary tumor model as well as an experimental metastasis model reveal significant radioactivity in the tumors.

Conclusions: We developed a novel CXCR4-PET radioligand as a companion diagnostic, which displays specific affinity to CXCR4 in vitro and in vivo preclinical assays. This novel PET radioligand could be a good companion diagnostics candidate to accompany CXCR4 therapeutics in clinical trials for guiding patient stratification and early evaluation of drug efficacy and safety.

References:

1. Muller, A.; et al. *Nature* **2001,** *410* (6824), 50-56.
2. Teicher, B. A.; et al. *Clin Cancer Res* **2010,** *16* (11), 2927-31.
3. Burger, J. A.; et al. *Expert Opin. Invest. Drugs* **2009,** *18* (4), 481-490.
4. Zhu, A.; et al. *J. Med. Chem.* **2010,** *53* (24), 8556-8568.
5. Debnath, B.; et al. *Theranostics* **2013,** *3* (1), 47-75.
6. Olsen, D.; et al. *Frontiers in Oncology* **2014,** *4*.
7. Mooring, S. R.; et al. *Heterocycl. Commun.* **2014,** *20* (3), 149-153.
8. Mooring, S. R.; et al. *ChemMedChem* **2013,** *8* (4), 622-632.
9. Tamamura, H.; et al. *Bioorg. Med. Chem. Lett.* **2001,** *11* (14), 1897-1902.
10. Liang, Z.; et al. *PLoS One* **2012,** *7* (4), e34038.

AUTHORS (LAST NAME, FIRST NAME): Oum, Yoon Hyeun[1]; Shetty, Dinesh[1]; Yoon, Younghyoun[1]; Liang, Zhongxing[1, 2]; Voll, Ronald J.[1]; Goodman, Mark M.[1, 2]; Shim, Hyunsuk[1, 2]

INSTITUTIONS (ALL):

1. Radiology and Imaging Sciences, Emory University, Atlanta, GA, United States.
2. Winship Cancer Institute of Emory University, Atlanta, GA, United States.

(No Image Selected)

CONTROL ID: 2222131

TITLE: Computational MR Model for Characterizing Atherosclerotic Plaques Morphology and Composition

PRESENTER: Michael Dada

ABSTRACT BODY:

Abstract Body: Introduction

Most studies of atherosclerotic plaques have focused on the assessment of degree of stenosis [1]. However, an anomaly has been noticed which suggests that plaque size is not always a determining factor in patient symptomatology and that other plaque features may play a significant role in plaque pathogenicity [1].
Recent clinical and patho-anatomic observations indicate that plaque composition and biology are more significant determinant than plaque size in the development of thrombus-mediated acute coronary syndromes [1]. Thus clinical risk may correlate more closely with plaque morphology and surface features than with size [1]. This possibility emphasizes the importance of developing non-invasive imaging methods for characterizing plaque morphology and composition in addition to determining lumen area and wall thickness.

Methods

For this study, we shall consider spin dynamics of arterial blood and surrounding tissues based on the time-independent Bloch NMR flow Eqn [2]. Within a rotating frame, Larmor condition holds (Eqn (1)) and provided that the bulk protons are moving at a variable velocity v(x), the NMR Bloch flow eqns is given[2] in Eqn (2). If the RF field $B_1(x)$ is applied such that M_y is sampled at max. magnitude, $M_0 \approx 0$. Eqn (2) therefore becomes Eqn (3). If the assumptions in Eqn (4) holds, we have a Bessel diff. Eqn (5). For M_y signal which is measurable at all points x and if C_1 is the amplification constant, solution to Eqn (5) is given in Eqn (6).

Results

From recent experimental studies [3, 4], arterial blood and plaque components have relaxation constants at 9.4T as presented in Table 1. From the results expressed in Eqn (6), we have developed a Python computer program. The resulting GUI is presented as Fig. 1. Figs. 2 give the M_y map of arterial blood and plague components at 9.4T.

Discussions

We have demonstrated possibility of performing computational MRI to spatially localize different components of atherosclerotic plaques in carotid arteries ex vivo. Using Table 1, we were able to obtain unique images for different plaque components and arterial blood. What is interesting in this work is that few NMR data are required for plaque imaging and the model is capable of interpolating for data points which are impossible because of NMR hardware restrictions.

Conclusion

The computer program may also prove to be very useful in monitoring the effects drugs for treatment of atherosclerotic lesions and in identifying, localizing and quantifying plaque components in 3D. It provides a time-friendly simulation platform for imaging, monitoring drug administration/testing and repetitive running of NMR data.

Acknowledgement

The authors would like to thank Fed. Univ. of Tech., Minna. The Supports of Prof. Silvio Aime and Dr. Simona Baroni (MBC, University of Torino, Turin, Italy) are highly appreciated.

References

[1] Morrisetta J. *et al.* (2003). Magn Reson Imaging 21: 465–474.
[2] Awojoyogbe OB, Dada OM, Faromika OP, Dada OE. CMRA 2011; Vol. 38A (3): 85–101.
[3] Dobre MC, Ugurbil K, Marjanska M (2007). Magn Reson Imaging 25:733–735 13.
[4] Lee SP, Silva AC, Ugurbil K et al (1999). Magn Reson Med 42:919–928.

AUTHORS (LAST NAME, FIRST NAME): Dada, Michael O.[1]; Awojoyogbe, Bamidele O.[1]; Ogbonna, Adimchinobi N.[1]; Jayeoba, Babatunde O.[1]

INSTITUTIONS (ALL):
1. Department of Physics , Federal University of Technology, Minna, Nigeria, Minna, Niger State, Nigeria.

$$f_0 = \gamma B - \omega = 0 \tag{1}$$

$$v^2(x)\frac{d^2M_y}{dx^2} + v(x)\left(T_0 + \frac{dv}{dx}\right)\frac{dM_y}{dx} + (\gamma^2 B_1^2(x) + T_g)M_y = \frac{M_0}{T_1}\gamma B_1(x);\ T_0 = \frac{1}{T_1} + \frac{1}{T_2};\ T_g = \frac{1}{T_1 T_2} \tag{2}$$

$$v^2(x)\frac{d^2M_y}{dx^2} + v(x)\left(T_0 + \frac{dv}{dx}\right)\frac{dM_y}{dx} + (\gamma^2 B_1^2(x) + T_g)M_y = 0 \tag{3}$$

$$v(x) = \frac{x}{\delta},\ \ B_1(x) = \frac{T_g}{T_0^2}Gx,\ \ \xi = \frac{T_g}{T_0^2}\gamma G\delta \tag{4}$$

$$x^2\frac{d^2M_y}{dx^2} + x(1+\delta T_0)\frac{dM_y}{dx} + (\xi^2 x^2 + \delta^2 T_g)M_y = 0 \tag{5}$$

$$M_y(x) = C_1 x^{\alpha} J_n(\xi x);\ \ \alpha = -\frac{\delta T_0}{2},\ \ n = \frac{\delta}{2}\sqrt{T_0^2 - 4T_g}, \tag{6}$$

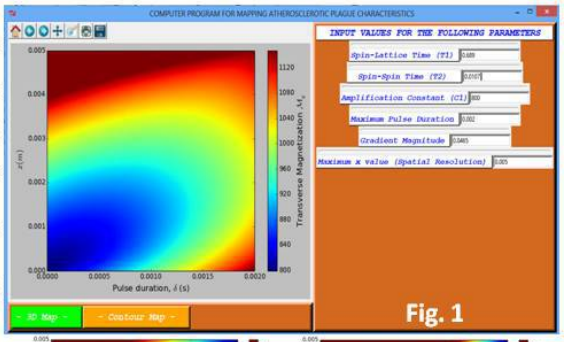

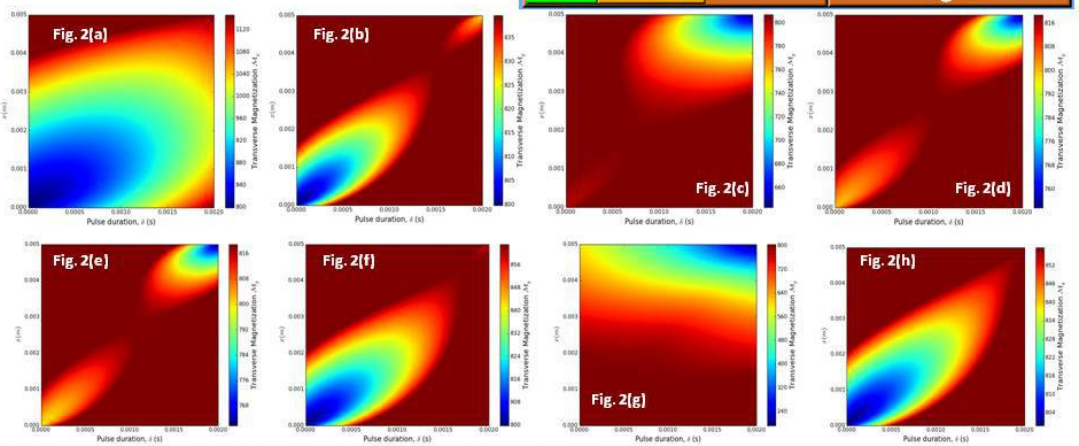

Fig.1: Python computer program graphic user interface (GUI) for mapping plaque components.
Fig.2: Transverse magnetization maps of (a) Calcification plaque component (b) Fibrous component (c) Intima (d) Media (e) Intima/media (f) Lipid-rich atheroma (g) Thrombus (h) Arterial blood.

CONTROL ID: 2222139

TITLE: Computational Model for Comparative Analysis of MRI Contrast Agents

PRESENTER: Michael Dada

ABSTRACT BODY:

Abstract Body: Introduction

The efficacy of MRI contrast agents (CAs) is not only determined by their pharmacokinetic properties but also by their magnetic properties as given by their T_1-and T_2-relaxivities [1,2]. It is very important to conduct comparative investigation on a large number of MRI CAs because their properties are dependent on different physiological environments (PEs) & binding to macromolecules in the blood [2]. Hence, different CAs are designed for different imaging objectives. However, the individual linearities of relaxation rates vs concentration is difficult to quantify using the experimental measurements in a wider concentration range due to the large amount of samples investigated at several magnetic field strengths and in different solvents [2]. Hence, we have developed a model and computer program for comparative analysis of NMR profiles of CAs in different PEs.

Methods

We consider spin dynamics of CAs & surrounding tissues based on Bloch NMR flow Eqn (BNFE) [3, 4]. Within a rotating frame, Larmor condition exists such according to Eqn (1). In the instance at which the molecules of the CAs are in motion at a variable velocity v(x) and the relaxation times of the solvent without the CA is T_{i0} (i = 1, 2) [2], the BNFE is [3, 4] given as Eqn (2). Note that C is the concentration of the CA while r_1 and r_2 are the relaxivities. Assuming that fluid velocity & the applied field have the forms expressed in Eqn (3), we then have Eqn (4). Because of the difficulties in obtaining analytical solution to Eqn (4), we employed Mathematica 9 software from where we got Eqn (5).

Results

A Mathematica code is also developed based on Eqn (5). Using relaxometric parameters of GADOVIST, MULTIHANCE & Gadomer in Plasma (T_{10} = 1.4493s, T_{20} = 0.3846s) & blood (T_{10} = 1.1111s, T_{20} = 0.2174s) at 37^0 C, B_0 = 1.5T [2]; setting C_1 = 2000, C_2 = 100 & M_0 = 100A/m, we have Figs. 1 & 2.

Discussions and Conclusion

It is worthy of note that for each of the CAs considered, the program showed unique M_y profiles & the model demonstrate the ease at which M_y of different CAs may be compared within different tissues/solvents. All that we require are the relaxometric & NMR parameters (such as gradient magnitude & pulse duration) of the CAs. In fact, large number of CAs may be compared in a very short time. In conclusion, we have developed a program which could make life easier for NMR scientists in terms of managing CAs for different physiological interests and they can now run as many simulations as possible before injecting the CAs into living systems.

Acknowledgement

The authors would like to thank Fed. Univ. of Tech., Minna. The Supports of Prof. Silvio Aime and Dr. Simona Baroni (both of Chemistry I.F.M. & MBC, University of Torino, Italy) are highly appreciated.

References

[1] Brix G., Kolem H., Nitz W.R., Bock M., Huppertz A., Zech C.J., Dietrich O. Springer Berlin Heidelberg, 2008.
[2] Rohrer M., Bauer H., Mintorovitch J., Requardt M., and Weinmann H. J. (2005). *Invest. radiology*, *40*(11), 715-724.
[3] Awojoyogbe OB, Dada OM, Faromika OP, Dada OE. CMRA 2011; 38A (3): 85–101.
[4] Gupta A, Stait-Gardner T, Ghadirian B, Price WS, Dada OM, Awojoyogbe OB. Science PG 2014; New York, USA.

AUTHORS (LAST NAME, FIRST NAME): Dada, Michael O.[1]; Awojoyogbe, Bamidele O.[1]; Jayeoba, Babatunde O.[1]

INSTITUTIONS (ALL):

1. Department of Physics , Federal University of Technology, Minna, Nigeria, Minna, Niger State, Nigeria.

$$f_0 = \gamma B - \omega = 0$$

$$v^2(x)\frac{d^2M_y}{dx^2} + v(x)\left(T_0 + \frac{dv}{dx}\right)\frac{dM_y}{dx} + (\gamma^2 B_1^2(x) + T_g)M_y = \frac{M_0}{T_1}\gamma B_1(x)$$

$$v(x) = \frac{x}{\delta},\quad B_1(x) = \frac{T_g}{T_0^2}Gx,\quad \xi = \frac{T_g}{T_0^2}\gamma G\delta$$

$$x^2\frac{d^2M_y}{dx^2} + x(1+\delta T_0)\frac{dM_y}{dx} + (\xi^2 x^2 + \delta^2 T_g)M_y = \frac{M_0}{T_1}\xi x\delta$$

$$M_y(x) = \frac{\pi M_0}{T_1}\xi x\delta 2^{-2-\alpha}(\xi x)^{-\alpha}\left\{\Gamma\left(\frac{\delta T_0}{4}+\frac{\alpha}{2}+\frac{1}{2}\right)(\xi x)^{2\alpha}Y_\alpha(\xi x)_1\tilde{F}_2\left[\left\{\frac{\delta T_0+2\alpha+2}{4}\right\};1+\alpha,\left\{\frac{\delta T_0+2\alpha+6}{4}\right\};-\frac{(\xi x)^2}{4}\right]\right\}$$

$$-\frac{\pi M_0}{T_1}\xi x\delta 2^{-2-\alpha}(\xi x)^{-\alpha}\left\{\cot(\alpha\pi)\Gamma\left(\frac{\delta T_0}{4}+\frac{\alpha}{2}+\frac{1}{2}\right)(\xi x)^{2\alpha}J_\alpha(\xi x)_1\tilde{F}_2\left[\left\{\frac{\delta T_0+2\alpha+2}{4}\right\};1+\alpha,\left\{\frac{\delta T_0+2\alpha+6}{4}\right\};-\frac{(\xi x)^2}{4}\right]\right\}$$

$$+\frac{\pi M_0}{T_1}\xi x\delta 2^{-2-\alpha}(\xi x)^{-\alpha}\left\{(2)^{2\alpha}\csc(\alpha\pi)\Gamma\left(\frac{\delta T_0}{4}-\frac{\alpha}{2}+\frac{1}{2}\right)J_\alpha(\xi x)_1\tilde{F}_2\left[\left\{\frac{\delta T_0-2\alpha+2}{4}\right\};1-\alpha,\left\{\frac{\delta T_0-2\alpha+6}{4}\right\};-\frac{(\xi x)^2}{4}\right]\right\}$$

$$+(x)^{-\frac{\delta T_0}{2}}\left(C_1 J_\alpha(\xi x)+C_2 Y_\alpha(\xi x)\right);$$

Where $\alpha = \frac{\delta}{2}\sqrt{T_0^2 - 4T_g}$; ${}_1\tilde{F}_2$ is the regularized generalized hypergeometric function.

(1)

(2)

(3)

(4)

(5)

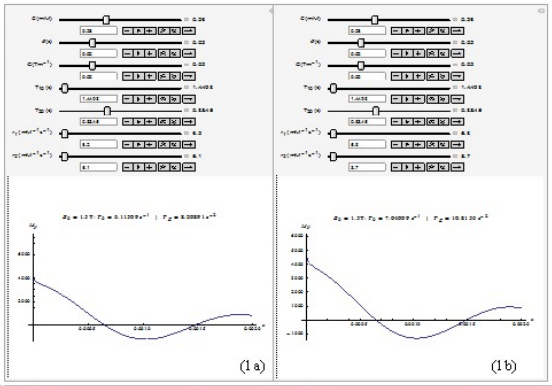

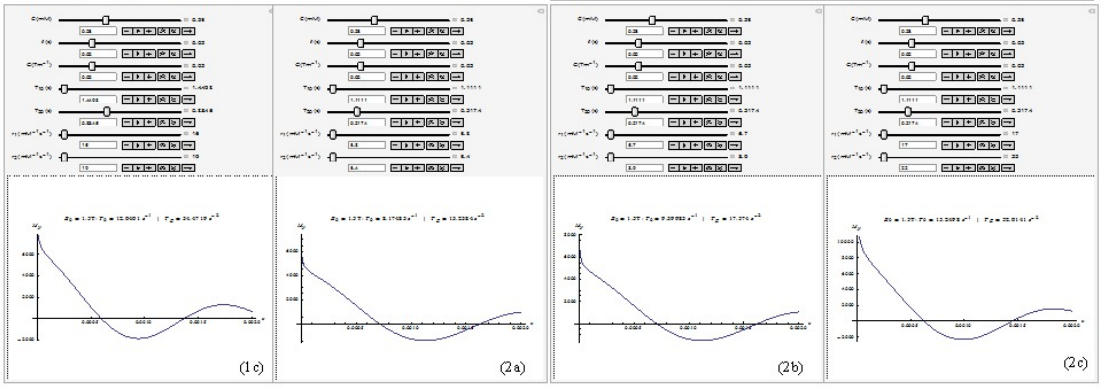

Fig.1: Executed program showing transverse magnetization profile of CA in plasma for (a) GADOVIST (b) MULTIHANCE (c) Gadomer.

Fig.2: Executed program showing transverse magnetization profile of CA in blood for (a) GADOVIST (b) MULTIHANCE (c) Gadomer.

CONTROL ID: 2224482

TITLE: Dual Tracer PET/MRI of Breast Tumors: Insights Into Tumor Biology

PRESENTER: Katja Pinker-Domenig

ABSTRACT BODY:

Abstract Body: Purpose:

To investigate combined multiparametric positron emission tomography/magnetic resonance imaging (PET/MRI) of breast tumors with dynamic contrast-enhanced MRI (DCE-MRI) for tumor neoangiogenesis, diffusion-weighted imaging (DWI) for assessment of tumor-microenvironment, the tracer ^{18}F-fluorodesoxyglucose (^{18}FDG) for detection of increased glycolysis and the tracer ^{18}F-fluoromisonidazole (^{18}FMISO) for detection of tumor hypoxia at 3T (3T MP ^{18}FDG/^{18}FMISO PET/MRI).

Methods and Materials:

In this IRB-approved prospective study, eight patients with suspicious breast lesions (BIRADS 4/5) underwent sequential 3T MP ^{18}FDG/^{18}FMISO PET/MRI. The MRI protocol included a high-resolution DCE sequence (0.1 mmol/kg Gd-DOTA, Dotarem) and a DWI rsEPI sequence b=50/850). All patients were subjected to ^{18}FDG/^{18}FMISO PET/CT scanning. CT data were used for attenuation correction. PET and MR images were registered using Mirada RTx (Mirada Medical, Oxford, UK, ver.1.4.0.23) software. 3T MP ^{18}FDG/^{18}FMISO PET/MRI was assessed for enhancement-kinetics, quantitative diffusivity and ^{18}FDG/^{18}FMISO avidity. Results were compared with pathological features grading, proliferation-rate (ki67), IHC and clinical endpoints (metastasis, death) using multiple correlation analysis. Histopathology was used as the standard of reference.

Results:

Seven invasive malignant and one benign fibrocystic lesion were identified. There were several moderate to excellent correlations identified between quantitative imaging markers, grading, receptor status and proliferation-rate. Multiparametric criteria provided independent information. DCE-MRI, ^{18}FDG- and ^{18}FMISO-avidity correlated with presence of metastasis [n=5; r=0.75 ($p<0.01$), 0.63 ($p=0.212$), 0.58 ($p=0.093$), respectively], while ADC and size did not (r=-0.26, 0.45). There was significant correlation of DCE-MRI with ^{18}FDG-avidity, but not ADC or ^{18}FMISO-avidity. DCE-MRI significantly positively correlated with grade, proliferation-rate and intrinsic molecular subtype and significantly negatively correlated ER/PR-receptor status.

Conclusion:

3T MP ^{18}FDG/^{18}FMISO PET/MRI in patients with breast tumors at 3T is feasible. 3T MP ^{18}FDG/^{18}FMISO PET/MRI reflects tumor biology and provides quantitative prognostic information in breast cancer patients.

AUTHORS (LAST NAME, FIRST NAME): Pinker-Domenig, Katja[1, 2]; Baltzer, Pascal A.[1]; Andrzejewski, Piotr[3]; Magometschnigg, Heinrich[1]; Georg, Dietmar[3]; Karanikas, Georgios[4]; Wadsak, Wolfgang[4]; Kapetas, Panagiotis[1]; Helbich, Thomas H.[1]

INSTITUTIONS (ALL):

1. Dept. of Biomedical Imaging and Image-guided Therapy, Division of Molecular and Gender Imaging, Medical University Vienna, Vienna, Austria.
2. Molecular Imaging and Therapy Services, Memorial Sloan-Kettering Cancer Center, New York, NY, United States.
3. Christian Doppler Laboratory for Medical Radiation Research for Radiation Oncology, Department of Radiation Oncology, Medical University Vienna, Vienna, Vienna, Austria.
4. Department of Biomedical Imaging and Image-guided Therapy, Division of Nuclearmedicine, Medical University Vienna, Vienna, Vienna, Austria.

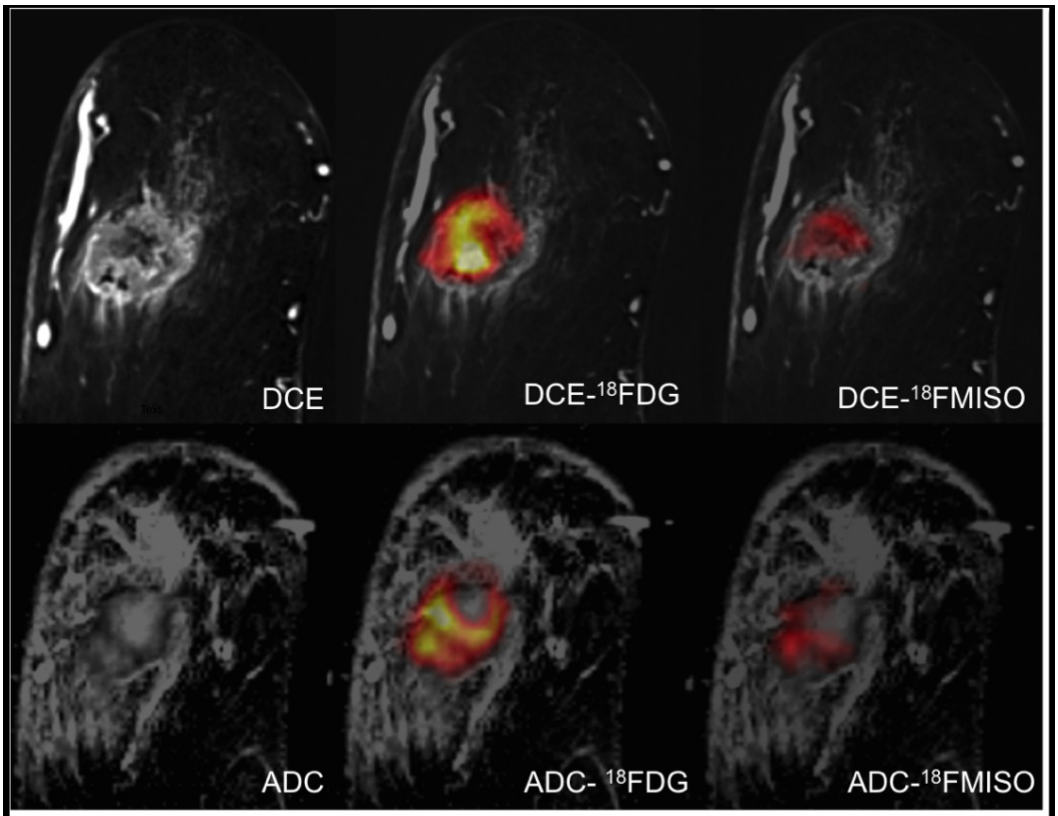

Figure1. Multiparametric ^{18}F-FDG/ ^{18}F-FMISO Positron Emission Tomography / Magnetic Resonance Imaging of the Breast at 3 Tesla (3T MP ^{18}F-FDG/ ^{18}F-FMISO PET/MRI) for visualizing intratumoral heterogeneity of breast cancer

Invasive ductal carcinoma G3 (ER pos., PR neg., Her2 pos, Ki67 80%) in a 56-year-old woman, laterally in the right breast. (A) In dynamic contrast-enhanced (DCE) magnetic resonance (MR) imaging the irregularly shaped and marginated lesion shows an initial fast rim-enhancement and in diffusion-weighted MR imaging the enhancing areas demonstrate restricted diffusivity with ADC values of 1.1 x 10^{-3} mm^2/sec. In combined ^{18}F-FDG/ ^{18}F-FMISO PET/MRI the tumor is highly FDG-avid (SUV_{max} 14.3) indicative of increased glycolysis. There are ^{18}FFMISO-avid parts within the ^{18}F-FDG-avid tumor indicative of areas of tumor

CONTROL ID: 2232311

TITLE: Relationship between extracellular glucose concentration and FDG uptake in sarcoma cell lines

PRESENTER: Katja Pinker-Domenig

ABSTRACT BODY:

Abstract Body: Objectives

For quantitative analysis of ^{18}F-FDG (FDG) PET/CT studies it has been recommended to multiply standardized uptake values (SUVs) with the plasma glucose concentration at the time of the scan, i.e glucose normalization. This normalization assumes that glucose metabolic rates of cancer cells do not change with plasma glucose concentrations. However, there is only scarce data to justify this assumption. Therefore the aim of this study was to investigate the relationship between glucose concentration in the culture media and FDG uptake in a panel of human sarcoma cell lines.

Methods

The sarcoma cell-lines of a gastrointestinal stroma tumor (GIST) 882, a malignant peripheral nerve sheet tumor (MPNST) 724 and an osteosarcoma (U2OS) were used for experiments. For the experiments, cells were plated in six-well plates at $5*10^5$ cells per well and incubated at 37 °C for 24 hours. Two uCi of FDG were added per milliliter (ml) of up-take media with different glucose concentrations, i.e 1, 2.5, 5.5, 7.2, 8.8, 10.6 and 11.7 mmol. Cells were incubated at 37 °C for 60min. After the respective incubation period, the up-take media was removed and the cells were washed with ice-cold phosphate buffered saline (PBS) twice. FDG uptake of cells was quantified as percent of the total activity bound to the cells.

Results

FDG uptake ranged between 0.21%-4.2% and decreased with increasing glucose concentrations in the incubation media. However the degree of change varied markedly between the three cell lines. In the U2OS cell line a more than 10-fold increase in glucose concentration only lead to a decrease in FDG uptake by 67%. In contrast, there was 90% decrease in the GIST cell line and a 83% decrease in the MPNST cell line. Consequently, the product of percentage FDG uptake and glucose concentration remained fairly constant for the GIST and MPNST cell line, whereas it increased 5 times for the U2OS cell line.

Conclusions

In the studied cell lines there was variable a relationship between glucose concentration and FDG uptake. These findings suggest that further studies are needed before glucose normalization is commonly used for quantitative analysis of FDG PET/CT studies in cancer patients.

AUTHORS (LAST NAME, FIRST NAME): Pinker-Domenig, Katja[1]; Desai, Pooja[1]; Weber, Wolfgang[1]

INSTITUTIONS (ALL):

1. Molecular Imaging and Therapy Service, Memorial Sloan Kettering Cancer Center, New York, NY, United States.

(No Image Selected)

CONTROL ID: 2216107

TITLE: Fluselenamyl: A Novel F-18 PET tracer for detection of Alzheimer's disease

PRESENTER: SUNDARAM GURUSWAMI

ABSTRACT BODY:

Abstract Body: Alzheimer's disease (AD) is a progressive neurodegenerative disorder characterized by decline in cognitive functions. Currently five million people are affected in the US, and the patient pool is projected to grow 4-fold by 2050 thus resulting into major healthcare issue in the 21st century. Among various biomarkers prevalent in AD, amyloid formation (Aβ) has been shown to precede decades prior to beginning of neurodegeneration phase, and the presence of senile plaques (SPs) and neurofibrillary tangles (NFTs) in non-demented older adults could also represent an earlier manifestation of AD prior to its clinical expression. Additionally, literature precedents indicate presence of three high-, moderate-, and modest- affinity binding sites on Aβ. Further, it is quite likely that orientation of these binding sites is also different at preclinical and clinical stages of the disease. Therefore, different PET tracers are desired to better understand Aβ pathophysiology *in vivo*, enable early diagnosis, monitoring disease progression, and tracking therapeutic response. Recently, Avid45, GE-067 (Flutemetamol) and AZD4694 (Florbetaben) have gained FDA approval for Aβ imaging. While showing promise as noninvasive imaging probes, these agents show high levels of nonspecific white matter binding, lack ability to detect diffuse Aβ plaques, and indicate low biological half-lives (Avid45 show two competing metabolites) thus potentially complicating image analysis. To further embellish imaging resources and enable disease-specific imaging without confounded effects, we have discovered a small heterocyclic and fluorescent molecule that demonstrates characteristics of translatable imaging agents. The PET counterpart was obtained via nucleophilic reaction using the precursor ligand and K^{18}F and Kryptofix in acetonitrile (35% yield; radiochemical purity >99%; specific activity (1700-2000 Ci/mmol). The PET tracer shows a concentration dependent and saturable binding with AD homogenates (Kd=1.70±0.05nM) and preformed $A\beta_{42}$ fibrils (Kd=1.58±0.05nM). Further, the agent demonstrates high first-pass extraction into brains (8.86 % ID/g; 2 min) of normal mice, followed by its clearance over 60 min. Additionally, the agent exhibits staining of fibrillar and diffuse plaques and detects cerebral amyloid angiopathy (CAA) in the hippocampal tissue sections of a neuropathologically confirmed AD patient. Preliminary multiphoton real-time imaging shows its ability to traverse the blood-brain barrier, detects CAA, and label parenchymal Aβ plaques in brains of transgenic mice within minutes post-intravenous injection. Finally, microPET/CT imaging (30 min post tail-vein injection) shows initial penetration and retention of the radiotracer in cortical regions of the brains of APP/PS1 mice compared with its clearance in their age-matched WT counterparts.

Conclusions: The lead agent demonstrates characteristic features of translatable imaging agents and provides a template scaffold for further optimization and development of Aβ-targeted probes.

AUTHORS (LAST NAME, FIRST NAME): GURUSWAMI, SUNDARAM[1]; Dhavale, Dhruva[2]; cirrito, john[2]; Lee, Jin-Moo[2]; Cairns, Nigel[2]; kotzbauer, paul[2]; sharma, vijay[1, 2]

INSTITUTIONS (ALL):

1. Radiology, washington university school of medicine, St louis, MO, United States.
2. Neurology, washington university school of medicine, Saint Louis, MO, United States.

(No Image Selected)

CONTROL ID: 2228985

TITLE: Targeting extracellular acidic tumor microenvironment in pancreatic adenocarcinoma: Multispectral Optoacoustic Tomography detects pH-low insertion peptide probes *in vivo*

PRESENTER: Lacey McNally

ABSTRACT BODY:

Abstract Body: Pancreatic ductal adenocarcinoma (PDAC) remains highly lethal because of its advanced stage at presentation, which is partly due to the lack of effective approaches to identify tumors early. pH-low Insertion Peptides (pHLIPs) can serve as a targeting moiety that enables pH-sensitive probes to detect solid tumors. Using these probes in conjunction with multispectral optoacoustic tomography (MSOT) is a promising approach to improve imaging for pancreatic cancer. A pH-sensitive pHLIP (V7) was conjugated to 750 NIR fluorescent dye and evaluated as a targeted probe for pancreatic adenocarcinoma. The pH-insensitive K7 pHLIP served as an untargeted control. Probe binding was assessed *in vitro* at pH 7.4, 6.8, and 6.6 using the human pancreatic cell lines S2VP10 and S2013. *In vitro,* the V7-750 probe demonstrated significantly higher fluorescence at pH 6.6 compared to pH 7.4 (S2VP10, p=0.0119; S2013, p=0.0160), while no difference was observed with the K7-750 control (S2VP10, p=0.8783; S2013, p=0.921). In vivo, Multispectral Optoacoustic Tomography was utilized to determine probe accumulation within the orthotopic pancreatic tumor and further confirmed using NIR-fluorescence (AMI). In the *in vivo* S2VP10 model, V7-750 probe signal was 147 times higher in the tumor than the K7-750 control (p= 0.0001). Similarly, V7-750 probe was 113 times higher than control in the S2013 model (p=0.0005). There was minimal off-target accumulation of the V7-750 probe within the liver or kidney, and probe distribution was confirmed with *ex vivo* imaging. Compared to pH-insensitive controls, the V7-750 pH-sensitive probe specifically targets pancreatic adenocarcinoma, and has minimal off-target accumulation. The non-invasive detection of pH-targeted probes by means of MSOT represents a promising modality to improve the detection and monitoring of pancreatic cancer.

AUTHORS (LAST NAME, FIRST NAME): Kimbrough, Charles[1]; Khanal, Anil[1]; McNally, Lacey R.[1]

INSTITUTIONS (ALL):

1. Medicine, University of Louisville, Louisville, KY, United States.

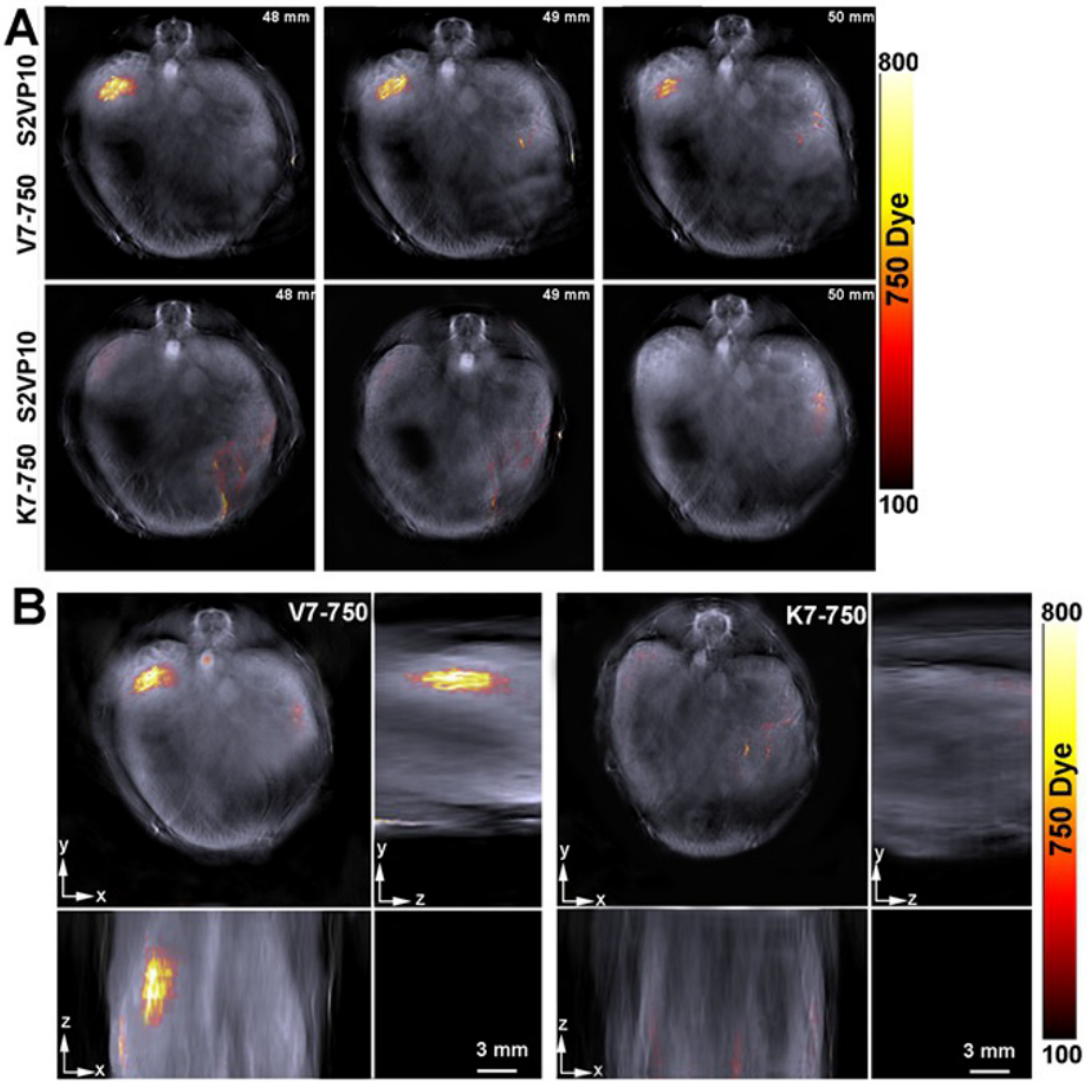

Axial tomographic slices of the S2VP10 mouse imaged using Multispectral Optoacoustic Tomography demonstrate localization of V7-750 probe signal to the region of the tumor bed, while similar signal is not observed with K7-750 probe (A). Orthogonal views of the pancreatic tumor bed at 4 hours demonstrate distribution of V7-750 probe signal throughout the tumor bed at 4 hours, while minimal accumulation is observed with K7-750. Peak intensity signal intensity with injection of V7-750 is 782.5 MSOT a.u., compared to 5.3 for the K7-750 probe. (B) Orthogonal images demonstrate 3D accumulation of V7-750 and K7-750 within the mouse in the xyz-plane.

CONTROL ID: 2232365

TITLE: Cyclic RGD micelles facilitate detection of ovarian cancer using multispectral optoacoustic tomography

PRESENTER: Lacey McNally

ABSTRACT BODY:

Abstract Body: Early detection and treatment of ovarian cancer cell is challenging due to limitations in both traditional imaging techniques (shallow depth penetration, low sensitivity and specificity, or the use of ionizing radiation) and insufficient efficacy of conventional chemotherapy *in vivo*. Here in, we constructed pH dependent tumor specific theranostic nanoparticle, which binds α5β3 integrin and releases contents in the presence of an acidic tumor microenvironment to enhance tumor detection via MSOT. The cRGD-pH responsive micelles were spherical in size (176 ± 10 nm) at pH 7.4 and were stable over the pH range of non-malignant tissue at pH 7.0-7.4, but dissociate in the acidic environment (pH 6.8) due to protonation. The paclitaxel (PTX) loading efficiency was 70% in cRGD-pH responsive micelles and released at the rate constant of 0.05 h^{-1} and 0.19 h^{-1} at pH 7.4 and pH 6.5, respectively. Cytotoxicity measurements revealed that PTX loaded cRGD-pH responsive micelles effectively killed ovarian cancer cells *in vitro* >92% at extracellular pH of 6.8 and >98% at 6.5, but < 10% at pH 7.4 by induction of apoptosis. In vivo, dye encapsulated cRGD-pH responsive micelles significantly accumulated in tumors at two hours post-injection as detected using multispectral optoacoustic tomography. cRGD-pH responsive micelles were observed in tumor vasculature and in areas of hypoxia. We reported for the first time that targeted theranostic cRGD-pH responsive micelles facilitate MSOT detection of ovarian cancer *in vivo* .

AUTHORS (LAST NAME, FIRST NAME): McNally, Lacey R.[1]; Khanal, Anil[2]

INSTITUTIONS (ALL):

1. Medicine, University of Louisville, Louisville, KY, United States.
2. Medicine, University of Louisvillie, Louisville, KY, United States.

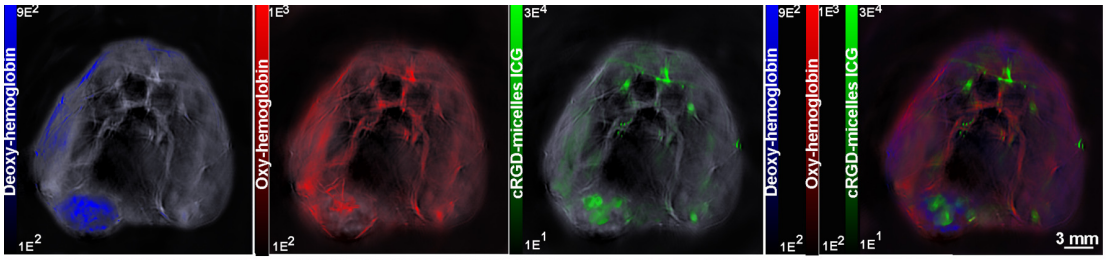

Localization of cRGD-pH responsive micelles in ovarian tumors as detected using multispectral optoacoustic tomography. ES-2 ovarian cancer cells were subcutaneously injected into athymic mice. 100 nM of cRGD-pH responsive micelles loaded with ICG dye were iv injected into tumor bearing mice. Two hours post injection mice were placed anesthetized using isoflurane and 0.8L medical air and 0.1 L O2 and imaged using Multispectral Optoacoustic Tomography. Images were taken simultaneously using 10 wavelenghts and spectrally unmixed using View MSOT. A single slice is depicted. Blue indicates deoxygenated hemoglobin, Red indicates oxygenated hemoglobin, Green indicates ICG dye.

CONTROL ID: 2231276

TITLE: Delivery of Syndecan-1 tagged liposomes into tumor cells via Insulin Growth Factor 1-Receptor-mediated endocytosis

PRESENTER: Wenyuan Yin

ABSTRACT BODY:

Abstract Body: Encapsulation of drugs within nanodelivery vehicles which selectively target malignant cells promises to mitigate toxic off-target effects of chemotherapy and to enable drug-delivery needed for personalized medicine. To realize this potential, however, targeted nanocarriers must simultaneously overcome multiple challenges, including identification of cargo release from the nanodelivery vehicle and tumor specificity. Here we constructed and characterized a Syndecan-1 tagged liposome (107 nm) which targets insulin growth factor 1 receptor (IGF1-R) encapsulating Propidium Iodide (PI) and/or indocynanine green. Because PI differentially fluoresces when bound or unbound to DNA, we exploited this property to determine release properties from the liposome. IGF1-R receptor mediated endocytosis of the targeted liposome was determined utilizing S2VP10 pancreatic cancer cells (IGF1-R positive) and SCC1 HNSCC cells (IGF1-R negative) via fluorescent microscopy. In vivo liposome accumulation and biodistribution was determined in orthotopic S2VP10 pancreatic cancer model utilizing multispectral optoacoustic tomogrpahy. While Syndecan-1 liposomes underwent endocytosis and released PI which bound to nuclear DNA resulting in red fluorescence in IGF1-R positive tumor cells, Syndecan-1 liposomes did not enter IGF1-R negative cells resulting in a green background fluorescence. Treatment of either IGF1-R positive or negative cells with untargeted control liposomes also failed to demonstrate red PI bound nuclear DNA. In vivo Syndecan-1 liposomes specificially targeted pancreatic cancer with 159.9 MSOT a.u. as compared to 15.6 MSOT a.u. in the kidney. The ability of the Syndecan-1 liposomes to specifically undergo IGF1-R mediated endocytosis is significant as IGF1-R is a highly expressed receptor in metastatic cancers and monoclonal antibody targeted therapies have previously demonstrated a lack of specificity. The combination of this particle promises to open new and exciting opportunities in detection and treatment of cancer.

AUTHORS (LAST NAME, FIRST NAME): Yin, Wenyuan[2]; Kimbrough, Charles[1]; McNally, Lacey R.[2]

INSTITUTIONS (ALL):

1. University of Louisville , Louisville, KY, United States.
2. Medicine, University of Louisville , Louisville, KY, United States.

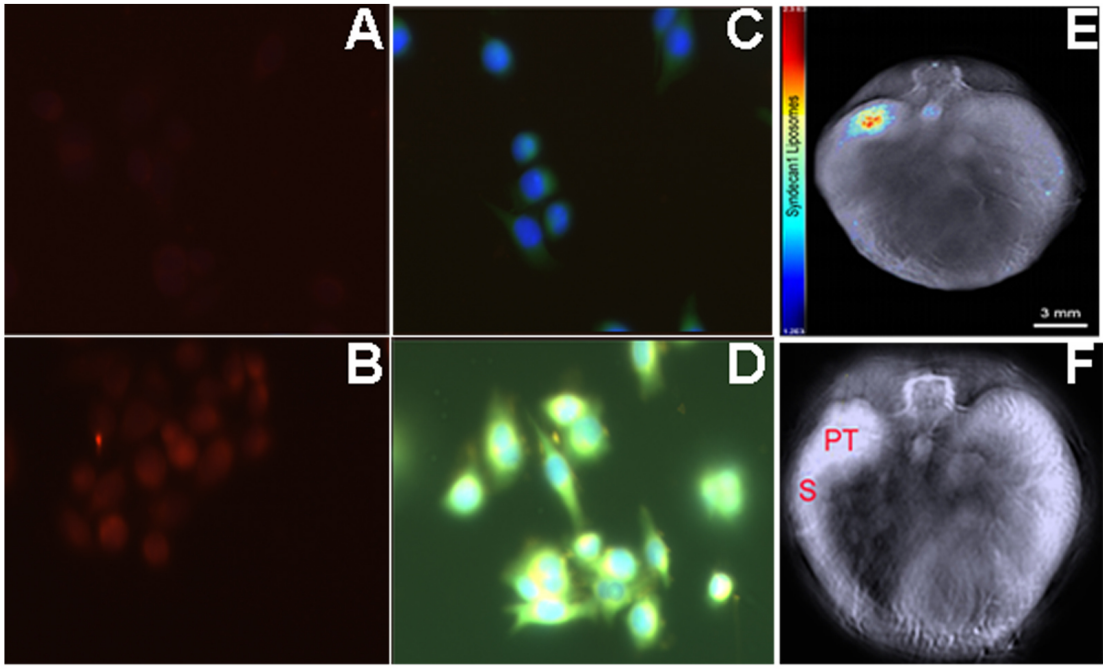

Images A-D demonstrate that Syndecan-1 tagged liposomes undergo IGF1-R mediated endocytosis. Propidium Iodide was encapsulated within untagged liposomes and Syndecan-1 tagged liposomes in IGF1-R positive S2VP10 cells (A-D) and SCC1 IGF1-R negative cells (not shown). Because DNA bound PI fluoresces red while unbound PI fluoresces green, red fluorescence indicates successful endocytosis of liposomes and delivery of encapsulated dye into the cell. Images A-B and C-D utilized identical exposures. S2VP10 cells treated with (A) Untagged liposomes (Texas Red filter); (B) Syndecan-1 tagged liposomes (Texas Red filter); (C) Untagged liposomes (DAPI, GFP, Texas Red filters); (D) Syndecan-1 tagged liposomes (DAPI, GFP, Texas Red filters). Positive red staining in B and co-localization (white) in D demonstrate PI binding to DNA.

To determine tumor specificity of Syndecan-1 tagged liposomes in vivo, S2VP10 cells were injected orthotopically in xenografts and detectedusing Multispectral Optoacoustic Tomography.

(E) A single axial slice demonstrates pancreatic tumor specific binding of Syndecan-1 tagged liposomes. (F) Demonstrates relative organ location (PT=pancreas tumor; S=Spleen).

CONTROL ID: 2229698

TITLE: Multispectral optoacoustic tomography detects orthotopic pancreatic tumors in vivo using a Syndecan-1 conjugated mesoporous silica-coated gold nanorod as a nano-contrast agent

PRESENTER: Lacey McNally

ABSTRACT BODY:

Abstract Body: Background: There have been very modest developments in pancreatic cancer detection and treatment with mortality essentially remaining unchanged in the last four decades. The major challenge for both early detection and treatment of pancreatic tumors lies in overcoming various biological barriers, especially poor perfusion, insufficient contrast agents/drugs uptake by the tumor, and limitations of traditional imaging modalities. The combination of accurate real-time imaging with tumor-specific nano-contrast agents could mitigate these impediments.

Methods: We constructed highly stable nano-contrast agents by encapsulating GNRs having aspect ratio 3:1 in PAA (1.5 ± 0.5 nm), and MS (6.25 ± 0.25 nm) shell, respectively and targeted to insulin growth factor 1 receptor (IGF1-R) positive pancreatic tumor cells via Syndecan-1 ligand. IGF1-R specific binding of Syndecan-MS-GNRs and Syndecan-PAA-GNR was determined using in an IGF1-R negative cell line (MiaPaca-2) or a blocking antibody to IGF1-R in S2VP10L pancreatic cancer cells determined via flow cytometry. In vivo, mice bearing orthotopic pancreatic tumors were iv injected with 100 nM of Syndecan-MS-GNRs and accumulation was determined four hours post injection via Multispectral Optoacoustic Tomography. Biodistribution was determined using a Region of Interest method.

Results: The cellular uptake of Syndecan-MS-GNRs significantly enhanced in the S2VP10L cells (503.4 counts) compared to MiaPaca-2 cells (64.1 counts), blocking agent (323.7counts) and untargeted MS-GNRs (average 47 counts) revealing that Syndecan-MS-GNRs enhanced both tumor specificity and OA signals by binding with IGF1-R in S2VP10L cells. *In vivo*,
Syndecan-MS-GNRs significantly accumulated in S2VP10L orthotopic pancreatic tumors (233.1 MSOT a.u.) with minimal accumulation in kidney (29.7 MSOT a.u.) and liver (31.4 MSOT a.u.). The Syndecan-MS-GNRs did not accumulate within the orthotopic MiaPaca-2 (IGF1-R negative) mouse model with the biodistribution of pancreas tumor (12.4 MSOT a.u.), kidney (114.3 MSOT a.u.), and liver (35.2 MSOT a.u.).

Conclusion: For the first time, we report the combination of MSOT with targeted nanocontrast agents (Syndecan-MS-GNRs) provide a high-resolution signal amplifier by minimizing off-target effect for successful detection of orthotopic pancreatic cancer cells *in vivo*.

AUTHORS (LAST NAME, FIRST NAME): Khanal, Anil[2]; McNally, Lacey R.[1]

INSTITUTIONS (ALL):

1. Medicine, University of Louisville, Louisville, KY, United States.
2. Medicine, University of Louisvillie, Louisville, KY, United States.

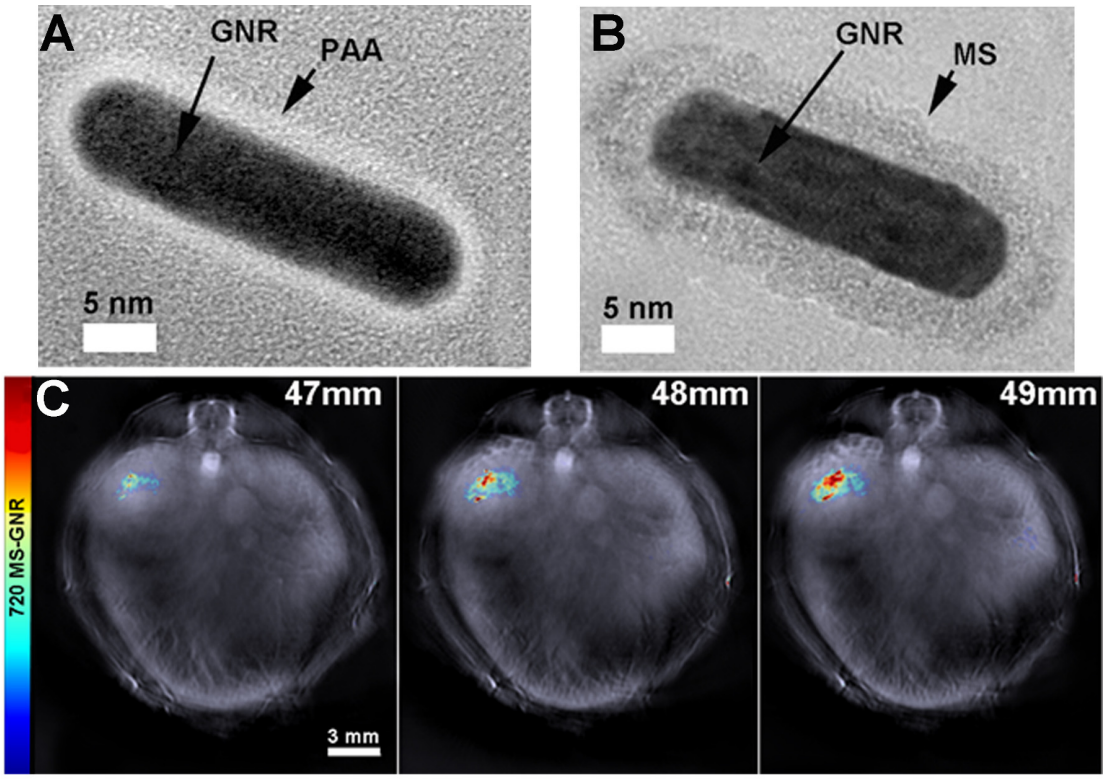

Mesoporous silica coated gold nanorods act as contrast agents to detect pancreatic cancer via Multispectral Optoacoustic Tomography. Gold nanorods coated with either PAA or MS were created and characterized. Transmission electron micrograph (TEM) shows gold nanorods (GNRs) with polyacrylic acid shell (PAA) and amine-functionalized mesoporous silica (MS) shell. (A) GNRs were coated with PAA shell (1.5 ± 0.5 nm) (B) GNRs were coated with MS shell (6.25±0.254 nm). The average length and width of GNRs were 22 ±3.15 nm and 7.0 ±0.33 nm in both cases.

Syndecan-1 tagged MS-GNRs were ultimately evaluated as contrast agents to facilitate detection of pancreatic cancer via multispectral optoacoustic tomography. (C) Identification of Syndecan-1 targeted MS-GNRs accumulation within S2VP10L pancreas tumor using multispectral optoacoustic tomography (MSOT). Serial images of a pancreatic tumor mass ranging illustrate the capability to precisely define the region of Syndecan-MS-GNRs distribution.

CONTROL ID: 2231103

TITLE: Al^{18}F-NOTA-Folate accumulates in inflamed atherosclerotic plaques and facilitates *in vivo* visualization by PET

PRESENTER: Johanna Silvola

ABSTRACT BODY:

Abstract Body: Purpose: The development of inflamed atherosclerotic plaques is a potential risk of future cardiovascular events. Therefore, detection of inflamed atherosclerotic plaques is crucially important. Folate receptor β (FR-β) is highly expressed in activated macrophages, also in atherosclerotic plaques [1]. Previously, it was shown that FR-β targeted imaging agent, ^{99m}Tc-EC20, accumulates aggressively in FR-β positive macrophages of atherosclerotic plaques in mice [2]. Purpose of this study was to explore the biodistribution of the novel FR-β targeted PET tracer, Al^{18}F-NOTA-Folate, in atherosclerotic mice and rabbit models.

Methods: Al^{18}F-NOTA-Folate was prepared by chelation of NOTA-folate to Al^{18}F at pH 4.0 with specific radioactivity of 130 GMq/μmol at the end of synthesis. Low-density lipoprotein receptor deficient mice expressing only apolipoprotein B100 and overexpressing insulin-like growth factor II in pancreatic β cells (IGF-II/LDLR$^{-/-}$ApoB$^{100/100}$, n=6) were fed with a high-fat diet for 4 months and C57BL control mice (n=9) were fed with normal chow. Al^{18}F-NOTA-Folate was *i.v.* injected (10±1 MBq), and the biodistribution was investigated *in vivo* by PET/CT and *ex vivo* by gamma counting and autoradiography. Furthermore, an atherosclerotic Watanabe rabbit with endothelial denudation in the aorta was studied with ^{18}F-FDG and Al^{18}F-NOTA-Folate.

Results: IGF-II/LDLR$^{-/-}$ApoB$^{100/100}$ mice demonstrated large and macrophage-rich atheromatous plaques. Al^{18}F-NOTA-Folate was rapidly cleared from blood circulation, excreted through kidneys to the urinary bladder and accumulated into inflamed atherosclerotic plaques. The *in vivo* PET/CT revealed significantly higher accumulation of Al^{18}F-NOTA-Folate in atherosclerotic aortic arch compared to controls (aorta-to-blood ratio 1.5±0.1 vs. 0.8±0.2, P=0.01). *Ex vivo* gamma counting confirmed the results; the atherosclerotic thoracic aorta uptake was significantly higher compared with controls (SUVs 1.0±0.4 vs. 0.6±0.2, respectively, P=0.01). Competitive binding assay with excess folic acid glucosamine reduced aorta uptake 89% and thus verified the specificity of tracer binding. In addition, the plaque-to-healthy vessel wall ratio was 2.6±0.7 (P<0.0001) based on autoradiography of aorta cryosections. In atherosclerotic rabbit, the Al^{18}F-NOTA-Folate clearly visualized metabolically active atherosclerotic plaque with aorta-to-blood ratio of 6.0. For comparison, the ^{18}F-FDG aorta-to-blood was 2.4 in the same area. *Ex vivo* Al^{18}F-NOTA-Folate analyses revealed even more significant plaque accumulation (aorta SUV 7.4, blood SUV 0.15, aorta-to-blood ratio 49).

Conclusion: Al^{18}F-NOTA-Folate, a novel FR-β targeted PET tracer, facilitates *in vivo* imaging of inflamed atherosclerotic plaques. Further studies in patients with atherosclerosis are warranted.

[1] Jager NA, Westra J, Golestani R, et al. J Nucl Med. 2014;55:1945-51.

[2] Ayala-López W, Xia W, Varghese B et al. J Nucl Med. 2010;51:768-74

AUTHORS (LAST NAME, FIRST NAME): Silvola, Johanna M.[1]; Li, Xiang-Guo[1]; Padmasola, Guru P.[1]; Virta, Jenni[1]; Marjamäki, Päivi[1]; Liljenbäck, Heidi[1]; Tarkia, Miikka[1]; Hytönen, Jarkko P.[2]; Saunavaara, Virva[1]; Ylä-Herttuala, Seppo[2]; Saraste, Antti[3]; Chen, Qingshou[4]; Low, Philip S.[4]; Knuuti, Juhani[1]; Roivainen, Anne[1]

INSTITUTIONS (ALL):

1. Turku PET Centre, University of Turku and Turku University Hospital, Turku, Finland.
2. A. I. Virtanen Institute for Molecular Sciences, University of Eastern Finland, Kuopio, Finland.
3. Heart Center, Turku University Hospital and University of Turku, Turku, Finland.
4. Department of Chemistry, Purdue University, West Lafayette, IN, United States.

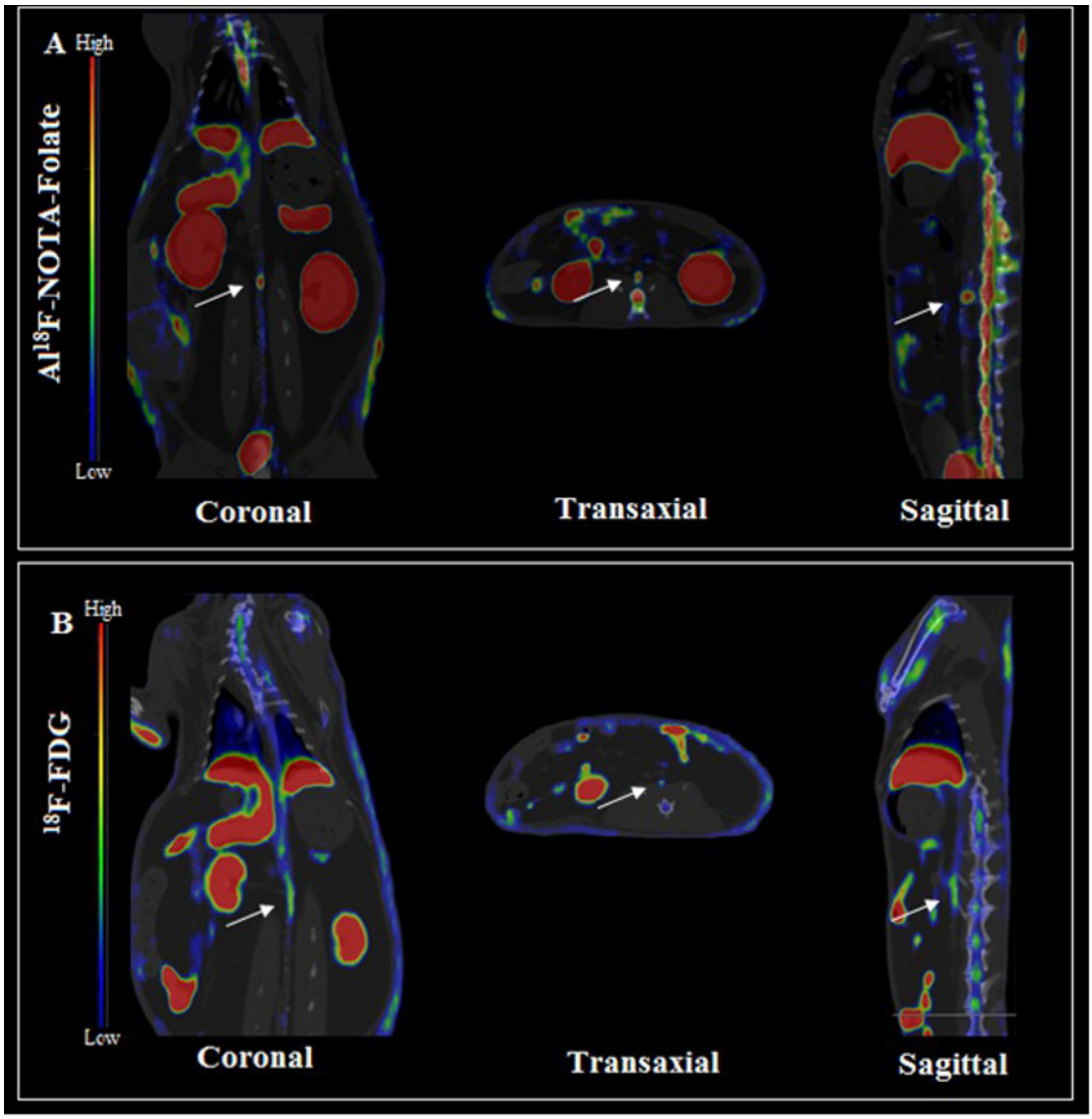

Figure 1. Al^{18}F-NOTA-Folate is highly accumulated in atherosclerotic plaque. A male Watanabe rabbit (3.5 years, 3.5 kg) with endothelial denudation injury was injected with 45 MBq/kg of ^{18}F-FDG and PET/CT scanned at 160 min post-injection (Discovery VCT, GE Medical Systems). In the next day, the same rabbit was injected with 45 MBq/kg of Al^{18}F-NOTA-Folate and a 90-min dynamic PET scan was performed. After imaging, rabbit was euthanized and tissue samples measured with a gamma counter. Target-to-background ratio (TBR; aorta SUV_{max}/vena cava SUV_{mean}) was determined at 160-170 min after ^{18}F-FDG injection and at 88-90 min after Al^{18}F-NOTA-Folate injection. The white arrows denote metabolically active plaque in the abdominal aorta with TBRs of 6.0 (Al^{18}F-NOTA-Folate) and 2.4 (^{18}F-FDG). Based on *ex vivo* gamma counting, the plaque-to-blood ratio of Al^{18}F-NOTA-Folate at the site of arrow/plaque was 49. (plaque SUV 7.4, blood SUV 0.15).

CONTROL ID: 2228835

TITLE: In vivo μSPECT imaging of ^{99m}Tc-mebrofenin to assess impaired hepatobiliary transport: a pharmacokinetic modeling study.

PRESENTER: Sara Neyt

ABSTRACT BODY:

Abstract Body: Purpose: ^{99m}Tc-Mebrofenin (MEB) is commonly used in nuclear medicine to investigate hepatic (dys)function by Single Photon Emission Computed Tomography (SPECT). After intravenous injection, MEB is taken up by hepatocytes through the organic anion transport protein (Oatp). MEB is then transported into bile by the active efflux transporter multidrug resistance protein 2 (Mrp2), finally entering the small intestine through the common bile duct. The goal of the current study is the implementation of a two compartment kinetic model (Ghibellini et al., 2008) of MEB to describe impaired hepatobiliary uptake and/or efflux caused by drugs or genetic disorders (Figure 1). Kinetic parameters of wild type (WT), rifampicin treated and Abcc2 knock-out (KO) mice are compared. Rifampicin is an Oatp and Mrp2 inhibitor and the Abcc2 gene encodes for the efflux transporter of ^{99m}Tc-mebrofenin, namely Mrp2. To calculate the kinetic parameters, the use of an image derived input function was investigated.

Methods: WT (n=5), rifampicin treated (n=3), and Abcc2 KO (n=4) mice were injected with 37 MBq of ^{99m}Tc-MEB. Dynamic SPECT images were acquired on a USPECT-II camera (Milabs) using 60 time frames of 15 seconds. Regions of interests (ROI) were manually drawn around the liver and gallbladder + intestines to determine the corresponding time activity curves. No activity was detected in the urinary bladder. To obtain an image derived input function, a static ^{99m}Tc-tetrofosmin scan was acquired, immediately after the dynamic MEB acquisition. Since the position of the mice was unaffected between the scans, a ROI drawn around the heart on the static tetrofosmin data, could be copied to the dynamic ^{99m}Tc-MEB images to obtain an image derived input function. Kinetic parameters of the 2-compartimental model were determined using MATLAB. Statistical analysis was performed in SPSS version 22 (Mann Witney U test; $p<0.05$ was considered as significant).

Results:

k_{12}, and k_{20} values were respectively 2- and 8-fold smaller in rifampicin treated mice compared to vehicle controlled mice (p-values of 0.034). k_{21} values were larger in rifampicin treated mice (300 fold). In Abcc2 KO mice, k_{12} and k_{21} values were similar to those of WT mice (0.221 and 0.806). K_{20} values, in contrast, were 10- fold lower in comparison with WT mice (p= 0.014) (Table 1).

Conclusion

In rifampicin treated mice, decreased k_{12} and k_{20} values were observed, since rifampicin is an Oatp and Mrp2 inhibitor (Neyt et al.; 2013). Additionally, the increase of k_{21} can be explained by the fact that there can be an upregulation of Mrp3 (Schrenk, 2001), which can also transport mebrofenin (Ghibellini, 2008). Abcc2 KO mice, in contrast, show a similar uptake in comparison with WT mice, which is reflected in similar k_{12} en k_{21} values. The efflux, in contrast, is decreased (lower k20 values), due to the absence of the efflux transporter. k_{21} is not increased, since Abcc2 knock-out mice have no induction of Mrp3 (Chu et al.,2006). In conclusion, kinetic parameters of the 2 compartment kinetic model of MEB is a useful tool to absolutely quantify (altered) hepatobiliary transport, which can be suitable during drug development.

AUTHORS (LAST NAME, FIRST NAME): Neyt, Sara[1]; Vanhove, Christian[2]; Mannens, Geert[3]; De Vos, Filip J.[1]

INSTITUTIONS (ALL):

1. Laboratory of Radiopharmacy, Ghent University, Ghent, Belgium.
2. IBITech-MEDISIP-INFINITY, Ghent University, Ghent, Belgium.
3. Drug Safety Sciences, Janssen Pharmaceutical Companies of Johnson & Johnson, Beerse, Belgium.

A

B

$$\frac{dC_c}{dt} = -k_{12} \times C_c + k_{21} \times \frac{X_{liver}}{V_c} \qquad C_c^0 = \frac{X_0}{V_c}$$

$$\frac{dX_{liver}}{dt} = k_{12} \times V_c \times C_c - k_{20} \times X_{liver} - k_{21} \times X_{liver} \qquad X_{liver}^0 = 0$$

$$\frac{dX_{bile}}{dt} = k_{20} \times X_{liver} \qquad X_{bile}^0 = 0$$

Scheme of the pharmacokinetic model describing the disposition and elimination of MEB in mice (A) and the differential equations describing the mebrofenin disposition in mice. X_0 represents the IV bolus; C_c is the concentration of MEB in the blood and V_c is the central compartment volume. All other compartments were modeled as amounts in MBq. All rate constants were assumed to be first order: k_{12} represents hepatic basolateral uptake; k_{21} represents hepatic basolateral excretion and k_{20} represents hepatic canalicular efflux.

CONTROL ID: 2230931

TITLE: Blood-Brain Barrier-Permeated Nanocomposites for Theranostic Molecular Imaging in Brain Tumor

PRESENTER: Chia-Hao Su

ABSTRACT BODY:

Abstract Body: Gliomas are the most aggressive and common intracranial tumors of the brain tumors and currently no better therapeutic methods can cure them. The survival periods of patients with gliomas are less than 15 months even after treatment of surgical excision or chemo-radiation therapy.[1] Many therapeutic agents are found that they can kill glioma cells effectively *in vitro*, but can not affect glioma cells *in viv*o due to the poor solubility and short half-life of therapeutic agents in the circulation. These critical obstacles can be overcomed by combining drug delivery of nanocarriers and targeting therapy. The drug-nanoparticle complexes can prolong blood circulation and enhance the local concentration of drugs in tumor region.[2] However, the physiological structure of blood-brain barrier (BBB) is the main hindrance to effectively treat brain-related disease by non-invasively therapeutic strategies because of BBB regulates the passage of only necessary substrates from blood circulation to brain tissues.[3] BBB provides a natural shield for brain against the invasion of various toxins and infected cells from circulating blood, so BBB also limits the brain uptake of diagnostic and therapeutic agents resulting in lower therapeutic efficiency.[4] Many methods have been used to nonspecifically disrupt the BBB to allow therapeutic agents entrance into brain, but these methods may allow circulating toxins from blood to get into the brain.[3] Thus, searching for safe and effective platforms that can delivery therapeutic drugs across the BBB to specifically kill glioma cells is under extensive and urgent investigation. Herein, we developed the biocompatible and BBB-permeated nanocomposites that were composed of paramagnetic iron oxide (Fe_3O_4) nanoparticles and biodegradable polymer (alginate; alg) as an nanocarrier for anticancer drug (doxorubicin; Dox) in brain cancer therapy. Furthermore, the alg-Fe_3O_4 NPs were conjugated with BBB-permeated G23 peptides that were able to increase the penetration of BBB for brain tumor treatment (shown in Scheme 1). As the results, we present this proof of concept that that G23 peptide-conjugated nanocomposites (G23-alg-Fe_3O_4 NPs) could cross the BBB successfully and enter the inside of brain tissue in the magnetic resonance imaging and immunohistochemistry (IHC). In addition, the *in vitro* and *in vivo* assays of brain cancer therapies also show significantly therapeutic efficiency when the C6 brain cancer cells (rat glioma) were treated with doxorubicin (Dox)-encapsulated nanocomposites (Dox/G23-alg-Fe_3O_4 NPs). These nanocomposites could be potentially used as a theranostic platform in brain-related diseases.

Reference:

[1] J. T. Huse, E. C. Holland, *Nat. Rev. Cancer* **2010**, *10*, 319-331.

[2] I. van Rooy, S. Cakir-Tascioglu, *et al.*, *Pharm. Res.* **2011**, *28*, 456-471.

[3] E. A. Neuwelt, *et al.*, *Nat. Rev. Neurosci.* **2011**, *12*, 169-182.

[4] R. Cecchelli, *et al.*, *Nat. Rev. Drug Discovery* **2007**, *6*, 650-661.

AUTHORS (LAST NAME, FIRST NAME): Su, Chia-Hao[1, 2]; Cheng, Fong-Yu[3]

INSTITUTIONS (ALL):

1. Center for Translational Research in Biomedical Sciences, Kaohsiung Chang Gung Memorial Hospital, Kaohsiung, Taiwan.

2. Department of Biomedical Imaging and Radiological Sciences, National Yang Ming University, Taipei, Taiwan.

3. Institute of Oral Medicine and Department of Stomatology, College of Medicine,, National Cheng Kung University and Hospital, Tainan, Taiwan.

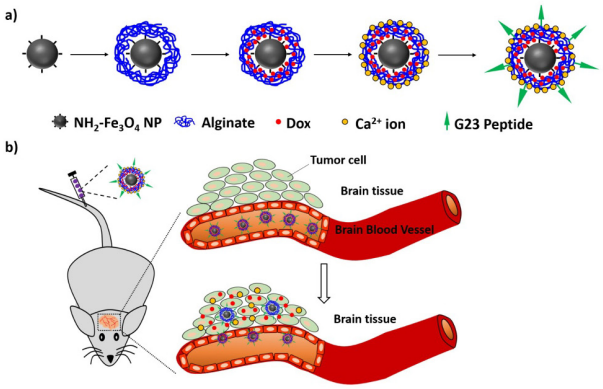

Scheme 1. a) Schematic synthesis process of bio-safety BBB-permeated nanocarriers. b) Schematic illustrating the mechanism of BBB-permeated nanocarriers across the BBB and Dox release from nanocarriers inside brain region to treat tumor cell.

CONTROL ID: 2216617

TITLE: Use of organic iron oxide nanoparticles in magnetically controlled embolization applications

PRESENTER: Dustin Osborne

ABSTRACT BODY:

Abstract Body: Introduction:

Some organically synthesized iron oxide nanoparticles have been shown to be highly magnetic compared to other synthetic methods of nanoparticle creation. Embolization is a technique by which the blood supply to a specific region is stopped. In some cases, it is necessary that this be permanent, while in others, it is desirable that the embolization be reversed. This work examines the use of highly magnetic organic iron oxide nanoparticles for creating controlled embolization events in a mouse tail vein model.

Materials and Methods:

All work was performed under the auspices of a University of Tennessee IACUC approved protocol.

Nanoparticles were grown using methods developed by Phelps, et. Al. Nanoparticles were isolated into a solution of PBS and injected via the tail vein. One set of mice were injected in the presence of a localized magnetic field with the edge of the magnets at the base of the tail. The other set of mice were controls injected with no magnetic field present. All mice were sacrificed after injection.

Visual inspection and microCT were used to determine if the magnetic field was able to create a controlled embolism at the site of the magnetic field due to aggregation of particles. Visual inspection examined the tail for any visual signs of embolism of the tail vein with and without the magnetic field in place.

microCT was performed using the Inveon Trimodality platform. Data nalysis was performed using the Inveon Research Workplace. CT scans of all mice were examined for signs of focal contrast in the tail vein corresponding to nanoparticle aggregation and the lack of enhancement in controls. Regions of interest (ROIs) were drawn on the sites of the embolus to assess the degree of contrast enhancement.

Results:

Visual inspection and microCT of mice injected using no magnetic field showed no signs embolism and no visible areas of contrast enhancement.

Visual inspection of nanoparticle injection sites in the presence of a magnetic field showed signs of embolization with focal regions of blood pool appearing in the tail vein indicative of a local embolus. microCT confirmed findings from visual inspection with focally enhanced contrast in the tail vein corresponding to magnetic field locations. ROI analysis indicated significant contrast enhancement at the site of embolism with maximum HU values of 86% of mean bone HU values in the tail.

Conclusions:

microCT analysis showed no focally enhanced regions of contrast in the tail vein following injection when no magnetic field was present, suggesting little or no aggregation of particles. In the presence of a magnetic field, the particles are visible as a locally enhanced region in the tail, indicating the formation of an embolus in the desired location. Visual inspection and microCT of iron nanoparticles injected in the presence of a magnetic field suggest that these nanoparticles may be used to create controlled embolic events by which temporary embolism may be achieved. Further work is underway to examine the temporary nature of these embolic events and to develop coatings that will prevent unwanted platelet aggregation around the particle clusters.

AUTHORS (LAST NAME, FIRST NAME): Osborne, Dustin[1]; Neveu, Melissa[1]; Kennel, Stephen[1]

INSTITUTIONS (ALL):

1. Graduate School of Medicine, University of Tennessee, Knoxville, TN, United States.

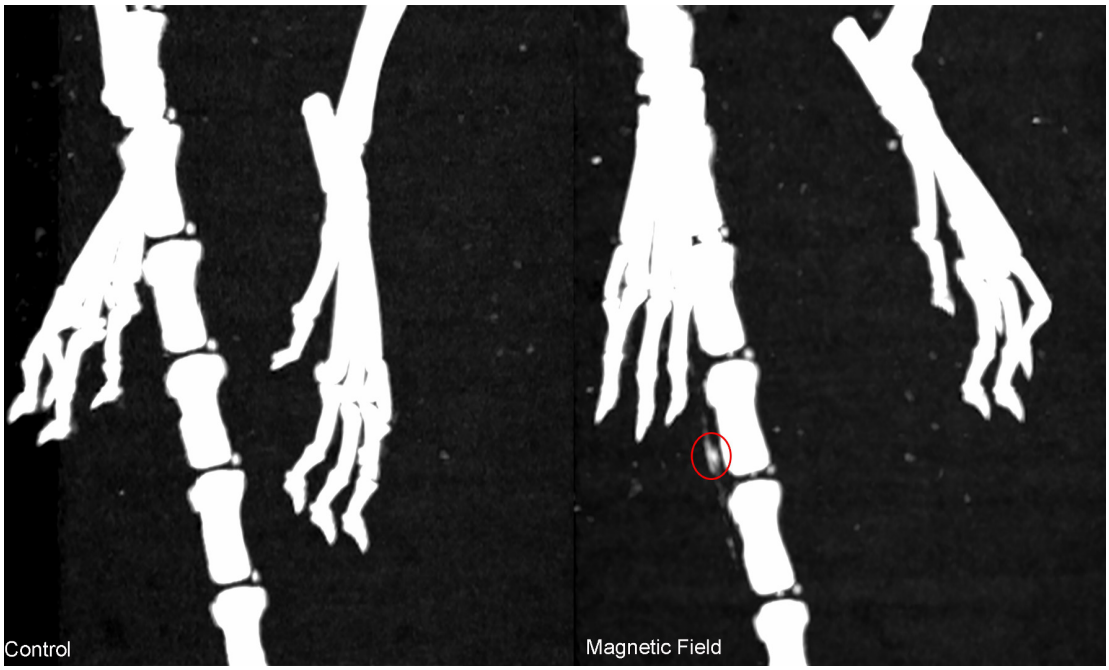
Control
Magnetic Field

CONTROL ID: 2233455

TITLE: Fluorescence imaging of lymph nodes and afferent lymph vessels in an in-vivo rat model differentiates normal from cancer-bearing nodes

PRESENTER: Alisha DSouza

ABSTRACT BODY:

Abstract Body: *Purpose:* Morbidity and complexity involved in lymph node staging via surgical resection and biopsy call for staging techniques that are less invasive. While visible blue dyes and lymphoscintigraphy are used to locate the sentinel lymph nodes from the draining lymphatic vessels near a tumor, they do not provide a metric to evaluate presence of cancer in those nodes.

Hypothesis: By interpreting relative fluorescence from methylene blue tracing through feeding lymphatic ducts relative to lymph nodes, quantitative differentiation would be possible between tumor-bearing and normal lymph nodes due to cancer-cell disruption of flow through nodes.

Innovation: In this work non-cancer specific lymphatic uptake differences in lymph nodes are quantitatively correct using fluorescence imaging of afferent lymph vessels.

Procedure: Planar fluorescence imaging of rats was used, with luciferase-expressing cancer cells injected directly into axillary lymph nodes. Cancer presence in nodes was confirmed by bioluminescence imaging before and after fluorescence imaging. Methylene blue was injected, and lymphatic uptake from the injection sites to lymph nodes was imaged at approximately 2 frames/minute. Kinetic analysis was performed using an afferent vessel input model approach. The lymphatic flow from injection sites to nodes was imaged and the relative kinetics from feeding lymphatic ducts relative to lymph nodes was quantified.

Results: Large variability existed in raw fluorescence and transport patterns within each cohort resulting in no systematic difference between average nodal uptake in normal, sham control and cancer-bearing nodes (See figure a–m). However, when the signal from the afferent lymph vessel fluorescence was used to normalize the signal of the lymph nodes, the high signal heterogeneity was reduced. Using a model, the lymph flow through the nodes (F_{LN}) was estimated to be 1.5 ± 0.6 ml/g/min in normal nodes, 1.5 ± 0.5 ml/g/min in sham control nodes, and reduced to 0.5 ± 0.2 ml/g/min in cancer-cell injected nodes. Thus showing significant difference ($p = 0.0002$) between cancer-free and cancer-bearing nodes in normalized flow (see figure n). This process of normalized flow imaging is promising and could potentially be used as an in situ tool to detect metastatic involvement in nodes.

Impact: This work demonstrates the ability to use fluorescence properties of a clinically approved blue dye, methylene blue, already in use in the sentinel lymph node procedure to identify cancer-bearing nodes based on changes in lymph flow rate through them. Sensitivity and specificity limits are yet to be established on this approach, but would potentially be helpful in identifying lymph nodes at advanced stages of metastasis.

AUTHORS (LAST NAME, FIRST NAME): DSouza, Alisha V.[1]; Elliott, Jonathan T.[1]; Gunn, Jason R.[1]; Barth, Richard J.[2]; Samkoe, Kimberley S.[1, 3]; Tichauer, Kenneth M.[4]; Pogue, Brian W.[1]

INSTITUTIONS (ALL):

1. Thayer School of Engineering, Dartmouth College, Hanover, NH, United States.
2. Department of Medicine, Geisel School of Medicine at Dartmouth, Hanover, NH, United States.
3. Department of Surgery, Geisel School of Medicine, Hanover, NH, United States.
4. Biomedical Engineering, Illinois Institute of Technology, Chicago, IL, United States.

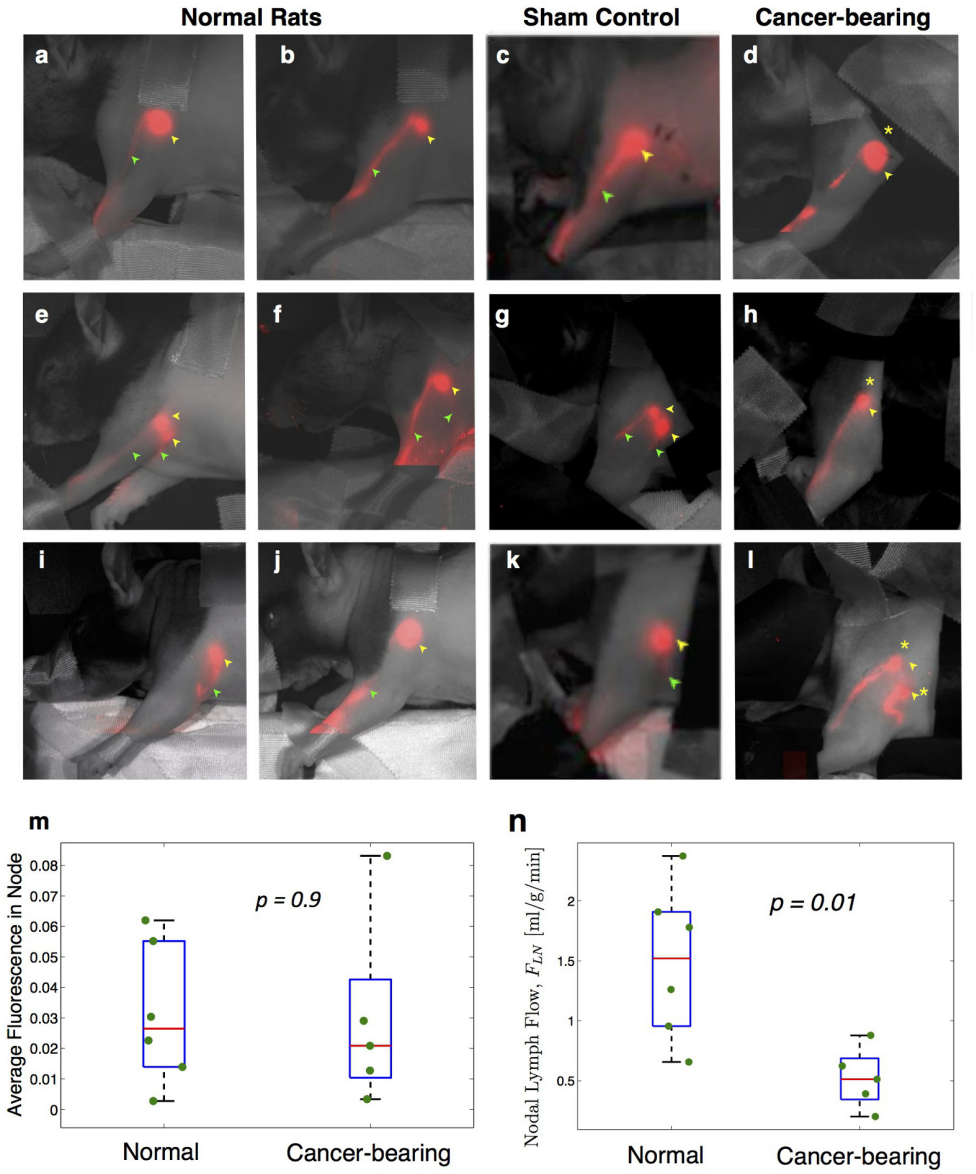

Figures a–l show uptake in rats, green arrow points to afferent lymph vessel and yellow arrow points to lymph node. **a,b,e,f,i,l** correspond to normal rats. Large variation is seen in uptake patterns**. c,g,k** shows sham control rats which had surgeries performed on them but PBS was injected in place of cancer-cells. **d,h,l** shows cancer-bearing rats. **m** shows that there is no significant difference in average fluorescence signal from nodes. **n** Nodal lymph flow estimated by a model-based approach shows that changes in lymph flow through nodes due to cancer presence are significant.

CONTROL ID: 2233618

TITLE: Dual Tracer Imaging implemented on a Hybrid Ultrasound-guided multi-spectral fluorescence tomography system to estimate lymph node tumor burden in-vivo

PRESENTER: Alisha DSouza

ABSTRACT BODY:

Abstract Body: *Background:* Morbidity and complexity involved in lymph node staging via surgical resection and biopsy call for staging techniques that are less invasive. While visible blue dyes, fluorophores and lymphoscintigraphy are routinely used to locate the sentinel lymph nodes from the draining lymphatic vessels near a tumor, they rarely provide a metric to evaluate presence of cancer in those nodes in vivo. Using Lymph Node Molecular Concentration Imaging (LN-MCI) with a dual tracer approach in an in-vivo mouse metastasis model Tichauer et al. [1] demonstrated the ability to quantify micro-metastasis in nodes; here a fluorescent tracer targeted to cancer-specific cell receptors was injected and imaged along with a reference tracer to correct non-specific uptake and delivery heterogeneity. In order to allow for migration of such approaches to the clinical or surgical environment, there is a need for subsurface fluorescence imaging techniques adapted to perform dual channel data acquisition.

Methods: A hybrid high-frequency multi-spectral ultrasound guided fluorescence tomography system has been under development. This system combines the ability of high frequency ultrasound to localize superficial lymph nodes with subsurface fluorescence quantification techniques. Both modalities are co-registered to allow sampling of a common imaging plane. Figure 1 shows a photograph of the hybrid system. The tomography system was described in detail in [2] and has been adapted to hold a 633nm and 785nm excitation lasers, and 655nm (used along with 633nm laser to acquire fluorescence in the 700nm channel), and 800nm long pass emission filters (used along with 785nm laser to acquire fluorescence in the 800nm channel); these are set up to sequentially acquire fluorescence data alternately from each imaging channel.

Results: Initial system characterization and validation tests with a 700nm channel fluorophore, protoporphyrin IX, demonstrate the ability to quantify fluorescence at concentrations as low as 45nM at 4-6mm depth in tissue phantoms and 76nM at depth of 4mm in tumor simulating subcutaneous matrigel inclusion phantoms in mice. System depth sensitivity is dependent on amount of autofluorescence and fluorescent inclusion size and further testing of this system needs to be performed to establish sensitivity limits using phantoms with lymph node-sized inclusions. Figure 2 shows a normal murine lymph node imaged using the ultrasound system on board.

Impact: The ultrasound guided fluorescence tomography system could be integrated into a clinical setting as part of routine ultrasound imaging on cancer patients.

References

Fig. 2 Ultrasound image of a murine axillary lymph node (white arrow)

[1] K. M. Tichauer, K. S. Samkoe, J. R. Gunn, and S. C. Kanick, "Microscopic lymph node tumor burden quantified by macroscopic dual-tracer molecular imaging," vol. 20, pp. 1348-53, Nov 2014.

[2] B. P. Flynn, A. V. Dsouza, S. C. Kanick, S. C. Davis, and B. W. Pogue, "White light-informed optical properties improve ultrasound-guided fluorescence tomography of photoactive protoporphyrin IX," *Journal of Biomedical Optics,* vol. 18, pp. 046008-046008, 2013.

AUTHORS (LAST NAME, FIRST NAME): DSouza, Alisha V.[1]; Gunn, Jason R.[1]; Tichauer, Kenneth M.[2]; Pogue, Brian W.[1]

INSTITUTIONS (ALL):

1. Thayer School of Engineering, Dartmouth College, Hanover, NH, United States.
2. Illinois Institute of Technology, Chicago, IL, United States.

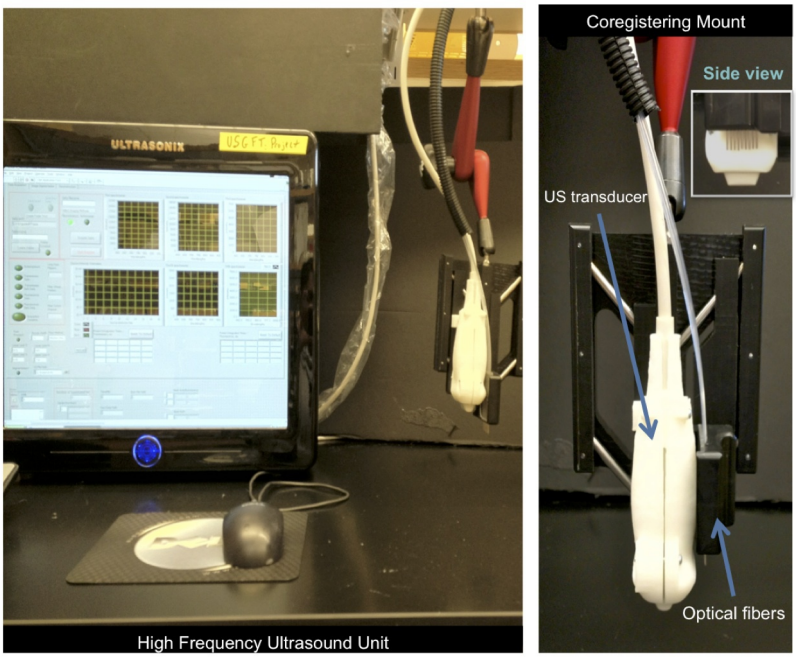

Fig. 1 UMSFT System

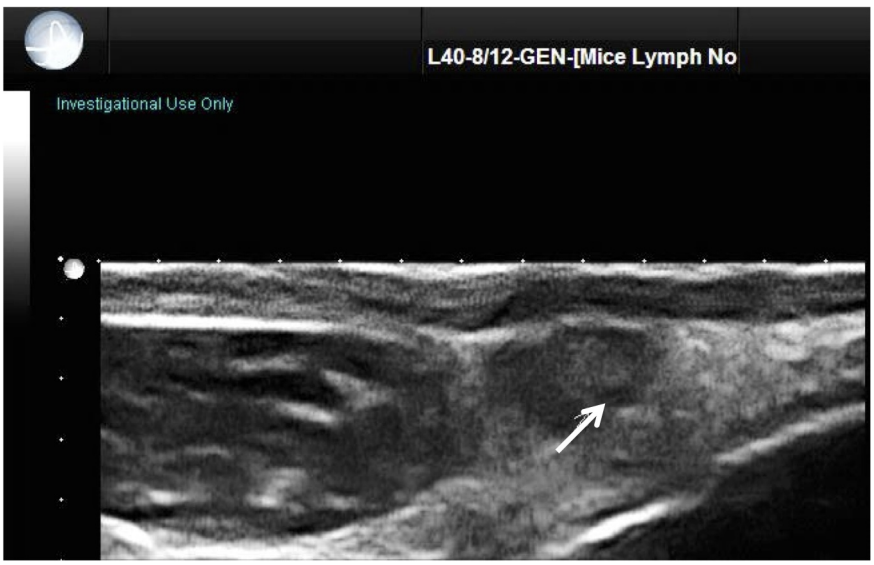

Fig. 2 Ultrasound image of a murine axillary lymph node (white arrow)

CONTROL ID: 2228344

TITLE: Tissue Biodistribution of Plasmonic Nanoparticles with Sub-Cellular Resolution Using Hyperspectral Microscopy and Machine Learning

PRESENTER: Orly Liba

ABSTRACT BODY:

Abstract Body: Plasmonic nanoparticles, such as gold nanorods (GNRs), are extensively used for molecular imaging and nanomedicine [1]. Measuring the biodistribution of the nanoparticles is important for understanding the efficiency and specificity of their binding and also for understanding their clearance mechanisms and circulation times.

Biodistribution of plasmonic nanoparticles is frequently done by using inductively-coupled plasma (ICP) techniques [2]. ICP provides the amount of gold atoms accumulated in the resected tissue, but is not able to spatially resolve the location of the particles due to its destructive nature to the tissue sample. Electron microscopy is often used to detect nanoparticles with a very high resolution [3], however, due to its small field of view (FOV) and lengthy sample preparation requirements, it is slow and labor intensive. Fluorescence and radioactivity tracing are also used but have limited sensitivity and spatial resolution, respectively. A more detailed picture of nanoparticles in tissue, including large FOVs, micron-scale spatial resolution and ultrahigh sensitivity, is imperative for understanding the mechanisms of biodistribution.

We propose a novel biodistribution method, based on hyperspectral dark-field microscopy combined with machine learning algorithms, to detect and localize plasmonic nanoparticles in the tissue anatomy with micron resolution. Unlike methods that asses the global amount of particles in a sample, this method is able to separate particles that are in circulation versus those that are bound to blood vessels or those that are in the extracellular space. The nanoparticles do not require any prior labeling and are detected only owing to their intrinsic plasmonic spectral peak. The automated nature of the detection algorithm provides an estimation of the quantity of nanoparticles, which can be measured by the ratio of pixels that contain nanoparticles to the total number of analyzed pixels.

We applied this method to perform a biodistribution study of GNRs in mice bearing ear tumors. We injected GNRs (Fig. a, b) intravenously to 20 mice with ear tumors. The ears were preserved 24h post injection, sectioned to 5 um slices and stained with H&E. We scanned the slices with a hyperspectral darkfield microscope (CytoViva HSI) with a 40x objective which provides a FOV of 200 um and pixel size of 400 nm. The scattering spectrum of each pixel was then pre-processed and classified as positive or negative for the existence of GNRs. Using this method we observed that significantly more GNRs appear in the tumor and around its blood vessels compared to the healthy tissue (Fig. c-i). We applied this method to slices of additional organs and were able to calculate the biodistribution of GNRs in the liver, spleen, lungs, muscle and kidney.

In summary, owing to its microscopic-level resolution, its efficient implementation and automated nature, this method provides valuable insight into biodistribution studies and can be a powerful tool for researchers.

[1] I. H. El-Sayed et al. Nano Letters 2005 5 (5)
[2] T. Niidome et al. J. of Controlled Release 2006 114 (3)
[3] B. D. Chithrani et al. Nano Letters 2006 6 (4)

AUTHORS (LAST NAME, FIRST NAME): Liba, Orly[1, 2]; SoRelle, Elliott[2, 3]; Shaviv, Dor[1]; Dalal, Roopa[4]; de la Zerda, Adam[2, 1]

INSTITUTIONS (ALL):
1. Electrical Engineering, Stanford University, Stanford, CA, United States.
2. Structural Biology, Stanford University, Stanford, CA, United States.
3. Biophysics Program, Stanford University, Stanford, CA, United States.
4. Ophthalmology, Stanford University, Stanford, CA, United States.

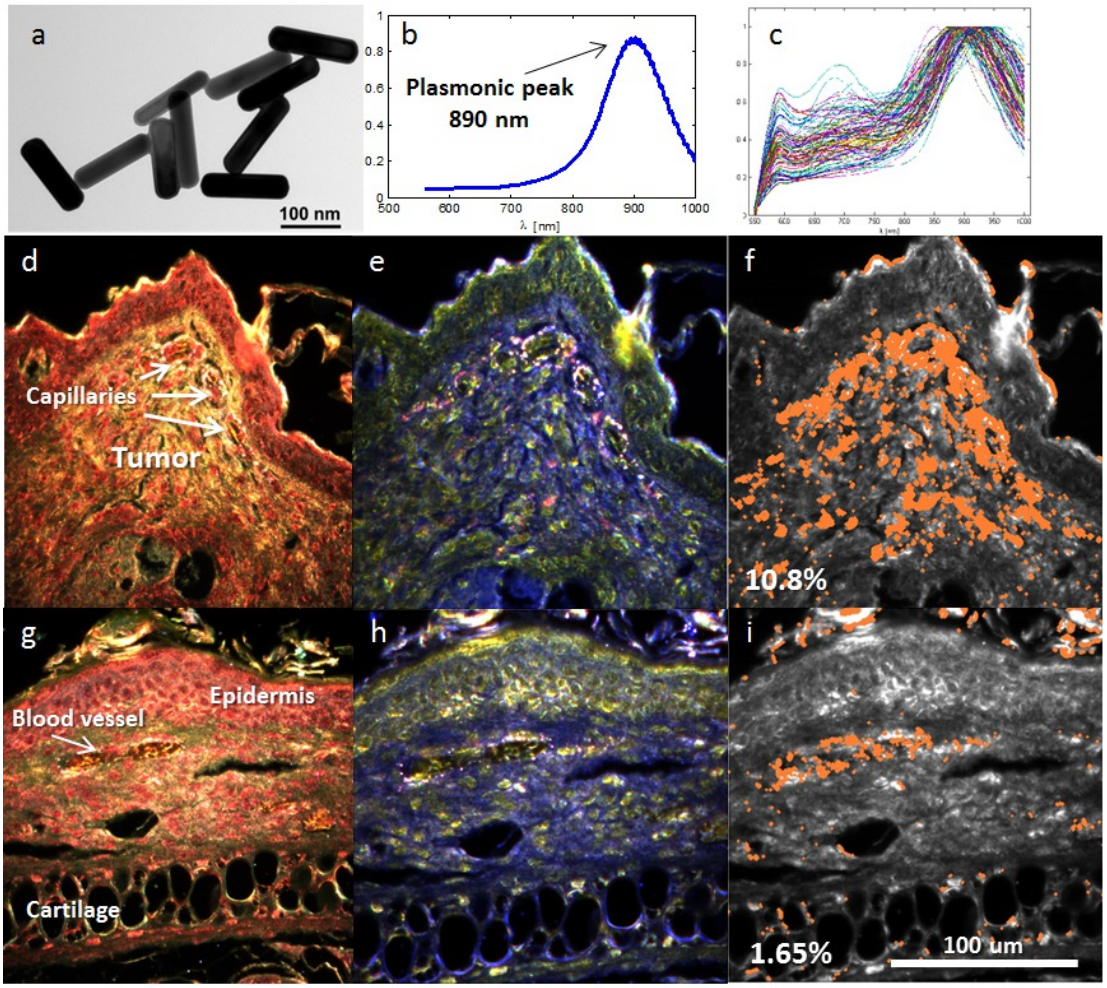

Figure: Detection of GNRs in healthy ear (g, h, i) and tumor (d, e, f). a) A TEM image of the injected GNRs. b) The average scattering spectrum of the GNRs in water, measured with the hyperspectral microscope. c) Normalized spectrums of the pixels classified as GNRs in f. d, g) Dark-filed images of the tissue slides. e, h) Representation of the hyperspectral data which highlights the GNRs. f, i) Detected GNRs shown in orange on top of the hyperspectral image. The ratio of pixels with GNRs to total processed pixels is 10.8% in tumor and 1.65% in the healthy tissue. The GNRs in the healthy tissue are still circulating in the blood while the GNRs in the tumor are both in the capillaries and inside the tumor mass.

CONTROL ID: 2218128

TITLE: Molecular imaging of polymer nanoparticles facilitated multi-microRNA therapy for triple negative breast cancer in small animal model

PRESENTER: Rammohan Devulapally

ABSTRACT BODY:

Abstract Body: Oncogenesis, in part, has been associated with dysregulated expression of various microRNAs (miRs). Therefore, targeting endogenous miRs is considered a unique molecularly targeted anticancer therapy. Anti-miRs are chemically modified small oligonucleotides, which are used to block the function of endogenous miRs that regulate various genes involved in major cellular processes. However, the systemic delivery of miRs and anti-miRs *in vivo* suffers from its poor stability in the nuclease rich blood circulation. Therefore, delivery vehicles that can protect and deliver intact miR- and anti-miR combinations to tumors *in vivo*, are needed for achieving successful therapeutic efficacy. Antagonizing endogenous miR-10b has been reported to inhibit tumor metastatic spread to the lungs, and miR-21 impairs tumor cell growth, induces apoptosis and reduces migration and invasion, in breast cancer cells highly expressing miR-10b and miR-21. The aim of the present study is to synthesize anti-miR-21 and anti-miR-10b co-loaded urokinase plasminogen activator receptor (uPAR) targeting peptide (uPA) conjugated PLGA-*b*-PEG nanoparticles (NPs) and evaluate its *in vitro* and *in vivo* efficacy in xenografts of human breast cancer in small animal model by molecular imaging. Here, we present the therapeutic outcome accomplished in triple negative breast cancer (TNBC) by concurrently antagonizing miR-10b-induced metastasis and miR-21-induced anti-apoptosis, using anti-miR-10b and 21 delivered by NPs. We synthesized the PLGA-*b*-PEG-uPA and optimized the anti-miRs co-loading using w/o/w method with highest loading efficiency of up to 1000 anti-miR molecules per NP (**Figure 1a**, **Table 1**). We characterized the PLGA-*b*-PEG-uPA using ^{1}H-NMR and MALDI-TOF techniques, and NPs size and shape using dynamic light scattering and TEM (**Figure 1b**). The results of qRT-PCR analysis indicate that co-loading of anti-miR-10b-21 in NPs was found to be at almost equimolar concentrations (**Figure 1c**). Subsequently, we have studied the anti-miRs release profile from NPs, cellular uptake, serum stability, and the following synchronous blocking of endogenous miR-21 and 10b function in MDA-MB-231-Fluc-eGFP cells in culture, and in tumor xenografts in mice using optical bioluminescence imaging. Results show that multi-target antagonization of endogenous miRNAs might be an efficient therapeutic approach for targeting metastasis and anti-apoptosis in the treatment of metastatic cancer. Anti-miR-21 and 10b individually loaded uPA-NPs showed 1.9 folds, ($p<0.05$) reduction in tumor growth compared to control uPA-NPs treated mice. Whereas anti-miR-21 and 10b co-loaded uPA-NPs treated mice showed nearly 3.2 folds ($p<0.001$) reduction in tumor growth compared to the control uPA-NPs treated mice, and 40% less tumor reduction compared to scrambled-uPA peptide conjugated NPs, thus signifying a potential new therapeutic strategy for TNBC (**Figure 1d-e**). In summary, we have successfully synthesized uPAR-targeting NPs and developed an effective procedure for co-loading anti-miRs with higher loading efficiency. The concurrent delivery of anti-miR-10b and 21 has a cumulative effect in decreasing TNBC cell proliferation.

AUTHORS (LAST NAME, FIRST NAME): Devulapally, Rammohan[1]; Sekar, Thillai V.[1]; Foygel, Kira[1]; Massoud, Tarik F.[1]; Willmann, Juergen K.[1]; Paulmurugan, Ramasamy[1]

INSTITUTIONS (ALL):

1. Radiology, Stanford University, Palo Alto, CA, United States.

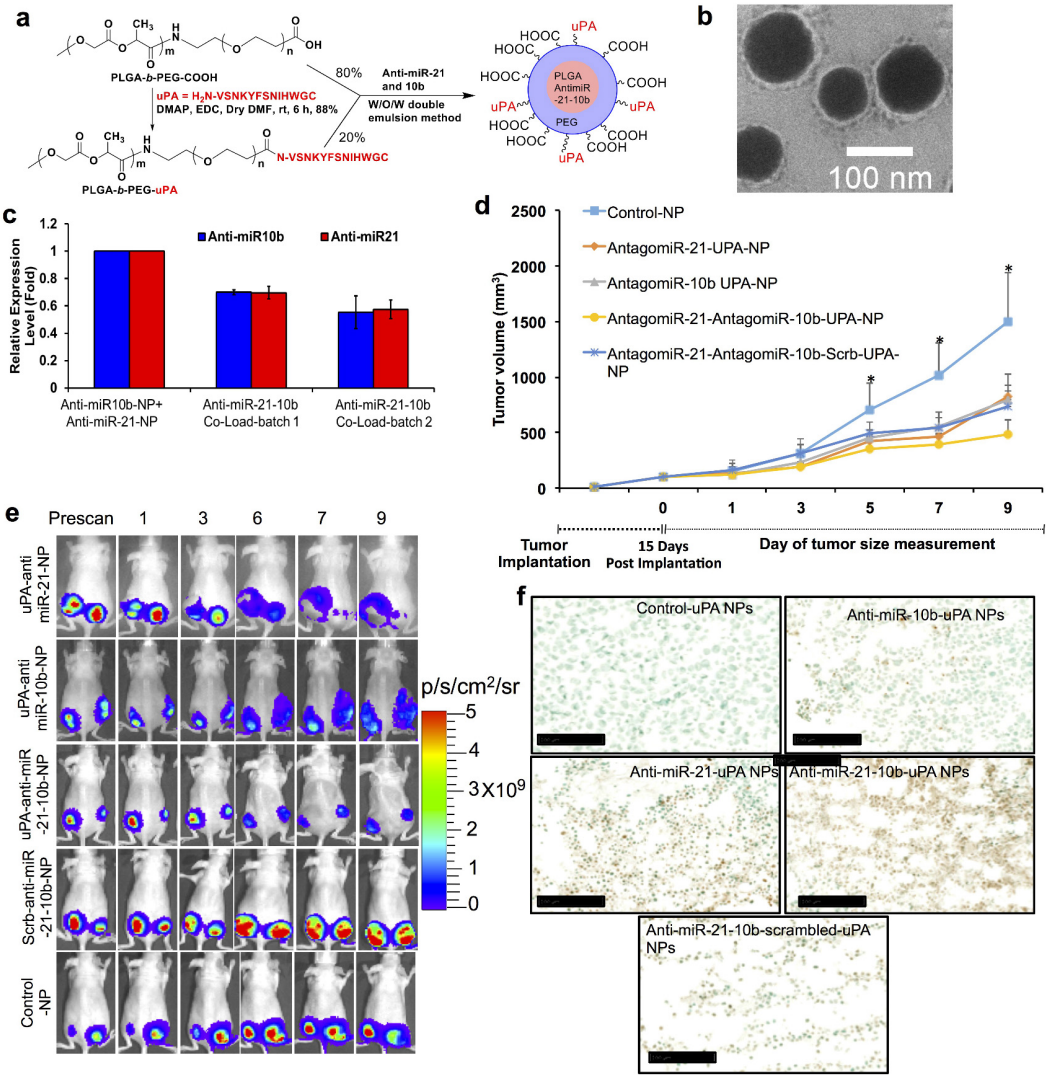

Figure 1. a) Synthesis of uPA peptide conjugated PLGA-*b*-PEG copolymer and anti-miR-10b and anti-miR-21 co-loaded nanoparticles (NPs) preparation using water-in-oil-in-water (w/o/w) method. **b**) Transmission electron microscopy (TEM) image of 1% phosphotungstic acid stained anti-miRs co-loaded PLGA-*b*-PEG NPs. **c)** Evaluation of anti-miR-10b and anti-miR-21 co-loading efficiency in PLGA-*b*-PEG-NPs by TaqMan-qRT-PCR analysis**. d-f**) *In vivo* tumor growth analysis and bioluminescence imaging of mice bearing MDA-MB-231-Fluc-eGFP tumors that were treated with anti-miR-10b and anti-miR-21 loaded or co-loaded PLGA-*b*-PEG-uPA, PLGA-*b*-PEG-Scrb-uPA and control uPA NPs. **d**) Tumors growth volume (mm^3) measured in different treatment groups over time. **e**) Bioluminescence images of animals (n = 10, 5 animals bearing two tumors, in each for each treatment group) treated with NPs over time. **f**) TUNEL staining of TNBC tumor tissues of animals treated with different NPs.

CONTROL ID: 2233580

TITLE: Synthesis of gemcitabine and anti-miR-21 coloaded polymer nanoparticles and its cytotoxicity evaluation in hepatocellular carcinoma cells

PRESENTER: Rammohan Devulapally

ABSTRACT BODY:

Abstract Body: Hepatocellular carcinoma (HCC) is a primary cancer of liver and its tumors are found to be with poor chemo-responsive to anticancer agents. Low permeability of drugs, inherent and acquired drug resistance are obstacles commonly encountered in HCC treatment. Superior treatment approaches, improved chemotherapeutic agents, and targeted drug delivery systems are desirable for improving chemotherapy in HCC. Gemcitabine (GEM) is a nucleoside analogue currently used as a chemotherapeutic agent for treating different types of cancers, including HCC. When administered as a free drug, GEM undergoes rapid enzymatic degradation and displays numerous side effects, including fever, nausea, and hair loss. To overcome some of these adverse side effects tumor specific targeted delivery of GEM is required. MiR-21 is an oncomiR, and its overexpression is associated with tumorigenesis and drug resistance in a variety of cancers, including HCC. Anti-miRs are small chemically synthesized single stranded oligonucleotides, which are used to block endogenous miRs function. Up-regulation of miR-21 has been reported to promote HCC cell proliferation, angiogenesis, invasion, and reduce cell death. Here, we present our results in synthesis of GEM-anti-miR-21 coloaded PLGA-*b*-PEG nanoparticles (NPs) and its *in vitro* therapeutic efficacy in HCC cells. We synthesized the PLGA-*b*-PEG NPs and optimized the GEM and anti-miR-21 co-loading efficiency using w/o/w method (**Figure 1a**). We characterized the NPs using DLS and TEM (**Figure 1b-1c**). The cellular uptake of NPs was studied using GEM-cy5-labelled-anti-miR-21 coloaded NPs in Hep3B cells. Results showed time dependent uptake of NPs in inside the cells; at 1 h - 4 h time points NPs were observed in the periplasmic space (**Figure 1d**), and later time points NPs entered into the cytoplasm of the cells. High level of NPs was observed in cytoplasm after 24 h. Since, GEM is a cytotoxic drug, we have studied the dose dependent toxicity analysis in Hep3B cells. Dose dependent cell viability analyses of free GEM, GEM and anti-miR-21 coloaded NPs were evaluated in Hep3B cells using MTT assay at 24 h, 48 h and 72 h post-treatment (**Figure 1e)**. Treatment with control NPs did not show any considerable cytotoxic effects. However, treatment with free GEM, GEM-anti-miR-21 coloaded or individually loaded NPs resulted in dose dependent cytotoxicity, and the highest cytotoxic effect was achieved in cells treated with NPs coloaded with GEM-anti-miR-21. GEM-anti-miR-21 coloaded NPs showed 1.7 ($p<0.001$), 1.4 ($p<0.01$), 1.3 ($p<0.005$) folds more cytotoxicity than free GEM, GEM-NPs, and anti-miR-21-NPs, respectively at 1 μM concentrations (**Figure 1e**). Complete cell death was observed in cells treated with NPs loaded with GEM (10 μM) and anti-miR-21 (50 nM). In summary, we have successfully synthesized PLGA-*b*-PEG NPs coloaded with GEM and anti-miR-21. Cytotoxicity evaluation in Hep3B cells showed increased treatment efficacy by NPs coloaded with GEM-anti-miR-21 compared to NPs with equal concentration of drug or anti-miR-21 separately, signifying that down-regulation of miR-21 can decrease Hep3B cell proliferation, invasion and viability.

AUTHORS (LAST NAME, FIRST NAME): Devulapally, Rammohan[1]; Sekar, Thillai V.[1]; Paulmurugan, Ramasamy[1]

INSTITUTIONS (ALL):

1. Radiology, Stanford University, Palo Alto, CA, United States.

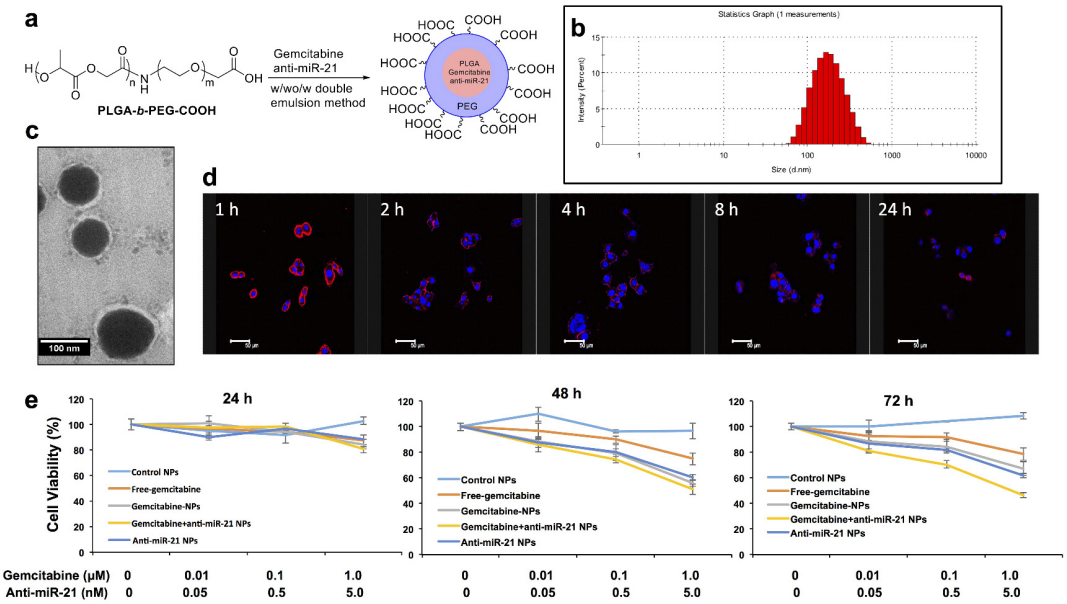

Figure 1. **a**) Synthesis of PLGA-*b*-PEG nanoparticles (NPs) using water-in-oil-in-water (w/o/w) double emulsion method. **b**) Dynamic Light scattering (DLS) image of NPs. **c**) Transmission electron microscopy (TEM) image of NPs taken after staining with 1% phosphotungstic acid. **d)** Cellular uptake of cy5-labelled-anti-miR-21 and GEM coloaded NPs in HeP3B cells, imaged by confocal fluorescent microscopy. **e**) Dose response of Hep3B cells (cells maintained in 2% MEM medium) treated with control NPs, free GEM, GEM NPs, GEM and anti-miR-21 coloaded NPs, and anti-miR-21 NPs for 24 h, 48 h, and 72 h by MTT assay. In case of control NPs, equal polymer weight of plain NPs (without ani-miR-21 and 4-OHT) related to drug loaded NPs for each concentrations was added.

CONTROL ID: 2218130

TITLE: Antiproliferative effect of microRNA and 4-hydroxytamoxifen coloaded urokinase plasminogen activator receptor (uPAR) targeted polymer nanoparticles in ER+ breast cancer cells

PRESENTER: Rammohan Devulapally

ABSTRACT BODY:

Abstract Body: Breast cancer is one of the leading cause of cancer death among women worldwide. Majority of breast cancers are estrogen receptor-positive (ER+) and hormone dependent. Neoadjuvant anti-estrogen therapy has been frequently employed to reduce tumor mass prior to surgery. Tamoxifen is widely used in the clinic for the treatment of ER+ breast cancers. However, most ER+ breast tumors develop tamoxifen resistance. 4-Hydroxytamoxifen (4-OHT) is an active metabolite of tamoxifen that displays higher affinity for estrogen receptors than tamoxifen. MicroRNA-21 (miR-21) is a small non-coding RNA that regulates several tumor suppressor and apoptotic genes, and contributes to chemoresistance in various cancers, including breast cancer. Anti-miRs are chemically synthesized small oligonucleotides that are used to inhibit the function of endogenous miRs. Since, tamoxifen resistant ER+ (MCF7) breast cancer cells significantly over-express urokinase plasminogen activator receptor (uPAR), we have selected uPA peptide as a targeting ligand. Here, we present the therapeutic outcome accomplished in ER+ breast cancer cells (MCF7 and 4T1) in response to the treatment of anti-miR-21 and 4-OHT coloaded uPA peptide conjugated PLGA-*b*-PEG nanoparticles (NPs). We synthesized the PLGA-*b*-PEG polymer and conjugated to uPA and scrambled (scrb) uPA peptides. Subsequently, we prepared the 4-OHT and anti-miR-21 individually, and co-loaded NPs using water-in-oil-in-water double emulsion method (**Figure 1a**). We have characterized the synthesis of PLGA-*b*-PEG-uPA and scrb-uPA by ^{1}H-NMR and MALDI-TOF, and NPs size and shape by Dynamic Light Scattering and Transmission Election Microscopy (**Figure 1b-1c**). Subsequently, we evaluated NPs for the 4-OHT induced anti-proliferation and anti-miR-21 induced apoptotic effect in ER+ breast cancer (MCF7, 4T1) cells (**Figure 1d**). Cell proliferation analysis indicated that control uPA NPs and anti-miR-21-uPA NPs did not show any considerable cell growth inhibition, whereas, anti-miR-21 and 4-OHT coloaded uPA-NPs significantly inhibited MCF7 and 4T1 cells growth compared to that of free 4-OHT (2.4 folds, $p<0.01$ and 2.2 folds, $p<0.01$) and untreated cells (6.0 folds, $p<0.001$; 2.3 folds, $p<0.001$) respectively at 1 μM concentration. However, 4-OHT-anti-miR-21 coloaded scrambled-uPA-NPs showed similar cell growth inhibitory effects as 4-OHT-anti-miR-21-uPA NPs. However, we expect uPA targeted NPs should show significant effect *in vivo* compare to non-targeted NPs, because of more targeted NPs uptake can occur in tumors. In summary, we have successfully synthesized uPAR-targeting peptide conjugated PLGA-*b*-PEG NPs and developed an efficient method for co-loading of 4-OHT and anti-miR-21. The simultaneous delivery of 4-OHT and anti-miR-10b has a collective effect in reducing ER+ cell proliferation. *In vivo* anti-proliferative effects of these NPs in small animal (mice) xenografts are currently under investigation.

AUTHORS (LAST NAME, FIRST NAME): Devulapally, Rammohan[1]; Foygel, Kira[1]; Sekar, Thillai V.[1]; Paulmurugan, Ramasamy[1]

INSTITUTIONS (ALL):

1. Radiology, Stanford University, Palo Alto, CA, United States.

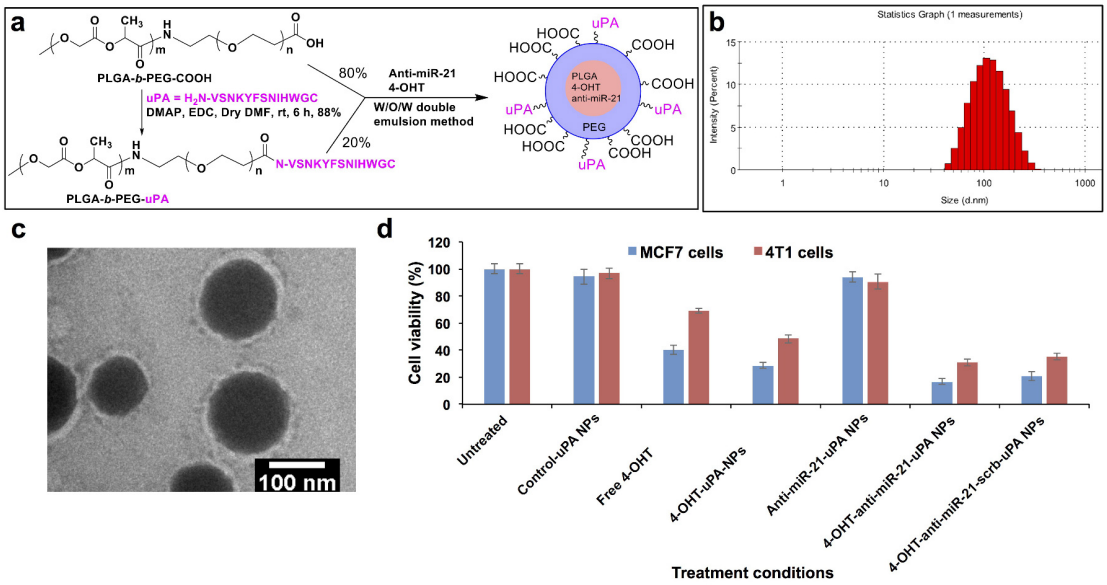

Figure 1. a) Synthesis of uPA peptide conjugated PLGA-*b*-PEG copolymer and anti-miR-21, 4-OHT individually or coloaded nanoparticles formulation. **b**) Dynamic Light Scattering image of NPs **c**) Transmission electron microscopy image of 1% phosphotungstic acid stained 4-OHT and anti-miR-21 coloaded PLGA-*b*-PEG NPs **d**) *In vitro* cell growth analysis of MCF7 and 4T1 cells that were treated with free 4-OHT, 4-OHT and anti-miR-21 loaded or co-loaded PLGA-*b*-PEG-uPA, PLGA-*b*-PEG-Scrb-uPA and control uPA NPs for 7 days.

CONTROL ID: 2228779

TITLE: Correlation of FDG-PET imaging with fibronectin expression in non-small cell lung cancer

PRESENTER: Bi Fang Lee

ABSTRACT BODY:

Abstract Body: FDG-PET is good for the evaluation and assessment of the extension, malignancy, and clinical stage. Because the lung cancer has the high glucose metabolism enough to accumulate t FDG to make the lesions visualize. Fibronectin (FN) is a biomarker of tumoral metastatic ability. It is a high-molecular-weight glycoprotein containing about 5% carbohydrate that binds to membrane spanning receptor proteins called integrins. The aim is to investigate whether FDG PET determines tumoral metastatic ability.

Under the approval of IRB in NCKU hospital, 46 patients had been studied. The average age was 61.45 ± 21.88 years-old (range: 21-78). There were 20 females and 26 males. There are 34 adenocarcinoma, 5 squamous cell carcinoma, 1 large cell carcinoma, and 5 bronchoalveolar cancer. The stroma FN expression via IHC staining show the correlation with pathological stage. The patients with positive stroma FN expression have worse outcome. As for positive stroma FN group, SUV via FDG-PET-CT is higher than negative stroma FN group. [positive stroma FN group (n=16): medium SUV=7.8; negative stroma FN group (n=19): medium SUV=3; $p<0.001$]

Stroma FN expression is correlated with uptake of FDG-PET in NSCLC lung cancer patients. The uptake of FDG-PET may have potential to predict stroma FN expression of tumor. FDG PET could determine tumoral metastatic ability.

AUTHORS (LAST NAME, FIRST NAME): Lee, Bi Fang[1]; Chiu, Nan-Tsing[1]

INSTITUTIONS (ALL):

1. National Cheng Kung University Hospital, Tainan, Taiwan.

(No Image Selected)

CONTROL ID: 2219595

TITLE: Prognostic surrogate markers for survival, a case series for a novel antiangiogenic therapy (Multi-targeted Epigenetic therapies/MTET)

PRESENTER: M. Nezami

ABSTRACT BODY:

Abstract Body: Quantitatively measured genomic imbalances (GI) identified in disseminated tumor cells by DNA genotyping (oncogenes or oncosuppressors), are recognized in literature to correlate with patient prognosis and survival. These imbalances have shown correlation with disease progression and relapse in variety of solid tumors, as an independent prognostic marker, beyond TNM grading. Therefore, therapeutic interventions geared accordingly to minimize the number of these circulatory tumor cells are speculated to reduce the residual disease as a target of therapy to improve survival. Here we hypothesize that the disease progression is quantitatively measurable, therefore, modifiable by a customized plan of care. We also show samples of treated cases with a novel anti angiogenic therapy targeting the disseminated tumor cells and incorporating this tool as a companion diagnostic to monitor clinical response.

Aggregated tumor cells are a prerequisite for metastases . That said, Majority of the antineoplastic agents fail to fully eradicate the disseminated tumor cells, therefore detection of minimal residual disease is vital to predict the future outcome. It is hypothesized that dissemination of cancer cells from the primary tumor occurs in nearly all patients, leading to the definition of cancer spread as a systemic disease. This theory becomes even more profoundly relevant considering the available literature showing that tumor Cells in metastases do not reflect the genotype of the matched primary tumor. These differences may be explained by the heterogeneity of primary tumors leading to extravastion of distinct subclones and/or by additional mutational events occurring in MRCC during circulation and retention in different organs leading eventually to sessile micro metastases and recirculation

Loss of heterozygosity due to loss of one allele in an oncosuppressor gene may uncover a phenotypic recessive mutational event on the other allele. Therefore genomic imbalances in such genes, can add to the mutational events in onco promoter genes also identifies through this method. The major genomic difference between primary tumor and MRCC favors the analysis of MRCC in the blood as the real target for systemic therapy. This system enables us to estimate prognosis and prediction of cancer patients leading to a new approach in cancer management. Here we review a summary of four cases with advanced disease treated with a novel therapy targeting the DNA genomic imbalances related to the disease progression and we show measurable efficacy on number and nature of such markers identified post therapy.

Conclusion: Summarizing our data we present a new novel therapy that aims to eradicate the detected disseminated tumor cells, especially the quantity and the composition of genomic imbalances which we were able to correlate with the actual clinical outcome of the patients.

AUTHORS (LAST NAME, FIRST NAME): Nezami, M.[1]; Gould-Simon, Aron [1]

INSTITUTIONS (ALL):

1. Pacific Medical Center of Hope, Fresno, CA, United States.

(No Image Selected)

CONTROL ID: 2222914

TITLE: Differential Kinetics of DNA Release in Myocardial Infarction and Ischemia-Reperfusion Injury

PRESENTER: Howard Chen

ABSTRACT BODY:

Abstract Body: Cardiomyocyte (CM) death and extracellular DNA release play a central role in the pathogenesis of acute ischemic heart disease. During ischemic stress, CMs undergoing acute necrotic cell death release DNA through their ruptured cell membranes into the extracellular space. The extracellular DNA present at the site of injury triggers a cascade of events leading to inflammation, immune infiltration, and further cell death. We have previously reported a Gadolinium-thiazole orange (TO) magnetic resonance (MR) contrast agent that targets extracellular DNA exposed during acute necrosis. In infarcted mice, DNA release begins within 2 hours (hrs), peaks between 9-18 hrs, and is cleared by 72 hrs after injury. The kinetics of DNA release in reperfusion injury, however, have yet to be characterized.

In this study we developed a dextranated TO nanoparticle (Dex-TO NP) to characterize the evolution of DNA release in vivo. We conjugated TO to a 40 kDa amine-dextran and similarly synthesized Dex-Cy5.5, as a well-matched, non-targeted control. The resulting Dex-TO NP has rapid blood clearance, multivalency, and enhanced DNA binding capabilities compared to plain TO. In cultured cells with induced cell death, Dex-TO specifically labels necrotic cells, but not apoptotic or healthy cells. In infarcted mice 24 hrs after permanent occlusion of the left coronary artery (LCA) (N=7), we co-injected Dex-TO and Dex-Cy5.5 intravenously, allowed the probe to circulate for 2 hrs, then harvested and sectioned the heart axially into 1-mm slices for triphenyltetrazolium chloride (TTC) staining and fluorescence reflectance imaging. Dex-TO, but not Dex-Cy5.5 specifically accumulated within the site of injury (Fig A). Furthermore, the area of Dex-TO uptake matched well with the area of infarction. Receiver Operating Characteristic (ROC) analysis confirmed the specificity and sensitivity of Dex-TO for detecting infarction, with an AUC of 0.88 (Fig B).

Ischemia-reperfusion (IR) injury was induced by transient occlusion of the LCA for 35 min followed by reperfusion (N=14). Prior to reperfusion, fluorescent microspheres were injected to delineate the area at risk (AAR). Fluorescent Annexin V (ANX) and Dex-TO were then co-injected 2 hrs prior to imaging at 3 time points: 2hr, 4hr and 6hr. ANX uptake occurred in over 90% of the AAR, and persisted from 2 to 6 hrs (Fig C-D). At 2 hrs, the fraction within the AAR positive for Dex-TO was 0.66 (±0.12), but decreased to 0.33 (±0.22, $p<0.05$) at 4 hrs, and to 0.28 (±0.14, $p<0.01$) at 6 hrs (Fig E). This suggests that DNA during IR is rapidly released within 2 hrs, and circulates within a wider area than the final necrotic infarct size. By 4-6 hrs the circulating DNA has washed out of the AAR and Dex-TO uptake at this time reflects final infarct size.

The kinetics of DNA release in myocardial infarction due to permanent coronary ligation differ from those seen in reperfusion injury. In IR, DNA release occurs rapidly and is widespread. Within 4-6 hrs after reperfusion, free DNA is confined to the area of infarction. This suggests that free DNA in ischemia-reperfusion is both rapidly released and washed out of the area of risk.

AUTHORS (LAST NAME, FIRST NAME): Chen, Howard H.[1, 5]; Yuan, Hushan[2]; Cho, Hoonsung[3, 2]; Ngoy, Soeun[4]; Liao, Ronglih[4]; Josephson, Lee[2, 1]; Sosnovik, David E.[1, 5]

INSTITUTIONS (ALL):

1. Martinos Center for Biomedical Imaging, Massachusetts General Hospital, Harvard Medical School, Boston, MA, United States.
2. Center for Advanced Medical Imaging Sciences, Massachusetts General Hospital, Harvard Medical School, Charlestown, MA, United States.
3. School of Material Science and Engineering, Chonnam National University, Gwangju, Korea (the Republic of).
4. Cardiovascular Division, Department of Medicine, Brigham and Women's Hospital and Harvard Medical School, Boston, MA, United States.
5. Cardiovascular Research Center, Cardiology Division, Massachusetts General Hospital, Harvard Medical School, Boston, MA, United States.

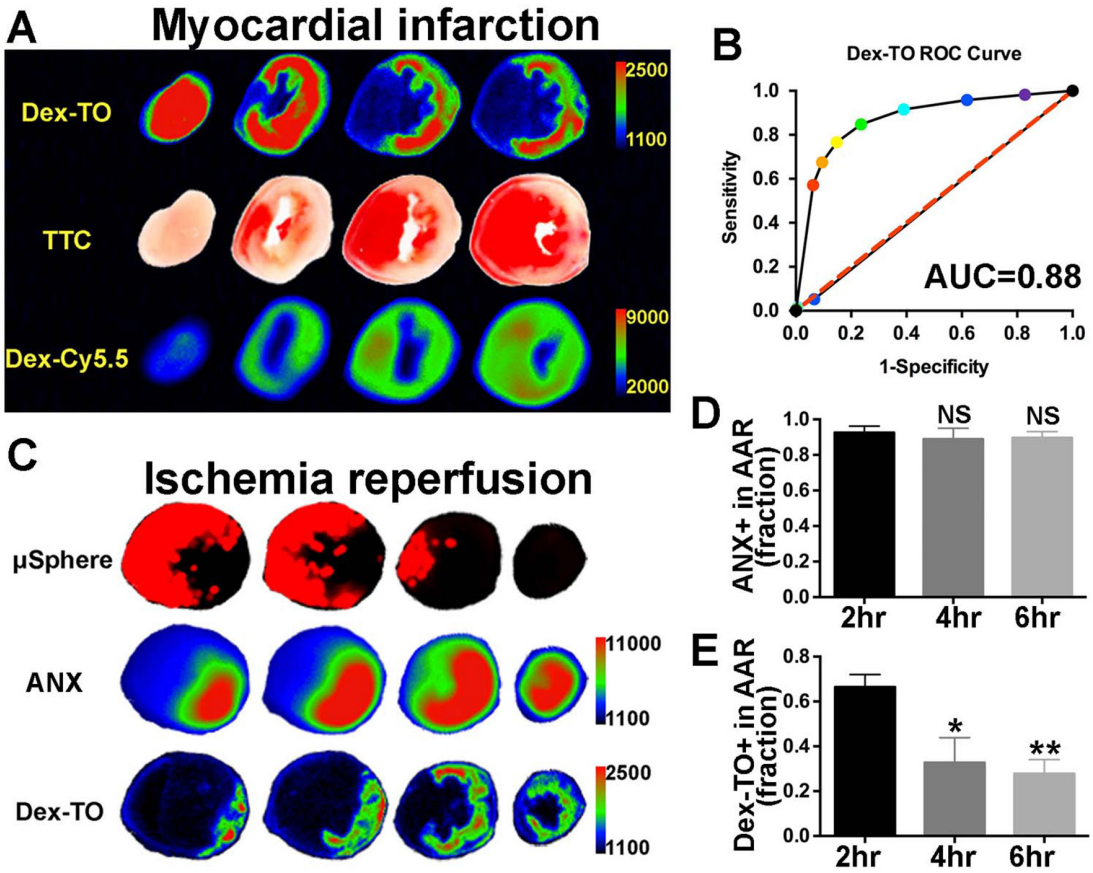

In vivo DNA release in myocardial infarction and ischemia-reperfusion injuries. (A) In myocardial infarction, Dex-TO, a DNA-binding nanoparticle (NP) injected intravenously, is confined to and matches with the area of injury, pale necrotic tissue devoid of triphenyltetrazolium chloride (TTC) staining. Dex-Cy5.5, a non-targeted control NP, is diffused throughout the myocardium. (B) Receiver Operating Characteristic (ROC) analysis confirms the specificity and sensitivity of Dex-TO for detecting infarction (AUC=0.88). (C) At 6 hrs post ischemia-reperfusion (IR) injury, Annexin V (ANX) uptake is prevalent within the area at risk (AAR), demarcated by the lack of microspheres. Only a smaller fraction of the AAR is Dex-TO positive. (D-E) In IR injury, ANX positive fraction within the AAR is >0.9, and persists from 2, 4 to 6 hrs post reperfusion. The fraction of Dex-TO positive area decreases from 0.66 at 2hr, to 0.33 at 4hr ($p<0.05$), and to 0.28 at 6hr ($p<0.01$). Free DNA in reperfusion injury is thus both rapidly released and washed out of the area of risk. *$p<0.05$, **$p<0.01$, ns=not significant, ANOVA.

CONTROL ID: 2220071

TITLE: First-in-Human study of [^{18}F]AA-7: A novel PET tracer for imaging L-type amino acid transporter 1 (LAT1)-positive tumors

PRESENTER: Satoshi Nozaki

ABSTRACT BODY:

Abstract Body: Background: [^{18}F]FDG PET is associated with false-positive findings due to rebound inflammation after chemotherapy and radiotherapy in clinical oncology. Radiolabeled amino acids including L-[methyl-^{11}C]methionine present higher specificity for cancer and are less influenced by inflammation than [^{18}F]FDG, though L-[methyl-^{11}C]methionine accumulates not only in tumor tissues but also in normal tissues. In surgical resection or radiotherapy of gliomas, accurate detecting the normal brain tissue–tumor boundary is critically important. However, as L-[methyl-^{11}C]methionine also accumulates in normal and inflamed tissues to some extent, it is impossible todetect precisely the normal brain tissue–tumor boundary. L-Type amino acid transporter 1 (LAT1) is highly expressed in a variety of human tumors including gliomas and a promising target for both imaging and therapy. The purpose of this study was to develop a novel tumor-specific PET tracer, targeting LAT1, to assess the safety, biodistribution, and dosimetric properties of the novel PET radiopharmaceutical agent, and to preliminarily evaluate its application in the diagnosis of gliomas.

Methods: We have developed a novel LAT1-specific tracer, [^{18}F]AA-7. In preclinical studies, PET imaging with [^{18}F]AA-7 was performed in mice bearing LNZ308 human glioblastoma cell line and also in two mice models of inflammation (turpentine oil-induced myositis model and collagen-induced arthritis model mice). In a clinical study, dosimetry estimations for [^{18}F]AA-7 in healthy volunteers were determined. Patients with glioma received 185 MBq of [^{18}F]AA-7 and underwent PET scan for 45 minutes after the injection. L-[methyl-^{11}C]methionine and [^{18}F]FDG were used as control tracers in both preclinical and clinical studies.

Results: In preclinical studies, accumulation of [^{18}F]AA-7 was higher than that of L-[methyl-^{11}C]methionine in LAT1 positive tumors [tumor to muscle ratio: 3.3±0.2 vs 2.1±0.4 (mean ± SD)]. Moreover, although [^{18}F]FDG was highly accumulated in inflamed regions, noticeable accumulation of [^{18}F]AA-7 was not observed in the two mice models of inflammation. The safety of AA-7 at microdosing condition was confirmed by the animal study along with the Japanese MHWL's guidance. In a clinical study, six healthy volunteers and seven patients were enrolled in the "first-in-human" trial. All the subjects had no significant problem. Upon visual examination, PET imaging using [^{18}F]AA-7 resulted in extremely clear images in patients with suspected glioblastoma.

Conclusions: [^{18}F]AA-7 may be useful as a novel PET tracer for LAT1-positive tumor imaging and imaging for the efficacy evaluation of therapies, which has low accumulation in inflamed tissues. It may be suitable for PET imaging in patients with suspected glioblastoma.

AUTHORS (LAST NAME, FIRST NAME): Nozaki, Satoshi[1, 2]; Oshita, Tomoko[1]; Nakatani, Yuka[2]; Sasano, Yumi[1, 5]; Yamamoto, Kenichiro[1, 5]; Hume, W. Ewan[1, 2]; Wada, Yasuhiro[2, 3]; Ishii, Akira[3]; Tanaka, Masaaki[3]; Shiomi, Susumu[6]; Tsuyuguchi, Naohiro[7]; Kodama, Kazuya[1, 4]; Watanabe, Yasuyoshi[2, 3]

INSTITUTIONS (ALL):

1. Novel PET Diagnostics Laboratory, RIKEN, Kobe, Hyogo, Japan.
2. Center for Life Science Technologies (CLST) , RIKEN, Kobe, Hyogo, Japan.
3. Department of Physiology, Osaka City University Graduate School of Medicine, Osaka, Osaka, Japan.
4. Research & Development Department, Nagase ChemteX Corporation, Tatsuno, Hyogo, Japan.
5. Life & Healthcare Products Department, NAGASE & CO., LTD., Kobe, Hyogo, Japan.
6. Department of Nuclear Medicine, Osaka City University Graduate School of Medicine, Osaka, Osaka, Japan.
7. Department of Neurosurgery, Osaka City University Graduate School of Medicine, Osaka, Osaka, Japan.

(No Image Selected)

CONTROL ID: 2232097
TITLE: DNase1 Decrease the Formation of the Size of Vegetation in Experimental Endocarditis Rat Model
PRESENTER: Jean-San Chia
ABSTRACT BODY:
Abstract Body: Title: DNase1 Decrease the Formation of the Size of Vegetation in Experimental Endocarditis Rat Model

Jeng-Wei Chen1, Ling-Yi Tseng2, Jean-San Chia, PhD3,4
1.Cardiac Surgical Division, Surgical Department, National Taiwan University Hospital Hsin-Chu Branch, Hsin-Chu, Taiwan
2.S-Sharp Corporation, New Taipei City, Taiwan
3.Graduate Institute of Microbiology, College of Medicine, National Taiwan University, Taipei, Taiwan
4.Graduate Institute of Immunology, College of Medicine, National Taiwan University, Taipei, Taiwan

Abstract
Background:
Neutrophil extracellular traps (NETs) are networks of extracellular fibers, primarily consisting of DNA from neutrophils. It is recognized as an important link between inflammation and thrombosis in host immune surveillance. DNase I is a nuclease that cleaves DNA. Using a Streptococcus mutans–induced experimental endocarditis rat model, we demonstrated that the NETs formation contributes directly to the expansion of vegetation formation.

Purpose:
This study aims to investigate the therapeutic effects of DNase I in decreasing vegetation formation from endocarditis rat model.

Materials and Methods:
In a Streptococcus mutans endocarditis rat model, DNase I was injected into the rats 30 minutes before or 4 hours after the inoculation of the bacteria. The ultrasonic investigation of aortic regurgitation with color Doppler-mode and PW Doppler-mode was performed by using single element transducer, center frequency 40MHz (Prospect, S-Sharp Corporation, Taipei, Taiwan). The effect of DNase I was evaluated by detecting the size of vegetation and the colonized bacteria density in the vegetation after ultrasonication and dilution with PBS. The NET formation stained with Hoechst 33258 was observed with a confocal microscope.

Results:
Prophylatic administration of DNase I intravenously before infection significantly improve the aortic insufficiency in PW Doppler-mode. DNase I treatment significantly reduced the size of the vegetation and the number of colonized bacteria in the vegetation. Immunostaining revealed that DNase I treatment also reduced the NET formation in the released DNA meshes.

Conclusion:
This in vivo study showed that the digestion of NETs with DNase I significantly reduced the number of bacteria and size of vegetation, which confirmed the role of NETs in the pathogenesis in infectious endocarditis.

AUTHORS (LAST NAME, FIRST NAME): Chen, Jeng-Wei[2]; Tseng, Ling-Yi[3]; Chia, Jean-San[1]
INSTITUTIONS (ALL):
1. Immunology, College of Medicine, Nartional Taiwan University, Taipei, Taiwan.
2. Surgery Department, National Taiwan University Hospital, Hsin-Chu Branch, Hsin-Chu, Taiwan, Taiwan.
3. S-Sharp Corporation, New-Taipei, Taiwan.
(No Image Selected)

CONTROL ID: 2229256

TITLE: Fluorescence imaging characteristics of the intravital tumor targeting agent BLZ-100 from a first in human skin cancer study

PRESENTER: Miko Yamada

ABSTRACT BODY:

Abstract Body: For many types of cancer, the accuracy of surgical resection directly influences patients' prognosis. The Tumor Paint™ product, BLZ-100, is a near-infrared (NIR) dye conjugated to a clinically validated tumor targeting peptide, Chlorotoxin. Preclinical data show BLZ-100 binding specifically to many animal tumours at well tolerated doses. The objective of the study was to evaluate the correlation between clinical fluorescence imaging and histological fluorescence imaging within the context of the histopathological diagnosis.

Human ethics approval was obtained prior to recruitment. BLZ-100 was administered as a single intravenous injection. A clinical fluorescence-imaging device (Fluobeam® 800, Fluoptics, Grenoble, France) was used to assess BLZ-100 accumulation in skin lesions prior to excision. This imaging device uses laser excitation at 750 nm, and has a long-pass filter for detection of emitted light at 800 nm and above. Five dose cohorts were carried out (3 patients each) and dose escalation was performed in a 3+3 design, starting from 1 to 18 mg of BLZ-100. Base-line (pre-dose) fluorescence images were taken to control for skin autofluorescence in lesion and peri-lesional skin. Additional images were taken at 2, 4, 24 and 48 hours after dose administration. Following surgical excision at 48 hours, 1/3 of each lesion was collected and the tissues were snap frozen. Serial sections were stained with H&E, and compared with the tissue NIR fluorescence (assessed using an Odyssey scanner) to characterise BLZ-100 specificity.

Fifteen subjects were enrolled in the dose escalation and yielded a total of 23 skin lesions for analysis. Seven cases of pathology confirmed basal cell carcinoma were identified and 5 of these cases showed clear increased signal, with highest signal occurring at 2 hours post infusion. A maximum 5-fold increase in the lesion over peri-lesional skin was observed in a subject receiving 3 mg BLZ-100. Cryosections revealed a high fluorescence signal from the excised lesion. The histopathology confirmed basal cell carcinoma (BCC) in the area. **Figure 1** shows the clear definition of BCC area by images taken by Fluobeam. By comparison, another patient with a clinically diagnosed squamous cell carcinoma (SCC) received 1 mg BLZ-100 and showed no visible signal from the lesion site, but did show diffuse fluorescence over the entire imaging area at early time points (2-4 hours). Imaged tissue sections showed a lack of signal from the sectioned lesion.

In conclusion, BLZ-100 has shown potential for tumour targeted imaging. Clinical fluorescence imaging has correlated well with microscopic fluorescence imaging of excised BCC lesions supporting the hypothesis that this approach could be beneficial when tumour margins need to be clearly defined.

AUTHORS (LAST NAME, FIRST NAME): Yamada, Miko[1]; Parrish-Novak, Julia[2]; Miller, Dennis[2]; Soyer, H. Peter[1]; Spelman, Lynda[3]; Prow, Tarl[1]

INSTITUTIONS (ALL):

1. Dermatology Research Centre, The University of Queenslad , Brisbane, QLD, Australia.
2. Blaze Bioscience, Inc, Seattle, WA, United States.
3. Specialist Connect, Brisbane, QLD, Australia.

(No Image Selected)

CONTROL ID: 2220310

TITLE: A novel design of fluorescence-guided surgical navigation system

PRESENTER: Yamin Mao

ABSTRACT BODY:

Abstract Body: Background: The fluorescence-guided surgery navigation system is introduced to clinical surgery for the purpose of distinguishing malignancy from norm tissue which is largely dependent on surgeon's experiences. However, the limit of most fluorescence imaging modals is detection depth, for example, the fluorescence molecular imaging (FMI) method can just detect about 1 cm distance. One advantage of endoscopic imaging is that it can move into the deep tissue to reach the regions which is undetectable by normal lens. To solve the problem of depth limitation, we develop a new molecular imaging system which employ an endoscope to detect deep regions and a wild-field lens to observe macro view.

Methods: One endoscope and one wild-field lens were used in our system for purpose of realizing the detection of macro facial view and micro deep regions on demand of surgery. This system integrate one color CCD camera and one near-infrared (NIR) camera to collect two spectrums of images which can guide surgeons to distinguish tumor margin in real time. Furthermore, white and NIR light sources were couple into one beam by one beamsplitter and three convex mirror for lighting up the surgery region. A Multi-Function Calibration Target (NT58-403, Edmund Optics, USA) test proven the system has highly resolution and a series of indocyanine green (ICG) experiments demonstrate the system has strong signal sensitivity.

Conclusion: The test results of the system's optical resolution is 0.1mm (10 lp/mm) which is enough for imaging demand. The minimum quantity of ICG been detected by the system is 0.195 ug which demonstrates the feasibility of our system. The system is feasible to detect fluorescence signal with both endoscope and wide-field lens for overcoming the limitation of detection depth exists in molecular imaging methods. Therefore, we hope our system can complete the clinical translation and be used in various surgical oncology in the near future.

AUTHORS (LAST NAME, FIRST NAME): Mao, Yamin[1]; Jiang, Shixin[4]; Ye, Jinzuo[2]; An, Yu[4]; Yang, Xin[1]; Chi, Chongwei[3]; Tian, Jie[1]

INSTITUTIONS (ALL):

1. Chinese Academy of Sciences, Institute of Automation, BeiJing, BeiJing, China.
2. Institute of Automation, Chinese Academy of Sciences, Beijing, China.
3. Key Laboratory of Molecular Imaging, Chinese Academy of Sciences, Institute of Automation, Chinese Academy of Sciences, Beijing, China.
4. School of Computer and Information Technology, Beijing Jiaotong University, BeiJing, BeiJing, China.

(No Image Selected)

CONTROL ID: 2220401

TITLE: Glymphatic Clearance Impaired In A Mouse Model of Tauopathy: Captured Using Contrast-Enhanced MRI

PRESENTER: Asif Machhada

ABSTRACT BODY:

Abstract Body: Background: Sleep disturbances are clinically associated with Alzheimer's disease (AD) [1]. Recent studies have demonstrated natural sleep results in an increased convective exchange between cerebrospinal and interstitial fluid compartments, the latter of which increases up to 60% in volume during this time) [1, 2]. This mechanism, referred to as the glymphatics system clears waste solutes including protein accumulations such as beta-amyloid (Aβ) [3], pathogenically associated with AD. Its remains an untested hypothesis as to whether impaired glymphatic clearance has a role in AD aetiology or whether AD pathology itself translates to an impairment of glymphatic clearance. Using an animal model of tauopathy, we quantify the extent of glymphatic clearance in the brain using contrast enhanced MRI to determine the effects of pathological tau accumulation on glymphatic clearance. This investigation is the one the first applications of a transgenic model to correlate decline in cognitive function with glymphatic clearance. Additionally, molecular and cellular analysis of animal brains was utilised to elucidate the mechanism by which glymphatic clearance is achieved and/or is impaired in this model.

Methods: Glymphatic clearance in 5 rTg4510 and 5 litter-matched wildtype mice was captured using contrast-enhanced MRI employing a 3D T1-weighted gradient echo sequence. Following implantation of an intrathecal catheter via puncture of the atlanto-occipital membrane and dura, Gadolinium was infused into the intracisternal space and its distribution through para-arterial glymphatic exchange channels followed in real time using MRI. Laser capture microdissection of astrocytes surrounding blood vessels and quantification of their aquaporin-4 expression was performed to help understand the involvement of this water channel in glymphatic clearance.

Results: In line with increased CSF tau, glymphatic ISF-CSF exchange was impaired in the brains of transgenic compared to wildtype animals. Expression levels of astrocytic aquaporin-4 highlight possible roles of this astrocytic water channel in the glymphatic clearance pathway.

Conclusions: Pathological accumulation of tau in this animal model of tauopathy is associated with impaired glymphatic clearance from the brain. This is the first investigation of glymphatic clearance in a tau model and warrants further investigation of the mechanisms involved. Furthermore, manipulation of the glymphatic clearance pathway may harbour new avenues of therapeutic intervention for AD.

References

1. Malkki, H., *Alzheimer disease: Sleep alleviates AD-related neuropathological processes.* Nature Reviews Neurolology, 2013. 9(12): p. 657.

2. Mendelsohn, A.R. and J.W. Larrick, *Sleep Facilitates Clearance of Metabolites from the Brain: Glymphatic Function in Aging and Neurodegenerative Diseases.* Rejuvenation research, 2013. 16(6): p. 518-523.

3. Iliff, J.J., et al., *A Paravascular Pathway Facilitates CSF Flow Through the Brain Parenchyma and the Clearance of Interstitial Solutes, Including Amyloid beta.* Science Translational Medicine, 2012. 4(147). p. 147ra111.

AUTHORS (LAST NAME, FIRST NAME): Machhada, Asif[1, 5]; Harrison, Ian F.[5]; Colgan, Niall[5]; Ismail, Ozama[5]; O'callaghan, James[5]; Holmes, Holly E.[5]; Wells, Jack[5]; Murray, Tracey[2]; Ahmed, Zeshan[2]; Johnson, Ross A.[4]; Collins, Emily C.[4]; O'Neill, Michael J.[3]; Gourine, Alexander[1]; Lythgoe, Mark F.[5]

INSTITUTIONS (ALL):

1. Neuroscience, Physiology and Pharmacology, University College London, London, United Kingdom.
2. Eli Lilly and Company, Windlesham, Surrey, United Kingdom.
3. Lilly Corporate Center, Eli Lilly and Company, Indianapolis, IN, United States.
4. Lilly Corporate Center, Eli Lilly and Company, Indianapolis, IN, United States.
5. Medicine, UCL Centre for Advanced Biomedical Imaging, London, United Kingdom.

(No Image Selected)

CONTROL ID: 2220531

TITLE: Using high resolution ultrasound to asssess direct parasympathetic control of ventricular contractility: A comparison a with pressure-clamped mode

PRESENTER: Asif Machhada

ABSTRACT BODY:

Abstract Body: Background: Parasympathetic efferent nerves are well known to control nodal tissues and atria [1]. However, the role of the vagal innervation of the ventricles remains controversial. The majority of physiology textbooks state that the vagal innervation of the ventricle is sparse and direct parasympathetic control of ventricular contractility is insignificant. This view persists in both the scientific and educational literature despite evidence obtained in various species (mouse, guinea pig, rat, cat, dog, pig, sheep and man) demonstrating the presence of choline acetyltransferase-positive nerve fibres, acetylcholinesterase and muscarinic receptors in both ventricles [2]. In the present study we used two novel anaesthetised rat models to determine the significance of tonic vagal influence on left ventricular (LV) contractility under different anaesthesia. In addition to this, vagal preganglionic neurones in the dorsal vagal motor nucleus (DVMN) were inhibited using microinjections of muscimol into the brainstem in order to identify the region responsible for the control of LV contractility as recent evidence that the activity of these neurones protects cardiomyocytes against acute ischaemia/reperfusion injury [3].

Pressure clamped model: Systemic atenolol administration, C1 transection and vasopressin infusion removes sympathetic influences and provides constant loading conditions and fixed filling times whilst pacing. This allows the maximal rate of change in LV pressure (LVd*P*/dt$_{max}$) to be used as a load independent measure of LV contractility.

Ultrasound left ventricular imaging: Whilst acquiring a parasternal long axis view, LV pressure measuremements was used to perform pressure-area loop analysis. Measurements were taken during atrial pacing, snaring the inferior cava to alter cardiac preload after atenolol adminstration. Using LV cross-sectional area (mm^2) as a surrogate measure of LV volume, the regression slope of the pressure-area relationship was used to determine the end-systolic elastance (Ees, mmHg mm^{-2}) to estimate changes in the LV inotropic state.

Results: Significant increases were measured in LVd*P*/dt$_{max}$ and end-systolic elasance in the pressure clamped model and with the pressure-area loop analysis resptively. Inhibition of the left caudal region of the DVMN using microinjections of muscimol significantly increase LVd*P*/dt max.

Conclusions: These data confirm the existence of a tonic restraining muscarinic influence on LV contractility. Neurones residing in the left caudal region of the DVMN exert direct load- and heart rate-independent tonic control of LV contractility.

References

1. Jones, J.F., *Vagal control of the rat heart.* Experimental Physiology, 2001. 86(6): p. 797-801.

2. Coote, J.H., *Myths and realities of the cardiac vagus.* Journal of Physiology, 2013. 591(17): p. 4073-4085.

3. Mastitskaya, S., et al., *Cardioprotection evoked by remote ischaemic preconditioning is critically dependent on the activity of vagal pre-ganglionic neurones.* Cardiovascular Research, 2012. 95(4): p. 487-94.

AUTHORS (LAST NAME, FIRST NAME): Machhada, Asif[1, 2]; Lythgoe, Mark F.[2]; Gourine, Alexander[1]

INSTITUTIONS (ALL):

1. UCL Centre for Cardiovascular and Metabolic Neuroscience, London, United Kingdom.

2. UCL Centre for Advanced Biomedical Imaging, London, United Kingdom.

(No Image Selected)

CONTROL ID: 2223192

TITLE: A new prototype pegylated gold nanoparticles: more uniform in size for fast, efficient bioconjugation

PRESENTER: Biying Xu

ABSTRACT BODY:

Abstract Body: Nanoparticle based technologies are becoming increasingly useful in biology and medicine. In particular, gold nanoparticles are well suited for a variety of applications. These applications range from diagnostic procedures such as the detection of specific proteins or pathogens to drug delivery and photothermal cancer therapy. In this study, we synthesized discrete PEG40 (m-dPEG40) and dPEG59-DBCO with lipoic acid (TA) group for grafting to the gold nanoparticles, all dPEGs were purified by RP-HPLC with purity over 95%. By using TA-dPEGs, we made pegylated gold nanoparticles with lower polydispersity index by dynamic lighter scattering analysis; in addition, the pegylated gold nanoparticles were more stable in the presence of DTT. As proof-of-concept study, we click reacted O6-benzylguanine with DBCO-dPEG59 to make O6-benzylguanine functionalized gold nanoparticles and did further functional testing using SNAP-Tag protein. Our results indicated that the O6-benzylguanine functionalized gold nanoparticles are readily reactive to SNAP-Tag; further biological studies are currently in progress.

AUTHORS (LAST NAME, FIRST NAME): Xu, Biying[1]; Swenson, Rolf[2]

INSTITUTIONS (ALL):

1. NIH, Rockville, MD, United States.
2. NIH, Rockville, MD, United States.

(No Image Selected)

CONTROL ID: 2230415

TITLE: 3D motion tracking, clinical fluorescence imaging and confocal microscopy aid drug delivery device development

PRESENTER: Tarl Prow

ABSTRACT BODY:

Abstract Body: The benefits and drawbacks of utilizing new forms of imaging and image analysis when developing topical drug delivery enhancement technologies will be discussed. In this laboratory we blend rapid prototyping and imaging technologies to underpin our device development programs with a focus on dermatology applications. We have found that the application of diverse, unconventional imaging technologies vastly improved our topical drug delivery enhancement technology development project. We have developed and patent a novel platform for lesion-directed drug delivery, Foroderm^{TM}. This technology is based on high-aspect ratio microparticles and involves painting the microparticles onto and into the skin using 3D printed applicators with microtexturing that has been optimised for the microparticle geometry.

Imaging and image analysis was used to quantify application, microparticle trajectory and topical drug delivery. Application parameters were assessed using an OptiTrack V120 Trio. The data were collected using a 3D printed applicator with calibrated reflective markers. Expert and novice users applied Foroderm^{TM} to excised skin while 3D tracking information was being collected at 120 frames per second. The 3D application parameters were then extracted. The treated skin was then assessed for microparticle direction, penetration depth, number per mm^2 and angle of penetration using reflectance confocal microscopy (RCM). **Figure 1** shows some examples of these data. Four expert applications and two novice applications were recorded while applying the mixture of 25 mg of Foroderm and 250 ug/ml of sodium fluorescein (NaF). The duration of application was 30 seconds and treatment area was 2cm square region. We avoided areas of skin where imperfections (cut or abrasions) that were identified by methylene blue staining. Once the recording was completed, treated skin was assessed under RCM with 840nm filter and fluorescence was used to assess NaF delivery. Each RCM images were taken from the centre and cardinal locations within the treatment area.

The data showed that the application parameters roughly correlated with some aspects of the microparticle and drug delivery profiles. However, the most striking finding was that there were significant differences in the intra- and inter-user application parameters that went beyond the level of training. These outcomes were only marginally present in the drug delivery assessments. In summary, the data indicated that an improved, simplified training protocol needed to be developed which could improve the inter-user variation observed in topical drug application. These data also helped to generate new hypotheses on the optimal mode of delivery but importantly the addition of 3D motion capture raised broad questions on how variable conventional topical drug delivery was being applied in the clinic and by patients at home. Our conclusion is that the integration of 3D motion capture into conventional dermatological research imaging modalities offers a vastly improved perspective that could be useful in many areas of research and development by better understanding human interactions with new and existing technologies.

AUTHORS (LAST NAME, FIRST NAME): Prow, Tarl[1]; Snoswell, Aaron J.[1]; Raphael, Anthony[2]; Dang, Nhung[1]; Yamada, Miko[1]; Hoang, Van[1]; Nufer, Kaitlin[1]; Singh, Surya[3]

INSTITUTIONS (ALL):

1. Dermatology Research Centre, The University of Queenslad , Brisbane, QLD, Australia.
2. Harvard Medical School, Centre for Systems Biology and Wellman Centre for Photomedicine, Boston, MA, United States.
3. School of Information Technology and Electrical Engineering, The University of Queensland, Brisbane, QLD, Australia.

(No Image Selected)

CONTROL ID: 2221064

TITLE: Correlation between crossed cerebellar diaschisis on brain perfusion SPECT and prognosis of functional ambulation in patients with stroke.

PRESENTER: Soonah Park

ABSTRACT BODY:

Abstract Body: Purpose: Crossed cerebellar diaschisis (CCD) is a common consequence of unilateral stroke patients and a decrease in regional cerebral blood flow (rCBF) in the contralateral cerebellar hemisphere to the affected cerebral hemisphere on brain perfusion single photon emission computed tomography (SPECT). Measurement of functional waking capacity for patients after stroke is important prognostic parameters. We investigated correlation between CCD on brain perfusion SPECT and the prognosis of functional ambulation in subacute-stroke patients.
Method: We enrolled 22 patients with first-ever stroke. The brain perfusion SPECT with ^{99m}Tc-hexamethyl-propylene amine oxime (HMPAO) was performed within three months after stroke. The presence and degree of CCD was evaluated by calculated asymmetry index (AI) that was measured on brain perfusion SPECT using region-of-interest (ROI) software for automated definition of ROIs in the anatomical cerebellar region. The functional status and recovery of ambulation was evaluated by using National Institutes of Health Stroke Scale (NIHSS), Functional Ambulation Category (FAC), Functional Independence Measure (FIM) and Berg Balance Scale (BBS) within 0, 1 and 3 months after stroke. We calculated correlation coefficient between the AI on brain perfusion SPECT and the result of functional ambulation tests.
Results: The patients with CCD at the time point of 3 months after stroke had significantly lower FAC and BBS scores than that of patients without CCD ($p<0.05$). Otherwise, there was a statistically non-significant correlation between the AI of CCD and clinical scales measured for functional ambulation at 0, 1 and 3 months ($r=-0.432$, $p<0.05$).
Conclusion: Our study suggested that the CCD observed on brain perfusion SPECT in 3 months after stroke may be considered prognostic parameter to predict the recovery degree of functional ambulation and risk category of falling down while walking in patient with the first-ever subacute stroke.

AUTHORS (LAST NAME, FIRST NAME): Park, Soonah[1]; Joo, Min Cheol [2]; Lim, Yu Hyun[2]; Kim, Myoung Hyoun[1]

INSTITUTIONS (ALL):

1. Nuclear Medicine, Wonkwang University Medical School, Iksan, Jeollabuk-do , Korea (the Republic of).
2. Rehabilitation, Wonkwang University Medical School, Iksan, Korea (the Republic of).

(No Image Selected)

CONTROL ID: 2220647

TITLE: Detection of mouse liver cancer by means of fluorescence molecular tomography after indocyanine green enhancement

PRESENTER: Jinzuo Ye

ABSTRACT BODY:

Abstract Body: Introduction: Fluorescence molecular tomography (FMT) is a promising imaging technique in preclinical research, enabling three-dimensionally resolve the fluorescence bio-distribution in small animals. In this study, we present quantitative optical images of mouse liver cancer *in vivo* based on a hybrid molecular imaging systems including micro-computer tomography and near-infrared fluorescence molecular tomography (Micro-CT/FMT) developed by us.

Methods: Green fluorescent protein (GFP) labeled human hepatocellular carcinoma cells was utilized to establish the orthotopic liver tumor model. The IVIS Imaging Spectrum System was then used to observe the growth process of the tumor cells. After the tumor cells were implanted 16~20 days, indocyanine green (ICG) was administered through an intravenous tail vein injection. About 72 hours after ICG injection, the hybrid Micro-CT/FMT imaging systems were used to obtain cone-beam micro-CT projection data and the fluorescence data. The FMT reconstruction of fluorescence bio-distribution was conducted using a nonmonotone spectral projected gradient pursuit method with structural priors. Multispectral epi-illumination cryoslicing imaging, which serves both as a method for accurately imaging the bio-distribution of ICG inside organisms and as a modality for the validation of FMT reconstruction, was carried out for the orthotopic liver cancer.

Results: The results demonstrate that the ICG uptake by the liver cancer was much higher than that by the normal liver tissue, especially about 72 hours after ICG injection. By using FMT, the mouse liver cancer was accurately located and the ICG bio-distribution inside organisms was accurately resolved. The FMT reconstruction results of ICG bio-distribution were validated by the multispectral epi-illumination cryoslicing imaging.

AUTHORS (LAST NAME, FIRST NAME): Ye, Jinzuo[1]; An, Yu[2]; Mao, Yamin[1]; Jiang, Shixin[2]; Yang, Xin[1]; Chi, Chongwei[1]; Tian, Jie[1]

INSTITUTIONS (ALL):

1. Chinese Academy of Sciences, Institute of Automation, BeiJing, BeiJing, China.
2. School of Computer and Information Technology, Department of Biomedical Engineering, Beijing, Beijing, China.

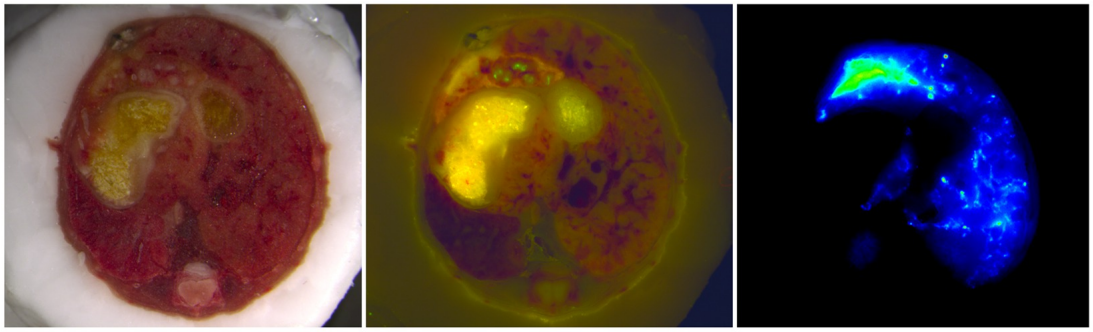

(a) (b) (c)

CONTROL ID: 2220648

TITLE: Preparation method of radiation sensitive copolymer carrier for coating radiated nanoparticles and chemotherapy drugs.

PRESENTER: Ming-Hsin Li

ABSTRACT BODY:

Abstract Body: Objectives : The primary object of the present invention is to provide a preparation method of radiation-sensitive copolymer carrier for coating nanoparticles and/or chemotherapy drugs.

Conclusions : The preparation method of the present invention that can be released from the opened nanosphere by protons penetrating tissue during proton therapy. The treatment effect of proton therapy is enhanced by two ways of using the radiated nanoparticles released from an opened nanosphere to produce nuclear fission with the protons for releasing electrons to destroy cancer cells of tumor and the chemotherapy drugs released from the opened nanosphere for distributing among tissue to kill the cancer cells of the tumor.

Results : Proton therapy that utilizes chemotherapy drugs made by the radiation-sensitive copolymer carrier of the present invention has decreasing proton energy in proportion with penetrated depth while the high-energy protons are hitting into the human body. The protons energy may decrease to one-third or one-fourth of primary energy while the protons are reaching to the cancer according to the penetration depth and incident energy of the protons. The incident protons having energy at 10-1000MeV will cause fission reaction of enrich heavy metal with certain probability while impacting the enrich heavy metal distributed on the cancer. FIG.1 shows the fission reaction while protons are impacting enrich heavy metal, wherein the fission yields varies with the mass distribution. These fission products are usually unstable nuclides and subject to continuing decay reactions.

Methods: The method includes utilizing polymer of diselenide and 3-aminopropylpoly to react with each other to obtain diselenide block copolymer as a nano pharmaceutical carrier having hydrophilicity and hydrophobicity for forming a nanosphere by self-assembling in emulsification. 1,2-Distearoyl-sn-Glycero-3-Phosphoethanolamine-PEG-biomarker (hereinafter referred to as DSPE-PEG-biomarker) is another polymer having hydrophilicity and hydrophobicity alike that can be added into the diselenide block copolymer during the emulsification. A stable structure of nanosphere is formed during self-assembling of the polymers, wherein hydrophobic groups of the polymers gathering is arranged by organic solvents, and hydrophilic groups of the polymers are exposed to external solution. The nanosphere produces water-repellent effect due to inner hydrophobicity after volatilization of the organic solvents. The water-repellent effect makes the nanosphere be indestructible by blocking water molecules into the nanosphere and stable in solution with the outer hydrophilic groups of the nanosphere.
The nanosphere produced by radiation-sensitive diselenide block copolymer of the present invention is stable in aqueous solution and preferable to be a potential nuclear pharmaceutical carrier for controlling collapse speed of the carrier by specific radiation.

AUTHORS (LAST NAME, FIRST NAME): Li, Ming-Hsin[1]; Chu, Han Hsiang[1]; Lee, Chien-Te[1]; CHANG, HAN-CHIH[1]

INSTITUTIONS (ALL):

1. Institute of Nuclear Energy Research, Taoyuan, Taiwan.

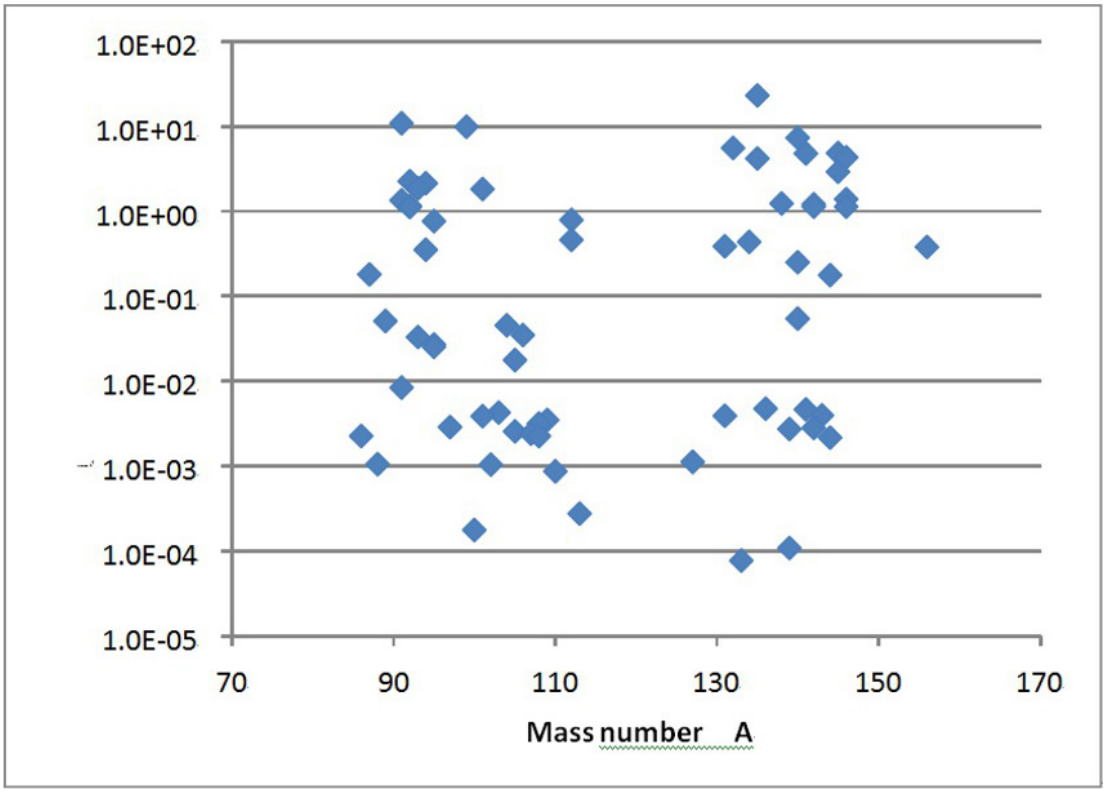
1.0E+02
1.0E+01
1.0E+00
1.0E-01
1.0E-02
1.0E-03
1.0E-04
1.0E-05
70
90
110
130
150
170
Mass number A

CONTROL ID: 2226284

TITLE: An automatic synthesizer for Gallium-68-DOTATATE PET radiopharmaceuticals

PRESENTER: Ming-Hsin Li

ABSTRACT BODY:

Abstract Body: Objectives:

Fast implementation of Ga-68-DOTATATE PET into clinical studies and research has resulted in high demands in the automated modules for the preparation of Ga-68-DOTATATE PET radiopharmaceuticals in a safe and reproducible process.

Methods:

The purpose of this study is to develop a fully automated controlled system for the synthesis of Ga-68-DOTATATE, with a compact synthesizer module. Main procedures of the process include: (1)absorption of Ga-68 cation; (2)reaction with DOTATATE ligand; (3) condition with C18 cartridge; (4)raw Ga-68-DOTATATE separation by C18 cartridge; (5) separation; (6)through 0.22um filter; and (7) collected in collection vial.

Results:

The advantages of this fabricated synthesizer module are illustrated as follows.

Firstly, the whole processes are operated in a closed system with a liquid nitrogen trapper used to condense the release gases of leaked radioactive material and organic solvent that can reduce the environmental radiation. Secondly, the assembly of the module is made as small as possible. Thirdly, this module is functioned with a fully automated control for synthesis of making Ga-68-DOTATATE. The process time is about 50mins.

Conclusions:

The products obtained with purity of greater than 95% is sufficient to meet the requirements of the specifications for Ga-68-DOTATATE PET in nuclear medicine applications. Other than the previous statements, the software designed can be used to execute the process step by step precisely under the command to be called. During the process performance, the temperature, pressure and variation of radiation dose can be monitored and recorded simultaneously to reflect the reaction situation at that time and compliant with the regulation of GMP.

AUTHORS (LAST NAME, FIRST NAME): Li, Ming-Hsin[1]; Chu, Han Hsiang[1]; CHANG, HAN-CHIH[1]; Lee, Chien-Te[1]

INSTITUTIONS (ALL):

1. Institute of Nuclear Energy Research, Taoyuan, Taiwan.

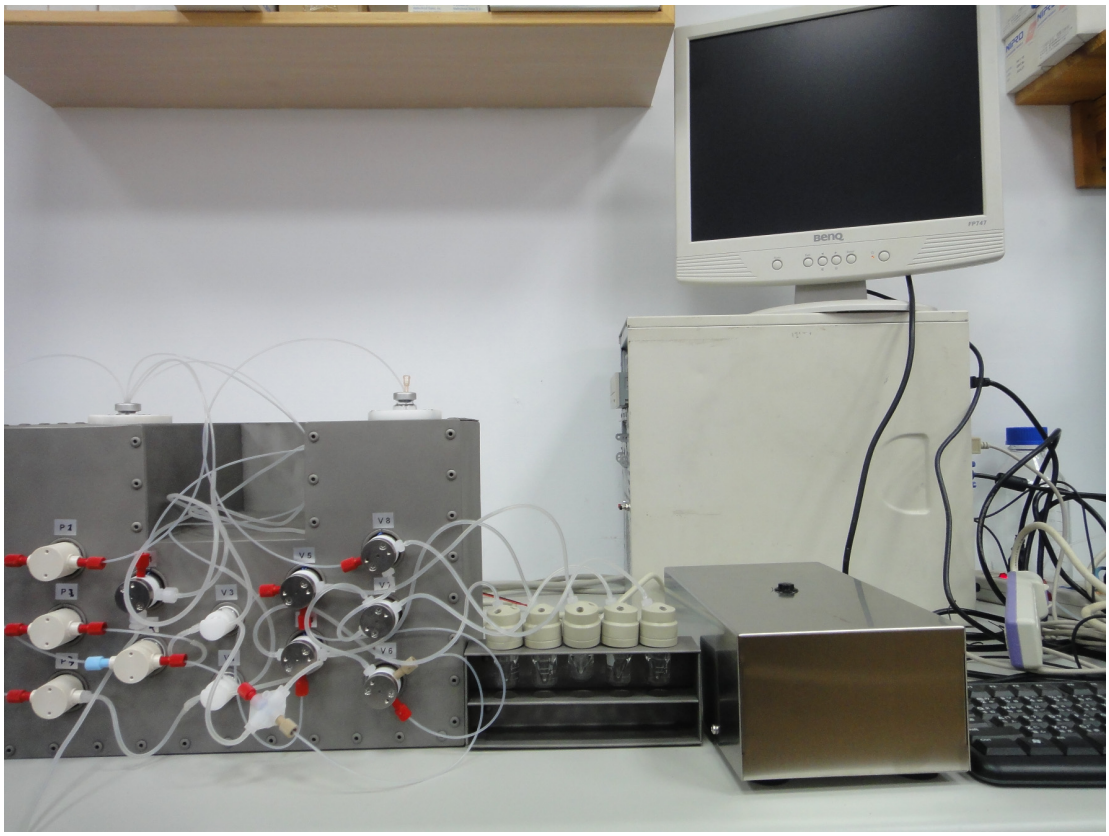
BenQ
P1
P1
P2
V8
V5
V3
V1
V6

CONTROL ID: 2226294

TITLE: Optimization and characterization of low frequency ultrasound sensitive liposomes with in vitro stability and drug release study and scintigraphic imaging study in xenograft brain tumor mouse

PRESENTER: Yi-Hsiu Chung

ABSTRACT BODY:

Abstract Body: The purpose of the study is to optimize the low frequency ultrasound (LFUS) sensitive liposomes with high stability in long circulation for cancer therapy. Liposomes encapsulating anti-chemotherapeutic drugs, a drug delivery system, have been widely used in clinic for cancer therapy. The reports have shown that LFUS can facilitate the drug release from a various of liposomes due to transit cavitation[1]. Saturated phospholipids and cholesterol can form the more rigid bilayer of liposomes and 5% PEG can improve the period of circulation in body. An optimized LFUS sensitive liposomal formulation by means of long circulation increases the amounts of anti-cancer drugs accumulate in target site following expose to LFUS, leading to efficient chemotherapy without harming normal tissue. Three liposomal formulation, dipalmitoyl-phosphatidycholine(DPPC)/Cholestrol(Chol)/1,2-distearoyl-sn-glycero-3-phosphoethanolamine-N-[methoxy(polyethylene glycol)-2000](DSPE-PEG2000) (45/50/5, 40/55/5 and 55/40/5) were manufactured by sonication. The longitudinal stability of liposomes in saline from day 0 to day 120 at 4°C were determined by particle size measurement using dynamic light scattering. The in vitro stability of liposomes incubating in saline and bovine serum albumin(BSA) at various time points were tested change of particle size. The 28kHz ultrasound with 1.07W/cm^2 was applied 60 seconds to the liposomes and then particle size and the release rate of doxorubicin encapsulating in liposomes were determined. In vivo study, liposomes labeled with Tc-99m for scintigraphic planar noninvasive image were performed at post injection 24h as the maximum accumulation of liposomes in U87MG tumor.

Three liposomal formulations are highly stable within 4 months without aggregation, only increasing 20% of particle size from original size. Incubating with saline and BSA, the particle size of DPPC/Chol(45/50), DPPC/Chol(40/55) and DPPC/Chol(55/40) are not significantly changed expect DPPC/Chol(40/55) in saline,107.08+/-6.5nm ($p<0.05$) and in BSA 106.6+/-2.5 nm at 20 h from baseline 95.07+/-1.12 nm. It indicated the liposomal formulation DPPC/Chol(45/50 and 55/40) were shown the better stability than other formulation in vitro study. The liposomal sizes are not altered after exposure to LFUS for all three formulation; however release rate of doxorubicin was 12.34%, 19.14% and 1.36% for DPPC/Chol/PEG-2000DSPE(45/50/5,40/55/5 and 55/40/5), respectively. The Tc-99m liposomes labeling efficiency were 66.32%, 76.69% and 63.40% for DPPC/Chol/DSPE-PEG2000 (45/50/5, 40/55/5 and 55/40/5). The ratio of tumor to muscle are 2.7+-/0.54,1.73+/-0.4,and 1.26+/-0.24 for DPPC/Chol/PEG-2000DSPE(45/50/5,40/55/5 and 55/40/5), respectively.

In conculsion, the liposomal formulation, DPPC/Chol/ DSPE-PEG2000(45/50/5) showed a good stability in vitro study and high drug accumulation in tumor as well as effectively release within ultrasound application. It could become a promising LFUS sensitive liposomes for cancer therapy.

[1] Avi Schroeder, Ultrasound, and drug delivery: principles for using ultrasound to control the release of drugs from liposomes, Chemistry and Physics of Lipids 162(2009)1-16

AUTHORS (LAST NAME, FIRST NAME): Chung, Yi-Hsiu[1]; Chang, Wen-Chi[1]; Hsu, Po-Hung[1]; Huang, Chiun-Wei[1]

INSTITUTIONS (ALL):

1. Center for Advanced Molecular Imaging and Translation, Chang Gung Memorial Hospital, Tao-yuan, Taiwan.

Scintigraphic,x-ray planar, and fusion images of DPPC/Chol/PEG-2000DSPE(45/50/5) liposomes labeled Tc-99m at 24 h post injection

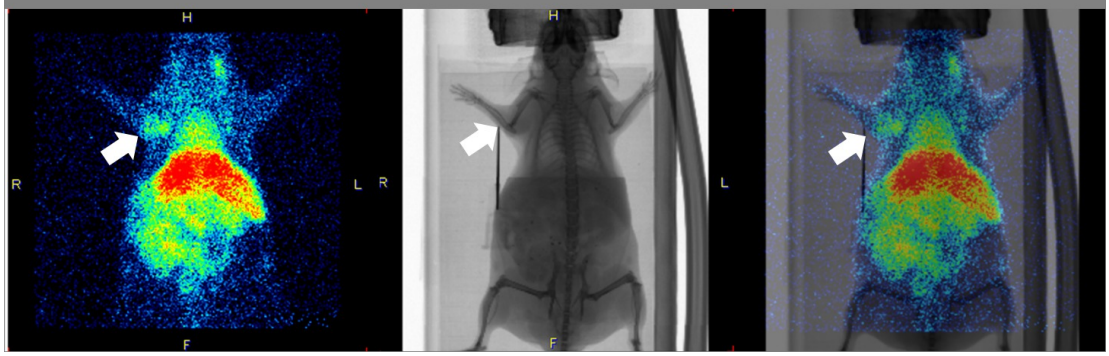

CONTROL ID: 2220706

TITLE: DUAL MODAL MR/FLUORESCENT ZINC SENSING PROBES FOR DIABETES IMAGING

PRESENTER: Graeme Stasiuk

ABSTRACT BODY:

Abstract Body: Magnetic Resonance (MR) imaging compared with other imaging modalities has excellent anatomical resolution; however, it suffers at the molecular scale due to its intrinsic low sensitivity. To produce a detectable change in water signal intensity, a relatively high concentration of contrast agent (0.01 - 0.1 mM) is required.[1] This creates problems when imaging at the molecular level, as the most interesting targets are present at much lower concentrations, typically in the nano- or pico-molar range. In order to overcome the inherent sensitivity problem of the NMR phenomenon,[2] dual modal contrast agents is an area of research that shows great promise. This is the attachment of a secondary imaging agent for e.g. PET, SPECT or fluorescence imaging to an MRI contrast agent. The goal is to overlay images from the different techniques, giving better image resolution and co-validation of the accumulation of targeted MR contrast agents at a specific site.

Despite the contribution of changes in pancreatic β-cell mass to the development of all forms of diabetes mellitus, few robust approaches currently exist to monitor these changes prospectively in vivo. Although MRI provides a potentially useful technique, targeting MRI-active probes to the β cell has proved challenging. Zinc ions are highly concentrated in the secretory granule, but they are relatively less abundant in the exocrine pancreas and in other tissues. We have therefore developed functional dual-modal probes based on transition-metal chelates capable of binding zinc. The first of these, Gd.1, based upon DOTA (1,4,7,10-tetraazacyclododecane -1,4,7,10-teraacetic acid) is proven to be an excellent chelate that can be functionalised for many biological imaging purposes.[3] Gd.1 binds Zn(II) directly by means of an amidoquinoline moiety (AQA), thus causing a large ratiometric Stokes shift in the fluorescence from λem=410 to 500 nm with an increase in relaxivity from r1=4.2 up to 4.9 mM-1s-1. The probe is efficiently accumulated into secretory granules in β-cell-derived lines and isolated islets, but more poorly by non-endocrine cells, and leads to a reduction in T1 in human islets. In vivo murine studies of Gd.1 have shown accumulation of the probe in the pancreas with increased signal intensity over 140 minutes.[4]

References:

[1] P. J. Endres, K. W. MacRenaris, S. Vogt, and T. J. Meade, ‘Cell-Permeable MR Contrast Agents with Increased Intracellular Retention’ Biocon. Chem. 2008, 19, 2049.
[2] P. Caravan, ‘Strategies for increasing the sensitivity of gadolinium based MRI contrast agents’, Chem. Soc. Rev., 2006, 35, 512.
[3] G. J. Stasiuk and N. J. Long, ‘The ubiquitous DOTA and its derivatives: the impact of 1,4,7,10-tetraazacyclododecane-1,4,7,10-tetraacetic acid on biomedical imaging’, Chem. Commun., 2013, 49, 2732
[4] G. J. Stasiuk, F. Minuzzi, M. Sae-Heng, C. Rivas, H-P. Juretschke, L. Piemonti, P. R. Allegrini, D. Laurent, A. R. Duckworth, A. Beeby, G. A. Rutter and N. J. Long, ’Dual-Modal Magnetic Resonance/Fluorescent Zinc Probes for Pancreatic β-Cell Mass Imaging’, Che. Eur. J., 2015

AUTHORS (LAST NAME, FIRST NAME): Stasiuk, Graeme J.[1, 2]; Long, Nicholas J.[2]; Rutter, Guy A.[3]

INSTITUTIONS (ALL):
1. Biological Sciences, University of Hull, Hull, United Kingdom.
2. Chemistry, Imperial College London, London, United Kingdom.
3. Medicine, Imperial College London, London, United Kingdom.

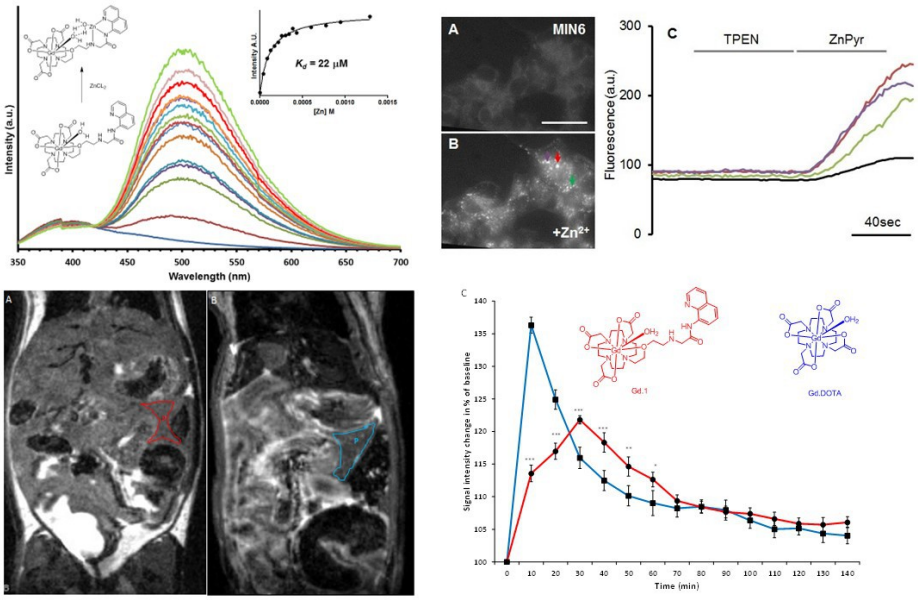

Figure 1. Gd.1 response in vitro and in vivo to zinc

CONTROL ID: 2233141

TITLE: Imaging L-lactate by CEST using paramagnetic shift reagents

PRESENTER: Lei Zhang

ABSTRACT BODY:

Abstract Body: Contrast agents are often used in magnetic resonance imaging (MRI) studies to enhance contrast between tissues. During the last decade, a new type of contrast mechanism based on chemical exchange saturation transfer (CEST) has been explored using a variety of diamagnetic and paramagnetic molecules. One advantage of CEST agents over typical T_1 or T_2 agents is that contrast can be turned “on” and “off” by use of selective radio frequency pulses[1]. Many endogenous molecules containing exchangeable –OH protons have been explored as potential CEST agents, including glucose and glycogen. Lactate also has an exchangeable –OH proton that could potentially be detected by CEST but the chemical shift of the lactate –OH proton is even closer to water than the –OH protons of glucose. Hence, it is quite difficult to detect lactate directly using CEST activation pulses. L-lactate is overproduced by most tumors even in the presence of abundant oxygen (the Warburg effect) so a method for direct imaging of lactate production by tumors could be a useful biomarker. We demonstrate here that one can shift the –OH resonance of L-lactate far downfield from tissue water protons using a paramagnetic shift reagent and then use the “on” versus “off” CEST response to quantify lactate produced by tumor cells growing in tissue culture (Fig 1). Depending upon which paramagnetic complex is used, the shifts can be quite large (40-50 ppm), moving the CEST signal of lactate well away from other confounding endogenous signals from tissues. Interestingly, the intensity of the lactate CEST signal is enhanced by ~50% under slightly acidic conditions (similar to that produced by tumors) and is higher at 37°C than at 25°C. These results provide the framework to develop a simple method to image lactate production in tumors by MRI.

References: (1)Woods, M.; Donald, E.W.C.; Sherry,A.D. *Chem. Soc. Rev.* **2006**, *35*, 500.

AUTHORS (LAST NAME, FIRST NAME): Zhang, Lei[1, 2]; Martins, Andre F.[1]; Wu, Yunkou[2]; Zhao, Piyu[1]; Sherry, A. D.[1, 2]

INSTITUTIONS (ALL):

1. Chemistry , University of Texas at Dallas, Richardson, TX, United States.

2. Advanced Imaging Research Center, The University of Texas Southwestern Medical Center, Dallas, TX, United States.

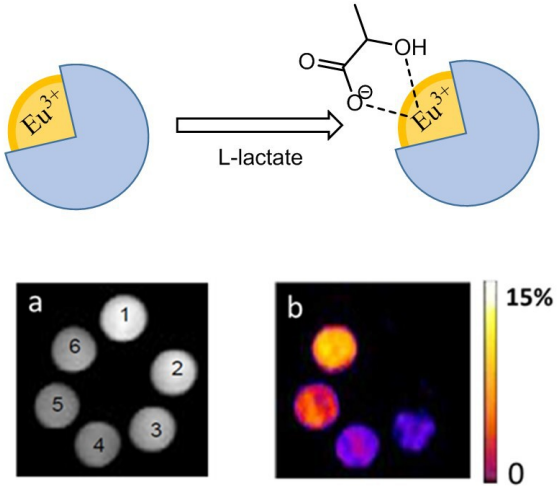

Fig 1: Proton density (a) and CEST (b) images of phantoms of media collected from A549 cells. 1) cell medium alone, 2) cell medium with shift reagent (EuDO3A), 3-6) increasing concentrations of shift reagent. Total [lactate] in the cell medium as assayed enzymatically was 14 mM.

CONTROL ID: 2221110

TITLE: Enhancement of Trastuzumab penetration using Atorvastatin and Cyclophosphamide to Her2+ NCI N87 xenograft mouse model

PRESENTER: KyungDeuk Cho

ABSTRACT BODY:

Abstract Body: Objectives: To investigate the effect of atorvastatin and cyclophosphamide for enhancement of Alexa Fluor 488 conjugated trastuzumab on the accumulation and the microdistribution of Alexa 488 trastuzumab. **Methods:** Groups of nude mice (n = 4-5 / group) were inoculated with Her2 positive NCI-N87 tumor cells. When the tumor size reached ~200 mm3, Alexa-488-Trastuzumab was intravenously injected single dose(150 μg) for control and cyclophosphamide (70 mg/kg) were intraperitoneally injected, and 12 μg/day of atorvastatin in a 0.2 ml volume (roughly equivalent to 40 mg/day in human treatment) was administered via oral gavage. Tumors were harvested, flash frozen and sliced (8 μm) 3 days after Alexa 488 trastuzumab injection. Microscopic imaging was performed using a EVOS FL auto cell imaging system. The penetration of Alexa-488-trastuzumab up to ~80 μm depth from the vessel and tumor surface was calculated by the area-under-curve (AUC) analysis. Circularity and fractal dimension were measured to identify the difference of morphological changes after treatment between groups. Overall micro-distribution of vessels was also assessed in terms of vascular density.

Results: Accumulation of Alexa-488-trastuzumab per tissue area was 1.72 ± 0.01 AU/μm^2 for the control group, 3.10 ± 0.05 AU/μm^2 for cyclophosphamide treatment group, and 2.76 ± 0.02 for the control group, 2.76 ± 0.02 ± 0.60 AU/μm^2 for cyclophosphamide treatment group, and 53.45 ± 0.20 AU/mm^2 for atorvastatin treatment group. The accumulation of Alexa-488-trastuzumab was 80.1% or 60.1% more when cyclophosphamide or atorvastatin was administered, respectively, than the control group ($P < 0.0001$). The penetration of Alexa-488-trastuzumab to 80-μm was 151% or 100% higher when cyclophosphamide or atorvastatin was administered, respectively, than the control group ($P < 0.0001$). Circularity near the vessel was significantly lower than the circularity far from the vessel for both the cyclophosphamide and atorvastatin groups ($P < 0.05$). There was no difference of circularity for the control group. The fractal dimension near the vessel was significantly higher than that of the far field region from the vessel for both the cyclophosphamide and atorvastatin treatment groups ($P < 0.05$). There was no difference of vascular density among the groups.

Conclusion: Co-administration of cyclophosphamide or atorvastatin with Alexa-488-trastuzumab resulted in significantly improved trastuzumab antibody penetration in the near field region from the vessel.

AUTHORS (LAST NAME, FIRST NAME): Cho, KyungDeuk[1]; kim, JIN SU[1]; Kim, Byung Il[1]; Kang, Joo Hyun[1]; Lim, Sang Moo [1]

INSTITUTIONS (ALL):

1. Korea Institute Radiological and Medical Sciences, Seoul, Korea (the Republic of).

(No Image Selected)

CONTROL ID: 2221302

TITLE: The urea transporter – an MRI gene reporter that can be detected using transmembrane water exchange measurements

PRESENTER: Franz Schilling

ABSTRACT BODY:

Abstract Body: INTRODUCTION:

Monitoring gene expression *in vivo* using non-invasive molecular imaging techniques could be used in the clinic to monitor gene therapy and for cell tracking in regenerative medicine. In the case of MRI, various reporter genes, with different underlying contrast mechanisms and substrates, have been developed (T_1,T_2,T_2*,chemical exchange saturation transfer (CEST), apparent diffusion coefficient (ADC)).[1,2] However, many of these approaches suffer from low sensitivity and would be difficult to translate into clinical use. Recently a urea transporter (UTB) has been described as an MRI gene reporter, where reporter expression was detected *in vivo* using ^{13}C MRS ADC measurements following injection of hyperpolarized ^{13}C urea. UTBs also transport water, at similar rates to aquaporin channels, and we show here that UTB reporter expression can also be detected using ^{1}H MRI measurements of water exchange.

METHODS:

An exchange-sensitive filtered-exchange imaging (FEXI) sequence was optimized on a 9.4 T animal scanner using a phantom with different sucrose concentrations (see suppl.).[5,6] HEK 293T cells that had been transduced with a UTB-expressing lentiviral vector were grown in DMEM. Four immune-deficient mice were implanted subcutaneously with 10 x 10^6 UTB-expressing cells on one flank and unmodified cells on the contralateral flank. Animals were imaged using FEXI, Inversion Recovery Turbo-FLASH for T_1 mapping, and diffusion-weighted EPI for ADC measurements. FEXI parameters were: diffusion filter *b*-values (b_f=(0;500)s/mm^2; detection *b*-values *b*=(36;517)s/mm^2; mixing times t_{mix} =(0.01;0.1;0.2;0.3)s; Δ=0.012 ms; δ=0.08ms; for other parameters see figure caption. Animal no. 4 received 0.1 ml of 0.1 mmol/ml Gd-DTPA via a tail-vein before additional T_1 mapping was performed for up to 90 min after injection.

RESULTS & DISCUSSION:

FEXI data yielded sufficient SNR in three of four animals to fit apparent exchange rates (AXRs) in xenograft ROIs (Fig. A,B). AXR values in the UTB-expressing xenografts were in the range of 1.8s^{-1} - 4.3s^{-1} (Fig. C,D) and were higher than in the control xenografts (AXR=0 for control tumours in animals 2 and 4). T_1 and ADC maps for the same ROIs did not show differences between UTB and control tumours (Fig. E,F). T_1 mapping after Gd-DTPA injection showed >15% T_1 reduction in UTB tumours compared to controls (Fig. G,H,I,J) between 20 to 60 min after injection. Modelling using the Bloch McConnell equations gave an intra- to extracellular water fraction of 0.55/0.45, exchange rates of k_{UTB} =0.6s^{-1} & $k_{control}$=0.1s^{-1}, and $T_{1,extra}$=0.29s & $T_{1,intra}$ =1.42s. Simulations demonstrate that either increasing the [Gd-DTPA] or k_{UTB}, via increased UTB expression, would lead to further improvements in image contrast (Fig. K).

ACKNOWLEDGEMENTS

This work was funded by a CRUK Programme Grant to KMB. FS is in receipt of funding from the Alexander von Humboldt Foundation.

REFERENCES

1. Weissleder, R. (2000) Nat Med 6:351 2. Vandsburger, M.H. (2013) NMR Biomed 26:827 3. Yang, B. (2002) J Biol Chem 277:36782 4. Patrick, P.S. (2015) Magn Res Med 5. Lasic, S. (2011) Magn Res Med 66:356 6. Nilsson, M. (2013) Magn Res Med 69:1573

AUTHORS (LAST NAME, FIRST NAME): Schilling, Franz[1]; Hu, De-En[1]; McGuire, Sarah[1]; Brindle, Kevin M.[1]

INSTITUTIONS (ALL):

1. Cancer Research UK Cambridge Institute, University of Cambridge, Li Ka Shing Centre, Cambridge, United Kingdom.

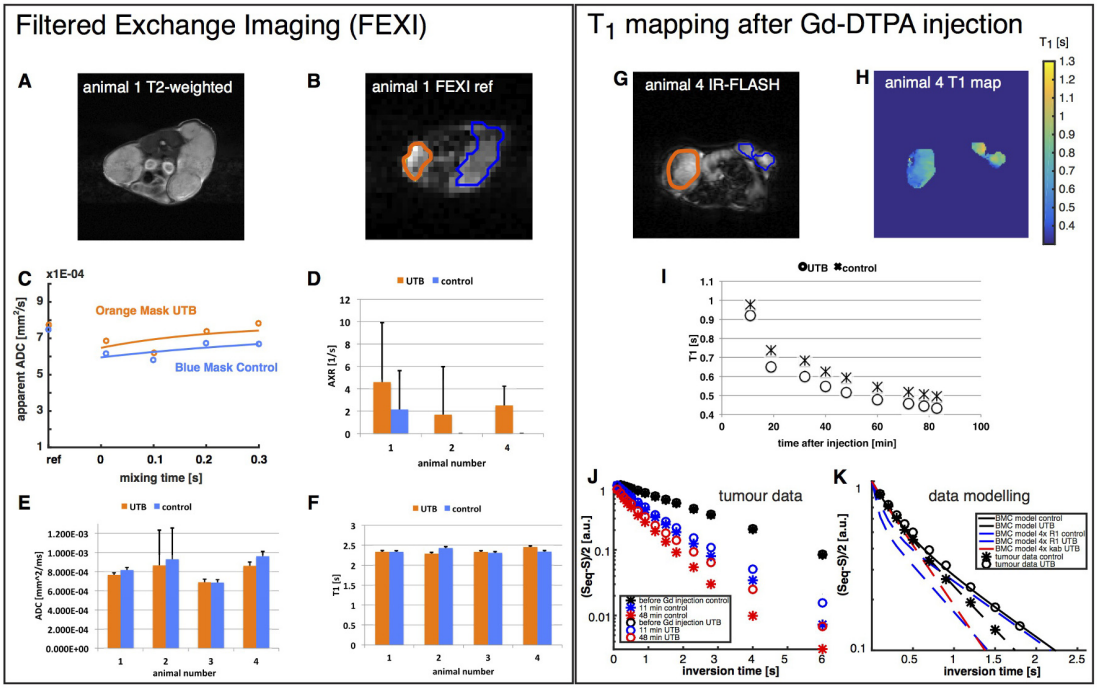

(A) T_2-weighted MRI highlighting UTB-expressing xenograft (left) and the control xenograft (right). **(B)** FEXI reference image **(C)** ADC values for FEXI dataset from animal1 (*b*-values: (37;517) s/mm^2, scan time ≈ 20 min). Fits of the apparent exchange rate (AXR) show faster recovery for UTB-expressing xenografts. **(D)** AXR values (+SD). **(E)** ADC maps (6 *b*-values). **(F)** T_1 maps (18 inversion times **(G)** IR-TFLASH image and ROIs. **(H)** T_1 map for animal 4. **(I)** Mono-exponential T_1 fits reveal reduced T_1 in UTB-expressing xenografts between 20 and 60 min after Gd-DTPA injection. **(J)** Semi-logarithmic plot of normalized ROI signal intensities from the IR-TFLASH experiments. **(K)** Bloch-McConnell equations based on two-site exchange models experiments (black line) and predicts improved contrast at higher UTB-expression (red line) and higher [Gd-DTPA] (blue lines).

CONTROL ID: 2221310

TITLE: Physiochemical, biological, and imaging performance of zwitterionic-coated TaO nanoparticles as CT contrast agents

PRESENTER: Jeannette Roberts

ABSTRACT BODY:

Abstract Body: Introduction

Current clinically-approved computed tomography (CT) contrast agents employ iodinated small molecules that are used to highlight vascular anatomy and pathology. (Cormode 2013) However, iodinated compounds have poor imaging efficacy in large patients and their use is contraindicated in a growing population of renally impaired patients who are hypersensitive to these contrast agents. (Cormode 2013) Nanoparticles have been explored as a potential new class of CT contrast agents. (Garcia 2014) In order to be clinically translatable as contrast agents, nanoparticles must have controlled physiochemical parameters and appropriate biological safety profiles. (Jakhmola 2012 & Garcia 2014) Tantalum oxide nanoparticles (TaO NPs) have high potential as CT contrast agents because of their promising biocompatibility and good radiopacity. (Bonitatibus 2010 & Torres 2012) In this study, we have identified a <5nm zwitterion-coated TaO nanoparticle that exhibits promising physiochemical, biological and CT imaging performance.

Methods and Results

A phosphonate-coated TaO NP (PHS, Bonitatibus 2010), a zwitterionic mixed siloxane-coated TaO NP (ZMS, Bonitatibus 2012) and a single-ligand zwitterion-coated TaO NP (CZ) were synthesized. Compared to the previously reported physiochemical properties of PHS, zwitterion-coated nanoparticles (ZMS, CZ) show lower viscosities at higher concentrations. (Figure 1a,b) To test organ retention of each TaO NP, naive rats were intravenously injected with the anticipated clinical dose (400 mg Ta/kg bodyweight) of each TaO NP. One week after injection, organs known to retain nanoparticles (liver, kidney and spleen) were removed and measured for Ta content (% injected dose/organ) by combustion followed by inductively-coupled plasma spectroscopy. Zwitterionic nanoparticles showed lower tantalum organ retention than PHS; CZ showing the lowest retention. (Figure 1c) To explore the safety performance of these nanoparticles, rats were intravenously injected with 3x anticipated clinical dose (1500 mg Ta/kg bodyweight) of each nanoparticle. To evaluate potential renal toxicity, kidneys were collected (day 7), sectioned, stained by H&E, and scored by a toxicologic pathologist (Charles River Labs). The kidney pathology that is observed with PHS was not observed by the zwitterionic nanoparticles (ZMS, CZ). (Figure 1d)

Tantalum-based contrast agents can provide improved vascular contrast and allow reduced radiation dose especially in larger patients. In Figure 1e, we show the image contrast produced by tantalum compared to iodine at the range of x-ray tube voltages (kVp) used in CT imaging. 80 kVp is used to scan the smallest adult patients. Tantalum provides higher image contrast than other elements at 100-140 kVp and could be used to improve image quality or to reduce radiation and/or contrast agent dose in most patients, with the highest improvement at 140 kVp, which is required for large patients.

Conclusions

In summary, zwitterionic coated TaO nanoparticles (ZMS, CZ) exhibit the best physiochemical, retention and safety profiles. These TaO nanoparticles may also reduce the radiation dose for CT imaging in larger patients.

AUTHORS (LAST NAME, FIRST NAME): Roberts, Jeannette[1]; Bonitatibus Jr, Peter J.[1]; Butts, Matthew[1]; Colborn, Robert E.[1]; Edic, Peter M.[1]; FitzGerald, Paul[1]; Lambert, Jack W.[2]; Marino, Michael[1]; Torres, Andrew[1]; Yeh, Benjamin M.[2]

INSTITUTIONS (ALL):

1. GE Global Research, Niskayuna, NY, United States.
2. University of California, San Francisco, CA, United States.

(a)

Name	Structure	Size (nm)	Si/Ta	Viscosity @ 250 Ta/kg (cps)
PHS	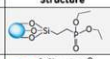	2.5	1.7	>25
ZMS	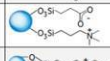	4.5	1.5	10
CZ	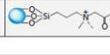	2.6	1.5	6

(b)

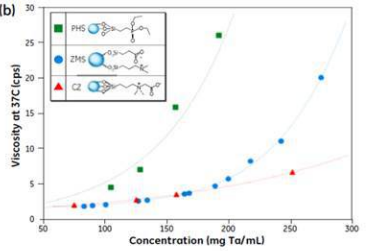

(c)

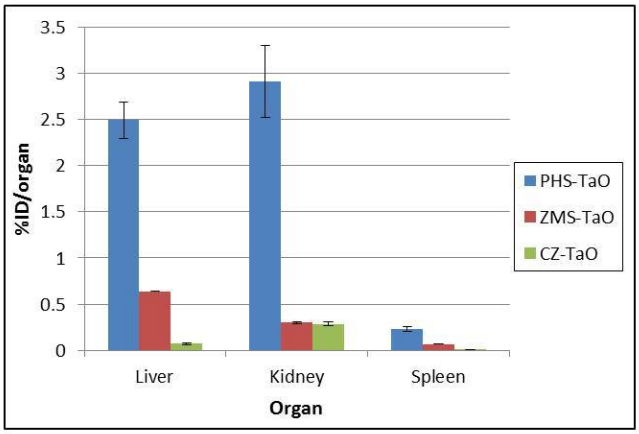

(d)

Key: N=Normal; 1=Minimal; 2=Mild; 3=Moderate; 4=Marked; >=Multifocal

Kidney Pathology Feature	Saline			PHS			ZMS			CZ		
Tubular epithelium, cortex- Degeneration	N	N	N	>3	>3	>2	N	N	N	N	N	1
Tubular epithelium, cortex- Regeneration	N	N	N	>3	>2	>2	N	N	N	N	N	N
Tubule, cortex - Dilatation	N	N	N	>2	>1	>1	N	N	N	N	N	N
Cortex - Infiltration, mononuclear cell	N	N	>1	N	>1	N	N	1	N	N	N	N
Tubular epithelium, cortex - cytoplasmic droplets	N	N	N	N	N	N	N	N	N	N	N	N

(e)

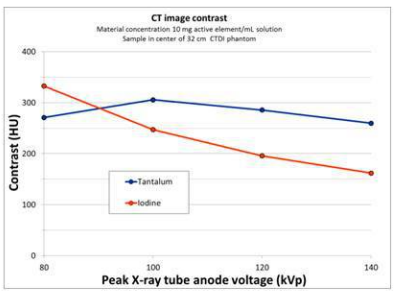

Figure 1: Properties of TaO nanoparticle CT contrast agents (a) Physical characteristics of synthesized TaO nanoparticles. (b) Viscosity of synthesized TaO nanoparticles. (c) Organ retention of TaO nanoparticle CT contrast agents. %ID/organ = % injected dose/organ. (d) Histopathology analysis of kidney tissue after injection with TaO nanoparticle CT contrast agents. (e) Measured imaging performance of tantalum versus iodine.

CONTROL ID: 2221432

TITLE: In vivo radiopharmaceutical excited fluorescence imaging for highly sensitive tumor detection

PRESENTER: Kun Wang

ABSTRACT BODY:

Abstract Body: Cerenkov luminescence imaging (CLI) has attracted more and more attentions recently, as it can provide in vivo distribution of radiopharmaceuticals through detection of Cerenkov light signals. This unique combination of nuclear medicine imaging and optical imaging indeed brought many benefits, such as well-developed radioactive tracers, high throughput, great superficial resolution, low cost, et al. However, the overall sensitivity of CLI is still one of the biggest challenges for in vivo diagnostic applications. The extremely weak luminescent signal and the blue weighted luminescent spectrum are the two essential problems. Here, we introduce a new imaging strategy, the radiopharmaceutical excited fluorescence imaging (REFI), which converts and Cerenkov radiation from radioisotopes into fluorescence through europium oxide (EO) nanoparticles. By injecting both radioactive tracer (^{18}F-FDG in this case) and EO nanoparticle intravenously, the internal dual radiation excited fluorescent signal was activated in the site where both tracers accumulate. The dual radiation excited fluorescence showed much higher signal intensity, and the spectrum was red weighted (characteristic peak: 620 nm) in comparison of conventional Cerenkov light. We applied this technique for in vivo tumor detection in U87MG xenografted mice. Comparing with CLI, REFI showed significantly greater ($P < 0.01$) signal in the tumor lesion region (Fig. 1) with the same dose of radio tracer (500 μCi). The mean intensity of REFI was about 25 times and 15 times greater than that of CLI with no filtering and 620 nm filtering, respectively. We believe that this new technique will facilitate the development of nuclear and optical molecular imaging for highly sensitive imaging applications.

AUTHORS (LAST NAME, FIRST NAME): Wang, Kun[1]; Hu, Zhenhua [1]; Tian, Jie[1]

INSTITUTIONS (ALL):

1. Institute of Automation, Chinese Academy of Sciences, Beijing, China.

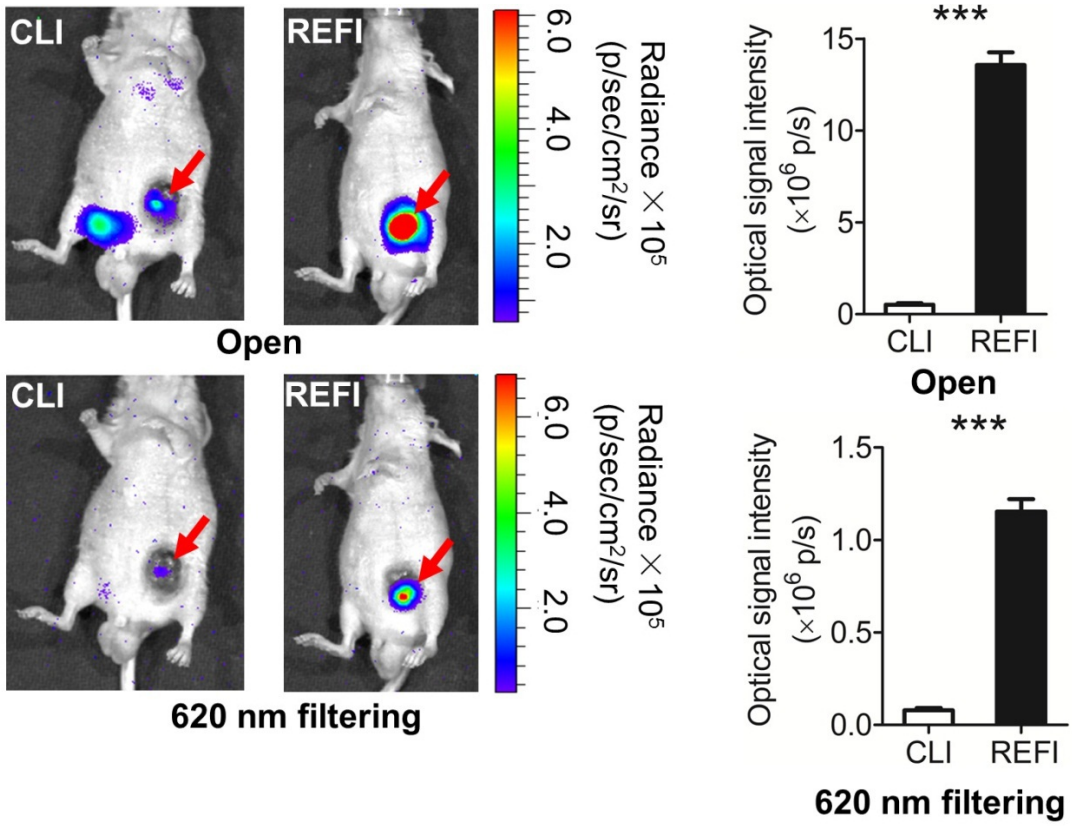
CLI
REFI
6.0
4.0
2.0
Radiance ×10^5 (p/sec/cm^2/sr)
Open
CLI
REFI
6.0
4.0
2.0
Radiance ×10^5 (p/sec/cm^2/sr)
620 nm filtering
***
Optical signal intensity (×10^6 p/s)
15
10
5
0
CLI
REFI
Open
***
Optical signal intensity (×10^6 p/s)
1.5
1.0
0.5
0.0
CLI
REFI
620 nm filtering

CONTROL ID: 2221490

TITLE: Bioluminescence tomography based on the linearized Bregman iterative with *Kicking*

PRESENTER: Chengcai Leng

ABSTRACT BODY:

Abstract Body: Bioluminescence tomography (BLT) is an important modality of optical molecular imaging, which has been widely used in physiology and pathology at cellular and molecular levels. The reconstruction problem of BLT is severely ill-posed. In this paper, we propose an effective reconstruction method based on the linearized Bregman iterative with *Kicking* for bioluminescence tomography. The proposed method can remove the stagnation periods and make it fast convergence to minimize the sparse regularization problem so as to achieve source reconstruction efficiently. The results on numerical simulation and *in vivo* experiment demonstrate the superiority of the proposed method.

AUTHORS (LAST NAME, FIRST NAME): Leng , Chengcai [1]; Zhang, Shuang[4]; Hu, Yifang[3]; Wang, Kun[1]; Tian, Jie[2]

INSTITUTIONS (ALL):

1. Institute of Automation, Chinese Academy of Sciences, Beijing, China.
2. Institute of Automation, Chinese Academy of Sciences, Beijing, China.
3. School of Computer and Information Technology, Beijing Jiaotong University, Beijing, China.
4. Sino-Dutch Biomedical and Information Engineering School, Northeastern University, Shenyang, China.

(No Image Selected)

CONTROL ID: 2221607

TITLE: A Fluorescent Delta-Opioid Receptor (DOR) Targeted Agent for Molecular Imaging and Intraoperative Guidance of Lung Cancer

PRESENTER: Allison Cohen

ABSTRACT BODY:

Abstract Body: Lung cancer is the leading cause of cancer deaths worldwide. Currently, the 5-year survival rate for this cancer is low. Better methods or tools for diagnosing and treating this disease are needed to improve patient outcomes. Targeted agents could be useful for molecular imaging and therapy of lung cancer. One of the major goals for cancer agent development is to target the tumor with high specificity and selectivity. The use of targeted agents to distinguish cancer from normal tissue during surgery by imaging is an area of great interest. Removal of the whole tumor without leaving behind microscopic pieces will reduce recurrence and increase patient survival. Fluorescently labeled targeted probes can be developed for real-time surgical guidance through the use of instruments with fluorescence capability. These agents can also be used to identify mediastinal lymph nodes for staging during surgery or for early detection of malignant lesions by fluorescence bronchoscopy. The goal of this work was to develop a targeted fluorescent agent for imaging of lung cancer and to evaluate it preclinically for utility in intraoperative guidance.

The delta opioid receptor (DOR) has been reported to be overexpressed in some lung cancers and we have validated its expression by immunohistochemical staining of a lung cancer tissue microarray. We have previously described the synthesis of a fluorescently-labeled DOR-targeted imaging agent (DORL-800) and showed that it has high affinity for the DOR *in vitro* (K_{i-} = 1.43 ± 0.24 nM, n = 3). We identified lung cancer cell lines with high (DMS-53) and no (H1299) endogenous expression of the DOR using qRT-PCR and verified protein expression using confocal microscopy. We have also fully evaluated the pharmacokinetics and biodistribution of this agent *in vivo* in a bilateral subcutaneous xenograft model using these lung cancer cell lines. In this work, we further evaluated this agent for imaging of the DOR *in vivo*. *In vivo* studies were performed under USF IACUC #R4125. To study DORL-800 in a more clinically relevant model, we developed an orthotopic model of lung cancer. In this model, the mice undergo a minor surgical procedure during which DMS-53 luc+ (DOR+) cells are injected directly in the left lung. The growth of the tumors is monitored using bioluminescence imaging (Figure 1A). The mice are imaged using fluorescence molecular tomography (FMT) following injection of DORL-800 at various time points post-injection. We have shown that DORL-800 accumulates specifically in the tumor. We have also performed preliminary studies using DORL-800 for intraoperative guidance. In these experiments, the Surgvision intraoperative imaging system was used to perform surgery on mice 6-8 hours post-injection of DORL-800. We were able to visualize the tumors intraoperatively with fluorescence imaging (Figure 1B). The presence of tumor in the lungs was confirmed by *ex vivo* fluorescence imaging (Figure 1C).

In conclusion, the fluorescent DORL-800 agent has high selectivity and affinity for the DOR. This agent could be useful for guidance during lung cancer resection. In the future, it can also be developed into a targeted therapeutic.

AUTHORS (LAST NAME, FIRST NAME): Cohen, Allison S.[1]; Jeune-Smith, Yolaine[1]; Khalil, Farah K.[2]; Enkemann, Steven A.[3]; Clark, Noel[4]; Johnson, Joseph 0.[5]; Chen, Tingan[5]; Bode, Aimee[6]; Casagni, Todd J.[6]; Baldwin, Margaret[6]; Budzevich, Mikalai[7]; Ruiz, Epifanio[7]; Patek, Renata[8]; Haura, Eric B.[9]; Vagner, Josef[8]; Morse, David L.[1]

INSTITUTIONS (ALL):

1. Department of Cancer Imaging and Metabolism, H. Lee Moffitt Cancer Center & Research Institute, Tampa, FL, United States.
2. Department of Anatomic Pathology, H. Lee Moffitt Cancer Center & Research Institute, Tampa, FL, United States.
3. Molecular Genomics Shared Resource, H. Lee Moffitt Cancer Center & Research Institute, Tampa, FL, United States.
4. Tissue Core Shared Resource, H. Lee Moffitt Cancer Center & Research Institute, Tampa, FL, United States.
5. Analytic Microscopy Core Shared Resource, H. Lee Moffitt Cancer Center & Research Institute, Tampa, FL, United States.
6. Department of Comparative Medicine, H. Lee Moffitt Cancer Center & Research Institute, Tampa, FL, United States.

7. Small Animal Imaging Laboratory Shared Resource, H. Lee Moffitt Cancer Center & Research Institute, Tampa, FL, United States.
8. Bio5 Institute, University of Arizona, Tucson, AZ, United States.
9. Department of Thoracic Oncology, H. Lee Moffitt Cancer Center & Research Institute, Tampa, FL, United States.

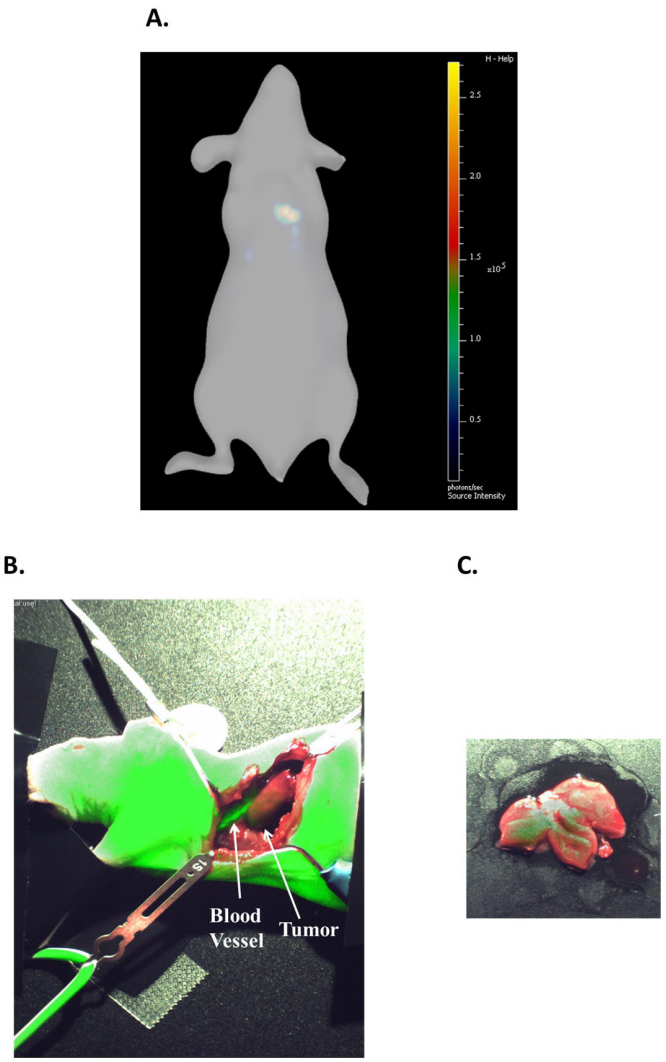

Figure 1. Intraoperative imaging of orthotopic lung tumor xenografts. The mouse was injected with DMS-53 luc+ (DOR+) cells and tumor growth was monitored by bioluminescence imaging on the IVIS 200. A) Representative 3D bioluminescence image acquired 7 weeks post-surgery. Fluorescence guided surgery was performed on the mouse with orthotopic lung tumor xenografts using a lung cancer specific imaging agent DORL-800 and the Surgvision intraoperative imaging system. The mouse was injected with 40 nmol/kg DORL-800 i.v. and the surgery was performed 7 hours post-injection. Shown are overlays of the white light and fluorescence images (shown in green). B) Representative real-time image of the mouse during surgery. The surgeon has exposed the lungs for visualization of the tumor. DORL-800 is present in the lung tumor and in a blood vessel. There is also background autofluorescence signal from the skin. Following intraoperative visualization, the mouse was euthanized and the lungs were removed. C) Representative ex *vivo* image of the lungs following surgery. The green fluorescence signal indicates the presence of a diffuse tumor.

CONTROL ID: 2231589

TITLE: Ultrasound Molecular Imaging using P- and E-selectin targeted microbubbles in a murine model of chronic inflammatory bowel disease with inducible acute inflammation.

PRESENTER: Steven Machtaler

ABSTRACT BODY:

Abstract Body: Introduction: Inflammatory bowel disease (IBD) is a complex group of relapse/remitting diseases (including Crohn's disease (CD) and ulcerative colitis (UC)) which involves gastrointestinal changes in mucosal immunity and physiology. Imaging plays an important role in the diagnosis and monitoring of IBD, specifically in the identification of disease extent along the length of the small and/or large bowel [1]. Ultrasound (US) molecular imaging (MI) utilizes micron-sized, gas-filled contrast agents (microbubbles; MBs) that are modified to bind to vascular proteins that are up-regulated due to disease or active biological processes, and has shown promise in imaging inflammation in preclinical murine models of IBD [2, 3]. However, these models initiate acute inflammation on previously normal colons, in contrast to patients with chronic IBD, where acute inflammation is often found in chronically inflamed regions that were in a quiescent state. In this study we explored the potential of dual P- and E-selectin targeted ultrasound molecular imaging for assessing acute inflammation on a quiescent chronic inflammatory background in order to replicate what would likely be encountered in a clinical setting.

Methods: Chronic IBD was induced using three cycles of 4% DSS in the drinking water of male FVB mice (n=47, 6-8 weeks of age). Acute inflammation was initiated 2 weeks after the final DSS cycle in a subset of mice with quiescent chronic IBD (n=18) through rectal administration of 1% 2.4.6-trinitrobenzenesulfonic acid (TNBS). Mice at different stages of inflammation were imaged using a small animal US system (Vevo2100; VisualSonics) following i.v. injection of clinical grade $5x10^7$ MB targeted to P- and E-selectin (MBselectin) or control MB (MBcontrol). *In vivo* imaging results were correlated with *ex vivo* immunofluorescence and histology.

Results: After validating quiescent and acute inflammation (Figure 1A), the USMI signal was obtained. Induction of acute inflammation on the chronic IBD background resulted in an increase in the USMI signal from 20.23 ± 21.23 arbitrary units (a.u.) at day 0 to 305.59 ± 293.75 a.u. ($P < 0.01$) at day1, 177.03 ± 192.3 a. u. ($P = 0.02$) at day 3, returning to levels similar to control at day 5 (Figure 1B and C). Control MB showed no significant binding. Expression of P- and E- selectin was validated on the colon vasculature (Figure 1D). After acute inflammation was initiated, there was a significant increase in the percentage of P- and E-selectin positive vessels at Day 1 (P-selectin: 21.0 ± 7.1% of vessels; $P < 0.05$; E-selectin: 16.4 ±3.7% of vessels; $P < 0.05$) compared to Day 0 (P-selectin: 10.3 ± 5.7% of vessels; E-selectin: 7.3 ± 7.0% of vessels).

Conclusion: Using a clinical-grade MB targeted to P- and E- selectin, acute inflammation on a chronic IBD background can be accurately measured in a clinically relevant murine IBD model. These findings suggest that USMI has the potential to accurately describe the inflammatory extent of IBD.

1. Duigenan, S., et al. (2012) *American Journal of Roentgenology.* **199**, 907-915. 2. Wang, H., et al. (2013) *Radiology.* **267**, 818-829. 3. Deshpande, N., et al. (2012) *Radiology.* **262**, 172-80.

AUTHORS (LAST NAME, FIRST NAME): Machtaler, Steven[2]; Knieling, Ferdinand[2]; Luong, Richard[3]; Bettinger, Thierry[1]; Tian, Lu[3]; Willmann, Juergen K.[4]

INSTITUTIONS (ALL):

1. Research, Bracco Suisse SA, Geneva, Switzerland.
2. Radiology, Stanford, Stanford, CA, United States.
3. Stanford, Stanford, CA, United States.
4. Radiology, Stanford, Stanford, CA, United States.

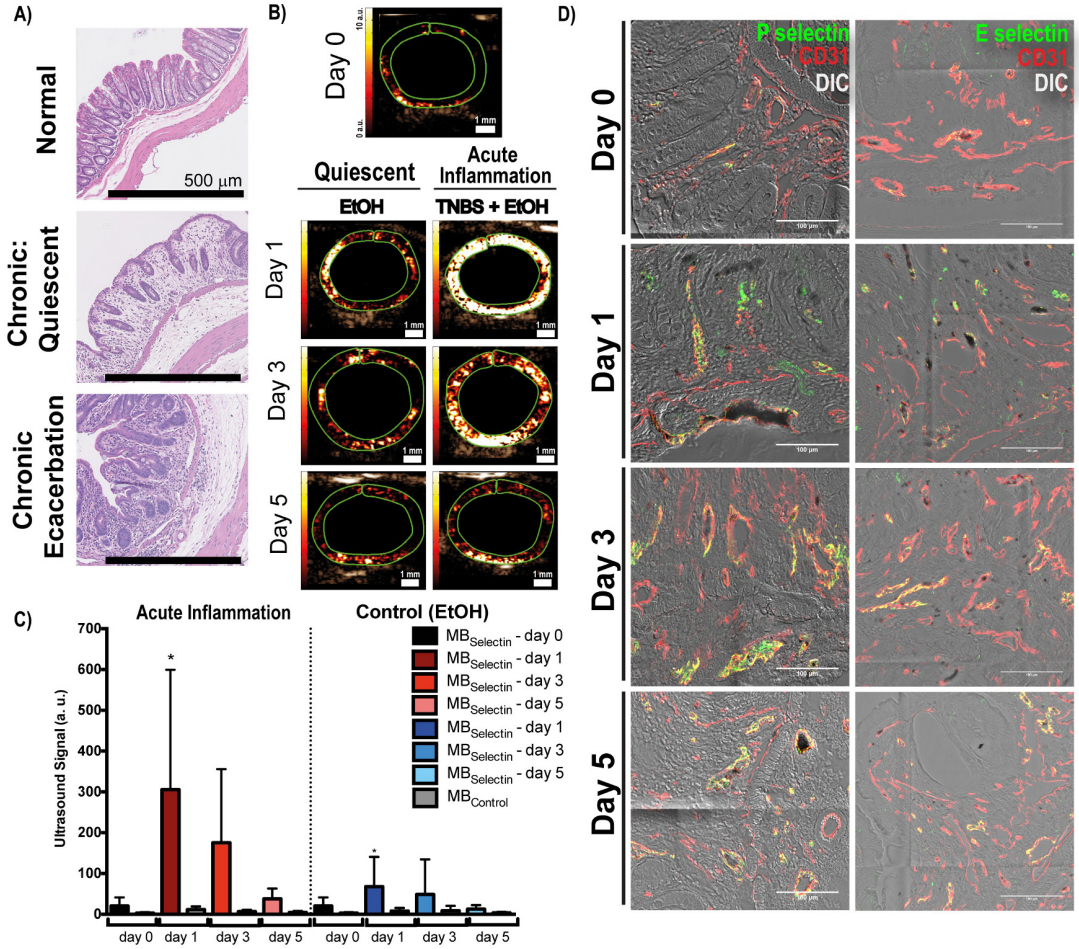

Figure 1: Example of US molecular imaging using MBselectin in a murine model of acute inflammation on a chronic IBD Background. A) H&E staining of normal (top), DSS-induced chronic IBD (Quiescent: middle), and a chronic IBD colon with TNBS-induced acute inflammation (bottom). B) Representative sonographs of the US molecular imaging signal obtained in chronic colitis after induction of acute inflammation using MBselectin (right panels) or EtOH control (left panels). C) Quantification US molecular imaging signal using MBselectin and MBcontrol. D) Representative micrographs of P-selectin (left) and E-selectin expression in the murine chronic IBD model after induction of acute inflammation (P-/ E-selectin = green, CD31 = red).

CONTROL ID: 2221789

TITLE: Prototype of an Awake Animal PET System

PRESENTER: Andrew Weisenberger

ABSTRACT BODY:

Abstract Body: We describe the development of a PET imaging system for imaging awake mice without the use of anesthesia. Earlier we have developed an Awake Animal SPECT/CT system for imaging the mouse brain using an optical motion tracking system. The system provides a unique tool for brain physiological studies and successfully has been imaging live mice without anesthesia. By leveraging our expertise in motion tracking techniques and image reconstruction, we built a prototype Awake Animal PET system using a motion tracking system and modular PET detectors. The system consists of a commercial motion tracking system that utilizes four CCD cameras equipped with near infra-red (NIR) light emitting diode strobes, retro-reflective markers, and a modular PET system consisting of 8 detector modules. The motion tracking system measures and provides the six degrees of freedom (x, y, z, roll, pitch, and yaw) of a moving target at 60 frames per second. The PET detector data acquisition system is based on a 32 channel flash ADC unit developed at Thomas Jefferson National Accelerator Facility. Each PET detector module is composed of a Hamamatsu H8500 5 cm x 5 cm position sensitive photomultiplier tube optically coupled to a 48 x 48 pixelated LYSO scintillator array that has a 1 mm pitch and is 10 mm thick. A custom electronic readout was built using Anger-logic to provide a 4-channel output for each detector module. Initial tests were performed with a ring-PET arrangement of the 8 detector modules resulting in a 5 cm axial field of view with a 20 cm diameter opening. Geometrical calibration was performed using ^{22}Na point source phantom using the same method used for Awake Animal SPECT. Initial tests were performed using a foam mouse phantom that had a ^{22}Na point source inserted inside the head region. During the PET scan, the foam mouse was moved and rotated through manual manipulations. An iterative image reconstruction with motion compensation provides a good point image while image reconstruction without motion compensation results is a blurred image because of the phantom motion.

Conclusion: The tracking system successfully provides 6 six degrees of freedom information of the foam mouse motion at 60 frames per second. We have demonstrated our technique has the capability of forming the basis of a future Awake Animal PET system to image moving mice.

AUTHORS (LAST NAME, FIRST NAME): Lee, Seungjoon[1]; Weisenberger, Andrew[1]

INSTITUTIONS (ALL):

1. Radiation Detector and Imaging Group, Thomas Jefferson National Accelerator, Newport News, VA, United States.

(No Image Selected)

CONTROL ID: 2233789

TITLE: A Method to Visualize Phosphorus Transport in Plant-Fungal Interactions in Soil

PRESENTER: Andrew Weisenberger

ABSTRACT BODY:

Abstract Body: We describe a new molecular imaging approach to following in a non-destructive manner the transport of phosphorus from soil to roots in plants for fungi studies using potted plants. Understanding the use of beneficial soil fungi to enhance plant productivity is critical to the sustainable production of crops and biofuels. Sustained high plant productivity depends on plant and fungal symbiosis and trade-offs in energy and nutrient exchange between interacting partners. Phosphorus (P) in phosphate salts (PO_4^{3-}), monohydrogen phosphate (HPO_4^{2-}), and dihydrogen phosphate ($H_2PO_4^-$) is a macronutrient that limits plant productivity globally. Several types of mycorrhizal fungi can provide plant hosts with phosphorus. Often researchers use ^{32}P and ^{33}P to study the P transport from soil to plants using ~100 kBq/g of soil. To quantify the amount and distribution of phosphorus the plant absorbed the plant is harvested and dissected, then portions of the plant are counted using a liquid scintillator counter. Both ^{32}P and ^{33}P are pure β particle emitters whose β particles travel a short distance before being absorbed. We are developing a ^{32}P / ^{33}P imaging detector capable of being used in the soil containing living plants in pots for plant-fungal interaction studies. The detector is based on a two-dimensional grid formed by two orthogonal planes of plastic scintillating fiber (PSF) to be readout by a photomultiplier such as a position sensitive photomultiplier tube or a collection of silicon photomultipliers. Several planes formed by the grids will be built into a root cuvette (pot) to allow below ground realtime measurement of the movement of ^{32}P or ^{33}P. Initial experiments with PSF coupled to SiPMs were carried out using a collimated bismuth-207 (^{207}Bi) sealed source. The source was used to illuminate with ^{207}Bi emitted β particles two 2 mm square PSF arranged on top of each other as a cross in which one end of each PSF is polished and optically coupled to a SiPM photon sensor. Only their cross-point is irradiated by β particles from ^{207}Bi through a single-hole polyethylene plastic collimator. The SiPM detected coincident signals and the results were displayed on a digital oscilloscope. A coincidence rate of 5.6% was measured.

Conclusion: Our early results indicate that a potentially useful molecular imaging methodology for phosphorus based studies of plant-fungi interactions can be based on PSF. We are continuing with the development and construction of a full plane of a grid of PSFs to be tested in soil.

AUTHORS (LAST NAME, FIRST NAME): Weisenberger, Andrew[1]; Kross, Brian[1]; Lee, Seungjoon[1]; Xi, Wenze[1]; Zorn, Carl[1]; Reid, Chantal D.[2]

INSTITUTIONS (ALL):

1. Radiation Detector and Imaging Group, Thomas Jefferson National Accelerator Facility, Newport News, VA, United States.

2. Biology, Duke University, Durham, NC, United States.

(No Image Selected)

CONTROL ID: 2221833

TITLE: In Vivo Optical Imaging of Immune Response

PRESENTER: Zhihong Zhang

ABSTRACT BODY:

Abstract Body: Optical molecular imaging is the most promising tools for investigating the function and motility of immune cells *in vivo*. Immuno-Optimaging as a new interdiscipline research area has been developed for a decade. Here, we developed a multi-scale optical imaging approach to evaluate the spatio-temporal dynamic behavior and properties of immune cells from the whole field of organs to the cellular level at the inflammatory site: the recruitment of leucocytes was directly visualized using whole-field fluorescent imaging at the organ and tissue levels; the dynamic distribution of the leukocytes was directly visualized using large-scale scanning microscopy at the single-cell level; the motility and migration dynamics of leukocytes were visualized in real time and analyzed using time-lapse confocal imaging or two-photon excitation microscopy at the single-cell level with high temporal resolution. Meanwhile, some multi-color labeling mouse models based on the exogenous labeling with fluorescent protein and the endogenous labeling with fluorescent dye were established. The dynamic properties and function of immunocytes in the immune response (e.g., the delayed type hypersensitivity reaction and tumor immunotherapy) were visually investigated using multi-scale optical imaging techniques combined with the multi-color labeling mice model.

AUTHORS (LAST NAME, FIRST NAME): Zhang, Zhihong[1]

INSTITUTIONS (ALL):

1. Huazhong University of Science and Technology, Britton Chance Center for Biomedical Photonics-Wuhan National Laboratory for Optoelectronics, Wuhan, China.

(No Image Selected)

CONTROL ID: 2221937

TITLE: Frequency of cisplatin induced severe renal injury in patients with solid tumors as determined by radionuclide renal scintigraphy

PRESENTER: Muhammad nouman

ABSTRACT BODY:

Abstract Body: Introduction:

Cisplatin is an effective chemotherapeutic drug for the treatment of solid tumors. However, its nephrotoxic side effects limit its optimal use and renal scintigraphy may be a reliable diagnostic tool for detecting, evaluating, and quantifying any cisplatin-induced nephrotoxicity.

Objective:

To determine the frequency of cisplatin induced severe renal injury by radionuclide renal scintigraphy in patients with solid tumors undergoing chemotherapy with cisplatin based regimens.

Study design:

Cross-sectional, observational study.

Setting:

Nuclear Medical Centre, Armed Forces Institute of Pathology (AFIP), Rawalpindi from Dec 2012 to Dec 2013.

Sample size:

62 patients

Materials and Methods:

Patients who were candidates for cisplatin based chemotherapy regimen with normal renal function as evidenced by normal serum urea and creatinine levels and a normal value of age adjusted GFR on Tc-99m-DTPA renal scintigraphy as per guidelines of National kidney foundation were subjected to a post chemotherapy Tc-99m-DTPA renal scintigraphy within 02 weeks of completion of 06 cycles cisplatin based chemotherapy. Post chemotherapy GFR was calculated.

Results:

Out of 62 patients, 48 (77%) were males and 14 (23%) were females. The age of the patients was between 26 and 70 years. The frequency of severe renal injury was calculated as 2/62(3.2%) as determined by radionuclide ^{99m}Tc-DTPA scintigraphy after completion of 6 cycles of chemotherapy.

Conclusion:

3.2% of all patients developed severe renal injury at the completion of 6 cycles of cisplatin based chemotherapeutic regimen. This included patients with severe renal injury (Severe renal injury= GFR 15 – 29 ml/min) as well as patients with severe renal injury leading to absolute renal failure (Renal failure=GFR<15 ml/min).

Keywords:

Cisplatin, Renal Injury, Renal scintigraphy, ^{99m}Tc-DTPA, Solid tumors

AUTHORS (LAST NAME, FIRST NAME): nouman, Muhammad I.[1]

INSTITUTIONS (ALL):

1. Nuclear medical centre, Armed forces institute of pathology, Rawalpindi, punjab, Pakistan.

(No Image Selected)

CONTROL ID: 2231826

TITLE: GPU-based prompt gamma ray imaging from boron neutron capture therapy

PRESENTER: Do-Kun Yoon

ABSTRACT BODY:

Abstract Body: Purpose: Purpose of this research is to realize the fast reconstruction of the prompt gamma ray image using the graphics processing unit (GPU) computation from boron neutron capture therapy (BNCT) simulation.

Methods: To evaluate an accuracy of the reconstructed image, a phantom including four boron uptake regions (BURs) was used in the simulation. After the Monte Carlo simulation of the BNCT, the modified ordered subset expectation maximization (OSEM) reconstruction algorithm using the GPU computation was used to reconstruct the images with fewer projections. The computation times for image reconstruction were compared between the GPU and the central processing unit (CPU). Also, the accuracy of reconstructed image was evaluated by the receiver operating characteristic (ROC) curve analysis.

Results: The image reconstruction time using GPU was 196 times faster than the conventional reconstruction time using the CPU. The four BUR's area under curve (AUC) values from the ROC curve were 0.6726 (A-region), 0.6890 (B-region), 0.7384 (C-region), and 0.8009 (D-region), respectively.

Conclusion: The tomographic image using the prompt gamma ray event from the BNCT simulation was acquired using the GPU computation in order to realize the fast reconstruction during treatment. We verified the feasibility of the prompt gamma ray image reconstruction using GPU computation for the BNCT.

AUTHORS (LAST NAME, FIRST NAME): Yoon, Do-Kun[1]; Jung, Joo-Young[1]; Shin, HanBack[1]; Kim, Moo-Sub[1]; Suh, Tae Suk[1]

INSTITUTIONS (ALL):

1. Biomedical Engineering, The Catholic University of Korea, Seoul, Korea (the Republic of).

(No Image Selected)

CONTROL ID: 2222162

TITLE: PET imaging of tumor glycolysis downstream of hexokinase through noninvasive measurement of pyruvate kinase M2

PRESENTER: Timothy Witney

ABSTRACT BODY:

Abstract Body: Cancer cells reprogram their metabolism in order to meet increased biosynthetic demands, commensurate with elevated rates of replication [1]. Aberrant tumor glycolysis has long been known to support the synthesis of metabolic precursors required to sustain this anabolic phenotype [2]. Pyruvate kinase catalyzes the final and rate-limiting step in glycolysis, with the M2 spliced isoform (PKM2) purported as a key regulator of aerobic glycolysis in tumors [3]. We report here the synthesis and evaluation of a novel positron emission tomography (PET) radiotracer, [^{11}C]DASA-23, that provides a direct measure of PKM2 expression for the first time, using preclinical models of glioblastoma multiforme (GBM). PKM2-23 was labeled with ^{11}C ($t_{1/2}$ = 20.4 min) at its aromatic methoxy moiety from the corresponding nor-methyl derivative of DASA-23 using the highly efficient methylation reagent [^{11}C]CH_3OTf. We obtained a radiochemical yield of 2.3 ± 0.8%, >99% radiochemical purity and a specific activity of 5.4 ± 2.8 Ci/μmol at end of synthesis (EOS; n = 7). [^{11}C]DASA-23 cell uptake strongly correlated with PKM2 protein expression in cultured tumor cells (R^2 = 0.83; P = 0.005; n = 3), assessed through target modulation by short inhibitory RNA (sense, CCAUAAUCGUCCUCACCAAUU; antisense, UUGGUGAGGACGAUUAUGGUU). *In vivo*, orthotopic U87 and patient-derived GBM39 tumors were clearly delineated from the surrounding normal brain tissue by PET imaging (n = 6 mice; Fig. 1). By 30 min post injection, [^{11}C]DASA-23 radioactivity in U87 tumors was 1.68 ± 0.47 %ID/g *versus* 0.78 ± 0.18 %ID/g in the contralateral background tissue (n = 6; P = 0.003). PET/MR co-registration confirmed precise correspondence of the [^{11}C]DASA-23 signal with the location of the intracranial tumors, further confirmed *ex vivo* by autoradiography, histopathology, and exclusive tumor-associated PKM2 expression. PKM1 expression was confined to the healthy brain and was not present in the tumor. In longitudinal studies, systemic treatment of orthotopic GBM39-tumored mice with the PKM2 agonist, TEPP-46, resulted in a reduction of tumor-associated [^{11}C]DASA-23 to background levels, from 1.61 ± 0.12 %ID/g to 0.88 ± 0.13 %ID/g (45% decrease; n = 4; P = 0.0002). Together, these data demonstrate that [^{11}C]DASA-23 annotates tumor-associated PKM2 in preclinical models of human GBM and provides the basis for clinical evaluation of imaging agents that target this important gatekeeper of tumor glycolysis. Given the great interest in targeting PKM2 for cancer therapy [4], [^{11}C]DASA-23 may also provide a means to measure the therapeutic efficacy of these novel agents.

[1] Cairns RA, Harris IS and Mak TW (2011) Regulation of cancer cell metabolism. Nat Rev Cancer 11: 85-95.
[2] Gatenby RA and Gillies RJ (2004) Why do cancers have high aerobic glycolysis? Nat Rev Cancer 4: 891-899.
[3] Wong N, De Melo J and Tang D (2013) PKM2, a Central Point of Regulation in Cancer Metabolism. Int J Cell Biol 2013: 242513.
[4] Anastasiou D, Yu Y, Israelsen WJ, Jiang JK, Boxer MB, et al. (2012) Pyruvate kinase M2 activators promote tetramer formation and suppress tumorigenesis. Nat Chem Biol 8: 839-847.

AUTHORS (LAST NAME, FIRST NAME): Witney, Timothy H.[1]; James, Michelle L.[1]; Shen, Bin[1]; Chang, Edwin[1]; Pohling, Christoph[1]; Arksey, Natasha[1]; Hoehne, Aileen[1]; Shuhendler, Adam[1]; Gowrishankar, Gayatri[1]; Rao, Jianghong[2]; Chin, Frederick T.[1]; Gambhir, Sanjiv S.[1]

INSTITUTIONS (ALL):
1. Department of Radiology, Stanford University, Stanford, CA, United States.
2. Department of Radiology, Stanford University, Stanford, CA, United States.

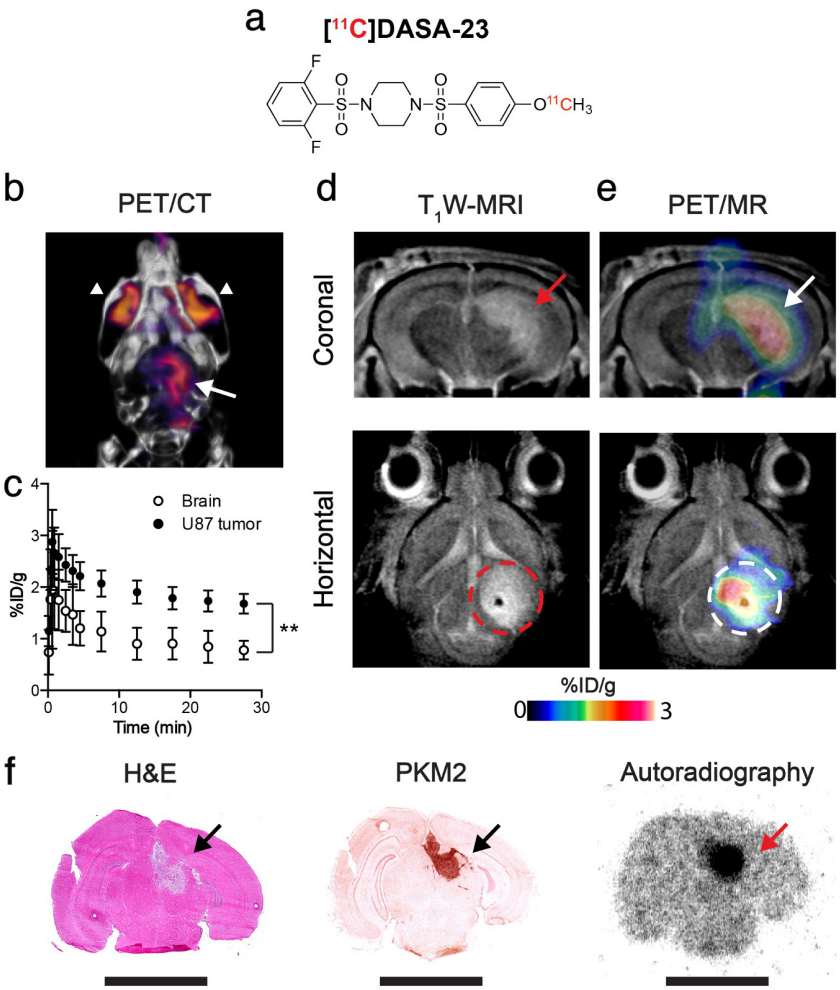

Fig 1. Non-invasive imaging of mice bearing orthotopic U87 human GBM. (**a**) Chemical structure of [^{11}C]DASA-23. (**b**) Representative fused [^{11}C]DASA-23-PET/CT (10 – 30 min summed activity) 3D volume rendering technique (VRT) image of the head of a mouse containing an orthotopically-grown U87 tumor. The long white arrow indicates the tumor. [^{11}C]DASA-23 accumulation in the harderian glands is indicated by white arrow heads. (**c**) Orthotopic U87 tumor and corresponding contralateral normal brain TAC taken from dynamic [^{11}C]DASA-23-PET/CT images. Data is mean ± SD (n = 6 animals). **, P<0.01. (**d**) Representative contrast-enhanced T1-weighted MR coronal and horizontal images of orthotopically-implanted U87 GBM. (**e**) Corresponding merged [^{11}C]DASA-23-PET/MR images. (**f**) Histopathological and *ex vivo* autoradiography analysis (20 min p.i.) of adjacent brain tissue sections. Arrows point to the tumor. Scale bar = 5 mm.

CONTROL ID: 2222570

TITLE: Fluorine-18 fluorocholine PET/CT reflects CDP-choline metabolism as one of the two major phosphatidylcholine synthesis pathways in the liver

PRESENTER: Sandi Kwee

ABSTRACT BODY:

Abstract Body: The cytidine-diphosphate choline (CDP-choline) pathway for phosphatidylcholine (PtC) synthesis is upregulated in liver cancer. This pathway generally results in PtC species containing highly saturated short to medium length fatty acids (HSFA). However, the liver can also produce PtC through hepatocyte-specific expression of phosphatidyl-ethanolamine N-methyltransferase (PEMT), leading to the generation of PtC species with longer polyunsaturated fatty acids (PUFA) (Delong et al. J Biol Chem, 1999). This study examined the relationship between tissue 18F-choline uptake and PtC composition in hepatomas.

High-resolution (+/- 5ppm) liquid chromatography – mass spectrometry (LCMS) was used to analyze liver and tumor specimen pairs from 20 patients with liver cancer who underwent liver 18F-choline PET/CT imaging prior to hepatectomy. The abundance of PtC species was quantified by exact mass, and the human metabolome database (hmdb.ca) was used to query the range of positive-mode electrospray ionization LCMS results to identify PtC species by their specific m/z ratios. In the m/z range 732.5537-760.5814 and m/z 786.6014-788.6101, a total of 54 PtC species were identified that predominantly contained –sn1 and –sn2 fatty acids 14 to 18 carbon long with up to 2 double bonds (most often at positions 9Z and 11Z). These HSFA-PtC species were consistent with products of the CDP-choline pathway. Over 150 other PtC species were identified with m/z 780.5573-784.5815 and m/z 806.5683-836.6099 that contained 18 to 22 carbon PUFAs with up to 6 double bonds consistent with products of the PEMT pathway. The relative amounts of HSFA-PtC and PUFA-PtC species were compared between tumor and liver tissue, and correlated with 18F-choline uptake on PET.

Tumors differed significantly from parenchymal liver tissue in the ratio of HSFA-PtC to long PUFA-PtC concentration (2.75 vs 1.91, p=0.0015), suggesting greater tumor reliance on the CDP-choline pathway for phospholipid membrane synthesis. PET SUV measurements of tumor 18F-choline uptake correlated significantly with HSFA-PtC levels and total PtC ($r = 0.71$, $p = 0.0005$ and $r = 0.72$, $p = 0.0004$, respectively), but not PUFA-PtC levels, supporting 18FC PET as being more reflective of CDP-choline pathway metabolism. Comparing tissue PtC profiles with liver histology, significant negative correlations were noted between Knodell histologic activity indices (particularly fibrosis score) and levels of all PtC species, which associates the clinical progression to cirrhosis with a global depletion of liver phospholipids. LCMS data from the aqueous extracts showed significantly higher levels of CDP-choline in tumors relative to parenchymal liver tissue (82.8 pmol/mg vs 51.4 pmol/mg, $p = 0.0014$) as well as a correlation between tumor CDP-choline level and 18F-choline uptake ($r = 0.47$, $p = 0.03$). These findings support the CDP-choline pathway as a target for molecular imaging of liver cancer, and 18F-choline PET/CT as a potential means to monitor treatments aimed at restoring the balance of phospholipid metabolism in liver cancer.

AUTHORS (LAST NAME, FIRST NAME): Kwee, Sandi A.[1, 2]; Franke, Adrian[3]; Custer, Laurie[3]; Li, Xingnan[3]; Miyazaki, Kyle[5]; Kuang, Yu[4]; Wong, Linda[1]

INSTITUTIONS (ALL):

1. School of Medicine, University of Hawaii, Honolulu, HI, United States.
2. Hamamatsu/Queen's PET Imaging Center, The Queen's Medical Center, Honolulu, HI, United States.
3. Natural Products and Experimental Therapeutics Program, University of Hawaii Cancer Center, Honolulu, HI, United States.
4. Medical Physics, University of Nevada, Las Vegas, Las Vegas, NV, United States.
5. Oncology Research Department, The Queen's Medical Center, Honolulu, HI, United States.

(No Image Selected)

CONTROL ID: 2222609

TITLE: Zirconium-89-Oxine Complex Enables Quantitative Monitoring of Systemic Bone Marrow Cell Trafficking by Positron Emission Tomography.

PRESENTER: Noriko Sato

ABSTRACT BODY:

Abstract Body: Bone marrow (BM) transplantation is used in the treatment of various malignancies and pathological conditions. Sufficient BM homing and engraftment of transferred hematopoietic stem cells is a critical determinant of the success of the treatment [1]. To this end, we employed zirconium-89 (^{89}Zr)-oxine complex cell labeling technique [2] to visualize and quantitate the BM cell migration by micro-positron emission tomography (PET)/computed tomography (CT) in a mouse BM transplantation model. ^{89}Zr-oxine successfully labeled BM cells without interfering with their differentiation function as demonstrated by their maturation into natural killer cells when cultured with IL-15, and to dendritic cells when cultured with granulocyte macrophage colony stimulation factor. Micro-PET/CT imaging revealed quick migrations of transferred BM cells to the BM, spleen, and liver. As high as 22% of donor cells homed to the BM within 4 h of administration. Interestingly, this rapid migration of the cells to the BM occurred irrespective of prior BM ablation. Inhibition of CXCR4 by plerixafor and plerixafor combined with G-CSF injection, prior to the transplantation, significantly blocked initial BM homing of the cells, indicating a crucial role of the CXCR4-CXCL12 system in the BM homing. Next, we injected plerixafor and G-CSF to mice pre-transferred with ^{89}Zr-oxine labeled BM cells, mimicking a cell mobilization process used for collection of hematopoietic stem cells from the circulation in BM transplantations in patients. The BM mobilization led to more than 3.5-fold increase of ^{89}Zr-labeled BM cells in the circulation compared to non-treated control, which was confirmed by imaging, radioactivity counts in the blood and flow cytometry. This also suggested that the ^{89}Zr-labeled cells homed to the BM were alive and functional. In fact, in BM ablated recipients, ^{89}Zr-oxine labeled donor BM cells engrafted and gave rise to mature peripheral mononuclear cells comparable to non-labeled donor cells. Collectively, ^{89}Zr-oxine PET/CT demonstrated BM homing kinetics of BM cells after transplantation, without impairing differentiation function of the cells, and could, therefore, be a useful method for optimizing BM transplantation.

References:

1. Jenq RR, van den Brink MR. Nat Rev Cancer. 2010;10(3):213-21

2. Sato N, Wu H, Asiedu KO, et al. Radiology. 2015. [Ahead of print]

AUTHORS (LAST NAME, FIRST NAME): Asiedu, Kingsley O.[1]; Koyasu, Sho[1]; Szajek, Lawrence[2]; Choyke, Peter L.[1]; Sato, Noriko[1]

INSTITUTIONS (ALL):

1. Molecular Imaging Program, National Cancer Institute, NIH, Bethesda, MD, United States.

2. Positron Emission Tomography Department, Warren Grant Magnuson Clinical Center, NIH, Bethesda, MD, United States.

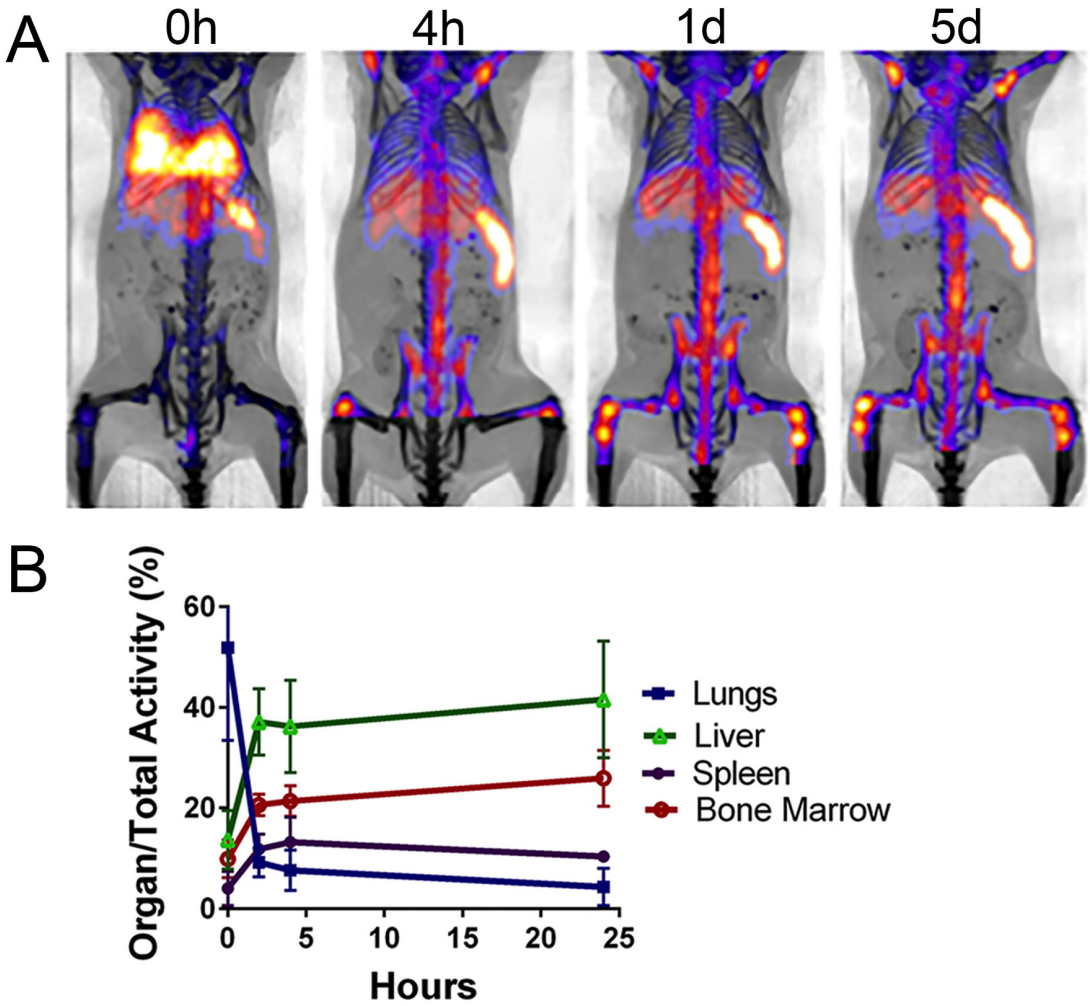

A. ^{89}Zr-oxine PET/CT imaging demonstrated bone marrow cell trafficking in mouse.

B. The kinetics analysis showed quick migrations of bone marrow cells to the bone marrow, spleen and liver.

CONTROL ID: 2231969

TITLE: PET Imaging Reveals a Greater Recruitment of Zirconium-89-oxine-labeled Monocytes to Cancer and Inflammation Compared to Macrophages.

PRESENTER: Sho Koyasu

ABSTRACT BODY:

Abstract Body: Cell-based therapies are becoming increasingly important in the treatment of cancers and inflammatory diseases. Therapies employing monocyte-macrophage-lineage cells are emerging [1, 2], although they have not been in the mainstream of cell-based therapies. To exploit the potential of these therapies, non-invasive cell tracking has a crucial role. Therefore, we employed the recently developed zirconium-89 (^{89}Zr)-oxine cell labeling method [3] for whole-body micro-PET imaging to visualize and investigate trafficking of monocytes and macrophages to cancerous or inflammatory lesions. Monocytes and macrophages were differentiated from the bone marrow of mice using macrophage-colony stimulating factor (M-CSF) and labeled with ^{89}Zr-oxine at 37 kBq/10^6 cells. Labeled cells retained the isotope and survived at comparable levels to the non-labeled cells. CMFDA dilution assay indicated that the labeled cells proliferated in response to M-CSF. Phagocytosis assays with pH-sensitive dye and migration assays using transwell inserts and MCP-1 showed that both cell types kept their phagocytic function after labeling, while monocytes exhibited higher migration potential than macrophages. We next intravenously transferred the ^{89}Zr-oxine labeled monocytes or macrophages to immunocompetent mice bearing melanoma tumor or granulomatous inflammation developed by polyacrylamide gel pellets mixed with lipopolysaccharide. Serial micro-PET images were acquired up to 7 days after the transfer. PET images demonstrated that transferred monocytes migrated to the tumor or inflammation, as well as the liver and the spleen, while macrophages distributed only to the liver and the spleen. We confirmed using flow cytometry that significantly more monocytes tracked to the tumor and inflammation than macrophages. In summary, the ^{89}Zr-oxine cell labeling method seems feasible for tracking monocytes and macrophages, and the PET imaging indicated that monocytes migrate to cancers and inflammation in greater numbers compared to macrophages.

1 Johnson CL, Green DS, Zoon KC. J Interferon Cytokine Res. 2015. 35:55-62

2 Wang Y, Wang YP, Zheng G et al. Kidney Int. 2007. 72:290-299

3 Sato N, Wu H, Asiedu KO et al. Radiology. 2015. (ahead of print)

AUTHORS (LAST NAME, FIRST NAME): Koyasu, Sho[1]; Asiedu, Kingsley O.[1]; Choyke, Peter L.[2]; Sato, Noriko[1]

INSTITUTIONS (ALL):

1. Molecular Imaging Program, National Cancer Institute, NIH, Bethesda, MD, United States.
2. Molecular Imaging Program, National Cancer Institute, NIH, Bethesda, MD, United States.

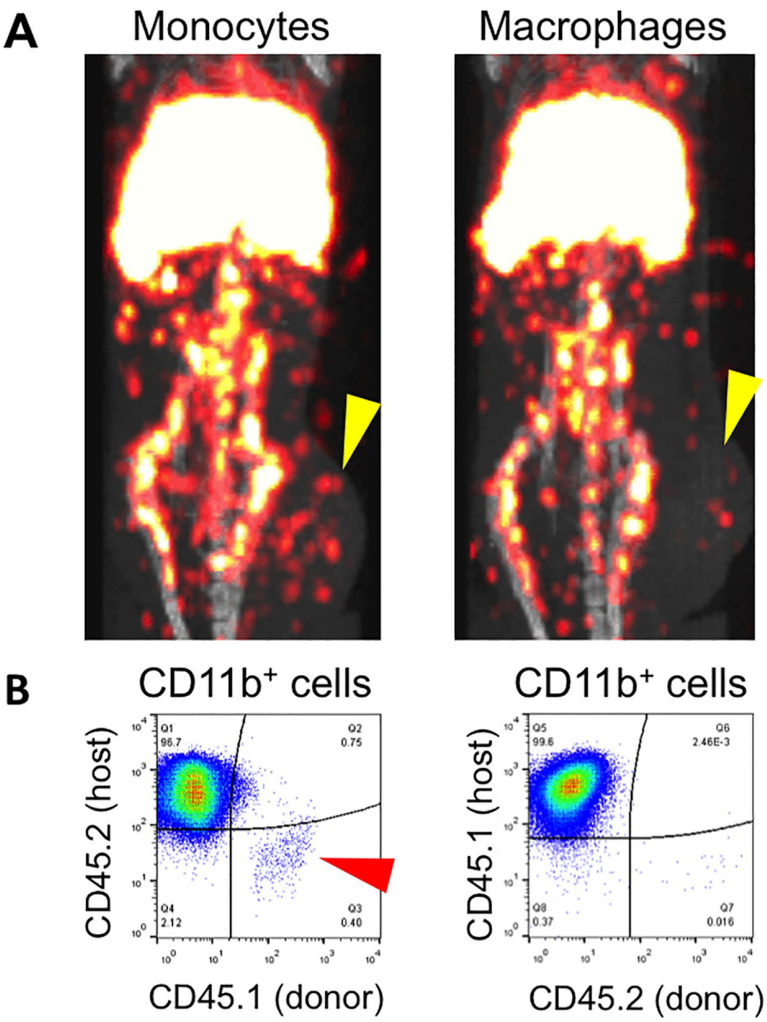

A: Cell tracking of ^{89}Zr-labeled monocytes and macrophages (8.5×10^6 cells) by PET in melanoma bearing mice. A moderate accumulation of the monocytes was observed in the tumor on day 4, but no comparable macrophage accumulation occurred (arrowheads).

B: Flow cytometry analysis of CD11b expressing cells collected from the tumors. Transferred monocytes (CD45.1+CD45.2-) were present in the tumor (arrowhead), but not the macrophages (CD45.2+CD45.1-).

CONTROL ID: 2222622

TITLE: FDG PET Imaging of the Brain in a Mouse Model of Dystonia

PRESENTER: Weibin Shi

ABSTRACT BODY:

Abstract Body: Objectives: Primary dystonia is a common but poorly understood movement disorder characterized by involuntary muscle contractions leading to abnormal movements and postures. A fraction of *Rcn2* knockout mice (30%) develop early onset overt dystonia though most of them are apparently normal. The purpose of this study is to detect potential functional or anatomic abnormalities in the brain of dystonic mice with fluorine-18 fluorodeoxyglucose (FDG) PET.

Methods: FDG was administered to Rcn2 knockout mice with or without dystonia and imaged for 60 min. The dynamic FDG PET data were analyzed in a 3-compartment kinetic model and compared to the standard of care SUV method. A model corrected blood input function (MCIF) was obtained from the LV blood pool corrected for partial volume averaging and spill-over contamination[1]. The MCIF was utilized in a 3-compartment kinetic model to obtain the rate constants K1-k4 and the net FDG influx constant, Ki (ml/min/g).

Results: Standard SUV analysis (imaging after 30 minutes post FDG injection for 20 minutes) did not show differences between dystonic and non-dystonic mice in the brain (Figure). In contrast, dynamic imaging showed that the Ki value for dystonic mice was much higher than non-dystonic ones. The Ki and K_1 plots were suggestive of leaky vasculature in the dystonic mouse brain. The average Ki for dystonic mouse brain were higher than the control brain.

Conclusions: Dynamic FDG PET imaging in a compartment model is able to differentiate the dystonic brain from the non-dystonic brain while the SUV analysis is not. Our finding also suggests vascular leakage in the brain of dystonic mice.

AUTHORS (LAST NAME, FIRST NAME): Shi, Weibin[1]

INSTITUTIONS (ALL):

1. Radiology & Medical Imaging, University of Virginia, Charlottesville, VA, United States.

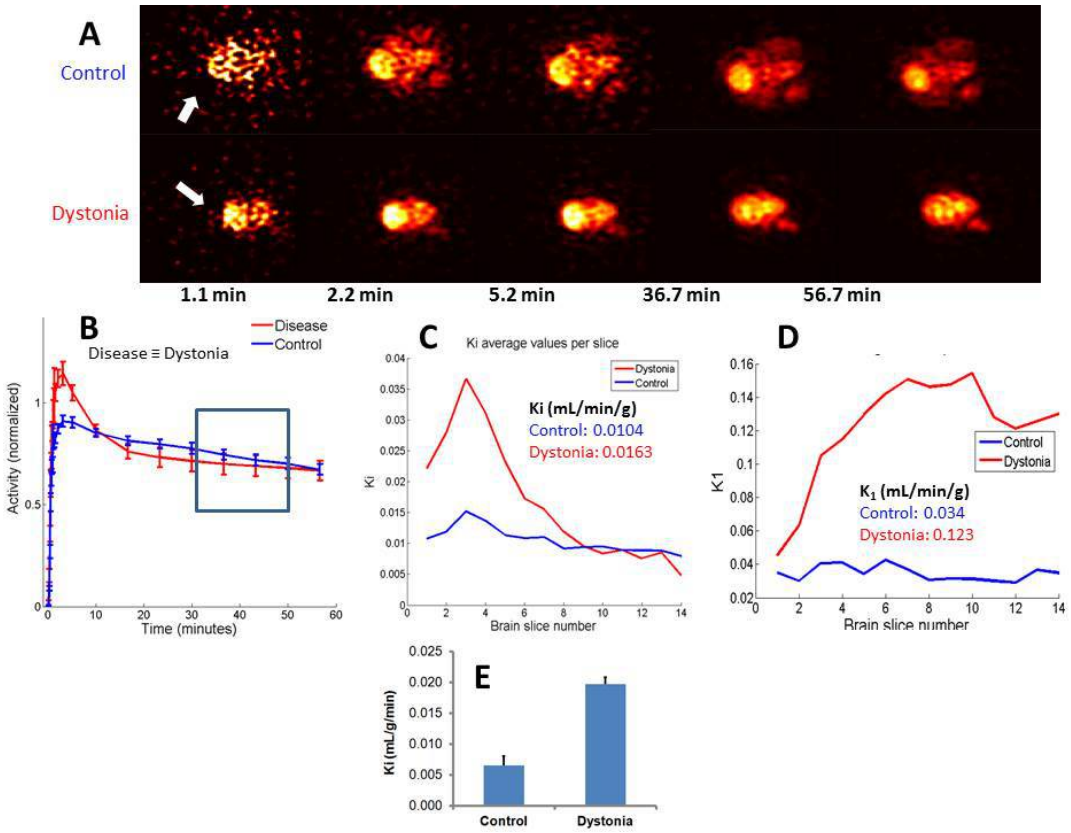
A
Control
Dystonia
1.1 min
2.2 min
5.2 min
36.7 min
56.7 min
B
Disease
Control
Disease ≡ Dystonia
Activity (normalized)
Time (minutes)
C
Ki average values per slice
Dystonia
Control
Ki (mL/min/g)
Control: 0.0104
Dystonia: 0.0163
Ki
Brain slice number
D
Control
Dystonia
K1 (mL/min/g)
Control: 0.034
Dystonia: 0.123
K1
Brain slice number
E
Ki (mL/g/min)
Control
Dystonia

CONTROL ID: 2222802

TITLE: Macrophage Cell Tracking PET imaging using mesoporous silica nanoparticles based on Bioorthogonal Strain-Promoted Cycloaddition.

PRESENTER: HyeonJin Jeong

ABSTRACT BODY:

Abstract Body: A nanoparticle is considered potentially cell tracer as an alternative gene manipulation tracer such as a reporter gene because it's able to labeling in the various cells by endocytosis and strain-promoted alkyne azide cycloaddition (SPAAC). An aza-dibenzocycloctyne-functionalized PEGylated mesoporous silica nanoparticles (ADIBO-PEG-MSN) were prepared, and these MSNs were successfully penetrated into rADSC and RAW264.7 cell by endocytosis. For cell tracking PET imaging study, we used U87MG-bearing mice models. The fluorine-18 labeled azido-PEG compound was injected into the mice given ADIBO-PEG-MSN in macrophage cell 1h early. We have obtained PET-CT image of tumor uptake by phagocytosis of macrophage cell using SPAAC conjugate reaction of ADIBO-PEG-MSN with fluorine-18 labeled azido-PEG synthon. In this study, we could visualize cell tracking by SPAAC reaction based pretargeting method using MSNs in tumor model.

AUTHORS (LAST NAME, FIRST NAME): Jeong, HyeonJin[1]; Kim, Dong Wook[1]

INSTITUTIONS (ALL):

1. Chemistry, INHA univ., Incheon, Other, Korea (the Republic of).

(No Image Selected)

CONTROL ID: 2222819

TITLE: Spectrum-based Calibration Method for Energy Discriminating X-ray Detectors Using Commercial X-ray Generators

PRESENTER: Xiaoman Xing

ABSTRACT BODY:

Abstract Body: Spectral Computed Tomography (CT) imaging needs a reliable measurement of energy-dependent attenuation coefficients for different materials. Current energy discriminating materials such as CZT have some significant disadvantages such as far higher density of defects in the crystal lattice, which leads to very different noise levels among pixels and vastly different spectral responses to the same gain setting. Due to non-uniformity in spectral responses, the detector's energy discriminating capability is severely limited. Traditionally, spectral calibration is done using at least two radioactive sources such as ^{99m}Tc and ^{57}Co. By locating multiple characteristic emission peaks, the correlation between incoming photon energy and its electronic yield for each pixel can be established. But radioactive sources are very expensive and not readily available to many laboratories. It would save researchers a lot of time and money if calibration can be done with commercial X-ray generators. We present a method to normalize the spectral response of the detector by gain and offset adjustment using spectral shape analysis, so that detectors can respond uniformly to the same X-ray photon flux. This method is robust, repeatable, and cheap. With minor adaptation, it can also be applied to other energy discriminating materials. Due to limitation of our experiments, exact correlation between photon energy and pulse height was not obtained. But our result strongly suggests its possibility. We hope our work can offer some insight into this area.

AUTHORS (LAST NAME, FIRST NAME): Xing, Xiaoman[1]; Xu, Pin[1]; Xia, Chun[1]; Sun, Mingshan[1]

INSTITUTIONS (ALL):

1. Medical Imaging, Suzhou Institute of Biomedical Engineering and Technology, China, China.

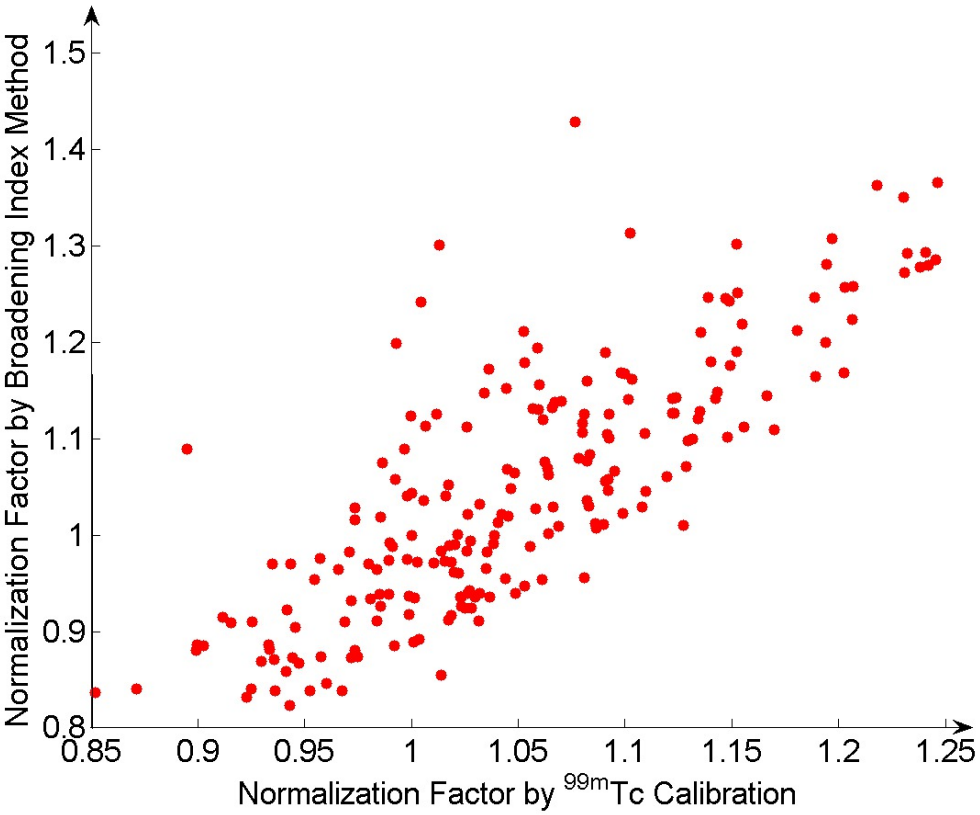
Normalization Factor by Broadening Index Method
1.5
1.4
1.3
1.2
1.1
1
0.9
0.8
0.85
0.9
0.95
1
1.05
1.1
1.15
1.2
1.25
Normalization Factor by 99mTc Calibration

CONTROL ID: 2222855

TITLE: *In-vivo* hyperpolarized ^{13}C flow-suppressed MRSI in mouse liver

PRESENTER: Hansol Lee

ABSTRACT BODY:

Abstract Body: Introduction Hyperpolarized ^{13}C MRI is an emerging *in-vivo* imaging technique for observing metabolic activities of various tissues. Typically, the conversion of substrates to metabolites in tissues can be measured by ^{13}C MRS/MRSI after intravenous injection of hyperpolarized substrates (Day *et al*, Nature, 2007). In mouse liver studies, the substrate signal can be contaminated by the large amount of substrate signal from blood flowing vessels due to the limited spatial resolution of MRSI, thus obstructing accurate quantifications (Fig.1(a-c)) (Yi-Fen *et al*, MRM, 2009). Therefore, this work presents a flow-suppressed MRSI method to remove artifacts from blood flow applied to *in-vivo* imaging of mouse liver.

Method *In-vivo* experiments were performed on a 9.4T small animal imaging system (Bruker BioSpin MRI GmbH, Germany) equipped with ^{1}H-^{13}C dual-tuned mouse volume transmit/receive coil. [1-13C] pyruvic acid doped with 15mM Trityl radical and 1.5M Dotarem was polarized using HyperSense DNP polarizer (Oxford Instruments, UK). After dissolution into aqueous state, a balb/c mouse was injected with approximately 380ul of the hyperpolarized pyruvate solution through a tail vein catheter. To suppress large amount of pyruvate signal in blood (caudal vena cava), flow suppression bipolar gradients were implemented after RF excitation in conventional MRSI sequence. The specifications of bipolar gradients such as strength, gap, and duration were experimentally adjusted by proton flow-suppressed MRI in mouse liver. B0 shimming was performed locally over the liver tissue (full width half max of ^{1}H~130Hz). Hyperpolarized ^{13}C flow-suppressed MRSI was acquired at 30s after pyruvate injection. Comparison was done with an examination on another mouse without any flow suppression. All animal procedures were approved by the local Animal Care and Use Committee.

Results The underlying anatomy and locations of each voxels are shown in Fig.1(a,d). ^{13}C spectra at caudal vena cava and liver tissue using conventional MRSI without flow-suppression are shown in Fig.1(b,c). In the highlighted tissue voxel, two peaks of pyruvate and a single peak of lactate were observed. Based on the single narrow peak of water in ^{1}H MRSI (data not shown), we presume that the two peaks of pyruvate did not originate from the voxel itself but was the result of contamination by signal from other voxels, especially blood vessels. As shown in Fig.1(e-f), signal in blood was greatly reduced in flow-suppressed MRSI. The signal of other metabolites in the liver tissue was not suppressed and had similar level of SNR as in the case without flow-suppression. Also, a single peak of pyruvate was observed.

Conclusion The influence of substrate signal in hyperpolarized ^{13}C MRSI coming from blood vessels can be large and complicated since in-flow effects continuously occur during the measurement. To reduce the influence of signal from blood vessel, a flow-suppressed MRSI method is presented. Bipolar gradients adjusted to suppress signal from moving spins within the range found in mouse studies were implemented for removing artifacts due to blood flow thus enabling more accurate quantification of metabolites.

AUTHORS (LAST NAME, FIRST NAME): Lee, Hansol[1]; Lee, Joonsung[2]; Joe, Eunhae[1]; Yang, Seungwook[1]; Choi, Young-suk[3]; Wang, Eunkyung[3]; Song, Ho-Taek[3]; Kim, Dong-Hyun[1]

INSTITUTIONS (ALL):

1. Department of Electrical & Electronic Engineering, Yonsei University, Seodaemun-gu, Korea (the Republic of).
2. Severance Biomedical Science Institute, Yonsei University, Seodaemun-gu, Korea (the Republic of).
3. Department of Radiology, Yonsei University College of Medicine, Seoul, Korea (the Republic of).

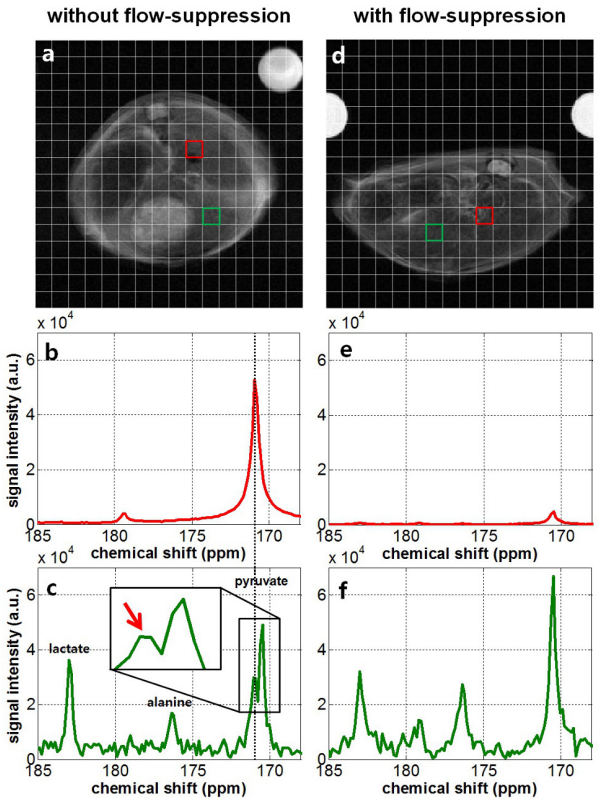

Fig. 1. Hyperpolarized ^{13}C MRSI without flow-suppression (a-c), and with flow-suppression (d-f). Anatomical information of mouse and location of MRSI voxels are overlaid. Blood vessel voxel (caudal vena cava) is highlighted with red box, and liver tissue voxel is highlighted with green box. The hyperpolarized ^{13}C spectra of each voxels are presented for comparison. The pyruvate has large amount of signal in blood vessel voxel (b). On the other hand, the peak of pyruvate with flow-suppression is reduced greatly in blood vessel voxel (e). In liver tissue, two peaks of pyruvate are observed without using flow-suppression (c). One of them is contaminated from blood vessel (red arrow). Using flow-suppression, single peak of pyruvate is achieved (f). The spectra of liver tissue were scaled 30-fold for presentation.

CONTROL ID: 2232428
TITLE: The Compatibility of Barcode Eartags for Automated Animal Identification in Small Animal Imaging Modalities.
PRESENTER: Eric Ibsen
ABSTRACT BODY:
Abstract Body: Accurate, reliable and unequivocal identification of research animals using methods compatible with common small animal imaging modalities, is essential to obtaining meaningful results in biomedical research studies and, to date, has been impossible using existing automated identification methods. The importance of unequivocal animal identification on longitudinal studies is self-evident, as identification errors commonly associated with non-automated identification methods, such as metal eartags, ear-punches, ear-notches, tattoos and others may seriously impact the integrity of study conduct and results. Currently two of the most popular identification methods used in pre-clinical research, RFID microchips and metal eartags, are completely incompatible with various small animal imaging systems due to their ferrous metal composition. In contrast, barcode eartags (RapID Tags produced by RapID Lab) are comprised of non-ferrous metal and a highly- advanced, biologically-inert polymer used in the medical device industry. Due to the novel material composition of the barcode eartags, they appear to offer the potential for compatibility with multiple small animal imaging methods while enabling automated and unequivocal animal identification. The results of tests performed by multiple research labs using a variety of methods are summarized here. RESULTS: In an initial test, it was demonstrated that the barcode eartags unattached to animals did not become attached to or react to the magnet of an MRI imaging system. In a test using a 7T Small Animal MRI System and a RapID tag taped between the eyes of a rat, no artifacts were observed in the brain. In a second MRI test using tags taped between the eyes and to the side of the head of mice some artifacts were observed in gradient echo and fast echo images, but were considered manageable for imaging the brain, spinal cord and areas away from the brain. In a test using an MRI system at a third lab where barcode eartags were applied to animals' ears, no artifacts were observed. In images acquired using a small animal microCT system with RapID Tags taped to a rat's shoulder, the tags could be seen, but no artifacts were produced. In a test at a second lab with CT, tags applied to the animals' ears produced minimal-to-no image

distortion. In a single test scanning an isolated barcode eartag using CT-attenuated PET scans, the eartag did affect the CT attenuation of the PETscan. No tests using PET imaging alone have been performed, but it is believed that no artifacts should be produced using barcode eartags in PETscans. CONCLUSION: The advent of barcode eartags provides the first automated and unequivocal small animal identification method available which is compatible with MRI and CT imaging in small animals. Further testing is needed to evaluate the compatibility with other imaging methods.

AUTHORS (LAST NAME, FIRST NAME): Swope, Brett[1]; Ibsen, Eric M.[1, 2]

INSTITUTIONS (ALL):

1. Research , RapidLab , Pacifica , CA, United States.
2. Studylog Systems, Inc., South San Francisco, CA, United States.

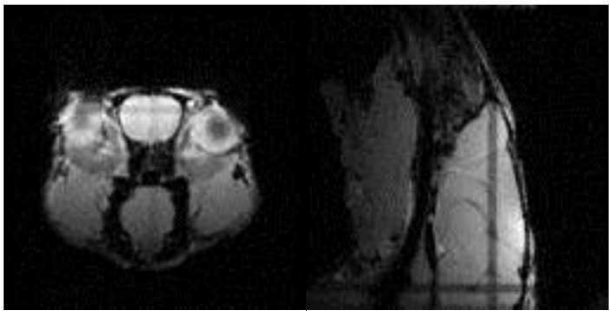

Image 1: Coronal MRI Image with tag affixed between the eyes

Image 2: Sagittal MRI Image with tag affixed between the eyes

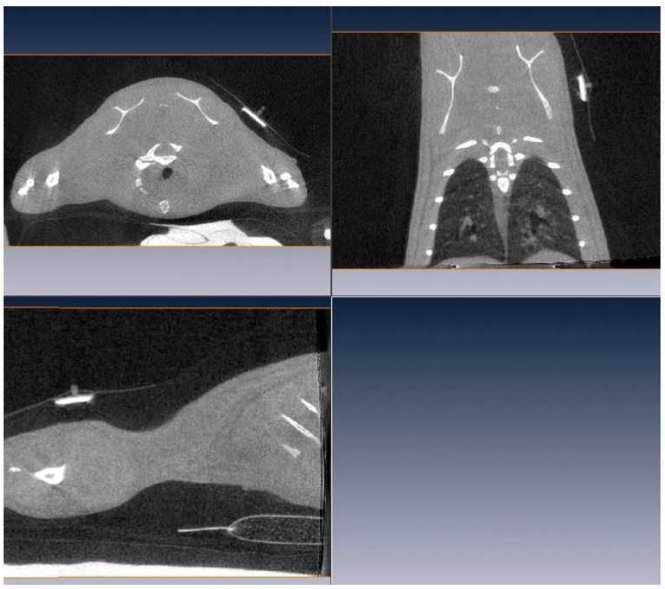

Image 3 (top left): Anterior MicroCT Image: tag affixed on the shoulder.

Image 4 (top right): Dorsal MicroCT Image: tag affixed on the shoulder.

Image 5 (bottom left): Orthagonal Cross-Section MicroCT Image: tag affixed between the eyes.

CONTROL ID: 2223756

TITLE: Biodistribution of ^{89}Zr-labeled ABT-806 in the cynomolgus macaque

PRESENTER: Sarah Mudd

ABSTRACT BODY:

Abstract Body: Purpose: Imaging the biodistribution of the parent mAb that makes up an antibody drug conjugate (ADC) may give insight into the distribution of the ADC and potential target-mediated toxicity liabilities. ABT-806, which binds human and cynomolgus macaques overexpressed WT and mutant EGFR, is the parent antibody of ABT-414, an ADC currently in phase 1/2 trials for glioblastoma.

Methods: Two, protein naïve female cynomolgus macaques were injected with approximately 1 mCi (0.07 mg/kg) ^{89}Zr-labeled ABT-806 and were imaged on Focus 220 PET and Ceretom CT scanners at 1 and 6 days post-injection. Images were analyzed to determine tissue concentrations of ^{89}Zr-labeled ABT-806.

Results: High uptake was observed in highly perfused tissues at 24 hours post-injection, but decreased at 144 hours post-injection. Uptake in the liver increased over time most likely due to clearance of ABT-806. Uptake of ABT-806 in the skin increased over time, most likely due to EGFR expression in this tissue.

Conclusion: The biodistribution of ABT-806 was determined in normal tissues using NHPs. Increased accumulation over time fit with our understanding of EGFR expression and mAb clearance.

Disclosures: All authors are employees of AbbVie. The design, study conduct, and financial support for this research were provided by AbbVie. AbbVie participated in the interpretation of data, review, and approval of the publication.

AUTHORS (LAST NAME, FIRST NAME): Mudd, Sarah R.[1]; Reuter, David R.[1]; Tovcimak, Ann[1]; Voorbach, Martin J.[1]; Giamis, Anthony M.[1]; Harlan, John[2]; Phillips, Andrew C.[3]; Reilly, Edward[3]; Beaver, John D.[1]

INSTITUTIONS (ALL):

1. Translational Imaging, AbbVie, North Chicago, IL, United States.
2. Protein Biochemistry, Abb, North Chicago, IL, United States.
3. Oncology Discovery, AbbVie, North Chicago, IL, United States.

(No Image Selected)

CONTROL ID: 2230811

TITLE: SPECT imaging of mouse xenografts expressing different levels of EGFR using ^{111}In-labeled ABT-806

PRESENTER: Sarah Mudd

ABSTRACT BODY:

Abstract Body: Purpose: ABT-806 is a therapeutic antibody targeting both vIII (de2-7) mutant and overexpressed wild-type Endothelial Growth Factor Receptor (EGFR). In this study the correlation between ABT-806 tumor uptake and EGFR expression was investigated. ^{111}In labeled ABT-806 tumor uptake was compared using SPECT/CT imaging in subcutaneous xenograft flank models with cell lines expressing a range of levels of EGFR.

Procedure: The xenograft tumor models expressing varying levels of wild type EGFR were grown in female immunodeficient mice. The relative EGFR expression level, as measured by IHC staining is indicated by parentheses, and the mouse strain is indicated by brackets. SW620 (-)[SCID] , LG0567 (-)[NSG], A549 FP3 (-)[SCID], NCI-H441 (+)[nude], FaDu (++)[SCID], SCC-15 (+++)[SCID], LG0476 (+++)[NSG], A-431 (++++)[nude], HCC 827 ER LMC (++)[SCID], U87MGde2-7 (+++)[nude]. The average tumor volume was approximately 200 mm^3 at the time of tracer injection. The animals underwent SPECT/CT imaging at 24, 48, 96, and 144 hrs. post intravenous injection of 500 µCi (50 µg) of ^{111}In-ABT-806.

Results: Analysis of tumor uptake was normalized to blood. Results showed significantly higher uptake ratios for the models that had high EGFR expression levels relative to the lower EGFR expressing models. The patient-derived LG0567 model showed moderate tumor uptake despite the fact that it has very low EGFR expression levels.

Conclusion: Tumors with high wild-type or mutant EGFR expression tend to have high ^{111}In-ABT-806 uptake as measured using SPECT, suggesting that ^{111}In-ABT-806 uptake may be useful for selecting patients with high wild-type or mutant EGFR expression.

*Disclosures: All authors are employees of AbbVie. The design, study conduct, and financial support for this research were provided by AbbVie. AbbVie participated in the interpretation of data, review, and approval of the publication.

AUTHORS (LAST NAME, FIRST NAME): Voorbach, Martin J.[2]; Palma, Joann[3]; Donawho, Cherrie K.[3]; Mishra, Sasmita[3]; Harlan, John[1]; Giamis, Anthony M.[2]; Reuter, David R.[2]; Buchanan, Fritz[3]; Luo, Yanping[2]; Fox, Gerard[2]; Beaver, John D.[2]; Mudd, Sarah R.[2]

INSTITUTIONS (ALL):

1. R43J, AbbVie, Inc, North Chicago, IL, United States.
2. iSAT Imaging, Abbvie, North Chicago, IL, United States.
3. In Vivo Tumor Biology, AbbVie, North Chicago, IL, United States.

(No Image Selected)

CONTROL ID: 2223815

TITLE: Long-term MR tracking and stereological quantification of ferumoxytol labeled human neural progenitor cells transplanted into the porcine spinal cord

PRESENTER: Jason Lamanna

ABSTRACT BODY:

Abstract Body: Transplantation of stem cells into the spinal cord has been explored as treatment for a range of diseases (Feldman et al. Ann Neurol, 2014). The post-transplantation fate of cellular therapeutics is poorly understood in both large animal models and in human studies because of limitations in cell graft detection. A minimally invasive technology for cellular graft tracking to visualize grafts *in vivo* is needed. However, it is important that the diagnostic marker does not impact engraftment of transplanted cells. We report on surgical transplantation of ferumoxytol labeled human neural progenitor cells into the spinal cord of a large animal with *in vivo* MRI graft tracking, quantification of cell engraftment post-mortem, and preliminary MR-guided delivery.

Human neural progenitor cells (Suzuki et al. PLoS One, 2007) were labeled with multiple concentrations of ferumoxytol ([0], [200], and [400 μg/mL]). For each of the three labeling conditions, four 250,000 cell grafts (n=12 grafts/pig) were transplanted into the ventral horn of the thoracolumbar spinal cord of minipigs via direct intraspinal microinjection using a spine-mounted platform following laminectomy. No post-operative deficits were observed and the pigs were maintained for 28 (n=3 pigs), 42 (n=3), and 105 days (n=5) after surgery. All [200] and [400] transplanted cell grafts (n=88) were visualized *in vivo* with 3T full-body MRI using a T2*-weighted gradient echo sequence 14 days after transplantation. 63.6% of grafts were 'on target' in the ventral horn. The grafts were tracked longitudinally with serial MRI and signal intensity quantified with a minimum threshold method. The mean volume after transplantation was 2.3 and 13.9 μL for [200] and [400] grafts. Furthermore, 75% of [200] and 100% of [400] grafts were identified at post-operative day 105 with a mean volume of 1.1 and 9.6 μL.

The pigs were sacrificed and the spinal cords harvested. The cords were sectioned at 50 μm intervals and every 6^{th} section immunostained for the human nucleus (HuNu). The engraftment of individual cell grafts was quantified using stereology for the 42-day cohort. The engraftment was calculated for [0] (mean 24.0% cell engraftment, range of 0.0-65.7%), [200] (17.1, 1.0-35.9), and [400] (25.0, 0.0-45.6) and no statistically significant difference was observed. Degradation of MR signal between 14 and 28 days for [200] and [400] grafts correlated with graft survival ($r=0.47$, $p=0.02$) in the 42-day cohort. Stereology is ongoing for the other cohorts. Prussian Blue-HuNu co-staining and transmission electron microscopy of tissue sections confirmed the presence of intracellular iron deposits.

Ferumoxytol labeling allows for immediate and long-term identification of cell grafts *in vivo* with MRI without impacting cell engraftment in a large animal xenograft model. The ferumoxytol nanoparticles were observed in the cytoplasm of transplanted, labeled cells. This approach has the potential to be used in ongoing and upcoming clinical trials to monitor cell-based therapies. Furthermore, ferumoxytol labeling allows for immediate visualization of stem cells transplanted into the spinal cord percutaneously under MR-guidance.

AUTHORS (LAST NAME, FIRST NAME): Lamanna, Jason J.[1, 2]; Gutierrez, Juanmarco[1]; Urquia, Lindsey N.[1]; Amador, Elman[1]; Federici, Thais[1]; Oshinski, John N.[3, 2]; Boulis, Nicholas M.[1, 2]

INSTITUTIONS (ALL):

1. Neurosurgery, Emory University, Atlanta, GA, United States.
2. Biomedical Engineering, Georgia Institute of Technology, Atlanta, GA, United States.
3. Radiology and Imaging Sciences, Emory University, Atlanta, GA, United States.

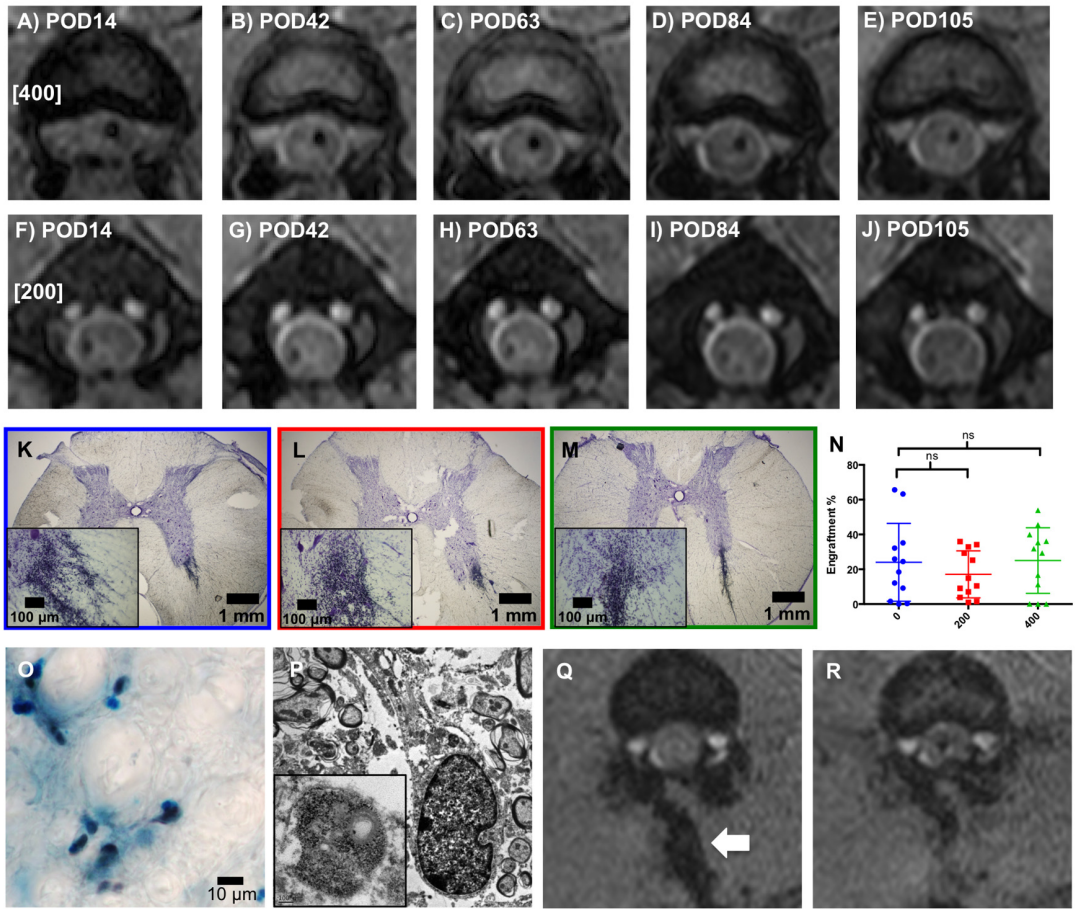

A representative [400 µg/mL] (**A – E**) and [200 µg/mL] (**F – J**) cell graft tracked with T2*-weighted gradient echo MRI from post-operative day (POD) 14 to 105 are shown. Representative micrographs of staining for intact human nuclei (black) of unlabeled [0] (**K**), and labeled [200] (**L**) and [400] (**M**) cell grafts are shown (4X magnification, 20X insert) for the 42-day cohort. Stereological quantification calculated no difference in survival between labeled and unlabeled cell grafts (n=12 grafts/condition, n=3 pigs) (**N**). Prussian blue and human nuclear antigen co-staining revealed co-localization of human nuclei and iron precipitates (**O**). Transmission electron microscopy with staining for the human nucleus revealed human cells with nanoparticle-laden lysosomes (**P**). Under the guidance of MRI, a cannula was advanced into the spinal cord of a live pig (**Q**). A 2.5e5 cell graft labeled with ferumoxytol was injected and the cannula was removed (**R**).

CONTROL ID: 2231396

TITLE: ^{18}F-Nifene: First-in-human PET studies for imaging nicotinic α4β2 receptors

PRESENTER: Jogeshwar Mukherjee

ABSTRACT BODY:

Abstract Body: Objectives: We have developed agonist ^{18}F-nifene for PET imaging studies of nicotinic α4β2 receptors related to tobacco abuse, lung cancer and neurodegeneration [1]. Animal (rodents and monkeys) PET imaging studies demonstrated the high selectivity of ^{18}F-nifene and rapid in vivo kinetics, suitable for a 1-hour scan time which is an advantage over existing technology for imaging this receptor system [2]. First-in-human studies have therefore been pursued. Here we report comparative brain distribution of ^{18}F-nifene in humans versus findings in animal models.

Methods: Acute multiple intravenous (IV) dose toxicity (1.6, 20, 40 μg/kg/day on days 1, 3 and 5) of nifene was measured in male and female Sprague-Dawley rats by SRI International. Radiosyntheses of ^{18}F-nifene was carried out with high specific activity ^{18}F-fluoride as reported previously [1,2]. Rodent, monkey and human studies were carried out either on an Inveon MicroPET/CT, MicroPET P4, or Siemen's ECAT EXACT HR+ scanner. Human ^{18}F-nifene studies were carried out under an FDA approved IND. All studies were carried out after an IV bolus injection of ^{18}F-nfiene (~0.2 for mice, ~0.7 mCi for rats, ~2-3 mCi for monkeys, ~5 mCi for humans) at a specific activity >2Ci/mmol. Isoflurane anesthesia (1.5-3%) was used for rodents and monkeys. Binding of ^{18}F-nifene to α4β2 receptor-rich regions were analyzed using reference regions cerebellum (CB; for rodents and monkeys) and corpus callosum (CC; for humans).

Results: Nifene was well tolerated in the rats and histopathology presented no dose-related findings. The maximum tolerated dose (MTD) and no observable adverse effect level (NOAEL) exceed 40 μg/kg/day. Rapid brain uptake of ^{18}F-nifene was observed in all brain regions across all species. Cerebellum (CB) was used as a reference region across all species, except humans. For humans (3 subjects: 1 M, 2 F), corpus callosum (CC) was used as a reference region because of significant ^{18}F-nifene binding in CB. Thalamus (TH) exhibited the highest levels of ^{18}F-nifene with a time to equilibration of ~45mins across all species. Extrathalamic regions such as cortical areas, lateral geniculate, cingulate gyrus and other brain regions were observed in all species and consistent with the known concentration of α4β2 receptors. At equilibrium, ^{18}F-nifene exhibited ratios of: TH/CC~3 (humans), TH/CB~3 (monkeys, rats and mice). Smaller nuclei in the mid-brain (substantia nigra/ventral tegmental area) were more prominent in the human brains.

Conclusion: Our first-in-human studies suggest ^{18}F-Nifene to be a safe and effective α4β2 nicotinic receptor imaging agent. Our findings with ^{18}F-nifene suggest homology of the α4β2 receptor-site across rodents, monkeys and humans. ^{18}F-Nifene may be reliably used to quantify α4β2 receptor distribution and pathology in animal models (such as lung cancer [3], learning and memory [4]) for translational human studies.

Research Support: NIH R01AG029479 (JM)

References:

1. Pichika et al. *Nucl. Med. Biol.*, **33**: 295-304, 2006.
2. Hillmer et al. *J. Nucl. Med.*, **53**:1471-1480, 2012.
3. Galitovskiy et al. *J. Cancer Res & Therapy*, **1**: 128-137, 2013.
4. Bieszczcad et al. *Synapse*, **66**: 418-434, 2012.

AUTHORS (LAST NAME, FIRST NAME): Mukherjee, Jogeshwar[1]; Lao, Patrick J.[2]; Betthauser, Tobey J.[2]; Hillmer, Ansel T.[2]; Pan, Min-Liang[1]; Patel, Ishani H.[1]; Kuruvilla, Sharon A.[1]; Higgins, Andrew T.[2]; Barnhart, Todd E.[2]; Stone, Charles K.[2]; Christian, Bradley T.[2]

INSTITUTIONS (ALL):

1. Radiological Sciences, University of California, Irvine, Irvine, CA, United States.
2. Medical Physics & Waisman Center, University of Wisconsin, Madison, WI, United States.

^{18}F-Nifene PET

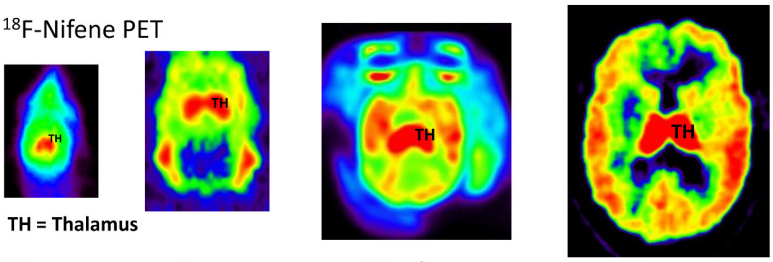

TH = Thalamus

Mouse	Rat	Monkey	Human
~25 g	~300g	~10,000g	~72,000g
Th/CB~3	*Th/CB~3*	*Th/CB~3*	*Th/CC~3*

Figure-1: Transaxial ^{18}F-Nifene PET brain slices of normal mouse, rat, rhesus monkey and human subject showing binding in thalamus (TH) and extrathalamic regions (CB=cerebellum; CC= corpus callosum).

CONTROL ID: 2223916

TITLE: In vivo quantification of ischemic memory following acute kidney injury using molecular ultrasound imaging

PRESENTER: Kenneth Hoyt

ABSTRACT BODY:

Abstract Body: The objective of this study was to evaluate the use molecular ultrasound (US) imaging for monitoring the early inflammatory effects following acute kidney injury and revealing any functional signs of ischemic memory.

A population of rats underwent 30 min of renal ischemia (acute kidney injury, N = 6) or sham injury (N = 4) using established surgical methods. Animals were divided and molecular US imaging was performed during the bolus injection of a targeted microbubble (MB) contrast agent to either P-selectin or VCAM-1. Imaging was performed before surgery and 4 and 24 h thereafter. After manual segmentation of renal tissue space, the molecular US signal was calculated as the difference between time-intensity curve data before MB injection and after reaching steady-state US image enhancement. All animal were terminated after the 24 h imaging time point and kidneys excised for immunohistochemical (IHC) analysis.

At baseline, there were no differences in the molecular US signals collected from control and injured renal tissue for either the P-selectin ($p = 0.74$) or VCAM-1 ($p = 0.59$) targeted US imaging studies. For animals imaged with P-selectin or VCAM-1 targeted MBs, the molecular US signal increased by nearly 600 % ($p = 0.07$) and 300 % ($p = 0.08$) and within 4 h for the acute kidney injury group animals, which subsided to increases of about 110 % ($p = 0.15$) and 90 % ($p = 0.21$) by 24 h, respectively. No such changes in the molecular US signal were observed in the control animals regardless of the inflammatory target ($p > 0.77$). While results using the P-selectin and VCAM-1 targeted MBs were comparable, it appears that the former was more sensitive to biomarker expression. Review of IHC tissue sections revealed that after ischemic injury, P-selectin was considerably upregulated in the glomerulus tufts as well as the intrarenal vasculature. In comparison, VCAM-1 upregulation was predominately localized to the peritubular capillaries and blood vessel endothelium. All molecular US imaging measures at animal termination had a positive correlation with IHC findings ($R^2 > 0.67$, $p < 0.05$).

Acute kidney injury is a serious disease in need of improved methods to help diagnose the extent of injury and monitor the tissue throughout disease progression. In this study, we explored the combination of targeted MBs and contrast-enhanced US for molecular US imaging of renal inflammation following acute kidney injury. Molecular US imaging revealed ischemic memory within 4 h of acute kidney injury and highlights a promising noninvasive strategy for the early diagnosis of impaired renal function.

AUTHORS (LAST NAME, FIRST NAME): Hoyt, Kenneth[1]; Warram, Jason[1]; Wang, Dezhi[1]; Ratnayaka, Sithira[1]; Traylor, Amie[1]; Agarwal, Anupam[1]

INSTITUTIONS (ALL):

1. University of Alabama at Birmingham, Birmingham, AL, United States.

(No Image Selected)

CONTROL ID: 2233312

TITLE: Quantification in molecular ultrasound imaging using a modified local density random walk model

PRESENTER: Kenneth Hoyt

ABSTRACT BODY:

Abstract Body: It is proposed that the modified local density random walk (mLDRW) model can be used to accurately describe the dilution process and binding activity of an intravascular contrast agent. The goal of this study was to evaluate the mLDRW function for modeling time-intensity curve data collected during molecular ultrasound (US) imaging studies.

Custom flow phantoms for molecular US imaging were created by pouring a heated solution of gelatin, corn starch and deionized water in a mold with three 2-mm diameter wires. Upon cooling, wires were removed and flow channels were incubated with biotin/water (0 to 5 mg/mL) for 12 h. The in-vitro setup involved a targeted flow phantom connected to a peristaltic pump and reservoir. A second peristaltic pump was used to continuously dilute the reservoir with uncirculated water. After introducing a biotin-targeted microbubble (MB) contrast agent (3×10^7 to 12×10^7 MBs; Targestar-SA, Targeson Inc), this unique flow setup mimicked the dynamic behavior of an in-vivo bolus injection whereas the first pump controlled the wash-in rate and the second pump governed the wash-out rate (MB dilution). RF data was collected for 10 min after MB dosing using a SONIX RP scanner with an L14-5 transducer (Ultrasonix Medical Corp) and a pulse-inversion harmonic imaging preset (transmit at 5 MHz, receive at 10 MHz). US data was processed using custom Matlab programs (Mathworks). After applying a Hilbert transform to the RF data, an ROI was defined using manual segmentation. A mean time-intensity curve was generated and local parameters were estimated by fitting the mLDRW function to the data. The parametric values were area under the curve (AUC), skewness (λ), mean transit time (MTT), MB accumulation (β) and onset of target binding (Δt). For comparison, intensity differences between baseline and images acquired at 10 min were used as a reference measure of the molecular US signal.

The mLDRW function accurately modeled time-intensity curve datasets collected in the vessel lumen ($R^2 > 96.0$) or at the vessel wall ($R^2 > 65.3$). No difference was found in molecular US signal measures from the control setup (0 mg/mL biotin) and between parametric estimates from the lumen or vessel wall ($p > 0.06$) except for the λ parameter ($p < 0.05$) due to variation in MB flow dynamics at the vessel boundary. In general, select molecular US parameters (*i.e.*, AUC and β) derived from data collected at the vessel wall increased with changes in target concentration ($p < 0.07$), which mimicked that observed in the reference molecular US signal ($p = 0.02$). Changes in volume flow rate had the largest impact on temporal features of targeted MB binding at the vessel wall (MTT and Δt, $p < 0.05$). After varying target concentration, there was a strong correlation between AUC and β-derived mLDRW measures and the reference molecular US signal ($R^2 > 0.99$). Importantly, model-based parametric measures exhibited considerably less variability.

A method based on mLDRW modeling of molecular US image data was developed. Preliminary validation with a series of in-vitro phantom materials highlighted the potential of this strategy and in-vivo animal studies are scheduled.

AUTHORS (LAST NAME, FIRST NAME): Hoyt, Kenneth[1]

INSTITUTIONS (ALL):

1. Radiology, University of Alabama at Birmingham, Bimingham, AL, United States.

(No Image Selected)

CONTROL ID: 2223930

TITLE: Quantitative assessment of angiogenic biomarkers with dynamic contrast-enhanced ultrasound imaging – A pilot study of human breast cancer

PRESENTER: Kenneth Hoyt

ABSTRACT BODY:

Abstract Body: The goal of this study was to investigate the use of quantitative tumor perfusion and vascular morphology measurements derived from dynamic contrast-enhanced ultrasound (DCE-US) images for detailing angiogenic biomarkers in breast cancer.

A new image processing strategy was developed for the simultaneous measurement of both tumor perfusion and neovascular morphology parameters from a sequence of DCE-US images. A computationally efficient technique for locally mapping tumor perfusion parameters was also developed. A series of binary images were constructed using Matlab for testing the neovascular morphology parametric estimation methods. Using a spatial combination of sinusoidal signals of varying frequency and length, these simulated images were characterized by vessel-like patterns with varying complexity and vascular width. The signal-to-noise ratio (SNR) was controlled by adding white Gaussian noise to the test images (SNR of 20 or 10 dB). For comparison, control images were uncorrupted and noise free (i.e., SNR of ∞ dB). A total of 50 iterations were performed for each test image pattern and average values for each neovascular morphology parameter were computed. Preliminary DCE-US image datasets were collected in 6 female patients diagnosed with invasive breast cancer. For this pilot imaging study, patients underwent US examinations with and without microbubble (MB) contrast media (Definity). For each DCE-US study, a 0.3 mL bolus of MBs was injected followed by a 10 mL saline flush. Ultrasound examinations were performed with a Phillips iU22 scanner equipped with a L9-3 MHz linear array probe using a MB contrast agent-sensitive harmonic imaging preset (transmit at 4 MHz and receive at 8 MHz) and at a low mechanical index (MI = 0.07) pre and post MB contrast agent destruction via a high MI image sequence (MI = 0.8). Uncompressed cine data in DICOM format was recorded for at least 60 sec at a frame rate of 17 Hz to capture both initial and late phases of tumor enhancement.

Simulation data demonstrates that neovascular morphology parametric estimation is highly reproducible. Notwithstanding, increased image noise levels can produce a corresponding increase in neovascular morphology parametric estimator variance suggesting that preprocessing and image filtering are critical to obtaining accurate parametric measurements. Experimental results indicate the feasibility of our approach to performing both tumor perfusion and neovascular morphology measurements from DCE-US images. Human breast cancer exhibits a high contrast perfusion profile as detailed in DCE-US acquisitions which is not evident from traditional grayscale ultrasound imaging results alone. Spatial maps of local tumor perfusion parameters depict the spatial heterogeneity in breast tumor perfusion.

In conclusion, image processing algorithms for analyzing sequences of DCE-US images to extract data on both tumor perfusion and neovascular morphological features were developed and preliminary results are encouraging.

AUTHORS (LAST NAME, FIRST NAME): Hoyt, Kenneth[1]

INSTITUTIONS (ALL):

1. University of Alabama at Birmingham, Bimingham, AL, United States.

(No Image Selected)

CONTROL ID: 2230425

TITLE: Hyaluronic Acid Conjugated Superparamagnetic Iron Oxide Nanoparticle for Cancer Diagnosis and Hyperthermia Therapy

PRESENTER: REJU THOMAS

ABSTRACT BODY:

Abstract Body: Recently, superparamagnetic iron oxide nanoparticles (SPIONs) have been prepared for magnetic resonance (MR) imaging and hyperthermia therapy. Here, we have developed hyaluronic acid (HA) coated SPIONs primarily for use in a hyperthermia application with an MR diagnostic feature. HA-coated SPIONs (HA-SPIONs) were prepared to target CD44-expressed cancer where the carrier was conjugated to PEG for analyzing longer circulation in blood as well as for biocompatibility (HA-PEG10 SPIONs). Characterization was conducted with TEM (shape), DLS (size), ELS (surface charge), TGA (content of polymer) and MRI (T2-relaxation time). The heating ability of both the HA-SPIONs and HA-PEG10-SPIONs was studied by AMF and SAR calculation. Cellular level tests were conducted using SCC7 and NIH3T3 cell lines to confirm cell viability and cell specific uptake. HA-SPIONs and HA-PEG10-SPIONs were injected to xenograft mice bearing the SCC7 cell line for MRI cancer diagnosis. We found that HA-SPION-injected mice tumors showed nearly 40% MR T2 contrast compared to the 20% MR T2 contrast of the HA-PEG10-SPION group over a 3 hr time period. Finally, *in vitro* hyperthermia studies were conducted in the SCC7 cell line that showed less than 40% cell viability for both HA-SPIONs and HA-PEG10-SPIONs in AMF treated cells.
In conclusion, HA-SPIONs were targeted specifically to the CD44, and the hyperthermia effect of HA-SPIONs and HA-PEG10-SPIONs was found to be significant for future studies.

AUTHORS (LAST NAME, FIRST NAME): THOMAS, REJU G.[1]; Moon, Myeong Ju[2]; Lee, Sejy[1]; Jeong, Yong Y.[1]

INSTITUTIONS (ALL):

1. RADIOLOGY, Chonnam National University Medical School, Gwangju, Korea (the Republic of).
2. BIOACTS, Incheon, -, Korea (the Republic of).

(No Image Selected)

CONTROL ID: 2230948

TITLE: Effectiveness of Losartan-loaded Hyaluronic Acid (HA) Micelles for the Reduction of Advanced Hepatic Fibrosis in C3H/HeN Mice Model

PRESENTER: REJU THOMAS

ABSTRACT BODY:

Abstract Body: Advanced hepatic fibrosis therapy using drug-delivering nanoparticles is a relatively unexplored area. Angiotensin type 1 (AT1) receptor blockers such as losartan can be delivered to hepatic stellate cells (HSC), blocking their activation and thereby reducing fibrosis progression in the liver. In our study, we analyzed the possibility of utilizing drug-loaded vehicles such as hyaluronic acid (HA) micelles carrying losartan to attenuate HSC activation. Losartan, which exhibits inherent lipophilicity, was loaded into the hydrophobic core of HA micelles with a 19.5% drug loading efficiency. An advanced liver fibrosis model was developed using C3H/HeN mice subjected to 20 weeks of prolonged TAA/ethanol weight-adapted treatment. The cytocompatibility and cell uptake profile of losartan-HA micelles were studied in murine fibroblast cells (NIH3T3), human hepatic stellate cells (hHSC) and FL83B cells (hepatocyte cell line). The ability of these nanoparticles to attenuate HSC activation was studied in activated HSC cells based on alpha smooth muscle actin (α-sma) expression . Mice treated with oral losartan or losartan-HA micelles were analyzed for serum enzyme levels (ALT/AST, CK and LDH) and collagen deposition (hydroxyproline levels) in the liver. The accumulation of HA micelles was observed in fibrotic livers, which suggests increased delivery of losartan compared to normal livers and specific uptake by HSC. Active reduction of α-sma was observed in hHSC and the liver sections of losartan-HA micelle-treated mice. The serum enzyme levels and collagen deposition of losartan-HA micelle-treated mice was reduced significantly compared to the oral losartan group.

Conclusion: Losartan-HA micelles demonstrated significant attenuation of hepatic fibrosis via an HSC-targeting mechanism in our in vitro and in vivo studies. These nanoparticles can be considered as an alternative therapy for liver fibrosis.

AUTHORS (LAST NAME, FIRST NAME): THOMAS, REJU G.[1]; Moon, Myeong Ju[2]; Lee, Sejy[3]; Jeong, Yong Y.[1]

INSTITUTIONS (ALL):

1. RADIOLOGY, Chonnam National University Medical School, Gwangju, Korea (the Republic of).
2. BIOACTS, Incheon, Korea (the Republic of).
3. Chonnam National University Medical School, Gwangju, Korea (the Republic of).

(No Image Selected)

CONTROL ID: 2224045

TITLE: Molecular targeted theranostic photoimmunotherapy combining two types of monoclonal antibodies targeting different epitopes of HER2: enhanced phototherapeutic effect based on fluorescence molecular imaging.

PRESENTER: Kimihiro Ito

ABSTRACT BODY:

Abstract Body: Introduction: Photoimmunotherapy (PIT) is a novel molecular imaging-guided cancer therapy that utilizes a monoclonal antibody (mAb) conjugated to a photosensitizer, IRDye700DX (IR700), in combination with near-infrared (NIR) light irradiation. The mAb-IR700 conjugate was subjected to target-specific binding and fluoresced with NIR light. Molecular target-selective tumor cell death was rapidly induced, without significant phototoxic effects for normal cells to which mAb-IR700 was not bound. A previous study showed that the HER2-specific monoclonal antibodies, trastuzumab and pertuzumab, induced a stronger antitumor effect on HER2-expressing tumors when treated in combination, than with either single agent. The aim of this study was to investigate the feasibility of HER2-targeted PIT, utilizing both trastuzumab-IR700 and pertuzumab-IR700 conjugates, in a preclinical setting.

Methods: NCI-N87 and NIH/3T3 were used as HER2-positive human cancer cells and HER2-negative control, respectively. Trastuzumab and pertuzumab, which bind to domain IV and II of HER2, respectively, were conjugated to IR700 and purified. The HER2-specific IR700 fluorescence, after addition of trastuzumab-IR700, pertuzumab-IR700, or both to the cells was examined by fluorescence microscopy and flow cytometric analysis. The phototoxicity of PIT was assessed by LIVE/DEAD assay, which can detect damaged cellular membranes. Xenograft tumor model mice bearing NCI-N87 cells were then created and examined for HER2-specific IR700 distribution over time, using the IVIS Imaging System. Lastly, HER2-positive tumors were subjected to NIR light irradiation treatment under the guidance of IR700 fluorescence, and the treatment effects were monitored.

Results: IR700 localization was observed (by fluorescence microscopy) to be HER2-specific, when treated with trastuzumab-IR700 or pertuzumab-IR700. Flow cytometric analysis showed that NCI-N87 cells produced a stronger IR700 signal when treated with both trastuzumab-IR700 and pertuzumab-IR700, than the treatment with either single agent (Fig. A). LIVE/DEAD assay revealed that the percentage of cell death when treated with a combination of trastuzumab-IR700 and pertuzumab-IR700 followed by NIR light irradiation was significantly increased, than the treatment with either single agent followed by NIR light irradiation (Fig. B). Xenograft tumors were visualized HER2-selectively using IR700 fluorescence, after injection of each mAb-IR700 conjugate. A stronger IR700 signal was observed 1 day after the injection of both trastuzumab-IR700 and pertuzumab-IR700, than when injected with either single agent (Fig. C, D). In addition, significant phototoxic effects were observed, depending on the IR700 fluorescence intensities.

Conclusion: The combination treatment of trastuzumab-IR700 and pertuzumab-IR700 enhanced IR700 signal intensities for HER2-positive tumor cells, resulting in a stronger PIT effect, than when treated with a single agent.

AUTHORS (LAST NAME, FIRST NAME): Ito, Kimihiro[1]; Mitsunaga, Makoto[1]; Nishimura, Takashi[1]; Tajiri, Hisao[1]

INSTITUTIONS (ALL):

1. Department of Gastroenterology and Hepatology, Jikei University School of Medicine, Tokyo, Minato, Japan.

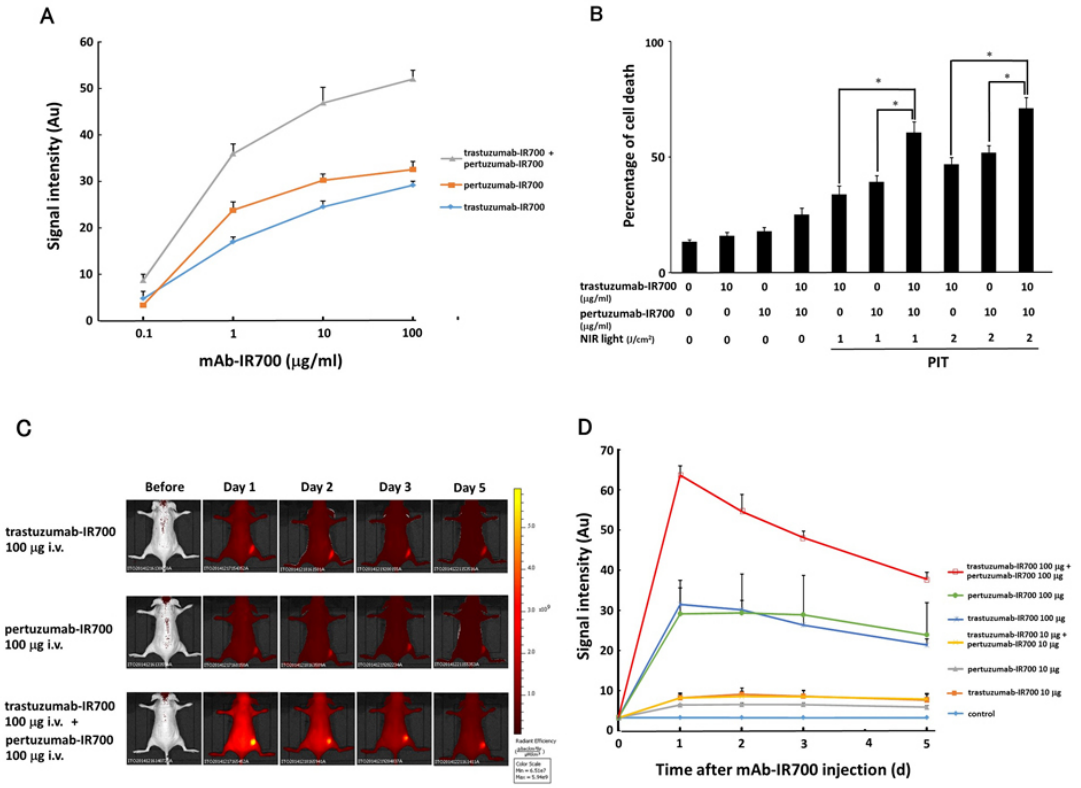

(A) Stronger HER2-specific IR700 fluorecence signal treated with trastuzumab-IR700 and pertuzumab-IR700, than the treatment with either single agent for HER2-positive NCI-N87 cells. (B) Cytotoxic effect in response to NIR light irradiation was dependent on HER2-specific IR700 signal intensity. (C, D) MAb-IR700 in vivo localizaion was HER2-selective, and stronger IR700 signal was observed 1 day after the injection of both trastuzumab-IR700 and pertuzumab-IR700, than when injected with either single agent. Treatment of NIR light irradiation was performed under the guidance of IR700 fluorescence signal.

CONTROL ID: 2229329

TITLE: Single Plane Illumination Microscopy (SPIM): a new tool for tumor cell detection in mouse brains

PRESENTER: Julia Bode

ABSTRACT BODY:

Abstract Body: During the last decades many new brain imaging techniques have been developed. The most prominent techniques for tumor volumetry on a macroscopic scale are computer tomography, magnetic resonance imaging (MRI) and positron emission tomography (PET). Confocal and two-photon microscopy with penetration depths of less than 1 mm cannot image the whole brain and therefore do not provide sufficient data for three dimensional reconstructions. Light sheet microscopy allows high-sensitivity detection and three dimensional optical sectioning [1]. With this kind of microscopy, the specimen is illuminated from two sides with a thin light sheet. In ultramicroscopy, optical sections are generated by stepping through the specimen in thin illumination planes. In comparison to confocal microscopy where planes above and below the imaging plane are permanently illuminated, leading to bleaching of fluorophores in out of focus planes, we obtained good optical sectioning also in macroscopic specimens without any bleaching of fluorophores during sample measurements.

We established single plane illumination microscopy (SPIM) for the investigation of tumor growth and single cell tumor invasion in the brain.

We have optimized organotypic hippocampal slice cultures with a tissue thickness of 300 µm from mice pups (p0 to 2). Tumorspheres from human glioma cells (i.e. LN229 or Hs683) stably expressing DsRed were grafted onto distint regions of hippocampus and cortex. An alternative technique was to use whole brains that allow for observation of single cell invasion with microscopic resolution. We either xenografted human tumor glioma cell lines in immunodeficient mice or generated high grade autochthonous fluorescent glioma models using the RCAS-mediated viral gene transfer in Nestin-Tva mice. Slices and whole brains were cleared using a modified 3DISCO protocol.

We were able to generate and establish novel mouse models for the evaluation of tumor growth and the volumetry of induced tumors in whole brains as well as brain slices with grafted tumorspheres. Infiltration of single tumor cells lentivirally transfected with DsRed can be evaluated. Tumor volumes can be evaluated by imaging the whole brain in z-stacks.

This method can be used to determine 3D structures of tumors in its surrounding tissue. Furthermore, treatment responses of cancer cells can be determined i) on single cell level in ii) different anatomical substructures and iii) correlated with various fluorescently labeled tumor supporting stroma cells.

1. Kim, S.Y., K. Chung, and K. Deisseroth, *Light microscopy mapping of connections in the intact brain.* Trends Cogn Sci, 2013. **17**(12): p. 596-9.

AUTHORS (LAST NAME, FIRST NAME): Bode, Julia[1]; Wirthschaft, Peter[1]; Breckwoldt, Michael[2]; Sharma, Rakesh[1]; Tews, Björn[1]

INSTITUTIONS (ALL):

1. Molecular Mechanisms of Tumor Invasion, German Cancer Research Center, Heidelberg, Germany.
2. Neuroradiology, University Hospital Heidelberg, Heidelberg, Germany.

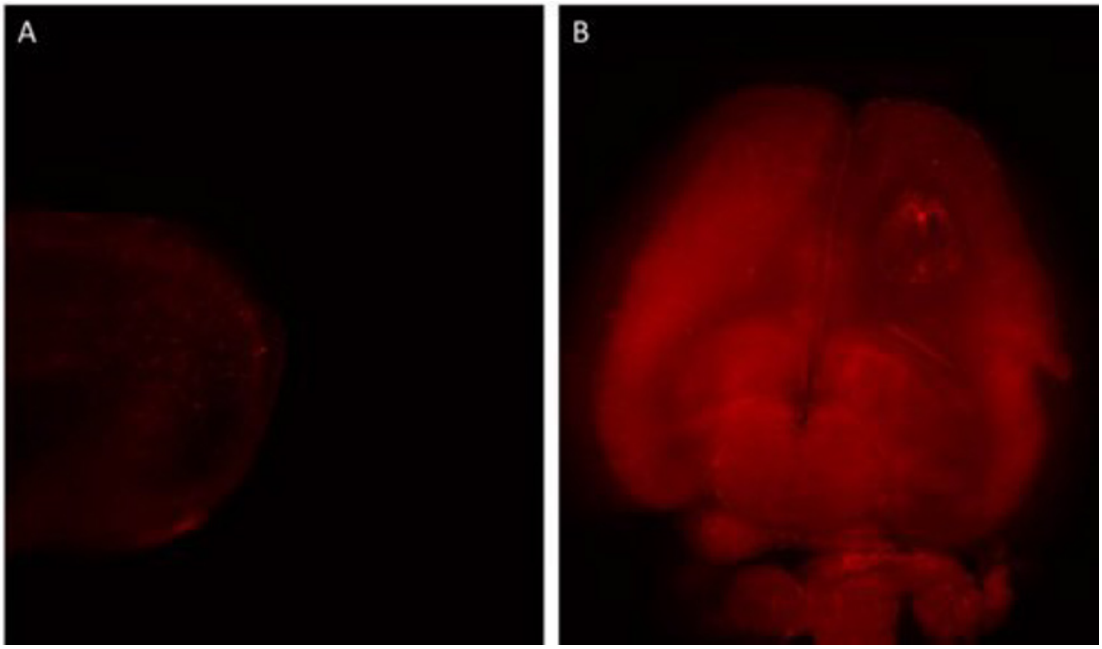

Figure 1: Human glioma cell line Hs683 lentivirally transfected with DsRed grafted onto a organotypic brain slice (A). Red dots implicate single tumor cells. Overwiew image of a mouse brain bearing a tumor in the right hemisphere (B). Tumor volume can be determined using a z-stack of the whole brain.

CONTROL ID: 2224214

TITLE: A Bio-Mimic Method for Labeling Stem Cells and Immune Cells with Ferumoxytol for Cell Tracking by Magnetic Resonance Imaging

PRESENTER: Li Liu

ABSTRACT BODY:

Abstract Body: **Background and Objective:** The success of cellular therapy depends on precise dosing, timing, and delivery of cells to the desired site. Tracking engrafted cells in an intact living organism is crucial. Cellular magnetic resonance imaging (MRI) combined with superparamagnetic iron oxide (SPIO) contrast agents is an effective and safe non-invasive cell-tracking method. Ferumoxytol (Feraheme) is currently the only FDA approved SPIO particles. Ferumoxytol is approved as an iron supplement for the treatment of iron deficiency anemia in adult patients with chronic kidney disease. However, Ferumoxytol does not effectively label cells *ex vivo* (in cell culture) without transfection agents (TA)[1]. Recently, it was found that mesenchymal stem cells (MSCs) can be labeled with Ferumoxytol *in vivo* (i.v. injection) [2]. MSCs are multipotent cells and are being explored clinically as a new therapeutic for treatment of many diseases. Macrophages (MØs), which are important players in organ transplantation and diseases, can also be labeled with Ferumoxytol *in vivo*, but not readily *ex vivo* [3]. The objective of this study is to develop an *ex-vivo* method, which mimics the *in-vivo* conditions, for labeling MSCs and MØs with Ferumoxytol, with no need of TA and/or electroporation.

Methods: The procedures are shown in the **Figure**. For MSCs labeling: (i) flush bone marrow cells from femurs and tibias of a BN rat and incubate for 24 hr at 37°C; (ii) remove the supernatant from the adherent cells; (iii) expand the number of MSCs for 7 days; (iv) prepare fresh supernatant by repeating step (i), using another BN rat; (v) trypsin-EDTA digest MSCs from step (iii) and wash MSCs with phosphate buffered saline (PBS); (vi) add Ferumoxytol (100 µg Fe/mL) to the cells and add the supernatant from step (iv); and (vii) allow the cells to incubate overnight, remove the supernatant, and allow the purification and expansion of the cells for 3 days. Steps iv, v, and vi are different from the traditional *ex-vivo* method. For MØ labeling, a similar procedure is conducted.

Results: The iron content of traditional-labeled cells, namely adding Ferumoxytol directly to the cell culture, was determined to be 0.16 ± 0.02 pg/MSC and 0.51 ± 0.02 pg/MØ. By our new method, the intracellular iron concentration increases to 2.50 ± 0.50 pg/MSC and 4.30 ± 1.42 pg/MØ. This result is comparable to that obtained with the use of heparin-protamine: 2.12 ± 0.11 pg/MSC and 2.56 ± 1.1 pg/monocyte [1]. The labeled cells exhibit over 95% viability. Labeling efficiency is verified by MR microscopy, transmission electron microscopy, and Prussian blue iron staining.

Conclusions: We have developed a simple method to label MSCs and MØs with Ferumoxytol, without the need of TA and/or electroporation, for MRI cell-tracking studies. Our method can be applied to cellular therapy.

References: **1**. Thu MS, *et al.* Nat Med 18, 463-67 (2012). **2**. Khurana A, *et al.* Radiology 269, 186-97 (2013). **3**. Alam SR, *et al.* Circ Cardiovasc Imaging 5, 559-65 (2012).

AUTHORS (LAST NAME, FIRST NAME): Liu, Li[1]; Tseng, Lanya[2]; Ye, Qing[1]; Wu, Yijen L.[1]; Bain, Daniel J.[3]; Ho, Chien[1]

INSTITUTIONS (ALL):

1. Department of Biological Sciences, Carnegie Mellon University, Pittsburgh, PA, United States.
2. Department of Statistics, Carnegie Mellon University, Pittsburgh, PA, United States.
3. Department of Geology and Planetary Science, University of Pittsburgh, Pittsburgh, PA, United States.

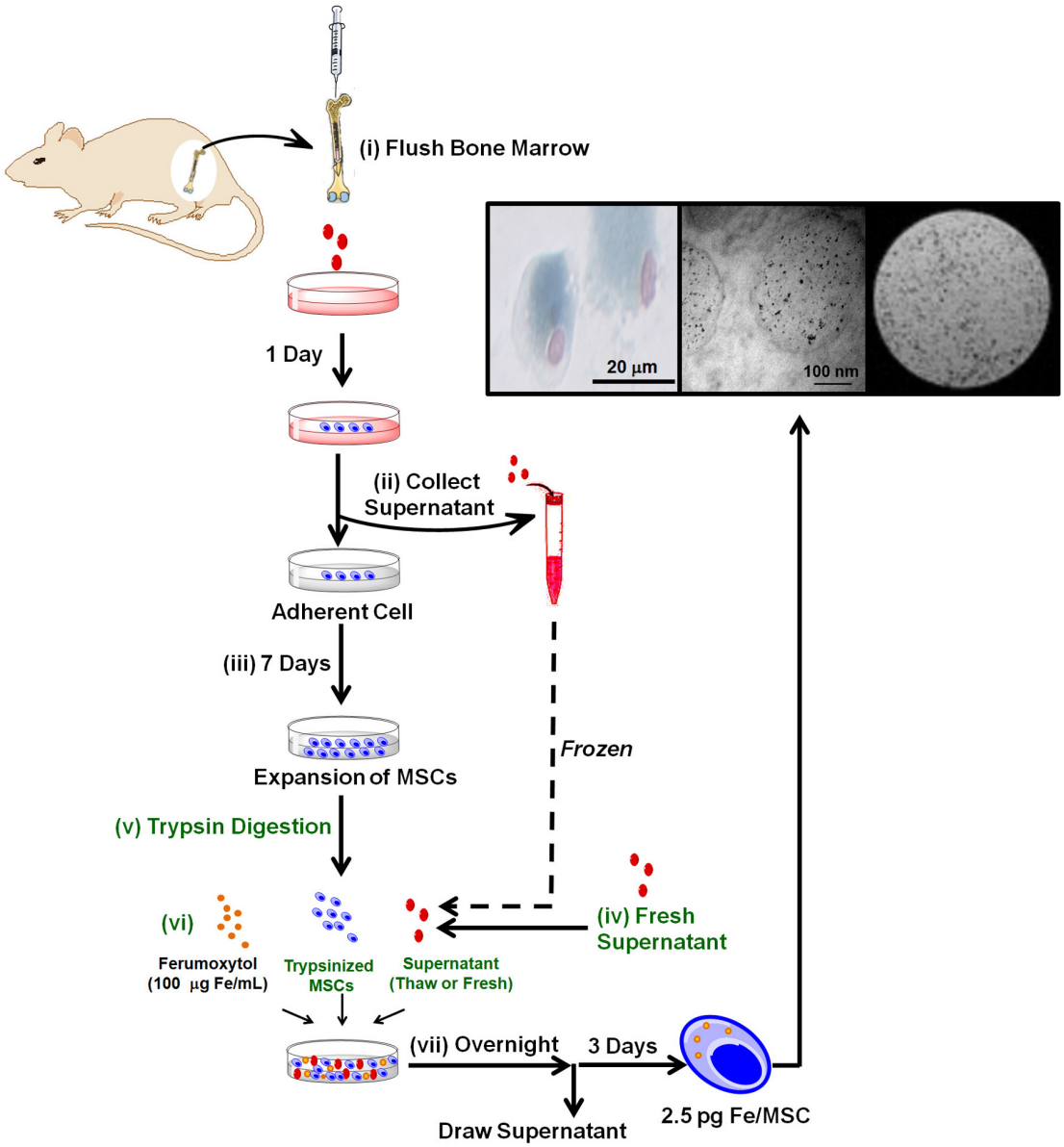

Figure Legend. Flow chart depicting our new method for labeling bone marrow MSCs with Ferumoxytol, with no need of transfection agents and/or electroporation.

CONTROL ID: 2229001

TITLE: How Improvements in *In-vivo* Cell Labeling by MRI Contrast Agents Led to Better Drug Delivery

PRESENTER: Li Liu

ABSTRACT BODY:

Abstract Body: Background and Objective: Nanotechnology-based imaging agents and chemotherapeutics have been investigated for more than 30 years. Their applications range from inflammation to cancer and regenerative medicine. A major challenge for translating nanomedicine to clinical applications is their rapid clearance by the reticuloendothelial system (RES), thus reducing efficacy and increasing toxic side effects on off-target organs. Many studies have been tried to decrease the RES clearance of nanoparticles by modifying nanoparticle characteristics, such as the size, charge, surface property, and composition. Unfortunately, the majority (40–80%) of the injected nanomedicines end up in the liver and spleen [1,2]. Our strategy is to target the RES to temporarily blunt the clearance and to increase the bioavailability of nanoparticles using a FDA approved agent, Intralipid. In the WMIC 2013, we presented our discovery that in rodents, Intralipid can reduce RES uptake ~50% and increase blood half-life ~3-fold of nano- and micron-sized particles in which magnetic resonance imaging (MRI) contrast agents (i.e., superparamagnetic iron-oxide) are loaded. Recently, we have applied this methodology to improve the delivery and reduce the toxic side effect of an anticancer nanodrug.

Methods: In our study, we have used an improved anticancer nanodrug, dichloro (1, 2-diaminocyclohexane) platinum (II)-loaded and hyaluronic acid polymer-coated nanoparticle (DACHPt/HANP), to test our hypothesis. A single dose of Intralipid (2 g/kg, clinical dosage) is administrated [intravenously (i. v.), clinical route] one hour before i.v. injection of DACHPt/HANP. Blood samples were collected at different time points to determine the changes in bioavailability of DACHPt/HANP upon Intralipid pre-treatment. At 5-, 24-, and 72-hour post injection of DACHPt/HANP, tissues (liver, spleen, and kidney) were collected to determine the changes in biodistribution of the nanodrug. Serum alanine aminotransferase (ALT) activities and creatine levels were determined to investigate the changes in liver and kidney functions. Tissue damages were further investigated by histological analysis

Results: We have found that Intralipid pre-treatment can significantly reduce the toxicities of DACHPt/HANP in liver, spleen, and kidney. Notably, Intralipid pre-treatment decreases spleen enlargement, which has been reported as a serious side effect of Abraxane®. Intralipid can decrease Pt accumulation in the liver, spleen, and kidney by 20.4%, 42.5%, and 31.2% at 24-hr post nanodrug administration, respectively. The bioavailability of DACHPt/HANP increases by 18.7% and 9.4% during the first 5 and 24 hr, respectively.

Conclusions: Our study shows that Intralipid can be used to improve the bioavailability and reduce the toxic side effects of DACHPt/HANP. Our approach is a general one applicable to any approved and in-development nanoparticle-based delivery system of imaging agents or therapeutic drugs to improve their bioavailability, without any new modification of the nanoparticles.

References: 1. Albanese A, *et al.* Annu Rev Biomed Eng 14, 1-16 (2012). **2**. Chow, E, *et al.* Sci Transl Med 5, 216rv214 (2013).

AUTHORS (LAST NAME, FIRST NAME): Liu, Li[1]; Ye, Qing[1]; Lu, Maggie[3]; Lo, Ya-Chin[3]; Hsu, Yuan-Hung[3]; Wei, Ming-Cheng[3]; Chen, Yu-Hsiang[2]; Lo, Shen-Chuan[2]; Wang, Shian-Jy[2]; Bain, Daniel J.[4]; Ho, Chien[1]

INSTITUTIONS (ALL):

1. Department of Biological Sciences, Carnegie Mellon University, Pittsburgh, PA, United States.
2. Material and Chemical Research Laboratories, Industrial Technology Research Institute, Hsinchu, Taiwan.
3. Biomedical Technology and Device Research Laboratories, Industrial Technology Research Institute, Hsinchu, Taiwan.
4. Department of Geology and Planetary Science, University of Pittsburgh, Pittsburgh, Pittsburgh, PA, United States.

(No Image Selected)

CONTROL ID: 2226530

TITLE: Imaging β-glucuronidase Activity in Human Breast Cancer Tumor Xenografts Using Fluorescein Substrate

PRESENTER: Li Liu

ABSTRACT BODY:

Abstract Body: Introduction: Detection of enzyme activity offers potential insight into developmental biology, disease progression, and potentially personalized medicine. The *Escherichia coli* β—glucuronidase encoded gene (GUS), has been proposed as a reporter gene system, and is widely used in plant molecular biology [1] and microbiology [2]. It has also been prosed and exploited as a reporter gene in transfected tumor cell lines [3]. Various chromogenic and fluorogenic substrates are available, but were limited to histology or *in vitro* assays. Human β-glucuronidase (β-Gluc) is mainly localized intracellularly in lysosomes in healthy tissues, but it is occurs extensively extracellularly in some human tumors, with expression being much higher than in normal tissues. We have now explored *in vivo* detection of β-Gluc using optical imaging to detect fluorescent signal following administration of Fluorescein Di-β-D-Glucuronide (FDGlcU).

Methods: Commercial reporter substrates were used. X-gluc solution was used to stain MCF7 cells, and FDGlcU was added wells of MCF7, which were observed using a small animal fluorescent imaging system. MCF7 ($1X10^6$) were implanted SC in the left and right flanks of female nude mice. When tumors reached about 8 mm diameter, FDGlcU was injected intravenously (3 mg in 100 µl). The anesthetized nude mice bearing MCF7 tumors were observed up to 400 mins after injection using blue emission and excitation filters. Tumors excised slices were observed under fluorescent microscopy and with H&E stain.

Results and Conclusion: β-Gluc activity was visualized in human wild type MCF7 cells with FDGlcU (Fig1. b) and more than 70% cell showed positive blue color signal with standard X-gluc stain (Fig1.a). After IV injection of FDGlcU, the β-Gluc enzyme activity was detectable from 5 min to 400 min, with maximum signal after 100 mins (Fig1. d & e) and also confirmed by histology (Fig1.c).This method offers a new paradigm for non-invasive in *vivo* imaging of glucuronidase gene expression. This observation provides a caveat for use of GUS as a reporter gene due to potential endogenous expression in wild type cells and suggests a possible method for detecting breast cancer.

Acknowledgment: Supported in part by U24 CA126608, P30 CA142543 and NIH 1S10RR024757

References:

1. Jefferson, R. A *et al.* (1987). "GUS fusions: Beta-glucuronidase as a sensitive and versatile gene fusion marker in higher plants". The EMBO J 6 (13): 3901–7.PMC 553867. PMID 3327686

2. Vande Broek, A *et al.* (1998). "Bacterial chemotactic motility is important for the initiation of wheat root colonization by Azospirillum brasilense". Microbiol. 144 (9): 2599–606. PMID 9782509.

3. Yu-Cheng S et al. (2014), PET Imaging of b-Glucuronidase Activity by an Activity-Based 124I-Trapping Probe for the Personalized Glucuronide Prodrug Targeted Therapy", Mol Cancer Ther; 13(12); 2852–63.

AUTHORS (LAST NAME, FIRST NAME): Liu, Li[1]; Mason, Ralph[1]

INSTITUTIONS (ALL):

1. Radiology, UT southwestern Medical Center, Dallas, TX, United States.

Fig.1

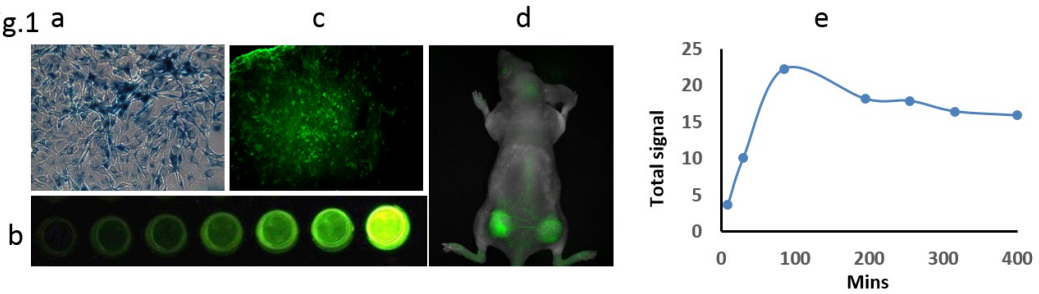

Figa: X-gluc staining of MCF7 cells; b: FDGlcU imaging for varying numbers of MCF7 cells (Left to right: 15625; 31250; 62500; 125000; 250000; 500000; 1000000); c: Fluorescent imaging for MCF7 left tumor slice; d: Representative image after IV injection FDGlcU in nude mouse with two MCF7 tumors; e: Fluorescent signal curve after injection.

CONTROL ID: 2224227

TITLE: 3-D characterisation of murine spleen and its response to the vascular disrupting agent ZD6126 using optical computed tomography.

PRESENTER: Ciara McErlean

ABSTRACT BODY:

Abstract Body: Optical computed tomography (OptCT) is an emerging imaging modality, delivering detailed 3-D maps of optical attenuation or fluorescence in optically cleared specimens. Here we present the first application of OptCT to image adult murine spleen. The spleen is a complex, hypervascular organ made up of several distinct tissue types, which standard 2-D imaging techniques can fail to interrogate accurately and quantitatively. We assessed the ability of OptCT to characterise the normal spleen, and to detect microvascular and volume changes induced by treatment with the vascular disrupting agent (VDA) ZD6126. Six-week-old female Balb/c mice were treated with either vehicle alone (n=3) or 200mg/kg ZD6126 i.p. (n=3). After 24 hours the spleens were excised and fixed in 70% ethanol in PBS overnight at 4˚C. Spleens were embedded in 0.75% agarose, dehydrated and optically cleared via immersion in a graded series of ethanol and 1:2 benzyl benzoate:benzyl alcohol over a one week period. This process reduces scattering attenuation in the tissue. OptCT imaging was performed using a previously characterised in-house scanner [1]. Each spleen was scanned twice, with each scan consisting of 1000 projection images of 512×512 pixels, acquired at 0.18˚ intervals over a 180˚ rotation, with a field-of-view of 13.3×13.3mm for whole-spleen visualisation and volume measurements, and 5.3×5.3mm for higher resolution images. Each dataset was reconstructed onto a matrix of 512^3 voxels. Projections were acquired at an illumination wavelength of 430nm, which is strongly absorbed by haemoglobin. The total volume of each spleen was calculated using segmentation tools in Osirix [2]. Textural features on the higher resolution scans were analysed using a grey-level co-occurrence matrix (GLCM) approach [3]. The analysis was extended to include three reference points in orthogonal planes. 3-D contrast and homogeneity measures were calculated for a range of pixel displacements [4]. High-contrast image volumes were acquired for each sample revealing the complex inner structure of the spleen (Fig1a). Significant (**p=0.001) shrinkage of total spleen volume was determined after ZD6126-treatment (Fig.1b). 3-D GLCM analysis showed contrast and homogeneity measures were significantly different between vehicle and ZD6126-treated cohorts over a range of length scales ($p<0.05$) (Fig1c-d). The ZD6126-treated cohort's peak mean 3-D contrast occurred at a smaller pixel displacement than for the vehicle cohort. All of these results support the hypothesis that the ZD6126-treatment induced a contraction of the spleen on a microvascular level. We have shown the ability of OptCT imaging, utilising endogenous haemoglobin contrast, to quantify the microvasculature of murine spleen and its response following treatment with the VDA ZD6126. This technique could be helpful in evaluating drug safety, for monitoring drug toxicity and off-target treatment effects.

[1] Doran, S.J. et al, Phys Med Biol, 2013, 58:6279-97

[2] Rosset, A., Spadola, L., Ratib, O., Journal of Digital Imaging, 2004

[3] Haralick, R.M., Shanmugam, K., Systems 1973

[4] Chen, W.S., Huang, R.H., Hsieh, L., Advances in Biometrics, 2009

AUTHORS (LAST NAME, FIRST NAME): McErlean, Ciara M.[1]; Boult, Jessica K.[1]; Collins, David J.[1]; Leach, Martin O.[1]; Robinson, Simon P.[1]; Doran, Simon J.[1, 2]

INSTITUTIONS (ALL):

1. CRUK Cancer Imaging Centre, Institute of Cancer Research, Sutton, United Kingdom.
2. Department of Physics, University of Surrey, Guildford, United Kingdom.

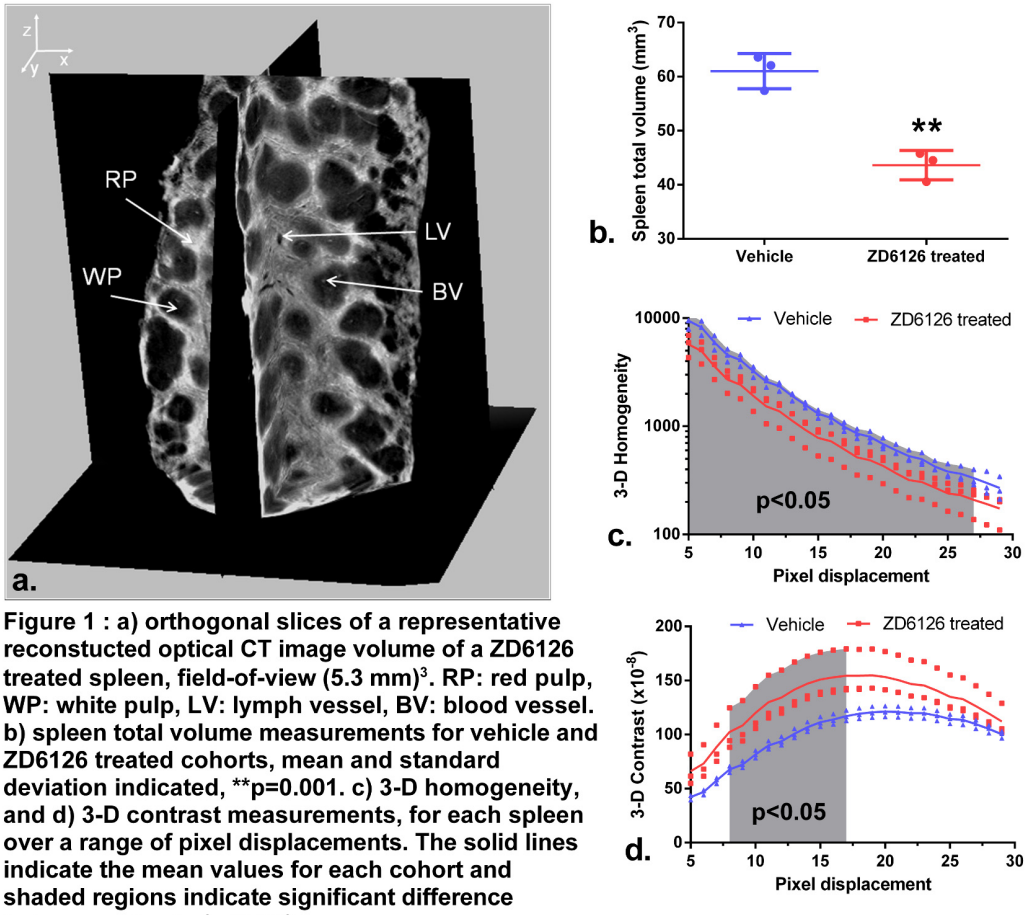

Figure 1 : a) orthogonal slices of a representative reconstucted optical CT image volume of a ZD6126 treated spleen, field-of-view (5.3 mm)^3. RP: red pulp, WP: white pulp, LV: lymph vessel, BV: blood vessel. b) spleen total volume measurements for vehicle and ZD6126 treated cohorts, mean and standard deviation indicated, **p=0.001. c) 3-D homogeneity, and d) 3-D contrast measurements, for each spleen over a range of pixel displacements. The solid lines indicate the mean values for each cohort and shaded regions indicate significant difference between cohorts (p<0.05).

CONTROL ID: 2229620

TITLE: Visualization of EGFR expressing mammary carcinomas in mice by SPECT applying $^{99m}Tc(CO)_3$-labeled single domain antibodies

PRESENTER: Thomas Krüwel

ABSTRACT BODY:

Abstract Body: A prerequisite for the application of targeted therapeutic strategies in oncology is to obtain accurate information on tumor load and spread as early as possible.

Single domain antibodies (sdAb) are small molecules (16kDa) consisting of a monomeric variable domain of a heavy chain antibody. Since sdAbs are only 1/10th in size compared to full immunoglobulins G (IgG), they are known to be faster removed from the blood pool than IgGs.

Hence, the aim of the study was to preclinically evaluate the suitability of sdAbs targeting the epidermal growth factor receptor (EGFR) as a tool for the detection of mammary carcinomas in mice.

SdAbs targeting EFGR (EGFR sdAb) and a non-binding control sdAb were produced in E. coli cultures, purified and analyzed by flow cytometry for their binding capacity to MDA-MB-468 cells which express high amounts of EGFR. The non-invasive detection of tumors with SPECT was investigated in an orthotopic MDA-MB-468 mammary carcinoma model in immunodeficient nude mice.

A CRS Kit was used to label the sdAbs with a $^{99m}Tc(CO)_3(OH_2)_3$ species via its hexahistidine tag. The radiochemical purity of the labeled sdAbs was analyzed by instant thin layer chromatography. From 30min to 270min post injection, in vivo SPECT scans (360°, 5min/frame, 50.6min total scan time) were performed at various time points in tumor bearing mice after intravenous application of 13.6 ± 1.1pmol of the control sdAb and 11.3 ± 1.0pmol of the EGFR sdAb corresponding to an initial activity of 1.8 ± 0.3MBq and 2.2 ± 0.4MBq, respectively. In order to correlate the obtained SPECT data to anatomical structures, CT scans in combination with an iodine-based based contrast agent were performed prior to SPECT. Following SPECT, the animals were sacrificed and the remaining activities in the organs were measured in a gamma counter.

In vitro, a strong binding of the EGFR sdAb to the MDA-MB-468 cells was determined by flow cytometry with a mean fluorescence index ten fold higher than the control sdAb being at baseline.

The sdAbs were labeled with $^{99m}Tc(CO)_3(OH_2)_3$ yielding a specific activity of 198 ± 19MBq/nmol and 136 ± 28MBq/nmol for the EGFR sdAb and for the control sdAb, respectively, both with a radiochemical purity above 99%.

In vivo, mammary tumors were visualized by SPECT with the EGFR sdAb with the highest uptake of approx. 2%ID/cm^3 30 min post injection. CT imaging confirmed the presence of the tracer within a tumor of 49.1mm^3. The tumor uptake decreased over time to approx. 1%ID/cm^3 at 150min and 0.5%ID/cm^3 at 270min post injection. Scans with the control sdAb showed no tumor uptake after 30min. Biodistribution analysis revealed a tumor uptake of 1.23 ± 0.47%ID/g compared to a remaining activity in the blood of 0.28 ± 0.08%ID/g resulting in a tumor-to-blood ratio of 4.4 for the EGFR sdAb. Since the sdAb is cleared via renal excretion from the body, high uptake was determined in the kidneys and the urine (214 ± 30%ID/g and 69 ± 31%ID/g, respectively).

These results demonstrate a favorable pharmacokinetic profile of the sdAb and indicate the suitability of the EGFR sdAb to specifically detect EGFR expressing tumors lesions in mice already 30 min post injection.

AUTHORS (LAST NAME, FIRST NAME): Krüwel, Thomas[1]; Nevoltris, Damien[2]; Chames, Patrick[2]; Dullin, Christian[1]; Baty, Daniel[2]; Stühmer, Walter[3]; Lotz, Joachim[1]; Alves, Frauke[1, 3]

INSTITUTIONS (ALL):

1. Department of Interventional and Diagnostic Radiology, University Medical Center Göttingen, Göttingen, Germany.
2. Antibody therapeutics and Immunotargeting, Cancer Research Center of Marseille, Marseille, France.
3. Molecular Biology of Neuronal Signals , Max-Planck-Institute for Experimental Medicine, Goettingen, Germany.

(No Image Selected)

CONTROL ID: 2224410

TITLE: Imaging HGF with ^{89}Zr-DFO-Rilotumumab as a Companion Diagnostic for Rilotumumab Treatment of Gastric Cancer

PRESENTER: Eric Price

ABSTRACT BODY:

Abstract Body: Introduction: The antibody Rilotumumab (AMG102) has been in clinical trials for treatment of several cancers, including gastric and brain. AMG102 is a fully human antibody that binds hepatocyte growth factor (HGF), preventing it from binding its receptor (MET) and therefore providing therapeutic benefit. A patient must ideally have elevated levels of HGF in tumors to benefit from AMG102 treatment, and clinical trials to date have had mixed results, perhaps due to poor patient selection. As a tool for patient selection, we aim to make a companion diagnostic from AMG102 by conjugating the chelator desferrioxamine (DFO) and radiolabeling with the PET imaging isotope ^{89}Zr ($t_{1/2}$ = ~3.3 d). The goal of this study is to prepare ^{89}Zr-DFO-AMG102 and study its properties, and determine if it can be used to specifically image cancers with elevated levels of HGF.

Methods: The chelator *p*-SCN-Bn-DFO was conjugated to AMG102 (PBS, pH 9.0) and purified. The modified antibody was then radiolabeled with ^{89}Zr under standard conditions (PBS, pH 7.4) with high radiochemical yields (>98%) and purity (>99%). The stability was evaluated by serum competition, being > 98% stable after 7 days (37°C). The brain cancer cell line U87-MG has been previous used to evaluate AMG102 therapeutically, as it is known to express high levels of HGF (autocrine production), and so was used as a proof-of-principle for PET imaging. Mice were xenografted with U87-MG cells on the right shoulder (n = 6) and imaged after 3 weeks. ^{89}Zr-DFO-AMG102 was injected (~160 µCi, 3 × 40 µg antibody, and 3 × 340 µg) and imaged by PET from 8 h to 120 h p.i. The gastric cancer cell line MKN-45 (high MET, low HGF) was also xenografted and imaged (n = 3). The MKN-45 mice were imaged by PET at 24 h and 72 h p.i (~140 µCi, 100 µg antibody).

Results: ^{89}Zr-DFO-AMG102 was successfully able to image U87-MG xenografts (high autocrine HGF expression), with a 120 h biodistribution showing the 40 µg injection (~160 µCi) provided tumor uptake of 24.6 ± 18.2 %ID/g, and the 340 µg injection (~160 µCi) 20.76 ± 5.6 %ID/g. The biodistribution error values were lower with the low specific activity group (340 µg), suggesting that co-injection or pre-injection of non-radioactive AMG102 may be required for optimum biodistribution. Experiments are in progress to determine the optimum dosage. The MKN-45 mouse xenografts acted as negative controls, and showed much lower tumor uptake of 5.1 ± 1.4 %ID/g (72 h p.i, by PET ROI), compared to 14.8 ± 6.7 %ID/g for U87-MG xenografts (72 h p.i, by PET ROI) (Figure 1).

Current and Future Work: The gastric cancer lines NCI-N87, GTL-16, and KATO-III are being evaluated and compared to U87-MG for MET and HGF production using western blot and ELISA. Full PET imaging and biodistribution studies will be performed using suitable cell lines with ^{89}Zr-DFO-AMG102 for imaging HGF.

Conclusions: We have successful synthesized ^{89}Zr-DFO-AMG102 and shown selective uptake in high-HGF expressing U87-MG mouse xenografts, and low uptake in low-HGF expressing MKN-45 xenografts, demonstrating the potential of this PET imaging agent for patient selection for AMG102 therapy.

Funding: NSERC PDF fellowship (E.W.P.).

AUTHORS (LAST NAME, FIRST NAME): Price, Eric W.[1, 2]; Sevak, Kuntal K.[1]; Edwards, Kimberly J.[1]; Carnazza, Kathryn E.[1]; Janjigian, Yelena Y.[1]; Lewis, Jason S.[1, 2]

INSTITUTIONS (ALL):

1. Radiology, Memorial Sloan Kettering Cancer Center, New York, NY, United States.
2. Molecular Pharmacology & Chemistry Program, Memorial Sloan Kettering Cancer Center, New York, NY, United States.

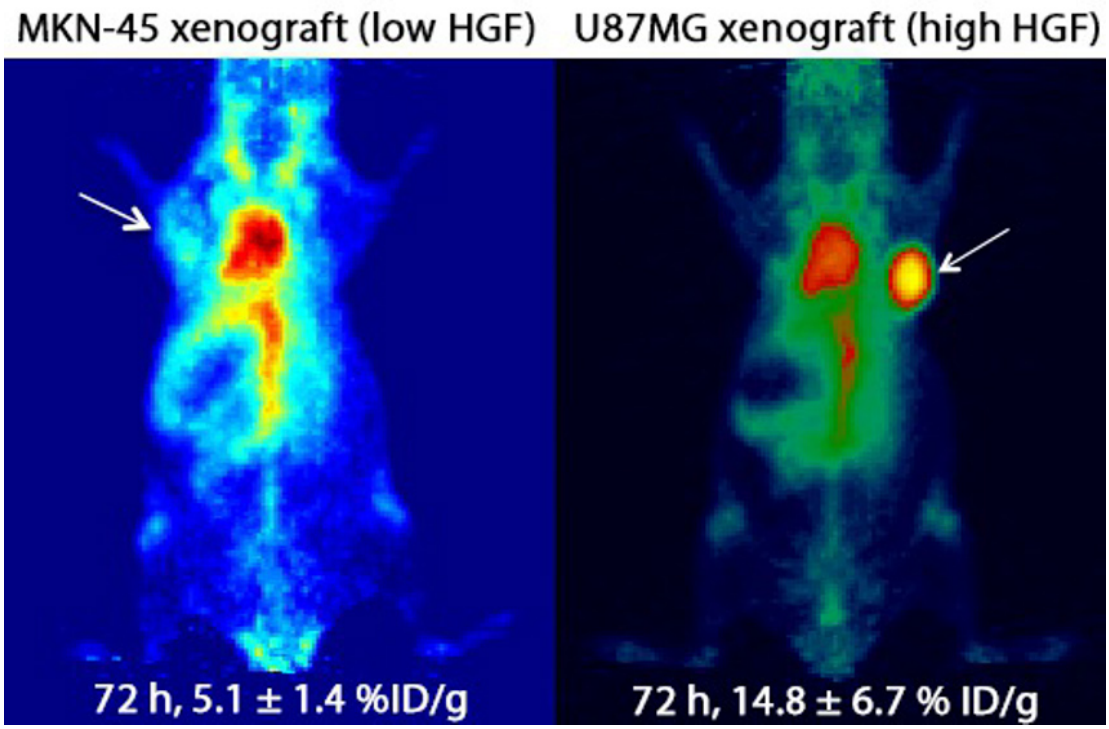

PET imaging of ^{89}Zr-DFO-AMG102 in MKN-45 (low HGF, left) and U87-MG (high HGF, right) mouse xenografts, demonstrating selective uptake in tumors with high HGF expression.

CONTROL ID: 2229204

TITLE: Discrepancy between tumor antigen distribution and antibody binding in nude mouse xenograft model of human melanoma

PRESENTER: Yong-il Kim

ABSTRACT BODY:

Abstract Body: Purpose: Biodistribution of antibody is critical in successful immunoscintigraphy and immunotherapy, and it is assumed to be similar to antigen distribution. We measured the pattern of radiolabeled antibody binding and compared to the distribution of tissue antigen in nude mouse xenograft model.

Methods: 10^7 of FEM-XII melanoma cells were transplanted at the right flank in 5 nude mice. As a control, $5X10^6$ of LS174T colon cancer cells were transplanted at the left flank. After 2 weeks, 10 μCi of I-131 labeled anti-melanoma monoclonal antibody 96.5 was injected intravenously. After sacrifice, antibody binding pattern in the tumors was evaluated using autoradiography (quantitative whole body autoradiography, QWBA). The adjacent tissue slices were incubated in solution dishes of various concentrations of I-125 labeled 96.5 antibody. In vitro quantitative autoradiography (QAR) was performed to measure the distribution and concentration of 9.2.27 antigen (antigen for 96.5 antibody).

Results: The tumor-to-blood ratio ranged from 1.48 to 10.89, and tumor-to-control ratio ranged from 0.74 to 8.3. The distribution of 9.2.27 antigen was generally homogeneous in the tumors (303-807 mg), but actual in vivo distribution of radiolabeled antibody was quite different among each mouse and according to location. We could not find any parameters related to the pattern of in vivo distribution of radiolabeled antibody.

Conclusion: We found the heterogenous features of target antibody distribution in human melanoma grafted nude mice. In vivo binding pattern of antibody cannot be expected by antigen distribution in tumor.

AUTHORS (LAST NAME, FIRST NAME): Kim, Yong-il [1]; Kim, Yong Joong [2]; Paeng, Jin Chul [1]; Cheon, Gi Jeong [1]; Kang, Keon Wook [1]; Lee, Dong Soo [1]; Chung, June-Key [1]

INSTITUTIONS (ALL):

1. Department of Nuclear Medicine, Seoul National University Hospital, Seoul, Korea (the Republic of).
2. Yesan Health Center, Yesan-gun, Korea (the Republic of).

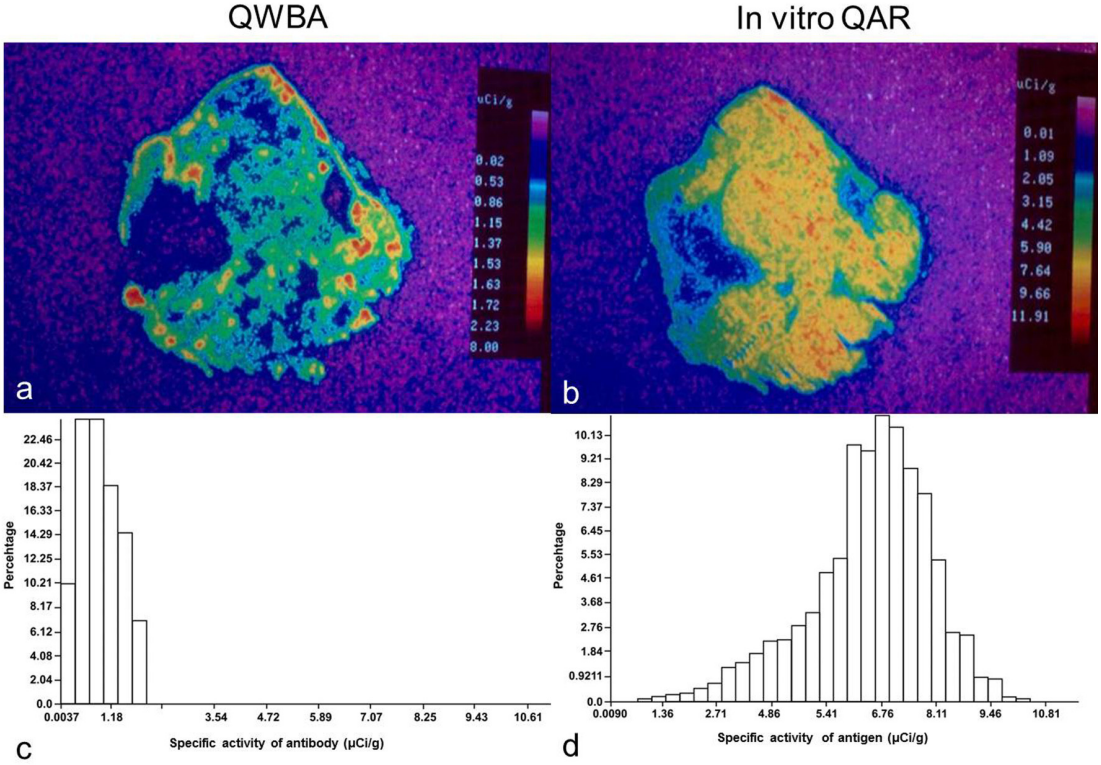

Comparison of QWBA and in vitro QAR case

CONTROL ID: 2224518

TITLE: Global and Local Non-rigid Registration in Sequential Quantitative SPECT/CT for Targeted Radionuclide Therapy

PRESENTER: Greta Mok

ABSTRACT BODY:

Abstract Body: Previously we showed that non-rigid registration on local organs in sequential SPECT images improved the 3D dosimetry for targeted radionuclide therapy. However, segmentation on each organ-of-interest on images at multiple time points is a very time consuming process and its accuracy depends on the operator's experience. This study aims to evaluate the performance of non-rigid registration on global whole-body and local organs in sequential SPECT/CT scans. We modeled 3 anatomical variations each with 3 In-111 Zevalin activity distributions, i.e., a population of 9 phantoms, at 1, 12, 24, 72 and 144 hrs post-injection using the digital 4D Extended Cardiac Torso (XCAT) phantom. Local deformation of the liver, kidneys, spleen and stomach were modeled of up to 5 pixels/degrees with <5% volume change, combined with whole body rigid motion of up to 5 pixels/degrees of translation/rotation. Realistic noisy projections were generated by an analytical projector, modeling attenuation, scatter and collimator-detector response and then reconstructed using OS-EM with 128 updates including full compensations. The corresponding attenuation maps of the phantoms served as the CT images. Affine+b-spline non-rigid registrations were performed on (i) whole-body SPECT and CT images; (ii) individual organs segmented semi-automatically on SPECT and CT images, using the 24-hr time point SPECT/CT images as the reference respectively. Voxel-by-voxel integration was performed on registered images over 5 time points, followed by convolution with a Y-90 dose kernel to generate dose images. Organ dose, differential and cumulative dose volume histograms (DDVH & CDVH) were generated for liver, spleen, kidneys and lungs. For liver dose, the %errors were -12.86%, 26.76% and -5.32% for no registration, whole-body and local registration on sequential SPECT images as compared to phantoms without misalignment, while the respective errors were -7.87%, 2.21% and -2.42% on sequential CT images. For DDVH, the normalized absolute errors were 25.78%, 44.07% and 21.11% for no registration, whole-body and local registration on sequential SPECT, while they were 20.78%, 15.24% and 14.03% for sequential CT. For CDVH, the difference between whole body and local liver registration was substantially smaller for sequential CT as compared to sequential SPECT images. Results were accordant for other organs. We conclude that organ-based segmentation is necessary to improve the 3D dosimetry when only sequential SPECT scans are available, while whole body registration is recommended for sequential CT scans.

AUTHORS (LAST NAME, FIRST NAME): Mok, Greta[2]; Leong, Ka Weng[2]; Li, Tiantian[2]; Ao, Edwin C.[2]; Liu, Ren-Shyan[1]

INSTITUTIONS (ALL):

1. Dept of Nuclear Medicine, Faculty of Medicine, National Yang-Ming University, Taipei, Taiwan.
2. Electrical and Computer Engineering, University of Macau, Taipa, Macao.

(No Image Selected)

CONTROL ID: 2233307

TITLE: A first in human study with the first tumor-specific agent with fluorescence in the NIR spectrum for image-guided surgery: a translational study.

PRESENTER: Charlotte Hoogstins

ABSTRACT BODY:

Abstract Body: Introduction

Intra-operative NIR fluorescence imaging of primary tumor and metastases may result in better patient outcomes in cancer surgery. OTL38 is an imaging agent that specifically binds to the folate receptor α (FRa) which is overexpressed by various tumors. FRa-positive cells become detectable by binding the NIR fluorescent agent, which fluoresces at 760nm. In this first-in-human study OTL38 was first administered to healthy volunteers (HVs), to assess tolerability and pharmacokinetics (PK). Subsequently, OTL-38 was administered to ovarian cancer patients to assess efficacy and the optimal dose.

Material and methods

HVs received a single iv dose in a randomized, placebo-controlled, ascending-dose study (0.025, 0.05, 0.1 and 0.2 mg/kg). Pharmacokinetics of OTL38 in blood, urine (by LC MS) and skin, (quantitated fluorescent signal) were assessed. The optimal doses were subsequently explored in 6 patients with metastasized ovarian cancer scheduled for cytoreductive surgery. Patients received a single ascending-dose of OTL38 intravenously 2-3 hours before surgery (0.025 and 0.05 mg/kg). The number of suspected lesions detected with fluorescence and concordance between fluorescence and FRa-status on histopathology was studied in addition to PK.

Results

In healthy volunteers OTL38 was well tolerated at low doses (0.025, 0.05 and 0.1 mg/kg) but the highest dose (0.2 mg/kg) caused hypersensitivity reactions. The plasma concentration-time profile showed bi-phasic elimination (elimination half-life: 26-160min). A dose-dependent fluorescent signal was observed in the skin, with a prolonged elimination half-life compared to blood. These data allowed definition of the optimal and safe starting doses in patients and an initial time window for intra-operative imaging (120 – 400 min after administration). In patients, OTL38 showed highly specific accumulation in FRa positive tumors. Mean Tumor-to-Background ratio was 3.8 (range 1.7 – 9.8). Fluorescence microscopy showed clear membranous and cytoplasmic accumulation of OTL-38 in tumor cells. In total, 35 fluorescent FRa positive malignant lesions were resected, of which 8 (23%) were not identified by inspection/palpation.

Conclusions

OTL38, the first tumor-specific agent with fluorescence in the NIR spectrum, was successfully used for intra-operative fluorescence imaging of FRa-positive tumors. It was well tolerated at doses that allowed identification of malignant lesions, even lesions that were otherwise undetectable.

AUTHORS (LAST NAME, FIRST NAME): Hoogstins, Charlotte E.[1, 2]; Tummers, Quirijn R.[1, 2]; Cohen, Adam F.[2]; van de Velde, Cornelis J.[1]; Low, Philip S.[3]; Vahrmeijer, Alexander L.[1]; Burggraaf, Jacobus[2]

INSTITUTIONS (ALL):

1. Surgery, Leiden University Medical Center, Leiden, Netherlands.
2. Centre for Human Drug Research, Leiden, Netherlands.
3. Purdue University, West Lafayette, IN, United States.

(No Image Selected)

CONTROL ID: 2228800

TITLE: Towards clinical validation of the tumor-specific near-infrared fluorescent agent cRGD-ZW800-1

PRESENTER: Hein Handgraaf

ABSTRACT BODY:

Abstract Body: Introduction

Accurate imaging of tumors during surgery remains challenging. Sensitivity of available imaging modalities is often inadequate with respect to margin or metastasis detection. Therefore, the surgeon currently relies mainly on visual and palpable feedback. Near-infrared (NIR) fluorescence imaging has been introduced to identify various structures in real-time during surgery. For tumor-specific imaging, fluorophores are conjugated to targeted ligands. The cRGD peptide targets integrins associated with (neo)angiogenesis (e.g. $\alpha_v\beta_3$) and has already successfully been used for nuclear imaging in oncologic patients. In this study, we describe the development and preclinical validation of cRGD conjugated to the NIR fluorophore ZW800-1.

Methods

cRGD–ZW800-1 was produced by current Good Manufacturing Practices (cGMP). Binding capacity was validated in vitro in a plate-assay competition experiment on cell lines HT29 (colon adenocarcinoma) and U87 (glioblastoma). In vivo, a dose optimization study was performed. After inducing orthotopic HT-29 tumors, mice were intravenously injected with 0.25, 1.00, 10 or 30 nmol cRGD–ZW800-1. After 4h, a small incision was made to image the tumor and adjacent intestines. Mice were sacrificed at 24 h. The abdomen was fully opened and imaged again. Subsequently, mice with orthotopic BXPC3 (pancreas adenocarcinoma) and OSC19 (oral squamous cell carcinoma) tumors were intravenously injected with 10 and 30 nmol cRGD-ZW800-1. After 4h, tumors and surrounding tissue were imaged, whereupon the mice were euthanized. Images were made with the IVIS, the Pearl® Impulse small animal imager, and the clinically validated FLARE™ imaging system. Biodistribution was studied by imaging the removed organs after euthanasia (4h and 24h after injection). Pharmacokinetics were studied in mice using the fluorescence signal in blood to estimate the concentration. Toxicology studies were performed in rats by injecting 100 and 300 times the anticipated human dose.

Results

cGMP synthesis resulted in a 99% pure product. In vitro, internalization of cRGD–ZW800-1 in tumor cells was observed. In vivo, tumor-to-background ratio (TBR) of HT29 tumors was sufficient 4h after injection of 10 and 30 nmol cRGD–ZW800-1 (2.8 ± 0.2 and 3.4 ± 1.0, respectively). The TBR remained satisfactory up to 24h (2.0 ± 0.4 and 2.3 ± 0.5, respectively). Similar results were found in BXPC3 and OSC19 tumors. In the biodistribution study at 4h, the highest signals were found in the kidneys, followed by the tumor and the bladder. In mice, the serum half-life was approximately 30 min. Toxicology studies did not show any clinical symptoms or other abnormalities up to a dose of 15 mg/kg.

Conclusions

This study describes the preclinical workup of a novel small peptide based NIR fluorescent agent, via cGMP production, PK/PD experiments, and toxicology studies. cRGD-ZW800-1 forms a powerful tool for tumor targeting and can be applicable in a broad variety of solid tumor types. The data obtained in this study will be used for the clinical translation of cRGD-ZW800-1 with first in-human results expected by next year.

AUTHORS (LAST NAME, FIRST NAME): Handgraaf, Hein[1]; Boonstra, Martin[1]; Prevoo, Marieke[1]; Boogerd, Leonora S.[1]; Tummers, Quirijn R.[1]; Valentijn, Rob P.[2]; Kuil, Joeri[2]; Burggraaf, Jacobus[3]; Vinkenburg - van Slooten, Maaike L.[1]; Sier, Cornelis F.[1]; de Boer, Theo[4]; Bordo, Mark W.[5]; Choi, Hak Soo[6]; van de Velde, Cornelis J.[1]; Frangioni, John V.[5, 6]; Vahrmeijer, Alexander L.[1]

INSTITUTIONS (ALL):

1. Surgery, Leiden University Medical Center, Leiden, Netherlands.
2. Clinical Pharmacy and Toxicology, Leiden University Medical Center, Leiden, Netherlands.
3. Centre for Human Drug Research, Leiden, Netherlands.
4. Analytical Biochemical Laboratory, Assen, Netherlands.

5. Curadel, LLC, Worcester, MA, United States.
6. Division of Hematology/Oncology, Department of Medicine, Beth Israel Deaconess Medical Center, Boston, MA, United States.
(No Image Selected)

CONTROL ID: 2224568

TITLE: Dedicated breast PET (dbPET) the extraordinary contribution of Molecular Imaging in the assessment response to neoadjuvant therapy in breast cancer.

PRESENTER: Michel Herranz

ABSTRACT BODY:

Abstract Body: Background: Breast cancer is one of the most common cancers in women. Approximately 232,670 new cases of breast cancer (14% of all new cancer cases) and 40,000 breast cancer deaths (6,8% of all cancer deaths) are expected to occur among US women in 2014. Since 1990, breast cancer death rates have dropped by 34%. Continued progress in the control of breast cancer will require sustained and increased efforts to provide high-quality screening, diagnosis, and treatment. Recently, the MAMmography with Molecular Imaging (MAMMI) dedicated breast PET (dbPET) has emerged as an additional imaging tool for breast cancer diagnosis, clarification of complex lesions and therapy follow-up. This study is aimed to determine whether correlations exist between physiological images with 18FDG of pre, post-2-cycles and post Neoadjuvant Chemotherapy, with a predictive value of response.

Methods: Twenty-five patients, and three scan points: pre, 2 cycle and post Neoadjuvant Chemotherapy were included in this analysis A prone position high-resolution dedicated breast PET (MAMMI-dbPET) was performed 60 min after administration of 90-120 MBq of 18F-FDG. Maximum standardized uptake value (SUVmax) quantification, volume characterization, positioning in all three space-axes, distances to reference points (proximal breast limit, nipple areola complex) were registered.

Results: When treatment was successful, a significant difference was found between pre and post neoadyuvant chemotherapy status and the SUVmax ($p < 0.001$) of breast tumors. Pre Neoadjuvant (mean SUVmax, 11.4) demonstrated a significantly higher SUVmax than did post 2 cycles tumors (median SUV, 4.7) ($p= 0.025$). No statistical significant difference was found for SUVmax of post-2 cycles vs. post lesions with a mean SUVmax of 4.7 and 3.9 ($p=0.25$) respectively. A statistically significant difference was found for volume measurement of pre vs. post-2 cycles vs post Neoadjuvant therapy lesions. A clear qualitative difference by three different observers has been reported among dbPET and MRI volume characterization. A 21% of volume (measurement) discrepancies were found, always with a volume over-estimation by magnetic resonance (structural vs functional imaging). An exquisite - and unexpected- millimetric correlation with post-surgical pathology at the end of neoadjuvant theraphy has been found in dbPET images.

Conclusions: dbPET MAMMI has proven to be an excellent tool for quantification, 3D spatial localization and monitoring of neoadjuvant therapy, showing, thanks to its functional nature, earlier and better precision and accuracy than conventional techniques (MRI). Post 2-cycle and Post Neodayuvant Chemotherapy breast cancer tumors consistently display lower 18FDG uptake than pre-treatment tumors when treatment is successful. This data suggest that SUVmax measurements of 18FDG-dedicated breast PET can provide valuable information about therapy efficiency. Such an association might be of relevant importance to treatment continuity or adjustement.

AUTHORS (LAST NAME, FIRST NAME): Herranz, Michel[1]; Argibay, Sonia[2]; Dominguez, Ines[2]; Garcia-Barredo, Anais[1]; Aguiar, Pablo[2]; Ruibal, Alvaro[2]

INSTITUTIONS (ALL):

1. Molecular Imaging , University Hospital Complex, Santiago , A Coruna, Spain.
2. Nuclear Medicine, University Complex Hospital, Santiago, Spain.

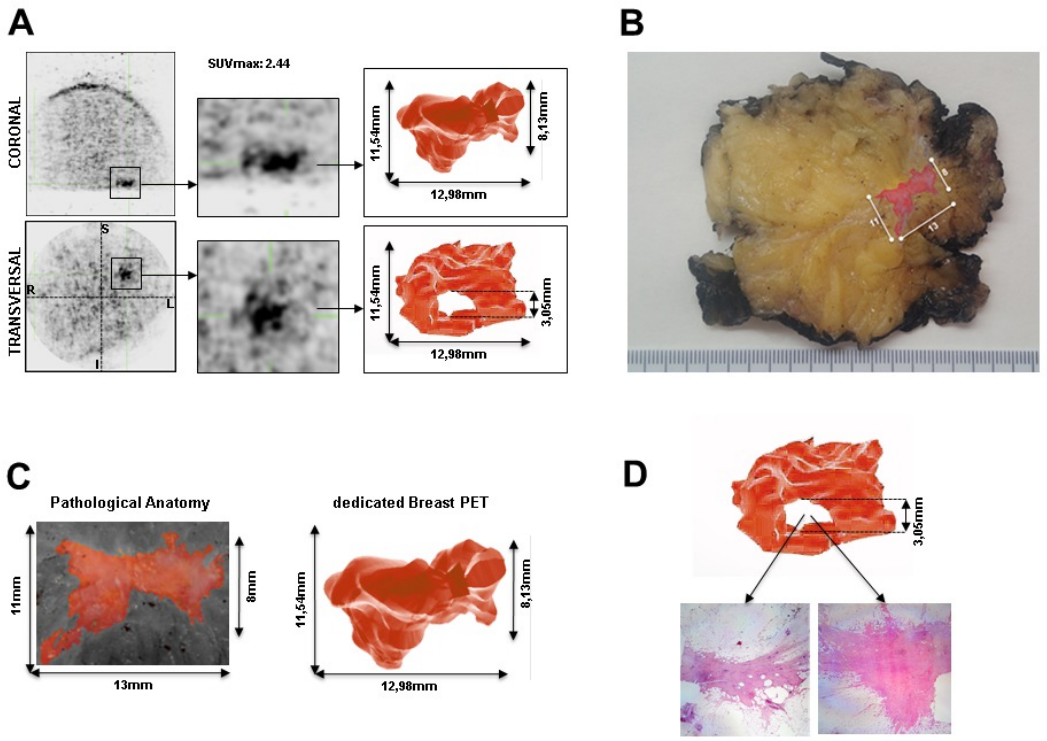
A
SUVmax: 2.44
CORONAL
TRANSVERSAL
S
R
L
I
11,54mm
8,13mm
12,98mm
11,54mm
3,05mm
12,98mm
B
C
Pathological Anatomy
dedicated Breast PET
11mm
8mm
13mm
11,54mm
8,13mm
12,98mm
D
3,05mm

CONTROL ID: 2224746

TITLE: Evaluation of CD4+ Cell Recovery *In Vivo* Using Single-Photon Emission Computed Tomography in Real Time Following $CD34^+$ Cell Transplantation in Rhesus Macaques.

PRESENTER: Robert Donahue

ABSTRACT BODY:

Abstract Body: Ionizing irradiation is used routinely to induce myeloablation and immunosuppression. However, it has not been possible to evaluate the extent of the ablation and subsequent recovery in tissues without invasive biopsy. For lymphoid recovery, investigators have had to rely on peripheral blood lymphocytes (PBLs) for analysis. PBLs, however, represent only a very small percentage of cells in lymphoid tissues (LTs). Using a combination of single-photon emission computed tomography (SPECT) and a radiotracer (^{99m}Tc-labeled rhesus IgG1 anti-CD4R1 $(Fab')_2$), we sequentially imaged CD4+ cell recovery in rhesus macaques following varying doses of total body irradiation (TBI) and reinfusion of vector transduced, autologous CD34+ cells. Eleven rhesus were used in this study. Two received a dose of 3Gy on two sequential days (3Gyx2days) of TBI (6Gy total), three received 4Gyx2days TBI, and three 5Gyx2days TBI. Two additional rhesus were evaluated several years post-transplant following 5Gyx2 days TBI, and one monkey was co-infected with SIV/SHIV lentivirus in chronic stage. For those animals transplanted, autologous CD34+ cells were immunoselected from a leukapheresis product following G-CSF and SCF mobilization over 5 days (Table 1). On the last day of TBI, CD34+ cells were reinfused after being transduced once (moi=50) with a SIV/HIV chimeric lentiviral vector expressing EGFP. SPECT/CT images were taken prior to transplant and at approximately 6, 30, 90, 150, 260 and 380 days post-TBI. Development of immunogenicity to the radiotracer was monitored using size exclusion HPLC and an *in vitro* cell binding assay. Following 3Gyx2days TBI, both animals rejected their CD34+ cell graft and developed an immune response to the radiotracer despite achieving a PBL nadir of <150 Lcs/mcL. SPECT/CT imaging revealed significant retention of CD4+ cells within LTs d.6 post-TBI (Fig. 1). At day 6 post-4Gyx2days TBI, all 3 rhesus experienced dramatic depletion of PBLs (88-95%) and CD4+ Lcs (93-97%), but SPECT imaging revealed variability in LT CD4 depletion, with more dramatic decreases observed in axillary lymph nodes (73-92%) and milder decreases in the spleen (36-40%). LT depletion was more profound in a chronically co-infected SIV/SHIV rhesus macaque. At 5Gyx2 days TBI differences in splenic depletion was more substantia l (Fig. 1). Unlike the 3Gyx2days TBI animals, no immunogenicity to the radiotracer was detected in the 4Gyx2days TBI rhesus monkeys until after d. 370-399 and 6 or 7^{th} exposure when all three animals developed an immune response to the radiotracer. No immune response has been observed so far at 5Gyx2 after one year. Our results present for the first time a sequential, real time, non-invasive method to evaluate CD4+ cell immune recovery in LTs following hematopoietic stem cell transplantation using SPECT imaging. Despite myeloablation of circulating leukocytes following TBI, total depletion of CD4+ cells in LTs such as the spleen is not achieved. The methodologies presented here have direct applications to the evaluation of immunosuppressive therapies and other immunosuppressive disorders, such as those associated with viral infections.

AUTHORS (LAST NAME, FIRST NAME): Donahue, Robert[1]; Srinivasula, Sharat[3]; Uchida, Naoya[2]; Kim, Insook[4]; St. Claire, Alexis[5]; Duralde, Gorka[5]; DeGrange, Paula[6]; St. Claire, Marisa[6]; Reba, Richard[7]; Bonifacino, Aylin[1]; Krouse, Allen[1]; Metzger, Mark[1]; Paik, Chang[8]; Lane, Clifford[9]; Tisdale, John[2]; Di Mascio, Michele[5]

INSTITUTIONS (ALL):

1. Hematology Branch, NHLBI, NIH, Bethesda, MD, United States.
2. Molecular and Clinical Hematology Branch, NHLBI, NIH, Bethesda, MD, United States.
3. Biostatistics Research Branch , Leidos Biomedical Research, Inc., FNLCR, Frederick, MD, United States.
4. Applied/Developmental Research Directorate, Frederick National Laboratory, Frederick, MD, United States.
5. Division of Clinical Research, NIAID, NIH, Bethesda, MD, United States.
6. Integrated Research Facility, NIAID, NIH, Frederick, MD, United States.
7. Center for Infectious Disease Imaging, Radiology and Imaging Sciences, CC, NIH, Bethesda, MD, United States.
8. Radiopharmaceutical Laboratory, Nuclear Medicine, Radiology and Imaging Sciences , Clinical Center, NIH, Bethesda, MD, United States.
9. Laboratory of Immunoregulation,, NIAID, NIH, Bethesda, MD, United States.

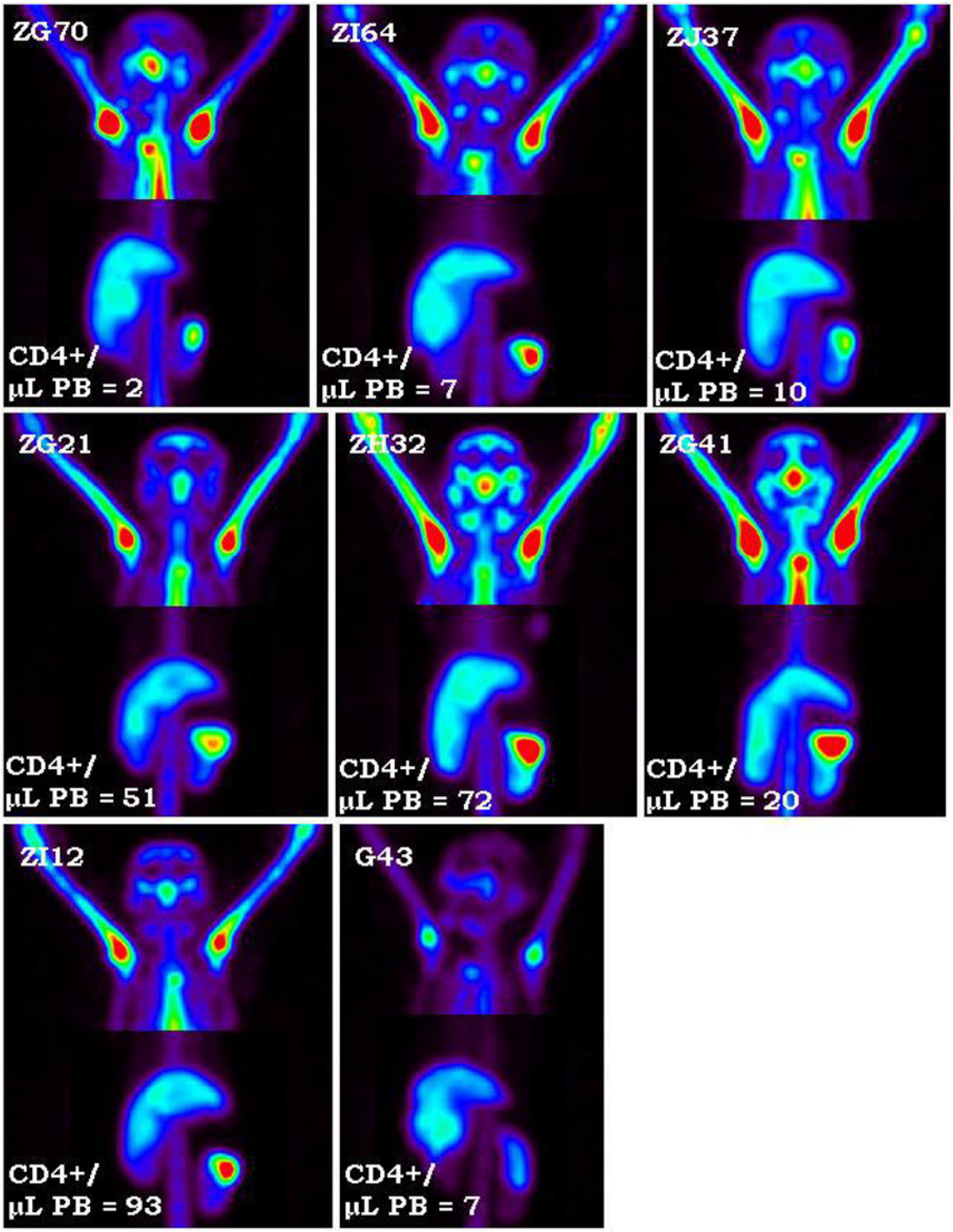

Fig. 1. SPECT maximum intensity projection images comparing 3Gyx2 (ZI12), 4Gyx2 (ZG21, ZH32, ZG41), and 5Gyx2 (ZG70, ZI64, and ZJ37) at day 6 post-TBI and a chronically infected SHIVDH12R/SIVmac239 rhesus macaque (G43). Despite low circulating levels of CD4+ cells in all animals, residual CD4+ cells remain within LTs such as the spleen following TBI.

CONTROL ID: 2224772

TITLE: Development of a Nanosponge Drug Delivery System Targeting the Pancreatic Beta Cell for Site-Directed Diabetes Therapeutics and Imaging

PRESENTER: John Virostko

ABSTRACT BODY:

Abstract Body: Approaches to deliver therapeutic agents to the insulin-producing pancreatic beta cell would have a major impact on the treatment of diabetes. Currently, there are a number of interventional strategies under development that seek to either prevent beta cell loss in type 1 diabetes or promote beta cell regeneration. However, these approaches cannot be applied because of the inability to specifically deliver these interventions to the beta cell or suffer from undesirable off-target effects on other cell types. We have developed a degradable nanoparticle, dubbed a “nanosponge”, that can sequester and solubilize therapeutics until delivery to tissues of interest [1] and adapted it to specifically target the beta cell. The glucagon-like peptide 1 (GLP-1) receptor is expressed on the beta cell and has previously been used as a target for several imaging ligands. Nanosponges were functionalized with a cysteine-40 modified exendin-4, as a targeting moiety, and the near-infrared dye iFluor750, for imaging purposes. In addition, nanosponges were specifically engineered with a size of 102nm in order to avoid hepatic clearance and accumulation in the liver, and allowing for improved bio-distribution and pharmacokinetic profile. In order to test in-vivo targeting of the derivitized nanosponges, we developed an imaging platform in which mice are engrafted with PC9 cells over-expressing the target molecule of interest, in this case the human GLP-1 receptor. After a period of engraftment, these cells develop into a discrete target rich niche. Beta cell-targeted, fluorescent nanosponges accumulated in GLP-1R expressing cell-grafts, but did not accumulate in control cell grafts lacking GLP-1R (Figure 1). Fluorescent signal in the GLP-1R expressing grafts persisted for over 48 hours. Following these initial promising results targeting GLP-1R expressing cell-grafts, we plan to assess nanosponge targeting to pancreatic islets. Therapeutic delivery of nanosponge payloads will also be evaluated in the context of diabetes relevant therapeutics.

[1] van der Ende, A., et al., *Tailored polyester nanoparticles: post-modification with dendritic transporter and targeting units via reductive amination and thiol-ene chemistry.* Soft Matter, 2009. 5(7): p. 1417-1425.

AUTHORS (LAST NAME, FIRST NAME): Virostko, John[1]; Phillips, Neil[2]; Gilmore, Kelly[3]; Beezer, Dain[3]; Harth, Eva[3]; Powers, Alvin C.[2]

INSTITUTIONS (ALL):

1. Institute of Imaging Science, Vanderbilt University, Nashville, TN, United States.
2. Department of Medicine, Vanderbilt University, Nashville, TN, United States.
3. Department of Chemistry, Vanderbilt University, Nashville, TN, United States.

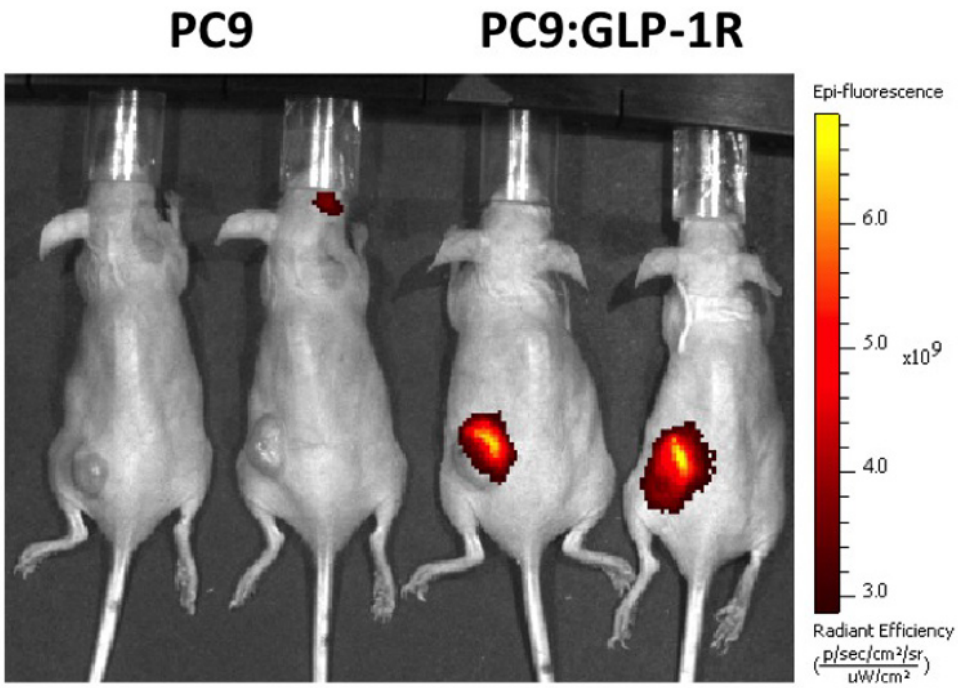

Beta cell-targeted, fluorescent nanosponges accumulate in GLP-1R expressing cell-grafts (right), but not in control cell grafts lacking GLP-1R (left).

CONTROL ID: 2224805

TITLE: Chemical Exchange Saturation Transfer (CEST) MRI of Cortical Gray Matter in Multiple Sclerosis

PRESENTER: Adrienne Dula

ABSTRACT BODY:

Abstract Body: PURPOSE: Cognitive impairment is a major manifestation seen in all subtypes of Multiple Sclerosis even more significantly, than motor function. It is estimated that cognitive dysfunction affects 40- 70% of patients with MS, typically including memory, concentration and attention, speed of processing information and executive functioning.

METHODS: Thirteen healthy subjects and two MS patients were scanned on the Philips 7T Achieva scanner. Six of the healthy subjects underwent repeat scans approximately two months after the initial scan. The protocol included two CEST scans. The first CEST acquisition included full-brain coverage (33 slices) using a 3D gradient echo with multi-shot EPI (factor = 7) readout, a 1.5 × 1.5 × 2.5 mm^3 resolution, TR/TE/flip = 65ms/7.2ms/5°, and binomial fat saturation. Saturation parameters were optimized for observation of the amide proton transfer (APT) at frequency offset of 3.5 ppm downfield (Δω=3.5ppm) resulting in a B1 = 2 μT and 25-ms duration swept between Δω= -5.0ppm to 5.0ppm with a Δω step of 0.2ppm and 14 reference (no CEST saturation, S_0) scans. The acquisition time was 9:10 min. The second CEST protocol was a single-slice (5-mm) scan optimized for observation of protons associated with glutamate and/or glutamine (gluCEST)[1] where Δω=3.0ppm. Imaging used a 2D gradient echo with multi-shot TFE (40 shots) readout with in plane resolution of 1.9 × 1.9 mm^2 on a slice located slightly superior to the corpus callosum. The CEST saturation parameters were B1 = 4.25 μT and 10-ms duration x 100 pulses at a 90% duty cycle swept between Δω= -5.0ppm to 5.0ppm, Δω step = 0.2ppm, for a total acquisition time of 11:36 min.

The CEST spectrum for each voxel is normalized, corrected and fit to a single-Lorentizian[2] and the minimum spectral intensity is shifted to an offset Δω=0ppm for B0 correction. The CEST effect from both acquisitions was quantified using both the typical asymmetry measure and the integration of the residuals of the Lorentzian fit around the resonance of interest. From a high-resolution MPRAGE acquisition, the gray and white matter were segmented and applied to the calculated CEST-derived indices.

RESULTS and DISCUSSION: CEST MRI results from 13 healthy subjects and two MS patients are shown in Figure 1. The normalized pixel frequency is shown as a function of the calculated CEST asymmetry for the resonances of 2.0 ppm (hydroxyl protons), 3.0 ppm (amine protons), and 3.5 ppm (amide protons). The black line indicates the grouped results from all healthy subjects while the red line represents an MS patient performing normally on cognitive tests. The cyan line demonstrates the CEST results of an MS patient performing significantly below the group average for the bulk of the cognitive test battery, suggesting that the measures derived from CEST MRI are reflective of differences in the biochemical environment which could be driving changes in cognitive function.

REFERENCES: 1. Cai K, et al., Nat Med. 22;18(2):302-6. 2. Jones CK, et al., NeuroImage 77:114-124.

AUTHORS (LAST NAME, FIRST NAME): Dula, Adrienne N.[1, 3]; Pawate, Siddharama[2]; Dethrage, Lindsey M.[3]; Conrad, Benjamin N.[3]; Smith, Seth A.[1, 3]

INSTITUTIONS (ALL):

1. Radiology and Radiological Sciences, Vanderbilt University Medical Center, Nashville, TN, United States.
2. Neurology, Vanderbilt University Medical Center, Nashville, TN, United States.
3. Vanderbilt University Institute of Imaging Science, Vanderbilt University Medical Center, Nashville, TN, United States.

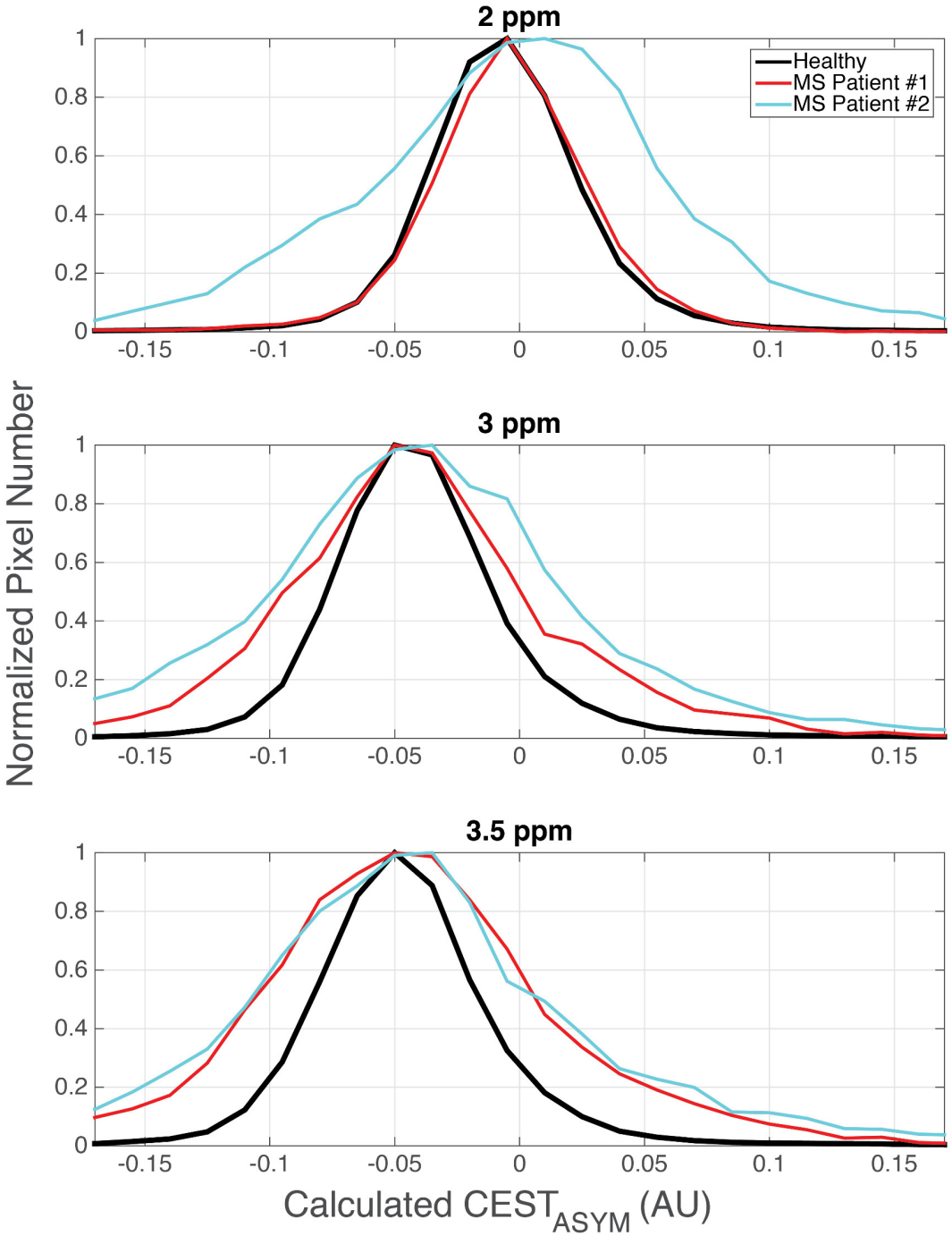
2 ppm
3 ppm
3.5 ppm
Healthy
MS Patient #1
MS Patient #2
Normalized Pixel Number
Calculated CEST$_{ASYM}$ (AU)
0
0.2
0.4
0.6
0.8
1
-0.15
-0.1
-0.05
0
0.05
0.1
0.15

CONTROL ID: 2225063

TITLE: Simultaneous and spectroscopic molecular imaging of multiple free radical intermediates using in vivo dynamic nuclear polarization-MRI

PRESENTER: Fuminori Hyodo

ABSTRACT BODY:

Abstract Body: The *in vivo* redox reaction plays a central role in living organisms. Mitochondria maintain redox homeostasis via the endogenous molecules such as flavin mononucleotide (FMN), flavin adenine dinucleotide (FAD), and coenzyme Q_{10} (CoQ_{10}), which have flavin or quinone moieties. The obligate one-electron transfer reactions convert FMN, FAD, and CoQ_{10} to the free radical intermediates FMNH and FADH, and $CoQ_{10}H$, respectively. These free radical intermediates, especially $CoQ_{10}H$, produce the superoxide anion radical, which is responsible for various oxidative diseases. The lipophilic vitamin E is a well-known antioxidant against lipid peroxidation in mitochondrial membranes[4]. Vitamin K_1, a fat-soluble derivative of 2-methyl-1,4-naphtoquinone, is a well-known anticoagulant; vitamin K_2 is reportedly involved in redox homeostasis. Both vitamins E and K are converted to free radical intermediates upon oxidation.

In vivo ESR spectroscopy and imaging have revealed how *in vivo* redox processes are involved in oxidative stress-mediated pathologies, but the spatiotemporal resolution of ESR imaging is much less than that of magnetic resonance imaging (MRI) because of the short T_2 of free radicals. *In vivo* DNP-MRI, also called proton electron double resonance imaging (PEDRI) or Overhauser-enhanced MRI (OMRI) , is a new imaging method for observing free radical species *in vivo*. Its main advantage is its high spatiotemporal resolution, which rivals that of conventional MRI. Most studies to date have been performed via *in vivo* DNP-MRI, where obtaining sufficient image intensity requires the use of synthetic stable radicals having simple and narrow resonance lines; nevertheless, these studies have provided unique information regarding redox processes in living animals. However, the ESR spectra of most endogenous free radical intermediates, such as FMNH, FADH, $CoQ_{10}H$, and radicals of vitamin E and K, exhibit multiple hyperfine splitting and inhomogeneous broadening. The imaging of these free radicals has not previously been attempted via *in vivo* DNP-MRI. If *in vivo* DNP-MRI offered the possibility of imaging free radical intermediates, it would demonstrate the potential to add metabolic/biochemical information to anatomic images.

Herein, we present a spectroscopic free radical imaging technique using *in vivo* DNP-MRI, which enables the imaging of multiple free radical intermediates that exhibit multiple hyperfine splitting and broad ESR spectra. DNP-MRI can simultaneously visualize and identify various endogenous free radical intermediates derived from redox transformations.

AUTHORS (LAST NAME, FIRST NAME): Hyodo, Fuminori[1]; Ito, Shinji[1]; Eto, Hinako[1]; Nakaji, Tomoko[1]; Yasukawa, Keiji[1]; Kobayashi, Ryoma[1]; Utsumi, Hideo[1]

INSTITUTIONS (ALL):

1. Kyushu Univ., Fukuoka, Japan.

(No Image Selected)

CONTROL ID: 2225523

TITLE: Molecular MRI With Engineered Physiology Enables High-Sensitivity Brain Imaging *In Vivo*

PRESENTER: Adrian Slusarczyk

ABSTRACT BODY:

Abstract Body: *In vivo* imaging of specific molecular activities across whole brains with high sensitivity and minimal invasiveness holds tremendous promise for earlier diagnosis of neurodegenerative disease, more effective drug evaluation, and for basic neuroscience, but it remains constrained by limitations of the available probes. MRI offers deeper tissue penetration than optical modalities and higher spatial resolution than radioactive probes, but current molecular MRI contrast agents require high concentrations in the micromolar to millimolar range for detection[1]. Techniques such as MRI with nuclear hyperpolarization[2] and accoustic imaging[3] resolve some challenges, but introduce other complications for imaging and for molecular probe design.

We present a conceptually novel molecular imaging approach which circumvents current limitations by relaying a molecular signal of interest into an evoked physiological response. We designed and validated molecular sensors which artificially actuate hemodynamic responses upon analyte detection, thus perturbing an endogenous source of abundant magnetic contrast. This decouples the concentration requirement for analyte and probe from the concentration requirement for MR detection and allows BOLD MRI detection of the probe in the low nanomolar range, *i.e.* below the intra-brain concentrations achievable for exogenous proteins via noninvasive delivery across the BBB[4].

Calcitonin gene-related peptide (CGRP)[5] is the most potent known human vasodilatory peptide. We conjectured that it could serve as the basis for peptidic probes that enable highly sensitive detection of specific molecular analytes with blood oxygenation-level dependent (BOLD) MRI. We demonstrated that nanomolar concentrations of exogenous CGRP evoke vasodilatory responses in the brains of live rats that can be readily imaged by BOLD MRI and other modalities, and that CGRP-evoked responses can be pharmacologically separated from NO-mediated BOLD contrast changes due to conventional neural stimulation. We further showed that caged variants of CGRP can serve as sensors for clinically and biotechnologically important proteases, with a ~250-fold improvement in potency upon cleavage by the protease of interest. We validated CGRP-based protease sensors *in vivo* by injection of nanomolar concentrations into the brains of live rats and BOLD MRI detection of their activity.

Our results demonstrate that vasoactive molecular MRI probes can detect specific biochemical events *in vivo* at sensor concentrations several orders of magnitude lower than for existing molecular MRI agents. We anticipate that imaging with engineered physiological responses will generalize to arbitrary analytes, allow for nonvasive sensor delivery across the BBB, and enable unprecedented *in vivo* molecular insights for biomedicine and neuroscience.

[1] VS Lelyveld, T Atanasijevic, A Jasanoff: *Int J Imaging Syst Technol* **20**, 71-79 (2010)
[2] A Viale, S Aime: *Curr Op Chem Biol* **14,** 90-6 (2010)
[3] J Yao, LV Wang: *IEEE Photonics J* **6**, 0701006 (2014)
[4] WM Pardridge, RJ Boado: *Meth Enzymol* **503**, 269-92 (2012)
[5] SD Brain, AD Grant: *Physiol Rev* **84**, 903-34 (2004)

AUTHORS (LAST NAME, FIRST NAME): Slusarczyk, Adrian L.[1]; Desai, Mitul[1]; Chapin, Ashley[1]; Barch, Mariya[1]; Jasanoff, Alan[1, 2]

INSTITUTIONS (ALL):
1. Biological Engineering, MIT, Cambridge, MA, United States.
2. Brain and Cognitive Sciences, MIT, Cambridge, MA, United States.

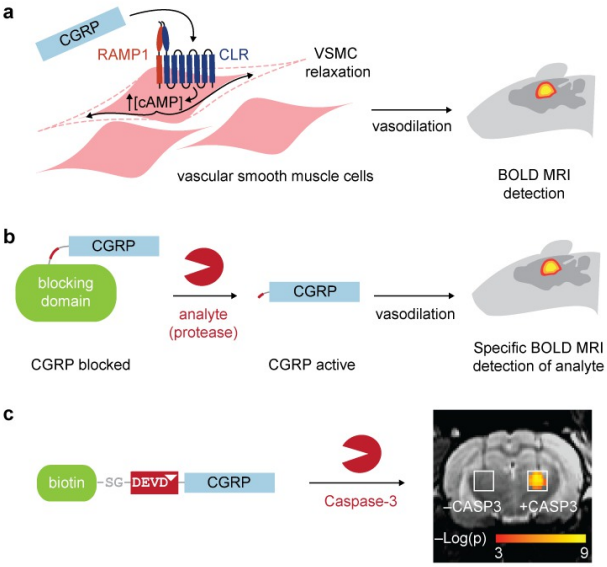

Molecular neuroimaging with evoked hemodynamic responses.

a) CGRP causes vasodilation by acting on a hetordimeric Class B GPCR, CLR:RAMP1, on the surface of vascular smooth muscle cells. Consequent elevation of cellular cAMP causes muscle relaxation and vasodilation, which is detectable by BOLD MRI and other modalities.

b) Design of molecular imaging probes for specific analytes based on CGRP, as exemplified by protease sensors. CGRP is fused to a blocking moiety via a cleavable linker. The blocking domain sterically interferes with CGRP receptor engagement; analyte-mediated cleavage liberates CGRP and gives rise to vasodilation and BOLD MRI contrast change.

c) Example of a molecular sensor for caspase-3 activity based on the design in (b) and validation in live rats. The caspase-3 probe is comprised of biotin as a blocking domain (green), a short linker (gray), a caspase-3 recognition site (red), and human CGRP (blue). Cleavage by caspase liberates CGRP and restores its potency. 100 nM of this sensor injected in the presence but not in the absence of caspase-3 evokes a strong BOLD MRI contrast change.

CONTROL ID: 2232400

TITLE: Noninvasive Imaging of Tuberculosis-Associated Neuroinflammation with Radioiodinated DPA-713 in an In Vivo Pediatric Rabbit Model

PRESENTER: Elizabeth Tucker

ABSTRACT BODY:

Abstract Body: Background:

Central nervous system (CNS) tuberculosis (TB), an extra-pulmonary form of TB, is a devastating disease that disproportionately affects young children. Extra-pulmonary TB is difficult to diagnose and CNS-TB is fatal without treatment. *Mycobacterium tuberculosis* (*M.tb*) preferentially infects microglial cells, the predominant immune cells of the brain. Due to the prolonged duration of therapy and inadequate tools for diagnosis/therapy monitoring, non-invasive imaging modalities could serve as excellent tools to monitor current or novel treatments for CNS-TB. Radioiodinated DPA-713, a synthetic ligand of TSPO, is highly expressed in activated microglia and macrophages, and has also been used to image tuberculosis-associated pulmonary inflammation (Foss et al JID 2013). We established a pediatric CNS-TB model using newborn rabbits and used [^{124}I] DPA-713 positron emission tomography (PET) to correlate the neuropathogenesis.

Objective:

To noninvasively demonstrate tuberculosis-associated neuroinflammation in a pediatric rabbit model.

Methods:

Neuroinflammation in newborn rabbits were established by injecting live *M.tb* (*H37Rv*) into the subarachnoid space. To determine TB associated neuroinflammation-(i) microglial activation (Iba-1) and cytokine analysis (TNF-α) was performed, (ii) Non-invasive imaging using [^{124}I] DPA-713 PET / computed tomography was performed in live animals within air-tight bio-containment devices. Neurobehavioral studies were conducted for cognitive/maturational deficits.

Results:

We demonstrated robust microglia activation (Iba-1) around the infection foci with a prominent tuberculoma in the brain as early as 14 days post-infection in the pediatric CNS-TB model. Bacterial burden in the brains were 2.76 $\log_{10}$ ±1 and 5.93 $\log_{10}$ ±0.59 colony forming units on day 1 and day 14 post infection respectively. Three weeks after infection, animals were imaged 1, 24 and 48 hours after an intravenous injection of 16.24MBq of [^{124}I] DPA-713 (3D Imaging, Maumelle, AR). Signal-to-noise was optimal at 48 hours after injection and PET imaging demonstrated accumulation of [^{124}I] DPA-713 in the tuberculoma with minimal accumulation in the brains of uninfected (control) animals. Maturation and cognitive testing demonstrate delayed ability to hop and eye opening in *M.tb*-infected kits.

Conclusions:

Pediatric CNS TB infection results in robust microglial activation and radioiodinated DPA-713 accumulates specifically in tuberculomas and correlates with neuroinflammation seen on gross pathology and histologically. Non-invasive radioiodinated DPA-713 imaging could be used to monitor disease progression as well as treatment responses in CNS-TB, a devastating disease and the most serious form of TB.

This work was funded by the NIH Director's Transformative Research R01-EB020539 (S.K.J.), New Innovator Award DP2-OD006492 (S.K.J.) and NIH R01HD069562 (S.K.).

AUTHORS (LAST NAME, FIRST NAME): Tucker, Elizabeth W.[1]; Pokkali, Supriya[2, 3]; DeMarco, Vincent P.[2, 3]; Klunk, Mariah[2, 3]; Zhang, Zhi[1, 5]; Nance, Elizabeth[1, 5]; Foss, Catherine A.[3, 4]; Kannan, Sujatha[1, 5]; Jain, Sanjay K.[6, 3]

INSTITUTIONS (ALL):

1. ACCM, Johns Hopkins University School of Medicine, Baltimore, MD, United States.
2. Center for Tuberculosis Research, Johns Hopkins University School of Medicine, Baltimore, MD, United States.
3. Center for Infection and Inflammation Imaging Research, Johns Hopkins University School of Medicine, Baltimore, MD, United States.

4. Russell H. Morgan Department of Radiology and Radiological Science, Johns Hopkins University School of Medicine, Baltimore, MD, United States.
5. Center for Nanomedicine, Johns Hopkins University School of Medicine, Baltimore, MD, United States.
6. Center for Tuberculosis Research, Johns Hopkins University School of Medicine, Baltimore, MD, United States.

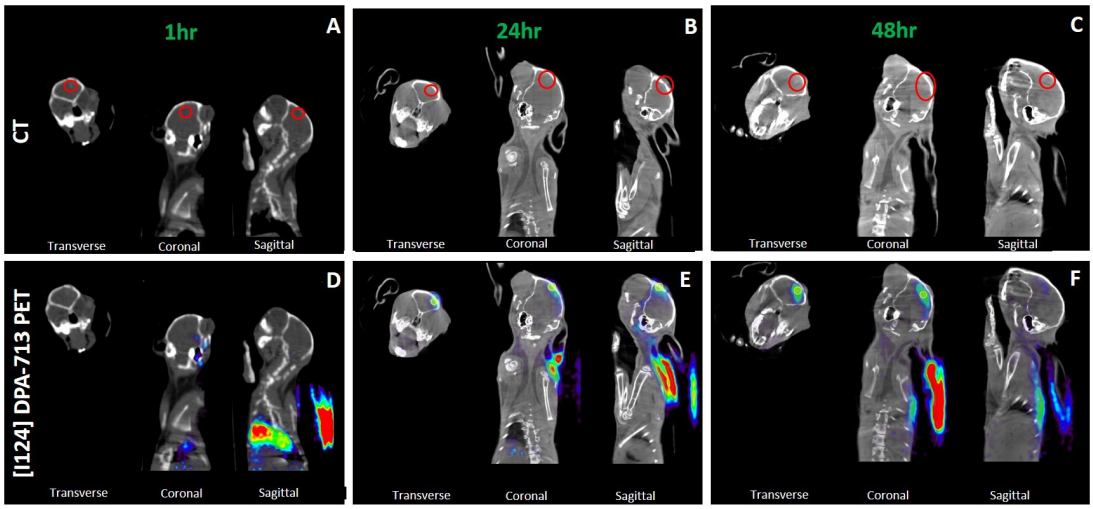

M.tb-infected rabbit at 1hr, 24hr and 48hrs post-tracer injection CT imaging (**A**, **B**, and **C** respectively) shows non-specific changes (red circles) associated with inflammatory exudate and tuberculoma formation on gross pathology. Coregistered [^{124}I] DPA-713 PET/CT (**D**, **E**, and **F** respectively) PET signal is noted at the site of the TB granuloma in the infected animal with optimal signal-to-noise ratio at 48 hours after tracer injection (panel **F**). Signal is also noted at the site of intravenous injection (ear vein).

CONTROL ID: 2225596

TITLE: Mass Spectrometry Imaging as a novel tool for monitoring the effects of 11β-hydroxysteroid dehydrogenase-1 deficiency and inhibition on region-specific glucocorticoid regeneration in mouse brain using stable isotope tracers

PRESENTER: Diego Cobice

ABSTRACT BODY:

Abstract Body: Introduction:

11β-Hydroxysteroid dehydrogenase type 1 (11β-HSD1) catalyses the glucocorticoids activation. It is an important tissue-specific regulator of glucocorticoid action in brain, liver, and adipose. However, key questions remain about the 11β-HSD1 expression patterns in the brain and consequences for local steroid regeneration.

Here, Mass Spectrometry Imaging has been used to measure the contribution of 11β-HSD1 to regional glucocorticoid regeneration in mice using a stable isotope tracer, 9,11,12,12[^{2}H]$_4$-cortisol (d_4F). This tracer is metabolised to d_3-cortisone with loss of the 11d and the subsequent formation of d_3F (labelled at 9,12,12), in vivo indicates reductase activity of 11β-HSD1.

Material and Methods:

Firstly, (male, 12 weeks) wild-type C57BL6/j mice or mice with targeted disruption of 11β-HSD1 (HSD1-KO) mice were infused with d_4F 1.75 mg/day for 6, 24 and 48h. C57BL6/j mice, infused with d_4F for 48h, were also studied 1, 2, 4h after administration (HPD) of an 11β-HSD1 inhibitor (UE2316; 25 mg/kg oral) or vehicle (n=3/group). Mass spectral images in brain sections (10μm) were obtained using a 12T MALDI-FTICRMS in positive ion at 150μm spatial resolution. Tissue glucocorticoid generation was assessed by rate of formation of d_3F and expressed as delta tracer:tracee ratio (ΔTTR d_4F/d_3F, corrected from plasma levels). Data are mean±SEM, *p<0.05.

Results:

d_4F was detected after 6h infusion except in adipose (48h). d_3F was detected at 6h in plasma and liver, 24h in brain, primarily in cortex, hippocampus and amygdala and 48h in adipose. The spatial distribution of d_3F generation in brain by MSI closely mapped 11β-HSD1 localization. In liver, generation of d_3F was detected, with a difference in d_4F/d_3F ratios of (ΔTTR* 0.18±0.03 (6h), 0.27±0.05 (24h) and 0.38±0.04 (48h)). A difference in TTR was also detected in the brain (ΔTTR* 0.09±0.03 (24h), 0.13±0.04 (48h)), with no detectable regeneration in adipose.

In HSD1-KO mice, d_3F was not detected, suggesting that 11β-HSD1 is the only enzyme carrying out d_3F generation. A similar pattern was seen after pharmacological inhibition. Plasma UE2316 peaked at 2h and declined by 4h, with same pattern in liver and brain. At 2HPD, the ΔTTR were lower compared with vehicle, in the liver (0.27± 0.08* vs. 0.45± 0.04) and brain (0.11± 0.02* vs. 0.19± 0.04), indicating less d_3F generation. In liver degree of inhibition paralleled circulating drug concentration, with ΔTTR returning to normal by 4HPD (0.38± 0.06). ΔTTR had not normalised 4HPD in brain (0.12± 0.02*), suggesting buffering of this pool. In adipose, UE2316 was not detected and TTR was not altered. Two potential phase I CYP450 metabolites were identified in the brain differing in spatial distribution.

Conclusion:

MALDI-FTICR-MSI is a powerful novel tool to assess region-specific turnover of glucocorticoids by 11β-HSD1 in murine brain. We have demonstrated its utility for measuring pharmacodynamic effects of small molecule inhibitors of 11β-HSD1; in combination with pharmacokinetic imaging, this will facilitate screening of the disposition of such drugs being developed to treat Alzheimer's disease.

AUTHORS (LAST NAME, FIRST NAME): Cobice, Diego F.[1]; Livingstone, Dawn E.[1]; McBride, Andrew[1]; MacKay, Logan[2]; Goodwin, Richard[3]; Webster, Scott P.[1]; Walker, Brian R.[1]; Andrew, Ruth[1]

INSTITUTIONS (ALL):

1. British Heart Foundation Centre for Cardiovascular Science, University of Edinburgh, Edinburgh, United Kingdom.
2. Chemistry, "Scottish Instrumentation and Resource Centre for Advanced Mass Spectrometry", Edinburgh, United Kingdom.
3. Drug Safety & Metabolism DMPK, AstraZeneca, Cambridge, United Kingdom.

(No Image Selected)

CONTROL ID: 2225620

TITLE: Molecular Imaging of Cancer Immunotherapy using Activated Antigen Presenting by Multivalent Polymer Nanocomplex

PRESENTER: Sun-Young Kim

ABSTRACT BODY:

Abstract Body: In this work, we designed and synthesized linear polymer-based nanoconjugates and nanocomplex bearing multivalent immunostimulatory ligands and also demonstrated that the synthetic multivalent nanocomplex led to the enhanced stimulation of immune cells in vitro and anti-tumor and systemic immune memory response in vivo. The authors have developed hyaluronic acid (HA)-based multivalent nanoconjugate and nanocomplex for enhanced immunostimulation through the combination of multivalent immune adjuvants with CpG ODNs (as a TLR9 ligand) and cationic poly(l-lysine) (PLL) (for the enhancement of cellular uptake). The multivalent HA-CpG nanoconjugate efficiently stimulated antigen-presenting cells and the multivalent PLL/HA-CpG nanocomplex also resulted in enhanced cellular uptake as well as continuous stimulation of endosomal TLR9. We examined the cellular internalization and uptake of the multivalent HA-CpG nanoconjugates and the PLL/HA-CpG nanocomplexes in BMDCs and RAW264.7 cells by fluorescence microscopy using CpG ODN labeled with the fluorophore FITC. To assess the migration of maturing DCs to the lymph node, we employed in vivo tracking of DCs to the lymph nodes using a near-infrared (NIR) optical imaging system. The DCs treated with the polymer nanocomplex and indocyanine green (ICG) were injected into the footpads of mice. Based on the NIR signals detected in the popliteal lymph nodes, we have evaluated the maturation and activation of DCs.The mice vaccinated with dendritic cells treated with the multivalent nanocomplex exhibited tumor growth inhibition as well as a strong anti-tumor memory response.

AUTHORS (LAST NAME, FIRST NAME): Kim, Sun-Young[2]; Cho, Sun-Hee[2]; Song, Chanyoung[1]; REN, Long[2]; Muhammad, Abrar[2]; Lim, yong T.[2]

INSTITUTIONS (ALL):

1. Sungkyunkwan University, Suwon-si, Gyeonggi-do, Korea (the Republic of).
2. SKKU Advanced Institute of Nanotechnology, Sungkyunkwan University, Suwon, Korea (the Republic of).

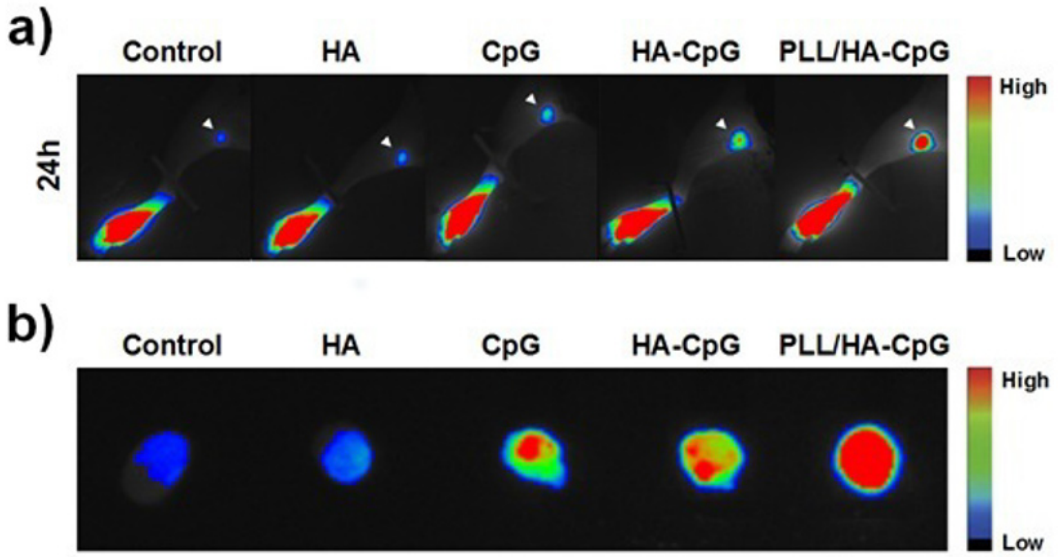

Figure 3. *In vivo* anti-tumor and memory response. a) *In vivo* tracking of DC migration to lymph nodes. NIR imaging of BMDCs treated with the indicated materials at 24 h after injection into the left footpads of mice (triangle: lymph node). b) NIR images of a dissected popliteal lymph node at 48 h.

CONTROL ID: 2231006

TITLE: Fluorescence Optical Imaging-based Evaluation of the Activation of Dendritic Cells by Protein Nanoparticles

PRESENTER: Chanyoung Song

ABSTRACT BODY:

Abstract Body: In this study, we evaluated the activation of dendritic cells (DCs) by soluble ovalbumin (OVA) and OVA nanoparticles using fluorescence optical imaging technique. Because OVA are glycoproteins and known to be sufficient immunogenic, they have been widely used as model proteins in immunology fields. Due to their low cell uptake efficiency, however, they were usually encapsulated into poly (lactic-co-glycolic acid) nanoparticles. The use of organic solvent during the synthesis of poly (lactic-co-glycolic acid) nanoparticles had an effect on antigenic properties of OVA. Here, we have fabricated OVA protein nanoparticles using desolvation method and their size ranged from 500 to 1000 nm. We used DQ-OVA and FITC-OVA to investigate the cell uptake and antigen processing of OVA in DCs. DQ-OVA is self-quenched conjugate of ovalbumin that exhibit bright green fluorescence upon proteolytic degradation and has been used as a fluorescence marker to check the antigen processing of OVA in DCs. Based on the fluorescence microscope image analysis, we have confirmed that more green fluorescence signal was detected in DCs treated with OVA nanoparticles rather than that treated with soluble OVA. The experimental results suggest that more OVA are delivered into DCs and processed efficiently when OVA nanoparticles were used as antigen source. Through the FACS analysis on the expression of MHC class I molecules, we could also verify the excellent immunogenicity of OVA nanoparticles. CD8+ OVA 1.3 T cells were stimulated by MHC class I molecule of bone marrow dendritic cells (BMDCs) and secreted Interleukin-2 (IL-2). The levels of IL-2 and MHC class I molecule expression value in BMDCs treated with OVA nanoparticles were 1.5-fold, and 10-fold higher than those treated with soluble OVA. Through the fluorescence optical imaging technique (fluorescence microscope and FACS analysis), we found that the OVA nanoparticles had great immunogenicity and mediated antigen cross-presentation by MHC class I pathway.

AUTHORS (LAST NAME, FIRST NAME): Song, Chanyoung[1]; Kim, Sun-Young[2]; Muhammad, Abrar[3]; REN, Long[4]; Cho, Sun-Hee[5]; Lim, yong T.[6]

INSTITUTIONS (ALL):

1. Sungkyunkwan University, Suwon-si, Gyeonggi-do, Korea (the Republic of).
2. SKKU Advanced Institute of Nanotechnology, Sungkyunkwan University, Suwon, Korea (the Republic of).
3. SAINT, Sungkyunkwan Univ., Suwon, Pakistan.
4. SAINT, Sungkyunkwan Univ., Suwon, Korea (the Republic of).
5. SAINT, Sungkyunkwan univ., Suwon, Korea (the Republic of).
6. Sungkyunkwan univ, Suwon, Korea (the Republic of).

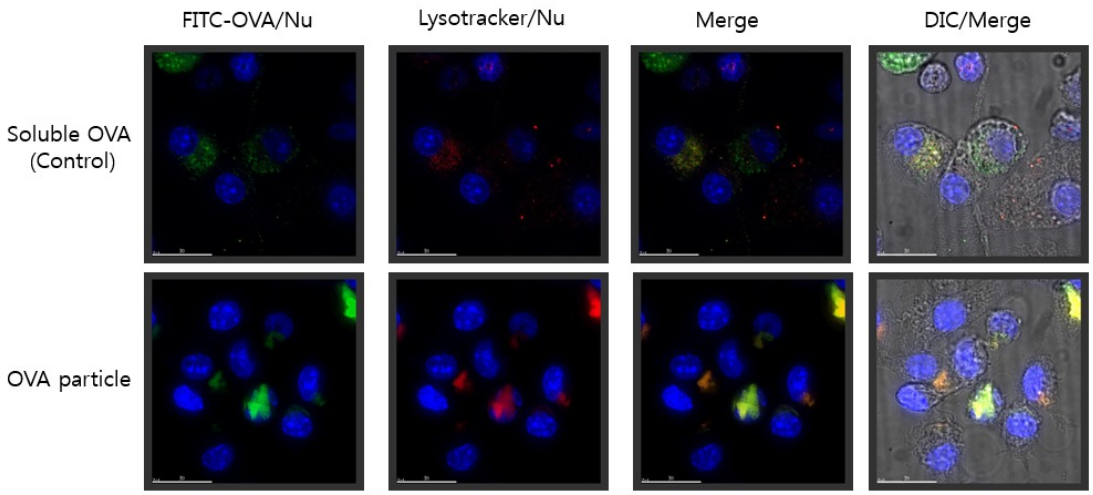
FITC-OVA/Nu
Lysotracker/Nu
Merge
DIC/Merge
Soluble OVA
(Control)
OVA particle

CONTROL ID: 2225739

TITLE: Synthesis and biological evaluation of a novel ^{18}F-labelled tetrazine for bioorthogonal chemistry

PRESENTER: Outi Keinänen

ABSTRACT BODY:

Abstract Body: Objectives: Phenyl substituted 1,2,4,5-tetrazines have exhibited the fastest reaction kinetics towards the most commonly used dienophiles in bioorthogonal reactions. We have developed an efficient synthesis method for preparation of a novel ^{18}F-labelled phenyl tetrazine, (*E*/*Z*)-N-(4-(1,2,4,5-tetrazin-3-yl)benzyl)-2-(((5-fluoro-2,3,4-trihydroxypentylidene)amino)oxy)acetamide ([^{18}F]TAF, compound **1** in Figure 1).

Methods: Compound (4-(1,2,4,5-tetrazin-3-yl)phenyl)methanamine was functionalized with an aminooxy functional group which has high reactivity towards aldose sugars, aldehydes and ketones. ^{18}F-labelling was achieved under mild reaction conditions with 5-deoxy-5-[^{18}F]fluororibose-based conjugation[1],[2]. Reactivity of [^{19}F]TAF was determined with several different dienophiles in methanol at r.t: *trans*-cyclooctenol (TCO-OH), (1*R*,8*S*,9*s*)-bicyclo[6.1.0]non-4-yn-9-ylmethanol (BCN-OH) and *exo*-5-norbornene-2-methanol (E5N2M). With TCO-OH the reaction kinetics were measured also in mouse plasma (in 50% PBS) at 37 °C. *In vitro* stability of [^{18}F]TAF in PBS (pH 7.41) at r.t and in mouse plasma (in 50% PBS) at 37 °C were assessed by HPLC. Lipophilicity of [^{18}F]TAF was determined with the shake flask method at pH 7.41. The biodistribution of [^{18}F]TAF was determined in BALB/c male mice at 4 time points in triplicate after *i.v.* administration of 3.0±1.2 MBq (specific radioactivity 12-16 GBq/μmol).

Results: [^{18}F]TAF was synthesized in more than 50% decay-corrected yield (n=5). The total duration of the synthesis was 2 hours. Radiochemical purity was ˃99% and the specific radioactivity varied between 12-70 GBq/μmol. TAF has an imine double bond and exists as *E*/*Z* isomers (*E*:*Z* = 3:1). In methanol the second-order rate constants (k_2) with TCO-OH, BCN-OH and E5N2M were 300±9 $M^{-1}s^{-1}$, 129±4 $M^{-1}s^{-1}$ and 0.35±0.04 $M^{-1}s^{-1}$, respectively. In mouse plasma k_2 with TCO-OH was 4500±400 $M^{-1}s^{-1}$. The logP values were -0.4315±0.0071 (*E*) and -0.0150±0.0174 (*Z*). The [^{18}F]TAF isomers have no difference in their stability in PBS or mouse plasma (50% in PBS). The proportion of the intact [^{18}F]TAF in PBS after 1 h and 3 h was >99%. The proportion of the intact [^{18}F]TAF in mouse plasma (50% in PBS) after 1 h and 3 h was 96.3% and 86.2%, respectively. *Ex vivo* results are presented in Figure 1.

Conclusions: [^{18}F]TAF was successfully synthesized under mild reaction conditions with high radiochemical yield and purity. TAF showed fast reaction kinetics towards the most commonly used dienophiles for bioorthogonal chemistry and sufficient stability under physiological conditions. The tracer showed fast elimination into urine accompanied by a relatively slow excretion via the hepatobiliary route. Biodistribution of [^{18}F]TAF exhibited sufficient blood circulation time considering its intended use as an *in vivo* biorthogonal reagent. The results indicate that [^{18}F]TAF is a promising candidate for *in vivo* bioorthogonal chemistry.

Acknowledgements: Supported by the Academy of Finland (272908) and Doctoral Program in Chemistry and Molecular Science (CHEMS).

References:

[1] X. G. Li et al. *Chemical communications* 2012, *48*, 5247-5249.

[2] X. G. Li et al. *Chemical communications* 2013, *49*, 3682-3684.

AUTHORS (LAST NAME, FIRST NAME): Keinänen, Outi M.[1]; Li, Xiang-Guo[2]; Chenna, Naveen K.[3]; Lumen, Dave[1]; Sarparanta, Mirkka[1, 4]; Helariutta, Kerttuli[1]; Vuorinen, Tapani[3]; Airaksinen, Anu J.[1]

INSTITUTIONS (ALL):

1. Laboratory of Radiochemistry, University of Helsinki, Helsinki, Finland.
2. Turku PET Centre, Turku University Hospital, Turku, Finland.
3. Department of Forest Products Technology, Aalto University School of Chemical Technology, Espoo, Finland.
4. Department of Radiology and Program in Molecular Pharmacology and Chemistry, Memorial Sloan Kettering Cancer Center, New York, NY, United States.

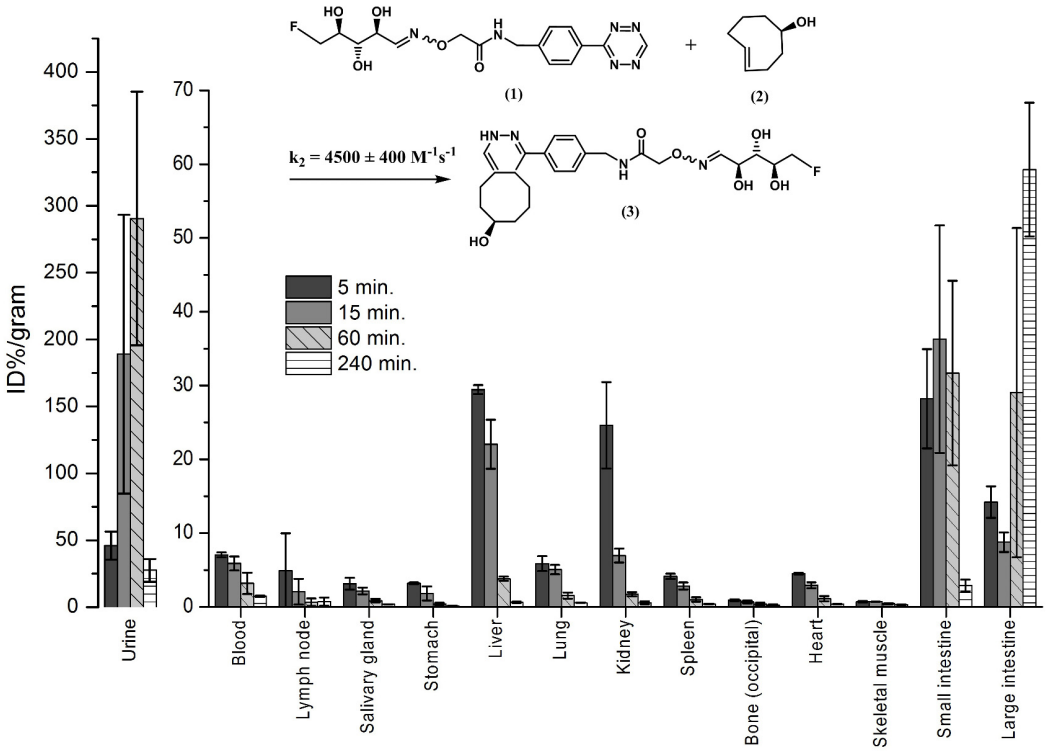

Figure 1. Click reaction between [^{18}F]TAF (**1**) and TCO-OH (**2**). Biodistribution of [^{18}F]TAF in BALB/c male mice at four time points (n=3) after *i.v.* administration of 3.0±1.2 MBq.

CONTROL ID: 2225833

TITLE: Design of a Ratiometric Fluorescent Probe Library for Specific Detection of Reactive Oxygen Species in Inflamed Intestine

PRESENTER: Diana Andina

ABSTRACT BODY:

Abstract Body: A well-established first line defense mechanism during intestinal inflammation is the oxidative burst of neutrophils. The specific detection of the reactive oxygen species (ROS) released in the gut lumen has, however, remained a challenge. A diagnostic tool aimed at monitoring ROS-rich areas quantitatively and selectively might help to understand the progress of inflammation and evaluate the efficacy of antioxidant therapies. Thus, a library of contrast agents to investigate extracellular ROS has been designed.

Our highly modular approach takes advantage of hydrocyanines to selectively detect superoxide and hydroxyl radicals [1], and a second ROS-insensitive dye (Chromis dyes, Cyanagen) to calibrate the system. Each fluorophore is conjugated to a peptidic linker, which is, additionally, connected to a complementary peptide nucleic acid (PNA) strand. Thanks to the PNA hybridization, any dye pair can virtually be combined in a single, chemically-stable contrast agent (Figure 1). In order to increase the hydrophilicity of the system and reduce the energy transfer between the fluorophores, a negatively charged peptide spacer was added between the hydrocyanine and the PNA strand. In general, Fmoc solid phase peptide synthesis coupling conditions were used for the construction of the PNA-spacer-cyanine and the hydrocyanine were obtained by a quantitative reduction step. The ROS-insensitive dye was reacted with a terminal lysine residue of the complementary PNA strand *via* NHS chemistry. Both strands were purified and fully characterized spectroscopically and by mass spectrometry. The hybridization was visualized by gel electrophoresis and high performance liquid chromatography. Furthermore, the hydrocyanines proved to be responsive to ROS in cell-free assays as well as to stimulated, differentiated Caco-2 monolayers.

Overall, a versatile platform to image ROS was designed, synthesized and tested. The strength of our approach is the flexible nature of the fluorescent probe, which enables easy adaption to experimental requirements while retaining the high selectivity for superoxide and hydroxyl radicals

[1]K. Kundu, S. F. Knight, N. Willett, S. Lee, W. R. Taylor, N. Murthy, *Angewandte Chemie* **2009**, *48*, 299-303.

AUTHORS (LAST NAME, FIRST NAME): Andina, Diana[1]; Brambilla, Davide[1]; Leroux, Jean-Christophe[1]; Luciani, Paola[1]

INSTITUTIONS (ALL):

1. Department of Chemistry and Applied Biosciences, Swiss Federal Institute of Technology Zurich (ETHZ), Zurich, Zurich, Switzerland.

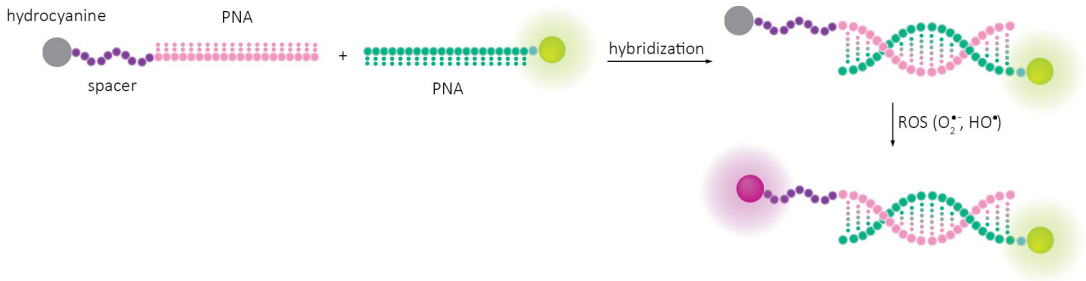

Figure 1: The basic principle of the library. A hydrocyanine-spacer-PNA is hybridized with a ROS-insensitive dye connected to the complementary PNA stand. Hydrocyanines are converted into cyanines upon encountering ROS. The ROS-insensitive dye allows to calibrate the system and to trace the probe even when there is no ROS.

CONTROL ID: 2225854
TITLE: Persistent luminescence in nanophosphors for long trem in vivo bioimaging
PRESENTER: Cyrille Richard
ABSTRACT BODY:
Abstract Body: Persistent luminescence in nanophosphors for long term *in vivo* bioimaging

E. Teston, T. Maldiney, D. Scherman, C. Richard

Unité de Technologies Chimiques et Biologiques pour la Santé; CNRS UMR 8258; Inserm U 1022; Université Paris Descartes; Chimie-ParisTech, Paris, F-75231 cedex France

Optical imaging constantly demands more sensitive tools intended for biomedical research and medical applications. However, tissue autofluorescence produces a substantial background signal that severely limits the quality of images, especially when very low concentrations of the fluorescent probe accumulate at the target site.[1]
Near-infrared persistent luminescence nanoparticles have recently been introduced in our group to enable highly sensitive *in vivo* optical detection and complete avoidance of tissue autofluorescence.[2] These nanophosphors have the ability to store the excitation light in traps, specifically introduce into the probe, and to emit light from minutes to hours after the end of the excitation.

The first generation of persistent luminescence nanophosphors pioneered by our group was a silicate which could be only excited by UV light before its injection, allowing to perform *in vivo* imaging for about 4 hours.[3] The search for new optical probes, with improved optical property, has led us to a new family of materials, a zinc gallate synthesized by a hydrothermal process. This non-toxic material has the advantage of emitting a particularly intense persistent luminescence signal situated in the infrared, after excitation through the tissues by visible photons.[4]

We will report several examples of the use of such persistent luminescence nanophosphors for *in vivo* optical imaging. We will show how this technology can be used either for tumour-targeting *in vivo*, or efficient cell tagging to track cells biological fate *in vivo*, without any acute toxicity in healthy mice.[5] We will also present our last results on bimodal optical and magnetic resonance imaging probe that can be perform with this new platform[6] and how magnetically attractable persistent luminescence nanophosphors can be prepared for preclinical applications.[7]

A novel nontoxic generation of optical nanoprobes based on red-excitable persistent luminescence nanophosphors have been prepared. Such unprecedented optical characteristics open alternatives to high sensitivity, long-term bioimaging in living animals. This technology should not only introduce and generalize persistent luminescence nanoparticles as one of the most versatile and user-friendly optical nanoprobes, but also be of wide applications to biologists and pharmacologists involved in cancer diagnosis, vascular biology, as well as cell tropism, cell homing, stem cell or cell therapy research.

References
1. G. Luo et al, Nature Communication 2012, 4:2326
2. Q. le Masne de Chermont et al, PNAS Proc. Natl. Acad. Sci. USA. 2007, 104, 9266-9271
3. T. Maldiney et al. J. Am. Chem. Soc. 2011, 133, 11810-11815
4. Patent, WOEP2013/051727
5. T. Maldiney et al. Nature Materials 2014, 13, 418-426
6. T. Maldiney et al. Adv Funct Mater 2015, 25, 331-338
7. E. Teston et al. Small 2015 in press
AUTHORS (LAST NAME, FIRST NAME): Richard, Cyrille[1]
INSTITUTIONS (ALL):
1. CNRS, Paris, France.

(No Image Selected)

CONTROL ID: 2225872

TITLE: Molecular Imaging of VCAM1 expression on the blood brain endothelium in animal model of MS

PRESENTER: Lode Goethals

ABSTRACT BODY:

Abstract Body: Introduction: The vascular endothelium of the brain has been identified as a key moderator in the maintenance of the brain microenvironment. Surface molecules, such as cell adhesion molecules (CAMs), mediate the functions of the vascular endothelium. CAMs mediate leucocyte rolling, adhesion, trans-migration across the BBB and their retention within the parenchyma during a relapse. These CAMs are rapidly up regulated in response to disease or injury. Amongst CAMs, in particular vascular cell adhesion molecule-1 (VCAM1) has been shown to be important in the development of experimental auto-immune encephalomyelitis (EAE) and multiple sclerosis (MS). Molecular imaging of this principle has been performed using MPIO labeled anti-VCAM1 antibodies. Within this study we tested our in house developed, GMP producible anti-VCAM1 nanobody, labelled with 99mTc as clinically translatable molecular imaging probe for SPECT detection and quantification of VCAM-1 expression in a mouse EAE model.

Materials and Methods: EAE was induced in 16 healthy, 11 week old, female C57bl/6 mice. Whole body triple pinhole SPECT/CT after intravenous injection of 99mTc labelled anti-VCAM1-nanobody was performed prior to induction, 7 days, 12 days, 15 days and 19 days after induction in 12 animals (EAE/VCAM1 group). All animals were scored clinically prior to scanning. 4 EAE animals underwent whole body SPECT/CT after injection of control nanobody cAbBIIc10 (EAE/cAbBIIc10 group). 4 control animals were scanned after injected with anti-VCAM1-nanobody (cô/VCAM1 group). Images were processed using AMIDE, mean activity within a ROI drawn in the brain parenchyma was calculated. After the final SPECT/CT, animals were killed and both gamma counting of all major organs and brain, together with autoradiography of brain tissue was performed.

Results: AMIDE image processing showed an increase in activity within the brain ROI, starting from 7 days, reaching a maximum from day 12 after induction, compared with baseline activity. These data corresponded with the classical evolution in clinical scoring in EAE animals. Autoradiography confirmed increased activity within the brain parenchyma of EAE/VCAM1 group compared to EAE/cAbBIIc10 and cô/VCAM1 animals. Dissection gamma counting further confirmed increased tracer binding in the brain parenchyma in EAE/VCAM1 group compared with both controls. In addition, dissection data showed significantly increased tracer binding in blood, heart, spleen and muscle samples in the EAE/VCAM1 compared with the EAE/cAbBIIc10 and the cô/VCAM1 groups.

Conclusion: Molecular imaging of VCAM1 expression in animal model of EAE showed markedly increased activity in brain tissue, but also in blood, muscle, spleen and heart samples, suggesting a widespread VCAM1 overexpression in the EAE model of MS. These findings show the feasibility of non invasively imaging VCAM1 overexpression in an EAE model of MS, using a GMP producible SPECT tracer.

AUTHORS (LAST NAME, FIRST NAME): Goethals, Lode R.[1, 4]; Van Royen, Arn [4]; Devoogdt, Nick[3]; De Geeter, Frank[4]; Lahoutte, Tony[2]

INSTITUTIONS (ALL):

1. Nuclear Medicine, Universitair Ziekenhuis Brussel, Brussel, Belgium.
2. Vrije Universiteit Brussel, Jette, Belgium.
3. ICMI, Vrije Universiteit Brussel, Brussels, Belgium.
4. In Vivo Cellular and Molecular Imaging Centre, Vrije Universiteit Brussel, Brussels, Brussels, Belgium.

(No Image Selected)

CONTROL ID: 2227599

TITLE: DCE-MRI Reveals The Role of Cellular Senescence in Placental Processing of Labeled-Albumin

PRESENTER: Marina Lysenko

ABSTRACT BODY:

Abstract Body:

Introduction

The placenta is an autonomous organ of embryonic origin intended for feeding the fetus during intrauterine life. In mammalian species with invasive placentation, including humans and mice, fusion of trophoblast-cells into a multinucleated cell layer, called the syncytiotrophoblast, is a key process of placenta morphogenesis [1]. The senescence program is regulated by complex interplay of molecular pathways where p16/19,p53 and p21 genes serve as important regulators [2] The purpose of this study was to gain an understanding of the functional role of senescence in the syncytiotrophoblast of the mammalian organism *invivo*, and to investigate whether the disruption of the senescence program leads to changes in placental functionality in mice.

Methods

Dynamic contrast enhanced (DCE) MRI was performed *in-utero* on four knockout genotypes with a C57Bl6 background: p16/p19$^{-/-}$,p16$^{-/-}$/p19$^{-/-}$;p53(+/-), p53$^{-/-}$ and p21$^{-/-}$ pregnant females mice on E14.5 (n=4) of gestation, using a 9.4 T Bruker scanner. C57Bl6 females were used as controls. T_1-weighted 3D-GE images were acquired during a 60-min period immediately following contrast-agent (biotin-BSA-Gd-DTPA,10mg/kg) administration. The mean signal intensity (SI) was derived for each placenta and for the vena-cava. Following MRI experiments, mice were euthanized and their placentas were retrieved for histological examinations.

Results

Contrast-agent administration to C57Bl6 mice produced an SI increase (3-9 min), which was followed by SI decrease (12-27 min) and then a second SI recovery 30-60 min post contrast agent injection [Fig.1B-C]. P16/p19$^{-/-}$, and p16/p19$^{-/-}$;P53$^{-/-}$ and p53-/- knockout mice had an altered SI Dynamic which resulted with reduced kinetic parameters, whereas no apparent change in the p21$^{-/-}$ mice dynamics was observed [Fig.1D]. The histological examination resulted with abnormal morphology in the labyrinth zone which appeared more cellular, had more nuclear condensation, and collapsed vasculature (arrowheads) in p16/p19$^{-/-}$, when compared to heterozygous placentas from the same litter [Fig.1E-F], p21$^{-/-}$ and WT placentas.

Discussion

The observed SI reduction in B6 mice placentas was previously demonstrated to result from the active uptake of the albumin-based contrast agent by the trophoblast cell compartment in the labyrinth [3]. This resulted in a T2* effect and a subsequent signal decrease in the T1-wighted images [Fig.1A]. The observed moderate SI reduction in the P16/p19$^{-/-}$, p16/p19$^{-/-}$;P53$^{-/-}$ and P53$^{-/-}$ knockout mice, suggests a defective cellular-uptake mechanism. The altered SI dynamics, together with the altered morphology suggests an impaired functionality that may result from abnormal placental development due to defective activation of cellular-senescence. By comparison, p21$^{-/-}$knockout analysis did not reveal any change in either the placental signal dynamics or in the histological analysis, suggesting p21$^{-/-}$KO compensational mechanisms in the placenta. These findings reveal that complex and unexplored senescence-related placental development provides a mechanism that influences both placenta morphology and functionality and can be non-invasively detected by DCE-MRI.

AUTHORS (LAST NAME, FIRST NAME): Lysenko, Marina[1]; Gal, Hilah[2]; Golani, Ofra[3]; Garbow, Joel R.[4]; Sameh, Youssef A.[5]; de Bruin, Alain[5]; Neeman, Michal[1]; Krizhanovsky, Valery[2]

INSTITUTIONS (ALL):

1. Biological Regulation , Weizmann Institute of Science, Rehovot, Israel.
2. Molecular Cell Biology, Weizmann Institute of Science, Rehovot, Israel.
3. Biological Services Unit, Weizmann Institute of Science, Rehovot, Israel.
4. Department of Surgery, Washington University in St. Louis, St. Louis, MO, United States.

5. Dutch molecular pathology center, College of veterinary medicine, Utrecht University, Utrecht , Netherlands.

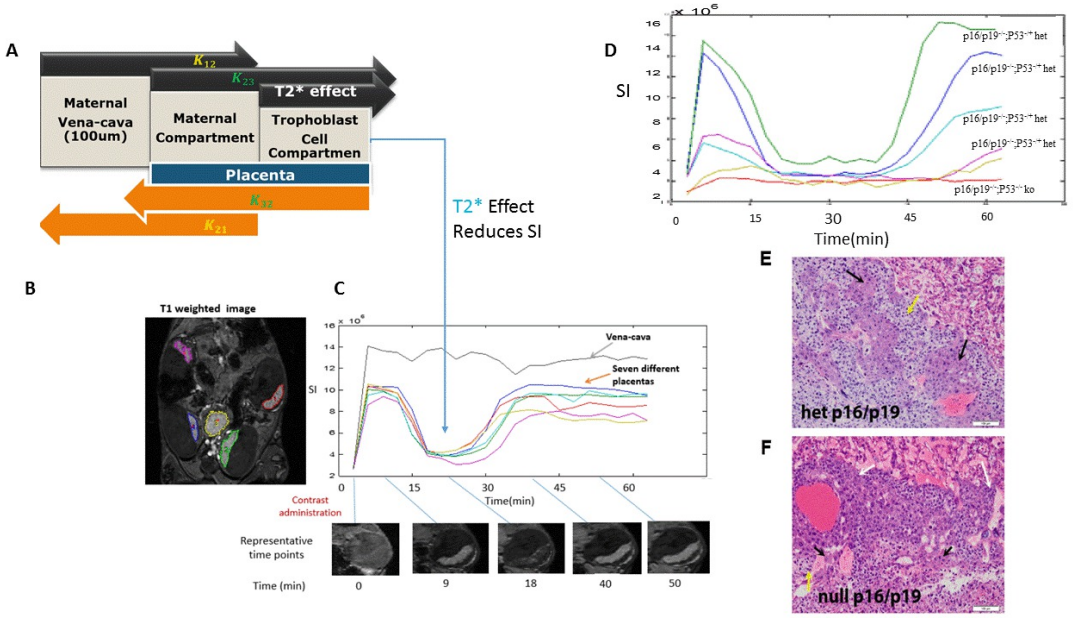

Figure 1: Altered signal intensity (SI) and compartmental composition was observed in p16/p19$^{-/-}$; P53$^{-/-}$ comparing with p16/p19$^{-/-}$; P53$^{-/+}$ and C57Bl6 E14.5 pregnant mice. (A) Suggested three-compartment model for biotin-BSA-Gd-DTPA kinetics during DCE-MRI scanning of mouse placenta. **(B-C)** Representative graph of SI calculation for seven different placentas (lower curves) and the maternal vena cava (VC, upper curve) of B6 placentas. **(D)** Representative graph of SI vs. time for six different placentas of p16/p19$^{-/-}$; P53$^{-/+}$ het and p16/p19$^{-/-}$; P53$^{-/-}$ null placentas. (E-F) H&E staining of the trophospongium zone of Het p16/p19$^{-/-}$; P53$^{-/+}$, compared with null p16/p19$^{-/-}$; P53$^{-/-}$ placentas.

CONTROL ID: 2225970

TITLE: Detection of metabolism in alginate biopsy mimics at 1T using hyperpolarized [1-^{13}C] pyruvate.

PRESENTER: Sui Seng Tee

ABSTRACT BODY:

Abstract Body: Introduction

Hyperpolarized magnetic resonance spectroscopy (MRS) using dissolution dynamic nuclear polarization (DNP) is a technique that has enhanced the sensitivity of detecting ^{13}C nuclei (Ardenkjaer-Larsen et al, 2003). This enables measurement of enzymatic fluxes non-invasively, in real-time. The most widely studied probe for DNP-MRS is [1-^{13}C] pyruvate; predominantly converted to [1-^{13}C] lactate in cancer cells catalyzed by lactate dehydrogenase (LDH). While this technique has been tested for safety in humans, it is important to understand its metabolism in human tissues, such as biopsies, to elucidate the mechanism *in vivo*. As this imaging modality is non-destructive, metabolic flux information can first be derived by DNP-MRS before sending the same specimen for further analysis using traditional methods such as histology and genomic studies.

As human tissues are scarce, it is critical to have human biopsy mimics to optimize MRS methodologies. To this end, we have developed a culture system using sodium alginate threads that are of similar dimensions to a clinical biopsy. These provide growth conditions that are more physiological than experiments performed in cell suspensions and physical dimensions that are more relevant compared to alginate beads.

Materials and Methods

UOK262 renal cancer cells were grown under standard conditions. 92 hr before imaging, cells were trypsinized, pelleted and resuspended in a sodium alginate solution in HBSS at a concentration of 1x10^{8} cells/ml. After thorough mixing, the cell suspension was extruded through a 23G needle to form threads of approximately 500um diameter. On the day of imaging, threads were wound around a custom-designed cartridge and inserted into a 5mm NMR tube placed in a 1T spectrometer (Magritek). [1-^{13}C] pyruvic acid was polarized in a SpinLab (GE) and injected into the NMR tube, as previously described (Keshari et al, 2013). Spectra were acquired using a 10^{o} excitation pulse every 10 seconds. A section of the alginate thread was fixed in 10% neutral buffered formalin for histology while the rest dissociated for trypan blue exclusion and cell counting.

Results

Visual examination of alginate threads under bright-field microscopy revealed alginate threads of approximately 50um in diameter (Fig 1A).

Histological examination of alginate threads with standard H&E (Fig 1C) and the proliferation marker Ki-67 (Fig 1D) clearly reveals the presence of proliferating cells within this 3D structure.

Administration of hyperpolarized [1-^{13}C] pyruvate resulted in the formation of [1-^{13}C] lactate (Fig 1A). Lactate formation represents metabolism of pyruvate catalyzed by LDH. The final concentration of pyruvate after dissolution was 40mM and pyruvate metabolism was facilitated by approximately 3x10^{6} cells that were in the active region of the coil.

Conclusion

Cells grown as alginate threads represent a simple method to mimic human biopsy tissue. The dimensions achieved are similar to clinical specimens and are metabolically active as evidenced using hyperpolarized MRS. Future work will compare metabolism of real human biopsies compared with alginate biopsy mimics to determine the fidelity of this model.

AUTHORS (LAST NAME, FIRST NAME): Tee, Sui Seng[1]; Truong, Steven[1]; Di Gialleonardo, Valentina[2]; Aldeborgh, Hannah N.[1]; Alvarez, Julio A.[1]; Poot, Alex J.[1]; Keshari, Kayvan R.[1]

INSTITUTIONS (ALL):

1. Memorial Sloan Kettering Cancer Center, New York, NY, United States.
2. Radiology, Memorial Sloan Kettering Cancer Center, New York, NY, United States.

(No Image Selected)

CONTROL ID: 2226205

TITLE: Imaging of immune checkpoints of PD-1 receptor expressing T cells using novel immunoPET tracer in an transgenic mouse model bearing melanoma

PRESENTER: Arutselvan Natarajan

ABSTRACT BODY:

Abstract Body: Purpose/b> It is well known that immune checkpoints play a key role in maintaining physiologic self-tolerance and have been more recently implicated in the down-regulation of anti-tumor immunity. Restoring suppressed anti-tumor immunity through immune checkpoint blockade is proving to serve as an effective immunotherapy. Many efforts are underway to develop antibody-based immune checkpoint interventions targeting the regulatory receptor programmed cell death protein 1 (PD-1) on regulatory T lymphocytes (Treg) and its ligand (PD-L1) expressed on tumor cells. Many anti PD-1 and PD-L1 antibodies have been approved by the FDA for clinical studies and are showing promising data against several tumor types. As several PD-1 targeted therapies are already on the market, there is a critical need for diagnostic and prognostic imaging tools to assess the PD-1 status of tumor infiltrating lymphocytes which will ultimately aid in determining whether a patient will benefit from immunomodulatory therapies and may help to improve patient management. Materials and Methods:/b> We have developed a novel immunoPET tracer to image PD-1 expressing effector T cells in a melanoma xenograft mouse model for the evaluation of PD-1 expressing T cells *in vivo*:/i>. We used an established transgenic mouse model which expresses GFP, luciferase and the diphtheria toxin receptor under control of the FoxP3 promoter as a marker of Treg (Foxp3.LuciDTR). Results:/b> These Foxp3.LuciDTR mice were implanted subcutaneously with B16-F10 mouse melanoma (n=10) in left shoulder and were scanned by Bioluminescence-based optical image (BLI) to detect Treg (+) cells at the tumor site (day 5, 10 and 15 post-tumor implantation) (Fig. A-B). A 64-Cu labeled anti-mouse (IgG) PD-1 immunoPET tracer was developed to detect PD-1expressing T cells by PET imaging. Quality control of the tracer showed >95% purity by HPLC and >70% immunoreactivity compared to unmodified PD1 antibody by *in vitro* /i>cell binding assay. Tumor bearing mice at day 16 after implantation (n=5) were tail-vein injected with anti-PD-1 tracer (200µCi/10µg/200µl). PET scans were performed at 1, 4, 18 and 24 h post-injection (Fig. C). PET-CT images of Treg-xenografted with melanoma mouse (1-24 h) indicated that the anti-PD-1 tracer was able to track PD-1 expressing effector T cells in tumor, thymus, and spleen (Fig. C). The tracer uptake (%ID/g ± SD, by ROI) in tumor at 1, 4, 18, and 24 h are 1.9 ± 0.5, 2.7± 0.7, 3.2 ± 0.7 and 3.5 ± 0.8.

Conclusion:/b> Comparison of the PET and BLI images suggests that we are able to image PD-1 expressing Treg cells within the tumor and lymphoid tissues with liver PET signal related to clearance of PET tracer. To the best of our knowledge, this data is the first report to image the PD-1 receptor using an immunoPET tracer to image tumor associated PD-1 expression *in living mice*. The tracer developed should be useful to image immune checkpoints in mouse models.

AUTHORS (LAST NAME, FIRST NAME): Natarajan, Arutselvan[1]; Gano, Jacob[1]; Reeves, Robert E.[1]; Gambhir, Sanjiv S.[1, 2]

INSTITUTIONS (ALL):

1. Radiology, Stanford University, Stanford, CA, United States.
2. Bioengineering, Materials Science and Engineering, Stanford University, Stanford, CA, United States.

Imaging of immune checkpoints of PD-1 receptor expressing T cells using novel immunoPET tracer in an transgenic mouse model bearing melanoma

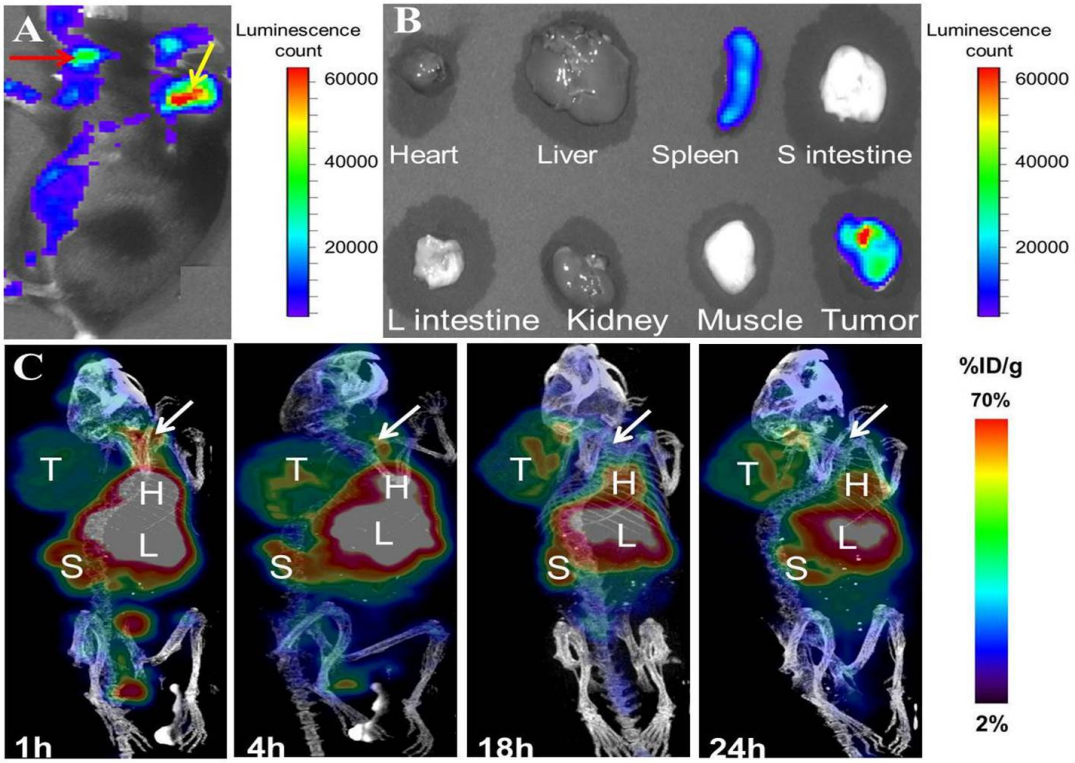

Fig A: Bioluminescence-based optical (BL) image (5 min after 4 mg of D-luciferin dose by IP, 1 min scan) of Treg transgenic mouse bearing melanoma tumor. Red arrow= thymus and Yellow arrow=tumor (16 th day post implantation).

Fig B: Representative BL image of Treg transgenic mouse bearing melanoma tumor ex-vivo organs image. Organs were dissected and kept in 200 µL of D-luciferin for 1minute and scanned for BL for 30 sec image.

Fig C: PET-CT images (1, 4, 18, 24 h) of anti-PD1 tracer [64-Cu-DOTA-mPD1 IgG antibody; 200µCi/10µg/200µl] on Treg transgenic mouse bearing melanoma tumor. T=Tumor; H= Heart; S= Spleen; L= Liver; White Arrow = Thymus.

CONTROL ID: 2231153

TITLE: [^{11}C]Methyl-JQ1; a novel PET probe for *in vivo* epigenetic imaging

PRESENTER: Kyoko Kakumoto

ABSTRACT BODY:

Abstract Body: Histone modifications play an important role in transcriptional regulation and are associated with abnormal gene expression in several diseases, such as cancer, inflammation and neuronal disorder. The bromodomain and extra-terminal domain (BET) protein family (BRD2/3/4 and BRDT) recognizes the ε-N-acetylation of lysine residues on histone tails and regulates chromatin accessibility to transcription factors. Since the expression of BET proteins have been shown to be upregulated in some cancers, inhibitors such as JQ1, which specifically inhibit the BET protein binding, have enormous potential both for the development of epigenetic anti-cancer drugs and diagnostic tools, such as PET probe.

To develop a novel PET probe for BET protein imaging, we have synthesized ^{11}C-labeled methyl-JQ1 ([^{11}C]Me-JQ1), which was designed based on computational approaches with target protein structure. Me-JQ1 showed a similar binding affinity to BET protein and pharmacological anti-cancer effects to JQ1. Cellular uptake assay showed that [^{11}C]Me-JQ1 was incorporated *in vitro* into both lung adenocarcinoma and glioma cells expressing BRD2 and BRD4 proteins. PET imaging and radio-labeled metabolites analysis with tumor bearing mouse showed that [^{11}C]Me-JQ1 was incorporated into these cancer cells-derived xenograft tumors without any degradation.

These results indicates that [^{11}C]Me-JQ1 can be effective as PET probes for imaging of BET proteins in cancer cells, and thus could be utilized for personalized cancer medicine and drug developments.

AUTHORS (LAST NAME, FIRST NAME): Kakumoto, Kyoko[1]; Mizuma, Hiroshi[1]; Sugiyama, Shimpei[1]; Mawatari, Aya[1]; Doi, Hisashi[1]; Honma, Teruki[2]; Minoda, Aki[3]; Umehara, Takashi[2]; Onoe, Hirotaka[1]

INSTITUTIONS (ALL):

1. Division of Bio-function imaging, RIKEN, Center for Life Science Techonologies (CLST), KOBE-city, Japan.
2. Division of Structural and Synthetic Biology, RIKEN, Center for Life Science Technolgies (CLST), YOKOHAMA-city, Japan.
3. Division of Genomic Technologies, RIKEN, Center for Life Science Technolgies (CLST), YOKOHAMA-city, Japan.

(No Image Selected)

CONTROL ID: 2227554

TITLE: Comparing Diffusion-Weighted Imaging and Positron Emission Tomography for Non-Small Cell Lung Cancer 1 to 3 cm

PRESENTER: Hiroaki Nomori

ABSTRACT BODY:

Abstract Body: Purposes: To examine whether diffusion-weighted magnetic resonance imaging (DWI) is as useful as fluorodeoxyglucose-positron emission tomography (FDG-PET) for discriminating between non-small cell lung cancer (NSCLC) and benign pulmonary nodules less than 3 cm, as well as for predicting tumor aggressiveness.
Methods: PET and DWI were carried out in 87 pulmonary nodules 1 to 3 cm in size (66 NSCLCs and 21 benign nodules). Signal intensity (SI) of DWI was measured by contrast ratio (CR) between lesions and spinal cord, i.e. SI-CR. Maximum standard uptake value (SUV) of PET was measured by CR between lesions and contralateral lung, i.e. SUV-CR.
Results: DWI can image NSCLC as well as PET. DWI and PET showed sensitivities of 0.86 and 0.71, and specificities of 0.90 and 0.81, respectively. While there was no significant difference in specificity between the two, DWI showed significantly higher sensitivity than PET (p=0.013). While the difference of sensitivity was significant in lung adenocarcinoma (p=0.012), there was no difference in the other histological types. Both the SI-CR and SUV-CR were significantly higher in tumors with histological invasiveness or lymphatic metastasis than in those without.
Conclusions: DWI could be useful not only to diagnose NSCLCs, especially in lung adenocarcinoma, but also to predict tumor aggressiveness as well as FDG-PET.

AUTHORS (LAST NAME, FIRST NAME): Nomori, Hiroaki[1]

INSTITUTIONS (ALL):

1. Thoracic Surgery, Kemeda Medical Center, Kamogawa, Chiba, Japan.

(No Image Selected)

CONTROL ID: 2226356

TITLE: Clinical significance of tau accumulation assessed by [^{11}C]PBB3 PET in diverse tauopathies

PRESENTER: Hitoshi Shimada

ABSTRACT BODY:

Abstract Body: Background and aims:

Tau neurofibrillary changes is considered to be a promising target for imaging and therapy in Alzheimer's disease (AD) and non-AD tauopathies such as progressive supuranuclear palsy (PSP), corticobasal syndrome (CBS) and frontotemporal dementia (FTD). In addition, some neuropathologists regard tau tangles in the brain as an inevitable consequence of aging even in cognitively healthy subjects. [^{11}C]PBB3 is a novel tau imaging PET ligand, which could visualize the tau deposition in AD and non-AD tauopathies. The aim of this study is to investigate the diagnostic utility and the clinical significance of tau PET imaging with [^{11}C]PBB3.

Methods:

Participants were 21 AD patients, 16 mild cognitive impairments (MCI) patients, ten PSP patients, nine CBS patients, six FTD patients, and 34 cognitively healthy controls (HC) consisted of 24 age-matched elderly control and 10 young HCs. We performed PET scans with [^{11}C]PBB3 and [^{11}C]Pib for imaging of tau and Aβ lesions, respectively, and metabolic radiotracer [^{18}F]FDG, along with MRI, neurological examination and psychological batteries. Voxel-based calculation of standardized uptake value ratio (SUVR) to the cerebellum was employed for quantification. We carried out a voxel-by-voxel correlation analysis between [^{11}C]PBB3 SUVR and age for Aβ-negative HC group, in order to explore brain regions exhibiting an age-related increase. We additionally performed voxel-based correlation analyses between SUVRs for each radiotracer and neuropsychological test scores.

Results:

All AD patients, ten of 16 MCI patients, one of nine CBS patient, one FTD patient, and three of 24 old HCs were Aβ-positive. Some Aβ-negative old HCs showed PBB3 uptake around medial temporal cortex. Furthermore, [^{11}C]PBB3 retention was positively correlated with age in a few areas including the bilateral medial to inferior temporal cortices in 31 Aβ-negative HCs. Distribution patterns of [^{11}C] PBB3 accumulation were different among each patient group, and [^{11}C]PBB3 uptake were observed in lesions associated with neurological symptoms in each disease. In AD spectrum, brain regions with higher [^{11}C]PBB3 binding expanded as a function of cognitive decline from Aβ-positive MCI to AD, whereas distribution of increased [^{11}C]Pib binding was unaltered. Mean cortical SUVR of [^{11}C]PBB3 was increased in Aβ-positive MCI and AD groups by 15% and 30%, respectively, relative to HCs. General clinical dementia scale was correlated with increased [^{11}C]PBB3 SUVR in extensive brain regions, and memory and frontal scores were associated with [^{11}C]PBB3 SUVR in reported functional regions in Aβ-positive MCI and AD groups. Spatial and temporal distribution of impaired [^{18}F]FDG uptake appeared to follow the increase of [^{11}C]PBB3 SUVR.

Conclusions:

Tau imaging with [^{11}C]PBB3 and PET is useful for pursuing pathological advancement from normal aging to MCI and from MCI to AD, and provides an objective index of the disease severity and molecular basis of neurologic and neuropsychological manifestations. Furthermore, Tau PET imaging using [^{11}C]PBB3 could help a differential diagnosis among HCs and a variety of AD and non-AD tauopathies.

AUTHORS (LAST NAME, FIRST NAME): Shimada, Hitoshi[1]; Suhara, Tetsuya[1]; Shinotoh, Hitoshi[1, 2]; Hirano, Shigeki[1, 3]; Yamada, Makiko[1, 4]; Kimura, Yasuyuki[1]; Sahara, Naruhiko[1]; Zhang, Ming-Rong[5]; Ito, Hiroshi[7, 6]; Kuwabara, Satoshi[3]; Higuchi, Makoto[1]

INSTITUTIONS (ALL):

1. Molecular Neuroimaging Program, Molecular Imaging Center, National Institute of Radiological Sciences, Chiba, Chiba, Japan.
2. Neurology Chiba Clinic, Chiba, Chiba, Japan.
3. Department of Neurology, Graduate School of Medicine, Chiba University, Chiba, Chiba, Japan.
4. Precursory Research for Embryonic Science and Technology, Japan Science and Technology Agency, Chiyoda-ku, Tokyo, Japan.
5. Molecular Probe Program, Molecular Imaging Center, National Institute of Radiological Sciences, Chiba, Chiba, Japan.
6. Advanced Clinical Research Center, , Fukushima Medical University, Fukushima, Fukushima, Japan.

7. Biophysics Program, Molecular Imaging Center, National Institute of Radiological Sciences, Chiba, Chiba, Japan.
(No Image Selected)

CONTROL ID: 2227062

TITLE: Synthesis, deuterium enrichment, and characterization of a novel biosensor for pH-imaging

PRESENTER: Christian Hundshammer

ABSTRACT BODY:

Abstract Body: Introduction:

pH plays an important role in many diseases, such as cancer and inflammation[1, 2]. A technique for non-invasive *in vivo* pH measurements could therefore facilitate diagnosis and benefit the monitoring of therapy in the clinic. Recently, magnetic resonance imaging based methods like CEST- pH-reporter molecules[3] and hyperpolarized ^{13}C-bicarbonate[4] have shown great potential for pH imaging. However, none of these techniques is easily translated to the clinic. Here, we present the molecular characteristics of hyperpolarized [1,5-$^{13}C_2$]zymonic acid (ZA)– a novel pH reporter for magnetic resonance spectroscopic imaging

Methods:

[1,5-$^{13}C_2$]zymonic acid was synthesized from [1-^{13}C]pyruvic acid by either acid or base catalyzed aldol condensation followed by dehydrogenation[5]. Further purification was carried out using C18 reversed phase HPLC (2% – 20% acetonitrile in water). Deuterium enrichment was achieved by a base catalyzed aldol condensation in D_2O.

4 M ZA in DMSO were doped with 15 mM trityl radical (Oxo63) and 5 mM Dotarem and hyperpolarized in a HyperSense polarizer. The dissolution was performed in 0.1 g/L EDTA and an adequate amount of NaOH in D_2O. T_1 measurements were performed on a SpinsolveCarbon benchtop NMR spectrometer (Magritek, B_0=1T) using a 10 degree flip angle and a repetition time of 3 s. Spin lattice time (T_1) decay curves were flip angle corrected and fitted by a mono-exponential decay curve.

Results and Discussion:

We synthesized non-deuterated and deuterated [1,5-$^{13}C_2$]zymonic acid in one step from [1-^{13}C]pyruvic acid, whose carboxyl carbon exhibits a long T_1 time. Its five-membered lactone ring bears a stable enol group with pKa in the physiological range (Fig. A). The deprotonation of the hydroxyl-group leads to chemical shift changes up to 4 ppm/ pH of neighboring ^{13}C atoms, which are fast on the NMR time scale (Fig. B, C).

The T_1 of $^{13}C_1$-ZA and $^{13}C_5$-ZA are pH dependent and are between 49 s and 81 s at pH<6 and pH>8. Around the pKa (6<pH<8), $^{13}C_1$ and $^{13}C_5$ exhibit T_1-values between 32 s and 53 s (Fig. C, D).

At 25 mM concentration, hyperpolarized $^{13}C_5$ of ZA has a T_1 of 50 s ± 0.1 s at pH7.0 ± 0.2. Deuterium enrichment increases the T_1 of $^{13}C_5$ of 25 mM ZA by 45 % to 72 s ± 2 s at pH7.5 ± 0.2 (n=2, data not shown).

Furthermore, the T_1 of ZA is concentration dependent and shows longest T_1-values at low concentrations most likely explained by weaker hydrogen bond formation in combination with decreased ZA concentration leading to a lower viscosity of the solution. A 12.5 mM hyperpolarized ZA solution has a T_1 of 55 s at pH 7.4 compared to 40 s for a 50 mM ZA solution at pH 7.4 (Table).

In summary we provide fundamental data for a novel pH biosensor, which has potential to be translated into the clinic.

Acknowledgements:

This work was funded by DFG (SFB824) and BMBF (FKZ 13EZ1114).

References:

[1] Schroeder, M. A. et al. (2008). PNAS. USA. **105**, 12051-12056.

[2] Gillies, R. J. et al. (2004) IEEE EMBS **23**, 57-64.

[3] Longo, D. L. et al. (2014) JACS. **136**(41), 14333-14336

[4] Gallagher, F. A. et al. (2008). Nature **453**, 940-943.

[5] Wolff, L. Liebigs Ann. Chem. (1899). **305**, 154-165.

AUTHORS (LAST NAME, FIRST NAME): Hundshammer, Christian[1, 2]; Düwel, Stephan[1, 2]; Gersch, Malte[2]; Feuerecker, Benedikt[1]; Schwaiger, Markus[1]; Glaser, Steffen[2]; Schilling, Franz[1, 2]

INSTITUTIONS (ALL):

1. Clinics and Polyclinics of Nuclear Medicine, Klinikum rechts der Isar/ Technical University Munich, München, Bavaria, Germany.

2. Department of Chemistry, Technische Universität München, Garching, Bavaria, Germany.

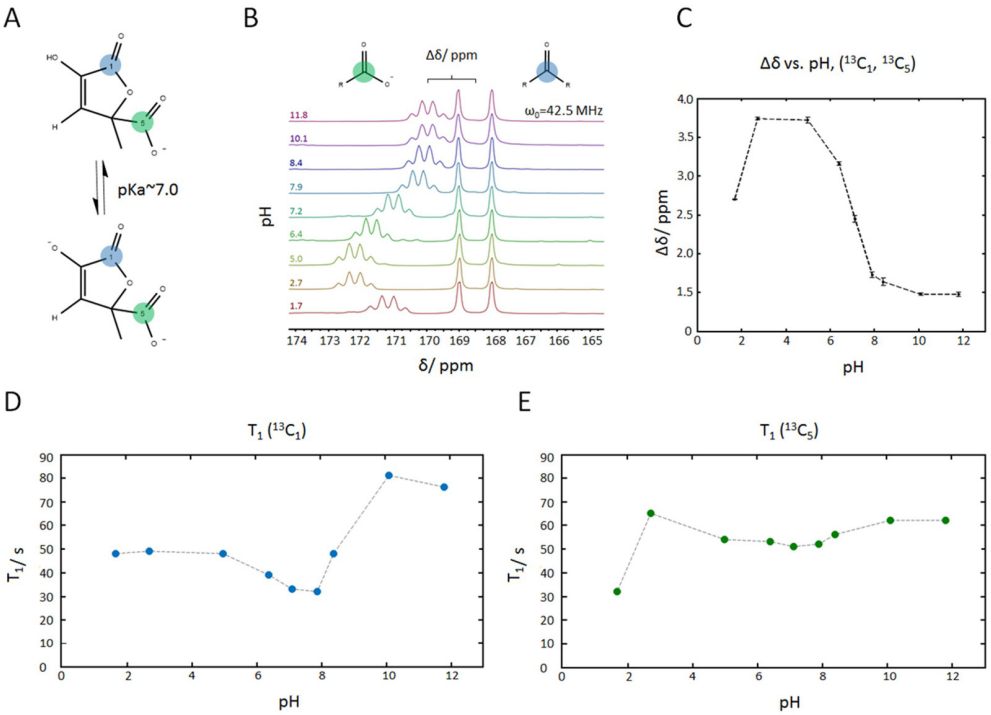

(A) Equilibrium reaction of ZA at pH~7.0. Protonation and deprotonation of the enol-hydroxyl group leads to chemical shift changes of neighbouring ^{13}C atoms. (B) Stacked spectra of hyperpolarized $^{13}C_{1,5}$ ZA at different pH. In order to allow for an easy calculation of the difference in chemical shift, all spectra were aligned by their $^{13}C_1$ resonances, even if the resonance signal of both ^{13}C labelled atoms exhibit a pH dependent chemical shift. (C) pH dependent chemical shift difference of $^{13}C_1$ and $^{13}C_5$ (n=50). (D) pH dependency of T_1 of $^{13}C_1$. Fast de- and re-protonation at pH=pKa leads to a decrease of T_1. At pH>pKa, di-anionic ZA exhibits longest T_1 due to reduced dipolar relaxation. (E) pH dependent T_1 of $^{13}C_5$ of ZA. At pH<pKa_{COOH} (~2.5), dipolar coupling between $^{13}C_5$ and the acid proton determines a short T_1. Deprotonation increases T_1 at pH~3, which decreases until pH~pka. At pH>pKa, reduced dipolar coupling of $^{13}C_5$ again increases T_1.

CONTROL ID: 2230053

TITLE: A highly efficient hyperpolarized ^{13}C xenobiotic for *in vitro* and *in vivo* evaluation of carboxylesterase activity.

PRESENTER: Federico Maisano

ABSTRACT BODY:

Abstract Body: Magnetic Resonance Spectroscopy (MRS) of ^{13}C-hyperpolarized molecules is a growing technology that is successfully applied to *in vivo* imaging of fast metabolic conversions, as those that take place in rapidly growing tumor cells. 1-^{13}C-pyruvate has been the first molecule to enter clinical trials, as a marker of lactate dehydrogenase activity in tumors [1]. Although several other endogenous moieties, such as TCA cycle substrates as well as aminoacids, have been investigated at preclinical level, many metabolic pathways remain unexplored due to lack of suitable hyperpolarized tracers. The idea of synthesizing *ad hoc* a metabolically active xenobiotic for metabolic imaging, with superior hyperpolarization features has not been exploited so far.

Carboxylesterases are a group of highly efficient, promiscuous enzymes, with rather broad specificity, often over- or under-expressed in tumor cells [2]. They are also responsible both of the detoxification of many exogenous compounds and of the activation of some chemotherapeutic prodrugs [3], *e.g.*, irinotecan and paclitaxel-2-ethylcarbonate, thus appearing as a clinically valuable target. It has been recently shown that hyperpolarized [1,3-$^{13}C_2$]ethyl acetoacetate is a useful metabolic marker of liver cancer [4], being preferentially hydrolyzed by the carboxylesterase isoform 1 (CE1).

We do now propose a novel xenobiotic molecule, namely 1,1-Cyclopropane-1-^{13}C-2,2,3,3-d_4-di(methan-d_2-ol), 1,1-diacetate (CDDA), specifically designed to probe carboxylesterase activity and optimized for MRS applications. It features very long ^{13}C longitudinal relaxation time (T_1), high solubility and very fast conversion into the corresponding monacetate (CDMA) and dimethanol (CDM) derivatives (Fig. 1).

CDDA was hyperpolarized using Dynamic Nuclear Polarization techniques under microwave irradiation at 94 GHz in a magnetic field of 3.35 T at a temperature of 1.2 K. Once the ^{13}C polarization reached an equilibrium value of 15%, the solid sample was suddenly dissolved to obtain a 3.5 mM (48 mM) solution, which was immediately used for *in vitro* (*in vivo)* assays.

The metabolic fate of CDDA was first investigated *in vitro* in a model of hepatoma (McA-RH7777). Strong signals were recorded for both the substrate and the hydrolyzed metabolites, which were readily generated by intracellular carboxylesterases. In Fig. 1 the build-up curves of the metabolites of CDDA and of 1-^{13}C-pyruvate in McA-RH7777 cells are compared.

CDDA metabolism was also appreciated in human prostate cancer cells (PC-3) and resulted to be approx. 6 times higher than in immortalized healthy human prostate cells.

Finally, a first *in vivo* experiment was performed in live rats, that allowed an unquestionable identification of CDDA, CDMA and CDM with notable chemical shift differences and signal intensities.

[1] Nelson S.J., Kurhanewicz J., Vigneron D.B., *et al.* Sci. Transl. Med. 2013; 5: 198.

[2] Xu G., Zhang W., Ma M.K., and McLeod H.L. Clin. Cancer Res. 2002; 8: 2605

[3] Hatfield J.M, Tsurkan L., Garrett M., *et al.* Biochem Pharmacol. 2011; 81(1): 24

[4] Jensen P.R., Serra S.C., Miragoli L., *et al.* Int. J. Cancer 2015; 136(4): E117

AUTHORS (LAST NAME, FIRST NAME): Maisano, Federico[2]; Cabella, Claudia[2]; Miragoli, Luigi[2]; Colombo Serra, Sonia[2]; Tedoldi, Fabio[2]; Jensen, Pernille R.[1]; Karlsson, Magnus[1]; Lerche, Mathilde H.[1]

INSTITUTIONS (ALL):

1. Albeda Research Aps, Copenhagen, Denmark.
2. Bracco Imaging SpA, Colleretto Giacosa, Torino, Italy.

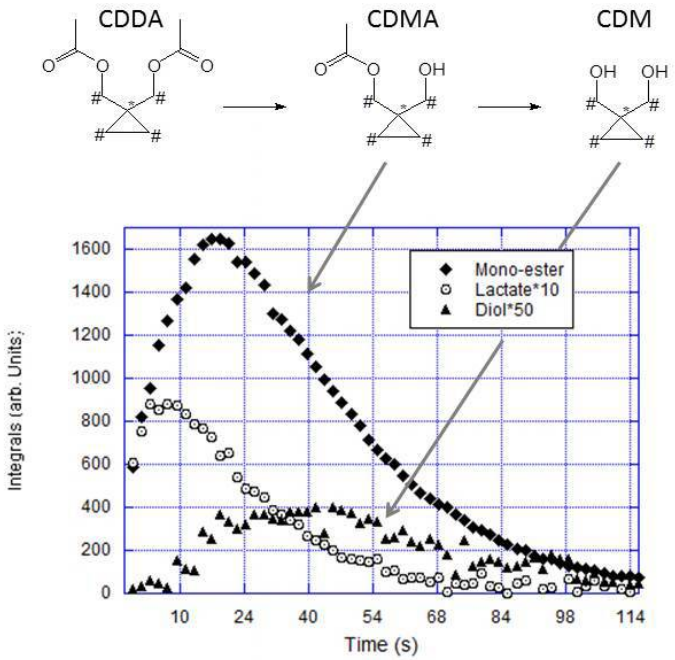

Figure 1. Top: Scheme of hydrolytic conversion of CDDA by carboxylesterases. * indicates the ^{13}C atom used as MRS probe, # indicate perdeuterated carbons. Bottom: Build-up of the metabolites CDMA (Mono-ester) and CDM (Diol*50) from injection of hyperpolarized CDDA and of [1-^{13}C]lactate (Lactate*10) from injection of hyperpolarized [1-^{13}C]pyruvate, respectively into whole rat liver cancer cells (McA-RH7777).

CONTROL ID: 2226463

TITLE: Resonance frequency-shifting nitroxide for probing proteolytic activity *in vivo* using the Overhauser-enhanced MRI technique

PRESENTER: Neha KOONJOO

ABSTRACT BODY:

Abstract Body: Molecular imaging of proteolysis is a challenging field. As compared to more sensitive imaging techniques, MRI needs new probe-design for high protease-specific biological contrast. Here, low MRI sensitivity was unveiled using Overhauser-enhanced MRI. The OMRI approach, based on the Overhauser effect between unpaired electrons of a nitroxide and surrounding water protons (^{1}H) after electron saturation (ES), enables high NMR signal enhancement, thus revealing the presence of unpaired electrons in MR images. The novelty of our study was to validate *in vivo* a line-shifting nitroxide probe-design, synthesized chemically with an acetyl group which can be hydrolyzed enzymatically to give a hydroxyl group. Upon hydrolysis, their nitrogen and phosphorus hyperfine coupling constants (a_N & a_P respectively) are changed (fig 1) allowing a distinct substrate (**A**) or product (**B**) visualization using OMRI. Nitroxides were evaluated *in vitro* and substrate hydrolysis was evaluated *in vivo* in mice.

Methods: Nitroxides - **A** (a_P=38.7G; a_N=15.6G; ES=5426MHz) has its peaks shifted by 8 MHz from **B** (a_P=43.1G; a_N =15.0G; ES=5418 MHz).

OMRI setup - A 0.2T MRI system (Siemens) and a Transverse-Electric-mode resonant cavity (Bruker) were used. ^{1}H-frequency=8.24MHz; electron frequency= 5.4GHz.

Animal Preparation - 200µl nitroxide (24mM) was orally administered (n=3).

Imaging Protocol - 1) 18-s images were acquired at 5426MHz using TrueFISP sequence (resolution=0.5×1×1 mm^3) with/out ES. 2) Similar data set was acquired at 5418MHz. 3) A TrueFISP image (0.5×0.5×0.5 mm^3) without ES was generated for keyhole reconstruction(KH). 4) A 3-minute gradient echo anatomical image (0.5×0.59×1.0 mm^3) was acquired.

Image Processing - 3D KH resulted in OMRI images with ES (OMRI-**on**) or without (OMRI- **off**). Overhauser enhancements were calculated as a ratio of signal intensity of OMRI-**on** images to that of OMRI-**off**.

Results: *In vitro*, no spontaneous hydrolysis from **A** to **B** was observed. Preliminary *in vivo* results (n=3) showed a clear Overhauser enhancement of the **A** immediately after gavage and later on **B**. At 5426MHz, a signal enhancement of 5.0 ± 0.8 was either observed in the stomach or in the small intestine; showing the presence of **A**. Simultaneously, at 5418MHz, an average signal enhancement of 4.8 ± 3.3 revealing B was obtained in the stomach. For the mouse (fig.2), a maximum Overhauser enhancement of 5.8 was observed at 15mins post-gavage at 5426MHz and of 8.5 at 36mins at 5418MHz. Both enhancements were seen inside the stomach as validated in the superimposed image (fig 2).

The feasibility in the use of this probe was clearly demonstrated *in vivo* through highly resolved OMRI. Even if this substrate had a low specificity as well as a low affinity with a certain class of enzymes, high signal amplifications undoubtedly showed an enzymatic process occurring in the stomach of the mice. This appealing molecular imaging strategy monitors and localizes both the substrate and its associated enzymatic product at two distinct frequencies. In conclusion, this line-shifting OMRI probe-design would be a good candidate to target abnormal proteolysis using specific peptide sequences.

AUTHORS (LAST NAME, FIRST NAME): KOONJOO, Neha[1]; Audran, Gérard[2]; Bosco, Lionel[2]; Brémond, Paul[2]; Franconi, Jean-Michel[1]; Marque, Sylvain R.[2]; Massot, Philippe[1]; Mellet, Philippe[1]; Parzy, Elodie[1]; Thiaudière, Eric[1]

INSTITUTIONS (ALL):

1. University of Bordeaux - CNRS - UMR5536, Bordeaux, France.
2. ICR - UMR CNRS 7273, Marseille, France.

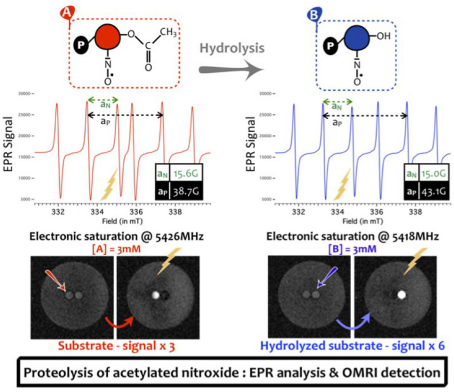

Figure 1 represents a rough sketch of the nitroxide molecule with the acetylated form (A) and the hydrolyzed form (B). The 6-EPR peaks of the nitroxide is also displayed with their different a_p and a_n values. The OMRI *in vitro* images of the selective Overhauser enhancements are also depicted in this figure.

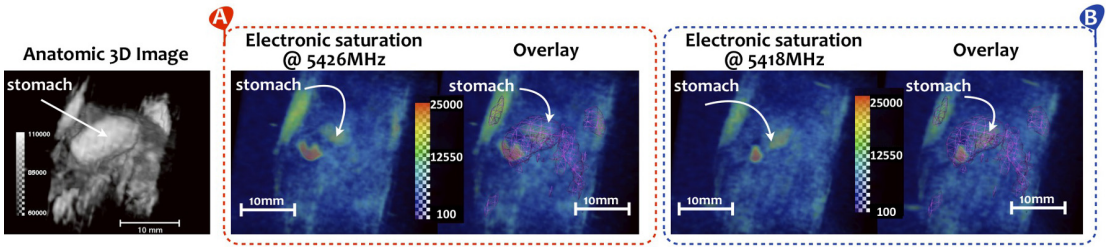

Figure 2: *In vivo* images. A Maximal-Intensity-Projection (MIP) of the T_1-weighted anatomic image (left). Box A – OMRI-on image at 5426MHz; Box B – OMRI-**on** image at 5418MHz. "Overlay" – superimposed image of the anatomic image and OMRI-**on** image to localize the presence of the probe.

CONTROL ID: 2231256

TITLE: *In vivo* Overhauser-enhanced MRI of Proteolytic Activity

PRESENTER: Neha KOONJOO

ABSTRACT BODY:

Abstract Body: Purpose: Molecular imaging is of increasing interest in the field of pathology diagnosis, prognosis and monitoring. Among the existing imaging techniques available, MRI is a promising method for future molecular imaging applications due to its noninvasive nature, excellent SNR, high spatial resolution and remarkable soft tissue contrast. However its sensitivity is quite low. To counteract this weakness, a new approach: the Overhauser-enhanced MRI (OMRI) technique was developed at 0.2T[1]. This technique is based upon the Overhauser effect occurring while unpaired electrons of a free radical species interact with surrounding water protons (^{1}H) after saturating electron spins. Nuclear ^{1}H polarization is then increased, thereby, revealing the presence of unpaired electrons in MR images. Here, our aim was to visualize a proteolytic activity happening inside living mice during digestion. In this perspective, a nitroxide-labeled macromolecule that can generate strong Overhauser enhancements upon cleavage was designed (Fig1). This current work would eventually be transposed into disease-bearing animal model with a view to early diagnosis.

Methods: OMRI Setup: It was composed of a 0.2T MRI system (Siemens - 8.25MHz ^{1}H frequency) and a TE011-mode resonant cavity (5.43GHz electron frequency, Bruker) at the centre of the magnet.

Animal Preparation: 200µl of nitroxide-labeled elastin at 18mM was orally administered in mice (n=7, CB57/CRL). They were anesthetized and placed on a thermostatic bed for imaging.

Imaging Protocol: **1)** A 17-min anatomical image (resolution = 0.5(mm)^3) was obtained. **2)** Successive 18-s images were acquired using a fully balanced steady-state sequence (resolution = 0.5*1*1 mm^3) **with/out** electron spin saturation. **3)** A 5-min TrueFISP3D image of resolution 0.5(mm)^3 without electron spin excitation was obtained for keyhole reconstruction.

Image Processing: 3D keyhole reconstruction resulted in OMRI images with electron spin saturation (OMRI-on) or without (OMRI-off). Parametric images of Overhauser enhancements were then calculated as a ratio of signal intensity of OMRI-**on** images to that of OMRI-**off**.

Results: Overhauser enhancements of 7.2 ± 2.4 (n=7) were observed at the opening of the duodenum about 20-30 minutes post-gavage where pancreatic juice is first secreted by the exocrine pancreatic cells (Fig 2). No Overhauser enhancements were observed in the stomach (Figure 2). The 3D superimposed images were obtained from the anatomical image and the reconstructed 3D OMRI-**on** image. This overlay validated correct localization of the Overhauser enhanced signal within the digestive tract of the mouse.

Discussion: In this study, highly resolved OMRI of the mouse's abdomen, with spatial resolution 0.5 (mm)^3 in less than 20s acquisition was achieved (5 times quicker than the previous article[2]). Specific pancreatic elastin proteolysis was observed in the duodenum with strong signal amplifications. In conclusion, the Overhauser effect clearly improved MRI sensitivity and localized precisely *in vivo* biological activity.

References: 1. Mellet.P et al. PLoS One 2009;4(4):e5244. 2. Massot.P et al. Contrast Media Mol Imaging 2012 Jan-Feb;7(1):45-50.

AUTHORS (LAST NAME, FIRST NAME): KOONJOO, Neha[1]

INSTITUTIONS (ALL):

1. University of Bordeaux - CNRS - UMR5536, Bordeaux, France.

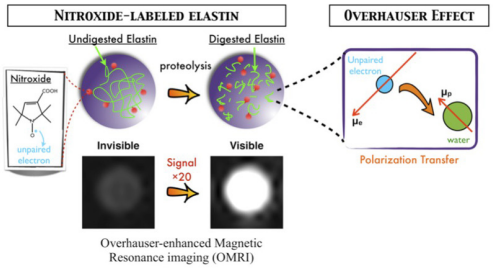

Figure 1: OMRI technique – *in vitro* imaging of the nitroxide-labeled elastin digestion (left) and the Overhauser effect taking place upon digestion after electron spin saturation (right).

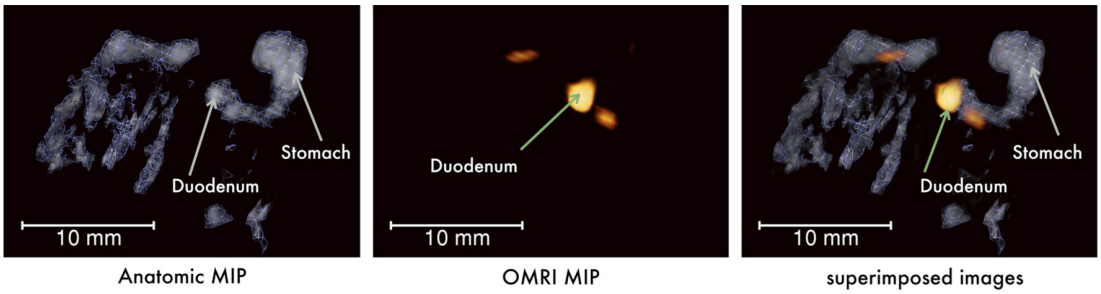

Figure 2: *In vivo* proteolysis 26 minutes post-gavage. Color maps of Maximal-intensity-projections (MIP) of anatomical 3D-FLASH image (left), the reconstructed 3D keyhole OMRI-on image (middle) and superimposed image (right).

CONTROL ID: 2226490

TITLE: A novel hyperpolarized biosensor for ^{13}C magnetic resonance spectroscopic imaging of pH

PRESENTER: Stephan Düwel

ABSTRACT BODY:

Abstract Body: Introduction

Local pH changes in the human body are triggered by pathologies which overrule natural pH regulatory mechanisms, in particular tumors, inflammation and ischemia[1]. A spatially resolved and non-invasive method for the measurement of local pH offers an immense potential for preclinical and clinical applications both for diagnostics as well as therapeutical purposes such as monitoring response-to-treatment. In the field of magnetic resonance (MR), various pH-sensitive molecules have been developed for different nuclei (^{1}H, ^{19}F, or ^{31}P)[2] based on several contrast mechanisms (e.g. chemical exchange saturation transfer CEST) or hyperpolarized ^{13}C-bicarbonate[3]. Even though some methods showed great promise, none of them has yet been translatable to the clinic. We introduce [1,5-$^{13}C_2$]zymonic acid (ZA), a novel pH biosensor for in-vitro (pH phantoms) and in-vivo (rat bladder, kidney, tumor) pH measurements based on MR spectroscopic imaging (MRSI) of pH sensitive ^{13}C chemical shifts. ZA is an endogenous, non-toxic compound, also used as a flavoring compound in the food industry[4].

Methods

ZA was synthesized[5] from [1-^{13}C]pyruvic acid, purified using reversed phase HPLC, and freeze dried. Its structure was confirmed using mass spectrometry and high-field NMR. ^{1}H and ^{13}C NMR titrations of zymonic acid were performed at 7 and 14.1T, chemical shifts recorded in H_2O and DMSO. Temperature stabilized traditional titrations were performed to determine $\Delta pKa/\Delta T$. ZA was hyperpolarized together with ^{13}C-urea in nitrogen frozen layers in a *HyperSense*. Hyperpolarized ZA, dissolved to a final concentration of 50mM and neutralized to pH≈7.4 in a dissolution agent consisting of D_2O, NaOD and EDTA, was injected into the tail vein at 37°C and a dose of ≈5mL/kg; rats (Lewis, Fischer) were anesthetized with 3-5% isoflurane. Imaging experiments were performed on a 7T small animal scanner using chemical shift imaging with FOV=6cm, matrix size=16x16, T_R=118ms, FA=3°.

Results & Discussion

^{13}C NMR chemical shifts of hyperpolarized ZA vs. pH conform to the theoretical titration model (A) and allow the determination of pH of different buffer phantoms (B and Table). pH measurements of hyperpolarized ZA injected directly into the rat bladder result in an acidic pH ≈ 6.90-6.95 confirmed by electrode pH = 6.8±0.1 of sampled urine (C, D). Hyperpolarized ZA injected via tail vein results in a pH difference of $\Delta pH \approx 0.5$ between the kidneys and its surroundings (E, F). Mat B III tumor cells seem to have a slightly more acidic environment ($\Delta pH \approx 0.1$) than healthy tissue (G, H).

In conclusion, we have shown that ZA represents an accurate pH reporter for *in vivo* MRSI showing great promise for clinical translation. Its large pH-sensitive chemical shift, evoked by rapid proton dynamics, is unique and does not rely on enzyme kinetics which is advantageous for hyperpolarized rapidly decaying nuclei.

Acknowledgements

EU Grant No. 294582 (MUMI), BMBF (FKZ 13EZ1114), DFG (SFB 824).

References

1 Gatenby, A. (2004) Nat Rev Cancer 4:892. **2** Gillies, R. (2004) IEEE Eng Med Biol Mag 23:57. **3** Gallagher, F. (2008) Nature 453:940. **4** Dietrich, P. (1973) patent CH532906. **5** Wolff, Liebigs Ann Chem (1901) 317:1.

AUTHORS (LAST NAME, FIRST NAME): Düwel, Stephan[2, 1]; Hundshammer, Christian[1, 2]; Gersch, Malte[2]; Feuerecker, Benedikt[1]; Haase, Axel[3]; Glaser, Steffen[2]; Schwaiger, Markus[1]; Schilling, Franz[2, 1]

INSTITUTIONS (ALL):

1. Department of Nuclear Medicine, Klinikum rechts der Isar, Technische Universität München , Munich, Germany.
2. Department of Chemistry, Technische Universität München, München, Germany.
3. Institute of Medical Engineering, Technische Universität München, Garching, Germany.

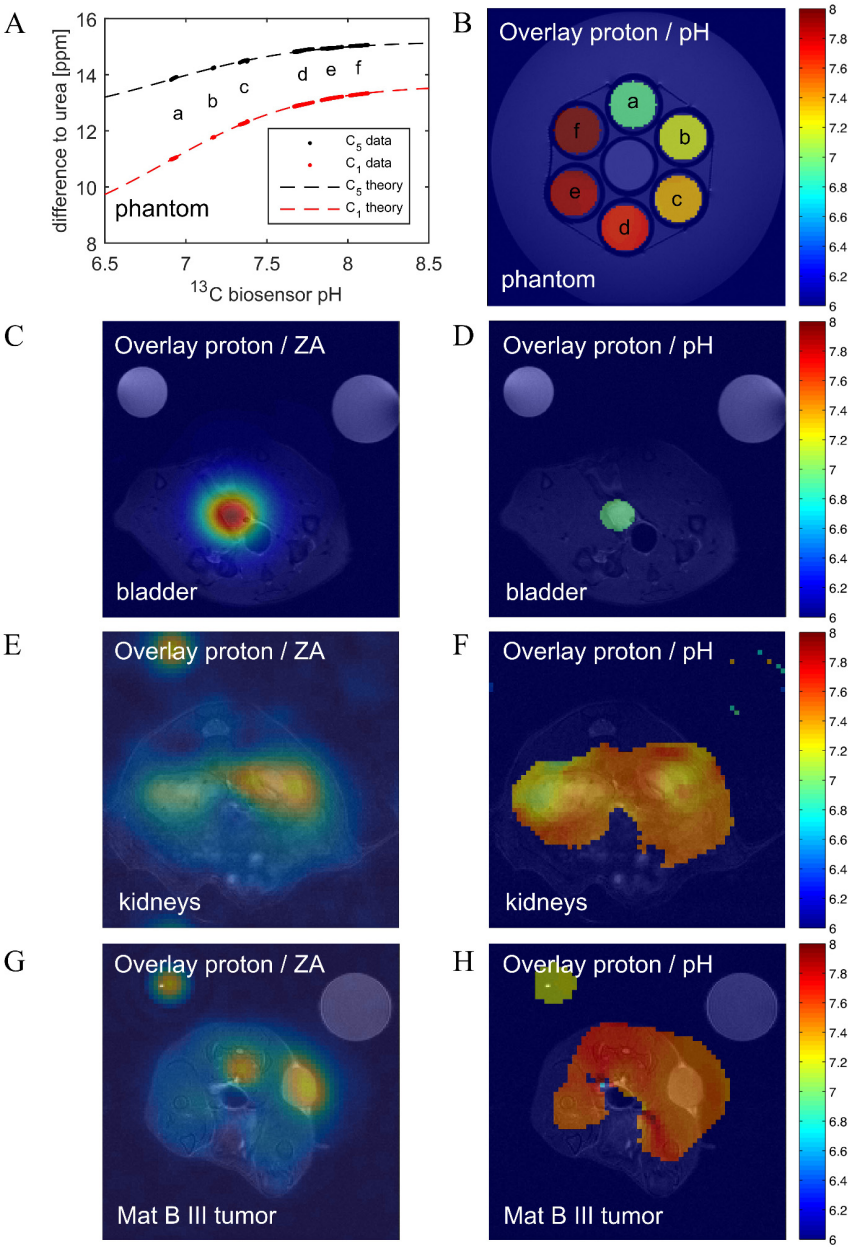

(A) Experimental ^{13}C NMR chemical shifts of hyperpolarized zymonic acid (ZA, pH sensitive) relative to hyperpolarized ^{13}C-urea (pH insensitive) with the theoretical curves used to calculate the pH in all other figures. **(B)** pH image resulting from hyperpolarized ZA added to six different pH phantoms of 80mM TRIS buffer. **(C)** Overlay of axial proton image and intensity of hyperpolarized ZA injected directly into the rat bladder. **(D)** ZA indicates an acidic pH of 6.90-6.95 in the rat bladder compared to pH 6.8 measured by a pH electrode within urine sampled after the hyperpolarized measurement. **(E)** Overlay of axial proton image and intensity of hyperpolarized ZA injected into the rat via tail vain. **(F)** ZA shows a pH difference of ΔpH≈0.5 between rat kidneys and outside of the kidneys. **(G)** Overlay of axial proton image and intensity of hyperpolarized ZA injected into the rat via tail vain. **(H)** ZA indicates a slightly more acidic Mat B III tumor environment (ΔpH≈0.1) compared to healthy tissue.

CONTROL ID: 2231603

TITLE: In vivo PET- lymphography imaging and Cerenkov guided resection of metastatic lymph nodes in a PC3-mouse model

PRESENTER: Hannah Lockau

ABSTRACT BODY:

Abstract Body: Objective

PET-lymphography using ^{18F}FDG followed by Cerenkov guided resection of lymph nodes in healthy mice has previously been shown (1). Our aim was to assess the feasibility and differences in imaging characteristics amongst metastatic versus non-metastatic nodes. Thus using PET-lymphography it was our goal to also visualize concomitant changes in lymphatic drainage. Essentially we wanted to test if metastatic nodes can be distinguished from normal nodes via optical means, in order to then be resected under Cerenkov imaging guidance.

Materials and Methods

A highly metastatic Luciferase-transduced PC3-cell line was implanted subcutaneously on the dorsal hind paw of nude mice (n=4). Accordingly, the contralateral side served as a negative control. Tumors were allowed to grow for 5-8 weeks until there was evidence of lymph node metastasis via bioluminescence imaging (or until an endpoint was reached). Dynamic PET/CT imaging was performed after injection of 80-150 µCI ^{18F}FDG peritumorally and into the contralateral footpad for one hour using an Inveon microPET/CT. After imaging, popliteal lymph nodes were exposed and sequential Cerenkov images were acquired using the IVIS Spectrum. Immunohistochemistry was done to verify the presence of metastasis in the lymph nodes.

Results

PET-lymphography using ^{18F}FDG was successfully performed on tumor-bearing and non tumor-bearing legs; the results clearly identified the sentinel lymph nodes and delineated the lymphatic drainage. Total lymph node volume determined by CT volumetry was significantly greater in tumor-bearing nodes compared to non tumor-bearing nodes. Time points of maximum tracer uptake in the lymph nodes did not relevantly differ between the side bearing the tumor and the control leg. Loss of activity over time occurred significantly faster in non-metastatic nodes when percent of injected dose per gram within the first minutes of each scan were compared to percentages within the last scan minutes. Based on these results after one hour, the contrast in detection and identification of metastatic lymph nodes was distinct and quantifiable using Cerenkov imaging after the removal of the skin.

Conclusion

Significantly longer retention of ^{18}F-FDG during ^{18F}FDG-lymphography is seen in metastatic versus non-metastatic lymph nodes in a PC3-mouse model, allowing for differentiation of the two and for the selective resection of tumor-bearing nodes using Cerenkov imaging.

1. Thorek DL, Abou DS, Beattie BJ, Bartlett RM, Huang R, Zanzonico PB, Grimm J. Positron lymphography: multimodal, high-resolution, dynamic mapping and resection of lymph nodes after intradermal injection of 18F-FDG. Journal of nuclear medicine : official publication, Society of Nuclear Medicine 2012;53:1438-45.

AUTHORS (LAST NAME, FIRST NAME): Lockau, Hannah[1]; Ogirala, Anuja[1]; Vilaseca, Antoni[1]; Shukla, Priyanka[1]; Grimm, Jan[1]

INSTITUTIONS (ALL):

1. Memorial Sloan Kettering Cancer Center, New York, NY, United States.

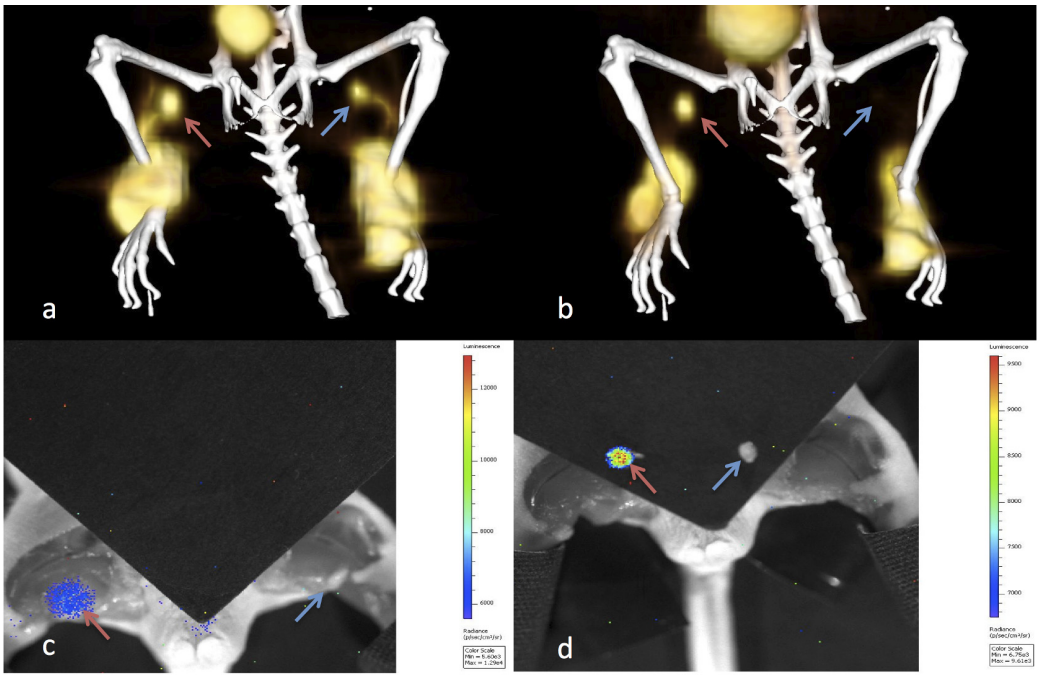

^{18F}FDG PET-lymphography followed by Cerenkov guided resection of tumor positive lymph nodes in a metastatic PC3 mouse model. (a) Acitivity is present in both, metastatic (red arrow) and non-metastatic (blue arrow) lymph nodes on early scans after peritumoral and contralateral footpad injections. (b) Prolonged retention of activity in metastatic nodes is evident in dynamic PET. (c) and (d) This finding can be utilized for identification and selective resection of tumor-positive lymph nodes using Cerenkov imaging.

CONTROL ID: 2226685

TITLE: Super-resolution molecular ultrasound imaging with laser-activated nanodroplets

PRESENTER: Geoffrey Luke

ABSTRACT BODY:

Abstract Body: Although ultrasound imaging has made great strides as a molecular imaging tool, the type of information it can provide is limited. First, its resolution is fundamentally constrained by the bandwidth and aperture of the transducer. Second, typical ultrasound contrast agents – gas-filled microbubbles – are too large to escape the vasculature and target extravascular molecules. We have simultaneously overcome both limitations by combining a new nano-sized optically triggered contrast agent with advanced image processing techniques. The contrast agent, known as a laser-activated nanodroplet (LAND), consists of a liquid perfluorohexane core, an encapsulated near-infrared dye, and a stabilizing shell, and it can be molecularly targeted via conjugation to antibodies. The LANDs were synthesized using a procedure developed for synthesis of similar previously published particles. Briefly, the particles were created by sonicating a solution containing 2.5 mL of water, 0.5 mL of 1% Zonyl Fluorosurfactant, 0.25 mL of perflurohexane, and 1 mg of Epolight 3072 dye for 1 hour at 3 °C. Upon exposure to a nanosecond pulsed laser, the LANDs undergo a liquid to gas phase transition, resulting in the formation of a transient microbubble. Because the boiling point of perfluorohexane (56 °C) is far above that of the surrounding tissue, the microbubbles recondense into their native liquid droplet state. The actual lifetime of the transient microbubbles is stochastic; it depends on the LAND size, the local temperature and pressure, and the tissue microenvironment. Using high-frame-rate ultrasound imaging, the recondensation of individual LANDs was captured. After the response of an individual LAND is isolated by taking the difference of successive frames, the ultrasound footprint of LAND is fit to the point spread function of the imaging system to localize its position with much greater precision than the system's resolution. We have successfully localized individual LANDs to within 5-12 μm in tissue-mimicking polyacrylamide phantoms thus improving the spatial resolution by 8 fold. Furthermore, we have demonstrated the ability to apply this technique *in vivo*. After undergoing a craniotomy, a CD-1 mouse was imaged using a 40-MHz linear array ultrasound transducer with simultaneous 1064-nm pulsed laser irradiation. The LANDS were visualized with high contrast in the microvasculature of the brain. Individual features as small as 7-15 μm were localized *in vivo* at centimeter depth using the super-resolution imaging procedure. These results pave the way for noninvasively obtaining molecular information *in vivo* at unprecedented spatial scales.

AUTHORS (LAST NAME, FIRST NAME): Luke, Geoffrey P.[1, 2]; Hannah, Alexander[1]; Emelianov, Stanislav Y.[1, 2]

INSTITUTIONS (ALL):

1. Biomedical Engineering, The University of Texas at Austin, Austin, TX, United States.
2. Department of Imaging Physics, MD Anderson Cancer Center, Houston, TX, United States.

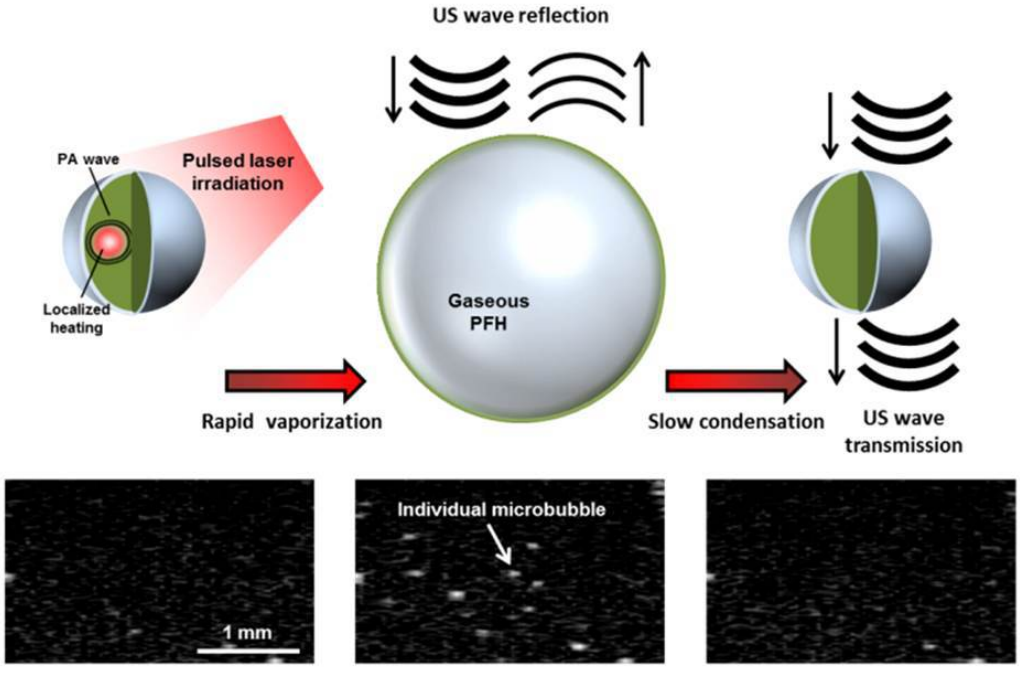
US wave reflection
PA wave
Pulsed laser irradiation
Localized heating
Gaseous PFH
Rapid vaporization
Slow condensation
US wave transmission
Individual microbubble
1 mm

CONTROL ID: 2226694

TITLE: Differential Impact of Ubiquitin-Activating Enzyme (UAE) Inhibition on 3'-Deoxy-3'-[^{18}F]Fluorothymidine (FLT) and 2-Deoxy-2-[^{18}F]Fluoro-D-Glucose (FDG) Uptake: Studies in Cells and Cell- or Patient-Derived Xenograft Tumor Models

PRESENTER: Nicolas Salem

ABSTRACT BODY:

Abstract Body: Background: Poly-ubiquitination is a post-translational modification that targets proteins for degradation by the proteasome. Mono- and poly-ubiquitination can also regulate DNA repair and protein localization.
The ubiquitin-activating enzyme (UAE) is the primary E1 enzyme responsible for activating ubiquitin. Subsequently, E2 ubiquitin-conjugating enzymes and E3 ubiquitin ligases complete the three-step process of covalently linking ubiquitin to a substrate protein. In this study, the acute and chronic impacts of treatment with a small molecule UAE inhibitor (UAEi) on FLT and FDG uptake were measured and compared *in vitro* and *in vivo*.

Methods: FLT and FDG uptake were measured in HCT-116 cells (colon) after exposure to a UAEi. Female severe combined immunodeficiency (SCID) mice were inoculated with WSU-DLCL2 (lymphoma) cells and either PHTX-24C (primary human tumor xenograft; colon) or PHTX-132Lu (lung) tumor fragments. Tumor-bearing animals were treated with vehicle or UAEi intravenously (IV). Tumor growth was monitored with calipers over a period of 21 days. Some tumors were collected approximately 8h and 24h after the first UAEi dose for analysis of cleaved caspase-3 (CC3) and protein poly-ubiquitination levels by immunohistochemistry. Other tumor-bearing animals were imaged with a Siemens Inveon positron emission tomography/computed tomography (PET/CT) system using FDG or FLT between 6 and 96 hours and between 6 and 8 days after the start of treatment. Data was analyzed using the InviCRO VivoQuant and iPACS software.

Results: A decoupling in the FLT and FDG response after treatment with UAEi was observed. Despite significant increases in CC3 levels and decreased protein poly-ubiquitination, we did not consistently observe modulation of FDG uptake (*in vitro* or *in vivo*). Interestingly, a significant increase in FDG uptake in treated PHTX-24C tumors was observed 8h after the first dose of UAEi (a time-point that preceded significant induction of apoptosis). In contrast, FLT uptake significantly decreased within hours of the first exposure to the UAEi in HCT-116 cells and in PHTX-24C and PHTX-132Lu tumors. Twenty-four hours after the first dose of UAEi, the FLT uptake decreased by 34% in the PHTX-24C model and by 78% in PHTX-132Lu model. However, treatment with UAEi resulted in similar treated to vehicle tumor volume ratio (T/C) in PHTX-24C and PHTX-132Lu xenografts at d21 (0.1 and 0.16, respectively). This may be due to the fact that PHTX-132Lu tumors had an exceptionally high baseline FLT uptake (SUV_{mean}@d0 = 2.4 ± 0.3) compared to that in PHTX-24C (SUV_{mean}@d0 = 0.9 ± 0.1). Of note, while the FLT uptake in PHTX-132Lu tumors at day 7 remained low if the mice received treatment on days 0, 3 and 6, it recovered to levels similar to that seen in vehicle-treated tumors if the mice were only treated on days 0 and 3.

Conclusions: These results highlight differences in the ability of FDG and FLT PET imaging to capture early biological changes associated with UAE inhibition. Whereas there was little change in FDG uptake, significant decreases in FLT uptake could be measured as early as 8 hours after the first exposure or dose of UAEi.

AUTHORS (LAST NAME, FIRST NAME): Salem, Nicolas[1]; Robertson, Robbie[1]; Saylor, Melissa[1]; Borland, Maria[1]; Huck, Jessica[1]; Traore, Tary[1]; Shi, Judy[1]; Hebert, Gustave[1]; Stringer, Bradley[1]; Wong, Tzu-Tshin[1]; Bharathan, Indu[1]; Ciavarri, Jeffrey[1]; Ishii, Yuko[1]; Hyer, Marc L.[1]; Bradley, Daniel P.[1]

INSTITUTIONS (ALL):

1. Millennium Pharmaceuticals, Inc., a wholly owned subsidiary of Takeda Pharmaceutical Company Limited, Cambridge, MA, United States.

(No Image Selected)

CONTROL ID: 2226698

TITLE: Towards Chemical Probes of ASCT2 (*SLC1A5*) As Precision Cancer Imaging Diagnostics

PRESENTER: Michael Schulte

ABSTRACT BODY:

Abstract Body: Cancer cells exhibit an altered metabolic profile compared to normal cells. In addition to increased utilization of glucose, they can become highly dependent on the amino acid glutamine. A sodium-dependent transporter of glutamine, ASCT2 (gene symbol *SLC1A5*), stands out as the major transporter for glutamine uptake making it a promising target for probe development. In cancer cells, *SLC1A5* expression is associated with oncogenic MYC and KRAS(1,2). While radiolabeled glutamine analogues have been developed and evaluated *in vivo,* these tracers are limited in their ability to measure ASCT2 directly due to the promiscuity of glutamine for multiple amino acid transporters. No imaging probes are currently available that specifically target ASCT2. Given the clinical relevance of ASCT2 in human cancer, we have undertaken the development of ASCT2-targeted PET probes that could be ultimately deployed clinically for precision cancer imaging.

To date, few compounds that target ASCT2 have been reported and most are derivatives of endogenous amino acid substrates of ASCT2. As an early entrant to the field, in 2004, Esslinger and co-workers described L-γ-glutamyl-*p*-nitroanilide (GPNA), a glutamine analog, as a probe of the ASCT2 amino acid binding site (3). Recently, this class of inhibitors was expanded and *N*-(2-(morpholinomethyl)phenyl)-L-glutamine was identified as a novel glutamylanilide with three-fold improved activity against ASCT2 compared to GPNA (4). To continue our efforts towards novel ASCT2 inhibitors, we focused on elaborating the glutamylanilide scaffold further and arrived at a series of substituted diaminobutanoic acid analogs, which stood out as a unique molecular scaffold with activity at ASCT2. This novel scaffold has been expanded further to afford compounds with significantly greater potency than GPNA including our best compound in this series to date which exhibits an IC_{50} = 19 mM. A molecular modeling approach was used to guide further medicinal chemistry and to elucidate novel structure activity relationships. Since a crystal structure of human ASCT2 has not been reported, a homology model was generated based on the structure of the bacterial neutral amino acid transporter GltPh in complex with an inhibitor (PDB ID 2NWW) (5). The best scoring poses for the most potent compounds identified demonstrated a compatible fit with the human ASCT2 model and, exhibited points of interaction with both the amino acid zwitterion binding site and an adjacent hydrophobic pocket. Ongoing studies are optimizing current novel ASCT2-selective leads for proof-of-principle PET imaging studies. References: 1) Dang, C.V., et. al *Cancer Res.*, **2010**, *70(3)*, 859-62. 2) Watanabe, T. et. al. Eur. J. Cancer, **2011**, *47(13)*, 1946-54. 3) Esslinger C.S., *et al. Bioorg. Med. Chem.* 2005. *13(4)*; 1111-18. 4) Schulte, M.L *et. al.* Bioorg. Med. Chem. Lett. **2015**, *25(1)*, 113-116. 5) Albers T,*et al. Mol. Pharmacol.* 2012. *81(3)*: 356-65.

AUTHORS (LAST NAME, FIRST NAME): Schulte, Michael L.[1]; Saleh, Sam A.[1]; Zhao, Ping[1]; Dawson, Eric S.[1]; Fu, Allie[1]; Cuthbertson, Madison L.[1]; Manning, H. Charles[1]

INSTITUTIONS (ALL):

1. Radiology and VUIIS, Vanderbilt University, Nashville, TN, United States.

(No Image Selected)

CONTROL ID: 2226732

TITLE: ^{18}F-FES PET/CT Estrogen Receptor Activity Imaging of Desmoid Tumors

PRESENTER: Karen Ayres

ABSTRACT BODY:

Abstract Body: Background and Specific Aims: Desmoid tumors are benign but locally aggressive fibrous tumors. Response to a number of available therapies is heterogeneous and unpredictable. Desmoid tumors express beta-estrogen receptors, and approximately half of the tumors will improve with anti-estrogen therapies. The aim of this pilot study is to determine the ^{18}F-FES avidity of these tumors, with the long-term goal of evaluating correlation between avidity and anti-estrogen therapy treatment response.

Methods: Ten adult patients with desmoid tumors will be imaged using standard PET/CT imaging protocols following the IV injection of approximately 6 mCi of ^{18}F-FES. Uptake of the radiotracer will be compared to the estrogen receptor expression as determined by immunohistochemical (IHC) analysis.

Results: We hypothesize desmoid tumors will be heterogeneously ^{18}F-FES-avid. There may not be a correlation with IHC as the IHC is based on a small biopsy specimen, and imaging will represent the entire tumor.

Conclusion: We hope to conclude that ^{18}F-FES PET/CT imaging will provide valuable information to clinicians when making treatment decisions regarding desmoid tumor therapy.

AUTHORS (LAST NAME, FIRST NAME): Ayres, Karen L.[1]; Manning, H. Charles[2]; Hartley, Kate[1]

INSTITUTIONS (ALL):

1. Radiology and Radiological Sciences, Vanderbilt University Hospital, Nashville, TN, United States.
2. Vanderbilt University Institute of Imaging Sciences, Nashville, TN, United States.

(No Image Selected)

CONTROL ID: 2226747

TITLE: Precision Visualization of Human Non-Melanoma Skin Cancer Ex Vivo: Implication for Rapid Detection of Surgical Margin and Surgery

PRESENTER: Ethan Walker

ABSTRACT BODY:

Abstract Body: Basal cell carcinoma (BCC) is the most common form of skin cancer; an estimated 2.8 million are diagnosed annually in the US. BCCs are rarely fatal, but can be highly disfiguring if allowed to grow. Squamous cell carcinoma (SCC) is the 2nd most common form of skin cancer. An estimated 700,000 cases of SCC are diagnosed each year in the US. Mohs micrographic surgery (MMS) is the treatment of choice for BCC/SCC. However, ¾ of skin cancer lesions are too large for their entire margins to be practically assessed for cancer using MMS. Non-MMS assesses ~1% of the margin with the results being available days after surgery resulting in re-excisions when margins are not clear (approximately 20% for SCC and 10% for BCC). Thus, there exists an unmet clinical need to more completely assess surgical margins to increase cure rates and minimize removal of normal tissue. To rapidly and globally detect cancer in skin samples here we test a quenched near infrared fluorescent contrast probe, GB119 [Nat Chem Biol. 2007(10):668].

Skin cancer samples obtained from debulking MMS were used to characterize the feasibility of *ex vivo* applied GB119 to penetrate human skin tissue and “find” BCC/SCC. Presence of the cancer was detected by increased fluorescence resulting from specific activation and de-quenching of GB119 as it encounters active cathepsin associated with BCC/SCC. Excised skin samples were pre-imaged and then, using an applicator pad, GB119 was topically applied onto the samples containing BCC/SCC for 5 min. Initially, activation of GB119 was measured (Maestro, PerkinElmer) and fluorescent “hot spots” on the surface of BCC (n=34) or SCC (n=21) samples were marked with pathology ink followed by snap freezing and slicing for histology and IHC. H/E staining confirmed presence of ink nearby of cancerous tissue and absence of ink marks at the cancer-free areas. Per ‘hot spot’ (n=90) analysis reveled a sensitivity 0.99 (95% CI: 0.940-1.00) and specificity 0.89 (95% CI: 0.769-0.965) of this method for all patients. Next, to more precisely correlate fluorescence with the presence and location of skin cancer the samples (n=7) were serially sectioned from top to bottom followed by H/E staining. Overlaying of GB119-fluorescent map onto H/E slide images revealed a tight correlation between Cy5/GB119 fluorescence and cancer nests as well as cancer-related inflammation. To microscopically visualize and correlate de-quenched GB119 with cancer cells an IHC assay was developed. Anti-Cy5 antibody (Sigma) binds to de-quenched GB119 approximately 5-fold better than to GB119 allowing us to discriminate de-quenched GB119 in tissue [Mol Imaging Biol. 2014(5):608]. Using this assay we detected low to zero levels of GB119 activation in normal skin and high levels of GB119 activation within/along “nests” of cancerous tissue and areas of cancer-related inflammation for BCC/SCC samples.

These data confirm the feasibility of topically applying GB119 to excised skin samples to rapidly detect the presence of cancer within the margins of the samples. If successful this technology could potentially provide MMS-like precision to non-MMS surgical techniques.

AUTHORS (LAST NAME, FIRST NAME): Walker, Ethan[1]; Mann, Margaret[3]; Honda, Kord[3]; Vidimos, Allison[4]; Schluchter, Mark [6]; Blum, Galia [5]; Bogyo, Matthew[2]; Basilion, James[1, 7]

INSTITUTIONS (ALL):

1. Biomedical Engineering, CWRU, Cleveland, OH, United States.
2. Pathology, Microbiology and Immunology, Stanford University, Stanford, CA, United States.
3. Dermatology, University Hospital, Cleveland, OH, United States.
4. Dermatology, Cleveland Clinic Foundation, Cleveland, OH, United States.
5. The Hebrew University, Jerusalem, Israel.
6. Epidemiology & Biostatistics, CWRU, Cleveland, OH, United States.
7. Radiology and NFCR Center for Molecular Imaging, CWRU, Cleveland, OH, United States.

(No Image Selected)

CONTROL ID: 2226775

TITLE: Characterization of Preclinical Intratumor Heterogeneity via Textural Analysis on ^{18}F- Fluorodeoxyglucose and ^{18}F-Fluorothymidine Positron Emission Tomography Images

PRESENTER: Ozlem Yardibi

ABSTRACT BODY:

Abstract Body: Positron emission tomography (PET) is now intensively used in oncologic imaging in the clinic primarily for diagnosis and staging, and progressively to determine the response to therapy in a predictive or prognostic manner. The normalized mean or maximum tumor activity concentration known as standardized uptake value (SUV_{mean} or SUV_{max}, respectively) of imaging tracer within a region of interest is the predominant index used for quantitative assessment of PET images. However, these relatively simple measurements of tumor uptake do not inform on spatial heterogeneity. It is increasingly recognized that evaluation of intratumor heterogeneity can better predict the fate of solid tumors before and after therapy [1]. The aim of the current study was to explore and evaluate new features derived by textural analysis on preclinical PET images for efficacy assessment and prediction of therapy in various colon cancer cell lines. Three-dimensional ^{18}F-Fluorodeoxyglucose (^{18}F-FDG) and ^{18}F-Fluorothymidine (^{18}F-FLT) PET images were separately acquired using an Inveon PET/CT scanner (Siemens Medical, Knoxville, TN, USA) in three different subcutaneous xenograft tumor models (RKO, HCT116 and Colo205) at days 0, 2, and 7 in the treatment cycle. Each study had twenty-four animals in three different groups; n=8/group with vehicle, medium and high dose groups. An experienced scientist manually segmented the tumor regions from the PET images (VivoQuant, inviCRO, Boston, MA, USA) and the resultant three-dimensional areas of interest containing tumor regions were analyzed using an in-house built software. A comprehensive list of features encompassing shape, intensity, textural, difference, run-length and size-zone features were compiled using the tracer uptake values in the tumor regions. The current work describes the relationships between conventional PET indices such as mean, maximum, or peak SUV voxels against characterizing tumor metabolic distribution or cellular proliferation; these advanced features were found to significantly differentiate the three treatment groups. In conclusion, it has been confirmed that textural analysis of tumor uptake distribution presents a subset of imaging biomarkers that can capture differences between 1/ tumours of different phenotype and 2/ degree of response to therapy, and may allow for better predictive, improved sensitivity, and prognostic assessment of treatment via characterization of intratumor heterogeneity.

References

[1] Davnall et al., Assessment of tumor heterogeneity: an emerging imaging tool for clinical practice? *Insights into imaging*, 3(6):573–589, December 2012.

AUTHORS (LAST NAME, FIRST NAME): Yardibi, Ozlem N.[1]; Saylor, Melissa[1]; Robertson, Robbie[1]; Borland, Maria[1]; Cvet, Donna[1]; Philip, Rohit C.[2]; Salem, Nicolas[1]; Bradley, Daniel P.[1]

INSTITUTIONS (ALL):

1. Biomedical Imaging, Takeda Pharmaceuticals Inc., Cambridge, MA, United States.
2. Electrical and Computer Engineering , The University of Arizona, Tucson, AZ, United States.

(No Image Selected)

CONTROL ID: 2226817

TITLE: Fluorescent imaging of prostate stem cell antigen in translational mouse models of cancer

PRESENTER: Ziyue Karen Jiang

ABSTRACT BODY:

Abstract Body: In cancer surgery, the inability to differentiate malignant tissues from normal structures contributes both to incomplete tumor removal and surgical side effects. So, our goal is to develop cancer-targeting fluorescent imaging probes that can provide the surgeon with a better visualization of tumor during surgery. To this end, over-expression of the prostate stem cell antigen (PSCA) has been discovered on the cell surface of various types of solid tumors, including pancreatic and prostate cancer. We previously reported the protocols for conjugating anti-PSCA antibody fragments (diabodies and minibodies (**Fig. S1**)) with far-red and NIR fluorophores for optical imaging in subcutaneous models. Here, we moved forward and established a series of translational models, in which the potentials of clinical application of these probes were carefully examined.

First, we tested the performance of an NIR-minibody probe in imaging orthotopic prostate tumors. Endogenous PSCA expresser LAPC-9 cells were implanted into the dorsal lateral lobe of the prostate of male nude mice 7-8 weeks before the i.v. administration of the probe. Mice were imaged 48 hours later. As shown in **Fig. 1a**, the cancerous prostate was successfully detected whereas cancer-free prostate exhibited the same level of fluorescence as the background.

Next, we assessed the performance of an NIR-diabody probe in an orthotopic pancreatic cancer model that expressed PSCA endogenously. As shown in **Fig. 1b**, the tumors were distinctly demarcated by the probe.

Finally, we asked whether the use of anti-PSCA optical probes could provide intra-operative fluorescent guidance for more complete tumor resection. Intramuscular tumors of PSCA-over-expressing 22Rv1 prostate cancer cells were established in male nude mice 21-22 days before i.v. injection of a Cy5-diabody probe. These tumors were highly infiltrative and difficult to remove completely (**Fig. S2**). Mice were then randomized into two cohorts to receive either just a white light surgery or an additional fluorescence surgery (**Fig. S3** shows the experimental design). Remarkably, the surgeon was blinded to the groupings while performing the white light surgery to ensure that all mice received the same unbiased operation, with the goal of removing as much tumor as possible while preserving adjacent normal tissues (akin to radical prostatectomy). Following first stage white light resection, the fluorescent light was turned on to assess margin status; and as expected, all mice (n=17) had residual fluorescent signals which correlated to unresected cancer tissues as was confirmed by histological analysis (**Fig. 1c**). Then, mice in the fluorescence cohort underwent secondary imaging-guided surgeries to remove remaining fluorescing tissues. Lastly, remaining thigh musculature was harvested and examined to determine the final margin status. Positive margins were found in all 8 mice in the white light only cohort but in 0 of the 9 mice assigned to receive the fluorescence-guided surgery (**Fig. 1d and Fig. S4**).

Overall, these data demonstrated excellent imaging capabilities and hence great translational potentials of anti-PSCA fluorescent probes

AUTHORS (LAST NAME, FIRST NAME): Jiang, Ziyue Karen[1]; Behesnilian, Andrew S.[1]; Bentolila, Laurent A.[2]; Wu, Anna M.[3]; Reiter, Robert[1]

INSTITUTIONS (ALL):

1. Urology, University of California, Los Angeles, Los Angeles, CA, United States.
2. Chemistry and Biochemistry, UCLA, Los Angeles, CA, United States.
3. Molecular & Medical Pharmacology, UCLA, Los Angeles, CA, United States.

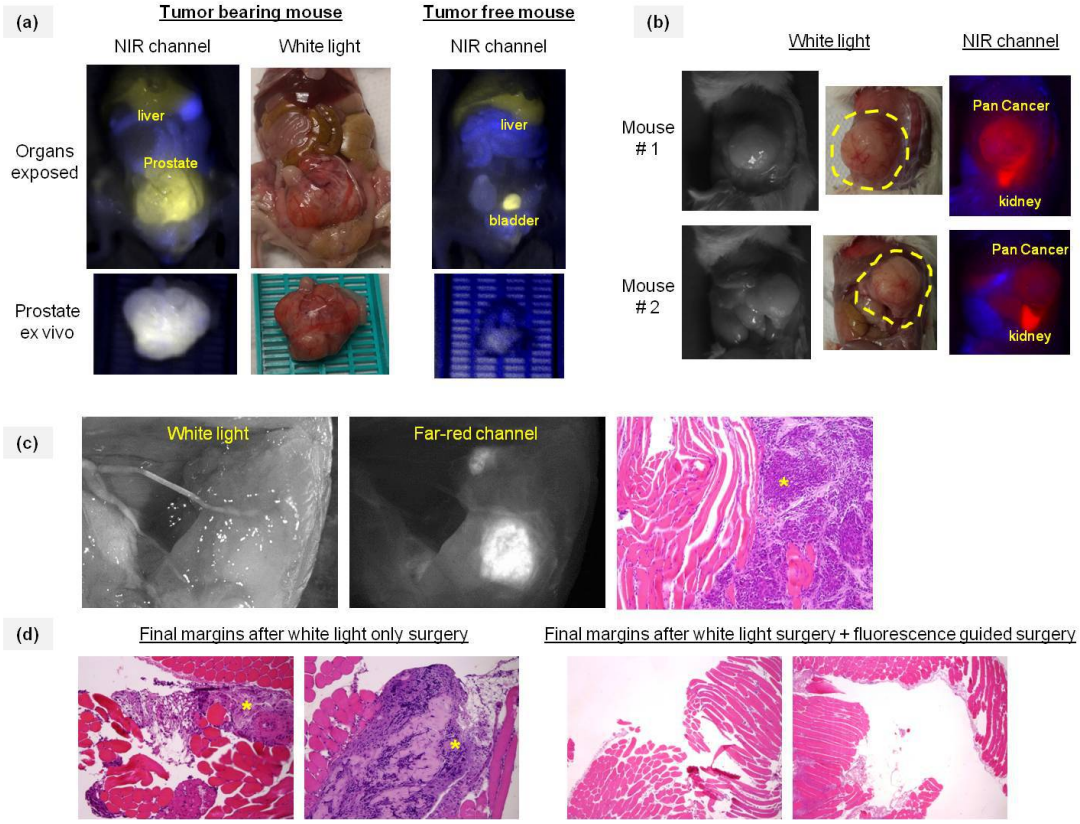

(a) NIR and white light images of mice with and without orthotopic prostate cancer. Upper panel: in vivo images with the animals' internal organs exposed. Lower panel: ex vivo images of the prostate. Liver and kidney fluoresced due to probe clearance and secretion. (b) Patient-derived pancreatic cancer xenografts were established orthotopically in NOD-SCID mice. IRDye800CW-diabody probe was administrated i.v. 24 hours prior to imaging. Shown are two representative mice with tumors highlighted by yellow dashed circles. (c) Representative white-light and fluorescent images of a tumor bed after white-light-only surgery. The residual fluorescent tissue proved to be cancer (*) by H&E staining (100X). (d) Histology staining of final margins revealed the presence of residual tumors (*; 100X) in mice from the white light surgery cohort and the absence of residual tumors from the fluorescence-guided surgery cohort (40X). Shown are two representative images from each group.

CONTROL ID: 2226851

TITLE: Six PET Tracers Target a Single Epitope of Integrin avb6 in Pancreatic Cancer

PRESENTER: Richard Kimura

ABSTRACT BODY:

Abstract Body: Integrin avb6 is overexpressed in pancreatic cancer, and is therefore an important imaging and therapeutic target. We are currently translating a ~4kDa cystine knot peptide to detect pancreatic cancer. However, to better understand the effect of molecule size on the pharmacokinetics of tumor targeting agents, we developed a set of six high affinity PET ligands in the ~4 kDa to ~150 kDa MW range. Importantly, each ligand recognizes the same epitope of integrin avb6 so that comprehensive head-to-head comparisons are possible for the first time in a single study. Because synthetic peptides have been effective as PET tracers and also because they are relatively inexpensive to clinically translate compared to biosynthesized entities, we have used a new cystine knot peptide ^{64}Cu-DOTA-$R_0$1-MG as the benchmark with which to make comparisons across the set of larger proteins that are not amenable to chemical synthesis, but may provide improved performance as diverse imaging or therapeutic agents. The cystine knot (~4 kDa), the monobody (~15 kDa) and the single chain variable fragment (scFv, ~30 kDa) were engineered for high affinity molecular recognition of integrin avb6 by way of directed evolution studies. The scFv served as the smallest unit from which the larger antibody-based ligands were engineered. Upon formatting, each ligand retained subnanomolar binding affinity to target epitope. As summarized in figure 1, PET tracers based in the cystine knot, monobody, scFv and scMinibody (~80 kDa) demonstrated comparable tumor uptake values of ~3-4%ID/g. Greatly improved uptake was evident in the scDiabody (~60 kDa, ~6%ID/g) and the full antibody (~150 kDa, ~19%ID/g). The peptide and the antibody demonstrated the best tumor-to-muscle ratios. Renal uptake was highly elevated for the monobody, and significantly lower for the full antibody due to its long circulation half-life. Liver uptake was lowest for peptide and monobody, but significantly higher for the antibody derivatives. In summary, these data show that the full antibody had the highest tumor uptake, lowest renal uptake, and excellent tumor-to-muscle ratios. However, its liver uptake was comparatively higher. The monobody and antibody fragments showed some benefit including a two-fold improvement in tumor uptake shown by the scDiabody. However, elevated kidney and liver uptake were liabilities in reformatted antibodies. This study represents unique opportunity to examine, in living animals, different classes of PET tracers that recognize the same oncological epitope. Due to unique pharmacokinetic profiles, large ligands such as the full IgG may better serve as therapeutics where very high tumor uptake is required. At the same time, small ligands such as cystine knot peptides, may be better suited as companion imaging agents that leverage lower overall radioactive exposure to patients, while providing enough contrast to yield critical molecular information about a tumor. Together, molecularly targeted ligand sets may fill important roles in theranostic management of cancer.

AUTHORS (LAST NAME, FIRST NAME): Kimura, Richard[1]; Zhang, Chao[1]; Gambhir, Sanjiv S.[1]

INSTITUTIONS (ALL):

1. Radiology, Stanford University, Stanford, CA, United States.

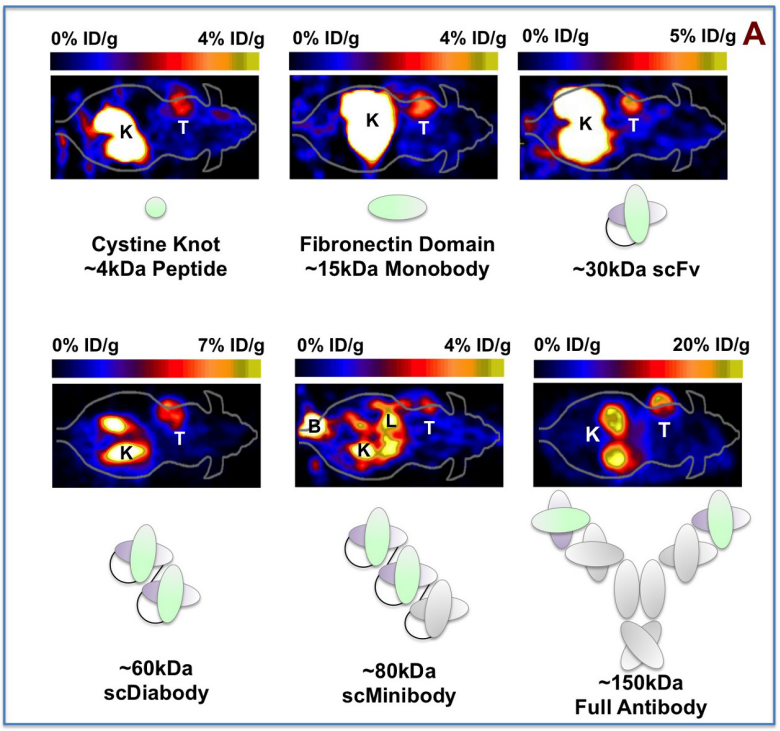

B

*Integrin αvβ6(+) A431 s.c. xenograft (n=3 mice/tracer, * p<0.05)*

TRACER	CLASS	Affinity	U(T)	U(K)	U(L)	T:M	uCi Inj.
^{64}Cu-DOTA-$R_0$1-MG	Cys-Knot Peptide	800 pM	3.1	30.3	2.3	8.9	76.6
^{64}Cu-DOTA-Monobody	Fibronectin	897 pM	3.4	101.3*	3.3	5.5*	87.3
^{64}Cu-DOTA-scFv	Ab Fragment	435 pM	4.3	66.9*	14.5*	5.4*	93.9
^{64}Cu-DOTA-scDb	Ab Fragment	468 pM	6.2*	33.6	24.4*	3.9*	101.7
^{64}Cu-DOTA-scMb	Ab Fragment	555 pM	3.1	27.9	14.9*	2.8*	115.5
^{64}Cu-DOTA-IgG	Full mAb	608 pM	18.6*	18.8*	10.4*	14.5*	230.2

Figure 1. Targeting a single epitope of integrin αvβ6 with 6 successively larger PET tracers. (A) Representative PET images accompany the schematic diagrams of six successively PET tracers starting in the upper left with a ~4 kDa small cystine knot peptide followed by a ~15 kDa fibronectin domain monobody, and a ~30 kDa single chain fragment variable domain (scFv) containing the complementarity determining region (CDR) loops responsible for binding to integrin αvβ6. This scFv resulted from yeast surface display directed evolution studies, and was used to build the larger constructs including the ~60 kDa single chain diabody (scDb), the ~80 kDa single chain minibody (scMb), and ~150 kDa the fully humanized IgG1 antibody. Each ^{64}Cu-DOTA-PET tracer, starting with the smallest cystine knot peptide to the largest full length antibody, target the same epitope of integrin αvβ6, a pancreatic cancer target. The letters T, K, L, B indicate tumor, kidneys, liver, and bladder, respectively. (B) This table describes each PET tracer and their class or type of ligand from which it was constructed. The binding affinity is shown as an average of three replicates. Average uptake values of three mice at 24 hours post injection for tumor (T), kidney (K), liver (L) are followed by the tumor-to-muscle ratio for each PET tracer. The average radioactive doses for each tracer are shown in the final column. The * indicates statistical significance $p<0.05$ compared to the cystine knot ^{64}Cu-DOTA-$R_0$1-MG.

CONTROL ID: 2234280

TITLE: [^{18}F]FP-R$_0$1-MG-F2, A Radiofluorinated Cystine Knot PET Tracer for Pancreatic Cancer Detection

PRESENTER: Richard Kimura

ABSTRACT BODY:

Abstract Body: We are currently translating a cysteine knot PET tracer (Figure 1A,B) for detection of pancreatic cancer through integrin avb6, a overexpressed and validated marker. Initial directed evolution studies resulted in the selection of a methionine residue that oxidizes during peptide processing. To facilitate clinical-grade production of PET tracer, additional rounds of site-specific directed evolution led to several high-affinity variants that substituted glycine (MG), arginine (MR) and tryptophan (MW) for methionine in the active loop. New PET tracers were evaluated to determine the best candidate for clinical translation. The original methionine-containing PET tracer (wt) and the variants were coupled to DOTA and radiolabeled with ^{64}Cu for PET imaging in avb6-positive sub-cutaneous A431 xenografts (n=3 per tracer). Data are summarized in Figure 1C. The MR variant demonstrated the highest tumor uptake, but suffered from greatly elevated renal uptake and retention compared to the wt and MG variants. The MW variant also demonstrated comparatively high binding affinity by yeast surface display, but it was not chemically synthesized because of its increased hydrophobicity, which can cause solubility issues during peptide processing, and increased hepatobiliary uptake as a PET tracer. With its shorter radioactive half-life, the ^{18}F-Fluorobenzyl (FB) variant would decrease off-target dose to patients compared to ^{64}Cu-DOTA cohorts, but its tumor uptake was low (~2%ID/g). Therefore, a different radiosynthon, [^{18}F]-Fluoropropyl (FP) was evaluated. FP-R$_0$1-MG produced two stereo chemical enantiomers via fluoropropyl's chiral stereo center (Fig 1B). The fractions, F1 and F2, were separated by ~1 minute using RP-HPLC methods. Both F1 and F2 were identical in mass and 3D-structure by MALDI, and 2D-NMR analysis, respectively. However, PET tracer F2 was chosen over F1, which co-eluted with an impurity upon closer evaluation. [^{18}F]FP-R$_0$1-MG-F2 was produced in high radiochemical purity (>95%) and yield with specific activity of ~1.2 Ci/mmol (details given in a separate abstract). Next, static (Fig 1D) dynamic PET (Fig 1E) studies revealed specific, rapid and high tumor uptake (~4%ID/g) in integrin avb6 positive tumors, a renal-bladder clearance route, and an excellent tumor-to-muscle ratio (~6:1) at 1 hr post injection. These imaging figures of merit bode well for clinical translation. Mouse dosimetry studies using OLINDA software predicted the dose limiting organ in human to be the kidneys which would be subjected to 1.1E-02 mGy/MBq, which indicates that up to ~45.5mCi/single dose can be used per FDA guidelines for exposure (5 Rem/dose). In clinical studies, ~20% of the maximum allowable dose will be used in human subjects. With these encouraging results we are optimizing the radiochemistry, finalizing rat toxicology studies and preparing an eIND to initiate phase 1 clinical trials after FDA approval.

AUTHORS (LAST NAME, FIRST NAME): Kimura, Richard[1]; Shen, Bin[1]; Witney, Timothy H.[1]; Devulapally, Rammohan[1]; Filipp, Fabian[2]; Ilovich, Ohad[1]; Natarajan, Arutselvan[1]; Cheng, Zhen[1]; Chin, Frederick T.[1]; Gambhir, Sanjiv S.[1]

INSTITUTIONS (ALL):

1. Department of Radiology, Stanford University, London, CA, United States.
2. Biology, UC Merced, Merced, CA, United States.

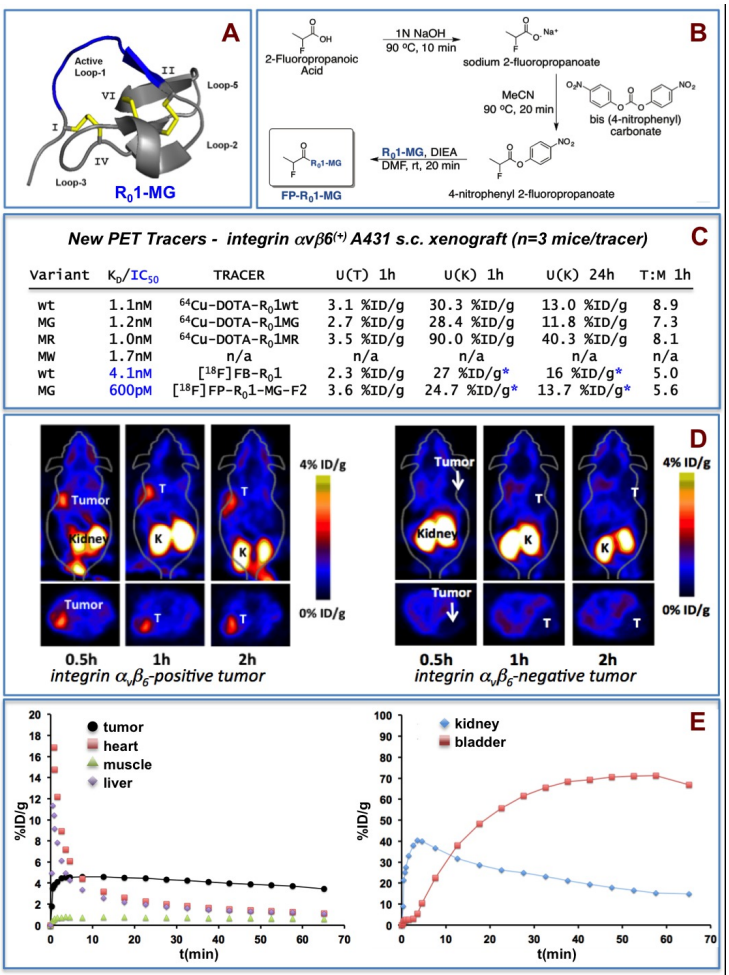

Variant	K_D/IC_{50}	TRACER	U(T) 1h	U(K) 1h	U(K) 24h	T:M 1h
wt	1.1nM	^{64}Cu-DOTA-R$_0$1wt	3.1 %ID/g	30.3 %ID/g	13.0 %ID/g	8.9
MG	1.2nM	^{64}Cu-DOTA-R$_0$1MG	2.7 %ID/g	28.4 %ID/g	11.8 %ID/g	7.3
MR	1.0nM	^{64}Cu-DOTA-R$_0$1MR	3.5 %ID/g	90.0 %ID/g	40.3 %ID/g	8.1
MW	1.7nM	n/a	n/a	n/a	n/a	n/a
wt	4.1nM	[^{18}F]FB-R$_0$1	2.3 %ID/g	27 %ID/g*	16 %ID/g*	5.0
MG	600pM	[^{18}F]FP-R$_0$1-MG-F2	3.6 %ID/g	24.7 %ID/g*	13.7 %ID/g*	5.6

Figure 1. Development of a Cystine Knot PET Tracer for Detection of Pancreatic Cancer. (A) Model structure of a cystine knot peptide, R$_0$1-MG, where the blue loop-1 contains the active sequence that binds integrin αvβ6. The gray loops represent the rest of the cystine knot framework. The yellow structures represent the three disulfide bonds that stabilize the peptide's three-dimensional fold and provides structural rigidity to the peptide's core. Cystine knot peptides are reported to be exceptionally stable in vivo, and resist biological, chemical and physical insult. (B) Labeling scheme for the production of fluoropropyl-labeled R$_0$1-MG detailing the steps for generation of the active fluoropropanoate ester and its subsequent coupling to the N-terminus of R$_0$1-MG to yield FP-R$_0$1-MG. (C) Table summarizing average binding affinities, average uptake (U) values in tumor (1h) and kidney (1h and 24h), and average tumor-to-muscle (T:M) ratio for each PET tracer used in studies comparing and selecting appropriate PET tracer for clinical translation. Due to the shorter half-life of ^{18}F compared to ^{64}Cu, the blue stars (*) indicate 30 minutes and 1 h for the fluorinated PET tracers. R$_0$1-MW was not pursued beyond directed evolution studies; n/a refers to data not available. (D) Static PET images at the indicated timepoints after administration of ~100uCi [^{18}F]FP-R$_0$1-MG-F2 in mouse xenograft models with integrin αvβ6-poitive A431 tumors (left) and integrin αvβ6-negative 293 tumors (right). At least three mice were used per PET tracer variant evaluated throughout this study. The letter T shows the location of the tumors in the models. The letter K identifies mouse kidneys in PET slices shown here. (E) Dynamic PET data for non-decay corrected images obtained with a small animal PET/CT scanner. These data were next decay-corrected, quantified, and entered into OLINDA to allometrically estimate human dosimetry for the eIND application.

CONTROL ID: 2226878

TITLE: Imaging of Nitric Oxide-Producing Macrophages with a Polymer Micelle-Based Fluorescent Probe

PRESENTER: Jun-ichiro Jo

ABSTRACT BODY:

Abstract Body: INTRODUCTION

Nitric oxide (NO) is an intracellular and intercellular messenger that plays an important role in cellular events in physiological and pathophysiological processes. NO is one of the inflammation markers and macrophages of an inflammatory cell produce large amount of NO compared with other cells. Non-invasive detection system of NO is highly required to realize an early therapeutic treatment considering the process of pathophysiological changes. Diaminorhodamine (DAR)-4M is one of the sensitive NO-detecting fluorescent dyes, but there are issues to be improved for the in vivo use. Due to the low molecular weight and water-insolubility of DAR-4M, it is practically difficult to maintain high concentrations at the site of NO to be detected. Therefore, a material approach for the efficient DAR-4M delivery is promising to address the issues. It has been reported that the hydrophobic derivatives of gelatin are effective in water-solubilization of water-insoluble and low-molecular-weight drugs and enhancing their biological activity. In this study, the water-solublization of DAR-4M by the hydrophobic derivative of gelatin was attempted to design an imaging agent for NO detection.

EXPERIMENTAL METHODS

Various amounts of L-α-phosphophatidylethanolamine distearoyl (DSPE) with an active ester were reacted to gelatin with an isoelectric point of 5.0 and the weight-average molecular weight of 10,000 to obtain DSPE-grafted gelatin derivatives (DSPE-g-gelatin) with different grafting extents. DMSO solution containing the DSPE-g-gelatin (20 mg) and DAR-4M (8.4 μg) was dialyzed against double-distilled water to obtain the DAR-4M water-solubilized by DSPE-g-gelatin micelle (DAR-4M micelle). The amount of DAR-4M water-solubilized in each micelle was determined by measuring the absorbance in DMSO solution at the wavelength of 370 nm.

A mouse model of acute interstitial nephritis was induced by the intraperitoneal injection of aristolochic acid (AA). DAR-4M micelle (DAR-4M concentration: 10 μM) was intravenously injected to the mice 1, 4, 7, 14, 21, and 35 days after AA injection. The mice were sacrificed and the inflamed kidneys were isolated 1 hr after micelle injection. The kidneys isolated was fluorescently imaged with the IVIS Spectrum at the excitation and emission wavelengths of 535 and 580 nm, respectively.

RESULTS AND DISCUSSION

The amount of DAR-4M water-solubilized in the micelles became larger with an increase in the extent of DSPE introduced. The apparent size of DAR-4M micelles was almost constant to be 100 nm.

Fluorescent intensity in the kidneys of AA-induced mice injected with the DAR-4M micelle was higher than that of normal mice and injected with free DAR-4M. The extent became large with time after AA induction. The flow cytometry analysis of isolated kidney revealed that the number of macrophages increased with time for nephritis mice induced with AA. The results can be explained by the efficient imaging ability. The DAR-4M micelle would be effectively delivered to the inflamed kidney, and the enough amount of DAR-4M in the micelle would react with NO produced by macrophages in the inflamed kidney.

AUTHORS (LAST NAME, FIRST NAME): Jo, Jun-ichiro[1]; Tatsutomi, Mikio[1]; Tabata, Yasuhiko[1]

INSTITUTIONS (ALL):

1. Institute for Frontier Medical Sciences, Kyoto University, Kyoto, Japan.

(No Image Selected)

CONTROL ID: 2233034

TITLE: In vitro and in vivo evaluation of mTOR inhibitor treatment in gastrointestinal stromal tumor using PET/MRI/^{13}C NMR

PRESENTER: Valentina Di Gialleonardo

ABSTRACT BODY:

Abstract Body: Objective: Imatinib mesylate (Gleevec) is a tyrosine kinase inhibitor used as a first line treatment for advanced and metastatic gastrointestinal sarcoma tumors (GISTs). 10-20% of all GISTs patients are gleevec resistant, additionally, 40-50% of patients that undergo treatment develop secondary (acquired) resistance. Various studies of different types of Imatinib-resistant tumors show a hyperactivation of the phosphatidylinositol 3-Kinase (PI3K) and mammalian target of Rapamycin (mTOR) pathway, in imatinib-resistant tumors. The goal of this study is to evaluate early metabolic changes following direct inhibition of the PI3K/mTOR pathway using a Rapamycin[1]. A multi-modality approach was used to assess both cellular metabolism and signaling *in vitro* and *in vivo*. **Methods:** *In vitro* ^{18}F-FDG uptake and [1,6-^{13}C]glucose NMR were performed in order to compare the metabolic changes in vehicle and 50nM Rapamycin treated GIST T1 cells. PET/MRI imaging as well *ex vivo* ^{13}C NMR were performed in vehicle and treated GIST T1 bearing mice (n=6)[2]. All treatment studies are conducted at 24 hours. **Results and Discussion:** Accumulation of ^{18}F-FDG in GIST T1 decreased 25.79% in Rapamycin treated cells compared to vehicle treated cells ($P<0.01$). In contrast, a larger decrease of [1,6-^{13}C]glucose consumption was observed in treated cells (86.89%, $P<0.01$). [1,6-^{13}C]glucose probes many pathways supplied by glucose, including glycolysis, the TCA cycle and biosynthesis of amino acids. ^{13}C-Lactate production from enriched glucose was reduced 50.6% when treated with Rapamycin from 0.017±0.002 to 0.0084±0.0007µmoles/10^6 cells ($P<0.001$). Total lactate decreased 22.5% from 0.0187±0.00007 to 0.0145 ± 0.0021 µmoles/10^6 cells. A shift in oxidation status after treatment ($NADH/NAD^+$ ratio: 1.65 ± 0.56 vs 3.48 ± 1.12, $p<0.05$) cells was observed as well. ^{18}F-FDG uptake in GIST T1 xenograft mice was of 4.85 ± 0.85 and 2.87 ± 0.31 %ID/g for vehicle and Rapamycin treated animals (41% reduction, $p<0.01$). Western blots for GLUT-1 demonstrate unchanged protein expression, however effective inhibition of pS6K, a key component of PI3K/mTOR pathway, both *in vitro* and *in vivo*. Rapamycin treated cells and animals showed a decrease of FDG uptake and even more pronounced ^{13}C glucose at 24 hrs of treatment, implying a change in glycolytic flux, potentially not captured by ^{18}FDG. This would be a promising target for future metabolic imaging studies in GIST and the potential for probing the lactate pool using novel approaches such as hyperpolarized pyruvate MRI.

1. S Bauer et al, *Oncogene*, 2007, 26, 7560-7568. **2.** I. Marin-Valencia et al, *Cell Metab*, 2012, 15, 827-837.

AUTHORS (LAST NAME, FIRST NAME): Di Gialleonardo, Valentina[1]; Aldeborgh, Hannah N.[1]; Poot, Alex J.[1]; Tee, Sui Seng[1]; Alvarez, Julio A.[1]; Tap, William D.[1, 2]; Lewis, Jason S.[1]; Weber, Wolfgang[1]; Keshari, Kayvan R.[1]

INSTITUTIONS (ALL):

1. Memorial Sloan Kettering Cancer Center, New York, NY, United States.
2. Medicine, Memorial Sloan Kettering Cancer Center, New York, NY, United States.

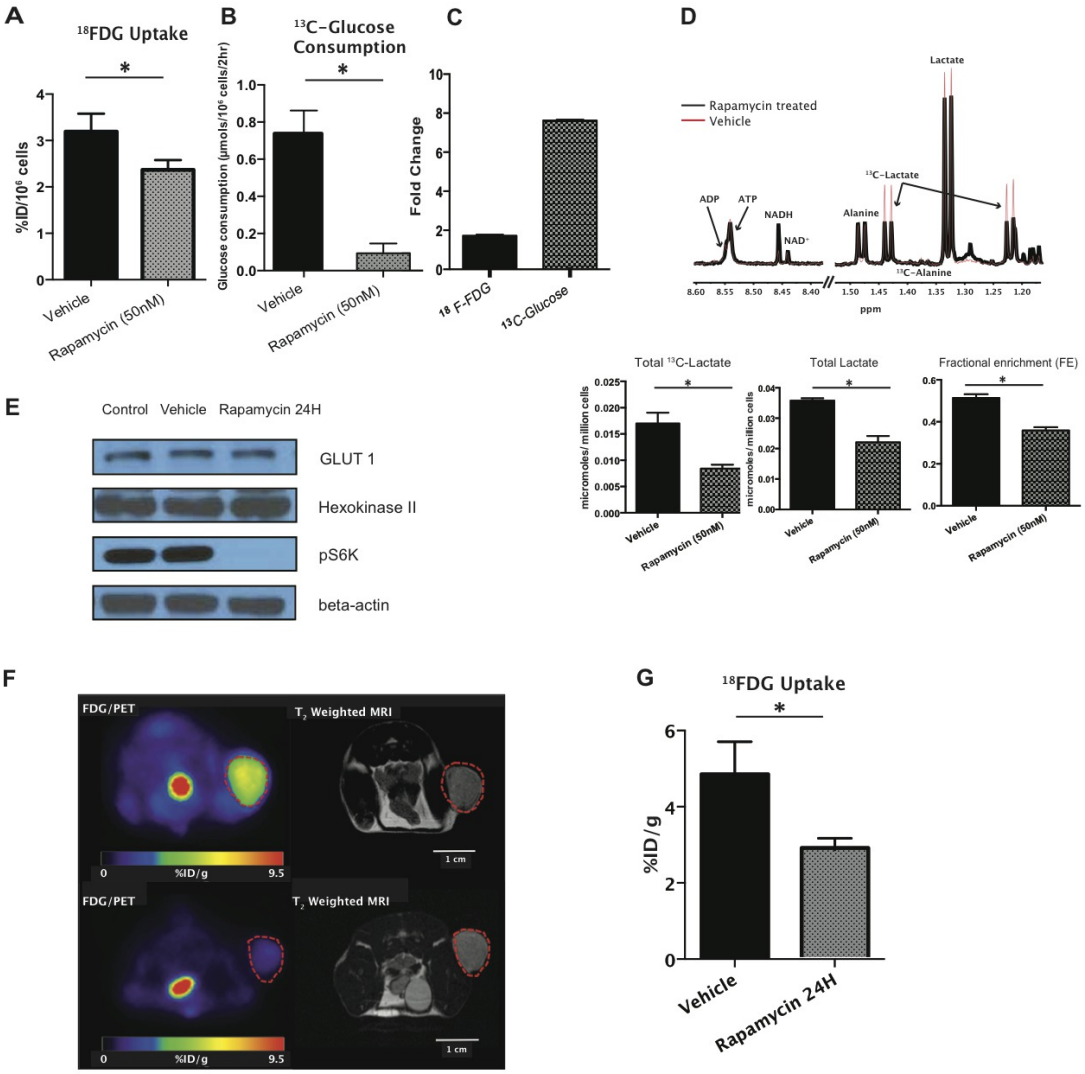

Figure 1. A) 18FDG uptake in vehicle and Rapamycin treated GIST T1 cells. A significant decrease in FDG uptake was observed after 24 hrs treatment (%injected dose/million cells was reduced from 3.19±0.39 to 2.37±0.21, p value <0.05). B) [1,6-13C]glucose consumption was reduce of 86.89% in Rapamycin treated of GIST T1 (0.0186 vs 0.0144 µmoles/million cells). C) Relative change in 18F-FDG and 13C glucose in vehicle and Rapamycin treated GIST T1. D) Representative 1H NMR spectrum of GIST T1 cell extracts of vehicle (red) and Rapamycin treated (black) cells scaled to cell density. 13C satellites are readily observed at chemical shifts indicating direct attachment to 1H moieties of interest. Production of 13C–lactate decreases 49.57% in Rapamycin treated sample as compared to DMSO vehicle. A reduction in total lactate was observed as well to a lesser extent (42.95%). The fractional enrichment (FE) of 13C-lactate is significantly different in treated cells, indicating that the lactate in the cell is potentially derived from alternative sources. 13C alanine labeling and ADP/ATP ratio remain unchanged with rapamycin treatment, while a dramatic increase in NADH as well as the NADH/NAD+ ratio is observed. E) Western blot analysis for GLUT 1, hexokinase II, pS6K. The target is efficiently inhibited in Rapamycin treated cells, while there is no effect on the glucose transporter. F) 18FDG-PET and MRI spectra of a xenografted GIST T1 tumor. The uptake of 18F-FDG pre (top) and post treatment (bottom) with accompanied T2-weighted MRI. No change in tumor size was observed in 24 hrs of treatment. G) Quantification of 18F-FDG-uptake vehicle and treated animals a significant decrease in FDG uptake was observed ($p<0.01$), mimicking in vitro cell studies.

CONTROL ID: 2227042

TITLE: Molecular imaging of drug delivery by using high resolution microscopic mass spectrometry

PRESENTER: Masahiro Yasunaga

ABSTRACT BODY:

Abstract Body: Microscopic mass spectrometry (MMS), in which a microscope is coupled with an atmospheric pressure matrix-assisted laser desorption/ionization (MALDI) and quadruple ion trap time-of-flight (TOF) analyser has been developed for the investigation of the distribution of molecules such as small peptides, metabolites and drugs. The matrix-coated drug sample is ionized and then separated on the basis of its mass-to-charge ratio (*m/z*). Images were acquired from imaging mass spectrometry (IMS) or tandem mass spectrometry (MS/MS) data.

Recently, pharmacokinetic (PK) and pharmacodynamic (PD) studies are important to evaluate the efficacy and toxicity of the drugs. In these analyses, tissue homogenates are generally used for the quantification by high-performance liquid chromatography (HPLC) or liquid chromatography mass spectrometry (LC-MS). However, they lack the information regarding the drug distribution in a specific anatomical area. The information of the drug distribution allows us to optimize the drug design enabling more efficient targeted delivery.

We studied the tissue distribution of paclitaxel (PTX) and its micellar formulation (NK105) using a MMS. (1) We established the drug imaging system with enhanced resolution and sensitivity. In the analysis, MS and MS/MS were used for quantification and validation, respectively. (2) NK105 showed much stronger antitumor effects on a human pancreatic cancer BxPC3 xenograft than PTX. In the drug imaging, we demonstrated that NK105 delivered more PTX to the whole tumor tissue (including the center lesion). In the mouse model, PTX caused the peripheral neurotoxicity but NK105 did not. Multiple high drug-signal areas surrounding and inside the caudal nerve were observed in the case of PTX, whereas the signals after NK105 injection were significantly low. We succeeded in corroborating the EPR effect using MMS. The data obtained by the drug imaging may be useful for facilitating DDS-drug development.

We also introduce some recent progress on MMS imaging and its applications.

[1] Yasunaga M, Furuta M, Ogata K, Koga Y, Yamamoto Y, Takigahira M, Matsumura Y. The significance of microscopic mass spectrometry with high resolution in the visualisation of drug distribution. *Sci Rep.* 3:3050. 2013.

AUTHORS (LAST NAME, FIRST NAME): Yasunaga, Masahiro[1]; Furuta, Masaru[2]; Ogata, Koretsugu[2]; Fujiwara, Yuki[1]; Koga, Yoshikatsu[1]; Matsumura, Yasuhiro[1]

INSTITUTIONS (ALL):

1. Decelopmental Therapeutics, National Cancer Center Hospital East, Kashiwa, Japan.
2. Analytical & Measuring Instruments Division, Shimadzu Corporation, Kyoto, Japan.

(No Image Selected)

CONTROL ID: 2227141

TITLE: Employing tariquidar for 5-HT2A receptor SPECT imaging with [123I]R91150: a rat study

PRESENTER: Philippe Millet

ABSTRACT BODY:

Abstract Body: Introduction P-glycoprotein-induced (Pgp, or MDR1 transporters) radiotracer efflux may hamper neurotransmitter quantification, as for 5-HT2A with [123I]R91150 (1). Tariquidar (TQD) is studied as a Pgp inhibitor that enhances radiotracer uptake in brain. However, region-specific effects of Pgp inhibition may compromise quantification (2). In this study, we compare *in vivo* and *ex vivo* imaging using tariquidar treatment and a *Mdr1a* knock-out (KO) rat model.

Methods 7 male Sprague-Dawley (wild-type, WT) and 8 *Mdr1a* KO rats were employed. *In vivo* dynamic SPECT imaging was performed in 3 WT, 30 min after a bolus 15 mg/kg TQD intravenous injection, in 4 *Mdr1a* KO rats and in 1 WT rat, without prior treatment, along with metabolite analysis and arterial input function measurement. *Ex vivo* autoradiography with [123I]R91150 was performed in 4 WT rats and 4 *Mdr1a* KO rats without prior treatment, 120 min after tracer intravenous injection and in the 3 TQD-treated WT rats (TW-TQD) right after the end of the SPECT session. In vivo SPECT images were analyzed using a (a) 1 tissue-compartment model (1TC) to calculate the whole distribution volume (V_T) and (b) specific tracer uptake ratio (SUR), using cerebellum as reference region. *Ex vivo* autoradiography images were analyzed for specific binding ratio (SBR) estimation. Statistical analysis of results was performed with factorial ANOVA (using “group” and Region-of-interest “ROI” as factors), and correlation analysis.

Results *In vivo* SPECT images of rat brains are shown in Figure 1 (bars represent standardized uptake values). WT rat presents minimal tracer uptake (Fig 1A) that is substantially elevated in *Mdr1a* KO (1B) and WT-TQD rats (1C). *Ex vivo* SBR values from the three groups correlate highly: Pearson’s r=0.962 and 0.979, for the comparison between WT-TQD and *Mdr1a* KO rats with WT rats, respectively, $p<0.001$ for both. However, WT-TQD rat SBR values are significantly higher than those of WT rats with augmentations being not uniform across brain regions ($p<0.001$ for main effect of group and $p<0.01$ for group x ROI interaction). A similar result was obtained with *in vivo* SUR. WT-TQD rats presented values, by average, 3.04±0.50 times higher than *Mdr1a* KO rats ($p<0.001$ for main effect of group). Again, the interaction of factors group and ROI was significant in factorial ANOVA pointing to a regionally varying difference ($p<0.001$). 1TC analysis of SPECT scans demonstrated cerebellum V_T values 2.020 times higher in *Mdr1a* KO rats compared to WT-TQD-rats proposing that differences in reference region’s kinetics may account for this effect.

Conclusion TQD pretreatment may induce non-uniform Pgp inhibition across brain regions. This is important when references tissue approaches are employed, as the cerebellum presents a significantly low V_T in WT-TQD rats compared to *Mdr1a* KO rats, probably due to a locally suboptimal inhibition of Pgp.

Dumas N., et al. Mol Imaging. 2014: 13(1)

Kroll T., et al. Nucl Med Biol. 2014: 41;1-9

AUTHORS (LAST NAME, FIRST NAME): Tsartsalis, Stergios[1, 2]; Tournier, Benjamin B.[1]; Huynh Gatz, Trinh[1]; Millet, Philippe[1]

INSTITUTIONS (ALL):

1. Department of Mental Health and Psychiatry, University hospitals of Geneva, Chêne-Bourg, Geneva, Switzerland.
2. Psychiatry Department, University of Geneva, Geneva, Switzerland.

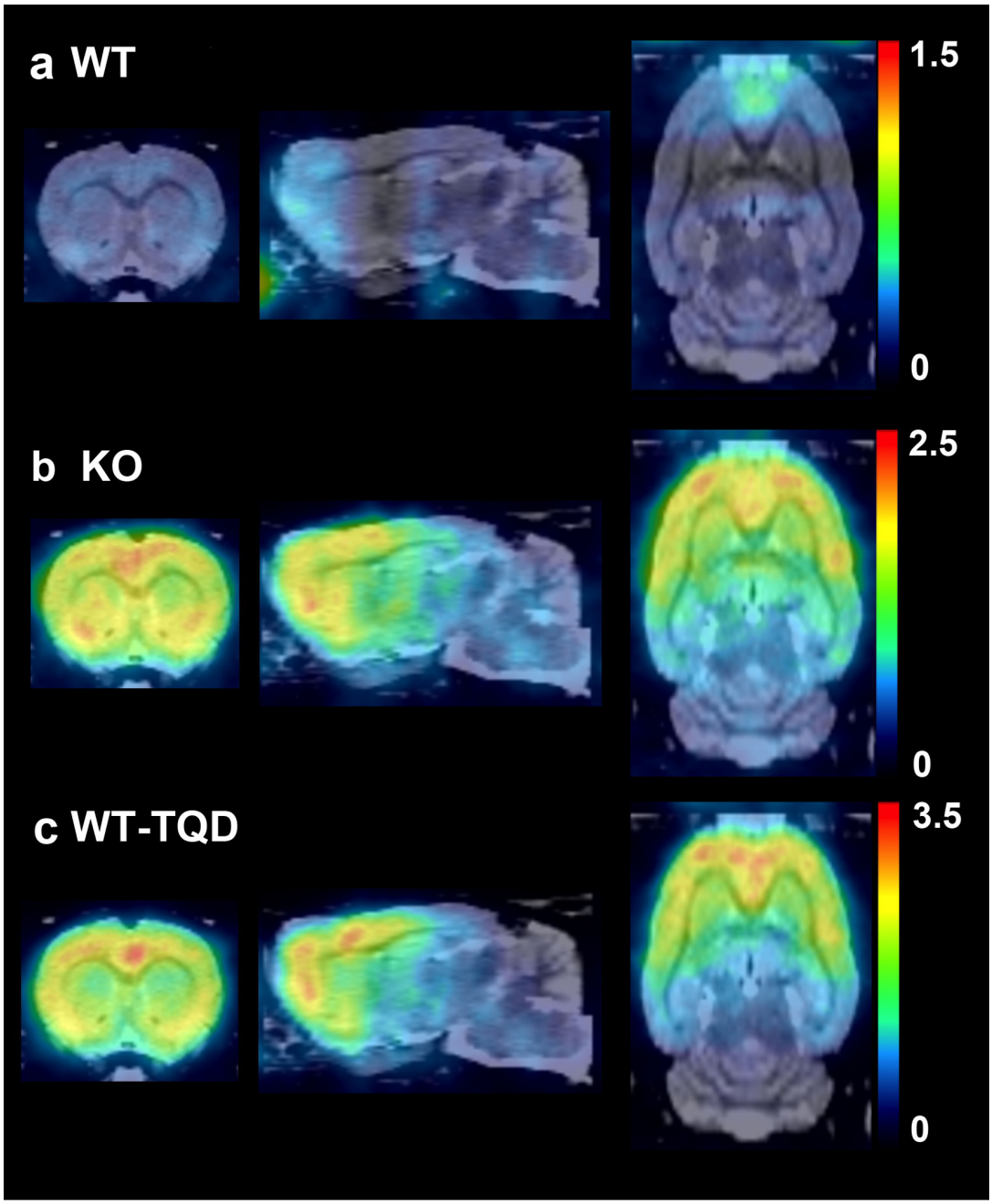

Figure 1. Representative SPECT images, averaged over frames corresponding to the last 60 minutes of the scans, from a WT (a9, a Mdr1a KO (b) and a WT-TQD rat (c). Colour bars represent SUV.

CONTROL ID: 2227142

TITLE: Poly(amidoamine) dendrimers as a tool for the design of functionalized iron oxide nanoparticles for multimodal MRI imaging and drug delivery

PRESENTER: Adriano Boni

ABSTRACT BODY:

Abstract Body: Magnetic nanoparticles are often synthesized by decomposition of organometallic precursors into hot surfactant solutions, a technique that results in highly crystalline iron oxide cores with a narrow size distribution. In order to use these nanoparticles for biomedical applications, replacement of the hydrophobic coating with a hydrophilic one is necessary to obtain stable and injectable aqueous solutions. Among the available hydrophilic coatings, dendrimers, highly monodisperse hyperbranched polymers with a repetitive and perfectly defined structure, have attracted considerable interest.[4-7]

Recently, we presented a novel and facile method to attach commercially available lipid-modified PAMAM dendrimers to the surface of iron oxide nanoparticles. Here we report the latest developments of this work.

By means of this platform, we have been able to tune the relaxometric properties of iron oxide nanoparticles, such as coating thickness and core size, to obtain the best relaxometric efficiency with a high degree of control. Also, we have performed *in vitro* biocompatibility tests and half-life *in vivo* measurements to demonstrate the possibility to use this materials as MRI negative contrast agents.Thanks to the versatility of the PAMAM base coating, we have been able to successfully modify the surface of the nanoparticles for specific applications. Lipophilic drugs, such as coumarin-6 and doxorubicin, could be easily loaded on the nanoparticles by entrapping them into the double lipidic shell formed by the oleic acid and the PAMAM C12 chains on the surface. These results are interesting in view of theranostic applications where the PAMAM coated nanoparticles are able to increase the diagnostic efficiency of MRI, and also to perform therapy by specific deliver and release of drugs.

AUTHORS (LAST NAME, FIRST NAME): Boni, Adriano[1]

INSTITUTIONS (ALL):

1. Center for Nanotechnology Innovation, Istituto Italiano di Tecnologia, Pisa, Italy.

(No Image Selected)

CONTROL ID: 2227204

TITLE: Pretargeted immunoPET imaging of CA19.9, a shed antigen, in murine models of pancreatic cancer

PRESENTER: Jacob Houghton

ABSTRACT BODY:

Abstract Body: *Rationale*: Pretargeted imaging has emerged as an effective way to combine the favorable pharmacokinetic properties of radiolabeled small molecules with the affinity and specificity of antibodies to reduce the radiation exposure during PET imaging. We recently reported that ^{89}Zr-DFO-5B1 exhibited exquisite tumoral uptake in xenografts but also had high retention in blood at 120 h (9.3±1.2 %ID/g), making it an ideal candidate for pretargeting (PreT).[1] We chose to adapt and evaluate a PreT system utilizing the bioorthogonal reaction of transcyclooctene (TCO) and tetrazine (Tz).[2] We used a multistep process in which TCO-conjugated 5B1 was injected and allowed to accumulate at the tumor while slowly clearing nontarget tissue. Then a ^{64}Cu labeled Tz-NOTA conjugate was injected which reacted with 5B1-TCO in the tumor and rapidly cleared nontarget tissues. Our goal was to optimize this system for 5B1, evaluate its utility in the clinically relevant context of shed, circulating CA19.9, and determine its potential for adaptation to pretargeted radioimmunotherapy.

Methods and results: 5B1 was incubated with the *N*-hydroxysuccinyl ester of TCO (30 eq.) in PBS (pH 8.5) to generate 5B1-TCO. Mice with subcutaneous BxPC3 xenografts were injected with the relevant radiolabeled Tz (320-450 µCi) 72 h after injection of the 5B1-TCO (225-250 µg), which was the optimal mass of 5B1 and lag time based on pilot studies.

To optimize the PK of the Tz-NOTA, we modified the previously reported molecule by appending PEG spacers (PEG $_{3,7, \text{ and } 11}$) between NOTA and Tz. Analysis of MIPs from pilot PET studies suggested a PEG_7 linker would give the best results. We then performed serial PET imaging to compare the previously reported ^{64}Cu-NOTA-Tz to ^{64}Cu-NOTA-PEG_7-Tz. Both iterations of the Tz-NOTA yielded excellent PET images as early as 6 h P.I., and MIPs clearly showed that addition of a PEG_7 linker expedited the clearance without decreasing overall uptake. This was corroborated by a biodistribution study, which showed increased uptake of ^{64}Cu-NOTA-PEG_7-Tz at 20 h (8.2±1.7 %ID/g, n=4) compared to ^{64}Cu-NOTA-Tz (7.2±0.7 %ID/g, n=4).

Subcutaneous and orthotopic CAPAN-2 xenograft models were used to evaluate the potential of PreT in the context of shed, circulating CA19.9. Although a biodistribution study indicated that the uptake was lower (3.2±0.4 %ID/g at 20h), tumors were clearly delineated using PET/CT, suggesting PreT is feasible in the context of shed/circulating antigen. Post imaging, tumor tissue was harvested and analyzed via autoradiography, immunohistochemistry, and H&E staining, revealing that uptake of the tracers was specific to areas of CA19.9 expression.

Conclusions: Our optimized PreT system yielded exceptional PET images with extremely high uptake for a PreT system, which is an important step towards using PreT for radioimmunothearpy. We also demonstrated the potential for using PreT in the clinically relevant and complicating context of shed, circulating antigen.

[1] Viola-Villegas et al. J. Nucl. Med. 2013, 54(11):1876-82.

[2] Zeglis et al. J. Nucl. Med. 2013, 54(8):1389-96.

AUTHORS (LAST NAME, FIRST NAME): Houghton, Jacob[2]; Zeglis, Brian M.[3]; Abdel-Atti, Dalya[2]; Sawada, Ritsuko[1]; Scholz, Wolfgang W.[1]; Lewis, Jason S.[2]

INSTITUTIONS (ALL):

1. Mabvax Therapeutics, San Diego, CA, United States.
2. Department of Radiology, Memroial Sloan Kettering Cancer Center, New York, NY, United States.
3. Department of Chemistry, Hunter College and the Graduate Center of the City University of New York, New York, NY, United States.

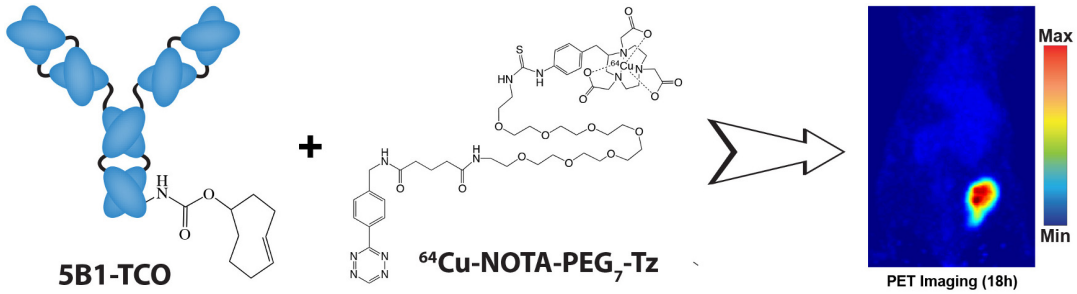
5B1-TCO
64Cu-NOTA-PEG7-Tz
Max
Min
PET Imaging (18h)

CONTROL ID: 2227208

TITLE: Detection of tumor macrophage recruitment by MRI following treatment with GSK2849330, an ADCC and CDC optimized anti HER3 mAb, in CHL-1 melanoma xenograft tumors

PRESENTER: Hasan Alsaid

ABSTRACT BODY:

Abstract Body:

Introduction

ErbB3/HER3 is a member of the epidermal growth factor receptor family of tyrosine kinases. In this study, we investigated the effects of GSK2849330, an anti-HER3 antibody with optimized antibody dependent cell cytotoxicity (ADCC) and complement dependent cytotoxicity (CDC) activity[1], on tumor macrophage recruitment in CHL-1 melanoma xenograft tumor using ferumoxytol-enhanced MRI. Ferumoxytol is an ultrasmall superparamagnetic iron oxide (USPIO) MRI contrast agent that is phagocytosed by macrophages; it has previously been used to measure tumor-associated macrophages in CHL-1 xenograft tumor[2].

Methods

All procedures were approved by the Animal Care and Use Committee of GlaxoSmithKline and were specifically designed to minimize animal discomfort. C.B-17 SCID female mice (age 9-10 weeks) bearing CHL-1 tumors were treated for 2 weeks with either vehicle (n=10) or GSK2849330 (25mg/kg, ip, 3 times/week, n=10). Imaging was performed on a 9.4 Tesla vertical MRI (Bruker Biospin GmbH) using a 30mm volume coil. MRI was performed pre and 24 hours post iv injection of 1.0mmol [Fe]/kg ferumoxytol (AMAG Pharmaceuticals, Inc) on day 16 post-treatment. Axial Multi Gradient Echo T_2^*-weighted (T_2^*-W) images were acquired: TR/TE=300/2.2ms, flip Angle =30º, NEX=4, FOV=3.5x3.5cm, Matrix =128x128, and slice thickness =1mm. Tumors were collected, formalin fixed and paraffin embedded for Immunohistochemistry (IHC): F4/80 macrophages and Prussian Blue for presence of ferric iron. MR Image analysis was performed using Jim 7.0 software (Xinapse Systems). Statistical analysis was performed with GraphPad Prism 5.0 using Two-Way ANOVA & t-test, and data are presented as Mean±SE.

Results

Compared to vehicle treatment, tumor growth (A) was significantly reduced by GSK2849330 treatment. MRI (B) showed differences in tumor signal intensity post USPIO injection compared to baseline. Signal/Noise (T_2^*-W) was decreased significantly post-USPIO injection compared to pre injection in the GSK2849330 treated group (C) (50.5±2.5 *vs* 39.6±2.1; $p<0.01$) indicating that ferumoxytol uptake was higher in the GSK2849330 treated group compared to the vehicle group. A qualitative review of IHC staining in CHL-1 tumors (D) confirmed the co-localization of ferumoxytol (iron) with a subset of F4/80+ve macrophages.

Conclusion

Treatment with GSK2849330 inhibited tumor growth and was associated with significant increase in tumor macrophage recruitment in CHL-1xenograft as determined by ferumoxytol-enhanced MRI. These results suggest that ferumoxytol-enhanced MRI can be used to monitor aspects of the immune system antitumor response to GSK2849330, potentially providing a clinically translatable technique to non-invasively assess ADCC in patients.

Reference

1- N. Clarke et al. Preclinical pharmacologic characterization of GSK2849330, a monoclonal AccretaMab® antibody with optimized ADCC and CDC activity directed against HER3. European Journal of Cancer, 2014, 50, 98-99.

2- H. Alsaid et al. Ferumoxytol-enhanced MRI of macrophages in CHL-1melanoma tumor model. Proc. Intl. Soc. Mag. Reson. Med. 21 (2013), #1712.

AUTHORS (LAST NAME, FIRST NAME): Alsaid, Hasan[1]; Rambo, Mary[1]; Skedzielewski, Tinamarie[1]; Hoang, Bao[3]; Long, Edward R.[1]; Tunstead, James[3]; Clarke, Neil J.[2]; Matheny, Christopher[2]; Jucker, Beat M.[1]

INSTITUTIONS (ALL):

1. Preclinical & Translational Imaging, LAS, PTS, GlaxoSmithKline, King of Prussia, PA, United States.
2. Biopharm R&D, GlaxoSmithKline, King of Prussia, PA, United States.
3. Molecular Discovery Research, PTS, GlaxoSmithKline, King of Prussia, PA, United States.

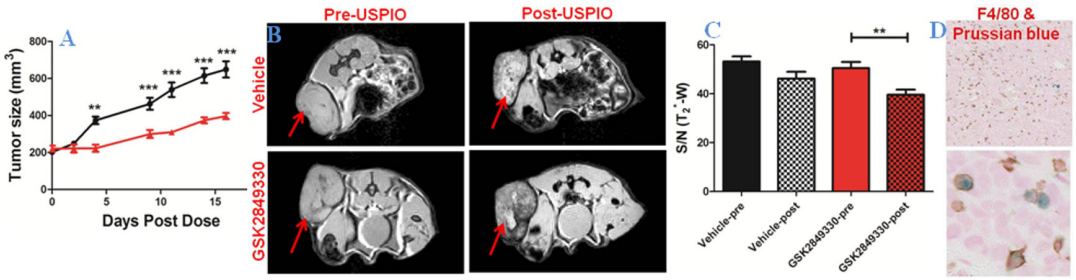

Figures Tumor growth (A) was significantly inhibited in the GSK2849330 treated group (red) compared to the vehicle group (black). Axial MRI slices (B) showing T_2^*-W images pre-USPIO and 24 hours post injection of ferumoxytol (Post-USPIO), red arrows indicate xenograft tumors. S/N (T_2^*-W) decreased significantly post-USPIO in the GSK2849330 treated group (C). IHC dual staining (D) reflects association of cytoplasmic iron staining with a sub population of plasma membrane F4/80 positive cells. **P<0.01, and ***P<0.001.

CONTROL ID: 2227267

TITLE: Development of Imaging Technologies to Track Tuberculosis in Live Animals

PRESENTER: Jeffrey Cirillo

ABSTRACT BODY:

Abstract Body: Tuberculosis afflicts one-third of the world's population and its slow growth rate of approximately one month greatly hinders research. Our laboratory has developed technologies that allow immediate quantitative assessment of the causative agent, *Mycobacterium tuberculosis* (Mtb). Beyond application in tuberculosis research, these technologies are geared toward clinical applications for diagnosis of infections and assessment of therapeutic outcomes. We have utilized three primary approaches to track Mtb; fluorescent proteins (FP), bioluminescence systems and reporter enzyme fluorescence (REF)(*1-7*). Both FP and bioluminescence require recombinant strains and therefore, are applicable to pre-clinical studies. REF, which uses endogenous enzymes combined with custom fluorogenic substrates to produce signal, can be applied clinically and demonstrate great promise when combined with microendoscopy. In the case of FP, we have constructed transcriptionally and translationally optimized plasmids. tdTomato, in particular, performs well in live animals, with a threshold of ~10^4 colony forming units (cfu) during pulmonary infection. Studies have suggested some impact on virulence using bacterial bioluminescence, but transcriptionally and translationally optimized firefly and click-beetle red reporter systems perform as well as FP, with thresholds of detection ~10^4 cfu. FP have the advantage that they allow microscopy post-fixation in animal models and bioluminescence systems allow the advantage of a more rapid readout of bacterial viability. These data led us to the conclusion that stable dual FP and bioluminescence systems are optimal for most pre-clinical studies. REF imaging demonstrated greater sensitivity than FP or bioluminescence imaging for Mtb in live animals, with a threshold of <10^3 cfu during pulmonary infections, but despite the development of sufficient probe specificity for clinical use(*8, 9*), most clinical applications are limited due to the greater tissue depth present in infected humans. We circumvented the impact of tissue depth using microendoscopy for illumination and detection, allowing detection of ~100 cfu during pulmonary infection. This greater sensitivity allows use of an integrated microendoscope with a whole body imaging system for pre-clinical imaging and microendoscopy using aerosol delivery of substrate for detection of infections directly in larger organisms, potentially including humans, infected with physiologically relevant bacterial numbers.

1. Y. Kong *et al.*, *Curr Protoc Microbiol* **Chapter 2**, Unit2C 3 (May, 2011).
2. Y. Kong, J. D. Cirillo, *Virulence* **1**, 558 (Nov-Dec, 2010).
3. Y. Kong *et al.*, *Curr Protoc Microbiol* **Chapter 2**, Unit2C 4 (May, 2011).
4. Y. Kong, S. Subbian, S. L. Cirillo, J. D. Cirillo, *Tuberculosis (Edinb)* **89 Suppl 1**, S15 (Dec, 2009).
5. Y. Kong *et al.*, *Proc Natl Acad Sci U S A* **107**, 12239 (Jul 6, 2010).
6. M. H. Chang, S. L. Cirillo, J. D. Cirillo, *J Vis Exp*, (2011).
7. M. Chang, K. P. Anttonen, S. L. Cirillo, K. P. Francis, J. D. Cirillo, R*PLoS One* **9**, e108341 (2014).
8. H. Xie *et al.*, *Nature chemistry* **4**, 802 (Oct, 2012).
9. Y. Cheng *et al.*, *Angew Chem Int Ed Engl* **53**, 9360 (Aug 25, 2014).

AUTHORS (LAST NAME, FIRST NAME): Yang, Hee-Jeong[1]; Kong, Ying[2]; Cheng, Yunfeng[3]; Nooshabadi, Fatemeh[4]; Janagama, Harish[1]; Hassounah, Hany A.[1]; Xie, Hexin[3]; Rao, Jianghong[3]; Maitland, Kristen C.[4]; Cirillo, Jeffrey[1]

INSTITUTIONS (ALL):

1. Microbial Pathogenesis and Immunology, Texas A&M Health Science Center, Bryan, TX, United States.
2. University of Tennessee Health Science Center, Memphis, TN, United States.
3. Stanford University, Stanford, CA, United States.
4. Texas A&M University, College Station, TX, United States.

(No Image Selected)

CONTROL ID: 2227292

TITLE: Uptake and retention of Mn and ^{52}Mn in the rat brain for PET/MRI in neurological applications

PRESENTER: Christina Lewis

ABSTRACT BODY:

Abstract Body: Objectives: Dual-modality manganese (Mn)-based imaging with PET and MRI has gained attention due to the recent production of the β^+-emitting radiometal ^{52}Mn by several groups. Mn-based PET/MRI may have a variety of applications, particularly in neurology, where Mn-enhanced MRI has been applied for anatomical and functional studies in rodents. In this work, we investigate the uptake and retention of Mn contrast agents for MRI (Mn^{2+}) and PET (^{52}Mn) in the rat brain with the aim of optimizing protocols for *in vivo* Mn-based PET/MRI.

Methods: $MnCl_2$ was prepared at a concentration of 66.7 mM and brought to pH 7 in 100 mM bicine. ^{52}Mn (29.4% β^+, 575 keV E_{max}, $t_{1/2}$=5.6 days) was cyclotron produced through irradiation of ^{nat}Cr with 16 MeV protons and separated via ethanolic anion exchange. ^{52}Mn was diluted either in saline to 1.5 mCi/mL or in $MnCl_2$ solution to 0.4 mCi/mL. Animals were delivered 30-60 mg/kg $MnCl_2$ and/or 2 mCi/kg ^{52}Mn via tail vein at a rate of 2 mL/hr. To observe Mn uptake with MRI, *in vivo* R_1 mapping was performed pre-contrast and at days 1, 2, 4, 7, and 14 post-contrast. ROI-based measurements of R_1 relaxation rate in the striatum were compared across doses and time points. To observe ^{52}Mn uptake, brains were excised at days 1 and 2 post-contrast and activity uptake was measured via gamma counting. One subject underwent PET/CT at 48 hours after infusion of no-carrier-added (NCA) ^{52}Mn.

Results: Striatal R_1 enhancement was observed at all time points and doses with MRI. The greatest R_1 increase of 84% was observed at the maximum delivered dose 48 hours after contrast delivery. Despite high levels of inter-subject variability in MRI, a trend of increased R_1 enhancement at higher doses was observed. In ^{52}Mn gamma counting experiments, an increase in brain uptake of 90-140% was observed in subjects delivered NCA ^{52}Mn (average 0.10%ID/g) compared to those delivered ^{52}Mn supplemented with $MnCl_2$ (average 0.05%ID/g). Again, increased uptake was observed at 48 hours compared to 24 hours, and this increase was greater when ^{52}Mn was supplemented with $MnCl_2$. *In vivo* PET/CT showed highest brain ^{52}Mn uptake in the pituitary and to a lesser extent in the cerebellum, with a whole-brain average of 0.16%ID/g.

Conclusions: These data lay the groundwork for optimizing Mn-based PET/MRI imaging protocols in rodent neurological applications. They indicate that maximum Mn uptake occurs 48 hours after contrast administration for both tracer (PET) and bulk (MRI) doses. They also support the previously established conclusion that R_1 relaxation rate increases with $MnCl_2$ dose, but contrast doses must be limited to a non-toxic range. The reduced ^{52}Mn uptake observed when ^{52}Mn was supplemented with $MnCl_2$ is likely due to the saturation of Mn transporters across the blood-brain barrier. The greater increase in ^{52}Mn uptake over time with supplemented $MnCl_2$ suggests that more circulating Mn may result in greater delayed uptake. Last, we observed low but detectable brain uptake of ^{52}Mn with *in vivo* imaging. Partial volume effects from other high signal regions of the head could obscure signal changes in the brain and should be taken into careful consideration.

AUTHORS (LAST NAME, FIRST NAME): Lewis, Christina[1]; Graves, Stephen[1]; Smit-Oistad, Ivy[2]; Nickles, Robert J.[1]; Meyerand, Mary E.[1, 3]; Suzuki, Masatoshi[2]

INSTITUTIONS (ALL):

1. Medical Physics, University of Wisconsin-Madison, Madison, WI, United States.
2. Comparative Biosciences, University of Wisconsin-Madison, Madison, WI, United States.
3. Biomedical Engineering, University of Wisconsin-Madison, Madison, WI, United States.

(No Image Selected)

CONTROL ID: 2227396

TITLE: Labeling monocytes with gold nanoparticles to track their recruitment in atherosclerosis

PRESENTER: Peter Chhour

ABSTRACT BODY:

Abstract Body: Introduction:

Monocytes play a key role in the progression of atherosclerosis. Monocytes are recruited into the arterial intima and differentiate into macrophages. These macrophages become foam cells leading to the development of a rupture prone plaque. A plaque rupture in a coronary artery can lead to an occlusion of the artery causing a heart attack. Computed tomography (CT) is one of the best non-invasive techniques to image the heart and coronary arteries. For CT, there has been an increasing interest in the use of gold nanoparticles (AuNP) as contrast agents due to their high biocompatibility and strong x-ray attenuation properties. We herein report the development of AuNP to label monocytes and non-invasively track their recruitment to atherosclerotic plaques.

Results:

AuNP of 15 nm diameter were synthesized by using the Turkevich method (Fig. 1A). We then proceeded to stabilize these particles for biological use by examining a library of thiol-ligands. Formulations found stable were further characterized with TEM (Fig. S1), UV/vis (Fig. S2A), DLS (Fig. S2B), and zeta potential (Fig. S2C). These AuNP formulations were evaluated *in vitro* with a monocyte cell line (RAW 264.7) for cytotoxicity, cytokine production, and AuNP uptake (Fig. S3, S4). AuNP formulations were found not to affect cell viability except for PEI coated particles (Fig. 1B). Additionally, monocyte cytokine production was not affected by AuNP except for PEI and 4-MB coatings (Fig. 1C). From these experiments, 11-MUDA coated AuNP were selected as a lead formulation due to their high uptake in monocytes and lack of effect on biological parameters.

We isolated primary monocytes from the spleens of mice. The purity of these monocytes was found to be >99% with flow cytometry (Fig. S5). The primary cells were examined *in vitro* with 11-MUDA coated AuNP. The effects of the 11-MUDA AuNP were found to be similar in primary cells as the monocyte cell line for viability (Fig. S6A), cytokine production (Fig. S6B), and cell uptake (Fig. 1D). For our *in vivo* studies, ApoE-/- mice were fed Western diet for 10 weeks to establish an atherosclerotic mice model. Primary monocytes were then labeled with 11-MUDA AuNPs and intravenously injected into atherosclerotic mice. The mice were scanned using a pre-clinical CT scanner (day 0, 3, 4, 5 post injection) to track the recruitment of the labeled monocytes to atherosclerotic plaques. Increasing CT intensities were found in the aortic region of the atherosclerotic mice (Fig. 1E). Such increases were not observed in the aortas of wild type mice or atherosclerotic mice injected with unlabeled monocytes.

Conclusion:

In this study, we identified AuNP formulations optimal for monocyte uptake. The formulation exhibiting the best *in vitro* properties was used for *in vivo* experiments. Hyperintensities in the CT scans were found in the aortas of the mice. In future experiments, we will seek to determine the monocyte accumulation in the plaque by correlating CT intensity and gold concentration in the tissue. Additionally, the accumulation of AuNP labeled monocytes will be confirmed via TEM on aortic sections.

AUTHORS (LAST NAME, FIRST NAME): Chhour, Peter[1]; Naha, Pratap C.[2]; Kim, Johoon[1]; O'Neill, Sean [1]; Reilly, Muredach P.[1]; Ferrari, Victor A.[1]; Cormode, David[2]

INSTITUTIONS (ALL):

1. University of Pennsylvania, Philadelphia, PA, United States.
2. Radiology, University of Pennsylvania, Philadelphia, PA, United States.

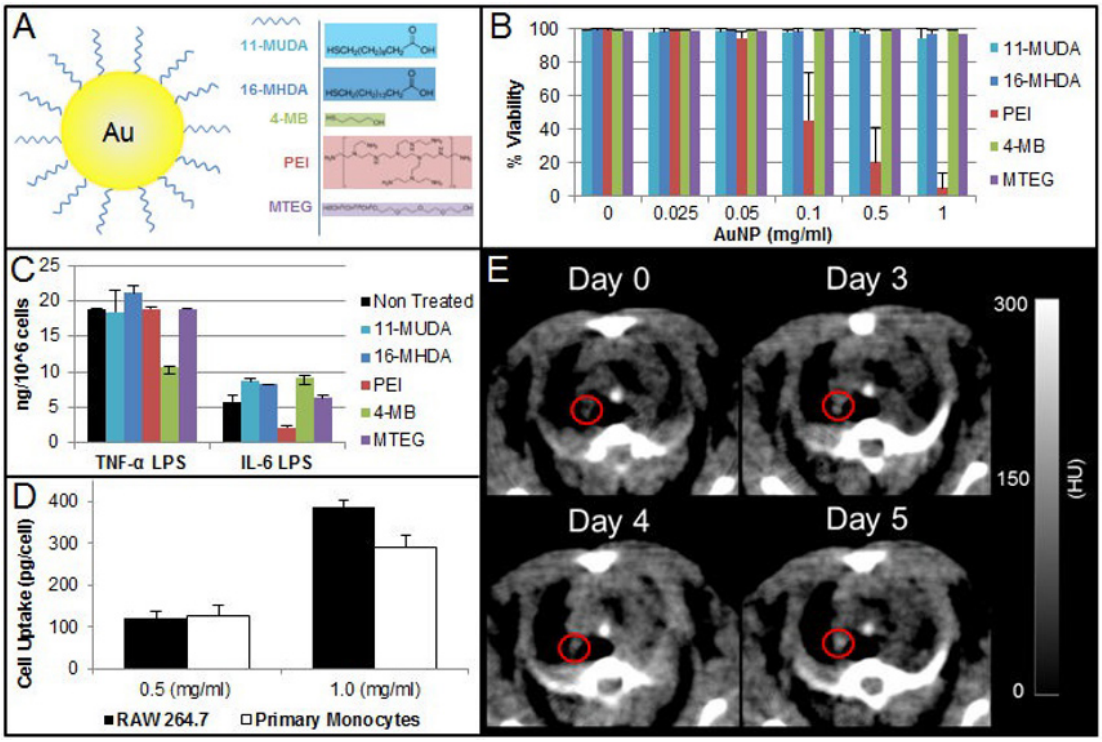
A
Au
11-MUDA
16-MHDA
4-MB
PEI
MTEG
B
% Viability
AuNP (mg/ml)
0
0.025
0.05
0.1
0.5
1
11-MUDA
16-MHDA
PEI
4-MB
MTEG
C
ng/10^6 cells
TNF-α LPS
IL-6 LPS
Non Treated
11-MUDA
16-MHDA
PEI
4-MB
MTEG
D
Cell Uptake (pg/cell)
0.5 (mg/ml)
1.0 (mg/ml)
RAW 264.7
Primary Monocytes
E
Day 0
Day 3
Day 4
Day 5
300
150
0
(HU)

CONTROL ID: 2227450

TITLE: Nanogels from Metal-Chelating Crosslinkers as Platforms for Bimodal MRI/PET Imaging: An Application to Copper-64 PET Imaging of Tumors and Metastases

PRESENTER: Jacques Lux

ABSTRACT BODY:

Abstract Body: Metal complexes are of considerable importance in medicine and are clinically applied to multiple imaging modalities[1] such as magnetic resonance imaging (MRI),[2] positron emission tomography (PET)[3] and X-ray imaging.[4] To create a versatile platform for the development of multifunctional agents combining imaging modalities and radiotherapy, we synthesized metal-chelating hydrogel nanoparticles (nanogels) with maximal chelation stability. These nanogels were formulated by incorporating metal-chelating crosslinkers, which both act as an imaging probe and hold the nanogels together. These nanoscale systems have high stability in aqueous solution,[5] high loading capacity for biomacromolecules[6] or smaller molecules,[7] and allow ample water access throughout the particle, which is important for MRI contrast agents, where the metal must interact with water to enhance signal.

Metal-chelating crosslinkers were first chelated with Gd^{3+} to yield stable MRI contrast agents. The nanogel structure decreases the chelator's tumbling frequency and grants fast water exchange, both of which enhance relaxivity. Polyacrylamide(PAA)-based nanogels (diameter 50 to 85 nm) incorporating these Gd^{3+}-chelating crosslinkers display higher relaxivity than clinically used contrast agents, such as Magnevist® (4.9-fold increase) or Dotarem® (6-fold increase). Importantly, this nanogel structure also stabilizes Gd^{3+} ions within the chelates against transmetallation, which should reduce toxicity associated with release of free Gd^{3+} ions.

To demonstrate the versatility of the platform, ^{64}Cu was incorporated instead of Gd^{3+} to obtain PET radiotracers. Radiolabeled nanogels stably retained ^{64}Cu in mouse serum. Upon intravenous injection in BALB/c mice with mammary 4T1 tumors or metastases, radiolabeled nanogels accumulated in tumors and metastases as detected by PET/CT imaging. Biodistribution studies confirmed high accumulation of the ^{64}Cu-labeled nanogels in tumors (12.3% ID/g and 16.6% ID/g) and metastases (29.9% and 30.4% ID/g) at 24 and 48 h after injection, and low accumulation in the liver and spleen (8.5% ID/g and 5.5% ID/g respectively after 24 h).

These promising results suggest that this strategy could be used to develop bimodal MRI/PET imaging platforms by using both the ^{64}Cu-NOTA crosslinkers (PET) and Gd^{3+}-DOTA crosslinkers (MRI), which would provide the high sensitivity and quantification of PET with the high resolution and anatomical precision of MRI.[8] We are currently incorporating our crosslinkers into nanogels composed of a biodegradable polymer backbone to accelerate clearance. We are also exploring the incorporation of ^{177}Lu chelates as crosslinkers to obtain theranostic nanogels for bimodal imaging MRI/PET and radiation therapy.

(1) Caravan et al, *Wiley Encyclopedia of Chemical Biology*; John Wiley & Sons, Inc.: 2007.
(2) Caravanet al, *Chem Rev* **1999**, *99*, 2293.
(3) Anderson et al, *Chem Rev* **1999**, *99*, 2219.
(4) Yu et al, *Chem Rev* **1999**, *99*, 2353.
(5) Kabanov et al, *Angew Chem Int Edit* **2009**, *48*, 5418.
(6) Kwon et al, *J Control Release* **2005**, *105*, 199.
(7) Bronich et al, *Nano Lett* **2001**, *1*, 535.
(8) Weissleder et al, *Nature* **2008**, *452*, 580.

AUTHORS (LAST NAME, FIRST NAME): Lux, Jacques[1]; White, Alexander G.[2]; Chan, Minnie[1]; Anderson, Carolyn J.[2]; Almutairi, Adah[1, 3]

INSTITUTIONS (ALL):
1. School of Pharmacy, UCSD, San Diego, CA, United States.
2. Departments of Radiology, Pharmacology & Chemical Biology and Bioengineering, University of Pittsburgh, Pittsburgh, PA, United States.
3. KACST-UCSD Center for Excellence in Nanomedicine and Engineering, La Jolla, CA, United States.

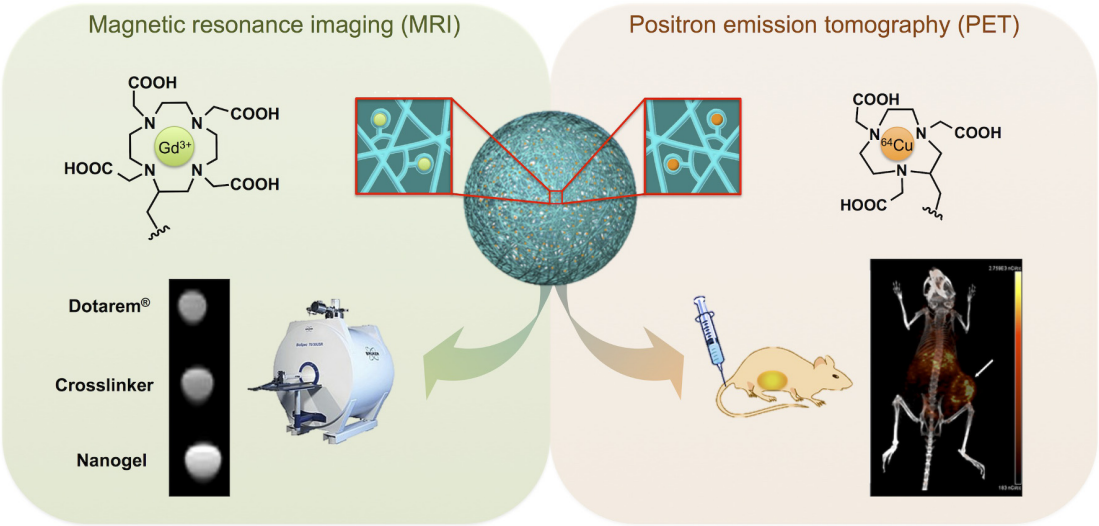
Magnetic resonance imaging (MRI)
Positron emission tomography (PET)
COOH
COOH
COOH
HOOC
Gd3+
COOH
COOH
64Cu
HOOC
Dotarem®
Crosslinker
Nanogel

CONTROL ID: 2227462

TITLE: Efficient preparation and pilot *in vivo* studies of hyperpolarized 1-^{13}C-phospholactate metabolic contrast agent

PRESENTER: Roman Shchepin

ABSTRACT BODY:

Abstract Body: BACKGROUND: Hyperpolarized (HP) ^{13}C-pyruvate (^{13}C-PYR) and ^{13}C-lactate (^{13}C-LAC) have been successfully used for molecular imaging of elevated glycolysis of cancer. The technology of using HP ^{13}C MRI (metabolic imaging) has progressed rapidly from the proof-of-principle *in vitro* and preclinical studies to clinical trials over the last decade (1). Dissolution-dynamic nuclear polarization (d-DNP) is the only HP technology used to efficiently hyperpolarize ^{13}C-PYR to date (2). Once injected, exogenous HP ^{13}C-PYR is converted to HP ^{13}C-LAC enzymatically using lactate dehydrogenase (LDH). Moreover, it has also been shown that the injection of exogenous HP ^{13}C-LAC can also be effectively used for detection on endogenous LAC pool using LDH-catalyzed exchange *in vivo* (3). While both approaches of injecting exogenous HP ^{13}C-PYR or HP ^{13}C-LAC reach the same goal of visualizing elevated glycolysis and endogenous LAC pool (an experiment with clinical potential in oncology), the use of exogenous HP ^{13}C-LAC (vs. HP ^{13}C-PYR) is advantageous, because HP ^{13}C-LAC can be used at physiological concentrations (3).

METHODS: Parahydrogen (pH_2) based hyperpolarization technique (4) is an ultra-fast alternative technology capable of producing a HP contrast agent within a minute. However, the requirement of having custom isotopically labeled molecular precursor with double or triple bond typically adjacent to the ^{13}C significantly dampened the development of this useful in vivo hyperpolarization technique (5). We have recently developed 1-^{13}C-phosphoenolpyruvate-d_2 (1-^{13}C-PEP-d_2), precursor for hyperpolarization of 1-^{13}C-phospholactate-d_2 (1-^{13}C-PLAC-d_2) via molecular addition of pH_2 across the double bond (Fig. 1) (6).

RESULTS/DISCUSSION: ^{13}C nuclear spin polarization of 1-^{13}C-PLAC-d_2 of > 15% was demonstrated using 1-^{13}C-PEP-d_2 molecular precursor corresponding to signal enhancement of > 30,000,000 fold at 5.75 mT – the magnetic field of the *hyperpolarizer* device (6). This new HP contrast agent is produced in aqueous medium. It has a relatively long lifetime: 58 ± 4 s at 47.5 mT, and it can be produced in sufficiently large quantities: ~50 micromoles in ~3 mL per each run, suitable for *in vivo* studies. Moreover, it was shown (using a MUC1 mouse model of breast cancer) that exogenous non-hyperpolarized 1-^{13}C-PLAC is converted 1-^{13}C-LAC by blood phosphatases within second even at higher dose. Therefore, this approach of injecting HP 1-^{13}C-PLAC and producing HP 1-^{13}C-LAC is potentially suitable for molecular imaging of elevated endogenous LAC (3) – the hallmark of cancer and other diseases. The pilot *in vivo* study using exogenous HP 1-^{13}C-PLAC-d_2 injected intravenously (via tail vein) proves the feasibility of *in vivo* detection of HP 1-^{13}C-PLAC-d_2 and potentially other metabolites.

REFERENCES: (1) Kurhanewicz, J. et al. *Neoplasia* **2011,** *13*, 81. (2) Ardenkjaer-Larsen, J. H. et al. *PNAS* **2003,** *100*, 10158. (3) Kennedy, B. et al. *JACS* **2012,** *134*, 4969. (4) Bowers, C. et al. *Phys. Rev. Lett.* **1986,** *57*, 2645. (5) Shchepin, R. et al. *JACS* **2012,** *134*, 3957. (6) Shchepin, R. et al. *Anal. Chem.* **2014,** *86*, 5601. (7) Shchepin, R. et al. *J. Labelled Comp. Radiopharm.* **2014,** *57*, 51.

AUTHORS (LAST NAME, FIRST NAME): Shchepin, Roman[1]; Coffey, Aaron M.[3]; Pham, Wellington[1]; Chekmenev, Eduard Y.[2]

INSTITUTIONS (ALL):

1. VUIIS, Vanderbilt Medical Center, Nashville, TN, United States.
2. Institute of Imaging Science, Vanderbilt University, Nashville, TN, United States.
3. VUIIS, Vanderbilt Medical Center, Nashville, TN, United States.

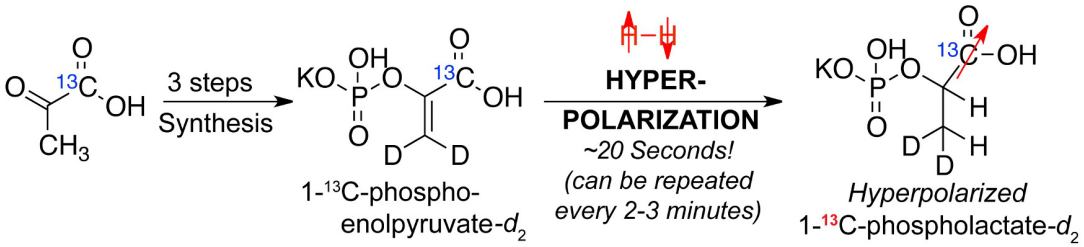
3 steps
Synthesis
1-13C-phospho-
enolpyruvate-d2
HYPER-
POLARIZATION
~20 Seconds!
(can be repeated
every 2-3 minutes)
Hyperpolarized
1-13C-phospholactate-d2

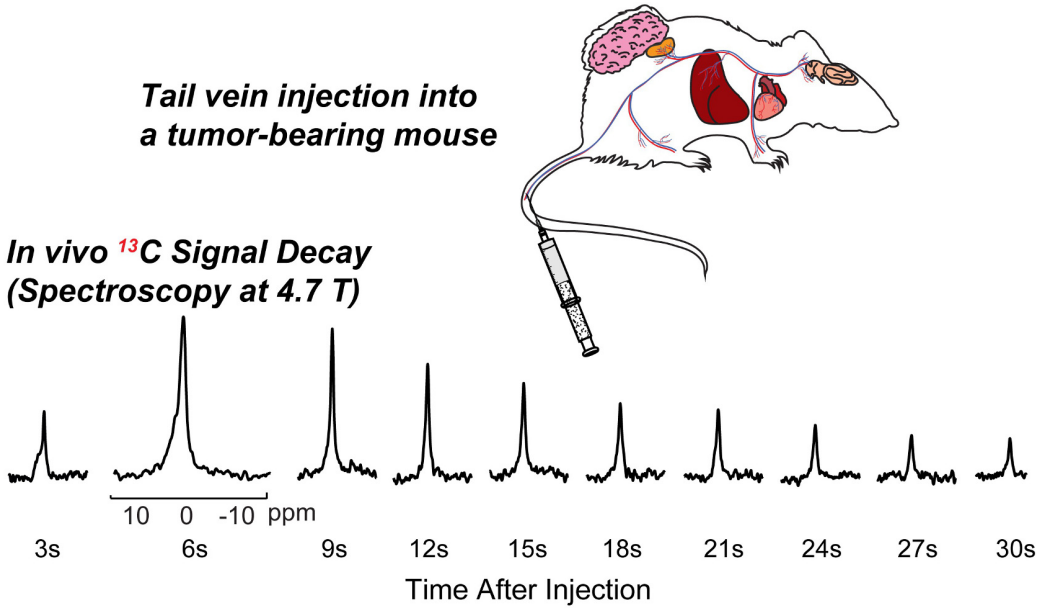
Tail vein injection into
a tumor-bearing mouse
In vivo 13C Signal Decay
(Spectroscopy at 4.7 T)
10 0 -10 ppm
3s
6s
9s
12s
15s
18s
21s
24s
27s
30s
Time After Injection

CONTROL ID: 2227172

TITLE: Imaging of arterial injury and healing in mice using VCAM-1 targeted ultrasound imaging

PRESENTER: Fabian Kiessling

ABSTRACT BODY:

Abstract Body: Radiological interventions can induce endothelial damage making anticoagulant therapy necessary. However, so far there is no tool available to monitor the extent of the defect and the process of re-endothelialization. For this purpose, we evaluated molecular ultrasound imaging using poly-n-butylcyanoacrylate microbubbles (MBs) targeted against the vascular cell adhesion molecule-1 (VCAM-1) in *ApoE*$^{-/-}$ mice subjected to wire-injury of the carotid artery. Before the intervention, animals were fed an atherogenic diet for 1 week or 12 weeks. Destruction-replenishment ultrasound imaging in contrast mode was applied to detect stationary MBs by the difference in the plateau levels before and after the destructive pulse, using a 55 MHz transducer (Vevo 770).

Flow chamber experiments on explanted carotids and *in vivo* molecular US imaging were performed at different time points (1, 3, 7 and 14 days) after endothelial denudation. Two-photon laser scanning microscopy (TPLSM) on fluorescent VCAM-1-targeted microbubbles (MB_{VCAM-1}) was employed for validation. In addition, the VCAM-1 expression pattern and the degree of re-endothelialization were investigated *ex vivo* by TPLSM and by immunofluorescence imaging of histological slices.

In the short-term, atherogenic diet group quantification of US grayscale intensity showed a ~8-fold increase in MB $_{VCAM-1}$-binding after 1 d, and a ~15-fold increase after 3 d, compared to the noninjured group ($p<0.001$ and $p<0.001$, respectively). At 7 d, MB_{VCAM-1}-binding dropped to a 2-fold increase compared to the noninjured group ($p>0.05$). Interestingly, in the long-term atherogenic diet group, enhanced MB_{VCAM-1}-binding was observed compared to the short-term atherogenic diet group: in comparison with untreated animals a ~9-fold increase in US grayscale intensity difference was observed after 1 d, a ~18-fold increase after 3 d and a ~8-fold increase after 7 d ($p<0.05$, $p<0.001$ and $p<0.001$, respectively). Thus, in mice fed for 12 weeks with atherogenic diet, vascular inflammation after wire-injury was enhanced and endothelial recovery was delayed, which translated into a prolongated binding of MB_{VCAM-1} up to 7 d after arterial denudation. Fourteen days after wire-injury, MB_{VCAM-1} binding dropped down to the level of control animals in both short-term and long-term atherogenic diet groups, showing that endothelial recovery was completed. Results were confirmed by TPLSM showing that 1 d after wire injury the endothelial layer was removed and VCAM-1 positive smooth muscle cells were exposed to the vessel lumen to which MB_{VCAM-1} bound. At later time points the vascular defect was increasingly covered with VCAM-1 positive endothelial cells (3 d and 7 d). After restoration of the endothelial coverage (14 d), endothelial VCAM-1 expression was dowregulated to the normal state.

In conclusion, endothelial injury and recovery after wire injury can be noninvasively visualized and quantified by US imaging using VCAM-1 targeted MBs.

AUTHORS (LAST NAME, FIRST NAME): Curaj, Adelina[3]; Wu, Zhuojun[3]; Fokong, Stanley[2]; Liehn, Elisa[2]; Weber, Christian[1]; Burlacu, Alexandrina[5]; Lammers, Twan[4]; Kiessling, Fabian[4]; van Zandvoort, Marc[2]

INSTITUTIONS (ALL):

1. LMU, Minic, Germany.
2. RWTH, Aachen, Germany.
3. ExMI, RWTH, Aachen, Germany.
4. Experimental Molecular Imaging, RWTH Aachen University, Aachen, NRW, Germany.
5. Laboratory of Stem Cell Biology , Institute of Cellular Biology and Pathology "Nicolae Simionescu", Bucharest, Romania.

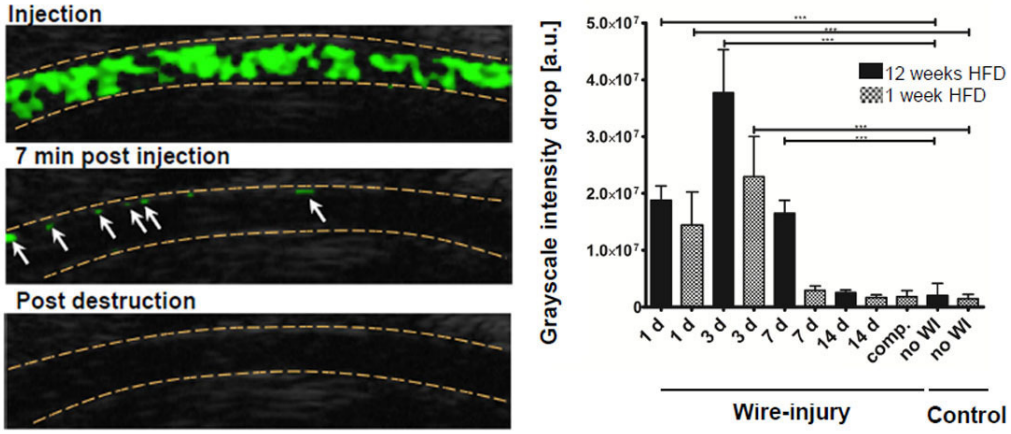

Left: *In vivo* molecular US imaging of denudated carotid arteries. In vivo contrast mode US images of murine carotids show circulating MB_{VCAM-1} directly after injection (upper panel), bound MB_{VCAM-1} before the destructive pulse (middle panel) and a MB-free lumen after the destructive pulse. MBs are color-coded in green; stationary MBs are indicated with white arrows.

Right: The quantification and statistical analysis of MB binding (n=4-5 animals per group) indicates specific binding of MB_{VCAM-1} to injured carotids. Competitive binding experiments (comp) were conducted in a separate group of animals 1 d after arterial injury. HFD: High fat diet.

CONTROL ID: 2233685

TITLE: Improved identification and quantification of cancer tissue with paired-agent fluorescence guided brain tumor surgery: finding an optimal control agent

PRESENTER: Xiaochun Xu

ABSTRACT BODY:

Abstract Body: The five-year survival rate for patients with high-grade brain tumor remains below 20% owing partially to obscure tumor margins resulting from the invasive nature of high-grade tumors. Fluorescence guided surgery has been proposed as a powerful new method of improving tumor-to-healthy margin contrast to improve the probably of achieving clean surgical margins during dissection. Current agents that have been applied off-label for use in brain surgery are Fluorescein and 5-ALA induced ppIX [1-3]. However, neither of these are truly tumor specific, and preferential aggregation of signal in the tumor area relies on leaky blood-brain barrier, higher metabolism and enhanced permeability and retention (EPR) effect, factors can be variable and are not ubiquitous to all brain tumors. Cancer-targeted imaging agents are being developed to improve differentiation of the tumor edge, especially in sparse and punctated tumor sites. Yet variable delivery and non-specific retention can significantly affect the quality of tumor-cell specific “staining”. To overcome these obstacles, so-called “paired-agent” methods employ coinjection of the targeted imaging agent with a control, untargeted agent that in turn is used to account for non-binding related mechanisms of agent delivery and retention, allowing quantification of targeted receptor concentrations to provide the ultimate contrast between tumor and healthy tissue.

Variability in the integrity of the blood brain barrier in invasive margins poses a complication to paired-agent compared to previous applications since ideal agent pairs should be chose to reach tumor tissue as well as healthy tissue with similar efficacy. Affibody-based epidermal growth factor receptor (EGFR) targeted fluorescent agents have demonstrated this ability (Sexton et al). In this study, various control imaging agent candidates were tested alongside anti-EGFR Affibody in orthotropic nude mouse models of brain tumor (U251 human glioblastoma) to identify an optimal control agent, with a specific focus on FDA approved agents (fluorescein, methylene blue, indocyanine green). With an ideal untargeted tracer to normalize the non-binding related retention, anti-EGFR Affibody is able to catch 93.7% tumor signal while fluorescein only labeled 53.6% tumor signal. Results from these studies indicate that all FDA approved imaging agents demonstrate very poor uptake in healthy brain and in tumor margins where fluorescence guided surgery would be most effective. This is likely attributable to a high potential for all of these agents to associate with large plasma proteins (predominantly albumin). On the other hand, free Alexa Fluor dyes demonstrated commensurate uptake to the targeted Affibody imaging agent in all tissue with neglible EGFR concentration suggesting that the new wave of imaging agents that are being GMP produced (e.g., IRDye-800CW), that do not bind to plasma proteins will offer suitable control agent pairs to smaller molecule targeted imaging agents.

AUTHORS (LAST NAME, FIRST NAME): Xu, Xiaochun[1]; Straus, David[2]; Brey, Eric[1]; Byrne, Richard[2]; Tichauer, Kenneth M.[1]

INSTITUTIONS (ALL):

1. Biomedical Engineering, Illinois Institute of Technology, Chicago, IL, United States.
2. Neurosurgery, Rush University Medical Center, Chicago, IL, United States.

(No Image Selected)

CONTROL ID: 2227511

TITLE: Use of Folate-Conjugated Multifunctional MR Imaging Agents to Target Activated Macrophages in ApoE$^{-/-}$ Mice

PRESENTER: Yuyu Yao

ABSTRACT BODY:

Abstract Body: ***Objective*—**Inflammation is important for the initiation and progression of atherosclerosis, research has found the folate receptor β (FR-β) highly expressed in activated macrophages in the plaque. We used multimodal imaging probe to examine FR-β expression as a function of carotid atherosclerosis formation in the apolipoprotein E–deficient (apo E$^{-/-}$) mouse.

Materials and Methods: Folate acid β receptor targeted dual-modal fluorescent magnetic nanoparticles (MNPs) were developed by composing of cores containing iron oxide nanocrystals and amphiphilic oligomers (OPE) shells, ending with folic acid (FA) as the targeted ligand, MNPs@OPE-PEG-FA, and untargeted MNPs@OPE-PEG-NH_2 as control. *In vitro* analysis of iron oxide uptake was performed in a FR-positive subclone of murine macrophage-derived RAW264.7 cells, whereas for *in vivo* experiments, partial ligation of the left carotid artery in apo E$^{-/-}$ mice were used. Partial ligation mice were randomly divided into an FA targeted MNPs@OPE-PEG-FA or untargeted MNPs@OPE-PEG-NH_2 groups (n = 6/group each) and imaged at 7.0T magnetic resonance imaging (MRI) prior to contrast administration and 24 h after administration. Perl's staining was performed to demonstrate MNPs deposition, whereas FR-β/MAC-3 was detected by immunohistochemistry.

Results: In vitro analysis showed higher uptake of MNPs in macrophages treated with MNPs@OPE-PEG-FA than those treated with untargeted MNPs@OPE-PEG-NH_2. Using *in vivo* MRI measurements, plaque formation in the carotid arteries of apo E$^{-/-}$ mice were induced 14 days after partial ligation. MNPs@OPE-PEG-FA injection exhibited significantly higher degrees of MNPs uptake, which was detected using MRI as a distinct loss of signal intensity. The contrast-to-noise ratio value decreased in proportion to an increase in the number of iron-laden macrophages in the plaque. Besides, in vitro studies also indicate that the dual-modal probes can serve as an effective two-photon fluorescent in plaque area.

Conclusion: This report shows that MNPs@OPE-PEG-FA detects FR-β-enriched inflammatory plaque in apo E$^{-/-}$ mice. Our study provides important information for monitoring early atherosclerotic plaque.

Keywords: Atherosclerotic plaque; Magnetic resonance imaging; FR-β; MNPs

AUTHORS (LAST NAME, FIRST NAME): Yao, Yuyu[1, 2]; Li, Bing[1]; Teng, Gao-jun[2]; Fan, Quli[3]

INSTITUTIONS (ALL):

1. department of cardiology, southeast university, Nanjing, China.
2. Jiangsu Key Lab of Molecular and Function Imaging, Department of Radiology, southeast university, Nanjing, China.
3. Key Laboratory for Organic Electronics & Information Displays and Institute of Advanced Materials, Nanjing University of Posts & Telecommunications, Nnanjing, China.

(No Image Selected)

CONTROL ID: 2227509

TITLE: Imaging of the response of Head and Neck Squamous Cell Carcinoma to irradiation using a Poly(ADP-ribose) Polymerase 1 targeted optical imaging agent

PRESENTER: Susanne Kossatz

ABSTRACT BODY:

Abstract Body: Purpose:

Molecular Imaging can offer innovative ways for an effective therapy monitoring, which remains a big challenge in cancer research, by imaging the expression dynamics of tumor specific markers during or after therapy. For oral cancers, particularly DNA damage response is an interesting target, since this is directly affected by common therapeutic interventions such as radiotherapy, and might therefore be a reliably stable biomarker for treatment success. Therefore, we investigated how the expression of the DNA damage repair enzyme Poly(ADP-ribose) Polymerase 1 (PARP1) is affected by radiation therapy in head and neck squamous cell carcinoma (HNSCC), and if changes in its expression can be imaged with the PARP1 imaging agent PARPi-FL.

Methods:

The basic PARP1 expression in FaDu and Cal27 HNSCC cell lines and mouse control tissues (tongue, trachea, muscle) was quantified using immunofluorescence (IF). Next, the effect of irradiation from 0 to 10 Gy on clonogenic potential and viable cell number was determined. For *in vitro* and *in vivo* imaging of PARP1 expression, we used PARPi-FL (MW: 640 g/mol), which is based on the PARP1 inhibitor Lynparza (Olaparib, Astra-Zeneca) and conjugated to the green fluorescent dye BODIPY-FL [1]. The nuclear uptake of PARPi-FL at different time points post irradiation was determined via flow cytometry. *In vivo*, athymic nude mice carrying FaDu tumors were irradiated with 10 Gy, while controls were not irradiated. Uptake of PARPi-FL 90 min p.i. was assessed with fluorescence reflectance imaging. PARP1 expression in tumors was assessed using IF PARP1 quantification. Lastly, we correlated the PARP1 expression and PARPi-FL uptake of the tumors.

Results:

We found a pronounced baseline expression of PARP1 in both cancer cell lines, which was higher in faster growing FaDu than in Cal27. Control tissues had a very low PARP1 expression. 10 Gy irradiation caused a strong decrease of viable cell number and surviving fraction (<5% FaDu, <1% Cal27). After 10 Gy irradiation *in vitro*, uptake of PARPi-FL into surviving cells increased significantly 24 and 48 h post irradiation by up to 50% in both cell lines. *In vivo* irradiation led to strong inhibition of tumor growth up to 30 days after irradiation. This was reflected in an increase in the uptake of PARPi-FL in irradiated tumors compared to non-irradiated ones and a corresponding increase in PARP1 expression in the tumors, which was rather to due an increase in the PARP1 positive tumor area than the PARP1 intensity of individual cells. The correlation of PARPi-FL nuclear uptake in tumor cells and PARP1 IF staining is very strong (mean r^2: 0.92), while stromal cells show neither PARPi-FL uptake nor PARP1 staining.

Conclusion:

PARPi-FL is a promising small molecule imaging agent to rapidly image the surviving tumor mass in tumors of the oral cavity after radiation therapy due to their high expression of the DNA repair enzyme PARP1. An increase of PARP1 expression can be monitored since the accumulation is quantitatively linked to the expression of the enzyme PARP1.

[1] Reiner, T., Lacy, J., Keliher, E. J., Yang, K. S., Ullal, A., Kohler, et al. (2012). Neoplasia, 14(3), 169–177.

AUTHORS (LAST NAME, FIRST NAME): Kossatz, Susanne[1]; Weber, Wolfgang[1]; Reiner, Thomas[1]

INSTITUTIONS (ALL):

1. Radiology, Memorial Sloan Kettering Cancer Center, New York City, NY, United States.

(No Image Selected)

CONTROL ID: 2240583

TITLE: Optical Imaging and Expression of PARP1 in mouse models and human tissue specimens

PRESENTER: Susanne Kossatz

ABSTRACT BODY:

Abstract Body: Purpose: Tumors of the oral cavity are often detected late, resulting in 5-year survival rates of only about 50%. A key strategy to improve prognosis and survival is early detection. Targeting DNA repair mechanisms is a promising approach for timely detection as well as intraoperative imaging of such tumors based on the widespread expression of DNA repair proteins, such as Poly(ADP-ribose)Polymerase 1 (PARP1). Here, we evaluated the fluorescent PARP1 inhibitor PARPi-FL for imaging of squamous cell carcinoma (SCC) of the oral cavity with the goal of improving the detection and surgical removal of malignant cells.

Methods: *In vivo* imaging was performed with PARPi-FL, a small molecule imaging agent, conjugated to BODIPY-FL (Exc./Em. max.: 503/512 nm) [1]. Uptake of PARPi-FL into subcutaneous SCC xenografts (FaDu, Cal27) in mice (n=6/group) was determined using Fluorescence Reflectance Imaging (FRI) and compared to their PARP1 expression, as assessed by IHC. Uptake of PARPi-FL was also evaluated in an orthotopic tongue tumor model by *in vivo* imaging with a fluorescence stereomicroscope. We performed imaging of excised tumors with a cellular resolution using an endomicroscope and a custom built dual-axis confocal microscope [2] (n=4/group). We assessed the correlation between PARP1 expression and PARPi-FL uptake as well as malignancy of the tissue histologically. Finally, we determined the presence and expression levels of PARP1 in human oral tongue tumor specimen (n=10) and adjacent healthy tissue.

Results: FaDu and Cal27 xenografts expressed high levels of PARP1 compared to mucosa and muscle, which correlated to the high uptake of PARPi-FL measured by FRI. Tumor to background ratios (FaDu: 4.5±1.4, Cal27: 2.8±1) allowed clear detection of tumors versus tongue tissue (0.8±0.3). Orthotopic FaDu tongue tumors were also clearly detectable *in vivo* using a stereomicroscope (Fig. 1). On the cellular level, we demonstrated real time non-invasive *in vivo* detection of tumors with a fluorescence endomicroscope. Confocal microscopy of whole excised tumors confirmed targeted delivery and retention of PARPi-FL within the PARP1 expressing nuclei of the tumors. In orthotopic tumors, areas of high PARPi-FL uptake were correlated to PARP1 expression. Normal mucosa and muscle did not show detectable PARPi-FL uptake. All human tongue tumors (stages T2-T4) were positive for PARP1 expression. The PARP1 positive area increased from 2.3±1.9% in normal tongue to 14.5±3% in malignant tissue, an increase of more than 600%.

Conclusion: High PARP1 expression in mouse models and human tongue tumors allows tumor detection and potentially intraoperative delineation. The specific nuclear accumulation of PARPi-FL and high tumor-to-background contrast in SCC *in vivo* on the macroscopic and microscopic scale is promising for clinical application.

Acknowledgements:

Supported by the Brain Tumor Center of MSKCC, the Imaging and Radiation Sciences Program of MSKCC, and the NIH/ NIDCR R01DE023497 (Liu).

[1] Reiner, T., Lacy, J., Keliher, E. J., Yang, et al. (2012). Neoplasia, 14(3), 169–177.

[2] Liu, J.T.C., Mandella, M. J., Crawford, J. M., et al. J Biomed Opt (2008) vol. 13 (3) pp. 034020

AUTHORS (LAST NAME, FIRST NAME): Kossatz, Susanne[1]; Riaz, Nadeem[3]; Katabi, Nora[3]; Yarusi, Brett[3]; Leigh, Steven Y.[4]; Wang, Danni[2]; Liu, Jonathan T.[4]; Lee, Nancy[3]; Weber, Wolfgang[1]; Reiner, Thomas[1]

INSTITUTIONS (ALL):

1. Radiology, Memorial Sloan Kettering Cancer Center, New York City, NY, United States.
2. Biomedical Engineering, Stony Brook University, New York, NY, United States.
3. Radiation Oncology, Memorial Sloan Kettering Cancer Center, New York, NY, United States.
4. Mechanical Engineering, University of Washington, Seattle, WA, United States.

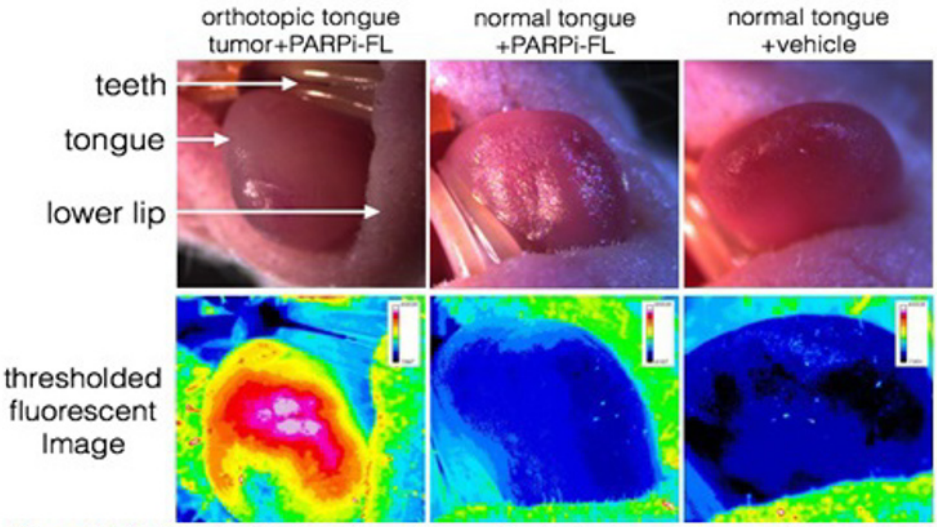

Figure 1. Optical *in vivo* imaging of an orthotopic human tongue tumor model (based on FaDu cells) with a fluorescence stereomicroscope (488 nm Laser, Lumar, Zeiss) in mice, following intravenous PARPi-FL dosage (75 nmol, 90 min prior to imaging).

CONTROL ID: 2227545

TITLE: Tunable Composite Nanocarriers for Magnetic Resonance Imaging, Multi-Modal Imaging and Theranostic Applications

PRESENTER: Robert Prud'homme

ABSTRACT BODY:

Abstract Body: MRI and NIR-active, multi-modal and theranostic Composite NanoCarriers (CNCs) have been developed using a simple one-step process, Flash NanoPrecipitation (FNP). The CNCs have higher MRI T2 contrast and drug loading than have been reported for carriers produced by more complex assembly processes. In the controlled precipitation process, 10 nm iron oxide-based nanocrystals (IONCs) were encapsulated into poly(ethylene glycol) stabilized CNCs to make biocompatible T2 contrast agents. By adjusting the formulation, the CNC size was tuned between 80 and 360 nm. Holding the CNC size constant at 99 nm ± 3 nm, the particle relaxivity varied linearly with encapsulated IONC content ranging from 66 to 533 $mM^{-1}s^{-1}$ for CNCs with 4 to 16 wt% IONCs. By functionalizing the CNC surface with hydroxyl groups, the CNCs targeted the liver. The CNCs darkened healthy liver tissue, which enabled the detection of 0.8 mm^3 non-small cell lung cancer metastases *in vivo*. Incorporation of the hydrophobic NIR dye, PZn3, into CNCs enabled visualization with long wavelength fluorescence at 800 nm as well as MRI imaging. Both the dye and IONC were encapsulated into the core of the CNCs. *In vivo* imaging demonstrated the ability of these particles to act both as MRI and fluorescent imaging agents and to circulate in the blood over 24 hours. To demonstrate the high drug-loading capabilities of CNCs formed via FNP, a theranostic CNC was created by the single step, block copolymer-directed assembly of IONCs and itraconazole. The CNC had an ITZ drug loading of 47%.

AUTHORS (LAST NAME, FIRST NAME): Prud'homme, Robert K.[1]; Pinkerton, Nathalie M.[1]; Pagels, Robert F.[1]; Gindy, Marian[1]; Adler, Derek S.[3]; Gao, Dayuan[3]; Li, Shike[3]; Zevon, Margot[3]; Yao, Nan[1]; Pacheco, Carlos[3]; Therien, Michael[4]; Rinaldi, Carlos[2]; Sinko, Patrick[3]

INSTITUTIONS (ALL):

1. Chem. and Biol. Engr., Princeton University, Princeton, NJ, United States.
2. University of Florida, Gainesville, FL, United States.
3. Rutgers University, New Brunswick, NJ, United States.
4. Duke University, Durham , NC, United States.

(No Image Selected)

CONTROL ID: 2232378

TITLE: Scaleable Production of Long Wavelength Fluorescent Nanoparticles to Enable Targeting and Multiplexed Imaging

PRESENTER: Robert Prud'homme

ABSTRACT BODY:

Abstract Body: Long wavelength (NIR) fluorescent dyes enable deep tissue penetration and avoidance of tissue autofluorescence. In diagnostic applications and therapeutic drug delivery, targeting is often required. Nanoparticles offer advantages in targeted delivery because avidity of binding can be enhanced by presenting multiple copies of the targeting ligand on the nanoparticle surface. The combination of long wavelength fluorescence and targeting presents challenges in the production and scaleup of nanoparticles with repeatable and quantifiable characteristics. We present a novel technology --Flash NanoPrecipitation – a controlled precipitation process that produces stable nanoparticles at high concentrations of encapsulated components using amphiphilic block copolymers to direct self-assembly. Uniform particles with tunable sizes from 50 – 500 nm can be prepared in an economical, scalable, and reliable manner.[2] The key to the process is the control of time scales for micromixing, self-assembly, and nucleation and growth. Stoichiometric encapsulation of components enables the assembly of complex nanoparticles with tailored optical and targeting properties.

Most bio-imaging, even for long wavelength dyes, has employed aqueous dyes that are conjugated onto the surfaces of nanoparticles. The long wavelength dyes are intrinsically large, conjugated structures and significant surface attachment may interfere with targeting. Instead we employ extremely hydrophobic dyes that remain sequestered in the cores. This enables higher loadings than are achievable with surface-attached dyes. Also, we show that several dyes which the community considers “hydrophobic” such as Nile red or ICG, partition out of nanoparticle cores to other lipid compartments and do not act as true reporters of the nanoparticle concentration or location. We report on two novel classes of NIR dyes: a hexacene based dye that has been first used in photo-voltaic applications, and a series of chlorin and bacteriochlorin dyes from Nirvana Sciences. The later dyes are particularly interesting because the wavelengths can be tuned at ~10nm intervals over the NIR window as shown in Fig. 1. The native form of these dyes is hydrophobic, so they are ideally suited for encapsulation in our nanoparticle constructs. The narrow emission spectra will allow multiplexing of these dyes so that multiple populations of dyes with different targeting ligands can be injected simultaneously and their location/fate *in vivo* can be ascertained.

We present targeting studies with these long-wavelength dyes to show ligand density can be easily varied to determine optimum ligand concentration on the nanoparticle surface.[3] We demonstrate targeting with mannose ligands to macrophages, folate ligands to cancer cells, and larger 10-14K peptide ligands with secondary structure.

AUTHORS (LAST NAME, FIRST NAME): Prud'homme, Robert K.[2]; Lu, Hoang D.[2]; Pansare, Vikram J.[2]; Wilson, Brian K.[2]; D’Addio, Suzanne M.[2]; Hejazi, Shahram[1]

INSTITUTIONS (ALL):

1. Optimeos Life Sciences LLC, Princeton, NJ, United States.
2. Chemical and Biological Engineering, Princeton University, Princeton, NJ, United States.

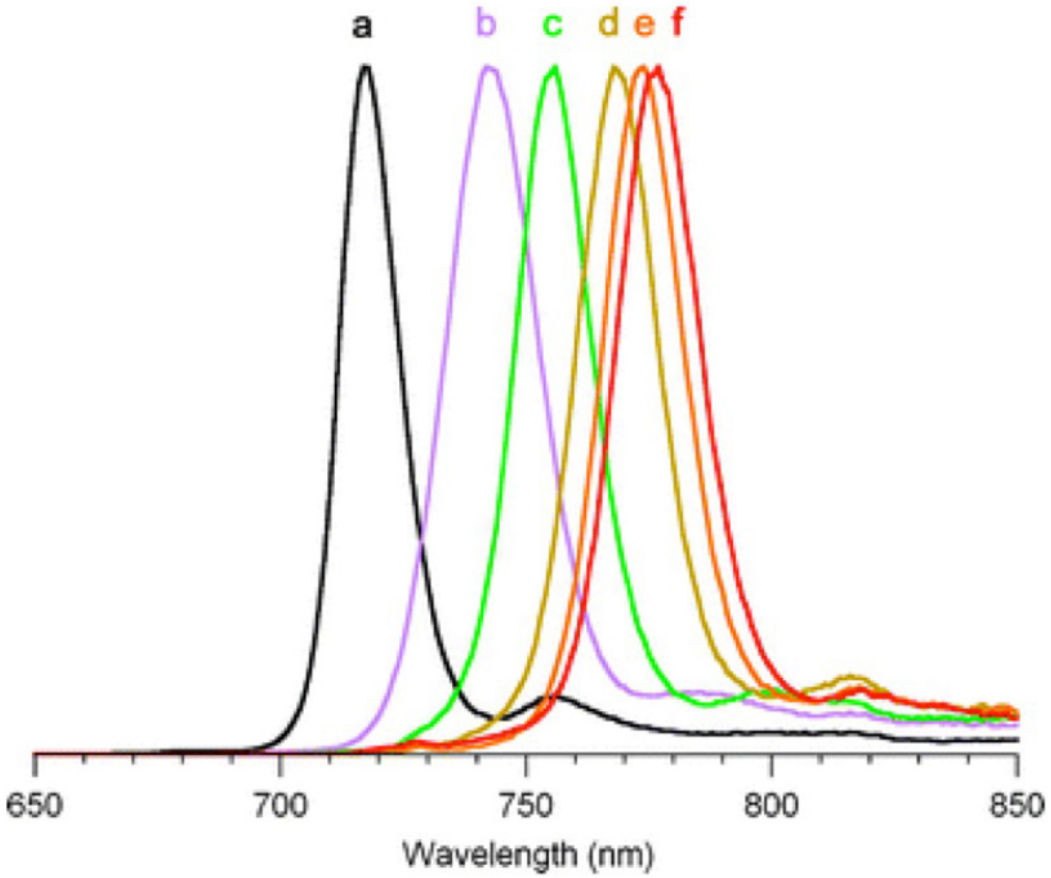

The long wavelength emission spectra of the family of bacteriochlorin dyes from Nirvana Sciences are shown. The incorporation of these hydrophobic dyes, with their sharp emission spectra enable the creation of a pallete of nanoparticles which enables multiplexed imaging with different targeting agents on each nanoparticle.

CONTROL ID: 2229924

TITLE: Development of Hexacene Based Nanoparticles for Optoacoustic imaging

PRESENTER: Robert Prud'homme

ABSTRACT BODY:

Abstract Body: Optoacoustic imaging is a rapidly developing imaging modality that uses NIR absorption to drive thermo-elastic pressure waves that are detected with ultrasound receivers. The Multispectral Optoacoustic Tomography (MSOT) Imaging optoacoustic embodiment of the technique provides in vivo structural, functional and molecular information at clinically relevant penetration depths. We present a new optoacoustic imaging agent based on encapsulating a hydrophobic dye based on hexacene -- a dye first introduced in photovoltaic applications. A key feature of the dye is a sharp absorption band in the NIR window that allows efficient background subtraction to obtain excellent image resolutions. The dye is encapsulated into nanoparticles of tunable sizes using the block-copolymer-directed rapid precipitation process, Flash NanoPrecipitation Nanoparticles. Particles between 35 nm and 200 nm with up to 80% wt dye loading are produced. Nanoparticles are decorated with dense PEG layers that provide steric stability, biocompatibility, and sites for targeting ligand attachment. *In vitro* measurement show the nanoparticles are non-toxic to concentrations of 1.5 mg/ml against MDA-231 mammalian tumor cells. The nanoparticles are evaluated with a screening protocol that we propose for the evaluation of all optoacoustic agents. The results of the MSOT experiments on phantom gels and ex-vivo with subcutaneous mouse injections demonstrate excellent imaging results to concentrations below 0.048 mg/ml of nanoparticles.

AUTHORS (LAST NAME, FIRST NAME): Prud'homme, Robert K.[1]; Nunes, Antonio[2]; Pansare, Vikram J.[1]; Beziere, Nicolas [2]; Reber, Josefine [2]; Bruzek, Matthew[3]; Anthony, John[3]; Ntziachristos, Vasilis[2]; Lu, Hoang D.[1]; Hejazi, Shahram[4]

INSTITUTIONS (ALL):

1. Chem. and Biol. Engr., Princeton University, Princeton, NJ, United States.
2. Institute for Biological and Medical Imaging, Neuherberg, Germany.
3. Chemistry, University of Kentucky, Lexington, KY, United States.
4. Optimeos Life Sciences, Princeton, NJ, United States.

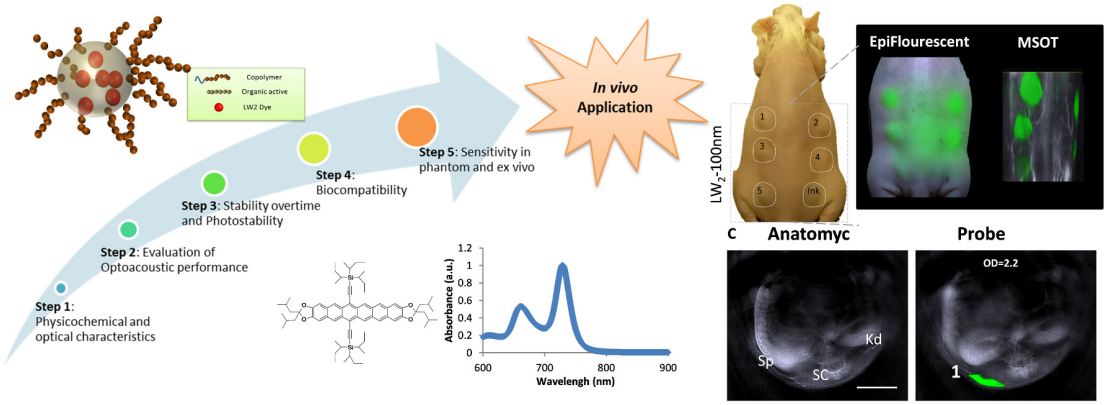
Copolymer
Organic active
LW2 Dye
Step 1: Physicochemical and optical characteristics
Step 2: Evaluation of Optoacoustic performance
Step 3: Stability overtime and Photostability
Step 4: Biocompatibility
Step 5: Sensitivity in phantom and ex vivo
In vivo Application
Absorbance (a.u.)
Wavelengh (nm)
LW2-100nm
EpiFlourescent
MSOT
Anatomyc
Probe
Kd
Sp
SC
OD=2.2
1

CONTROL ID: 2233933

TITLE: Image-guided Drug Delivery to Macrophages for Targeting Inflammation

PRESENTER: Carolyn Anderson

ABSTRACT BODY:

Abstract Body: Targeting macrophages for therapeutic and diagnostic purposes is an attractive approach applicable to multiple diseases, and nanoemulsions have shown promise for delivery of low solubility, lipophilic drugs. A theranostic perfluorocarbon nanoemulsion platform (Patel et al, PLOS One 2013, Patel et al, JBO 2013, Janjic et al Biomaterials 2014) was developed for simultaneous delivery of a cyclooxygenase-2 (COX-2) inhibitor (celecoxib) to macrophages and monitoring of changes in macrophage migration patterns by optical imaging using the DiD near-infrared dye. A mouse paw inflammation model was employed, where Complete Freund's Adjuvant was injected in the base of the footpad, with inflammation occurring within hours. Nanoemulsions showed greater accumulation in the inflamed vs. control paw, with histology confirming their specific localization in CD68 positive macrophages expressing COX-2 compared to minimal uptake in neutrophils. With a single dose administration of the celecoxib-loaded theranostic agent, we observed a reduction in fluorescence in the paw over time to nearly baseline, corresponding to a reduction in macrophage infiltration. Our data show that drug delivery to infiltrating macrophages at sites of inflammation can be monitored by optical imaging *in vivo*. Studies are ongoing to monitor drug delivery using radiometal-labeled nanoemulsions by PET/CT imaging.

AUTHORS (LAST NAME, FIRST NAME): Beaino, Wissam[1]; Patel, Sravan K.[2]; Herneisey, Michele[2]; Anderson, Carolyn J.[1]; Janjic, Jelena M.[2]

INSTITUTIONS (ALL):

1. Radiology, University of Pittsburgh, Pittsburgh, PA, United States.
2. Pharmaceutical Sciences, Duquesne University, Pittsburgh, PA, United States.

(No Image Selected)

CONTROL ID: 2227570

TITLE: Temporal analysis of hippocampal glucocorticoid receptor activity in the therapeutic action of fluoxetine

PRESENTER: Song Her

ABSTRACT BODY:

Abstract Body: Previous studies have shown inconsistent results regarding the actions of antidepressants on glucocorticoid receptor (GR) signalling. To resolve these inconsistencies, we used a lentiviral-based reporter system to directly monitor rat hippocampal GR activity during stress adaptation. Acute stress significantly induced not only GR activity but also its intra-individual variability, showing a temporal GR activation. However, these increases were dampened by exposure to chronic stress, which were partly restored by fluoxetine treatment without affecting glucocorticoid secretion. Immobility in the forced swim test was negatively correlated with the intra-individual variability, but was not correlated with the quantitative GR activity during fluoxetine therapy; this highlights the temporal variability in the neurobiological links between GR signalling and the therapeutic action of fluoxetine. Furthermore, we demonstrated sequential phosphorylation between GR (S224) and (S232) following fluoxetine treatment, showing a molecular basis for hormone-independent nuclear translocation and transcriptional enhancement. Collectively, these results suggest a neurobiological mechanism by which fluoxetine treatment confers resilience to the chronic stress-mediated attenuation of hypothalamic-pituitary-adrenal axis activity.

AUTHORS (LAST NAME, FIRST NAME): Her, Song[1]; Kim, Young-Han[1]

INSTITUTIONS (ALL):

1. Bioimaging, Korea Basic Science Institute, Chuncheon, Gangwon-Do, Korea (the Republic of).

(No Image Selected)

CONTROL ID: 2232512

TITLE: Imaging of reactive oxygen species in mouse brain by using [^{3}H]Hydromethidine as a potential radical trapping radiotracer

PRESENTER: Nozomi Takai

ABSTRACT BODY:

Abstract Body: An excessive amount of reactive oxygen species (ROS) causes the imbalance of redox state and damages cell function in living tissue and organs. We previously reported [^{3}H]-labeled *N*-methyl-2,3-diamino-6-phenyl-dihydrophenanthridine ([^{3}H]Hydromethidine) as a radical trapping radiotracer, and showed its potential for detection of in vivo ROS generated by sodium nitroprusside microinjection into the striatum of mice. In the present study, we investigated the spatiotemporal changes of ROS generation after ischemia/reperfusion in mice using [^{3}H]Hydromethidine.

The reactivity of [^{3}H]Hydromethidine with ROS was evaluated using in vitro ROS-generation systems. Mice after transient middle cerebral artery occlusion (tMCAO) were used as models with ROS generated in the brain, and radioactivity accumulation after [^{3}H]Hydromethidine injection was assessed by autoradiography. We also examined the effect of treatment with dimethylthiourea (DMTU), a hydroxyl radical scavenger, on the brain ROS generation.

In vitro studies showed that [^{3}H]Hydromethidine is oxidized by a superoxide radical, a hydroxyl radical, and peroxynitrite but not hydrogen peroxide. In the mouse brain, radioactivity accumulation was observed in the ipsilateral striatum and cortex at 1, 5, and 7 hr after tMCAO, and was significantly attenuated by the treatment with DMTU. Brain infarct volumes were also reduced in DMTU-treated mice at 24 hr after tMCAO. These results suggested that [^{3}H]Hydromethidine could be a useful radiotracer for ROS detection in relation to neural damage in ischemic brain.

AUTHORS (LAST NAME, FIRST NAME): Takai, Nozomi[1]; Abe, Kohji[1]; Fukumoto, Kazumi[1]; Imamoto, Natsumi[1]; Tonomura, Misato[1]; Ito, Miwa[1]; Kanegawa, Naoki[1]; Sakai, Katsunori[1]; Morimoto, Kenji[1]; Todoroki, Kenichiro[2]; Inoue, Osamu[3]

INSTITUTIONS (ALL):

1. Research Laboratory for Development, Shionogi & Co. Ltd., Toyonaka, Osaka, Japan.
2. Laboratory of Analytical and Bio-Analytical Chemistry, School of Pharmaceutical Sciences University of Shizuoka, Shizuoka, Japan.
3. Hanwa Intelligent Medical Center, Hanwa Daini Senboku Hospital, Sakai, Osaka, Japan.

(No Image Selected)

CONTROL ID: 2230860

TITLE: Image-guided Drug Delivery across the Blood-Brain Barrier using Theranostic Microbubbles

PRESENTER: Twan Lammers

ABSTRACT BODY:

Abstract Body: INTRODUCTION: The blood-brain barrier (BBB) is the primary obstacle for treating disorders of the central nervous system (CNS). Several different strategies have been evaluated to improve drug delivery across the BBB, including pharmacological interventions, such as mannitol-based hyper-osmotic treatment, and physical treatments, such as sonoporation. Sonoporation refers to combined use of ultrasound (US) and microbubbles (MB). When exposed to externally applied US pulses, MB cavitate, resulting in phenomena such as microstreaming, shock waves and jet formation, which permeate cell membranes and vascular endothelium, including that in the brain. The main problem associated with BBB permeation, however, is toxicity, resulting e.g. in hemorrhages, inflammation and edema formation. To attenuate the toxicity of sonoporation-based BBB opening, we incorporated iron oxide nanoparticles (USPIO; for T2/T2*-based magnetic resonance imaging (MRI)), as well as other contrast agents, into the MB shell, and we investigated whether such theranostic MB can be employed to at the same time mediate and monitor BBB permeation.

EXPERIMENTAL METHODS: MB based on poly(butyl cyanoacrylate) (PBCA) were prepared and loaded with contrast agents according to previously established procedures. These theranostic MB were administered to healthy mice, via tail vein infusion, and the brains of the mice were concomitantly exposed to transcranial US pulses for 1, 5 and 30 minutes. Using US, MRI, optical and photoacoustic imaging, the destruction of the MB and the deposition of the contrast agents into the CNS were visualized and quantified. BBB opening and efficient macromolecular model drug delivery to the brain were verified using 2D and 3D microscopy, as well as using hybrid computed tomography - fluorescence molecular tomography (CT-FMT).

RESULTS AND DISCUSSION: Microbubbles could be efficiently loaded with different types of contrast agents. Figure 1A-G shows examples for MB loaded with USPIO nanoparticles for MRI, and with fluorophores for optical and photoacoustic imaging. Up to 2 million tracer molecules could be entrapped within the ~50 nm-thick shell of a single MB. For image-guided BBB opening, USPIO-loaded MB were exposed to destructive US pulses (16 MHz, MI 0.9) while circulating through the blood vessels in the brain (Figure 1H-I). MRI was performed before and 2 hours after MB+US-mediated sonoporation, and clearly confirmed USPIO disposition across the permeabilized BBB (Figure 1J-K). The ΔR2* values increased by up to 20% at 2 hours post MB destruction and sonoporation. Immediately after MRI, the mice were sacrificed, brains were isolated, and the extravasation and penetration of 70 kDa FITC-dextran was visualized and quantified using two-photon microscopy. As shown in Figure 1L-M, sonoporation very prominently enhanced the extravasation and the penetration of model drug molecules across the BBB and into the CNS. Such theranostic materials and methods are considered to be useful for tailoring drug delivery to the brain, and for enabling safe and efficient treatment of CNS disorders.

AUTHORS (LAST NAME, FIRST NAME): Lammers, Twan[1]; Koczera, Patrick[1]; Kiessling, Fabian[1]

INSTITUTIONS (ALL):

1. Experimental Molecular Imaging, RWTH Aachen University, Aachen, Germany.

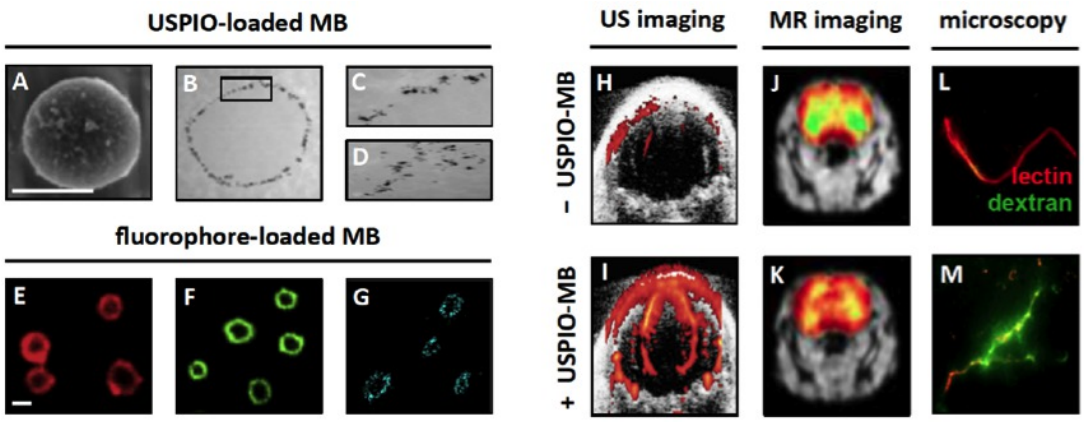

FIGURE 1 *: Contrast agent-loaded microbubbles for image-guided blood-brain barrier permeation. A-G: MB were loaded with USPIO nanoparticles for magnetic resonance imaging (A: SEM image; B-D: TEM images before (B-C) and after exposure to destructive US pulses (D)) and with fluorophores for optical (E: rhodamine; F: coumarine) and photoacoustic imaging (G: methylene blue). Scale bar: 1 µm. H-M: BBB permeation upon MB+US-mediated sonoporation. H-I: Power Doppler US imaging before and after USPIO-MB infusion, exemplifying efficient perfusion of brain blood vessels. J-K: R2*-weighted MR imaging before and after exposing USPIO-MB to destructive US pulses, confirming the release of USPIO nanoparticles from the MB shell, and their subsequent deposition into the brain (Note that the half-life time of MB is in the order of 1-2 minutes, and that the bottom MR image was obtained 2 hours after MB infusion). L-M: Microscopic validation of BBB permeation. Blood vessels in the brain were stained using rhodamine-lectin (red), and the extravasation and penetration of 70 kDa FITC-dextran (green; macromolecular model drug) was visualized and quantified using two-photon microscopy.*

CONTROL ID: 2227604

TITLE: Co-transplantation of Mesenchymal Stem Cells Improves Neural Stem Cell Survival in a Mouse Model of Amyotrophic Lateral Sclerosis.

PRESENTER: Amit Srivastava

ABSTRACT BODY:

Abstract Body: Neural stem cells (NSCs) are being investigated as a possible treatment for ALS through intraspinal transplantation. However, progressive inflammation in the ALS spinal cord creates a microenvironment that could impair survival of engrafted cells. Mesenchymal stem cells (MSCs) are known to release pro-survival trophic and immunomodulatory factors and when co-transplanted may modify the spinal cord microenvironment. In this study, a total of 29 animals were used and divided into four cohorts. Cohort #1: $SOD1^{G93A}$ transgenic ALS mice (n=9) transplanted with allogeneic Luc^{+}-NSCs; cohort #2: $SOD1^{G93A}$ transgenic ALS mice (n=6) co-transplanted with allogeneic Luc^{+}-NSCs and syngeneic MSCs; cohort #3: wild type littermates (n=8) transplanted with Luc^{+-}-NSCs; and control cohort #4: $SOD1^{G93A}$ transgenic ALS mice (n=6) injected with saline. Each mouse received two grafts (bilaterally at the C5 ventral horn) of 100,000 NSCs in 2 µL saline/site (cohort # 1 and 2) or 100,000 NSCs + 50,000 MSCs/site (cohort #3). Mice were immunosuppressed with FK506/rapamycin (1 mg/kg, i.p.) daily. Bioluminescence imaging (BLI) and computed tomography (CT) were performed for several weeks post-transplantation using a dual-mode Perkin Elmer Spectrum/CT IVIS system. Rota-rod test was performed to determine motor deficits. Upon normalization of BLI signal intensity to day 1 we observed that, at week 4 post-transplantation, signal intensity only decreased by 38% in ALS mice transplanted with MSC+NSC versus 71.7% in ALS mice transplanted with Luc^{+}-NSCs alone ($p<0.05$). At week 5 post-transplantation, BLI signal intensity further declined to 56% in ALS mice transplanted with Luc^{+}-NSC+MSC versus 81.7% in ALS mice transplanted with Luc^{+}-NSC alone ($p<0.05$). After week 6 post-transplantation, signal intensity rapidly declined in both cohorts and reached background levels by the time of ALS mice entered into the late stage of disease. In wild type littermates, the BLI signal was still detectable (42.14%) at 6 weeks confirming that transplanted cells were able to survive in normal mice. The survival of graft in wild type mice was further confirmed by histology. Compared to saline-injected animals, in mice engrafted with NSCs alone, a transient improvement in motor performance was observed at the very early stage of disease. However, the decrease of cell survival preceded the decline in motor performance. Mice transplanted with NSCs+MSCs showed significant improvement in motor performance in the symptomatic stage of disease compared to both saline injected and NSC alone-engrafted mice ($p <0.05$). Thus, co-transplantation of MSCs can significantly improve engrafted cell survival in the early symptomatic stage of ALS. These data demonstrate a first proof-of-principle of the use of MSCs to modify the microenvironment of ALS spinal cord for enhanced NSC survival.

AUTHORS (LAST NAME, FIRST NAME): Srivastava, Amit K.[1, 2]; Gross, Sarah K.[3]; Almad, Akshata[3]; Bulte, Camille A.[1, 2]; Maragakis, Nicholas J.[3]; Bulte, Jeff W.[1, 2]

INSTITUTIONS (ALL):

1. Radioloy, Johns Hopkins University, Baltimore, MD, United States.
2. Cellular Imaging Section and Vascular Biology Program, Institute for Cell Engineering, Baltimore, MD, United States.
3. Neurology , The Johns Hopkins University, Baltimore, MD, United States.

(No Image Selected)

CONTROL ID: 2227610

TITLE: Fluorescent Activatable Ferritin Nanocomplex for Real-Time Monitoring of Apoptosis during Photodynamic Therapy (PDT)

PRESENTER: LEI ZHU

ABSTRACT BODY:

Abstract Body: Photodynamic therapy (PDT) is clinically approved for the treatment of various diseases, including cancers. It utilizes thermoneutral light of specific wavelengths to excite non-toxic photosensitizers to produce toxic reactive oxygen species (ROS) and/or singlet oxygen (SO), leading to selective tissue destruction and vascular damage. The advantages of PDT over other conventional cancer treatments are the superiority of non-invasive, low systemic toxicity and therefore minimal side effects. Many studies have reported that apoptosis is initiated during PDT, but few of those works clarify the details of apoptosis during the therapy.

Herein, we present a novel theranostic nanocomplex that can enable effective PDT treatment of MDA-MB-435 tumors and provide real-time imaging of caspase-3 activation (Figure 1a). The complex is based on a biocompatible ferritin nanoparticle (FRT), a major iron storage protein composed of 24 subunits of L- and H-chains with varied proportion. FRT subunits can self-assemble into a cage-like structure at neutral conditions and disassemble at acidic conditions. In this work, FRT was modified with NIR dye labeled caspase-3 specific substrates and black hole quencher-3 (BHQ-3) on the outer layer and denoted as FABP. A metal based photosensitizer, Zinc(II) phthalocyanine (ZnPc), was embedded inside the nanosenor for a therapeutic role and named as FABP/ZnPc (Figure 1a). Upon NIR laser irradiation, the built-in photosensitizer ZnPc will be activated and generate ROS/SO to induce apoptosis. Then, the caspase-3 specific peptide substrate labeled on the outside of the FABP will be cleaved by activated caspase-3 and boost strong fluorescence signals in a time-dependent manner (Figure 1b). This PDT-responsive nanocomplex (FABP/ZnPc) is able to ensure simultaneous real-time imaging of PDT-induced apoptosis and therefore is helpful for understanding PDT-induced apoptosis mechanisms and also predicting therapeutic outcomes.

In summary, we successfully engineered ferritin nanocages that can effectively and simultaneously induce PDT of tumors and image PDT-induced apoptosis *in vitro* and *in vivo*. By tuning the ratio of dye/quencher labeled FRTs, we were able to optimize the composition of a hybrid FRT with effective sensitivity and specificity to caspases-3. The feasibility of such a hybrid ferritin nanocomplex for caspase-3 imaging during PDT was confirmed in living cells as well as a tumor bearing model. Our strategy may not only facilitate the understanding of the mechanisms of PDT-induced apoptosis, but also may be helpful for screening and evaluating new photosensitizers. The engineered ferritin platform in our report can be extended to target other proteinases or even multiple targets for other practical applications.

Acknowledgements

This work was supported by National High Technology Research and Development Program of China (863 Program) (No. 2014AA020708), National Science Foundation of China (NSFC) (81201129 and 51373144).

Reference

Zhu L, *et al.* Real-time monitoring of caspase cascade activation in living cells. *J Control Release.* 2012 Oct 10;163(1):55-62.

AUTHORS (LAST NAME, FIRST NAME): ZHU, LEI[1]; Wang, Jingjing[1]; Zhang, Liwen[1]

INSTITUTIONS (ALL):

1. Center for Molecular Imaging and Translational Medicine, Xiamen, Fujian, China.

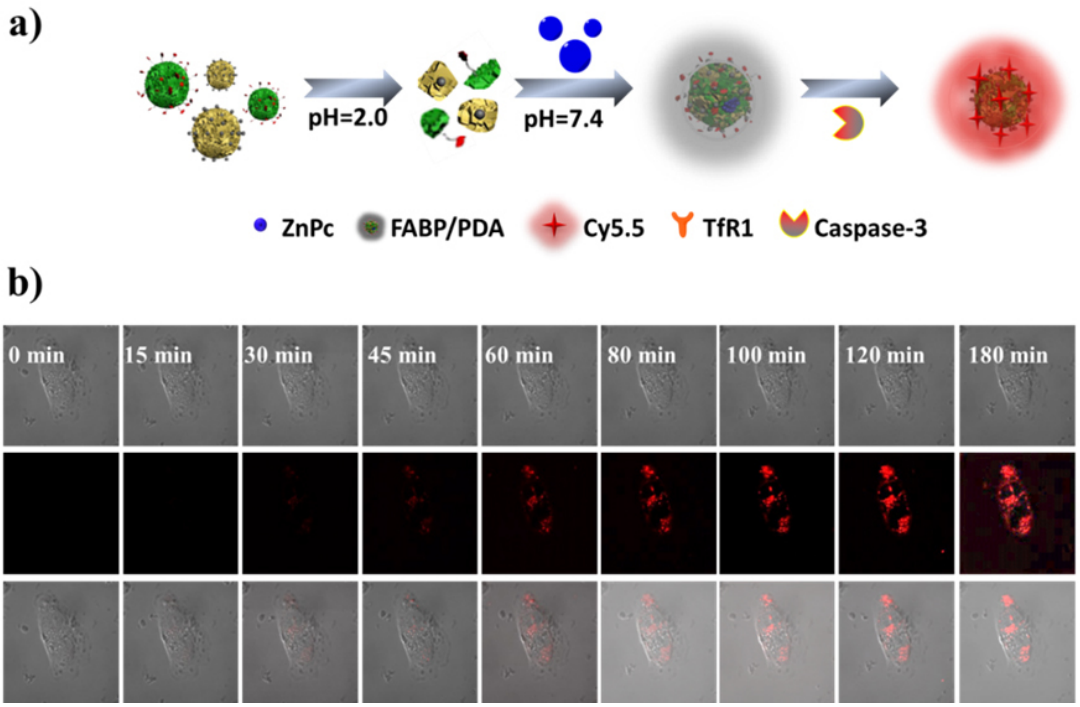

Figure 1. a). Design and preparation of FABP/ZnPc. b). Real-time visualization of caspase-3 activation in MDA-MB-435 cells during PDT. Images were collected at different time points after laser irradiation over 3 h by confocal laser scanning microscopy.

CONTROL ID: 2231139

TITLE: Using Multimodal Imaging to Study Mode of Action of Therapeutic Antibodies

PRESENTER: Daniel Gutierrez

ABSTRACT BODY:

Abstract Body: INTRODUCTION:

Multimodal in-vivo imaging is widely used to visualize immune cell infiltration to tumours in a spatiotemporal manner. We are generating in-vitro and in-vivo imaging readouts to understand the mode of action (MOA) of glycoengineered antibodies (Ab) and characterize their mediated immune cell infiltration to tumours. In particular we used bioluminescence (BLI) and confocal imaging to visualize events of antibody dependent cellular phagocytosis (ADCP) and ROS production by macrophages, as well as antibody dependent cellular cytotoxicity (ADCC) mediated by NK92 cells and their ability to activate caspases in cancer cells.

A recent investigation showed that macrophages mediate ROS production by regulating enzymatic expression, where they rely only on phagocyte NADPH oxidase (Phox) localized at the cellular membrane to produce superoxide (1).

METHODS:

Animals: SCID FcgR3a tg

Tumour model: MDA-MB231Fluc mammary tumour cells injected in the mammary fat pad.

Tumour cell lines for confocal: MDA-MB231 RFP and A549 Fluc.

Effector cell lines: NK92 and M1 macrophages.

Therapy: in-house produced Ab which binds to EGFRs on tumour cells and FCγ receptors on immune cells.

Imaging probes: Lucigenin (Sigma Aldrich), a non-membrane permeable BLI indicator of macrophage-dep ROS production; PhRodo (Life Technologies), an AM-ester fluorescent pH indicator; VivoGlo (Promega), a BLI reporter of caspase 3/7 activation.

Imaging system: IVIS (Perkin Elmer) for BLI. Confocal microscope (Zeiss LSM 700).

RESULTS:

Pre-incubating tumour cells with PhRodo allowed monitoring in-vitro ADCP. Only phagocyted tumour cells will carry the indicator inside macrophages where low pH within phagosomes would make it fluorescent. Not only had we observed a higher increase in fluorescence upon phagocytosis, but also an enhanced number of phagocytic events when applying our Ab. Alternatively, using VivoGlo we monitored apoptosis via caspase activation on A549Fluc lung tumour cells using NK92 as effector cells. In-vitro we observed that our Ab significantly increased caspase 3/7 activity after 20 min of its application, showing as well a reduced percentage of cell viability compared to ctrl.

In-vivo administration of Lucigenin to tumour-carrying mice displayed a weak Lucigenin-dep ROS signal around the tumour region. Upon administration of our Ab, we observed a significant increase in macrophage-dep ROS activity in the therapy group compared to vehicle.

DISCUSSION:

This data shows that we could in-vivo monitor macrophage infiltration to tumours by measuring ROS-dep enzymatic activity. Furthermore administration of a therapeutic Ab led to higher levels of ROS and reduced tumour size. In-vitro the occurrence of ADCP could be followed using pH-sensitive fluorescent tracers and ADCC by a caspase reporter. Taking together our data suggests that we could use multimodal imaging readouts to screen different therapies, study Ab's mode of action and add to the understanding of how to fight against cancer development.

REFERENCES:

In Vivo Imaging of Inflammatory Phagocytes; Jen-Chieh Tseng and Andrew L. Kung; Chemistry & Biology, 19, 1199–1209, 2012.

AUTHORS (LAST NAME, FIRST NAME): Gutierrez, Daniel[1, 2]; Perro, Mario[2]; Colombetti, Sara[2]; Sam, Johannes[2]; Nicolini, Valeria[2]; Gerdes, Christian[2]; Rudin, Markus[1]

INSTITUTIONS (ALL):

1. Institute for Biomedical Engineering, ETH Zurich, Zurich, Zurich, Switzerland.

2. Pharmacology, Roche, Schlieren, Zurich, Switzerland.
(No Image Selected)

CONTROL ID: 2227704

TITLE: Longer-Lived Hyperpolarized Propane Gas for Biomedical Imaging Application

PRESENTER: Eduard Chekmenev

ABSTRACT BODY:

Abstract Body: Background: Hyperpolarization technologies have lead to MRI sensitivities greater than conventional MR or MRS by several orders of magnitude improving functional MR imaging and spectroscopy. Hyperpolarized (HP) ^{129}Xe is the leading HP contrast agent for functional lung MRI: it has a relatively low cost compared to ^{3}He and significantly longer T_1 and detection sensitivity compared to ^{131}Xe and ^{83}Kr. However, HP MRI using ^{129}Xe is associated with two main translational barriers: (i) expensive hyperpolarizer is required for production of a few liters/h of HP agent, and (ii) MRI requires the use of a multi-nuclear scanner.

Methods: Proton-based HP gases can be successfully produced for imaging applications in principle using metal (e.g. Rh) nanoparticle heterogeneous supported catalysts (2). However, the level of polarization (P) was low for high-resolution gas MRI. It was recently demonstrated that significantly higher levels of HP propane ($\%P_H$ ~ 1%) can be achieved using advanced Rh/TiO_2 catalysts enabling ultra-fast (seconds) high-resolution (as low as 0.5×0.5×0.5 mm^3 pixel size) 3D MRI of flowing HP propane gas using conventional high-field MRI scanner and pulse sequences (3,4). Despite these significant leaps in development of new catalysts and HP gas production, HP propane T_1 is < 1 s at high magnetic field (e.g. 9.4 T) (4,5), which limits the use of this potential HP contrast agent to applications of MR of flowing gas (Fig. 1).

Results/Discussion: We show that long-lived spin states (LLSS) can be induced in HP propane gas using parahydrogen and detection at low magnetic field in the regime when $(\delta_{Ha}-\delta_{Hb})/2\pi < J_{Ha-Hb}$. As a result, LLSS can preserve the produced proton hyperpolarization significantly longer with T_{LLSS} ~ 4.7 s (4) for non-deuterated propane and T_{LLSS} ~ 6.0 s (5) for propane-d_6. As a result, high-resolution MRI of stopped propane gas is feasible (Fig. 1) over a time window of > 10 s, which is now sufficient for potential *in vivo* administration by gas inhalation. The use of low-field MRI for propane imaging offers additional advantages including (i) significantly lower thermal proton tissue signal background, and (ii) potentially greater detection sensitivity at low field vs. that at high magnetic fields for HP contrast agents (7).

Conclusion: Despite nominally lower $\%P_H$ of HP propane achieved to date, it has multiple advantage over HP ^{129}Xe: (i) HP production is low-cost and scalable to large volumes pure from heterogeneous catalyst, (ii) MR imaging can be done on conventional proton scanner with already available sequences. Propane is a non-toxic asphyxiating anesthetic gas, which can be potentially safely administered to humans for functional imaging of the lung and other molecular imaging applications.

References: (1) M.G. Pravica and D.P. Weitekamp, *Chem. Phys. Lett.* 1988, **145**, 255. (2) L.S. Bouchard, *et al. Science* 2008, **319**, 442. (3) K.V. Kovtunov, *et al. Chem. Eur. J.* 2014, **20**, 11636. (4) K.V. Kovtunov, *et al. Chem. Eur. J.* 2014, **20**, 14629. (5) K.V. Kovtunov, *et al. J. Phys. Chem. C* 2014, **118**, 28234. (6) S.J. DeVience, *et al. Phys. Rev. Lett.* 2013, **111**, 5. (7) A.M. Coffey, *et al. J. Magn. Reson.* 2013, **237**, 169.

AUTHORS (LAST NAME, FIRST NAME): Kovtunov, Kirill V.[2]; Barskiy, Danila A.[2]; Coffey, Aaron M.[1]; Truong, Milton L.[1]; Koptyug, Igor V.[2]; Chekmenev, Eduard Y.[1]

INSTITUTIONS (ALL):

1. Institute of Imaging Science, Vanderbilt University, Nashville, TN, United States.
2. International Tomography Center, Novosibirsk, Russian Federation.

Hyperpolarized (%P_H~1%) propane-d_6 3D MRI
voxel size 0.5×0.5×0.5 mm^2 (flowing gas)

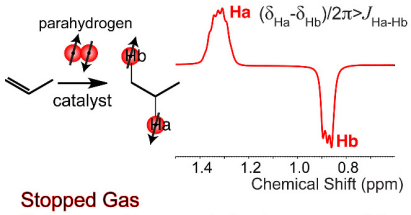

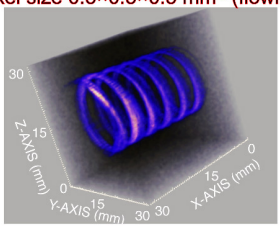

Relaxation Time	perdeuterated propene precursor	nondeuterated propene precursor
High field (9.4T) (δ_{Ha}-δ_{Hb})/2π>J_{Ha-Hb}	< 1 s	< 1 s
Low field (0.05T) (δ_{Ha}-δ_{Hb})/2π<J_{Ha-Hb}	~ 6 s	~ 4.7 s*

* requires RF pulse sequence to unlock long-lived spin states

Stopped Gas
Sub-second hyperpolarized propane-d_6 imaging (single average) at 0.05 T: pixel size 0.88×0.88 mm^2

H_2O reference
(8 averages)

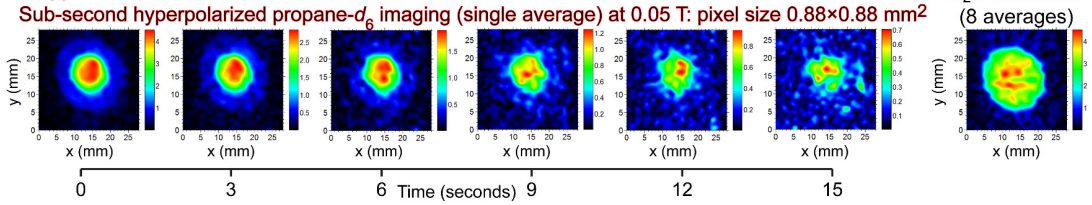

CONTROL ID: 2227827

TITLE: *In vivo* Detection of miRNA expression in tumors using an activatable nanosensor

PRESENTER: Anna Moore

ABSTRACT BODY:

Abstract Body: Introduction:

MicroRNAs (miRNAs or miRs) are well-known key regulators in carcinogenesis. Here we describe technology that provides the capability to detect them in an *in vivo* setting. Specifically, we have developed dual-modality nanosensors capable of detecting miRNA expression *in vivo*. The nanosensors are based on magnetic nanoparticles conjugated to activatable fluorescent sensor oligos sensitive to individual miRNA-mediated RNA interference. In these initial studies we focused on detecting miRNA-10b, which plays a major role in metastasis[1].

Methods:

The nanosensor was synthesized by conjugating miRNA sensor oligos to amine-derivatized dextran-coated iron oxide nanoparticles. The sensor oligos were designed to be perfectly complementary to miR-10b[2] and modified with Cy5 (a fluorescent dye) at the 5´-end and Iowa Black RQ (a quencher) at the 3'-end. For monitoring miR-10b, two animal models were generated: model **1** in which miR-10b expression in MDA-MB-231-luc-D3H2LN breast tumors was either left active or inhibited, as described in[3] and model **2** in which invasive MDA-MB-231 and non-invasive MCF-7 cells were implanted bilaterally. After i.v. injection of the nanosensors, tumor-associated fluorescence was monitored for upto 40 hrs. Bioluminescence imaging (BLI) was used as a reference for tumor delineation.

Results and Discussion:

Animal model **1** was used to evaluate the feasibility of miR-10b detection in breast tumors. Animal model **2** allowed for discrimination between poorly and highly invasive tumors based on miR-10b expression. In animal model 1, we observed a clear enhancement of the miR-10b-active primary tumors after an accumulation of the nanosensors, consistent with cleavage of the sensor oligos, separation of the Cy5 dye from the quencher, and fluorescence activation (Figure). This effect was specific for miR-10b, since in the miR-10b inhibited tumors, the radiant efficiency was significantly lower ($p < 0.05$, $n = 3$). The maximum difference in fluorescence between miR-10b-inhibited and miR-10b-active tumors was achieved 18 hrs after nanosensor injection. Ex vivo examination of the tumor tissues confirmed that fluorescence in the miR-10b active tumors was associated with tumor cells. In animal model 2, the radiant efficiency was significantly higher in the MDA-MB-231 tumors than the MCF-7 tumors and reflected a difference in the expression levels of miR-10b between the invasive MDA-MB-231 and noninvasive MCF-7 tumors (not shown).

Conclusion:

We showed that the described nanosensors are capable of accurately reporting on target miRNA expression in tumors. Because the nanosensors are based on superparamagnetic nanoparticles, it is possible in the future to monitor nanosensor delivery to the tumors by noninvasive MRI. This information can then be correlated to the fluorescence output from the nanosensor to more accurately determine target miRNA expression. The described technology has broad implications and can be utilized in any model system or clinical scenario to answer questions related to microRNA function.

AUTHORS (LAST NAME, FIRST NAME): Yoo, Byunghee[1, 2]; Kavishwar, Amol[1, 2]; Medarova, Zdravka[1, 2]; Moore, Anna[1, 2]

INSTITUTIONS (ALL):

1. Massachusetts General Hospital, Charlestown, MA, United States.
2. Harvard Medical School, Boston, MA, United States.

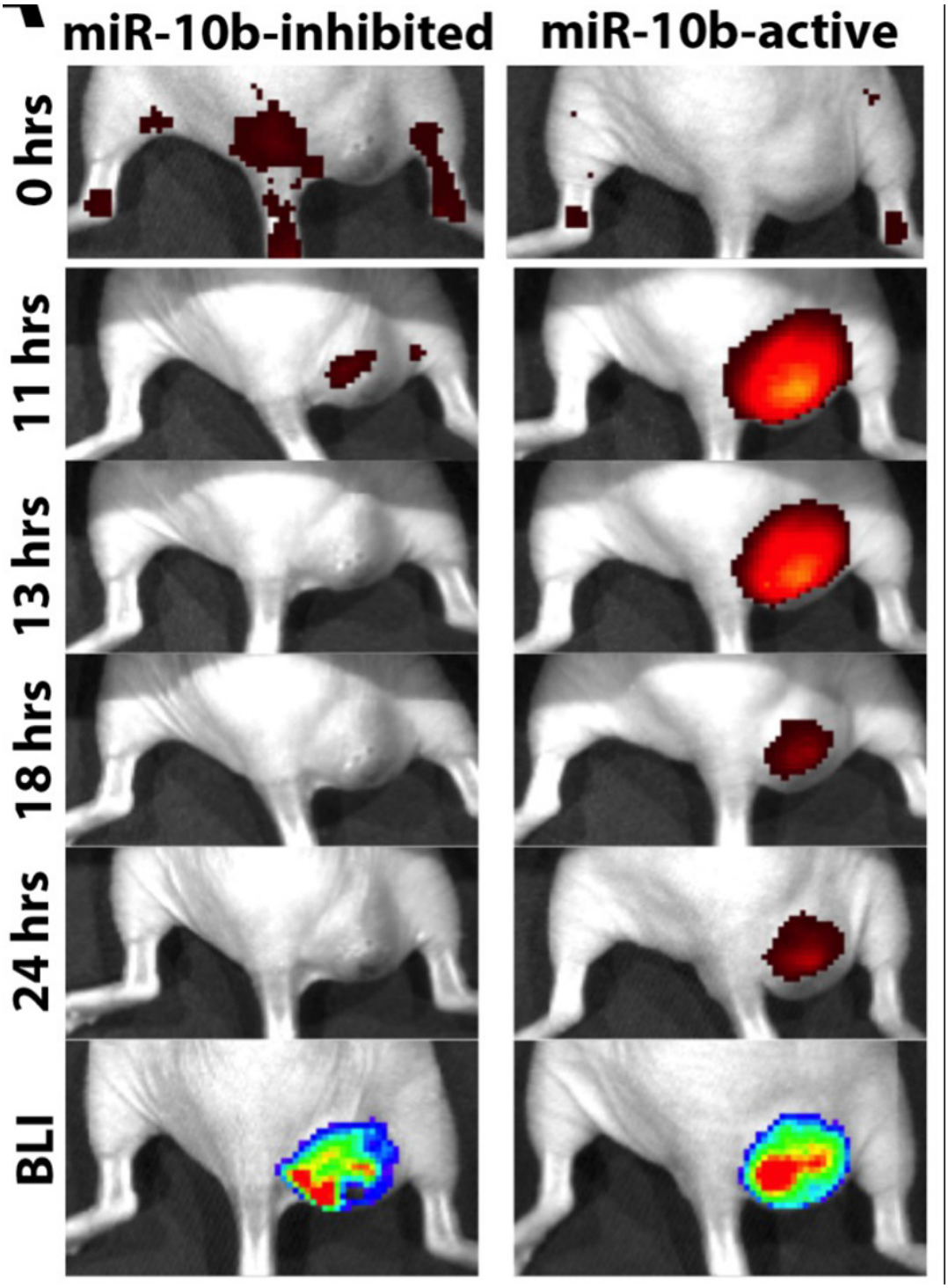

Fluorescence optical imaging showing visibly higher fluorescence intensity in the tumors in which miR-10b was left active over the miR-10b inhibited controls.

References

1. Ma, L., *et al.* Tumour invasion and metastasis initiated by microRNA-10b in breast cancer. *Nature* **449**, 682-688 (2007).

2. Yoo, B.*, et al.* Detection of miRNA expression in intact cells using activatable sensor oligonucleotides. *Chemistry & Biology* **21**, 199-204 (2014)

3. Yigit, M.V.*, et al.* Context-dependent differences in miR-10b breast oncogenesis can be targeted for the prevention and arrest of lymph node metastasis. *Oncogene* **32**, 1530-1538 (2012)

CONTROL ID: 2227919

TITLE: Towards a universal tumor-imaging agent: surface-enhanced resonant Raman spectroscopy (SERRS) nanostars for high-precision cancer imaging

PRESENTER: Ruimin Huang

ABSTRACT BODY:

Abstract Body: The inability to visualize the true extent of cancers represents a significant challenge in many areas of oncology. Furthermore, the multifocal microscopic satellite lesions represent a major reason for tumor local recurrences and metastatic spread. An imaging method to reveal the tumor extent is desired clinically and surgically. To this end, a surface-enhanced resonance Raman scattering (SERRS) nanoparticles (SERRS-nanostars), which feature a star-shaped gold core, a Raman reporter resonant in the near-infrared spectrum, and a primer-free silication method, has been developed (Science Translational Medicine, Jan 21;7(271):271ra7, 2015) (Fig.1).

SERRS-nanostars enabled the visualization of the full tumor extent in state-of-the-art mouse models of breast cancer (Fig.2), pancreas cancer (Fig.3), sarcoma (Fig.4&5), and prostate cancer (Fig.6), without requiring a dedicated targeting moiety; in other words, a “one-probe-fits-all” concept. Tumor-bearing animals were injected with SERRS-nanostars (30 fmol/g) via tail vein. After 16 to 18 hours, Raman imaging was performed at 10 to 100 mW laser power, 1.5-s acquisition time, a 5× objective using an inVia Raman microscope with a 785 nm laser.

The precise visualization of tumor margins, microscopic tumor invasion, multifocal loco-regional tumor spread, and even premalignant lesions using SERRS-nanostars Raman imaging was demonstrated. In a representative example of the MMTV-PyMT breast cancer mouse, two primary tumors were resected by a surgeon with white light illumination only, being blinded to the Raman signal (Fig.2A&B). No residual tumor tissue could be identified with white light imaging (Fig.2C). However, when a Raman image of the resection bed was acquired (Fig.2C, upper panel), multiple submillimeter foci were identified that were positive for the Raman spectral fingerprint of the SERRS-nanostars. Hematoxylin and eosin (H&E) staining and overexpression of PyMT (Fig.2C, lower panel) confirmed the presence of microscopic tumor cell deposits in these SERRS-nanostar-positive foci. In the KPC pancreatic cancer mouse model, Raman imaging of the exposed pancreas was performed in situ. This not only delineated the bulk tumor but also detected smaller, submillimeter SERRS-nanostar-positive foci in the body and tail of the pancreas (Fig.3A&B). Histological examination of the bulk tumor (Fig.3B, arrow 1) demonstrated that the SERRS-nanostars accumulated both in the tumor stroma and within epithelial tumor cells. Examination of the small scattered foci (Fig.3B, arrow 2) demonstrated the presence of pancreatic intraepithelial neoplasia (PanIN), a precursor of invasive pancreatic cancer, confirmed by histology (Fig.3C). Notably, these lesions were also detected in situ in a simulated intraoperative scenario without Raman signal interference from liver or spleen (Fig. 3A). Macropinocytosis has been demonstrated to be involved in the SERRS-nanostar uptake by tumor cells (Fig.7).

High sensitivity (1.5 femtomolar limit of detection) and broad applicability, in conjunction with their inert gold-silica composition, render SERRS-nanostars a promising imaging agent for more precise cancer imaging and resection.

AUTHORS (LAST NAME, FIRST NAME): Huang, Ruimin[1]; Harmsen, Stefan[1]; Wall, Matthew[1, 2]; Karabeber, Hazem[1]; Samii, Jason M.[1]; Spaliviero, Massimiliano[12]; White, Julie R.[3, 4]; Monette, Sébastien[3, 4]; O’Connor, Rachael[5]; Pitter, Kenneth L.[3]; Sastra, Stephen A.[6, 7]; Saborowski, Michael [3]; Holland, Eric C.[8]; Singer, Samuel [5]; Olive, Kenneth P.[6, 7]; Lowe, Scott W.[3, 9]; Blasberg, Ronald G.[10, 1]; Kircher, Moritz F.[1, 11]

INSTITUTIONS (ALL):

1. Radiology, Memorial Sloan Kettering Cancer Center, New York, NY, United States.
2. Chemistry, Hunter College of the City University of New York, New York, NY, United States.
3. Cancer Biology and Genetics Program, Memorial Sloan Kettering Cancer Center, New York, NY, United States.
4. Tri-Institutional Laboratory of Comparative Pathology, Memorial Sloan Kettering Cancer Center, The Rockefeller University, Weill Cornell Medical College, New York, NY, United States.
5. Surgery, Memorial Sloan Kettering Cancer Center, New York, NY, United States.
6. Medicine, Columbia University Medical Center, New York, NY, United States.
7. Pathology and Cell Biology, Columbia University Medical Center, New York, NY, United States.
8. Human Biology Division and Solid Tumor Translational Research, Fred Hutchinson Cancer Research Center, Seattle, WA, United States.
9. Howard Hughes Medical Institute, New York, NY, United States.

10. Neurology, Memorial Sloan Kettering Cancer Center, New York, NY, United States.
11. Center for Molecular Imaging and Nanotechnology, Memorial Sloan Kettering Cancer Center, New York, NY, United States.
12. Urology, Memorial Sloan Kettering Cancer Center, New York, NY, United States.
(No Image Selected)

CONTROL ID: 2227940

TITLE: A novel synthesis of 6-[^{18}F]fluoromaltotriose as a PET tracer for imaging bacterial infection

PRESENTER: Mohammad Namavari

ABSTRACT BODY:

Abstract Body: Purpose: The goal of this study is to develop a positron emission tomography (PET) tracer to visualize and monitor the therapeutic response to bacterial infections. There have been several publications on the use of maltose and maltohexose PET Probes for imaging bacterial infections (Gowshankar et al, PLOS one 2014 and Ning et al, Angew. Chem. Int. 2014). In our continuing efforts to find the second generation of maltose based PET tracers that can image all bacterial infections, we have designed, successfully prepared and evaluated 6-[^{18}F]fluoromaltotriose as a the next generation bacterial infection PET imaging agent.

Method: 6-[^{18}F]fluoromaltotriose was synthesized from precursor per-O-acetyl-6-deoxy-6-nosyl-maltotriose (**1**). Precursor 1 was prepared from per-O-acetyl-6-hydroxymaltotriose via a nosylation reaction. This method utilizes the reaction between the leaving group nosylate in precursor **1** and anhydrous [^{18}F]KF/Krytofix 2.2.2 in acetonitrile at 85 ^{o} C for 15 min to give per-O-acetyl-6-deoxy-6-[^{18}F]fluoromaltotriose (**2**). Basic hydrolysis of the acetyl protecting groups in **2** yielded 6-[^{18}F]fluoromaltotriose (**3**). Also, cold 6-fluoromaltotriose (for comparison with 6-[^{18}F]fluoromatotriose) was prepared from per-O-acetyl-6-hydroxymaltotriose via a DAST reaction followed by a basic hydrolysis. *Escherichia-coli* uptake of 6-[^{18}F]fluoromaltotriose was evaluated in bacterial culture.

Results: We have successfully synthesized 6-[^{18}F]fluoromaltotriose in 4-7 % radiochemical yield (decay corrected) with 95 % chemical and radio-chemical purities. Total synthesis time was 125 min. Preliminary bacteria uptake experiments showed that *E-coli* takes up 6-[^{18}F]fluoromaltotriose and the uptake is time dependent. Competition assay indicated that the uptake was blocked by co-incubation with 1 mM of cold maltose (90 % blocking, $p<0.0003$, Fig 1), the natural substrate of the maltose transporter. This observation is consistent with 6-[^{18}F]fluoromaltotriose being recognized and transported by the bacteria in a manner similar to maltose .

Conclusion: To the best of our knowledge, for the first time we have synthesized 6-[^{18}F]fluoromaltotriose by a direct fluorination of a protected maltotriose precursor. This methodology can be also used for synthesis of 1-[^{18}F]fluoromaltotriose and 2-[^{18}F]fluoromaltotriose. Preliminary bacterial uptake and competition assay experiments in *E-coli* suggest a possible application of 6-[^{18}F]fluoromaltotriose as a new PET tracer to track and image bacterial infection.

AUTHORS (LAST NAME, FIRST NAME): Namavari, Mohammad[1]; Gowrishankar, Gayatri[1]; Srinivasan, Ananth[1]; Gambhir, Sanjiv S.[1]

INSTITUTIONS (ALL):

1. Radiology, Stanford University, Stanford, CA, United States.

(No Image Selected)

CONTROL ID: 2227941

TITLE: [^{11}C]MeDAS-PET Imaging of Myelination for Efficacy Evaluation of Novel Myelin Repair Therapies

PRESENTER: Chunying Wu

ABSTRACT BODY:

Abstract Body: Objectives: Destruction or changes associated with myelin in the CNS play a key role in the pathogenesis of multiple sclerosis (MS) and related neurodegenerative disorders. Novel therapies are currently under development to prevent demyelination and promote remyelination. For efficacious evaluation of these myelin-targeted therapies, a major challenge is assessing and quantifying changes in myelin content *in vivo*. To meet this unmet need, we have developed a PET probe ([^{11}C]-MeDAS) that readily enters the CNS and selectively binds to myelin membranes. Here we reported its application in image-guided myelin repair therapies in an animal model of MS.. **Methods:** 1)EAE rats were induced using MOG 1-125; 2) The EAE rats were treated with a mesenchymal stem cell-based hepatocyte growth factor (HGF) to promote remyelination. 3) The time course of myelin changes were quantitatively monitored by longitudinal microPET imaging and correlated with histological analysis. **Results**: 1) Demyelination was induced by MOG 1-125; 2) HGF treatment showed significant remyelination; 3) Quantitative imaging analysis showed that the uptake and retention of [^{11}C] MeDAS correlated well with the level of myelin content. **Conclusions**: [^{11}C]MeDAS-PET is a promising imaging marker to monitor the changes in myelination in vivo, which is capable of monitoring myelin-targeted drug effects.

AUTHORS (LAST NAME, FIRST NAME): Wu, Chunying[1]; Zhu, Junqing[1]; Miller, Robert [2]; Wang, Yanming[1]

INSTITUTIONS (ALL):

1. Radiology, Case Western Reserve University, Cleveland, OH, United States.
2. Neuroscience, Case Western Reserve University, Cleveland, OH, United States.

(No Image Selected)

CONTROL ID: 2227999

TITLE: Specific tumor imaging and therapy by activatable fluorescent and therapeutic agents based on internalizing RGD (iRGD) peptide

PRESENTER: Sehoon Kim

ABSTRACT BODY:

Abstract Body: Tumor homing peptides containing RGD sequence, named internalizing RGD (iRGD, c(CRGDK/RGPD/EC)), were reported to enhance vascular and tissue penetrating efficacy with active targeting.[1] Using iRGD peptide, we designed and synthesized an activatable fluorescence turn-on iRGD peptide by the combination of a dye and a quencher for highly specific tumor imaging. To construct this quenched system, we conjugated a fluorescent dye on the *N*-terminal of iRGD which is a part of the internalizing sequence (CendR motif), and a quencher on the *C*-terminal of iRGD. The activatable dequenching with the synthetic iRGD peptide (Fl-iRGD-Qu) was examined by treating with DTT and trypsin. Under the exposure of both DTT and trypsin, the Fl-iRGD-Qu was activated to be cleaved, resulting in fluorescence turn-on. In cellular assay, dequenched fluorescent signal from the Fl-iRGD-Qu were detected in U-87 MG and PC-3 cells containing both αvβ3 integrin and neuropilin-1, whereas the fluorescence from a control sequence peptide was still quenched. When administered to mice bearing U-87 MG xenografts by intravenous injection, Fl-iRGD-Qu demonstrated more efficient tumor imaging with higher contrast than that of the fluorescent iRGD without a quencher.

For specific tumor therapy using iRGD, we applied a photosensitizer on iRGD system (Ppa-iRGD-Qu) with dye-quencher combinations to attain activatable photodynamic therapy (PDT). Activatable optical and singlet oxygen ($^1O_2$) generation properties of the Ppa-iRGD-Qu were confirmed under both DTT and trypsin condition. The Ppa-iRGD-Qu showed better cellular uptake than that of control peptide sequence, leading to efficacious phototoxicity in tumor cell. To enhance the therapeutic efficiency of Ppa-iRGD-Qu for in vivo PDT, molecular depots composed of the quenched Ppa-iRGD-Qu were formulated near the tumor environment by peritumoral injection. The molecular depots contained stable quenched state of the Ppa-iRGD-Qu and provided sustained release of the Ppa-iRGD-Qu, enabling multiple PDT treatments with a single injection. The released Ppa-iRGD-Qu was well internalized inside the tumor allowing in vivo detection of the fluorescence signal of Ppa and also effective generation of singlet oxygen. The quintuple PDT treatment with a single injection and selective laser irradiation suppressed the tumor volume efficaciously with clinician-friendly use.

1. K. N. Sugahara, T. Teesalu, P. P. Karmali, V. R. Kotamraju, L. Agemy, O. M. Girard, D. Hanahan, R. F. Mattrey and E. Ruoslahti, Cancer Cell, 2009, 16, 510-520.

AUTHORS (LAST NAME, FIRST NAME): Cho, Hong-Jun[1]; Park, Sung-Jun[2, 1]; Lee, Sang-Myung[3]; Lee, Yoon-Sik[2]; Kim, Sehoon[1]

INSTITUTIONS (ALL):

1. Center for Theragnosis, Korea Institute of Science and Technology, Seoul, Korea (the Republic of).
2. School of Chemical and Biological Engineering, Seoul National University, Seoul, Korea (the Republic of).
3. Department of Chemical Engineering, Kangwon National University, Chuncheon, Korea (the Republic of).

(No Image Selected)

CONTROL ID: 2228022

TITLE: Correlation Study between Choline and β-catenin Molecular Pathways in Breast Cancer using in-vivo MR Spectroscopy and ELISA

PRESENTER: Naranamangalam Jagannathan

ABSTRACT BODY:

Abstract Body: Introduction: In vivo MRS studies have documented elevated total choline [(tCho; comprising of free choline, glycerophosphocholine and phosphocholine (PC)], as a biomarker for differentiating malignant and benign breast tissues[1]. β-catenin protein is an important component of Wnt signalling pathway. Regulation of β-catenin stability and consequently its T-cell factor (TCF)–mediated transactivation are critical for tumor proliferation. In the present study we investigated the correlation if any, between increased tCho levels observed through in-vivo ^{1}H MRS and β-catenin in malignant and benign breast tissues to get an insight into the connectivity between two molecular pathways i.e., choline synthesis and β-catenin.

Patient and Methods: 20 malignant and 10 benign subjects were recruited and in vivo ^{1}H MRS was performed at 1.5 T (Avanto, Siemens) using PRESS sequence (TR=1500 ms, TE=100 ms, averages=128) with water and lipid suppression. Spectrum without suppression from same voxel was obtained for tCho quantification[2]. Tissue samples were collected and snap frozen in liquid nitrogen immediately after surgery from same subjects and lysates (cytosolic and nuclear fractions) were prepared[3]. Total protein was measured using Bradford assay. ELISA was done in duplicate as per manufacturer guidelines (Cloud-clone Corp.). β-Catenin concentrations were determined from the resultant standard curve.

Results and Discussion: Malignant tumors showed significantly higher levels of tCho (4.3 ± 1.4 mmol/Kg) compared to benign lesions (1.7 ± 0.6 mmol/Kg; Figure 1A). A significant increase in both cytosolic (5.1 ± 1.5 pg/ml) and nuclear (15.2 ± 12.7 pg/ml) β-catenin concentrations of malignant compared to benign lesions (4.0 ± 1.6 pg/ml and 7.2 ± 5.8 pg/ml) was observed (Figure 1B & 1C). A significant positive Pearson correlation was seen between tCho and cytosolic β-catenin concentrations in malignant (r=0.7) compared to benign lesions (r=0.2), which indicated the relationship between the two molecular pathways during malignancy. Further a weak positive correlation (p=0.4) between tCho and nuclear β-catenin concentrations in malignant compared to benign lesions (r=-0.05) was seen. Phosphatidylcholine-specific phospholipase D is a ubiquitous enzyme involved in the hydrolysis of PtdCho to phosphatidic acid and Cho, also acts as a positive regulator for β-catenin synthesis. It is documented that increase in cytoplasmic and/or, nuclear β-catenin is related to poor prognosis in breast cancer patients [4]. A significant increase in tCho and β-catenin concentrations in malignant tumors indicates the increased proliferation rate compared to benign tissues. Our results imply a link between the choline synthesis and β-catenin pathways that play a significant role in breast cancer. Therapeutic interventions targeted against these pathways may be of clinical benefit. This finding needs to be verified in large cohort of patients.

References: (1) Sah et al. MRM 2012; 13: 1973-80 (2) Sah RG et al. JMRI 2013 (3) Pu YS et al. J Biomed Science 2009; 16: 82 (4) Dolled-Filhart M et al. Cancer Res. 2006; 66: 5487-94.

AUTHORS (LAST NAME, FIRST NAME): Agarwal, Khushbu[1]; Hariprasad, Gururao[2]; Rani, Komal[2]; Sharma, Uma[1]; Hari, Smriti[3]; Seenu, Vurthaluru[4]; Parshad, Rajinder[4]; Jagannathan, Naranamangalam R.[1]

INSTITUTIONS (ALL):

1. Department of NMR & MRI Facility, All India Institute of Medical Sciences, New Delhi, Delhi, India.
2. Department of Biophysics, All India Institute of Medical Sciences, New Delhi, Delhi, India.
3. Department of Radio-diagnosis, All India Institute of Medical Sciences, New Delhi, Delhi, India.
4. Department of Surgical Disciplines, All India Institute of Medical Sciences, New Delhi, Delhi, India.

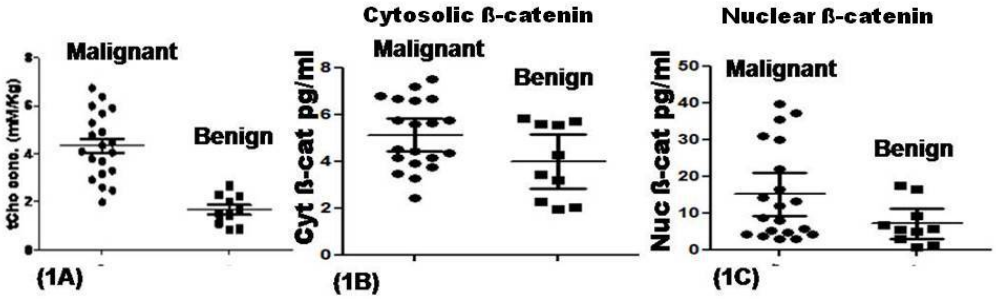

Figure 1A: Shows the difference in tCho concentration in malignant and benign breast tissues; Figure 1B: Shows the difference in cytosolic ß-catenin concentrations in malignant and benign breast tissues; Figure 1C: Shows the difference in nuclear ß-catenin concentrations in malignant and benign breast tissues.

CONTROL ID: 2228052

TITLE: Pulsed radiotherapy alters dynamic tumor contrast enhancement in a mouse model of glioblastoma

PRESENTER: Sarah Krueger

ABSTRACT BODY:

Abstract Body: Purpose/Objectives: Recent studies have demonstrated that pulsed radiotherapy (PRT) may be associated with greater sparing of vasculature and decreased levels of tumor hypoxia compared to standard radiotherapy (SRT) (2-4). PRT divides a standard 2-Gy fraction into ten 0.2-Gy pulses that are delivered every three minutes. It is hypothesized that this type of delivery may exploit the therapeutic ratio via differential effects on DNA damage recognition, allowing for greater repair of radiation-induced damage in normal tissue (5). In this study, it is shown that a short course of PRT in a mouse model of glioblastoma may promote changes in vasculature which can be visualized by dynamic MRI.

Materials/Methods: *Nu/nu* mice were injected intracranially with U87MG cells to establish orthotopic tumors. Whole brain irradiation (WBI) was given by either SRT (one continuous fraction) or PRT (10 pulses with a 3-minute pulse interval) and comprised of a 2-Gy dose delivered for five consecutive days. Treatment was given as a single planar beam via a 160 kVp Faxitron x-ray machine. Tumors were imaged with dynamic contrast enhanced (DCE) MRI before and after treatment. Semi-quantitative analysis was done on dynamic images examining changes in signal intensity (SI) over time (1). Following post-treatment imaging, animals were injected with Hoechst 33342 and pimonidazole to evaluate perfusion and hypoxia. Brain tissue was then collected and snap frozen. Tissue sections were stained to evaluate hypoxia and vascularity.

Results: Compared to contralateral normal brain, tumors in all groups at all time-points demonstrated significant contrast enhancement. After treatment, PRT treated tumors showed little change in tumor SI (Maximum relative enhancement=7.7%) while SRT and control tumors both showed increased enhancement, (27.7 and 27.2% respectively). In addition, the time to 90% maximum SI (T90) was unchanged in PRT treated tumors, but increased 20% following SRT and 50% in control animals. The rate of enhancement was also increased 150% in control animals, 43.6% in SRT treated animals but dropped 6.2% in PRT treated mice. Histopathology to confirm changes in vasculature and perfusion are ongoing.

Conclusions: Previous work in this animal model has demonstrated that PRT may be less damaging to normal brain tissue, particularly in terms of vascular sparing (2,3). The data from this study suggests a normalization of vasculature following PRT that is absent after SRT. Utilization of this type of RT, either alone or as a part of a standard schedule, could potentially improve tumor response to radiation via reduction of hypoxia and spare normal tissue (4). Because only 10 Gy was delivered in this study, there was little effect on tumor growth; studies are currently in progress to look at the effects of longer courses of treatment on tumor vascularity and tumor response.

1. Gordon Y, Partovi S, et al. *Cardiovasc Diagn Ther* 2014.
2. Dilworth JT, Krueger SA, et al. *Radiother Oncol* 2013.
3. Lee DY, Chunta JL, et al. *Int J Radiat Oncol Biol Phys* 2013.
4. Adkison JB, Tome W, et al. *Int J Radiat Oncol Biol Phys* 2011.
5. Marples B Collis SJ. *Int J Radiat Oncol Biol Phys* 2008.

AUTHORS (LAST NAME, FIRST NAME): Krueger, Sarah[1, 2]; Kane, Jonathan L.[1, 3]; Dabjan, Mohamad[1]; Wilson, George D.[1, 2]; Marples, Brian[1, 2]

INSTITUTIONS (ALL):

1. Radiation Oncology, Beaumont Health System, Royal Oak, MI, United States.
2. Oakland University-William Beaumont School of Medicine, Rochester, MI, United States.
3. Oakland University, Rochester, MI, United States.

(No Image Selected)

CONTROL ID: 2228059

TITLE: Targeting Apoptotic Cells In Vivo in Ischemia Stroke by a Novel Small-molecule Probe

PRESENTER: Cheng Qian

ABSTRACT BODY:

Abstract Body: ***Background*** Stroke is one of the leading causes of serious long-term disabilities and even death around the world. Focal ischemia results in changes compatible with apoptosis in regions of penumbra. It has been proved that attenuating apoptosis pathway could ameliorate ischemic injury. Therefore, detecting apoptosis would make a lot of senses. Molecular imaging of apoptosis in vivo may have important implications for clinical practice, assisting in early detection of disease, monitoring of disease course, assessment of treatment efficacy, or development of new therapies. Although a probe for clinical imaging of apoptosis would be highly desirable, this is yet an unachieved goal, mainly because of the required challenging integration of various features, including sensitive and selective detection of the apoptotic cells, clinical aspects such as favorable biodistribution and safety profiles. A novel small-molecule probe targeting various steps of the apoptotic cascade has been developed to address this challenge.
Aims The purpose of this study was to test the applicability of this probe as a diagnostic imaging agent for the detection of apoptotic cells in ischemia stroke.
Methods Using fluorescein isothiocyanate-cystine or Cy5.5-cystine, we evaluated cell apoptosis in vitro and in vivo. Hela cells were induced apoptosis by incubating with doxil for 24 hours. Probes were then added in after drug administration. Cytotoxicity was also evaluated in Hela cells with various concentrations of probes by cell counting kit-8. Ischemia stroke was induced in mice by photothrombotic proximal middle cerebral artery occlusion. Probes were injected intravenously after occlusion. Fluorescent images were obtained with the Maestro in vivo imaging system (CRi, Woburn, MA, USA) at predetermined time points for assessment of probes uptake. At 24 hours, both fluorescent and magnetic resonance images were acquired to make an image fusion. Then animals were sacrificed, and brain tissue was subjected to fluorescent microcopy ex vivo, in correlation with the hallmark of apoptosis (Annexin-V binding) and neuron markers (MAP2 and NeuN).
Results Marked and selective uptake of probes could be seen in the doxil-induced Hela cells, while non-induced cells rarely uptook the probes. There was no significant cells death even with a high concentration of probes (2500ug/ml). Selective uptake of probes was observed at the primary site of injury. Fluorescent images matched well with the magnetic resonance images. Uptake was at the cellular level, with accumulation in the cytoplasm. Cells manifesting probes uptake were confirmed as apoptotic cells by detection of the characteristic apoptotic hallmark Annexin-V.
Conclusions Our study proposes fluorescein isothiocyanate-cystine and Cy5.5-cystine as useful tools for selective targeting and detection in vivo. Such imaging of apoptosis, following future radiolabeling the probe, may advance care for patients, by allowing real-time evaluation of the extent of tissue damage, assessment of novel therapeutic strategies, and optimization of treatment for the individual patient.

AUTHORS (LAST NAME, FIRST NAME): Qian, Cheng[1, 2]; Liu, Dong-Fang[1]; Teng, Gao-jun[1, 2]; Jiao, Yun[1]

INSTITUTIONS (ALL):

1. Jiangsu Key Laboratory of Molecular and Functional Imaging, Southeast University, Nanjing, Jiangsu, China.
2. Radiology, Zhongda Hosipital, Nanjing, Jiangsu, China.

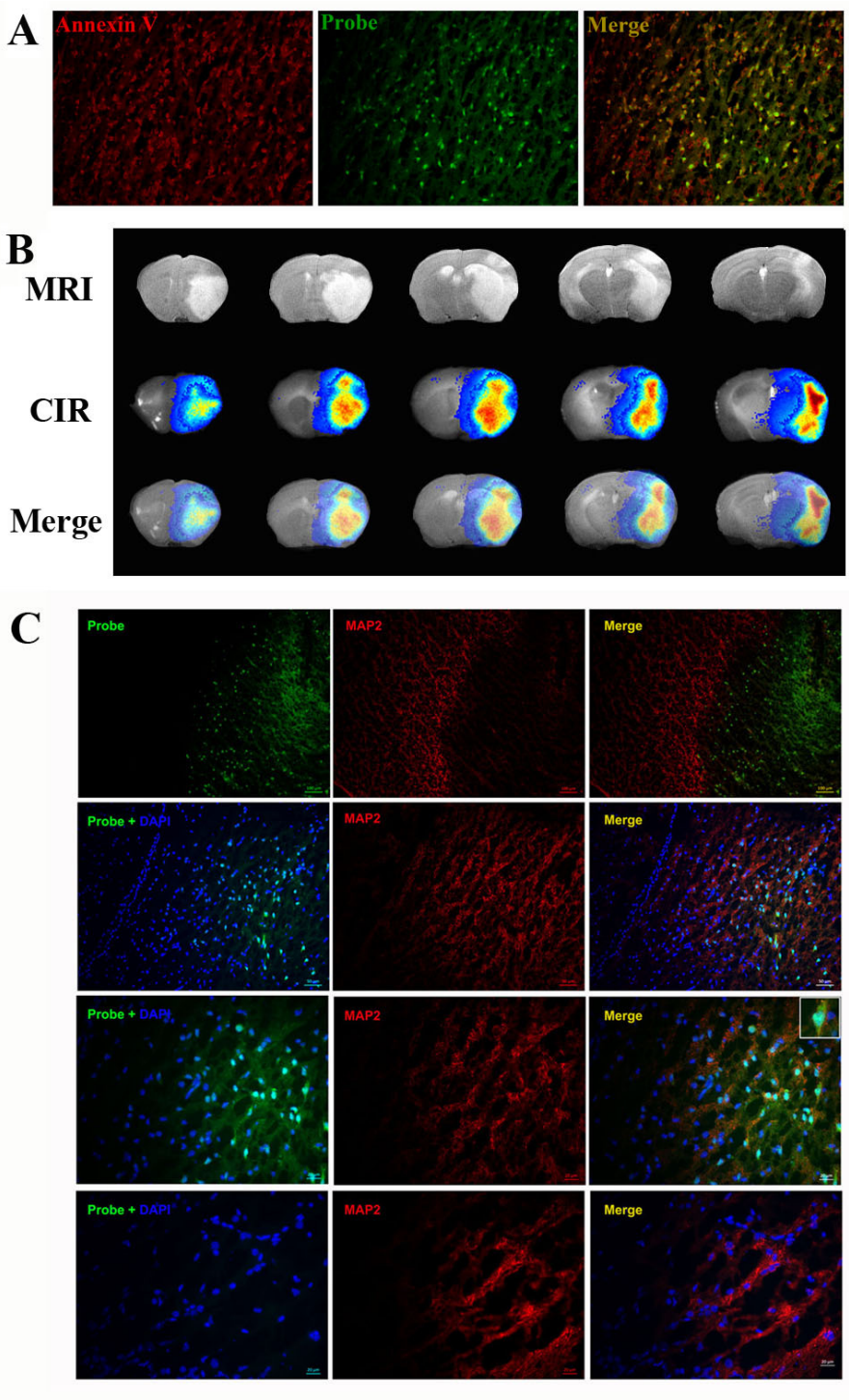
A
Annexin V
Probe
Merge
B
MRI
CIR
Merge
C
Probe
MAP2
Merge
Probe + DAPI
MAP2
Merge
Probe + DAPI
MAP2
Merge
Probe + DAPI
MAP2
Merge

CONTROL ID: 2228197

TITLE: Imaging tumor microenvironment with ^{125}I-iodinated hyaluronan

PRESENTER: Zhonglin Liu

ABSTRACT BODY:

Abstract Body: Hyaluronan or hyaluronic acid (HA) is an anionic, nonsulfated glycosaminoglycan distributed widely throughout connective, epithelial and neural tissues. HA is a major component of the extracellular matrix and contributes to cell proliferation, and migration. It plays key roles in skin wound healing and in tumor microenvironment (TME) remodeling. HA interacts with the transmembrane receptor CD44 and hyaluronan-mediated motility receptor (RHAMM) on tumor cells, endothelial cells, and macrophages in cancers, such as breast cancer. Those tumors typically grow in an extensively remodeled TME to sustain tumor cell proliferation, angiogenesis, and invasion. ^{125}I-iodinated HA (^{125}I-HA) has been used previously to study HA metabolism. However, ^{125}I-HA has not been characterized as a radioligand for detecting CD44 expression and assessing HA-CD44 interactions in TME by *in vivo* imaging. This study was designed to study ^{125}I-HA uptake in skin would healing in mice as well TME remodeling in mice with xenografted human breast cancer. **Methods**: HA (MW 10-20 KDa) was activated with cyanogen bromide (CNBr) and reacted with tyrosine (Tyr). Tyr-bound HA (Tyr-HA, 100 μg) was then iodinated with 1.0 mCi [^{125}I]NaI in a tube coated with 50 μg IODO-GEN Reagent. After purification, ^{125}I-HA radiochemical purity was greater than 97% for animal injection. The feasibility and specificity of ^{125}I-HA uptake in skin wound-healing lesions was determined in two groups of ICR mice with 12-O-tetradecanoylphorbol-13-acetate (TPA)-induced skin injury on right ears. The mice in Group 1 received overdose injection of non-radiolabeled HA and Group 2 had saline (carrier vehicle) injection before ^{125}I-HA administration. Tumor uptake of ^{125}I-HA was studied in five BALB/C nude mice with xenografted MDA-MB-231 tumors, which exhibit high CD44 expression, and four mice carrying human MCF-7 xenografts with low CD44 expression. ^{125}I-HA uptake in target tissues was imaged at 3-24 hours after intravenous injection of ^{125}I-HA (~200 μCi) using an intensified quantum imaging detector [iQID] camera, a custom-built planar imager that offers ~200 μm resolution and high sensitivity to low energy ^{125}I photons. The ears and tumors were excised for biodistribution measurements, *ex vivo* autoradiography, and immunohistochemical analysis. **Results**: *In vivo* imaging demonstrated that ^{125}I-HA clearly localized in the wound-healing skin lesions with high CD44 expression. Biodistribution data (%ID/g) showed that the radioactive ratio of injured ears to control ears was reduced significantly from 8.2±1.9 in the saline control group to 3.9±0.2 ($P < 0.05$) in the HA blockade group. ^{125}I-HA uptake was increased and readily detectable in the MDA-MB-231 tumor, but was undetectable in the MCF-7 site. Postmortem analyses indicated that ^{125}I-HA selectively accumulated in the MDA-MB-231 tumor with upregulated CD44 expression but not in the MCF-7, in which CD44 was not detectable by Western blot assay. **Conclusion**: ^{125}I-HA tumor distribution can be used to specifically measure HA-CD44 metabolic status. Imaging with ^{125}I-HA may provide a direct, real-time method to estimate TME remodeling and modulation in cancer research.

AUTHORS (LAST NAME, FIRST NAME): Liu, Zhonglin[1]; Barber, Christy[1]; Wan, Li[1]; Han, Ling[1]; Furenlid, Lars R.[1]; Woolfenden, James M.[1]

INSTITUTIONS (ALL):

1. Medical Imaging, The University of Arizona, Tucson, AZ, United States.

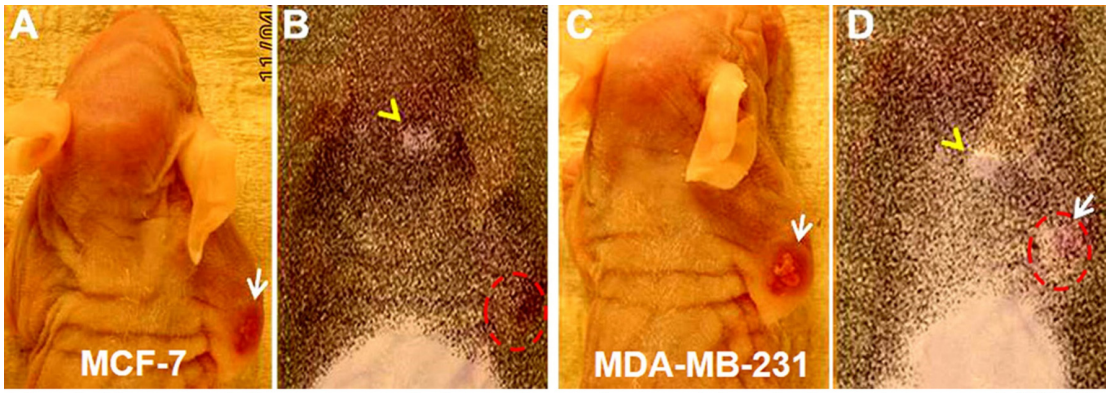

Fig. 1. Representative mouse photographs and co-registered planar images of ^{125}I-HA from two mice with xenografted MCF-7 (A and B) and MDA-MB-231 (C and D) tumors marked by arrows. Focal radioactive uptake was visualized in the MDA-MB-231 tumor (arrow), but not in the MCF-7. The thyroid (arrowhead) shows accumulation of free ^{125}I.

CONTROL ID: 2229682

TITLE: Novel large gold nanorods for ultrahigh contrast and molecular sensitivity in biomedical applications

PRESENTER: Elliott SoRelle

ABSTRACT BODY:

Abstract Body: The vast majority of gold nanorods (GNRs) used in biomedical therapy and imaging studies are ~50x15nm particles produced by methods developed over a decade ago [1,2]. Recently, methods have been developed to produce larger-than-usual GNRs (~100x30nm) in higher purity and monodispersity [3]. Large GNRs are also predicted to have better optical properties than small GNRs [4]. Despite clear advantages, large GNRs are virtually absent from biomedical literature. Prior to such use, large GNRs must be surface coated to achieve stability in biological environments. Moreover, the ability to conjugate the particle surface with targeting biological moieties (such as antibodies) is highly desired for molecularly targeted studies. While coating methods exist for small GNRs [5], these methods have not been tested rigorously for large GNRs. Here we report significant flaws in common surface functionalization methods for gold nanorods (GNRs) of larger-than-usual sizes.

Small (~50x15nm) and large (~100x30nm) GNRs were produced using two published methods [1,3]. Particle morphology and size distribution were characterized using Transmission Electron Microscopy (TEM), and spectra were measured by Vis-NIR Spectrometry. Colloidal stability of each GNR was assayed at various stages of functionalization with different surface coatings using zeta potential and Vis-NIR measurements. Unlike small GNRs, large GNRs functionalized with PEG undergo irreversible aggregation and crash out of solution after minimal washing by centrifugation. In contrast to PEG, incubation with poly(sodium 4-styrenesulfonate) (PSS) made large GNRs extremely stable in aqueous solution. The stability of large GNRs in biological serum was also assessed and it was found that PSS-coated large GNRs remain highly stable in the presence of serum proteins. In addition to developing a strategy for large GNR stability, a novel platform to enable molecular targeting of large GNRs was also designed and validated through binding specificity experiments. Finally, large GNRs were shown to produce 32 times greater signal in Optical Coherence Tomography (OCT) than small GNRs *in vitro* (see figure). We also found that large GNRs exhibited 8 times greater extinction coefficient than small GNRs, making them superior photoacoustic contrast agents.

This work enables the use of large GNRs in biomedical applications for the first time through rigorous characterization and development of new surface chemistry approaches. This study also demonstrates tremendous advantages (e.g. increased particle contrast, signal sensitivity) that large GNRs possess compared to the current standards set by small GNRs. Our results also indicate that colloidal stability of large and small particles of similar chemical composition is predicated on different fundamental mechanisms. Importantly, the biomedical advantages of novel nanoparticle synthesis methods may not be realized without concurrent customized surface functionalization methods.

[1] Nikoobakht & El-Sayed, *Chem Mater* (2003)
[2] Jana *et al*, *J Phys Chem B* (2001)
[3] Ye *et al*, *Nano Lett* (2013)
[4] Jain *et al*, *J Phys Chem B* (2006)
[5] Niidome *et al*, *J Control Release* (2006)

AUTHORS (LAST NAME, FIRST NAME): SoRelle, Elliott[1, 3]; Liba, Orly[1, 2]; Hussain, Zeshan M.[1]; Gambhir, Milan[1]; de la Zerda, Adam[1, 2]

INSTITUTIONS (ALL):
1. Structural Biology, Stanford University, Stanford, CA, United States.
2. Electrical Engineering, Stanford University, Stanford, CA, United States.
3. Biophysics, Stanford University, Stanford, CA, United States.

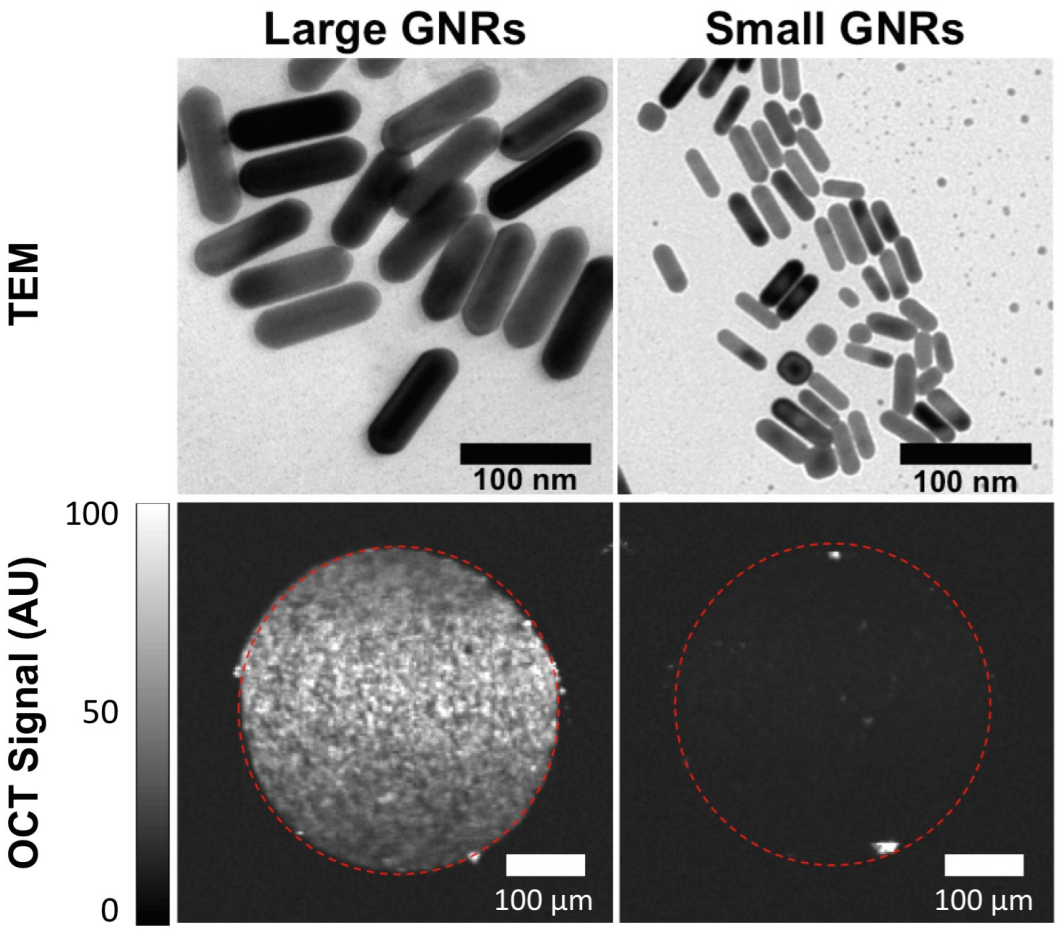

Figure: Large GNRs exhibit 32x stronger OCT signal than commonly-used small GNRs.

CONTROL ID: 2231660

TITLE: Novel TSPO Ligands for Optical Imaging and High-throughput Screening

PRESENTER: Jun Li

ABSTRACT BODY:

Abstract Body: Translator protein (TSPO) is an 18 kDa protein typically localized to the outer mitochondrial membrane whose primary role is to facilitate cholesterol metabolism. Within that context, TSPO expression and function tend to be linked with steroid biosynthesis, cellular proliferation, and apoptosis. TSPO represents an attractive target for non-invasive imaging given that elevated levels of TSPO are observed in many human cancers and other diseases.[1] Whereas the majority of our prior studies have focused on the development and characterization of high-affinity positron emission tomography (PET) ligands, this study focused on the development of an optimized series of fluorescence-based TSPO tracers suitable for cellular-resolution imaging and high-throughput small molecule screening. We envision that such molecular probes could be useful for elucidating the role of TSPO in various human diseases and for aiding the discovery of future TSPO ligands.

Leveraging prior structure-activity relationships (SAR) on a series of novel pyrazolopyrimadines[2], we developed a series of new TSPO ligands with appended FITC fluorescence easily detectable by conventional optical imaging and microscopy. A library of candidate ligands were rapidly expanded and subjected to competitive binding assays that explored the effects of fluorescent selection and linker length (n= 2-8). The best candidate probe, which exhibited exceptional TSPO affinity (K_d = 0.22 nM) and negligible CBR activity, exhibited suitable *in vitro* imaging characteristics and was found useful for small molecule screening studies in multi-well plate format. At *in vitro* fluorescence imaging, fluorescent probe accumulation co-localized with Mito Tracker Red in C6 rat glioma cells and its specificity was confirmed by functional displacement using its parent TSPO ligand. [3]

This work lays the foundation for the development of a battery fluorescence-based TSPO ligands that could be potentially translated to *in vivo* studies, especially with further refining of the fluorescence properties. In addition, we envision a role for these probes as precision, point-of-care diagnostics, given the important role of TSPO in many human diseases.

Reference: [1] Batarseh, A. et al., Molecular and cellular endocrinology, 2010. **327**(1): 1-12; [2] Tang, D., et al., Journal of medicinal chemistry, 2013. **56**(8): 3429-3433; [3] Denora, N., et al., Pharmaceutical research, 2011. **28** (11): p. 2820-2832.

AUTHORS (LAST NAME, FIRST NAME): Li, Jun[2, 3]; Tang, Dewei[2]; Buck, Jason R.[2]; Schulte, Michael L.[2]; Watchmaker, Jennifer M.[2]; Hight, Matthew[2]; Manning, H. Charles[1]

INSTITUTIONS (ALL):

1. Radiology and VUIIS, Vanderbilt University, Nashville, TN, United States.
2. Vanderbilt University Institute of Imaging Science, Nashville, TN, United States.
3. Vanderbilt University Interdisciplinary Materials Science Program, Nashville, TN, United States.

(No Image Selected)

CONTROL ID: 2228353

TITLE: ICG conjugated Trastuzumab as an Agent for Fluorescence Guided Cancer Surgery and Photoimmunotherapy

PRESENTER: Insoo Park

ABSTRACT BODY:

Abstract Body: During the last decade, tremendous advances in preoperative molecular imaging modalities such as positron emission tomography, ultrasonography, computed tomography and magnetic resonance imaging have facilitated earlier and more accurate detection and stage determination of cancer. However, intraoperative tumor surgery still relies on the surgeon's naked eye, which is impossible to detect cancer lesions less than 50 mm. The precise detection of primary and metastatic lesions and complete resection of them with their margins at the time of surgery are essential to reduce the rate of recurrence. We developed an antibody based cancer specific fluorescent imaging agent, ICG conjugated trastuzumab (Tra-ICG), and tested its ability using KPL4, KATO III and SKOV3 tumor xenograft models in mice. Trastuzumab (Herceptin), a 148 kDa recombinant humanized monoclonal antibody that binds to the extracellular domain of human epidermal growth factor receptor 2 (HER2), which is overexpressed in several cancer types including breast, gastric/gastroesophageal, ovary, endometrium, bladder, lung, colon and head and neck cancers. Herceptin received FDA approval for use in women with HER2 positive breast cancer in 1998. ICG is an FDA approved near infrared (NIR) fluorescence dye whose maximum excitation light wavelength is at 780 nm and the highest emission light wavelength is at ~800 nm. Fluorescence in this range of wavelengths has limited autofluorescence and generates low background signals. In this study, we demonstrated that Tra-ICG is a useful agent to visualize small diseased lesions, which are normally undetectable with the surgeon's naked eye. Over 90 fold fluorescence quenched Tra-ICG was dequenched within 10 min when it binds to the HER2 expressing plasma membrane and very slowly endocytosed into the cells and ICG fluorescence was palpably detectable at the tumor sites over 28 days. In addition, Tra-ICG induced rapid necrosis of cancer tissues after exposure to NIR light. Tra-ICG may serve as an agent for helping surgeons to accurately localize tumor tissues and their margins during operations and for enhancing HER2 positive cell necrosis with NIR light irradiation to eradicate all residual diseased lesions.

AUTHORS (LAST NAME, FIRST NAME): Park, Insoo[1]; Kim, Seungwon[1]; Kim, Seok-Ki[1]

INSTITUTIONS (ALL):

1. Molecular Imaging & Therapy Branch, National Cancer Center, Goyangsi, Gyeonggido, Korea (the Republic of).

(No Image Selected)

CONTROL ID: 2232226

TITLE: A mixture of ICG, Macroaggregated Albumin and Hyaluronic Acid, as a Tracing Agent for Fluorescence Guided Cancer Surgery

PRESENTER: Insoo Park

ABSTRACT BODY:

Abstract Body: Precise determination of cancer lesions and their positive margins during operations is critical in the success of surgical outcomes because residual tiny tumor tissues usually lead to recurrent diseases. Various tracing methods, ultrasound (US) guided needle location, US guided blue dye injection, colloidal charcoal tracer injection, radioisotype injection, have been developed to help surgeons efficiently identify any cancer lesions in the operating field. However, each method has its own disadvantages such as diffusion, migration into the nearby tissues, risk of pain and bleeding, and leaving permanent staining on the skin and subcutaneous tissues. To improve these drawbacks, we have developed a safe and convenient near infrared (NIR) fluorescent imaging tracer using three Food and Drug Administration (FDA) approved materials, indocyanine green (ICG), macroaggregated human serum albumin (MAA), and hyaluronic acid (HY), and named ICG-MAA-HY. ICG, an NIR fluorescent dye, has a short blood half-life of 150 to 180 seconds and is rapidly removed from circulation. However, its stability and fluorescence intensity were dramatically increased in the presence of MAA without altering initial activities of both ICG and MAA. MAA has an average particle size of 10-90 mm. MAA prevents ICG-MAA-HY from diffusing into surrounding tissues and from undergoing phagocytosis by local macrophages, while HY helps to increase its viscosity, so that MAA is maintained in a suspended form without settling down on the syringe wall during injection. This method could be easily translated to the clinic as a tracing agent for fluorescence guided cancer surgery.

AUTHORS (LAST NAME, FIRST NAME): Park, Insoo[1]; Kim, Seungwon[1]; Noh, Jinhee[1]; Kim, Seok-Ki[1]

INSTITUTIONS (ALL):

1. Molecular Imaging & Therapy Branch, National Cancer Center, Goyangsi, Gyeonggido, Korea (the Republic of).

(No Image Selected)

CONTROL ID: 2228364

TITLE:

Long term tracking of human neural progenitor cells derived from pluripotent stem cells using mitochondrial ferritin as an MRI reporter gene

PRESENTER: Kazim Narsinh

ABSTRACT BODY:

Abstract Body: Introduction

An unmet challenge to successful translation of stem cell therapies into patients is the ability to non-invasively monitor cellular behavior and movement following transplantation. Imaging tools can potentially provide critical information regarding the homing, engraftment, and proliferation of the delivered cells. MRI can track cells by direct labeling with iron-oxide nanoparticles or gadolinium chelates, but these agents become diluted after mitotic cellular divisions, thereby limiting long-term visualization, and may fail to discriminate between living versus dead cells. Genetically-engineered ferritin constructs can be used as MRI reporter genes to overcome these limitations (1). Upon cellular expression, ferritin forms a superparamagnetic iron core that generates hypointensity in T2- and T2*-weighted images. Because the ferritin gene cam be stably passed to daughter cells, long-term tracking studies of cellular therapeutics may be performed. Here, we report the use of a modified mitochondrial ferritin construct, with improved MRI sensitivity over wild-type ferritins, to monitor the engraftment and survival of human neural progenitor cells after their transplantation into rat striatum.

Materials and Methods

We inserted an engineered human mitochondrial ferritin gene (2) into a lentiviral construct already containing green fluorescent protein (GFP) under a human ubiquitin promoter. We then transduced human embryonic stem cell-derived neural progenitor cells (hESC-NPCs) with the lentiviral construct to generate hESC-NPC lines that stably expressed mtFt. Twenty adult male athymic nude rats underwent stereotactic implantation of mtFt-expressing hESC-NPCs into their striata, while nontransduced hESC-NPCs were stereotactically implanted into the contralateral striata as a control. On day 7, 14, 21, 60, and 120 after implantation, in vivo MRI was performed at 11.7 T using gradient-recalled echo (GRE) and multislice multiecho (MSME) sequences. *Ex vivo* GRE imaging at 11.7 T was also performed using 50 μm pixels. Immunohistochemistry was performed on the fixed rat brain tissue using rabbit polyclonal antibody against mtFt, mouse anti-nuclear protein/h-nuc antibody (anti-hNUMA) specific to a human antigen, and goat anti-GFP antibody.

Results and Discussion

After injection into rat brain cortex, hESC-NPCs expressing mtFt were clearly detected as hypointense regions on T2*-weighted GRE images. The contralateral side demonstrated normal signal intensity. Immunohistochemical analysis confirmed that the hypointense regions contained transplanted cells expressing GFP. Truncated mtFt localized to the cytoplasm and loaded more iron than wild-type mtFt or human ferritin. The ferritin-expressing cells identified by MRI were confirmed as hESC-NPCs by immunohistochemical staining for a human specific nuclear antigen. This optimized MRI reporter gene has significant potential for long-term monitoring of the success of stem cell transplantation studies.

References

1. Genove G, DeMarco U, Xu H, Goins WF, Ahrens ET. *Nat Med.* 2005 (43):450–4.

2. Iordanova B, Hitchens TK, Robison CS, Ahrens ET. *PLoS One*. 2013 8(8):e72720.

AUTHORS (LAST NAME, FIRST NAME): Narsinh, Kazim[1, 2]; Navarro, Michael[2, 3]; Weber, Thomas G.[1, 2]; Xu, Hongyan[1, 2]; Marsala, Martin[2, 3]; Ahrens, Eric T.[1, 2]

INSTITUTIONS (ALL):

1. Radiology, UC San Diego School of Medicine, La Jolla, CA, United States.
2. Sanford Consortium for Regenerative Medicine, La Jolla, CA, United States.
3. Anesthesiology, UC San Diego School of Medicine, La Jolla, CA, United States.

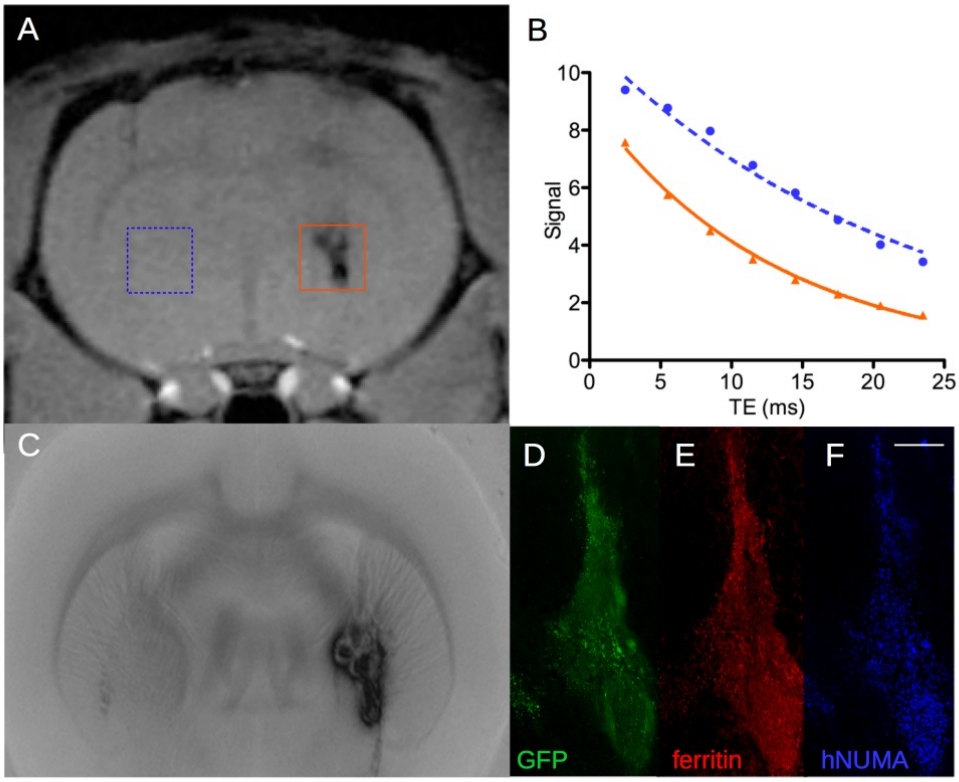

Long term tracking of human embryonic stem cell-derived neural progenitor cells using a mitochondrial ferritin reporter gene. (A) In vivo MRI at 11.7T after 28 days of engraftment shows distinct hypointensity in the left striatum on GRE images. **(B)** Marked T2* shortening (orange) due to the presence of ferritin-expressing cells relative to the contralateral striatum (blue) injected with untransduced cells. **(C)** Ex vivo MRI confirming presence and location of ferritin-expressing cells. Panels **(D-F)** show postmortem histologic staining of the same rat with anti-GFP, ferritin, and hNUMA (human specific nuclear antibody), demonstrating clear expression of ferritin in the grafted hNUMA+ cells in the same location as the MRI. Scale bar in **F** is 500 μm.

CONTROL ID: 2228393

TITLE: Sortase-mediated site-specific labeling of Nanobodies: a generic method for multiple imaging modalities

PRESENTER: Sam Massa

ABSTRACT BODY:

Abstract Body: Nanobodies, the recombinantly produced antigen-binding domains of camelid heavy-chain antibodies, have already proven to be proficient probes for non-invasive molecular imaging (1). To safeguard their intrinsically high binding specificity and affinity and to ensure the tracer's homogeneity, methods to site-specifically label them have been developed (2,3). We investigated the use of Sortase A, a transpeptidase enzyme derived from *Staphylococcus aureus* that catalyzes the conjugation between an LPXTG-tagged protein and an oligoglycine-functionalized probe (4), as a generic strategy for site-specific labeling of Nanobodies for use in nuclear and optical imaging.

The chelating agents CHX-A''-DTPA (for radiolabeling with indium-111 for SPECT) and NOTA (for radiolabeling with gallium-68 for PET), and the fluorescent dye Cy5 (excitation: 650nm, emission: 670nm) were functionalized with an N-terminal triglycine. The sortase-recognition sequence LPETG (sortag) on the other hand was introduced at the C-terminal end of the Nanobody, upstream of the hexahistidine-tag.
The HER2-targeting Nanobody 2Rs15d was generated with a sortag and conjugated to the triglycine-functionalized chelating agents or dye. After a straightforward IMAC and SEC purification strategy, a yield of 30-50% single-conjugated product was obtained and confirmed by ESI-Q-TOF mass spectrometry analysis. The enzymatic conjugation did not negatively influence the radiolabeling efficiency: radiolabeling with indium-111 or gallium-68 resulted in a high radiochemical yield (> 97%) and purity (≥ 98%).
After *in vitro* validation (surface plasmon resonance, cell binding study, stability in serum) the new tracer construct was validated *in vivo* in a HER2-expressing tumor model. *Ex vivo* biodistribution analysis showed that the radiolabeled Nanobodies were able to target the HER2-positive tumor specifically (^{111}In-CHX-A''-DTPA-2Rs15d-sortag: 12.57 ± 4.44 %IA/g vs. 0.90 ± 0.51 %IA/g for a non-targeting control Nanobody; ^{68}Ga-NOTA-2Rs15d-sortag: 12.63 ± 3.51 %IA/g vs. 0.99 ± 0.53 %IA/g for a non-targeting control Nanobody) at 90 min post injection in BT474M1-xenografted mice. In all three modalities (SPECT, PET and FRI) the tumor was visualized with high contrast at early time points post injection.

These results provide a versatile and standardized strategy for the site-specific labeling of Nanobodies. Using the sortase-mediated conjugation strategy any oligoglycine-functionalized label or chelating agent could be attached to the targeting probe, resulting in a homogeneous population of tracers for use in molecular imaging with multiple modalities.

References:

(1) De Vos *et al*. (2013) Expert Opin. Biol. Ther. 13, 1149-1160.
(2) Xavier *et al*. (2012) Methods Mol. Biol. 911, 485-490.
(3) Massa *et al*. (2014) Bioconjug. Chem. 25, 979-988.
(4) Popp *et al*. (2007) Nature Chem. Biol. 3, 707-708.

AUTHORS (LAST NAME, FIRST NAME): Massa, Sam[1, 2]; Vikani, Niravkumar[2]; Gorsen, Santina[1]; Vanderhaegen, Saskia[5, 3]; Steyaert, Jan[5, 3]; Bartz, Christian[4]; Betti, Cecilia[4]; Ballet, Steven[4]; Bunschoten, Anton[7]; van Leeuwen, Fijs[7]; Descamps, Benedicte[8]; Vanhove, Christian[8]; Caveliers, Vicky[1, 6]; Lahoutte, Tony[1, 6]; Hernot, Sophie[1]; Muyldermans, Serge[2]; Xavier, Catarina[1]; Devoogdt, Nick[1, 2]

INSTITUTIONS (ALL):
1. In vivo Cellular and Molecular Imaging laboratory, Vrije Universiteit Brussel, Brussels, Belgium.
2. Laboratory of Cellular and Molecular Immunology, Vrije Universiteit Brussel, Brussels, Belgium.
3. Structural Biology Research Center, VIB, Brussels, Belgium.
4. Laboratory of Organic Chemistry, Vrije Universiteit Brussel, Brussels, Belgium.
5. Structutral Biology Brussels, Vrije Universiteit Brussel, Brussels, Belgium.
6. Nuclear Medicine Department, Universitair Ziekenhuis Brussel, Brussels, Belgium.

7. Interventional Molecular Imaging Laboratory, Department of Radiology, Leiden University Medical Center, Leiden, Netherlands.
8. Infinity-MEDISIP-iMinds Medical IT, Department of Electronics and Information Systems, Ghent University, Ghent, Belgium.

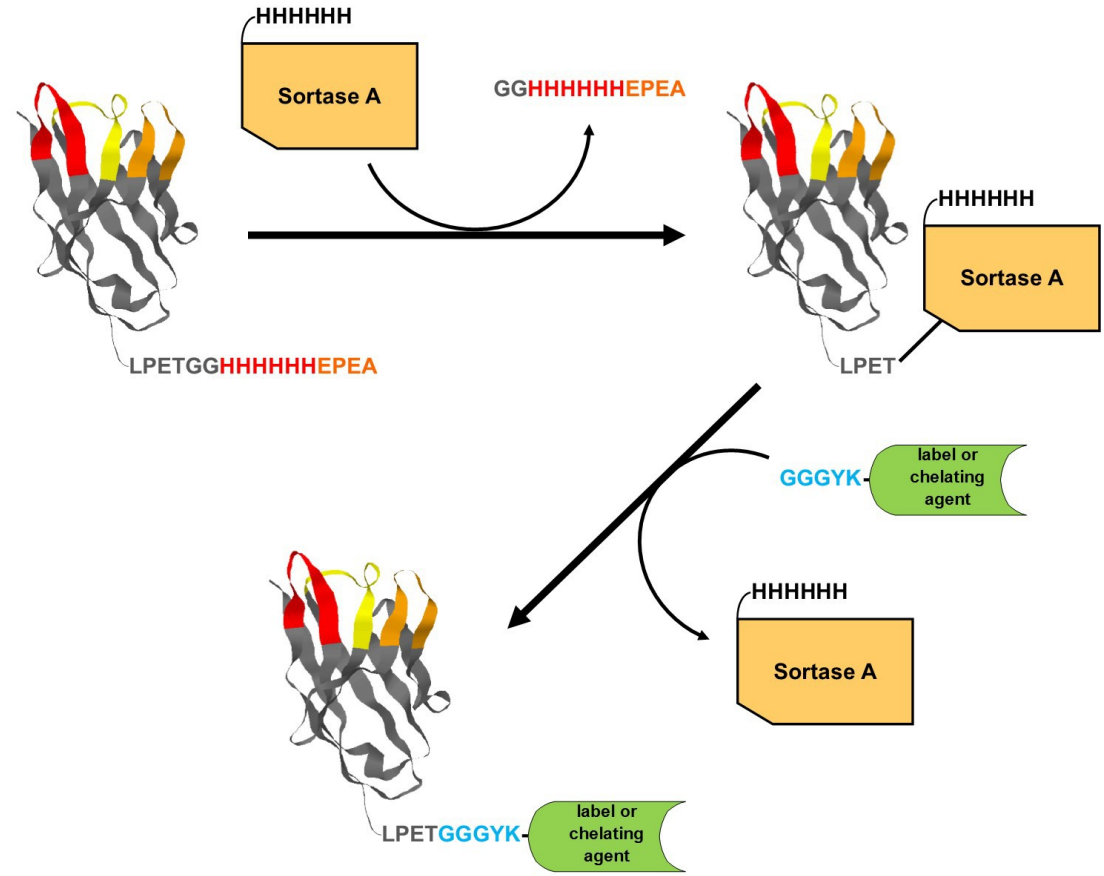

Scheme 1 - Sortase-mediated conjugation reaction mechanism

CONTROL ID: 2231239

TITLE: Development and Evaluation of a Small [^{11}C]-Tetrazine as Bioorthogonal PET Probe

PRESENTER: Christoph Denk

ABSTRACT BODY:

Abstract Body: Slow tracer accumulation of imaging probes can be circumvented by pretargeting using bioorthogonal ligations. These fast and biocompatible *"click"* reactions are capable of forming a covalent linkage between a pre-administered marker and a labeled pull down reagent (PDR) *in vivo*.[1] Due to particular high ligation rates the inverse electron demand Diels-Alder reaction (IEDDA) of strained dienophiles with 1,2,4,5-tetrazines (Tz) has gained interest in nuclear medicine.[2]

In addition to fast ligation rates PDRs must exhibit homogenous biodistribution, sufficient *in vivo* stability and fast excretion. The use of ^{11}C for PET pretargeting is beneficial due to its particular high specific activity and comparatively low production costs. Moreover, the short $t_{1/2}$ is still compatible with IEDDA reaction rates and allows for PDR administration at multiple time points to evaluate marker accumulation kinetics. By now the synthesis of one ^{11}C-Tz has been described in literature, however no *in vivo* data is available for this compound.[3]

We aimed to develop a small ^{11}C-Tz that exhibits good pharmacokinetics as well as sufficient IEDDA reactivity. *N*-Methylation was chosen as straight-forward method to introduce ^{11}C, but 3-aminotetrazines were excluded as precursors due to their limited IEDDA reactivity as estimated *in silico*.

Herein we present the (radio)synthesis, reaction kinetics, biodistribution and metabolic profile of *N*-([^{11}C]methyl)-1-(6-methyl-1,2,4,5-tetrazin-3-yl)methanamine (**^{11}C-1**). Precursor **2** was obtained via metal-catalyzed tetrazine synthesis and subsequent deprotection in 23% yield.[4] Reference material **1** exhibited fast reaction rates with s-TCO (**3**) as the dienophile ($k = 89.6\ M^{-1}s^{-1}$) in 1,4-dioxane. **^{11}C-1** was obtained in >98% radiochemical purity by reacting **2** with [^{11}C]CH_3OTf in a GE TRACERLab FX Pro module and subsequent HPLC purification. **^{11}C-1** was synthesized in a decay-corrected radiochemical yield of 30±2%, based on [^{11}C]CH_3I, in a total synthesis time of 30 min.

Whole body dynamic PET/MR scans (t=60 min) of female BALB/c mice (n=3) showed rapid renal clearance of **^{11}C-1** and homogenous biodistribution in most body regions (~1 SUV). The brain and medulla showed increased uptake of approx. 3 SUV which indicates the ability of **^{11}C-1** or metabolites to pass the blood brain barrier. Following imaging, PET data was confirmed by *ex vivo* biodistribution results. Metabolite analysis revealed up to 45% intact PDR in plasma and up to 87% unchanged **^{11}C-1** in urine.

^{11}C-1, a small IEDDA click reactant is accessible by straight-forward ^{11}C-radiochemistry and thus easy to establish in PET centers. Our *in vitro* and *in vivo* investigations indicate the suitability of **^{11}C-1** as either PDR for *in vivo* click chemistry or as prosthetic group for biomolecule labeling. In summary this versatile tool should allow for many applications in the field of bioorthogonal PET imaging and biomedical research.

(1) Rossin, R. *et al. ACIE* **2010**, *49*, 3375.
(2) Rossin, R. *et al. JNM* **2013**, *54*, 1989.
(3) Herth, M. M. *et al. Chem.Comm.* **2013**, *49*, 3805.
(4) Yang, J. *et al. ACIE* **2012**, *51*, 5222.

AUTHORS (LAST NAME, FIRST NAME): Denk, Christoph[1]; Mairinger, Severin[2]; Stanek, Johann[2]; Wanek, Thomas[2]; Filip, Thomas[2]; Svatunek, Dennis[1]; Fröhlich, Johannes[1]; Kuntner, Claudia[2]; Mikula, Hannes[1]

INSTITUTIONS (ALL):
1. Institute of Applied Synthetic Chemistry, Vienna University of Technology, Vienna, Austria.
2. Austrian Institute of Technology (AIT), Seibersdorf, Austria.

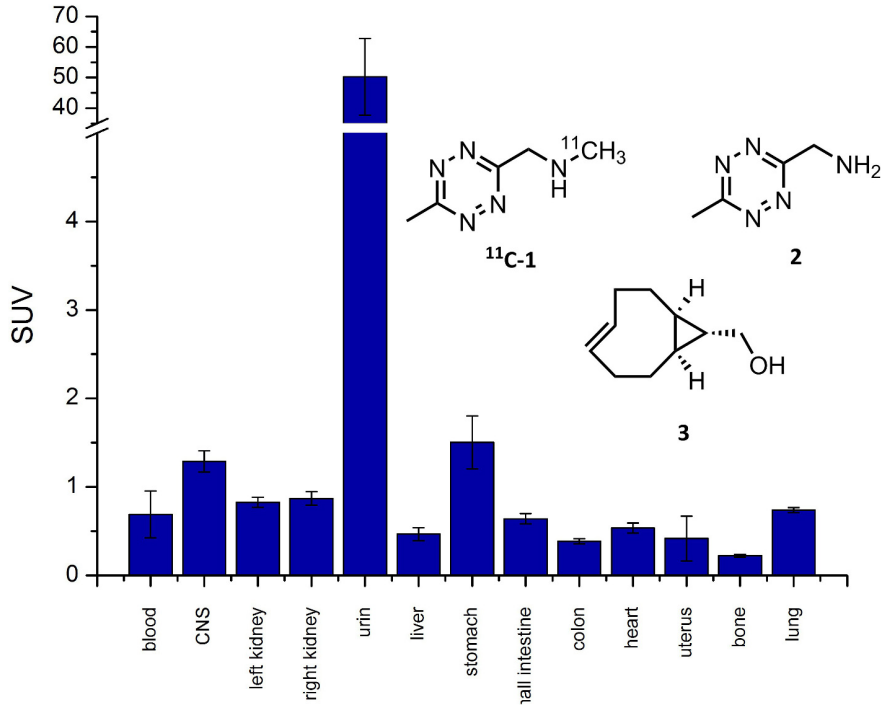
SUV
70
60
50
40
4
3
2
1
0
blood
CNS
left kidney
right kidney
urin
liver
stomach
all intestine
colon
heart
uterus
bone
lung
^{11}C-1
2
3
OH
H
H

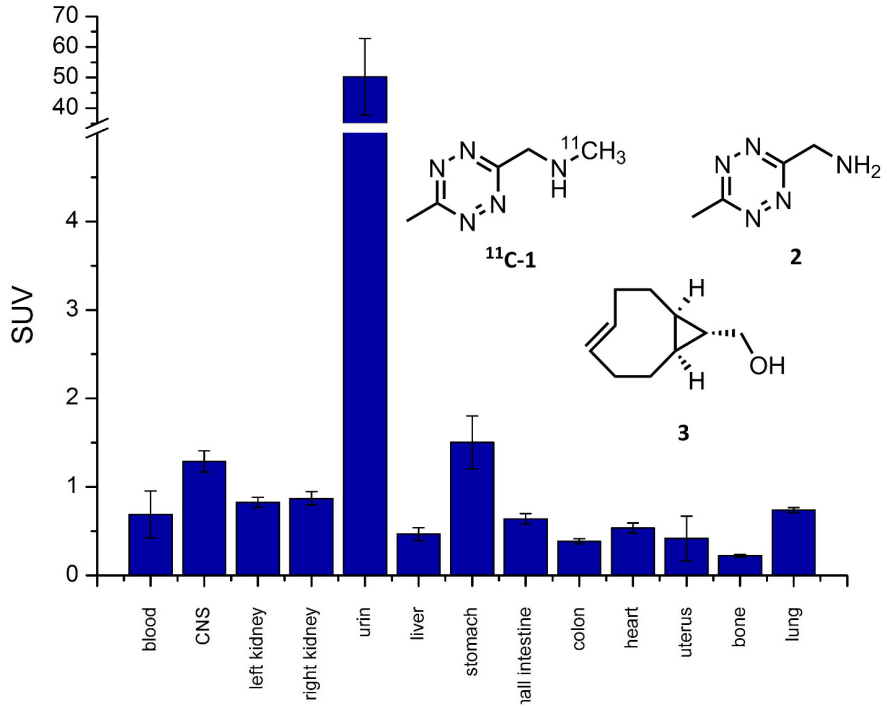

Ex vivo biodistribution data of **^{11}C-1** in female BALB/c mice 60 min after tracer administration

CONTROL ID: 2228410

TITLE: ^{64}Cu-DOTATATE PET for Somatostatin Receptor Imaging of Neuroendocrine Tumor Patients: a Prospective Head-to-Head Comparison with ^{111}In-DTPA-octreotide in 112 patiens.

PRESENTER: Andreas Kjaer

ABSTRACT BODY:

Abstract Body: BACKGROUND: Neuroendocrine tumors can be visualized using radiolabeled somatostatin analogs. We have previously shown the potential of a Copper-labeled compound in a small feasibility study. The aim of present study was, in a large prospective study, to compare on a head-to-head basis the performance of ^{64}Cu-DOTATATE and ^{111}In-DTPA-OC as basis for implementing ^{64}Cu-DOTATATE as a routine.

METHODS: The study prospectively enrolled 112 patients with pathologically confirmed neuroendocrine tumors of gastro-entero-pancreatic or pulmonary origin. All patients underwent both PET/CT with ^{64}Cu-DOTATATE and SPECT/CT with ^{111}In-DTPA-octreotide (^{111}In-DTPA-OC) within 60 days. PET scans were acquired 1 hour post-injection of 202 MBq (range 183 – 232 MBq) ^{64}Cu-DOTATATE following a diagnostic contrast-enhanced CT scan. Patients were followed for 42-60 months for confirmation of discrepant imaging findings. McNemar's test was used to compare the diagnostic performance.

RESULTS: 87 patients were congruent PET and SPECT positive. No SPECT positive cases were PET negative, while 10 false-negative SPECT cases were identified using PET. Diagnostic sensitivity and accuracy of ^{64}Cu-DOTATATE (97% for both) were significantly better than ^{111}In-DTPA-OC (87% and 88% respectively), p = 0.017. In 84 patients (75%) ^{64}Cu-DOTATATE identified more lesions than ^{111}In-DTPA-OC and always at least as many. In total, twice as many lesions were detected using ^{64}Cu-DOTATATE compared to ^{111}In-DTPA-OC. Moreover, in 40 of 112 cases (36%) lesions were detected by ^{64}Cu-DOTATATE in organs not identified as disease-involved by ^{111}In-DTPA-OC.

CONCLUSION: With these results, we demonstrate that ^{64}Cu-DOTATATE is far superior to ^{111}In-DTPA-OC for diagnostic performance in NET patients. Therefore, we do not hesitate to implement ^{64}Cu-DOTATATE as routine for replacement of ^{111}In-DTPA-OC.

AUTHORS (LAST NAME, FIRST NAME): Pfeifer, Andreas[1]; Knigge, Ulrich[2]; Binderup, Tina[2]; Mortensen, Jann[2]; Oturai, Peter [2]; Berthelsen, Anne Kiil[2]; Langer, Seppo[2]; Rasmussen, Palle [3]; Elema, Dennis[3]; von Benzon, Eric[2]; Hojgaard, Liselotte[2]; Kjaer, Andreas[1]

INSTITUTIONS (ALL):

1. Nuclear Medicine & PET, Rigshospitalet & University of Copenhagen, Copenhagen, Denmark.
2. Rigshospitalet, Copenhagen, Denmark.
3. DTU, Lygby, Denmark.

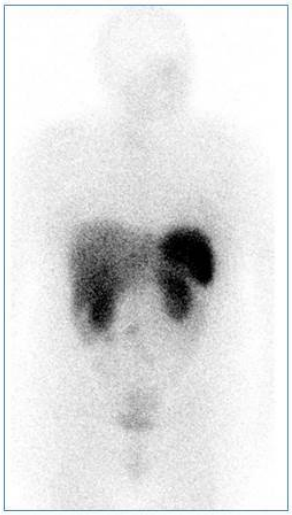

^{111}In-DTPAOC (24h)

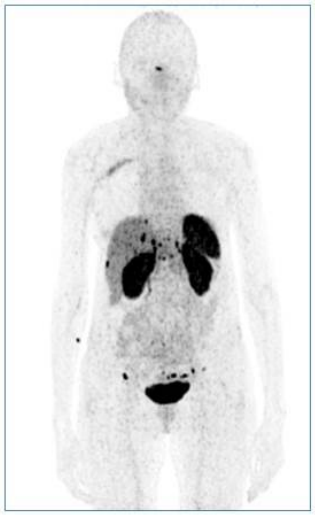

^{64}Cu-DOTATATE (1h)

CONTROL ID: 2234118

TITLE: Imaging of the invasive prostate cancer phenotype: a first-in-human study using uPAR PET/CT

PRESENTER: Andreas Kjaer

ABSTRACT BODY:

Abstract Body: Urokinase-type plasminogen activator receptor (uPAR), a proteolytic system involved in cancer invasion and metastatic diseases, is present in prostate cancer (PC). Studies using immunohistochemistry and in situ hybridization have shown low expression levels of uPAR in normal prostate tissue, compared to high expression in malignant prostate cancer. Also, high plasma levels of uPAR have been associated with advanced PC stage and bone metastasis. Finally, preoperative plasma uPAR levels are associated with early progression. Therefore, since uPAR seems closely related to the aggressive phenotype it seems an attractive target for molecular imaging of the aggressive PC phenotype. We suggest that non-invasive PET/CT imaging and quantification of uPAR expression could provide a reliable method for early identification of aggressive PC. This information can be used for treatment planning Our objective was therefore to perform the first proof-of-concept phase 1 PET imaging study of uPAR in PC patients.

I total, 4 patients with localized prostate cancer and a PSA level from 7.7 to 150 and a Gleason score of 7 (n=1) or 9 (n=3), were enrolled in the study. Patients were PET/CT scanned after 1, 3 and 24 hrs post injection of the uPAR PET ligand ^{64}Cu-DOTA-AE105. Primary endpoints were safety and biodistribution. Secondary endpoints were tumor uptake and tumor-to-background ratio analysis.

No safety issues following the uPAR PET imaging procedures were found in any patients. A fast clearance of the PET ligand was observed in vivo, generating a fine contrast already after 1 hr post injection. In all 4 PC patients, a high uptake in the tumor lesions were found, with a SUVmax value of 9.6±2.1, 9.9±2.3 and 3.3±0.8 after 1, 3 and 24 hr, respectively. A tumor-to-liver, tumor-to-kidney, tumor-to-muscle and tumor-to-blood ratio of 0.7, 0.8. 4.5 and 1.6 were found 1 hr post injection.

In summary, we performed a first-in-human uPAR PET study in PC. No safety issues were reported. Background uptake was low and PC uptake high leading to a high contrast. Further studies are justified to investigate the full potential of uPAR PET Imaging for early identification of aggressive PC.

AUTHORS (LAST NAME, FIRST NAME): Persson, Morten[1]; Skovgaard, Dorthe[1]; Jacob, Madsen[1]; Nielsen, Carsten H.[1]; Loft, Annika[1]; Brandt-Larsen, Malene[1]; Christensen, Camilla [1]; Hojgaard, Liselotte[1]; Brasso, Klaus[2]; Kjaer, Andreas[1]

INSTITUTIONS (ALL):

1. Nuclear Medicine & PET, Rigshospitalet & University of Copenhagen, Copenhagen, Denmark.
2. Department of Urology, Rigshospitalet, Copenhagen, Denmark.

uPAR PET/CT of prostate cancer. For comparison also immunohistochemistry of uPAR is shown.

CONTROL ID: 2228454

TITLE: An Integrated Imaging and MicroRNA-based Blood Reporter Strategy for Cell Tracking in Mice

PRESENTER: Aloma D'Souza

ABSTRACT BODY:

Abstract Body: Precise tracking of the effectiveness of cell-based therapies can become a reality if technologies for measuring transplanted cell numbers, viability, location(s) and cell state are utilized in the clinic. An exciting prospect is to tag cells with imaging reporter genes to serially monitor their fate with imaging. Potential limitations of this are the frequency that a patient can be imaged and the sensitivity to detect small numbers of cells. Thus combining imaging reporter assays with a complementary and relatively cheap blood-based reporter assay might be ideal. Bioluminescence imaging (BLI) is a highly sensitive optical technique used for non-invasive cell tracking in animals. MicroRNAs (miR) are short (18-22 base pairs) non-coding RNAs that regulate mRNA translation and have been identified as relatively stable blood-based biomarkers. Here we show that a novel complement of BLI together with a unique miR-based reporter adds an *in vitro* blood-based diagnostic to enhance the monitoring of transplanted cells. The potential advantages of our new miR-based blood reporter are: no unwanted biological effects, low/no background expression and the ability to use PCR-based detection to amplify low levels of the reporter in the blood.

We established a Hela cell line (Hela-luc2/miR) that stably expressed Firefly luciferase (luc2) and the miR driven by the elongation factor-1 promoter. We chose a miR sequence of 21 base pairs that does not bind to any known vertebrate-mRNA. In culture Hela-luc2/miR cells secreted significant levels of miR in the media over two days, compared to the background of naïve Hela cells ($p<0.006$). Separately, naïve and Hela-luc2/miR cells were implanted subcutaneously into the flank of nu/nu mice (n=5/group). We monitored tumor growth over 35 days by measuring tumor volume by caliper measurement, performing BLI, and measuring the miR levels in blood at various time points (Day 7, 14, 21, 28 and 35) (Fig. A). BLI signal was detected at all time points and, as expected, tumor volume correlated with BLI signal over time ($R^2=0.6508$; $p=0.0015$). Significantly ($p<0.05$) increased miR blood levels in Hela-luc2/miR versus naïve cell mice were detected on day 21 and 28 after implantation. Some mice (n=3) were euthanized before day 35 preventing statistical comparison at this time point. Importantly, the levels of miR in the blood of the individual mice correlated well with both tumor volume ($R^2=0.6949$; $p=0.0008$) and BLI signal ($R^2=0.8228$; $p<0.0001$) (Fig. B), indicating that miR levels can be used to complement BLI measures.

This proves the capability of this system to potentially be used for monitoring of cellular viability and numbers in a preclinical setting. The sensitivity of the miR reporter system was found not to be as sensitive as BLI in living mice, however we hypothesize it will be more sensitive than clinically-relevant PET reporter imaging systems. Future work will test this hypothesis as well as explore ways to optimize expression and secretion of our miR reporter into the blood. This is the first work exploring the development of an RNA-based blood reporter to complement imaging reporters for cell tracking.

AUTHORS (LAST NAME, FIRST NAME): D'Souza, Aloma L.[1]; Ronald, John[1]; Chuang, Hui-Yen[1]; Gambhir, Sanjiv S.[1, 2]

INSTITUTIONS (ALL):

1. Radiology, Stanford University, Stanford, CA, United States.

2. Departments of Bioengineering and Materials Science & Engineering, Stanford University, Stanford, CA, United States.

A. BLI image and miR expression levels

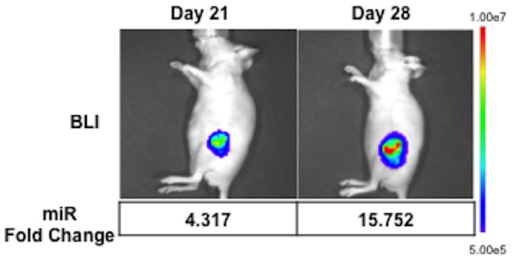

B. Correlation of miR levels and BLI radiance

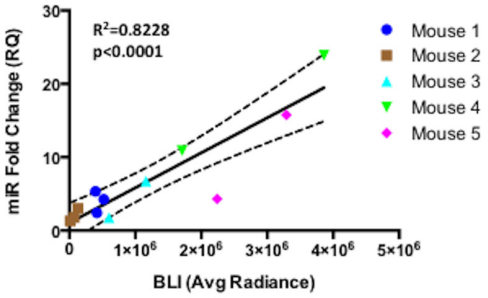

CONTROL ID: 2228474

TITLE: Styrylbenzoxazole and curcumin derivatives that have preferred features of a fluorine-19 MRI probe for amyloid imaging

PRESENTER: Ikuo Tooyama

ABSTRACT BODY:

Abstract Body: Amyloid β (Aβ) deposition in the brain is generally considered to be the initial phase in Alzheimer's disease (AD). Amyloid imaging is widely studied in diagnosing AD and evaluating disease stage, with considerable advances achieved in recent years. Several types of probes have been developed in positron emission tomography (PET). However, little information is available about ligands for amyloid detection with magnetic resonance imaging (MRI). We have developed two types of potential imaging agents using fluorine (^{19}F)-MRI: ^{19}F-containing styrylbenzoxazole derivative (named Shiga-X22) and ^{19}F-containing curcumin derivative (named Shiga-Y5). Following injection of Shiga-Y5 or Shiga-X22 compounds into the tail vein of a transgenic mouse model of AD or control wild-type mice, MR signals were measured using a 7.0 T horizontal-bore MR scanner. After MR measurement, brain sections were prepared for fluorescence microscopy. Both compounds showed marked ^{19}F-MR signals in the area corresponding to the brain of the AD mouse but not controls. Under fluorescence microscopy, AD model mice injected with Shiga-Y5 or Shiga-X22 showed massive fluorescence co-localized with amyloid plaques. Quartz crystal microbalance (QCM) analysis and histochemical examination demonstrated that both Shiga-X and Shiga-Y compounds bound to Aβ aggregates (with β-sheet) and senile plaques in the brain of AD mice and human subjects. Moreover, QCM analysis showed significant frequency decreases in oligomer-immobilized electrodes following the addition of Shiga-Y5, but not Shiga-X22. These results indicate that we have two types of probes: Shiga-Y5 detects Aβ oligomers as well as Aβ aggregates, while Shiga-X22 only detects Aβ aggregates.

AUTHORS (LAST NAME, FIRST NAME): Tooyama, Ikuo[1]; Yanagisawa, Daijiro[1]; Taguchi, HIroyasu[1]; Ibrahim, Nor F.[1]; Durani, Lina Wati[1]; Hamezah, Hamizah Shahirah[1]; Hirao, Koichi[2]; Shirai, Nobuaki[2]; Sogabe, Takayuki[3]; Morikawa, Shigehiro[1]

INSTITUTIONS (ALL):

1. Molecular Neuroscience Research Center, Shiga University of Medical Science, Otsu, Shiga, Japan.
2. Northeastern Industrial Research Center of Shiga Prefecture, Nagahama, Shiga, Japan.
3. Otsuka Pharmaceutical Co., Ltd, Kawauchi-cho, Tokushima, Japan.

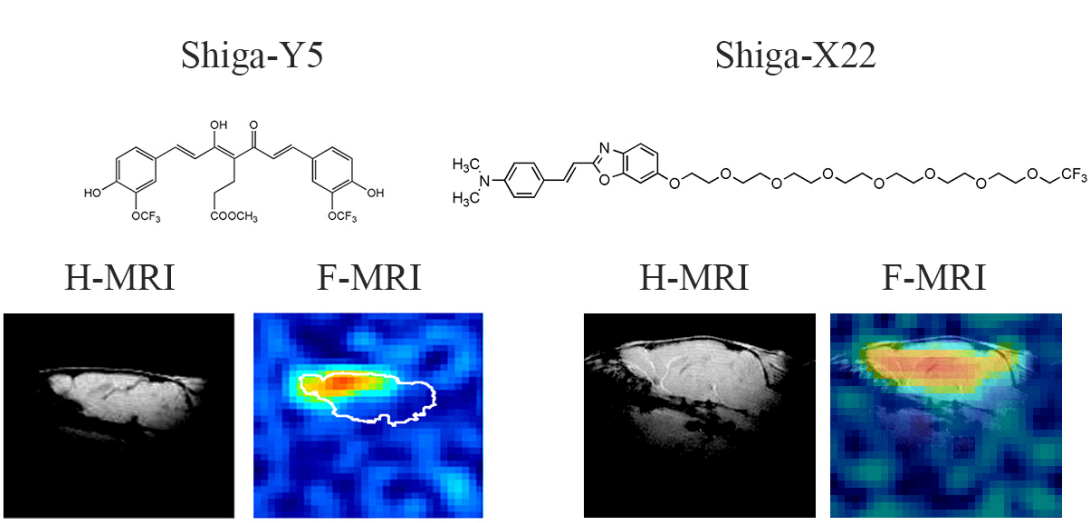

In vivo amyloid imaging of the brain of transgenic mouse model of Alzheimer's disease with 19F-MRI using Shiga-Y5 (left) and Shiga-X22 (right)

CONTROL ID: 2228529

TITLE: Intraoperative optical imaging of peritoneal carcinomatosis of colorectal origin using a VEGF targeted fluorescent tracer – Results of the Hi-Light study

PRESENTER: Niels Harlaar

ABSTRACT BODY:

Abstract Body: Introduction

Optimal cytoreduction in addition to a Hyperthermic IntraPEritoneal Chemotherapy (HIPEC) procedure is of essential value in the curative treatment of peritoneal carcinomatosis of colorectal origin. Currently, the maximum size of detection of peritoneal lesions with tactile and visual inspection is only several millimeters. Surgeons sometimes doubt if they have removed all the malignant lesions due to the limitations of detection accuracy by the naked eye and palpation. Better detection of small metastases could lead to improved radical cytoreduction and enabling a way to distinguish between benign and malignant lesions, improving the efficacy of hyperthermic chemotherapy preventing over- and under-treatment.

Methods

Peritoneal metastases of colorectal origin were detected using bevacizumab-IRDye800CW, a near-infrared fluorescent tracer targeting VEGF-A, in combination with an intra-operative camera system. After exposure of the abdominal cavity, two surgeons independently calculated the PCI (peritoneal cancer index). Initially with palpation and visual inspection, followed by using the fluorescence imaging platform. Biopsies were taken from fluorescent and non-fluorescent areas for ex vivo analysis by H&E staining and fluorescence microscopy.

Results

This Proof-of-Concept study comprises 10 patients. Currently, six patients are included. There were no adverse events related to the use of the tracer. At this moment a total of 70 lesions were imaged and histologically analyzed. In 25 out of 45 fluorescent lesions (55%) cancerous cells were found during histological analysis. Twenty fluorescent lesions (44%) were false positive. All 25 non-fluorescent lesions were cancer negative. Additionally, in two patients the method detected cancer tissue that was initially missed by inspection and palpation. In one patient this concerned a positive resection margin and in another case a para-aortal lymph node metastasis was found.

Conclusion

Intraoperative near-infrared fluorescence imaging of peritoneal carcinomatosis during the HIPEC procedure is technically feasible and safe. The high sensitivity (100%) gives the surgeon potentially a real-time tool for intraoperative decision making. Additionally, the technique enables the evaluation of possible positive resection surfaces, which might be of use on a future study concerning locally advanced rectal cancer. The results of the Hi-Light study look promising. We will present our final results and conclusions during the WMIC meeting.

AUTHORS (LAST NAME, FIRST NAME): Harlaar, Niels[1]; Koller, Marjory[1]; van Leeuwen, Barbare[1]; Hemmer, Patrick H.[1]; Been, Lukas[1]; Kats-Ugurlu, Gursah[2]; Lub-de Hooge, Marjolijn[3]; Linssen, Matthijs[3]; Jorritsma, Annelies[3]; Nagengast, Wouter[4]; Reyners, An[5]; Ntziachristos, Vasilis[6]; van Dam, Gooitzen M.[1]

INSTITUTIONS (ALL):

1. Surgery, University Medical Center Groningen, Groningen, Groningen, Netherlands.
2. Pathology, University Medical Center Groningen, Groningen, Netherlands.
3. Pharmacy, University Medical Center Groningen, Groningen, Netherlands.
4. Gastroenterology, University Medical Center Groningen, Groningen, Netherlands.
5. Medical Oncology, University Medical Center Groningen, Groningen, Netherlands.
6. Institute for Biological and Medical Imaging, Helmholtz Zentrum München, Neuherberg, Germany.

(No Image Selected)

CONTROL ID: 2228540

TITLE: Assessment and precise quantification of post-infarction scar remodeling using a collagen-targeted magnetic resonance contrast agent and T1 mapping techniques

PRESENTER: Fabian Lohoefer

ABSTRACT BODY:

Abstract Body: Purpose: The aim of this study is to evaluate molecular magnetic resonance imaging (MRI) at high field strength using a collagen-targeted contrast agent to analyze and quantify mechanisms of myocardial remodeling and scar formation in a murine myocardial infarction model.

Methods: In-vivo accumulation of Gadofluorine P, targeting collagen, tenascin and proteglycans within the infarct scar, was investigated in a mouse model of myocardial infarction. C57BL/6J mice were scanned by in-vivo MRI at 7 Tesla 1 and 6 weeks after coronary artery ligation. Gadofluorine P was injected at a dose of 0.1mmol/kg body weight and compared to conventional Gd-DTPA. Contrast enhancement of infarcted myocardium was assessed using Late Gadolinium Enhancement (LGE) and T1 mapping. T1/R1 values were calculated from T1 maps based on a Look-Locker sequence. T1 images were calculated from source images based on a 3-parameter Levenberg-Marquardt curve fitting procedure with a correction for read-out-induced attenuation of the relaxation curve. Cardiac function parameters were assessed by volumetric analysis based on short axis views in CINE sequences. Mice from each time point were sacrificed after completion of imaging. The heart was removed and further processed for immunohistochemistry and matrix-assisted laser desorption ionization imaging (MALDI) to quantify Gadofluorine P accumulation ex-vivo.

Results: R1 values in myocardial infarction peaked 10min after Gadofluorine P injection. A slow linear decrease was seen over a time period of 2h. CNR between infarcted and healthy myocardium in LGE reached baseline values after 90 min, whereas R1 values of infarcted tissue were still significantly increased. Especially mice with high initial R1 values following Gadofluorine P injection developed progressive heart failure with extensively reduced ejection fraction after 6 weeks.

Conclusion: MR imaging using the collagen-targeted contrast agent Gadofluorine P allows capturing of extracellular matrix components in remodeling and scar formation after myocardial infarction. T1 mapping at high field strength enables a more precise quantification of signal enhancement and imaging over a prolonged time period compared to conventional LGE.

AUTHORS (LAST NAME, FIRST NAME): Lohoefer, Fabian[1]; Hoffmann, Laura[1]; Glinzer, Almut[1]; Kosanke, Katja[1]; Schilling, Franz[2]; Rummeny, Ernst J.[1]; Wildgruber, Moritz[1]

INSTITUTIONS (ALL):

1. Department of Radiology, TU München, München, Germany.
2. Department of Nuclear Medicine, TU München, Munich, Germany.

(No Image Selected)

CONTROL ID: 2228560

TITLE: Improved radiation dosimetry for lung ventilation scintigraphy

PRESENTER: Martin Andersson

ABSTRACT BODY:

Abstract Body: Objectives: Lung scintigraphy in the form of ventilation and perfusion scintigraphy or both, is an important examination in nuclear medicine to evaluate pulmonary and cardiovascular disorders. Ventilation scintigraphy is performed with gases or aerosols. Aerosol ventilation scintigraphy records the *bronchopulmonary* distribution of an inhaled radionuclide (e.g. Technegas) within the lungs. Gas ventilation scintigraphy records the pulmonary distribution of a radioactive gas (e.g ^{81m}Kr, ^{127}Xe or ^{133}Xe) during breathhold or continuous breathing. The current dose estimations of these radiopharmaceuticals by the International Commission on Radiological Protection (ICRP) have adopted a simplified model that assumes an initial uniform lung distribution of the radiopharmaceutical. A fraction of aerosols or gases is assumed to be uniformly distributed throughout the entire body or treated as orally administered radiopharmaceuticals. The ICRP has later published the Human Respiratory Tract (HRT) model to generate more realistic dose estimations for inhalation of radionuclides. Together with the introduction of the new generation of adult reference phantoms there is now a possibility for more detailed dose estimations.
Methods: The new dose assessments for Technegas, krypton-81m and xenon-127 and -133 are based on the biokinetic model published in ICRP Publications 53 and 80. The calculations were made with the ICRP/ICRU computational adult male and female voxel phantoms and the effective dose was calculated with the tissue weighting factors from ICRP Publication 103. The biokinetic model was modified to fit the HRT-model using standardized parameters for soluble and reactive gases. The new reference phantoms also enable the use of the Human Alimentary Tract (HAT) model, which requires additional adjustments of the ICRP biokinetic model. Absorbed dose and effective dose calculations were performed using the computer program IDAC 2.0. The results of the new calculations were compared with the doses published in the ICRP Publications 80 and 128 (in press). A comparison was also made with doses calculated with the ICRP/ICRU computational adult male and female voxel phantoms together with the published biokinetic model given by the ICRP without the HRT-model.
Results and conclusion: The result shows that there is a minor increase in effective dose for Technegas and krypton 81m, while for the xenon radionuclides there is an effective dose reduction compared with earlier dose estimations performed without the HRT-model. Compared with the published values of ICRP there is an effective dose reduction for all radiopharmaceuticals. For Technegas the reduction is as high as 40 %. In the comparison with the published ICRP values the reduction is explained by change to the voxel phantoms, HRT- and HAT-model as well as the new organ tissue weighting factors.

AUTHORS (LAST NAME, FIRST NAME): Andersson, Martin[1]; Minarik, David[1]; Johansson, Lennart[2]; Mattsson, Sören[1]; Leide-Svegborn, Sigrid[1]

INSTITUTIONS (ALL):

1. Medical Radiation Physics, Malmö, Lund University, Malmö, Sweden.
2. Institutionen för strålningsvetenskaper, Radiofysik, Umeå universitet, Medicinska fakulteten, Umeå, Sweden.

(No Image Selected)

CONTROL ID: 2232418

TITLE: Cetuximab-IRDye700DX Tissue Levels and IRDye700DX Histologic Locations in Cynomolgus Macaques Following i.v. Cetuximab-IRDye700DX

PRESENTER: Esther de Boer

ABSTRACT BODY:

Abstract Body: Aim: Anti-EGFR (epidermal growth factor receptor) antibody has been successfully applied to treat head and neck squamous cell carcinoma. The use of receptor-targeted antibodies conjugated to cytotoxic therapeutics is actively being explored to enhance treatment efficacy. Antibody targeted photodynamic therapy (i.e. photoimmuntherapy) combines the tumor-specificity of antibodies with the toxicity induced by photosensitizers (e.g. IRDye700DX), but the safety of this approach in humans remains unknown. To facilitate clinical testing we evaluated cetuximab conjugated to IRDye700DX (IR700) in cynomolgus macaques.

Methods: Tissues (n=52) were collected at 2d after i.v. 40 mg/kg cetuximab-IR700, 14d after i.v. 80 mg/kg cetuximab-IR700, or 14d after i.v. cetuximab. All 3 groups had 2 animals each sex; 12 total. Tissue sections were scanned with the Odyssey (LiCor) to determine IR700 locations. The fluorescence images were compared to high resolution scans of the H&E stained slides to allow precise localization of IR700 in each tissue section, with background from sections from cetuximab-dosed animals **(Fig 1a)**. Fluorescence signal in tissue sections was further quantified as mean counts/pixel. Separate frozen samples were homogenized and subjected to gel electrophoresis (LDS-PAGE) to measure intact cetuximab-IR700.

Results: By histologic exam the IR700 at 2d and 14d was predominantly located in connective tissue, such as the submucosa of the larynx and trachea, digestive tract and urinary bladder; perivascular and peribronchial connective tissue of the lung; perivascular and peripelvic connective tissue of the kidney; wall of the gall bladder; and stroma of the salivary gland, thymus, and testis; and the medulla of lymph nodes. The liver was a singular exception to this pattern; strong IR700 accumulation was indicated in portal areas, and moderate diffuse accumulation in the hepatic parenchyma. IR700 was predominantly in the dermis and was multifocal to diffuse in distribution and mild to strong in intensity. At 2d after dosing the sections with highest fluorescence were axillary lymph node, vagina, gall bladder, skin, mammary gland, and liver (range=599->184 mean counts/pixel) **(Fig 1b)**. At 14d the sections with highest fluorescence were gall bladder, bladder, duodenum, skin, sternum, and liver (range=93->46 mean counts/pixel) **(Fig 1c)**. Intact cetuximab-IR700 at 2d averaged 35.6$\pm$1.1, 14.8$\pm$0.6, and 9.8$\pm$1.9 µg/mL, in blood, lung and liver, respectively, whereas all brain tissues were <0.8 µg/mL. At this time the liver and lymph nodes had <10% of fluorescence as intact cetuximab-IR700, 2-3 fold less than other tissues. At 14d the intact cetuximab-IR700 levels declined to between 0.25-2 µg/g in all tissues.

Discussion and Conclusions: To our knowledge this is first study utilizing fluorescence imaging to detect the precise location of IR700 in primate tissue sections, and determine tissue levels of intact cetuximab-IR700. Also, our data provides support for the hypothesis that metabolized dye accumulating in the sinuses of the lymph nodes could be the main responsible reason for nonspecific uptake of imaging tracers.

AUTHORS (LAST NAME, FIRST NAME): de Boer, Esther[1, 2]; Rosenthal, Eben[5]; Samuel, Sharon[3]; Warram, Jason M.[1]; French, David N.[3]; Schoeb, Trenton R.[4]; Zinn, Kurt R.[3]

INSTITUTIONS (ALL):

1. Surgery, University of Alabama at Birmingham, Birmingham, AL, United States.
2. Surgery, University Medical Center Groningen, Groningen, Netherlands.
3. Radiology, University of Birmingham Alabama, Birmingham, AL, United States.
4. Genetics, University of Alabama at Birmingham, Birmingham, AL, United States.
5. Otolaryngology, Stanford University, Stanford, CA, United States.

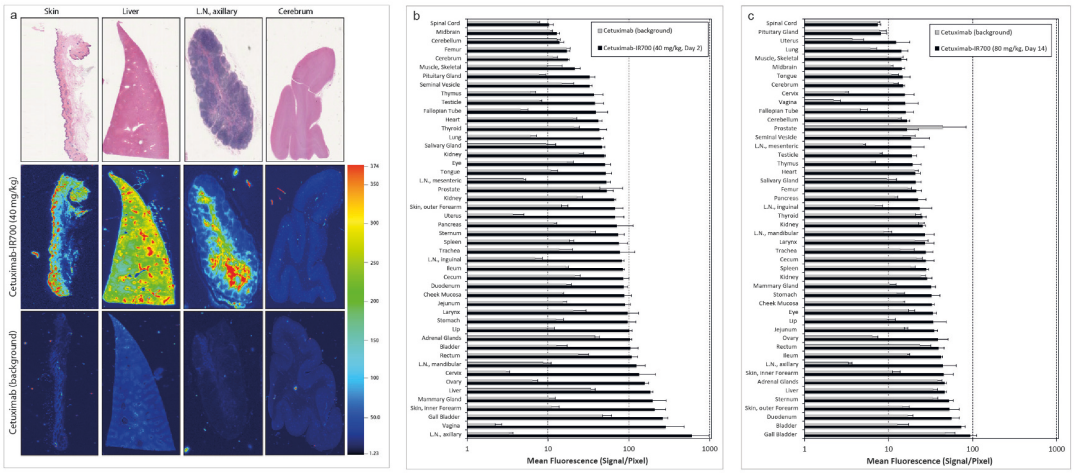

Figure 1 Histology. Representative H&E of skin, liver, L.N., axillary and cerebrum is shown with corresponding fluorescence image of an animal dosed with cetuximab-IR700 at 40 mg/kg and cetuximab at 16 mg/kg (a). Mean fluorescence signal per pixel, corrected for background, in tissue sections is shown for tissue sections at Day 2 after dosing with cetuximab-IR700 at 40 mg/kg (b) and Day 14 after dosing with cetuximab-IR700 at 80 mg/kg (c). Error bars are standard error, with n=4/tissue, except female or male tissues that have n=2/tissue. L.N. Lymph node

CONTROL ID: 2232590

TITLE: Biodistribution of IRDye700DX in Cynomolgus Tissues Following i.v. Cetuximab-IRDye700DX

PRESENTER: Esther de Boer

ABSTRACT BODY:

Abstract Body: Aim: Antibody-based photodynamic therapy is a novel targeted cancer therapy, which can serve as both a diagnostic and a therapeutic agent. In this approach, antibodies are conjugated to a fluorescent photosensitizer, such as IRDye700DX (IR700), and act as targeting agents to specifically deliver the photosensitizer to the tumor. Preclinical rodent studies have explored EGFR-targeted antibodies conjugated with IR700 to provide a tumor-specific mechanism to improve detection and treatment of (subclinical) disease. As our goal is human translation for therapy, we assessed the biodistribution of an EGFR-targeted antibody (cetuximab-IR700) in non-human primates (NHP) since the antibody cross-reacts with endogenous EGFR in NHP tissues, and not with rodent EGFR.

Methods: Spectral analyses determined IR700 bound to cetuximab-IR700; immunoreactivity was evaluated by specific binding to recombinant EGFR on beads. Four cynomolgus macaques (2 each per sex per time point per Group) received i.v. cetuximab-IR700 at 40 mg/kg (Group 1) or 80 mg/kg (Group 2) with termination at 2d or 14d after dosing, respectively; Group 3 received cetuximab alone (no IR700) and was terminated 14d later; tissues served as controls. IR700 levels in tissues were measured with a Pearl Impulse Imaging System (LI-COR, Lincoln, NE). A standard curve converted the fluorescence counts to µg of cetuximab-IR700, with normalization to tissue weight. Total recovered organ/tissue µg was determined using necropsy organ weights or published tissue estimates as % of body weight [4].

Results: There was a mean 2.5 IR700 per cetuximab-IR700; immunoreactivity was 82 ± 2%, with 10 ± 3% non-specific binding. For Group 1 (40 mg/kg cetuximab-IR700 terminated on day 2), the highest levels of IR700 were found in liver, gall bladder, and axillary lymph node; the lowest levels in this group were found in brain tissues, and spinal cord (**Fig. 1a)**. For Group 2 (80 mg/kg cetuximab-IR700 terminated on day 14), the highest levels of IR700 were found in mesenteric lymph node, inguinal lymph node and prostate; the lowest levels in this group were found in brain tissues, and spinal cord (**Fig. 1b)**. The total cetuximab-IR700 accounted for in all tissues collected from the animals terminated on day 2 (40 mg/kg cetuximab-IR700) averaged 45,925 µg (*n=4*) or 38.4 ± 1.6% of the dose. Similarly, the total accounted for cetuximab-IR700 in all tissues collected from animals in Group 2 (80 mg/kg cetuximab-IR700 terminated on day 14) averaged 7,130 µg (*n=4*) or 2.84 ± 0.75% of the total dose. The background arising from autofluorescence from all tissues averaged 683 µg (*n=4*) as determined from the total of all tissues from the cetuximab group.

Discussion and Conclusions: This is the first study to assess the biodistribution of an IR700-conjugate administered by i.v. infusion to cynomolgus monkeys. The IR700 levels were consistent with known EGFR expression, and changes between 2d and 14d was consistent with rapid metabolism and excretion of the cetuximab-IR700.

AUTHORS (LAST NAME, FIRST NAME): de Boer, Esther[2, 6]; Rosenthal, Eben[1]; Samuel, Sharon[3]; Warram, Jason M.[2]; French, David N.[4]; Zinn, Kurt R.[5]

INSTITUTIONS (ALL):

1. Otolaryngology, Stanford University, Stanford, AL, United States.
2. Surgery, University of Alabama at Birmingham, Birmingham, AL, United States.
3. Radiology, University of Alabama at Birmingham, Birmingham , AL, United States.
4. Radiology, University of Alabama at Birmingham, Birmingham , AL, United States.
5. Radiology, University of Alabama at Birmingham, Birmingham , AL, United States.
6. Surgery, University Medical Center Groningen, Groningen, Netherlands.

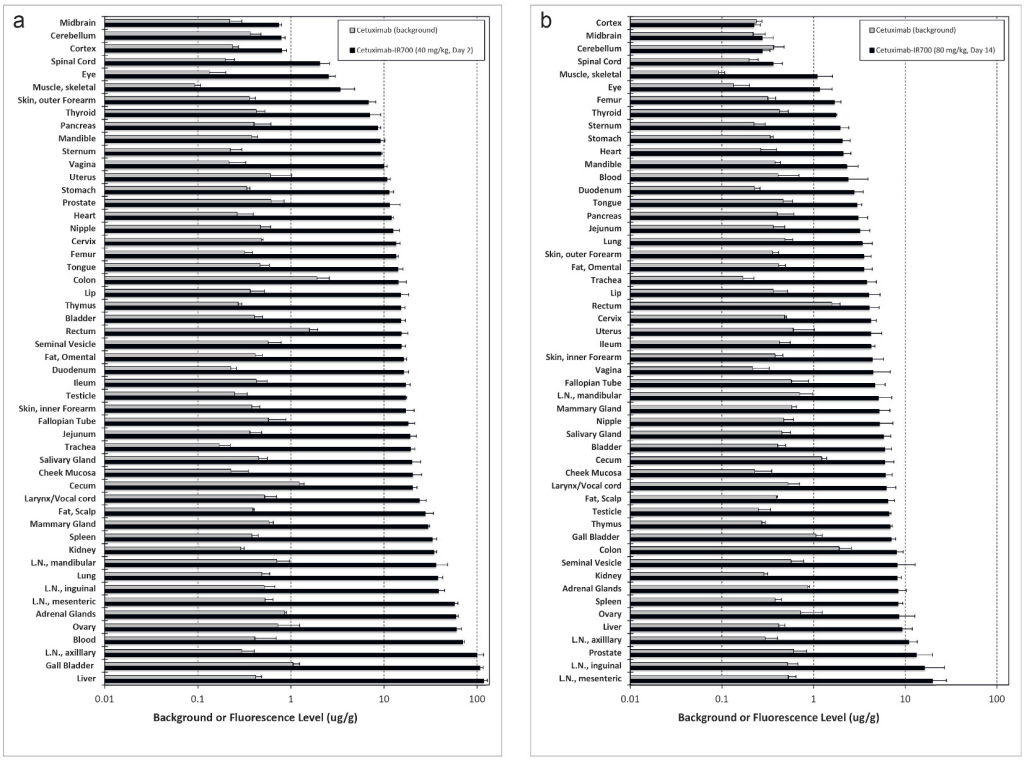

Figure 1 Biodistribution in tissues as mean microgram (ug) of antibody per gram of tissue at Day 2 (a) and Day 14 (b) post cetuximab-IR700 intravenous infusion. Error bars are standard error, with n=4/tissue, except female or male tissues that have n=2/tissue

CONTROL ID: 2228614

TITLE: Pretargeting Cancer with TCO-derivatized pH (Low) Insertion Peptide (pHLIP): Syntheses, Biophysical Studies, and In Vitro Analysis.

PRESENTER: Dustin Demoin

ABSTRACT BODY:

Abstract Body: The pretargeting approach to imaging and treating cancers with radiopharmaceuticals capitalizes on the tumor-specific targeting of the biological vector while allowing the radioactive tracer to be introduced after the biological vector has localized. Pretargeting cancer with peptides requires peptides that are not internalized, have bioorthogonal reactive groups on the extracellular/non-inserting domain, and remain bioavailable at the cell long enough for the second injection. The pH (low) insertion peptides (pHLIPs) are a group of membrane peptides that fold and insert into the cellular membrane in the presence of low pH extracellular environments, such as those in tumors, in order to insert into the cellular membrane. Three variants of pHLIP (WT, var3, and var7) have been derivatized with *trans*-cyclooctene (TCO) on the cysteine residue (non-inserting end) of pHLIP (83 %, 38.4 % and 56 % yield, respectively) for pretargeting with ^{64}Cu-SarAr-tetrazine (80 % radiochemical yield, 667 ± 61 mCi/mg) via the inverse electron-demand Diels-Alder click reaction. Biophysical studies indicate that the conjugation of the TCO moiety to pHLIP results in folding and insertion behavior similar to that of pHLIP alone, but indicate an increase of the pH at which the peptide inserts (pKa of insertion) and a change in cooperativity (Table 1) (e.g., the pK_a of insertion shifts from 5.94 ± 0.09 (WT-pHLIP) to pH 6.25 ± 0.04 (TCO-WT-pHLIP) or to pH 6.98 ± 0.06 (TCO-Bn-WT-pHLIP)). In vitro studies pretargeting 4T1 cells incubated with the TCO-pHLIP variants (0.8-8.6 %ID/mg protein) show 5-10 times the radioactivity uptake of cells incubated without the TCO-pHLIP variants (0.14-0.20 %ID/mg protein). Of the 4T1 cell cultures incubated with either TCO-WT-pHLIP (0.77 ± 0.12 % ID/mg protein), TCO-var3-pHLIP (1.17 ± 0.13 % ID/mg protein), or TCO-var7-pHLIP (2.0 ± 0.2 % ID/mg protein) at physiological pH (pH 7.4), cells showed greater uptake of TCO-var7-pHLIP than the other two variants. These studies indicate that the TCO-derivatized pHLIP analogs of WT, var3, and var7 (1) retain the three-state folding behavior observed in the underivatized peptides and (2) react in biological media with the tetrazine component of the radioactive tracer. Additionally, the greater uptake of the TCO-var3 and TCO-var7 analogs indicates that these two variants might be the best suited for pretargeting 4T1 cancer cells. In vivo studies to investigate the pretargeting ability of these analogs are planned.

AUTHORS (LAST NAME, FIRST NAME): Demoin, Dustin W.[1]; Wyatt, Linden[2]; Edwards, Kimberly J.[1]; Emmetiere, Fabien[1]; Zeglis, Brian M.[1, 3]; Cook, Brendon[3]; Brand, Christian[1]; Andreev, Oleg A.[2]; Reiner, Thomas[1]; Reshetnyak, Yana K.[2]; Lewis, Jason S.[1, 4]

INSTITUTIONS (ALL):

1. Department of Radiology, Memorial Sloan Kettering Cancer Center, New York, NY, United States.
2. Physics Department, University of Rhode Island, Kingston, RI, United States.
3. Department of Chemistry, Hunter College of the City University of New York, New York, NY, United States.
4. Program in Molecular Pharmacology and Chemistry, Memorial Sloan Kettering Cancer Center, New York, NY, United States.

(No Image Selected)

CONTROL ID: 2228641

TITLE: Selective cell elimination with near infrared photoimmunotherapy in 2D and 3D mixed cultures and in a mixed tumor model

PRESENTER: Kazuhide Sato

ABSTRACT BODY:

Abstract Body: Innovation/ Impact/ Objectives:

Cell cultures and tissues often contain cellular subpopulations that potentially interfere with or contaminate other cells of interest. However, it is difficult to eliminate unwanted cells without damaging the very cell population one is seeking to protect, especially in established tissue [1]. Near infrared photoimmunotherapy (NIR-PIT) is a new, highly selective cancer treatment that combines the specificity of intravenously injected antibodies that target tumors with the toxicity induced by photosensitizers activated by NIR-light [2]. Here, we present a method of eliminating specific subpopulations of cells from a mixed 2D or 3D cell culture or a tumor model with NIR-PIT. Using the optical reporters, RFP, GFP and luciferase, it could be demonstrated that the selected cell population could be eliminated by NIR-PIT without damaging adjacent non target cells.

Materials/ Methods:

In vitro and *in vivo* experiments were conducted with an EGFR, luciferase and GFP expressing cell line (A431-luc-GFP) as a target, and EGFR negative, RFP expressing cell line (Balb/3T3-RFP) as background. An antibody-photosensitizer conjugate (APC) consisting of panitumumab and a phthalocyanine dye, IRDye-700DX, was synthesized (pan-IR700). NIR-PIT cytotoxicity for 2D and 3D A431-luc-GFP cell cultures was confirmed with dead staining, luciferase activity, and GFP fluorescence intensity. In a mouse model, the effect of NIR-PIT was confirmed with bioluminescence image (BLI), and fluorescence imaging (FLI). Specific cell elimination from almost confluent *in vitro* 2D mixed culture (A431-luc-GFP and 3T3-RFP) and *in vitro* mixed 3D (spheroids) were evaluated with luciferase activity and GFP/RFP fluorescence intensity. Specific cell elimination from *in vivo* mixed tumor was also assessed with BLI and FLI.

Result:

In vitro NIR-PIT cytotoxicity for A431-luc-GFP cells followed a light-dose dependence. Repeated NIR-PIT eradicated whole cells within 3D spheroids and within *in vivo* tumors, which was confirmed with BLI and FLI. Elimination of A431-luc-GFP from an almost-confluent 2D mixed cell culture was demonstrated after NIR-PIT. Repeated NIR-PIT resulted in a decrease in size due to complete target cell elimination from the mixed 3D cell culture without damaging non-target cells. Repeated NIR-PIT also led to complete elimination of target-expressing cells from mixed tumors with minimal damage to non-target cells. All these data were demonstrated with BLI and FLI, and quantified by luciferase activity and fluorescence intensity. BLI and FLI of *ex vivo* tumor confirmed the results.

Conclusions:

NIR-PIT is a practical method for eliminating a selective set of cells from cell culture or tissue without damaging the remaining cells. Local cell-specific elimination by NIR-PIT has the potential for applications in many fields, for instance, regenerative medicine, immunomodulation, and tumor immunity.

References

Ben-David, et al. *Nat. Commun.* **4,** 1992 (2013).

Mitsunaga, M. et al. *Nat. Med.* **17,** 1685–1691 (2011).

AUTHORS (LAST NAME, FIRST NAME): Sato, Kazuhide[1]; Nagaya, Tadanobu[1]; Harada, Toshiko[1]; Nakamura, Yuko[1]; Choyke, Peter L.[1]; Kobayashi, Hisataka[1]

INSTITUTIONS (ALL):

1. Molecular Imaging program, National Cancer Institute, Bethesda, MD, United States.

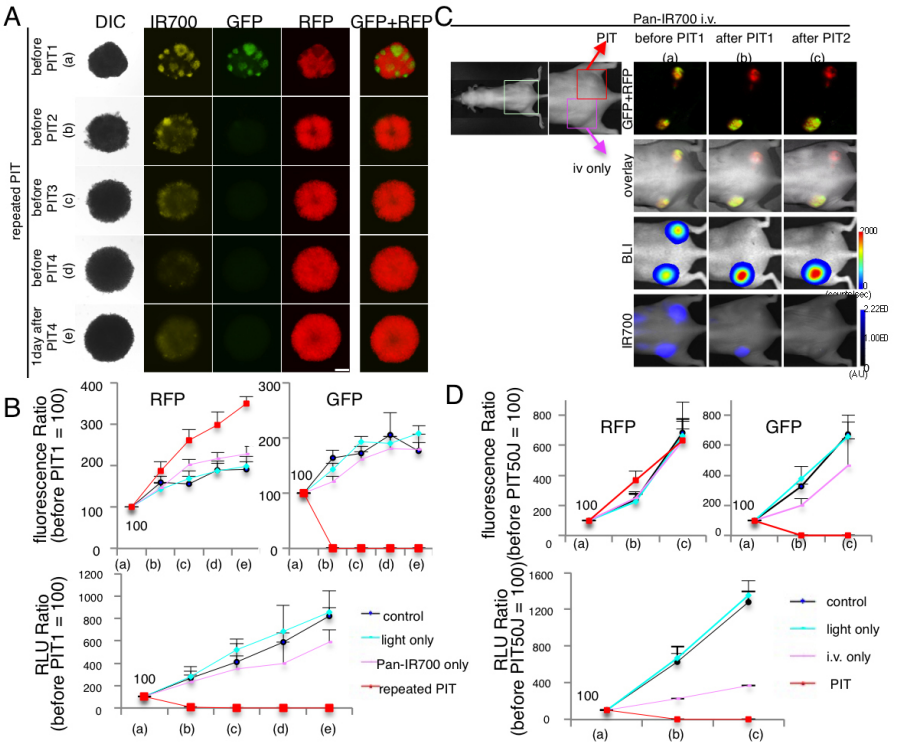

Demonstration of specific cell elimination from mixed 3D cultures and a mixed tumors.
(A) Repeated NIR-PIT completely eliminated target cells with no harm to non-target cells, in a mixed 3D spheroid. Bar = 200 μm. (B) Quantification of fluorescence ratios/ RLU ratio showed complete elimination of target cells and no damage on non-target cells. (n = 10 spheroids in each group). (C) Repeated NIR-PIT completely eliminated target cells from mixed tumors *in vivo*. (D) Quantification of fluorescence ratios/ RLU ratio showed complete elimination of target cells in mixed tumors (n = 10 mice in each group).

CONTROL ID: 2228687

TITLE: Efficient and Site-specific Labeling of Iodine Radioisotope using Copper-Free Click Reaction

PRESENTER: Jongho Jeon

ABSTRACT BODY:

Abstract Body: Recently strain-promoted copper-free click reaction has been extensively investigated and used for the bioorthogonal and biocompatible labeling of a variety of biomolecules and living cells. Due to its excellent specificity and rapid reaction rate, copper-free click reaction has been employed to labeling of radioisotopes such as ^{18}F and ^{64}Cu for synthesis of PET imaging tracers.[1] In addition to *in vitro* radiolabeling applications, it has also been investigated for *in vivo* chemistry for pre-targeted imaging of tumor.[2]

Herein, we present an efficient and site-specific labeling method of iodine radioisotope using copper-free click reaction. For this study, radioiodination using the tin precursor **2** and [^{125}I]NaI was carried out at room temperature to give ^{125}I labeled azide ([^{125}I]**1**) with high radiochemical yield (85-90%) and excellent radiochemical purity (>99%) (Figure 1). Specific radioactivity of the product ([^{125}I]**1**) was 40.7 GBq/μmol. We then prepared dibenzylcyclooctyl (DBCO) group functionalized small molecule **3**, cRGD peptide **4**, and 13 nm size gold nanoparticle **5**. The labeling reactions of substrates (**3**-**5**) using [^{125}I]**1** were conducted at 37 ^{o}C for 30 min to give triazoles **6**-**8** respectively with good radiochemical yields (67-95%) which could be detected by radio HPLC (for **6** and **7**) and radio TLC (for **8**). In all cases, radiochemical purities of the products were more than 95%.

We next carried out tissue biodistribution study of [^{125}I]**1** in normal ICR mice to investigate the level of organ accumulation which needs to be considered when applying [^{125}I]**1** for *in vivo* pre-targeting imaging. As shown in figure 2, large amount of [^{125}I]**1** distributed rapidly in liver and kidney from bloodstream and underwent rapid renal and hepatobiliary clearance. Moreover [^{125}I]**1** was found to be quite stable (>90%) in mouse blood for 24 h. Therefore [^{125}I]**1** would be potentially useful to apply *in vivo* pre-targeting strategy for specific imaging of tumor cells.

Those results clearly indicated that current method using copper free click reaction will be quite useful for both *in vitro* and *in vivo* labeling of iodine radioisotopes.

References

[1] *Angew. Chem. Int. Ed.* **2011**, *50*, 11117-11120.

[2] *Angew. Chem. Int. Ed.* **2013**, *52*, 10549-10552.

AUTHORS (LAST NAME, FIRST NAME): Jeon, Jongho[1]; Choi, Dae Seong[1]; Jang, Beom-Su[1]; Lee, Dong Eun[1]; Kang, Jung Ae[1]; Nam, You Ree[1]; Park, Sang Hyun[1]

INSTITUTIONS (ALL):

1. Advanced Radiation Technology Institute, Korea Atomic Energy Research Institute, Jeongeup, Jeonbuk, Korea (the Republic of).

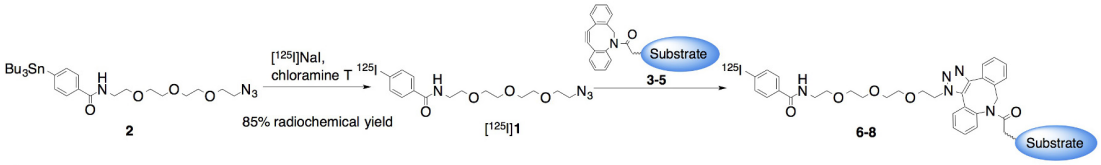

Substrate	Conditions	Product	Radiochemical yield (%)
DBCO-NH_2 **3**	37 °C, 30 min, mouse plasma/DMSO	**6**	84
DBCO-cRGD peptide **4**	37 °C, 30 min, DMSO	**7**	67
DBCO-Gold nanoparticle **5**	37 °C, 30 min, water	**8**	95

Figure 1. In vitro radiolabeling results using [^{125}I]**1**

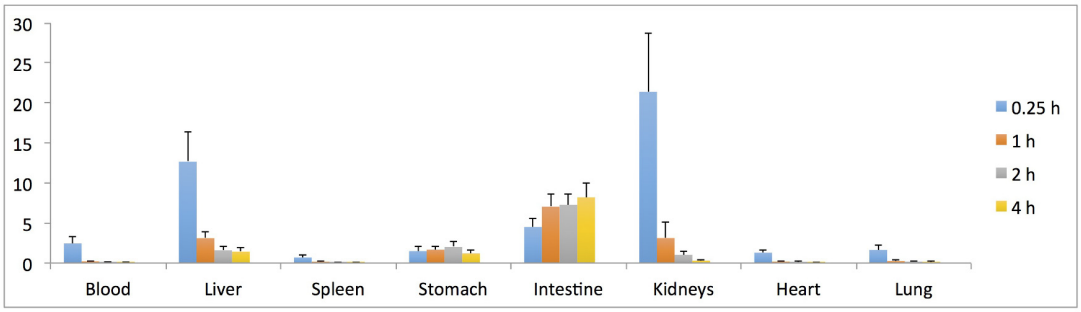

Figure 2. Organ distribution result of [^{125}I]**1**

CONTROL ID: 2230022

TITLE: Usefullness of 3D Fast Spin-Echo Protcol for Vessel Wall Imaging in Cerebral Main Artery Stenosis.

PRESENTER: Michiya Igase

ABSTRACT BODY:

Abstract Body: [Background]
Strokes are the leading cause of disability and the third leading cause of death in Japan. Strokes are subdivided into two major classifications: ischemic (80 percent) and hemorrhagic (20 percent). Especially in Ischemic strokes, in cerebral main artery steno-occlusive lesion are based on the atherosclerosis. However, it has been even difficult to delineate a local atherosclerotic focus, because of that smallness of relevant arteries and the thinness of that vessel wall. Recently 3 tesla (3T) MRI has shown up, which has a superior S/N ratio and a frequency resolution, enabling cerebral main artery steno-occlusive lesion to be more clearly delineated. In this study, we have tried to visualize the arterial wall and the atherosclerotic local lesion with use of a brand-new sequence of 3T MRI.
[Methods]
Thirteen cases suspected to have a stenosis of unilateral middle cerebral artery (MCA) on TOF-MRA were collected as a stenosis group. For the vessel wall analysis, we performed non-contrast-enhanced 3D fast spin-echo T1 imaging with variable flip angles, T1-cube, using 3T MRI (SIGNA HDxt: GE healthcare), and images were reformatted to observe both short and long axis directions of bilateral M1 portion of MCA, on which the maximal wall thickness on a short axis following after the observation on a long axis in each case was measured. Besides, 12 cases without cerebral artery stenosis were recruited as a normal group and the wall thickness of both sides was also measured.
[Results]
The arterial wall was apparently delineated as high signal intensity on the image obtained with T1-cube sequence. In a stenosis group, Mean thickness of the arterial wall in a healthy side was 1.20±0.09 mm, whereas that in a lesion side was 1.60±0.30 mm, where a significant difference was seen between both sides ($p<0.05$). Meanwhile, the mean arterial wall thickness in a normal group was 0.86±0.25 mm, which was significantly smaller than that in both healthy and lesion side of a stenosis group ($p<0.05$, $p<0.001$, respectively).
[Conclusion]
Given these results, the arterial wall at the stenotic region of cerebral main artery stenosis might have an atherosclerotic change like carotid atheromatous plaque. For the next step, it would be crucial to evaluate contents of the atherosclerotic plaque.

AUTHORS (LAST NAME, FIRST NAME): Igase, Michiya[2]; Igase, Keiji[1]; Sadamoto, Kazuhiko[1]

INSTITUTIONS (ALL):
1. Department of Neurosurgery, Washokai Sadamoto Hospital, Matsuyama, Japan.
2. Department of Geriatric Medicine and Neurology, Ehime University Graduate School of Medicine , Ehime, Japan.

(No Image Selected)

CONTROL ID: 2230292

TITLE: Dynamic 3D (4D) microscopic imaging of cancer cell death during near infrared photoimmunotherapy.

PRESENTER: Hisataka Kobayashi

ABSTRACT BODY:

Abstract Body: Innovation/ Impact/ Objectives:

Near infrared photoimmunotherapy (NIR-PIT) is a new, highly selective cancer treatment that combines the specificity of intravenously injected antibodies with the toxicity of photosensitizers activated by NIR-light [1]. NIR-PIT induces rapid cell death within minutes due to profound cell membrane damage resulting in highly selective necrosis. In this work, we depict the process of cell death with dynamic 3D (4D) live cell microscopic images using a low-coherence quantitative phase microscope (LC-QPM) and a dual-view inverted selective plane (sheet) illuminating microscope (diSPIM) to better understand the mechanism of cell killing with NIR-PIT.

Materials/ Methods:

In vitro and *in vivo* experiments were conducted with 3T3/HER2 cells and a GFP expressing cell line (3T3/HER2-GFP). An antibody-photosensitizer conjugate (APC) consisting of traztuzumab and a phthalocyanine dye, IRDye-700DX, was synthesized (tra-IR700). NIR-PIT targeting HER2 was performed in vitro with or without tra-IR700 and cells were serially imaged with either a LC-QPM (Hamamatsu Photonics Co.) or a fiber-coupled diSPIM (in house) [2] before, during and after exposure to NIR light. Volumetry of cells, concentration of cytoplasmic GFP and movement of various molecules ($^{3}H_{2}O$, Propidium Iodide, Calcein-AM, and Ethidium Homodimer-1 (EthD-1)) across the membrane were analyzed to investigate the potential causes of necrotic cell death induced by NIR-PIT.

Result:

Dynamic images obtained with LC-QPM and diSPIM clearly showed that NIR-PIT treated cells immediately increased in volume after NIR light exposure. Cellular volumetry of cells demonstrated up to a 2-fold increase in volume within 1 min. Dynamic images showed that >90% of cells initially increased in volume, burst and then decreased in volume within 30 min. High osmolality media containing 50 mM dextran completely inhibited the expansion of cells induced by NIR-PIT. Tritiated water entered into cells during expansion. However, other fluorescent molecules tested in this study crossed the membrane only after cell membranes were clearly disrupted. The results suggested that NIR-PIT damaged the cell membrane, allowing fluid to enter the cells due to unbalanced osmotic pressures across the membrane inducing necrotic cell death.

Conclusions:

NIR-PIT induced cell membrane damage and unbalanced osmotic pressure between the inner and outer surface of the membrane. Therefore, after NIR-PIT, treated cancer cells dramatically expand, then burst, leading to pure necrotic cell death.

References:

1. Mitsunaga, M. et al. Nat Med. 17, 1685–1691 (2011).

2. Kumar, A. et al. Nat Protoc.11, 2555-2573 (2014).

AUTHORS (LAST NAME, FIRST NAME): Kobayashi, Hisataka[1]; Ogawa, Mikako[2]; Yamauchi, Toyohiko[3]; Nakamura, Yuko[1]; Nagaya, Tadanobu[1]; Sato, Kazuhide[1]; Kumar, Abhishek[4]; Shroff, Hari[4]; Choyke, Peter L.[1]

INSTITUTIONS (ALL):

1. Molecular Imaging Program, NCI/NIH, Bethesda, MD, United States.
2. Medical Photonics Research Center, Hamamatsu Medical University, Hamamatsu, Japan.
3. Central Research Laboratory, Hamamatsu Photonics K. K., Hamamatsu, Japan.
4. NIBIB/NIH, Bethesda, MD, United States.

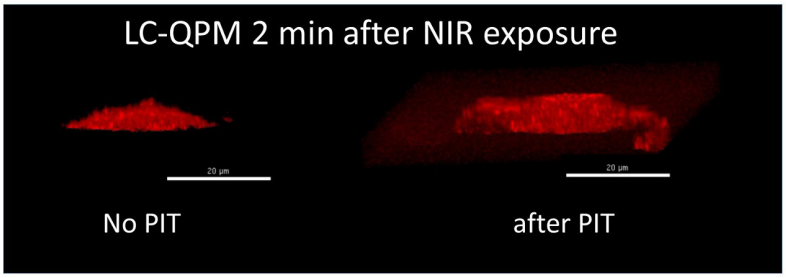

LC-QPM: Volumetry of cells 1

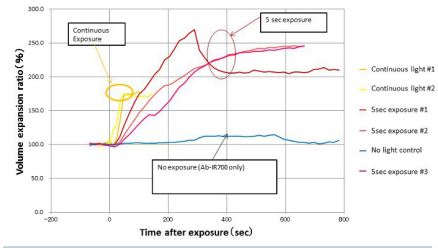

LC-QPM: Volumetry of cells 2

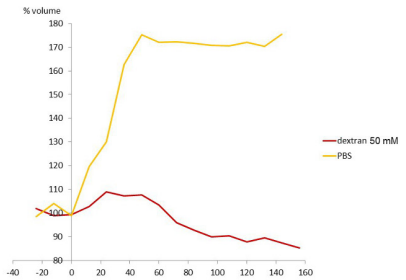

diSPIM: Volumetry vs GFP FL signal

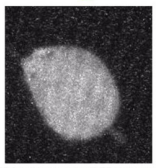

3T3/HER2 cell expressing GFP in the cytoplasm
Plane selective (sheet light) illumination microscope

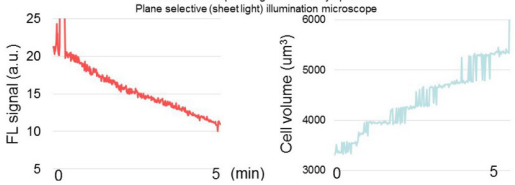

LC-QPM 4D images of a NIR-PIT treated cell

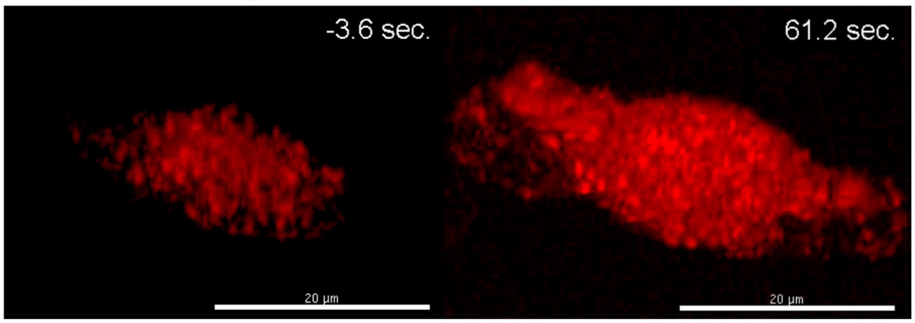

CONTROL ID: 2228734

TITLE: Optical Imaging of Angiogenesis and MMP Activity in a Murine Model of Vascular Remodelling

PRESENTER: Holly Stott

ABSTRACT BODY:

Abstract Body: Introduction: Matrix Metalloproteinases (MMPs) contribute to a number of vascular remodelling processes although their precise roles are unclear. MMP-12 activity is suggested to inhibit angiogenesis.

Hypothesis: MMP-12 activity inhibits angiogenesis in a murine model.

Aims: To determine the relationship between MMP-12 activity and new vessel formation by imaging MMP activity and angiogenesis *in vivo*.

Methods: Two polyurethane sponges were inserted under the dorsal skin of male C57/Bl6 mice (age 8-10 wks).[1] Angiogenesis and MMP activity within the sponges were imaged 7, 14 and 21 days (d) after surgery (n=5-6/group) using commercial agents (AngioSense® 680, MMPSense® 750 FAST) and fluorescence molecular tomography (FMT).

Sponges were also removed 7, 14, 21, 28 or 35 d after surgery (n=6/group). Vessel density was assessed via histologically-stained sections of sponge using antibodies to detect endothelial cells (platelet endothelial cell adhesion molecule-1; PECAM-1) and smooth muscle (smooth muscle α-actin) cells. Inflammatory cell infiltration was determined by counting neutrophils (H&E) and measuring macrophage infiltration (F4/80). The expression profiles of MMPs (2, 9, 10, 12 & 13); markers for vascular endothelial cells (PECAM-1) and vascular mitogens (platelet-derived growth factor (PDGF); vascular endothelial growth factor (VEGF) were determined in sponges using RTqPCR. The protein expression of MMP-12 and TIMP-1 were measured by ELISA. MMP-12 activity was assessed using zymography.

Results and Discussion: Subcutaneous implantation of the sponges stimulated an angiogenic response. This process was successfully imaged in the sponges (*in vivo* & *ex vivo*) using AngioSense®. Consistent with this, there was an apparent increase in transcript levels of PECAM-1 and PDGF levels whereas VEGF levels fell over the timecourse of the study. Transcript levels of TNFα remained steady but histological analysis showed neutrophil content and macrophage infiltration.

MMP activity was detected in sponges (*in vivo* & *ex vivo*) using MMPSense® which supports other evidence that MMP activity is necessary during the angiogenic remodelling process. Transcript levels of MMP-9, 10, and 13 fell over the time course of the study but, strikingly, MMP-12 increased progressively. Interestingly the MMP-12 (and TIMP-1) was most active at earlier time-points and levels decreased over the experiment.

Conclusion: Angiogenesis and MMP activity can be imaged non-invasively *in vivo* using this model. The profiles for MMP-12 transcript number, protein and activity were distinctively different. MMP-12 activity peaks within the sponge as macrophage infiltration begins, and diminishes after angiogenesis peaks, despite the continued presence of macrophages. Ongoing investigations will clarify the relationship between MMP-12 activity and angiogenesis by applying this model to MMP-12 knockout mice and novel MMP-12 selective inhibitors.

1) Small *et al.* (2005) *PNAS*, **102 (34)**: 12165-70

AUTHORS (LAST NAME, FIRST NAME): Stott, Holly R.[1]; Dhaliwal, Kev[2]; Bradley, Mark[3]; Hadoke, Patrick W.[1]

INSTITUTIONS (ALL):

1. Centre for Cardiovascular Science, The University of Edinburgh, Edinburgh, lothian, United Kingdom.
2. MRC Centre for Inflammation Research, The University of Edinburgh, Edinbrugh, United Kingdom.
3. School of Chemistry, The University of Edinburgh, Edinburgh, United Kingdom.

(No Image Selected)

CONTROL ID: 2232469

TITLE: Validation of capsapse-3 biosensor to assess the dynamic function of natural killer cells

PRESENTER: Ho Won Lee

ABSTRACT BODY:

Abstract Body: Objective: Biosensor with high sensitivity to visualize apoptosis activation would facilitate the biological understanding of complex mechanism of cellular death mediated by NK killing, but few have been reported until now. Here, we validated the feasibility of caspase-3 biosensor to assess the apoptosis mediated by dynamic NK function in its several biological experiment setting.

Materials and Methods: Several stable cancer cells such as glioma D54 cell, anaplastic thyroid cancer ARO cell and colon carcinoma RKO cell that express caspase-3 biosensor (Ref) was established, which it will be referred as D54/C, ARO/C and RKO/C, respectively. We compared caspase-3 sensor with lactate dehydrogenase (LDH) assay as well-established and non-radioactive cytotoxicity assay, upon treatment of NK92 cells to each cancer cells in a different ratio of target to effect. To determine whether caspase-3 sensor can reveal the different susceptibility of NK92 cells to several cancer cells, BLI activity of caspase-3 sensor was monitored serially after treatment of NK92 cells to each cancer cells, and phenotype expression levels such as FAS, DR5, MIC A/B and HLA-ABC were also determined. To assess whether caspase-3 sensor can show the modulated cytotoxic effects of NK92 against drug-treated cancer cells, NK92 cells were co-incubated to RKO/C cells treated with or without bortezomib and BLI signals from caspase-3 sensor were measured. At the same time, phenotype expression levels such as FAS, DR5, MIC A/B and HLA-ABC was also determined in cancer cells treated with or without bortezomib by FACS analysis.

Results:NK92 treatment leads to a time- and effector number- dependent increase of BLI activity in caspase-3 sensor. LDH assay also showed the increase of LDH activity in a time- and effector cell number-dependent manner, but its less sensitivity was observed in LDH assay than caspase-3 sensor based assay. Treatment of NK92 cells to each cancer cells exhibited the 3.4-, 12.8- and 16.9-maxium fold increase of BLI activity in ARO/C, RKO/C and D54/C cells. Parallel with the results from caspase-3 sensor, FACS analysis demonstrated that the expression levels of Fas, DR5 and MIC A/B is significantly higher in D54/C cells compared with ARO/C and RKO/C cells, with more increased expression of Fas and MIC A/B in RKO/C cells than ARO/C cells. Upon treatment of NK92 cells to RKO/C cells, bortezomib-treated cells showed more fast increase of BLI activity than vehicle-treated cells. Consistent with BLI activity, the expression level of Fas, MIC A/B and HLA-ABC was higher in bortezomib-treated cells compared with vehicle-treated cells.

Conclusions: We successfully evaluated the usefulness of caspase-3 sensor to serially measure the apoptosis activation by dynamic NK activity in various experimental setting by the comparison with conventional cytotoxic assay method and simple and easy monitoring of different susceptibility of NK cells to either several cancer cells or drug-treated cancer cells.

AUTHORS (LAST NAME, FIRST NAME): Lee, Ho Won[1]; Singh, Thoudam Debraj[1]; Lee, Sang Bong [1]; Ahn, Su-Bi [1]; Oh, Seul-Gi[1]; Jeong, Shin Young[1]; Lee, Sang-Woo[1, 4]; Ha, Jeoung-Hee [2]; Ahn, Byeong-Cheol[1]; Rehemtulla, Alnawaz[5]; Jeon, Yong Hyun[1, 4]; Lee, Jaetae[1, 3]

INSTITUTIONS (ALL):

1. Nuclear Medicine, School of Medicine, Kyungpook National University, Daegu, Korea (the Republic of).
2. Department of Pharmacology,, Kyungpook National University, Daegu, Korea (the Republic of).
3. Daegu-Gyeongbuk Medical Innovation Foundation (DGMIF), Daegu, Korea (the Republic of).
4. Leading-edge Research Center for Drug Discovery and Development for Diabetes and Metabolic Disease, Kyungpook National University Hospital, Daegu, Korea (the Republic of).
5. Department of Radiation Oncology, University of Michigan, Ann Arbor, MI, United States.

(No Image Selected)

CONTROL ID: 2232662

TITLE: Evaluation of migration ability of bone marrow-derived dendritic cells induced with different cytokine condition using *in vivo* fluorescent imaging

PRESENTER: Su-Bi Ahn

ABSTRACT BODY:

Abstract Body: Objective:

Non-invasive imaging tools with simple and easy labeling have been strongly required to validate the migration levels of DC induced by appropriate cytokines to draining lymph nodes, which facilitate the protocol optimization of DC-based immunotherapy.

Here, the aim of this study is to evaluate the migration ability of BMDC induced with different cytokine condition (either GM-CSF or GM-CSF/ IL-4) to draining lymph nodes using *in vivo* fluorescent imaging.

Materials and Methods:

To generate the bone marrow-derived dendritic cells (BMDCs), bone marrow cells from C57BL/6 mice were differentiated with either GM-CSF or with GM-CSF plus IL-4 for 7days. To characterize the differentiated BMDC with different cytokine conditions, phenotype marker analysis (CD11c, MHC class I and II, CD54, CD86 and CCR7) and antigen uptake assay and transwell migration test were performed. For *in vivo* DC tracking, respective BMDCs were labeled with *in vivo* compatible fluorescent dye (DiD, Ex/Em: 644/665, Invitrogen) and labelled cells were subcutaneously injected to footpad of mice. *In vivo* fluorescent imaging (FLI) were conducted from 2h until 72h post-injection of labelled DCs. To further determine the existence of migrated BMDCs, draining popliteal lymph nodes (DPLN) were excised and then both ex vivo BLI and flow cytometry analysis were done.

Results:

No significant difference of phenotype expression level, antigen uptake level and migration ability was shown between GM-CSF-induced BMDC and GM-CSF/IL-4-induced BMDCs. *In vivo* FLI imaging revealed that the migration of GM-CSF-induced BMDC to DPLNs was detected at as early as 2h and FLI signals emitted from labeled cells gradually increased at 24h, showing that it reached peak at 72h (Supporting Fig.1A, upper panel). Contrary to GM-CSF-induced BMDC, the movement of GM-CSF/IL-4-induced BMDCs was identified at 24h and FLI signals reached peak at 48h (Supporting Fig.1A, bottom panel). Furthermore, the migration level was approximately two fold higher in GM-CSF-induced BMDC than GM-CSF/IL-4-induced BMDC (Supporting Fig.1B), which is consistent with *ex vivo* FLI of excised DPLN. Subsequently, using FACS analysis, we can further confirm that DiD-positive population is about two fold higher in the DPLN from mice receiving GM-CSF-induced BMDC than mice receiving GM-CSF/IL-4-induced BMDC.

Conclusions:

We successfully monitored the different migration ability of BMDC differentiated with either GM-CSF or GM-CSF/IL-4 to draining lymph nodes using a simple and easy labeling methods with *in vivo* fluorescent imaging in living mice.

AUTHORS (LAST NAME, FIRST NAME): Ahn, Su-Bi [1]; Lee, Ho Won [1]; Singh, Thoudam Debraj [1]; Oh, Seul-Gi [1]; Lee, Sang Bong [1, 3]; Jeong, Shin Young [1]; Lee, Sang-Woo [1, 3]; Ha, Jeoung-Hee [2]; Ahn, Byeong-Cheol [1]; Jeon, Yong Hyun [1, 3]; Lee, Jaetae [1, 4]

INSTITUTIONS (ALL):

1. Nuclear Medicine, School of Medicine, Kyungpook National University, Daegu, Korea (the Republic of).
2. Department of Pharmacology , Kyungpook National University, Daegu, Korea (the Republic of).
3. Leading-edge Research Center for Drug Discovery and Development for Diabetes and Metabolic Disease, Kyungpook National University Hospital, Daegu, Korea (the Republic of).
4. Daegu-Gyeongbuk Medical Innovation Foundation (DGMIF) , Daegu, Korea (the Republic of).

Supporting Figure 1.

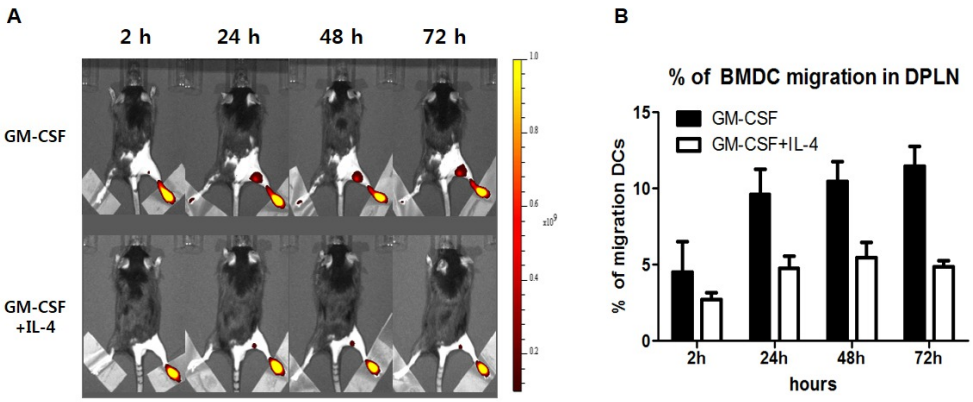

CONTROL ID: 2232603

TITLE: Radionuclide embedded Gold Nanoparticles as a high sensitive and stable nuclear medicine imaging platform for *in vivo* DCs tracking

PRESENTER: Sang Bong Lee

ABSTRACT BODY:

Abstract Body: Objective: The aim of this study is to develop a novel nuclear medicine imaging probe with combination of gold nanoparticles and radionuclides which have high sensitivity and long-term stability, and to demonstrate its feasibility as an imaging platform for DC tracking in living subjects.

Material and Methods: Radionuclide embedded gold nanoparticles (RIe-AuNPs) was developed as illustrated in Supporting Fig. 1. The stability of RIe-AuNPs was evaluatedin human serum and various pHs for 24h. A bone marrow derived dendritic cells (BMDCs) prepared from C57BL/6 mice was labeled with RIe-AuNPs to determine the efficiency of cell uptake in a dose- and time-dependent manner. The effects of RIe-AuNPs on DC function was examined in BMDCsby cell viability, phenotype marker, antigen uptake ability.For in vivo imaging, RIe-AuNPs labeled BMDCs was injected to footpad of mice and animal PET/CT imaging was done once a day for 4 days. Draining popliteal lymph nodes (DPLN) were excised at day 4 post-transfer of labeled cells, followed by *ex vivo* imaging.

Results:RIe-AuNPs exhibitedhigh stability in human serum and various pHs for 24h. Dose- and time-dependent increase of RIe-AuNPs uptake was shown in BMDC, revealing the saturation of its cellular uptake within as early as 3h and at 2 nM. Cellular labeling with RIe-AuNPs did not affect cell proliferation, phenotype marker and antigen uptake ability. The intense radioactive signals were detected in DPLN of mice injected with RIe-AuNPslabeled DCs at as early as 1 day, and the radioactivity at DPLN reached peak at day 3 with slight decrease of radioactivity at day 4 (Supporting Fig. 2). Consistently, ex vivo PET/CT imaging showed distinct radioactivity signal in excised DPLN.

Conclusions: We successfullytracked the BMDC migration to draining lymph nodes with newly developed RIe-AuNPs and PET/CT imaging, and these data support the feasibility of RIe-AuNPs as a potential imaging probe for cell tracking such as immune cells and stem cells.

AUTHORS (LAST NAME, FIRST NAME): Lee, Sang Bong [1, 2]; Ahn, Su Bi[1]; Lee, Ho Won[1]; Oh, Seul-Gi [1]; Singh, Thoudam Debraj [1]; Jeong, Shin Young[1]; Lee, Sang-Woo[1, 2]; Ahn, Byeong-Cheol[1]; Lim, Dong-Kwon[4]; Jeon, Yong Hyun[1, 2]; Lee, Jaetae[1, 3]

INSTITUTIONS (ALL):

1. Nuclear Medicine, School of Medicine, Kyungpook National University, Daegu, Korea (the Republic of).
2. Leading-edge Research Center for Drug Discovery and Development for Diabetes and Metabolic Disease, Kyungpook National University Hospital, Daegu, Korea (the Republic of).
3. Daegu-Gyeongbuk Medical Innovation Foundation (DGMIF), Daegu, Korea (the Republic of).
4. KU-KIST Graduate School of Converging Science and Technology, Korea university, Seoul, Korea (the Republic of).

Supporting Fig. 1

1. Gold nanoparticles (AuNPs,20 nm) were modified with adenine-rich oligo nucleotide.
2. Sulfo-SHPP was conjugated for iodination.
3. The modified AuNPs were radiolabeled with $Na^{124}I$ or $Na^{125}I$ using chloramines-T.
4. Finally seed-mediated gold shell growth (11 nm thickness growth).

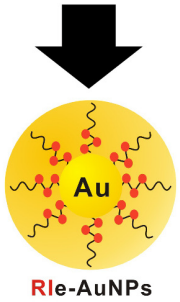

RIe-AuNPs

Supporting Fig. 2

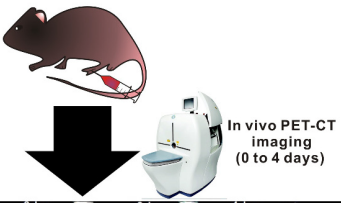

In vivo PET-CT imaging (0 to 4 days)

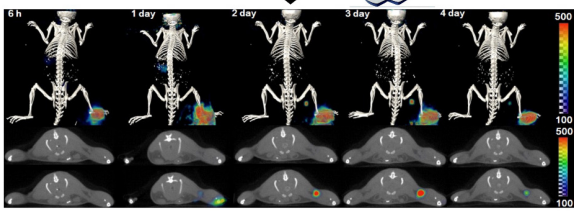

CONTROL ID: 2232562

TITLE: Noninvasive imaging of macrophage migration to tumor lesion and their promotion of tumor growth in living mice with colon cancer using *in vivo* dual optical imaging

PRESENTER: Seul-Gi Oh

ABSTRACT BODY:

Abstract Body: Objective: The aim of this study is to not only track the macrophage migration to tumor lesion with an enhanced firefly luciferase but also evaluate the effect of migrated macrophage on tumor growth with mcherry gene as an fluorescent reporter in living mice with colon cancer.

Methods: Murine macrophage Raw264.7 cells expressing an enhanced firefly luciferase and Thy1.1 genes (Raw264.7/effluc-Thy1.1) and murine colon cancer CT26 cells expressing a mcherry gene (CT26/mCherry) were established. For *in vivo* tracking of macrophage, tumor model were established by challenge of CT26/mCherry cells to Balb/c mice. When tumor mass were detected, either PBS or Raw264.7/effluc cells was intravenously transferred to tumor-bearing mice. Thereafter, bioluminescence (BLI, for macrophage imaging) was conducted once a day from day 1 to until day 4 post-transfer of macrophage. *In vivo* fluorescent imaging (FLI, for tumor imaging) was done daily from day 1 to until day 11 post-transfer of macrophage. To further determine the level of migrated macrophage in tumor, tumor was excised and single cells were isolated, followed by FACS analysis with anti-Thy1.1 Ab (as surrogate for effluc gene).

Results: Upon transfer of macrophage, early distribution of infused macrophage was detected at lung within 1 h. The migration of macrophage to tumor lesion was detected at day 1 and BLI signals were distinct at tumor lesion until day 4. The location of macrophage migrated to tumor was well matched with fluorescent signals from CT26/mCherry tumor. In consistent with *in vivo* BLI, *ex vivo* imaging of excised tumor exhibited strong signals of BLI, and subsequently lots of Thy1.1-positive population from tumor was determined by FACS analysis. Interestingly, *in vivo* fluorescent imaging of tumor progression demonstrated that the rate of tumor growth is significantly more increased in tumor-bearing mice with Raw264.7/effluc than tumor-bearing mice cells, suggesting that Raw264.7/effluc promote the growth of colon cancer ($P<0.05$).

Conclusions: We successfully tracked the macrophage migration toward tumor lesion with enhanced firefly luciferase in living mice, and furthermore serially monitor enhanced tumor growth by macrophage migrated to tumor lesion using mcherry gene as an *in vivo* fluorescent reporter.

AUTHORS (LAST NAME, FIRST NAME): Oh, Seul-Gi [1]; Ahn, Su-Bi [1]; Lee, Ho Won [1]; Singh, Thoudam Debraj [1]; Lee, Sang Bong [1]; Jeong, Shin Young [1]; Lee, Sang-Woo [1]; Ha, Jeoung-Hee [2]; Ahn, Byeong-Cheol [1]; Jeon, Yong Hyun [1, 3]; Lee, Jaetae [1, 4]

INSTITUTIONS (ALL):

1. Nuclear Medicine, School of Medicine, Kyungpook National University, Daegu, Korea (the Republic of).
2. Department of Pharmacology, Kyungpook National University, Daegu, Korea (the Republic of).
3. Leading-edge Research Center for Drug Discovery and Development for Diabetes and Metabolic Disease,, Kyungpook National University Hospital, Daegu, Korea (the Republic of).
4. Daegu-Gyeongbuk Medical Innovation Foundation (DGMIF), Daegu, Korea (the Republic of).

(No Image Selected)

CONTROL ID: 2228764

TITLE: Characterization of two patient derived colon cancer tumor models in mice

PRESENTER: Marcel Krueger

ABSTRACT BODY:

Abstract Body: Introduction

Tumors do not only consist of neoplastic cells, but are instead a complex structure including stromal cells like fibroblasts, immune cells and mesenchymal stem cells. Recently these components have been shown to be crucial for tumor progression and metastasis. Classical subcutaneous xenograft tumor models lack an extensive stroma. Therefore, clinically more relevant models like endogenous and patient derived tumor models are gaining importance and need to be characterized. Here, we have characterized the two patient derived colorectal tumor models CR-LRB-018P and CR-IC-0002P by multimodal imaging as well as metabolomics, proteomics and histology. Both models differ in terms of sensitivity to the two commonly used anti-cancer drugs Irinotecan and Cetuximab.

Methods

Tumor bearing mice were imaged with [^{18}F]FDG-, [^{18}F]FLT-, [^{18}F]FMISO-, [^{68}Ga]RGD-, [^{11}C]Choline- and [^{11}C]Methionine-PET at an early stage and again with [^{18}F]FDG, [^{18}F]FLT and [^{18}F]FMISO at a late stage. Volumes of interest (VOI) were defined and the %ID/cm³ in tumors was calculated. Furthermore apparent diffusion coefficients (ADC) were determined by MR imaging. Immediately after the last PET/MR scan the animals were killed and tumors were dissected and frozen. Tumors were apportioned and samples were prepared for solid state NMR, mass spectrometry (MS) based metabolomics, proteomics and slices for autoradiography and H&E staining were prepared.

Results

[^{11}C]Choline, [^{11}C]Methionine and [^{68}Ga]RGD showed only very low uptake in both tumor models and these tracers were excluded from the study after a first round of imaging. There was no significant difference in [^{18}F]FLT (0.6 +/-0.13 vs 0.62 +/-0.05) and [^{18}F]FMISO SUV (0.41 +/-0.11 vs 0.61+/-0.13) between models CR-LRB-018P and CR-IC-0002P respectively, while [^{18}F]FDG showed significantly higher uptake in CR-IC-0002P tumors (0.76 +/-0.07 vs 1.3+/-0.02). NMR analysis revealed increased phosphocholine levels in CR-IC-0002P tumors. Autoradiography showed large necrotic areas in CR-LRB-018P tumors which was supported by H&E staining. MS based metabolomics and proteomics data are currently analyzed in detail.

Conclusion

We have here characterized two patient derived tumor models to generate a holistic tumor profile. Multimodal imaging data were combined with NMR metabolomics, MS metabolomics and proteomics data. These studies are the basis for future studies with Irinotecan and Cetuximab treatment regimens and will allow us to correlate imaging data with proteomics and metabolomics data. In general, we gain a deeper understanding of imaging data by correlation with metabolomics and proteomics.

Acknowledgments

The research leading to these results has received funding from the European Research Council under the European Union's Seventh Framework Programme (FP/2007-2013) / ERC Grant Agreement n. [323196].

AUTHORS (LAST NAME, FIRST NAME): Krueger, Marcel A.[1]; Disselhorst, Jonathan A.[1]; Pichler, Bernd J.[1]

INSTITUTIONS (ALL):

1. Preclinical Imaging, University Hospital Tuebingen, Tuebingen, Baden-Wuerttemberg, Germany.

(No Image Selected)

CONTROL ID: 2228771

TITLE: Ex-vivo light attenuation quantitation in the mouse brain: a comparison of three optical clearing techniques

PRESENTER: Angela d'Esposito

ABSTRACT BODY:

Abstract Body: Introduction

Optical clearing allows the reduction of light scattering in biological tissue, enabling 3D morphological information to be obtained deep within tissue using techniques such as optical projection tomography and light sheet microscopy. However, the extent of the clearing is dependent on the technique that is used. There is therefore a need for methods to quantify the quality of the clearing process and thereby to compare clearing techniques. In this study, such a method was developed using a custom spectroscopy system to compare three techniques that were applied to mouse brain: BABB (Murray's clear)[1], pBABB (a modification of BABB which includes the use of hydrogen peroxide), and passive CLARITY[2].

Methods

For spectroscopic light attenuation measurements, harvested brains from perfused mice were sliced to obtain sagittal slices that were 2 mm in thickness. Tissue clearing was performed with established procedures. Spectroscopic light attenuation measurements were performed with a custom system in three areas within the brain: the olfactory bulb, the cerebellum and the pons. Transmittance spectra in the range of 400 to 1100 nm were acquired with a spectrometer using a program written in Labview.

Results

Light attenuation spectra acquired in the brain samples varied with the clearing technique, and these variations depended on the tissue region (Fig.1). For all brain regions, samples that were cleared with pBABB and BABB resulted in lower attenuation coefficients than samples that were cleared with CLARITY. For example, for the pons, the mean attenuation coefficients, as calculated across the entire measured wavelength range, were $1.09 \pm 0.28\ mm^{-1}$ and $0.75 \pm 0.10\ mm^{-1}$ for BABB and pBABB, respectively, and they were $1.89 \pm 0.19\ mm^{-1}$ for CLARITY. Moreover, the maximum attenuation occurred at a higher wavelength for CLARITY than for BABB- and pBABB-cleared samples.

Discussion

The study demonstrated a novel method to quantify the efficacy of optical clearing protocols, which is an essential step in choosing a clearing protocol and for the evaluation of imaging data. The results showed that the degree of clearing obtained with pBABB methodology is greater than those given by BABB and CLARITY, and that differences exist in the shape of absorption spectra, particularly at wavelengths greater than 600nm. It is also been shown that the level of optical clearing varies within the brain, most likely due to the structure and composition of each particular area, which may have implications for quantitation of fluorescence. The study focussed on three optical clearing techniques and on optical clearing of brain but could easily be applied to any other clearing method or tissue.

References

Dodt, H., Nature Methods (2007)

Tomer, R., Nature Protocols (2014)

AUTHORS (LAST NAME, FIRST NAME): d'Esposito, Angela M.[2]; Nikitichev, Daniil I.[1]; Desjardins, Adrien E.[1]; Walker-Samuel, Simon[2]; Lythgoe, Mark F.[2]

INSTITUTIONS (ALL):

1. Medical Physics and Biomedical Engineering, UCL, London, United Kingdom.
2. Centre for Advanced Biomedical Imaging, UCL, London, United Kingdom.

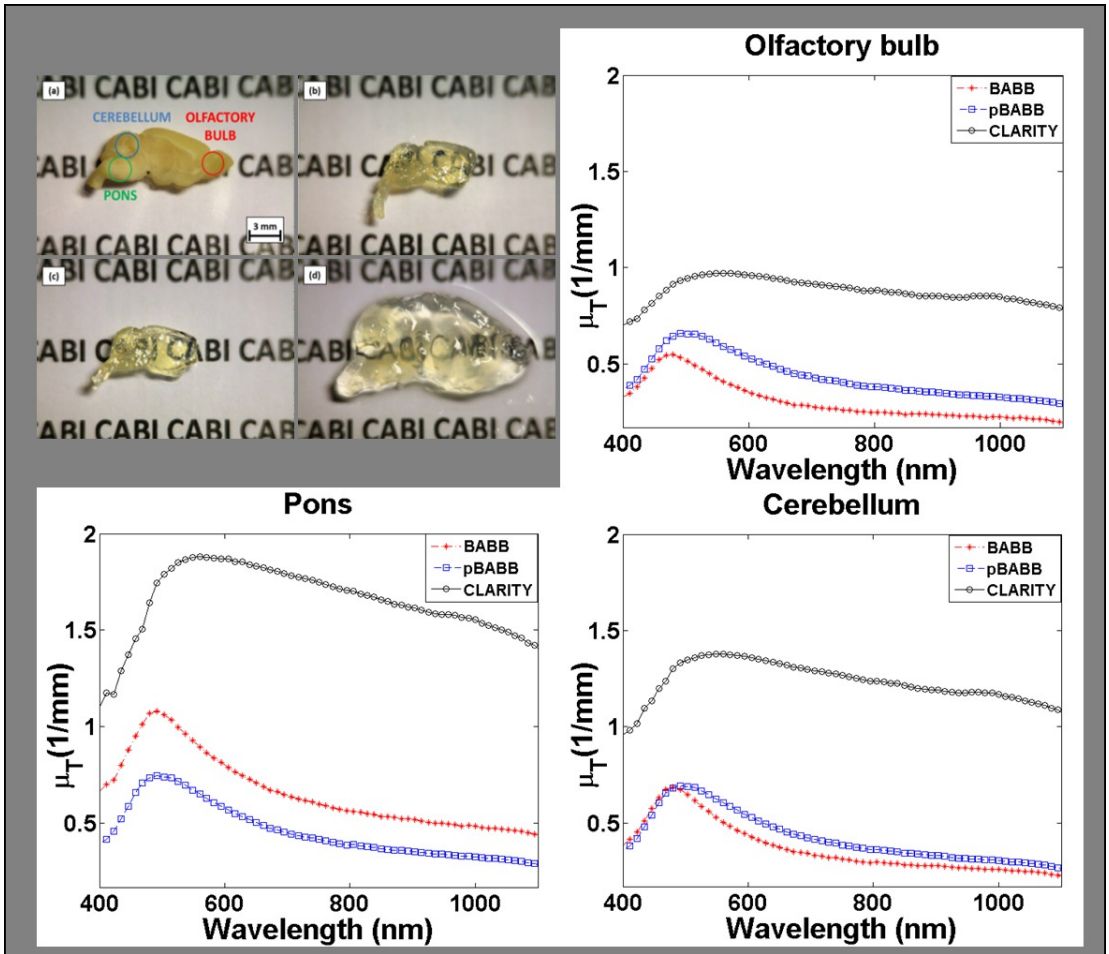

Figure 1: Images of cleared and uncleared mouse brain slices acquired with white light and light attenuation spectra averaged over all measured brains. Prior to optical clearing, the tissue was opaque **(a)**. Optical clearing with **(b)** BABB, **(c)** pBABB, and **(d)** CLARITY significantly increased tissue transparency. The areas where spectroscopic light attenuation measurements were performed were the same in all slices; they are shown in **(a)**. The graphs show post- processed attenuation spectra averaged over data acquired in all measured brains. Each curve represents a clearing method. The wavelength for which the attenuation coefficient was a maximum, λ_{MAX}, varied with brain region and clearing technique, as did the corresponding attenuation coefficients, $\mu_T(\lambda_{MAX})$.

CONTROL ID: 2233262

TITLE: Three dimensional *in vivo* and *ex vivo* visualization of metastatic liver vasculature with Magnetic Resonance Imaging and Optical Projection Tomography

PRESENTER: Angela d'Esposito

ABSTRACT BODY:

Abstract Body: Introduction

The liver has a complex dual-blood supply from portal vein and hepatic artery, and the ratio of inflowing blood from these two vessels is of diagnostic value[1]. In this study, we report on the development of a three-step pipeline for studying drug delivery to tumours in the liver, which is based on biomedical imaging data: 1) Magnetic Resonance Imaging (MRI) was used to non-invasively monitor tumor growth *in* vivo, with a spatial resolution of 156 μm; 2) tumor morphologic and biologic information were then acquired *ex vivo* with Optical Projection Tomography (OPT), which allowed three-dimensional, high resolution fluorescence imaging of the tumor microvasculature; 3) the data obtained is then analyzed *in silico* to create a digital model of the vasculature in order to simulate the delivery of anti-cancer therapies [2].

Methods

Animal model: Colorectal carcinoma cells were injected intrasplenically at a concentration of $1x10^6$ cells in 100 μl in serum free media into three MF1 *nu*/*nu* mice[3]. Cells were allowed to wash through to the liver for 5 minutes followed by splenectomy. Mice were imaged 2 weeks after surgery.

MRI: Anatomical scans were acquired at 9.4T (*Agilent Technologies*): Respiratory-triggered, axial, 2D, fast spin echo, resolution 0.11 x 0.11 x 0.5 mm^3, effective TE 19 ms, TR 2 s, 3 averages.

***Ex-vivo* Preparation:** Animals were perfuse-fixed following intravenous injection of 100 μg of lectin-Alexa 647. Optical clearing of the livers was achieved with BABB (1:2 benzyl alcohol: benzyl benzoate).

OPT: Transmission (white light) and emission (NIR: exciter 655/40 nm, emitter 716/40 nm), isotropic resolution 5 μm, 0.9 degree angular increments, exposure times 200÷400 ms.

Image Analysis: Liver and tumour volumes were determined by manual segmentation of the MRI data. OPT images were reconstructed with NRecon software. 3D anatomical representations were generated using Amira 5.4 (*FEI, Oregon, USA*).

Results

A 3D rendering of the segmented MRI data can be seen in figure 1: liver (red), metastases (yellow) and major vasculature (blue) were analysed for co-localisation with OPT images. Mean (± SD) final tumour volume detected by MRI was 0.24 ± 0.02 mm^3, with a doubling rate of 4.6 ± 0.5 days (n = 3). Multispectral fluorescence OPT imaging of the livers allowed visualization of tumour morphology and metastatic vascular network (Fig. 1).

Conclusion

In this study, an orthotopic mouse model of colorectal liver metastasis was investigated *in vivo* to characterise tumour growth and vascular development, and *ex vivo* to analyze metastases and their vascular network in three-dimensions and at cellular resolution. Comparison of the virtual data sets created by MRI and OPT proved an excellent morphologic correlation between the techniques. The data acquired will be utilized to create a mathematical model of the blood supply in the metastatic liver, which can be validated by further in-vivo MRI measurements of blood flow[4] and cell-sizes[5] and which could prove useful in cancer treatment.

References

1. Ballantyne, Nucl Med Commun, 1990
2. Shipley, Microcirculation, 2015
3. Fidarova, Clin Cancer Res, 2008
4. Ramasawmy, NMR Biomed, 2014
5. Panagiotaki, Cancer Res, 2014

AUTHORS (LAST NAME, FIRST NAME): d'Esposito, Angela M.[1]; Ramasawmy, Rajiv D.[1]; Roberts, Thomas[1]; Johnson, Sean P.[1]; Desjardins, Adrien E.[2]; Lythgoe, Mark F.[1]; Walker-Samuel, Simon[1]

INSTITUTIONS (ALL):

1. Centre for Advanced Biomedical Imaging, UCL, London, United Kingdom.
2. Medical Physics and Biomedical Engineering, UCL, London, United Kingdom.

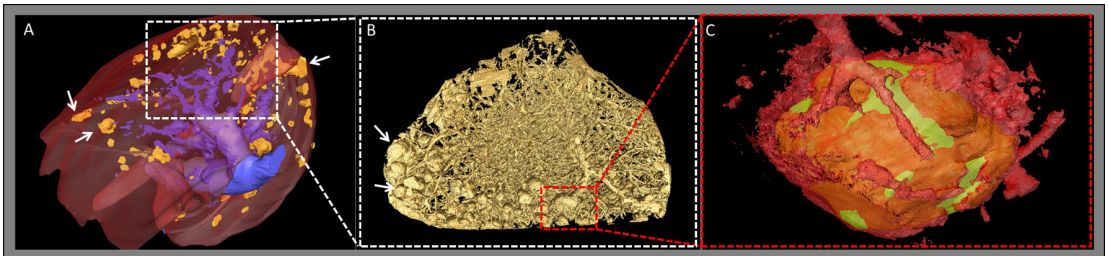

Figure 1: (A) MRI image of liver (red) and metastases (yellow). White arrows point to some of the metastases. (B) 3D-reconstruction of the metastatic liver microvascular architecture (single lobe), OPT acquisition, 5 µm resolution. The endothelium of the hepatic vasculature was labelled with lectin-Alexa 647 fluorophore. (C) Zoom-in of one liver metastasis (yellow), showing vasculature around the tumour (red).

CONTROL ID: 2228789

TITLE: Magnetic Resonance Imaging (MRI) of Adipose-Derived Mesenchymal Stem Cell Enhanced Tropism For Brain Tumors

PRESENTER: Lina Alon

ABSTRACT BODY:

Abstract Body: Brain tumor and in particular glioblastoma (GB) is a devastating malignancy with an extremely poor prognosis. Stem cell therapy using mesenchymal stem cells (MSCs) has been suggested as a novel therapeutic paradigm, giving hope to patients. These cells have the natural ability to migrate to tumors by following cues of proteins secreted by the tumor cells, and can be engineered to carry an anti-tumor cargo such as drugs and therapeutic genes. To enhance cell migration, it is crucial to understand the molecular pathways leading to cell recruitment. The goal of this study is to investigate the genes that promote stem cell tropism for brain tumor in vivo using non-invasive monitoring technique for visualizing of gene expression and MSCs migration to tumor site. The stromal cell-derived factor 1 α (SDF-1 α) also known as C-X-C motif chemokine 12 (CXCL12), is a constitutively secreted chemokine. CXCL12 and its receptor CXCR4 are known to play an important role in the recruitment of stem cells to the bone marrow and to sites of injury. Our hypothesis is that tumor cells secret the CXCL12, which in turns, is sensed by the MSCs expressing CXCR4 receptor, resulting in MSCs chemotaxis toward tumor site.

In the current study, we used two different cell-labeling techniques to be imaged by MRI: 1. 9L glioblastoma cells were engineered to express a lentivral vector encoding for the enzyme herpes simplex virus type 1 - thymidine kinase (HSV1-TK) that can be used as a magnetic resonance imaging (MRI) reporter gene[1], under the regulation of the CXCL12 promoter (pLenti-CXCL12prom::HSV1-TK-V5). 2. Human adipose-derived MSCs (hADMSCs, Invitrogen) were labeled with mesoporous silica-coated hollow manganese oxide (MnO) magnetic nanoparticles[2].

First, we demonstrated that different tumor cell lines (9L and SH-SY5Y) express CXCL12 and that the hADMSCs express the CXCL12 receptor, CXCR4, by using RT-PCR and western blot analysis, respectively. Second, we were able to image, both *in vitro* and *in vivo*, MnO labeled hADMSCs by MRI. And third, we demonstrated that 9L glioblastoma cells infected with pLenti-CXCL12prom::HSV1-TK-V5 showed expression of the HSV1-TK using western blot and furthermore, ^{125}IFIAU radioactive bio-distribution assay demonstrated the enzyme activity in the transduced cell.

We have taken the first steps to prove our hypothesis that hADMSCs expressing the CXCR4 receptor will migrate toward the glioma following a gradient of the chemokine CXCL12 that is secreted by the tumor cells. We have developed a genetically encoded system that can report on the expression of CXCL12 using a surrogate MRI reporter gene. Using these imaging technologies, we will determine the potential to increase stem cell tropism to brain tumors. The findings using this approach could be directly translated to enhance the delivery of therapeutic agents by engineered cells to the tumor site.

Acknowledgments: Supported by MSCRFII-0042.

References: 1. Bar-Shir, A., Liu, G., Greenberg, M.M., Bulte, J.W.M. & Gilad, A.A. *Nat. Protocols* **8**, 2380-2391 (2013). 2. Kim, T.*, et al. J. Am. Chem. Soc.* **133**, 2955-2961 (2011).

AUTHORS (LAST NAME, FIRST NAME): Alon, Lina[1, 2]; Bar-Shir, Amnon[1, 2]; Cortez, Angel[1]; Xiaolei, Song[1, 3]; Xu, Jiadi[1, 3]; McMahon, Michael[1, 3]; Bulte, Jeff W.[1, 2]; Gilad, Assaf A.[1, 2]

INSTITUTIONS (ALL):

1. Radiology , Johns Hopkins University School of Medicine, Baltimore, MD, United States.
2. Cellular Imaging Section, Institute for Cell Engineering, Baltimore, MD, United States.
3. F.M. Kirby Research Center for Functional Brain Imaging, Kennedy Krieger Institute, Baltimore, MD, United States.

(No Image Selected)

CONTROL ID: 2228873

TITLE: Imaging the interaction between cellular adhesome and degradome molecules in breast cancer metastasis

PRESENTER: Asif Rizwan

ABSTRACT BODY:

Abstract Body: Although primary breast tumors are detected early in most cases, it is inevitable that many patients remain at risk for future recurrence and death due to micrometastases. We investigated the metastatic process with a focus on matrix metalloproteases (MMPs) within the degradome and on integrins and E-cadherin within the adhesome. We have performed comparative studies with a set of non-metastatic (BT-474, T47D, MCF7) *versus* metastatic (MDA-MB-231, SUM149, SUM159) human breast cancer cell lines and xenografts. Experiments were carried out to measure growth rate, migration and invasion, and colony formation. By utilizing immunoblotting and immunohistochemistry, we demonstrated higher expression levels of MMPs and the heterophilic cell adhesion molecule integrin β1 (ITGB1) and lower expression of the homophilic cell adhesion molecule E-cadherin in metastatic cancer cells and xenografts. Zymography and noninvasive imaging of MMPs revealed that metastatic cancer cells and xenografts had higher degradome activity. All metastatic breast cancer models consistently displayed higher heterophilic cell-extracellular matrix (ECM) and lower homophilic cell-cell adhesion compared to those of non-metastatic models. Inhibition of MMPs in metastatic cells led to reduced expression levels of ITGB1, and stimulation of ITGB1 resulted in higher MMP activities in metastatic cancer cells. Re-expression of E-cadherin (CDH1) resulted in reduced expression levels of active ITGB1. Circulating breast cancer cells and breast cancer cells from lung metastatic nodules of metastatic breast cancer xenografts had lower expression levels of active ITGB1 and a reduced amount of the epithelial-to-mesenchymal transition (EMT) marker protein fibroblast specific protein1 (FSP1/S100A4). Overall, our results point towards a dependence of MMPs, ITGB1, and CDH1 on each other that is critical for the transformation from benign to invasive carcinoma and for all steps of metastasis.

AUTHORS (LAST NAME, FIRST NAME): Rizwan, Asif[1]; Cheng, Menglin[1]; Jiang, Lu [1]; Krishnamachary, Balaji[1]; Bhujwalla, Zaver[1]; Glunde, Kristine[1]

INSTITUTIONS (ALL):

1. Radiology, Johns Hopkins Medicine, Baltimore, MD, United States.

(No Image Selected)

CONTROL ID: 2228803

TITLE: *In-vivo* DCE-MRI for the discrimination between glioblastoma and radiation necrosis.

PRESENTER: Julie Bolcaen

ABSTRACT BODY:

Abstract Body: Introduction: Discrimination between glioblastoma (GB) and radiation necrosis (RN) remains a diagnostic challenge because both entities have similar imaging characteristics on conventional magnetic resonance imaging (MRI) [1]. Both GB and RN lesions are heterogeneously hyperintense on T2-weighted MR images and contrast enhancing on T1-weighted images (Fig1a-d). A correct diagnosis is important for patient management because RN may require steroid administration while tumor recurrence requires second-line treatment [2]. Currently, a correct diagnosis can only be achieved by brain biopsy. In this study the potential of semi-quantitative analysis of dynamic contrast-enhanced (DCE) MRI was investigated to differentiate GB from RN in rats.

Methods:

We developed a GB rat model by inoculating F98 GB cells into the right frontal region (n=15). From 8 to 23 days post-inoculation fast tumor growth was seen on follow-up MRI. Induction of RN was achieved by irradiating the right frontal region with 60 Gy using three non-coplanar arcs. RN lesions developed 6-8 months post-irradiation (n=10). DCE-MRI of GB and RN lesions were acquired in 12 min using a fast low angle shot (FLASH) sequence in a single slice (1mm) with an in-plane spatial resolution of 312 μm^2 and a temporal resolution of 1.34 s (Fig1e,f). The raw time series of the DCE signal intensity within each ROI are plotted in Fig1g. The curves were fitted to the function $f(t)=c+a(1-e^{-kt})-dt$. Semiquantitative DCE parameters of the raw (r) and fitted (f) curves were compared between GB and RN using the Mann-Whitney U test, including the area under the curve (AUC_r), maximal intensity ($Imax_r$, $Imax_f$), time to peak (TTP_r, TTP_f) and function variables c, a, k and d. Furthermore, ROC analysis was performed to find an optimal cut-off value for discriminating GB from RN.

Results:

Mean curves of GB and RN lesions are visible in Fig 1g. The wash-in rate of the fitted curves, represented by k, and the washout rate of the fitted curves, represented by d, are significantly higher in GB than in RN (p=0.016 and p=0.014, respectively). Thirdly, the TTP_f is significantly lower in GB compared to RN (p=0.001). A threshold k-value of 0.016 yields a 80% sensitivity and a 80% specificity in discriminating GB from RN. Furthermore, both a threshold d-value of -0.03 and a threshold TTP_f-value of 581.3 yield a 86.7% sensitivity and a 80% specificity in defining the presence of GB or RN.

Conclusion:

Based on our results we can conclude that GB and RN can be discriminated using the washout-rate of the DCE time-intensity curve and the TTP_f (86.7% sensitivity and 80% specificity). These findings can be explained by a difference in vascular density, vascular permeability, blood flow, composition of the extravascular extracellular space and the interstitial pressure between GB and RN [3].

Acknowledgements: This work is supported by Stichting Luka Hemelaere.

Christian Vanhove is supported by the GROUP-ID consortium.

[1]. Alexiou GA, et al. J Neurooncol 2009;95:1-11.

[2]. Van Laere K, et al. Eur J Nucl Med Mol Imaging 2005;32:39-51.

[3]. Zahra MA, et al. Int J Radiation Oncology Biol Phys 2009;74(3):776-73.

AUTHORS (LAST NAME, FIRST NAME): Bolcaen, Julie[1]; Descamps, Benedicte[2]; Deblaere, Karel[3]; Hallaert, Giorgio[4]; Kalala, Jean-Pierre[4]; Vanhove, Christian[2]; Goethals, Ingeborg[1]

INSTITUTIONS (ALL):

1. Nuclear Medicine, Gent University Hospital, Gent, Belgium.
2. Department of Electronics and Information Systems, Ghent University, iMinds Medical IT - MEDISIP - Infinity lab, Ghent, Belgium.
3. Radiology, Gent University Hospital, Ghent, Belgium.
4. Neurosurgery, Gent University Hospital, Ghent, Belgium.

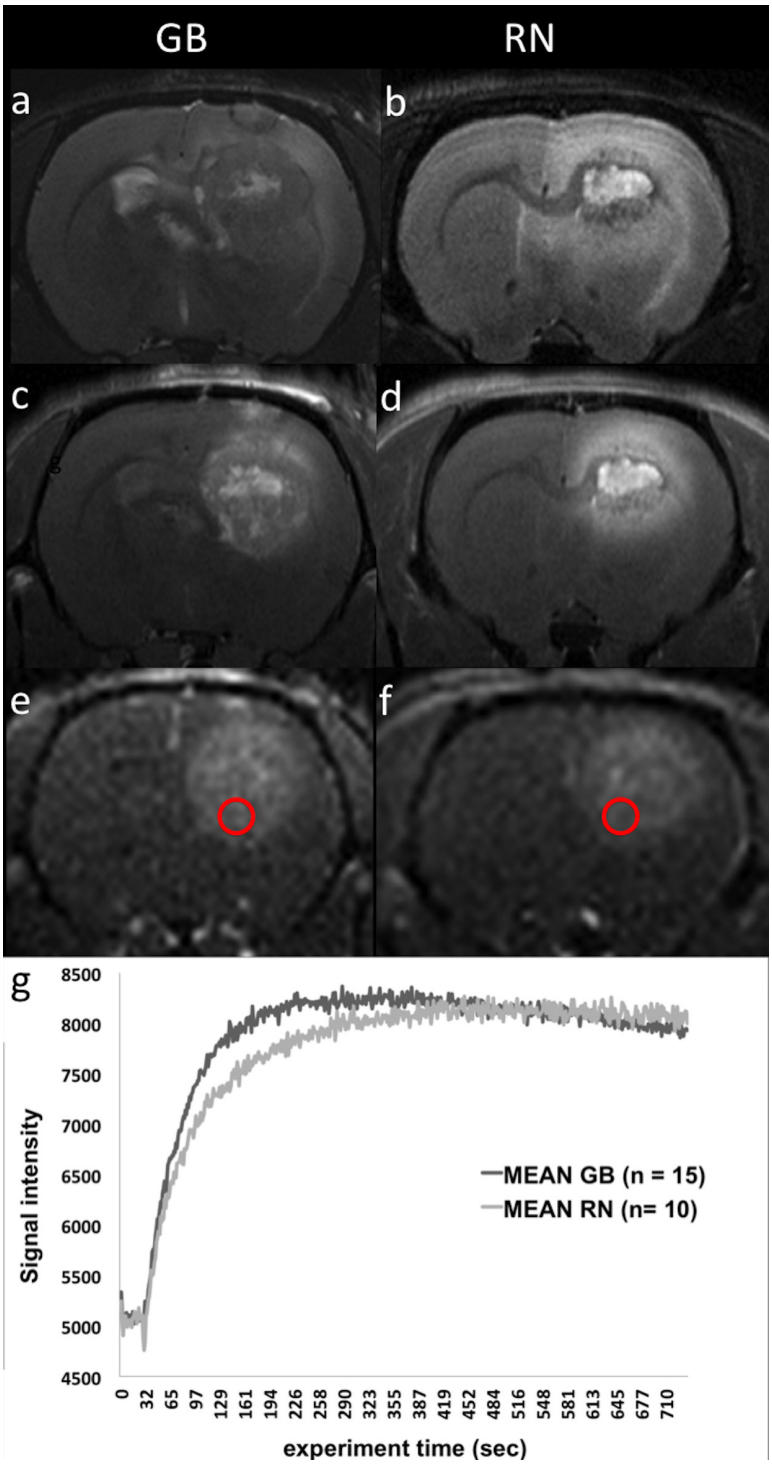
GB
RN
a
b
c
d
e
f
g
Signal intensity
8500
8000
7500
7000
6500
6000
5500
5000
4500
0
32
65
97
129
161
194
226
258
290
323
355
387
419
452
484
516
548
581
613
645
677
710
experiment time (sec)
MEAN GB (n = 15)
MEAN RN (n= 10)

CONTROL ID: 2228816

TITLE: *In vivo* Monitoring of Sevoflurane-induced Neuronal Injury in Neonatal Nonhuman Primates using Small-animal Positron Emission Tomography

PRESENTER: Xuan Zhang

ABSTRACT BODY:

Abstract Body: Background: In surgical procedures for human infants, sevoflurane is the most widely used volatile general anesthetic. Early exposure to sevoflurane may induce neuronal cell death in the developing brain. In this study, in vivo microPET/CT imaging with ^{18}F-labeled fluoroethoxybenzyl-N-(4-phenoxypyridin-3-yl) acetamide (FEPPA), a sensitive biomarker for the detection of neuronal damage/inflammation, was utilized to monitor sevoflurane-induced neuronal injury in neonatal rhesus monkeys.

Methods: On postnatal day (PND) 5 or 6, animals (4-6/group) were exposed to 2.5% sevoflurane mixed with oxygen, or acetyl-L-carnitine (ALC) (100mg/kg given i.p.) plus this mixture for 8 hours; control monkeys with and without ALC were exposed to room air only. One day later, [^{18}F]-FEPPA (56 MBq) was injected into the lateral saphenous vein and microPET/CT images were obtained over the next 2 hours. MicroPET/CT scans were repeated for each monkey one week, three weeks and 6 months after the anesthetic exposure.

Results: The radiotracer quickly distributed into the brains of both treated and control monkeys on all scan days. One day after anesthetic exposure the uptake of [^{18}F]-FEPPA was significantly increased in the frontal and temporal lobes. One week after exposure the uptake of [^{18}F]-FEPPA in the frontal lobe of treated animals was significantly greater than that in controls. Sevoflurane-induced neural damage was morphologically confirmed by EM observations. No significant increases were found in radiotracer uptake in the brains of treated monkeys three weeks or 6 months after exposure. Co-administration of ALC effectively blocked the increase in FEPPA uptake in both the temporal and frontal lobes.

Conclusions: These findings suggest that early exposure to sevoflurane may trigger neurotoxicity in the nonhuman primate brain. Volatile anesthetic-induced brain damage in different brain regions can be dynamically detected using microPET imaging. In addition, ALC appears to be a potential protective agent against at least some of the adverse effects associated with such exposures.

AUTHORS (LAST NAME, FIRST NAME): Zhang, Xuan[1]; Newport, Glenn D.[1]; Paule, Merle G.[1]; Thompson, James[1]; Liu, Shuliang[1]; Berridge, Marc S.[2]; Apana, Scott M.[2]; Slikker, William[1]; Wang, Cheng[1]

INSTITUTIONS (ALL):

1. NCTR, Jefferson, AR, United States.
2. 3DImagingLLC, Little Rock, AR, United States.

(No Image Selected)

CONTROL ID: 2228842

TITLE: Ultrasound mediated siRNA and Chemotherapeutic Drug Delivery in treatment of Prostate cancer: *In vivo* and *in vitro* Evaluation

PRESENTER: Hak Jong Lee

ABSTRACT BODY:

Abstract Body: Purpose: To evaluate the effectivity of intracellular delivery of small interfering RNA (siRNA) and chemotherapeutic drug using microbubble-liposome complex (MLC)

Materials and Methods: To target prostate cancer, MLC conjugated with anti-Her2 antibody were synthesized. For the evaluation of delivery into the prostate tumor cell lines, intracellular delivery of MLC was evaluated under confocal microscopy with or without ultrasound flashing. The delivery of MLC conjugated with survivin-targeted siRNA and doxorubicin was also evaluated by cell viability study with or without ultrasound flashing. Xenograft prostate tumor models were generated, and survivin-targeted siRNA was delivered to *in vivo* model using MLC, and the subsequent suppression of survivin was evaluated.

Results: Under confocal microscopy, significant intracellular uptake of the MLC was confirmed in LNCaP cells which expressed high level of Her2. In LNCaP cells, the delivery of MLC conjugated with siRNA and doxorubicin increased cell apoptosis after the exposure of ultrasound. In xenograft prostate tumor model, the level of survivin expression was reduced in LNCaP tumors to which the MLC conjugated with siRNA were delivered. There was also combined effect of siRNA and chemotherapeutic agent delivery *in vivo* study.

Conclusions: Using ultrasound, MLC can effectively target prostate cancer cells, enabling intracellular delivery of siRNA and doxorubicin. Ultrasound mediated delivery of survivin-targeted siRNA and doxorubicin can induce prostate cell apoptosis and block survivin expression *in vitro and in vivo* models

AUTHORS (LAST NAME, FIRST NAME): Lee, Hak Jong[1, 2]; Yoon, Young Il[2]; Yoon, Tae-Jong[3]; Bae, Yun Jung[1]

INSTITUTIONS (ALL):

1. Radiology, Seoul National University Bundang Hospital, Seongnam-si, Gyeonggi-do, Korea (the Republic of).
2. Program in Nanoscience and Technology, Seoul National University, Suwon, Korea (the Republic of).
3. Applied science, CHA university, Seongnam, Korea (the Republic of).

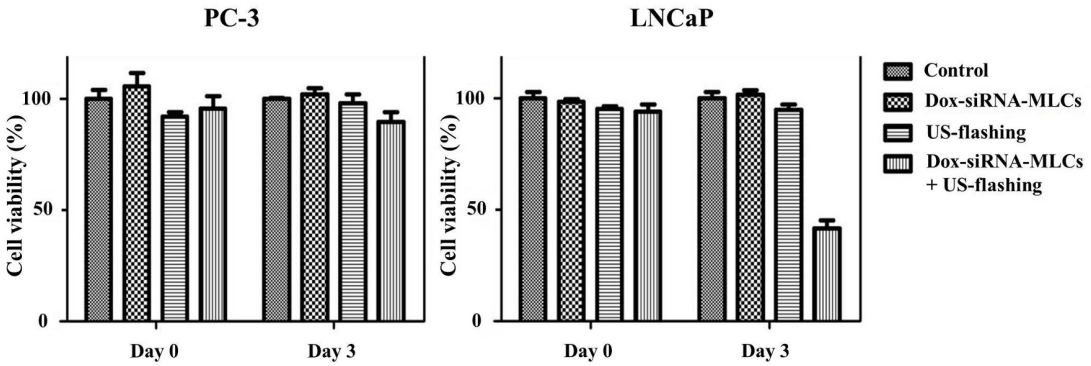
PC-3
LNCaP
Cell viability (%)
100
50
0
Day 0
Day 3
Control
Dox-siRNA-MLCs
US-flashing
Dox-siRNA-MLCs
+ US-flashing

CONTROL ID: 2228844

TITLE: Multimodality imaging in Von Hippel-Lindau (vHL) Syndrome with emphasis on the value of new molecular imaging agents

PRESENTER: Vani Vijayakumar

ABSTRACT BODY:

Abstract Body: PURPOSE/AIM

von Hippel Lindau disease (vHL) is a rare, autosomal dominantly inherited multisystem disorder characterized by benign and malignant tumors including retinal and central nervous system hemangioblastomas, endolymphatic sac tumors, renal cysts and tumors, pancreatic cysts and tumors, pheochromocytomas, and epididymal cystadenomas. To discuss different imaging modalities with emphasis on molecular imaging help in the diagnosis and surveillance of vHL.

CONTENT ORGANIZATION

Screening for VHL Disease

A multidisciplinary approach to screening includes a geneticist, urologists, gastroenterologists, neurologists, ophthalmologists, and radiologists with dedicated clinic. Screening protocols include

1. Renal screening: annual abdominal US is performed from the age of 10 years which may be followed up with CT or MR imaging, based on the US findings with optional annual CT or MR imaging to screen the kidneys. However, CT has the risk of ionizing radiation, screening asymptomatic patients or at-risk relatives and MR may be preferable at higher cost.
2. CNS screening: baseline MR imaging of the brain and spine is performed at age 20 years followed by annual neurologic examinations, for any suspicious signs or symptoms. Annual MR imaging to screen the CNS is optional.
3. Adrenal screening: which consists of 24-hour measurement of urinary vanillylmandelic acid level annually. No imaging is warranted unless this is abnormal. Nevertheless, incidental pheochromocytomas may be detected during routine screening for renal lesions with CT.
4. Ophthalmic screening: consists of annual direct and indirect ophthalmoscopy from the age of 5 years.
5. Additionally an auditory screening tool may be helpful. An audiogram is obtained; if abnormal, MR imaging of the internal auditory canal is performed to look for endolymphatic sac tumors.

Molecular Imaging:

New Ga-68 somatostatin receptor PET/CT is also very useful for the detection of the different tumors associated with VHL syndrome and have an impact in the management of the disease, detecting malignant lesions not usually identified by other imaging modalities. Ga 68 PET/CT also provides important information on the tumor differentiation, i.e., the expression of somatostatin receptors, that is essential for considering peptide receptor radionuclide therapy. Ga-68 somatostatin receptor PET/CT has the potential to become an integral part in the management of VHL disease to help in early diagnosis, recurrence and treatment response of various tumors.

SUMMARY

Although genetic testing is available, imaging plays a major role in the localization of disease process, follow up, in the screening of asymptomatic gene carriers, and patient long-term surveillance. Imaging screening is emphasized because the lesions in vHL disease are treatable; early detection enables conservative therapy and may enhance the patient’s length and quality of life. Molecular Imaging with Ga-68 PET/CT is useful for the detection of a variety of different tumors in the vHL syndrome and provides clinical impact in the management of the disease, detecting malignant lesions not identified by other imaging modalities and further therapy.

AUTHORS (LAST NAME, FIRST NAME): Vijayakumar, Vani[2]; VIJAYAKUMAR, SRINIVASAN[1]

INSTITUTIONS (ALL):

1. RADIATION ONCOLOGY/CANCER INSTITUTE, UNIVERSITY OF MISSISSIPPI MEDICAL CENTER, Jackson, MS, United States.
2. Dept of Radiology, University of Mississippi Medical Center, Jackson, MS, United States.

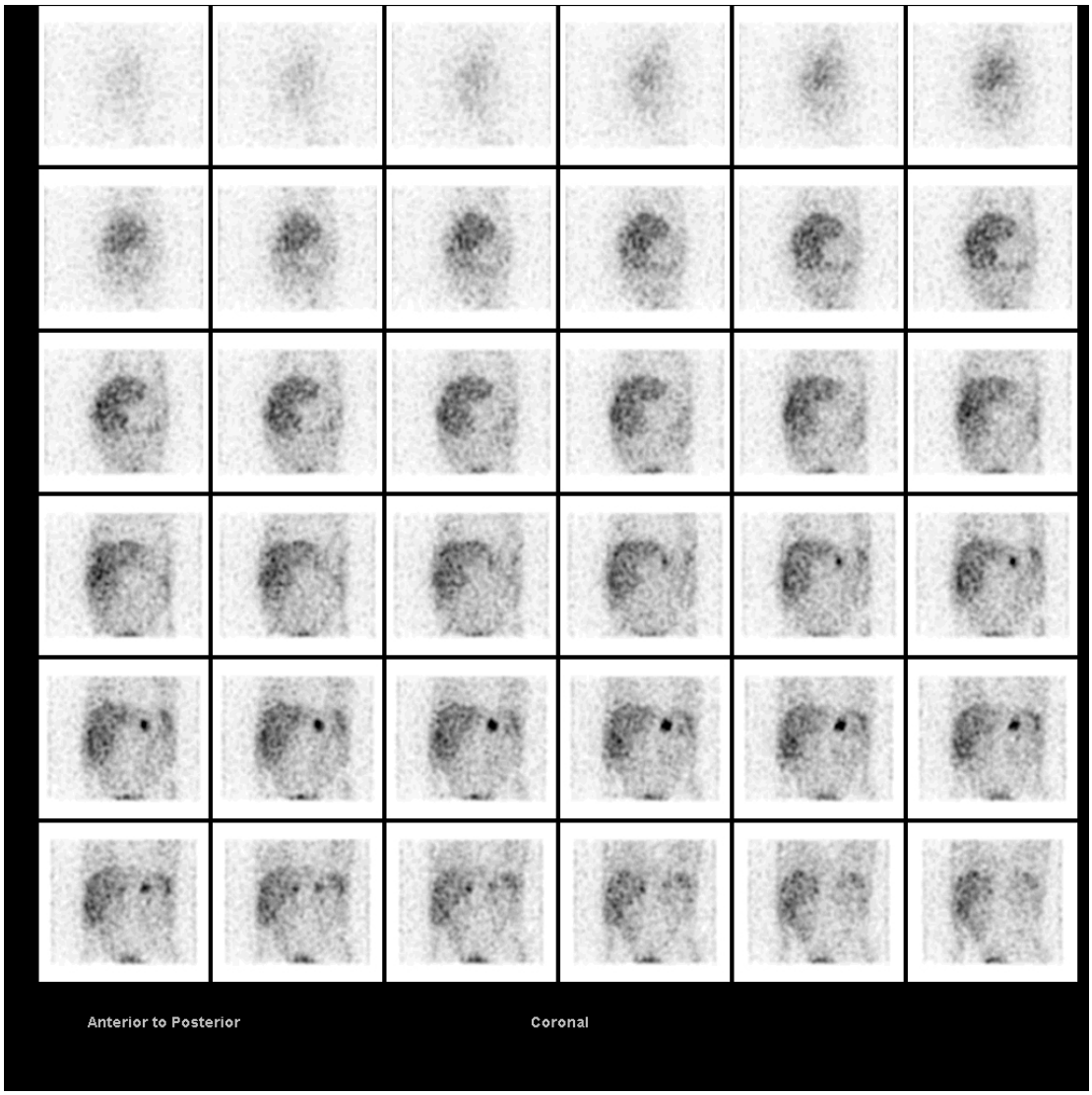
Anterior to Posterior
Coronal

CONTROL ID: 2229457

TITLE: Image Registration and Integration of PET-CT and SPECT functional imaging with Anatomic MRI fusion as an alternative to hybrid imaging in localizing epileptogenic cortex, tumors and Radiation Therapy Planning

PRESENTER: Vani Vijayakumar

ABSTRACT BODY:

Abstract Body:

PURPOSE/AIM

To demonstrate the role of image fusion in seizure disorders and tumor imaging to improve the diagnostic accuracy of nuclear and molecular imaging. Also demonstrate image registration in radiation therapy planning

CONTENT ORGANIZATION

PET-CT has been used in the evaluation of seizure disorders and PET– MRI is not readily available. Anatomic localization with MRI is crucial in the preoperative evaluation of refractory seizures. Fusion of brain PET- CT with MRI using commercial software is proven very helpful in the surgical planning. Similarly, fusion of SPECT with CT or MRI helps the anatomic localization of certain tumors. Image registration also helps Radiation Treatment (RT) Planning
There is growing interest in integration of Anatomic imaging with Nuclear metabolic Imaging, In modern radioon oncology practice, to distinguish between viable tumor and necrosis is of great importance, since toxicity, due to repeated treatment, could worsen, particularly in brain disease. CT and MR images can evidence an anatomic tumor area without giving the distribution of the viable residual tumor portion, whereas SPECT and PET studies can give such information but lack anatomic and spatial resolution of CT and MR. Therefore, the association of different imaging capabilities, by means of image registration techniques, would improve the localization of neoplasms and provide a more accurate disease localization and tumor for radiotherapy treatment planning.
The term “image registration” means the process of integration of the geometric relationship between multiple image studies. Image registration and fusion techniques were first applied successfully in neurology, especially for brain studies, in stereotactic radiosurgery, and stereotactic radiotherapy of cerebral lesions. In neurologic application, it is reasonable to assume a coordinate transformation of a rigid body, consisting only of a three-dimensional translation and rotation. Nine parameters must be estimated to establish the transformation: three rotation angles, three translation values, and three scaling factors to take into account the different pixel sizes of the imaging devices

SUMMARY:

PET-MRI is not readily available. MRI is the commonly used imaging modality in seizure evaluation. As the associated metabolic defect is often larger than any anatomical defect, adding metabolic data improves sensitivity for detection of epileptogenic cortex. Similarly, fusing SPECT with CT and MRI helps the anatomic localization and preoperative management of tumors.
Image fusion and integration also plays an important role in anatomic localization of viable tumors and Radiation Treatment Planning of various Tumors. Fusing anatomic and functional images using the different commercial software systems is cost-effective, accurate, serves as a good teaching tool, and improves diagnostic accuracy with anatomic localization.

Figure 1. Fused Abdominal Octreoscan SPECT and CT demonstrating NET pancreatic Tail (Submitted)

Figure 2: Fused Brain PET CT with MRI Brain showing the hypometabolic seizure focus (Not Submitted)

AUTHORS (LAST NAME, FIRST NAME): Vijayakumar, Vani[2]; Thaggard, Anson[2]; VIJAYAKUMAR, SRINIVASAN[1]

INSTITUTIONS (ALL):

1. RADIATION ONCOLOGY/CANCER INSTITUTE, UNIVERSITY OF MISSISSIPPI MEDICAL CENTER, Jackson, MS, United States.

2. Dept of Radiology, University of Mississippi Medical Center, Jackson, MS, United States.

Figure 1: Fused SPECT and CT Abdomen

Carcinoid tail of Pancreas (Red arrow)

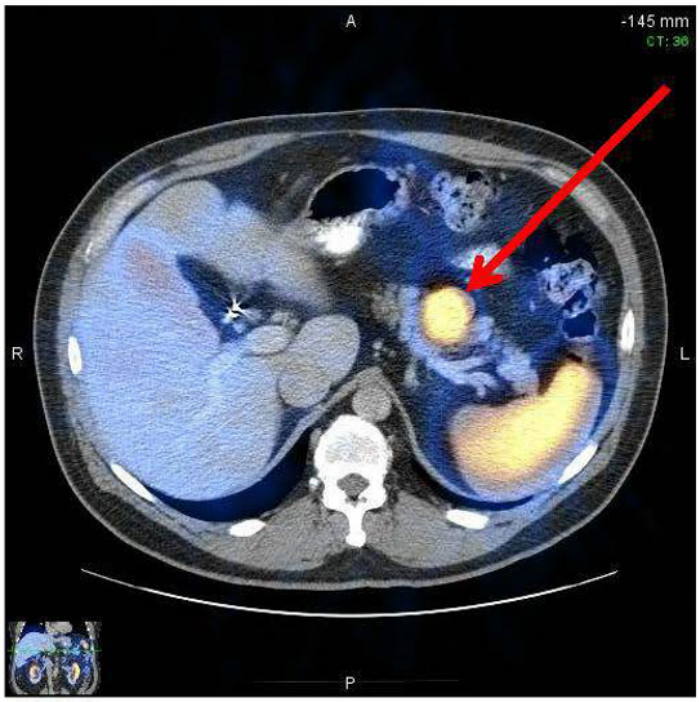

CONTROL ID: 2228856

TITLE: Hyaluronic Acid-Based Nanoplatform for Prostate Cancer Therapy

PRESENTER: Magdalena Swierczewska

ABSTRACT BODY:

Abstract Body: The goal of this project is to develop a prostate cancer-targeted nanoplatform for imaging and drug delivery using hyaluronic acid (HA)-based nanoparticles. Despite the significant enhancements in the detection and diagnosis of cancer, prostate cancer is the second leading cause of cancer death in American men. Unfortunately, it is estimated that about 1 out of 36 patients diagnosed with prostate cancer will die from it. A significant challenge is predicting cancer progression and to determine when it will lead to metastasis. Although most patients with metastatic prostate cancer respond to androgen ablation, relapse is common and can lead to castration-resistant prostate cancer. It has been reported that prostate cancer progression can be predicted by the imbalance between HA and the HA-degrading enzyme, hyaluronidase (HYAL1).

In this study, we utilize self-assembling, hydrophobically modified HA to form HA-based nanoparticles that can carry imaging agents on their surface and anti-cancer drugs in their center cores. By exploiting the excess HYAL1 in the metastatic tumor microenvironment, as opposed to that in slow-progressing prostate tumors, the nanoparticles can be enzymatically degraded to release chemotherapeutics from their core specifically at the metastatic tumor site. In addition, because HA's endogenous receptor, CD44, is expressed on metastatic cancer cells and cancer stem cell-like cells, these cells can be targeted by HA-based nanoparticles.

We demonstrate that the HA-based nanoparticles can serve as targeted imaging and drug delivery agents by taking advantage of the imbalance between HA and HYAL1 in the prostate tumor microenvironment. HA-based nanoparticles maintain the CD44 targeting ability of HA and therefore have specificity for cancerous cells over non-cancerous cancer cells. Next, HA nanoparticles are degraded in a concentration-dependent manner by HYAL1 and can therefore deliver their drug cargo in response to the prostate tumor environment and into prostate cells. Finally, HA-based nanoparticles deliver the conventional anti-cancer drug, docetaxel, to the tumor site with lower drug doses and lower systemic side effects that free drug in an animal cancer model.

By using a nanomedicine approach, the proposed strategy can localize drugs at the progressive tumor site, thereby reducing side effects on healthy tissue. Because the average age of prostate cancer diagnosis is 67 years old, lower side effects are particularly important in the elderly patient population that may have comorbidities. HA nanoparticles can firstly target the tumor site through the enhanced permeation and retention effect, then target the specific metastatic cancer cells via the CD44 receptor, and finally can deliver drugs encapsulated in the nanoparticle by excessive HYAL1 concentration present in the prostate cancer tumor microenvironment and inside cells. The HA-based nanoplatform is an effective approach to image HYAL1 overexpression in metastatic prostate cancer and deliver drugs at the tumor site.

AUTHORS (LAST NAME, FIRST NAME): Swierczewska, Magdalena[1]; Lee, Sangmin[1]; Oh, Yumin[1]; Pomper, Martin[1]; Lee, Seulki[1]

INSTITUTIONS (ALL):

1. Radiology, Johns Hopkins University, Baltimore, MD, United States.

(No Image Selected)

CONTROL ID: 2228897

TITLE: PROGNOSTICATING OUTCOMES AND DOSE PAINTING IN LUNG CANCER USING FDG-PET IN THE ERA OF 4-D COMPUTERIZED TOMOGRAPHY BASED RADIOTHERAPY TREATMENT PLANNING

PRESENTER: SRINIVASAN VIJAYAKUMAR

ABSTRACT BODY:

Abstract Body: Introduction: FDG-PET's role in staging and identifying new disease sites not otherwise detected has been well established. However, less well known is the use of FDG-PET in radiation therapy [RT] treatment planning. RT has also improved in terms of the techniques being used in the past decade. In this presentation, we will discuss:
RT treatment planning using FDG-PET and 4D computerized tomography [CT]
Details of target volume delineation such as Gross Tumor Volume [GTV], Clinical Target Volume [CTV], Metabolic Target Volume [MTV] and Planning Target Volume]PTV
The benefits of using FDG-PET and 4D CT in dose escalation to selected targets and decreasing normal tissue doses and thus decreasing toxicity and improving quality of life
Use of FDG-PET in the middle of RT course to help:
Help identify sub-targets for dose escalation and dose painting in an adaptive RT mode
Review current evidence to support such a dose painting adaptive RT
Methods: RT treatment planning was done in supine position after making customized molds for each patient [VakLoc®]. 4D frame was set for each patient's body over the thorax and then CT scans without contrast were obtained. The CT images were obtained extending from chin to Lumbar 4 vertebral body, with a narrower field selection over the lesion of interest for the 4D image capturing. Image Fusion was done with FDG-PET using Mims Software®. GTV, CTV, MTV and PTV were outlined followed by RT treatment planning. All treatments were delivered using Low-Modulation IMRT.
Results based on the review of the literature:
Target volumes accuracy was improved with the use of PET-fusion, especially in identifying mediastinal structures and atelectasis
4D CT helps avoid missing the target during RT treatments by taking in to account target and organ motion due to breathing
Use of FDG-PET in the middle of RT course improves identifying sub-population of patients who will respond well versus those who are likely to fail within the RT treatment volumes; this enables adaptive RT-dose painting for dose escalation of radio-resistant sub-targets
Conclusions: Use of FDG-PET and 4D CT planning has already shown improved targeting as well as decreasing doses to normal tissues. Use of FDG-PET in the middle of RT course will further help adaptive-RT and dose painting.

AUTHORS (LAST NAME, FIRST NAME): VIJAYAKUMAR, SRINIVASAN[1]; Packianathan, Satyaseelan[1]; Dugger, William N.[1]; Kanakamedala, Madhava[1]; Green, Edward D.[2]; Thigpen, James[1]; Puneky, Louis[1]; Vijayakumar, Vani[2]

INSTITUTIONS (ALL):

1. RADIATION ONCOLOGY/CANCER INSTITUTE, UNIVERSITY OF MISSISSIPPI MEDICAL CENTER, Jackson, MS, United States.
2. Dept of Radiology, University of Mississippi Medical Center , Jackson, MS, United States.

(No Image Selected)

CONTROL ID: 2229144

TITLE: Critical Decision Points in Screening and Diagnosis of Prostate Cancer and the Role of Molecular Biomarkers: Implications for the Imaging Community

PRESENTER: SRINIVASAN VIJAYAKUMAR

ABSTRACT BODY:

Abstract Body: In the US, there will be an estimated 221,000 new cases of prostate cancer [PC] in 2015; there will be about 27,500 deaths from PC. With Prostate Specific Antigen [PSA] based **population screening** programs of the past 20 years, the overall mortality from PC has declined, there is a stage migration to more favorable risk groups, and survival rates have improved. Yet, the population based screening programs are under great scrutiny. This is because of the over-diagnosis and over treatment among those who are diagnosed with PC. For example, about 1 million prostate gland biopsies are performed per year; only 50% of them are positive for PC. In repeat biopsies, another 20% are diagnosed with PC. The United States Preventive Task Force recommended against routine PSA screening. American Cancer Society [ACS] has changed its years of screening recommendations and the need for a robust informed decision and team approach to screening decisions, are being emphasized. Given the controversy and confusion, a 'Melbourne Consensus Statement' has been developed; even this statement is inadequate to 'personalize' the PC Screening Recommendations.

The past decade also has seen a revolution in genomics and bioinformatics. 'Precision Medicine' and 'Personalized Medicine' have been added to our vocabulary. $1000 genomic profile of individuals is not far away.

Based on the above, we hypothesized the following:

1. There are a number of critical forked decision points in the screening, prevention, early diagnosis, staging and treatment of PC. The current clinical algorithms to make decisions are inadequate.

2. Such an inadequacy has led to over-diagnosis, over-treatment, a high Number Needed to Treat [NNT] and a loss of Quality of Life [QOL] for PC patients.

3. The genomics and bioinformatics revolution can be brought to bear upon under these circumstances and help personalize decision makings in PC.

4. Such an approach will need a robust analysis of the published literature and new innovative clinical trials.

Our above hypotheses are based on the following:

1. Approximately 100 SNPS are associated with an increased risk of PC diagnosis

2. In the 'REDUCE' clinical trial, adding a 'Genetic Score' improved the Receiver Operated Curve [ROC] statistics in the diagnosis of PC

3. Close to 10 genomic-biomarker tests / panels have been discovered for PC in the past two years

4. In a Genome Wide Survey analysis, Hicks et al demonstrated many functionally related and relevant patterns in PC

In this presentation we will review the relevant literature and propose new models in the use of molecular biomarkers in the critical fork-points of decision making in PC.

AUTHORS (LAST NAME, FIRST NAME): VIJAYAKUMAR, SRINIVASAN[1]; Hicks, Chindo[1]; Gomez, Christian[1]; Lewin, Jack[1]; Gonzalez-Fernandez, Federico[3]; Vijayakumar, Vani[2]

INSTITUTIONS (ALL):

1. RADIATION ONCOLOGY/CANCER INSTITUTE, UNIVERSITY OF MISSISSIPPI MEDICAL CENTER, Jackson, MS, United States.
2. Dept of Radiology, University of Mississippi Medical Center, Jackson, MS, United States.

3. RESEARCH, VAMC, Jackson, MS, United States.
(No Image Selected)

CONTROL ID: 2228908

TITLE: Temporal weighting and angular rebinning for artifact-free single-rotation restrospectively gated 4D cardiac micro-CT

PRESENTER: Daniele Panetta

ABSTRACT BODY:

Abstract Body: Introduction. Rats and mice are the most used models for the study of cardiovascular diseases. The detection of early regional cardiac dysfunction in these animals with high heart rate requires volumetric time-resolved (4D) imaging at sub-millimeter spatial resolution and very high temporal resolution (Espe et al, J Card Mag Res 2013;15:82). Retrospectively gated micro-CT is promising, but it suffers of severe artifacts due to sparse and irregular angular sampling and noise (Clark et al, Physica Medica 2015;30(6):619-34). Hence, there is strong interest in developing high-speed instrumentation and optimal data utilization strategies. Here, we evaluated a retrospective micro-CT cardiac gating method based on a high frame-rate, slow single-turn rotation acquisition and weighted temporal/angular rebinning allowing 4D reconstruction of the heart with an arbitrary partitioning of the cardiac cycle. **Materials and Methods.** The micro-CT images were acquired with a micro-PET/CT scanner (IRIS™, raytest GmbH, Germany), which is equipped with a microfocus X-ray source and a high-speed CMOS+CsI(Tl) X-ray detector with exposure times >11 ms using hardware rebinning. Healthy Wistar rats were anesthetized (isoflurane) and injected with a contrast agent (Iomeron®, Bracco, Italy), 200 mg/mL, 0.4 mL/min in a tail vein. The scanning protocol consisted of a multi-arc rotating acquisition with 3600-20000 projections over 360°, with a total scan time of 2 to 6 minutes. The tube setting was 80 kV, 1 mA, and the dose was <0.5 Gy in all experiments. For 4D reconstruction, cardiac and respiratory signals were derived from raw projection data (Dinkel et al, Circ Cardiovasc Imaging. 2008;1:235-243); each projection was assigned to one or more cardiac phases with weighting factors depending on the amount of intersection of its exposure interval with each gate (Figure 1a). Each rebinned projection in the gated datasets was calculated by weighted angular rebinning (AR) using a triangular weighting window centered at the median angle. Datasets of all gates were reconstructed with a standard FDK algorithm. **Results.** We have successfully obtained 4D cardiac images of rat hearts (165-330 bpm) with temporal bin duration down to 8 ms. The temporal weighting allowed to minimize data loss when dense partitioning of the cardiac cycle was used, and appropriate width of weighted AR allowed to keep the streak artifacts at minimum (Figure 1b); when the heart was close to the CFOV, there was no visible loss of spatial resolution. In rats, a voxel size of 240 μm was sufficient to delineate myocardial walls (Figure 1c) and to take advantage of the detector shortest exposure time which allowed a more precise detection of cardiac and respiratory phases from the intrinsic gating signal. The best compromise between cardiac cycle partitioning and image quality was such that (N. gates)x(exp.time)/(RR interval) ≈ 1. **Conclusion.** Retrospectively gated multi-phase imaging of the rat heart is feasible with good quality by proper utilization of the projection data, even using standard FDK reconstruction and without physiological sensors. Experiments with mice are ongoing and will be also presented.

AUTHORS (LAST NAME, FIRST NAME): Panetta, Daniele[1]; Belcari, Nicola[2]; Burchielli, Silvia[3]; Pelosi, Gualtiero[1]; Tripodi, Maria[1]; De Simone, Mariarosaria[1]; Iozzo, Patricia[1]; Del Guerra, Alberto[2]; Salvadori, Piero A.[1]

INSTITUTIONS (ALL):

1. CNR Institute of Clinical Physiology, Pisa, Italy.
2. Department of Physics "E.Fermi" - University of Pisa, Pisa, Italy.
3. Fondazione CNR/Toscana "G. Monasterio", Pisa, Italy.

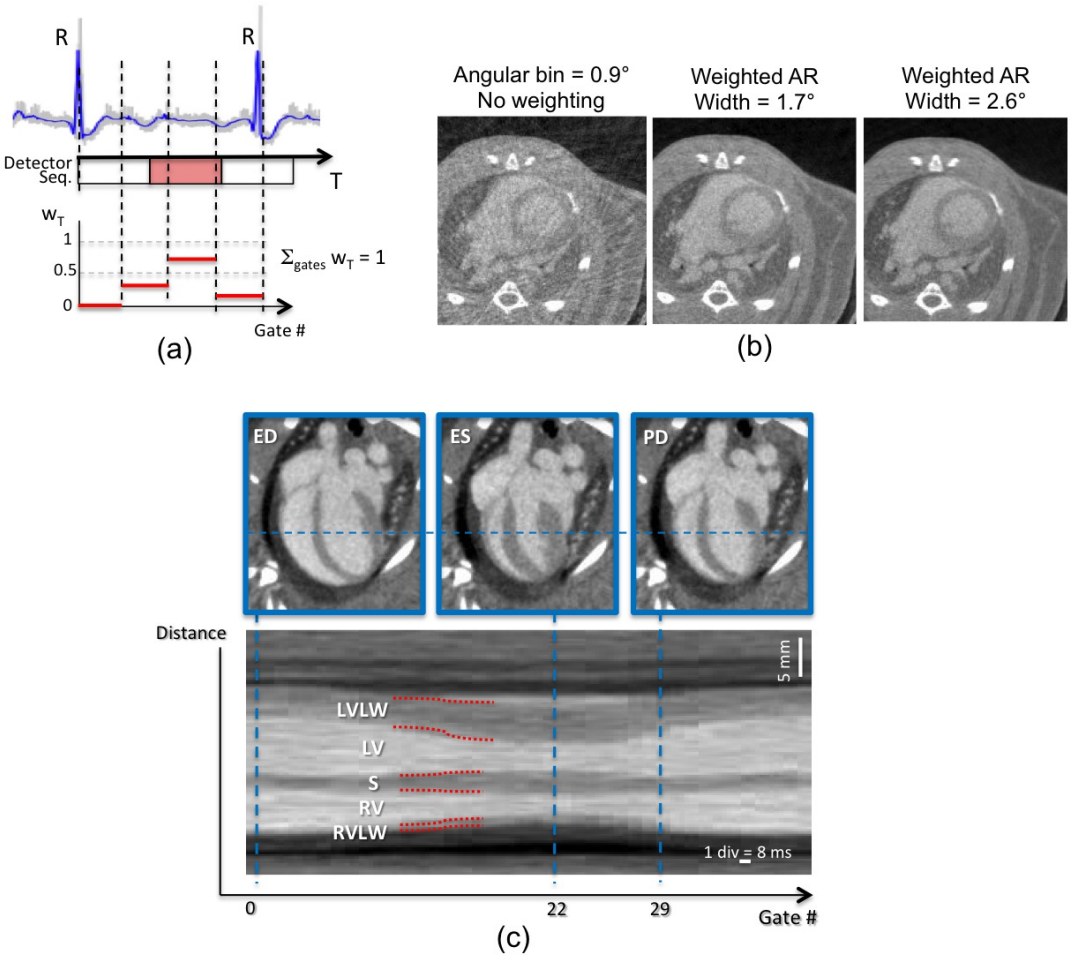

Figure 1 – (a) Temporal weighting function. Each raw projection (red rectangle) is assigned to one or more cardiac phases to optimally distribute all the data between gates, thus minimizing the number of empty bins in the gated datasets. (b) Rat transaxial images at end-diastole (RR = 366 ms, T_{gate} = 23 ms), showing the weighted angular rebinning effect at various widths. (c) M-mode-like representation of a rat beating heart (RR = 335 ms, T_{gate} = 8 ms) reconstructed from 20000 projections (6 min scan time) with 40 equally-spaced gates; the vertical dashed lines intersect the heart at end-diastole (ED), end-systole (ES) and proto-diastole (PD). LVLW: left-ventricle lateral wall; LV: left-ventricle; S: interventricular septum; RV: right ventricle; RVLW: right ventricle lateral wall.

CONTROL ID: 2228977

TITLE: Bone Marrow Derived Myeloid Cells Orchestrate Resistance to Anti-angiogenic Therapy in Novel Chimeric Mouse Model of Glioblastoma

PRESENTER: Ali Arbab

ABSTRACT BODY:

Abstract Body: Glioblastoma (GBM) is considered as hypervascular form of brain tumors. Anti-angiogenic therapies (AAT) were used as an adjuvant against VEGF-VEGFR pathway to normalize blood vessels. Surprisingly, AAT resulted into marked hypoxia and recruited bone marrow derived cells (BMDCs) to the tumor microenvironment (TME). Nonavailability of *in vivo* model limits investigation of BMDCs in AAT resistance. We established a novel chimeric mouse model using as low as $5x10^6$ BM cells from GFP+ transgenic mice, administered through *i.v* route in athymic nude mice following whole body irradiation, which resulted in >70% engraftment within 14 days. We exploited chimeric mouse model to develop orthotopic U251 tumor and tested receptor tyrosine kinase inhibitors and CXCR4 antagonist against GBM using both optical and magnetic resonance imaging. Increased infiltration of GFP+ BMDCs acquiring suppressive myeloid and endothelial phenotypes in TME, and increased tumor growth were observed following treatments. Inhibition of CSFR1+ myeloid cells using GW2580 reduced tumor growth by decreasing myeloid and angiogenic cells in TME. This was followed by decreased inflammatory, proangiogenic and immune suppressive factors compared to vehicle and other treated groups. In conclusion, we developed preclinical chimeric model of GBM and role of tumor infiltrated BMDCs were investigated in context of resistance of AATs by utilizing state of art multispectral optical and MR imaging. Study suggests that inhibiting immune suppressive myeloid cells could provide a better therapeutic benefit in GBM.

AUTHORS (LAST NAME, FIRST NAME): Achyut, Bhagelu R.[1]; Shankar, Adarsh[1]; Iskander, Asm[1]; Ara, Roxan[1]; Angara, Kartik[1]; Arbab, Ali S.[1]

INSTITUTIONS (ALL):

1. Cancer Center, Georgia Regents University, Augusta, GA, United States.

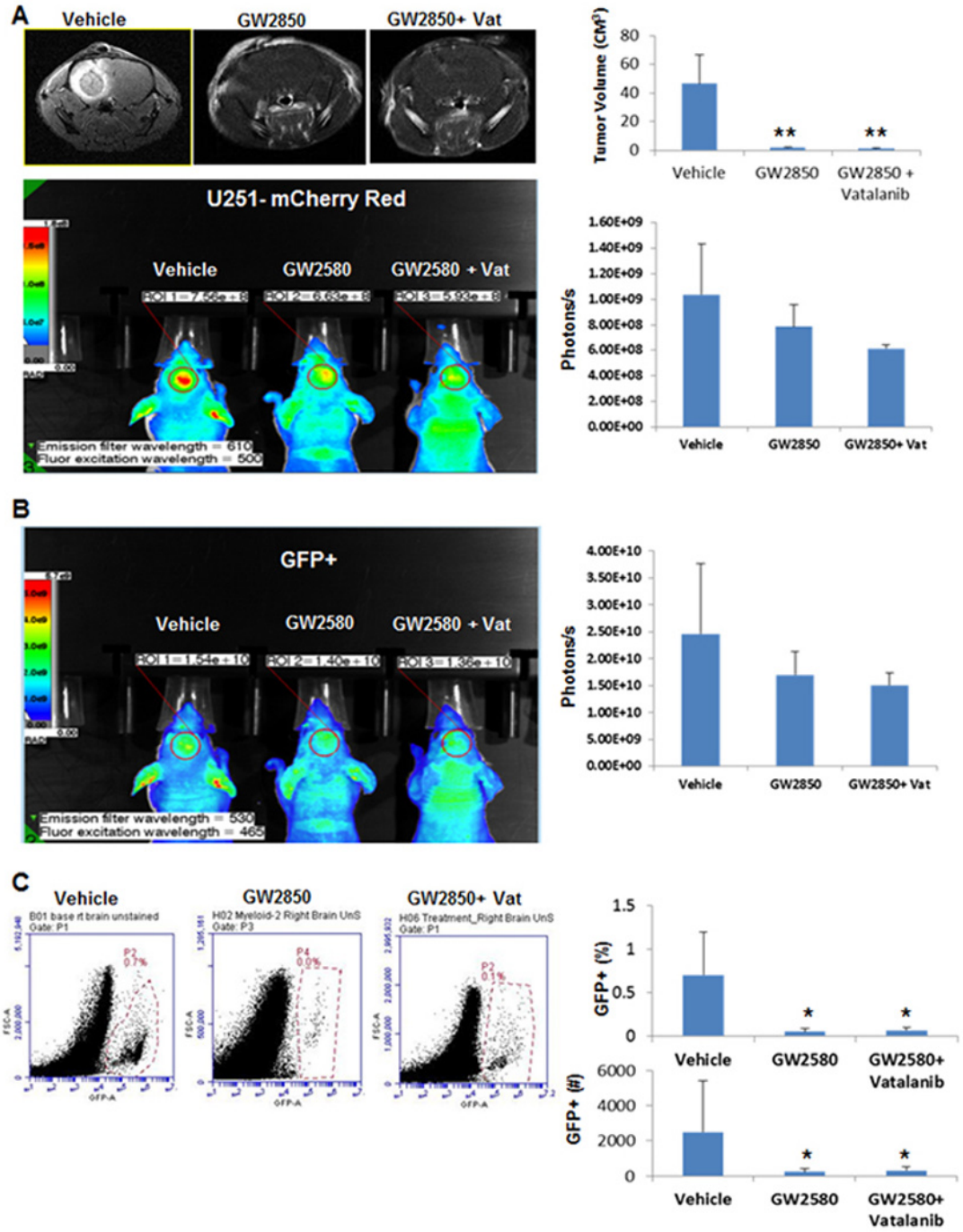

Figure 1: MRI and optical imaging (mCherry) indicate the growth of orthotopic GBM in mice following treatments with vehicle, GW2580 and GW2580 plus vatalanib. Optical imaging (GFP) indicate accumulation of GFP+ cells in the tumors. Tumor volume and photon intensity measurements indicate the effect of GW2580. Flowcytometric analysis indicate the lower number of GFP+ bone marrow cell in the treated animals. It is to be noted that vatalanib alone does not decrease the tumor.

CONTROL ID: 2228979

TITLE: NMR Metabolomics and Hyperpolarized Magnetic Resonance Imaging Reveal Altered- Metabolism in Patient-derived Pancreatic Ductile Adenocarcinoma (PDAC) Mouse Xenografts

PRESENTER: Prasanta Dutta

ABSTRACT BODY:

Abstract Body: Pancreatic ductal adenocarcinoma (PDAC) is an aggressive and lethal disease that develops relatively symptom-free. The absence of early symptoms and effective treatments has created a critical need for identifying and developing new noninvasive biomarkers and therapeutic targets for patient management. Hyperpolarized magnetic resonance imaging (HP-MRI) provides a >10,000-fold signal enhancement for detecting of endogenous, nontoxic, nonradioactive substances to monitor metabolic fluxes through multiple key biochemical pathways including glycolysis and citric acid cycle [1]. In particular, conversion between hyperpolarized ^{13}C-labeled pyruvate and lactate, catalyzed by lactate dehydrogenase (LDH), has been shown to have a number of potential applications such as diagnosis, staging tumor grade and monitoring therapy response [2]. Genetic mutation is evident in causing tumorigenesis and often time these mutations trigger the signaling pathways that are associated with “metabolic transformations”. There is currently tremendous research interest in dissecting the mechanisms and impact of metabolic transformation for effective therapeutic intervention. In this effort, we are applying high-resolution NMR (nuclear magnetic resonance spectroscopy) metabolomics and the real-time *in-vivo* hyperpolarized metabolic imaging of patient-derived xenograft tumors for probing the underlying mechanism of altered-metabolism and correlate genomics to downstream metabolomics. The protocol detailing heterotopic engraftment of patient tumors into immunodeficient mice and expansion of direct xenograft tumors was recently reported elsewhere [3].The fresh-frozen tumor samples were homogenized, lyophilized, and resuspended in D_2O and NMR spectroscopy (Image 1) was employed to characterize the water-soluble portion of the metabolome. The NMR metabolomics data suggest that alterations in choline metabolism and elevated glycolysis (production of high level lactate) may arise in PDAC development (Persuasive Data-Figure 1). Also, the metabolite concentrations are distinct among the four tumor types. The real-time metabolic imaging shows the immediate conversion of lactate after injection (i.v.) of hyperpolarized ^{13}C pyruvate and probe the upregulated LDH activity (Persuasive Data-Figure 2,). Real-time *in-vivo* choline uptake and transport study using hyperperpolarized ^{15}N-choline imaging is underway. This model system provides an excellent platform where mutational status of these patient tumors can be correlated with both high resolution and hyperpolarized dynamical metaboloimics data for characterizing individual tumor phenotypes.

1. P. Dutta et. al. “A New Horizon of DNP Technology: Application to In-vivo ^{13}C Magnetic Resonance Spectroscopy and Imaging” ***Biophysical Reviews,* 5,** 271-281, 2013.

2. P. Dutta et. al. “*In-vivo* assessment of LDH-A and glutaminase inhibition in tumor xenografts using hyperpolarized ^{13}C-pyruvate magnetic resonance spectroscopy” ***Cancer Research,* 73,** 4190-4195, 2013.

3. X. Li et. al. “Extracellular lumican inhibits pancreatic cancer cell growth and is associated with prolonged survival after surgery” ***Clinical Cancer Research***, **20**, 6520-6540, 2014.

AUTHORS (LAST NAME, FIRST NAME): Dutta, Prasanta[1]; Zhang, Ran[2]; Kang, Yaan[2]; McCullough, Christopher R.[1]; Zacharias, Niki[1]; Maitra, Anirban[3]; Fleming, Jason B.[2]; Bhattacharya, Pratip[1]

INSTITUTIONS (ALL):

1. Cancer Systems Imaging, M.D. Anderson Cancer Center, Houston, TX, United States.
2. Surgical Oncology, M.D Anderson Cancer Center, Houston, TX, United States.
3. Pathology, M. D. Anderson Cancer Center, Houston, TX, United States.

Representative High-resolution NMR Spectrum of the patient-derived xenograft tumor sample (MDA-PATX104)

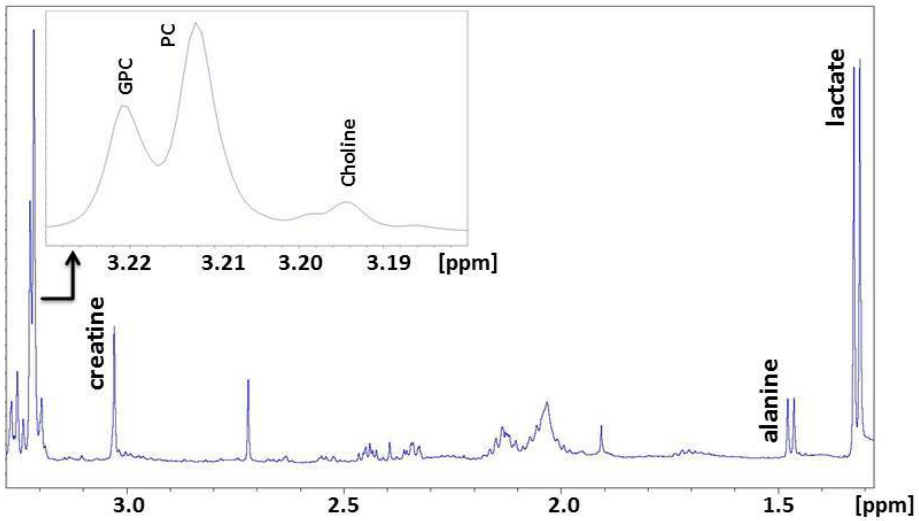

PC: Phosphocholine
GPC: Glycerophosphocholine

Prasanta Dutta et.al

CONTROL ID: 2228986

TITLE: Synthesis, characterization and application of monofluorinated resazurin, a selective Cerenkov absorbing viability and redox dye

PRESENTER: Alejandro Arroyo

ABSTRACT BODY:

Abstract Body: Cerenkov radiation occurs when β-particles, emitted from decaying radionuclides such as ^{18}F, travel faster than the speed of light in a medium. This phenomenon produces photons along the path travelled by the β-particles. These Cerenkov photons are multispectral and continuous throughout the visible wavelengths. The presence of a chromophore or fluorophore in the vicinity of the emission will cause a disruption of the Cerenkov radiation within a particular wavelength range, associated with the absorption (and emission, if applicable) maxima of the molecule. In the presence of a functional chromophore, this disruption in emission spectra can be correlated to the measurement of a biological parameter. The objective of this project is to develop a feasible and robust method to utilize the emission of Cerenkov photons in conjunction with functional fluorinated chromophores to determine the redox status in cells and tissues. Resazurin (RA), also known as Alamar Blue, is a commonly used viability dye and redox sensor. When reduced in cells, RA is converted into resorufin (RA_{red}), a highly fluorescent molecule. RA was successfully labeled with fluorine using electrophilic fluorination under acidic conditions. The resulting mixture of fluorinated derivatives was purified using preparative HPLC; 5 fractions were identified and collected. Mass spectrometry analysis on the fractions confirmed the synthesis of mono and difluorinated compounds. ^{1}H-NMR and ^{19}F-NMR analysis confirmed the presence of two isomers of monofluorinated resazurin (FRA) in one of the fractions. After determination of absorption maxima in basic conditions, titration curves were constructed to determine the pK_a of each fraction. The pK_a decreased to higher acidity with increased degree of fluorination. To assess the capability of FRA and FRA_{red} to differentially attenuate Cerenkov radiation, a chemical reduction experiment, with sodium dithionite, was run to demonstrate this phenomenon. Analysis of the Cerenkov emissions using optical imaging determined that both FRA (with the addition of FDG as photon source) and ^{18}FRA could be reduced chemically and that their reduced compound is highly fluorescent. The difference in photonic emission between FRA and FRA_{red} was greatest using 620-660 nm emission filters and suggests that these are the best wavelengths to use for *in cellulo* and/or *in vivo* applications. On the best performing filter (620 nm), the ratio of emission between FRA and FRA_{red} was >3.5. The fluorescent capability of FRA_{red} detected by optical imaging is due to Cerenkov Radiation Energy Transfer (CRET). Preliminary cell studies show that DU145 prostate cancer cells are also able to reduce FRA. The detection of redox stress, be it reductive or oxidative, is a potential tool to non-invasively detect several medically relevant scenarios including measurement of cell viability, antioxidant studies, inflammation and potentially in neurodegenerative diseases. The eventual impact of this technique lies in the ability to translate it to the clinic coupled with PET for a dual imaging modality.

AUTHORS (LAST NAME, FIRST NAME): Arroyo, Alejandro D.[1]; Kachur, Alexander[1]; Browning, Elizabeth[1]; Blankemeyer, Eric[1]; Popov, Anatoly V.[1]; Delikatny, Edward J.[1]

INSTITUTIONS (ALL):

1. Radiology, University of Pennsylvania, Philadelphia, PA, United States.

(No Image Selected)

CONTROL ID: 2228997

TITLE: Differentiating bacterial infection from inflammation in mouse lung using 2-[^{18}F]-fluorodeoxysorbitol (^{18}F-FDS)

PRESENTER: Junling Li

ABSTRACT BODY:

Abstract Body: Introduction: Our previous studies demonstrated the uptake of ^{18}F-FDS was proportional to bacterial growth and correlated well with the degree of infection in mouse lung, thus ^{18}F-FDS might be used as an imaging biomarker to monitor disease progression and to assess treatment efficacy of bacterial infection. Early differential diagnosis of infection and inflammation is of utmost importance for the optimal management of patients. ^{18}F-FDG is considered as a gold standard in clinical PET/CT imaging, but lacks the differential diagnostic ability of infection and inflammation. Thus the objective for this study was to determine whether ^{18}F-FDS is a pathogen-specific imaging biomarker in differentiating bacterial infection from inflammation caused by heat-killed bacteria in mouse lung.

Methods: *In vitro* uptake of ^{18}F-FDS or ^{18}F-FDG in 6 different concentrations of heat-killed *Klebsiella* (*K.*) *pneumoniae* (n=3 each, 10^4 to 10^9 CFU/ml in an increment of 10 folds) was performed. For *in vivo* studies, 10 Albino C57 female mice received intratracheal challenge with $10^{8.3}$ heat-killed *K. pneumoniae* per mouse. From day 1 to day 4 post inoculation of dead bacteria, PET/CT imaging was performed sequentially on 5 mice with ^{18}F-FDS and then another 5 mice with ^{18}F-FDG. 200-250 μCi of each tracer was injected intravenously into each mouse via tail vein. PET scan was performed for 20 min 1 h post injection, followed by CT for another 10 min. The mice were sacrificed after all the scans were finished on day 4 and then biodistribution studies were performed. % ID/g was used to compare the radioactivity accumulation among multiple tissues and organs of interest.

Results: Neither ^{18}F-FDS nor ^{18}F-FDG was taken up by dead bacteria *in vitro*. However, PET imaging with ^{18}F-FDS demonstrated a completely different uptake pattern from that of ^{18}F-FDG, especially in the lung. The majority of ^{18}F-FDS was accumulated in the gut, kidney, and bladder, but little uptake was detected in the brain and lung from day 1 to day 4 post inoculation of dead bacteria. The average uptake in the lung was about 0.48±0.12 % ID/g and the average ratio of inoculated lung/baseline lung was 1.3±0.3. PET imaging showed major accumulation of ^{18}F-FDG in the brain, heart, and lung. Uptake of ^{18}F-FDG in the lung was 13-20 folds higher than that of ^{18}F-FDS, with % ID/g of 6.7±0.9, 9.1±3.0, 9.9±1.3, and 7.2±1.0 for day 1, 2, 3, and 4, indicating the peak of lung inflammation on days 2 and 3. Uptake of ^{18}F-FDS was previously found to be 2.5 % ID/g in mouse lung on day 3 post inoculation of live bacteria; thus, the ratio between lung inoculated with live bacteria and lung inoculated with dead bacteria on day 3 was 5.3. Biodistribution data were consistent with PET imaging results for both ^{18}F-FDS and ^{18}F-FDG, showing the uptake of ^{18}F-FDG in lung was substantially higher than that of ^{18}F-FDS.

Conclusions: Our preliminary data showed that uptake of ^{18}F-FDS could differentiate bacterial infection from inflammation while that of ^{18}F-FDG could not. Thus ^{18}F-FDS is a promising pathogen-specific imaging biomarker which might provide a useful noninvasive tool for an accurate diagnosis of bacterial infection in the lung.

AUTHORS (LAST NAME, FIRST NAME): Li, Junling[1]; Zheng, Huaiyu[1]; Fodah, Ramy A.[2]; Warawa, Jonathan M.[2, 3]; Ng, Chin K.[1]

INSTITUTIONS (ALL):

1. Radiology, University of Louisville, Louisville, KY, United States.
2. Microbiology & Immunology, University of Louisville, Louisville, KY, United States.
3. Center for Predictive Medicine, University of Louisville, Louisville, KY, United States.

(No Image Selected)

CONTROL ID: 2233274

TITLE: Targeting phospholipids with ^{68}Ga-DOTA-duramycin and ^{68}Ga-DOTA-DPA for imaging apoptosis in cancer

PRESENTER: Junling Li

ABSTRACT BODY:

Abstract Body: Introduction: Phosphatidylethanolamine (PE) and phosphatidylserine (PS) are two major phospholipids that account for about 25% and 10% of the phospholipid content respectively in mammalian cellular membranes. Both PE and PS are externalized to the surface of apoptotic cells, making them excellent targets for apoptotic imaging. Duramycin is a polypeptide that has been shown to bind specifically to PE on cell surfaces with high affinity. On the other hand, DPA is a small synthetic organic molecule that binds specifically to PS on apoptotic cells. Therefore the objective of this study was to assess whether ^{68}Ga DOTA-duramycin and ^{68}Ga DOTA-DPA could be used for predicting apoptotic response in cancer cells pretreated with different doses of camptothecin.

Methods: Human leukemia U937 cells were incubated with 4 different concentrations of camptothecin (CTP: 0, 0.1, 1, and 50 μM with n=5 each) for 48 h. DOTA-duramycin and DOTA-DPA were labeled with ^{68}Ga at pH 5.0 and 5 μCi of each radiotracer was then added into each well. After the cells had been incubated for 1 h at 37 ^{o}C; the cells were harvested, centrifuged, washed, and then measured for radioactivity. Percent uptake was calculated by counts in cells divided by total counts. The degree of cell apoptosis was measured by flow cytometry using a commercially available assay kit of annexin-V/PI.

Results: The labeling yields of ^{68}Ga-DOTA-duramycin and ^{68}Ga-DOTA-DPA were greater than 95%. Cell apoptosis was measured to be 4.99±1.23, 14.49±3.56, 25.99±3.87, and 67.38±6.58% for 0, 0.1, 1, and 50 μM of CTP, respectively. The induction of apoptosis by CTP in U937 cells appeared to be biphasic, with the inflection point at 26 μM. The uptake of both Ga-68 radiotracers also increased in a biphasic dose-dependent relationship with CTP concentration-3.42±0.49, 6.92±0.60, 8.32±0.42, and 9.78±0.38% for ^{68}Ga-DOTA-duramycin; and 4.45±0.45, 5.02±0.41, 6.29±0.54, and 7.59±0.64% for ^{68}Ga-DOTA-DPA at 0, 0.1, 1 and 50 μM of CTP, respectively. After normalizing to their respective control group at 0 μM of CTP, the uptake ratio of ^{68}Ga-DOTA-duramycin to ^{68}Ga-DOTA-DPA was estimated to be 1.73±0.06, with the maximal uptake of 2.8 and 1.7 for ^{68}Ga-DOTA-duramycin and ^{68}Ga-DOTA-DPA.

Conclusions: Our preliminary data showed that both tracers might be used as an imaging biomarker for predicting apoptotic response in cancer cells. PE-targeting ^{68}Ga-DOTA-duramycin was shown to be more sensitive than PS-targeting ^{68}Ga-DOTA-DPA in imaging apoptosis, probably due to the fact that the amount of PE present in the cell membrane is at least twice that of PS.

AUTHORS (LAST NAME, FIRST NAME): Li, Junling[1]; Guo, Haixun[3]; Gray, Brian D.[2]; Pak, Koon Y.[2]; Ng, Chin K.[1]

INSTITUTIONS (ALL):

1. Department of Radiology, University of Louisville, Louisville, KY, United States.
2. Molecular Targeting Technologies, Inc. , West Chester , PA, United States.
3. Department of Radiology, and Center for Predictive Medicine for Biodefense and Emerging Infectious Diseases, University of Louisville, Louisville, KY, United States.

(No Image Selected)

CONTROL ID: 2239356

TITLE: Transurethral photoacoustic endoscopy: making moves into the clinic

PRESENTER: Liangzhong Xiang

ABSTRACT BODY:

Abstract Body: *Purpose/Objective(s)*

Photoacoustic imaging (PAI) is a newly emerging strategy for applications in cancer detection, diagnosis and therapy monitoring, which essentially lets us “hear” light. The trick of PAI is to convert light absorbed at depth to sound waves, which scatter a thousand times less than light, for transmission back to the surface. This thermoelastic expansion converts photons to sound waves that are used to form images with the resolution associated with the ultrasound wavelength, at tissue depths never before possible.

The goal of this work is to move photoacoustic (PA) imaging from bench to bedside. We are developing a transurethral catheter with a PA/US endoscope allows accurate prostate cancer detection and real-time biopsy guidance.

Materials/Methods

The PA/US endoscope imaging system comprises three major hardware components: (i) a tunable (680-970 nm) OPO laser beam pumped by Nd:YAG laser delivers < 10 ns duration pulses (OPOTEK Inc., Carlsbad, CA, USA) through an optical fiber bundle to the prostate with repetition frequency of 20 Hz, (ii) a 128 elements US array (20-MHz central frequency and 80% bandwidth); and (iii) a 128 channels signal processing and data acquisition system(SonixDAQ, Ultrasonix Corp., Canada). The ultrasound probe has been integrated with a custom-designed fiber optic assembly for *in vivo* detection and characterization of human prostate tissue. A synchronization signal generated from the laser system was used to coordinate the data acquisition system. Using the spatial phase-controlled algorithm, the 2D tomograms were reconstructed. We then used the 2D tomograms to localize the prostate tumor and real-time guide the biopsy.

Results

We present the coregistered US and photoacoustic imaging system structure, the optimal design of the PC interfacing software, and the reconfigurable field programmable gate array operation and optimization. Data acquisition, beamforming, scan conversion, and display are implemented in real-time at 20 frames per second which only limited by the laser repetition rate. Phantom experiments of system lateral resolution and axial sensitivity evaluation, examples of the scanning of a molecular imaging contrast agent, NIR dye IRdye800CW, and *ex vivo* human prostate tissue studies are demonstrated.

Conclusions

PAI is a natural complement to existing ultrasonography and should enlarge the scope of US in diagnostic imaging and therapeutic monitoring of prostate cancer by providing additional information. The transurethral light delivery provides a reasonable imaging penetration depth (>3 cm) in photoacoustic imaging for clinical usage compared to the external or transrectal light delivery. The high frequency ultrasound transducers (>20 MHz) used will result in higher resolution (<100 μm) imagery which will improve diagnostic capabilities. The ability to image both vasculature and molecular profile outside the blood vessels gives molecular PAI a unique advantage over currently used imaging techniques. The imaging method presented here can find application both in diagnosis and in image-guided biopsy.

AUTHORS (LAST NAME, FIRST NAME): Tang, Shanshan [3]; Liu, Hong [1]; Xiang, Liangzhong [2]

INSTITUTIONS (ALL):

1. University of Oklahoma, Norman, OK, United States.
2. School of Electric and Computer Engineering , University of Oklahoma, Norman, OK, United States.
3. School of Electric and Computer Engineering, , University of Oklahoma, Norman, OK, United States.

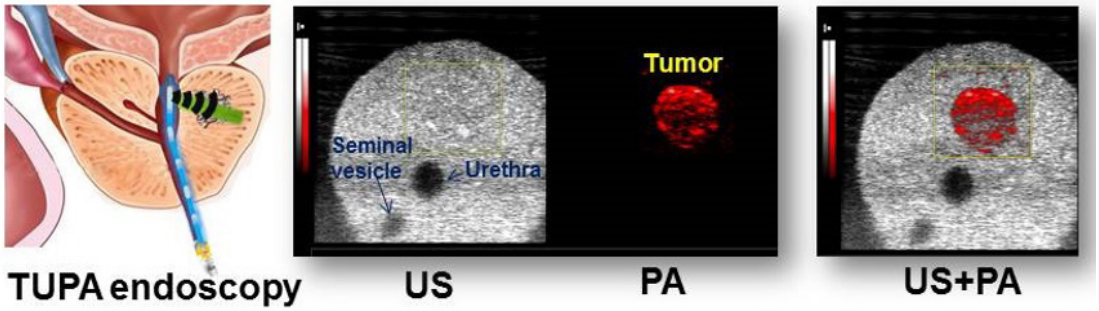
Tumor
Seminal vesicle
Urethra
TUPA endoscopy
US
PA
US+PA

CONTROL ID: 2229010

TITLE: Volumetric MR Spectroscopic Imaging Identifies Infiltrating Margin in Glioblastoma for 5-ALA Intraoperative Fluorescence-Guided Surgery

PRESENTER: James Cordova

ABSTRACT BODY:

Abstract Body: PURPOSE: Glioblastoma (GBM) resection based on T1 contrast-enhanced MRI (T1CE) results in high rates of local recurrence (<2 cm from resection cavity), as infiltrating tumor is known to extend beyond contrast enhancement **[1]**. Metabolite maps generated from MR spectroscopic imaging (MRSI) have been shown to identify high-risk tumor infiltration zones outside of T1CE regions more specifically than T2 imaging **[2,3]**. Accordingly, coupling preoperative MRSI with real-time fluorescence-guided surgery (FGS) using 5-aminolevulinic acid (5-ALA) may facilitate safe removal of occult tumor tissue beyond the enhancing tumor margin.

MATERIALS/METHODS: In an ongoing Phase II trial for new and recurrent GBM patients (n=18, at the time of this abstract), 3D full-brain MRSI metabolite volumes, including maps of total choline (tCho), creatine (tCr), N-acetylaspartate (tNAA) and their ratios, were acquired, co-registered with surgical planning MRI, and imported into a neuronavigation system to guide resection. Patients were administered 5-ALA orally 3-5h before surgery. Biopsies were collected from regions of elevated Cho/NAA values within T1CE and/or T2/FLAIR-hyperintense regions before proceeding to bulk resection to prevent error due to brain shift. To account for potential navigation error, MRSI data was sampled from interpolated metabolite volumes using an 8 mm^3 region-of-interest centered on the recorded location of tissue extraction. Tissue samples were immunostained for SOX2, a tumor-specific marker, and the proportion of SOX2-positive cells was quantified using an adaptive, automated digital pathology image analysis tool. Quantitative tumor segmentation was used to evaluate extent-of-tumor resection (EOR) on postoperative MRI.

RESULTS: One-hundred percent of tissue samples from regions with MRSI abnormalities contained SOX2-positive cells (range: 3 – 96% of total cells). SOX2-positive cells were also found in tissue devoid of T2/FLAIR abnormality. Cho/NAA, Cho/Cr, and tCho values showed strong, statistically significant correlation with the percentage of SOX2-positive cells (Pearson correlation of 0.70, 0.66, and 0.60, respectively, $p < 0.05$). Intraoperative tumor fluorescence was confirmed *ex vivo*, and showed less pronounced, yet statistically significant correlations with Cho/NAA and tCho values (0.365 and 0.404, $p<0.05$). Median EOR in MRSI/5-ALA cases was found to be 97.5% whereas that found in a separate Phase II clinical trial utilizing 5-ALA only was found to be 94.2%.

CONCLUSION: The trends that MRSI metabolic abnormalities exhibit with histopathology and quantitative intraoperative fluorescence support the use of MRSI for identifying regions of tumor infiltration outside of T1CE. This is the first time that 5-ALA-induced tumor fluorescence has been shown to correlate with MRSI-derived metabolic markers in GBM. The combination of MRSI-neuronavigation with 5-ALA FGS in this trial results in more complete resections and may potentially prolong progression-free survival and overall survival in GBM.

[1] Stummer W, et al. (2006) ***Lancet Oncology*****, *7*(5), 392-401**

[2] Lin A, et al. (1999) ***JNO*****, *45*(1), 69-81**

[3] Schlemmer HP, et al. (2001) ***AJNR*****, *22*(7), 1316-24**

AUTHORS (LAST NAME, FIRST NAME): Cordova, James S.[2]; Hadjipanayis, Constantinos G.[3, 1]; Liang, Zhongxing[2, 1]; Cooper, Lee A.[5, 6]; Kairdolf, Brad A.[6]; Neill, Stewart G.[4]; Appin, Christina L.[4]; Olson, Jeffrey J.[3, 1]; Holder, Chad A.[2]; Shim, Hyunsuk[2, 1]

INSTITUTIONS (ALL):

1. Winship Cancer Institute, Atlanta, GA, United States.
2. Radiology, Emory University, Atlanta, GA, United States.
3. Neurosurgery, Emory University, Atlanta, GA, United States.
4. Pathology, Emory University, Atlanta, GA, United States.
5. Biomedical Informatics, Emory University, Atlanta, GA, United States.
6. Biomedical Engineering, Georgia Institute of Technology, Atlanta, GA, United States.

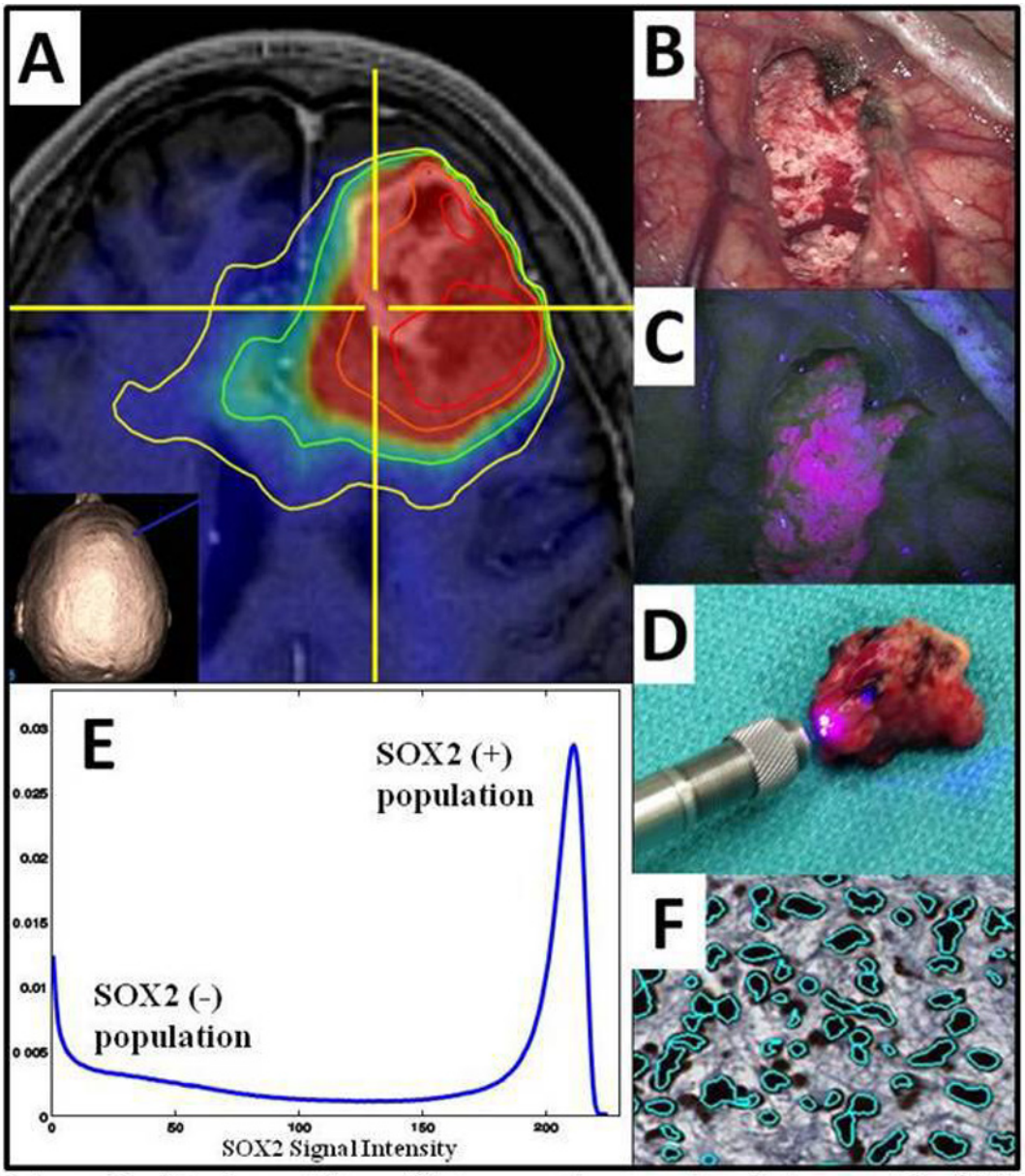

Schematic of study workflow. A) Intraoperative targeting of abnormal Cho/NAA region. Red, orange, green, and yellow contours demarcate 10X, 5X, 2X, and 1.5X normal Cho/NAA values. **B & C)** Resection cavity under white and 400 nm blue light, respectively. **D)** *Ex vivo* measurement of fluorescence. **E & F)** Bimodal distribution of SOX2 staining cells and nuclear segmentation result.

CONTROL ID: 2242859

TITLE: A Machine-Learning Approach for Automated Classification of Spectral Quality and Metabolic Abnormality in High-Resolution, 3D MR Spectroscopic Imaging of Gliomas

PRESENTER: James Cordova

ABSTRACT BODY:

Abstract Body: PURPOSE: Magnetic resonance spectroscopy imaging (MRSI) has emerged as a robust molecular imaging modality capable of assessing therapeutic response in glioma by localizing metabolically-active tumor without exogenous tracers [1]. Whole-brain, 3D volumes for visualization can be constructed with each voxel representing certain spectral components, including the signals from metabolites like choline (Cho), creatine (Cr), and N-acetylaspartate (NAA). However, accuracy of these metabolite volumes are dependent on the quality of acquired spectra with poor quality leading to erroneous volumetric results [2]. Therefore we have developed an objective approach for determining spectral quality (SQ) based on quantitative curve-fitting metrics using machine-learning techniques ultimately resulting in an accurate, data-driven method for evaluating SQ in MRSI.

METHODS/MATERIALS: MRSI was performed on glioma patients using a 3D echo-planar, parallel imaging sequence on a 3T Siemens scanner with a 32-channel head coil array. Whole-brain, volumetric maps exhibit 4.4 mm x 4.4 mm x 5.7 mm nominal voxel size. A spectrosopic analysis tool was used to visually review and label each spectrum as having adequate (A) or inadequate (I) SQ. MRSI curve-fitting parameters describing 115 characteristics from each spectrum were used as features to train random forest classifiers to determine SQ in 6243 voxels from 7 patients. Classifiers were trained on the following scenarios: 1) A vs I in tumor & normal voxels; 2) A vs I in tumor voxels only; and 3) A vs I in normal voxels only. Strict cross-validation was performed to evaluate generalizability, training each classifier on six patients and evaluating on the seventh in a rotating, leave-one-out manner. Classifiers were also trained to discriminate between tumor and normal tissue in 1) voxels with adequate SQ and 2) voxels with inadequate SQ. Classifier performance was evaluated using ROC analysis to determine area-under-the-curve (AUC), and feature salience was evaluated by summing the split criterion for each variable over all trees in each forest of the classifier.

RESULTS: AUC values from classification of SQ ranged from 0.92 to 0.89. The most salient features for SQ included the Cramer-Rao bounds for Cho frequency and area as well as the Lorentzian and Guassian components of the NAA peak. The AUC for classifying tumor versus normal in A voxels was 0.76 and in I voxels was 0.48. The most salient features for this classification included Cho/NAA, Cho/Cr, and NAA/Cr ratios: three values used for identification of tumor tissue clinically [1].

CONCLUSIONS: The high AUC values for SQ classification suggest that machine-learning approaches are able to determine SQ with a very high degree of accuracy. More advanced methods are needed to improve discrimination between tumor and normal, particularly where SQ is low. However, the > 0.70 AUC observed for adequate voxels supports the use of curve-fit metrics as features for MRSI tumor classification. Histological evidence will be essential for determining tumor versus normal ground-truth in this case.

[1] Lin A, et al. *JNO* 1999;45(1):69-81.

[2] Posse S, et al. JMRI 2013;37:1301-25

AUTHORS (LAST NAME, FIRST NAME): Cordova, James S.[3]; Shu, Hui-Kuo G.[1, 2]; Shim, Hyunsuk[3, 2]; Cooper, Lee A.[4, 5]

INSTITUTIONS (ALL):

1. Radiation Oncology, Emory University, Atlanta, GA, United States.
2. Winship Cancer Institute, Atlanta, GA, United States.
3. Radiology, Emory University, Atlanta, GA, United States.
4. Biomedical Informatics, Emory University, Atlanta, GA, United States.
5. Biomedical Engineering, Georgia Institute of Technology, Atlanta, GA, United States.

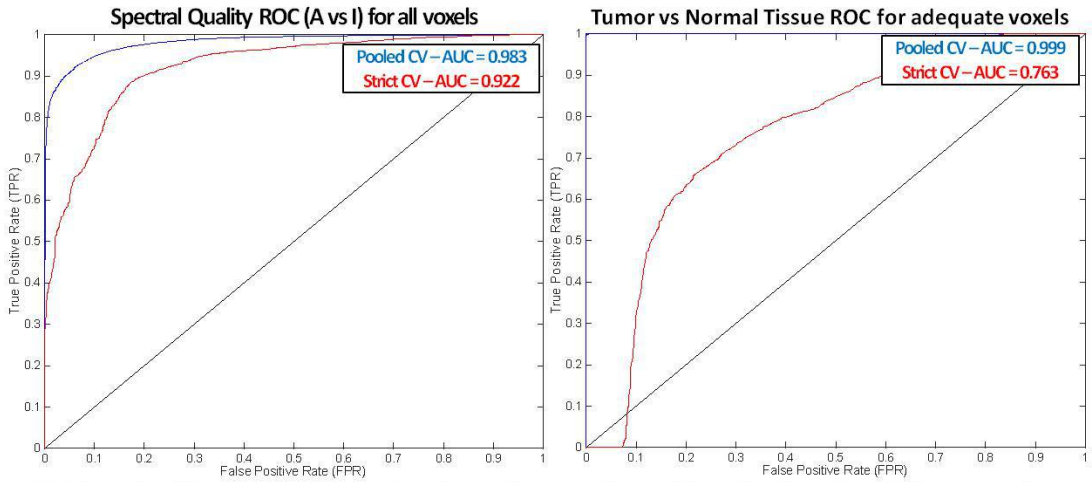

ROC Analysis of Classifiers for Spectral Quality and Tumor vs Normal Tissue Discrimination. AUC measures for two cross-validation (CV) methods are shown: voxels are pooled and sampled randomly for 10-fold CV (Pooled CV) and voxels from 6 patients are pooled to test against the seventh patient in a rotating, leave-one-out manner (Strict CV). High AUC for spectral quality ROC (left) means high accuracy for differentiating voxels with adequate (A) and inadequate (I) spectra. Moderate AUC for Tumor vs Normal ROC (right) suggests use of curve-fit measures as potential features for automated identification of metabolic abnormalities.

CONTROL ID: 2230110

TITLE: Integrating Histology with MR Spectroscopic Imaging Using Digital Whole-Slide Image Analysis

PRESENTER: James Cordova

ABSTRACT BODY:

Abstract Body: PURPOSE: MR spectroscopy (MRS) is a promising technique for detecting brain regions containing infiltrating glial tumor cells **[1]**. However, validation of MRS ultimately requires the correlation of *in vivo* imaging measurements with histology to determine the power with which MRS measurements can predict extent of tumor infiltration **[2]**. In this investigation we developed a histology analysis pipeline for quantifying the extent of tumor infiltration in excised tissues for validation of spatially coregistered, quantitative MRS maps. This pipeline consists of three components: 1. Segmentation 2. Feature Extraction 3. Classification.

METHODS/MATERIALS: In this study, tissues are obtained from glioblastoma (GBM) surgical specimens using MR neuronavigation. Tissues are fixed, embedded and cut to 5 microns, stained with SOX2 antibody to specifically identify neoplastic cell nuclei, and counterstained with hematoxylin (HXN) to identify normal nuclei. Each stained tissue specimen is scanned into whole-slide images at 40X magnification. Automatic segmentation to delineate nuclear boundaries is performed by first digitally deconvolving HXN (all nuclei) and SOX2 (neoplastic nuclei) signals into separate image channels. Randomly sampled $1mm^2$ fields in each slide are then initialized and locally adapted using prior knowledge constraints to accommodate local color variations without overfitting. A graph-cuts approach is used to identify and split any closely clumped nuclei into individual objects. Ultimately, robust statistical models of HXN and SOX2 intensities are generated. Feature extraction is then performed on segmented nuclei to quantify the max, min, and average SOX2 intensity within each cell. These features are used to classify each cell into SOX2-positive or negative populations. The absolute number, percentage, and percent area of SOX2-positive cells is then calculated for validation of MRS data.

RESULTS: This pipeline was applied to a set of 85 slides representing 65 tissue samples from 11 patients. A total of 6.8 million cells were analyzed to give a well-separated, biomodal distribution with respect to SOX2 intensity. Fourteen values for SOX2 intensity thresholds were evaluated exhibiting only 15% change in the percent tumor-MRSI metabolite value correlation coefficient (Choline/NAA) from highest to lowest.

CONCLUSIONS: This algorithm is currently being integrated into The Cancer Digital Slide Archive (cancer.digitalslidearchive.net), a web-based portal hosting > 22,000 whole-slide images of cancer tissues. This system enables users to browse and interact with nuclear segmentation and classification results from billions of cells rendered automatically from an image analysis database. This type of system is essential to the quantitative histological validation of MRSI and other advanced imaging modalities.

[1] Lin A, et al. Efficacy of proton magnetic resonance spectroscopy in clinical decision making for patients with suspected malignant brain tumors. *JNO*. 1999;45(1):69-81.

[2] McKight A, et al. Histopathological validation of 3D magnetic resonance spectroscopy index as predictor of tumor presence. *JNS*. 2002; 97(4), 794-802

AUTHORS (LAST NAME, FIRST NAME): Cordova, James S.[3]; Nalisnik, Michael[6]; Liang, Zhongxing[3, 2]; Brat, Dan[1, 2]; Hadjipanayis, Constantinos G.[4, 2]; Olson, Jeffrey J.[4, 2]; Shu, Hui-Kuo G.[5, 2]; Holder, Chad A.[3]; Shim, Hyunsuk[3, 2]; Cooper, Lee A.[6, 7]

INSTITUTIONS (ALL):

1. Pathology, Emory University, Atlanta, GA, United States.
2. Winship Cancer Institute, Atlanta, GA, United States.
3. Radiology, Emory University, Atlanta, GA, United States.
4. Neurosurgery, Emory University, Atlanta, GA, United States.
5. Radiation Oncology, Emory University, Atlanta, GA, United States.
6. Biomedical Informatics, Emory University, Atlanta, GA, United States.

7. Biomedical Engineering, Georgia Institute of Technology, Atlanta, GA, United States.

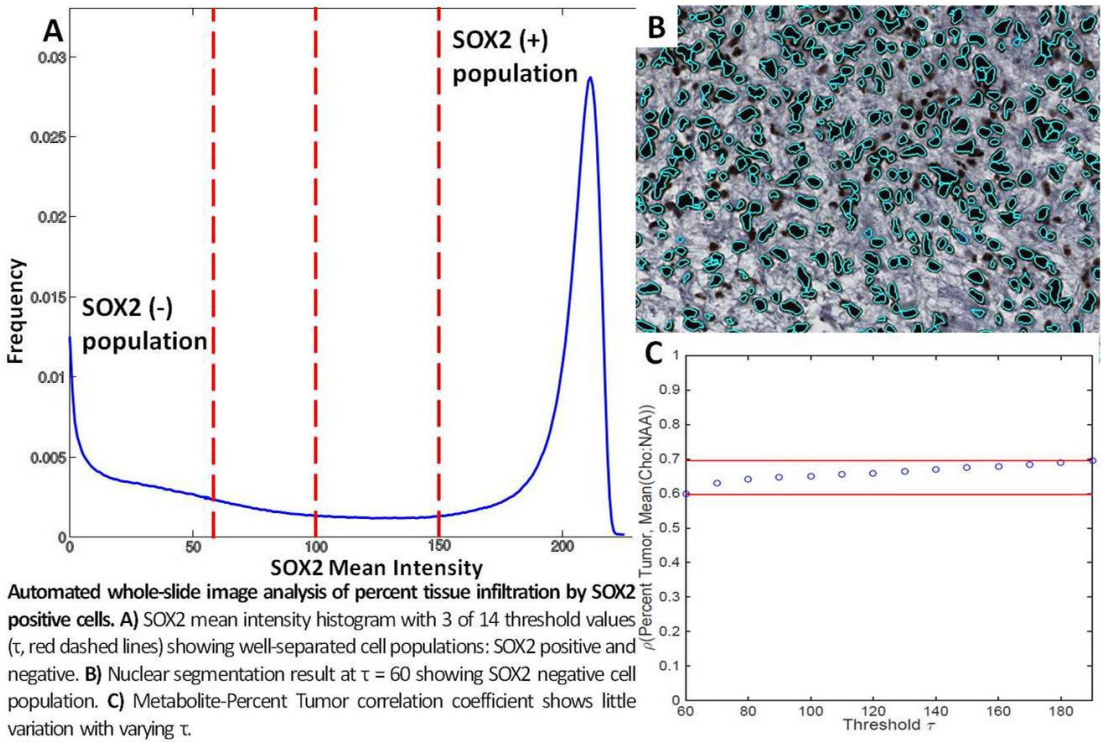

Automated whole-slide image analysis of percent tissue infiltration by SOX2 positive cells. A) SOX2 mean intensity histogram with 3 of 14 threshold values (τ, red dashed lines) showing well-separated cell populations: SOX2 positive and negative. **B)** Nuclear segmentation result at τ = 60 showing SOX2 negative cell population. **C)** Metabolite-Percent Tumor correlation coefficient shows little variation with varying τ.

CONTROL ID: 2230096

TITLE: Fluorescence-guided resection of newly-diagnosed glioblastoma: A tumor morphology and survival benefits analysis of Phase II clinical trial data

PRESENTER: James Cordova

ABSTRACT BODY:

Abstract Body: Introduction: The standard-of-care for glioblastoma (GBM) is maximum safe tumor resection followed by chemoradiation; however, the survival benefit conferred by surgery remains under debate. Standard resection utilizing contrast-enhanced T1-weighted (CE-T1W) MR images for neuronavigation results in approximately 80% of patients having local recurrences (<2 cm from the resection cavity), and a 5-year survival rate of <5% **[1]**. Fluorescence-guided surgery (FGS) using 5-aminolevulinic acid (5-ALA) has been shown to improve the extent-of-resection (EOR) beyond the CE-T1W margins, and help prevent surgical injury to non-infiltrated brain **[2]**. Oral administration of 5-ALA leads to the selective accumulation of a fluorescent metabolite in malignant tumor cells, allowing the neurosurgeon to see the fluorescent tumor margins intraoperatively. The current investigation expands upon the previous efficacy studies by incorporating validated morphological tumor analyses.

Methods: A Phase II clinical trial is currently underway evaluating the use of 5-ALA FGS for newly-diagnosed GBM resection. Patients are administered 5-ALA orally 3-5 hours before FGS. Pre- and post-operative tumors are delineated with a previously described semi-automated segmentation method to evaluate EOR, residual tumor volume (RTV), and morphological tumor features, including surface area and component volume [3]. Patients are then followed to determine progression-free survival (PFS) and overall survival (OS) benefits using univariate analysis.

Results: Median EOR and RTV in 31 newly-diagnosed GBMs were found to be 94.3% (interquartile range 14.47%) and 0.82 cm^3 (interquartile range 7.45 cm^3), respectively. Preoperative tumor surface area to volume ratio showed a statistically significant negative correlation with RTV (correlation coefficient of -0.419 with $p = 0.02$), while preoperative necrosis volume to total volume ratio exhibited a positive, yet non-significant, correlation with EOR (correlation coefficient 0.302 with $p = 0.10$). The proportion of patients with PFS at six months was higher (41.9%) than historical non-FGS controls (28.3%) **[2]**. Age, preoperative functionality status (KPS), and PTEN gene deletion were found to be significant predictors of OS, while age and MGMT gene promoter methylation status were found to be significant predictors of PFS.

Conclusions: This investigation indicates that 5-ALA FGS is more effective than conventional neuronavigation in decreasing RTV and increasing EOR for patients with GBM. The current work not only validates previous efficacy studies, but also supports the need to establish multi-center clinical trials for a larger-scale study of 5-ALA to evaluate survival outcomes more definitively.

[1] Sanai N, et al. Neurosurgery 2008; 62,753-64

[2] Stummer W, et al. Lancet Oncology 2006; 7(5):392-401

[3] Cordova, J S, et al. Transl Oncol 2014; 7(1):40-7

AUTHORS (LAST NAME, FIRST NAME): Cordova, James S.[2]; Holder, Chad A.[2]; Olson, Jeffrey J.[3, 1]; Schreibmann, Eduard[4]; Guo, Ying[5]; Shu, Hui-Kuo G.[4, 1]; Shim, Hyunsuk[2, 1]; Hadjipanayis, Constantinos G.[3, 1]

INSTITUTIONS (ALL):

1. Winship Cancer Institute, Atlanta, GA, United States.
2. Radiology, Emory University, Atlanta, GA, United States.
3. Neurosurgery, Emory University, Atlanta, GA, United States.
4. Radiation Oncology, Emory University, Atlanta, GA, United States.
5. Biostatistics and Bioinformatics, Emory University, Atlanta, GA, United States.

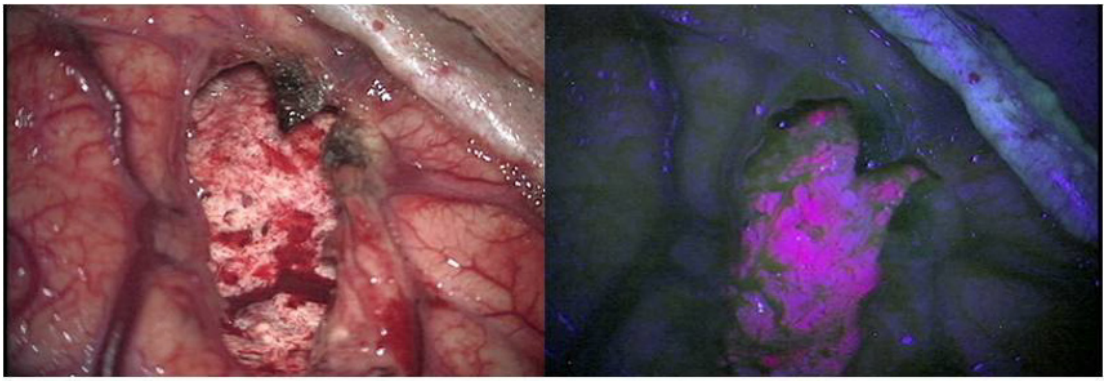

Tumor infiltrated brain tissue visualized intraoperatively using 5-ALA fluorescence. Left) Resection cavity visualized under white light. Right) Resection cavity visualized under 400 nm blue light shows clear fluorescence indicating infiltrated white matter.

CONTROL ID: 2229020

TITLE: ^{18}F-labeled anti-CD20 cys-diabody for same day immuno-PET of B-cells malignancies in transgenic mice

PRESENTER: Kirstin Zettlitz

ABSTRACT BODY:

Abstract Body: ^{18}F-FDG is the current standard for clinical PET for many malignancies; however, some lesions show low avidity for FDG. The majority of B-cell malignancies express CD20, making it a valuable target both for antibody-based therapy and imaging. Immuno-PET could be an efficacious diagnostic tool for initial diagnosis, therapy management and follow-up.

We previously developed novel PET tracers based on engineered antibody fragments of the humanized anti-CD20 mAb GA101 (obunituzumab). The smallest bivalent fragment, the cys-diabody (50 kDa) with a peak uptake at 1-2 h p.i. and a biological half-life of 3-5 h, is compatible with short-lived positron emitters such as ^{18}F ($t_{1/2}$ 110 min), allowing high-contrast, same-day imaging.

The prosthetic group *N*-succinimidyl-4-[^{18}F]fluorobenzoate ([^{18}F]SFB) was used to conjugate [^{18}F] to the anti-CD20 cys-diabody with highly reproducible labeling efficiencies of 35.5 ± 4.8 % (n=6). [^{18}F]FB-GA cDb had a mean specific activity of 429 ± 181 MBq/mg and a radiochemical purity of 97.4 ± 2.8 %. The immunoreactivity of [^{18}F]FB-GA cDb was 60.9 ± 5.3 % (n≥4) as determined by cellular association with excess CD20 expressing A20 cells (mouse B cell lymphoma transfected with human CD20).

[^{18}F]FB-GA cDb was used to image transgenic mice expressing human CD20 on B cells (huCD20TM) and a disseminated, syngeneic model of B cell lymphoma based on the A20 cell line that forms liver metastases upon i.v. implantation. Mice were imaged with [^{18}F]FDG (after 1 hour unconscious uptake) and the following day received immunoPET/CT scans (dynamic 0-120 min and static 4 h) post injection of [^{18}F]FB-GA cDb (20 µg, 4.8-5.5 MBq). In huCD20TM dynamic scans showed rapid tracer localization to B cell containing organs and clearance of [^{18}F]FB-GA cDb through the kidneys, as expected. Peak uptake in the kidneys was seen around 1 h p.i. and decreased quickly while uptake in target organs was retained resulting in high contrast images at 4 h p.i.. Ex vivo biodistribution confirmed the spleen as the organ with the highest uptake (22.5 ± 10.2 %ID/g) and the average uptake in the liver was 1.7 ± 0.9 %ID/g. In tumor bearing mice both [^{18}F]FDG and [^{18}F]FB-GA cDb showed high uptake in the liver. However, while [^{18}F]FDG accumulates in tissues with high metabolic rates nonspecifically (brain, heart, kidney and tumor cells), [^{18}F]FB-GA cDb showed only marginal background and specific uptake in all CD20 expressing tissues (liver metastases, spleen, lymph nodes). Ex vivo biodistribution confirmed higher uptake of [^{18}F]FB-GA cDb in the liver (4.1 ± 1.5 %ID/g) while uptake in the spleen decreased (8.4 ± 3.1 %ID/g) due to the antigen sink effect.

In conclusion, the novel immunoPET tracer [^{18}F]FB-GA cDb specifically targets human CD20 expressing metastases in the context of normal tissue expression of human CD20 and enables same-day imaging. In contrast to FDG it could provide not only information about extent of disease but also about presence and localization of therapeutic target, and response to therapy. Because [^{18}F]FB-GA cDb is based on a humanized mAb and [^{18}F] is widely available it has great potential for translation into the clinic.

AUTHORS (LAST NAME, FIRST NAME): Zettlitz, Kirstin A.[2]; Yamada, Reiko E.[1]; Tavaré, Richard[2]; Salazar, Felix B.[2]; Collins, Jeffrey[2]; van Dam, R. Michael[2]; Timmerman, John M.[1]; Wu, Anna M.[2]

INSTITUTIONS (ALL):

1. Department of Medicine, University of California, Los Angeles, Los Angeles, CA, United States.
2. Department of Molecular and Medical Pharmacology, University of California, Los Angeles, Los Angeles, CA, United States.

(No Image Selected)

CONTROL ID: 2229034

TITLE: TSPO PET to Visualize Patient-Derived Glioma

PRESENTER: James Harty

ABSTRACT BODY:

Abstract Body: Precision imaging diagnostics remain a major clinically unmet need in glioma. Positron emission tomography (PET) imaging with radiopharmaceuticals represents a unique opportunity for early detection, diagnosis and grading of gliomas. Despite this, PET is not routinely used for evaluation of glioma due to lack of a good radiotracer. Magnetic resonance imaging (MRI), the current standard of care, has significant limitations in this setting, including insensitivity to glioma's metabolic activity and microscopic infiltration of tumor cells into normal brain, a leading cause of post treatment recurrence.

Elevated levels of translocator protein (TSPO) are frequently observed in human cancers and tend to correlate with aggressivity in certain clinical settings; we evaluated TSPO immunohistochemistry (IHC) in 17 low-grade and 37 high-grade human gliomas in a tissue microarray developed from patients treated at our institution. In low-grade glioma, TSPO levels were moderately elevated in greater than half the tissue specimens; while in high-grade gliomas, TSPO levels were more uniformly elevated to greater extents, suggesting TSPO PET could serve as an indicator of tumor grade in this setting. To simulate clinical use of TSPO PET within the context of high-grade human glioma, microPET imaging studies featuring a second generation TSPO PET ligand, [^{18}F]PBR06, were carried out in rat primary orthotopic human xenograft models derived from WHO grade III and IV gliomas. In agreement with TSPO immunoreactivity, PET imaging demonstrated significant and selective accumulation of [^{18}F]PBR06 in the engrafted tumor, with ≥ 3:1 tumor-to-normal brain ratios, resulting in superior visualization compared to [^{18}F]FDG PET. Interestingly, infiltrative growth of gliomas into white matter tracks, which was undetectable by MRI, appeared to be observable with TSPO PET, suggesting that TSPO PET could enable improved detection of tumor extent and assessment of white matter infiltration. This finding could be of particular clinical importance as defining tumor cell margins more effectively could significantly improve surgical and radiation therapy planning to treat the entire tumor to prevent recurrence. This study lays the framework for evaluating brain tumors clinically with TSPO PET ligands.

AUTHORS (LAST NAME, FIRST NAME): Harty, James[2]; Buck, Jason R.[1]; McKinley, Eliot[5]; Fu, Allie[5]; Abel, Ty[5]; Thompson, Reid[5]; Cooper, Michael[5]; Watchmaker, Jennifer M.[4]; Manning, H. Charles[3]

INSTITUTIONS (ALL):

1. VUIIS, Nashville, TN, United States.
2. Radiology and Radiological Sciences, Vanderbilt University, Nashville, TN, United States.
3. Radiology and VUIIS, Vanderbilt University, Nashville, TN, United States.
4. Vanderbilt University Institute for Imaging Science, Vanderbilt University , Nashville, TN, United States.
5. Vanderbilt University, Nashville, TN, United States.

(No Image Selected)

CONTROL ID: 2229070

TITLE: Co-polarization of HP001 and pyruvic acid for hyperpolarized 13C studies

PRESENTER: Albert Chen

ABSTRACT BODY:

Abstract Body: Introduction: While most hyperpolarized ^{13}C MR studies using the DNP-dissolution method have focused on metabolic substrates to investigate cellular metabolism[1], using metabolically inactive and primarily intra-vascular molecules to study perfusion have also been demonstrated[2-3]. The feasibility of simultaneously probing perfusion and metabolism has been shown by co-polarizing [1-^{13}C]pyruvic acid and ^{13}C urea[3]. However, the preparation of combined pyruvic acid and urea samples require freezing the two components separately in layers, since urea is not soluble in the neat pyruvic acid. The frozen-layer method may not be practical if the instrument/sample-cup setup does not allow the sample to be kept frozen prior to sample insertion. HP001 (bis-1,1-(hydroxymethyl)-[1-^{13}C]cyclopropane-d_8) is a neat liquid and has been shown to be suitable for hyperpolarized ^{13}C angiographic and perfusion studies *in vivo*[2-3]. The feasibility of using a mixture of [1-^{13}C]pyruvic acid and HP001 for hyperpolarized ^{13}C studies was investigated.

Methods: All studies were performed using a 3T GE scanner and a SPINLab polarizer (GE). Neat [1-^{13}C] pyruvic acid and neat HPOO1 was each doped with 15mM of OX63 radical (Oxford Instruments) and 1mM Gd chelate (Bracco International). 30µl of the pyruvic acid mixture and 15µl of the HP001 mixture were pipetted into the sample vial at room temperature. The sample was polarized at a 3.35 T and 0.8 K. A H_2O/EDTA solution was used as the dissolution media and the sample was neutralized with a NaOH/TRIS buffer post dissolution. ^{13}C spectra were acquired from a 3 ml (80 mM pyruvate + 28 mM HP001) aliquot of the hyperpolarized media (n = 2) using a pulse-acquire pulse sequence just after dissolution (~15-20s sample transfer) and at thermal equilibrium.

Results and discussion: Hyperpolarized spectra of [1-^{13}C]pyruvate and HP001 in solution from a co-polarized [1-^{13}C]pyruvic acid + HP001 sample are shown in Fig. 1. [1-^{13}C]pyruvate resonance had a much larger initial signal than HP001 due to its higher concentration and higher polarization, but it decayed faster due to its shorter T_1 (65s vs. 90s). The polarizations in solution from two samples (@ ~15-20s post dissolution) were 26.7 and 21.1% for pyruvate, and 18.7 and 14.5% for HP001. The polarizations for [1-^{13}C]pyruvate from the co-polarized samples were similar but a bit lower than polarizations obtained from samples of pyruvic acid alone using the same protocol (~30%). The polarizations for HP001 were similar to reported values[2-3]. The unknown resonance observed at 7.3 ppm up-field from HP001 may be an impurity in the sample or a product of pyruvic acid–HP001 reaction, and will require further investigation.

Conclusions: Co-polarization of [1-^{13}C]pyruvic acid and HP001 for production of hyperpolarized [1-^{13}C]pyruvate + HP001 in solution was demonstrated in this study and high levels of polarization were achieved. This preparation may be suitable for simultaneous ^{13}C MR imaging of tissue metabolism and perfusion with a single injection.

References: 1. Keshari KR et al. Chem Soc Rev 2014. 2. Svensson J et al. MRM 2003. 3. Von Morze C et al. MRI 2012.

AUTHORS (LAST NAME, FIRST NAME): Chen, Albert P.[1]; Lau, Justin Y.[2]; Cunningham, Charles H.[2, 3]

INSTITUTIONS (ALL):

1. GE Healthcare, Toronto, ON, Canada.
2. Medical Biophysics, University of Toronto, Toronto, ON, Canada.
3. Imaging Research , Sunnybrook Health Sciences Centre, Toronto, ON, Canada.

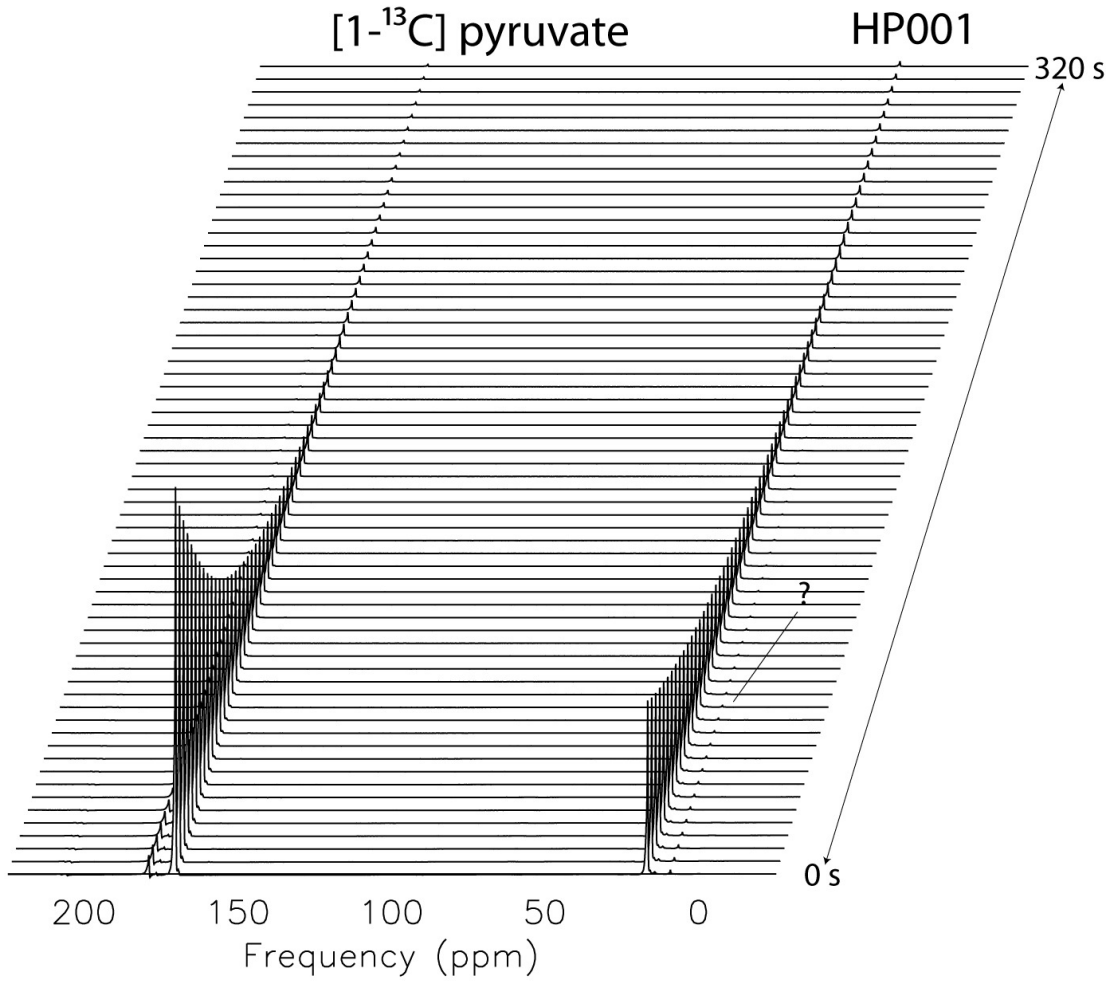

Figure 1. ^{13}C MR spectra acquired from hyperpolarized [1-^{13}C]pyruvate and HP001 in solution (from co-polarized pyruvic acid + HP001). An unknown resonance was observed up-field from HP001.

CONTROL ID: 2229105

TITLE: A Practical Depth-of-Interaction Detector for PET/CT and PET/MR Using Dichotomous-Orthogonal-Symmetry Readout Decoding

PRESENTER: Wai-Hoi Wong

ABSTRACT BODY:

Abstract Body: Clinical PET images suffer from count-deprivation. There are three ways to alleviate this signal-deprivation: (i) increase the depth of the scintillators, (ii) increase the axial field-of-view of the PET, and (iii) decrease the diameter of the detector ring. Combining all three options can enhance the signal-detection sensitivity by an order of magnitude or more. However, each of these options causes significant degradation in image resolution due to the depth-of-interaction (DOI) in the thick PET detectors. The lack of DOI measurement in clinical PET is due to the high cost of implementing DOI readout in the large detector system with 20K-100K detectors. Conventional DOI PET detector using "dual-end readout" requires two 2-dimensional SiPM arrays for each scintillator array. With top and bottom SiPM reading the same scintillator pixel, there is information redundancy. We proposed a dichotomous-orthogonal-symmetric (DOS) dual-end DOI readout method to eliminate this redundancy to significantly reduce SiPM usage, electronic channels, and heat load. Reflecting films are novelistically arranged within a scintillator array (SA) to channel light exiting the SA top only along the X-direction, while light exiting the SA bottom is channeled along the orthogonal Y-direction only. Despite the unidirectional channeling on each end, the top readout can deduce both X and Y information using **two** 1-dimensional SiPM arrays; similarly, the bottom readout also provides X and Y information with two 1-dimensional (1D) SiPM arrays. The difference in signals between the top and bottom readout determines the depth (Z). Thus four 1-D SiPM arrays (using 4N SiPM) are used to decode XYZ to replace two 2D SiPM arrays (with $2N^2$ SiPM); SiPM usage is reduced from $2N^2$ to 4N. Monte Carlo (MC) simulations using GATE were performed to study the XY decoding resolution, energy resolution, and DOI resolution. Coupling the DOS design with a channel-decoding scheme, an array of 15x15 LSO (2.4x2.4x20mm pixels) can be decoded by 18 SiPMs (2 rows of nine 3x3mm SiPM) on top and 18 SiPMs at bottom, thus achieving a 10X reduction in SiPM usage, electronic channels and heat load. For BGO with lower light output than LSO, an 8x8 array (2.4x2.4x20mm pixels) can be achieved with 6.4X reduction. MC simulations show 5-6mm DOI resolution, 0.45-0.96mm XY-decoding blurring, 20-24% energy resolution. This MC study shows the feasibility of the DOS-DOI design. Even comparing to non-DOI detectors, there is a 5X/3X SiPM reduction for LSO/BGO. The proposed detector may yield practical ultrahigh-resolution PET/MR systems with depth-of-interaction with a production cost below current non-DOI PET. For PET/CT, the DOS design can also be modified by replacing the bottom 1D SiPM arrays with two large PMT in a half-staggered configuration, if PMT is more cost effective. This low-cost DOS-DOI detector design when coupling with the low-cost BGO scintillators may enable the realization of affordable long axial-field-of-view (1-m) PET that may perform whole-body cancer staging in 1-2 minutes or image the head-and-torso simultaneously to study wholebody dynamic physiological functions and treatment responses.

AUTHORS (LAST NAME, FIRST NAME): Zhang, Yuxuan[1]; Yan, Han[1]; Baghaei, Hossain[1]; Wong, Wai-Hoi[1]

INSTITUTIONS (ALL):

1. Cancer Systems Imaging, University of Texas MD Anderson Cancer Center, Houston, TX, United States.

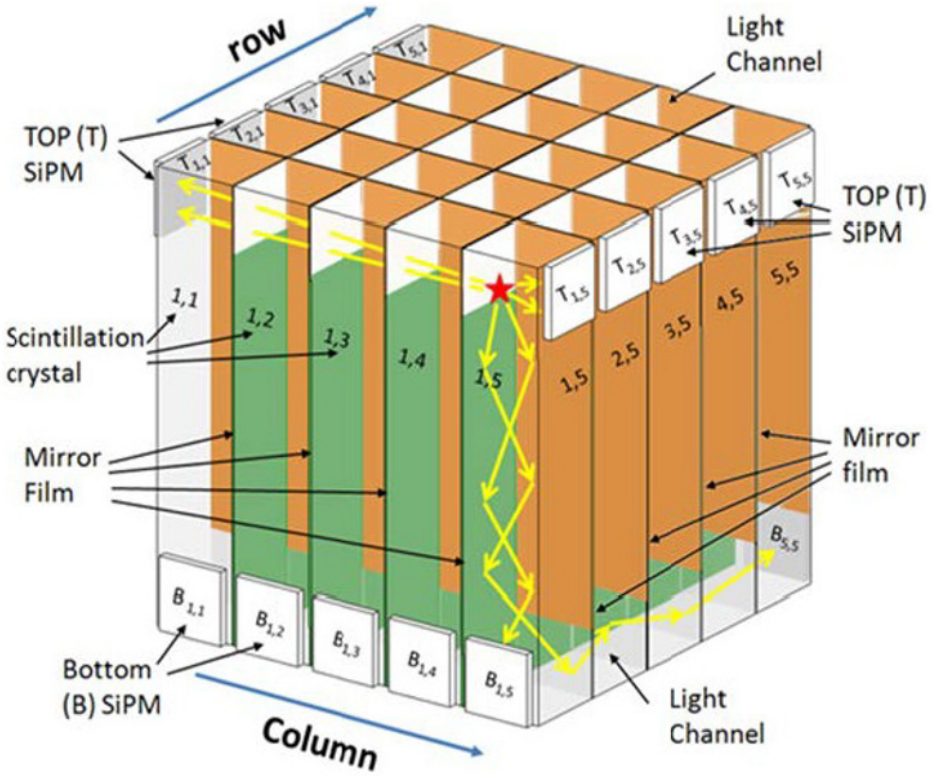

Dichotomous-Orthogonal-Symmetry Depth-of-Interaction PET Detector

CONTROL ID: 2231508

TITLE: Characterization of site-selective single and dual-conjugated antibodies for in vivo imaging and therapeutic applications

PRESENTER: Brian Agnew

ABSTRACT BODY:

Abstract Body: We previously presented a novel site-specific antibody labeling technology that can be applied to essentially any existing antibody with Fc-domain N-linked glycans. We recently demonstrated application of the technology to the production of site-selective radioimmune-PET imaging probes, both single- and dual-conjugated fluorescent forms, compatible with multimodal imaging platforms. We also demonstrated application of the technology to the production of trastuzumab antibody-drug conjugates (ADCs) and fluorescent dual-conjugated species thereof. Here, we describe the full analytical characterization of trastuzumab single- and dual-conjugated antibodies with respect to degree of labeling, site-specificity, and heterogeneity of the conjugated species.

In the enzyme-based conjugation approach, a mutant beta-galactosyltransferase activates heavy chain-specific antibody glycans by transferring an azide-activated N-acetyl-galactosamine sugar (GalNAz) onto terminal N-acetyl-glucosamine (GlcNAc) residues on the Fc domain glycans. The azide tag is then conjugated to essentially any alkyne-bearing molecule in a “lego-like” fashion. The technology ensures preservation of antigen binding activity, is highly reproducible between different antibodies, and allows for easy characterization of the sites of labeling.

In our past work, single and dual-labeled antibody conjugates were characterized using a variety of indirect methods including spectroscopic absorbance, radioactive binding assays, enzymatic cleavage, and gel electrophoresis. However, there still remained the requirement to unequivocally demonstrate site-specific conjugation to the heavy chain Fc domain glycans and to quantitatively determine the number of tags per glycan. Also, in the case of the dual-conjugated species, we wanted to determine the ratio of each respective tag per antibody, as well as characterize the extent of heterogeneity of antibody species in the final purified mixture.

To that effort, a number of single- and dual-conjugated trastuzumab conjugates were prepared using site-specific conjugation. Singly-conjugated constructs were prepared with desferrioxamine (DFO) chelator, a fluorescent dye, a di-tyrosine compound (for site-specific iodine labeling), and the ADC toxin, vc-PAB-MMAE (vedotin). Site-specific dual-conjugated constructs thereof were prepared that include DFO/vc-PAB-MMAE, di-tyrosine/vc-PAB-MMAE, and vc-PAB-MMAE/fluorescent dye species. After conjugation the antibodies were purified and prepared for mass spectrometric analyses.

Our results show that first; the primary activation of the antibody glycans is highly efficient in that all available terminal GlcNAc residues are azide-activated with GalNAz. Secondly, after DIBO modification with the tags of choice, all of the terminal azide residues are fully reacted. In most cases, the major antibody species contain 4 sites of modification (2 per heavy chain). And finally, the mass analyses show, unequivocally, that the modifications are specifically located to the antibody Fc domain while the F(ab)2 fragments remain completely unaltered.

AUTHORS (LAST NAME, FIRST NAME): Aggeler, Robert[1]; Viner, Rosa[3]; Zhang, Terry[3]; Wang, Jessica[4]; Zeglis, Brian M.[2]; Agnew, Brian J.[1]

INSTITUTIONS (ALL):

1. Biosciences Division, Thermo Fisher Scientific, Eugene, OR, United States.
2. Department of Chemistry, Hunter College , New York, NY, United States.
3. Chromatography and Mass Spectrometry Division, Thermo Fisher Scientific, San Jose, CA, United States.
4. Chromatography and Mass Spectrometry Division, Thermo Fisher Scientific, San Jose, CA, United States.

(No Image Selected)

CONTROL ID: 2229176

TITLE: Quantitative Susceptibility Mapping Based Microscopy of Magnetic Resonance Angiography (QSM-mMRA) for *In Vivo* Morphological and Functional Assessment of Cerebromicrovascular

PRESENTER: Meng-Chi Hsieh

ABSTRACT BODY:

Abstract Body: Introduction

While abnormal structure and blood oxygen saturation (SO_2) of cerebromicrovascular is a critical feature of brain disorder, characterizing unusual microvascular change and extraordinary SO_2 might be useful for the diagnosis and prognosis of cerebrovascular diseases (e.g., stroke and glioma). Hence, in this study, we aim to propose a novel technique called QSM-mMRA to morphologically and functionally assess cerebromicrovascular of rats.

Materials and Methods

Control rats: Three healthy rats were performed MRI 3D T2*-weighted images using flow-compensated gradient-echo sequence. Each MR data of rat brain was processed offline to calculate a quantitative susceptibility map (QSM). An average venous oxygen saturation (SvO_2) of cerebromicrovasculars was estimated using the relationship between SvO_2 and susceptibility. Furthermore, the vessel density and size were used to compare with conventional susceptibility-weighted image (SWI).

Stroke rat: A MCAO stroke rat was used to demonstrate the ability of QSM-mMRA to longitudinally monitor the rehabilitation after reperfusion. A pulse oxygen saturation measures (SpO_2) by a standard metric pulse oximeter was also used to compare with our results.

Results

First of all, we optimized the regularized QSM algorithm to obtain a high contrast-to-noise ratio of QSM. Then, the average SvO_2 of healthy rats cerebromicrovascular was estimated by QSM-mMRA (Table 1). Compared to conventional SWI, QSM-mMRA can simultaneously provide structural and quantitative information of cerebrovascular. Finally, the QSM-mMRA was used to longitudinally monitor the rehabilitation of the cerebrovascular of a post-stroke rat (Figure A-D). The SvO_2 estimates by the QSM-mMRA in a post-stroke rat were comparable with the SpO_2 measures by a pulse oximeter standard metric (Figure E & F).

Conclusion

We have described a QSM-based microscopic MRA combined with QSM reconstruction for *in vivo* quantitative visualization of the architecture of small blood vessels. The approach simultaneously offers cerebral anatomy, *in vivo* microvascular structure, and SvO_2 measures, which can be used to evaluate the physiological and functional characteristics of microvascular changes over time. This technique might be further applied to monitor the animal models or clinical patients with cerebrovascular disease.

AUTHORS (LAST NAME, FIRST NAME): Hsieh, Meng-Chi[1, 2]; Su, Chia-Hao[3]; Chen, Jyh-Horng[1, 2]

INSTITUTIONS (ALL):

1. Graduate Institute of Biomedical Electronics and Bioinformatics, National Taiwan University, Taipei, Taiwan.
2. Molecular Imaging Center, National Taiwan University, Taipei, Taiwan.
3. Center for Translational Research in Biomedical Sciences, Kaohsiung Chang Gung Memorial Hospital, Kaohsiung, Taiwan.

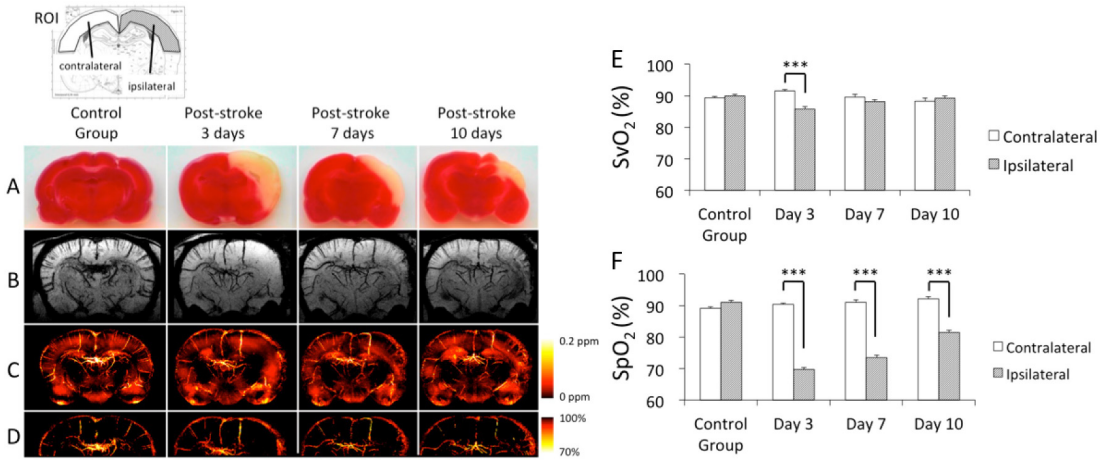
ROI
contralateral
ipsilateral
Control Group
Post-stroke 3 days
Post-stroke 7 days
Post-stroke 10 days
A
B
C
D
0.2 ppm
0 ppm
100%
70%
E
SvO2 (%)
100
90
80
70
60
***
Control Group
Day 3
Day 7
Day 10
Contralateral
Ipsilateral
F
SpO2 (%)
100
90
80
70
60
***
***
***
Control Group
Day 3
Day 7
Day 10
Contralateral
Ipsilateral

CONTROL ID: 2229193

TITLE: The effect of Apolipoprotein E ε4 allele on the morphological and functional neuroimaging in late onset Alzheimer's disease.

PRESENTER: Seiju Kobayashi

ABSTRACT BODY:

Abstract Body: *Objective:* APOE ε4 allele is a risk factor for developing Alzheimer's disease (AD), however its impact on cerebral morphological/functional changes in AD remains controversial. Previous studies had the opposite results each other or failed to confirm any association. It may be because many previous studies failed to consider either the effect of patient age at onset or that of clinical stage. We performed neuroimaging studies using current improved techniques to re-examine the effect of APOE ε4, taking both the age at onset and clinical stage into account.

Methods: *145* Subjects were divided into two groups, the early onset AD (EOAD) 16 subjects and late onset AD (LOAD) 129 subjects. The LOAD group was further divided into 3 subgroups based on MMSE score. We investigated the influence of ε4 allele on structural/functional cerebral changes in each group of LOAD by using cutting-edge analysis software: VSRAD, vbSEE, and 3DSRT.

Results: The APOE ε4 was significantly associated with pronounced atrophy in the medial temporal lobe and relatively preserved atrophy and cerebral blood flow in the cerebral cortices.

APOE ε4 does not seem to exacerbate cerebral cortex in mild stage, while it does so in moderate stage. This study may help resolve the uncertainties of previous studies. The involvement of the Apolipoprotein E ε4 allele in the brain atrophy and rCBF may influence therapy at each clinical stage of AD.

Conclusions: Dividing AD subjects into subgroups based on the severity as well as the age at onset is important for precise outcomes. This study may help resolve the uncertainties of previous studies.

AUTHORS (LAST NAME, FIRST NAME): Kobayashi, Seiju[1]; Tateno, Masaru[6]; Utsumi, Kumiko[2]; Sohma, Hitoshi[3, 4]; Kokai, Yasuo[4]; Morii, Hidetoshi[5]; Kawanishi, Chiaki[1]

INSTITUTIONS (ALL):

1. Neuropsychiatry, Sapporo Medical University, Saporo, Hokkaido, Japan.
2. Department of Psychiatry, Sunagawa City Medical Center, Sunagawa, Japan.
3. Department of Educational Development, Sapporo Medical University Center for Medical Education, Sapporo, Japan.
4. Department of Biomedical Engineering, Sapporo Medical University, School of Medicine, Sapporo, Japan.
5. Psychiatry, Sunagawa Jikeikai Hospital, Sunagawa, Japan.
6. Tokiwa Child Development Center, Tokiwa Hospital, Sapporo, Japan.

(No Image Selected)

CONTROL ID: 2229222

TITLE: Cognitive, Emotional and Motor-related Cortical Regions Involved in Spinocerebellar Ataxia Type 3 using Copula modularity

PRESENTER: Yu-Te Wu

ABSTRACT BODY:

Abstract Body: Background:

Spinocerebellar ataxia type 3(SCA3) is an inherited ataxic disorder, which is characterized as progressive ataxia, parkinsonism, dysarthria and a variable pattern of other neurological deficits. In addition to motor-related deficits, patients with SCA3 exhibit higher-order dysfunctions, including cognitive and affective impairments (Zawacki, Grace et al. 2002, Klinke, Minnerop et al. 2010, Braga-Neto, Pedroso et al. 2011, Jacobi, Bauer et al. 2011). Although growing evidence shows widespread involvements in entire brain of SCA3 (Soong and Liu 1998, Wullner, Reimold et al. 2005, Yamada, Sato et al. 2008), it is unclear where are the corresponding brain areas being affected. Investigations of alterations in structural connectivity in SCA3 may help to clarify the cause of cognitive and affective impairments.

Methods:

In this study, the three-dimensional fractal dimension (3D-FD) method was applied to quantify the changes of cortical complexity in SCA3 patients. We attempt to investigate the supratentorial involvement of SCA3 by measuring significant atrophy in relatively focal regions. Since we observed that joint distributions over the atrophic brain regions are often dependent and the marginal distributions in atrophic brain regions maybe not completely normal distribution, the use of Pearson correlation to calculate the region-to-region connectivities can be problematic. Instead, we used the copula correlation to measure the correlation, which is similar to nonparametric rank-based correlation coefficient estimators, and has the advantage in preventing the bias based on asymmetric distributions. Based on the region-to-region connectivities, we utilized the hierarchical modular analysis to modularize the altered regions of SCA3 and established the Copula modular network. By comparing the structural connectivity pattern between SCA3 and healthy controls, the variation of Copula modular network may allow us to measure the inherently mental state of SCA3 patients.

Results:

We recruited forty-eight genetically confirmed SCA3 patients and 50 gender- and age-matched control persons in this study. Using the 3D-FD method, we found that the cortical involvement was more extensive than involvement of traditional olivopontocerebellar regions and the corticocerebellar system. Moreover, the significant correlation between decreased 3D-FD values and disease duration may indicate atrophy of the cerebellar cortex and cerebral cortex in SCA3 patients. Additionally, the copula modularity network of SCA3 exhibited primary three modules, which were corresponded to cognitive-related regions (See Figs. A, B), parkinsonism-related regions (See Figs. C, D) and emotion-related regions (See Figs.E, F), separately. The results of modular connectivity network may reveal the potential cause of mental decline in SCA3.

AUTHORS (LAST NAME, FIRST NAME): Wang, Tzu-Yun[2]; Jao, Chii-Wen[3]; Wang, Po-Shan[1]; Wu, Yu-Te[1]

INSTITUTIONS (ALL):

1. Institute of Biophotonics, Taipei, ROC, Taiwan.
2. Department of Biomedical Imaging and Radiological Sciences, National Yang-Ming University, Taipei, ROC, Taiwan.
3. Department of Recreation Sports and Health Promotion, Asia-Pacific Institute of Creativity, Tao-Fen, ROC, Taiwan.

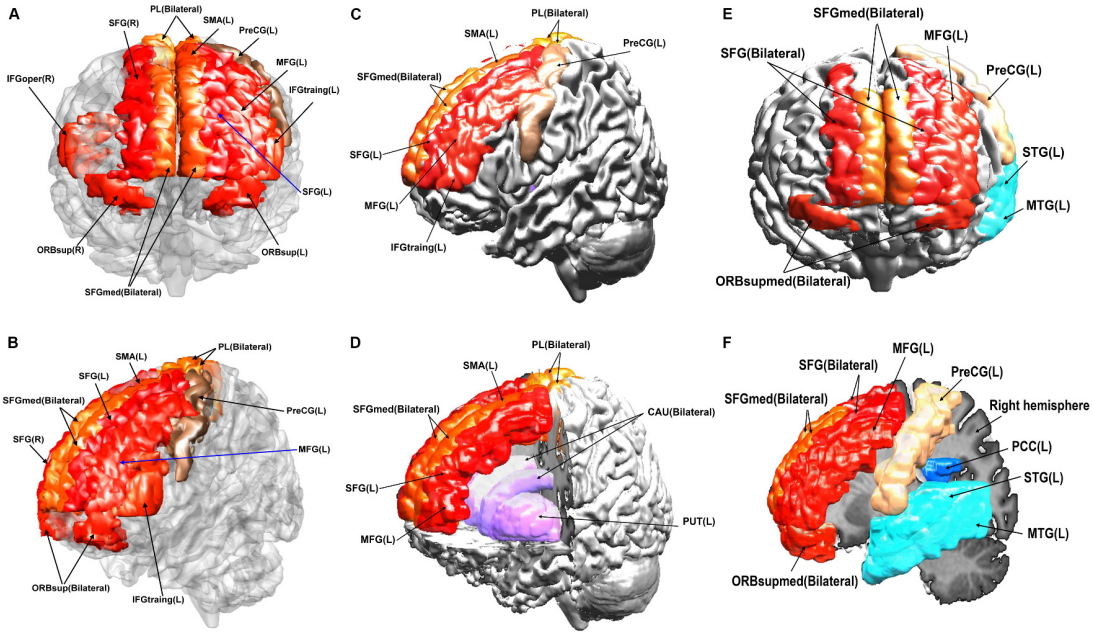
A
PL(Bilateral)
SFG(R)
SMA(L)
PreCG(L)
MFG(L)
IFGoper(R)
IFGtraing(L)
SFG(L)
ORBsup(R)
ORBsup(L)
SFGmed(Bilateral)
C
PL(Bilateral)
SMA(L)
PreCG(L)
SFGmed(Bilateral)
SFG(L)
MFG(L)
IFGtraing(L)
E
SFGmed(Bilateral)
MFG(L)
SFG(Bilateral)
PreCG(L)
STG(L)
MTG(L)
ORBsupmed(Bilateral)
B
PL(Bilateral)
SMA(L)
SFG(L)
SFGmed(Bilateral)
PreCG(L)
SFG(R)
MFG(L)
ORBsup(Bilateral)
IFGtraing(L)
D
PL(Bilateral)
SMA(L)
SFGmed(Bilateral)
CAU(Bilateral)
SFG(L)
PUT(L)
MFG(L)
F
MFG(L)
SFG(Bilateral)
PreCG(L)
SFGmed(Bilateral)
Right hemisphere
PCC(L)
STG(L)
MTG(L)
ORBsupmed(Bilateral)

CONTROL ID: 2229228

TITLE: Multiplexed molecular imaging with targeted SERS nanoparticles for intraoperative guidance of tumor resection

PRESENTER: Yu Wang

ABSTRACT BODY:

Abstract Body: In order to guide the complete resection of tumors, intraoperative imaging techniques are needed to identify residual tumor at the surgical margins. A highly specific means of identifying tumor is to image disease-related biomarkers. However, due to the heterogeneity of biomarker expression in tumors, assessing a panel of relevant biomarkers is advantageous for accurate tumor detection. Surface-enhanced Raman-scattering (SERS) nanoparticles (NPs), a contrast agent with great multiplexing capabilities, have attracted interest in recent years [1]. Although basic experiments to assess the sensitivity [2, 3], targeting ability [4, 5] and multiplexing potential [6] of SERS NPs have been performed, there is a need to demonstrate that multiplexed biomarker imaging is possible with SERS NPs topically applied on fresh tissues under time-limited clinical settings.

Here, we demonstrate that the topical application and quantification of a multiplexed cocktail of biomarker-targeted SERS NPs offers the potential for rapid (15 min) molecular phenotyping of the freshly excised tissues to determine the presence of tumor. A topical-staining procedure as well as a raster-scanned fiber-optic imaging system were developed to comprehensively image fresh tissue specimens. To distinguish biomarker-specific binding from nonspecific binding caused by off-target accumulation and uneven delivery, a ratiometric strategy was employed [3, 5].

Ex vivo studies with tumor xenografts (Persuasive data) and human breast tissues (Fig. 1) were performed to demonstrate the SERS-NP-based molecular imaging technique. For breast tissue imaging, each tissue specimen was stained with an equimolar mixture of HER2-NPs and isotype-NPs (10 min), followed by a quick rinse in PBS (20 s). After that, the stained tissue surface was raster-scanned within 2 min. The entire procedure was performed in less than 15 min, a time frame that is consistent with current intraoperative guidance techniques such as X-ray CT examination of surgical excisions and frozen-section pathology. Figure 1b shows that the HER2 vs. isotype ratio measured from 4 tumor specimens is significantly elevated compared to the ratio from 4 normal specimens, clearly revealing the HER2 expression. Figs. 1d–1g show images of one tissue specimen that contained both tumor and normal regions. Measurements of absolute NP concentrations are misleading due to nonspecific accumulation of the topically applied NPs (Fig. 1e): HER2-NPs accumulate more on normal tissue regions than on tumor regions. However, the ratiometric image (Fig. 1f) accurately quantifies HER2 expression levels in agreement with IHC validation data (Fig. 1g).

In summary, we have demonstrated that the topical application and quantification of receptor-targeted SERS NPs allows for rapid (< 15 min) molecular phenotyping at the surface of freshly resected tissues, and that the unambiguous detection of biomarkers is achievable through the ratiometric quantification of targeted NPs vs. untargeted NPs. These tools have the potential to enable the accurate intraoperative detection of residual tumors at the resection margins.

References (see Persuasive data)

AUTHORS (LAST NAME, FIRST NAME): Wang, Yu[2]; Khan, Altaz[1]; Leigh, Steven Y.[1]; Murray, Melissa[3]; Abeytunge, Sanjeewa[4]; Peterson, Gary[5]; Rajadhyaksha, Milind[6]; Liu, Jonathan T.[2]

INSTITUTIONS (ALL):

1. Biomedical Engineering, Stony Brook University, Seattle, WA, United States.
2. Department of Mechanical Engineering, University of Washington, Seattle, WA, United States.
3. Memorial Sloan Kettering Cancer Center, New York, NY, United States.
4. Memorial Sloan Kettering Cancer Center, New York, NY, United States.
5. Memorial Sloan Kettering Cancer Center, New York, NY, United States.
6. Memorial Sloan Kettering Cancer Center, New York, NY, United States.

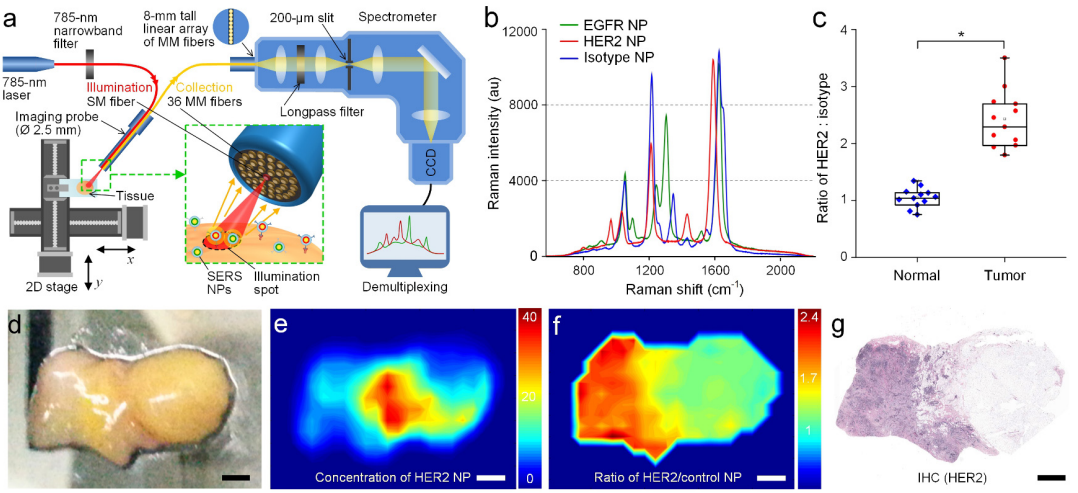

Figure 1. Multiplexed molecular imaging of fresh breast tissues *ex vivo* with targeted SERS nanoparticles. **(a)** Schematic illustration of a customized raster-scanned imaging system to detect bioconjugated NPs topically applied on a tissue surface (zoom-in panel: distal end of fiber bundle for Raman spectral measurements). **(b)** Raman spectra of the three NP contrast agents used in this study. **(c)** Concentration ratio of targeted vs. untargeted NPs topically applied on normal breast tissues and HER2+ tumors (4 tissue samples from two patients). *p<0.001. **(d)** Photograph of a breast tissue sample containing both tumor and normal tissue regions (tissue size: 1×1.8 cm^2). Images showing **(e)** concentration of HER2-NPs (ambiguous due to nonspecific accumulation), **(f)** concentration ratio of HER2-NPs vs. isotype-NPs and **(g)** IHC staining with an anti-HER2 mAb. The scale bars are 2 mm.

CONTROL ID: 2229231

TITLE: Near infrared quantum dot and ^{89}Zr dual-labeled nanoparticles for in vivo Cerenkov imaging

PRESENTER: Yiming Zhao

ABSTRACT BODY:

Abstract Body: Introduction

Cerenkov luminescence (CL) is generated when charged particles (e.g. e^+ or e^-) travel faster than the light in a dielectric medium, and is observed for many medically relevant isotopes. Making use of this faint self-luminescent light CL allows background-free imaging and therefore is sparking increasing interest for biomedical purposes. [1] However, as the emission of CL is most dominant in the UV-blue region, the intensity and penetration depth of CL greatly suffers from scattering and tissue absorption. A possible solution is to use an *in vivo* spectrum converter to down-convert the high energy CL to near infrared (NIR) light. NIR quantum dots (QDs) have a broad spectral overlap with CL and a high quantum yield that make them excellent spectrum converters. Therefore, a biocompatible nanoplatform that could efficiently co-deliver radioisotopes and QDs to the targeted area is of great interest. To realize this concept, we here developed three types of NIR-QD and ^{89}Zr due-labeled nanoparticles (NPs) and evaluated their properties for Cerenkov luminescence imaging (CLI) for lymph node mapping and tumor visualization in a mouse model.

Methods and Results

QD-^{89}Zr micelles (QD-MC-^{89}Zr) consist of a hydrophobic QD core and PEGlyated-lipid coating, in which there are desferrioxamine (DFO) functionalized lipids, which allow radiolabeling of ^{89}Zr through complexion. QD-containing nanoemulsions (QD-NE-^{89}Zr) consist of lipid stabilized medium chain triglycerides with high payloads of QDs dispersed in the oil phase. ^{89}Zr can be transferred into this NP platform using DFO-NCS as a phase transition agent. A third platform is based on an amphiphilic block copolymer coated QD (QD-BP-^{89}Zr). PEG and DFO can be readily conjugated on the hydrophobic polymer backbone. All three QD-containing NPs can be pre-synthesized and then labeled with ^{89}Zr at the last step with over 80% of labeling efficiency. *In vitro* experiments show that either increasing QD concentration or radioactivity will increase the total emission intensity in the NIR range, while an increased QD concentration increase the conversion efficiency of UV-blue to NIR light.

Injecting these QD-^{89}Zr NPs in the footpad of nude mice allows lymph node CLI, epi-fluorescence imaging, and positron emission tomography (PET) imaging. CLI results in significantly better signal to noise ratios than direct fluorescence imaging. After injecting NPs in the periphery of solid tumors, we observed the accumulation of NPs in the sentinel lymph node (SLN), and were able to remove the SLN under the guidance of CLI. Among these NPs, QD-BP-^{89}Zr has the best serum stability and suitable for tumor imaging. After i.v. injecting QD-BP-^{89}Zr, the extravasation of NPs into the tumor could be visualized as soon as 1 h post-injection by CLI. [2]

Conclusion

We have developed three types of QD and ^{89}Zr dual-labeled NPs. The conversion of UV-Blue CL into near infrared light by QDs increases the output signal intensity and tissue penetration depth. We demonstrated the application of the different NP platforms for lymph node CLI and tumor imaging.

1. Thorek *et al*. Nat. Med. 2013, 19, 1345.

2. Zhao *et al*. ACS Nano 2013, 7, 10362.

AUTHORS (LAST NAME, FIRST NAME): Zhao, Yiming[1]; Shaffer, Travis[3]; Perez Medina, Carlos[4, 2]; Das, Sudeep[2, 3]; Mulder, Willem J.[1]; Grimm, Jan[3, 2]

INSTITUTIONS (ALL):

1. Translational and Molecular Imaging Institute, Icahn School of Medicine at Mount Sinai, New York, NY, United States.

2. Molecular Pharmacology and Chemistry Program/Radiology, MSKCC, New York, NY, United States.

3. Radiology, Memorial Sloan Kettering Cancer Center, New York, NY, United States.

4. Radiology, Mount Sinai, New York, NY, United States.

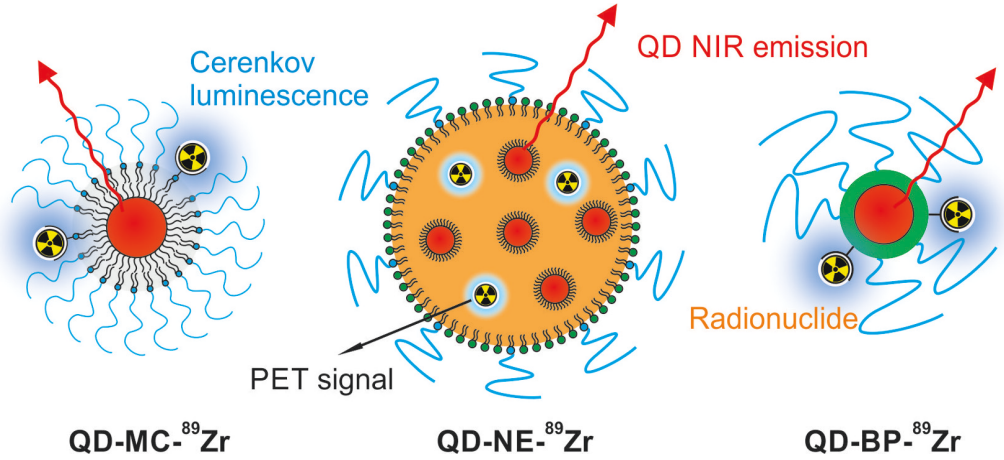
Cerenkov
luminescence
QD NIR emission
Radionuclide
PET signal
QD-MC-^{89}Zr
QD-NE-^{89}Zr
QD-BP-^{89}Zr

CONTROL ID: 2229232

TITLE: A novel ultrahigh resolution imaging mass spectrometry visualizes distribution of sphingomyelin molecular species in the mouse tissue section

PRESENTER: Masayuki Sugimoto

ABSTRACT BODY:

Abstract Body: Background: It is important to obtain the histological information to elucidate the molecular functions of lipids. Matrix assisted laser desorption/ionization (MALDI) imaging mass spectrometry (IMS) is expected as a powerful tool to visualize the distribution of endogenous low molecular metabolites including lipids, which are hard to detect by the immunohistochemistry. Especially, fourier transform-ion cyclotron resonance (FT-ICR)-MS is expected to identify the target molecules specifically since it has an ultrahigher mass resolution compared with conventional time-of-flight MS. Sphingomyelins (SMs) are important sphingolipids which maintain the structure of biological membranes and regulate signal transductions. Because SMs contain sphingoid base and different-length acyl-chains, they consist of multiple molecular species by the length of acyl-chains. However, it is not well known their molecular functions and distributions within tissues. Thus, IMS analysis of each SM molecular species was performed with MALDI-FT-ICR-MS to visualize their distribution in the brain and to quantify their amount within liver sections for understanding of their molecular functions.

Methods: IMS study of SM standards with FT-ICR-MS was performed and evaluated the correlation between their concentrations and their signal intensities. The collision-induced dissociation-fragmentation of SM standards was performed to obtain their structural information. The brain tissues were collected from C57BL/6N mice (5 weeks of age, n=3) and sectioned after frozen. IMS analysis was performed and distribution of each SM molecular species was analyzed after 2,5-dihydroxybenzoic acid (DHB) was sprayed as the matrix compound on the tissue section. Next, C57BL/6N mice fed normal diet or high-fat diet (HFD) (10 weeks of age, n=3 in each) were sacrificed and the liver tissues were collected. The tissues were frozen, and lipids were extracted by modified bligh & dyer methods. Hepatic SM concentrations were measured by liquid chromatography-tandem mass spectrometry (LC/MS/MS). The frozen sections derived from the same liver tissues were splayed DHB and performed IMS analysis.

Results: FT-ICR-MS identified each SM molecular species (shown as sphingoid-base/acyl-chain) and showed a good correlation between concentrations and signal intensities of SM standards. FT-ICR-MS also revealed that SM (d18:1/18:0) was distributed in the neuronal cell-rich gray matter, while SM (d18:1/24:1) was distributed in the white matter or in the region containing the myelin sheath in the brain (Fig. 1). In addition, it was also revealed that HFD increased SM (d18:1/22:0) and decreased SM (d18:1/24:1), while each SM species did not show specific distribution in the liver. These results were correlated with the results obtained using LC/MS/MS. Thus, it was speculated that each SM molecular species might have different functions in each organ.

Conclusions: IMS with FT-ICR-MS reveals that distributions of SMs in the brain and the HFD-induced changes in the liver are different among the lengths of their acyl-chain. Thus, IMS with FT-ICR-MS would be a useful tool for exploration of SMs distributions and functions.

AUTHORS (LAST NAME, FIRST NAME): Sugimoto, Masayuki[2, 3]; Shimizu, Yoichi[1, 2]; Wakabayashi, Masato[3]; Yoshioka, Takeshi[3]; Tanaka, Yukari[4]; Higashino, Kenichi[3]; Numata, Yoshito[3]; Sakai, Shota[5]; Kihara, Akio[6]; Igarashi, Yasuyuki[5]; Kuge, Yuji[1, 2]

INSTITUTIONS (ALL):

1. Central Institute of Isotope Science, Hokkaido University, Sapporo, Hokkaido, Japan.
2. Graduated School of Medicine, Hokkaido University, Sapporo, Japan.
3. Discovery Research Laboratory for Innovative Frontier Medicines, SHIONOGI & CO., LTD., Sapporo, Japan.
4. Research Laboratory for Development, SHIONOGI & CO., LTD., Toyonaka, Japan.
5. Faculty of Advanced Life Science, Hokkaido University, Sapporo, Japan.
6. Faculty of Pharmaceutical Science, Hokkaido University, Sapporo, Japan.

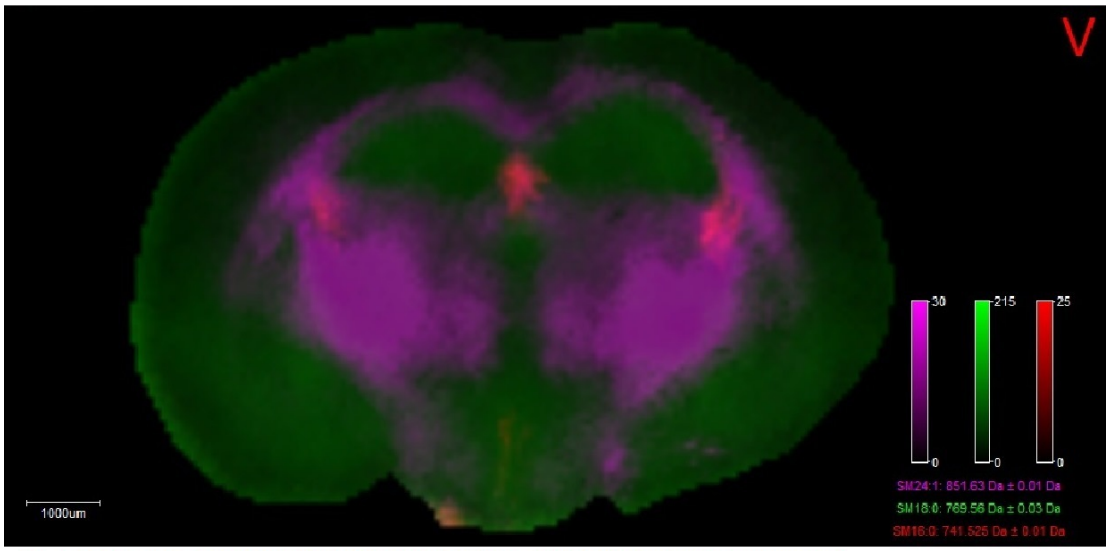

Fig. 1. Distribution of SM (d18:1/16:0), SM (d18:1/18:0) and SM (d18:1/24:1) in the mouse brain.

CONTROL ID: 2229234

TITLE: Amine-terminated Polyethylene Glycol Functionalized Gold Nanostars for X-ray/CT Imaging and Photothermal Therapy In Vivo Animal <script>(function hold() {var videoElement = document.querySelector('#CTPmediaElement1'); if (videoElement == null) return;var position = -1;videoElement.addEventListener('play', function() {if (position > 0) { videoElement.currentTime = position;}position = -1;});document.addEventListener('visibilitychange', function() {if (document.visibilityState === 'hidden' && videoElement.paused) {position = videoElement.currentTime;}}); })(window);</script>

PRESENTER: Shouju Wang

ABSTRACT BODY:

Abstract Body: Computed tomography (CT) is one of the most widely used imaging modalities for tumor diagnosis. However, the lack of intrinsic anti-tumor activity makes iodine unsuitable for developing multifunctional theranostic agents. Therefore new materials are needed to develop next generation of theranostic contrast agents for X-ray/CT guided anti-tumor therapy.

We herein report amine-terminated polyethylene glycol (PEG) functionalized gold nanostars (GNSs) as theranostic probes for X-ray/CT imaging and photothermal therapy (PTT). We found that, compared with methoxy-terminated PEG (mPEG), amine-terminated PEG (PEG-NH_2) can increase the cellular uptake of GNSs and enhance the corresponding photothermal therapeutic effect. In animal models, injection of amine-terminated PEG functionalized GNSs (GNS-PEG-NH_2) resulted in remarkably positive X-ray/CT contrast between tumors and normal tissues. Moreover, the growth of GNS-PEG-NH_2 treated tumors was completely suppressed after laser irradiation.

Bare GNSs were synthesized using a CTAB-free method. mPEG and PEG-NH_2 was introduced on the surface of GNSs by Au-S bonds to obtain GNS-mPEG and GNS-PEG-NH_2, respectively. TEM revealed that both GNS-mPEG and GNS-PEG-NH_2 exhibited protruding sharp branches with an average diameter of ~60 nm. The hydrodynamic sizes of GNS-mPEG and GNS-PEG-NH_2 were 85.3 ± 1.3 nm and 86.5 ± 1.4 nm. Both of them exhibited broad plasmon spectra peaked at ~730 nm. GNS-mPEG showed a slightly negative zeta potential at -12.75 ± 2.84 mV, while the zeta potential of GNS-PEG-NH_2 was 38.25 ± 3.48 mV. For in vitro studies, MCF-7 cells were incubated with nanoparticles for 4 h. It was revealed that both GNS-PEG-NH_2 and GNS-mPEG showed great biocompatibility. The result of inductively coupled plasma mass spectrometry (ICP-MS) indicated that the cellular uptake of GNS-PEG-NH_2 was significantly higher than that of GNS-mPEG (0.38 ± 0.05 ng Au/ng protein vs. 0.04 ± 0.01 ng Au/ng protein, $p < 0.01$). MTT assays showed that after 3 min of irradiation, the viability of cells treated with GNS-mPEG was 57 ± 2.3%, while the viability of GNS-PEG-NH_2 treated cells dropped to 3.2 ± 0.2%. These results indicated that PEG-NH_2 may increase the cellular uptake of GNSs and enhance the corresponding photothermal therapeutic effect. We then tested the X-ray/CT imaging ability and photothermal efficiency of GNS-PEG-NH_2 in vivo. Subcutaneous MCF-7 tumor model was established on nude mice. After intratumoral injection of GNS-PEG-NH_2, both X-ray and CT images showed positive contrast between tumors and normal tissues. After irradiated with laser for 5 min, the temperature of tumors treated with GNS-PEG-NH_2 increased up to 53 ℃. The volume of GNS-PEG-NH_2 treated tumor also significantly shrunk after two weeks. Moreover, the GNS-PEG-NH_2 didn't induce any noticeable side effect to treated mice even 15 days after treatment.

In conclusion, by functionalized GNSs with PEG-NH_2, we successfully increased the cellular uptake and photothermal efficiency of GNSs. The animal studies showed that GNS-PEG-NH_2 could be used as potential theranostic probes for X-ray/CT imaging and PTT treatment. <script>(function hold() {var videoElement = document.querySelector('#CTPmediaElement1');if (videoElement == null) return;var position = -1; videoElement.addEventListener('play', function() {if (position > 0) {videoElement.currentTime = position;}position = -1; });document.addEventListener('visibilitychange', function() {if (document.visibilityState === 'hidden' && videoElement.paused) {position = videoElement.currentTime;}});})(window);</script>

AUTHORS (LAST NAME, FIRST NAME): Wang, Shouju[1]; Tian, Ying[1]; Lu, Guangming[1]

INSTITUTIONS (ALL):

1. Jinling Hospital, Nanjing, China.

(No Image Selected)

CONTROL ID: 2229239

TITLE: *Ex Vivo* Assessment of Perfluorocarbon Emulsion as a Theranostic Agent of ^{19}F MR-guided Focused Ultrasound

PRESENTER: ChangKi Min

ABSTRACT BODY:

Abstract Body: Introduction: Focused ultrasound (FUS) is considered as a potential non-invasive therapy to thermally ablate tumors. It is usually aided by MR thermometry and perfluorocarbon (PFC) emulsions in order to monitor the temperature during treatment and to nucleate cavitation activity[1]. We hypothesized that PFC emulsions can be used not only for increasing thermal dose but also for tracking tumor sites using ^{19}F MRI. We tested the feasibility of using PFC emulsions as theranostic agents of ^{19}F MR-guided FUS and quantitatively analyzed the dynamics of temperature profile to optimize FUS conditions.

Methods: PFC emulsions were prepared by sonicating 30 mg/ml of Poloxamer 188, 20% perfluoro-15-crown-5-ether and ddH_2O[2]. Phantoms were made by previous formulation[3]: 33% v/v of 30% acrylamide, 0.1% v/v TEMED, 0.5% v/v 10% ammonium persulfate solution, 35% v/v egg white and 31.4% v/v ddH_2O were mixed, degassed, and crosslinked. For the phantom with emulsions, 10% v/v ddH_2O was replaced by the same volume of PFC emulsions. Phantoms were exposed to FUS (f = 1MHz) for 20 seconds at the acoustic pressure of 2.58 or 3.44 MPa. Each position in phantoms was exposed twice, and temperature was recorded every second. Before and after FUS exposure, ^{1}H and ^{19}F images were acquired using a 7T MR scanner and a volume coil tunable to ^{1}H and ^{19}F (Bruker). ^{1}H images were acquired using RARE (TR/TE = 2500/35ms, RARE factor = 8, slice thickness = 0.7mm), and ^{19}F images were acquired using FLASH (TR/TE = 100/2.5ms, NA = 50, slice thickness = 2mm). For quantitative analysis of temperature profile, a mathematical model $\Delta T[1-e^{-t/\tau}]+T_0$ was used to fit the data (ΔT = maximum temperature rise, T_0 = initial temperature). Values of ΔT and τ that minimize mean squared error was found to estimate the rate and magnitude of temperature rise.

Results: ^{19}F MRI showed that PFC emulsions were homogeneously distributed throughout the phantom. ^{1}H images showed thermally ablated lesions that coincide with positions sonicated with the pressure of 3.44 MPa. No difference in ^{19}F signal intensity was detected after FUS treatment, indicating that PFC molecules remained in the phantom (Fig.1A). The dynamics of temperature profile is well represented by the proposed model (Fig.1B). Table 1 shows that PFC emulsions generated 1.5 - 2.7 fold increase in magnitude and 2.2 – 4.6 fold increase in rate of temperature rise.

Discussions & Conclusions: We showed the feasibility of using ^{19}F MRI to track PFC emulsions which simultaneously enhance thermal dose. ^{19}F MRI will visualize intratumoral distribution of PFC emulsions and quantify their accumulation in tumors so that emulsion dosage and delivery route can be optimized. Our model successfully captures the temperature profile and quantifies the effect of PFC emulsions. This model can be utilized to precisely control sonication conditions and target temperature depending on types and statuses of tumors. We believe ^{19}F MR-guided FUS will be a powerful theranostics for tumor treatment.

References: 1. Kopechek et al., *Phys Med Biol*, 2014, 59:3465-3481. **2.** Wang et al., *Quant Imaging Med Surg*, 2013, 3(3):132-140. **3.** Zhang et al. *Acad Radiol*, 2011, 18(9):1123-1132.

AUTHORS (LAST NAME, FIRST NAME): Shin, Soo Hyun[1]; Min, ChangKi[1]; Jeon, SoYeon[1]; Park, Eun-Joo[3, 4]; Kim, Daehong[1, 2]

INSTITUTIONS (ALL):

1. Molecular Imaging & Therapy Branch, National Cancer Center, Goyang, Gyeonggi-do, Korea (the Republic of).
2. Department of Radiology, National Cancer Center, Goyang, Gyeonggi-do, Korea (the Republic of).
3. Biomedical Research Institute, Seoul National University Hospital, Seoul, Korea (the Republic of).
4. Department of Radiology, Seoul National University Hospital, Seoul, Korea (the Republic of).

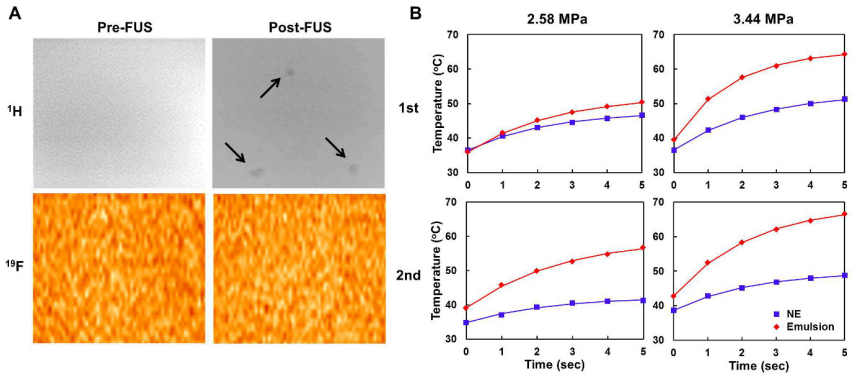

Figure 1. (A) MR images of an emulsion-incorporated phantom. Post-FUS ^{1}H image shows thermally ablated lesions, which coincide with positions sonicated with FUS of 3.44 MPa pressure (black arrows). There are no differences in ^{19}F images taken before and after FUS treatment. **(B)** First 5-second data points were fitted in the proposed model to assess initial temperature burst and maximum temperature rise. Phantoms with emulsions show faster and larger temperature rise than those without emulsions (NE). No difference in temperature profile was observed between first and second insonation at the same position.

CONTROL ID: 2231808

TITLE: Dynamic PET evaluation of the increased FLT uptake level after sorafenib treatment in mice bearing a human renal cell carcinoma xenograft

PRESENTER: Naoyuki Ukon

ABSTRACT BODY:

Abstract Body: Introduction:

Sorafenib shows significant clinical activity against renal cell carcinoma (RCC). It is used as an oral multikinase inhibitor and has anti-tumor proliferation and anti-angiogenetic effects. Recently, we have evaluated the early tumor response to sorafenib treatment in a RCC xenograft on the basis of ^{3}H-fluorothymidine (^{3}H-FLT) uptake level. Contrary to our expectation, the results showed that ^{3}H-FLT uptake level in the tumor significantly increased after the sorafenib treatment. In this study, to clarify the reason for the increased FLT uptake level after the sorafenib treatment, we evaluated the dynamic pattern of ^{18}F-FLT uptake level in tumors by positron emission tomography (PET) in mice bearing a RCC xenograft (A498).

Materials and methods:

A498 xenograft was established in nude mice, and the mice were assigned to the control (n=5) and sorafenib-treated (n=5) groups. Mice in the sorafenib- treated group were administered sorafenib (20 mg/kg/day p.o.) once daily for 3 days. Twenty-four hours after the treatment, dynamic PET was performed up to 120 min after injection with ^{18}F-FLT (7.63 ±1.87 MBq). The 3D region of interest (ROI) was manually defined for tumor on a 120 min image with the threshold of one half of the maximum standardized uptake value (SUV) applied to the tumor. A three-compartment model fitting was carried out to estimate four rate constants (K_1:the forward transport of FLT, k_2:the reverse transport, k_3:the phosphorylation and k_4:dephosphorylation) using the measured ^{18}F-FLT blood clearance rate and the time activity curve (TAC). A cuboid ROI was drawn on the left ventricle region on a CT image and projected to all dynamic PET images to obtain ^{18}F-FLT blood clearance rate which was used as the input function for modeling analysis. Repeated ANOVA was carried out to assess each the TACs. The SUV of ^{18}F-FLT in tumors at 120 min postinjection and each rate constants were compared using the unpaired t-test ($p<0.05$).

Results:

In the control group, the tumor TAC peaked immediately after injection and then diminished. In the sorafenib-treated group, the tumor TAC gradually increased with time. The dynamic pattern of ^{18}F-FLT uptake level was significantly different between the control and sorafenib-treated groups ($p<0.05$). The SUV of sorafenib-treated group (1.65±0.30) was significantly higher than that of the control group (0.60±0.22, $p<0.05$). The K_1, k_2, and k_4 were significantly decreased in the sorafenib-treated group than in the control group. The k_3 was significantly higher in the sorafenib-treated group (0.111±0.027) than in the control group (0.082±0.009, $p<0.05$). No significant changes were observed in the distribution volume (K_1/k_2) between the control and sorafenib-treated groups.

Conclusion:

The dynamic pattern of ^{18}F-FLT uptake level in the tumor was significantly changed after sorafenib treatment. The rate constant k_3, representing FLT phosphorylation, significantly increased after sorafenib treatment, while distribution volume did not changed. These findings indicate that the increase in FLT uptake level may be caused by FLT phosphorylation in the tumor after sorafenib treatment in mice bearing a RCC xenograft.

AUTHORS (LAST NAME, FIRST NAME): Ukon, Naoyuki[2]; Zhao, Songji[2]; Yu, Wenwen[2]; Shimizu, Yoichi[1, 3]; Nishijima, Ken-ichi[1, 3]; Kubo, Naoki[1, 3]; Tamaki, Nagara[4]; Kuge, Yuji[1, 3]

INSTITUTIONS (ALL):

1. Central Institute of Isotope Sience, Hokkaido University, Sapporo, Hokkaido, Japan.
2. Tracer Kinetics and Bioanalysis, Hokkaido University, Sapporo, Hokkaido, Japan.
3. Integrated Molecular Imaging, Hokkaido University, Sapporo, Hokkaido, Japan.
4. Nuclear medicine, Hokkaido University, Sapporo, Hokkaido, Japan.

(No Image Selected)

CONTROL ID: 2229242

TITLE: MR thermometry for thermal therapy using frequency map

PRESENTER: ChangKi Min

ABSTRACT BODY:

Abstract Body: Introduction: Safe and efficient thermal therapy requires accurate temperature monitoring. Among several methods, proton resonance frequency (PRF)-based phase mapping is preferred in many *in vivo* applications for its excellent linearity with temperature regardless of tissue types. However, temperature maps from conventional PRF-based method are vulnerable to errors from phase unwrapping and phase noise. Since PRF method is based on the resonance frequency change of water proton depending on the temperature, we hypothesized that the resonance frequency map will accurately represent the temperature. In this study, we propose a new method of PRF-based temperature mapping by calculating resonance frequency maps from multiple phase images.

Methods: A 7T MR scanner (Bruker) with multi echo gradient echo (MGE) pulse sequence was used to obtain the resonance frequency map (TR/TE: 1500/7 ms, # of echo: 12, FOV: 1.5 cm *1.5 cm, matrix resolution: 64 * 48, slice thickness: 1 mm). The frequency was calculated using the phase difference between the echoes. A home-made program with IDL (Interactive Data Language) was built for frequency map. A 2% agar phantom was heated by warm air and its temperature was monitored by a non-magnetic thermo-couple probe.

Results: The temperature of the phantom was steadily increased from 30 ℃ to 40 ℃. The frequency maps were obtained with MGE images and the home-made program (Fig.2). The temperature changes were calculated using the frequency maps. The calculated temperature changes from the frequency map were compared with the measured temperature changes from the thermo-couple probe (Fig.1). Figure 1. shows that the slope of line is almost one and this means those values are almost same.

Conclusions & Discussion: In this study, the temperature change was accurately measured with the new method. This new method calculates temperature from resonance frequency mapping, which does not need the phase unwrapping process and reduces the phase error. The methods will be applied to the MR-guided thermal therapy such as focused ultrasound (FUS) and RF ablation.

References: Rieke V et al., J Magn Reson Imaging, 2008 Feb; 27(2): 376-90

AUTHORS (LAST NAME, FIRST NAME): Min, ChangKi[1]; Jeon, SoYeon[1]; Shin, Soo Hyun[1]; Kim, Daehong[1, 2]

INSTITUTIONS (ALL):

1. Molecular Imaging & Therapy Branch, National Cancer Center, Goyang, Gyeonggido, Korea (the Republic of).
2. Department of Radiology, National Cancer Center, Goyang, Gyeonggido, Korea (the Republic of).

Fig. 1

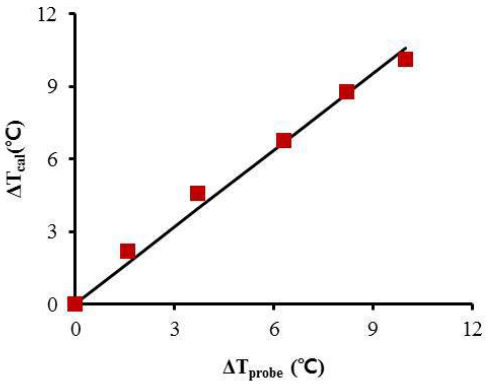

Fig. 1. The graph of probe temperature change versus calculated temperature change (vertical axis: calculated temperature change, horizontal axis: probe temperature change). The Black line is fitted by the least-squared method. The slope of the line is 1.06135 (y = 1.06135x).

Fig. 2

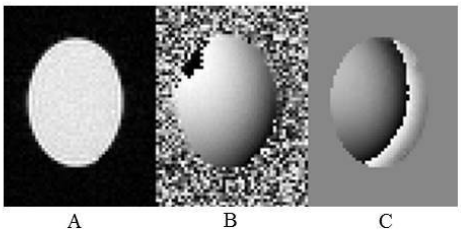

Fig. 2. MR images at temperature of 30 ℃.
A, B: magnitude image and phase image from first echo,
C: frequency map calculated using all echoes images

CONTROL ID: 2229244

TITLE: Evaluating Natural Products against Human Gliomas through Molecular Imaging

PRESENTER: Edwin Chang

ABSTRACT BODY:

Abstract Body: INTRODUCTION: Glioblastoma multiforme (GBM) is a malignant cancer having median survival time (with treatment) of 15 months (1). Interventions consist of surgical resection and then standardized radiotherapy with chemotherapy. But prognosis remains poor (1) and there is a need for mechanism-specific drugs. Within Ayurvedic medical tradition, extracts from the roots and leaves of the winter cherry plant (*Withania sominifera*) are applied to numerous health problems (2). A specific extract from this plant, AshwaMAX, is concentrated (4.3%) for Withaferin A, a steroidal lactone inhibiting cancer cells by several possible anti-oncogenic mechanisms (3). We hypothesized that this extract could treat glioblastoma (as effectively, at least, as Withaferin A) and that bioluminescent molecular imaging (BLI) would be a good modality to track oral therapy in orthotopic xenografts of glioblastoma in nude mice. METHODS: Human parietal-cortical glioblastoma cells (pcGBM2, GBM39, U87-MG) were isolated from primary tumors. pcGBM2 was transduced with lentiviral vectors that express a GFP/firefly luciferase fusion protein. Mutational and expression status of relevant targets such as EGFRviii was studied. Proliferative potential of these cells was assessed by the alamar blue bioassay. Intracranial xenografts of glioblastomas was grown in the right parietal regions of female, nude mice (n=3-5 per experiment). Tumor growth was followed through bioluminescent imaging of injected D-Luciferin. RESULTS: Both wild type and EGFRviii were present. GBM39 expressed EGFRviii 20-fold higher than pcGBM2 but U87-MG had virtually no EGFRviii. Neurosphere cultures of U87-MG, pcGBM2 and GBM39 were inhibited by AshwaMAX at IC_{50} of 1.4, 0.19 and 0.22 uM equivalent respectively and by Withaferin A with IC_{50} of 0.31, 0.28 and 0.25 µM respectively (Figures 1A-B). These data led to preclinical studies with pcGBM2 xenografts in nude mice. Daily oral gavage of a non-toxic dosage of AshwaMAX (80mg/kg per day) significantly reduced bioluminescence signal (n=3 mice, $p<0.02$, four parameter non-linear regression analysis). After 30 days, bioluminescent signal increased suggesting the onset of resistance (Figures 1C-D). In contrast to AshwaMAX-treated mice, the BLI signal for control, untreated mice increased and then plateaued. CONCLUSION: AshwaMAX killed human GBM cells at nanomolar concentrations. We conclude that our approaches then would be useful for high-throughput analysis of other natural products. Pioneering preclinical studies confirmed, for the first time, that AshwaMAX (and Withaferin A) could be effective against GBM in living mice. AshwaMAX is thus a promising candidate for future clinical translation in GBM.

1. Johnson DR, O'Neill BP. Glioblastoma survival in the United States before and during the temozolomide era. J Neurooncol. 2012;107:359-64.

2. Mirjalili MH, Moyano E, Bonfill M, Cusido RM, Palazon J. Steroidal lactones from Withania somnifera, an ancient plant for novel medicine. Molecules. 2009;14:2373-93.

3. Vanden Berghe W, Sabbe L, Kaileh M, Haegeman G, Heyninck K. Molecular insight in the multifunctional activities of Withaferin A. Biochem Pharmacol. 2012;84:1282-91.

AUTHORS (LAST NAME, FIRST NAME): Chang, Edwin[1, 2]; Pohling, Christoph[2]; Kaur, Jasdeep[2]; Murty, Surya[2]; Xu, Lingyun[1]; van de Ven, Stephanie M.[1]; Natarajan, Arutselvan[1]; Gowrishankar, Gayatri[2]; D'Souza, Aloma L.[2]; Schick, Sophie[1]; Chan, Liyin[1]; Wu, Nicholas H.[1]; Kyaw, Phoo[1]; Mischel, Paul[3]; Abbasi, Taher[4]; Mallick, Parag[1]; Gambhir, Sanjiv S.[2]

INSTITUTIONS (ALL):

1. Radiology, Canary Center, Stanford University, Stanford, CA, United States.
2. Radiology, Stanford University, Stanford, CA, United States.
3. Medicine, UCSD, Ludwig Center, La Jolla, CA, United States.
4. Cell Works Inc., San Jose, CA, United States.

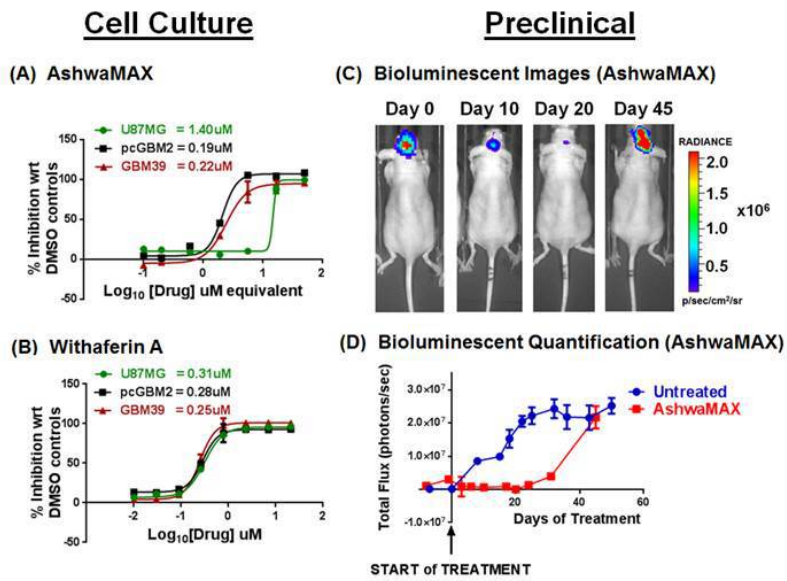

Figure 1: (A) Dosage-dependent inhibition of cellular proliferation of several human glioblastoma cell lines by AshwaMAX. IC_{50}'s were at 14.8ug/ml (U87MG), 2.1ug/ml (pcGBM2) and 2.4ug/ml (GBM39) or, if assuming 4.3% Withaferin A in AshwaMAX: 1.4, 0.22 and 0.19 uM equivalent respectively. (B) Dosage-dependent inhibition of cellular proliferation of several human glioblastoma cell lines by Withaferin A. IC_{50}'s were at 0.31uM (U87MG), 0.28uM (pcGBM2) and 0.25uM (GBM39). (C) Representative BLI scans for mice with orthotopic xenografts of pcGBM2 expressing GFP/Luciferase and given daily oral gavage of AshwaMAX (80 mg/kg/day). (D) Representative graphical quantification of murine BLI for control, untreated mice (blue) and mice given daily oral gavage of AshwaMAX (red) at 80 mg/kg/day (n=3 readings per experiment, slope of plot significantly different from zero (P<0.02) as assessed via four parameter non-linear regression analysis). All mice implanted orthotopically with pcGBM2/GFP/Luciferase.

Effect of Withaferin A and AshwaMAX on Glioblastoma Neurospheres and Xenografts

CONTROL ID: 2229246

TITLE: Optimization of non-invasive [^{18}F]fluoromethyl-PBR28 PET study for quantification of neuroinflammation using alternative reference compartments in rat Parkinson's disease model

PRESENTER: Hyun Soo Park

ABSTRACT BODY:

Abstract Body: The absence of the reference tissue causes substantial inefficiency in the preclinical stage of the PET radioligand development for neuroinflammation imaging. We performed [^{18}F]fluoromethyl-PBR28 PET studies to identify a suitable alternative reference compartment for simplifying the data acquisition and the quantification of the neuroinflammation in rat Parkinson's disease (PD) model.

LPS-induced PD rat models were underwent dynamic [^{18}F]fluoromethyl-PBR28 PET studies. The image-derived input function (IDIF) using the left ventricle (LV) and contralateral side of LPS-infusion in the striatum were selected as alternative reference compartments. Distribution volume (DV) and binding potential (BP_{ND}) were estimated for each reference compartment using 2-tissue compartment model and non-invasive graphical analysis, respectively. Time-activity curves were rebinned and target to reference compartment concentration ratio (CR) of each binning were calculated. The correlation between DV, BP_{ND} and CR were statistically tested.

DV (5.5±1.6) and BP_{ND} (2.8±0.9) of [^{18}F]fluoromethyl-PBR28 in the ipsilateral striatum of LPS-infusion were significantly correlated (R^2=0.970, P<0.05). A significant correlation between CR of 40–60 min binning of the time-activity curves and BP_{ND} was found (R^2=0.997, P<0.05).

Data demonstrated that contralateral side of LPS-infusion in the striatum in PD rat model is an alternative reference compartment for quantification of neuroinflammation using non-invasive graphical analysis for [^{18}F]fluoromethyl-PBR28 PET studies. And semi-quantification of 20 min-static image data acquired 40 min after the injection provides reliable results represent BP_{ND} of [^{18}F]fluoromethyl-PBR28.

AUTHORS (LAST NAME, FIRST NAME): Park, Hyun Soo[2]; Moon, Byung Seok[1]; Jung, Jae Ho[1]; Lee, Byung Chul[1]; Kim, Sang Eun[2]

INSTITUTIONS (ALL):

1. Department of Nuclear Medicine, Seoul National University Bundang Hospital, Seoul National University College of Medicine, Seongnam, Korea (the Republic of).

2. Department of Transdisciplinary Studies, Graduate School of Convergence Science and Technology, Seoul National University, Seoul, Korea (the Republic of).

(No Image Selected)

CONTROL ID: 2229253

TITLE: Upconversion nanoprobes for efficient *in vivo* sentinel lymph node mapping and quantitative analysis

PRESENTER: Hye Sun Park

ABSTRACT BODY:

Abstract Body: Lanthanide-based upconversion nanoparticles (UCNPs) have gathered great attention due to their photostability and biocompatibility. In the field of *in vivo* optical imaging, UCNPs do not make an issue of noise caused by autofluorescence background, providing a great signal-to-noise ratio. Especially, UCNPs allow sensitive detection and quantitative analysis of target regions by optical imaging in the face of repeated and prolonged exposure to excitation source without photobleaching.

One of the most promising cancer-related applications of UCNPs is sentinel lymph node (SLN) mapping because lymphatic mapping and biopsy of SLN techniques have been widely used in the diagnosis of cancer metastasis, investigating lymph node metastasis as one of the most important prognostic signs. Transport and retention of water soluble and surface functionalized UCNPs in lymphatic mapping were evaluated with sensitive and well-resolved mapping images. We characterized their kinetic luminescence profiles in lymph node mapping for injection sites as well as axillary lymph nodes with several types of surface modified UCNPs. In the earlier time after injection, the UCNPs showed different transport behaviours with their surface characters. We quantified the localization of the UCNPs within the lymph node by *in vivo* optical imaging and *ex vivo* quantitative analysis after lymph node resections. In addition, we also observed luminescence signals in the injection area for a long time to investigate the efficient excretion of the nanoparticles from the initially injected region. These results indicate a potential application of the UCNPs with high quality images and non-invasive quantitative *in vivo* optical imaging.

AUTHORS (LAST NAME, FIRST NAME): Park, Hye Sun[1]; Nam, Sang Hwan[2]; Cho, Jee-Hyun[1]; Suh, Yung Doug[2, 3]; Hong, Kwan Soo[1]

INSTITUTIONS (ALL):

1. Bioimaging Research Team, Korea Basic Science Institute, Cheongju-si, Cheongwon-gu, Korea (the Republic of).
2. Laboratory for Advanced Molecular Probing (LAMP), Research Center for Convergence Nanobiotechnology, Korea Research Institute of Chemical Technology , Daejeon, Korea (the Republic of).
3. School of Chemical Engineering, Sungkyunkwan University, Suwon, Korea (the Republic of).

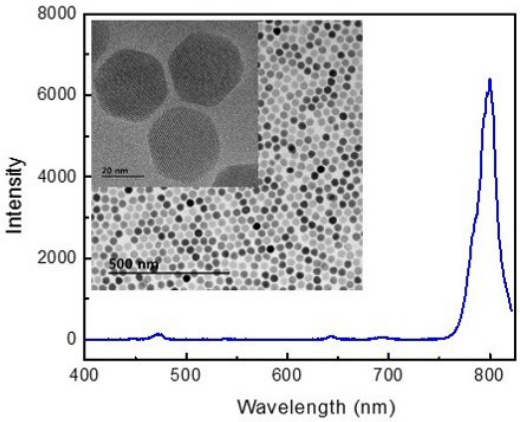
8000
6000
4000
2000
0
Intensity
400
500
600
700
800
Wavelength (nm)
20 nm
500 nm

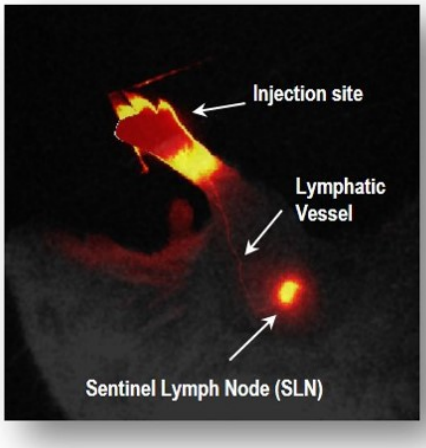
Injection site
Lymphatic
Vessel
Sentinel Lymph Node (SLN)

CONTROL ID: 2229277

TITLE: Radiofrequency Hyperthermia Enhanced Herpes Simplex Virus-Thymidine Kinase Gene Therapy of Hepatocellular Carcinoma:Monitored by Dual-Modality Imaging

PRESENTER: Jianfeng Wang

ABSTRACT BODY:

Abstract Body: Purpose: To determine the possibility of using radiofrequency hyperthermia (RFH) to enhance therapeutic effect of herpes simplex virus thymidine kinase/ganciclovir (HSV-TK/GCV) on hepatocellular carcinoma (HCC).

Materials and Methods: Human HCC cells (HepG2) were first transfected with lentivirus/luciferase. For both in-vitro confirmation and in-vivo validation, Luciferase-labeled HCC cells and HCC tumor xenografts on mice received different treatments: (i) combination therapy of intratumoral HSV-TK/GCV-mediated gene therapy plus MR imaging-heating-guidewire (MRIHG)–mediated RFH; (ii) gene therapy only; (iii) RFH only; and (iv) phosphate-buffered saline (PBS) as control. Cell proliferation was quantified by MTS assay. Tumor changes were monitored by ultrasound imaging and bioluminescence optical imaging before and at days 7 and 14 after treatments, which were correlated with subsequent histology.

Results: Of in vitro experiments, MTS assay demonstrated the lowest cell proliferation in combination therapy group compared with those in three control groups (29±6% VS 56±9%, 93±4%, and 100±5%, $\rho<0.05$). Of in vivo experiments, ultrasound imaging showed smaller relative tumor volume in combination therapy group than those in three control groups (0.74±0.19 VS 1.79±0.24, 3.14±0.49 and 3.22±0.52, $\rho<0.05$). Optical imaging demonstrated significant decrease of bioluminescence signals of tumors in the combination therapy group, compared to those in three control groups (1.2±0.1 VS 1.9±0.2% VS 3.3±0.6% VS 3.5±0.4%, $\rho<0.05$)(Figure). These imaging findings were correlated well with histologic confirmation.

Conclusion: RF-hyperthermia can enhance HSV-TK/GCV-mediated gene therapy of human hepatocellular cancer, which may open new avenues for efficient management of hepatocellular carcinoma using MR/RF-hyperthermia integrated interventional gene therapy.

AUTHORS (LAST NAME, FIRST NAME): Wang, Jianfeng[1, 2]; Zhang, Feng[1]; Shi, Yaoping[1]; Bai, Zhibin[1]; Qiu, Longhua[1]; Li, Longgang[1]; Zhai, Renyou[2]; yang, xiaoming[1]

INSTITUTIONS (ALL):

1. Radiology, University of Washington, School of Medicine, Seattle, WA, United States.
2. Radiology, Beijing Chaoyang Hospital, Beijing, Beijing, China.

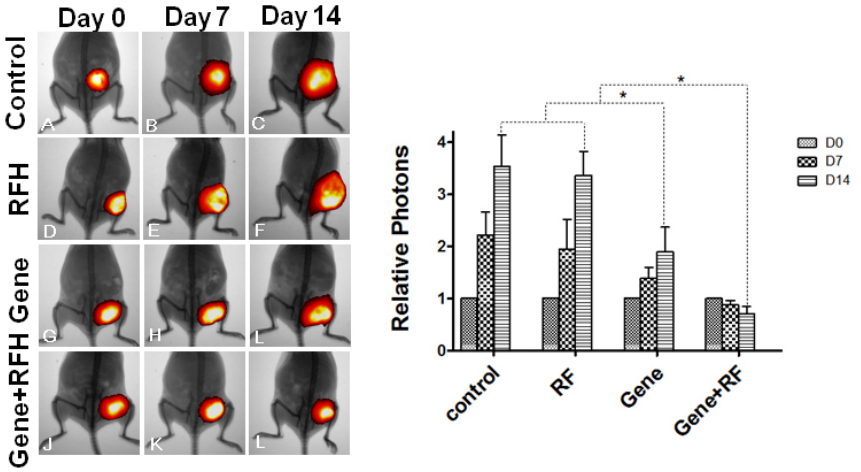

Figure. Representative molecular optical images of hepatocellular carcinomas in four animal groups with different treatments. (A-C) control with saline, (D-F) HSV-TK/GCV gene therapy only, (G-I) radiofrequency hyperthermia (RFH) only, and (J-L) combination therapy with gene therapy plus RFH. The optical signal intensity and size of the tumor in the combination therapy group significantly decrease 14 days after the treatment, in comparison to those in other three control groups (*=$p<0.05$).

CONTROL ID: 2229300

TITLE: Quantitative simultaneous acquisition of dual tracer using ^{99m}Tc and ^{123}I-labeled radiotracers in preclinical SPECT scanner with CZT detector

PRESENTER: Asuka Mizutani

ABSTRACT BODY:

Abstract Body: Purpose: Several recent scanners incorporate semiconductor materials such as cadmium zinc telluride (CZT). The CZT-based scanners improve energy and spatial resolution, as compared with sodium iodide scintillation detectors, which are used in conventional SPECT scanners. In this study, simultaneous acquisition of a dual tracer with ^{99m}Tc and ^{123}I was evaluated using a preclinical SPECT scanner with a CZT-based semiconductor detector.
Methods: Two 10-ml syringes contained 100 or 300 MBq ^{99m}Tc-tetrofosmin (^{99m}Tc-TF) and 100 MBq 15-(p-iodophenyl)-3R,S-methyl pentadecanoic acid (^{123}I-BMIPP), respectively. A rat-sized cylindrical phantom contained both 100 or 300 MBq ^{99m}Tc-TF and 100 MBq ^{123}I-BMIPP. SPECT scan data were acquired in rats after transient coronary occlusion and injection of 300 MBq ^{99m}Tc-TF. After the first scan, the same rats were injected with 100 MBq ^{123}I-BMIPP and rescanned using the same protocols. After reconstruction with distance-dependent collimator response correction with or without scatter correction (SC) for single-tracer imaging, and without SC for dual-tracer imaging, radioactive counts were measured using the SPECT images.
Results: In the syringes, downscatter contaminations of ^{123}I-BMIPP in 125–150 keV were respectively 3.5% and 13.2% of the radioactive counts for 100 MBq ^{99m}Tc-TF with and without SC, whereas it was 4.1% for 300 MBq ^{99m}Tc-TF without SC. There was no upscatter contamination of ^{99m}Tc-TF in 150–175 keV. In the rat-sized cylindrical phantom including both 300 MBq ^{99m}Tc-TF and 100 MBq ^{123}I-BMIPP, the radioactive count ratio decreased to 1.08 in ^{99m}Tc-TF images in 125–150 keV, and to 0.98 in ^{123}I-BMIPP images in 150–175 keV. In the rat model of myocardial infarction, the ^{99m}Tc-TF images with the dual tracer were identical to those of ^{99m}Tc-TF with the single tracer. In normal and myocardial infarction areas, the radioactive counts of ^{99m}Tc-TF in dual tracers were not much different from those in the single tracer.
Conclusion: Dual-tracer imaging of ^{99m}Tc-TF and ^{123}I-BMIPP is feasible in a preclinical SPECT scanner with CZT detectors. Radioactivity of the injected ^{99m}Tc-TF tracer should be increased as much as possible to improve quantification of ^{99m}Tc-TF in dual-tracer imaging if the correction methods cannot be appropriately applied.

AUTHORS (LAST NAME, FIRST NAME): Mizutani, Asuka[3]; Kobayashi, Masato[1]; Matsunari, Ichiro[2]; Nishi, Kodai[4]; Miyazaki, Yoshiharu[2]; Kawai, Keiichi[3]

INSTITUTIONS (ALL):

1. Wellness Promotion Science Center, Institute of Medical, Pharmaceutical and Health Sciences, Kanazawa University, Kanazawa, Japan.
2. Clinical Research Department, The Medical and Pharmacological Research Center Foundation, Hakui, Japan.
3. School of Health Science, College of Medical, Pharmaceutical and Health Sciences, Kanazawa University, Kanazawa University, Kanazawa, Japan.
4. Department of Radioisotope Medicine, Atomic Bomb Disease Institute, Nagasaki University, Nagasaki, Japan.

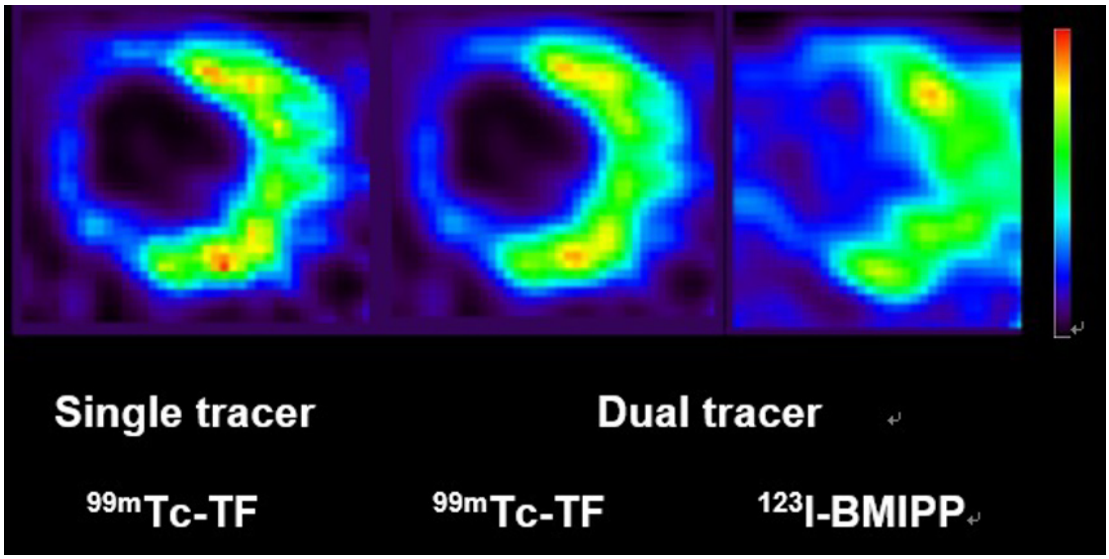
Single tracer
Dual tracer
99mTc-TF
99mTc-TF
123I-BMIPP

CONTROL ID: 2243697

TITLE: Comparison of image quality with ^{62}Cu and ^{64}Cu-radiotracers in whole body tumor imaging

PRESENTER: Masato Kobayashi

ABSTRACT BODY:

Abstract Body: Introduction: Copper (Cu)-labeled radiotracers have been used in some basic science research and for clinical PET. PET imaging is possible with Cu isotopes, ^{60}Cu, ^{61}Cu, ^{62}Cu and ^{64}Cu. In particular, ^{62}Cu and ^{64}Cu labeled radiotracers has highly been used for preclinical and clinical PET studies. In this study, we compare image quality between ^{62}Cu and ^{64}Cu imaging with different acquisition mode and reconstruction algorithm using whole body phantom.

Methods: In a NEMA 2001 whole-body phantom, the concentration of ^{62}Cu-ATSM and ^{64}Cu-ATSM was, respectively, approximately 270 and 180 kBq/mL in all the spheres and approximately 90 and 60 kBq/mL in the background. Two-dimensional (2D) and three-dimensional (3D) PET scan data were acquired for 10 min. These phantom experiments were repeated three times. The data were reconstructed using filtered back projection (FBP) and the ordered subset expectation maximization (OSEM) algorithm. Image quality of ^{62}Cu and ^{64}Cu was compared using recovery coefficient (RC), sphere-to-background ratio (SBR) and coefficient of variation (%COV).

Results: There were no significant differences between ^{62}Cu and ^{64}Cu imaging, visually. RCs of ^{64}Cu images were higher than those of ^{62}Cu images. RC of ^{64}Cu images with 3D acquisition mode and OSEM was the highest in all experiments. SBR values were not significantly different from the true value of 3.0 in 2D acquisition and FBP, but 3D acquisition and OSEM slightly might yield overestimation. %COV values of ^{64}Cu were lower than those of ^{62}Cu, and then OSEM produced lower %COV than FBP.

Conclusions: ^{64}Cu-radiotracers provide higher image quality than ^{62}Cu-radiotracers in whole-body tumor imaging. Although ^{64}Cu imaging may be better image quality using a 3D acquisition mode and OSEM algorithm, the quantitative values slightly might be overestimated.

AUTHORS (LAST NAME, FIRST NAME): Kobayashi, Masato[3]; Mori, Tetsuya[4]; Tsujikawa, Tetsuya[4]; Mizutani, Asuka[2]; Kiyono, Yasushi[4]; Okazawa, Hidehiko[4]; Kawai, Keiichi[1]

INSTITUTIONS (ALL):

1. Faculty of Health Sciences, Kanazawa University, Kanazawa, Japan.
2. Health Science, Kanazawa University, Kanazawa, Japan.
3. Wellness Promotion Science Center, Institute of Medical, Pharmaceutical and Health Sciences, Kanazawa University, Kanazawa, Japan.
4. Biomedical Imaging Research Center , University of Fukui, Fukui, Japan.

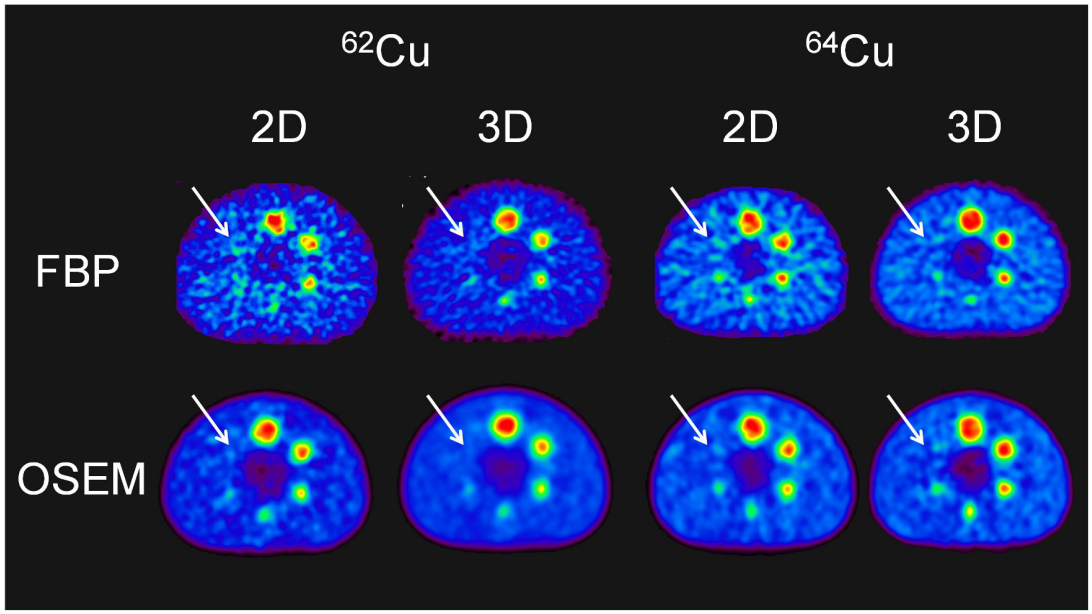

Fig. Images of the whole-body phantom

CONTROL ID: 2229321

TITLE: Delineation of tumor margins *in vivo* with an uPAR-targeted NIR optical imaging probe, using the fluorophor Indocyanine green.

PRESENTER: Karina Juhl

ABSTRACT BODY:

Abstract Body: Introduction/Background:

Near infrared intra-operative optical imaging is an emerging new technique with clear implications for improved cancer surgery by enabling more distinct delineation of tumor margins during resection. This modality has the potential to increase the number of patients with tumor free margin after intended radical tumor resection with an expected increase in survival. Invasive solid human carcinomas express high level of uPAR in the tumor-stromal interface of invasive lesions and are therefore considered an ideal target for intra-operative imaging. In the present study a new urokinase plasminogen activator receptor (uPAR)-targeted probe ICG-Glu-Glu-AE105 synthesized by us was investigated and validated by *in vivo* and *ex vivo* studies.

Methods:

The affinity for human uPAR of our new optical probe, comprising a linear uPAR targeting peptide (AE105) conjugated with indocyanine green (ICG), was measured using surface plasmon resonance. For further characterization the probe was investigated *in vivo* in a human glioblastoma xenograft model. The mice received either 10 nmol AE105:ICG (n=5) or 10 nmol ICG (n=5) i.v. and were imaged 15 hr post injection. Additionally, imaging the mice was also performed using an approved clinical camera to illustrate the potential of clinical translation. All tumors were analyzed for uPAR expression using a validated ELISA method. Finally a group of mice (n=4) was either injected with 10 nmol AE105:ICG or 10 nmol AE105:ICG + 6.7 nmol uPA, the natural ligand for uPAR, and a dynamic scan over 15 hr was performed.

Results:

ICG-Glu-Glu-AE105 affinity for uPAR (IC_{50}=134nM) was reduced compared with the core peptide AE105, but still potent as a specific uPAR targeting probe. Comparing the two groups receiving ICG-Glu-Glu-AE105 and ICG a significant ($p<0.001$) difference between the signals were observed. In the group receiving ICG-Glu-Glu-AE105 a tumor-to-background (TBR) of 3.52 ± 0.17 was observed while the group receiving ICG alone had a TBR at 1.04 ± 0.04. The uPAR expression in the groups was equal. When injecting uPA as blocking agent, together with ICG-Glu-Glu-AE105 a significant reduced ($p<0.0001$) signal was observed over time with a mean decrease in fluorescent signal of 46.7%±3.7%.

Conlusion:

We demonstrated a specific binding to uPAR of a new optical probe synthesized in our laboratory. The probe showed high TBR when used together with a clinically approved camera, which underlines the translational potential for this probe. Our data supports the hypothesis that the optical probe ICG-Glu-Glu-AE105 can be used to delineate tumors expressing high uPAR from healthy tissue and that it has a high potential for intra-operative optical imaging.

AUTHORS (LAST NAME, FIRST NAME): Juhl, Karina[1]; Christensen, Anders[1, 2]; Persson, Morten[1]; Ploug, Michael[3]; Kjaer, Andreas[1]

INSTITUTIONS (ALL):

1. Department of Clinical Physiology, Nuclear Medicine & PET and Cluster for Molecular Imaging, Rigshospitalet and University of Copenhagen, Copenhagen, Denmark.
2. Department of Otolaryngology , Head & Neck Surgery and Audiology, Rigshospitalet, Copenhagen, Denmark.
3. Finsen Laboratory, Rigshospitalet & Biotech Research and Innovation Centre (BRIC), Copenhagen, Denmark.

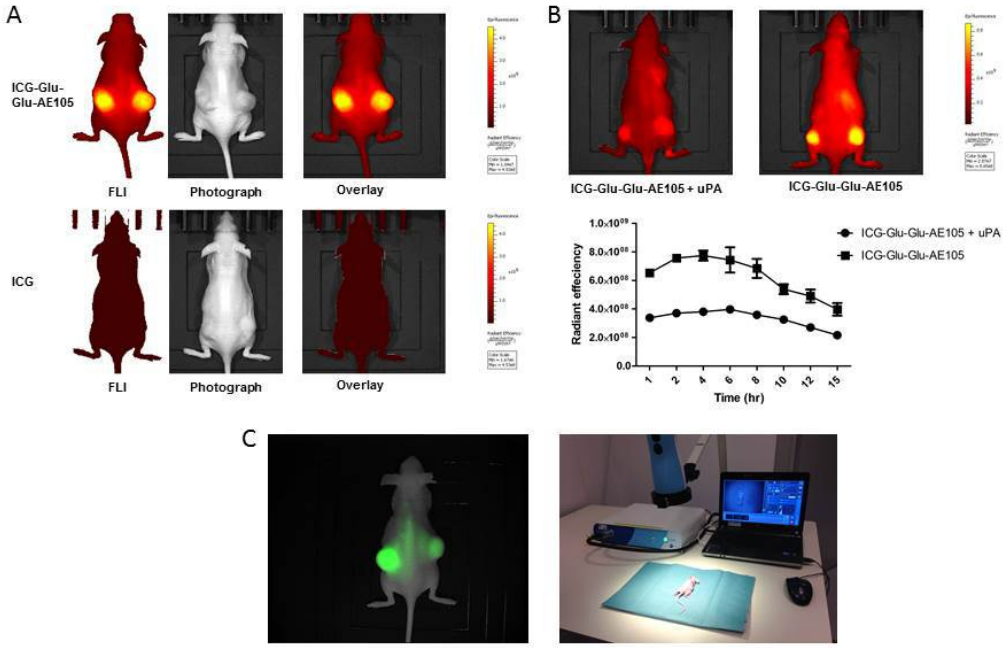

Figure 1. Optical imaging of human glioblastoma xenograft mouse model. (A) A representative image of mice receiving either the uPAR targeted optical probe (ICG-Glu-Glu-AE105) or ICG alone. The images show a significant difference ($p<0.001$) in fluorescent signal 15 hr post injection (TBR for ICG-Glu-Glu-AE105 was 3.52±0.17 and for ICG 1.04±0.04) (B) By blocking with the natural ligand for uPAR, uPA, the signal was significant reduced ($p<0.0001$) over a time period of 15 hr. (C) A representative image of a mouse receiving the optical probe and imaged with the clinical camera (Fluobeam® 800) TBR with clinical camera showed similar TBR values (3.58±0.29).

CONTROL ID: 2229325

TITLE: The assessment of tumor’s malignant-behavior with MR ferritin reporter imaging mediated by hTERT promoter

PRESENTER: Dong ZHANG

ABSTRACT BODY:

Abstract Body: Background and Objectives: The malignant behavior assessment of tumor is very important for the patient’s therapy and outcome evaluation. Telomerase activity is a marker for majority of malignant tumors. In this study, we report that MR ferritin reporter imaging mediated by human telomerase reverse transcriptase (hTERT) promoter could be used to detect malignant tumors noninvasively.

Methods: The lentiviral vector Lenti-hTERT-Fth1-3flag-Puro, in which the expression of ferritin heavy chain gene (Fth) was controlled by malignant tumor-specific hTERT promoter, was constructed firstly. And another lentiviral vector Lenti-CMV-Fth1-3flag-Puro, controlling by nonspecific CMV promoter, was used as a control. In vitro study, telomerase-positive and negative cells were transfected with the two lentiviral vectors respectively, and then their intracellular Fth protein content, iron accumulation, transverse relaxation rate (R2*) and T2* weighted imaging (T2*WI) signal intensity were examined. In vivo study, telomerase-positive and negative tumor models were established and then intratumorally injected with lentiviral vectors. T2*WI and T2WI images of tumors were acquired and their signal intensity changes were validated by examining Fth/flag expression and iron accumulation.

Results: In vitro study, when transfected with Lenti-hTERT-Fth1-3flag-Puro, only telomerase-positive cells had significantly more Fth protein content and iron accumulation than the untransfected ones, and correspondingly had higher R2* value and showed remarkable hypointensity on T2* weighted images, but the telomerase-negative cells did not. Similarly, in vivo study, after intratumorally injected with Lenti-hTERT-Fth1-3flag-Puro, only telomerase-positive tumor showed remarkable hypointensity on T2* weighted images, which in line with the increase of Fth/flag expression and iron accumulation in tumor tissues, while the telomerase-negative tumor did not. In contrast, when experimented with Lenti-CMV-Fth1-3flag-Puro, all telomerase-positive and negative cells and tumors showed strong hypointensity on T2* weighted images. Conclusion: These results suggested that with the usage of hTERT promoter-driven ferritin lentiviral vector, malignant tumors can be detected by MR imaging without the help of any exogenous contrast agents, which provides a new research idea and method for molecular imaging research of malignant tumor.

AUTHORS (LAST NAME, FIRST NAME): ZHANG, Dong[1]; Yang, Yan[1]

INSTITUTIONS (ALL):

1. Department of Radiology, Xinqiao Hospital, Third Military Medical University, ChongQing, China.

(No Image Selected)

CONTROL ID: 2233059

TITLE: PET/MR multimodal theranostics: Direct gallium-68 radiolabelling of silica coated iron oxide nanorods for use in multimodal liver imaging and hyperthermia therapy

PRESENTER: Benjamin Burke

ABSTRACT BODY:

Abstract Body: The commercial availability of combined magnetic resonance imaging (MRI)/positron emission tomography (PET) scanners for clinical use has increased demand for agents which offer signal or contrast in both modalities.[1, 2] The aim of this work is to develop silica coated iron oxide nanorods (NRs) for final step radiolabelling with ^{68}Ga to form PET/MRI multimodal imaging agents with therapeutic applications via magnetic hyperthermia.

Uncoated iron oxide nanorods were synthesised via co-precipitation and functionalised with varying ratios of siloxane derivatised polyethylene glycol (PEG) and the tetrazamacrocycle, DO3A. The isolation of the iron oxide NRs was confirmed by transmission electron microscopy which showed that the iron oxide core is universally rod-like and is unchanged after coating. NR lengths are in the range of 80-130 nm and mean hydrodynamic sizes between 99 – 155 nm making them suitable for *in vivo* applications. All the NR constructs produced had a similar, negative surface potential and are stable in aqueous solution with no visible precipitation of the NRs observed after 2 months. The magnetic behaviour of the NRs was measured *in vitro* at 3 T. All constructs were shown low T_1 relaxivity and high T_2 relaxivity (up to mM^{-1} 175 s^{-1}) with the highest values correlating to the increased PEG content of the NR coating. Preliminary magnetic hyperthermia evaluation indicated the capability of the NRs to absorb the energy of an oscillating magnetic field and convert it to heat, with a specific absorption rate for the PEG coated NRs of 15.8 W/g, indicating their potential use as therapeutic agents.

Radiolabelling studies with the positron emitting radioisotope gallium-68 ($t_{1/2}$ = 68 min) were carried out with quantitative radiochemical yields in 15 min at 90 ˚C.[3] Stability assays showed no significant difference between the three coatings containing 0, 50 and 100 % of the macrocyclic bifunctional chelating unit using *in vitro* in competition binding assays with apo-transferrin and human serum over 3 h. ^{68}Ga radiolabelling results indicated that, surprisingly, the absence of a bifunctional chelator does not influence the radiometal complexation kinetics or *in vitro* stability. *In vivo* PET-CT and MR imaging studies show the expected high liver uptake of gallium-68 radiolabelled nanorods with no significant release of the radiometal ions, validating this novel simple approach to the radiolabelling of iron oxide NRs with in the absence of a chelator to allow high sensitivity liver imaging with the potential to be hyperthermia therapeutic agents.

1. R. T. M. de Rosales, *J. Labelled Compd. Radiopharm.,* 2014, 57, 298; **2.** R. Thomas *et al.*, *Int. J. Mol. Sci.*, 2013, 14, 15910; **3.** B. P. Burke *et al.*, *Faraday Discussions,* 2015, 175, 59.

AUTHORS (LAST NAME, FIRST NAME): Burke, Benjamin P.[1, 2]; Baghdadi, Neazar[1]; Kownacka, Alicja E.[1]; Nigam, Shubhanchi[1, 2]; Clemente, Gonçalo S.[2, 3]; Domarkas, Juozas[1, 2]; Lorch, Mark[1]; Pickles, Martin D.[4]; Gibbs, Peter[4]; Tripier, Raphaël[5]; Bakandritsos, Aristides[6]; Cawthorne, Christopher[2, 3]; Archibald, Steve[1, 2]

INSTITUTIONS (ALL):

1. Department of Chemistry, University of Hull, Hull, East Riding of Yorkshire, United Kingdom.
2. Positron Emission Tomography Research Centre, University of Hull, Hull, United Kingdom.
3. School of Biological, Biomedical and Environmental Sciences, University of Hull, Hull, United Kingdom.
4. Centre for Magnetic Resonance Investigations, University of Hull, Hull, United Kingdom.
5. UFR Sciences et Techniques, Université de Brest, Brest, France.
6. Materials Science Department, University of Patras, Patras, Greece.

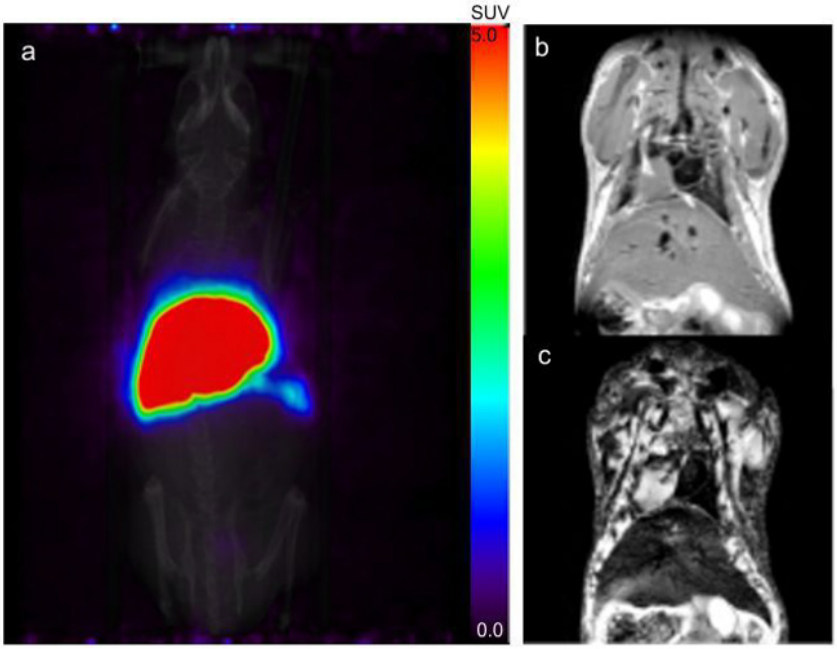

Figure 1 - *In vivo* mouse images of Gallium-68 labelled PEG coated iron oxide nanorods (a) PET/CT (b) T1 weighted MR and (c) T2 weighted MR showing liver signal in both modalities

CONTROL ID: 2229387

TITLE: Bidirectional 6 thin light-sheet fluorescence microscopy:
Three-dimensional insight into tumor biology and whole mouse organ morphology

PRESENTER: Michael Dobosz

ABSTRACT BODY:

Abstract Body: Introduction

Over the last decades light-sheet fluorescence microscopy in combination with optical tissue clearing became a very powerful technique for the three-dimensional (3D) analysis of large tissue specimen at cellular resolution. Different light-sheet geometries have been developed to increase homogenous light penetration and reduce interfering scattering and photobleaching artifacts to a minimum. In this regard, we applied bidirectional 6 thin light-sheet microscopy for high-resolution multicolor imaging of cleared and fluorescently labeled tissue samples, with a focus on cancer research.

Methods

AlexaFluor750 labeled anti-HER2 antibody was injected i.v. into a tumor bearing SHO mouse (orthotopic breast cancer cell line - KPL4, Tumor volume: 80 mm3) and six hours thereafter, we intravenously applied the vessel marker Lectin-AlexaFluor647. After five minutes the tumor and different organs were removed. Specimens were formalin-fixed, dehydrated and incubated for at least two days in a clearing solution (benzyl alcohol / benzyl benzoate). Optical transparent samples were scanned with bidirectional 6 thin light-sheet fluorescence microscope (Ultramicroscope II, LaVision BioTec) at different magnification (0.63x to 12.6x) and fluorescent channels. The received virtual tumor data were quantified with a set of custom-developed image analysis algorithms (Definiens). Visualization and volume rendering was performed with Osirix software. Following 3D scanning, the cleared tumor tissue was also analyzed by conventional histology (H&E, Ki67 & HER2 staining).

Results

Bidirectional 6 thin light-sheet fluorescence microscopy combined with our novel set of image analysis algorithms enables the fully automatic segmentation and quantification of multiple tumor parameters at cellular resolution. Besides detecting tumor tissue morphology and different tumor vessel parameters, such as vessel volume, length, diameter and number of segments and branch points, we were also able to quantify the 3D penetration behavior of AlexaFluor750 labeled anti-HER2 antibody from tumor border to center and from tumor vasculature to the surrounding tissue (Fig.1). In addition to multispectral 3D tumor analysis, optically cleared specimen showed also excellent staining results in conventional histology. The combination of both methods provides a detailed and profound insight into tumor biology and the pharmacokinetic behavior of fluorescent labeled drugs. Furthermore, the new bidirectional 6 thin light-sheet geometry enables the 3D visualization of cleared whole mouse organs from mesoscopic down to cellular resolution.

Conclusion

Combining bidirectional 6 thin light-sheet fluorescence microscopy with our novel set of algorithms enables the 3D visualization and automatic quantification of multiple tumor parameters and drug penetration on a cellular level. Furthermore, this technology bridges the gap between common macroscopic and microscopic imaging modalities and opens up new three-dimensional insights into biology.

AUTHORS (LAST NAME, FIRST NAME): Dobosz, Michael[1]; Scheuer, Werner[1]

INSTITUTIONS (ALL):

1. Roche Diagnostics GmbH, Penzberg, Germany.

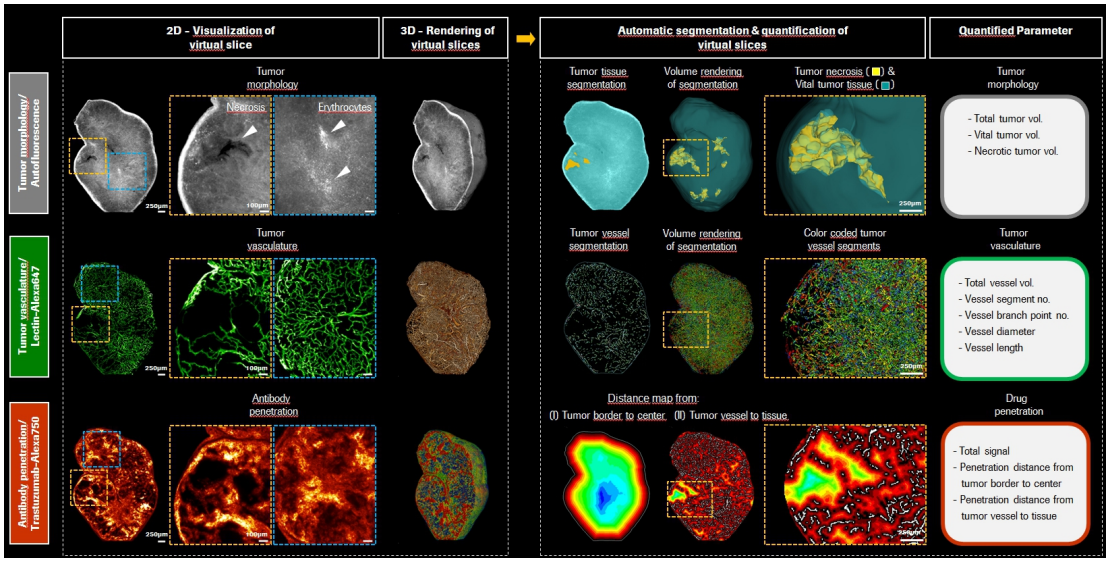

Three-dimensional visualization and quantification of tumor morphology, tumor vasculature and antibody penetration in an orthotopic breast cancer xenograft.

CONTROL ID: 2229361

TITLE: Discovery and Evaluation of SPARC-targeted Peptides for Detection of Prostate Cancer

PRESENTER: Julien Dimastromatteo

ABSTRACT BODY:

Abstract Body: Background. Prostate cancer is the second leading cause of cancer death in the United States. Currently, there is a clinical need to identify which patients should undergo radical prostatectomy versus watchful waiting. Secreted Protein Acidic and Rich in Cysteine (SPARC) is a matricellular protein expressed by stromal cells and tumor cells and is a hallmark of aggressive cancers. SPARC expression has been shown to correlate with increased Gleason score and poor prognosis and as such, SPARC represents a potential marker for the treatment stratification of patients. Since clinical tools that accurately predict the tumor's metastatic potential are lacking, we hypothesized that SPARC-targeted small peptides for PET imaging may enable imaging of aggressive prostate cancer.

Methods. Chinese hamster ovary (CHO) cells were transfected using a plasmid construct designed to induce SPARC expression on the cell surface. The construct included Tobacco Etch Virus (TEV) Protease cleavage site and transmembrane domain. Cells were incubated with M13 phage PhD 7 library for 30min, washed and incubated with TEV Protease to release the phage/SPARC protein from the cell surface. Supernatant was collected and DNA corresponding to the phage clones sequenced. Using a unique algorithm developed in our lab, the top four peptide sequences were selected based on the frequency of appearance corrected from known bias. The four peptide sequences were chemically synthesized and labeled with I125. Iodination quality control was performed using thin layer chromatography. After selection by binding assay, 50μCi of the lead compound was injected into nude mice bearing C4-2b SPARC-positive xenograft tumors (n=3). 60min p.i., mice were euthanized. The main organs including tumor were harvested, weighed and the gamma activity counted. Blood samples were collected at 1, 2, 5, 10, 30 and 60min p.i. to evaluate peptide blood clearance.

Results. SPARC transfection was successfully achieved as determined by immunofluorescence. Incubation with TEV protease resulted in 40% decrease in fluorescence intensity demonstrating the presence of SPARC in supernatant (0.023±0.003 *vs* 0.014±0.002 AU, $p<0.001$, respectively). We chose the four peptides with the top representation in the library after selection for chemical synthesis. The four peptide sequences were successfully iodinated with >93% efficiency. *In vitro*, I125-SPARC-targeted Peptide #2 (I-Clone#2) showed the highest binding to rhSPARC (4947±211 *vs* 761±53, 342±65 and 533±59 cpm for #2 *vs* #1, #3 and #4, $p<0.05$, respectively). *In vivo*, at 60 min p.i., I-Clone#2, tumor-to-muscle activity ratio was 3.0±0.4. There was slow I-Clone #2 blood pool clearance with 27.2±5.0% initially at 60 min p.i. Additionally, I-Clone#2 was mainly renally excreted (7.8±0.7 *vs* 0.9±0.2 %ID/g in the liver, $p<0.05$).

Conclusion. We performed phage display selection and identified four peptide sequences that are specific for SPARC binding. Clone #2 had the highest affinity in vitro and therefore was chosen for *in vivo* experiments. Based on the *in vivo* experiments, SPARC-targeted Peptide #2 has potential for development into a F18 PET tracer.

AUTHORS (LAST NAME, FIRST NAME): Dimastromatteo, Julien[1]; Bauknight, Dustin[1]; Brinton, Lindsey T.[1]; Gutknecht, Michael F.[1]; Kelly, Kimberly A.[1]

INSTITUTIONS (ALL):

1. Biomedical Engineering, University of Virginia / CVRC, Charlottesville, VA, United States.

(No Image Selected)

CONTROL ID: 2229422

TITLE: Gadolinium-Gold nanoparticles for non-invasive detection of transplanted cells using MRI

PRESENTER: Michel Modo

ABSTRACT BODY:

Abstract Body: Non-invasive, *in vivo* monitoring of transplanted cells for applications like cell therapy and tissue reconstruction is vital to ensure the safety and efficacy of such strategies. However, when native image contrast in insufficient, particularly with regard to small cell populations, Gd(III) based contrast agents can augment positive, T_1 contrast. Using this approach requires pre-labeling of transplanted cells with agents. Current research indicates that a major challenge with the use of Gadolinium (Gd)-based agents for this purpose has been the relatively low cellular tolerance and relaxivity (r_1) of available agents. To generate sufficiently high contrast to noise ratios that cells are visible by MRI, high agent concentrations are required. Here we show that conjugation of monomeric Gd chelates to DNA gold nanoparticles (Gd(III)-DNA AuNP) can dramatically increase the cellular uptake and r_1 of Gd(III) relative to the clinical standard ProHance (PH) in human neural stem cells (hNSC). Furthermore, using Gd(III)-DNA AuNP, we visualize NSCs transplanted into rat brains. In an extensive study to ensure a sufficient and safe cell uptake, NSCs were incubated *in vitro* with different concentrations of Gd(III)-DNA AuNP, and quantified using fluorescence histology and inductively coupled plasma mass spectrometry to measure intracellular concentrations of Gd(III) (Figure 1A). An intracellular concentration of up to 0.2 fmol Gd/cell was achieved without a measurable detriment to cell survival or proliferation over 7 days. *In vitro* MRI afforded the visualization of a cell pellet with 50% signal increase in T_1 compared to unlabelled control cells. To test the *in vivo* efficacy of this approach, transplantation of labelled cells into control animals, was performed, followed by MR imaging at 24 hours post-injection. Imaging of these animals at 9.4 T showed positive identification of labeled cell populations relative to controls in T_1-weighted images (Figure 1B). Histological validation of these results was obtained using a human-specific antibody and the red fluorescence of the Gd(III)-DNA AuNP, confirming that the labelling of NSCs selectively affords their detection by T_1-weighted MRI. To ensure the specificity of the detection, the number of double-labeled cells (human-specific antibody+Gd(III)-DNA AuNP) were counted and compared with cells that were only positive for the human antibody (false negatives), as well as host cells that contained Gd(III)-DNA AuNP. There was a neglible amount of false positive (<1%), but a significant proportion of false negatives (~25%). Overall, this approach hence provides a specific imaging of transplanted cells with a risk of underestimation the number of cells based on T_1-weighted images. These results are encouraging as they indicate that it is possible to specifically visualize transplanted cells using T_1 imaging. The ultimate aim of this approach is to link the location, migration and survival of cells with behavioural recovery in preclinical models, and thereby informing the design of clinical trials to provide optimal cell placement relative to the injury site.

AUTHORS (LAST NAME, FIRST NAME): Nicholls, Francesca J.[1]; Rotz, Matthew[2]; Ling, Wen[1]; MacRenaris, Keith[2]; Meade, Thomas J.[2]; Modo, Michel[1]

INSTITUTIONS (ALL):

1. Department of Radiology & McGowan Centre for Regenerative Medicine, University of Pittsburgh, Pittsburgh, PA, United States.

2. Northwestern University, Chicago, IL, United States.

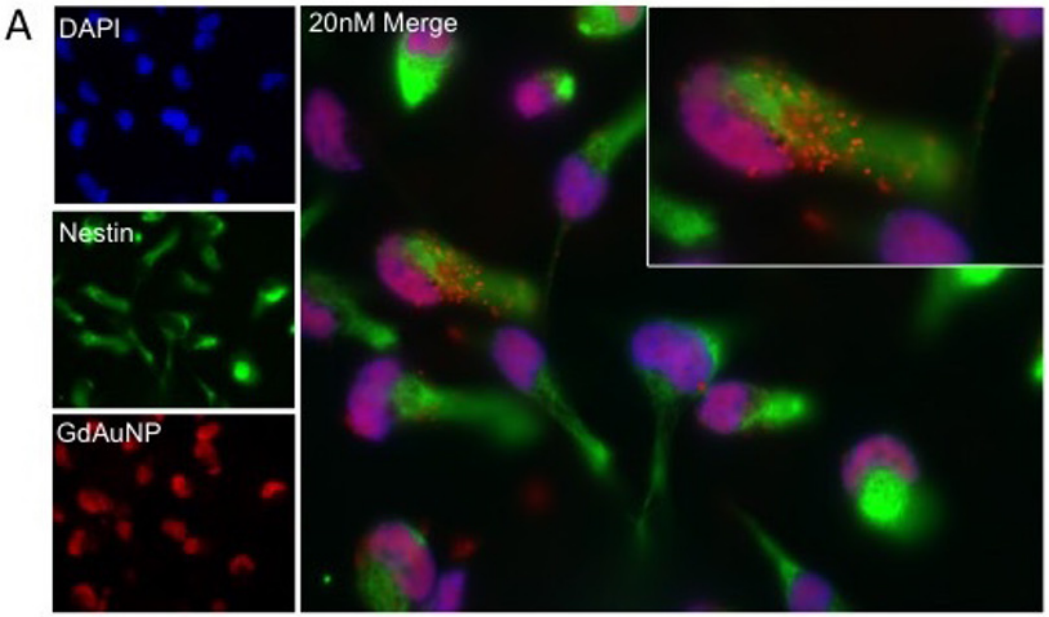
A
DAPI
Nestin
GdAuNP
20nM Merge

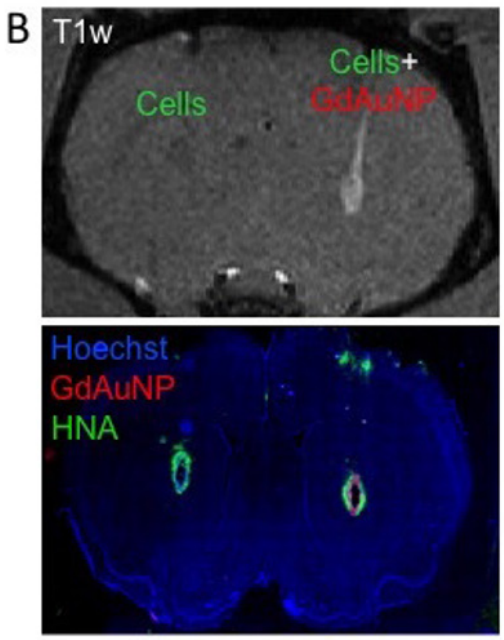
B
T1w
Cells
Cells+
GdAuNP
Hoechst
GdAuNP
HNA

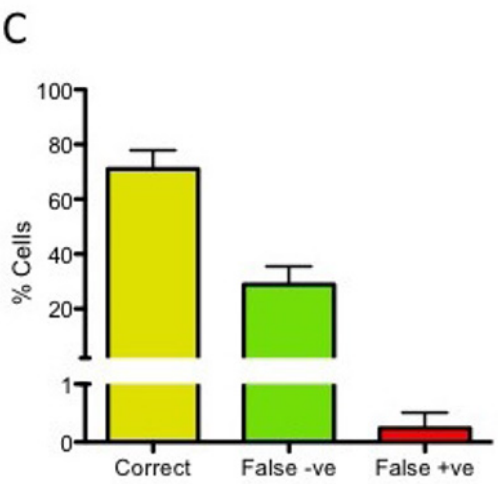
C
100
80
60
40
20
1
0
% Cells
Correct
False -ve
False +ve

CONTROL ID: 2229509

TITLE: Simultaneous in vivo MR imaging of neural stem cells and endothelial cells in a rat model of stroke.

PRESENTER: Michel Modo

ABSTRACT BODY:

Abstract Body: Non-invasive in vivo monitoring of regenerative medicine approaches for tissue and organ reconstruction will be an important technological development to ensure the safety and efficacy of such strategies. However, the involvement of multiple cell types complicates in vivo monitoring that is dependent on a single contrast mechanism. Herein we explore the use of paramagnetic chemical exchange saturation transfer (paraCEST) MRI contrast agents to specifically visualize two transplanted cell populations used for an in situ regenerative medicine approach for the treatment of the stroke-damaged brain. In order to promote the long term survival of transplanted cells within the lesion, vascularization is vital. One potential avenue to achieve this would be through co-transplantation of neural stem cells with endothelial cells. The ability to simultaneously monitor both populations in vivo is important to correlate the survival and distribution of each cell type with eventual outcome measures, such as neo-vascularization and behavioral recovery. In this study, human neural stem cells (NSCs) and human brain endothelial cells (ECs) were labelled using the paraCEST agents Eu-HPDO3A and Yb-HPDO3A, respectively. Electroporation of Yb-HPDO3A in ECs resulted in a higher intracellular concentration compared to Eu-HPDO3A for NSCs. Both were detectable in vitro using MRI. MRI parameters were adjusted to ensure physiological levels that afforded long scan times to ensure sufficient signal could be detected in vivo. In animals (n=3) with stroke damage, 160,000 Eu-HPD03A-labeled neural stem cells and 40,000 Yb-HPDO3A-labeled ECs per ul were transplanted into the lesion cavity two weeks post-occlusion. Pre-transplant and 24 hour post-transplant MRI scans were acquired to visualize the lesion cavity as well as both paraCEST labels. A comparison between unlabelled and labelled cells indicated a 3% signal change for Eu-HPDO3A- and 1% change for Yb-HPDO3A-labeled cells. These images afforded the visualization of the distribution of both populations of cells within the lesion cavity and this was further verified using fluorescent immunohistochemistry. These results provide proof-of-principle that the simultaneous non-invasive imaging of two populations of cells in the brain is feasible. The development of non-invasive imaging will be a key technology to ensure the efficient development of in situ tissue engineering in neurological conditions.

AUTHORS (LAST NAME, FIRST NAME): Nicholls, Francesca J.[2]; Ling, Wen[3]; Ferrauto, Guiseppe[4]; Delli Castelli, Daniela[4]; Aime, Silvio[4]; Modo, Michel[1]

INSTITUTIONS (ALL):

1. Department of Radiology & McGowan Centre for Regenerative Medicine, University of Pittsburgh, Pittsburgh, PA, United States.
2. University of Pittsburgh, Pittsburgh, PA, United States.
3. University of Pittsburgh, Pittsburgh, PA, United States.
4. University of Turin, Turin, Italy.

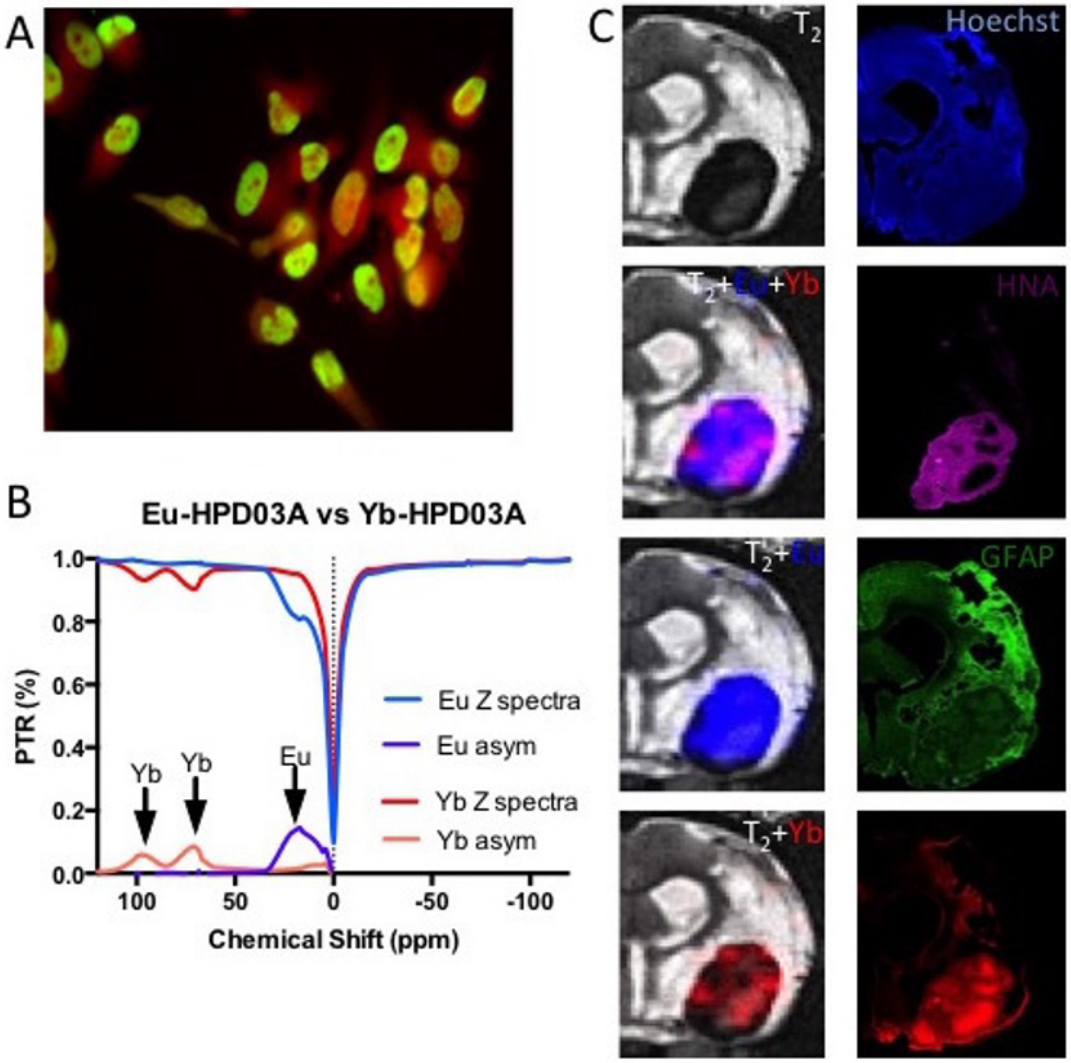

Figure 1. A. Eu-HPD03A's inherent fluorescence can be exploited to determine its uptake into neural stem cells indicating a cytoplasmic distribution after electroporation. B. The chemical exchange properties of Eu-HPD03A and Yb-HPD03A result in z spectra asymmetries that afford their distinction. C. These distinct imaging characteristics can be exploited to visualize the distribution of NSCs (Eu-HPD03A-labeled) and ECs (Yb-HPD03A) after implantation into the stroke cavity. Immunohistochmistry validate in vivo MR imaging indicating that only the area detected on paraCEST images contains transplanted human cells (human nuclei antigen). Glial fibrillary acid protein (GFAP) present in NSCs and CD31 present in ECs revealing the two distinct population of cells and their correspondence to their respective paraCEST images.

CONTROL ID: 2229429

TITLE: Photo-Acoustic Imaging Enables Real-time, Non-invasive Detection of Microvascular Disease and Local Oxygenation Defects in Patients with Chronic Lower Limb Ischemia

PRESENTER: Petra Korpisalo

ABSTRACT BODY:

Abstract Body: Introduction and Aims Despite improvements in revascularization treatments and disease prevention, ischemic complications of cardiovascular and metabolic diseases such as atherosclerosis and diabetes continue to cause major disability, heath care costs and deaths in the Western countries (1). It is known that besides blockages in large arteries, a microvascular disease (MVD) is associated to tissue ischemia (2) and might not be cured only by revascularization of arterial blockages. Furthermore, the lack of suitable imaging methods to detect or locate the microvascular complications has restricted the possibilities of developing or testing specific treatments for the ischemic MVD. We tested photo-acoustic imaging as a tool to study MVD and localize muscle oxygenation defects in patients with chronic lower limb ischemia. **Methods** 15 patients with chronic lower limb ischemia according to Fontaine or Rutherford classification and 5 healthy male volunteers imaged with Vevo® LAZR (Fujifilm Visual Sonics Inc.) equipped with a highly sensitive photo-acoustic transducer at a central frequency of 21 MHz (3). Oxygenation images were acquired by imaging with a sequential laser pulses at 750 nm and 850 nm. As a validation study, we have investigated the drop in tissue oxygenation on calf muscles of a volunteer, by performing imaging while inhaling normal room air and then breathing through a paper bag for 5 minutes. Ischemic calf muscles and an asymptomatic control muscle were imaged from patients.t. Ethical approval and licenses for the study and its equipment were obtained from the Ethical Committee of Kuopio University Hospital, Kuopio University Hospital organization and the Finnish Supervisory Authority “Valvira”. **Results** With volunteers a 9 %units drop was observed in calf muscle sO_2 (Figure, a) providing proof-of principle of the system function as correlating values were also obtained from finger pulse oximeter. In patients photo-acoustic imaging was useful in non-invasive and real-time detection and localization of calf muscle oxygenation defects (Figure, b) that varied in intensity (up to 20 %units drops in sO_2 as compared to control tissue) according to disease severity. **Conclusions** Photo-acoustic imaging provides an interesting novel imaging modality for the detection and characterization MVD and local oxygenation defects in patients with ischemic complications with advantages in ease of use, non-invasiveness, real-time diagnostics and being radiation free. Its applications could easily vary from diagnosis and treatment follow-up of diabetic and ischemic tissue complications to wound healing and further to surgical tissue viability analysis in e.g. skin flaps or amputation stumps. Importantly, tissue level localization of the microvascular complications will help design and target specific treatment for the ischemic MVD. **References** 1) Norgren L et al *Eur J Vasc Endovasc Surg* 33 Suppl 1:S1-75. 2007. 2) Petersen JW et Pepine CJ. Trends Cardiovasc Med. Feb;25(3):98-103. 2015 3) Needles A et al *IEEE Trans Ultrason Ferroelectr Freq Control* 60: 888-897, 2013.

AUTHORS (LAST NAME, FIRST NAME): Korpisalo, Petra[1, 2]; Tarvainen, Santeri[1]; Wirth, Galina[1]; Mäkinen, Kimmo[2]; Laitinen, Tomi[2]; Ylä-Herttuala, Seppo[1]

INSTITUTIONS (ALL):

1. Dept. Molecular Medicine and Biotechnology, Univeristy of Eastern Finland, Kuopio, Finland.
2. Kuopio University Hospital, Kuopio, Finland.

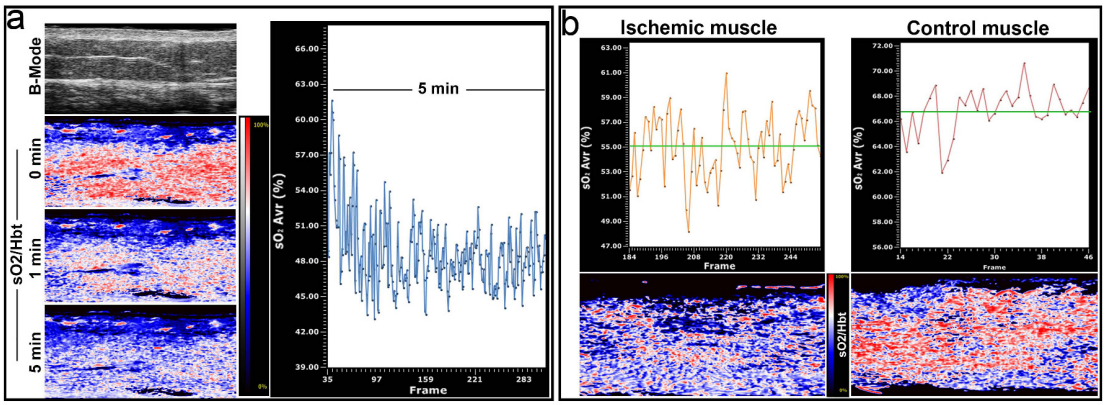

a) Photo-acoustic imaging of calf muscle oxygenation change (sO2/Hbt) in a healthy volunteer breathing through a paper bag for 5 minutes. Representative images at different time points on the left and quantification of the signal on the right.
b) Photo-acoustic imaging of calf muscle oxygenation defects (sO2/Hbt) in a patient with chronic lower limb ischemia. On the top signal quantification and on the bottom the corresponding images.
Colors in PA images: Red signal = 100% sO2/Hbt. Black signal = 0% sO2/Hbt.

CONTROL ID: 2230507

TITLE: Assessing Kidney Function with Magnetic Resonance Imaging of Hyperpolarised 15N-Glutamine

PRESENTER: Markus Durst

ABSTRACT BODY:

Abstract Body: Assessment of the renal function is a vital need for many diseases such as renal insufficiency, renovascular disease, and metabolic disorders. Furthermore, it is required after renal transplantation as well as abdominal trauma. A wide range of non-invasive tests of renal function have been developed (1-3), however all of them have serious drawbacks such as ionising radiation, lack of precision or nephrotoxicity.

Recently, the advent of dynamic nuclear polarisation (DNP) allowed to measure physiologic concentrations of endogenous biomarkers in vivo for the first time by using NMR spectroscopy (4-6). Using DNP, the NMR signal of a labelled molecule can be increased by up to several 10.000 times. Several 13C labelled compounds have been proposed to measure perfusion and transport (8-10). However, their T1 relaxation times are about 30s in vivo (at 3T), which is too short for many physiological processes. We have developed a new molecule for hyperpolarisation, [α-15N(CD3)3]glutamine (7) which exhibits an especially long T1 time (120s in vitro at 3T) on the 15N label because of the deuteration and the low gyromagnetic ratio. Due to the deuterated methyl-group, it is metabolically inactive which was confirmed by in vitro tests. To measure the hyperpolarised 15N signal, we have modified our clinical 3T HDx system (GE Healthcare) with a custom-built TR switch (RAPID Biomedical) to receive and send on the 15N frequency. Furthermore, we have built a small animal 15N butterfly transmit and receive coil.

We have conducted first in vivo tests in healthy rats after injection of a 90-112 mM hyperpolarised solution of our 15N-glutamine compound. A single-shot spiral readout (FOV 8cm, nominal resolution 32x32) was used to acquire images every 5 seconds with a flip angle of 10°.

Time curves from a region of interest within the kidneys show the buildup of the hyperpolarised molecule within the kidneys. The decay was slow enough to obtain a quantifiable signal even after 5 minutes. Mass spectrometry analysis of tissue, blood and urine samples taken at different time intervals shows a quick filtration and excretion within the time scale of the measurement.

Compared to other hyperpolarised molecules which have been introduced to measure perfusion and transport (8-10) our compound exhibits T1 times which are two to three times longer. In addition to perfusion measurements, this could allow the determination of filtration rates and tubular properties, as well as characterisation of the collecting system for the first time using hyperpolarised agents.

References

1. Journal of hypertension 1999;17(3):309-317.
2. Kidney international 1992;41(6):1595-1598.
3. Clinical pharmacology and therapeutics 1990;48(5):503-508.
4. Proc Natl Acad Sci U S A 2003;100(18):10158-10163.
5. Cancer Res 2006;66(22):10855-10860.
6. Nat Med 2007;13(12):1521-1521.
7. Contrast media & molecular imaging 2013;8(5):417-421.
8. American Journal of Physiology-Renal Physiology 2012;302(12):F1658-F1662.
9. Magn Reson Imaging 2012;20(3):305-311.
10. J Magn Reson Imaging 2011;33(3):692-697

Acknowledgements: Co-funding by BMBF grant number 13EZ1114.

AUTHORS (LAST NAME, FIRST NAME): Durst, Markus[1]; Chiavazza, Enrico[2]; Haase, Axel[1]; Aime, Silvio[2]; Schwaiger, Markus[4]; Schulte, Rolf F.[3]

INSTITUTIONS (ALL):
1. IMETUM, Technical University of Munich, Garching, Bavaria, Germany.
2. University of Torino, Turin, Italy.
3. GE Global Research, Garching, Germany.
4. Technical University of Munich, München, Germany.

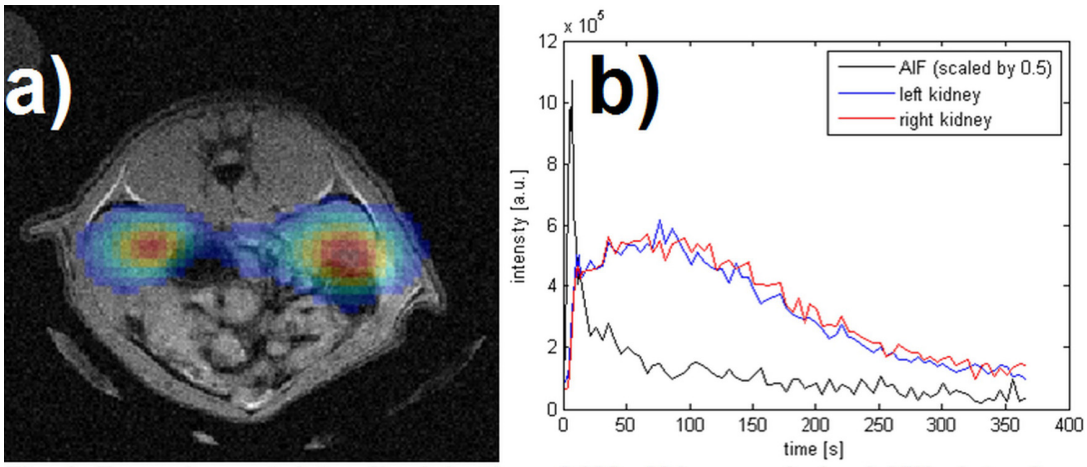

Fig. 1: Exemplary rat data after injection of 100mM hyperpolarised 15N-glutamine. a) Overlay of hyperpolarised image data with anatomical proton MRI scans. b) time curves of hyperpolarised signal within kidney and artery ROI.

CONTROL ID: 2242042

TITLE: Quantifying Lactate Secretion in Tumours using Hyperpolarised Nuclear Magnetic Resonance

PRESENTER: Markus Durst

ABSTRACT BODY:

Abstract Body: Introduction

Most tumours exhibit a high rate of glycolysis and predominantly produce energy by lactic acid fermentation. In order to maintain energy production and prevent self-poisoning, the generated lactate needs to be rapidly transported out of the cell. This is achieved by monocarboxylate transporters (MCTs) [1] which therefore play an important role in cancer pathogenesis [2]. Excessive lactate secretion is also linked to metastasation, radioresistance, lowered immune reaction, vascularisation and many other crucial steps in the progress of cancer [3]. This work is the first demonstration of noninvasive quantitative measurement of MCT activity in vivo by using hyperpolarised 13C pyruvate in combination with a tailored relaxation agent.

Materials and Methods

We used a coordinatively unsaturated Gd(III)DO3A complex which selectively binds to pyruvate and its metabolites to destroy the extracellular hyperpolarisation almost instantaneously. Furthermore, a frequency-selective saturation pulse was programmed so that the intracellular pyruvate magnetisation could be destroyed after a sufficient amount of lactate was formed to exclude effects arising from further pyruvate to lactate conversion.

In vivo experiments were performed on male Fisher F344 rats (n=3) with subcutaneous MAT BIII tumour (neck) in a clinical 3T system. 80mM hyperpolarised [1-13C]pyruvate solution was injected into the tail vein. For each animal, two separate injections were applied: The first without and the second with administration of highly concentrated GdDO3A solution (1:5 compared to pyruvate) 16s after the pyruvate injection. After 20s, pyruvate magnetisation was quenched and spectra of lactate and alanine were acquired in an axial tumour slice (see Fig. 1.). Since only the intracellular metabolite hyperpolarisation is left, the difference in signal decay between the two measurements must be due to transport out of the cell, where the hyperpolarised metabolite is quenched immediately when GdDO3A is present.

Results and Discussion

A considerable difference between the two measurements was observed for lactate (T1 without GdDO3A: 9.3 +- 2.0s, T1 with GdDO3A: 2.51 +- 0.40s). This indicates that lactate is rapidly transported out of the cell and probably that there is a big vascular lactate compartment. The transporter rate was calculated to be 0.33 +- 0.06s^-1. For alanine, the curves are virtually identical within the SNR limits (T1 = 13.3 +- 1.7s), which means alanine stays mostly within the cells, consistent with literature.

Conclusion

Cancer cell membrane transporter rates for lactate efflux could be quantified for the first time in vivo. This could allow a better understanding of tumour metabolism and progression; and enables treatment response measurements for MCT-targeted cancer therapies.

References

[1] Biochem. J. (1999) 343, 281–299

[2] J Bioenerg Biomembr (2012) 44:127–139

[3] Cancer Res 2011;71:6921-6925

Acknowledgements Co-funding by BMBF grant #13EZ1114

AUTHORS (LAST NAME, FIRST NAME): Durst, Markus[3]; Koellisch, Ulrich[6]; Reineri, Francesca[5]; Daniele, Valeria[5]; Aime, Silvio[5]; Menzel, Marion I.[2]; Haase, Axel[4]; Schulte, Rolf F.[1]

INSTITUTIONS (ALL):

1. GE Global Research, Garching, Germany.
2. Diagnostics, Imaging and Biomedical Technologies Europe, GE Global Research, Garching, Germany.
3. IMETUM, Technical University of Munich, Garching, Bavaria, Germany.
4. IMETUM, Technische Universitaet Muenchen, Garching, Germany.
5. University of Torino, Turin, Italy.
6. IMETUM, Technical University of Munich, Garching, Germany.

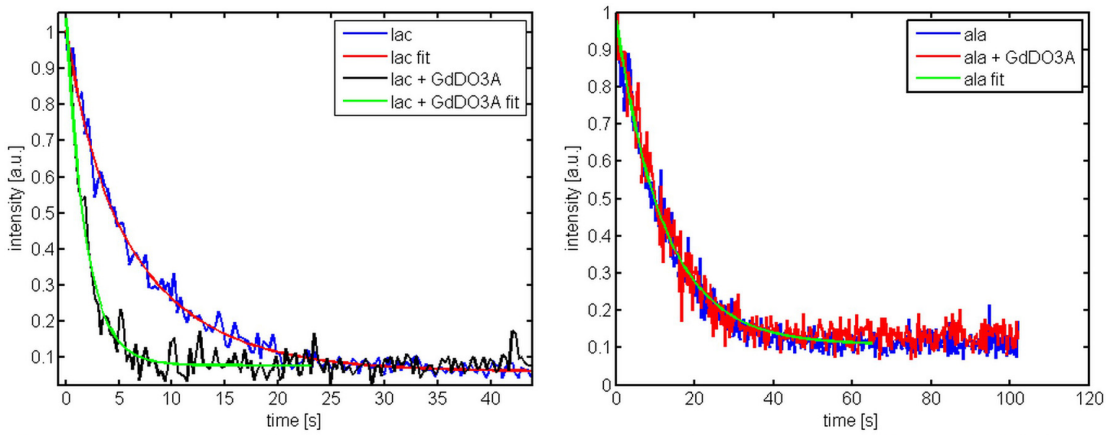

Fig. 1. Lactate and alanine curves in Mat BIII tumour slice with and without additional GdDO3A injection. Lactate efflux from the tumour cells manifests as additional relaxation whereas alanine remains intracellular.

CONTROL ID: 2232273

TITLE: Comparison of Acquisition Schemes for Hyperpolarised 13C Magnetic Resonance Imaging

PRESENTER: Markus Durst

ABSTRACT BODY:

Abstract Body: Introduction

Dynamic nuclear polarisation has enabled magnetic resonance imaging studies with endogenous biomarkers (1). Four of the most widely used encoding types were chosen for an in-depth comparison: FIDCSI (2), EPSI (3), IDEAL spiral CSI (4), and spiral CSI (5). The goal of this work is to facilitate the selection of optimal imaging parameters for a specific purpose and to provide a basis for identifying potential candidates for clinical applications.

Materials and Methods

Two groups of sequences with a spatial resolution of 8×8 and 16×16 pixels (FOV of 8x8cm²) were created. Simulations were performed to evaluate the signal-to-noise ratio (SNR), point spread function (PSF) and artefact behaviour (gradient errors, motion, off-resonance).The sequences were then directly compared in 11 male Fisher F344 rats (Charles River) bearing a subcutaneous Mat BIII tumour in the kidney region after injection of hyperpolarised 80mM [1-13C]pyruvate solution. Experiments were performed in a clinical 3T HDx MRI Scanner (GE Healthcare) using a dual-tuned 13C-1H birdcage volume coil.

Results and Discussion

While FIDCSI delivered adequate image quality, its low encoding efficiency prevents dynamic or multi-slice imaging. The main advantages of FIDCSI are its robustness and benign artefact behaviour. For dynamic acquisitions, the correct approach depends on the desired application. EPSI showed a solid performance for both 16×16 and 8×8 acquisitions, with a better SNR efficiency for 8×8 due to lower gradient demands. Since a full spectrum is obtained, it is stable against off-resonance effects, and the Cartesian sampling scheme reduces errors due to gradient imperfections. IDEAL spiral CSI and spiral CSI have a higher encoding efficiency and can theoretically achieve slightly higher SNR values. However, non-Cartesian encoding has worse artefact behaviour in respect to both off-resonance effects as well as gradient imperfections. This is most likely also the reason why the experimental IDEAL spiral CSI SNR in the tumour is lower than predicted by simulation, which is also supported by the corresponding B0 map.

Conclusion

It was demonstrated in simulations and in tumour-bearing rats that comparable SNR and image quality can be achieved with all of the examined sequences, given that they are used with appropriate parameters. The choice therefore depends on secondary parameters such as encoding efficiency and artefact behaviour. If acquisition time is not critical, EPSI is a robust choice for many applications. For multi-slice imaging or a high time resolution, IDEAL spiral CSI or spiral CSI should be considered. FIDCSI is only an option when no time resolution is needed. With regard to clinical applications, the achievable spatial resolution will be severely limited by sensitivity. Under these conditions, EPSI or spiral CSI are the appropriate choices.

References

[1] Proc Natl Acad Sci USA 2003;100(18):10158-10163. [2] Nature medicine 2007;13(11):1382-1387. [3] Magnetic Resonance in Medicine 2009;62(1):1-10. [4] Magnetic Resonance in Medicine 2012;68(1):8-16. [5] Magnetic Resonance in Medicine 2006;56(4):932-937.

Acknowledgements: Co-funding by BMBF grant #13EZ1114

AUTHORS (LAST NAME, FIRST NAME): Durst, Markus[5]; Koellisch, Ulrich[5]; Rancan, Giaime[4]; Menzel, Marion I.[2]; Schwaiger, Markus[3]; Haase, Axel[6]; Schulte, Rolf F.[1]

INSTITUTIONS (ALL):

1. GE Global Research, Garching, Germany.
2. Diagnostics, Imaging and Biomedical Technologies Europe, GE Global Research, Garching, Germany.
3. Nuklearmedizinische Klinik und Poliklinik, Klinikum rechts der Isar, Technische Universität München, München, Germany.
4. Technical University Munich, München, Germany.
5. IMETUM, Technical University of Munich, Garching, Bavaria, Germany.
6. IMETUM, Technische Universitaet Muenchen, Garching, Germany.

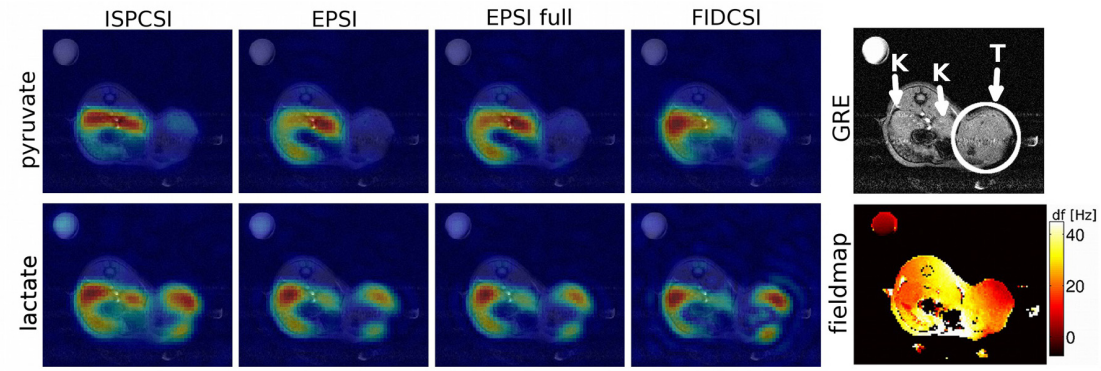

Pyruvate and lactate maps at 16x16 resolution. The proton reference images show the tumour (T) and the kidney (K) ROI. The field maps illustrate the off-resonance for 13C in Hz.

CONTROL ID: 2229473

TITLE: Imaging Patients with Breast and Prostate Cancers Using Combined ^{18}F NaF/^{18}F FDG and TOF simultaneous PET/ MRI

PRESENTER: Andrei Iagaru

ABSTRACT BODY:

Abstract Body: Introduction: We previously reported the pilot evaluation of a simultaneous PET/MRI scanner with TOF capability, as well as the use of combined ^{18}F NaF/^{18}F FDG PET/CT in cancer patients. Here we prospectively compared the combined ^{18}F NaF/^{18}F FDG PET/ MRI against ^{99m}Tc-MDP in patients with breast and prostate cancers for the detection of metastatic disease.

Methods: Fifteen patients referred for ^{99m}Tc-MDP bone scans were prospectively enrolled from Oct 14 - Feb 15. The cohort included 7 men with prostate cancer and 8 women with breast cancer, 41 – 85 year-old (average 62 ± 13). ^{18}F NaF (0.7-2.2 mCi, mean: 1.33 mCi) and ^{18}F FDG (3.9-5.2 mCi, mean: 4.6 mCi) were subsequently injected from separate syringes. The PET/MRI was done 6-12 days (average 9.3 ± 3.2) after bone scan. The whole body MRI protocol consisted of T2-weighted, DWI, and contrast-enhanced T1-weighted imaging. Lesions detected with each test were tabulated and the results were compared.

Results: All patients tolerated the PET/MRI exam, and PET image quality was diagnostic despite the marked reduction in the administered dosage of radiopharmaceuticals (80% less for ^{18}F NaF and 67% less for ^{18}F FDG). Eight patients had no bone metastases identified on either scans. Bone scintigraphy and PET/MRI showed osseous metastases in 7 patients, but more numerous bone findings were noted on PET/MRI than on bone scintigraphy in 3 patients. Lesions outside the skeleton were identified by PET/MRI in 2 patients.

Conclusion: The combined ^{18}F NaF/^{18}F FDG PET/MRI is superior to ^{99m}Tc-MDP scintigraphy for evaluation of skeletal disease extent. Further, it detected extra-skeletal disease that may change the management of these patients, while allowing a significant reduction in radiation exposure from lower dosages of PET radiopharmaceuticals administered. A combination of ^{18}F NaF/^{18}F FDG PET/MRI may provide the most accurate staging of patients with breast and prostate cancers prior to the start of treatment.

AUTHORS (LAST NAME, FIRST NAME): Iagaru, Andrei[1]; Barkhodari, Amir[1]; Jamali, Mehran[1]; Minamimoto, Ryogo[1]; Gambhir, Sanjiv S.[2]; Vasanawala, Shreyas[2]

INSTITUTIONS (ALL):

1. Radiology, Nuclear Medicine, Stanford Hospital and Clinics, Stanford, CA, United States.
2. Radiology, Stanford University, Stanford, CA, United States.

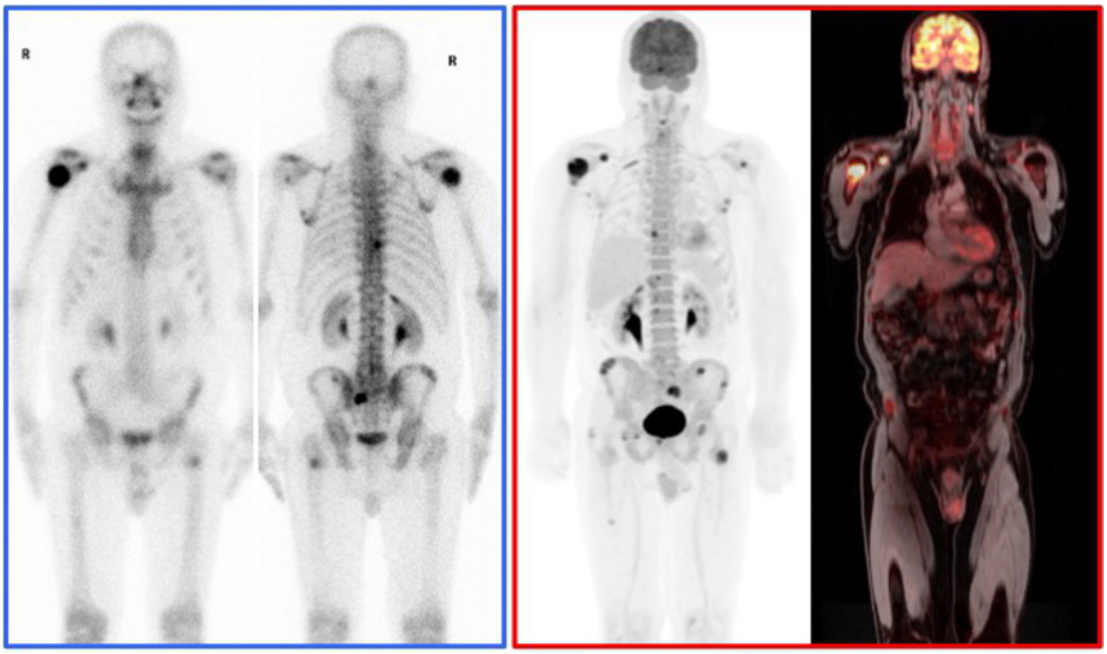

^{99m}Tc MDP Bone Scan

^{18}F NaF (2 mCi) / ^{18}F FDG (5 mCi)
PET/MRI
83 min post-injection

BMI: 27.6

CONTROL ID: 2229488

TITLE: Understanding *Francisella* infection *in vivo* using non-invasive optical imaging

PRESENTER: Charlotte Hall

ABSTRACT BODY:

Abstract Body: *Francisella tularensis* is a highly infectious, gram-negative, intracellular bacterium and is the etiological agent of tularemia. Tularemia has a low aerosol infectious dose (ID_{50} <10 CFU) and a high mortality rate if untreated and, as such, maybe considered a potential biothreat agent. Optical imaging allows infection to be monitored non-invasively both longitudinally and in real time. Genes encoding luciferases such as *lux* can be engineered into pathogens to enable the generation of light which can be visualized through the tissues of a live animal. Additionally optical imaging can be used to sequentially image dissemination of infection in the same animal and can therefore reduce the number of animals used. This technology has enabled the study of host-bacteria interactions and the identification of factors which facilitate bacterial replication and dissemination in the host. Moreover, this methodology will have an application in the evaluation of therapeutics.

The shuttle vector pEDL41 encoding the *luxCDABE* operon was introduced into *F. tularensis* subsp. *tularensis* strain Schu S4 by electroporation. Fitness of Schu S4-*lux*, in terms of growth, stability and virulence, compared to wild-type Schu S4 was assessed *in vitro*. For longitudinal pathogenicity studies BALB/c mice were infected by the aerosol route with wild-type F. tularensis Schu S4 or F. tularensis Schu S4-lux and infection was imaged sequentially using an IVIS Spectrum whole body imaging system until humane end point was reached. Organs were imaged post mortem and bacteriology was conducted to determine bacterial load. All experiments including imaging were conducted within a containment level 3 facility.

This study has found that luciferase reporter strains of Schu S4 suitable for imaging Francisella infection. The virulence of Schu S4-lux in a mouse inhalational challenge model was equivalent to that of the wild-type Schu S4. Bioluminescent signal was detectable from 3 days post-challenge until the humane endpoint with strong signal in the lungs, liver, spleen and lymph nodes. Longtiduinal imaging studies have identified that the lungs serve merely as a gateway for infection rather than the primary site. Following aerosol challenge F. tularensis rapidly disseminates to the spleen and lymph nodes with infection in lung establishing as a secondary infections. Bacterial burden in organs was comparable between F. tularensis-lux to wild-type strains. Additionally the plasmid bearing the lux operon was stably replicated in the absence of antibiotic selective pressure. These data demonstrate non-invasive optical imaging is suitable for the study of F. tularensis pathogenesis in vivo and the evaluation of therapeutic approaches for tularemia.

AUTHORS (LAST NAME, FIRST NAME): Hall, Charlotte[1]

INSTITUTIONS (ALL):

1. University of Exeter, Salisbury, United Kingdom.

(No Image Selected)

CONTROL ID: 2231269

TITLE: 4-[^{18}F]Fluoroglutamine PET to Assess ASCT2 Expression in Lung Cancer

PRESENTER: Jason Buck

ABSTRACT BODY:

Abstract Body: With over 150,000 deaths annually, lung cancer remains the leading cause of cancer-related deaths in the United States (1). This is due largely to a lack of specific and sensitive diagnostic methods, as more than 60% of patients remain undiagnosed until the disease has progressed to an advanced or metastatic state (2). Currently, 2-[^{18}F]fluoro-2-deoxy-D-glucose (^{18}F-FDG) positron emission tomography (PET) remains the only molecular imaging approach clinically approved for the detection and diagnosis of lung cancer. While ^{18}F-FDG PET has proven sensitive towards the detection of glucose-avid tumors, its specificity is limited in the context of lung cancer due to an inability to distinguish cancerous lesions from inflammatory and benign nodules (3). As such, there exists a pressing clinical need to develop improved non-invasive imaging diagnostics of lung cancer.

Emerging evidence suggests that glutamine uptake in cancer cells is regulated by oncogenic signaling pathways (4). In lung cancer, pharmacological inhibition of glutamine uptake has been shown to suppress cell growth *in vitro* and induce regression of primary and metastatic tumors *in vivo* (5). In previous works, expression of the sodium-dependent, neutral amino acid transporter ASCT2, was identified as a candidate biomarker of lung cancer (6). Moreover, the role of ASCT2 in carcinogenesis was validated as an essential glutamine transporter that influences lung cancer cell metabolism, growth, and survival (7).

Given these findings, we hypothesized that a quantitative PET measure of ASCT2 expression may serve as a precision imaging diagnostic of lung cancer. In these studies we evaluated a previously described ^{18}F-labeled analogue of glutamine, 4-[^{18}F]fluoroglutamine (^{18}F-4F-Gln) (8), as a quantitative measure of ASCT2 expression in human cell line xenografts of varying transporter levels and a genetically engineered mouse model of lung cancer. Comparisons were also made to the current clinical standard, ^{18}F-FDG.

Uptake of ^{18}F-4F-Gln, but not ^{18}F-FDG, agreed with relative ASCT2 levels in the xenograft tumors. In the genetically engineered mice, ^{18}F-4F-Gln accumulation was sufficiently elevated in lung tumor, relative to normal lung, and cardiac tissue. ^{18}F-4F-Gln PET appears to provide a non-invasive measure of ASCT2 expression. Given the potential of ASCT2 as a lung cancer biomarker, this and other tracers reflecting ASCT2 levels could emerge as novel, precision imaging diagnostic in this setting.

References: (**1**) Edwards BK *et al.* (2014) *Cancer* 120:1290. (**2**) Parkin DM *et al.* (2005) *CA Cancer J Clin* 55:74. (**3**) Deppen S *et al.* (2011) *Ann Thorac Surg* 92:428; discussion 433. (**4**) Liu W *et al.* (2012) *P Natl Acad Sci USA* 109:8983. (**5**) Shelton LM *et al.* (2010) *Int J Cancer* 127:2478. (**6**) Shimizu K *et al.* (2014) *Brit J of Cancer* 110:2030. (**7**) Hassanein M *et al.* (2013) *Clin Cancer Res* 19:560. (**8**) Qu W *et al.* (2011) *J Am Chem Soc* 133:1122.

AUTHORS (LAST NAME, FIRST NAME): Buck, Jason R.[2, 3]; Hight, Matthew[2, 3]; Hassanein, Mohamed[4]; Tantawy, Mohammed N.[2, 3]; Nickels, Michael L.[2, 3]; Harris, Bradford K.[4]; Pao, William[5]; Watchmaker, Jennifer M.[2]; Massion, Pierre P.[4, 6]; Manning, H. Charles[1, 3]

INSTITUTIONS (ALL):

1. VUIIS, Nashville, TN, United States.
2. Vanderbilt University Institute for Imaging Science, Vanderbilt University, Nashville, TN, United States.
3. Department of Radiology and Radiological Sciences, Nashville, TN, United States.
4. Division of Allergy, Pulmonary and Critical Care Medicine, Nashville, TN, United States.
5. Department of Medicine, Nashville, TN, United States.
6. Vanderbilt-Ingram Cancer Center, Nashville, TN, United States.

(No Image Selected)

CONTROL ID: 2229522

TITLE: Quantification of the endolymphatic hydrops in Ménière's disease using contrast enhanced small animal MRI

PRESENTER: Julia Mannheim

ABSTRACT BODY:

Abstract Body: Morbus Ménière is a disease of the inner ear, which is characterized by hearing loss, tinnitus and vertigo. Its cause is currently unknown. It is assumed that the expansion of volume in the endolymphatic system can cause symptoms of Ménière's disease. The hydrops usually affects the ductus cochlearis and the sacculus in the labyrinthine membrane. In the past the endolymphatic hydrops could only be diagnosed by post-mortem analysis. Recent advances in MR imaging have allowed the volumetric quantification of the endolymphatic hydrops and hence allow *in vivo* diagnosis. A common animal model to study potential therapies is the surgical obliteration of the ductus and saccus endolymphaticus.

Eight guinea pigs underwent a unilateral obliteration. The other ear served as control. To quantify the volume change of the fluid spaces in the inner ear, guinea pigs were *i.v.* injected with a gadolinium based contrast agent. Animals were scanned using a 7 T small animal MR scanner 1.5 h after contrast agent application. MR images were acquired using a proton weighted turbo spin echo sequence and a voxel size of 0.102 x 0.102 x 0.3 mm^3. Orientation was aligned planar to the nervus cochlearis to acquire lateral plane images. The contrast agent is taken up by the scala tympani and scala vestibuli. The scala media does not show an uptake, hence the volume change of the scala media can be monitored by the volume change of the scala vestibuli. MR imaging was performed one week before, 1, 3, 5 & 7 weeks after obliteration. ROIs were drawn in the scala vestibuli & the scala tympani. After the last MRI scan, the inner ear function of the animals was examined using electrocochleography. Then animals were sacrificed and inner ears were fixed for histological analysis.

1 week after surgical obliteration the volume of the scala media was increased in 5 out of 9 animals at the expense of the volume of the scala vestibuli (max. decrease 3.1 to 1.5 mm^3). 3 weeks after obliteration 2 out of those 6 animals showed still an increase of the volume of the scala media compared to the volume before obliteration. For one animal that didn't show a volume change in week 1, an increase of volume has been detected in week 3 (decrease of scala vestibuli 2.7 to 1.1 mm^3). For the remaining 4 animals, that showed a volume increase in week 1, the volume decreased back to baseline levels. 5 and 7 weeks after obliteration 2 animals did show an enlargement in the scala media. Volume of the scala tympani was stable over time. The electrophysiological examination didn't show a significant difference between the control and the obliterated ear. Histological staining showed a good correlation with the MRI results.

It was shown that the hydrops was able to be resolved and to be quantified just one week after the surgical obliteration. To our knowledge this is the first *in vivo* study showing the onset of the endolymphatic hydrops one week after surgical obliteration. However further studies are required to optimize the surgery to obtain a more stable hydrops. Nevertheless this animal model showed a high potential of being a suitable tool to study potential therapies for Ménière's disease.

AUTHORS (LAST NAME, FIRST NAME): Mannheim, Julia G.[1]; Müller, Marcus[2]; Schmid, Andreas M.[1]; Kumagami, Hidetaka[3]; Vollmer, Sonja[4]; Gottwald, Ulrich[4]; Pichler, Bernd J.[1]; Löwenheim, Hubert[2]

INSTITUTIONS (ALL):

1. Department of Preclinical Imaging and Radiopharmacy, Eberhard Karls University Tübingen, Werner Siemens Imaging Center, Tübingen, Germany.
2. Carl von Ossietzky Universität Oldenburg, Universitätsklinik für Hals-Nasen-Ohrenheilkunde, Oldenburg, Germany.
3. Department of Otolaryngology-Head and Neck Surgery, Nagasaki University Graduate School of Biomedical Sciences, Nagasaki, Japan.
4. Global Drug Discovery, Bayer Pharma AG, Berlin, Germany.

(No Image Selected)

CONTROL ID: 2229533

TITLE: Clinical prognosis of patients with discordance result of sestamibi myocardial perfusion SPECT and NH_3 PET

PRESENTER: Eun-jung Kong

ABSTRACT BODY:

Abstract Body: Purpose: We retrospectively evaluated the clinical prognosis of patients with perfusion defects of ^{99m}Tc - sestamibi myocardial perfusion SPECT (MPS) and/or ^{13}N - NH_3 PET (PET).

Materials and Methods:
We reviewed 27 patients(60.4±11.8 y-o; male 21) who undertook both adenosine stress PET and MPS within 2 days, from March 2005 to February 2006. We assessed the concordance and discordance between the PET and MPS images, then compared imaging results with their clinical prognosis; We identified the coronary stenosis on angiography and their reversibility on follow-up imaging study (echocardiography, MPS or FDG PET) and checked the development of chest pain.

Results: Coronary angiography was performed in 24 patients. Ultimately, 22 patients had coronary artery disease, 5 patients had no coronary artery stenosis; 2 dilated cardiomyopathy, 1 hypertrophy cardiomyopathy, 1 congestive heart failure and 1 repetitive syncope. MPS showed reversible or irreversible perfusion defects on 19 patients, 4 equivocal defects and 4 negative scan. Overall 21 patients got benefit from PET; 14 patients with irreversible or partially reversible in MPS turned to reversible defect on PET, and their wall motion or perfusion improvement were confirmed in follow-up imaging study, moreover 2 of 14 also were diagnosed additional ischemic lesion. Four equivocal perfusion defects on MPS turned to definite defects on PET. Two of 4 negative scan on MPS turned to left main disease and multivessel disease, respectively. In 2 dilated cardiomyopathy patients, MPS showed perfusion defect however, PET revealed one negative scan and one equivocal defect. The MPS and PET showed same results in 2 myocardial infarction and 2 negative scan. During follow-up, 1 patient died from nasopharyngeal cancer, 2 patients were done intervention due to restenosis.

Conclusion: Adenosine stress ^{13}N - NH_3 PET showed more reversible perfusion defects with higher accuracy than ^{99m}Tc - sestamibi MPS. ^{13}N -ammonia PET offer better assessment of myocardial ischemia and viability.

AUTHORS (LAST NAME, FIRST NAME): Kong, Eun-jung[1]; Cho, Ihn Ho[1]

INSTITUTIONS (ALL):
1. Yeungnam Univ Hospital, Daegu, Korea (the Republic of).

(No Image Selected)

CONTROL ID: 2231819

TITLE: Diagnostic Performance of Hybrid PET/MR for Determination of Preoperative axillary Lymph Node Status in Patients with invasive breast cancer

PRESENTER: Eun-jung Kong

ABSTRACT BODY:

Abstract Body: Objective: The aim of the study was to evaluate diagnostic performance of hybrid PET/MRI for determining preoperative axillary lymph node(ALN) status in patients with invasive breast cancer.

Materials and methods:

Two hundred thirty-six women with histologically proven breast cancer were recruited to undergo preoperative PET/MR imaging. Among them, 184 patients fulfilled the inclusion criteria (invasive carcinoma, no previous operation, no neoadjuvant chemotherapy). MR Imaging of the breast including a dynamic contrast enhanced series and diffusion weighted imaging (DWI) was performed with a dedicated breast coil according to ACR guidelines. PET data was acquired simultaneously for 8 minutes. ALNs were identified on obtained images and following parameters were evaluated: long axis, cortical thickness, shape, presence of fat hilum, apparent diffusion coefficient (ADC) and maximum standardized uptake value (SUV). Histology served as the gold standard.

Results:

Sentinel lymph node biopsy was performed in 122 cases, axillary dissection in 62 cases. 70 patients exhibited ALN metastases, of whom 15 were classified as micrometases. Mean size of breast mass was 2.1 ±1.5 cm. Macrometastatic ALN showed high FDG uptake, longer axis, thicker cortex, more frequent morphologic abnormalities, higher signal intensity at DWI and higher ADC values with statistical significance. No significant difference between micrometastatic ALN and benign ALN in PET/MR imaging. The sensitivity, specificity and accuracy of PET for determining ALN metastasis were 84%, 58% and 68%, respectively. Those are 77%, 84% and 82% in considering both PET with morphologic change and 81%, 66% and 72% in considering PET, morphologic change and DWI, respectively.

Conclusion

PET/MR imaging techniques showed high accuracy in the preoperative evaluation of axillary status in patients with breast cancer. Additional information by DWI is unlikely to be useful in predicting metastatic ALN.

AUTHORS (LAST NAME, FIRST NAME): Kong, Eun-jung[1]; Cho, Ihn Ho[2]

INSTITUTIONS (ALL):

1. Yeungnam Univ Hospital, Daegu, Korea (the Republic of).
2. Nuclear Medicine, Yeungnam University Hospital, Daegu, Korea (the Republic of).

(No Image Selected)

CONTROL ID: 2229539

TITLE: *In vivo* PET imaging of inflammation in rheumatoid arthritis (RA) using the platelet-collagen binding tracer [^{64}Cu]NOTA-GPVI

PRESENTER: Kerstin Fuchs

ABSTRACT BODY:

Abstract Body: The platelet glycoprotein VI (GPVI), a type I transmembrane glycoprotein which belongs to the immunoglobulin superfamily, has been identified as the major platelet collagen receptor *in vivo*. GPVI an important platelet adhesion receptor plays a critical role in the process of thrombosis for example at sites of atherosclerotic lesions and is expressed exclusively by megakaryocytes and platelets. It mediates integrin activation via non-covalent interaction with the γ-chain of the Fc receptor. [^{64}Cu]NOTA-GPVI has been used by our group for imaging of atherosclerotic lesions in mice, but unexpectedly during *in vivo* imaging studies of atherosclerotic lesions in humans tracer accumulation was observed at sites of inflammation. The aim of this study was to investigate [^{64}Cu]NOTA-GPVI as potential PET tracer for *in vivo* non-invasive imaging of inflammation using an experimental animal mouse model of RA.

We labelled the soluble dimeric form of the human GPVI conjugated to an Fc-fragment with NOTA and radiolabeled the complex using [^{64}Cu]. BALB/c mice were injected *i.p.* with glucose-6-phosphate isomerase containing serum (100µL) to induce arthritic inflammation, or control serum for control animals. On day 5 after arthritis induction, mice were injected with 10.6±0.5 MBq [^{64}Cu]NOTA-GPVI and PET scans were performed 1h, 24h and 48h after tracer injection. To test specificity of tracer binding, 1mg unlabelled GPVI was injected *i.v.* simultaneous to tracer solution. To analyse blood clearance of [^{64}Cu]NOTA-GPVI, samples were collected 1h, 24h and 48h after tracer injection in blocked and unblocked mice and analysed using a γ-counter. Collagen-, histological staining, biodistribution and autoradiography studies were performed on day 7 after serum injection to confirm *in vivo* PET results.

Analysis of the different imaging time points in arthritic ankles revealed an enhanced [^{64}Cu]NOTA-GPVI uptake already 1h after *i.v.* tracer injection in arthritic ankles (13.7±2.25 %ID/g) compared to control ankles (1.5±0.2 %ID/g). [^{64}Cu]NOTA-GPVI uptake increased and reached a tracer uptake with a maximum level 24h and 48h after tracer injection in arthritic joints (33.0±3.5 %ID/g), 48h (33.9±3.4 %ID/g). Blocking experiments revealed a statistic significant reduced tracer uptake after 24h (23.0±1.8%ID/g) and 48h (20.8±2.0 %ID/g) compared to unblocked PET investigations at 24h and 48h ($p<0.01$). In addition PET data correlated well with *ex vivo* biodistribution, autoradiography and histological analysis. Analysis of blood and plasma clearance revealed a high tracer concentration in plasma 1h after tracer injection, but nearly no tracer after 24h and 48h in blood or blood-plasma, at time points with the maximum tracer uptake in inflamed ankles.

Our data clearly show that [^{64}Cu]NOTA-GPVI is a new powerful tool for non-invasive imaging of inflammation in experimental-induced RA *in vivo*, as our results correlated well with ankle thickness, histopathological changes, biodistribution and autoradiography analysis, and the fast blood and blood-plasma clearance qualify this tracer for translation into clinics. We are currently evaluation the GPVI PET tracer for other types of inflammation.

AUTHORS (LAST NAME, FIRST NAME): Fuchs, Kerstin[1]; Ehrlichmann, Walter[1]; Harant, Maren[1]; Kohlhofer, Ursula[2]; Quintanilla-Martinez, Leticia[2]; Kneilling, Manfred[1, 3]; Pichler, Bernd J.[1]

INSTITUTIONS (ALL):

1. Department of Preclinical Imaging and Radiopharmazy, Eberhard Karls Univsersity of Tuebingen, Germany, Werner Siemens Imaging Center, Tuebingen, Germany.
2. Department of Pathology, Eberhard Karls University of Tuebingen, Tübingen, Germany.
3. Department of Dermatology, Eberhard Karls University of Tuebingen, Tübingen, Germany.

(No Image Selected)

CONTROL ID: 2244255

TITLE: In vivo Manganese enhanced Magnetic Resonance imaging (MEMRI) as new tool to evaluate rat bone marrow cellularity

PRESENTER: Francesca Rosa

ABSTRACT BODY:

Abstract Body: Purpose:

Despite their relevance in clinical medicine, extension and activity of red bone marrow (rBM) cannot be directly evaluated in vivo.

The purpose of this exhibit is to explore the feasibility of High-resolution Mn^{2+}enhanced MRI (MEMRI) for in vivo assessments of red bone marrow distribution by a clinical 3T MR scanner.

Material and Methods:

In vivo experiments were approved by the Institutional Review Committee of the National Cancer Institute, and were performed in accordance to the National Regulation on Animal Research Resources (D.L. 116/92). Six months old male rats (n=2) were inoculated i.v. with 250 mmol solution of $MnCl_2$. Rats were positioned in a wrist coil, applied to a clinical 3T MR scanner. Before and 24 hours after Mn^{2+} i.v. injection, T1-3D-SPGR-weighted sequences with a slices thickness of 230 micron, were performed. Qualitative and quantitative analysis were performed by setting ROIs, respectively on left and right, proximal and distal femur, proximal tibia and humerus, acetabolum and lumbar vertebrae in order to evaluate BM cellularity. Specimens were then paraffin-embedded and processed for histological analysis according to standard techniques.

Results:

Contrast enhancement at BM site was analised around 24 hours after $MnCl_2$ injection on T1-3D-SPGR weighted images in order to evaluate intracellular accumulation: Mn^{2+} uptke was different in each bone segment at qualitative and quantitative analysis.

Paired Student's t-test analysis of SNR values before and 24 hours after Mn^{2+}administration yielded a significant P value for red bone marrow ($P<0,05$).

To correlate manganese-enhanced MR images with BM cellularity, histological analysis were performed in each bone specimens.

The highest presence of Hematopoietic Stem Cells (HSCs) was found at the proximal humerus and femur diafisis, according to Mn^{2+} uptake observed at MR imaging.

Discussion:

The biology of Mn^{2+} ion combined with its ability to act as an MR contrast agent opens the possibility of using MEMRI to visualise tissue functions. Manganese can enter into the cells via a certain number of transport systems, which can be regulated by the plasma membrane calcium sensing receptor. Quantitative analyses demonstrated an increase in ΔSI 24 hours after manganese administration. The complete lack of RBCs in the half part of distal tibia may therefore be responsible for the absence of ΔSI increase.

ΔSI was not the same for each examined bone segments, but it was correlated to histological data which describe BM cells distribution in relation with anatomic site as described by Cline et al. The mean percentage of available marrow space occupied by hematopoietic cells showed a correlation with ΔSI: the SI tended to increase according to cellularity.

In conclusion, this first preliminary investigation points out the feasibility of MEMRI of BM by a 3T scanner. Manganese, as contrast, allows a quantitative whole-body evaluation of HSCs distribution. This method opens the opportunity to evaluate the activity of BM in pathological conditions and to investigate HSCs engraftment in transplanted patients.

AUTHORS (LAST NAME, FIRST NAME): Rosa, Francesca[2]; Basso, Luca[2]; Pace, Daniele[2]; Prono, Valentina[2]; Salvi, Sandra[1]; Neumaier, Carlo Emanuele[2]; Baio, Gabriella[3]

INSTITUTIONS (ALL):

1. Anatomical Pathology, IRCCS San Martino IST Hospital, Genova, Italia, Italy.

2. radiology, IRCCS IST- San Martino, Genova, Genova, Italy.
3. Aberdeen Biomedical Imaging Centre, University of Aberdeen, Aberdeen, United Kingdom.

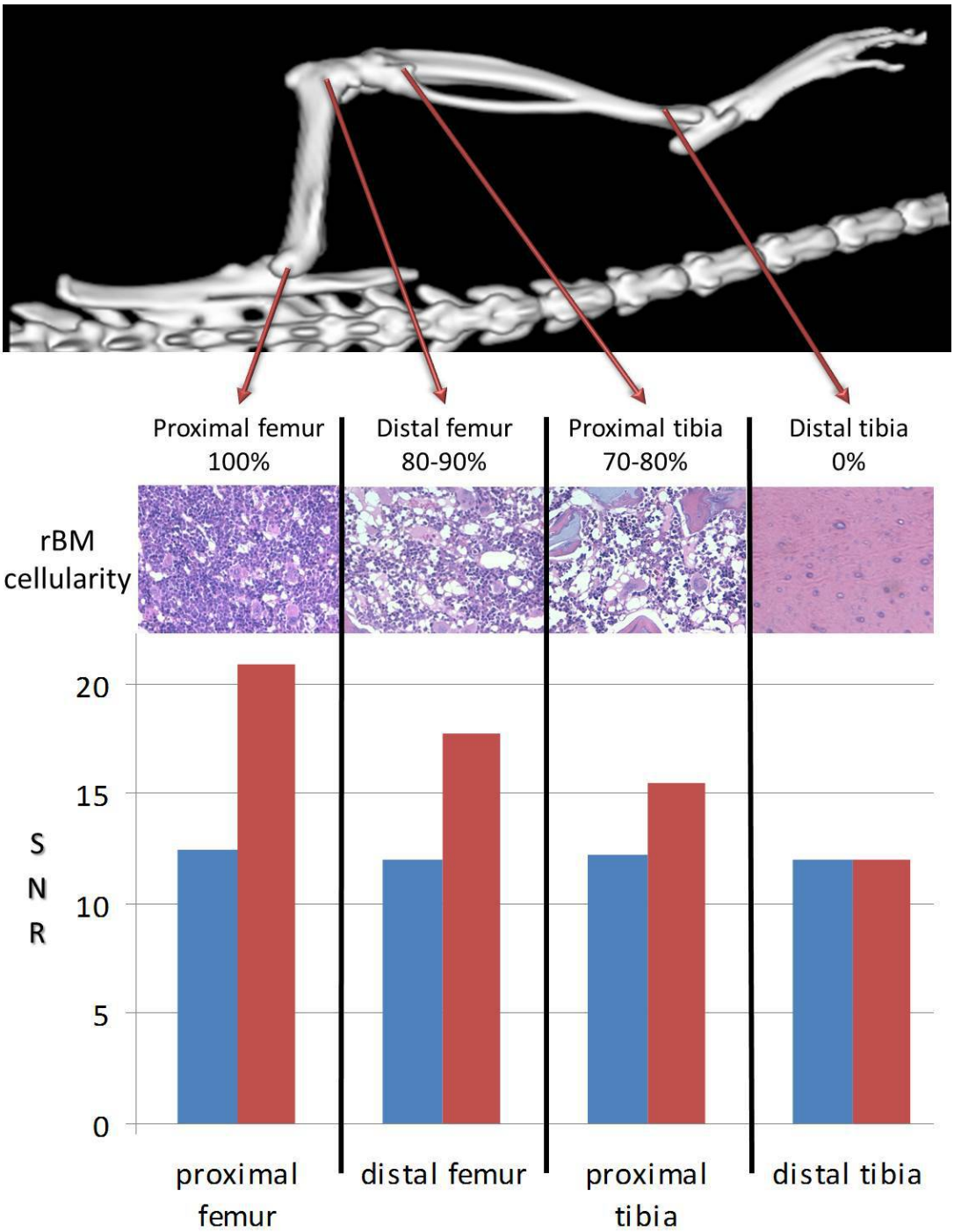

The mean percentage of available marrow space occupied by hematopoietic cells showed a correlation with SI: where cellularity increased also the SI tended to increase.

CONTROL ID: 2244652

TITLE: In Vivo Non-invasive Detection of Brown Adipose Tissue through Manganese Enhanced Magnetic resonance Imaging (MEMRI)/b>

PRESENTER: Francesca Rosa

ABSTRACT BODY:

Abstract Body: Introduction

Obesity is rapidly spreading across most developed countries . At a fundamental level, obesity is the result of an imbalance between energy intake and energy expenditure. The latter is very difficult to quantify and recent work suggests that it can be altered by the function of Brown Adipose Tissue (BAT).

The recent discovery of active BAT in adult humans has opened new avenues for obesity research and treatment, as reduced/increased BAT activity seems to be implicated in development of diabetes, hypertension and cancer cachexia.

However, clinical applications are currently limited by the lack of non-invasive tools for measuring mass and function of this tissue in humans. Here we show a new magnetic resonance imaging method based on biology of manganese and its accumulation in cells via calcium channels. With this method we can explore the characteristic cellular structure of BAT to selectively image it. We demonstrate and validate this method in mice using histology.

Objectives To demonstrate that Mn^{2+} can visualise BAT in human breast/prostate cancer murine model and healthy Adult Spraque-Dawley rats, as assessed by clinical 3T magnetic resonance (MR).

Methods

In vivo experiments were approved by the Institutional Review Committee of the National Cancer Institute (IST), and were performed in accordance to the National Regulation on Animal Research Resources (D.L. 116/92).

Human MDA-MB-231-Luc breast cancer cells (n=2) and PC3 prostate cancer cells (n=2) were orthotopically grown in NOD/SCID mice to a minimum mass of 5 mm. Mice and health Spraque-Dawley Male rats (n=2) were evaluated on T1- weighted sequences before and after intravenous injection of $MnCl_2$.

T1-3D-SPGR-weighted sequences before $MnCl_2$ i.v. inoculation and 20 minutes and 20 hours after, were performed.

Both qualitative and quantitative analysis by using a clinical functool software 9.4.05a were performed.

Results 20 minutes and 20 hours after Mn^{2+} administration, on T1-3D-SPGRWI, we observed a significant increase in Signal Intensity (SI). Paired Student's t-test analysis of SNR values before and 20 hours after Mn^{2+} administration yielded a significant P value for BAT ($P<0,05$).

Conclusion

Many literature reports have investigated the BAT physiology in animals and humans. The activity of this tissue and its relation to metabolism has led to implications of BAT as a preventive mechanism against weight gain and obesity.

On the other side, the activation of brown fat has been described in rodent models of cachexia and in certain cachectic patients.

Human breast cancer cell line MDA-MB-231 which give rise to tumours if transplanted in immunocompromised mice, secrete PTHrP upon stimulation which triggers adipose tissue browning and cancer cachexia.

Thus, neutralization of PTHrP might hold promise for ameliorating cancer cachexia and improving patient survival.

MEMRI can visualise BAT in both physiological and pathological condition, opening up possibilities for a new MRI contrast agent able to evaluate BAT response to future target therapy and its activity in oncological animal models.

AUTHORS (LAST NAME, FIRST NAME): Rosa, Francesca[2]; Basso, Luca[3]; Pace, Daniele[1]; Secondini, Lucia[3]; Boccardo, Simona[5]; Neumaier, Carlo Emanuele[6]; Baio, Gabriella[4]

INSTITUTIONS (ALL):

1. Radiology, IRCCS AZIENDA OSPEDALIERA UNIVERSITARIA SAN MARTINO IST - ISTITUTO NAZIONALE PER LA RICERCA SUL CANCRO, Genoa, Italy.
2. radiology, IRCCS IST- San Martino, Genova, Genova, Italy.
3. Radiology, IRCCS San Martino IST Hospital, Genova, Italia, Italy.
4. Aberdeen Biomedical Imaging Centre, University of Aberdeen, Aberdeen, United Kingdom.
5. anatomical pathology, AOU IRCCS IST San Martino, Genova, Genova, Italy.
6. Radiology, AOU IRCCS IIST San Martino, Genova, Genova, Italy.

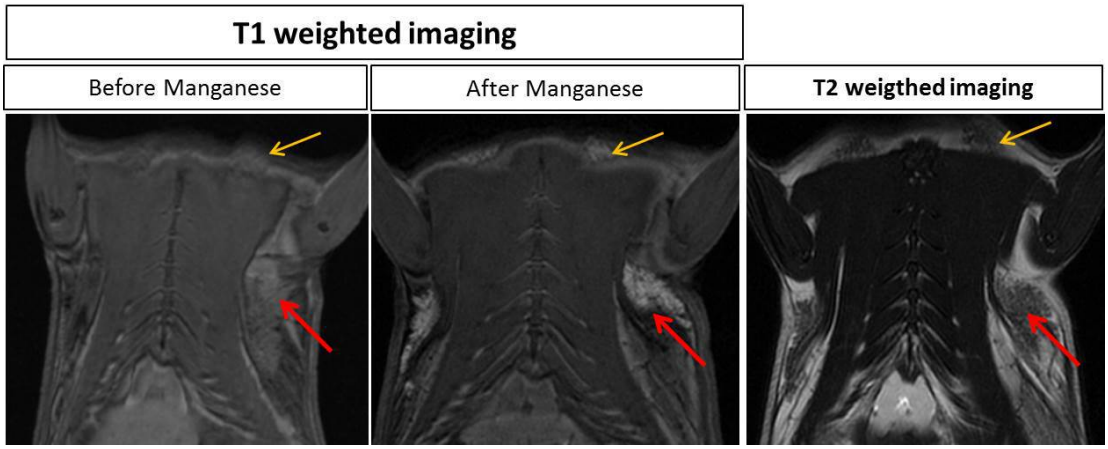
T1 weighted imaging
Before Manganese
After Manganese
T2 weigthed imaging

CONTROL ID: 2229640

TITLE: Tumor Progression and Regression Monitoring using Hyperpolarized [1-^{13}C]Pyruvate Metabolic Imaging in a Breast Cancer Murine Model

PRESENTER: Peter Shin

ABSTRACT BODY:

Abstract Body: Purpose: A major challenge in cancer biology is to monitor altered cancer metabolism in vivo in a non-invasive way, preferrably prior to any observable morphologic changes [1]. We used hyperpolarized [1-^{13}C]pyruvate metabolic imaging to monitor the tumor progression and regression in a breast cancer murine model that conditionally expresses the human *c-MYC* oncogene in a doxycycline regulated way. Previously, it was shown that the model further develops secondary tumor even after c-MYC deinduction [2]. Hence, our purpose was to monitor altered glycolytic metabolism in this multi-stage mammary tumorigenesis animal model.

Method: Tumor grafts derived from a human *c-MYC* transgenic mouse were transplanted into a mammary gland of a female FVB mouse. Following the transplant, we fed the mouse with chows containing doxycycline (doxy-chow) for deregulated c-MYC expression from the onset. After a baseline [1-^{13}C]pyruvate imaging study, the doxy-chow was removed (off-doxy) from her diet and four other follow up studies were performed at different time points (4, 16, 33, and 49 days after the off-doxy time point). ^{1}H images were also acquired to monitor morphological changes and to spatially register the ^{13}C data.

Result: Five ^{13}C measurements from the animal were acquired in the span of 7 weeks before and after the withdrawal of doxycycline (Figure). Morphological regression of the tumor was observed as fast as 4 days after off-doxy (c-MYC deinduction) together with a decreased lactate-to-pyruvate ratio. Lactate production further decreased until the 16th day as shown in the ^{13}C spectra. Then, on the 33rd day, an increase in the lactate-to-pyruvate ratio was observed. However, there were no apparent changes in the tumor size at this point. Finally, a full-blown tumor mass was observed after 49 days post off-doxy with further increase in lactate production.
From a different animal, we observed possible metastatic lesions forming in the mouse liver (44 days post off-doxy). The primary tumor site at the implanted mammary gland showed severe heterogeneity (Persuasive Data 1). In the liver, a marked lesion was observed indicating a possible metastasis (Persuasive Data 2). Interestingly, ^{13}C data showed high levels of alanine production in the liver voxels, suggesting a link between the liver metastasis and the alleviated alanine production. Previously, high rate of conversion from pyruvate to alanine has been observed in pre-tumor stage of c-*MYC*-induced liver cancer mice [3].

Conclusion: In this work, we used hyperpolarized [1-^{13}C]pyruvate metabolic imaging to examine in vivo glycolytic alterations at different stages of mammary tumor formation. The data show that pyruvate-to-lactate conversion tightly reflects the regression of the primary tumor. Furthermore, we were able to observe a change in the conversion rate prior to secondary tumor formation. A possible metastatic lesion distal from the transplanted site was also detected.

References:

[1] Kurhanewicz J et al., Neoplasia 2011;13:81-97.
[2] D'Cruz CM et al., Nat. Med. 2001;7:235-239.
[3] Hu S et al., Cell Metabol. 2011;14:131-142.

AUTHORS (LAST NAME, FIRST NAME): Shin, Peter J.[1]; Zhu, Zihan[1, 2]; Camarda, Roman[3]; Bok, Robert[1]; Zhou, Alicia Y.[4]; Goga, Andrei[3, 4]; Vigneron, Daniel[1, 2]

INSTITUTIONS (ALL):
1. Radiology and Biomedical Imaging, UCSF, San Francisco, CA, United States.
2. The UC Berkeley - UCSF Graduate Program in Bioengineering, San Francisco, CA, United States.
3. Biomedical Sciences Graduate Program, UCSF, San Francisco, CA, United States.
4. Department of Cell and Tissue Biology, UCSF, San Francisco, CA, United States.

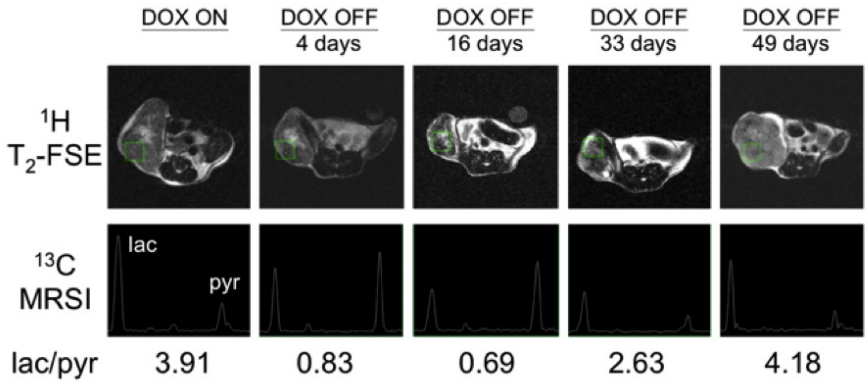

1-¹³C monitoring of tumor progression and regression. Note the change in lac/pyr value between the 16 days and 33 days data showing altered metabolism that precedes morphological change in the tumor.

CONTROL ID: 2230718

TITLE: ^{18}F Sodium Fluoride Uptake in PET/MR is Associated with Pain and Cartilage Degeneration in Knee Osteoarthritis

PRESENTER: Dragana Savic

ABSTRACT BODY:

Abstract Body: Purpose

Osteoarthritis (OA) is a degenerative joint disease and a leading cause of disability in the US. Knee OA Outcome Score (KOOS) is used to assess the patient's symptoms including pain. MRI derived $T_{1/b>}$ and T_2 relaxation times in the cartilage are used to quantify early signs of OA[1]. The clinically used Whole Organ MRI Scores (WORMS[2]), that range from 0-4, assess the focal lesions, where WORMS>0 indicate a lesion. Na^{18}F is used to assess subchondral bone remodeling in OA[3], but the relationship of subchondral bone remodeling, cartilage changes, and clinical parameters has not been previously investigated. PET/MRI is a combined modality that enables the investigation of both the cartilage(MRI) and bone remodeling (PET) simultaneously. The purpose of this study is to investigate if pain and cartilage degenerations are associated with bone remodeling in OA patients as demonstrated by Na^{18}F uptake.

Method

Seven patients (KL_{avg}=1)[1] were imaged with PET/MRI (GE HC) and were IV administered 10mCi Na^{18}F at scan onset. The MR sequences included a 3D FSE (CUBE) and a quantitative combined $T_{1\rho}/T_2$[1]. Maps were reconstructed by fitting $T_{1\rho}$ and T_2 weighted images voxel-by-voxel. PET was acquired in list mode for 60min and dynamic multiframes were reconstructed using an iterative algorithm. Standardized uptake values [SUV_{bw} g/ml] were examined in bone regions located next to the cartilage (Fig. 1). KOOS scores and WORMS grades were assessed.

Results

SUVs ranged from 0.2-1.9 depending on the knee compartment. Interestingly patients without KOOS pain, the SUVs in patella, trochlea (TRO) and medial tibia (MT) was consistently higher than in those patients with pain. $T_{1/b>}$ in patella correlated with pain, and the range of $T_{1\rho}$ and T_2 values in the cartilage were higher for the patients with pain, compared to patients without pain. Patients with low Na^{18}F uptake in the patella and TRO had pain and showed high WORMS grade=3. Patients with high Na^{18}F uptake in the patella had low WORMS grade≤1 and no pain. Finally patients who had low WORMS grade=1 in the patella, TRO and MT showed high Na^{18}F uptake in the regions but no specific trend of pain.

Conclusion

Na^{18}F uptake in bone regions is related to KOOS pain and cartilage lesions. Patients with pain showed high WORMS and low Na^{18}F uptake in the patella suggesting no trend of bone remodeling with high-grade cartilage lesions. But patients with low-grade lesions all showed higher Na^{18}F uptake in the corresponding bone but with varying pain. This study indicates that low-grade lesions may be associated with Na^{18}F uptake and it is speculated that increased Na^{18}F bone uptake happens prior to the cartilage lesion. Total joint characterization may be better evaluated on PET/MRI scanners, where subchondral bone changes can be studied simultaneously with $T_{1/b>}$, T_2 values and WORMS to assess the morphological and biochemical properties of cartilage. Further research is required to elucidate the exact etiology of the relationship of osteoblastic activity in these regions to patient related outcomes and cartilage lesions.

Reference

1. Li *Osteoar Cart 20*07 15:7 789-97

2. Link *Osteoar Cart 2010 18:6 776-86*

3. Lajeunesse *Rheum* 2003 15:5 628-33

AUTHORS (LAST NAME, FIRST NAME): Savic, Dragana[1]; Mazur, Courtney M.[1]; Venkatachari, Anand K.[1]; Pedoia, Valentina[1]; Seo, Youngho[1]; Franc, Benjamin L.[1]; Majumdar, Sharmila[1]

INSTITUTIONS (ALL):

1. Radiology and Biomedical Imaging, University of California, San Francisco, San Francisco, CA, United States.

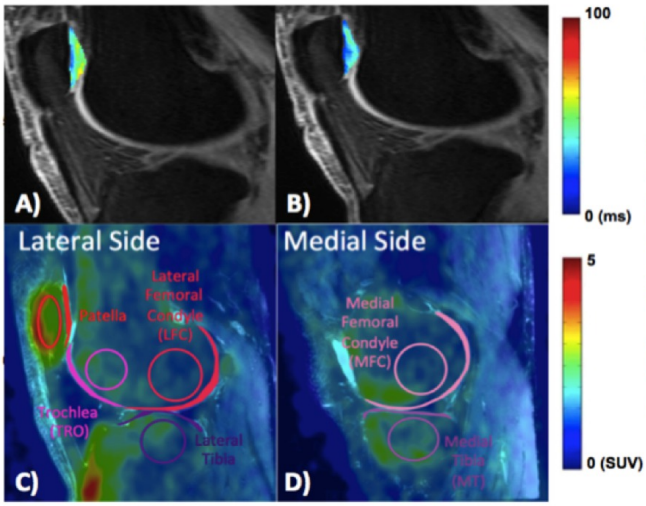

Figure 1. Sagittal view of lateral side of knee. **A)** $T_{1\rho}$ map of patella overlaid on the first echo. The color map indicates higher $T_{1\rho}$ relaxation times in the patella. **B)** T_2 map of patella overlaid on the first echo. The color map shows slightly increased T_2 relaxation times in the patella. **C) & D)** show PET/MRI fused images of MR FSE CUBE with $Na^{18}F$ PET uptake at 60min post injection, SUV (0-5). Cartilage ROIs and corresponding bone ROIs are shown on the lateral side of the knee **(C)** and on the medial side of the knee **(D)**. Increased uptake is observed in Patella and Lateral tibia.

CONTROL ID: 2229656

TITLE: Developing a molecularly targeted T_2-exchange MRI contrast agent for the early detection and diagnosis of primary and recurring thyroid cancers

PRESENTER: Mark Milne

ABSTRACT BODY:

Abstract Body: Introduction: The problem with thyroid nodules (i.e., tumors) is that about 50% of the population has them. Yet only 5% to 8% of these are malignant. Also, the standard diagnostic suite for thyroid nodules (i.e., ultrasound, iodine-131 SPECT/CT, fine-needle biopsy, and genetic markers) is costly, takes several months to complete, and still leads to a high level of indeterminacy. Currently, the only method for a 100% accurate diagnosis is surgical removal of the entire thyroid for pathological examination. Yet this leads to thousands of unnecessary surgeries per year, where the nodules turn out to be benign. What is needed is a single, whole-body test that could offer both high-resolution anatomic information as well as functional information in order to determine if a thyroid nodule is malignant. In contrast to SPECT/CT, MRI offers superior anatomic resolution and soft tissue contrast with zero ionizing radiation, making it an excellent tool for cancer detection and monitoring. The effectiveness of MRI in the functional and molecular imaging regime is currently limited due to the lack of highly sensitive molecularly targeted contrast agents. Creating such agents, like the one described here, would greatly improve the use of MRI for the early detection and diagnosis of thyroid and other cancers.

Hypothesis: It was recently shown that Ln^{3+}DOTA-based chelates create enhanced T_2 contrast (i.e., image darkening) in MRI through the chemical exchange of water molecules (1,2). The level of this "T_2-exchange" contrast (T_{2ex}) is proportional to the bound water molecule chemical shift and reaches a maximum at a specific water molecule exchange rate, which the Dy^{3+}DOTA-based chelate has been successfully "tuned" to (1). It was also previously demonstrated that T_{2ex} contrast could be increased by several orders of magnitude through simple linear polymerization of the Ln^{3+}DOTA chelate (3). We hypothesize that by using these methods, a highly sensitive T_{2ex} MRI contrast agent can be created for improved biological targeting and molecular imaging of thyroid cancer with MRI. In addition, this technique could also be combined with MR spectroscopy of the choline peak of the tumor to increase cancerous tissue specificity (4).

Innovation and Impact: If successful, this research has the potential to significantly improve thyroid and other cancer diagnostics by accurately imaging the location and size of cancerous lesions and, by using cell receptors as prognostic indicators, differentiate between indolent and aggressive forms, thereby performing disease characterization entirely non-invasively (i.e., without FNA biopsy). Also, in contrast to SPECT/CT, disease diagnostics and therapy monitoring would be performed on a single-modality MRI instrument without the risk of ionizing radiation. This would reduce patient stress by eliminating unnecessary thyroid resections, finding recurrence earlier, and accelerating the time for diagnosis.

References: **(1)** Soesbe TC, et al. MRM 2014;71:1179-1185. **(2)** Soesbe TC, et al. MRM 2011;66:1697-1703. **(3)** Wu Y, Soesbe TC, et al., JACS 2008;130:13854-13855. **(4)** Mountford C, et al. JMRI 2006;24:459-477.

AUTHORS (LAST NAME, FIRST NAME): Soesbe, Todd C.[1, 2]; Milne, Mark[1]; Nwariaku, Fiemu[3]; Lenkinski, Robert E.[2]; Sherry, A. D.[1]

INSTITUTIONS (ALL):

1. Advanced Imaging Research Center, UT Southwestern Medical Center, Dallas, TX, United States.
2. Department of Radiology, UT Southwestern Medical Center, Dallas, TX, United States.
3. Department of Surgery, UT Southwestern Medical Center, Dallas, TX, United States.

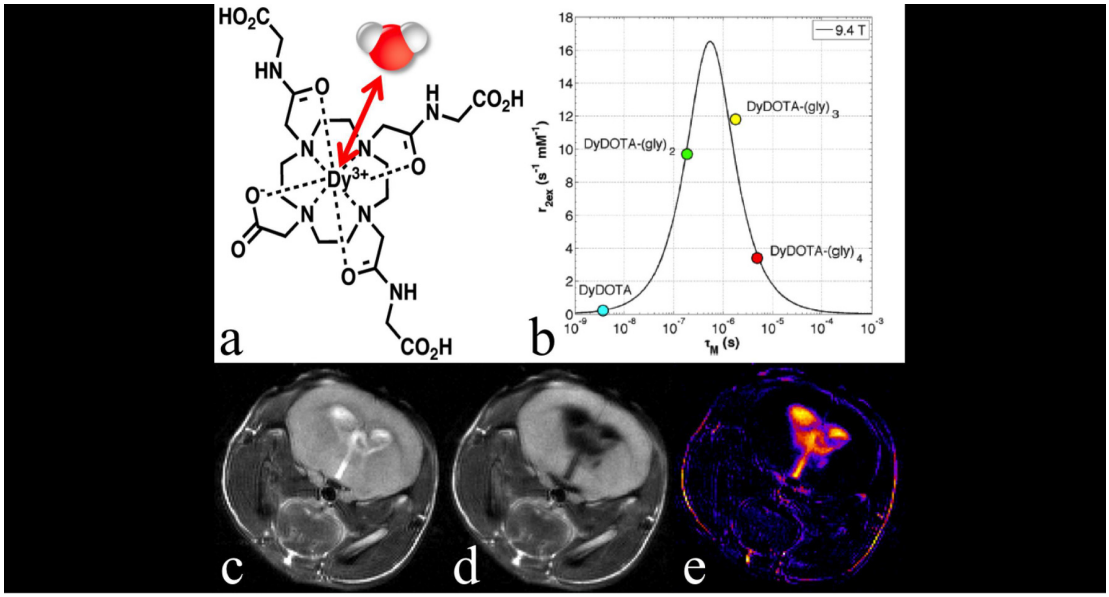

Fig. 1: **a)** A schematic of the DyDOTA-$(gly)_3$ chelate showing that three of the four possible sidearm locations have been populated with glycinate (gly), which slows down the water molecule exchange rate between the Dy^{3+} ion and the bulk water (red arrow). By attaching different numbers of glycinate sidearms (i.e., 0 to 4) to the DyDOTA chelate, different water molecule exchange rates (and thus different levels of T_{2ex} contrast) were achieved.

b) A Swift-Connick plot (solid line) showing the theoretical relationship between the transverse relaxivity due to water molecule exchange (r_{2ex}, y-axis) and the $Dy3^+$ bound water lifetime (τ_M, x-axis) at 9.4 T. The measured data for the different DyDOTA-based chelates we synthesized (circular markers, taken at 37 °C) are in excellent agreement with Swift-Connick theory. While the water molecule exchange rates ($k_{ex} = \tau_M^{-1}$) for DyDOTA (blue circle) and DyDOTA-$(gly)_4$ (red circle) are too fast and too slow respectively, the exchange rates for DyDOTA-$(gly)_2$ (green circle) and DyDOTA-$(gly)_3$ (yellow circle) place them near the peak of the Swift-Connick plot (τ_M=545 ns).

To show the negative contrast capabilities of these new T_{2ex} contrast agents, small doses were directly injected into mice brain areas to simulate uptake due to molecular targeting. **c)** Axial MRI of a healthy house brain. **d)** The same axial slice after intracranial injection of 0.03 mmol/kg of DyDOTA-$(gly)_3$ in 20 μL. Note the darkening of the ventricle cerebrospinal fluid due to T_{2ex}. **e)** The difference image (c minus d) showing regions of agent uptake.

CONTROL ID: 2229691

TITLE: angioCEST: using TmDOTMA encapsulated liposomes and chemical exchange saturation transfer for enhanced MRI angiography

PRESENTER: Todd Soesbe

ABSTRACT BODY:

Abstract Body: Introduction: Liposomal encapsulation of paramagnetic chemical exchange saturation transfer (paraCEST) agents creates enhanced contrast in MRI by shifting the resonance frequency of the water molecule protons inside the liposome away from the bulk water frequency by 2 ppm to 10 ppm (lipoCEST) (1). Radio-frequency saturation at this shifted proton resonance, along with water molecule exchange across the liposome membrane, causes enhanced negative contrast (image darkening) in areas of liposome uptake. LipoCEST greatly increases the relative sensitivity of paraCEST contrast agents by using the approximately 10^6 to 10^9 shifted protons contained within the liposome for CEST. In this research, we investigate the idea of utilizing the high CEST sensitivity and the long blood circulation half-life (~18 hours) (2,3) of polyethylene glycol (PEG) coated “stealth” liposomes encapsulating TmDOTMA to perform CEST-based MRI angiography for vascular space imaging and quantitative blood volume measurements (angioCEST).

Methods: A 67 mM aqueous solution of TmDOTMA was encapsulated inside of 135 nm diameter liposomes. The total intra-liposome water was 27% of the stock solution volume, giving an effective Tm^{3+} concentration of 18 mM. *In vitro* z-spectrum of the stock solution were measured at 37 °C on an Agilent 9.4 T small animal MRI system using a 38 mm diameter birdcage coil and the gradient-echo pulse sequence with centric k-space ordering. A 5 second long saturation pulse was used with varied power (0.3, 0.6, 1.3, 2.5, 5, and 10 μT) in order to find the optimal power and saturation frequency settings. These ideal settings were then used to image the abdominal vasculature of healthy female Black-6 mice that were tail vein injected with 500 μL of the 18 mM TmDOTMA liposome solution (i.e., a 0.4 mmol[Tm^{3+}]/kg dose).

Conclusion: These preliminary data show that liposomal TmDOTMA angioCEST can image the vascular space with zero signal from background tissue using low-power saturation (2.5 μT). This technique could be used to evaluate therapeutic efficacy of cancer agents by measuring tumor blood volume before and after treatment. Further work includes incorporating B_o corrections using the WASSR method (4), speeding up acquisition using 3D gradient-echo and shorter saturation pulses, and improving chemical shift and sensitivity by increasing the Tm^{3+} concentration inside the liposome through chelate polymerization techniques.

References: (1) S. Aime, et al., MRM, 44:5513-5515, 2005. (2) K. B. Ghaghada, et al., AJNR, 28:48-53, 2007. (3) A. L. Ayyagari, et al., MRM, 55:1023-1029, 2006. (4) M. Kim, et al., MRM, 61:1441-1450, 2009.

AUTHORS (LAST NAME, FIRST NAME): Soesbe, Todd C.[1, 3]; Ghaghada, Ketan B.[2]; Ratnakar, S. J.[1]; Sherry, A. D.[1]; Lenkinski, Robert E.[3]

INSTITUTIONS (ALL):

1. Advanced Imaging Research Center, UT Southwestern Medical Center, Dallas, TX, United States.
2. Texas Children's Hospital, Houston, TX, United States.
3. Department of Radiology, UT Southwestern Medical Center, Dallas, TX, United States.

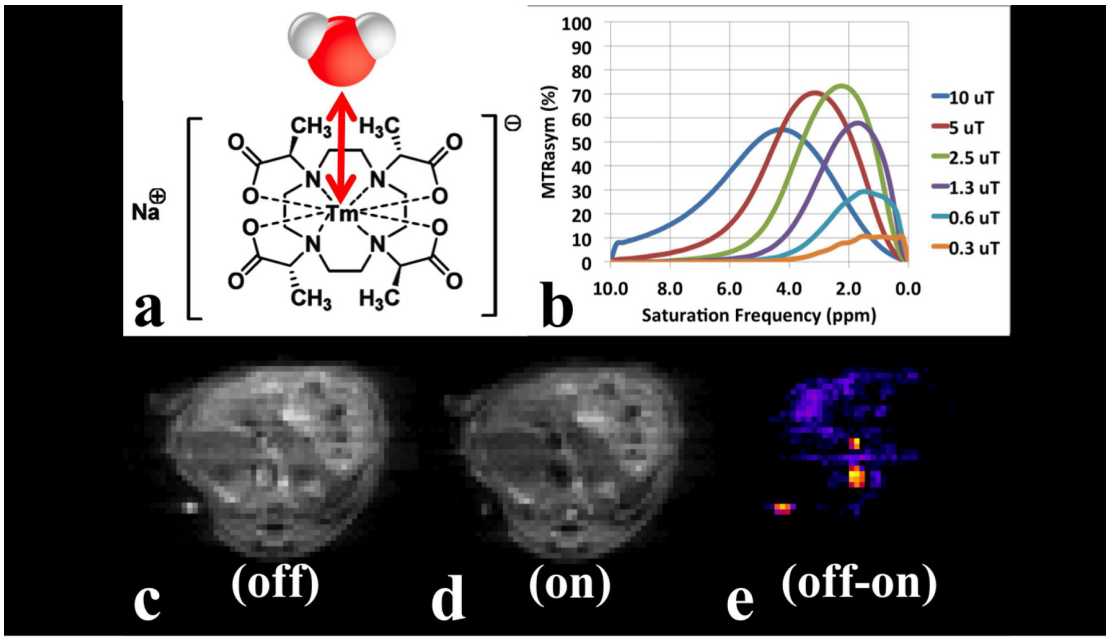

Fig.1: a) A schematic of the TmDOTMA chelate illustrating the water molecule exchange between the Tm^{3+} ion and the bulk water (red arrow). **b)** In vitro MTRasym plots of the TmDOTMA encapsulated liposomes. These data were taken at 9.4 T and 37 °C using a 1 second long saturation pulse and six different saturation powers. Note that for 2.5 μT (green line) there is a large 75% MTRasym at 2.2 ppm. These data have been B_o corrected using the WASSR method. **c)** Axial gradient-echo MRI of a healthy house abdomen taken with the saturation pulse (1 second/2.5 μT) at the "off" frequency (-2.2 ppm). **d)** The same slice with the saturation pulse (1 second/2.5 μT) at the "on" frequency (+2.2 ppm). **e)** The difference image (c minus e) showing an approximately 50% MTRasym in the vascular space (orange areas) due to the presence of the TmDOTMA liposomes.

CONTROL ID: 2229725

TITLE: Development of novel tracers for positron emission tomography and single photon computed tomography of poly(ADP-ribose) polymerase-1.

PRESENTER: Filip Zmuda

ABSTRACT BODY:

Abstract Body: Background: Poly(ADP-ribose) polymerase-1, PARP-1, is involved in the repair of DNA breaks[1] and is overexpressed in a wide variety of tumours.[2] These tumours can be sensitsed to conventional chemotherapy by introducing a PARP-1 inhibitor (PARPi) such as olaparib. However, such combinations are highly toxic to bone marrow.[3] Nuclear imaging using a radiolabelled PARPi could be used to monitor PARPi retention in different tissues with the aim of optimising dosing such that bone marrow sensitisation is minimised. To date, there are no clinical PARP-1 molecular imaging tracers in existence.

Aims: This work aimed to develop Single Photon Emission Computed Tomography (SPECT) and Positron Emission Tomography (PET) tracers based on olaparib that can be used to establish PARPi tumour and bone marrow retention profiles and subsequently optimal PARPi and chemotherapy dosing schedules.

Methods: A total of 19 target SPECT and PET compounds were synthesised in their cold form and screened for lipophilicity (Log P_{oct}), percentage plasma protein binding (%PPB) and PARP-1 inhibitory properties using high performance liquid chromatography and a cell-free Trevigen^{TM} colorimetric assay. Lead candidates were assessed for plasma and microsomal stability by incubation in mouse plasma and pooled human liver microsomes followed by liquid chromatography mass spectroscopy analysis. All assays were based on validated literature methodology. Radiolabelling of lead candidates was performed as per Figure 1. The biodistribution of the SPECT tracer was investigated in subcutaneous U87MG tumour bearing nude mice at 30 minutes (n=3) and 120 min (n=4) post-injection by gamma-counting of harvested organs.

Results: The screening procedure identified FZ044 (cell-free IC_{50} 3.3 nM, log P_{oct} 3.00 and %PPB 96.2%) and FZ236 (cell-free IC_{50} 2.0 nM, log P_{oct} 2.51 and %PPB 87.7%) as lead SPECT and PET candidates respectively; olaparib was used as a gold standard (cell-free IC_{50} 11.9 nM, log P_{oct} 1.95 and %PPB 75.9%). Both FZ044 and FZ236 were stable in plasma after 20 hours and showed rapid intrinsic clearance of 85 ± 4 and 82 ± 11 µL/mL/min respectively, compared to 29 ± 8 µL/mL/min for olaparib. Radiochemistry allowed for 88 ± 1% ^{123}I incorporation with an end of synthesis (EOS) yield of 42 ± 4% (n=3) and 63 ± 10% ^{18}F incorporation with an EOS yield of 8 ± 2% (n=2) to generate [^{123}I]-FZ044 and [^{18}F]-FZ236 respectively. At 120 minutes post injection [^{123}I]-FZ044 showed a tumour to muscle ratio of 5.6 and a tumour to femur ratio of 1.0 with some evidence of hepatobiliary clearance.

Conclusion: SPECT and PET candidates for non-invasive molecular imaging of PARP-1 have been developed and synthesised in respectable radiochemical yields. The initial *in vivo* data for the SPECT tracer is promising, as it showed retention in both tumour and bone tissue. Further *in vivo* characterisation of both imaging tracers is currently underway.

References:

Wang Z, *et al*. *Front Med* 2012, **6**, 156–164

Ossovskaya V, *et al. Genes & Cancer* 2010, **1**, 812–821

Plummer R, *et al*. *Clin Cancer Res* 2008, **14**, 7917–7923

AUTHORS (LAST NAME, FIRST NAME): Zmuda, Filip[1, 2]; Blair, Adele[2]; Champion, Susan[3]; Chahal, Sandeep[4]; Malviya, Gaurav[5]; Anderson, Kurt I.[6]; Sutherland, Andrew[2]; Chalmers, Anthony[4]; Pimlott, Sally[3, 1]

INSTITUTIONS (ALL):

1. College of Medical, Veterinary and Life Sciences, University of Glasgow, Glasgow, United Kingdom.
2. School of Chemistry, University of Glasgow, Glasgow, United Kingdom.
3. Department of Clinical Physics, Western Infirmary, Glasgow, United Kingdom.
4. Wolfson Wohl Cancer Research Centre, Glasgow, United Kingdom.
5. Department of Nuclear Imaging, The Beatson Institute for Cancer Research, Glasgow, United Kingdom.
6. Beatson Advanced Imaging Resource, The Beatson Institute for Cancer Research, Glasgow, United Kingdom.

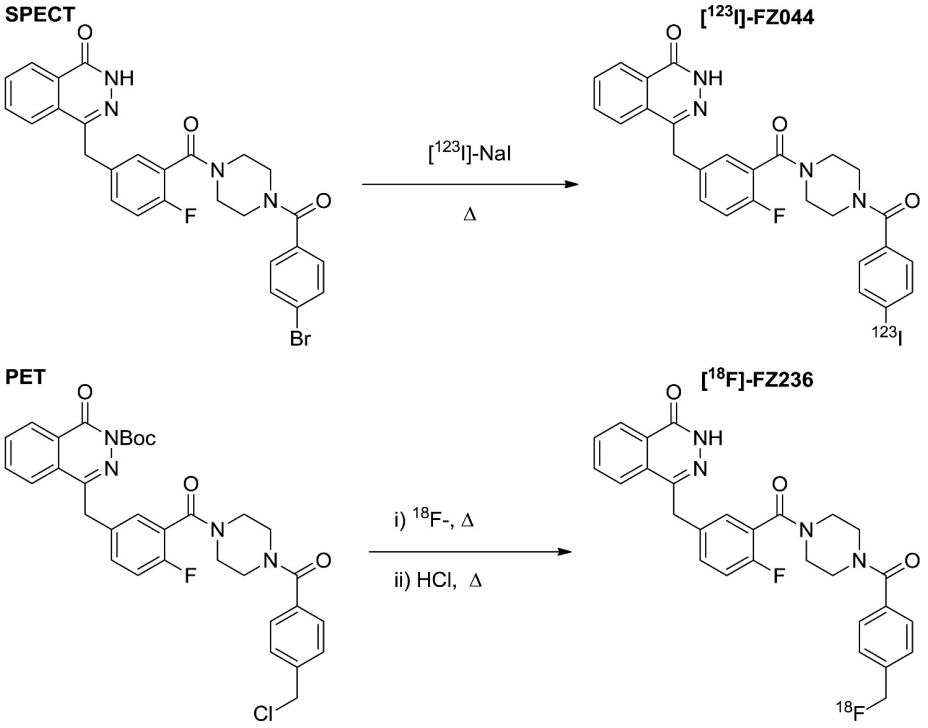

Figure 1. Radiochemical approaches used to generate the target SPECT ([^{123}I]-FZ044) and PET ([^{18}F]-FZ236) tracers.

CONTROL ID: 2229740

TITLE: Nanoreporter technology allows imaging-facilitated prognoses of anti-cancer nanotherapy efficacy

PRESENTER: Carlos Perez Medina

ABSTRACT BODY:

Abstract Body: Nanomedicine is a blooming field of research in which preclinical successes have propelled the FDA approval of clinical products, like Doxil® or Abraxane®. Nanotherapeutic formulations of cytotoxic agents are becoming increasingly integrated in patient cancer care. Unfortunately, nanotherapy treatment response varies immensely between individuals, likely related to tumor permeability heterogeneity[1]. A method to non-invasively evaluate tumor-targeting efficacy would have tremendous impact on patient care and nanotherapy success rate, as it facilitates adaptation of dosing regimen to individual needs, as well as assessing therapeutic safety[2]. Here we present a new nanoreporter strategy to evaluate pegylated liposomal drug delivery to tumors in vivo by PET imaging.

Methods: We developed an ^{89}Zr-labeled nanoreporter system (^{89}Zr-NRep) as surrogate imaging agent for pegylated liposomal doxorubicin (Doxil). In female NCr nude mice bearing 4T1 breast cancer tumors, Doxil (10 mg/kg) and ^{89}Zr-NRep were intravenously co-injected and ex vivo quantification of radioactivity and doxorubicin concentration was performed at three time points (6, 24 and 48 h post injection, p.i.) in digested tumor tissues. Nanoreporter standardized uptake values (SUVs) derived from in vivo PET imaging were correlated with doxorubicin concentration in digested tumor tissues obtained after imaging at 24 h p.i. To test the predictive value of our nanoreporter we performed a therapeutic study in which mice were co-injected with Doxil (dosed at 20 or 10 mg/kg) and ^{89}Zr-NRep. A PET imaging session was performed at 24 h p.i. and the size of tumors was monitored three times weekly. Control animals received either saline or ^{89}Zr-NRep.

Results: A strong correlation was found between ex vivo quantified radioactivity and doxorubicin concentration in tumors at all time points (R^2 = 0.90, 0.95 and 0.93 at 6, 24 and 48 h, respectively) as well as for all time points combined (R^2 = 0.93, figure 1A). A similar strong correlation was observed between SUVs obtained by in vivo PET imaging and doxorubicin concentration in tumor tissues (R^2 = 0.93, figure 1B and 1C). A significant inverse correlation between SUVs at 24 h p.i. and tumor growth rates was observed by the end of treatment effect (R^2 = 0.45, $p < 0.0001$ and R^2 = 0.53, $p < 0.0001$, at 9 and 12 days p.i., respectively), indicative of the ability of ^{89}Zr-NRep imaging to predict treatment response. Moreover, the median survival values of animals in which more than 50 mg/kg doxorubicin accumulated in the tumor, as determined by in vivo PET imaging, increased from 19 to 23 days (figure 1D).

Conclusion: We have developed a nanoreporter technology that allows in vivo monitoring and predicting the efficacy of pegylated liposomal doxorubicin. Our technology represents a valuable in vivo biodistribution visualization tool, without the need to modify the nanotherapy. This approach can be readily adapted for other nanoparticle drug formulations and be applied for a variety of diseases.

1) Prabhakar et al. *Cancer Res* **2013**, *73*, 2412-7.

2) Sanhai et al. *Nat Nanotechnol.* **2008**, *3*, 242-4.

AUTHORS (LAST NAME, FIRST NAME): Perez Medina, Carlos[1, 2]; Abdel-Atti, Dalya[3]; Fayad, Zahi A.[1]; Lewis, Jason S.[4]; Mulder, Willem J.[1]; Reiner, Thomas[5, 6]

INSTITUTIONS (ALL):

1. Translational and Molecular Imaging Institute, Mount Sinai, New York, NY, United States.
2. Centro de Investigación en Red de Enfermedades Respiratorias, Madrid, Spain.
3. Radiology, Memorial Sloan Kettering Cancer Center, New York, NY, United States.
4. Radiology, Memorial Sloan Kettering Cancer Center, New York, NY, United States.
5. Radiology, Memorial Sloan Kettering Cancer Center, New York, NY, United States.
6. Weill Cornell Medical College, New York, NY, United States.

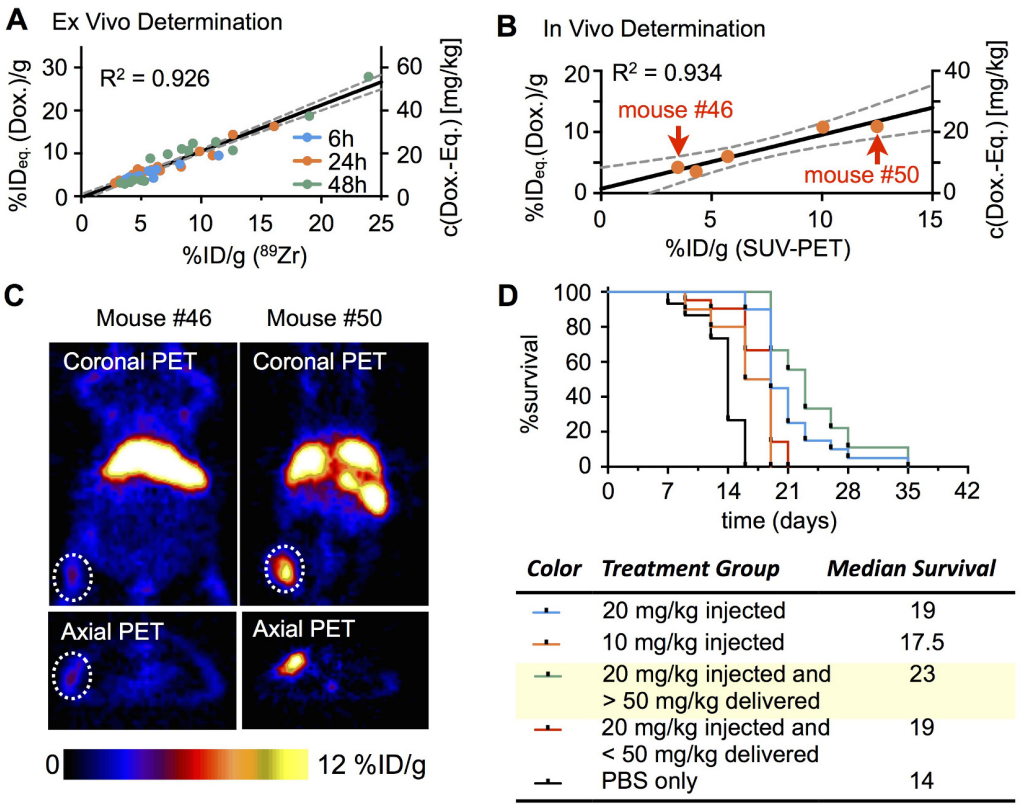

Color	Treatment Group	Median Survival
	20 mg/kg injected	19
	10 mg/kg injected	17.5
	20 mg/kg injected and > 50 mg/kg delivered	23
	20 mg/kg injected and < 50 mg/kg delivered	19
	PBS only	14

Figure 1. ^{89}Zr-NRep mirrors doxorubicin concentration in tumors as determined A) ex vivo, and B) in vivo by PET imaging. C) Representative PET images of two mice at 24 h p.i. demonstrating variability in tumor uptake. D) Survival curves for the different groups.

CONTROL ID: 2229771

TITLE: Advanced Cardiac Chemical Exchange Saturation Transfer (cardioCEST) – MRI for *In Vivo* Multi-color Cell Tracking and Myocardial Creatine Imaging.

PRESENTER: Ashley Pumphrey

ABSTRACT BODY:

Abstract Body: Purpose To apply a recently developed cardiac chemical exchange saturation transfer (CEST) pulse sequence[1] to track paraCEST labeled cells in the mouse heart, and to identify changes in myocardial creatine in obese mice. Methods ***Pulse Sequence***: CardioCEST imaging was validated against standard spin-echo CEST imaging (supplemental). CEST encoding used a 2s train of 8.8ms Gaussian saturation pulses prior to a constant TR (7.3ms) cardio-respiratorty gated cine gradient echo readout. Following saturation, 4 averages of one phase-encode step were acquired for each cardiac phase with dummy pulses used to maintain steady state magnetization during respiratory motion. All imaging was performed on a 7T Clinscan (Bruker, Ettlingen, Germany) scanner with a cylindrical volume coil for excitation and a 4-channel phased-array surface coil for reception. ***CEST Cell Tracking***: 10^6 cells labeled with either the paraCEST agent Eu-HPDO3A ($\Delta\omega$ = 15ppm, n=4) or saline (n=2, control) were implanted in the anterior-lateral wall of the left ventricle. CardioCEST was performed 24 hours after cell implantation with saturation offsets of ±15ppm (at 37 °C) in 2 slices: 1 at the site of injection and 1 apical slice as an internal control. ***Creatine CEST***: Mice were fed either a high-fat diet (60% kCal from fat, n=5) or a low-fat diet (10% kCal from fat, n = 5) for 14 weeks. Creatine CEST imaging[2] was performed via the acquisition of cardioCEST image pairs at ±1.8ppm. ***Analysis***: CEST contrast was quantified as $MTR_{asym}=(S_{OFF}-S_{ON})/S_{OFF}*100(\%)$, where S_i represents the signal intensity for saturation at ± the resonant frequency of the CEST agent. Results Calculation of MTR_{asym} maps enabled the visualization of Eu-HPDO3A labeled cells (Figure). The fraction of voxels with MTR_{asym} > 30% was significantly higher in slices containing Eu-HPDO3A labeled cells than saline labeled cells and control slices (8.9 ± 5.6% Eu-HPDO3A, 1.4 ± 2.0% saline, 0.4 ± 0.8% control, $p<0.05$ Eu-HPDO3A vs. all). Despite significantly higher body mass in high-fat diet mice (45±1g high-fat vs. 31±1g low-fat, $p<0.05$), creatine MTR_{asym} (Figure) was significantly lower compared to low-fat diet mice (2.7 ± 1.5% high-fat vs. 7.8 ± 3.3% low-fat, $p<0.05$). Septal wall thickness, ventricular geometry, and fractional shortening were all unchanged between groups. Conclusion CardioCEST imaging enabled the selective visualization of cell survival without disturbing underlying image contrast, and can be multiplexed with measurements of ventricular structure and function in cell therapy models. In a mouse model of diet induced obesity, significantly reduced myocardial creatine was measured in the absence of structural or functional changes, reflecting early metabolic failure before overt heart failure. Future applications of cardioCEST can include in vivo imaging of cell fate decisions in cell therapy, or the efficacy of targeted interventions for heart failure with preserved ejection fraction. References 1. Vandsburger et al. Circ. Cardiovasc. Imaging 2015; 8: e002180. 2. Haris et al. Nat. Med. 2014; 20: 209.

AUTHORS (LAST NAME, FIRST NAME): Pumphrey, Ashley L.[1]; Yang, Zhengshi[1]; Ye, Shaojing[3]; Vandsburger, Moriel[1, 2]

INSTITUTIONS (ALL):

1. Saha Cardiovascular Research Center, University of Kentucky, Lexington, KY, United States.
2. Biomedical Engineering, University of Kentucky, Lexington, KY, United States.
3. Saha Cardiovascular Research Center, University of Kentucky, Lexington, KY, United States.

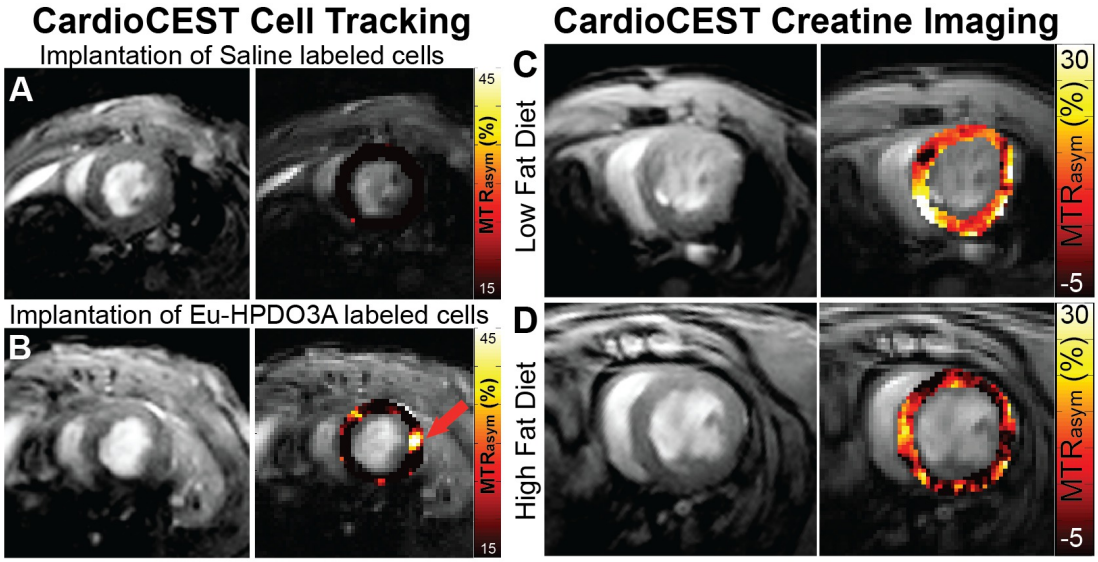

Figure. (A) Magnitude (left) and super-imposed left ventricular MTRasym maps (right) generated using cardioCEST reveal uniformly low MTRasym patterns in a mouse receiving saline labeled cells. **(B)** In a mouse receiving cells labeled with Eu-HPDO3A, the location of transplanted cells (red arrow) demonstrates significantly elevated MTRasym values. **(C)** Mice fed a control low-fat diet demonstrate robust creatine CEST contrast throughout the left ventricle. **(D)** In comparison, mice fed a high-fat diet for 14 weeks demonstrate similar ventricular structure but attenuated creatine CEST contrast as observed through reduced MTRasym at 1.8ppm.

CONTROL ID: 2229774

TITLE: Bimodal liposomes carrying NMR contrast agent and zinc phthalocyanine for MR imaging and photodynamic therapy of cancer.

PRESENTER: Paulina Skupin-Mrugalska

ABSTRACT BODY:

Abstract Body: Recently, liposomes have been attracting much attention as a potential theranostic delivery system due to its ability to encapsulate molecules of different hydrophobic character. Liposomes also possess a variety of opportunities to alter lipid composition and surface modification. Lipid vehicles can be thus developed into multifunctional nanoplatforms combining diagnostic and therapeutic modalities.
Above features have been employed to evolve gadolinium incorporated liposomes for simultaneous delivery of MRI contrast agent and a drug substance and for image-guided drug delivery.

The objective of this study was to develop novel type of liposomes (GdLip) that can provide contrast in a convenient MR image guidance for photodynamic therapy (PDT). GdLip were composed of 1-palmitoyl-2-oleoyl-*sn*-glycero-3-phosphocholine and L-*α*-phosphatidyl-D,L-glycerol (chicken egg, PG) or N-[1-(2,3-dioleoyloxy)propyl]-N,N,N-trimethylammonium chloride and had incorporated bis(1,2-dipalmitoyl-*sn*-glycero-3-phosphoethanolamine)-N-N'-diethylenetriaminepentaacetic acid gadolinium salt (Gd2-DTPA, 0.05 – 0.75 mM) and zinc phthalocyanine, ZnPc (50 μM) as a model photosensitizer. GdLip vehicles were prepared by a standard thin layer evaporation method. Thin layers were hydrated in buffer or normal saline solution and subsequently extruded through polycarbonate filters (pore diameter 100-200 nm). Size and concentration of GdLip vehicles was determined using nanoparticle tracking analyzer, showing the diameter of prepared liposomes in the range of 100-200 nm, depending on composition.
To confirm usefulness of GdLip liposomes as a contrast agent, relaxivity parameters r_1 and r_2 were obtained for 3 proton resonance frequencies (16.5 MHz, 200 MHz, 400 MHz). The highest values of r_1 (103.2 $mM^{-1}s^{-1}$) and r_2 (269.7 $mM^{-1}s^{-1}$) were observed for GdLip containing gadolinium at concentration of 0.05 mM, at 16.5 and 400 MHz, respectively. This suggests that GdLip vehicles present promising properties as a potential contrast agent at T_1 and T_2 images at magnetic field used in humans and T_2 images at higher magnetic fields. T_2 weighted MRI images showed very high contrast between GdLip vehicles and a blank sample (normal saline, Figure 1).
In vitro study was performed using cancer cell line (HeLa) and human fibroblasts, and was divided into two experiments involving photocytotoxicity and cytotoxicity assay. Cell viability was evaluated following 24-hour incubation in media containing 10-fold dilution of GdLip samples and reference vehicles as a control. For photocytotoxicity test, cells were exposed to light (λ_{act} = 660 nm) obtained from a High Power LED Multi Chip Emitter for 30 minutes. The light intensity at the surface of the plate was 1.0 mW/cm^2 according to Thorlabs TM100A Optical Power Meter, giving the total light dose as 1.8 J/cm^2. The results showed no cytotoxicity of GdLip under dark conditions but a decrease in cell viability following light irradiation (all experiments were performed in triplicates, Chart 1).

Acknowledgements
The authors acknowledge the financial support for the project from the Polish National Science Centre, No 2012/07/N/NZ7/04325.

AUTHORS (LAST NAME, FIRST NAME): Skupin-Mrugalska, Paulina[1]; Sobotta, Lukasz[1]; Wereszczynska, Beata[2]; Warowicka, Alicja[2]; Zalewski, Tomasz[2]; Mielcarek, Jadwiga[1]; Gapinski, Jacek[2]; Jurga, Stefan[2]

INSTITUTIONS (ALL):
1. Department of Inorganic and Analytical Chemistry, Poznan University of Medical Sciences, Poznan, Greater Poland, Poland.
2. NanoBioMedical Centre, Adam Mickiewicz University, Poznan, Greater Poland, Poland.

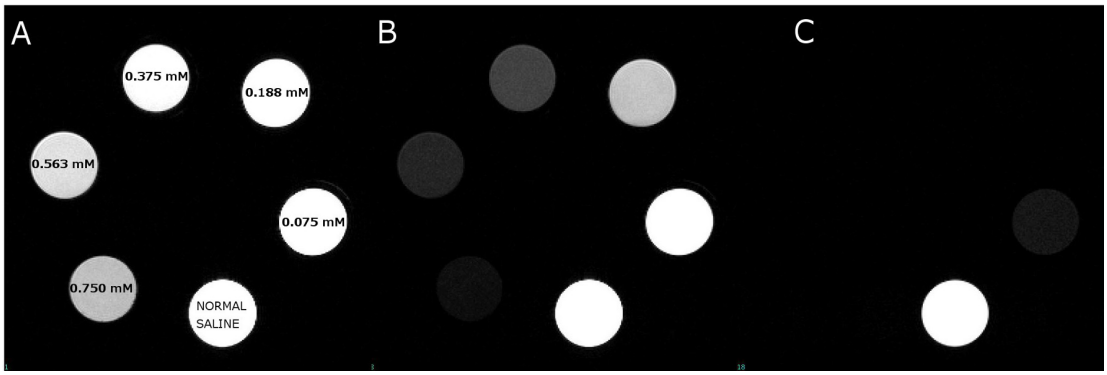
A
B
C
0.375 mM
0.188 mM
0.563 mM
0.075 mM
0.750 mM
NORMAL
SALINE

CONTROL ID: 2230057

TITLE: Dual Functional Probes for Targeted-Near Infrared Imaging and Targeted-Photodynamic Therapy of Prostate Cancer

PRESENTER: Xinning Wang

ABSTRACT BODY:

Abstract Body: Prostate cancer represents the second most common cause of cancer-related deaths in American men. Prostatectomy has been the mainstay treatment for men with localized prostate cancer. Surgery however often results in major side effects including incontinence and impotence, which are caused from damage and removal of nerves and muscles surrounding the prostate. There is an urgent need for a technology that can help surgeons distinguish the invasion of prostate cancer, perform more complete prostatectomy and simultaneously reduce surgery-related morbidities in localized cancers. Prostate-specific membrane antigen (PSMA) is a type II membrane antigen. It is highly expressed by prostate cancer, especially in more advanced tumors. PSMA has been an attractive target for imaging and therapy. Photodynamic therapy (PDT) is a non-invasive therapy which is used clinically in the treatment of various cancers and other diseases. Most PDT drugs are fluorescent, making them easy to track and useful for image-guided tumor resections. However, a main challenge for PDT is selective delivery of photosensitizing agents to cancer tissues without accumulation within normal tissues. Non-specific accumulation and activation of the photosensitizer will lead to cell death in normal tissue.

The objective of this study is to develop low molecular weight PSMA-targeted PDT agents which would provide image-guidance for prostate tumor resection and allow for subsequent PDT to eliminate un-resectable or “missed” cancer cells. Based on our previously developed PSMA ligand named PSMA-1, we synthesized two conjugates named PSMA-1-Pc413 and PSMA-1-IR700. Both PSMA-1-Pc413 (IC_{50}=2.1nM) and PSMA-1-IR700 (IC_{50}=2.2nM) showed improved binding affinity compared to the parent ligand Cys-Co-Glu (IC_{50}=9.75nM) in in vitro competition binding studies. In in vitro cellular uptake experiments the two probes demonstrated selective and specific uptake in PSMA-positive PC3pip cells, but not in PSMA-negative PC3flu cells. In in vivo imaging studies using nude mice bearing both PC3pip and PC3flu tumors, both probes showed selective tumor uptake in PC3pip tumors. Finally, the two PSMA-1-PDT probes were injected into mice bearing PSMA-positive PC3pip tumors and the tumor was irradiated with 690 nm light to activate the agents. Tumor volume was significantly reduced after the treatment and the response was dose-dependent. For example, on day 21-post treatment, the average tumor weight in the no treatment control group was 1.01±0.24 g, while it was reduced to 0.06±0.02 g in the group received 0.5 μg/g of PSMA-1-Pc413 and 150J of light. PSMA-1-IR700 required triple treatment on days 0, 4 and 8 to achieve significant tumor regression and average tumor weight was 0.13±0.03g on day 21-post treatment. In summary, both PSMA-1-Pc413 and PSMA-1-IR700 demonstrated high selectivity and specificity to PSMA-positive cells and they could effectively inhibit tumor growth when activated by light. They may have the potential to aid in the diagnosis and resection of prostate cancers. It may also allow for the identification of unresectable cancer tissue and PDT ablation of such tissue after surgical resection.

AUTHORS (LAST NAME, FIRST NAME): Wang, Xinning[1]; Tsui, Brian[1]; Ramamurthy, Gopolakrishnan[1]; Ren, Xiaoyi[1]; Basilion, James[1]

INSTITUTIONS (ALL):

1. Case Western Reserve University, Cleveland, OH, United States.

In vivo image in mice at 4-hour postinjection of 1 nmol PSMA-1-IR700

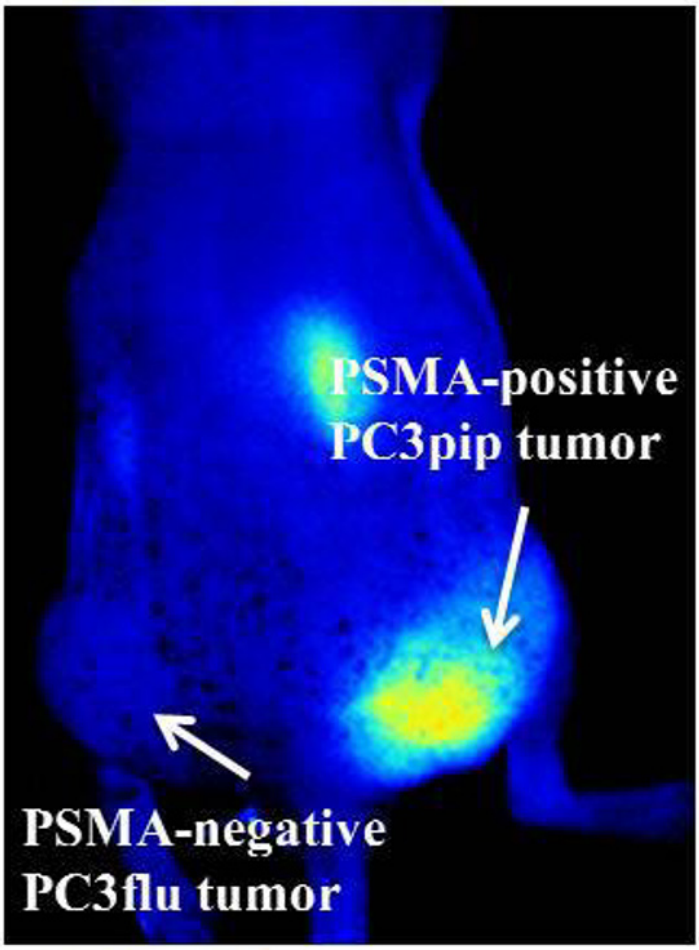

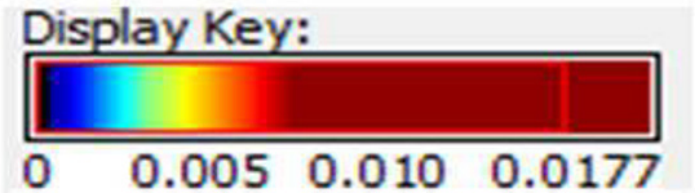

CONTROL ID: 2232622

TITLE: 5-hydroxytryptamine receptor 2A (5-HT_{2A}) expression and [^{18}F]altanserin accumulation in rodent brain under long-term light/dark environments

PRESENTER: Mei-Hui Wang

ABSTRACT BODY:

Abstract Body: Introduction: 5-hydroxytryptamine receptor 2A (5-HT_{2A}) is a main excitatory neurotransmitter receptor in the central serotonin system and plays an important role in psychiatric disorders. It has been reported that the expression level of 5-HT_{2A} is influenced by photo-cycle period (Ushijima K. et al. Mol. Pharmacol. 2012; 82:264-270). However, there is no report on the effects of long-term light exposure (i.e. lighten or darken for 48 h) on the 5-HT_{2A} expression. We report herein the results of the effect of long-term light exposure on the 5-HT_{2A} expression using [^{18}F]altanserin microPET and western blotting.

Methods:

Western Blotting: Three groups of mice were used for this study (i.e. 48h-light, 48h-dark and normal photo-cycle period, n=3 for each group). Proteins extracted from mouse thalamus (THA), striatum (STR), midbrain (MID), cerebellum (CB), and cortex (CTX) were analyzed using MBS 175200 anti-HTR_{2A} antibody and the 43 kD HTR_{2A} band was quantified with Multi Gauge (FUJIFILM).

Imaging: The [^{18}F]altanserin was prepared by the reported method (Sadzot B. et al. J Cereb Blood Flow Metab. 1995; 15:787-797). The brain uptake of [^{18}F]altanserin in mice were determined using a microPET/MR scanner with a resolution of 0.7 mm^3. Sixty min post i.v. injection of [^{18}F]altanserin (400 ~ 450 mCi/mouse), static imaging was conducted for 30 min. Regions of interest (ROIs) were drawn manually. The average values from the pixels within ROIs were divided by total injection dose.

Results: The uptake of [^{18}F]altanserin is significantly higher in CTX, THA, STR and CB, but lower at MID for long-term light exposure mice compared to the controls (Table1). In contrast, results from western blotting assay showed lower 5-HT_{2A} expression in CTX, THA, STR, and CB but higher in MID for mice under long-term light/dark environments than those of the controls (Fig.1).

Conclusions: The results showed long-term light exposure affected 5-HT_{2A} expression in mice.

AUTHORS (LAST NAME, FIRST NAME): Ho, Chung-Hsien[1]; Yang, Chung-Huang[1]; Chan, Po-Fan[1]; Wang, Mei-Hui[1]; Ma, Kuo-Hsing[2]; Cheng, Cheng-Yi[2]; Shiue, Chyng-Yann[2]; Lin, Wuu-Jyh[1]; Huang, Wen-Sheng[3]; Chen, Mu-Kuan[3]

INSTITUTIONS (ALL):

1. Institute of Nuclear Energy Research, Taipei, Taiwan.
2. Tri-Service General Hospital, National Defense Medical Center, Taipei, Taiwan.
3. Nuclear Medicine, Changhua Christian Hospital, Changhua, Taiwan.

(No Image Selected)

CONTROL ID: 2234151

TITLE: The Novel Radiofluorination Strategy of [^{18}F]FBEM as a Thiol Active Prosthetic Group

PRESENTER: Mei-Hui Wang

ABSTRACT BODY:

Abstract Body: Purpose: Radiolabeled peptides and proteins are being investigated with increasing interest as imaging probes to target cancer cells and to evaluate biological processes. PET imaging with [^{18}F] is clinically attractive due to its nuclear decay properties (b^+ 0.635 MeV, 97% abundance, $t_{1/2}$ 109.8 min). Peptides or proteins are usually labeled with [^{18}F] by an indirect strategy via conjugating [^{18}F]-labeled prosthetic group to the peptides or proteins. It was reported that [^{18}F]FBEM is a typically used prosthetic group to conjugated with peptides or proteins. The usual preparation of [^{18}F]FBEM that was in three steps required 83~110 min. The radiochemical yield is 10.2~24.4% (uncorrected). In this study, we aimed to develop a novel one-step radiosynthesis strategy of [^{18}F]FBEM that result in shorter synthesis time and higher radiochemical yield.

Method: N-[2-(4-N,N,N-trimethylammoniumbenzoate triflate)ethyl]maleimide which was used as [^{18}F]FBEM precursor was synthesized by 4-dimethylbenzoic acid conjugated with N-(2-aminoethyl)maleimide and further reacted with nitro methane and methyl triflate. [^{18}F]FBEM was radiofluorinated via [$^{18}F^-$]/K222/K_2CO_3 in one step and purified by HPLC.

Results: [^{18}F]FBEM precursor was prepared via a two-step synthesis with high chemical purity (> 95%) and the chemical yield is about 10~15% after purified by silica normal phase column chromatography. The [^{18}F]FBEM was prepared by a one-step synthesis with high radiochemical purity (> 98%) within only 40~60 min. The radiochemical yield is about 10~15% (uncorrected) after HPLC purification.

Conclusion: In this study, we successfully developed a one-step radiosynthesis strategy to prepare [^{18}F]FBEM. According to the result, comparable radiochemical yield and radiochemical purity but reduced preparation time (about 20~70 min) could be achieved by this method. With this novel strategy, we can get a simplified method for synthesis of [^{18}F]-labeled peptides and proteins.

AUTHORS (LAST NAME, FIRST NAME): Ho, Chung-Hsien[1]; Chen, Jyun-Hong[2]; Wang, Mei-Hui[2]; Yu, Hung-Man[2]; Lin, Wuu-Jyh[2]

INSTITUTIONS (ALL):

1. Institute of Nuclear Energy Research, Taipei, Taiwan.
2. Division of Isotope Applications, Institute of Nuclear Energy Research, Taoyuan, Taiwan.

(No Image Selected)

CONTROL ID: 2229883

TITLE: Perfluorocarbon nanodroplets for oxygen delivery and ultrasound image-guided release

PRESENTER: Daniela Santiesteban

ABSTRACT BODY:

Abstract Body: Stem cell (SC) angiogenic therapies are used to promote angiogenesis needed for restoration of injured ischemic tissue. Initial angiogenic SC studies showed promise in reducing infarct region and improving tissue function.1 However, in clinical translation, SC therapies proved ineffective due to high amounts of SC death upon implantation into ischemic tissue. A main factor contributing to cell death is the severe hypoxia of the injury site. While slight levels of hypoxia promote secretion of SC angiogenic factors, extreme hypoxia results in cell death and further inflammation. Therefore, a system capable of delivering controlled amounts of oxygen (O2) at levels that minimize cell death while promoting angiogenesis would greatly improve current SC-based angiogenic therapies.

Previously, perfluorocarbon (PFC) compounds have been used as blood substitutes due to their ability to carry high payloads of O2. More recently, PFCs were explored as contrast agents in ultrasound (US) and photoacoustic (PA) imaging. Our research aims to combine the O2 loading capabilities of PFCs with US/PA imaging to develop a controlled O2 delivery system that will increase cell viability and thus the efficacy of SC angiogenic therapies.

The current system consists of O2 saturated perfluorocarbon nanodroplets (PFCnDs) and an optically absorbing dye (Epolight 3072), stabilized by a protein shell. Oxygen release from the PFCnDs occurs in two ways: 1) passive diffusion and 2) laser activated release. The extent of passive diffusion was determined by measuring the dissolved O2 (dO2) in solutions of PFCnDs over time. Solutions of O2-loaded PFCnDs showed significantly increased dO2 levels proportional to the PFCnD concentration. Studies of the laser-activated release mechanism indicated that amount of O2 released from the PFCnDs is dependent on the concentration of particles as well as laser energy (Fig 1a), suggesting a higher degree of user control over existing O2 delivery methods. In vitro studies, in which SCs were cultured under severely hypoxic conditions (1% O2) for 48 hours, showed that the presence of O2-loaded PFCnDs significantly increased SC viability. Thus, PFCnDs may provide sufficient oxygen to counteract the harsh effects of low O2 environments on SC viability. The PFCnDs also act as an imaging contrast agent (Fig 1b). Upon laser activated O2 release, the phase change of the PFCnDs can be observed using US imaging, which provides spatiotemporal visualization of successful activation and information regarding where molecular O2 is released.

In conclusion, we developed a system to allow for spatiotemporal control of O2 release, a vital tool to treat the widely variable patient-specific ischemic injuries. Current work is being done to advance the design of the system by developing Multi-colored Oxygen Saturated Activatable and Injectable nanoCapsules (MOSAICs) that would further increase the user's ability to control O2 release under US image guidance. Future studies will focus on designing PFCnD with shells that can provide optimal stability and O2 release from the nDs.

1 Shim, W.et al. Cytotherapy (2013). 15(4):399-415.

AUTHORS (LAST NAME, FIRST NAME): Santiesteban, Daniela Y.[1]; Hannah, Alexander[1]; Suggs, Laura[1]; Emelianov, Stanislav Y.[1]

INSTITUTIONS (ALL):

1. Biomedical Engineering, The University of Texas at Austin, Austin, TX, United States.

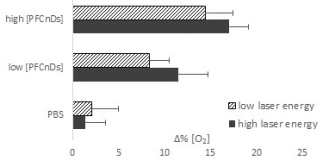

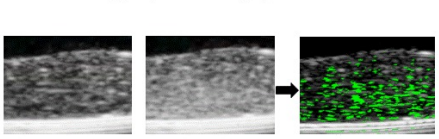

Figure 1. (A) Solutions containing PFCnDs were irradiated with laser light at high and low energies. Those irradiated at higher energies experienced greater O_2 release, as did solutions with higher concentrations of PFCnDs. (B) US images before and after pulsed laser irradiation. These images were processed to show the locations of activated PFCnDs (green).

CONTROL ID: 2229985

TITLE: Classification Study of 99mTc-TRODAT-1 SPECT Image by Skewness and Dopamine Transporter Activity Volume

PRESENTER: Yun-Hsuan Hsu

ABSTRACT BODY:

Abstract Body: The 99mTc-TRODAT-1 single photon emission computed tomography (SPECT) is used to diagnose the dopamine neurotransmitter diseases. However, the diagnostic results were difficult to quantify according to the pixel intensity. In this study, the retrospective experiment was applied to collect effective cases. The skewness and dopamine transporter activity volume of images were utilized to quantify and classify negative (n=6) and positive (n=196) cases as Parkinson's disease. Two hundred and two of 99mTc-TRODAT-1 SPECT images were involved in this study. The features of image are defined as skewness of whole brain images and dopamine transporter activity volume. The skewness and dopamine transporter activity volume (DTAV) were shown statistically significant difference between negative and positive groups by Mann-Whitney U Test ($P<0.05$). The SPECT image was classified as positive group as the skewness is smaller than 0.39 and DTAV is smaller than 24.5. Both 0.39 and 24.5 were selected according to the maximum of Youden's J statistic. Therefore, the sensitivity, specificity and accuracy were (97%, 83%, 92%) and (97%, 83%, 97%) with respective to the skewness and DTAV. The areas under receiver operating characteristic curve (AUC) were 84% and 99% with respectively to the skewness and DTAV. The Kappa statistic of the skewness and DTAV were 0.36 and 0.61. Hence, the skewness and DTAV of SPECT not only provide potentially significant features to classify negative and positive groups, but shows feasible and reasonable quantitative values between positive and negative groups. The distribution of skewness computed from SPECT images will be discussed in the future. The classified model contributed by the skewness and DTAV will be surveyed for the future work.

AUTHORS (LAST NAME, FIRST NAME): Hsu, Yun-Hsuan[1]

INSTITUTIONS (ALL):

1. Nuclear Medicine, E-DA Hospital, I-Shou University, Kaohsiung, Taiwan.

(No Image Selected)

CONTROL ID: 2229931

TITLE: Classification Study of ^{99m}Tc-TRODAT-1 SPECT Image by Skewness and Dopamine Transporter Activity Volume

PRESENTER: Yun-Hsuan Hsu

ABSTRACT BODY:

Abstract Body: The ^{99m}Tc-TRODAT-1 single photon emission computed tomography (SPECT) is used to diagnose the dopamine neurotransmitter diseases. However, the diagnostic results were difficult to quantify according to the pixel intensity. In this study, the retrospective experiment was applied to collect effective cases. The skewness and dopamine transporter activity volume of images were utilized to quantify and classify negative (n=6) and positive (n=196) cases as Parkinson's disease. Two hundred and two of ^{99m}Tc-TRODAT-1 SPECT images were involved in this study. The features of image are defined as skewness of whole brain images and dopamine transporter activity volume. The skewness and dopamine transporter activity volume (DTAV) were shown statistically significant difference between negative and positive groups by Mann-Whitney U Test ($P<0.05$). The SPECT image was classified as positive group as the skewness is smaller than 0.39 and DTAV is smaller than 24.5. Both 0.39 and 24.5 were selected according to the maximum of Youden's J statistic. Therefore, the sensitivity, specificity and accuracy were (97%, 83%, 92%) and (97%, 83%, 97%) with respective to the skewness and DTAV. The areas under receiver operating characteristic curve (AUC) were 84% and 99% with respectively to the skewness and DTAV. The Kappa statistic of the skewness and DTAV were 0.36 and 0.61. Hence, the skewness and DTAV of SPECT not only provide potentially significant features to classify negative and positive groups, but shows feasible and reasonable quantitative values between positive and negative groups. The distribution of skewness computed from SPECT images will be discussed in the future. The classified model contributed by the skewness and DTAV will be surveyed for the future work.

AUTHORS (LAST NAME, FIRST NAME): Tu, Po-Wei[1, 3]; Hsu, Yun-Hsuan[1]; Chen, Huei-Yung[1]; Lin, Ming-Chia[1]; Wu, Yi-Chen[1]; Huang, Yung-Hui[2]; Chen, Tai-Been[2]

INSTITUTIONS (ALL):

1. Nuclear Medicine, E-DA Hospital, I-Shou University, Kaohsiung, Taiwan.
2. Medical Imaging and Radiological Sciences, I-Shou University, Kaohsiung , Taiwan.
3. Information Engineering, I-Shou University, Kaohsiung , Taiwan.

(No Image Selected)

CONTROL ID: 2229936

TITLE: The prognostic value of total lesion glycolysis via ^{18}F-fluorodeoxyglucose PET-CT in surgically treated esophageal squamous cell carcinoma

PRESENTER: Joon-Kee Yoon

ABSTRACT BODY:

Abstract Body: In addition to staging, the identification of prognostic factors is important for predicting survival in patients with esophageal cancer after esophagectomy. The present study was performed to document the prognostic role of total lesion glycolysis (TLG) in postoperative patients.

Methods: We retrospectively reviewed the records of 50 patients with esophageal squamous cell carcinoma who underwent surgical resection and complete lymph node dissection after positron emission tomography–computed tomography (PET-CT). A region of interest was drawn on the primary lesion and suspected metastatic lymph nodes, and the maximum standardized uptake value (SUVmax), TLG of the primary lesion (TLGp), and whole-body TLG (TLGwb) were measured using an SUV cutoff of 2.5.

Results: The study population included 50 patients with a mean age of 63.14 ± 8.18 years: 12 (24%) were reported as stage I, 13 (26%) as stage II, and 25 (50%) as stage III. The median follow-up period was 20.46 months, and recurrences occurred in 17 patients. The mean SUVmax, TLGp, and TLGwb were 11.11 ± 6.40, 122.54 ± 180.98, and 129.37 ± 193.66, respectively. On the multivariate analysis, TLGp was a risk factor for disease-free survival (DFS) [hazard ratio (HR) = 1.002, p = 0.026], and TLGwb was a risk factor for overall survival (OS) (HR = 1.002, p = 0.021) and DFS (HR = 1.002, p = 0.044). The 3-year OS rates were 66.1% in patients with low TLGwb (≤41.45) and 33.3% in those with high TLGwb (>41.45; p = 0.004). The concordance index of the TLGwb was 0.752 (95%CI: 0.659–0.845).

Conclusions: TLGwb is a significant prognostic factor for OS and DFS in patients with surgically treated esophageal squamous cell carcinoma.

AUTHORS (LAST NAME, FIRST NAME): Park, Seong Yong[2]; Lee, Su Jin[1]; Yoon, Joon-Kee[1]

INSTITUTIONS (ALL):

1. Nuclear Medicine & Molecular Imaging, Ajou University Medical School, Suwon, Korea (the Republic of).
2. Thoracic and Cardiovascular Surgery, Ajou University School of Medicine, Suwon, Korea (the Republic of).

(No Image Selected)

CONTROL ID: 2243522

TITLE: Clinicopathologic factors associated with F-18 FDG uptake of early gastric cancer

PRESENTER: Joon-Kee Yoon

ABSTRACT BODY:

Abstract Body: F-18 fluorodeoxyglucose (FDG) PET/CT has been widely used in the evaluation of various cancers. However, because of the low detection rate, F-18 FDG PET/CT is not generally recommended for staging of early gastric cancer (EGC). In this study, clinicopathologic factors associated with F-18 FDG uptake were investigated.
Methods: A total of 220 patients (137 men, 53 women, age = 61 years) who underwent preoperative F-18 FDG PET/CT were enrolled retrospectively. Pathologic information was obtained through gastrectomy (n = 157) or endoscopic mucosal dissection (n = 33). Univariate and multivariate analyses were performed to evaluate the association between clinicopathologic factors (age, sex, multiplicity, relation to adenoma, location, gross type, WHO classification, Lauren classification, size, depth of invasion, involvement of resection margin and lymphatic/venous/perineural invasion) and F-18 FDG uptake of primary tumors.
Results: Seven patients had multiple EGCs and 16 were related to adenoma. The most common location of primary tumors was lower third (51.3%). The two most common gross types were IIc (43.9%) and IIb (33.9%). pT1b was more frequent (52.6%) than pT1a (47.4%). F-18 FDG uptake was observed in 17.4%, 40/230) of patients with EGCs. On univariate analysis, the location of tumor, gross type, WHO classification, Lauren classification, depth of invasion and lymphatic invasion were significant variables affecting on F-18 FDG uptake. A subsequent multivariate analysis with these factors revealed that the location of tumor (*p = 0.024*, exp(B) = 2.115), gross type (*p 001*, exp(B) = 0.47) and the depth of invasion (*p = 0.036*, exp(B) = 2.901) were significantly associated with F-18 FDG uptake. Tumors located in the lower third of stomach showed more FDG avidity (23.7%) than those in the upper third (6.7%) and the middle third (12.3%). Gross type I (75.0%) and IIa (40.0%) had higher FDG avidity. Tumors with submucosal invasion (25.8%) showed FDG uptake more frequently than those limited in mucosa (8.3%).
Conclusion: F-18 FDG uptake in EGC is dependent on the location, gross type and the depth of invasion of primary tumors. This result would help clinicians to decide which patients are eligible for F-18 FDG PET/CT in EGC.

AUTHORS (LAST NAME, FIRST NAME): Jo, Kyung Sook[1]; Yoon, Joon-Kee[1]; Lee, Su Jin [1]; Lee, Dakeun[2]; Kim, Young Bae[2]; Lim, Seon Kyo[4]; Lee, Kee Myung[4]; Byun, Cheulsu [3]; Huh, Hoon[3]; Han, Sang-Wook [3]

INSTITUTIONS (ALL):

1. Nuclear Medicine & Molecular Imaging, Ajou University Medical School, Suwon, Korea (the Republic of).
2. Pathology, Ajou University School of Medicine, Suwon, Korea (the Republic of).
3. Surgery, Ajou University School of Medicine, Suwon, Korea (the Republic of).
4. Gastroenterology, Ajou University School of Medicine, Suwon, Korea (the Republic of).

(No Image Selected)

CONTROL ID: 2233160

TITLE: A preliminary study for radioimmunotherapy targeting F0F1 ATP synthase in stomach cancer xenograft model using I-131 ATP synthase mAb

PRESENTER: Joon-Kee Yoon

ABSTRACT BODY:

Abstract Body: Objectives: F0F1 ATP synthase is present on the extracellular surface of many tumor cells and plays a role as an angiostatin receptor, thus it is a potential therapeutic target of tumor angiogenesis. Previously, we labeled I-125 to monoclonal antibody (mAb) of ATP synthase successfully and showed its biodistribution in wild-type mice and tumor-bearing mice. In the present study, we evaluated the therapeutic efficacy of I-131 labeled ATP synthase mAb in tumor xenograft model.

Methods: I-131 ATP synthase mAb was prepared using iodogen tube method, and then cellular uptake was tested in 7 different cancer cell lines in vitro. The cell line with the highest uptake was chosen for xenograft model. Vehicle and I-131 ATP synthase mAb were injected intravenously to control (n=6) and treated group (n=7) for 4 weeks, respectively, and then the tumor size was measured once a week for comparison. F-18 FDG PET images were acquired before and after therapy.

Results: The labeling efficiency of I-131 ATP synthase mAb was dependent on the dose of mAb and was over 50% at 80μg. Among 7 cancer cell lines, MKN-45 human gastric cancer cells showed the highest I-131 ATP synthase mAb uptake (%uptake/g cell) in vitro. The tumor size increased significantly at 4 week after starting treatment in both groups (6.44 mm -> 13.89 mm for control, 7.17 mm -> 11.64 mm for treated group, all $p < 0.01$). However, the tumor size of treated group was significantly smaller than that of control ($p = 0.05$) at 4 week. F-18 FDG PET imaging showed a marked decrease of tumor uptake after treatment.

Conclusion: I-131 labeled ATP synthase mAb slowed down tumor growth significantly in MKN-45 xenograft model, which indicates that it could be used as an anti-cancer treatment. This result needs to be validated in further experiments with different models.

AUTHORS (LAST NAME, FIRST NAME): Park, Bok-Nam[1]; Lee, Su Jin[2]; Hong, Ka-Young[1]; Yoon, Joon-Kee[1]

INSTITUTIONS (ALL):

1. Nuclear Medicine & Molecular Imaging, Ajou University Medical School, Suwon, Korea (the Republic of).
2. Nuclear Medicine, Ajou University School of Medicine, Suwon, Korea (the Republic of).

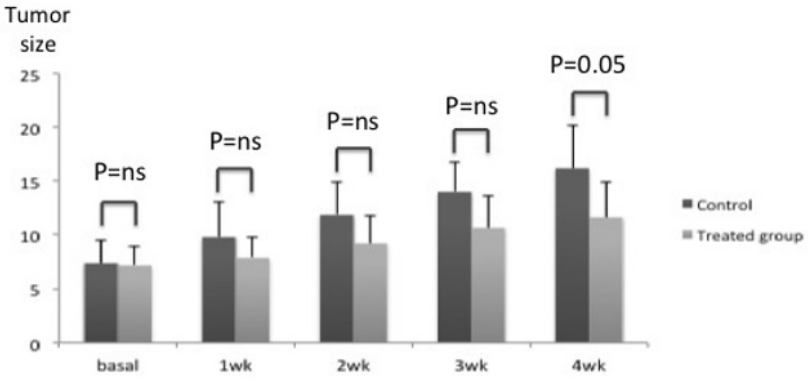
Tumor size
25
20
15
10
5
0
P=ns
P=ns
P=ns
P=ns
P=0.05
basal
1wk
2wk
3wk
4wk
Control
Treated group

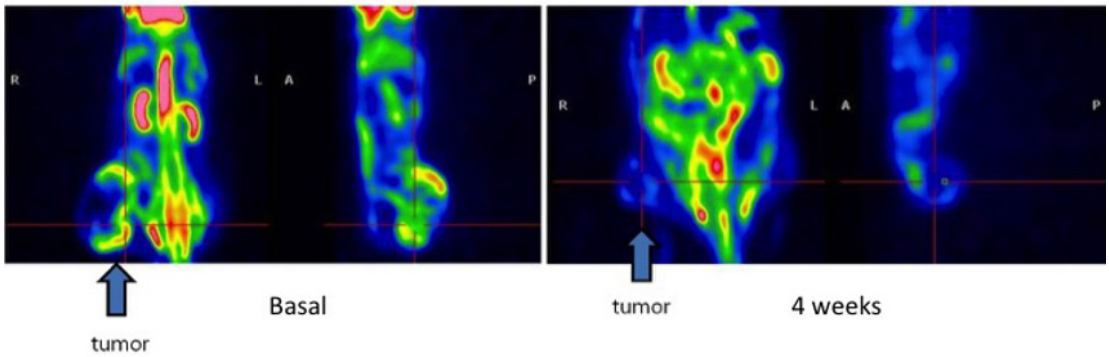
R
L
A
P
tumor
Basal
R
L
A
P
tumor
4 weeks

CONTROL ID: 2230456

TITLE: Improvements of Radiation Treatment Planning Using Interpolated Average CT Technology

PRESENTER: Yu-Rou Chiou

ABSTRACT BODY:

Abstract Body: **Objectives**: An interpolated average CT (IACT) method for attenuation correction in PET (PET_{IACT}), which is a good low-dose approximation of cine average CT to reduce misalignments and improve quantification in PET/CT. This study aims to evaluate the potential benefit in the radiation treatment of lung cancer patients by comparing the dose distributions and dosimetric parameters between the targets contours using PET and PET_{IACT} on IMRT plans.

Materials and Methods: Four lung cancer patients who underwent radiotherapy were retrospectively included in this study. All patients had undergone the standard procedure of PET/CT scanning. The original data in each case included a series of helical CTs, two extreme phases CTs: the full-expiration and the full-inspiration CTs, a whole body PET and generated PET_{IACT} based on the deformable image registration and two extreme phases CTs. All PET/CT images were registered with the simulation CT for treatment planning. Two IMRT plans based on PET and PET_{IACT} were designed and compared in each patient. Dosimetric parameters of the two different plans were compared in terms of tumor coverage and avoidance of normal tissues and critical organs.

Results: Better conformity indices and homogeneity indices were observed in the plans incorporated with PET_{IACT} as compared to the plans using conventional PET. The median reductions in the mean doses to lung, heart, and spinal cord in the plan using PET_{IACT} were 1.8, 1.3 and 3.2 Gy, respectively, compared with those in the plans using PET. Most plans using PET_{IACT} demonstrated significant improvement in lung dose including V_5, V_{20} and mean dose.

Conclusions: IACT-guided IMRT planning appears to be effective in preserving lung in lung cancer patients.

AUTHORS (LAST NAME, FIRST NAME): Chiou, Yu-Rou[2]; Yang, Shih-Neng[4]; Zhang, Geoffrey G.[3]; Huang, Tzung-Chi[1]

INSTITUTIONS (ALL):

1. Biomedical Imaging and Radiological Science, China Medical University, Taichung, Taiwan.
2. China Medical University, Taiwan, Taichung, Taiwan.
3. Radiation Oncology, Moffitt Cancer Center, Tampa, FL, United States.
4. Department of Radiation Oncology, China Medical University Hospital, Taiwan, Taichung, Taiwan.

(No Image Selected)

CONTROL ID: 2229966

TITLE: Feasibility study of the hair growth enhancements with ultrasound mediated minoxidil loaded microbubbles cavitation

PRESENTER: Ai-ho Liao

ABSTRACT BODY:

Abstract Body: Background, Motivation and Objective

A first commercially available formulation of minoxidil improves its poor water solubility and increase permeability by chemical enhancement methods (ethanol, propylene glycol). The commercially products require at least two times a day to ensure its pharmacological effect, because the products is made of chemical formulations (ethanol, propylene glycol) to increase the ability of transdermal drug delivery so it will often occur atopic dermatitis for long-term use. In this study, a new ultrasound contrast agent, minoxidil loaded microbubbles (MBs) were created and combined with US energy in water-phase to enhance hair growth and reduce the side effects of skin.

Statement of Contribution/Methods

The MBs which are layer by layer (LbL) assembly of chitosan oligosaccharide lactate (COL) shell which absorbed minoxidil on this cationic carriers. The zeta potential and size distribution of the minoxidil loaded MBs in suspension were measured by DLS. The in vitro and in vivo experimental parameters will be randomly divided into four groups (n=5 animals per group): (1) only penetrating minoxidil (2) commercially formulations of minoxidil (3) US combines MBs mixed with minoxidil (4) US combines minoxidil-COL-MBs.

Results/Discussion

The cationic MBs were modified by chitosan. The mean diameters of MBs, MBs coated with COL, and minoxidil loaded COL-MBs were 1.48, 4.15, 4.50 μm. The loading efficiency of minoxidil on cationic MBs was 14.5% (n=5). The zeta potentials of MBs coated with COL and minoxidil loaded COL-MBs were 24.13±0.44 and 11.78 ±1.24 mV, respectively. The release kinetics of minoxidil from minoxidil loaded COL-MBs were determined by dynamic dialysis method. After US treatment, the released rate increased 33% at 2 hour. For the in vivo experiments, the minoxidil loaded MBs would be expected to promote hair growth rapidly, reduced the treatment dose and side effects.

AUTHORS (LAST NAME, FIRST NAME): Liao, Ai-ho[1]

INSTITUTIONS (ALL):

1. Institute of Biomedical Engineering, National Taiwan University of Science and Technology, Taipei, Taiwan.

(No Image Selected)

CONTROL ID: 2231844

TITLE: Research on Sensitivity Improvement of Semiconductor PET Scanner with the use of event data by multiple interaction: A Simulation Study

PRESENTER: Yohei Kikuchi

ABSTRACT BODY:

Abstract Body: We performed a simulation study to investigate about improvement in sensitivity of PET scanners that employ semiconductor detectors. Instead of nonorganic scintillation detectors employed in current scanners, the application of semiconductor detectors has a potential to improve scanner's performances, particularly in spatial resolution. However, the candidate PET detectors' detection efficiency and event ratio of photoelectric (PE) absorption against 511 keV γ-ray are lower than those of scintillation detectors, thereby achievement of good sensitivity is difficult.

The detection efficiency is improved by an increase of the detector assembly's volume. However, the event ratio of PE is an intrinsic material property of the detector. The small PE ratio indicates the low event probability of full-energy (511 keV) absorption by just one interaction inside a detector, so that the amount of valid data obtained for image creation is reduced in conventional detection methods. To solve this problem, we propose the efficient use of full-energy absorption events by multiple interactions including single/multiple Compton scattering (SC) and PE through several detectors inside the assembly. Such detection events are irrelevant data in current systems, however, to identify the first interaction allows to utilize the events as valid data. In this study, we evaluated scanner's sensitivity with consideration in the use of the multiple interaction. In our previous study, a kind of two-dimensional position sensitive CdTe detector (2D CdTe PSD) which has the volume of 19.1 x 20.0 x 1.00 mm^3 have been developed with the aim of PET applications. Our simulations assume the use of the detector.

The detection efficiency obtained with a detector assembly was evaluated. The assembly assumes the 100-layer stack of 2D CdTe PSDs and the size is 20.0 x 20.0 x 100 mm^3. 1.0 x 10^6 511 keV-photons were emitted into the center of the 20.0 x 100 mm^2 plane. Approximately 1.1 x 10^5, 1.5 x 10^5, 0.9 x 10^5, 0.3 x 10^5 and 0.09 x 10^5 photons, out of 3.9 x 10^5 total interacting photons, are fully-absorbed by just one interaction (no SC before PE), two (one SC before PE), three (two SC before PE), four (three SC before PE) and more than five interactions respectively. The result indicates that 89.7 % or 97.6 % of the total detection events can be obtained as valid data by the use of up to three or four interaction event. These values suggest achievement of 35 % or 38 % detection efficiency. Compared with 11% in the current detection method (no SC before PE), higher detection efficiencies can be obtained. The values are equivalent to that of LSO detectors which are employed as one of representative detectors in current scanners. Moreover, we proposed a method to identify the first interaction point and applied it to the detection event data by two interactions. The scattering angle depends on the deposited energy at the interaction point. The relationship is expressed by Klein-Nishina formula and our method is based on it. As a result, it was confirmed that the probability of successful identification considerably varies with detector performances, energy resolution and position resolution.

AUTHORS (LAST NAME, FIRST NAME): Kikuchi, Yohei[1]

INSTITUTIONS (ALL):

1. Graduate School of Engineering, Tohoku University, Sendai, Miyagi, Japan.

(No Image Selected)

CONTROL ID: 2229991

TITLE: Development of Small-molecule Fluorescence Probes to Detect Hypoxia *in vivo*

PRESENTER: Kenjiro Hanaoka

ABSTRACT BODY:

Abstract Body: Inadequate supply of oxygen is deeply related to various pathologies such as cancer, cardiopathy and vascular diseases and provokes unique biological phenomena. So, chemical tools to detect and visualize hypoxia are highly required to investigate its biological effects. Especially, hypoxia sensor with high oxygen sensitivity is preferred to detect the mild hypoxic regions where hypoxia inducible factor 1a (HIF-1a) starts to be activated. It is known that the increase of reductive stress is one of the features in hypoxia and several compounds including azo and nitro aromatic compounds are also selectively reduced under hypoxic conditions. Besides this hypoxia-dependent reduction, azo dyes are known to be nonfluorescent because of their ultrafast photoisomerization process to quench photoexcitation energy. Taking advantage of these phenomena, novel hypoxia-sensitive fluorescence probes, mono azo rhodamine (**MAR**) and mono azo Si-rhodamine (**MASR**), based on two different colored fluorophores, have been developed (see Supporting Figure) [1]. They contain azo group conjugated to the xanthene moiety of rhodamine derivatives. Under normoxic conditions, the probes are nonfluorescent due to ultrafast conformational change around the N=N bond, on the other hand, under hypoxia, their azo group is selectively reduced by reductases, releasing strongly fluorescent rhodamine derivative. Interestingly, the live cell fluorescence imaging revealed that **MAR** and **MASR** showed different hypoxia detection thresholds, i.e., their fluorescence intensity increased as the oxygen concentration fell below 5% and 1%, respectively. This indicates that **MAR** is a useful tool to detect mild hypoxia region. Since their detection wavelength is different, simultaneous usage of two probes enabled to monitor the relative hypoxia severity by multicolor imaging. Moreover, we successfully visualized retinal hypoxia with **MAR** in a rat model of retinal artery occlusion. Moreover recently, in order to develop a fluorescence probe for *in vivo* imaging, we paid attention to the fluorophore, which has near-infrared (NIR) absorption and emission, because tissue penetration is best in this wavelength range. NIR is relatively poorly absorbed by biomolecules including hemoglobin as the principal absorber of visible light, water and lipids as the principal absorber of infrared light, and so it can penetrate deeply into tissues. So, we designed and synthesized NIR fluorescence probe, **diMe azoSiR640**, by utilizing our new NIR fluorophore based on the same design strategy as the above. We then applied it to fluorescence imaging. We applied it to living mice, and successfully achieved real-time imaging of ischemia of their liver and kidney. Thus, these probes would provide an innovative approach for researchers to work on many challenges related to hypoxia.

[1] Wen Piao, Satoru Tsuda, Yuji Tanaka, Satoshi Maeda, Fengyi Liu, Shodai Takahashi, Yu Kushida, Toru Komatsu, Tasuku Ueno, Takuya Terai, Toru Nakazawa, Masanobu Uchiyama, Keiji Morokuma, Tetsuo Nagano, Kenjiro Hanaoka *Angew. Chem. Int. Ed.*, vol.52, pp13028-13032 (2013).

AUTHORS (LAST NAME, FIRST NAME): Hanaoka, Kenjiro[1]; Piao, Wen[1]; Nagano, Tetsuo[2]; Urano, Yasuteru[3, 4]

INSTITUTIONS (ALL):

1. Graduate School of Pharmaceutical Sciences, The University of Tokyo, Tokyo, Japan.
2. Open Innovation Center for Drug Discovery, The University of Tokyo, Tokyo, Japan.
3. Graduate School of Pharmaceutical Sciences, The University of Tokyo, Tokyo, Japan.
4. Graduate School of Medicine, The University of Tokyo, Tokyo, Japan.

(No Image Selected)

CONTROL ID: 2229996

TITLE: Comparison of *In Vivo* Distribution of ^{64}Cu-labeled Trastuzumab Fragments Conjugated with DOTA, NOTA, and NODAGA in PET Imaging of Tumor-bearing Mice.

PRESENTER: Yousuke Kanayama

ABSTRACT BODY:

Abstract Body: PET imaging of antibody drugs are expected to be highly useful for diagnosis of target expression, selection of applicable patient, and treatment planning. In the antibody imaging, because of the long circulating half-life of whole antibody, it takes more than 2 days for the timing of enough tumor-to-non-tumor contrast. Although using long-lived radionulclides such as ^{89}Zr is one of the most popular ways for high contrast imaging of antibody, it takes 4-5 days for imaging and may cause high radiation exposure.

In the previous study, we successfully visualized the HER2 expression using ^{64}Cu-DOTA-Trastuzumab in clinical PET trial with the breast cancer patients in collaboration with National Cancer Center Hospital, Japan (*J. Nucl. Med.* 2013;54(11):1869-75). Copper-64 has half-life of 12.7 h and the calculated exposure from ^{64}Cu-DOTA-Trastuzumab was low level, similar to ^{18}F-FDG-PET. To reduce radiation exposure and the strain on patients, faster blood clearance and tumor accumulation are required for the PET probes. Fragmented antibody may have shorter circulation and be useful for the imaging in the shorter time. In this study, we investigated *in vivo* distribution of Fab or F(ab')2 fragments of Trastuzumab labeled with ^{64}Cu using three different chelator DOTA, NOTA, NODAGA in the PET imaging of tumor-bearing mice.

Fragmented Trastuzumab was obtained by proteolytic digestion with pepsin or papain.

Each fragments were confirmed the conjugation of the similar number of chelator and affinity. Preparing tumor-bearing mice, HER2-overexpressed A431 cells and negligibly low-expressed C6 cells were inoculated in nude mice. After injection of respective probes, PET data was acquired for 1 h, and then 30 min acquisition was performed in 4, 8, 12, 24, 48 h.

As the result, DOTA- or NODAGA-labeled probes showed the increasing liver accumulation after the radioactivity in the heart (blood pool) was almost disappeared. The behavior of liver accumulation might be influenced by ^{64}Cu dissociated from chelators. On the contrary, NOTA-labeled probes didn't show such behavior. ^{64}Cu-NOTA-F(ab')2 showed the best tumor contrast in 4-24 h. ^{64}Cu-NOTA-labeled F(ab')2 fragment might be useful to reduce the imaging time of immuno-PET.

AUTHORS (LAST NAME, FIRST NAME): Kanayama, Yousuke[1]; Zochi, Riyo[1]; Hayashinaka, Emi[1]; Yamazaki, Asumi[1]; Wada, Yasuhiro[1]; Watanabe, Yasuyoshi[1]

INSTITUTIONS (ALL):

1. RIKEN Center for Life Science Technologies, Kobe, Japan.

(No Image Selected)

CONTROL ID: 2229995

TITLE: A new method for the visualization and quantification of targeted microbubbles in ultrasound molecular imaging

PRESENTER: Peter Frinking

ABSTRACT BODY:

Abstract Body: Introduction

In ultrasound molecular imaging (USMI), detection of bound microbubbles (MB) is a prerequisite for accurately quantifying target expression. Despite natural clearance of the freely circulating unbound MB, late-phase enhancement, typically assessed minutes after injection (5-10 min.), still may comprise substantial amounts of unbound MB. A classical approach for differentiating between bound and unbound MB destroys all the MB in the field of view using high mechanical index (MI) pulses, and compares late-phase enhancement pre and post destruction. This differential targeted enhancement (dTE) approach suffers from limitations, *viz.* the binding cannot be repeatedly assessed after destruction and the signal from circulating MB might be under/over-estimated. To avoid these limitations, we developed an image processing method, based on the analysis of low MI data that improves the conspicuity of bound MB by suppressing the echoes originating from remaining circulating MB.

Objective

To validate the quantitative aspect of the new image processing method, and to compare its results with the classical dTE method in an in vivo model.

Material and Methods

An in-house developed flow-cell was used to assess the quantifiability of bound MB using the new image processing method. The bottom plate of the flow cell was coated with mouse P-selectin-Fc receptor at different concentrations. P-selectin-targeted MB were bound to the plate following incubation by decantation. Bubble density was measured optically, and imaging was subsequently performed using a Sequoia ultrasound system. In vivo imaging was performed in the colorectal HCT116 tumor mouse model using BR55, a clinically translatable VEGFR2-targeted agent. Late-phase enhancement (10 min. post-injection) of BR55 MB was compared pre- and post-inhibition of VEGFR2. Qualitative and quantitative analysis of late-phase enhancement was performed using the new method and the dTE approach.

Results

Bubble density measured optically increased linearly with receptor concentration (R^2 = 0.99). Moreover, the USMI signal measured with the new method was directly proportional to receptor concentration (R^2 = 0.96), indicating the quantifiability of the method. In the mouse tumor model, the new method improved the qualitative assessment of BR55 significantly, offering better delineation of the tumoral lesion compared to the dTE method. Next, late-phase enhancement of BR55 was quantified within the same mice pre- and post-inhibition of VEGFR2 after 1 h. Analyses results obtained with the new method indicated that inhibition was highly reproducible, and late-phase enhancement of BR55 decreased by more than 98%, whereas with dTE results were more variable, and the decrease of late-phase enhancement due to inhibition was only 70% (Figure 1).

Conclusion

The new image processing method improves the detection of bound MB by effectively suppressing echoes originating from remaining circulating MB, an added value for the identification and quantification of target expression during USMI.

AUTHORS (LAST NAME, FIRST NAME): Frinking, Peter J.[1]; Hyvelin, Jean-Marc[1]; Gaud, Emmanuel[1]; Costa, Maria[1]; Henrioud, Sylvie[1]; Fresneau, Thomas[1]; Bettinger, Thierry[1]; Tranquart, François[1]

INSTITUTIONS (ALL):

1. Global Research and Development, Bracco Suisse SA, Plan-les-Ouates / GE, Switzerland.

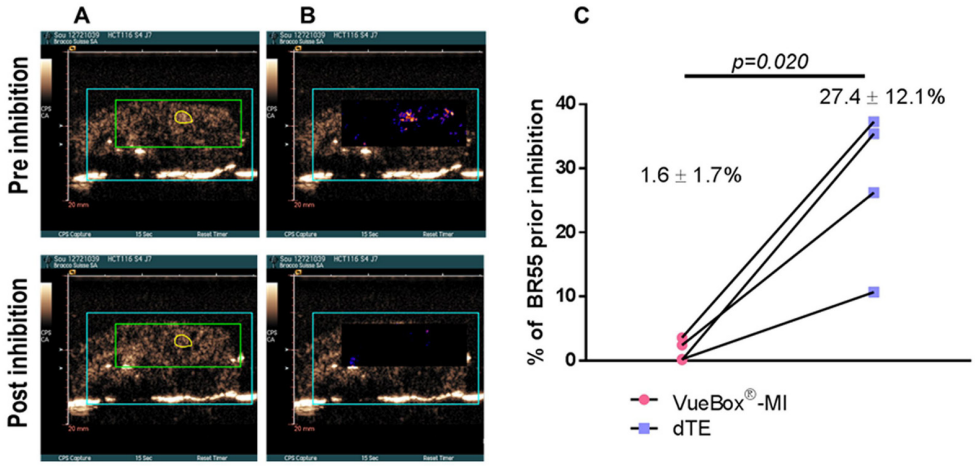

Figure 1. A) Typical late-phase ultrasound images of BR55 in HCT116 colorectal tumor (yellow region), pre- (top) and post (bottom) inhibition of VEGFR2. B) Processed images obtained with the new method pre- and post inhibition (top and bottom row, respectively). Note the improved delineation of the colorectal tumor in the processed image pre inhibition (B-top). C) Quantitative analysis results of bound BR55 microbubbles post-inhibition of VEGFR2, obtained with the new method (purple) and dTE (blue).

CONTROL ID: 2230002

TITLE: FDG PET/CT total lesion glycolysis predicts prognosis in patients with operable extrahepatic cholangiocarcinoma

PRESENTER: Eun Jeong Lee

ABSTRACT BODY:

Abstract Body: Purpose: We investigated clinicopathologic factors to predict prognosis in patients with operable extrahepatic cholangiocarcinoma. **Materials and Methods:** This retrospective study included 25 consecutive newly diagnosed patients with extrahepatic bile duct adenocarcinoma who underwent fluorine-18 fluorodeoxyglucose positron emission tomography/computed tomography (FDG PET/CT) before surgery. Maximum standardized uptake value (SUV), metabolic tumor volume (MTV), total lesion glycolysis (TLG, MTV ´ mean SUV), and pathologic size of primary tumor was measured. Preoperative level of tumor marker (CA 19-9), TNM stage, and presence of adjuvant chemotherapy were also evaluated. Survival analysis was performed for progression free survival and overall survival using the Kaplan-Meier method. Cox proportional hazard models were used to determine independent prognostic factors. **Results:** Univariate survival analysis identified high TLG (≥8.8), high MTV (≥2.9), and large primary tumor size (>2.0) as significant predictors of poor progression-free survival. Preoperative level of CA 19-9, maximum SUV, adjuvant chemotherapy, T-stage, N-stage, and stage were not a significant prognostic predictor for progression-free survival. For overall survival, high TLG (≥12.0), high MTV (≥3.5), high maximum SUV (≥4.2) were significant poor prognostic predictors. Preoperative level of CA 19-9, primary tumor size, adjuvant chemotherapy, T-stage, N-stage, and stage were not a significant prognostic predictor for overall survival. After multivariate survival analysis, no independent prognostic predictor for poor progression-free survival was found. For overall survival, only high TLG (P = 0.03) was an independent poor prognostic predictor. **Conclusions:** Assessment of TLG by FDG PET/CT in patients with operable extrahepatic cholangiocarcinoma provides a useful information regarding prognosis.

AUTHORS (LAST NAME, FIRST NAME): Lee, Eun Jeong[1]; Chung, Hyun Woo[2]; So, Young[2]

INSTITUTIONS (ALL):

1. Nuclear Medicine, Seoul Medical Center, Seoul, Korea (the Republic of).
2. Nuclear Medicine, Konkuk University Medical Center, Seoul, Korea (the Republic of).

(No Image Selected)

CONTROL ID: 2230013

TITLE: Pancreas cancer cell metabolic measurement using hyperpolarized [1-^{13}C] pyruvic acid in a bioreactor system

PRESENTER: Lotte Bertelsen

ABSTRACT BODY:

Abstract Body:

Purpose: To use a newly developed MR-compatible bioreactor system for measuring metabolic fluxes in pancreas cancer cells grown in a scaffold using hyperpolarized [1-^{13}C] pyruvic acid.

Materials and methods: The pancreas cancer cell line BxPC-3 was seeded on scaffolds made from polycaprolactone (PCL) and fabricated by fused deposition modeling with a BioScaffolder (Sys+Eng GmbH, Germany). Five mm porous mats were made by a layered deposition of 200 µm thick fibers of PCL melt with an edge-edge distance of 600 µm. The scaffolds with BxPC-3 cells were placed in a bioreactor chamber with a 4.2 mm inner diameter and a 5.0 mm outer diameter. The DNP injection is constituted by a Fluorinated Ethylene Propylene (FEP) tube with a 0.25 mm inner diameter fluid path and has a low dead space volume of 0.2 ml. When the bioreactor chamber is removed from the incubator and placed in the RF solenoid coil, it is mounted in a 3D printed socket made with a 6% luer female conical fitting allowing direct coupling with the bioreactor chamber. The socket is designed as a fluid outlet for the bioreactor chamber, but also provides an easy and quick way to ensure that the scaffold is positioned accurately and reproducibly in the coverage area of the RF coil and in the 9.4 MRI magnet isocenter every time it is used. The RF coil is a part of a double tuned NMR Probe and the [1-^{13}C] pyruvic acid were polarised using a SpinLab (GE Healthcare, Milwaukee, WI, USA).

Results: The design of the bioreactor is highlighted in Figure 1(A-B) and a SEM image of the scaffold structure is shown in Figure 1C. Injection of 10 mM [1-^{13}C] pyruvate was performed and a NMR spectrum is shown in Figure 1D where the green curve represents a control scaffold with only medium loaded and the pink curve represents a scaffold containing approx. 10 million human pancreas cancer cells. Development of lactate is clearly seen in the cancer cells.

Conclusion: This study demonstrates the use of a newly developed five mm bioreactor system for a horizontal 9.4T MRI system. The bioreactor system is designed to measure cell metabolism of cells in suspension or of cells grown in scaffolds with relatively low cell numbers. The scaffold system facilitates a dynamic cell culture environment with controlled nutrient flow, oxygen supply and a large surface area for growth of adherent cells with minimal disturbance of the cells. Ongoing studies are focusing on evaluation of cell numbers in suspension and scaffold in this bioreactor design.

AUTHORS (LAST NAME, FIRST NAME): Bertelsen, Lotte B.[1]; Lauritsen, Simon H.[1]; Laustsen, Christoffer[1]; Daugaard, Preben[1]; Nielsen, Nathalie[1]; Zhang, Xiaolu[1]; Ringgaard, Steffen[1]; Stødkilde-Jørgensen, Hans[1]

INSTITUTIONS (ALL):

1. The MR Research Centre, Department of Clinical Medicine, Aarhus University, Aarhus, Select, Denmark.

Figure 1

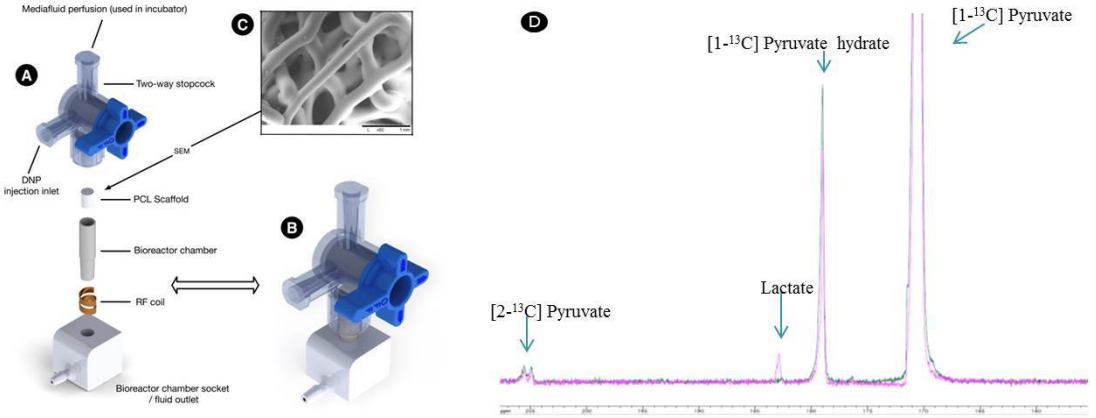
Mediafluid perfusion (used in incubator)
A
Two-way stopcock
DNP
injection inlet
C
SEM
PCL Scaffold
Bioreactor chamber
RF coil
Bioreactor chamber socket
/ fluid outlet
B
D
[1-13C] Pyruvate
[1-13C] Pyruvate hydrate
Lactate
[2-13C] Pyruvate

CONTROL ID: 2230018

TITLE: TGFβRI Inhibition Produces Dual Cardioprotective Actions through Increasing Survivin and Inhibiting Wnt Expressions in Cardiac Progenitors

PRESENTER: Wen-Pin Chen

ABSTRACT BODY:

Abstract Body: *Introduction*

A83-01, a TGFβRI inhibitor, could facilitate cardiac self-repair in post-MI mice via expanding Nkx2.5+ cardiomyoblast. The detailed signaling mechanism remains to be clarified. This study aimed to investigate the autocrine/paracrine factors regulated by A83-01 and the mechanistic link to A83-01-mediated cardioprotective action.

Methods and Results

Using transgenic Nkx2.5 enhancer-GFP reporter mice to isolate cardiac Nkx2.5-GFP+ (Nkx2.5+), sca1+ and Nkx2.5+/sca1+ cells, A83-01 was demonstrated to proliferate the three subpopulations mainly through increasing Birc5 expression in MEK/ERK-dependent pathway. Survivin, encoded by Birc5, could directly proliferate Nkx2.5+ cells and enhance cultured cardiomyocytes viability. Moreover, in post-injured mice hearts, Wnt3a was up-regulated but Birc5 was down-regulated. Wnt3a inhibited Nkx2.5+ cell growth, which could be reversed by A83-01 partly through inhibiting Fzd6 and WISP1 expressions. Using inducible αMHC-cre/mTmG mice to label cardiomyocytes with GFP and non-myocytes with RFP, more survived myocytes and few renewed RFP+ myocytes in parallel with less cardiac fibrotic were found in isoprenaline-injected mice treated with A83-01, indicating the prominent benefit of paracrine survivin in supporting myocyte survival. The effect of A83-01 treatment also was confirmed by echocardiography using Prospect small animal ultrasound system (S-Sharp Corporation, New Taipei City, Taiwan). The ultrasound result showed that A83-01 treatment could significantly improve cardiac function.

Conclusions

TGFβRI inhibition in cardiac progenitors could both stimulate the autocrine/paracrine of survivin to mediate cardioprotective action and attenuate Wnt-induced cell depletion.

AUTHORS (LAST NAME, FIRST NAME): Ho, Yu-Sian[1]; Lin, Fen-Chiung[2, 3]; Tsai, Wan-Hsuan[1]; Chen, Wen-Pin[1]

INSTITUTIONS (ALL):

1. Institute of Pharmacology, College of Medicine, National Taiwan University, Taiwan., Taipei, Taiwan.
2. Graduate Institute of Clinical Medicine, Taipei Medical University, Taiwan., Taipei, Taiwan.
3. Division of Cardiology, Linkou Chang Gung Memorial Hospital, Taiwan., Taoyuan, Taiwan.

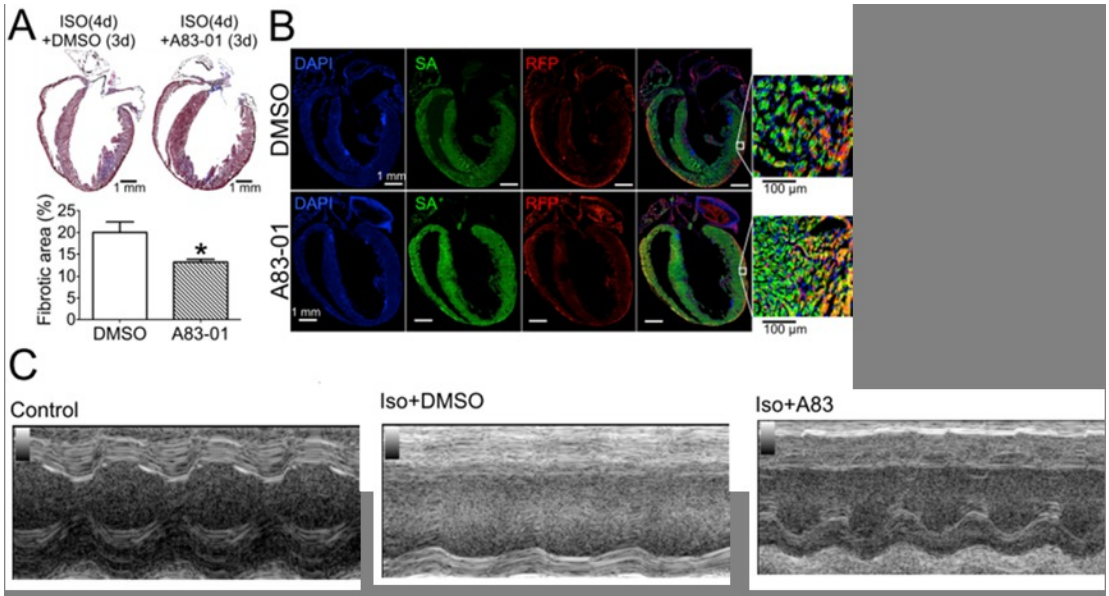

Fig. 1 (A) Masson's Trichrome stain shows the decrease of cardiac fibrotic area in post-injured hearts subjected to four consecutive doses of isoprenaline and followed by the treatment of DMSO or A83-01. The hearts were harvested on day 14. The fibrotic region was indicated by blue, muscle region by red, and nuclei by black. (B) The fluorescent immunostaining was performed to identify cardiomyocytes and non-myocytes genetically labeled with tdTomato. (C) Representative echocardiographic images of the cardiac motion under M-mode via assessing the parasternal views of longitudinal axis in mice with the indicated treatments.

CONTROL ID: 2232671

TITLE: Therapeutic Efficacy Evaluation and Underlying Mechanism of Quetiapine in Collagen Induced Arthritis Animal Model

PRESENTER: Tzu-Yao Huang

ABSTRACT BODY:

Abstract Body: Quetiapine, an atypical antipsychotic drug, is widely used to treat the symptoms of schizophrenia and other psychotic disorders. Quetiapine has been shown to exert anti-inflammatory effect, however, its underlying mechanism in collagen-induced arthritis remains ambiguous. Here whether the release of proinflammatory cytokines such as IL-6, TNFα and IL-1β can be inhibited by quetiapine in LPS-stimulated RAW 264.7 macrophages are investigated. The results show that quetiapine could inhibit CREB and NF-κB signaling pathways *via* suppressions of ERK and AKT phosphorylation, respectively. The therapeutic efficacy of quetiapine in collagen-induced arthritis (CIA) mouse model was also assayed. The results show that proinflammatory cytokines are decreased while immunosuppressor factors are increased in CIA mice. Furthermore, the inflammatory activity in the joints was monitored by the accumulation of ^{18}F-FDG/microPET. Significantly lower uptakes of ^{18}F-FDG were found compared with that of the celecoxib group, and further verified by *ex-vivo* autoradiography. Micro-CT imaging was also performed to demonstrate the severity of bone erosion, no or minor bone erosion was found in the quetiapine group compared with that of the celecoxib group. Taken together, these results suggest that quetiapine could be a potential anti-inflammatory drug, and may be used for the treatment of rheumatoid arthritis.

AUTHORS (LAST NAME, FIRST NAME): Huang, Tzu-Yao[1]; Hwang, Jeng-Jong[1]

INSTITUTIONS (ALL):

1. Biomedical imaging and radiological science, National Yang-Ming University, Taipei, Taiwan.

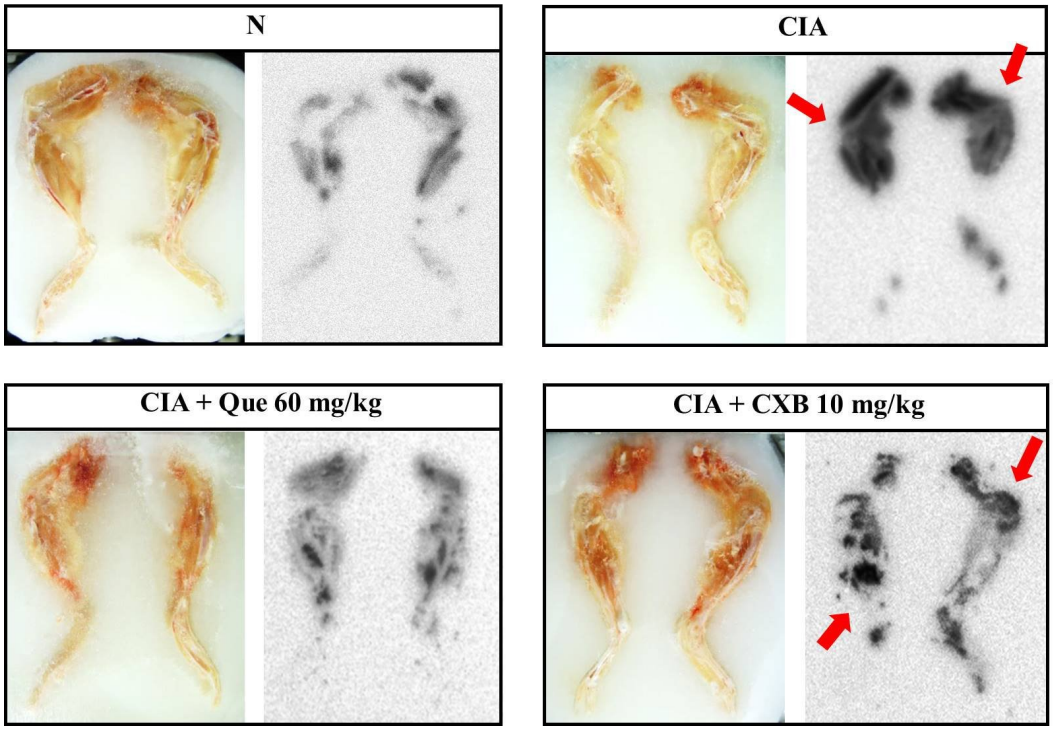
N
CIA
CIA + Que 60 mg/kg
CIA + CXB 10 mg/kg

CONTROL ID: 2232860

TITLE: A physiological based model for tracer concentration time curves in blood vessels measured by dynamic imaging

PRESENTER: Dennis Cheong

ABSTRACT BODY:

Abstract Body: Background

Tracer kinetic or pharmacokinetic analysis of dynamic imaging requires the tracer concentration profile in the incoming blood plasma, usually called the arterial input function and recently also called the vascular input function (VIF). It is beneficial to fit a curve to VIF and most attempts constructed empirical mathematical expressions to do so. Very few describe VIF physiologically as it can be too complex [1] for curve fitting. A recent attempt by Horsfield et al. [2] can fit both VIFs in aorta and portal vein, but is limited to DCE MRI because of assumptions specific to Gd-based tracer. Here, we present a physiological based model that is independent from modality and tracer to describe the tracer concentration over time in any blood vessel.

Theory

We consider 3 contributing physiological factors. First, the delay and dispersion of the injected tracer as it travels from the injection point to the measurement point, resulting in the first bolus. We use the vascular transport operator, VTO, with 2 parameters representing the time delay and the relative dispersion as described by King et al. [3]. This VTO provides good descriptions for the intravascular mass transport and has been successfully used in other physiological models [1].

Second, widening boluses of tracer pass through the same measurement point repeatedly, commonly referred to as recirculation. We describe each of the subsequent boluses by applying a second VTO to the previous one, assuming each recirculation has the same minimum recirculation time and has the same relative dispersion.

Finally, to account for the amount of tracer remaining in the vascular space, we scaled the n^{th} recirculation bolus by a fraction, q(n) derived from a three-compartment exchange system that models the tracer distribution after each bolus circulation in the vascular, interstitial, and excretion spaces. Thus, the n^{th} bolus may be modeled by convolving the second VTO with the previous unscaled bolus and scale it down by q(n). We termed our model as MultiVTO model.

Methods

Curve fitting using our model and the Horsfield model was performed using MATLAB® LSQCURVEFIT on VIFs measured at 5 locations and 2 modalities. DCE MRI data from descending aorta (n=34), vertebral artery (n=8), hepatic artery (n=3), and portal vein (n=3), and DCE CT data from iliac artery (n=43).

Results

Our model successfully fitted the different VIFs at slightly better performance than the Horsfield model. Fig. 1 shows the typical fitted curves. Table 1 compares the goodness of fit between the models.

Discussions and Conclusion

This physiological model is able to fit different VIFs measured by both DCE MRI and DCE CT, and at different blood vessel locations. It should be applicable to VIFs acquired by different imaging modalities such as PET, SPECT, DCE CT, DSC and DCE MRI, for both human and animal studies. In addition, its parameters have physiological meanings and may assist in validating measured VIFs, especially in MRI where quantification is problematic.

References

[1] van Osch MJP et al.; Magn Reson Med 2003, 50, 614

[2] Horsfield MA et al.; Phys Med Biol 2009, 54, 2933

[3] King RB et al Am. J. Physiol. 1993 265 H2196

AUTHORS (LAST NAME, FIRST NAME): Cheong, Dennis L.[1]

INSTITUTIONS (ALL):

1. Clinical Imaging Research Centre, Singapore, Singapore.

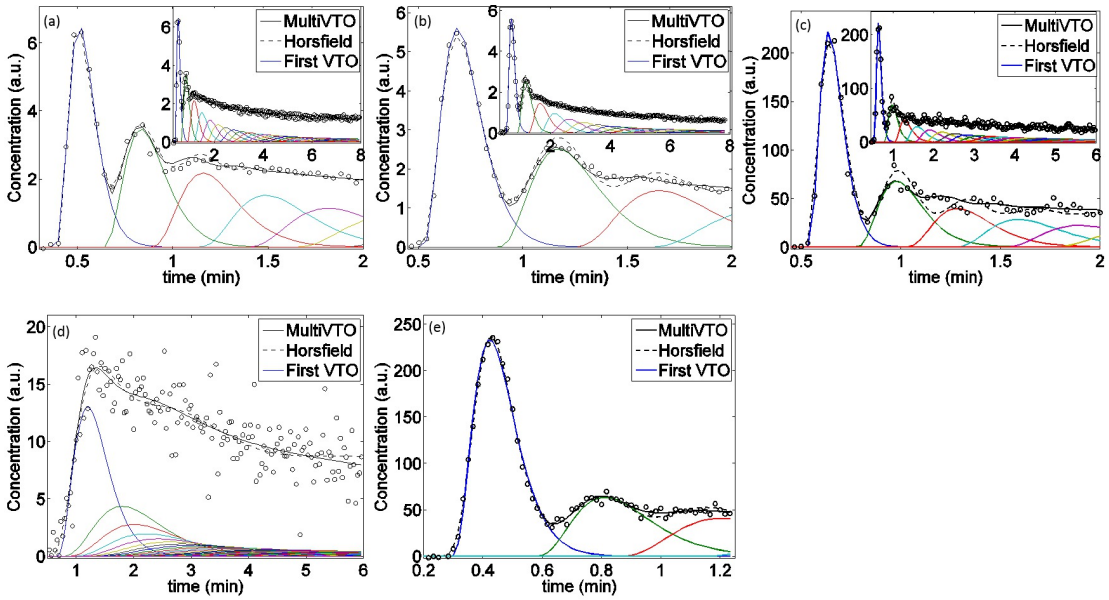

Figure 1. Typical VIFs measured by DCE MRI at descending aorta (a), vertebral artery (b), hepatic artery (c), portal vein (d), and by DCE CT acquired at iliac artery (e). VIFs are fitted using MultiVTO (black solid line) and Horsfield model (black dashed line). Colored sold lines are the individual VTO curves. Insets in (a-c) show the full VIF to allow zoom-in view in the main plot.

CONTROL ID: 2230026

TITLE: *In vivo* optical imaging of stem cells delivered with injectable, thermosensitive extracellular matrix-methylcellulose hydrogels

PRESENTER: Jun Sung Kim

ABSTRACT BODY:

Abstract Body: Stem cell-based regenerative medicine has emerged as a potential therapeutic alternative for many diseases. Despite their rapid transition from animal studies to clinical applications, a number of questions remain unanswered, particularly regarding *in vivo* behaviors of stem cells transplanted into target tissues including issues about their survival, distribution, migration, and engraftment [1,2]. *In situ* forming hydrogels that can undergo sol-gel transitions in response to temperature are attractive as vesicles for stem cell delivery because of easy incorporation of cells, simplicity of implantation by injection, long-term retention of delivered cells, and improvement of cell viability by providing the chemical and physical cues of extracellular matrix (ECM) [3]. Recently, intact ECMs derived from various living tissues have been used for developing thermosensitive hydrogels. These tissue-derived ECMs are considered to be effective in providing a niche for controlling cellular behaviors and tissue regeneration because of well-preserved original tissue's 3-D ultrastructure, mechanical integrity, protein composition, and biologic activity. In this study, we investigated the bio-distribution and engraftment of stem cells using injectable, thermosensitive hydrogels based on human adipose-derived ECM and methylcellulose (MC). The ECM was isolated from human adipose tissue [4] and was solubilized using urea and guanidine-HCl buffer. The ECM solution (6 wt%) was blended with the MC solution (6 wt%) at low temperatures. Human adipose-derived stem cells (hASCs) were labeled with lipophilic 1,1'-dioctadecyl-3,3,3',3',-tetramethylindotricarbocyanine iodide (DiR), which can strongly bind to cell membranes [5]. The ECM-MC pre-gel solution (50 μL) containing DiR-conjugated hASCs (2.5×10^5 cells) was subcutaneously injected into the backs of nude mice using an 28-gauge needle. The bio-distribution and engraftment efficacy of DiR-labeled hASCs were monitored for 7 days by IVIS imaging system under 750 nm of excitation and 782 nm of emission. The injected hydrogel rapidly formed a transparent hydrogel at the injection site. *In vivo* imaging showed that DiR-hASCs were well entrapped within the hydrogel, while the fluorescent signals of hASCs were rarely observed in the PBS group on day 7. Overall results suggest that the ECM-MC hydrogel is a promising stem cell delivery system which can improve the engraftment of transplanted stem cells and enhance the therapeutic efficacy of stem cell therapy.

[1] Ballios BG, Cooke MJ, van der Kooy D, Shoichet MS, **Biomaterials** *2010* 31(9) 2555-2564

[2] Choi YC, Choi JS, Woo CH, Cho YW, **J Control Release** *2014* 10 42-50

[3] Dai M, Xu P, Hou M, Teng Y, Wu Q, **Exp Ther Med** *2015* 9(2) 372-376

[4] Choi JS, Kim BS, Kim JY, Kim JD, Choi YC, Yang HJ, Park K, Lee HY, Cho YW, **J Biomed Mater Res A**, *2011* 97(3) 292-299

[5] Kalchenko V, Shivtiel S, Malina V, Lapid K, Haramati S, Lapidot T, Brill A, Harmelin A, **J Biomed Opt** *2006* 11(5) 050507

AUTHORS (LAST NAME, FIRST NAME): Kim, Jun Sung[1]; Kim, Eun Ji[1]; Choi, Ji Suk[1]; Kim, In-San[2]; Cho, Yong Woo[1]

INSTITUTIONS (ALL):

1. Hanyang University, Ansan, Korea (the Republic of).
2. Korea Institute of Science and Technology, Seoul, Korea (the Republic of).

(No Image Selected)

CONTROL ID: 2230044

TITLE: Combined PET-MRI: Correlating FET and Gd-DTPA perfusion for advanced pharmacokinetic modelling

PRESENTER: Marie Anne Richard

ABSTRACT BODY:

Abstract Body: Introduction The kinetics of ^{18}F-fluoroethyltyrosine (FET) can be described by a 2-tissue compartment model (Fig. 1-A) in which perfusion through the capillary walls (k_1 and k_2) and uptake by amino acid transporters (k_3 and k_4) are coupled. Uncoupling these parameters would allow quantitative comparisons of metabolism between differently perfused tumors. This can be achieved using a compound with similar perfusion kinetics as FET, but no metabolism.

Hypothesis Outside of the blood-brain barrier (BBB), perfusion is governed by passive diffusion through capillary pores, a process modulated by the radius of the molecule and its chemical properties [1]. A correlation between the k_1 of Gd-DTPA and FDG was found in previous unpublished work. Therefore, FET, another water-soluble, low-molecular-weight compound, may also share a relation of the form $k_{FET} = f(k_{Gd\text{-}DTPA})$ for k_1 and k_2.

Protocol Eight Fischer rats with F98 glioma were scanned sequentially by MRI followed by PET according to a previously published protocol [2]. Table 1 shows the doses of Gd-DTPA and FET injected for each scan. Scans were separated by a 30 minute interval. A T_1 map (gradient echo with multiple flip angles) and DCE-MRI images (gradient echo keyhole) were acquired on a 7 T small animal system (Varian) with a 4 s temporal resolution. PET images were acquired on a LabPET4 scanner (Gamma Medica/GE Healthcare) and reconstructed with variable temporal resolution. The arterial input function (AIF) was determined with two methods: (1) by blood sampling trough the caudal artery during the PET scan and (2) using a tissue of reference [3]. Plasma FET was dosed by gamma counter and Gd-DTPA by ICP-MS. Manual co-registration of MRI and PET images (Fig. 1-B) and pharmacokinetic analysis were performed using an in-house MATLAB program. Statistical analysis was performed in GraphPad Prism.

Results and discussion A significant correlation between and was found when using the tissue of reference AIF (Fig 1-C) (Pearson's test). Brain regions were excluded from this analysis because transport across the BBB does not rely on passive diffusion as in the muscles or in abnormal tumor vasculature. No significant correlation was found for, which is consistent with different elimination mechanisms for these compounds. The blood AIF yielded large inter-subject variations attributed to difficulties in performing consistent manual blood sampling and repeating an identical Gd-DTPA injection for dosing during the PET scan. Statistical analyses using the blood sampled AIF were deemed inconclusive (data not shown).

Conclusion Gd-DTPA and FET appear to have similar perfusion kinetics outside of the BBB, but their elimination from tissue is unrelated. These results suggest that it would be possible to determine the k_1 parameter of FET from the Gd-DTPA MRI data and use this information to distinguish between metabolism and perfusion.

References [1] Pandit, *Introduction to the Pharmaceutical Science,* (Baltimore: LLW, 2007), 126. [2] Poulin *et al.* Magn Reson Med. 2013;69(3):781-792. [3] Yankeelov *et al.* Magn Reson Imaging. 2005;23:519–529.

AUTHORS (LAST NAME, FIRST NAME): Richard, Marie Anne[1]; Turgeon, Vincent[1]; Fouquet, Jérémie P.[1]; Tremblay, Luc[1]; Lebel, Réjean[1]; Lepage, Martin[1]

INSTITUTIONS (ALL):

1. CIMS, Université de Sherbrooke, Sherbrooke, QC, Canada.

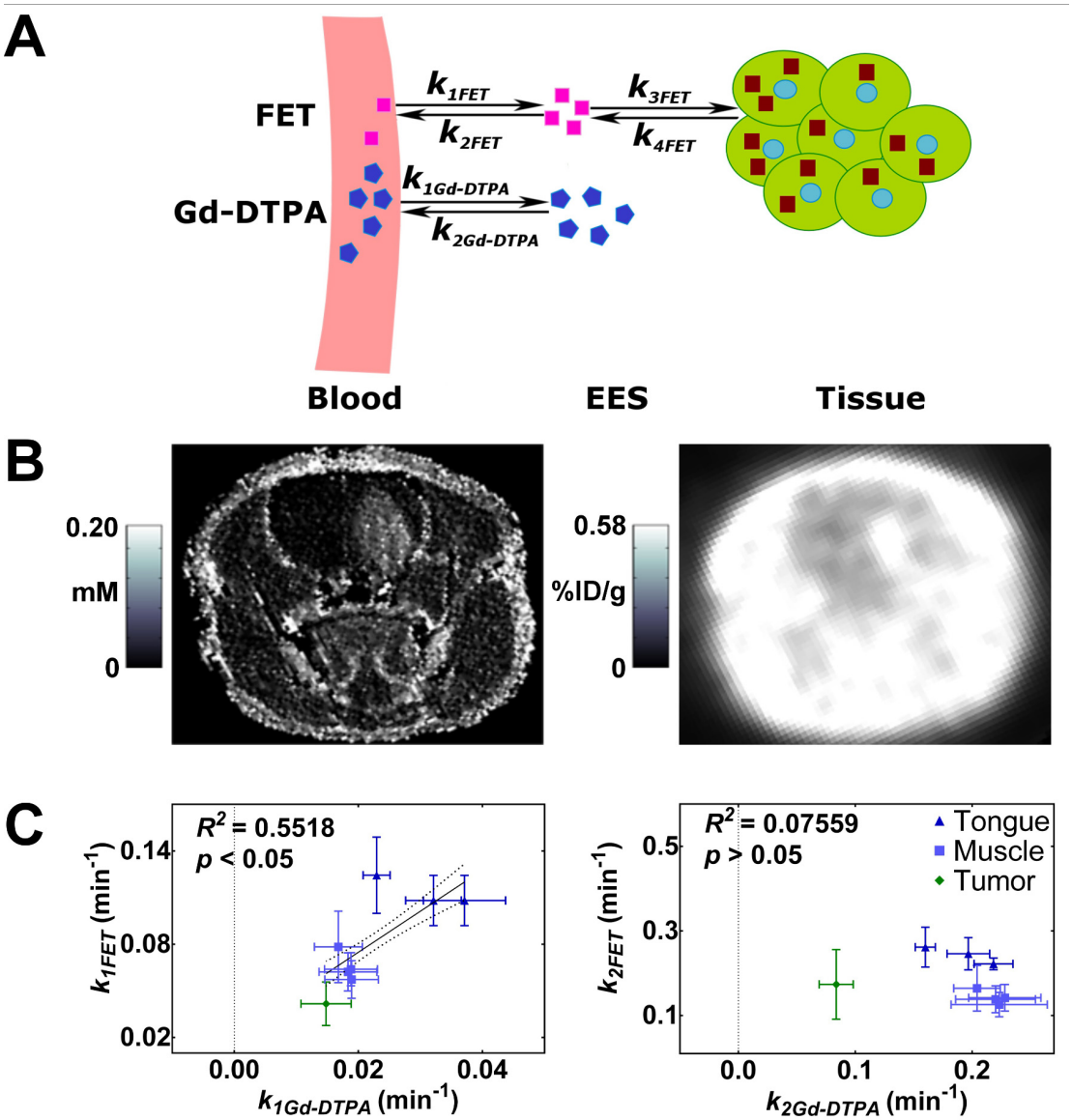

Figure 1. A) Compartment model showing perfusion (k_1 and k_2) and metabolism (k_3 and k_4). EES: extracellular-extravascular space. B) Coregistered Gd-DTPA and FET concentration maps used for pharmacokinetic modelling. C) Significant linear correlation between $k_{1Gd-DTPA}$ and k_{1FET} but not between $k_{2Gd-DTPA}$ and k_{2FET} in the muscles, the tumor and the tongue.

CONTROL ID: 2230052

TITLE: Hepatic Metabolomic Analysis in Patients with Non-alcoholic Steatohepatitis using ^{1}H MR spectroscopy with Long echo time

PRESENTER: Kwon-Ha Yoon

ABSTRACT BODY:

Abstract Body: Purpose: Early diagnosis of non-alcoholic steatohepatitis (NASH) can prevent the potential development of cirrhosis and hepatocellular carcinoma. Until now, it is difficult to differentiate from hepatic steatosis and NASH, if not liver biopsy. The aim of this study was to evaluate the hepatocellular metabolic difference between patients with non-alcoholic steatosis and NASH using ^{1}H-MR spectroscopy (MRS) with long echo time (TE).

Methods: Eight patients with non-alcoholic steatosis (age 40.5±11.6 years) and three patients with NASH (age, 25.3 ± 7.9 years) were enrolled, which were pathologically proven. Both groups have no history of liver diseases. The subjects were studied using a 3.0T MRI scanner (Achieva; Philips Healthcare) with a 32-channel body coil. Together with breath-hold technique, the ^{1}H-MRS measurements were performed using a point-resolved spectroscopy (PRESS) sequence with following parameters: TR/TE= 2000/288ms, 6 acquisitions and 2×2×2cm^{3} size on a localized voxel of the right lobe. MRS data were analyzed with jMRUI. Major hepatocelluar metabolites were assigned as follows: alanine (Ala, 1.50ppm), lactate/triglyceride (Lac/TG, 1.33ppm) and triglyceride (TG, 0.90ppm). The residual water peak at 4.70ppm was used as an internal reference for the metabolite quantification. All the patients were measured based on the body mass index (BMI). Liver function tests including of aspartate aminotransferase (AST) and alanine aminotransferase (ALT) were performed. Statistical analysis was performed with two sample *t*-test.

Results: On ^{1}H-MRS, Ala concentration showed significantly difference between two groups (steatosis: 0.8±0.1 vs NASH: 73.92±37.1, $p<0.01$). On the contrary, Lac/TG concentration (430.3±144.4 vs1121.8±793.0, $p>0.05$), and TG concentration (51.4±7.0 vs 584.2±512.1, $p>0.05$) were not significantly different. The BMI was not significantly different between two groups (28.8 ± 2.5 vs 31.4 ±5.7, $p>0.05$). On laboratory test, the AST and ALT level were not significantly different between two groups.

Conclusions: ^{1}H-MRS with long TE would provide a useful biomarker for non-invasive diagnosis in patients with the NASH.

References

1. Lomonaco R, et al. *Hepatology* 2012; 55: 1389-97.
2. Farrell GC and Larter CZ. *Hepatology* 2006; 43: S99-S112.
3. Rector RS, et al. *World J Gastroenterol* 2008; 14: 185-192.
4. Browning JD, et al. *Hepatology* 2004; 40: 1387-1395.

AUTHORS (LAST NAME, FIRST NAME): Kim, Tae-Hoon[1]; Jun, Hong Young [1]; Yoon, Kwon-Ha[1]

INSTITUTIONS (ALL):

1. Radiology, Wonkwang University, Iksan, Korea (the Republic of).

(No Image Selected)

CONTROL ID: 2230334

TITLE: Reproducibility over time of 4DCT derived ventilation distribution data

PRESENTER: Geoffrey Zhang

ABSTRACT BODY:

Abstract Body: Deriving lung ventilation distribution from 4-dimensional CT (4DCT) using deformable image registration is a recent technical development. Several studies have shown that this technique reasonably agrees with other established techniques such as SPECT/CT. Theoretically, one could determine regions of high lung ventilation in thoracic cancer patients and use these regions as avoidance structures in radiotherapy treatment planning, without the need of an additional imaging procedure such as SPECT/CT. In this study, we evaluated the serial reproducibility of ventilation data derived from two separate 4DCT data sets, collected at different time points. A total of 33 lung cancer patients were retrospectively analyzed following a protocol approved by our institutional review board. All patients had two lung cancer stereotactic body radiotherapy treatment courses (different isocenters) with a median interval between them of 9.6 months (range: 0.7-39 mo). Sets of 4DCT were acquired for treatment planning for each treatment course. Seven patients were excluded due to artifacts in the 4DCT data sets. The ventilation distributions in the lungs for each patient were calculated using the two sets of 4DCT data, with the tumor volumes excluded. The Diffeomorphic Morphons (DM) method was applied for the deformable image registration (DIR) between the expiration and inspiration phases in each 4DCT data set. The generated deformation matrices were used to generate ventilation distributions using the ΔV method which is a direct geometrical calculation of the volume change. In each case, the 2nd set of ventilation distributions was mapped onto the 1st set using DM DIR and the two ventilation distributions were compared. Since radiation dose can alter regional lung ventilation, these dose regions were excluded to prevent introduction of systemic error in the ventilation calculations. We chose to analyze lung regions that received less than 1 Gy of radiation dose. The Spearman correlation coefficient (SCC) between the ventilation data sets in each case was calculated. The Dice similarity coefficient (DSC) was also calculated between the upper 30% ventilation regions of the two sets. For the 26 cases, the median SCC value was 0.31 (range 0.18 to 0.52, p value < 0.01 for all cases). The median DSC value was 0.75 (range 0.71 to 0.81, Figure 1). Mushroom artifacts often appear in 4DCT data due to irregular diaphragmatic motion. This imaging artifact introduces errors in DIR and consequently errors in the derived ventilation distributions. Because of these errors, the SCC value could be very low, close to 0. Based on the SCC and DSC values of all the cases, we can conclude that the two ventilation data sets in each case correlated and the reproducibility over time, especially for the high ventilation regions, was reasonably good when there were no obvious artifacts in the 4DCT. High quality 4DCT is essential for good reproducibility in ventilation distributions.

AUTHORS (LAST NAME, FIRST NAME): Alsyed, Emad M.[2]; Latifi, Kujtim[1]; Moros, Eduardo G.[1]; Feygelman, Vladimir[1]; Dilling, Thomas J.[1]; Zhang, Geoffrey G.[1]

INSTITUTIONS (ALL):

1. Radiation Oncology, Moffitt Cancer Center, Tampa, FL, United States.
2. Physics, University of South Florida, Tampa, FL, United States.

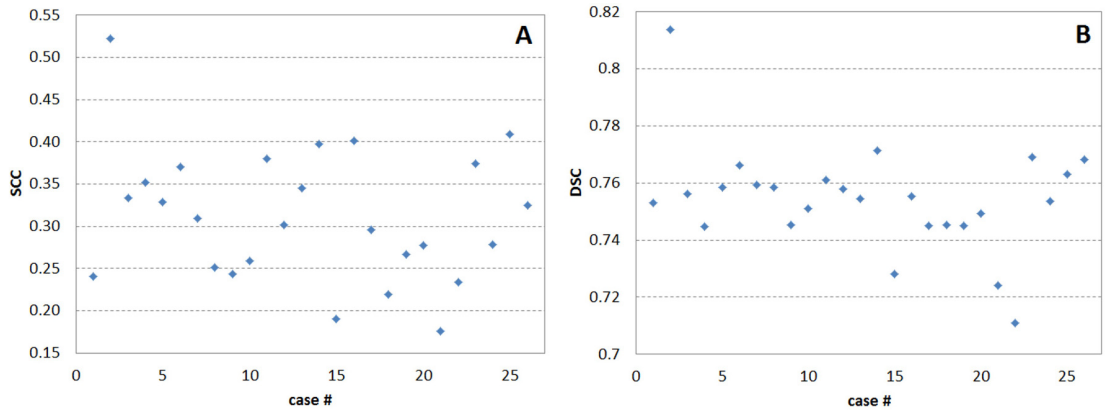

Figure 1. (A) Spearman correlation coefficients (SCC) and (B) Dice similarity coefficients (DSC) for all 26 cases.

CONTROL ID: 2230115

TITLE: 2-(2-[^{18}F]fluoroethyl)-L-phenylalanine (2-[^{18}F]FELP) versus [^{18}F]FET for peripheral tumor imaging: comparative uptake in various tumor cell lines

PRESENTER: Ken Kersemans

ABSTRACT BODY:

Abstract Body: Introduction: At present, the best established amino acid analogue for brain, head and neck tumor imaging with PET is [^{18}F]FET. However, [^{18}F]FET accumulates poorly in peripheral tumors, a finding that is linked to its aspecific transport characteristics. Therefore, the development of new radiofluorinated amino acid analogues has focussed on LAT1 specific compounds [1]. Recently, 2-(2-[^{18}F]fluoroethyl)-L-phenylalanine (2-[^{18}F]FELP) was identified as a LAT1-selective tumor tracer with a high affinity towards LAT1 and with a favourable biodistribution and tumor uptake in a R1M rhabdomyosarcoma model [2]. In order to evaluate the potential of 2-[^{18}F]FELP as a peripheral tumor imaging agent, it was evaluated in several relevant tumor cell lines and compared to [^{18}F]FET.

Methods: 2-[^{18}F]FELP and [^{18}F]FET were obtained by means of an automated radiosynthesis that was previously described [3]. The tracers were evaluated *in vitro* using human A549 (lung carcinoma), C6 (glioma), Capan2 (pancreas adenocarcinoma) and HT29 (colon carcinoma) cells and compared to the R1M (rat rhabdomyosarcoma) model in HEPES buffer with (HEPES+) and without sodium ions (HEPES-) and in MEM buffer. Transport type characterization, time dependency, inhibition, trans-stimulation and efflux were studied according to the method described by Kersemans et al. [4].

Results: The influx of 2-[^{18}F]FELP could be inhibited almost quantitatively by BCH (8mM) and L-Phenylalanine (8mM) independent of sodium ions while MeAIB (methyl-amino-butyric acid; 8mM) did not show any effect on the uptake, indicating LAT1 specific transport. In the same assay, 2-[^{18}F]FELP and [^{18}F]FET showed a Km of 10 +/- 3µM and 249 +/- 41 µM respectively. The time dependent uptake for both tracers showed similar uptake kinetics up to 15 minutes, after which [^{18}F]FET reached its maximum and started to wash out slowly, while 2-[^{18}F]FELP uptake remained constant or kept increasing, depending on the cell line. The ratio of the cellular uptake per million cells of 2-[^{18}F]FELP over [^{18}F]FET after 120 minutes was lowest for R1M (HEPES+ = 0.97; HEPES- =2.0) and highest for HT29 (HEPES+ = 2.6; HEPES- = 2.9).

Conclusion: The *in vitro* uptake studies showed 2-[^{18}F]FELP had a high accumulation after 2 hours and a good retention in the studied cell lines in comparison with [^{18}F]FET, which would be beneficial for imaging. Based on the encouraging results, additional studies are warranted to characterize 2-[^{18}F]FELP *in vivo*.

References:

[1] Wang L, Nucl Med Biol. 2011;38(1):53-62

[2] Kersemans K. WMIC 2014, Seoul, Poster Presentation.

[3] Kersemans K, J Label Compd Radiopharm. 2010; 53(2): 58-62

[4] Kersemans V. Nucl Med Biol. 2004; 31: 739–746

AUTHORS (LAST NAME, FIRST NAME): Kersemans, Ken[1]; Dumolyn, Caroline[1]; De Vos, Filip J.[1]

INSTITUTIONS (ALL):

1. Radiopharmacy, Ghent University, Ghent, Belgium.

(No Image Selected)

CONTROL ID: 2230131

TITLE: A modular dual labeling approach for multimodal agent development

PRESENTER: Sukhen Ghosh

ABSTRACT BODY:

Abstract Body: Objective: Growing clinical evidence suggests that multimodality imaging can improve surgical outcomes in cancer (van den Berg, N.S. *et al*., Radiology, 2014, 140322). Accordingly, interest in the development of multimodal agents possessing nuclear and optical reporters has increased in efforts to combine real-time surgical guidance and non-invasive nuclear imaging capabilities into a single agent. Alongside conventional dual labeling methods, modular schemes have recently been introduced to facilitate the design, synthesis, and optimization of multimodal agents (Ghosh, S.C. *et al*. J Med Chem, 2013, 406-16), (Brand, C. *et al*., Bioconjug Chem, 2014, 1323-30). The modular constructs can reduce the likelihood of over-modification during the labeling process, and potentially offer improved selectivity through site-specific conjugation. Here, different dual labeling methods are compared using a multimodal chelator (MMC) for enhanced production of immunoconjugates for PET/NIRF imaging.

Methods: A DOTA mimetic was functionalized with reactive groups for NHS, sulfhydryl, and click chemistry and conjugated to the epithelial cell adhesion molecule (EpCAM)-specific antibody, mAb7. For samples using sulfhydryl chemistry, mAb7 was treated with varying amounts of the reducing agent, dithiothreitol (DTT), to partially reduce interchain disulfides for site-specific conjugation. Fluorescence intensity was monitored by HPLC and NIR detection to identify differences in optical properties between the labeling methods. Efficiency of ^{64}Cu labeling was examined, and MMC/mAb ratios were quantified by isotopic dilution and confirmed by spectrophotometry. Immunoreactivity was assessed by ELISA and flow cytometry. *In vivo* imaging was assessed by PET/NIRF using a sulfhydryl-produced immunoconjugate in a prostate tumor model.

Results: MMC-immunoconjugates synthesized by sulfhydryl chemistry had 1-8 MMC/mAb and correlated with the amount of DTT used, while NHS and click chemistry schemes yielded 1-3 MMCs/mAb. Immunoreactivity was retained with each method as indicated by ELISA and flow cytometry, and ^{64}Cu labeling showed >60% yield and >95% purity for all agents. Specific activity ranged from 0.11-0.30 MBq/μg, with the sulfhydryl compound having the highest values. The fluorescence intensity of the NHS and sulfhydryl-produced agents were reduced following conjugation to MMC and mAb7, suggesting possible quenching of IRDye800 during the multistep synthesis. This was not observed for the click analog which involved dye conjugation to MMC-mAb7 in the final step. Multimodal imaging with a sulfhydryl-produced immunoconjugate containing 2 MMCs provided excellent delineation of primary and metastatic tumor sites. *Ex vivo* analysis and PET quantitation confirmed high tracer uptake with tumor/muscle ratios ranging from 9.01-22.7.

Conclusions: Multiple dual-labeling strategies can be used to produce MMC-immunoconjugates for hybrid imaging. Preliminary *in vivo* findings revealed excellent imaging properties and could be further improved through dye labeling in the final step to maximize fluorescence intensity for intraoperative use.

AUTHORS (LAST NAME, FIRST NAME): Ghosh, Sukhen[1]; Pinkston, Kenneth L.[1]; Wilganowski, Nathaniel[1]; Harvey, Barrett R.[1]; Sevick-Muraca, Eva M.[1]; Azhdarinia, Ali[1]

INSTITUTIONS (ALL):

1. Center for Molecular Imaging, UT Health Science Center-Houston, Houston, TX, United States.

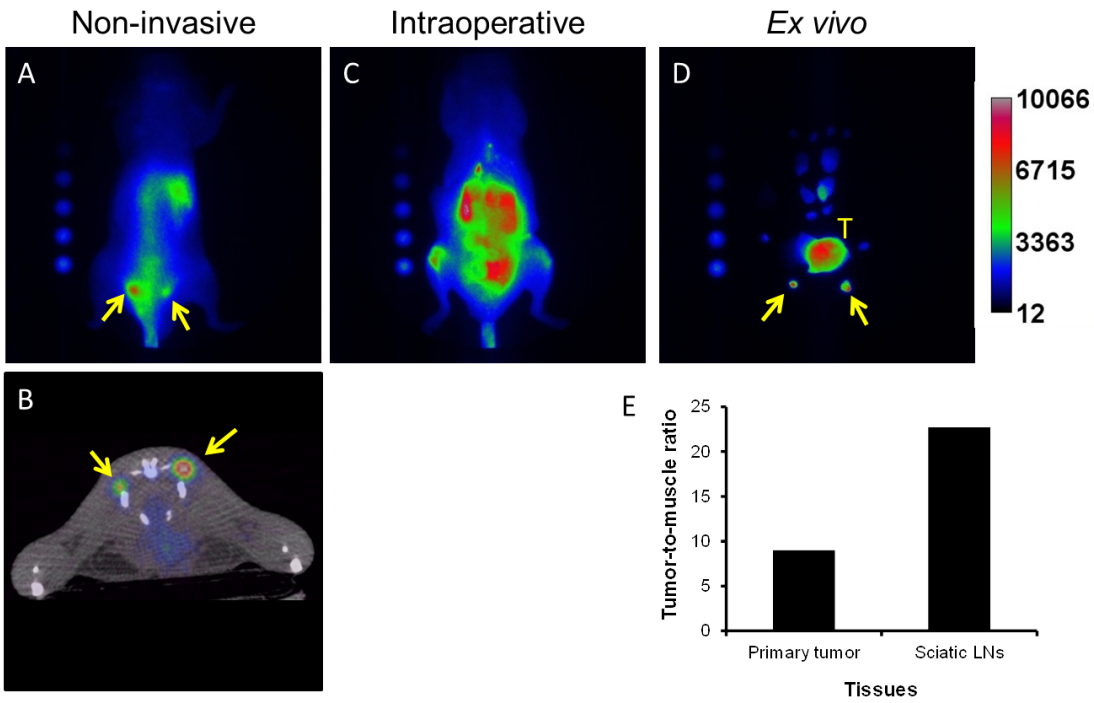
Non-invasive
Intraoperative
Ex vivo
A
B
C
D
T
10066
6715
3363
12
E
Tumor-to-muscle ratio
25
20
15
10
5
0
Primary tumor
Sciatic LNs
Tissues

CONTROL ID: 2230147

TITLE: ***In vivo*** **magnetic resonance imaging and microscopy of vessel permeability and endovascular inflammation using targeted microparticles of iron oxide**

PRESENTER: Lisa Whittingstall

ABSTRACT BODY:

Abstract Body: Introduction: The vascular cell adhesion molecule 1 (VCAM-1) is an inducible endothelial membrane protein that is often used as a marker in studies of inflammatory conditions. Here we present a method combining *in vivo* MRI and microscopy using fluorophore labelled, VCAM-1 antibody-conjugated microparticles of iron oxide (MPIOs) in order to *non-invasively* study cerebro-vascular inflammation and blood vessel permeability.

Methods: *In vivo MRI* Lipopolysaccharide (LPS) injections of 1 µg into the right hemisphere (RH) of female Balb/c mice were used to induce inflammation. MR imaging was conducted on a small animal 7T scanner with a dedicated mouse head-coil. **(1)** The effect of inflammation on vessel permeability was studied 7.5 h post LPS injection using T_1-weighted dynamic contrast-enhanced (DCE)-MRI with Gd-DTPA. A pre-contrast T_1 map was acquired, followed by gradient-echo multislice T_1-weighted MRI (resolution: 156 x 156 µm^2', slice thickness 1mm, temporal resolution: 14 s, total acquisition time 28 min) before, during and after the injection of Gd-DTPA. **(2)** The distribution of VCAM-1 on activated endothelial cells was subsequently studied using VCAM-1 targeted MPIOs as first described by McAteer et al. [1] with a T_2*-weighted sequence (resolution: 78 x 78 x 104 µm^3, 41 min). Immunohistochemistry was performed to validate imaging results. *Image analysis* **(1)** The area under the curve of GD-DTPA concentration vs. time curves across the dynamic range was calculated voxel-wise. **(2)** Negative contrast volume was computed for both hemispheres with negative contrast voxels empirically determined to be all voxels with intensity below three standard deviations of the mean signal in the brain. Moreover, the minimum intensity projection (mIP) was calculated for coronal slices corresponding to the slices from the DCE-MRI data set. *In vivo microscopy* Mice with cranial windows were injected i.p. with 10 µg LPS to induce systemic inflammation and were imaged using a confocal microscope (FV1000, Olympus). Cerebral vessels were visualized using FITC-labeled dextran (150 kDa) followed by injection of VCAM-MPIO labelled with Cy5. Dynamic fluorescence imaging (resolution: 0.28 x 0.28 µm^2, temporal resolution 2.45 s) was performed over 5 min per region.

Results and conclusion: Specific retention on inflamed vasculature is visible in the RH post VCAM-MPIO injection with almost absent contrast effect in the control hemisphere (LH)**(A)**. Such accumulation was not observed with MPIOs labelled with a control antibody. Comparison of negative contrast volume indicates a significant decrease in contrast in the RH vs LH (**B**). IHC shows MPIO lining a vessel on the injected side of the brain **(C).** VCAM-MPIO binding inside a vessel is observed in real-time with i*n vivo* microscopy **(D).** Integrated concentration maps indicate increased vascular permeability in the RH as compared to the LH which appears to be co-localized with areas of inflammation **(E).** Taken together, this approach allows for an extensive, *non-invasive* study of cerebro-vascular inflammation and its effect on vessel permeability.

References:

[1]M.A. McAteer et al., *Nat Med*, vol 13, pp 1253-1258, 2007

AUTHORS (LAST NAME, FIRST NAME): Whittingstall, Lisa[1]; Fouquet, Jérémie P.[1]; Sikpa, Dina[1]; Lebel, Réjean[1]; Tremblay, Luc[1]; Lepage, Martin[1]

INSTITUTIONS (ALL):

1. Centre d'imagerie moléculaire de Sherbrooke (CIMS), Université de Sherbrooke, Sherbrooke, QC, Canada.

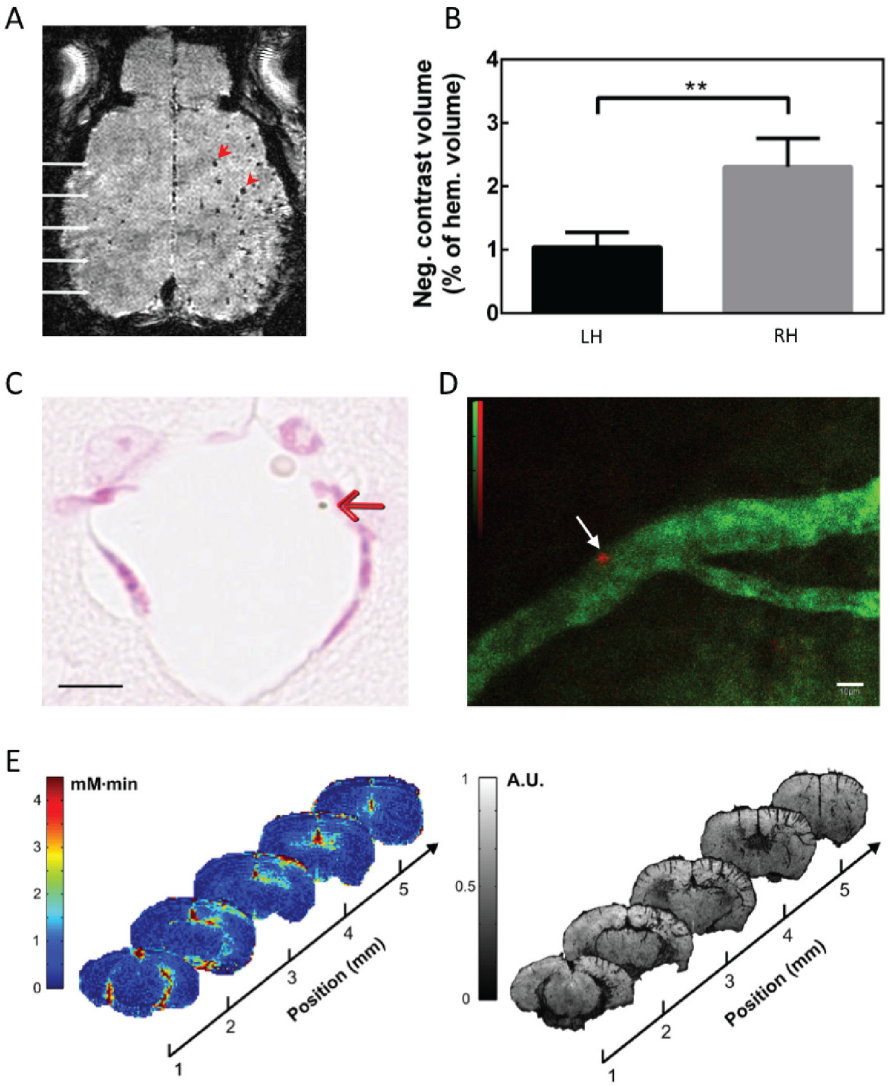

Figure (A) In vivo T2*-weighted axial image of a treated mouse brain obtained with the proposed method Specific retention on acutely activated vasculature is reflected as signal voids (red arrowheads) (B) Comparison of negative contrast volume (n=4) in the LH and RH. Data given in % of hemisphere volume ± SEM, $p < 0.005$. (C) Postmortem light micrographs of the mouse brain. Perl staining shows MPIO lining a vessel on the injected side of the brain (red arrow, scale bar represents 10 µm).
(D) Image from in vivo dynamic microscopy of cortical vasculature of a mouse shows binding of VCAM-MPIO inside the vessel (white arrow, scale bar represents 10 µm). (E) Integrated concentration maps for 1mm-thick coronal slices from in vivo dynamic T1- weighted MRI (positions indicated by white lines in A) and mIP of the corresponding coronal images from the GE3D data set in A, suggest a co-localization of increased vascular permeability and areas of inflammation in the mouse brain.

CONTROL ID: 2230172

TITLE: In-vivo magnetic resonance imaging of neurotransmitter reuptake

PRESENTER: Aviad Hai

ABSTRACT BODY:

Abstract Body: Molecular imaging of dynamic processes in the brain is highly challenging and currently relies on modalities such as positron emission tomography (PET) which offers high specificity but relatively low temporal and spatial resolution and requires the use of radio-labeled ligands. We present the use of a novel protein-based serotonin binding MRI sensor for the detection of serotonin reuptake kinetics in vivo. Brain injection of the sensor with and without serotonin into the striatum of anesthetized rats, demonstrates a clear difference in MRI signal kinetics as a result of unbinding of serotonin from the sensor. Systemic injection of the serotonin transporter inhibitor (SSRI) fluoxetine blocks reuptake and reverses the MRI signal increase. Spatial maps of serotonin reuptake in conjunction with kinetic modeling allow for the first time to explore neurotransmitter transport and inhibition by anti-depressant drugs using MRI.

AUTHORS (LAST NAME, FIRST NAME): Hai, Aviad[1]; Cai, Lili[1]; Lee, Taekwan[1]; Lelyveld, Victor S.[1]; Jasanoff, Alan[1]

INSTITUTIONS (ALL):

1. Massachusetts Institute of Technology, Cambridge, MA, United States.

(No Image Selected)

CONTROL ID: 2230238

TITLE: Development of ^{18}F-labeled arginine for *in vivo* PET imaging of asthma treatment

PRESENTER: Tang Tang

ABSTRACT BODY:

Abstract Body: Asthma is a chronic inflammatory airway disease and debilitates millions of patients with symptoms such as wheezing, coughing and shortness of breath. Studies have shown that L-arginine supplementation or arginase inhibition can decrease measures of allergic airway inflammation and airway hyper-responsiveness - the two hallmarks of asthma in animal models. Though several arginase inhibitors have been developed in recent years, there is no current method to study arginase *in situ* and track inhibitors *in vivo* to investigate their potential clinical translations. Herein, we report a development of fluorinated arginine, which will be able to track arginase *in vivo* by positron emission tomography (PET) to better understand its distribution, kinetics and potential as a therapeutical target. Fluorinated arginine was synthesized with fast fluorination at the last step and demonstrated to be stable and nontoxic to mammalian cells. Tissue homogenates were incubated with fluorinated arginine to show substrate-enzyme binding and functional metabolism by urea production and was compared with non-fluorinated arginine. ^{18}F-labeled arginine was injected to mouse via tail vein and provided a biodistribution pattern of the probe. This pilot study offers valuable information and guidance for our future development of radiolabeled arginase inhibitors for *in vivo* PET imaging of asthma treatment.

AUTHORS (LAST NAME, FIRST NAME): Tang, Tang[1]; Tu, Chuqiao[2]; Kukis, David L.[3]; Bratt, Jennifer M.[4]; Louie, Angelique[2]

INSTITUTIONS (ALL):

1. Chemistry, University of California, Davis, Davis, CA, United States.
2. Biomedical Engineering, University of California, Davis, Davis, CA, United States.
3. Center for Molecular and Genomic Imaing, University of California, Davis, Davis, CA, United States.
4. Internal Medicine- Division of Pulmonary, Critical Care and Sleep Medicine, University of California, Davis, Davis, CA, United States.

(No Image Selected)

CONTROL ID: 2230255

TITLE: Effects of Respiratory-gated ^{18}F-FAZA PET-CT on Hypoxic Fraction in patient and phantom

PRESENTER: Douglass Vines

ABSTRACT BODY:

Abstract Body: Purpose: Respiratory gated (4D) PET has been shown to quantitate radioactivity more accurately in the presence of motion. The purpose of this study was to evaluate the feasibility and potential benefit of using the 4D method in ^{18}F-Fluoroazomycin arabinoside (FAZA-PET) lung imaging with respect to the estimation of hypoxic fraction (HF) in phantom and patient-derived datasets.

Methods: The uptake of FAZA in patient tumor (T) and erector spinae muscle (M) were used to guide the amount of ^{18}F placed into phantom compartments that simulate T and M. The phantom had 3 compartments simulating T, M, and lung and was moved with a known respiratory cycle and amplitude.
Attenuation correction (AC) was performed using a helical CT (hCT) for both non-gated and 4D PET data (6 bin). A 4D-CT was also used to reconstruct the matching phase of the 4D PET to create phase-matched AC 4D PET data (PM-AC). PET-CT images of all 6 bins in the phantom were assessed quantitatively for both AC methods by manually placing a 3D volume-of-interest over T and M to measure FAZA uptake. HF was then estimated according to the method of Mortensen et al, 2012. Comparison of the effects of 4D PET using AC by both PM-AC and hCT-AC methods to non-gated was performed by calculating the differences in HF. Using the same methods, and only the exhale bin in the patient, a retrospective study from the first patient of the planned 20 patients (non-small cell lung cancer) was also performed. The patient was imaged 2h post-injection with FAZA using 4D PET and both hCT and 4D-CT.

Results: The amount of FAZA in the patient T (maximum) and M (mean) for exhale PM-AC were 4.0 and 2.1 kBq/ml. This compared closely to the phantom experiment using 4.2 and 2.1 kBq/ml for simulated T and M, respectively.
The phantom HF was greater for PM-AC than hCT-AC for all 6 bins, and both 4D PET methods had higher HF than the non-gated method (see table). In the 6 bins, the average increase in HF from PM-AC compared to hCT-AC was 0.071 (range 0.028-0.102). PM-AC increased HF by 0.099, a change of 61% compared to the non-gated scan of the same time frame, while hCT-AC increased HF by 0.027, a change of 17%.
In the patient who had tumor motion of 1.7 cm, both PM-AC and hCT-AC methods showed an increase in HF compared to non-gated. The increase in patient HF for exhale PM-AC compared to the same time frame of non-gated scan was from 0.10 to 0.17, the increase for exhale hCT-AC was from 0.10 to 0.18. Although there was little difference in the numerical value of HF between PM-AC and hCT-AC, there may be differences in the spatial location and distribution of the hypoxia.

Conclusions: The phantom study demonstrated that 4D PET was both feasible and beneficial with PM-AC having consistently higher values of HF compared to hCT-AC and non-gated. In the patient, 4D PET was feasible, however the potential benefit was not as evident as the phantom data. Additional patient datasets with tumor motion are required to determine the usefulness of 4D PET in the context of FAZA lung imaging.

AUTHORS (LAST NAME, FIRST NAME): Vines, Douglass C.[1, 2]; Driscoll, Brandon D.[1, 3]; Yeung, Ivan[1, 2]; Publicover, Julia[1, 3]; Sun, Alexander[1, 2]; Jaffray, David A.[1, 2]

INSTITUTIONS (ALL):

1. Radiation Medicine Program, Princess Margaret Cancer Centre, Toronto, ON, Canada.
2. University of Toronto, Toronto, ON, Canada.
3. The Techna Institute, Toronto, ON, Canada.

(No Image Selected)

CONTROL ID: 2230288

TITLE: PET quantification of specific and nonspecific VMAT2 binding with ^{18}F-FP-(+)-DTBZ and ^{18}F-FP-(-)-DTBZ in baboons, and healthy volunteers and T1DM patients

PRESENTER: Gary Cline

ABSTRACT BODY:

Abstract Body: Hypothesis:

Recent studies suggest that positron emission tomography (PET) and the ligand ^{18}F-Fluoropropyl-(+)-dihydrotetrabenazine (^{18}F-FP-(+)-DTBZ) can be used to noninvasively estimate human β-cell mass (BCM) via targeting of the vesicular monoamine transporter type 2 (VMAT2).[1] ^{18}F-FP-(+)-DTBZ signal in the pancreas consists of specific VMAT2 binding, primarily from β-cells with a modest contribution from other VMAT2-expressing cells, and nonspecific binding. This study tested the hypothesis that the lower pancreatic binding of ^{18}F-FP-(+)-DTBZ in T1DM patients compared to healthy controls can be attributed to a decrease in specific binding to β-cells of the endocrine pancreas, and not to changes of nonspecific binding within the exocrine pancreas.

Innovation:

To accurately estimate specific binding to VMAT2, we must measure nonspecific binding of ^{18}F-FP-(+)-DTBZ in the pancreas, or in a suitable reference tissue. However, since the β-cells are dispersed throughout the pancreas, no reference tissue (free of VMAT2) can be defined within the pancreas. Because binding of ^{18}F-FP-(+)-DTBZ to VMAT2 is stereospecific, and the (-)-enantiomer has little affinity for VMAT2, the nonspecific binding of ^{18}F-FP-(+)-DTBZ in the pancreas can potentially be determined from the binding of ^{18}F-FP-(-)-DTBZ.[2] We compared the enantiomers in nonhuman primates (NHP) and in healthy and T1DM volunteers.

Results and Conclusion:

In NHP, for each enantiomer, a control scan and displacement scans by cold FP-(-)-DTBZ and cold FP-(+)-DTBZ were performed to assess binding. 3-hr emission scans were acquired. Three regional time–activity curves (TACs) were generated (Figure 1A, B) and distribution volume (VT) was estimated. Pancreatic uptake of ^{18}F-FP-(-)-DTBZ was substantially lower than ^{18}F-FP-(+)-DTBZ. Uptake of ^{18}F-FP-(-)-DTBZ peaked at ~5 min, followed by rapid clearance in all regions. The highest initial uptake was in the renal cortex, followed by the pancreas, with lowest uptake was in the spleen. Uptake of ^{18}F-FP-(+)-DTBZ, on the other hand, showed the highest uptake in the pancreas (peak at 30~50 min) with relatively slow washout. These displacement studies indicate that FP-(-)-DTBZ displays low binding affinity with VMAT2 in baboons, and hence is suitable for measuring nonspecific binding in human pancreas.

In humans, nonspecific binding in the pancreas, measured by ^{18}F-FP-(-)-DTBZ, was similar in healthy controls (VT=23.1±3.4 ml/cm^3, n=5) and T1DM patients (VT=18.2±5.8 ml/cm^3, n=3). The nonspecific background signal was estimated to account for ~12% of total pancreatic binding of ^{18}F-FP-(+)-DTBZ in healthy controls, and ~16% in T1DM patients (Figure 1C,D). Thus, the marked reduction in pancreatic binding of ^{18}F-FP-(+)-DTBZ in T1DM patients[1] cannot be attributed to a reduction of nonspecific binding of ^{18}F-FP-(+)-DTBZ in the exocrine pancreas, but is consistent with a loss of specific binding to the endocrine pancreas in tandem with the loss of pancreatic β-cell mass.

References:

1. Normandin MD (2012) J Nucl Med
2. Harris PE (2013) Nucl Med Biol

AUTHORS (LAST NAME, FIRST NAME): Naganawa, Mika[2]; Lim, Keunpoong[2]; Shu-fei, Lin[2]; Labaree, David C.[2]; Harris, Paul E.[3]; Huang, Yiyun[2]; Carson, Richard[2]; Cline, Gary W.[1]

INSTITUTIONS (ALL):

1. Internal Medicine, Yale University School of Medicine, New Haven, CT, United States.
2. Diagnostic Radiology, Yale University, New Haven, CT, United States.
3. Columbia University, New York City, NY, United States.

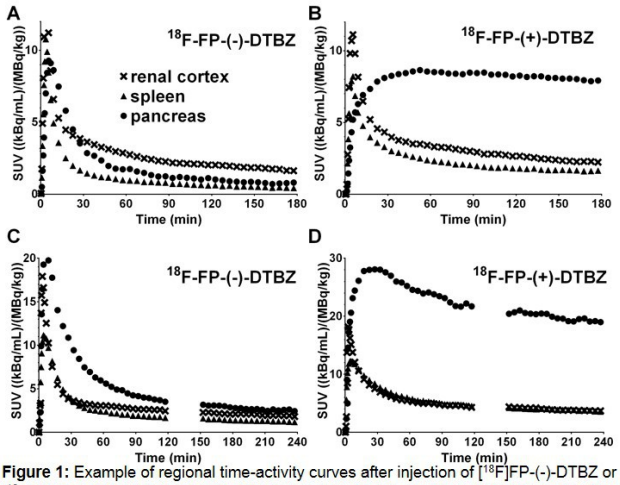

Figure 1: Example of regional time-activity curves after injection of [^{18}F]FP-(-)-DTBZ or [^{18}F]FP-(+)-DTBZ in baboons (**A, B**) and humans (**C, D**). **Panel A**: 179 MBq (4.8 mCi) of [^{18}F]FP-(-)-DTBZ (baboon A). **Panel B**: 181 MBq (4.9 mCi) of [^{18}F]FP-(+)-DTBZ (baboon C). **Panel C**: 290 MBq (7.8 mCi) of [^{18}F]FP-(-)-DTBZ (Healthy Control #8). **Panel D**: 298 MBq (8.1 mCi) of [^{18}F]FP-(+)-DTBZ (Healthy Control #8). Pancreatic uptake level (circles) of [^{18}F]FP-(-)-DTBZ was between the renal cortex (x) and spleen (triangles), while [^{18}F]FP-(+)-DTBZ pancreas uptake was highest among the three regions of interest.

CONTROL ID: 2237413

TITLE: SPECT-CT imaging to study the pharmacokinetics of radiolabelled antisense oligonucleotides (AONs) in vivo

PRESENTER: Evita van de Steeg

ABSTRACT BODY:

Abstract Body: Aim: For drug development, determining the biodistribution of compounds is extremely important. SPECT-CT imaging is a non-invasive technique, allowing repeated measurement of biodistribution in vivo. Currently, availability of dedicated non-invasive technologies to evaluate pharmacokinetics of DNA-/RNA-based therapeutics (e.g. antisense oligonucleotides (AONs)) is still limited. We aimed to set-up and validate novel minimally-invasive methods to trace AONs in vivo.

Methods: An AON developed for Duchenne Muscular Dystrophy (DMD) treatment was radiolabeled with either ^{123}I or ^{111}In. The pharmacokinetics of [^{123}I]-AON or [^{111}In]-AON after subcutaneous administration (100mg/kg) to Mdx mice, a DMD model, were assessed with SPECT-CT imaging. Subsequently, tissues were collected, radioactivity counted and AONs quantified by an ELISA-based method.

Results: SPECT-CT imaging showed that both [^{123}I]-AON and [^{111}In]-AON could be used to determine in situ tissue levels of the AON up to 48 hours after administration. Scan data matched well with results from the invasive biodistribution.

Conclusions: Quantitative SPECT-CT imaging with radiolabelled AONs provides a powerful approach to non-invasively assess AON pharmacokinetics. Radiolabelling with ^{111}In appears preferable for oligonucleotides. Imaging can significantly improve translation to humans, and reduce the number of animals used in preclinical drug development.

AUTHORS (LAST NAME, FIRST NAME): van de Steeg, Evita[1]

INSTITUTIONS (ALL):

1. TNO, Zeist, Netherlands.

(No Image Selected)

CONTROL ID: 2230443

TITLE: Redox- and pH-sensitive polymeric micelles based on poly(β-amino ester)-grafted-disulfide methylene oxide poly(ethylene glycol) for anti-cancer drug delivery

PRESENTER: Moon-Sun Jang

ABSTRACT BODY:

Abstract Body: For decades, stimulus-responsive polymeric micelles have gained a huge interest formulating medicines especially in cancer chemotherapy to overcome the challenges of hydrophobic therapeutic agents. In this report, a redox- and pH-sensitive poly(β-amino ester)-grafted-disulfide methylene oxide poly(ethylene glycol) was synthesized which showed not only a sharp pH-dependent assembly-disassembly transition but also a quick shell shading in high concentration of reducing agent by Michael addition polymerization. 1H-NMR, dynamic light scattering, transition electron microscope were combined to characterize the redox- and pH-responsibility in various triggered conditions. Hydrophobic drug doxorubicin (DOX) was used as model drug to investigate the encapsulation and delivery ability of polymeric micelles both *in vitro* and *vivo* experiments. Notably, anti-tumor experiment on tumor-bearing mice showed the DOX-loaded polymeric micelles effectively enhanced the therapeutic efficacy in comparing to the free-DOX which was further confirmed by histopathological examinations. All of results suggested that PAE-g-DSMPEG could be a potential hydrophobic drug delivery vehicle.

AUTHORS (LAST NAME, FIRST NAME): Jang, Moon-Sun[1]; Im, Geun Ho[1]; Bui, Quang N.[2]; Yi, Li [2]; Lee, Jung Hee[1]; Lee, Doo Sung[2]

INSTITUTIONS (ALL):

1. Department of Radiology, Samsung Medical Center, Sungkyunkwan University School of Medicine and Center for Molecular and Cellular Imaging, Samsung Biomedical Research Institute, Seoul, Korea (the Republic of).
2. Theranostic Macromolecules Research Center, School of Chemical Engineering, Sungkyunkwan University, Suwon, Korea (the Republic of).

(No Image Selected)

CONTROL ID: 2230407

TITLE: ROS-responsive Activatable Prodrug for the Treatment of Metastatic Tumors

PRESENTER: Eun-Joong Kim

ABSTRACT BODY:

Abstract Body: Reactive oxygen species (ROS)-induced oxidative stress plays a significant role in several pathological processes during cancer progression. Especially, metastatic tumors have been found to have high levels of ROS such as hydrogen peroxide (H_2O_2). In this study, prodrug **7** was designed to be activated by H_2O_2-mediated boronate oxidation, resulting in activation of the fluorophore for detection and release of the therapeutic agent. Drug release from prodrug **7** was investigated by monitoring fluorescence after addition of H_2O_2 to the cancer cells. Prodrug **7** activated by H_2O_2, selectively inhibited tumor cell growth. Furthermore, intratracheally administered prodrug **7** showed effective antitumor activity in a mouse model of metastatic lung disease. Thus, this H_2O_2-responsive prodrug has therapeutic potential as a novel treatment for metastatic cancer via cellular imaging with fluorescence as well as selective release of the anticancer drug.

AUTHORS (LAST NAME, FIRST NAME): Kim, Eun-Joong[1]

INSTITUTIONS (ALL):

1. KBSI, Cheungbuk, Korea (the Republic of).

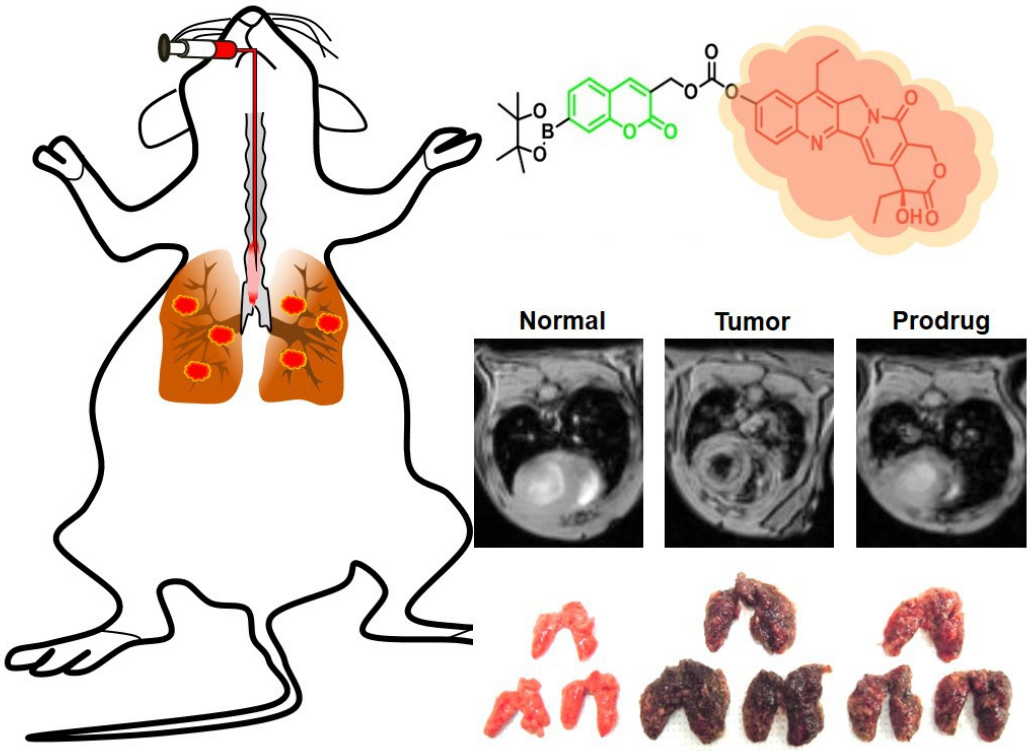
Normal
Tumor
Prodrug

CONTROL ID: 2230405

TITLE: NanoAu-Cocktail-pulsed Dendritic Cells Preferentially Homing to Liver-Draining Lymph Nodes and Inducing Anti-Viral CD8+ T Cell Responses monitored by Bioluminescence imaging

PRESENTER: linsheng zhan

ABSTRACT BODY:

Abstract Body: The lack of efficient antigens and activators delivery systems, as well as the restricted migration of dendritic cells (DCs) to secondary lymph organs, dramatically limits DCs-based adoptive immunotherapy. We selected two spherical gold nanoparticles (AuNPs)-based vehicles of optimal size for activator and antigen delivery. Their combination (termed the NanoAu-Cocktail) was associated with dual-targeting of CpG oligonucleotides (CpG-ODNs) and OVA peptide (OVAp) to DCs subcellular compartments, inducing enhanced antigen cross-presenting, up-regulated expression of costimulatory molecules (CD40,CD80 and CD86) and elevated T helper1 (Th1) cytokine secretion (e.g., IL-12p70, TNF-α). In particular, taking advantage of the high specificity and sensitivity of the bioluminescence imaging, we systematically depicted the dynamic distribution and homing map of ENMs pulsed DCs in vivo. Data showed that circulating NanoAu-Cocktail pulsed DCs preferentially targeted liver-draining lymph nodes (LLNs) and were distributed in the T cell area. The improved homing ability of NanoAu-Cocktail pulsed DCs to local LNs were associated with high expression of chemokine receptor 7 (CCR7) and rearrangement of the cytoskeleton. Increased IFN-γ secretion from LLN cells was observed upon ex vivo restimulation, indicating that a strong antigen-specific CD8+ T cell response was elicited. The activated T cells in the LLNs protected the liver from invasion by OVAp-expressing adenovirus. These findings highlight the feasibility of AuNPs-based antigen and activator delivery systems to target adoptive DCs and to modulate their trafficking patterns in vivo and, more importantly, support the possibility of using engineered gold materials for organ-targeted immunotherapy.

AUTHORS (LAST NAME, FIRST NAME): zhan, linsheng [1]

INSTITUTIONS (ALL):

1. Beijing Institute of Transfusion Medicine, Beijing, China.

(No Image Selected)

CONTROL ID: 2230412

TITLE: Fluorescent Turn-on chemodosimeter Probe for KCN and Bioimaging

PRESENTER: Sankarprasad Bhuniya

ABSTRACT BODY:

Abstract Body: The KCN is highly toxic chemical entity that produces HCN inside the body and accelerates pathogenesis of CF lung disease. The cyanide anions interferes cellular respiratory process by dysfunctions of cytochrome c. Additionally cyanide anion induces Ca^{2+} ions level in intracellular region which accelerates enzymatic cascade changes for producing ROS in cells; [1] that causes disruption of oxidative defense system. The assessment for detriment of HCN to CF patients and cyanide level in cellular milieus is not an easy task.[2] Thus, fluorogenic probes are needed to easy way to detect cyanide ions in biological system.

A new probe (**IND-1**) was developed to assess the cyanide anion is aqueous and biological milieus. It undergoes intramolecular crossed-benzoic reaction in presence of KCN at ambient temperature and subsequently produced fluorescent signal with visual changes from colorless to pink color. Rsult depicted that the selectivity of the probe toward the CN^- over other competitive anions under the physiological relevant condition.

Before proceeding to evaluate the efficacy of the probe to detect CN^- in biological system, cytotoxicity of the **IND-1** has been tested by MMT assay. Results implied that **IND-1** is nontoxic as much as high to conc. 20 μM. The result indicated that **IND-1** can be used to assess the cyanide ions in cellular milieus.

Finally, fluorescent image of HeLa cells in the presence CN^- ions was recorded as shown in Figure 1. It indicated that the probe, **IND-1** is capable to detect the CN^- ions in cellular level as low as to 0.5 ppm.

In conclusion, the probe, **IND-1** is specific reaction based CN^- ions sensor, nontoxic and capable to detect cyanide ions in vitro cellular level. It displays sensitivity toward CN^- as low as to 4 nM in aqueous medium; which is remarkably lower than any previously reported results.

References:

1. M. A. Acheampong, R. J. W. Meulepasa and P. N. L. Lens, *J. Chem. Technol. Biotechnol.*, 2010, **85**, 590

2. H. J. Kim, K. C. Ko, J. H. Lee, J. Y. Lee and J. S. Kim, *Chem. Commun.,* 2011. **47**, 2886

AUTHORS (LAST NAME, FIRST NAME): Bhuniya, Sankarprasad[1]

INSTITUTIONS (ALL):

1. Amrita Centre for Industrail Research & Innovation, Amrita Vishwa Vidyapeetham, Coimbatore, Tamil Nadu, India.

Confocal laser fluorescence microscopic images of HeLa cells treated with **IND-1** (2 uM). The cells were pre-incubated with media containing CN- of various concentrations (0, 0.5, and 1.0 ppm) for 30 min at 37 °C. Cell images were obtained using excitation wavelengths of 543 nm, and emission wavelengths of 570–630 nm, green signal, respectively.

CONTROL ID: 2230414

TITLE: In vivo fluorescence and MR imaging of delivery of IL-4 receptor-targeted Bcl-xL siRNA/BPEI-SPION complexes to tumor for anti-tumor therapy

PRESENTER: Guruprasath Padmanaban

ABSTRACT BODY:

Abstract Body: Targeted delivery of imaging agents and therapeutics to tumors would provide early detection and increased therapeutic efficacy against cancer. Interleukin-4 receptor (IL-4R) is over-expressed on many types of cancer cells including breast cancer. Interaction of IL-4 and IL-4R up-regulates anti-apoptotic proteins such as Bcl-xL in tumor cells. Here we exploited an IL-4R-targeted small interfering RNA (siRNA) carrier complexes by grafting the IL4RPep-1 (IL-4R-targeting peptide-1), CRKRLDRNC, to branched polyethyleneimine-superparamagnetic iron oxide (BPEI-SPION) nanoparticles. IL4RPep-1-grafted Bcl-xL siRNA/BPEI-SPION complexes more efficiently knocked down Bcl-xL expression and increased the chemosensitivity of MDA-MB231 breast tumor cells in response to etoposide treatment compared to untargeted Bcl-xL siRNA/BPEI-SPION complexes. *In vivo* fluorescence imaging showed higher levels of accumulation of near infrared fluorescence (NIRF) dye-labeled IL4RPep-1-Bcl-xL siRNA/BPEI-SPION complexes, compared to untargeted complexes, to MDA-MB231 tumor xenografts on nude mice as early as 3 h after injection. Little accumulation of the complexes to control organs including the liver and spleen were observed. Also, accumulation of IL4RPep-1-Bcl-xL siRNA/BPEI-SPION complexes to MDA-MB231 tumor after intratumoral injection were detected by MR imaging. Anti-tumor treatment with IL4RPep-1-Bcl-xL siRNA/BPEI-SPION complexes (3 times i.v. injection/week for 4 weeks) in combination with doxorubicin (one time i.p. injection/week for 4 weeks) synergistically increased anti-tumor activity in MDA-MB231 tumor-bearing mice compared to doxorubicin alone. These results suggest that IL4RPep-1-grafted siRNA/BPEI-SPION complexes could be a useful tool for imaging and targeted delivery of siRNA to IL-4R over-expressing tumors.

AUTHORS (LAST NAME, FIRST NAME): Padmanaban, Guruprasath[1, 2]; Chi, Lianhua[1, 2]; Sri Murugan, Poongkavithai Vadevoo[1, 2]; Namgung, Ran[3]; PARK, IN KYU[4]; Kim, Won Jong[3]; Lee, Byung-Heon[1, 2]

INSTITUTIONS (ALL):

1. Department of Biochemistry and Cell Biology, Kyungpook National University, Daegu, Korea (the Republic of).
2. BK21 Plus Biomedical Convergence Program, Kyungpook National University, Daegu, Korea (the Republic of).
3. Department of Chemistry, Polymer Research Institute, POSTECH, Pohang, Korea (the Republic of).
4. Department of Biomedical Sciences, Chonnam National University, Hwasun, Korea (the Republic of).

(No Image Selected)

CONTROL ID: 2230417

TITLE: Development of I-131 single gamma correction after I-131 labeled monoclonal antibody during F-18 FDG PET follow up

PRESENTER: JIN SU kim

ABSTRACT BODY:

Abstract Body: F-18 FDG PET was widely used for the monitoring the tumor response. I-131 emitted the single gamma (284, 364, 637, and 723 keV). In this study, we assessed the effect of single gamma from I-131 in FDG PET and feasibility of our proposed single gamma correction method for actual mouse model.

Methods: The effect of single gamma due to I-131 was assessed within various energy windows (350-600, 350-650, 450-600, and 450-650 keV) and various activities. The single gamma was corrected from the sinogram space during PET reconstruction. We applied single gamma correction method to both phantom and *in vivo* mouse model. For animal model, CD20+ Raji cell xenografted lymphoma model and her2+ NCI-N87 cell xenografted gastric cancer model were used. I-131 Rituximab for lymphoma model or I-131 Trastuzumab was administered.

Results: The single gamma fraction (SGF) was 12% when 300 μCi of I-131 and 100 μCi of FDG were administered. The SGF exponentially increased with increasing I-131 activity for all energy windows. Our developed single gamma photon correction method was applied to both phantom and in vivo mouse model. Difference of SOR was reduced to <5% after I-131 single gamma correction. When our developed single gamma photon correction method was applied to *in vivo* mouse model, SUV of tumor region was 2.74 for FDG PET only (served as a goldstandard), 3.17 after single gamma photon correction, and 3.78 before single gamma photon correction, respectively. In addition, contrast was improved by 18% after single gamma photon correction.

Conclusions: We developed the I-131 single gamma photon correction method for FDG PET after I-131 mAb therapy and applied to actual in-vivo mouse model. Our developed single gamma correction method would be helpful to monitor therapeutic efficacy for newly developed drug in FDG PET follow up after I-131 therapy or I-131 labeled mAb therapy.

AUTHORS (LAST NAME, FIRST NAME): Lee, Young Sub [1]; kim, JIN SU[1]; Cho, Kyung Deuk [1]; Lim, Sang Moo [1]

INSTITUTIONS (ALL):

1. Korea Institute Radiological and Medical Sciences, Seoul, Korea (the Republic of).

Schematic of the single gamma photon correction method

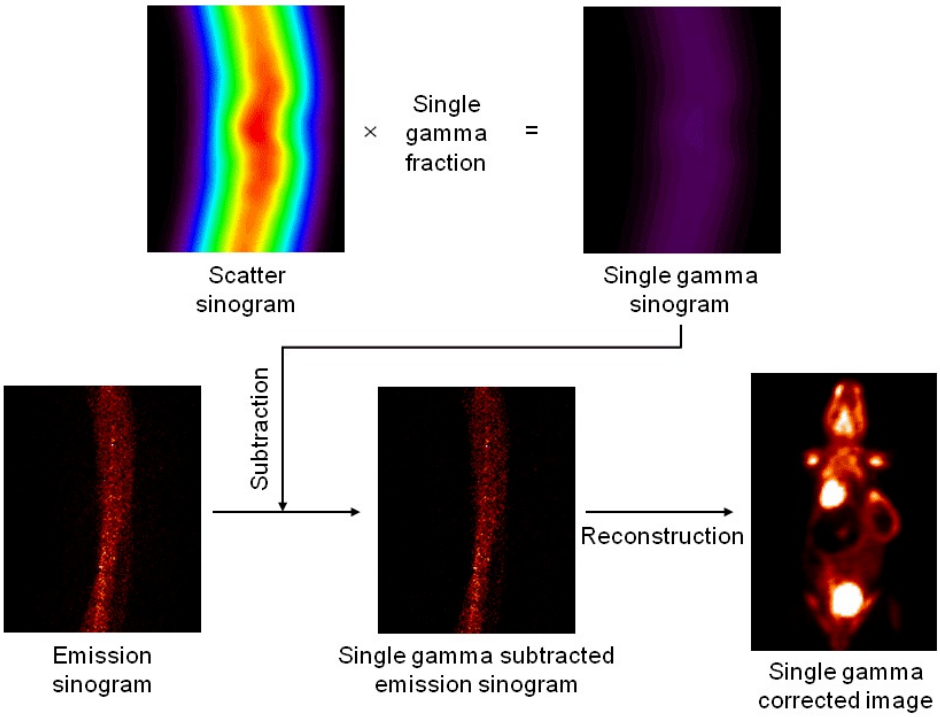

CONTROL ID: 2230419

TITLE: Novel contrast agents for detection of hypoxia with optical and magnetic resonance (MR) imaging

PRESENTER: Karolina Jankowska

ABSTRACT BODY:

Abstract Body: When oxygen demand outweights its supply, a reducing chemical environment is produced, which is commonly called hypoxia. Hypoxia is suspected to underlie various medical conditions including strokes [1], heart ischemia [2] and solid hypoxic tumours. [3], and pinpointing the location and severity of hypoxia will assist in treatment of these conditions.

We are interested in developing new methods for the imaging of hypoxia and oxidative stress *in cellulo* and *in vivo*, using both optical and magnetic resonance (MR) imaging. To achieve this, we are developing responsive imaging agents, whose output (whether emission or contrast) is a function of the redox environment.

We have developed a first generation MRI contrast agent, FGdR1, which has a two-fold greater relaxivity in oxidised than reduced form, making it one of the first fully-reversible MRI sensors of redox state. FGdR1 can detect biologically-relevant changes in the GSH:GSSG ratio. In addition to its MR behaviour, FGdR1 is fluorescent in its oxidised form, and non-fluorescent in the reduced form. Based on these preliminary results, we are now developing new Gd-based complexes with altered reduction potentials and superior fluorescence behaviour.

Our second generation of hypoxia-responsive MRI contrast agents are hypoxia-responsive, and is harnessing the unique properties of cobalt. The Co^{3+} to Co^{2+} reduction is well tuned to the redox potentials of tissue hypoxia.[4] Diamagnetic Co^{3+} is MR silent, while paramagnetic Co^{2+} will give an MR signal, making this a true off-to-on switch; rare for an MR sensor. Based on this theory, we have synthesized various cobalt complexes, and demonstrated a clear “turn-on” of relaxation rate as the complex is reduced. We are now tuning the properties of our Co complexes to maximise the dynamic range and sensitivity of the systems.

[1] M. a Moskowitz, E. H. Lo, C. Iadecola, *Neuron* **2010**, *67*, 181–98.

[2] J. Neuzil, B. S. Rayner, H. C. Lowe, P. K. Witting, *Redox Rep.* **2005**, *10*, 187–97.

[3] W. R. Wilson, M. P. Hay, *Nat. Rev. Cancer* **2011**, *11*, 393–410.

[4] N. Yamamoto, A. K. Renfrew, B. J. Kim, N. S. Bryce, T. W. Hambley, *J. Med. Chem.* **2012**, *55*, 11013–21.

AUTHORS (LAST NAME, FIRST NAME): Jankowska, Karolina[1]; O'Neill, Edward S.[1]; Bonnitcha, Paul[2]; New, Elizabeth J.[1]

INSTITUTIONS (ALL):

1. School of Chemistry, The University of Sydney, Sydney, NSW, Australia.

2. The Kolling Insitute of Medical Research, The University of Sydney, Sydney, NSW, Australia.

(No Image Selected)

CONTROL ID: 2232401

TITLE: Synthesis and evaluation of Förster Resonance Energy Transfer (FRET) probes detecting changes in cellular redox state

PRESENTER: Karolina Jankowska

ABSTRACT BODY:

Abstract Body: Oxidative stress is causally linked to many diseases such as obesity [1], cancer [2] and neurodegeneration. [3] It is therefore pertinent to monitor the oxidative capacity of human tissues on cellular and subcellular levels. The only modality able to provide such spatiotemporal resolution is optical imaging enhanced by the use of fluorescent probes.

An ideal optical contrast agent should address certain criteria, including rapid localisation within cells, reversibility and responsiveness to biological changes. Our group has developed FRET agents that, unlike existing probes, satisfy these requirements. These agents contain two fluorophores chemically linked via carbon chains: one containing a redox-sensitive group, and the other a FRET donor or acceptor.

Using combinations of flavin, a widely used redox sensor, with a range of fluorophores, we have synthesised some effective redox probes. The first generation of compounds contained coumarin as a FRET donor. Fluorimetry studies have shown an emission shift to a longer wavelength in increasingly oxidative conditions, while the emission peak of coumarin is unchanged in reducing conditions. Biological studies performed in HeLa cells using confocal microscopy, fluorescence lifetime imaging microscopy and flow cytometry confirm utility of our agents. More recently developed agents employ rhodamine as a FRET acceptor and targeting vector simultaneously.

[1] Rupérez, A. I.; Gil, A.; Aguilera, C. M. Int. J. Mol. Sci. 2014, 15, 3118.

[2] Wang, X.; Wang, W.; Li, L.; Perry, G.; Lee, H.; Zhu, X. Biochim. Biophys. Acta 2014, 1842, 1240.

[3] Sosa, V.; Moliné, T.; Somoza, R.; Paciucci, R.; Kondoh, H.; LLeonart, M. E. Ageing Res. Rev. 2013, 12, 376.

AUTHORS (LAST NAME, FIRST NAME): Jankowska, Karolina[1]; Kaur, Amandeep[1]; Bonnitcha, Paul[2]; New, Elizabeth J.[1]

INSTITUTIONS (ALL):

1. School of Chemistry, The University of Sydney, Sydney, NSW, Australia.
2. The Kolling Insitute of Medical Research, The University of Sydney, Sydney, NSW, Australia.

(No Image Selected)

CONTROL ID: 2230428

TITLE: Velocity estimation for mucociliary transit studies using purpose written software

PRESENTER: Alice Cottee

ABSTRACT BODY:

Abstract Body: Aim: Nuclear medicine imaging is a novel modality for assessing tracheal mucociliary velocity (TMV), with previous reports in obstructive airways disease (COPD). The current study aimed to refine the direct injection methodology and improve the quantitative computer assessment to account for the complex pathways of radiopharmaceutical tracer movement within in the trachea. This was evaluated by the addition of an extra plane of nuclear imaging acquisition and modifying and updating the purpose-written data analysis software (ciliaC). Patients were imaged in the anterior and lateral planes to improve tracking of the radiopharmaceutical and to enhance the computer analysis.

Method: The study group was a cohort (n=19) of patients (11M, 8F, Age range: 60-90) with mild to moderate COPD (FEV1 < 80% predicted), who were clinically stable. After upright injection into a predefined tracheal space, dynamic images were immediately acquired with the patients supine using a dual head gamma camera configured for two planes of imaging. The dynamic images were visually assessed for quality and analysed using ciliaC for TMV. ciliaC software allows for loading of data sets at different time points and projections. It then estimates velocity using automated or manual peak tracking.

Results: Each patient was imaged on two separate occasions, four patients were imaged on three occasions resulting in a total of 45 separate studies. Studies were considered unsuitable for analysis (11%) for several reasons including injection into the tracheal wall, coughing the droplet out through the vocal cords immediately after injection and excessive patient movement. Tracheal mucociliary clearance (TMC) was always antegrade, directed towards the vocal cords and observed to be in a right-handed spiral pattern as opposed to the previously assumed linear movement. Patterns of movement were designated as a "slug trail" of activity characterized by a poorly defined peak or a discrete bolus of activity which could be automatically tracked. The lateral plane of images helped delineate tracheal movement from oesophageal movement.

Conclusion: The addition of the lateral plane in imaging combined with refinements in the analysis software adds to the understanding of TMV and TMC in this cohort of patients with COPD, significantly improving sensitivity. The pattern of spiral and vertical movement in what had been previously considered to be an unusual variant would suggest that spiral clearance is the dominant pattern of clearance in the trachea which has not been described before. Analysis by single subjects rather than pooled data has highlighted the importance of patient positioning, cough and movement as significant acquisition factors. Imaging in both anterior and lateral planes improves visualisation of the radiopharmaceutical transit. It contributes to a more accurate software estimation of specific time points for velocity analysis.

AUTHORS (LAST NAME, FIRST NAME): Pearson, Mark A.[1]; Frater, Clayton[2]; Abelson, David[2, 3]; Cottee, Alice M.[3]; Morgan, Lucy C.[3, 2]

INSTITUTIONS (ALL):

1. Nuclear Medicine, Concord Hospital, Concord, NSW, Australia.
2. Concord Campus, Sydney University, Concord, NSW, Australia.
3. Respiratory Medicine, Concord Hospital, Concord, NSW, Australia.

(No Image Selected)

CONTROL ID: 2230438

TITLE: Clinical value of FAZA-PET/CT in advanced lung cancer patients: comparison with FDG-PET/CT

PRESENTER: Tsuneo Saga

ABSTRACT BODY:

Abstract Body: Objective: The presence of hypoxia in cancer tissue is known to increase not only their refractoriness to treatment, but also their malignant potential. The information of cancer hypoxia, therefore, is important for the management of cancer patients such as prediction of treatment response and the selection of appropriate treatment strategy. The aim of the present study was to evaluate the clinical value of PET/CT with FAZA, a PET probe to detect cancer hypoxia, in advanced non-small cell lung cancer patients, in comparison to FDG-PET/CT, especially on the prediction of patients' prognosis. **Methods:** Thirty eight patients with advanced non-small cell lung cancer (clinical stage: stage III - 23 patients and stage IV - 15 patients; histology: squamous cell carcinoma (SCC) - 11 patients, adenocarcinoma (Adeno) - 19 patients, large cell carcinoma (LC) - 8 patients) received FAZA- and FDG-PET/CT before treatment. Patients were followed to determine the treatment response and survival. Uptake parameters of FAZA (tumor-muscle ratio at 2h (T/M)) and FDG (SUVmax at 1h (SUV)) in primary lesion and lymph node (LN) metastasis were compared with various clinical parameters (histology, clinical stage, etc.). Progression-free survival (PFS) periods and overall survival (OS) periods were compared with various clinical and FAZA/FDG uptake parameters. Kaplan-Meier analyses with Log Rank test were performed for all (stage III + IV) patients and for stage III (IIIA + IIIB) patients. Study protocol was approved by the institutional review board, and informed consent was obtained from all patients. **Results:** There was a weak correlation between FAZA T/M and FDG SUV of primary lesion ($p = 0.040$), but intra-tumoral distribution patterns of FAZA and FDG for individual patients were not identical for three histological subtypes, SCC, Adeno and LC. There was a significant difference in FAZA T/M among histological subtypes ($p = 0.036$). As for the prognosis, clinical stage (stage IV vs. III, $p = 0.017$; stage IIIA vs. IIIB, $p = 0.046$) and FAZA T/M in LN metastasis (> 1.800 vs. </= 1.800, $p = 0.007$ in stage III + IV patients; > 1.800 vs. </= 1.800, $p = 0.018$ in stage IIIA + IIIB patients) were significant predictors of PFS, while other parameters including FDG uptake parameters were not. Cox's proportional hazard analysis had shown that clinical stage (stage IV vs. III, $p = 0.002$, HR = 4.610, stage IIIA vs. IIIB, $p = 0.024$, HR = 3.595) and FAZA T/M in LN metastasis (> 1.800 vs. </= 1.800, $p < 0.001$, HR = 5.985 in stage III + IV, $p = 0.009$, HR = 6.338 in stage IIIA + IIIB patients) were significant predictors of PFS. For OS, FAZA T/M in LN metastasis was an only significant predictor in stage IIIA + IIIB patients (> 1.800 vs. </= 1.800, $p = 0.034$). No significant predictor of OS was detected in stage III + IV patients. **Conclusion:** FAZA T/M in LN metastasis was a strong predictor of survival of advanced lung cancer patients. PET/CT with FAZA is expected to afford useful information on the management of lung cancer patients.

AUTHORS (LAST NAME, FIRST NAME): Saga, Tsuneo[2]; Inubushi, Masayuki[1]; Koizumi, Mitsuru[3]; Yoshikawa, Kyosan[4]; Zhang, Ming-Rong[2]; Horiike, Atsushi[3]; Yanagitani, Noriko[3]; Ohyanagi, Fumiyoshi[3]; Nishio, Makoto[3]

INSTITUTIONS (ALL):

1. Department of Nuclear Medicine, Kawasaki Medical School, Kurashiki, Japan.
2. Molecular Imaging Center, National Institute of Radiological Sciences, Chiba, Japan.
3. Cancer Institute Hospital, Tokyo, Japan.
4. Research Center for Charged Particle Therapy, National Institute of Radiological Sciences, Chiba, Japan.

(No Image Selected)

CONTROL ID: 2232933

TITLE: Evaluation of the Effect of High Intensity Focused Ultrasonic (HIFU) treatment with Liposome Encapsulated Doxorubicin on CT26 tumor model: drug release in vitro and therapeutic effect in vivo

PRESENTER: Jeongil Kwon

ABSTRACT BODY:

Abstract Body: Purpose

HIFU is used usually in thermal therapy and increasing of drug release. We concern with the use of HIFU in drug release for tumor therapy excluding thermal effect. This study is focused on the evaluation of drug release from liposome by HIFU treatment in low acoustic intensity *in vitro* and therapeutic effect by HIFU-mediated liposome encapsulated doxorubicin on mice model of CT26 tumor *in vivo*.

Method

Prepared the long circulating liposome (LCLP) with 1,2-distearoyl-sn-glycero-3-phosphoethanolamine-N-methoxy (polyethyleneglycol)-2000 (DSPE-PEG-$_{2000}$), LCLP encapsulated indocyanine green (ICG) (LCLP-ICG) or doxorubicin (LCLP-Dox). LCLP was prepared with amine-N-(4-nitrobenzo-2-oxa-1,3-diazole**) (**NBD-PE) for study in to ascertain the rupture of liposome structure. We studied the release of drug encapsulated in liposome and the change of liposome structure by HIFU treatment in change of intensity of ICG or NBD dye *in vitro*. The drug release was also demonstrated by exposure mice bearing CT26 tumor to HIFU in low acoustic intensity after intratumoral injection of LCLP-ICG and obtained optical image by IVIS system *in vivo*. To evaluate therapeutic effect by HIFU treatment in low acoustic intensity after tail vein injection of LCLP-Dox, prepared mice model of CT26 tumor and divided into three groups (n=7); HIFU treatment after injection of PBS (PBS+HIFU group), administered LCLP-Dox only (Dox group) and HIFU treatment after administration of LCLP-Dox (Dox+HIFU group). We measured tumor volume to determine the therapeutic effect in the three treatment groups. The treatments were performed three times on every third day from Day 11 after implantation of CT26 cell to mice.

Result

Prepared LCLP with the same molar ratio had similar mean diameter and size distribution (116 ± 30 nm). The fluorescence intensity of encapsulated ICG (15 μM) in LCLP-ICG in liposome was decreased about 30% by HIFU treatment but only 7% decrease for NBD dye *in vitro*. The fluorescence intensity of ICG (1 mM) of LCLP-ICG *in vitro* and *in vivo* studies was increased due to recovery of signal loss and quenching in high concentration by released free ICG, although HIFU treatment was performed in low acoustic intensity (Isata=83.35 W/cm^2). The tumor growth rate was decreased with statistically significance ($p < 0.05$) in the Dox+HIFU group compared with other groups. The HIFU exposure to mice administered LCLP-Dox in low acoustic intensity caused increasing of accumulation of liposome and uptake of released doxorubicin from liposome, having effective concentration in tumor that consequently exhibited high efficacy of therapy.

Conclusion

The encapsulated drug in liposome could be released in the procedure of liposome reforming by HIFU treatment in low acoustic intensity, excluding thermal effect. The HIFU treatment in low acoustic intensity combined with administration of liposome encapsulated doxorubicin showed high efficiency of chemotherapy on CT26 solid tumor with potential

AUTHORS (LAST NAME, FIRST NAME): Kwon, Jeongil[6]; Jeong, Hwan-Seok[5]; Hwang, Hyosook[3]; Kim, Eun-Mi[4]; Kim, Dong Hyun[7]; Lee, Tai Kyoung[2]; Oh, Philsun[8]; Kim, MinJoo[1]; Kim, HyunSoo[9]; Kim, Eun ji[10]; Choi, Ji-Hae[11]; Lim, Seok Tae[12]; Sohn, Myung-Hee[13]; Jeong, Hwan-Jeong[14]

INSTITUTIONS (ALL):

1. Nuclear Medicine, Chonbuk National University, Jeonju, Korea (the Republic of).
2. Nuclear Medicine, Chonbuk National University Hospital, Jeonju, Korea (the Republic of).
3. Chonbuk National University Medical School and Hospital, Jeonju, Korea (the Republic of).
4. nuclear medicine, Chonbuk national university medical school, Jeonju-si, Korea (the Republic of).
5. Nuclear Medicine, chonbuk National University Medical School and Hospital, Jeonju, Korea (the Republic of).

6. Nuclear Medicine:Molecular Imaging & Therapeutic Medicine Research Center:Cyclotron Research Center:Institute for Medical Sciences:Biomedical Research Institute, chonbuk National University Medical School and Hospital, Jeonju, Jeonbuk, Korea (the Republic of).
7. Nuclear Medicine:Molecular Imaging & Therapeutic Medicine Research Center:Cyclotron Research Center:Institute for Medical Sciences:Biomedical Research Institute, chonbuk National University Medical School and Hospital, Jeonju, Jeonbuk, Korea (the Republic of).
8. Nuclear Medicine:Molecular Imaging & Therapeutic Medicine Research Center:Cyclotron Research Center:Institute for Medical Sciences:Biomedical Research Institute, chonbuk National University Medical School and Hospital, Jeonju, Jeonbuk, Korea (the Republic of).
9. Nuclear Medicine:Molecular Imaging & Therapeutic Medicine Research Center:Cyclotron Research Center:Institute for Medical Sciences:Biomedical Research Institute, chonbuk National University Medical School and Hospital, Jeonju, Jeonbuk, Korea (the Republic of).
10. Nuclear Medicine:Molecular Imaging & Therapeutic Medicine Research Center:Cyclotron Research Center:Institute for Medical Sciences:Biomedical Research Institute, chonbuk National University Medical School and Hospital, Jeonju, Jeonbuk, Korea (the Republic of).
11. Nuclear Medicine:Molecular Imaging & Therapeutic Medicine Research Center:Cyclotron Research Center:Institute for Medical Sciences:Biomedical Research Institute, chonbuk National University Medical School and Hospital, Jeonju, Jeonbuk, Korea (the Republic of).
12. Nuclear Medicine:Molecular Imaging & Therapeutic Medicine Research Center:Cyclotron Research Center:Institute for Medical Sciences:Biomedical Research Institute, chonbuk National University Medical School and Hospital, Jeonju, Jeonbuk, Korea (the Republic of).
13. Nuclear Medicine:Molecular Imaging & Therapeutic Medicine Research Center:Cyclotron Research Center:Institute for Medical Sciences:Biomedical Research Institute, chonbuk National University Medical School and Hospital, Jeonju, Jeonbuk, Korea (the Republic of).
14. Nuclear Medicine:Molecular Imaging & Therapeutic Medicine Research Center:Cyclotron Research Center:Institute for Medical Sciences:Biomedical Research Institute, chonbuk National University Medical School and Hospital, Jeonju, Jeonbuk, Korea (the Republic of).

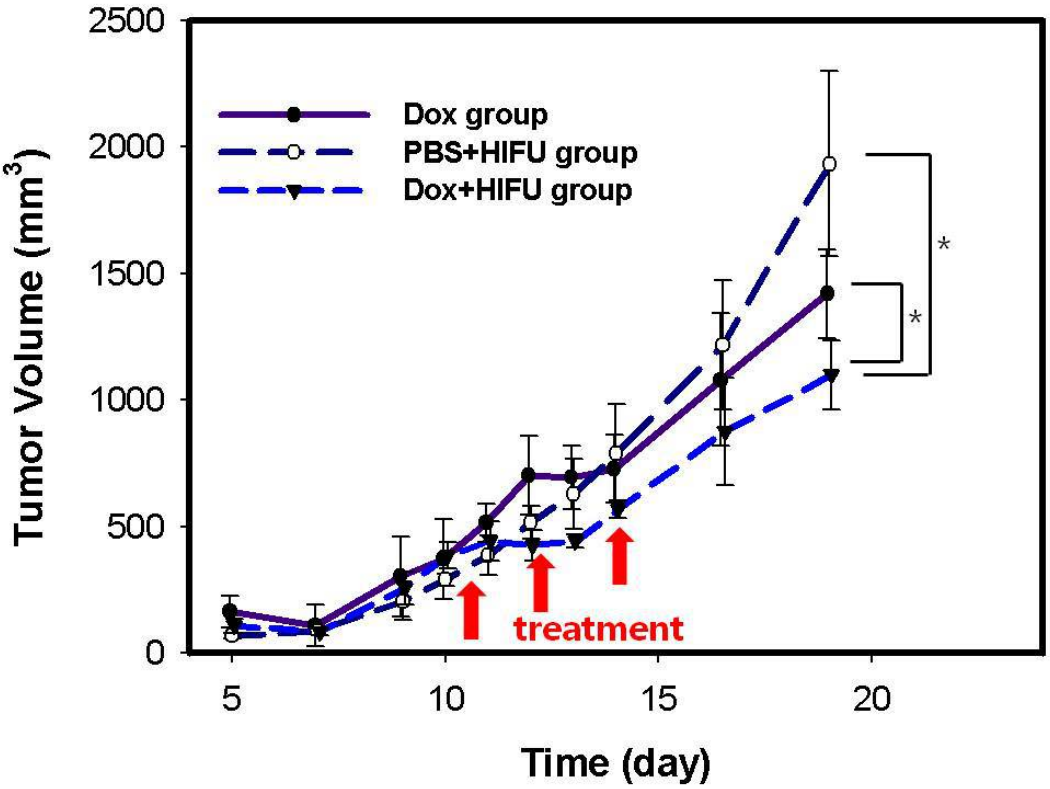
2500
2000
1500
1000
500
0
Tumor Volume (mm3)
Dox group
PBS+HIFU group
Dox+HIFU group
*
*
treatment
5
10
15
20
Time (day)

CONTROL ID: 2232944

TITLE: Development of Selective Released Chitosan Nanohydrogels for Ischemic Therapy and Radioactive Tracer.

PRESENTER: Jeongil Kwon

ABSTRACT BODY:

Abstract Body: Objectives

Chitosan based nanohydrogels was useful for drug delivery system. This vehicle was able to drug loading by encapsulation method. However, encapsulated small molecules were fast released before reach target site. In order to solve this problem, we were development of selective release formation of chitosan, chitosan-N-Succinimidyl 6-(3-[2-pyridyldithio]-propionamido)hexanoate-vascular endothelial growth factor receptor peptide (CHI-SPDP-VEGF). Disulfide group of CHI-SPDP-VEGF was reduced by biological reduction agent as a glutathione (GSH) and then released VEGF peptide. Also, CHI-SPDP-VEGF was able to Tc-99m labeling. The ultimate goal of this study is clinical testing with dual effect of ischemic therapy through the released VEGF and radioactive tracer by labeled Tc-99m.

Methods

CHI-SPDP was synthesized of the NHS ester group of LC-SPDP with the amine group of chitosan. Disulfide group of CHI-SPDP was substitution reaction with sulfide group of VEGF peptide thiol. Chitosan nanohydrogels was prepared by ionotropic gelation. TPP was added dropwise to a CHI-SPDP-VEGF solution (0.1%) under stirring at room temperature for 2 hours. The hydro dynamic diameter of hydrogels was obtained from dynamic light scattering (DLS) measurement. Formulated nanohydrogels was purification by dialysis method using cellulose membrane (3~600 Da). Remained TPP and acetic acid were removed from the hydrogels by dialysis. Dialyzed chitosan nanohydrogels were evaluated pH, DLS and HPLC or Mass analysis. Also, synthesized CHI-SPDP-Cy 5.5 was prepared same method as CHI-SPDP-VEGF that VEGF peptide thiol was exchanged Cy 5.5 thiol. CHI-SPDP-Cy 5.5 was formulated to nanohydrogels and then it was storage in three solutions (GSH, human serum, human serum and GSH). Also, Tc-99m labeled chitosan nanohydrogels were measure of radiolabeling efficiency by Radio TLC scanner every one hour. At last, Tc-99m labeled hydrogels were injected to hindlimb ischemia rat model and then identified by gamma imaging.

Results

Characterization of CHI-SPDP-VEGF was evaluated ^{1}H NMR and FT-IR analysis. Hydrodynamic diameter of chitosan nanohydrogels was 100 ~ 130 nm. In purification of dialysis, pH of the hydrogels was changed pH of 7 at 2 hours, after this hydrogels were aggregation. In Cy 5.5 reduction test, the hydrogels show about zero intensity in GSH and highest intensity in mixture of GSH and human serum. Tc-99m labeling efficiency of nanohydrogels was 99% and the radiolabeling stability was more than 99 % for 4 hours. Also, Tc-99m labeled nanohydrogels were injected to hindlimb ischemia rat model and then identified on the ischemic zone.

Conclusions

Synthesis of CHI-SPDP-VEGF was improved encapsulation method. This selective reduction hydrogels were reduced by biological reduction agent of GSH and human serum. This reduction has the potential to clinical testing. Also, Tc-99m labeling was able to on site labeling in Tc-99m supplier and more elaborated evaluation by gamma imaging system. In molecular imaging system, chitosan nanohydrogels of CHI-SPDP-VEGF may be effective diagnostic and therapeutic vehicle for ischemic injury.

AUTHORS (LAST NAME, FIRST NAME): Kwon, Jeongil[2]; Lee, Chang-Moon[7]; Kim, Eun-Mi[5]; Hwang, Hyosook[4]; Jeong, Hwan-Seok[6]; Kim, Dong Hyun [4]; Lee, Tai Kyoung[3]; Oh, Philsun[4]; Kim, MinJoo[1]; Kim, HyunSoo[6]; Kim, Eun ji [6]; Choi, Ji-Hae[6]; Lim, Seok Tae[6]; Sohn, Myung-Hee [6]; Jeong, Hwan-Jeong[6]

INSTITUTIONS (ALL):

1. Nuclear Medicine, Chonbuk National University, Jeonju, Korea (the Republic of).
2. Chonbuk National University Hospital, Jeonju-si, Korea (the Republic of).
3. Nuclear Medicine, Chonbuk National University Hospital, Jeonju, Korea (the Republic of).
4. Chonbuk National University Medical School and Hospital, Jeonju, Korea (the Republic of).
5. nuclear medicine, Chonbuk national university medical school, Jeonju-si, Korea (the Republic of).
6. Nuclear Medicine, chonbuk National University Medical School and Hospital, Jeonju, Korea (the Republic of).
7. Department of Biomedical Engineering, Chonnam National University, Yeosu, Korea (the Republic of).

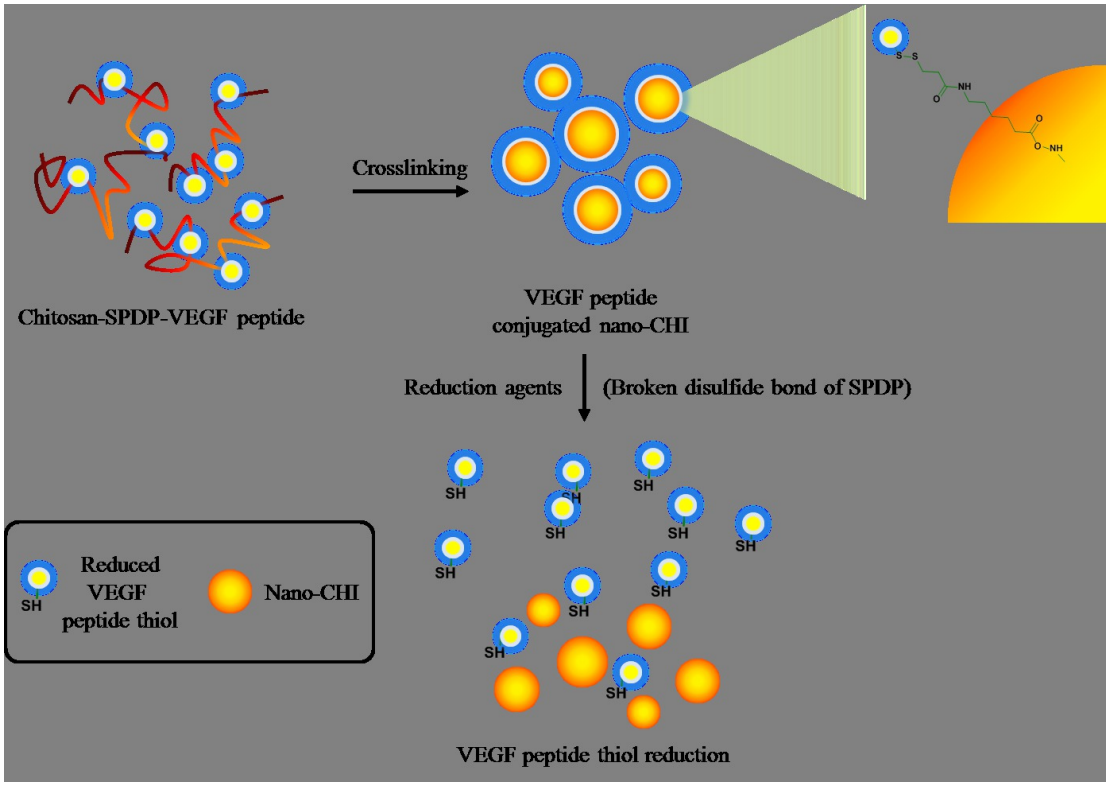
Crosslinking
Chitosan-SPDP-VEGF peptide
VEGF peptide
conjugated nano-CHI
Reduction agents
(Broken disulfide bond of SPDP)
Reduced
VEGF
peptide thiol
Nano-CHI
SH
VEGF peptide thiol reduction

CONTROL ID: 2230450

TITLE: PET Imaging of Dopamine Dynamics in Romantic Love

PRESENTER: Kayo Takahashi

ABSTRACT BODY:

Abstract Body: What happens in the brain when we fall in love? An fMRI study by Bartels and Zeki (2000) indicated that there is engagement of medial insula, anterior cingulate cortex, and striatum, structures known to be high in dopaminergic activity, during romantic experiences. To investigate dopaminergic activity during such experiences we performed a positron emission tomography (PET) study with ^{11}C-raclopride, a dopamine D_2/D_3 receptor antagonist, during visual excitation produced by the loved partner's portrait. Ten subjects viewed pictures of partners to whom they were romantically attached and, as a control, of friends of the same sex for whom they had neutral feelings during PET study. The visual stimuli (pictures) were presented 15 min before the dopamine antagonist, ^{11}C-raclopride, was administered, and lasted for 30 min. The binding potential (BP_{ND}) was calculated using the simplified reference tissue model 2 and BP_{ND} images were generated. Using Statistical Parametric Mapping 8 software, whole-head structural BP_{ND} images were statistically compared between the love and control conditions. The results demonstrated a statistically significant increase in dopaminergic activity in two regions, the medial orbitofrontal cortex and medial prefrontal cortex, the former of which has been strongly implicated in a variety of rewarding experiences, including that of beauty. The positive correlation in medial orbitofrontal cortex between excitement levels and dopaminergic activity was evident only in the love, not in the control, condition.

AUTHORS (LAST NAME, FIRST NAME): Takahashi, Kayo[1, 2]; Mizuno, Kei[1, 2]; Sasaki, Akihiro T.[1, 2]; Wada, Yasuhiro[1, 2]; Tanaka, Masaaki[2]; Ishii, Akira[2]; Tajima, Kanako[1]; Tsuyuguchi, Naohiro[2]; Watanabe, Kyosuke[1]; Zeki, Semir[3]; Watanabe, Yasuyoshi[1, 2]

INSTITUTIONS (ALL):

1. Center for Life Science Technologies, RIKEN, Kobe, Japan.
2. Graduate School of Medicine, Osaka City University, Osaka, Japan.
3. Wellcome Laboratory of Neurobiology, University College London, London, United Kingdom.

(No Image Selected)

CONTROL ID: 2234285

TITLE: Innovation of New Luciferin Analog for *in vivo* Imaging

PRESENTER: Ryohei Saito

ABSTRACT BODY:

Abstract Body: 【Introduction】

We are innovating new imaging technologies by using organic chemistry. For making advanced medicinal technology, *in vivo* imaging is needed. So, we have been developing compounds suitable for deep *in vivo* imaging.

【Background】

It is very difficult for deep *in vivo* imaging to be absorbed and scattered light in living tissue. But, it is well known that the light in the near infrared region (NIR) has high permeability for the living tissue. It is a challenge to visualize *in vivo* deep imaging by developing an imaging material that has NIR emission. We have got structure-activity relationship data on the firefly luciferin luciferase reaction. According to the structure-activity relationship data on luciferin analogues, we have designed and marked NIR probe “Akalumine®, (WAKO pure chemical LTD.). Akalumine® gives a higher brightness compared with the natural firefly luciferin because of high permeability Akalumine® in tissue.

【Purpose】

We try to rise concentration of the firefly luciferin for high dose. But we faced difficulty that Akalumine® has low water-soluble.

For various applications, “high dose” is key technology on *in vivo* imaging.

Based on the Akalumine®structure, new luciferin analogues have designed and synthesized three types.

【Result and conclusion】

We made the substances of three new luciferin analogues. One of these emits in the NIR and another has water-solubility increased by 15 fold for Akalumine®.

We will apply new probe to the animal for conforming practical ability and discuss these new luciferin analogues for *in vivo* imaging technology.

AUTHORS (LAST NAME, FIRST NAME): Saito, Ryohei[1]; Kiyama, Masahiro[1]; Kitada, Nobuo[1]; Iwano, Satoshi[1]; Obata, Rika[3]; Niwa, Haruki[2]; Maki, Shojiro[1]

INSTITUTIONS (ALL):

1. Dept. of Engineering and Science , The University of Electro - Communications, Chohu, Tokyo, Japan.
2. Brain Science Inspired Life Support Research Center, The University of Electro-communications, Chofu, Tokyo, Japan.
3. Keio Univ., Kanagawa, Japan.

(No Image Selected)

CONTROL ID: 2230458

TITLE: Quantification constraints for preclinical PET systems at high background radioactivity from therapeutic radionuclides

PRESENTER: Emma Mellhammar

ABSTRACT BODY:

Abstract Body: Objective:

In radionuclide therapies high activities are administrated to deliver high absorbed dose to tumors. Activities in the order of 10-50 MBq are commonly administrated to the experimental animal. Many therapeutic radionuclides besides particle emission also emit photons, which result in a high photon fluence rate. Imaging with different PET probes can be used to monitor tumor response intra-therapeutically. The high photon fluence may influence the quantification capabilities due to count losses and image distortion. The aim of this study was to investigate three preclinical PET systems with various detector design and different radionuclide combinations.

Method:

The PET systems evaluated included two with stationary block ring systems and one with four-detectors-in-a-box-geometry system. Studies were performed with ^{99m}Tc ($T_{1/2}$ 6.02 h) to mimic a therapeutic radionuclide and contributing with high photon fluence rate. As PET sources ^{18}F ($T_{1/2}$ 109.8 m) and ^{22}Na ($T_{1/2}$ 2.6 y) were used. Different combinations of sphere phantoms (9.5-15.9 mm Ø) filled with ^{18}F and ^{99m}Tc were used. The ^{18}F-filled phantom was imaged alone and together with the ^{99m}Tc phantom. Also, an in-house made mouse phantom (dimensions 90 x 30 x 20 mm^3) with silicon tubes 15 mm apart was filled with ^{99m}Tc. Inside a channel of the phantom, a ^{22}Na point source was placed. The count rate capability was evaluated from the single and coincidence count rates and the image distortion from Full with half maximum (FWHM) and Full with tenth maximum (FWTM) measurements of the reconstructed ^{22}Na point source. These studies are now being complemented with experiments using the therapeutic radionuclide ^{177}Lu responsible for the background activity.

Result:

In all of the systems effects on count rate capability could be seen with the additional high photon fluence rates, resulting in changes in the single and coincidence rates detected, leading to erroneous quantification compared to the case with no background activity. Effects could be seen already at activity levels below 1 MBq. The dead-time corrections made in one of the PET systems were able to correct the coincidence count rates to closely the same rates as detected without background activity. The spatial resolution measured with the ^{22}Na point source was negatively affected at higher background activities. These results will be compared with results from the therapeutic radionuclide ^{177}Lu.

Conclusion:

By adding additional radioactivity in the field of view of the preclinical PET systems investigated both count rate losses and image distortions were detected. These results clearly show that intra-therapeutically imaging has to consider these effects for accurate quantification. The dead-time corrections currently implemented in one of the preclinical PET systems investigated was able to correct the coincidence count rate, but the reduced spatial resolution at high background activity remains a limiting factor for intra- therapeutically PET measurements.

Research Support:

Swedish Cancer Foundation, Swedish Research Council, Mrs. Bertha Kamprad Foundation, Gunnar Nilsson Cancer Foundation and Medical Faculty ALF grant, Lund University.

AUTHORS (LAST NAME, FIRST NAME): Mellhammar, Emma M.[5]; Axelsson, Johan[1]; Dahlbom, Magnus[2]; Tran, Thuy A.[3]; Strand, Sven-Erik[4]

INSTITUTIONS (ALL):

1. Department of Physics, Lund University, Lund, Sweden.
2. Department of Molecular and Medical Pharmacology, UCLA School of Medicine, Los Angeles, CA, United States.
3. Lund University BioImaging Center, Lund University, Lund, Sweden.
4. Department of Clinical Sciences Lund, Medical Radiation Physics, Lund, Sweden.
5. Department of Clinical Sciences Lund, Oncology and Pathology, Lund, Sweden.

(No Image Selected)

CONTROL ID: 2230467

TITLE: Molecular Imaging of Microcalcifications

PRESENTER: Inneke Willekens

ABSTRACT BODY:

Abstract Body: Introduction:

Mammographic microcalcifications are routinely used for the early detection of breast cancer. The morphology of microcalcifications is the most important factor in deciding whether the microcalcifications are typically benign or either suspicious (intermediate concern) or of a high probability of malignancy.

The aim of our study was to evaluate the 3D shape of breast microcalcifications using micro-computed tomography (micro-CT) in comparison with the anatomopathological analysis.

Materials and Methods:

Breast biopsy samples with findings of suspicious microcalcifications on routine mammograms were analyzed. The samples were imaged using a micro-CT (SkyScan 1076) at a resolution of 35 μm. Images were reconstructed using filtered back-projection and analyzed in 3D using surface rendering. The samples were subsequently analyzed by anatomopathology. Reconstructed 3D images were compared with the corresponding histological slices.

Results:

Malignant microcalcifications tended to be thinner and to have a smaller volume and surface area, while their surface area-to-volume ratio was greater than that of benign microcalcifications. The structure model index values were the same for malignant and benign microcalcifications.

Conclusions:

This was the first analysis of microcalcifications in 3D using micro-CT. This application is promising in the evaluation of the morphologic characteristics of malignant and benign microcalcifications.

AUTHORS (LAST NAME, FIRST NAME): Willekens, Inneke[1]; Van de Casteele, Elke[2]; Buls, Nico[1]; Temmermans, Frederik[3]; Jansen, Bart[3]; Deklerck, Rudi[3]; de Mey, Johan[1]

INSTITUTIONS (ALL):

1. UZ Brussel, Brussels, Belgium.
2. KULeuven, Leuven, Belgium.
3. Vrije Universiteit Brussel, Brussels, Belgium.

(No Image Selected)

CONTROL ID: 2233748

TITLE: Investigation of the ExiTron imaging agents.

PRESENTER: Inneke Willekens

ABSTRACT BODY:

Abstract Body: Introduction:

To investigate the contrast enhancement in liver, spleen, and heart of Exitron P, U, V, nano 6000, and nano 12000.

Materials and Methods:

All contrast agents were intravenously injected in C57bl/6 mice (n=37). We started at a dose of 0.1 ml/25g (n=22), as indicated on the manual. When the mouse died a dose of 0.05/25g was injected (n=15). Animals were anesthetized with Isoflurane. Imaging was performed using micro-CT at a resolution of 83 µm before contrast injection, immediately after contrast injection and at 15 min, 30 min, 45 min, 1h, 2h, 3h, 4h, 24h and 48h after contrast (scan duration: 121 sec). Images were analysed using Amide. Regions of interest were drawn in spleen, liver, and left ventricle. The contrast enhancement was measured and expressed in function of time.

Results:

The dose of 0.1 ml/25g of ExiTron P, ExiTron nano 6000, and ExiTron nano 12000 and the dose of 0.05 ml/25g of ExiTron P were lethal. Maximum contrast enhancement of the spleen was reached just after injection of ExiTron U and ExiTron V, while maximum liver enhancement occurs at 1h after ExiTron V and at 3h after ExiTron U. Maximum contrast enhancement of the spleen after injection of ExiTron nano 6000 and ExiTron nano 12000 occurs after 48h, while maximum liver enhancement is after 4h for ExiTron nano 6000 and after 24h for ExiTron nano 12000. Enhancement in the cardiac cavity is the highest after ExiTron nano 12000.

Conclusion:

ExiTron nano 6000 and 12000 are able to provide strong contrast enhancement of liver, spleen, and heart at a low injection volume.

AUTHORS (LAST NAME, FIRST NAME): Willekens, Inneke[1]; Buls, Nico[2]; Lahoutte, Tony[3]; de Mey, Johan[4]

INSTITUTIONS (ALL):

1. UZ Brussel, Brussels, Belgium.
2. Radiology, UZ Brussel - VUB, Brussels, Belgium.
3. Vrije Universiteit Brussel, Jette, Belgium.
4. UZ Brussel, Brussels, Belgium.

(No Image Selected)

CONTROL ID: 2230468

TITLE: Identification and improvement of a linear peptide specific for the Notch-ligand delta-like ligand (Dll) 4

PRESENTER: Annette Altmann

ABSTRACT BODY:

Abstract Body: Peptides are useful tools for the targeted delivery of radionuclides or chemotherapeutic drugs to their site of action within an organism. Since angiogenesis plays a fundamental role during tumor development and metastatic spread, targeting vascular development could represent a new therapeutic approach for the treatment of cancer. The endothelial cell membrane protein and Notch-ligand delta-like ligand 4 (Dll4) is predominantly expressed by tumor endothelial cells and has, therefore, been suggested a highly relevant target for the development of novel binding agents for diagnosis and therapy of angiogenesis.

Methods: A 12 amino-acid peptide phage display system was applied to identify a new peptide binding to Dll4. The biopanning was performed in solution-phase by exposure of the peptide library to streptavidin beads coated with the biotinylated extracellular domain of Dll4 fused to Fc-Protein. The linear binding motif was modified by N-acetylation (AcDll4Pep2) and grafting into the scaffold structure of the sunflower trypsin inhibitor (SFTI)-1 (SFDll4Pep2). The binding specificity of the peptide and derivates against Dll4 was verified by surface plasmon resonance spectrometry (SPR) and by *in vitro* cell binding, competition and internalization experiments employing the iodine-125 labeled peptide and Dll4-expressing tumor cells human prostate tumor cells PC-3 and rat pancreatic tumor cells AR42J. For the determination of the proteolytic stability radiolabeled peptides were incubated in human serum and subsequently analysed by HPLC. Small animal PET-imaging was performed in the AR42J tumor-bearing rat model using DOTA Ga^{68}-labeled peptide.

Results: After 4 selection rounds, the Dll4-binding motif Dll4Pep2 (LHFGQPNFGIVL) was identified. The modification of the linear peptide motif by acetylation (AcDll4Pep2) and grafting into the SFTI-1 scaffold (SFDll4Pep2) increased the proteolytic stability of Dll4Pep from 1.5 min to 12 hours and more than 8 hours, respectively, without affecting the binding specificity. Dll4Pep2, SFDll4Pep2 and AcDll4Pep2, but not the binding motif modified by ^{1}dLeu or the unmodified SFTI scaffold displayed a significant binding to the surface of Dll4-expressing tumor cells but only at triple-digit nanomolar affinity (SFDll4Pep2: K_D 604 nM).

PET-imaging performed in the AR42J tumor-bearing rat model after injection of DOTA Ga^{68}-labeled Dll4Pep2 revealed a moderate tumor uptake.

Conclusion: Chemical modifications increasing the proteolytic stability of the linear peptide transform Dll4Pep to a highly attractive peptide candidate targeting tumor vasculature. However, for diagnostic or therapeutic applications of tumor angiogenesis additional modifications are needed to improve the affinity.

AUTHORS (LAST NAME, FIRST NAME): Altmann, Annette[1]; Lindner, Thomas[1]; Sauter, Max B.[1]; Markert, Annette[1]; Mier, Walter[1]; Haberkorn, Uwe[1]

INSTITUTIONS (ALL):

1. Nuclear Medicine, University Hospital Heidelberg, Heidelberg, Germany.

(No Image Selected)

CONTROL ID: 2230476

TITLE: Identification and evaluation of a Dll4-binding peptide based on the cystine-knot miniprotein Min23 scaffold

PRESENTER: Annette Altmann

ABSTRACT BODY:

Abstract Body: Angiogenesis plays a fundamental role during tumor development and metastatic spread. Therefore, the development of novel binding agents for diagnosis and therapy of angiogenesis could represent a new therapeutic approach for the treatment of cancer. In this context, the Notch-ligand delta-like ligand 4 (Dll4) has been suggested a highly relevant target, which is predominantly expressed by tumor endothelial cells and on distinct some tumor cells. Owing to the remarkable stability and the tolerance of sequence mutagenesis of cystine-knot miniproteins we designed a phage display library based on the scaffold structure of the Ecballium elaterium trypsin inhibitor (EETI-II, Min23) to identify a binding entity against Dll4.

Methods: The biopanning was performed in solution-phase by exposure of the peptide library to streptavidin beads coated with the biotinylated extracellular domain of Dll4 fused to Fc-protein. The binding specificity of the peptide against Dll4 was verified by surface plasmon resonance spectrometry (SPR) and by *in vitro* cell binding, competition and internalization experiments employing the iodine-125 labeled peptide and Dll4-expressing tumor cells. Small animal PET-imaging was performed in PC-3 tumor-bearing mice using iodine-124 labeled peptide. The serum stability of the radiolabeled peptide was determined by radio-HPLC analysis.

Results: After 4 panning rounds the screening hit Dll4Min3 (H_2N-LMRCKQDSDCLAGSVC-**LFHLFIYI**-FCG-COOH) was identified and characterized by a proteolytic stability in human serum of more than 8 hours. A specific binding of ^{125}I-Dll4Min3 but not of the unmodified radiolabeled Min23 scaffold to the Dll4-expressing human prostate tumor cells PC-3 and rat pancreatic tumor cells AR42J was measured which was inhibited up to 67% by the unlabeled peptide. In PC-3 and AR42J cells 75% and 54% of the bound activity was internalized after 60 min incubation. Alanine scanning of the binding domain indicated the influence of individual amino acids on binding and affinity for Dll4. Substitution of ^{1}Leu and ^{4}Leu by Ala reduced the binding to PC-3 by 51% and 63% and to AR42J by 35% and 64% but increased the affinity to Dll4 from K_D 702 nM (Dll4Min3) to K_D 74.1nM (^{1}Ala) and 39.8 nM (^{4}Ala) as determined by SPR analysis. PET-imaging performed in the PC-3 tumor-bearing nude mouse model after injection of ^{124}I-labeled Dll4Min3 revealed a significant tumor uptake, however a high liver accumulation was observed.

Conclusion: These results accentuate the potential of Dll4Min3 generated by phage display as molecular diagnostic agent in cancer research. However, further optimization of the peptide is required for improvement of tumor uptake and reduction of liver accumulation.

AUTHORS (LAST NAME, FIRST NAME): Altmann, Annette[1]; Lindner, Thomas[1]; Sauter, Max B.[1]; Markert, Annette[1]; Mier, Walter[1]; Haberkorn, Uwe[1]

INSTITUTIONS (ALL):

1. Nuclear Medicine, University Hospital Heidelberg, Heidelberg, Germany.

(No Image Selected)

CONTROL ID: 2230470

TITLE: Functional MRI of the visual system of *Chamaeleo Chameleon*: binocular and monocular stimulation

PRESENTER: Inbal Biton

ABSTRACT BODY:

Abstract Body: Vision is a field in which the relationships between overt behavior patterns and underlying neural structures and activities can be clearly demonstrated. Because the architecture of chameleons' nervous system and visual behavior combines both typical ectotherm / reptilian features and specialized oculomotor / optical capacities [1], it is of great interest to use them as "non-mammlian" model of visually related patterns of brain activity. The aim of this study is to understand the morphological and functional structure of the common chameleons' visual pathway, using MRI and CT techniques. Specifically, we ask: What are the patterns of neural activation in the ipsilateral and the contralateral optic tecta under monocular and binocular visual stimulation, as obtained by functional-MRI (fMRI)? We focus on two techniques: Manganese enhanced-MRI (MEMRI) [2-3] and fMRI. MEMRI allows a large field-of-view, high resolution mapping of the entire visual pathway [1] that is difficult to acquire using the fMRI technique. fMRI opens new, non-invasive venues to advance our understanding of brain organization and function. The technique has been used, to our knowledge, only on endothermic vertebrates, e.g., dogs, cats, pigeons, rats and mice [4-5] but not on ectotherms.

We developed a specially-built MRI compatible closed chamber system for anesthetized chameleons that allows the entering of the MRI room in the SPF facility. We tested different anesthetic procedures and established that Medetomidine is highly reliable for longitudinal experiments. The 3D CT imaging provided information about the morphology of the bony structures in the chameleons' skull (Fig. 1A), while the conventional MRI images provided information about the structure of the visual pathways in the chameleon brain (Fig. 1B). The unique structure of the optic nerve and the visual brain pathways are marked with color, overlaid on a gray-scale MEMRI image (Fig. 1C). We measured the activity in the optic tecta, with both eyes open, in the dark or when both were exposed to flickering white light. The fMRI activation time course (Fig. 1D) showed a significant bilateral BOLD signal in the tecta, corresponding to the flickering light stimuli. Our current experiments test for tectal activation under monocular stimulations.

References

Lustig A., et al. (2012). Anim. Cogn. 15, 609-621.

Pautler, R. G., et al. (1998). *Magn. Reson. Med* 40(5), 740-748.

Takashi, W., et al. (2004). *NMR in biomedicine* 17(8), 554-568.

Watanabe, T., et al. (2001). *Magn. Reson. Med* 46(3), 424–429.

Duong, T. Q. (2007). *Brain Research* 1135, 186-194.

Groof, G. D., et al. (2013). *Behav. Brain Res.* 239, 43-50.

AUTHORS (LAST NAME, FIRST NAME): Biton, Inbal E.[1]; Stettner, Noa[1]; Dafni, Hagit[1]; Lev Ari, Tidhar[2]; Ketter katz, Hadas[3]; Harmelin, Alon[1]; Katzir, Gadi[2]

INSTITUTIONS (ALL):

1. Department of Veterinary Resources, Weizmann Institute of Science, Rehovot, Israel.
2. Department Environmental and Evolutionary Biology, University of Haifa, Haifa, Israel.
3. Department of Neurobiology and Ethology, University of Haifa, Haifa, Israel.

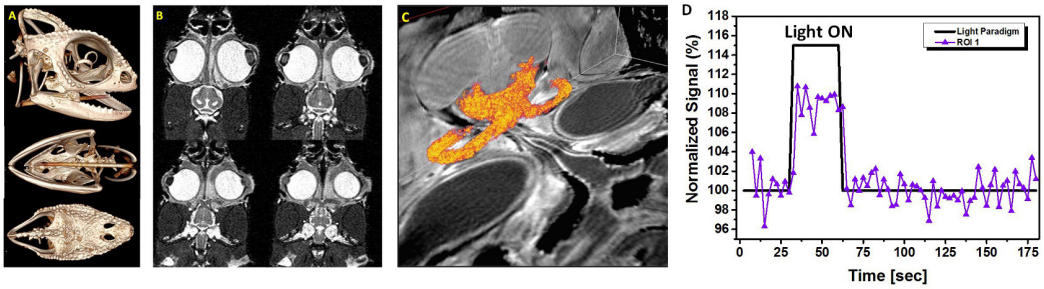
A
B
C
D
Light ON
Light Paradigm
ROI 1
Normalized Signal (%)
Time [sec]
118
116
114
112
110
108
106
104
102
100
98
96
0
25
50
75
100
125
150
175

CONTROL ID: 2230511

TITLE: Comparison of the PET imaging agents for atherosclerotic plaque detection

PRESENTER: Mikako Ogawa

ABSTRACT BODY:

Abstract Body: Background:

Vulnerable plaques in atherosclerotic lesions can cause acute myocardial infarction and stroke. Macrophage infiltration is characteristics for atherosclerotic vulnerable plaques, and energy metabolism and cell proliferation are elevated in these macrophages. At the same time, the calcification is often detected in atherosclerotic lesions. [^{18}F]FDG is the most common tracer for vulnerable plaque imaging by PET, but blood sugar affects the tracer accumulation. It is previously reported that [^{11}C]choline, can be applied for plaque imaging by visualizing the cell proliferation, and [^{18}F]NaF for calcification. In this study, we compared [^{18}F]FDG, [^{11}C]choline and [^{18}F]NaF as atherosclerotic plaque imaging agents.

Methods:

For *in vitro* studies, macrophages were isolated from the mice peritoneum (M0), and polarized to M1 or M2 phenotype by LPS/IFNg or IL-4/IL-13, respectively. Then, [^{18}F]FDG (2hr) or [^{11}C]choline (0.5hr) uptake level was investigated in high glucose (4000 mg/L) or low glucose (1000 mg/L) condition. PET imaging studies were performed in an atherosclerotic animal model, WHHL rabbits. [^{18}F]FDG (74 MBq), [^{11}C]choline (136 MBq) or [^{18}F]NaF (136 MBq) was injected into the rabbits (16 m.o., n=4, fasted for 16 hr) and PET imaging studies were performed from 120 to 150 min post injection for [^{18}F]FDG and [^{18}F]NaF, and from 30 to 90 min for [^{11}C]choline. CT images were obtained before each PET scan. For direct comparison of the tracers, each rabbit was investigated with all three tracers on separate days.

Results:

[^{18}F]FDG uptake to M0 macrophages was largely affected by glucose (low glucose: 37, high glucose: 3 %dose/mg protein). In contrast, the effect was small in [^{11}C]choline (low glucose: 10, high glucose: 8 %dose/mg protein). [^{18}F]FDG uptake was higher in proatherogenic M1 than anti-inflammatory M2 macrophages, but polarization did not affect [^{11}C]choline uptake. In PET studies, the atherosclerotic plaques were detected by [^{18}F]FDG and [^{18}F]NaF, but the radioactivity localization was different between these tracers. [^{11}C]choline showed fairly weak signal in the aorta, and the high radioactivity accumulation to the liver obscured the plaque visualization.

Conclusions:

Our *in vitro* studies indicated that [^{18}F]FDG is the preferable tracer in glucose level controllable patients, and [^{11}C]choline can be used as an alternative tracer in such as diabetes patients. However, the *in vivo* studies showed that the accumulation of [^{11}C]choline is not enough for PET imaging. In contrast, the small lesions were clearly detectable with [^{18}F]NaF, due to the low background signal except for the bone. Historical studies with the rabbit aortic sections are now undergoing to elucidate the different localizations of [^{18}F]FDG and [^{18}F]NaF.

AUTHORS (LAST NAME, FIRST NAME): Ogawa, Mikako[1, 2]; Kosugi, Mutsumi[1]; Ishiguro, Haruka[1]; Magata, Yasuhiro[1]

INSTITUTIONS (ALL):

1. Medical Photonics Research Center, Hamamatsu University School of Medicine, Hamamatsu, Japan.
2. Graduate School of Pharmaceutical Sciences, Hokkaido University, Sapporo, Japan.

(No Image Selected)

CONTROL ID: 2230471

TITLE: Development of polyethylene glycol conjugated with indocyanine green as a photoacoustic tumor imaging probe

PRESENTER: Kohei Sano

ABSTRACT BODY:

Abstract Body: Objectives: Photoacoustic (PA) imaging, which detects ultrasonic waves thermoelastically induced by photon absorption of light absorber, can provide *in vivo* biomedical information. Some fluorescence dyes and metal nanoparticles have been proposed as PA contrast agents because they show absorptions in the near-infrared window. Among them, indocyanine green (ICG) is a FDA-approved diagnostic agent, and the potential as a PA signal emitter has been reported. In this study, we developed an ICG-based PA contrast agent using polyethylene glycol (PEG), which were also FDA-approved for use in pharmaceuticals. The influence of molecular weight of PEG on PA tumor imaging was evaluated.

Methods: Propylamine terminal methoxy PEGs (molecular weight: 5, 10, 20, 40 kDa) were conjugated with ICG-sulfo-OSu. Each PEG conjugated with ICG (PEG-ICG) was referred to as PEG5-ICG, PEG10-ICG, PEG20-ICG, and PEG40-ICG, respectively. PA signal of PEG-ICG conjugate generated by titanium sapphire pulsed laser was measured. In *in vivo* fluorescence imaging study, colon26 (mouse rectal tumor)-bearing mice intravenously administrated with PEG-ICG conjugate were imaged, and the fluorescence of PEG-ICG accumulated in the tumor and blood was measured. ^{111}In-labeled DTPA-PEG-ICGs were intravenously administrated into colon26 tumor-bearing mice, and *in vivo* biodistribution was evaluated. In order to confirm the feasibility of PA tumor imaging, colon26 tumor-bearing mice administrated with PEG20-ICG (26 nmol) were imaged before and 24 h after probe injection by PA imaging system.

Results: The conjugation ratios of ICG to PEG were approximately 1 for each PEG-ICG conjugate. PA signal intensity of PEG-ICG conjugates was comparable with that of ICG. In the fluorescence imaging study, PEG20-ICG and PEG40-ICG provided significantly higher signals in the tumor than PEG5-ICG and PEG10-ICG. The fluorescence signals of PEG5-ICG and PEG10-ICG were decreased with time, whereas PEG20-ICG and PEG40-ICG showed maximum accumulation in the tumor at 24-48 h after administration. PEG20-ICG and PEG40-ICG showed prolonged half life in the blood compared with the others. The biodistribution of ^{111}In-labeled DTPA-PEG-ICGs was similar to the results of the fluorescence measurement in the tumor and blood. There was no remarkable accumulation of ^{111}In-labeled DTPA-PEG-ICGs in normal tissues except liver, kidneys, and spleen. Each ^{111}In-labeled DTPA-PEG-ICG was mainly excreted in the urine until 24 h after administration. In PA imaging, the tumor of the mice injected with PEG20-ICG was clearly visualized 24 h post-injection (152% signal increase) with high background ratios. Furthermore, the PA signal in the tumor region produced by PEG20-ICG increased in proportion with the injected dose (13-104 mol).

Conclusion: PEG-ICG showed a high accumulation in the tumor and excretion in the urine in both fluorescence and radiolabeled study. PEG20-ICG enabled PA tumor imaging *in vivo*. These results suggest that PEG-ICG has a capability as a PA contrast agent for diagnosis of tumor.

AUTHORS (LAST NAME, FIRST NAME): Sano, Kohei[1, 2]; Kanazaki, Kengo[1, 3]; Makino, Akira[1, 4]; Takahashi, Atsushi[3]; Yamauchi, Fumio[3]; Homma, Tsutomu[3]; Watanabe, Hiroyuki[1]; Temma, Takashi[1, 5]; Ono, Masahiro[1]; Saji, Hideo[1]

INSTITUTIONS (ALL):

1. Graduate School of Pharmaceutical Sciences, Kyoto University, Kyoto, Japan.
2. Kyoto University Hospital, Kyoto, Japan.
3. Medical Imaging Project, Corporate R&D Headquarters, Canon Inc., Tokyo, Japan.
4. Biomedical Imaging Research Center, University of Fukui, Fukui, Japan.
5. Department of Investigative Radiology, National Cerebral and Cardiovascular Center, Suita, Japan.

(No Image Selected)

CONTROL ID: 2231100

TITLE: In vivo HER2-Targeted Magnetic Resonance Tumor Imaging Using Iron Oxide Nanoparticles Conjugated with Anti-HER2 Single Chain Antibody

PRESENTER: Kohei Sano

ABSTRACT BODY:

Abstract Body: Objectives: HER2, closely related to poor prognosis, is highly expressed in various cancers including breast, ovarian and gastric cancer. Thus, we have planned to develop a HER2-targeted magnetic resonance imaging (MRI) probe by utilizing the ability of MRI in the diagnosis, staging and follow-up of many tumors with high spatial resolution. Iron oxide nanoparticles (IONPs), whose surface is flexible for modifying, were FDA-approved as MR contrast agents. In our previous studies, anti-HER2 single chain antibody conjugated IONPs (scFv-IONPs) showed high affinity to HER2 as well as a potential of photoacoustic (PA) imaging both *in vitro* and *in vivo*. In this study, we investigated the feasibility of tumoral HER2-targeted MRI with anti-HER2 scFv-IONPs as contrast agents.

Methods: scFv-IONPs were prepared by conjugating the sulfhydryl groups of reduced scFv to the maleimide groups on the surface of Nanomag®-CLD-spio (20nm in diameter). The scFv-IONP solution with a IONP concentration in the range of 0.05 to 0.2 mM was prepared and the transverse relaxivity (*r*2) was measured based on spin-echo images. The binding affinity of scFv-IONPs to HER2 was evaluated by cell binding assay using human gastric carcinoma NCI-N87 (HER2 positive). *In vitro* MR study was performed by incubating NCI-N87 and SUIT2 (HER2 negative) cells with scFv-IONPs or IONPs, and MR signals of the cells were measured by MRmini SA imaging system. To validate the specific binding of scFv-IONPs, excess Herceptin was used for blocking. For *in vivo* MRI, NCI-N87 and SUIT2 tumor-bearing mice intravenously injected with scFv-IONPs or IONPs were imaged before and 24 h after probe injection. Berlin blue staining was performed for the excised tumors after MR imaging studies to confirm the uptake of IONPs.

Results: About nine reduced scFv molecules were introduced to an IONP. The scFv-IONPs showed 47.5 nm particle size and 3.2 mV z-potential, respectively. The *r*2 of scFv-IONPs was 0.186 $mM^{-1}ms^{-1}$. The scFv-IONPs showed high affinity to NCI-N87 cells (Kd = 11.6 nM). In an i*n vitro* MRI, NCI-N87 cells exhibited significant reduction (44.6%) in MR signals of scFv-IONP than SUIT2 cells (6.8%), and the specific binding to HER2 was demonstrated by the blocking study. In an *in vivo* MRI, the decrease of MR signals in the NCI-N87 tumor (21.2%) was more notable than that in SUIT2 tumor (2.1%), which was also confirmed by Berlin blue staining. On the other hand, in both *in vitro* and *in vivo* MRI, control IONPs showed a slight signal decrease for both cells and tumors.

Conclusion: The scFv-IONPs showed the high affinity to HER2-expressing cells and enabled HER2-specific MR imaging of tumors *in vivo*. These results suggest that scFv-IONPs could be a robust MR contrast agent and also serve as a PA/MR dual imaging agent for diagnosis of malignant tumors.

AUTHORS (LAST NAME, FIRST NAME): Sano, Kohei[1, 2]; Ding, Ning[1]; Kanazaki, Kengo[1, 3]; Ono, Masahiro[1]; Saji, Hideo[1]

INSTITUTIONS (ALL):

1. Graduate School of Pharmaceutical Sciences, Kyoto University, Kyoto, Japan.
2. Kyoto University Hospital, Kyoto, Japan.
3. Canon Inc., Tokyo, Japan.

(No Image Selected)

CONTROL ID: 2230486

TITLE: Multi-modal imaging assessment of glioma growth, glioma associated microglial activation, and active matrix metalloproteinases *in vivo*.

PRESENTER: Bastian Zinnhardt

ABSTRACT BODY:

Abstract Body: *Introduction*

Glioma growth and glioma-associated microglial activation are characterized by the 18 kDa translocator protein TSPO and matrix metalloproteinases (MMPs). These molecular parameters are both considered to be key factors of tumor invasion and malignancy. Non-invasive imaging of TSPO and MMPs, as disease-specific alterations, was studied *in vivo*. Tumor growth, tumor associated microglial activation, and MMP activation were assessed in relation to a clinically established marker of active tumor volume with PET and MRI.

Methods

17 mice (n=11 for the experimental group; n=6 for the sham group) underwent sequential PET and MRI studies after implantation of a Gli36ΔEGFR-LITG glioma cell line. All mice were subjected to triple PET imaging (13±1 days) with [^{18}F]DPA-714 (TSPO; 20 MBq; 60-90 min p.i.), [^{18}F]BR-351 (MMPs; 20 MBq; 90-110 min p.i.) and [^{18}F]FET (amino acid transport 10 MBq, 20-30 min p.i.). Tumor-to-normal brain (T/B) ratios were calculated. T2w-μMRI was conducted for anatomical localization of the tumor. Immunohistochemistry for TSPO, MMP-9, and Iba-1 was performed. Additional *in situ* and gel zymography were used for visualizing activated MMPs.

Results

All radiotracers showed increased T/B uptake ratios of the maximum %ID/cc. [^{18}F]DPA-714 signal appeared within and around the tumor as determined by T2w-μMRI (T/B: 1.52 ± 0.28; $p<0.001$; t-test; n=11), [^{18}F]BR-351 uptake appeared to be restricted to the center of the tumor (T/B: 1.46 ± 0.30; $p<0.05$; t-test; n=11). [^{18}F]FET uptake was also significantly increased in the tumor compared to the contralateral side (T/B: 2.29 ± 0.46; $p<0.001$; t-test; n=7). Spatial comparison of [^{18}F]DPA-714 and [^{18}F]BR-351 PET with immunohistochemistry for TSPO and *in situ* zymography, respectively, revealed good spatial agreement of tracer uptake with histology for TSPO and *in situ* zymography for activated MMPs. Additional gel zymography revealed MMP-2 as the major contributor of the [^{18}F]BR-351 uptake. Strikingly, detailed analysis of TSPO sources indicated that [^{18}F]DPA-714 uptake reflects a mixture of human tumor-derived TSPO, and murine microglia-derived TSPO.

Conclusion

For the first time, multi-modal imaging based on PET and MRI revealed insight into the spatial distribution of important markers of glioma growth, and glioma-associated inflammation. These findings and methods will allow future evaluation of novel treatment paradigms targeting and subsequently modulating the inflammatory reaction in glioma.

Acknowledgements

This research was partly funded by a fellowship of the 'Cells-in-Motion Cluster of Excellence (EXC1003 - CiM) Graduate School, and the International Max-Planck Research School – Molecular Biomedicine (IMPRS-MBM) Joint Graduate Program to B. Zinnhardt, and the EU 7th Framework Programme (FP7/2007-2013) under grant agreement n° 278850 (INMiND), and by the Interdisciplinary Center for Clinical Research (IZKF core unit PIX), Münster, Germany.

AUTHORS (LAST NAME, FIRST NAME): Zinnhardt, Bastian[1]; Winkeler, Alexandra[2]; Thézé, Benoit[2]; Viel, Thomas[1]; Wachsmuth, Lydia[3]; Wagner, Stefan[4]; Breyholz, Hans-Jörg[4]; Faust, Andreas[1, 4]; Hermann, Sven[1]; Dollé, Frédéric[2]; Faber, Cornelius[3]; Kuhlmann, Michael T.[1]; Schäfers, Michael[1, 4]; Jacobs, Andreas H.[1, 5]

INSTITUTIONS (ALL):

1. European Institute for Molecular Imaging, University of Münster, Münster, Germany.
2. Laboratoire d'Imagerie Moléculaire Expérimentale, CEA-DSV-I2BM-SHFJ, Orsay, France.
3. Clinical Radiology, University of Münster, Münster, Germany.
4. Department of Nuclear Medicine, University of Münster, Münster, Germany.
5. Department of Geriatrics, Johanniter Hospital, Evangelische Kliniken, Bonn, Germany.

(No Image Selected)

CONTROL ID: 2230488

TITLE: CASE REPORT: GLIOBLASTOMA IMAGING AND THERAPY WITH $^{64}CuCl_2$

PRESENTER: Gianluca Valentini

ABSTRACT BODY:

Abstract Body: Glioblastoma is one of the most malignant and aggressive type of brain tumors with an average life expectance of less than 15 months. Our aim is to demostrate $^{64}CuCl_2$ capability to obtain both diagnosis and therapy in PET/CT imaging for a radiotargeted molecular therapy in patients with glioblastoma.

We introduced this new product according to following reasons: as showed in previous experimental data, glioblastoma needs copper for cellular metabolic activities and ^{64}Cu is able to link DNA and to destroy tumor cells thanks to its Auger effect. In fact, it is characterized by high Linear Energy Transfer (LET) in a small spatial region that can crash the cell. We report a particular case of a 71-year-old man with cerebral craniotomy (November, 2010) for a glioblastoma in the left rolandic region. In spite of surgery, the patient showed severe epilepsy with difficult gait (lower limb palsy) and non fluent speech with urinary incontinence. Moreover, he had not exact and real thought-movement nexus. He underwent a complete radiation therapy and a partial chemo treatment due to his pharmaceutical intolerance. Prior patient's consent, $^{64}CuCl_2$ PET/CT has been evaluated in four different treatments, planned every 3 months. Two to 3 hours after 80 mCi dose injection, PET/CT acquisition was made according to cerebral protocol 15 min length with 128x128 matrix (*Biograph 6 Truepoint PET/CT, Siemens*). $^{64}CuCl_2$ scans showed a markedly volume reduction along all three sections (axial, coronal, sagittal): 1.42 cm, 2.6 cm and 1.5 cm. It's also verified $^{64}CuCl_2$ capability to cross the blood-brain barrier (BBB) and to link cellular DNA. Patient's life expectancy has been carried up to 15 months after tumor diagnosis with enhanced quality of life. Actually, the man is able to walk, to munch and swallow, to have a speech and his epilepsy crisis are shorter, milder and few and far between. These results are very promising but we need to extend this study to other patients to evaluate $^{64}CuCl_2$ real usefulness in glioblastoma diagnosis and therapy, mainly in pediatric population where it would be possible to obtain three-time greater efficacy.

AUTHORS (LAST NAME, FIRST NAME): Valentini, Gianluca[1]; Panichelli, Paola[1]; Villano, Carlo[2]; Pigotti, Gioia[1]; Martini, Domenico [1]; Giacobbi, Beatrice[1]; Coccetti, Daniela[1]

INSTITUTIONS (ALL):

1. ACOM Advanced Center Oncology Macerata SpA, Montecosaro (MC), N.A., Italy.
2. U.O.C. Medicina Nucleare e Terapia Radiometabolica, Ospedale Civile "Spirito Santo", Pescara, Italy.

(No Image Selected)

CONTROL ID: 2230492

TITLE: Nanotechnologies for Molecular Probes and Quantitative Sensors

PRESENTER: Daniel Heller

ABSTRACT BODY:

Abstract Body: Two major promising applications of nanotechnology towards the treatment of cancer are the control over molecular binding sites and the detection of binding phenomena, which could lead to better therapies, earlier cancer detection, and better tools for cancer research. For these pursuits, new methods are needed to quantify disease biomarkers and other bioanalytes. The real-time and spatially-resolved detection and identification of analytes in biological media present important goals for next-generation nanoscale sensors. To this end, we employ the intrinsic near-infrared fluorescence of single-walled carbon nanotubes. The emission of semiconducting nanotubes is photostable yet sensitive to the immediate environment. Analyte identification is achieved by modulation of the nanotube's spectral response, resulting in distinct optical fingerprints. The responses can be spatially mapped in live cells and tissues, and measured in real-time with sensitivity down to the single-molecule level, facilitating unprecedented bioanalytical studies.

AUTHORS (LAST NAME, FIRST NAME): Heller, Daniel A.[1, 2]

INSTITUTIONS (ALL):

1. Memorial Sloan-Kettering Cancer Center, New York, NY, United States.
2. Weill Cornell Medical Colege, New York, NY, United States.

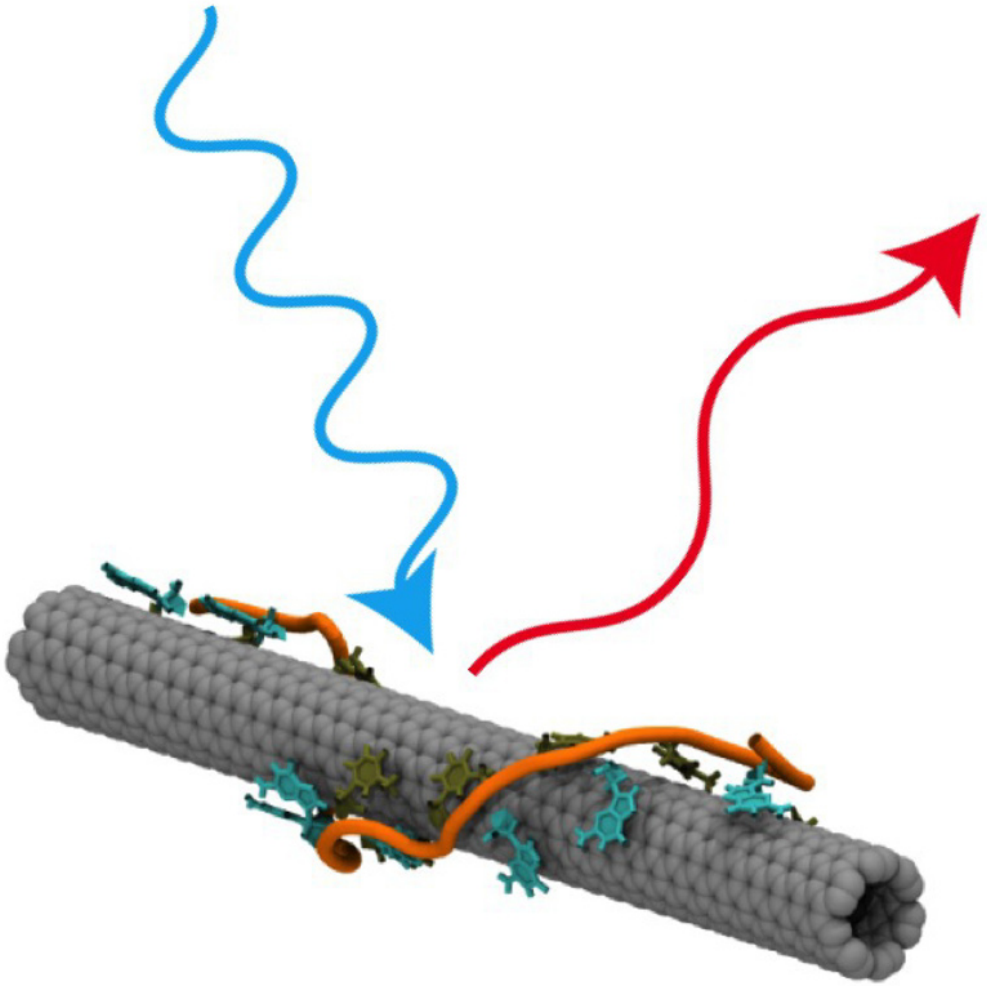

CONTROL ID: 2230495

TITLE:

Multimodal imaging of 6-hydroxydopamine induced neurodegeneration and its impact on neuroinflammation and neurogenesis

PRESENTER: Inga Fricke

ABSTRACT BODY:

Abstract Body:

Introduction

Parkinson's disease (PD) is a slowly progressing neurodegenerative disorder caused by loss of dopaminergic neurons in the substantia nigra (SN), leading to severe impairments in motor and non-motor function. Endogenous neural stem cells of the subventricular zone (SVZ) constantly give birth to new cells which might serve as a possible source for regeneration in the adult brain. However, neurodegeneration (ND) is accompanied by neuroinflammation (NI) potentially compromising regeneration.

This study aims to non-invasively monitor ND, NI, and progenitor cell migration in a mouse model of PD by multimodal molecular imaging employing small animal SPECT, PET, MRI, and BLI.

Methods

C57Bl6 mice received unilateral intranigral injections of 6-hydroxydopamine (6-OHDA) or vehicle. Multimodal imaging was performed at various time points post injection (p. i.), including [^{18}F]DPA-714-PET to assess microglia activation (d7 n=14; d14 n=25; d21 n=21), [^{123}I]Ioflupane-SPECT to determine nigrostriatal degeneration (d3 n=8; d7 n=5; d18 n=16) as well as T2-weighted MRI in order to obtain anatomical information. *In vitro* autoradiography with [^{18}F]DPA-714-PET was performed 2 wpi of 6-OHDA into the left striatum (n=7). A lentiviral-based reporter construct carrying the firefly luciferase gene under the control of the cytomegalovirus promoter was injected into the SVZ of FVB mice and progenitor cell migration was followed weekly using BLI. After reaching a signal plateau, unilateral 6-OHDA (n=5) and vehicle infusion (n=4) was carried out and signal distribution was examined over six weeks.

Results

At all studied time points, neurotoxin injection leads to a highly significant decrease in dopamine transporter ligand accumulation in the left striatum, compared to the normal right striatum ($p<0.001$). PET with the TSPO ligand [^{18}F]-DPA-714 reveals an increase in tracer accumulation in the lesioned SN two weeks p.i. (wpi) compared to control SN ($p<0.05$), which abates 3 wpi. Autoradiography at 2 wpi of 6-OHDA into the striatum confirmed nigral inflammation ($p<0.01$). Two to three weeks after reporter vector injection into the SVZ, first progenitor cell migration towards the olfactory bulb (OB) could be observed using BLI with significantly increased OB/SVZ signal ratio after 7.5 weeks. Unilateral injection of 6-OHDA/vehicle led to no BLI detectable change in signal distribution or regional signal intensity. Immunohistological analysis revealed acute nigral microgliosis, nigral and striatal astrogliosis, but unchanged SVZ neuroblast numbers.

Conclusions

The use of multimodal molecular imaging techniques enables us to study ND, NI and progenitor cell migration in experimental Parkinsonism. Induced degeneration in the nigrostriatal system leads to acute microgliosis in the SN and astrogliosis in SN and striatum, without compromising neuroblast generation in the SVZ.

Acknowledgement

The research leading to these results has received funding from the Interdisciplinary Center for Clinical Research (IZKF); Muenster; Germany (project SchwJ3/001/11), and the European Union's Seventh Framework Programme (FP7/2007-2013) under grant agreement n° 278850 (INMiND).

AUTHORS (LAST NAME, FIRST NAME): Fricke, Inga B.[1, 3]; Viel, Thomas[4, 1]; Worlitzer, Maik M.[3]; Collmann, Franziska M.[1, 5]; Vrachimis, Alexis[1, 2]; Faust, Andreas[1]; Wachsmuth, Lydia[6]; Faber, Cornelius[6]; Boutin, Hervé[7]; Dollé, Frédéric[8]; Schwamborn, Jens C.[3, 9]; Jacobs, Andreas H.[1, 10]

INSTITUTIONS (ALL):

1. European Institute for Molecular Imaging (EIMI), University of Muenster, Muenster, Germany.
2. Nuclear medicine, University Hospital of Muenster, Muenster, Germany.
3. ZMBE, Institute of Cell Biology, Stem Cell Biology and Regeneration Group, University of Muenster, Muenster, Germany.

4. PARCC, Inserm UMR 970, Université Paris Descartes, Sorbonne Paris Cité, Assistance Publique-Hôpitaux de Paris, Hôpital Européen Georges Pompidou, Paris, France.
5. In-vivo-NMR, Max Planck Institute for Metabolism Research, Cologne, Germany.
6. Department of Clinical Radiology, University Hospital Muenster, Muenster, Germany.
7. Wolfson Molecular Imaging Centre, University of Manchester, Manchester, United Kingdom.
8. Service Hospitalier Frédéric Joliot, I2BM, CEA, Orsay, France.
9. Luxembourg Centre for Systems Biomedicine (LCSB), University of Luxembourg, Esch-Belval, Luxembourg.
10. Department of Geriatric Medicine, Evangelische Kliniken, Johanniter Krankenhaus Bonn , Bonn, Germany.

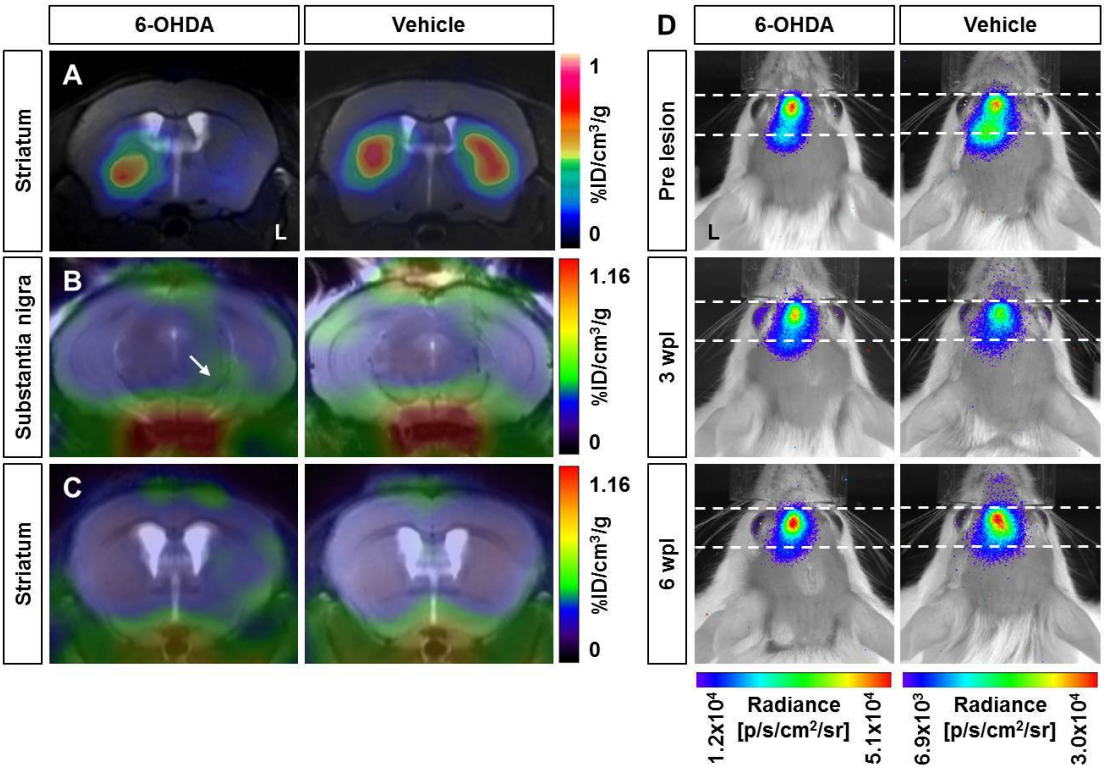

Figure 1: *In vivo* imaging of neurodegeneration, neuroinflammation and progenitor cell migration after 6-hydroxydopamine/vehicle injection: (A) Representative images of [^{123}I]loflupane-SPECT/T2w MRI at 7 days post injection in axial projections of the striatum. (B-C) [^{18}F]DPA-714-PET/T2w MRI at 14 days post injection in axial views of the substantia nigra (B) or the striatum (C). (D) BLI signal distribution pre- and post lesion (wpl: weeks post lesion).

CONTROL ID: 2233776

TITLE: Asialoglycoprotein receptor imaging for functional liver reserve using [^{68}Ga]GSA PET

PRESENTER: Andreas Schmid

ABSTRACT BODY:

Abstract Body: Introduction: The quantification of the functional liver reserve is of great interest in several medical settings, including steatosis, transplantation and therapy monitoring of cancer. In the past ^{99m}Tc-labelled galactosyl human serum albumin ([^{99m}Tc]DTPA-GSA) was used. Meanwhile, also [^{68}Ga] was introduced using the advantages of PET. Here we compare the performance of [^{68}Ga]DTPA-GSA and [^{68}Ga]NOTA-GSA using small animal PET.

Methods: ^{68}Ga was eluted from a ^{68}Ge-based generator using 0.1 M HCl and buffered to pH 5-6 with sodium acetate. 1 µg of DTPA-GSA or NOTA-GSA per MBq ^{68}Ga was added and incubated for 60 min at room temperature. Radio-TLC and Radio-HPSEC were performed to assess the radiolabeling success. Ten healthy male Fischer rats (254 ± 10 g) were injected with 4.9 ± 0.2 MBq either [^{68}Ga]NOTA-GSA or [^{68}Ga]DTPA-GSA. PET measurements were performed on a dedicated small animal tomograph, followed by MRI measurements on a 7 T small animal MRI scanner. During the experiments, animals were anesthetized with 1.5 % isoflurane evaporated in medical oxygen. After the imaging sessions, the animals were sacrificed and dissected and activity concentration analyzed. Dynamic PET data were analysed by drawing regions of interest in heart (176 mm³), kidney (163 mm³), liver (273 mm³) and spleen (31 mm³). Time activity curves (TAC) were extracted and the times for reaching 50% (T50) and 90% (T90) of maximal uptake were determined from linear interpolation as well as the slope of the TAC from 0.5 – 1.5 minutes after tracer injection for liver tissue.

Results: Both NOTA- and DTPA-conjugated GSA was successfully labeled with comparable radiochemical purity of ~93.5 %. The NOTA-labeled derivative reached a pseudo-plateau of 6.5%ID/mL after approximately 8 min, but continued to rise slowly for the remaining measurement time. The DTPA-labeled tracer achieved slightly higher plateau of 7.7 %ID/mL after 3 ¾ minutes followed by a slight decrease. The initial slope of the liver uptake showed a faster increase for DTPA-GSA (NOTA: 3.31 ± 0.36 %ID/ml/min vs DTPA 3.75 ± 0.12 %ID/ml/min), also resulting in shorter T50 and T90 values.

Conclusions: Overall, the behavior of both tracers is similar, even though the uptake of DTPA-GSA is faster. For quantification of functional liver reserve, however, the initial rise in the TAC is of interest. Here, both tracers provide comparable values, and thus are promising markers for functional liver reserve. Furthermore, for the quantification of T50 and T90, the absolute max value was used; shorter values can be reached for the NOTA-GSA, if the onset of the pseudo-plateau is used. Future studies will reveal the value of the tracers by quantifying functional liver reserve in disease models, e. g. hepatic steatosis or liver cancer.

AUTHORS (LAST NAME, FIRST NAME): Schmid, Andreas M.[1]; Maurer, Andreas[1]; Pichler, Bernd J.[1]; Virgolini, Irene J.[2]; Haubner, Roland[2]

INSTITUTIONS (ALL):

1. Department of Preclinical Imaging and Radiopharmacy, University Hospital Tübingen, Tübingen, Germany.
2. Department of Nuclear Medicine, Medical University of Innsbruck, Innsbruck, Austria.

(No Image Selected)

CONTROL ID: 2230504

TITLE: Preclinical *in vivo* evaluation of a novel PET/SPECT genetic reporter system for imaging T-cells in the brain

PRESENTER: Louise Kiru

ABSTRACT BODY:

Abstract Body: Introduction: Chimeric antigen receptor (CAR) T-cell therapy is emerging as an effective strategy in neuro oncology. Currently, there is no established method to longitudinally image the fate of CAR T cells in the brain of clinical subjects irrespective of blood brain barrier integrity. The aim is to develop a PET/SPECT genetic reporter to image homing of T cells to the brain. This study proposes the use the human dopamine transporter (hDAT) as a genetic reporter in combination with clinically approved radioligand, [^{123}I]-FP-CIT. The objectives are; (1) to demonstrate hDAT engineered T cells directly injected into the brain can be imaged with [^{123}I]-FP-CIT and (2) to visualise trafficking of aCD19 CAR T cells in a CNS lymphoma mouse model.

Methods: *Proof of concept:* The T cell line, SupT1 was engineered with hDAT and FLuc. [^{123}I]-FP-CIT binding and specificity was evaluated *in vitro*. NSG mice (n=5) were intracranially inoculated with hDAT(+) cells. BLI verified cell viability and MRI was used to normalise tumour sizes. Dynamic brain scans were acquired post injection of [^{123}I]-FP-CIT. Manual ROIs were drawn on co-registered MRI-SPECT data to determine binding potential (BP). *CNS lymphoma model:* PBMCs co-transduced with aCD19 CAR and FLuc were injected via tail vein at two weeks post intracranial injection of lymphoma. Tumour progression was assessed by MRI and T cell distribution visualised by BLI. Immunohistochemical staining was performed.

Results: *Proof of concept:* hDAT(+) SupT1 cells (Fig. 1a(i)) demonstrated 80 fold higher [^{123}I]-FP-CIT binding (25.08% ± 1.14) compared to hDAT(-) cells (0.31% ± 0.04). Co-incubation of hDAT(+) cells with [I]-FP-CIT significantly reduced binding (1.01% ± 0.22) (Fig. 1a(ii)). BLI confirmed hDAT(+) SupT1 cell viability (Fig. 1b(i)). Tumour volumes were normalised to 22.86 ± 4.98 mm^3. hDAT(+) cells were visualised by SPECT as early as 0.25 and up to 6h post [^{123}I]-FP-CIT injection (Fig. b(ii)). BP peaked at 2h (6.73 ± 2.13), with a decrease at 4h (5.09 ± 1.18), and 6hr (4.61 ± 1.16) (Fig. 1b(iii)). *CNS lymphoma model:* BLI demonstrated homing of aCD19 CAR T-cells to CNS lymphoma in treated group with no signal observed in the T cell only group. MRI revealed oedema at the tumour site in the treated group whilst hydrocephalus was observed in the tumour only group. Histology confirmed co-localisation of aCD19 CAR T-cells and lymphoma (Fig. 1c).

Conclusion: This study demonstrates for the first time that T-cells can be visualised in the brain using the unique combination of hDAT and [^{123}I]-FP-CIT as a genetic reporter system. T cells were transduced with hDAT with high efficiency and purity without hampering cell function. hDAT(+) T cells bound [^{123}I]-FP-CIT with high affinity and specificity *in vitro* and *in vivo*. T-cells were detected as early as 15 min p.i. with an optimal imaging window at 2h. Homing of aCD19 CAR T-cells to CNS lymphoma post systemic administration was visualised via BLI and histology. The work above paves the path for studies currently underway to determine whether T cell trafficking can be imaged using the hDAT/[^{123}I]-FP-CIT reporter system and to quantify the sensitivity of the technique.

AUTHORS (LAST NAME, FIRST NAME): Kiru, Louise[1, 2]; Badar, Adam[1]; Philip, Brian[2]; Kalber, Tammy L.[1]; Ramasawmy, Rajiv D.[1]; Ricciardelli, Ida[3]; Siow, Bernard[1]; Shende, Vishvesh[4]; Marafioti, Teresa[4]; Pule, Martin [2]; Lythgoe, Mark F.[1]

INSTITUTIONS (ALL):

1. Medicine, UCL Centre for Advanced Biomedical Imaging , London, United Kingdom.
2. Haematology , UCL Cancer Institute, London, United Kingdom.
3. Molecular & Cellular Immunology , UCL Institute of Child Health, London, United Kingdom.
4. Celluar Pathology and Histopathology, University College London, London, United Kingdom.

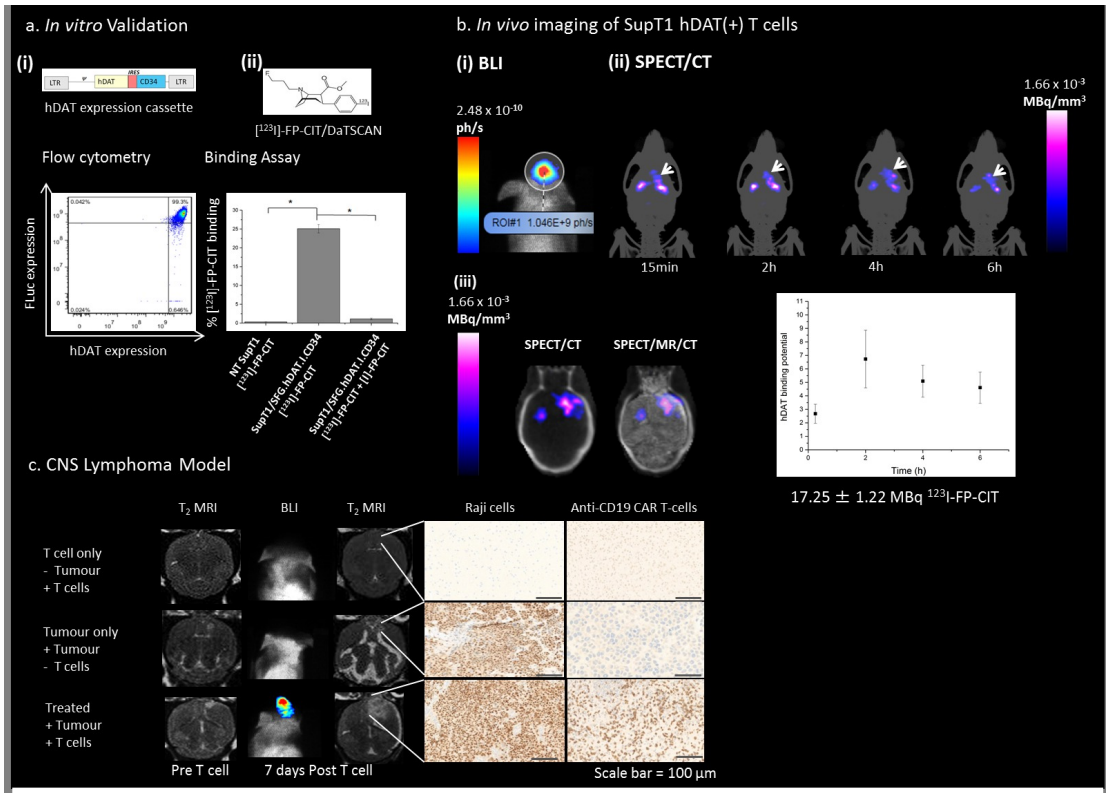

Figure 1: In vitro and in vivo evaluation of the hDAT/[^{123}I]-FP-CIT reporter system

(A) Cell engineering (i) and [^{123}I]-FP-CIT cell binding (ii). (B) BLI (i) dynamic SPECT/CT showing the maximum intensity projections (ii) coregistered SPECT/MR/CT used to determine the binding potential measurements (iii). (C) MR and co-localised histology of aCD19 CAR T cells trafficking to lymphoma in the brain.

CONTROL ID: 2230506

TITLE: Combined Endogenous Chemical Exchange Saturation Transfer and Hyperpolarized ^{13}C-Pyruvate Metabolism Imaging in Subcutaneous Tumours in Rats

PRESENTER: Geoffrey Topping

ABSTRACT BODY:

Abstract Body: Lactate/Pyruvate ratio (LPR) and chemical exchange saturation transfer (CEST) exchange rate dependent contrast are important biomarkers of tumour metabolism. In this work, we acquire CEST and LPR data of tumours in rats.

Four Fischer rats (mass approx. 150 g) were subcutaneously injected with 10^6 Mat B III rat mammary carcinoma cells. After 1-2 weeks tumour growth to 0.5 to 1.0 cm diameter, rats were anesthetized with isoflurane for imaging. Tumours were extracted for histological examination (not shown here).

Hyperpolarization was achieved with a HyperSense DNP Polarizer (Oxford Instruments). [1-^{13}C]pyruvic acid was polarized for approximately 1 hour, then rapidly dissolved in hot buffered solvent, resulting in 80 mM hyperpolarised [1-^{13}C]pyruvate solution, which was injected via tail vein catheter while animals were in the magnet, with a volume of approximately 1 ml over 5 seconds.

Proton and ^{13}C MRI data were acquired acquired using General Electric / Agilent Discovery 901 7T small animal MRI system. ^{13}C data were acquired using an IDEAL spiral chemical shift imaging (CSI) sequence with a repetition time (TR) of 3.6 s. Proton T1 maps were acquired using an inversion recovery fast spin echo (FSE) sequence with inversion times (TI) ranging from 50 to 4000 ms. Endogenous CEST Z-spectra were acquired with a 4 s continuous-wave 70 Hz amplitude pre-saturation, with offset frequencies from -2400 to +2400 Hz, followed by an FSE readout with effective TR of approximately 13.5 s.

Proton and ^{13}C data were processed in MatLab (The Mathworks), including ^{13}C reconstructions of pyruvate and lactate, and fitting of proton magnitude images to produce T1 maps, to determine Z-spectra B_0 shift corrections, and to generate endogenous CEST exchange-rate-dependent contrast images (Zaiss et al., 2014, NMR Biomed). Pyruvate and lactate images were summed for timepoints acquired after 2 s, where lactate became substantially visible. The per-voxel ratios of lactate and pyruvate were calculated, and averaged within regions of interest consisting of voxels that were within 67% of the tumour lactate peak intensity. Regions of interest on the CEST map were drawn by hand where the tumour appeared (which was not possible for ^{13}C images that lacked structural details). Average CEST contrast was calculated with these ROIs. Results are listed in the table.

There is a trend at lower Lactate/Pyruvate ratios (LPR) for positive correlation with endogenous CEST exchange rate contrast, but this breaks down at high LPR, where the CEST contrast is low. This may indicate potential for the combination of Lactate/Pyruvate metabolism and endogenous CEST to provide complimentary information for tumour characterization.

AUTHORS (LAST NAME, FIRST NAME): Topping, Geoffrey[1]; Rancan, Giaime[1]; Durst, Markus[2]; Skuratovska, Iryna[3]; Braren, Rickmer[3]; Schwaiger, Markus[1]

INSTITUTIONS (ALL):

1. Nuclear Medicine, Technische Universität München , München, Bayern, Germany.
2. Institute of Medical Engineering, Technische Universität München, München, Bayern, Germany.
3. Institut für Röntgendiagnostik, Technische Universität München, München, Bayern, Germany.

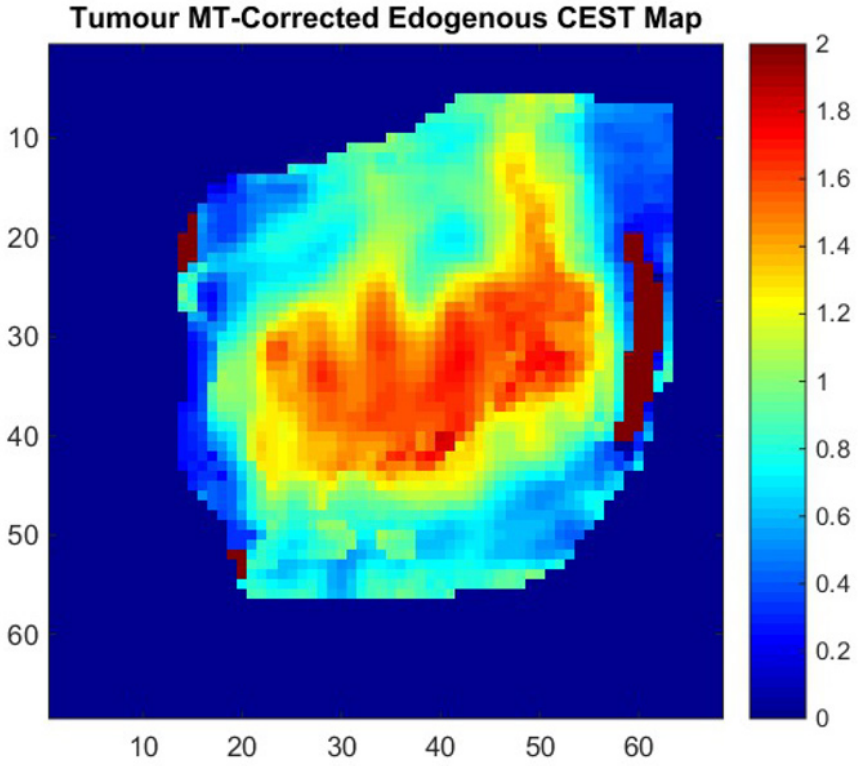
Tumour MT-Corrected Edogenous CEST Map
10
20
30
40
50
60
10
20
30
40
50
60
2
1.8
1.6
1.4
1.2
1
0.8
0.6
0.4
0.2
0

CONTROL ID: 2230561

TITLE: Multispectral Optoacoustic Tomography (MSOT) Sensitivity in Detecting Melanoma-derived Cells in Phantoms

PRESENTER: David Bates

ABSTRACT BODY:

Abstract Body: Introduction

Melanoma accounts for most of skin cancer-related deaths. Metastatic cells originating from the primary cancer travel to sentinel lymph nodes before spreading to distant sites in the body. Sentinel lymph node biopsy is the current preferred surgical diagnostic procedure for metastasis, however this method is invasive, suffers from a high false negative rate and the majority of biopsies are found to be histologically negative. Therefore a technique that can improve on this would be key in the early detection of metastasis and promoting increasing survival rates.

MSOT provides high resolution imaging in deep tissue with high molecular specificity. In a recent yet unpubblished clinical study (Stoffels et al.) MSOT has proved to be an unprecedented imaging modality that has the potential to increase lymph node metastasis detection rate and reduce excision-related morbidity, thanks to the detection of the optoacoustic signature of melanin in melanoma metastatic cells.

In the current study we have investigated the sensitivity of MSOT in detecting melanotic melanoma cells in scattering phantoms in a controlled and reproducible experimental setting and have shown that it is possible to detect as few as 4 cells.

Methods

B16-F10 melanoma and HCT 116 colorectal carcinoma control cells were grown to confluency and harvested. Cells were re-suspended in low melting agarose. Gel tubiform structures containing the cells were cut under an inverted bright-field Leica microscope into very small blocks ($<1.8 \times 10^{-2}$ mm^3) in order for cells to be within the same voxel. The number of cells inside the agarose blocks were counted. The blocks were placed over a 2 cm diameter cylindrical scattering phantom (1.5% agar, 0.5% intralipid) and then covered by low melting agarose (0.5% intralipid). The phantom was placed inside the MSOT inVision 128 small animal scanner. The mean signal of each block was quantified following imaging at 730 nm.

Results

Panel A in Fig 1 shows individual measurements (n=55, blue circles) including non-pigmented control cells (black triangles, n=6) and a linear fit, displaying linear relationship between cell number and optoacoustic signal. Panel B shows the MSOT signal as a function of cell number for those cell numbers for which replicates were available. There was a statistically significant difference between control and melanin-containing cell populations (as indicated by *) as determined by a one way anova (P = 0.0117). The statistical analysis revealed the ability to detect 4 cells.

Conclusions

MSOT has recently proved to be an optimal diagnostic imaging modality for lymph node metastasis. In the current study MSOT has shown to have a high sensitivity, being able to detect as low as 4 cells at depth in a scattering phantom. This finding is of high relevance for early detection of lymph node metastasis.

Association of multispectral optoacoustic imaging and metastatic node detection in malignant melanoma. Stoffels I., Helfrich I., Hillen U., Lehy J., Morscher S., Burton NC, Sardella TCS, Claussen J, Schadendorf D, Gunzer M, Klode J. Submitted for publication

AUTHORS (LAST NAME, FIRST NAME): Sardella, Thomas[1, 2]; Morscher, Stefan[3, 2]; Hupple, Clinton[1]; Burton, Neal C.[1, 2]; Bates, David[1]; Ntziachristos, Vasilis[3, 2]; Razansky, Daniel[3, 2]

INSTITUTIONS (ALL):

1. iThera Medical, Munich, Germany.
2. IBMI, Helmholtz Centre, Munich, Germany.
3. Technical University, Munich, Germany.

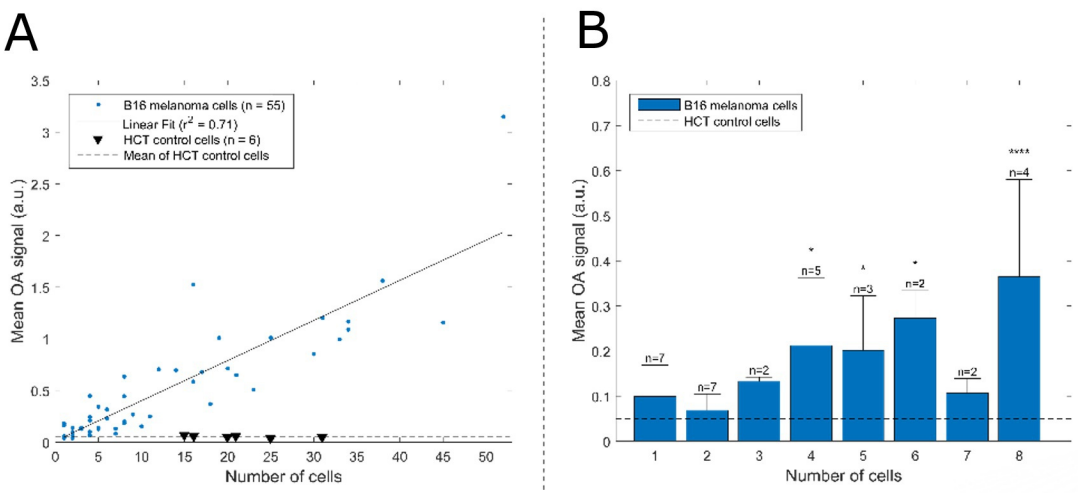
A
B16 melanoma cells (n = 55)
Linear Fit (r^2 = 0.71)
HCT control cells (n = 6)
Mean of HCT control cells
Mean OA signal (a.u.)
Number of cells
B
B16 melanoma cells
HCT control cells
Mean OA signal (a.u.)
Number of cells
n=7
n=7
n=2
n=5
n=3
n=2
n=2
n=4
****

CONTROL ID: 2231678

TITLE: Functional Mapping of Regional Hematocrit by Simultaneous Imaging of F-18 Albumin and Tc-99m Labeled Red Blood Cells: A Demonstration Study in the Mouse

PRESENTER: Michael Green

ABSTRACT BODY:

Abstract Body: Regional plasma and red blood cell (RBC) volumes are affected by a wide-variety of conditions encountered both clinically and experimentally. These volumes can, in principle, be quantified simultaneously *in vivo* if images of the distributions in the body of labeled plasma and labeled RBCs can be somehow separated from one another and if the ratio of plasma to RBC concentrations of the respective labels in the blood can be determined. An experimental whole-body mouse projection imaging system was created to test the potential of simultaneous imaging of single photon-emitting and positron-emitting compounds. We here test the hypothesis that we can use this system to simultaneously image F-18 labeled albumin (F-18 ALB) and Tc-99m labeled red blood cells (Tc-99 RBC) in the mouse, separate these image data into plasma-only and RBC-only images, and from these images create a "functional map" of the distribution of hematocrit throughout the mouse body. This study is intended only as a demonstration of these concepts and (very) many improvements to, and applications of, a "final" methodology are possible.

Rat serum albumin was labeled with F-18 as described by Basuli, et al. (*Nuc Med Biol 42; (3): pp 215-233, March 2015).* A pooled whole blood sample was created from blood drawn from three nude mice (NcR-nu/nu). The RBC fraction was labeled using the Tc-99m kit (UltraTag®) developed for human use. The F-18 ALB and Tc-99m RBC were mixed together and 0.2 ml of this mixture (130 uCi F-18, 210 uCi Tc-99m) injected into an anesthetized mouse (31 g body weight, pentobarbital, 60 mg/kg) via tail vein. Ten minutes were allowed for mixing to occur followed by projection imaging for 20 minutes. At the end of the imaging period, the animal was sacrificed and an arterial blood sample was obtained directly by capillary tube. The capillary tube was centrifuged to physically separate the plasma from the RBC fraction and to determine the arterial hematocrit. This same capillary tube was then imaged in projection for 60 minutes. The Tc-99m count rate/mm imaged along the RBC portion of the capillary tube divided by the F-18 (coincidence) count rate/mm along the plasma portion of the same tube provides the (constant) concentration ratio (C_{RBC}/C_P) required to make the regional hematocrit (H_i) calculation:

(1) $H_i = 1/[1 + (R_P/ R_{RBC})_i(C_{RBC}/C_P)]$

where R_P/ R_{RBC} is the F-18 count rate at image pixel "i" in the separated F-18 image divided by the Tc-99m rate at the same image pixel "i" in the separated Tc-99m image. A functional image of regional hematocrit was then constructed using Eqn. 1 applied to every image point.

Despite being a projection image, the resulting functional hematocrit image showed major mouse organ hematocrits similar to those reported in the literature for the spleen, liver, kidney and arterial blood. These results suggest that a system capable of simultaneous single photon and positron coincidence imaging may yield additional insights into various physiological processes requiring paired measurements, e.g. glucose metabolism/blood flow, hematocrit, etc.

Funded by NCI Contract HHSN261200800001E.

AUTHORS (LAST NAME, FIRST NAME): Green, Michael V.[2, 1]; Seidel, Jurgen[2, 1]; Williams, Mark[1, 4]; Jagoda, Elaine M.[1]; Basuli, Falguni[3]; Choyke, Peter L.[1]

INSTITUTIONS (ALL):

1. Molecular Imaging Program, NIH/NCI , Bethesda, MD, United States.
2. Contractor to Leidos Biomedical Research, Inc. (formerly SAIC-Frederick), NCI-Frederick, Frederick, MD, United States.
3. Imaging Probe Development Center, NIH/NHLBI, Bethesda, MD, United States.
4. Leidos Biomedical Research Inc. (formerly SAIC-Frederick), Frederick, MD, United States.

(No Image Selected)

CONTROL ID: 2230613

TITLE: Characterization of a high-resolution PET insert for small animal PET/MRI imaging

PRESENTER: Andrew Goertzen

ABSTRACT BODY:

Abstract Body: Introduction

We have recently completed a PET insert system for simultaneous PET/MRI imaging of small animals with a 7T animal MRI system. We present here a description of the PET system and initial results from PET system characterization and preliminary PET and PET/MRI imaging results.

Methods

PET System Design: The PET insert is a single ring of 16 detector modules, each with a dual-layer offset LYSO scintillator array with crystal pitch 1.27 mm and 28.3 mm axial field of view (FOV). The detector uses two SensL SPMArray4B SiPM arrays mounted on a custom readout board. The detectors are mounted on an ABS gantry attached to a 60 mm inner diameter carbon fiber cylinder with a 113 mm diameter carbon fiber cylinder as an outer cover. PET system dimensions were chosen so that it fits within the Bruker BGA-12S gradient coil and accommodates the Bruker 35 mm RF volume coil for the 7T Bruker Avance III MRI system installed at our centre. PET acquisition uses the OpenPET data acquisition system. At present, the system firmware can support a singles rate of 280kcps, allowing imaging with ~1MBq of activity. Future OpenPET firmware upgrades will increase the singles rate capability to >5Mcps.

PET System Characterization: PET calibration data were acquired using a ^{68}Ge line source positioned at the centre of the FOV, allowing creation of crystal and energy lookup tables. A first image was acquired for the PET system using an off-centre ^{68}Ge line source. Data were sorted into sinograms and reconstructed using the 3DRP algorithm implemented in STIR.

MR compatibility: The fully assembled and powered PET insert was tested in a 7T Bruker MRI. Spin echo (SE), RARE, FLASH and single-shot echo planar images (EPI) MRI sequences were acquired with the 35 mm RF volume coil using a 25 mm diameter cylinder phantom. Three MRI acquisitions were acquired: MRI only, MRI with PET insert present but not operating, MRI with PET insert present and operating. Detector level PET data were acquired and evaluated for flood image quality and energy resolution with and without the MR operating.

Results

PET System Characterization: PET data quality are sufficient to resolve >99% of all crystals in the flood histograms. Average energy resolution for the 6,544 crystals in the system was 11.94% +/- 1.77% FWHM. Initial sinograms and reconstruction images acquired with the ^{68}Ge line source were artefact free.

MR compatibility: No obvious MRI image artefacts were introduced by the PET insert system. Only the EPI sequence showed a small change in SNR (-15%). There were no significant differences for the B_1 field caused by the PET insert while for the B_0 field, $\Delta\omega/\omega$ increased slightly with the PET system operating (0.27 ppm vs. 0.16 ppm for MRI only). There were no significant differences in PET detector flood image quality or energy resolution for the detector outside the MRI or inside the MRI with the MR system acquiring data.

Conclusions

Construction and initial characterization work has been completed for a new PET insert for PET/MRI imaging of small animals. Initial phantom and mouse imaging will be conducted in March, together with preliminary evaluation using the NEMA NU4-2008 standard.

AUTHORS (LAST NAME, FIRST NAME): Goertzen, Andrew[1, 3]; Stortz, Greg[2]; Thiessen, Jonathan D.[4, 5]; Bishop, Daryl[6]; Khan, Muhammad Salman[7]; Khilani, Jatin[8]; Kozlowski, Piotr[9]; Retiere, Fabrice [6]; Schellenberg, Graham[8]; Shams, Ehsan[10]; Sossi, Vesna[2]; Thompson, Christopher J.[11]

INSTITUTIONS (ALL):

1. Department of Radiology, University of Manitoba, Winnipeg, MB, Canada.
2. Department of Physics & Astronomy, University of British Columbia, Vancouver, BC, Canada.
3. PET/CT Imaging Program, Health Sciences Centre, Winnipeg, MB, Canada.
4. Imaging Program, Lawson Health Research Institute, London, ON, Canada.
5. Department of Medical Biophysics, Western University, London, ON, Canada.
6. Detector Development Group, TRIUMF, Vancouver, BC, Canada.

7. Department of Electrical & Computer Engineering, University of Manitoba, Winnipeg, MB, Canada.
8. Department of Physics & Astronomy, University of Manitoba, Winnipeg, MB, Canada.
9. Department of Radiology, University of British Columbia, Vancouver, MB, Canada.
10. Biomedical Engineering Graduate Program, University of Manitoba, Winnipeg, MB, Canada.
11. McConnell Brain Imaging Centre, Montreal Neurological Institute, Montreal, QC, Canada.
(No Image Selected)

CONTROL ID: 2230616

TITLE: Molecular biomarkers in human pathologies from Fast Field-Cycling MRI

PRESENTER: Lionel Broche

ABSTRACT BODY:

Abstract Body: Fast Field-Cycling (FFC) is an NMR technique that involves changing the main magnetic field during the pulse sequence, which provides an extra dimension to the experimenter. It is a rich technique that is well known to characterise molecular dynamics with various applications already demonstrated in polymer matrices, porous media, liquid crystals and many other systems [1]. However, much work remains to be been done on the applications of FFC NMR in medical applications.

Our research group is working on translating FFC techniques to MRI [2]. We have developed three innovative FFC MRI scanners with that aim, two of which are whole-body scanners. This presentation exposes how FFC MRI may be used to find molecular biomarkers of clinical relevance through the results obtained from several research projects using FFC MRI on human tissues, mainly on cancer, osteoarthritis [3], muscle damage and thrombosis.

The table below summarises the studies done so far by our team. Preliminary analyses were made on a benchtop FFC NMR relaxometer (SMATracer, Stelar s.r.l., Italy) when possible using field-cycled inversion recovery sequences and were followed by FFC MRI using mainly FC-PRESS, field-cycled spin echo and field cycled gradient echo. All the work performed here has been reviewed by ethics committees (CERB and NoSREC).

Several biomarkers appeared from our studies: the shape of the dispersion curve, which varies dramatically in breast tissues around carcinomas, the presence of the so-called quadrupolar signal [4], which was shown to quantify the amount of fibrin and to characterise the state of the collagen matrix in osteoarthritis, and the offset of the dispersion curve, which is closely related to tumour grade.

FFC MRI shows a general trend to detect protein modifications quantitatively and in particular variations of collagen content. Several biomarkers have been extracted so far that are closely linked to biologically relevant information. More work is ongoing in order to explore other pathologies and to better explain the pathways that connect the biomarkers and the diseases.

AUTHORS (LAST NAME, FIRST NAME): Broche, Lionel M.[1]; Ross, James[1]; Davies, Gareth[1]; Lurie, David[1]

INSTITUTIONS (ALL):

1. ABIC, Univeristy of Aberdeen, Aberdeen, Aberdeenshire, United Kingdom.

(No Image Selected)

CONTROL ID: 2234112

TITLE: Evaluation of a DOTA-conjugated RGD/Bombesin-antagonist as a potential theranostic agent for prostate cancer using ^{86}Y and ^{90}Y

PRESENTER: Nilantha Bandara

ABSTRACT BODY:

Abstract Body: The gastrin-releasing peptide receptor (GRPR) and $\alpha_v\beta_3$ intergrin are two well established tumor targeting methods known to be overexpressed on human prostate cancer. In this study, a novel approach is taken by combing the above biomarkers to produce a heterodimeric peptide to enhance the tumor uptake and retention. Furthermore, by utilizing yttrium radionuclides, this dual receptor targeted agent has the potential as a diagnostic and therapeutic agent for prostate cancer.

The ability of GRPR agonists to internalize and target prostate tumors has been previously reported by our group and others. In this study RM2, an antagonist, which has shown improved tumor uptake compared to most agonistic peptides was utilized to target GRPR. A cyclic RGD motif was incorporated to specifically target $\alpha_v\beta_3$ intergrins in tumors. Radiolabeling studies were conducted using the matched pair radionuclides of ^{86}Y and ^{90}Y. ^{86}Y ($t_{1/2}$ = 14.7 h, β^+ = 33%, E_{avg} = 664 keV) is used as the PET imaging isotope and will provide a dosimetry partner for the ^{90}Y therapeutic isotope ($t_{1/2}$ = 64.1 h, β^- = 99.9%, E_{β^-} = 1.3 MeV).

Successful radiosynthesis of RGD-Glu-[$^{86/90}$Y-DO3A]-6-Ahx-RM2 was achieved with >95% purity. In vitro stability studies demonstrated that these tracers were stable in serum for up to 24 h with both being 100% intact. Competitive binding assays were conducted to evaluate binding affinities of this dual receptor system. IC_{50} values for the RGD-Glu-[DO3A]-6-Ahx-RM2 and RGD-Glu-[^{nat}Y-DO3A]-6-Ahx-RM2 in PC-3 cells were 9.26 ± 0.01 nM and 5.65 ± 0.00 nM, while in U87-MG glioblastoma cells IC_{50} values were 321 ± 82.0 nM and 346 ± 5.30 nM, respectively. Preliminary evaluation in SCID mice bearing PC-3 xenografts have shown a rapid and specific tumor uptake with 8.5 - 9.0 % ID/g for both ^{86}Y and ^{90}Y at 1 h. Specificity was demonstrated by co-injection of an excess of bombesin that reduced the tumor uptake by 47%. Comparison of the *in vivo* biodistributions of the ^{86}Y and ^{90}Y-radiolabelled analogs and results of ^{86}Y preclinical PET imaging studies will be presented.

AUTHORS (LAST NAME, FIRST NAME): Bandara, Nilantha[1]; Krieger, Stephanie S.[1]; Diebolder, Philipp J.[1]; Reynolds, Tamila J.[2]; Schehr, Rebecca[2]; Smith, Charles J.[2]; Rogers, Buck E.[1]

INSTITUTIONS (ALL):

1. Radiation Oncology, Washington University School of Medicine, Saint louis, MO, United States.
2. Department of Radiology, University of Missouri School of Medicine, Columbia, MO, United States.

(No Image Selected)

CONTROL ID: 2230653

TITLE: Preliminary evaluation of ^{18}F-labeled flexible benzyloxybenzenes for PET imaging of *β*-amyloid plaques

PRESENTER: Yanping Yang

ABSTRACT BODY:

Abstract Body: ***Objectives:*** Neurotoxic *β*-amyloid (A*β*) plaque in the brain has been recognized as the central histological characteristic that defines Alzheimer's disease (AD). Breaking the extended π-conjugated systems of the well-known rigid flat A*β* binding probes, a novel class of radioiodinated flexible benzyloxybenzene analogs was developed for lighting up the A*β* plaques [1]. Based on the benzyloxybenzene scaffold, we synthesized and evaluated two fluoro-pegylated benzyloxybenzene derivatives for PET visualization of A*β* plaques.

Procedures: Binding affinities were tested through in vitro competition binding assay using Aβ_{42} aggregates. Radiosynthesis of ^{18}F-labeled ligands was achieved using corresponding tosylate precursors for nucleophilic substitution with [^{18}F]fluoride. Specific binding to A*β* plaques was verified by in vitro autoradiography on brain sections from AD patient (male, 91 years old). In vivo biodistribution was conducted on normal ICR mice (20-22 g, male).

Results: In competition binding assay, two fluoro-pegylated benzyloxybenzenes displayed high binding affinities to Aβ_{42} aggregates (**5**, K_i = 25.7 ± 2.6 nM; **9**, K_i = 21.0 ± 4.9 nM), slightly higher than that of well-known IMPY (K_i = 32.2 ± 2.1 nM) and PIB (K_i = 38.8 ± 2.6 nM). [^{18}F]**5** and [^{18}F]**9** were obtained in 25-32% of decay corrected radiochemical yeild with approximate 200 GBq/*μ*mol of specific activity. Specific plaque labeling was verified by *in vitro* autoradiography on brain sections from AD patients. In biodistribution, [^{18}F]**9** exhibited high initial brain uptake (9.14 %ID/g at 2 min p.i.) and rapid washout rate (brain$_{2min}$/brain $_{60min}$ = 5.1), superior to the results of U.S. FDA approved [^{18}F]AV-45 (florbetapir) gained under the same procedure (6.59 %ID/g at 2 min p.i., brain$_{2min}$/brain $_{60min}$ = 3.3).

Conclusions: As fluoro-pegylated benzyloxybenzene [^{18}F]**9** combined a potent binding to A*β* plaques and excellent pharmacokinetics with high initial brain uptake and fast clearance from normal brain regions, we believe that [^{18}F]**9** is a promising candidate as PET probe for the early detection of A*β* plaques in AD brains.

Corresponding Author: cmc@bnu.edu.cn (Mengchao Cui)

Acknowledgements: Supported by NSFC (21201019)

References: [1] Yang, Y. *et al. J. Med. Chem.* **57**, 6030-6042 (2014).

AUTHORS (LAST NAME, FIRST NAME): Yang, Yanping[1]; Cui, Mengchao[1]; Liu, Boli[1]

INSTITUTIONS (ALL):

1. College of Chemistry, Beijing Normal University, Beijing, China.

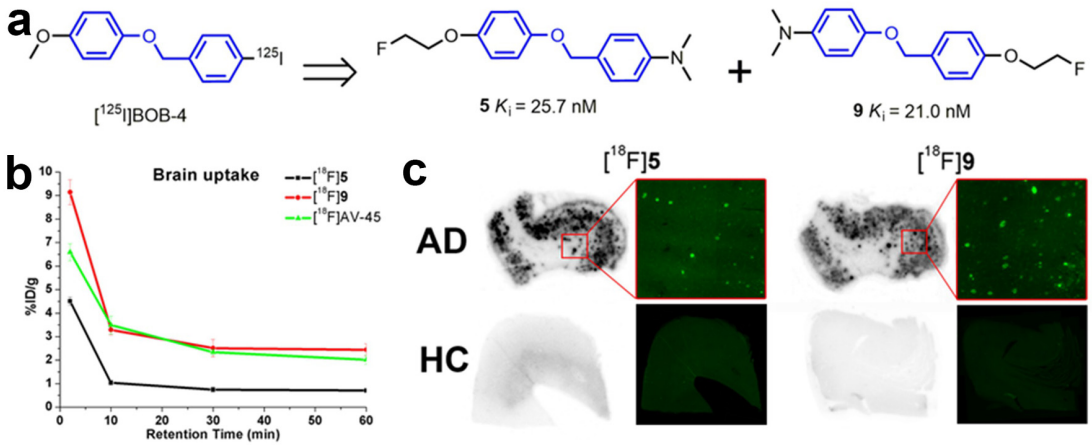

Figure 1. (**a**) Chemical structures and inhibition constants of the designed fluoro-pegylated benzyloxybenzene derivatives. (**b**) Plots of brain uptake of [^{18}F]**5**, [^{18}F]**9** and [^{18}F]AV-45 in normal ICR mice at different post-injection time points. (**c**) *In vitro* autoradiography of [^{18}F]**5** and [^{18}F]**9** in AD human brain sections (male, 91 years old) and normal brain sections (male, 74 years old). The presence and distribution of plaques in the sections were confirmed with Thioflavin-S.

CONTROL ID: 2230681

TITLE: Imaging reporter labeled degradable dextran nano-polymer as a COX-2 siRNA carrier for cancer therapy

PRESENTER: Zhihang Chen

ABSTRACT BODY:

Abstract Body: Cyclooxygenases (COX-1 and COX-2) are key enzymes in the biosynthetic pathway of conversion of arachidonic acid to prostaglandins (PGs). COX-1 is expressed at relatively constant levels in numerous tissues. COX-2 is normally low or absent in most nomal cells, but up-regulated by proinflammatory cytokines and tumor promoters. COX-2 is an important target in cancers that are COX-2 dependent, and may be a useful target in triple negative breast cancer. Unlike pharmacological COX-2 inhibitors that have significant side-effects, COX-2 small interfering RNA (siRNA) provides specific and effective downregulation of COX-2. However, because artificial polymers can induce proinflammatory signals that increases COX-2 expression, there are few if any reports about the use of artificial polymers as a carrier to deliver COX-2 siRNA in cancer cells.

Here we present an imaging reporter labeled biodegradable nano-polymer based on dextran as the carrier for COX-2 siRNA in cancer therapy. Cy5.5, used as an optical imaging probe, was labeled to the 40 kDa dextran which underwent oxidation, Schiff base formation, and reductive amination. A small number of positively charged functional amine groups that electrostatically bind siRNA were conjugated to the Cy5.5 labeled dextran platform with acetal bonds that were easily cleaved under acidic conditions. Rhodamine was labeled to these amine group as a second imaging probe to detect degradation and removal from the cell. When this nano-polymer was delivered within cancer cells, the acetal bond was broken under the weak acid condition. The amine group was released from the cells rapidly, minimizing the proinflammatory side-effects of the positively charged amine group.

The mechanism of this biodegradable nano-polymer carrier are presented in Figure 1A. The hydrodynamic radius of this dextran compound is about 7 nm. The ratio of absorbance of rhodamine to absorbance of Cy5.5 was used to evaluate the degradation of the nano-polymer at pH 5.5 and pH 7.4 buffer, and the results indicated that most of amine group was cleaved after 24h reaction in pH 5.5 buffer, although this compound was stable after 48h reaction in pH 7.4 buffer. Optical microscopy of cancer cells (Figure 1B) demonstrated that this nano-polymer delivered siRNA into cells efficiently, and the polymer degraded almost completely after 24h *in vitro* incubation. RT-PCR studies demonstrated that this COX-2/dextran complex efficiently reduced COX-2 mRNA levels in triple negative MDA-MB-231 breast cancer cells. Our data demonstrate the feasibility of using this dextran nano-polymer as a safe, reproducible, and biocompatible siRNA carrier that effectively reduces COX-2 expression in cancer cells.

This work was supported by NIH P50 CA103175 and R01 CA82337.

AUTHORS (LAST NAME, FIRST NAME): Chen, Zhihang[1]; Krishnamachary, Balaji[2]; Bhujwalla, Zaver[3]

INSTITUTIONS (ALL):

1. Johns Hopkins University, Baltimore, MD, United States.
2. Johns Hopkins University, Baltimore, MD, United States.
3. Johns Hopkins University, Baltimore, MD, United States.

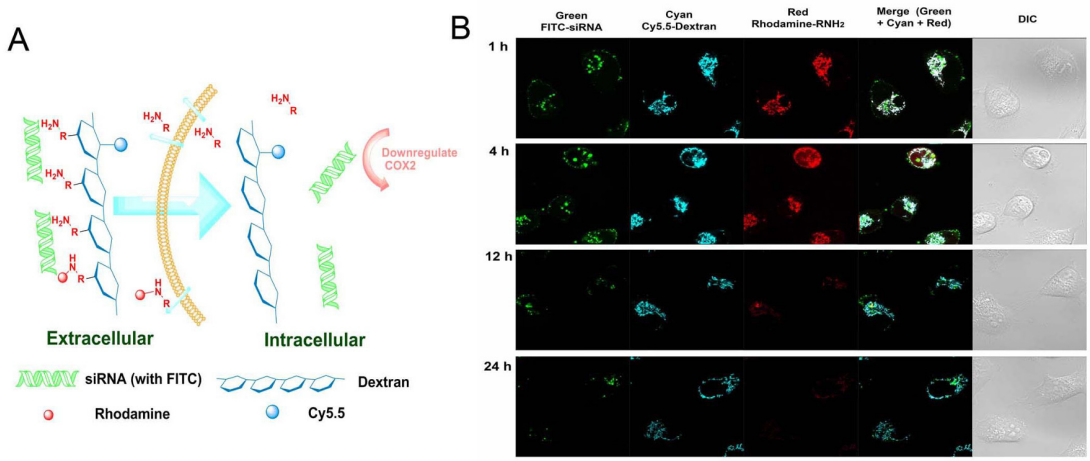

Figure 1. (**A**) Mechanism of biodegradable dextran nano-polymer. (**B**) Laser confocal fluorescence microscopy of MDA-MB-231 cells with siRNA/dextran nano-polymer. Cells were treated with FITC-siRNA/dextran nano-polymer (concentration of siRNA: 100 nM; N/P ratio: 50).

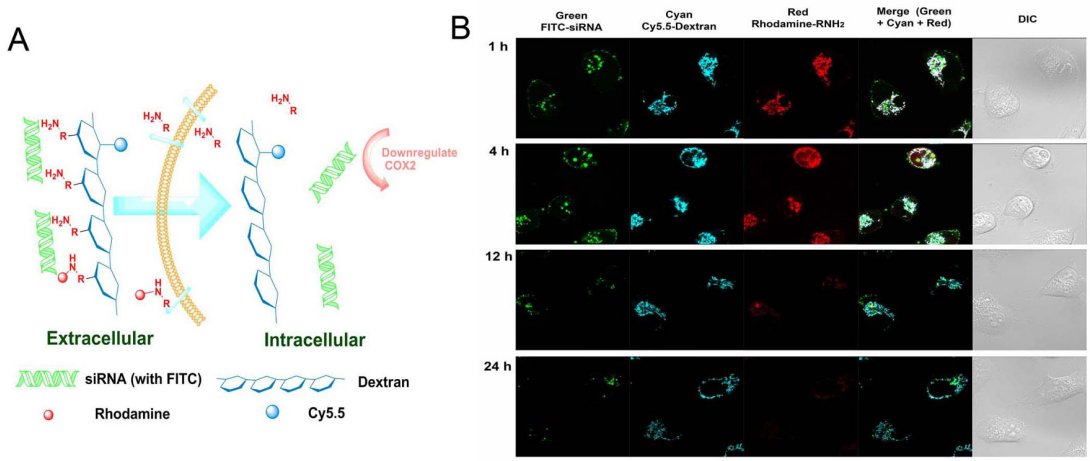

Figure 1. (**A**) Mechanism of biodegradable dextran nano-polymer. (**B**) Laser confocal fluorescence microscopy of MDA-MB-231 cells with siRNA/dextran nano-polymer. Cells were treated with FITC-siRNA/dextran nano-polymer (concentration of siRNA: 100 nM; N/P ratio: 50).

Figure 1 **A** and **B**

CONTROL ID: 2230717

TITLE: PET Imaging of [^{11}C]ascorbic acid in a murine rheumatoid arthritis model

PRESENTER: Bin Shen

ABSTRACT BODY:

Abstract Body: Objective: Reactive oxygen species (ROS) are chemically reactive molecules containing oxygen such as $OH^{\cdot}$, O_2^{-}, and H_2O_2. ROS dysregulation results in oxidative damage to various biological molecules and is implicated in many diseases including cardiovascular disease, cancer, inflammation/autoimmune disease [1]. Non-Invasive imaging of ROS in a living subject has proven to be extremely challenging. Currently most efforts are focused on *ex vivo* fluorescence imaging or indirectly measurement of ROS level in blood sample. Ascorbic acid (AA) acts as an antioxidant that can scavenge ROS resulting in the oxidized structure of dehydroascorbic acid (DHAA). DHAA is known to be transported into cells via GLUT 1-4 and recycled to reform ascorbate [2]. By exploiting this intracellular AA recycling and trapping mechanism, we can potentially use ^{11}C-radiolabeled AA ($t_{1/2}$ = 20.4 min) as a PET imaging tool to visualize ROS *in vivo*. We have previously reported the first radiosynthesis of [^{11}C]AA [3]. Herein we report the evaluation of [^{11}C]AA in a murine arthritis model.

Methods: [^{11}C]AA was synthesized using a GE TRACERlab FX $_{FN}$ module in conjunction with a GE Process Cabinet (Figure 1a). Inflammation was induced in the right hind paw of mice with Freund's complete adjuvant [4] and the other untreated paws served as internal controls. Severity of arthritis was monitored by measuring swelling as changes in the lateral dimension of the paw. At the height of acute inflammation at 7 d after induction, [^{11}C]AA dynamic PET/CT imaging on Siemens Inveon Scanner was performed over 1 h and tissues subsequently harvested for gamma counting.

Results: [^{11}C]AA was prepared in 35 min from end of bombardment (EOB) with a radiochemical yield of 18.1 ± 2.6% (n=7, decay corrected to EOB) and specific radioactivity of 412.8 ± 101.6 mCi/μmol (n=5, d.c. to EOB). In the PET/CT image (Figure 1b), more uptake of radioactivity was clearly observed in the inflamed paw compared to the control paw. *Ex vivo* counting of both dissected paws also confirmed a significant difference in uptake (30% increase, n=4, p <0.05) between inflamed *vs*. control paws. In addition, a trend was found between arthritis severity and radioactivity uptake (n=4, R^2=0.48, Figure 1c). At 1h post injection, we can see major uptake in liver (42.6 ± 3.6% ID/g) and kidney (27.7 ± 6.9 %ID/g) due to high toxin/ROS expression and renal excretion respectively (Figure 1d).

Conclusions: To the best of our knowledge, this is the first study to demonstrate *in vivo* PET imaging study with [^{11}C]AA. Our fully automated radiosynthesis process can produce >30 mCi/mL [^{11}C]AA, which is more than adequate to provide for *in vivo* PET studies. [^{11}C]AA PET imaging shows potential for localizing inflammation with ROS-rich regions *in vivo* and [^{11}C]AA PET may be further explored in other different ROS-related disease models.

[1] M Diehn *et al*. *Nature* **2009**, 458: 780-3. [2] Y Wang *et al. Proc. Natl. Acad. Sci. USA* **1997**, 94: 13816-9. [3] V Carroll *et al*. Abstract accepted, ISRS 2015, Columbia, MO, USA. [4] JD MacKenzie *et al*. *Radiology* **2011**, 259: 414-20.

AUTHORS (LAST NAME, FIRST NAME): Shen, Bin[1]; Palner, Mikael[1]; Carroll, Valerie N.[2]; shao, xia[3]; Scott, Peter J.[3]; MacKenzie, John D.[2]; Wilson, David M.[2]; Chin, Frederick T.[1]

INSTITUTIONS (ALL):

1. Radiology, Stanford University, Stanford, CA, United States.
2. Radiology, University of California San Francisco, San Francisco, CA, United States.
3. Radiology, University of Michigan, Ann Arbor, MI, United States.

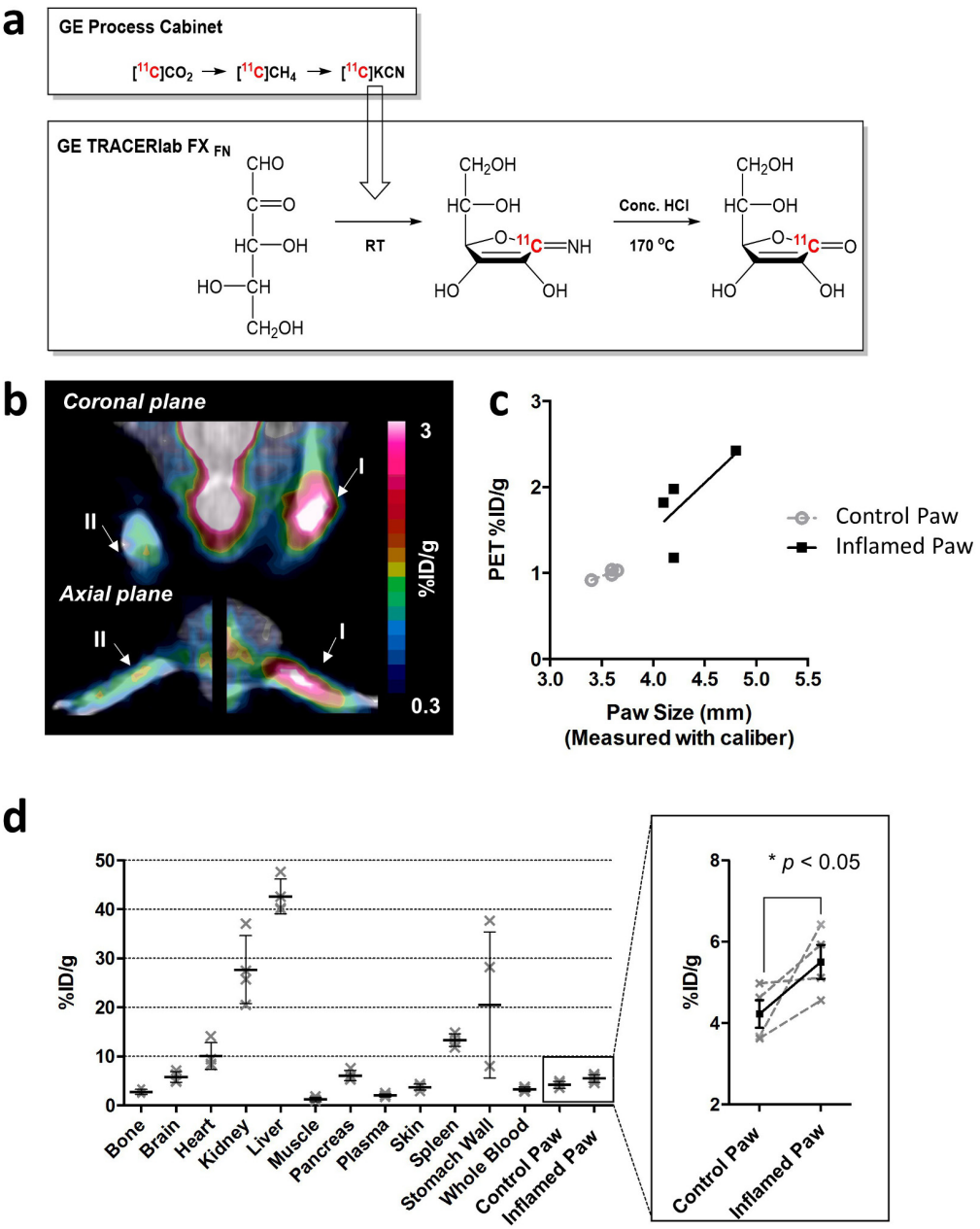

Figure 1. (**a**) Automated radiosynthesis of [^{11}C]ascorbic acid. (**b**) Representative [^{11}C]ascorbic acid PET images in arthritis mouse model (sum of 45-60 min scan, 294 ± 27 µCi/mouse of [^{11}C] ascorbic acid via a catheter in the tail vein), **I** = Inflamed Paw, **II** = Control Paw. (**c**) Correlation between paw size (severity of arthritis) and PET signals. (**d**) Ex vivo [^{11}C]ascorbic acid biodistribution in arthritis model (1h post injection).

CONTROL ID: 2232805

TITLE: Clinical-grade [^{18}F]FP-R$_0$1-MG-F2: Radiosynthesis of $\alpha_V\beta_6$ Integrin ligand for human PET studies

PRESENTER: Bin Shen

ABSTRACT BODY:

Abstract Body: Objective: A known cell surface receptor, $\alpha_V\beta_6$ integrin, is overexpressed in many cancer cells and has been evaluated as a novel clinical biomarker. Molecular imaging of $\alpha_V\beta_6$ integrins may be used to visualize receptor expression levels in order to determine prognosis and guide therapy. In general, $\alpha_V\beta_6$-binding peptides (either linear peptides or even simple disulfide-bonded peptides) have poor *in vivo* stability unlike engineered cystine knot peptides (R$_0$1-MG) with rigid molecular scaffold of 3-4 kDa that has shown exceptionally high stability and is more suitable for PET imaging. Our novel radioligand [^{18}F]FP-R$_0$1-MG-F2 has been developed and evaluated in mouse pancreatic tumor model. High specific tumor uptake presents excellent $\alpha_V\beta_6$ imaging potential for early cancer detection (described in a separate abstract). Herein, we are describing a procedure of radiosynthesizing clinical grade [^{18}F]FP-R$_0$1-MG-F2 for clinical translation (Figure 1).

Methods: [^{18}F]FP-R$_0$1-MG-F2 was synthesized in a modified automated radiochemistry system (GE TRACERLab FX F-N Pro plus an adjacent customized module). In addition, this system is equipped with a 6-port column selector (VICI) to facilitate multiple purification steps with different HPLC columns. Briefly, ^{18}F-prosthetic group 4-nitrophenyl-2-[^{18}F]fluoropropionate ([^{18}F]NPE) was synthesized from methyl 2-bromopropionate through three steps: ^{18}F-labeling, esterification and hydrolysis. The HPLC-purified anhydrous [^{18}F]NPE was added to the R$_0$1-MG knottin precursor to generate [^{18}F]FP-R$_0$1-MG-F2 in our adjacent customized module. The crude reaction mixture was transferred back into GE TRACERLab FX$_{F\text{-}N\ Pro}$ and purified on a second HPLC column. The [^{18}F]FP-R$_0$1-MG-F2 HPLC fraction was formulated in 0.9% NaCl containing no more than 10% ethanol via sterile filtration. Quality control criteria were set and the tests were performed according to USP 823. A 14-day single IV dose toxicity study of [^{19}F]FP-R$_0$1-MG-F2 in Sprague Dawley rats was submitted for testing at 1.1 mg/kg, equivalent to 250x the anticipated clinical dose (SoBran Bioscience).

Results: [^{18}F]FP-R$_0$1-MG-F2 was obtained in 0.5 ±0.2% radiochemical yield with a specific radioactivity of 4.2±2.2 Ci/μmol (n=3, decay-corrected to EOS, total synthesis is 3.5 h). Both radiochemical and chemical purities were > 99%. Stability tests also showed that prepared doses were stable for 4 h at ambient temperature. All other QC test results met specified criteria and the radiochemistry protocols were set for our future clinical studies. Finally, there were no treatment findings in the toxicity studies 3 or 15 days after a single IV dose of [^{19}F]FP-R$_0$1-MG-F2.

Conclusions: We have performed 3 consecutive validation runs for preparing clinical-grade, highly $\alpha_V\beta_6$ -selective radiotracer [^{18}F]FP-R$_0$1-MG-F2. An eIND application with the completed validation runs and final toxicity report has been submitted for FDA review. We plan to perform our first-in-human studies to examine [^{18}F]FP-R$_0$1-MG-F2 biodistribution in healthy human subjects and cancer patients after we have received all regulatory approvals for human administration.

AUTHORS (LAST NAME, FIRST NAME): Shen, Bin[1]; Kimura, Richard[1]; Cheng, Zhen[1]; Gambhir, Sanjiv S.[1]; Chin, Frederick T.[1]

INSTITUTIONS (ALL):

1. Radiology, Stanford University, Stanford, CA, United States.

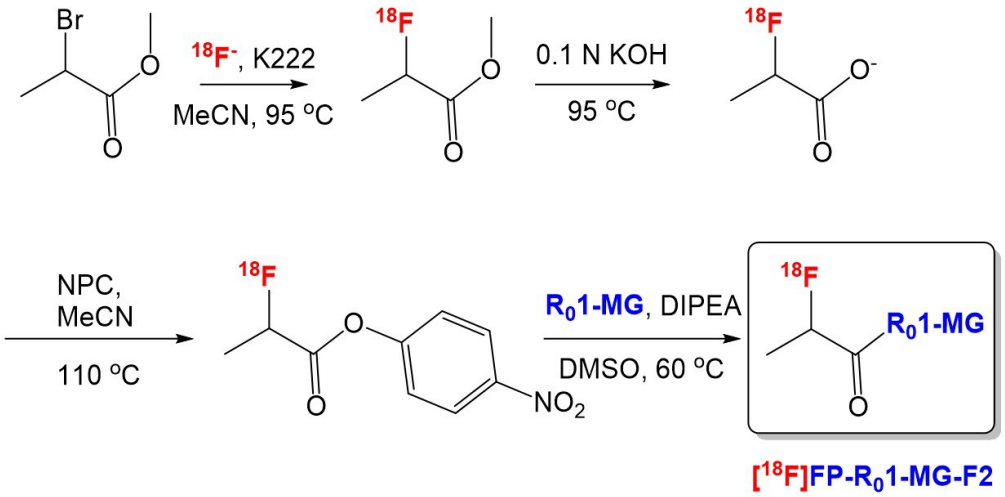

Figure 1. Radiosynthesis of [^{18}F]FP-R$_0$1-MG-F2

CONTROL ID: 2230719

TITLE: Novel segmentation of dynamic ^{18}F-FDG PET bypasses the need of arterial plasma input function, delivering a robust quantification of the tumor microenvironment

PRESENTER: Prateek Katiyar

ABSTRACT BODY:

Abstract Body: Introduction: Non-invasive imaging has greatly enriched our understanding of the factors underlying cancer progression. ^{18}F-FDG PET plays a pivotal role in tumor characterization and treatment planning in many cancer subtypes. Although compartmental modeling extracts the crucial information about blood flow and receptor status, estimation of kinetic parameters not only relies upon the acquisition of time activity curves (TACs) with low noise, but also on a precise measurement of the arterial input function (AIF). Accurate measurement of the AIF is an invasive and tedious procedure in humans and highly challenging in mice, nearly prohibiting applications in longitudinal studies. We propose a new algorithm for accurate mapping of the tumor micro-environment without the necessity of an AIF. We show that our method is robust to varying levels of noise, and, thus, can be used for the voxel-wise characterization of dynamic PET data. We also present exhaustive simulations to compare the proposed algorithm with standard compartmental modeling, and assess the kinetic parameter variability caused by various distortions in the AIF.

Methods: Several (n=12, 4 mice x 3 scans) ^{18}F-FDG dynamic PET scans were acquired using the Inveon small-animal PET scanner for 60 min with 27 frames. The plasma input curves of all the measurements were approximated using a minimal blood-sampling scheme [1]. A two tissue compartmental model was applied to the mean TAC of the entire tumor for each measurement. The observed kinetic parameter range was used to simulate the TACs of three tumor tissue classes. All the tumors were excised into 2-3 mm thin slices parallel to the axial field of view and processed for histological staining. The TACs of the simulated and real example were segmented using a novel clustering algorithm.

Results: To perform an objective evaluation, simulated TACs were corrupted with different levels of noise and segmented using the suggested algorithm. The proposed method showed substantial prediction accuracy in comparison to SUV based clustering. Spectral clustering derived segmented regions of the real example showed a significant correlation with histology slides stained with CD31. Cluster-wise averaged time activity curves were also in congruence with histology, with well perfused areas characterized by a higher activity concentration in contrast to that of remaining tumor regions. Kinetic modeling rate constants were underestimated with decrease and overestimated with increase in the peak amplitude of the plasma input function. The rate constants also showed substantial variability with the increase in amount of noise.

Conclusion: Unlike compartmental modeling, spectral clustering is independent of the AIF, thus eliminates the need of arterial blood sampling and associated sampling errors. The variability in the estimation of kinetic rate constants indicates its sensitivity for voxel level analysis and stresses the need of robust models for precise quantification of the tumor microenvironment.

[1] Estimation of the ^{18}F-FDG input function in mice by use of dynamic small-animal PET and minimal blood sample data, *JNM* 2007

AUTHORS (LAST NAME, FIRST NAME): Katiyar, Prateek[1]; Divine, Mathew R.[1]; Pichler, Bernd J.[1]; Disselhorst, Jonathan A.[1]

INSTITUTIONS (ALL):

1. Department of Preclinical Imaging and Radiopharmacy, Werner Siemens Imaging Center, Eberhard Karls University Tübingen, Tübingen, Baden Württemberg, Germany.

(No Image Selected)

CONTROL ID: 2230721

TITLE: Ultrasound Molecular Imaging of Inflammation in a Porcine Acute Terminal Ileitis Model

PRESENTER: Ismayil Guracar

ABSTRACT BODY:

Abstract Body: Purpose

Inflammatory bowel disease (IBD) primarily affects young patients, and the terminal ileum is the most commonly affected segment of the bowel. Disease monitoring should be noninvasive, inexpensive, widely available, and radiation-free. Ultrasound molecular imaging (USMI) has been shown to allow accurate noninvasive quantification of inflammation in murine IBD models by visualizing various adhesion molecules including both P-and E-selectin (1, 2, 3). The purpose of this study was to further translate USMI from small to large animals by assessing feasibility and reproducibility of USMI using dual P- and E-selectin targeted microbubbles ($MB_{Selectin}$) for assessment of inflammation in a porcine terminal ileitis model.

Materials and Methods

Acute terminal ileitis was established in 19 pigs by intraluminal TNBS/ethanol installation; 4 pigs without inflammation served as controls. USMI was performed in contrast pulse sequencing mode using a clinical machine (Acuson Sequoia 512; 15L8W, 7MHz; Siemens) after i.v. injection of clinical grade $MB_{Selectin}$ at increasing doses (0.5x, 1x, 2.5x, 5x, 10x, and $20x10^8$/kg b.w.) and non-targeted MBs ($MB_{Control}$). To test reproducibility, scans were repeated twice following $MB_{Selectin}$ and $MB_{Control}$ injection. Four minutes after MB injection, US datasets were acquired for 10 sec, followed by a 5-sec high power destruction pulse; this was followed by another 10-sec data acquisition. Linearized imaging signal was expressed as intensity ratio (IR), defined as average pre-destruction signal intensity divided by post-destruction signal intensity. After imaging, ileal segments were analyzed *ex vivo* for both inflammation grading on H&E staining and for expression of selectins using quantitative immunofluorescence.

Results

IR with $MB_{Selectin}$ increased linearly ($P<0.001$) between 0.5-$5.0x10^8$/kg and plateaued between 10-$20x10^8$/kg. Using a dose of 5×10^8/kg, imaging signals were well reproducible (ICC=0.70). Administration of $MB_{Selectin}$ in ileitis resulted in a significantly higher (P=0.03) IR (3.0±1.3) compared to control ileum (1.2±0.1). Also, IR using $MB_{Selectin}$ was significantly higher ($P<0.001$) compared to $MB_{Control}$ (1.2±0.3) in ileitis. In control ileum, IR was not significantly different (P=0.19) with $MB_{Selectin}$ or $MB_{Control}$ (Fig.1). *Ex vivo* inflammation histological grading correlated well with *in vivo* US signal (r=0.79), and both P-selectin (37.4%±14.7 of vessels positive; $P<0.001$) and E-selectin expression levels (31.2%±25.7) in vessels in the bowel wall of ileitis segments were higher compared to control ileum (5.1%±3.7 for P-selectin, 4.8%±2.3 for E-selectin, respectively).

Conclusion

USMI with dual selectin-targeted MB can be translated from small to large animal imaging in an acute terminal ileitis model in pigs using current clinical ultrasound equipment. Quantitative measurements of inflammation obtained by USMI are reproducible and correlate well with the extent of inflammation on histology in a porcine acute ileitis model as a next step towards clinical translation.

References

1. Bachmann. Gastroenterology 2006;130:8-16
2. Deshpande. Radiology 2012;262:172-80
3. Wang. Radiology 2013;267:818-29

AUTHORS (LAST NAME, FIRST NAME): Wang, Huaijun[1]; Felt, Stephen[2]; Machtaler, Steven[1]; Guracar, Ismayil[3]; Bettinger, Thierry[4]; Tian, Lu[5]; Willmann, Juergen K.[1]

INSTITUTIONS (ALL):

1. Department of Radiology, Molecular Imaging Program at Stanford, Stanford University, School of Medicine, Stanford, CA, United States.
2. Department of Comparative Medicine, Stanford University, Stanford, CA, United States.
3. Siemens Healthcare, Ultrasound Business Unit, Mountain View, CA, United States.
4. Bracco Suisse SA, Geneva, Switzerland.
5. Department of Health, Research & Policy, Stanford University, Stanford, CA, United States.

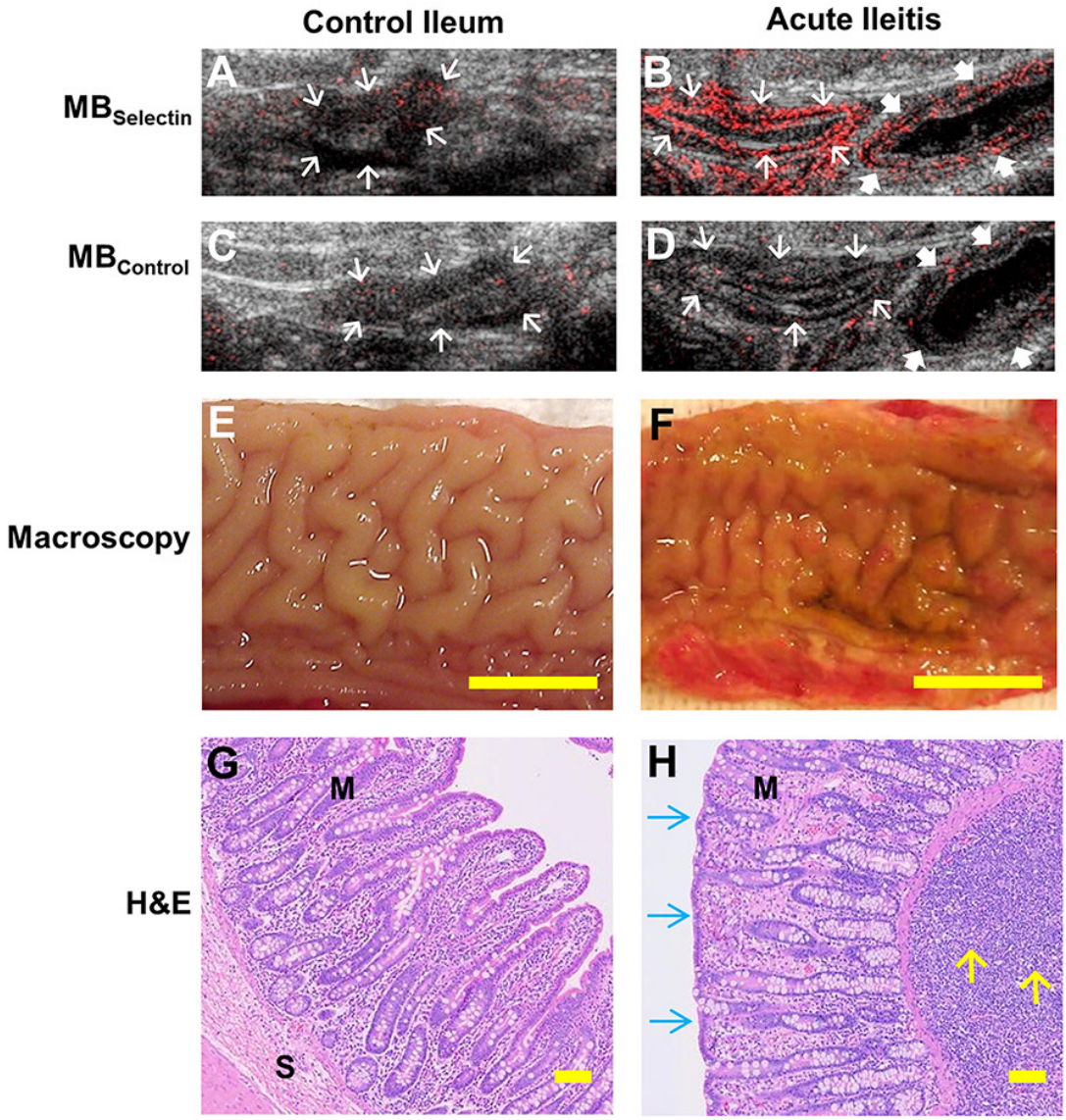
Control Ileum
Acute Ileitis
MB Selectin
MB Control
Macroscopy
H&E
A
B
C
D
E
F
G
H
M
M
S

CONTROL ID: 2230760

TITLE: Volumetric Molecular Ultrasound Imaging of Tumor Angiogenesis: Intra-Animal Comparison with Dynamic Contrast-Enhanced Imaging

PRESENTER: Huaijun Wang

ABSTRACT BODY:

Abstract Body: Purpose

Three-dimensional (3D) ultrasound molecular imaging (USMI) and dynamic contrast-enhanced (DCE)-US are promising imaging techniques for quantifying tumor angiogenesis and assessing treatment response to targeted therapies (1). The purpose of this study was to perform an intra-animal comparison between 3D USMI using clinical grade vascular endothelial growth factor receptor 2 (VEGFR2)-targeted contrast microbubble (MB_{VEGFR2}) and 3D DCE-US using non-targeted microbubbles ($MB_{Nontargeted}$) for assessing tumor angiogenesis and anti-angiogenic treatment effects in a murine model of human colon cancer.

Materials and Methods

Subcutaneous human colon cancers were induced in 19 mice and randomized to either anti-angiogenic treatment (n=11; i.v. single dose of anti-angiogenic agent, bevacizumab at 10mg/kg) or vehicle treatment (n=8; saline treatment). In all animals, 3D US imaging was performed with a clinical system (IU22 xMATRIX; Philips) and a matrix array transducer (X6-1; 3.2MHz) using two techniques: 1) 3D USMI was performed 4min after i.v. injection of 5×10^7 MB_{VEGFR2}; and 2) DCE-US images were continuously acquired with the steady state (4min)-destruction (5sec)-replenishment (3min) approach by constantly infusing $MB_{Nontargeted}$ at 40μL/min. VEGFR2-targeted signal intensity (SI) was quantified from USMI and the two perfusion parameters, relative blood volume (rBV) and flow (rBF) were calculated from DCE-US data sets. VEGFR2 expression levels and the percent area of blood vessels (PABV) were assessed *ex vivo* using immunofluorescence (IF) and correlated with correponding *in vivo* US parameters.

Results

Both 3D US imaging techniques showed strong anti-angiogenic treatment effects. All three parameters including VEGFR2-targeted USMI SI (58%, P=0.002), rBV (52%, P=0.002) and rBF (38%, P=0.02) significantly decreased following a single anti-angiogenic treatment compared to the control group. IF showed significantly diminished VEGFR2 expression (P=0.03) and PABV (P=0.03) in treated tumors, while no significant change was observed in control tumors (Fig.1). SI was highly correlated with VEGFR2 expression (Pearson coefficent r=0.95, P=0.001), and rBV (r=0.71, P=0.08) or rBF (r=0.82, P=0.02) showed good correlation with PABV.

Conclusions

Both 3D USMI and 3D DCE-US provide complementary *in vivo* information on anti-angiogenic treatment effects and allow accurate quantification of tumor angiogenesis in human colon cancer xenografts compared to *ex vivo* reference standard techniques.

References

1. Streeter JE, et al. *Mol Imaging*. 2011;10:460-468.

AUTHORS (LAST NAME, FIRST NAME): Wang, Huaijun[1]; Hristov, Dimitre[2]; Tian, Lu[3]; Willmann, Juergen K.[1]

INSTITUTIONS (ALL):

1. Department of Radiology, Molecular Imaging Program at Stanford, Stanford University, School of Medicine, Stanford, CA, United States.
2. Department of Radiation Oncology, Stanford University, Stanford, CA, United States.
3. Department of Health, Research & Policy, Stanford University, Stanford, CA, United States.

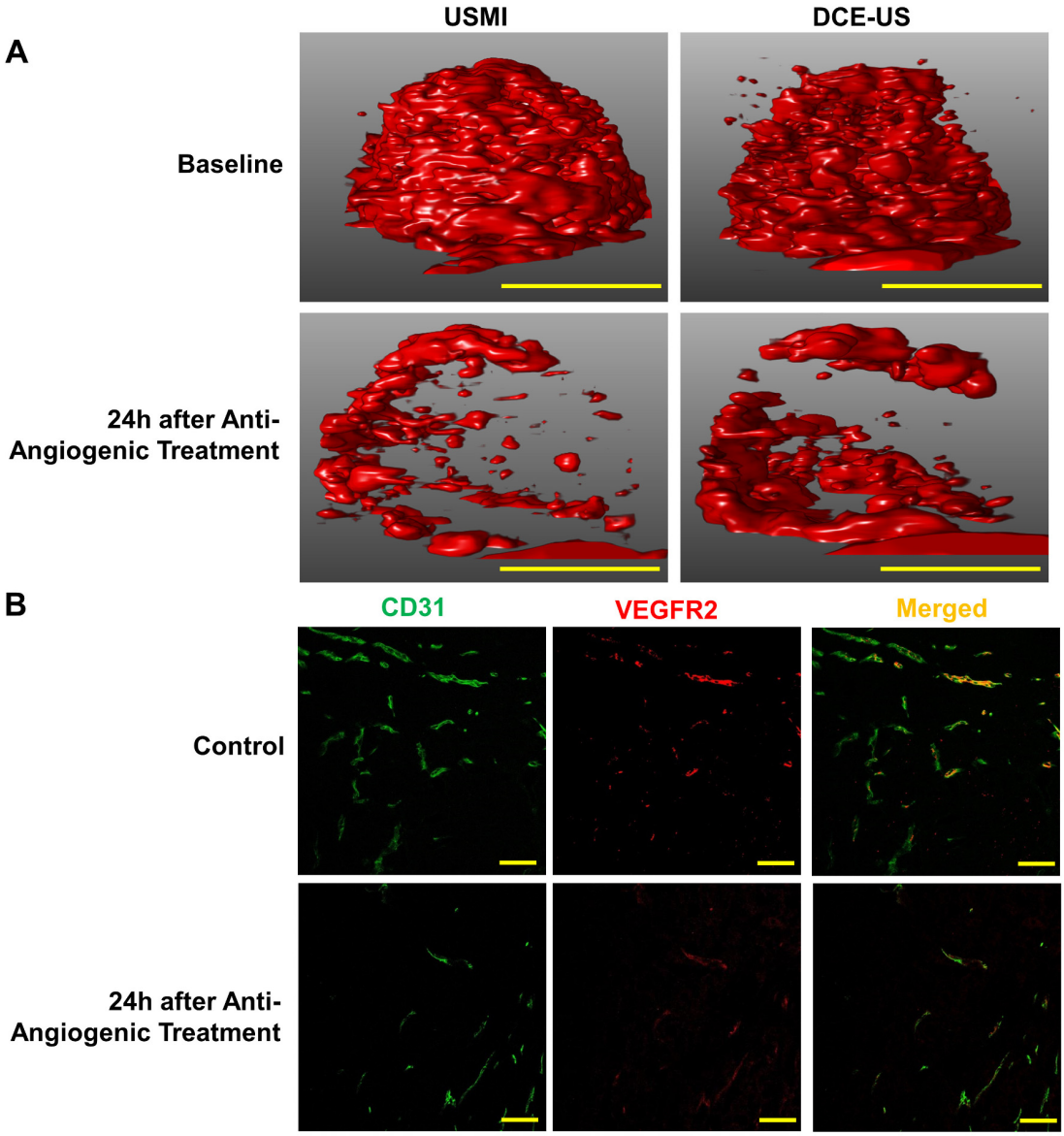
A
USMI
DCE-US
Baseline
24h after Anti-Angiogenic Treatment
B
CD31
VEGFR2
Merged
Control
24h after Anti-Angiogenic Treatment

CONTROL ID: 2230751

TITLE: Feasibility and Reproducibility of Three-dimensional Ultrasound Molecular Imaging of Tumor Angiogenesis using a Clinical Matrix Array Ultrasound Transducer

PRESENTER: Huaijun Wang

ABSTRACT BODY:

Abstract Body: Purpose

Ultrasound molecular imaging (USMI) is a promising imaging modality for evaluating treatment response to targeted therapies at the molecular level (1). However, heterogeneity in tumor tissue can lead to sampling errors with two-dimensional (2D) imaging approaches (2). The purpose of this study was to assess the feasibility and reproducibility of 3D USMI of vascular endothelial growth factor receptor 2 (VEGFR2) expression in tumor angiogenesis using a clinical matrix array transducer and a clinical grade VEGFR2-targeted contrast microbubbles (MB_{VEGFR2}) in a murine model of human colon cancer.

Materials and Methods

Subcutaneous human colon cancers were induced in 33 mice and randomized into 1) control group without treatment for imaging reproducibility test (n=19); 2) a treatment group (n=7; i.v. single dose of anti-angiogenic agent, bevacizumab at 10mg/kg); and 3) a vehicle group (n=7; saline treatment). Mice were scanned with a clinical US system and transducer (Philips IU22; X6-1 transducer) following i.v. injection of either MB_{VEGFR2} or non-targeted control microbubbles ($MB_{Control}$) at a dose of $5x10^7$. Group 1 mice were scanned twice to assess reproducibility of 3D USMI. Group 2 and 3 mice were scanned before and 24h after treatment. 3D volumetric imaging signal intensity (SI) was quantified. To simulate 2D imaging, the 3D USMI datasets were retrospectively reconstructed into multiple consecutive 1-mm thick planes. Vascular VEGFR2 expression was assessed *ex vivo* using immunofluorescence.

Results

3D USMI was highly reproducible for both MB_{VEGFR2} (ICC=0.83; 95% CI, 0.62-0.93) and $MB_{Control}$ (ICC=0.83; 95% CI, 0.60-0.93). SI with MB_{VEGFR2} ($1.1\times10^6\pm5.7\times10^5$) was significantly higher ($P<0.001$) compared to MB $_{Control}$ ($2.8\times10^5\pm2.7\times10^5$) in mice of group 1. VEGFR2-targeted USMI SI significantly (P=0.02) decreased by 57% following anti-angiogenic treatment compared to the control group, which correlated well with *ex vivo* VEGFR2 expression on immunofluorescence (Spearman coefficient r=0.93, P=0.003; Fig.1). USMI SIs reconstructed from multiple 2D 1-mm planes showed substantial spatial heterogeneity within tumors before treatment (coefficient of variation=0.43; 95% CI, 0.35-0.51). This spatial heterogeneity further increased significantly (P=0.006) after anti-angiogenic treatment (coefficient of variation=1.1; 95% CI, 0.45-1.77). If only central 1-mm tumor planes were analyzed to assess anti-angiogenic treatment response, the USMI signal change was significantly (P=0.006) overestimated by an average of 27% (range, 2-73%) compared to 3D USMI.

Conclusions

3D USMI is technically feasible and highly reproducible for assessing tumor angiogenesis in a human colon cancer xenograft model in mice and shows good correlation with *ex vivo* VEGFR2 expression. 3D imaging capabilities of US may further expand its future clinical role in molecular imaging of cancer. 3D USMI using a clinical grade VEGFR2-targeted contrast agent allows non-invasive quantification of anti-angiogenic therapeutic effects and may better account for heterogeneity of tumor angiogenesis compared to traditional 2D USMI.

References

1.Pysz. Radiology. 2010;519-27.

2.Hoyt. Invest Radiol. 2012;167-74.

AUTHORS (LAST NAME, FIRST NAME): Wang, Huaijun[1]; Kaneko, Osamu F.[1]; Tian, Lu[2]; Hristov, Dimitre[3]; Willmann, Juergen K.[1]

INSTITUTIONS (ALL):

1. Department of Radiology, Molecular Imaging Program at Stanford, Stanford University, School of Medicine, Stanford, CA, United States.

2. Department of Health, Research & Policy, Stanford University, Stanford, CA, United States.

3. Department of Radiation Oncology, Stanford University, Stanford, CA, United States.

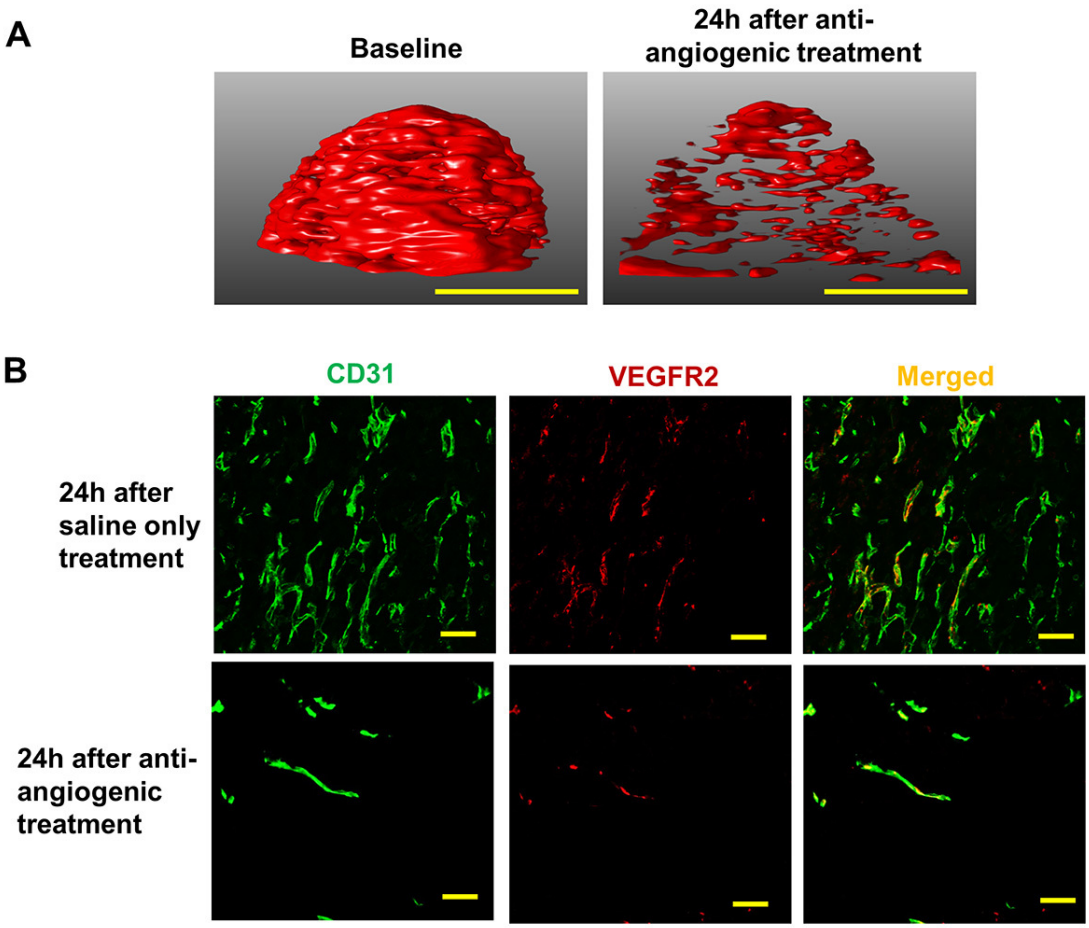
A
Baseline
24h after anti-angiogenic treatment
B
CD31
VEGFR2
Merged
24h after saline only treatment
24h after anti-angiogenic treatment

CONTROL ID: 2230826

TITLE: Tumor-targeting with *Salmonella typhimurium* A1-R decoys cancer cells to cycle and become chemosensitive demonstrated by FUCCI imaging

PRESENTER: Robert Hoffman

ABSTRACT BODY:

Abstract Body: The major problem for cancer chemotherapy is that the majority of cancer cells within a tumor are in G_0/G_1 and thereby chemoresistant. Fluorescence ubiquitination-based cell cycle indicator (FUCCI) imaging was used to identify the cell-cycle phase of each cell within tumors in vivo. *Salmonella typhimurium* A1-R decoyed cancer cells within tumors in nude mice to cycle from G_0/G_1 to $S/G_2/M$, thereby making them sensitive to cytotoxic agents. After decoy of *S. typhimurium* A1-R tumors became much more sensitive to cisplatinum and paclitaxel than to either drug alone. These results suggest a new paradigm of decoy cancer therapy that overcomes quiescent chemoresistant cancer cells within tumors.

AUTHORS (LAST NAME, FIRST NAME): Hoffman, Robert M.[1, 2]; Yano, Shuya[1, 2]; Miwa, Shinji[1, 2]; Bouvet, Michael[2]; Fujiwara, Toshiyoshi[3]

INSTITUTIONS (ALL):

1. AntiCancer, Inc., San Diego, CA, United States.
2. Department of Surgery, University of California San Diego, San Diego, CA, United States.
3. Department of Gastroenterological Surgery, Okayama University Graduate School of Medicine, Okayama, Japan.

(No Image Selected)

CONTROL ID: 2230953

TITLE: Tumor-targeting *Salmonella typhimurium* A1-R inhibits spontaneous and experimental lung metastasis of soft-tissue sarcoma

PRESENTER: Robert Hoffman

ABSTRACT BODY:

Abstract Body: Tumor-targeting therapy with the genetically-modified auxotrophic strain of *Salmonella typhimurium*, termed A1-R, was evaluated on orthotopic mouse models of primary soft tissue sarcoma produced by intra-muscular injection of HT1080-RFP human fibrosarcoma cells. *S. typhimurium* A1-R was administered from day 14, once a week for two weeks. On day 28, lung samples were excised and observed with a fluorescence imaging system for lung metastasis. The number of lung metastasis was 8.8 ± 3.4 in the untreated group and 0.8 ± 0.8 in the treated group (P = 0.024). A mouse model of experimental lung metastasis was obtained by tail vein injection of HT1080-RFP cells. The mice were treated with *S. typhimurium* A1-R (i.v.) on day 7, once a week for three weeks. *S. typhimurium* A1-R significantly reduced lung metastases and improved overall survival (P = 0.004). *S. typhimurium* A1-R bacterial therapy has future potential for treating advanced soft tissue sarcoma and improving prognosis of patients with lung metastasis.

AUTHORS (LAST NAME, FIRST NAME): Miwa, Shinji[1, 2]; Zhang, Yong[1]; Bouvet, Michael[2]; Tsuchiya, Hiroyuki[3]; Hoffman, Robert M.[1, 2]

INSTITUTIONS (ALL):

1. AntiCancer, Inc., San Diego, CA, United States.
2. Department of Surgery, University of California San Diego, San Diego, CA, United States.
3. Department of Orthopaedic Surgery, Kanazawa University, Kanazawa, Japan.

(No Image Selected)

CONTROL ID: 2230943

TITLE: Fluorescence-guided surgery inhibits recurrent and increases survival in an orthotopic osteosarcoma nude-mouse model

PRESENTER: Robert Hoffman

ABSTRACT BODY:

Abstract Body: 143B human osteosarcoma cells expressing red fluorescent protein (RFP) were injected into the intramedullary cavity of the tibia in nude mice. The fluorescent areas of residual tumors after bright-light surgery (BLS) and fluorescence-guided surgery (FGS) were 10.2 ± 2.4 mm^2 and 0.1 ± 0.1 mm^2, respectively ($p<0.001$). BLS-treated mice and BLS+cisplatinum (CDDP)-treated mice had significant recurrence. In contrast, the FGS mice and FGS+CDDP mice had very little recurring tumor growth. Disease-free survival (DFS) in the BLS group was 12.5%, BLS+CDDP group was 37.5%, FGS group was 75.0%, and the FGS+CDDP-group was 87.5%. The FGS-treated mice had a significantly higher DFS group rate than the BLS-treated mice ($p=0.021$). The FGS+CDDP-treated mice had significantly higher DFS rate than the BLS+CDDP-treated mice ($p=0.043$). FGS significantly reduced the recurrence of the primary tumor but did not reduce lung metastasis. The combination of FGS and adjuvant CDDP reduced tumor recurrence and prevented multiple metastases.

AUTHORS (LAST NAME, FIRST NAME): Miwa, Shinji[2, 3]; Hiroshima, Yukihiko[2, 3]; Yano, Shuya[1, 3]; Zhang, Yong[2]; Bouvet, Michael[3]; Tsuchiya, Hiroyuki[4]; Hoffman, Robert M.[2, 3]

INSTITUTIONS (ALL):

1. AntiCancer, San Diego, CA, United States.
2. AntiCancer, Inc., San Diego, CA, United States.
3. Department of Surgery, University of California San Diego, San Diego, CA, United States.
4. Department of Orthopaedic Surgery, Kanazawa University, Kanazawa, Japan.

(No Image Selected)

CONTROL ID: 2230940

TITLE: Fluorescence-guided surgery of prostate cancer bone metastasis in combination with Zoledronic acid increases disease-free survival in nude mouse models

PRESENTER: Robert Hoffman

ABSTRACT BODY:

Abstract Body: Nude mouse models of experimental bone metastasis of prostate cancer were made with tibial injection of PC-3-GFP cells. The percentage of residual tumor after bright-light surgery (BLS) and fluorescence-guided surgery (FGS) was 9.9 ± 2.2% and 0.9 ± 0.3%, respectively ($P < 0.001$). FGS reduced recurrent tumor growth in the tibia compared with BLS ($P < 0.005$). Although FGS alone had no significant effect on inguinal lymph node metastases, lung metastasis or disease-free survival (DFS), zoledronic acid (ZOL) in combination with FGS significantly increased DFS ($P = 0.01$) in comparison with the combination of BLS and ZOL.

AUTHORS (LAST NAME, FIRST NAME): Miwa, Shinji[2, 3]; Matsumoto, Yasunori[5]; Hiroshima, Yukihiko[2, 3]; Yano, Shuya[1, 3]; Bouvet, Michael[3]; Tsuchiya, Hiroyuki[4]; Hoffman, Robert M.[2, 3]

INSTITUTIONS (ALL):

1. AntiCancer, San Diego, CA, United States.
2. AntiCancer, Inc., San Diego, CA, United States.
3. Department of Surgery, University of California San Diego, San Diego, CA, United States.
4. Department of Orthopaedic Surgery, Kanazawa University, Kanazawa, Japan.
5. Dept. of Frontier Surgery, Chiba University, Chiba, Japan.

(No Image Selected)

CONTROL ID: 2230819

TITLE: Cancer-specific killer-reporter adenovirus for curative fluorescence-guided surgery of soft-tissue sarcoma

PRESENTER: Robert Hoffman

ABSTRACT BODY:

Abstract Body: Fluorescence-guided surgery (FGS) of cancer has not yet been shown to be curative due to residual microscopic disease. The present study aimed to overcome this problem with use of a killer-reporter cancer-specific adenovirus to label tumors in vivo. Human fibrosarcoma HT1080 expressing red fluorescent protein (RFP) was implanted orthotopically in the quadriceps femoris muscle of nude mice. After tumor growth, the tumor-bearing mice were injected with high and low-dose telomerase-dependent, green fluorescent protein (GFP)-containing adenovirus OBP-401, which labeled the tumor with GFP. Fluorescence-guided surgery (FGS) or bright light surgery (BLS) was then performed. OBP-401 could label soft-tissue sarcoma (STS) with GFP *in situ*, concordant with RFP. OBP-401-based FGS resulted in superior resection of STS in the orthotopic model of soft-tissue sarcoma (STS), compared to BLS. High-dose administration of OBP-401 enabled FGS without residual sarcoma cells or local or metastatic recurrence, due to its dual effect of cancer-cell labeling with GFP and killing. High-dose OBP-401 based-FGS improved disease free survival (p = 0.0013) as well as preserved muscle function compared with BLS. High-dose OBP-401-based FGS could cure STS, a presently highly-treatment-resistant disease. Since the parent virus of OBP-401, OBP-301, has been previously proven safe in a Phase I clinical trial, it is expected the OBP-401-FGS technology described in the present report should be translatable to the clinic in the near future for fluorescence-guided surgery.

AUTHORS (LAST NAME, FIRST NAME): Yano, Shuya[1, 2]; Miwa, Shinji[1, 2]; Urata, Yasuo[4]; Bouvet, Michael[2]; Fujiwara, Toshiyoshi[3]; Hoffman, Robert M.[1, 2]

INSTITUTIONS (ALL):

1. AntiCancer, Inc., San Diego, CA, United States.
2. Department of Surgery, University of California San Diego, San Diego, CA, United States.
3. Department of Gastroenterological Surgery, Okayama University Graduate School of Medicine, Okayama, Japan.
4. Oncolys BioPharma, Inc., Tokyo, Japan.

(No Image Selected)

CONTROL ID: 2230806

TITLE: Variable-magnification and spectral-separation fluorescence imaging systems are complementarity for noninvasive detection of metastasis and intravital detection of single cancer cells in mouse models

PRESENTER: Robert Hoffman

ABSTRACT BODY:

Abstract Body: Imaging of tumor growth, progression and metastasis with fluorescent proteins in mouse models has many applications, due to the multiplier of spectrally-distinct colors and very high extinction coefficient. A limit to fluorescent protein imaging has been for non-invasive deep-seated tumors, such as those in the lung. In the present study, the Maestro spectral-separation fluorescence imaging system with a liquid-tunable filter and the OV100 variable-magnification imaging system were compared for noninvasive detection of metastasis in fluorescent protein-expressing orthotopic lung, liver, pancreas, and colon cancer in nude mouse tumor models, as well as for intravital single-cell imaging. Sensitivity, multispectral capability, contrast, and single cell resolution were investigated. The Maestro system outperformed the OV100 for noninvasive imaging of primary and metastatic tumors. The Maestro system detected brain tumor metastasis five days earlier than did the OV100. Maestro had greater depth of detection compared with the OV100. By separating skin and food autofluorescence, Maestro provided high-contrast images. The Maestro system was able to produce composite images with more unmixed components and detected more different color signals simultaneously than did the OV100. However, the OV100 system had higher resolution and was able to detect single cells *in vivo*. The present study demonstrates that the two instruments are complementary for imaging of all stages of cancer in mice, including single-cell trafficking and that fluorescent-protein in vivo imaging is superior to luciferase photon counting.

AUTHORS (LAST NAME, FIRST NAME): Zhang, Yong[1]; Hiroshima, Yukihiko[1, 2]; Ma, Huaiyu[1]; Zhang, Nan[1]; Zhao, Ming[1]; Hoffman, Robert M.[1, 2]

INSTITUTIONS (ALL):

1. AntiCancer, Inc., San Diego, CA, United States.

2. Department of Surgery, University of California San Diego, San Diego, CA, United States.

(No Image Selected)

CONTROL ID: 2230782

TITLE: UVC irradiation cures metastatic human pancreatic cancer by killing residual disease remaining after fluorescence-guided surgery in orthotopic mouse models

PRESENTER: Robert Hoffman

ABSTRACT BODY:

Abstract Body: Fluorescence-guided surgery has shown to have important benefits but has not been curative. The aim of this study was to determine if ultraviolet light (UVC) irradiation in combination with fluorescence-guided surgery (FGS) can eradicate metastatic human pancreatic cancer in orthotopic nude–mouse models. Two weeks after orthotopic implantation of human MiaPaCa-2 pancreatic cancer cells, expressing green fluorescent protein (GFP), in nude mice, bright-light surgery (BLS) was performed on tumor-bearing mice. The residual tumors remaining after BLS were resected using a hand-held portable imaging system under fluorescence navigation. The surgical resection bed was irradiated with 2700 J/m^2 UVC (254 nm). The average residual tumor area after FGS was significantly smaller than after BLS only (0.135 ± 0.137 mm^2 and 3.338 ± 2.929 mm^2, respectively; $p = 0.007$). The BLS treated mice had significantly reduced survival compared to FGS- and FGS-UVC-treated mice for both relapse-free survival (RFS) ($p < 0.001$ and $p < 0.001$, respectively) and overall survival (OS) ($p < 0.001$ and $p < 0.001$, respectively). FGS-UVC-treated mice had increased RFS and OS compared to FGS-only treated mice ($p = 0.008$ and $p = 0.025$, respectively); with RFS lasting at least 150 days indicating the animals were cured. The results of the present study suggest that UVC is a powerful adjuvant therapy following FGS.

AUTHORS (LAST NAME, FIRST NAME): Hiroshima, Yukihiko[1, 2]; Maawy, Ali[2]; Zhang, Yong[1]; Bouvet, Michael[2]; Endo, Itaru[3]; Hoffman, Robert M.[1, 2]

INSTITUTIONS (ALL):

1. AntiCancer, Inc., San Diego, CA, United States.
2. Department of Surgery, University of California San Diego, San Diego, CA, United States.
3. Department of Gastroenterological Surgery, Yokohama City University Graduate School of Medicine, Yokohama, Japan.

(No Image Selected)

CONTROL ID: 2230766

TITLE: Individual chemosensitive and chemoresistant cancer cells distinguished by cell-cycle fate-monitoring in drug-treated heterogeneous populations demonstrated by real-time FUCCI imaging

PRESENTER: Robert Hoffman

ABSTRACT BODY:

Abstract Body: Tumor heterogeneity is currently an intractable obstacle for chemotherapy. The cell-cycle phase of a cancer cell determines in large part chemosensitivity or resistance. In the present study, we utilized the fluorescence ubiquitination-based cell cycle indicator (FUCCI) imaging system to investigate the correlation between cell-cycle behavior and apoptosis after treatment of cancer cells with chemotherapeutic drugs. HeLa cells expressing FUCCI were treated with doxorubicin (DOX) (5 μM) or cisplatinum (CDDP) (5 μM) for 3 h. Cell-cycle progression and apoptosis were monitored by time-lapse FUCCI imaging for 72 h. Time-lapse FUCCI imaging demonstrated that both DOX and CDDP could induce cell cycle arrest in $S/G_2/M$ in almost all the cells, but a subpopulation of the cells could escape the block and undergo mitosis. The subpopulation which went through mitosis subsequently underwent apoptosis, while the cells arrested in $S/G_2/M$ survived. The present results demonstrate that chemoresistant cells can be readily identified by FUCCI imaging in a heterogeneous population of cancer cells by $S/G_2/M$ arrest, which can serve in future studies as a visible target for novel agents that kill cell-cycle-arrested cells.

AUTHORS (LAST NAME, FIRST NAME): Miwa, Shinji[1, 2]; Yano, Shuya[1, 2]; Bouvet, Michael[2]; Fujiwara, Toshiyoshi[4]; Tsuchiya, Hiroyuki[3]; Hoffman, Robert M.[1, 2]

INSTITUTIONS (ALL):

1. AntiCancer, Inc., San Diego, CA, United States.
2. Department of Surgery, University of California San Diego, San Diego, CA, United States.
3. Department of Orthopaedic Surgery, Kanazawa University, Kanazawa, Japan.
4. Department of Gastroenterological Surgery, Okayama University Graduate School of Medicine, Okayama, Japan.

(No Image Selected)

CONTROL ID: 2230732

TITLE: Real-time fluorescence imaging of the DNA damage repair response during mitosis imaged in real-time by 53BP1-GFP focus formation

PRESENTER: Robert Hoffman

ABSTRACT BODY:

Abstract Body: DNA damage may occur during mitosis which may result in mitotic catastrophe. The response to DNA damage during mitosis of cancer cells was visualized using real-time fluorescence imaging of focus formation by the DNA-damage repair (DDR) response protein 53BP1 linked to green fluorescent protein (GFP) (53BP1-GFP) in MiaPaCa-2$^{Tet\text{-}On}$ pancreatic cancer cells. To observe 53BP1-GFP foci during mitosis, MiaPaCa-2$^{Tet\text{-}On}$ 53BP1-GFP cells were imaged every 30 min by confocal microscopy. Time-lapse imaging demonstrated that 11.4 $\pm$ 2.1% of the mitotic MiaPaCa-2$^{Tet\text{-}On}$ 53BP1-GFP cells had increased focus formation over time. Non-mitotic cells did not have an increase in 53BP1-GFP focus formation over time. Some of the mitotic MiaPaCa-2$^{Tet\text{-}On}$ 53BP1-GFP cells with focus formation became apoptotic. The results of the present report suggest that DNA strand breaks occur during mitosis and undergo repair demonstrated by 53BP1-GFP focus formation, which may cause some of the mitotic cells to enter apoptosis in a phenomenon possibly related to mitotic catastrophe.

AUTHORS (LAST NAME, FIRST NAME): Miwa, Shinji[1, 2]; Yano, Shuya[1, 2]; Efimova, Elena V.[3]; Bouvet, Michael[2]; Tsuchiya, Hiroyuki[4]; Hoffman, Robert M.[1, 2]

INSTITUTIONS (ALL):

1. AntiCancer, Inc., San Diego, CA, United States.
2. Department of Surgery, University of California San Diego, San Diego, CA, United States.
3. Ludwig Center for Metastasis Research, The University of Chicago, Chicago, IL, United States.
4. Department of Orthopaedic Surgery, Kanazawa University, Kanazawa, Japan.

(No Image Selected)

CONTROL ID: 2230960

TITLE: Experimental human breast cancer bone metastasis in nude mice is prevented by tumor-targeting *Salmonella typhimurium* A1-R

PRESENTER: Robert Hoffman

ABSTRACT BODY:

Abstract Body: High bone-metastatic variants of human breast cancer cells were selected in nude mice by cardiac injection whereby all untreated mice had experimental bone metastases compared to only 20% with parental cells. Treatment with tumor-targeting *Salmonella typhimurium* A1-R completely prevented experimental bone metastasis of the high metastatic variant in nude mice ($P < 0.001$). After injection of the highly bone-metastatic breast cancer variant to the tibia of nude mice, *S. typhimurium* A1-R treatment significantly reduced tumor growth in the bone ($P < 0.001$).

AUTHORS (LAST NAME, FIRST NAME): Miwa, Shinji[2, 4]; Yano, Shuya[1, 4]; Zhang, Yong[2]; Bouvet, Michael[4]; Tsuchiya, Hiroyuki[3]; Hoffman, Robert M.[2, 4]; Zhao, Ming[2]

INSTITUTIONS (ALL):

1. AntiCancer, San Diego, CA, United States.
2. AntiCancer, Inc., San Diego, CA, United States.
3. Department of Orthopedic Surgery, Kanazawa University, San Diego, CA, United States.
4. Department of Surgery, University of California San Diego, San Diego, CA, United States.

(No Image Selected)

CONTROL ID: 2230742

TITLE: Design and Syntheses of Novel Fluorescent and Biotinylated Tocopherol Probes

PRESENTER: Zhen-Dan Shi

ABSTRACT BODY:

Abstract Body: Niemann–Pick type C (NPC) is a lysosomal storage disease caused by mutations of the NPC1 and NPC2 genes, which results in accumulation of unesterified cholesterol in lysosomes by the malfunctions of NPC1 and NPC2 proteins. Currently there are no FDA-approved therapies for NPC. Recent studies showed that d-tocopherol effectively decreased lysosomal cholesterol accumulation, reduced lysosomal volume and alleviated NPC pathological phenotype, while it also increased cholesterol efflux. These results indicated that d-tocopherol would represent a new class of drugs for treating lysosomal storage disease. Preliminary studies show that d-tocopherol may be mediated through an induced intracellular Ca^{2+} response and subsequent increment of lysosomal exocytosis. In order to further investigate mechanisms of cell cholesterol trafficking, multiple new fluorescent tocopherol probes and biotinylated tocopherol probes were designed and synthesized by conjugation to different dyes and biotin. Some of the probes are cellular permeable and maintain pharmacological effects. The structural activity relationships we observed, on method and location of dye attachment, could lead to more specific compounds for the treatment of NPC, without some of the other side effects of d-tocopherol. Herein we present the detailed design, syntheses and biological testing results of the tocopherol probes.

AUTHORS (LAST NAME, FIRST NAME): Shi, Zhen-Dan[1]; Xu, Biying[1]; Griffiths, Gary[1]; Zheng, Wei[2]; Swenson, Rolf[3]

INSTITUTIONS (ALL):

1. National Heart, Lung, and Blood Institute, National Institutes of Health, Rockville, MD, United States.
2. National Center for Advancing Translational Sciences, National Institutes of Health, Rockville, MD, United States.
3. National Heart, Lung, and Blood Institute, National Institutes of Health , Rockville, MD, United States.

(No Image Selected)

CONTROL ID: 2230756

TITLE: Imaging Cellular Pharmacokinetics of ^{18}F-FDG in Inflammatory Cells

PRESENTER: Raiyan Zaman

ABSTRACT BODY:

Abstract Body: Objectives: Atherosclerosis is a progressive inflammatory condition that underlies coronary artery disease (CAD)—the leading cause of death in the USA and worldwide. Thus, understating the metabolism of inflammatory cells can be a valuable tool for investigating CAD. In this study, we imaged the pharmacokinetics of [^{18}F]fluoro-deoxyglucose (^{18}F-FDG) uptake into macrophages and compared with induced pluripotent stem cells (iPSCs) and mesenchymal stem cells (MSCs). A novel imaging technique, radioluminescence microscopy initially developed to image glucose uptake in single living cancer cell was used for the first time in this study to visualize radiotracer uptake in living cells of macrophage, iPSCs, and MSCs.

Methods: For imaging with this technique, live cells were cultured sparsely on Matrigel in a glass-bottom dish and starved for an hour before incubation with 250 µCi of ^{18}F-FDG radiotracer for 45 minutes. The cells were then washed with DMEM medium without glucose (3×1 mL) to remove excess radiotracer. Before imaging, DMEM (1 mL) was added to the cell culture and a 100 µm-thin $CdWO_4$ scintillator plate was placed on top of the cells. Light produced following beta decay was measured using a highly sensitive microscope (LV200, Olympus), with 300 ms exposure time, an inverted microscope fitted with a 40x/1.3 high-NA oil objective, and an electron-multiplying charge-coupled device (EM-CCD, Hamamatsu) cooled to -70˚C. The images were collected over 18000 frames with 4×4 binning and 1200 MHz EM Gain. These frames were collected over 90-99 minutes. Custom-written software developed in MATLAB was used for image processing. For each cell type, 20 different region-of-interests (ROIs) were selected to perform statistical analysis on the average observed decay in each cell.

Results: Figure 1A shows bright-field images for all three different cell types before ^{18}F-FDG was introduced. The corresponding fusion images (Figure 1B) were generated from 18000 frames. Although, there were significant variance identified in the average observed decay for all three cell lines, the relationship between cell-to-cell comparisons was found to be linear for macrophages unlike iPSCs and MSCs, which were best fitted with moving or rolling average (Figure 1C). The average observed decay of ^{18}F-FDG in a single cell of MSCs per second (0.067) was 20% and 36% higher compared to iPSCs (0.054) and macrophages (0.043), respectively (Figure 1D).

Conclusion: Although, all the parameters for these experiments were constant for each cell type examined, MSCs was found to be 2-3× more sensitive to glucose molecule. To the best of our knowledge, we are the first to successfully investigate the pharmacokinetics of ^{18}F-FDG in macrophages and stem cells using this novel imaging technique.

AUTHORS (LAST NAME, FIRST NAME): Zaman, Raiyan[1]; Tuerkcan, Silvan[2]; MAHMOUDI, Morteza[3]; Saito, Toshinobu[3]; Kosuge, Hisanori[3]; Yang, Phillip[3]; Chin, Frederick T.[4]; McConnell, Michael V.[3]; Xing, Lei[2]

INSTITUTIONS (ALL):

1. Departments of Medicine and Radiation Oncology, Stanford University School of Medicine, Stanford, CA, United States.
2. Department of Radiation Oncology, Stanford University School of Medicine, Stanford, CA, United States.
3. Department of Medicine, Stanford University School of Medicine, Stanford, CA, United States.
4. Department of Radiology, Stanford University School of Medicine, Stanford, CA, United States.

(No Image Selected)

CONTROL ID: 2230758

TITLE: Quantitative molecular imaging of ACL grafts by FDG PET/MRI

PRESENTER: Katherine Binzel

ABSTRACT BODY:

Abstract Body: Objectives: Injury to the anterior cruciate ligament (ACL) is common, particularly among young athletes. In cases of a complete tear, reconstruction with a graft is frequently performed to restore stability and function. The rate at which graft ligamentization occurs is not well delineated by magnetic resonance imaging (MRI). In a first-in-human study, we proposed and demonstrate the feasibility of an integrated quantitative molecular and morphologic imaging approach to evaluate whether combined MR imaging with dynamic positron emission tomography (PET) data could provide insight into the graft healing process following reconstructive surgery.

Methods: 10 patients post-ACL graft reconstruction underwent standard of care MRI on a Philips 3T Achieva (Cleveland, OH). Proton density and T1 weighted sequences were acquired on all three planes, with a 3D high resolution image acquired on the sagittal plane. Patients were grouped according to time since surgery, 0-6 months, 6-12 months, 12-24 months, and 24 months or greater. Dynamic PET was acquired on a Philips Gemini TF 64 (Cleveland, OH). An in-house fabricated foam device was used to place both knees in an identical position to that of the dedicated MRI knee coil. A single bed position centered on the knees was acquired continuously for 75 minutes, with an average injection of 111 MBq ^{18}F-fluorodeoxyglucose (FDG) occurring 15-30 seconds into the acquisition. PET images were co-registered to the MRI for quantification. Regions of interest (ROIs) were placed over the proximal, middle, and distal portions of the graft, in the femoral and tibial tunnels, and in the posterior cruciate ligament (PCL) and quadriceps muscle for reference. Matched ROIs were drawn in the contralateral knee. Dynamic maximum standardized uptake values (SUV_{max}) were measured on 5 minute frames and a static SUV_{max} was measured on images reconstructed as a 15 minute frame from 60-75 minutes post-injection.

Results: Dynamic PET images were readily co-registered to MRI series for all patients. In the 0-6 month group, the average slope of the metabolic uptake curve was 0.14 in the distal graft, 0.22 in the mid graft, 0.29 in the proximal graft, and 0.27 in the femoral tunnel. In the 24+ month group the averages were 0.06, 0.05, 0.07, and 0.03, respectively. The SUV_{max}'s of the ROIs approached healthy values with increased time since surgery. The average SUV_{max} of each time group can be seen in Table 1. The patients with longer recovery times were again seen to have SUVs more comparable to those in healthy knees than those who had more recently had ACL repair.

Conclusions: Metabolic PET imaging of the ACL and surrounding tissues enables quantitative evaluation of ligamentization and graft healing. In dynamic imaging, the rate of FDG uptake in the graft and bone tunnels appears to correlate with time since surgery; as did the SUV_{max} measured at 75 minutes post-injection. The proposed PET/MRI approach appears to be a promising molecular imaging methodology to assess the viability of ACL grafts.

AUTHORS (LAST NAME, FIRST NAME): Binzel, Katherine[2]; Kaeding, Christopher[1]; Flanigan, David C.[1]; Magnussen, Robert A.[1]; Knopp, Michelle I.[2]; Wei, Wenbo[2]; Knopp, Michael V.[2]

INSTITUTIONS (ALL):

1. Sports Medicine, The Ohio State University Wexner Medical Center, Columbus, OH, United States.
2. Wright Center of Innovation, The Ohio State University Wexner Medical Center, Columbus, OH, United States.

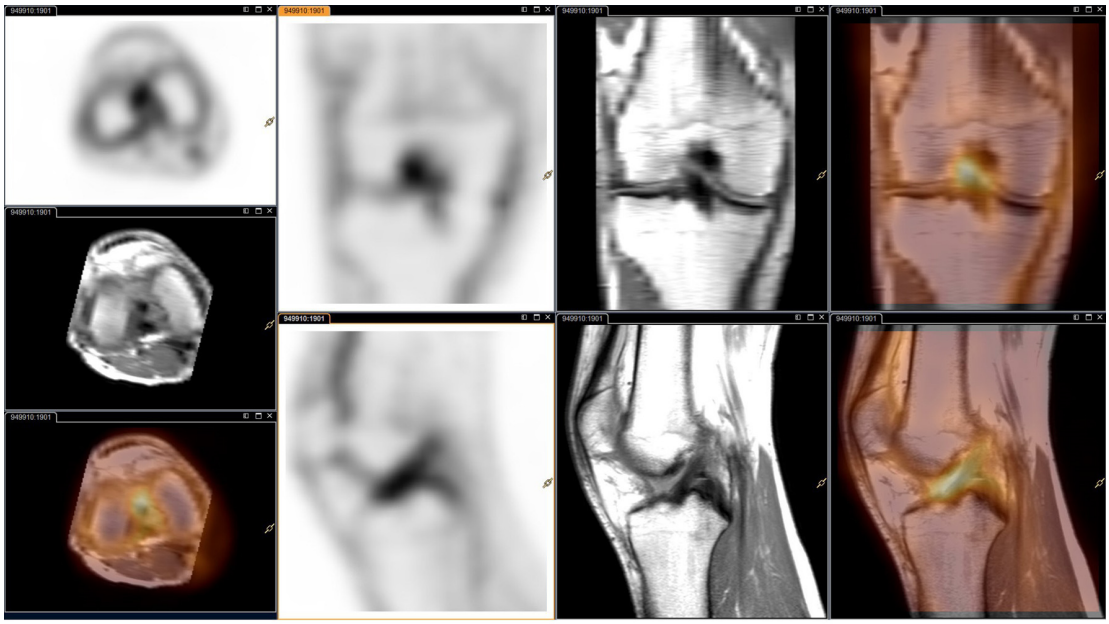

Image 1: Co-registered PET and MRI for dynamic evaluation of ACL graft and bone tunnel uptake, focused on the area of the graft, showing marked metabolic uptake less than 6 months post-reconstructive surgery.

CONTROL ID: 2245144

TITLE: Molecular Imaging to assess and monitor tissue proliferation by 18F-FLT PET/CT during investigational Breast Cancer Therapy

PRESENTER: Michael Knopp

ABSTRACT BODY:

Abstract Body: Objectives:

To demonstrate the utility of 3'-deoxy-3'[^{18}F]-fluorothymidine (FLT) as a non-invasive PET/CT imaging biomarker of cellular proliferation to characterize breast tumors and monitor changes during investigational therapy. Additionally, to assess the appropriate quantification approach and observable changes in bone marrow and liver during therapy.

Methods: FLT-PET/CT was performed using a 370 MBq /10 mCi target dose at baseline (BL), day 7 (F1), day 14 (F2) and after three cycles (F3) of an investigational breast cancer therapy. A dynamic acquisition of 45 min over the target region was performed prior to whole body PET/CT imaging. A Gemini 64 TF PET/CT (Philips Healthcare, Cleveland) was acquired as part of a comprehensive investigational protocol. 28 patients had complete FLT imaging data sets at the four imaging time points. An intraindividual comparison assessment to FDG PET/CT was also available for the examination at baseline and after three cycles (F3). The images were visually and quantitatively analyzed by ROI by three blinded, independent readers. A separate analysis was performed on the lumbar spine at the location of L1, L3 and L5 as well as of the liver to assess the proliferation activity.

Results: A total of 112 FLT-PET/CT exams were performed from 28 patients undergoing investigational breast cancer therapy. All imaging studies had satisfactory image quality and were acquired according to protocol. No adverse event occurred nor did we identify unforeseen imaging findings. Statistically significant changes ($p<0.01$) in FLT uptake were noted between baseline and day 7 (F1) follow up. Comparing the changes between baseline and post cycle 3 between FLT and FDG PET/CT reveal a consistent trend. Standard 3D ROI placement was impacted in > 20% of FLT lesions assessments due to strong and physiologic bone marrow or liver uptake. Based on those findings, several modified assessment and quantification approaches were explored and found to be feasible. A quantitative bone marrow assessment was semi-automated and revealed changes consistent with hemopoetic markers. A strong concordance between the three vertebrae was found unless there was malignant bone marrow infiltration.

Conclusions: 18F-FLT PET/CT appears to be a feasible methodology to assess and monitor proliferative biologic activity in breast cancer lesions and the RES. The proliferative activity and its change during therapy revealed a heterogenous pattern of lesions and lymphnodes. Due to different biodistribution than the commoly used FDG, both the visual approach to reading and qualitative as well as the most effective quantitative analysis had to be refined. The demonstrated capabilities and assessment approaches indicate that FLT PET/CT can be used for early monitoring of biologic activity in breast cancer response assessment of lesions as well as the RES.

AUTHORS (LAST NAME, FIRST NAME): Knopp, Michael V.[1]; Binzel, Katherine[1]; Lan, Xiaoli[1]; Subramanian, Preethi[1]; Bhatia, Prayna[1]; Hall, Nathan[1]; Ramaswamy, Bhuvaneswari[2]; Zhang, Jun[1]

INSTITUTIONS (ALL):

1. Wright Center of Innovation, The Ohio State University Wexner Medical Center, Columbus, OH, United States.
2. Division of Medical Oncology, The Ohio State University Comprehensive Cancer Center, Columbus, OH, United States.

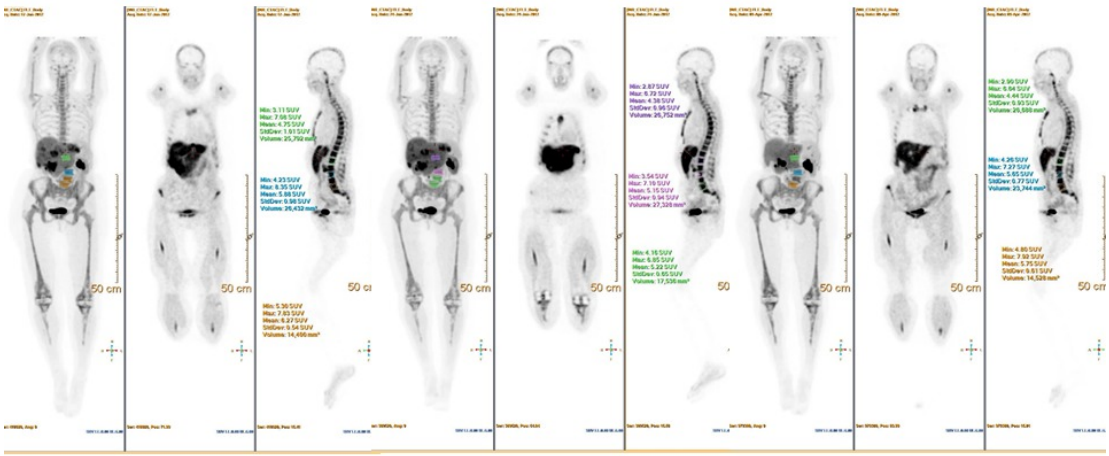

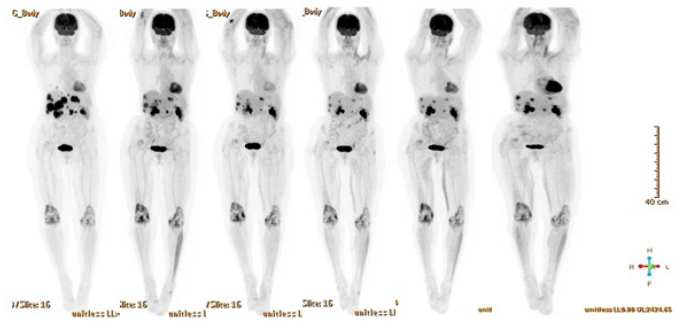

^{18}FLT-PET/CT above displayed at baseline, F1 and F3 using a semi automated methodology to assess the proliferation in the bone marrow of L1,L3 and L5.

On the left, long term FDG follow up in this patient with initial response to therapy

CONTROL ID: 2243603

TITLE: Feasibility of ultra-low dose FDG PET imaging for nutrition and metabolism studies and beyond

PRESENTER: Michelle Knopp

ABSTRACT BODY:

Abstract Body: Objectives: In vivo visualization and objective quantification of specific tissues such as brown adipose tissue (BAT) is highly desirable for nutrition and metabolism studies. However, current clinical FDG doses (avg. 480 MBq / 13 mCi) lead to undesirable radiation exposure levels for such uses. We therefore embarked upon a methodology development to perform ultra-low dose FDG PET/CT imaging for such applications.

Methods: As part of a clinical study, we performed low dose (avg. 93 MBq / 2.5 mCi) FDG PET/CT studies on 18 subjects using a Gemini 64 time of flight PET/CT system (Philips Healthcare, Cleveland). In order to activate BAT, the subjects were exposed to cold temperatures for 2 hours. All acquisitions were performed with 360 s per bed/ volume position 60 to 70 min p.i. and in list mode which enables the subsampling to simulate lower count densities or dosing levels. Data sets were additionally reconstructed using only 240s, 120s, 90s, 60s and 15s list mode events representing dose reductions by 33%, 66%, 75%, 83% and 96%. The images were visually and quantitatively analyzed by ROI by three blinded, independent readers. A receiver operator curve (ROC) was determined for each case, reader and cumulative.

Results: The blinded assessment concluded that a 66% dose reduction from the 93 MBq / 2.5 mCi could be implemented without impact on visual or quantitative assessment thereby facilitating an effective dose requirement of only 30 MBq / 0.8 mCi FDG on current generation systems and using current reconstruction approaches. Based on investigational work using the next generation solid state detector PET system, we were able to further simulate that a dose of 15 MBq 0.4 mCi appears achievable for ultra-low dose PET. This can be combined also with ultra-low dose attenuation CT using <50mAs and potentially also with no CT attenuation scanning.

Conclusions: Ultra-low dose FDG PET imaging to assess metabolism of tissue such as brown adipose tissue has been demonstrated to be possible at 30 MBq / 0.8 mCi FDG on current generation systems and are predicted to be possible at 5-15 MBq / 0.1 - 0.4 mCi on new solid state digital detector system potentially also without CT attenuation scanning. This paves the way for innovative and safe use of FDG PET for nutrition and metabolism evaluations in health population studies. These findings further support the exploration of lowering clinical FDG dosing schedules as these have not kept up with improvements of PET modalities.

AUTHORS (LAST NAME, FIRST NAME): Knopp, Michelle I.[1, 2]; Zhang, Jun[1]; Binzel, Katherine[1]; Lan, Xiaoli[1]; Cole, Patricia[1]; Hall, Nathan[1, 3]; Knopp, Michael V.[1]

INSTITUTIONS (ALL):

1. Wright Center of Innovation, The Ohio State University Wexner Medical Center, Columbus, OH, United States.
2. College of Medicine, The Ohio State University, Columbus, OH, United States.
3. Radiology, University of Pennsylvania, Philadelphia, PA, United States.

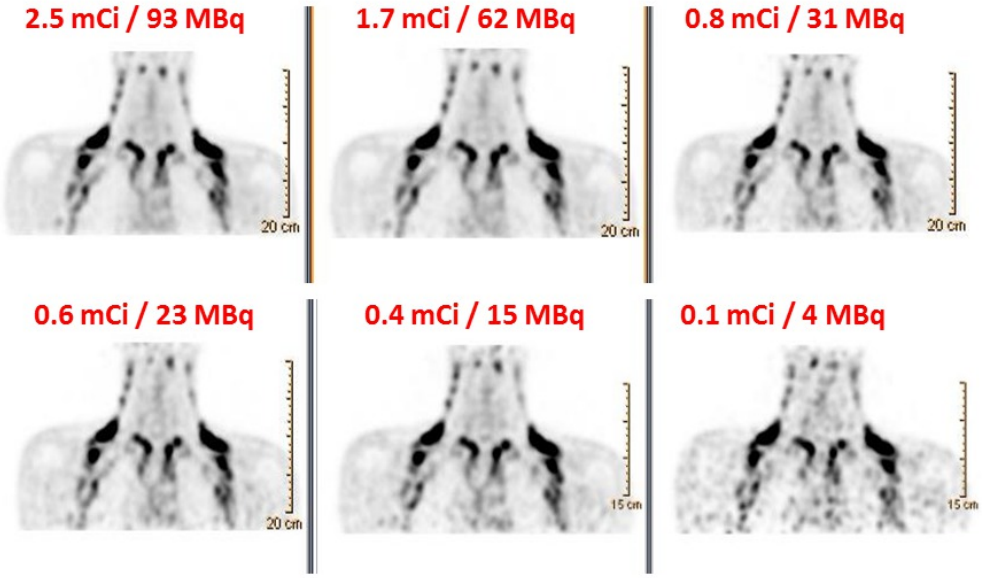

18F-FDG PET/CT Dose simulation by segmented reconstruction of the 2.5mCi / 93 MBq BAT acquisition. Image quality was not affected as determined by blinded review up to a dose of 0.8 mCi / 31 MBq. Lower doses appear even feasible with modified reconstruction approaches.

CONTROL ID: 2234354

TITLE: First clinical experience of solid state digital PET/CT in oncologic FDG imaging

PRESENTER: Michael Knopp

ABSTRACT BODY:

Abstract Body: Objectives:

To present first clinical experience of the next generation digital PET/CT in clinical oncologic ^{18}F-FDG PET/CT imaging evaluated by intra-individual comparison with current photomultiplier TOF PET/CT.

Methods:

A next generation, solid state, digital PET/CT system (Vereos, Philips Healthcare, Cleveland) operating in pre-factory release, investigational Phase I mode was used to compare imaging characteristics in 25 clinical care patients to current photomultiplier detector based time of flight PET/CT. Standard of care (SOC) imaging was performed at 75 min with the investigational digital imaging at 55 or 95 min p.i.. Image characteristics were assessed by three blinded readers using a scoring system and blinded quantitative ROI analysis. CT attenuation scans were acquired using 120KV, 50 mAS using iterative iDose4 reconstruction. PET emission was acquired with 90s per bed position and all image data sets were reconstructed using TOF with different voxel volumes 64mm^3 (4x4x4) or 8mm^3 (2x2x2) using point spread function (PSF) with Gaussian filtering.

Results:

All matched exams were rated evaluable with decay corrected higher count intensity on all digital PET images. Image quality and detection ability was consistently rated significantly higher ($p<.01$) on the digital PET images. Comparing different reconstruction approaches, 2mm whole body, PSF with Gaussian filtering achieved the highest image quality score. The confidence of lesion detection increased on the digital PET/CT exams with decreased voxel volume, with significant ($p\leq0.05$) improved lesion characterization between the conventional and digital PET acquisitions. Most pronounced differences were noted in small and intense lesions such as pulmonary and lymph node metastases.

Conclusions:

Our first in human Phase I trial of the next generation digital PET/CT system demonstrated higher count sensitivity, improved spatial and contrast resolution that led to better lesion detection and improved quantification of small, metabolic active lesions. Digital PET/CT appears to advance visual and quantitative capabilities in oncologic PET and improves our ability to detect and characterize. The improved capabilities appear to lead to higher resolution oncologic PET imaging, better quantitative precision and potentially substantially lower tracer doses than currently being used for standard of care, all important aspects to further advance clinical molecular PET imaging.

AUTHORS (LAST NAME, FIRST NAME): Knopp, Michael V.[1]; Zhang, Jun[1]; Binzel, Katherine[1]; Bardos, Philip[1]; Knopp, Michelle I.[1]; Wright, Chadwick L.[1]; Nagar, Veena[1]; Maniawski, Piotr[2]

INSTITUTIONS (ALL):

1. Wright Center of Innovation, The Ohio State University Wexner Medical Center, Columbus, OH, United States.
2. Philips Healthcare, Cleveland, OH, United States.

Table 1: Differences in detector elements and further characteristics between the first generation digital TOF PET/CT system and current PMT detector-based systems.

	Vereos	Gemini TF 64
Detectors	Direct Photon Counting	PMT Anger Logic
Crystal Material	LYSO	LYSO
Crystal Size (mm)	4 x 4 x 19	4 x 4 x 22
# of Detector	23,040	420 PMT
Crystal - Detector Coupling	1 : 1	multi : multi
Transaxial FOV (cm)	57.6 (up to 67.6)	57.6 (up to 67.6)
Axial FOV (cm)	16.4	18
Energy resolution (%)	11	11.7
Energy calibration	1 : 1	multi : multi
Timing Resolution (ps)	320	550
Timing Calibration	1 : 1	multi : multi
NEMA NU 2 Spatial Resolution		
Transverse at 1 cm (mm FWHM)	4.1	4.7
Tangential at 10 cm (mm FWHM)	4.5	5.2
Radial at 10 cm (mm FWHM)	4.5	5.2
Axial at 1 cm (mm FWHM)	4.1	4.7
Axial at 10 cm (mm FWHM)	4.3	5.2
NEMA NU 2 Sensitivity at center of FOV (kcps/MBq)	NA	7
Time-of-Flight Effective True Count Rate (kcps)	>3,500 at 60kBq/mL	<500 when >20kBq/mL

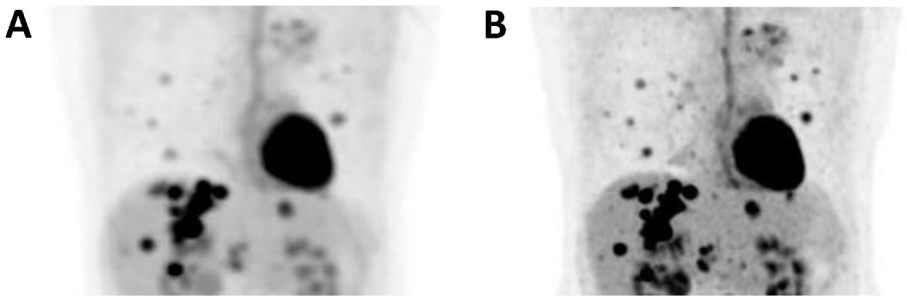

Figure 1: Intra-individual comparison between (A) PMT Gemini PET and (B) digital Vereos PET of a patient with extensive metastatic disease. The lesion conspicuity as well as lesion detection in the lung and liver is considerably improved in the digital PET.

CONTROL ID: 2233652

TITLE: Optimization of tri-contrast microCT for detection of colon lesions in a longitudinal murine model

PRESENTER: Michelle Williams

ABSTRACT BODY:

Abstract Body: Objectives : Investigate and improve evaluation of longitudinal colorectal tumor burden in-vivo utilizing clinically available exogenous as well as endogenous contrast.

Methods : The tumor bearing animals were given a soft, high calorie diet (Clear H2O Diet Gel Boost) doped with barium sulphate (8% by mass EZpaste) twenty-four hours prior to an overnight fast. Immediately prior to scanning, an intraperitoneal (IP) injection of 1 mL iohexol (300 mg/cc 20% dilution by volume in isotonic saline) was administered. The IP injection was immediately followed by inhaled anesthesia induction of 2% vaporized isoflurane. Lying supine on a thermal pad, the subject had 2 mL of air delivered rectally. This was accomplished using surgilube, a sterile 18 G gavage needle on a 3mL luer lock syringe, and very minimal penetration (no more than 0.5 cm). The plunger was depressed in three to four increments of its full travel followed by abdominal massage to distribute the air evenly. The animal was then transferred to the microCT for a quick high resolution scan.

Results : Provided are three views of intestine where the lumen was quite visibly deliniated either between air and injected/ingested contrast (red) or ingested contrast and injected contrast (green). The food contents (yellow) show up quite nicely throughout the entire tract and should be easily discerned from possible lesions.

Conclusions : The introduced methodology allows for easier lesion identification and quantification via microCT without inducing physiologic ileus. This use of contrast allows for discrimination of fecal material, invaginations, lesions and local thickening of the intestinal wall within the lumen as well as the intraperitoneal space. The dilution sets of contrast were the most recently optimized compromise for reduction of beam hardening artifacts, motion, and resolution.

AUTHORS (LAST NAME, FIRST NAME): Williams, Michelle M.[1]; Briley, Karen[1]; Knopp, Michael V.[1]

INSTITUTIONS (ALL):

1. Wright Center of Innovation, The Ohio State University, Columbus, OH, United States.

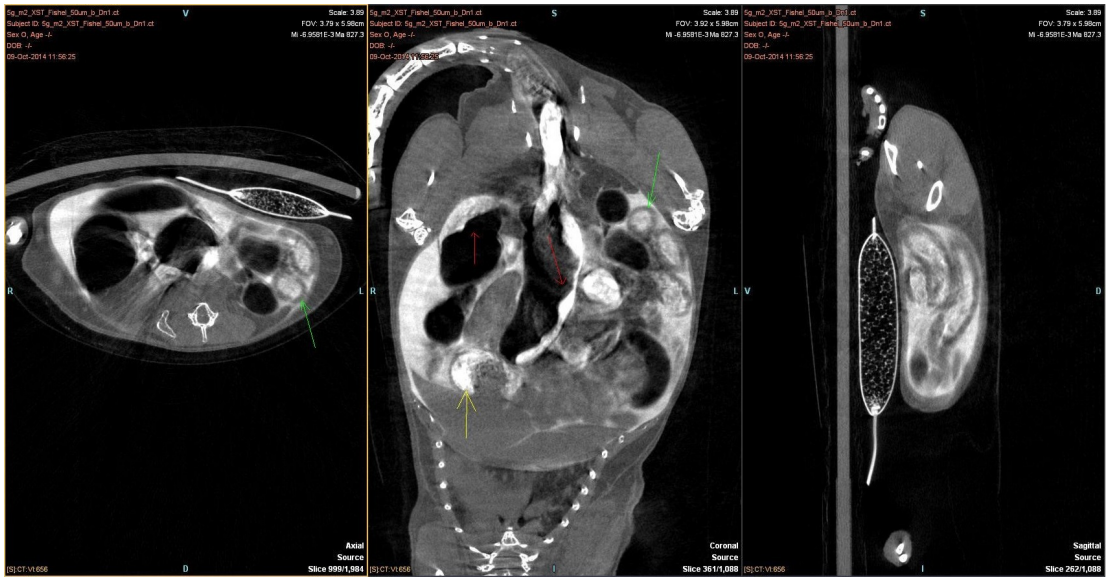
Sg_m2_XST_Fishel_50um_b_Dn1.ct
Subject ID: Sg_m2_XST_Fishel_50um_b_Dn1.ct
Sex O, Age -/-
DOB -/-
09-Oct-2014 11:56:25
Scale: 3.89
FOV: 3.79 x 5.98cm
MI -6.9581E-3 Ma 827.3
Axial
Source
Slice 999/1,984
Coronal
Source
Slice 361/1,088
Sagittal
Source
Slice 262/1,088

CONTROL ID: 2232782

TITLE: ^{18}F-Labeled thymidine analogues as potent and selective PET probes for imaging of human mitochondrial thymidine kinase.

PRESENTER: Kai Chen

ABSTRACT BODY:

Abstract Body: Objectives: In an effort to increase the potency and selectivity of substrate-based probes of human mitochondrial thymidine kinase 2 (TK-2), we reported the design, synthesis, and biological evaluation of new ^{18}F-labeled thymidine analogues.

Methods: Molecular modeling techniques were used to simulate the interaction-binding between a series of thymidine analogues and the homology-based model of TK-2. The potent candidates, having favorable binding modes, were selected, synthesized, and characterized. The potency and selectivity of new thymidine analogues were measured by enzyme based assays. The lead compounds were radiolabeled with ^{18}F and subject to biological evaluations.

Results: Molecular modeling data suggested that the new thymidine analogues, containing a 1,2,3-triazol-1-yl substituent at the 3'-position of the 2'-deoxyribofuranosyl ring, occupy the substrate-binding site in a TK-2−ATP complex. These analogues were successfully prepared by Cu-catalyzed cycloadditions of 3'-azido-3'-deoxythymidine and the appropriate alkynes. Selected analogues showed nanomolar binding activity for TK-2, while minimally affecting thymidine kinase 1 (TK-1). The ^{18}F labeling of new analogues was achieved by using click chemistry approach. The cellular uptake studies revealed that the new ^{18}F-labeled thymidine analogues strongly bind to A549 lung cancer cells.

Conclusions: A rational approach to the design and synthesis of new radiolabeled thymidine analogues is being advanced. Molecular modeling techniques aid in the selection of agents that have good binding potency and selectivity for TK-2. The approach is general and can be applied to the development of other diagnostic and therapeutic radiopharmaceuticals for specific enzyme and receptor.

Research Support: This work was supported by the SNMMI Mitzi & William Blahd Research Grant, the Whittier Grant for Translational Research, and the USC Department of Radiology.

AUTHORS (LAST NAME, FIRST NAME): Chen, Kai[1]; Zhu, Yizhou[1]; Huang, Rui[1]; Yap, Li-Peng[1]; Conti, Peter S.[1]

INSTITUTIONS (ALL):

1. Radiology, University of Southern California, Los Angeles, CA, United States.

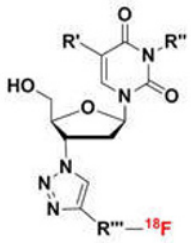

Thymidine Analogues	Ki (μM)	
	TK-2	TK-1
FMAU	4.9 ± 0.3	70 ± 4
T07	0.017 ± 0.001	192.2 ± 8.0

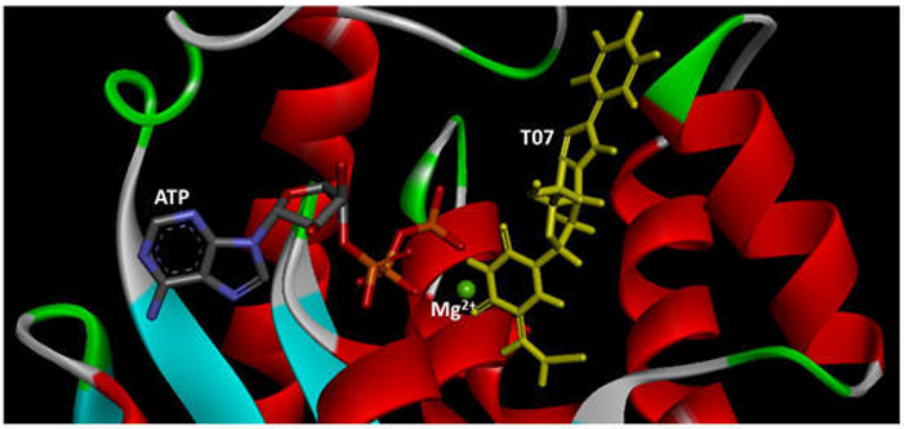

Figure 1. Development of ^{18}F-labeled thymidine analogues as potent and selective PET probes for imaging of human mitochondrial thymidine kinase.

CONTROL ID: 2232865

TITLE: Monitoring tumor response to chemotherapy by near-infrared fluorescence imaging of cell death using PSVue-T-643.

PRESENTER: Kai Chen

ABSTRACT BODY:

Abstract Body: Objectives: Anionic phosphatidylserine (PS) exposure is one of the most ubiquitous fingerprints of dying cells, making it an attractive target for molecular imaging. This study aims to utilize near-infrared fluorescence imaging (NIRF) with a molecular probe (PSVue-T-643) to visualize and evaluate PS expression during chemotherapy treatment in a mouse tumor model.

Methods: *In vitro* confocal microscopy study was performed to determine the binding of PSVue-T-643 to human glioblastoma U87MG cells with or without treatment of 10 nM paclitaxel for 16 h. The expression level of cleaved caspase-3 was evaluated by western blot analysis. Subcutaneous U87MG xenograft mouse model was selected for *in vivo* optical imaging. PSVue-T-643 (12.5 nmol) was administrated *via* tail vein for each mouse before and after the paclitaxel treatment (45 mg/kg) at Day 2 and 5. *In vivo* optical imaging was performed at various post-injection time points. The tumor, major tissues, and organs were dissected and subjected to *ex vivo* fluorescence imaging.

Results: Confocal microscopy demonstrated enhanced binding of PSVue-T-643 to paclitaxel-treated U87MG cells as compared to the untreated group. The western blot analysis showed that cleaved caspase-3 was increased significantly after treatment, suggesting that paclitaxel induced apoptosis in U87MG cells. *In vivo* NIRF imaging showed the maximum tumor uptake of PSVue-T-643 was at 4 h pi. At Day 0, 2, and 5 of treatment, the tumor-to-muscle (T/M) ratio of PSVue-T-643 at 4 h pi was calculated to be 1.25±0.35, 1.65±0.51, and 3.65±0.62, respectively. The results from *ex vivo* imaging were consistent with the *in vivo* findings. TUNEL assay confirmed that significantly more tumor cell death was observed in the tumor sections from the treated group as compared to the untreated group.

Conclusions: PSVue-T-643 has been successfully applied for visualization and quantification of PS expression. The optical imaging with PSVue-T-643 provides highly sensitive and target-specific evaluations of cell death associated with tumor response to chemotherapy.

Research Support: This work was supported by the Robert E. and May R. Wright Foundation and the USC Department of Radiology.

AUTHORS (LAST NAME, FIRST NAME): Chen, Kai[1]; Huang, Rui[1]; Ma, Wenhui[1]; Gray, Brian D.[2]; Pak, Koon Y.[2]; Conti, Peter S.[1]

INSTITUTIONS (ALL):

1. Radiology, University of Southern California, Los Angeles, CA, United States.
2. Molecular Targeting Technologies, Inc., West Chester , PA, United States.

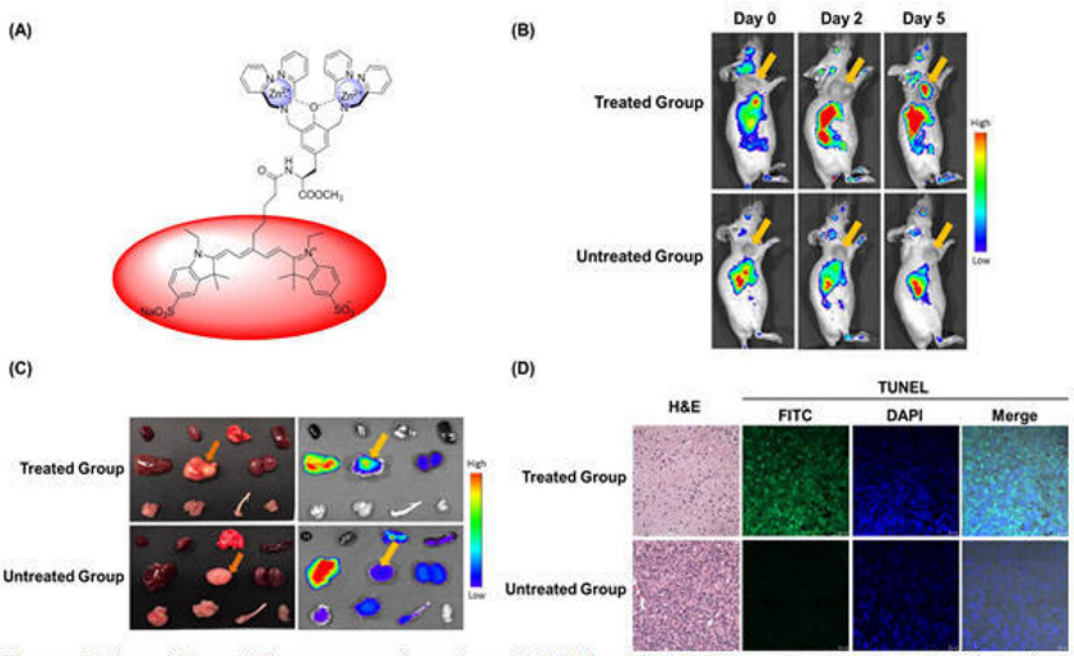

Figure 1. Near-infrared fluorescence imaging with PSVue-T-643 for monitoring phosphatidylserine-targeted cell death induced by chemotherapy. **(A)**: Chemical structure of PSVue-T-643. **(B)**: Fluorescence imaging of subcutaneous U87MG tumor-bearing nude mice at Day 0, 2, and 5 after paclitaxel treatment (45 mg/kg). The images were shown at 4 h pi of PSVue-T-643 (12.5 nmol). Tumors are indicated by arrows. **(C)**: *Ex vivo* fluorescence imaging of U87MG tumor and normal tissues with PSVue-T-643 in treated and untreated groups at 4 h pi on Day 5 after treatment. Tumors are indicated by arrows. **(D)**: H&E (Magnification 40×) and TUNEL staining (Magnification 63×; Scale bar: 20 μm) of tumor sections from the treated and untreated groups on Day 5 after treatment.

CONTROL ID: 2232845

TITLE: PET imaging with a novel phosphatidylserine-targeted molecular probe for monitoring cell death induced by chemotherapy.

PRESENTER: Kai Chen

ABSTRACT BODY:

Abstract Body: Objectives: This study aimed to apply PET imaging with a novel DPA-containing probe (^{18}F-PSVue-T) to evaluate cell death induced by paclitaxel in a U87MG tumor xenograft model.

Methods: The tyrosine-containing DPA derivative was conjugated with a dibenzocyclooctyne (DBCO) moiety to provide a precursor, which was then mixed with an ^{18}F-labeled azide synthon (^{18}F-N_3) to afford ^{18}F-PSVue-T via catalyst-free click chemistry. Established U87MG tumors in nude mice were treated daily with a combination of All-Trans Retinoic Acid (ATRC) (1.5 μg/kg) and paclitaxel (45 μg/kg). Longitudinal PET imaging was performed with ^{18}F-PSVue-T before treatment and at Day 3, 6, and 9 after treatment. Following PET imaging, a direct tissue biodistribution study was performed to confirm the accuracy of PET quantification. H&E staining and TUNEL assay were performed on the tumor sections to evaluate tumor morphology and apoptosis.

Results: The total synthesis time for ^{18}F-PSVue-T was about 120 min. The decay-corrected radiochemical yield was 28±5% (n = 6). For cellular uptake studies, about 4.16% of ^{18}F-PSVue-T uptake in paclitaxel-treated U87MG cells was determined after 1 hr incubation, which is significantly higher than the 2.62% (p<0.05) observed for untreated cells, suggesting that ^{18}F-PSVue-T specifically binds to the apoptotic and necrotic cells. Daily treatment with ATRC and paclitaxel effectively inhibited the growth of U87MG tumors by inducing cell death and cell death was clearly visualized by ^{18}F-PSVue-T PET. The tumor uptake, which was observed at Day 9 after treatment, was significantly higher than that in the untreated tumors (3.93±0.38 vs. 1.21±0.25%ID/g, p<0.05) at 2 h post-injection. The biodistribution results were consistent with the quantitative analysis of PET imaging. TUNEL assay confirmed that extensive tumor cell death was observed in the tumor sections from the treated group, whereas tumor cell death remained at a minimal level in the untreated group.

Conclusions: PET imaging with ^{18}F-PSVue-T is sensitive enough to allow visualization of paclitaxel induced cell death in a U87MG tumor xenograft model. Fully quantitative imaging of tumor response to therapy with ^{18}F-PSVue-T may provide early assessment of cancer treatment efficacy leading to individually tailored therapeutic plans with improved outcomes.

Research Support: This work was supported by the Robert E. and May R. Wright Foundation and the USC Department of Radiology.

AUTHORS (LAST NAME, FIRST NAME): Chen, Kai[1]; Huang, Rui[1]; Ma, Wenhui[1]; Gray, Brian D.[2]; Pak, Koon Y.[2]; Zhu, Yizhou[1]; Liu, Zhenwei[1]; Conti, Peter S.[1]

INSTITUTIONS (ALL):

1. Radiology, University of Southern California, Los Angeles, CA, United States.
2. Molecular Targeting Technologies, Inc., West Chester , PA, United States.

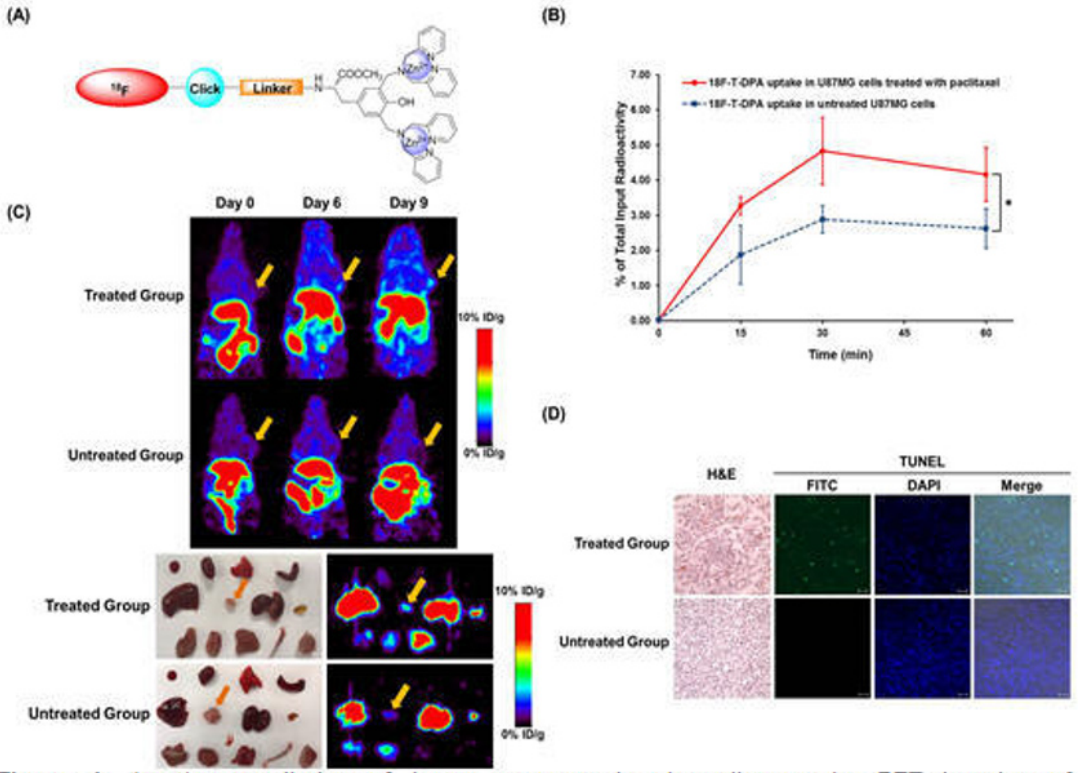

Figure 1. *In vivo* monitoring of tumor response to chemotherapy by PET imaging of phosphatidylserine exposure using ^{18}F-PSVue-T. **(A)**: Schematic representation of ^{18}F-PSVue-T. **(B)**: Cellular uptake assay: time-dependent uptake of ^{18}F-PSVue-T in untreated and treated U87MG (25 nM of paclitaxel for 16 h) (n = 3, mean ± SD). **(C)**: (TOP) Decay-corrected whole-body coronal microPET images of nude mice bearing U87MG tumor (n = 6/group) at 2 h post-injection of ^{18}F-PSVue-T (7.4 MBq) before and after the daily combination treatment of All-Trans Retinoic Acid (ATRC) (1.5 µg/kg) and paclitaxel (45 µg/kg), with tumors indicated by arrows. (Bottom) *Ex vivo* microPET imaging of U87MG tumor and normal tissues with ^{18}F-PSVue-T (7.4 MBq) after euthanizing the mice at 4 h pi. **(D)**: H&E and TUNEL staining of tumor sections from the treated and untreated groups on Day 9 post-treatment (Magnification 40×; Scale bar: 20 µm).

CONTROL ID: 2232836

TITLE: Screening thymidine analogues as potent and selective PET probes of human thymidine kinases.

PRESENTER: Kai Chen

ABSTRACT BODY:

Abstract Body: Objectives: The aim of this study was to develop a methodological platform for the screening of novel thymidine analogues that can be used as PET probes targeted to the measurement of thymidine kinase level in tumor proliferation.

Methods: Human recombinant TK-1 and TK-2 protein were expressed in *E. coli* as fusion protein containing an *N*-terminal His-tag and a thrombin cleavage site, and purified by using metal affinity chromatography. Kinetic binding parameters of thymidine analogues (FMAU as a control) were determined by using a phosphotransferase assay with ^{32}P-ATP as a labeled substrate. The data were fitted into the Michaelis-Menten equation. The K_m, V_{max}, and k_{cat} values were calculated using subunit molecular weight of the enzymes. Inhibition assays were performed using the DE-81 filter paper with ^{3}H-dT as a substrate. The mode of inhibition and K_i values were derived from the Dixon plots.

Results: The specific activity of TK-1 and TK-2 was measured to be 2637±132 and 1872±95 nmol/min/mg, respectively. The phosphotransferase assay showed that FMAU is a substrate for both TK-1 (K_m=32.5±1.2μM) and TK-2 (K_m=72.3±3.7μM), whereas a new thymidine analogue (T07) is a good substrate of TK-2 (K_m=44.6±5.0μM) but not TK-1. As determined by the inhibition assay, FMAU inhibited the phosphorylation of ^{3}H-dT for both TK-1 (Ki=70±4μM) and TK-2 (K_i=4.9±0.3μM). However, T07 showed excellent potency and selectivity for TK-2. T07 was determined to be an uncompetitive inhibitor of ^{3}H-dT for TK-1 (K_i=192.2±8μM), and an excellent inhibitor for TK-2 (K_i =0.017±0.001μM).

Conclusions: A reliable and efficient method for the screening of thymidine analogues has been successfully developed. The hits identified from the assays can be used as PET probes for specifically measuring thymidine kinase level in tumor proliferation.

Research Support: This work was supported by the SNMMI Mitzi & William Blahd Research Grant, the Whittier Grant for Translational Research, and the USC Department of Radiology.

AUTHORS (LAST NAME, FIRST NAME): Chen, Kai[1]; Huang, Rui[1]; Yap, Li-Peng[1]; Conti, Peter S.[1]

INSTITUTIONS (ALL):

1. Radiology, University of Southern California, Los Angeles, CA, United States.

(A)

Kinetic Parameters of FMAU and T07 with TK-1 and TK-2

Thymidine Analogues	TK-1			TK-2		
	K_m (μM)	V_{max} (nmol/min/mg)	k_{cat} (s^{-1})	K_m (μM)	V_{max} (nmol/min/mg)	k_{cat} (s^{-1})
FMAU	32.5 ± 1.2	99 ± 6	0.045±0.003	72.3 ± 3.7	255.4 ± 5.8	0.12±0.003
T07	ND	ND	ND	44.6 ± 5.0	17.3 ± 4.1	0.008±0.002

ND: No detectable activity.

(B)

Inhibitory effect of FMAU and T07 on dT phosphorylation by TK-1 and TK-2

Thymidine Analogues	TK-1		TK-2	
	K_i (μM)	Mode of inhibition	K_i (μM)	Mode of inhibition
FMAU	70 ± 4	Competitive	4.9 ± 0.3	Competitive
T07	192.2 ± 8.0	Uncompetitive	0.017 ± 0.001	Competitive

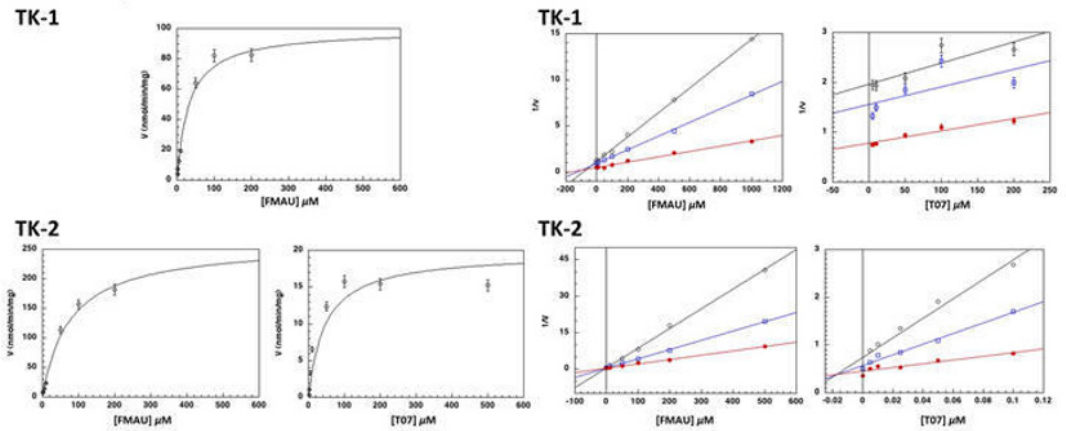

Figure 1. Development of biological assays for screening thymidine analogues as potent and selective PET probes of human thymidine kinases. **(A)** Kinetic binding parameters of FMAU and T07 with TK-1 and TK-2. **(B)** Inhibitory effect of FMAU and T07 on ^{3}H-dT phosphorylation by TK-1 and TK-2.

CONTROL ID: 2230774

TITLE: MENGA: a comprehensive tool for the integration of brain imaging modalities and Allen brain genomic atlas

PRESENTER: Gaia Rizzo

ABSTRACT BODY:

Abstract Body: Introduction. Brain-wide mRNA mappings (as derived from Allen Brain Atlas, ABA [1]) have a great potential for integration with neuroimaging studies: they can predict protein levels in unrelated control populations for systems where translational mechanisms predominantely regulate expression [2]. This work presents MENGA (Multimodal Environment for Neuroimaging and Genomic Analysis), a platform which explores the similarities between the spatial patterns of ABA mRNA expressions and brain imaging data of unrelated subjects.

Material and methods. ABA is used as source of mRNA data [3], with more than 29,000 genes (on average 2.0 ± 1.4 probes per gene) sampled throughout the brain of 6 healthy donors (5 males, 1 female, age: 42.5 ± 13.4, range 24-57 yrs, with 617 ± 242 samples per subject). ABA data were preprocessed in order to select for each gene the most reliable and consistent probes across subjects to define a unique mRNA expression profile per gene. The gene profiles are stored in a database that is accessed at each MENGA query.

The spatial coordinates of each sample were converted in MNI coordinates in order to derive a biunivocal relationship to match ABA with the image data for each donor. Additionally, the anatomical classification of the sample labels were moved on the image space to obtain a brain segmentation consistent with the *sample*/*structure*/*coarse* levels of resolution, as defined in ABA.

Based on this structure, MENGA takes the input image, queries the database and re-samples the image into each donor's space to have a 1:1 sample-to-image correspondance. At the analysis stage, it returns the genomic-imaging cross-correlation weighted for gene donors' autocorrelation. The package has been developed in a Matlab® environment (The Mathworks Inc., Natick, MA, USA).

Results. The main outcome of MENGA is the genomic-imaging cross-correlation (as Pearson's or Spearman's correlation). It also returns the gene auto-correlation value as a measure of the variability of the process. This can be interpreted as an upper bound for the cross-correlation. MENGA works at various levels of resolution, which are user-defined, based on the anatomical ABA labels.

MENGA can work with all brain image modalities (functional or anatomical), provided they are aligned in standardized MNI space (181x217x181, 1mm voxel size).

As proof of principle, we tested MENGA in some representative cases of positron emission tomography and magnetic resonance imaging (Figure).

Conclusion. MENGA is an integrated system which allows the comparison of genomic and imaging data. The software investigates the relationship between a given image modality and the corresponding biological process that is investigated. Specifically, it evaluates whether the spatial mRNA expression patterns can explain the image phenotype.

References.

[1] Hawrylycz et al, Nature, 2012

[2] Rizzo et al, JCBFM, 2014

[3] *downloaded from* http://www.brain-map.org

AUTHORS (LAST NAME, FIRST NAME): Rizzo, Gaia[1]; Veronese, Mattia[2]; Expert, Paul[2]; Turkheimer, Federico E.[2]; Bertoldo, Alessandra[1]

INSTITUTIONS (ALL):

1. Department of Information Engineering, University of Padova, Padova, Italy.

2. Department of Neuroimaging, Institute of Psychiatry, Psychology & Neuroscience, King's College , London, United Kingdom.

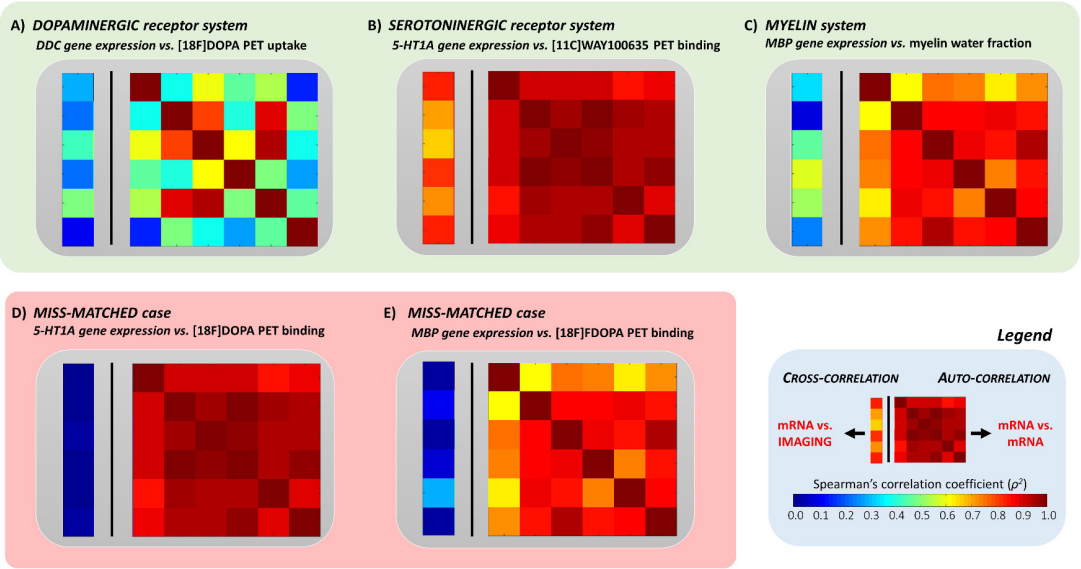

Example of MENGA application. *Panel A-E reports the genomic-imaging correlation values along with genomic auto-correlation. In the results matrix, each element represents the correlation between couples of donors (for the auto-correlation) or between one donor's mRNA levels and the image sampled in the same donor's space. MENGA has been tested considering both matched and miss-matched genomic information, with the following positron emission tomography tracers and magnetic resonance imaging:*
Matched cases: (A) Dopamine system with [18F]DOPA PET imaging vs. dopa decarboxylase (DDC) mRNA expression, (B) Serotoninergic system with [11C]WAY100635 PET imaging vs. 5-HT1A receptor mRNA expression, (C) Myelin water fraction MR imaging vs. myelin-basic protein (MBP) mRNA expression.
Miss-matched cases: (D) [18F]FDOPA PET imaging (dopamine system) vs. 5-HT1A mRNA expression (serotonin system), (E) [18F]FDOPA PET imaging (dopamine system) vs. MBP mRNA expression (myelin system).
Notably while in the matched cases cross-correlation and auto-correlation are comparable, in the miss-matched cases the cross-correlation is significantly lower than the gene auto-correlation indicating the absence of any correspondence between imaging and genomic analysis.

CONTROL ID: 2231917

TITLE: Use of a Variational Bayesian inference method for the quantification of brain PET data at the voxel level

PRESENTER: Gaia Rizzo

ABSTRACT BODY:

Abstract Body: Introduction

Full kinetic modelling of dynamic PET images at the voxel level can be challenging due to the low signal-to-noise ratio of the voxel activities. Bayesian approaches, which incorporate prior information on the tissue kinetic, have been shown to provide robust estimates also at the voxel level [1-2]. However, these methods either require the linearization of the kinetic model, not always possible, or are computationally demanding, not appropriate for clinical practice. Here we apply Variational Bayes (VB), an approach for the statistical inference of the model parameters previously used in magnetic resonance studies [3]. VB is here used for the first time with PET data in order to assess its performance in the voxel-wise quantification of model parameters including the volume of distribution (V_T).

Methods

VB was implemented as in [3], accounting for a time-variant measurement error as standard practice in PET [4].
VB was tested on 3 different radioligands: [11C](*R*)-rolipram (3 healthy subjects), [11C]WAY100635 (3 healthy subjects) and [11C]PBR28 (1 healthy subject). [11C]PBR28 was included to assess VB performance when a model more complex than the “classical” two-compartmental model is used (i.e. including a vascular component [5]). The priors (mean and variance) were derived from the regional model estimates following a hierarchical approach. Estimates of V_T [mL/cm^3] were corrected for failures and outliers (i.e. values with a coefficient of variation > 100% or with less than 5% difference from the priors). VB values were then compared with those obtained voxel-wise by using a weighted non-linear least square estimator (WNLLS), considered as reference values. The comparison was carried out in the intersection of voxels where both methods gave reliable estimates. The results were compared in terms of correlation (Pearson’s coefficient R^2), slope and intercept of the regression analysis and mean relative difference (MRD).

Results

As expected, WNLLS had the highest percentage of outliers (56.3%±4.8% for [11C]WAY100635, 23.6%±9.2% for [11C](R)-rolipram and 63% for [11C]PBR28, Table). On the contrary, VB showed a remarkable improvement both in terms of outliers (2.7%±0.2%, 0.16%±0.03% and 5.9% for the three tracers respectively, Table) and in terms of parametric maps quality (Figure). Computationally, it was at least 40% faster than WNLLS, completing a single brain analysis in less than 40 min.
In all datasets, VB showed an excellent agreement with the reference WNLLS values ([11C]WAY100635: MRD=2.9%±2.2%, R^2 = 0.91±0.02; [11C](R)-rolipram: MRD = -2.8%±0.5%, R^2=0.77±0.03; and [11C]PBR28: MRD = 16.3%, R^2=0.8).

Conclusions

VB is applied for the first time to PET data. It provides robust and accurate parameter estimates with low percentage of outliers and reduced computational time. VB is compatible with clinical practice, even when complex compartmental model are employed.

References

[1] Rizzo et al. (2012) Neuroimage
[2] Zanderigo et al. (2010) Nucl Med Biol
[3] Chappell et al. (2009) IEEE Trans Sign Proc
[4] Mazoyer et al. (1986) J Comp Ass Tomography
[5] Rizzo et al. (2014) JCBFM

AUTHORS (LAST NAME, FIRST NAME): Rizzo, Gaia[1]; Tonietto, Matteo[1]; Zanoni, Simone[1]; Chappell, Michael A.[2]; Castellaro, Marco[1]; Bertoldo, Alessandra[1]

INSTITUTIONS (ALL):

1. Department of Information Engineering, University of Padova, Padova, Italy.
2. Institute of Biomedical Engineering, University of Oxford, Oxford, United Kingdom.

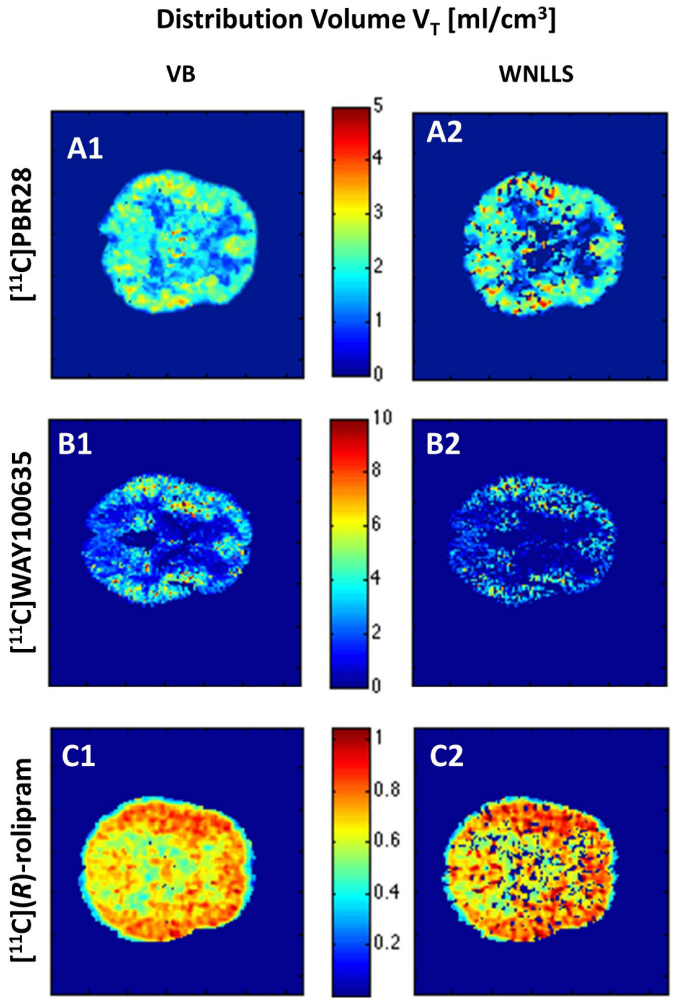

Figure: Parametric map of the volume of distribution obtained with VB and WNLLS on the three different tracers ([11C]PBR28, A1-A2; [11C]WAY100635, B1-B2; [11C](R)-rolipram, C1-C2).

CONTROL ID: 2230787

TITLE: Performance of a 2D vs. 3D Hand-Held Multispectral Optoacoustic Tomography (MSOT) System in a Melanoma Brain Metastasis Model

PRESENTER: Volker Neuschmelting

ABSTRACT BODY:

Abstract Body: Objective: The development of a handheld approach to optoacoustic imaging is essential for the potential clinical translation of this emerging technique. Distinct 2- and a 3-dimensional handheld multispectral optoacoustic tomography (MSOT) devices have recently been developed by iTheraMedical. We aimed to compare their intrinsic optoacoustic contrast performance in vitro and in vivo in a mouse model of melanoma metastatic to the brain.

Methods: In vitro, imaging performance of both devices was determined in a dilution series of B16F10 live cell suspensions in a tissue mimicking phantom. For in vivo experiments, seven albino B6 mice were stereotactically implanted with $2x10^5$ B16F10-luc melanoma cells into the right frontal lobe. Isovoxel T1-WI MR images were aquired for anatomical reference. MSOT images were aquired in vivo on day 6, 8, 10, 13 with the use of a 2-D arc shaped prototype detector (center frequency 4MHz, angular coverage 135°, center illumination) and a 3-D cup shaped detector (center frequency 4MHz, angular coverage 120°, center-only and center- plus side illumination). After sacrificing the animals, histological examination of the brains was performed.

Results: In vitro, the limit of detection of melanoma cells was significantly lower using the prototype 2D-arc device than the commercially available 3D-cup with the center illumination only. Within the field of view the signal decreased more profoundly in relation to depth in the 3D-cup than the 2-D approach. This observation was confirmed in vivo as well. In vivo, both approaches were capable of imaging the melanoma tumors at all time points qualitatively. Quantatively, the 2D approach allowed closer anatomical resemblance of the tumor compared to the 3D-cup in reference to the MRI and histological examination, particularly at depths beyond 3 mm. The additional side illumination in the 3D approach at constant total laser power enabled MSOT signal detection at greater depths. The test-retest reliability was significantly higher for the 2D than the 3D approach. On the other hand, the 3D-image aquisition was less time consuming than the 2D approach due to less image sets needed based on the 3rd dimension.

Conclusion: The current version of the 2D-arc MSOT prototype handheld device proved to be more suitable than the center illuminated 3D-cup MSOT handheld device for optoacoustic imaging of tissue targets at greater depths. Using additional side illumation, the 3D-cup device demonstrated the promise to overcome this limitation and save imaging time, but more work is needed to improve its test-retest-reliability.

AUTHORS (LAST NAME, FIRST NAME): Neuschmelting, Volker[1]; Burton, Neal C.[3]; Lockau, Hannah[1]; Harmsen, Stefan[1]; Huang, Ruimin[1]; Hupple, Clinton[3]; Grimm, Jan[1, 2]; Kircher, Moritz F.[1, 2]

INSTITUTIONS (ALL):

1. Department of Radiology, Memorial Sloan Kettering Cancer Center, New York, NY, United States.
2. Center for Molecular Imaging and Nanotechnology (CMINT), Memorial Sloan Kettering Cancer Center, New York, NY, United States.
3. iThera Medical GmbH, Munich, Germany.

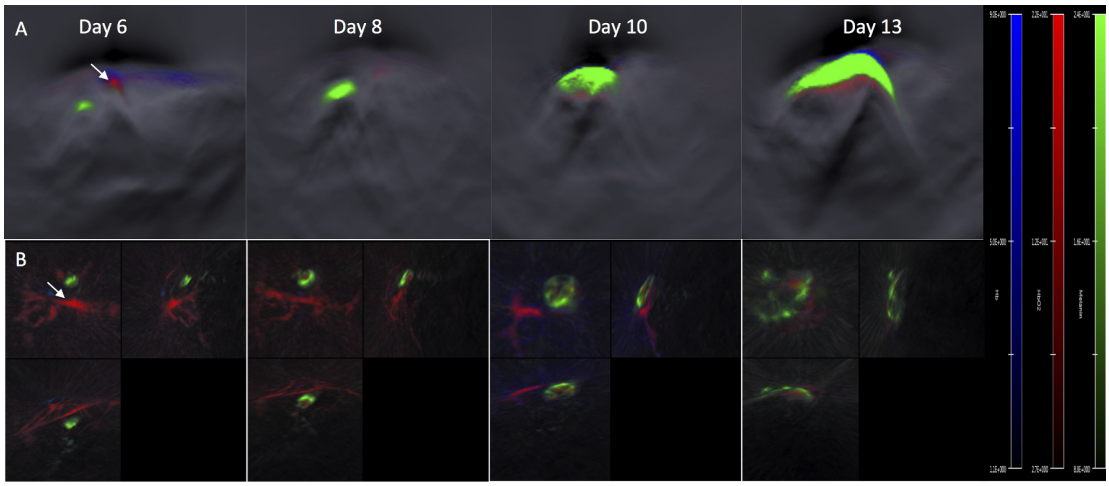

Longitudinal MSOT follow up of melanoma metastasis bearing mouse brain with the use of (A) 2D arc-shaped and (B) 3D cup detector in comparison (green: melanin; red: HbO2: blue: HbdeOx; arrow: sagittal venous sinus).

CONTROL ID: 2230791

TITLE: Simultaneous *In Vitro* and *In Vivo* Diagnosis of Bacterial Infections in Living Mice

PRESENTER: Gayatri Gowrishankar

ABSTRACT BODY:

Abstract Body: Background: Despite advance in molecular diagnostics & imaging, the rapid diagnosis of bacterial infections has continued to pose a challenge to the medical community. The last few years have seen the emergence of various positron emission tomography (PET) tracers to image bacterial infection pre-clinically. These tracers are specific to a certain class of bacteria ([^{18}F Fluorodeoxysorbital for enterobacteriaceae) or can be used to image any bacterial infection like the 6-[^{18}F]-fluoromaltose [1, 2 and 3]. While these tracers would enable physicians to determine the location(s) and the spread of bacterial infections in patients, they would still not inform on the identity of the bacterial strain that has infected a given individual. In this study we report on the development of a novel PET tracer -6-[^{18}F] fluoromaltotriose- that can be used to image all bacterial infections and a blood based method utilizing the diagnostic potential of exosomes, that would enable the simultaneous identification of the specific bacterial strain causing the infection **Results** 6-[^{18}F]-fluoromaltotriose (Figure 1B) was synthesized as described in detail in another abstract. The uptake of 6-[^{18}F]-fluoromaltotriose was evaluated in *E.coli.* The accumulation of 6-[^{18}F]-fluoromaltotriose in the *E. coli* increased over time. The uptake in *E.coli* could also be blocked by a co-incubation with 1mM of cold maltose (98% blocking, $p < 0.0003$), the natural substrate of the transporter, confirming that the tracer was a substrate of the bacterial maltose transporter. 10^8 colony-forming units (CFU) of *E.coli* was then inoculated in the right thigh muscle of nude mice (n=4). 24h later, 200uCi of the 6-[^{18}F]-fluoromaltotriose was administered via tail vein and dynamic PET/CT scans were obtained over the course of 1h. Figure 1A shows a representative PET/CT image at 1 hour. The tracer clearly accumulated in the infected leg. ROI analysis showed that infected muscle had an average uptake of 4.7 ± 1.3 % ID/g (mean ± SD), 3.1-fold higher than the contra-lateral muscle ($p<0.05$). The route of clearance of the tracer is renal which makes it suitable for clinical translation. At the end of the imaging study, the mice were euthanized and their blood was collected. Exosomes were prepared from the serum of these mice using a standard protocol. Reverse-transcriptase PCR was performed using *E.coli* specific 23s ribosomal RNA primers. A clear PCR product was seen from the serum of the mice that had been infected (Figure 1C). **Conclusions:** In this study a novel tracer that can be used to image all bacterial infections has been synthesized and tested. This tracer has been shown to have exquisite sensitivity and specificity and a clearance pattern that makes it amenable for clinical translation. This tracer combined with an exosome based *in vitro* diagnostic platform will enable clinicians to determine not just the extent of the infection but also identify the pathogen causing the infection, greatly improving the clinical management of infectious diseases

References

1) Weinstein EA et al, Science Translational medicine 2014

2) Gowrishankar G et al, Plos One 2014

3) Ning X et al, Angewandte Chemie 2014

AUTHORS (LAST NAME, FIRST NAME): Gowrishankar, Gayatri[1]; Namavari, Mohammad[1]; Srinivasan, Ananth[2]; Ravi, Neeraja[3]; Reeves, Robert E.[4]; Gambhir, Sanjiv S.[5, 6]

INSTITUTIONS (ALL):

1. Radiology, Stanford University, Stanford, CA, United States.
2. Radiology, Stanford University, Stanford, CA, United States.
3. Bioengineering, University of California San Diego, San Diego, CA, United States.
4. Radiology, Stanford University, Stanford, CA, United States.
5. Radiology, Stanford University, Stanford, CA, United States.
6. Bioengineering, Stanford University, Stanford, CA, United States.

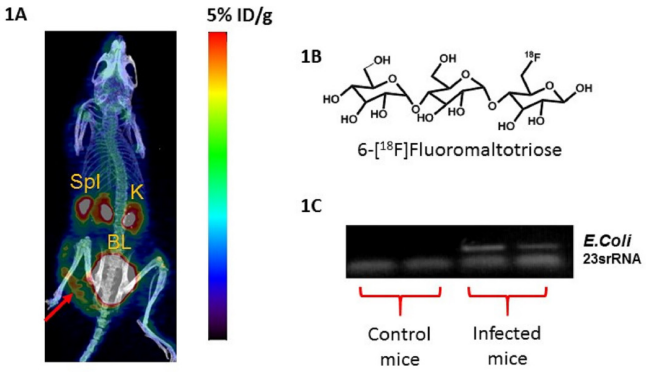

Figure 1: A) Maximum intensity projection from a dynamic PET/CT scan of a mouse that had been injected with 200µCi of 6-[^{18}F]-fluoromaltotriose. The red arrow indicates the site of infection. Kidney (K), Bladder (BL) and spleen (Spl) are also seen in the figure. B) Structure of 6-[^{18}F]-fluoromaltotriose C) Agarose gel chromatogram showing *E.coli* specific 23s rRNA PCR products in the blood of the infected mice. Blood from uninfected control mice is shown for comparison.

CONTROL ID: 2230790

TITLE: Transparancy, the tool for 3D light microscopy of the blood vasculature in mouse brain.

PRESENTER: Tonny Lagerweij

ABSTRACT BODY:

Abstract Body: Introduction

Light microscopy is still the golden standard for diagnosis of a variety of diseases. The standard way of histological analysis is however hampered by the fact that this results only in 2D analysis and may result in large selection bias because only a thin slice of the sample will be diagnosed. Furthermore this analysis lacks insight into the 3D architecture. This could be circumstanced by slicing and analyzing consecutive slices, but this is technically challenging and laborious.

The last decade, clearing techniques including 3DISCO (Ertürk et al., 2012), CLARITY (Chung et al., 2013) and iDISCO (Renier et al., 2014) have become available to enable 3D imaging of whole tissues. We have explored the CLARITY and iDISCO clearing techniques for the visualization and quantification of blood vasculature architecture in mouse brain tissue.

Methods

Mouse brains were processed by CLARITY or iDISCO procedures and stained by fluorescently labeled Lycopersicon Esculentum (Tomato) lectin together with a nuclear staining. Both clearing techniques allowed imaging by 2-photon microscopy along the entire working distance length of the objective. The obtained images were processed by the commercially visualization and quantification software package IMARIS for 3D representation. The blood vessel architecture was analyzed after semi-automatic computational reconstruction of the blood vasculature and correlated to the number of nuclei in both dense cellular areas and sparse cellular areas.

Conclusion

Clearing of adult mouse brain by CLARITY or iDISCO procedures, results in transparent tissue and allowed light microscopy imaging of the vasculature up to an imaging depth of several millimeters. Computational analysis allowed the quantification of the number of nuclei and the vasculature. We show an equilibrium between number of cells and number of blood vessels: The blood vessel surface in a certain brain region correlates directly with the number of brain cells present in this region.

AUTHORS (LAST NAME, FIRST NAME): Lagerweij, Tonny[1]; Dusoswa, Sophie[2]; Wurdinger, Thomas[1, 3]

INSTITUTIONS (ALL):

1. Neuro-oncology Research Group, VU university medical center, Amsterdam, Netherlands.
2. MCBI, VU university medical center, Amsterdam, Netherlands.
3. Massachusetts General Hospital, Harvard Medical School, Boston, MA, United States.

(No Image Selected)

CONTROL ID: 2230802

TITLE: Assessing Changes in Tumor Extracellular pH during Metabolism-Targeting Therapies with acidoCEST MRI

PRESENTER: Paul Akhenblit

ABSTRACT BODY:

Abstract Body: Introduction: Cancer cells employ a high rate of aerobic glycolysis as their main pathway for energy production instead of oxidative phosphorylation, commonly referred to as the Warburg Effect.[1] This shift in metabolism yields a high overproduction of lactic acid, which is excreted into the tumor extracellular space, lowering the extracellular pH (pHe) from physiological levels of ~7.2 to ~7.4 to acidic levels, ~6.6 to ~6.8.Tumor acidity has been shown to desensitize tumors to weak-base chemotherapy agents, such as doxorubicin, and lowering patient survival.[2] Therefore there is merit to studying metabolism-targeting therapies meant to neutralize tumor acidosis, which may re-sensitize tumors to weak-base chemotherapies and increase patient survival.

Key to the production of lactic acid is lactate dehydrogenase A (LDHA), which has been shown to be inhibited by gossypol.[3] We developed a robust, non-invasive imaging method called acidoCEST MRI.[4] Using an FDA-approved CT contrast agent, we can accurately and precisely measure tumor pHe levels in mouse tumor models. We hypothesized that acidoCEST MRI can detect an increase in tumor pHe following treatment with gossypol.

Methods: Seven nude mice were prepared by injecting MDA-MB-231 cells in the right rear flank, and the subcutaneous flank tumor was allowed to grow for 3 weeks. Mice were injected with 15 mg/kg of gossypol in a 10% ethanol vehicle i.p. with a volume of 200 mL. Mice were imaged 24 hours prior to treatment and again 24 hours post treatment. Just prior to acidoCEST MRI, a 200 mL bolus of iopamidol (370 mg iodine/mL Isovue™, Bracco Diagnostics, Germany) was administered i.v., followed by infusion of the agent at 400 mL/hr. AcidoCEST MR images were acquired using a Bruker 7T Biospec MRI scanner with a 72 mm-diameter quadrature transceiver coil (Bruker Biospin, Inc., Billerica, MA). A total of 38 saturation frequencies were collected from -10 to 10 ppm, with a 3.5 μT Half-Gauss 5000 ms pulse. Each mouse was maintained at 37 °C while imaging. The acidoCEST MRI images were processed with Matlab® R2013a (Mathworks, Inc., Natick, MA).

Results/Discussion: The mean pHe value increased from 6.63 ± 0.07 (n=7) before treatment to 6.67 ± 0.05 (n=6) after treatment. The average standard deviation did not vary from between the acidoCEST MRI scans, and the percent uptake of the tumors varied little from 51.65% to 50.67%. Tumor volume did not show a decrease in size between the imaging sessions. The increase was mild. Future studies are warranted to evaluate the tumor pHe after 72 hours of continuous treatment.

1. DeBerardinis, Ralph J., et al. *Cell Metabolism* 7.1 (2008): 11-20.
2. Mahoney, Brent P., et al *Biochemical Pharmacology* 66.7 (2003): 1207-1218.
3. Tuszynski, George P., and Giulio Cossu. *Cancer Research* 44.2 (1984): 768-771.
4. Chen, Liu Qi, et al *Magnetic Resonance in Medicine* 72.5 (2014): 1408-1417.

AUTHORS (LAST NAME, FIRST NAME): Akhenblit, Paul J.[1]; Howison, Christine[2]; Pagel, Mark[2, 3]

INSTITUTIONS (ALL):
1. Cancer Biology GIDP, University of Arizona, Tucson, AZ, United States.
2. Biomedical Engineering, University of Arizona, Tucson, AZ, United States.
3. Medical Imaging, University of Arizona, Tucson, AZ, United States.

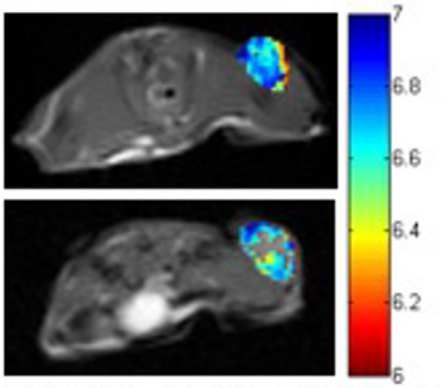

Figure 1. A parametric map of tumor pHe before and 1 day after treatment with gossypol. The drug treatment caused a mild increase in average tumor pHe.

CONTROL ID: 2230829

TITLE: Zinc responsive MRI Contrast Agents for *in vivo* Imaging

PRESENTER: Andre Martins

ABSTRACT BODY:

Abstract Body: Zn(II) is an essential mineral in the organism, responsible for the secretory function of several tissues including the pancreas, mammary glands, and prostate (1). The healthy human prostate has been reported to have the highest levels of free zinc (2) while malignant prostate cells undergo a metabolic transformation that results in a reduced accumulation of Zn(II) (3). Such a disparity in tissue Zn(II) concentration between normal prostate and prostate cancer cells offers the potential to distinguish malignancy from normal tissue, benign prostatic hyperplasia (BPH), prostatic intraepithelial neoplasia (PIN), and inflammation. Here, we report several gadolinium-based contrast agents capable of detecting free Zn(II) ions by MRI at physiological concentrations. In the absence of Zn(II), GdDOTA-bisBPEN derivatives have little to no affinity for albumin but after binding to 2 or 1 equivalents of free Zn(II), the resulting complexes then bind to human serum albumin (HSA) which in turn results in an increase in r_1 relaxivity as high as 57 $mM^{-1}s^{-1}$ (860% increase) (4). The rate of water exchange was optimized and analysed by ^{17}O NMR (high resolution NMR techniques) in a series of BPEN derivatives by introduction of different functional groups as spacers (phosphinate groups, extra methylene carbons, piperazine units, one arm BPEN) and interesting binding properties were observed for the new derivatives. Depending on the individual structure, these new agents demonstrate significantly improved longitudinal relaxivities (r_1) and exhibit highly sensitive MRI detection of Zn(II) and nicely enhance the mouse prostate *in vivo* by MRI only after co-injection of glucose. This suggests a mechanism involving stimulated release of Zn(II) from the prostate, similar to that observed previously for the pancreas (5). These results demonstrate that it is possible to design and optimize functional MRI contrast agents that respond to alterations of important biological ions *in vivo* at an acceptable dose relevant for translation to human imaging.

References

[1] S.L. Kelleher et al., *American Society for Nutrition. Advances in Nutrition*, **2**, 101-111 (2011)

[2] L.C. Costello, R.B. Franklin, *The Prostate*, **35**, 285-296 (1998)

[3] R.B. Franklin, L.C. Costello, *Archives of Biochemistry and Biophysics*, **463**, 211-217 (2007)

[4] A.C. Esqueda et al., *Journal of the American Chemical Society*, **131**, 11387-11391 (2009)

[5] A.J.M. Lubag, A.D. Sherry, *Proceedings of the National Academy of Science*, **108**, 18400-18405 (2011)

AUTHORS (LAST NAME, FIRST NAME): Martins, Andre F.[1]; Yu, Jing[1]; Preihs, Christian[2]; Clavijo, Veronica[2]; Zhao, Piyu[1]; Wu, Yunkou[2]; Sherry, A. D.[2]

INSTITUTIONS (ALL):

1. Chemistry, UT Dallas, Richardson, TX, United States.

2. Advanced Imaging Research Center, University of Texas Southwestern Medical Center, Dallas, TX, United States.

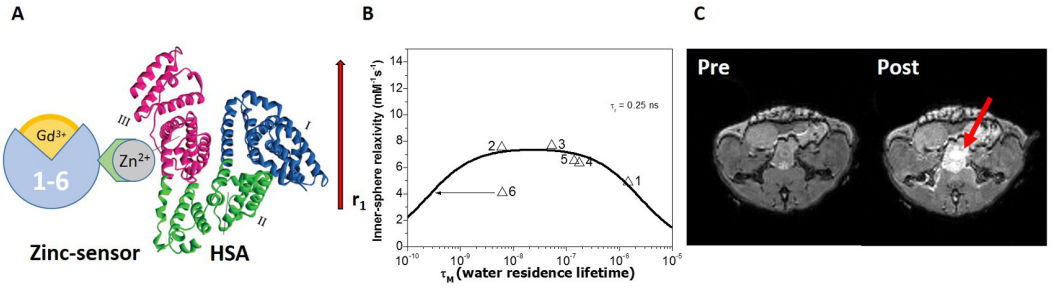

Figure 1. A) Gd^{3+}-complexes (1-6) bind to human serum albumin (HSA) only when free Zinc is present in solution. The r_1 relaxivity is enhanced due to the slow rotation of the agglomerate. **B)** Fine-tuned water exchange properties for all sensors measured by ^{17}O NMR and analysed with Solomon-Bloembergen-Morgan theory. **C)** The zinc sensors enhance the mouse prostate *in vivo* by MRI only after co-injection of glucose.

CONTROL ID: 2231870

TITLE: Crossectional and Test-Retest Characterization of PET with ^{18}F-FP-(+)-DTBZ for β-Cell Mass Estimates in Diabetes

PRESENTER: Paul Harris

ABSTRACT BODY:

Abstract Body: Objective of Study.

Molecular imaging of vesicular monoamine transporter, type 2 (VMAT2) offers the possibility of obtaining precision/personalized medical information in the form of anatomical estimates of β-cell mass (BCM) needed for individualized therapy of both type 1 and type 2 diabetes [1-5]. VMAT2 is expressed by insulin producing β-cells and was evaluated as a biomarker of BCM by positron emission tomography (PET) with 18F-fluoropropyl-dihydrotetrabenazine (18F-FP-(+)-DTBZ).

Methods.

The feasibility of longitudinal pancreatic PET VMAT2 quantification in the pancreas was evaluated in two studies with healthy controls and patients with type 1 or type 2 diabetes. VMAT2 binding potential (BP_{ND}) in the body and tail of the pancreas was estimated voxelwise using a reference tissue method in a crossectional study, followed by assessment of reproducibility using a test-retest paradigm. Metabolic function was evaluated by stimulated c-peptide measurements.

Innovation.

The test retest characteristics of BCM estimates in the human pancreas has not been previously reported.

Results.

Pancreatic BP_{ND} was significantly decreased in patients with T1DM relative to control subjects, confirming previous results [1,3] and the test retest variability was 9.4%. An additional metric was examined: the product of PET defined ROI volume and the mean BP_{ND} (PET ROI_{vol} x BP_{ND}) or functional binding capacity (FBC). The FBC was signiciantly reduced in the body and tail of pancreata of patients with T1DM relative to controls (to 37%, p=0.001). The mean variability of FBC was 16.6%, the intraclass correlation coefficient (ICC) of the FBC was 0.88 and the minimal detectable change (95% CI) for FBC was 18. β-cell mass as estimated by a metabolic functional test (i.e. peak c-peptide production) correlated significantly (p =0.011) with FBC.

Conclusions.

Pancreatic VMAT2 content is significantly reduced in long-term diabetes patients relative to controls and repeat scans are sufficiently reproducible to suggest the feasibility of VMAT2 measurements in longitudinal studies of new onset diabetes.

References cited.

1. Goland R, et al. 2009. 11C-dihydrotetrabenazine PET of the pancreas in subjects with long-standing type 1 diabetes and in healthy controls. J Nucl Med 50: 382-9.

2. Freeby, M, et al. 2012 Vesicular Monoamine Transporter, Type 2 (VMAT2) Expression as it Compares To Insulin and Pancreatic Polypeptide in the Head, Body and Tail of the Human Pancreas. Islets 4:393-7 .

3. Normandin, M, et al. 2012. In Vivo Imaging of Endogenous Pancreatic β-Cell Mass in Healthy and Type 1 Diabetic Subjects Using ^{18}F-Fluoropropyl-Dihydrotetrabenazine and PET. J Nucl Med 53:908-91.

4. Harris, PE, et al. 2013. PET quantification of pancreatic VMAT 2 binding using (+) and (-) enantiomers of [18F]FP-DTBZ in baboons. Nuclear Medicine and Biology 40(1):60-4

5. Ichise, M, et al. 2010. Imaging of β-cell mass and function. J Nucl Med 51:1001-4.

AUTHORS (LAST NAME, FIRST NAME): Harris, Paul E.[1]

INSTITUTIONS (ALL):

1. Medicine/Endocrinology, Columbia University, New York City, NY, United States.

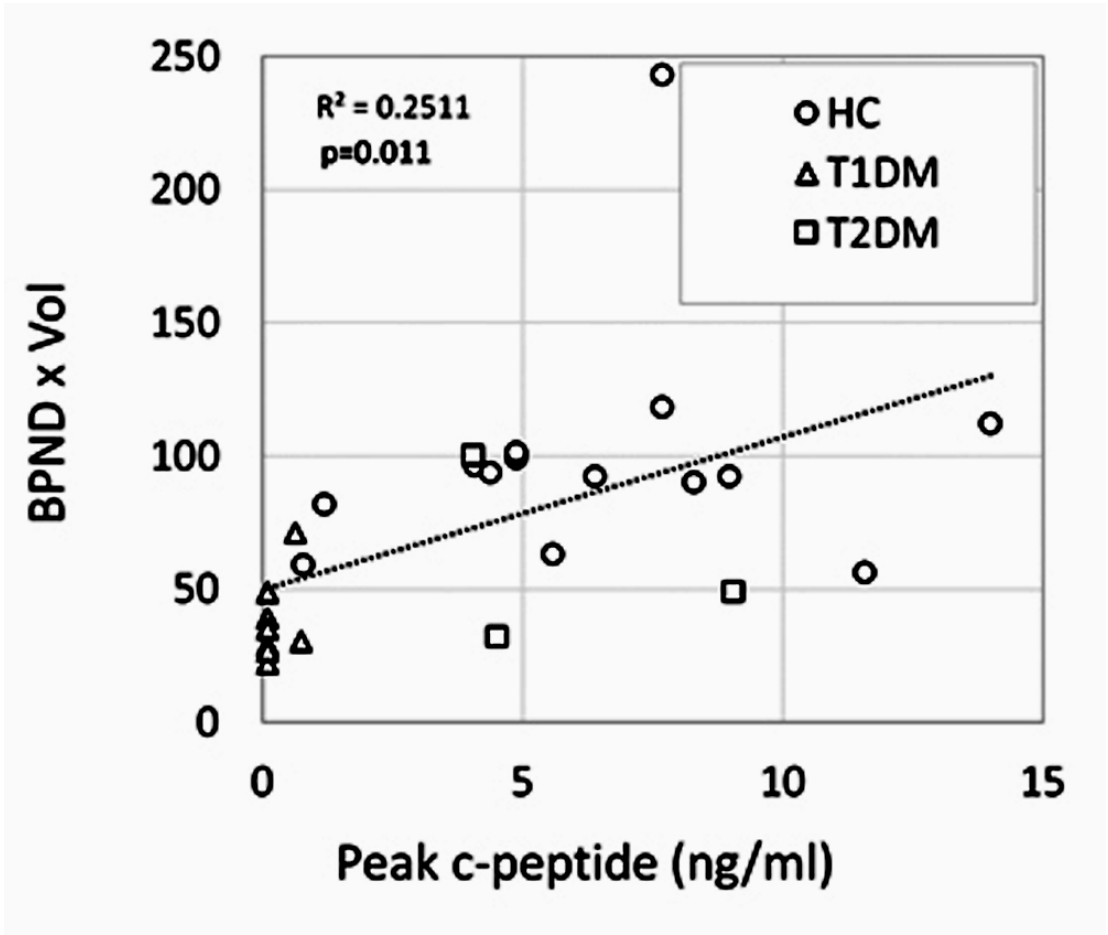
250
200
150
100
50
0
BPND x Vol
R² = 0.2511
p=0.011
HC
T1DM
T2DM
0
5
10
15
Peak c-peptide (ng/ml)

CONTROL ID: 2230875

TITLE: Optimized ^{52}Mn Production for Long-lived PET Applications

PRESENTER: Stephen Graves

ABSTRACT BODY:

Abstract Body: Introduction

^{52}Mn ($t_{1/2}$ =5.59 d, ß$^{+}$ = 29.6%, Eß$_{max}$ = 0.58 MeV) presents itself as an excellent candidate for a variety of PET applications. Chelation of ^{52}Mn would allow for radiolabelled antibody imaging 2-4 weeks post-injection, and free ^{52}Mn^{2+} has shown promise as a reporter gene probe in stem cell tracking applications [1]. The goals of this work were to develop an efficient ^{52}Mn production target, to optimize separation chemistry, and to demonstrate effective chelation.

Methods

^{52}Mn was produced by 16 MeV proton irradiation of natural chromium metal (approximately 750 mg, 99.999%, GFS chemicals) hydraulically pressed into 0.5 mm thick silver disk. With direct jet water cooling on the rear face, these targets were shown to withstand 60 µA of beam current for one hour without failure. Targets were etched by 2 mL 12.1M HCl and then diluted with 48 mL ethanol and 0.5 mL of 12.1M HCl. ^{52}Mn was radiochemically isolated from the target solution (96% Ethanol, 0.12M HCl) by loading the activity onto approximately 150 mg of AG-1x8 strong anion exchange resin, followed by rinsing. ^{52}Mn was eluted in 1 mL of 6M HCl, before repeating the purification with two additional separation cycles. The final product was eluted in approximately 500 µL of 0.1M HCl. DOTA labeling was performed at pH 4 using 0.25M pH 4.5 NaOAc to buffer the activity.

Results

Average end of bombardment ^{52}Mn yield was 0.14 ± 0.05 mCi/µAh (n=4). Radionuclidic purity was measured to be greater than 99% by high-purity germanium analysis. Target etching resulted in approximately 450 mg of chromium metal dissolution. An average radiochemical separation yield of 72 ± 17% (n=2) has been observed. Total chromium mass in the separated product was measured to be 1.1 ± 0.1 µg (n=1) by microwave plasma atomic emission spectrometry, corresponding to an overall separation factor of approximately 1.6 x 10^{5}. DOTA chelation of ^{52}Mn was found to be complete after one hour at room temperature, resulting in a measured effective specific activity of 0.05 Ci/µmol (n=1).

Conclusions

Production, separation, and chelation of ^{52}Mn have been demonstrated with very simple targetry and chemistry. These methods significantly improve over previous techniques [2-3] by improving Cr target purity from 99.95% to 99.999% and by allowing for a trap-and-release chromatographic separation. With such an approach, specific activities have been increased and the ^{52}Mn production process can be automated to reduce radiation dose to personnel. These developments will allow for rapid translation into imaging applications.

This work was supported by the NIH Radiological Sciences Training Grant, the DOE (DE-FG02-12ER41882), and the NCI (5 T32 Ca009206-34).

References

[1] CM Lewis, SA Graves, *et al.*, Theranostics, 5(3): 227-239, 2015.

[2] S Lahiri, *et al.*, Anal Chem, 78: 7517–21, 2006.

[3] GJ Topping, *et al.*, Med Phys, 40: 042502, 2013.

AUTHORS (LAST NAME, FIRST NAME): Graves, Stephen[1]; Severin, Gregory W.[2]; Valdovinos, Hector F.[1]; Fonslet, Jesper[2]; Ellison, Paul[1]; Barnhart, Todd E.[1]; Engle, Jonathan W.[3]; Cai, Weibo[1]; Nickles, Robert J.[1]

INSTITUTIONS (ALL):

1. Medical Physics, University of Wisconsin - Madison, Madison, WI, United States.
2. Center for Nuclear Technologies, Technical University of Denmark, Roskilde, Denmark.
3. Los Alamos National Laboratory, Los Alamos, NM, United States.

(No Image Selected)

CONTROL ID: 2230880

TITLE: Motexafin Gadolinium-Enhanced Molecular MR and Optical Imaging of Rat Gliomas for Potential Intraoperative Determination of Tumor Margins

PRESENTER: Longhua Qiu

ABSTRACT BODY:

Abstract Body: Purpose: Malignant glioma is an extremely aggressive neoplasm known for its highly infiltrative growth and dissemination. Identification of the real tumor margin during surgery plays a pivotal role in ensuring the complete eradication of tumors. The aim of this study was to investigate the possibility of using motexafin gadolinium (MGd)-enhanced molecular MR imaging and optical imaging to identify the genuine margins of gliomas.

Method and Materials: Rat glioma model was created by inoculating C6 glioma cells in right caudate nucleuses of male Sprague-Dawley rats (160g ± 20g). Thirty six rats with tumors were randomized into six groups (n=6/group). Five groups were euthanized at different time points of 15, 30, 60, 120 and 240 minutes after intravenous administration of 6-mg/kg MGd (Pharmacyclics, Inc.) respectively, while one group received saline as a control. After a craniotomy, ex vivo optical imaging was performed to identify the tumors featuring as MGd-emitting red fluorescence. Then, the whole brains were harvested for ex-vivo T1-weighted MRI (T1WI). Optical photon intensities and MRI signal-to-noise ratio (SNR) were quantified for plotting the times to photon/SNR curves. Tumor extent was demarcated on both optical and MR imaging. Subsequently, confocal microscopy of brain tissues was performed to confirm the intracellular uptake of MGd by tumor cells and correlate the tumor margins determined on both optical and MR images.

Results: Fluorescent optical imaging could sensitively detect the deep-seated tumors with red fluorescence in rat brains and clearly outlined the tumor margins. The photon intensity reached the peak at 15 minutes after MGd administration. T1WI showed the tumors heterogeneous enhancement, and the maximal enhancement on T1WI was measured at 15 minutes after MGd administration. Confocal microscopy confirmed the intracellular localization of MGd, which was well correlated with imaging findings (Figure).

Conclusion: Both MGd-enhanced optical imaging and molecular MR imaging can sensitively determine rat glioma tumor margin within the optimal time window of 15~30 minutes post-MGd administration, which pose the potential clinical application for aiding the complete removal of gliomas at a hybrid surgical setting with intraoperative optical and MR imaging capabilities.

AUTHORS (LAST NAME, FIRST NAME): Qiu, Longhua[2]; Zhang, Feng[5]; Shi, Yaoping[3]; Bai, Zhibin[1]; Wang, Jianfeng[4]; Lee, Donghoon[2]; Feng, Xiaoyuan[7]; yang, xiaoming[6]

INSTITUTIONS (ALL):

1. Radiology, University of Washington, Seattle, WA, United States.
2. University of Washington School of Medicine, Seattle, WA, United States.
3. Radiology, University of Washington School of Medicine, Seattle, WA, United States.
4. Radiology, University of Washington, School of Medicine, Seattle, WA, United States.
5. University of Washington School of Medicine, Seattle, WA, United States.
6. University of Washington School of Medicine, Seattle, WA, United States.
7. Huashan Hospital, Fudan University, Shanghai, China.

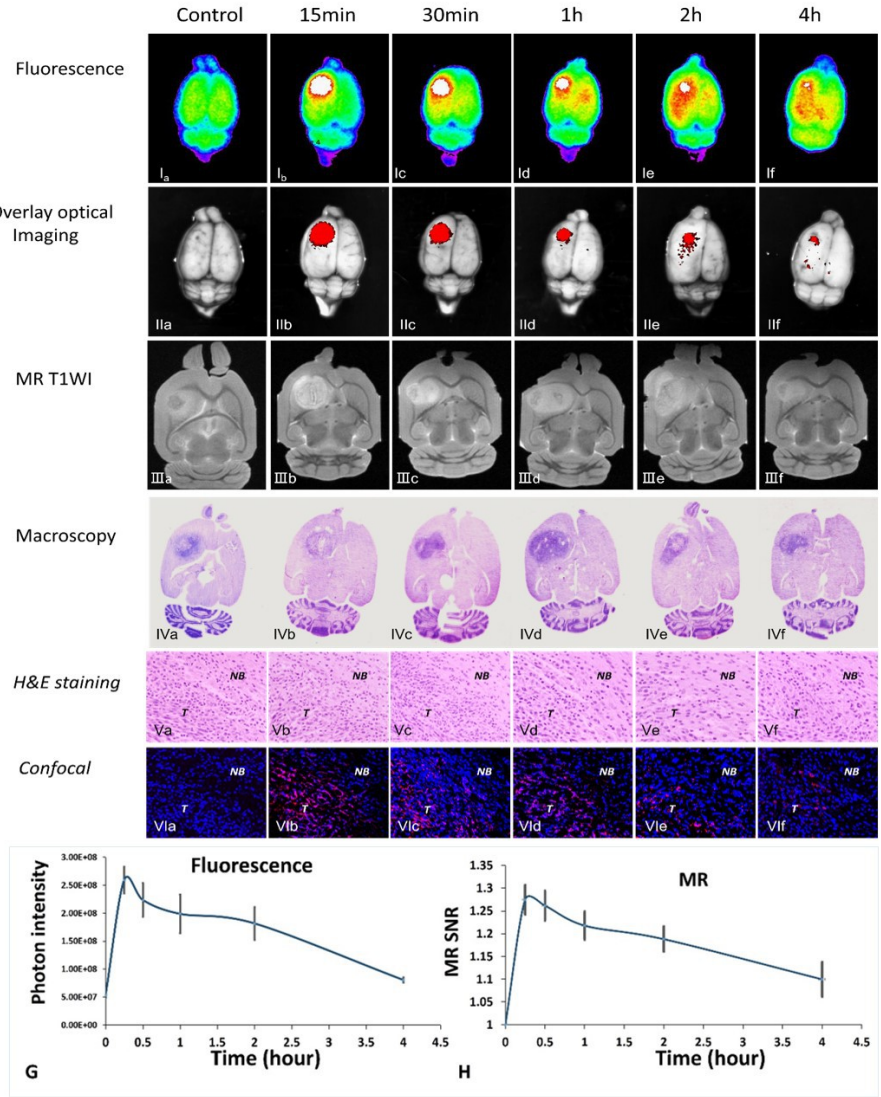

Fig. Ex vivo fluorescent optical imaging and MGd-enhanced T1WI of rat glioma tumors collected at different time points after the MGd administrations. (Ⅰa~f) Tumors optical images and (Ⅱa~f) overlay optical images show that tumors have the highest signal at the time point 15 mins after MGd administration and the signal becomes weak over times of 4 hours. (Ⅲa~) Axial T1WIs show the highest enhancement of tumors at 15 mins and the signal intensity of MGd-enhanced tumors decreased over times. (IVa~f) Cross-sectional macroscopic view of H&E-stained sections confirmed the brain tumors. (Ⅴa~f) Confocal microscopies of MGd-treated tumors show that MGd are specifically taken up by glioma cells and the highest signal is depicted at 15mins. There is a clear margin between MGd-containing tumor cells and normal brain cells, which is highly consistent with microscopy (Ⅵa~f). (NB = normal brain, T = tumor). Time to photon intensity (G) and time to SNR (H) curve show a steep increase of signal at 15 mins followed by a gradual signal decline.

CONTROL ID: 2230916

TITLE: Image-guided focused ultrasound ablation enhances drug accumulation and modulates immune cell profiles in a murine breast cancer model

PRESENTER: Elizabeth Ingham

ABSTRACT BODY:

Abstract Body: Thermal ablation is rapidly advancing as a promising minimally-invasive treatment for tumors in multiple organs[1]. Tumor-ablative heating strategies appear to directly induce acute coagulative necrosis as well as enhance periablational drug uptake at the site of the tumor[2]. Additionally it is thought that the anti-cancer effects of ablation may be due to a synergy between direct cytotoxicity and upregulation of anti-tumor immunological responses[3]. Here we evaluated the ability of a single-point MR-guided focused ultrasound ablation strategy to enhance drug accumulation as well as modulate changes in immune cell profiles in an aggressive murine breast cancer model.

Methods: Thirteen female FVB mice bearing bilateral mammary fat pad NDL tumors were separated into four groups (Control, n = 3; Ablation, n = 4; ^{64}Cu-LCL, n=3; Ablation + ^{64}Cu-LCL, n=3). Tumors (one tumor per mouse) were ablated with MR-guided focused ultrasound (Image Guided Therapy, France) for either 7 or 20 seconds with 7.6 or 5.6 MPa peak negative pressure and reached a maximum temperature of 60 or 75°C, respectively. Nanoparticle accumulation at the tumor site was assessed over 48 hrs post-ablation via injection of ^{64}Cu-labeled long-circulating liposomes (LCL) and PET imaging. After 48 hrs, tumors were excised for histological evaluation and autoradiographical detection of ^{64}Cu. To investigate ablation-induced immunological responses, one week post ablation treatment, tumors were extracted and enzymatically digested. Single-cell suspensions from each tissue were stained with anti–mouse antibodies to identify immune cells and FCS data files were collected using a Fortessa cell analyzer with FACSDiva software (BD). All datasets were analyzed using FlowJo software (Treestar).

Results: With single-point image-guided ultrasound ablation, accumulation of ^{64}Cu-LCL was dramatically increased compared to non-ablated control tumors (maximum accumulation after 3 hrs was 27.39 ± 2.14 vs. 8.55 ± 0.75 %ID/cc, respectively, Figure a,b). In comparison, the average accumulation of free drug in a mouse tumor model in the absence of interventions such as ultrasound is expected to be approximately 1 %ID/cc[4]. Regional ablative heating also induced significant increases in immune cell recruitment to the treated-tumor site compared to non-treated tumors (Figure c,d). The numbers of macrophages, dendritic cells, natural killer cells, and CD8+ T cells in ablation-treated tumors were all significantly increased with respect to the no-treatment controls ($p < 0.05$).

Conclusion: Ultrasound-ablation dramatically enhances localized particle uptake, indicating that chemotherapeutic-loaded liposome accumulation can be more than doubled at the tumor site using this thermal technique. This enhanced accumulation can translate to reduced systemic drug toxicity as well as enhanced tumor cytotoxicity. Further, the significant increase in immune cell number within the tumor may play a role in the underlying anti-tumor mechanisms of a localized ablation treatment strategy.

1. Radiology (2011); 258(2):351-69.

2. PLoS One (2014); 9(8): e102727.

3. Cancer Res (2004); 64(11):4024-9.

4. J Control Release (2008); 132(3): 171-83.

AUTHORS (LAST NAME, FIRST NAME): Ingham, Elizabeth S.[1]; Wong, Andrew[1]; Mirsoian, Annie[2]; Sckisel, Gail D.[2]; Watson , Katherine D.[1]; Liu, Yu[1]; Fite, Brett[1]; Mahakian, Lisa M.[1]; Tam, Sarah M.[1]; Seo, Jai Woong[1]; Kheirolomoom, Azadeh[1]; Murphy, William J.[2]; Ferrara, Katherine[1]

INSTITUTIONS (ALL):

1. Biomedical Engineering, University of California, Davis, Sacramento, CA, United States.

2. Dermatology, University of California, Davis, Sacramento, CA, United States.

(No Image Selected)

CONTROL ID: 2230926

TITLE: Novel Integrated Parameter Based Stopping Criterion for Iterative Reconstruction Methods

PRESENTER: Shih-Chun Jin

ABSTRACT BODY:

Abstract Body: Computed tomography (CT) has evolved into an indispensable imaging method in clinical routine for a long time. It gives us high resolution, high contrast and non-invasive tomographic images in brief scan time. In recent years, some manufactures have developed iterative reconstruction (IR) algorithms because dose reduction becomes a very important issue in CT scan. Another important reason is owing to the noisy nature of the measured projections. The latter one is also a big issue that we are interested because it has a very important influence on the ill-posed inverse problem of IR methods.

Most IR methods used minimized L_1-norm error between reconstructed image and referenced image to be the stopping criterion, and combined lots of figures-of-merit (FOMs): root-mean-square-error (RMSE), signal-to-noise ratio (SNR), contrast-to-noise ratio (CNR), coefficient of variation (CV), peak signal-to-noise ratio (PSNR) and universal quality index (UQI) to maintain the image quality. But here we simplify integrate all of these items to be an integrated parameter based criterion, which maximizes the integrated point (IP) by averaging PSNR and UQI.

In practice, testing codes were implemented in the image processing workstation (Precision T5600, Dell co.) with two CPUs (Intel® Xeon® E5-2620, 2.0 GHz). The reconstruction volume was 864 × 864 × 1536 without binning from flat-panel detector (Dexela1207, Perkin Elmer® Inc., USA). All IR algorithms: algebra reconstruction technique (ART), simultaneous ART (SART), maximum-likelihood expectation-maximization (MLEM), ordered-subsets EM (OSEM) and OS-SART, and FOMs were addressed by parallel computing toolbox on MATLAB® platform (ver. R2014b). A modified Sheep-Logan phantom was used to validate the results of all IR algorithms. Also, there were some physical phantoms and a real animal data, which were scanned by our homemade dual-modality micro-FT/CT system which can provide 50 kVp, 100 μA characteristic x-ray beams from transmission type tube (NS081505, NanoRay Biotech. Co., Taiwan). Those data were used to evaluate the iterative reconstructed image quality in real world. All IR reconstruction methods used fully 360-degree projections with two different sampling intervals: 1 degree/projection and 5 degree/projection. The OS conditions were maintained as 24 projections in each subset (3 and 15 subsets of two sampling intervals). Our data shows that the image quality was better in statistical IR (MLEM: 13 iterations, 73.004 sec/slice, IP=2.6132) than algebraic IR (ART almost diverges; SART: 19 iterations, 103.472 sec/slice, IP=2.5708). Considering optimization between integrated parameter based criteria, reconstruction time and iteration number, our data shows that OSEM method can produce better image quality when we used conventional FBP method to be the initial guess in full scan (4 iterations, 10.496 sec/slice, IP=1.8407) but OS-SART can produce better image quality under uniform initial guess (12 iterations, 17.214 sec/slice, IP=1.7502). Finally, this paper also provides good tips for robust stopping criteria choices of the IR reconstructions to maintain the trade-off between image quality and computing cost.

AUTHORS (LAST NAME, FIRST NAME): Jin, Shih-Chun[1]; Chen, Jyh-Cheng[1, 2]

INSTITUTIONS (ALL):

1. Biomedical Imaging and Radiological Sciences, National Yang-Ming University, Taipei, Taiwan.
2. Biophotonics and Molecular Imaging Research Center, National Yang-Ming University, Taipei, Taiwan.

(No Image Selected)

CONTROL ID: 2230935

TITLE: Reveal of accumulation mechanism of hypoxia imaging probe “FMISO” in tumors by imaging mass spectrometry: A possible involvement of low-molecular metabolite

PRESENTER: Yoichi Shimizu

ABSTRACT BODY:

Abstract Body: Objectives: 2-nitro imidazole-based compounds have been developed for agents with the features of accumulating specifically in hypoxic areas. Among them, ^{18}F-fluoromisonidazole (FMISO) has been expected to use as a hypoxia imaging probe for PET diagnosis. FMISO has been supposed to bind covalently with macromolecules in the hypoxic cells followed by reduction of nitro group in the imidazole ring; however it is difficult to distinguish the metabolic states of FMISO in tumor by conventional radio isotope analysis methods such as autoradiography (ARG), which makes the understanding of its detail mechanism complicated. To reveal the mechanism of accumulation in hypoxic area of FMISO, we investigated the chemical forms of FMISO and their distributions in tumor hypoxic area by imaging mass spectrometry (IMS). IMS is the technique to visualize directly the distribution of molecules on tissue sections, therefore IMS is considered to be useful to help us deepen our understanding of the accumulation mechanism of FMISO.

Methods: Balb/c nu/nu mice xenografted FaDu human pharyngeal squamous-cell carcinoma cells were injected intravenously with ^{18}F-FMISO (10 MBq, 550 mg/kg), and the tumors were excised at 4 h after injection. After radioactivity measurement, the tumor tissues were homogenized and divided into covalent-binding fraction to macromolecules and low-molecular fraction by solvent extraction. The molecular characteristics of the low-molecular fractions were analyzed by radio-HPLC. ARG, IMS and histologic studies were also performed with the serial tumor sections.

Results & Discussions: The distribution ratio of the radioactivity to covalent-binding fraction to macromolecules was 32.2±4.0% (n=4) in tumor homogenates, which suggests that the most part of radioactivity derived from ^{18}F-FMISO and its metabolites existed as low molecules. In the radio-HPLC analysis of the low-molecular fraction, unknown fractions which could not assign their chemical forms were observed mainly in addition to unchanged FMISO and amino-FMISO whose nitro group in the imidazole ring was reduced to an amino group. Therefore, the acquired ARG images were considered to be strongly reflected the distribution of these unknown fractions. The IMS analysis revealed that amino-FMISO was uniformly distributed in tumor and its distribution pattern did not correspond to the ARG images acquired from serial sections. In the IMS search of molecules contained specifically in the FMISO dosed tumors, a low-molecular metabolite of FMISO whose distribution pattern corresponded to ARG images was discovered. Its distribution was also correlated with the positive area of Pimonidazole (a marker of hypoxia) immunohistochemical staining.

Conclusion: Our IMS study reveals that a low-molecular metabolite of FMISO in addition to covalent-binding to macromolecules has been closely involved in accumulation of FMISO in tumor hypoxic area.

AUTHORS (LAST NAME, FIRST NAME): Masaki, Yukiko[1]; Shimizu, Yoichi[2, 4]; Yoshioka, Takeshi[1]; Tanaka, Yukari[3]; Higashino, Kenichi[1]; Sakamoto, Shingo[3]; Numata, Yoshito[1]; Yamaguchi, Yoshitaka[3]; Nishijima, Ken-ichi[2, 4]; Zhao, Songji[4]; Tamaki, Nagara[4]; Kuge, Yuji[2, 4]

INSTITUTIONS (ALL):

1. Discovery Research Laboratory for Innovative Frontier Medicines, SHIONOGI & CO., LTD., Sapporo, Japan.
2. Central Institute of Isotope Science, Hokkaido University, Sapporo, Japan.
3. Research Laboratory for Development, SHIONOGI & CO., LTD., Toyonaka, Japan.
4. Graduate School of Medicine, Hokkaido University, Sapporo, Japan.

Mass Spectrometric Image of a low-molecular metabolite of FMISO	18F-FMISO ARG
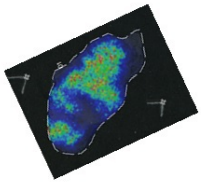	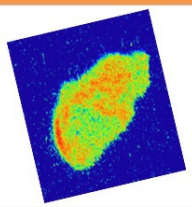

CONTROL ID: 2230998

TITLE: In Vivo Quantitative Analysis with PET of the Dopamine Transporter in the KI-G2019S and KI-R1628P LRRK2 mice with [^{18}F]FE-PE2I

PRESENTER: Zhimin WANG

ABSTRACT BODY:

Abstract Body: Background and Objectives:
Small animal models for leucine-rich repeat kinase 2 (LRRK2) have received great attention recently. Several successful small animal disease models have been developed, for example the LRRK2^{G2019S}, which showed age-dependent decrease in striatal DA content and decreased striatal DA release and uptake in G2019S mice[1]. However, there is no significant differences in striatal TH, and dopamine transporter (DAT) by Western blot analysis[1].

Recently, [^{18}F]FE-PE2I, a DAT radioligand, provides the possibility of quantifying the DAT density using the Positron Emision Tomography (PET) neuroimaging. The main objectives of the present study were (i) to evaluate whether PET imaging allowed reliable quantification of the DAT density changes *in vivo* in a rodent disease model of PD, and (ii) whether there are any demonstrable DAT density changes observed with PET in the KI-G2019S and KI-R1628P (LRRK2 risk variant, which was mainly found in the Asian population) mice models.

Materials and Methods:
A total of 9KI-G2019S and 4 KI-R1628P mice at ages 8.5 to 21.2 months were used for this study. They were categorized as Young group (3KI-G2019STg and 3 KI-G2019S NTg, all 8.5 months), and Ageing group (1KI-G2019STg, 2 KI-G2019S NTg, 2 KI-R1628P Tg, and 2 KI-R1628P NTg, 17.2-21.2 months). 3D dynamic PET scans were performed using the nanoScan PET/MRI scanner (Mediso, Hungary) at SingHealth Experimental Medicine Centre (SEMC). The injected radioactivity was 6.5-16 MBq. The specific radioactivity (SA) was 5.6-24.6 (11.2±5.5) GBq/mmol.

Image and kinetic analyses were performed using the image fusion tool in PMOD (version 3.5; PMOD Technologies, Switzerland), and the [^{18}F]FE-PE2I binding was quantified using the simplified reference tissue model with the cerebellum as reference region. Microsoft Excel was used to assess whether the obtained binding potential (BPnd) values were statistically different or not (t-Stats).

Results:
For the Young group, KI-G2019S Tg mice have higher BPnd values in both right striatum (2.51±0.38) and left striatum (2.46±0.45) as compared to the KI-G2019S NTg mice (2.39±0.34, 2.29±0.29, respectively). However, the changes were not statistically significant (p=0.71and p=0.62). Similarly, In the Ageing group, the BPnd values in KI-R1628P Tg mice was not different from KI-R1628P NTg mice (p=0.70 and p=0.61). Unfortunately, we were not able to make comparisons between the Aging KI-G2019S Tg and NTg mice as the sample size was too small.

Conclusions:
Although there are variations in the BPnd values for all the groups, our results demonstrated that it is possible to quantify the DAT changes with PET imaging with [^{18}F]FE-PE2I. Meaningful (statistical significance) comparisons could be achieved if more mice can be included.

References:
1. X Li *et al*. Enhanced striatal dopamine transmission and motor performance with LRRK2 overexpression in mice is eliminated by familial Parkinson's disease mutation G2019S. J Neurosci. 2010 Feb 3;30(5):1788-97.

AUTHORS (LAST NAME, FIRST NAME): WANG, Zhimin[1]; ZENG, Li[2]; LIM, Christina[2]; CAO, Zhen[2]; TAN, Eng King[2]; Padmanabhan, Parasuraman[1]; Yang, Changtong[1]; Ghosh, Krishna Kanta[1]; Halldin, Christer[1, 3]; Gulyas, Balazs[1, 3]

INSTITUTIONS (ALL):

1. LKC School of Medicine, Nanyang Technological University, Singapore, Singapore.
2. National Neuroscience Institute, Singapore, Singapore.
3. Clinical Neuroscience, Karolinska Institutet, Stockholm , Sweden.

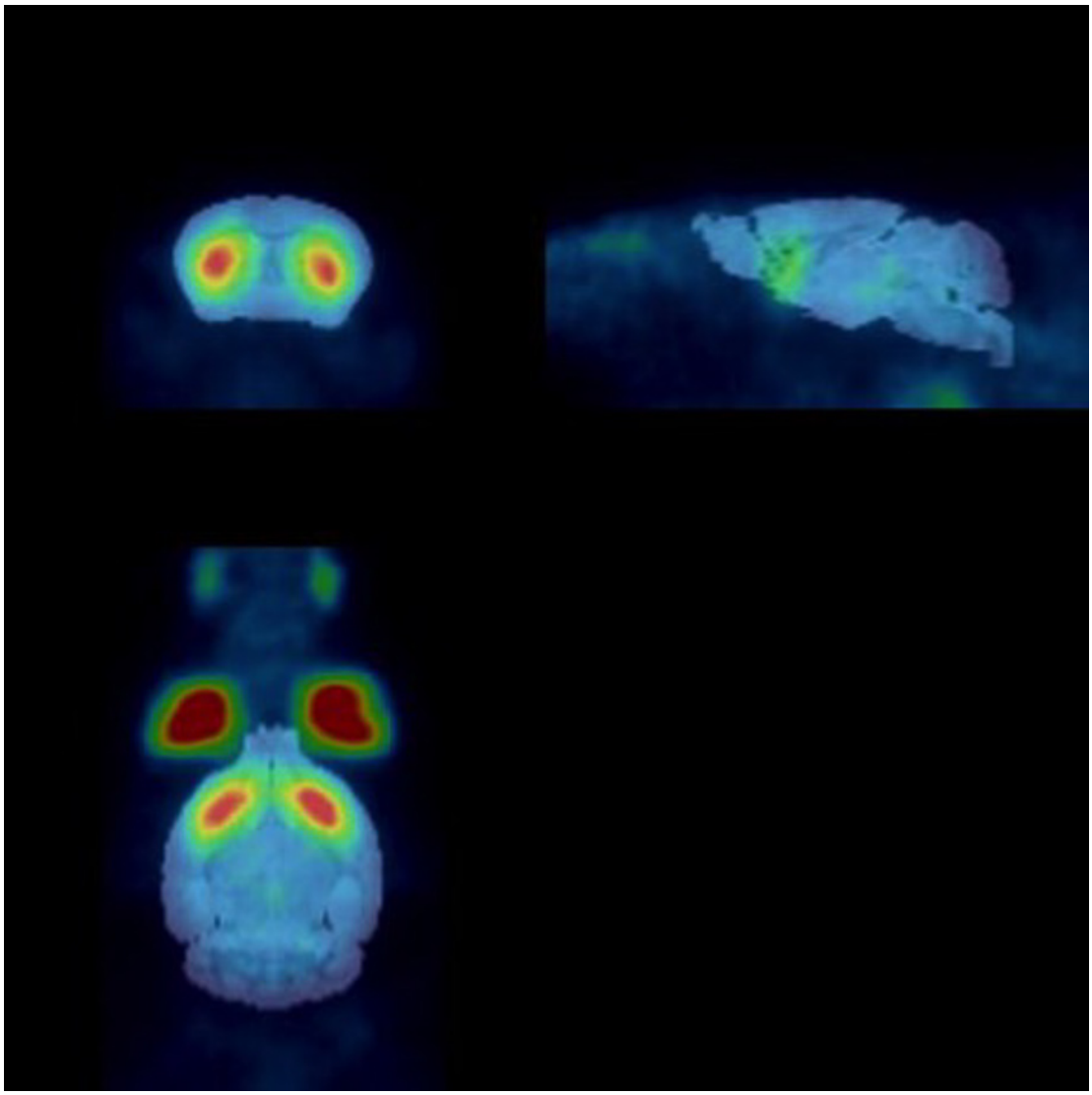

CONTROL ID: 2231019

TITLE: Quantitative evaluation of bone-anatomy compensation methods for MR-based attenuation correction for brain PET imaging in a time-of-flight PET/MRI system

PRESENTER: Jaewon Yang

ABSTRACT BODY:

Abstract Body: Purpose: An atlas-CT-based bone-anatomy compensation for MR-based attenuation correction (MRAC) is a current standard in brain PET/MR imaging. In general, MRAC is achieved by segmenting MR images into three classes with known attenuation properties (sinus/tissue/bone). Among the classes, bone structures are derived from the atlas-CT as Dixon-type water-fat separation does not depict the bone anatomy (1); however, proton-density weighted Zero TE (ZTE) MR bone imaging has demonstrated bone structure segmentation (2). For this reason, this study aims to evaluate and compare the impact of two bone-anatomy compensation methods (MRAC-atlas vs. MRAC-pseudoZTE) for PET quantitation, simulating ZTE-driven pseudoCT using a patient-specific CT.

Methods and Materials: Whole-body FDG-PET/CT followed by PET/MRI were performed for twelve patients. Using the same PET raw data from PET/MRI, time-of-flight (TOF) iterative reconstruction was performed with MRAC-atlas, MRAC-pseudoZTE, and CTAC. In the MRAC-atlas method, the bone structures of *pseudoCT* were extracted from an atlas-CT registered to MR-InPhase; while, in the MRAC-pseudoZTE, the bone structures of *pseudoCT* were derived from a patient-CT registered to MR-InPhase and assigned with a mean value of intensities (HU 500 and above) of the bone structures for simulating ZTE-based bone classification. For quantitative evaluation, CTAC using the patient-CT was considered as gold standard, and PET mean activity concentration values were measured and compared in eight 10 ml volumes-of-interest (VOIs) throughout the brain.

Results: PET activity concentrations were systematically underestimated, compared to CTAC, on average by 0.63±0.34 kBq/ml (4.0±2.2%) and 0.50±0.26 kBq/ml (3.2±1.6%) for the MRAC-atlas and the MRAC-pseudoZTE, respectively ($p < 0.00001$). The MRAC-pseudoZTE provided improved AC accuracy by 0.13±0.29 kBq/ml (0.82±1.85%), compared to that of the MRAC-atlas. However, the error reduction was patient-dependent (highest: 3.4% vs. lowest: -1.9%) and VOI-dependent (highest 1.8% vs. lowest: 0.1%). In both MRAC approaches, the worst result was occurred at the VOI contained in the cerebellum surrounded by the mixture of air, tissue, and bone.

Discussion and Conclusion: For the first time, two distinct bone-anatomy compensation methods (MRAC-atlas vs. MRAC-pseudoZTE) for brain PET imaging in an integrated TOF PET/MRI system were evaluated and compared, simulating ZTE-based MRAC. Overall, the MRAC-pseudoZTE achieves quantification accuracy similar to CTAC within a small but measurable difference of 3.2% on average, which is 1% smaller than the error of the MRAC-atlas. Since the skull has the greatest contribution to the PET quantitative difference, as shown in our simulation, a patient-specific cortical bone anatomy that could be derived from ZTE, if an appropriate single value could be assigned to the bone, would replace an atlas-CT and improve the accuracy of PET quantification.

References

1. S.D. Wollenweber, *et al.*, "Evaluation of an atlas-based PET head attenuation correction using PET/CT & MR patient data," 2012 IEEE NSS/MIC

2. F. Wiesinger, *et al.*, "Zero TE MR bone imaging in the head," 2015 Magn. Reson. Med.

AUTHORS (LAST NAME, FIRST NAME): Yang, Jaewon[1]; Jian, Yiqiang[2]; Tohme, Michel[2]; Behr, Spencer[1]; Vigneron, Daniel[1]; Majumdar, Sharmila[1]; Seo, Youngho[1]

INSTITUTIONS (ALL):

1. Radiology and Biomedical Imaging, UCSF, San Francisco, CA, United States.
2. GE Healthcare, Greater Milwaukee Area, WI, United States.

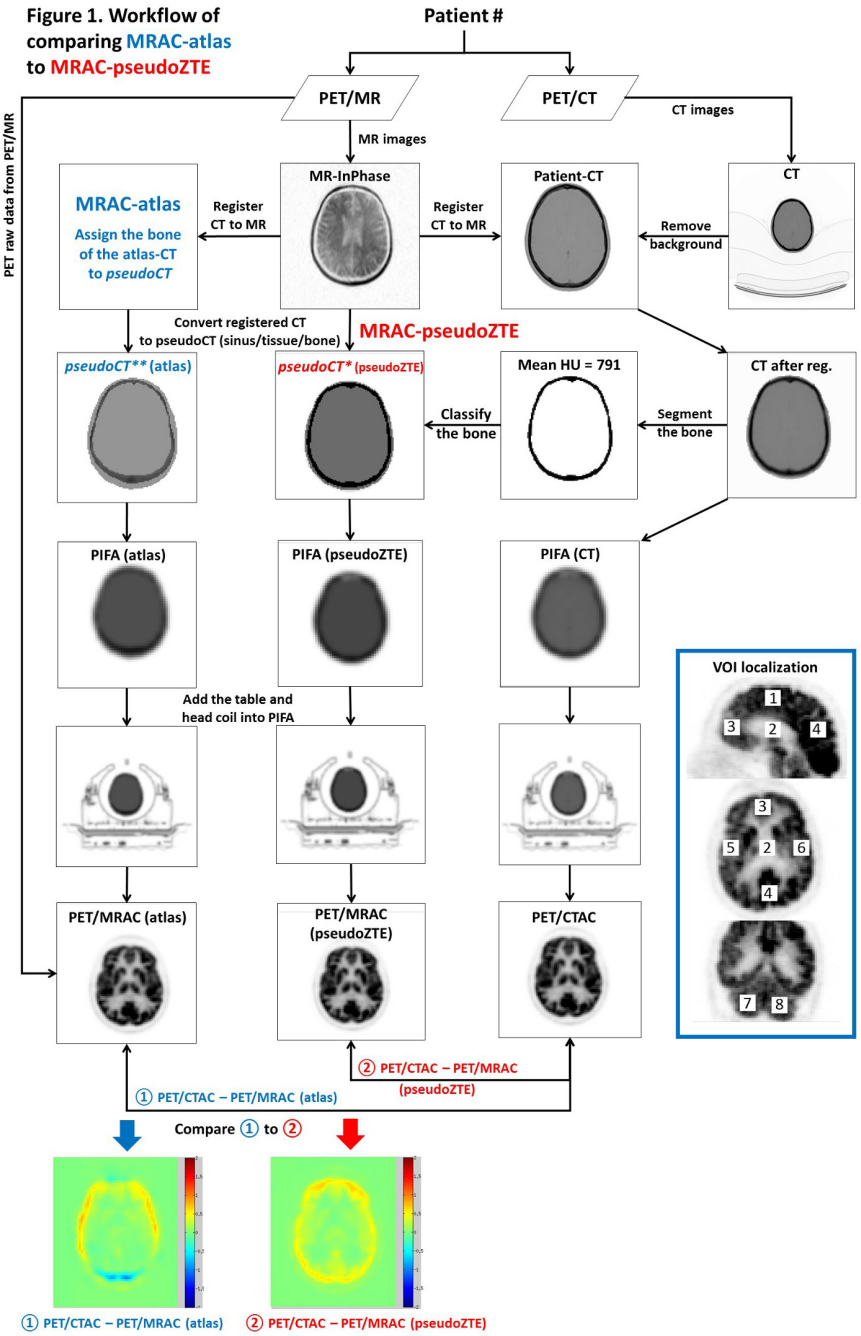

- pseudoCT consists of three classes (sinus/tissue/bone).
- **pseudoCT** (atlas)** : bone structures are extracted from the atlas-CT and has continuous values.
- pseudoCT* (pseudoZTE) : bone structures are extracted from a patient-CT, to which the mean value of the segmented bone is assigned. ZTE-driven pseudoCT** is simulated through using patient-specific CT.

CONTROL ID: 2231037

TITLE: In vivo two-photon imaging of neural activity for small animals

PRESENTER: Hui Hui

ABSTRACT BODY:

Abstract Body: Introduction: The ability of observing *in vivo* neural activity plays central role in neural engineering. In this work, two-photon calcium imaging of spontaneous and sensory-evoked neural activities at L2/3 depth to the cortex is presented. The results show that this method can be applied to observe the activities of neural population with both high spatial and temporal resolution. **Experimental Setup:** AOD based high-speed two-photon microscope was used in this experiment [1]. The image rate can reach up to 200 Hz. A tunable Ti: Sapphire pulsing laser with wave length from 690~1040nm was chosen as excitation source. Water immersion microscope objective with long work distance (×40/0.8NA, WD 3.5 mm) was equipped. **Craniotomy:** Wild type mice C57BL/6 was used for making a small craniotomy (approximately 2x2.5 mm) using a high-speed drill with a small-tip steel burr, centered at 4.5 mm lateral to the midline and 2.5 mm posterior to bregma. A craniotomy preparation process was carefully conducted [2]. **Calcium indicator injection:** With the guidance of two-photon imaging and avoid damaging any blood vessels, the tip of the pipette was navigated to penetrate dura and reach the depth to L4 (~420μm) [3]. By using a micromanipulator, neural population of L2/3 was labeled by calcium indicator OGB-1 AM via patch pipette injection with ~5μL of pipette solution [4]. **Two-photon calcium imaging:** In vivo two-photon calcium imaging was performed after 3 mins of the injection. An appropriate region (200x200 μm^2) of the neural population was chosen for two-photon imaging, see Figure 1 (a). The region of interest (ROI) in the center of the FOV was placed to observe spontaneous and sensory-evoked neural activities. The activities of these recorded neurons can be imaged, allowing for mapping of sensory inputs and imaging calcium transient of cortical neurons, as shown in Figure 1(b).

The proposed technique has been used for studying the functions of neural population by imaging the calcium signals. It is also can be used for mapping the local cortical circuits. It is believed that this technique may help the researchers to understand the mechanisms of brain diseases in the near future. **References:** [1] Grewe, B. F. and F. Helmchen, 2014 Cold Spring Harb Protoc (6). [2] Chen, X., et al., 2012 Nat Protoc 7(10). [3] Stosiek, C., et al., 2003 PNAS, 100(12). [4] Grienberger, C. and A. Konnerth, 2012. Neuron 73(5). **Acknowledgement**: The authors would like to thank Laboratory Members of Brain Research Center, Third Military Medical University for help with performing two-photon imaging experiments. This work was supported in part by the National Basic Research Program of China (973 Program) Grant 2011CB707700, the National Natural Science Foundation of China under Grant Nos. 81227901, 61231004, 81471739, 81301346, the Chinese academy of sciences, scientific research and equipment development project under Grant No. YZ201457.

AUTHORS (LAST NAME, FIRST NAME): Hui, Hui[1]; Dong, Di[1]; Ma, Xibo[1]; Yang, Xin[1]; Tian, Jie[1]

INSTITUTIONS (ALL):

1. Key Laboratory of Molecular Imaging, Institute of Automation, Beijing, China.

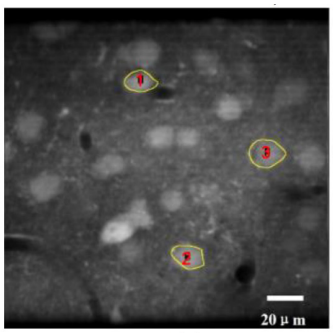
1
3
2
20 μ m

(a)

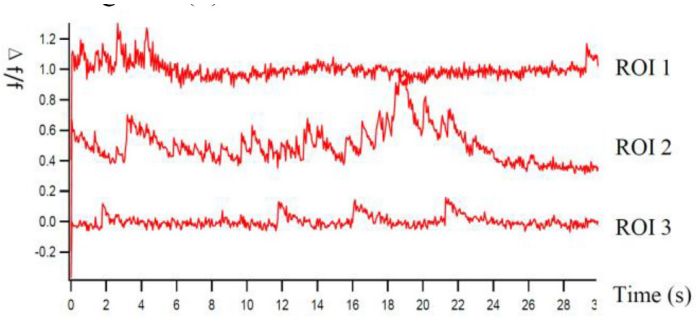
ΔF/F
1.2
1.0
0.8
0.6
0.4
0.2
0.0
-0.2
0
2
4
6
8
10
12
14
16
18
20
22
24
26
28
ROI 1
ROI 2
ROI 3
Time (s)

(b)

CONTROL ID: 2231041

TITLE: F-18 PET/CT findings of Helicobacter pylori-positive and Helicobacter pylori-negative gastric mucosa-associated lymphoid tissue lymphoma

PRESENTER: YE YOUNG SEO

ABSTRACT BODY:

Abstract Body: Background: Helicobacter pylori (H. pylori) infection is suggested to be causally associated with primary gastric mucosa-associated lymphoid tissue (MALT) lymphoma. This study evaluates the F-18 PET/CT findings of low-grade gastric mucosa-associated lymphoid tissue lymphoma depending on Helicobacter pylori positivity.

Methods: From January 2007 to December 2010, a total of 30 patients with gastric MALT lymphoma were enrolled. To assess the differences in clinical characteristics and PET/CT findings between H. pylori-positive (n=17, 57%) and H. pylori-negative (n=13, 43%) cases, we compared these 2 types of lymphoma.

Results: Abnormal gastric FDG uptake was observed in 41% of tumors in the H. pylori-positive group and 39 % of cases in the H. pylori-negative group. The mean maximum standardized uptake values for H. pylori-positive patients and H. pylori-negative patients were 3.8 and 4.5, respectively, no significant differences were observed between the 2 groups. There was no significant correlation between the 2 groups in terms of age or staging.

Conclusions: No significant differences in PET/CT findings were observed between the H. pylori-positive and H. pylori-negative groups.

AUTHORS (LAST NAME, FIRST NAME): SEO, YE YOUNG[1]; Sohn, Hyung Sun[1]; Kim, Sung Hoon[2]

INSTITUTIONS (ALL):

1. Department of Radiology, Yeouido St Mary's Hospital, College of Medicine, The Catholic University of Korea, Seoul, Korea (the Republic of).
2. Department of Radiology, Seoul St Mary's Hospital, College of Medicine, The Catholic University of Korea, Seoul, Korea (the Republic of).

(No Image Selected)

CONTROL ID: 2232480

TITLE: Ductal carcinoma in situ and ductal carcinoma in situ with microinvasion: correlation of F-18 FDG uptake with histological and biological prognostic factors

PRESENTER: YE YOUNG SEO

ABSTRACT BODY:

Abstract Body: Purpose

The aim of this study was to assess the correlation between FDG uptake values on PET/CT with histological and biological prognostic factors in ductal carcinoma in situ (DCIS) and ductal carcinoma in situ with microinvasion (DCIS-Mi).

Materials and Methods

PET/CT images for initial staging of confirmed DCIS and DCIS-Mi patients, taken between July 2004 and December 2009, were reviewed retrospectively. Maximum standardized uptake values (SUVmax) and tumor background count density ratio (TBCDR) on PET/CT were compared with tumor characteristics. Histological and biological prognostic factors included tumor size, nuclear grade, Van Nuys Prognostic index (VNPI), estrogen receptor, progesterone receptor, c-erbB2, and Ki-67 index.

Results

In total, 87 lesions from 83 patients (all females; mean age 51±9 years) were studied. The VNPI group was 1 in 25 lesions, 2 in 36, and 3 in 26. On statistical analysis, significant differences in SUV max and TBCDR were seen between the VNPI groups and according to tumor size and c-erbB2. The correlation between SUV max and Ki-67 was significant. However, the correlation between TBCDR and Ki-67 was not statistically significant.

Conclusions

In DCIS and DCIS-Mi cases, significant correlations were found between increased FDG uptake and several histological and biological factors for poor prognosis (tumor size, VNPI, and c-erbB2).

AUTHORS (LAST NAME, FIRST NAME): SEO, YE YOUNG[1]; Yoo, Ie Ryung[3]; Sohn, Hyung Sun[2]

INSTITUTIONS (ALL):

1. Department of Radiology, Yeouido St Mary’s Hospital, College of Medicine, The Catholic University of Korea, Seoul, Korea (the Republic of).

2. Department of Radiology, Yeouido St Mary’s Hospital, College of Medicine, The Catholic University of Korea, Seoul, Korea (the Republic of).

3. Department of Radiology, Seoul St Mary’s Hospital, College of Medicine, The Catholic University of Korea, Seoul, Korea (the Republic of).

(No Image Selected)

CONTROL ID: 2231715

TITLE: Hybrid Poly Acrylate Nanoparticles as Novel Photoacoustic Imaging Probes

PRESENTER: Yihong Li

ABSTRACT BODY:

Abstract Body: Introduction: Photoacoustic imaging (or optoacoustic imaging) is a dual imaging modality that overcomes the depth limitation of the current traditional optical imaging techniques while preserving relatively high contrast. Contrast agents can been used to achieve contrast-enhanced photoacoustic imaging at a molecular and cellular level which has presently attracted a great deal of attention. Herein we introduce exogenous hybrid photoacoustic imaging probes capable of detecting biological processes more concisely and conveniently. **Method**: Poly acrylate-based hybrid nanoparticles were constructed via emulsification to encapsulate methylene blue(MB) along with acrylate polymerization. The particle size distribution and zeta potential were examined by using dynamic light scattering (Malvern NANO ZS and NANOSIGHT 300), and the embedding structure was characterized by scanning electron microscopy (SEM), transmission electron microscopy (TEM). MB loading and encapsulation efficiency were determined in triplicate using an ultraviolet-visable (UV-Vis) spectrophotometer at an excitation wavelength λ_{MB}=664nm. **Results:** The mean diameter of pure poly acrylate nanoparticles was 338.7nm (PDI=0.158), while after the encapsulation of MB, the diameter of hybrid nanoparticles was 525.1nm (PDI=0.112), and the zata potential was approximately -4.52mV, which indicated that a negative charge was formed on the surface of the hybrid nanoparticles. Moreover, SEM images show that the hybrid poly acrylate-MB nanoparticles exhibited a smooth and uniform spherical morphology. In addition, the concentration of encapsulated MB is 7.6μg/mL, which afforded the encapsulation efficiency of MB was approximately 1%. Even at this low concentration, the photoacousitc phantom imaging showed a satisfactory sensitivity that as-constructed poly acrylate nanoparticles demonstrated good imaging response at the laser exposure wavelength of 680nm. **Conclusions:** We have successfully developed an MB-loaded poly acrylate photoacoustic imaging probes for photoacoustic imagining. Our in vitro experiment demonstrated that these hybrid probes could enhance the sensitivity as an exogenous photoacoustic contrast agent. Further functionalization with targeting moieties and biomedical applications as vehicles for image-guided diagnostics and therapy are under investigation. **Acknowledgment:** This work was financially supported by Scientific Research Foundation for Returned Scholars, Ministry of Education of China and Start-up funding of Wenzhou Institute of Biomaterials and Engineering (Grant WIBEZD2014005-02).

AUTHORS (LAST NAME, FIRST NAME): Li, Yihong[1]; Song, Yuanhui[1]; Shi, Changcan[1]; Wang, Jie[1]; Liu, Zhe[1]

INSTITUTIONS (ALL):

1. Wenzhou Institute of Biomaterials and Engineering, Chinese Academy of Sciences, Wenzhou, Zhejiang, China.

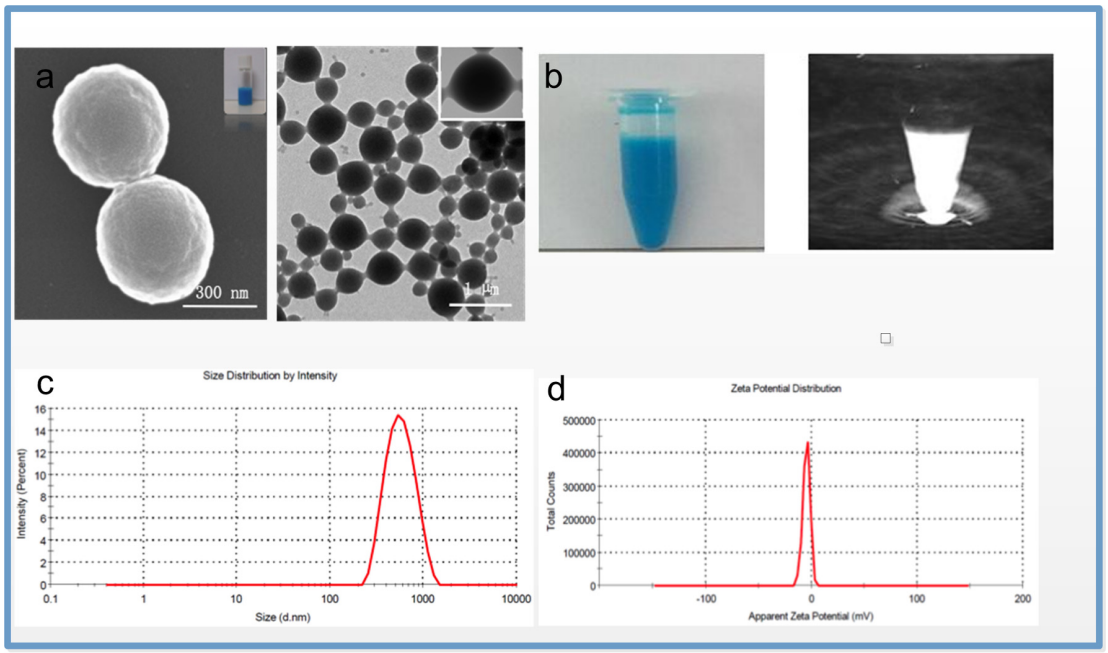

(a)TEM and SEM images of hybrid nanoparticles; (b) Photograph of hybrid nanoparticles and phantom imaging at the laser excition of wavelength 680nm ([MB] = 7.6μg/mL); Measurement of (c) size distribution and (d) zeta potential of hybrid nanoparticles.

CONTROL ID: 2231046

TITLE: Glutathione responsive anti-proliferative nanoparticle for efficient delivery of therapeutic gene in colon cancer xenograft mouse model

PRESENTER: IN KYU PARK

ABSTRACT BODY:

Abstract Body: In cancer gene therapy, one of the major concerns is to improve the therapeutic efficacy of the gene and minimize non specific targeting. Hence, nanoparticle based gene delivery happens to be the most effective method of delivering therapeutic genes in tumor cells. In cells, anti-oxidising agent Glutathione happens to be cleaving disulfide bonds in the cytoplasmic protein and also its concentration in most cancer cells are higher compared to the normal cells. Considering this fact, a disulfide crosslinked cationic polymer linked with a therapeutic siRNA through disulfide bonding was designed aiming for high transfection as well as proper release. Therefore for the current study, disulfide crosslinked polyethylenimine (ssPEI) was conjugated with thiolated Akt1 protein kinase siRNA (SH-Akt siRNA) and improvement in the therapeutic efficacy of the Akt1 siRNA in colon cancer xenograft mouse model was studied. Akt1 is one of the key components of PIK3/Akt1 signalling pathway, which signals the downstream molecules that controls the elements responsible for cancer cell proliferation and apoptotic inhibition. It is considered to be one of the prime targets for preventing tumor development. Silencing of Akt1 protein using siRNA in many cancer cells has shown reduction in cell proliferation and induction of apoptosis. The physiochemical characterization of the nanoparticle has shown that the disulfide bonding between SH-Akt siRNA and ssPEI has enhanced the complexation and reduced surface charge with smaller average particle sizes even at lower N/P ratio compared to the branched PEI/SH-Akt siRNA polyplex. And also the cellular uptake of the nanoparticle in CT-26 mouse colon cancer cells is enhanced. In in-vitro condition, this increase in cellular uptake and siRNA release from nanoparticle in the cytoplasm has lead to reduction in cell proliferation as well as induction of apoptosis in CT-26 colon cancer cell line. Downregulation of Akt1 expression and Tumor volume reduction was observed in invivo mouse tumor model. Overall, the Akt1 silencing using ssPEI/SH-Akt siRNA have improved both in vitro and invivo mouse tumor model.

AUTHORS (LAST NAME, FIRST NAME): PARK, IN KYU[1]; Muthiah, Muthunarayanan[1]; Che, Hui-Lian[1]; Rajendrakumar, Santhosh K.[1]

INSTITUTIONS (ALL):

1. Department of Biomedical Sciences, Chonnam National University, Hwasun, Korea (the Republic of).

(No Image Selected)

CONTROL ID: 2231053

TITLE: Therapeutic microRNA 145/osmotically active sorbitol modified PEI nanoparticle suppresses cell proliferation in breast cancer cell line

PRESENTER: IN KYU PARK

ABSTRACT BODY:

Abstract Body: In cancer gene therapy, developing a safe and accelerated gene transfer system to deliver nucleic acids have been focussed a lot nowadays. Previously, studies have been shown that the polysorbitol modified PEI have improved the transfection efficiency as well as selective particle intake via caveolea endocytosis in cancer cells. In cancer cells, MicroRNAs (miRNA) which are basically short oligonucleotides of endogenous origin involved in post-transcriptional regulation are altered. miRNA 145 is a novel tumor suppressor gene involved in cell suppression, invasion and migration of cancer cells; it is downregulated in most of the cancer cells. Hence for cellular delivery of miRNA 145, polysorbitol-mediated transporter (PSMT) was used and since it has polysorbitol backbone that osmotic property, it will lead to enhanced cellular uptake. PSMT delivers genes into cells by a caveolea-mediated endocytic pathway. Caveolea expression is usually altered in transformed cancer cells. Physicochemical characterization, transfection efficiency and transgene expression capability of PSMT/reporter plasmid DNA nanoparticles, were determined. GFP-tagged miRNA 145 delivery with PSMT was confirmed by confocal microscopy and Western blotting. The functional effects of miRNA 145 delivered with PSMT were analyzed by confocal microscopy, as well as in apoptosis, proliferation and wound healing assays. Finally, the expression of a miRNA 145 target protein, c-myc, was determined by Western blotting after intracellular delivery of PSMT/miRNA 145 nanoparticle (NP). Therefore in in-vitro condition, microRNA 145 delivered by PSMT in breast cancer cells have shown reduction in cell proliferation better than the control carrier.

AUTHORS (LAST NAME, FIRST NAME): PARK, IN KYU[1]; Muthiah, Muthunarayanan[1]; Lee, Hwa-Jeong[1]

INSTITUTIONS (ALL):

1. Department of Biomedical Sciences, Chonnam National University, Hwasun, Korea (the Republic of).

(No Image Selected)

CONTROL ID: 2232251

TITLE: Role of p38 MAPK on MMP Activity in Ischemic Stroke as Measured by a Novel Fast MMP Activatable Nanoprobe

PRESENTER: Di Chang

ABSTRACT BODY:

Abstract Body: Matrix metalloproteinases (MMPs) exert a deleterious role in ischemic stroke by acutely disrupting blood-brain barrier (BBB) and promoting edema and hemorrhage, representing an ideal therapeutic target in ischemic stroke. However, to date nearly all clinical trials regarding MMP inhibitors have failed and new treatments to inhibit MMP activity with fewer side-effects are required. Emerging evidences suggest that p38 mitogen-activated protein kinase (MAPK) signal transduction pathway may be involved in the regulation of MMP activity. Therefore, we used a p38 MAPK inhibitor RWJ67657 to test whether the down-regulation of p38 MAPK can produce therapeutic effects through the suppression of MMP activity in ischemic stroke. More importantly, a novel fast and ultrasensitive MMP activatable optical probe was used for the real-time visualizing of MMP activity in stroke mice non-invasively and dynamically. This new strategy for the first time enables a fast and direct visualizing of MMP activity and effectively monitoring of the decreased MMP activity during treatment. Using this probe, we observed that RWJ67657 significantly reduced the MMP activity in ischemic stroke model. Further analysis, we found that this inhibitor specifically reduced MMP-9 but not MMP-2 activity. These findings implied that MMP-9 activity is involved in p38 MAPK mediated stroke damage.

AUTHORS (LAST NAME, FIRST NAME): Chang, Di[1]; Ju, Shenghong[1]

INSTITUTIONS (ALL):

1. Department of Radiology, Zhongda Hospital, Medical School of Southeast University, Nanjing, jiangsu, China.

Figure 1

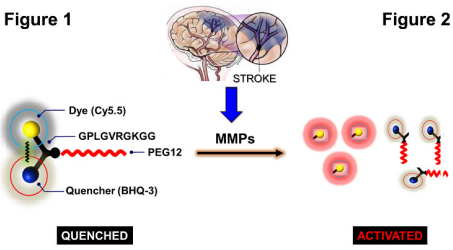

Figure 1. Chemical structure of MMP-P12 probe.

Figure 2

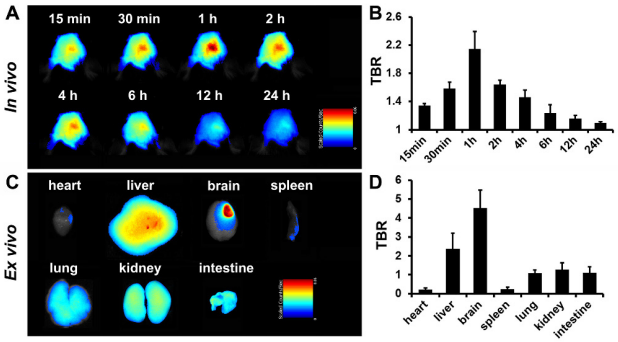

Figure 3

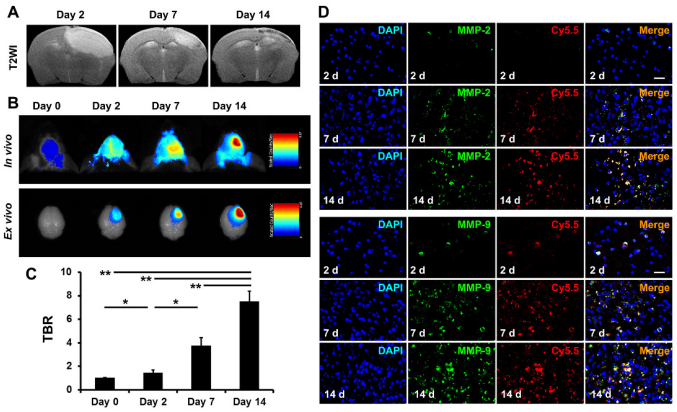

Figure 4

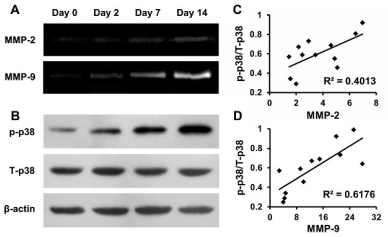

Figure 5

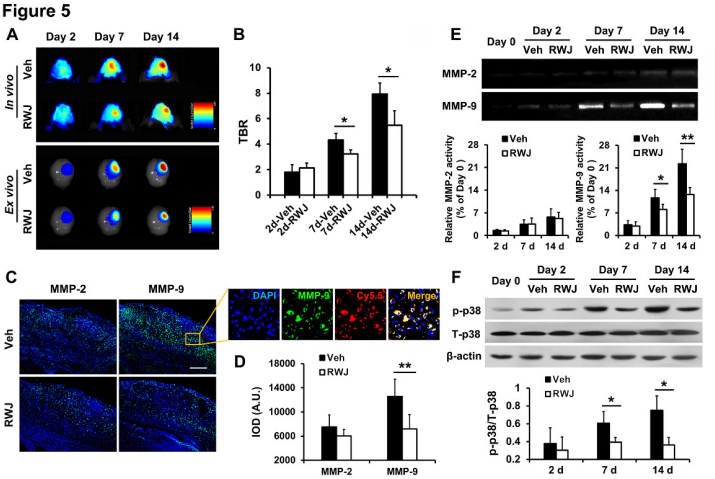

Figure 1. Chemical structure of MMP-P12 probe.

Figure 2. *In vivo* NIRF imaging and *ex vivo* biodistribution of MMP-P12 probe.

Figure 3. Time course evaluation of MMP activity correlating with stroke development.

Figure 4. Correlation of MMP expression to p38 MAPK activation.

Figure 5. P38 MAPK inhibition reduced MMP activities.

CONTROL ID: 2231068

TITLE: Development of a multi-purpose low-profile γ-ray imaging detector

PRESENTER: Young-Jun Jung

ABSTRACT BODY:

Abstract Body: The imaging performance of γ-ray detectors for nuclear medicine is highly dependent on the optimization of the detector specifications for radioisotopes (RIs). For tomographic systems, expandability and compatibility are also key factors for detector development. In almost the entire development of PET/MRI and SPECT/MRI, PET or SPECT gantry is inserted into the bore of MRI. Therefore, keeping the detector as slim as possible is an important issue in designing an MRI-insert PET to widen the bore size. Regardless of the energy targeted, acquiring a high-resolution image is an important issue, especially for SPECT, to enable the use of various types of RIs. In this regard, this study aims to develop a multi-purpose low-profile γ-ray detector that is practically applicable to most nuclear medicine imaging systems.

The scintillator is a pixelated Ce:GAGG (Furukawa Co., Ltd.) array, which has a high density (6.63 g/cm^3), excellent light yield (57,000 photon/MeV), and no emission of background radiation. The size of the scintillator array is 26.7 mm × 26.7 mm (31 × 31 pixels), and the pixel dimension is 0.7 mm × 0.7 mm × 5 mm (Fig. 1(a)). The photo-sensor is MPPC (Hamamatsu S11830-3344MF), which has a small dead area, low dark current, and thin FPC-type connector for the signal readout. The sensor is tiled into 2 × 2, and the dimension is 28.6 mm × 27.2 mm (Fig. 1 (b)). An acrylic light guide (2 mm) was coupled between the MPPC and the scintillator (Fig. 1 (c)). The readout electronics are composed of a resistive chain and a charge-sensitive preamplifier circuit. The resistive chain was created by modification of the discretized positioning circuit for efficient channel reduction and positioning. To acquire flood images, an FPGA-based data acquisition (DAQ) board with 12-bit serial ADCs and DAQ firmware, which was developed by our research group, was used in the study.

The flood map of the scintillator array for Na-22 and Ba-133 is shown in Fig. 2 (a) and (c). The profiles (marked with a black line on the figure) of both RIs are shown in Fig. 2 (b) and (d). The peak-to-peak distance between the pixels is 0.8 mm. The Na-22 flood image represents more peaks than the Ba-133 image. Moreover, the average pixel value for the peaks is also higher in the Na-22 flood image than in the Ba-133 image. Although the flood image of Ba-133 is worse, the separations are sufficient to set the position boundaries for both RIs, except for the edge. The total height of the detector is about 1 cm, including the readout circuit. The DAQ board will be replaced with an Ethernet-based data communication-type FPGA board, which has the merit of system extension.

AUTHORS (LAST NAME, FIRST NAME): Jung, Young-Jun[3]; Min, Eungi[1]; Lee, Hakjae[4]; Cha, Hyemi[3]; Jeong, Sang-Goo[4]; Kim, KyeongMin[2]; Lee, Kisung[4]

INSTITUTIONS (ALL):

1. Department of IT convergence, Korea University, Seoul, Korea (the Republic of).
2. Molecular Imaging Research Center, Korea Institute of Radiological and Medical Sciences, Seoul, Korea (the Republic of).
3. Department of Bio-convergence Engineering, Korea University, Seoul, Korea (the Republic of).
4. School of Biomedical Engineering, Korea University, Seoul, Korea (the Republic of).

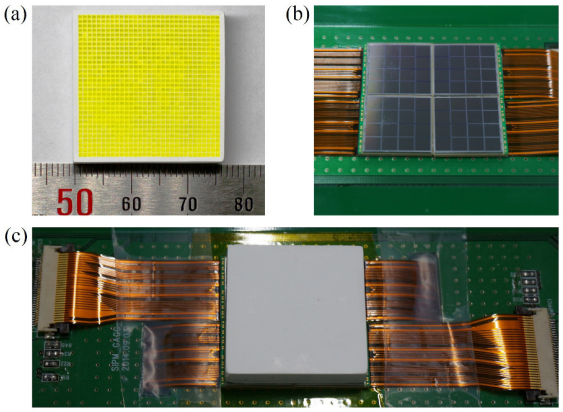

Figure 1. Low profile gamma ray imaging detector based on (a) 0.7 mm pixel Ce:GAGG scintillator, (b) 2×2 MPPC array, and (c) detector assembly with 2 mm acrylic plate for the light guide.

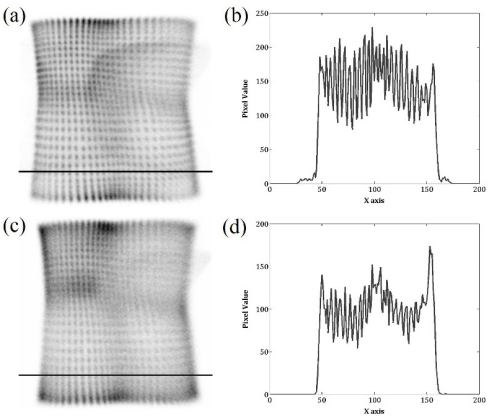

Figure 2. The flood map image of (a) Na-22 (511 keV) and (b) the line profile, and the flood map image of (c) Ba-133 (356 keV) and (d) the line profile of the low profile γ-ray imaging detector with a standard radiation sources.

CONTROL ID: 2236360

TITLE: Two Level Multi-pinhole Collimator for a Small Field of View Gamma Imaging System

PRESENTER: Jaekeon Bae

ABSTRACT BODY:

Abstract Body: Image resolution and system sensitivity are major performance indicators in single-photon emission computed tomography. The multi-pinhole (MP) collimator is used for high resolution small-animal and clinical organ-specific imaging. We have been developing an 8-hole MP collimator for a high resolution rectangular shaped small field of view gamma camera. The FOV size of 8-hole collimator is 90 mm (diameter), and each hole covers exactly one-eighth of the entire detector. The sensitivity of 8-hole collimator increased six times higher than that of single-pinhole collimator. However, the image resolution of 8-hole collimator is 15% less because the 8-hole collimator has a one-third magnification factor [1].

This study aims to design a high-resolution and high-sensitivity collimator for a gamma-ray imaging system. To increase the resolution and sensitivity of the 8-hole collimator, we propose the use of a 5-hole collimator. The collimator has two types of holes: the center hole and four surrounding holes. The use of two types of holes has different aims. The center hole is designed mainly to increase collimator resolution and sensitivity. It has a maximized magnification factor up to 1.2 and has a closer object-to-collimator distance than the surrounding holes have. These surrounding holes are optimized to increase sensitivity. To cover the remaining area of the detector outside of the center hole, he surrounding holes have a smaller coverage than the center hole has. The surrounding holes have a smaller magnification factor and farther object-to-collimator distance than the center hole has, so that the efficiency of the detector is maximized. The 5-hole collimator is illustrated in Figure 1, and the specifications of the two types of holes are listed in Table 1. Figure 1(a) shows conceptual illustration of the 5-hole collimator and figure 1(b) displays the top view of pinhole coverage area on the detector.

To evaluate the performance of the proposed collimator, a simulation model was built with the geant4 application for tomographic emission simulation tool. Figure 1(c) shows the results of the 8-hole collimator and 5-hole collimator. Nine spherical phantoms that have an inter-phantom distance of 30 mm, as shown in Fig. 1(c), were used. The each phantom diameter is 5 mm. The activity of each source is 5mCi. The total angle coverage is 360°, and the projection angle intervals are 3°. The total number of projections is 120, and each acquisition time is 5 seconds. In the case of the 5-hole collimator, the full width at half maximum of a central phantom is 5.0 mm while that of 8-hole collimator is 9.7mm. The total counts of a projection are 72k and 237k for 8-hole collimator and 5-hole collimators, respectively. Up to the conference, we will verify the suitability of our proposed MP collimator to small-animal and organ-specific applications by more simulation studies.

Reference

Jaekeon Bae, Seungbin Bae, Kisung Lee, Yong Choi, Yongkwon Kim, Jinhun Joung, "Design and Performance Investigation of Multi-pinhole Collimator for a Small Field of View Gamma Imaging System", Journal of the Korean Physical Society, Vol. 64, No. 7, pp. 970-975, 2014.

AUTHORS (LAST NAME, FIRST NAME): Bae, Jaekeon[1]; Jung, Young-Jun[1]; Min, Eungi[1]; Chun, Jaehee[1]; Joung, Jinhun[2]; Kim, Yongkwon[2]; Lee, Kisung[3]

INSTITUTIONS (ALL):

1. Department of Bio-convergence Engineering, Korea University, Seoul, Korea (the Republic of).
2. Nucare Medical Systems, Yeonsu-gu, Incheon, Korea (the Republic of).
3. School of Biomedical Engineering, Korea University, Seoul, Korea (the Republic of).

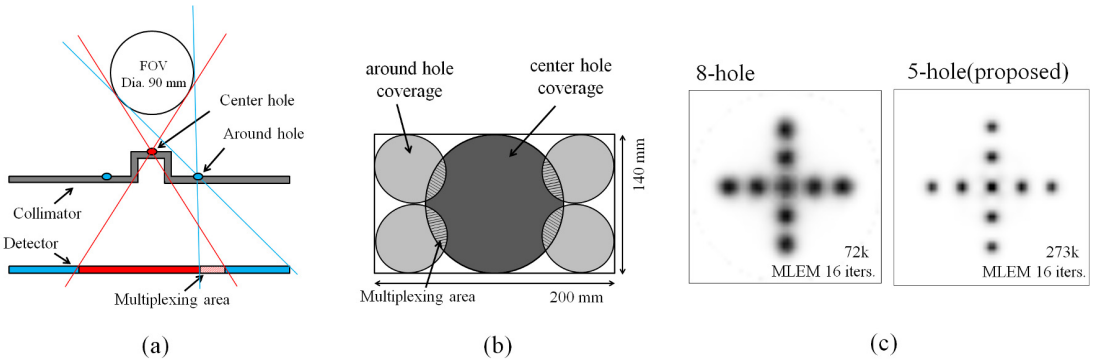

Figure 1. (a) is conceptual illustration of 5-hole collimator, (b) is the top view of pinhole coverage area on the detector, and (c) is the reconstruction images of 8-hole collimator and 5-hole collimator.

CONTROL ID: 2231082

TITLE: Molecular ultrasound imaging using targeted contrast agents and signal quantification based on the law of mass action

PRESENTER: Sithira Ratnayaka

ABSTRACT BODY:

Abstract Body: The objective of this study was to develop a novel algorithm for evaluating and defining perfusion parameters using contrast enhanced molecular ultrasound (US). The algorithm describes the US signal produced by the perfusion of microbubble contrast agents (MB) in a flow environment, and provides physically relevant units as parameters.

Custom flow phantoms for US imaging were made by pouring heated gelatin, corn starch, and water in a mold with three 2-mm diameter wires. Upon cooling wires were removed and channels were incubated with biotin/water solution (1-10 mg/ml) for 12 h. A flow pump pushed biotin-targeted MB's (Targestar-SA) from a reservoir through the flow phantom. A second pump added diluted the MB solution with water. US signal was acquired using a SONIX RP scanner with a L14-5 transducer (Ultrasonix) and a pulse-inversion harmonic imaging preset (transmit/receive at 5/10 MHz). A novel algorithm was developed using parameters observed using the flow phantom setup via US imaging. Construction of the algorithm was initiated using the laws of mass-action binding and chemical mass balance. The algorithm's variables were: initial MB concentration (MB/ml), MB decay rate (MB/ml), flow speed (ml/min), binding affinity (binding %) and reversible binding (binding %). All parameters were observed as a function of time (s). Matlab software was developed for both US image processing and initial development and testing of the algorithm.

When applying the algorithm to the in vitro model, it was found that, using curve-fitting, the algorithm provided a good fit ($R^2 > 0.8$). Individual algorithm parameters also showed close association; for an initial contrast agent injection of 10^5 MB/ml, the algorithm estimated $1.05*10^5$±5% MB/ml (5% difference, $p = 0.14$). For an observed flow speed of 1 ml/min, it projected 1.08±9% ml/min (8% difference, $p = 0.3$). For a sample decay rate of 100 MB/min, the calculated speed was 103.12±5% (3% difference, $p = 0.43$). Binding showed a positive correlation with the molecular US signal using digital subtraction (intensity of last data point subtracted from the background/first data point), ($R^2 > 0.8$, $p < 0.05$). The reversible binding rate had a negative correlation with the digital subtraction ($R^2 > 0.69$, $p < 0.05$).

In conclusion, a novel algorithm for perfusion parameters using contrast enhanced molecular US was developed. This algorithm can provide clinically relevant measurements, which can in turn be used for exploring phenomena highlighted by contrast enhanced US.

AUTHORS (LAST NAME, FIRST NAME): Ratnayaka, Sithira[1]; Hoyt, Kenneth[2, 1]

INSTITUTIONS (ALL):

1. Biomedical Engineering, University of Alabama at Birmingham, Birmingham, AL, United States.
2. Radiology, University of Alabama at Birmingham, Bimingham, AL, United States.

(No Image Selected)

CONTROL ID: 2231102

TITLE: Comparison of tumor uptake of the radiotracers targeting cancer metabolism

PRESENTER: Takako Furukawa

ABSTRACT BODY:

Abstract Body: The distinct metabolism of cancer cells relying on glycolysis is gaining renewed attention as a “hallmark of cancer” (1) since its close connection to alteration in oncogenes and signaling pathways has been revealed. Why cancer cells rely on glycolysis, an inefficient process to produce ATP, is not fully understood, however, a probable cause proposed is that the products of glycolysis can be used to meet the need for large amount of substrate to support the rapid proliferation (2). The importance of glutamine metabolism, in addition to glucose, has been reported recently. Various pharmaceuticals targeting the cancer metabolism have been developed both for therapy and diagnosis. As PET radiopharmaceuticals, 2-deoxy-2-[^{18}F]fluoro-D-glucose ([^{18}F]FDG) for glucose metabolism is widely used in clinics, along with 3’-deoxy-3’-[^{18}F]fluorothymidine ([^{18}F]FLT) reflecting DNA synthesis and [^{11}C]acetate for fatty acid synthesis. The development of PET radiopharmaceuticals for glutamine metabolism is also quite active. The tumor accumulation of these pharmaceuticals is expected to predict prognosis, although there still is some controversy and the relation of their accumulation to each other needs more examination.

In this study, to examine the above relation, we compared tumor accumulation and intratumoral distribution of FDG, FLT, acetate and glutamine, administering two radiotracers with different half-lives in combination, [^{18}F]FLT and [^{14}C]FDG for example, into tumor bearing mice. In the double tracer biodistribution study, positive correlation was only observed between FDG and glutamine, and FLT and acetate. The intratumoral distributions of the two tracers in the above two combinations showed similarity, but in the other combinations the two tracers often showed different pattern. From our observation, accumulation and intratumoral distribution of the four PET pharmaceuticals or tracers, FDG, FLT, acetate and glutamine, could be different, although they are all supposed to reflect tumor cell proliferation. Some caution may be necessary when we are interpreting their tumor accumulation.

References

Hanahan D, Weinberg RA. Hallmarks of cancer: the next generation. Cell. 2011, 1445:646-74.

Vander Heiden MG, Cantley LC, Thompson CB. Understanding the Warburg effect: the metabolic requirements of cell proliferation. Science. 2009, 3245930:1029-33.

AUTHORS (LAST NAME, FIRST NAME): Furukawa, Takako[1]; Yuan, Qinghua[1]; Jin, Zhao-Hui[1]; Aung, Winn[1]; Saga, Tsuneo[1]

INSTITUTIONS (ALL):

1. Molecular Imaging Center, National Institute of Radiological Sciences, Chiba, Japan.

(No Image Selected)

CONTROL ID: 2231109

TITLE: Intravascular molecular-structural NIRF-OCT assessment of stent fibrin deposition and tissue coverage in coronary stents in vivo

PRESENTER: Jason McCarthy

ABSTRACT BODY:

Abstract Body: Background: Unhealed stents, characterized by fibrin deposition and de-endothelialized stent struts, are at risk for stent thrombosis. In addition, bare metal stents (BMS) and drug-eluting stents (DES) heal differentially, but their integrated molecular-structural signatures and timecourses have not been characterized in vivo.

Objectives: To assess *in vivo* fibrin deposition and persistence on BMS and DES using near-infrared fluorescence (NIRF) molecular imaging, and understand fibrin deposition in the context of stent coverage simultaneously assessed by optical coherence tomography (OCT).

Methods: New Zealand white rabbits underwent implantation of one BMS and one DES without overlap in the infrarenal aorta (N=24 3.5x12mm stents). At 7 or 28 days post stenting, the fibrin-targeted NIRF molecular imaging agent (FTP11-CyAm7) was intravenously injected. Two hours later, intravascular NIRF-OCT was performed. Subsets of rabbits underwent serial imaging at day 7 and day 28. Ex vivo imaging, NIRF and OCT image analysis, and histopathology were performed.

Results: Intravascular NIRF-OCT enabled accurate and high-resolution imaging of fibrin overlying stent struts in vivo, as confirmed by microscopy. Compared to BMS, DES evolved greater fibrin deposition and fibrin persistence at both day 7 and day 28 ($p<0.01$ vs. BMS), with the highest fibrin signals noted at the stent edges. Remarkably, for edge stent struts identified as “covered” by OCT, 92.8±2.7% of DES and 55.8±6.3% of BMS struts were NIRF fibrin-positive at day 7. At day 28, 18.6±3.8% (DES) and 5.1±3.1% (BMS) of struts remained NIRF fibrin-positive.

Conclusions: Intravascular NIRF-OCT fibrin molecular-structural imaging markedly improves the identification of unhealed stents compared to standalone OCT . demonstrates that DES evolve greater fibrin deposition and fibrin persistence than BMS in vivo. Fibrin molecular imaging further demonstrates that OCT stent coverage is not necessarily benign. These findings support the concept that NIRF-OCT fibrin molecular imaging could provide new insights into stent healing using coronary translatable technology.

AUTHORS (LAST NAME, FIRST NAME): Hara, Tetsuya[1]; Ughi, Giovanni J.[2]; McCarthy, Jason[3]; Erdem, Sibel[3]; Mauskapf, Adam[1]; Tearney, Guillermo[2]; Jaffer, Farouc[1]

INSTITUTIONS (ALL):

1. Cardiovascular Research Center, Massachusetts General Hospital, Boston, MA, United States.
2. Wellman Center for Photomedicine, Massachusetts General Hospital, Boston, MA, United States.
3. Center for System Biology, Massachusetts General Hospital, Boston, MA, United States.

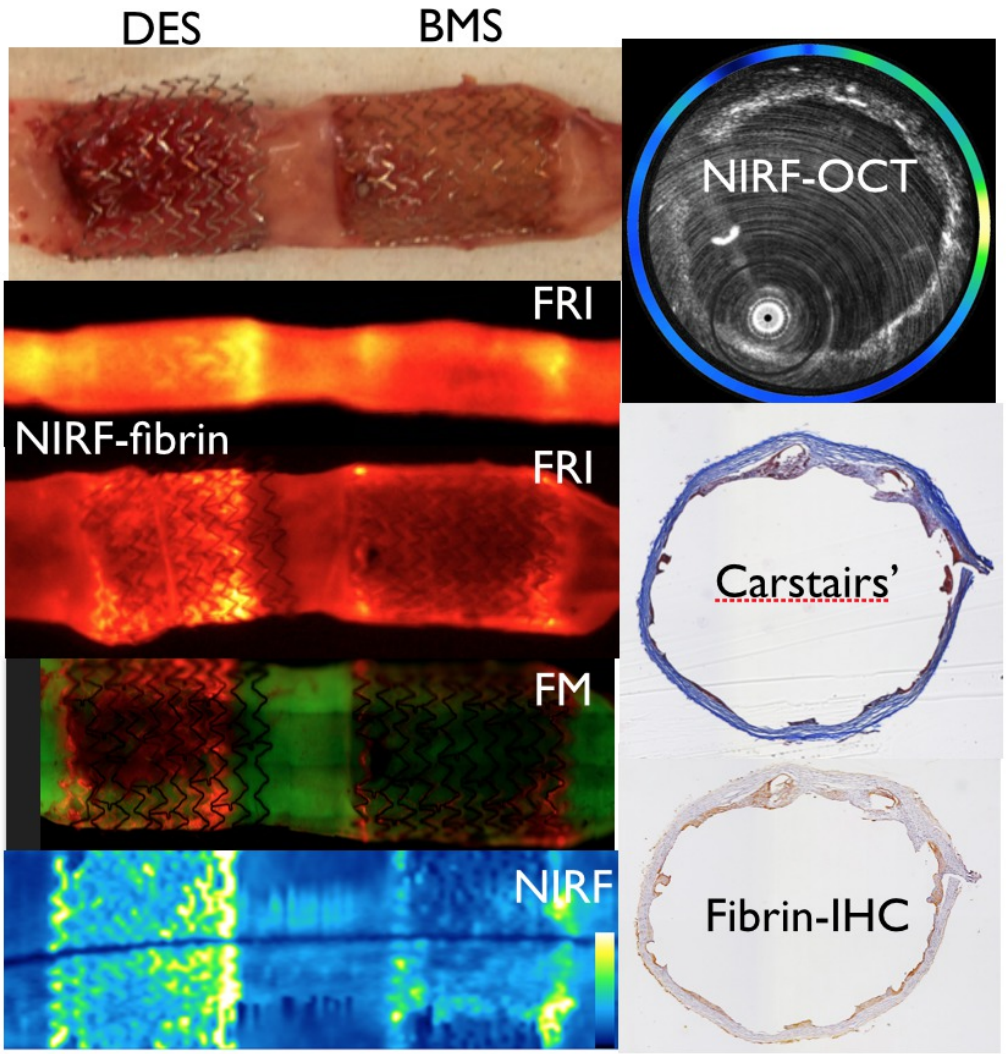
DES
BMS
NIRF-OCT
FRI
NIRF-fibrin
FRI
Carstairs'
FM
NIRF
Fibrin-IHC

CONTROL ID: 2232772

TITLE: Low kidney uptake of [^{18}F]exendin-4 and high beta cell binding in rat and human pancreatic islet

PRESENTER: Kirsi Mikkola

ABSTRACT BODY:

Abstract Body: Background and Aims

A reliable method for non-invasive quantification of beta cell mass *in vivo* in humans will enhance our understanding of the pathophysiology of both type 1 and type 2 diabetes. Several radiometal-labelled exendin based tracers ([^{64}Cu], [^{68}Ga], [^{99m}Tc] and [^{111}In]exendin) have been intensively explored for beta cell imaging. The obstacle with these has been high uptake in the kidneys. The aim of this study is to develop a novel [^{18}F]exendin-4 tracer for clinical imaging of beta cells with PET (positron emission tomography) with reduced tracer uptake in the kidneys.

Materials & Methods

[^{18}F]exendin-4 was produced *via* Cu(I)-mediated click reaction between the exendin-4-azide and alkyne derivatized [^{18}F]-ethylene glycol precursor. Isolation and radiochemical analysis of [^{18}F]exendin-4 was performed using HPLC and TLC. Biodistribution and kinetics of [^{18}F]exendin-4 was evaluated in rats (N=3–9 per time point, weighing 250−300 g) and pigs (N=1–2 per time point, weighing 31–36 kg). Animals were injected intravenously with [^{18}F]exendin-4 (19±3 MBq/kg, mass 0.3±0.2 nmol/kg rats, 1.2±0.2 MBq/kg, mass 0.02±0.003 nmol/kg pigs) and thereafter rats were sacrificed at 15 and 30 min, and at 1, 2, 4 and 6 h and pigs at 1 h and 4 h. In rats, the GLP-1R specificity was assessed using cold exendin-3 (N=1). In addition, sections of human pancreas were incubated with [^{18}F]exendin-4 at various ligand concentrations (range 2.5−20 nM) *in vitro*. Distribution of radioactivity in pancreas and kidney was assessed using autoradiography. Islet labelling was verified by immunohistochemistry and islet-to-exocrine tissue ratios were analysed. For PET scans, rats were imaged up to six hours and pigs up to four hours using Inveon Multimodality PET/CT and Discovery 690 hybrid PET/CT scanner, respectively. The organ-specific radioactivity is reported as a percentage of the injected dose per gram of tissue (%ID/g) or tissue ratios.

Results

Islet labelling was observed in rats after tracer injection into living animals and in human pancreatic sections *in vitro* (Figure 1). Blocking studies with rats indicated GLP-1R specific uptake in the islets. Autoradiography analysis of pancreatic sections showed that the islet-to-exocrine tissue ratio was in rats 78±29 at 1 h p.i. In human sections, the binding in the islets was 13 times higher compared to the exocrine pancreas. In line with other exendin based tracers, [^{18}F]exendin-4 uptake by rat kidneys was high at 1 hour (16.7±3.0 %ID/g), but thereafter its clearance was fast and retention decreased to 1.5±0.4 %ID/g, at 6 h p.i. In pigs, the radioactivity uptake in kidneys was observed to be three times less at four hour time point compared to one hour time point. No specific uptake was observed in pig pancreatic islets. Both in rats and pigs the radioactivity in bone was low, indicating low defluorination of the tracer.

Conclusion

We found specific and sustained uptake of [^{18}F]exendin-4 in the pancreatic islets in rats and in human tissues. Both in rats and in pigs, the renal clearance of the tracer was rapid. These indications are promising for the development of novel [^{18}F]exendin-4 towards clinical imaging of beta cells.

AUTHORS (LAST NAME, FIRST NAME): Mikkola, Kirsi[1]; Yim, Cheng-Bin[1]; Lehtiniemi, Paula[1]; Rajander, Johan[2]; Solin, Olof[2]; Nuutila, Pirjo[1, 3]

INSTITUTIONS (ALL):

1. Turku PET Centre, University of Turku, Turku, Finland.
2. Accelerator Laboratory, Åbo Akademi University, Turku, Finland.
3. Department of Endocrinology, Turku University Hospital, Turku, Finland.

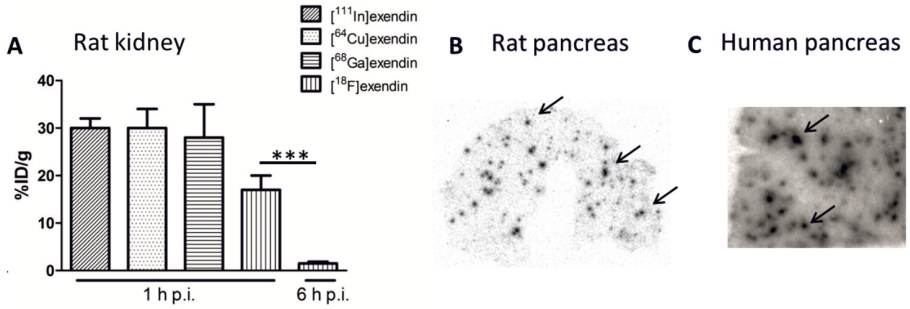

Figure 1. Radioactivity uptake of several exendin based tracers in kidney and pancreas. The uptake of [^{111}In], [^{64}Cu] and [^{68}Ga]exendin in rat kidney was found in similar levels one hour after tracer injection (**A**). The uptake of [^{18}F]exendin was significantly decreased at 6 h time point compared to 1 h time point. Autoradiography image of rat pancreas one hour after tracer injection (**B**) and human pancreas after *in vitro* incubation (**C**). Islet labelling (black dots indicated by arrows) were clearly visible both in rat and human pancreas. Two-tailed, unpaired Student's *t* test was used for the analyses of statistical differences between groups. %ID/g percentage injected dose per gram of tissue.

CONTROL ID: 2231128

TITLE: A fluorescence resonance energy transfer labeling method to study dissociation kinetics of lipid-based nanoparticles

PRESENTER: Sjoerd Hak

ABSTRACT BODY:

Abstract Body: Introduction

Lipid-based nanoparticles (LBNs) are applied extensively for a variety of biomedical applications, including targeted drug delivery and molecular imaging. Their specificity can be modulated by targeting ligand surface-functionalization. Using our window chamber mouse model and intravital fluorescence resonance energy transfer (FRET) imaging we have recently demonstrated that LBNs are dynamic structures that rapidly exchange lipids with plasma constituents, such as lipoproteins and albumin (1). As this can also result in the loss of imaging labels, drugs, or targeting ligands before the target site is reached it will be crucial to obtain insights in the exchange dynamics of ligand-targeted nanoparticles. Moreover, the ability to monitor LBN dissociation dynamics at the target site will provide valuable insights in drug delivery applications as well as aid in the interpretation of imaging data.

Over the last years we have optimized a lipid-based oil-in-water nanoemulsion platform (NEP) to target tumor angiogenesis through an $\alpha_v\beta_3$-specific RGD peptide (2). In the current study we have equipped this platform with two fluorophores which form a FRET pair, optimized fluorophore content, and characterized its FRET features.

Methods and results

The NEP consists of soybean oil droplets (approx. 100 nm diameter) stabilized by a lipid mixture (DSPC/cholesterol/PEG2000-DSPE at molar ratios of 1.85/1/0.15, respectively) (2). To obtain an NEP with FRET features we incorporated the lipophilic donor fluorophore p-HTAM (methyl ester of p-HTAA (3), excited at 405 nm, emission max at 490 nm) and acceptor fluorophore NR668 (4) (excitation max at 515, emission max at 590 nm), see figure A-B. Confocal microscopy was used to demonstrate that both fluorophores were dissolved in the soybean oil droplets in the crude emulsion (persuasive data). By varying the molar donor to acceptor fluorophore ratio, we found FRET to be most efficient when this ratio was smaller than or equalled one (persuasive data). As the FRET signal was highest in the 1:1 preparation we used this ratio for kinetic experiments. In these experiments, different amounts of fetal bovine serum (FBS) were added to the NEP and FRET was monitored as a function of time (persuasive data). We observed that increasing amounts of FBS resulted in faster dissociation, which could be monitored in real time.

Conclusion

We have developed a FRET labeling method that allows real time NEP dissociation imaging. We are currently conducting experiments where we study intracellular dissociation of RGD-conjugated vs non-targeted nanoemulsion in vitro. Finally, we aim to study nanoparticle dissociation in vivo in our window chamber set-up.

References

Zhao et al. 2013, ACS Nano **7**, p10362
Hak et al. 2012, ACS Nano **6**, p5648
Åslund et al. 2009, ACS Chem Biol **4**, p673
Klymchenko et al. 2012, RSC Advances **2**, p11876

AUTHORS (LAST NAME, FIRST NAME): Hak, Sjoerd[4]; Åslund, Andreas K.[1]; Zhao, Yiming[2]; Mulder, Willem J.[3]; Haraldseth, Olav[4]; Davies, Catharina[1]

INSTITUTIONS (ALL):

1. Department of physics, Norwegian University of Science and Technology, Trondheim, Norway.
2. Translational and Molecular Imaging Institute, Icahn School of Medicine at Mount Sinai, New York, NY, United States.
3. Translational and Molecular Imaging Institute, Icahn School of Medicine at Mount Sinai, New York, NY, United States.
4. Department of circulation and medical imaging, Norwegian University of Science and Technology, Trondheim, Norway.

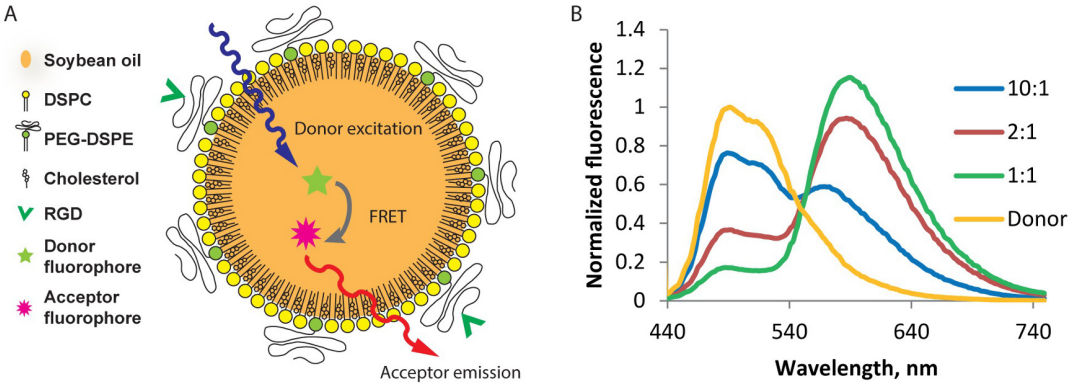

Figure. A: Cartoon of the NEP with FRET features. B: Fluorescence spectra of nanoemulsions with constant donor concentration and the indicated donor:acceptor ratios, excited at 405 nm.

CONTROL ID: 2231144

TITLE: Synthesis and characterization of Ga-68 labeled water dispersible Fe_3O_4 NPs for dual applications as diagnostic imaging agent in PET/ MRI

PRESENTER: Bo-Bae Cho

ABSTRACT BODY:

Abstract Body: Radioisotope labeled magnetic nanoparticles (NPs) for dual modality imaging like Positron Emission Tomography/ Magnetic Resonance Imaging (PET/MRI) provides an opportunity to combine the power of MRI and PET, which has better anatomical resolution with high sensitivity. In this present work, we designed the nano-bio composite of ^{68}Ga radioisotope labeled Fe_3O_4 nanoparticles (NPs) for dual applications of diagnostic imaging agent in PET/MRI. The ^{68}Ga-SCN-NOTA-Hydrazine-Fe_3O_4 NPs (^{68}GaNHFCNP) composite was fabricated via surface modified Fe_3O_4 NPs and NOTA as bi-functional chelating agent with ^{68}Ga radioisotope from an in-house generator. The obtained ^{68}GaNHFCNP exhibits synergic property such as magnetic behavior and radio activity. The structural and morphological properties of ^{68}GaNHFCNPs were characterized by XRD, TEM, IR analysis. Radio-TLC analysis showed the formation of ^{68}GaNHFCNPs via radiolabeling of ^{68}Ga-NOTA complex. The cell viability of ^{68}GaNHFCNPs were almost 100% in SK-BR-3 and CT-26 cell line. Moreover, the cellular uptake of ^{68}GaNHFCNPs shows higher effective for SK-BR-3 than CT-26 cell line. The values of cellular uptake was increases with respect to time and attained a maximum of 8.778 % at 120 min for CT-26 and 15.491 % at 120 min for SK-BR-3 cell line. These detailed studies established that ^{68}GaNHFCNP exhibits potential application for cancer contrast.

AUTHORS (LAST NAME, FIRST NAME): Cho, Bo-Bae[2]; Yu, Kook Hyun[1, 3]

INSTITUTIONS (ALL):

1. Dongguk university, Seoul, Korea (the Republic of).
2. chemistry, Dongguk university, Seoul, Korea (the Republic of).
3. Korea institute of radiological and medical sciences, Seoul, Korea (the Republic of).

(No Image Selected)

CONTROL ID: 2231148

TITLE: Lung-imaging in a rodent model of COPD: A comparison of CT and MRI at 15.2 Tesla

PRESENTER: Wolfram Stiller

ABSTRACT BODY:

Abstract Body: *Purpose:* The purpose of this study was to evaluate ultra high-field magnetic resonance imaging (MRI), especially zero-echo-time (ZTE) MRI, for assessment of chronic obstructive pulmonary disease (COPD) in a rodent model, and to compare it to computed tomography (CT).

Materials and Methods: Respiratory-triggered MR imaging of mouse lungs was conducted on a 15.2 T BioSpec (Bruker BioSpin MRI, Ettlingen) with a transmit-receive RF coil using a fast imaging with steady-state precession (FISP) sequence (TE/TR 0.9ms/10ms, acquisition matrix: 200x200x200, field of view: 2.5×2.5x2.0cm^3, acquisition time: 3min 48s), a rapid acquisition with relaxation enhancement (RARE) sequence (TE/TR 2.1ms/450ms, acquisition matrix: 200x200x40, field of view: 2.5×2.5x2.0cm^3, acquisition time: 6min), as well as a ZTE sequence (TE/TR 0µs/8ms, acquisition matrix: 256x256x256, field of view: 3.5×3.5x4.5cm^3, acquisition time: 8min 13s) in healthy and βENaC-Tg mice with COPD-like lung disease. CT images of the same mice were acquired with a SkyScan 1176 (Bruker microCT, Kontich) at 50 kV, 500 mA and 60 ms for 9 x 258 projections at a step angle of 0.7° for a total orbit of 180°, 9 frames per step for retrospective synchronization. Prior to manual analysis, CT rawdata was reconstructed (reconstruction matrix: 1000x1000x568, field of view: 3.6x3.6x2.0cm^3). Mean and standard deviation of signal intensities (SI) were evaluated in regions-of-interest (ROI) manually placed in affected lung regions showing air-trapping (L1 (COPD)), unaffected regions within the same lung (L1 (w/o)), and unaffected regions of the opposite lung (L2 (w/o)).

Results: CT and MRI, except FISP MRI, provided good image quality for the lung parenchyma. ZTE MRI, RARE MRI, and CT also allowed detailed assessment of the lungs' structure (Figure, A-C). For comparing COPD-mice with non-COPD-mice, ZTE and RARE were superior to all other techniques (Figure, D). In healthy wildtype mice, the SI of L1 (w/o) and L2 (w/o) did not differ for all imaging modalities (data not shown). In COPD-mice, unaffected lung regions (L1 (w/o), L2 (w/o)) did not differ significantly (Figure, D), only ZTE was able to detect a SI decrease of L1 (w/o) vs. L2 (w/o). Affected lung regions showing air-trapping, however, expressed a significantly lower SI than unaffected regions (e.g. ZTE: L1 (COPD)=0.49 +/- 0.05, L1 (w/o)=0.64 +/- 0.04, L2 (w/o)=0.71 +/- 0.05; RARE: L1 (COPD)=0.20 +/- 0.09, L1 (w/o)=0.42 +/- 0.12, L2 (w/o)=0.42 +/- 0.16). In terms of the depiction of anatomy CT performed best and offered shortest acquisition times, followed by ZTE and RARE. Both of the latter, however, were more sensitive to COPD-induced air-trapping causing minute spin-density differences in lung parenchyma.

Conclusion: CT, ZTE MRI, and RARE MRI are suitable for imaging in small animal models of lung disease. Whereas CT was superior in terms of resolution, ZTE and RARE at 15.2 T performed better regarding lung tissue contrast for detection of COPD-affected regions showing air-trapping.

AUTHORS (LAST NAME, FIRST NAME): Weis, Christian[1]; Triphan, Simon M.[1]; Duerr, Julia[2]; Zhou-Suckow, Zhe[2]; Basse-Lüsebrink, Thomas[3]; Strobel, Klaus[3]; Mall, Marcus[2]; Kauczor, Hans-Ulrich[1]; Stiller, Wolfram[1]

INSTITUTIONS (ALL):

1. Radiology, University Hospital Heidelberg, Heidelberg, Germany.
2. Department of Translational Pneumology, University Hospital Heidelberg, Heidelberg, Germany.
3. Bruker BioSpin MRI GmbH, Ettlingen, Germany.

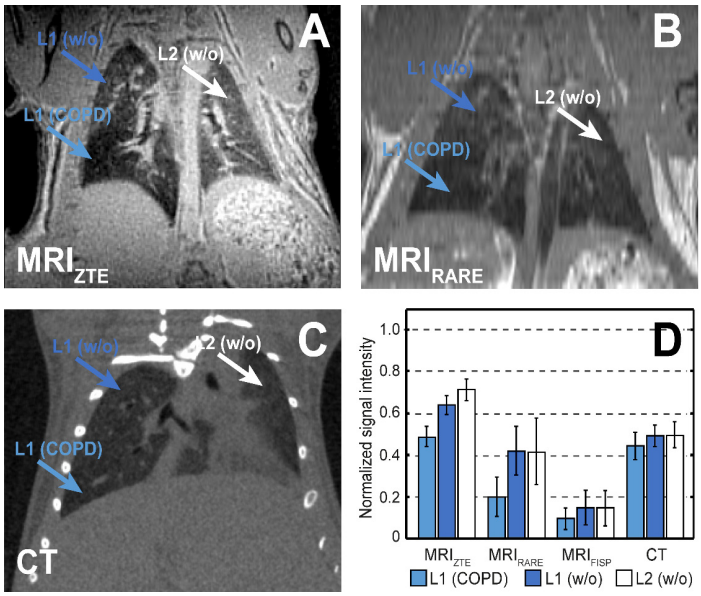

Representative images of a mouse lung acquired with CT and ultra high-field MRI for a study in a rodent model of COPD. Zero-Echo-Time (A), RARE (B), FISP, and CT (C) were evaluated in terms of their ability to image COPD. Affected lung regions showing air-trapping (L1 (COPD)) were compared to unaffected regions within the same lung (L1 (w/o)), and unaffected regions of the opposite lung (L2 (w/o)). Compared to unaffected regions, ZTE and RARE detected a significant decrease in signal intensity for L1 (COPD), whereas FISP and CT only detected a weak signal drop for the affected region (D).

CONTROL ID: 2232240

TITLE: Evaluation of polymeric micelle MR contrast agent for mice MR imaging: comparison with gadofluorine M

PRESENTER: Shigeru Kiryu

ABSTRACT BODY:

Abstract Body: Due to its high structural stability in the blood, polymeric micelles are expected to stay in the blood for a long period of time. The self-assembling property in a selective solvent makes polymeric micelles be comprehensively used as nano-sized drug carriers for drug targeting. The purpose of this study is to evaluate the potential of polymeric micelle contrast agent, a new PEG-poly(L-lysine)-based gadolinium magnetic resonance contrast agent, compared with gadofluorine M.

MR imaging was performed before and after intravenous injection of polymeric micelle contrast agent or gadofluorine M in mice using 1-Tesla permanent magnet compact MR system. The kinetics of both agents were assessed. The visualization of the blood vessels in maximum intensity projection images was also assessed.

In comparison with gadofluorine M, contrast enhancement in the blood was more remarkable for polymeric micelle contrast agent. According to the P-interaction analysis, the enhancement in the liver was similar between two contrast agents, and it differed significantly in the vein, kidney and spleen. In MIP images, prominent enhancement was demonstrated in the blood 24 hours after delivery of polymeric micelle contrast agent, while only slight enhancement was visible 1 hour after the injection of gadofluorine M. The degree of enhancement of the aorta and intrahepatic vein was significantly higher in polymeric micelle contrast agent until 24 hours after injection of it.

The enhancement of the blood was strong and lasted long after the injection of polymeric micelle contrast agent. This contrast agent appears promise as both blood pool imaging agent and drug-delivery system.

AUTHORS (LAST NAME, FIRST NAME): Kiryu, Shigeru[1]; Wang, Fang[1, 2]; Shiraishi, Kouichi[3]; Yokoyama, Masayuki[3]; Nojima, Masanori[4]; Inoue, Yusuke[5]; Ohtomo, Kuni[6]

INSTITUTIONS (ALL):

1. Radiology, Institute of Medical Science, The University of Tokyo, Tokyo, Japan.
2. Radiology, Qi Lu Hospital of Shandong University, Jinan, China.
3. Medical Engineering Laboratory, Research Center for Medical Sciences, The Jikei University School of Medicine, Tokyo, Japan.
4. Division of Advanced Medicine Promotion, The Advanced Clinical Research Center, The Institute of Medical Science, University of Tokyo, Tokyo, Japan.
5. Diagnostic Radiology, Kitasato University School of Medicine, Kanagawa, Japan.
6. Radiology, Graduate School of Medicine, University of Tokyo, Tokyo, Japan.

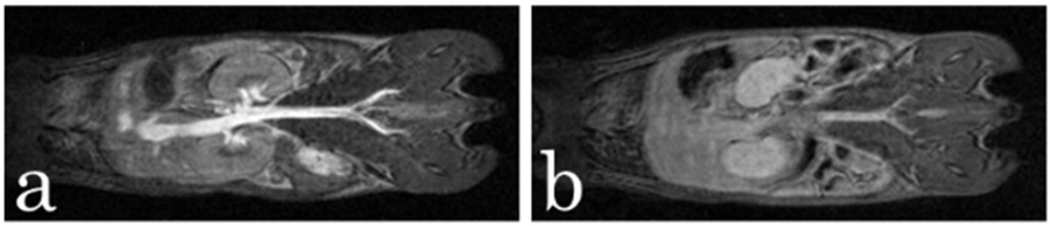

Coronal MR images acquired 24 hours after injection of contrast agents (a, polymeric micelle; b, gadofluorine M).

CONTROL ID: 2231230

TITLE: Improving the efficiency of preclinical pulmonary disease and therapy studies: MicroCT-derived biomarkers reveal marked changes throughout lung infection, inflammation, fibrosis and treatment

PRESENTER: Greetje Vande Velde

ABSTRACT BODY:

Abstract Body: Because it provides longitudinal information, in vivo microCT is increasingly embraced in the pulmonary research field where ex vivo assessment of experimental disease models is nevertheless still the gold standard. To optimize the quantitative monitoring of lung diseases and their therapy in vivo, we evaluated longitudinal changes in four different microCT-derived biomarkers describing the time course of bleomycin-induced lung inflammation and fibrosis followed by therapy (imatinib), pulmonary cryptococcosis and invasive aspergillosis, compared to longitudinal changes in healthy adult mouse lungs.

After induction of lung disease and therapy, free-breathing mice were scanned regularly with longitudinal microCT and lung biomarkers (total lung volume, aerated lung volume, lung tissue (including lesions) volume and mean lung density) quantified. After the last time point, we performed pulmonary function tests and isolated the lungs for histological validation.

We show that the lungs of adult healthy mice keep growing, with none of the studied lung biomarkers remaining stable during longitudinal follow-up. Absolute values should therefore always be compared with age-matched controls when evaluating how lung biomarkers change after an intervention.

Inflammation and fibrosis lead to a significant increase in total lung volume that affects the interpretation of aerated lung volume, tissue volume and mean lung density (Fig.1A). Therapy of lung fibrosis improved lung air content and hence function, but the enlargement of the lung remained (Fig.1B). Also in fast and slowly progressing lung infections a marked increase in lung volume is observed, further supporting that the net decrease in air spaces due to an increase of the lesion burden in the lung underestimates the progression of disease when evaluated on its own. This suggests that some of the total lung volume changes reflect a compensatory mechanism and should be considered as an indirect marker of disease.

Our findings underscore the importance of quantifying not only aerated lung volume or lesion volumes but also total lung volume to document growth as well as potential compensatory mechanisms in mouse models of lung disease, in order to fully describe and better understand the different dynamic processes during lung disease progression and therapy in preclinical trials. This is relevant as the imperfections of mouse models mimicking human disease are likely to account for at least some of the many discrepancies found when translating therapy evaluation results from mouse studies to human patients. Non-invasive, longitudinal imaging and accurate quantification of disease progression and therapy effects will likely be indispensable tools in this regard.

AUTHORS (LAST NAME, FIRST NAME): Vande Velde, Greetje[1]; Poelmans, Jennifer[1]; De Langhe, Ellen[2, 3]; Hillen, Amy[1]; Vanoirbeek, Jeroen[4, 5]; Lories, Rik[2, 3]; Himmelreich, Uwe[1]

INSTITUTIONS (ALL):

1. Imaging and Pathology, KU Leuven, Leuven, Flanders, Belgium.
2. Development and Regeneration, KU Leuven, Leuven, Belgium.
3. Rheumatology, University Hospitals Leuven, Leuven, Belgium.
4. Public Health and Primary Care, KU Leuven, Leuven, Belgium.
5. Pneumology, KU Leuven, Leuven, Belgium.

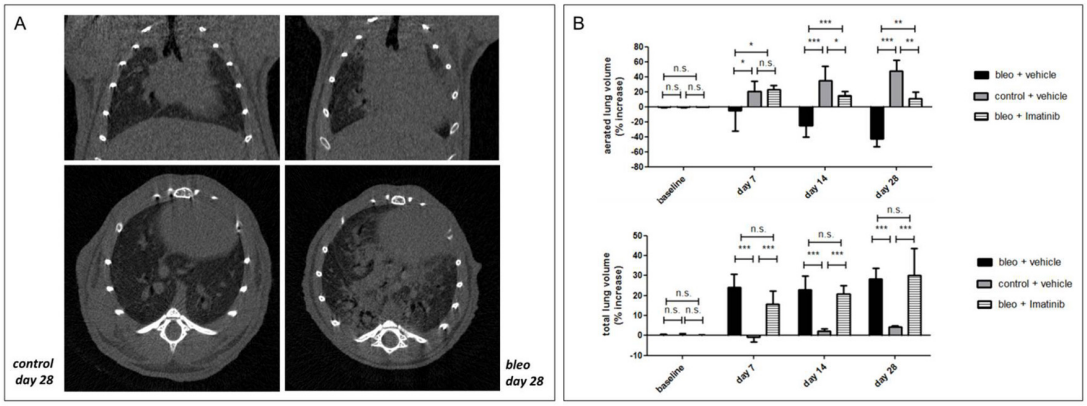

Figure 1: Longitudinal in vivo lung micro-CT biomarkers for mice with bleomycin-induced lung pathology and upon treatment with imatinib. *(A) Coronal (top) and transversal (bottom) micro-CT images acquired from C57BL/6 mice at 28 days after PBS- ('control', left panels) and bleomycin-instillation ('bleo', right panels). (B) Graphs of the increase in aerated lung volume and total lung volume relative to baseline, quantified from the longitudinal micro-CT scans acquired at baseline and at 7, 14 and 28 days p.i. for bleomycin- ('bleo') or PBS-instilled C57BL/6 mice ('control', n = 3), treated with imatinib (n = 6) or vehicle (n = 6). (Error bars indicate SD of replicate samples; *: $p < 0.05$, **: $p < 0.01$, ***: $p < 0.005$).*

CONTROL ID: 2234025

TITLE: Differentially and non-invasively characterizing brain lesions by use of multimodal MRI, MRS and fibered confocal fluorescence microscopy in a mouse models of cerebral cryptococcosis

PRESENTER: Greetje Vande Velde

ABSTRACT BODY:

Abstract Body: *Cryptococcus neoformans* and *C. gattii* are encapsulated yeasts that cause life-threatening infections, mainly affecting immune-compromised individuals. The main route of infection is by inhalation, but *Cryptococcus* can subsequently spread from the lung to the brain. The exact mechanism of how and why these pathogens manage to breach through the blood-brain-barrier to disseminate into the CNS is still largely unknown. Thereby, they may cause brain lesions that are often difficult to distinguish from other pathologies like cystic brain tumors. We aimed at longitudinal follow-up and characterization of cerebral cryptococcomas in mice and the identification of biomarkers to enable early differential diagnosis.

Cryptococcus strains (*C. neoformans* H99, 1841D and *C. gattii* R265, GFP+) were stereotactically injected into the right striatum of female BALB/c mice. Mice were scanned 1-3 times a week during a period of 2-4 weeks using a 9.4 T MRI scanner (Bruker Biospin). We have acquired anatomical (T2-weighted), diffusion and perfusion MRI as well as single-voxel ^{1}H MR spectra of the lesions. Intravital microscopy using fibered confocal fluorescence microscopy (FCFM) was performed to visualize the lesions at a cellular level. Afterwards, the brains were isolated for validation with histology and fungal load quantification.

Disease progression, associated with an increase in lesion size, could be monitored longitudinally with MRI. MRI parameters of cryptococcomas were similar to those found in glioblastoma models (1) with marginally larger ADC values (Fig.1) and reduced perfusion. ^{1}H MR spectra of the lesion area showed a characteristic trehalose signal (1), indicating the lesions can be classified as cryptococcomas. This was confirmed by the visualization of individual cryptococci within the lesion by FCFM. MRS was therefore able to identify marker metabolites that not only enabled to distinguish the abscesses from glioblastoma, but are specific to the lesion-causing pathogen. For the first time, this study presents a method for non-invasive follow-up and characterization of cerebral cryptococcomas in a mouse model. The combination of these techniques has the potential to assist in non-invasive differential diagnosis and could contribute to the unraveling of the pathogenesis of infectious diseases.

1. Himmelreich et al. Radiology 2001; 220:122–8 2.

AUTHORS (LAST NAME, FIRST NAME): Vande Velde, Greetje[1]; Vanherp, Liesbeth[1]; Hillen, Amy[1]; Lagrou, Katrien[2]; Himmelreich, Uwe[1]

INSTITUTIONS (ALL):

1. Imaging and Pathology, KU Leuven, Leuven, Belgium.
2. Microbiology and Immunology, KU Leuven, Leuven, Belgium.

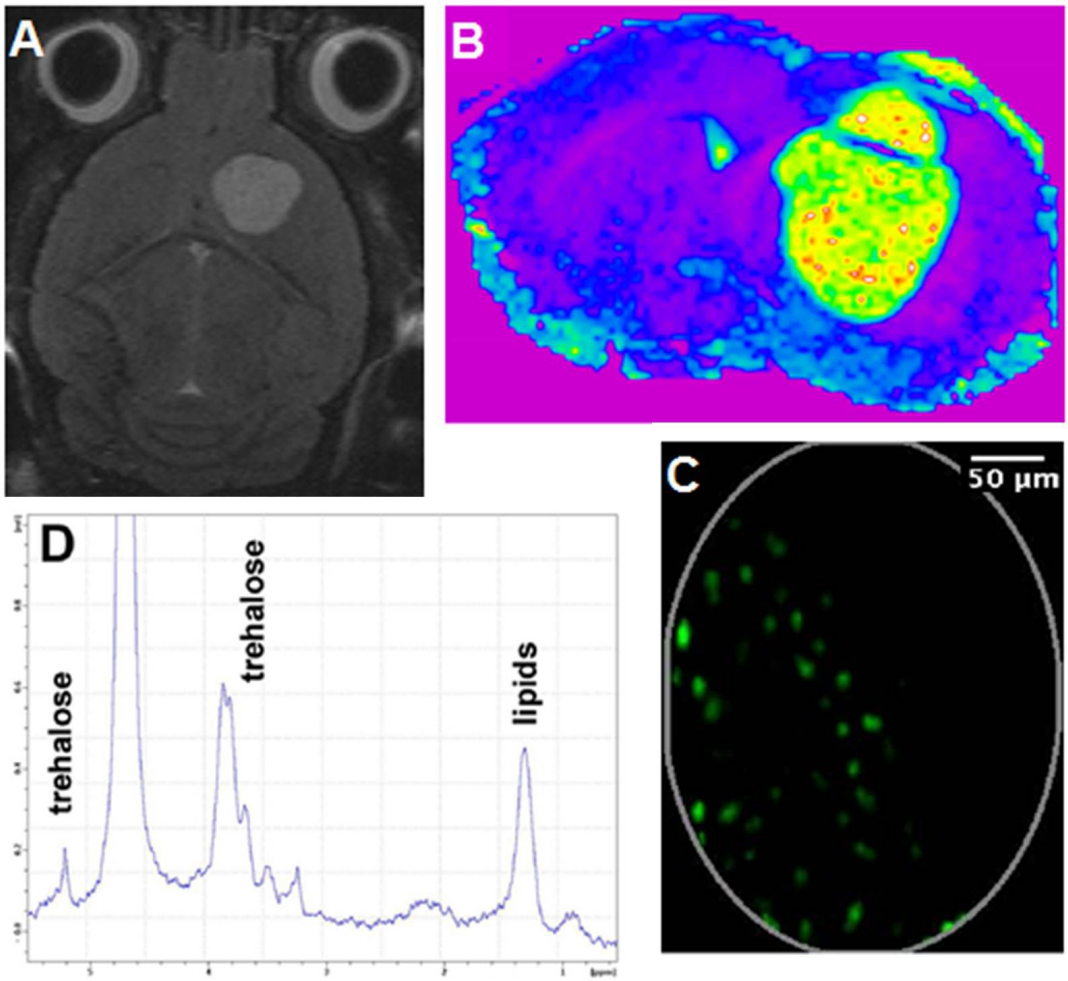

Figure1: Multimodal imaging of a mouse with cerebral cryptococcosis: *(A)T2-weighted MRI; (B) ADC-map; (C) IVM; (D) localized MRS of the lesion.*

CONTROL ID: 2233182

TITLE: Longitudinal bioluminescence imaging to increase the in vitro and in vivo screening efficiency of antifungal activity against Candida albicans biofilms

PRESENTER: Greetje Vande Velde

ABSTRACT BODY:

Abstract Body: Fungal infections are a major problem in hospitals, in particular for the increasing number of immune-compromised patients. Candida albicans is an important human pathogen causing mucosal and deep tissue infections of which the majority is associated with biofilm formation on medical implants. Such biofilms have a huge impact on public health, as they are highly resistant against most antimycotics. Animal models of biofilm formation are indispensable for the investigation of biofilm antifungal resistance, the interaction with the host immune system and novel antifungal strategies that are effective in combatting biofilms. Currently, evaluation of the efficacy of antifungal prevention or treatment of biofilms is limited to ex vivo analyses, requiring the sacrifice of many animals in order to reach sufficient statistical power. As an alternative, we investigated the feasibility to perform non-invasive, dynamic imaging and quantification of in vitro and in vivo C. albicans biofilm formation and its treatment by using a bioluminescent C. albicans strain in a subcutaneous catheter model in mice.

Mature 24h-old in vitro biofilms were formed on the bottom of 96-well plates by wild-type and gLuc-expressing C. albicans, washed twice and further incubated for 24 and 48h with different antifungals (fluconazole, amphotericin-B, anidulafungin, micafungin, caspofungin) in a concentration range from 64 µg/ml to 0,125 µg/ml. The resulting fungal load was quantified in parallel with BLI and CFU counting. For screening of antifungal activity against biofilms formed in vivo, gLuc-expressing C. albicans-inoculated catheter pieces were implanted on the lower back of immune-suppressed Balb/C mice ([1, 2]), allowed to form mature biofilms for 2 days after which antifungal treatment was started (daily during 7 days; fluconazole 125, amphotericin-B 5, anidulafungin 10, micafungin 30, caspofungin 10 mg/kg/day i.v.). The mice were imaged with BLI 2 (baseline), 6 and 9 days after implantation. After the last imaging time point the mice were sacrificed, catheters explanted and CFUs quantified for validation of the results.

In vitro BLI of antifungal activity against C. albicans biofilms resulted in a sufficiently high signal compared to background that allowed immediate, fast, reproducible and quantitative output regarding the dose and activity of different compounds, consistent with gold standard CFU results. Longitudinal monitoring of biofilms formed and treated with different antifungals in vivo using BLI allowed to evaluate and compare the efficacy of antifungal compounds against mature biofilms (Fig.1), thereby overcoming statistical issues with inherently highly variable baseline values. In vivo BLI results regarding the efficacy of amphotericin-B and echinocandins at the evaluated concentrations in mice was consistent with CFU counts. This imaging platform allows more powerful and efficient screening of efficacy, dose range, fungistatic versus fungicidal activity etc… of therapy options against mature biofilms, thereby refining preclinical studies.

1. Vande Velde G. et al. Methods Mol Biol 2014, 1098: 153-67.

2. Vande Velde G. et al. Cell Microbiol 2014, 16: 115-30.

AUTHORS (LAST NAME, FIRST NAME): Vande Velde, Greetje[1]; Kucharíková, Sona[2]; Van Dijck, Patrick[2]; Himmelreich, Uwe[1]

INSTITUTIONS (ALL):

1. Imaging and Pathology, KU Leuven, Leuven, Flanders, Belgium.

2. Molecular Microbiology and Biotechnology, KU Leuven/ VIB, Heverlee, Belgium.

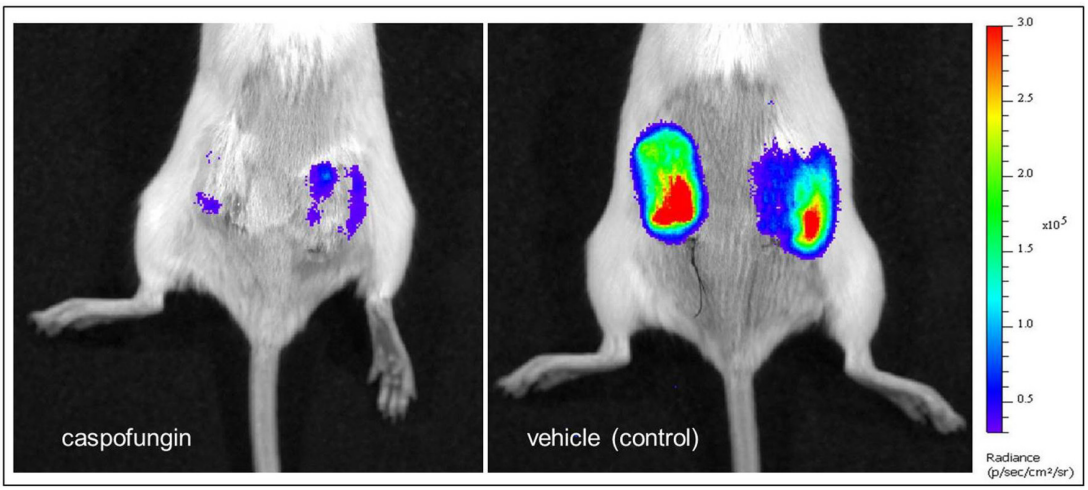

Figure 1: Longitudinal BLI of antifungal activity against biofilms under in vivo conditions. *Typical in vivo BLI images from a mouse treated with caspofungin and a mouse treated with placebo, imaged 9 days after catheter implantation.*

CONTROL ID: 2231154

TITLE: Integrin expression and angiogenesis in Non Small Cell Lung Cancer (NSCLC): A in vivo hybrid Fluciclatide PET/ CT perfusion molecular imaging study.

PRESENTER: thida Win

ABSTRACT BODY:

Abstract Body: The PET Tracer ^{18}F-Fluciclatide has high affinity for the αvβ3 integrin receptor, which shows increased expression in tumour angiogenesis. Angiogenesis depicted by tumor vascularity measurements derived from dynamic contrast enhance CT (DCE-CT) has been shown to predict survival in patients with non-small cell lung cancer (NSCLC). We hypothesize that we can demonstrate a relationship between in vivo measurements of tumor uptake of ^{18}F-Fluciclatide on PET with

1 Measurements of vascularity using DCE-CT in patients with NSCLC

2 Glucose metabolism using ^{18}F-FDG PET in patients with NSCLC.

METHODS: Eleven patients >40 years (female=5, male=6; mean age 78 years, range 50-86) with suspected primary NSCLC underwent ^{18}F-FDG PET/CT followed on a separate day by combined ^{18}F-Fluciclatide PET/DCE-CT. Tumor uptake of ^{18}F-Fluciclatide and ^{18}F-FDG was assessed qualitatively by visual assessment and also semi-quantitatively using the maximum standard uptake value (SUV_{max}). Using DCE-CT, the tumor vascular parameters of mean transit time (MTT) and permeability were then derived. Statistical analysis was performed using Pearson correlation.

RESULTS:

All patients demonstrated an ^{18}F-Fluciclatide PET signal by visual assessment. The tumor ^{18}F-Fluciclatide semi-quantitative assessment showed a Mean SUV_{max} 4.3, SD 1.27, range 7.49-107.23) in comparison the mean ^{18}F-FDG SUV_{max} was13.60 (range 1.5 – 26.1).

DCE CT results showed a mean transit time of 5.38 (range 3.22 –8.23) and a Mean permeability of 20.08 (range 0.07-38.89).

There was significant correlation between ^{18}F-Fluciclatide uptake (SUV max) and permeability (r=.634, p=0.036) but there was no correlation between Permeability and ^{18}F-FDG.

CONCLUSION:

^{18}F-Fluciclatide PET uptake is associated with tumor permeability as derived by DCE-CT, independent of tumour glucose metabolism. The relationship between ^{18}F-Fluciclatide uptake and permeability may be accounted for by the improved specificity of ^{18}F-Fluciclatide in demonstrating tumor neovasculaturity compared to that when using ^{18}F-FDG.

AUTHORS (LAST NAME, FIRST NAME): neriman, deena[2]; Win, thida[2]; Hoath, John[2]; Shortman, Robert I.[2]; Endozo, Raymond[2]; John, Dickson[2]; Ganeshan, Balaji[2]; Miles, Kenneth[2]; Groves, Ashley[1]; Janes, Sam[1]

INSTITUTIONS (ALL):

1. UCL, London, United Kingdom.

2. Institute of Nuclear Medicine, University College London, London, London, United Kingdom.

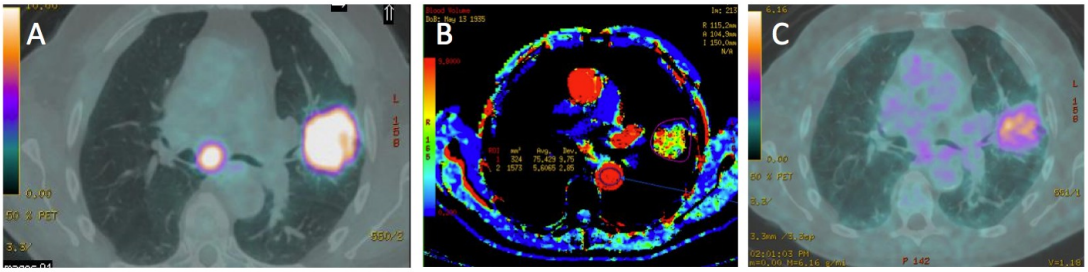

A – Axial fused 18F FDG PET-CT showing avid uptake, B – Perfusion map and C – Axial fused 18F Fluciclatide PET-CT showing avid uptake in a left upper lobe carcinoma.

CONTROL ID: 2232806

TITLE: Immune-modulating effects of the FDA approved iron oxide nanoparticle ferumoxytol inhibit tumor growth

PRESENTER: saeid zanganeh

ABSTRACT BODY:

Abstract Body: Purpose: During our imaging evaluations of adenocarcinomas with the FDA-approved superparamagnetic iron oxide nanoparticle (USPIO) compound ferumoxytol (Feraheme), we observed a surprising therapeutic effect of USPIO that resulted in significant tumor growth inhibition. The purpose of this study was to elucidate underlying pathophysiological mechanisms that lead to the observed USPIO-induced tumor growth inhibition.

Materials and Methods: Murine macrophages were co-cultivated with MMTV-PyMT breast carcinoma cells in a transwell co-culture system with 0.4 and 3 μm-sized microporous membranes, with or without addition of USPIO. Macrophage migration, M1/M2 polarization, and cancer cell apoptosis were evaluated by migration assays, quantitative real-time PCR, and caspase 3 immunocytochemistry, respectively.

Next, 63 FVB/N mice were implanted with MMTV-PyMT cancer cells and randomly divided into 5 experimental groups: 1) bilateral tumor implantations with or without co-implanted USPIO, 2) single tumor implantations with of without USPIO, 3) different USPIO doses, 4) different USPIO compounds; 5) different tumor cell quantities. Tumor volume, MRI iron signal, histological analyses and FACS analyses were compared between different tumor groups using Student's t-test and a $p<0.05$.

Results: In vitro, USPIO or macrophages alone showed no significant cytotoxic effects on cancer cells, while cancer cells co-incubated with USPIO and macrophages showed significant caspase expression ($p<0.05$). USPIO exposure led to upregulated M1-associated TNFa, iNOS, CD68 gene expression and downregulated M2-associated IL-10, CD206 gene expression in macrophages. In vivo studies revealed a significantly suppressed cancer growth for USPIO-co-injected cancers compared to controls ($p<0.05$). The tumor volume increased with locally decreasing iron signal on MRI. At 21 days after implantation, USPIO-co-injected cancers demonstrated 60% decreased volume compared to untreated controls, which corresponded to significantly increased quantities of monocytes and macrophages on FACS and significantly increased CD80 positive macrophages on immunohistochemistry.

Conclusion: Intra-tumoral administration of FDA-approved iron oxide nanoparticles significantly inhibits tumor growth due to the increased attraction of macrophages to tumors and polarization into pro-inflammatory M1 macrophages. This intrinsic effect could have broad implications for diagnostic and therapeutic iron oxide nanoparticles applications.

Acknowledgments:

The authors acknowledge support from the NIH/NCI, grant number R21CA156124.

Key words:

Ferumoxytol, Macrophage, MRI, Molecular Imaging, Cancer

AUTHORS (LAST NAME, FIRST NAME): zanganeh, saeid[1]; Lenkov, Olga D.[4]; Moseley, Michael[3]; Daldrup-Link, Heike E.[2]

INSTITUTIONS (ALL):

1. Radiology, Stanford Medical School, Palo Alto, CA, United States.
2. Radiology, Stanford University, Stanford, CA, United States.
3. radiology, stanford university, Palo Alto, CA, United States.
4. Department of Radiology, Stanford University, Stanford, CA, United States.

Supplementary Data:

Immune-modulating effects of the FDA approved iron oxide nanoparticle ferumoxytol inhibit tumor growth

Saeid Zanganeh, PhD[1], Olga Lenkov, BS[1], Michael Moseley, PhD[1], Heike E. Daldrup-Link, MD, PhD[1]
[1] *Department of Radiology, Molecular Imaging Program at Stanford, Stanford University*

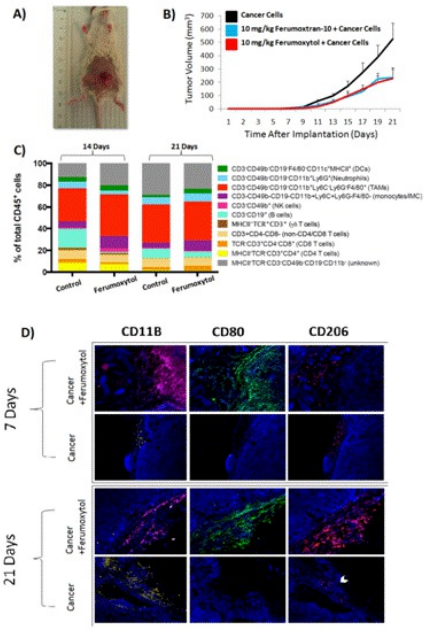

Supplementary Data:
Ferumoxytol inhibits tumor growth: (A) Decreased size of a representative mammary cancer on day 16 after co-implantation with ferumoxytol (right flank) compared to an untreated cancer (left flank). (B) Tumor volumes at different time points after implantation of cancer cells treated with different doses of ferumoxytol and untreated controls (mean data of 7 tumors in each group with SD). (C) Immune cell composition of USPIO-treated MMTV PyMT cancers and untreated controls demonstrates increased quantities of TAM and NK cells in USPIO-treated tumors. D) Immunohistochemistry demonstrates higher quantity of CD 80 expressing macrophages (M1 phenotypes) and lower quantity of CD206 expressing macrophages (M2 phenotypes) in USPIO-treated tumors compared to untreated controls.

CONTROL ID: 2231163

TITLE: Imaging Arthritis Disease Activity By Targeting S100A9 and Gelatinases Expression In A Mouse Model Of Inflammatory Arthritis

PRESENTER: Mahesh Kondapuram

ABSTRACT BODY:

Abstract Body: Damage associated molecular pattern molecules (DAMPs) are the key players in the initiation and maintenance of inflammation in many acute and chronic inflammatory diseases. S100A9, one subunit of the S100A8/S100A9 complex is one such DAMP involved in maintaining inflammation in rheumatoid arthritis (RA). Elevated serum and synovial fluid levels of S100A8/S100A9 correlate well with rheumatoid arthritis disease activity. A recent study based on labeled S100A9 antibodies demonstrated S100A9 as a good biomarker for *in vivo* imaging of local inflammatory activity in various inflammatory diseases[1].

In arthritis, local joint inflammation is accompanied by joint destruction. Serum and synovial gelatinase (MMP-2 and MMP-9) levels serve as a good biomarker to study cartilage and joint destruction in arthritic patients. In this study we demonstrate two novel compounds (CES-271 (S100A9) and AF-443 (MMP2/9)) labeled with fluorescent dyes as potential candidates for imaging inflammation and joint destruction by targeting S100A9 and gelatinase expression, respectively, in a murine model of rheumatoid arthritis.

Dba/J (n=10) mice were immunized with type II collagen for induction of arthritis (CIA). A booster injection was conducted 21 days after the first immunization. One week later, all mice started to developed signs of arthritis mainly in the fore and hind paws (visually scored by erythema, edema, and stiffness of limbs on a scale of 0-3). Optical imaging was performed using the MS-FX pro imaging station by injecting CES-271 conjugated to Cy7 and AF-443 conjugated to Cy5.5 in both healthy controls and CIA mice. The imaging results were further validated against the severity of disease using macroscopic clinical scoring, histological assessment of paws localizing S100A9, MMPs distribution and the systemic S100A8/S100A9 level by ELISA.

All CIA mice developed clear signs of arthritis when compared to healthy controls. The mean fluorescence signal obtained from CIA mice using both tracers showed high signal intensities when compared to those of healthy controls. The fluorescence imaging data also correlated well with the bright light images. Furthermore, the local and systemic expression of S100A9, MMP2, and MMP9 levels obtained using histology, ELISA and western blot correlated well with florescence imaging data.

Our data suggest that both CES-271 and AF-443 have the potential to image local disease activity and its progression by targeting S100A9 and gelatinase expression respectively. The involvement of S100A9 in early stages of RA disease activity and the elevation of gelatinases during the chronic disease phase make these tracers valuable for use in the clinic to assess the ongoing disease activity and its severity in RA patients.

Acknowledgements

This project is funded by 7th Framework program of the EU, SP3-People, Training/Career Development Network for Initial Training (ITN), FP7-PEOPLE-2011-ITN, under Marie Skłodowska-Curie grant agreement No 289903.

Reference:

Vogl T. *et al. Nat. Commun.* **2014**, 5, 4593

AUTHORS (LAST NAME, FIRST NAME): Kondapuram, Mahesh K.[1]; Zenker, Stefanie[2]; Vogl, Thomas[2]; Faust, Andreas[1]; Roth, Johannes[2]; Schäfers, Michael[1]; Hermann, Sven[1]

INSTITUTIONS (ALL):

1. European Institute for Molecular Imaging , University of Münster, Münster , Germany.
2. Institute of Immunology , University of Münster , Münster, 48149, Germany.

(No Image Selected)

CONTROL ID: 2231165

TITLE: Targeted imaging of the KISS1 receptor for oncological bone disease in breast cancer and multiple myeloma

PRESENTER: Robert Tower

ABSTRACT BODY:

Abstract Body: Bone formation and resorption is a tightly regulated process. Invasion of tumor cells within the bone marrow alters this balanced bone remodeling and results in either excessive bone loss (osteolytic lesion) or gain (osteosclerotic lesion). Current diagnosing strategies typically rely on radiological imaging approaches which monitor changes in bone mineral, meaning that bone lesions are not detectable until well after initial metastases formation and excessive bone loss or gain has occurred. Alternative scintigraphic methods are also possible, but frequently are more efficient at identifying osteosclerotic lesions, while lytic lesions remain difficult to identify at early stages. A more sensitive imaging method which could serve as a biomarker for both lytic and sclerotic skeletal metastases, either through direct binding to tumor cells and/or to the stromal cells comprising the tumor niche, would greatly increase the possibilities of identifying bone lesions at early stages where existing therapies are most effective. To this end, the KISS1 receptor (KISS1R), a G-coupled receptor known to play a role in the regulation of endocrine function, was identified as a target gene known to be upregulated in some breast cancer cells and found to also be upregulated on mesenchymal stem cells (MSCs) and osteoprogenitor cells (OPCs) when cultured with multiple myeloma (MM) cells. We hypothesized that a labeled Kisspeptin conjugate targeting the KISS1R should permit labeling of tumor cells and resulting bone microenvironment alterations thus providing a sensitive marker of tumor progression with potential also for therapeutic targeting.

To develop this target as a potential new biomarker, the KISS1R ligand, kisspeptin, was synthesized and conjugated with a fluorescent dye. *In vitro* fluorescent microscopy showed binding of the conjugated kisspeptin to MCF-7 breast cancer cells, as well as to both MM and MSCs under direct co-culture conditions. To determine the functionality of the KISS1R to serve as a biomarker for tumor-mediated bone diseases, conjugated kisspeptin was injected into immune-deficient mice carrying primarily osteosclerotic MCF-7 bone lesions or into immune-competent mice containing osteolytic MM bone lesions and marker distribution assessed over time in accordance with the guidelines of institutional authorities and approved by the ethics committee for animal experiments at the Christian Albrechts University. Tumor-burdened limbs in both MCF-7 and MM disease models showed significantly increased peak fluorescence *in vivo* compared to contralateral control limbs (increases of 34.1±7.8% and 28.1±8.2% respectively). These data suggests the utility of the KISS1R as a new biomarker in two different *in vivo* models of osteosclerotic and osteolytic bone disease resulting from breast cancer or MM skeletal metastases, capable of targeting both the tumor cells and host cells of the tumor microenvironment overcoming existing limitations in scintigraphy. This new biomarker approach could potentially serve as a new targeting strategy for future diagnostic and therapeutic approaches in these difficult to treat diseases.

AUTHORS (LAST NAME, FIRST NAME): Tower, Robert[1, 4]; Dotterweich, Julia[2]; Müller, Marc[1, 4]; Brandl, Andreas[3]; Penate-Medina, Oula[1, 4]; Beilhack, Andreas[3]; Ebert, Regina[2]; Tiwari, Sanjay[1, 4]; Schütze, Norbert[2]; Jakob, Franz[2]; Glüer, Claus C.[1, 4]

INSTITUTIONS (ALL):

1. University Hospital Schleswig-Holstein, Kiel, Germany.
2. Orthopedic Center for Musculoskeletal Research, University of Würzburg, Würzburg, Germany.
3. Ceneter for Interdisciplinary Clinical Research, University of Würzburg, Würzburg, Germany.
4. MOIN CC, Section Biomedical Imaging, Kiel, Germany.

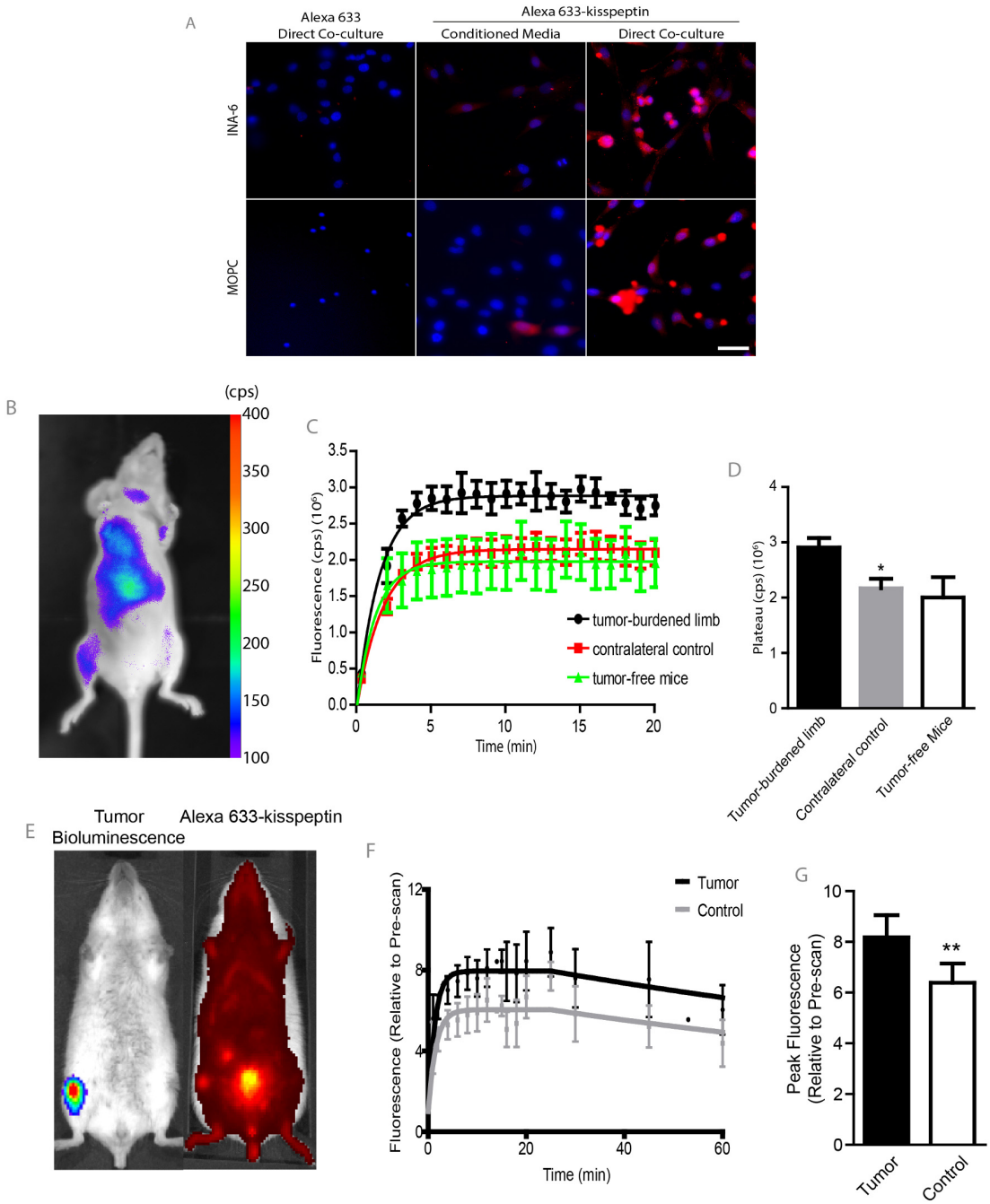

Conjugated kisspeptin probe was found to bind to MM and MSCs *in vitro* after direct co-culturing (A). *In vivo*, conjugated probe was found to bind to a significnatly greater extenet to limbs burdened with osteosclerotic MCF-7 breast cancer lesions (B-D) or lytic MM lesions (E-G)

CONTROL ID: 2232275

TITLE: Imaging tumor hypoxia using infrared fluorescent protein (iRFP) reporter under control of hypoxia driven HRE-promoter

PRESENTER: Martin Schneider

ABSTRACT BODY:

Abstract Body: In treatment of cancer the oxygenation state of the cancer tissue constitutes a crucial element. Low oxygen concentrations are associated with poor prognosis and poor responsiveness to radio-and chemotherapy. Not surprisingly major efforts have been invested to better understand the occurrence of hypoxia and how tumor cells (and the microenvironment) behave under hypoxic conditions in response to treatment. There are a considerable number of reporter gene assays that have been developed to study hypoxia related events [1]. Yet many of these approaches are limited as they rely on fluorescent or bioluminescent reporters, the value of which is compromised by poor light penetration in tissue. Recently a novel infrared fluorescent protein (iRFP) has been described [2]. Here we report on a novel hypoxia reporter gene assay based on iRFP expressed under the control of hypoxia responsive elements (HREs). In addition, cells were marked with constitutively expressed GFP.

Methods:
Lentivirus entry-vectors were received from the lab of I.Frew (University of Zürich) and the iRFP gene under the control of a HRE-promoter as well as GFP under the control of the CMV promoter inserted. Human DLDwt, DLDmut, RKOwt, RKOmut colon tumor cells and mouse B16F10 melanoma tumor cells were then stably transduced with this viral construct. Upregulation of iRFP under hypoxic conditions was evaluated in vitro via Leica DMI6000 microscope and CRI MAESTRO and in vivo via CRI MAESTRO after injection of 2.5x10^6 tumor cells(DLDwt/mut, RKOwt/mut and B16F10) subcutaneously into the flank of BALB/c-nu/nu mice.

Results:
We successfully transfected 4 human cancer cell lines and 1 mouse cancer cell line. All cell lines showed constant levels of expression of GFP and while the expression of iRFP could be triggered either through administration of DMOG (inhibiting proteasomal HIF1a degradation) or hypoxic conditions in a hypoxic chamber. In vivo studies in subcutaneous tumor models in mice revealed increasing volume-normalized iRFP levels with increasing tumor volumes for all tumor lines tested. In contrast, volume normalized GFP remained constant.

Discussion:
These results indicate a reliable, cell number independent, readout of iRFP expression under hypoxic conditions in vitro and in vivo. In view of the favorable optical parameters of iRFP, i.e. reduced absorptions compared to fluorescent proteins in the visible domain of the spectrum, the use of iRFP as a hypoxia marker is attractive for studying deeper lying, orthotopic tumors. The possibility to normalize the increasing iRFP signal according to the cell number makes these transduced cells a perfect target for analyzing drug or radiation influences.

1 Lehmann, S. *et al.* Longitudinal and multimodal in vivo imaging of tumor hypoxia and its downstream molecular events. *Proceedings of the National Academy of Sciences of the United States of America* **106**, 14004-14009, doi:10.1073/pnas.0901194106 (2009).
2 Filonov, G. S. *et al.* Bright and stable near-infrared fluorescent protein for in vivo imaging. *Nature biotechnology* **29**, 757-761, doi:10.1038/nbt.1918 (2011).

AUTHORS (LAST NAME, FIRST NAME): Schneider, Martin K.[1, 2]; Germanier, Catherine[1, 2]; Rudin, Markus[1, 2]

INSTITUTIONS (ALL):
1. Biomedical Engineering, ETH Zürich, Zurich, Switzerland.
2. Pharmacology & Toxicology, University Zurich, Zürich, Zürich, Switzerland.

iRFP expression under hypoxia driven HRE- promoter

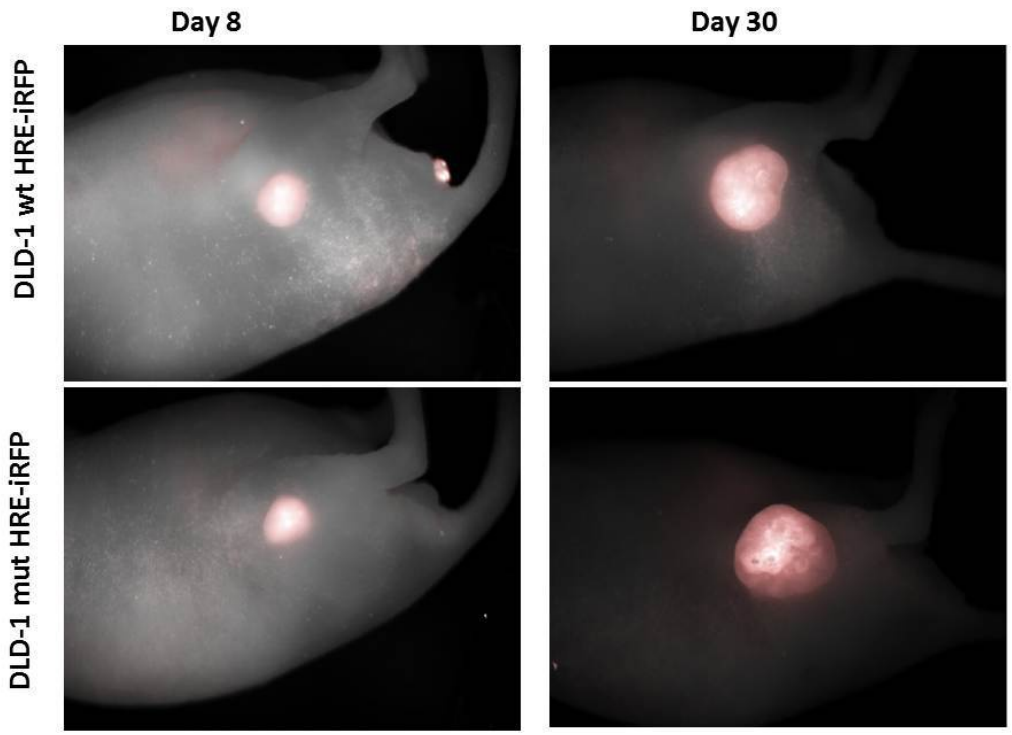

CONTROL ID: 2233948

TITLE: Translation fMRI in rheumatoid arthritis: Investigating the interlock of the imune system and brain function.

PRESENTER: Andreas Hess

ABSTRACT BODY:

Abstract Body: Arthritis is one of the most frequent and severe diseases in humans. This inflammation of the locomotor system causes pain, stiffness and swelling, resulting in decreased physical function and disability associated with premature death. Arthritic pain, the pivotal disease manifestation, is elicited by the nociceptive effects of inflammatory mediators such as cytokines and prostaglandins, triggering the activation of peripheral nerve ends and allowing the transmission of the pain signal to the dorsal root ganglia and via the thalamus into higher cortical areas. The sensation of pain is mediated by a complex network of neural circuits in the peripheral and central nervous systems. Major advancement in understanding how this network at the level of the CNS processes nociceptive signals was provided by human functional MRI studies over the last decade. Aimed at a deeper mechanistic insight and investigation of new treatment options, here particular anti-TNF treatments, animal experiments play and will play a major role because mice allow for specific genetic modifications affecting key players if the immune system like TNF. We therefore adapted functional BOLD MRI imaging to mice overexpressing human TNF (hTNFtg) allowing us to measure 3D brain activity maps of heat-induced nociception in this model of rheumatoid arthritis. We first could demonstrate the pathophysiological changes going along with the chronic pain in hTNFtg mice compared to wild-type mice and second how successful treatment with anti-TNF Infliximab results in unexpected fast changes of the brain network dynamics, in particular reducing the strong connections between thalamus and PAG. Due to the non-invasiveness of BOLD fMRI we were able to translate these findings to the human brain of rheumatoid patients. The success of a therapy for the patient could be confirmed with different anti-TNF drugs (Infliximab and Certolizumab Pegol) by significantly reduced overall brain activity as well as reduced connectivity strength between thalamus and PAG.

References:

Rech, J. et al. Association of brain functional magnetic resonance activity with response to tumor necrosis factor inhibition in rheumatoid arthritis. Arthritis Rheum 65, 325-333, doi:10.1002/art.37761 (2013).

Hess, A. et al. Blockade of TNF-alpha rapidly inhibits pain responses in the central nervous system. Proc Natl Acad Sci U S A 108, 3731-3736, doi:1011774108

AUTHORS (LAST NAME, FIRST NAME): Hess, Andreas[1]; Rech, Juergen[2]; Kreitz, Silke[1]; Schett, Georg[2]

INSTITUTIONS (ALL):

1. I. of Pharmacology, FAU Erlangen Nürnberg, Erlangen, Germany.
2. Department of Internal Medicine 3, FAU Erlangen Nuernberg, Erlangen, Germany.

(No Image Selected)

CONTROL ID: 2231203

TITLE: ^{44}Sc labelling of DOTA-PSMA DKFZ-617 for dosimetry and therapy of prostate cancer

PRESENTER: Ana de la Fuente

ABSTRACT BODY:

Abstract Body: OBJECTIVES

Radiolabelling of the prostate-specific membrane antigen (PSMA) inhibitor, Glu-NH-CO-NH-Lys (Ahx), using DOTA as chelator, a broad pool of radionuclides becomes available for labelling. These possible variations allow the visualization of the biological behavior over different periods of time depending on the half-life of the used radionuclide (^{68}Ga $t_{1/2}$ = 68 min; ^{44}Sc $t_{1/2}$= 3.9 h). Additionally, the usage of different imaging modalities or endoradiotherapies can be applied depending on the employed radionuclide.

METHODS

DKFZ-PSMA-617 was obtained from ABX (Radeberg, Germany). ^{44}Sc was obtained from a ^{44}Ti/^{44}Sc generator in Mainz, where ^{44}Ti decays with a half-life of 60 a to no-carrier-added (n.c.a) ^{44}Sc. Radiolabelling with ^{44}Sc was performed in 3 mL 0.25 M ammonium acetate buffer with varying amount of ligand at 95°C. Quality control was performed using radioHPLC and radioTLC.

RESULTS

^{44}Sc-DKFZ-PSMA-617 and ^{177}Lu-DKFZ-PSMA-617 were effectively labeled at 95 °C. Subsequent cartridge-based solid-phase-extraction (C-18) resulting in a radiochemical purity of the final tracers of ≥98%. Stability studies and small animal imaging with ^{44}Sc-DKFZ-PSMA-617 were performed. Radiochemical purity could be analyzed effectively using radioHPLC and radioTLC.

CONCLUSIONS

The radiolabelling of DKFZ-PSMA-617 with the new generator-derived PET radionuclide ^{44}Sc was investigated in detail. ^{44}Sc-DOTA-PSMA was investigated *in vitro* and *in vivo*. Small animal μPET studies were performed to investigate pharmacological *in vivo* characteristics adequate to long-term (up to one day) molecular imaging studies.

AUTHORS (LAST NAME, FIRST NAME): de la Fuente, Ana[1]; Eppard, Elisabeth[2]; Roesch, Frank[1]; Essler, Markus[2]

INSTITUTIONS (ALL):

1. Nuclear chemistry, Johannes Gutenberg University, Mainz, Germany.
2. Klinik und Poliklinik für Nuklearmedizin, Bonn , Bonn, Germany.

(No Image Selected)

CONTROL ID: 2231206

TITLE: SDF-1/CXCR7/β-catenin signaling promotes mesenchymal stem cell therapy for rheumatoid arthritis via tissue immunomodulation

PRESENTER: chia-ching lin

ABSTRACT BODY:

Abstract Body: Rheumatoid arthritis (RA) is a chronic symmetrical autoimmune disease caused by loss of immunologic self tolerance and characterized by chronic joint inflammation. Mesenchymal stem cells (MSCs) were recently used to repair injured tissues through immune-suppression and cell replace mechanisms. However, a significant barrier to MSC therapy is less tissue regeneration or insufficient immunomodulation after cell transplantation. The purpose of this study was to investigate the therapeutic efficiency of human bone marrow-derived mesenchymal stem cells (hMSCs) overexpressing CXCR7 on collagen-induced arthritis (CIA) and to explore the underlying mechanisms. Here, we show that enforced expression of CXCR7 in hMSCs could induce β-catenin activation. CXCR7 overexpression and SDF-1 treatment of hMSCs promote chondrogenesis and osteogensis that are inhibited by blocking of T-cell factor (TCF)/β-catenin signaling. In splenocyte or macrophage co-cultured with hMSCs, CXCR7 overexpression in hMSCs increased splenocyte or macrophage apoptosis compared to control hMSCs. Overexpression of CXCR7 in hMSCs increased the transcripts and secreted proteins of immunomodulatory cytokines such as IL-10 relative to levels in control hMSCs. The therapeutic benefits of transplanting engineered CXCR7-overexpressing MSCs were superior to those of control MSCs in collagen-induced arthritis. Taken together, cell transplantation of genetically modified hMSCs overexpressing CXCR7 inhibits experimental arthritis not only by promoting tissue regeneration via TCF/β-catenin signaling but also by suppressing autoimmune response via immunomodulatory cytokines, and thus would be a new strategy for treating rheumatoid arthritis.

AUTHORS (LAST NAME, FIRST NAME): lin, chia-ching[1]; Hsieh, Chia-Hung[1]

INSTITUTIONS (ALL):

1. China Medical University , Basic Medical Science, Sandy Springs, GA, United States.

(No Image Selected)

CONTROL ID: 2231257

TITLE: *In vivo* quantifying molecular specificity of Cy5.5-GX1 with dynamic fluorescence imaging

PRESENTER: Yunpeng Dai

ABSTRACT BODY:

Abstract Body: GX1, a cyclic 9-mer peptide of CGNSNPKSC that binds specifically to blood vessels of gastric cancer, has been conjugated with the NIR fluorescent dye of Cy5.5 (Cy5.5-GX1) to supervise angiogenesis of gastric cancer. In this work, a study of quantifying molecular specificity of Cy5.5-GX1 in the BGC823 subcutaneous tumor models was presented. The tumor models were established by injecting 1×10^7 BGC823 cells into the right mammary fat pad of the female athymic nude mice at the age of 4-6 weeks. After the tumors are palpable, tumor growth was monitored by caliper measurements three times a week. The mice were used for optical imaging when the tumor volume reached about 300 mm^3 (about 14 days after tumor inoculation). In the experiments, mice were randomly divided into four groups. In the first group, the mice were received 1nmol/mice Cy5.5-GX1; only Cy5.5 was injected in the second group; in the third and fourth groups, the mice were received 20mg/kg GX1 before 1 hour or 24 hours injecting Cy5.5-GX1 of 1nmol. One hour dynamic imaging were performed immediately following the intravenous injection of Cy5.5-GX1. Typically, 12s/frame was used for the first 900s, 18s/frame for the second 900s, and 24s/frame for the last 1800s. The acquired fluorescent images were combined with a pharmacokinetic model to determine kinetic properties of normal and tumor tissues. Preliminary results are described in Fig. 1. Some useful conclusions can be addressed from the results. First, the molecular specificity of Cy5.5-GX1 was confirmed by blocking the tumor uptake with excess GX1. Second, very similar kinetic properties of Cy5.5-GX1 were obtained as Cy5.5-c(KRGDf), including the kinetics time activity curves (TACs) and the summation of pharmacokinetic rate constants k_{total} (Cy5.5-GX1: k_{total}=0.21, Cy5.5-c(KRGDf): k_{total}=0.28). Results revealed that Cy5.5-GX1 is a promising molecular probe for fluorescence imaging of tumor vasculature.

AUTHORS (LAST NAME, FIRST NAME): Dai, Yunpeng[1]; Chen, Xueli [1]; Yin, Jipeng[2]; Zhang, Xianghan[1]; Liang, Jimin[1]

INSTITUTIONS (ALL):

1. School of Life Science and Technology,, Xidian University, Xi’an, Shaanxi, China.
2. State Key Laboratory of Cancer Biology, Xijing Hospital, Xi'an, Shaanxi, China.

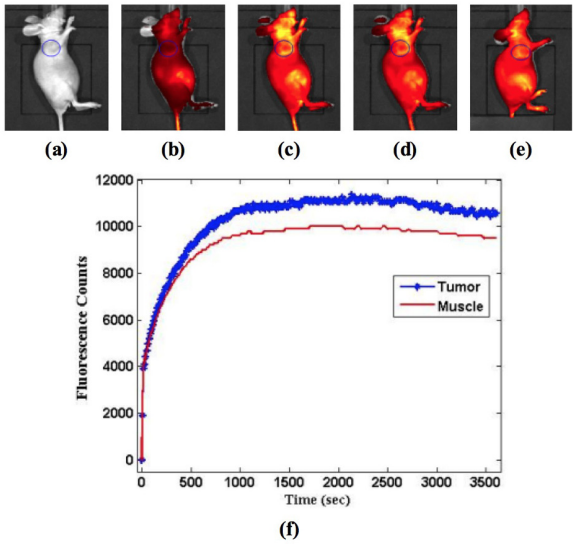

Fig. 1 Preliminary results for in vivo quantifying molecular specificity of Cy5.5-GX1. (a) White light image of a mouse that indicates the location of the tumor; (b)-(e) Fluorescence images obtained 1min, 30min, 60min and 120min after the administration of Cy5.5-GX1; (f) Time activity curve generated from 1h dynamic fluorescence imaging.

CONTROL ID: 2231311

TITLE: Multimodal imaging of breast cancer metastasis targeting and antimetastatic nanotherapy

PRESENTER: Larissa Rizzo

ABSTRACT BODY:

Abstract Body: INTRODUCTION: As opposed to the routine use of nanomedicines for drug targeting to solid tumors, the highest medical need refers to targeting and treating metastasis. Little is known regarding the accumulation of polymers, liposomes and micelles in metastases, and no systematic analyses have been performed comparing drug targeting to different types (and sizes) of metastases. We here employ three different nanocarriers, an optically imageable metastatic mouse model and several different imaging techniques, to assess drug targeting and drug treatment of metastasis. With fluorophore-labeled nanomedicines, we show that metastases can be more efficiently targeted than primary tumors. In addition, we provide convincing proof-of-principle that docetaxel-loaded micelles are able to inhibit metastasis, also providing initial insights into the vascularity of different types of metastases within different organs.

METHODS: Female Nu/Nu mice were orthotopically implanted with $2x10^5$ 4T1-iRFP cells (exc 680 nm). Mice were non-invasively monitored for local tumor growth and metastatic colonization using hybrid 3D computed tomography - fluorescence molecular tomography (CT-FMT). Upon metastastic detection, fluorophore-labeled (488/750) polymers, liposomes and micelles were i.v. injected. At 72h, primary tumors and metastases were harvested for ex vivo fluorescence reflectance imaging (2D FRI), assessing the colocalization between metastases (680nm) and nanocarriers (750nm). In an initial therapy study, 4T1-iRFP bearing mice were i.v. treated with vehicle, free docetaxel (Taxotere 30 mg/kg), and core-crosslinked polymeric micelles containing docetaxel (CriPec 30 mg/kg). In addition, a single CriPec 90 mg/kg was administered. Animals were CT-FMT scanned for metastasis colonization, organs were harvested for histology and 1 mouse/group was perfused with the vascular casting agent Microfil (for high-resolution ex vivo CT imaging of blood vessels in tumors and metastases).

RESULTS AND DISCUSSION: Metastatic colonization was sensitively detected using CT-FMT (Fig.1A-C). Fluorophore-labeled polymers and liposomes efficiently colocalized with metastases (overlap between 680 and 750 signals, Fig.1B-C), with no accumulation in healthy areas in lungs, lymph nodes and ovary (Fig.1C). The therapeutic efficacy of docetaxel-loaded core-crosslinked polymeric micelles was found to be higher than that of the free drug, with smaller primary tumors and less lung metastases, as visualized and quantified using optical imaging, CT imaging and histology (Fig.1D-E). A single 90 mg/kg micelle dose was found to be more efficient than three 30 mg/kg doses of free drug. High-resolution ex vivo μCT provided initial insights on the microvascular network in different types of metastases, showing that those are more extensively and more homogenously vascularized than primary tumors (Fig.1F).

CONCLUSION: In summary, we here systematically show that different types of metastases - in particular lung, lymph node, bone and ovary - can be efficiently targeted and treated using nanomedicines. Initial evidence correlating vascular characteristics with metastatic drug targeting is also provided.

AUTHORS (LAST NAME, FIRST NAME): Rizzo, Larissa[1]; Rijcken, Cristianne[2]; Pola, Robert[3]; Storm, Gert[4, 5]; Ehling, Josef[1, 6]; von Stillfried, Saskia[1, 6]; Kiessling, Fabian[1]; Lammers, Twan[1, 4]

INSTITUTIONS (ALL):

1. Experimental Molecular Imaging, RWTH Aachen University, Aachen, Germany.
2. Cristal Therapeutics, Maastricht, Netherlands.
3. Institute of Macromolecular Chemistry, Academy of Sciences, Prag, Czech Republic.
4. Department of Pharmaceutics, Utrecht University, Utrecht, Netherlands.
5. Department of Targeted Therapeutics, University of Twente, Enschede, Netherlands.
6. Department of Pathology, RWTH Aachen University Hospital, Aachen, Germany.

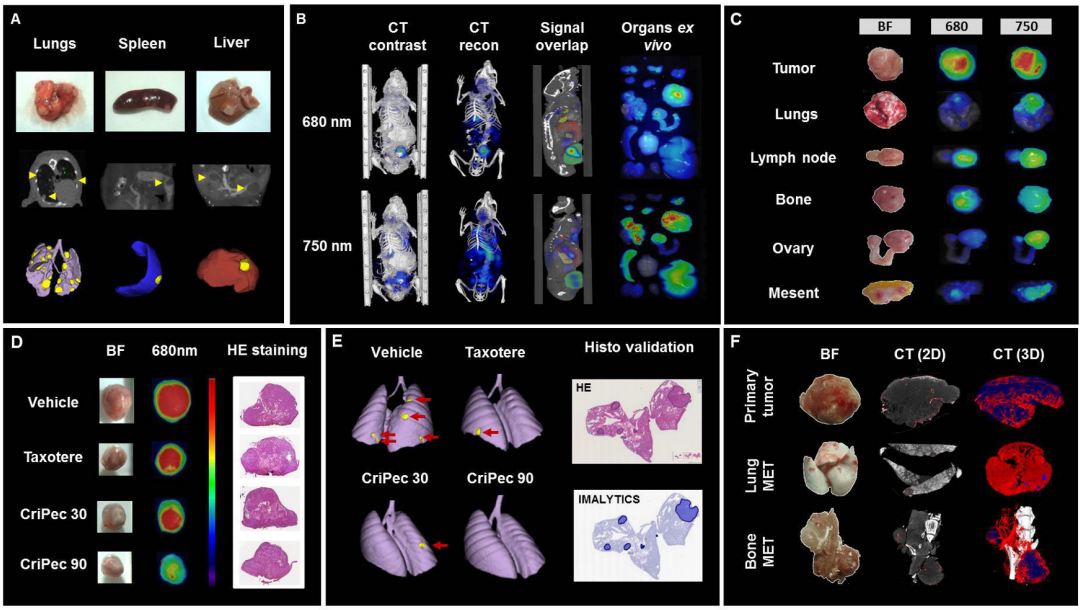

Figure 1: Imaging, targeting and treating breast cancer metastases using nanomedicine formulations. A: In vivo CT imaging of 4T1-iRFP breast cancer metastases in lung (top panels), spleen (middle panels) and liver (bottom panels). Metastases are segmented in yellow in the in vivo CT images, the respective organs (excised post-mortem) are shown on the left. B-C: Efficient and specific targeting of fluorophore-labeled polymers and liposomes to metastatic lesions in several different tissues, non-invasively in vivo in (B) and ex vivo 2D FRI (C). iRFP-expressing cancer cells are shown at 680 nm, fluorophore-labeled nanocarriers at 750 nm. Note the overlap between the 680 and 750 signals. BF: Bright-field images. D-E: Efficient anti-metastatic therapy using docetaxel-loaded core-crosslinked polymeric micelles (CriPec), exemplifying smaller primary tumors upon drug targeting (D) and less metastatic lung lesions (E), as also validated through histology by less necrotic areas upon treatment and also less lung metastases (lower number of lung metastases nodules, as well as lower relative area covered by the nodules (%)). F: High-resolution ex vivo CT imaging of blood vessels (red) in orthotopic breast cancer tumors and in lung and bone metastases upon Microfil perfusion. Analyses to correlate the efficiency of tumor and metastasis targeting with anatomical and functional blood vessel characteristics are currently ongoing. All images are based on own unpublished findings.

CONTROL ID: 2231229

TITLE: Radioiodinated 1,2,4,5-Tetrazine (Radio)Synthesis and in vivo Evaluation for Therapeutic Pretargeting

PRESENTER: Mitchell Duffy

ABSTRACT BODY:

Abstract Body: Bioorthogonal chemistry is a powerful tool for forming covalent linkages within living organisms.[1] Poor pharmacokinetics of radiolabeled probes can be circumvented using a two-step-process: First, a marker is accumulated in target tissue, second, a radiolabeled Pull Down Reagent (PDR) is ligated to this marker *in vivo*. Out of several reported bioorthogonal ligations the rapid reaction between strained alkenes and 1,2,4,5-tetrazines (Tz) proved highly suitable for radiolabeled agents.[1]

Several diagnostic Tz-based PDRs labeled with ^{11}C, ^{18}F and various radiometals have been reported.[1-4] Pretargeting using a therapeutic PDR could reduce radiation doses to healthy tissues and organs in radionuclide therapies.[4] The choice of readily available therapeutic radionuclides consists mainly of metals requiring bulky chelating agents for labeling. Resulting polar, high molecular weight molecules are unlikely to internalize making them unsuitable for intracellular targets. We aim to develop a therapeutic PDR with the potential to cross cell membranes, leading to flexibility regarding the targeting marker. ^{131}I was selected as nuclide due to its availability, low cost and favorable decay properties. Additionally, substitution of ^{131}I for ^{124}I or ^{123}I gives rise to PET and SPECT probes.

Electrophilic aromatic iodination was chosen as a well established way to introduce radioiodine. A methyl-terminated Tz scaffold was selected due to sufficient reaction kinetics and excellent *in vivo* stability. Herein, we describe the (radio)synthesis and *in vivo* evaluation of 3-(4-hydroxy-3-iodophenyl)-N-((6-methyl-1,2,4,5-tetrazin-3-yl)methyl)propanamide **(1).** Precursor **2** was readily accessible from EDCI coupling of **3** and **4** in 66% yield. Radioiodination using the Iodo-Gen© method followed by purification afforded ^{131}**I-1** in 74%, ^{124}**I-1** in 58% and ^{123}**I-1** in 22% radiochemical yield.

^{131}**I-1** exhibited excellent plasma stability over 7 days at 37°C. The log D value of 0.96 is in range of potential cell internalization. Dynamic SPECT/CT scanning with ^{123}**I-1** over 6.5 hours in CD1 nude mice (n=2) bearing a Human Thyroid Carcinoma K1 tumor xenograft on their breast revealed rapid renal and hepatobiliary excretion. Thyroid uptake at the 3 h and 5 h time point suggests *in vivo* deiodination of **1**. The SPECT data was in good agreement with data obtained from the *ex vivo* biodistribution conducted 6.5 h post PDR injection. Analysis of plasma and urine samples taken at 30 and 90 min post administration indicated rapid degradation and formation of polar metabolites.

To the best of our knowledge, ^{123}**I-1**, ^{124}**I-1** & ^{131}**I-1** are the first described radioiodinated Tz derivatives. Our investigations show that **1** may be used as prosthetic group for rapid radiolabeling, but limited metabolic stability disproves its use as a PDR for pretargeting applications. However, a therapeutic Tz- PDR based on ^{131}**I** is still of high significance and further derivatives with improved metabolic stability are currently under investigation.

(1) Rossin, R. *et al. ACIE* **2010**, 49, 3375
(2) Herth, M. M. *et al. Chem.Comm.* **2013**, 49, 3805
(3) Denk, C. *et al. ACIE* **2014**, 53, 9655
(4) Rossin, R. *et al. JNM* **2013**, 54, 1989

AUTHORS (LAST NAME, FIRST NAME): Denk, Christoph[1]; Duffy, Mitchell[2, 3]; Hermann, Sven[2]; Faust, Andreas[2]; Svatunek, Dennis[1]; Fröhlich, Johannes[1]; Schäfers, Michael[2, 4]; Mikula, Hannes[1]

INSTITUTIONS (ALL):
1. Institute of Applied Synthetic Chemistry, Vienna University of Technology, Vienna, Austria.
2. European Institute for Molecular Imaging, Westfälische Wilhelms Universität, Münster, NRW, Germany.
3. Cells-in-Motion Cluster of Excellence (EXC 1003 – CiM), Westfälische Wilhelms Universität, Münster, NRW, Germany.
4. Department of Nuclear Medicine of the University Hospital, Westfälische Wilhelms Universität, Münster, NRW, Germany.

(No Image Selected)

CONTROL ID: 2231235

TITLE: Human sodium iodide symporter as an imaging reporter gene for developing an animal MERS-CoV model

PRESENTER: Svetlana Chefer

ABSTRACT BODY:

Abstract Body: Introduction: Middle East Respiratory Syndrome Coronavirus (MERS-CoV) is an emerging pathogen associated with a severe respiratory disease (MERS) with a roughly 40% case fatality rate. Thus far, an animal model that recapitulates MERS has not been established. Non-human primate models demonstrated limited respiratory tract pathology associated with MERS-CoV exposure [1]. Furthemore, MERS-CoV-receptor-transduced mice support transient virus replication and demonstrate lung pathology [2]. The expression of human sodium iodide symporter (hNIS) gene in virus-infected cells can visualize temporal and spatial virus dissemination through the accumulation of radioactive tracers. Therefore, monitoring virus replication and dissemination in a live animal by nuclear medicine imaging can promote the development of animal models for MERS-CoV and other viruses. In this study, a recombinant MERS-CoV that expresses the hNIS was generated (MERS-CoV/hNIS). The goal of this study is to determine the stability and fitness of recombinant MERS-CoV/hNIS and to evaluate the functionality of the hNIS reporter gene in cell culture by planar scintigraphy.

Material and Methods: Parental MERS-CoV and MERS-CoV/hNIS were grown in cell culture on Vero E6 cells. One-step (multiplicity of infection [MOI] =3) and multi-step (MOI=0.01) kinetic studies were conducted in parallel to demonstrate fitness of both viruses with serial sampling up to 96 hrs after infection. HNIS reporter gene stability was evaluated by reverse transcription-polymerase chain reaction (RT-PCR). Functionality of hNIS gene was assessed by hNIS-mediated accumulation of ^{99m}Tc-pertechnetate using a Philips Precedence single photon emission computed tomography/computed tomography (SPECT/CT) scanner. Infected cells were incubated with 0.5 mCi of ^{99m}Tc-pertechnetate for 30 and 60min at 24 and 96hrs after infection and images of the plates were acquired by planar scintigraphy.

Results: The growth of MERS-CoV/hNIS was not attenuated compared with that observed with parental virus, as indicated by the similarity of the one-step (r=0.90, p=0.03) and multi-step growth curves (r=0.96, p=0.0082) of both viruses. RT-PCR confirmed hNIS gene maintenance in the MERS-CoV/hNIS. Scintigraphy was able to visualize and quantitate hNIS-associated accumulation of ^{99m}Tc-pertechnetate in MERS-CoV/hNIS-infected cells. The uptake of radioisotope by the cells infected with MERS-CoV/hNIS was as much as 100-fold higher (mean radioactivity of 89.8±5.6 µCi) compared with that observed in uninfected cells (0.57±0.04 uCi) and cells infected with MERS-CoV (0.77±0.15 µCi) after 96hrs, Fig.1.

Conclusion: MERS-CoV/hNIS demonstrated kinetics and fitness similar to the parental MERS-CoV and was functional in cell culture as measured by planar scintigraphy. We conclude that an application of MERS-CoV/hNIS in animal models and subsequent SPECT imaging with ^{99m}Tc-pertechnetate is feasible. Such a virus can be used for localization of the virus in infected animals and can provide real-time evidence of viral dissemination and the effects of treatment.

References:

1. Falzarano,D et al.*PLoS Pathog.***2014,**10(8).

2. Zhao,J et al. *Proc.Natl.Acad.Sci.USA.***2014,**111.

AUTHORS (LAST NAME, FIRST NAME): Chefer, Svetlana[1]; Seidel, Jurgen[2]; Thomasson, David[1]; Bartos, Christopfer[1]; Sayre, Philip[1]; Yount, Boyd[3]; Kumar, Mia[4]; Hagen, Katie R.[1]; Sims, Amy[3]; Dyall, Julie[1]; Holbrook, Michael[1]; Olinger, Gene G.[1]; Hensley, Lisa[1]; Jahrling, Peter[1, 4]; Baric, Ralph S.[3]; Johnson, Reed[4]

INSTITUTIONS (ALL):

1. Integrated Research Facility, NIAID, NIH, Frederick, MD, United States.
2. Molecular Imaging Program, NIH/NCI , Bethesda, MD, United States.
3. Department of Microbiology and Immunology, University of North Carolina, Chapel Hill, NC, United States.
4. Emerging Viral Pathogens Section, Integrated Research Facility, NIAID, NIH, Frederick, MD, United States.

(No Image Selected)

CONTROL ID: 2231262

TITLE: Effects of Fenbendazole on Tumor [^{18}F]FDG-PET Imaging

PRESENTER: Yun Lin

ABSTRACT BODY:

Abstract Body: Fenbendazole (FBZ) is a widely used antiparasitic drug. It can eliminate a variety of helminths by preventing their growth by inhibiting polymerization of the tubulin. Since a FBZ-containing diet is a common treatment against parasitic infection in laboratory animals, the aim of this study was to investigate how this diet influences tumor glucose consumption quantified by *in vitro* and *in vivo* [^{18}F]FDG measurements.

In *in vitro* studies, CT26 and U87MG tumor cells were incubated with a series of FBZ concentrations. Seven days after incubation, tumor cell growth was evaluated, and the [^{18}F]FDG uptake of the cells was measured by using γ-counter assays. For the *in vivo* study, balb/c mice received a standard FBZ-containing diet or a control diet (n= 4-5/group). Two weeks later, 10^6 CT26 tumor cells were injected subcutaneously at the right flank of each mouse. Non-fasting and overnight fasting [^{18}F]FDG-PET scans were performed on the same animals 14 and 17 days after tumor inoculation respectively. After intravenous administration of [^{18}F]FDG, 15-min PET acquisitions were started after 60-min sleeping uptake. The tumor to muscle ratio (T/M) of [^{18}F]FDG was evaluated. The 50% of maximum [^{18}F]FDG uptake was further analyzed in $T_{50\%}$/M.

In vitro, tumor cell growth of CT26 and U87MG was inhibited at high FBZ concentrations (>1μM), whereas the [^{18}F]FDG uptake of the cells increased after the normalization of cell numbers. The *in vitro* tumor cell growth and [^{18}F]FDG uptake were much less sensitive to low FBZ concentrations. The subcutaneous CT26 tumors tended to grow faster in the FBZ group without affecting body weight. An increased development of tumor necrosis was observed in the FBZ group at the final PET measurements. The T/M of non-fasting (control: 5.02±1.13, FBZ: 6.42±0.99) or fasting (control: 6.49±1.74, FBZ: 5.04±1.28) status did not differ between the FBZ and the control group. The $T_{50\%}$/M of non-fasting (control: 6.92± 1.22, FBZ: 8.82± 1.81) or fasting (control: 11.73± 3.43, FBZ: 9.08± 1.37) status didn't differ between these two groups as well. However, the control group revealed a significantly higher $T_{50\%}$/M at fasting state compared to non-fasting state ($p<0.05$), whereas no change was found in the FBZ group.

The *in vitro* experiments demonstrated cytotoxic effects of the antiparasitic drug on tumor cell growth and glucose consumption at high concentrations but not in low concentrations. The FBZ group showed a tendency of faster tumor growth with increased necrosis development. The control group had higher T/M at fasting state compared to non-fasting state, whereas this result was inverted in the FBZ group. The later phenomenon in the FBZ group may be due to necrosis occurrence which led to a lowered global tumor [^{18}F]FDG uptake on the day of fasting PET scans. To rule out the null uptake in the necrotic regions, the $T_{50\%}$/M was evaluated; nevertheless, the FBZ group revealed a different [^{18}F]FDG utilization compared to the control group. Although standard FBZ-containing diet has been considered a nontoxic treatment to lab animals, caution should be taken if tumor studies are performed at different treatment periods and dietary states.

AUTHORS (LAST NAME, FIRST NAME): Lin, Yun[1]; Calaminus, Carsten[1]; Pichler, Bernd J.[1]

INSTITUTIONS (ALL):

1. Werner Siemens Imaging Center, Department of Preclinical Imaging and Radiopharmacy, Eberhard Karls University, Tuebingen, Germany.

(No Image Selected)

CONTROL ID: 2231263

TITLE: AUTOMATED PRODUCTION AND QUALITY TESTING OF ^{18}F-LABELLED RADIOTRACERS USING THE BG75 SYSTEM

PRESENTER: Atilio Anzellotti

ABSTRACT BODY:

Abstract Body: The BG75 system comprises a small, positive ion cyclotron (7.5 MeV), synthesis and quality control modules. All modules are self-shielded and automated with the possibility of being controlled by one operator from one control console. Every radiotracer is produced in a single-use card that is sterile and represents a close system (DOSE ON DEMAND); ultimately the final product is delivered aseptically into a sterile syringe.
Automated tests for quality control are performed in parallel to the dose manufacture and have been validated according to ICH guidelines.
The system has consistently produced clinical grade [^{18}F]FDG doses since March 2013 in Sveta Marina University Hospital (Bulgaria) passing all required Quality Control criteria. In addition [^{18}F]FDG and [^{18}F]NaF have been produced in the University of Oklahoma – College of Pharmacy (USA) and other sites all around the world since 2012.
A summary of the results obtained for [^{18}F]FDG and [^{18}F]NaF in our sites in addition to proof of concept for other tracers such as [^{18}F]FMISO and [^{18}F]FLT, will be also presented.

REFERENCES

A.I. Anzellotti, A. R. McFarland, D. Ferguson, K.F. Olson, Curr. Org. Chem. 17 (2013) 2153.
V. Awasthi, J. Watson, H. Gali, G. Matlock, A. McFarland, J. bailey, A. Anzellotti, Appl Rad. Isot. 89 (2014) 167.
V. Awasthi, H. Gali, A. McFarland, A. Anzellotti, J Nucl Med. 55 (2014) 1243.

AUTHORS (LAST NAME, FIRST NAME): Anzellotti, Atilio I.[1]; Brown-Proctor, Clive[1]; Bailey, James D.[1]; McFarland, Aaron[1]; Khachaturian, Mark H.[1]

INSTITUTIONS (ALL):

1. ABT Molecular Imaging, Louisville, TN, United States.

(No Image Selected)

CONTROL ID: 2231361

TITLE: Impaired kidney development in mice with a mutation in the planar cell polarity protein Celsr1

PRESENTER: Hortensja Brzoska

ABSTRACT BODY:

Abstract Body: Epithelial cell alignment and co-ordinated organisation are essential for the development and maintenance of healthy organs and tissues. Planar cell polarity (PCP) is a signalling pathway regulating polarisation of cells along a plane orthogonal to the apical-basal axis.[1] PCP is required for vertebrate processes including directional cell movement, polarised cell division, ciliary orientation, neural tube closure, heart development and lung branching and is largely controlled by two groups of proteins referred to as the “core” planar polarity pathway and the Fat/Dachsous (Ds) system.[2,3] In the developing kidney, it has been previously shown that mice with a mutation in Vangl2, a core PCP component, have impaired glomerular maturation and ureteric bud branching.[4] In this study we sought to determine the role of another core PCP protein, Celsr1, in kidney development. Celsr1 is expressed in the ureteric bud and early nephron structures during development [1,4]; therefore, we hypothesised that a mutation in this core PCP molecule would lead to impaired ureteric bud branching and disrupted oriented cell division.

Using optical projection tomography (OPT) and quantitative image analysis (Tree Surveyor software)[5] we examined kidney branching in E13.5 *Celsr1*^{Crsh} mice, which harbour a single-point mutation in *Celsr1* gene. Orientation of mitotic chromosomes was assessed with use of confocal microscopy scanning of E17.5 kidney cryosections (30μm) stained with anti phospho-histone H3 (mitotic chromosomes) and entactin (tubular basement membrane). Mitotic angles were measured using Imaris software. Renal histology and gene expression of PCP genes using quantitative PCR were also assessed.

At embryonic day (E) 13.5 the total kidney volume of *Celsr1*^{Crsh} mutants was significantly smaller compared to wild-type littermates ($p<0.05$, n=3-5 for each genotype). *Celsr1*^{Crsh} mutants contained a reduced number of ureteric bud tips ($p<0.05$) compared to their wild-type littermates. The size of the bud tips and the angle at which they branched were unchanged. At E17.5, orientation of mitotic chromosomes was significantly disrupted in *Celsr1*^{Crsh} mutants compared to wild-type embryos ($p<0.0002$) but we did not observe an overt-cystic phenotype or any compensatory changes in the mRNA expression of other PCP genes (*Celsr2, Vangl2*, *Vangl1*, *Scrib*, *Pk1 and Pk2*) between *Celsr1*^{Crsh} and wild-type littermates.

This data highlights that Celsr1 plays a critical role in kidney tubular branching and is involved in oriented cell division. Our findings confirm the importance of the PCP signalling pathway during kidney morphogenesis.

References:

1. Carroll, T. J. and Das, A. (2011). Organogenesis 7(3): 180-190.
2. Papakrivopoulou, E. et al (2014). Nephrol Dial Transplant Jul;29(7):1320-6.
3. Lienkamp, S.S. et al (2012). Nat Genet 44: 1382-1387.
4. Yates L.L. et al (2010). Hum Mol Genet. Dec 1;19(23):4663-76.
5. Short, K. et al (2013). Development 140, 471-478.

AUTHORS (LAST NAME, FIRST NAME): Brzoska, Hortensja L.[2]; d'Esposito, Angela M.[1]; Lythgoe, Mark F.[1]; Woolf, Adrian S.[3]; Papakrivopoulou, Eugenia[2]; Long, David A.[2]

INSTITUTIONS (ALL):

1. Medical Physics and Biomedical Engineering, UCL, London, United Kingdom.
2. Developmental Biology and Cancer, UCL Institute of Child Health, London, United Kingdom.
3. Institute of Human Development, University of Manchester, Manchester, United Kingdom.

(No Image Selected)

CONTROL ID: 2231288

TITLE: Detection and differentiation of breast cancer sub-types using a cytosolic phospholipase A_2 Near-Infra Red (NIR) activatable fluorophore.

PRESENTER: Michael Chiorazzo

ABSTRACT BODY:

Abstract Body: Cytosolic phospholipase A_2 ($cPLA_2$) is signaling enzyme responsible for the liberation of esterified arachidonic acid from the *sn*-2 position of phospholipids. Release of arachidonic acid is the initial step in the eicosanoid signaling pathway, which has been studied extensively for its involvement in cancer. In breast cancer, a correlation of $cPLA_2$ to disease burden has been demonstrated. Lower grade, luminal-like breast cancer expresses low levels of $cPLA_2$ mRNA and protein compared to high grade, basal-like breast cancer [1]. Furthermore, resistance to estrogen receptor therapy in luminal-like cancer has been shown to involve the activation of $cPLA_2$ [1]. Therefore, a means of detecting $cPLA_2$ activity *in vitro* and *in vivo* would be useful for cancer detection, staging, and evaluation of therapeutic response.

Previously, we have reported the synthesis and characterization of a $cPLA_2$ activatable fluorophore, DDAO arachidonate, and demonstrated its ability to activate selectively by $cPLA_2$ in breast cancer cells. In this study, we investigate the potential to detect and differentiate breast cancer subtypes *in vitro* and *in vivo* based on $cPLA_2$ expression. Three cell lines were analyzed: MDA-MB-231, 4175Luc+, and MCF-7. MDA-MB-231 cells are a human triple negative breast (basal-like) cancer cell line, shown in the literature to express high levels of $cPLA_2$ mRNA and protein [2]. 4175Luc+ is a mouse adapted MDA-MB-231 line, expected to have similar protein expression. MCF-7 cells are a human estrogen receptor positive (luminal-like) cancer cell line, shown to express significantly lower levels of $cPLA_2$ [2]. DDAO arachidonate was added to these cell lines and time-dependent changes in fluorescence were measured (ex/em 600/660). At 3.5 h, fluorescence between 4175Luc+ and MDA-MB-231 cells was similar. However, fluorescence of MCF-7 cells was significantly lower than the basal-like cancer lines indicating lower $cPLA_2$ activity. To control for non-$cPLA_2$ mediated cleavage. a control probe, DDAO palmitate, was added and the fluorescence activation of DDAO arachidonate was adjusted by subtracting that from DDAO-palmitate. Following adjustment, the significance between cell lines was retained, indicating that the observed differences are a direct result of $cPLA_2$ activity. *In vivo*, 4175Luc+ tumor bearing mice were tail vein injected with DDAO arachidonate or DDAO palmitate and fluorescence generation was measured with time over multiple wavelengths. Spectral un-mixing was used to resolve probe fluorescence from background. A significant tumor activation of DDAO arachidonate versus DDAO palmitate was observed at 4 and 6 hours following injection. *Ex vivo* analysis of tumor fluorescence at 6 hours was also performed and demonstrated a significant activation of DDAO arachidonate compared to control. These data demonstrate the ability to differentiate breast cancer sub-types based upon $cPLA_2$ activity. Furthermore, we show that this $cPLA_2$ activated fluorescence can be observed *in vivo* either with whole body spectral un-mixing or with *ex vivo* tumor analysis

1. Caiazza *et al.* British Journal of Cancer (2011)

2. Caiazza *et al.* Mol Endocrinol (2010)

AUTHORS (LAST NAME, FIRST NAME): Chiorazzo, Michael[1]; Popov, Anatoly V.[2]; Delikatny, Edward J.[2, 1]

INSTITUTIONS (ALL):

1. Pharmacology, University of Pennsylvania, Philadelphia, PA, United States.

2. Radiology, University of Pennsylvania, Philadelphia, PA, United States.

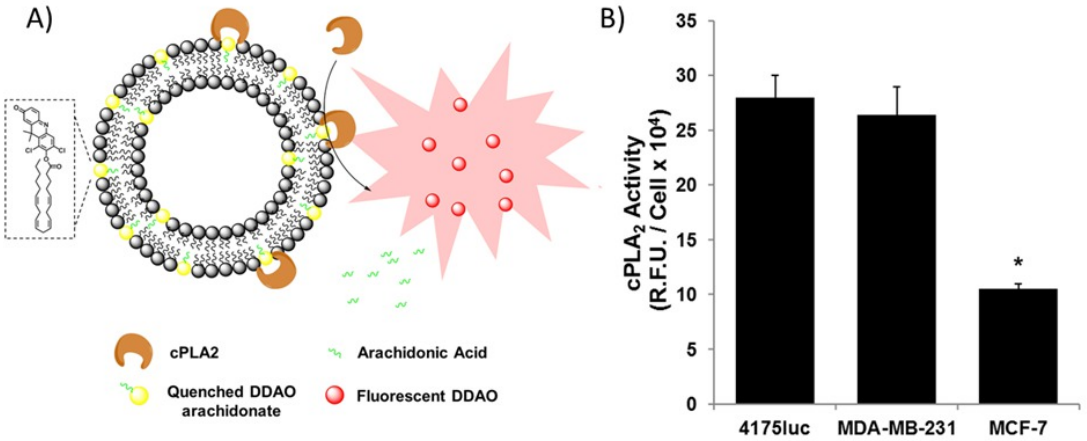

Figure 1. DDAO arachidonate: a novel tool for measuring cPLA$_2$ activity in breast cancer. A) DDAO arachidonate is packaged into phosphatidylcholine liposomes at a mole fraction of 0.05. Once added to cells in culture, or tumor tissue *in vivo*, cPLA$_2$ binds selectively to DDAO arachidonate and hydrolyzes the fluorophore from arachidonic acid. Once hydrolyzed, the fluorophore is no longer quenched and can fluoresce at an ex/em of 600-650/660. B) Fluorescence measurement of three breast cancer cell lines with known cPLA$_2$ activity. Fluorescence (ex/em 600/660) was measured after 3.5 hours of incubation in a 96 well plate. Quantitation showed similar fluorescence between the triple negative MDA-MB-231 cells and 4175Luc+ cells. However, significantly decreased fluorescence was observed in MCF-7 cells indicating lower activity of cPLA$_2$.

CONTROL ID: 2231297

TITLE: Orthotopic Canine Prostate Cancer Model for Molecular Imaging of Human Cancer Receptors

PRESENTER: Michael Tweedle

ABSTRACT BODY:

Abstract Body: Radical resection/ablation of in situ prostate cancer (PCA) is effective but causes impotence and incontinence. Active surveillance avoids or delays radical treatment but at high cost. Focal therapy enabled by US-MRI fusion guided HiFu will not treat multifocal disease. Systemic targeted chemo and radiation therapies carry unacceptable side effects in early stage.

Objective. To couple new theranostic agents with an innovative delivery technology for ultra low dose use in in situ prostate cancer. We transfected huGRPr (a known human prostate cancer cell marker) into an ACE-1 canine prostate cancer cell line (Prost. 2006, 66, 1213). A mouse xenograft ACE-1 / huGRPr-ACE-1 dual tumor model was generated to identify IR800-Abz4-t-BBN, a huGRPr-avid Optical agent (DOI: 10.1007/s11307-014-0727-2). Herein we develop a dog model, and demonstrate a dramatic pharmacologic dose advantage for a practical local delivery method.

Methods. IR800-Abz4-t-BBN was competed with 125I-BBN in huGRPr-ACE-1 cells with and without iodixanol, the angiographic agent. 3-5-year-old, sexually intact beagles (12-16 kg) have a ~ 20-30 g prostate that naturally develops BPH. 3 dogs were immunocompromised with cyclosporine (200-300 mg/d; nadir blood levels of 400 ng/mL). In Dogs 2 and 3 we added azathioprine (25 mg every other day), prednisolone (1 mg/kg/d), and methylprednisolone (10 mg/kg IM at time of cell implantation). 5 million huGRPr-ACE-1 cells were injected either into the medial region of a lateral prostate lobe from the inguinal region under ultrasound guidance, or into the sub cutis of the flank. After tumors were visualized by ultrasonography (4-5 wk) the prostatic artery (on the side of tumor cell injection) was catheterized via the carotid artery, guided by iodixanol fluoroscopy. 800-Abz4-t-BBN (20 nmol, 2 mL) was infused followed by 1- 2 h incubation, saline flush, then either euthanasia (Dogs 1 -2) or (Dog 3) single carotid artery ligation, 24 h recovery, then euthanasia. US, MRI and optical images were collected, and histopathology performed.

Results. Iodixanol had only a minor effect on IR800-Abz4-t-BBN binding to huGRPr-CE-1 cells. Dog 1, cyclosporine only (The Prost 1999, 39, 187): At 4 wk there was no visible tumor; tumor cells were rejected by a local immune response in the prostate. Dog 2: new immunosuppressive protocol for 4 wk; 1–2 mm tumors were present on the prostate capsule, and > 5 cm tumors in the flanks from xenograft injections. Dog 3: new immunosuppressive protocol for 6 wk; multinodular tumors (1-2 cm) in the prostate gland, on the capsule and along the injection tract visualized by US and MRI. High tumor to background (BPH) signal in optical images resulted from the 1.5 nmol/kg dose, compared to 500 nmol/kg needed intravenously in the mouse xenograft.

Conclusion. Orthotopic huGRPr-ACE-1 canine prostate cancer is viable with a new immunosuppression protocol. huGRPr-ACE-1 was targeted and imaged with IR800-Abz4-t-BBN. Local delivery through the prostatic artery could enable targeted chemo- and radio-therapy agents to be used safely for treatment of in situ prostate cancer.

AUTHORS (LAST NAME, FIRST NAME): Ding, Haiming[2, 1]; Drost, willliam T.[2]; Gong, Li[2, 1]; Kothandaraman, Shankaran[2, 1]; menendez, maria[2]; nguyen, Huyen[2]; phelps, mitch[2]; Dowell, Joshua[1]; Bahnson, Robert R.[3]; Knopp, Michael V.[2, 1]; Rosol, Thomas J.[4]; Tweedle, Michael F.[1, 2]

INSTITUTIONS (ALL):

1. Radiology, The Ohio State University, Columbus, OH, United States.
2. Wright Center of Innovation, The Ohio State University, Columbus, OH, United States.
3. Urology, Ohio State University, Columbus, OH, United States.
4. Veterinary Biosciences, Ohio State University, Columbus, OH, United States.

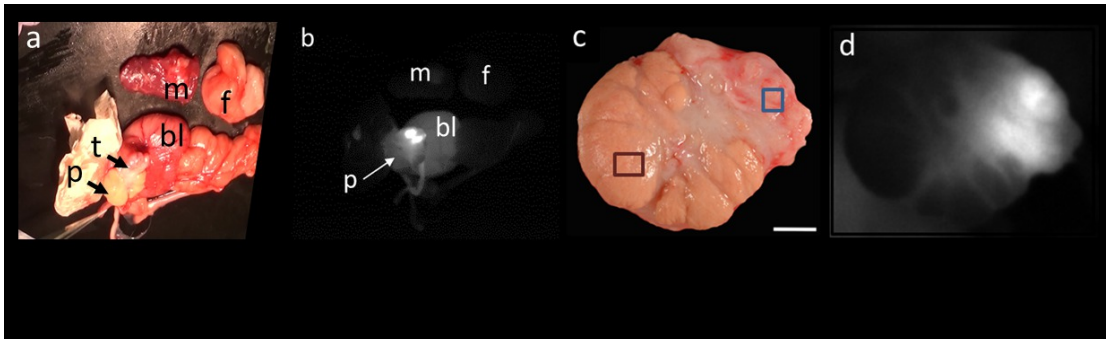
a
m
f
bl
t
p
b
m
f
bl
p
c
d

CONTROL ID: 2233813

TITLE: Early time point *in vivo* PET/MR is a promising biomarker for determining efficacy of a novel Db(αEGFR)-scTRAIL fusion protein therapy in a colon cancer model

PRESENTER: Mathew Divine

ABSTRACT BODY:

Abstract Body: The novel αEGFR diabody-single-chain-TRAIL Fusion Protein, developed by the group at the University of Stuttgart, is a potent apoptosis-inducing agent that benefits from EGF receptor targeting giving way to superior *in vivo* anti-tumoral effects. We present work on assessing the feasibility of using serial PET/MR to predict early changes in the tumor microenvironment.

NMRI nu/nu mice (n = 24) were subcutaneously injected with 4.5 x 10^6 COLO205 tumor cells and allowed to grow for 14 days before being randomized into either treatment or control groups. Baseline and 4 subsequent [18F]FDG or [18F]FLT scans were performed over the course of nine days using small animal PET. After PET scans, mice were moved to a 7 T Clinscan small animal MRI where Diffusion Weighted (DW) images were acquired. After baseline PET/MR measurements, mice were either injected with 100 µg of fusion protein in combination with 5 µg of the proteasome inhibitor Bortezomib or PBS and saline solution in equivalent volumes. Mice were measured on day 2,4,7, and 9 after baseline using the same PET/MR protocol. In a second cohort, the same mouse model was used, but this time only MRI measurements were performed on sham and treated mice at 24h or 72h after 1 or 2 treatments. This was done in order to gauge early changes in ADC, T2 and T2* maps before and after injection of USPIO particles. At the end of the last imaging experiment, mice were sacrificed by cervical dislocation and tumors were harvested for immunohistochemistry (IHC) for correlation to imaging.

In the first cohort the superior anti-tumoral effect of the fusion protein was apparent just 2 days after induction of therapy in MR images due to tumor shrinkage ($P<0.05$). Changes in glucose metabolism in the treated tumors as assessed by [18F]FDG and ADC scans were not significantly different from controls throughout imaging experiments. [18F]FLT uptake in treated tumors showed a downward trend throughout the course of imaging experiments. The H&E staining shows that treatment groups have more extracellular matrix, possibly altering water diffusion, and the treated tumors show signs of fibrous tissue build up. Apoptosis induction was higher in control tumors compared to treated tumors as seen in Activated Caspase 3 stainings, and Ki-67 staining revealed little to no difference in tumor groups. In the second cohort, early time point, MR imaging revealed significant differences in the T2pre images in the 24h treatment group compared to all other groups ($p<0.05$) and was also significantly different in T2* pre and T2*difference images in the 72h treatment group compared to all other groups ($p<0.05$). Parametric maps were highly correlated to histological findings, and inter-tumoral heterogeneity was very high in tumor images. Histology identified that mass apoptosis was induced in the 24hr treatment group, followed by large amounts of fibrous tissue buildup in the 72hr treatment group. TK-1 staining was greatly reduced in treatment groups.

Intra-tumoral heterogeneity is a confounding factor in PET/MR biomarker determination necessitating parametric imaging, early time point imaging, and direct histological comparison.

AUTHORS (LAST NAME, FIRST NAME): Divine, Mathew R.[1]; Harant, Maren[1]; Katiyar, Prateek[1]; Disselhorst, Jonathan A.[1]; Bukala, Daniel[1]; Aidone, Sandro[1]; Siegemund, Martin[2]; Pfizenmaier, Klaus[2]; Kontermann, Roland[2]; Pichler, Bernd J.[1]

INSTITUTIONS (ALL):

1. Department of Preclinical Imaging and Radiopharmacy, Werner Siemens Imaging Center, Eberhard Karls University Tübingen, Tübingen, Baden Württemberg, Germany.
2. University of Stuttgart, Stuttgart, Germany.

(No Image Selected)

CONTROL ID: 2232394

TITLE: PET-CT Imaging Of Tumor Angiogenesis And Metabolism For Evaluation Of Complementary And Alternative Medicine (CAM) Treatment Of Breast Cancer.

PRESENTER: Iwona Dobrucka

ABSTRACT BODY:

Abstract Body: Introduction

Complementary and alternative medicines (CAM) such as extract from black cohosh (BC) are often used by breast cancer patients subjected to doxorubin-based (DOX) chemotherapy. Major goal of this study was to evaluate synergistic effects of BC and DOX on in vitro viability of human breast cancer cells (MCF-7) and in vivo tumor growth, metabolism and angiogenesis assessed with PET-CT imaging in preclinical model of MCF-7 xenografts.

Methods

MCF-7 (~10^6) were incubated with 1-100uM DOX alone or with BC extract, washed and incubated with both calcein-AM and propidium iodide for flow cytometry (FC) to distinguish live from apoptotic cells. Treated MCF-7 were cultured to form colonies, then fixed, stained with crystal violet and imaged for clonogenic assay. For in vivo studies 6-wks old overiectomized athymic nude mice injected with MCF-7 in both flanks and estradiol pallets to promote tumor growth. After 6-wks of tumor growth measured with a digital caliper, animals were divided into three groups: treated with DOX (4mg/kg/wk), DOX and BC (20mg/kg/d), and untreated control. Mice were imaged with ^{18}F-FDG (tumor metabolism at baseline, 1 and 3 wks) and ^{64}Cu-cRGD$_2$ (angiogenesis at 2 wks) using small animal dedicated Inveon PET-CT scanner. PET-CT images were reconstructed, analyzed by segmentation of tumor mass, and activities expressed in %ID/g.

Results

Combined DOX and BC incubation resulted in doubling the number of apoptotic cells as compared with control. Treatment with DOX altered the potential of MCF-7 to form colonies, however BC treatment did not affect this process. Tumor growth was reduced by 12% in BC, 20% in DOX and 57% in DOX+BC groups. Tumor metabolism assessed with 18F-FDG was significantly attenuated in DOX (-40%) and BC (-20%) treated animals but there was no synergistic effect observed. Tumor angiogenesis was found reduced in all groups. On average the DOX+BC group had 16% less ^{64}Cu-cRGD$_2$ uptake than control animals.

Conclusions

Using various molecular biology and targeted imaging techniques we successfully demonstrated that BC exerts synergistic effects on DOX cytotoxicity resulting in significant reduction in tumor size and angiogenesis, but this change is independent of in vitro ability of MCF-7 to form colonies and in vivo tumor glucose metabolism. Additional studies will be needed to establish which mechanism underlies observed effects that could result in potential clinical implications on how breast cancer patients are managed.

AUTHORS (LAST NAME, FIRST NAME): Dobrucka, Iwona T.[1]; Schuh, Sarah[1, 2]; Ploska, Agata[1, 3]; Hedhli, Jamila[1, 2]; Helferich, William[4]; Kalinowski, Leszek[3, 1]; Dobrucki, Wawrzyniec L.[2, 1]

INSTITUTIONS (ALL):

1. Beckman Institute, University of Illinois at Urbana-Champaign, Urbana, IL, United States.
2. Bioengineering, University of Illinois at Urbana-Champaign, Urbana, IL, United States.
3. Medical Laboratory Diagnostics, Medical University of Gdansk, Gdansk, Poland.
4. Division of Nutritional Sciences, University of Illinois at Urbana-Champaign, Urbana, IL, United States.

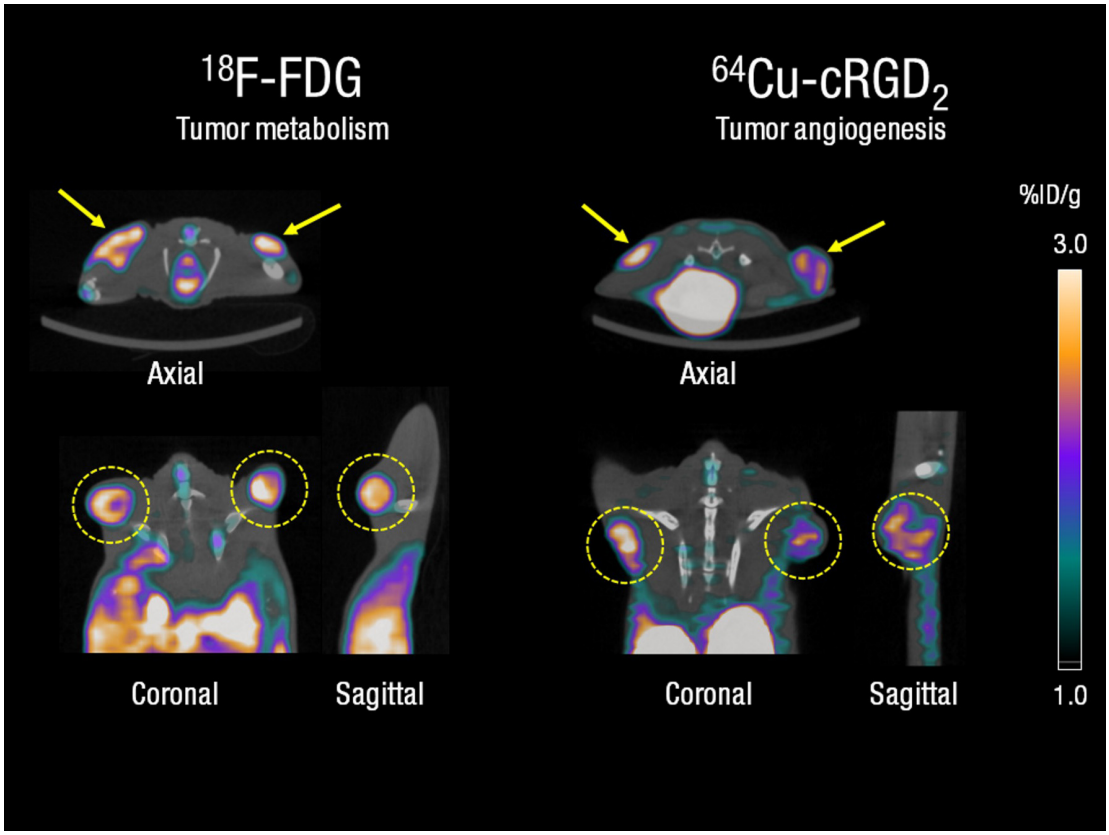
18F-FDG
Tumor metabolism
64Cu-cRGD2
Tumor angiogenesis
%ID/g
3.0
1.0
Axial
Axial
Coronal
Sagittal
Coronal
Sagittal

CONTROL ID: 2231355

TITLE: Tumor pO2 and glycolytic activity in pancreatic cancer xenografts as biomarkers to guide treatment.

PRESENTER: Murali Cherukuri

ABSTRACT BODY:

Abstract Body: Pancreatic cancer is a malignant neoplasm with an extremely poor prognosis. The 5-year overall survival rate is below 10%. A new drug TH-302 in combination with gemcitabine was approved for Phase 3 clinical trial in locally advanced or metastatic pancreatic adenocarcinoma in December 2012. The TH-302 is a kind of drugs known as hypoxia-activated prodrug (HAP), which activated under hypoxia (low concentration of oxygen) and exhibits anti-tumor effect. A question derived is how clinicians select patients who receive most benefit from treatment with this hypoxia targeting new drug, instead of classical radiation therapy or gemcitabine monotherapy. Electron paramagnetic resonance imaging (EPRI) can non-invasively provide 3D absolute oxygen images. Here, we investigated if the EPR oxygen imaging can predict treatment benefit of oxygen dependent or independent therapies in three different pancreatic cancer xenografts.

Three human pancreatic cancer cells Hs766t, MiaPaca2, and Su8686 were subcutaneously inoculated in hind leg of athymic nude mice. The tumor bearing mice were treated with TH-302 (80mg/kg, ip, 5 days), X-radiation (3Gy, 5 days), or gemcitabine (150mg/kg, ip, twice a week). Tumor oxygen imaging was conducted by a homemade 300 MHz pulsed EPRI scanner using an oxygen sensitive triarylmethyl probe OX063, followed by anatomic MRI scan.

Three pancreatic cancer cell lines showed large difference in tumor oxygenation. Tumor median pO_2 values are 9.1+/-0.7 mmHg for Hs766t, 11.1+/-1.0 mmHg for MiaPaca2, and 17.6+/-1.1 mmHg for Su8686. TH-302 treatment provided survival benefic of 28.6 days in hypoxic Hs766t tumors but only 1.0 days in the most oxygenated Su8686 tumors. In contrast, tumor growth delay by radiotherapy was 10.3 days in Hs766t, 18.6 days in MiaPaca2, and 19.3 days in Su8686 tumors. Gemcitabine treatment was effective in both hypoxic and oxygenated tumors but there seemed to be most effective against the hypoxic Hs766t tumors.

Quantitative oxygen images by EPRI can predict difference in the benefit from oxygen-dependent anti-tumor treatments in individual pancreatic tumor cell lines that may help properly choose the best treatment in patients with pancreatic cancer if EPRI is available in clinic.

AUTHORS (LAST NAME, FIRST NAME): Matsumoto, Shingo[4]; Saito, Keita[2]; Devasahayam, Nallathamby[1]; Munasinghe, Jeeva P.[3]; Mitchell, James B.[1]; Cherukuri, Murali K.[1]

INSTITUTIONS (ALL):

1. Center for Cancer Research, NCI, Bethesda, MD, United States.
2. National Cancer Institute, Bethesda, MD, United States.
3. Neurological Disorders and Stroke, National Institutes of Health, Bethesda, MD, United States.
4. Hokkaido University, Sapporo, Japan.

(No Image Selected)

CONTROL ID: 2233002

TITLE: Advanced fluorescence nano particles for live cells, *in vivo* imaging, and fluorescence analysis.

PRESENTER: Dong hwi Shim

ABSTRACT BODY:

Abstract Body: Highly stable bead type fluorescent nanoparticles for efficient molecular imaging were developed. These novel nanomaterials can be conjugated to various biomaterials (antibodies, proteins, peptides, etc.) and proved their capability and applicability.

Fluorescent dyes have been widely used in the elucidation of the active information of biomolecules. However, low intensity and instability of dyes limit their utilization to being fully exploited in the bimolecular research. Thus, many researchers have developed stable and long-lasting fluorescent nanoparticles as efficient alternatives of dyes. However, their application in the body has to be cautious due to poor pharmacokinetic property. We synthesized new nanoparticles based on low-toxic polymer that derived from a living body and coated them with the fluorescent dyes to achieve strong fluorescence intensity. For binding to various biomolecules, several different reaction moieties were applied to the particle.

AUTHORS (LAST NAME, FIRST NAME): Shim , Dong hwi[2]; Moon, Myeong Ju[2]; Park, Jin Woo[1]; Jeong, Eun Ae[1]

INSTITUTIONS (ALL):

1. BioActs, Incheon, Korea (the Republic of).
2. DKC coporation (BIOACTS), Incheon, Korea (the Republic of).

(No Image Selected)

CONTROL ID: 2231379

TITLE: Molecular Magnetic Resonance Imaging of Breast Cancer using Core/Shell Nanoparticles

PRESENTER: Barbara Blasiak

ABSTRACT BODY:

Abstract Body: Breast cancer is the most frequently diagnosed cancer in women.Unfortunately, the sensitivity of the mammography, the standard diagnostic method,is relatively low and decreases when breast tissue is dense. Ultrasound and PET are also used but the detection of small tumors (<5-10 mm) is poor andthe spatial resolution is not accurate enough to exclude breast cancer in patients with abnormal mammograms or palpable breast masses. Magnetic Resonance Imaging (MRI) has excellent spatial resolution but low specificity. Thus we have appliedmolecular MRI for the early diagnosis of malignant triple negative breast cancer.We have developed new core/shell $NaDyF_4$/$NaGdF_4$ nanoparticlesand conjugated them with the tumor specific antibodies (1-3). The relaxation times (T_1 and T_2) of the nanoparticles with various score/shell sizes were measured at 9.4T to find the optimum T_1/T_2 ratiofor MRI. An animal model of the breast cancer was used. The infra-red (IR),T_1-, T_2-weighted and synergetic T_1/T_2MR images were collected before and after injection of the contrast agent. The agents consisting of the targeted nanoparticleswith the controlled core and shell sizes providedimproved tumor contrast when the synergetic T_1/T_2 MR pulse sequencewas applied. This allowed better tumor delineation and positive, tumor-specific contrast in MR images. A 9.4T MRI system was used for *in vivo* experiments.The results have shown the efficacy of the new contrast agents, thus potential suitability for the early detection of cancerous tissues.

References:

1. Das GK, et al.$NaDyF_4$ Nanoparticle as T_2 Contrast Agent for Ultra-High Field Magnetic Resonance Imaging. *J. Phys. Chem. Lett.* **3**:524-529, 2012.

2. Dong C, et al.Cation exchange: a facile method to make $NaYF_4$:Yb,Tm-$NaGdF_4$ core-shell nanoparticles with a thin, tunable, and uniform shell. *Chemistry of Materials.* **24**:1297–1305, 2012.

3. Blasiak B et al Comparison of T2 and T2*-weighted MR molecular imaging of a mouse model of glioma. *BMC Medical Imaging*, **13**:20-28, 2013.

AUTHORS (LAST NAME, FIRST NAME): Blasiak, Barbara[1]; van Veggel, FrankC. J. M.[2]; Gautam, Anurag[2]; Zhang, Xinghua[2]; Corluka, Slavisa[3]; Abulrob, Abedelnasser[3]; Tomanek, Boguslaw[1, 4]

INSTITUTIONS (ALL):

1. Department of Clinical Neurosciences, University of Calgary, Calgary, AB, Canada.
2. Department of Chemistry, University of Victoria, Victoria, BC, Canada.
3. Department of Cellular and Molecular Medicine, Univerity of Ottawa, Ottawa, ON, Canada.
4. Department of Oncology, University of Alberta, Edmonton, AB, Canada.

(No Image Selected)

CONTROL ID: 2231377

TITLE: Clinical Study of *ex vivo* Photoacoustic Imaging in Endoscopic Mucosal Resection Tissues

PRESENTER: Liang Lim

ABSTRACT BODY:

Abstract Body: Accurate endoscopic detection and dysplasia in patients with Barrett's esophagus (BE) remains a major unmet clinical need. Current diagnosis use multiple biopsies under endoscopic image guidance, where up to 99% of the tissue remains unsampled, leading to significant risk of missing dysplasia.

We conducted an *ex vivo* clinical trial using photoacoustic imaging (PAI) in patients undergoing endoscopic mucosal resection (EMR) with known high-grade dysplasia for the purpose of characterizing the esophageal microvascular pattern, with the long-term goal of performing *in vivo* endoscopic PAI for dysplasia detection and therapeutic guidance. 13 tissue samples from 8 patients were analyzed, and these spanned a range of pathological classifications including non-dysplastic BE (12), low grade dysplasia (3), high grade dysplasia (4), intramucosal carcinoma (2), and adenocarcinoma (2). EMR tissues were mounted immediately on an agar layer and covered with ultrasound gel. Digital photography guided the placement of the PAI transducer (40 MHz center frequency). The luminal side of the specimen was scanned over a 3D field of view of 14 mm (width) by 15 mm (depth) strips at 680, 750, 824, 850 and 970 nm. Acoustic images were simultaneously acquired. Tissues were then sliced along a pre-defined short axis with spacing approximately 2 mm and fixed in formalin for histopathology with H&E staining. Analysis consisted of co-registration and correlation between the intrinsic PAI features and the histological images.

From the acoustic images, we can create 3D reconstruction of the full *ex vivo* tissue volume (Figure *1A*), and calculate the relative hemoglobin concentrations (oxy-, deoxy-, and total), and oxygen saturation (Persuasive Data Figure S1). Ongoing analysis includes co-registration and correlation between the intrinsic PAI features and the corresponding histological images as illustrated in Figures 1B and 1C. The photoacoustic signal distribution within the tissue appears to coincide with the distribution of blood (dark pink on the H&E section), the main absorber in the tissue.

The initial PAI + ultrasound images have demonstrated the technical feasibility of this approach and point to the potential of PAI to reveal the microvascular pattern within EMR specimens. Photoacoustic signals were obtained in all 13 samples to a depth of approximately 2 mm and analysis of total hemoglobin is currently being assessed against histologically measured vessel areas from H&E stained sections for each dysplasia categories. Results of these investigation will be reported and discussion of the limitations of this type of photoacoustic mapping of BE will be discussed.

AUTHORS (LAST NAME, FIRST NAME): Lim, Liang[1]; Foster, F. Stuart[2]; Streutker, Catherine J.[3]; Marcon, Norman[4]; Cirocco, Maria[4]; Iakovlev, Vladimir[3]; DaCosta, Ralph[1]; Wilson, Brian C.[1]

INSTITUTIONS (ALL):

1. Princess Margaret Cancer Centre, University Health Network, Toronto, ON, Canada.
2. Sunnybrook Research Institute, Sunnybrook Health Sciences Centre, Toronto, ON, Canada.
3. Surgical Pathology, St. Michael's Hospital, Toronto, ON, Canada.
4. Gastroenterology, St. Michael's Hospital, Toronto, ON, Canada.

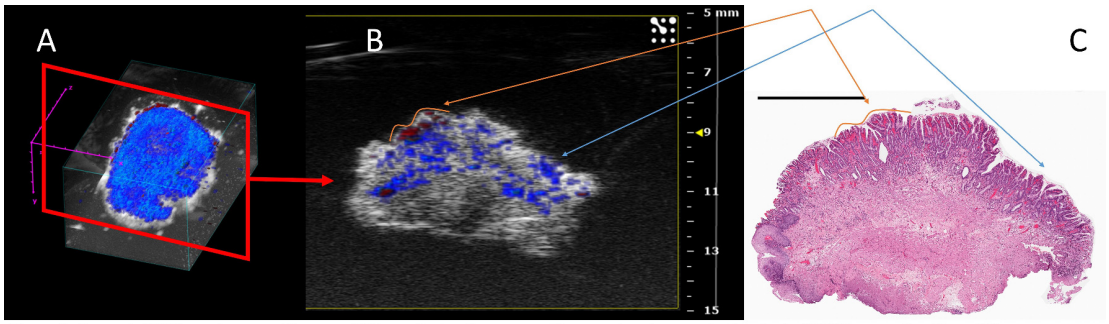

Figure 1: Example EMR specimen and images. This particular tissue was diagnosed as low grade dysplasia. (A) 3D reconstruction of the photoacoustic signal (blue – 750 nm, red – 850 nm) overlaid on top of the ultrasound (greyscale), using maximum intensity projection. (B) A slice of from the 3D reconstruction. The vertical scale (in mm) is the distance from the front face of the transducer probe. (C) Histopathology of the closest corresponding slice. Similar physical features have been highlighted. Horizontal scale bar is 2 mm in length.

CONTROL ID: 2231388

TITLE: Nanosponges as Activatable Magnetic Resonance Imaging Contrast Agents and Stimuli-responsive Chemotherapeutic Vehicles

PRESENTER: Charalambos Kaittanis

ABSTRACT BODY:

Abstract Body: Sensitive diagnosis and effective therapy are critically needed for the management of cancer, ideally based on the innovative use of imaging platforms. Since Nature widely employs multivalency in order to convert weak interactions to high affinity and fidelity molecular associations, we developed valency-engineered magnetic nanoparticles with small molecule ligands. These magnetic nanosensors rapidly detected a single cancer cell in unprocessed clinical samples, via the changes in the spin-spin (T2) magnetic resonance signal. Further studies, revealed that the nanosensors could serve as a facile platform for the ultrasensitive identification and characterization of novel interactions between small molecules and overexpressed transmembrane proteins, having major ramifications in the development of new diagnostics and therapeutics. We subsequently utilized a multivalent nanoparticle for the *in vivo* delivery of cancer chemotherapeutics to prostate tumors that expressed the prostate-specific membrane antigen (PSMA); a protein that is found in >90% of prostatic lesions and correlates to disease stage. The nanoparticles allowed visualization of the tumors through magnetic resonance imaging (MRI, **Figure 1a**) and fluorescence molecular tomography (**Figure 1b**). Histological studies using fluorescence microscopy and iron-specific staining confirmed the in vivo imaging findings (**Figure 1c**). In prostate cancer, similar to many other cancers, one signaling pathway may modulate the output of another signaling cascade. Specifically, it was recently reported that inhibition of the androgen receptor pathway in prostate cancer causes activation of the PI3K pathway, which may lead to resistance and metastasis. Therefore, we loaded the PSMA-specific nanoparticles with the anti-androgen enzalutamide and the PI3K inhibitor BEZ235, achieving complete tumor regression in mice that had AR-positive, PSMA-positive xenografts (**Figure 1d**). Furthermore, we identified that a clinical iron oxide nanoparticle could serve as a versatile drug delivery nanosponge, which retains multiple chemotherapeutics within its coating. Besides being stable in serum, the drug-loaded nanosponges retained their cargo at physiological pH, but released it at slightly acidic conditions (pH ≤6.8). We discovered that the nanosponges were able to accommodate chemotherapeutics, like Taxol, Doxorubicin and enzalutamide, via weak electrostatic interactions between the nanosponges' coating and the drugs' functional groups, which were perturbed in lower pH. Intriguingly, these drugs among others were able to quench the nanosponges' MRI signal, allowing real-time monitoring of drug release *in vivo* with MRI and optimization of cancer treatment. Notably, release of the drugs by the nanosponges resulted in recovery of the nanosponges' T2 signal *in vivo* (**Figure 1e**), whereas continuous nanosponge tracking was achieved by recording the T2* signal, which was unaffected by the cargo's presence (**Figure 1f**). Overall, we foresee the use of these systems in the development of disease stratification strategies and patient-tailored imaging-driven therapies for solid tumors that improve survival.

AUTHORS (LAST NAME, FIRST NAME): Kaittanis, Charalambos[1]

INSTITUTIONS (ALL):

1. Memorial Sloan Kettering Cancer Center, New York, NY, United States.

(No Image Selected)

CONTROL ID: 2231411

TITLE: Microfluidic-based production of narrow size distribution freeze-dried microbubbles for ultrasound imaging and cancer therapy: Synthesis and *in vivo* characterization

PRESENTER: Siqi Zhu

ABSTRACT BODY:

Abstract Body: Introduction. There is great interest in evaluating narrow size distribution, lipid-stabilized, microbubbles to increase the frequency-dependent response of microbubbles for ultrasound imaging and targeted cancer treatment. A promising method to synthesize single-sized microbubbles is through microfluidics, but the resulting slow bubble generation rate (~10^3 bubbles/sec), the specialized expertise required, and the significant challenges in storing and transporting unstable bubbles make it challenging for such monodisperse microbubbles to be evaluated *in vivo*. We hypothesize that monodisperse lipid stabilized droplets, which can be produced at very high generation rates compared to the direct microfluidic generation of microbubbles, can be dehydrated and used as precursors of stable, narrow size distribution microbubbles after on-site reconstitution with saline.

Methods. Monodisperse, lipid-stabilized precursor hydrocarbon droplets were synthesized using three-inlet, flow-focusing, quartz microfluidic devices. The precursor droplets were heated above the lipids' transition temperatures followed by controlled cooling, lyophilization, and infusion with perfluorocarbon gas. The precursor droplets and bubbles post-reconstitution were sized with optical microscopy and a Coulter Counter. The frequency-dependent response and shell properties of the final bubbles were characterized using attenuation measurements from 1.5 to 39 MHz. The bubbles were assessed *in vivo* after tail vein injection into CH3/HeJ mice with KHT sarcoma tumor xenografts, using a Philips iU22 clinical ultrasound scanner equipped with a L9-3 probe.

Results. Monodisperse lipid-stabilized droplets of controlled sizes ranging from 2 to 10 microns and coefficient of variations (CVs) below 8% were produced at generation rates of up to ~10^6 droplets/s, up to 10^3 times faster than the direct generation of bubbles using microfluidics. After reconstitution, although the bubble size distribution increased (CVs >13%), microbubbles were highly stable with no change in the normalized bubble size distribution and only ~10% decrease in bubble concentration after 30 minutes. *In vitro* ultrasound measurements show that after reconstitution, the shell stiffness and viscosity were similar to polydisperse, commercially available freeze-dried microbubbles. *In vivo*, the persistence and echogenicity of the narrow size distribution microbubbles in the tumor was evaluated and found to be appropriate for ultrasound imaging and cancer therapy.

Conclusions. High yield, transportable, and stable, lipid-stabilized microfluidic-generated microbubbles were successfully synthesized and evaluated. *In vivo* studies in tumor mouse models showed that the final saline-reconstituted, narrow size distribution microbubbles are promising for ultrasound cancer imaging and therapy applications.

AUTHORS (LAST NAME, FIRST NAME): Seo, Minseok[2]; Zhu, Siqi[2]; Leung, Ben[2]; Goertz, Dave[2]; Matsuura, Naomi[1]

INSTITUTIONS (ALL):

1. University of Toronto, Toronto, ON, Canada.
2. Sunnybrook Research Institute, Toronto, ON, Canada.

(No Image Selected)

CONTROL ID: 2232404

TITLE: Targeted PET Imaging of COX-1 in Ovarian Cancer

PRESENTER: Jashim Uddin

ABSTRACT BODY:

Abstract Body: Companion imaging diagnostics that predict patients likely to respond to precision medicine represent a critically unmet need in ovarian cancer. Noninvasive imaging plays a critical role in the management of ovarian cancer by confirming sites of disease, informing surgical intervention (upfront surgery versus chemotherapy followed by surgery), and determining the effectiveness of treatment. Imaging modalities include transvaginal ultrasound (TVUS), computed tomography (CT), magnetic resonance imaging (MRI), ^{18}F-fluorodeoxyglucose positron emission tomography (FDG-PET), and FDG-PET combined with CT (PET/CT). All of these imaging strategies have limitations in predicting response to treatment. The folate receptor radiotracer is the only diagnostic modality that has shown promise in predicting response to a molecular targeted therapy. Cyclooxygenase-1 (COX-1) is a promising molecular target in ovarian cancer. Our results indicate that COX-1 is overexpressed in high-grade serous ovarian cancer (HGSOC), which is significantly higher than other tumor types and normal tissues. RNAseq experiments comparing isogenic COX-1 knockdown to COX-1 overexpressing HGSOC cells demonstrate coordinated inhibition of multiple oncogenic pathways associated with vascular endothelial growth factor (VEGF) and angiogenesis, proliferation, and cell migration/invasion. Functional *in vitro* assays paralleled the observed changes in gene transcripts. Taken together, our results corroborate multiple lines of evidence to support the concept that COX-1 is a unique and attractive molecular target for ovarian cancer, particularly HGSOC tumors. To image COX-1 in ovarian cancer by PET/CT, we designed, synthesized, and evaluated a series of new compounds based on 5,5-dimethyl-3,4-diarylfuran-2(5H)-one scaffold, and optimized a lead fluorine-containing COX-1-selective inhibitor. We developed a novel method for the radiosynthesis of the lead *^{18}F-COX-1 probe*. We used a subcutaneous athymic nude mouse xenograft model to validate the target specificity of the ^{18}F-COX-1 probe using COX-1 overexpressing SKOV3 cells transfected with PTGS1 (SKOV3/COX-1) and low COX-1 expressing parental SKOV3 cells. At 2 h post-injection, ^{18}F-COX-1 probe (500~800 μCi, retro-orbital) accumulated in the high COX-1-expressing SKOV3/COX-1 xenografts in greater levels than in the low COX-1-expressing SKOV3 xenografts, detected by microPET/CT. Further, to evaluate the ability of our ^{18}F-COX-1 probe to target ovarian cancer under physiologically relevant conditions, we used a SKOV3/COX-1 peritoneal tumor model in female nude mice. The animals bearing peritoneal tumors were dosed with ^{18}F-COX-1 probe (600~700 μCi, retro-orbitally) and imaged in the microPET/CT for 30 min (PET) and 5 min (CT) post-injection of the radiotracer. The ^{18}F-COX-1 probe accumulated sufficiently in peritoneal tumors, which facilitated non-invasive detection in this ovarian cancer model. These results illustrate that this ^{18}F-probe is a promising novel tracer of COX-1 activity that warrants further translational development as new modality suitable for imaging ovarian cancer and predicting its response to targeted therapy.

AUTHORS (LAST NAME, FIRST NAME): Uddin, Jashim[1]; Crews, Brenda C.[1]; Ghebreselasie, Kebreab[1]; Daniel, Cristina M.[1]; Wilson, Andrew[3]; Nickels, Michael L.[4]; Tantawy, Mohammed N.[2]; Manning, H. Charles[4]; Khabele, Dineo[3]; Marnett, Lawrence J.[1]

INSTITUTIONS (ALL):

1. Department of Biochemistry, Chemistry, and Pharmacology, Vanderbilt University School of Medicine, Nashville, TN, United States.
2. Radiology and VUIIS, Vanderbilt University Medical Center, Nashville, TN, United States.
3. Department of Obstetrics & Gynecology, Vanderbilt University School of Medicine, Nashville, TN, United States.
4. Department of Radiology and Radiological Sciences, Vanderbilt University School of medicine, Nashville, TN, United States.

(No Image Selected)

CONTROL ID: 2231799

TITLE: Longitudinal *in vivo* monitoring of cancer cachexia development points towards browning of white adipose tissue and enhanced utilization of fatty acids in brown adipose tissue

PRESENTER: Wolfgang Thaiss

ABSTRACT BODY:

Abstract Body: Introduction:

Cancer cachexia (CC) is a devastating concomitant effect in a variety of malignancies with loss of weight, fat and muscle tissue (1). Recent advances identified brown adipose tissue (BAT) and browning of white adipose tissue (WAT) as main drivers for energy expenditure (2,3). Here, we aimed to longitudinal monitor CC development in two established mouse models in order to identify changes in glucose and fatty acid metabolism with *ex vivo* verification.

Methods:

C57BL/6 wild-type mice were injected with B16 melanoma or Lewis Lung Cells (LLC) subcutaneously or sham treated (n=3 per group). We performed ^{18}F-FDG-PET measurements of tumor bearing mice 6, 11 and 18 days after injection and ^{18}F-fluoro-6-thia-heptadecanoic acid (^{18}F-FTHA-PET) measurements after 10 and 16 days. 10 min static PET scans were acquired with a small animal PET scanner 1 hour after ^{18}F-FDG injection (8.14 ± 0.9 SD MBq); 10 min static PET scans 30 minutes after ^{18}F-FTHA injection (9.9 ± 2 SD MBq). Mice were anaesthetized with 1.5% isoflurane; body temperature was maintained in all experiments at 37°C. Tumor volume and regions of interest were determined based on T2 weighted MR images (using a 7T small animal MRI). Finally we performed biodistribution studies and analyzed cachexia-related serum markers.

Results:

As fundamental basis, weight development over time corrected for tumor weight confirmed the cachectic phenotype (19.8 ± 1.4 g in B16, 19.5 ± 0.4 g in LLC and 20.9 ± 0.3 g in control animals). PET analysis displayed a significantly increase in ^{18}F-FDG uptake over time in LLC (4.4 ± 1.5 %ID/cc (day 6), 8.2 ± 2.4 %ID/cc (day 11) to 7.6 ± 0.4 %ID/cc (day 18, $p<0.05$) while the ^{18}F-FTHA tumor uptake did not change significantly over time.

^{18}F-FTHA uptake increased ~25% from day 10 (3.4 ± 0.2 %ID/cc) to 16 (4.3 ± 0.5 %ID/cc) in the BAT of B16 melanoma bearing mice and BAT of LLC bearing mice (day 10: 2.6 ± 0.2 %ID/cc; day 16: 3.7 ± 0.2 %ID/cc), while no change was observed in controls (day 10: 3.2 ± 0.1 %ID/cc, day16: 3.2 ± 0.8 %ID/cc). ^{18}F-FDG uptake in the BAT did not exhibit these differences.

Biodistribution analysis revealed increased ^{18}F-FDG uptake in inguinal WAT (7.5 ± 3 %ID/cc (LLC), 2.0 ± 1.3 %ID/cc (control), $p<0.05$) as correlate for browning of WAT during cachexia development. Serum parameters were strongly increased for cholesterol, LDL, TAG, and GOT in cachectic animals.

Conclusion:

^{18}F-FDG Uptake increased significantly over the time in CC development in LLC while no significant difference in ^{18}F-FTHA uptake was detected. Inguinal white adipose tissue showed higher FDG uptake over time as correlate for browning of WAT. Fatty acid uptake increased over time in brown adipose tissue in B16 melanoma and LLC bearing mice compared to controls. Taken together, we demonstrate first noninvasive evidence of WAT browning in cancer cachexia and changes in fatty acid metabolism as correlate for energy expenditure.

1. Fearon et al. Nature reviews Clinical oncology. 2013; 10(2):90-9.
2. Kir et al. Nature. 2014; 513(7516):100-4.
3. Petruzzelli et al. Cell metabolism. 2014; 20(3):433-47.

AUTHORS (LAST NAME, FIRST NAME): Thaiss, Wolfgang M.[1, 2]; Ehrlichmann, Walter[1]; Sartorius, Tina[3]; Peter, Andreas[3]; Nikolaou, Konstantin[2]; Pichler, Bernd J.[1]; Kneilling, Manfred[1, 4]

INSTITUTIONS (ALL):

1. Department of Preclinical Imaging and Radiopharmacy, Eberhard Karls University, Werner Siemens Imaging Center, Tübingen, Germany.
2. Department of Radiology, Eberhrad Karls University, Diagnostic and Interventional Radiology, Tübingen, Germany.

3. Department of Internal Medicine IV, Eberhard Karls University, Tübingen, Germany.
4. Department of Dermatology, Eberhard Karls University, Tübingen, Germany.
(No Image Selected)

CONTROL ID: 2231992

TITLE: Ketamine/Xylazine anesthesia reveals superior signal-to-noise ratios in ^{18}F-FAZA-PET tumor hypoxia imaging when compared to Isoflurane anesthesia

PRESENTER: Wolfgang Thaiss

ABSTRACT BODY:

Abstract Body: Introduction

Hypoxia within carcinomas is associated with poor prognosis. Thus, non-invasive *in vivo* detection of tumor hypoxia with ^{18}F-fluoro-azomycine arabinoside (18F-FAZA), a positron emission tomography (PET) biomarker is an important issue. We recently have demonstrated the impact of different anesthesia regimes on the mouse physiology and on invasive *in vivo* oxygen probe and static ^{18}F-FAZA-measurements. The aim of this study was to compare the dynamics of ^{18}F-FAZA-uptake as well as the tracer washout in Ketamine/Xylazine (K/X)- or Isoflurane (IF)-anesthetized CT 26 colon carcinoma bearing mice and to uncover the distinct advantages and disadvantages for dynamic and static PET measurements.

Material and Methods

Female BALB/c mice were inoculated with CT26 colon carcinomas *s.c.* at the right upper flank 15-18 days prior to dynamic (180 min) static ^{18}F-FAZA PET studies using a small animal PET system. Tumor volumes in the two experimental groups were similar (~ 300 mm³). H&E histology of CT26 colon carcinomas excluded necrosis. We anesthesized mice 20 min before dynamic PET acquisition and during the PET measurements with either IF (1.5%) or K/X (100 and 5 mg/kg body weight, n = 4 per group). K/X was maintained via *i.p.* administration on the PET bed. We administered 13.0 ± 0.09 MBq ^{18}F-FAZA *i.v.* in spontaneouslybreathing mice and maintained the body temperature at 37°C. Hot spot analysis was used for analysis of our ^{18}F-FAZA-PET data set.

Results

^{18}F-FAZA time activity curves (TACs) revealed an emphasized initial perfusion peak in the CT26 colon carcinomas and muscle tissue of K/X-anesthetized mice compared to IF-anesthetized littermates (1 h: ^{18}F-FAZA-uptake: IF: 185.7 ± 45.4 kBq/mm^3 vs. K/X: 426.1± 45.4 kBq/mm^3). Accordingly, 3h TACs revealed an increased ^{18}F-FAZA uptake in tumors of K/X-anesthetized mice when compared to IF-anesthetized mice
(3 h: IF: 86.1 ± 50.1 kBq/mm^3 vs. K/X 256.4 ± 59.1 kBq/mm^3). ^{18}F-FAZA muscle TACs revealed and enhanced uptake in K/X-anesthetized mice only until 90 min post [^{18}F]FAZA injection when compared to IF-anesthetized littermates. Tumor ^{18}F-FAZA washout kinetics revealed a trapping for 1h after ^{18}F-FAZA injection in tumors of K/X-anesthetized mice (after the perfusion peak). At 1h, 94% of the maximum ^{18}F-FAZA uptake was reached in tumors of K/X-anesthetized mice whereas ~60% of the maximum ^{18}F-FAZA uptake was reached in tumors of IF-anesthetized littermates. In tumors of IF-anesthetized mice, the ^{18}F-FAZA activity dropped down to 28% 3h after tracer injection compared to 56% in tumors of K/X-anesthetized mice. In contrast, we observed a comparable ^{18}F-FAZA washout in the muscle tissue.

Conclusion

Dynamic ^{18}F-FAZA analyses in CT26 colon carcinoma bearing mice revealed a strong dependency on the used anesthesia regime on ^{18}F-FAZA-uptake in carciomas and muscle tissue. ^{18}F-FAZA tumor uptake was strongly enhanced in K/X anesthetized mice when compared to IF anesthetized littermates. Thus, K/X reveals superior signal-to-noise ratios in PET hypoxia imaging when compared to IF, the most widely used preclinical anesthetic.

AUTHORS (LAST NAME, FIRST NAME): Thaiss, Wolfgang M.[1, 2]; Mahling, Moritz[1]; Fuchs, Kerstin[1]; Maier, Florian C.[1]; Pichler, Bernd J.[1]; Kneilling, Manfred[1]

INSTITUTIONS (ALL):

1. Department of Preclinical Imaging and Radiopharmacy, Eberhard Karls Univsersity, Werner Siemens Imaging Center, Tuebingen, Germany.

2. Department of Radiology, Eberhard Karls University, Diagnostic and Interventional Radiology, Tuebingen, Germany.

(No Image Selected)

CONTROL ID: 2231415

TITLE: An Optical Imaging Threshold to Detect Head and Neck Cancer during Fluorescence-Guided Surgery

PRESENTER: Lindsay Moore

ABSTRACT BODY:

Abstract Body: During fluorescence-guided surgery, a cancer-specific optical probe is injected and then visualized using a compatible device intraoperatively to provide visual contrast between disease and normal tissues. However, the current classifications used to define the extent of fluorescence within tissues are often purely qualitative, undefined, and lacking distinct criteria for fluorescence comparison (Nat Med. 2011;17:1315-9). A quantitative reporting criterion using standardized methods is necessary for widespread approval and advancement of this technique. Here, we introduce a ratiometric value as a novel method for assessing tissue fluorescence in real-time to objectively distinguish between normal and cancerous tissue during fluorescence-guided surgery. Imaging was performed on punch biopsy tissues from resected primary tumors of head and neck cancer during a phase 1 dose-escalation trial evaluating the safety and tumor-specificity of cetuximab-IRDye800. In this study, 97 punch biopsies of tumor (n=50) and normal (n=47) tissue were collected from areas of high and low fluorescence intensity in 12 resected primary tumors from patients who received the study probe. Two fluorescent imaging devices, an open-field (LUNA) and a closed-field (Pearl) device, were used to evaluate the approach and assess the variability of a ratiometric threshold between different imaging devices. Punch biopsy tissues were imaged using both imaging devices and mean fluorescence intensity (MFI) was calculated. Additionally, skin and muscle samples were collected and imaged to serve as internal anatomic controls for each patient and to establish a patient-matched “background” fluorescence to ensure the ratiometric value would account for inherent variability between patient tissues. For each specimen, a fluorescence ratio was calculated by dividing the specimen’s MFI by the MFI of patient-matched background tissues (muscle or skin). Ratios were correlated to pathological assessment in order to determine a ratiometric threshold to predict the presence of malignant tissue with fluorescence imaging. For the open-field intraoperative device, when the muscle-normalized ratiometric value was less than 2.7, the negative predictive value (NPV) was 89.2%. When skin-normalized values were less than 1.1, the NPV was 92.0%. With the closed-field device, the muscle-normalized NPV was 89.8% using a threshold of 3.2 and skin-normalized NPV was 90.7% using a threshold of 1.5. Table 1 shows the sensitivity and specificity of each imaging device to accurately detect disease using a corresponding threshold. Receiver operator characteristic (ROC) analysis was performed to assess the accuracy of the diagnostic test, which demonstrated a significantly ($p<0.01$) greater AUC than the chance diagonal with a 95% confidence interval for both skin and muscle normalized ratios using both open- and closed-field imaging devices. This proof of concept study yielded a highly sensitive, semi-quantitative threshold for objective determination of the presence of cancer using fluorescence imaging. Furthermore, statistical assessments of the ratiometric threshold confirmed the accuracy of the diagnostic tool.

AUTHORS (LAST NAME, FIRST NAME): Moore, Lindsay S.[4]; de Boer, Esther[4]; Schmalbach, Cecelia E.[2]; Carroll, William R.[3]; Morlandt, Anthony[5]; Young, Erik S.[6]; Rosenthal, Eben[1]; Warram, Jason M.[4]

INSTITUTIONS (ALL):

1. Otolaryngology, Stanford University, Stanford, AL, United States.
2. Surgery, Univ of Alabama at Birmingham, Birmingham, AL, United States.
3. Surgery, University of Alabama - Birmingham, Birmingham, AL, United States.
4. Surgery, University of Alabama at Birmingham, Birmingham, AL, United States.
5. Surgery, Univerity of Alabama at Birmingham, Birmingham, AL, United States.
6. Pathology, University of Alabama at Birmingham, Birmingham, AL, United States.

(No Image Selected)

CONTROL ID: 2242887

TITLE: Dose Ranging of Anti-Lymphangiogenic Treatment for Enhanced Antibody-based Therapy in an Animal Model of Head and Neck Cancer

PRESENTER: Lindsay Moore

ABSTRACT BODY:

Abstract Body: The vascular endothelial growth factor receptor-3 (VEGFR3) has been shown to play a role in the development of abnormal blood and lymphatic vessels in many solid tumors, which contribute to increased intratumoral interstitial pressure and impaired fluid mechanics.[1-4] Normalization of these vessels with anti-angiogenic agents has demonstrated enhancement in the delivery of small molecule anti-cancer agents by decreasing interstitial pressure and improving intratumoral fluid transport to maximize the delivery and extravasation of therapeutic agents.[1,2,5] In this study, we demonstrate that the normalization of tumor associated lymphatics through neoadjuvent treatment with an anti-VEGFR3 agent, 31C1 (Eli Lilly and Company), increases the tumor-specific delivery of the therapeutic antibody Cetuximab (200μg/mouse, systemic) to head and neck squamous cell carcinoma flank xenografts (OSC-19) in a mouse model. Additionally, we studied a range of anti-angiogenic agent doses (5mg/kg, 10mg/kg, 20mg/kg, and 40mg/kg) to optimize the enhancement of therapeutic drug delivery in this mouse model (n=5/group). To evaluate Cetuximab uptake over time, Cetuximab was fluorescently labeled with IRDye800, and the conjugate was imaged daily post-administration using both a closed-field (Pearl Impulse) and open-field (Luna) fluorescence imaging system. At day 14, tumors were resected, serially bisected, weighed and imaged to determine correlation in fluorescence uptake between treatment groups. Immunohistochemistry was performed to confirm the presence of vascular normalization in neoadjuvant groups. Size-normalized tumor fluorescence was found to be dose-dependent and significantly ($p<0.05$) greater in all dose groups compared to the control group (Cetuximab-IRDye800 alone). A 4.17-fold increase in fluorescently-labeled drug delivery was demonstrated in the 40mg/kg dose group compared to the group that received no neo-adjuvant treatment ($p=0.008$). Furthermore, this increase in drug delivery was specific to the tumor, as there were no significant differences between the background fluorescence values in any of the treatment or control groups. Additionally, the 40mg/kg group demonstrated the smallest percent increase in tumor area (17.4%, $p= 0.02$) over time, further validating the optimal dose of neoadjuvant treatment to enhance the therapeutic effect of anti-tumor antibodies. Immunohistochemical analysis to confirm vessel normalization revealed a significantly ($p<0.02$) greater percentage of NG2 in all treatment groups compared to the control, and an NG2:CD31 ratio of 0.67 in the 40mg/kg group compared to 0.24 in the control group ($p=0.02$).This study demonstrated a dose-dependent increase in the tumor-specific delivery of a fluorescently-labeled therapeutic antibody through neoadjuvent anti-lymphangiogenic treatment with the anti-VEGFR3 agent 31C1.

1. *Journal of Clinical Oncology*. 2013; 31(17):2205-2218.
2. *Cancer Res*. 2007; 67(6): 2729-2735.
3. *Journal of National Cancer Institute*. 2002; 94(6):417-421.
4. *Cancer Res*. 2000; 60: 4324-4327.
5. *Cancer Res.* 2006; 66(5): 2650-2657.

AUTHORS (LAST NAME, FIRST NAME): Moore, Lindsay S.[4]; Patel, Neel G.[4]; Schmalbach, Cecelia E.[2]; Carroll, William R.[3]; Rosenthal, Eben[1]; Warram, Jason M.[4]

INSTITUTIONS (ALL):

1. Otolaryngology, Stanford University, Stanford, AL, United States.
2. Surgery, Univ of Alabama at Birmingham, Birmingham, AL, United States.
3. Surgery, University of Alabama - Birmingham, Birmingham, AL, United States.
4. Surgery, University of Alabama at Birmingham, Birmingham, AL, United States.

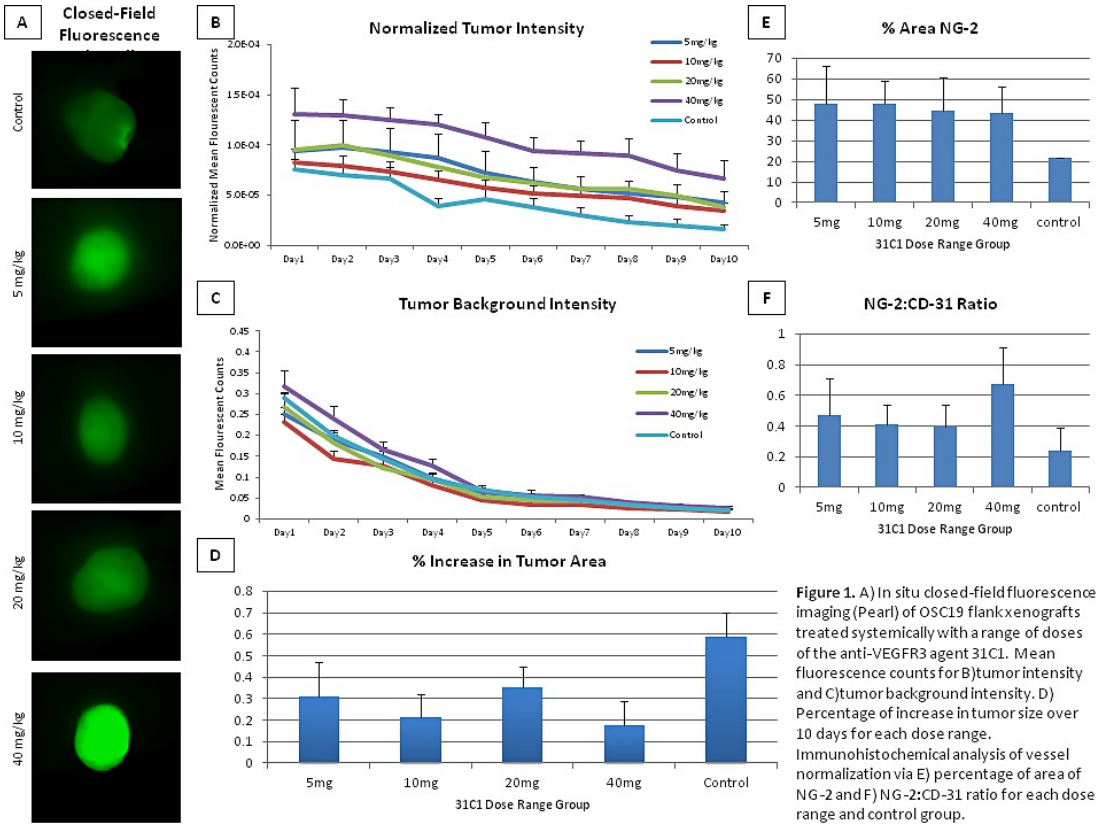

Figure 1. A) In situ closed-field fluorescence imaging (Pearl) of OSC19 flank xenografts treated systemically with a range of doses of the anti-VEGFR3 agent 31C1. Mean fluorescence counts for B)tumor intensity and C)tumor background intensity. D) Percentage of increase in tumor size over 10 days for each dose range. Immunohistochemical analysis of vessel normalization via E) percentage of area of NG-2 and F) NG-2:CD-31 ratio for each dose range and control group.

Figure 1. A) In situ closed-field fluorescence imaging (Pearl) of OSC19 flank xenografts treated systemically with a range of doses of the anti-VEGFR3 agent 31C1. Mean fluorescence counts for B)tumor intensity and C)tumor background intensity. D) Percentage of increase in tumor size over 10 days for each dose range. Immunohistochemical analysis of vessel normalization via E) percentage of area of NG-2 and F) NG-2:CD-31 ratio for each dose range and control group.

CONTROL ID: 2231419

TITLE: Phage Display Selection of ErbB2/ErbB3 Targeting Peptides

PRESENTER: Susan Deutscher

ABSTRACT BODY:

Abstract Body: The EGFR family of receptors propels numerous carcinomas including those on breast, ovary, and prostate via homo- and hetero-dimerization with other EGFR family receptors. Of the four known EGFR family members ErbB2 has received the most attention in terms of viable tumor targets. ErbB2 heterodimerizes with other family members, most notably ErbB3. ErbB3 upon activation with neuregulin (NRG) will heterodimerize with ErbB2 activating several signaling pathways resulting in increased tumor growth and decreased apoptosis. ErbB-3 has now been linked to progression of cancer and resistance to several therapies. ErbB3, usually present at low to moderate receptor numbers, can be upregulated through inhibition of other ErbB family members and certain cellular stresses, including chemotherapeutics. Even though it has become clear that ErbB3 and the heterodimer, ErbB2/ErbB3 (B2/B3), play a critical role in signaling and cancer, the only currently available clinical assays for assessment of ErbB3 or B2/B3 status require invasive biopsies. The ability to detect ErbB3 and/or B2/B3 status could provide diagnosis of high risk carcinomas. To this end, we hypothesized that bacteriophage (phage) display could be exploited to select for peptide sequences specific for ErbB3 and/or B2/B3 heterodimer. Parallel phage display selections were employed against purified ErbB3 extracellular domain (ECD) or B2/B3 -ECD heterodimer. First, the affinity and specificity of the phage selected against ErbB3-ECD for ErbB3-ECD and human ErbB3 expressing cell lines was investigated. MSP3 and MSP4 phage bound 9.3 fold and 20 fold more to ECD than wild type (WT) phage, respectively. Binding to ErbB3 expressing cell lines was 200X greater than WT phage. Phage were then labeled with either NHS-Dylight680 for direct imaging or NHS-PEG-Biotin for three-step pretargeted imaging in SCID mice bearing MDA-MB-435 human breast carcinomas tumors was performed. Optical imaging of phage labeled with Dylight680 in MDA-MB-435 breast tumor xenografted mice showed tumor accumulation of phage at 4 h post-injection (Figure 1A). Ex vivo quantification of fluorescent signal at 4 h post-injection revealed MSP4 intensity of $2.55x10^6$ RFU within the tumor, and was double that of the MSP3 signal. A three-step pretargeted protocol was performed using biotinylated phage, neutravidin, and ATTO-680 labeled biotin. The fluorescent signal from the regions of interest were $2.77x10^6$ RFU and $3.42x10^6$ RFU for MSP3 and MSP4, respectively, compared to that of $1.47x10^6$ RFU for ATTO680-biotin only (Figure 1B). MSP3 in biotinylated peptide form bound to ErbB3-ECD protein and ErbB3-overexpressing human cultured cancer cells with high nanomolar affinity (MDA-MB-435 K_D=336nM, MDA-MB-231 K_D=106nM). The second phage display selection against B2/B3 heterodimer resulted in a six amino acid motif sequence derived from 13 sequences, of which four have been validated. Future work will include in vitro and in vivo characterization of the selected anti-ErbB2/B3 peptides.

AUTHORS (LAST NAME, FIRST NAME): Newton-Northup, Jessica[1]; Cabrara, Mirel[3]; Dickerson, Marie[2]; Quinn, Thomas[1]; Deutscher, Susan L.[2, 1]

INSTITUTIONS (ALL):

1. Department of Biochemistry, University of Missouri, Columbia, MO, United States.
2. Research Service, Harry S. Truman Veterans Memorial Hospital, Columbia, MO, United States.
3. Centro de Investigaciones Nucleares, Universidad de la República, Montevideo, Uruguay.

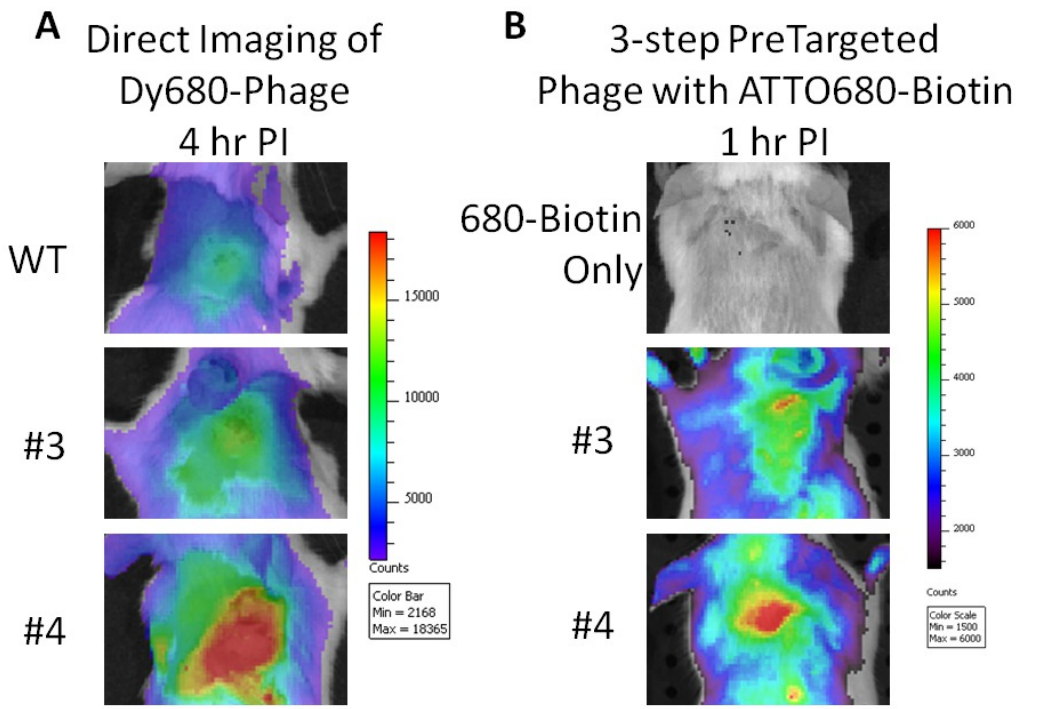
A
Direct Imaging of
Dy680-Phage
4 hr PI
WT
#3
#4
15000
10000
5000
Counts
Color Bar
Min = 2168
Max = 18365
B
3-step PreTargeted
Phage with ATTO680-Biotin
1 hr PI
680-Biotin
Only
#3
#4
6000
5000
4000
3000
2000
Counts
Color Scale
Min = 1500
Max = 6000

CONTROL ID: 2231434

TITLE: Do Carotid MR Surface Coils Affect PET Quantification in PET/MR Imaging?

PRESENTER: Venkatesh Mani

ABSTRACT BODY:

Abstract Body: Aim: To evaluate the effect of surface coils for carotid MR imaging on PET quantification in a clinical simultaneous whole-body PET/MR scanner.

Methods and materials: A cylindrical phantom was filled with a homogeneous 2 liters mixture of water and fluorodeoxyglucose (FDG) at a starting dose of 301.2 MBq. Clinical PET/MR and PET/CT systems were used to acquire PET-data without a coil (reference standard) and with two carotid MRI coils (Siemens Special Purpose 8-Channel and Machnet 4-Channel Phased Array). Attenuation of the PET-signal was evaluated with Osirix using using 51 (PET/MR) and 37 (PET/CT) circular regions of interest (ROIs). Mean and maximum standardized uptake values (SUVs) were quantified for each ROI. Furthermore, SUVs of PET/MR and PET/CT were compared. For validation, a patient was scanned with an injected dose of 407.7 MBq on both a PET/CT and a PET/MR system without a coil and with both coils. Time difference between both scans was 26 minutes.

Results: PET/MR underestimations were -2.2% (Siemens) and -7.8% (Machnet) for SUV_{mean}, and -1.2% (Siemens) and -3.3% (Machnet) for SUV_{max}, respectively. For PET/CT, underestimations were -1.3% (Siemens) and -1.4% (Machnet) for SUV_{mean} and -0.5% (both Siemens and Machnet) for SUV_{max}, respectively using no coil data as reference. Except for PET/CT SUV_{max} values all differences were significant. SUVs differed significantly between PET/MR and PET/CT with SUV_{mean} values of 0.51-0.55 for PET/MR and 0.68-0.69 for PET/CT, respectively. The patient examination showed that median SUV_{mean} values measured in the carotid arteries decreased from 0.97 without a coil to 0.96 (Siemens) and 0.88 (Machnet).

Discussion - Conclusion: Carotid surface coils do affect attenuation correction in both PET/MR and PET/CT imaging. PET quantification is underestimated in PET/MR and for SUV_{mean} values in PET/CT, whereas SUV_{max} was not affected in PET/CT. Furthermore, SUVs differed significantly between PET/MR and PET/CT.

AUTHORS (LAST NAME, FIRST NAME): Willemink, Martin J.[2, 3]; Eldib, Mootaz[1, 3]; Leiner, Tim[2]; Fayad, Zahi A.[1, 3]; Mani, Venkatesh[1, 3]

INSTITUTIONS (ALL):

1. Department of Radiology, Icahn School of Medicine at Mount Sinai, New York, NY, United States.
2. Department of Radiology, University Medical Center, Utrecht, Netherlands.
3. Translational and Molecular Imaging Institute, Icahn School of Medicine at Mount Sinai, New York, NY, United States.

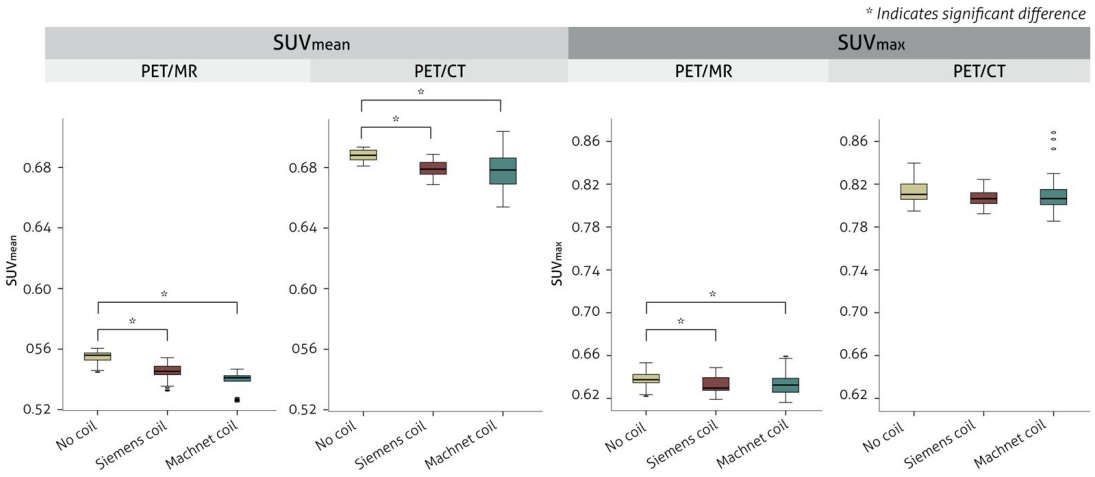

Figure 3: Results of the phantom study

CONTROL ID: 2234314

TITLE: Micro-embolic risk at elective revascularization and its relationship with 3D multi-contrast MRI

PRESENTER: Venkatesh Mani

ABSTRACT BODY:

Abstract Body: BACKGROUND: Management of asymptomatic carotid stenosis must balance the benefits of intervention against the risks of peri/post-operative cerebrovascular events. The pre-operative identification of high-risk plaque characteristics with MRI may assist in assessing embolic potential of carotid plaque. 3D multi-contrast (MC) Black Blood turbo spin echo (TSE) sampling perfection with application-optimized contrast using different flip angle evolution (SPACE) sequence is a convenient method to evaluate high risk plaque characteristics non-invasively. Due to higher SNR, decreased susceptibility of volume averaging artifacts, and ability to obtain isotropic voxels thereby enabling multi-planar reformatting of images, 3D approaches are preferred to 2D plaque evaluation. The purpose of this study was to examine the relationship between vulnerable plaque characteristics detected by 3D MC MRI and micro-embolic risk during elective revascularization.

METHODS: This study was approved by the local institutional review board. All participating subjects signed written informed consent. 20 patients (symptomatic, stenosis>50% or asymptomatic, stenosis>70%) undergoing either carotid artery stenting (CAS) or carotid endarterectomy (CEA) were enrolled. A pre-operative Mini-Mental Status Exam (MMSE), 3D MC SPACE MRI, and cerebral diffusion-weighted (DW) MRI were obtained 1-3 days prior to intervention on a 3T scanner. Carotid plaque burden and composition were determined from MC-MRI and carotid plaques were classified according to AHA criteria. Intraoperatively, transcranial Doppler was performed to monitor for microembolic signals (MES). Plaque specimen and filter debris were analyzed histologically for high-risk characteristics and correlated with MRI. A post-operative DW-MRI and MMSE were performed within 72 hours to examine for microinfarcts and changes in neurocognitive function. Sample images obtained using 3D MC SPACE and corrsponding histology after endarterectomy are shown in the Figure.

RESULTS: Results demonstrated an increase in ipsilateral microembolic signals (MES) detected intra-operatively in patients with AHA Type VI plaque as detected on pre-operative carotid 3D SPACE MC MRI. MES were predominantly detected in CEA patients during the placement of the shunt and subsequent to internal carotid release, and during filter deployment and stent deployment in CAS patients. Decrease in MMSE scores was seen in patients with intra-plaque hemorrhage and necrotic lipid-core, and less so in patients with stable fibrous cap and calcification as determined by MRI and confrimed by plaque histology.No changes were observed on the DW-MRI.

CONCLUSIONS: Preliminary results suggest that high-risk carotid atherosclerotic lesions are identifiable by 3D MC SPACE MRI and are associated with increased MES and neurocognitive changes as measured by a MMSE in patients undergoing carotid revascularization. The information in this study may allow for a better understanding of high-risk plaque as seen on 3D MC SPACE MRI and their embolic potential intra-operatively, thus refining the guidelines for the management of asymptomatic plaque and improving patient outcomes.

AUTHORS (LAST NAME, FIRST NAME): Li, Jennifer[3]; Giannarelli, Chiara[3]; Faries, Peter[3]; Wiley, Jose[3]; Fayad, Zahi A.[4, 1]; Mani, Venkatesh[2, 1]

INSTITUTIONS (ALL):

1. Translational and Molecular Imaging Institute, Icahn School of Medicine at Mount Sinai, New York, NY, United States.
2. Department of Radiology, Icahn School of Medicine at Mount Sinai, New York, NY, United States.
3. Department of Medicine, Icahn School of Medicine at Mount Sinai, New York, NY, United States.
4. Department of Radiology, Icahn School of Medicine at Mount Sinai, New York, NY, United States.

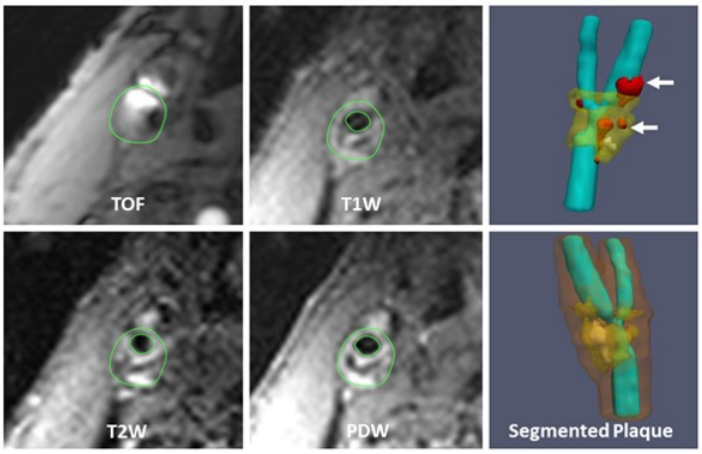

Figure 1: Sample 3D MC SPACE images (TOF, T1, T2 and PD weighted images) of right carotid of a 65 year old subject prior to carotid endarterectomy with corresponding segmented plaque showing lipid rich necrotic core (yellow) and intra-plaque hemorrhage (red)

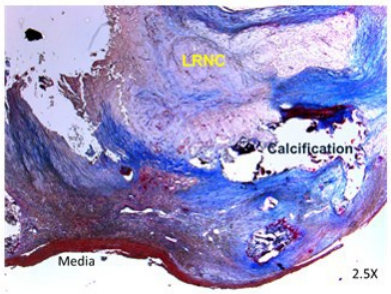

Figure 2: Masson's trichrome staining of atherosclerotic plaque of same subject shown in Figure 1

CONTROL ID: 2232315

TITLE: Feasibility of 18F-Fluorodeoxyglucose Radiotracer Dose Reduction in Simultaneous Carotid PET/MR Imaging

PRESENTER: Venkatesh Mani

ABSTRACT BODY:

Abstract Body: Purpose: The purpose of this study was to develop and validate low dose 18F-FDG-PET acquisition protocols for detection of inflamed carotid plaques specifically for simultaneous PET/MR imaging. The hypothesis was that increasing the duration of the PET acquisition to match that of the MR acquisition might allow for the use of lower levels of the radiotracer, while preserving quantification and image quality.

Methods: Seven subjects were scanned twice at least one week apart on a simultaneous PET/MR scanner using either the standard clinical dose of 18F-FDG (373 ± 63 MBq) for 8 minutes or a low dose (93 ± 17 MBq) for 75 minutes.

Results: A maximum absolute difference of only 4.17% and 7.49% in the left and right carotid TBR was found between the standard dose and four time points of the low dose acquisitions (8, 24, 45, 75 minutes). Only the 8-minute low dose PET data was significantly different in terms of SNR (P=0.009; % difference = -51%) and qualitative image quality evaluation (P=0.0005; % difference = -45%).

Conclusions: Our preliminary findings indicate that up to 75% reduction of the clinical standard 18F-FDG dose could be achieved using the proposed acquisition scheme while maintaining accurate quantification and SNR.

AUTHORS (LAST NAME, FIRST NAME): Eldib, Mootaz[1, 2]; Bini, Jason[1, 2]; Lairez, Olivier[1, 2]; Faul, David D.[3]; Oesingmann, Niels[3]; Fayad, Zahi A.[1, 2]; Mani, Venkatesh[1, 2]

INSTITUTIONS (ALL):

1. Department of Radiology, Icahn School of Medicine at Mount Sinai, New York, NY, United States.
2. Translational and Molecular Imaging Institute, Icahn School of Medicine at Mount Sinai, New York, NY, United States.
3. Siemens Healthcare, New York, NY, United States.

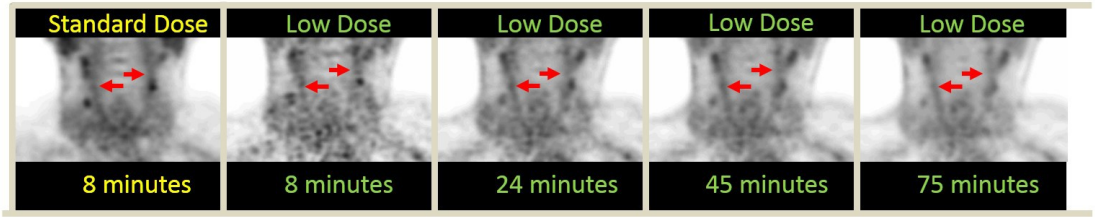

Representative coronal PET images in the same subject using the clinical standard dose of 18F-FDG acquired for 8 minutes compared to the low dose images acquired for 8,25,45 and 75 minutes.

CONTROL ID: 2231476

TITLE: Synthesis and initial PET imaging evaluation of 18F-FDGamines for imaging the acidic tumor microenvironment in PC3 xenograft mice

PRESENTER: Robert Flavell

ABSTRACT BODY:

Abstract Body: Background: Solid tumors are poorly perfused and secrete acids, resulting in an interstitial microenvironment which is mildly acidic, with pH typically ranging from 6.5 – 7.0. We hypothesized that a pro-drug approach could be used to image this property, in which FDG is conjugated with an acid labile protecting group. We selected conjugation with amines on the basis of prior reports demonstrating acid lability of N-aryl-glycosylamines (Fig 1A). In this report, we describe the synthesis of a series of 18F-fluorodeoxyglycosylamines (FDGamines), evaluation in a PC3 cell culture model of malignancy, and initial PET imaging in PC3 xenograft mice.

Results: Radiosynthesis of FDGamines was accomplished in one step from 18F-FDG by incubation with various amines. We found that FDGamines were relatively stable at pH 7.4, but decomposed to FDG at pH 6.5 in an in vitro HPLC degradation assay. Overall, the rate of decomposition is inversely proportional to the pKa of the parent amine (table 1). Uptake of the resulting prodrugs was assessed in a PC3 cell culture assay by incubating the indicated compounds with cells in RPMI at pH 7.4 or 6.5, with or without the inhibtors of FDG uptake, cytochalasin b and glucose, and harvesting the cells and counting the cell-associated activity. In PC3 cells, uptake of FDGamine 3 was reduced at pH 7.4 in comparison with FDG, but not at pH 6.5 (Fig 1B). Furthermore, uptake of both FDG and FDGamines were blocked by both glucose and cytochalasin b, suggesting that uptake of both compounds requires glucose transporters. We performed PET imaging in PC3 xenograft mice using 4-phenylbenzylamine FDG, and compared against imaging using FDG (Fig 1C, D). We found that both compounds had similar uptake in the tumor. However, 4-phenylbenzylamine-FDG had reduced uptake in tissues which normally have high FDG uptake in mice, such as heart and brain.

Conclusions : We have demonstrated the radiosynthesis, in vitro evaluation, and initial PET imaging evaluation of FDGamines. These are a promising class of compounds for imaging the acidic tumor interstitial environment.

AUTHORS (LAST NAME, FIRST NAME): Flavell, Robert R.[1]; Truillet, Charles[1]; Ganguly, Tanushree[1]; Regan, Melanie[1]; Blecha, Joseph E.[1]; Evans, Michael J.[1]; VanBrocklin, Henry[1]; Wilson, David M.[1]

INSTITUTIONS (ALL):

1. Radiology and Biomedical Imaging, University of California, San Francisco, San Francisco, CA, United States.

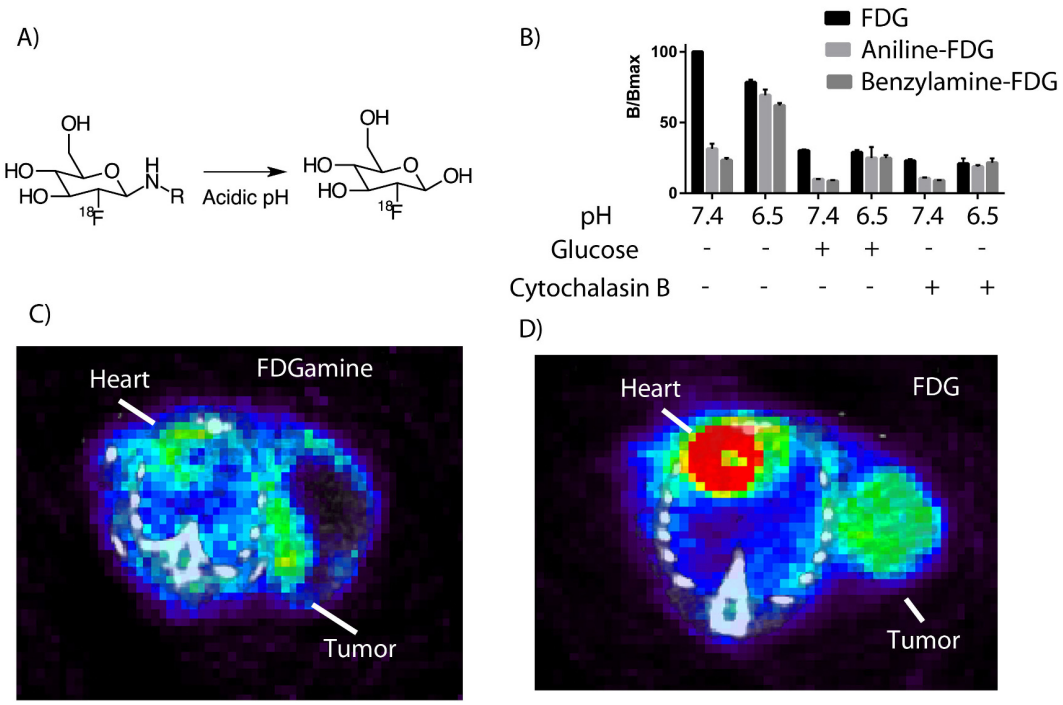

Figure 1 A) Chemical structure of FDGamines, which degrade to form FDG upon exposure to acid. B) PC3 cell assay demonstrates that uptake of FDGamines are blocked at neutral, but not acidic pH, while uptake of FDG is similar at pH 6.5 and 7.4. C&D) Axial micro-PET/CT image through the tumor and heart following administration of 4-Phenylbenzylamine-FDG (C) and FDG (D). Scale of tissue uptake is the same in both images, where the maximum is 8% ID/g.

CONTROL ID: 2231479

TITLE: Mouse dosimetry studies for ^{64}Cu-DOTA-B-Fab - an immunoPET companion diagnostic for antibody-drug conjugates targeting CA6

PRESENTER: Ohad Ilovich

ABSTRACT BODY:

Abstract Body: ^{64}Cu-DOTA-B-Fab, a novel immunoPET imaging agent, was developed as a companion diagnostic for an antibody-drug conjugate (SAR566658) which targets the tumor-associated MUC1-sialoglycotope, CA6. In preparation of using this tracer in humans as a tool for stratifying ovarian cancer patients according to their expression of CA6, imaging studies in mice were performed to evaluate the in vivo biodistribution and estimate human dosimetry of ^{64}Cu-DOTA-B-Fab.

Four female nude mice were injected with ^{64}Cu-DOTA-B-Fab (137±1.2 µCi) and scanned in a µPET/CT at 2, 4, 8, 17, 24, 48 and 72 hours post-injection (Figure 1). Volumes of interest were manually drawn around the brain, heart, lung, liver, kidney bladder and whole body based on the CT scan and centered on the peak of activity profile. Radioactivity distribution in the liver was homogenous and therefore a large representative ROI was deemed sufficient for analytical purposes. ROIs for all other organs were maximized to the size of the organ. The activity concentrations in the mentioned mouse organs [%ID/g] were extrapolated to human using the popular scaling method described by Kirshner et. al. [1]. Human organ weights and body weight were taken from the dosimetry software (OLINDA/EXM) with some modifications [2]. A dynamic bladder voiding model was not necessary due to the residualizing nature of copper-64 and its retention in kidneys. The scaled and extrapolated values were then implemented into OLINDA/EXM for computation of the human absorbed doses.

Female human estimates of ^{64}Cu-DOTA-B-Fab show the kidneys to receive the highest dose (0.303 rem/mCi) followed by the osteogenic cells (0.165 rem/mCi) and heart wall (0.133 rem/mCi) with slightly lower doses in male patients. The mean effective dose of ^{64}Cu-DOTA-B-Fab was estimated to be 0.081 rem/mCi. This favorable dosimetry combined with the ability of ^{64}Cu-DOTA-B-Fab to stratify tumors according to CA6 expression in vivo fully support human testing of ^{64}Cu-DOTA-B-Fab.

References

1. Kirschner, A.S., R.D. Ice, and W. Beierwaltes, *Radiation dosimetry of 131I-19-iodocholesterol: the pitfalls of using tissue concentration data—reply.* Journal of Nuclear Medicine, 1975. **16**(3): p. 248-249.

2. Singh, D., et al., *Weights of human organs as autopsy in Chandigarh zone of north-west India.* JIAFM, 2004. **26**(3): p. 0971-0973.

AUTHORS (LAST NAME, FIRST NAME): Ilovich, Ohad[1]; Gambhir, Sanjiv S.[2]

INSTITUTIONS (ALL):

1. Radiology, Stanford University, Palo Alto, CA, United States.
2. Radiology, Stanford University, Stanford, CA, United States.

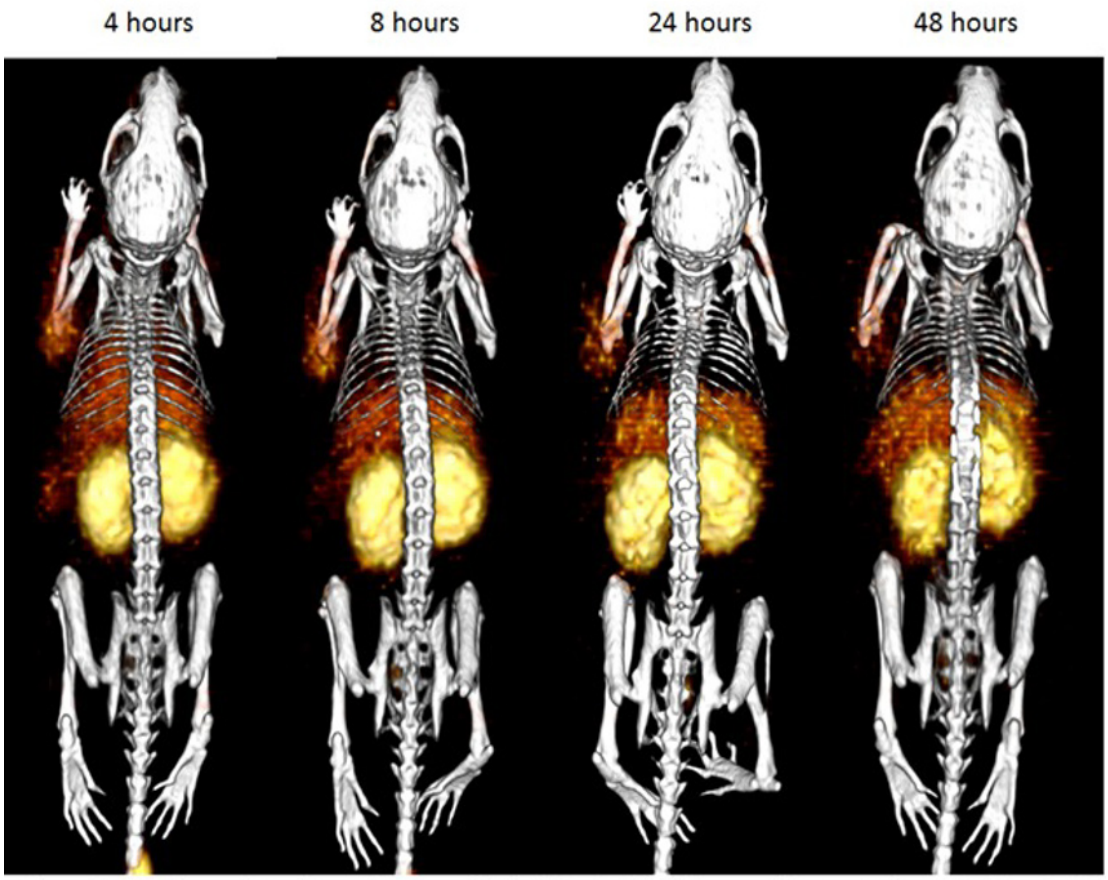

Figure 1 - Maximum intensity projections of whole-body PET/CT coronal images taken 4, 8, 24 and 48 hours after injection of 64Cu-DOTA-B-Fab to mice bearing WISH subcutaneous tumors on their left shoulder.

CONTROL ID: 2231526

TITLE: In vivo CA6-antigen stratification using ^{64}Cu-DOTA-B-Fab – a companion diagnostic for antibody-drug conjugate (SAR566658) therapy

PRESENTER: Ohad Ilovich

ABSTRACT BODY:

Abstract Body: Patient tumor stratification according to the expression of membrane-bound antigens which are not shed efficiently into the blood typically requires invasive biopsies. Repeat biopsies involve increased risk for complication just like any invasive procedure while archived biopsies do not necessarily reflect antigen expression at the time of therapy nor give information regarding metastatic processes. The use of ImmunoPET companion diagnostics may overcome these difficulties. ^{64}Cu-DOTA-B-Fab, a recently published companion diagnostic to SAR566658 (an antibody-drug conjugate targeting the tumor-associated MUC1-sialoglycotope, CA6) is able to differentiate between CA6-positive and CA6-negative cells (Figure 1a). Here we evaluated for its ability to stratify xenograft tumors according to their expression of CA6 in vivo.

Tumor xenografts were established in nude female mice by combining different ratios of WISH (CA6+) and A2780 (CA6-) cells. Six groups of animals (n=4 per group) were implanted with varying percentage of CA6+ cells (100, 80, 60, 40, 20, 0). Animals were imaged 10 days post-implantation and biodistribution was performed (n=2 per group) to both confirm imaging results and investigate CA6 expression via immunohistochemistry (IHC). IHC was performed by a pathologist who was blinded to both implanted cell mixtures and imaging results. IHC results for pure WISH tumors show that WISH cells spontaneously lose CA6 expression over time as 10 and 17 days post implantation only 60% and 25%, respectively, of all non-necrotic tumor tissue expressed CA6. Despite this CA6 correlation between implanted and expressing cells was high (r^2=0.91 at day 10). In imaging studies, highly necrotic tumors (>40%) showed uncharacteristically high accumulation of ^{64}Cu-DOTA-B-Fab making imaging and IHC data less correlative (r^2=0.69). Removal of the highly necrotic tumors increases correlation significantly (r^2=0.86) (Figure 1b).

Many novel PET tracers provide proof-of-concept in simple antigen-positive versus antigen-negative systems. Patient tumors represent a wider range of expression variation, making in-vivo antigen stratification a necessary step for tracers headed for clinical translation. Despite using a challenging tumor system, ^{64}Cu-DOTA-B-Fab was able to distinguish between different levels of antigen expression in vivo with extrapolation predicting a fourfold difference between antigen positive and antigen negative tumors. Although necrosis makes image analysis challenging with ^{64}Cu-DOTA-B-Fab, FDG photopenia should be able to locate necrotic tumor cores in human subjects, simplifying analysis. ^{64}Cu-DOTA-B-Fab is a promising PET companion diagnostic which holds promise for clinical translation

AUTHORS (LAST NAME, FIRST NAME): Ilovich, Ohad[1]; Hori, Sharon S.[1]; Caron, Anne[2]; Sarkar, Susanta K.[3]; Gambhir, Sanjiv S.[4]

INSTITUTIONS (ALL):

1. Radiology, Stanford University, Palo Alto, CA, United States.
2. Sanofi, Vitry-sur-Seine, France.
3. Imaging, Sanofi, Cambridge, MA, United States.
4. Radiology, Stanford University, Stanford, CA, United States.

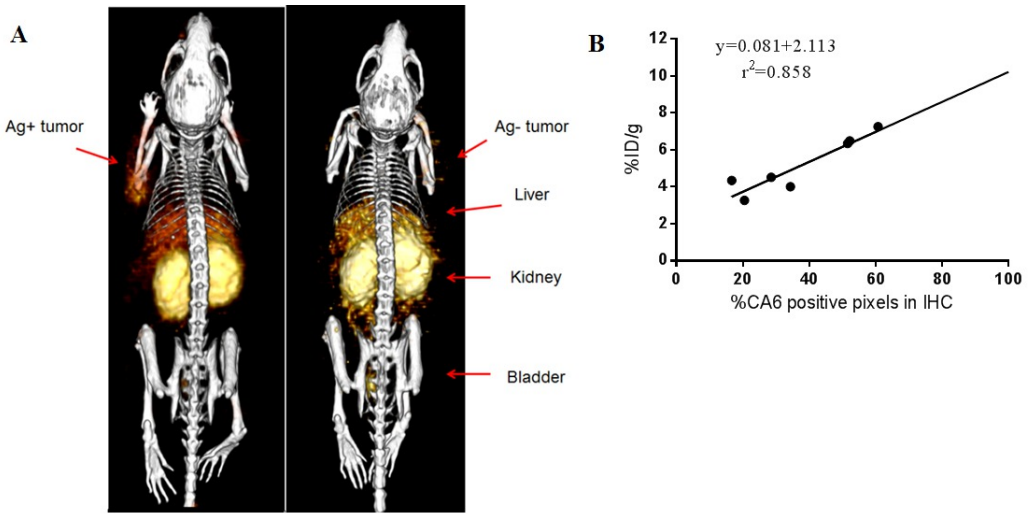

Figure 1 – (A) Maximum intensity projections of whole-body PET/CT coronal images taken 6 hours after injection of 64Cu-DOTA-B-Fab to mice bearing either WISH (left) or A2780 (right) subcutaneous tumors. The tumors, liver, kidneys and bladder are labeled. (B) Correlation between %ID/g of 64Cu-DOTA-B-Fab in subcutaneous tumors in mice and the %CA6 positive pixels seen in immunohistochemical analysis.

CONTROL ID: 2231507

TITLE: The Development and Evaluation of PSMA-targeted Microbubbles using Bioorthogonal Chemistry for Prostate Cancer Ultrasound Imaging

PRESENTER: Aimen Zlitni

ABSTRACT BODY:

Abstract Body: There is an urgent need for new tools to identify and determine the extent and aggressiveness of prostate cancers. This includes being able to better visualize the disease during diagnosis, and to assess early response to therapy.

Prostate specific membrane antigen (PSMA) is a glycoprotein known to be highly expressed in prostate carcinoma as well as the neovasculature in other solid tumors. It has been an attractive target for optical and nuclear imaging methods, which have shown the utility of PSMA imaging in prostate cancer. Access to a PSMA targeted microbubble contrast agents would create the opportunity to use ultrasound imaging to localize prostate tumors. This requires the development of microbubbles (MBs) capable of selectively targeting PSMA positive tumors.

Targeted MBs have traditionally been prepared by linking ligands to their outer shell either covalently or through biotin-streptavidin binding. We have previously demonstrated it is possible to target MBs to vascular endothelial growth vector receptor 2 (VEGFR2) through the use of a bioorthogonal coupling reaction between tetrazine functionalized MBs and trans-cyclooctene (TCO) tagged cells[1]. We have subsequently adapted this new strategy to create actively targeted PSMA-binding MBs.

A TCO-conjugated anti-PSMA antibody (TCO-J591) was prepared by adding (E)-cyclooct-4-enyl-2,5-dioxopyrrolidin-1-yl carbonate (TCO-NHS) to J591; an established anti-PSMA antibody. Tetrazine-coated MBs (MB_{Tz}) were prepared in parallel by adding a biotinylated derivative of a tetrazine to streptavidin-coated MBs (MicroMarker Target-Ready contrast agents, VisualSonics). The ability of MB_{Tz} to bind PSMA-expressing PC3 cells *in vitro* was assessed in a flow chamber adhesion assay using two approaches. The first involves the incubation of the cells with TCO-J591 for 30 min before introducing MB_{Tz}. While in the second approach, TCO-J591 was incubated with MB_{Tz} ($MB_{Tz\text{-}TCO\text{-}J591}$) before introduction to the cells as a way to create an actively targeted PSMA-MBs. From the microscopy images and the semi-quantitative analysis, we found lower binding of MB_{Tz} to PSMA-expressing PC3 cells when the cells were pre-incubated with TCO-J591 prior to the assay. This observation is probably due to the internalization of TCO-J591 in the cells[2]. For the actively targeted MBs, the results showed around 5 fold higher binding of $MB_{Tz\text{-}TCO\text{-}J591}$ to PSMA-expressing cells compared to controls, which included PSMA-negative PC3 cells as well as MB_{Tz} in the absence of TCO-J591 and unfunctionalized MBs. The approach was further evaluated *in vivo* in a PSMA expressing LNCaP derived xenograft. After imaging with non-targeted MB_{Tz}, $MB_{Tz\text{-}TCO\text{-}J591}$ was injected and following a destruction replenishment sequence preliminary *in vivo* data shows meaningful difference in the signal enhancement between $MB_{Tz\text{-}TCO\text{-}J591}$ and MB_{Tz} images. Description of the MBs preparation, *in vitro* and *in vivo* studies, including quantitative analysis versus histology, and potential clinical utility will be presented.

References:

[1] A. Zlitni *et al. Angew. Chem. Int. Ed. Engl.* **2014**, *53*, 6459–6463.

[2] H. Liu *et al. Cancer Research* **1998**, *58*, 4055–4060.

AUTHORS (LAST NAME, FIRST NAME): Zlitni, Aimen[2]; Yin, Melissa[1]; Yan, Judy[1]; Foster, F. Stuart[3, 1]; Valliant, John[2]

INSTITUTIONS (ALL):

1. Sunnybrook Research Institute, Toronto, ON, Canada.
2. Chemistry and Chemical Biology, McMaster University, Hamilton, ON, Canada.
3. Department of Medical Biophysics, University of Toronto, Toronto, ON, Canada.

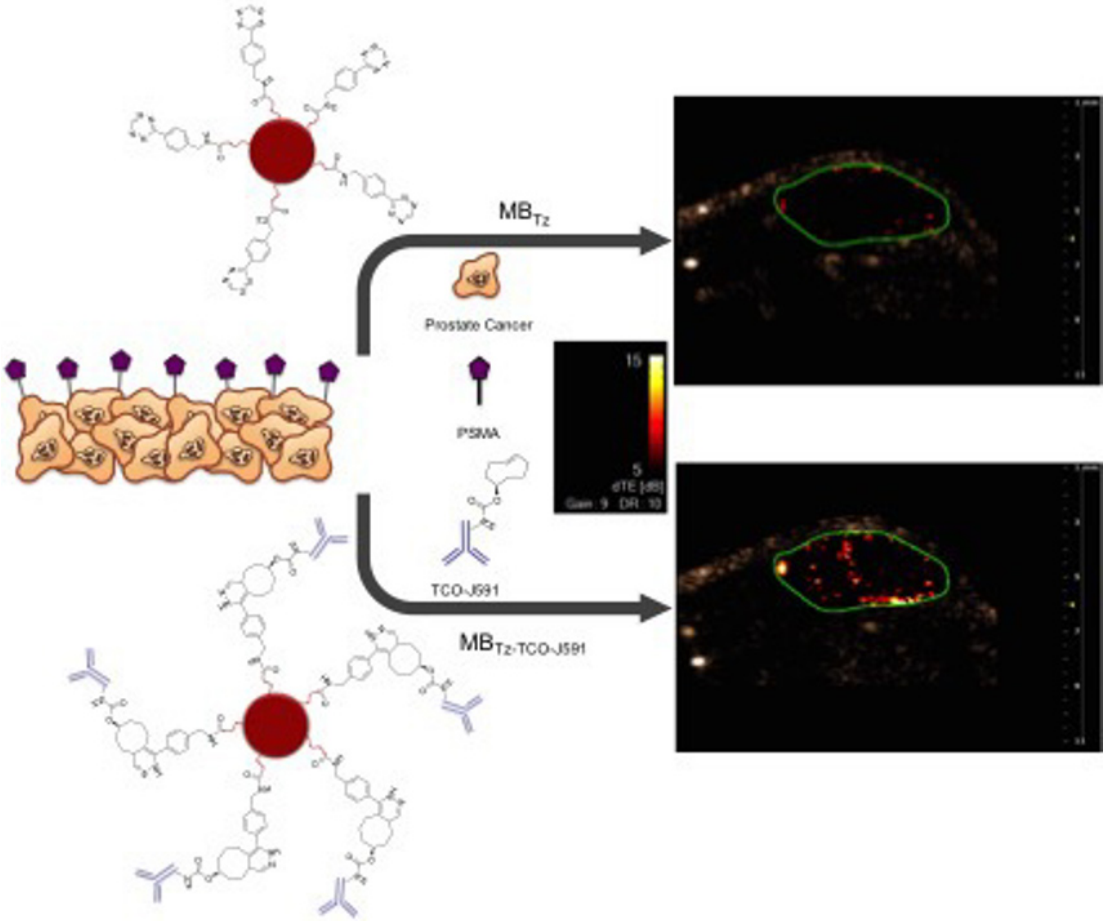
MBTz
Prostate Cancer
PSMA
TCO-J591
MBTz-TCO-J591
15
5
dTE [dB]
Gain 9 DR 10

CONTROL ID: 2233942

TITLE: Accumulation of 20 nm ^{64}Cu-micelles is enhanced in rat glioblastoma model as compared with ^{64}Cu-liposomes

PRESENTER: Jai Woong Seo

ABSTRACT BODY:

Abstract Body: Glioblastoma multiforme (GBM) is the most common and aggressive malignant brain tumor, comprising 70% of all malignant gliomas. A small drug carrier that effectively accumulates throughout the brain lesion is desirable. Recently, long circulating ~20 nm self-assembled micelles were engineered based on a 3-helix peptide-PEG conjugate. Here, the accumulation of ^{64}Cu-labeled long circulating liposomes [1] (119 nm) and micelles [2] (20 nm) was compared in glioblastoma within the rat brain to elucidate their ability to accumulate following intravenous injection (Image).

Method

Long circulating liposomes and micelles, incorporating 6-BAT lipids and 6-BAT-1coi-dC18, respectively, were labeled with Cu-64 in ammonium citrate buffer (pH 5.5), isolated through size exclusion chromatography, and intravenously administered to rats (n =11) with intracranially transplanted U87 glioblastoma multiforme (GBM) in the right striatum. PET and MR images were acquired at 0, 3.5, 7, and 21 hours, and after perfusion with saline at 22h, the radioactivity in the left and right brain, and major organs were assayed with a well counter. Tumor blood volume and uptake of both nanoparticles were calculated from a region of interest (ROI) on PET/MR coregistered images. Autoradiography was performed to localize the accumulation of each nanoparticle. Sliced brain H&E and immunohistochemistry with CD31 were employed to compare the tumor vascularization.

Result and discussion

The average mean diameters and zeta-potential of the liposomes and micelles were 111.9 ± 5.7 and 19.6 ± 7.4 nm, and -30.4 ± 0.75 and 22.8 ± 3.9 mV, respectively. The blood circulation of both ^{64}Cu-labeled nanoparticles in blood was similar (Figure a). Tumor blood volumes (TBV) between small (<100 mm^3) and large glioblastoma (>100 mm^3) were similar (Figure b). The accumulation of the ^{64}Cu-micelles in the tumor was significantly higher (1.7 times) than ^{64}Cu-lipsomes (Figure c) and coregistered PET/MR images showed the higher accumulation of the micelles within the lesion (Figure d). Similarly, on biodistribution the accumulation of micelles in the glioblastoma-bearing right brain was significantly higher that that of liposomes in small and large glioblastoma (Figure e).

Conclusion

Our observation demonstrates that micelles with a diameter 5 times smaller than that of liposomes accumulate within glioblastoma. We expect that 3-helix peptide-PEG micelles carrying chemotherapeutic drugs may improve the treatment of glioblastoma. PET imaging analyses can assist in the design of nanoparticles for the treatment of glioblastoma.

(1) Seo, J. W., Zhang, H., Kukis, D. L., Meares, C. F., and Ferrara, K. W. (2008) A Novel Method to Label Preformed Liposomes with ^{64}Cu for Positron Emission Tomography (PET) Imaging. *Bioconjugate Chem. 19*, 2577-2584.

(2) Dong, H., Dube, N., Shu, J. Y., Seo, J. W., Mahakian, L. M., Ferrara, K. W., and Xu, T. (2012) Long-Circulating 15 nm Micelles Based on Amphiphilic 3-Helix Peptide-PEG Conjugates. *Acs Nano 6*, 5320-5329.

AUTHORS (LAST NAME, FIRST NAME): Seo, Jai Woong[2]; Ang, JooChuan[3]; Mahakian, Lisa M.[2]; Tam, Sarah M.[2]; Fite, Brett[2]; Ingham, Elizabeth S.[2]; Jiang, Yufeng[3]; Beyer, Janine[1]; Forsayeth, John[1]; Xu, Ting[3]; Ferrara, Katherine[2]

INSTITUTIONS (ALL):

1. Neurological Surgery, UCSF, San Francisco, CA, United States.
2. Biomedical Engineering, University of California, Davis, Davis, CA, United States.
3. Department of Materials Science & Engineering, University of California, Berkeley, Berkeley, CA, United States.

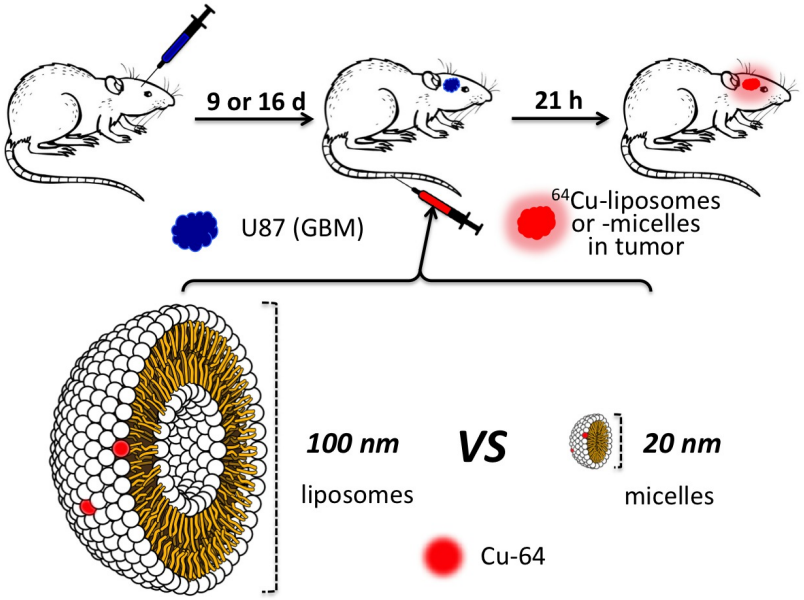

Figure Schematic figure of experimental procedure, which compares the accumulation of liposome and micelles within Glioblastoma multiforme in rat brain. Nanoparticles were intravenously injected through tail vein

CONTROL ID: 2231529

TITLE: Optical Imaging-Monitored Intra-Esophageal Radiofrequency Hyperthermia-Enhanced Local Chemotherapy of Esophageal Cancers

PRESENTER: Yaoping Shi

ABSTRACT BODY:

Abstract Body: Purpose: To investigate the possibility of using bioluminescent optical imaging to monitor intra-esophagus radiofrequency hyperthermia (RFH)-enhanced local chemotherapy of rat models with orthotopic esophageal squamous cancers (ESCs).

Materials and Methods: Human ESC cells were transduced with lentivirus/luciferase. Orthotopic ESC masses were established by inoculating luciferase-ESC cells into cervical esophagus walls of nude rats via a specifically designed transesophageal approach. Twenty four rats with ESC cancers were divided into four study groups (n=6/group) receiving various treatments: i) combination therapy of intraesophageal MR imaging-heating-guidewire (MRIHG)-mediated RFH (42^0C) plus local chemotherapy (cisplatin and 5-fluorouracil); ii) chemotherapy-only; iii) RFH-only; and (iv) phosphate-buffered saline (PBS). Bioluminescent optical imaging and transcutaneous ultrasound imaging were used to follow up bioluminescence signal and size changes of tumors among the groups over a time period of two weeks, which were correlated with subsequent histology.

Results: Optical imaging demonstrated a significantly decreased bioluminescence signal in the combination therapy group, compared to those in three control groups (0.51±0.18 VS 1.6±0.4 VS 3.18±0.9 VS 3.5±0.96, $p<0.05$). Ultrasound imaging showed the smallest tumor volumes of the combination therapy group, in comparison to those of other control groups (0.62±0.16 VS 1.25±0.19 VS 2.28±0.25 VS 2.64±0.26, $p<0.05$). Both imaging findings were confirmed by histologic correlation (Figure).

Conclusion: Optical imaging is a useful tool for monitoring intra-esophageal RFH-enhanced chemotherapy of ESCs, which may provide a new opportunity for efficient management of esophageal malignancies.

AUTHORS (LAST NAME, FIRST NAME): Shi, Yaoping[2]; Zhang, Feng[4]; Wang, Jianfeng[3]; Bai, Zhibin[5]; Qiu, Longhua[1]; Li, Yonggang[1]; yang, xiaoming[1]

INSTITUTIONS (ALL):

1. University of Washington School of Medicine, Seattle, WA, United States.
2. Radiology, University of Washington School of Medicine, Seattle, WA, United States.
3. Radiology, University of Washington, School of Medicine, Seattle, WA, United States.
4. Radiology, University of Washington School of Medicine, Seattle, WA, United States.
5. Radiology, University of Washington School of Medicine, Seattle, WA, United States.

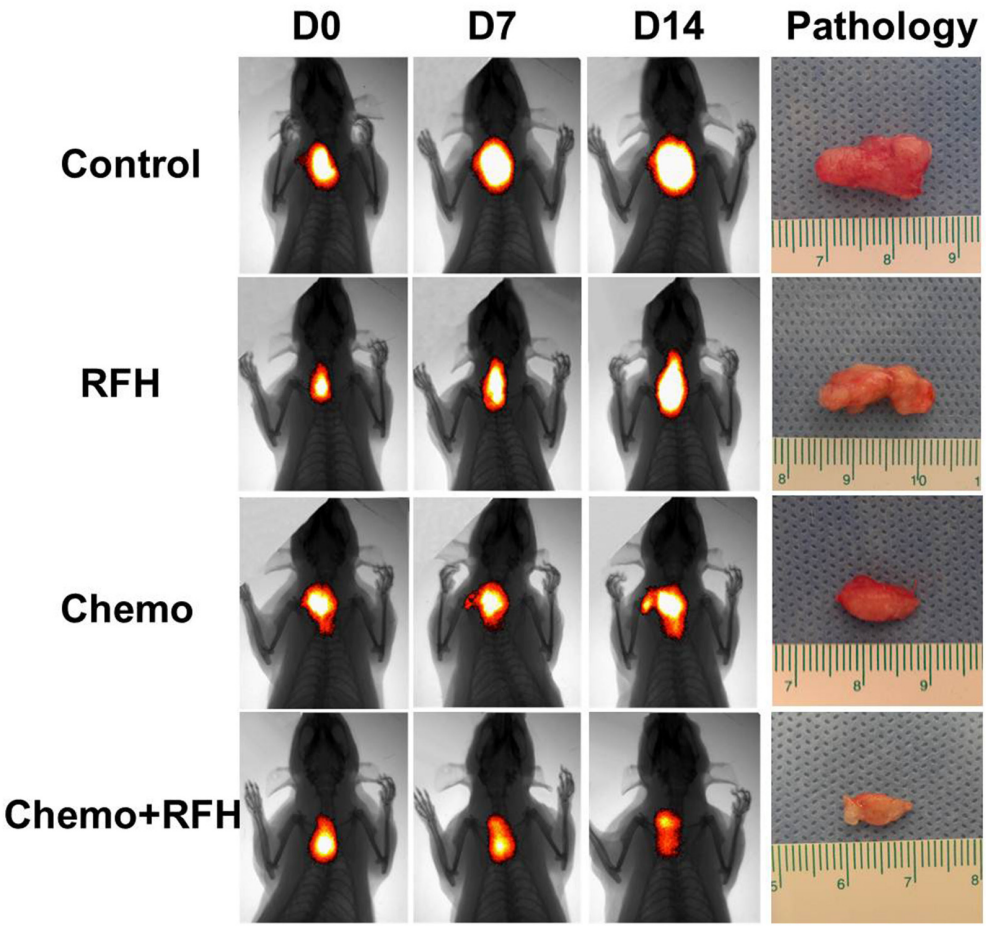

Figure. Follow-up optical/x-ray images obtained from four animal groups at days 0, 7 and 14 after different treatments, showing decreased bioluminescence signals (yellow-red color) of luciferase-tumors in the animal group treated by combination therapy (Chemo +RFH), compared to three control animal groups. Optical imaging findings are confirmed by histology.

CONTROL ID: 2231554

TITLE: Assessment of brain tissue damage in the Sub-Acute Stroke Region by Multiparametric Imaging using [89-Zr]-Desferal-EPO-PET/MRI.

PRESENTER: Salvador Castaneda Vega

ABSTRACT BODY:

Abstract Body: Ischemic stroke (IS) is the third cause of death worldwide. Erythropoietin (EPO) mediates neuroprotection in the stroke area by coupling to its receptor (EPOr) (Buemi et al. JNEN 2003). EPOr has been shown to be overexpressed in neurons in the presence of hypoxia (Sirén et al. AN 2001). The aim of this study was to target EPOr using [89-Zr]-Desferal-EPO-PET to positively identify the stroke area in combination with Apparent Diffusion Coefficient (ADC) and Perfusion Maps (PWI). In addition, using a Gaussian Mixture Model (GMM), we aimed to produce clusters of the stroke areas according to their response to hypoxia, perfusion and edema characteristics.
We injected Stroke and Sham Sprague Dawley rats (n=3 to 4) with 7MBq [89-Zr]-Desferal-EPO I.V. 3 hours after stroke induction. We induced IS using the Middle Cerebral Artery Temporary Occlusion (MCAO) stroke model while Sham animals underwent surgery with no occlusion. The rats were scanned 24, 48 and 72 hours after on-set of stroke using sequential PET/MRI including ADC, PWI and T2 weighted images (T2WI). The acquisitions were then coregistered to each other and regions of interest (ROIs) were drawn on the stroke hemisphere. The multiparametric dataset was segmented into biologically distinct regions using GMM. Furthermore, in order to investigate spatial significance, the identified clusters were overlaid on the T2WI. In addition, at 72h, we performed immunohistochemistry for EPO and HIF1a, H&E staining and autoradiography of the rat brains.
We confirmed our previous findings of [89-Zr]-Desferal-EPO uptake on the stroke volume (SV) on a different animal species. The %ID of [89-Zr]-Desferal-EPO on the SV (according to vasogenic edema ROIs) at 72 hours was 0.46 ± 0.06% while it was 0.22 ± 0.02% on Sham rats (P=<0.01). We looked for three clusters using GMM on both hemispheres which produced a mean silhouette value of 0.38 in strong contrast to 0.15 for the contralateral hemisphere. We found a cluster of interest on the stroke hemisphere which was characterized by having sub-acute stroke imaging hallmarks such as reduced ADC and perfusion. In addition this cluster presented high [89-Zr]-Desferal-EPO uptake. Mismatches were found between the cluster of interest and the T2WI SV. Focalization of [89-Zr]-Desferal-EPO on the SV was confirmed by autoradiography and histology of all rat brains. EPO immunohistochemistry and HIF1a confirmed hypoxia on the stroke regions.
In this report we present a novel method for assessing and differentiating ischemic damage in the sub-acute stroke area by targeting EPOr. The mismatch between the T2WI SV and the cluster of interest suggests different levels of ischemic damage and a true overestimation of the SV produced by T2WI. The addition of [89-Zr]-Desferal-EPO to the multiparametric MR imaging of IS provides crucial information on the discrimination between vasogenic edema with and without a hypoxic response component. These findings have a direct impact on the assessment of IS damage evaluation for therapies aimed at the sub-acute stroke time point in preclinical or clinical therapeutic trials.

AUTHORS (LAST NAME, FIRST NAME): Castaneda Vega, Salvador[1]; Katiyar, Prateek[1]; Russo, Francesca[2]; Disselhorst, Jonathan A.[1]; Calaminus, Carsten[1]; Poli, Sven[2]; Maurer, Andreas[1]; Ziemann, Ulf[2]; Pichler, Bernd J.[1]

INSTITUTIONS (ALL):

1. Werner Siemens Imaging Center, Department of Preclinical Imaging and Radiopharmacy, Eberhard Karls University Tuebingen, Tuebingen, Baden-Wurttemberg, Germany.
2. Department for Neurology, Hertie Institute for Clinical Brain Research, University Clinic Tuebingen, Tuebingen, Germany.

(No Image Selected)

CONTROL ID: 2231567

TITLE: Modulation of nanoparticle targeting by surface-switching technology

PRESENTER: Francois Fay

ABSTRACT BODY:

Abstract Body: Purpose: Surface functionalization of nanoparticles (NPs) with targeting ligands such as antibodies, peptides or nucleic acids has shown significant advantages in preclinical cancer nanotherapy studies[1]. Disadvantageously, those moieties may also cause elevated NP recognition by the mononuclear phagocyte system and off-target binding. To overcome these limitations, we have developed a matrix metalloproteinase-2 (MMP-2) cleavable polyethylene glycol (PEG) coating to prevent NP/cell interaction in the bloodstream. Once exposed to MMP-2, i.e. when the NPs accumulate within the tumor microenvironment, the PEG coating will be cleaved. The resulting surface exposure of the targeting moieties (RGD peptide) facilitates NP association with αvβ3 integrin expressing tumor cells.

Methods: Surface-switchable NPs are composed of a near infrared fluorescent (NIRF) poly(lactic-co-glycolic acid) (PLGA) core and a paramagnetic PEG-lipid coating. These hybrid NPs were synthesized by dripping a PLGA/acetonitrile mixture into a hot water/ethanol solution containing specific combinations of phospholipids, including a custom made cleavable PEG-phospholipid[2] in which PEG2000 is conjugated via a MMP-2 cleavable peptide unit. Paramagnetic properties were introduced by the inclusion of 25 mol% Gd-DTPA-BSA. NPs were incubated with various cell lines, and cell uptake was measured *in vitro* by fluorescent microscopy, flow cytometry and cell pellet magnetic resonance imaging (MRI). NPs were injected in mice bearing orthotopic MDA-MB-231 human breast tumors then their biodistributions were assessed by MRI and NIRF imaging. The NP/cell interaction within the tumor was determined *ex vivo* by flow cytometry.

Results: *In vitro* fluorescence microscopy demonstrated that unshielded RGD decorated NPs had a stronger interaction with αvβ3 integrin expressing MDA-MB-231 breast cancer cells compared to control NPs. *In vitro* flow cytometry data and cell pellet MRI corroborated the aforementioned and confirmed the specificity of the mPEG-MMP2p-DSPE shielding. *In vivo* MRI revealed T1 and T2 to be lowered from 2148 to 1877 ms and 66 to 60 ms respectively indicative of NP tumor accumulation. *Ex vivo* NIRF imaging confirmed NP biodistribution and accumulation in the rim of the tumors while *ex vivo* flow cytometry measurements revealed the association of the accumulated NPs with tumor cells and tumor associated macrophages.

Conclusion: We developed a hybrid nanoparticle platform with a MMP-2 cleavable PEG-lipid corona. *In vitro* and *in vivo* models demonstrated that upon incubation with MMP-2 the PEG coating is cleaved and targeting ligands become available to bind αvβ3 expressing cells. Our new surface-switching coating approach ensures a high NP targeting specificity without compromising favorable NP pharmacokinetics.

References: 1) Fay et al, Immunotherapy 2011; 2) Gianella et al, Chem Commun. 2013;

AUTHORS (LAST NAME, FIRST NAME): Fay, Francois[1]; Hansen, Line[2, 1]; Hectors, Stefanie J.[3]; Tang, Jun[1]; Gianella, Anita[1]; Sanchez-Gaytan, Brenda[1]; Zhao, Yiming[1]; Mieszawska, Aneta J.[1]; Langer, Robert [5]; Calcagno, Claudia[1]; Strijkers, Gustav[3]; Fayad, Zahi A.[1]; Mulder, Willem J.[1, 4]

INSTITUTIONS (ALL):

1. Translational and Molecular Imaging Institute, Icahn School of Medicine at Mount Sinai, New York, NY, United States.
2. Interdisciplinary Nanoscience Center, Aarhus University, Aarhus, Denmark.
3. Biomedical NMR, Department of Biomedical Engineering, Eindhoven University of Technology, Eindhoven, Netherlands.
4. Department of Vascular Medicine, Academic Medical Center, Amsterdam, Netherlands.
5. Department of Chemical Engineering, Massachusetts Institute of Technology, Cambridge, MA, United States.

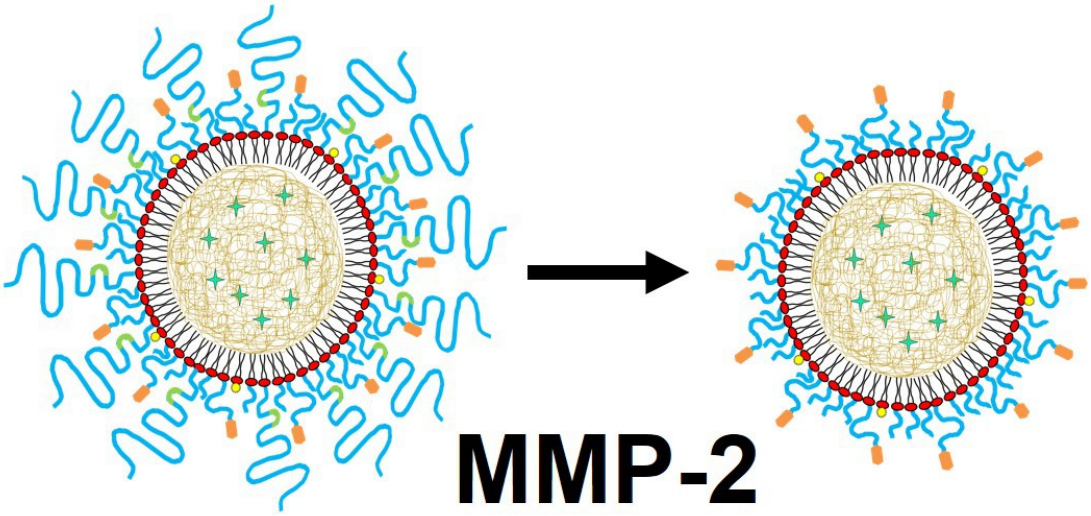

The nanoparticle platform is composed of a PLGA polymeric core shielded by a phoshopholipid corona that contains a mixture of specific mPEG-DSPE molecules. Upon tumor accumulation, nanoparticles are exposed to secreted MMP-2. This results in the cleavage of the long PEG coating and the surface exposure of RGD targeting peptides, which enables tumor cell binding and internalization.

CONTROL ID: 2231570

TITLE: OKN-007 decreases free radicals levels in a preclinical F98 rat glioma model

PRESENTER: Rheal Towner

ABSTRACT BODY:

Abstract Body: Free radicals are involved in several cancers, including gliomas. Here, we report the free radical scavenging effect of an anticancer nitrone compound, OKN-007 [Oklahoma Nitrone 007; a disulfonyl derivative of α-phenyl-tert-butyl nitrone (PBN)] in a F98 rat glioma model using combined molecular magnetic resonance imaging (mMRI) and immuno-spin trapping (IST) methodologies. Free radicals can be trapped with the spin trapping agent, 5,5-dimethyl-1-pyrroline *N*-oxide (DMPO), to form DMPO-nitrone radical adducts, which can then be further tagged by immuno-spin trapping, a method that utilizes an antibody against DMPO-adducts. In this study, we combined mMRI with a biotin-Gd-DTPA-albumin-based contrast agent for signal detection with the specificity of an antibody for DMPO nitrone adducts (anti-DMPO probe), to detect in vivo free radicals in OKN-007 treated rat F98 gliomas. OKN-007 was found to significantly decrease ($p < 0.05$) free radicals levels detected in treated animals compared to the untreated group, both of which were administered with the anti-DMPO probe. Immunoelectron microscopy was used with gold-labeled anti-biotin to detect the anti-DMPO probe within the plasma membrane of F98 tumor cells from rats administered anti-DMPO *in vivo*. This is the first attempt at detecting *in vivo* levels of radicals in a rat glioma model and assessing the free radical scavenging capability of an anticancer nitrone. The results indicate that OKN-007 effectively scavenges free radicals associated with glioma tumor growth. Furthermore, this method can potentially be applied towards other types of cancers for the *in vivo* detection of macromolecular free radicals and the assessment of antioxidants.

AUTHORS (LAST NAME, FIRST NAME): Towner, Rheal[1]; Coutinho de Souza, Patricia[1]; Smith, Nataliya[1]; Saunders, Debra[1]; Lerner, Megan[2]; Meek, Bill[3]; Ehrenshaft, Marilyn[4]; Mason, Ronald[4]

INSTITUTIONS (ALL):

1. Advanced Magnetic Resonance Center, Oklahoma Medical Research Foundation, Oklahoma City, OK, United States.
2. Univ. of Oklahoma Health Sciences Center, Oklahoma City, OK, United States.
3. Oklahoma State University Center for Health Sciences, Tulsa, OK, United States.
4. NIEHS, Research Triangle Park, NC, United States.

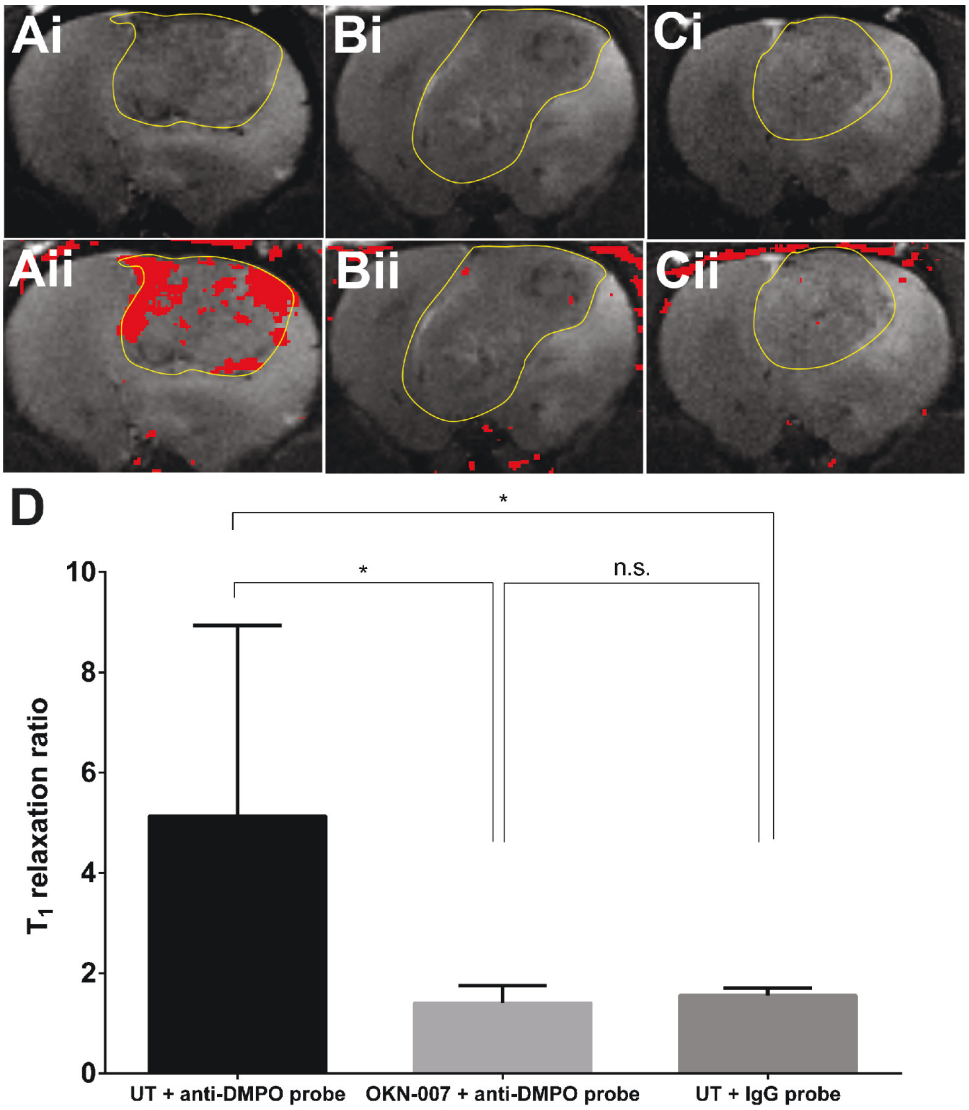

Figure 1: mMRI detection of free radical adducts in a F98 rat glioma model. Representative MR images from: (A) Untreated + anti-DMPO probe, (B) OKN-treatment + anti-DMPO probe, (C) Untreated + IgG probe, treated F98 rat gliomas. (A-Ci) T_2-w images of F98 glioma. (A-Cii) T_2-w images overlayed with a difference T_1-w image (red), which was the subtraction between the 2 hr post-contrast and the pre-contrast images after injection of either the anti-DMPO probe or the IgG contrast agent. (D) Histogram of T1 relaxation ratios for F98 glioma-bearing rats treated with the anti-DMPO probe alone, OKN-007 + anti-DMPO probe, or the IgG non-specific contrast agent. OKN-007 was found to significantly decrease (p<0.05, n=5) the levels of free radicals in the treated group compared to the untreated animals (n=7), which both received the anti-DMPO probe. There was no significant difference between the OKN-007 treated group and the untreated animals that received the IgG contrast (negative control group). Values are represented as means ± SD. Asterisks indicate statistically significant differences (*p < 0.05). UT: untreated animals.

CONTROL ID: 2231665

TITLE: In Vivo Targeted Molecular Magnetic Resonance Imaging of Free Radicals in Diabetic Cardiomyopathy in Mice

PRESENTER: Rheal Towner

ABSTRACT BODY:

Abstract Body: Evidence suggests that free radicals contribute to the pathogenesis of diabetic cardiomyopathy. Here we report on a method to observe free radical events in vivo. This study reports on in vivo imaging of protein/lipid radicals using molecular MRI (mMRI) and immune-spin trapping (IST) in diabetic cardiac muscle. Mice were treated with streptozotocin (STZ), and assessed for diabetes when glucose levels were >300 mg/dl. For control groups, non-diabetic mice were given the radical trapping agent, 5,5-dimethyl-pyrroline-N-oxide (DMPO) (non-disease control), and administered an anti-DMPO probe (biotin-anti-DMPO antibody-BSA (bovine serum albumin)-Gd-DTPA), or diabetic mice were given DMPO but administered a non-specific IgG contrast agent (contrast agent control; mouse-IgG conjugated to biotin-BSA-Gd-DTPA) instead of the anti-DMPO probe. For detection of free radicals in diabetic cardiomyopathy, STZ-exposed mice were given DMPO and administered an anti-DMPO probe. DMPO administration started at 7 weeks following STZ treatment for 5 days, and then the anti-DMPO probe was administered one week later. MR experiments were carried out on a 7T imaging spectrometer. Mice were imaged at 8 weeks following STZ administration. Mouse hearts were imaged at 0 (pre-contrast) and at 90-100 min post-contrast agent injection. Relative MR signal intensities were calculated for selected regions-of interest (ROIs), and difference images were obtained between before and 90 min after injection of the anti-DMPO probe or IgG contrast agent. MRI was used to detect the presence of the anti-DMPO adducts by a significant sustained increase ($p<0.001$) in MR signal intensity. The biotin moiety of the anti-DMPO probe was targeted with fluorescently-labeled streptavidin to locate the anti-DMPO probe in excised cardiac tissues, indicating elevated fluorescence only in cardiac muscle from mice administered the anti-DMPO probe. It was found that diabetic mice have more radicals in cardiac tissue, as measured by the presence of the anti-DMPO probe with targeted molecular MRI, than non-diabetic mice.

AUTHORS (LAST NAME, FIRST NAME): Towner, Rheal[1]; Smith, Nataliya[1]; Saunders, Debra[1]; Carrizales, Jorge[1]; Lupu, Florea[2]; Silasi-Mansat, Robert[2]; Ehrenshaft, Marilyn[3]; Mason, Ronald[4]

INSTITUTIONS (ALL):

1. Advanced Magnetic Resonance Center, Oklahoma Medical Research Foundation, Oklahoma City, OK, United States.
2. Cardiovascular Biology, Oklahoma Medical Research Foundation, Oklahoma City, OK, United States.
3. NIEHS, Research Triangle Park, NC, United States.
4. NIEHS, Research Triangle Park, NC, United States.

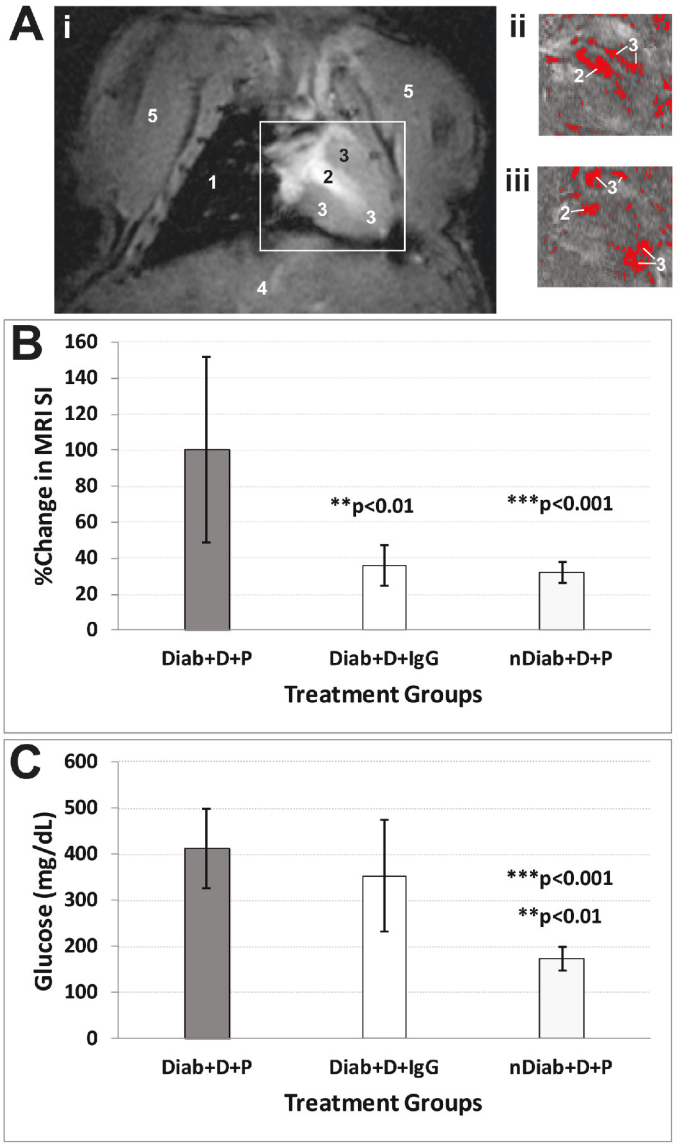

Figure 1: Molecular MRI detection of DMPO-trapped radical adducts in hearts of diabetic mice. (A) T_1-w images of STZ mouse hearts with difference images (ii and iii) obtained from 120 min post-administration of anti-DMPO probe minus pre-administration image [raw MR image (i), and thresholded images (ii) and (iii)]. (B) Percent (%) change in MRI signal intensities (SI) in the left ventricle cardiac muscle of mice that were either diabetic (Diab) or non-diabetic (nDiab) and treated with DMPO (D) and either the anti-DMPO probe (P) or an IgG isotype contrast agent (IgG). There was a significant increase in MRI SI for the diabetic mice given DMPO and the anti-DMPO probe, compared to the probe control (IgG) ($p<0.01$) or the non-diabetic control ($p<0.001$). (C) Blood glucose levels (mg/dL) in diabetic and non-diabetic mice. There was a significant increase in blood glucose in diabetic mice either given DMPO and the anti-DMPO probe ($p<0.001$) or given DMPO and the IgG contrast agent ($p<0.01$), compared to non-diabetic mice given DMPO and the anti-DMPO probe. Glucose (mg/dL) from STZ-induced diabetic mice (n=13) and non-diabetic (normal). Significant differences (**p>0.001 for IgG control; ***p>0.001 for anti-DMPO probe) were found between IgG controls and non-diabetic anti-DMPO administered mice.

CONTROL ID: 2231648

TITLE: OKN-007 decreases VEGRF-2 levels in a preclinical GL261 mouse glioma model

PRESENTER: Rheal Towner

ABSTRACT BODY:

Abstract Body: Angiogenesis is essential to tumor progression, and the precise imaging of the angiogenic marker vascular endothelial growth factor receptor 2 (VEGFR2) may provide an accurate evaluation for angiogenesis during a therapeutic response. In this study, we assessed VEGFR2 levels in untreated and OKN-007-treated GL261 mouse gliomas using molecular magnetic resonance imaging. OKN-007 was found to decrease significantly the levels of VEGFR-2 ($p < 0.05$) compared to the untreated group. Furthermore, OKN-007 was also able to decrease significantly the tumor volumes ($p < 0.01$) and increase survival ($p < 0.001$) in treated animals. Immunofluorescence imaging for the VEGFR-2 probe indicated that there was colocalization with the endothelial marker CD31 in an untreated tumor bearing mouse and decreased levels for an OKN-007-treated animal. Immunoelectron microscopy was used with gold-labeled anti-biotin to detect the anti-VEGFR-2 probe within the plasma membrane of GL261 tumor endothelial cells. This is the first attempt at detecting in vivo levels of VEGFR-2 in a mouse GL261 glioma model and assessing the anti-angiogenic capability of an anticancer nitrone. Our study confirmed that in vivo VEGFR2 levels can be monitored and can be used to assess the efficacy of an anti-angiogenic therapy. This method can potentially be applied towards other types of cancers for the in vivo assessment of VEGFR-2 levels, and assess various anti-angiogenic agents. The results indicate that OKN-007 treatment substantially decreased VEGFR-2 levels in a GL261 glioma model, and can be considered as an anti-angiogenic therapy in human gliomas.

AUTHORS (LAST NAME, FIRST NAME): Towner, Rheal[1]; Coutinho de Souza, Patricia[1]; Smith, Nataliya[1]; Saunders, Debra[1]; Chen, Hong[2]; Dong, Yunzhou[2]; Lupu, Florea[2]; Silasi-Mansat, Robert[2]

INSTITUTIONS (ALL):

1. Advanced Magnetic Resonance Center, Oklahoma Medical Research Foundation, Oklahoma City, OK, United States.
2. Cardiovascular Biology, Oklahoma Medical Research Foundation, Oklahoma City, OK, United States.

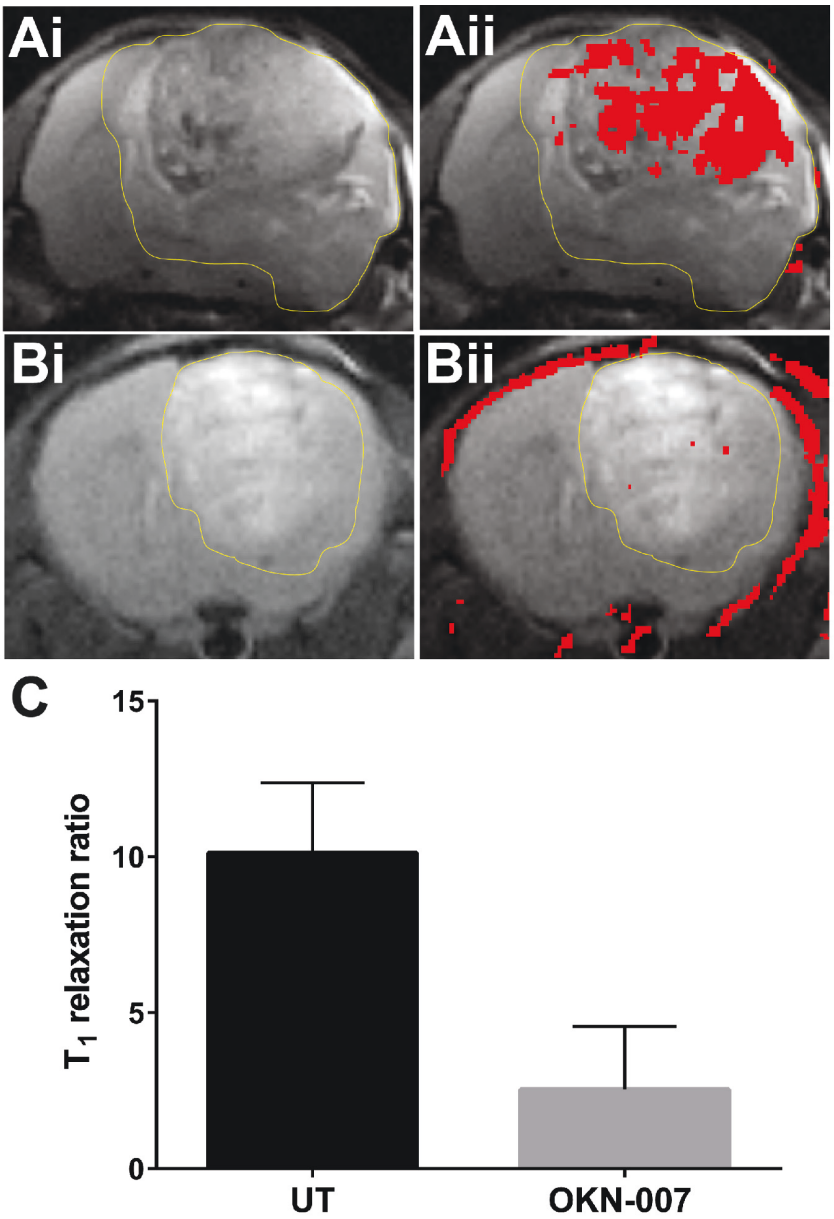

Figure 1: mMRI detection of VEGFR-2 in a GL261 mouse glioma model. Representative MR images from: (A) Untreated and (B) OKN-007 treated GL261 mouse gliomas. (Ai-Bi) T_2-weighted images of GL261 glioma. (Aii-Bii) T_2-weighted images overlayed with a difference T_1-weighted image (red), which was the subtraction between the 2 hr post-contrast and the pre-contrast images after injection of either the anti-VEGFR-2 probe contrast agent. (C) Histogram of T1 relaxation ratios in GL261-bearing mice treated with the anti-VEGFR2 probe alone or OKN-007 + anti-DMPO probe. OKN-007 was found to significantly decrease (p = 0.4137) (2.54 ± 2.02) the levels of VEGFR-2 in the treated group compared to the untreated animals (10.12 ± 2.25). Values are represented as means ± SD. Asterisks indicate statistically significant differences (*p < 0.05). UT: untreated animals.

CONTROL ID: 2233945

TITLE: New class of high-relaxivity Mn^{III}-based contrast agents as platforms for targeted intracellular magnetic resonance molecular imaging

PRESENTER: Ali Barandov

ABSTRACT BODY:

Abstract Body: Magnetic resonance imaging (MRI) offers unique potential for noninvasive molecular imaging with high spatial and temporal resolution. A major barrier in the application of molecular MRI agents for imaging intracellular targets is the difficulty of delivery across cell membranes. Most MRI contrast agents are complexes of gadolinium with aminopolycarboxylic acid chelators; a high number of carboxylic acid residues is crucial for stabilizing metal ions with no ligand field stabilization energy, but inherently restricts the cell permeability of the complexes. Here we have addressed these limitations by designing a new class of contrast agents based on high-spin Mn(III) complexes with planar tetradentate chelators derived from 1,2-phenylenediamine. All complexes have two axially coordinated water molecules (q = 2) with elongated Mn-O(H_2) bond distances due to Jahn-Teller distortion. Despite the modest spin number of Mn(III) (S = 2), the T_1-relaxation rate of the new diamido complexes is comparable with standard S = 7/2 Gd-based contrast agents at 7 T and is up to 2.5-fold higher than previously reported Mn(III) compounds. The amphiphilic nature of the new contrast agents confers both water solubility and unprecedented cell permeability, resulting in substantial changes in the R_1 of cells incubated with submicromolar probe concentrations. Variants incorporate additional functionality to enable cell-specific labeling or analyte detection while preserving their relaxivity and cell-permeability properties. This novel class of contrast agents therefore provides a powerful platform from which to develop reagents for *in vivo* molecular imaging of diverse processes inside cells.

AUTHORS (LAST NAME, FIRST NAME): Barandov, Ali[1]; Bartelle, Benjamin B.[2]; Jasanoff, Alan[1]

INSTITUTIONS (ALL):

1. Biological Engineering, Massachusetts Institute of Technology, Cambridge, MA, United States.
2. Biological Engineering, Massachusetts Institute of Technology, Cambridge, MA, United States.

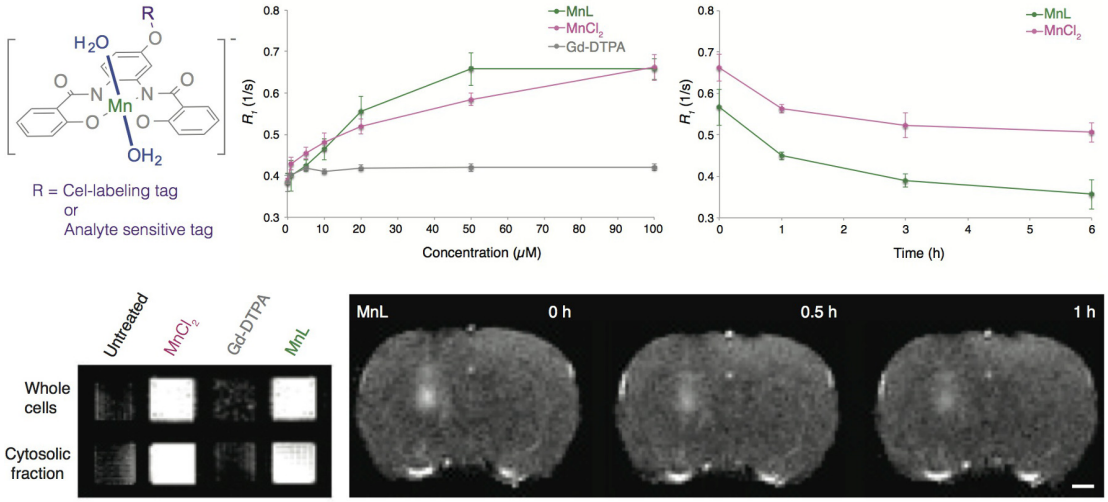

Figure 1. Manganese complexes with diamido chelators present versatile potential for molecular imaging of intracellular targets. (a) Molecular structure of a representative cell-permeable MnIII-complex of diamido chelator, showing attachment point for functional groups associated with intracellular targeting or analyte sensing. (b) Longitudinal relaxation rate (R1) measured from cells pre-incubated with a MnIII-complex (MnL, where L is a bifunctional diamido chelator) or with contrast agents expected remain excluded (Gd-DTPA) from cells. Cellular contrast achieved with the planar chelator persists over washing steps extending over 6 hours, indicating suitability for long-term cellular imaging applications. (c) MRI scans from fractionated cell samples associated with the conditions in (b), indicating cytosolic localization of the diamido complex. (d) T1-weighted images demonstrating retention of a diamido contrast agent in tissue following intracranial administration of MnL (14 μM). Scale bar = 2 mm.

CONTROL ID: 2231582

TITLE: A Method for the Reduction of Respiratory Motion Blur in Small Animal Computed Tomography

PRESENTER: Richard Taschereau

ABSTRACT BODY:

Abstract Body: Abstract

Small-animal Computed Tomography (CT) is used both as a complementary or a stand-alone imaging modality. Reconstructed images are affected by a number of artifacts that can be more or less easily corrected. One of those is image blurring caused by respiratory motion. Blurring can be observed in the guts, heart, lungs, diaphragm, etc.
The thorax of a properly anesthetized mouse, with a breathing frequency between 40 to 120 breaths per minute, can be in motion 50% of the time or more. A technique known as prospective gating, can synchronize data acquisition with the respiratory cycle, therefore eliminating motion blur. The technique requires respiratory sensors and a gating-capable scanner. The mouse setup time is also longer than with no gating. Another approach, retrospective gating[1], does not need specialized equipment but rather analyses and processes data post acquisition to minimize blurring.
In this paper, we describe a software retrospective gating technique that can identify, reject and/or replace projections affected by motion in such a way that motion blur is greatly reduced.

Method

Data was acquired on a prototype continuous rotation CT scanner that can collect 360, 720 or 1080 projections over 360 degrees. The first step is to identify projections at the apogee of the inhale phase. Pixel values in the central column of each projection are collected (that column goes through the center of the mouse in the cranio-caudal direction) and one of those pixels is selected as a surrogate for the respiratory signal. The selected pixel is the one for which the Fourier Transform is maximum in the likely frequency range of 40-120 breaths per minute. The time series (i.e. throughout the scan) of all values for that pixel provides the surrogate respiratory signal.
The signal is low-pass filtered and differentiated. Zero crossings identify frames located at the peak of the inhale phase.
At this point, three strategies can be used for the replacement of the “peak” frame:
1) the data frame at the peak (n) is replaced by the previous projection (n-1);
2) like (1) in addition to having the frame following the peak (n+1) replace by frame (n+2);
3) the peak frame (n) is replaced by the corresponding “light” frame (effectively removed), frame (n-1) is replaced with (n-2) and frame (n+1) is replace by (n+2).

Images were reconstructed using the Feldkamp algorithm[2] with a post-reconstruction median filter (3x3x3) applied.

Results

In Fig. 1 are shown coronal sections of a mouse scan with no gating (left) and with gating (right) using the third strategy. The upper boundary of the diaphragm is better delineated with gating.

Conclusion

The retrospective gating method described is simple and effective. It can be easily incorporated with existing software; no special hardware is required. Motion blur is reduced as a function of the breathing frequency of the mouse: the faster the breathing, the more the blurring is reduced.

[1]Paul J Schleyer et al, Retrospective data-driven respiratory gating for PET/CT, Phys. Med. Biol. 54, pp. 1935-1950 (2009)
[2]L. A. Feldkamp, L. C. Davis, and J. W. Kress, Practical cone-beam algorithm, JOSA A, Vol. 1, Issue 6, pp. 612-619 (1984)

AUTHORS (LAST NAME, FIRST NAME): Taschereau, Richard[1]; Chatziioannou, Arion F.[1]

INSTITUTIONS (ALL):

1. Molecular and Medical Pharmacology, Crump Institute for Molecular Imaging, UCLA, Los Angeles, CA, United States.

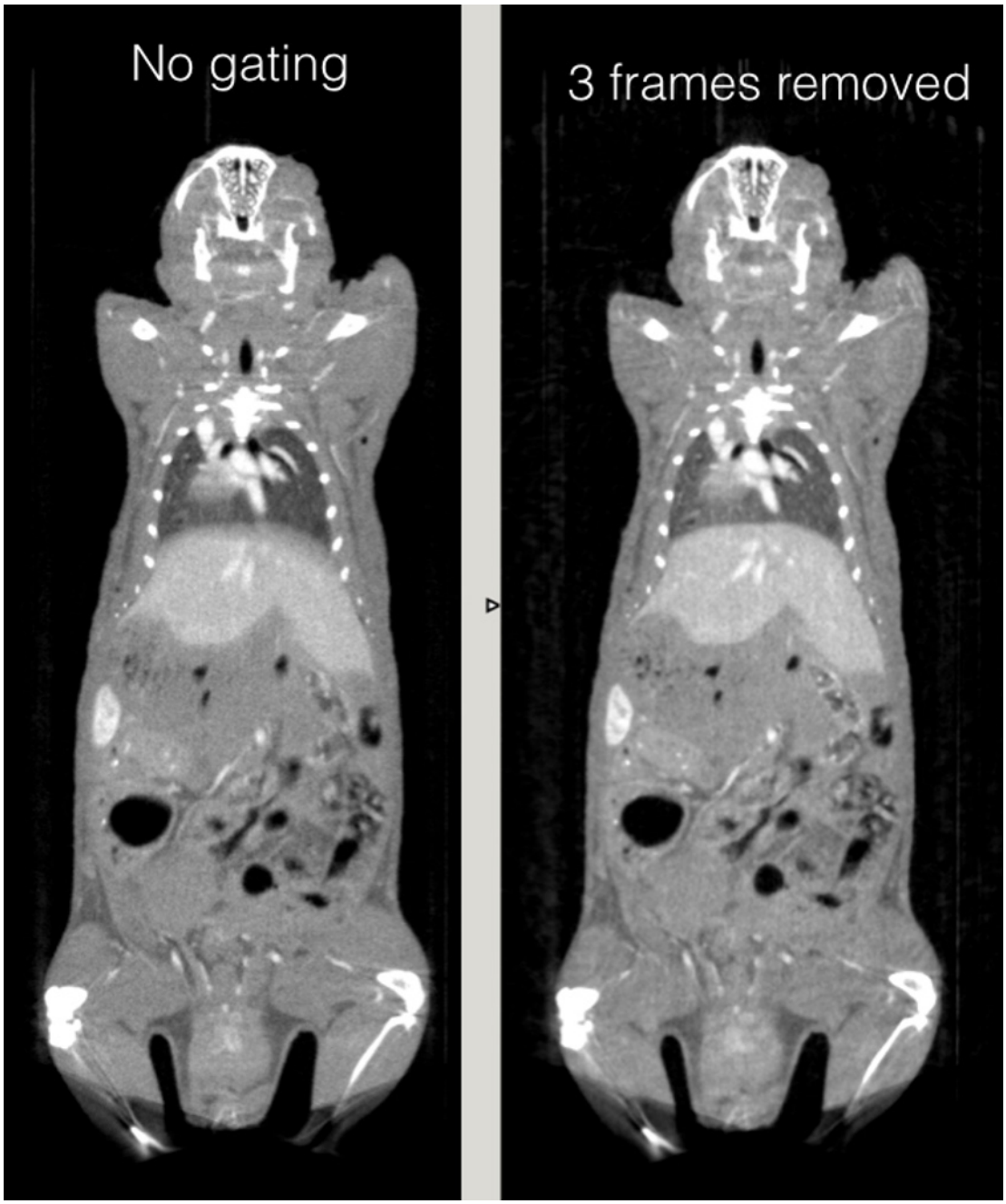
No gating
3 frames removed

CONTROL ID: 2231599

TITLE: Gold encapsulated polyphosphazene nanospheres as biodegradable contrast agents for computed tomography and photoacoustic imaging

PRESENTER: Rabee Cheheltani

ABSTRACT BODY:

Abstract Body: Introduction:

Gold nanoparticles (AuNP) have been proposed as novel contrast agents for medical imaging. Although large AuNP (>5nm) are desirable for their longer circulation and accumulation in diseased tissue, small AuNPs (<5nm) are required for swift excretion via the kidneys. We present a novel contrast agent platform where small AuNP are encapsulated into biodegradable poly-di(carboxylatophenoxy)phosphazene (PCPP) nanospheres. We hypothesize these larger nanoparticles will perform their function as contrast agents, subsequently break down into harmless byproducts and release the AuNP for swift excretion (A). We have examined these particles as contrast agents for computed tomography (CT) and photoacoustic imaging (PAI), and evaluated their biodegradability and biocompatibility in vitro.

Methods and results:

AuNP CT attenuation increases linearly with dose (S1). Small gold nanocrystals are synthesized via reduction of gold chloride with sodium borohydride, capped with a ligand for stabilization in biological media and purified via centrifugation. This results in ligand coated AuNP that are stable in PBS and have diameters tunable between 2-5 nm (B). These small AuNP are excreted swiftly (S2). Various capping ligands such as glutathione and 11-mercaptoundecanoic acid (11-MUA) were evaluated (S3). AuNP biocompatibility was studied by incubation for 4 hours with four cell lines; HepG2 (hepatocytes), SVEC4 (endothelial), J774A.1 (macrophages) and Reneca (kidney epithelial) and cell viability was assessed by MTS assay at a range of concentrations. These incubations did not reduce viability at concentrations as high as 1 mg/ml (D & S4), indicating very high biocompatibility

Gold encapsulated PCPP nanoparticles (Au-PCPP) are synthesized by mixing the polymer and gold, cross-linking with spermine, capping with PEG-polylysine (PEG-PLL), hardening in calcium chloride and purification by centrifugation. A microfluidic device is used for uniform polymer and cross-linker mixing conditions that produce homogeneously sized Au-PCPP. Synthesis of PCPP nanoparticles and encapsulation of AuNP in PCPP have been confirmed using TEM (C). Furthermore, the size of the Au-PCPP can be controlled by the amount of PEG-PLL added to the formulation (S5). The Au-PCPP nanoparticles can produce strong CT contrast (E). Inclusion of varying amounts of AuNP in PCPP tunes their UV-Vis absorption peak into the near infrared region (S6), making them potent contrast agents for PAI (F). Au-PCPP are biocompatible when studied by incubation with cells and MTS assay (S7). To evaluate biodegradability, the gold core release was studied by incubating Au-PCPP in 10% serum in PBS at 37 °C and measurement of gold in the supernatant with ICP-MS. A 59% release of AuNP over 7 days (G) and other evidence (S8-10) provided strong proof for the biodegradability of Au-PCPP.

Conclusion:

We have developed a novel approach to synthesize polyphosphazene nanoparticles loaded with AuNP. These formulations have the dual advantage of large size and high potency as contrast agents, are biocompatible and biodegradable, and thus represent a platform with potential for clinical translatability.

AUTHORS (LAST NAME, FIRST NAME): Cheheltani, Rabee[1]; Ezzibdeh, Rami M.[2]; Chhour, Peter[1, 2]; Jurcova, Martina[1]; Blundell, Cassidy[2]; Litt, Harold I.[1]; Ferrari, Victor A.[4]; Allcock, Harry R.[3]; Sehgal , Chandra M.[1]; Cormode, David[1, 2]

INSTITUTIONS (ALL):

1. Radiology, University of Pennsylvania, Philadelphia, PA, United States.
2. Bioengineering , University of Pennsylvania, Philadelphia, PA, United States.
3. Chemistry , Pennsylvania State University, University Park, PA, United States.
4. Medicine, University of Pennsylvania, Philadelphia, PA, United States.

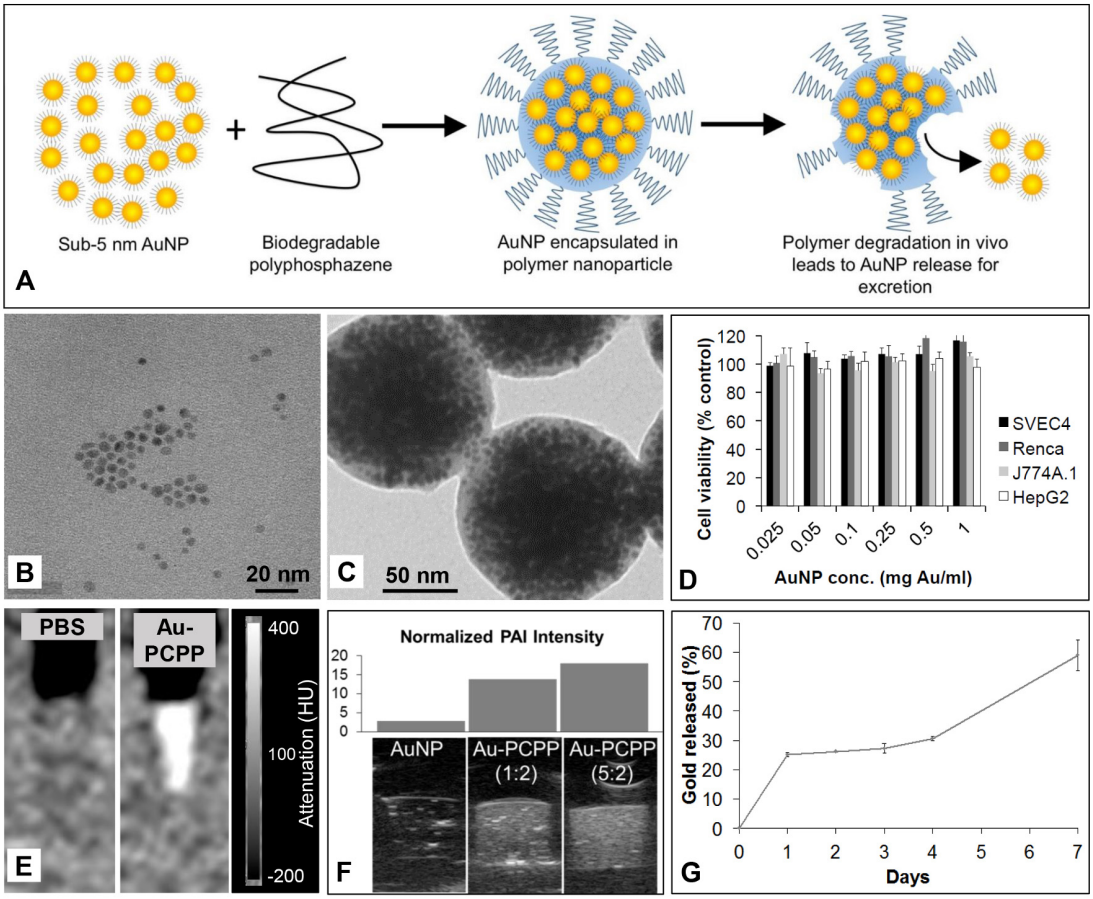

Figure 1 Biodegradable gold core polyphosphazene contrast agents (Au-PCPP). **A)** Schematic depiction of Au-PCPP. **B)** TEM of 5 nm gold nanoparticles. **C)** TEM of Au-PCPP. **D)** Effect of glutathione coated AuNP on cell viability. **E)** CT image of Au-PCPP. **F)** PA image of 11-MUA coated Au-PCPP. **G)** Degradation of Au-PCPP in 10% serum (37 ℃).

CONTROL ID: 2231606

TITLE: Basal dopamine occupancy estimation with simultaneous PET/fMRI

PRESENTER: Christin Sander

ABSTRACT BODY:

Abstract Body: Objectives: Basal receptor occupancy by endogenous neurotransmitter cannot be measured with PET without depleting the entire neurotransmitter population, which has major side effects[1]. We have previously shown that occupancy and fMRI signal are linearly related for a D2/D3 antagonist[2], from which relative basal dopamine (DA) levels can be inferred. For this study, we propose to derive *absolute* basal DA levels occupancies *in vivo* using an antagonist-agonist pair and simultaneous PET/fMRI.

Methods: Simultaneous PET/fMRI was acquired in two anesthetized non-human primates with the radiotracer [^{11}C]raclopride and graded D2/D3 pharmacological challenges: antagonist raclopride (0.4, 1.4, 4.5, 16, 41 μg/kg) and agonist quinpirole (0.1, 0.2, 0.3 mg/kg). fMRI data were analyzed with the GLM and signals converted to cerebral blood volume (CBV)[3]. PET kinetic modeling was performed with SRTM2[4] using a time-dependent binding parameter[5], from which occupancies were derived. A generalized neurovascular coupling model was established to compute absolute basal DA occupancy levels.

Results & Discussion: Dose-dependent signal changes were observed for both agonist and antagonist, albeit with different response patterns. Fig. 1 shows a plot of CBV vs. occupancy (θ), demonstrating a monotonically increasing/decreasing function but with distinct slopes for antagonist/agonist. The voxelwise maps on the right show that the relative CBV magnitude in putamen and caudate is reversed for agonist and antagonist. Interestingly, CBV magnitudes of antagonist were larger compared to agonist at matching occupancies, and shorter fMRI timecourses were observed for the latter. These experimental observations are consistent with agonist-induced internalization and suggest that neurovascular coupling constants (N) cannot be assumed to be constant between antagonist/agonist. Our proposed coupling model shows that CBV signal is $\propto N_{Ant}\varepsilon_{Ant}(\theta^{(0)}_{DA}\theta_{Ant})$ in the antagonist case, but $\propto N_{Ag}((\varepsilon_{Ag} - \theta^{(0)}_{DA})\theta_{Ag})$ in the agonist case, with $\theta^{(0)}_{DA}$ the basal occupancy and ε the efficacy of the drug. Since a direct application of the model to estimate absolute basal DA occupancies from one drug and anatomical region is not possible without assuming $N_{Ant}=N_{Ant'}$, we employed ratios of the neurovascular coupling expressions between regions and injected drugs. $\theta^{(0)}_{DA}$ was thus determined as ~10% in caudate and ~20% in putamen, which is consistent with reported literature values[6].

Conclusion: Our approach using ratios of an agonist/antagonist pair and anatomical regions enables the estimation of *absolute* basal neurotransmitter occupancies. This method is not affected by distinct function-occupancy relationships of agonists/antagonists. Further studies with varying efficacies of ligands can further validate this technique. The ability to measure basal DA occupancies non-invasively and without major side effects is important for its application as a clinical biomarker in psychiatric and neurologic disease.

References: [1]Abi-Dargham *et al. PNAS* (2000). [2]Sander *et al. PNAS* (2013). [3]Mandeville *et al. MRM* (1998). [4]Ichise *et al. JCBFM* (2003). [5]Normandin et al. *NeuroImage* (2012). [6]Pifl et al. *Neurochem. Int.* (2006).

AUTHORS (LAST NAME, FIRST NAME): Sander, Christin Y.[1, 2]; Hooker, Jacob M.[1, 2]; Catana, Ciprian[1, 2]; Rosen, Bruce R.[1, 2]; Mandeville, Joseph B.[1, 2]

INSTITUTIONS (ALL):

1. A. A. Martinos Center for Biomedical Imaging, Department of Radiology, Massachusetts General Hospital, Charlestown, MA, United States.
2. Harvard Medical School, Boston, MA, United States.

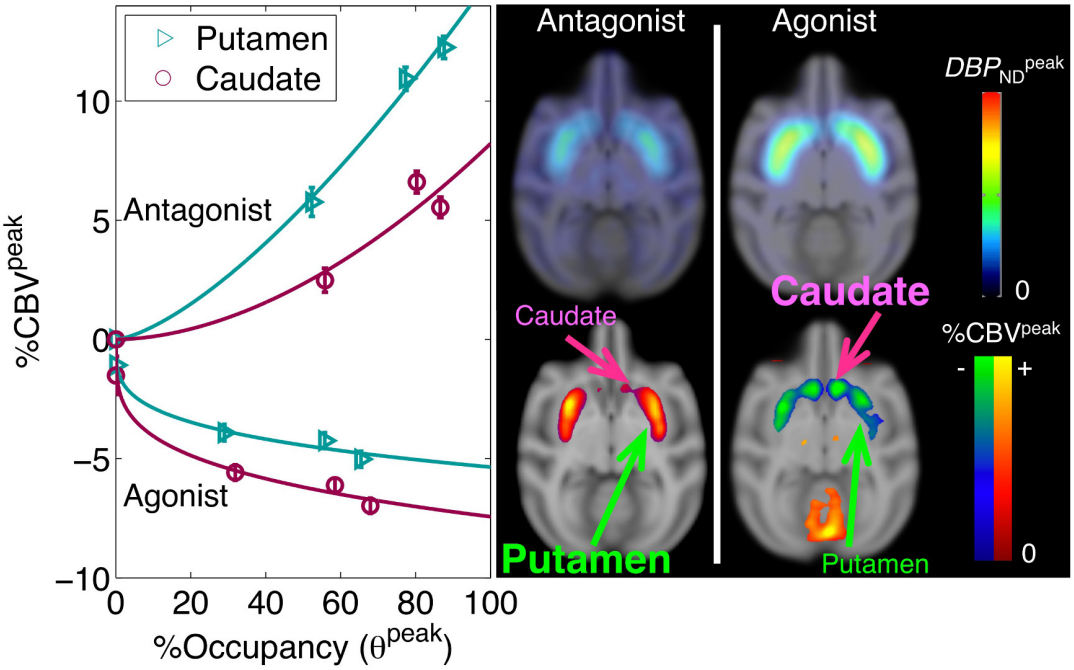

Figure 1: *Left:* Plot of CBV versus occupancy for the D2/D3 pair of antagonist/agonist challenges, showing the function-occupancy relationship for the two drugs in the putamen and caudate. *Right:* Dynamic binding potential maps derived from PET (*upper*) and CBV maps (*lower*) for a representative dose of antagonist (16 ug/kg raclopride) and agonist (0.2 mg/kg quinpirole). Putamen shows a larger CBV signal with the antagonist, whereas for the agonist, a larger magnitude is observed in the caudate. This regional difference forms the basis for the basal dopamine occupancy estimation.

CONTROL ID: 2231611

TITLE: Pharmacologically-induced epileptic seizures involve focal, but not global rCBF-changes – relationship of activated brain clusters and $GABA_A$-R density assessed with combined [$^{15}O]H_2O$-PET- and [^{11}C]flumazenil-PET/MRI

PRESENTER: Florian Maier

ABSTRACT BODY:

Abstract Body: The complex etiology of generalized tonic-clonic seizures includes dynamic changes of brain physiology (e.g. of regional cerebral blood flow, rCBF) during seizures, and the regional distribution of $GABA_A$-receptors ($GABA_A$-R). Using a combination of [$^{15}O]H_2O$ and [^{11}C]flumazenil PET/MRI, we aimed at quantifying rCBF-changes, the regional distribution of $GABA_A$-R density and their correlation. To obtain complementary information for $GABA_A$-R antagonistic/agonistic effects, we employed bicuculline and diazepam as pharmacological stimuli.

Three-month-old C57BL/6 wildtype mice were injected intravenously (*i.v.*) with 26±3MBq [$^{15}O]H_2O$ at baseline and 1 or 2min after pharmacological challenges (separated by 30 min; PET-scan duration: 180s). Mice were *i.v.*-challenged with 1.5mg/kg bicuculline 1 min prior [$^{15}O]H_2O$- (1min p.B.i., n=7), 2min prior [$^{15}O]H_2O$- (2min p.B.i., n=4) or with 1.5mg/kg diazepam 2min prior [$^{15}O]H_2O$-injections (2min p.D.i., n=4). Additionally, the 2min p.B.i. group underwent a second bicuculline challenge cycle 1h later (2min p.2ndB.i.). Mice were anesthetized with 1.5% isoflurane, body temperature was maintained at 37±0.5°C. A subset of the mice underwent [^{11}C]flumazenil scans before the [$^{15}O]H_2O$ acquisitions were conducted (60 min, *i.v.*-injection of 8.5±2.3MBq, n=8). [$^{15}O]H_2O$ and [^{11}C]flumazenil data were reconstructed with FBP2D. After the calculation of parametric rCBF maps using an image derived arterial input function, [$^{15}O]H_2O$-scans were coregistered and analyzed for activated clusters with SPM12b (cluster size 50 voxel=0.5 mm³, $P<0.05$, two-sided, paired *t*-test). Parametric [^{11}C]flumazenil-BPnd maps were calculated with PMOD3.2 using the *MRTM0*-approach and the pons as reference region. All PET-images were coregistered to T_2-MR images, and significantly activated [$^{15}O]H_2O$ clusters were analyzed for [^{11}C]flumazenil-BPnd.

The 2min p.B.i. group displayed significantly inactivated clusters (n=13) focally in S2,CPu,AcbC,RSG, hippocampus (Hi) and thalamus (Th) (t-value: $2.78<t<12.2$), the second challenge resulted in widespread activation throughout the entire forebrain (t-value: $2.78<t<12.3$; n=25 clusters). The 2min p.D.i. group displayed significantly activated clusters (n=6) in the S1,S2,RSG,RSA,PMCo and Pir (t-value: $2.78<t<5$). No significant changes were observed in the 1min p.B.i. group (t-value: $t<2.37$). [^{11}C]flumazenil-BPnd ranged from 0.19±0.06 (PMCo) to 1.49±0.19 (RSG) and correlated with the [$^{15}O]H_2O$-PET-activation in S2 (pearson: -0.81; $R^2=0.65$), CPu and AcbC (pearson: 0.78; $R^2=0.60$) of the 2min p.B.i. group. The 2min p.D.i. group displayed an inverse correlation in S1 (pearson: -0.94; $R^2=0.88$). All remaining groups and conditions showed no correlation between [^{11}C]flumazenil and [$^{15}O]H_2O$ (detailed results: supplementary information).

Elucidating the complex mechanisms underlying generalized tonic-clonic seizures remains difficult. However, our results support the theory, that these seizures are not affecting the entire brain, but rather involve focal regions. The only partial correlation with [^{11}C]flumazenil-BPnd might be due to the complexity of the GABAergic system, and warrants further studies.

AUTHORS (LAST NAME, FIRST NAME): Maier, Florian C.[1]; Harant, Maren[1]; Ehrlichmann, Walter[1]; Pichler, Bernd J.[1]

INSTITUTIONS (ALL):

1. Department of Preclinical Imaging and Radiopharmacy, Eberhard Karls University Tuebingen, Tuebingen, Germany.

(No Image Selected)

CONTROL ID: 2233624

TITLE: Ultrasound and Microbubble Mediated Therapeutic Modulation of Hepatocellular Carcinoma using Two Complementary MicroRNAs

PRESENTER: Sayan Mullick Chowdhury

ABSTRACT BODY:

Abstract Body: Introduction: Hepatocellular carcinoma (HCC), characterized by late detection, poor prognosis, drug resistance and high mortality rate has limited treatment options and new strategies for its therapy are critically needed [1]. MicroRNAs (miRNAs) are potent gene expression regulators that when aberrantly expressed, play a profound role in cancer development and progression. The purpose of this study was to explore a novel treatment approach for HCC by simultaneously delivering into tumor cells two miRNA modulating therapeutic agents: 1) miRNA-122, a miRNA-122 mimic designed to supplement under-expressed endogenous miRNA-122; and 2) antimiR-21, which binds and inhibits overexpressed miRNA-21. An image-guided ultrasound (US) and microbubble (MB) delivery platform was used to increase therapeutic delivery of miRNA loaded Poly(lactic-co-glycolic acid) nanoparticles(PLGA NP).

Methods: PLGA NP synthesis and miRNA loading were performed using a double emulsion method [2]. Doxorubicin resistant HepG2 cell lines were created and characterized. Sequencing was used to quantitate altered miRNA expression profile of human HepG2 HCC cells *in vivo* on miRNA delivery. Live cell counting was used to assess cell proliferation in resistant and non-resistant HCC after miRNA and drug treatment. Confocal microscopy was used to visualize Cy5-tagged miRNA in vitro and qRT-PCR was used to quantitate delivered miRNA in vitro and in vivo. Western blots were performed to confirm up/down-regulation of miRNA targets in vitro. Ex vivo, Tunnel staining and Transmission electron microscopy (TEM) was used to confirm therapeutic effects of delivered miRNA in subcutaneous human HCC xenografts in mice.

Results: In vitro assays, sequencing data and western blots established that combined delivery of both miRNA-122 and antimiR-21 was more effective in decreasing cell proliferation and sensitizing doxorubicin-resistant human HCC cells versus delivery of either miRNA-122 or antimiR-21 alone. Electron microscopy confirmed that our US and MB-mediated delivery platform could successfully deliver miRNA-loaded PLGA-NP within tumor cells of HCC xenografts. The delivered intracellular miRNA-122 and antimiR-21 were intact and functional, as confirmed by qRT-PCR and apoptosis assay. A single miRNA modulation treatment, using a dose of 14nmol/kg b.w. of both miRNA-122 and antimiR-21, resulted in strong therapeutic effect with substantial areas of apoptosis in human HCC xenografts in mice. (Figure 1).

Conclusion: Therapeutic US and MB mediated delivery of miRNA-loaded PLGA-NP in HCC results in substantial therapeutic effects in human HCC xenografts in mice. The combined delivery of miRNA-122 and antimiR-21 can sensitize resistant HCC to doxorubicin and potentially overcome the current therapeutic void for HCC patients.

References:

[1] Forner, A et al. *The Lancet* 379, 1245-1255(2012).
[2]Cohen-Sela, E et al. *Journal of controlled release* **133**, 90-95 (2009).

AUTHORS (LAST NAME, FIRST NAME): Mullick Chowdhury, Sayan[3]; Wang, Tzu-Yin[2]; Bachawal, Sunitha[4]; Devulapally, Rammohan[3]; Paulmurugan, Ramasamy[3]; Willmann, Juergen K.[1]

INSTITUTIONS (ALL):
1. Radiology, Stanford , Stanford, CA, United States.
2. Stanford University, Palo Alto, CA, United States.
3. Radiology, Stanford University, Palo Alto, CA, United States.
4. Radiology/MIPS, Stanford University, School of medicine, Stanford, CA, United States.

(No Image Selected)

CONTROL ID: 2231635

TITLE: Monitoring Tumor Hypoxia Following High Dose Radiation Therapy Using Oxygen Sensitive MRI on a Lung Cancer Xenograft Rat Model

PRESENTER: Heling Zhou

ABSTRACT BODY:

Abstract Body: Introduction: Tumor hypoxia is an important biomarker affecting tumor treatment response especially for radiation therapy [1]. Hypofractionated stereotactic body radiation therapy (SBRT) has attracted great attention in recent years and some promising results have been reported. Hypofractionated SBRT requires fewer patient visits and customized treatment planning has become a possibility. In this study, we applied blood oxygen level dependent (BOLD) and tissue oxygen level dependent (TOLD) MRI together with dynamic contrast enhanced (DCE) MRI to explore the longitudinal effects of hypofractionated SBRT on tumor re-oxygenation and development using human lung cancer xenografts in a subcutaneous rat model.

Methods: A549 human lung cancer cells were implanted subcutaneously in the thigh of ten nude rats. MRI was performed at 4.7 T. Interleaved BOLD (multi-echo gradient echo) and TOLD (gradient echo) MRI were acquired with the intervention of an oxygen challenge (from air to 100% O_2). DCE was performed with IV injection of gadolinium contrast (Gadavist) at a dose 0.1 mmol/kg body weight. T_1 maps were also acquired for pharmacokinetic analysis of DCE prior to contrast injection. MRI was performed on the day prior to, and 24 hours after radiation. Seven tumors received 12 Gy with oxygen breathing 30 minutes pre and during the irradiation, and three tumors received no radiation and served as control. Data were processed using Matlab. Semi-quantitative percentage signal intensity changes (%ΔSI) of BOLD and TOLD and quantitative T_1 and T_2* maps were calculated. Initial area under the curve (IAUC), time-to-maximum (TTM) and slope were calculated from DCE. The Yankeelov model was used for the quantitative analysis to obtain K^{trans} and v_e [2].

Results: Intra-tumor heterogeneity was seen on multi-parametric maps, especially in BOLD, T_2* and DCE, which may indicate the special growth pattern of A549 subcutaneous tumors (Fig. A). Most tumors at baseline showed a positive BOLD signal response (%ΔSI) and increased T_2* indicating increased oxygenation in response to oxygen challenge. Similar observations were found on control tumors 24 hours later. However, the irradiated tumors showed a significantly decreased T_2* (-2.5±1.8ms) after 24 hours, which may imply decreased oxygenation. Muscle values from both irradiated and control tumors were also obtained for reference (Fig. B). DCE also revealed the heterogeneity in the tumor.

Conclusions: Multi-parametric MRI revealed longitudinal changes in the tumor microenvironment. The changes in BOLD and TOLD may allow optimized timing of hypo-fractionated SBRT. Further exploration with more animals and different time points will be valuable to better understand the effect of radiation therapy and help optimize the interval of the treatments.

Acknowledgement: The study was supported in part by funds from the Cancer Prevention and Research Institute of Texas (CPRIT MIRA RP120670) and Cancer Center Resource facilities under 1P30 CA142543 and P41- EB015908.

References:

1. Tatum, J.L., *et al. Int. J. Radiat. Biol.*, 2006. **82**(10): p. 699-757

2. Faranesh, A.Z., *et al., Phys. Med. Biol.*, 2008. **53**(10): p. 2617-2631

AUTHORS (LAST NAME, FIRST NAME): Zhou, Heling[1]; Denney, Rebecca[1]; Zhang, Zhang[2]; Saha, Debabrata[2]; Mason, Ralph[1]

INSTITUTIONS (ALL):

1. Radiology, UT Southwestern Medical Center, Dallas, TX, United States.

2. Radiation Oncology, UT Southwestern Medical Center, Dallas, TX, United States.

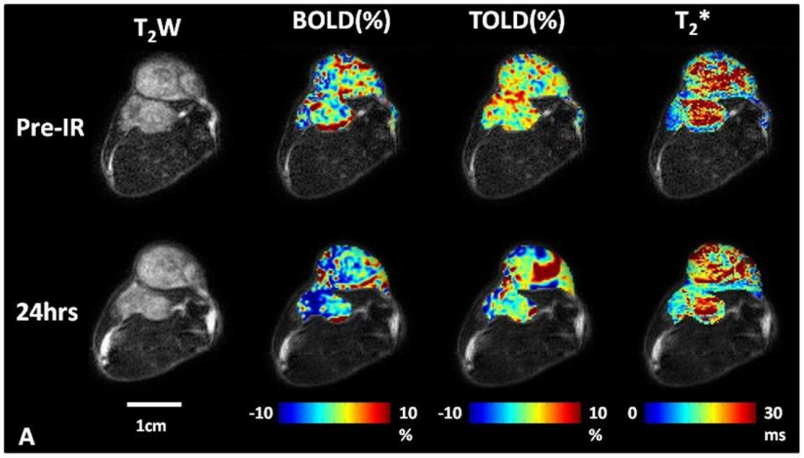

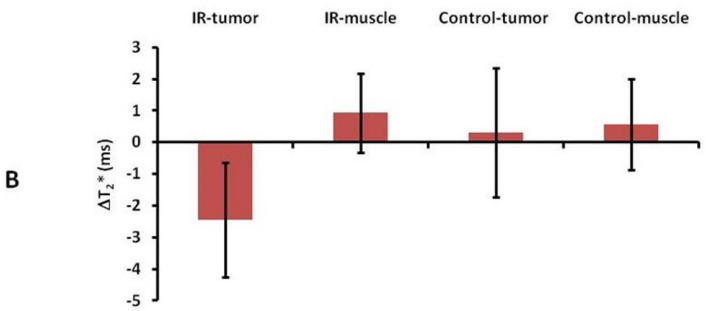

A. T_2-weighted image, %ΔSI of BOLD and TOLD and T_2* map (left to right) of one representative s.c. A549 tumor before and 24 hours after 1st dose of radiation). Tumor appeared to be multi-nodular on T_2-weighted image. Distinct heterogeneity was observed in all the functional maps at both time points. Each parameter appeared to decrease progressively following radiation indicating hypoxiation. B. Summary of changes of T_2* values from pre IR to 24 hours post radiation of tumor and muscle of the irradiated (IR) (n = 7) and the control rats (n = 3). Bars represent standard error.

CONTROL ID: 2232706

TITLE: Assessing Tumor Oxygenation and Perfusion in Response to a Novel Vascular Disrupting Agent OXi6197 Using Color-Doppler Ultrasound, Multi-parametric MRI and Bioluminescence Imaging

PRESENTER: Heling Zhou

ABSTRACT BODY:

Abstract Body: Purpose: Vascular disrupting agents (VDAs), a new class of anti-cancer drugs, selectively damage the endothelial cells of tumor blood vessels, inducing ischemia which leads to hypoxia and cell death (*Integr. Biol.*, 2011. 3(4): 375). In this study, we investigated the impact of a novel VDA (OXi6197) on tumor perfusion and oxygenation using bioluminescence imaging (BLI), color-Doppler ultrasound and MRI of lung cancer animal models. OXi6197 is a water-soluble phosphate prodrug of OXi6196, a newly developed dihydronaphthalene-based VDA inspired by combretastatin A-4 phosphate (CA4P) and colchicine.

Methods: A549 human lung cancer cells were implanted in the thigh (subcutaneously) or lung (orthotopically) of nude rats (pre-treated with whole body radiation). MRI was performed at 4.7 T including interleaved BOLD (blood oxygen level dependent R_2*: multi-echo gradient echo) and TOLD (tissue oxygen level dependent T_1w: gradient echo) with respect to an oxygen challenge (from air to 100% O_2). With continued oxygen breathing DCE-MRI (dynamic contrast enhanced) was performed with IV injection of gadolinium contrast (Gadavist; 0.1 mmol/kg). T_1 maps (spin echo) were also acquired for pharmacokinetic analysis of DCE-MRI prior to contrast injection. Then color-Doppler ultrasound was performed using a Vevo2100 before and 2 hrs after administration of OXi6197 IP (15 mg/kg). Oxygen enhanced MRI was repeated 24 hours later. Data were processed using Matlab. Semi-quantitative percentage signal intensity changes (%ΔSI) of BOLD and TOLD and quantitative T_1 and T_2* maps were calculated. Initial area under the curve (IAUC), time-to-maximum (TTM) and slope were calculated from DCE-MRI. A reference tissue model was used for the quantitative analysis to obtain K^{trans} and v_e (*Phys. Med. Biol*, 2008. 53(10): 2617). For comparison, dynamic BLI of a rat with A549-luc orthotopic (o.t.) lung tumor was acquired at baseline, 2, 6 and 24 hours with respect to OXi6197 at 30mg/kg.

Results and Discussion: The subcutaneous A549 tumor model developed significant muscular invasion in multiple cases. Color-Doppler showed reduction in blood flow two hours post injection of the VDA, OXi6197 (Figure 1). Intra-tumor heterogeneity was revealed on multi-parametric maps using MRI. %ΔSI of BOLD and TOLD decreased significantly 24 hours after receiving VDA, which may imply decreased oxygenation in tumor (Figure 2). DCE-MRI also showed reduction in contrast. Maximum signal enhancement was observed after a significantly longer time especially for the central tumor regions. K^{trans} decreased while v_e increased after receiving VDA. The orthotopic lung tumor showed 86% reduction in total BLI flux 2 hours after administration of VDA and maintained at 55% reduction at 24 hours (Figure 3).

Conclusions: Both color-Doppler and DCE-MRI showed decreased blood flow after administration of VDA. Oxygen sensitive MRI, BOLD and TOLD, suggested progressive hypoxiation at 24 hours. DCE and BLI showed changes of perfusion after treatment.

Acknowledgement: The study was supported in part by R01 CA140674, 1P30 CA142543 and P41 EB015908.

AUTHORS (LAST NAME, FIRST NAME): Zhou, Heling[1]; Lopez, Ramona[1]; Zhang, Zhang[2]; Saha, Debabrata[2]; Denney, Rebecca[1]; Trawick, Mary Lynn[3]; Pinney, Kevin[3]; Mason, Ralph[1]

INSTITUTIONS (ALL):

1. Radiology, UT Southwestern Medical Center, Dallas, TX, United States.
2. Radiation Oncology, UT Southwestern Medical Center, Dallas, TX, United States.
3. Chemistry and Biochemistry, Baylor University, Dallas, TX, United States.

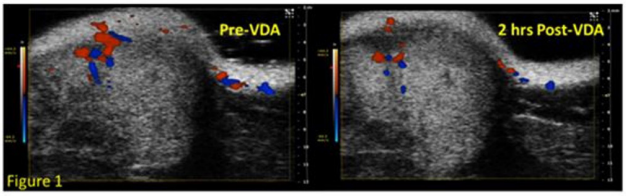

Figure 1

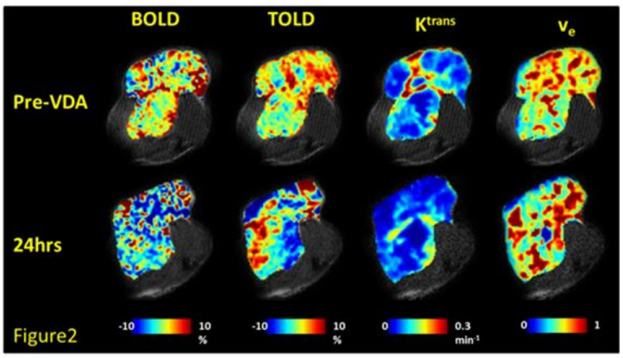

Figure2

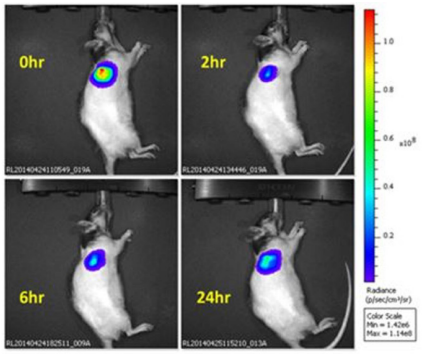

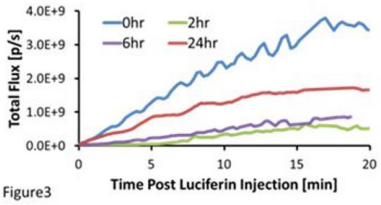

Figure3

Figure 1- Color Doppler ultrasound images show reduction of blood perfusion 2 hours after the administration of Oxi6197 vascular disrupting agent. Figure 2- Multi parametric MR images showing tumor physiological changes following the injection of VDA. Significant decrease in oxygenation is suggested by both BOLD and TOLD oxygen breathing challenge response maps. Decreased permeability and increased extracellular extravascular space seen the DCE-derived parameter maps for K^{trans} map and v_e, suggest cell death. Figure 3 – BLI monitoring orthotopic lung tumor in response to OXi6197. Top: Maximum BLI signal was observed around 15 minutes post SC injection of luciferin at baseline and 2, 6 and 24 hours post VDA. Bottom: Corresponding dynamic time courses of total flux obtained at the four time points.

CONTROL ID: 2231639

TITLE: Ultrasound Molecular Imaging of Angiogenesis using Engineered Scaffold Ligands

PRESENTER: Lotfi Abou-Elkacem

ABSTRACT BODY:

Abstract Body: Objective: The introduction of novel molecularly-targeted contrast microbubbles are increasingly being recognized as a powerful technique for the detection and quantification of disease processes that are characterized by a differential expression of molecules on the vasculature, such as a tumor angiogenesis markers like vascular endothelial growth factor receptor type 2 (VEGFR2). Since the development of hybridoma technology, a multitude of antibodies have been created and explored for medical purposes. However, the development and production of antibodies against a specific target is challenging, costly, and time-consuming. Alternatively, the evolving engineered protein scaffold (EPS) technique paves the way for developing novel binders to a target of interest. Multiple EPSs such as knottins, scFvs, nanobodies, and peptides have been designed and used for molecular imaging [1]. Recently, a novel engineered scaffold, the 10_{th} type III domain of human fibronectin (FN3s) has been shown to be a promising platform for designing binding ligands for molecular imaging [2]. The purpose of this study was to test a new class of targeted microbubbles to detect tumor angiogenesis in a transgenic breast cancer mouse model using an engineered VEGFR2–binding FN3 coupled to a microbubble (VEGFR2-FN3-MB).

Material and Methods: VEGFR2-FN3-MB were created by attaching VEGFR2-FN3 [3] to a PEG200-spacer using carboxyl-amine-conjugation chemistry which was attached to the shell of synthesized perfluorobutane-filled phospholipid MBs. FN3s with a scrambled sequence (scra-FN3) and non-targeted MBs were used as controls. The MB construct was also compared to a standard MB decorated with anti-VEGFR2 antibodies (VEGFR2-MB). The binding of VEGFR2-FN3-MB, VEGFR2-MB, and control-MBs to a soluble VEGFR2 was assessed by flow cytometry (FACS). Finally, all microbubble constructs were tested for their molecular imaging capabilities in a transgenic mouse model (FVB/N Tg(MMTV/PyMT634Mul) of breast cancer development.

Results: Compared to non-targeted and scra-FN3-MB, FACS analysis showed high affinity binding to soluble 10nM VEGFR2 using VEGFR2-FN3-MB and VEGFR2-MB, respectively. *In vivo* ultrasound molecular imaging showed significantly higher signal following VEGFR2-FN3-MB ($p<0.001$) and VEGFR2-MB ($p<0.001$) administration compared to the two controls scra-FN3 and non-targeted MB. After *in vivo* blocking of VEGFR2 receptors with free VEGFR2-FN3, VEGFR2-FN3-MB imaging signal significantly decreased ($p=0.0244$). Imaging signal using VEGFR2-FN3-MB and VEGFR2-MB was not significantly different. *Ex vivo* immunofluorescence analysis confirmed VEGFR2 expression on neoangiogenic tumor vessels.

Conclusion: Alternative scaffolds represent an emerging platform with the advantage of generating small, stable, cost-effective, and reproducible binding ligands for molecular imaging. Our results demonstrate that engineered VEGFR2-FN3 constructs coupled to MBs provides a novel alternative class of clinically translatable molecularly-targeted ultrasound contrast agents.

References:

[1] Willmann JK et al. J Nucl Med. 2010

[2] Hackel BJ et al. Radiology. 2012

[3] Getmanova EV et al. Chem Biol. 2006

AUTHORS (LAST NAME, FIRST NAME): Abou-Elkacem, Lotfi[1]; Wilson, Katheryne E.[1]; Bachawal, Sunitha[2]; Johnson, Sadie[3]; Hackel, Benjamin J.[3]; Willmann, Juergen K.[4]

INSTITUTIONS (ALL):

1. Radiology, Stanford University, Palo Alto, CA, United States.
2. Radiology, Stanford University, Stanford, CA, United States.
3. Department of Chemical Engineering and Materials Science, University of Minnesota, Minneapolis, MN, United States.
4. Radiology, Stanford University, Stanford, CA, United States.

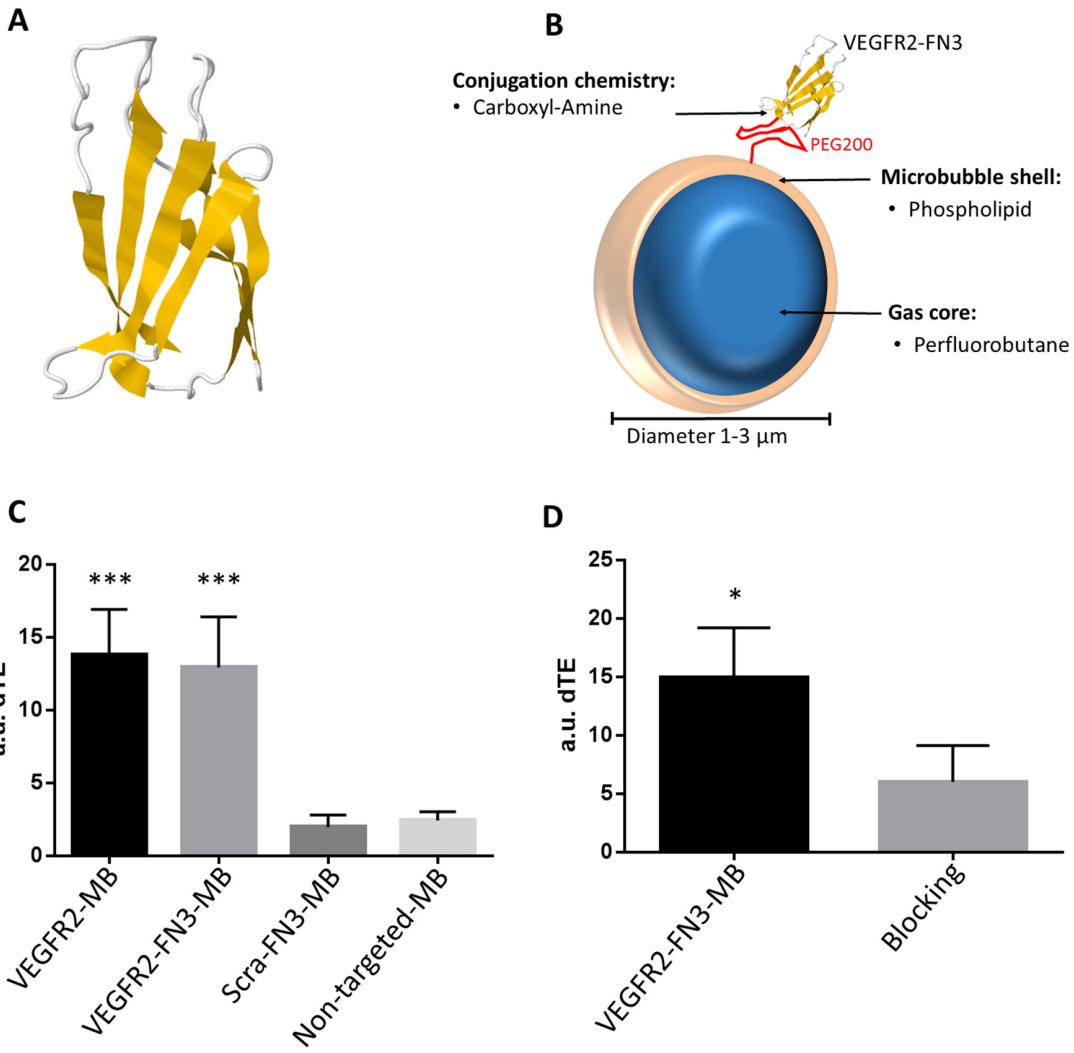
A
B
VEGFR2-FN3
Conjugation chemistry:
• Carboxyl-Amine
PEG200
Microbubble shell:
• Phospholipid
Gas core:
• Perfluorobutane
Diameter 1-3 µm
C
a.u. dTE
20
15
10
5
0
***
***
VEGFR2-MB
VEGFR2-FN3-MB
Scra-FN3-MB
Non-targeted-MB
D
a.u. dTE
25
20
15
10
5
0
*
VEGFR2-FN3-MB
Blocking

CONTROL ID: 2231637

TITLE: Spatial distribution and intracellular delivery of therapeutic microRNA loaded nanocarriers in tumors using ultrasound induced microbubble cavitation

PRESENTER: Tzu-Yin Wang

ABSTRACT BODY:

Abstract Body: Introduction: Ultrasound (US) induced microbubble (MB) cavitation can facilitate targeted delivery of therapeutic microRNAs (miRs) loaded in an FDA approved drug carrier, poly(lactic-*co*-glycolic acid)-nanoparticles (PLGA-NP) into tumors [1]. However, critical information on how far PLGA-NP penetrate into tumors and whether they are internalized into tumor cells, triggering desired therapeutic outcomes, is unavailable. This study evaluated the spatial distribution and intracellular delivery efficiency of the miR-loaded nanocarriers in tumors *in vivo*. Specifically, the penetration depth and intracellular uptake of the nanocarriers, and percentage of cells transfected with miR after US and MB treatment were investigated.

Method: Two types of nanocarriers (semiconducting polymer nanoparticles (SPN) and PLGA-NP) of 115 nm diameter were synthesized and studied for delivery into subcutaneous human LS174T colon cancer or HepG2 hepatocellular cancer xenografts in mice using US and MB. The highly fluorescent SPN were used for spatial localization of nanocarriers in tumors while the PLGA-NP served as clinically translatable carrier for therapeutic miR delivery. A total of 3.5×10^{8} lipid-shelled gas-filled MB were mixed with 6×10^{11} nanocarriers and intravenously injected into each animal. A total of 57 tumors on 41 animals were treated with 5 cycles of 1.8-MHz US pulses at pulse repetition rate of 100Hz and various pressures from 0 to 6.9 MPa. The tumors were extracted at 4h or 24h post treatment and processed for *ex vivo* 3D confocal microscopy (to assess penetration depth), TEM microscopy (to assess intracellular uptake), and FACS (to assess percentage of cells transfected with miRs).

Results: 3D confocal micrographs confirmed substantial extravasation of nanocarriers into tumor parenchyma in LS174T tumors at 4h and 24h post treatment **(Fig. A)**. As the pressure increased from 0 to 6.9 MPa, the median penetration depth of the extravasated nanocarriers increased from 4.9 μm (range:0.5–15.2μm) to 13.5 μm (range:4.6–43.9μm) at 4h (N=54 each), and from 9.5 μm (range:4.1–24.2μm) to 25 μm (range:12.2–58.2μm) at 24h (N=36 each). TEM micrographs showed that the miR-loaded PLGA-NP were internalized into tumor cells in HCC xenografts by endocytosis at 24h after US (5.4 MPa) and MB treatment **(Fig. B)**. Additionally, extensive accumulation of PLGA-NP was seen per single cells in tumors treated with US and MB **(Fig. C)** but not in the control with administration of PLGA-NP but without US and MB treatment (N=2 each). FACS analysis showed approximately 9% of cells in a tumor were transfected with miR at 24h after US (5.4 MPa) and MB treatment, while only 0.5% of cells were transfected in the control with administration of miR-loaded PLGA-NP but without US and MB treatment.

Conclusions: Our results suggest that tuning acoustic parameters can substantially enhance delivery efficiency and penetration depth of nanocarriers during ultrasound-guided drug delivery *in vivo* which will be of paramount importance when translating this drug delivery platform from small to large animals as well as patients in the future.

[1] Wang, T.Y., et al., J Control Release, 2015. **203**(10): p. 99-108.

AUTHORS (LAST NAME, FIRST NAME): Wang, Tzu-Yin[2]; Mullick Chowdhury, Sayan[2]; Bachawal, Sunitha[2]; Choe, Jung Woo[1]; Devulapally, Rammohan[2]; Pu, Kanyi[2]; Abou-Elkacem, Lotfi[2]; Khuri-Yakub, Butrus[1]; Rao, Jianghong[2]; Paulmurugan, Ramasamy[2]; Willmann, Juergen K.[2]

INSTITUTIONS (ALL):

1. Stanford University, Palo Alto, CA, United States.
2. Radiology, Stanford University, Palo Alto, CA, United States.

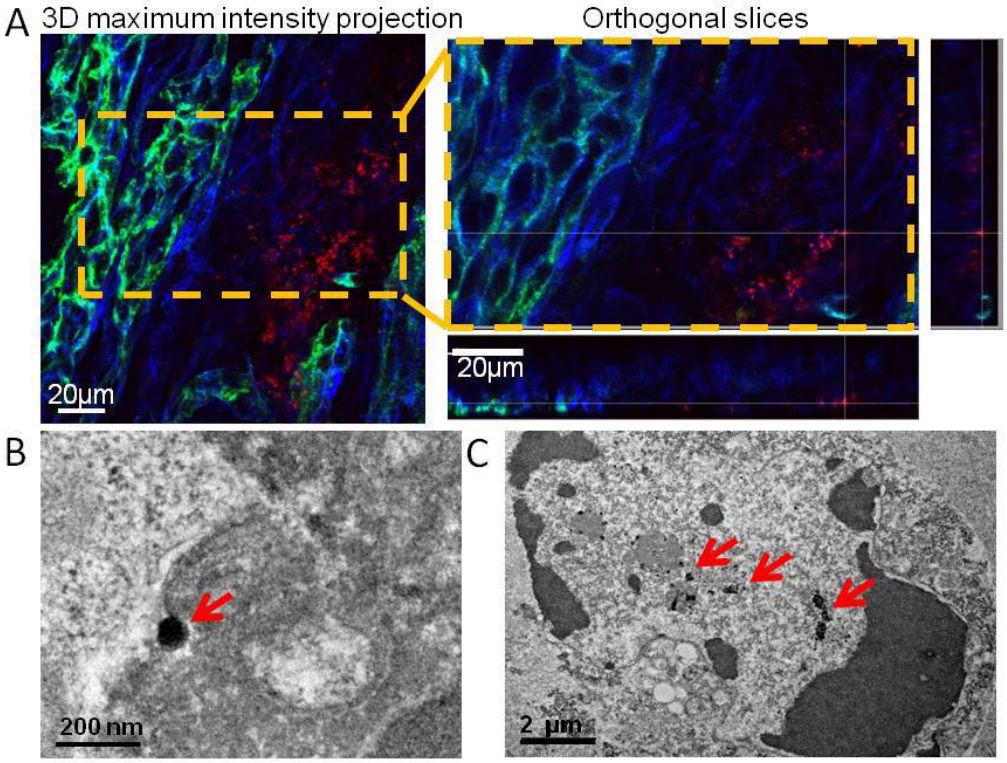

Figure: (A) Representative maximum intensity confocal immunofluorescence image reconstructed from 3D confocal microscopy data sets of human colon cancer xenograft treated with US and MB (6.9 MPa) shows extravasated SPN *(red)* compared to tumor vessels *(green)* in the imaged volume. Orthogonal slices indicated by the gray dashed lines further confirmed presence of SPN in tumor parenchyma *(blue)* and away from the vessel lumen (contoured in *green*). (B, C) TEM micrographs after a single treatment of US and MB mediated delivery of miR-loaded PLGA-NP in human HCC xenograft in mice. (B) PLGA-NP is internalized into an HCC cell by endocytosis (red arrow). (C) Extensive accumulation of miR-loaded PLGA-NP (black dots) in an HCC cell (arrows point to multiple PLGA-NP delivered within the cytoplasm).

CONTROL ID: 2231651

TITLE: A novel photoacoustic agent for imaging prostate-specific membrane antigen (PSMA) in prostate tissue

PRESENTER: Jelena Levi

ABSTRACT BODY:

Abstract Body: Current clinical diagnosis of prostate cancer, including biopsy, can be greatly improved by utilization of an imaging modality that allows better characterization of the disease through evaluation of functional and molecular status in a detected lesion. Molecular photoacoustic imaging, with relatively good depth penetration in combination with high contrast and resolution has a great potential to be clinically utilized for non-invasive, non-ionizing visualization of prostate lesions.

We report here a photoacoustic imaging (PAI) agent capable of assessing the localization of prostate specific membrane antigen (PSMA) within a prostate lesion. PSMA is expressed in a vast majority of prostate cancers (95%) and is correlated to tumor grade and aggressiveness[1]. A few PSMA–targeted PET agents have already been applied in the clinic with great success for imaging recurrent prostate cancer[2-4]. In this study we evaluate the utility of a PSMA photoacoustic imaging agent in the primary diagnosis of prostate cancer. Since normal prostate epithelium expresses PSMA it was of outmost importance to test the agent in a model that accurately depicts normal prostate and primary prostate adenocarcinoma. For that reason we chose to evaluate the agent in tissue slice cultures (TSC)[5], thin slices of human prostate tissue that maintain cellular heterogeneity and thus allow interrogation of binding to cancer and normal prostate epithelium often within the same tissue core.

This new PAI agent consists of a urea based PSMA inhibitor and a dye that provides high photoacoustic signal, ATTO-740. The agent shows strong binding to PSMA expressing cells, PC3 PIP (Kd=6.015 nM), and minimal binding to PC3 Flu cells that lack PSMA. The specificity to PSMA was further confirmed by the blocking of the agent binding using a well-known PSMA inhibitor, 2-PMPA. The agent was mostly binding to the surface of the PC3 PIP cells with 25% internalization at 30 minutes post-incubation. TSCs from freshly excised human prostate tissue from a single patient were incubated with 1.5 nmol of the agent for 30 minutes and imaged photoacoustically using 750 nm excitation wavelengths. The PAI agent could clearly differentiate between normal and tumor tissue, which was also confirmed by fluorescence imaging (Figure 1). Additionally, PAI allowed visualization of the areas of high and low signal reflecting heterogeneity of the tissue and intermingling of cancer with benign areas as further confirmed by immunohistochemistry.

This is the first report of a small molecule PSMA-directed PAI agent. The agent demonstrated good binding to cancer and minimal binding to normal tissue. The PAI method using a PSMA-targeted agent shows promise for application in diagnosis as well as in image guided biopsy. Prostate imaging using PAI has a great potential for clinical translation and this study warrants further investigations in that direction.

1. Minner S, et al. Prostate. 2011;71: 281-288.
2. Cho SY, et al. J Nucl Med. 2012;53: 1883-1891.
3. Beheshti M, et al. Mol Imaging Biol. 2014.
4. Afshar-Oromieh A, et al. Eur J Nucl Med Mol Imaging. 2013;40: 486-495.
5. Maund SL, et al. Lab Invest. 2014;94: 208-221.

AUTHORS (LAST NAME, FIRST NAME): Levi, Jelena[1]; Ramakrishnan, Sindhuja[1]; Ilovich, Ohad[2]; Peehl, Donna[4]; Gambhir, Sanjiv S.[3, 1]

INSTITUTIONS (ALL):
1. Canary Center at Stanford, Palo Alto, CA, United States.
2. Radiology, Stanford University, Palo Alto, CA, United States.
3. Radiology, Stanford University, Stanford, CA, United States.
4. Urology, Stanford University , Stanford, CA, United States.

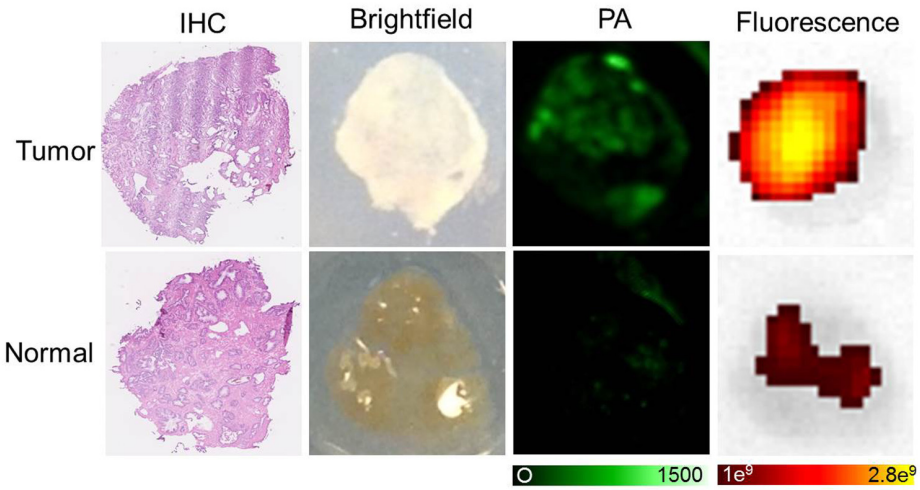

Figure 1. Binding of the PSMA-targeted photoacoustic agent in human prostate tissue. Normal tissue or cancer was grossly identified in the fresh radical prostatectomy specimen and a core of tissue, 8-mm in diameter, was aseptically bored and precision-cut at 300-μm (brightfield). After one hour recovery from slicing, tissue slices were incubated with 1.5 nmol PSMA-targeted photoacoustic agent, washed three times with PBS and immediately imaged both optically and photoacoustically. Both fluorescent and photoacoustic images revealed clear distinction between normal and tumor tissue. The presence and Gleason grade of cancer as well as normal tissue was validated by H&E staining.

CONTROL ID: 2233910

TITLE: Radiofluorinated PARPi-FL as PET/Optical tool for Glioblastoma imaging

Giuseppe Carlucci[1], Brandon Carney[1], Christian Brand[1], Edmund J. Keliher[3], Wolfgang A. Weber[1,2], Thomas Reiner[1,2]

[1] Memorial Sloan Kettering Cancer Center, New York, New York 10065, United States, [2] Weill Cornell Medical College, New York, New York 10065, United States, [3] Center for Systems Biology, Massachusetts General Hospital, Boston, Massachusetts 02114, United States

PRESENTER: Giuseppe Carlucci

ABSTRACT BODY:

Abstract Body: Objectives: PARP1 is a DNA repair enzyme that is overexpressed in multiple forms of brain malignancies. Here, ^{18}F-PARPi-FL, a bimodal fluorescent/positron emission tomography (PET) imaging agent, is presented. The tracer was produced via isotopic exchange with one of the ^{19}F fluorine atoms of PARPi-FL, a previously described PARP1 targeted fluorescent imaging agent that is capable of delineating glioblastoma in mouse models of cancer [1]. Methods: ^{18}F-PARPi-FL was obtained by the replacing of one of the boron-bound ^{19}F with an ^{18}F in the presence of $SnCl_4$ at 35 °C for 30 min [2, 3] (Figure 1). PET imaging and biodistribution studies as well as *ex-vivo* IVIS imaging and autoradiography were performed in U87 MG bearing mice (n=20). Results: ^{18}F-PARPi-FL was obtained with a radiochemical yield of 34.8 ± 1.1%, a radiochemical purity >98% and optimized specific activity of ~0.8 ± 0.1 Ci/μmol. ^{18}F-PARPi-FL uptake in U87 MG xenografts was 0.8 ± 0.1 % ID/g at 90 min p.i. and correlated using both PET and optical imaging modalities. The agent's accumulation was efficiently blocked after pre-injection of 50-fold excess Olaparib. The uptake of ^{18}F-PARPi-FL in the tumor was higher than the observed accumulation in brain and muscle in both optical imaging (tumor to brain ratio was 7-fold) and *ex-vivo* phosphor autoradiography (tumor to brain ratio was 9-fold higher). Olaparib-blocked U87 MG xenografts showed reduced tumor uptake (74 ± 12% reduction for optical imaging and 66 ± 9% for autoradiography). Conclusion: ^{18}F-PARPi-FL is a novel PARP1 targeting agent that can be used as an intraoperative fluorescent tool for glioblastoma as well as PET imaging agent for detection of deep-seated lesions. The fluorescent component of ^{18}F-PARPi-FL allows cellular-resolution point-of-care imaging, whereas the radiolabeled component is useful for the detection of brain malignancies and might be useful in planning radiation treatment. Ultimately, this agent may fulfill unmet clinical needs and assist in the clinical decision making process.

Acknowledgments: Supported by the Brain Tumor Center of MSKCC, the Imaging and Radiation Sciences Program of MSKCC, the American Italian Cancer Foundation and NIH P30-CA08748.

References: [1] Irwin CP, Portorreal Y, Brand C, et al. PARPi-FL - a Fluorescent PARP1 Inhibitor for Glioblastoma Imaging. Neoplasia 2014;16:432-40. [2] Keliher EJ, Klubnick JA, Reiner T, et al. Efficient acid-catalyzed ^{18}F/^{19}F fluoride exchange of BODIPY dyes. ChemMedChem 2014;9:1368-73. [3] Liu S, Lin TP, Li D, et al. Lewis acid-assisted isotopic ^{18}F-^{19}F exchange in BODIPY dyes: facile generation of positron emission tomography/fluorescence dual modality agents for tumor imaging. Theranostics 2013;3:181-9.

AUTHORS (LAST NAME, FIRST NAME): Carlucci, Giuseppe[1]; Carney, Brandon[1]; Brand, Christian[2]; Keliher, Edmund J.[5]; Weber, Wolfgang[3]; Reiner, Thomas[4]

INSTITUTIONS (ALL):

1. Memorial Sloan Kettering Cancer Center, New York, NY, United States.
2. Memorial Sloan Kettering Cancer Center, New York, NY, United States.
3. Memorial Sloan Kettering Cancer Center, New York, NY, United States.
4. Memorial Sloan Kettering Cancer Center, New York, NY, United States.
5. Massachusetts General Hospital, Boston, MA, United States.

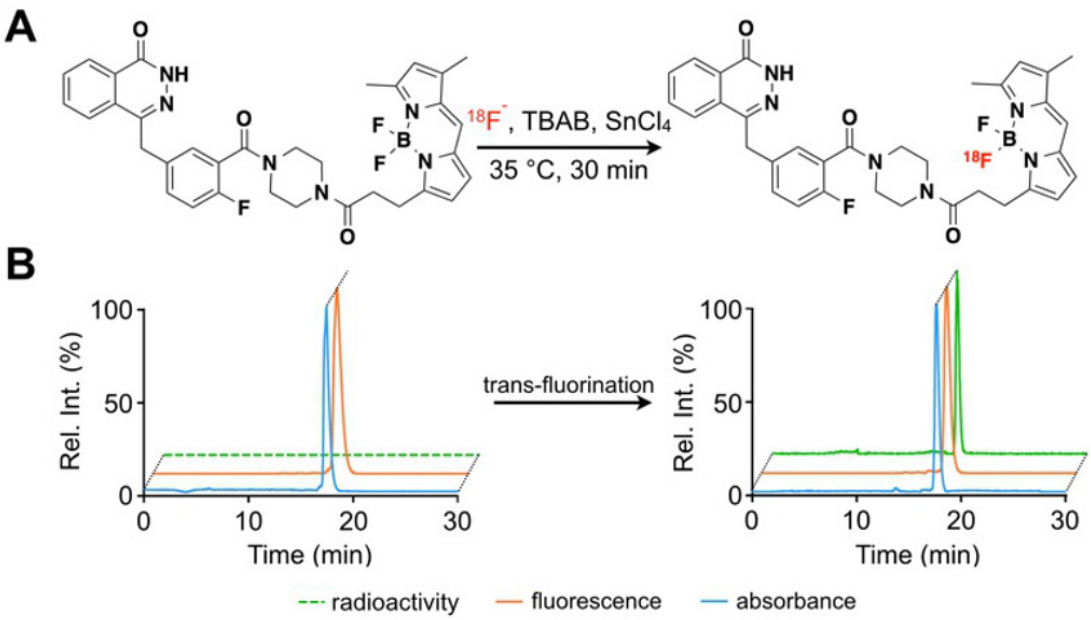
A
$^{18}F^-$, TBAB, $SnCl_4$
35 °C, 30 min
B
Rel. Int. (%)
Time (min)
trans-fluorination
radioactivity
fluorescence
absorbance

CONTROL ID: 2231677

TITLE: Glutamine Metabolism as a Target in the Evaluation of Colorectal Cancer Development and Therapeutic Response

PRESENTER: Matthew Hight

ABSTRACT BODY:

Abstract Body: Energy production in cancer cells is abnormally dependent on aerobic glycolysis, the Warburg effect, and is routinely analyzed by positron emission tomography (PET) using 2-[^{18}F]fluoro-2-deoxy-D-glucose ([^{18}F]FDG). Beyond a predilection for glycolysis, cancer cells have other atypical metabolic characteristics, such as increased fatty acid synthesis and an increased dependency on the natural amino acid glutamine as a fuel source; a phenomenon commonly described as glutamine addiction. Furthermore, emerging evidence suggests that glutamine uptake in cancer cells is controlled by oncogenic signaling pathways, such as *MYC* (1) and *KRAS* (2). Given this, quantitative measures of glutamine uptake may reflect critical processes in oncology that are difficult to measure using existing imaging metrics. To address this clinical need, these studies sought to elucidate the feasibility of [^{18}F]4-fluoroglutamine ([^{18}F]4-F-GLN), a reported radiolabeled derivative of glutamine (3), and PET imaging to evaluate the inhibition and activation of oncogenic pathways in colorectal cancer (CRC). Initially, [^{18}F]4-F-GLN PET was evaluated in preclinical models of *BRAF*^{V600E}-expressing CRC as a means of detecting molecular response to targeted therapeutics. Simulating a clinical trial at our institution, the regimen included an inhibitor of mutant BRAF, a PI3K/mTOR inhibitor, and a combination thereof. In human xenograft tumor bearing mice simulating these cohorts, decreased [^{18}F]4-F-Gln accumulation was observed in response to combination BRAF and PI3K/mTOR inhibition and not to single agent therapies. Interestingly, [^{18}F]4-F-GLN PET was found to be sensitive to pathways of drug response that were not observed by [^{18}F]FDG, which was down for all cohorts. Given the increasingly reported phenomena of oncogenic MYC-regulated glutamine addiction, it is possible, at least in this setting, that [^{18}F]4-F-Gln PET acts as a measure of molecular events that are downstream to PI3K/mTOR and BRAF pathway blockage. Expanding these investigations to a CRC model of mutant *KRAS*, a mutation found in 30-50% of colon cancers, [^{18}F]4-F-Gln showed decreased accumulation in combined MEK/BCL-XL treated xenograft tumors and agreed with previous reports that support this combination as a therapeutic approach for treating *KRAS* mutant cancers. Further exploring [^{18}F]4-F-GLN as a diagnostic marker of the *Kras* oncogene, PET imaging studies were performed in a genetically engineered mouse model that recapitulates the sequence of genetic mutations and loss of function that leads to colonic tumors in humans. In this setting, expression of Asct2, a neutral amino acid transporter of glutamine, as well as cellular [^{18}F]4-F-GLN uptake were associated with activation of mutant *Kras*. Conclusively, we believe these findings illuminate [^{18}F]4-F-GLN PET as a precision and companion imaging diagnostic for discerning critical oncogenic pathways in human CRC. References: 1) Wise DR, et al. PNAS. **2008**. 105: 18782-87. 2) Son J*, et al. Nature.* **2013**. 496(7443):101-5. 3) Qu W, *et al. JACS*. **2011**. 133:1122-33.

AUTHORS (LAST NAME, FIRST NAME): Hight, Matthew[1]; Zhao, Ping[1]; Poulin, Emily J.[1]; Coffey, Robert[1]; Manning, H. Charles[1]

INSTITUTIONS (ALL):

1. Vanderbilt University, Nashville, TN, United States.

(No Image Selected)

CONTROL ID: 2231698

TITLE: *In vivo* optical imaging of the regulatory dynamics of reactive oxygen species-stress and NF-kB-activation during delayed type hypersensitivity reactions

PRESENTER: Johannes Schwenck

ABSTRACT BODY:

Abstract Body: NF-kB is an essential regulator of inflammation and is driven by different stimuli such as reactive oxygen species (ROS). We recently have shown that the ROS scavenger N-acetylcysteine is capable of suppressing acute and chronic delayed type hypersensitivity reactions (DTHR). The aim of this study was to uncover the temporal dynamics of ROS stress and NF-kB-activation during both acute and chronic DTHR.

C57BL/6 wild-type mice and C57BL/6 NF-kB-luciferase-reporter mice were sensitized at the abdomen with 5% trinitrochlorobenzene (TNCB) and challenged at the right ear seven days later with 1% TNCB to elicit acute DTHR. To induce chronic DTHR mice were repetitively TNCB-challenged every 48h for up to five times. We measured the ear thickness (ET) and performed *in vivo* optical imaging (OI) at 4h, 12h and 24h after the 1^{st}, 3^{rd} and 5^{th} challenge. To measure *in vivo* NF-kB-activation we injected luciferin *i.p.* into NF-kB-luciferase-reporter mice 5 min before *in vivo* OI. For *in vivo* ROS-detection we injected C57BL/6 mice with L-012 *i.p.* 5 min before OI. Additionally we performed H&E histology of inflamed ears and RT-PCR analysis of ROS-driven (hemoxygenase-1 HO-1) and NF-kB-driven (IL-1β, IL-6) genes.

Despite an increase in ET of 50±18 µm 4h after the 1^{st} challenge (acute DTHR) we could not detect ROS-stress or NF-kB-activity. In contrast, we observed strong ROS-stress and NF-kB-activity accompanied with an increase in ET of 80±16 µm after 12h. ROS-stress reached its maximum 12h after the 1^{st} challenge and decreased to 50% after 24h while the ET further increased another 71±12 µm. NF-kB-activity reached a maximum at 12h and remained at a similar level until 24h after the 1^{st} challenge. Contrary to acute DTHR, we detected a strongly enhanced ROS-stress and NF-kB-activity already 4h after the 3^{rd} challenge. The highest NF-kB-activity was determined 12h after the 3^{rd} challenge followed by a decrease (to 50%) after 24h, while the ET further increased (+63±25 µm) 24h after the 3^{rd} challenge. ROS-stress remained at a similar level until 12h and dropped down to 20% at 24h. After five challenges ROS-stress and NF-kB-activity peaked at 12h while the strongest increase in ET was measured 4h after the 5^{th} challenge (30±20 µm).

Whereas NF-kB-activity increased two-fold from acute to chronic DTHR, we found no differences in the maximum ROS-stress levels between acute and chronic DTHR. H&E histology revealed strong edema and was dominated by neutrophils during acute DTHR and tissue remodelling, angiogenesis and a dense leukocyte infiltrate during chronic DTHR. Even 4h after 1^{st} challenge we detected enhanced HO-1 mRNA expression values followed by a slight increase after the 3^{rd} challenge. We measured a slight increase in IL-1β and IL-6 mRNA expression after the 1^{st} challenge, an impressive increase after the 3^{rd} challenge followed by a decrease after the 5^{th} challenge.

In vivo OI uncovered that ROS and NF-kB yield different expression patterns and temporal dynamics during acute and chronic DTHR. This knowledge is a basic prerequisite for unraveling new windows of opportunity for innovative treatment approaches in T-cell dependent DTHR, like rheumatoid arthritis.

AUTHORS (LAST NAME, FIRST NAME): Schwenck, Johannes[2, 1]; Thaiss, Wolfgang M.[2, 3]; Schörg, Barbara F.[2]; Fuchs, Kerstin[4]; Griessinger, Christoph[2]; Mucha, Natalie[2]; Bukala, Daniel[2]; Brück, Jürgen[5]; Carlsen, Harald[6]; Röcken, Martin[5]; Pichler, Bernd J.[2]; Kneilling, Manfred[4, 5]

INSTITUTIONS (ALL):

1. Department of Nuclear Medicine, Eberhard Karls University Tübingen, Tübingen, Germany.
2. Werner Siemens Imaging Center, Department of Preclinical Imaging and Radiopharmacy, Eberhard Karls University Tübingen, Tübingen, Germany.
3. Department of Diagnostic and Interventional Radiology, Eberhard Karls University Tübingen, Tübingen, Germany.
4. Werner Siemens Imaging Center, Department of Preclinical Imaging and Radiopharmacy, Eberhard Karls University Tübingen, Tübingen, Germany.
5. Department of Dermatology, Eberhard Karls University Tübingen, Tübingen, Germany.
6. Department of Chemistry, Biotechnology and Food Science, Norwegian University of Life Sciences, Ås, Norway.

(No Image Selected)

CONTROL ID: 2231721

TITLE: Comparison of specific ^{68}Ga-labelled PSMA-ligand and ^{11}C-Choline in the detection of metastasis from primary and recurrent prostate cancer by PET/CT

PRESENTER: Johannes Schwenck

ABSTRACT BODY:

Abstract Body: Prostate specific membrane antigen (PSMA) is a carboxypeptidase which is considered to be expressed ubiquitously on the membrane of prostate tumors and its metastasis. While PET/CT using ^{11}C-choline was considered as the gold standard in the staging of prostate cancer, recently PET with radiolabelled PSMA-ligands was introduced into the clinic. Our aim was to compare the PSMA-ligand ^{68}Ga-HBED-CC-PSMA (^{68}Ga-PSMA) with ^{11}C-choline in the detection of metastases from primary and recurrent prostate cancer.

In total, 68 patients underwent a whole body PET/CT examination 60 min p.i. of 165±14 MBq ^{68}Ga-PSMA as well as 5 min p.i. of 624±25 MBq ^{11}C-choline on the same day. For the latter, additional pelvic images were acquired 20 min p.i. Suspicious lesions were evaluated visually and semiquantitatively (SUVavg). Out of these 68 patients, 55 suffered from a confirmed biochemical relapse after prostatectomy and/or radiotherapy (mean PSA level of 4.5 ng/ml), while 13 patients underwent primary staging.

In 38 patients, we detected lymph nodes suspicious for metastasis. PET using ^{68}Ga- PSMA showed a SUVavg of 11.4 in these lymph nodes, which was significantly higher than in ^{11}C-choline-PET (SUVavg 4.0). Consequently, the detection rate was higher in the ^{68}Ga-PSMA-PET (87%) as compared to ^{11}C-choline (74%).

In patients with primary cancer, the detection rate of ^{68}Ga-PSMA-PET was 91%, while in patients suffering from biochemical relapse we observed a detection rate of 84%. The lymph nodes which were detected additionally in ^{68}Ga-PSMA-PET showed an average size of 6.5 mm and were significantly smaller than the detected ^{11}C-choline-positive lymph nodes (11.4 mm). Interestingly, we found 7% of the patients with only ^{68}Ga-PSMA-positive and 4% patients with only ^{11}C-choline-positive lymph nodes. In 12% of the patients, both tracers discovered additional regions (pararectal/praesacral, iliacal, paraaortal) with suspicious lymph nodes, which were only positive for one of the tracers.

In 17 patients, we revealed bone lesions suspicious for prostate cancer metastasis. In the PET examinations using ^{68}Ga-PSMA, the bone lesions showed a significantly higher uptake (14% vs 6%) and as a consequence a detection rate which was superior to ^{11}C-choline-PET (96% vs. 74%). In patients with primary tumors, the detection rate for ^{68}Ga-PSMA-PET turned out to be higher than in biochemical relapse (98% vs. 94%). In 3% of the patients, we found only ^{68}Ga-PSMA-positive bone lesions, while 1% of the patients had only ^{11}C-choline-positive bone lesions. One patient with primary prostate cancer showed exclusively ^{68}Ga-PSMA-positive lesions, while among the patients with biochemical relapse, one patient with solely ^{68}Ga-PSMA-positive and one with only ^{11}C-choline-positive lesions was detected.

PET using ^{68}Ga-PSMA showed a higher detection rate than ^{11}C-choline-PET for lymph nodes as well as bone lesions. Especially for small lymph nodes we could show clear advantages of the PSMA-ligand ^{68}Ga-PSMA. However, we found lymph nodes and bone lesions which were not concordant applying both tracers. Further studies are needed to clarify the characteristics of these findings.

AUTHORS (LAST NAME, FIRST NAME): Schwenck, Johannes[4, 1]; Rempp, Hansjoerg[2]; Reischl, Gerald[3]; Nikolaou, Konstantin[2]; Pfannenberg, Christina[2]; la Fougere, Christian[4]

INSTITUTIONS (ALL):

1. Werner Siemens Imaging Center, Department of Preclinical Imaging and Radiopharmacy, Eberhard Karls University Tübingen, Tübingen, Germany.
2. Department of Diagnostic and Interventional Radiology, Eberhard Karls University Tübingen, Tübingen, Germany.
3. Department of Preclinical Imaging and Radiopharmacy, Eberhard Karls University Tübingen, Tübingen, Germany.
4. Department of Nuclear Medicine, Eberhard Karls University Tübingen, Tübingen, Germany.

(No Image Selected)

CONTROL ID: 2231704

TITLE: A PET/MR study of cartilage-bone interactions in osteoarthritis using $T_{1\rho}$ dispersion

PRESENTER: Dragana Savic

ABSTRACT BODY:

Abstract Body: Purpose: Osteoarthritis (OA) is a degenerative cartilage disease leading to pain and disability. Quantitative MRI techniques are in development to detect OA as early as possible. $T_{1\rho}$ imaging detects proton exchange between water and macromolecules such as glycosaminoglycans (GAG), which degrade in the early stages of OA[1]. $T_{1\rho}$ increases as spinlock frequency (FSL) increases, giving a $T_{1\rho}$ dispersion curve as a function of FSL. $R_{1\rho}$ ($1/T_{1\rho}$) dispersion can provide information about chemical and diffusive exchange in tissue[2]. ^{18}F sodium fluoride (NaF) is used to assess subchondral bone remodeling in OA. Here we hypothesize that $T_{1\rho}$ and $R_{1\rho}$ dispersion curves will be associated with NaF uptake and patient-reported metrics of function and pain.

Methods: Eight patients with KL scores 0-3 were imaged on a 3T PET/MRI. The MR sequences included quantitative combined $T_{1\rho}/T_2$ with: $T_{1\rho}$ TSL = 0/10/40/80 ms, FSL = 200 and 500 Hz, T_2 preparation TE = 0/12.87/25.69/51.39 ms (equivalent to FSL = 0 Hz). 10mCi of NaF was IV administered at scan onset, and PET was acquired in LIST dynamic mode for 60 minutes. Patients completed the Knee Osteoarthritis Outcome Score (KOOS) questionnaire on the scan day. Slopes of $R_{1\rho}$ between 0-200 Hz and 200-500 Hz were calculated for each knee compartment in all patients (MT, LT, MFC, LFC, TRO, PAT). Standardized uptake values (SUV; bw-g/ml) were examined in bone regions adjacent to cartilage.

Results: $T_{1\rho}$ relaxation times at 500 Hz in the patella were correlated with patient-reported stiffness (WOMAC, r =-0.889, p=0.007) and pain (KOOS, r=-0.712, p=0.072; WOMAC, r=-0.686, p=0.089). Dispersion was observed for all patients as FSL increased from 0 to 500 Hz. For all patients, $T_{1\rho}$ and $R_{1\rho}$ slopes were higher between 0-200 Hz than between 200-500 Hz. Dispersion curve shapes were variable between patients of the same KL grade and the same reported pain. For each patient, dispersion varied in different compartments. The medial tibia, femur and the lateral femur cartilage showed similar dispersion that differed from the patella, trochlea and lateral tibia. Averaged across all patients, the greatest $R_{1\rho}$ slopes and the least NaF uptake were observed in the patella and trochlea. The patient with the greatest observed dispersion averaged across all compartments also had the highest reported pain.

Conclusions: $T_{1\rho}$ dispersion has been observed using three frequencies on a PET/MR scanner. These observations depend on low-frequency $T_{1\rho}$ quantification and would not have been apparent with just T_2 and $T_{1\rho}$ imaging at 500 Hz. The dispersion observed in all patients indicates exchanging protons possibly related to GAG degradation. The dispersion does not seem to be associated with KL grade, and relationship to patient-reported pain is uncertain, implying that early OA may not be well-represented by these metrics. Our study suggests a relationship between NaF uptake and dispersion. Additional testing of intermediate FSL and more patients may provide specific biomarkers to differentiate tissue characteristics in OA.

[1] Li X and Majumdar S, *J Magn Reson Imaging* 2013, 38(5) 991-1008.

[2] Wang P, et al. *Magn Reson Imaging* 2015, 33(1) 38-42.

AUTHORS (LAST NAME, FIRST NAME): Mazur, Courtney M.[2]; Savic, Dragana[1]; Pedoia, Valentina[1]; Venkatachari, Anand K.[1]; Seo, Youngho[1, 2]; Franc, Benjamin L.[1]; Majumdar, Sharmila[1, 2]

INSTITUTIONS (ALL):

1. Radiology and Biomedical Imaging, University of California, San Francisco, San Francisco, CA, United States.
2. UC Berkeley and UC San Francisco Graduate Program in Bioengineering, San Francisco, CA, United States.

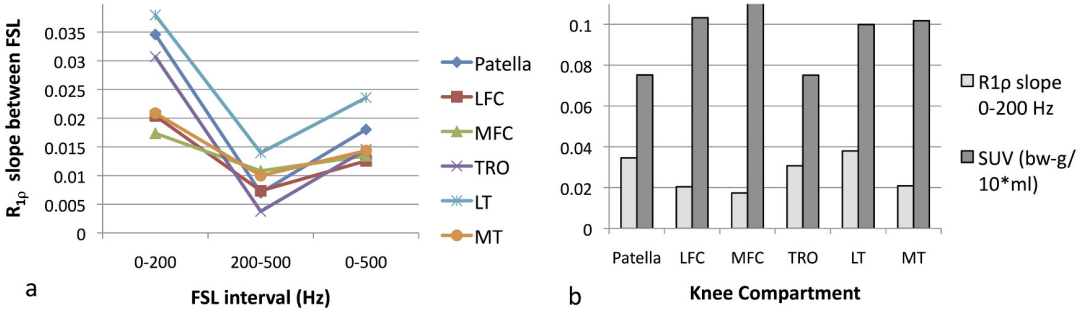

a) Absolute value of slope of the $R_{1\rho}$ dispersion curve between each of the FSL investigated. Slopes were calculated from the average $R_{1\rho}$ of 8 patients in each compartment. b) The slope of the $R_{1\rho}$ dispersion between 0-200 Hz and the NaF uptake varied between patients and compartments. Averaged across all patients, the greatest $R_{1\rho}$ slopes were observed in the compartments with the least NaF uptake.

CONTROL ID: 2231705

TITLE: Multiplexed transfer of immune genes into an allogeneic transplant model and in vivo screening by bioluminescence imaging demonstrates short-term protection from acute rejection

PRESENTER: Michael Bachmann

ABSTRACT BODY:

Abstract Body: Transplantation of MHC-mismatched cells and organs triggers a powerful immune response in the recipient that requires therapy with potent immunosuppressive drugs to prevent graft rejection. While drug regimens for protecting allogeneic transplants have been greatly improved over the last four decades, the generalized immunosuppression still carries systemic risks, such as infection and cancer. Surprisingly, in rare allograft recipients who cease immunosuppressive therapy, the rejection reaction fails to develop for unclear reasons, giving rise to a metastable state of "operational transplant tolerance" (OTT). We are therefore seeking to emulate OTT by genetically modifying cell and tissue grafts so that these are no longer rejected but become locally tolerated over long periods of time.

While some of the genes and signaling pathways involved in transplant tolerance are already known and well studied, the full identity and complex nature of the genetic network responsible for graft tolerance remain unresolved. To address this we have developed a multiplexed, non-viral gene transfer and in vivo analysis approach using bioluminescent mouse models of human transplantation. NIH3T3 fibroblasts (MHC H-2^q) are modified with up to five *Sleeping Beauty* transposon vectors to express a) combinations of cDNAs that encode immunomodulatory proteins, and b) firefly luciferase to non-invasively monitor cell survival in vivo with bioluminescence imaging (BLI). 1 million gene modified cells are injected s.c. into each Balb/c mouse (H-2^d) and periodically assessed by BLI. Bioluminescent control NIH3T3 cells modified with empty vectors steadily decline in numbers and are eliminated within 8-14 days. Transfer of single genes (encoding murine TGFb, IL4, SDF1, and IDO1), and transfer of eight genes (TGFb, IL4, IL10, IL1RN, SDF1, CCL17, IDO1, and CD47) in two vectors did not extend cell survival significantly beyond that of control cells. However, multiplexed transfer of fourteen genes in three transposon vectors (previous eleven plus Timp3, FasL, PD-L1, B7-H4, and human Galectin-1) blocked the immediate cell depletion and extended the survival of the transplanted cells for a brief but statistically significant time period (mean survival: p=0.0124, area under the curve: p=0.0068). While this extension is insufficient for clinical translation and the minimally necessary combination needs to be defined, the result represents the first milestone in a multi-step process of uncovering the complex, cooperative gene network that can shift the immune response away from transplant rejection towards localized long-term tolerance without life-long, drug-mediated immunosuppression.

AUTHORS (LAST NAME, FIRST NAME): Bachmann, Michael H.[1]; Kusy, Sophie[1]; Wey, Winston[1]; Creusot, Remi[3, 4]; Roedder, Silke[7, 1]; Wilber, Andrew[5, 6]; McIvor, R. Scott[6]; Sarwal, Minnie[7, 1]; Fathman, Garrison[4]; Contag, Christopher H.[2]

INSTITUTIONS (ALL):

1. Pediatrics, Stanford University, Stanford, CA, United States.
2. Pediatrics, Stanford Universtiy, Stanford, CA, United States.
3. Columbia Center for Translational Immunology, Columbia University, New York, NY, United States.
4. Dept. of Medicine, Division of Immunology and Rheumatology, Stanford University, Stanford, CA, United States.
5. Department of Medical Microbiology, Immunology and Cell Biology, Southern Illinois University School of Medicine, Springfield, IL, United States.
6. Dept. of Genetics, Cell Biology and Development, University of Minnesota School of Medicine, Minneapolis, MN, United States.
7. Division of Multi Organ Transplantation, Department of Surgery, University of California San Francisco, San Francisco, CA, United States.

(No Image Selected)

CONTROL ID: 2231739

TITLE: Indocyanine green-embedded Nanoparticles as Novel Photoacoustic and Fluorescent Contrast Agents

PRESENTER: Yuanhui Song

ABSTRACT BODY:

Abstract Body: Introduction: Photoacoustic imaging (PAI) is a non-invasive and nonionizing imaging modality relying on the photoacoustic effect. PAI provides high detection sensitivity and high spatial and temporal resolution which are at least an order of magnitude below traditional cell imaging techniques. However, the utilization of this potential imaging technology is greatly limited by the lack of PAI contrast agents, particularly activatable PAI probes. Indocyanine green (ICG) is an FDA-approved tricarbocyanine dye with strong absorbance in the near infrared (NIR) region, which has been extensively used for fluorescence imaging in vivo. Herein, we introduce a poly(butyl cyanoacrylate) (PBCA) nanoparticle-based nanocarrier that was particularly designed to carry the negatively charged ICG molecules and used as contrast agents for molecular photoacoustic imaging. **Methods:** 1% (v/v) butyl cyanoacrylate monomer and ICG was added slowly dropwise to a 1% (w/v) solution of dextran 70,000 in 0.001 M HCl (pH 3). This mixture was stirred for 4 h with a magnetic stirrer to promote polymerizationat room temperature. Afterwards the polymerization was completed by neutralization of the mixture with 1 N sodium hydroxide. The polymerized PBCA nanoparticles were separated from residual monomers by centrifugation. The particle size distribution and zeta potential was evaluated using Malvern Zetasizer, and the surface tomography was characterized using SEM and TEM. Endra Nexus 128 small animal imaging system was employed to capture the multi-wavelength photoacoustic and fluroscent images. **Results:** ICG-embedded PBCA nanoparticles can be successfully fabricated using emulsion method. These hybrid nanoparticals exhibits a narrow size distribution of 272 nm (Pdi=0.016) in diameter, and zeta potential of approximately -5.98mV. The SEM and TEM images showed an uniform smooth sphere morphology. The contrast agents shows awavelength-dependent photoacoustic signal, and the signal intensity irradiated at 805nm is slightly stronger than that at 680nm, which indicates that ICG-embedded PBCA nanoparticles can be used as a new class of PA contrast agents (Figure 1). **Conclusions:** We have successfully developed a ICG-embedded PBCA based contrast agents and used to demonstrate proof-of-principle, non-invasive multiplex PAI *in vitro*. The fabricated contrast agents exhibited good aqueous stability and remarkable optical absorption in near-infrared wavelengths, and could provide excellent photoacoustic signals *in vitro*, which shows the potential application to the stem cell labeling and tracing. **Acknowledgment:** This work was financially supported by Scientific Research Foundation for Returned Scholars, Ministry of Education of China and Start-up funding of Wenzhou Institute of Biomaterials and Engineering (Grant.WIBEZD2014005-02, WIBEZD2014005-04).

AUTHORS (LAST NAME, FIRST NAME): Song, Yuanhui[1]; Shi, Changcan[1]; Li, Yihong[1]; Wang, Jie[1]; Liu, Zhe[1]

INSTITUTIONS (ALL):

1. Wenzhou Institute of Biomaterials and Engineering, Chinese Academy of Sciences, Wenzhou, Zhejiang, China.

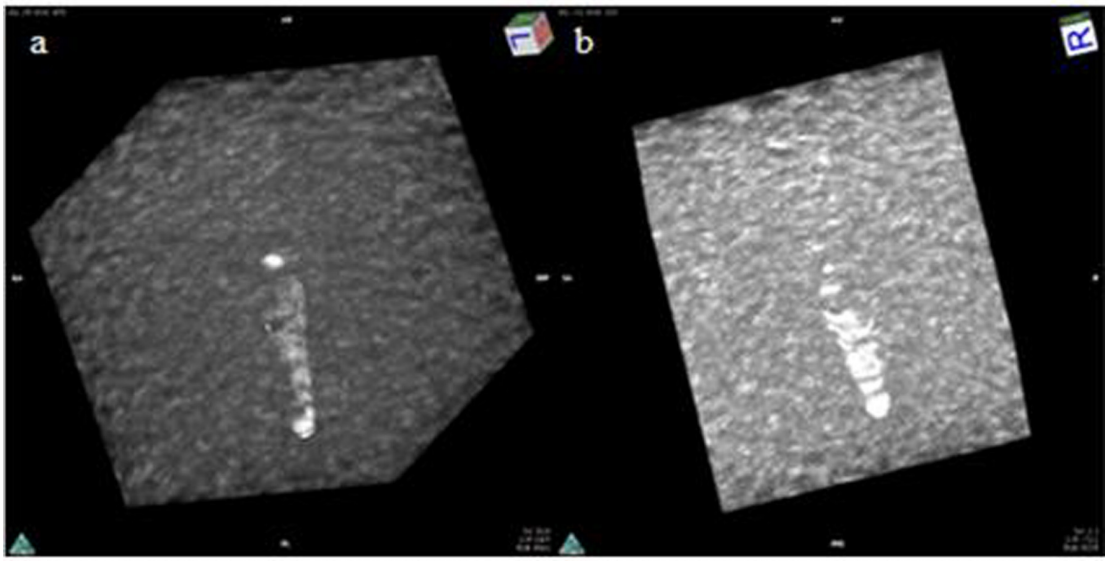

Figure 1. PA imaging of ICG-embedded PBCA nanoparticles at different irradiation wavelength: a) 680nm, b) 805nm.

CONTROL ID: 2231731

TITLE: In vivo Kinetics PET/CT Imaging of Angiogenesis by ^{68}Ga-NOTA-PRGD2 Probe in Porcine Heart post Myocardial Infarction

PRESENTER: Bo Tao

ABSTRACT BODY:

Abstract Body: Objectives: The $\alpha_v\beta_3$ integrin represents as a promising target for noninvasive imaging for angiogenesis. This study is designed to investigate the dynamic angiogenesis formation in porcine infarcted heart tracking by $\alpha_v\beta_3$ targeted positron emission tomography (PET) probe. (^{68}Ga-NOTA-PRGD2)

Methods: Acute myocardial infarction (AMI) in ten minipigs weighing between 25 and 30 kilograms were established by double embolization containing half angioplasty balloon and sponge block in left anterior descending coronary. Myocardial infarction was confirmed by electrocardiogram, echocardiography and ^{18}F-fluorodeoxyglucose (FDG) PET/CT imaging pre-MI and post-MI. Before PET/CT scan, minipigs were intravenously injected with ^{68}Ga-NOTA-PRGD2 solution at the dose of approximately 1.85 MBq (0.05 mCi) per kilogram body weight. Cardiac PET/CT scan was performed to evaluate the standard uptake value (SUV) of region of interest (ROI) with ^{68}Ga-NOTA-PRGD2 at pre-MI , 3 days, 1 week, 3 weeks, 6 weeks, 12 weeks and 24 weeks post operation. Syngo MI software and MIM 6.4 software were used to analyze the single and series plane imaging results respectively. Contralateral myocardium was considered as non ROI.

Results: 8 out of 10 minipigs underwent the MI operation alived. Patchy ^{68}Ga-NOTA-PRGD2 uptake occurring in the ischemic regions around the apical and septal myocardial infarction region was demonstrated by ^{18}F-FDG PET/CT imaging. The regional accumulation of ^{68}Ga-NOTA-PRGD2 can be detected at 3 days (0.78 ± 0.23 vs. 0.47 ± 0.19, $p < 0.05$) and peaked between 1 and 3 weeks (1.01 ± 0.32 vs. 0.59 ± 0.25, $p < 0.05$ and 1.55 ± 0.30 vs. 0.91 ± 0.25, $p < 0.01$, respectively). The focal accumulation decreased but still kept at a higher level at 6 weeks and 12 weeks post operation (0.86 ± 0.28 vs. 0.50 ± 0.25, $p < 0.05$ and 0.80 ± 0.29 vs. 0.43 ± 0.22, $p < 0.05$). Until 24 weeks post operation, the standard uptake value of ROI were still higher than non ROI, but statistical difference were not found (0.59±0.17 vs 0.41±0.19, $p>0.05$).Meanwhile, SUVmax in single plane, SUVmean and SUVmax in series plane remained the same trend. In addition, the volume of ROI presented dynamic changes and peaked at the time point of 3 weeks post-operation, with the value of 7.00 ± 1.05 cubic centimeter.

Conclusion: PET imaging of ^{68}Ga-NOTA-PRGD2 can be applied to noninvasive visualization of longitudinal myocardial angiogenesis after infarction, which could be used to evaluate the efficacy of revascularization therapy in chronic occlusive cardiovascular diseases.

AUTHORS (LAST NAME, FIRST NAME): Tao, Bo[2]; Gao, Haokao[2]; Ma, Sai[2]; Fan, Miaomiao[2]; Luo, Zhenli[2]; Wang, Shengjun[4]; Liang, Jimin[3]; Wang, Jing[4]; Cao, Feng[1]

INSTITUTIONS (ALL):

1. Cardiology, Chinese PLA General Hospital, Beijing, China.
2. Cardiology, Xijing Hospital , Xi'an, Shaanxi, China.
3. School of Life, Xidian University, Xi'an, shaanxi, China.
4. Nuclear Medicine , Xijing Hospital, Xi’an, Shaanxi, China.

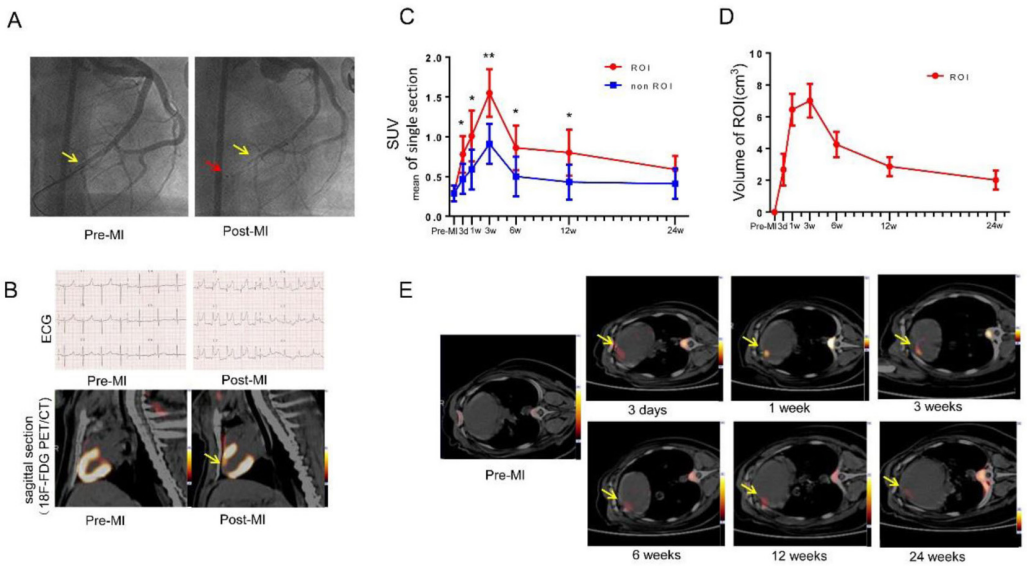

Figure:(A)Selective CAG determines the location of embolism (pre-MI, yellow arrow).Blood flow is completely blocked after double embolism of the distal LAD coronary artery, while the blood flow of second diagonal branch is still normal and clear (post-MI, yellow arrow). The red arrow indicates the location of distal part of embolized half balloon and sponge block. (B) 12-lead ECG confirm ST segment sharp elevation of anterior wall leads. Hybrid imaging of ^{18}F-FDG PET/CT. The apical and septal myocardial infarction is indicated by yellow arrow. (C-D) Semi-quantitative analysis of SUV_{mean} in single plane and volume of ROI of series plane. (*$p<0.05$; **$p<0.01$). (E)Representative ^{68}Ga-NOTA-PRGD2 PET/CT images of one minipig at different times.Patchy uptake occurs in the ischemic regions around the apical and septal myocardial infarction region demonstrated by^{18}F-FDG PET/CT imaging.Yellow arrows indicate the location of ROI and the accumulation of uptake present dynamic changes in different phases.

CONTROL ID: 2231766

TITLE: Molecular imaging of atherosclerotic plaque *via* osteopontin targeted Cy5.5 labeled Fe_3O_4 magnetic nanoparticle probe

PRESENTER: HongYu Qiao

ABSTRACT BODY:

Abstract Body: Background

Rupture of vulnerable atherosclerotic plaque is the principal pathological cause of luminal thrombosis in acute coronary syndromes including the cardiac arrest. Lots of studies showed that macrophage infiltration in vulnerable plaque was almost 4-fold higher than that in stable plaque. Osteopontin (OPN), an extracellular matrix protein, can promote the adhesion, migration and activation of macrophages that have been identified as prominent components of human atherosclerotic lesions. This study is to construct a novel osteopontin targeted nanoparticle conjugated Cy5.5 covalently in series to monitor atherosclerotic plaque *via* noninvasive molecular imaging.

Methods

OPN antibody and Cy5.5 dye were conjugated to DMSA-MNPs by carboxyl and amine condensation. The probe was characterized by transmission electron microscopy (TEM) and dynamic light scattering (DLS) respectively. Twenty C57BL/6J $ApoE^{-/-}$ mice were fed with high fat diet for 16 weeks. Fluorescence signals were detected using Xenogen In Vivo Imaging System at 24h, 48h, 72h after tail vein injection of the probe respectively and MRI was performed before and after the probe was injected. Prussian blue staining was applied to confirm the localization of MNPs *ex vivo.*

Results

Atherosclerotic lesions in the abdominal aorta of $ApoE^{-/-}$ mice were confirmed by oil red histological staining. The TEM image showed that DMSA-MNPs were well dispersed. The mean hydrodynamic size of DMSA-MNPs was 26.8 nm, while anti-OPN-DMSA-MNPs was 30.1 nm. *In vivo* fluorescence imaging revealed that after the OPN antibody conjugated DMSA-MNPs injection, the area of atherosclerotic plaques in carotid and aortic arch exhibited significant higher signals in model mice in comparison with control group. *In vivo* 7.0T MRI demonstrated that after anti-OPN-DMSA-MNPs injection, the area of atherosclerotic plaque in carotid and aortic arch exhibited lower T2 signal intensity. Histology of Prussian blue confirmed that anti-OPN-DMSA-MNPs mainly localized in the atherosclerotic plaques.

Conclusion

As a novel molecular imaging probe, OPN antibody labeled DMSA-MNPs provides potential for noninvasive monitoring of atherosclerotic plaque targeted macrophage *in vivo.*

AUTHORS (LAST NAME, FIRST NAME): Qiao, HongYu[2]; Qiao, Ruirui[3]; Wang, Yabin[4]; Huang, Xu[1]; Zhang, Yan[1]; Gao, Mingyuan[3]; Cao, Feng[1, 2]

INSTITUTIONS (ALL):

1. Cardiology, Chinese PLA General Hospital, Beijing, China.
2. Cardiology, Xijing Hospital, Xi'an, Shaanxi, China, Xi'an, Shannxi, China.
3. Institute of Chemistry, Chinese Academy of Sciences, Bei Yi Jie 2, Zhong Guan Cun, Beijing, China.
4. Xijing Hospital, Xi'an, Shaanxi, China, Xi'an, Shaanxi, China.

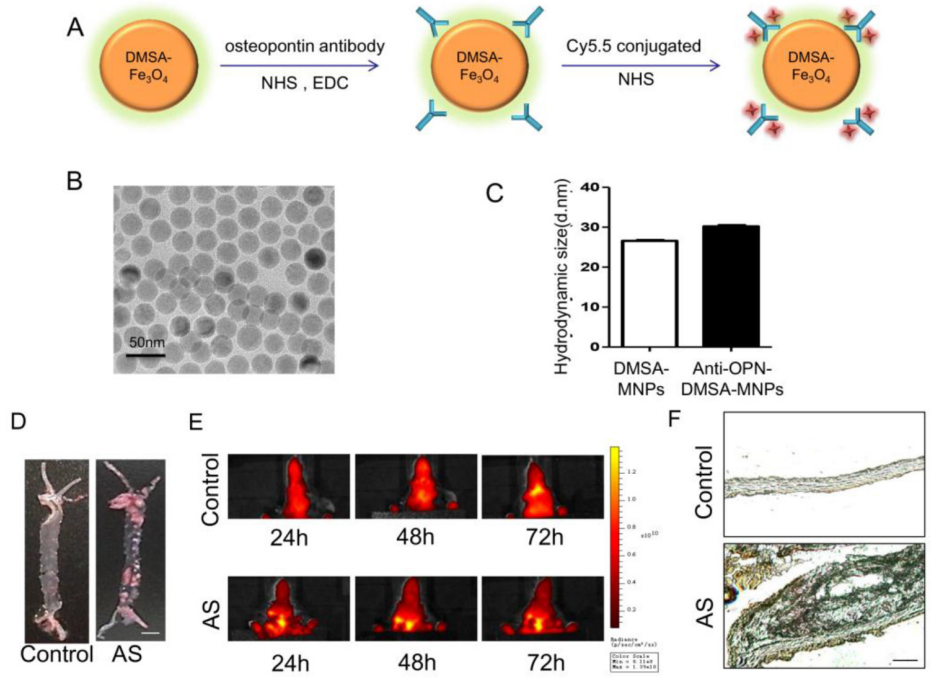

Figure: Characterization of anti-OPN-DMSA-MNPs, in vivo fluorescence imaging studies and histological staining of atherosclerotic plaques.

A. Schematic process of OPN antibody and activated Cy5.5 conjugated to DMSA-MNPs; B. Transmission electron microscopy (TEM) image of anti-OPN-DMSA-MNPs, bar=50nm; C. Hydrodynamic size of DMSA-MNPs and anti-OPN-DMSA-MNPs. D. Oil red staining of arties of control group and atherosclerosis group; E. In vivo fluorescence imaging of control and atherosclerosis groups respectively, bar=100μm; F. Prussian blue staining of arteries of control and atherosclerosis groups ex vivo respectively, bar=10μm.

CONTROL ID: 2231725

TITLE: Highly specific inflammation detection using activatable fluorescent nanoprobes

PRESENTER: Adah Almutairi

ABSTRACT BODY:

Abstract Body: Conventional fluorescence imaging agents are “always on,” resulting in low target-to-background signal ratios. Although activatable probes promise to overcome this limitation, most consist of small molecules, whose low sensitivity and specificity limit signal activation and rapid clearance from the circulation limits the time available for imaging. To create an inflammation-detecting agent with much greater on-off signal ratios and longer circulation time, we designed activatable fluorescent nanoprobes that would allow simultaneous activation of many dye molecules upon encountering reactive species present at higher than normal levels in inflamed tissue, specifically H^+ and H_2O_2. As packing many dye molecules within a nanoparticle quenches their fluorescence, we encapsulated the infrared dye IR780 at high concentrations in nanoparticles composed of dextran modified with acid- and H_2O_2-hydrolyzable groups (specifically acetals and aryl boronic esters). These modifications make the carbohydrate polymer more hydrophobic, allowing formulation into nanoparticles; cleavage of the triggering groups by H^+ and H_2O_2 increases hydrophilicity. In intact particles, IR780 fluorescence is mostly quenched because of close proximity among dye molecules, but upon solubilization, they spread farther apart and their fluorescence is activated. Though IR780 does fluoresce slightly within particles, this signal is red-shifted relative to the signal from free dye molecules (825 nm vs. 790 nm), allowing spectral unmixing of ‘off’ and ‘on’ signals.

We investigated whether these inflammation-activated fluorescent nanoprobes allow detection of disease in three settings: subcutaneous human breast tumor grafts, the K/BxN serum-transfer model of arthritis, and lipopolysaccharide-induced paw edema (all in mice). Spectral unmixing yielded disease-specific ‘on’ signal in tumors, arthritic paws, and inflamed paws, with negligible background in organs where nanoparticles accumulate (liver, spleen) or are cleared (kidneys).

Given its high specificity, this system promises clinical relevance in detection of inflammatory conditions at subclinical stages. We are currently examining whether it allows visualization of low-grade inflammation. This principle could be extended to activation of MRI signal upon development of extremely high-relaxivity Gd nanoparticles that could be silenced within hydrophobic assemblies.

AUTHORS (LAST NAME, FIRST NAME): Viger, Mathieu L.[1]; Lux, Jacques[1]; Collet, Guillaume[1]; Nguyen Huu, Viet Anh[1]; Guma, Monica[1]; Garcia, Arnold[1]; Bartok, Beatrix[1]; Firestein, Gary[1]; Almutairi, Adah[1]

INSTITUTIONS (ALL):

1. UC San Diego, La Jolla, CA, United States.

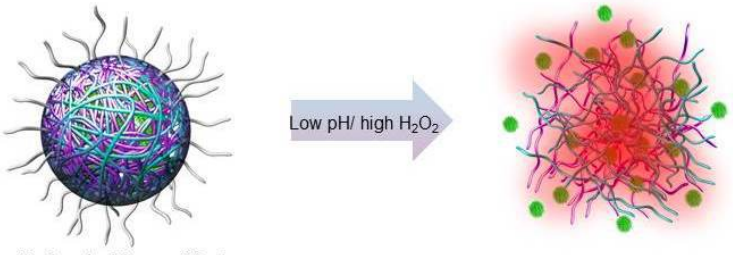

Hydrophobic modified dextran
'OFF' state

Hydrophilic dextran
'ON' state

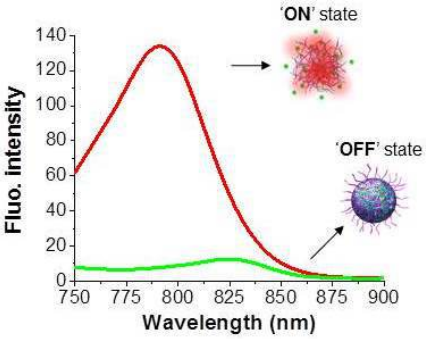

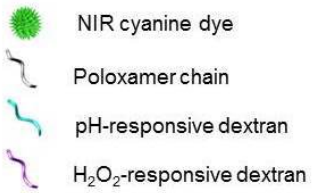

pH- and H_2O_2-responsive polymeric materials control the activity and spectral profile of multiple NIR fluorescent contrast agents. Above, schematic; below, emission spectra of free IR780 ('on' state) and non-activated responsive nanoprobes ('off' state).

CONTROL ID: 2231718

TITLE: Radiolabeling of functionalized pyrazoles on the heteroaromatic moiety: potential PET agents for imaging of COX-2 expression.

PRESENTER: Artem Lebedev

ABSTRACT BODY:

Abstract Body: Background: Several attempts at developing ^{18}F labeled COX-2 imaging agents were reported in the literature[1]. All of them relied on classic SN2 reactions of organic precursors with radioactive ^{18}F-fluoride. Due to the limitations of existing strategies, fluoride could only be attached to the positions vulnerable to the in vivo degradation.

Results: Recently we reported a method for radiolabeling of aromatic compounds via electrochemical fluorination on platinum electrodes. Building up on this method we developed a method expanding this technique on radiolabeling of functionalized heteroaromatic molecules. The method was used for radiolabeling of previously described[2] COX-2 inhibitor based on substituted arylpyrazole.

To achieve this result, we have developed a precursor suitable for electrochemical radiolabeling (**1**) and utilized it to produce ^{18}F labeled COX-2 inhibitor using an automated set up. Molecule **^{18}F-1** was isolated in a radiochemically pure form. Other radioactive products of the reactions, were also isolated and characterized.

Conclusions: Electrochemical radiofluorination is a method suitable for radiolabeling of heteroaromatic compounds, including pyrazole-based COX-2 inhibitors. In vitro validation and in vivo evaluation of the resulting agents is underway.

Research Support: UCLA Scholars in Oncologic Molecular Imaging program (NIH grant R25T CA098010); ICMIC Developmental Award (NIH grant P50 CA086306).

References: 1) Pacelli, A.; Greenman, J.; Cawthorne, C.; et al Label. Compd. Radiopharm. 2014, 57, 317
2) Penning, T.D.; Talley, J.J.; Bertenshaw, R. et al. Journal of Medicinal Chemistry, 1997, 40(9), 1347-1365

AUTHORS (LAST NAME, FIRST NAME): Lebedev, Artem[1]; Herschman, Harvey[1]; Sadeghi, Sam[1]

INSTITUTIONS (ALL):

1. Molecular Pharmacology, UCLA, Los Angeles, CA, United States.

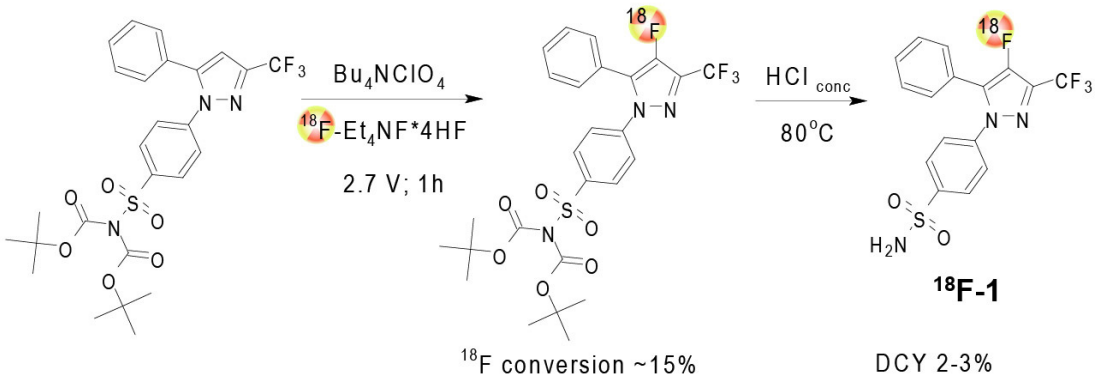
Bu4NClO4
18F-Et4NF*4HF
2.7 V; 1h
HCl conc
80°C
18F conversion ~15%
18F-1
DCY 2-3%

CONTROL ID: 2231737

TITLE: Multifunctional Nanocomplex for Controlled Manipulation and Dynamic Imaging of Sequential mRNA Expression in the Neural Stem Cells Differentiation

PRESENTER: Zhongliang Wang

ABSTRACT BODY:

Abstract Body: Achieving a controlled and reproducible means to direct the stem cell differentiation and simultaneously determine dynamics of mRNA is the most critical concern scientists have been trying to address since the discovery of stem cells. In this regard, we created a multifunctional nanocomplex, which integrated Sox9 siRNA shell as a stimulating unit and a fluorescence probe as core for dynamic imaging of a specific mRNA (**Figure 1a**). This probe is a gold nanoparticle modified with a dense layer of DNA oligonucleotides hybridized with fluorophore-capped 'reporter' sequences. The fluorophore does not fluoresce when it is attached to the gold nanoparticle as a quencher, but it reactivates when it attaches to mRNA. The mRNA competitively hybridizes with the DNA oligonucleotides on the nanocomplex, and it is more attracted to this DNA than are the existing reporter genes. This nanocomplex showed improved enzymatic stability, fast recognition kinetics, and high specificity. Under the stimulation by reducible glutathione, this nanocomplex realized successive stimulating motif (Sox9-siRNA) release and the dynamic imaging of chronological mRNA (*Tubb3* and *Fox3*, **Figure 1c**) expression during neural stem cell differentiation without the use of transgenetic manipulation. Therefore, this nanocomplex not only provides a platform to effectively delivery siRNA molecules into stem cells for genetic manipulation, but also is highly amenable as an alternative tool to explore the dynamics of intricate mRNA activities in various physiological and pathological conditions.

AUTHORS (LAST NAME, FIRST NAME): Wang, Zhongliang[1]

INSTITUTIONS (ALL):

1. School of Life Science and Technology, Xidian University, Xi'an, Shaanxi, China.

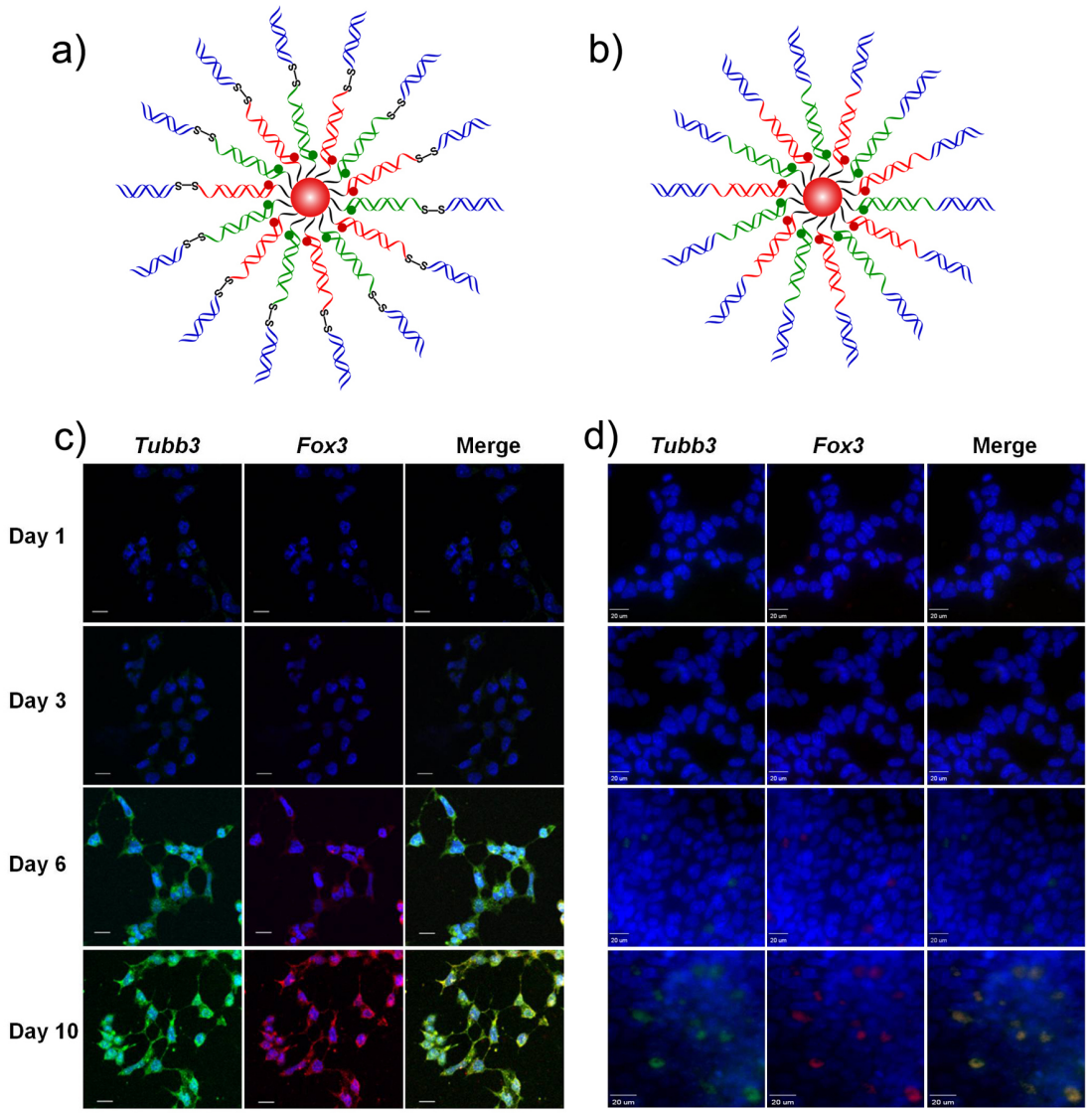
a)
b)
c)
Tubb3
Fox3
Merge
Day 1
Day 3
Day 6
Day 10
d)
Tubb3
Fox3
Merge

CONTROL ID: 2231830

TITLE: In vivo Bioluminescence Imaging (BLI) Tracking of Mesenchymal Stem Cells (MSCs) Survival and Proliferation in Injured Liver

PRESENTER: Dan Li

ABSTRACT BODY:

Abstract Body: Purpose: The purpose of this study was to track the fate of mesenchymal stem cells (MSCs) in mice with acute liver injury using bioluminescence imaging (BLI).

Procedures: Lentivirus was used for stable labeling of MSCs (derived from both mouse and human) with the Luc2-mKate2 dual-fusion reporter gene. 2.5×10^5 MSCs were delivered into liver via the superior mesenteric vein (SMV) in NOD/SCID mice with acute liver injury. Cellular fate was tracked through in vivo BLI.

Results: The percentage of reporter gene labeled MSCs was more than 90% after lentiviral transduction and further fluorescence-activated cell sorting. After SMV infusion, MSCs were dispersedly distributed in the liver. In mice transplanted with mouse MSCs, the liver BLI signal increased with time (1 d – 4 w), which indicated that MSCs was able to proliferate in the injured liver. In mice transplanted with human MSCs, the liver BLI signal declined at first (1 d – 3 w) but increased at late time points (4 w – 16 w), which implied that delivered MSCs were initially cleared by the body and the remaining cells could proliferate in the liver. The in vivo imaging results were further validated by tissue analysis.

Conclusions: Collectively, BLI enables us to noninvasively and dynamically investigate MSCs survival and proliferation in the injured liver. Further studies are needed to explore the relationship between MSCs proliferation and subsequent therapeutic efficacy on injured liver.

Acknowledgments

This work was supported by the National Natural Science Foundation of China (No. U1032002, 81271621) and Key Clinical Research Project of Public Health Ministry of China 2010 – 2012 (No. 164).

AUTHORS (LAST NAME, FIRST NAME): Li, Dan[1]; Li , Zhengran [1]; Shan, Hong[1, 2]

INSTITUTIONS (ALL):

1. Radiology, The Third Affiliated Hospital of Sun Yat-sen University, Guangzhou, Guangdong, China.
2. Interventional Radiology Institute, Sun Yat-sen University, Guangzhou, Guangdong, China.

(No Image Selected)

CONTROL ID: 2231750

TITLE: Using *Mce4* Molecular Beacons for the Detection and Attenuation of Mycobacterial Infection in Macrophages

PRESENTER: REMO GEORGE

ABSTRACT BODY:

Abstract Body: Tuberculosis (TB) continues to pose a significant threat to today's society and is mediated by the pathogen *Mycobacterium tuberculosis* (*Mtb*). The ability of *Mtb* to invade and survive within macrophages of the pulmonary granuloma is attributed to the product of the mammalian cell entry *(mce)* genes whose operon, *mce4*, encodes a cholesterol transporter that helps transport host lipids into the bacterium that allows the bacterium to survive for years during chronic infection. Currently, there are no rapid and reliable tests for the detection and complete eradication of latent TB.

Therefore, we propose and tested the hypothesis that mycobacterial infection in macrophages can be detected and eradicated using short interfering RNA (*siRNA)* molecular beacons against *mce4* operon mRNA.

This hypothesis was tested in U937 cells infected or not infected with *Mycobacterium smegmatis (Ms)* using a microplate reader to detect infection and with *E. coli* expressing *mce4* genes from *Ms (E.Ms)* or with *Ms* itself using invasion assay to measure degree of infection.

Our results showed that *mce4A* conferred the greatest degree of infection to host *E. coli*. Therefore, a *siRNA* molecular beacon was designed against a region of the *mce4A* gene. Using this *mce4A siRNA* molecular beacon our studies showed that this molecular beacon can detect mycobacterial infection in U937 cells that were infected with *Ms* . In addition, our results showed that this *mce4A siRNA* molecular beacon can attenuate infection in macrophages after infecting with *E.coli* expressing *mce4A* gene or *M. smegmatis*. Attenuation of infection was attributed to a decrease in *mce4A* mRNA expression.

In conclusion, our results showed that a *mce4A siRNA* molecular beacon could be designed and used to detect and eradicate mycobacterial infection in macrophages.

AUTHORS (LAST NAME, FIRST NAME): GEORGE, REMO[1]; Bolus, Norman[1]; Waugh, Jonathan B.[2]; Unlap, M T.[3]

INSTITUTIONS (ALL):

1. Nuclear Medicine Technology, Clinical & Diagnostic Sciences, University of Alabama at Birmingham, Birmingham, AL, United States.
2. Respiratory Therapy, Clinical & Diagnostic Sciences, University of Alabama at Birmingham, Birmingham, AL, United States.
3. Biotechnology, Clinical & Diagnostic Sciences, University of Alabama at Birmingham, Birmingham, AL, United States.

(No Image Selected)

CONTROL ID: 2232742

TITLE: Multi-modality patho-physiological imaging of orthotopic glioblastoma in mouse brain

PRESENTER: Chris Jun Hui Ho

ABSTRACT BODY:

Abstract Body: *Aim*: Tumor growth and progression involves a lot of factors (e.g. hypoxia) that promote angiogenesis and thus the growth of tumors. Physiological biomarkers are crucial to understand the response of solid tumor to therapy (RECIST). In this study, a growth evaluation of an orthotopic glioma model was done using Multi Spectral Optoacoustic Tomography (MSOT) and Magnetic resonance imaging (MRI). ***Methods***: Orthotopic model was developed by stereotaxic injection of U87MG glioma cells in the brain of nude mice. MRI and MSOT imaging were done before and after tumor implantation. MRI was acquired on a 7T (Bruker Biospin GmbH) scanner which included T2 weighted fast spin echo imaging for tumor volume and arterial spin labelling (FAIR) based perfusion imaging. MSOT (iThera Medical GmbH) measurements were obtained for the oxy-haemoglobin (HbO2) and deoxy-hemoglobin (Hb) in the infra-red range. ***Results and Discussion***: The orthotopic glioma model had an initial slow growing lag phase (8 days), followed by an exponential growth phase (post-implantation 8 to 20 days; rate of growth = 0.46 mm^3/day) (Figure A). Glioblastoma/astrocytoma tumors are greatly influenced by the oxygenation levels that under hypoxic condition the VEGF/VPF are increased several folds and promotes angiogenesis. MSOT measures showed that during the exponential growth phase Hb levels were higher at the core compared to the rim of the tumor and opposite to the HbO2 levels (Figure B and C). Perfusion MRI revealed low blood flow in the tumor core compared to the rim of the tumor. The oxygenation and perfusion had a very good correspondence across regions (figure E and F). *Conclusion:* The preliminary results show the potential of quantitative imaging of perfusion and Hb/HbO2 with MRI and MSOT, respectively, and their correlation depending on the tumor area inspected. The multimodality approach would provide non-invasive biomarkers for monitoring of tumor growth and response to treatment.

AUTHORS (LAST NAME, FIRST NAME): Chandrasekharan, Prashant[1]; Ho, Chris Jun Hui[1]; Attia, Amalina Binte Ebrahim[1]; Tay, Hui Chien[1]; Balasundaram, Ghayathri[1]; Olivo, Malini[1]; Chuang, Kai Hsiang[1]

INSTITUTIONS (ALL):

1. A*STAR, Singapore Bioimaging Consortium, Singapore, Singapore.

A) Tumor growth curve

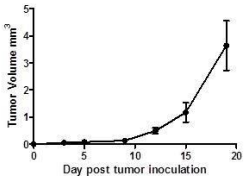

B) Hb/HbT

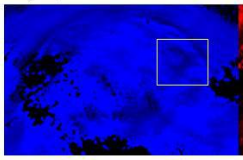

C) HbO2/HbT

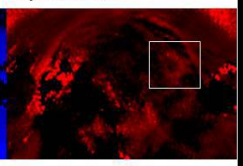

D) Perfusion map

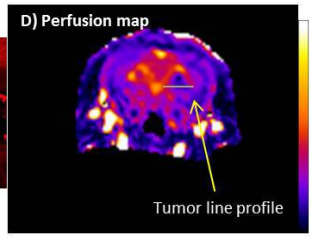

E) Perfusion map over the diameter of tumor

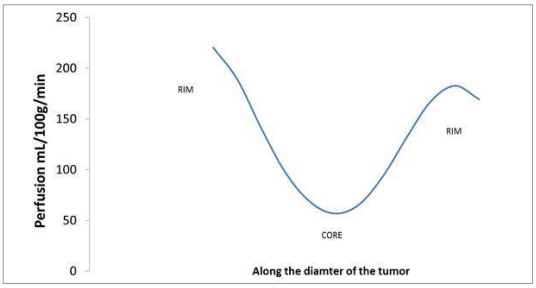

F) Variation of Hb and HbO2/HbT over the diameter of tumor

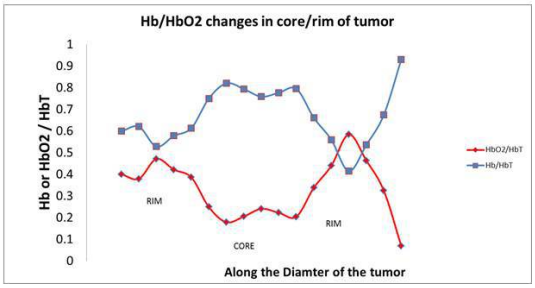

CONTROL ID: 2231759

TITLE: Glutathione Peroxidase 3 (GPx3) suppressed HCC invasiveness through JNK-cJun-MMP2 signaling pathway - Application of in vivo real-time molecular imaging

PRESENTER: Kwan Man

ABSTRACT BODY:

Abstract Body: Objective

Our recent study [1] showed that GPx3 possessed prognostic and therapeutic value in HCC. With the latest development of in vivo imaging modality, it allows us to kinetically observe the process of tumor invasion in a micro-view and directly see the cells in a living animal. We here intended to explore the suppressive role of GPx3 in HCC invasiveness using in vivo imaging platform.

Methods

The correlation of GPx3 expression with tumor recurrence was investigated in a rat orthotopic liver transplantation model and further validated in clinical samples from 106 HCC recipients. The ectopic liver cancer model with dorsal window chamber was established to kinetically observe the effect of GPx3 on tumor invasion using in vivo imaging system. The suppressive effect of GPx3 on lung metastasis was also investigated. The mechanism was further explored.

Results

GPx3 was significantly down-regulated (day1: 33 vs 1147; day3: 3209 vs 4459; day7: 303 vs 2506; mU/mL, $P<0.05$) in the rat with small-for-size graft, which provided favourable micro-environment for tumor recurrence. Consistently, lower plasma GPx3 significantly correlated with more tumor recurrence of HCC patients post-transplantation (day1: 4.16 vs 8.99 μg/mL; day7: 3.86 vs 9.99 μg/mL; $P<0.01$). The lower plasma GPx3 indicated poor overall and disease-free survival outcome. The in vitro study showed that over-expression of GPx3 significantly inhibited wound healing and Matrigel invasion of HCC cells. The in vivo imaging showed that over-expression of GPx3 significantly suppressed the capacity of HCC cells invading into surrounding connective tissues at different time points after tumor established (Fig 1). The lung metastasis was also significantly inhibited upon GPx3 over-expression. The suppressive effect of GPx3 on tumor invasion was mediated through inhibition of JNK-cJun-MMP2 pathway.

Conclusion

GPx3 suppressed HCC invasiveness through JNK-cJun-MMP2 pathway. The in vivo imaging platform provided the direct evidences of tumor behavior in a living animal.

[1] Qi, et al. Oncotarget, 2014

AUTHORS (LAST NAME, FIRST NAME): Qi, Xiang[1]; Man, Kwan[1]

INSTITUTIONS (ALL):

1. Surgery, The University of Hong Kong , Hong Kong, China.

Figure 1. Over-expression of GPx3 suppressed liver tumor invasiveness

CONTROL ID: 2231763

TITLE: A novel PET tracer enabling *in vivo* imaging of poly(ADP ribose) polymerase-1 activity for precision cancer medicine.

PRESENTER: Adam Shuhendler

ABSTRACT BODY:

Abstract Body: Objectives: Poly(ADP ribose) polymerase-1 (PARP-1) is an enzyme that monitors DNA integrity, where PARP-1 activity acts as an intracellular signal selecting between DNA repair or cell death[1]. Therefore PARP-1 enzymatic activity, not protein expression level, is prognostic of both the DNA damage response common to an array of cancer therapies[2], and the utility of PARP-1 inhibition as targeted therapeutic, just approved for human use in 2015[3]. While PARP-1 activity plays a central role in cancer therapy, no biomarker for its activity currently exists. To this end, and towards the goal of precision medicine through imaging, our objective was to develop an ^{18}F-labelled substrate-based PARP-1 activity PET tracer (^{18}F-SuPAR) in order to determine PARP-1 activity in living subjects for the first time, and to monitor radiation therapy response and determine PARP-1 inhibitor efficacy in mouse models of human cervical and breast cancers. **Results:** Rational tracer development based on the endogenous PARP-1 substrate yielded ^{18}F-SuPAR with high substrate activity. Enzyme-based structure activity relationships were rationalized through *in silico* modeling of probe candidate binding to PARP-1. Radiolabelling occurred by ligand-assisted copper-catalyzed click chemistry (RCY = 8.2%). Radiation therapy response was successfully detected in mice bearing human cervical or breast tumors as early as 8 hours following 5 Gy or 10 Gy radiation. ^{18}F-SuPAR provided the non-invasive measurement of PARP-1 activity in living subjects and identified a differential response to radiation therapy between tumor types. In a mouse model of breast cancer metastasis to the brain, ^{18}F-SuPAR showed uptake in metastatic but not healthy brain tissue, suggesting its application to imaging secondary brain cancers. PARP-1 inhibition by BMN673, a new chemical entity currently in Phase III clinical trial[4], was also investigated. PARP-1 activity was significantly inhibited in breast tumors following administration of BMN673, but not in cervical tumors. Importantly, ex vivo autoradiography and immunofluorescence of the endogenous product of PARP-1 activity indicated that ^{18}F-SuPAR signal correlated strongly with PARP-1 activity in breast ($r=0.93$, $p<0.05$) but not in cervical tumors ($r=0.46$, n.s.). **Conclusion**: ^{18}F-SuPAR uniquely measures PARP-1 activity *in vivo*, with target specificity confirmed through PARP-1 inhibition and *ex vivo* analysis. Breast but not cervical cancer was identified to benefit from PARP-1 inhibition therapy, mimicking clinical data[5]. **Innovation and Impact:** The ability to measure PARP-1 activity in living subjects has been elusive until the development of ^{18}F-SuPAR. This novel tracer may enable precision medicine through selection of patients benefiting from PARP-1 inhibitor therapy based on measurements of PARP-1 activity, and may allow for clinical mapping of radiation therapy response over the volume of the tumor early after administration.

1.Ganesan S. Sci Signal (2011) 4:pe15; 2. Dent RA & Bristow RG J Clin Oncol (2011) 29:2130 ; 3. Cancer Discovery (2015) Jan 23; 4. Liu JF et al., Gynecol Oncol (2014) 133:362; 5. Tangutoori S et al. Maturitas (2015) Feb 7.

AUTHORS (LAST NAME, FIRST NAME): Shuhendler, Adam[1]; Cui, Lina[1]; Lin, Jianguo[2]; Shen, Bin[1]; James, Michelle L.[3]; Witney, Timothy H.[1]; Bazalova-Carter, Magdalena[1]; Chattopadhyay, Niladri[1]; Gambhir, Sanjiv S.[4]; Chin, Frederick T.[5]; Graves, Edward[1]; Rutt, Brian[6]; Rao, Jianghong[7]

INSTITUTIONS (ALL):

1. Radiology, Stanford University, Stanford, CA, United States.
2. Jiangsu Institute of Nuclear Medicine, Key Laboratory of Nuclear Medicine, Wuxi, China.
3. Radiology, Stanford University, Stanford, CA, United States.
4. Radiology, Stanford University, Stanford, CA, United States.
5. Radiology, Stanford University, Stanford, CA, United States.
6. Radiology, Stanford University, Stanford, CA, United States.
7. Radiology, Stanford University, Stanford, CA, United States.

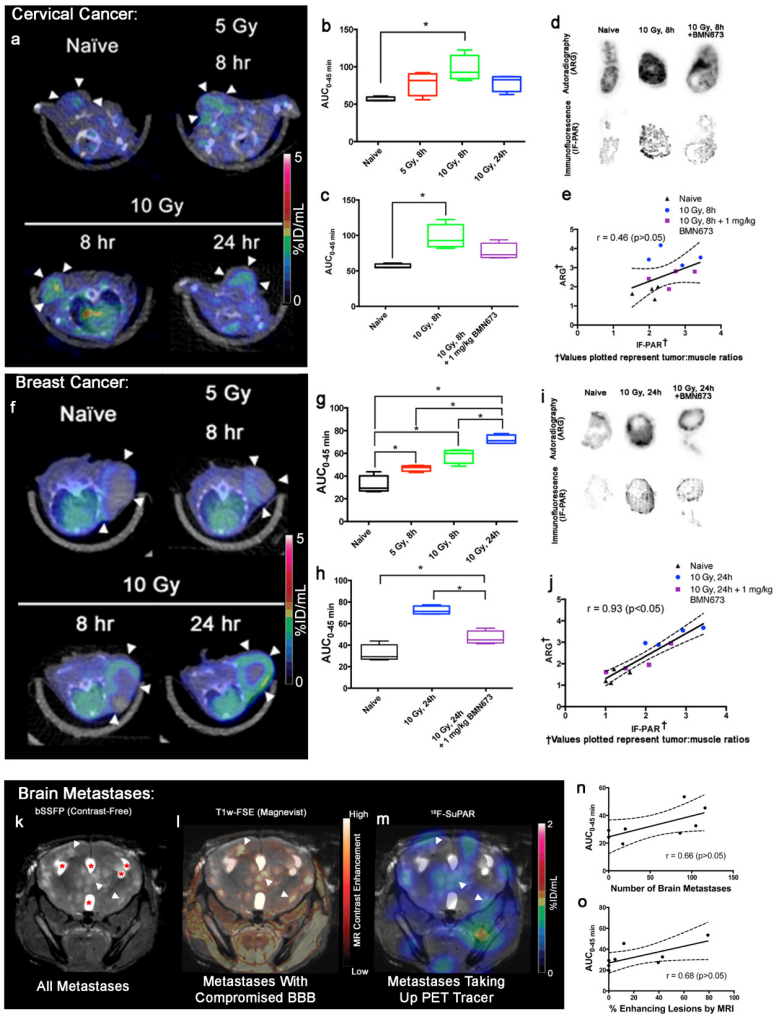

Representative axial images of mice bearing human cervical (a) or breast (f) tumors (white arrowheads) remaining untreated (top left), 8 h after 5 Gy irradiation (top right), and 8 h (bottom left) or 24 hr (bottom right) following 10 Gy irradiation. Corresponding boxplots of area under the time activity curve (AUC) for cervical (b) or breast (g) tumor uptake of ^{18}F-SuPAR are shown. Inhibition of PARP-1 by BMN673 is shown for cervical (c) or breast (h) tumors, with purple box indicating effect of inhibition. Autoradiography (top row) and PAR localization by immunofluorescence (bottom row) for untreated tumors (left), treated with 10 Gy radiation 8 h (cervical, d) or 24 h (breast, i) prior to resection (middle), and treated tumors given BMN673 (right). The correlation of ^{18}F-SuPAR retention (ARG) and production of PAR (IF-PAR) for cervical (e) and breast (j) tumors. Solid line = regression, dashed line = 95% confidence interval. * $p<0.05$ by ANOVA. Brain metastasis of breast cancer was investigated with balanced steady-state free procession (bSSFP) MRI, indicating total tumor burden (k). Overlaid on bSSFP images are T1-weighted Fast Spin Echo (T1wFSE) MRI 60 min after contrast agent administration (Magnevist) showing regions of blood-brain barrier compromise (l), and ^{18}F-SuPAR PET images showing tumor uptake of tracer (m). Neither the number of brain lesions as per bSSFP images (n), nor the percent of brain lesions showing Magnevist enhancement (o) correlate with ^{18}F-SuPAR uptake ($p>0.05$), implicating other mechanisms of tracer uptake, such as those related to tumor DNA repair status. Red asterisks = brain ventricles; White arrowheads = brain metastases.

CONTROL ID: 2231779

TITLE: First-in-human study of a cysteine cathepsins activity-based PET probe

PRESENTER: Shaobo Yao

ABSTRACT BODY:

Abstract Body: Objectives: ^{68}Ga-BMV101 is a novel positron emission tomography (PET) probe designed to recognize cysteine cathepsins activity, which are highly expressed in antigen presenting cells such as macrophages. This study aims at radiolabelling of BMV101, evaluating its biodistribution in normal mice and performing a first-in-human clinical application in two patients with pulmonary fibrosis.

Methods: ^{68}Ga-BMV101 was prepared by incubation of 10μL BMV101 (1mM in DMSO) with 4-7 mCi of $^{68}GaCl_3$ elution, pH was adjusted to 4.5 with sodium acetate buffer (1.25 M), and the mixture was incubated at 37 ºC for 30 minutes. The reaction solution was analyzed by RP-HPLC, and 3-h stability was evaluated. For the biodistribution assays in normal female balb/c mice, series of microPET scans were performed at 1, 2, 3 and 4 h respectively after intravenous injection of 3.7−7.4 MBq ^{68}Ga-BMV101. In acute toxicity study, 20 g mice were injected with 18.5 MBq ^{68}Ga-BMV101 in 0.3 mL saline and raised for another 48 h before the dissection for the visceral injury inspection. For clinical evaluation, two patients diagnosed with pulmonary fibrosis, characterized as bilateral ground-glass opacities on CT, underwent ^{68}Ga-BMV101 PET/CT. Whole-body images were acquired at 1 h and 2.5 h respectively after intravenous injection of 48.1-55.5 MBq ^{68}Ga-BMV101. The standardized uptake values (SUVs) was measured for semi-quantitative evaluation.

Results: The decay-corrected yield of ^{68}Ga-BMV101 was 78%. According to radio-HPLC analysis, the radiochemical purity was 91-95% and no less than 90% for 3 h at 37 ºC. Moderate uptake was found in liver and spleen in normal mice, which decreased within 4 h. No acute toxicity was found to the mice with the 1000-time dose used in human in this study. The human studies showed that ^{68}Ga-BMV101 was mainly excreted through the urinary system. Moderate tracer accumulation was found in blood pool, liver, and spleen. SUV_{max} of the lung lesions were 2.20, 2.13 at 1 h and 2.06, 1.90 at 2.5 h, and the lesion-to-normal lung ratios were 3.79, 4.73 and 4.58, 4.32, respectively for the two patients. No adverse effect was reported related to the intravenous tracer injection.

Conclusions: This study preliminarily indicates the safety of ^{68}Ga-BMV101 as a PET probe targeting cysteine cathepsin and its effectiveness in evaluation of pulmonary fibrosis. Further optimization of the probe may be needed to reduce the blood-pool distribution.

AUTHORS (LAST NAME, FIRST NAME): Yao, Shaobo[1]; Wang, Hanping[2]; Zhu, Wenjia[1]; Wu, Peilin[1]; Zhang, Jingjing[1]; Wu, Chenxi[1]; Xu, Kai-Feng[2]; Withana, Nimali P.[3]; Bogyo, Matthew[3]; Cheng, Zhen[4]; Zhu, Zhaohui[1]

INSTITUTIONS (ALL):

1. Department of Nuclear Medicine, Peking Union Medical College Hospital, Chinese Academy of Medical Science & Peking Union Medical College, Beijing, China.
2. Department of Respiratory Disease, Peking Union Medical College Hospital, Chinese Academy of Medical Science & Peking Union Medical College, Beijing, China.
3. Department of Pathology, Radiology, Microbiology and Immunology, Stanford University School of Medicine, Stanford, CA, United States.
4. Department of Radiology, Stanford University School of Medicine, Stanford, CA, United States.

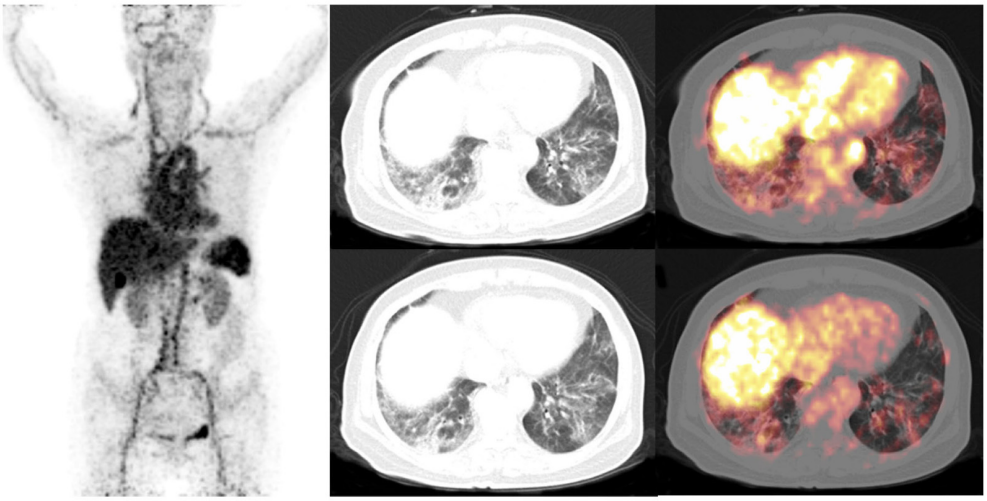

Figure legends

Maximum intensity projection image of ^{68}Ga-BMV101 PET (left) and transaxial CT and PET/CT fusion images at 1 h (upper) and 2.5 h (lower) in a patient (F, 67 y) with pulmonary fibrosis.

CONTROL ID: 2231802

TITLE: Synthesis and evaluation of a ^{18}F-labled 1,3,5-triazine-substituted benzenesulfonamide for imaging carbonic anhydrase IX expression in tumors with positron emission tomography

PRESENTER: Jinhe Pan

ABSTRACT BODY:

Abstract Body: Introduction: Sulfonamides are a class of carbonic anhydrase (CA) inhibitors that have shown antitumor activity *in vitro* and *in vivo.* Despite their high affinity, a major shortcoming of these compounds is the lack of isoform specificity. 1,3,5-triazine-substituted aromatic sulfonamides have enhanced efficacy and specificity towards CA-IX, an enzyme overexpressed in hypoxic tumors. To our knowledge, neither the radiochemistry nor imaging studies of 1,3,5-triazine-substituted sulfonamides have been reported. Herein, we synthesized a ^{18}F-labeled 1,3,5-triazine-substituted benzenesulfonamide and evaluated its potential for imaging CA-IX expression with positron emission tomography (PET).

Method: A 1,3,5-triazine-substituted sulfonamide P04150 was synthesized in three steps: coupling of 4-aminobenzensulfonamide with cyanuric chloride in 1:1 ratio, reaction with excess azidoethanol, and click reaction of the azido group of the intermediate with excess of an ammoniomethyl-trifluoroborate-conjugated alkyne. The cold compound was radiolabeled via the ^{18}F-^{19}F isotope exchange reaction. Stability of the tracer was assessed in mouse plasma with HPLC and $LogD_{7.4}$ was determined using a modified shake flask method. Imaging and biodistribution studies were performed at 1 h post-injection using HT-29 tumor-bearing immunocompromised mice.

Results: The overall yield for P05140 was 3.3%. ^{18}F-labeled P05140 was obtained in 14-29% decay-corrected radiochemical yields in 45 min with 4.4 Ci/mmol specific activity and > 99% radiochemical purity. ^{18}F-labeled P05140 was fairly hydrophilic with a $LogD_{7.4}$ value of -2.72 ± 0.02 and was stable in mouse plasma with negligible decomposition after 2 h incubation at 37°C. From the PET and biodistribution data, it was observed that the tracer was excreted mainly through the hepatobiliary pathway. More than 40% injected dose (ID) was retained in the gastrointestinal tract at 1 h post-injection. At the same time point, tumor uptake was 0.54 ± 0.09 %ID/g for the tracer and tumors were visible on PET images with moderate contrast. The uptake ratios of tumor-to-blood and tumor-to-muscle were 1.67 ± 0.46 and 5.44 ± 1.36, respectively.

Conclusions: [^{18}F]P05140 was radiolabeled in good radiochemical yield, purity and specific activity. Derivatization of 1,3,5-triazine-substituted benzenesulfonamide successfully targeted CA-IX expressing tumor xenografts with moderate contrast. Our preliminary results suggest that 1,3,5-triazine-substituted sulfonamides may serve as promising pharmacophores for targeting CA-IX expressing tumors.

AUTHORS (LAST NAME, FIRST NAME): Pan, Jinhe[1]; Lau, Joseph[1]; Hundal-Jabal, Navjit[1]; Zhang, Zhengxing[1]; Zhang, Chengcheng[1]; Bénard, François[1]; Lin, Kuo-Shyan[1]

INSTITUTIONS (ALL):

1. BC Cancer Agency, Vancouver, BC, Canada.

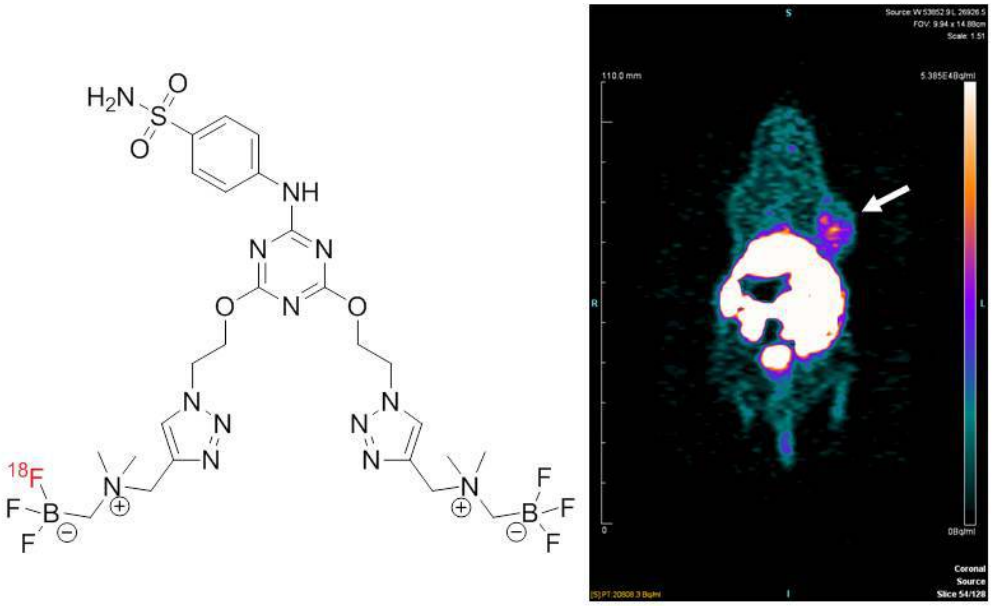

Chemical structure of [^{18}F]P05140 and its imaging (1 h post-injection) in immunocompromised mice bearing HT-29 tumor (white arrow).

CONTROL ID: 2231889

TITLE: Radiofrequency Hyperthermia-Enhanced Local Chemotherapy of Pancreatic Cancers: Monitored by Dual Modality Imaging

PRESENTER: Zhibin Bai

ABSTRACT BODY:

Abstract Body: Purpose: To investigate the feasibility of using molecular optical imaging and ultrasound imaging to assess radiofrequency hyperthermia (RFH)-enhanced therapeutic effect of gemcitabine (Gem) on rat models with orthotopic pancreatic carcinomas.

Materials and Methods: Lentivirus/luciferase-labeled rat pancreatic adenocarcinoma cells (DSL-6A/C1, 10^7) were subcutaneously inoculated into flanks of donor immunocompetent Lewis rats. We collected the subcutaneous tumor tissues from donor rats, and then transplanted the tissues into the pancreatic tails of recipient Lewis rats, to create orthotopic cancer models. Twenty-four rats with orthotopic pancreatic cancers were received various treatments in four groups: (i) combination therapy with intratumoral MR imaging-heating-guidewire (MRIHG)-mediated local RFH (42^0C) plus local chemotherapy (Gem); (ii) chemotherapy-only; (iii) RFH-only; and (iv) phosphate- buffered saline (PBS). Tumors sizes were followed-up by ultrasound imaging at days 0, 7 and 14 after the treatments. Bioluminescence signals of the tumors were measured via a laparotomy approach. Imaging results were correlated with subsequent histology analysis.

Results: Ultrasound imaging showed the smallest relative tumor volume in the combination therapy group compared to those in three control groups (0.62±0.18 VS 1.31±0.30,1.61±0.28, 1.71±0.29, $p<0.05$). Optical imaging demonstrated a decrease of bioluminescence signals of tumors in the combination therapy group, in comparison to those of three control groups (0.18±0.06 VS 0.41±0.12 VS 0.89±0.26 VS 1.0±0.32), which were well correlated with histologic confirmation (Figure).

Conclusion: Local radiofrequency hyperthermia can enhance the regional chemotherapeutic effect on orthotopic pancreatic carcinomas, which has established the groundwork to develop new interventional oncological techniques for effective management of human pancreatic malignancies.

AUTHORS (LAST NAME, FIRST NAME): Bai, Zhibin[2]; Zhang, Feng[4]; Shi, Yaoping[4]; Wang, Jianfeng[3]; Qiu, Longhua[1]; Teng, Gao-jun[5]; yang, xiaoming[6]

INSTITUTIONS (ALL):

1. University of Washington School of Medicine, Seattle, WA, United States.
2. Image-guided Bio-Molecular interventions Section, Department of Radiology, University of Washington School of Medicine, Seattle, WA, United States.
3. Radiology, University of Washington, School of Medicine, Seattle, WA, United States.
4. Radiology, University of Washington School of Medicine, Seattle, WA, United States.
5. Zhongda Hospital of Southeast University, Nanjing, China.
6. Radiology, university of Washington School of Medicine, Seattle, WA, United States.

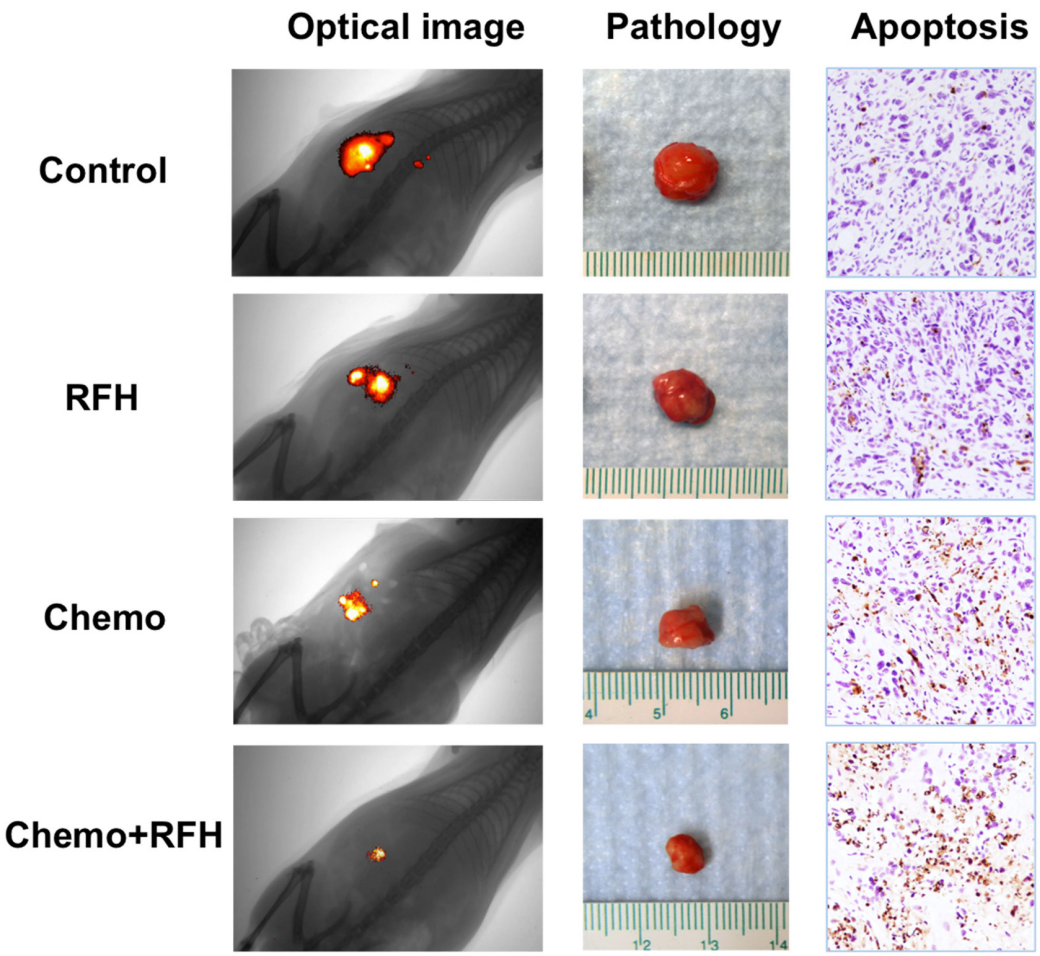

Figure. Optical/x-ray images obtained from four animal groups after laparotomy at days 14 showing decreased bioluminescence signals (yellow-red color) of luciferase-tumors in the animal group treated by combination therapy (Chemo +RFH), compared to three control animal groups. Optical imaging findings are confirmed by histology, showing more apoptosis cells (brown-color spots) in the combination therapy group.

CONTROL ID: 2231817

TITLE: Non-invasive Molecular Imaging Of Tumor Metastasis Affected By MicroRNA Let-7 Family

PRESENTER: man-jyun Liao

ABSTRACT BODY:

Abstract Body: Cofilin-1 is an actin binding protein belonging to the actin depolymerizing factor (ADF)/cofilin family. Cofilin-1 causes depolymerization at the minus end of actin filaments, thereby replenishes the actin pools in cytosol for building up more actin filaments. We previously found that over-expressed cofilin-1 led to destabilization of actin cytoskeleton and inhibition of invasion in human non-small cells lung cancer. However, the underlying mechanism remains unclear. Using a tetracycline inducible system to over-express cofilin-1 in H1299 lung cancer cells, we found that let-7 family members are up-regulated by over-expressed cofilin-1 after investigation of the microRNA expressive profiles. The hsa-let7 microRNA family is known to exhibit a tumor suppressive property. We also found that let-7b and let-7e are mostly up-regulated when cofilin-1 is over-expression in this cell line. Use of locked nucleic acid (LNA) to inhibit let-7b and let-7e in cofilin-1 over-expressing cells, cell growth and metastatic ability were recovered. Here, we further i.v. injected the LNA transfected cells cofilin-1 over-expressing cells into nude mice, based on the experimental metastatic animal model. To noninvasively monitor the effects of let-7 inhibitors on over-expressed cofilin-1 suppressed tumor accumulation in lungs, we have stably infected a LT-3R reporter gene construct that can be used for optical imaging and radionucleotide based reporter gene imaging. The result showed that the tumor signals (as determined using bioluminescent imaging) in lungs were reduced by over-expression of cofilin-1 after animals were fed with doxycycline, but co-transfection of let-7 inhibitors recovered the tumor signals. We will follow up this experiment about 7 days. This study suggests that let-7 is required for cofilin-1 mediated inhibition of tumor metastasis in vitro and in vivo. It will be of interest to further investigate whether this signaling pathway is dependent or independent of actin cytoskeletal reorganization and destabilization.

AUTHORS (LAST NAME, FIRST NAME): Liao, man-jyun[1]

INSTITUTIONS (ALL):

1. yang-ming university, Taipei, Taiwan.

(No Image Selected)

CONTROL ID: 2231832

TITLE: Construction and in vitro Characterization of Dual-modality SPECT/MR Nanoprobes Targeting HAb18G/CD147 in Breast Tumors

PRESENTER: Mingru Zhang

ABSTRACT BODY:

Abstract Body: Purpose: It is reported that 64.36% breast cancer patients overexpress cell membrane antigen HAb18G, which has been confirmed to be homologous with CD147. The overexpression of HAb18G is closely related to the development and metastasis of tumors, as well as the sensitivity of patients to radiotherapy and chemotherapy. This study aims at preparing dual-modality nanoprobes of SPECT/MR to target tumors overexpressing HAb18G/CD147, and preliminarily investigating the physicochemical and biological properties of the nanoprobes in vitro.

Materials and Methods: Superparamagnetic iron oxide nanoparticles (SPIOs) were prepared by one-pot reaction method. The single-chain antibody fragments HAb18F(ab')$_2$, were conjugated to SPIOs via chemical method and then labeled with ^{125}I by Iodogen method. The final ^{125}I-SPIO-HAb18F(ab')$_2$ nanoprobes were purified by a desalting column. Preliminary physicochemical and biological evaluations were carried out on the nanoprobes in vitro. Two breast tumor cell lines, mda-mb-231 and mda-mb-468, were used in the biological evaluations. The expression of HAb18G/CD147 is predominant on the former while low on the latter.

Results: The SPIOs were fairly homogeneous with an average core size of 10.32 ± 1.3 nm; SPIOs and SPIO-HAb18F(ab')$_2$ had a hydrodynamic diameter of 44.80 nm and 52.64 nm. MRI scanning showed that the transverse relaxation efficiency (r_2) of SPIOs and SPIO-HAb18F(ab')$_2$ were 38.79 and 106.73 $mM^{-1}\cdot s^{-1}$, respectively. The radio chemical yield (RCY) of ^{125}I-SPIO-HAb18F(ab')$_2$ and ^{125}I-HAb18F(ab')$_2$ were 41.9% and 85.8%, after purification the radio chemical purity (RCP) of those two nanoprobes were both greater than 95%. The logP value of ^{125}I-SPIO-HAb18F(ab')$_2$ and ^{125}I-HAb18F(ab')$_2$ were -0.99 ± 0.03 and -1.49 ± 0.08, respectively, and the two agents were both stable while incubated in PBS and murine serum for 3 hours. The IC_{50} values of ^{125}I-SPIO-HAb18F(ab')$_2$ and ^{125}I-HAb18F(ab')$_2$ were 48 nM and 1.6 nM respectively (Fig-1A). The accumulation of ^{125}I-SPIO-HAb18F(ab')$_2$ in mda-mb-231 cell increased moderately over time, with a binding rate of 10.52 ± 2.04% at 4 h, while in mda-mb-468 cell, the cell binding rate of ^{125}I-SPIO-HAb18F(ab')$_2$ remained at 6% among the 4 hours incubation (Fig-1B).

AUTHORS (LAST NAME, FIRST NAME): Zhang, Mingru[1]; Liu, Xianping[2]; Wang, Jing[2]

INSTITUTIONS (ALL):

1. Nuclear Medicine, First Affiliated Hospital of the Fourth Military Medical University, Xi'an, Shaanxi, China.
2. first affiliated hospital of the Forth Military Medical University, Xi’an, Shaanxi, China.

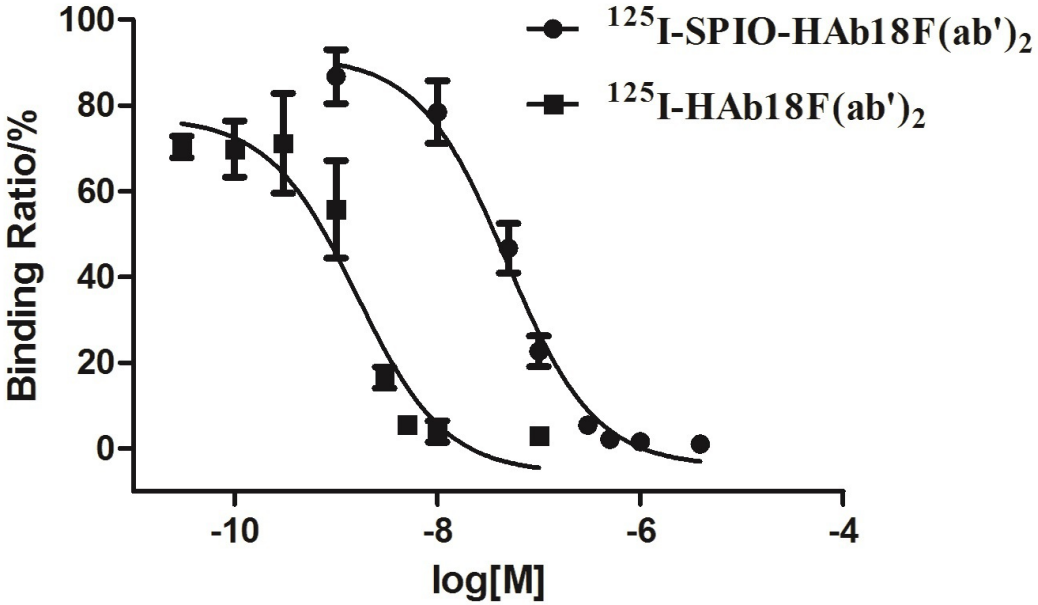
100
80
60
40
20
0
Binding Ratio/%
-10
-8
-6
-4
log[M]
^{125}I-SPIO-HAb18F(ab')$_2$
^{125}I-HAb18F(ab')$_2$

CONTROL ID: 2231835

TITLE: Linking imaging to omics: Image-guided extraction of frozen tissue samples

PRESENTER: Jonathan Disselhorst

ABSTRACT BODY:

Abstract Body: Phenotypic heterogeneity is a common feature of tumors, in both clinical and preclinical setting. With imaging technologies such as PET and MRI, some of these intratumoral variations can be observed. Proteomics and metabolomics can help to characterize the biological background of the heterogeneity and understand their significance. This requires fast and accurate sample preparation methods. Therefore, a milling machine for the precise extraction of tissue samples was developed. These samples can be delineated on PET/CT scans as volumes of interest (VOIs). The samples remain cooled throughout the procedure, facilitating subsequent analysis in NMR or mass spectrometry (MS). This method will allow a deeper understanding of tumor metabolism by correlating imaging to omics data.

Materials

A 3-axis computer numerical control (CNC) milling machine was augmented with a liquid nitrogen bath. To keep the object cold, gaseous nitrogen is blown in this liquid to create nitrogen vapor during milling. The machine is controlled based on VOIs delineated on PET/CT.

Mice were injected with FDG, followed by a 1h uptake period. Subsequently, PET/CT images were acquired, after which the animals were killed. The mice were immediately frozen to quench metabolism, by submerging them in a mixture of isopropyl alcohol and dry ice cooled to –55°C. Afterwards, the mice were embedded in ice in a polymer holder. A second scan, acquired from the frozen mice, was used to define VOIs. These VOIs were converted to machine instructions, and milled from the mice. A CT scan acquired after milling was used to investigate the accuracy of the procedure. Finally, tissue samples were collected for NMR, MS and histology. Spatial coherency between pre- and post-freezing PET scans was achieved by manual segmentation of the tumor using isocontour VOIs and subsequent non-rigid automatic registration. R^2 values and scatter plots between the registered scans were generated and used for assessment of global registration accuracy.

Results

Alignment of the CT-scans acquired pre and post milling proved that extraction of the defined VOIs could be performed with sub-mm accuracy. High quality data could be generated from the prepared samples using NMR metabolomics, MS proteomics or histology. Temperature measurements around the frozen animal during milling showed that –30°C was not exceeded. R^2 between 6 co-registered pre- and post-freezing PET images was 0.62±0.15. The mean volume change for all 6 animals was 16.1±20.0%.

Conclusion

This is the first time that different regions within a tumor can be observed with preclinical imaging and subsequently analyzed with high spatial accuracy using proteomics and metabolomics. This strategy is highly promising to link imaging to the underlying protein expression and metabolic processes, and gain a deeper understanding of the resulting imaging phenotypes.

In future studies we aim to further improve the accuracy of the milling process and apply our strategy in a range of different tumor models and therapeutic settings.

Acknowledgement

We thank Fraunhofer IPA for developing the machine. The research has received funding from the European Research Council (323196).

AUTHORS (LAST NAME, FIRST NAME): Disselhorst, Jonathan A.[1]; Krueger, Marcel A.[1]; Bezrukov, Ilja[1]; Pichler, Bernd J.[1]

INSTITUTIONS (ALL):

1. Werner Siemens Imaging Center, Eberhard Karls University Tuebingen, Tuebingen, Germany.

(No Image Selected)

CONTROL ID: 2231839

TITLE: A translational awake rodent pharmacological MRI imaging model: a report investigating central effects of MK-801

PRESENTER: Sakthivel Sekar

ABSTRACT BODY:

Abstract Body: One of the major hurdles in early drug discovery, especially in the neuro-psychopharmacology, is the lack of appropriate pre-clinical models and techniques for screening psycho-active compounds. Hence, in-light of high attrition rate in drug development, there is a need for translational endpoints/models, which are crucial, & where pre-clinical imaging techniques, such as pharmacological magnetic resonance imaging (phMRI) has a vital role to play in the arena. However, these studies have translational limitations due to the use of anaesthesia during animal imaging. The potential confound introduced by the drug-anaesthetic interaction, as well as the anaesthetic agents' effect on neuronal activations, affects the translational scope of basic research findings from imaging studies. Therefore, the use of ‘awake animal imaging’ is particularly attractive for studies investigating central drug effects. Through this investigation we have established an awake rodent imaging model which encompasses comprehensive acclimation procedures [with custom-built restrainer & RF coil for acclimation (for a duration of 9 days: day 1 (5 mins), day 2 (10 mins), day 3 & 4 (30 mins), day 5 to 9 (60 mins)] & imaging at ultra-high field 9.4T (Bruker Biospec) on day 10 for 60 mins, respectively) and robust phMRI protocols, including unique algorithms for motion correction and statistical parametric map generation, across 174 segmented rodent brain structures. Classical NMDA antagonist MK-801 (at a behaviourally effective dose of 0.18 or 0.3 mg/kg, SC) was employed to evoke a central drug response. The composite of six drug treated subjects (male Wistar rats), analyzed against six saline treated controls was used to generate statistical parametric maps. Briefly, the location of every voxel in any subject whose p value was <0.05 after false-positive filtering for +/- BOLD signal change was included in the composite analysis & located within the region of interest. Results: The effectiveness of this acclimation procedure in minimizing the stress experienced by the animal as assessed by alterations in serum cortisol levels has been explored. Results confirm the significant reduction in stress levels following this acclimation procedure. The significantly activated voxels which are the composite of all subjects overlaid on the MIVA atlas, with 174 delineated brain structures, were characterised across three temporal analysis-windows (16 to 30 mins, 31 to 45 mins, 46 to 60 mins post treatment). Interestingly localized response of high significance ($p<0.01$) were apparent toward the third temporal analysis-window (46-60 mins) in the primary somatosensory, motor and visual cortex; further parietal and rostral piriform cortex, facial nucleus, inferior olivary complex, ventral posteriolateral thalamic nucleus, central gray & medial septum reflected statistical significance ($p<0.05$). These observations are of potential importance in understanding the translatability of pre-clinical pharmacological MRI and this awake imaging approach will contribute significantly in the development of more efficacious clinically active psycho-active compounds.

Acknowledgement: JCO DP Grant, A*Star

AUTHORS (LAST NAME, FIRST NAME): Sekar, Sakthivel[1]; Garnell, Joanne[1]; Seramani, Sankar[1]; Bhakoo, Kishore[1]

INSTITUTIONS (ALL):

1. Translational Imaging Industrial Lab (TIIL), Singapore Bioimaging Consortium (SBIC), Agency for Science, Technology & Research (A*STAR), Singapore, Singapore.

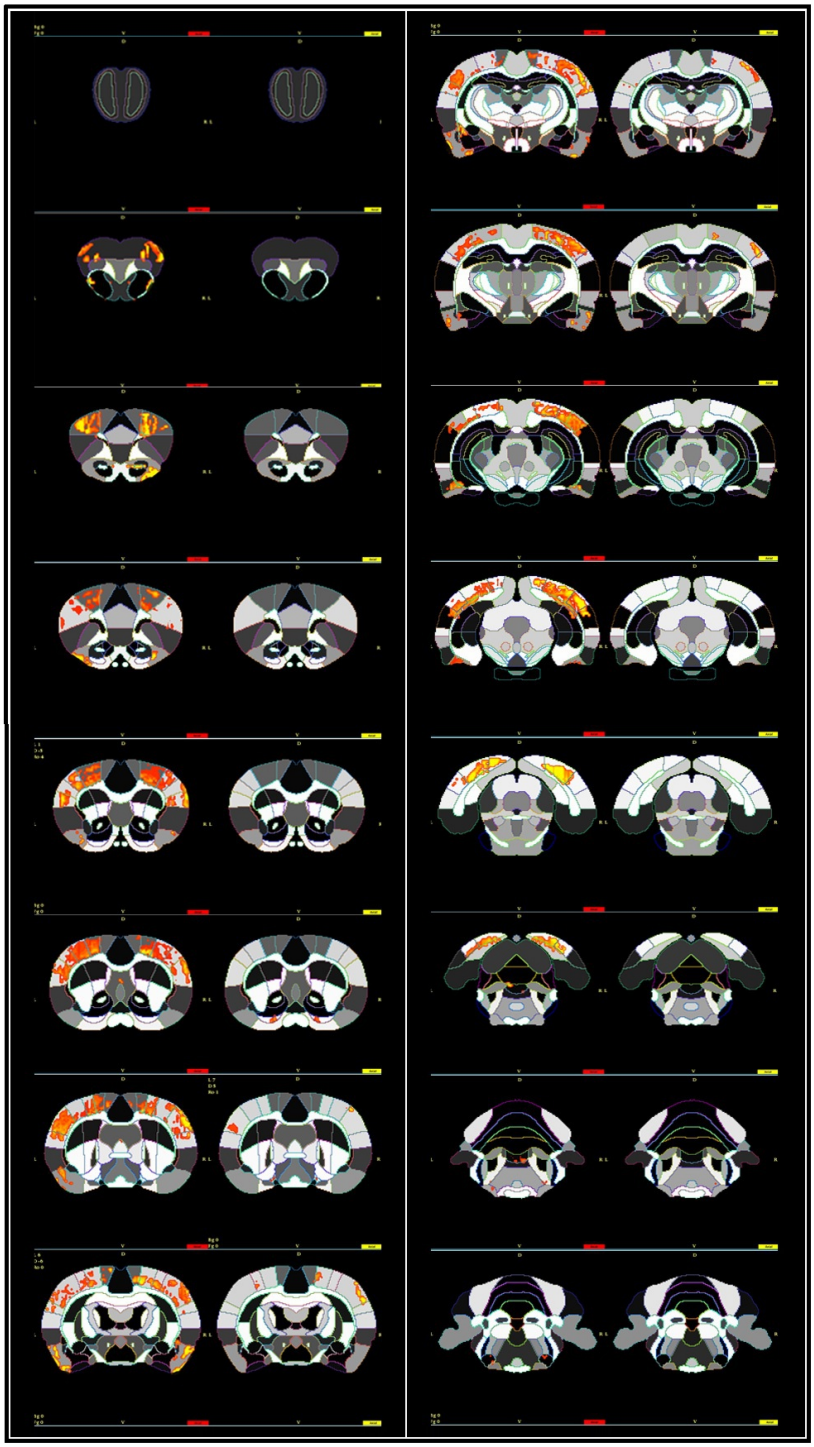

CONTROL ID: 2233090

TITLE: Ultrasmall theranostic nanoparticles for bimodal scintigraphy/MRI imaging in oncology

PRESENTER: Eloïse Thomas

ABSTRACT BODY:

Abstract Body: Nanoparticles in medicine have shown their interest since more than two decades thanks to their advantages in comparison with molecular agents: (i) enhancement of the number of active species per object, (ii) multimodality by combining complementary imaging modalities or imaging and therapy, (iii) original biodistribution with longer blood circulation time and potential targeting of tumor by enhanced permeability and retention effect (EPR effect) or grafting of targeting molecules on the nanoparticle's surface. Toxicity is of course a critical issue for clinical applications. In order to avoid it, it seems preferable that the particles are exclusively eliminated by renal excretion, which implies hydrodynamic diameter inferior to about 5-10 nm.

Our lab has developed such kind of nanoparticle for theranostic application. It is made of gadolinium chelates (DOTA, 1,4,7,10-tetraazacyclododecane-1,4,7,10-tetraacetic acid) covalently grafted to a polysiloxane core. It displays a hydrodynamic diameter below 5 nm providing exclusively renal excretion. This nanodevice has shown its interest in the context of radiotherapy guided by MRI. Indeed, the presence of gadolinium enables the nanoparticles to be used as positive MRI contrast agent (r_1=11.9 $s^{-1}.mM^{-1}$ per Gd at 60 MHz) and provides them radiosensitizing properties.[1,2] So far, no toxicity has been noticed during regulatory toxicity tests on rodents.

Adding a SPECT or PET modality on this nanoparticle is really interesting. The nanodevice obtained combines the advantages (for example MRI resolution and scintigraphy sensitivity) and overcome the drawbacks of both technics. It would then make medical diagnosis in clinic more reliable, lead to accurate detection of disease sites, help to the determination of the optimal injection dose and improve treatment monitoring.

To get such a structure, the nanoparticles described above have first been modified by adding specific chelates available for radiolabelling. DOTA or NODA (1,4,7-triazacyclononane-N,N',N"-triacetic acid) derivatives have thus been grafted on the nanoparticles. After characterizations, the synthesized particles have been successfully radiolabelled with high purity for SPECT with ^{111}In or for PET with ^{64}Cu or ^{68}Ga.[2,3] Size remains below 5 nm leading to exclusive renal excretion and limiting toxicity after intravenous injection. Quantitative biodistributions have been obtained on healthy animals and on tumor bearing animals. It demonstrates the interest of such kind of nanoparticles for new fused instruments combining scintigraphy and MRI and for imaging guided radiotherapy.

1 A. Mignot et al, Chem. Eur. J., **2013**, *19,* 6122-6136

2 F. Lux et al, Angew. Chem. Int. Ed., **2011**, *50,* 12299-12303

3 C. Truillet et al, Contrast Media Mol. I., DOI: 10.1002/cmmi.1633

AUTHORS (LAST NAME, FIRST NAME): Thomas, Eloïse[2]; Truillet, Charles[1]; Sancey, Lucie[2]; Denat, Franck[3]; Moreau, Mathieu[3]; Bernhard, Claire[3]; Collin, Bertrand[3]; Boschetti, Frederic[4]; Brunotte, François[5]; Oudot, Alexandra[6]; Roux, Stéphane[7]; Bouziotis, Penelope[8]; Lux, François[2]; Tillement, Olivier[2]

INSTITUTIONS (ALL):

1. Radiology, UCSF, San Francisco, CA, United States.
2. Institut Lumière Matière, Université Lyon 1, Villeurbanne, France.
3. Institut de chimie moléculaire de l'Université de Bourgogne, Université de Bourgogne, Dijon, France.
4. CheMatech, Dijon, France.
5. Nuclear imaging department, Centre Georges François Leclerc, Dijon, France.
6. Nuclear medicine department, Centre Georges François Leclerc, Dijon, France.
7. Institut Utinam, Besançon, France.
8. National Center for Scientific Research "Demokritos", Athens, Greece.

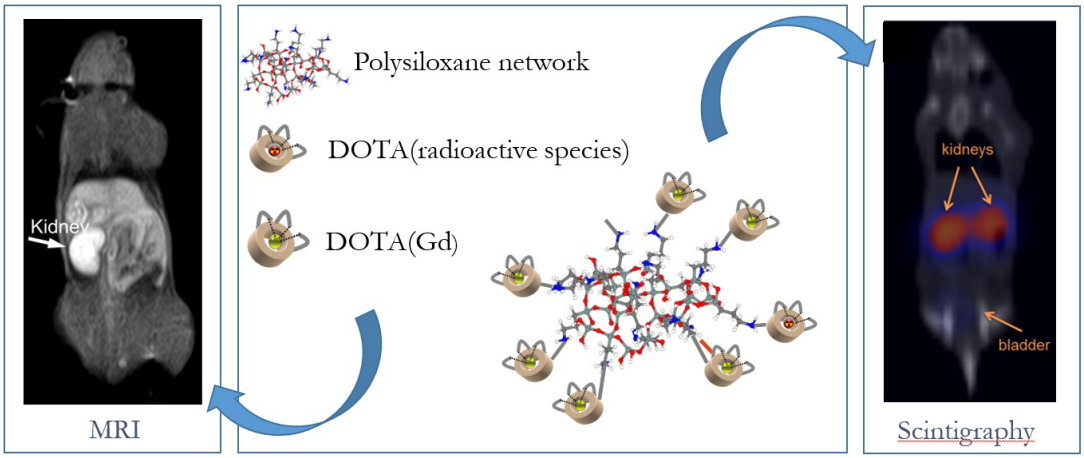

MRI and PET/CT images of mouse with ^{68}Ga radiolabelled nanoparticles

CONTROL ID: 2231867

TITLE: Spatial resolution recovery utilizing multi-ray tracing and graphic processing unit in PET image reconstruction

PRESENTER: HAO PENG

ABSTRACT BODY:

Abstract Body: We aim to implement resolution modeling utilizing multi-ray tracing on the GPU platform to reduce the depth-of-interaction (DOI) effect and improve processing speed.The concept of multi-ray tracing was used to trace multiple rays from the virtually created DOI layers considering the effect of crystal penetration to calculate the coincidence point spread function. Each ray was processed by a processing unit on the GPU in parallels to increase processing speed. The proposed method was tested on a breast-dedicated PET ring insert being developed in our group (Phys. Med. Biol. 60, 1217–1236, 2015). Three different cases were tested: 1) no physical DOI and no resolution modeling (case 1); 2) two physical DOI layers and no resolution modeling (case 2) ; and 3) no physical DOI design but with different number of virtual DOI layers (case 3). The proposed method was first validated against the Monte Carlo simulation, including the dependency of accuracy on the number of virtual DOI layers. Second, the spatial resolution performances were compared among the 3 cases, in terms of the resolution FWHM of the sphere phantoms across the field-of-view. Third, contrast and noise performances were studied. The results based upon the analytical modeling are in good consistency with the Monte Carlo simulation results. The spatial resolution of the image was improved with the modeling, especially when more virtual DOI layers were modeled. Similar effect was observed for the contrast result, and the noise could be reduced with the modeling. The results indicate that the proposed method has the potential to be used as an alternative to other physical DOI designs and achieve comparable imaging performances, while reducing detector/system design cost and complexity. The implementation using the GPU platform and CUDA programming helps speed up the system matrix modeling task and PET image reconstruction on-the-fly.

AUTHORS (LAST NAME, FIRST NAME): Liang, Yicheng[2]; PENG, HAO[1]

INSTITUTIONS (ALL):

1. Medical Physics, Electrical Enigineering, McMaster University, Hamilton, ON, Canada.
2. Medical Physics, McMaster University, Hamilton, ON, Canada.

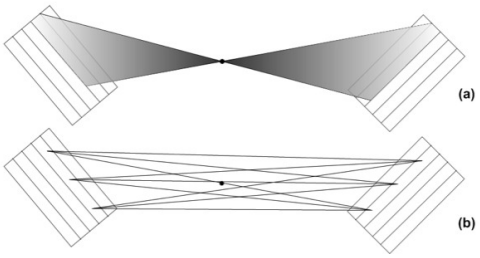

Figure 1. (a) Coincidence point spread function (CPSF) modeling for each crystal pair. (a) Single crystal element and no DOI based on the location of point source and solid angle coverage. (b) 9 sub-LORs based on three virtual crystal layers inside each crystal element, independent of the location of point source.

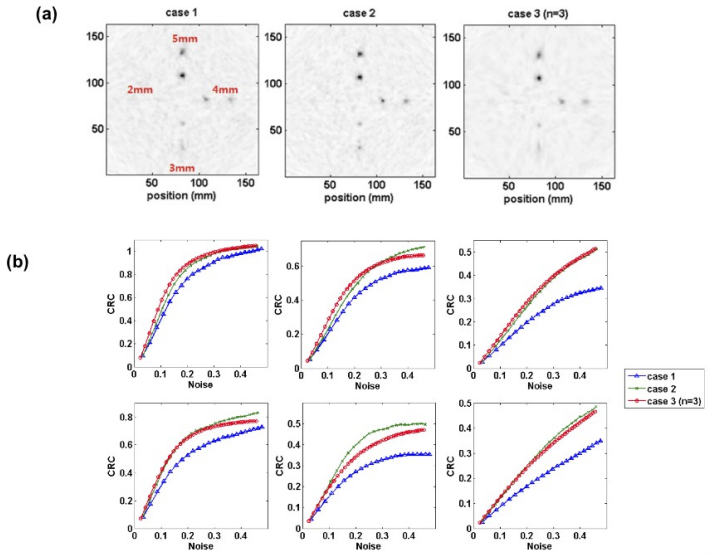

Figure 2. (a) Reconstructed images of the contrast phantom for three cases. (b) Noise vs. Contrast Recovery Coefficient (CRC) for the inner spheres (top) and the outer spheres (bottom).

CONTROL ID: 2231876

TITLE: Method development of a 3D reconstruction of the murine aortic arch

PRESENTER: Almut Glinzer

ABSTRACT BODY:

Abstract Body: Purpose:

This study aims establishing a 3D-reconstruction of the murine aortic arch combining histological techniques and magnetic resonance imaging (MRI). This reconstruction can provide the base of a predictive mathematical multiscale model of the mechanobiology of atherosclerosis.

Methods:

Contrast enhanced high resolution MRI-angiography at 7 Tesla, using a 3D gradiend echo sequence, was performed on low density lipoprotein receptor deficient mice (LDLr $^{-/-}$). Gd-DTPA was injected at a dose of 0.6 mmol/kg body weight. Mice were sacrificed after completion of imaging. After paraffin embedding of the aortic arch navigated serial histological sections of 5 µm were established at a microtome. Followed by Haematoxylin and Eosin staining histological images were acquired. The histological data set was processed for image registration with MATLAB© scripts. The MRI data set was used for pixel-segmentation of the aortic arch region.

Results:

Establishing a method to reconstruct the murine aortic arch with histological section was determined by information about the geometry of the arch. MRI imaging followed by pixel segmentation offered a centerline, which shows the focal point of the vessel. After image registration the created 3D-Object, based on histological sections, was adjusted to this centerline.

A 3D-Object of the murine aortic arch was successfully generated in the shape of the aortic arch.

Conclusion:

Combination of conventional histology and high resolution MRI, offering exact geometrical information, enables the establishment of a 3D-reconstruction of the murine aortic arch.

This 3D-reconstruction can serve as the basis for verification of mathematical modeling of biological factors that determine progression of atherosclerosis.

AUTHORS (LAST NAME, FIRST NAME): Glinzer, Almut[1, 3]; Thon, Moritz[2]; Lohoefer, Fabian[1]; Eckstein, Hans H.[3]; Rummeny, Ernst J.[1]; Gee, Michael W.[2]; Wildgruber, Moritz[1]; Zernecke, Alma[4]

INSTITUTIONS (ALL):

1. Department of Radiology, TU München, München, Germany.
2. Mechanics & High Performance Computing Group, Technische Universität München, Munich, Germany.
3. Department of Vascular and Endovascular Surgery, Technische Universität München, München, Germany.
4. Institute for Clinical Biochemistry and Pathobiochemistry, Universitätsklinikum Würzburg, Würzburg, Germany.

(No Image Selected)

CONTROL ID: 2232270

TITLE: Molecular imaging of atherosclerosis using the novel magnetic resonance contrast agent Gadofluorine P and T1 mapping techniques

PRESENTER: Almut Glinzer

ABSTRACT BODY:

Abstract Body: Purpose:

Evaluation of Gadofluorine P, a novel amphiphilic contrast agent, by molecular magnetic resonance imaging (MRI) in a mouse model of atherosclerosis and improved analysis of progression and precise quantification of atherosclerotic plaques using T1 mapping techniques at high field strength.

Methods:

In this longitudinal study low density lipoprotein receptor deficient mice ($LDLr^{-/-}$) were fed a Western Type diet. After 4, 8 and 16 weeks mice were imaged by high-field 7 Tesla MRI after injection of Gadofluorine P at a dosage of 0.1mmol/kg body weight. Age matched C57BL/6 mice on a chow diet were used as control group. Imaging planes were planned in line with the aortic arch and perpendicular at the branch point of the left common carotid artery (CCA). Black blood imaging using a double inversion recovery fast spin echo sequence was used for high resolution anatomical depiction of the aortic arch. Vessel wall contrast enhancement was assessed by Late Gadolinium Enhancement (LGE) and quantified by T1-mapping. T1/R1 values were calculated from T1 maps based on a Look-Locker sequence. T1 images were calculated from source images based on a 3-parameter Levenberg-Marquardt curve fitting procedure with a correction for read-out-induced attenuation of the relaxation curve. Mice from each time point were sacrificed after completion of imaging. The aortic arch was further processed for immunohistochemistry and matrix-assisted laser desorption ionization imaging (MALDI) to quantify Gadofluorine P accumulation ex-vivo.

Results:

R1 values in atherosclerotic plaques located in the inner curvature of the aortic arch peaked 30min after Gadofluorine P injection. A kinetic study showed that R1 values of the vessel wall returned to baseline levels after ~5h.
R1 values in the aortic wall in $LDLr^{-/-}$ mice were significantly higher compared to the control group. Contrast enhancement of the vessel wall increased over the time period of the high fat diet.

Conclusion:

MR imaging using the novel contrast agent Gadofluorine P allows capturing of plaques even at early stages of atherosclerosis in mice. T1 mapping at high field strength allows precise quantification of contrast agent accumulation in plaques. The combination of Gadofluorine P with T1 mapping enables a precise and quantitative analysis of atherosclerosis in a mouse model.

AUTHORS (LAST NAME, FIRST NAME): Glinzer, Almut[1]; Lohoefer, Fabian[1]; Hoffmann, Laura[1]; Kosanke, Katja[1]; Rummeny, Ernst J.[1]; Zernecke, Alma[2]; Schilling, Franz[3]; Wildgruber, Moritz[1]

INSTITUTIONS (ALL):

1. Department of Radiology, Klinikum Rechts der Isar, Technische Universität München, München, Germany.
2. Institute for Clinical Biochemistry and Pathobiochemistry, Universitätsklinikum Würzburg, Würzburg, Germany.
3. Department of Nuclear Medicine, Klinikum Rechts der Isar, Technische Universität München, München, Germany.

(No Image Selected)

CONTROL ID: 2231880

TITLE: Assessing implant wear- induced inflammation using PET [^{11}C]PK11195 imaging in a rat model

PRESENTER: Weiping Ren

ABSTRACT BODY:

Abstract Body: INTRODUCTION: The early diagnosis of aseptic loosening (AL) is difficult. AL is characterized by the tissue accumulation of wear debris-activated macrophages. PK11195 is a ligand for peripheral benzodiazepine receptor (PBR) expressed on the surface of macrophages. The purpose of this study is to develop a positron emission tomography (PET) technology using a [11C]PK11195 tracer to assess implant wear- induced inflammation in a rat model.

MATERIALS AND METHODS: Rat model of knee joint replacement SD rats were used to prepare the tibial intramedullary canal. Then 100 ul of UHMWPE particles was injected into bone marrow cavity, followed by implantation of a titanium pin into the proximal parts of rat tibiae. The right hind limb was used as control (sham surgery); uCT data acquisition μCT image was used as a volumetric frame to assess the periprosthetic tissue pathology; PET data acquisition Rats were injected with [11C]PK11195 [2 nmol/kg] via the tail vein. The initial 30 min scan was binned into one time frame and reconstructed using measured attenuation, scatter correction and the OSEM2D iterative algorithm yielding an isotropic resolution of about 2mm FWHM; Co-registration of PET images and CT images. uCT and microPET image volumes were coregistered using the MPItool software by matching the position of the three fiducial markers in both data sets. Following coregistration, regions of interest (ROIs) were defined in the uCT image volume.

RESULTS: mCT scans confirmed the position of the implantation and record of the initial bone density data. We noticed that the titanium pin shadow obscures the surrounding bone density on CT image, and this shadow was disappeared after data modeling using our spline simplex software. Representative images of both mCT scan and PET image showed the accumulation of the [11C]PK11195 tracer in the challenged knee joint with UHMWPE particle stimulation, as compared with the sham-operated left limbs.

DISCUSSION: The PET [11C] PK11195 has been used clinically to monitor macrophage-mediated inflammation in the brain and lung. Using a rat model, our pilot study demonstrated that [11C]PK11195 tracer concentration is significantly higher in rat knee joints with UHMWPE particle injection, as compared with unchallenged knee joints in a rat model. These data supported our hypothesis that the real time changes of periprosthetic tissue macrophage kinetics in response to implant wear stimulation can be measured, mapped, and dynamically monitored using PET [11C] PK11195 technology, where repeated invasive tissue pathology analysis is rarely available. PET [11C]PK11195 imaging may reflect the real time status of macrophage-dominant periprosthetic tissue inflammation, and is an “early warning tool” for patients with total joint replacements who are at high risk of later AL development. A time course study is underway in our laboratory.

AUTHORS (LAST NAME, FIRST NAME): Ren, Weiping[1, 2]; Muzik, Otto[1]; Jackson, Nancy[2]; Flynn, Jeffrey C.[2]; Gelovani, Juri G.[1]; Markel, David C.[2]

INSTITUTIONS (ALL):

1. Biomedical Engineering, Wayne State University, Detroit, MI, United States.
2. Orthopaedics , Providence Hospital, Southfield, MI, United States.

(No Image Selected)

CONTROL ID: 2231881

TITLE:

Integrin-targeted fluorescence molecular imaging of neoangiogenesis in a small-cell lung cancer model

PRESENTER: Valerie Phi van

ABSTRACT BODY:

Abstract Body:

Purpose: Small lung cell cancer (SCLC) is a fast-growing tumor that is not commonly treated by surgery, but by chemotherapy and especially targeted therapy aiming to reduce tumor vasculature. The characteristic of SCLC is their high potential of neoangiogenesis. This could be a target for anti-angiogenetic therapy via VEGF inhibition. Purpose of the study was to evaluate integrin-targeted molecular imaging as a promising platform for monitoring those novel targeted tumor therapies.

Material and Method: Lewis lung cell carcinoma cell were implanted endotracheally in C57BL/6J mice. Mice were screened for tumor growth using T2 weighted MRI and upon reaching a tumor size>2mm mice underwent avß3 Integrin imaging with Integrisense using hybrid fluorescence molecular tomography/x-ray computed tomography (FMT-CT). Mice were followed by molecular imaging for 14 days and sacrificed after the last imaging session and subsequently processed for cryoslicing, immunohistochemistry and flow cytometry. To investigate in-vivo specificity, mice blocked with cilengitide before Integrisense imaging were additionally investigated.

Result: Immunoflourescence staining confirms the expression of avß3 Integrin on Lewis Lung Cells. In-vivo fluorescence signal increased steadily over the three consecutive scans correlating with the growing volume of the tumor. The specificity of IntegreSense was confirmed by blocking *avß3* via cilengitide, a specific RGD-based ligand for avß3, which decreased the Integrisense flourescence signal. Cryoslicing confirmed accumulation of IntegriSense in the pulmonal lesions ex-vivo.

Conclusion:

Integrin targeted FMT-CT imaging allows a faithful visualization of angiogenesis in avß3 expressing lung cancer for detection and therapy monitoring in murine model.

AUTHORS (LAST NAME, FIRST NAME): Phi van, Valerie[1]; Ma, Xiaopeng [2]; Kosanke, Katja[1]; Kimm, Melanie[1]; Rummeny, Ernst J.[1]; Braren, Rickmer[1]; Ntziachristos, Vasilis[2]; Wildgruber, Moritz[1]

INSTITUTIONS (ALL):

1. Department of Radiology, TU München, München, Germany.
2. Chair for Biological Imaging, Helmholtz Zentrum München , Munich , Germany.

(No Image Selected)

CONTROL ID: 2231883

TITLE: A Modified Clinical Endoscope for Fluorescence-based Colonoscopies using Pathology-targeted Nanoplatforms

PRESENTER: Jeffrey Souris

ABSTRACT BODY:

Abstract Body: To determine the utility of targeting aberrant glycosylation for the *in vivo* imaging of nascent colorectal cancers and polyps, we have recently designed, synthesized, and evaluated targeted, ultra-bright fluorescent mesoporous silica nanoparticles (MSNs) for *in vivo* use as endoscopic contrast agents. In conjunction with our nanoprobe development we have modified a commercially available clinical endoscope so as to enable its use for both white-light and fluorescence wide-field imaging – with light sources and optics that have been optimized for use with our pathology-targeted fluorescent MSNs. *In vitro* testing of the endoscope's performance, with the endoscope affixed to an inexpensive compact CMOS camera, revealed 1-10 ng/ml (~ 1-10 nM) detection of free/unconjugated fluorophore (ATTO647N: MW = 843 g/mol) in distilled water for exposure times of < 35 msec: a framerate suitable for *in vivo* studies. Quantitative assessment of the endoscope's detection sensitivity was achieved via correlating images of phantoms bearing milli- to pico- molar concentrations of aqueous suspensions of ATTO647N +/- MSN derived from endoscope examination to those obtained from a calibrated commercial *in vivo* fluorescence/bioluminescence imaging system. *In vivo* endoscopic exams were then performed using fasted, colonically prepped A/J male mice that had been subjected to azoxymethane (AOM) / dextran sodium sulfate (DSS) treatments – a standard model for colitis-associated colorectal tumor development. Endoscopic imaging of ATTO647N-MSNs targeting alpha-L-fucose and tumor-associated glycoprotein 72 (TAG72) expression, topically delivered during examination via one of the endoscope's working channels, demonstrated significant nanoprobe binding and specificity to polyps and tumors in AOM/DSS-treated animals but not +/- control animals. Semi-quantitative endoscopic comparison of PEGylated to unPEGylated nanoparticles revealed significantly greater binding of the former, suggesting that PEGylation can greatly enhance the transport of nanoparticles through colonic mucosa. Following *in vivo* endoscopic examination at 4-week intervals, colons of select mice were harvested, longitudinally opened, and sectioned into 5 mm strips for immediate endoscopic re-examination as well as subsequent quantitative fluorescence imaging and histopathology. Ongoing studies are aimed at quantifying and further enhancing both our endoscope's sensitivity and our nanoplatform's targeting specificity and transport through colon mucus.

AUTHORS (LAST NAME, FIRST NAME): Souris, Jeffrey S.[1]; Chen, Nai-Tzu[1]; Cheng, Shih-Hsun[1]; Konda, Vani[3]; Bissonnette, Marc[3]; Lo, Leu-Wei[1, 2]; Chen, Chin-Tu[1]

INSTITUTIONS (ALL):

1. Department of Radiology, The University of Chicago, Chicago, IL, United States.
2. Institute of Biomedical Engineering and Nanomedicine, National Health Research Institutes, Zhunan, Miaoli, Taiwan.
3. Department of Medicine, The University of Chicago, Chicago, IL, United States.

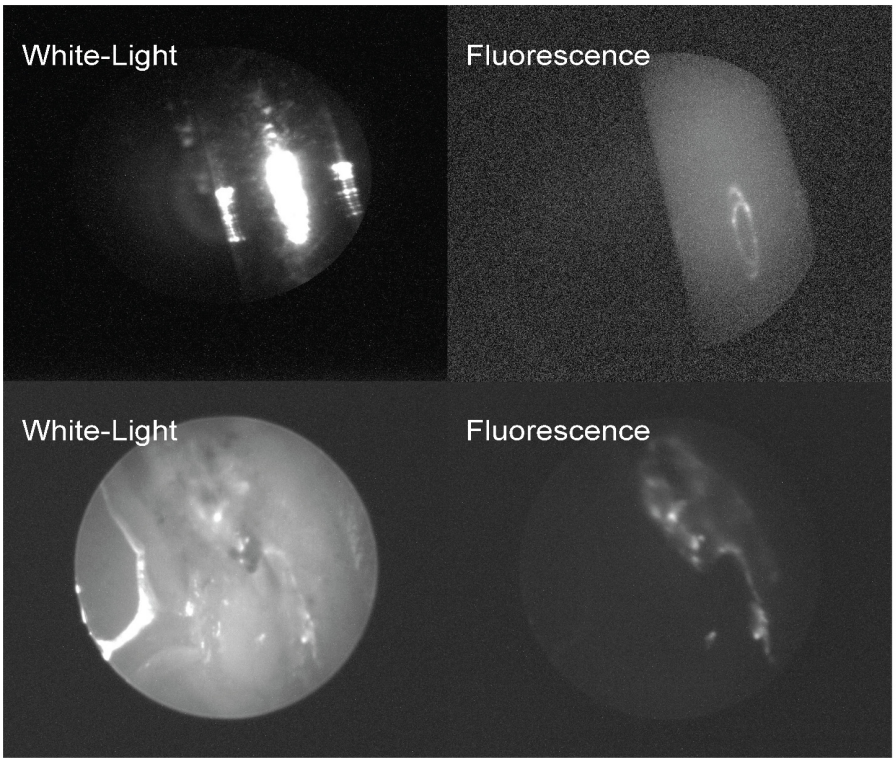

Figure 1. (Top) Captured white-light (left) and fluorescence (right) endoscopic images of a 2 mm OD thin-walled glass capillary tube containing 100 ng/ml free ATTO647N in H_2O (~100 nM). **(Bottom)** Captured white-light (left) and fluorescence (right) endoscopic *in vivo* images of ATTO647N-MSN-TAG72 nanoparticles associated with induced colorectal polyps in a male A/J mouse whose AOM/DSS treatment commenced 14 weeks prior.

CONTROL ID: 2233782

TITLE: Radioluminescence Characterization of Europium-doped Yttrium Oxide Nanoparticles for X-ray Dosimetry

PRESENTER: Jeffrey Souris

ABSTRACT BODY:

Abstract Body: We have developed Europium-doped Yttrium Oxide (Y_2O_3:Eu) nanoparticles that exhibit surprisingly bright, stable luminescence upon their exposure to x-rays. Spectroscopic analyses of their radioluminescent response reveal marked linearity with changes in x-ray flux and energy, making them potentially well suited for dosimetric applications. Synthesis of the Y_2O_3:Eu nanoparticles was accomplished by general urea homogeneous precipitation methods and particle morphology characterized by high-resolution transmission electron microscopy (HRTEM), operating at an acceleration voltage of 80 kV. A typical HRTEM image of the resulting Y_2O_3:Eu nanoparticles appears in the upper-left inset of Figure 1(a), with particle diameters averaging 150 nm. X-ray induced luminescence studies were conducted using a Small Animal Intensity Modulated Radiation Therapy System operating at 25-225 kVp tube potential and 1-25 mA tube current, both with and without Cu (0.3 mm thick) filtering of lower energy photons. The emergent x-ray beam was collimated to a diameter of 15 mm so as to fully bathe the Y_2O_3:Eu phantom yet prevent scattering and radioluminescence from neighboring support structures. For x-ray induced spectroscopic studies 10 mg of Y_2O_3:Eu nanoparticles were placed in a 1 ml cuvette containing 250 µl distilled water that had been situated vertically, 7.5 cm directly beneath the x-ray beam collimator's exit aperture. Emitted phosphorescence was collected by a 600 µm diameter glass bundle optical fiber positioned orthogonal to the x-ray beam and cuvette, just outside the beam path and connected to a highly compact, fluorescence spectrophotometer. A typical radioluminescence spectra derived from this experimental configuration appears in Figure 1(b). For each tube potential selected, complete radioluminescence spectra were collected and subsequently curve-fitted (Gaussian) – to establish the peak wavelength, height, and area-under-curve (AUC) for the 590 nm, 610 nm, and 627 nm peaks, as shown in Figure 1(b). A plot of these various AUC integrals and their summations (ΣAUC) appear in Figure 1(c), for tube currents of 5, 10, and 20 mA. As can be seen in that figure, the integrated AUC of both the dominant 610 nm peak and the summation of the integrated AUCs of the 590 nm, 610 nm, and 627 nm peaks reveal highly linear behavior with changes in peak tube voltage (kVp) and thus, by extension, mean x-ray energy. As such we posit that these radioluminescent nanoparticles could be used *in situ*, to provide real-time dosimetry during radiotherapy.

AUTHORS (LAST NAME, FIRST NAME): Souris, Jeffrey S.[1]; Cheng, Shih-Hsun[1]; Pelizzari, Charles[2]; Chen, Nai-Tzu[1]; La Riviere, Patrick[1]; Lo, Leu-Wei[1, 3]; Chen, Chin-Tu[1]

INSTITUTIONS (ALL):

1. Department of Radiology, The University of Chicago, Chicago, IL, United States.
2. Department of Radiation and Cellular Oncology, The University of Chicago, Chicago, IL, United States.
3. Institute of Biomedical Engineering and Nanomedicine, National Health Research Institutes, Zhunan, Miaoli, Taiwan.

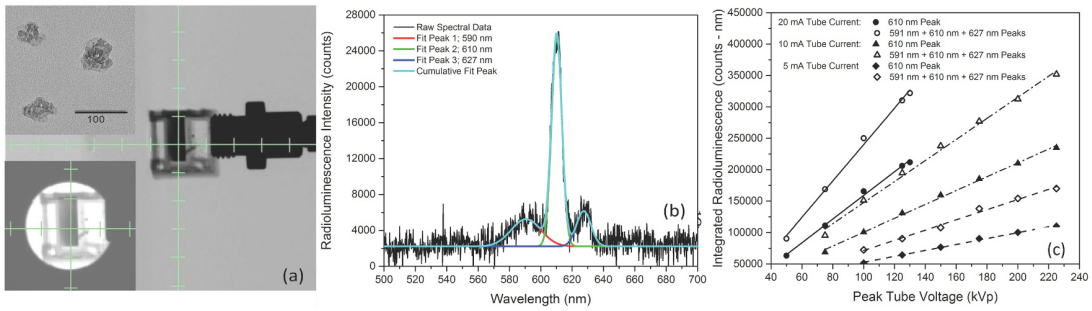

Figure 1. (a) Uncollimated, axial projection x-ray image of Y_2O_3:Eu filled cuvette, abutted to optical bundle fiber for spectra collection during irradiation. Insets: (upper-left) HRTEM image of Y_2O_3:Eu nanoparticles with 100 nm scale bar and (lower-left) collimated view of same cuvette. **(b)** Typical radioluminescence spectra showing dominant emission peaks at 590 nm, 610 nm, and 627 nm – and their corresponding, independent Gaussian curve-fits. **(c)** AUC of 610 nm (solid symbols) and summed (open symbols) 590 nm + 610 nm + 627 nm (open) radioluminescence spectra peaks – as a function of peak tube voltage (proportional to x-ray energy) – for various fixed tube currents (proportional to x-ray flux), showing excellent linearity.

CONTROL ID: 2239321

TITLE: Design of Protein-based MRI Contrast Agents (ProCAs) for Molecular Imaging of Cancer Metastasis

PRESENTER: Jenny Yang

ABSTRACT BODY:

Abstract Body: The major barriers limiting the application of MRI to detect small lesions and metastasis at the early stage and patient selection for targeted therapy based on molecular imaging of disease biomarkers, are due to the lack of desired MRI contrast agents capable of enhancing the contrast between normal liver tissues and tumors with high relaxivity, tumor targeting, high intra-tumoral distribution and no toxicity. To address the critical need, we have developed a novel class of protein-based MRI contrast agents (ProCAs) with significant improvement of both r_1 and r_2 relaxivities and *in vivo* dose efficiency in mouse models. Several key factors for relaxivitysuch as correlation time, exchangeable water numbers from first coordination shell and secondary/ outer sphere are improved by protein design of Gd^{3+} binding site(s) in stable proteins and protein modification. Our recent studies have shown that the Gd^{3+} binding constant of ProCAs is comparable to DTPA but metal selectivity for Gd^{3+} over physiological metal ions such as Ca^{2+}, Mg^{2+} and Zn^{2+} are >10000 fold than DTPA and there is no detectable cellular and animal toxicity. It enables non-invasive early detection primary liver tumors and metastatic tumors at 0.2 mm from the current threshold of 20 mm or larger. In addition, our developed ProCAs enable the 100 fold increase of detection size of metastatic liver tumors by MRI from the current threshold of 20 mm or larger with high confidence using our established melanoma metastatic mouse model. Furthermore, we have designed several MRI contrast agents that specifically targeting to cancer biomarkers including HER2, EGFR, GRPR, VEGFR, and CXCR4 that expressed on various types of cancers using animal models. These new classes of targeted MRI probes exhibit advantages in crossing the endothelial boundary, tissue distribution, and tumor tissue retention as demonstrated by even distribution of the imaging probe across the entire tumor mass. The capability to spatially and temporally visualize intratumoral distribution as well as quantification of the levels of major disease biomarkers would greatly improve our ability to track the change of the biomarkers during tumor progression, monitor treatment efficacy, aid in patient selection, and further develop novel targeted therapies for clinical application.

AUTHORS (LAST NAME, FIRST NAME): Yang, Jenny J.[3]; Xue, Shenghui[3]; Qiao, Jingjuan[3]; Pu, Fan[3]; Salarian, Mani[3]; Tan, Shanshan[4]; Patel, Anvi[1]; Liu, Zhi-ren[2]

INSTITUTIONS (ALL):

1. Georgia State University, Atlanta, GA, United States.
2. Biology, Georgia State University, Atlanta, GA, United States.
3. Chemistry, Georgia State University, Atlanta, GA, United States.
4. chemistry, Georgia state university, Atlanta, GA, United States.

(No Image Selected)

CONTROL ID: 2231888

TITLE: DCA promotes tumor progression in vitro and in vivo

PRESENTER: Benedikt Feuerecker

ABSTRACT BODY:

Abstract Body: INTRODUCTION Even in the presence of oxygen most cancer cells convert glucose to lactate via pyruvate instead of performing oxidative phosphorylation (aerobic glycolysis - Warburg effect). Therefore it has been considered to shift pyruvate - the entry metabolite of aerobic glycolysis - to acetylCoA by activation of pyruvate dehydrogenase (PDH). AcetylCoA will then be metabolized by oxidative phosphorylation. DCA has been described to alter the glucose metabolism of cancer cells by inhibition of pyruvate dehydrogenase kinase (PDK), which is a negative regulator of pyruvate dehydrogenase (PDH).[1,2,3,4] Therefore, the purpose of this study was to shift tumor cells from aerobic glycolysis to oxidative phosphorylation using dichloroacetate (DCA), an inhibitor of PDH-kinase.

METHODS The effects of DCA on proliferation/viability and PDH activity were assayed in vitro in Neuro-2a (murine neuroblastoma), Kelly and SK-N-SH (human neuroblastoma) as well as SkBr3 (human breast carcinoma) cell lines. The effects of DCA on tumor development were investigated in vivo using a xenograft model in which NMRI nu/nu mice were bearing subcutaneous Neuro-2a tumors. For that purpose animals were treated continuously with DCA (300 mg/l) in the drinking water or received normal drinking water. Tumor volumes and development were monitored using caliper measurements and via F-18-FDG-positron emission tomography.

RESULTS & DISCUSSION In this study we showed that DCA treatment increased viability/proliferation in Neuro-2a and SkBr3 cells, but did not cause significant alterations of PDH activity, whereas no significant effects of DCA were observed in Kelly and SK-N-SH cells. In mice bearing Neuro-2a xenografts, DCA significantly increased tumor proliferation compared to mock-treated mice. Thus, we could demonstrate that DCA – an indicated inhibitor of tumor growth[3,4] – efficiently promotes tumor growth in Neuro-2a cells in vitro and in vivo. In conclusion, our results indicate that therapeutic application of DCA should be carefully pondered with regard to the treated tumor type and possible adverse effects in vivo.

AUTHORS (LAST NAME, FIRST NAME): Feuerecker, Benedikt[1]; Seidl, Christof[3]; Pirsig, Sabine[1]; Bruchelt, Gernot[2]; Senekowitsch-Schmidtke, Reingard[1]

INSTITUTIONS (ALL):

1. Department of nuclear medicine, Technische Universität München, München, Germany.
2. Department of Pediatrics, Universitätsklinikum Tübingen, Tübingen, Germany.
3. Department of Obstetrics and Gynecology, Technische Univeristät München, Munich, Germany.

(No Image Selected)

CONTROL ID: 2233998

TITLE: Hyperpolarized 13C diffusion MRS of copolarized pyruvate and fumarate in the light of monitoring lactate export in different cancer cells

PRESENTER: Benedikt Feuerecker

ABSTRACT BODY:

Abstract Body: INTRODUCTION In the light of upregulation of glycolysis in tumors and acidification of tumor microenvironment, hyperpolarized ^{13}C-labelled metabolic tracers can be used to probe fast metabolic pathways in real-time. However, little has been known from these measurements about their presence in intra- or extracellular compartments, a distribution that is largely influenced by the expression of monocarboxylate transporters (MCT). NMR and MRSI can provide information about the metabolites' microenvironment as well as about the intactness of the plasma membrane (grade of necrosis).[1,2,3] The aim of this study is to examine whether hyperpolarized ^{13}C diffusion NMR can be used to detect differences in lactate export between tumor cell lines and to compare the sensitivity for diffuse necrosis between ADC measurements and enzymatic conversion from fumarate to malate.

METHODS ADCs of ^{13}C-metabolites were measured in MCF-7 tumor cells and 8932 pancreas carcinoma cells on a 14.1T NMR spectrometer. After injection of hyperpolarized [1-^{13}C]pyruvate and [1,4-$^{13}C_2$]fumarate at a final concentration of 2 mM each, the metabolites are taken up by the cells. The hyperpolarized label from pyruvate is intracellularly exchanged to lactate by LDH activity. In cells that are subject to necrosis the enzyme fumarase converts fumarate to malate. An established diffusion-weighted NMR pulse sequence based on a pulsed gradient spin echo sequence in combination with an 8 mm NMR tube in-vitro setup was used for measuring ADCs of hyperpolarized ^{13}C nuclei.[3] Approximately 20 Mio cells were used per experiment; for necrotic stage studies, some cultures of 8932 tumor cells were incubated with 1% Triton X-100 in the assay medium.

RESULTS & DISCUSSION ADCs of pyruvate, lactate and fumarate were detected in both breast cancer and pancreas carcinoma cells in-vitro and correlated to the degree of necrosis (Fig. 1A,B). In viable cells lactate ADC is lower than pyruvate ADC for both cell lines reflecting its intracellular origin, whereas pyruvate (at this comparatively high, injected dose) is predominantly distributed extracellularly. The ADC_{lac}/ADC_{pyr} ratio showed differences between the two cell lines with the ratio being higher in 8932 cells (range: [0.64:0.86]) compared with MCF-7 (range: [0.51:0.56])(Fig. 2A). This might reflect a lower MCT transport of lactate out of the cell in MCF-7 cells as compared to the pancreatic cancer cells which are known for their fast export of lactate (Fig. 2B,C).[4] Measurable amounts of malate were only detected in cells that were entirely necrotic after addition of Triton X-100 (Fig. 1C). In this state, no lactate was observed. Most likely LDH activity is hindered by the dilution of the coenzyme NADH. At the same time the ADCs of all metabolites were showing no large differences reflecting a blending of compartments. Thus, by using this co-polarized agent two essential states of a cell can be characterized simultaneously: a) The ADC_{lac}/ADC_{pyr} ratio reveals information about the microenvironmental differences between lactate and pyruvate being influenced by lactate transport rates and b) malate detects a fast and immediate process of cell death.

AUTHORS (LAST NAME, FIRST NAME): Feuerecker, Benedikt[1]; Durst, Markus[1]; Düwel, Stephan[1]; Saur, Dieter[3]; Menzel, Marion I.[2]; Schwaiger, Markus[1]; Schilling, Franz[1]

INSTITUTIONS (ALL):

1. Department of nuclear medicine, Klinikum rechts der Isar, Technische Universität München, München, Germany.
2. GE Global Research, Garching, Germany.
3. Department of internal medicine, Klinikum rechts der Isar, Technische Universität München, München, Germany.

(No Image Selected)

CONTROL ID: 2231899

TITLE: Administration route dependent effects of tumor-associated antigen specific Th1 cells during immunotherapy of cancer

PRESENTER: Christoph Griessinger

ABSTRACT BODY:

Abstract Body: Tumor-associated antigen specific Interferon-γ producing $CD4^+$ T helper cells (TAA-Th1) induce strong antitumoral effects and represent a promising alternative for $CD8^+$ T cell immunotherapies against cancer. T cell immunotherapies require well characterized treatment schemes including the right administration route, dosage and injection frequency. So far antitumoral mechanisms of TAA-Th1 cells are poorly understood. We previously showed the therapeutic efficiency of Tag2-Th1 cells after intra-venously (*i.v.*) or intra-peritoneally (*i.p.*) transfer in an endogenous insular cell carcinoma model (RIP1-Tag2) over 17 weeks by MRI. In subsequent studies we performed comprehensive studies to characterize Tag2-Th1 homing dynamics and influences on the immune system of the treated animals.

5 weeks old RIP1-Tag2-mice were initially irradiated with 2Gy and injected once weekly *i.v.* or *i.p.* with 10^7 Tag2-Th1 cells or PBS (SHAM) until 15 weeks of age. We monitored the treatment efficiency by determination of the blood glucose levels (BGL; marker for tumor burden) and MRI in 13 weeks old mice. For cell tracking studies we labelled Tag2-Th1 cells with the fluorescence dye DiD, injected 10^7 DiD-Tag2-Th1 *i.v.* or *i.p.* in 14 weeks old treated RIP1-Tag2 mice and performed *in vivo* and *ex vivo* optical imaging (OI). Additionally, we performed H&E histology and immunohistochemistry of the carcinomas as well as flow cytometry of the T cell homing sites.

14 weeks old *i.v.* treated RIP1-Tag2 mice exhibited 13% higher BGL (93±4 mg/dl) compared to *i.p.* treated animals (82±5 mg/dl) whereas the BGL in SHAM-treated animals dropped to 41±3 mg/dl. *In vivo* MRI of 13 weeks old mice revealed a reduced volume and number of insular carcinomas after *i.v.* when compared to *i.p.* treatment. OI cell tracking studies revealed a striking homing of the *i.p.* transferred DiD-Tag2-Th1 cells to the carcinomas, whereas only faint homing was observed after *i.v.* administration. After *i.v.* administration Tag2-Th1 cells homed into the lung, liver, and spleen and after *i.p.* administration into the spleen, the perithymic and mesenteric lymph nodes. H&E histology of the pancreatic tissue yielded smaller tumors after *i.v.* treatment. In the thymus *i.v.* treatment induced atrophy, *i.p.* treatment thymus depletion, whereas the thymus of SHAM-treated animals appeared normal. No histological alterations were observed in other homing sites. CD3- and B220-immunohistochemistry revealed T- and B-cells at the margins and in the carcinomas after *i.v.* and *i.p.* treatment. Flow cytometry uncovered a reduced number of $CD8^+$ T cells and an increased number of $CD4^+$ T cells within the pancreatic lymph nodes and the spleens of both treatment regimes. Up to 50% of the $CD4^+$ T cells were identified as Tag2-Th1 cells. Both treatment regimes provoked an increased expression of dendritic and myeloid derived suppressor cells. Our results uncovered that both Tag2-Th1 cell administration routes induced impressive antitumoral effects with enormous alterations of the host immune system. In summary, *i.v.* treatment exhibited a slightly higher antitumoral efficiency compared to *i.p.* treatment despite a reduced homing to the carcinomas.

AUTHORS (LAST NAME, FIRST NAME): Griessinger, Christoph M.[1]; Schmid, Andreas M.[1]; Schörg, Barbara F.[1]; Krüger, Dominik B.[1]; Bukala, Daniel[1]; Kohlhofer, Ursula[2]; Quintanilla-Martinez, Leticia[2]; Röcken, Martin[3]; Pichler, Bernd J.[1]; Kneilling, Manfred[1, 3]

INSTITUTIONS (ALL):

1. Werner Siemens Imaging Center, Department of Preclinical Imaging and Radiopharmacy, Eberhard Karls University Tübingen, Tübingen, Germany.
2. Department of Pathology, Eberhard Karls University Tübingen, Tübingen, Germany.
3. Department of Dermatology, Eberhard Karls University Tübingen, Tübingen, Germany.

(No Image Selected)

CONTROL ID: 2231935

TITLE: Age-related changes in CSF dynamics assessed with PET/MR imaging of simultaneous intra-cisternal Gd-DTPA and ^{89}Zr-DTPA infusion in young and old beagle dogs

PRESENTER: Tyler Wellman

ABSTRACT BODY:

Abstract Body: A hallmark of many neurodegenerative diseases is the accumulation of misfolded protein aggregates such as amyloid-beta (Aβ) with increasing age. The recently discovered “glymphatic system” appears to play a critical role in the clearance of metabolic waste products such as Aβ from the brain[1]. This system shows increased activity during sleep[2] and reduced activity with aging in mice[3]. Although cerebrospinal fluid (CSF) dynamics in the glymphatic system are thought to play a role in pathogenic protein aggregation, changes in glymphatic function with aging have yet to be quantitatively mapped or studied in a model similar in size and structure to the human brain.

In this study, we used dynamic PET/MR imaging of simultaneous intra-cisternal (IC) infusion of Gd-DTPA and ^{89}Zr-DTPA to quantify regional CSF dynamics in young and old beagle dogs as a model for the aging human brain. Three young (4.4±0.3 years old) and three old (15.8±2.5 years old) dogs were anesthetized and imaged with PET/MR for 4.5 hours following the start of a 20 min IC infusion of a mixture of ~0.125M Gd-DTPA (Magnevist) and 33.7±8.6 MBq ^{89}Zr-DTPA via surgically-placed catheter. T1-weighted MR images were acquired every 5 min, and PET data were reconstructed into frames corresponding to 5 min bins. For each animal, all images were co-registered to the baseline MR image, and a 45-region symmetric brain atlas was fit to the MR data. ^{89}Zr-DTPA kinetics were assessed in each atlas region as well as in the retropharyngeal lymph nodes, which were demarcated in the MR images.

In all dogs, both tracers moved rapidly up the ventral midline of the brain following convective glymphatic flow (Figure 1A). Brain regions close to the injection site on the ventral side of the brain (e.g., pons; Figure 1B) showed similar kinetic behaviors between young and olds dogs, with early influx in the first hour followed by slower efflux rates as the tracer spread throughout the CSF volume and into the parenchyma. Penetration of ^{89}Zr-DTPA into the dorsal brain regions (e.g., coronal gyrus; Figure 1C) was observed in young dogs, whereas old dogs showed tracer distribution limited to the ventral side of the brain even at 4 hours after infusion. Lymphatic outflow of ^{89}Zr-DTPA resulting from CSF-ISF exchange was also different between young and old dogs (Figure 1D). Progressively increasing lymphatic ^{89}Zr-DTPA concentration was observed in all 3 young dogs, while no lymphatic ^{89}Zr-DTPA was detected in old dogs.

In conclusion, using a multi-modal approach which allowed us to quantify absolute tracer concentrations in precisely delineated anatomical regions of the brain, we found significantly limited CSF penetration and reduced glymphatic flow in aged dogs, with a preponderance of dysfunction toward dorsal regions. These findings support a role of impaired CSF flow in the pathogenesis of neurodegenerative disorders, and emphasize the importance of CSF dynamics for delivery of therapeutic drugs to specific regions of the aging brain.

References

1. Iliff et al. *Sci Transl Med*. 2012;4(147)

2. Mendelsohn AR, Larrick JW. *Rejuvenation Res.* 2013;16(6):518-523

3. Kress et al. *Ann Neurol*. 2014;76(6):845-861

AUTHORS (LAST NAME, FIRST NAME): Wellman, Tyler J.[1]; Dobson, Howard[1, 2]; Sullivan, Jenna M.[1]; Biernaski, Heather[3]; Butler, John R.[3]; Deans, Lela[3]; Sykes, Jane[3]; Hoppin, Jack[1]; Verma, Ajay[4]

INSTITUTIONS (ALL):

1. inviCRO LLC, Boston, MA, United States.
2. InterVivo Solutions, Toronto, ON, Canada.
3. Lawson Health Research Institute, Western University, London, ON, Canada.
4. Biogen Idec, Cambridge, MA, United States.

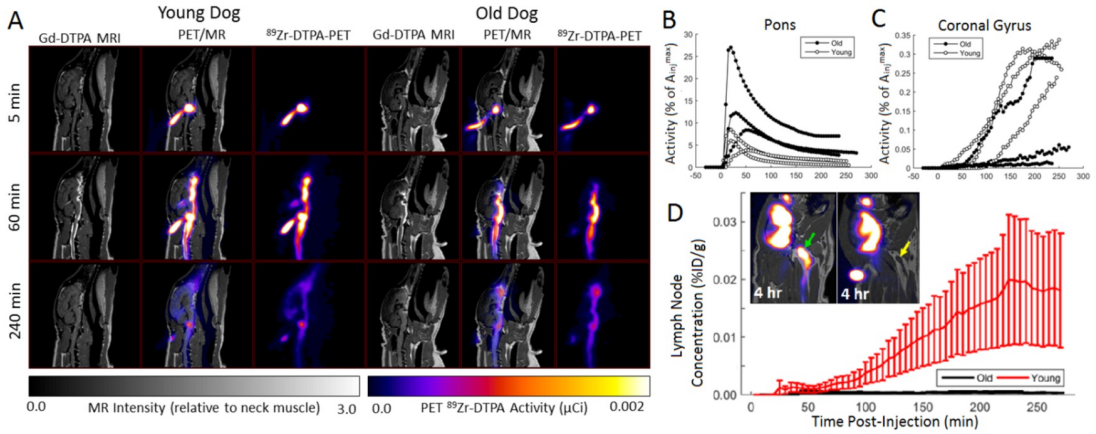

Figure 1. PET/MR imaging of CSF dynamics in young versus old beagle dogs. (A) Following co-infusion of Gd-DTPA and ^{89}Zr-DTPA, dogs were imaged every 5 minutes for 4.5 hours. Differences in tracer distribution developed over time, with significantly higher tracer delivery in dorsal brain regions of young (<5 year-old) compared to old (>14 year-old) dogs. ^{89}Zr-DTPA kinetics were similar in regions close to the injection site such as the pons (B), but distinct in dorsal brain regions such as the coronal gyrus (C). Lymphatic outflow resulting from CSF-ISF exchange in the glymphatic system was significantly more active in young than in old animals (D).

CONTROL ID: 2231944

TITLE: Workflow of sequential *in vivo* Magnetic Particle Imaging and *in vivo* Magnetic Resonance Imaging in mouse

PRESENTER: Michael Kaul

ABSTRACT BODY:

Abstract Body: Purpose: For the first time a commercial preclinical magnetic particle imaging scanner is available. It was our goal to organize a workflow between MPI and magnetic resonance imaging (MRI) and to generate the first fused MR-MP images.

Materials and Methods: The MPI examinations of five mice were performed with the Philips Preclinical MPI Package, consisting of a Bruker Preclinical MPI system and dedicated MPI- and MRI-compatible Minerve animal handling equipment. MRI reference imaging was performed on a 7 Tesla MRI scanner (ClinScan, Bruker). The mice were anaesthetized with isoflurane, a catheter for a tail vein tracer injection was prepared. Then it was placed on a bench that can be easily attached to technical support unites (TSU) located at the positioning systems of the scanners. The TSUs provided connectors for isoflurane, air heating, and for sensors to detect vital signals.

First, MRI for anatomic referencing was performed (T2w 2D turbo spin echo sequence coronal, sagittal, and transverse orientation: FOV 32 mm, matrix 256x256, slices 28, thickness 0.8 mm (no gap), TR 1100 (triggered on every respiratory cycle), TE 28, turbo factor 8, NSA 3. Then the mouse was transferred to the MPI scanners located 10 meters away. Static and dynamic MPI scans were performed with a drive field amplitude of 10 mT and a selection field gradient of 1.0 T/m covering a volume of 40x40x20mm³. A bolus injection of 50 µL ferucarbotran (Bayer Schering, Japan) was performed during the dynamic scan with a temporal resolution of 21.5 msec per 3D volume. Finally, a MRI scan was repeated to prove the successful SPIO injection.

Later on, MPI images were reconstructed with a temporal resolution of 2.15 sec und 3.0x3.0x1.5 mm³ voxel size (ParaVision 6.0/MPI, Bruker). The images of the injection phase were co-registered with the MRI data (Imalytics, Philips).

Results: We established a practical workflow of a combined preclinical MRI and MPI examination. A successful injection of ferucarbotran was proven by MPI and MRI. By registration of the image data sets the signal increase in the MPI images shortly after the injection could be allocated to the vena cava and the heart. The pre and post injection MRI did not show any dislocation of the mouse.

Our measurements clearly point out the need of a combined MR–MPI workflow. In our case, we performed sequential measurements using the MRI before and after the MPI scan. A limitation of this study is the high trace dose of 0.9 mmol/kg that was applied. Based on this proposed workflow, in future we will examine aspects of sensitivity and dosage form on the reconstruction performance.

Conclusion: MPI is an imaging technology with high potential, due to the absence of ionizing radiation and its speed for imaging the distribution of the applied tracers. It is a new tool for angiography and perfusion measurements and suggests itself for tracer analytics as applied in molecular imaging.

AUTHORS (LAST NAME, FIRST NAME): Kaul, Michael G.[1]; Ittrich, Harald[1]; Jung, Caroline[1]; Mummert, Tobias[1]; Reitmeier, Aline[2]; Knopp, Tobias[1, 3]; Adam, Gerhard[1]

INSTITUTIONS (ALL):

1. Department of Diagnostic and Interventional Radiology, University Medical Center Hamburg-Eppendorf, Hamburg, Germany.

2. Animal Care Unit, University Medical Center Hamburg-Eppendorf, Hamburg, Germany.

3. Hamburg University of Technology, Hamburg, Germany.

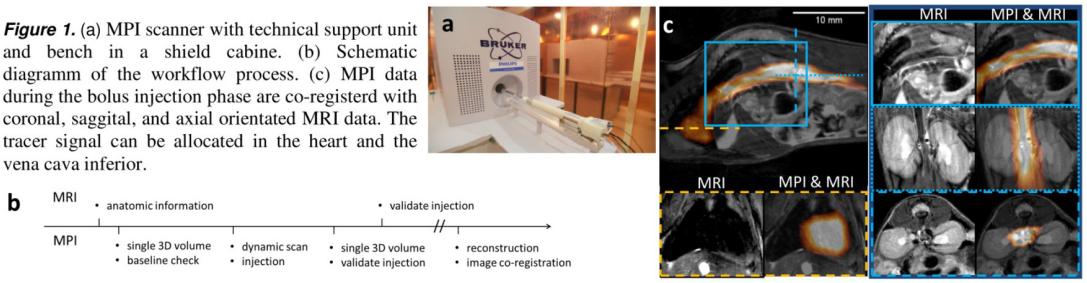

Figure 1. (a) MPI scanner with technical support unit and bench in a shield cabine. (b) Schematic diagramm of the workflow process. (c) MPI data during the bolus injection phase are co-registerd with coronal, saggital, and axial orientated MRI data. The tracer signal can be allocated in the heart and the vena cava inferior.

CONTROL ID: 2231947

TITLE: Targeting CA19.9 for Radioimmunotherapy and Therapeutic Monitoring in Pancreatic Cancer

PRESENTER: Ryan Lanning

ABSTRACT BODY:

Abstract Body: Objective: Outcomes for locally advanced or metastatic pancreatic cancer (PCa) are dismal with survival measured in months. Treatment options are limited to systemic chemotherapy and radiation therapy, which only modestly improve survival. There is an unmet need for new therapies and diagnostic imaging modalities. We adapted 5B1 an anti-CA19.9 human antibody, which showed exquisite tumor uptake in PET studies[1], to serve as a radioimmunotherapy (RIT) construct.

Materials/Methods: As candidates for RIT, we selected the radioisotopes Yttrium-90 (^{90}Y) and Lutetium-177 (^{177}Lu) for their biologically relevant β-emission path lengths and half-lives. 5B1 was functionalized with either DOTA or CHX-A”-DPTA and radiolabeled with ^{90}Y or ^{177}Lu. Immunoreactivity (IR) of each RIT construct was assessed by Lindmo assay using CA19.9-positive BxPC3 PCa cells. *In vivo* biodistribution (bioD) and therapy studies were performed in nude mice bearing BxPC3 xenografts on the right flank. Therapy studies using 4 different doses for both ^{90}Y and ^{177}Lu were initiated when tumors reached ~100mm^3. Tumor size was measured manually using calipers. At completion of therapy, animals were randomly selected for positron emission tomography (PET) and bioD studies using ^{89}Zr-labeled 5B1 (^{89}Zr-DFO-5B1).

Results: The CHX-A”-DPTA constructs demonstrated significantly better IR than the DOTA-5B1 constructs (95.3% vs 85.6%, P<0.0001). The DOTA-5B1 constructs showed excellent tumor localization at 48 and 120 hours post-injection (^{90}Y-DOTA-5B1: 79±6 & 77±27 %ID/g; ^{177}Lu-DOTA-5B1: 23±6 & 38±14 %ID/g; n=5). The DOTA constructs had elevated reticuloendothelial system uptake so preclinical therapy studies were performed with the CHX-A”-DPTA conjugates. Control groups consisted of both saline (n=8) and 5B1 (250µg, n=8). Doses for each ^{90}Y-CHX-A”-DPTA-5B1 treatment group were 25, 50, 100, and 250 µCi (n=8 each). The estimated tumor absorbed dose matched activities for ^{177}Lu-CHX-A”-DPTA-5B1 were 75, 150, 300, and 450 µCi. By 2 weeks after administration, all RIT treatment groups demonstrated significant tumor growth delay and regression compared to the control groups. After 3 weeks, the 25 µCi ^{90}Y cohort no longer exhibited a significant growth delay. Mice from the 2 middle RIT doses for each construct were injected with 130µCi of ^{89}Zr-DFO-5B1 on day 60 (n=4 each). PET imaging demonstrated uptake in both the treated and control tumors. Post-PET necropsy revealed higher tumor ^{89}Zr-DFO-5B1 uptake for all the treated mice versus the controls (5B1: 55±53 %ID/g; Saline: 122±53 %ID/g), statistically higher for the 150µCi ^{177}Lu (314±148 %ID/g) and 50µCi ^{90}Y (334±199 %ID/g) groups.

Conclusion: RIT scaffolds targeting CA19.9 in preclinical models demonstrate significant tumor cytotoxicity with either ^{90}Y or ^{177}Lu. Tumor selectivity of 5B1 constructs remained elevated over controls at the completion of therapy indicating possible continued high expression of CA19.9 and a potential benefit from fractionated RIT, proving versatile for both delivering and monitoring therapy in pancreatic cancer.

[1] Viola-Villegas et al. J. Nucl. Med. 2013, 54(11):1876-82

AUTHORS (LAST NAME, FIRST NAME): Lanning, Ryan M.[1]; Houghton, Jacob[2]; Abdel-Atti, Dalya[2]; Gupta, Simran[2]; Sawada, Ritsuko[3]; Scholz, Wolfgang W.[3]; Lewis, Jason S.[2]

INSTITUTIONS (ALL):

1. Radiation Oncology, Memorial Sloan Kettering Cancer Center, New York, NY, United States.
2. Radiology, Memorial Sloan Kettering Cancer Center, New York, NY, United States.
3. MabVax Therapeutics, Inc, San Diego, CA, United States.

(No Image Selected)

CONTROL ID: 2231971

TITLE: Spiropyran Sensors of Glutathione and Cysteine: Substituent Effects on Thiol Selectivity.

PRESENTER: Brandon Tautges

ABSTRACT BODY:

Abstract Body: Background: Oxidative stress has been shown to precede and contribute to the progression of diseases including cancer, cardiovascular disease, and neurodegenerative disorders.[1] Promising markers of oxidative stress include biothiols, such as glutathione and cysteine, which are found in high cellular (1-10 mM) and extracellular (3-21 μM) concentrations as well as in the cytosol.[2] Current methods to measure biothiols levels require expensive instrumentation and sample pretreatment before these analytical techniques can be performed, limiting their applicability. *In vivo* imaging of thiol levels promises temporal and spatial resolution of regions of oxidative stress that current quantfication techniques cannot provide. This information is crucial to understanding disease pathogenesis and early detection. It has previously been shown that spiropyrans can be adapted for magnetic resonance imaging, creating an magnetic resonance imaging (MRI) probe sensitive to NADH.[3] Herein, we present the synthesis and characterization of spiropyran sensors for quanitification of biothiol levels. These spiropyran probes were developed with a functional hydroxyl linker for future conjugation to an MRI contrast agent for *in vivo* imaging of thiol levels. **Methods:** Spiropyran sensors were synthesized via condensation reaction of dinitrosalicylaldehyde with a substituted Fischer's base which was accessed via Sandmeyer reaction and subsequent Fischer indole synthesis. Solutions of the photoswitches were made in a 50/50 Ethanol/PBS (pH 7.4) mixture and incubated with one equivalent of an amino acid to evaluate colorimetric sensing. Isomerization of molecular switches response to thiols was monitored using UV-vis spectroscopy. The change in absorbance at the λ_{max} of the merocyanine form of spiropyrans was used to determine photoswitch response to thiols. **Results:** By modifying substituent patterns it was possible to modulate selectivity of spiropyran molecular switches towards different thiol species. Selective placement of a hydroxyl linker on a dinitro spiropyran was capable of inducing cysteine selectivity over other competing thiol species, namely glutathione and homocysteine. Modifying the substitution pattern of the chromene ring also accessed a glutathione selective probe. While thiol selective probes have been reported in the literature, there are only a few examples of colorimetric or fluoresecent probes that can distinguish among cysteine, homocysteine, and gluthatione species. This work demonstrates the utility of spiropyrans for the quantification of specific thiols in the presence of competing thiol species, making them attractive probes for conjugation to MRI contrast agents for *in vivo* redox imaging. [1] Drake, J.; Link, C.D.; Butterfield, A. Oxidative stress precedes fibrillar deposition of Alzheimers disease amyloid β-peptide (1-42) in a transgenic *Caenorhabditis elegans* model. *Nuerology of Aging*. **2003**. *24*. 415-420. [2] Meister, A.; Anderson, M.E.; Glutathion. *Ann. Rev. Biochem.* **1983**. *52*. 711-760 [3] Tu, C.; Nagao, R.; Louie, A.Y. Multimodal Magnetic-Resonance/Optical-Imaging Contrast Agent Sensitive to NADH. *Angewandte Chemie*. **2009**. *48*. 6547-6551

AUTHORS (LAST NAME, FIRST NAME): Tautges, Brandon[1]; Or, Victor W.[1]; Louie, Angelique[2]

INSTITUTIONS (ALL):

1. Chemistry, University of California, Davis, Davis, CA, United States.
2. Biomedical Engineering, University of California, Davis, Davis, CA, United States.

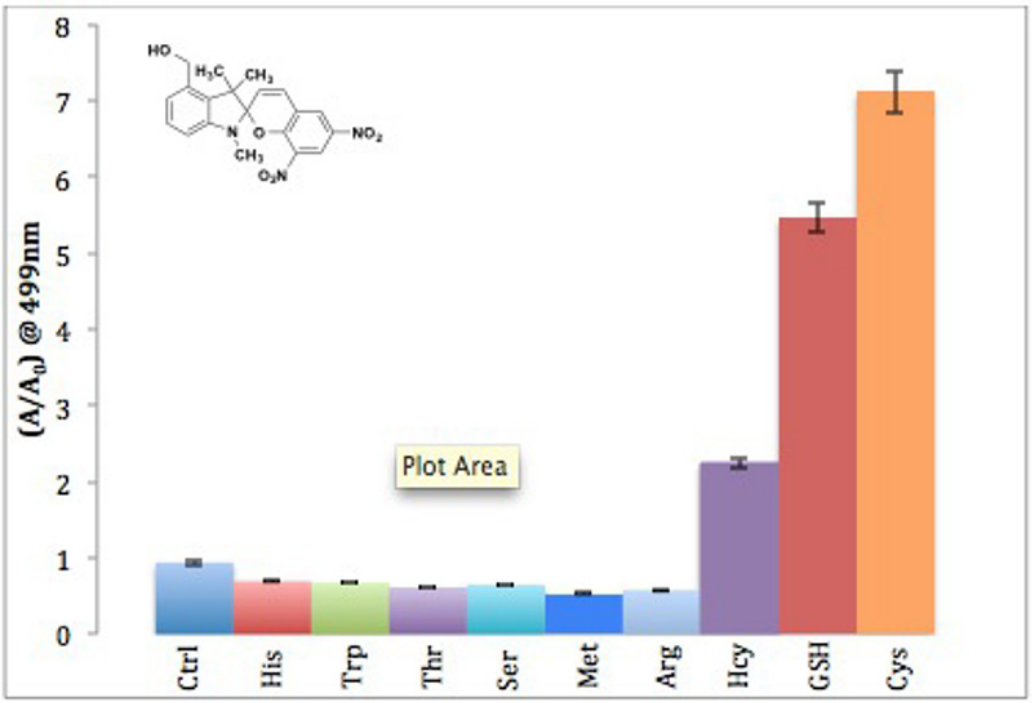
8
7
6
5
4
3
2
1
0
(A/A0) @ 499nm
Plot Area
Ctrl
His
Trp
Thr
Ser
Met
Arg
Hcy
GSH
Cys

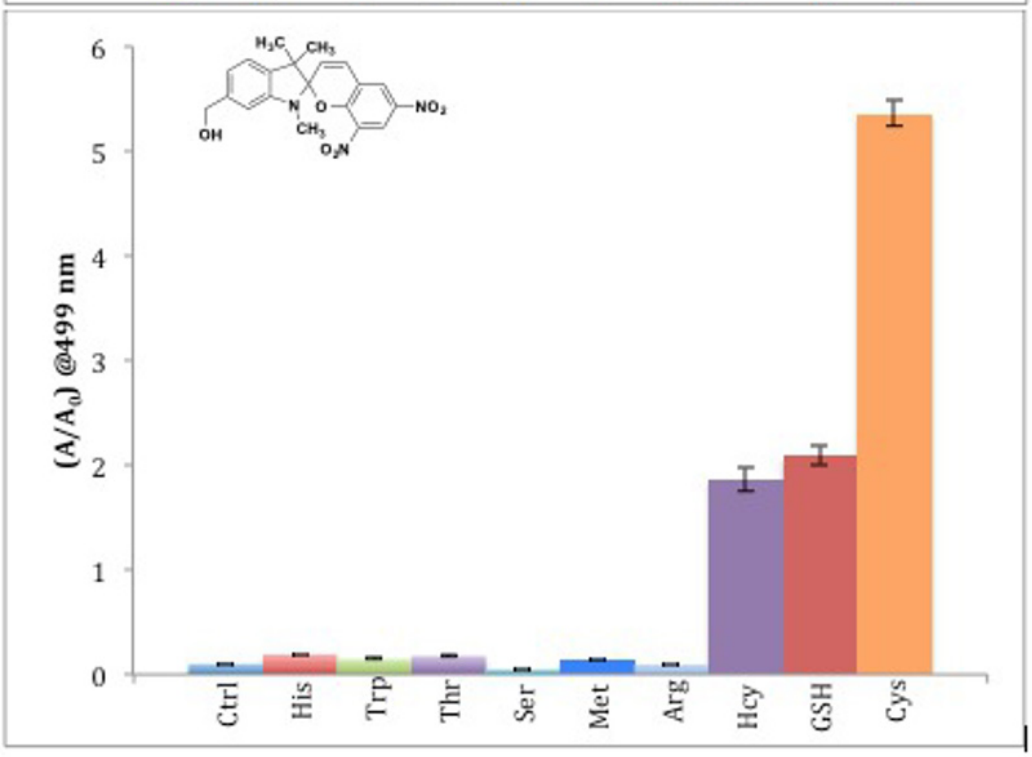
6
5
4
3
2
1
0
(A/A0) @499 nm
Ctrl
His
Trp
Thr
Ser
Met
Arg
Hcy
GSH
Cys

CONTROL ID: 2231977

TITLE: Micro- and nano- bubble based dual modality ultrasound and photoacoustic contrast agents for *in vivo* prostate cancer detection

PRESENTER: Sri Rajasekhar Kothapalli

ABSTRACT BODY:

Abstract Body: Transrectal ultrasound (TRUS)-guided random prostate biopsy prompted by elevated serum prostate specific antigen (PSA) levels is the standard screening method for prostate cancer but has limited diagnostic capabilities. Novel imaging technologies that simultaneously visualize anatomical, functional and molecular information of the tissue are an attractive choice for disease screening and therapy monitoring. Synergizing TRUS and photoacoustic imaging (PAI) approaches, we recently developed and translated an integrated transrectal ultrasound and photoacoustic (TRUSPA) device for dual-modality human prostate imaging. Our first-in-human results (n>10) demonstrated that TRUSPA can simultaneously display structural information of the prostate in ultrasound mode, and hemoglobin absorption derived intrinsic optical contrast of the prostate in photoacoustic mode. These clinical results motivated us to investigate clinically translatable extrinsic molecular contrast agents that would be administered to patients and improve the sensitivity and specificity of TRUSPA for the prostate cancer detection.

Using FDA approved ultrasound and optical contrast agents, poly lactic-*co*-glycolic acid (PLGA) microbubbles and Indocyanine green (ICG), we developed dual modality ICG-encapsulated microbubbles (~ 1.5 μm in size with PDI 0.6) that provide both ultrasound and photoacoustic contrast. Because micron size bubbles are limited to vascular targeting, we also developed ICG-encapsulated nanobububles (~200 nm in size with PDI 0.094) that extravasate tumor vasculature. We optimized ICG concentration and size of these micro- and nano- bubbles. While the peak absorption wavelength of pure ICG changed from 780 nm to 700 nm with concentrations of 0.005 to 1 mg/mL, ICG-encapsulated-bubbles demonstrated narrow spectral profiles with peak optical absorption around 780 nm. Our phantom experiments showed that quantified PA and US signal intensities vary linearly (R^2=0.96) with the concentration of the respective bubbles. The limit of detection of these bubbles were found to be 0.03125 mg/ml. In addition, our *in vivo* longitudinal experiments with subcutaneous PC3 tumor bearing mice (n=6) demonstrated that these dual modality micro- and nano-bubbles increase in tumor vascular PA signal with ICG-encapsulated microbubbles and increase intra- and extra-vascular PA signal with nanobubbles. The peak imaging time was 60 minutes. In addition, our *in vitro* cell toxicity showed that toxicity increases with increasing concentrations of these agents. We also synthesized these bubbles with IR800 and Atto740 to further improve photostability and molecular targeting capabilities of these bubbles and the results are.

To our knowledge, this data is the first reported *in vivo* application of such dual modality bubbles for ultrasound and photoacoustic imaging. Biomarker-specific molecular targeting approaches with these bubbles have high potential to predict the prognosis of the prostate cancer.

AUTHORS (LAST NAME, FIRST NAME): Kothapalli, Sri Rajasekhar [1]; Lin, Vincent[3]; Jokerst, Jesse V.[1]; Chang, Huan-Yu D.[1]; Gambhir, Sanjiv S.[2]

INSTITUTIONS (ALL):

1. Radiology, Stanford University, Palo Alto, CA, United States.
2. Radiology Department, Stanford University, Stanford, CA, United States.
3. Harvard, Cambridge, MA, United States.

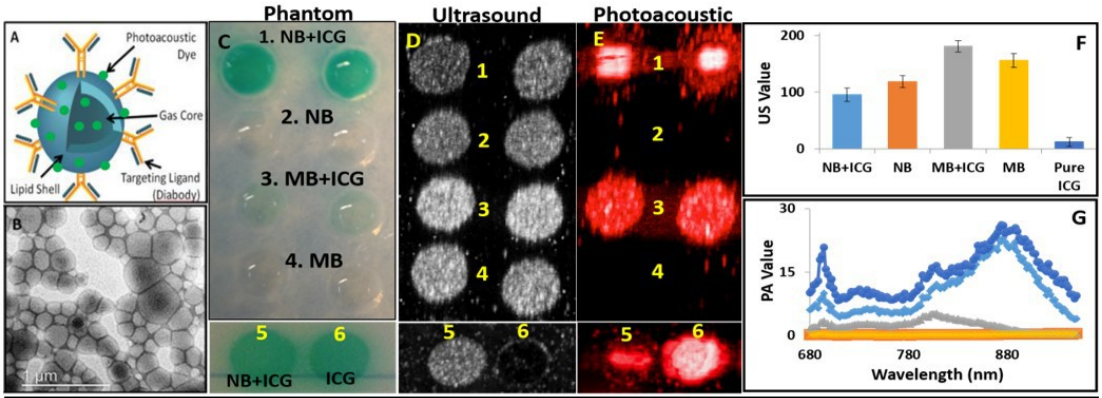

Figure 1: Indocyanine green (ICG)-encapsulated micro- and nano- bubble molecular imaging agents. A) Schematic representation of micro- or nano- bubbles consisting of a gaseous core for ultrasound, indocyanine green (ICG) dye for photoacoustics, and a lipid shell for stabilization. These agents can be further functionalized to bind to cancer cells using targeting ligands. Photoacoustic/fluorescent dyes, e.g., IR800 and Atto740 were also placed in the shell. B) Electron microscopy (EM) images of 225 nm sized nanobububles. The non-spherical shape is due to the high vacuum of EM imaging and does not reflect the nanobubble's hydrated morphology. C-E) Ultrasound and photoacoustic (PAI) signal of nanobubbles (NB) and microbubbles (MB) with and without ICG imaged in a phantom. F-G) US and PA signals of these dual modality micro- and nano- bubble agents and pure ICG were quantified. We used Vevo LAZR small animal imaging system for this experiment.

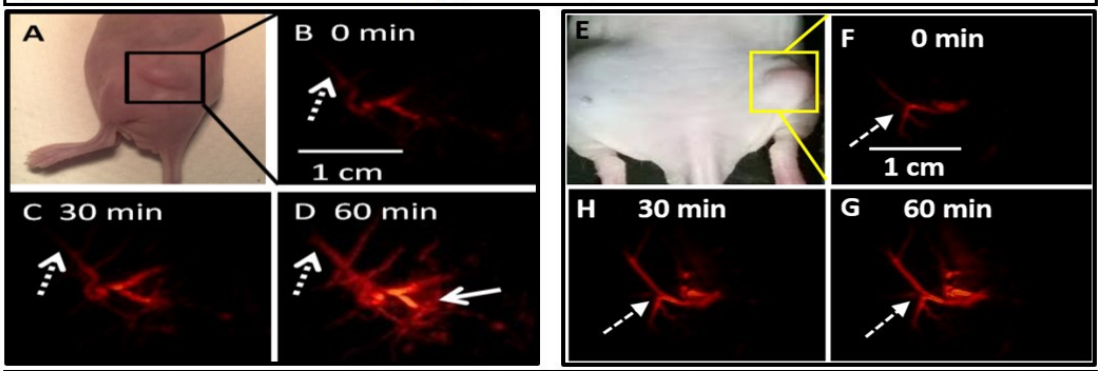

Figure 2: In vivo Photoacoustic Imaging of ICG-encapsulated micro- and nano- bubbles in prostate cancer mice models. Mice carrying xenograft prostate tumors from PC3 cells were injected by tail vein with ICG-encapsulated nanobubbles (A-D) and ICG encapsulated micro bubbles (E-G) and imaged at different time points of injection. Images represent a sagittal maximum intensity projection. Even in the pre-injection images (0 min) there is some photoacoustic signal in the vasculature (dashed arrow) due to absorption from hemoglobin molecules. This vascular signal increases with time for both micro- and nano- bubbles. However, for the ICG-encapsulated nanobubbles an increase in extra-vascular PA signal (solid arrow in D) also occurs at the later time point due to extravasation. A tomographic small animal photoacoustic imaging scanner was (Endra, Inc.) used for these longitudinal imaging studies. Scale bar in B and F apply to all images.

CONTROL ID: 2234065

TITLE: Multimodal Nano Probe for *in vivo* Cell Tracking.

PRESENTER: Manuela Ventura

ABSTRACT BODY:

Abstract Body: Introduction: Cell-based therapies hold great promise for treatment of a variety of diseases including cancer. The ability to inertly label cells of interest for non-invasive tracking of their *in vivo* delivery and distribution has the potential to improve our understanding of the mechanisms of disease development and optimize cell-based therapies. Our study reports the successful labeling and image-based tracking of breast cancer (BC) cells *in vitro* and i *n vivo* using a dual-modality near-infrared (NIR) fluorescence and computed tomography (CT) liposome-based nano probe (CF800). **Methods:** CF800 is a liposome formulation co-encapsulating iohexol (50mg/mL of iodine) and 100mg/mL indocyanine green (ICG). It was used to label the triple-negative human BC cell line MDA-MB231-Luc. The cell uptake efficiency and retention of CF800 were quantified and cell viability and proliferation was closely monitored. *In vitro,* 24h after cell seeding, the CF800 liposomes were added to the cells at 0, 1, 2, 5 and 10% of the total culture media volume and were incubated for 1, 6 and 24h. *In vivo*, a 24h incubation period with $10\%_{vol}$ CF800 was selected. Female SCID mice were injected with $4x10^6$ of either CF800-labeled (n=3) or unlabeled (n=3) MDA-MB231-Luc cells into their inguinal mammary fat pad (MFP). Mice were imaged with bioluminescence (IVIS, Perkin-Elmer), NIR fluorescence (Maestro, Perkin-Elmer) and CT (Locus Ultra, GE) on days 0, 1, 3, 6, 8, 10 and 14 post-inoculation. **Results:** *In vitro* cell labeling with CF800 was both time and dose-dependent. The uptake efficiency measured by NIR fluorescence ranged from 3.17±0.5% after 1h incubation to 28.5±0.2% after 24h incubation with $10\%_{vol}$ liposome concentration. The 24h incubation period was the most efficient in terms of uptake percentage and cellular retention, at all tested liposome concentrations. Specifically, it yielded a mean signal per cell that is 3.5±1.6 times higher compared to 1h incubation, and 1.8±0.2 times greater compared to 6h incubation, without affecting cell viability or proliferation. CF800 labeling also achieved prolonged intracellular retention. Although a decrease in the mean fluorescence signal-per-cell was observed over the 3-day period as a result of cell division, no significant changes were measured in the total fluorescence signal at 96h, indicating robust intracellular retention of CF800. *In vivo*, longitudinal CT and NIR fluorescence tracking of the labeled cells was possible for at least 14 days. The labeled tumor sites showed significantly higher fluorescence signal compared to muscle (signal ratio of 32.4±15.1). No detectable signal was measured at the tumor site of mice that received the unlabeled tumor cells. CT imaging showed significant contrast at the tumor site formed from labeled cells with mean HU values of 123.1±14.5 vs. 67.7±5.7 measured in the unlabeled tumors and 54.4±2.5 in muscle at 14 days post-inoculation. **Conclusion:** CF800 has demonstrated to be a suitable imaging agent for *in vitro* cell labeling and longitudinal *in vivo* cell tracking applications. The feasibility of using the same nano agent to label and track therapeutic cells is currently under investigation.

AUTHORS (LAST NAME, FIRST NAME): Ventura, Manuela[1]; Fan, Linyu[1]; Zheng, Jinzi[1, 2]

INSTITUTIONS (ALL):

1. TECHNA Institute for the Advancement of Technology for Health, University Health Network, Toronto, ON, Canada.

2. Institute of Biomaterials & Biomedical Engineering, University of Toronto , Toronto, ON, Canada.

(No Image Selected)

CONTROL ID: 2231993

TITLE: Detection of anti-PD-L1 responders using anti-CD8 immunoPET in a mouse model of colon carcinoma.

PRESENTER: Richard Tavaré

ABSTRACT BODY:

Abstract Body: Programmed death-ligand 1 (PD-L1) and its receptor PD-1 are immune checkpoints that have been implicated in promoting immune evasion in the tumor microenvironment. Antibodies that block the PD-1/PD-L1 interaction restore anti-tumor activity and have shown tumor responses in patients with a variety of cancers. In mouse models, it has been shown that response to checkpoint blockade therapy is $CD8^+$ T cell dependent. A technique to noninvasively detect alterations in systemic and tumor-infiltrating $CD8^+$ lymphocytes, such as anti-CD8 immunoPET (1), could help guide the success of immunotherapies, including checkpoint blockade.

In this study, Balb/c mice bearing syngeneic CT26 colon carcinoma xenografts were treated with anti-PD-L1 therapy that has been shown to cause regression of CT26 tumors in ~30 % of treated mice (2). Anti-CD8 immunoPET was used to detect changes in cytotoxic $CD8^+$ tumor infiltrating lymphocytes. Specifically, an anti-mouse CD8 cys-diabody (cDb; scFv dimer) engineered from the parental rat anti-mouse CD8 depleting YTS169 hybridoma was site-specifically conjugated to maleimide-DFO for subsequent ^{89}Zr radiolabeling and immunoPET acquisition (radiolabeling efficiency: 98.8 ± 1.2 %; specific activity: 4.6 ± 0.2 μCi/μg; immuno-reactive fraction: 86.6 ± 1.6 %).

Mice bearing week old CT26 xenografts were treated with anti-PD-L1 therapy and subsequently divided into three groups for anti-CD8 immunoPET imaging at day 8 post-therapy induction: (1) no anti-PD-L1 treatment, (2) anti-PD-L1 non-responders (tumor average diameter > 8 mm), and (3) anti-PD-L1 responders (tumor average diameter < 8 mm). ImmunoPET images show increased intratumoral probe accumulation in the anti-PD-L1 responder group compared to both the control and anti-PD-L1 non-responder group. Biodistribution studies confirm the immunoPET data showing the anti-PD-L1 responders, anti-PD-L1 non-responders, and control mice had uptake of 11 ± 2.7 %ID/g, 6.4 ± 1.0 %ID/g, and 6.0 ± 0.83 %ID/g, respectively. Flow cytometry was used to confirm an increase of $CD45^+/CD8^+$ tumor infiltrating T cells in anti-PD-L1 responding mice. This work demonstrates the feasibility of detecting $CD8^+$ tumor infiltrating lymphocytes in models of checkpoint blockade therapy and was shown to distinguish between responding and non-responding mice. Importantly, anti-CD8 immunoPET can be expanded to alternative therapeutic strategies to monitor efficacy.

REFERENCES:

1. Tavaré R, McCracken MN, Zettlitz KA, et al. (2014) Engineered antibody fragments for immuno-PET imaging of endogenous $CD8^+$ T cell expression in vivo. *Proc Natl Acad Sci U.S.A.* 111;1108-1113.

2. Duraiswamy J, Kaluza KM, Freeman GJ, et al. Dual blockade of PD-1 and CTLA-4 combined with tumor vaccine effectively restores T-cell rejection function in tumors. *Cancer Res.* 2013;73(12):3591-3603.

AUTHORS (LAST NAME, FIRST NAME): Tavaré, Richard[1, 2]; Escuin-Ordinas, Helena[3]; McCracken, Melissa N.[2]; Zettlitz, Kirstin A.[1, 2]; Salazar, Felix B.[1, 2]; Witte, Owen N.[4, 2]; Ribas, Antoni[3, 2]; Wu, Anna M.[1, 2]

INSTITUTIONS (ALL):

1. Crump Institute for Molecular Imaging, UCLA, Los Angeles, CA, United States.
2. Molecular & Medical Pharmacology, UCLA, Los Angeles, CA, United States.
3. Department of Medicine, Division of Hematology-Oncology, UCLA, Los Angeles, CA, United States.
4. Howard Hughes Medical Institute, UCLA, Los Angeles, CA, United States.

(No Image Selected)

CONTROL ID: 2232017

TITLE: Microscopic Imaging Reveals Preferential Tumor Cellular Uptake and Retention of Indocyanine Green for *In Vivo* Imaging

PRESENTER: Nobuhiko Onda

ABSTRACT BODY:

Abstract Body: Introduction: Molecular imaging using exogenous tumor-specific fluorescent agents can be applied to endoscopic systems and laparoscopic systems as well as open-surgery imaging systems. For this reason, it is an attractive method for early cancer detection and minimal-invasive image-guided surgery. Indocyanine green (ICG) is a fluorescent contrast agent approved by the Food and Drug Administration and European Medicines Agency for clinical applications. Recently, several studies have reported the availability of intravenously administered ICG for tumor detection in mouse xenograft models of a variety of tumors and a variety of clinical cancers. However, the tumor imaging mechanism by ICG has not been elucidated. The aim of the present study was to clarify the tumor imaging mechanism by intravenously administered ICG. **Materials and Methods:** Microscopic approaches [1] that enable spatio-temporal analysis as well as high-magnification analysis were employed to clarify the imaging mechanism of ICG. To investigate the *in vivo* kinetics of intravenously administered ICG, HT-29 human colon cancer xenografts in athymic nude mice were used. To investigate the tumor imaging mechanism by ICG at cellular level, six phenotypically different human colon cancer cell lines were used in cultured cell experiments. **Results:** *In vivo* study showed that ICG enabled high-sensitive detection of HT-29 xenograft tumors, even under millimeter-sized tumors, owing to a rapid preferential tumor cellular uptake of ICG within 30 min and long retention at least for one day in parallel with rapid excretion from normal tissues. Cultured cell experiments revealed that the internalization of ICG in the HT-29 cells is mediated mainly by endocytosis. Furthermore, ICG readily internalized in colon cancer cells that form aberrant tight junctions, such as HT-29, HCT-116, LoVo and COLO-320-DM, but not in colon cancer cells that form tight junctions, such as DLD-1 and T84. **Conclusions:** Current data suggest that rapid extravasation of ICG, sequential tumor cellular uptake and long retention are the main mechanism of tumor imaging by ICG in the HT-29 mouse xenograft model. The preferential tumor cellular uptake of ICG is likely the result of the disruption of tight junctions, which is one of the hallmarks of cancer. These data suggest that ICG can be used as a tumor-specific imaging agent for clinical cancers.

[1] Transl Oncol. 6: 628-37, 2013

AUTHORS (LAST NAME, FIRST NAME): Onda, Nobuhiko[1, 2]; Shibutani, Makoto[2]

INSTITUTIONS (ALL):

1. Corporate R&D Center, Olympus Corporation, Hachioji-shi, Tokyo, Japan.
2. Laboratory of Veterinary Pathology, Tokyo University of Agriculture and Technology, Fuchu-shi, Tokyo, Japan.

(No Image Selected)

CONTROL ID: 2232022

TITLE: A luciferin analog achieves highly sensitive deep-tissue tumor imaging using near-infrared bioluminescence

PRESENTER: Takahiro Kuchimaru

ABSTRACT BODY:

Abstract Body: In preclinical cancer research, bioluminescence imaging (BLI) using firefly luciferase (Fluc) and D-luciferin has become a standard to monitor tumor growth, protein-protein interactions and specific molecular activity in mouse tumor models. However, the emission maximum (λmax) produced by D-luciferin is 558 nm, at which absorption of visible light by hemoglobin (Hb) and melanin restricts signal penetration and image resolution, hiding the detection of signals from deep tissues. Previous works therefore have made efforts to develop a BLI system that utilizes near-infrared (NIR) wavelengths to improve signal penetration through biological tissues. We here demonstrate that first-time practical synthetic luciferin which can emit NIR-shifted bioluminescence (λmax = 677 nm) with native Fluc, greatly improving detection sensitivity of tumors in deep-tissue over D-luciferin.

We previously synthesized luciferin analog named Akalumine (denoting red-shifted luminescence in Japanese) by substitution of benzothiazole moiety to aromatic structure in D-luciferin (Tetrahedron 2013, 69, 3847). Although Akalumine robustly emits NIR-shifted bioluminescence, high hydrophobic property causes poor water solubility (<2 mM), which is a major drawback for its use in vivo. We thus newly synthesized Akalumine hydrochloride (Akalumine-HCl) and confirmed its high solubility in water (up to 40 mM). NIR bioluminescence emitted by Akalumine-HCl showed >10-fold light penetration in a biological tissue (8-mm thickness) as compared to that by D-luciferin. In addition, Akalumine-HCl has a unique property that its concentration (2.5 μM – 250 μM) does not influence bioluminescence output in the reaction with cancer cells expressing Fluc probably due to its small *Km* value and high cell-membrane permeability. These properties of Akalumine-HCl greatly improved detection sensitivity of cancers in deep-tissue of living mice. Injection of Akalumine-HCl (50 mg/kg) yielded over 10-fold higher bioluminescence signal from lung metastasis than equivalent amount of D-luciferin. Akalumine-HCl is compatible with D-luciferin in current BLI system with native Fluc including cell transplantation models and transgenic mice. Therefore, Akalumine-HCl immediately improves a wide range of applications of BLI in biological studies with small animals.

AUTHORS (LAST NAME, FIRST NAME): Kuchimaru, Takahiro[1]; Iwano, Satoshi[2]; Kiyama, Masahiro[2]; Mitsumata, Shun[1]; Kadonosono, Tetsuya[1]; Niwa, Haruki[2]; Maki, Shojiro[2]; Kizaka-Kondoh, Shinae[1]

INSTITUTIONS (ALL):

1. Tokyo Institute of Technology, Yokohama, Japan.
2. The University of Electro-Communications, Tokyo, Japan.

(No Image Selected)

CONTROL ID: 2232034

TITLE: Liposomal Nano-constructs for Image-guided Delivery in Tumor Vasculature

PRESENTER: Sudath Hapuarachchige

ABSTRACT BODY:

Abstract Body: Noninvasive image-guided drug delivery associated with nano-scale components is highly important in cancer drug development, and allows to visualize the delivery and to predict the outcome. Although superparamagnetic iron oxide nanoparticles (SPIONs) are highly sensitive MRI contrast agents, use of SPIONs as delivery platform is problematic because of their rapid clearance. In this study, we investigate if the delivery of SPIONs to tumors can be enhanced by encapsulating them in liposomes for either “passive” delivery via the enhanced permeability and retention effect (EPR) or “active” delivery via the receptors for vascular endothelial growth factor (VEGF). The MDA-MB-231/luc tumor xenografts mouse models were imaged following i.v. administration of either free (SPIONs) or non-targeted Lip(Gd/Fe) and VEGF receptor targeted scVEGF-Lip(Gd/Fe) liposomal SPIONs dual labeled with SPIO and GdDTPA to detect liposome degradation (Fig. 1A).[1] Lip(Gd/Fe) were designed for passive targeting strategy. Microscopic uptake of fluorescence-labeled constructs was detected *in vivo* by multiphoton intravital microscopy (Fig. 1B). At 4 and 24 h. post-injection non-targeted liposomal formulation of SPIONs provides improved tumor accumulation in comparison to SPIONs or liposomal constructs targeted to VEGF receptors. The uptake index, used as a measure of the tumor uptake of SPIONs, indicated that the highest uptake occurred 4 h after the administration in all three groups; however, only Lip(Gd/Fe) resulted in statistically significant hypo-intense tumor signals at 4 h time point (Fig. 1C). Intravital microscopy images of the distribution of the fluorescent scVEGF probe in the tumor vasculature (Fig. 1D). The clearance of the probe from the blood stream and binding to the blood vessel walls was also detected. The fusion of the probe with vascular dextran marker is shown in Fig. 1D. Intravital microscopy images of the distribution of control untargeted and scVEGF targeted fluorescent liposomes in the vasculature of MDA-MB-231 tumors using different magnifications (Fig. 1E). High magnification images demonstrate extravasation of the untargeted liposomes due to EPR effect (red arrow) whereas no extravasation was detected for the targeted liposomes. The delivery of SPIONs to MDA-MB-231 tumors was improved by encapsulating them into non-targeted and targeted liposomes. The EPR effect provided better tumor accumulation of liposomal SPIONs than their presumably more transient retention via binding to VEGF receptors in the tumor vasculature. We hypothesize that VEGFRs expressed on tumor endothelium, in effect, might act as a barrier for targeted liposomes and therefore interfere with EPR-mediated extravasation and accumulation. On the other hand, the decoration of liposomes with scVEGF could by itself change their pharmacokinetics and the ability to extravasate. Blood vessels constitute only a small fraction of the total tumor volume, and high expression of VEGFR-2 receptors on the tumor endothelial cells was reported only for a subset of those cells[2].

(1) Onuki Y, et al. *Biomaterials* 2010; 31(27): 7132. (2) Imoukhuede PI, et al. *Cancer Medicine* 2014; 3(2): 225.

AUTHORS (LAST NAME, FIRST NAME): Hapuarachchige, Sudath[1]; Kato, Yoshinori[4]; Zhu, Wenlian[1]; Backer, Joseph M.[3]; Backer, Marina[3]; Sarkar, Susanta K.[2]; Artemov, Dmitri[1]

INSTITUTIONS (ALL):

1. Radiology and Radiological Science, Johns Hopkins University School of Medicine, Baltimore, MD, United States.
2. Oncology, Sanofi, Cambridge, MA, United States.
3. Sibtech, Inc. , Brookfield, CT, United States.
4. Life Science Tokyo Advanced Research Center, Hoshi University School of Pharmacy, Tokyo, Japan.

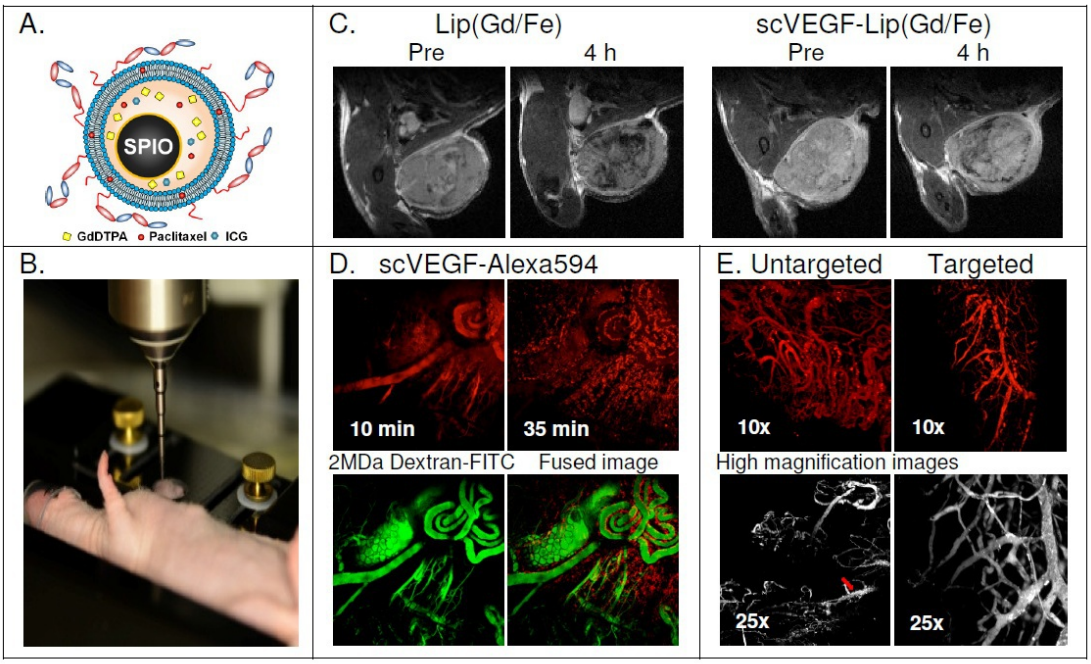

Figure 1. A. Schematics of dual magnetic labeled liposomal nano-constructs. **B.** Experimental setup for multiphoton intravital fluorescence microscopy in mouse tumor models. **C.** *T2*-weighted MR images of orthotopic MDA-MB-231/luc tumors before and after intravenous administration of untargeted and targeted liposomal nano-construct formulations. **D.** Intravital microscopy images of the distribution of fluorescent scVEGF probe in the tumor vasculature. Complete clearance of the probe from the blood stream and binding to the blood vessel walls was detected 35 min after administration. Images on the right demonstrate fusion of the probe with vascular dextran marker. **E**. Intravital microscopy images of the distribution of control untargeted and scVEGF targeted fluorescent liposomes in the vasculature of MDA-MB-231 tumors 1.5 h after administration. High magnification images (bottom) demonstrate extravasation of the untargeted liposomes due to EPR effect (red arrow) whereas no extravasation was detected for the targeted liposomes presumably due to high-affinity binding to the endothelial cells via VEGFR2 receptors.

CONTROL ID: 2232035

TITLE: Modular Synthesis of Peptide-based Single and Multi-modal Targeted Molecular Imaging Agents

PRESENTER: Hans Schmitthenner

ABSTRACT BODY:

Abstract Body: Objective: The development of a practical synthesis of multimodal targeted molecular imaging agents (TMIAs) combining NIR dyes (for OMI or PAI) and chelated metals (for MRI or PET) would be a significant benefit for molecular imaging scientists. There are few methods for combining two different dyes, metals, or dyes with metals, and following this with the conjugation of a variety of targeting groups to use a given imaging system for multiple targets.[1] Peptides have been utilized as scaffolds for dyes and metals used in PET, MRI and NIR.[2,3] The aim was to reassemble these through a modular method by coupling together amino acids with imaging agents on their side chains to form "imaging peptides". Linkers could then be attached for conjugating targeting groups in the final steps to create a versatile and broadly applicable route to compact multi-modal, multi-metal, or multi-dye agents for a diverse range of single, dual or tri-modal targeted imaging modalities. Method: The synthesis utilizes a modular or “puzzle piece” approach in which pre-formed lysines with imaging groups on their side chains are synthesized first, then coupled together and extended using peptide methodology. The approach is elegant in its simplicity, but made possible by several discoveries. A key finding revealed that when a metal for MRI or PET is introduced early it can serve as a protecting group for DOTA during synthesis. This eliminates the need for separate protection and harsh deprotection in final steps.[2] Secondly, this allows combining metals (such as in PET-MRI) or combining different NIR dyes together (for OMI or PAI) or mixing metals with dyes (NIR-PET, NIR-MRI). A third feature is the ability to gently conjugate sensitive targeting groups in the final steps. A fourth feature results from a discovery that the lanthanide metals La or Ce may be readily replaced by Cu, as a model for PET, in the last step. A unique procedure in mild acid, designed for a clinical setting, was developed for this transmetalation to afford the final PET agent in 2-4 hours starting with the La-TMIA. Results: TMIAs utilizing the integrin seeking peptide RGDyK[4] and a PSMA inhibitor[5] as targeting groups have been synthesized with bimodal agents for NIR (PAI)-MRI and NIR (PAI)-PET, agents with two NIR dyes and a di-Gd agent for MRI. The modular synthesis, shown in Figure 1, provides versatile TMIAs. Single and dual-modal agents containing Cy5.5 have been shown to target A549 cancer cells through the use of confocal microscopy (CFM). Efficacy in MRI was verified by spin-lattice relaxation time (T_1) in NMR. Transmetalation kinetics to form PET agents has also been measured. This new family of TMIAs is advantaged due to the inherent features of small peptides in bioavailability, biodistribution, and clearance, including optimization for proteolytic stability using D-amino acids. In addition they can be readily purified by SPE or by HPLC and fully characterized.

1.Azhdarinia A, Mol Imaging Biol. 2012,14(3):261

2.De Leun-Rodriguez, Chem. Eur. J. 2004,10:1149

3.Sancey L, Molecular Therapy,2009,17:837

4.Cheng Z, Bioconjugate Chemistry, 2005,16(6):1433

5. Banerjee SR, J. Med. Chem 2008,51:4504

AUTHORS (LAST NAME, FIRST NAME): Schmitthenner, Hans F.[1, 2]; Barrett, Taylor M.[1]; Beach, Stephanie[1]; Heese, Lauren[1, 3]; Weidman, Chelsea J.[1]; Sweeny-Jones, Anne M.[1]; Becker, Amy E.[2]; Hornak, Joseph P.[1, 2]; Ophardt, Henry[3]; Evans, Irene[3]

INSTITUTIONS (ALL):

1. Chemistry and Materials Science, Rochester Institute of Technology, Rochester , NY, United States.

2. Center for Imaging Science , Rochester Institute of Technology, Rochester, NY, United States.

3. School of Life Sciences, Rochester Institute of Technology, Rochester, NY, United States.

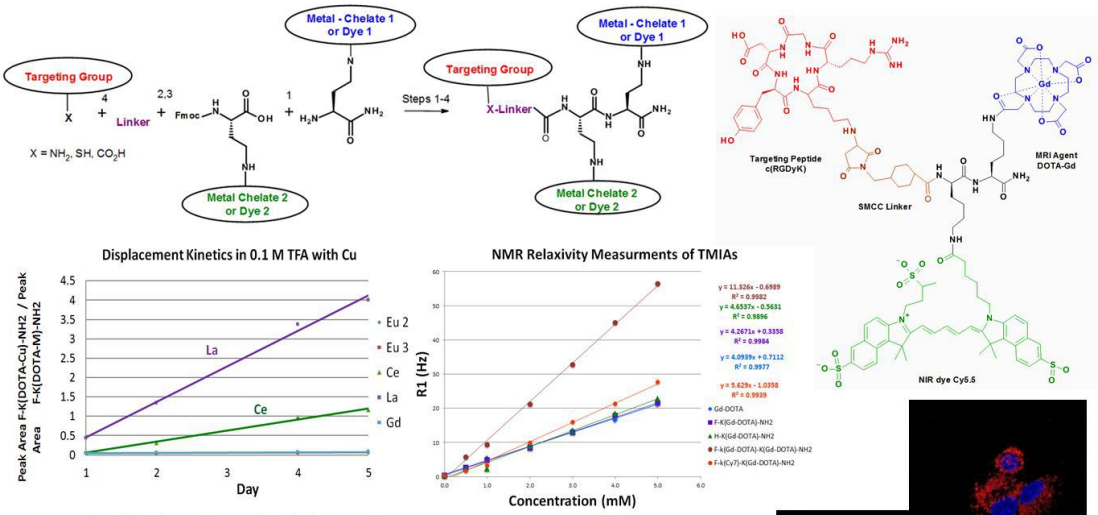

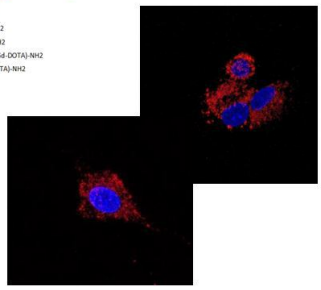

Figure 1a. Modular synthesis of RGdyK targeted mixed single or mult-imodal TMIAs: RGDyK-SMCC-dLys(Cy5.5)-Lys(Gd)-NH_2, RGDyK-SMCC-dLys(Cy7)-Lys(Gd)-NH_2, RGDyK-SMCC-dLys(Gd)-Lys(Gd)-NH_2, RGDyK-SMCC-dLys(Cy5.5)-Lys(Cy7)-NH_2, And precursors for PET SMCC-dLys(La)-Lys(Gd)-NH_2, SMCC-dLys(Cy5.5)-Lys(La)-NH_2,

Figure 1b. Structure of RGDyK-SMCC-dLys(Cy5.5)-Lys(Gd)-NH_2 for MRI-OMI, MRI-PAI or CFM,

Figure 1c. Transmetalation kinetics of La, Ce, Eu and Gd by Cu (optimized separately for synthesis),

Figure 1d. Measurement of T_1 relaxation times by NMR of single and di-Gd TMIAs,

Figure 1d. CFM images of TMIA 1b targeting live A549 cells: amplification of signal is via endocytosis.

CONTROL ID: 2232044

TITLE: Simultaneous Detection of Glutathione and Lactate using Spectral Editing at 3T

PRESENTER: Peter Barker

ABSTRACT BODY:

Abstract Body: Introduction: In brain MR spectroscopy (MR), spectral editing is often used to selectively detect signals from lower concentration metabolites (such as GABA, or glutathione (GSH)) that overlap with those of other, more abundant compounds. Usually, one compound is observed at a time, however there have been examples of editing sequences designed to simultaneously detect 2 compounds at the same time (1,2). This abstract describes the optimization of the 'MEGA-PRESS' editing sequence to simultaneously detect GSH and lactate (Lac) in a single acquisition.

Methods: Experiments and numerical simulations were performed to determine the optimum TE and editing pulse frequencies for simultaneous GSH and Lac editing. Spectra were acquired on a Philips 'Achieva' 3T scanner using a 32-channel receive head coil. The PRESS sequence was used with frequency-modulated slice selective refocusing pulses ('fm_ref07', 2.2 kHz bandwidth) in order to minimize chemical shift displacement effects. Phantom spectra were collected in a phantom containing 50 mM GSH and 25 mM sodium lactate in phosphate-buffered saline (pH = 7.2). In the PRESS experiments, TE was varied from 70 to 280 ms in 10 ms increments. In the MEGA-PRESS experiments using TE 140 ms, the 'on' editing pulse frequency was varied from 4.1 to 4.56 ppm in increments of 0.05 ppm, with the 'off' pulse placed at 10 ppm. The editing pulse duration was 20 ms (75 Hz bandwidth). Finally, a MEGA-PRESS experiment was performed with an 'on' editing pulse at 4.35 ppm with 10 ms duration (150 Hz bandwidth). Simulations of the MEGA-PRESS experiment for the GSH spin system were performed using MATLAB, including spatially-resolved modulation effects, using the chemical shifts and coupling constants given by Govinderaju et al. (3).

Results: In the phantom, the optimum TE for editing (i.e. most negative signal in the 'off' scan) for both GSH and Lac was in the range of 140-150 ms, which was in good agreement with the simulations (Figure 1A). As expected, maximum GSH signal was obtained with an editing pulse frequency of 4.56 ppm, while maximum Lac was observed at 4.10 ppm. By increasing the editing pulse bandwidth (to 150 Hz), and placing it symmetrically between the coupled resonances of Lac and GSH (4.35 ppm), it was possible to edit both resonances simultaneously with ~90% sensitivity of the individual measurements (FIgure 1B).

Discussion: Simultaneous editing of Lac and GSH is possible at 3T. Compared to sequential measurements, simultaneous editing results in a 50% reduction in the scan time while retaining nearly the same sensitivity. Note that the optimization performed here did not consider T_2 relaxation effects *in vivo*, which will tend to shorten the optimal TE. The simultaneous measurement of Lac, an indicator of non-oxidative glycolysis, and GSH (a major anti-oxidant) may be of interest in various brain pathologies, including schizophrenia.

References

1. Terpstra et al., MRM 56:1192-9 (2006)
2. Snoussi et al., ISMRM (2015)
3. Govindaraju et al., NMR Biomed 13:129–53 (2000)

AUTHORS (LAST NAME, FIRST NAME): Chan, Kimberly[1]; Snoussi, Karim[1]; Edden, Richard[1]; Barker, Peter[1]

INSTITUTIONS (ALL):

1. Radiology, Johns Hopkins University, Baltimore, MD, United States.

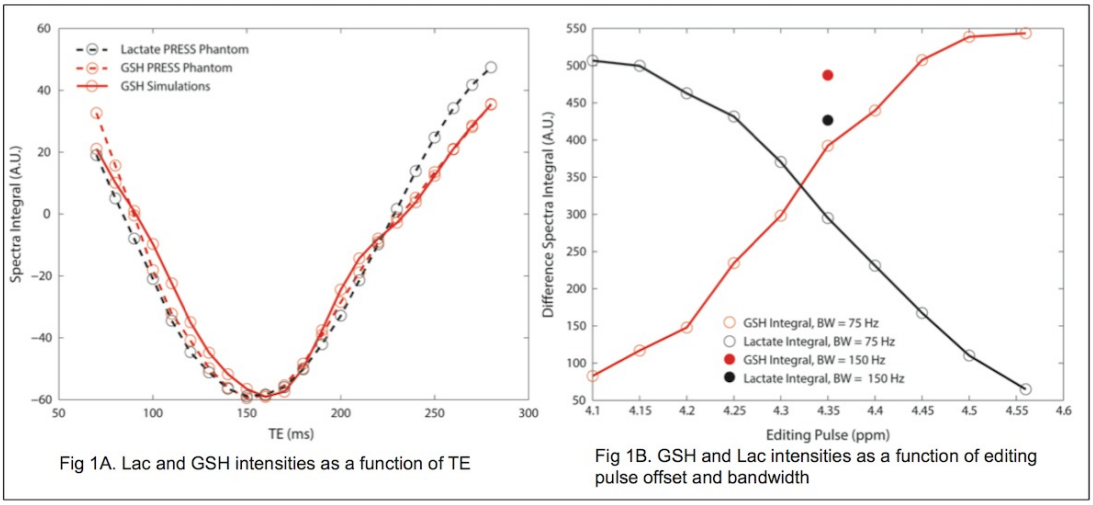

Fig 1A. Lac and GSH intensities as a function of TE

Fig 1B. GSH and Lac intensities as a function of editing pulse offset and bandwidth

CONTROL ID: 2232065

TITLE: Ultrasound Molecular Imaging with anti-VCAM-1 Antibody-Targeted Microbubbles: Sequential Use of Thiol-Maleimide Coupling and Amalgamation for a One-Pot Microbubble Contrast Formulation.

PRESENTER: Alexander Klibanov

ABSTRACT BODY:

Abstract Body: Introduction. Ligand-decorated microbubbles expand ultrasound contrast imaging from anatomy and physiology to molecular diagnostics. Preparation of antibody-decorated targeted microbubbles is cumbersome and lengthy. In a preclinical setting, biotinylated antibodies are often attached to microbubbles via a streptavidin link; this approach is not applicable for clinical translation. With the rapid progress of the humanized antibody technology, covalent attachment of monoclonal antibodies to microbubbles should be investigated. The use of active ester coupling for covalent attachment of antibodies to pre-formulated microbubbles requires extremely high concentrations of reactants, or offers a very low coupling yield. Attachment of thiolated proteins to maleimide-carrying microbubbles is only somewhat better. In this study we use tris(2-carboxyethyl)phosphine (TCEP), a reducing agent that provides a rapid and selective generation of thiols in the hinge region of the antibody molecule, to generate antibody-carrying microbubbles in a quick and efficient one-pot preparation: TCEP does not directly react with maleimide, so its removal from the reaction media is not required. In vivo testing of this formulation for ultrasound molecular imaging in a murine tumor model demonstrates successful targeting to VCAM-1 expressed on vascular endothelium in the tumor.

Methods. A monoclonal antibody MVCAM.A (rat IgG, anti-mouse VCAM-1) was reduced with TCEP in 0.1 M HEPES buffer solution; in 30 min, micellar solution of maleimide-PEG-DSPE was added and thioether coupling performed. Without further purification, micellar solution of DSPC and PEG stearate in aqueous propylene glycol was added, vials sealed under perfluorobutane gas headspace and amalgamated for microbubble preparation (45s x 5, Vialmix apparatus). Formulation lacking the antibody was used as a control. Microbubbles were diluted with degassed saline and injected intravenously to C57BL/6 mice with MC38 tumor cells (a generous gift of Dr. J. Schlom, NIH) grown subcutaneously in the hind leg. Contrast ultrasound imaging of the tumor vasculature was performed with a Sequoia 512 scanner (15L8 probe, Cadence CPS multipulse contrast mode, 7 MHz, MI 0.2). In 10 min, ultrasound transmit power was increased to maximum MI (1.9) to destroy targeted microbubbles and determine the background concentration of circulating microbubbles. Ultrasound images were transferred to a PC and contrast intensities of the tumor ROI and contralateral leg muscle wwere analyzed with ImageJ (NIH).

Results. Selective accumulation of anti-VCAM-1-targeted but not control microbubbles in the tumor vasculature was observed 10 min following intravenous bolus administration ($n=6$, $p<0.001$). Targeted microbubbles selectively accumulated in the tumor but not in the contralateral control leg tissue ($n=6$, $p<0.004$). At 10 min, residual level of circulating microbubbles in the vasculature (following destruction of targeted bubbles) was low.

Conclusions. A one-pot preparation of anti-VCAM-1 antibody-decorated targeted microbubbles was tested. Successful ultrasound molecular imaging of VCAM-1 overexpressed on vascular endothelium was demonstrated.

AUTHORS (LAST NAME, FIRST NAME): Klibanov, Alexander L.[1, 2]; Du, Zhongmin[2]; Diakova, Galina[2]

INSTITUTIONS (ALL):

1. Department of Medicine, Cardiovascular Division, University of Virginia, Charlottesville, VA, United States.
2. Robert M. Berne Cardiovascular Research Center, University of Virginia, Charlottesville, VA, United States.

(No Image Selected)

CONTROL ID: 2234375

TITLE: Ultrasound Treatment of Doxorubicin-Liposome-Microbubble Complexes in the Tumor Vasculature Enhances Drug Delivery in the Tumor Tissue and Suppresses Tumor Growth

PRESENTER: Alexander Klibanov

ABSTRACT BODY:

Abstract Body: Introduction: Triggered release of drugs from carrier systems is widely investigated for targeted tumor therapy. Ultrasound-sensitive liposome-microbubble pendant drug carrier systems have been developed. Due to low drug load, those particles were only successful for suppressing tumor cell growth in cell culture in vitro so far. In this study, we prepare particles with high doxorubicin load, using liposomes larger than the standard 80 nm Doxil/Caelyx formulation, and achieve successful inhibition of tumor growth in a subcutaneous murine tumor model.

Methods: Decafluorobutane microbubbles were stabilized with DSPC, PEG stearate and biotin-PEG-DSPE. Liposomes carrying ammonium citrate were prepared from DOPC, cholesterol and biotin-amidocaproyl-DSPE and purified by centrifugation. Remote loading of citrate-containing liposomes with doxorubicin was performed to achieve efficient drug uptake into the liposome aqueous core. Streptavidin was used to place biotinylated liposomes on biotinylated microbubbles. Pendant complex formation was confirmed by fluorescence microscopy. Subcutaneous hind leg tumor model in C57BL/6 mice (MC38 colon adenocarcinoma cells, J. Schlom, NIH) was used. Therapy started when tumors reached 4-5 mm. Doxorubicin-liposome-microbubble complexes were injected intravenously (doxorubicin dosage 6 mg/kg). Contrast ultrasound imaging with Sequoia 512 (15L8 probe, CPS, 7 MHz, MI 0.2) was used to monitor particles in the tumor vasculature. Therapeutic ultrasound treatment was initiated immediately and performed for 10 min (0.6 W/cm^2, 1 MHz sine wave applied repeatedly for 3 s with 10 s intervals, Birtcher Megason ultrasound). Drug deposition in the insonated and control untreated tumors was assessed by fluorescence microscopy.

Results and Conclusions: Doxorubicin-liposome-microbubble complexes have been prepared; they demonstrated excellent drug load (>1 pg doxorubicin per complex, an order of magnitude higher than demonstrated earlier with Doxil-like liposome-based complexes). Treatments were performed repeatedly, two or three times a week, for the course of two weeks; ultrasound imaging confirmed tumor perfusion with drug carrier. Mice demonstrated normal behavior during the course of the treatments. Doxorubicin-liposome-microbubble pendant complex particle administration combined with insonation showed significant suppression of tumor growth, as compared with control untreated animals ($p<0.05$). Some of the tumors have reduced size in response to the combination treatment. Untreated control animals, as well as mice receiving doxorubicin-liposome microbubble complexes but not insonated, have all demonstrated rapid tumor growth. Fluorescence microscopy confirmed doxorubicin deposition in the tumor in response to ultrasound treatment.

Conclusion. Repeated administrations of doxorubicin-liposome-microbubble pendant particles combined with ultrasound treatments of the tumor under ultrasound imaging guidance resulted in suppression of tumor growth in a subcutaneous murine tumor model.

Acknowledgements. Supported in part via NIH R21/33 CA102880, R21 EB016752.

AUTHORS (LAST NAME, FIRST NAME): Klibanov, Alexander L.[1, 2]; Du, Zhongmin[2]; Diakova, Galina[2]

INSTITUTIONS (ALL):

1. Department of Medicine, Cardiovascular Division, University of Virginia, Charlottesville, VA, United States.
2. Robert M. Berne Cardiovascular Research Center, University of Virginia, Charlottesville, VA, United States.

(No Image Selected)

CONTROL ID: 2232074

TITLE: PERCIST guidelines is better than EASL and RRECIST in assessing the short-term response in primary hepatocellular carcinoma after interventional therapy

PRESENTER: Shengjun Wang

ABSTRACT BODY:

Abstract Body: Purpose: To compare EASL guidelines and PERCIST and RRECIST in assessing the short-term response in primary hepatocellular carcinoma after interventional therapy.**Methods:** In this prospective study, 22 patients (18 males and 4 females; mean age, 48.8) with primary hepatocellular carcinoma which was confirmed by biopsy were enrolled. Except 5 patients who had 18F-FDG PET/CT examinations before interventional therapy and one month afterward, the other 17 patients underwent the third time PET/CT scan three months after the therapy. Abdominal enhanced CT scans were done in all 22 cases one month after PET/CT scans. All images were analyzed by two radiologists according to the RECIST and EASL methods based on enhanced CT, and two PET/CT physicians according to the PERCIST. The results were finally confirmed by comprehensively analyzing the AFP, enhanced CT scans and PET/CT results by physicians. Chisquare test was used to compare the response rate andsensitivity, specificity, accuracy, PPV and NPV.

Results: According to RECIST, EASL and PERCIST, patients achieved complete response, partial response, stable disease,progressive disease 1 month after the interventional therapy were 10, 5, 5, 2;8,4,8,2 and 3,16,1,2 respectively.The sensitivity, specificity, accuracy, PPV and NPV were 90%, 8.3%, 45.5%, 45% and 50% with RICIST, 70%, 8.3%, 36.4%, 38.9% and 25% with EASLand 95%, 50%, 90.9%, 95% ,50% with PERCIST(p =0.036,0.003,0.000,0.000,0.223). After 3 months after therapy, the complete response, partial response, stable disease,progressive disease were 5, 2, 4, 6; 4, 1, 5, 7 and 2, 2, 1, 12 respectively according to RECIST, EASL and PERCIST. The sensitivity, specificity, accuracy, PPV and NPV were 91.7%,20%,70.6%,73.3%,50%; 90.9%,16.7%,64.7%,66.7%,50%; 93.3%,50%,88.2%,93.3%,50% respectively.(p=0.036,0.003,0.000,0.000,0.223).

Conclusion: PERCIST should be accepted in predicting short-term response in primary hepatocellular carcinoma after interventional therapy because it provide more accurate information. PERCIST guidelines is better than EASL and RRECIST.

AUTHORS (LAST NAME, FIRST NAME): Wang, Shengjun[1]; Yi, Jingwei[1]; Wang, Jing[1]

INSTITUTIONS (ALL):

1. Fourth Military Medical University, Xi'an, Shaanxi, China.

(No Image Selected)

CONTROL ID: 2232080

TITLE: SWIFT MR Imaging of Grafted Mesenchymal Stem Cells in Bone Tissue

PRESENTER: Sergio Wong

ABSTRACT BODY:

Abstract Body: Introduction: Mesenchymal stem cells (MSCs) have high potential in the treatment of bone loss diseases such as osteoporosis and fracture [1,2]. To facilitate preclinical research and accelerate translation of this therapy to clinic, a noninvasive method of monitoring of transplanted cells is needed. Previous studies indicate that iron labeled cells can be successfully detected *in vivo* with gradient echo (GE) MR imaging [3-4]. However labeled cells and bones appear dark on GE images, which makes implementation of this technique for bone disorders challenging. SWIFT pulse sequence can produce a positive MRI signal from structures with short T2, such as iron labeled cells. In this study, parameters of SWIFT MR imaging and cell labeling protocols were optimized for *in vivo* tracking MSCs in stem cells therapy of bone diseases.

Methods: *Cell Culture and labeling:* Human MSCs were maintained on uncoated flasks in media with αMEM, 10% FBS, and 1% PSA. At 70-80% confluence 25, 50 or 200μg/ml of Fe and 375ng/ml poly-L-lysine mixture were added into incubation media for ~12 hrs. *Cells Injection:* 50μl of 50μg/ml Fe labeled MSCs were injected into rat femur. 20μl of 25, 50, 200μg/ml Fe labeled MSCs were injected into muscles close to mouse femur. *SWIFT MR Imaging*: Three-dimensional (3D) radial *in vivo* and *ex vivo* SWIFT images were acquired with 2.6μs duration segmented RF pulse with excitation bandwidth of 100kHz. Data was acquired with TR=1.3ms and TE=2.6μs.

Results: Fig1 shows SWIFT MR image of femur before (A) and after (B) injection of MSCs labeled with 50μg/ml of iron oxide. Bright signal from grafted cells was observed. To determine a concentration of iron oxide particles, which will produce highest contrast between grafted cells and surrounding tissue, we imaged cells labeled with different (25, 50, 200μg/ml) iron concentration. Fig1C depicts dependence of the signal intensity (SI) vs. excitation flip angle from cells labeled with different iron concentrations and muscular tissue. A strong dependence of SI on excitation flip angle was observed for grafted cells while signal from muscle simply deceased. The largest difference in SI between grafted cells and muscle was detected for cells labeled with 50μg/ml of Fe and 6 degree excitation flip angle.

Discussion and conclusion: The long-term goal is to develop a method to monitor stem cell therapy of bone diseases. In this study a capacity of SWIFT MRI pulse sequence was tested to identify grafted cells. Distinct “positive” signal was detected from iron labeled grafted cells in bone and muscle tissue. Measurements of SIs at different excitation flip angles revealed that labeling cells with 50μg/ml of iron oxide and acquisition with 6 degree flip angle produce strongest contrast between tissue and grafted cells. *In vivo and ex vivo experiments show* that SWIFT has a high potency for the detection of grafted MSCs in bone tissue, which was not achievable with conventional MR imaging.

References: 1.Guan, M.,et al..Nat Med,2012.**18**(3):p.456-62. 2.Yao,W.,et al.,Stem Cells,2013. 3.Magnitsky, S.,et al.,Neurodegenerative Diseases,2007.**4**(4):p.314-21. 4.Magnitsky, S., et al..Academic Radiology,2008.**15**(10):p.1269-81.

AUTHORS (LAST NAME, FIRST NAME): Wong, Sergio B.[1]; Idiyatullin, Djaudat S.[2]; Corum, Curtis A.[2]; Lane, Nancy E.[3]; Majumdar, Sharmila[1]; Magnitsky, Sergey[1]

INSTITUTIONS (ALL):

1. Radiology and Biomedical Imaging, University of California, San Francisco, San Francisco, CA, United States.
2. Department of Radiology, University of Minnesota, Minneapolis, MN, United States.
3. Department of Internal Medicine, University of California at Davis, Davis, CA, United States.

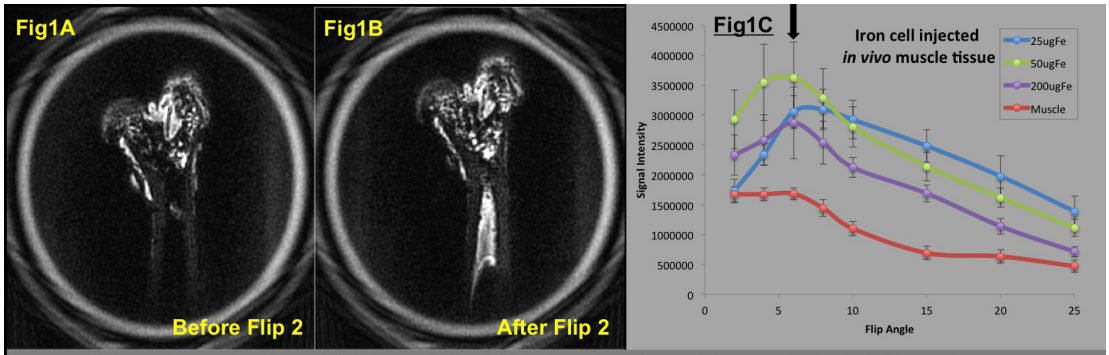

Fig1A-B: SWIFT MR image of rat femur (A) before and after (B) injection of 2x10^6 MSCs labeled with 50µg/ml of iron oxide*. Images were acquired with 1 hrs after injection. Acquition parameters: 2 degree excitation flip angle, 100kHz bandwidth, TR=1.3ms and TE=2.6µs.* ***SWIFT pulse sequence generates hyperintense signal from iron oxide labeled cells***

Fig1C: MRI signal intensity from grafted cell and muscle tissue at different excitation flip angle*. MSCs labeled with 25,50, and 200µg/ml of iron oxide were injected into muscle and SWIFT MR images were acquired 1hrs after injection .* ***Maximal signal contrast found at 50µg/ml grafted cells at 6° flip (arrow)***

CONTROL ID: 2233412

TITLE: ImmunoPET imaging of murine T helper lymphocytes with an anti-CD4 cys-diabody

PRESENTER: Amanda Freise

ABSTRACT BODY:

Abstract Body: Investigating the immune system presents a unique challenge because immune cells traffic and localize among multiple sites throughout the entire body. Current methods of monitoring this dynamic system include biopsies, which are site-specific, and blood draws, which sample only the circulating component of the lymphoid population. A functional immune system depends in part on proper signaling, numbers, and trafficking of $CD4^+$ T cells, the “master regulators” of immunity. $CD4^+$ T cells circulate to and from lymphoid organs and sites of inflammation; abnormal cell numbers or trafficking can lead to an inappropriate immune response, resulting in serious infections, autoimmunity, or induction of tolerance to cancer. As such, noninvasive imaging of the presence and localization of $CD4^+$ T cells throughout the body would be an improvement upon current methods of analysis. Selective imaging of $CD4^+$ T cells can be accomplished with antibody-based probes, which have exquisite specificity and affinity for their cognate ligands. Engineering antibodies to produce fragments allows customization of pharmacokinetics, clearance route, and conjugation to suit *in vivo* imaging applications such as positron emission tomography (PET). Based on the well-characterized GK1.5 rat anti-mouse CD4 antibody, we have developed a cys-diabody (cDb) fragment for the purpose of imaging T cells *in vivo*. The cDb (GK1.5 cDb; ~50 kDa) is comprised of two single-chain variable fragments joined by a linker and lacks the Fc domain of the parental antibody, resulting in increased rate of clearance and removal of Fc-mediated functionality. A C-terminal cysteine was introduced to enable site-specific conjugation to maleimide-Alexa488 (mal488) or maleimide-DFO (malDFO), a radiometal chelator. Binding specificity was shown *in vitro* with flow cytometry by isolating primary cells from murine peripheral blood, spleen, lymph nodes (LN), and thymus and staining with mal488-GK1.5 cDb or a commercial anti-CD4 antibody. An ELISA binding curve using immobilized murine CD4 as antigen gave an estimated dissociation constant of ~7.44 nM. *In vivo* binding specificity was demonstrated by radiolabeling malDFO-GK1.5 cDb with ^{89}Zr and injecting 10-16 µg (25-35 µCi) into untreated mice, mice that underwent CD4 depletion with intact GK1.5 (25 mg/kg daily for 3 days), or mice that received a bolus injection of 3 mg/kg unlabeled cDb. Mice were PET scanned at 4, 8, and 22 hours post-injection, followed by biodistribution studies. Axillary LNs and spleen showed high uptake of cDb in untreated mice (45, 30% ID/g respectively), in contrast to CD4-depleted mice (3.9, 4.1% ID/g) and those that received a blocking injection (7.1, 6.1% ID/g). A subsequent dose escalation study showed that the lowest protein dose (2 µg/7 µCi) gave the highest signal:noise ratio and better targeting of spleen and LN compared to a higher protein and radiation dose (40 µg/136 µCi). In conclusion, radiolabeled GK1.5 cDb provided an effective imaging agent for CD4 expressed in lymphoid organs in wild type mice and is a promising agent for future studies, including T cell imaging in autoimmune disease.

AUTHORS (LAST NAME, FIRST NAME): Tavaré, Richard[1]; Freise, Amanda C.[1]; Salazar, Felix B.[1]; Wu, Anna M.[1]

INSTITUTIONS (ALL):

1. Crump Institute for Molecular Imaging, Department of Molecular and Medical Pharmacology, David Geffen School of Medicine, UCLA, Los Angeles, CA, United States.

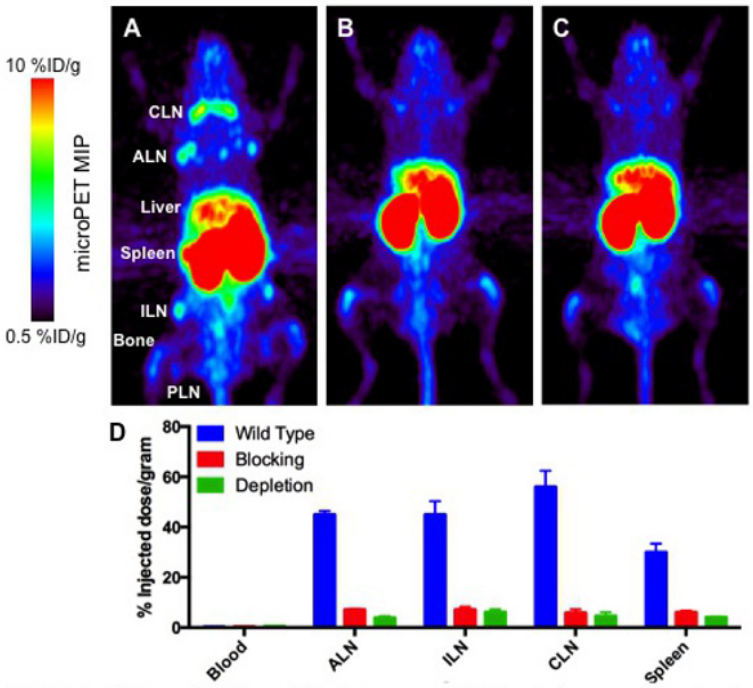

Radiolabeled GK1.5 anti-CD4 cys-diabody targets CD4$^+$ T cells in secondary lymphoid organs including spleen and lymph nodes (LN) in a wild type mouse (A) (n=3). Blocking with unlabeled cys-diabody (B) (n=4) and depletion with parental antibody (C) (n=4) as well as quantitative biodistribution analysis 24h post-injection (D) confirm that imaging is CD4-specific. MIP: maximum intensity projection; CLN: cervical LN; ALN: axillary LN; ILN: inguinal LN; PLN: popliteal LN.

CONTROL ID: 2232094

TITLE: Comparing alkylphosphocholine analogs NM346 & NM397 in a breast cancer murine model

PRESENTER: Justin Jeffery

ABSTRACT BODY:

Abstract Body: Introduction:Alkylphosphocholine (APC) analogs selectively target a broad spectrum of solid tumors largely due to an over-abundance of phospholipid ethers on malignant cell membranes. APC analogs, developed by Cellectar Biosciences, consist of a targeting ligand and a diapeutic moiety. Due to the long biological half-lives of APCs, long-lived radioiodine such as I-124 for PET imaging and I-131 for radiotherapy serve as complementary diapeutic moieties that possess similar biodistribution and pharmacokinetics when radiolabeled to APCs. I-124-NM404, a first generation APC analog currently in clinical trials, is designed for diagnostic PET imaging of malignant tumors. Through structure activity analysis and preliminarily preclinical studies, 2 second generation APCs, NM346 and NM397, have shown similar tumor uptake as NM404 despite slight structural differences. Although the differences in chemical structure do not seem to affect tumor targeting, their respective biodistributions and pharmacokinetics ultimately determine the utility of each agent as diagnostic or therapeutic. An ideal diagnostic agent has a large tumor-to-normal tissue ratio ($TNOR_{tissue}$) at an optimal imaging time point. In contrast, an ideal therapeutic agent has a large ratio of residence times (area-under-the-curve (AUC)) between tumor and the dose-limiting normal organ (ie. blood, kidneys, liver). For these reasons, we aim to compare NM346 and NM397 as potential diagnostic imaging or therapeutic agents using biodistribution and pharmacokinetic data derived from imaging.

Methods:8 female NUDE mice were inoculated with 2 x 10^6 2LMP breast cancer cells in the right flank. 3 weeks post inoculation, mice were pair matched into 2 groups of 4. Groups were intravenously injected with 266 ± 6.47 uCi (mean ± SD) of I-124-NM346 or I-124-NM397. Mice were scanned at 0hr, 24hr, 48hr, 72hr, and 96hr post-injection with an Inveon microPET/CT scanner. 40 million counts per mouse were acquired for all time points. MicroPET data were 3D histogrammed and reconstructed using OSEM3D/MAP without scatter correction and with CT attenuation correction. Image analysis was conducted using Inveon Research Workplace. All data were decay corrected. Percent injected dose per gram (%ID/g) was measured in the tumor, liver, kidneys, muscle, blood and whole body (excluding tumor). 3 equivalent-sized ROIs were drawn in the boundary of each tissue and averaged. To determine therapeutic potential, time points were normalized to the 0hr injected activity and the ratios of the AUC of the tumor to the AUC of the blood, kidneys, and liver were compared. To determine the diagnostic potential, the max tumor-to-muscle ratios at each time point were compared.

Results:The max $TNOR_{muscle}$ occurred at 96hrs post injection for NM346 and NM397; 3.73 ± 1.32 (SD) and 3.44 ± 1.32, respectively. See table for therapy potential results.

Conclusions:Our data suggest that NM346 may serve as a better diagnostic agent than NM397 due to higher $TNOR_{muscle}$. Furthermore, our data suggest that NM397 may be preferential over NM346 for radiotherapy due to an increased payload of the agent in the tumor relative to the normal dose-limiting tissue.

AUTHORS (LAST NAME, FIRST NAME): Jeffery, Justin[3, 1]; Pinchuk, Anatoly[1]; Zhang, Ray[1]; Mehta, Tej[1]; Muhowski, Elizabeth[1]; Larrabee, Jason[2]; Weichert, Jamey[1, 2]; Grudzinski, Joseph J.[4, 2]

INSTITUTIONS (ALL):

1. Radiology, University of Wisconsin-Madison, Madion, WI, United States.
2. Cellectar Biosciences, Inc, Madison, WI, United States.
3. Carbone Cancer Center, University of Wisconsin-Madison, Madison, WI, United States.
4. Medical Physics, University of Wisconsin-Madison, Madison, WI, United States.

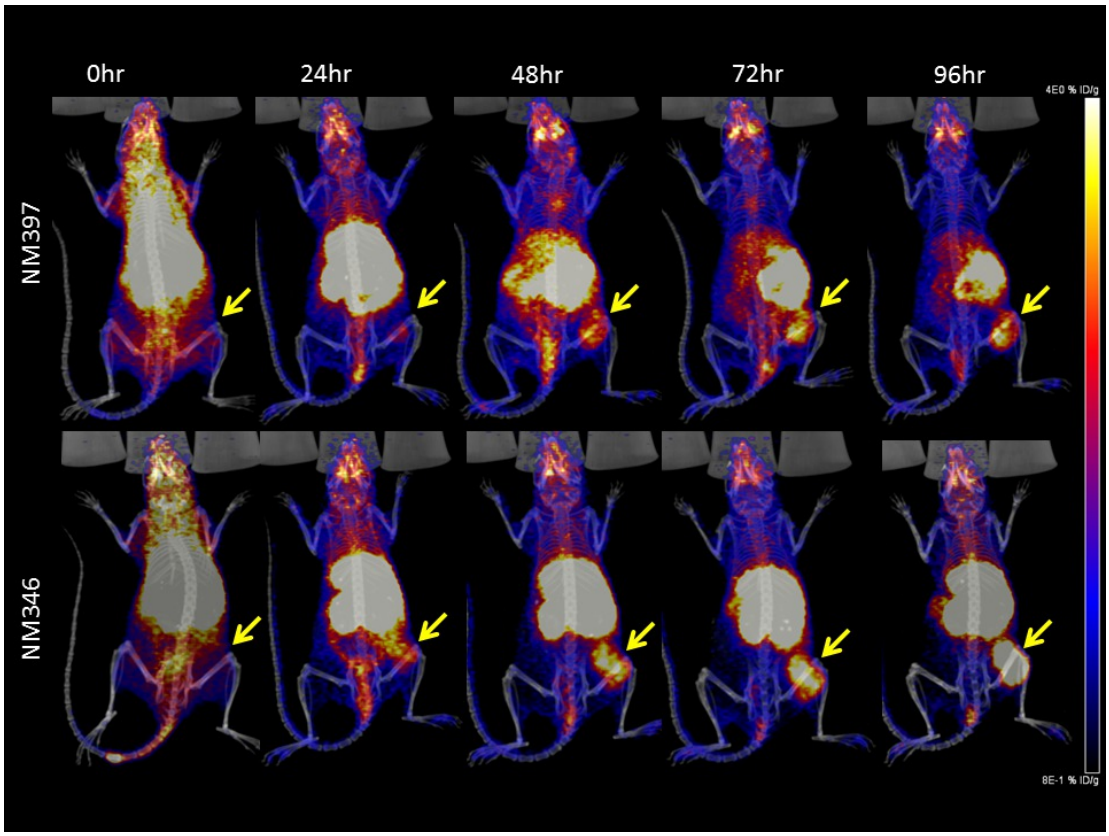
0hr
24hr
48hr
72hr
96hr
NM397
NM346
4E0 % ID/g
8E-1 % ID/g

CONTROL ID: 2232200

TITLE: Early monitoring of tumor response to photothermal therapy delivered by nano-graphene oxide through T2*-weighted and Diffusion-weighted MRI

PRESENTER: Fan Zhang

ABSTRACT BODY:

Abstract Body: Abstract

Background: Graphene with unique physical and chemical properties have been widely explored as graphene-based contrast agents in different imaging modalilties and drug delivery vehicles for potential cancer photothermal therapy (PTT) [1-2]. PTT effect is determined by several parameters which include temperature regimens and heating time. It is valuable if a technique can be used to monitor the tumor response to PTT and predict treatment efficacy at an early time; thereby, immediate prognosis and early consideration of adjuvant treatment are allowed. In the present study, we evaluate the capability of T2*-weighted MRI and DW MRI for early detection of tumor response to PTT induced by nano-graphene oxide in an animal model [3].

Methods: 4T1 cells (2×10^6 cells/each mouse) were subcutaneously transplanted into the right hip of female BALB/C mice. When the tumors reached a size of 100 mm^3, GO-PEG (200ul) was injected intravenously into the mice. Subsequently, the tumors received photothermal therapy (PTT). The tumor volumes were measured to evaluate the anticancer efficacy of different temperature and heating time. T2*-weighted MRI and DW MRI were acquired by using high-field (9.4 Tesla, Bruker). Small animal MRI was performed pre PTT and 30 min, 2h, 6h, 12h, 1d, 3d and 7d and 10d after PTT. Tumor size, apparent diffusion coefficients (ADC) and T2* value (ms) were calculated at different time points to examine the treatment effect. Final tumor responses, as determined by changes of tumor size or volume on MRI, were correlated with tumor T2* values and ADC values at different time points.

Results: In photothermal treated tumors, hemorrhage was observed 30 min after PTT as dark signal in T2*-weighted MRI and increased necrosis which is high signal in ADC-map with increasing PTT temperature at 24h. There is an overall decrease in tumor volume proportional to the increase in PTT temperature. Tumor T2* values showed significant hemorrhage 30 min after PTT. Changes observed in water diffusion by ADC value after PPT showed significantly positive correlation with cancer killing efficacy and later tumor growth rate. These results were validated by immunohistochemistry and H&E staining.

Conclusions: T2*-weighted MRI and DW MRI have potential use for the early detection of tumor response to photothermal therapy delivered by nano-graphene oxide and for predicting treatment outcome.

References

Kai Yang, Shuai Zhang, Guoxin Zhang, et al. Graphene in Mice: Ultrahigh In Vivo Tumor

Uptake and Efficient Photothermal Therapy. Nano Lett. 2010; 10, 3318–3323

Xiaoze Shi, Hua Gong, Yingjie Li, et.al. Graphene-based magnetic plasmonic nanocomposite for dual bioimaging and photothermal therapy. Biomaterials. 2013; 34: 4786-4793

Hamstra DA, Rehemtulla A, Ross BD. Diffusion magnetic resonance imaging: a biomarker for treatment response in oncology. J Clin Oncol. 2007; 25:4104–4109.

AUTHORS (LAST NAME, FIRST NAME): Zhang, Fan[1]; Cao, Jianbo[1]; Fu, Guifeng[1]

INSTITUTIONS (ALL):

1. center for molecular imaging and translational medicine, Xiamen University , Xiamen, China.

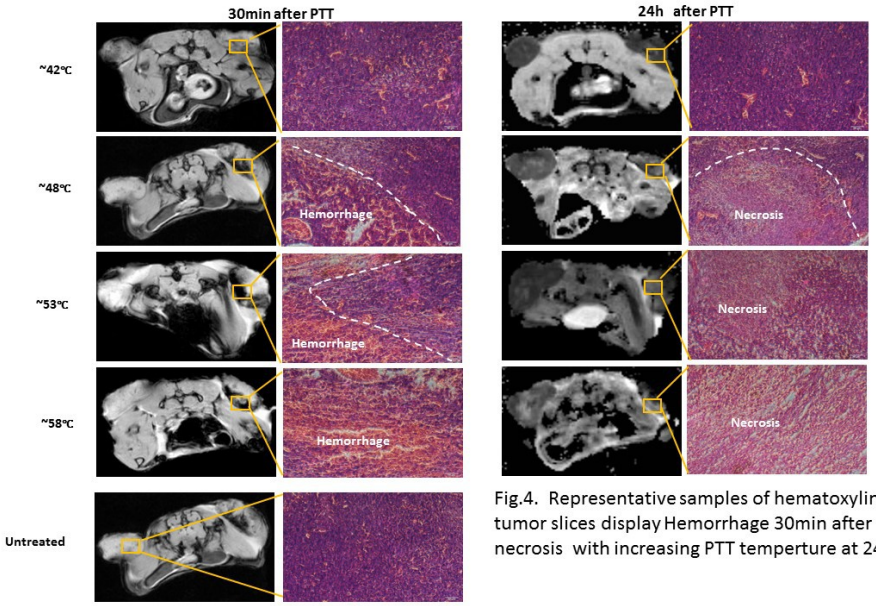

Fig.4. Representative samples of hematoxylin and eosin–stained tumor slices display Hemorrhage 30min after PTT and increase necrosis with increasing PTT temperture at 24h.

CONTROL ID: 2232101

TITLE:

68Ga labeled iNGR with tumor penetrating motif has better PET imaging performance than NGR in CD13 positive tumor

PRESENTER: Fei Kang

ABSTRACT BODY:

Abstract Body:

Objectives : To compare the performance of the cancer targeting peptides 68Ga-NGR and 68Ga-iNGR containing CendR tumor penetrating motif for the imaging of the CD13 angiogenesis maker.

Methods : NGR and iNGR peptides both conjugated with NOTA were synthesised. CD13 of HT1080 and HT29 cells was confirmed by western blot and immunofluorescence. NGR and iNGR peptides were labeled by 68Ga and assayed by HPLC and stability tests. In vitro affinity to cancer cells of the two peptides was compared by competitive cell binding assays. In vivo imaging of 68Ga-NGR and 68Ga-iNGR was compared by mricoPET imaging of the same nude mouse bearing HT1080 and HT29 tumors. The in vivo CD13 affinity was verified by competitive PET imaging of the same mouse with or without cold NGR blocking. The mechanism of the theoretically improved performance of iNGR via NRP1 was verified by comparison imaging by using blockade NRP1 antibody. Tumor uptake was measured by ROI method and quantified by SUV.

Results : CD13 was overexpressed in HT1080 cells but not in HT29 cells. Both probes exhibited high radiochemical purity and high stability in mouse serum or saline. The CD13 binding affinity of iNGR was comparable to that of NGR.The uptake of 68Ga-iNGR in HT1080 cells increased with incubation time, and the maximum uptake ratio was about 1.78±0.04% in HT1080 cells after 2h incubation, about 2-fold higher than that of 68Ga-NGR. In vivo imaging showed that the HT-1080 tumors were of higher contrast to HT29 tumors at all time points after injection of 68GaiNGR or 68Ga-NGR. The HT1080 tumor uptake of 68Ga-iNGR was significantly higher than that of 68Ga−NGR. Moreover, tumor 68Ga-iNGR uptake could be completely blocked by cold NGR and partly blocked by NRP1 antibody. Immunohistochemistry confirmed CD13 and NRP1 overexpression in HT1080 tumor neovasculature.

Conclusions : 68Ga-iNGR demonstrated higher tumor uptake and better tumor retention than 68Ga-NGR through NRP1, indicating the CendR motif modification is a promising way for improving NGR peptides performance.

AUTHORS (LAST NAME, FIRST NAME): Zhao, Mingxuan[1]; Kang, Fei[1]; Zhang, Mingru[1]; Wang, Shengjun[1]; Yang, Weidong[1]; Wang, Jing[1]

INSTITUTIONS (ALL):

1. Department of Nuclear Medicine, Xijing Hospital, Xi'an, Shaanxi, China.

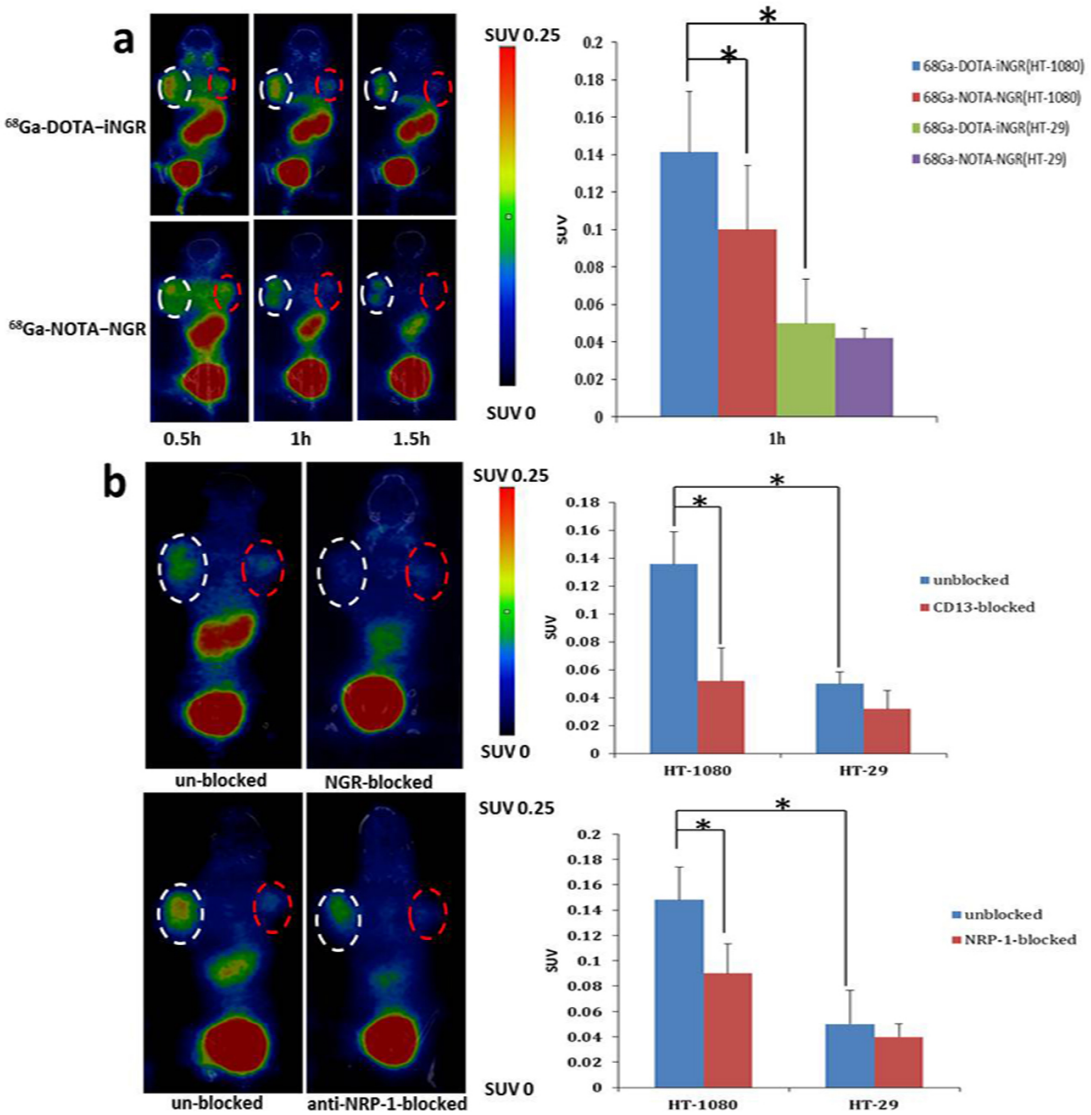
a
^{68}Ga-DOTA–iNGR
^{68}Ga-NOTA–NGR
0.5h
1h
1.5h
SUV 0.25
SUV 0
SUV
1h
68Ga-DOTA-iNGR(HT-1080)
68Ga-NOTA-NGR(HT-1080)
68Ga-DOTA-iNGR(HT-29)
68Ga-NOTA-NGR(HT-29)
b
un-blocked
NGR-blocked
HT-1080
HT-29
unblocked
CD13-blocked
un-blocked
anti-NRP-1-blocked
unblocked
NRP-1-blocked

CONTROL ID: 2232102

TITLE: PET imaging of ^{18}F labeled PZA in *M. tuberculosis*-infected animals to quantify drug concentrations in infected tissues

PRESENTER: Zhuo Zhang

ABSTRACT BODY:

Abstract Body: In our study, the front-line tuberculosis (TB) drug, pyrazinamide (PZA), was radiolabeled with fluorine-18 (5-^{18}F-PZA) and imaged in *M. tuberculosis (M.tb)*-infected mice by Positron Emission Tomography (PET). The biodistribution and real-time concentration of 5-^{18}F-PZA in multiple organs including infected tissues was detected and measured by PET imaging non-invasively. Concentrations of 5-^{18}F-PZA at infected and uninfected sites were quantified by PET and compared. The signal observed in bones suggested that free fluoride was produced by de-fluorination of 5-^{18}F-PZA. Significantly higher SUV of 5-^{18}F-PZA in infected lungs in *M.tb*-infected animals than in lungs of healthy animals was observed. Although a non-specific blood-pooling effect could contribute to the higher accumulation in the organs of the infected animals, *M.tb*-infection-specific drug accumulation was supported by the much higher ratio of uptake in infected lungs to healthy lungs than that of *M.tb*-free tissues such as the heart and brain. In summary, our study utilized PET as a non-invasive imaging tool to profile real-time *in vivo* tissue pharmacokinetics (PK) of the TB drug analog, 5-F-PZA, in *M. tuberculosis*-infected animals. Such data are difficult to measure using other techniques. The results can help understand the anti-TB mechanism of PZA, and also provide important information to guide the PZA regimen for TB treatment.

Acknowledgement. This work was supported by NIH grants DP2-OD006492 (SJ) and GM102864 (PJT), and an ACTG Novel Formulations subcontract from Brigham and Women's Hospital

AUTHORS (LAST NAME, FIRST NAME): Wang, Hui[1, 2]; Ordoñez, Alvaro A.[3]; Zhang, Zhuo[1, 2]; DeMarco, Vincent P.[3]; Jain, Sanjay K.[3]; Tonge, Peter[1, 2]

INSTITUTIONS (ALL):

1. Chemistry, Stony Brook University, Stony Brook, NY, United States.
2. Institute of Chemical Biology and Drug Discovery, Stony Brook University, Stony Brook, NY, United States.
3. Center for Infection and Inflammation Imaging Research, Johns Hopkins University, Baltimore, MD, United States.

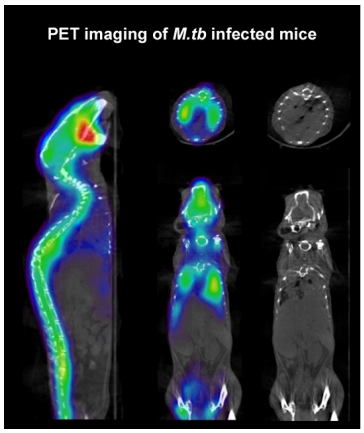
PET imaging of *M.tb* infected mice

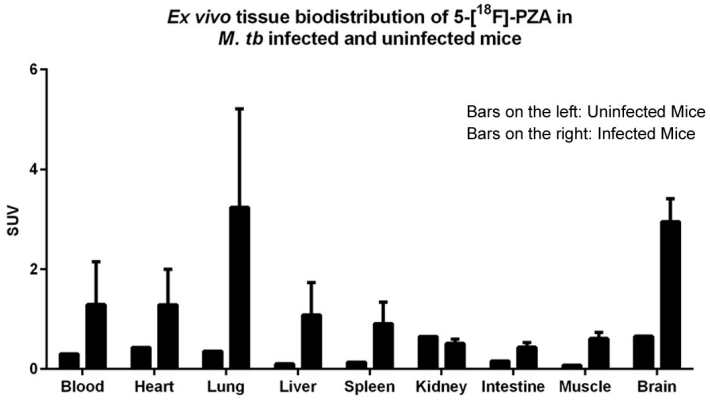
Ex vivo tissue biodistribution of 5-[^{18}F]-PZA in *M. tb* infected and uninfected mice
Bars on the left: Uninfected Mice
Bars on the right: Infected Mice
SUV
0
2
4
6
Blood
Heart
Lung
Liver
Spleen
Kidney
Intestine
Muscle
Brain

CONTROL ID: 2232113

TITLE: Multiscale photoacoustic microscopy for *in vivo* preclinical imaging

PRESENTER: Xiaoquan Yang

ABSTRACT BODY:

Abstract Body: System biology studies call for imaging data collected on multiple scales. The interpretation and transfer of data from different scales are challenging, since they are generally acquired by different imaging modalities and based on varied contrast. Fortunately, photoacoustic microscopy (PAM) can obtain scalable resolutions based on the same imaging mechanism and has been used to image biological structures at scales from organelles to organs *in vivo*.

By making full use of the potential multiscale imaging capability of PAM, a multiscale photoacoustic microscope for in vivo preclinical imaging is developed. The scalable imaging capability is achieved by delivering light through an electrical varifocal lens and an optical fiber bundle. The varifocal lens is used to generate a focused laser spot with tunable size on the tip of the fiber bundle. Laser beams emerging from the other end of the fiber bundle formed a “sampled” copy of the incident spot and then imaged into the biological tissues to excite photoacoustic signals. Based on this imaging principle, continuously tunable lateral resolution ranging from optical diffraction limited focus to acoustic focus can be achieved. The resolution tuning range is verified as large as from ~1 μm to more than 44.8 μm. Moreover, *in vivo* images under three different scales of a mouse ear are otained, demonstrated the feasibility of the multiscale *in vivo* imaging capability of our system.

AUTHORS (LAST NAME, FIRST NAME): Jiang, Bowen[1]; Yang, Xiaoquan[1]; Luo, Qingming[1]

INSTITUTIONS (ALL):

1. Wuhan National Lab for Optoelectronics, Huazhong Univ. of Sci. & Tech., Wuhan, Hubei, China.

(No Image Selected)

CONTROL ID: 2232115

TITLE: The effect of moderate endurance exercise during doxorubicin-treatment in tumor-bearing mice

PRESENTER: Chia-Ying Lien

ABSTRACT BODY:

Abstract Body: Doxorubicin (DOX), a highly effective chemotherapeutic medicine, is associated with cardiac dysfunction. Several evidences indicate that endurance exercise during DOX-treatment can preserve cardiac function against DOX cardiotoxicity in non-tumor bearing rats. However, it is less clear whether exercise during chemotherapy in a tumor model is efficacious. To our knowledge, the effects of concurrent endurance exercise training and DOX treatment on cardiac function in tumor bearing animals has never been investigated. Furthermore, clinical recommendations from physicians to cancer patients regarding exercise during DOX treatment are inconsistent and complete avoidance of exercise is a common suggestion regardless of the current evidence base. PURPOSE: To determine the effect of involuntary exercise (treadmill) during DOX treatment on the antineoplastic efficacy of DOX. If the anti-cancer properties of DOX are unadulterated by concurrent endurance training, a secondary goal is to investigate the cardioprotective or e*xacerbative* effects of involuntary exercise on DOX-induced myocardial dysfunction. METHOD: Eight week old C57BL/6 (B6) female mice were randomly assigned to either receive a subcutaneous injection of $5x10^5$ cells of B16F10 melanoma (tumor group, n=27) or an equivalent volume of saline (non-tumor group, n=18). Three weeks following the tumor cell inoculation, mice received (7 days apart) two injections (i.p.) of cumulative dose of 12 mg DOX/kg body weight (Non-tumor+DOX, n=9; Tumor+DOX, n=18) or an equivalent volume of saline (Non-tumor+SAL, n=9; Tumor+SAL, n=9). During DOX treatment, animals in Tumor+DOX group were randomly assigned to either sedentary (Tumor+DOX+SED, n=9) or treadmill exercise (Tumor+DOX+TM, 4d/wk, 30min/day, n=9) for two weeks. All other groups remained sedentary and *in vivo* cardiac function was assessed two weeks later. RESULTS: B16F10 melanoma was a malignant tumor. All animals in Tumor+SAL were dead before the assessment (5 weeks post tumor inoculation). DOX-treatment improved overall survival rate (4/9, 44% survived 5 weeks). DOX alone did not affect cardiac function when Non-tumor+SAL was compared to Non-tumor+DOX or Tumor+DOX+SED ($p>0.05$). However, involuntary exercise resulted in a reduction in survival rate (2/9, 22%). Additionally, involuntary exercise resulted in reduced mitral flow velocity MV (452±88mm/s), increased ejection time (129±61ms, and isovolumic relaxation time IVRT (36.4±7.1ms) when compared to controls ($p<0.05$). CONCLUSIONS: The current study is in conflict with previous research utilizing concurrent exercise training and DOX treatment to attenuate DOX cardiotoxicity in non-tumor bearing animals. Interestingly, concurrent endurance exercise training and DOX treatment altered anti-neoplastic efficacy and exacerbated cardiotoxicity in tumor-bearing mice.

AUTHORS (LAST NAME, FIRST NAME): Chuang, Tai-Yuan[1]; Jensen, Brock T.[2]; Chen, Mei-Li[1]; Cheng, Hu[3]; Lien, Chia-Ying[1]

INSTITUTIONS (ALL):

1. Athletic Department, National Taiwan University, Taipei, Taiwan.
2. Exercise and Rehabilitative Sciences, Slippery Rock University,, Slippery Rock , PA, United States.
3. Physical Education, Chinese Culture University, Taipei, Taiwan.

(No Image Selected)

CONTROL ID: 2232120

TITLE: Ultra-high-resolution SPECT using variable pinhole collimator—a simulation study

PRESENTER: Hakjae Lee

ABSTRACT BODY:

Abstract Body: The two major factors that determine the quality of a single photon emission computed tomography(SPECT) is spatial resolution and sensitivity. Usually, the pinhole collimator is used when high resolution image is required. However, pinhole collimator requires much more imaging time and radiation dose than the other types of collimators because of its intrinsically low sensitivity.

In general, the field-of-view(FOV) of pinhole collimator is designed to achieve the whole body image of the target. However, the region-of-interest(ROI) is much smaller than the FOV, in many cases. If the FOV of SPECT can be focused to the ROI, spatial resolution can be enhanced dramatically. Some researchers have been developed the ROI-focused collimators to achieve high resolution images.

In spite of these efforts, there were several limitations of conventional pinhole collimators. The size and the position of the ROI are not always same for different target objects. Furthermore, for each rotation angle, the stationary acceptance angle of conventional pinhole collimator is not optimal even in a target object.

In order to achieve the best performance of SPECT, we propose a novel pinhole collimator which can change its shape in real-time. The proposed variable pinhole collimator, modeled on the conventional pinhole by piling several tungsten layers of different apertures, is shown in Figure 1(a). These apertures are drilled into thin tungsten sheets, as displayed in Figure 1(b) and the movement of each tungsten sheet is controlled by its designated motor driving unit, to align the optimal aperture of each layer with the pinhole center, as shown in Figure 1(c). When the thickness of tungsten sheets is thin enough, the cross-sectional diagram of the piled holes can imitate various conventional pinholes. In the proposed SPECT, the size of ROI and the distance of the collimator from object can be varied for each rotation angle. The variance in acceptance angle of the proposed collimator helps the size of the reflection image for every rotation angle can be optimized to cover the full area of the scintillator.

The performance of the proposed SPECT has been verified by Monte-carlo simulation. To compare the resolution and the sensitivity of proposed system with the conventional SPECT systems(whole body SPECT and ROI-focused SPECT), quantitatively, we designed a micro-Derenzo like digital phantom. The result of phantom study shows that the sensitivity of the proposed system is higher by about 192% than the conventional whole body SPECT and about 341% than the conventional ROI-focused SPECT. In reconstructed images of the conventional whole body SPECT and ROI-focused SPECT, 1.2 mm and 0.8 mm diameter of hot rods were barely distinguished, respectively, while 0.6 mm diameter of hot rods were clearly distinguished in the image of proposed system.

In this study, we designed a novel pinhole collimator and showed preliminary results of proposed system. Currently, we are pursuing strategies to realize the proposed system, in order to develop high sensitivity and high resolution SPECT.

AUTHORS (LAST NAME, FIRST NAME): Lee, Hakjae[1, 2]; Bae, Seungbin[3]; Bae, Jaekeon[3]; Cha, Hyemi[3]; Chun, Jaehee[3]; Lee, Kisung[1, 3]

INSTITUTIONS (ALL):

1. School of Biomedical Engineering, Korea University, Seoul, 0, Korea (the Republic of).
2. Research Institute of Global Health Technologies at Korea University, Seoul, Korea (the Republic of).
3. Bio-convergence Engineering, Korea University, Seoul, Korea (the Republic of).

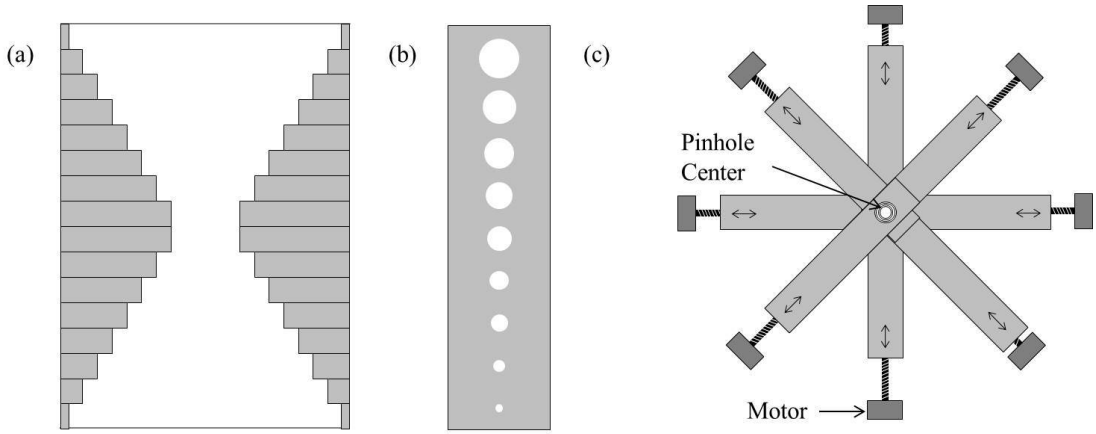

Fig. 1. (a) Cross-sectional diagram of the variable pinhole collimator, which has been designed by piling tungsten layers having different apertures. (b) Different apertures which are drilled into a tungsten sheet. (c) The movements of stacked tungsten sheets are guided by motor controlled sliding units.

CONTROL ID: 2232122

TITLE: Modified method for labeling of 5-fluorouracil with ^{99m}Tc and study of its in-vivo behavior in animal.

PRESENTER: Naseer Ahmed

ABSTRACT BODY:

Abstract Body: Introduction: 5-fluorouracil is an antimetabolite used as an antineoplastic agent in solid tumors like colon, rectum, breast, stomach and pancreas. The aim of this study was to develop modified method for labeling of 5-fluorouracil with ^{99m}Tc which rapidly accumulate and excrete from different organs without altering the normal bio-distribution of 5-fluorouracil. Method: In this study EDDA-5-FU-^{99m}Tc precursor was synthesized using 2.5 mg of EDDA as a co-ligand and stannous chloride as a reducing agent.. Its radiochemical analysis method was developed with the help of butane-2-one and acetonitrile: water used for ascending type of chromatography. Its stability study was done and found that it was stable for 04 hours with 92% purity. It's in vivo distribution was measured using dual head gamma camera. Results: It was observed that within 30 minutes, 35.8% of injected dose cross the blood-brain barrier. After 04 hours, its brain activity reduced to 17.2%. In-vivo distribution showed that within 04 hours, maximum activity was excreted through the kidney. During the whole study, no sign of toxicity was observed. Conclusion: It was concluded that this modified method was an efficient labeling method for development of 5-fluorouracil-^{99m}Tc radiopharmaceutical and can be used as a diagnostic probe for further study of imaging of solid tumors.

AUTHORS (LAST NAME, FIRST NAME): Ahmed, Naseer[1, 2]; Saeed, Adnan[1]; Fatima, Shazia[1]; Irfan, Javaid[1]

INSTITUTIONS (ALL):

1. Nuclear Medicine, Nuclear Medicine, Oncology and Radiotherapy Institute NORI, Islamabad, Pakistan.
2. Biotechnology, Quaid -I-Azam University, Islamabad, Pakistan.

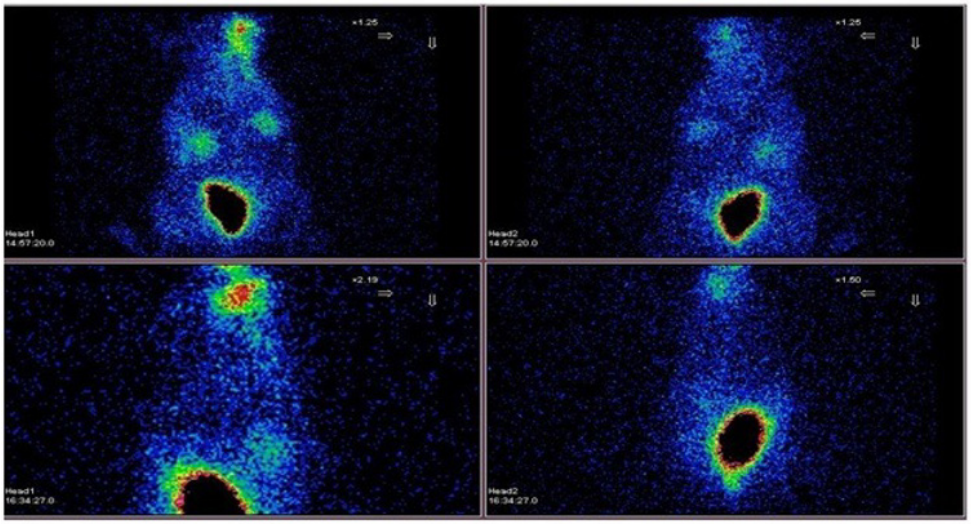

50MBq Injected, 30 and 60 minutes Anterior (left) and posterior (right) Scintigraphic Images (valium was used for sedation of animal)

FIG. B: 30 and 120 mins. Scintigraphic images [Planer and static] of rabbit taken by Dual head gamma camera after injected EDDA-5FU-TcO_4

CONTROL ID: 2232126

TITLE: The Monitoring Value of PET in Huaier Extract to Therapy of Nude Mice Bearing Human Breast Cancer Xenografts

PRESENTER: chen yao

ABSTRACT BODY:

Abstract Body: objective Current treatments are difficult to accomplish the individualized treatment of breast cancer patient's require.Huaier is a famous medicinal fungi in Chinese traditional medicine and its anticancer efficacy is being extensively studies. This experiment using small animal PET imaging surveillance to analysis different of the imaging features and metabolic activity on the treatment of Huaier extract to different molecular subtypes of breast cancer in nude mice. **Methods** BT474(HER2+) and MDA-MB-231(HER2-) human breast cancer cell lines were harvested in vitro. Using CCK8 cell proliferation experiment evaluated Huaier on the therapeutic effect of two different subtypes of breast cancer cells. Xenografts were established in nude mice. Mice were randomized into treatment and control groups (n=10) once tumors' diameter had reached 5mm. At mean time all mice underwent small-animal PET (the day 1) and mice were treated with Huaier extract diluted in saline (loading dose 50mg/μl) or the same volume saline (control) administered orally daily over the next 20 days. Small-animal PET was repeated on the 2nd,8th,15th and 21st day after treatment. The tumors were measured and the mice were weighted every week. The region of interest (ROI) analysis was performed qualitatively and the tumor uptake was expressed as the tumor/normal ratio. After the last PET imaging, all nude mice were sacrificed, the tumor tissues were isolated for immunohistochemical analysis. **Results** CCK8 experiment indicated when the concentration of Huaier extract was 8mg/ml, growth inhibition on two tumor cell began to appear. The treatment of mice with Huaier, compared with control , resulted in a significant decrease in tumor uptake of ^{18}F-FDG in BT474 xenografts since the treatment of the 2nd week ($p<0.01$). At the 2nd week, MDA-MA-231 xenografts mice treated with Huaier group as well resulted in significant decrease in tumor uptake of ^{18}F-FDG($p<0.05$), whereas no significant difference was observed for MDA-MB-231 xenografts from the 3rd week when the tumor tissue was ruptured. Notwithstanding the uptake of ^{18}F-FDG had no correlation with the changes of all two breast cancer tumor volume. Two cancer tumor size before and after treatment showed no significant differences. Immunohistochemical indicated the positive percentage was higher in the treatment group than in the control group of the apoptosis factor Caspase-3, whereas the cell proliferation associated Antigen Ki67 in the treatment was opposite. **Conclusion** Huaier in lowering metabolism rate of tumor, inducing tumor cell apoptosis, and inhibiting proliferation of breast cancer has a certain role. PET has certain value in monitoring of Huaier in different molecule classification of breast cancer.

AUTHORS (LAST NAME, FIRST NAME): yao, chen[1]

INSTITUTIONS (ALL):

1. nuclear medicine, Hangzhou, China.

(No Image Selected)

CONTROL ID: 2232127

TITLE: Antibody mimics, fibronectin domain III for EphA2-targeting as a probe in murine tumor model

PRESENTER: Seung-Hwan Park

ABSTRACT BODY:

Abstract Body: Specific binder proteins are developed on diagnosis and therapy for *in vitro* and *in vivo* applications. As an antibody mimics, human fibronectin domain III (Fn3) of small, stable and single-domain is well studied as a scaffold protein which is capable to be easily engineered with specificity and affinity. EphA2 is well-known early detection marker of various tumors such as lung, breast and colon cancer. In this study, we isolated EphA2 targeting peptides (E1 and E10) with Fn3 scaffold through the screening of yeast surface display library. They showed high affinities (Kd~2nM) against recombinant human EphA2 (hEphA2). In ELISA against EphA2 and their homologs, they only bound hEphA2 and mEphA, although binding to hEphA2 binding is 2-fold higher than mEphA2. Also they showed similar binding to the cells and tumor tissue with EphA expression on the cell surface. In vivo optical imaging showed a strong targeting of Cy5.5-labled E1 in EphA2 over-expressing xenograft models (PC3 cells). Therefore, Fn3 proteins isolated from this study show specifically binding to EphA2 with enough affinity. Altogether, high affinity Fn3 against EphA2, E1 would be useful as a candidate for EphA2 probe for *in vivo* diagnosis and therapy.

AUTHORS (LAST NAME, FIRST NAME): Park, Seung-Hwan[1]; Hong, Yeongjin[3]; Park, Sukho[1]; Park, Yong Dae[5]; Kimura, Richard[2]; Min, Jung-Joon[1]; Gambhir, Sanjiv S.[4]

INSTITUTIONS (ALL):

1. Nuclear Medicine, Chonnam National University Medical School, Gwangju, Korea (the Republic of).
2. Stanford University, Palo Alto, CA, United States.
3. Microbiology, Chonnam National Universityn, Gwangju, Korea (the Republic of).
4. Radiology, Molecular imaging Program, Stanford, CA, United States.
5. Korea Atomic Energy Research, Jeongup, Korea (the Republic of).

Figure 6

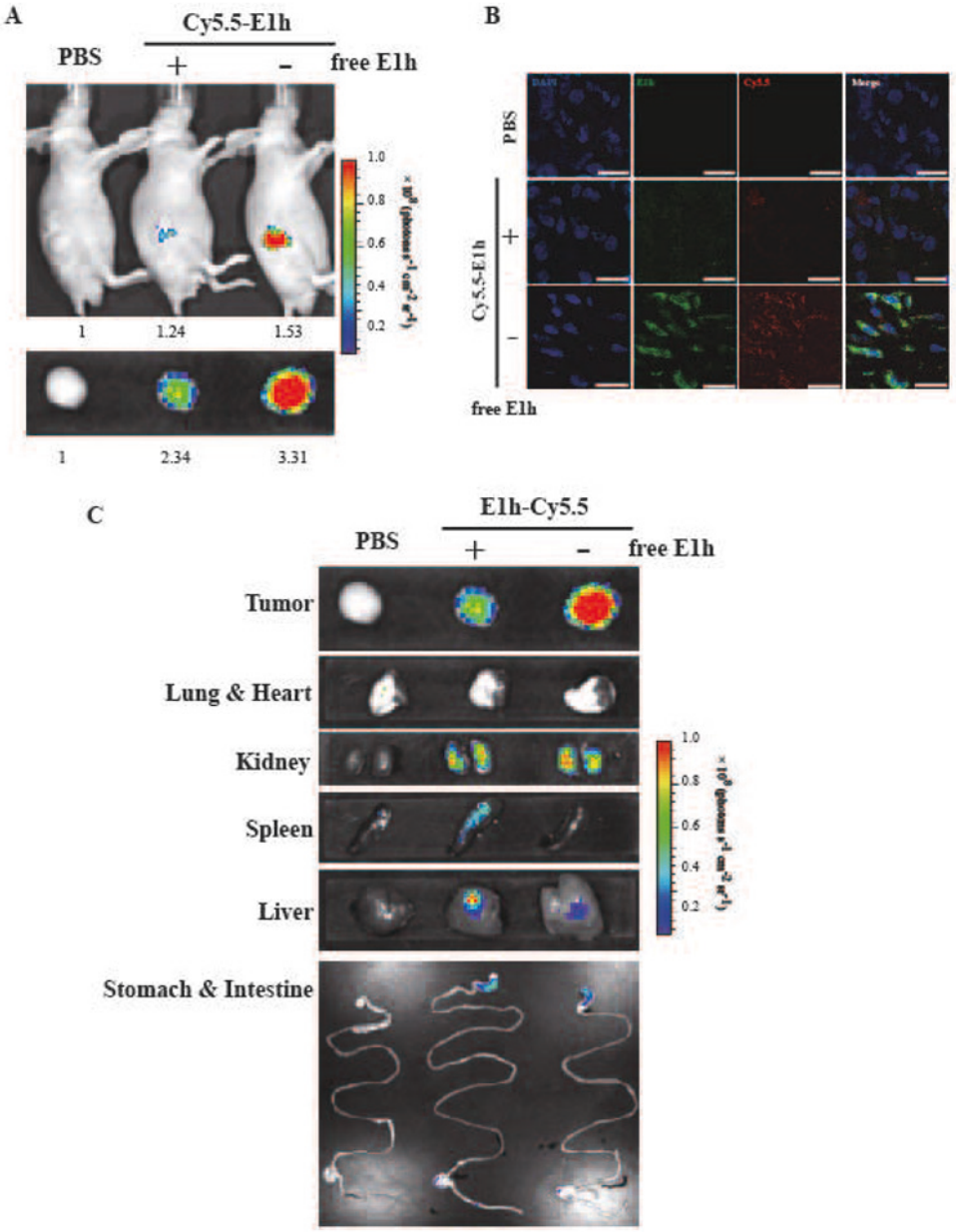
A
Cy5.5-E1h
PBS
+
-
free E1h
1
1.24
1.53
1
2.34
3.31
B
PBS
Cy5.5-E1h
+
-
free E1h
C
E1h-Cy5.5
PBS
+
-
free E1h
Tumor
Lung & Heart
Kidney
Spleen
Liver
Stomach & Intestine

CONTROL ID: 2232129

TITLE: Study of Tumor Suppressive Response of microRNA let-7i in Rhenium-188 Liposomal Drug Treated Head and Neck Squamous Cell Cancer

PRESENTER: Chun-Yuan Chang

ABSTRACT BODY:

Abstract Body: Over 90% of the head and neck cancers are categorized as squamous cell cancers (HNSCC), and the surgical dissection is the most effective treatment currently. However, the locations of HNSCC limit the surgical procedures by the surrounding organs and functions, and severe side effects of chemotherapy worsen the life quality of patients. Recently, PEGylated liposomal drugs have been developed for the prolonged residence in tumors through the enhanced permeability and retention (EPR) effect. Despite the well-characterized DNA damage repair response, the underlying tumor suppressive mechanism from close-ranged crossfire of internal radiotherapy is still unclear. Herein, we aim to investigate if ^{188}Re-liposome provides a better outcome in treating HNSCC as well as the significance of *let-7i* in tumor protective role. Radioactive ^{188}Re was embedded into PEGylated liposome following our previous study. We orthotopically implanted human hypopharyngeal cancer cell, FaDu, in nude mice, and intravenously injected the ^{188}Re-liposome. After the ^{188}Re-liposome administration, the accumulation of drug was detected by nanoSPECT/CT. Within 4-week treatment, growth of tumor was significantly suppressed, and the survival of the treated mice was prolonged. Moreover, we screened tumor suppressive mechanism triggered by ^{188}Re-liposome. Unlike the external radiotherapy, using microarray and gene set enrichment analysis (GSEA), we found a cluster of let-7-regulated genes were significantly changed after ^{188}Re-liposome administration. Additionally, we found that ^{188}Re-liposome drastically suppressed the Twist1, HOTAIR, and let-7 family gene expression. Suggesting that the close-range and crossfire mode of radiotherapy may be more effective than the external beams. In addition, modulation of let-7 family dramatically altered the radiosensitivity of HNSCC cells; moreover, the implanted HNSCC with let-7 over-expression drastically inhibited the malignancy of tumors. In summary, our findings suggest that ^{188}Re-liposome has a great potential in treating HNSCC by not only retarding the growth but also triggering a tumor suppressive machinery by the let-7 regulatory axis.

AUTHORS (LAST NAME, FIRST NAME): Chang, Chun-Yuan[1]; Lin, Liang-Ting[1]; Chang, Chih-Hsien[2]; Wang, Hsin-Ell[1]; Liu, Ren-Shyan[1]; Lee, Te-Wei[2]; Lee, Yi-Jang[1]

INSTITUTIONS (ALL):

1. Department of Biomedical Imaging and Radiological Sciences, National Yang Ming University, Taipei, Taiwan.
2. Institute of Nuclear Energy Research, Taoyuan, Taiwan.

(No Image Selected)

CONTROL ID: 2232130

TITLE: In vivo photoacoustic microscopy of nanocarrier-enhanced chemotherapy response in small animal.

PRESENTER: Liming Nie

ABSTRACT BODY:

Abstract Body: At present, conventional medical imaging modalities are difficult to monitor chemotherapy response in a timely way. In our work, photoacoustic tomography and microscopy with theranostic nanoformulation was designed to noninvasively monitor the therapy response. Photoacoustic tomography was applied to visualize blood vessel, quantify vascular number, diameter and signal strength. Photoacoustic microscopy was used to image subtle blood vessels, capillary growth change and even a single red blood cell. Graphene oxide nanosheets were also designed as both drug loading vehicle and photoacoustic signal amplifier to the tumor. The subtle microvascular changes of the chemotherapy response in tumor were advantagely revealed by our imaging system, which was much earlier than the morphological measurement by standard imaging techniques. Combined with exogenous functional molecular probes, multiscale photoacoustic imaging technology is expected to achieve early diagnosis and timely efficacy monitoring.

AUTHORS (LAST NAME, FIRST NAME): Nie, Liming[1]; Huang, Peng[2]; Chen, Xiaoyuan[2]

INSTITUTIONS (ALL):

1. School for public health, Center for Molecular Imaging and Translational Medicine, Xiamen, Fujian, China.
2. National Institutes of Health, Bethesda, MD, United States.

(No Image Selected)

CONTROL ID: 2232131

TITLE: *In vivo* tracking of ^{64}Cu-NOTA-CD11b-labeled granulocytic myeloid-derived suppressor cells in PyMT breast cancer by PET

PRESENTER: Sabrina Eilenberger

ABSTRACT BODY:

Abstract Body: Cancer and cancer metastasis rank among the leading causes of mortality worldwide. Tumor growth and metastasis are supported by the immunosuppressive properties of granulocytic myeloid-derived suppressor cells (G-MDSCs). As immature progenitor cells of macrophages, dendritic cells and neutrophilic granulocytes, G-MDSCs suppress both innate and adaptive immune responses and thereby inhibit tumor rejection. The depletion of immunosuppressive G-MDSCs should therefore be considered when developing novel immunotherapeutic anti-cancer approaches. In previous studies from our group, we have visualized the homing of DiD-labeled G-MDSCs to primary tumors and metastases by optical imaging (OI). Moreover, our group has established an antibody-based T cell labeling strategy that allows *in vivo* T cell tracking by combined PET/CT. Using a similar approach, this work shows that *in vitro* generated, adoptively transferred G-MDSCs can be tracked *in vivo* in an orthotopic PyMT breast cancer mouse model by combined PET/MRI.

Bone marrow cells were isolated from femura and tibiae of wild-type C57BL/6 donor mice, and supplemented with IL-6 and GM-CSF to generate G-MDSCs *in vitro* which were purified according to the expression of Ly6G using a magnetic cell separation kit. Radiolabeling of purified G-MDSCs was achieved employing an affinity purified, ^{64}Cu-NOTA-modified anti-CD11b monoclonal antibody (mAb) derived from M1/70 hybridoma cell lines. At 6 weeks of age, C57BL/6 mice were injected orthotopically with 0.5x10^{6} PyMT breast cancer cells into the 4th mammary fat pad. Migration of 2x10^{6} ^{64}Cu-radiolabeled G-MDSCs was tracked *in vivo* in tumor-bearing mice (n=5) and control littermates (n=3) after i.v. injection. In a preliminary approach, one tumor-bearing mouse was i.v. injected with 5x10^{6} ^{64}Cu-radiolabeled G-MDSCs. Trafficking of G-MDSCs was visualized by 20 min static PET scans and anatomical T2-weighted MR scans 24 h and 48 h post injection.

Utilization of the ^{64}Cu-NOTA-CD11b mAb allowed for successful G-MDSC labeling accompanied by a cell loss of approximately 30% during 30 min of labeling. Uptake values ranged between 0.02-0.03 MBq per 2x10^{6} cells. Comparable to other lymphocytes after i.v. transfer, early homing sites of G-MDSCs were the lung, liver and spleen. The homing of G-MDSCs could be tracked to the liver (15.1±4.7 %ID/cc) and spleen (16.8±6.6 %ID/cc) of tumor-bearing mice and control littermates (6.9±1.4 %ID/cc and 5.45±1.2 %ID/cc, respectively) *in vivo* 24 h post injection. G-MDSCs accumulated locally in the tumor (2.2±0.3 %ID/cc) 48 h post injection, infiltration of the whole tumor could not be detected. Ex vivo biodistribution analysis confirmed the results obtained by PET.

This study shows for the first time that G-MDSCs migration can be tracked by PET using an antibody-based labeling approach, NOTA as a chelator and [^{64}Cu] as a radioisotope. While PET allows for the *in vivo* 3D cell detection for 48 h, OI allows for 2D cell tracking only but over a longer period of time. For further studies, long-lived isotopes such as ^{89}Zr and MR labeling strategies will be considered to survey G-MDSC recruitment to the tumor microenvironment.

AUTHORS (LAST NAME, FIRST NAME): Eilenberger, Sabrina H.[1]; Sceneay, Jaclyn E.[2]; Wong, Christina S.[3]; Kneilling, Manfred[4]; Möller, Andreas[3]; Pichler, Bernd J.[1]; Griessinger, Christoph M.[1]

INSTITUTIONS (ALL):

1. Werner Siemens Imaging Center, Department of Preclinical Imaging and Radiopharmacy, Eberhard Karls University Tübingen, Tübingen, Germany.
2. Department of Hematology, Brigham and Women's Hospital, Boston, MA, United States.
3. Tumour Microenvironment Laboratory, QIMR Berghofer Medical Research Institute, Herston, QLD, Australia.
4. Department of Dermatology, Eberhard Karls University Tübingen, Tübingen, Germany.

(No Image Selected)

CONTROL ID: 2232147

TITLE: Tumor-associated macrophage imaging to delineate the margins of glioblastoma using a triple-modality PET-MRI-fluorescent nanoparticle

PRESENTER: Jung Sun Yoo

ABSTRACT BODY:

Abstract Body: Glioblastoma multiforme (GBM) is the most aggressive and lethal type of human brain cancer. Most patients survive no longer than 1 year after diagnosis despite optimal treatment of currently available therapies, including surgery, radiation and chemotherapy. One challenge in treating GBM is diffusely infiltrating characteristics of glioma cells that makes complete removal by surgical resection impossible. GBM typically consists of the highly cellular core with abundant neo-vessels and the diffuse edematous margin with a complex mixture of glioma cells and non-neoplastic brain cells. Complete surgical resection especially for the infiltrative boundary region is pivotal to prevent recurrence and improve survival. Abundant macrophage infiltration is a key feature of GBM margins. Recent studies showed that tumor-associated macrophages (TAMs) actively promote GBM progression in multiple aspects. In addition, several pioneering approaches to target TAMs have already shown initial promise for GBM treatment. Therefore, accurate imaging of TAMs which are enriched in GBMs may provide a new option for improved diagnosis and prognosis, related treatment decisions, and intraoperative guidance of GBM resection. Here we present a triple-modality positron emission tomography (PET)-magnetic resonance imaging (MRI)-near infrared fluorescence (NIRF) imaging nanoparticles for TAM targeting. Nanoparticle is a favorite imaging agent for macrophages given their naturally high endocytosis activity. Based on this avidity, we synthesized superparamagnetic iron oxide nanoparticles with strong MRI contrast and conjugated with near-infrared fluorophore Cy5.5 for NIRF imaging and azide molecules for ^{18}F PET isotope labeling. It is noteworthy that the developed nanoparticles have superior long-term water stability by active introduction of polyethylene glycol MW 600 (PEG) which have been a major obstacle of iron oxide nanoparticles for biomedical use. *In vivo* NIRF imaging with U87-MG GBM xenograft models demonstrated excellent tumoral uptake by nanoparticles and immunofluorescence staining analysis confirmed that the accumulated nanoparticles were exclusively co-localized with CD68^{+} TAMs, but not tumor cells and other stromal cells including CD31^{+} endothelial cells. The adverse effects of the nanoparticles on cell viability were minimal. This nanoprobe allows preoperative planning with PET and MRI and intraoperative resection of GBM with sensitive NIRF imaging by a single injection. The presented novel triple-modality-nanoparticle approach targeting TAMs may facilitate the development of effective options for GBM treatment to circumvent previous failure of most therapeutics targeting glioma cells.

AUTHORS (LAST NAME, FIRST NAME): Yoo, Jung Sun[1]; Lee, Chaedong[1]; Yoon, Juhwan[1]; Jung, Jae Ho[3]; Lee, Byung Chul[3]; Piao, Yuanzhe[1]; Kim, Sang Eun[2]

INSTITUTIONS (ALL):

1. Department of Transdisciplinary Studies, Seoul National University, Suwon, Korea (the Republic of).
2. Department of Nuclear Medicine , Seoul National University College of Medicine, Seongnam, Korea (the Republic of).
3. Nuclear Medicine, Seoul National University College of Medicine, Seoul National University Bundang Hospital, Bundang-gu, Seongnam-si, Korea (the Republic of).

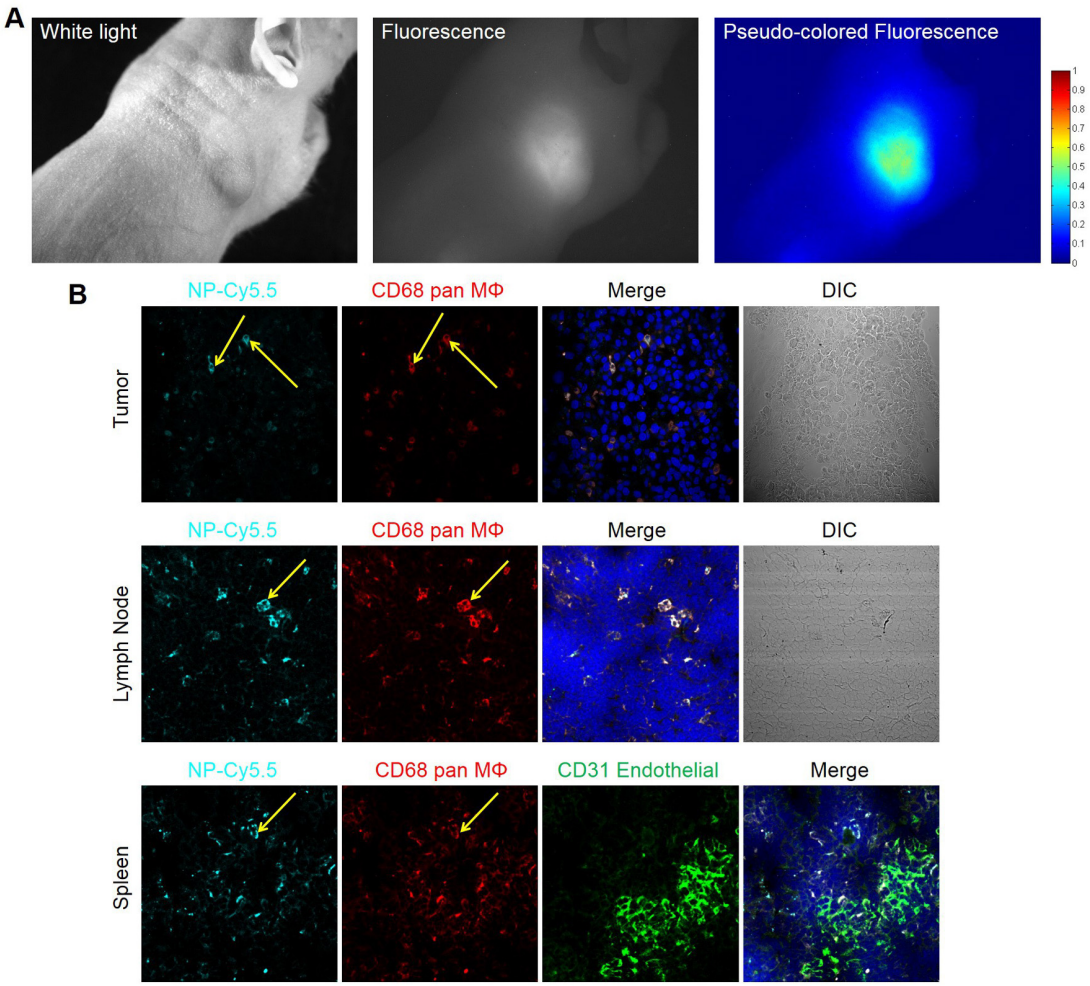

A, *In vivo* fluorescence imaging of a glioblastoma xenograft model using Cy5.5-labeled iron oxide nanoparticles. A strong fluorescence signal was detected in tumor tissue. **B,** Histologic assessment of *in vivo* targeting by Cy5.5-labeled iron oxide nanoparticles. Shown are immunostained sections of tumor, lymph node, and spleen of the xenograft 24 h after intravenous injection of the nanoparticles. All sections were counterstained with Hoechst33342 to show nuclei (blue). Most cells containing nanoparticles (cyanine) expressed macrophage marker, CD68 (red) but not endothelial cell marker, CD31 (green). Arrows denote representative coexpressed cells with CD68 and nanoparticles.

CONTROL ID: 2232158

TITLE: Optimized Image Generation with Hybrid Optoacoustic Ultrasound System using Concave Arrays

PRESENTER: Elena Mercep

ABSTRACT BODY:

Abstract Body: It has not been a long time since optoacoustic imaging started drawing the interest of the research and medical communities and there is still room to improve on quantification capabilities of the technique, as well as to exploit the potential of hybrid imaging solutions such as ultrasound (US) and multispectral optoacoustic (OAT) tomography for real-time probing of tissue. Thanks to complementary anatomical and functional information delivered by these two methods, an integrated solution is foreseen to become a valuable diagnostic tool. However, different physical origins of the generated contrast impose challenges on optimal tomographic data acquisition and reconstruction when combining the two modalities[1].

In this study, the performance of several transducer geometries commonly employed in ultrasound and optoacoustic imaging was investigated with respect to image quality of the generated hybrid images. It has been shown that accurate image reconstruction in OAT is achieved by collecting optoacoustic responses from as many angles around the imaged object as possible. On the other hand, the established beamforming techniques result in unsatisfactory quality of pulse-echo US images when using tomographic arrays solely tailored for optimal OA image acquisition. To address this problem, optimized beamforming strategies for the curved array design were proposed with improvements showcased in both optoacoustic and pulse-echo ultrasound images acquired from tissue-mimicking phantoms and mice.

Experimental validation was performed on an MSOT system[2] upgraded to incorporate a custom-made multiplexer unit for switching between optoacoustic and ultrasonography modes using the same transducer array. A tunable pulsed OPO laser illuminated the sample in a wavelength range of 680–980nm at a repetition rate of 10Hz. Several transducer types were employed in the study, including tomographic cross-sectional and handheld probes with 270° and 135° angular coverage, respectively, as well as a conventional linear array US probe. For generation of ultrasound pulses a 128-channel transmitter with transmit voltage up to 80 Vpp was used. Experiments were performed on a solid polyurethane-based phantom and post-mortem mice. For generation of the pulse-echo US images, the synthetic transmit aperture (STA) technique was employed, which enables rendering of images at a high frame rate[3,4] in combination with spatial compounding technique[5]. Optimal size of a single sub-aperture for STA imaging and the overlap between multiple sub-apertures for spatial compounding were chosen by means of numerical simulations and quantification metrics such as peak-to-side-lobe ratio and full width of the main lobe of the beam profile.

It has been demonstrated that optimal selection of the array pitch size, tomographic coverage and parameters of the beamforming achieves an accurate hybrid imaging performance. The presented techniques serve as a roadmap towards successful integration and increase in the diagnostic significance of stand-alone imaging modalities.

[1] Bouchard et al. 2014 [2] Morscher et al. 2014 [3] Karaman et al. 1995 [4] Jensen et al. 2006 [5] Mohana et al. 1985

AUTHORS (LAST NAME, FIRST NAME): Mercep, Elena[1, 3]; Jeng, Gency[4]; Morscher, Stefan[1, 3]; Li, Pai-Chi L.[5, 6]; Razansky, Daniel[1, 2]

INSTITUTIONS (ALL):

1. Institute for Biological and Medical Imaging (IBMI), Helmholtz Center Munich, Neuherberg, Germany.
2. Faculty of Medicine, Technical University of Munich, Munich, Germany.
3. iThera Medical GmbH, Munich, Germany.
4. S-Sharp Corporation , New Taipei City 231, Taiwan.
5. Graduate Institute of Biomedical Electronics and Bioinformatics, National Taiwan University, Taipei, Taiwan.
6. Department of Electrical Engineering, National Taiwan University, Taipei, Taiwan.

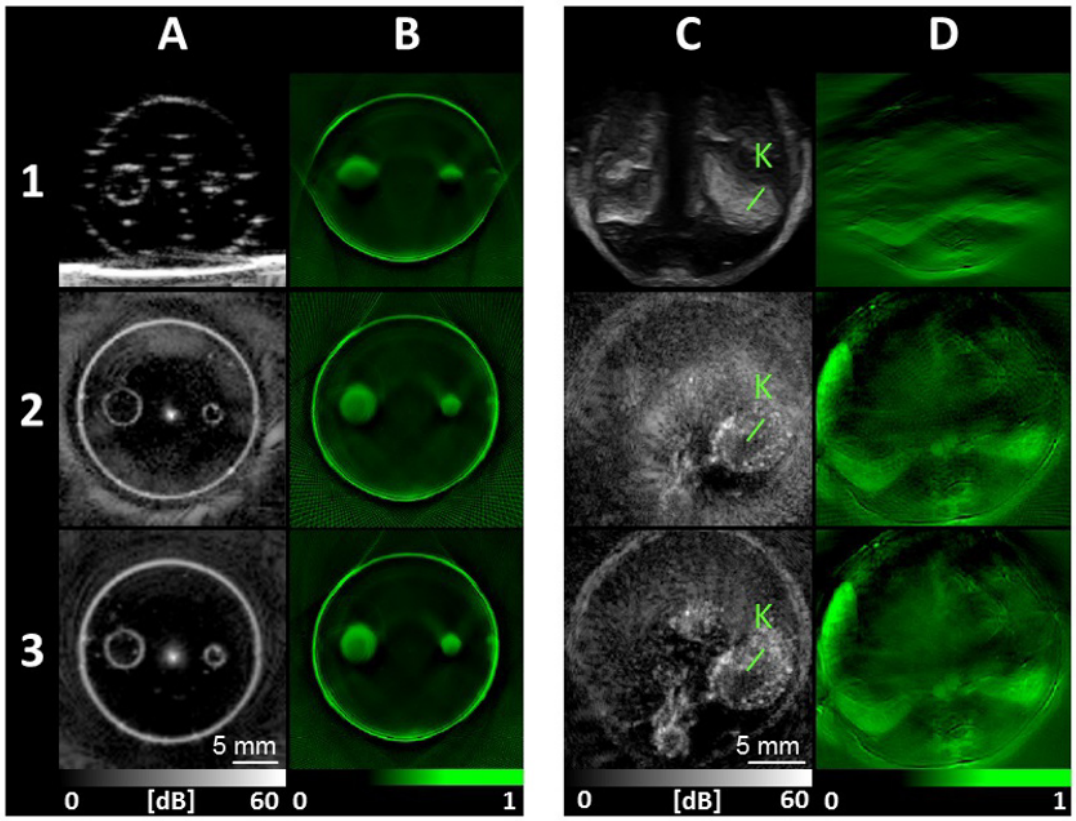
A
B
C
D
1
2
3
K
K
K
5 mm
5 mm
0
[dB]
60
0
1
0
[dB]
60
0
1

CONTROL ID: 2233797

TITLE: The Role of USPIO in Evaluating the Dignity of a Lesion

PRESENTER: Perla Seyfer

ABSTRACT BODY:

Abstract Body: Introduction:

Early distinction of malignant and benign lesions is essential regarding the decision of the appropriate therapy. The value of Ultrasmall superparamagnetic iron oxide particles (USPIO)-enhanced MRI as a diagnostic tool for differentiating abscesses from the rabbit VX2-carcinoma has been confirmed earlier.

The aim of the present study was to determine, whether Ferumoxtran-labeled MRI can differentiate intramuscular tumors of implanted HeLa cells from abscesses.

Methods and materials:

This experiment was approved by the local animal care committee. HeLa-cells and bacteria were implanted into the hind thighs of athymic mice leading to tumors and intramuscular abscesses, respectively. Two weeks after the injection of tumor cells, MR imaging was performed with a 7 Tesla magnet pre contrast and serially for 24 hours after injecting USPIO (Ferumoxtran). Harvested abscesses and HeLa-tumors were stained with Hematoxylin-eosin and Prussian blue (Fig1 C D) and evaluated using a light microscope. Radiologic-histologic correlations were performed between the MR images and the corresponding histologic slices.

Results:

24h after the Ferumoxtran-injection, no remarkable changes were observed in HeLa-carcinomas (Fig1), whereas a mean reduction of the signal-to-noise ratio (SNR) of approximately 84% was noticed in abscesses. On histopathologic examination, abscesses demonstrating a signal drop were found to include iron-containing macrophages indicating that the reduction in SNR was caused by USPIO-tagged monocytes.

Conclusion:

USPIO-enhanced MRI is able to differentiate a malignant human cancer from an inflammation, based on iron-positive macrophages. The results of our study confirm the value of USPIO-enhanced MRI as a diagnostic tool for early detection of carcinoma and therefore for prompt treatment.

AUTHORS (LAST NAME, FIRST NAME): Seyfer, Perla[1]; Hengl, Carina[1]; Heverhagen, Johannes T.[2]

INSTITUTIONS (ALL):

1. Diagnostic and Interventional Radiology, University Hospital of Marburg, Marburg, Germany.
2. Department of Diagnostic, Interventional and Pediatric Radiology, University Hospital of Bern, Bern, Switzerland.

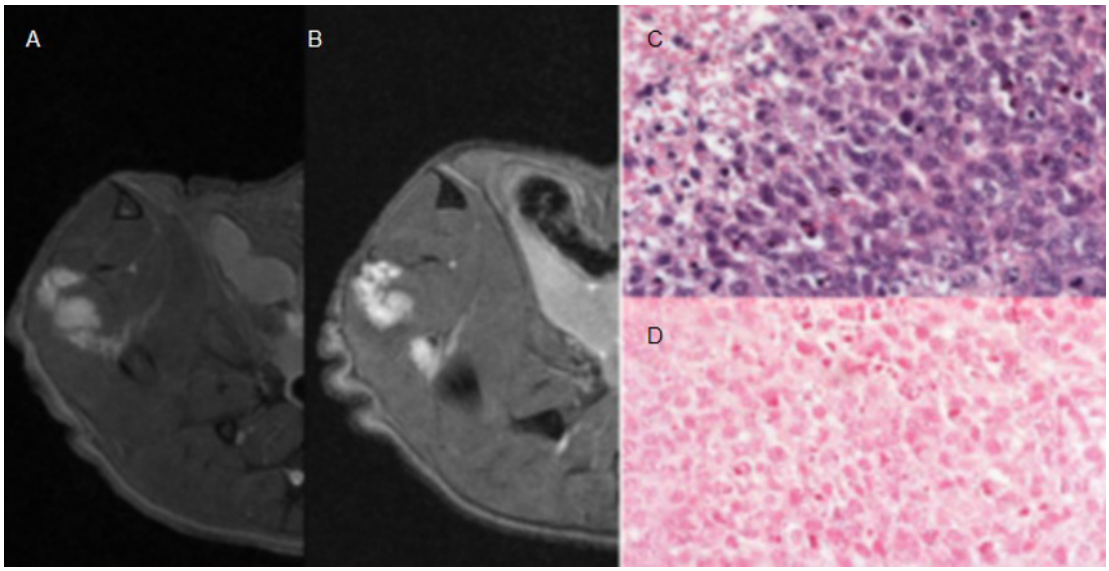
A
B
C
D

CONTROL ID: 2232186

TITLE: Adefovir dipivoxil-induced Fanconi syndrome and hypophosphatemic osteomalacia in patients with chronic hepatitis B

PRESENTER: Ying Zhang

ABSTRACT BODY:

Abstract Body: Background: Adefovir dipivoxil (ADV) is commonly used for treatment of chronic hepatitis B (CHB), that is widely distributed in China. The renal toxicity of ADV is both dose and time related. Generalised proximal, type 2, Renal Tubular Acidosis, also known as Fanconi syndrome, is a generalised dysfunction of the proximal renal tubule characterized by impaired reabsorption and increased urinary loss of phosphate and other solutes such as uric acid, glucose, amino acids and bicarbonate. Chronic hypophosphatemia is the second most common cause of osteomalacia after vitamin D deficiency in adult patients. It can have a heterogeneous presentation ranging from mild symptoms such as muscle weakness and skeletal pain to more severe presentation such as disabling myopathy, severe bone and joint pain, difficult walking, and even bone fractures. This rare condition may be life-threatening and mimic other bone metabolic disorders that are treated with drugs which may further impair phosphate balance. Objective: this report describes three cases of severe hypophosphatemic osteomalacia with multiple fragility fractures induced by adefovir and potassium phosphate administration. Results and conclusions: we highlight the limited diagnostic value of radiology and the possible clinical application of bone scintigraphy in this challenging diagnosis. Conclusion: Bone metabolism should be always assessed in patients treated with adefovir for early detection of osteomalacia due to Fanconi Syndrome.

AUTHORS (LAST NAME, FIRST NAME): Zhang, Ying[1]

INSTITUTIONS (ALL):

1. Zhejiang University, Hangzhou, Zhejiang, China.

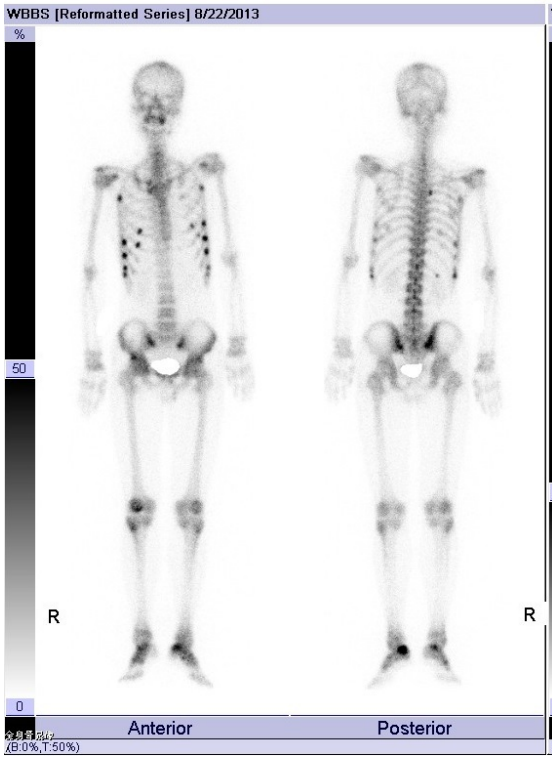
WBBS [Reformatted Series] 8/22/2013
%
50
0
R
Anterior
Posterior
(B:0%,T:50%)

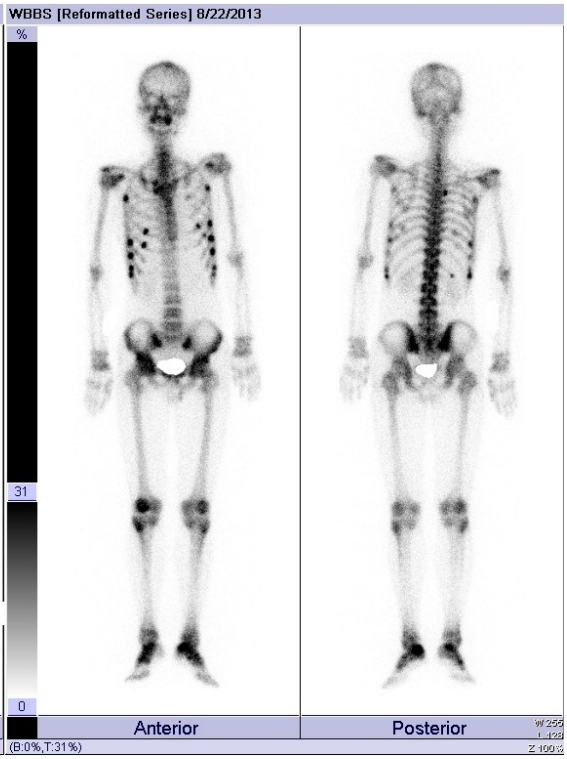
WBBS [Reformatted Series] 8/22/2013
%
31
0
R
Anterior
Posterior
(B:0%,T:31%)

CONTROL ID: 2232182

TITLE: Multiparametric contrast enhanced ultrasound with VEGFR-2 targeted microbubbles and DCE-MRI for monitoring the effects of regorafenib on colorectal adenocarcinoma xenografts in rats with immunohistochemical validation

PRESENTER: Ralf Eschbach

ABSTRACT BODY:

Abstract Body: Purpose:

To investigate contrast enhanced ultrasound with VEGFR-2 targeted microbubbles for monitoring the effects of regorafenib on experimental colon carcinomas in rats with correlation to DCE-MRI and immunohistochemical validation.

Methods and Material:

Human colorectal adenocarcinoma xenografts (HT-29) were implanted subcutaneously in n=20 female athymic nude rats (Hsd: RH-Foxn1^{rnu}) randomized to either therapy or control group. The animals were imaged at baseline and after a one-week daily treatment with regorafenib or a placebo, using contrast enhanced ultrasound (CEUS) with VEGFR-2 targeted microbubbles (BR55) and multiparametric DCE-MRI with Gadobutrol.

In CEUS with BR55, both functional and molecular parameters were quantified: Tumor perfusion (peak enhancement, wash-in-rate, mean transit time, relative blood volume, relative blood flow) during an early vascular phase and VEGFR-2-specific binding of the microbubbles (signal intensity of bound microbubbles) during a late phase up to 10 minutes after contrast injection, using a high-end ultrasound system with a 15 MHz probe and dedicated software. In DCE-MRI, functional parameters of plasma flow (PF, mL/100 mL/min) and plasma volume (PV, %) were calculated based on a two-compartment kinetic model. For validation purposes, CEUS parameters were correlated with DCE-MRI parameters and immunohistochemical CD31 (microvascular densisty), TUNEL (apoptosis) and VEGFR-2 stainings.

Results:

CEUS parameters of tumor perfusion decreased siginficantly ($p<0.05$) under regorafenib therapy from day 0 to day 7, while there were no significant changes ($p>0.05$) in the control group. Additionally the number of bound microbubbles in the late phase declined significantly ($p<0.05$) from baseline to follow-up in therapy group and was significantly ($p<0.05$) lower in therapy than in control group at day 7. In Regorafenib treated animals DCE-MRI parameters PF and PV decreased significantly ($p<0.05$) between day 0 and day 7 with no significant changes ($p>0.05$) in the control group. PF and PV were significantly lower ($p<0.05$) in the therapy than in the control group at day 7. Immunohistochemistry revealed significantly fewer ($p<0.05$) CD31, TUNEL and VEGFR-2 positive cells in therapy group. CEUS parameters showed moderate, but significant ($p<0.05$) correlations to DCE-MRI parameters PF and PV as well as to immunohistochemical stainings CD31, TUNEL and VEGFR-2.

Conclusion:

Regorafenib therapy significantly suppressed tumor perfusion assessed by CEUS and DCE-MRI. Additionally a significant lower number of bound BR55 microbubbles was detected in the regorafenib therapy group, consistent with a significantly reduced expression of VEGFR-2 in immunohistochemistry. Thus a multiparametric CEUS imaging protocol with VEGFR-2-targeted microbubbles allowed for monitoring regorafenib therapy effects on experimental colorectal adenocarcinomas with significant correlations to DCE-MRI parameters and immunohistochemistry.

AUTHORS (LAST NAME, FIRST NAME): Eschbach, Ralf S.[1]; Clevert, Dirk-Andre[1]; Kazmierczak, Philipp M.[1]; Schneider, Moritz[1]; Havla, Lukas[1]; Hirner-Eppeneder, Heidrun[1]; Schuster, Jessica[1]; Tadros, Dina[1]; Moser, Matthias[1]; Cyran, Clemens C.[1]

INSTITUTIONS (ALL):

1. Department for clinical radiology, University Hospital Munich LMU, Munich, Bavaria, Germany.

Contrast-enhanced Ultrasound (CEUS) mit BR55 (Bracco)

Functional Imaging Biomarker
Tumor perfusion

Molecular Imaging Biomarker VEGFR-2 expression

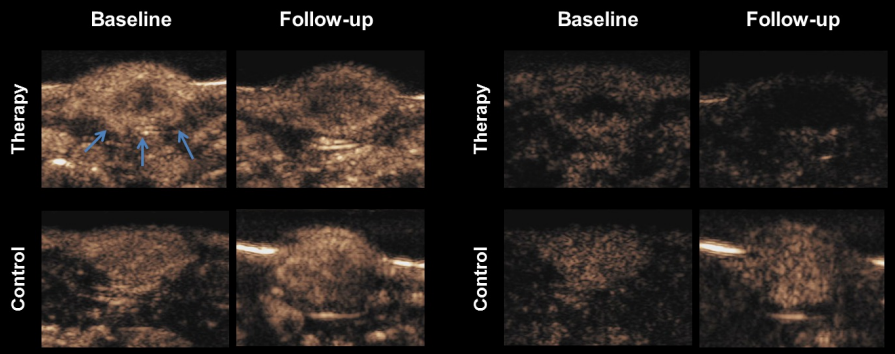

Subcutaneous human colon carcinoma xenografts (HT-29) under regorafenib therapy (1 week)

CONTROL ID: 2232185

TITLE: In vitro evaluation of a novel ^{18}F-labelled P2X$_7$ receptor antagonist for an improved PET detection of neuroinflammation

PRESENTER: Enrico Fantoni

ABSTRACT BODY:

Abstract Body: Background

P2X$_7$ receptor expression is required to sustain chronic neuroinflammation. At present, PET imaging of neuroinflammation is restricted by the low sensitivity and/or selectivity of the available radiotracers. Thus, we envisage that a P2X$_7$ radiotracer could act as a promising new imaging agent for neuroinflammation. Starting from the known antagonist A-804598, we developed and evaluated *in vitro* a novel ^{18}F-labelled PET ligand targeting P2X$_7$.

Methods

The radiotracer was synthesised via a new 4-step procedure and radiofluorinated by copper-catalysed alkyne-azide cycloaddition (Supplementary Figure A). We preformed radiotracer incubations with live BV-2 microglia in the presence or absence of Brilliant Blue G (BBG) blockade. Mouse brains were fixed in cold acetone, cut into coronal sections and mounted onto microscope slides. The slices were later incubated with the radiotracer in the presence or absence of BBG.

Results

We synthesised a novel P2X$_7$ radiotracer with 9-33% DC RCY and >99% RCP (Supplementary Figure B). A preliminary tracer evaluation in BV-2 microglia expressing the target receptor (Supplementary Figure C) delivered encouraging results (Figure 1), prompting us to investigate the *in vitro* uptake in hypoxic ischemic mouse brain tissues (Supplementary Figure D).

Conclusion

The work carried out forms the basis for the development of a novel PET tracer targeting P2X$_7$. Here, we report the synthesis of the ^{18}F tracer ^{18}F-AFA and its preliminary *in vitro* evaluation in cell and mouse tissue models of neuroinflammation. The tracers could form an important part of a drug discovery programme targeting the P2X$_7$ receptor and serve for early diagnosis, monitoring and treatment of neuroinflammation.

References

[1] Donnelly-Roberts, D L, *et al.* (2009), Neuropharmacology, 56, 223-9. [2] Able, S L, *et al.* (2011), Br. J. Pharmacol., 162, 405-14. [3] Glaser, M, *et al.* (2007), Bioconjugate Chem., 18, 989-993.

AUTHORS (LAST NAME, FIRST NAME): Fantoni, Enrico R.[1]; Fleiss, Bobbi[4, 3]; Lovestone, Simon[2]; Gee, Antony[1]

INSTITUTIONS (ALL):

1. Division of Imaging Sciences and Biomedical Engineering, King's College London, London, United Kingdom.
2. Department of Psychiatry, University of Oxford, Oxford, United Kingdom.
3. Institut national de la santé et de la recherche médicale (INSERM), Paris, France.
4. Department of Perinatal Imaging and Health, Division of Imaigng Sciences and Biomedical Engineering, King's College London, London, United Kingdom.

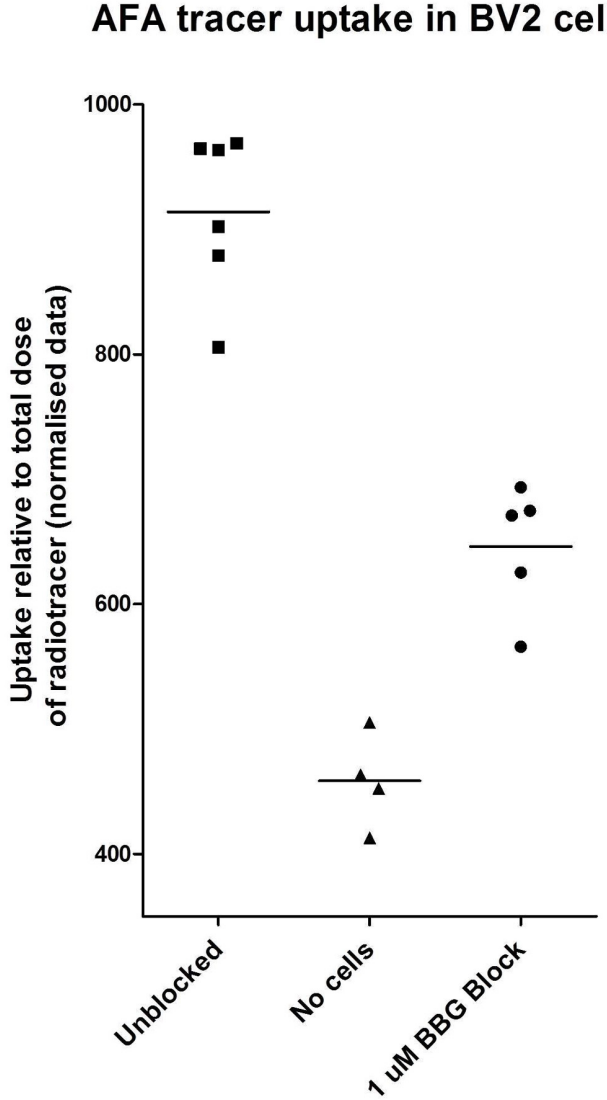

Figure 1 - ^{18}F-AFA tracer uptake after 1hr incubation at 4°C by BV-2 cells expressing the target receptor $P2X_7$. Uptake was higher in untreated cells compared to empty wells and to cells pre-treated with the $P2X_7$-selective blocker Brilliant Blue G.

CONTROL ID: 2232188

TITLE: Phototoxic effects of nanosecond laser exposure in optoacoustic microscopy on cells expressing genetic fluorescence reporters

PRESENTER: Sven Gottschalk

ABSTRACT BODY:

Abstract Body: Nanosecond-duration laser pulses are exploited in a plethora of therapeutic and diagnostic applications, such as optoacoustic imaging. But, phototoxic effects of such pulsed radiation in living cells, in particular those expressing genetic reporters, is not well understood. Here, a three dimensional (3D) fluorescent protein expressing cellular model was established in order to reliably investigate the extent and major exposure parameters responsible for both photobleaching and phototoxicity under pulsed laser exposure. A variety of possible effects on living cells was discovered, from reversible photobleaching to cytotoxicity and cell death. Significant cellular toxicity, as assessed by loss of fluorescence intensity, was identified when exposing the cells to illumination conditions considered safe under common safety standards of human exposure in diagnostic imaging applications.

A 3D cell culture, more closely representing normal cellular functions and mimicking in vivo architecture of natural tissues, was developed based on murine osteosarcoma (MOS) cells and expressing the fluorescent protein mCherry. MOS cells grow as multi-cellular spheroids in suspension culture. For experiments, spheroids were embedded in agar and exposed to various illumination conditions. Bleaching, phototoxicity and cell viability were assessed by loss of fluorescence intensity.

Bleaching of protein-expressing cells occurred already at relatively low laser fluence levels of 1 mJ/cm^2 under exposure times of around tens of seconds, which are considered safe under standards of human exposure for diagnostic imaging applications. However, when using focused scanning beams with fluence levels in the order of 1 J/cm^2, it was even proven sufficient to deposit single laser pulses to cause irreversible photobleaching. Furthermore, toxic effects were estimated from fluorescene intensity measurements after a potential recovery period of 24 hours. While lower energies had no toxic effect, laser pulse energies being commonly used in certain high-performance optoacoustic imaging systems may exhibit significant cellular toxicity.

In conclusion, the use of photolabile fluorescent proteins and their in vivo exposure parameters have to be considered carefully for all applications using pulsed nanosecond laser pulses. Especially, a loss of signal due to bleaching of the fluorescent proteins may significantly alter signals in longitudinal studies, thus hindering data quantification.

Figure Caption:

Bleaching effects of low laser fluence levels (A), focused scanning beams (B) and fast bleaching kinetics of selective illumination (C).

AUTHORS (LAST NAME, FIRST NAME): Gottschalk, Sven[1]; Estrada, Hector[1]; Degtyaruk, Oleksiy[1]; Klymenko, Olena[2]; Rosemann, Michael[2]; Razansky, Daniel[1, 3]

INSTITUTIONS (ALL):

1. Institute for Biological and Medical Imaging, Helmholtz Zentrum München, Neuherberg, Germany.
2. Institute of Radiation Biology, Helmholtz Zentrum München, Neuherberg, Germany.
3. Faculty of Medicine, Technical University of Munich, München, Germany.

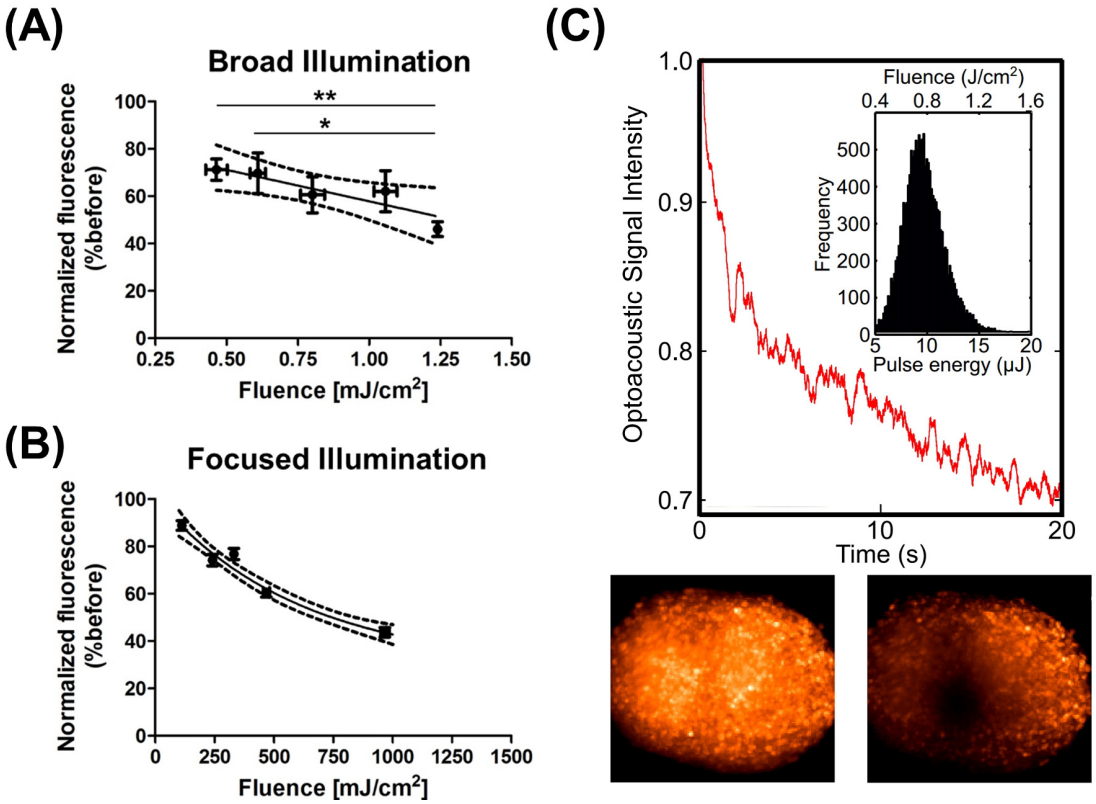
(A)
Broad Illumination
**
*
Normalized fluorescence (%before)
100
80
60
40
20
0
0.25
0.50
0.75
1.00
1.25
1.50
Fluence [mJ/cm2]
(B)
Focused Illumination
Normalized fluorescence (%before)
100
80
60
40
20
0
0
250
500
750
1000
1250
1500
Fluence [mJ/cm2]
(C)
Optoacoustic Signal Intensity
1.0
0.9
0.8
0.7
0
10
20
Time (s)
Fluence (J/cm2)
0.4
0.8
1.2
1.6
Frequency
500
400
300
200
100
0
5
10
15
20
Pulse energy (μJ)

CONTROL ID: 2232201

TITLE: Pilot study of a novel peptide targeting GPC3 for HCC

PRESENTER: Xiaohua Zhu

ABSTRACT BODY:

Abstract Body: Purpose: Glypican-3 (GPC3) is a heparan-sulfate proteoglycan over-expressed in most hepatocellular carcinoma (HCC). A peptide binds to GPC3 with high specificity and affinity will facilitate targeted diagnosis and/or therapy of HCC.

Methods: A Ph.D.-12^{TM} phage display library was used to screen the high affinity peptide against the human recombinant GPC3 protein. A 12-mer peptide GPC3-TJ12P1 was synthesized according to the DNA sequence of selected GPC3 binding phage. ELISA test was used to determine the binding affinity between GPC3-TJ12P1 and the human recombinant GPC3 protein. Specificity of GPC3-TJ12P1 to GPC3 was confirmed by western blot and cell florescent on cells with (HepG2) or without (PC3) GPC3 expression. In vivo, near-infrared fluorescent (NIRF) imaging and biodistribution studies were performed in nude mice bearing HepG2 and PC3 tumor xenografts to evaluate the target ability of Cy5.5-GPC3-TJ12P1 to GPC3.

Results: The binding of GPC3-TJ12P1 to GPC3 gradually increased and came to saturation when the concentration of biotin-GPC3-TJ12P1 reached 1.17 μM. Western blotting confirmed that GPC3-TJ12P1 was able to effectively detect GPC3 expression in HepG2 and PC3 cells. Based on gray scale analysis, GPC3 expression level in HepG2 cells was 55% ± 7.6% compared with internal reference (β-actin), while that was 14% ± 2.5% in PC3 cells. Cy5.5-GPC3-TJ12P1 mainly attached to HepG2 cells surface under confocal microscopy, while there were less fluorescent on the PC3 cells membrane. A weak signal was observed when GPC3 expressed on HepG2 cells were blocked by free GPC3-TJ12P1 before Cy5.5-GPC3-TJ12P1 labeling. In vivo NIRF study showed that HepG2 xenograft tumors had a higher accumulation of Cy5.5-GPC3-TJ12P1 than that of control group, blocking group and PC3 xenograft tumors (n=3 or 4), respectively. Tumor/muscle fluorescent intensity ratio reached 3.98 ± 0.36 at 4h post-injection in HepG2 tumor models. Ex vivo study also confirmed that an enrichment of Cy5.5-GPC3-TJ12P1 at 4h in the HepG2 dissected tumors.

Conclusions: A novel peptide, GPC3-TJ12P1, targeting GPC3 was obtained using phage display library and identified in vitro and in vivo. It can be applied for further studies, such as peptide mediated multifunctional molecular imaging and drug deliveries as well as a new promising molecular probe for early HCC diagnosis and intervention.

AUTHORS (LAST NAME, FIRST NAME): Zhu, Dongling[1]; Qin, Yushuang[1]; Zhang, Liwen[2]; Wang, Jingjing[2]; Zhu, Lei[2]; Zhu, Xiaohua[1]

INSTITUTIONS (ALL):

1. Nuclear Medicine & PET, Tongji Hospital, Tongji Medical College, Huazhong University of Science and Technology, Wuhan, Hubei, China.

2. State Key Laboratory of Molecular Vaccinology and Molecular Diagnostics & Center for Molecular Imaging and Translational Medicine, School of Public Health, Xiamen University, Xiamen, China.

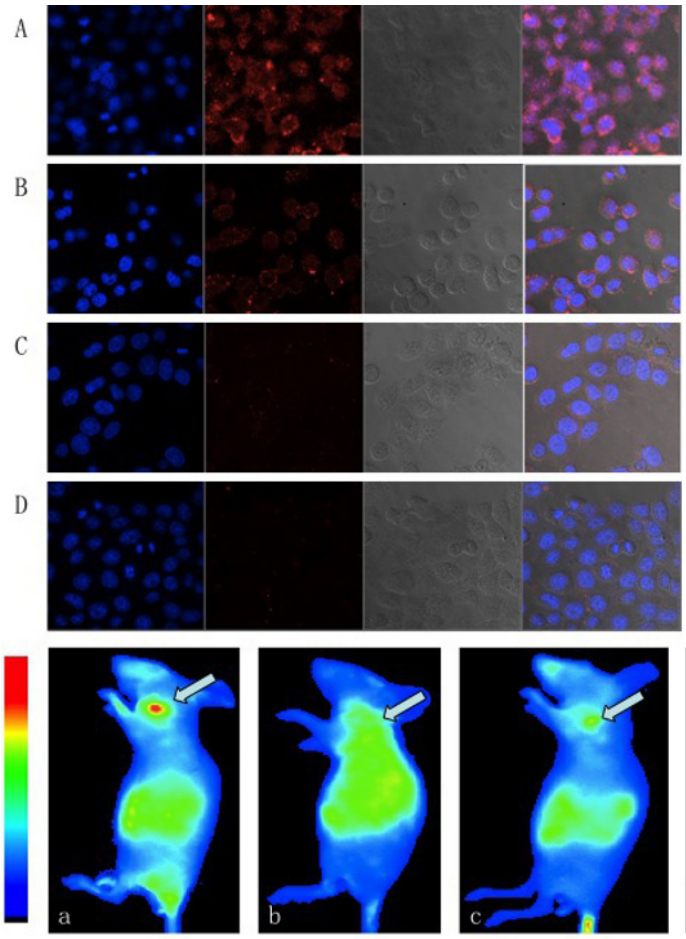

Left: Cy5.5-peptide targeting cells under confocol microscopy. Red color: Cy5.5-peptide, blue color: DAPI for nuclei visualization. (A. HepG2-4h, B. HepG2-2h, C. Blocking-2h, D. PC3-2h)
Bottom: Near-infrared optical imaging in different tumor models. Representative sagittal views of tumor-bearing mice at different time points after intravenous injection of Cy5.5-GPC3-TJ12P1. (a. HepG2, b. HepG2-blocking, c. PC3, d. HepG2-scr, e. HepG2-injection of Cy5.5)

CONTROL ID: 2232233

TITLE: A pretargeted strategy employing Technetium-99m and Rhenium -188 based on bioorthogonal Diels-Alder Click Chemistry for SPECT imaging and radioimmunotherapy

PRESENTER: Lynn Francesconi

ABSTRACT BODY:

Abstract Body: Objectives:The specificity and affinity of antibodies render them highly attractive as cancer therapeutics. Their long biologic half-lives restrict their use to radioisotopes with long physical half-lives. The selective and fast kinetics of the biorthogonal Diels-Alder click reaction between tetrazine (Tz) and antibody-transcyclooctene (TCO) components forms the basis of an *in vivo* pretargeting strategy for PET that allows short lived isotopes to be used for immunoPET.[1] The short half-life of Technetium-99m, ^{99m}Tc, presently the most widely used radioisotope for diagnostic imaging using SPECT, precludes its use in covalently radiolabeled antibody approaches. Given that SPECT is available to more hospitals in the US and globally than PET and recent advances have improved its resolution, the objective of this study is to develop a pretargeting strategy for SPECT employing ^{99m}Tc. A further innovation includes expansion of the study to identify stable ^{188}Re (therapy "partner" for ^{99m}Tc) scaffolds upon which to build ^{188}Re-tetrazine constructs for pretargeted radioimmunotherapy (RIT) with potential to produce very high therapeutic ratios. **Methods**: A ^{99m}Tc-tetrazine construct was prepared by reaction of the tripeptide ^{99m}Tc complex [^{99m}Tc-phe-lys-cys (Tc-FKC)][2] with NHS-Tz in DMSO to form ^{99m}Tc-FKC-Tz. The "cold" Re standard was synthesized and characterized by routine analytical techniques. The huA33 antibody was conjugated with transcyclooctene (A33-TCO)[1]. In a pretargeting study, mice bearing huA33 antigen-expressing SW1222 colorectal cancer xenografts were injected with A33-TCO via tail vein. After allowing 24 h for accumulation of the antibody in the tumor, the mice were injected with ^{99m}Tc-FKC-tetrazine (900 μCi) for SPECT imaging. In anticipation of pretargeted RIT, ^{188}Re-FKC (Tc analog) and ^{188}Re N_2S_2 complexes were prepared by reaction of the ligands with ^{188}Re glucoheptonate followed by prep HPLC.

Results: Co-elution of ^{99m}Tc FKC-Tz with the characterized "cold" Re FKC-Tz complex demonstrates the expected structure (Fig.1). *Ex vivo* reaction of Tc FKC-Tz with A33-TCO is rapid and specific. Injection of the ^{99m}Tc FKC- Tz construct 24 h after administration of the antibody A33-TCO in mice bearing SW1222 tumors shows significant uptake of ^{99m}Tc activity in the tumor and fecal excretion. In anticipation of development of ^{188}Re-labeled tetrazine radioligands, we demonstrated that the tracer ^{188}Re FKC analog (N_3S donor group) and ^{188}Re N_2S_2 complex maintain their integrity over a period of hours.

Conclusion: A new Tc FKC-tetrazine construct based on a peptide scaffold was prepared and characterized. Tc FKC-Tz reacts with A33-TCO *in vivo* demonstrating pretargeted ^{99m}Tc SPECT imaging based on biorthogonal Diels Alder click chemistry. The ^{188}Re FKC scaffold provides requisite stability showing that tripeptides should be excellent scaffolds for pretargeting RIT where short term stability of the tetrazine radioligand is required.

Acknowledgments: NSF: DGS-0965983 (IGERT), DOE: FG02-09ER16097; NIH: CA008748, K99CA178205

References: [1] Zeglis, B.M., et al (2013) J. Nucl. Med. 54, 1389-1396. [2] Cantorias, M.V., et al. Inorg. Chem. (2007) 46, 7326-7340.

AUTHORS (LAST NAME, FIRST NAME): Walsh, Justin[1]; Sanders, Vanessa[2]; Groveman, Samuel[1]; Zeglis, Brian M.[1, 3]; Lewis, Jason S.[3]; Francesconi, Lynn C.[1]

INSTITUTIONS (ALL):

1. Chemistry, Hunter College and the Graduate Center of the City University of New York, New York, NY, United States.
2. Radiochemistry, University of Nevada Las Vegas , Las Vegas, NV, United States.
3. Radiology, Memorial Sloan Kettering Cancer Center, New York City, NY, United States.

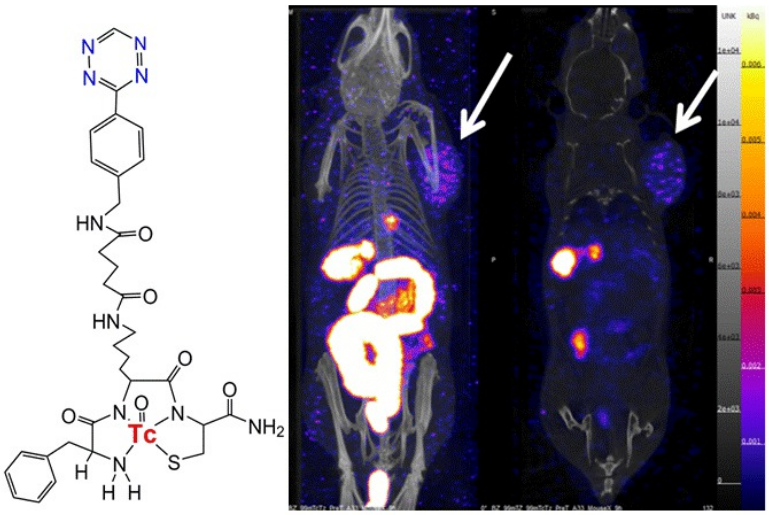

Left: ^{99m}Tc phe-lys-cys-Tetrazine (^{99m}Tc FKC-Tz). **Right**: Pretargeted SPECT images of ^{99m}Tc FKC-Tz. Mice bearing subcutaneous huA33-expressing SW1222 xenografts were injected with huA33-TCO (100 µg) via the tail vein, followed 24 h later with ^{99m}Tc-FKC-Tz (~ 1.0 mCi), also via tail vein injection. Image taken at 9 h p.i. of the ^{99m}Tc-FKC-Tz construct. Left to right: Maximum Intensity Projection (MIP), coronal view. White arrow marks tumor.

CONTROL ID: 2234238

TITLE: *In vivo* investigations of restorative neuronal functions during the circadian rhythm applying diffusion MRI

PRESENTER: Mario Amend

ABSTRACT BODY:

Abstract Body: Introduction:

Sleep is conserved across all mammalian species, however it remains unknown why sleep is a restorative process. A possible metabolic clearance mechanism of waste products such as Aβ [1] is the interchanging process of cerebrospinal fluid (CSF) and interstitial fluid (ISF) via the glymphatic system [2]. Therefore a higher diffusivity could be expected after prolonged phases of sleep. To investigate this hypothesis the influence of the circadian rhythm on brain diffusivity was investigated by MR imaging

Methods:

MR imaging was performed on a 7 T small animal scanner with a 300 mT/m gradient system (ClinScan, Bruker) and a 2x2 rat brain receive coil. Male lewis rats (n=4, 350±50 g) were anesthetized (1.2% isoflurane in air) and body temperature stabilized at 37.0 ±0.5°C. An EPI DTI Sequence (b-values: 0, 150, 400, 800, 1200 s mm^{-2}, TE: 60 ms, TR: 5500 ms, FoV read: 53.0 mm, Voxel-Size: 0.4x0.4x0.8 mm^3, 26 slices, b-values: 0, 150, 400, 800, 1200 s mm^{-2}, 64 diffusion directions) was acquired at two time points: 7a.m. and 7p.m. Between measurements, rats were allowed to recover for two days in order to avoid changes in the circadian rhythm. DTI data were analyzed for total ADC value as well as ADC in the b-value intervals 150-400, 400-800, 800-1200 s mm^{-2} – in order to discriminate different compartments. Additionally, the signal decay as a function of the b-value to calculate ADC_{fast} and ADC_{slow} values was analyzed according to the biexponential function of the form:

$S(b)/S(0)=f_{slow}exp(-b*ADC_{slow})+(f_{fast}exp(-b*ADC_{fast})$

Results:

ADC (in mm^2 s^{-1}) calculations of cortical (7a.m.: 7.16E-04 ± 1.42E-04/ 7p.m.: 6.65E-04 ± 3.72E-05; p=0.381), thalamic (7a.m.: 6.46E-04 ± 6.64E-05/ 7p.m.: 6.75E-04 ± 4.26E-05; p=0.259) and ventricular (7a.m.: 1.02E-03 ± 9.78E-05 / 7p.m: 1.06E-03 ± 4.28E-05; p=0.521) regions showed no significant differences in brain diffusivity of rats measured at 7a.m. compared to 7p.m. Furthermore the bioexponential ADC calculation did not reveal significant differences in any of the ADC_{slow} (7a.m.: 0.396 ± 0.187 /7p.m.: 0.488 ± 0.212), ADC_{fast} (7a.m.: 0.015 ± 0.150/7p.m.: 0.071 ± 0.024), f_{slow} and f_{fast} values. However, ADC values were significantly higher for small b-values (150-400 s mm^{-2}) compared to middle (450-800 s mm^{-2}) and high b-values (800-1200 s mm^{-2}) revealing an at least compartmentation of diffusion signal in the rat brain.

Discussion:

Our results did not reveal a significant change of diffusivity as a function of the circadian rhythm in the rat brain. A possible explanation for this is that either CSF-ISF-interchange is independent from the circadian rhythm, but rather is depending on the acute the sleep-wake state itself, or does not alter brain diffusivity in general. Furthermore, also the use of anesthesia could have offset the expected effect of the circadian rhythm on diffusivity. The observed higher diffusivity at small b-values indicates a compartmentation of diffusivity mainly to extracellular, interstitial areas.

[1] Sleep drives metabolite clearance from the adult brain. Science 2013

[2] Brain-wide pathway for waste clearance captured by contrast-enhanced MRI. J Clin Invest 2013

AUTHORS (LAST NAME, FIRST NAME): Amend, Mario[1]; Thielcke, André[1]; Leibfritz, Dieter[1]; Pichler, Bernd J.[1]; Wehrl, Hans F.[1]

INSTITUTIONS (ALL):

1. Department of Preclinical Imaging and Radiopharmacy, University of Tuebingen, Tuebingen, Deutschland, Germany.

(No Image Selected)

CONTROL ID: 2244753

TITLE: Simultaneous PET/MR imaging of sustained whisker stimulation in rats applying [^{18}F]FDG-PET and BOLD-fMRI using a novel, single scanning session, protocol

PRESENTER: Mario Amend

ABSTRACT BODY:

Abstract Body: Introduction:

Combined positron emission tomography (PET) and functional magnetic resonance imaging (fMRI) is an ideal tool to study functional and metabolic processes in the brain. Here we study rat brain function in response to a sustained barrel-field stimulus simultaneously using [^{18}F]FDG-PET, which traces changes in glucose metabolism on a slow time scale, and functional MRI (fMRI) using the blood oxygen level dependent (BOLD) effect, which assesses vascular and oxygenation changes during activation. We aimed on establishing a protocol mapping changes in glucose metabolism (CMRGlu) and BOLD effect within one single scanning session. This single session protocol has the benefit that activation and baseline conditions can be evaluated in the same animals during the same anesthesia setting.

Materials and Methods:

Simultaneous PET/MRI was performed on a 7 T small animal scanner with a 300 mT/m gradient system (ClinScan, Bruker) and a 2x2 rat brain receive coil combined with small animal PET insert (Bruker). Male lewis rats (n = 4, 290 ± 5g) were anesthetized (1.1% isoflurane in air) and body temperature stabilized at 37.0 ± 0.5°C. Blood glucose levels were measured before and after the scan. An EPI BOLD Sequence (TE: 18ms, TR: 2000ms, Voxel size: $0.5\times0.5\times1mm^3$, FoV 102×102mm, slice thickness: 1mm, 8 slices) was acquired over 60min. Simultaneously, rats were continuously infused with [^{18}F]FDG-PET (dose at infusion start 111mBq) via a tail vain catheter and PET images were acquired. Three sustained electrical stimulation intervals of the left whisker pad were applied at 20-30min, 40-45min and 55-60min. Data were analyzed using statistical parametric mapping (SPM 12, GLM) as well as a region of interest analysis.

Results:

We found spatial and quantitative correlations between the PET and the fMRI activation data. Accordingly to a stimulation of the left whisker pad the fMRI analysis revealed significant BOLD signal ($T = 4.36$; $p_{uncorr} = 0.004$) in the right barrelfield cortex S1BF. PET data showed also significant activation ($T = 3.17$; $p_{uncorr} = 0.001$) and a spatial shift compared to BOLD data (Euclidean distance = 0.41 mm). Both, BOLD as well as PET data revealed also ipsilateral S1BF activation in the left hemisphere together with additional activation centers in thalamus, cingulate and insular cortex regions. Venous glucose levels showed no significant difference pre and post [^{18}F]FDG-infusion (pre: 104.25mg/dL, post: 109.25mg/dL, $p = 0.74$).

Conclusions:

To our knowledge, this is the first small animal study reporting a spatial and quantitative correlation of PET and fMRI activation data based on baseline and sustained stimulation within one single scanning session. The established protocol has clear evidence for the characterization of functional and metabolic changes during brain activation on the basis of stable animal physiology and experimental setup, since baseline and activation measurements were taken at the exact same experimental conditions. This paves the way also to studies using different short and long half life tracers, and is ultimately also transferable to a clinical setting.

AUTHORS (LAST NAME, FIRST NAME): Amend, Mario[1]; Thielcke, André[1]; Pichler, Bernd J.[1]; Wehrl, Hans F.[1]

INSTITUTIONS (ALL):

1. Department of Preclinical Imaging and Radiopharmacy, University of Tuebingen, Tuebingen, Deutschland, Germany.

(No Image Selected)

CONTROL ID: 2232223

TITLE: Inhomogeneity in myocardial perfusion gated SPECT of heart transplant recipientsis is associated with the development of systolic allograft dysfunction

PRESENTER: Christian Wenning

ABSTRACT BODY:

Abstract Body: Purpose: Development of cardiac allograft vasculopathy (CAV) is a crucial factor for the long-term survival of heart transplant (HTx) recipients. Myocardial perfusion gated SPECT can be used for non-invasive detection of hemodynamically relevant coronary artery stenosis. The prognostic relevance of the frequently observed finding of inhomogeneous myocardial perfusion in HTx patients is unclear so far. Thus, the long-term prognosis of patients with homogeneous versus inhomogeneous perfusion was evaluated.

Methods: 104 HTx patients (mean 3.6 ± 2.9 years after HTx) without significant ischemia (Summed Stress Score ≤3) in gated SPECT and without CAV in coronary angiography were included. Myocardial perfusion was visually assessed as homogeneous or inhomogeneous (further sub-classified as moderately and severely inhomogeneous). The follow-up period after SPECT imaging was 9.4 ± 3.1 years. Endpoints were the diagnosis of CAV in coronary angiography, major cardiac events (MACE) or death and the development of systolic allograft dysfunction (left ventricular ejection fraction (EF) < 45%).

Results: 24% of the patients (n=25) presented with inhomogeneous myocardial perfusion. Compared to the patients with homogeneous perfusion the patients with inhomogeneity were at higher risk for development of systolic allograft failure in the follow-Up ($p<0.01$; Hazard Ratio (HR) = 4.4). As to the development of CAV, the occurrence of MACE or death no statistical differences were observed. Furthermore, there was no correlation between myocardial perfusion pattern and prior cardiac allograft rejections.

Conclusion: Inhomogeneous myocardial perfusion in gated SPECT by HTx patients without known CAV indicates a higher risk for development of allograft systolic dysfunction.

AUTHORS (LAST NAME, FIRST NAME): Wenning, Christian[1]; Vrachimis, Alexis[1]; Penning, Alvyda[1]; Stypmann, Jörg[2]; Schäfers, Michael[1]

INSTITUTIONS (ALL):

1. Nuclear Medicine, University Hospital Münster, Muenster, Germany.

2. Cardiovascular Medicine, University Hospital Münster, Münster, Germany.

(No Image Selected)

CONTROL ID: 2234154

TITLE: In vivo PET imaging of ^{64}Cu-NOTA-aptide targeting tumor-associated fibronectin extra domain B

PRESENTER: Mi Jeong Kim

ABSTRACT BODY:

Abstract Body: Purpose: Fibronectin extra domain B (ED-B) is expressed in cancer-associated blood vessels, which has been suggested as an attractive cancer targeting marker for cancer imaging and therapy. In this study, NOTA-conjugated ED-B-specific high affinity peptide (aptide) was labeled with ^{64}Cu and cancer targeting ability for specific ED-B was evaluated using animal PET imaging.

Methods: Low ED-B-expressing cell line (B16F1 and U373) and high ED-B-expressing cell lines (LLC and U87MG) were used. ED-B mRNA and protein expressions were measured by real-time RT PCR and western bolt. ED-B aptide was conjugated with SCN-NOTA in c-term or lysine part and their affinity was analyzed by surface plasmon resonance (SPR) assay. NOTA-conjugated ED-B aptide was labeled with ^{64}Cu for 1 h at 42 °C and the labeling efficiency was analyzed using instant thin-layer chromatography in 0.1 M sodium citrate solution. For in vivo experiment, LLC and U87MG cell lines were inoculated to BALB/c nude mice and ^{64}Cu-NOTA-ED-B aptide was injected intravenously. Animal PET imaging was performed at 10 min, 2 h, and 22 h using GENISYS PET scanner.

Results: ED-B mRNA expression in LLC cells and U87MG was higher to 29 times and 10 times than in B16F1 cells and U373 cells, respectively. ED-B protein expression in LLC cells and U87MG was higher to 5.7 times and 3.7 times than in B16F1 cells and U373 cells, respectively. Each Kd value of ED-B aptide NOTA-conjugated in c-term and in lysine part was 84 nM and 233 nM, and we chose c-term form. Labeling efficiency of ^{64}Cu-NOTA-ED-B was 100% and the stability was 100% in human serum at 37 °C until 52 h. Animal PET imaging showed kidney uptake and rapid excretion through urine as well as both tumor (LLC and U87MG) uptake. LLC and U87MG tumor uptake was 0.95 ± 0.35 %ID/g and 0.97 ± 0.43 %ID/g at 2 h after IV injection.

Conclusion: We confirmed that stable ^{64}Cu-NOTA-ED-B aptide was targeted in ED-B positive tumor using in vivo PET imaging. ^{64}Cu-NOTA-ED-B aptide could be used as a promising agent for imaging and targeted therapy of cancer angiogenesis.

AUTHORS (LAST NAME, FIRST NAME): Kim, Mi Jeong[1, 2]; Kim, Hyungjun[3]; Jang, Sol-Ah[1, 2]; Song, Myung Geun[1, 2]; Lee, Yun-Sang[1, 4]; Youn, Hyewon[1, 5]; Chung, June-Key[1, 6]; Lee, Dong Soo[1, 7]; Jon, Sangyong[3]; Kang, Keon Wook[1, 2]

INSTITUTIONS (ALL):

1. Nuclear Medicine, Seoul National University, Seoul, Korea (the Republic of).
2. Laboratory of Molecular Imaging and Therapy, Cancer Research Institute, Seoul National University, Seoul, Korea (the Republic of).
3. Biological Sciences, KAIST Institute for the BioCentury, Korea Advanced Institute of Science and Technology, Daejeon, Korea (the Republic of).
4. Medical Research Center, Institute of Radiation Medicine, Seoul National University College of Medicine, Seoul, Korea (the Republic of).
5. Laboratory of Molecular Imaging and Therapy, Cancer Research Institute, Tumor Microenvironment Global Core Research Center, Seoul National University, Cancer Imaging Center, Seoul National University Cancer Hospital, Seoul, Korea (the Republic of).
6. Laboratory of Molecular Imaging and Therapy, Cancer Research Institute, Tumor Microenvironment Global Core Research Center, Biomedical Sciences, Seoul National University, Seoul, Korea (the Republic of).
7. Molecular Medicine and Biopharmaceutical Sciences, WCU Graduate School of Convergence Science and Technology, Seoul National University, Seoul, Korea (the Republic of).

(No Image Selected)

CONTROL ID: 2232245

TITLE: PET-based pharmacokinetics of IV injected ^{89}Zr nanoparticles reveals monocyte trafficking

PRESENTER: Lee Josephson

ABSTRACT BODY:

Abstract Body: *Background:* Monocytes trafficking to atherosclerotic lesions (*1*), tumors (*2*) and sites of infection (*3*) play a key role in these common pathologies. The often-used ex-vivo loading of monocytes with a radioactive tracers (*4*), followed by SPECT, requires handling monocytes in vitro. After an IV injection of a ^{89}Zr-nanoparticle, we used a PET-based pharmacokinetic (PK) analysis to distinguish slow monocyte trafficking to the spleen and lymph nodes in normal mice.

Objectives: Our objectives were to (i) to prepare ^{89}Zr-Feraheme nanoparticles (^{89}Zr-FH) with a heat induced radiolabeling technique (*5*) and, (ii) to demonstrate that after IV injection of ^{89}Zr-FH, the time dependence of PET-based standard uptake values (SUVs) would show the slow the trafficking of ^{89}Zr-FH loaded monocytes.

Methods: Heat induced radiolabeling was used to obtain ^{89}Zr-FH. With BALB/c mice, PET derived SUV's were obtained on a GE VISTA small animal PET/CT, A Rhesus monkey was injected with FH and blood drawn at 3 h. A monocyte rich buffy coat was obtained by Ficoll centrifugation and analyzed by relaxometry (0.47 T).

Results: Liver and spleen showed biexponential SUV increases, with fast components ($t_{1/2}$'s of 1.27 & 1.24 h, respectively), corresponding to the clearance of ^{89}Zr-FH's from plasma by blood sampling ($t_{1/2}$ = 1.02 h). A slow increase in SUVs by popliteal and axillary lymph nodes ($t_{1/2}$'s = 21.2 h & 20.2 h, respectively), and by spleen (36.3 h) occurred. The magnitude of nodal SUVs was high, comparable to those of the liver and spleen. After injection of FH into a monkey, monocyte uptake of FH was confirmed from T2 relaxation times of a buffy coat preparation.

Conclusion: PK analysis of ^{89}Zr-FH indicated a vascular phase, a fast hepatic and splenic uptake phase (direct ^{89}Zr-FH phagocytosis from plasma), and a slow splenic and nodal uptake phase (from ^{89}Zr-FH loaded monocyte trafficking). PK analysis of IV injected ^{89}Zr-FH can be used to visualize monocyte tracking, adding to our knowledge of key players of immune function.

(1) Kircher, M. F. (2008) Noninvasive in vivo imaging of monocyte trafficking to atherosclerotic lesions. *Circulation 117* , 388-95.

(2) De Palma, M. (2013) Macrophage regulation of tumor responses to anticancer therapies. *Cancer cell 23*, 277-86.

(3) Shi, C.(2011) Monocyte recruitment during infection and inflammation. *Nature reviews. Immunology 11*, 762-74.

(4) Van Hemert, (2009) Labeling monocytes for imaging chronic inflammation. *The quarterly journal of nuclear medicine and molecular imaging 53*, 78-88.

(5) Boros, E. (2014) Chelate-free metal ion binding and heat-induced radiolabeling of iron oxide nanoparticles. *Chemical Science*, DOI: 10.1039/c4sc02778g.

AUTHORS (LAST NAME, FIRST NAME): Wilks, Moses Q.[1, 2]; Yuan, Hushan[1, 2]; Normandin, Marc D.[1, 2]; El Fakhri, George[1, 2]; Josephson, Lee[1, 2]

INSTITUTIONS (ALL):

1. Massachusetts General Hospital, Charlestown, MA, United States.

2. Center for Advanced Medical Imaging Sciences, Mass Gen Hospital , Charlestown, MA, United States.

(No Image Selected)

CONTROL ID: 2232225

TITLE: Click Chemistry For Targeting Group Attachments to Heat Induced Radiolabeled (HIR) Feraheme Nanoparticles

PRESENTER: Lee Josephson

ABSTRACT BODY:

Abstract Body: The use of nanoparticles (NPs) in biology and medicine can involve two general types of chemistries, a surface functionalization reaction to obtain in vivo targeting, often using so-called click chemistry (*1*), and a radiolabelling reaction, so the NP fate can be imaged by PET or SPECT (*2*). Heat induced radiolabeling (HIR) is a chelateless method that employs heat (120°C, 2 h) to radiolabel Feraheme (FH) nanoparticles (NPs) with any of three radioisotopes (^{89}Zr or ^{64}Cu for PET, ^{111}In for SPECT) (*3*). By exploiting the unique temperature stability of the FH NPs, HIR produces radiolabeled NPs that are identical to the starting NP, an approved drug, except for the addition of trace amounts of radiometal. FH is safe and widely available NP drug, evident from its approval for treating iron anemia in many countries. We postulated the value of the HIR method would be greatly enhanced if a facile surface modifications using click chemistry were compatible with it.

We attached the azide and the alkyne groups of click chemistry to the FH NP, and showed that these functional groups survived the heating used with the HIR method. This enabled the preparation of a nonradioactive azide-FH, followed by a HIR of the NP with ^{89}Zr, followed by a copperless click reaction with a DBCO-bearing cyclic RGD peptide. (DiBenzoCycloOctyl = DBCO) Similarly, an alkyne-FH was prepared, followed by the HIR radiolabeling with ^{89}Zr, and this was followed by a copper mediated click reaction with an azide-bearing folate. FH surface chemistry was monitored by a technique termed “fluorochrome reaction quantitation,” where NPs were reacted with alkyne-Cy5.5 or azide-Cy5.5 fluorochromes and the NP analyzed by Cy5.5 absorbance. Thus we show that the FH NP can be surface functionalized with azides or alkynes, submitted to a HIR reaction, and the surfaces of the now radioactive NPs functionalized with a cyclic RGD peptide or Folate using rapid click chemistries. The temperature stability of the FH NP drug, and the alkyne-FH and azide-FH NPs we prepared from it, indicate that HIR, a multi-isotope NP radiolabeling method that uses heat rather than covalent reactions, can yield surface functionalized magnetic/radioactive NPs which might be used in targeting imaging applications.

(1) Li, N. (2011) Click-chemistry for nanoparticle-modification. *J. Mater. Chem. 21*, 16717.

(2) Sapsford, K. E. (2013) Functionalizing nanoparticles with biological molecules *Chemical reviews 113*, 1904.

(3) Boros, E. (2014) Chelate-free metal ion binding and heat-induced radiolabeling of iron oxide nanoparticles. *Chem. Sci.*, DOI: 10.1039/c4sc02778g.

AUTHORS (LAST NAME, FIRST NAME): Wilks, Moses Q.[1]; Yuan, Hushan[1]; Normandin, Marc D.[1, 2]; Josephson, Lee[1, 2]

INSTITUTIONS (ALL):

1. Massachusetts General Hospital, Charlestown, MA, United States.

2. Harvard Medical School/MGH, Boston, MA, United States.

(No Image Selected)

CONTROL ID: 2232229

TITLE: Temporally unmixed multispectral optoacoustic tomography (tuMSOT) enables high contrast reporter imaging in vertebrate model systems.

PRESENTER: Gil Westmeyer

ABSTRACT BODY:

Abstract Body: We have recently shown [1] how temporal unmixing of photocontrolled time courses [3] obtained from reversibly switchable fluorescent proteins enables high-contrast optoacoustic detection of these proteins in the presence of dominant spectrally overlapping absorbers such as blood *in vitro*.

We now show the sensitivity gain of employing this detection method in cell and tissue culture as well as *in vivo* in a zebrafish model. We demonstrate how reversibly switchable fluorescent proteins (RSFP) [2] can be temporally unmixed in mammalian cell culture as well as in zebrafish in the presence of dominant non-switchable absorbers. Our data show how specific detection is possible also under very low fluence conditions.

We furthermore discuss, supported by simulations and experimental data, how the optimal photocontrol schedule can be determined to maximize the contrast to noise for a given *in vivo* tuMSOT imaging session of live organisms exhibiting strong time-varying background signals.

In conclusion, we show how tuMSOT enables high contrast *in vivo* reporter imaging by optoacoustics via exploiting the information from photocontrolled temporal signal trajectories in addition to the information contained in the absorbance spectra. These data demonstrate the value of tuMSOT for high-contrast and multiplexed *in vivo* detection of photochromic molecules available in several synthetic and genetically encoded variants.

References:

[1] Stiel AC, Deán-Ben XL. *et al.,* Optics Letters **40(3)**, 367-370 (2015)

[2] Stiel, A. C. *et al.*, The Biochemical journal **402**, 35–42 (2007).

[3] Marriott, G. *et al.*, PNAS **105**, 17789–17794 (2008).

Acknowledgments:

G.G.W. acknowledges support by Technische Universität München, the Helmholtz Association of German Research Centers and Helmholtz Alliance ICEMED. We furthermore acknowledge support from the European Research Council under grant agreements ERC-2010-StG-260991 (D.R.) and ERC-2012-StG-311552 (G.G.W).

AUTHORS (LAST NAME, FIRST NAME): Jiang, Yuanyuan[3]; Dean-Ben, Xose Luis[6]; Stiel, Andre C.[4]; Cappetta, Michele[1, 3]; Rolbieski, Hannes[3]; Ntziachristos, Vasilis[5, 3]; Razansky, Daniel[2]; Westmeyer, Gil G.[1, 3]

INSTITUTIONS (ALL):

1. Nuclear Medicine, Technical University Munich, Munich, Germany.
2. Institute for Biological and Medical Imaging, Technical University of Munich and Helmhotlz Center Munich, Neuherberg, Germany.
3. IBMI / IDG, Helmholtz Center Munich, Munich, Germany.
4. Research Group Protein Design, Max-Planck-Institute for Developmental Biology, Tuebingen, Germany.
5. Chair for Biological Imaging,, Technical University Munich, Munich, Germany.
6. IBMI, Helmholtz Center Munich, Munich, Germany.

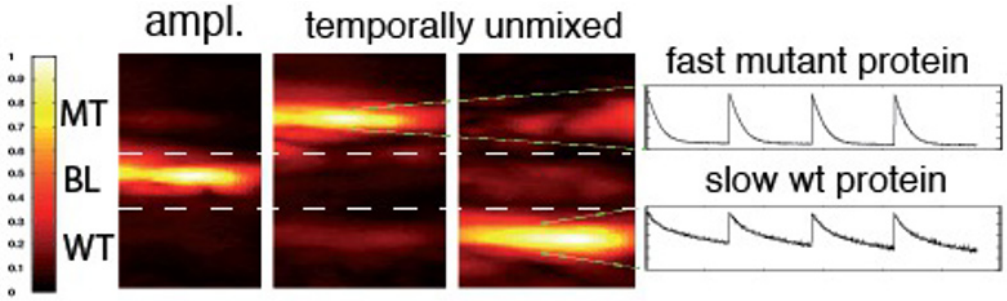

Fig. 1. Temporally unmixed Multispectral Optoacoustic Tomography (tuMSOT). The optoacoustic amplitude image is juxtaposed with the temporally unmixed optoacoustic images and corresponding temporal profiles from the reversibly switchable proteins Dronpa (lower trace) and a fast switchable mutant Dronpa-M159T (upper trace) demonstrating the strong gain in contrast over non-switchable blood as background absorber displaying an order of magnitude higher amplitude.

CONTROL ID: 2233466

TITLE: Non-invasive fast calcium neuroimaging of zebrafish behavior with complementary light-field and selective plane illumination microscopy

PRESENTER: Gil Westmeyer

ABSTRACT BODY:

Abstract Body: The zebrafish larva allows for whole-organism multiplexed molecular imaging at cellular resolution using genetically encoded molecular sensors in conjunction with advanced fluorescent imaging equipment.
This genetic model organism thus offers unique opportunities for molecular imaging to reveal the function of cell-circuits in the context of *e.g.* cardiovascular, metabolic or neuroscientific biomedical questions [1,2].
We here demonstrate the complementary use of state-of-the art confocal, light-field and selective plane illumination microscopy to study neuronal activity in reporter zebrafish during rest, in response to different photostimuli and during visually induced behavior.
We first show an analysis of the resting activity of zebrafish expressing different genetically encoded calcium indicators (GECIs) employing time series analysis based on diffusion maps as compared with standard clustering algorithms [3,4]. This description of the default activity then allows us to investigate how visual stimuli perturb the default activity to different degrees and on different time scales.
We next demonstrate neural activity during light-induced avoidance behavior in partially restrained and freely swimming fish using dedicated fast imaging setups. The analysis of these complementary datasets starts to reveal neural circuits that are activated just before and after the fish initiate swimming bouts and may be associated with photoaversion as opposed to spontaneous pre-motor activity.
In summary, we present a comprehensive approach to molecular neuroimaging of entire vertebrate brains using new fast fluorescence imaging setups and corresponding state of the art computational analysis tools. The systematic analysis of circuit dynamics with cellular precision in vertebrate models such as the zebrafish will help decipher principle elements for interpreting brain network activity accessible only at a much coarser level in more complex mammalian brains with important implications also for neuropsychiatric diseases.

References:

[1] Mickoleit et al. Nat. Methods (2014)
[2] Ahrens, et al. Nat. Methods (2013)
[3] Freeman et al. 2014; Nature America, 10.1038
[4] Coifman et al. 2005; PNAS, 102(21), 7426.

AUTHORS (LAST NAME, FIRST NAME): Lauri, Antonella[1, 2]; Symvoulidis, Panagiotis[2]; Cappetta, Michele[1]; Cruz Perez, Carlos[2]; Haghverdi, Laleh[3]; Myklatun, Ahne[2]; Marr, Carsten[3]; Theis, Fabian[3, 4]; Westmeyer, Gil G.[1, 2]

INSTITUTIONS (ALL):
1. Nuclear Medicine, Technical University Munich, Munich, Germany.
2. IBMI / IDG, Helmholtz Center Munich, Munich, Germany.
3. ICB, Helmholtz Center Munich, Munich, Germany.
4. Mathematics, Technical University Munich, Munich, Germany.

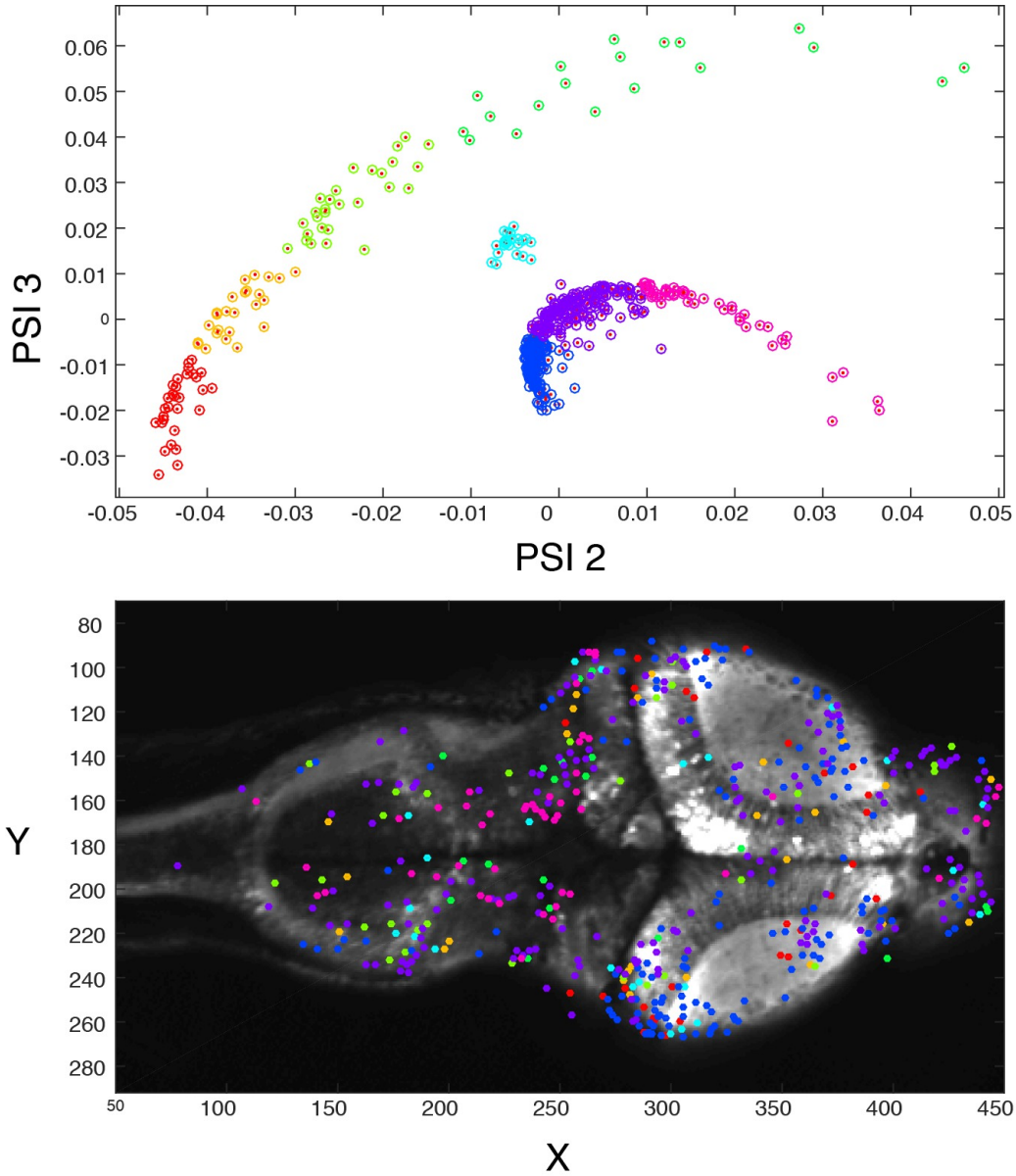

Figure 1. Analysis of resting calcium activity in the zebrafish Diffusion maps showing clustering of neuronal ROIs based on the temporal patterns of calcium transients (upper panel) and the corresponding spatial coordinates of the color-coded neurons (lower panel).

CONTROL ID: 2232897

TITLE: BNCT as alternative radiation therapy---an application on radioresistance GBM

PRESENTER: Hui-Hsien Lin

ABSTRACT BODY:

Abstract Body: Glioblastoma multiforme (GBM) is the most malignant primary brain tumor worldwide (grade IV in WHO classification), and its prognosis still remains extremely dismal despite a conventional treatment associating surgical resection and subsequent radio-chemotherapy. The radioresistance in GBM is one of the most important clinical issue and researches have attributed this to a subpopulation of cancer stem cells (CSCs) which may be responsible for tumor recurrence following treatment. Accumulated evidence indicated that GBM CSCs exhibit higher DNA damage repair ability and are more resistant to radiation than that of parental GBM cells. Recently, boron neutron capture therapy (BNCT) has been developed for the purpose of efficiently treating cancers. BNCT is a molecular radiation treatment based on the 10B (n, α) 7Li nuclear reaction in cancer cells, while the 10B concentration in tumor is critical. Herein, we expect BNCT can provide more treatment efficiency against the radioresistant GBM CSCs than that of other radiation sources. In this study, we investigated the diverse ability of radioresistance in GBM cell lines between non-CSCs and CSCs. Our results demonstrated that GBM CSCs were more radioresistant than non-CSC population by clonogenic assay and comet assay. Both non-CSCs and CSCs were irradiated (10 Gy) and immunofluorescent staining for γ-H2AX and 53BP1 foci to quantify double-strand break repair events, which demonstrated GBM CSCs was rapidly repair than that of non-CSCs. In addition, GBM CSCs also enhanced activation of the G2/M checkpoint following irradiation and repair DNA double strand breaks (DSBs) more efficiently than their counterparts. Using BNCT, we found a close therapeutic effect between GBM CSCs different pairs of tumor cells even in the radioresistant GBM CSCs. In addition to in vitro study, we established tumor-bearing mice underwent conventional radiotherapy and BNCT, respectively. Clinically, PET tracer 4-borono-2-18F-fluoro-phenylalanine (18F-FBPA) has been used for BPA-fr accumulation prediction before BNCT. Therefore, animal model were screened by 18F-FBPA imaging. Eventually, BNCT provided a better therapeutic outcome than the conventional linear accelerator, which indicated that BNCT could effectively suppress the malignant cancer stem cells. Despite BNCT possesses great potential for cancer treatment, it is still necessary to elucidate the underlying effect on CSCs and to raise the boron concentration as high as possible in tumor lesion prior to the thermal neutron irradiation. Although the application of BNCT treated in the radioresistant GBM clearly needs further exploration, but these results illustrated the potential of BNCT as a possible treatment strategy for radioresistant GBM CSCs.

AUTHORS (LAST NAME, FIRST NAME): Lin, Hui-Hsien[1]; Yen, Sang-Hue[1]; Chou, Fong-In[2]; Chen, Yi-Wei[1]

INSTITUTIONS (ALL):

1. Division of Radiation Oncology, Cancer Center, Taipei Veterans General Hospital, Taipei, Taiwan.
2. National Tsing Hua University, Hsinchu city, Taiwan.

(No Image Selected)

CONTROL ID: 2232288

TITLE: Sodium iodide symporter (NIS)-based reporter gene imaging with [^{18}F]-tetrafluoroborate allows *in vivo* metastasis tracking by PET

PRESENTER: Gilbert Fruhwirth

ABSTRACT BODY:

Abstract Body: Purpose: The aim of this work was to evaluate dual modality reporter gene-based non-invasive tracking of metastasis in a murine breast cancer model using PET. The principle of the radionuclide-optical fusion protein approach was previously shown (Ref.1). Metastasis tracking has not been shown before using NIS-based PET imaging. The purpose of this study was to compare the PET radiotracer [^{18}F]-BF_4^- (Ref.2) with the SPECT radiotracer [^{123}I]-iodide for NIS reporter gene imaging-afforded detection and monitoring of metastasis. A second goal was to compare metastasis detection and tracking of this NIS-RFP-afforded PET approach with [^{18}F]-FDG PET in this preclinical model.

Methods: Rat breast adenocarcinoma cells (MTLn3E) were engineered to stably express the sodium iodide symporter (NIS) fused on its C-terminus to the red fluorescent protein TagRFP (RFP) for multi-modal imaging. Furthermore, we transduced MTLn3E.NIS-RFP cells with the full-length or truncated chemokine receptor CXCR4 that was fused to green fluorescent protein (GFP) (3E.FL-NIS and 3E.Δ-NIS, respectively). The resultant cell lines served as a model for tumor xenografts that showed a low or very high propensity for spontaneous metastasis (Ref.3). Xenografts were established orthotopically in the lower mammary fat pad of female SCID/Beige mice. Dynamic radionuclide scanning using [^{18}F]-BF_4^-, [^{123}I]-iodide and/or [^{18}F]-FDG tracers was performed by PET/CT and SPECT/CT as appropriate. Specificity and sensitivity of metastasis detection were measured by comparing radionuclide scans with confocal fluorescence microscopy of biopsied lymph node tissues.

Results: Uptake of both [^{18}F]-BF_4^- and [^{123}I]-iodide in primary tumors was rapid, reaching 12.1 and 11.0 %ID/g for [^{18}F]-BF_4^- and [^{123}I]-iodide, respectively, after 12min, and 56.9 and 60.5 %ID/g, respectively, after 120min. Clearance of [^{18}F]-BF_4^- from the blood was faster (falling to 0.06 %ID/g at 36 min) than clearance of [^{123}I]-iodide (3.1 %ID/g at 36 min). 100% of lymph nodes (LN) that were detected via [^{18}F]-BF_4 PET were also confirmed positive for 3E.Δ-NIS tumor cells using confocal fluorescence microscopy of biopsied material. Furthermore, all LNs that were not detected by [^{18}F]-BF_4 PET were confirmed to be free of metastasis. LNs detected by [^{18}F]-BF_4^- and confirmed to be positive for tumor metastases were not detected using [^{18}F]-FDG in >95% of the cases.

Conclusion: [^{18}F]-BF_4^- PET showed more favorable tracer kinetics and signal-to-background as compared to [^{123}I]-iodide SPECT. Furthermore, it showed much higher sensitivity and specificity for metastasis detection as compared to [^{18}F]-FDG. This preclinical model is particularly useful for studying spontaneous cancer metastasis and for evaluating the treatment response of anti-cancer and particularly anti-metastatic therapeutics.

References:

(1) Fruhwirth GO et al. J Nuc Med 2014; 55(4):686-94.

(2) Jauregui-Osoro M et al. Eur J Nucl Med Mol Imaging, 2010; 37(11):2108-16.

(3) Vermeer LS et al. J Proteome Res 2012; 11(5):2996-3003.

AUTHORS (LAST NAME, FIRST NAME): Diocou, Seckou[1]; Fruhwirth, Gilbert O.[1]; Chuamsaamarkkee, Krisanat[1]; Jauregui-Osoro, Maite[1]; Livieratos, Lefteris[1]; Ng, Tony[2, 3]; Blower, Philip J.[1]; Mullen, Greg E.[1]

INSTITUTIONS (ALL):

1. Deptartment for Imaging Chemistry and Biology, King's College London, London, United Kingdom.
2. Division of Cancer Studies and Randall Division, King's College London, London, United Kingdom.
3. UCL Cancer Institute, University College London, London, United Kingdom.

(No Image Selected)

CONTROL ID: 2233021

TITLE: Characterizing Cavitary Lesions in a Murine Model of Tuberculosis using High Resolution Computer Tomography

PRESENTER: Alvaro Ordoñez

ABSTRACT BODY:

Abstract Body: Mice are widely used to study the pathogenesis of tuberculosis (TB) and efficacy of therapeutic agents. However, standard mouse strains do not develop caseous necrosis or cavities, key features of human TB associated with transmission, poor treatment outcomes and resistance. Occasional observations of cavities in mice prompted us to use high resolution computer tomography (CT) to evaluate cavity formation and characterize it further.

C3HeB/FeJ mice, that develop well defined necrotic and hypoxic lesions, were aerosol infected with *Mycobacterium tuberculosis.* A cohort of these animals received combination drug treatment with rifampin, isoniazid and pyrazinamide (RHZ regimen) to evaluate the effects of treatment on cavity formation. Live *M. tuberculosis*-infected mice were imaged within a sealed bio-containment bed modified in-house to comply with biosafety level-3 (BSL-3) containment. Each animal was weighed and imaged using a NanoSPECT/CT small animal imager. Images were reconstructed and visualized using VivoQuant 1.23.

Initial pulmonary bacterial burden (day 1 post-infection) was 2.00 ± 0.13 $\log_{10}$ colony forming units (CFU). At 2-4 weeks post-infection, consolidations were observed by CT in the lung fields of infected animals. In some animals the central area of these consolidations underwent liquefaction and was evacuated to form a cavity within the lesions. Cavitation was evident by CT and confirmed by gross pathology and histology in 61% of treated and 60% of untreated *M. tuberculosis*-infected mice. CT imaging and subsequent post-mortem histological analyses clearly demonstrated that the necrotic contents of the liquefying granuloma are expelled into the airways, as in human TB.

Serial pulmonary CT imaging was able to non-invasively identify cavity formation in live *M. tuberculosis*-infected mice, and provided novel insights into the pathogenesis of cavity formation. This is the first systematic demonstration of cavity formation in a mouse model of TB. C3HeB/FeJ mice display key pathological features of human TB and could therefore serve as an important preclinical model for the development of novel therapeutics.

A.A.O. and R.T. contributed equally to this work. E.L.N. and S.K.J. also contributed equally. This work was funded by the NIH Director's Transformative Research Award (R01-EB020539) (S.K.J.), NIH Director's New Innovator Award (DP2-OD006492) (S.K.J.), the Bill & Melinda Gates Foundation (OPP 1037174) (E.L.N) and the U.S. FDA (U18-FD-004004) (E.L.N.).

AUTHORS (LAST NAME, FIRST NAME): Ordoñez, Alvaro A.[1, 2]; Tasneen, Rokeya[3, 4]; Converse, Paul J.[3, 4]; Klunk, Mariah[1, 2]; Pokkali, Supriya[1, 2]; Nuermberger, Eric L.[3, 4]; Jain, Sanjay K.[1, 2]

INSTITUTIONS (ALL):

1. Center for Infection and Inflammation Imaging Research, Johns Hopkins University School of Medicine, Baltimore, MD, United States.
2. Department of Pediatrics, Johns Hopkins University School of Medicine, Baltimore, MD, United States.
3. Center for Tuberculosis Research, Johns Hopkins University School of Medicine, Baltimore, MD, United States.
4. Department of Medicine, Johns Hopkins University School of Medicine, Baltimore, MD, United States.

(No Image Selected)

CONTROL ID: 2232258

TITLE: Engineered Antibody Fragments for PSMA-targeted Imaging and Therapy of Prostate Cancer

PRESENTER: Liang Shan

ABSTRACT BODY:

Abstract Body: Monoclonal antibodies have long been attractive for molecular imaging of cancer because of their high specificity and potential to impart molecular specificity into existing imaging modalities. However, two major issues, including long circulation time and poor tissue penetration, form a critical barrier for antibodies to achieve efficient imaging. To overcome the issues of using antibodies for molecular imaging, three different formats of antibody fragments were designed, including single-chain variable fragment (scFv, 27 kDa), bivalent tandem scFv (biscFv, 54.6 kDa), and bivalent scFv fold-back diabody (scfbDb, 54.6 kDa). These fragments were generated by fusing the variable regions of the heavy and light chains of prostate-specific membrane antigen (PSMA)-specific J591 antibody. Competition assay showed that the binding affinity of scfbDb was 7-fold and 2.5-fold higher than that of scFv and biscFv formats, respectively. To test the delivery efficiency of scfbDb, a recombinant immunotoxin was then generated by fusing the scfbDb with a mutated diphtheria toxin moiety (DT390) using a diphtheria toxin-resistant *P. pastoris* expression system. *In vitro*, fluorescent microscopy and flow cytometry demonstrated that scfbDb efficiently mediated the entry of DT390 into the PSMA-positive LNCaP prostate cancer cells but not into the PSMA-negative PC-3 cells, inducing LNCaP cell apoptosis and growth arrest (IC_{50}, 0.57 nM). *In vivo*, fluorescent optical imaging confirmed the PSMA-targeting specificity of scfbDb, showing specific accumulation in LNCaP tumor xenografts. The drug-delivery efficiency of scfbDb was also confirmed with anti-tumor efficacy test, showing that systemic administration of the scfbDb-based immunotoxin significantly inhibited the growth of LNCaP, but not the PC-3 tumor xenografts (0.27±0.09 g *vs.* 0.67±0.11 g; $P < 0.05$). These results indicate that the engineered antibody fragments, especially the scfbDb, could serve as a springboard to develop PSMA-targeted imaging and therapeutic agents with high sensitivity and specificity against prostate cancer.

AUTHORS (LAST NAME, FIRST NAME): Shan, Liang[1]; Lin, Stephen[1]; Wang, Paul C.[1]

INSTITUTIONS (ALL):

1. Radiology, Howard University , Washington DC, DC, United States.

(No Image Selected)

CONTROL ID: 2232259

TITLE: Modulation of metabolic parameters and antioxidant enzymes in diabetic aging female rat brains: Beneficial role of Metformin.

PRESENTER: Pardeep Kumar

ABSTRACT BODY:

Abstract Body: Objective: The objective of this study was to investigate beneficial effects of metformin on membrane bound enzymes (monoamine oxidase, Na^+ K^+ ATPse,) and antioxidant enzymes (sueroxidase dismutase, glutathione S-transferases), lipid peroxidation, neurolipofuscin, DNA degradation in diabetic aging female rats.
Methods: Young (3 months) adult (12 months) and aged (24 months) rats will be diabetic by using alloxan monohydrate. Metformin was administered i.p. at a dose of 200 mg/kg/day for 30 days to both control and diabetic aging rats. Learning was tested in a Morris water maze. A detailed study was carried on membrane linked enzymes, membrane fluidity, neurolipofuscin, antioxidant enzymes and DNA degradation to identify the antidiabetic and antiaging role of metformin using biochemical ,molecular and histiochemical study.
Results: Present study shows that there was a similar pattern of increased lipid peroxidation, neurolipofuscin, DNA degradation and monoamine oxidase activity and a decrease in membrane fluidity, Na^+ K^+ ATPse, antixodant enzymes activities in both aging and diabetes. Metformin was found to be an effective treatment in stabilizing and normalizing the membrane functions; therefore this therapy can be considered an alternative to be explored further as a means of diabetic and aged related disorders control. Metformin treatment also helped to reverse the age related changes studied, to normal levels, elucidating an anti-aging, antidiabetic and neuroprotective action.
Conclusions: The results of this study will be useful for pharmacological modification of the aging process and applying new strategies for control of age related disorders including metabolic syndrome.

AUTHORS (LAST NAME, FIRST NAME): Kumar, Pardeep[1]; Baquer, Najma[1]

INSTITUTIONS (ALL):

1. School of Life Sciences, Jawaharlal Nehru University, New Delhi, India.

(No Image Selected)

CONTROL ID: 2232266

TITLE: Title: Transcriptional activation of endogenous retroviruses in response to age and stress

PRESENTER: Somnath Mukherjee

ABSTRACT BODY:

Abstract Body: Objectives

Basic objectives were to analyze the transcriptional regulation of endogenous retrovirus in response to age and stresses.

Methods

Real time PCR analysis using RNA isolated from various brain regions and various tissues from old and young wistar rats was carried out to determine the change in endogenous retrovirus transcripts.

Results

There was no significant change in the expression of endogenous retrovirus in various brain regions of 2 month old and 18 month old rats except cerebral cortex.

The heavy metals nickel, cadmium, lead, mercury and aluminum upregulates the expression of endogenous retrovirus in tissue specific and age dependent manner.

Conclusions

The results of this investigation conclusively prove that endogenous retrovirus are transcriptionally activated in response to stress.

AUTHORS (LAST NAME, FIRST NAME): Mukherjee, Somnath[1]; Upadhyaya, Prof K.C[1]; Kumar, Deepak[1]

INSTITUTIONS (ALL):

1. School of Life Sciences, Jawaharlal Nehru University, New Delhi, New Delhi, India.

(No Image Selected)

CONTROL ID: 2232279

TITLE: ^{68}Ga-NODAGA-Exendin-4 for the imaging of upregulated glucagon-like peptide-1 receptor expression after experimental myocardial infarction

PRESENTER: Mia Ståhle

ABSTRACT BODY:

Abstract Body: Purpose: Therapies activating glucagon-like peptide-1 (GLP-1) signalling are increasingly used in the treatment of diabetes. Although these therapies have influence on cardiovascular function, the expression of GLP-1 receptor (GLP-1R) in the heart is still unclear. [1-3] We evaluated ^{68}Ga-NODAGA-Exendin-4 for monitoring the level of GLP-1R expression in the heart after experimental myocardial infarction (MI).

Methods: Rats were studied at 3 d (n=6), at 1 wk (n=7) and at 12 wk (n=9) after induction of MI by permanent ligation of the left coronary artery or at 1 wk and 12 wk after sham-operation (n=9 and n=9, respectively). Rats were injected with 52±3 MBq of ^{68}Ga-NODAGA-Exendin-4 and a 60-min dynamic PET and a contrast-enhanced CT were performed. After imaging, left ventricle (LV) was cut into serial short axis cryosections for autoradiography, histology and immunohistochemistry. A subset of rats was studied with cardiac MRI.

Results: MI size measured as percentage of LV circumference was 48±7 % at 3 d, 42±7 % at 1 wk and 35±14 % at 12 wk. In vivo cardiac MRI and PET/CT showed ^{68}Ga-NODAGA-Exendin-4 uptake at the infarcted anterior wall of the LV in all time-points. Compared with the myocardium of sham-operated rats, autoradiography revealed significantly increased ($p<0.001$) tracer uptake in the infarct scar and in the surrounding border zone myocardium at 3 d and 1 wk post-MI (0.8±0.4 vs. 11.1±2.7 and 3.7±1.1, and vs. 6.6±2.3 and 2.2±0.5 PSL/mm^2, respectively) as well as at 12 wk post-MI (1.0±0.4 vs. 4.3±1.2 and 2.5±0.6 PSL/mm^2, respectively). Tracer uptake was slightly increased ($p<0.05$ vs. sham) also in the remote, non-infarcted myocardium at 3 d, 1 wk and 12 wk post-MI (1.4±0.7, 1.4±0.5 and 1.5±0.4 PSL/mm^2, respectively). GLP-1R expression at MI was confirmed by immunohistochemistry and specificity of tracer uptake by in vivo competition experiment.

Conclusions: This study provides evidence that GLP-1R is expressed in the heart in response to ischemic myocardial injury. The uptake of ^{68}Ga-NODAGA-Exendin-4 was the highest early after MI, but extended up to 3 months. Imaging of GLP-1R may help to study the functions and potential of GLP-1-based therapies in the heart.

References: [1] Ussher JR. & Drucker DJ. Circ Res. 2014;114:1788–1803, [2] dos Santos L. et al. Circ Heart Fail. 2013;6:1029–1038, [3] Ban K. et al. Circulation. 2008;117:2340–2350.

AUTHORS (LAST NAME, FIRST NAME): Ståhle, Mia[1]; Kytö, Ville[2]; Liljenbäck, Heidi[1, 3]; Kiugel, Max[1]; Metsälä, Olli[1]; Käkelä, Meeri[1]; Virta, Jenni[1]; Koskensalo, Kalle[1]; Saukko, Pekka[4]; Knuuti, Juhani[1]; Roivainen, Anne[1, 3]; Saraste, Antti[1, 2]

INSTITUTIONS (ALL):

1. Turku PET Centre, University of Turku, Turku, Finland.
2. Heart Center, Turku University Hospital, Turku, Finland.
3. Turku Center for Disease Modeling, University of Turku, Turku, Finland.
4. Department of Pathology and Forensic Medicine, University of Turku, Turku, Finland.

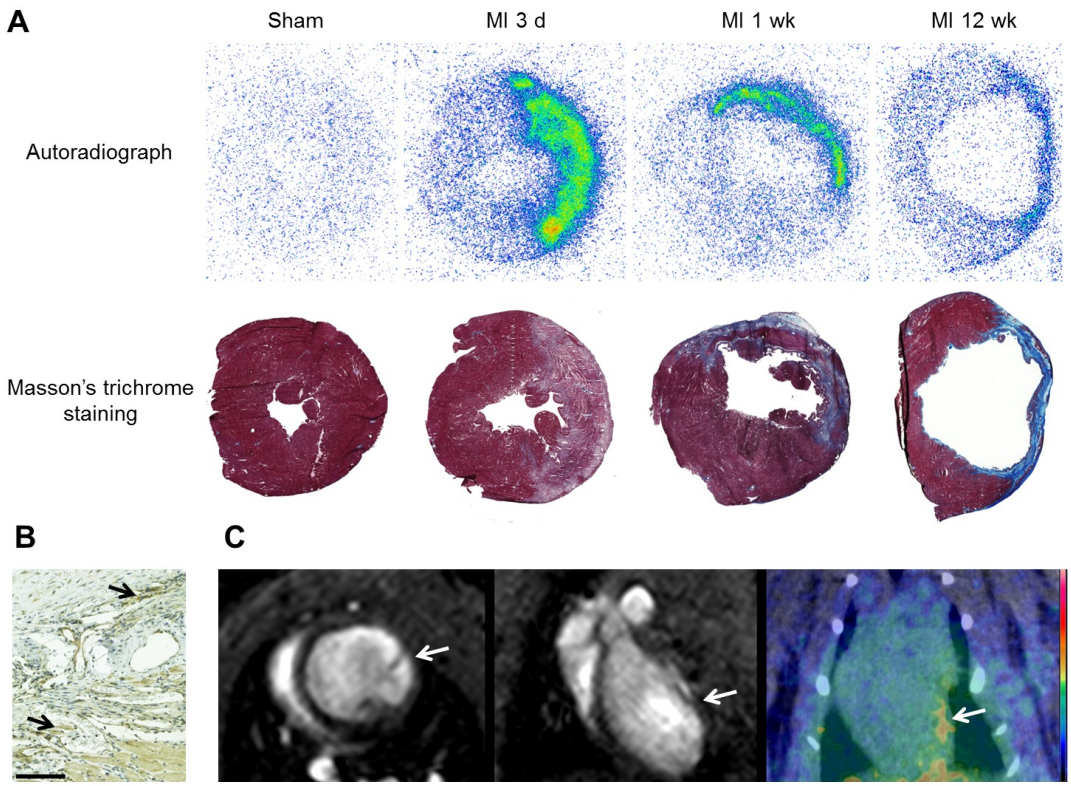

A. Representative autoradiographs of myocardial ^{68}Ga-NODAGA-Exendin-4 uptake and corresponding Masson's trichrome staining at different time-points after MI or after sham-operation. **B.** Immunohistochemical staining of GLP-1R (arrows) in the infarcted myocardium (scale bar 100 µm). **C.** Example of infarcted anterior wall of the LV by cardiac MRI and corresponding ^{68}Ga-NODAGA-Exendin-4 PET/CT (arrows) at 1 wk post-MI.

CONTROL ID: 2232280

TITLE: An EDB Fibronectin Targeting MRI Contrast Agent for Molecular MRI of Breast Cancer Micrometastases

PRESENTER: Zheng Han

ABSTRACT BODY:

Abstract Body:

Objectives

The objective of this study is to develop targeted MRI contrast agent for molecular imaging of breast cancer metastases. Metastasis is one of the main causes of mortality of breast cancer patients. Molecular imaging of metastasis and breast cancer with metastatic potential has a potential to detect the life threatening disease earlier and to timely monitor therapeutic response, which is essential for tailoring more efficacious treatment for better therapeutic outcome. It is suggested that early metastases substantially overexpress extradomain-B fibronectin (EDB-FN), which supports the outgrowth of metastases. Thus, we developed an MRI contrast agent based on an EDB-FN targeting peptide and tested the agent for high-resolution molecular MRI of small metastases in mice.

Methods

A peptide of 7 amino acids, ZD2, specific to EDB-FN targeting peptide was developed using phage display and synthesized in solid phase. MRI imaging agent, ZD2-Gd(HP-DO3A), was synthesized by conjugating Gd(HP-DO3A) to the peptide using click chemistry. A fluorescence imaging probe, ZD2-Cy5, was also synthesized by labeling ZD2 with Cy5. Metastatic breast cancer model was developed by intracardially injecting 0.2×10^6 4T1-GFP-Luc2 cells, which were treated with TGFβ for 3 days prior to injection. Development of metastases was monitored with bioluminescence imaging. MRI images of whole mice were acquired at 1 week, 2 weeks and 3 weeks following tumor injection using a three-dimensional T_1 weighted gradient echo sequence with respiratory gating (Sequence details: TR = 25 ms, TE = 2.8 ms, average = 3, 15° flip angle. Resolution: 0.12 × 0.1 × 0.56 mm). A dose of 0.2 mmol Gd/kg was used in all MRI studies. At three weeks, 10 nmol ZD2-Cy5 was intravenously injected into mice and organs of the mice were examined for fluorescent signals after three hours. Western blot analysis was further used to validate the overexpression of EDB-FN in metastatic tumors from different locations.

Results

Our results indicated that micrometastatic tumors with a diameter of < 1 mm can be detected at day 7 using MRI following injection of 0.2 mmol-Gd/kg ZD2-Gd(HP-DO3A). Successful detection can be further validated by monitoring the growth of detected metastases at day 14 and day 21. Fig. 1a shows the contrast enhancement of a lymph node metastasis above the kidney. To examine the co-localization of peptide probe with tumor, fluorescent images of metastases in the same location were acquired after ZD2-Cy5 injection. As shown in Fig. 1b the lymph node metastases above the kidney showed significant enhancement using ZD2-Cy5. Western blot analysis, as shown in Fig. 1c, confirmed the overexpression of EDB-FN in metastases.

Discussion and Conclusion

We have developed a targeted MRI contrast agent specific to EDB-FN for effective molecular MRI of of breast cancer micrometastases. The preliminary results have demonstrated that targeted MRI contrast agent has potential for early treatment of small breast cancer and micrometastases.

AUTHORS (LAST NAME, FIRST NAME): Han, Zheng[1]; Zhou, Zhuxian[1]; Lu, Zhengrong[1]

INSTITUTIONS (ALL):

1. Biomedical Engineering, Case Western Reserve University, Cleveland, OH, United States.

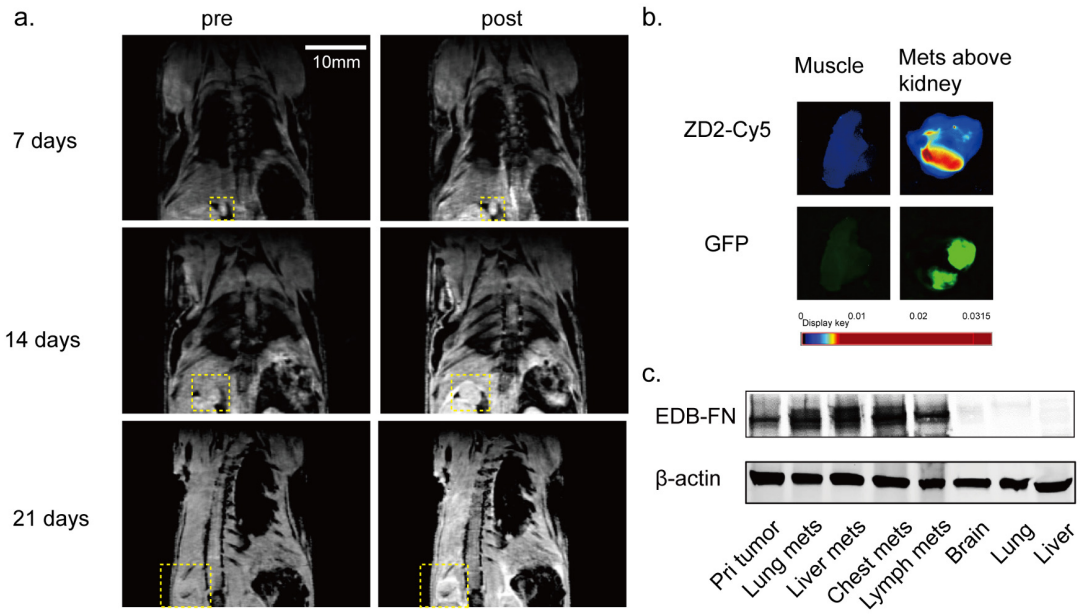

Fig. 1. a. Representative images of a mouse with a metastatic tumor located above the kidney (indicated with dashed box). Pre-contrast image (pre) and post-contrast image (post) are shown for 7 days, 14 days and 21 days after cancer cell inoculation. b. ZD2-Cy5 signal in lymph node metastases located above the kidney compared with that in muscle. Fluorescent signals of Cy5 are presented as jet-black colormaps (see display keys below). GFP signals indicate the location of tumor. c. Western blot analysis of EDB-FN expression in metastases in different organs.

CONTROL ID: 2232285

TITLE: Non-invasive PET-based diagnostic for precision HSP90 therapy in glioblastomas

PRESENTER: Alexander Bolaender

ABSTRACT BODY:

Abstract Body: Background

Glioblastoma multiforme (GBM) is a highly aggressive brain tumor with poor prognosis and few therapeutic options. Recent studies on Heat-shock protein 90 (HSP90) propose this protein as a potential target in GBMs.(1, 2) Specifically, significant antitumor activity was noted with HSP90 inhibitors in several GBM cell lines, subcutaneous xenografts, genetic GBM models and primary GBMs in culture, proposing HSP90 as a therapeutic target in a subset of GBMs. A brain permeable HSP90 inhibitor, PU-GBM, is currently aimed for clinical translation in GBM.

Hypothesis

We hypothesize that the introduction of non-invasive imaging based diagnostics that enable for the detection of target-expressing and drug-accessible tumors will accelerate the rational application of PU-GBM in CNS tumors. This approach has been successfully applied to the non-CNS targeted HSP90 agent PU-H71 (3,4).

Methods

PU-GBM, like PU-H71, contains an endogenous iodine atom which can be isotopically substituted for PET with the long-lived positron emitter iodine-124 (^{124}I), without changing its affinity, selectivity or biodistribution profile. We thus investigated several routes for the transformation of radiochemical precursors of PU-GBM into [^{124}I]-PU-GBM. We also optimized its recovery and purification aiming for consistent and reliable production of radiotracer. To investigate the ability of [^{124}I]-PU-GBM to image GBMs by PET, we established primary GBM xenografts in mice. These were derived by intracranial transplantation of patient derived glioma stem cells. Tumor establishment and size were monitored by MRI. For PET, tumor bearing mice were imaged at different time points following tracer administration and brains were eventually excised to verify specific tumor uptake.

Results

We successfully synthesized the radiochemical precursor of PU-GBM and developed a one-step radioiodination method to obtain [^{124}I]-PU-GBM from its precursor by reaction with [^{124}I]-NaI and Chloramine-T as oxidant. [^{124}I]-PU-GBM was synthesized from its precursor in a single step, in > 60% (isolated) yield. The obtained tracer was over 96% pure. *In vivo* PET imaging of [^{124}I]-PU-GBM in tumor-bearing mice provided visualization of intracranial GBMs. Specific tumor uptake and retention of [^{124}I]-PU-GBM was confirmed by autoradiography and H&E staining.

Significance

To our knowledge there are no diagnostic tools to aid in the development of HSP90 inhibitors in CNS tumors and [^{124}I]-PU-GBM PET could be poised to fill this gap.

1. Jhaveri K, et al. (2014) Heat shock protein 90 inhibitors in the treatment of cancer: current status and future directions. Expert opinion on investigational drugs 23(5):611-628.
2. Siegelin MD, et al. (2010) Global targeting of subcellular heat shock protein-90 networks for therapy of glioblastoma. Molecular cancer therapeutics 9(6):1638-1646.
3. Dunphy, M. PET Imaging of Cancer Patients Using [^{124}I]-PU-H71: A Pilot Study available from: http://clinicaltrials.gov; NCT01269593.
4. Gerecitano, J. The First-in-human Phase I Trial of PU-H71 in Patients with Advanced Malignancies available from: http://clinicaltrials.gov; NCT01393509.

AUTHORS (LAST NAME, FIRST NAME): Bolaender, Alexander[1]; Shimizu, Fumiko[1]; Pillarsetty, Naga Vara Kishore[2]; Ochiana, Stefan O.[1]; Longo, Valerie A.[4]; Tabar, Viviane[3]; Zanzonico, Pat[2]; Chiosis, Gabriela[1]

INSTITUTIONS (ALL):

1. Molecular Pharmacology and Chemistry, Memorial Sloan Kettering Cancer Center, New York, NY, United States.

2. Department of Radiology, Memorial Sloan Kettering Cancer Center, New York, NY, United States.
3. Department of Neurosurgery, Memorial Sloan Kettering Cancer Center, New York, NY, United States.
4. Animal Imaging Core Facility, Memorial Sloan Kettering Cancer Center, New York, NY, United States.
(No Image Selected)

CONTROL ID: 2232295

TITLE: Atherosclerotic plaque permeability: in vivo quantification in the aortic root of ApoE-/- mice using DCE-MRI

PRESENTER: Claudia Calcagno

ABSTRACT BODY:

Abstract Body: *Introduction*: Inflammation is a hallmark of atherosclerotic plaques at high risk for rupture and thrombosis[1]. Monocyte recruitment[2], macrophage proliferation[3], death[4], and exit[5] have recently been identified as key processes that modulate plaque inflammation. In mouse models, it has been proven that certain stimuli, such as psychosocial stress[6] and myocardial infarction[7], aggravate plaque inflammation through these pathways. These phenomena are tightly linked to increased plaque endothelial permeability, which sustains cells' turnover in the vessel wall. Developing techniques to measure plaque permeability *in vivo* may greatly contribute to our understanding of plaque biology, the identification of vulnerable plaques and the development of novel anti-inflammatory drugs. Recently, we have demonstrated the use of semi-quantitative, contrast enhanced (CE) MRI as a non-invasive, *in vivo* read-out of decreased endothelial permeability in the aortic root of atherosclerotic mice after intervention with anti-inflammatory nanoparticles (**Fig 1**). Building upon these results, we propose a robust, fully quantitative protocol to measure endothelial permeability in the mouse aortic root using non-invasive dynamic contrast enhanced (DCE) MRI[8]
.

Methods: DCE-MRI of the root was performed on 6 ApoE -/- mice for 15 minutes after injection of Gd-DTPA, using a novel, self-gated, fast low angle shot (FLASH) MR sequence with weighted k-space filling and compressed sensing acceleration[9] (**Fig 2A-B**), which acquires data continuously and asynchronously with the periodic cardiac and respiratory motion (**Fig 2A**). After acquisition, data were reconstructed into 15 cardiac phases and 10 temporal dynamic frames, for a total of 150 images. A region of interest (ROI) encompassing the aortic root was selected in one cardiac frame, and propagated throughout the 10 dynamic frames to extract enhancement curves.

Results: In each mouse at least one cardiac phase clearly showing the vessel wall of the aortic root could be identified. **Fig 2B** shows 3 temporal frames of a representative cardiac phase. Signal enhancement can be clearly seen in post-contrast temporal frames 5 and 10, with respect to pre-contrast frame 1. This pattern was found to be consistent across all animals. **Fig 2D** depicts ROI concentration curves from each animal (one cardiac phase).

Conclusion: We demonstrate the feasibility of self-gated DCE-MRI with prospective compressed sensing acceleration to quantify endothelial permeability in the aortic root of atherosclerotic mice. In the future, quantitative in vivo measures of permeability will be correlated with genetic, molecular and cellular assays in the root, and will serve as read-outs of plaque progression or regression after anti-atherosclerotic therapy.

References: 1. Virmani R, J Am Coll Cardiol 2006; 2. Swirski F, J Clin Invest 2007; 3. Robbins CS, Nat Med, 2013; 4. Moore KJ, Cell, 2011; 5. Moore KJ, Nat Rev Immunol, 2013; 6. Heidt T et al, Nat Med 2014; 7.Dutta P et al, Nature 2012; 8.Calcagno C et al ATVB 2008; 9.Motaal AG et al NMR in biomedicine 2012

AUTHORS (LAST NAME, FIRST NAME): Calcagno, Claudia[1]; Giannarelli, Chiara[2]; Mootal, Abdallah[3]; Nahrendorf, Matthias[4]; Mulder, Willem J.[1]; Fayad, Zahi A.[1]; Strijkers, Gustav[3]

INSTITUTIONS (ALL):

1. Radiology, Icahn School of Medicine at Mount Sinai, New York, NY, United States.
2. Cardiology, Icahn School of Medicine at Mount Sinai, New York, NY, United States.
3. Biomedical Engineering and Physics, Academic Medical Center, Amsterdam, Netherlands.
4. Center for Systems Biology, Massachusetts General Hospital, Boston, MA, United States.

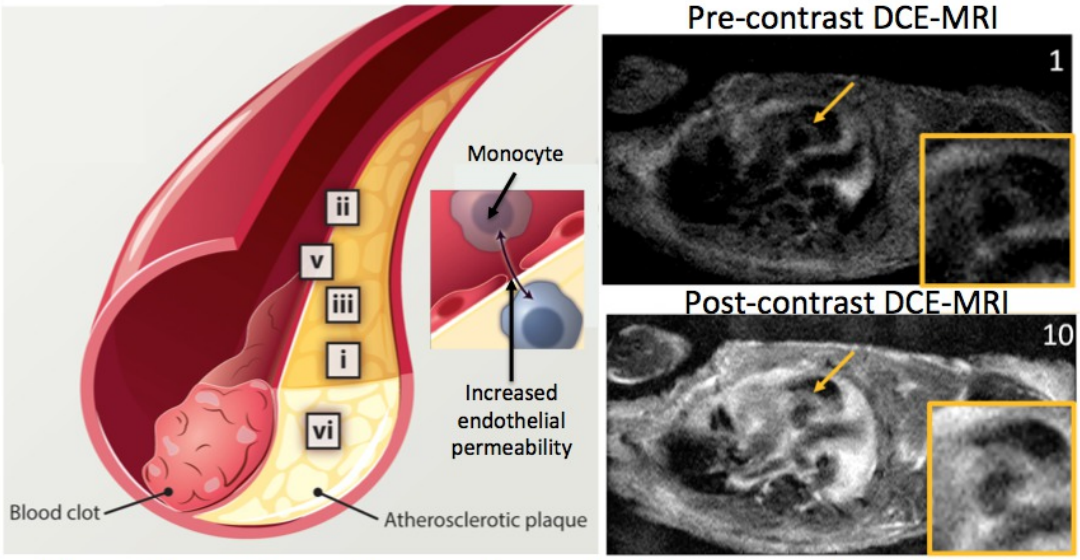

Plaque inflammation and increased permeability: in vivo monitoring by DCE-MRI

CONTROL ID: 2232297

TITLE: Set up and MR-PET imaging of a *S. aureus* vascular graft infection model in mice

PRESENTER: Hélène Van de Vyver

ABSTRACT BODY:

Abstract Body: Introduction: *Staphylococcus aureus* readily binds to the plastic surface of implanted catheters forming thick biofilm layers, this causes rare but serious vascular graft infections. These biofilm layers are difficult to detect, seeing as they are often accompanied by nonspecific clinical symptoms and are very tough to eradicate with antibiotics. Therefore, these infections usually result in the removal of the foreign material and are associated with a high morbidity and mortality(1). Thus, it is essential to improve the detection methods in order to treat the patient as quickly as possible. To study new detection methods it is necessary to have a representative *in vivo* model which closely mimics the situation in patients.

Aim: The aim of this study was to create a mouse model to realistically study vascular graft infections as well as combining MRI and PET imaging to allow early detection and non-invasive follow-up of the biofilm formation. MRI imaging was used for *in vivo* velocity measurements of the carotid arteries, with the aim of detecting a reduced blood flow due to biofilm formation on the graft. ^{18}F-FDG PET imaging has been shown to be a reliable tool for the detection of vascular graft infections(2,3) and by combining this imaging modality with the MRI measurements it is possible to substantially improve the specificity of detection.

Methods: A Teflon catheter was inserted into the right carotid artery of mice to act as a vascular graft, subsequently flow velocities in the carotid arteries and inflammation were measured. Mice were infected intravenously via the tail vein with *S. aureus*, in order to mimic the mode of infection in patients. 10 days after infection flow velocities in the carotid arteries and inflammation were measured again and 14 days post infection mice were sacrificed and organs were analyzed for bacterial load.

Results: This murine model showed that after infection with a high dose of *S. aureus*, the mice develop a sepsis followed by biofilm formation on the catheter, this was confirmed using electron microscopy. MRI imaging showed that the flow velocity in the right carotid artery is strongly reduced after infection compared to before infection, implying that this is a promising tool to non-invasively detect biofilm formation. Also, MR-PET revealed that there is a high level of inflammation specific to the site of the catheter after infection, proving that combing these two imaging modalities could be a valuabel tool for the early detection of vascular graft infections. This mouse model also provides a solid platform for studying underlying mechanims of biofilm formation and finding more effective treatment options.

1. Infect. Dis. Clin. N. Am. 2012; 26:41–56

2. J Nucl Med 2007; 48:1230–1236

3. Semin Nucl Med 2009; 39:36-51

AUTHORS (LAST NAME, FIRST NAME): Van de Vyver, Hélène[1]; Bovenkamp, Philipp R.[2]; Hoerr, Verena[2]; Hansen, Uwe[3]; Peters, Georg M.[1]; Löffler, Bettina[4]

INSTITUTIONS (ALL):

1. Institute for Medical Microbiology, University of Münster (Germany), Münster, NRW, Germany.
2. Institute for Clinical Radiology, Münster, Germany.
3. Institute of Physiological Chemistry and Pathobiochemistry, Münster, Germany.
4. Institute for Medical Microbiology, Jena, Germany.

(No Image Selected)

CONTROL ID: 2232305

TITLE: FMT imaging in the development of targeted liposomes for cell-specific delivery of small molecule drugs to the infarct border zone after myocardial infarction

PRESENTER: Alexander Klibanov

ABSTRACT BODY:

Abstract Body: Introduction: Coronary artery disease is the leading cause of morbidity in the world with only limited treatment options available to prevent heart failure after myocardial infarction (MI). Long-term medications following successful reperfusion include beta-blockers, ACE inhibitors and aldosterone antagonists, but these can only slow the progression of heart failure. Given that most strategies for preventing heart failure post-MI would benefit from targeted delivery of therapeutic agents to the infarct border zone, we hypothesized that suitable targeting ligands could be identified by biopanning a phage display library in vivo in a mouse model of MI. We were able to combine phage display screening with optical imaging of phage by fluorescence molecular tomography (FMT) to enable rapid and efficient screening of targeted, pharmacologically relevant phage clones. Peptides identified through this screen were conjugated to liposomes and used to study their target specificity by in vivo and ex vivo imaging. **Methods**: After three rounds of in vivo biopanning, FMT imaging was used to compare the biodistribution/specificity of selected clones against a negative control phage clone. Fluorescence microscopy of labeled phage clones in cardiac tissue, combined with immunofluorescent detection of cell-type specific markers then enabled us to identify peptides targeting cell types of interest in the infarct zone. Liposomes were targeted using peptides for activated endothelial cells, cardiomyocytes and c-Kit+ cells. Liposomal preparations included DiR, a lipophilic near infrared dye, that was incorporated in the lipid bilayer and peptide sequences included a FAM molecule on their C-terminal linker sequence. These tags facilitated the characterization of the pharmacokinetics and tissue distribution of targeted liposomes. **Results:** With FMT, we were quickly able to differentiate between specific and non-specific groups of phage clones. Similarly, we were able to identify individual clones with high specificty from the phage groups. Liposomes with DiR and FAM allowed us to identify peptides with high specificity for the post-infarct heart, and at the same time monitor the stability of the peptide-liposome conjugates in vivo. Cardiomyocyte-specific liposomes loaded with a small molecule inhibitor of PARP-1 (AZ7379) were 9-fold more efficient than negative control (NCP) liposomes in ex vivo bioassays of PARP activity. **Conclusions:** FMT imaging enabled our lab to perform phage clone validation at high efficiency while at the same time providing valuable information about the distribution of these clones in the infarct area in relation to the associated cell types. The combination of an organ-level biodistribution screen (provided by FMT) with a tissue-level analysis of peptide-targeted phage and liposomes proved to be a powerful imaging strategy that expedited biopanning in post-MI mice and also provided information on the stability of peptide-liposome conjugates.

AUTHORS (LAST NAME, FIRST NAME): Dasa, Siva Sai Krishna[1]; Suzuki, Ryo[3]; Brinton, Lindsey T.[4]; Tian, Yikui[5]; Michaëlsson, Erik[6]; Lindfors, Lennart[7]; Klibanov, Alexander L.[2, 1]; French, Brent A.[4, 2]; Kelly, Kimberly A.[4, 1]

INSTITUTIONS (ALL):

1. Cardiovascular Research Center, University of Virginia, Charlottesville, VA, United States.
2. Dept. of Medicine, Cardiovascular Div., University of Virginia, Charlottesville, VA, United States.
3. Faculty of Pharma-Sciences, Teikyo University, Tokyo, Japan.
4. Department of Biomedical Engineering, University of Virginia, Charlottesville, VA, United States.
5. Department of Surgery, University of Virginia, Charlottesville, VA, United States.
6. iMed CVMD, Bioscience, AstraZeneca, Molndal, Sweden.
7. Pharmaceutical Development, AstraZeneca, Molndal, Sweden.

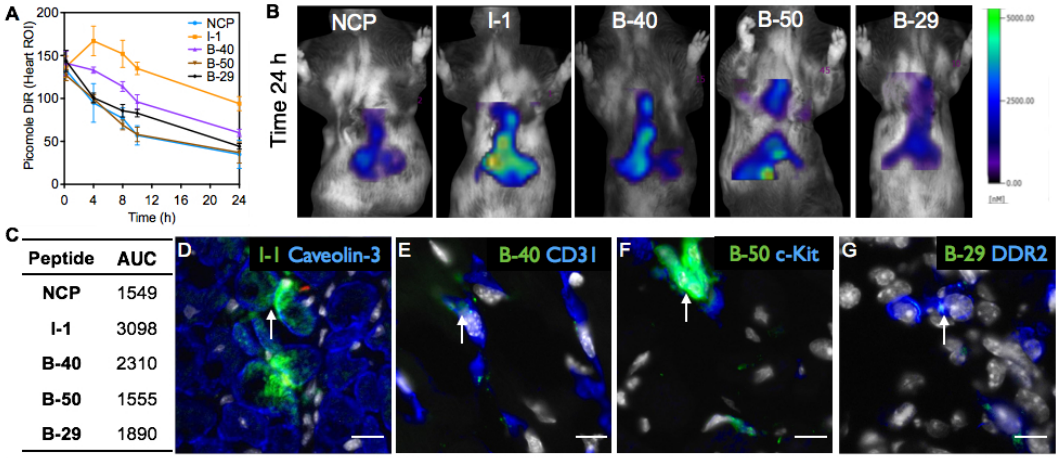

C

Peptide	AUC
NCP	1549
I-1	3098
B-40	2310
B-50	1555
B-29	1890

Figure. 1. Peptide-modified liposomes display specificity for cell types of interest in the infarct border zone. A) Graph showing pharmacokinetics of five different peptide-conjugated liposomes obtained using FMT imaging followed by image analysis using the heart as the region of interest (ROI). FMT imaging of the liposome preparations was performed in live mice on day 4 post-MI. Liposomes conjugated to a negative control peptide (NCP) were included to compare random vs. targeted liposome kinetics. In this instance, targeted liposome accumulation was largely consistent with the abundance of available cellular targets. B) FMT images at 24 h post-injection of four peptide-conjugated liposomes. C) Using a two-compartment model fit, areas-under-the-curve (AUC) were determined for the five different peptide-conjugated liposomes. Peptides identified in the phage screen were specific for cellular targets present in the border zone: D) Peptide I-1 was specific for cardiomyocytes (caveolin-3, arrow), E) B-40 specific for endothelial cells (CD31, arrow), F) B-50 specific for c-Kit+ cells (c-Kit, arrow), and G) B-29 specific for myofibroblasts (DDR2, arrow). Peptides are pseudo-colored green and cell markers (caveolin-3, CD31, c-Kit, DDR2) are shown in blue (scale bar; 20 μm).

CONTROL ID: 2232322

TITLE: Comparison of ^{1}H and ^{13}C Apparent Diffusion Coefficient Values of Mice Liver *in vivo* using Dynamic Nuclear Polarization and Magnetic Resonance Imaging at 14T

PRESENTER: Irene Marco-Rius

ABSTRACT BODY:

Abstract Body: Introduction: Diffusion weighted MRI measuring water molecule movement and tissue microstructure is frequently used to characterize both diffuse and focal liver disease. In liver fibrosis, for instance, increased collagen formation is associated with restricted diffusion of water[1]. However, the majority of water within the liver is either in the vascular or intracellular space, making the diffusion of water a potentially poor marker for fibrosis, which is an extracellular process. Hyperpolarized ^{13}C-substrates have been previously used to image perfusion[2] and metabolism [3]. Here, we investigated using an exogenously injected extracellular agent, hyperpolarized ^{13}C-urea, as a potentially more sensitive probe of the extracellular space in the liver. As a preliminary step to evaluate hyperpolarized urea in fibrotic mice, we first optimized and tested a diffusion weighted protocol in normal mice, computing the ADCs of ^{13}C-urea and water in the liver.

Methods: Images were acquired using a 14T MRI scanner (Varian, Inc) with a 98mm bore size, and dedicated coils for ^{13}C and ^{1}H imaging. A total of four mice were imaged. The protocol was approved by the local institutional animal care and use committee. A single central slice was used in both cases. ^{1}H diffusion weighted spin echo images were acquired with the following parameters: 128x128 matrix, 40mm FOV, slice 2mm, b=20,183,325,509s/mm^{2}. Combined cardiac and respiratory gating was employed. Diffusion-weighted ^{13}C images were acquired using an echo planar sequence with diffusion-compensated variable flip angle[4] following a tail-vein injection of a solution containing hyperpolarized ^{13}C-urea (110mM). Images were acquired approximately 33s after injection with 32x32 matrix, 32mm FOV, slice 8mm, b=50, 500, 700s/mm^{2}. Only respiratory triggering was used. ADC maps were calculated and a mean value determined over a ROI chosen in the liver.

Results: Figure 1 demonstrates the feasibility of rapidly acquiring ^{13}C-urea ADC maps in the liver with coregistration to ^{1}H ADC maps. Respiratory gating was crucial in obtaining this image quality. Both the ^{13}C-urea and water ADC values are larger near the major vasculature, and smaller in the liver tissue. The ^{13}C-urea ADC is also relatively homogeneous across the liver tissue.

We noted that the ^{13}C-urea ADC is consistently higher than the water ADC (table). A possible explanation would be that while the hyperpolarized urea remains extracellular, water is mainly intracellular, which makes it more restricted. Miscalibration of the RF variable flip angles, and hyperpolarized slice profile effects[5] can also result in inaccurate measurements of hyperpolarized ^{13}C ADCs. Further investigation will be required to further separate these potential effects.

Future experiments will use these methods to investigate the effects of multiple CCl4 doses that is expected to lead to a fibrotic response in the liver.

1. Annet *et al. J Magn Reson Imaging* **25,** 122–8 (2007)
2. Von Morze *et al. Magn Reson Med* **72,** 1599–609 (2014)
3. Dzien *et al. Magn Reson Med* (2014) doi: 10.1002/mrm.25286
4. Koelsch *et al. Magn Reson Med* (2014) doi:10.1002/mrm.25422
5. Deppe *et al. J Magn Reson* **202**, 2 (2010), 180–9

AUTHORS (LAST NAME, FIRST NAME): Marco-Rius, Irene[1]; Gordon, Jeremy W.[1]; Bok, Robert[1]; Larson, Peder E.[1]; Sukumar, Subramaniam[1]; Zhu, Zihan[2]; von Morze, Cornelius[1]; Vigneron, Daniel[1]; Kurhanewicz, John[1]; Ohliger, Michael A.[1]

INSTITUTIONS (ALL):

1. Radiology and Biomedical Imaging, University of California San Francisco, San Francisco, CA, United States.
2. University of California, San Francisco , San Francisco, CA, United States.

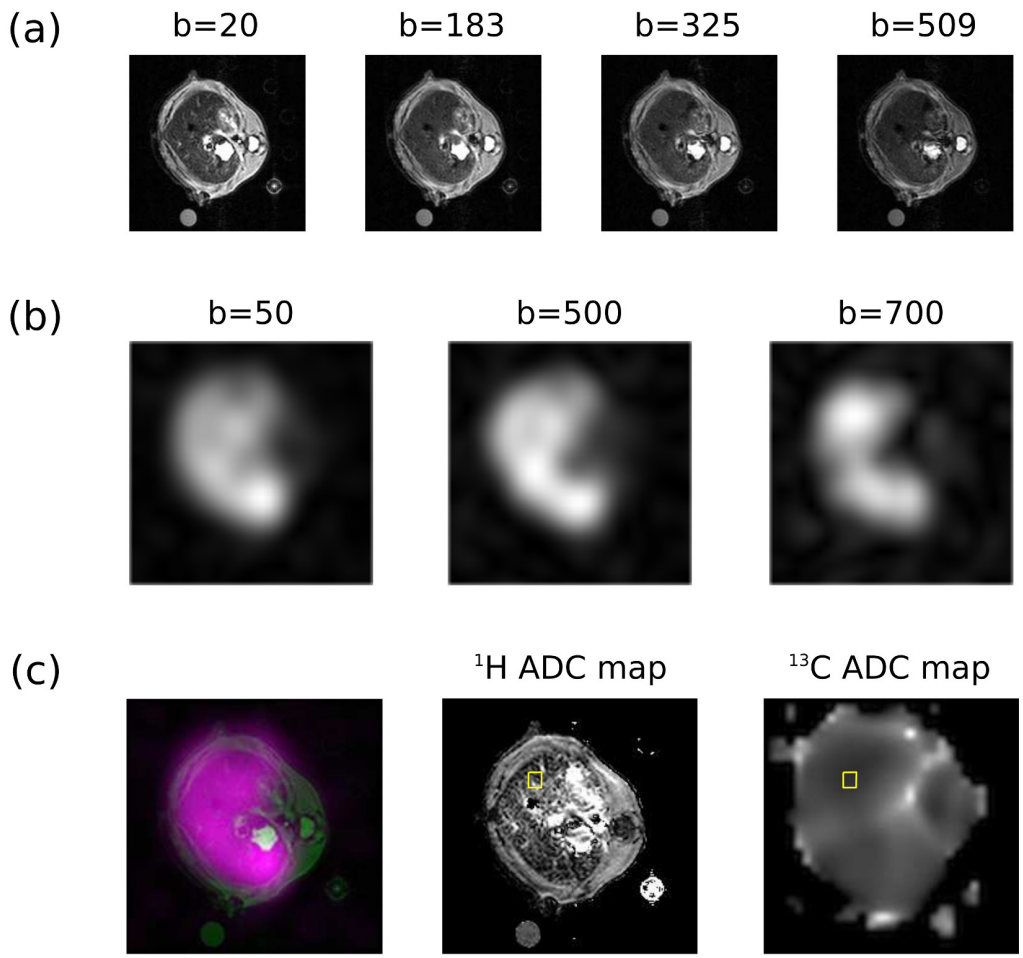

Figure 1. Images obtained from Mouse #2 in study. (a) Water diffusion images. (b) ^{13}C-urea diffusion images, individually scaled. b-values in units of s/mm^2. (c, left) Water diffusion image (b=20 s/mm^2, green) merged with ^{13}C-urea diffusion image (b=50 s/mm^2, pink). (c center & c right) ADC maps, ROI contour shown in yellow.

CONTROL ID: 2232330

TITLE: A Temperature Sensitive, Cobalt-based PARACEST Agent for MR Thermometry

PRESENTER: Joseph Spernyak

ABSTRACT BODY:

Abstract Body:

Background:

Unlike most conventional MRI contrast agents, chemical exchange saturation transfer (CEST) agents can be responsive to environmental changes such as pH (1-2), redox status (3) and temperature (4). Inclusion of a chelated paramagnetic metal to create PARACEST agents can dramatically shift the resonant frequency of associated water and/or exchangeable protons in ligand pendant groups. Recently, a cobalt (II) PARACEST complex with multiple CEST peaks was shown to register pH by ratiometric imaging (1). Here we report the further development and characterization of cobalt-based PARACEST agents for potential use in MR thermometry.

Methods:

A cobalt-based PARACEST agent was synthesized through the incorporation of Co(II) into the amide-appended macrocycle, 1,4,8,11-tetrakis(carbamoylmethyl)-1,4,8,11-tetraazacyclotetradecane (Co(**L1**), Figure 1A). Temperature dependent Z-spectra were acquired on a 500MHz NMR spectrometer at 5 temperatures ranging from 25-50°C using a 2s presaturation pulse of 24μT at each ppm offset. Similarly, imaging-based MR thermometry was performed on a 4.7T preclinical MR scanner utilizing a series of five 1s, 12μT saturation pulses followed by a fast-spin echo acquisition. CEST imaging consisted of six images acquired with CEST saturation pulses at frequencies surrounding the furthest shifted CEST peak of Co(**L1**) (112ppm at 37°C) with temperatures ranging from 27-42°C. CEST signal was calculated as the ratio of signal between images acquired with the presaturation pulse on resonance and off resonance of the exchangeable protons, e.g. +112 (on) / -112ppm (off). The offset frequency which yielded maximum CEST signal during imaging was determined at each temperature by fitting the CEST signal vs. ppm offset to a Lorentzian curve.

Results:

The resonant frequency of the Co(**L1**) demonstrated a linear dependence on temperature for all four CEST peaks in the positive ppm range (Table 1). Due to a moderate rate constant of exchange of 510 s^{-1} (1), no significant line-broadening was observed over a temperature increase of 25°C. Temperature dependence for the furthest shifted CEST peak using CEST-based MR thermometry demonstrated strong agreement with the NMR spectroscopic method (-0.586 ppm/°C vs. -0.564 ppm/°C, respectively).

Discussion:

The pH and temperature dependence of cobalt-based PARACEST agents have considerable potential for unique applications for *in vivo* imaging. The large chemical shift of 112 ppm is advantageous for increased sensitivity of detection *in vivo* as it is considerably shifted from the bulk of magnetization transfer signal arising from endogenous protein–water interactions. As the ppm offsets of the CEST peaks are independent of pH and concentration, Co(**L1**) offers the potential to measure temperature and pH with a single compound in one MR imaging session.

References

[1] Dorazio SJ et. al., Chem Commun (Camb). 2013 Nov 4;49(85):.

[2] Liu G et. al., Mol Imaging. 2012 Feb;11(1):47-57.

[3] Tsitovich PB et. al., Angew Chem Int Ed Engl. 2013 Dec 23;52(52).

[4] Li, AX et. al., Magn Reson Med. 2008 Feb;59(2).

AUTHORS (LAST NAME, FIRST NAME): Spernyak, Joseph[1]; Olatunde, Abiola[2]; Bond, Christopher[3]; Dorazio, Sarina J.[4]; Daddario, Michael[1]; Morrow, Janet[3]

INSTITUTIONS (ALL):

1. Dept. of Cell Stress Biology, Roswell Park Cancer Institute, Buffalo, NY, United States.
2. Dept. of Radiology, Harvard Medical School, Boston, MA, United States.

3. Dept. of Chemistry, SUNY at Buffalo, Buffalo, NY, United States.
4. Dept. of Chemistry, University of Connecticut, Storrs, CT, United States.

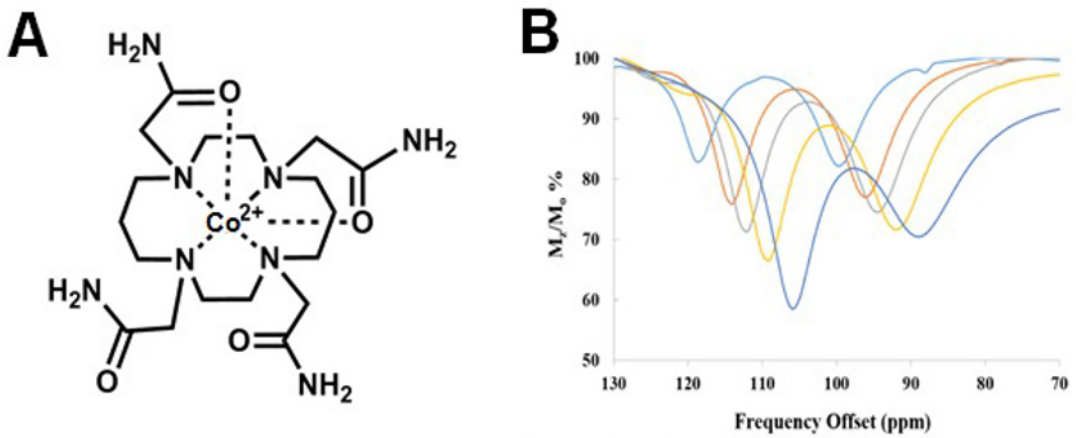

Figure 1. (A) Chemical structure of Co(L1). (B) Downfield Z-spectra demonstrating an upfield, temperature dependent shift of Co(L1) from 25°C (light blue) to 50°C (dark blue).

CONTROL ID: 2232338

TITLE: Pre-clinical evaluation of a novel CEA-targeting near-infrared fluorescent tracer delineating colorectal and pancreatic tumors

PRESENTER: Martin Boonstra

ABSTRACT BODY:

Abstract Body: Introduction:

Surgery is the cornerstone of oncologic therapy with curative intent. However, identification of tumor cells in the resection margins is difficult, resulting in non-radical resections, increased cancer recurrence and subsequent decreased patient survival. Novel imaging techniques that aid in demarcating tumor margins during surgery are needed. Overexpression of carcinoembryonic antigen (CEA) is found in the majority of gastro-intestinal carcinomas, including colorectal and pancreas. We developed ssSM3E/800CW, a novel CEA-targeted near-infrared fluorescent (NIRF) tracer, based on a disulphide stabilized single-chain antibody fragment (ssScFv), to visualize colorectal and pancreatic tumors in a clinically translatable setting.

Material and Methods:

The applicability of the tracer was tested for cell and tissue binding characteristics and dosing using immunohistochemistry, flow cytometry, cell-based plate assays and orthotopic colorectal (HT-29, well differentiated) and pancreatic (BXPC-3, poorly differentiated) xenogeneic human-mouse models. NIRF signals were visualized using the clinically compatible FLARE^{TM} imaging system.

Results:

Calculated clinically relevant doses of ssSM3E/800CW selectively accumulated in colorectal and pancreatic tumors, with highest tumor-to-background ratios of 5.1±0.6 at 72 h post-injection, which proved suitable for intra-operative detection and delineation of tumor boarders and small (residual) tumor-nodules in mice, between 8 h and 96 h post-injection. *Ex vivo* fluorescence imaging and pathologic examination confirmed tumor-specificity and the distribution of the tracer.

Conclusion:

Our results indicate that ssSM3E/800CW shows promise as a diagnostic tool to recognize colorectal and pancreatic cancers for fluorescent-guided surgery applications. If successful translated clinically, this tracer could help improve the completeness of surgery and thus survival.

AUTHORS (LAST NAME, FIRST NAME): Boonstra, Martin[2]; Tolner, Berend[3]; Schaafsma, Boudewijn[2]; Boogerd, Leonora S.[2]; Prevoo, Marieke[2]; Guarav, Bhavsar[3]; Kuppen, P.J.K.[2]; Sier, Cornelis F.[2]; Bonsing, Bert[2]; Frangioni, John V.[1]; van de Velde, Cornelis J.[4]; Chester, Kerry[3]; Vahrmeijer, Alexander L.[2]

INSTITUTIONS (ALL):

1. Curadel, LLC, Worcester, MA, United States.
2. Surgery, Leiden University Medical Center, Leiden, Netherlands.
3. Royal Free & University College Medical School, London, United Kingdom.
4. Leiden University Medical Center, Leiden, Netherlands.

(No Image Selected)

CONTROL ID: 2232342

TITLE: Noninvasive detection of lymph node metastasis in rats using targeted fluorescence molecular imaging with indocyanine green as a paired control agent

PRESENTER: Chengyue Li

ABSTRACT BODY:

Abstract Body: The involvement of axillary lymph node is recognized as a prognostic factor for determining the stage and guiding adjuvant treatment of breast cancer[1]. Currently, invasive surgical dissection and histology of lymph nodes is performed to assess node metastases because no noninvasive methods exist[2]. However, dissection and biopsy is associated with overtreatment concerns and considerable morbidity, including lymphedema, pain, numbness and restricted arm mobility[3] , and at least 70% of cases result in metastases-free nodes[4]. Molecular imaging has great potential to noninvasively assess tumor burden; nonetheless, variable delivery and nonspecific uptake of imaging agents in lymph nodes can significantly confound sensitivity and specificity[5]. A previous study presented a new lymph node imaging method employing a second untargeted, “control” imaging agent to correct for nonspecific uptake of a cancer-targeted imaging agent in lymph nodes, demonstrating a sensitivity to fewer than 200 cells[6].

Previous work with this highly sensitive, “paired-agent” approach employed two imaging agents that are not currently FDA approved, yielding a substantial barrier towards clinical adaptation of this methodology. This study tests the feasibility of using the FDA approved dye, Indocyanine Green (ICG), as the control imaging-agent to allow quantification of cancer targeted antibody-based imaging agent binding (which can be made targetable to many cancer-specific receptors). To compare the lymph node delivery and retention of antibody-based targeted agents we chose to compare kinetics of ICG and a non-targeted antibody protein, rat IgG, which was bound to IRDye-700DX (LICOR), so the kinetics of antibody-based agents could be compared to ICG in the absence of binding. The cocktail of the two agents were co-injected intradermally into a rear footpad of rats. The uptake and retention dynamics of both agents were then imaged in the popliteal lymph node behind the knee of the rat using a two-wavelength fluorescence imaging system (Pearl Imaging, LICOR Biosciences, Lincoln, NE) every 45 s for 35 min. Results are presented in the persuasive data file. In summary, the kinetics of the ICG and the IRDye-700DX-IgG demonstrated a strong correlation with each other in the absence of binding ($r = 0.99$, $p < 0.001$) and the measured binding potential (see persuasive data file) of the antibody agent was found to be -0.03 ± 0.01 after 20 min injection, which compares well to values determined in the previous study, indicating that ICG indeed could fill the role of a control for paired-agent methods that have demonstrated unprecedented levels of cancer sensitivity in mouse studies of lymph node metastasis[6].

1. Kissin, M.W., et al., Lancet, 1982. **1**(8283): p. 1210-2.
2. Chen, S.L., et al., CA Cancer J Clin, 2006. **56**(5): p. 292-309; quiz 316-7.
3. Schrenk, P., et al., Cancer, 2000. **88**(3): p. 608-14.
4. Tabar, L., et al., Radiol Clin North Am, 1992. **30**(1): p. 187-210.
5. Reilly, R.M., et al., Clin Pharmacokinet, 1995. **28**(2): p. 126-42.
6. Tichauer, K.M., et al., Nat Med, 2014. **20**(11): p. 1348-53.

AUTHORS (LAST NAME, FIRST NAME): Li, Chengyue[1]; Xu, Xiaochun[1]; McMahon, Nathan[1]; Tichauer, Kenneth M.[1]

INSTITUTIONS (ALL):

1. Biomedical Engineering, Illinois Institute of Technology, Chicago, IL, United States.

(No Image Selected)

CONTROL ID: 2232349

TITLE: Modular Synthesis of Near Infrared Agents for Targeted Photoacoustic Imaging of Cancer

PRESENTER: Lauren Heese

ABSTRACT BODY:

Abstract Body: Objective: Photoacoustic imaging (PAI) is a sensitive, non-invasive means of detecting cancer and is poised to become a transformative method for early screening, targeted biopsies and monitoring disease progression.[1] A key innovation needed in PAI is the design of 'high-gain" imaging agents which can readily be prepared and conjugated to groups which target biomarkers in diseased cells.[1,2] The current technology relies on using endogenous dyes such as deoxyhemoglobin or oxy-hemoglobin. There is a precedent for the use of a targeted NIR dye, IR800CW, conjugated to a peptide specific for neutropilin yielding a photoacoustic signal in a breast cancer model.[2] The goal is to provide a versatile and broadly applicable synthesis of peptide-based agents combining high-gain exogenous NIR dyes that may be conjugated to a PSMA inhibitor for the early detection of prostate cancer by PAI. Method: A broadly applicable method was developed for the modular construction of "NIR peptides" by coupling together pre-formed amino acids with NIR dyes on their side chains. Linkers were attached for conjugating targeting groups in the final steps of the synthesis. The literature synthesis of a urea based inhibitor, "DCL", reported to bind strongly to the active site of PSMA,[3,4] was revised to provide robust preparation which will be shown. This was followed by conjugation of the PMSA inhibitor to various modular "imaging peptides" shown in Figure 1. The targeted molecular imaging agents (TMIAs) containing NIR dyes will be evaluated *in-vitro* by confocal fluorescent microscopy (CFM), and phantom studies for PAI and *in-vivo* in mouse models for prostate cancer. Results: A practical, modular synthetic method to NIR TMIAs based on a peptide approach was developed. Pre-formed lysines containing Cy 5.5, Cy7 and IR800CW were prepared then coupled together to form mono, di and tri-dye agents which are ready for conjugation. Because of the limitations of the CFM laser at RIT, the Cy5.5, λmax 633 nm, was utilized. For *in-vivo* screening in photoacoustic spectroscopy the higher wavelength dye Cy7, and IR800CW λmax 750, 780 nm, was utilized. In order to ensure that the TMIAs binds to cancer cells that express PSMA, a dual Cy5.5- Cy7 agent will be used to definitively prove that the dual dye agent binds to the *in-vitro* and *in-vivo* cells by the same mechanism in CFM and in PAI. The next aim is to increase the gain (loudness) of ultrasound signal by the use of two Cy7 dyes shown, then three Cy7 dyes. These have been synthesized and will be evaluated and compared by photoacoustic spectroscopy. Conclusion: A novel modular approach to multi-NIR dye imaging agents is described that enables binding of two or three of the same dyes or different dyes on the side chains of "imaging peptides". A revised synthesis of a PSMA inhibitor is described followed by its conjugation to targeting agents. The synthesis, absorbance, fluorescence and photoacoustic spectra are shown in Figure 1.

1. Zackrisson S, Cancer Res, 2014;74(4):979

2. Stantz KM, SPIE Proceedings, 2019 7564,756410

3. Banerjee SR, J. Med. Chem, 2008; 51:4504

4. Chen Y, Biochem Biophys Res Commun, 2009; 390(3):624

AUTHORS (LAST NAME, FIRST NAME): Heese, Lauren[1, 2]; Schmitthenner, Hans F.[1, 4]; Akporji, Nnamdi[1]; regan, michael[1]; Chinni, Bhargava[3]; Rao, Navalgund A.[4]; Dogra, Vikram[3]

INSTITUTIONS (ALL):

1. Chemistry and Materials Science , Rochester Institute of Technology , Rochester , NY, United States.

2. School of Life Sciences, Rochester Institute of Technology, Rochester, NY, United States.

3. School of Medicine and Dentistry , University of Rochester, Rochester, NY, United States.

4. Center for Imaging Science , Rochester Institute of Technology , Rochester, NY, United States.

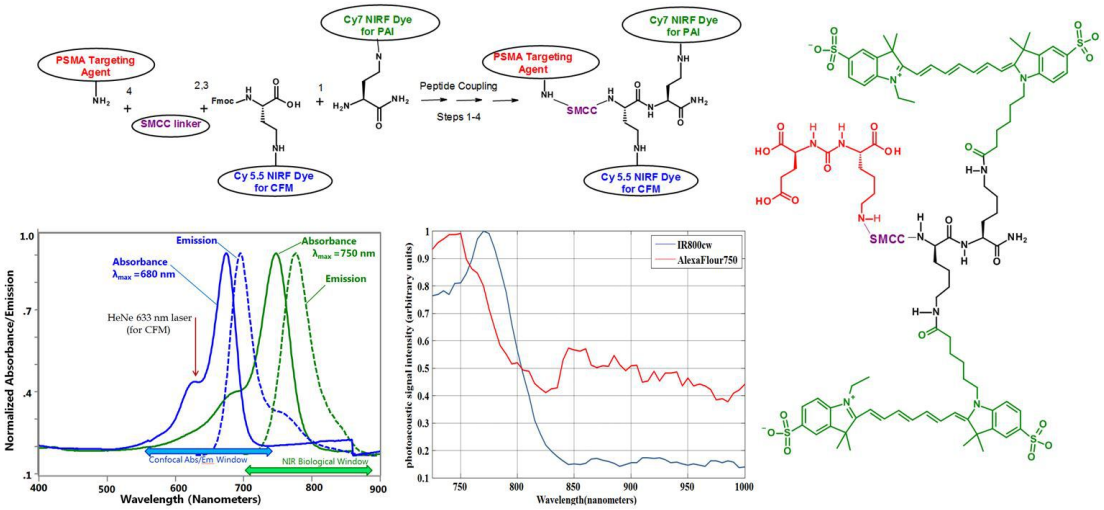

Figure 1a. Modular Synthesis of PMSA targeted Cy-Cy5.5 dual dye imaging agent,
Figure 1b. Structure of di-Cy7 imaging agent DCL-SMCC-dLys(Cy7)-Lys(Cy7)-NH_2,
Figure 1c. Absorbance and Fluorescence spectra for Cy5.5 and Cy7 agents,
Figure 1d. Photoacoustic spectroscopy of Alexafluor 750 (Cy7 analog) and IR800CW.

CONTROL ID: 2232358

TITLE: A novel ^{68}Ga-labeled c(CGRRAGGSC) for microPET imaging of IL-11 receptor expression

PRESENTER: Jin Sun

ABSTRACT BODY:

Abstract Body: Interleukin-11 (IL-11) and the IL-11 receptor (IL-11R) have been reported for the relationship of tumor progression and may play a significant role in bone metastases. Gallium-68(^{68}Ga) is suitable for labeling for small molecule peptides. **0bjective** In this study, we radiolabeled c(CGRRAGGSC) with ^{68}Ga to monitoring the IL-11 receptor expression. The nonapeptide structure c(CGRRAGGSC) is a phage-display-selected IL-11 mimic binding to IL-11R. **Methods** The molecular probe ^{68}Ga-NOTA-c(CGRRAGGSC) was radiolabeled with 68Ga using the 1,4,7-triazacyclononane-1,4,7-triacetic acid (NOTA) chelate. The binding characteristics of the labeled probe was analyzed using radioreceptor analysis. The biodistribution of the probe was studied using ICR normal mice. Positron emission tomography imaging of the probe were investigated using MDA-MB-231 tumors xenografts. A competitive inhibition imaging was performed using unlabeled c(CGRRAGGSC). **Results** NOTA-c(CGRRAGGSC) was purified by High Performance Liquid Chromatography. After 15 minutes reaction at room temperature, The labeling efficiency of ^{68}Ga-NOTA-c(CGRRAGGSC) reached to 91.4%. The radiochemical purity o in normal saline solution was (90.59±0.24) %, (88.95±0.58)% and (86.67±0.51) % respectively, after 1h, 2h and 4h at room temperature. The labeling compounds were excreted mainly through the kidney. The radioactivity distribution in the major organs was low at each time points for observation, especially in the regions of muscle and brain. One-hour dynamic microPET imaging showed heart and bladder had physiologic uptake and liver has quite low uptake. The tumor had high uptake relative to homolateral skeletal muscle. The mean values and the maxium values of uptake were 80.17±2.13 and 93.90±4.56 respectively for tumors, and 51.37±2.37 and 56.11±5.17 respectively for muscle. The tumor-to-non tumor (T/NT) ratio was up to 2.0. The results of the competitive inhibition imaging showed obviously decreased uptake in tumor regions. **Conclusion** ^{68}Ga-NOTA-c(CGRRAGGSC) was successfully analyzed and had good stability. The data showed acceptable biodistribution in vivo and relatively high uptake in tumor. ^{68}Ga-NOTA-c(CGRRAGGSC) may be furtherly used for IL-11 receptor expression studies.

AUTHORS (LAST NAME, FIRST NAME): Sun, Jin[1]; Li, Tiannv[1]; Wang, Tongxing[3]; Liu, Lu[2]

INSTITUTIONS (ALL):

1. Jiangsu Province Hospital, Nanjing, Jiangsu, China.
2. Southeast University, Nanjing, China.
3. Nanjing First Hospital Affiliated to Nanjing Medical University, Nanjing, China.

(No Image Selected)

CONTROL ID: 2233330

TITLE: Acoustic Radiation Force Decorrelation Weighted Pulse Inversion (ADW-PI) Method for Ultrasound Molecular Imaging

PRESENTER: Frank Mauldin

ABSTRACT BODY:

Abstract Body: Objective: Ultrasound molecular imaging with targeted microbubbles is a promising approach for early detection and treatment monitoring of cancer. In this technique, ligand-conjugated microbubbles bind to disease markers on the endothelium, providing contrast between normal and pathological tissue. Strategies such as pulse inversion (PI) and contrast pulse sequence (CPS) are often used to visualize microbubble signal. These methods take advantage of the non-linear acoustic responses from microbubbles. However, insufficient suppression of tissue signal is often exhibited at highly echogenic tissue interfaces that generate significant harmonic signal. Here we present a microbubble imaging approach that combines non-linear imaging with a new method using acoustic radiation force (ARF) to generate and subsequently measure microbubble motion via signal decorrelation. The new technique, termed ARF-decorrelation-weighted PI (ADW-PI), was validated in a mouse tumor model.

Methods: Images were acquired with a programmable scanner (Verasonics) and a linear array transducer (ATL L12-5) using a combination of synthetic aperture virtual source element imaging and PI. For the purpose of ensuring microbubble motion (non-bursting) and obtaining a measurable decorrelation signal, ARF was applied at low mechanical index (MI< 0.1). Images (PI and B-mode; Freq = 11 MHz) were acquired directly before and after each train of ARF pulses (Freq = 4.4 MHz, Duration = 875 μs, , Ten 15-cycle pulses, PRF = 11.4 kHz). For comparison, CPS images of the same tumor were acquired with a clinical scanner (Siemens Sequoia).

C57BL/6 mice with subcutaneous tumors on the hindlimb were used in the study and vascular endothelial growth factor receptor 2 (VEGFR2) was targeted with lipid-shelled microbubbles conjugated to anti-VEGFR2 antibody. Microbubbles were administered intravenously and allowed to circulate and bind for 10 min. Images were acquired for 5 s.

Decorrelation maps were generated by measuring correlation coefficients between image pairs before and after transmission of ARF. A Gaussian mapping function was used to map decorrelation values to an ADW image. The final ADW-PI image was generated by multiplying the ADW image and the corresponding PI image. Regions of interest were selected within the tumor and tissue regions to compare the decorrelation values.

Results: Tumor regions with bound microbubbles exhibited significantly higher signal decorrelation relative to normal tissue. The decorrelation coefficient in bound microbubble regions was 0.024 without ARF and 0.028 with ARF. Corresponding decorrelation values for tissue regions were about six-fold lower ($p < 0.02$, $n = 4$). Combining ADW with the PI image suppressed tissue effectively (Fig. 1) and improved contrast. ADW-PI was demonstrated to suppress PI signal in tissue regions (> 80 dB reduction), thus increasing the microbubble-to-tissue contrast by at least 50 dB compared to the CPS images of the same tumor.

Conclusions: ADW-PI is an effective technique that addresses the limitations of current non-linear microbubble imaging methods by eliminating false positive image signal from harmonic-generating tissue interfaces.

AUTHORS (LAST NAME, FIRST NAME): Herbst, Elizabeth[1]; Unnikrishnan, Sunil[1]; Wang, Shiying[1]; Klibanov, Alexander L.[1, 2]; Hossack, John A.[1]; Mauldin, Frank W.[1]

INSTITUTIONS (ALL):

1. Biomedical Engineering, University of Virginia, Charlottesville, VA, United States.
2. Dept. of Medicine, Cardiovascular Div., University of Virginia, Charlottesville, VA, United States.

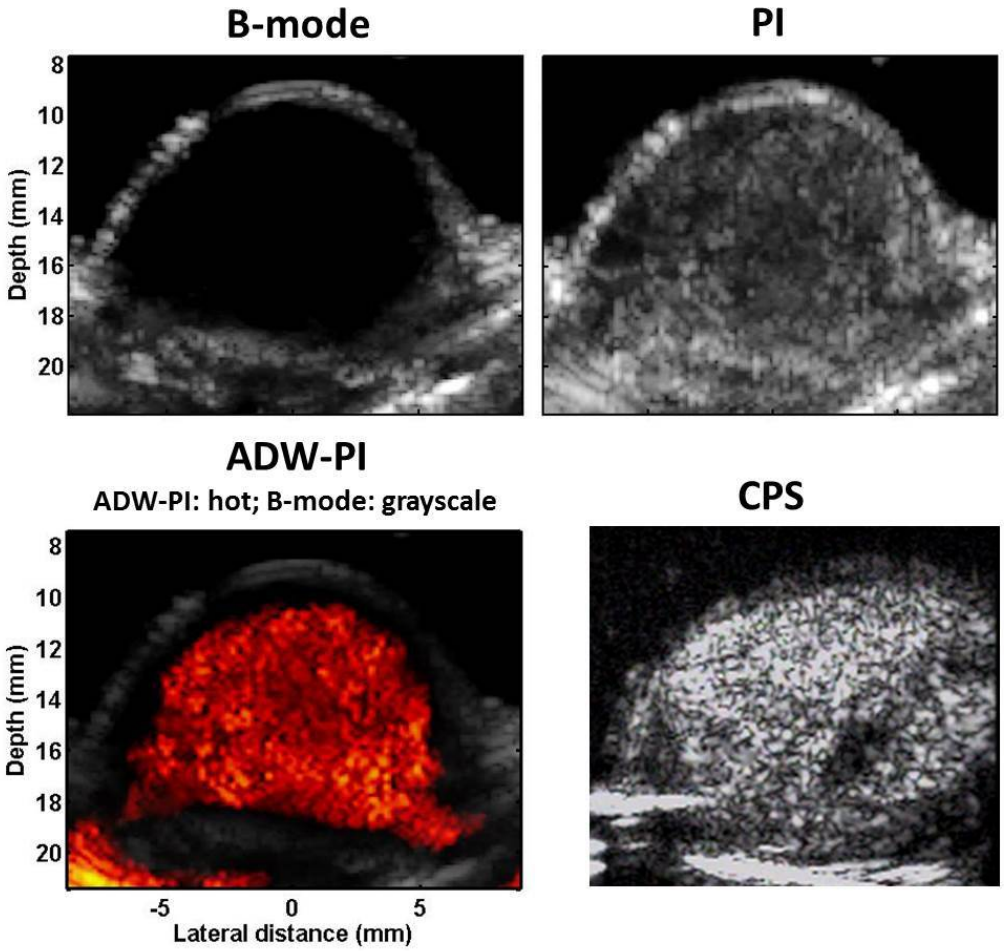

Figure 1: Demonstration of the ability of ADW-PI to suppress tissue signal while preserving microbubble signal. Both the PI and CPS images show significant harmonic signal at the echogenic surface of the mouse femur, below the bubble-perfused tumor. By applying a bilateral filter and multiplying PI intensity with B-mode decorrelation, the low-decorrelation, high-intensity signal from the femur is cancelled out while the high-decorrelation, high-intensity microbubble signal is highlighted. The filtered image is then displayed in a heatmap overlaying the original B-mode image.

CONTROL ID: 2243105

TITLE: Evaluating Targeted Molecular Imaging Agents Using Two- and Three-Dimensional Cell Culture Cancer Models

PRESENTER: Irene Evans

ABSTRACT BODY:

Abstract Body: Objective: Improved treatment of cancer requires knowing where the tumor is located as well as its outlines and metastases. In order to achieve ever-increasing spatial resolution, improved targeted molecular imaging agents are necessary.[1-2] The goal of this research is to develop specific targeted molecular probes for specific target cancers. These multimodal targeted molecular imaging agents (TMIAs) would be advantageous if agents bound well to cancerous cells illuminating them. Thus, the best imaging agents must be selected using sensitive screening techniques. In order to compare the binding and uptake of TMIAs, 2D cell models were compared with 3D cell models. An ever increasing body of literature indicates significant differences in cell morphology, gene expression, proliferation, and migration between 2D and 3D cultured cells, with 3D culture more accurately representing live animal models *in vivo*.[3-4] **Methods:** In order to evaluate TMIA agents, several human cell lines were cultured using traditional two-dimensional methods as well as several three-dimensional matrices including Matrigel, Geltrex, Collagen type I, and Agarose. Fluorescent confocal microscopy was used with multiple fluorescent dyes. In addition, a Cy5.5-RGDyk conjugate, which specifically targets αvβ3 integrins, shown to be overexpressed on the surface of some cancer cell strains, was employed as a TMIA. **Results:** The differences in morphology between a 2D and 3D cell model of lung cancer are dramatic with the 2D cell culture forming a flattened monolayer structure versus the spheroid-like structure formed in the 3D structure. The images show the presence and cellular location of the TMIA which is present on the surface of the cells as well as endocytosed into the tumor cells. Three dimensional tumor models utilizing Matrigel formed spheroid-like structures and more closely resembled a tumor mass than did 2D cultured cells. We also observed that the TMIA agents penetrated 3D cancer models and stained cells buried inside the spheroid tumor model indicating the agents tested had good penetrability characteristics. **Conclusion:** The use of 3D cellular models which mimic more closely *in vivo* tumors should facilitate development of TMIAs and result in molecules which target to metastatic tumors illuminating their presence, size, and structure thus allowing better clinical treatment and hopefully enhanced cancer survival.

This work was supported in part by NIH grant 1R15CA192148-01

Weissleder R. Science, 312: 170-174 (2006)

Weissleder R, Pittet MJ. Nature, 452: 580–589 (2008)

Ghosh S, Spagnoli GC, Martin I, Ploegert S, Demougin P et al. J Cell Physiol, 204: 522-531 (2007)

Pampaloni F, Reynaud EG, Stelzer EH. Nat Rev Mol Cell Biol, 8: 839-45 (2007).

AUTHORS (LAST NAME, FIRST NAME): Evans, Irene M.[3]; Ophardt, Henry[1]; Heese, Lauren[3, 2]; Schmitthenner, Hans F.[2, 4]

INSTITUTIONS (ALL):

1. Gosnell School of Life Sciences, Rochester Institute of Technology, Rochester, NY, United States.
2. Chemistry and Materials Science , Rochester Institute of Technology , Rochester , NY, United States.
3. Gosnell School of Life Sciences, Rochester Institute of Technology, Rochestern, NY, United States.
4. Center for Imaging Science, Rochester Institute of Technology, Rochester, NY, United States.

(No Image Selected)

CONTROL ID: 2232385

TITLE: Quantitative modeling of effect of radiation therapy on [^{18}F]Dasatinib tumor uptake in a glioma xenograft model

PRESENTER: Edward Fung

ABSTRACT BODY:

Abstract Body: Introduction:

Dasatinib is a Src family tyrosine kinase inhibitor for patients with CM leukemia and potentially for those with prostate cancer. Radiation-induced activation of Src may mediate internalization and nuclear transport of EGFR [1], suggesting a role for dasatinib as a radiosensitizer. We performed quantitative compartment analysis to investigate the effect of irradiation on dasatinib pharmacokinetics using the positron emission tomography (PET) imaging agent [^{18}F]Dasatinib [2].

Materials & Methods:

We inoculated nude mice with U251-TGL human glioma cell xenografts in both shoulders creating a bilateral preclinical model with an intrinsic control (i.e. the unirradiated tumor). Mice were imaged at 3 time points: 24 h pre-treatment for baseline, then 24 and 48 h post-radiation (p.rad). We injected the mice with 150 μCi of [^{18}F]Dasatinib immediately at the start of each PET scan on an Inveon microPET scanner. Emission data were acquired for 40 minutes post-injection (p.i.) for each scan and reconstructed into dynamic 3D data sets. Radiation (12, 18, or 24 Gy in one fraction) was delivered using an X-rad 225Cx irradiator to one of the two xenografts.

3D volumes of interest (VOIs) were drawn for treated and control tumors in each mouse on full-scan duration images. Heart VOIs drawn on early summed images (0-1 min p.i) were used to generate whole-blood input functions. Time activity curves (TACs) were extracted from the highest activity 2 x 2 cube clusters in each VOI. We fit the TACs to a one-tissue (1T) compartment model and estimated kinetic parameters. Pairwise comparison was performed on each tumor with its intrinsic control.

Results:

K_1 values, indicative of tissue uptake, were found to be higher for irradiated tumors (0.047 ± 0.006 mL/g/min, std. err.) than for controls (0.036 ± 0.01 mL/g/min) at 48 h p.rad. (n = 10). At baseline, K_1 values were similar for treatment and control tumors (0.031 ± 0.009 and 0.032 ± 0.011). Tissue clearance, indicated by k_2, was not appreciably different between treatment (0.028 ± 0.006 min^{-1}) and control (0.026 ± 0.01 min^{-1}) at 48 h p.rad. The difference between estimated parameters for the irradiated tumors and matched controls was greatest for the 24 Gy dose group. At baseline, estimated K_1 values for controls subtracted from treatment side tumors was -0.002 ± 0.004 mL/g/min. At 48 h p.rad., the difference was 0.018 ± 0.007 mL/g/min.

Conclusion:

[^{18}F]Dasatinib uptake was increased in xenografts that were irradiated when compared to control xenografts on the same mouse. This may indicate that dasatinib is binding Src family kinases activated by radiotherapy. We have shown that [^{18}F]Dasatinib PET can be used to analyze the pharmacokinetics of this anti-cancer drug both in control and radiotherapy-treated tumors. Further study using parametric images could elucidate binding changes as opposed to altered enhanced perfusion and retention due to radiation exposure. Pre-irradiation may also be a practical approach to increasing tumor concentrations and thus therapeutic effectiveness of dasatinib.

[1] Kahn EM, et al. (2006) J Biol Chem, 281: 14486-14493

[2] Veach DR, et al. (2007) J Med Chem, 50: 5853-5857

AUTHORS (LAST NAME, FIRST NAME): Fung, Edward K.[1, 2]; Longo, Valerie A.[4]; Veach, Darren R.[5]; Chen, Qing[2]; Akkari, Leila[3]; Joyce, Johanna A.[3]; Zanzonico, Pat[2]

INSTITUTIONS (ALL):

1. Molecular Pharmacology and Chemistry Program, Memorial Sloan Kettering Cancer Center, New York, NY, United States.
2. Medical Physics, Memorial Sloan Kettering Cancer Center, New York, NY, United States.
3. Cancer Biology and Genetics Program, Memorial Sloan Kettering Cancer Center, New York, NY, United States.
4. Animal Imaging Core Facility, Memorial Sloan Kettering Cancer Center, New York, NY, United States.
5. Radiochemistry and Imaging Sciences Service, Radiology, Memorial Sloan Kettering Cancer Center, New York, NY, United States.

(No Image Selected)

CONTROL ID: 2232386

TITLE: A miniature handheld line-scanned dual-axis confocal (LS-DAC) microscope for early detection and surgical guidance

PRESENTER: Jonathan Liu

ABSTRACT BODY:

Abstract Body: The microscopic observation of histologically processed tissue specimens is regarded by the medical community as a highly reliable standard-of-care method for the diagnosis of disease. Through advances in optical design and miniaturization, it is possible to move this type of analysis into the clinic and to provide *in vivo* analyses of tissue micro-anatomy and molecular markers of disease. We are developing a portable line-scanned dual-axis confocal (LS-DAC) microscope for high-speed (10 - 15 Hz) microscopic imaging of superficial (<150-μm deep) tissue surfaces for examining suspicious lesions in the oral cavity as well as for guiding the resection of brain tumors. The line-scanned DAC architecture enables fast frame rates that will mitigate motion artifacts during clinical use.

Unlike first-generation miniature MEMS-scanned DAC microscopes [1-3], the handheld LS-DAC microscope incorporates conventional achromatic lenses (rather than a parabolic reflector) and a pair of 45-deg reflective prisms for the alignment of low-NA illumination and collection beams (Figs. 1a and 1b). A cylindrical lens placed in the illumination path (Fig. 1a) creates a focused line in tissue, which is imaged onto a linear detector array. A commercial MEMS scanner (see Persuasive data file) from Mirrorcle Technologies (Richmond, CA) scans the focal line orthogonally to construct an image in a line-by-line fashion. A custom 3X magnifying relay objective (Fig. 1c and Persuasive data file), developed in collaboration with Photon Gear Inc., increases the numerical aperture (NA) and crossing angle of the dual-axis beams for high-resolution imaging of tissues (1-3 μm resolution) in reflectance or fluorescence mode for oral cancer detection and for guiding brain tumor resection, respectively. Ray-trace simulations (see Persuasive data file) demonstrate the potential of a miniature LS-DAC design to image with near-diffraction-limited performance over a field of view of 400 μm. Initial axial-response measurements have been made to validate the performance of the device (FWHM axial resolution < 3 μm), with the goal of obtaining images similar to what has been previously acquired with a tabletop LS-DAC device (see Persuasive data).

In summary, a miniature line-scanned DAC microscope is being developed for two applications in point-of-care *in vivo* pathology. First, we will use this device to image suspicious lesions in the human oral cavity as an initial screening tool to guide physical biopsies and subsequent histopathology (NIDCR-funded project). Second, for brain-tumor resection (NCI-funded project), we plan to use our device to quantify the expression of 5-ALA-induced PpIX in low-grade gliomas, and to provide neurosurgeons with an objective and reproducible metric by which to optimize the extent of resection and improve patient outcomes.

1. Liu, J.T.C., *et al. Analytical cellular pathology*, Vol. 34 81-98 (2011).
2. Liu, J.T.C., *et al. J Biomed Opt*, Vol. 15 026029 (2010).
3. Leigh, S.Y. & Liu, J.T.C., *Opt Lett*, Vol. 37 2430-2432 (2012).

AUTHORS (LAST NAME, FIRST NAME): Mandella, Michael J.[1, 2]; Pillai, Prasanth C.[3]; Yin, Chengbo[3]; Leigh, Steven Y.[3, 4]; Abeytunge, Sanjeewa[5]; Peterson, Gary[5]; Rajadhyaksha, Milind[5]; Liu, Jonathan T.[3]

INSTITUTIONS (ALL):
1. Molecular Imaging Program at Stanford (MIPS), Stanford, CA, United States.
2. Pediatrics, Stanford University School of Medicine, Stanford, CA, United States.
3. Mechanical Engineering, University of Washington, Seattle, WA, United States.
4. Biomedical Engineering, State University of New York (SUNY) at Stony Brook, Seattle, WA, United States.
5. Dermatology Service, Memorial Sloan-Kettering Cancer Center, New York, NY, United States.

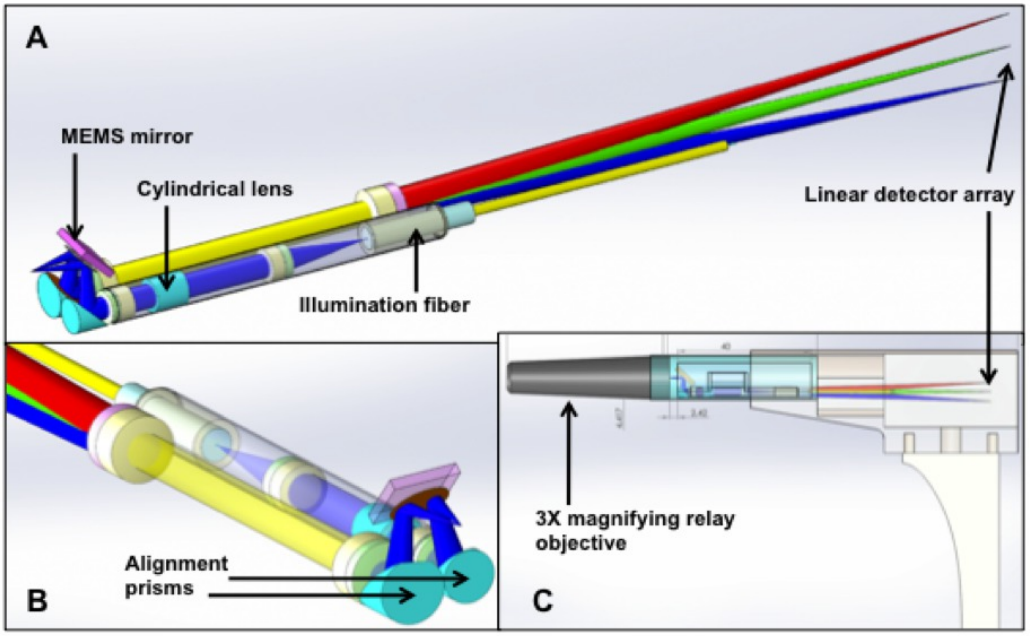

Figure 1 | CAD drawings of a miniature line-scanned dual-axis confocal (LS-DAC) microscope device. (A) Scan head design: the optical path contains a cylindrical lens to create a focal line for illumination, and a linear detector array at the proximal end for collection of fluorescence. **(B)** The alignment prisms are rotated and translated in the axial direction for independent alignment of the illumination and collection beams. **(C)** A custom 3X magnifying relay objective allows for high-resolution sub-cellular imaging (~1 μm lateral resolution). The diameter of the distal tip of the relay in contact with the tissue of interest is 10 mm.

CONTROL ID: 2232387

TITLE: A screening assay in the search of an alpha-synuclein PET radioligand

PRESENTER: Mathieu Verdurand

ABSTRACT BODY:

Abstract Body: Introduction

The accumulation of aggregated α-synuclein (α-syn) in multiple brain regions is a neuropathological hallmark of synucleinopathies like Parkinson's disease, dementia with Lewy bodies and multiple system atrophy. A pre-mortem diagnosis tool would improve early diagnosis, monitor disease progression and therapeutic efficacy. While suitable amyloid-β (Aβ) PET radioligand have been developed like [11C]PIB and [18F]AV45, no selective α-syn PET ligand has been identified to date. One PET tracer, BF227, labelled with carbon-11 or fluor-18, has demonstrated interesting binding properties towards α-syn fibrils in vitro (Fodero-Tavoletti et al., Eur J Pharmacol, 2009) and α-syn glial inclusions in MSA patients (Kikuchi et al., Brain, 2010). The aim of this work was to develop a simple screening assay to find a selective α-syn ligand using competitive autoradiography with [18F]BF227 and candidate molecules.

Methods

α-syn and Aβ fibrils were obtained by incubating commercial human recombinant proteins at 200µM, 37°C, 250rpm. Rats were stereotaxically injected with 5µL (200µM) of α-syn or Aβ fibrils. Animals were euthanasized shortly after injection, their brains frozen and cryostat cut into 20-µm sections encompassing the injected striata.
[18F]BF227 (Specific Activity always >1Ci/µmol) was used for competitive in vitro autoradiography using fixed nanomolar concentration of radiotracer and 1-10µM BF227, PIB or Thioflavine T. After [18F]BF227 incubation with or without cold competitors, sections were washed in ethanol/water solutions before exposition on phosphorimaging plates.

Results

Competitive [18F]BF227 autoradiography on rat brain sections injected with either α-syn or Aβ fibrils showed a dose dependent competition of cold BF227 towards [18F]BF227. Thioflavine T was ineffective at competing with [18F]BF227 binding sites on either types of fibrils, while PIB at 1µM efficiently competed with [18F]BF227 binding sites. Figure 1 shows representative results obtained with α-syn fibrils. Quantification is in progress.

Conclusion

We have set up an in vitro autoradiography screening assay that will enable testing the capacity of several original candidate molecules to compete with [18F]BF227 binding sites on Aβ and α-syn fibrils. The next steps of this project will include (i) in vitro filter binding assay on isolated fibrils to measure affinity, (ii) ex vivo autoradiography and in vivo small animal PET imaging on injected rats and transgenic mice overexpressing α-syn.

AUTHORS (LAST NAME, FIRST NAME): Verdurand, Mathieu[1]; Mendjel, Meriem[1]; Levigoureux, Elise[1]; Lancelot, Sophie[1]; Billard, Thierry[2]; ZIMMER, Luc[1]; Chauveau, Fabien[1]

INSTITUTIONS (ALL):

1. University of Lyon, Lyon Neuroscience Research Center (CNRS UMR5292; INSERM U1028, Univ. Lyon 1), Lyon, France.
2. University of Lyon, Institute of Chemistry and Biochemistry (ICBMS); CNRS UMR5246; INSA-Lyon, Lyon, France.

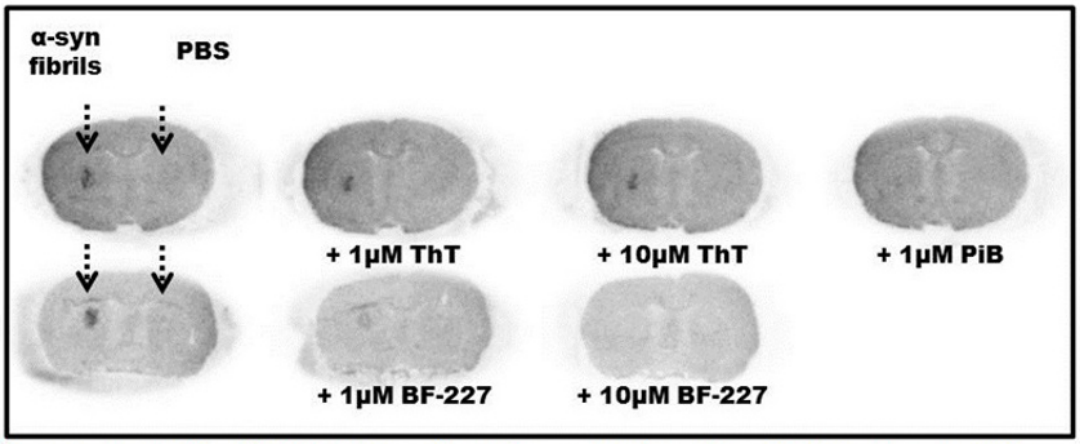

Figure 1. Competitive [^{18}F]BF227 autoradiography on rat brain sections injected with α-syn fibrils.

CONTROL ID: 2233062

TITLE: Molecular Imaging of Non-Small Cell Lung Cancer (NSCLC) using ^{82}Rubidium and ^{18}FDG PET/CT

PRESENTER: thida Win

ABSTRACT BODY:

Abstract Body: Background: ^{82}Rubidium-82 (^{82}Rb), a short half-life radio nucleotide is routinely used in the assessment of myocardium perfusion with quantification using flow modelling to predict cardiovascular events. ^{82}Rb has shown uptake in mainly animal neoplasms, but may have potential to provide a method to assess perfusion in human tumors.

In this study we hypothesize that we can

1 Demonstrate ^{82}Rb uptake in patients' with non-small cell lung cancer (NSCLC);

2 Identify a comparison between ^{82}Rb uptake and ^{18}FDG PET uptake in NSCLC.

3 Show a relationship between ^{82}Rb flow quantification and tumor vascularity using dynamic contrast enhanced CT (DCE-CT) in tumors of patients with NSCLC

Methods

Eight patients who underwent clinical (static) ^{18}FDG PET CT for lung cancer staging were prospectively imaged with low-dose CT for attenuation correction followed by a dynamic PET study to map the kinetics of a ^{82}Rb infusion. Patients then underwent dynamic contrast enhanced CT (DCE-CT). Visual agreement between ^{82}Rb and ^{18}FDG uptake was assessed. One compartmental model K1 and blood flow quantification (adiabetic parameter analysis) were used to assess respectively ^{82}Rb and CT perfusion.

Results

All 8 patients showed tumor uptake with both ^{18}FDG and ^{82}Rb tracers.

Tumor tracer uptake was more intense with ^{18}FDG than with ^{82}Rb.

With ^{82}Rb PET, the average derived k1 in the lung tumors was 0.53 ml/g/min (Range: 0.11 – 2.07). Tumor blood flow as derived from DCE-CT was 0.76 ml/g/min (Range 0.13 – 1.99).

There was no significant correlation between k1 and blood flow measured on DCE-CT.

Conclusion

We demonstrate successful *in vivo* multimodal PET/CT with ^{18}FDG and ^{82}Rb derived tumor flow quantification coupled with DCE-CT of tumors in patients with NSCLC.

Combining ^{82}Rb and ^{18}FDG PET CT may provide further information on the relationship between tumor glucose metabolism and perfusion/vascularity.

The lack of correlation between k1 using ^{82}Rb and blood flow using DCE CT may suggest that ^{82}Rb uptake is not simply be related to blood flow and could reflect other parameters such as tumor cell Na/K ATPase activity.

AUTHORS (LAST NAME, FIRST NAME): neriman, deena[2]; Fraioli, Francesco [2]; Win, thida[3]; Hoath, John[2]; Dickson, John C.[2]; Endozo, Raymondo[2]; Janes, Sam[1]; Groves, Ashley[1]

INSTITUTIONS (ALL):

1. UCL, London, United Kingdom.
2. Institute of Nuclear Medicine, University College London, London, London, United Kingdom.
3. Respiratory, East and North Herts NHS Trust, Stevenage, United Kingdom.

(No Image Selected)

CONTROL ID: 2233162

TITLE: FDG PET: A prognostic biomarker in Non IPF interstitial lung disease patients

PRESENTER: thida Win

ABSTRACT BODY:

Abstract Body: *Rationale:* There is a lack of prognostic biomarkers for patients with interstitial lung disease (diffuse parenchymal lung disease) excluding patients with Idiopathic pulmonary fibrosis (IPF).
We hypthothesize ^{18}F-FDG PET/ CT can be used to predict survival in patients with Non IPF ILD.
Methods: A total of 71 (39 male, 32 female; mean age 65.3±11.3 years) prospectively and consecutively consented patients with interstitial lung disease (excluding IPF patients) were recruited for ^{18}F-FDG PET/CT. Quantification of baseline pulmonary function test (PFT), quality of life (QOL) scores and blood markers were also performed.

Main Measurements and Results: The maximum pulmonary uptake of ^{18}F-FDG (SUVmax), the background lung activity (SUVmin,) and target-to-background ratio (TBR = SUVmax/ SUVmin) were quantified. Baseline PFT included FVC, KCO, TLC, TLCO and FEV1. Baseline QOL scores included activity, impact, symptoms and total scores. Baseline blood markers included haemoglobin (Hb) and haematocrit (HCT). Kaplan-Meier survival analysis assessed the performance of these biomarkers as survival risk classifiers. Multivariate Cox regression was used to determine if the most significant PET parameter was independent of the most significant PFT, QOL, blood markers in predicting patient survival (also their interactions were included in the Cox model).

Mean duration of follow-up was 34.7±24.9-months. There were 18 deaths. SUVmax (p=0.0057), SUVmin (*p*=0.0008), FVC (*p*=0.031), KCO (*p*=0.016), TLC (*p*=0.0087) FEV1 (*p*=0.039), Symptom-score (*p*=0.0013) and Hb (*p*=0.0009) were associated with mortality. Cox Regression showed that the interaction between SUVmin and TLC (HR: 24.5, 95% CI: 3.2-189.8, p=0.002) as well as an interaction between Hb and Symptom score (HR: 8.5, 95% CI: 1.3-53.8, p=0.024) were the two independent survival factor in these patients.

Conclusion: Pulmonary uptake of ^{18}F-FDG quantified using PET is associated with mortality in patients with non-IPF interstitial lung disease.

AUTHORS (LAST NAME, FIRST NAME): Win, thida[1]; Screaton, Nicholas[5]; Porter, Joanna C.[2]; Maher, Toby[4]; Ganeshan, Balaji[3]; Millner, Lynn[2]; Groves, Ashley[2]

INSTITUTIONS (ALL):

1. Respiratory, East and North Herts NHS Trust, Stevenage, United Kingdom.
2. UCL, London, United Kingdom.
3. UCL, London, London, United Kingdom.
4. Brompton, London, United Kingdom.
5. papworth, Cambridge, United Kingdom.

(No Image Selected)

CONTROL ID: 2232415

TITLE: Ring-closing synthesis of dibenzothiophene sulfonium salts and their use as precursors for aromatic [18F]fluorination – Application to direct labeling of the mGluR5 PET tracer [18F]FPEB

PRESENTER: Thibault Gendron

ABSTRACT BODY:

Abstract Body: Objectives: Aromatic [18F]fluorination of small molecule PET tracers is attractive as it can result in improved pharmacological profile. However, direct introduction of fluorine into aromatic groups remains challenging for complex drug-like molecules. We recently discovered that dibenzothiophene sulfonium salts are highly reactive precursors for direct aromatic [18F]fluorination. To explore this new class of precursors, we aimed to develop a practical synthetic method for the formation of dibenzothiophene sulfonium salts and investigate their reactivity as leaving groups for reaction with [18F]fluoride.

Methods: Structurally diverse dibenzothiophene sulfonium salts were synthesized through an unprecedented intramolecular cyclization of their respective thioethers. The ring-closure was optimized by screening different activating agents, Lewis acids (LA) and solvents. The effect of the dibenzothiophene substitution on the labeling efficiency was also investigated. As a first proof of concept, the structurally optimized dibenzothiophene sulfonium salt was used as leaving group for aromatic [18F]fluorination of the mGluR5 tracer [18F]FPEB (Figure 1).

Results: The introduction of dibenzothiophene sulfonium groups in precursors of interest was achieved by ring-closure of the corresponding diaryl thioethers. Our initial results highlighted two critical steps in that reaction: *i*) electrophilic sulfur activation *via* an umpolung and *ii*) ring-closure mediated by a Lewis acid. Further optimizations resulted in the selection of *N*-chlorosuccinimide (NCS) as activating agent and bismuth or lanthanide triflates as Lewis acids. Using these conditions, the desired salts were obtained in 65-85% yield after flash chromatography and proved highly stable. [18F]Fluorination of these novel precursors proceeded smoothly (15 min, 50-110 ºC) in 20-80% analytical radiochemical yield (RCY). Using this method, the mGluR5 tracer [18F]FPEB was obtained in 60 ± 2% decay corrected isolated RCY under mild conditions (50 °C, 15 min, 2 mg precursor). In contrast, the established method for labeling of [18F]FPEB results in RCYs as low as 2-5%.[1]

Conclusions: A novel synthetic route to dibenzothiophene sulfonium salts *via* a ring-closing reaction has been developed and optimized. This new strategy allows straightforward preparation of reactive precursors for direct aromatic [18F]fluorination. Applicability for PET has been demonstrated by highly efficient labeling of the mGluR5 tracer [18F]FPEB.

References: [1] Sullivan, J. M.; Lim, K.; Labaree, D.; Lin, S.; McCarthy, T. J.; Seibyl, J. P.; Tamagnan, G.; Huang, Y.; Carson, R. E.; Ding, Y.-S.; Morris, E. D. *Journal of Cerebral Blood Flow & Metabolism* **2013**, *33*, 532-541

AUTHORS (LAST NAME, FIRST NAME): Gendron, Thibault[1]; SANDER, Kerstin[1]; Cybulska, Klaudia[2]; Gray, Vincent[1]; Arstad, Erik[1, 2]

INSTITUTIONS (ALL):

1. Institute of Nuclear Medicine, University College London, London, United Kingdom.
2. Department of Chemistry, University College London, London, United Kingdom.

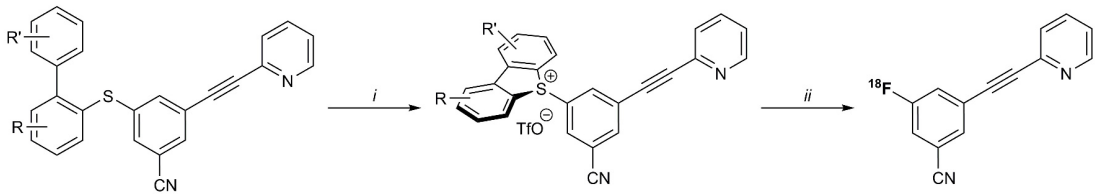

Novel cyclization reaction

[^{18}F]FPEB
RCY 73 ± 4% (60 ± 2%)

Figure 1: Synthesis of the dibenzothiophene sulfonium precursors by intramolecular cyclization and labeling of mGluR5 tracer [^{18}F]FPEB. *Reagents and conditions: i*) NCS (1 equiv.), LA (1 equiv.), MeCN, 80 °C, 30 min, 65 % yield. *ii*) 18-fluoride, $K_{2.2.2.}$, $KHCO_3$, DMSO, 50 °C, 15 min. Results given as decay corrected analytical (isolated) radiochemical yield (RCY) ± Standard deviation (n = 4)

CONTROL ID: 2232414

TITLE: Magnetic Resonance Imaging of the Intracellular/Extracellular pH Gradient in Glioma

PRESENTER: Heeseung Lim

ABSTRACT BODY:

Abstract Body: Objective: The goal of this study is to map the intracellular/extracellular pH gradient in a rodent glioma model. Chemical exchange saturation transfer (CEST) magnetic resonance imaging (MRI) was used for intracellular pH (pH_i) measurement and hyperpolarized ^{13}C-bicarbonate magnetic resonance spectroscopic imaging (MRSI) used for extracellular pH (pH_e) measurement.

Methods: A Wistar rat was surgically implanted with one million C6 glioma cells in the right caudate nucleus of the brain. The pH_i and pH_e were mapped in the tumour and contralateral brain tissue 14 days after implantation. pH_i was measured using CEST MRI on a 9.4T small animal MRI scanner (Agilent, Santa Clara, CA). CEST spectra were acquired using a standard fast spin echo (FSE) pulse sequence (TR/TE = 7000/7 ms, ETL = 32, ETE = 7 ms, matrix = 64 x 64, FOV = 40 mm x 40 mm, 2 prescans, slice thickness = 2.0 mm, pre-image saturation pulse = 1.5 μT and 4-s duration). On the same day, extracellular pH was measured using hyperpolarized ^{13}C bicarbonate MRSI on a Discovery MR750 3.0T scanner (GE Healthcare, Waukesha, WI). The animal received a single bolus injection of 150-mM hyperpolarized ^{13}C sodium bicarbonate solution through the tail vein and ^{13}C spectra of the rat brain were acquired using an optimized 2D FID-CSI sequence (TR = 80 ms, matrix = 8 x 8, FOV = 60 mm x 60 mm, slice thickness = 12.0 mm and BW = 5000Hz).

Results: pH_i and pH_e maps of the rat brain are shown in Figures 1b) and 1c) respectively. At 14 days post-surgery, pH_i and pH_e were measured in the tumour to be 7.27 ± 0.08 and 6.63 ± 0.10 respectively. pH_i and pH_e in the contralateral brain tissue were 7.14 ± 0.06 and 6.83 ± 0.10 respectively. The pH gradient ($\Delta pH = (pH_i - pH_e)$) was 0.64 ± 0.12 in tumor and 0.31 ± 0.11 in contralateral brain tissue.

Discussion: The acid-base balance in the brain is tightly controlled by endogenous buffers such as bicarbonate and phosphate. An alkaline tumour pH_i increases the activity of several metabolic enzymes that drive cellular proliferation [1]. In contrast, an acidic tumour pH_e is established due to increased lactic acid production and the subsequent active transport of protons out of the cell. In this study, the results showed a consistent agreement of increased ΔpH in tumour compared with the contralateral tissue. Furthermore, the heterogeneity of tumour pH can be observed in the regional pH_i and pH_e maps. These regional measurements may be useful to assess therapeutic response and predict local areas of treatment resistance.

Conclusion: In this preliminary study, the intracellular/extracellular pH gradients in a rodent glioma model were non-invasively measured to a precision of ~0.1 pH units. A large difference in ΔpH was observed between tumour and contralateral brain. Since most therapeutic agents are weak acids or bases, *a priori* knowledge of the pH gradient may help guide choice of therapeutic agents. In future experiments, the pH gradient of tumours at multiple time points will be measured during tumour growth.

Reference:

[1] McLean LA, et al. Malignant gliomas display altered pH regulation by NHE1 compared with non-transformed astrocytes. Am J Physiol-Cell Ph 2000

AUTHORS (LAST NAME, FIRST NAME): Lim, Heeseung[1]; Albatany, Mohammed[1]; Martinez-Santiesteban, Francisco M.[1]; Bartha, Robert[1, 2]; Scholl, Timothy J.[1, 2]

INSTITUTIONS (ALL):

1. Medical Biophysics, Western University, London, ON, Canada.
2. Robarts Research Institute, Western University, London, ON, Canada.

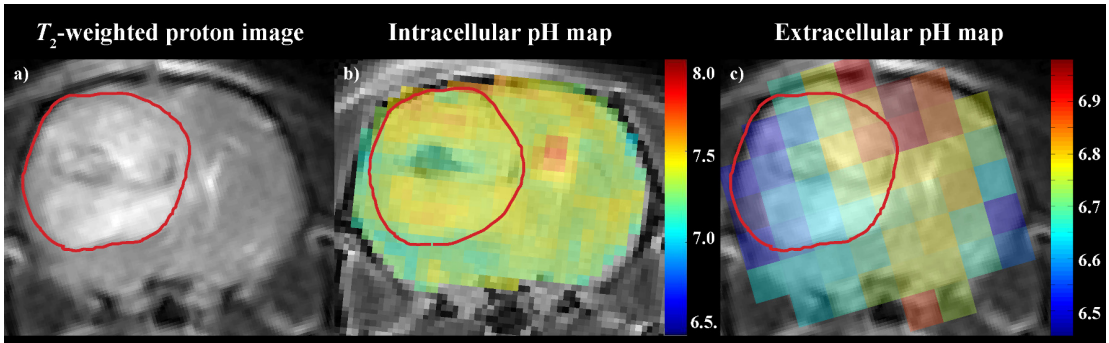

Figure1. pH maps of rat brain with tumour. a) *T*2-weighted image showing the anatomy of rat brain. Tumour is outlined in red b) CEST pH_i map overlaid on the top of proton anatomy image. c) Hyperpolarized ^{13}C pH_e map overlaid on the proton anatomy image.

CONTROL ID: 2232426

TITLE: Combined PET–ME-MR imaging to quantify β-cell mass and function in a Rip1-Tag2 mouse model

PRESENTER: Filippo Michelotti

ABSTRACT BODY:

Abstract Body: Introduction

In order to monitor diabetes progression, innovative imaging technologies are developed to quantitatively monitor beta cell mass and function in vivo. We combined [64Cu]-NODAGA-Exendin-4 based PET and Manganese (Mn2+) enhanced (ME-) MRI in a dedicated animal PET/MRI setup which allowed simultaneous data acquisition using transgenic Rip1-Tag2 mice and healthy control animals.

Thus, beta cell mass (BCM) can be revealed by GLP1-receptor expression on the cell surface and [64Cu]-NODAGA-Exendin-4-PET, while function of beta cells is directly linked to Mn2+ transport through Ca2+- channels.

Material and Methods

All MR images were acquired using a 7T dedicated small animal MRI scanner, while all PET data were acquired using a MRI-compatible PET insert. This imaging set-up enabled the acquisition of temporally and spatially correlated data. For the measurements, animals were anesthetized using 1.5% isoflurane and placed on temperature controlled animal beds.

Static PET images were acquired 1h, 24h and 48h after i.v. injection of 3,7±0,5 MBq of [64Cu]-NODAGA-Exendin-4 in Rip1-Tag2 mice at a late stage of insulinoma progression (13 weeks). Reference T2-weighted whole body anatomical images were acquired and co-registered with PET images to define the regions of interest.

ME-MR images were acquired before and after i.p. injection of ~15mg/kg of MnCl2, two minutes after glucose stimulation. Rapid 3D-T1maps were obtained using an optimized two angles method through the acquisition of two FLASH images (TR/TE=10ms/1.5ms; α1/α2=4°, 23°).

Ex vivo autoradiography and biodistribution at 48h after tracer injection were subsequently performed to validate the in vivo results.

Results

While overall [64Cu]NODAGA-Exendin-4 uptake signal was lower at 24h, and 48h, compared to 1h post injection (p.i.), the pancreas-to-liver ratio from transgenic RIP1-Tag2 mice showed a 50% increase from 1±0,5 at 1h p.i. to 1,6±0,2 at 48h p.i. compared with the kidney-to-liver ratio, which remained stable (1,9±0,6 at 1h to 2,1±0,3 at 48h), indicating a specific tracer accumulation for the targeted tissue. Notably, transgenic mice had a twofold increase in tracer uptake at 48h p.i. compared with control mice (co: 0,9±0,1). T1maps showed a decrease of the relaxation time of the pancreas in both groups from ~1500ms to ~500ms already after 1h. While no more Mn2+ was visible in the kidney at 48h, the pancreas still displayed shorter T1 values over time.

Ex vivo biodistribution confirmed an increased tracer uptake of approximately four times in pancreata of transgenic RIP1-Tag2 mice compared to the healthy pancreas of control animals.

Conclusion

Our studies confirm that [64Cu]-NODAGA-Exendin-4 is a promising biomarker to assess non-invasively BCM in pancreata of RIP1-Tag2. A decrease in the T1 relaxation time was still visible 48h after Mn2+ injection, suggesting a stable uptake of Mn2+ over the time. A later scan time point may be required to determine appreciable differences in tissue functionality. Thus, combined PET–ME-MRI can likely be used as a reliable tool to assess simultaneously mass and functionality.

AUTHORS (LAST NAME, FIRST NAME): Michelotti, Filippo C.[2]; Bowden, Gregory[2]; Schmid, Andreas M.[1]; Pichler, Bernd J.[3]

INSTITUTIONS (ALL):

1. Department of Preclinical Imaging and Radiopharmacy, University Hospital Tübingen, Tübingen, Germany.
2. Department of Preclinical Imaging and Radiopharmacy, Werner Siemens Imaging Center, University of Tuebingen, Tuebingen, Saint Barthélemy.
3. Department of Preclinical Imaging and Radiopharmacy, Werner Siemens Imaging Center, University of Tuebingen, Tübingen, Germany.

(No Image Selected)

CONTROL ID: 2232432

TITLE: Gold-198 Nanocluster for Cerenkov Luminescence Transfer Imaging and Tumor Therapy

PRESENTER: Xiaowei Ma

ABSTRACT BODY:

Abstract Body: Objectives: In this study, we designed Gold-198 (^{198}Au, βmax = 0.96 MeV, half-life = 2.7d) doped gold nanoclusters (AuNC) for in vivo fluorescence imaging (FLI), Cerenkov luminescence transfer imaging (CLTI) and tumor radiation therapy.

Methods: The non-radioactive AuNC and ^{198}Au doped AuNC (^{198}AuNC) were synthesized and coated with human serum albumin (HSA) by adding NaOH to the mixture of HSA and $HAuCl_4$ (or $H^{198}AuCl_4$) at 37℃. The particle size, fluorescence spectrum, and Cerenkov luminescence (CL) spectrum of ^{198}AuNCs and AuNC were tested. For cell studies, U87MG cells were cultured with 20μCi ^{198}AuNC (0.1mg) or 0.1 mg AuNC for 2, 4, and 12h, and then they were imaged with fluorescent microscope for cell imaging and livability evaluation. For in vivo studies, U87MG xenograft mice (n=4 per group) were injected with ^{198}AuNC, AuNC, or saline through tail vein, respectively. Then the mice were imaged with an optical imaging system at 500nm excitation and 680 nm emission filters and CL imaging at 2h, 4h, and 24h after injection. The tumor size was measured every day for 7 days after injection of the nanoparticles.

Results: AuNC were well dispersed with diameter of 1.2±0.2 nm in transmission electron microscopy (TEM) and 2.9±1.1 nm in dynamic light scattering (DLS). The fluorescence spectrum showed a strong peak at 680 nm with 500 nm excitation while luminescence spectrum showed two significant peaks at 520 nm and 680 nm, which were correspondent to the CL and AuNC fluorescence excited by CL, respectively. The in vitro results demonstrated intensive fluorescence from the U87MG cells at different time points. The cell livability was only 34.5±3.2% when incubated with ^{198}AuNC compared with 95.6±2.4% of control for 12h (P>0.05). The in vivo imaging displayed significant luminescence and fluorescence signal from the tumor at 680 nm. The therapy studies indicated that the tumor growth rate at day 7 of the ^{198}AuNC, AuNC, and saline control groups were 27.4±6.2%, 97.3±19.5%, and 103.9±22.8%, respectively, demonstrating the significant higher in vivo treatment efficacy of the ^{198}AuNC than both of AuNC and saline.

Conclusions: The ^{198}Au-doped theranostic ^{198}AuNC can serve as an efficient radio-optical multi-function agent for tumor multimodal imaging and radionuclide therapy.

ACKNOWLEDGMENT: This work was supported by the Office of Science (BER), U.S. Department of Energy (DE-SC0008397) and the National Natural Science Foundation of China (81230033).

AUTHORS (LAST NAME, FIRST NAME): Ma, Xiaowei[1, 2]; Cheng, Kai[1]; Sun, Yao[1]; Cutler, Cathy S.[3]; Kang, Fei[2]; Yang, Weidong[2]; Wang, Jing[2]; Cheng, Zhen[1]

INSTITUTIONS (ALL):

1. Molecular Imaging Program at Stanford (MIPS), Bio-X Program, and Department of Radiology, Canary Center at Stanford for Cancer Early Detection, Stanford University, Stanford, CA, United States.
2. Department of Nuclear Medicine, Xijing Hospital, The Fourth Military Medical University, Xi'an, Shaanxi, China.
3. University of Missouri Research Reactor, Columbia, MO, United States.

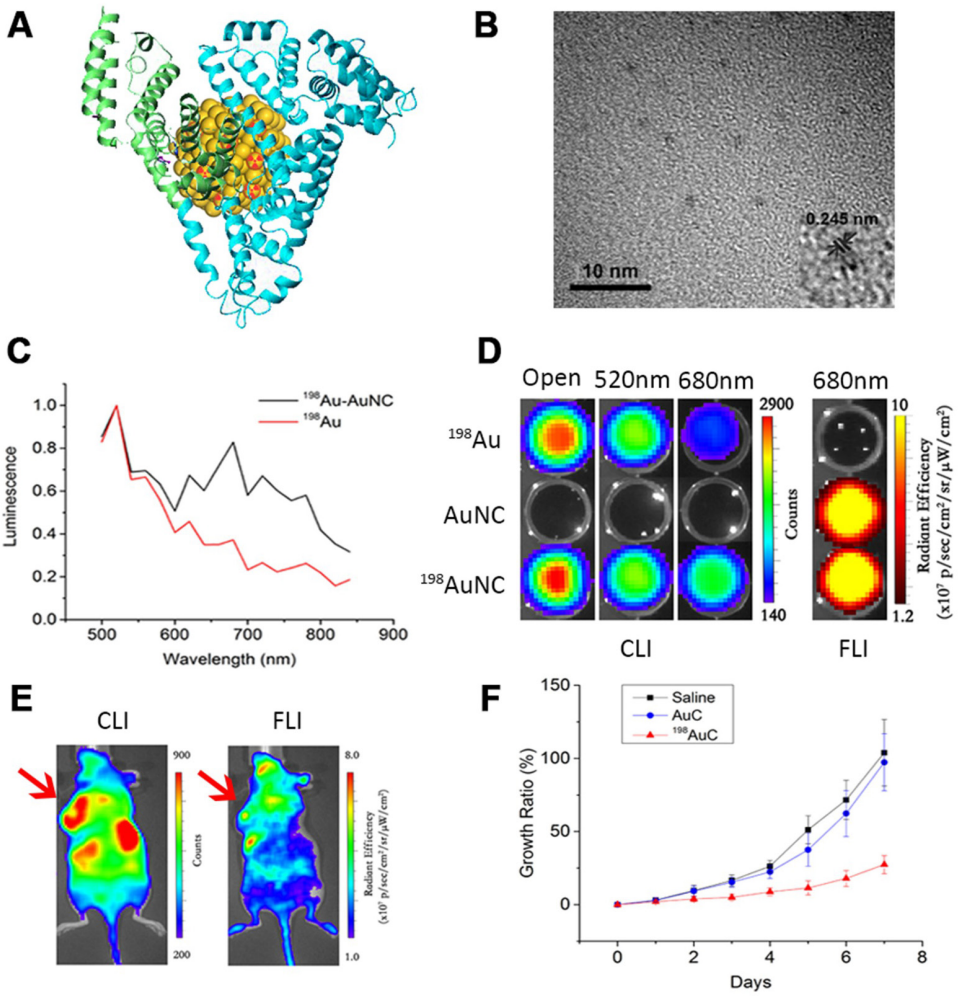

Figure 1. (a) The schematic structure of 198AuNC; (b) TEM images of AuNC; (c) Luminescence spectrum of 198AuNC and 198AuHCl4; (d) The CLI and FLI of 198AuHCl4, AuNC and 198AuNC; (e) The CLI and FLI imaging of the U87MG xenograft (left flank) mice; (f) The treatment efficacy of 198AuNC, AuNC, and saline from day 1 to day 7 after injection.

CONTROL ID: 2232448

TITLE: Gd-Free T_1 MRI contrast agents based on Mn(III)Porphyrin: a sensitive and versatile platform for diverse applications at high magnetic fields

PRESENTER: Xiao-an Zhang

ABSTRACT BODY:

Abstract Body: Since Magnevist®, a Gd(III)-chelate (GdDTPA) was approved as the 1st clinical MRI contrast agent (CA) in 1987, an array of Gd-based contrast agents (GBCAs) have been developed and play increasingly important roles in modern diagnostic imaging. Despite their dominant success in clinics, most GBCAs share two major limitations: low sensitivity (T_1 relaxivity, or r_1), particularly at high magnetic fields, and Gd-toxicity associated with nephrogenic systemic fibrosis (NSF). To fundamentally address these challenges, a series of novel Mn(III)porphyrins (MnPs) have been developed in our group as Gd-free T_1 CAs with optimized sensitivity and biocompatibility. As a micronutrient, Mn is intrinsically safer than Gd, and forms highly stable complex with porphyrin to prevent metal release. The unique electron relaxation properties make MnPs possible to achieve higher r_1 than GBCAs, even though Mn(III) has less unpaired electrons than Gd(III) (4 *vs* 7). Through rational structural modifications, different classes of new MnPs have been constructed with distinct pharmacokinetics tailored for diverse applications. Among them, MnTCP was designed as an extracellular fluid (ECF) agent. As the smallest water-soluble MnP known to date, MnTCP is highly polar, exhibiting higher r_1 than GdDTPA (Fig 1a).[1] In fact, MnTCP has the highest r_1 in high clinical fields among all small CAs with MW below 600. MnTCP exhibits rapid extravasation and renal clearance upon *i.v.* injection in rats.[2] With this pharmacokinetics of typical ECF agent, MnTCP was successfully applied for detecting breast cancer in rodent model by monitoring the abnormal vascularity.[3] The 2nd type of MnP was designed as blood-pool agent (BPA) for MR angiography (MRA), a type of techniques for imaging the structure and function of vascular system, widely applicable for different organs. Towards this goal, a dimeric porphyrin, MnP2 was developed, containing a rigid biphenyl-linker for non-covalent interaction with serum albumin (SA). Binding to SA can elongate the retention of MnP2 in the blood stream, desirable for MRA. As monitored by optical methods, such as UV-vis, fluorescence and CD spectroscopies, MnP2 forms a reversible interaction with HSA with sub-mmol affinity.[4] As a result, MnP2 offers long intravascular enhancement for more than 24 h. Moreover, due to slower tumbling rate, dimeric construct and fast electron relaxation, MnP2 shows a high molar r_1 of 20 mM^{-1} s^{-1} at 3 T, twice as strong as Ablavar®, the only FDA approved BPA. With long circulation and high r_1, MnP2 was successfully used for imaging lung, an organ difficult to image with regular MRI methods.[5] The 3rd class MnP is designed for cell-labeling. Based on a pro-drug strategy, the cell impermeable MnTCP was converted to a lipophilic form, which can cross the cell membrane freely. Upon intracellular enzyme activation, it is converted to MnTCP, and trapped inside the cell for long-term MRI labeling.[6] Overall, MnP is a versatile platform ideal for developing Gd-free CAs for diverse applications.

Ref: 1. *J Med Chem* **2014**(57)516; 2. *JMRI* **2014**(40)1474; 3. *JMRI* **2015**(41)397; 4. *J Biol Inorg Chem* **2014**(19)229; 5. *Mol Imaging* **2014**(13)1 ; 6. Unpublished.

AUTHORS (LAST NAME, FIRST NAME): Zhang, Xiao-an[1, 2]; Cheng, Weiran[1, 2]; Haedicke, Inga E.[1, 2]

INSTITUTIONS (ALL):

1. Chemistry, University of Toronto, Toronto, ON, Canada.
2. Department of Physical & Environmental Sciences, University of Toronto Scarborough, Toronto, ON, Canada.

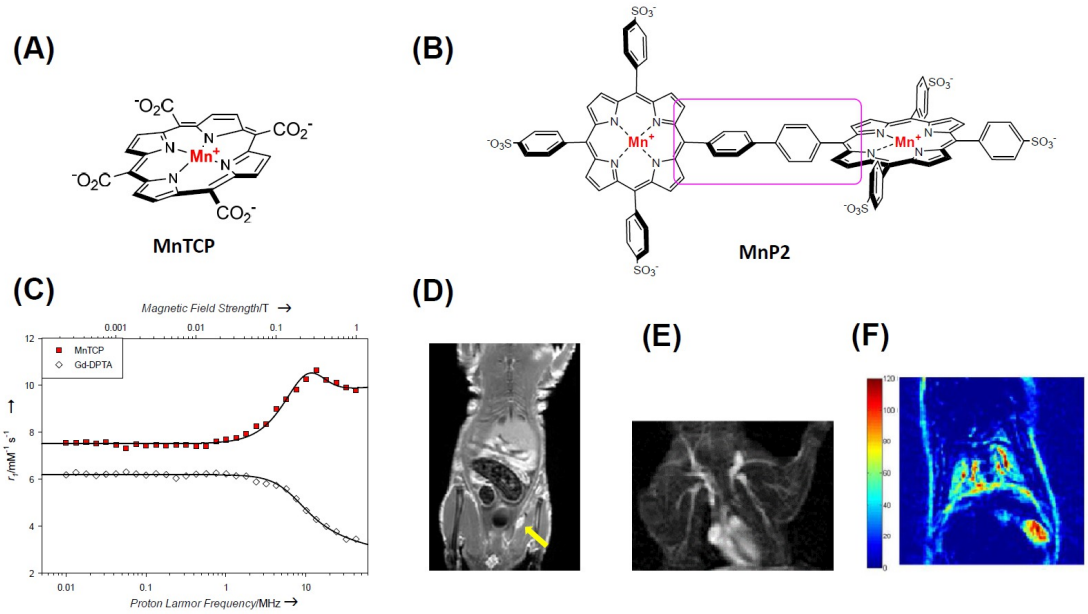

Figure Representative novel Mn(III)porphyrins (MnPs) as sensitive Gd-free contrast agents tailored for diverse applications: (A) MnTCP, a small and polar extracellular fluid (ECF) agent;[1] (B) MnP2, a blood-pool agent (BPA) with high r_1 and long circulation in vascular system. The plausible HSA binding site is highlighted in the frame;[4] (C) Field-dependent r_1 (NMRD profile) shows MnTCP a higher relaxivity than GdDTPA, particularly at high field regions;[1] (D) Using MnTCP to detect breast cancer (yellow arrow) by contrast enhanced MRI;[3] (E) T_1–weighted MR angiography of a rat injected with MnP2, selectively highlighting the vascular system;[4] (F) Application MnP2 for lung MR imaging using ultrashort echo time.[5]

CONTROL ID: 2232465

TITLE: Non-invasive, ultrasensitive, and early detection of myocardial ischemia using activated platelet-targeted PET/CT imaging

PRESENTER: Karen Alt

ABSTRACT BODY:

Abstract Body: Background: Platelets have an established role in haemostasis but it is becoming increasingly clear that they also have inflammatory functions. This makes molecular PET of platelets very attractive as it opens up the possibility to detect not only acute thrombotic events in diseases such as myocardial infarction and stroke but also acute and chronic inflammation. We previously generated a single-chain antibody (scFv) that specifically binds to the highly abundant platelet surface receptor GPIIb/IIIa in its active, ligand bound form (LIBS). The presented work reports on the use of a novel ^{64}Cu MeCOSar labeled $scFv_{anti\text{-}LIBS}$ towards early detection of myocardial ischemia. Our work has the potential to detect ischemia very early on and guide clinical interventions.

Methods: Different time periods of ischemia were induced in C57BL/6 mice by temporary ligation of the left anterior descending (LAD) coronary artery. Activated platelets were targeted with a ^{64}Cu metal ligand conjugated scFv directed against LIBS epitopes on activated glycoprotein (GP)IIb/IIIa. A single PET/CT scan was performed after injection of $scFv_{anti\text{-}LIBS}$-^{64}CuMeCOSar at several time points after reperfusion. To support our PET findings, histology staining against platelets was performed.

Results: Activated platelets were detectable by PET depending on the duration of ischemia and time points after reperfusion. After 1 h ischemia, platelets were detected as early as 5 min after reperfusion; the signal peaked 2 h after reperfusion. Even very short periods of ischemia (10 and 20 min) resulted in detectable levels of platelet accumulation as shown by strong PET signals. Furthermore, biodistribution analysis confirmed the PET results and indicated a significantly higher radioactive uptake of $scFv_{anti\text{-}LIBS}$-^{64}CuMeCOSar in the ischemic myocardium compared to the non-ischemic myocardium as well as the muscle as control. Our results demonstrate the excellent sensitivity of PET and the suitability of platelets as a novel marker of myocardial ischemia.

Conclusions: PET/CT imaging targeting the PET-tracer isotope ^{64}Cu to activated platelets facilitates the early and sensitive detection of myocardial ischemia. This ultrasensitive and non-invasive imaging strategy is of clinical interest for both diagnostic and prognostic purposes, and highlights the potential of molecular imaging using PET for the characterizing of myocardial ischemia.

AUTHORS (LAST NAME, FIRST NAME): Alt, Karen[1]; Ziegler, Melanie[1]; Hagemeyer, Christoph E.[1]; Peter, Karlheinz[1]

INSTITUTIONS (ALL):

1. Baker IDI Heart and Diabetes Institute, Melbourne, VIC, Australia.

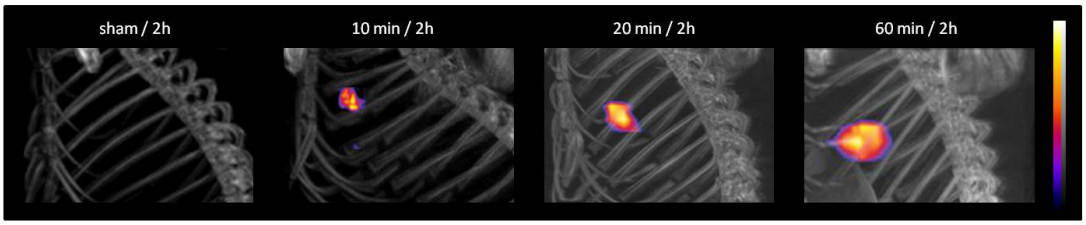

Figure 1: PET/CT imaging of activated platelets within the ischemic myocardium.
Comparison of representative maximum-intensity projection PET/CT images after sham-operation and different time periods of ischemia (10, 20 and 60 min of temporary LAD ligation). The colour scale shows radiotracer uptake with white corresponding to the highest activity and blue to the lowest activity.

CONTROL ID: 2232466

TITLE: Establishment of an Optical/Magnetic Dual-modality Probe for Targeted Gastric Cancer In Vivo Imaging

PRESENTER: Changhao Liu

ABSTRACT BODY:

Abstract Body: Gastric cancer is one of the malignancies that severely threatens human health. Delayed diagnosis attributed to its high mortality rate, thus early detection is the key to improve survival. However, current clinical methods are ineffective in early diagnosis because of lacking sensitivity and specificity. Optical/Magnetic dual-modality imaging probes with diagnostic capabilities have drawn considerable attention for their potential application in oncology. Thus in our study, a novel gastric cancer specific dual-modality probe comprised of Fe_3O_4 magnetic nanoparticle (MNP), Cy5.5 and gastric cancer specific monoclonal antibody MGb2 was designed and fabricated. During the probe fabrication, we adopted two conjugating strategies named Parallel and Series strategy. Further tests showed that series probe had a hydrosize of 77.3 ± 1.1 nm and Zeta potential of -19.6 ± 1.2 mV; while parallel probe's hydrosize wass 87.7 ± 0.3 nm and Zeta potential was -19.3 ± 0.5 mV. Through parallel strategy, one MNP could be conjugated with 1.4 MGb2 antibodies while series strategy could increase this number to 3. Fluorescence excitation assay revealed that at the same concentration, series probe's fluorescent intensity was twice as much of the parallel probe's. Magnetic resonance scanning and T_2 calculation suggested the probe's relaxation rate was 231.1 $mM^{-1}s^{-1}$. As for in vivo imaging, we built nude mouse tumor xenograft models and injected our probe at a 15 mg Fe/kg dosage through tail vein. The dual-modality probe achieved enhanced imaging contrast in both magnetic resonance imaging and fluorescence imaging. Living animal optical imaging displayed that the tumor was best imaged at 24 h after specific probe injection. Then the signal attenuated and became a little higher than pre-injection condition at the 72 h time point. The unspecific probe group's signal was slightly increased and quickly restored to normal. Same tendency was detected by magnetic resonance imaging and T2* calculation. At the time point of 6 h, 24 h, 48 h and 72 h post probe injection, the T_2* value of tumor region was 86.91%, 68.95%, 82.37% and 90.17% of the same region before probe injection. In the negative control group, these data were 97.39%, 90.17%, 95.88% and 101.59% and in the competition group, the T_2* values of tumor region were 91.83%, 85.90%, 98.77% and 106.57% of pre-injection conditions. Biodistribution assay implicated the probe mainly metabolized through liver.

In conclusion, we have successfully established a new dual-modality probe for gastric cancer imaging, which has satisfactory imaging capability that could bind and detect gastric cancer cells specifically and sensitively. It could be a promising probe for clinical gastric cancer early diagnosis. And if further modified, such as coupled with anti-cancer drugs, the probe's application would expand and achieve the theranostic goal.

AUTHORS (LAST NAME, FIRST NAME): Liu, Changhao[1]; Qiao, Ruirui[2]; Yin, Jipeng[1]; Gao, Mingyuan[2]; Wu, Kaichun[1]

INSTITUTIONS (ALL):

1. State Key Laboratory of Cancer Biology, Department of Gastroenterology, Xijing Hospital, Fourth Military Medical University, Xi'an, Shaanxi, China.

2. Institute of Chemistry, Chinese Acadamy of Sciences, Beijing, China.

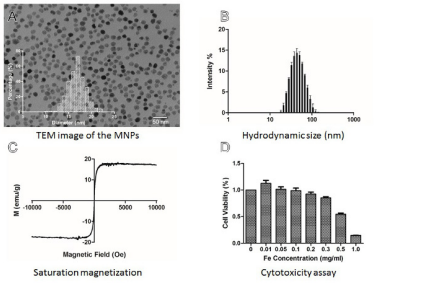

Figure 1 Magnetic Nanoparticle Characterization

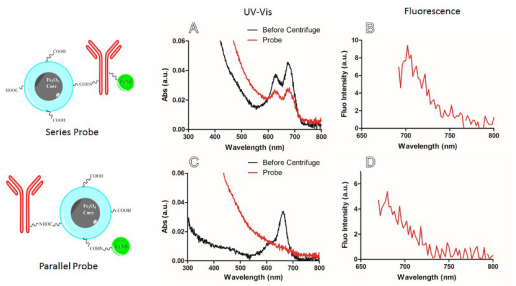

Figure 2 Schematic Diagram of Probes and Optical Characters

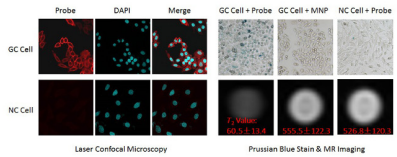

Figure 3 In Vitro Probe Binding Assays

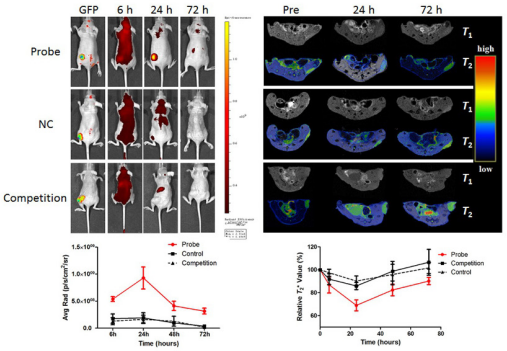

Figure 4 In Vivo Gastric Cancer Optical & MR Imaging

CONTROL ID: 2232467

TITLE: The relationship between Adenine Nucleotide Translocase2 expression and ^{18}F-FDG uptake in anaplastic thyroid cancer

PRESENTER: Chul-Hee Lee

ABSTRACT BODY:

Abstract Body: Objectives: Anaplastic thyroid carcinoma, one of the most aggressive tumors, has been known to show intensive uptake signals in ^{18}F-FDG PET. Adenine nucleotide translocase 2 (ANT2) imports glycolytic ATP into mitochondria and prevents apoptosis. Although ANT2 expression has been suggested as a marker of cell proliferation and carcinogenesis, the correlation between ANT2 expression and ^{18}F-fluorodeoxyglucose (^{18}F-FDG) uptake was not reported. We investigated the association of ANT2 expression with ^{18}F-FDG uptake in thyroid cancer cells.

Methods: Human thyroid cell lines such as N-thy-ori (normal), TPC-1 (papillary cancer) and FRO (anaplastic cancer) were used for this research. ANT2 expression was measured by RT-PCR and western blot. 2'-methoxy (2'-OMe) modified siRNAs were used for down-regulating ANT2 expression. A gamma counter was used for measuring ^{18}F-FDG uptake. Luciferase-expressing FRO cells were subcutaneously grafted in a BALB/c nude mouse, and siRNA was directly injected into the tumor. ^{18}F-FDG PET and *in vivo* bioluminescent imaging were obtained using animal PET and IVIS 100.

Results: ^{18}F-FDG uptake rate in FRO was 3.5-fold and 1.5-fold higher than N-thy-ori and TPC-1, respectively ($P<0.001$). FRO was chosen to investigate the role of ANT2 in ^{18}F-FDG uptake because ANT2 mRNA and protein expressions were the highest among thyroid cells. FRO cells treated with ANT2 siRNA for 48 hr showed that reduced ANT2 expression and ^{18}F-FDG uptake as concentration dependently. Especially, ^{18}F-FDG uptake in 200 nM ANT2 siRNA treatment was significantly decreased in 0.55-fold ($P<0.001$) of the scramble siRNA treatment. In the xenografted mouse model, 48 hr treatment of 5 nmole ANT2 siRNA reduced ^{18}F-FDG tumor uptake at 0.75-fold ($P<0.01$) of the scramble treatment.

Conclusion: We demonstrated that higher ANT2 expression is related with higher ^{18}F-FDG uptake in the anaplastic thyroid cancer cells by modulating ANT2 expression. Though further studies are required to solve the questions regarding the effect of ANT2 on the mitochondrial bioenergetics of tumors, our result suggesting that the evaluation of ANT2 expression can be used as a possible biomarker for ^{18}F-FDG PET positive tumor.

Keyword: Adenine nucleotide translocase 2, ^{18}F-fluorodeoxyglucose uptake, anaplastic thyroid carcinoma, siRNA

AUTHORS (LAST NAME, FIRST NAME): Lee, Chul-Hee[1, 2]; Kim, Mi Jeong[1, 3]; Youn, Hyewon[4, 5]; Kang, Keon Wook[1, 3]; Chung, June-Key[1, 2]

INSTITUTIONS (ALL):

1. Nuclear Medicine, Seoul National University, Seoul, Korea (the Republic of).
2. Biomedical Sciences, Seoul National University, Seoul, Korea (the Republic of).
3. Cancer Research Institute, Seoul National University, Seoul, Korea (the Republic of).
4. Tumor Microenvironment Global Core Research Center, Seoul National University, Seoul, Korea (the Republic of).
5. Cancer Imaging Center, Seoul National University Cancer Hospital, Seoul, Korea (the Republic of).

(No Image Selected)

CONTROL ID: 2232470

TITLE: ^{18}F-sodium fluoride uptake is a marker of active calcification and disease progression in patients with aortic calcification: Compared with ^{18}F-fluorodeoxyglucose.

PRESENTER: Seigo Fujita

ABSTRACT BODY:

Abstract Body: Aims and objectives

^{18}F-Sodium fluoride (^{18}F-NaF) and ^{18}F-fluorodeoxyglucose (^{18}F-FDG) are promising novel biomarkers of disease activity in aortic calcification. We compared ^{18}F-NaF and ^{18}F-FDG uptake with calcium score of Abdominal aorta and assessed whether they predicted disease progression.

Methods and materials

Six patients with aortic calcium underwent early nad delayed combined positron emission and computed tomography using ^{18}F-NaF and ^{18}F-FDG radiotracers. We correlated with calcium score and ^{18}F-NaF and ^{18}F-FDG uptake in Mann-Whitney U-test with Bonferroni correction.

Results

Many parameters (calcium score, early and delayed ^{18}F-NaF uptake and early ^{18}F-FDG uptake) did not accept the clear correlation by the comparison between all groups. Only delayed ^{18}F-FDG uptake was correlated with calcium score of CT and disease progression. So ^{18}F-NaF uptake was a better marker of active calcification than ^{18}F-FDG uptake.

Conclusion

^{18}F-NaF uptake identifies active tissue calcification and predicts disease progression in patients with calcific aortic calcification.

AUTHORS (LAST NAME, FIRST NAME): Fujita, Seigo[1]

INSTITUTIONS (ALL):

1. Radiology, Miyazaki Prefectural Nichinan Hospital, Miyazaki, Japan.

(No Image Selected)

CONTROL ID: 2232474

TITLE: Multimodal ultrasound-photoacoustic imaging for longitudinal monitoring of tissue engineering scaffolds

PRESENTER: Yahfi Talukdar

ABSTRACT BODY:

Abstract Body: Introduction: Polylactic-co-glycolic acid 50:50 (PLGA) has gained much prominence in this field of tissue engineering due to its desirable biocompatible and biodegradable properties that allow tissue to penetrate into the scaffold. Real-time *in vivo* imaging of this regeneration process has been a major challenge. Current methods of investigating the scaffold architecture, and neo-vascularization include microCT that uses ionizing radiation, and post-mortem histological analysis have significant limitations. Poor contrast in microCT for wet scaffolds limits its usage in *in vivo* studies and histological analysis is only suitable for end point analysis and does not allow longitudinal imaging of the regenerative process including neo-vascularization. Thus, to follow the fate of the scaffolds, and to understand tissue development within these scaffolds *in vivo*, it is crucial to develop methods of non-ionizing, and non-invasive imaging. In this study, we investigate the use of ultrasound (US)-photoacoustic (PA) multi-modal imaging to detect tissue-engineering scaffolds and monitor the process of neovascularization *in vivo* in a rat model.

Methods: Single-walled carbon nanotube (SWCNT), that provides PA contrast, was incorporated into the PLGA (0.5 wt%) to make composite scaffolds (SWCNT-PLGA). Porous PLGA and SWCNT-PLGA scaffolds were made using NaCl porogen. The scaffolds were embedded in varying thickness of chicken breast tissue *ex vivo* and imaged with Vevo LAZR. For *in vivo* imaging, the scaffolds were implanted in subcutaneous pockets of rats. US and PA imaging was done simultaneously 7 and 14 days after implantation. Differential absorption of oxy-and-deoxyhemoglobin at 750nm and 850nm wavelengths was used to measure oxygen saturation of the scaffolds to monitor the process of vascularization. The scaffolds with surrounding tissue were extracted for histological analysis and microCT imaging.

Results: The scaffolds were detected *in vivo* using the high temporal and spatial resolution (720fps and 45μm) ultrasound images. The nanocomposites have a strong PA signal and can be imaged up to 6 mm deep in the chicken breast tissue. PLGA scaffolds generate no PA signals, and cannot be imaged using PA imaging. MicroCT images of subcutaneous tissue containing PLGA or SWCNT-PLGA scaffolds had poor contrast and the scaffolds could not be distinguished from background. Small blood vessels and capillaries were observed in the histological sections of the explanted scaffolds confirming the oxygen saturation data obtained from PA imaging.

Conclusion: US and PA imaging can be used to detect nanocomposites *in vivo* up to 6 mm deep and oxygen saturation measurements can be used to determine the extent of tissue regeneration and vasculogenesis within the scaffolds. These results taken together with results on SWCNT-incorporated PLGA scaffolds obtained using photoacoustic microscopy indicate that the PA imaging could multiscale imaging of tissue engineering scaffolds. Additionally, US imaging provides the appropriate contextual anatomic information for useful localization of the photoacoustic imaging signals within the animal.

AUTHORS (LAST NAME, FIRST NAME): Sitharaman, Balaji[1]; Talukdar, Yahfi[1]

INSTITUTIONS (ALL):

1. Biomedical Engineering, Stony Brook University, Stony Brook, NY, United States.

(No Image Selected)

CONTROL ID: 2232476

TITLE: PET Imaging of Tumor-Targeting Salmonella typhimurium using [^{18}F]Fluorodeoxysorbitol in small animal models

PRESENTER: Dong-Yeon Kim

ABSTRACT BODY:

Abstract Body: Optical imaging techniques such as bioluminescence or fluorescence were utilized for quantitative and noninvasive imaging of attenuated *Salmonella typhimurium (aSL)* that have a propensity to naturally accumulate and replicate in a wide range of solid tumors. However, optical imaging techniques have a limitation to apply large animals or human due to shallow penetration depth (<1 cm). Herein, we report a novel PET imaging study to track and visualize intravenously injected *aSL* in mouse tumor models using ^{18}F labeled sorbitol (2-deoxy-2-[^{18}F]fluorosorbitol, [^{18}F]FDS), which is a metabolic substrate for Enterobacteriaceae.

Methods: [^{18}F]FDS was obtained from commercially available [^{18}F]FDG. [^{18}F]FDG was reduced with sodium borohydride at 35°C for 30 min and the product was passed through an n-alumina Sep-Pak cartridge. For identification radio-TLC was performed and [^{18}F]FDS was passed through a 0.20 μm membrane filter into a sterile multidose vial for in vitro and in vivo experiments. *aSL* defective in the synthesis of ppGpp (ΔppGpp strain) expressing bacterial luciferase (*lux*) gene were routinely grown overnight in Luria–Bertani (LB) medium. Probe uptake assays were performed by incubating bacterial cultures (alive and heat-killed) with [^{18}F]FDS (20 kBq/ml) at 37°C with rapid agitation. The mice bearing about 300 mm^3 s.c. tumors (CT26) were injected intravenously with sterile PBS or 4.5x10^7 cfu ΔppGpp strain resuspended in 100μl of sterile PBS. IVIS images were obtained before microPET studies. MicroPET studies were performed at 1h after [^{18}F]FDS injection (7.4 MBq) from 0 to 4 days postinoculum (dpi). Finally, we compared and analyzed IVIS images with microPET images.

Results: [^{18}F]FDS was synthesized easily and non-decay corrected radiochemical yield was around 60 %. With only one peak based on radio-TLC reader with Rf=0.51 (80% acetonitrile with 20% water as eluent, Rf=0.60 for [^{18}F]FDG). [^{18}F]FDS showed high accumulation at 2 h after incubation with *aSL* however, heat-killed bacteria did not incorporate [^{18}F]FDS for 2 h. Bioluminescence imaging confirmed bacterial targeting and proliferating in tumor tissue between 0 and 4 dpi. [^{18}F]FDS PET also showed tracer accumulation in bacterial colonized tumor like bioluminescence imaging. [^{18}F]FDS PET imaging revealed high tumor uptake demonstrating high tumor-to-background ratio (0 dpi: 1.97 ± 0.48, 1 dpi: 2.62 ± 0.59, 2dpi: 2.75 ± 0.33, 3 dpi: 2.13 ± 0.29) (Fig. 1).

Conclusion: [^{18}F]FDS PET study demonstrated stable uptake in tumor from 1 to 4 dpi and rapid clearance from the blood and other organs within 1 h. It may be a useful tool that allows visualization of injected bacteria for targeted cancer therapy using *aSL*.

AUTHORS (LAST NAME, FIRST NAME): Kim, Dong-Yeon[1]; Nguyen, Vu H.[1]; Kim, Hyeon Sik[1]; Pyo, Ayoung[1]; Bom, Hee-Seung[1]; Min, Jung-Joon[1]

INSTITUTIONS (ALL):

1. Nuclear Medicine, Chonnam National University Hwasun Hospital, Hwasun, Korea (the Republic of).

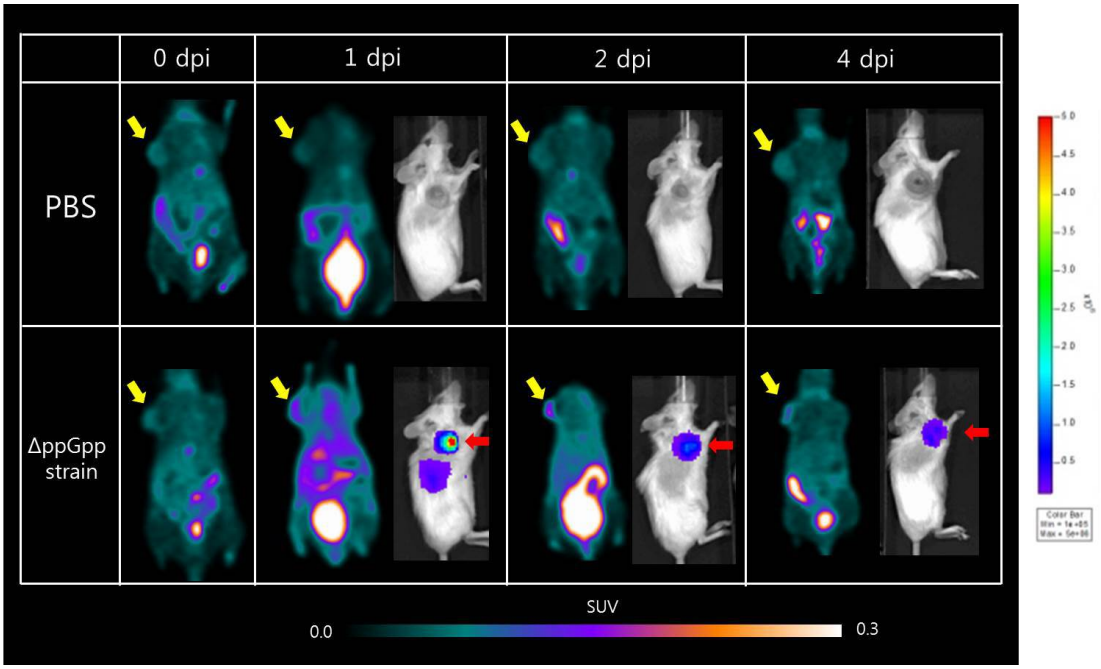
0 dpi
1 dpi
2 dpi
4 dpi
PBS
ΔppGpp strain
SUV
0.0
0.3

CONTROL ID: 2232484

TITLE: Comparison of probe efficacy for Cherenkov excited luminescence imaging in tissue from linear accelerator radiation

PRESENTER: Huiyun Lin

ABSTRACT BODY:

Abstract Body: Ionizing radiation delivered by a medical linear accelerator (LINAC) generates Cherenkov emission in treated tissue, which could be used to excite optical molecular reporters *in vivo*, allowing imaging of tissue response. This approach will allow high resolution molecular imaging dictated by the ionizing beam, with sensitive detection at biologically relevant concentrations *in vivo*. Detection is done by spectrally resolving or time-domain gating of the signal, and the luminescence signal can be isolated from the Cherenkov background to varying degrees, depending on which probe is used, with the strongest additional factors being the concentration of the probes and the radiation level used. The signal decays with depth below the tissue surface.

In this paper, near-infrared fluorophores from IRDye®, i.e. IRDye® 680RD NHS Ester, IRDye® 700DX NHS Ester and IRDye® 800CW (LI-COR Biosciencs, Nebraska, USA) and oxygen-sensitive phosphorescent probe Oxyphor G4 (PtG4) were used for the detectability study in the tissue equivalent phantom, which composed by the phosphate buffered saline (PBS) solution with 1% v/v Intralipid© and 1% v/v whole blood. The ionizing radiation was from a Varian Clinic 2100CD linear accelerator (LINAC, Varian Medical Systems, Palo Alto, CA). The probe tube included in the tissue equivalent phantom was irradiated by a 6 MV square (10×10 mm^2) ionizing beam. The Cherenkov excited luminescence of probes was detected by a fiber-optic coupled intensifier-gated CCD camera (PI-MAX3, Princeton Instruments, USA) interfaced to a spectrometer (Acton Insight, Princeton Instruments, Acton, USA). The concentration of IRDye® and PtG4 was varied from 0.1 to 100 μM. In the detectable depth experiments, the concentration of IRDye® and PtG4 was kept to 6.25 μM, and the distance from the optical detector to the radiation beam were varied from 0 to 25 mm with 5 mm increments.

Major results including minimum detectable concentrations and largest detectable depth were summarized in the table for investigated probes. Results from continuous wavelength (CW) and time domain gating (Gated) acquisition were compared for PtG4. The results showed that under CW acquisition the lowest detectable concentration for IRDye® 700DX was 1.6 μM, which was 2 times lower than IRDye® 680RD, and the largest detectable distance was about 20 mm. The lowest detectable concentration for PtG4 was 0.2 μM with gated acquisition, which was about 8 times lower than CW measurement results, while the largest detectable depth showing an improvement about 5 mm (20 mm for CW and 25 mm for Gated).

In conclusion, excited by the Cherenkov emission induced by LINAC radiation, the luminescence from IRDye® and PtG4 can be detected. In terms of detectable concentration and depth, IRDye® 700DX would be more suitable for fluorescence imaging combined with ionizing radiation. Gated acquisition can increase the detectability in terms of concentration and depth for probes with lifetime in μs level.

AUTHORS (LAST NAME, FIRST NAME): Lin, Huiyun[1, 2]; Zhang, Rongxiao[3]; Vinogradov, Sergei A.[4]; Gladstone, David J.[5]; Pogue, Brian W.[1, 3]

INSTITUTIONS (ALL):

1. Thayer School of Engineering, Dartmouth College, Hanover, NH, United States.
2. MOE Key Laboratory of OptoElectronic Science and Technology for Medicine, Fujian Provincial Key Laboratory for Photonics Technology, Fujian Normal University, Fuzhou, Fujian, China.
3. Physics and Astronomy, Dartmouth College, Hanover, NH, United States.
4. Department of Biochemistry and Biophysics, Perelman School of Medicine, University of Pennsylvania, Philadelphia, PA, United States.
5. Department of Medicine, Geisel School of Medicine, Dartmouth College, Hanover, NH, United States.

(No Image Selected)

CONTROL ID: 2232486

TITLE: Atherosclerosis Ischemia Markers in Coronary Artery Disease [CAD]: Regulatory Approval Pathway Implications for Routine Clinical Applications versus Development [Surrogate] Marker Applications

PRESENTER: Norman LaFrance

ABSTRACT BODY:

Abstract Body: Hypothesis:
Are alternative Regulatory approaches required for either routine clinical appications of atherosclerosis or ischemic markers versus utilization for development programs[surrogate markers]?

Abstract innovation:
This poster will review pathways for diagnostic and/or prognostic information and required product performance in CAD. (Manolio 2004 NEJM). This approach needs to prove a significant impact on patient management, is more effective than alternative options and have excellent imaging with quantification capabilities.

Impact for current/future applications:
One of the most active and exciting areas of CAD research are in markers of atherosclerosis/vulnerable plaque and ischemia. More than 100 potential athersclerotic plaque markers have been identified (High Country Nuclear Medicine Conference, March 1, 2015). Current debates are ongoing between the emphasis on measuring ischemia and blood flow [weel proven] versus identifying and characterizing vulnerable plaque and plaque burden [ongoing].The real requirement is to identify the vulnerable patient, rather than a vulnerable lesion, and is consistent with CAD being recognized as a diffuse, multisystem and chronic inflammatory disorder involving vascular, metabolic and immune systems with various local and systemic manifestations. It is essential to assess total patient vulnerability and not just search for a single vulnerable plaque. (Spagnoli et al JNM 2007)

Current Options and Discussion:
Establishing an atherosclerotic marker(s) via classic regulatory guidances are well described in FDA guidance documents (FDA Guidance for Approval of Diagnostic Imaging Drugs-three parts 2004). Phase 1 studies showing Proof of Mechanis, Phase 2 for preliminary efficacy and safety and to direct Phase 3 design and define image timing, acquistion and quantification parameters. And, finally, two well controlled Phase 3 studies of [at least] N=300-500 patients and additional Phase 3 or Phase 4 studies for evaluating outcomes and/or pharmacoeconomics. A development program to take a novel atherosclerotic marker agent to approval could easily reach $200MM or more and take 8-10 years and, even if approved may not reach routine or primary tier utilization. Elegant biochemical or pathophysiological markers may not always translate into a successful development program.

Conclusion:
Because of expense, time and the uncertain probability of success for claasic diagnostic drug development approval process, alternative pathways of atherosclerosis marker develpment as a markers of a vulnerable plaque, and more importantly the vulnerable patient, are required.

AUTHORS (LAST NAME, FIRST NAME): LaFrance, Norman D.[1]

INSTITUTIONS (ALL):
1. Medical & Regulatory Affairs, Jubilant DraxImage, Hudson, QC, Canada.

(No Image Selected)

CONTROL ID: 2232487

TITLE: Low cost, high spatial resolution, depth of interaction PET detector designs using position sensitive sparse sensor (PS3) arrays and dual sided (DS) readout.

PRESENTER: Robert Miyaoka

ABSTRACT BODY:

Abstract Body: Objectives: The overall goal of this work is to develop low-cost, high spatial resolution, depth-of-interaction (DOI) PET detectors for organ specific imaging systems, such as human brain and breast. For these types of systems image resolution of <2 mm and DOI resolution of <4 mm is desirable. Position sensitive sparse sensor (PS3) arrays will be used to enable low-cost designs. PS3 arrays use a sparse arrangement of silicon photomultiplier (SiPM) devices coupled with custom light guide designs to significantly lower cost versus detectors using tightly packed SiPM sensor arrays. For this work, a sparsity factor of at least 4 will be used for each detector design where sparsity is defined as the area of the crystal array surface being decoded divided by the total surface area of the SiPM devices. A sparsity factor of 4 reduces the cost of SiPM sensors by 75%, where the cost of SiPM sensors is a significant fraction of the total cost of the detector module. Photosensor size, placement, and optical light-guide design are important design considerations in optimizing this sparse readout design.

Methods: DETECT, Monte Carlo light ray tracing software, was used to simulate LYSO and BGO detector modules using dual sided PS3 array readout. Both detector module designs used 2x2x20 mm^3 crystals. Simulations were conducted for a 15x15 array of LYSO crystals and a 14x14 array of BGO crystals. Dual-sided symmetric and complementary sensor patterns were evaluated. The dimensions of the SiPM sensors are 3x3 mm^2 active area and 3.4x3.4 mm^2 package size. For the LYSO detector, a dual-sided, symmetric pattern with 13 sensors per side and a dual-sided, complementary pattern with 13 sensors on one side and 12 on the other were investigated, see figure 1(b) for illustration of complementary style pattern. For the BGO detector, a dual-sided, symmetric pattern with 16 sensors per side was simulated. The BGO detector had a sparsity rating of 4 while the LYSO detectors had sparsity ratings of >5.5. After running DETECT simulations, noise was added to the acquired photon counts according to a dark count rate of 2Mcps/channel and an appropriate acquisition time window for LYSO (120 nsec) or BGO (600 nsec). The effect of SiPM saturation was also modeled. The X and Y positions of the sensors were used as weights and the crystal maps were formed using the weighted signals from both sides of the crystal array. The DOI was determined from the ratio of the sum of the signals from the top set of sensors to the sum of the signals from all of the sensors.

Results: The crystal decoding characteristics for all tested PS3 patterns for the simulated LYSO and BGO detectors were excellent. Each crystal element could easily be individually resolved. The complementary readout pattern provided a more linear crystal map. The average DOI positioning resolution for both simulated LYSO detectors was ~3 mm FWHM. The average DOI positioning resolution for the BGO detector was ~4 mm FWHM.

Conclusions: The use of PS3 arrays can significantly reduce the cost of high performance PET detector modules as simulation results for DS-PS3 LYSO and BGO detector blocks yielded very promising results.

AUTHORS (LAST NAME, FIRST NAME): Miyaoka, Robert[1]; Hunter, William C.[1]

INSTITUTIONS (ALL):

1. Radiology, University of Washington, Seattle, WA, United States.

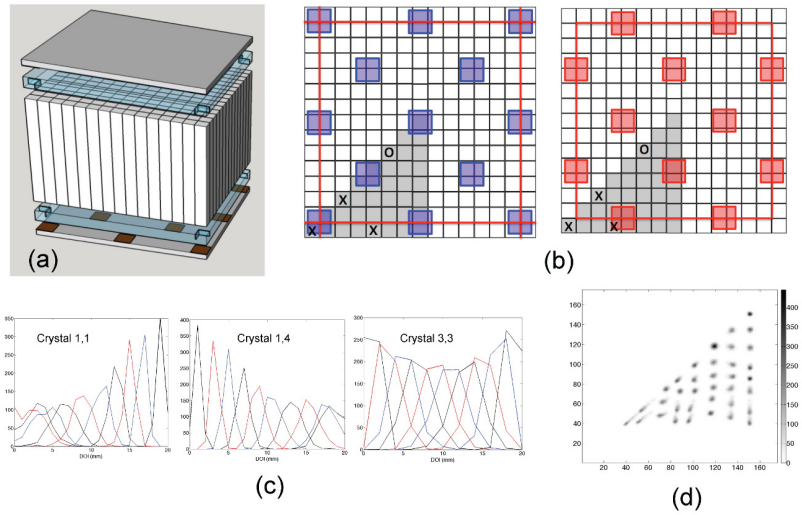

Fig. 1. (a) Drawing of DS-PS3 LYSO PET detector. (b) Example of 25 sensor, complementary dual-sided PS3 pattern (13 on one side and 12 on the other). The red lines indicate where slots were placed in a 2mm thick light guide to optimize crystal decoding. (c) Plots of depth of interaction positioning performance for three crystals identified with X's as shown in (b). (d) Plot of crystal decoding performance for gray crystals in as shown in (b). Crystal map has been zoomed for better visualization.

CONTROL ID: 2232497

TITLE: Immunofluorescent labeling of cancer marker *Her-2* with Iodoemodin

PRESENTER: Jeong Hoon Park

ABSTRACT BODY:

Abstract Body: last study, we have confirmed that iodine labeled emodin is specific bind to *HER-2* receptor overexpressing breast cancer cells. In this study, a stable isotope of 2-iodoemodin by introducing a fluorescence immunoassay method using a breast cancer cell line (SK-BR-3) were measured for cell-uptake. The labeling of Iodine was performed in sodium iodide solution, chloramine T with emodin solution in DMF then stirring for 60 minutes. The compound was purified by RP-HPLC. The synthesis of 2-iodoemodin was confirmed by ^{1}H-NMR spectroscopy and MS spectrometer. Purification of 2-iodoemodin was carried out by a RP-HPLC using 0.1% TFA and acetonitrile. As a result, the peak was found about 25 minutes. The breast cancer cells SK-BR-3 cell lines were seeded at 1×10^{5} in 24 well plates at 1 mL per well and incubated at 37 degree in a 5% CO_2 for 24 h for an adherence and growth. To each well in 2-iodoemodin and emodin were added. Cells were washed twice in cold phosphate buffered saline (PBS) at designated time point (15 min, 30 min, 60 min and 120 min). The cell pellets were measured by microplate fluorometer. The cellular uptakes of 2-iodoemodin increased in a time dependent manner for breast cancer cell line (SK-BR-3). The uptake of 2-iodoemodin was higher than that of emodin. This preliminary study suggests 2-iodoemodin are potent breast cancer imaging probe.

AUTHORS (LAST NAME, FIRST NAME): Lee, Jun Young[1]; Park, Jeong Hoon[1]; Hur, Min Goo[1]; Yang, Seung Dae[1]; Kim, Sang Wook[2]

INSTITUTIONS (ALL):

1. Radiation Instrumentation Research Division, Korea Atomic Energy Research Institute, Jeongeup si, Jeollabuk do, Korea (the Republic of).
2. Advanced material chemistry, Dongguk University, Gyeongju, Korea (the Republic of).

(No Image Selected)

CONTROL ID: 2232499

TITLE: Construction of a Novel uPAR targeted Multimodal Imaging Probe Using Strained Cyclooctyne Scaffold and Thiol-Yne Chemistry

PRESENTER: Yao Sun

ABSTRACT BODY:

Abstract Body: Objectives:

Small molecule based multimodal imaging probes play prominent roles in biomedical research and has high clinical translation ability. In this study, we designed a novel dual-modality (PET/NIRF) uPAR targeted imaging probe (^{64}**Cu-CHS1)** based on the thiol-yne chemistry and strained cyclooctyne. The ^{64}**Cu-CHS1** was evaluated in U87MG cells and tumor-bearing mice models *in vivo*.

Methods: The **CHS1** was constructed by installing the thiol modified NOTA and Cy5.5 motif into the strained cyclooctyne *via* base-catalyzed thiol-yne chemistry. **CHS1** was labeled with ^{64}Cu at ambient temperature within 30 min and was purified by RP-HPLC to produce ^{64}**Cu-CHS1**. The cell-uptake and receptor specificity of ^{64}**Cu-CHS1** were evaluated *in vitro* by uPAR positive U87MG cells using fluorescent microscope and γ-counter. The *in vivo* studies of ^{64}**Cu-CHS1** were then performed in U87MG xenografted mice (n = 4 per group) using micro PET/CT and an optical imaging system.

Results: The thiol-yne reaction can be effectively catalyzed by organic bases at ambient temperature and aqueous medium, and it can tolerate a wide range of functional groups (Figure 1A). Based on this imaging platform, ^{64}**Cu-CHS1** was easily and reliably produced and exhibited targeting specificity and high stability *in vitro*. From both NIRF and PET imaging, the U87MG tumor could be clearly visualized from the surrounding background tissue even at 1 h p.i.(Figure 1B), with good tumor contrasts for all-time points investigated. The tumor uptake values of ^{64}**Cu-CHS1** were gradually increased from 1 to 2 h and were reduced at 24 h after injection, with 3.55±0.30, 3.69±0.21, 3.45±0.20 and 0.91±0.14% ID/g at 1, 2, 4 and 24 h, respectively. Significantly lower tumor uptakes for the blocking-dose group were observed, with the value of 0.42±0.04, 0.43±0.02, 0.45±0.05 and 0.18±0.02% ID/g at 1, 2, 4 and 24 h, respectively. The highest PET signal intensity ratio between the tumor and normal tissue (T/N) for ^{64}**Cu-CHS1** was obtained at 2 h time point with the T/N value of 8.86±0.43. At all-time points, the NIRF intensity ratios (T/N) for ^{64}**Cu-CHS1** alone were significantly higher than those of the blocking group (P>0.05).

Conclusions: The novel strained cyclooctyne scaffold and thiol-yne chemistry have been developed and then successfully applied for construction multimodality imaging probes. Especially the ^{64}**Cu-CHS1** has demonstrated excellent imaging characteristics *in vivo* and has high clinical and translational potential.

Acknowledgment: This work was supported by the Office of Science (BER), U.S. Department of Energy (DE-SC0008397).

AUTHORS (LAST NAME, FIRST NAME): Sun, Yao[3, 1]; Ma, Xiaowei[2]; Cheng, Kai[4]; Cheng, Zhen[5]

INSTITUTIONS (ALL):

1. Stanford University, Palo alto, CA, United States.
2. Radiology, Stanford University, Stanford, CA, United States.
3. wuhan university, Wuhan, China.
4. Stanford University, Stanford, CA, United States.
5. Stanford University, Stanford, CA, United States.

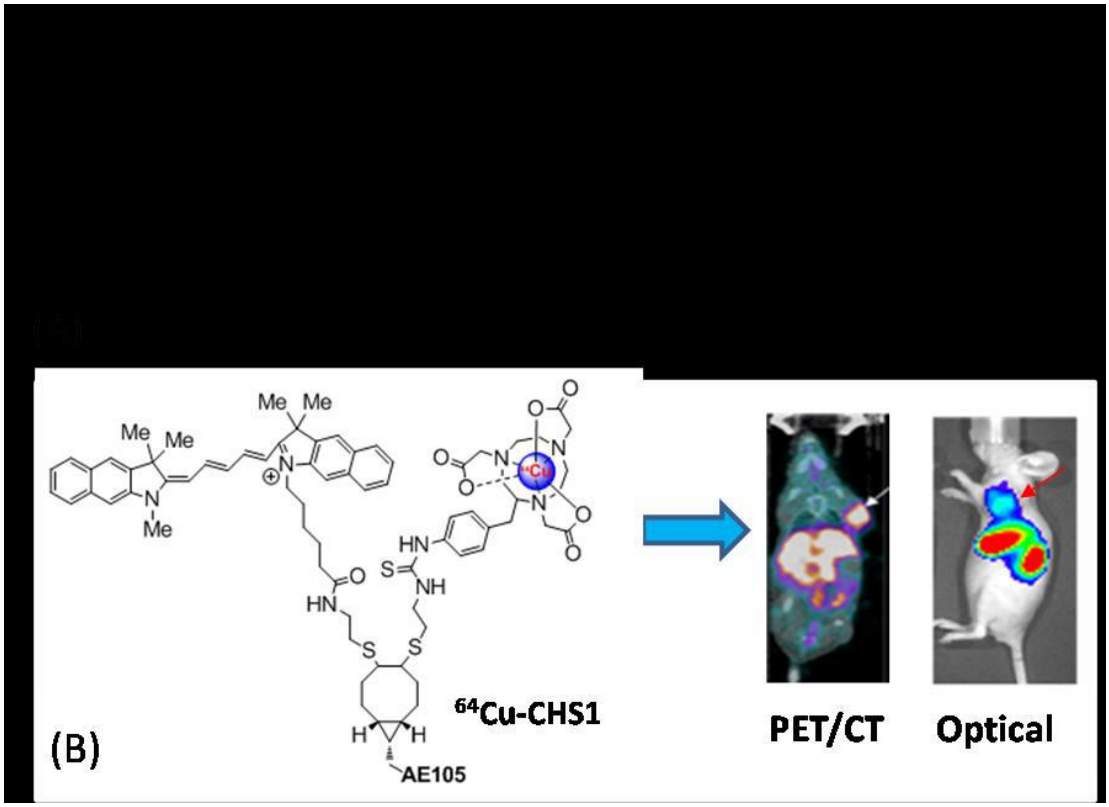
(B)
Me Me
Me Me
N
Me
HN
S
NH
HN
S
S
H
H
AE105
64Cu-CHS1
PET/CT
Optical

CONTROL ID: 2243549

TITLE: Labeling and stability studies for a tetrameric cyclic RGD peptide based radiopharmaceutical $^{64/67}$Cu-cyclam-RAFT-c(-RGDfK-)$_4$

PRESENTER: Zhao-Hui Jin

ABSTRACT BODY:

Abstract Body: We have developed an $\alpha_V\beta_3$ integrin-targeted tetrameric cyclic RGD peptide based radiopharmaceutical $^{64/67}$Cu-cyclam-RAFT-c(-RGDfK-)$_4$ ($^{64/67}$Cu-cyclam-RAFTRGD) (1). ^{64}Cu-cyclam-RAFTRGD shows a strong and positive correlation between the tumor uptake of this probe and the corresponding tumor $\alpha_V\beta_3$ expression levels (2), and PET imaging with this probe is potentially applicable for the diagnosis of $\alpha_V\beta_3$ positive pancreatic cancers (3), and for *in vivo* angiogenesis imaging and monitoring of anti-angiogenesis therapy (4). Despite the successful results, the question about the stability of Cu-cyclam could easily arise since the stability of radio-copper complex is still an extensively studied issue. Considering that $^{64/67}$Cu-cyclam-RAFTRGD would be a promising PET probe and radiotherapeutic agent, we aimed to optimize the Cu-radiolabeling, evaluate and verify the stability of $^{64/67}$Cu-cyclam-RAFTRGD by using several analytical techniques. **Methods:** Radiolabeling reaction, in terms of time, temperature, solvent, and molar ratio, was assessed by reversed phase -high-performance-liquid-chromatography (RP-HPLC) or radio-thin-layer chromatography (radio-TLC). *In vitro* plasma stability of $^{64/67}$Cu-cyclam-RAFTRGD was analyzed by RP-HPLC and radio-TLC, and *in vivo* stability and metabolism in blood, urine, liver, and kidney in normal mice injected with ^{64}Cu-cyclam-RAFTRGD were determined by radio-TLC and size exclusion chromatography (SEC). **Results:** All the parameters, including time, temperature, solvent, molar ratio, and the specific activity of $^{64/67}$Cu, may influence the Cu-labeling efficiency for RAFTRGD. Cyclam-RAFTRGD can be radiolabeled with $^{64/67}$Cu with ~100% labeling efficiency and ~100% radiochemical purity at room temperature within 10 minutes. The specific radioactivity can be achieved at 74 MBq/nmole for ^{64}Cu-cyclam-RAFTRGD, and 5.55 MBq/nmole for ^{67}Cu-cyclam-RAFTRGD. Both radio-TLC and RP-HPLC analyses demonstrated that $^{64/67}$Cu-cyclam-RAFTRGD was quite stable in mouse and /or human plasma, remaining in intact form after 48 hours at 37^{o}C. Both radio-TLC and SEC showed the high *in vivo* stability of ^{64}Cu-cyclam-RAFTRGD, with only the intact probe detected in plasma and urine at 1 hour post-injection. SEC analysis clearly showed that more than 70% of radioactivity and around 50% of radioactivity in the kidney and liver, respectively, corresponded to the intact probe. **Conclusion:** RAFTRGD can be efficiently radiolabeled with $^{64/67}$Cu through the bifunctional chelator cyclam, with ~100% radiochemical purity and excellent biostability.

AUTHORS (LAST NAME, FIRST NAME): Jin, Zhao-Hui[1]; Furukawa, Takako[1]; Degardin, Mélissa[2]; Boturyn, Didier[2]; Zhang, Ming-Rong[1]; Fujibayashi, Yasuhisa[1]; Dumy, Pascal[3]; Saga, Tsuneo[1]

INSTITUTIONS (ALL):

1. Molecular Imaging Center, National Institute of Radiological Sciences, Chiba, Japan.
2. Département de Chimie Moléculaire, Université Grenoble-Alpes - CNRS, Grenoble, France.
3. École Nationale Supérieure de Chimie de Montpellier, Montpellier, France.

(No Image Selected)

CONTROL ID: 2234173

TITLE: Feasibility of Bubble liposomes as ultrasound contrast agent; in vivo animal study

PRESENTER: Yusuke Oda

ABSTRACT BODY:

Abstract Body: [Purpose]

Ultrasound contrast agents (microbubbles) have been used for ultrasonography in tumor imaging. Flash Replenishment Imaging (FRI) in which the microbubbles in the scanning volume are destroyed by high intensity ultrasound and the following re-perfusion of the bubbles is detected, is an important method for real time imaging. Micro Flow Imaging (MFI) is also an important technique for visualization of branched narrow tumor blood vessels. MFI is an accumulative imaging technique by maximum intensity projection method.

We previously developed sub-micron sized Bubble liposomes which are lipid-coated perfluoropropane nanobubbles encapsulated in liposomes. In this study, we examined the feasibility of Bubble liposomes as ultrasound contrast agent for FRI and MFI method.

[Methods]

Liposomes consisting of 1,2-distearoyl-sn-glycero-phosphatidyl choline (DSPC), 1,2-distearoyl-sn-glycero-3-phosphatidyl-ethanolamine-methoxypolyethylene glycol (DSPE-PEG(2k)–OMe) 94: 6, were prepared by reverse-phase evaporation method. Sterilized vials containing 2 ml of the liposome suspension (lipid concentration: 1 mg/ml) were filled with perfluoropropane, capped, and then supercharged with another 7.5 ml of perfluoropropane. The vials were placed in a bath-type sonicator for 5 minutes to form the Bubble liposomes.

Mouse melanoma cells (B16/BL6: 1×10^6 cells/mouse) were inoculated to HR-1 mice. After 10 days, the tumor tissue was monitored with ultrasound imaging device (Vevo® 2100 system: FUJIFILM VisualSonics, Inc.). Then, Bubble liposomes (lipid 300 μg) were infused for 3 minutes, and monitored with contrast mode. For taking a FRI, after the infusion, flash ultrasound was exposed to tumor tissue, and the re-perfusion of Bubble liposomes was monitored. For taking a MFI, 540 frames during Bubble liposomes infusion were overlaid into on projection.

[Results & Discussion]

When the the tumor was exposed to flash echo, the contrast mean power decreased. After the flash echo, the contrast mean power returned to the same level as before exposure. These results indicate that Bubble liposomes were collapsed responding to the flash echo, and returned by re-perfusion of blood containing bubbles. Additionally, the structures of tumor vessels were clearly drawn by MFI.

[Conclusion]

This study shows that Bubble liposomes can be applied as an ultrasound contrast agent for FRI and MFI.

[Acknowledgement]

This study was supported by MEXT-Supported Program for the Strategic Research Foundation at Private Universities (2013-2017), the Programs for Promotion of Fundamental Studies in Health Sciences of the National Institute of Biomedical Innovation (NIBIO) and JSPS KAKENHI (25860397)

AUTHORS (LAST NAME, FIRST NAME): Oda, Yusuke[1]; Suzuki, Ryo[1]; Omata, Danki[1]; Unga, Johan[1]; Uruga, Hitoshi[1]; Sugii, Mutsumi[1]; Maruyama, Kazuo[1]

INSTITUTIONS (ALL):

1. Faculty of Pharma-Sciences, Teikyo University, Tokyo, Japan.

(No Image Selected)

CONTROL ID: 2232515

TITLE: Visualization of colon and NSCL cancer using Novel Protein Scaffold, anti-EGFR Repebody

PRESENTER: Misun Yun

ABSTRACT BODY:

Abstract Body: Purpose : Repebody is a binding scaffold based on variable lymphocyte receptors, which are nonimmunoglobulin antibodies composed of leucine-rich repeat modules in jawless vertebrates. Repebody can be developed against variety of epitopes by module engineering. The epidermal growth factor receptor (EGFR, HER1) autocrine pathway contributes to a number of highly relevant processes in cancer development and progression, including cell proliferation, regulation of apoptotic cell death, angiogenesis and metastatic spread. In this study, EGFR-specific repebody was developed to visualize the status of receptor expression and to prevent ligand binding that may inhibit autophosphorylation and downstream intracellular signaling.

Methods : We developed anti-EGFR repebody by phage display. We selected human non-small cell lung cancer (H1650) and human colon cancer (HT29) highly expressing EGFR for in vitro and in vivo experiments. Human melanoma (MDA-MB-435) was selected as a negative control. Specific binding of anti-EGFR repebody to cells and cancer tissue was determined by immunoflourescence (IF) staining and/or FACs analysis. In vivo imaging was done by i.v. injection of Cy5.5 labeled anti-EGFR repebody (30 μg/mouse) or ^{64}Cu-NOTA-repebody (7.4 MBq/mouse) in H1650- and HT29-bearing mouse models using cooled CCD camera or microPET, respectively.

Results : In vitro and in vivo IF staining demonstrated that strong binding of anti-EGFR repebody to H1650 and HT29, but not to MDA-MB-435. In vivo near infrared (NIR) imaging demonstrated specific targeting of Cy5.5-labeled anti-EGFR repebody to grafted H1650 and HT20 tumor in mice. A strong fluorescence signals were detected at the grafted tumors from day 1, and continuously to day 10 after injection. The ^{64}Cu-NOTA-repebody was detected at the implanted tumor from 1 h (SUVmax: 1.34±0.12) after the injection, peaked at 6 h (1.75±0.18), maintained to 24 h (1.33±0.17), and declined at 48 h (1.11±0.05). To verify the specificity of the anti-EGFR repebody binding to the EGFR-expressing tumor, the tumor-bearing mice were injected with 10 mM naïve EGFR repebody 1 day before injection of ^{64}Cu-NOTA-EGFR repebody. The radioactivity decreased 50%, indicating the specificity of EGFR repebody binding *in vivo*.

Conclusion : The anti-EGFR repebody could be developed for imaging and therapy of cancer overexpressing EGFR. Our work provides a basis to develop potential strategy of targeted immuno detection of cancers which may replace monoclonal antibodies.

AUTHORS (LAST NAME, FIRST NAME): Yun, Misun [1]; Kim, Dong-Yeon[1]; Kim, Hyeon Sik[1]; Zheng, Jin Hai[1]; Pyo, Ayoung[1]; Hong, Yeongjin[2]; Min, Jung-Joon[1]

INSTITUTIONS (ALL):

1. Nuclear Medicine, Chonnam National University Hwasun Hospital, Hwasun, Korea (the Republic of).
2. Microbiology, Chonnam National University Medical School, Gwangju, Korea (the Republic of).

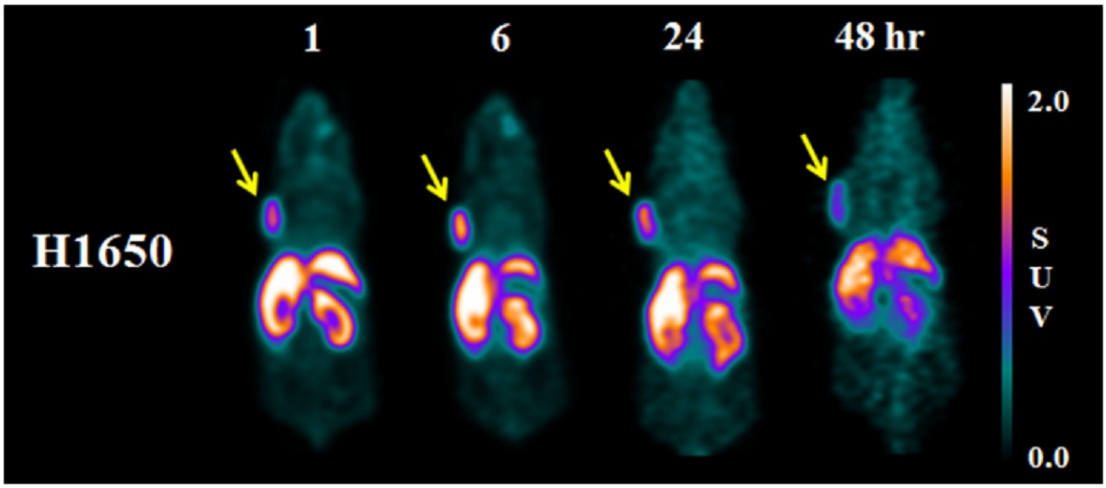
1
6
24
48 hr
H1650
2.0
S
U
V
0.0

CONTROL ID: 2232534

TITLE: Near Infrared Fluorescent Image Based Evaluation of Gastric Tube Perfusion after Esophagectomy in Preclinical Model

PRESENTER: Minji Kim

ABSTRACT BODY:

Abstract Body: Background; This study was to evaluate the feasibility of near infrared (NIR) fluorescent images as a tool for evaluating the perfusion of the gastric tube after esophagectomy. In addition, we investigated the time required to acquire enough signal to confirm the presence of ischemia in gastric tube after injection of indocyanine green (ICG) through peripheral versus and central venous route.

Methods; ICG (0.6mg/kg) was used as a NIR fluorescent tracer and the fluorescence signal-to-background ratios (SBR) were measured by using the intraoperative color and fluorescence imaging system (ICFIS). 4 porcine underwent esophagogastrostomy and their right gastric arteries were ligated to mimic ischemic condition of gastric tube. Then we evaluated perfusion of gastric tubes by comparing their SBR with esophageal SBR. In addition, we measured the time required to acquire enough signal in 10 porcine which underwent esophagectomy after peripheral (n=6) or central (n=4) venous injection of ICG.

Results; In ischemic models, SBR of esophagus was higher than that of gastric tube (2.8±0.54 vs. 1.7±0.37, $p<0.05$). It showed high esophagus-stomach signal to signal ratio. (SSR, 1.8±0.76). We also could observe recovery of blood perfusion in few minutes after releasing the ligation of right gastric artery. In comparison study according to the injection route of ICG, The time to acquire signal stabilization was faster in central than in peripheral route (119 ± 65.1 seconds in central route vs. 295±130.4 in peripheral route, $p<0.05$).

Conclusion: NIR fluorescent images could provide the real-time information if there was ischemia or not in gastric tube during operation. And, central injection of ICG might give that information faster than peripheral route.

AUTHORS (LAST NAME, FIRST NAME): Kim, Minji[1]; Quan, Yuhua[3]; Choi, Byeong Hyeon[3]; han, Kooknam[3]; Lee, Kisung[1]; Eo, Jae Seon[2]; Choi, Yeong ho[2]; Choi, Yeonho[1]; Park, Ji Ho[4]; Kim, Hyun Koo[2]; Kim, Beop-min[1]

INSTITUTIONS (ALL):

1. Biomedical Engineering, Korea University, Seoul, Korea (the Republic of).
2. Korea University Guro Hospital, Korea University College of Medicine, Seoul, Korea (the Republic of).
3. Thoracic and Cardiovascular Surgery, Korea University Guro Hospital, Korea University College of Medicine, Seoul, Korea (the Republic of).
4. KAIST, Daejeon, Korea (the Republic of).

(No Image Selected)

CONTROL ID: 2232517

TITLE: High resolution micro-endoscopy for the diagnosis of gastric carcinoma and precancerous lesions

PRESENTER: Haifeng Liu

ABSTRACT BODY:

Abstract Body: Objectives

In this study, experiments were designed and conducted to explore the value of high resolution micro-endoscopy (HRME) to the diagnosis of gastric cancer and precancerous lesions in clinics.

Methods

Firstly, HRME was examined in the gastric biopsy specimens of 5 gastric cancers, 5 gastric precancerous lesions, 5 normal gastric antrum mucosae, and 5 normal gastric fundus mucosae obtained by endoscopy. Secondly, the characteristics of the HRME images were analysed. Diagnostic criteria of HRME were summed up for the normal gastric mucosa, gastric cancer and gastric precancerous lesion. Thirdly, the 15 human gastric cancer specimens obtained during surgery were imaged for HRME. Each gastric cancer specimen has 4 imaging positions. 60 HRME images were analysed. Based on the diagnostic criteria, HRME results were obtained. Lastly, the results were compared with the pathological findings. The value of HRME to the diagnosis of gastric cancer and precancerous lesions was evaluated.

Results

Diagnosis was realized by analysing the nucleus size, shape, arrangement, gland, the structure of the glandular tube, and calculating the nucleo-cytoplasmic ratio in the ROI. Normal gastric mucosa has the following characteristics: the nuclei were in the same size, regular shape, neat structure of the glands and the glandular tube. Gastric pit openings were tubular or elliptic shaped, and cells around gastric pit arranged regularly.

Gastric fundus mucosa is showed in Figure 1(a). A large number of closely packed glands were seen. Gastric pit openings were oval or long branching, fracture was linear, and the nuclei were arranged regularly. HRME of gastric antrum mucosa is shown in Figure 1(b). Gastric pit openings were irregular or tubular shaped, glandular cavity was fissure shaped. Cells around gastric pit arranged regularly, and the nuclei were small and densely distributed. Figure 1(d) is the HRME of the gastric cancer. Nuclei were more irregularly sized, arranged disorderly. Gland size difference was very big, and structure was not clear or unable to discern glands. Gastric pit structure was destroyed, and normal gastric pit structures disappeared. The characteristics of precancerous lesion are between the gastric cancer and the normal gastric mucosa, as shown in Figure 1(c).

HRME results indicated that the number of normal gastric mucosa, gastric precancerous lesions, and gastric cancer was 18, 14, and 28, respectively. Pathological results showed that 21 normal gastric mucosa, 16 gastric precancerous lesions, and 23 gastric cancers. After statistical analysis, diagnostic accuracy, specificity, sensitivity, negative predictive value and positive predictive value of HRME for gastric carcinoma and precancerous lesions are shown in the Table 1.

Conclusions

Data showed that HRME this novel imaging method had great value in the detection of gastric cancer and precancerous lesions.

AUTHORS (LAST NAME, FIRST NAME): Hu, Zhenhua[1]; Tan, Tao [2]; Qu, Yawei [2]; Zhang, Xiaojun[3]; Liu, Haifeng [2]; Tian, Jie[1]

INSTITUTIONS (ALL):

1. Key Laboratory of Molecular Imaging of Chinese Academy of Sciences, Institute of Automation, Beijing, China.
2. Department of Gastroenterology, General Hospital of Chinese Armed Police Forces, Beijing, China.
3. Department of nuclear medicine, Chinese PLA General Hospital, Beijing, China.

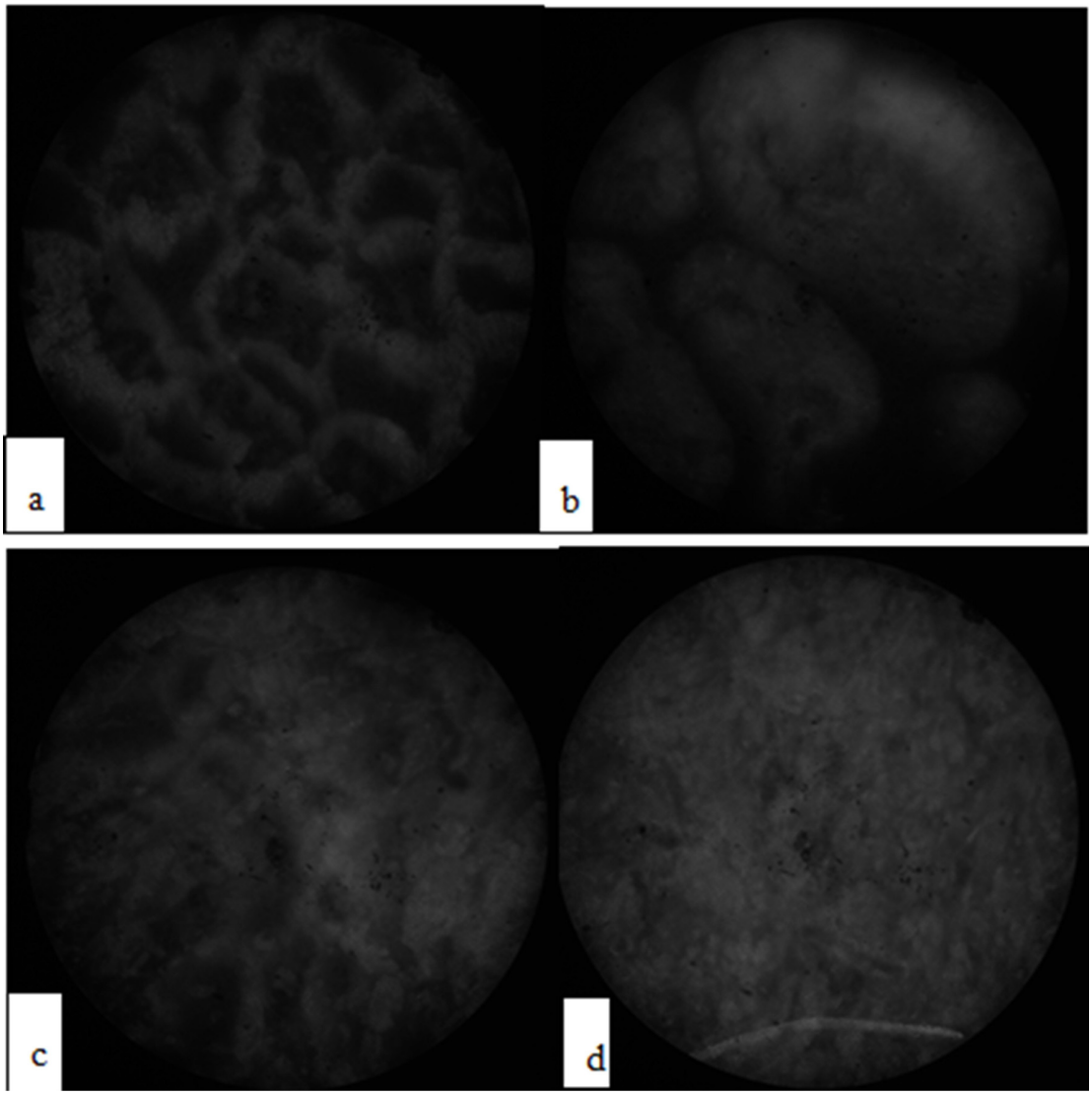
a
b
c
d

CONTROL ID: 2232813

TITLE: *In Vivo* Imaging of Transplanted Stem Cells by Near Infrared Region-II (NIR-II) Fluorescence

PRESENTER: Hiroshi Yukawa

ABSTRACT BODY:

Abstract Body: We have studied *in vivo* fluorescence imaging of transplanted stem cells by using Quantum dots (QDs) that show the absorption and fluorescence in near infrared region-I (NIR-I) (700-900 nm) named as biological window [1-4]. However, the sensitivity was not sufficient for *in vivo* imaging of transplanted stem cells in mice, because the optical transparency in the NIR-I to the body is not sufficiently-high. In this study, we investigated the usefulness of the fluorescence in near infrared region-II (NIR-II : over-1000 nm) as the second biological window, showing a very high optical transparency to the body [5], for *in vivo* imaging of transplanted stem cells.

The fluorescence in NIR-II range under 980 nm excitation was detected by using a portable *in vivo* fluorescent imaging system (SAI-1000, Shimadzu). Yttrium oxide and yttrium-based nanoparticles (Y_2O_3-PEG-PA_2 and NaYF4-PEI) were prepared by Katayama Chemical Industries Co.,Ltd. and were used as over-1000 nm NIR fluorescent nanoparticles. The fluorescence intensity of the nanoparticles was measured in the transduction medium (FD medium + 20% FBS). The efficiency of the cellular uptake was investigated using adipose tissue-derived stem cells (ASCs) collected from C57BL/6 mice. The ASCs labeled with the nanoparticles were transplanted subcutaneously into the backs of mice or into mice through the tail vein.

The strong NIR-II fluorescence derived from Y_2O_3-PEG-PA2 and $NaYF_4$-PEI could be detected in the transduction medium by using SAI-1000. ASCs could be labeled with both nanoparticles of Y_2O_3-PEG-PA2 and $NaYF_4$-PEI, however the labeling efficiency of $NaYF_4$-PEI was much higher than that of Y_2O_3-PEG-PA2. Thus, $NaYF_4$-PEI was used for *in vivo* fluorescence imaging of transplanted ASCs. The subcutaneously transplanted ASCs labeled with $NaYF_4$-PEI (> about 6,250 cells) could be detected on the back of mice with the high efficiency in comparison to previous method using QDs. Next, the transplanted ASCs labeled with $NaYF_4$-PEI through tail vein could be detected in the lungs and liver in mice as with previous results. On the other hand, the accumulation of transplanted ASCs into spleen could be confirmed, which was previously undetectable. These data suggested that *in vivo* fluorescence imaging by using NIR-II fluorescence is useful for detecting and diagnosis of transplanted stem cells.

References

1. Yukawa, H. et al. *Cell Transplant.,* **2009**, *18*, 611-618.
2. Yukawa, H. et al. *Biomaterials,* **2010**, *31(14)*, 4094-4103.
3. Yukawa, H. et al. *Biomaterials,* **2012**, *33(7)*, 2177-2186.
4. Yukawa, H. et al. *Cell Medicine,* **2013**, *6,* 83-90.
5. Guosong, H. et al. Nature Photonics, **2014**, *8*, 723-730.

AUTHORS (LAST NAME, FIRST NAME): Yukawa, Hiroshi[1]; Onoshima, Daisuke[2]; Takeuchi, Tsukasa[3]; Ishikawa, Tetsuya[4]; Baba, Yoshinobu[5]

INSTITUTIONS (ALL):

1. FIRST Research Center for Innovative Nanobiodevice, Nagoya University, Nagoya, Aichi, Japan.
2. Institute of Innovation for Future Society, Nagoya University, Nagoya, Japan.
3. Analytical & Measuring Instruments Division, Shimadzu Corporation, Tokyo, Japan.
4. Department of Medical Technology, Nagoya University, Nagoya, Japan.
5. Department of Applied Chemistry, Graduate School of Engineering, Nagoya University, Nagoya, Japan.

(No Image Selected)

CONTROL ID: 2232523

TITLE: Surface Engineered Quantum Dots, their Conjugates, and Amphiphilic Polyethyleneimine Polymer Wrapped Composites for Biomedical and Imaging Applications

PRESENTER: Joonhyuck Park

ABSTRACT BODY:

Abstract Body: Semiconductor nanocrystal quantum dots (QDs) with unique optical properties and surface functionalization capability have emerged as an alternative for fluorescence proteins or organic dyes in bio-imaging applications.

A new QD ligand chemistry is introduced that can provide zwitterionic surface QDs. Zwitterionic QDs are compact with the ligand hydrodynamic(HD) thickness less than 2 nm, colloidally very stable over broad pH and even in saturated NaCl solution, and shows minimal non-specific adsorptions. Mixed zwitterionic and other functional groups on QD surface allows simple conjugations for highly specific targeting while retaining the advantages of zwitterionic QD surface. Streptavidin(SA) or antibody QD conjugates using the mixed QD surface ligand system have been demonstrated that can show over 4000 times higher signal-to-noise ratio over the unconjugated mixture control case. Surface-engineered semiconductor QDs have been demonstrated to act as a signal amplifiable reporter in immunoassays *via* self-assemblies using SA and biotin QD conjugate pair. Typical sandwich-type immunoassay procedures were adopted, and the targeted protein-binding events were effectively transduced and amplified by the fluorescence of the SA-biotin QD conjugates. The detection limit of myoglobin in 100% serum was determined to be at the sub-attomolar level. The assay can be highly miniaturized and multiplexed, and parallel and rapid detection of 4 different cancer markers has been successfully demonstrated. To demonstrate that this QD signal amplification can be a universal platform, sensitive imaging and early detection of apoptotic cells were also showcased.

Polyethyleneimine(PEI) based amphiphilic polymers (amPEIs) were synthesized by derivatizing amines with alkylisocyanates and demonstrated as a platform technology for QD cellular labeling and imaging. As-synthesized QDs were wrapped by amPEIs *via* hydrophobic interaction between alkyl moieties of the polymers and QDs' original surface ligands, retaining the unreacted amines of PEI backbone at outside of the surface of wrapped QDs. For maximizing intracellular delivery of amPEI wrapped QDs (QD-amPEI), their HD sizes (~100 nm) and zeta potential value (~60 mV) were delicately optimized. Quantitative and comparative studies of intracellular delivery of QD-amPEI were investigated by flow cytometry, confocal microscopy, and cross-sectional transmission electron microscopy. For specific cellular labeling, hyaluronic acid (HA)-QD-amPEI composites were synthesized *via* electrostatic self-assembly and their specific-to-non-specific fluorescence signal ratio was around 120. Green fluorescent protein (GFP) gene silencing was performed by delivering QD-amPEI-siRNA to GFP transfected cells, which was 20 times more efficient than Lipofectamine^{TM}-siRNA complexes. Oxygen sensing probes were synthesized by wrapping both oxygen sensitive ruthenium(II)-based phosphorescence dyes and QDs with amPEI (QD-Ru-amPEI). The QD-Ru-amPEI composites were demonstrated as reversible and oxygen-sensitive probes in normoxic and hypoxic condition by ratiometric PL measurements *in vitro*, in cultured monolayer cell level, and a mouse dorsal model.

AUTHORS (LAST NAME, FIRST NAME): Park, Joonhyuck[1]; Park, Youngrong[1]; Lee, Junhwa[1]; Kwag, Jungheon[1]; Kim, Bumju[2]; Kim, Ki Hean[2]; Bok, Seoyeon[3]; Ahn, G-one[3]; Kim, Sungjee[1]

INSTITUTIONS (ALL):

1. Chemistry, POSTECH, Pohang, Gyeong-buk, Korea (the Republic of).
2. Mechanical Engineering, POSTECH, Pohang, Gyeong-buk, Korea (the Republic of).
3. Division of Integrative Biosciences and Biotechnology, POSTECH, Pohang, Gyeong-buk, Korea (the Republic of).

(No Image Selected)

CONTROL ID: 2232521

TITLE: Imaging the impact of eosinophil cationic protein in breast cancer progression

PRESENTER: Mei-Ling Hsieh

ABSTRACT BODY:

Abstract Body: Eosinophils mediate their immune function via degranulation and production of various molecules including cytotoxic granule proteins, cytokines, chemokines, lipid mediators, neurotransmitters. One of granule proteins with cytotoxic activity against bacteria, parasites, viruses, respiratory and epithelium is the eosinophil cationic protein (ECP). Although in vitro studies have shown that ECP has growth-inhibitory effect in cancer cells, in vivo role of ECP in cancer progression is still unclear. Here, we observe in vivo effect of ECP in breast cancer progression via ECP bone marrow chimeric mice and orthotopic breast cancer model. The bioluminescence imaging studies demonstrated that control mice implanted with 4T1-luc cells had lung metastases, whereas ECP bone marrow chimeric mice showed no metastases. The tumor sizes in ECP bone marrow chimeric mice were smaller than in control mice. There was a significant growth delay in ECP bone marrow chimeric mice compared to control mice. Furthermore, survival analysis showed that ECP bone marrow chimeric mice with 4T1-luc cells implantation had a significantly longer survival than the control mice with 4T1-luc cells implantation. Immunohistochemical studies revealed ECP-positive staining 4T1 tumor tissues could be detected in ECP bone marrow chimeric mice but not in control mice, suggesting ECP is able to accumulate in breast cancer from bone marrow cells. Taken together, these results provide an evidence that ECP inhibits tumor growth and metastasis in breast cancer progression. These findings also provide a novel concept that ECP is a natural and non-cytotoxic component involved in innate immunity against the malignant progression

AUTHORS (LAST NAME, FIRST NAME): Hsieh, Mei-Ling[1]; Hsieh, Chia-Hung[2]

INSTITUTIONS (ALL):

1. Graduate Institute of Immunology, China Medical University, Taichung , Taiwan.
2. Graduate Institute of Basic Medical Science, China Medical University, Taichung, Taiwan.

(No Image Selected)

CONTROL ID: 2232525

TITLE: Gold Nanopaticle Assembly Systems as Theranostic agent for Selective Cancer therapy and Imaging *in Vitro* and *in Vivo.*

PRESENTER: Jaejung Song

ABSTRACT BODY:

Abstract Body: Assembled gold nanoparticles (AuNPs) have been used for many biomedical applications, which includes photothermal effect, CT imaging contrast, and radio-sensitization. Properly tuning the plasmonic wavelength for photothermal therapy typically results in the nanostructures such as nanorods, nanoshells, and nanocages of which hydrodynamic sizes typically reach ~100 nm. We innovatively designed platforms for AuNP assemblies using DNA hydrogel or pH-responsive surface ligand.

The assembled AuNPs in Dgel showed strongly coupled plasmon modes, and Dgel vehicle can co-load anticancer drugs, such as Doxorubicin (Dox), as a light-controlled releasing cargo by DNA intercalations. Upon laser excitation, local heat shock generation was accompanied by the Dox release. Highly synergistic thermo chemo combination cancer therapy was demonstrated at cellular and also at animal model. Our Dgel vehicle can be fragmented after the excitation-induced heat generations, which subsequently renders dispersion of AuNPs. Our system allows the usage of small AuNPs that can be inherently less toxic. The Dgel vehicle is designed to fragment by the plasmon-induced heat, which can subsequently render the dispersion of AuNPs for rapid clearance and mitigation of toxicity.

A ‘smart’ gold nanoparticle (SAN) consists of ~10 nm gold sphere and pH-responsive surface ligands that can convert their charges from negative to positive under mild acidic environment. Triggered by pH change, the nanoparticle (NP) surfaces are engineered to have both positive and negative charges. Electrostatic attractions between the NP can rapidly form aggregates. The pH-induced formation of aggregates shifts the absorption to near-infrared region which can show maximal penetrations of tissue. The SANs show highly specific accumulations in cancer cells due to the enhanced phagocytic activity of cancer cells and the exocytosis which was efficiently blocked by the increased size of the aggregates. Thanks to the acquired properties, the SANs have been demonstrated as versatile cancer-specific imaging/therapy agents including phtotothermal therapy, photothermal-optical coherence tomography, and photoacoustic imaging. SANs can be further conjugated with anticancer drug Dox at the terminal of surface molecules via carbodiimide coupling reaction. The high synergistic effect of chemo and photothermal combination cancer therapy was demonstrated in vitro and in vivo level. Theragnostic SAN was also demonstrated by the surface co-decoration with the pH-responsive ligand and a Raman-active molecule. The theragnostic agents can form aggregate and simultaneously provide hot spots for surface enhanced Raman scattering with the enhanced factor reaching $1.3x10^4$. Moreover, the phothermal effect of gold nanoparticle was applied to photoacosutic tomography. By selective photoacoutic conversion efficiency, significant signal enhancement is confirmed with the 20-fold *in vitro* and 4-fold increment *in vivo* than normal cell or tissue.

We expect that these assembly systems of gold nanoparticle can show powerful multimodal properties for diagnostic and therapeutic application when integrating several modalities.

AUTHORS (LAST NAME, FIRST NAME): Song, Jaejung[1]; Hwang, Sekyu[2]; Nam, Jutaek[2]; Jung, Sungwook[1]; Kim, Jeesu[4]; Ahn, G-one[3]; Kim, Ki Hean[3]; Kim, Chulhong[4, 5]; Park, Nokyoung[6]; Kim, Sungjee[1, 2]

INSTITUTIONS (ALL):

1. School of Interdisciplinary Bioscience and Bioengineering, Pohang University of Science & Technology (POSTECH), Pohang, Gyeongsangbuk-do, Korea (the Republic of).
2. Department of Chemistry, Pohang University of Science & Technology (POSTECH), Pohang, Korea (the Republic of).
3. Division of Integrative Biosciences and Biotechnology, Pohang University of Science & Technology (POSTECH), Pohang, Gyeong-buk, Korea (the Republic of).
4. Department of Electrical Engineering, Pohang University of Science & Technology (POSTECH), Pohang, Gyeong-buk, Korea (the Republic of).
5. Department of Creative IT Engineering, Pohang University of Science & Technology (POSTECH), Pohang, Korea (the Republic of).
6. Department of Chemistry, Myongji University, Yongin, Korea (the Republic of).

(No Image Selected)

CONTROL ID: 2232535

TITLE: Spraying Quantum Dot Conjugates for Rapid and Multiplex Cancer Diagnosis Using Endoscopy

PRESENTER: Sungjee Kim

ABSTRACT BODY:

Abstract Body: The detection of colon cancer using endoscopy is widely used but the interpretation of the diagnosis is based on the clinician's naked eye. This is subjective and can lead to false detection. Here we developed a rapid and accurate molecular fluorescence imaging technique using antibody-coated quantum dots (Ab-QDs) sprayed and washed simultaneously on colon tumor tissues inside live animals, subsequently excited and imaged by endoscopy. QDs were conjugated to matrix metalloproteinases (MMP) 9, MMP 14 or carcinoembryonic antigen (CEA) Abs with zwitterionic surface coating to reduce non-specific bindings. The Ab-QD probes can diagnose tumors on sectioned mouse tissues, fresh mouse colons stained *ex vivo* and also *in vivo* as well as fresh human colon adenoma tissues in 30 minutes and can be imaged with a depth of 100 μm. The probes successfully detected not only cancers that are readily discernible by bare eyes but also hyperplasia and adenoma regions. Sum and cross signal operations provided post-processed images that can show complementary information or regions of high priority. This multiplexed quantum dot, spray-and-wash, and endoscopy approach provides a significant advantage for detecting small or flat tumors that may be missed by conventional endoscopic examinations and bestows a strategy for the improvement of cancer diagnosis.

AUTHORS (LAST NAME, FIRST NAME): Kim, Sungjee[1]; Park, Youngrong[1]; Ryu, Yeon-Mi[2]; Jung, Yebin[1]; Wang, Taejun[4]; Baek, Yeonggyeong[3]; Yoon, Yeoreum[5]; Bae, Sang Mun[2]; Park, Joonhyuck[1]; Hwang, Sekyu[1]; Kim, Jaeil[6]; Do, Eun-Ju[2]; Kim, Sang-Yeob[2]; Chung, Euiheon[7]; Kim, Ki Hean[4]; Myung, Seung-Jae[2]

INSTITUTIONS (ALL):

1. Chemistry, POSTECH, Pohang, Korea (the Republic of).
2. Asan Institute for Life Sciences, Asan Medical Center, Seoul, Korea (the Republic of).
3. School of Interdisciplinary Bioscience and Bioengineering,POSTECH, Pohang, Korea (the Republic of).
4. Division of Integrative Biosciences and Biotechnology,POSTECH, Pohang, Korea (the Republic of).
5. POSTECH, Pohang, Korea (the Republic of).
6. Health Screening and Promotion Center, Asan Medical Center, Seoul, Korea (the Republic of).
7. Gwangju Institute of Science and Technology, Gwangju, Korea (the Republic of).

(No Image Selected)

CONTROL ID: 2232536

TITLE: Preclinical Safety and Efficacy of Graphene Based High Performance Magnetic Resonance Imaging Contrast Agent for Diagnosis and Monitoring of Renal Abnormalities

PRESENTER: Balaji Sitharaman

ABSTRACT BODY:

Abstract Body: Introduction: The etiology of patients with advanced renal insufficiency include kidney specific and non-specific conditions.[1,2] The use of Gd^{3+}-based contrast agents (GBCA) in magnetic resonance imaging (MRI) offers a unique possibility for both non-invasive morphological and functional imaging at early stage of the disease. However, the retention of GBCA impose a greater risk of developing debilitating and possibly life-threatening disease of nephrogenic systemic fibrosis in patients with renal insufficiency. Thus, there is a need for a T_1 MRI CA that is safer, more efficacious, and can allow the same clinical MRI performance at substantially lower dosages than GBCAs. We have developed a novel high-performance carbon nanostructure-based MRI CA from graphene nanoplatelets (small stacks of graphene sheets) intercalated with trace amounts of manganese (~0.06 wt%), and non-covalently functionalized with the FDA-approved polymer dextran (a.k.a. Mangradex (disk shaped, thickness=3-4 nm, diameter ~100 nm)).[3,4] The r_1 relaxivity of Mangradex is 92 $mM^{-1}s^{-1}$ (22 MHz proton Larmor frequency); ~20-30 fold greater than clinical MRI CAs.[4] These nanoparticles are hydrophilic, hemocompatible, iso-osmol and is-viscous to blood and form stable colloidal dispersions in biological fluids.[3,4] In this work, we report their *in vivo* pre-clinical safety and efficacy evaluation in small animals.

Methods: ***Toxicity***: Mangradex was injected at 1, 25, 50, 125, 250, 500 mg/kg (n=8/dose) by IV injection for acute toxicity, at dosages between 1-100 mg/kg (n=8/dose) 3X/week for three weeks for chronic toxicity study in healthy rats, and at potential therapeutic dosages between 1-50 mg/kg (n=8/dose for 15 and 30 days) for Nephrotoxicity in a 5/6 Nephrex rat model. Blood pressure, body weight, cardiac output, clinical blood chemistry and tissue histopathology were analyzed. ***MR Imaging***: *In vivo* T_1-weighted MRI was performed using a 7 T Bruker Biospec 7.0T/20-cm USR horizontal magnet (Bruker, Billerica, MA) in 5/6 nephrex rats to compare Mangradex at dose = 25 mg/kg or 60 nanomoles Mn^{2+}/kg with FDA-approved agent Ablavar® at equivalent Gd^{3+} concentration. T_1 relaxation time, signal to noise ratio (SNR) and contrast to noise ratio (CNR) were calculated in the region of interest (ROI).

Results and Discussion: The table (fig 1B) summarizes the major findings of the toxicity study on rodents**.** *In vivo* MRI (fig 1A) showed significant contrast enhancement in kidneys, drop in T_1 relaxation time (fig 1C) and substantial (>100%) increase in SNR and CNR up to 85 minutes in kidneys and 25 minutes in renal artery compared to Ablavar® (fig 1D).

Conclusion: *In vivo* studies indicate that Mangradex formulations are safe over large range of dosages and do not show any toxic effect in healthy and 5/6 Nephrex rats. Preliminary MRI examination of 5/6 Nephrex rats at 7 T show significant and sustained contrast in kidney and renal artery. Taken together these results indicate the exciting possibility of their development for diagnosis of renal failure.

References: **1.** *Neph Clin Practice, 2012; 12: c179-c184* **2.** *JABFM, 2010;* 23: *542-550* **3**. PloS one. 2012; 7(6):e38185; **4**. *Int J of Nanomed*, 2013; 8: 2821–2833.

AUTHORS (LAST NAME, FIRST NAME): Kanakia, Shruti[1]; Toussaint, Jimmy[3]; Kulkarni, Praveen [2]; Lee, Stephen[1]; Khan, Slah[1]; Mulick Chowdhury, Sayan[1]; Shroyer, Kenneth R.[1]; Moore, William[4]; Sitharaman, Balaji[1]

INSTITUTIONS (ALL):

1. Biomedical Engineering, Stony Brook University, Port Jefferson, NY, United States.
2. Northeastern University, Boston, MA, United States.
3. Stony Brook University, Stony Broook, NY, United States.
4. Stony Brook University, Stony Brook, NY, United States.

(No Image Selected)

CONTROL ID: 2232544

TITLE: Next Generation Digital PET/CT – First in Human Assessment of New Capabilities and Potential for Neuroimaging

PRESENTER: Jun Zhang

ABSTRACT BODY:

Abstract Body: Objectives:

To evaluate and demonstrate the potential capabilities of the next generation solid state digital photon counting PET/CT in clinical ^{18}F-FDG PET imaging of the brain.

Methods:

A next generation digital PET/CT system (Vereos, Philips Healthcare, Cleveland OH) was used in a pre-commercial release investigational Phase I trial. Replacing the conventional photomultiplier tube (PMT) detectors with solid state increase the number of discrete detectors from 420 to 23,040. Another important aspect is the improved timing resolution of time-of-flight (TOF) from current 550 ps to 320 ps. 10 clinical patients, whose standard of care (SOC) wholebody PET/CT (75±15kg; 1.7±0.1m; 13.1±0.6mCi FDG; 75±5min PET uptake time) was performed on a conventional PMT PET/CT system (Gemini TF 64, Philips Healthcare), were consented to have an additional dedicated brain PET acquisition on the digital PET/CT system (50-100min uptake time) before or after SOC using an ultrafast 90 seconds acquisition time. The digital PET/CT was reconstructed using system default high (2mm) and ultra-high (1mm) resolution protocols with combinations of ordered subsets expectation maximization (OSEM), TOF, point spread function (PSF) and Gaussian filter (GF). Blinded image reviews were assessed by radiologists, nuclear medicine physicians and medical physicists. Image quality was compared to conventional 10-minute brain PET imaging. Additionally phantom experiments were performed to assess quantitative accuracy.

Results:

Brain image quality was consistently scored higher and preferable on digital PET compared to conventional PMT PET ($p<0.01$). Digital PET was found to be quantitatively more accurate in the comparative phantom experiments. Even using ultrashort acquisition time of 90s, it revealed preferable anatomic details in all brain regions and including delineation of the optical nerves. PSF on digital PET improved image spatial resolution (>10%) and contrast (>15%), and together with Gaussian filter the signal-to-noise (SNR) was improved about >20%.

Conclusions:

Our first in human observation using the next generation digital PET/CT system indicates that neuroimaging is considerably improved compared to current generation photomultiplier systems. The high detection efficiency enables either much shorter acquisition times and/or substantial dose reduction. Higher spatial resolution was readily achievable. The concurrently improved timing resolution of time of flight appears to translate to more precise localization of neuro-anatomic structures. The digital detector technology appears to enable considerable improvements for molecular neuro PET imaging.

Research Support:

This project was enabled by the Ohio Third Frontier Scholars, Wright Project and Innovation Platform project grants, the Wright Center of Innovation in Biomedical Imaging and Philips Healthcare providing the investigational pre-commercial release system.

AUTHORS (LAST NAME, FIRST NAME): Zhang, Jun[1]; Binzel, Katherine[1]; Bardos, Philip[1]; Knopp, Michelle I.[1]; Nagar, Veena[1]; Wright, Chadwick L.[1]; Scharre, Douglas[2]; Rezai, Ali[3]; Maniawski, Piotr[4]; Knopp, Michael V.[1]

INSTITUTIONS (ALL):

1. Wright Center of Innovation & Radiology, The Ohio State University Wexner Medical Center, Columbus, OH, United States.
2. Neurology, The Ohio State University Wexner Medical Center, Columbus, OH, United States.
3. Neurological Surgery, The Ohio State University Wexner Medical Center, Columbus, OH, United States.
4. Philips Healthcare, Cleveland, OH, United States.

Figure 1. Initial phantom digital PET demonstration. An Esser Jaszczak ACR PET phantom with rod inserts (4.8mm to 12.7mm diameters) was used. PET/CT was performed on the digital PET/CT system with 90sec/bed in 60min after an administration of 1.3mCi FDG. While current PMT PET/CT systems may identify rods in 7.9mm (the 4th largest) and larger rods, even the smallest rod in 4.8mm can be identified on the digital PET

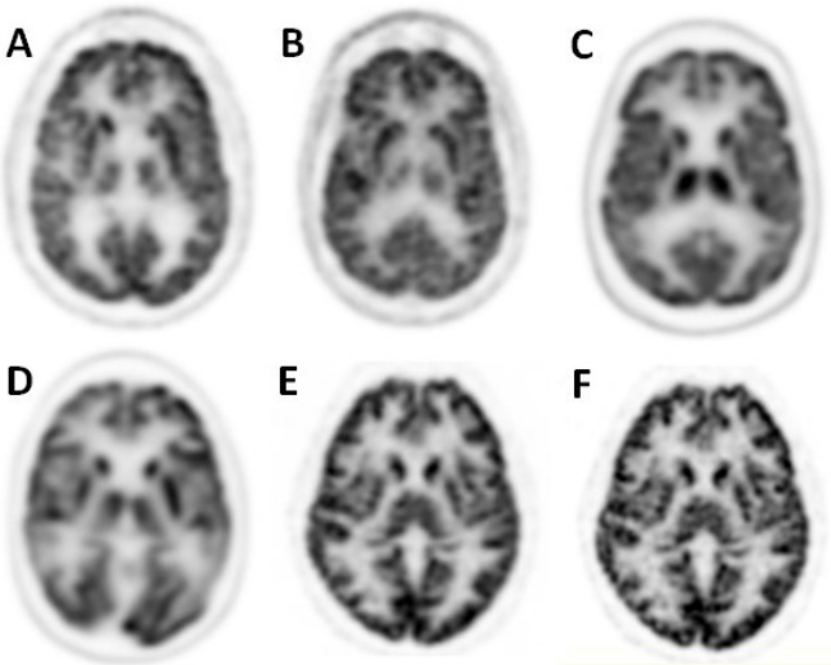

	A	B	C	D	E	F
PET/CT	Gemini TF 64	Gemini TF 64	mCT	mCT	Vereos	Vereos
XY resolution	2mm	2mm	1mm	1mm	2mm	1mm
Slice Thickness	2mm	2mm	3mm	3mm	2mm	1mm
FDG Injected	4.3mCi	5.0mCi	10.0mCi	12.0mCi	13.9mCi	13.9mCi
Uptake time	45min	45min	50min	49min	118min	118min
Acquisition Time	10min	10min	10min	10min	**90sec**	**90sec**

Figure 2. Comparison of four clinical standard of care 10-minute PET cases (A-D) performed on conventional PMT PET/CT systems (Gemini, mCT) with one 90-second PET (E-F) performed on the digital PET/CT system (Vereos).

CONTROL ID: 2232547

TITLE: Molecular Imaging the Impact of Disrupted-In-Schizophrenia 1 in Glutamatergic Transmission

PRESENTER: Wei-Ling Chen

ABSTRACT BODY:

Abstract Body: Disrupted-In-Schizophrenia 1 (DISC1), a multifunctional scaffolding protein that regulates cyclic adenosine monophosphate (cAMP) signaling via interactions with phosphodiesterase 4 (PDE4), has been studied extensively in the context of neurodevelopment and is a risk factor for major mental illnesses. However, the role of DISC1 in glutamatergic neurotransmission, particularly in N-methyl-D-aspartate receptor (NMDAR) activation that occurs in response to glutamate, which is implicated in numerous psychiatric disorders, remains elusive. Here, we synthesized a positron emission tomography (PET) radiotracer, ^{18}F-labelled alkylthiophenyl guanidine (^{18}F-FSAG), for imaging the PCP site of the NMDA ion channel, to observe deficient DISC1-mediated changes in activation of NMDAR in DISC1 knockout (DISC1$^{-/-}$) mice. *Ex vivo* biodistribution and PET imaging studies demonstrated that an appreciably lower accumulation of radioactive substances was found in the hippocampus in DISC1$^{-/-}$ than in wild-type mice. Moreover, the microdialysis together with glutamate assays were further utilized to determine the extracellular glutamate in hippocampus. The extracellular glutamate level in hippocampal was significantly decreased in DISC1$^{-/-}$ compared with wild-type mice. Taken together, these results suggest loss of DISC1 has hypofunction of glutamatergic transmission in the hippocampus. These findings may explain why patients with DISC1 mutations may have the mental disorders.

AUTHORS (LAST NAME, FIRST NAME): Chen, Wei-Ling[1, 2]; Hsieh, Chia-Hung[3, 4]

INSTITUTIONS (ALL):

1. Department of Psychiatry, Taichung Veterans General Hospital, Taichung, Taiwan.
2. Aging Medicine Program, China Medical University, Taichung, Taiwan.
3. Graduate Institute of Basic Medical Science, China Medical University, Taichung, Taiwan.
4. Department of Medical Research, China Medical University Hospital , Taichung, Taiwan.

(No Image Selected)

CONTROL ID: 2232713

TITLE: Development of an awake mouse MR imaging method using soft immobilization for a cryogenic probe system

PRESENTER: Shunsuke Kusanagi

ABSTRACT BODY:

Abstract Body: Introduction: In order to suppress blurring in MR images due to animal movements, treatments with anesthesia and fixing apparatuses are usually required. However, the physiological conditions are reportedly different between anesthetized and awake animals, and thus methods for awake MRI without anesthesia are attracting increased attention. In the current awake brain-imaging MR methods, fixing apparatuses implanted in the brain by surgery [1] and acclimation procedures by training [2] have been applied to suppress head movement in the scanner, and thus these methods require technical proficiency and days for recovery from surgery or for training. To overcome these drawbacks, we developed an easily implemented method for awake MRI using designed clothes, without surgery and training. Recently, a cryogenic transceive coil system (cryo coil), which greatly enhances the SNR of MR images, has become commercially available, and is now widely used [3]. To our knowledge, there are no reports of an awake mouse imaging method applicable to the cryo coil system.
The aim of this study is to improve our awake MRI method for application to the cryo coil system, through refinement of the designed mouse clothes.

Methods: MRI experiments were performed with a 7.0 Tesla Bruker Biospec 70/20 scanner and a mouse brain 2-channel phased array surface cryogenic coil or a mouse brain 4-channel phased array surface room temperature coil (r.t. coil) (Bruker BioSpin). Mouse clothes were designed to fit the mouse body and were used for the MRI measurements. The experiments were performed on adult male C57BL/6 mice. Under awake conditions, MR images were acquired for 30 minutes. Standard deviations (SDs) of the mouse brain movements in the three directions of Left–Right, Superior–Inferior, and Anterior–Posterior were calculated using SPM8, based on the acquired MR images. Throughout the experiments, the mice were kept at 37±1°C by a heating pad, and respiration and heart rates were monitored.

Results: The respiration and heart rates during the awake MRI experiments remained within the ranges normally observed in the awake mice under both conditions, using the cryogenic coil and the r.t. coil. The SDs of the mouse head movements were less than 0.15 mm under the cryogenic coil conditions, and 0.06 mm under the r.t. coil conditions in all three directions. The SDs under the cryogenic coil conditions were slightly larger than those under the r.t. coil conditons, but were lower than the spatial resolution of the MR images (0.2 mm). The images of the awake mice acquired with the cryo coil had a higher SNR than the image acquired with the r.t. coil.

Conclusions: We successfully improved the awake MRI method using soft immobilization by the designed clothes, for application to a cryogenic transceive coil system. Our method will greatly contribute to brain function studies by combined use with fMRI methods.

References: [1] Desai, M. *et al.*, *J. Neurophysiol.* **105**, 1393–1405 (2011), [2] King, J.A. *et al.*, *J. Neurosci. Methods* **148**, 154–160 (2005), [3] Haueisen, R. *et al.*, *Proc. Eur. Soc. Mag. Reson. Med. Biol.* **22**, 80 (2005)

AUTHORS (LAST NAME, FIRST NAME): Kusanagi, Shunsuke[1]; Kimura, Kazunari[1]; Funatsu, Hirotsugu[1]; Hirakane, Makoto[1]; Iwamoto, Shigeto[1]; Araki, Rikita[2]; Yoshinaga, Sosuke[1]; Terasawa, Hiroaki[1]

INSTITUTIONS (ALL):

1. Kumamoto University, Kumamoto, Japan.
2. Bruker BioSpin K.K., Yokohama-shi, Japan.

(No Image Selected)

CONTROL ID: 2232559

TITLE: PEGylated Nanoliposomes to Treat Myocardial Ischemia

PRESENTER: Hyosook Hwang

ABSTRACT BODY:

Abstract Body: Although liposomes hold promise for cancer therapy, the effectiveness for treating myocardial ischemia has yet to be proved. Nanoliposomes can effectively direct therapeutic agents to ischemic myocardium via the mechanism involving the enhanced permeability and retention effect. PEGylation can further facilitate the effective delivery by prolonging the circulation time. The present study tested the hypothesis that PEGylated nanoliposomes can be an effective treatment strategy for myocardial ischemia. Rats (~300 g) subjected to 30 minutes of myocardial ischemia received ^{99m}Tc HMPAO-labeled liposomes (mean diameter; 100, 300, and 600 nm) with or without PEGylation via apical puncture. Myocardial liposome uptakes and the tissue distribution were determined at 90 minutes post-injection. The liver exhibited the largest capacity for liposome uptakes followed by the spleen. The relatively greater liver and spleen uptakes were shown with 600 nm vesicles vs. 100 nm. Conversely, increased myocardial uptakes were shown with smaller sizes of vesicles (100 nm, 0.8 ± 0.25%; 600 nm, 0.2 ± 0.07 %; p=0.08). PEG modification augmented the liposomal uptakes in ischemic myocardium. The effect was greater with 100 nm vesicles (3.1 ± 1.53 %) vs. 300 nm (1.3 ± 0.75 %; p=0.019 vs. 100 nm) or 60 nm (1.5 ± 0.33 %; p=0.014 vs. 100 nm). To investigate the therapeutic effectiveness, ischemic hearts received PEGylated nanoliposomes (~100 nm) encapsulated with angiogenic peptides. Autoradiographic analysis by ^{99m}Tc tetrofosmin studied 7 days later revealed that PEGylated nanoliposomes loaded with angiogenic peptides improved myocardial perfusion (Control, 52 ± 13%; PEG, 71 ± 11%; p=0.006 vs.), whereas without PEG modification, no appreciable effects on perfusion were observed (unPEG, 54 ± 10%; p=0.700 vs. Control). These results establish the relative importance of liposomal size control and PEG modification for treating myocardial ischemia and the optimal design for drug delivery.

AUTHORS (LAST NAME, FIRST NAME): Hwang, Hyosook[1]; Jeong, Hwan-Seok[3]; Lee, Tai Kyoung[2]; Na, Kyung Suk[1]; Oh, Philsun[1]; Kwon, Jeongil[1]; Kim, Eun-Mi[1]; Kim, HyunSoo[1]; Kim, MinJoo[1]; Kim, Dong Hyun[1]; Lim, Seok Tae[1]; Sohn, Myung-Hee[1]; Jeong, Hwan-Jeong[1]

INSTITUTIONS (ALL):

1. Department of Nuclear Medicine, Molecular Imaging & Therapeutic Medicine Research Center, Cyclotron Research Center, Institute for Medical Sciences, Biomedical Research Institute, Chonbuk National University Hospital, Jeonju-si, Korea (the Republic of).

2. Department of Nuclear Medicine, Molecular Imaging & Therapeutic Medicine Research Center, Cyclotron Research Center, Institute for Medical Sciences, Biomedical Research Institute, Chonbuk National University Medical School and Hospital, Jeonju, Korea (the Republic of).

3. Department of Nuclear Medicine, Molecular Imaging & Therapeutic Medicine Research Center, Cyclotron Research Center, Institute for Medical Sciences, Biomedical Research Institute, chonbuk National University Medical School and Hospital, Jeonju, Korea (the Republic of).

(No Image Selected)

CONTROL ID: 2232787

TITLE: Improving Cerebral Blood Flow through Liposomal Delivery of Angiogenic Peptides: Potential of ^{18}F-FDG PET Imaging in Ischemic Stroke Treatment

PRESENTER: Hyosook Hwang

ABSTRACT BODY:

Abstract Body: The purpose of the study was to determine whether liposomal delivery of angiogenic peptides with known biological activity of vascular endothelial growth factor benefits cerebral ischemia and to examine the potential of ^{18}F-FDG PET imaging in ischemic stroke treatment.

Rats (n=40) were subjected to 40 minutes of middle cerebral artery occlusion. After 15 minutes of reperfusion, the rats (n=10) received angiogenic peptides incorporated into liposomes. Animals receiving phosphate-buffered solution served as controls (Control). One week later, ^{18}F-FDG PET imaging was carried out to examine regional changes in glucose utilization in response to the angiogenic therapy. The following day, ^{99m}Tc HMPAO autoradiography was performed to determine changes in cerebral perfusion after angiogenic therapy. Corresponding changes in angiogenic markers, including von Willebrand factor and angiopoietin-1 and -2, were determined by immune-staining and PCR analysis, respectively.

A 40-minute period of middle cerebral artery occlusion decreased blood perfusion in the ipsilateral ischemic cortex of the brain compared to that in the contralateral cortex, as measured by ^{99m}Tc HMPAO autoradiography. Liposomal delivery of angiogenic peptides to the ischemic hemisphere of the brain attenuated the cerebral perfusion defect (median, 1.0-fold of the contralateral; IQR, 0.9-.12; P=0.028 vs. non-treated controls) compared to non-treated controls (median, 0.9-fold of the contralateral; IQR, 0.8-1.0). In line with these results, vascular density evidenced by von Willebrand factor-positive staining was increased (median, 16 vessels per high power field; IQR, 15.5-20, P=0.039 vs. controls) in response to angiogenic therapy compared to that of the controls (median, 13 vessels per high power field; IQR, 12-15). This was accompanied by an early increase in angiopoietin-2 expression, a gene participating in angiogenesis (median, 3.7-fold of the normal without ischemia; IQR, 2.3-8.4; P=0.043 vs. control). ^{18}F-FDG PET imaging measured at seven days post-treatment revealed that liposomal delivery of angiogenic peptides facilitated glucose utilization (median, 1.038-fold of the contralateral; IQR, 1.021-1.090; P=0.018 vs. controls) in the ipsilateral ischemic cortex of the brain compared to that in the controls (median, 1.014-fold of the contralateral; IQR, 0.980-1.028). Furthermore, the change in regional glucose utilization was correlated with the extent of improvement in cerebral perfusion (r=0.742, P=0.035). Liposomal delivery of angiogenic peptides benefits cerebral ischemia. ^{18}F-FDG PET imaging holds promise as an indicator of the effectiveness of angiogenic therapy in cerebral ischemia.

AUTHORS (LAST NAME, FIRST NAME): Hwang, Hyosook[2]; Jeong, Hwan-Seok[3]; Lee, Tai Kyoung[4]; Na, Kyung Suk[5]; Oh, Philsun[6]; Kwon, Jeongil[1]; Kim, Eun-Mi[7]; Kim, HyunSoo[11]; Kim, MinJoo[10]; Kim, Dong Hyun[8]; Lim, SeokTae[1]; Sohn, Myung-Hee[9]; Jeong, Hwan-Jeong[1]

INSTITUTIONS (ALL):

1. Department of Nuclear Medicine, Molecular Imaging & Therapeutic Medicine Research Center, Cyclotron Research Center, Institute for Medical Sciences, Biomedical Research Institute, Chonbuk National University Hospital, Jeonju-si, Korea (the Republic of).
2. Department of Nuclear Medicine, Molecular Imaging & Therapeutic Medicine Research Center, Cyclotron Research Center, Institute for Medical Sciences, Biomedical Research Institute, Chonbuk National University Medical School and Hospital, Jeonju, Korea (the Republic of).
3. Department of Nuclear Medicine, Molecular Imaging & Therapeutic Medicine Research Center, Cyclotron Research Center, Institute for Medical Sciences, Biomedical Research Institute, chonbuk National University Medical School and Hospital, Jeonju, Korea (the Republic of).
4. Department of Nuclear Medicine, Molecular Imaging & Therapeutic Medicine Research Center, Cyclotron Research Center, Institute for Medical Sciences, Biomedical Research Institute, Chonbuk National University Medical School and Hospital, Jeonju, Korea (the Republic of).
5. Department of Nuclear Medicine, Molecular Imaging & Therapeutic Medicine Research Center, Cyclotron Research Center, Institute for Medical Sciences, Biomedical Research Institute, Chonbuk National University Medical School and Hospital, Jeonju, Korea (the Republic of).
6. Department of Nuclear Medicine, Molecular Imaging & Therapeutic Medicine Research Center, Cyclotron Research Center, Institute for Medical Sciences, Biomedical Research Institute, Chonbuk National University Medical School

and Hospital, Jeonju, Korea (the Republic of).
7. Department of Nuclear Medicine, Molecular Imaging & Therapeutic Medicine Research Center, Cyclotron Research Center, Institute for Medical Sciences, Biomedical Research Institute, Chonbuk National University Medical School and Hospital, Jeonju, Korea (the Republic of).
8. Department of Nuclear Medicine, Molecular Imaging & Therapeutic Medicine Research Center, Cyclotron Research Center, Institute for Medical Sciences, Biomedical Research Institute, Chonbuk National University Medical School and Hospital, Jeonju, Korea (the Republic of).
9. Department of Nuclear Medicine, Molecular Imaging & Therapeutic Medicine Research Center, Cyclotron Research Center, Institute for Medical Sciences, Biomedical Research Institute, Chonbuk National University Medical School and Hospital, Jeonju, Korea (the Republic of).
10. Department of Nuclear Medicine, Molecular Imaging & Therapeutic Medicine Research Center, Cyclotron Research Center, Institute for Medical Sciences, Biomedical Research Institute, Chonbuk National University Medical School and Hospital, Jeonju, Korea (the Republic of).
11. Department of Nuclear Medicine, Molecular Imaging & Therapeutic Medicine Research Center, Cyclotron Research Center, Institute for Medical Sciences, Biomedical Research Institute, Chonbuk National University Medical School and Hospital, Jeonju, Korea (the Republic of).
(No Image Selected)

CONTROL ID: 2232704

TITLE: Synthesis of ^{11}C-Labeled Fumaric Acid: A Potential New Imaging Tracer for Fumarate Respiration

PRESENTER: Daisuke Kano

ABSTRACT BODY:

Abstract Body: In recent years, cancer cells have been linked to making the fumarate respiration that does not occur in the normal mammalian cells of the mammalian cells are reported. Visualization of the fumarate respiration by should be promising a new PET probe is promising beacause of based on unique accumulation mechanism. In this study, we aimed to develop new imaging tracer for the fumarate respiration, ^{11}C-labeled fumaric acid was synthesized.

The carboxylations by Grignard reagents have been werewidely used for synthesis of carboxylic acids. However But for successful outcomes, these reactions require great care, such as the exclusion of moisture, and diligent control of reagent stoichiometry. Riss et al. whoelaborated novel carboxylation methods for the synthesis of ^{11}C-labeled carboxylic acids by using boronic acid esters. In this approach, boronic acid esters are quite stable to air and moisture and therefore are easily handled and stored. Consequently, this approachit is relevant to fully automated PET tracer synthesis.

The synthesis of ^{11}C-labeled fumaric acid was performed as follows. The precursor compound was prepared by copper-catalyzed mono-boration of ethyl propiolate (commercialy available). Radiosynthesis was achieved by copper-catalyzed ^{11}C carboxylation of boronic acid ester. No-carrier-added $^{11}CO_2$ was produced by a HM-12 cyclotron. (Sumitomo Heavy Industries, ltd.) Production of ^{11}C-fumaric acid was performed at the automated multipurpose synthesizer CFN-MPS100. (Sumitomo Heavy Industries, ltd.)

Cyclotron-produced $^{11}CO_2$, trapped on a column cooled with liquid N_2, was released by purging the column with N_2 gas at room temperature and directed into a reaction vessel containing (E)-ethyl 3-(4,4,5,5, -tetramethyl-1,3,2-dioxaborolane-2-yl) acrylate, CuI, Kryptofix-2.2.2, KF and TMEDA in DMF. The reaction mixture was, heated at 100 ℃ for 5 min, and thenrapidly cooled to room temperature, and then quenched with formic acid. The crlude product was directed with water. Then, the diluted solution was loaded onto two Sep-Pak Plus PS-2 cartridges connected in series. The cartridges were washed with water and the yielded ester was eluted with MeCN to second reaction vessel. To the reaction vessel was added aqueous NaOH and heated at 80 ℃ for 2 min. After coolinged to room temperature, the reaction mixture was neutralized with KH_2PO_4 buffer. The resulting crude ^{11}C-fumaric acid was then loaded onto a semi-preparative HPLC column. The HPLC fraction containing ^{11}C-fumaric acid was collected into a product vial. The product obtained as an aqueous solution which can be administered directly. The overall reaction takes about 25 min from the end of bombardment. The optimization of the reaction conditions resulted in radiochemical yield of 4.2%–8.6%. No radiochemical impurities were detected by HPLC.

For the pilot study, biodistribution patterns in tumor-bearing mice were examined. Furthermore, in vivo images were obtained by using a small animal PET scanner (GENISYS4 Summit Pharmaceuticals International, Japan). ^{11}C-fumaric acid showed high uptake in the tumor tissue.

AUTHORS (LAST NAME, FIRST NAME): Kano, Daisuke[2]; Kojima, Yoshiki K.[2]; Muramatsu, Yoshihisa[2]; Saito, Shinichiro[2]; Fujii, Hirofumi[1]; Kusumoto, Masahiko[2]; Nakagami, Yoshihiro[2]

INSTITUTIONS (ALL):

1. Division of Functional Imaging, National Cancer Center, Kashiwa, Chiba, Japan.
2. National Cancer Center Hospital East, Kasiwa, chiba, Japan.

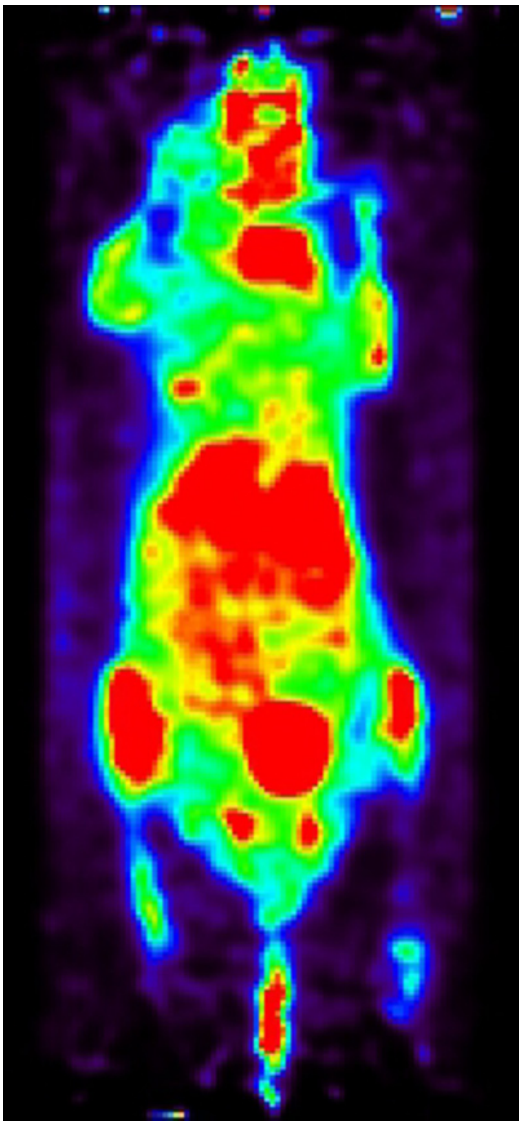

CONTROL ID: 2232578

TITLE: Anti-EGFR affibody molecules labeled with IRDye 800CW developed for Neurosurgical Fluorescence Image Guidance in a Phase 0 Human Study

PRESENTER: Brian Pogue

ABSTRACT BODY:

Abstract Body: Molecular-guided oncologic surgery could transform the decision making process for resection, allowing decisions to be informed with cellular receptor expression information, in addition to the structural features now used. Yet development of contrast agents which truly report on this have been inhibited by major financial barriers preventing commercial backing. We hypothesize that development of such agents in the standard biological therapeutic paradigm is not viable, due to the high up front financial investment needed and the limitations in the revenue models of contrast agents for imaging. The proposed solution to this problem is to develop small molecular biologicals tagged with an established fluorescent reporter, through the chemical agent approval pathway, targeting a phase 0 trials initially, such that the initial startup phase can be completely funded by a single NIH grant. In this way, fast trials can be completed to de-risk the development pipeline, and advance the idea of fluorescence-guided surgery (FGS) reporters into human testing.

This strategy is being tested with anti-EGFR affibody molecules, labeled with near-infrared emitting dye, IRDye® 800CW, termed ABY-029. This agents is being developed and tested in academic and industrial laboratories with well-established records for GMP production, fill & finish, toxicity testing, and early phase clinical trials with image guidance. The initial test synthesis shows reasonable affinity levels to human, rat and mouse EGF of 0.89, 0.95 and 0.73 nM. The plasma clearance lifetime in mouse was ~20 mins. This moderate affinity level combined with the high plasma clearance rate allows for effective localization in glioma tumors with high permeability, with imaging to occur as soon as 1 hour after injection.

The localization of the dye in the glioma was verified with dual-tracer imaging, using orthotopic U251 glioma tumors in nude rats, with injection at the microdose level required for a Phase 0 trial (200 ug/human or 0.58 ug/rat). This was done to confirm that at expected microdose levels, that there is substantial uptake in the bulk of the cancer. Imaging was done in vivo, as well as ex vivo in frozen sections. Quantitative analysis of this was completed for the standard dose levels as well as 2X and 4X lower doses.

As with biological therapies the potential successes of each agent are still moderate, but this process will allow the field to advance in a more stable and productive manner, rather than relying upon isolated molecules developed at high cost and risk. A key observation in this work is that with microdose delivery that the fluorescence from receptor-targeted reporter can be see within a glioma tumor, using standard fluorescence methods.

AUTHORS (LAST NAME, FIRST NAME): Pogue, Brian W.[1]; Samkoe, Kimberley S.[1]; Gunn, Jason[1]; Paulsen, Keith[1]; Draney, Daniel[2]; Feldwisch, Joachim[3]

INSTITUTIONS (ALL):

1. Engineering, Dartmouth College, Hanover, NH, United States.
2. LI-COR Biosciences, Lincoln, NE, United States.
3. Affibody AB, Solna, Sweden.

(No Image Selected)

CONTROL ID: 2232595

TITLE: Fixed dose of radioiodine (5 mCi) for the treatment of Graves' disease: is it possible to predict outcome before therapy?

PRESENTER: Haifeng Hou

ABSTRACT BODY:

Abstract Body: Background: Although radioiodine therapy (RIT) is well established for definitive treatment of Graves' disease (GD), the factors that might influence the outcomes of RIT remain unknown. The aim of this study is to explore the potential factors influencing the success rate of a fixed-dose RIT (5 mCi) for treatment of GD.

Methods: This is a retrospective study of 157 GD patients who received RIT with a single fixed 5 mCi of radioiodine (RAI). The thyroid function outcome (hyperthyroidism or euthyroidism/hypothyroidism) was verified at least 1 year after RIT retrospectively and compared with presenting clinical characteristics and pre-RIT parameters.

Results: Post-therapy follow-up revealed that RIT was successful in104 patients (70.7%) and failed in 43 (29.3%). Of the 104 patients in whom RIT was successful, 50 developed hypothyroidism and 54 developed euthyroidism. The outcomes of RIT were found to be significantly associated with the adjusted thyroid ^{99m}Tc–pertechnetate uptake (ATTU). The patients with ATTU ≤ 0.34 were 4.75 times (95% CI = 2.20—10.25) as likely to obtain success with treatment.

Conclusion: ATTU is a simple index that may be used to predict the patients in whom fixed low-dose RIT (5mCi) may fail or succeed. This approach seems to be practical and effective for treating GD patients with ATTU ≤ 0.34. But high failure rates are expected in patients with higher ATTU, particularly those with estimated ATTU > 0.34. These patients should be better candidates for receiving higher RAI doses or to be referred for thyroidectomy.

AUTHORS (LAST NAME, FIRST NAME): Hou, Haifeng[1]; Hu, Shu [2]; Fan, Rong [2]; Sun, Wen [3]; Sun, Taotao[2]

INSTITUTIONS (ALL):

1. Department of Nuclear Medicine, the Second Affiliated Hospital of Zhejiang University School of Medicine, Hangzhou, China.

2. Department of Nuclear Medicine, Peking University Shenzhen Hospital,, Shenzhen, China.

3. Department of Nuclear Medicine,, Affiliated Hospital of Hainan Medicinal College,, Haikou, China.

(No Image Selected)

CONTROL ID: 2232619

TITLE: A Receptor-Targeted Contrast Agent for Fluorescence-Enhancement of Gastrointestinal Adenomas: A Preliminary Study in a Mouse Model

PRESENTER: David Vera

ABSTRACT BODY:

Abstract Body: Background: There is an unmet clinical need for contrast enhancement of gastrointestinal adenomas during endoscopy. It is well known that M2 macrophages and dendritic cells invade adenomas. This function is consistent with the role of CD206, the receptor for Tc-99m-*tilmanocept* (FDA approval 2013). The objective of this study is to test the hypothesis that adenomas can be fluorescently detected after an intravenous injection of Tc-99m-*tilmanocept* covalently labeled with *IRDye800CW*.

Methods: In this preliminary study, two mice (14 wks of age; APC+/delta716 mutation (an adenoma model) or APC+/delta716/Smad4+- mutation (an adenocarcinoma model)) and two mice (27 wks of age; adenoma model or adneocarcinoma model) received an intravenous injection of fluorescent-labeled *tilmanocept* (1 nmol, 2.2 *IRDye800CW* dyes per *tilmanocept*). Each mouse was euthanized 30 min after injection and the small intestine was excised. After a longitudinal excision, the bowel was cleaned, positioned with the exterior of the organ facing a black non-reflective surface, and imaged (1 sec) with a *Fluorbeam800* imager. Each intestine was inspected for polyps, and if fluorescent sampled for radioactivity and histology. Microhistographs were prepared in the following manner: 4% paraformaldehyde (5 min), wash with PBS containing 0.2 M $CaCl_2$ (5 min), blocking (10 min), primary antibody (anti-CD206) (overnight), wash (5 min x 3), secondary antibody (anti-Rat *AlexaFluor594*) (30 min), wash (5 min x 3), and mounting with DAPI. A Keyence microscope fitted with a near infra-red filter set (Texas Red (Ex 560/40, Dichroic 585, Em 630/75) for CD206, *IRDye800CW*-specific filter (Ex 747/33, Dichroic 776, Em 776LP) for *IRDye800CW-tilmanocept*) was used to determine if the fluorescent-*tilmanocept* co-localized with its receptor, CD206. An adjacent H&E-stained section was used to confirm adenoma.

Results: As expected, no intestinal lesions were detected visually or by fluorescence imaging in both 14-wk old mice. Multiple polyps were detected visually and by fluyorescence imaging in the jejunrm and ileum of the 27-wk old mice. Of the polyps assayed for radioactivity, the percent-of-injected dose was 0.01 - 0.05 %, which was approximately 50 pmol of *IRDye800CW* per lesion. Multi-channel microscopy confirmed co-localization of the in vivo administered *IRDye800CW-tilmanocept* and *AlexaFluor594*, labeled the CD206 receptor.

Conclusion: This preliminary study confirmed the detectability of adenomas via the intravenous administration of fluorescent-*tilmanocept*. Althought a more extensive study using the APC animal model is warranted, a human trial will be required to valid our clinical goal, which is to increase the rate of adenoma detection without increasing procedure-time or patient discomfort.

AUTHORS (LAST NAME, FIRST NAME): Mendez, Jeanette[1]; Itatani, Yoshiro[1]; Qin, Zhengtao[1]; Hall, David J.[1]; Pestonjamasp, Kersi[1]; Valasek, Mark A.[1]; Taketo, Mark[2]; Vera, David R.[1]

INSTITUTIONS (ALL):

1. Moores UCSD Cancer Center, La Jolla, CA, United States.
2. Kyoto University, Kyoto, Japan.

(No Image Selected)

CONTROL ID: 2234336

TITLE: *In vivo* biodistribution of ^{64}Cu labeled human serum albumin tagging different number of azide (N_3)- or DBCO-functional groups for click chemistry approach

PRESENTER: Myung Geun Song

ABSTRACT BODY:

Abstract Body: Objectives: Click chemistry is a powerful chemical reaction with excellent bioorthogonality features. Conjugation methods using click chemistry is a simple and highly efficient strategy to prepare radiolabeled human serum albumin (HSA) with ^{64}Cu preserving the characteristics of HSA. We investigated in vivo biodistribution of ^{64}Cu labeled human serum albumin with the various number of azide (N_3)- or DBCO-functional groups.

Methods: HSA was conjugated with NHS-DBCO (dibenzyl cyclooctyne) or NHS-N_3 (molar ratio of HSA:NHS-DBCO(or -N_3) = 1:1, 5, 10 or 20). And DBCO or N_3 conjugated with NOTA chelator was synthesized for preparing the pre-radiolabeled alkyne complex with ^{64}Cu in PBS. Radio-TLC, MALDI-TOF-MS and DLS were used for analysis. After injection of ^{64}Cu-HSA to BALB/c nude mice, in vivo biodistribution of ^{64}Cu-HSA were quantitatively evaluated by PET images.

Results: Following incubation with the ^{64}Cu-radiolabeled DBCO or N_3 complex (DBCO- or N_3-PEG4-NOTA-^{64}Cu), the DBCO or N_3-functionalized HSA were radiolabeled successfully with ^{64}Cu, with a high radiolabeling efficiency and yield (>95%). In addition, Size of DBCO or N3-tagged HSA were about 7 - 9.4nm dependent on molar ratio of HSA and NHS-DBCO(or -N_3). And zeta-potential of DBCO or N_3-functionalized HSA were measured. Serial PET imaging revealed that the ratio of heart-to-liver activity were higher in the condition with one to five ratio of HSA to DBCO or N_3 (HSA:DBCO(or N_3) = 1:5) than others. However, ^{64}Cu labeled DBCO-HSA was more rapidly cleared than N_3-HSA via liver and intestine after 24 h.

Conclusions: Both DBCO- and N_3-functionalized HSA showed similar blood circulation time and liver uptake, but DBCO-HSA was more rapidly cleared, suggesting that DBCO-functionalization is more useful for in vivo imaging.

AUTHORS (LAST NAME, FIRST NAME): Song, Myung Geun[1]; Park, Ji Yong[5]; Youn, Hyewon[2]; Lee, Dong Soo[3]; Chung, June-Key[6]; Lee, Yun-Sang[4]; Jeong, Jae Min[7]; Kang, Keon Wook[3]

INSTITUTIONS (ALL):

1. Nuclear Medicine, Cancer Research Institute, Seoul, Korea (the Republic of).
2. Cancer Imaging Center, Seoul National Univ, Seoul, Jongno-Gu, Korea (the Republic of).
3. Nuclear Medicine, Seoul National University, Seoul, Korea (the Republic of).
4. Department of Nuclear Medicine, Seoul National University College of Medicine, Seoul, Korea (the Republic of).
5. Radiation Medicine, Seoul, Korea (the Republic of).
6. Nuclear Medicine, Cancer Research Institute, Seoul, Korea (the Republic of).
7. Radiation Medicine, Seoul, Korea (the Republic of).

(No Image Selected)

CONTROL ID: 2236484

TITLE: ^{64}Cu-lactosaminated human serum albumin as a promising probe for asialoglycoprotein receptor-positive tumor PET imaging

PRESENTER: Myung Geun Song

ABSTRACT BODY:

Abstract Body: Purpose: A selective delivery of drugs to liver cells can be obtained by conjugation with galactosylated macromolecules, which have ability to internalize into the hepatocytes by the specific interaction of the galactose residues and the asialoglycoprotein receptor (ASGPR). This receptor was also found on the cells of the large majority of well differentiated hepatocarcinomas (HCCs). Recently, asialoglycoprotein receptor (ASGPR) became one of the most important theranostic biomarkers for hepatocellular carcinoma. Here, we evaluated targeting ability of ^{64}Cu labeled human serum albumin (^{64}Cu-Ln-HSA) with various numbers of lactosamine residues in the ASGPR expressing tumor models.

Methods: Human serum albumin was conjugated with various numbers of lactosamine residues (Ln-; L0-, L8-, L26-, L56) to generate Ln-HSA. The FITC-labeled Ln-HSA was also produced for confocal microscopy. For PET imaging, Ln-HSA was conjugated with SCN-NOTA for generating ^{64}Cu-Ln-HSA. For ^{64}Cu labeling, NOTA conjugated Ln-HSA was radiolabeled with $^{64}CuCl_2$ in sodium acetate buffer (0.1 N, pH 6.0) at 37°C for 1 h, which purified using a PD-10 column. Labeling efficiencies of ^{64}Cu-Ln-HSA were determined by ITLC. ^{64}Cu-Ln-HSA (50 uCi/mouse) was injected to nude mice having HepG2 (ASGPR+) and HT29 (ASGPR-) tumors and PET images were obtained.

Results: FITC-lactosaminated HSA was detected in HepG2 cells, but not detected in HT29 cells. The FITC signal was dependent on increasing lactosamine residues on HSA surface (L56>L26>L8>L0). Labeling efficiency of ^{64}Cu-Ln-HSA was over 95%, and in vitro uptake test using ^{64}Cu-Ln-HSA showed its specificity in HepG2 cells. Serial PET imaging revealed that HepG2 tumor uptake of ^{64}Cu-L26-HSA was 7.5, 7.9 and 7.3 %ID/g at 10, 22, and 46 h post-injection, respectively. Autoradiography also showed that ^{64}Cu-L26-HSA was accumulated more than other conjugates in HepG2 tumors.

Conclusions: Lactosaminated HSA enhanced the targeting ability to ASGPR positive cells by addition of 26 lactosamine residues on the surface of HSA. We propose ^{64}Cu-lactosaminated HSA as a promising probe for ASGPR specific imaging.

AUTHORS (LAST NAME, FIRST NAME): Song, Myung Geun[1, 7]; Jang, Sol-Ah[8]; Youn, Hyewon[2, 1]; Lee, Yun-Sang[4, 7]; Jeong, Jae Min[5, 7]; Lee, Dong Soo[3]; Chung, June-Key[6, 7]; Krats, Felix[9]; Kang, Keon Wook[3, 2]

INSTITUTIONS (ALL):

1. Nuclear Medicine, Cancer Research Institute, Seoul, Korea (the Republic of).
2. Cancer Imaging Center, Seoul National Univ, Seoul, Jongno-Gu, Korea (the Republic of).
3. Nuclear Medicine, Seoul National University, Seoul, Korea (the Republic of).
4. Department of Nuclear Medicine, Seoul National University College of Medicine, Seoul, Korea (the Republic of).
5. Nuclear Medicine, Seoul National University College of Medicine, Seoul, Korea (the Republic of).
6. Nuclear Medicine, Seoul National University Hospital, Seoul, Korea (the Republic of).
7. Institute of Radiation Medicine, Medical Research Center, Seoul, Korea (the Republic of).
8. Department of Nuclear Medicine, Cancer Research Institute, Seoul, Korea (the Republic of).
9. Tumor Biology Center, University of Freiburg, Freiburg, Germany.

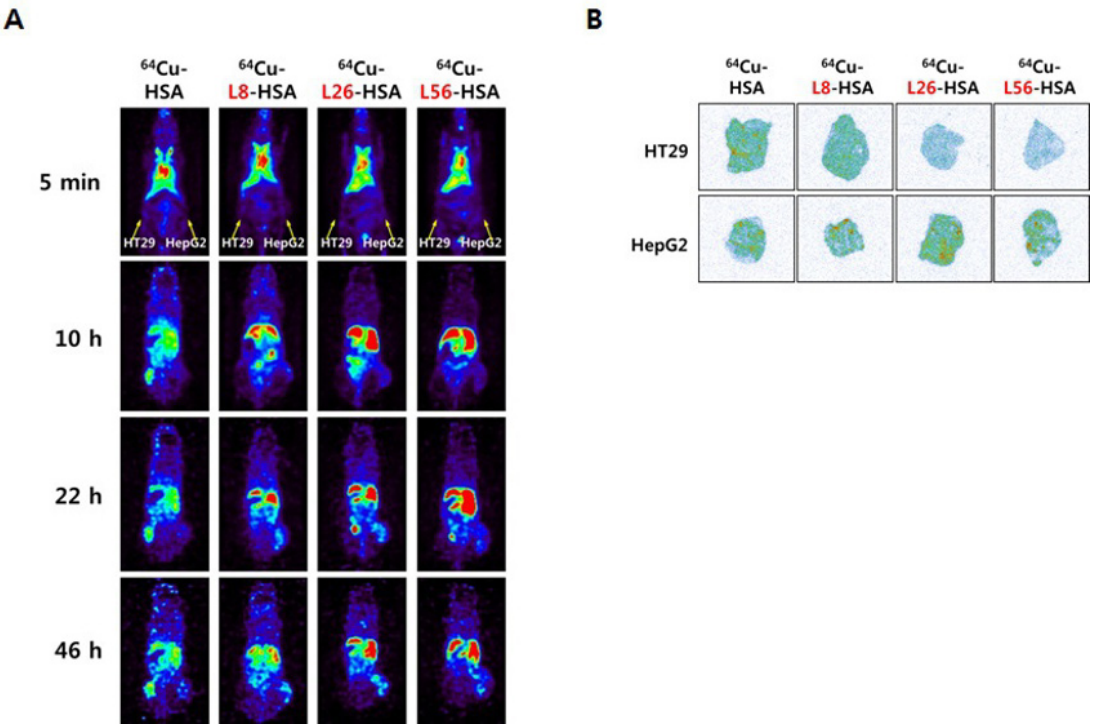

Serial PET imaging and autoradiography using ^{64}Cu-Ln-HSA

CONTROL ID: 2232626

TITLE: Diffusion kurtosis imaging and white matter modeling improves the characterization of white and grey matter pathology following demyelination and remyelination

PRESENTER: Caroline Guglielmetti

ABSTRACT BODY:

Abstract Body: INTRODUCTION

Although magnetic resonance imaging is the gold standard for the diagnosis of multiple sclerosis, current techniques often fail to detect cortical alterations and provide little information about gliosis, axonal damage and myelin status of lesions. Diffusion tensor (DTI) and kurtosis imaging (DKI), for which a white matter modeling (WMM) method has been developed[1], provide sensitive and complementary measures of the tissue microstructure. In the present work we used the cuprizone (CPZ) mouse model[2] of central nervous system demyelination to assess the temporal evolution of DKI-derived metrics following acute inflammatory demyelination and spontaneous remyelination.

METHODS

C57BL6/J mice (n= 20) received a diet supplemented with 0.2% CPZ for a period of 6 weeks and then were returned to standard chow. Mice were imaged on a 9.4T scanner at key time points for white matter inflammation and demyelination (3 weeks of CPZ), cortical demyelination (6 weeks of CPZ) and remyelination (6 weeks of CPZ followed by 6 weeks recovery period). Control mice (n=16) were imaged at the same time points. The DKI protocol included 7 non-DW images and 210 DW images with the use of 7 b -values and 30 noncollinear diffusion gradient directions. Axial (AD), radial (RD) and mean diffusivity (MD); axial (AK), radial (RK) and mean kurtosis (MK); axonal water fraction (AWF) and diffusivity inside the axons (D_a) were computed from the somatosensory cortices (SS), splenium and genu of the corpus callosum. For each metric we fitted a linear mixed model with time, treatment, and the interaction between time and treatment as fixed factors. In case of significant interaction ($p \leq 5\%$), groups were compared using the estimates from the interaction model. Quantitative immunofluorescence for myelin, microglia and astrocytes was performed.

RESULTS

While DTI metrics were unable to detect CPZ-induced cortical alterations, MK, RK and AK were found decreased in the SS. In white matter, DTI, DKI and WMM metrics enabled the detection of CPZ-induced changes according to the stage and the severity of the lesion. MK, RK and AWF were sensitive for the detection of CPZ-induced changes in the genu, a region less affected by CPZ diet. Additionally, microgliosis was associated with an increase of MK and RK during acute inflammatory demyelination. In the severely affected splenium, MD and RD were among the best discriminators between CPZ and control groups, highlighting their ability to detect both acute and long lasting changes. WMM metrics were able to distinguish between the different stage of the disease, for instance, D_a and AWF were found decreased in the CPZ treated group, D_a during the acute inflammatory demyelinating phase, indicating axonal damage whereas AWF was associated to the remyelination period.

CONCLUSION

Our results demonstrate that DKI is sensitive to alterations of cortical areas and provides, along with WMM metrics, information which is complementary to DTI metrics for the characterization of white matter integrity and subsequent inflammatory processes associated to a demyelinating event.

References [1] Fieremans, NeuroImage, (2011),[2] Gudi, Brain Res, (2009).

AUTHORS (LAST NAME, FIRST NAME): Guglielmetti, Caroline[2]; Veraart, Jelle[1]; Roelant, Ella[3]; Mai, Zhenhua[2]; Daans, Jasmijn[4]; van audekerke, johan[2]; Naeyaert, Maarten[2]; Vanhoutte, Greetje[2]; Delgado y Palacios, Rafael[2]; Praet, Jelle[2]; Fieremans, Els[5]; Ponsaerts, Peter[4]; Sijbers, Jan[1]; VAN DER LINDEN, Annemie[2]; Verhoye, Marleen[2]

INSTITUTIONS (ALL):

1. Department of Physics, University of Antwerp, iMinds Vision Lab, Antwerpen, Belgium.
2. Department Pharmaceutical, Veterinary and Biomedical Sciences - University of Antwerp, Bio-Imaging Lab , Antwerpen, Belgium.
3. University of Antwerp, StatUa Center for Statistics, Antwerpen, Belgium.
4. University of Antwerp, Experimental Cell Transplantation Group, Laboratory of Experimental Hematology, Vaccine and Infectious Disease Institute (Vaxinfectio), Antwerpen, Belgium.
5. NYU School of Medicine, New York, NY, United States.

(No Image Selected)

CONTROL ID: 2232638

TITLE: Coupling of non-invasive bioluminescence imaging (BLI) and giant magnetoresistor-Biosensor (GMRB) for longitudinal monitoring of antibodies-mediated spontaneous lymphoma cells regression in living subjects.

PRESENTER: Carmel Chan

ABSTRACT BODY:

Abstract Body: Background: Lymphoma is a systemic disease involving multiple organs and lymph nodes (LNs). BLI allows non-invasive longitudinal tracking of lymphoma cells labeled with a Firefly Luciferase (FL)-enhanced green fluorescent protein (GFP) fusion reporter within living mice. However, use of a reporter, in immune-competent mice, may sometimes lead to spontaneous tumor regression. The origins of this regression are not currently well understood. In one Burkitt's Lymphoma system, we have observed tumor regression in 16% of the syngenic C57/BL6 mice injected with the FL-GFP labeled lymphoma cells, but not in mice injected with unlabeled cells.

Method: To determine the role of antibody responses in lymphoma regression, we have developed a highly sensitive (detection limit of 0.5 nM) GMRB for detection of FL antibodies (total IgG and 4 individual isotype) with relatively small quantities of serum (5 µl). The levels of FL antibodies were used to correlate the BLI signals at each imaging time point for regression and non-regression mice (5 representative mice per group out of 25 mice in the cohort).

Results: Tumor regression in inguinal and axillary LN (ILN and ALN) (determined by caliper measurements) and decreases in BLI signals was observed in spleen, kidney and renal LN, ILN, ALN starting from Day 14 (Figure 1). The level of total IgG2a on Days 18, 20 and 24 were elevated by 2.4-, 3.9- and 9.8-fold, compared to that of non-regression mice ($p < 0.004$, 0.001 and 0.002, respectively). Total levels of FL IgG (including all isotypes) were elevated by 2.3-, and 4.3-fold in mice with tumor regression on Days 20 and 24, compared to that of non-regression mice ($p < 0.01$ and 0.0001 respectively). The levels of IgG1 was elevated by 3.0-fold in the regression mice on Day 24, compared to that of non-regression mice ($p < 0.001$) (Table 1). The levels of IgG2b and IgG3b were similar between regression and non-regression mice ($p > 0.05$) at all time points.

Conclusion: By coupling whole body BLI of lymphoma cells with GMRB, we were able to longitudinally monitor spontaneous site-specific tumor regression as well as the systemic levels of FL antibodies. Elevated serum levels of FL IgG2a (involved in complement -dependent cell cytotoxicity (CDC) and antibody-dependent cell cytotoxicity (ADCC) and IgG1 (involved in CDC) correlated with tumor regression in this model. This combined approach allows sensitive detection of antibodies and can be extended for monitoring efficacy of tumor immunotherapy and vaccination when coupled with molecular imaging. Our results also caution that utilization of reporter genes can sometimes lead to the triggering of an immune response in immunocompetent animals.

AUTHORS (LAST NAME, FIRST NAME): Chan, Carmel T.[1, 8]; Lee, Jung-Rok[3]; Ruderman, Daniel[2]; Chuang, Hui-Yen[1, 4]; Sathirachinda, Ataya[1, 8]; Mallick, Parag[5]; Lowe, Scott W.[6]; Wang, Shan X.[3, 9]; Gambhir, Sanjiv S.[7, 8]

INSTITUTIONS (ALL):

1. Radiology, Stanford University, Stanford, CA, United States.
2. Molecular Medicine, University of Southern California, Los Angeles, CA, United States.
3. Materials Science and Engineering, Stanford University , Stanford, CA, United States.
4. Biomedical Imaging and Radiological Sciences, National Yang-Ming University, Taipei, Taiwan.
5. Radiology, Stanford University, STanford, CA, United States.
6. Cancer Biology and Genetics Program, Memorial Sloan Kettering Cancer Center, New York, NY, United States.
7. Radiology, Stanford University, Stanford, CA, United States.
8. Molecular Imaging Program in Stanford (MIPS), Stanford University, CA, United States.
9. Electrical Engineering, Stanford University, Stanford University, CO, United States.

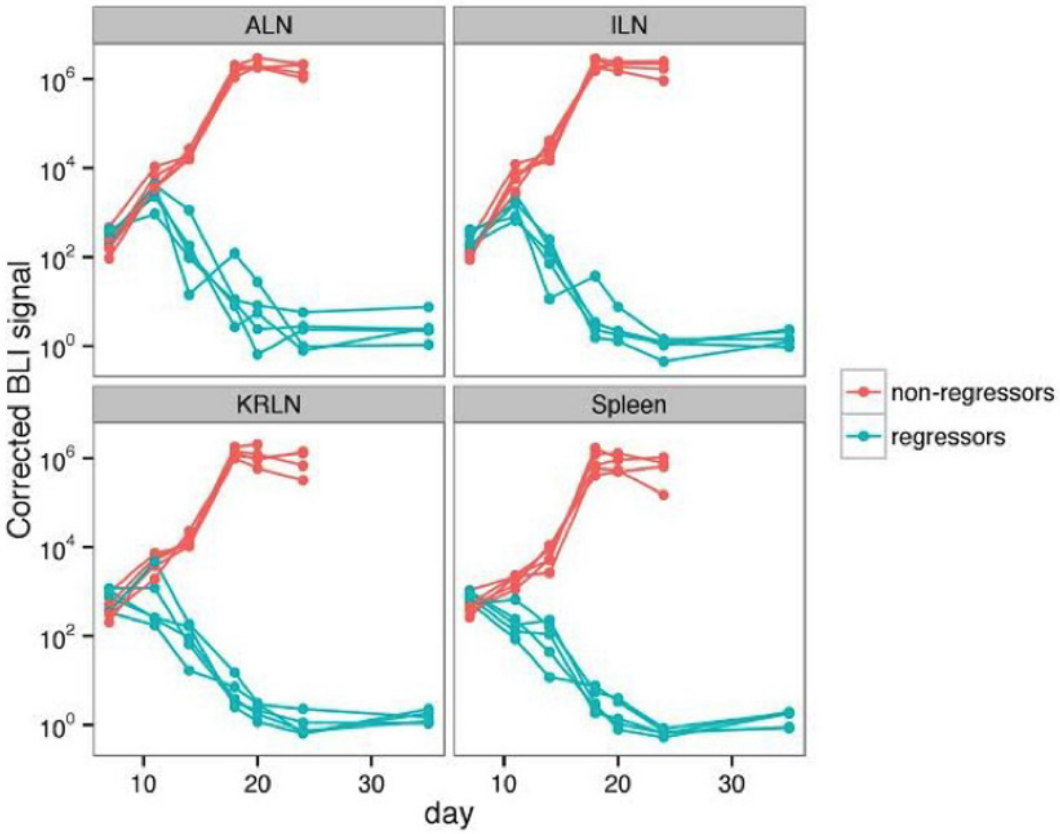

Figure 1: Decrease in bioluminescence (BLI) signals in mice that exhibit lymphoma regression. Burkitt's Lymphoma cells were labeled with a Firefly Luciferase (FL)-enhanced green fluorescent protein (GFP) fusion reporter prior to injection into syngenic C57/BL6 mice. BLI signals (expressed in average radiance) at different time points post cell injection in spleen, axiliary lymph nodes (ALN), inguinal lymph nodes (ILN), kidney with renal lymph nodes (KRLN) from mice injected with equal number of unlabeled cells was subtracted from that of mice injected with labeled cells. The BLI signals in spleen and lymph nodes decreased dramatically in regression mice, compared to that of non-regression mice starting on Day 14. All the non-regressors mice died by Day 24 post cell injection.

CONTROL ID: 2232642

TITLE: Paramagnetic small size mesoporous silica nanoparticles for targeted fluorescence and magnetic resonance imaging of tumor

PRESENTER: He Hu

ABSTRACT BODY:

Abstract Body: 1. **Introduction**

The widespread use of magnetic resonance imaging (MRI) technology in clinical and scientific research has attracted great interest in designing high relaxivity contrast agents to improve their sensitivity for the early stage detection of cancer. Mesoporous silica nanoparticles (MSNs) have been considered an attractive multifunctional platform for diagnosis and therapy based on their fantastic properties such as: high surface area, large pore volume, uniform and tunable pore size, and facile functionalization. the relaxivity of Gd-complex could be dramatically increased by immobilize it with nanostructured materials upon slowing down its molecular tumbling motion insofar as its water residence time is closed to optimal.

2. Methods

In our protocol, a PEG-silane free, one-pot, soft-templating sol-gel technique was adopted to fabricate the fluorescein-doped and amino-functionalized MSNs (MSNs-NH_2) by using cetyl-trimethylammonium bromide (CTAB) as the templating surfactant and triethanolamine (TEAH3) as the mineralizing agent under mild condition. The MSNs were further surface modified with macrocyclic Gd-complexes: Gd-DOTAGA and a_vb_3 integrin targeting ligands: cyclic arginine-glycine-aspartic (RGD) peptide. The ^{1}H relaxometric properties of this MR-enhanced nanoprobe were systematic investigated. The Gd-MSNs-RGD nanoprobe were used to target integrin a_vb_3 of U87MG human glioblastoma cell line *in vitro* and T_1-weighted MR imaging of xenografts tumor modal *in vivo*.

3. Results:

The fluorescein-doped and amino-functionalized small size mesoporous silica nanoparticles (MSNs) (~ 30 nm) were synthesized as multifunction nanoplatform. The final nanoprobe Gd-MSNs-RGD shown good physiological stability, low cytotoxicity and high relaxivity (37.6 $mM^{-1}s^{-1}$ at 21.5 MHz). *In vitro* fluorescence and MR imaging demonstrated their good targeting capability with U87MG cells, and further *in vivo* T_1-weighted MR imaging also highlighted the xenografts tumor modal.

4. Conclusions:

We have successful fabricated high r_1-relaxivity targeting contrast agents. Findings from this study indicated that the small size Gd-MSNs-RGD can be used for high sensitive multifunctional imaging study from the cellular scale to small-animal whole-body evaluation.

5. Acknowledgement:

National Natural Science Foundation of China (51102171), the Marie Curie Action of the Seventh Framework Programme of Europe Union (PIIF-GA-2011-298821).

AUTHORS (LAST NAME, FIRST NAME): Hu, He[1, 2]; Arena, Francesca[1]; Gianolio, Eliana[1]; Aime, Silvio[1]

INSTITUTIONS (ALL):

1. Molecular imaging center, University of Torino, Torino, Italy.
2. Department of Chemistry, Shanghai Normal University, Shanghai, China.

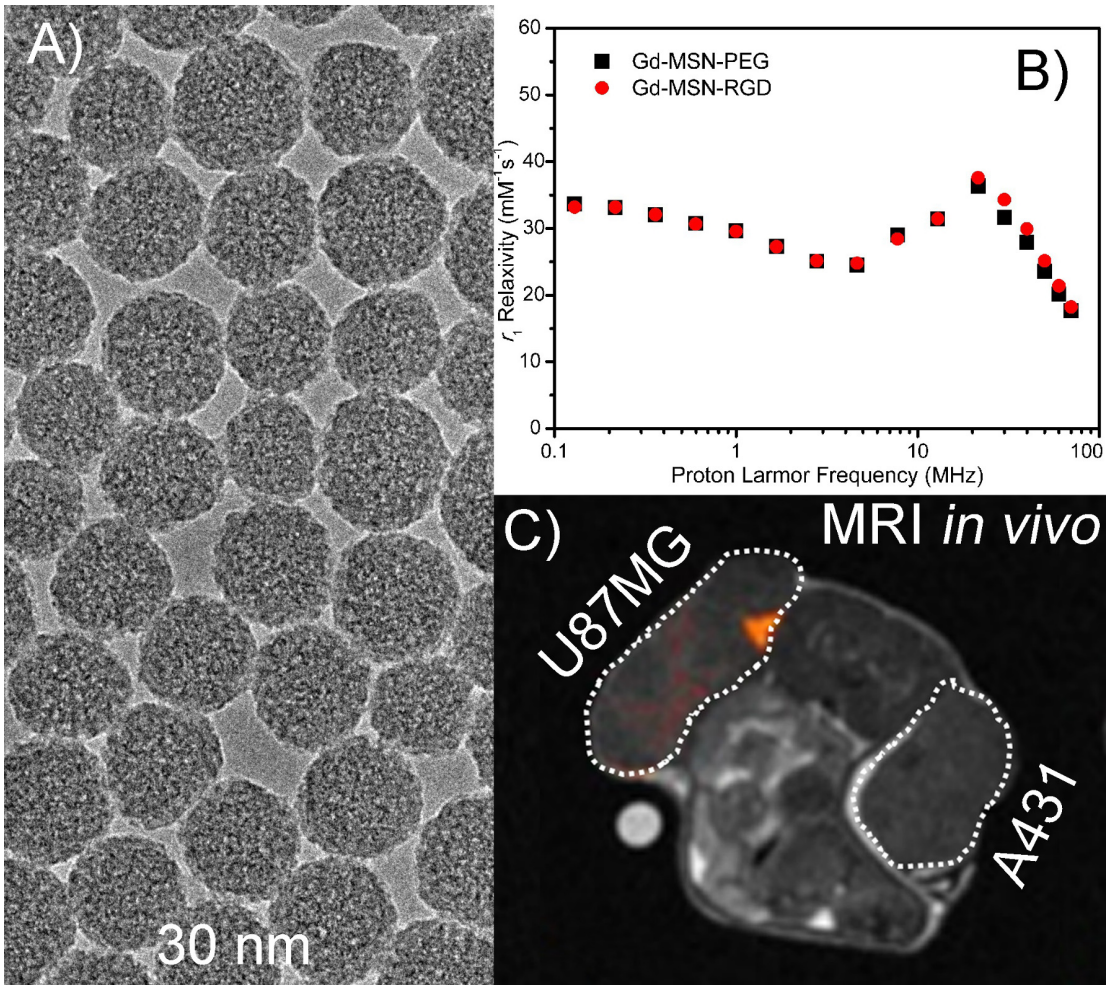
A)
30 nm
B)
Gd-MSN-PEG
Gd-MSN-RGD
r_1 Relaxivity ($mM^{-1}s^{-1}$)
Proton Larmor Frequency (MHz)
0
10
20
30
40
50
60
0.1
1
10
100
C)
MRI *in vivo*
U87MG
A431

CONTROL ID: 2232647

TITLE: Stimulation of endothelin B receptors increases [^{18}F]FDG uptake in cancerous lesions in mice

PRESENTER: Svetlana Selivanova

ABSTRACT BODY:

Abstract Body: Objectives: Positron emission tomography (PET) imaging with fluorine-18 labelled fluorodeoxyglucose ([^{18}F]FDG) became a major clinical technique for cancer diagnosis. [^{18}F]FDG concentrates in tissues that over-consume sugars due to their high metabolism, including cancer. However, [^{18}F]FDG lacks specificity and cannot always differentiate malignant cancer cells from a benign condition, which involves increased cell metabolic rate. We hypothesized that such differentiation could be possible with a concomitant administration of endothelin receptor type B (ET_B) agonist. ET_B is expressed in several cell types, including endothelial cells of the blood vessels. Stimulation of ET_B results in the production of nitric oxide and prostaglandins, which promote vasodilation. [1] Fast growing tumour blood vessels differ in structure from normally formed vasculature. In one instance, hastily formed underdeveloped smooth muscle layer, which controls blood flow at normal conditions, cannot provide required autoregulation in cancer cells. [2] There is evidence that selective and transient vasodilation of cancer vasculature can be achieved by activating ET_B receptors. [3] The goal of this study was to evaluate in a mouse tumor model whether pre-treatment with an ET_B agonist could increase [^{18}F]FDG uptake in cancer lesions.

Methods: BALB/c mice were inoculated with MC7-L1 mouse mammary carcinoma cell line (subcutaneous, 1×10^6 cells per mouse) and tumors were allowed to grow for approximately one month until they reached ~4 mm^3 in diameter. Mice were randomly divided in groups and injected with either, phosphate buffered saline or selective ET_B agonist IRL-1620 (Suc-Asp-Glu-Glu-Ala-Val-Tyr-Phe-Ala-His-Leu-Asp-Ile-Ile-Trp, 3 nmol/kg) followed by [^{18}F]FDG (12-14 MBq per mouse). Small animal PET imaging was used to monitor tissue distribution of [^{18}F]FDG after tracer administration. ROIs were drawn over the tumors and contralateral muscle tissue and the radioactivity uptake was quantified. Two animals were subjected to a continuous infusion of [^{18}F]FDG while IRL-1620 was administered to observe its effect in real time.

Results: The uptake of [^{18}F]FDG in tumors increased by 38% on average when administered 15 minutes after the treatment with IRL-1620 (Figure 1) and this was statistically significant ($p<0.0001$). In two animals tested during infusion, [^{18}F]FDG uptake rate increased 1.6 and 1.8 fold potentiated by IRL-1620.

Conclusions: Treatment of mice with selective ET_B agonist IRL-1620 enhanced [^{18}F]FDG uptake in tumors. Administration of the selective ET_B agonist together with [^{18}F]FDG could be a promising strategy to increase sensitivity of [^{18}F]FDG PET imaging.

References: [1] H. F. Galley HF and Webster NR (2004) Brit J Anaesth, 93,105-113. [2] Jordan BF and Sonveaux P (2012) Front Pharmacol, 3, Article 94. [3] Rai A and Gulati A (2003) Cancer Chemother Pharmacol, 51, 21-28.

AUTHORS (LAST NAME, FIRST NAME): Yatsyna, Anna[1]; Ladrie, Jordan[1]; Lebel, Réjean[1]; Sarrhini, Otman[1]; Bentourkia, M'hamed[1]; Lecomte, Roger[1]; Selivanova, Svetlana V.[1]

INSTITUTIONS (ALL):

1. Sherbrooke Molecular Imaging Centre, CRCHUS, Unviersité de Sherbrooke, Sherbrooke, QC, Canada.

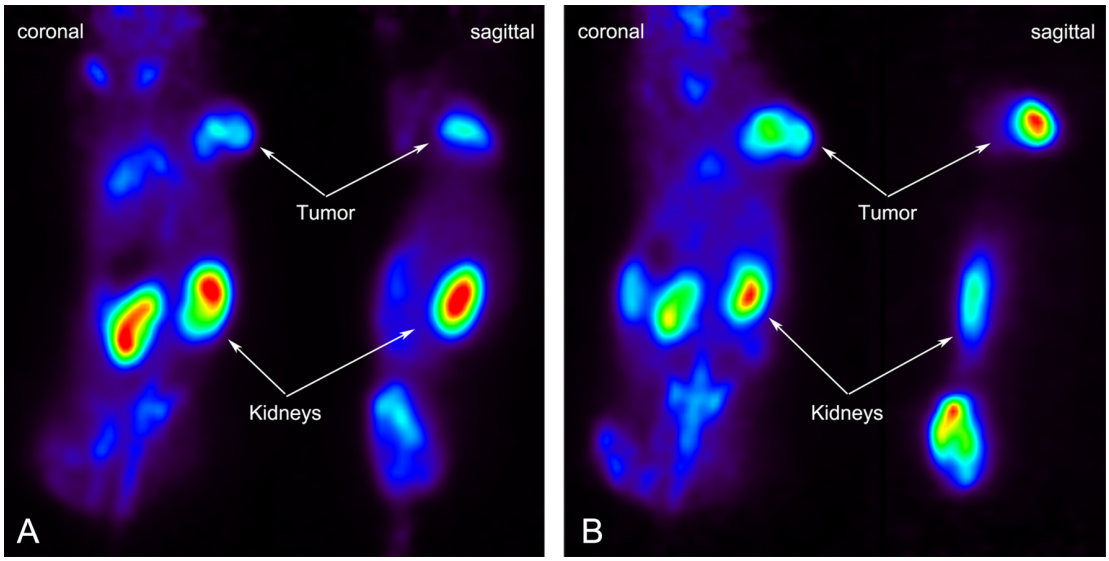

Figure 1. Accumulation of [^{18}F]FDG in tumor without (panel A) and with (panel B) administration of selective ET_B agonist IRL-1620. Coronal and sagittal slices are shown. Images are averaged 40-60 min after injection of [^{18}F]FDG and normalized.

CONTROL ID: 2243351

TITLE: Near-Infrared Dye-Albumin Conjugates as Imageable Photothermal Theranostics for Imaging-Guided Cancer Therapy

PRESENTER: Peng Huang

ABSTRACT BODY:

Abstract Body: Background: Development of imageable photothermal theranostics has attracted a great deal of attention for imaging guided photothermal therapy (PTT) with high tumor ablation efficacy and little collateral damage. **Methods:** Firstly, we synthesized the fluorescent near-infrared (NIR) dye CySCOOH, and then conjugated with human serum albumin (HSA) to form the final product HSA@CySCOOH. *In vivo* NIR fluorescence and photoacoustic (PA) imaging studies were carried out on 4T1 tumor-bearing mice by intravenous injection. Both *in vitro* and *in vivo* PTT were also investigated. **Results:** The as-prepared HSA@CySCOOH nanoparticle exhibits intense fluorescence for NIR fluorescence imaging, and strong NIR absorption for PA imaging and PTT. HSA can improve tumor accumulation efficiency of CySCOOH via the enhanced permeability and retention (EPR) effect over free CySCOOH. Most intriguingly, 100% *in vivo* tumor elimination was achieved by intravenous injection of HSA@CySCOOH without weight loss, noticeable toxicity, or tumor recurrence. **Conclusion:** This imageable photothermal HSA@CySCOOH theranostics, with high water dispersibility and solubility, good biodegradability and biocompatibility, were developed for NIR fluorescence/photoacoustic/thermal trimodality imaging and photothermal tumor ablation. Most importantly, HSA@CySCOOH, like “Abraxane”, raises fewer concerns for clinical translation than synthetic carriers.

AUTHORS (LAST NAME, FIRST NAME): Huang, Peng[1]; Chen, Xiaoyuan[2]

INSTITUTIONS (ALL):

1. NIBIB, NIH , Bethesda, MD, United States.
2. National Institute of Biomedical Imaging and Bioengineering, National Institutes of Health, Bethesda, MD, United States.

(No Image Selected)

CONTROL ID: 2232649

TITLE: Acid-Induced Collagen Remodeling Study in the Microenvironment of Tumors Using Window Chamber Model

PRESENTER: mehdi damaghi

ABSTRACT BODY:

Abstract Body: Combination of poor vascular perfusion, regional hypoxia and increased glycolysis makes the physical microenvironment of solid tumors heterogeneously acidic.

We recently showed that lysosomal turn over and lysosomal proteins play major role in responding of cancer cells to acid and adaptation to their acidic microenvironment. Lysosomal enzymes such as cathepsin B, L, and K have optimal activity in acidic pH and can digest or remodel collagen fibers such as collagen I in the tumor microenvironment and help the cancer cells to grow, migrate and invade out. Other proteinases in the tumor microenvironment such as MMP9 that also have optimal activity in low pH contribute in tumor stroma remodeling. Therefore, cancer cells can remodel their surrounding habitat by producing acid and acid-induced or -activated enzyme.

To study this phenomenon we developed a dorsal window chamber model using a collagen binding protein that is fluorescently tagged. The accuracy of this technique is better than SHG and enabled us to monitor several target at the same time with multiphoton microscope. Using SNARF-1, which is a pH sensitive fluorescent dye we create the acidity map of the wound area. Superposition of all the images from different channels of the microscope helped us to unravel the structural changes of collagen in different acidic regions. IHC staining of the same tumor with the target antibody enabled us to understand the molecular mechanism of acid-induced collagen remodeling.

Using this method we found different structures of collagen in acidic regions than neutral ones that facilitates cancer ells invasion. We also validated the role of TG2, that we discovered in a SILAC-proteomics approach on breast cancer cell lines, in collagen remodeling in acidic regions.

AUTHORS (LAST NAME, FIRST NAME): damaghi, mehdi[1]; Chent, Tinjan[1]; Johnson, Joe[1]; Gillies, Robert[1]

INSTITUTIONS (ALL):

1. Moffitt Cancer Center, Tampa, FL, United States.

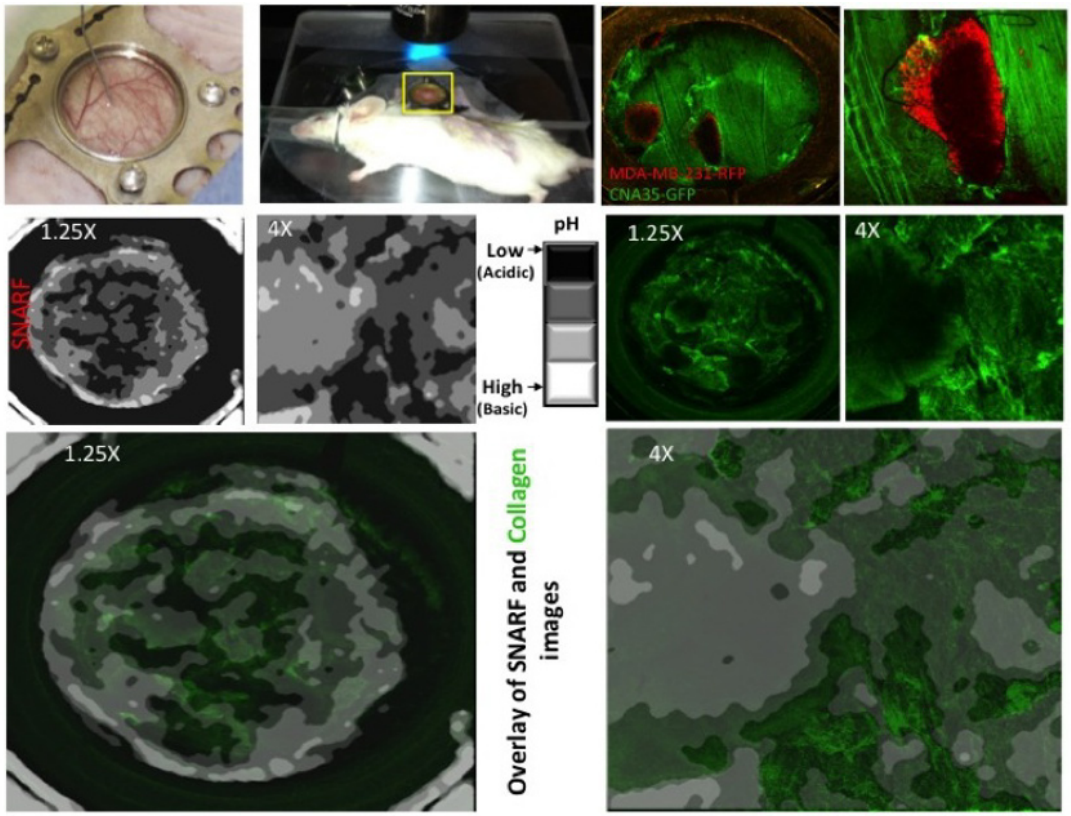
MDA-MB-231-RFP
CNA35-GFP
1.25X
SNARF
4X
pH
Low
(Acidic)
High
(Basic)
1.25X
4X
1.25X
Overlay of SNARF and Collagen images
4X

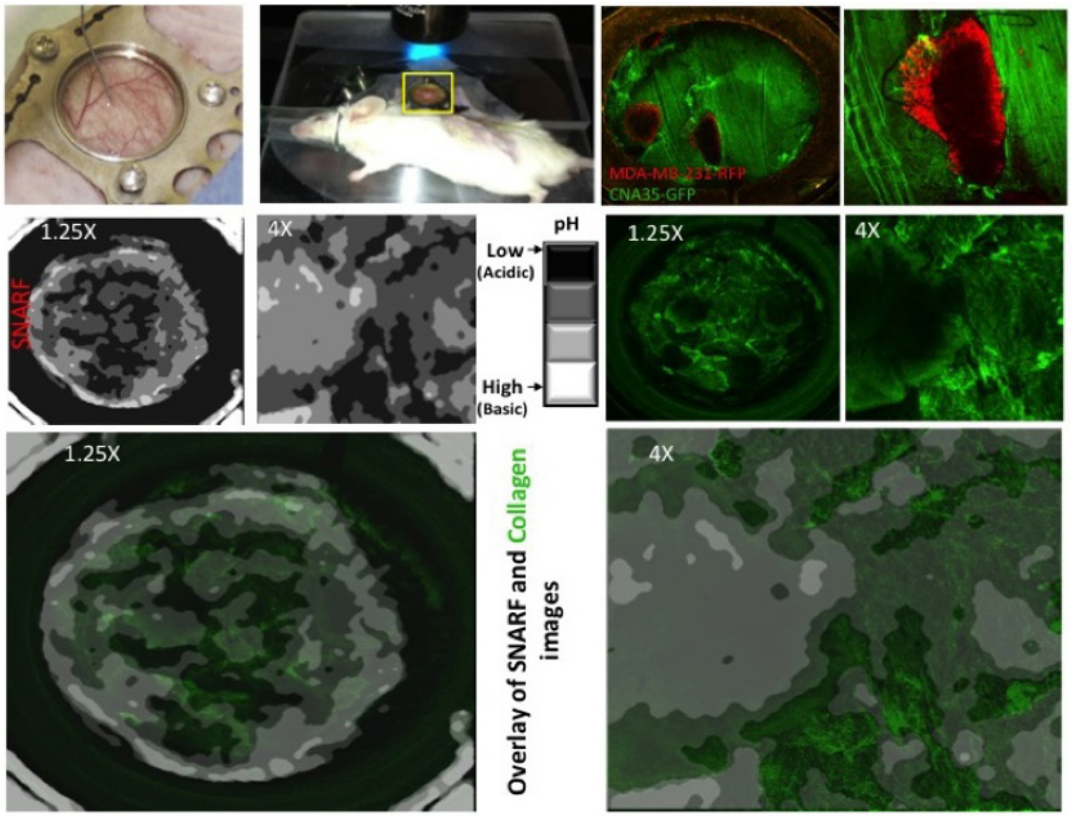

Fig1. Development of window chamber model for simultaneous imaging of collagen and acidity map: After adding the 3D spheroid tumor to the wound area, the host collagen is marked with a fluorescent label (green structures). Injection of SNARF while doing the intravital imaging using a Multiphoton microscope gives us the ability of making the pH map and collagen structure at each time point. Collective images over time reveals the collagen remodeling in areas with different acidity.

CONTROL ID: 2244206

TITLE: Biomarker Discovery for Acid-adapted Cancer Cells and Their Acidic Microenvironment.

PRESENTER: mehdi damaghi

ABSTRACT BODY:

Abstract Body: The physical microenvironment of tumors is heterogeneous. A combination of poor vascular perfusion, regional hypoxia and increased glycolysis leads to an acidic microenvironment. Chronic acidosis selects for phenotypic alterations and changes in protein expression. The tumor cells that acquire resistance to acid-mediated cytotoxicity have a growth advantage over non-adapted stromal cells and hence acquire an invasive and metastatic phenotype.

As a consequence of its importance to cancer progression, there has been a concerted effort to develop molecular imaging probes to measure tumor and tissue pH. An alternative approach is to develop probes to target tissue response to acidosis. As a precursor to developing such probes, we have used proteomic approaches to identify proteins that are expressed in cells that have been adapted to growth in acidic conditions.

Stable Isotope Labeling by Amino acids in Culture (SILAC) techniques provide an efficient method for quantitative analysis of whole proteome of paired biological samples. In this study we SILAC labeled MCF-7 breast cancer cells grown in neutral pH and adapted for growth at pH 6.7, which required more than 3 months. The whole proteomes of neutral and acid-adapted samples were compared in a 2 set parallel “flipping” experiments, which reduces the false positive rate and increases the reliability of the data set. Selected Reaction Monitoring (SRM) re-confirmed the differences in the expression levels of three of the proteins that had increased expression in acidic pH: viz. LAMP2, S100A6, and HSP72. qRT PCR and Western blots confirmed overexpression, with LAMP2 and S100A6 showing a higher increase than HSP72.

In spheroid 3D cell culturing and tumor xenografts in mice followed by Immunohistochemistry (IHC), LAMP2 showed very interesting pattern close to the hypoxic area of the spheroid that is comparable to Glut1 expression pattern. Using a Dorsal Window Chamber (DWC) we showed the overexpression of LAMP2 in more acidic area of the actual tumor inside the chamber. Finally, IHC analyses of Tissue Micro Array (TMA) of breast cancer patient samples showed staining patterns for LAMP2 that were consistent with areas suspected to be acidic. We thus suspect that LAMP2 specific ligands may be useful targeted molecular imaging probes for biological acidosis. Such agents may have potential to serve broadly for the non-invasive detection of tumor acidity, which would be a valuable in prognosis, prediction and monitoring therapy response.

AUTHORS (LAST NAME, FIRST NAME): damaghi, mehdi[4]; Tafreshi, Narges K.[5]; Estrella, Veronica C.[1]; Lloyd, Mark[3]; Morse, David L.[2]; Gatenby, Robert[3]; Gillies, Robert[3]

INSTITUTIONS (ALL):

1. CNacer Imaging and Metabolism, H. Lee Moffitt Cancer Center, Tampa, FL, United States.
2. Cancer Imaging and Metabolism, H. Lee Moffitt Cancer Center and Research Institute, Tampa, FL, United States.
3. Moffitt Cancer Center, Tampa, FL, United States.
4. Cancer Imaging and Metabolism , Moffitt Cancer Center, Tampa, FL, United States.
5. Imaging, Moffitt Cancer Center, Tampa, FL, United States.

Fig. 6.

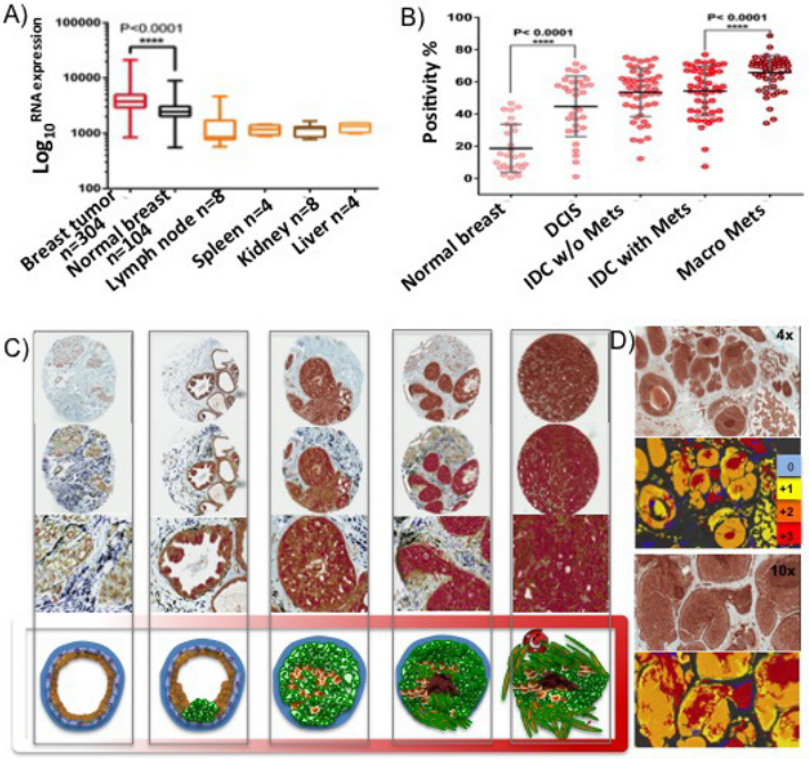
A)
Log10 RNA expression
100000
10000
1000
100
P<0.0001
****
Breast tumor n=304
Normal breast n=104
Lymph node n=8
Spleen n=4
Kidney n=8
Liver n=4
B)
Positivity %
100
80
60
40
20
0
P< 0.0001
****
P< 0.0001
****
Normal breast
DCIS
IDC w/o Mets
IDC with Mets
Macro Mets
C)
D)
4x
0
+1
+2
+3
10x

CONTROL ID: 2234240

TITLE: Integrated Optical Tools Using Molecular Imaging for In Vivo Pathology in an Orthotopic Xenograft Model of Colon Cancer

PRESENTER: Stephan Rogalla

ABSTRACT BODY:

Abstract Body: Introduction

Colorectal cancer remains the third most common and the second most deadly cancer occurring in western countries despite the widespread preventive screening by white light endoscopy. This current screening standard has a high specificity for dysplastic or malignant neoplasia in the colon. Removal of such lesions has both diagnostic and preventive values. Polyps are precancerous and could further progress into invasive cancer if not removed. Nonetheless, up to 25% of lesions are not detected. The most commonly missed lesions by this method are typically difficult to image due to their flat morphology, small size (<2 mm in diameter), or location (e.g., behind folds). Moreover, standard white-light endoscopy does not offer any molecular information. Thus, additional information such as expression of certain key proteins, that can indicate malignancy or the genetic subtype of cancer, is not obtained. Emerging fluorescence-based imaging devices, coupled with molecular probes that target specific biomarkers of dysplasia and cancer, may offer improved sensitivity and specificity over white-light colonoscopy for detection of these often overlooked lesions. For this purpose, we have created a dual modality microendoscope comprised of a clinical fiberscope modified for fluorescence imaging and a dual-axis confocal (DAC) microscope. Together these tools offer wide-field macroscopic and high-resolution microscopic fluorescence imaging capabilities. BMV109 is a molecular probe that targets the cathepsin activity arising from both cancer cells and macrophages in the tumor microenvironment. It was designed as a pan-cathepsin quenched probe that is activated by direct covalent modification of target cathepsins, releasing a quenching molecule and producing a durable fluorescent signal that is permanently attached to the target protease.

Methods

The human colon cancer cell line, HCT116, was labeled with GFP and luciferase prior to the in vivo experiment. Endoscopically assisted injections of 10^6 cells directly into the colonic wall of nude mice were performed. Tumor growth was monitored using luciferase expression from the engineered HCT116 cells and imaged by an IVIS Spectrum system. For fluorescence imaging, BMV109 was intra-rectally applied, and after 45-min colon lesions were imaged using a novel combined fluorescence fiberscope. Afterwards the bowel was removed and findings were confirmed using the IVIS Spectrum and DAC microscope. Anatomical findings of the probe were compared to GFP labeling of the tumor cells.

Results

We found the tumors fluorescent with sticking contrast to surrounding normal mucosal tissue. The fiberscope was able to detect polyp-specific fluorescence both *in vivo* and *ex vivo*. The findings could be verified using an IVIS Spectrum system for fluorescence imaging. We confirmed the cellular uptake of BMV109, and excluded the possibility of noise arising from random pooling of the probe on the surface of tissue or in mucus using a DAC microscope.

Conclusion

We could show that integrated optical tools enable in vivo pathology in this small animal model.

References

Verdoes M. *et al. J. Am. Chem. Soc.* (2013)

Siegel R. *et. al.* (2014)

AUTHORS (LAST NAME, FIRST NAME): Rogalla, Stephan[1, 6]; Zavaleta, Cristina L.[4, 6]; Loewke, Nathan O.[1, 6]; Mandella, Michael J.[3, 6]; Segal, Ehud[5]; Oresic Bender, Kristina[5]; Bogyo, Matthew[5, 6]; Contag, Christopher H.[2, 6]

INSTITUTIONS (ALL):

1. Pediatrics and Neonatology, Stanford University, Stanford , CA, United States.
2. Pediatrics, Stanford Universtiy, Stanford, CA, United States.
3. Pediatrics, Stanford University, Stanford, CA, United States.
4. Radiology, Stanford University, Stanford, CA, United States.
5. Pathology, Stanford University, Stanford, CA, United States.
6. Molecular Imaging Program at Stanford (MIPS), Stanford University, Stanford, CA, United States.

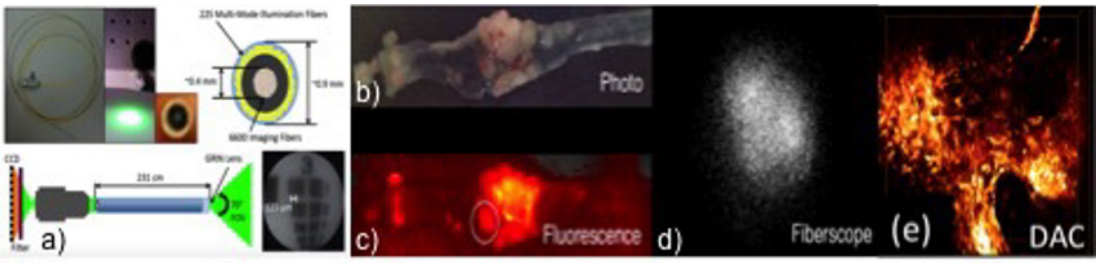

Fig. 1 (a) Custom fluorescence endoscope for mouse colonoscopy. **(b)** Photo of excised colon tissue from carcinogen-induced colon cancer mouse model. **(c)** Wide-field fluorescence image (IVIS) of excised tissue showing fluorescence signal from activatable pan-cathepsin-targeting molecular probe. **(d)** Wide-field fluorescence image from miniature fiberscope [field of view circled in (c)]. **(e)** *Ex-vivo*, dual-axis-confocal microscope image of a colon polyp after treatment with pan-cathepsin probe [different tissue from (b)-(d)].

CONTROL ID: 2234392

TITLE: Surgical Navigation in Real-Time Using Multimodality Optical Tools for Improved Resection and In Vivo Pathology of Medulloblastoma

PRESENTER: Stephan Rogalla

ABSTRACT BODY:

Abstract Body: Introduction

Medulloblastoma is the most common pediatric brain cancer and located in the motoric center of the brain – the cerbellum. Although the current standard of treatment for medulloblastoma has significantly improved survival rates, more than 30% of these young patients still die of their disease. Additionally, 20% of the survivors sustain severe neurological damage due to resection of normal brain tissue or due to the side effects of radiation or chemotherapy. However, survival of children suffering from this devastating disease correlates only with the extent of surgical resection. Hence there is impetus for aggressive resections without damaging healthy tissue through image guidance. Sensitive and specific molecular probes are still needed for such guidance. BMV109 is a quenched fluorescent probe that can be activated through cleavage of a covalently bound quencher by cathepsin proteases B, L, S, and X leading to restored fluorescence capability of the Cy5 molecular component. Cathepsin as proteases can be found in the environment of inflamed and neoplastic areas.

Methods

In 2 different xenograft models, nude mice were injected with 10^6 human medulloblastoma cells subcutaneously in the shoulder and intracerebellarly left of the frontal fissure through the bone at a depth of 2 mm. Human medulloblastoma cells expressing GFP and luciferase were used to enable tumor visualization and localization. Tumor growth was observed weekly using luciferase labeling of the cells. After 6 to 10 weeks, the brain was exposed and the probe was applied topically. Subsequently tumors were visualized in vivo using a dual-axis confocal microscope enabling in vivo pathology and guided resection. Results were confirmed using the IVIS Spectrum system and a standard surgical microscope across a range of spatial resolutions.

Results

We showed that the highly specific molecular fluorescent probe, BMV109, in combination with a DAC microscope can visualize tumor margins in real-time. BMV109 was able to show precise anatomic localization of the tumor compared to GFP labeling. We were able to guide resection using a DAC microscope to differentiate cancer from healthy tissue. Post-resection findings could be validated using a FDA-approved, standardized surgical resection microscope.

Conclusion

BMV109, in combination with a DAC microscope, is able to discriminate medulloblastoma from healthy brain tissue. This builds a foundation for image-guided resection of brain tumors in children as well as in adults.

Acknowledgement

We are grateful for the continuously generous support of the *Chambers Family*.

References

Verdoes M. *et al.* Improved Quenched Fluorescent Probe for Imaging of Cysteine Cathepsin Activity. *J. Am. Chem. Soc.* 135, 14726–14730 (2013)

Ra H. *et. al.* In vivo Imaging of Human and Mouse Skin with a Handheld Dual-Axis Confocal Fluorescence Microscope. J. Invest. Dermatol. 131(5), 1061-6 (2011)

Li K. K.-W. Signaling pathway and molecular subgroups of medullobalstoma. *Int J Clin Exp Pathol* 1–12 (2013).

Crawford J. R. *et. al.* Medulloblastoma in childhood: new biological advances. *The Lancet Neurology* 6, 1073–1085 (2007).

AUTHORS (LAST NAME, FIRST NAME): Rogalla, Stephan[1, 3]; Haag, Simone M.[1, 3]; Zavaleta, Cristina L.[4, 3]; Loewke, Nathan O.[1, 3]; Mandella, Michael J.[1, 3]; Oresic Bender, Kristina[5]; Bogyo, Matthew[5]; Contag, Christopher H.[2, 3]

INSTITUTIONS (ALL):

1. Pediatrics and Neonatology, Stanford University, Stanford , CA, United States.
2. Pediatrics, Stanford Universtiy, Stanford, CA, United States.
3. Molecular Imaging Program at Stanford (MIPS), Stanford University, Stanford, CA, United States.

4. Radiology, Stanford University, Stanford, CA, United States.
5. Pathology, Stanford University, Stanford, CA, United States.

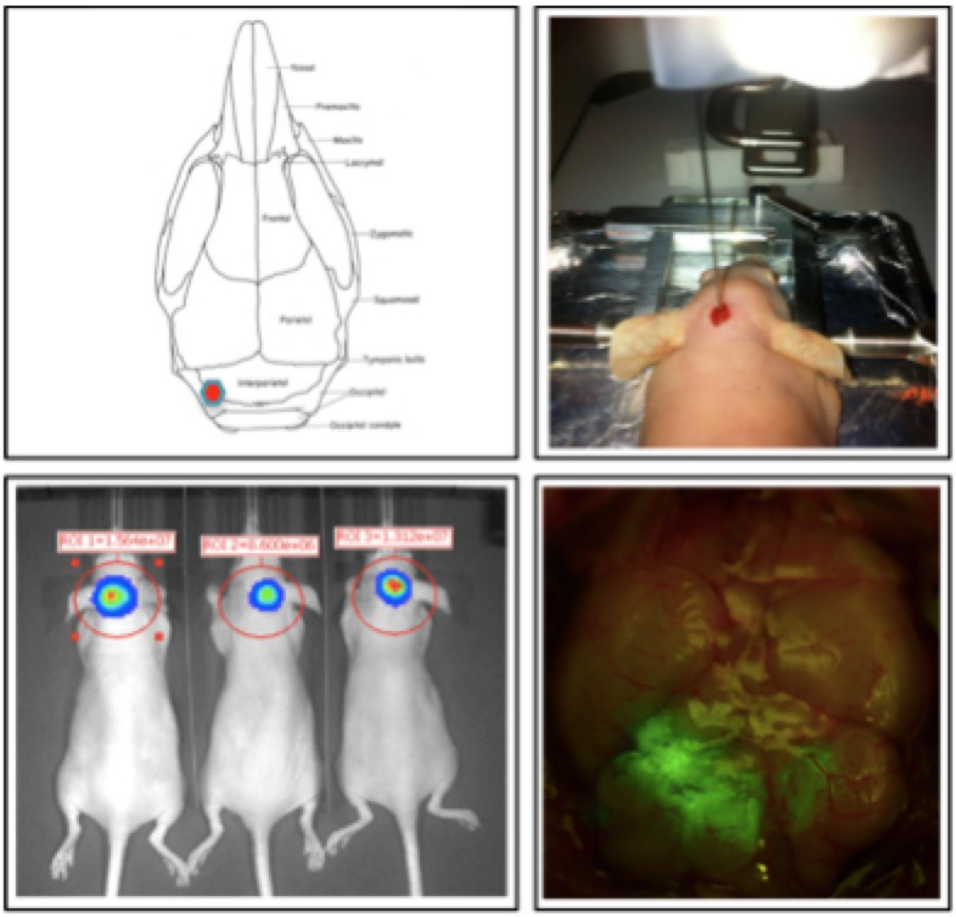

Schematic presentation of anatomic location of tumor cell injection (upper row). The tumor growth was controlled using luciferase labeling of human medulloblastoma cells, Daoy (lower left) and later in vivo using GFP-labeling of the cells (lower right).

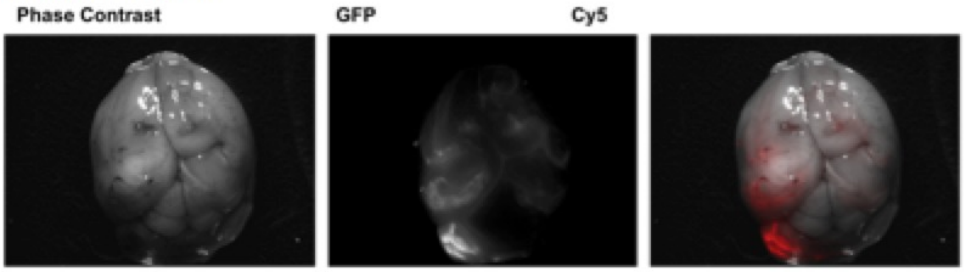

Regular phase contrast microscopic picture of excised mouse brain; the tumor site is barely visible (left). The GFP signal (middle) shows location of the tumor using fluorescence microscopy. This overlaps 1:1 with the signal shown by Cy5-labeled probe (right).

CONTROL ID: 2232656

TITLE: New Insights into the Radiosynthesis of the DAT Imaging PET Tracer [^{18}F]FE-PE2I

PRESENTER: Yiu-Yin Cheung

ABSTRACT BODY:

Abstract Body: The PET radioligand [^{18}F]FE-PE2I (**2**) has recently been used for quantifying dopamine transporters (DAT) in healthy adult humans. The advantages of using **2** over other known PET ligands, such as [^{18}F]FECNT, for DAT quantification include both higher affinity and selectivity for DAT, faster kinetics, and the formation of fewer radiometabolites that could potentially permeate the blood-brain-barrier. Initially a challenging two step production, recent optimization of the [^{18}F]FE-PE2I radiolabeling process led to the development of a straight forward, one step procedure.[1]

In this presentation, we report our development of the clinical production of **2** from tosylate **1** using an automated module (Tracerlab FX_{FN}). During this process, we identified and further optimized several labeling determinants that encouraged consistent yields, resulting in productions with high radiochemical purity (>98%) and suitable specific activity (1000-2000 Ci/mmol).

Initial attempts to produce **2** started with 3.48-3.94 Ci of fluoride, which furnished 170-332 mCi of final product with radiochemical purity 68-84%. A comparison of the radio HPLC traces from the semi-prep purification and final HPLC analysis indicated that the resulting high concentrations of **2** led to degradation of radiochemical purity through radiolysis. An additional issue identified was that selection of the final sterilizing filter was a critical determinant, given that certain brands led to significant retention of the final product.

We found that starting with ca. 500 mCi of fluoride and switching from saline to PBS in the final formulation with a final volume of 15 mL (1.5 mL EtOH; 13.5 mL 1X PBS) aided in both reduced radiolysis and greater overall yields. The final product, after filtration through a Millipore 22 micron filter, was obtained in final yields of 25-50 mCi with radiochemical purities >98% and found to meet all acceptance criteria up to 2 hours post EOS. Specific activities for these runs were in the range of 1000 - 2000 Ci/mmol. The use of less starting fluoride aided in shortening the overall production time both in terms of bombardment time and semi-preparative HPLC purification.

In addition to the radiolysis complication we found that sterile 1X PBS is not currently available for commercial purchase in the USA. Consequently 1X PBS had to be prepared as a ‘in-process-material’ from a pre-prepared sterile solution of 5X PBS and sterile water for injection. We also discovered that the quantification of a specific reaction by-product, the free acid of the drug product which is equipotent to the desired drug, required a second HPLC unit be used to determine if all release criteria are met prior to release of the drug product.

While taking these synthetic and technical issues into consideration, we have been successful in qualifying [^{18}F]FE-PE2I for clinical production. Thus we have enhanced our ability to produce [^{18}F]PE-PE2I for clinical studies at our institution.

Ref 1: J. Label. Compd. RadioPharm. 2012, 55, 206-210

AUTHORS (LAST NAME, FIRST NAME): Cheung, Yiu-Yin[1]; Zald, David H.[2]; Nickels, Michael L.[1, 3]; Manning, H. Charles[1, 3]

INSTITUTIONS (ALL):

1. Vanderbilt University Institute of Imaging Science, Vanderbilt University Medical Center, Nashville, TN, United States.
2. Department of Psychology, Vanderbilt University, Nashville, TN, United States.
3. Department of Radiology and Radiological Sciences, Vanderbilt University Medical Center, Nashville, TN, United States.

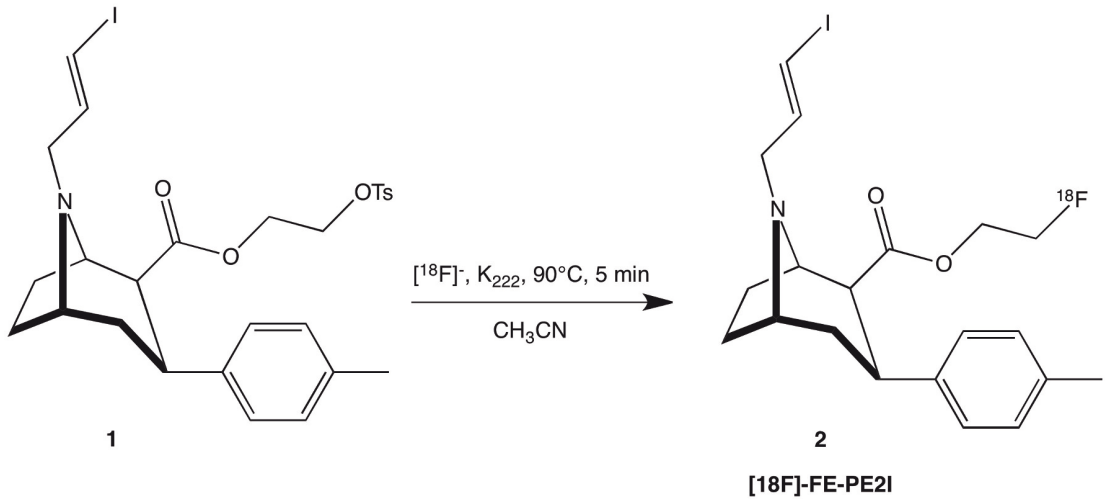

1 **2**

[18F]-FE-PE2I

CONTROL ID: 2232667

TITLE: A Novel 5 kDa Protein Scaffold for Robust Evolution of Ligands for PET

PRESENTER: Benjamin Hackel

ABSTRACT BODY:

Abstract Body: Protein scaffolds provide a platform for engineering ligands for molecular imaging. Relative to antibodies, small scaffolds can provide superior pharmacokinetics, tissue penetration, and ease of site-specific conjugation. While numerous scaffolds have proven effective for ligand engineering, including for molecular imaging, the optimal scaffold remains unclear as shortcomings are present for all scaffolds in particular applications. The aim of the current study was to push the limits on the combination of small size and robust evolution of stable, high affinity ligands. Through a systematic computational analysis of domains within the Protein Data Bank, the 45-amino acid gene 2 protein (Gp2) domain was identified as a candidate protein scaffold for molecular recognition. A combinatorial library of 10^8 mutants – via diversification of twelve amino acids in two adjacent loops within this scaffold – was displayed on the surface of yeast and screened for binders to five protein targets. Novel ligand discovery and directed evolution yielded binders with affinities as strong as 200±100 pM and no observable nonspecific binding. Circular dichroism demonstrated that evolved ligands have secondary structure comparable to the wild-type protein. Midpoints of thermal denaturation ranged from 65±3ºC to 80±1ºC for evolved ligands. Thus, Gp2 is an efficient source for ligand discovery in a small (45-residue) domain.

A Gp2 domain was evolved to target epidermal growth factor receptor (EGFR) with 18 ±8 nM affinity, receptor-specific binding on a host of tumor cell lines, and high thermal stability with refolding after denaturation. Site-specific conjugation of radiometal chelator DOTA to the N-terminal lysine was achieved without impacting binding affinity. ^{64}Cu radiolabeling was efficiently performed to enable positron emission tomography (PET) of subcutaneously xenografted A431 (EGFR^{high}) tumors in mice (n=3). PET at 45 minutes and 120 minutes after intravenous injection of ^{64}Cu-DOTA-Gp2$_{E2.2.3}$ revealed clear uptake in tumor as well as kidneys and bladder with minimal retention in muscle or the blood pool. Excised tissue gamma counting at 2 h post-injection corroborates the PET analysis and indicates tumor uptake of 6.4 ±3.6 %ID/g, tumor:blood ratio of 13 ±2, and tumor:muscle ratio of 27 ± 4. In addition, control studies, including non-targeted Gp2 domains and MDA-MB-435 (EGFR^{low}) tumors, will be presented. Along with the EGFR PET studies, ongoing studies with Gp2 domains targeting MET will be discussed.

AUTHORS (LAST NAME, FIRST NAME): Kruziki, Max A.[1]; Duong, Vandon T.[1]; Hackel, Benjamin J.[1]

INSTITUTIONS (ALL):

1. Chemical Engineering and Materials Science, University of Minnesota - Twin Cities, Minneapolis, MN, United States.

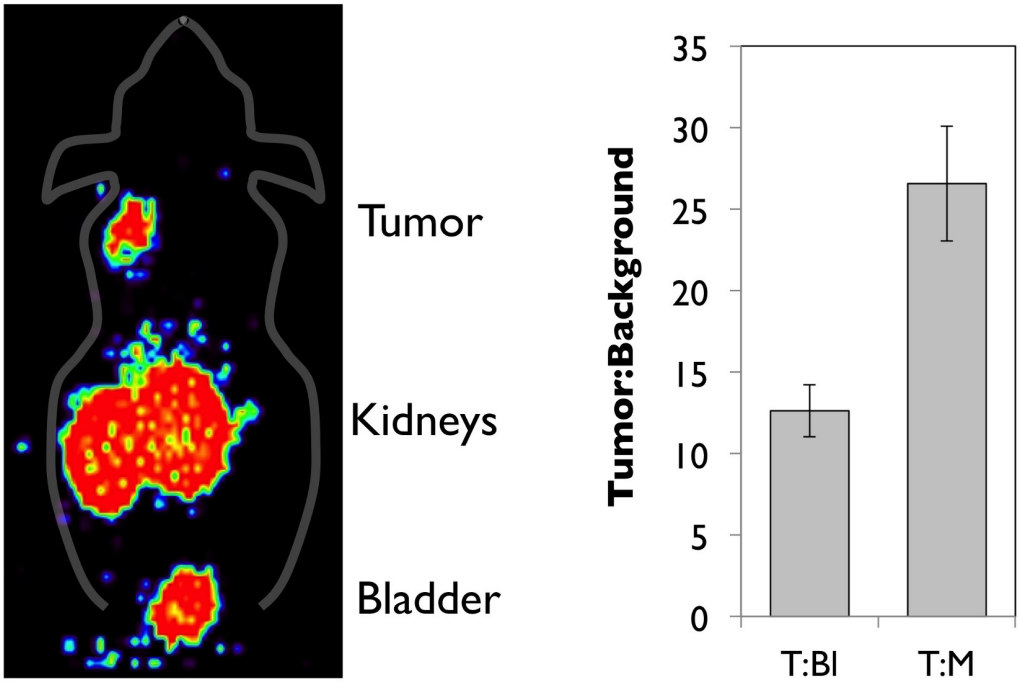

Figure 1. A Gp2 domain evolved to bind EGFR with 18 ±8 nM affinity was conjugated site-specifically with DOTA and radiolabeled with ^{64}Cu. ^{64}Cu-DOTA-Gp2$_{E2.2.3}$ was injected intravenously into mice with subcutaneous A431 tumors. Five minute PET scans were acquired at 2 h post-injection (left). Mice were euthanized and dissected to enable gamma counting of tissues and fluids. Tumor:blood ratio of 13 ±2 and tumor:muscle of 27 ±4 were observed as well as tumor uptake of 6.4 ±3.6 %ID/g.

CONTROL ID: 2232688

TITLE: Removing the Noise induced by High-energy Radiation in Optical Imaging using a Rank-ordered Mean Filter

PRESENTER: Xu Cao

ABSTRACT BODY:

Abstract Body: *Purpose*

Cerenkov luminescence imaging (CLI), radio luminescent imaging (RLI) and X-ray luminescent imaging (XLI) are optical imaging approaches involving high-energy radiation. Their optical signal acquisitions with CCD camera suffer from high level noises when high-energy rays reach the CCD chip. This study proposed a rank-ordered mean (ROM) filter method to remove this kind of noises.

Procedures

Unlike the traditional optical imaging strategy collecting only one image with long exposure time about several minutes, the proposed method uses a sequence of images captured with a litter shorter exposure time about dozens of seconds. Finally, ROM filter is used to filter out these noises and acquire a high quality image based on the sequence of images. A XLI experiment was performed based on a powder of terbium doped Gd_2O_2S to verify the proposed method.

Results

The proposed ROM filter method performs significantly better in terms of noise suppression and detail preservation than traditional mean filter and median filter algorithm.

Conclusions

The ROM filter method can effectively filter out the noises caused by high-energy rays in optical imaging involving high-energy radiation and improve image quality.

AUTHORS (LAST NAME, FIRST NAME): Cao, Xu[1]; Zhan, Yonghua[1]; Chen, Xueli[2]; Liang, Jimin[1]

INSTITUTIONS (ALL):

1. School of Life Science and Technology, Xidian University, Xi'An, China.
2. School of Life Science and Technology, Xidian University, Xi'an, Shaanxi, China.

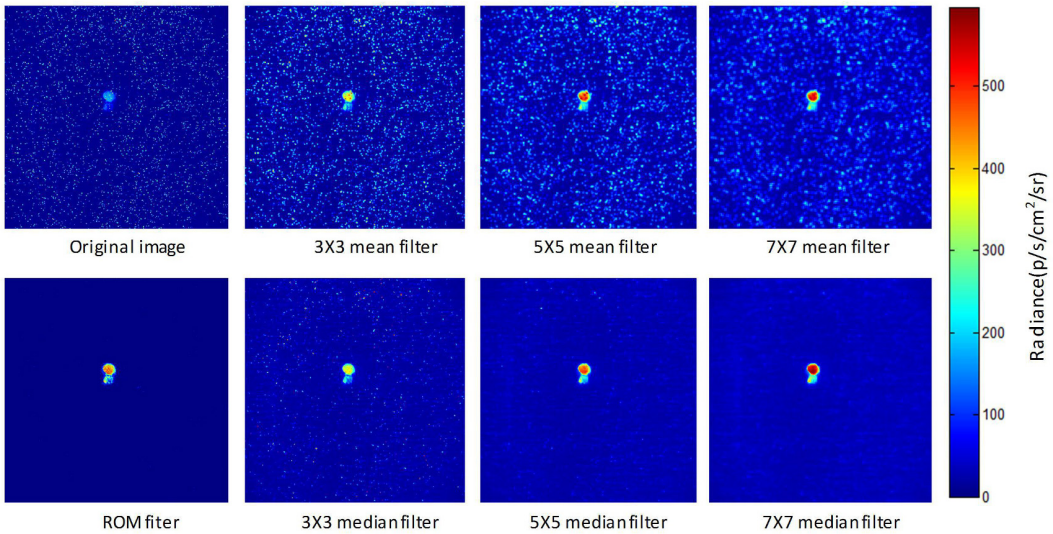
Original image
3X3 mean filter
5X5 mean filter
7X7 mean filter
ROM fiter
3X3 median filter
5X5 median filter
7X7 median filter
500
400
300
200
100
0
Radiance(p/s/cm^2/sr)

CONTROL ID: 2232692

TITLE: Peptide heterodimer for the uPAR-$\alpha_v\beta_3$ dual-targeted cancer imaging

PRESENTER: Dexing Zeng

ABSTRACT BODY:

Abstract Body: The clinical utility of monovalent imaging probes is often limited by a variety of factors, including receptor density, binding affinity, and *in vivo* pharmacokinetics. Recently, hetero-bivalency rapidly emerged as a novel promising approach for molecular imaging and therapy due to increased receptor density by combining two receptors), significantly improved binding affinity, and possibly enhanced pharmacokinetics. Therefore, a heterodimeric ligand that simultaneously associates two linked ligands targeting uPAR-$\alpha_v\beta_3$ respectively was designed specifically for the PET imaging of cancer in early stage when the amount of receptor is relatively low.

Integrin $\alpha_v\beta_3$ serves as a receptor for extracellular matrix proteins with exposed arginine-glycine-aspartic (RGD) tripeptide sequence. Its restricted expression during tumor growth, invasion, and metastasis present an interesting molecular target for diagnosis and treatment of the rapidly growing and metastatic tumors, and therefore is selected as one of the targeting receptor. uPAR is believed to be another important biomarker for the cancer imaging, since both clinical studies and laboratory research revealed that overexpression of uPA/uPAR is strongly correlated with poor prognosis in malignant tumors. Moreover, uPAR is overexpressed in various malignancies (normally expresses several thousand receptors per cell), but absent or very poorly expressed in normal and adjacent tissues. In this particular study, by using metal-free click chemistry, RGDyK and AE105 peptides targeting uPAR-$\alpha_v\beta_3$ respectively was linked covalently *via* a recently developed TACN-based chelator. The resulting peptidic heterodimer was purified by HPLC, and was then radiolabeled with Cu-64, Ga-68 and F-18. The Cu-64 incorporated heterodimer was evaluated in the nude mice xenograft with human breast cancer cell line (MBA-MD-231), and the quantitative data were compared to the other related Cu-64 radiolabled tracers, including peptidic monomer and peptidichomodimer.

Rendered by the triazole formation after the metal-free click reaction, the prepared heterodimer (AE105-NOTA-RGD) has been successfully radiolabeled with ^{64}Cu, ^{68}Ga and Al (^{18})F at 37 °C, 70 °C and 90 °C respectively. Compared to the ^{64}Cu-labeled monomer (^{64}Cu)CB-TE2A-AE105 and homodimer (^{64}Cu)NODAGA-E[c(RGDyK)]2, our heterodimer AE105-(^{64}Cu)NOTA-RGD showed significantly higher tumor uptake and increased blood retention, and greatly enhanced signal to background ratio (such as, tumor/muscle, tumor/liver and tumor/kidney).

Therefore, our newly developed heterodimer-based PET tracers showed greater potential for early detection of cancer by PET imaging, due to the greatly enhanced *in vivo* performance.

AUTHORS (LAST NAME, FIRST NAME): Zeng, Dexing[1]; Gai, Yongkang[1, 2]; Xiang, Guangya[2]; Ma, Xiang[2]; Sun, Lingyi[1]

INSTITUTIONS (ALL):

1. Radiology, University of Pittsburgh, Pittsburgh, PA, United States.
2. School of Pharmacy, Tongji Medical College, Huazhong University of Science and Technology, Wuhan, Hubei, China.

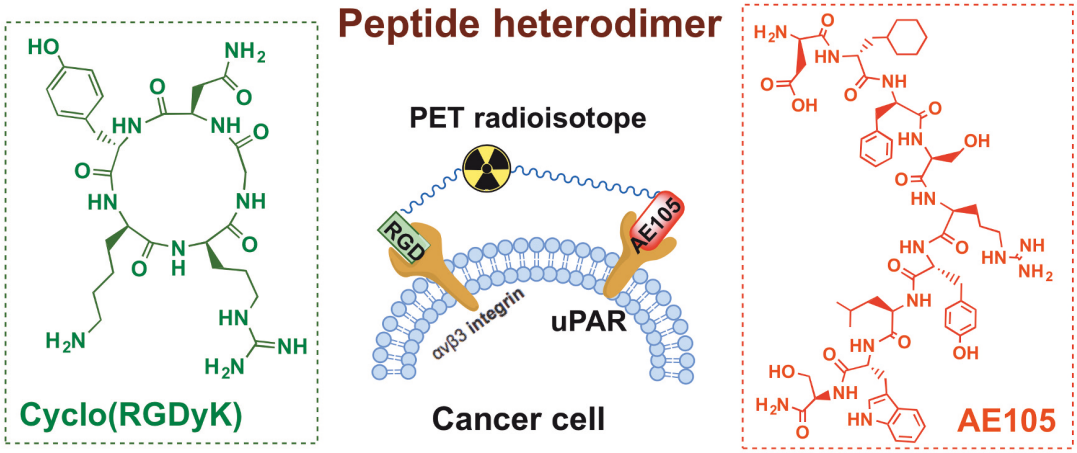

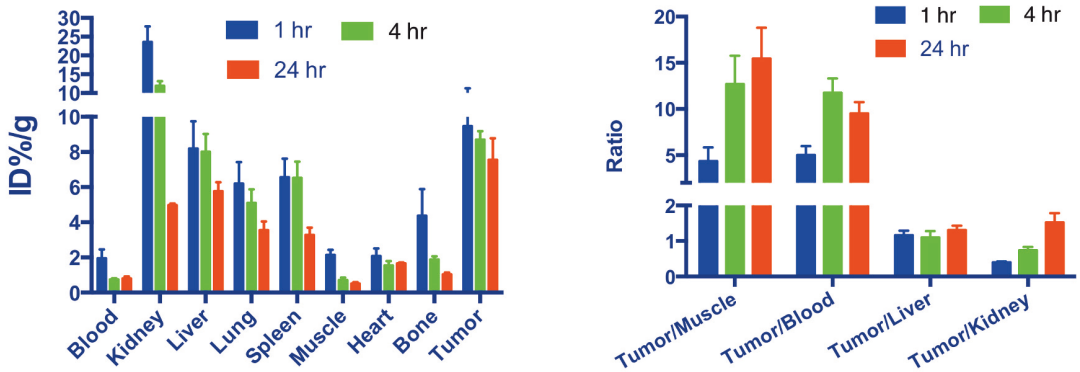

Ex vivo **biodistribution of heterodimer AE105-(^{64}Cu)NOTA-RGD, and tumor-to-nontumor ratio of the uptake**

CONTROL ID: 2232694

TITLE: Development of a fluorescent probe targeting folate receptors for fluorescence lifetime imaging (FLIM)

PRESENTER: Koji NUMASAWA

ABSTRACT BODY:

Abstract Body: Folate receptors (FRs) are membrane proteins which have a role in taking in folic acid, and it is reported that they are overexpressed in ovarian and endometrium cancer. It is also expressed at the stage of neural tube closure. Therefore, FRs have been attracted much attention in both fields of life science and clinical medicine. In this study, we developed a fluorescent probe selective for FRs to visualize FR-overexpressed cells by fluorescence lifetime imaging.

We first selected four xanthene-based fluorophores (rhodamines and fluorescein), and synthesized four fluorescent probes by conjugating these fluorophores to folic acid via the peptide linker. We then applied them to live KB cells, which express FRs, and succeeded in visualization of FRs on the cell membrane. However, we also observed the fluorescence signal inside OVCAR-3 cells which don't express FRs when rhodamine-based probes were applied to them. Therefore, it was considered that they were nonspecifically taken into cells, irrespective of FRs. On the other hand, we successfully observed the specific binding of the folate conjugate to FRs on the cell surface only when fluorescein was used as a fluorophore for folate conjugates. Based on this result, we developed a red fluorescent probe with DichloroTokyoMagenta (DCTM), which is a red fluorescein analogue, in which an O atom at the 10 position of the xanthene moiety of fluorescein is replaced with a Si atom. When DCTM-based folate conjugate was applied to KB cells, its FR-independent binding to the cell surface was successfully observed by fluorescence imaging in red region. Thus, we succeeded in visualizing FR-expressing live cells by fluorescence imaging in red region.

Moreover, when we examined photophysical properties of synthesized folate conjugates, we interestingly found that these probes showed weaker fluorescence intensity and shorter fluorescence lifetime than those of fluorophores without folate conjugation. We hypothesized that the folate moiety in the structure worked as a quencher for the fluorophore, i.e., it photophysically interacted with the fluorophore. To further examine the behavior of these folate conjugates in aqueous solution, we measured fluorescence lifetime of the fluorescein-folate conjugate in aqueous solution including various concentrations of CHAPS, a kind of surfactant. Interestingly, we found that its fluorescence lifetime became longer in the condition. Based on reports that folic acids form tetramers in aqueous solution (*Chem. Commun.*, **2011**, *47*, 4439 and *Eur. Biophys. J.*, **2011**, *40*, 1225), we thought that the fluorescein-folate conjugate also formed tetramer by hydrogen bonds the same as folic acids, thereby, it showed a shorter fluorescence lifetime by dynamic quenching between the folate moiety and the fluorophore. We then applied this folate conjugate to the fluorescence lifetime imaging microscopy (FLIM). As a result, we successfully observed a longer fluorescence lifetime in the cell membrane than that in the extracellular region, thus demonstrating the real time imaging of FR-expressing live cells by the fluorescence lifetime imaging.

AUTHORS (LAST NAME, FIRST NAME): NUMASAWA, Koji[1, 2]; Hanaoka, Kenjiro[1]; Nagano, Tetsuo[3]; Urano, Yasuteru[1, 4]

INSTITUTIONS (ALL):

1. Graduate School of Pharmaceutical Sciences, The University of Tokyo, Tokyo, Japan.
2. JST CREST, Tokyo, Japan.
3. Open Innovation center for drug discovery, Tokyo, Japan.
4. Graduate School of Medicine, The University of Tokyo, Tokyo, Japan.

(No Image Selected)

CONTROL ID: 2232695

TITLE: A platform-technology for systemic delivery of siRNA to tumors using rolling circle transcription and its applications for optical imaging probes

PRESENTER: Hyung Jun Ahn

ABSTRACT BODY:

Abstract Body: For therapeutic applications of siRNA, there are technical challenges with respect to targeted and systemic delivery. We here report a new siRNA carrier, RNAtr NPs, in a way that multiple tandem copies of RNA hairpins as a result of rolling circle transcription (RCT) can be readily adapted in tumor-targeted and systemic siRNA delivery. RNAtr NPs provide a means of condensing large amounts of multimeric RNA transcripts into the compact nanoparticles, especially without the aid of polycationic agents such as polyethylenimine, and thus reduce the risk of immunogenicity and cytotoxicity by avoiding the use of synthetic polycationic reagents. The highly condensed RNAtr NPs showed resistance to nucleases and polyanions, facilitated high cargo capacity, and finally resulted in robust gene silencing in vivo. This strategy allows the design of a platform-technology for systemic delivery of siRNA to tumor sites and also provides an alternavtive optical imaging probe for tumor visualization. Therefore, RNAtr NPs suggest great potentials as the siRNA therapeutics and imaging probes for cancer treatment.

AUTHORS (LAST NAME, FIRST NAME): Ahn, Hyung Jun[1]

INSTITUTIONS (ALL):

1. Center for Theragnosis, Biomedical Research Center, Korean Institute of Science and Technology, Seoul, Korea (the Republic of).

(No Image Selected)

CONTROL ID: 2232703

TITLE: Intraoperative Identification of Metastasis in Sentinel Lymph Nodes Using Macrophage Targeted Fluorescent; Indocyanine Green:Neomannosyl Human Serum Albumin

PRESENTER: Yuhua Quan

ABSTRACT BODY:

Abstract Body: OBJECTIVE and BACKGROUND: The presence of metastasis in sentinel lymph node (SLN) was important to decide whether the invasive lymph node dissection should be carried out or not during the surgery for many solid cancers. We developed a CD 206 targeting fluorescent which is one of marker of tumor associated macrophage. This study is to evaluate if a new macrophage targeting near infrared fluorescent (indocyanine green:neomannosyl human serum albumin, ICG:MSA) could identify the presence of metastasis in SLN through a custom-made intraoperative color and fluorescence merged imaging system (ICFIS) during surgery.

METHODS: The CD 206 targeting ability of ICG:MSA or ICG was compared in vitro by using differentiated monocytes cell line (U937). Metastatic SLN in mouse with Lewis Lung Cancer (LLC) cell and rabbit with VX2 cancer cell were confirmed on positron emission tomography/computed tomography (PET/CT) imaging two weeks after the tumor inoculation. The ICG:MSA or ICG was injected at peritumoral area of these animal models and measured the fluorescent intensity of the lymph nodes to detect SLN under ICFIS. And, the fluorescent intensity of these SLNs were compared between the animal models injected with ICG:MSA and ICG. The metastasis and expression of CD 206 in SLN were detected by hematoxylin and eosin and immunohistochemistry.

RESULTS: The fluorescence signal of U937 cells treated by ICG:MSA was almost 7 times higher than that of ICG. The ICG:MSA provided 3 times higher fluorescent intensity of metastatic SLN than ICG in animal tumor model (Figure). And, the ICG:MSA remained in metastatic SLN until 4h after injection, while ICG could not detected after 2 h injection. The SLN was successfully detected in all of the ICG:MSA injected VX2 rabbit tumor model while the ICG just detected in 3 of 5. The pathological findings showed that all of the dissected SLN have metastasis.

CONCLUSIONS: The new fluorescent (ICG:MSA) have specific targeting property of tumor associated macrophage in metastatic SLN. We hope that it could identify the presence of metastasis in SLN during cancer surgery without frozen biopsy.

AUTHORS (LAST NAME, FIRST NAME): Quan, Yuhua[5]; Kim, Minji[2]; Choi, ByeongHyeon[5]; Park, Ji Yong[4]; Eo, Jae Seon[3]; Park, Ji Ho[6]; Lee, Yun-Sang[4]; Jeong, Jae Min[4]; Choi, Yeonho[2]; Lee, Kisung[1]; Kim, Beop-min[2]; Kim, Hyun Koo[5]

INSTITUTIONS (ALL):

1. Biomedical Engineering, Korea University, Seoul, Korea (the Republic of).
2. Department of Bio-convergence Engineering, Korea University, Seoul, Korea (the Republic of).
3. Korea University Guro Hospital, Seoul, Korea (the Republic of).
4. Department of Nuclear Medicine, Seoul National University College of Medicine, Seoul, Korea (the Republic of).
5. Thoracic and Cardiovascular Surgery, Korea University Guro Hospital, Korea University College of Medicine, Seoul, Korea (the Republic of).
6. Department of Bio and Brain Engineering, Korea Advanced Institute of Science and Technology, Daejeon, Korea (the Republic of).

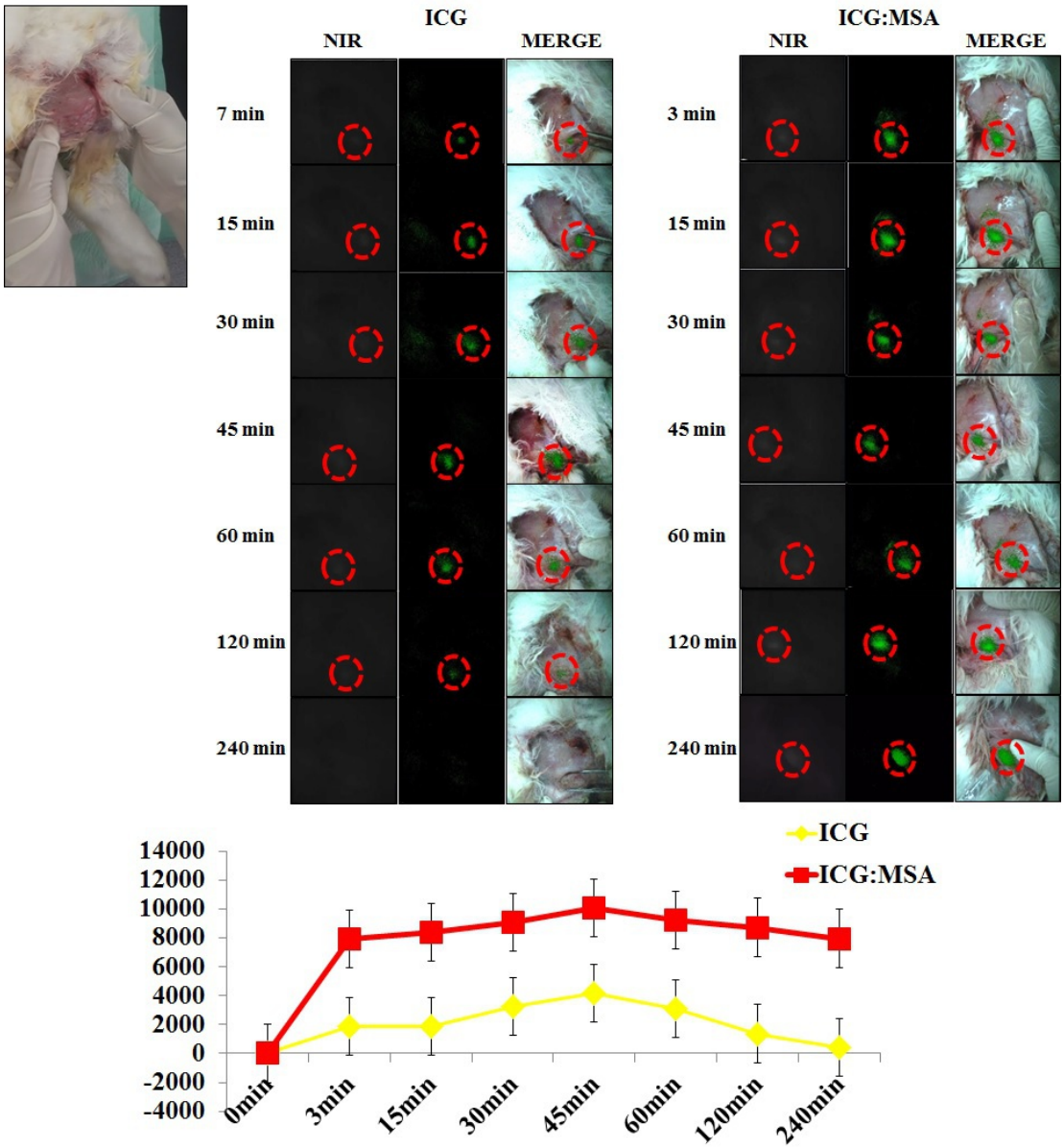

Comparison of metastatic SLN targeting effects of ICG and ICG:MSA in VX2 tumor model.

CONTROL ID: 2232707

TITLE: αVβ3 Integrin Targeted Tumor Theragnosis by Using Camptothecin Loaded c-RGD Conjugated Microbubbles in a Mouse Allograft Tumor Transplantation Model

PRESENTER: Wei-Tsung Chen

ABSTRACT BODY:

Abstract Body: Purpose: The aim of this study was to validate a camptothecin loaded cRGD-conjugated microbubble (cRGD-CPT-MB), for its ability to target αVβ3 integrin and its theragnostic effects in vitro and in an allograft mouse tumor model.

Procedures: αVβ3 integrin positive U87 cells and αVβ3 integrin negative KB cells, were incubated with NBD-labeled cRGD-CPT-MBs and cRAD-CPT-MBs for 2 hours. The cellular attachment of the cRGD-CPT-MBs and cRAD-CPT-MBs was observed by using fluorescent microscopy and was evaluated by flow cytometry. An agar phantom containing cRGD-CPT-MBs was used to test whether the cRGD-CPT-MBs can be visualized and destroyed by a commercial available ultrasound unit. Cell viabilities of U87 cells were evaluated after a 5 minutes treatment with blank MBs, CPT-MBs, cRGD-CPT-MBs, CRAD-CPT-MBs or free CPT with or without ultrasound exposure. The allograft tumor model was developed by embedding a polyvinyl alcohol sponge loaded with mouse breast cancer 4T1 cells ($1x10^6$) into an subcutaneous Matrigel bed. Theragnostic ultrasound was then performed on the mice 10 days later, and was repeated every 3 days till 30 days after tumor implantation (n=6). The cRGD-CPT-MBs or cRAD-CPT-MBs ($5x10^9$) were injected via retro-orbital venous plexus and the contrast enhancement patterns were observed by a commercial ultrasound unit under low acoustic pressure (mechanical index 0.1) for 10 minutes and the MBs were then destroyed by using higher acoustic pressure (mechanical index 1.2).

Results: The NBD-labeled cRGD-CPT-MBs attached to U87 cells, but did not adhere to KB cells. The cRAD-CPT-MBs had no attachment to neither cells (supplement 1). The cRGD-CPT-MBs loaded in the agar phantom can be visualized and destroyed by a commercial available ultrasound unit. The cell viabilities were decreased in the cRGD-CPT-MBs treatment group with ultrasound exposure in a dose-dependant relationship (supplement 2). In the contrast-enhanced ultrasound, a persistent contrast enhancement pattern was observed in the 4T1 tumors (n=6) injected with cRGD-CPT-MBs (figure 1), but a gradually washout pattern was seen in the cRAD-CPT-MBs injection group. The tumor growth rate was significantly decreased in the cRGD-CPT-MBs treatment group, as compared to the control group.

Conclusions: αVβ integrin-targeted tumor theranostics has been successfully implemented with cRGD-CPT-MBs and a clinical US unit. The ligand-directed and EPR mediated accumulation provides active and passive targeting capabilities, permitting the antitumor effects of cRGD-CPT-MBs to be exerted selectively to tumor angiogenesis and simultaneously providing targeted US imaging capabilities.

AUTHORS (LAST NAME, FIRST NAME): Chen, Wei-Tsung[1, 2]; Kang, Shih-Tsung[3]; Chen, Ran-Chou[1, 4]; Yeh, Chih-Kuang[3]

INSTITUTIONS (ALL):

1. Radiology Department, Taipei City Hospital, Taipei, Taiwan.
2. Radiology Department, National Taiwan University, School of Medicine, Taipei, Taiwan.
3. Department of Biomedical Engineering and Environmental Sciences, National Tsing Hua University, Taiwan, Hsinchu, Taiwan.
4. Department of Biomedical Imaging and Radiological Sciences, National Yang-Ming University, Taipei, Taiwan, Taipei, Taiwan.

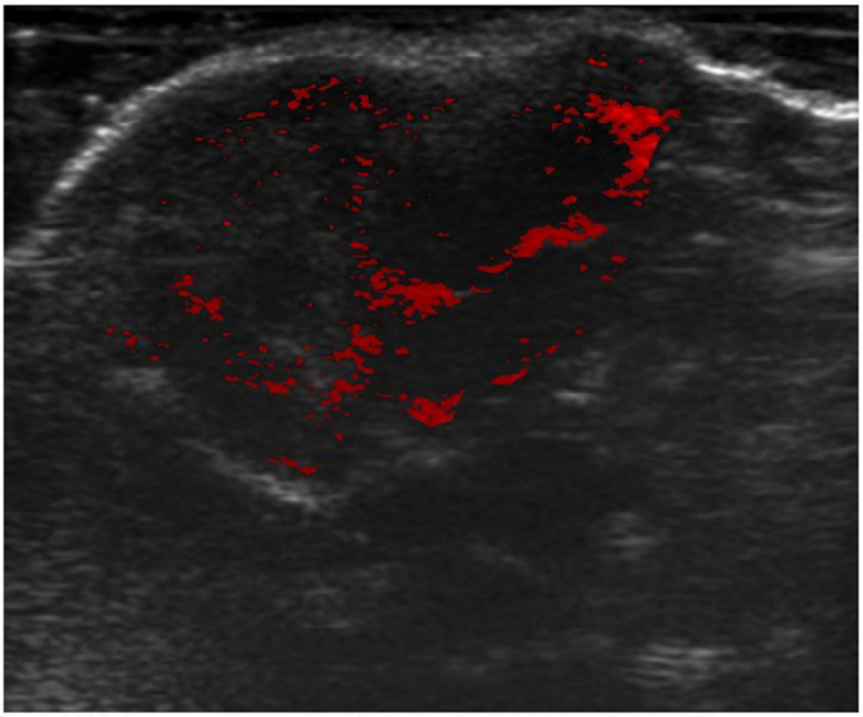

Figure 1 The αVβ3 integrin-targeted ultrasound imaging of the 4T1 mouse breast cancer tumor. A persistent contrast enhancement pattern was observed as the red color-coded zones within the tumor, 5 minutes after cRGD-CPT-MBs injection.

CONTROL ID: 2232827

TITLE: Combination Effects of Sorafenib with Ionizing Radiation on Orthotopic Human Oral-Bearing Mice Model

PRESENTER: Hui-Yen Chuang

ABSTRACT BODY:

Abstract Body: Objectives:

Oral squamous cell carcinoma (OSCC) is one of the leading cancers worldwide, especially in Asia. Most patients with OSCC have extremely poor quality of life due to bone invasion. In this study, we aimed to study whether sorafenib, a multikinase inhibitor, could enhance the therapeutic efficacy of radiotherapy (RT) and decrease the bone erosion using an *in situ* human OSCC-bearing mouse model. The underlying mechanisms involved in augmenting treatment outcomes were studied both *in vitro* and *in vivo*. Furthermore, the tumor progression and facial bone integrity were visualized by *in vivo* bioluminescent imaging (BLI) and micro-CT, respectively.

Materials and Methods:

Human oral carcinoma SAS cell line was transfected with p*CMV-luc2*, and renamed as SAS/*luc2*. Expressions of NF-kB and its downstream proteins and NF-kB activity in various groups (i.e. control, RT, sorafenib and combination) were studied by Western blotting and EMSA assay. For *in vivo* studies, 1.5×10^6 SAS/*luc2* cells were inoculated into the right masseter muscle of six-week-old male nude mice. Two weeks later, mice were randomly separated into six groups: (a) normal (i.e. no tumor); (b) control; (c) sorafenib alone; (d) radiation alone; (e) pretreatment (i.e. sorafenib prior to radiation), (f) concurrent treatment. The tumor growth and body weight were tracked by bioluminescent imaging (BLI) for another three weeks. Five weeks after tumor cell inoculation, mice were sacrificed, and subjected to micro-CT scanning to evaluate facial bone destruction of mice. The tumors were harvested for *ex-vivo* Western blot, *ex-vivo* EMSA, and IHC staining for mechanistic studies.

Results:

In vivo BLI showed that tumor growth was suppressed most significantly in the combination groups (i.e. pretreatment and concurrent groups), and are strongly related to the down-regulation of NF-kB and its effector proteins as detected by *ex vivo* EMSA and Western blotting. Notably, the expression level of p65 in tumor tissues of mice was suppressed most significantly in the pretreatment group. No or minor damage in the mandible and zygoma bones was found in the combination groups as demonstrated by reconstructed micro-CT images.

Conclusion:

The better control of human oral carcinoma could be achieved by combination of sorafenib with ionizing radiation, especially with the pretreatment of sorafenib. The underlying mechanism may through the suppression of NF-kB and its downstream effector proteins. In addition, bone destruction could also be reduced by the combination treatment, indicating that this may be a potential treatment strategy for human OSCC in clinic.

AUTHORS (LAST NAME, FIRST NAME): Chuang, Hui-Yen[1]; Hwang, Jeng-Jong[1]

INSTITUTIONS (ALL):

1. National Yang-Ming University, Taipei, Taiwan.

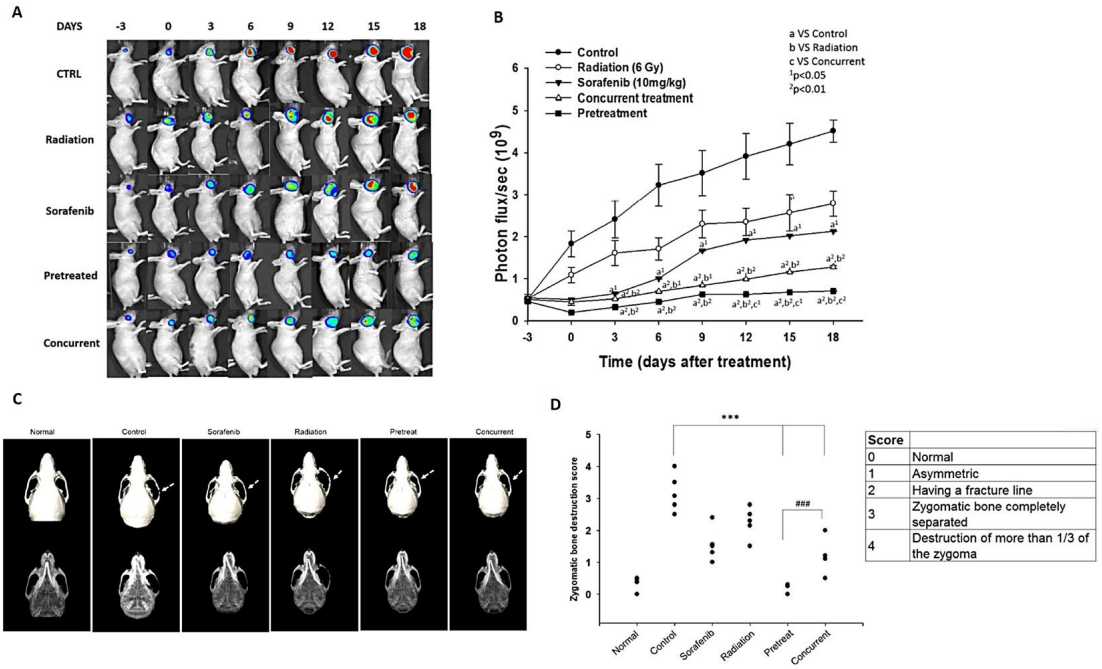

Score	
0	Normal
1	Asymmetric
2	Having a fracture line
3	Zygomatic bone completely separated
4	Destruction of more than 1/3 of the zygoma

CONTROL ID: 2233057

TITLE: NanoScan SPECT/CT Imaging of Tumor Acidic Microenvironment with ^{99m}Tc-labeled A Novel pH Low Insertion Peptide

PRESENTER: Jiyun Shi

ABSTRACT BODY:

Abstract Body: Objectives: The pH low-insertion peptides (pHLIPs) have received significant attention since their discovery due to the ability to target acidic tumor microenvironment. Studies of the wild type pHLIP (WT-pHLIP) showed a good contrast and tumor-to-blood ratio at 24 h postinjection (p.i.). However, a more rapid background signal reduction is absolutely essential for its application in clinical imaging. pHLIPv7 is one of the truncated versions of WT-pHLIP, which could be appropriate for PET/SPECT imaging, since the fluorescently labeled pHLIPv7 demonstrated fast tumor targeting and blood. Here, for the first time, this truncated pHLIP was radiolabeled with ^{99m}Tc for NanoScan SPECT/CT imaging of tumor acidic microenvironment.

Methods: The pHLIPv7 peptide was conjugated with 6-hydrazinonicotinyl (HYNIC) and then radiolabeled with ^{99m}Tc using TPPTS and tricine as coligands to obtain a radiotracer ^{99m}Tc-HYNIC-pHLIPv7 (^{99m}Tc-V7H). The *in vitro* stability of ^{99m}Tc-V7H was studied in 10% FBS solution. Metabolic stability, biodistribution and NanoScan SPECT/CT imaging were performed in MDA-MB-435S human breast tumor bearing nude mice to study the *in vivo* characteristics of ^{99m}Tc-V7H. The pH sensitivity of ^{99m}Tc-V7H was validated with control peptide ^{99m}Tc-HYNIC-K-pHLIPv7 (^{99m}Tc-KV7H) by performing biodistribution and NanoScan SPECT/CT imaging in pH modulated group, which were receiving bicarbonate-buffered drinking water (pH = 8.0).

Results: ^{99m}Tc-V7H was prepared by a non-$SnCl_2$ one-step method with more than 98% radiochemical purity. The radiotracer showed admirable in vitro and in vivo stability. The MDA-MB-435S tumor was clearly visualized by ^{99m}Tc-V7H NanoScan SPECT/CT imaging with low background except relatively high kidney uptake at all detected time points (1 h, 4 h and 8 h p.i.). The biodistribution results consistent with the imaging results, showing tumor uptake was second highest uptake among all detected organs (1.28 ± 0.10, 1.85 ± 0.09 and 1.62 ± 0.06 %ID/g at 1 h, 4 h and 8 h p.i., respectively). The selectivity of the pHLIP was shown by the modulation of pHe in MDA-MB-435S-bearing mice in which more acidic MDA-MB-435S tumors had greater uptake (1.85 ± 0.09 %ID/g at 4 h p.i.) of ^{99m}Tc-V7H than the less acidic (bicarb-modulated) MDA-MB-435S tumors (0.86 ± 0.03 %ID/g at 4 h p.i.). Compared to ^{99m}Tc-V7H, the control peptide ^{99m}Tc-KV7H showed relatively low tumor uptake (0.73 ± 0.14 %ID/g at 4 h p.i.), and non-responding to pH modulation (0.75 ± 0.09 %ID/g at 4 h p.i.).

Conclusions: In summary, we have synthesized and evaluated the optimized novel pHe-sensitive peptide SPECT agents for the delineation of low pHe in tumors. Our results suggest that SPECT/CT with ^{99m}Tc-V7H would provide an effective approach for the noninvasive detection of acidic tumors.

AUTHORS (LAST NAME, FIRST NAME): Shi, Jiyun[2, 1]; Yang, Li[1]; Zhai, Luoping[1]; Zhao, Haitao[1]; Gao, Hannan[1]; Zhao, Huiyun[1]; Jia, Bing[1]; Wang, Fan[1, 2]

INSTITUTIONS (ALL):

1. Medical Isotope Research Center, Peking University, Beijing, China.
2. Institute of Biophysics, Chinese Academy of Sciences, Beijing, China.

(No Image Selected)

CONTROL ID: 2232717

TITLE: Changes in cerebral glucose metabolism after non-invasive electrical stimulation of mild cognitive impairment patient

PRESENTER: Yong-An Chung

ABSTRACT BODY:

Abstract Body: Mild cognitive impairment (MCI) is a syndrome that disrupts an individual's cognitive function but preserves activities of daily living. MCI is thought to be a prodromal stage of Alzheimer's disease, which disrupts patients' daily lives and causes severe cognitive dysfunction. Although extensive clinical trials have attempted to slow or stop the MCI to Alzheimer's disease conversion, the results have been largely unsuccessful. Here, using transcranial direct current stimulation (tDCS) and Positron-Emission Tomography (PET), we showed that regular and relatively long-term use of tDCS significantly increased regional cerebral metabolism in MCI patients. Furthermore, subjective memory satisfaction and improvement of the memory strategies of participants were observed only in the real tDCS group after 3 weeks of stimulation. Our findings suggest that neurophysiological intervention at the early stage of MCI could improve transient memory function in MCI patients and even delay the progression to Alzheimer's disease.

AUTHORS (LAST NAME, FIRST NAME): Song, In-Uk[2]; Chung, Yong-An[1]

INSTITUTIONS (ALL):

1. Department of Radiology, Incheon St. Mary's Hospital, The Catholic University of Korea, Incheon, Korea (the Republic of).

2. Department of Neurology, Incheon St. Mary's Hospital, The Catholic University of Korea, Incheon, Korea (the Republic of).

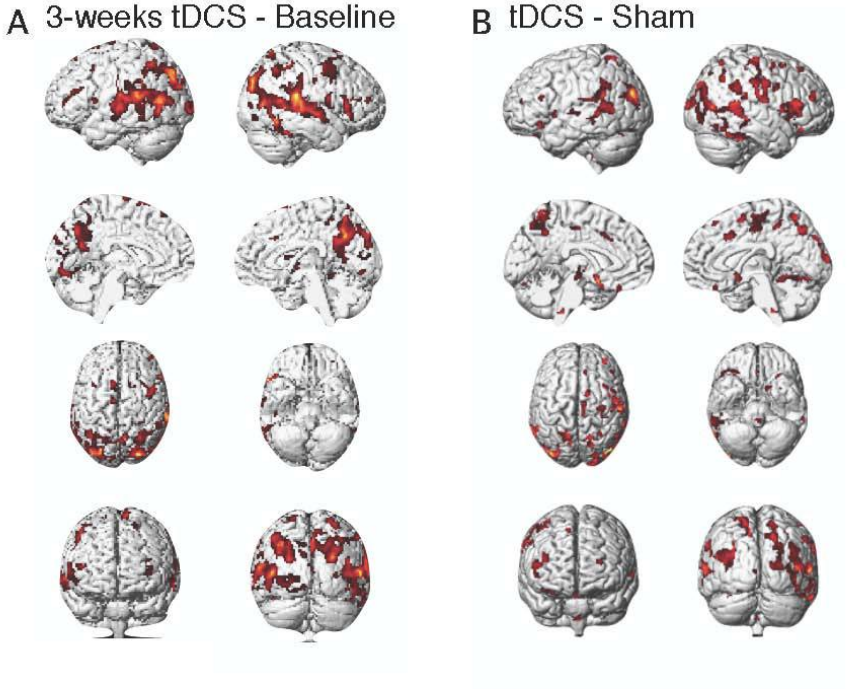
A 3-weeks tDCS - Baseline
B tDCS - Sham

CONTROL ID: 2232722

TITLE: Ablation rate and thyroglobulin decrease after low-dose ^{131}I in differentiated thyroid carcinoma post-total thyroidectomy

PRESENTER: Binh Duong

ABSTRACT BODY:

Abstract Body: Objective: The aim of this study is to evaluate the therapeutic success rate and serum thyroglobulin change after ^{131}I ablation therapy in patient with differentiated thyroid carcinoma post-total thyroidectomy.

Methods: Thirty four patients of differentiated thyroid carcinoma post-total thyroidectomy treated with low-dose ^{131}I ablation therapy (32 patients with 30 mCi and 2 patients with 60 mCi) between March 2011 and April 2014 were involved in this retrospective study. The imaging results of ^{131}I whole body scintigraphy and the change of serum thyroglobulin before and six months later after therapy were analyzed.

Result: Twenty seven (79%) out of 34 patients were found to have no thyroid uptake on their ^{131}I whole body scintigraphy image after ^{131}I ablation therapy and six months later. 7 patients (21%) were found to have thyroid uptake on their WBS.

Serum thyroglobulin had significantly decreased from the time of treatment to six months follow up later (Wilcoxon Signed Rank Test $P < 0.001$). Serum thyroglobulin was significantly decreased in successful cases (N = 27, Wilcoxon Signed Rank Test $P < 0.01$,). There was no significantly decreased of serum thyroglobulin in unsuccessful cases (N=7, Wilcoxon Signed Rank Test $P=0.612$)

Conclusion: Our finding suggests that the low therapeutic dose of ^{131}I is useful for the ablation to the differentiated thyroid carcinoma post total thyroidectomy with the successful rate is 79%. High serum thyroblobulin level group unlikely to be successful and need more dose of ^{131}I.

AUTHORS (LAST NAME, FIRST NAME): Duong, Binh D.[1]

INSTITUTIONS (ALL):

1. Diagnostic Radiology and Nuclear Medicine, Gunma University, Maebashi-shi, Gunma ken, Japan.

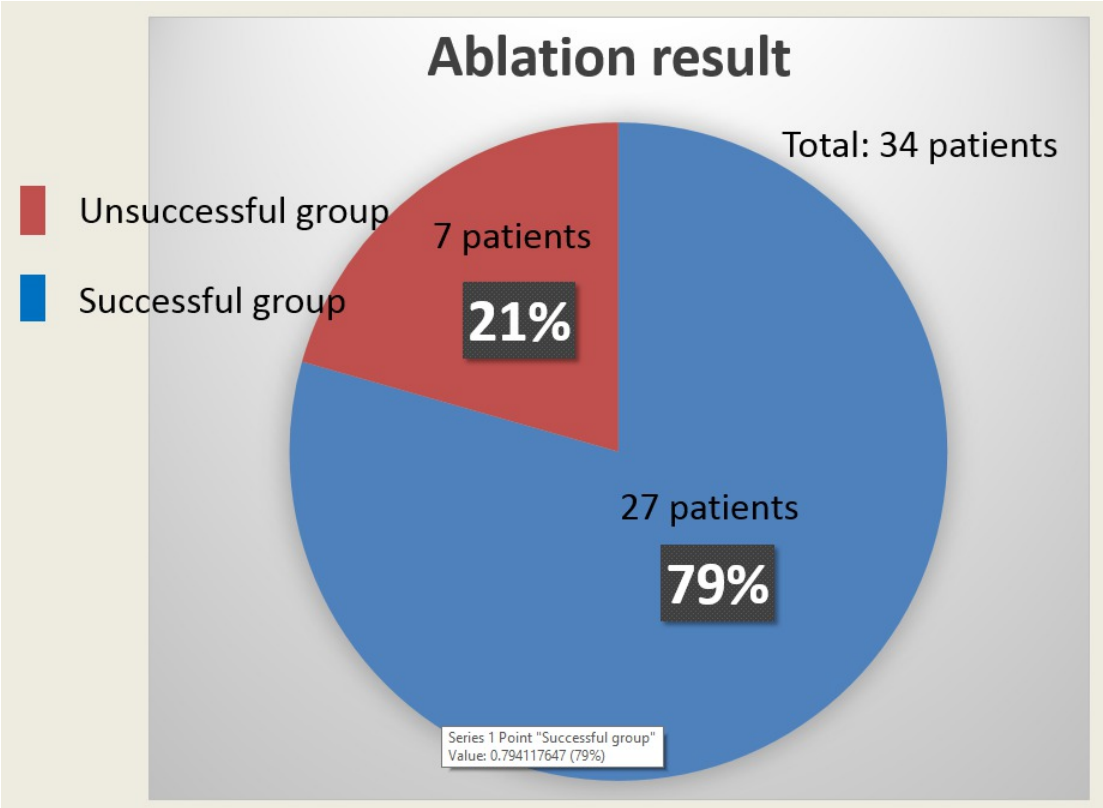
Ablation result
Total: 34 patients
Unsuccessful group
Successful group
7 patients
21%
27 patients
79%
Series 1 Point "Successful group"
Value: 0.794117647 (79%)

CONTROL ID: 2232723

TITLE: Effect of Curcumin on Breast Cancer Cell Glucose Metabolism and Formulation of EGF-Conjugated Curcumin-Lipid Nanoparticles and Anti-Cancer Therapy

PRESENTER: Kyung-Ho Jung

ABSTRACT BODY:

Abstract Body: Objective: Curcumin is a natural bioactive compound with multitargeting properties that have benefits on cancer treatment, but its therapeutic use is limited by poor stability and bioavailability. This could be overcome by nanoparticle carriers that improve stability and allow controlled drug delivery. In addition, introduction of specific targeting moiety can further elevate therapeutic outcome. In this study, we evaluated the effect of curcumin on cancer cell glucose metabolism, and prepared lipid nanoparticles (NPs) loaded with curcumin and conjugated with EGF ligands for anti-cancer therapy. **Methods:** MCF-7 breast cancer cells were treated with curcumin and evaluated for influence on ^{18}F-FDG uptake, lactate production, and hexokinase activity. For nanoparticle formulation, EGF was incubated with NHS-PEG-DSPE in 0.1 M HEPES solution for 24 h. After purification, curcumin was loaded into EGF-conjugated NPs (M.W. 10000) by the lipid film hydration method. Synthesized NPs was analyzed characterization including size, net charge and images using TEM and evaluated specific targeting of EGF to membrane-expressed EGFR. MDA-MB-468 breast cancer cells were treated with graded concentrations of native or non-targeted or targeted curcumin-NPs. In vitro cell survival was evaluated by sulforhodamine B (SRB) and colony formation assays. Furthermore, favorable targeted therapeutic effects of EGF conjugated curcumin-NPs were performed with micro-PET imaging in tumor bearing mice. **Results:** Curcumin treatment increased 24 h MCF-7 cell ^{18}F-FDG uptake in a dose and time-dependent manner. Cell growth was synergistically suppressed by 2-DG, a glycolytic inhibitor, when combined with curcumin. EGF conjugated curcumin-NPs were successfully prepared and their physicochemical characteristics were showed similar to between curcumin-NPs and EGF curcumin-NPs. Cell cytotoxicity based on SRB assays showed that vehicle and empty NPs had minimal effect on MDA-MB-468 cells survival. In contrast, specific targeted curcumin-NPs with EGF ligand demonstrated significantly dose-dependent reductions of surviving cell number compared to non-targeted curcumin-NPs. Calculation of half inhibitory concentration (IC50) of EGF curcumin-NPs revealed as 620.2 nM on MDA-MB-468 cells. Colony formation assays showed that cells treated with 5 μM EGF curcumin-NPs for 72 h had markedly reduced colony forming capacity. **Conclusion:** EGF curcumin-lipid NPs have specific and powerful therapeutic effects on MDA-MB-468 cells. Combination therapy with curcumin and 2-DG can enhance inhibition of MCF-7 cell survival. These results provide and encouraging outlook on the potential of ligand conjugated lipid NPs as an effective method for curcumin-specific delivery in vivo.

AUTHORS (LAST NAME, FIRST NAME): Jung, Kyung-Ho[1, 2]; Lee, Jin Hee[1, 2]; Park, Jin Won[1, 2]; Moon, Seung-Hwan[1]; Cho, Young Seok[1]; Lee, Kyung-Han[1, 2]

INSTITUTIONS (ALL):

1. Nuclear Medicine, Samsung Medical Center, Seoul, Korea (the Republic of).
2. Samsung Advanced Institute for Health and Sciences and Technology at Sungkyunkwan University, Seoul, Korea (the Republic of).

(No Image Selected)

CONTROL ID: 2232854

TITLE: Development of application program based on Fuzzy logic to enhance the image contrast on PET Scan

PRESENTER: Anil Pandey

ABSTRACT BODY:

Abstract Body: Introduction: A low contrast PET image requires image enhancement before it is subjected to either human interpretation or computer analysis. It is done by manipulating pixels either in spatial or frequency domain. In spatial domain pixels are directly manipulated, whereas in frequency domain, frequencies of the pixels are manipulated.

During the PET image reconstruction process, digital filters are applied to remove high frequency components that represent noise in the image. Since high frequency component also represents edge, therefore edges are blurred and this introduces the vagueness in terms of imprecise boundary. The images are further manipulated using window level adjustment tool during the process of scan reporting. This tool further increases the vagueness in identifying edges in the images. The vagueness in terms of imprecise boundary in the image can be solved by the fuzzy sets theory. We have developed an application program based on fuzzy logic algorithm to enhance the image contrast on PET Scans.

Material and Methods: Fuzzy logic technique is based on the modification of pixel in the fuzzy property plane of an image. The property of the domain is extracted from the spatial domain using fuzzifiers which play the role of creating different amount of fuzziness in the plane. An image I of M x N dimensions can be considered as an array of fuzzy singletons, each with a value of membership denoting the degree of brightness level L, L = 0,1,2, .. L-1 (e.g. a range of densities from L = 0 to L = 255). Using fuzzy set notations we can write:

$I = \{ \mu_{mn} / x_{mn} \}$;

Where m = 1, 2, 3...M and n = 1, 2, 3, N. μ_{mn} / x_{mn} denotes the fraction of the maximum intensity (gray level) possessed by the (m,n)the picture element x_{mn}. Here μ_{mn} = 0 denotes black and μ_{mn} = 1 denotes bright. Any intermediate value indicates the grade of maximum grey value of the pixel. Now for each μ in x we give a transformation of the form (equation 1)

……. (1)

The operator T (μ_{mn}) is known as contrast intensifier (INT) of a fuzzy set. This transformation reduces the fuzziness of X by increasing the values of μ_{mn} which are above 0.5 and decreasing those which are below it.

To enter into the fuzzy plane from the x_{mn} plane we defined an expression

Finally enhanced image was converted into spatial domain.

The algorithm was implemented using MATLAB R2013a. Fifteen PET images were processed with this application.

Results: Figure-1 shows an input and output image along with their histogram. We compared the effect of fuzzy logic and window level adjustment techniques. Fuzzy logic algorithm provided better image contrast. However, this method is computationally expensive.

Conclusion: The developed application program based on Fuzzy logic algorithm provided better image contrast in comparison to window level adjustment.

AUTHORS (LAST NAME, FIRST NAME): Pandey, Anil K.[1]; Sharma, Akshima[1]; Nazar, Aftab H.[1]; Patel, Chetan D.[1]; Bal, C.S.[1]; Kumar, Rakesh[1]

INSTITUTIONS (ALL):

1. Dept of Nuclear Medicine, All India Institute of Medical Sciences, New Delhi, Delhi, Delhi, India.

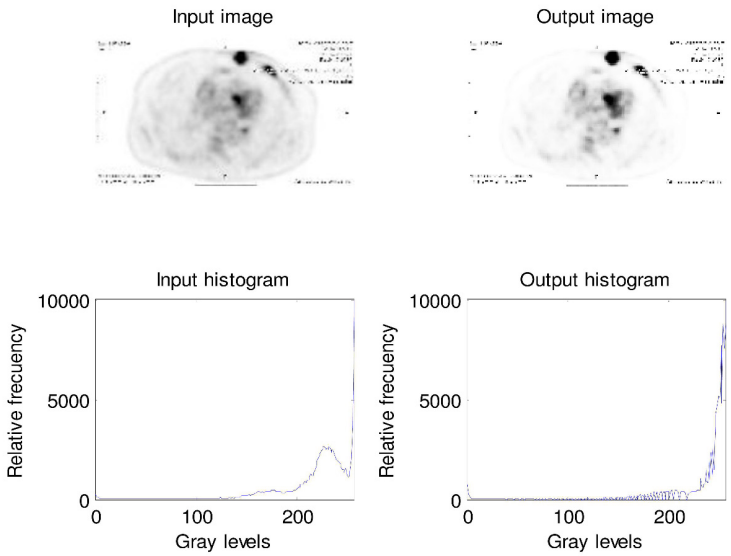

Figure 1: Shows input and output image and their corresponding histogram.

CONTROL ID: 2232726

TITLE: Near-Infrared Dye-Conjugated Hyaluronic Acid Nanoparticles for In Vivo Multimodal Imaging Guided Photothermal Therapy

PRESENTER: Xiaolong Liang

ABSTRACT BODY:

Abstract Body: Photothermal therapy (PTT) using PTT agents and near infrared (NIR) light has gained increasing attention as a minimally invasive approaches for cancer treatment. However, for effective and safe PTT treatment, the location and size of the tumors, distribution of in vivo photothermal agents and monitoring of post-treatment therapeutic effectiveness with appropriate imaging techniques are crucial to optimize personalized PTT treatment. In addition, the lack of targeting function of PTT agents also hampers its practical application. So theranostic agents with functions of both therapy and imaging that can actively targeted into tumor tissue are still needed urgently.[1]

However, single-modality imaging technique usually provide insufficient information for diagnosis. Considering each imaging modality possesses its own advantages and limitations, multiple-modality imaging can provide more comprehensive information for accurate diagnosis.[2] For examples, X-ray computed tomography (CT) takes advantages in illustrating biological structures with high resolution but low sensitivity. Near-infrared fluorescence (NIRF) imaging in the window of 700-900 nm holds much promise due to minimal autofluorescence and tissue scattering, showing high sensitivity but lower resolution. In contrast, photoacoustic imaging (PAI) combined both spectral selectivity of laser light and high resolution of ultrasound detection. Therefore, it is undoubted that the combination of CT, NIRF and PA imaging would conduce to accurate locating of cancerous tissue for more precise guidance of PTT.

Herein, a near-infrared fluorescent of indocyanine green derivatives (IR825) was conjugated to the naturally occurring polysaccharide hyaluronic acid (HA), obtaining amphiphilic polymers, which further self-assemblied into a nanoparticle (IR825-HA), followed by loading a CT contrast agent of perfluoroctyl bromide (PFOB), resulting in a tumor active targeting IR825-HA/PFOB nanocomposite with diameter around 100 nm. In this system, HA can strongly bind to its receptor (CD44), which is over-expressed in various cancer cells. IR825 with strong NIR absorbance appears to be an excellent contrast agent for photoacoustic (PA) imaging and an effective PTT agent. In vitro phototoxicity study show significantly phototoxic effect of IR825-HA/PFOB on the cultured HT-29 cells. After intravenous administration of the nanoparticle into HT-29 tumor-bearing mice, high fluorescence, CT and PA signals could be clearly observed in the tumor area over time, which peaked at the 24 h time point. The tumors growth could be effectively inhibited after treatment with R825-HA/PFOB in combination with laser irradiation, showing great potential for cancer diagnosis and therapy.

References:

[1] M. P. Melancon, M. Zhou, C. Li, Acc. Chem. Res. 2011, 44, 947.

[2] A. Louie, Chem. Rev. 2010, 110, 3146.

AUTHORS (LAST NAME, FIRST NAME): Liang, Xiaolong[1]; Fang, Lei[2]; Shi, Jiyun[1]; Dong, Chengyan[1]; Wang, Fan[1, 2]

INSTITUTIONS (ALL):

1. Institute of Biophysics, Chinese Academy of Science, Beijing, China.

2. Medical Isotopes Research Center, Peking University, Beijing, China.

(No Image Selected)

CONTROL ID: 2232739

TITLE: Small Molecule Dye based Probes for Near Infrared Window II Fluorescent Imaging of Tumor and Image-guided Surgery

PRESENTER: Xuechuan Hong

ABSTRACT BODY:

Abstract Body: Objectives: Second near-infrared window (NIR-II; 1000-1700 nm) fluorescent imaging is a newly emerging optical imaging technique which shows many advantages over conventional NIR window I (650-950 nm) imaging. But until now there is no small molecule dyes developed suitable for NIR-II imaging which seriously hampers its translation into clinical application. In this study, we designed and synthesized a novel small molecule dye (CH1055, MW 0.97kD, λex ~750nm, λem ~1080nm) which is capable of emitting fluorescence within NIR-II. CH1055 was further used for conjugation with different biomolecules for tumor imaging and image-guided surgery.

Methods: CH1055 was obtained through 8 steps of chemical synthesis. To demonstrate its in vivo use, two derivatives CH1055-PEG and CH1055-Affibody were prepared by conjugating CH1055 with PEG2000 and anti-EGFR Affibody, respectively (Figure 1a). The resulting bioconjugates were then characterized by MALDI-TOF-MS and tested in cells and in vivo. Specifically, CH1055-PEG was intravenously injected into mice bearing subcutaneous or orthotopic U87MG xenografts (n=4 per group). NIR-II imaging was performed at different time points and urine, feces, and blood of the mice were collected by time. Similarly CH1055-Affibody with or without anti-EGFR Affibody were injected in mice bearing EGFR positive SAS xenograft mice (n=4 per group). All of them were imaged at NIR II at 1h, 6h, 24h after injection. Real-time NIR-II image-guided surgery was also performed using SAS xenograft mice.

Results: All the probes were prepared successfully. CH1055-PEG was excreted ~90% within 24 hours. Importantly, CH1055-PEG displayed much better imaging quality than NIR I dye, indocyaninegreen (ICG), in resolving mouse brain vasculature (Figure 1b). High accumulation and imaging contrast of CH1055-PEG were observed in mouse brain tumors, suggesting its capability of imaging orthotopic tumor at a depth of ~4 mm (Figure 1b). CH1055-Affibody showed excellent tumor imaging contrast at both 1 and 6 h post-injection and tumor uptakes were specifically blocked by anti-EGFR Affibody (Figure 1C). Furthermore, the tumor-to-background signal ratio was over 15 at 24 h post-injection which afforded precise image-guided tumor removal surgery (Figure 1D).

Conclusions: We have successfully synthesized the first NIR-II small molecule dye with capability for conjugation with a variety of biomolecules. The resulting probes can show high stability and be quickly cleared through kidneys. These probes can be applied to image blood vasculature and tumors which were detected through both passive and targeted imaging. The small NIR-II probes developed can be used for precise image-guided surgery, and they could shift the paradigm of optical imaging in the clinic.

Acknowledgment: This work was supported by the Office of Science (BER), U.S. Department of Energy (DE-SC0008397).

AUTHORS (LAST NAME, FIRST NAME): Chen, Hao[2, 1]; Cheng, Kai[3]; Sun, Yao[4]; Hong, Xuechuan[2]; Cheng, Zhen[5]

INSTITUTIONS (ALL):

1. Molecular Imaging Program at Stanford and Bio-X Program, Stanford University, Stanford, CA, United States.
2. School of Pharmaceutical Sciences, State Key Laboratory of Virology, Key Laboratory of Combinatorial Biosynthesis and Drug Discovery , Wuhan, Hubei, China.
3. Department of Radiology, Molecular Imaging Program at Stanford (MIPS), Bio-X Program, Stanford, CA, United States.
4. Department of Radiology, Molecular Imaging Program at Stanford (MIPS), Bio-X Program, Stanford, CA, United States.
5. Department of Radiology, Molecular Imaging Program at Stanford (MIPS), Bio-X Program, Stanford, CA, United States.

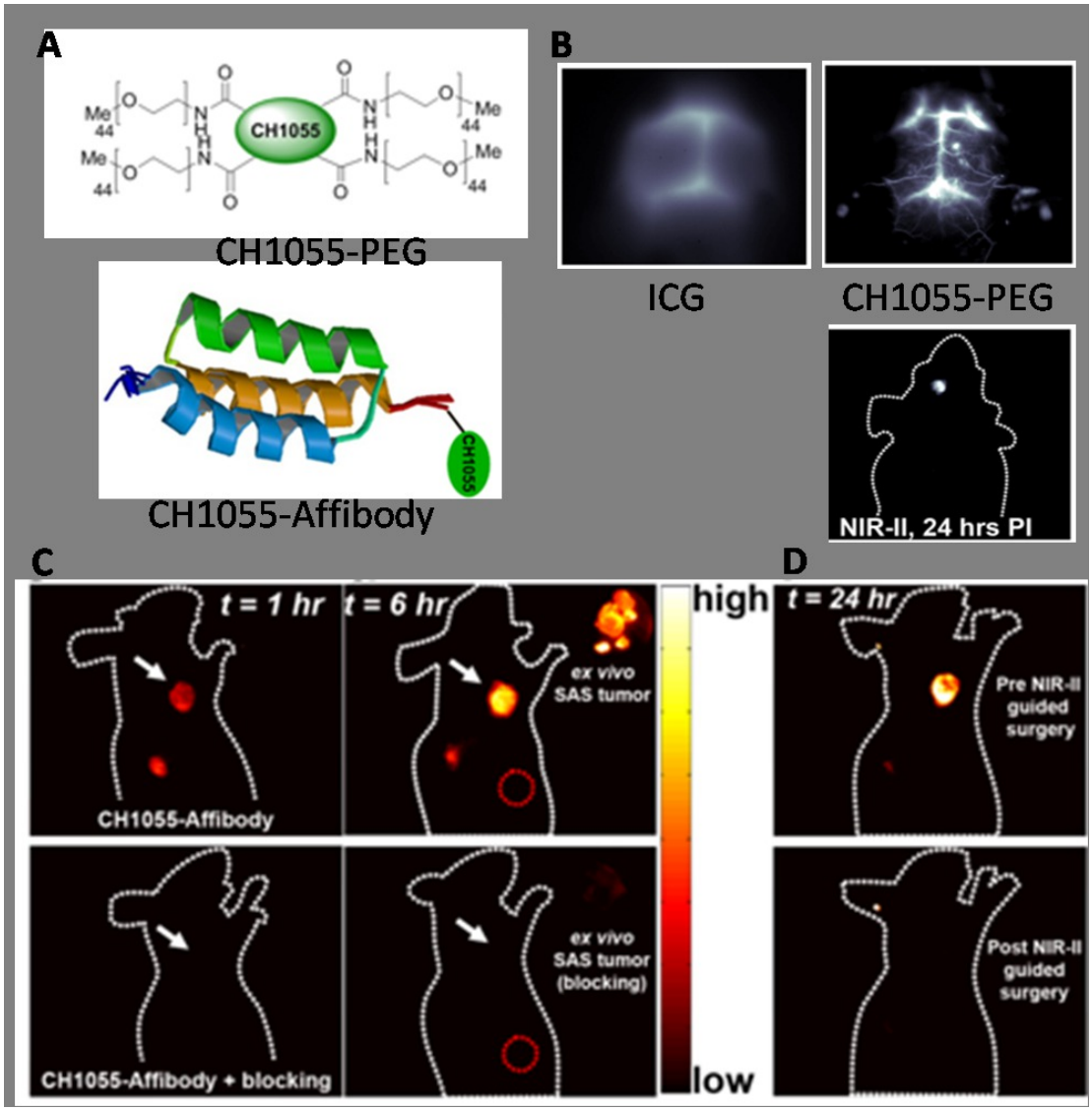
A
CH1055
Me
44
CH1055-PEG
CH1055
CH1055-Affibody
B
ICG
CH1055-PEG
NIR-II, 24 hrs PI
C
t = 1 hr
t = 6 hr
ex vivo
SAS tumor
high
low
CH1055-Affibody
ex vivo
SAS tumor
(blocking)
CH1055-Affibody + blocking
D
t = 24 hr
Pre NIR-II
guided
surgery
Post NIR-II
guided
surgery

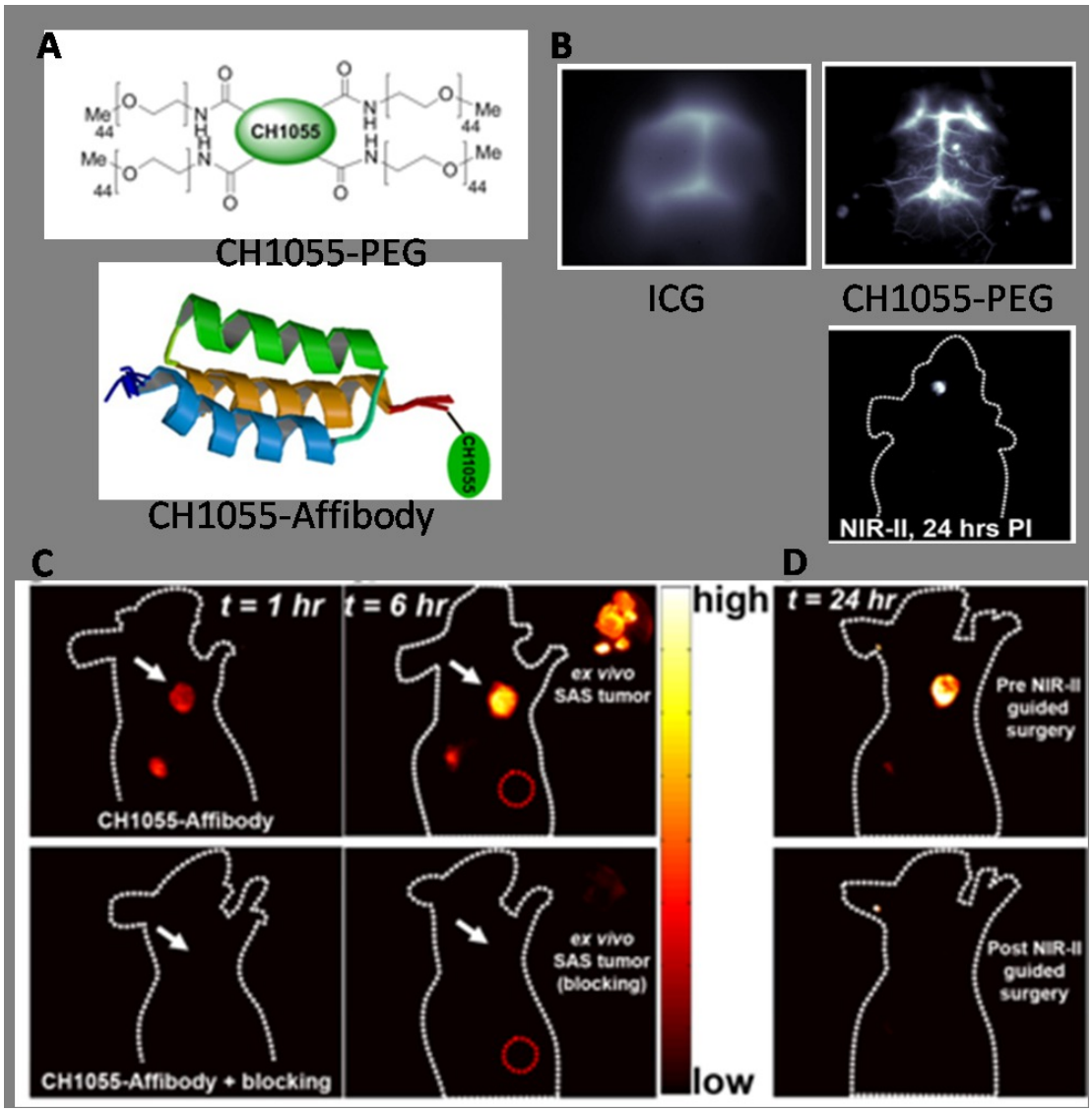

Figure 1: (**A**):Schematic structure of CH1055-PEG and CH1055-Affibody; (**B**)Brain vasculature imaging through the scalp and skull in C57BL/6 mice with shaved heads using either ICG (left) with a 100 ms exposure time (850-900 nm) and CH1055-PEG (right-top) with a 1s exposure time (1300 nm). Whole-body NIR-II fluorescence imaging at 24 h post-injection (right-bottom); (**C**)NIR-II fluorescence time-points taken at 1 h and 6 h after an intravenous injection of CH1055-affibody (60 μg). The upper panel shows clear tumor targeting and the bottom panel shows mice injected with a blocking dose consisting of CH1055-affibody plus free affibody concomitantly intravenously injected. Insert shows the SAS tumor *ex vivo* after excision in both a targeted and blocked mouse; (**D**) Images of a mouse 24 h post-injection of CH1055-Affibody before and after performing NIR-II fluorescence image-guided surgery to excise the tumor.

CONTROL ID: 2232747

TITLE: Clinical application of noninvasive and nonradioactive determination of microscopic lymph node tumor status by multispectral optoacoustic imaging

PRESENTER: Ingo Stoffels

ABSTRACT BODY:

Abstract Body: Background

Sentinel lymph node (SLN) staging is included in various cancer guidelines. This complex, time- and cost-intensive procedure requires radioactive tracing and could be avoided if noninvasive and nonradioactive assessment of nodal involvement was available. Multispectral optoacoustic tomography (MSOT) could help overcome the diagnostic drawbacks of SLNE using its potential to detect and stage SLNs noninvasively utilizing nonradioactive tracer.

Methods

We analyzed 506 excised SLNs from 214 melanoma patients with MSOT and subsequent histopathological assessment, either of sections containing the melanin positive region determined by MSOT, or applying the EORTC Melanoma Group histopathological protocol. We translated this into a clinical application combining MSOT with indocyanine green (ICG) as a fluorescent contrast agent to visualize SLNs. MSOT-guided ICG-based SLN detection followed by MSOT determination of SLN status was directly compared to standard 99mTc-guided SLNE and conventional pathological analysis of the SLNs.

Results

MSOT-guided histology improved the detection rate of SLN metastases in comparison to the EORTC Melanoma Group protocol (22.9% vs 14.2% p=0.019). In the clinical study all 99mTc-marked SLNs (n=41) visualized by lymphoscintigraphy and SPECT/CT were also ICG-labeled and detected by MSOT, for a concordance rate of 100% (Figure). MSOT visualized SLN in all anatomic regions with a penetration depth of 5 cm. MSOT identified tumor-free SLN *in vivo* without a single false negative.

Conclusions

We present for the first time a novel, noninvasive strategy, which has a high potential to eliminate the complex, radioactive and invasive SLN procedure for a significant number of melanoma patients.

AUTHORS (LAST NAME, FIRST NAME): Stoffels, Ingo[1, 5]; Morscher, Stefan[2]; Helfrich, Iris[1, 5]; Leyh, Julia[1, 5]; Burton, Neal C.[2]; Sardella, Thomas[2]; Claussen, Jing[2]; Poeppel, Thorsten D.[3]; Roesch, Alexander[1, 5]; Griewank, Klaus[1, 5]; Schadendorf, Dirk[1, 5]; Gunzer, Matthias[4]; Klode, Joachim[1, 5]

INSTITUTIONS (ALL):

1. Department of Dermatology, University Hospital Essen, Essen, Germany.
2. iThera Medical, Munich, Germany.
3. Department of Nuclear Medicine, University Hospital Essen, Essen, Germany.
4. Institute for Experimental Immunology and Imaging, Imaging Center Essen (IMCES), University Hospital Essen, Essen, Germany.
5. West German Cancer Center, University Duisburg-Essen, Essen, Germany.

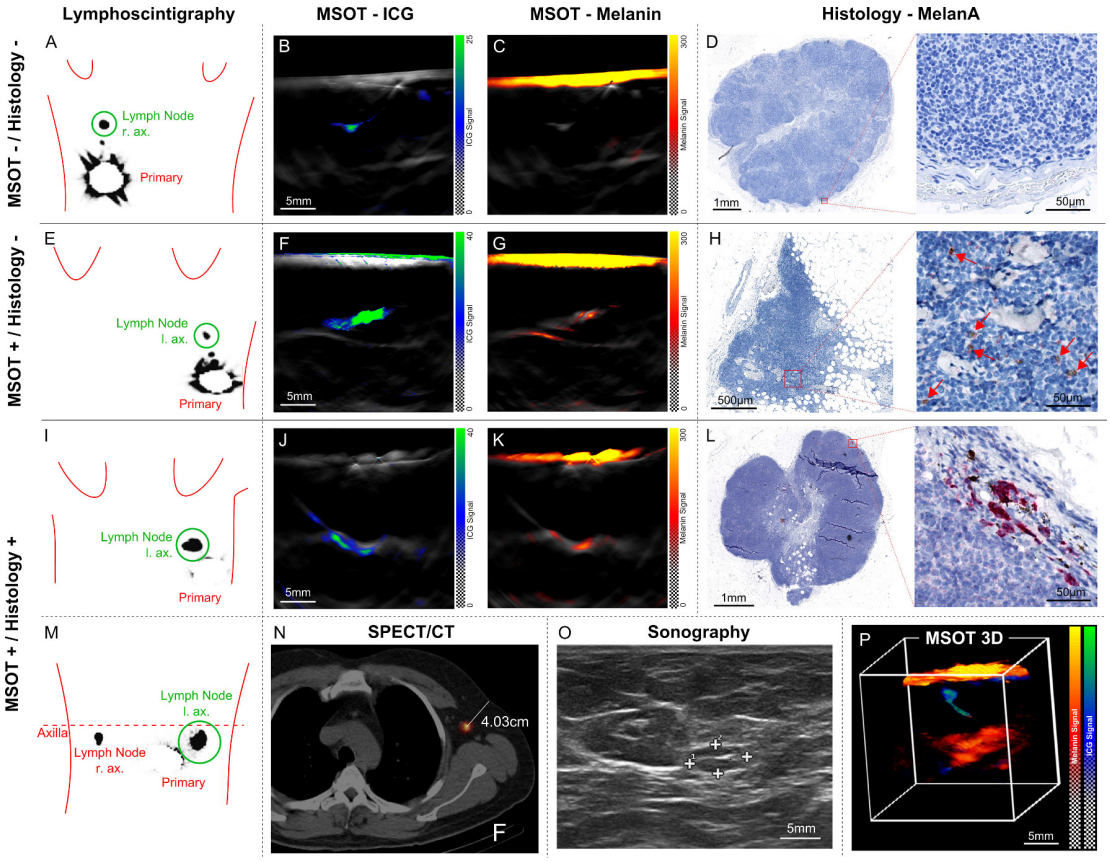
Lymphoscintigraphy
MSOT - ICG
MSOT - Melanin
Histology - MelanA
MSOT - / Histology -
MSOT + / Histology -
MSOT + / Histology +
A
B
C
D
E
F
G
H
I
J
K
L
M
N
O
P
Lymph Node
r. ax.
Primary
Lymph Node
l. ax.
Primary
Lymph Node
l. ax.
Primary
Axilla
Lymph Node
r. ax.
Lymph Node
l. ax.
Primary
SPECT/CT
4.03cm
Sonography
MSOT 3D
ICG Signal
Melanin Signal
5mm
1mm
500µm
50µm

CONTROL ID: 2232775

TITLE: Inhaled near infrared Itrybe nanoparticles for non-invasive tracking of macrophages in a mouse model of allergic airway inflammation.

PRESENTER: Joanna Napp

ABSTRACT BODY:

Abstract Body: Molecular imaging of lung diseases such as asthma in preclinical models is limited up to date. Allergic asthma is a chronic inflammatory disease, characterized by broncho-obstruction, airway hyper-responsiveness and increased mucus production. The acute asthma attack includes a considerable infiltration of immune cells in the lung, among others alveolar macrophages, the first line of defence. This study exploits these cells for *in vivo* and *ex vivo* imaging purposes, using inhaled near infrared fluorescence (NIRF)-Itrybe loaded 100 nm nanoparticles (Itrybe-NPs) in an ovalbumin (OVA)-induced model of allergic airway inflammation (AAI).

Itrybe-NPs uptake was analysed *in vitro* using MH-S mouse alveolar macrophage cell line. Here, NIRF microscopy revealed a strong internalisation already within 5h of incubation of the cells with 100 ng/ml NPs at 37°C, which was almost completely inhibited, when the cells were grown at 4°C.

In vivo, a severe OVA-based model was used to induce AAI in immunocompetent SKH-1 hairless mice, involving 4 challenges with OVA. Histological analysis of lung sections as well as broncho-alveolar lavage (BAL) revealed significant accumulation of immune cells including macrophages and eosinophils, development of bronchus-associated lymphoid tissue (BALT), mucus hyper production, and goblet cell hyperplasia, showing that the SKH-1 mice are receptive to the induction of AAI by OVA and represent an excellent model for asthma research.

24h after the last challenge, AAI and control mice intranasally received 160 µg of Itrybe-NPs and were imaged *in vivo* 1h, 5h and 24h after application using the OptixMX2 system. At all scan points, significantly higher fluorescence intensities were measured *in vivo* in lungs of AAI mice compared to controls (2.9, 1.7 and 1.4 times higher at 1h, 5h and 24h, respectively), with peak intensities obtained at 5h post NPs application. *In vivo* imaging results were confirmed by *ex vivo* lung scans and the development of AAI was validated by eosinophilia in the BAL and by histology.

Immunostaining of cytospins from BALs as well as extensive analyses of lung cryosections from entire lungs explanted 24h after NP instillation revealed the uptake of Itrybe-NPs predominantly by $CD68^{+}CD11c^{+}ECF\text{-}L^{+}MHCII^{low}$ cells, identifying them as alveolar M2 macrophages in the peribronchial and alveolar areas. We never found any Itrybe-NPs in proSP-C^{+} (prosurfactant protein C) alveolar type II (AT2) cells, but we occasionally observed some Itrybe-NPs within the cytoplasm of podoplanin^{+} alveolar epithelial type I (AT1) cells.

In summary, we demonstrate that fluorescence imaging in combination with bright NIR-emissive Itrybe-NPs is a promising method to preclinically assess allergic inflammation in the respiratory system *in vivo*. In addition, we show that Itrybe-NPs provide an excellent tool to track lung macrophages and further elucidate the alveolar M2 macrophages as the most efficient phagocytes.

AUTHORS (LAST NAME, FIRST NAME): Napp, Joanna[2, 3]; Markus, Andrea M.[3]; Behnke, Thomas[1]; Mitkovski, Miso[4]; Dullin, Christian[5]; Kilfeather, Stephen[6]; Resch-Genger, Ute[1]; Alves, Frauke[2, 3]

INSTITUTIONS (ALL):

1. Biophotonics, BAM Federal Institute for Materials Research and Testing, Berlin, Germany.
2. Molecular Biology of Neuronal Signals, MPI for Experimantal Medicine, Goettingen, Germany.
3. Department of Hematology and Medical Oncology, University Medical Center Göttingen, Goettingen, Germany.
4. MPI for Experimental Medicine, Goettingen, Germany.
5. Department of Diagnostic and Interventional Radiology, University Medical Center Göttingen, Goettingen, Germany.
6. Aeirtec Limited, Newcastle upon Tyne , United Kingdom.

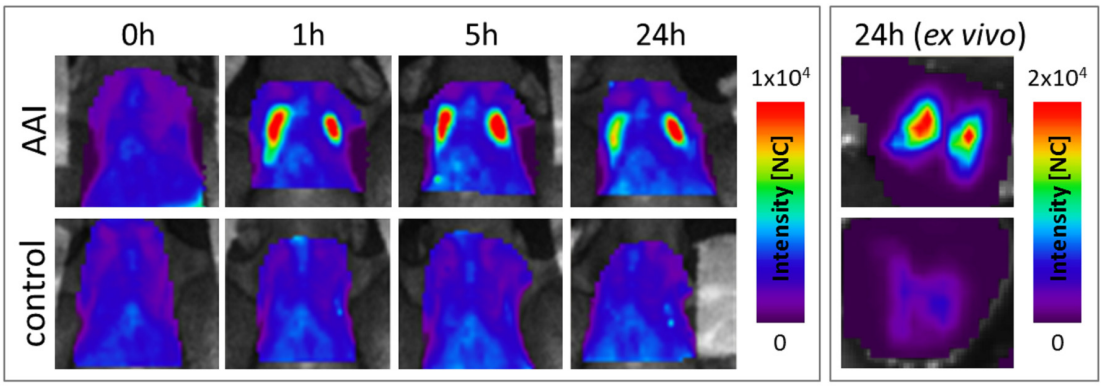

Fig. 1 *In vivo* (left) and *ex vivo* (right) imaging of lungs from AAI (upper panel) and control (lower panel) SKH-1 mice. NIRF loaded Itrybe nanoparticles were intranasally applied and fluorescence was measured as normalized counts [NC] using an Optix MX2 at the given time points post application.

CONTROL ID: 2232843

TITLE: Phosphate-based inorganic-organic hybrid nanoparticles with high potential for simultaneous treatment and diagnostics of inflammatory disease.

PRESENTER: Joanna Napp

ABSTRACT BODY:

Abstract Body: Hybrid nanomaterials combine properties and functions such as controlled drug release together with monitoring treatment delivery. Here, we present the synthesis of novel, phosphate-based inorganic-organic hybrid nanoparticles (IOH-NPs) with a composition $[ZrO]^{2+}[BMP]^{2-}[DUT]^{2-}$ and their preclinical evaluation. These ~70nm NPs are composed of an anti-inflammatory agent (betamethasonphosphate, BMP), routinely applied in the clinic, and a near-infrared (NIR) fluorescent dye (DY-647, DUT).

In vitro, an efficient uptake of IOH-NPs by two types of macrophages, mouse immortalized alveolar macrophages from the MH-S cell line and peritoneal macrophages, within 5h of incubation at 37°C was shown using NIR fluorescence microscopy. The uptake was even more prominent after 24 h and did not occur, upon incubation at 4°C.

The anti-inflammatory potential of $[ZrO]^{2+}[BMP]^{2-}$ $[DUT]^{2-}$ was tested *in vitro* with MH-S cells and with peritoneal macrophages, treated with the endotoxine, lipopolysaccharide (LPS, 200 ng/mL), in order to provoke an inflammatory response. Cells were simultaneously incubated with the IOH-NPs (1×10^{-10} to 1×10^{-5} M) or with dexamethasone as control (DM; 1×10^{-7} M) for 48 h. The release of tumor necrosis factor alpha (TNFα), interleukin 6 (IL-6) and NO into the culture medium was measured with ELISA. In both, a dose-dependent reduction in TNFα, IL-6 and NO secretion was observed in response to IOH-NPs, with the efficacy of 1×10^{-5} M $[ZrO]^{2+}[BMP]^{2-}[DUT]^{2-}$ comparable to 1×10^{-7} M of dissolved molecular DM, confirming the efficient release of BMP as well as the anti-inflammatory activity of IOH-NPs.

To study the *in vivo* efficacy of IOH-NPs, a sterile inflammation was induced by injecting Zymosan-A (500 µg/50 µl) into left the hind paw of BalbC mice and 50 µl PBS into the right paw as control. Two hours later, mice were treated intraperitoneally for 4 days either with $[ZrO]^{2+}[BMP]^{2-}[DUT]^{2-}$ (10 mg/kg; n=7) or with 0.9% NaCl (n=6). Treatment efficacy was assessed *in vivo* by measurement of paw volumes using µCT as well as *ex vivo*, via assessment of paw weights during section. Volumes of Zymosan-A treated left paws were significantly lower in mice treated with IOH-NPs (181 +/- 38 mm^3) than in the control group (222 +/- 33 mm^3). Volumes of the right control paws were similar in the two groups (154 +/- 7 mm^3 and 150 +/- 20 mm^3). In accordance, the average paw weights were decreased from 0.23 +/- 0.02 g to 0.19 +/- 0.3 g in untreated and IOH-NPs-treated mice, respectively. No differences in the right control paws were observed between treated (0.15 +/- 0.01g) and untreated mice (0.16 +/- 0.01 g).

These results clearly show that treatment with $[ZrO]^{2+}[BMP]^{2-}[DUT]^{2-}$ significantly reduces inflammatory response *in vitro* and *in vivo*.

To test the potential of the IOH-NPs for optical imaging, nude mice were subcutaneously injected with $[ZrO]^{2+}[BMP]^{2-}$ $[DUT]^{2-}$ and scanned with IVIS system. Spectral un-mixing allowed clear *in vivo* detection of the injected probe.

In summary, our results show that IOH-NPs can effectively be applied to combine therapy (drug release) and diagnostics (optical detection) and might have the potential to reach clinical application.

AUTHORS (LAST NAME, FIRST NAME): Napp, Joanna[1, 2]; Heck, Joachim G.[3]; R, Holger M.[4]; Feldmann, Claus[3]; Alves, Frauke[1, 2]

INSTITUTIONS (ALL):

1. Molecular Biology of Neuronal Signals, MPI for Experimantal Medicine, Goettingen, Germany.
2. Department of Hematology and Medical Oncology, University Medical Center Göttingen, Goettingen, Germany.
3. Institute for Inorganic Chemistry , KIT, Karlsruhe Institute of Technology, Karlsruhe, Germany.
4. Cellular and Molecular Immunology, University of Göttingen Medical School, Goettingen, Germany.

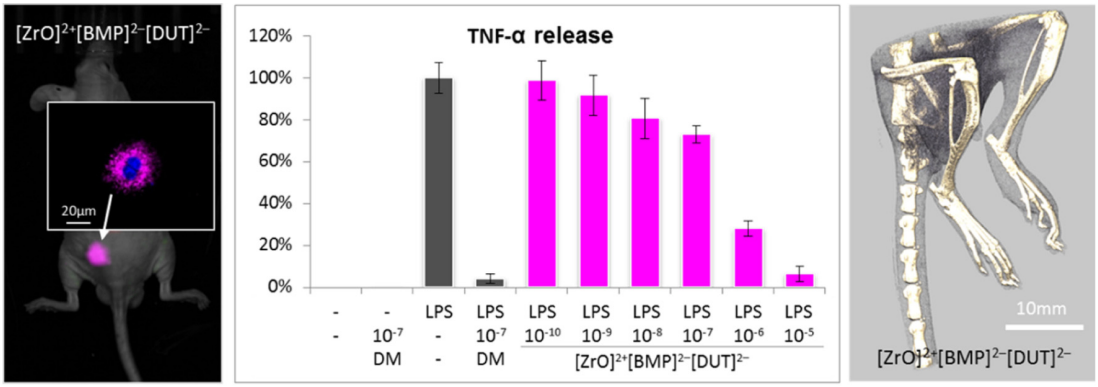

Fig. 1. $[ZrO]^{2+}[BMP]^{2-}$ $[DUT]^{2-}$ nanoparticles for optical imaging and drug delivery.

CONTROL ID: 2232754

TITLE: Imaging of atherosclerotic plaques in mice with somatostatin receptor 2-targeting PET tracer ^{68}Ga-DOTANOC

PRESENTER: Sanna Hellberg

ABSTRACT BODY:

Abstract Body: Introduction: Atherosclerosis is a chronic inflammatory disease of arterial walls that can eventually lead to plaque rupture and thrombosis. Rupture-prone atherosclerotic plaques are characterized by accumulation of inflammatory cells, especially macrophages, which have shown to express somatostatin type 2 receptors (SSTR-2) [1]. SSTR-2-targeted PET imaging of atherosclerotic plaques with ^{68}Ga-DOTATATE has been shown to be feasible [2, 3]. We aimed to investigate, whether SSTR-2-targeting PET tracer ^{68}Ga-DOTANOC can detect inflamed atherosclerotic plaques.

Methods: Atherosclerotic + diabetic IGF-II/LDLR$^{-/-}$ApoB$^{100/100}$ mice and healthy C57Bl/6N mice were studied in vivo and ex vivo for uptake of ^{68}Ga-DOTANOC into atherosclerotic plaques. Accumulation of the tracer into plaques and healthy vessel wall areas was studied by autoradiography at 60 minutes post-injection. Furthermore, tracer uptake was compared with plasma cytokine and metabolic hormone levels. The expression of SSTR-2 was analyzed by immunohistochemistry of mouse aortic and human carotid artery sections.

Results: Immunohistochemical stainings of mouse and human arteries were positive for both macrophages and SSTR-2. In vivo PET imaging revealed increased focal uptake of ^{68}Ga-DOTANOC in the aortic arch of atherosclerotic mice. Ex vivo uptake of the tracer in the whole thoracic aorta was higher in atherosclerotic mice compared to healthy controls (SUV values 1.02 ± 0.36 vs. 0.43 ± 0.18, p<0.001). There was, however, no difference in the aorta-to-blood ratios between the strains (1.2±0.3 vs. 1.3±0.3, p=0.14). In the autoradiography, ^{68}Ga-DOTANOC showed increased uptake to atherosclerotic plaques compared to healthy vessel wall areas (plaque-to-wall ratio 1.7 ± 0.3, p<0.001). Binding of ^{68}Ga-DOTANOC into atherosclerotic plaques was directly associated with plasma interleukin-6 levels (R^2 =0.53, p=0.01) as well as with insulin (R^2=0.70, p=0.01) and leptin (R^2=0.46, p=0.01).

Conclusions: ^{68}Ga-DOTANOC showed feasible properties for the detection of inflamed atherosclerotic plaques in mice. The results further strengthen the concept of SSTR-2-based imaging to identify rupture-prone plaques in high-risk patients.

References:

[1] Armani et al. J Leukoc Biol. 2007; 81(3):845-855.

[2] Rominger et al. J Nucl Med. 2010; 51(2):193-197.

[3] Li et al. Atherosclerosis. 2013; 230(1):33-39.

AUTHORS (LAST NAME, FIRST NAME): Hellberg, Sanna[1]; Rinne, Petteri[1]; Kiugel, Max[1]; Virta, Jenni[1]; Luoto, Pauliina[1]; Liljenbäck, Heidi[1, 2]; Hakovirta, Harri[3]; Gardberg, Maria[4]; Knuuti, Juhani[1]; Saraste, Antti[1, 5]; Roivainen, Anne[1, 2]

INSTITUTIONS (ALL):

1. Turku PET Centre, University of Turku, Turku, Finland.
2. Turku Center for Disease Modeling, University of Turku, Turku, Finland.
3. Department of Surgery, University of Turku, Turku, Finland.
4. Department of Pathology, Turku University Hospital and University of Turku, Turku, Finland.
5. Heart Center, Turku University Hospital and University of Turku, Turku, Finland.

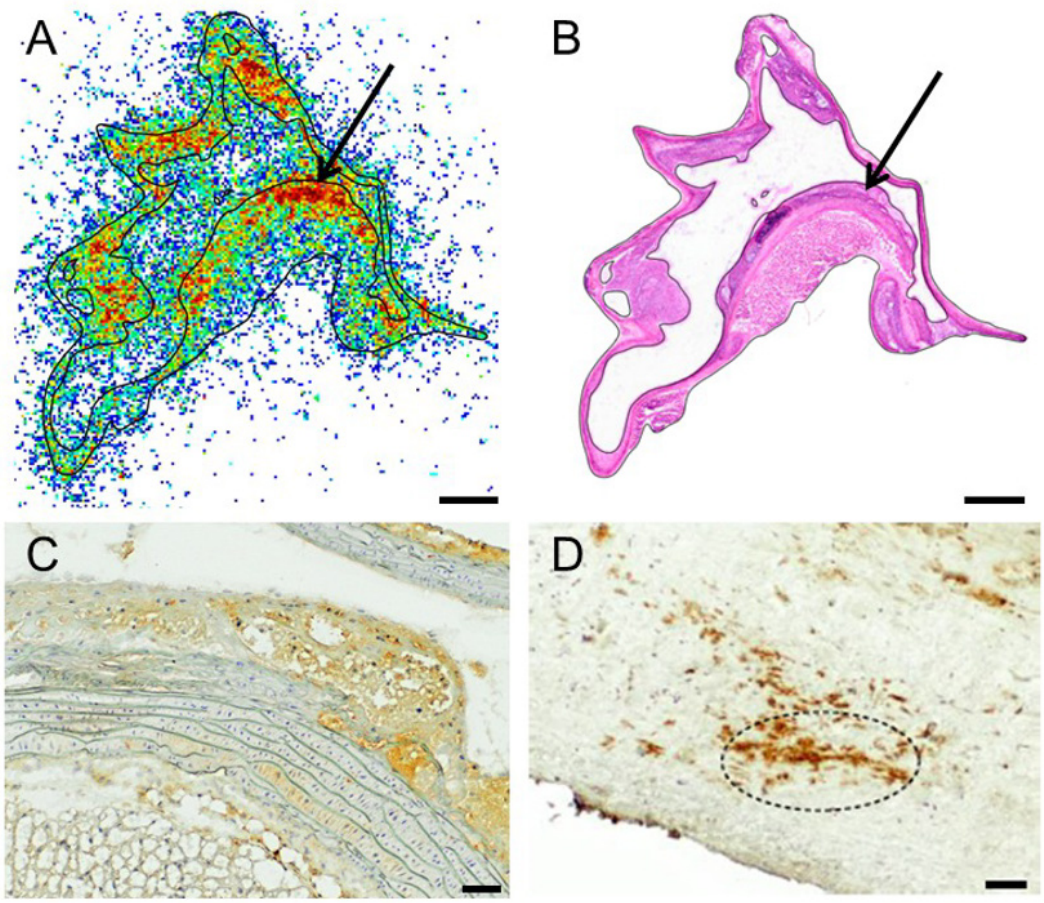

A. ^{68}Ga-DOTANOC autoradiography of atherosclerotic mouse aorta shows high uptake (red) in plaques. **B.** Corresponding aortic section stained with hematoxylin and eosin. **C.** Macrophage immunostain of aortic arch plaque (arrow in A and B). **D.** SSTR-2 immunohistochemistry shows positive staining in human endarterectomy section. Scale bar in A and B: 500 µm, C and D: 50 µm.

CONTROL ID: 2232795

TITLE: Peptide-guided in vivo optical imaging and targeted delivery of therapeutics to lung tumor in a transgenic mouse model

PRESENTER: HyunKyung Jung

ABSTRACT BODY:

Abstract Body: The lack of molecular targets for lung cancer remains a major drawback for effective chemotherapies and results in dose-limiting toxicities. In this study, we employed in vivo phage display to identify novel peptide ligands that homes to autochthonous lung tumor of K-ras^{LA2} transgenic mouse model in tumor microenvironment. After five rounds of screening, four candidate peptides were chosen based on the frequency of the sequences. When intravenously administered into a 12 week-old K-ras^{LA2} transgenic mouse, fluorescence dye-labeled rasLT-4 peptide was accumulated at tumor nodules in the lung at higher levels than other peptides, as determined by ex vivo fluorescence imaging of isolated lungs. Non-invasive in vivo imaging of rasLT-4 peptide homing was achieved using photoacoustic tomography(PAT), which demonstrated accumulation of the rasLT-4 peptide at the lung tumor at higher levels than other peptides. Microscopic analysis also demonstrated the localization of the rasLT-4 peptide at tumor tissue. The rasLT-4 peptide-labeled liposomal doxorubicin, when intravenously injected into tumor-bearing K-ras^{LA2} transgenic mice, more efficiently decreased total lung weight and number of tumor nodules with sizes above 3 mm. These results suggest that the rasLT-4 peptide is a promising targeting ligand for the delivery of anti-cancer therapeutics to lung cancer in its microenvironment.

AUTHORS (LAST NAME, FIRST NAME): Jung, HyunKyung[1, 2]

INSTITUTIONS (ALL):

1. kyungpook national university, Daegu, Korea (the Republic of).
2. Tumor Heterogeneity and Network Research Center, Daegu, Korea (the Republic of).

(No Image Selected)

CONTROL ID: 2232763

TITLE: Identification of the Role of Autophagy in *Salmonellae*-mediated Cancer Imaging and Therapy

PRESENTER: Mai Duong

ABSTRACT BODY:

Abstract Body: In bacteria-mediated cancer therapy, *Salmonellae* is one of the potential candidates to suppress the tumor growth. However, it has still remained unclear which mechanism of *Salmonellae* –induced tumor cell death could provoke anticancer immunogenicity. Autophagy is one of well-known cellular survival strategies which degrades proteins and unwanted organelles in the cytoplasm under stress conditions. Recent studies have provided new insights that autophagy in host cells plays as a defense mechanism in against to invasive bacteria[1,2]. Herein, we demonstrated that non-invasive *Salmonellae* induced autophagy in cancer cells in a dose and time- point dependent manner. Lipopolysaccharides derived from *Salmonellae* treatment also triggered autophagy through TLR4 expression on cellular membrane. This finding suggested a possible pathway that non-invasive *Salmonellae* triggered autophagic signaling pathway in cancer cells via the up-regulation of LPS/TLR4 pathway. Moreover, in response to bacteria-mediated cancer therapy, autophagy–competent, not autophagy-deficient cancer cell model, showed better tumor suppression effect. The exposure of calreticulin (CRT) and the release of high-mobility group box 1 protein (HMGB1), which required for immunogenicity, were significantly decreased in autophagy-deficient cancer cells as compared to autophagy-competent cells after bacterial infection. Thus, the release of HMGB1 and exposure of CRT from autophagic dying tumor cells are important factors that determine the therapeutic efficacy in bacteria-mediated cancer therapy.

In conclusion, our findings proposed a model of how autophagic cancer cell death plays an important role in determining therapeutic efficacy after bacterial treatment via the regulation of immunogenic signals release in tumor microenvironment, suggesting more promising approaches for bacteria-mediated cancer therapy.

AUTHORS (LAST NAME, FIRST NAME): Duong, Mai T.[1]; Nguyen, Vu H.[1]; Phan, Thuy X.[1]; Jo, Eun-Kyeong[2]; Min, Jung-Joon[1]

INSTITUTIONS (ALL):

1. Nuclear Medicine, Chonnam National University, Gwangju, Gwangju, Korea (the Republic of).
2. Department of Microbiology, Chungnam National University School of Medicine, Deajeon, Korea (the Republic of).

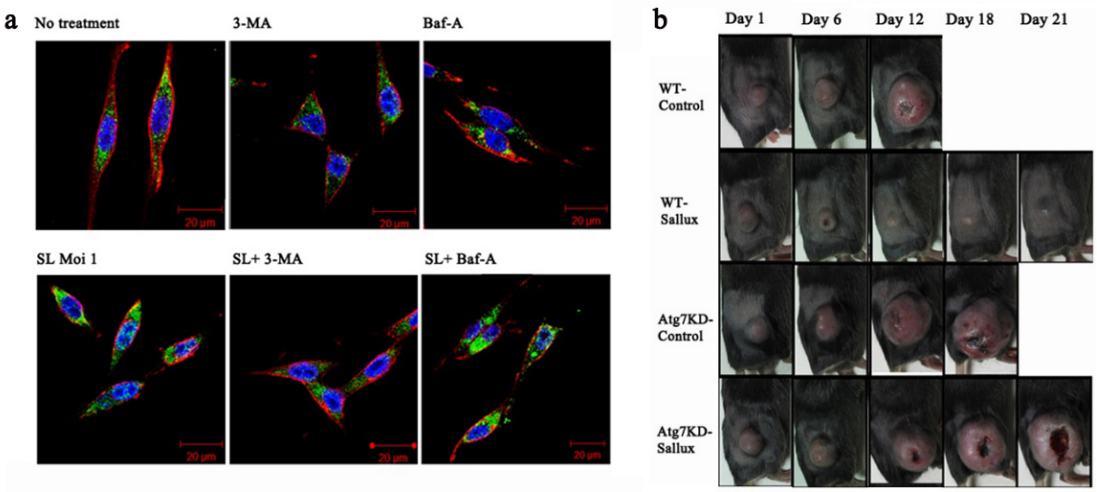
a
No treatment
3-MA
Baf-A
SL Moi 1
SL+ 3-MA
SL+ Baf-A
20 μm
b
Day 1
Day 6
Day 12
Day 18
Day 21
WT-Control
WT-Sallux
Atg7KD-Control
Atg7KD-Sallux

CONTROL ID: 2232764

TITLE: Comparison between Tumor heterogeneity and PET imaging features in non-small cell lung cancer

PRESENTER: Hyeon Sik Kim

ABSTRACT BODY:

Abstract Body: Purpose: Previous research provides evidence of pre-treatment PET measurements being predictors for treatment outcome in non-small cell lung cancer (NSCLC). The area under the curve of the cumulative SUV-volume histograms (AUC-CSH) was known to reflect the tumor heterogeneity. In the PET imaging features, the first order statistics describe the distribution of voxel intensities within the PET image and the gray level co-occurrence matrix based features (GLCM) provides any information regarding the relative position of the various gray levels over the image. We aim to compare the tumor heterogeneity with the PET imaging features. **Materials and methods:** We measured the AUC-CSH and the PET imaging features in 5 NSCLC patients. For calculation of AUC-CSH, volume of interest (VOI) of which boundaries have SUV intensity greater than 3.0 was drawn in the PET image of NSCLC. A cumulative SUV-volume histogram (CSH) was obtained by plotting the percent volume of a tumor with an SUV above a certain threshold against that threshold, which was varied from 0 to 100 % of SUV_{max}. The original PET images of VOI were extracted and decomposed into 8 decompositions (LLL, LLH, LHL, LHH, HLL, HLH, HHL and HHH filter) by three dimensional wavelet transform. For each decomposition, we computed the first order statistics (FOS, n=14) and textural features (GLCM, n=20). The values of calculated PET imaging features were transformed to a z-score level. AUC-CSH and the PET imaging features were compared by the Spearman correlation analysis. **Results:** We obtained AUC-CSH values (2954, 3870.1, 4692.2, 5668.2 and 6086.6) and 272 PET imaging features for each patient. In the LHH and HLH filtering image, the mean and variance features of first order statistics and AUC-CSH values showed the specific high correlation (r=1.000, p<0.001). In the LLL, LLH, LHL and HHH filtering image, uniformity of first order statistics and difference entropy, inverse difference moment normalized (IDMN) and sum entropy of GLCM and AUC-CSH values showed a high correlation (r=0.9, p=0.037). In the HHH filtering image, the correlation coefficient between AUC-CSH values and cluster shade and energy of GLCM was -0.9 (p=0.037) and -1.0 (p<0.001), respectively. **Conclusion:** We found PET imaging features which can predict the tumor heterogeneity in NSCLC. PET imaging features were the mean of FOS in LHH filtering image, variance of FOS in HLH filtering image, difference entropy of GLCM in LLH filtering image, IDMN of GLCM in LLL filtering image, sum entropy of GLCM in LHL filtering image, and uniformity of FOS, cluster shade and energy of GLCM in HHH filtering image. We thank that degree of tumor heterogeneity is found in the PET imaging features.

AUTHORS (LAST NAME, FIRST NAME): Kim, Hyeon Sik[1]; Kang, Sae-Ryoung[1]; Lee, Byeong-il[3]; Bom, Hee-Seung[1]; Min, Jung-Joon[2]

INSTITUTIONS (ALL):

1. Chonnam National University Hwasun Hospital, Jeollanam-do, Korea (the Republic of).
2. Channam National University Hwasun Hospital, Gwangju, Korea (the Republic of).
3. Korea Photonics Technology Institute, Gwangju, Korea (the Republic of).

(A)

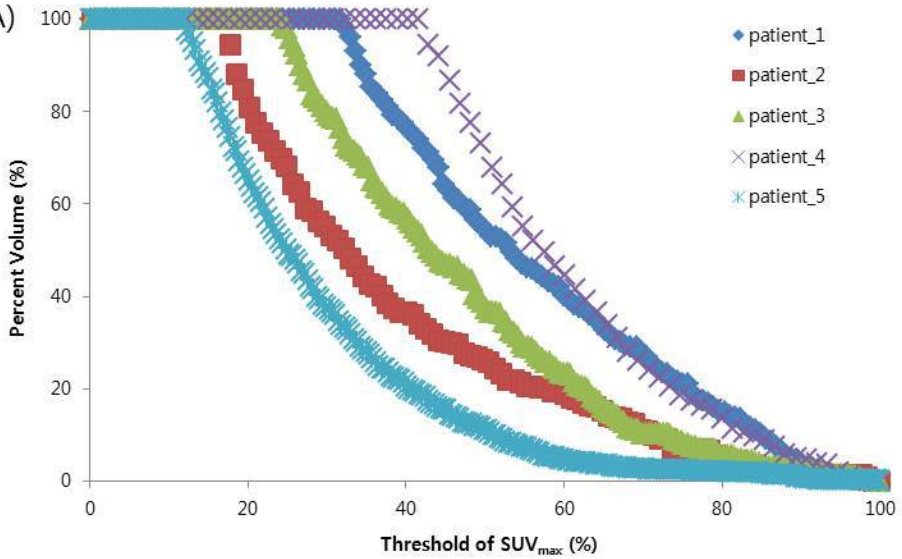

(B) Original tumor shape

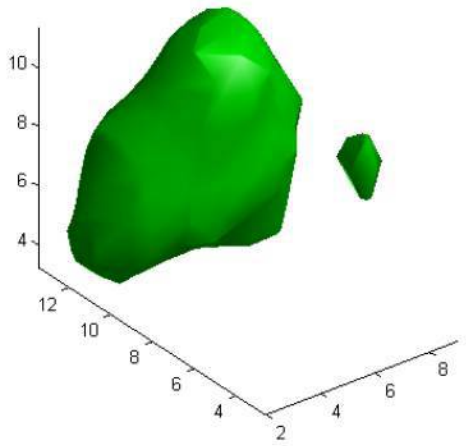

(C)

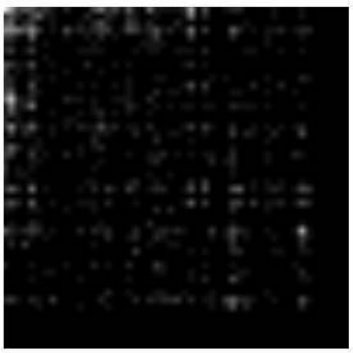

the mean of the GLCM features for each of the 13 directions

(D) n=5

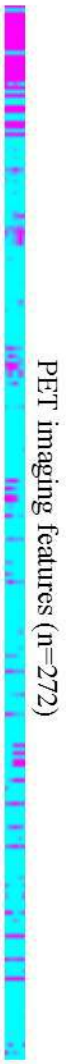

PET imaging features (n=272)

CONTROL ID: 2233401

TITLE: Preclinical PET/CT imaging of nitroreductase reporter gene with ^{18}F-FMISO

PRESENTER: Endre Stigen

ABSTRACT BODY:

Abstract Body: Introduction: Molecular imaging of preclinical murine models is an important tool in drug discovery and monitoring of disease development. It is non-invasive and can provide evidence of biological processes. Within cancer research, more representative orthotopic models have put a great emphasis on the development on fluorescent probes in the near infrared (NIR) spectrum. Our group have previously reported such a reporter platform where Nitroreductase (NTR), a bacterial flavoprotein that reduces aromatic nitro-groups in the presence of NAD(P)H, was used to activate the fluorescently quenched dye CytoCy5S in metastatic cancer models (1). Mostly associated with the prodrug CB1954 in Gene-directed Enzyme Prodrug Therapy (GDEPT)(2), the broad substrate acceptance has shown nitroreductase to be applicable as a preclinical multimodal imaging reporter gene. Although bioluminescence and fluorescence imaging undoubtedly has proven to be a valuable tool in preclinical models, they both lack the quantitative and translatable qualities of PET/CT imaging.

Methods: In this project we introduced ^{18}F-FMISO as a novel NTR probe for preclinical imaging and investigated the use of the NTR enzyme as an imaging agent for PET/CT. ^{18}F-FMISO, a previously described positron emitting hypoxia tracer (3), was evaluated *in vivo* in a panel of mice with NTR positive and negative subcutaneous xenografts. For this, NCI-H460 cell lines and MDA-MB-231 cell lines was used. Orthotopic models of triple-negative breast cancer were further used to evaluate ^{18}F-FMISO during aggressive metastasis.

Results: *In vivo* results show that ^{18}F FMISO have a significantly higher signal in NTR+ compared to NTR- tumours (Fig A). *Ex vivo* results support these *in vivo* data. *In vivo* data also shows that ^{18}F-FMISO is able to detect NTR positive breast cancer metastasis.

Conclusion: Our findings suggest that NTR can be used as a novel preclinical imaging strategy for the visualisation of metastatic cancer using the PET-tracer ^{18}F-FMISO.

References:

1. McCormack E, Silden E, West RM, Pavlin T, Micklem DR, Lorens JB, et al. Nitroreductase, a near-infrared reporter platform for in vivo time-domain optical imaging of metastatic cancer. Cancer research. 2013 Feb 15;73(4):1276-86. PubMed PMID: 23233739. Epub 2012/12/13. eng.

2. Patel P, Young JG, Mautner V, Ashdown D, Bonney S, Pineda RG, et al. A phase I/II clinical trial in localized prostate cancer of an adenovirus expressing nitroreductase with CB1954 [correction of CB1984]. Molecular therapy : the journal of the American Society of Gene Therapy. 2009 Jul;17(7):1292-9. PubMed PMID: 19367257. Pubmed Central PMCID: PMC2835198. Epub 2009/04/16. eng.

3. Williamson DJ, Ejaz S, Sitnikov S, Fryer TD, Sawiak SJ, Burke P, et al. A comparison of four PET tracers for brain hypoxia mapping in a rodent model of stroke. Nuclear medicine and biology. 2013 Apr;40(3):338-44. PubMed PMID: 23294900. Epub 2013/01/09. eng.

AUTHORS (LAST NAME, FIRST NAME): Lund, Kjetil B.[1, 3]; Stigen, Endre[1]; Popa, Mihaela[2, 1]; Rygh, Cecilie Brekke[4]; Adamsen, Tom Christian H.[5]; Kvernenes, Ole Heine[6]; Haug, Bengt Erik[7]; Mc Cormack, Emmet[1, 2]

INSTITUTIONS (ALL):

1. Clinical science, University of Bergen, Bergen, Norway.
2. KiNN Therapeutics AS, Bergen, Norway.
3. Virologisk Seksjon, Haukeland Universitetssykehus, Bergen, Norway.
4. Depatrment of Biomedicine, University of Bergen, Bergen, Norway.
5. Depatrment of Chemistry, University of Bergen, Bergen, Norway.
6. Department of radiology, Haukeland univeristy Hospital, Bergen, Norway.
7. Depatrment of Chemistry, University of Bergen, Bergen, Norway.

(No Image Selected)

CONTROL ID: 2232778

TITLE: Imaging of neuronal associated miRNA expression using transgenic mouse model via reporter system

PRESENTER: Yoori Choi

ABSTRACT BODY:

Abstract Body: MicroRNA (MiRNA) is known as a small non-coding RNA molecule and functions in transcriptional and post-transcriptional regulation of gene expression. miRNA responsive element-based reporter gene system has been widely applied to detect miRNA expression in cellular level. In this study, to track the expression of miRNA in vivo, we established a transgenic mouse model containing luciferase-IRES-GFP-miRNA-3xPT that luciferase signals were changed by miRNA activity.

Luciferase expression in luciferase vector containing miRNA-3XPT significantly reduced after treatment of miRNA oligomer. In vivo bioluminescence image results revealed that luciferase activity was seen in widespread organs of transgenic mouse. The miRNA expression from qPCR and luciferase activity were correlated in alteration of miRNA expression to validate reporter expression in the brain of a transgenic mouse. Furthermore, bioluminescence intensity of the brain from transgenic mouse dramatically decreased between the embryonic day 13 and 16, and the brain maintained decreasing bioluminescence signal in postnatal stage.

Herein, our results suggest that this transgenic reporter mouse is a suitable model for following dynamics of miRNA expression in vivo. And this method is useful for monitoring miRNA dynamics and validation for delivery tools of miRNA or siRNA in vivo.

AUTHORS (LAST NAME, FIRST NAME): Choi, Yoori[1]; Hwang, Do Won[1]; Lee, Dong Soo[1]

INSTITUTIONS (ALL):

1. Nuclear Medicine, Seoul National University, Seoul, Korea (the Republic of).

(No Image Selected)

CONTROL ID: 2232779

TITLE: Validation of neuronavigation as a tool to improve coil positioning in rodent rTMS studies

PRESENTER: Nick Van Laeken

ABSTRACT BODY:

Abstract Body: Introduction: Compared to the growing number of clinical studies reporting putative therapeutic properties of rTMS in a broad range of disorders, the number of preclinical studies investigating the neurological mechanisms involved is still scarce and the results of them are often contradictory. Besides the lack of appropriately sized coils and problems of heat dissipation, tightly controlling the coil position is described as one of the main obstacles that hampers research in rodents. In human studies, coil positioning is controlled by neuronavigation, which combines an MR image with a position sensor system to track the location of a patient's head and the operational tools. This study explains how to easily adapt neuronavigation for use in rats and aims to define its accuracy.

Methods: Making use of low-cost materials we created a wooden frame which contained a fixed bed position for the anesthetized rat and 3 fixed reference marker balls, which can be detected by the position sensor system. The accuracy of the neuronavigation system was investigated under ideal and real conditions. For the ideal conditions we developed a 3D printed plastic phantom with the dimensions of a rat head, which also contained 8 pins (d 1mm, h 5mm) representing several positions spread across the brain. An MR image was acquired on a Bruker Pharmascan 70/16 7T system by submerging the phantom in a water-filled container and by using a TX/RX rat whole body coil and a spin echo sequence (RARE, 200 µm isotropic resolution, TR/TE 8570/8.9ms, NA 9, TA 43min42s). To map the actual position on the MR image a tracked hand-held pointer was placed on 5 dots (1x1 mm) which represented several positions on the rat's head with a fixed distance to the brains: top of the nose, inner corner of the eyes and middle of the base of the ears. Subsequently, the pointer was placed perpendicular on each of the pins and both the Euclidean distances between the measured and the real (indicated on MRI) coordinates, and the degrees of deviation from perpendicular were calculated. For the real conditions 8 little MRI compatible screws (h 3.7 mm, shaft diameter 1.4 mm) were glued (Vetbond^{TM}, 3M) upside down on several positons spread across the skull of an anesthetized rat and an MR image (parameters previously mentioned) was acquired by adding Aquagel to the screws to provide negative contrast.

Results: The Euclidean distance (mean ± SD) between the measured and real coordinates was 0.80 ± 0.35 mm and 1.89 ± 0.36 mm for the ideal and real conditions respectively. The upper limit of the 95% confidence interval of this distance represents the minimal distance between two spots on the brain to be able to distinguish them from each other and was 0.91 mm and 2.00 mm respectively. Using the tangent of the measured angles and supposing a target region located 5 mm below the skull, an additional error of 0.44 mm and 0.77 mm needs to be taken into account for the ideal and real conditions respectively.

Conclusion: As the total surface area of the cerebral cortex of a rat is ± 6 cm², the neuronavigation tool can be used to differentiate between different areas of the rat brain.

AUTHORS (LAST NAME, FIRST NAME): Van Laeken, Nick[1]; Duprat, Romain J.[2]; Descamps, Benedicte[3]; Vanhove, Christian[3]; Hallaert, Giorgio[4]; Deprez, Karel[5]; Goethals, Ingeborg[6]; Baeken, Chris[2]; De Vos, Filip J.[1]

INSTITUTIONS (ALL):

1. laboratory of radiopharmacy, Ghent University, Ghent, Belgium.
2. Psychopathology and affective neuroscience lab, Ghent University, Ghent, East Flanders, Belgium.
3. Infinity-Medisip-Iminds medical IT, Ghent University, Ghent, Belgium.
4. Neurosurgery, Ghent University Hospital, Ghent, East Flanders, Belgium.
5. Medisip - Iminds Medical IT, Ghent University, Ghent, East Flanders, Belgium.
6. Department of Radiology and nuclear medicine, Ghent University Hospital, Ghent, East Flanders, Belgium.

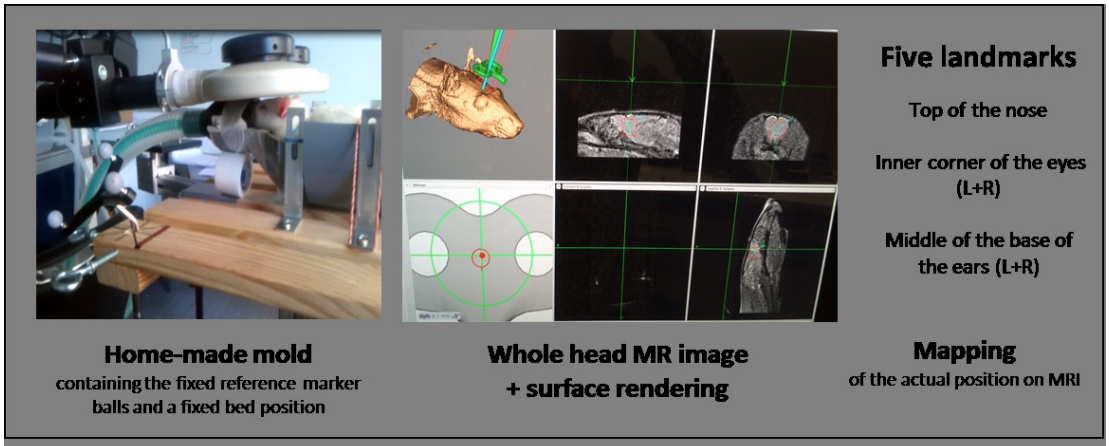

Figure 1: Neuronavigation in the rat

CONTROL ID: 2232786

TITLE: Radiosynthesis and In Vivo evaluation of ^{64}Cu Labeled Repebody for EGFR-mediated tumor Imagingin Small Animals

PRESENTER: Ayoung Pyo

ABSTRACT BODY:

Abstract Body: Objectives: The epidermal growth factor receptor(EGFR) is known as a member of the HER family and expressed in many kinds of tumors. Anti-EGFR repebodyusing this study is a newly designed protein scaffold for tumor targeting that hasleucine rich repeat modules. Radioisotope ^{64}Cu has been widely used to explore and develop to label antibodies due to proper half-life (12.7 h). In this study, we performed microPET studies with two kinds of ^{64}Cu labeled complexes (repebody with DOTA-NHS ester and ρ-SCN-Bn-DTPA) and evaluated characteristics in H1650 (human non-small cell lung cancer cell line) bearing nude mice.

Methods:DOTA-NHS ester and ρ-SCN-Bn-DTPA were dissolved in water and pH was adjusted to 9.0 by adding 1 M of NaOH. This solutions were added to the repebody in a 1:5 mole ratio (repebody : DOTA-NHS ester, ρ-SCN-Bn-DTPA)[1]. The resulting DOTA-repebody and DTPA-repebody conjugate were purified by HPLC and lyophilized. Purified compounds were radiolabeled with ^{64}Cu by addition of $^{64}CuCl_2$ in 0.1 N NaOAc (pH5.5) buffer followed by incubation for 1 h at 40 °C. The radiolabeled complexes were purified by a PD-10 column. The mircoPET images were obtained at 1,6, and 24 h after i.v.injection of ^{64}Cu labeled repebody (7.4 MBq) in H1650 (EGFR positive) bearing nude mice. The static images at 1 and 6 h were acquired for 10 min and 24 h was acquired for 20 min. The ROIs were drawn in the tumor and liver.The tumor-to-liver ratio (T/L) were obtained from max SUV of ROI.

Results: Radiochemical yields of ^{64}Cu-DOTA-repebody and ^{64}Cu-DTPA-repebody were approximately 60~70%. H1650 tumor was clearly visible after injection of each repebody, with high tumor-to-background ratio for whole time points. ^{64}Cu labeled repebody was accumulated specifically at 1 h after i.v. injection and retained in H1650. Uptake of ^{64}Cu-DOTA-repebody(1, 6 h SUV_{max}: 1.80, 2.20) and ^{64}Cu-DTPA-repebody(1, 6 h SUV_{max}: 2.23, 2.80)were increased from 1 h to 6 h. Both ^{64}Cu-DOTA- and ^{64}Cu-DTPA-repebodyshowed slow clearance from liver as T/Ls were 0.49, 0.59, 0.43 and 0.55, 0.97, 0.82 respectively at 1, 6 and 24 h.

Conclusions:^{64}Cu-DOTA-repebody and ^{64}Cu-DTPA-repebody demonstrated specific and comparable uptake in H1650 tumor bearing mouse model and might have a potential to be utilized as a novel EGFR targeting agent for PET.

AUTHORS (LAST NAME, FIRST NAME): Pyo, Ayoung[2]; Yun, Misun [2]; Kim, Hyeon Sik[2]; Kim, Dong-Yeon[1]; Min, Jung-Joon[1]

INSTITUTIONS (ALL):

1. Nuclear Medicine, Chonnam National University Hwasun Hospital, Hwasun, Korea (the Republic of).
2. Chonnam National Unversity Hwasun Hospital , Hwasun, Korea (the Republic of).

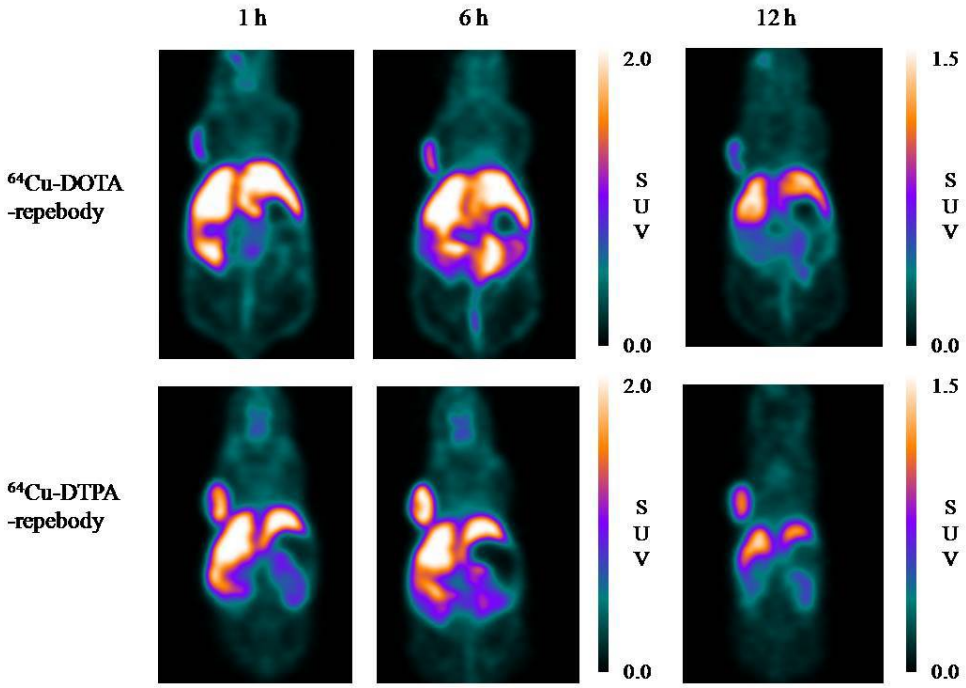
1 h
6 h
12 h
64Cu-DOTA
-repebody
64Cu-DTPA
-repebody
2.0
S
U
V
0.0
1.5
S
U
V
0.0
2.0
S
U
V
0.0
1.5
S
U
V
0.0

CONTROL ID: 2232889

TITLE: Predictive Estimation of Therapeutic Effects of Liposomal Anti-cancer Agents by SPECT/CT Imaging of Radiolabeled Liposomes in Mouse Xenograft Models

PRESENTER: Izumi Umeda

ABSTRACT BODY:

Abstract Body: Objectives: Although liposomal drugs encapsulating anti-cancer agents are promising in the light of enhanced drug delivery to tumors and reduced side effects, they are not effective to all malignant tumors. Development of biomarkers to identify responder patients is crucial. Here, we generated radiolabeled liposomes; i.e., liposomes encapsulating ^{111}In-DTPA, with lipid composition and size identical to Doxil®, liposomes encapsulating doxorubicin, and evaluated their usefulness to predict therapeutic effect of Doxil by SPECT/CT tumor images before the initiation of the treatment.

Methods: Human ovarian cancer xenograft models (Caov-3, SK-OV-3, KURAMOCHI, and TOV-112D) were used. Anti-tumor effects of Doxil to these implanted tumors were evaluated though comparison of the tumor size suppression with free doxorubicin. Histopathological studies were also performed. ^{111}In-labeled liposomes were prepared by using remote loading method and they were injected to tumors models. The tumor accumulation was determined quantitatively by measurement of their radioactivities and by *in vivo* SPECT/CT tests by using a SPECT/CT scanner dedicated for small animals.

Results: Anti-tumor activities of Doxil was drastically enhanced in Caov-3, moderate in SK-OV-3, and minimum in other two tumors. Doxil-perfusion assay, by observation of the autofluorescence of Doxil in the tumor, suggested that the tumor accumulation of Doxil was much higher in Caov-3 and relatively higher in SK-OV-3 than in others. The microvessel density and vascular perfusion were high in Caov-3 and SK-OV-3. The tumor accumulation of ^{111}In-labeled liposomes at 72 h after administration was high in Caov-3 and SK-OV-3 (4.0 – 4.3 % of administered dose/g of tumor, %AD/g), while it was less than 1.5 %AD/g in other two tumors. Area under the curve (AUC) values over 72 h was the highest in Caov-3, followed by SK-OV-3. It was very low in other two tumors. These results were consistent with the aforementioned retention and therapeutic efficacy of Doxil in these 4 tumors. Furthermore, since both therapeutic efficacy of Doxil® and tumor accumulation of ^{111}In-labeled liposomes varied greatly among SK-OV-3 tumor groups, this unique observation led us to the next step. We individually obtained SPECT/CT images of each SK-OV-3 bearing mouse (n=11) with ^{111}In-labeled liposomes, and then intravenously administered Doxil to each mouse, and evaluated therapeutic efficacy as suppression of tumor growth. A clear correlation (R^2=0.73) between the tumor accumulation of radioactive liposomes and the anti-tumor activities of Doxil was found.

Discussion: These results indicated that anti-tumor activities of Doxil depended on its tumor accumulation which was closely related to the microvessel density and vascular perfusion. Tumor accumulation of radiolabeled liposomes evaluated in SPECT images should predict the anti-tumor activities.

Conclusions: Radiolabeled liposomes would be a promising imaging biomarker to predict the therapeutic efficacy of liposomal anti-cancer drugs, such as Doxil.

AUTHORS (LAST NAME, FIRST NAME): Umeda, Izumi O.[1]; Ito, Ken[1, 2]; Hamamichi, Shusei[1]; Asano, Makoto[2]; Iwata, Masao[2]; Matsui, Junji[2]; Hori, Yusaku[1, 2]; Funahashi, Yasuhiro[2]; Fujii, Hirofumi[1]

INSTITUTIONS (ALL):

1. National Cancer Center, Kashiwa, Chiba, Japan.

2. Eisai, Co., Ltd., Tsukuba, Ibaraki, Japan.

(No Image Selected)

CONTROL ID: 2232797

TITLE: linically Applicable Magnetic-Labeling of Natural Killer Cells for MRI of Transcatheter Delivery to Liver Tumors: Preclinical validation for clinical translation

PRESENTER: Kangan Li

ABSTRACT BODY:

Abstract Body: Aim: To test the hypothesis that MRI can monitor of intra-portal vein (IPV) transcatheter delivery of clinically applicable heparin-protamine-ferumoxytol (HPF) nanocomplex–labeled NK cells to liver tumor. **Materials and methods:** Liver tumor rat models were underwent catheterization for IPV infusion of HPF-labeled NK cells (NK-92MI cell line). MRI measurements within tumor and adjacent liver tissues were compared pre and post NK cell infusion. Histology studies were used to identify NK cells in the target tumors. **Results:** for first time, we demonstrated that MRI track HPF-labeled NK cells migration within liver following IPV delivery. **Conclusion:** IPV transcatheter infusion permitted selective delivery of NK cells to liver tissues and MRI allowed tracking NK cell biodistributions within the tumors.

AUTHORS (LAST NAME, FIRST NAME): Li, Kangan[1]

INSTITUTIONS (ALL):

1. Department of Radiology, Shanghai General Hospital,Shanghai Jiaotong University School of Medicine, Shanghai, China.

(No Image Selected)

CONTROL ID: 2232828

TITLE: Noninvasively track Schwann cells repair of peripheral nerve injury *in vivo with MRI*

PRESENTER: Kangan Li

ABSTRACT BODY:

Abstract Body: Objective: This study investigated the feasibility of using Magnetic resonance imaging (MRI) to noninvasively track Schwann cells (SCs) repair of peripheral nerve injury *in vivo*. **Methods:** SCs were isolated, expanded, and subsequently labeled with superparamagnetic iron oxide nanoparticles (SPIONs). The morphological and functional properties of the SCs were assessed using immunohistochemistry. The intracellular stability, proliferation, and viability of the labeled cells were evaluated *in vitro*. Using a microsurgical procedure, the labeled SCs were then seeded into sciatic nerve conduits in C57/BL6 mice to repair a 1-cm sciatic nerve gap. A clinical 3T MRI was performed to investigate the SCs *in vitro* and the transplanted SCs inside the sciatic nerve conduits *in vivo*. **Results:** The SCs were efficiently labeled with SPIONs, without affecting their viability and proliferation. The labeled cells implanted into the mice sciatic nerve conduit exhibited a significant increase in axonal regeneration compared with the empty conduit and could be detected by MRI. Fluorescent microscopic examination, histological analysis and immunohistochemistry confirmed the axon regeneration and MRI results. **Conclusions:** These data will illuminate the neuroplasticity of SCs and provide a new protocol for *in vivo* tracking of them that are seeded to repair injured peripheral nerves.

AUTHORS (LAST NAME, FIRST NAME): Li, Kangan[1]

INSTITUTIONS (ALL):

1. Department of Radiology, Shanghai First People's Hospital,Shanghai Jiaotong University School of Medicine, Shanghai, China.

(No Image Selected)

CONTROL ID: 2232809

TITLE: *RGD peptide-modified PEGylated dendrimer-entrapped gold nanoparticles for targeted CT imaging of breast carcinoma*

PRESENTER: Kangan Li

ABSTRACT BODY:

Abstract Body: We report the synthesis and characterization of cyclo (Arg-Gly-Asp-D-Phe-Lys) peptide (RGD)-modified PEGylated dendrimer-entrapped gold nanoparticles (Au DENPs) for targeted computed tomography (CT) imaging of integrin-rich breast carcinomas. In this study, generation-5 amine-terminated poly (amidoamine) dendrimers (G5.NH_2) were modified with methoxyl polyethylene glycol acid (*m*PEG-COOH) and RGD-PEG-COOH peptides, and the products G5.NH_2-$(PEG\text{-}RGD)_7$-*m*PEG_8 were then used as templates to entrap gold nanoparticles (AuNPs). Following acetylation of the remaining dendrimer terminal amines, integrin $\alpha_v\beta_3$-targeted {$(Au^0)_{300}$-G5.NHAc-$(PEG\text{-}RGD)_7$-*m*PEG_8} DENPs (PEGylated Au DENPs-RGD) were obtained. The formed PEGylated Au DENPs-RGD probes were characterized via different techniques. We demonstrate that PEGylated Au DENPs-RGD with an AuNP core size of 2.8 nm are water dispersible, stable at different pH and temperature conditions, and biocompatible at the given concentration range. With the presence of Au NPs, the PEGylated Au DENPs-RGD displayed high X-ray attenuation intensity. The conjugated RGD ligand can specifically identify and target over-expressed integrins on both endothelial and cancer cells. Moreover, the half-decay time demonstrated by pharmacokinetic studies is sufficiently long to ensure accumulation of the NPs in the target area. These properties of the particles enable them to be used as nanoprobes for targeted CT imaging of integrin-rich breast carcinoma cells *in vitro* and xenograft tumor model *in vivo* via an integrin-mediated pathway. These findings suggest that the designed PEGylated Au DENPs-RGD can be used as targeted nanoprobes with good biocompatibility for targeted CT imaging and diagnosis of integrin-positive tumors.

AUTHORS (LAST NAME, FIRST NAME): Li, Kangan[1]

INSTITUTIONS (ALL):

1. Department of Radiology, Shanghai First People's Hospital,Shanghai Jiaotong University School of Medicine, Shanghai, China.

(No Image Selected)

CONTROL ID: 2232800

TITLE: A glycogen-based multimodal imaging nanoprobe is effectively internalised into human melanoma metastatic cells

PRESENTER: Frits Thorsen

ABSTRACT BODY:

Abstract Body: *Purpose:* Metastatic cancer is a significant cause of death worldwide, despite continuing advances in research on diagnostics and therapy [1]. To overcome unsuccessful drug delivery to the tumor tissue, several different nanoprobes have been designed, of which some have combined diagnostic and therapeutic properties [2]. It is an advantage to use non-toxic, biodegradable materials in the design of nanoprobes, as such compounds are easily eliminated from the body [3]. In this work we report for the first time the use of glycogen in a recently developed multimodal, theranostic nanoprobe. We labeled melanoma metastatic cell lines, and used multimodal imaging to show cellular uptake and efficiency of the probe.

Materials: The nanoprobe was developed in our laboratory, and consisted of a backbone of glycogen, where the red fluorescent marker Dyo-615 for fluorescence microscopy and Gadolinium for MRI were incorporated [4]. Therapeutic compounds can also be attached, however this was not done in our study. Fluorescence microscopy, high throughput imaging, confocal microscopy and resazurin viability assays were used to study cell labeling and cell viability in three human metastatic melanoma cell lines. MRI was used to study T_1 relaxivity *in vitro*, as well as T_1 contrast enhancement in subcutaneous tumors in NOD/SCID mice.

Results: Fluorescence microscopy demonstrated an effective labeling of human melanoma metastatic cells during 24 hours (Fig. 1a), and cell viability was unchanged after cell labeling (Fig 1b). The nanoprobe was localized in the cytoplasma of the cells, and accumulation of nanoprobe inside the lysosomes was demonstrated (Fig 1c). *In vitro* MRI relaxivity showed significant reduction in T_1 mapping times after cell labeling (Fig. 1d). *In vivo* MRI studies demonstrated that subcutaneous melanoma tumors in mice were effectively visualized with T_1 weighted MRI after intravenous injection of the nanoprobe, and the contrast enhancement was comparable to the enhancement seen after injecting standard Omniscan contrast agent (Fig. 1e).

Conclusions: Our biodegradable glycogen nanoprobe shows a high potential to be used further as a theranostic entity. The nanoprobe may offer additional advantages over MRI contrast agents, as tumor uptake of pharmaceuticals attached to the nanoprobe can be traced in real-time *in vivo*.

References

1. Daphu I, Sundstrøm T, Huszthy PC, Niclou SP, Sakariassen P, Immervoll H, Miletic H, Bjerkvig R, Thorsen F. *In vivo* animal models for
studying brain metastasis: value and limitations. Clin Exp Metastasis 30:695-710, 2013.

2. Khemtong C, Kessinger CW, Gao J. Polymeric nanomedicine for cancer MR imaging and drug delivery. Chem Commun 24:3497-3510, 2009.

3. Muthu MS, Leong DT, Mei L, Feng SS. Nanotherantostics - application and further development of nanomedicine strategies for advanced
theranostics. Theranostics 4:660-677, 2014.

4. Filippov SK, Sedlacek O, Bogomolova A, Vetrik M, Jirak D, Kovar J, Kucka J, Bals S, Turner S, Stepanek P, Hruby M. Glycogen as a
biodegradable construction nanomaterial for in vivo use. Macromol Biosci 12:1731-1738, 2012.

AUTHORS (LAST NAME, FIRST NAME): Aasen, Synnøve Nymark[1]; Pospisilova, Aneta[2]; Eichler, Tilo W.[3]; Hruby, Victor[2]; Stepanek, Petr[2]; Spriet, Endy[4]; Jirak, Daniel[5]; Skaftnesmo, Kai Ove[1]; Thorsen, Frits[1, 4]

INSTITUTIONS (ALL):

1. NorLux Neuro-Oncology Laboratory, Department of Biomedicine, University of Bergen, Bergen, Norway.
2. Institute of Macromolecular Chemistry AS CR, Prague, Czech Republic.
3. Department of Clinical Medicine K1, University of Bergen, Bergen, Norway.
4. Molecular Imaging Center, Department of Biomedicine, University of Bergen, Bergen, Norway.
5. Institute for Clinical and Experimental Medicine, Prague, Czech Republic.

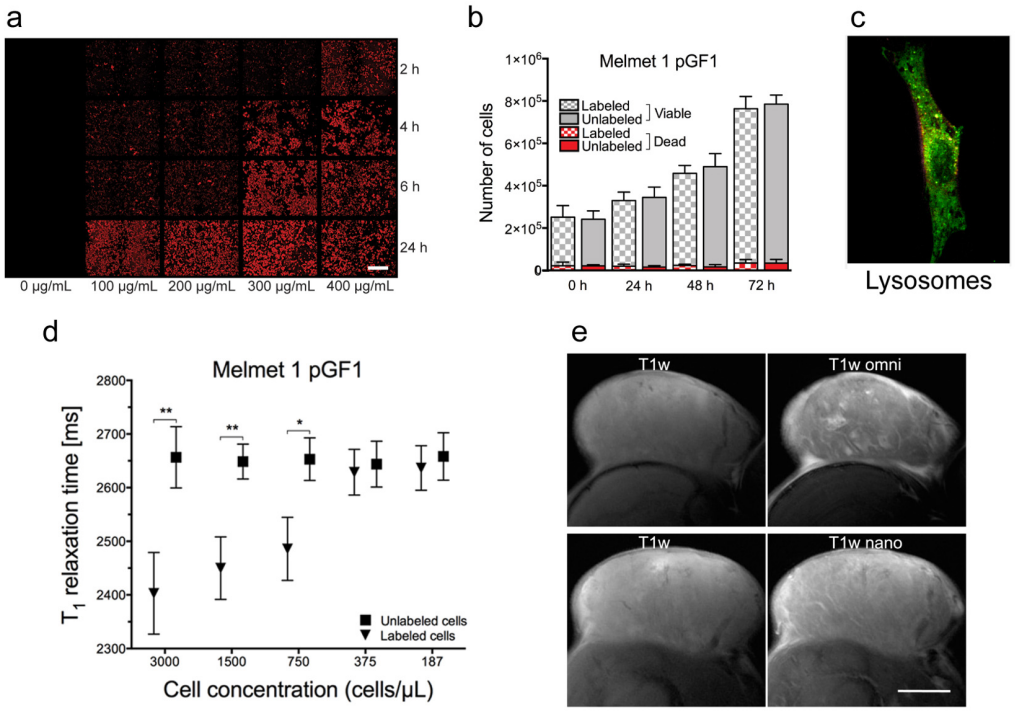

Fig 1. In vitro and in vivo characteristics of the glycogen nanoprobe. a) High throughput fluorescence microscopy, showing effective *in vitro* uptake of the glycogen nanoprobe into human H1_DL2 melanoma brain metastatic cells with increasing concentration of nanoprobe. **b)** *In vitro* cell viability was unchanged after cell labeling, as seen in the human metastatic cell line Melmet 1 pGF1. **c)** The nanoprobe was taken up into lysosomes in the cells. Red: nanoprobe, green: lysosome staining, yellow: colocalization of nanoprobe with lysosomes. **d)** *In vitro* MRI T*1* relaxation studies of agar phantoms with cells revealed that as little as 750 cells/uL could be detected. **e)** *In vivo* T1 weighted MRI of a subcutaneous tumor in a NOD/SCID mouse. The results indicated that contrast enhancement using the nanoprobe was comparable to the contrast enhancement seen after using Omniscan.

CONTROL ID: 2232807

TITLE: Hepatobiliary excretion study using *in vivo* optical and PET imaging of ^{64}Cu-labeled lanthanide-doped upconverting nanoparticles

PRESENTER: Sang Hwan Nam

ABSTRACT BODY:

Abstract Body: In recent years applications on nano-diagnosis and therapy have accelerated but long term accumulation and toxicity of nanomaterials *in vivo* are the major issues. Lanthanide-doped upconverting nanoparticles (UCNP) with unique optical properties that are non-bleaching and infrared excitation radiation are suitable for research fields of them. Here we carried out *in vivo* optical and positron emission tomography (PET) imaging using ^{64}Cu-labeled PEG-coated UCNPs ($NaYF_4$:Yb^{3+}, Er^{3+}). In the optical and PET images, it was observed that the nanobioprobes are not accumulated in the liver but excreted through feces after 4 hours. *Ex vivo* biodistribution study showed that approximately 80% of initial hepatic uptake was cleared in 72 hours through intestine. We also confirmed the hepatobiliary excretion via transmission electron microscopy (TEM) examination.

AUTHORS (LAST NAME, FIRST NAME): Nam, Sang Hwan[1]; Seo, Hyo Jung[3, 2]; Im, Hyung-Jun[3, 2]; Hwang, Do Won[3, 2]; Lee, Dong Soo[2, 3]; Suh, Yung Doug[1, 4]

INSTITUTIONS (ALL):

1. Laboratory for Advanced Molecular Probing (LAMP), Korea Research Institute of Chemical Technology, Daejeon, Korea (the Republic of).
2. Department of Nuclear Medicine, Seoul National University, Seoul, Korea (the Republic of).
3. Department of Molecular Medicine and Biopharmaceutical Sciences, Graduate School of Convergence Science and Technology, Seoul, Korea (the Republic of).
4. School of Chemical Engineering, Sungkyunkwan University, Suwon, Korea (the Republic of).

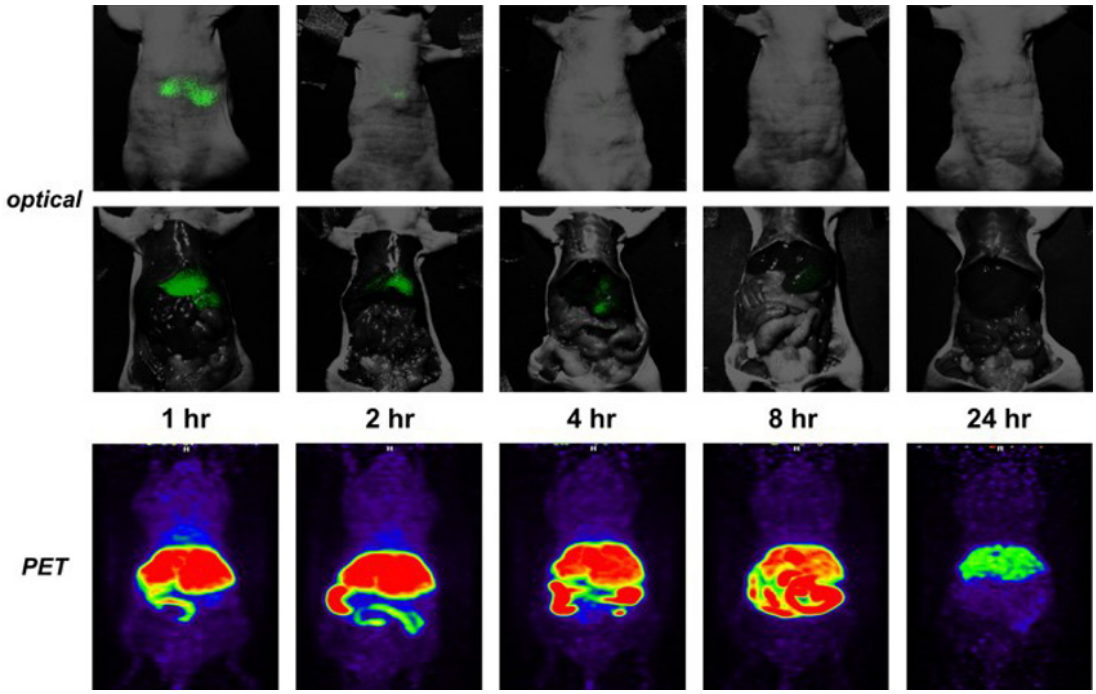
optical
1 hr
2 hr
4 hr
8 hr
24 hr
PET

CONTROL ID: 2232811

TITLE: The Warburg Effect in Cancer Stem Cells and Targeting of Mitochondrial Glucose Metabolism for Cancer Stem Cell Therapy

PRESENTER: Jin Won Park

ABSTRACT BODY:

Abstract Body: Enhanced glycolytic metabolism is a key cancer hallmark and the basis for F-18 FDG PET imaging of tumors. Recent studies indicate that tumors are hierarchically organized, where cancer stem cells (CSCs) play a central role in tumor growth and drug resistance. CSCs are predicted to have distinct metabolic properties, but how the Warburg effect is reprogramed in CSCs remains unclear. Furthermore, it has been recently suggested that mitochondria-targeting agents may have potential therapeutic effect on CSCs. In this study, we tested the hypothesis that CSCs have increased dependency on mitochondrial oxidative phosphorylation, and further investigated whether suppression of mitochondrial respiration with metformin with or without uncoupling protein-2 (UCP2) blocking using genipin may have therapeutic efficacy. Human MCF7 breast cancer and HT29 colon cancer cells engineered to stably express ZsGreen fused to the carboxylterminal region of ornithine decarboxylase (ZsGreen-cODC) were grown in CSC selection media for 7-14 days. Stemness was confirmed by ZsGreen fluorescences due to low 26S proteasome activity, as well as by CD133 and CD44 immunoblotting. The results showed that, compared to MCF7 cancer cells, FDG uptake of MCF7-derived CSCs was decreased 41.5 ± 5.1% (P <0.005). Furthermore, MCF7 CSCs had a 32.6 ± 2.9% decrease of lactate production (P <0.005), and 31.0 ± 9.15% decrease of oxygen consumption rate (OCR; P <0.05). Compared to HT29 cancer cells, HT29-derived CSCs displayed minimal change in FDG uptake, 39.2 ± 3.1% decreased lactate secretion (P <0.0001), and a marked 126.3 ± 31.1% increased OCR (P <0.0001). These findings are consistent with a metabolic shift to mitochondrial oxidative phosphorylation. When the effect of metformin was tested on H29 cells, the drug acutely stimulated FDG uptake and lactate production of cancer cells (7.7 fold), likely due to suppressed mitochondrial respiration. CSCs also showed increased FDG uptake, but to a lower magnitude. Metformin also increased ROS production in cancer cells, as well as CSCs (240.1 ± 16.9% of controls; P < 0.0001). CSC viability was decreased to about 50% by metformin, and further decreased by combining metformin and genipin (P <0.05). In conclusion, our study demonstrates that CSCs are metabolically reprogrammed in a manner shifted to less glycolysis-dependent phenotypes. Metformin suppresses mitochondrial respiration and increase ROS production, leading to reduced survival of these cells, and blocking of uncoupling protein-2 with genipin may help enhance this effect.

AUTHORS (LAST NAME, FIRST NAME): Park, Jin Won[1, 2]; Jung, Kyung-Ho[1, 2]; Lee, Jin Hee[1, 2]; Moon, Seung-Hwan[1]; Cho, Young Seok[1]; Lee, Kyung-Han[1, 2]

INSTITUTIONS (ALL):

1. Nuclear Medicine, Samsung Medical Center, Seoul, Korea (the Republic of).
2. Samsung Advanced Institute for Health Science and Technology at SungKyunKwan University, Seoul, Korea (the Republic of).

(No Image Selected)

CONTROL ID: 2232810

TITLE: Prospective Study of ^{68}Ga-NOTA-NFB: Radiation Dosimetry in Healthy Volunteers and First Application in Glioma Patients

PRESENTER: Zhe Wang

ABSTRACT BODY:

Abstract Body: Purpose: The chemokine receptor CXCR4 is overexpressed in various types of human cancers. As a specific imaging agent of CXCR4, ^{68}Ga-NOTA-NFB was investigated in this study to assess its safety, biodistribution and dosimetric properties in healthy volunteers, and to preliminarily evaluate its application in glioma patients.

Methods: Six healthy volunteers underwent whole-body PET scans at 0, 0.5, 1, 2, and 3 h after ^{68}Ga-NOTA-NFB injection (mean dose, 4.93 ± 0.10 mCi). For time-activity curve calculations, 1 mL blood samples were obtained at 1, 3, 5, 10, 30, 60, 90, 120, 150, and 180 min after the injection. The estimated radiation doses were calculated by OLINDA/EXM software. Eight patients with glioma were enrolled and performed with both ^{68}Ga-NOTA-NFB and ^{18}F-FDG PET/CT scans before surgery. The expression of CXCR4 on the resected brain tumor tissues were determined by immunohistochemical staining.

Results: ^{68}Ga-NOTA-NFB was safe and well tolerated by all subjects. A rapid activity clearance was observed in the blood circulation. The organs with the highest absorbed doses were spleen (193.8 ± 32.5 μSv/MBq) and liver (119.3 ± 25.0 μSv/MBq). The mean effective dose was 25.4 ± 6.1 μSv/MBq. The maximum standardized uptake values (SUV_{max}) and the maximum target to non-target ratios (T/NT_{max}) of ^{68}Ga-NOTA-NFB PET/CT in glioma tissues were 4.11 ± 2.90 (range, 0.45-8.21) and 9.21 ± 8.75 (range, 3.66-24.88), respectively, while those of ^{18}F-FDG PET/CT were 7.34 ± 2.90 (range, 3.50-12.27) and 0.86 ± 0.41(range, 0.35-1.59). The histopathological staining confirmed that CXCR4 was overexpressed on resected tumor tissues with prominent ^{68}Ga-NOTA-NFB uptake.

Conclusion: With a favorable radiation dosimetry profile, ^{68}Ga-NOTA-NFB is safe for clinical imaging. Compared to ^{18}F-FDG PET/CT, ^{68}Ga-NOTA-NFB PET/CT is more sensitive in detecting glioma and could have potential value in diagnosing and treatment planning for CXCR4 positive patients.

AUTHORS (LAST NAME, FIRST NAME): Wang, Zhe[1]; Zhang, Mingru[3]; Wang, Liang[4]; Wang, Jing[2]

INSTITUTIONS (ALL):

1. Nuclear Medicine Department, Xijing Hospital, Fourth Military Medical University , Xi'an, Shaanxi, China.
2. Department of nuclear medicine, Xijing hospital, Xi’an, Shaanxi, China.
3. the Forth Military Medical University, Xi'an, China.
4. Department of Neurosurgery, , Tangdu Hospital, Fourth Military Medical University, Xi'an, China.

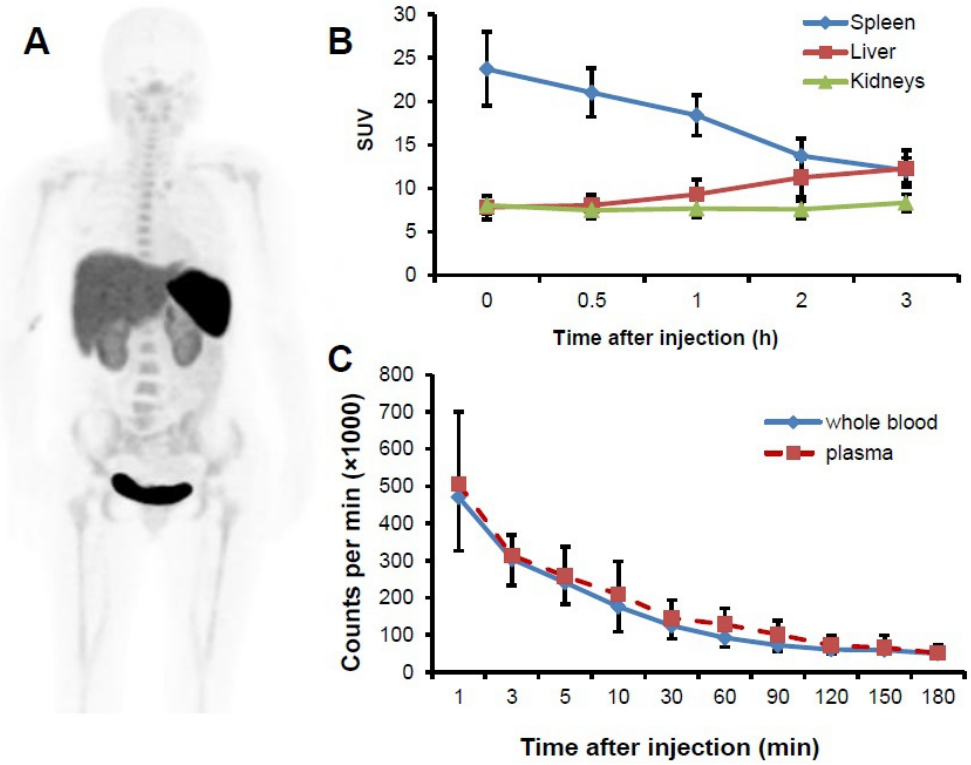

Fig. 1 A, PET image of distribution of ^{68}Ga-NOTA-NFB at 1 h post-injection in a healthy volunteer (subject 3). The uptake is mainly in the spleen, liver, kidneys and urinary bladder. B, Decay corrected averaged time-activity curves of ^{68}Ga-NOTA-NFB in the liver, kidneys and spleen for all healthy volunteers, error bars indicate standard deviations (n = 6). C, Decay corrected averaged time-activity curves for ^{68}Ga-NOTA-NFB in the whole blood and plasma, error bars indicate standard deviations (n = 6).

CONTROL ID: 2232814

TITLE: Optical imaging visualized anti-metastatic effect of TSAHC, an inhibitor of TM4SF5, in nude mouse orthotopic liver cancer model.

PRESENTER: Juri Na

ABSTRACT BODY:

Abstract Body: Objectives: Previous study showed that hepatic TM4SF5 promotes epithelial-mesenchymal transition for malignant tumor cell growth and migration. A synthetic compound, 4'-(p-toluenesulfonylamido)-4-hydroxychalcone (TSAHC) was reported to antagonize both the TM4SF5-mediated multilayer growth and migration/invasion. Here, we investigated anti-metastatic effect of TSAHC in mouse orthotopic model.

Methods: Human-optimized firefly luciferase was transfected into SNU449T cells (TM4SF5 over-expressing human hepatocellular carcinoma) for bioluminescence imaging. Luciferase- expressing SNU449T7 cells (10^6 cells) were injected in the liver of BALB/c nude mice to generate orthotopic tumor xenograft. Those mice were divided into 2 groups for control (DMSO-treated) and experimental group (TSAHC-treated), and imaged by IVIS LUMINAR. TSHAC was dissolved in 60% DMSO, and 25 mg/kg of TSHAC was intra-peritoneally injected to the mouse every weekday. IVIS images were followed up once a week. After a 3 week-treatment, the abdomen was opened for autopsy and imaged. Total photon flux of region of interest (ROI) from the primary and metastatic tumor was measure for further analysis.

Results: After 2-week, all of control mice (n=8) showed metastasis in the distal region from the primary injection site. However, in TSAHC-treated mice, only 3 of 8 mice (37.5%) showed metastasis. Lower levels of total photon flux from the tumors were observed in TSAHC-treated animals compared with control mice. TSAHC-treated animals also showed less metastasis. The metastatic regions were mostly found in the intestine area. After autopsy, similar results were also observed from the images of primary and the metastatic region.

Conclusion: TM4SF5-triggered metastasis was successfully inhibited by TSAHC, suggesting that TSAHC can be used as a new anti-metastatic drug (Hepatology. 2015 Accepted. Jan 27).

References:

Hepatology. 2009 Apr;49(4):1316-25

AUTHORS (LAST NAME, FIRST NAME): Na, Juri[1, 2]; Lee, Doohyung[3]; Chung, June-Key[4, 5]; Lee, Jung Weon[3, 6]; Youn, Hyewon[7, 6]

INSTITUTIONS (ALL):

1. Biomedical Science, Seoul National University, Seoul, Korea (the Republic of).
2. Nuclear Medicine, Seoul National University Hospital, Seoul, Korea (the Republic of).
3. Pharmacy, Seoul National University, Seoul, Korea (the Republic of).
4. Cancer Research Institute, Seoul National University, Seoul, Korea (the Republic of).
5. Nuclear Medicine, Seoul National University Hospital, Seoul, Korea (the Republic of).
6. Tumor Microenvironment Global Core Research Center, Seoul, Korea (the Republic of).
7. Cancer Imaging Center, Seoul National University Hospital, Seoul, Korea (the Republic of).

(No Image Selected)

CONTROL ID: 2232978

TITLE: The More Efficient Radioiodine Therapy Induced by BRG1 Bromodomain Dominant Negative Effect has been Visualized *in vivo* mouse.

PRESENTER: Juri Na

ABSTRACT BODY:

Abstract Body: Objectives: More than half of all people with cancer are treated with radiation therapy, a type of treatment that is used to stop the growth of cancer cells. However, some types of cancer cells become resistant to radiation after therapy. Therefore, stronger therapeutic effect is desired and this study is designed for radiation sensitization. Brahma-related gene 1 (BRG1), the catalytic subunit of SWI/SNF chromatin-remodeling complex functions DNA double strand breaks (DSB) repair. If the site of BRG1 bromodomain overexpressed, BRG1 is not able to induce DNA repair mechanism and broken states are remained. The strategy of this study is increasing I-131 therapeutic effect by overexpressing BRG1 bromodomain (BRD) as a competitor resulting inefficient DSB repair.

Methods: FRO anaplastic thyroid cancer cells which containing a luciferase reporter gene (effluc) were transfected with human sodium iodide symporter gene (pMSCV-oNIS) for radioiodine therapy. **pMX-BRG1-BRD retro-viral vector was used to establish BRG1-BRD overexpressing FRO-oNIS cells. BRG1-BRD overexpression in FRO-oNIS cells was confirmed by western blot. Tumor cells were subcutaneously implanted into BALB/c nude mice. Animal SPECT/CT imaging was performed at 1 hr after I-131 treatment (2 doses; 500, 60 μCi).** To investigate the effect of BRD on I-131 therapy, t*umor size* was measured with caliper and optical images were acquired by IVIS imaging system.

Results: Clonogenic assay indicated that radiation sensitizing effect of BRG1-BRD in FRO-oNIS-BRD cells. The luciferase signal of FRO-oNIS tumors which do not overexpressing BRD are continued to increase 32 fold until 18 days. However, the luciferase signal of FRO-oNIS-BRD decreased until 6 days when 500 **μCi of I-131 treated**. Thereafter, the signal of these tumors increased, indicating that the FRO-oNIS-BRD tumors regrowth from 6 days after I-131 treatment. The luciferase signal of the FRO-oNIS-BRD tumors showed 4.9 times lower than the FRO-oNIS tumors at 10 days. Also, the size of the tumors measured as same pattern to images. **The size of FRO-oNIS tumors and FRO-oNIS-BRD increased 13.7 and 1.2 fold, respectively.** Similarly, 60 **μCi** of I-131 treated mice bearing FRO-oNIS-BRD tumors have shown slower proliferation (1.97 times) than mice bearing FRO-oNIS tumors on day 10.

Conclusion: We have shown that radio-sensitizing effect induced by BRG1-BRD overexpression on radioiodine therapy, and our results indicating that BRG1-BRD overexpression could be used as a therapeutic gene by combination with NIS for reducing therapeutic dose of radioiodine. Also, making an attempt to treating relatively lower dose of I-131 (60 **μCi)** have shown successful differences, and this potential abilities can prevent the occurrence of secondary disease after radiation treatment.

Reference: Molecular Cancer Therapeutics. 2015 Feb 12;14(2):597-607.

AUTHORS (LAST NAME, FIRST NAME): Na, Juri[2, 3]; Youn, Hyewon[4, 5]; Kim, Mi Jeong[4]; Kang, Keon Wook[1]; Lee, Dong Soo[1]; Chung, June-Key[4, 3]

INSTITUTIONS (ALL):

1. Nuclear Medicine, Seoul National University, Seoul, Korea (the Republic of).
2. Biomedical Science, Seoul National University, Seoul, Korea (the Republic of).
3. Laboratory of Molecular Imaging and Therapy, Cancer Research Center, Seoul, Korea (the Republic of).
4. Nuclear Medicine, Seoul National University Hospital, Seoul, Korea (the Republic of).
5. Tumor Microenvironment Global Core Research Center, Seoul, Korea (the Republic of).

(No Image Selected)

CONTROL ID: 2232945

TITLE: *Nanoparticles optimized for efficient stem cell labeling and possessing optimal contrast properties for MRI and MPI*

PRESENTER: Alexander Kraupner

ABSTRACT BODY:

Abstract Body: Alexander Kraupner[1], Anne Kirchherr[1], Stefanie Runge[1], David Heinke[1], Florian Fidler[2] and Andreas Briel[1]

[1]nanoPET Pharma GmbH, Berlin, Germany, [2]MRB Research Center for Magnetic-Resonance-Bavaria, Würzburg, Germany

Objectives: Stem cell research in the field of regenerative medicine has increased significantly over the past few years because of the cells' healing capacities in neurodegenerative diseases such as Parkinson's or Alzheimer's disease. Monitoring of stem cells *in vivo* is essential for improved understanding of their interactions within the organism and their therapeutic effects. In this work, we present iron oxide nanoparticles, which are optimized for efficient stem cell labeling and possess optimal contrast properties for magnetic resonance imaging (MRI) as well as for magnetic particle imaging (MPI). *Methods:* Dextran-coated iron oxide nanoparticles were synthesized using an aqueous precipitation process [1]. The particles were functionalized by crosslinking and amination of the dextran surface to obtain particles with a positive surface potential. Subsequently, the particle dispersions were fully characterized and cytotoxicity tests were performed. Relaxation times were measured at 0.94 T @ 39 °C using a Bruker MiniSpec and the magnetic particle spectra (MPS) were recorded with a commercial MPS system (Pure Devices). *In vitro* labeling of mesenchymal stem cells was performed by incubation of the cells under standard cell culture conditions for 24 hours with the respective particle dispersion having an iron concentration of 0.1 mg/mL. *Results:* Nanoparticles with a mean hydrodynamic diameter of 170 nm and a zeta-potential of +25 mV @ pH = 7.0 were used for *in vitro* labeling experiments. Compared to the commercially available and negatively charged particles, FeraSpin^{TM} R, an iron uptake of ca. 22x higher was found for the positively charged particles (20 vs. 450 pg/cell). The contrast properties were found to be highly improved compared to FeraSpin R and the MPS data showed an increase up to a factor of 3 for the amplitude of the third harmonic. *Conclusion:* In this study we report on highly effective and biocompatible iron oxide nanoparticles for *in vitro* stem cell labeling with optimized contrast properties for MRI and MPI. The particle characteristics allow a direct labeling without the use of transfection agents or other additional treatments, which is favorable for the future development of clinical applications. The exceptionally high iron uptake enables the use of external magnetic fields to influence the labeled cells, allowing not only their homing to a specific target but also capturing of the labeled stem cells *in vivo*.

[1] N. Gehrke, D. Heinke, D. Eberbeck and A. Briel, "The Potential of Clustered Core Magnetic Particles for MPI," IEEE XPlore, DOI 10.1109/IWMPI.2013.6528368, 2013.

Acknowledgements: This work was supported by the European Commission's Seventh Framework Programme – Health.2011.1.4-2 - Contract no. 279288 - IDEA

AUTHORS (LAST NAME, FIRST NAME): Kraupner, Alexander[1]; Kirchherr, Anne[1]; Runge, Stefanie[1]; Heinke, David[1]; Fidler, Florian[2]; Briel, Andreas[1]

INSTITUTIONS (ALL):

1. nanoPET Pharma GmbH, Berlin, Germany.
2. MRB Research Center for Magnetic-Resonance-Bavaria, Würzburg, Germany.

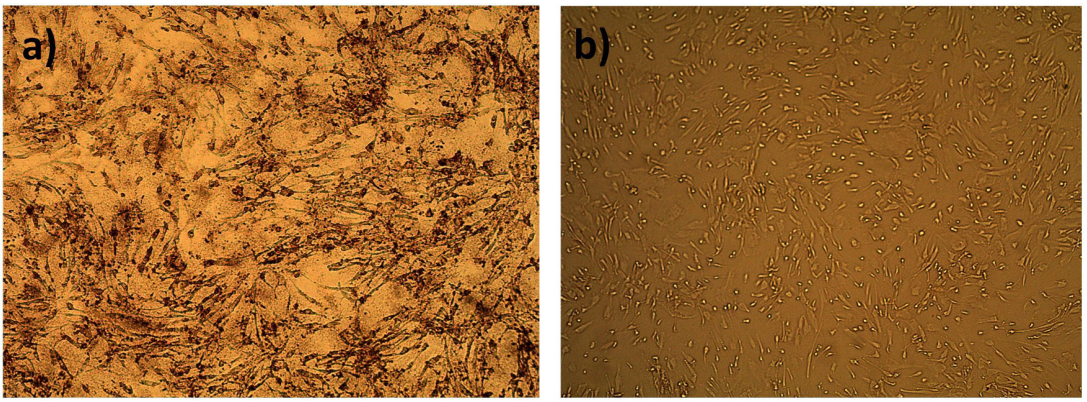

Fig. 1: Microscopic images of MSCs after labeling with a) positively charged and b) negatively charged particles, clearly showing the exceptionally high iron uptake of the positively charged particles.

CONTROL ID: 2232815

TITLE: *In vivo* bio-distribution of systemically injected exosomes derived from breast cancer cells using NIR and PET imaging

PRESENTER: Kyung Oh Jung

ABSTRACT BODY:

Abstract Body: Purpose: Breast cancer cells release exosomes to communicate with tumor microenvironment cells, promoting angiogenesis and metastasis. Physiologic distribution of the exosomes was not clarified until now. To monitor the biodistribution of exosomes, we performed fluorescence and PET imaging in mice.

Methods: Exosomes were isolated using ExoQuick^{TM} from cultured medium of 4T1, mouse breast cancer cell line. Exosomes were characterized by western blot and TEM. Purified exosomes were labeled with Cy7 and ^{64}Cu. Radio-labeled exosomes were systemically injected through tail vein. Fluorescence and PET images were obtained by IVIS and PETBOX, respectively. Radio-activities of major organs were measured with Gamma counter, and compared to the numbers from SUV of PET images.

Results: The macrocyclic bifunctional chelator pSCN-NOTA were used to make a bond with amine groups of exosomes, and then ^{64}Cu was labeled in the Exosome-NOTA. Thin layer chromatography showed that 95% of exosomes were labeled with ^{64}Cu. PET images showed that most of free ^{64}Cu were accumulated in liver and NOTA-^{64}Cu was mainly accumulated in kidney in PET images at 4 hr and cleared at 24 hr, whilst radiolabeled-exosomes showed higher uptake in the lung, liver, and spleen at 4 hr. Fluorescence images and the radio-activity measured by gamma counter of excised organs showed the similar pattern of exosomes bio-distribution with PET images, showing higher uptake in the lung, liver, and spleen.

Conclusions: Tumor exosomes were successfully labeled and visualized by fluorescence and PET imaging, showing that the exosomes initially accumulated in the RES (reticular endothelial system) after i.v. injection. This is the first PET study on exosome bio-distribution, and could provide indispensable information for in vivo application of exosomes as a therapeutic vehicle.

AUTHORS (LAST NAME, FIRST NAME): Jung, Kyung Oh[4, 3]; Youn, Hyewon[1, 2]; Kang, Keon Wook[3, 2]; Chung, June-Key[5, 4]

INSTITUTIONS (ALL):

1. Cancer Imaging Center, Seoul National Univ, Seoul, Jongno-Gu, Korea (the Republic of).
2. Cancer Research Institute, Seoul National University , Seoul, Korea (the Republic of).
3. Nuclear Medicine, Seoul National University, Seoul, Korea (the Republic of).
4. Biomecical Sciences, Seoul National University, Seoul, Korea (the Republic of).
5. Tumor Microenvironment Global Core Research Center, Seoul National University, Seoul, Korea (the Republic of).

(No Image Selected)

CONTROL ID: 2232820

TITLE: ^{18}F-FEDAC, a radiolabeled ligand targeting Translocator protein, as a PET tracer to image Rheumatoid Arthritis in a mouse model

PRESENTER: Seock-jin Chung

ABSTRACT BODY:

Abstract Body: PURPOSE: Translocator protein (TSPO) is abundant in activated macrophages which play an important role in the early phase of rheumatoid arthritis (RA) pathogenesis. ^{18}F-FEDAC (*N*-Benzyl-*N*-methyl-2-[7,8-dihydro-7-(2-[18F]fluoroethyl)-8-oxo-2-phenyl-9*H*-purin-9-yl] acetamide) is a radiolabeled ligand that recognizes TSPO, and we evaluated the targeting ability of ^{18}F-FEDAC as a possible PET tracer for TSPO in a mouse RA model.

METHODS: Lipopolysaccharide (LPS) was used to stimulate Raw264.7 mouse macrophage cells for in vitro experiments. RNA and protein expression levels of TSPO were measured by RT-PCR and western blotting. The ^{18}F-FEDAC cellular uptake was measured with gamma counter. PK11195, as known as a traditional TSPO ligand, was used to compete with FEDAC for testing specificity. A RA model in DBA/1 mouse was established by intradermal injections of Freund's adjuvant and type II collagen mixture. PET images were acquired at various time point in a RA mouse using ^{18}F-FEDAC. Immunohistochemistry stainings using anti-CD86 antibody and anti-TSPO antibody were performed to evaluate the distribution of infiltrated macrophages and TSPO expression in inflammation site.

RESULTS: TSPO was highly expressed in the LPS-stimulated (activated) RAW 264.7. Uptake of ^{18}F-FEDAC in activated RAW 264.7 cells was 1.5 fold higher than that in non-activated cells ($p<0.05$). In addition, uptake of ^{18}F-FEDAC in activated RAW 264.7 was successfully blocked by PK11195 demonstrating its specific binding to the activated macrophages. At 1 hr after injection of ^{18}F-FEDAC, PET signals in arthritic paws were significantly increased at 2 to 3 folds more than that in normal paws. The ^{18}F-FEDAC uptake in arthritic paws from PET imaging was closely associated with the clinical severity score. Immunohistochemistry images showed higher expression of macrophage marker (CD86) and TSPO in arthritic paws than in normal ones.

CONCLUSION: We demonstrated that ^{18}F-FEDAC specifically bind to activated macrophages and ^{18}F-FEDAC-PET showed strong uptake in arthritis areas. Our results indicated that ^{18}F-FEDAC-PET images have a potential to visualize RA activity by targeting TSPO.

AUTHORS (LAST NAME, FIRST NAME): Chung, Seock-jin[11]; Yoon, Haijeon[4]; Cheon, Gi Jeong[5]; Youn, Hyewon[2, 6]; Kim, Mi Jeong[7]; Lee, Yun-Sang[3, 8]; Chung, June-Key[9, 8]; Kang, Keon Wook[10, 8]; Zhang, Ming-Rong[1]; Jeong, Jae Min[3, 8]; Xie, Lin[1]

INSTITUTIONS (ALL):

1. National Institute of Radiological Sciences, Chiba, Japan.
2. Nuclear Medicine, Seoul National University, Seoul, Korea (the Republic of).
3. Nuclear Medicine, Seoul National University College of Medicine, Seoul, Korea (the Republic of).
4. Nuclear Medicine, Ewha Womans University School of Medicine, Seoul, Korea (the Republic of).
5. Nuclear Medicine, Biomedical science, Tumor biology program, Cancer research institute, Seoul National University, Seoul, Korea (the Republic of).
6. Cancer Research Institute, Tumor Microenvironment Global Core Research Center, Cancer Imaging Center, Seoul National University, Seoul, Korea (the Republic of).
7. Nuclear Medicine, Cancer Research Institute, Seoul National University, Seoul, Korea (the Republic of).
8. Institute of Radiation Medicine, Medical Research Center, Seoul, Korea (the Republic of).
9. Nuclear Medicine, Biomedical Sciences, Tumor Biology Program, Cancer Research Institute, Tumor Microenvironment Global Core Research Center, Seoul National University, Seoul, Korea (the Republic of).
10. Nuclear Medicine, Biomedical Sciences, Tumor Biology Program, Cancer Research Institute, Cancer Imaging Center, Seoul National University, Seoul, Korea (the Republic of).
11. Nuclear Medicine, Tumor Biology Program, Cancer Research Institute, Seoul National Unversity, Seoul, Korea (the Republic of).

(No Image Selected)

CONTROL ID: 2232824

TITLE: ^{99m}Tc-Labeled CWXY9 peptide for integrin α6 targeted tumor imaging

PRESENTER: Chengyan Dong

ABSTRACT BODY:

Abstract Body: Objectives: Overexpression of integrin α6 is associated with metastasis of multiple tumor types, and correlated with reduced patient survival and worse prognosis. Developing agents for non-invasive imaging of integrin α6 expression could provide a tool for early diagnosis and treatment planning of tumors. A 9-residue cyclic peptide named CWXY9 was discovered, and the novel radiotracer ^{99m}Tc-HYNIC-CWXY9 was prepared and evaluated in integrin α6 positive tumor model.

Methods: Flow cytometric analysis were performed in CNE2^{wild} (integrin α6-positive) and CNE2^{ITGA6-} (integrin α6-negative) nasopharyngeal carcinoma cells to verify the specificity of CWXY9 to integrin α6. HYNIC-CWXY9 was conjugated and labeled with ^{99m}Tc by using tricine and EDDA as coligands. SPECT/CT imaging and biodistribution studies in nude mice bearing CNE2^{wild} and CNE2^{ITGA6-} tumor xenografts were performed to investigate the in vivo performance of the probe.

Results: Results of flow cytometry demonstrated different expression of integrin α6 in CNE2^{wild} and CNE2^{ITGA6-} tumor cells and a good specificity of CWXY9 to integrin α6. The radiotracer ^{99m}Tc-HYNIC-CWXY9 was produced in 95% radiochemical yield analyzed with HPLC. In SPECT/CT imaging studies, ^{99m}Tc-HYNIC-CWXY9 exhibited specific tumor imaging with high contrast to the background in CNE2^{wild} tumor bearing animals. Compared with CNE2^{ITGA6-} tumors, CNE2^{wild} tumors had much more ^{99m}Tc-HYNIC-CWXY9 uptake, and could be imaged more clearly. Biodistribution studies showed a rapid in vivo clearance from whole body and low uptake in all organs (< 1.0 %ID/g except for kidneys ~6.91 ± 0.54 %ID/g at 1 h p.i.).

Conclusion: Our results suggested that SPECT/CT with ^{99m}Tc-HYNIC-CWXY9 would provide an effective approach for the noninvasive detection of integrin α6 expression.

AUTHORS (LAST NAME, FIRST NAME): Dong, Chengyan[1]; Wu, Yue[2]; Feng, Guokai[3]; Li, Liqiang[2]; Zhong, Qian[3]; Zeng, Musheng[3]; Wang, Fan[1, 2]

INSTITUTIONS (ALL):

1. Interdisciplinary Laboratory, Institute of Biophysics, Chinese Academy of Sciences, Beijing, China.
2. Medical Isotopes Research Center, Peking University, Beijing, China.
3. Sun Yat-sen University Cancer Center, State Key Laboratory of Oncology in South China, Collaborative Innovation Center for Cancer Medicine, Guangzhou, Guangdong, China.

(No Image Selected)

CONTROL ID: 2232866

TITLE: SPECT/CT Imaging of a Novel HER2-targeted Peptide ^{99m}Tc-HYNIC-YLF8 in a Breast Cancer Mouse Model

PRESENTER: Chengyan Dong

ABSTRACT BODY:

Abstract Body: Objectives: Human epidermal growth factor receptor-2 (HER2) is overexpressed in many human cancers, especially breast cancer. Nuclear imaging of HER2 expression in tumors might guide HER2-targeted therapies for patients. With this perspective, we aimed to develop a HER2-targeted peptide probe for breast cancer imaging. A novel SPECT imaging probe ^{99m}Tc-HYNIC-YLF8 was prepared and then evaluated in breast cancer animal models.

Methods: The HER2-targeted peptide YLF8 (YLFFVFER) was discovered by the high-throughput screening, synthesized by solid phase peptide synthesis and conjugated with a bifunctional chelator HYNIC. Binding specificity for HER2 was determined in a cell uptake assay using breast cancer cell line. ^{99m}Tc-HYNIC-YLF8 was prepared and the in vitro stability was tested. The SPECT/CT imaging was performed in nude mice bearing MDA-MB-435 breast cancers.

Results: YLF8 and HYNIC-YLF8 were characterized by HPLC analysis and mass spectrometry to confirm the structure and purity. While incubation with ^{125}I-YLF8, HER2-positive MDA-MB-453 cells accumulated much more radioactivity than HER2-negetive MDA-MB-231 cells. The ^{125}I-YLF8 binding could be inhibited by overdose of non-labeled YLF8. By a standard tricine/TPPTS labeling procedure, the radiochemical purity is over 98%. ^{99m}Tc-HYNIC-YLF8 displayed excellent in vitro stability in saline and cysteine buffer. The SPECT/CT imaging showed that the MDA-MB-453 tumors were clearly visualized (3.58 ± 0.01 %ID/g at 30 min p.i.) while the signals in HER2-negetive MDA-MB-231 tumors were much lower (0.73 ± 0.22 %ID/g at 30 min p.i.). The tumor uptake of MDA-MB-453 was blocked by the co-injection of overdose of YLF8.

Conclusion: ^{99m}Tc-HYNIC-YLF8 peptide probe specifically accumulated in HER2 positive tumor, which made it a promising probe for diagnosis of HER2 positive cancers and guiding HER2-targeted therapies.

AUTHORS (LAST NAME, FIRST NAME): Dong, Chengyan[1]; Li, Liqiang[2]; Wang, Zihua[3]; Wu, Yue[2]; Hu, Zhiyuan[3]; Jia, Bing[2]; Wang, Fan[4, 1]

INSTITUTIONS (ALL):

1. Interdisciplinary Laboratory, Institute of Biophysics, Chinese Academy of Sciences, Beijing, China.
2. Medical Isotopes Research Center, Peking University,, Beijing, China.
3. National Center for Nanoscience and Technology, Chinese Academy of Sciences,, Beijing, China.
4. Medical Isotopes Research Center, Peking University, Beijing, China.

(No Image Selected)

CONTROL ID: 2232831

TITLE: Targeting glucose regulated protein 78 using a cell penetrating peptide, Pep42, for glioblastoma imaging and therapy.

PRESENTER: Taemoon Chung

ABSTRACT BODY:

Abstract Body: Purpose:

Glucose regulated protein 78 (GRP78) is a multifunctional chaperone protein which is commonly overexpressed in malignant cancer cells. Because GRP78 has an important role in radio- and chemo-resistance of cancer, therapy targeting GRP78 may be useful in cancer treatment. In this study, we developed theranostic probe using GRP 78 targeting peptide (Pep42).

Methods:

Pep42 is a cyclic 13-mer GRP78 targeting and cell penetrating peptide developed by phage display. In human glioma cell lines (U87MG, U251) and primary glioma cells from one patient (GBM28, GBM37; before and after Temozolomide-radiation therapy), GRP78 expression levels were measured by microarray, RT-PCR and immunoblotting. After the glioma cells were incubated with red fluorescence labeled Pep42 (Pep42-R) for 2 hours, targeting by Pep42 were observed using a confocal fluorescence microscope. Pep42 labeled with I-125 was used to investigate the GRP78 targeting and cellular uptake. For in vivo GRP78 targeted imaging, Pep42-R was conjugated with Cu^{64} labeled human serum albumin (Cu^{64}–HSA-Pep42). Cu^{64}–HAS-Pep42 was intravenously injected into the mice xenografted U87MG, and images were obtained by an animal PET-BOX.

Results:

Confocal microscope showed the specific binding of Pep42-R at the cytoplasm as well as membrane of glioma cells. GRP 78 targeted miRNA expression in U87 and GBM37 was lower than in U251 and GBM28. RT-PCR and immunoblotting assay revealed higher GRP78 expression in U87MG cells than in U251 cells. GRP78 expression was also higher in GBM37 than in GBM28. Pep42-R images showed that U87MG fluorescent signals were 1.98 times more intense than U251 and GBM37 fluorescent signals were 2.04 times more intense than GBM28. Therefore, Pep42-R image successfully showed that the expression of GRP78 in U87MG and GBM37 was higher than that of U251 and GBM28. Labeling efficiency of ^{125}I-Pep42 and Cu^{64}–HSA-Pep42 were over 95%, and in vitro uptake test showed its specificity in U87MG cells. Serial PET imaging revealed that liver uptake of Cu^{64}–HSA-Pep42 was reduced dramatically and GRP78 positive tumor uptake was increased significantly. Therefore, Cu^{64}–HSA-Pep42 successfully visualized targeting GRP78 positive tumors in U87MG xenograft model using animal PET-BOX.

Conclusion:

We could evaluate the expression level of GRP78 on glioma cell lines and primary cultured glioma cells. Pep42 imaging probes specifically visualize GRP78 expression in glioma models, and could validate the malignant glioma cells. Therefore, this imaging probe could be useful as a theranostic probe for malignant cancers.

AUTHORS (LAST NAME, FIRST NAME): Chung, Taemoon[1, 4]; Youn, Hyewon[1, 6]; Song, Myung Geun[1]; Park, Ji Yong[2, 4]; Lee, Yun-Sang[2]; Jeong, Jae Min[2, 4]; Kang, Keon Wook[3, 4]; Chung, June-Key[3, 5]

INSTITUTIONS (ALL):

1. Nuclear Medicine, Cancer Research Institute, Seoul, Korea (the Republic of).
2. Department of Nuclear Medicine, Seoul National University College of Medicine, Seoul, Korea (the Republic of).
3. Nuclear Medicine and Cancer Research institute, Seoul National University College of Medicine, Seoul, Korea (the Republic of).
4. Biomedical sciences, Seould National Universitiy college of medicine , Seoul, Korea (the Republic of).
5. Tumor microenvironment global core research center, Seoul National University, Seoul, Korea (the Republic of).
6. Cancer imaging center, Seoul National University Cancer Hospital, Seoul, Korea (the Republic of).

(No Image Selected)

CONTROL ID: 2232822

TITLE: Remnant living tumor cells exhibit cancer stem cells-like characteristics in histone deacetylase inhibitor resistant xenograft of lung cancer in mouse model

PRESENTER: Wei-Ying Kuo

ABSTRACT BODY:

Abstract Body: Objectives: Cancer stem cells (CSCs) are usually resistant to chemotherapy and/or radiotherapy and responsible for the relapse. Although CSCs can be generated in vitro by non-adherent suspension culture in serum-free medium, the biologic characteristic of tumorspheres was far from CSCs in real tumors due to the distinct environmental factors, such as stroma cells, inflammation and hypoxia within tumor, which may profoundly reprogram CSCs. Previous studies reported that histone deacetylase inhibitors (HDACIs) may induce epithelial-to-mesenchymal transition (EMT) and CSC-enriched characteristics during treatment course. This study aimed to determine the role of suberoylanilide hydroxamic acid (SAHA) in the mediation of CSCs in lung cancer.

Methods: A H1299 stable clone which stably expressed a triple fused reporter gene (DsRedm-Fluc-tTKsr39) under the control of CMV promoter was used to establish a xenograft mouse model in the present study. Tumor cells were tracked by in vivo luminescence imaging after continuous SAHA treatment of tumor-bearing mice. Using the Aldefluor assay, viable CSCs were isolated from xenograft tumors which co-express the reporter gene and ALDH activity. The stem cell phenotype of CSCs was assessed by a cell invasion assay, by analyzing CSC-related gene expression, and by immunohistochemical staining for ALDH1A1 and other stem cell marker in vitro.

Results: Tumor tissues from SAHA-treated mice had increased CSC population which enrich by continuous administration of SAHA (percent increase in SAHA-treated mice relative to vehicle-treated control mice — xenograft tumors: 4.14%, controls: 1.50%). The microarray analysis showed that genes involved in the maintenance of CSCs, self-renewal and metastasis were upregulated in these isolated CSCs which obtained from SAHA-treated mice. Moreover, when compared to controls, an elevated invasive ability of these SAHA-induced CSCs was also observed.

Conclusions: In this study, we successfully isolated and characterized the in vivo CSCs, rather than in vitro tumorspheres, by using self-developed reporter gene system and Aldefluor assay. These results may improve our understanding on the molecular mechanism of CSCs and facilitate the discovery of specific targets against CSCs clinically.

AUTHORS (LAST NAME, FIRST NAME): Kuo, Wei-Ying[2]; Hwu, Luen[3]; Wu, Chun-Yi[4]; Wang, Hsin-Ell[1]; Chang, C. Allen[1]; Liu, Ren-Shyan[2, 3]

INSTITUTIONS (ALL):

1. Department of Biomedical Imaging and Radiological Sciences, National Yang-Ming University, Taipei , Taiwan.
2. Dept of Nuclear Medicine, Faculty of Medicine, National Yang-Ming University, Taipei, Taiwan.
3. National PET/Cyclotron Center, Taipei Veterans General Hospital, Taipei, Taiwan.
4. China Medical University, Taipei, Taiwan.

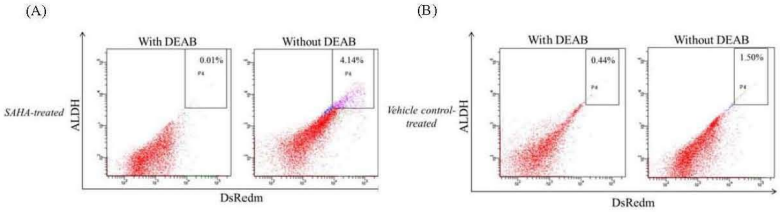

Figure 1. The expression of ALDH in primary H1299 xenografts. Flow cytometry analysis of (A) SAHA-treated and (B) controls. Single cell suspensions were made from each of primary H1299 xenografts. Viable cells were stained with Aldefluor without or with DEAB. To exclude contamination with murine cells, single cell suspensions were isolated with reporter gene expression (DsRed) and high ALDH enzymatic activity. SAHA treatment enhances the population of CSC-like cell.

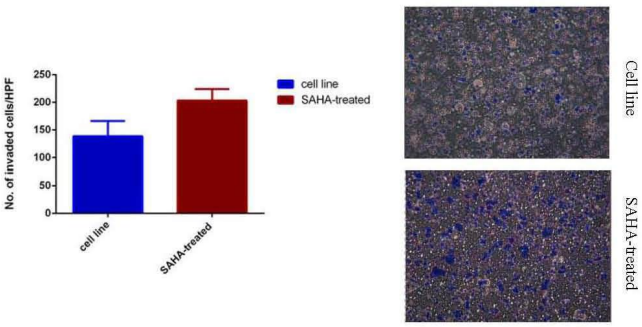

Figure 2. Continuous administration of SAHA increased the migration ability in H1299 cells. Right: phase-contrast images of H1299 cell line, xenograft tumors from SAHA-treated mice. Left: quantification of invasion assay.

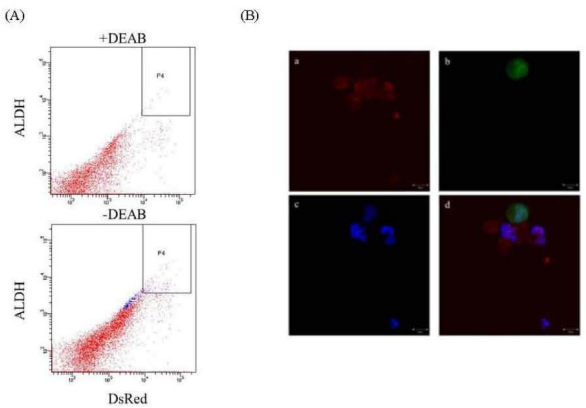

Figure 3. ALDH-positive cells detected in H1299 lung tumor xenografts. (A) Flow cytometry analysis of a xenograft samples using the Aldefluor assay. Baseline fluorescence was established by inhibiting ALDH activity with DEAB (upper panel) and use to generate a gate that will identify $ALDH^+$ cells in tumor xenografts that have not been incubated with DEAB (lower panel). (B) $ALDH^+$ cells can be observed by microscopy through accumulation of BAA (green, arrows) with nuclei identified by DAPI (blue). Scale bars=10 μm in each panel.

CONTROL ID: 2234332

TITLE: Evaluation of metabolic change of photochemically-induced brain ischemia by FDG/PET

PRESENTER: Chien-Chih Ke

ABSTRACT BODY:

Abstract Body: Objectives: Photochemical (PC) induction of brain ischemia is a relatively easy technique without manipulation of cerebral blood vessels. However, it generates small lesion size with minor sensorimotor deficits in comparison to other stroke models. As the result, it is difficult to evaluate therapeutic effect by behavior scoring. This study aims to investigate whether ^{18}F-FDG μPET imaging can be a tool for evaluating metabolic change of this stroke model.

Method: The skull of rat was exposed and photosensitive dye-rose bengal was i.v. injected followed by 560 nm-laser illumination of the motor cortex region (M1, M2) for 30 min. On day 1, day 5~7 and day 14, ^{18}F-FDG μPET imaging was performed to analyze the change of glucose metabolism of the brain after ischemia induction. % ID/cc of ^{18}F-FDG was measured from the region of interests of ischemic lesion and contralateral region and the metabolic difference index (MDI) was calculated by the equation: [(ROI(%ID/cc) of contralateral site – ROI(%ID/cc) of lesion site) x 100%] / [ROI(%ID/cc) of contralateral site]

Result: Brain ischemia was confirmed by tetrazolium chloride (TTC) and hematoxylin/eosin staining. MicroPET image on day 1 showed obvious decrease of ^{18}F-FDG uptake in motor cortex. MDI of rat after ischemia induction was 31.4±15.8% vs MDI of control rat 2.4±0.8%. On day 5~7 and day 14, MDI dropped to 18.1±11.3% and 14±4.2%, respectively.

Conclusion: Although PC induction of brain ischemia generates relatively small lesion (about 2x2mm^2), the PET image showed a ~30% decrease of ^{18}F-FDG uptake in the ischemic region as compared to contralateral normal brain. The metabolic difference between lesion and normal brain was decreasing with time, suggesting reversible ischemia. ^{18}F-FDG microPET imaging could be a tool for monitoring the metabolic change of PC-induced brain ischemia model, and is potentially useful for evaluating the therapeutic outcome of stroke on small animal.

AUTHORS (LAST NAME, FIRST NAME): Ke, Chien-Chih[6]; Liu, Nei-Wei[7]; Chen, You-Yin [8]; Hsieh, Ya-Ju[1]; Mok, Greta[2]; Zhao, Yong-Hua [7]; Chang, C. Allen[3]; Liu, Ren-Shyan[4, 5]

INSTITUTIONS (ALL):

1. 1.Department of Medical Imaging and Radiological Sciences, Kaohsiung Medical University, Kaohsiung, Taiwan.
2. Electrical and Computer Engineering, University of Macau, Taipa, Macao.
3. Biological Imaging and Radiological Sciences, National Yang Ming Univ., Taipei, Taiwan.
4. Dept of Nuclear Medicine, Faculty of Medicine, National Yang-Ming University , Taipei, Taiwan.
5. National PET/Cyclotron Center, Taipei Veterans General Hospital, Taipei, Taiwan.
6. Institute of Clinical Medicine, School of Medicine, National Yang-Ming University, Taipei, Taiwan.
7. Macau University of Science and Technology, Macau, Macao.
8. Biomedical Engineering, National Yang-Ming University, Taipei, Taiwan.

(No Image Selected)

CONTROL ID: 2234328

TITLE: Combined IUdR and enriched characteristic X irradiation for Auger electron cancer therapy

PRESENTER: Chien-Chih Ke

ABSTRACT BODY:

Abstract Body: Introduction: 5-iododeoxyuridine (IUdR) is one type of radiosensitizers categorized as halogenated pyrimidine which can incorporates into nascent DNA during DNA synthesis. Recently, many investigators attempt to treat cancer with combined IUdR and synchrotron radiation with energy slightly above K-edge of iodine to generate Auger electrons. The linear energy transfer (LET) of an Auger electron can be as high as 100 keV/μm which is capable of inducing an enormous DNA damage leading to cell death. This study aims to use an alternative radiation source, a transmission X-ray tube equipped with Tantalum target (NanoRay) which generate 33-40 keV- enriched photons to induce Auger electrons from iodine.

Method: With different settings, the NanoRay produces X-ray with different proportion (10% , 20% and 30%) of 33-40 keV- enriched photons. NG4TL4 fibrosarcoma cell line was used in this study. After treatment of IUdR combined with X-ray of 3 settings or Co-60 irradiation, cell survival was measured using colony formation assay, DNA damage was assayed by comet assay and γ-H2AX immunofluorescent staining. Metabolism of intra tumorally injected ^{123}IUdR was assessed μSPECT/CT imaging. Auger electron therapy of tumor was carried out by tumoral injection of IUdR followed by NanoRay irradiation.

Result: IUdR+NanoRay irradiation resulted in higher cell killing effect and DNA damage than irradiation alone or IUdR treatment alone. Compared with IUdR+Co-60 irradiation, IUdR+NanoRay showed better cell killing effect and higher DNA damage, indicating better therapeutic potential of Auger effect than that of radiosensitization. Further, when comparing the therapeutic results from IUdR+NanoRay with 3 settings, NanoRay with highest proportion of 33-40 keV (30%) induced most severe DNA damage. For in vivo tumor treatment, IUdR+NanoRay irradiation significantly inhibited tumor growth as compared to IUdR treatment or NanoRay irradiation alone.

Discussion and conclusion: This preliminary study validated the therapeutic effect of Auger electron therapy for cancer by combining IUdR treatment and X-irradiation with enriched 33-40 keV photons. This treatment regimen not only increased the DNA damage, cell killing but also inhibited tumor growth. In conclusion, this treatment model possesses high potential to be developed for future clinical cancer therapy.

AUTHORS (LAST NAME, FIRST NAME): Ke, Chien-Chih[4]; Kuo, Wen-Wang[2]; Li, Jia-Je[1]; Wang, Hsin-Ell[1]; Hsu, Shih-Ming[1]; Chen, Fu-Du[5]; Wang, Chia-Gee[6]; Liu, Ren-Shyan[2, 3]

INSTITUTIONS (ALL):

1. Department of Biomedical Imaging and Radiological Sciences, National Yang-Ming University, Taipei, Taiwan.
2. Dept of Nuclear Medicine, Faculty of Medicine, National Yang-Ming University, Taipei, Taiwan.
3. National PET/Cyclotron Center, Taipei Veterans General Hospital, Taipei, Taiwan.
4. Institute of Clinical Medicine, School of Medicine, National Yang-Ming University, Taipei, Taiwan.
5. Hwa Hsia University of Technology, New Taipei, Taiwan.
6. NanoRay Biotech, New York, NY, United States.

(No Image Selected)

CONTROL ID: 2234320

TITLE: Detection of thyroid function by in vivo I-131 Cerenkov luminescence imaging

PRESENTER: Chien-Chih Ke

ABSTRACT BODY:

Abstract Body: Objectives: Radioiodide and nuclear imaging instrument are regularly applied to detect thyroid-related disease in clinical practice. It has been reported that Cerenkov radiation can be observed from numerous radionuclides including radioiodide using optical imaging devices, and its signal intensity correlates linearly with radionuclide activity. This study aims to evaluate the feasibility of Cerenkov luminescence imaging (CLI) in assessment of thyroid function.

Methods: To know whether radioiodide activity in thyroid correlates the signal detected by CLI, mice were intraperitoneally (i.p.) injected with I-131 with serious doses (0~2 mCi) followed by imaging using IVIS 50 24 hours later. To correlate the signal of Cerenkov radiation and γ-ray from radioiodide in mouse thyroid, 0.5 mCi I-131 was injected i.p. into normal mice or mice with TSH-induced hyperthyroidism, and 24 hours later the γ-scintigraphy and CLI were performed to measure the thyroid uptake.

% uptake = (Thyroid activity - Bkg) / Injection dose activity x 100%

Activity measured from γ-scintigraphy is counts/s/pixel and from CLI is photons/s/area. The hyperthyroidism status was confirmed by determination of serum T4 by ELISA.

Results: Signal of CLI in the thyroid was highly correlated with I-131 dose injected ($R2=0.9$, $p<0.05$). For mice with hyperthyroidism, the % I-131 uptake in thyroid was 5.8±3.2 (range: 2.1-9.9) measured by CLI and 44.5±12.5 (range: 29.3-61.7) by γ-scintigraphy. The % I-131 uptake in thyroid of control mice was 1.6±0.6 (range: 1.1-2.6) measured by CLI and 22.1±6.9 (range:10.9-28.1) by γ-scintigraphy. Correlation of signals detected by γ-scintigraphy and CLI was 0.9, $p<0.05$.

Conclusion: Measurement of I-131 uptake function of mouse thyroid using CLI and γ-scintigraphy exhibit high correlation, indicating the potential of CLI as an alternative tool instead of γ-scintigraphy in measuring the thyroid uptake function of iodide.

AUTHORS (LAST NAME, FIRST NAME): Ke, Chien-Chih[4]; He, Zi-Ming[2]; Huang, Chia-Wen [3]; Hsieh, Ya-Ju[5]; Chang, C. Allen[1]; Liu, Ren-Shyan[2, 3]

INSTITUTIONS (ALL):

1. Biological Imaging and Radiological Sciences, National Yang Ming Univ., Taipei, Taiwan.
2. Dept of Nuclear Medicine, Faculty of Medicine, National Yang-Ming University, Taipei, Taiwan.
3. National PET/Cyclotron Center, Taipei Veterans General Hospital, Taipei, Taiwan.
4. Institute of Clinical Medicine, School of Medicine, National Yang-Ming University, Taipei, Taiwan.
5. Department of Medical Imaging and Radiological Sciences, Kaohsiung Medical University, Kaohuiung, Taiwan.

(No Image Selected)

CONTROL ID: 2232876

TITLE: PET Imaging Evaluation for Induced Pluripotent Stem Cell Transplantation in a Rat Model of Myocardial Infarction

PRESENTER: shuang wu

ABSTRACT BODY:

Abstract Body: The purpose of this study was to use small animal positron emission tomography (micro-PET) combined with echocardiography to evaluate and compare the therapeutic responses to pluripotent stem cells (iPSCs) and embryonic stem cells (ESCs) transplantation in a rat model of myocardial infarction (MI).

Methods: Twenty-eight rats were divided into 3 groups: phosphate-buffered saline (PBS) control, ESCs or iPSCs group. Serial ^{18}F-FDG micro-PET and echocardiography studies were performed weekly for 4 weeks. Autoradiography and immunohistochemical staining were conducted after the final micro-PET studies.

Results: Compared to the PBS control group, significantly higher left ventricular ejection fractions (LVEF) and increased ^{18}F-FDG accumulation in the peri-infarct area were observed in the stem cell (both iPSCs and ESCs) transplanted groups over the 4-week study period ($P < 0.05$ and $P < 0.001$, respectively). From weeks 3 to 4, peri-infarct ^{18}F-FDG uptake was higher in the iPSCs than in the ESCs group ($P < 0.05$). Immunohistochemical staining demonstrated survival of transplanted stem cells at the injection sites and migration to the infarct area.

Conclusion: ^{18}F-FDG PET imaging and echocardiography demonstrated metabolic and functional recovery after iPSCs and ESCs transplantation in the rat model of MI.

AUTHORS (LAST NAME, FIRST NAME): wu, shuang[1]; Shen, Yehua[1]; Song, Fahuan[1]; Liu, Hao[1]; Tian, Mei[1]; Zhang, Hong[1]

INSTITUTIONS (ALL):

1. Department of Nuclear Medicine, The Second Affiliated Hospital of Zhejiang University School of Medicine, Hangzhou, China.

(No Image Selected)

CONTROL ID: 2232825

TITLE: Systems and Materials Development for Second Biological Window of Small Animal Fluorescence Imaging

PRESENTER: Kohei Soga

ABSTRACT BODY:

Abstract Body: The second biological window (SBW), 1000-1700 nm near infrared, has attracted interests of the researchers and system developers as a biological window for deeper fluorescence bioimaging depth than currently used one. Especially, the longer the wavelength is, the weaker the scattering loss is around visible and near infrared wavelength range to provide much clearer images. The observation depth for fluorescence imaging is normally limited to be several mm at the currently used wavelengths. Some literature data tells us that the depth can be extended to be several cm by moving the excitation and fluorescence wavelengths into the SBW. The fact has been known since 1980s. However, the use of silicon-based camera has limited the observation wavelength to be less than 1000 nm. Recently, InGaAs CCD camera, to cover 800-1700 nm, has come into market for the observation in the SBW. The authors has built up a prototype small animal fluorescence imaging system for the SBW by using the InGaAs CCD. One of the candidate fluorescent materials for the bioimaging in the SBW is rare-earth doped ceramic nanophosphors (RED-CNPs). Since 2005, the authors has demonstrated cellular and small animal fluorescence bioimaging in the SBW. The observation depth was truly proved to reach several cm by animal imaging experiments with the RED-CNPs. The materials development for the SBW fluorescence boimaging includes photonic design, particle size control of the ceramic particles and design of organic-inorganic conjugate for biofunctionalizing the ceramic phosphors. Simultaneously, both of the microscopic imaging system for cells and macroscopic one for small animals has been developed. Our group of Tokyo University of Science and Shimadzu co. has collaborated together to develop both of the materials and systems to launch the SBW small animal fluorescence imaging system into market. In the end of 2014, the development is complete and now in Japan, the system is commercially available. For the SBW fluorescence bioimaging purposes, not only the RED-CNPs but some other phosphors such as quantum dots or organic dyes can be used. The presentation aims to review the whole picture of the materials and system development for the SBW fluorescence small animal bioaimgiing including some demonstrative imaging works by using the new system, “Shimadzu SAI-1000.” The demonstrative works cover blood vessel imaging, tumor imaging, digestive system imaging and so on, which can be applied for DDS tracing, biological researches and medical diagnosis.

AUTHORS (LAST NAME, FIRST NAME): Soga, Kohei[2]; Kamimura, Masao[2]; Takeuchi, Tsukasa[1]

INSTITUTIONS (ALL):

1. Shimadzu Corporation, Tokyo, Japan.
2. Materials Sci. and Tech., Tokyo Univ. of Science, Katsushika, Tokyo, Japan.

(No Image Selected)

CONTROL ID: 2232829

TITLE: Scattering Correction of SPECT by Fourier Transformation on Projection Data

PRESENTER: Huei-Yung Chen

ABSTRACT BODY:

Abstract Body: The single photon emission computed tomography (SPECT) had been applied to image gene therapy, estimated the growth of tumor, detected neural function of brain, diagnosed disease of cardiac coronal artery, and etc. However, the scattering of photons (noise) always cause of inaccurate SPECT images. In this study, the Fourier transformation (FT) approach will be used to investigate, correct, and estimate the noise fractions in SPECT. This study was fully supported by E-DA Hospital, Taiwan (No. EDAHP103022).

The SPECT scanner (Siemem Symbia S ECAM) was adopted to undergo experiments. The 32 step-and-shots of parallel detectors, scanning 10 minutes, injected ^{99m}Tc 40.7 MBq, and reconstructed by filtering-back projection with size 128×128 pixels were used for those experiments (i.e., Resolution and Uniform Phantoms). The Fourier transformation (FT) on projection data was used to correct the scattering events for uniform and resolution phantoms. The absolutely values of Fourier domain smaller than the critical values were set to zero and then applied inverse FT. The critical values (CV) on Fourier domain were investigated by half, one, two, three, and four times of the maximum intensity of original projection data. The reconstructed images after scattering correction by FT were compared signal-to-noise ratio (SNR) and full width at half maximum (FWHM) with original SPECT images. The experimental results were shown the SNR and FWHM were (4.706, 5.050), (4.662, 5.144), (5.235, 5.031), (7.974, 5.230), (8.725, 5.427) and (8.934, 5.734) with respectively to original image and presented method on five critical values. In general, the CV, two times of the maximum of original projection data, had provided the accepted SNRs and low FWHMs tested on phantoms. Moreover, the SNR provide by proposed method had improved over 10% than those of original images tested on resolution phantom.

The real animal study and complicated phantoms should be investigated in the future.

AUTHORS (LAST NAME, FIRST NAME): Hsu, Shih-Yen[2]; Hsu, Yun-Hsuan[1]; Lin, Ming-Chia[1]; Wu, Yi-Chen[1]; Huang, Yung-Hui[2]; Chen, Tai-Been[2]; Chen, Huei-Yung[1]

INSTITUTIONS (ALL):

1. Nuclear Medicine, E-DA Hospital, I-Shou University, Kaohsiung , Taiwan.
2. Medical Imaging and Radiological Sciences, I-Shou University, Kaohsiung, Taiwan.

(No Image Selected)

CONTROL ID: 2232826

TITLE: Different ^{18}F-FDG accumulation according to glucose-6-phosphatase expression in cancer cells and activated macrophages

PRESENTER: Youngeun Lee

ABSTRACT BODY:

Abstract Body: Objectives: Although increased ^{18}F-FDG uptake is widely used as an unique characteristic of cancer in clinical PET, it is also shown at the sites of various inflammations. Some investigators showed rapid washout pattern in a case of inflammation, and suggested different activity of glucose-6-phosphatase. We investigated the difference in ^{18}F-FDG uptake pattern and the glucose uptake-related proteins in cancer cells and activated macrophages.

Methods: *In vitro* ^{18}F-FDG uptake assay and ^{18}F-FDG efflux assay were performed in human breast cancer (MDA-MB231), human hepatocellular carcinoma (HepG2) and mouse macrophages (Raw264.7). For in vivo inflammatory model, BALB/c nude mouse was injected with 100 mL turpentine oil or PBS (control) in the right thigh muscle. After 4 days, the progress of inflammation was longitudinally monitored by animal PET Raw264.7 cells were stimulated with 100 ng/ml lipopolysaccharide (LPS) for 6 hour. Cellular uptake of ^{18}F-FDG was measured after 2×10^5 cells were incubated with ^{18}F-FDG (5 uCi) for 10, 60, 120, 240, 360 min. To investigate efflux of the ^{18}F-FDG, the cells were incubated with ^{18}F-FDG (5 uCi) for 60 min. After replacement of medium, ^{18}F-FDG uptake of the harvested supernatants was measured at 10, 20, 30, 60, 90, 120 min using gamma counter. Expression levels of glucose transport-1 (Glut-1), hexokinase II (HK II) and glucose-6-phosphatase (G6Pase) were evaluated by western blot analysis.

Results: Activated macrophages showed increased ^{18}F-FDG uptake until 240 min and decreased after then. In inflammatory mouse model, SUVmax of ^{18}F-FDG uptake showed a peak as 1.8 at 90 min, which was 2.5-fold higher than control, and decreased after then. After LPS stimulation, G6Pase expression was increased compared with the inactivated macrophages, although Glut-1, HK II expression was increased a little. To confirm the effect by G6Pase expression, among various cancer cell lines, glucose-6-phosphatase (G6Pase) high-expressing HepG2 and G6Pase low-expressing MDA-MB231 were chosen. ^{18}F-FDG uptakes in G6Pase low-expressing MDA-MB231 cells increased continuously and those of G6Pase high-expressing HepG2 cells showed the saturated pattern from 60 min. In efflux analysis indicating G6Pase activity, approximately 65% of radioactivity was released from activated macrophages, whereas 54% of radioactivity was released from MDA-MB231 at 120 min.

Conclusion: We found decrease of ^{18}F-FDG accumulation and increase of G6Pase activity in activated macrophages. Our data showed that evaluation of glucose metabolism might be useful to distinguish between cancer and inflammation on FDG PET.

AUTHORS (LAST NAME, FIRST NAME): Lee, Youngeun[1, 3]; Kim, Mi Jeong[4, 6]; Lee, Chul-Hee[1, 9]; Youn, Hyewon[5, 6]; Cheon, Gi Jeong[3, 4]; Kang, Keon Wook[4, 6]; Lee, Dong Soo[2, 4]; Alavi, Abass N.[8]; Chung, June-Key[4, 7]

INSTITUTIONS (ALL):

1. Nuclear medicine, Seoul National University, Seoul, Korea (the Republic of).
2. Molecular Medicine and Biopharmaceutical Sciences, Seoul National University, Seoul, Korea (the Republic of).
3. Tumor Biology Program, Seoul National University, Seoul, Korea (the Republic of).
4. Nuclear Medicine, Seoul National University College of Medicine, Seoul, Korea (the Republic of).
5. Cancer Imaging Center, Seoul National University Cancer Hospital, Seoul, Korea (the Republic of).
6. Laboratory of Molecular Imaging and Therapy, Cancer Research Institute, Seoul, Korea (the Republic of).
7. Tumor Microenvironment Global Core Research Center, Seoul National University, Seoul, Korea (the Republic of).
8. Radiology, Division of Nuclear Medicine, Hospital of the University of Pennsylvania, Philadelphia, PA, United States.
9. Biomedical Sciences, College of Medicine, Seoul National University, Seoul, Korea (the Republic of).

(No Image Selected)

CONTROL ID: 2233186

TITLE: Core-shell Fe_3O_4/Gd_2O_3 nanocube as T1- T2 Dual-Modal Contrast Agent

PRESENTER: Fenfen Li

ABSTRACT BODY:

Abstract Body: In molecular imaging and tumor diagnosis, magnetic resonance imaging(MRI) holds extremely important position due to its non-invasive character, superior resolution and non-limited penetration depth. Currently, there are two types of clinically prevalent contrast agents. One is paramagnetic gadolinium chelates (such as Gd-DTPA) as T1 positive contrast agents and the other is superparamagnetic iron oxide(SPIO) nanoparticles as T2 negative contrast agents. T1 contrast agents are preferred over the T2 agents because their high signal intensity can be differentiated from the signal of other biological conditions. However, the significant drawbacks of clinically used gadolinium chelates such as Gd-DTPA are their short body circulation time and low local contrast. On the other hand, the SPIOs are the predominant ultrasensitive T2 contrast agents. However, the clinical applications of T2 contrast agents are still quite limited because of the darkening contrast effect and magnetic susceptibility artifacts. Because each type of contrast agents has its own strengths and limitations, the T1–T2 dual-modal strategy for MRI may be a good solution which can offer complementary diagnostic information and lead to more precise diagnosis. Herein, we report a novel core-shell Fe_3O_4/Gd_2O_3 nanocube as T1-T2 dual-mode contrast agent. Report has indicated that only the surface Gd (III) ions in gadolinium oxide nanoparticles cooperatively and significantly contribute to the longitudinal relaxation of the water proton. Therefore, the strategy that Gd species are collected near the surface of one nanoparticle may bring their function into full play and further lead to a great enhancement of T1 contrast effects. To obtain biocompatible T1-T2 dual mode nanoparticles, the small molecule dopamine (DA) is a good candidate to make nanoparticles water-soluble and to allow further functionalization due to the free amine group. Therefore, a small-sized T1-T2 dual contrast agents were developed.

Characterization. The nanoparticles showed a cubic shape with round edges with an edge length of about 9 nm. The energy-dispersive X-ray (EDX) element mapping indicated that the distribution of Gd element is mainly collected on the surface of the nanocube and Fe element in concentrated in the core.
Relaxivity Measurements. To validate the potential of the nanocubes as a dual contrast agent, the magnetic resonance imaging was performed and the relaxation rates were measured on a 1.5 T MRI scanner. The results showed that the nanocubes exhibited much better T1 positive contrast and T2 negative contrast than Gd-DTPA and iron oxide nanocubes respectively. For T1 contrast ability, the r1 value of the nanocubes was determined to be 45.24 $mM^{-1}s^{-1}$, about 7.5-fold higher than Gd-DTPA which was 6.01 $mM^{-1}s^{-1}$. For T2 contrast ability, the r2 value was 186.51 $mM^{-1}s^{-1}$, about 2-fold higher than the iron oxide nanocubes.

In summary, we developed a novel core-shell Fe_3O_4/Gd_2O_3 nanocube as T1-T2 dual-mode contrast agent. With good positive and negative contrast effect, this novel nanomaterials could be potentially utilized as molecular imaging probes for a wide range of diagnostic and therapeutic applications.

AUTHORS (LAST NAME, FIRST NAME): Li, Fenfen[1]; Qiu, Bensheng[1]

INSTITUTIONS (ALL):

1. School of Information Science and Technology, University of Science and Technology of China, Hefei, Anhui, China.

(No Image Selected)

CONTROL ID: 2232841

TITLE: Intrinsically Radioactive [64Cu] Self-Illuminating ^{64}Cu-Doped CaS:Eu@CaS Nanocrystals for *in Vivo* PET and Optical Tumor Imaging

PRESENTER: Tianye Cao

ABSTRACT BODY:

Abstract Body: Functionalized luminescence lanthanide nanocrystals (LNs) have attracted much attention recently due to their potential as highly sensitive optical probes for biological imaging applications. Here, we prepared a self-illuminating LNs system by doping positron-emitting radionuclide ^{64}Cu into CaS:Eu@CaS core/shell LNs. Attaching positron-emitting radioisotopes onto LNs not only endows their positron emission tomography (PET) functionality, but also results in self-illuminating LNs, with no need for an external light source, by Cerenkov resonance energy transfer (CRET). The signal of ^{64}Cu can accurately reflect the biodistribution of the LNs during circulation with no dissociation of ^{64}Cu from the nanoparticles. We also explored this system conjugated with transferrin for *in vivo* tumor imaging. This nanoprobe showed high tumor-targeting ability in a mouse 4T1 breast tumor xenograft model and feasibility for *in vivo* luminescence imaging of tumor in the absence of excitation light. The availability of these self-illuminating integrated LNs provides an accurate and convenient tool for *in vivo* tumor imaging and detection.

AUTHORS (LAST NAME, FIRST NAME): Cao, Tianye[1]

INSTITUTIONS (ALL):

1. Department of Nuclear Medicine, Fudan University,Fudan University Shanghai Cancer Center, ShangHai, China.

(No Image Selected)

CONTROL ID: 2232891

TITLE: Two-stage combined imaging method to detect sentinel lymph node metastasis using ^{99m}Tc phytate and Affibody fluorescent probes in animals

PRESENTER: Makoto Tsuchimochi

ABSTRACT BODY:

Abstract Body: In this study, we investigated a 2-stage combined imaging method to detect sentinel lymph node metastases using ^{99m}Tc phytate and Affibody fluorescent probes. Sentinel lymph node biopsy is a standard procedure used to examine micrometastases in N0 cancers, such as breast cancer and melanoma. Typically, radiopharmaceuticals and/or blue dyes are used for sentinel lymph node detection. In a previous study, we tested the feasibility and utility of a new dual-modality imaging probe in which polyamidoamine (PAMAM)-coated silica nanoparticles (PCSNs) loaded with ^{99m}Tc and indocyanine green (ICG) were used to detect sentinel lymph nodes in animals (EJNMMI Res. 2013 Apr 25; 3(1); 33.). This probe was unable to confirm the existence of metastatic cells within the sentinel lymph node. In the current study, we investigated the efficacy of a two-stage combination probe based on lymph node scintigraphy and near-infrared Affibody imaging to detect metastatic tumor cells within the sentinel lymph node. The anti-HER2 Affibody molecule was dissolved in PBS to obtain a final concentration of 1 mg/ml, after which 0.3 mg dithiothreitol (DTT) was added to achieve a final concentration of 20 mM at pH > 7.5. After incubation, the solution was centrifuged prior to labeling with ICG-sulfo-OSu. After desalting the solution, the near-infrared fluorescence of the labeled Affibodies was verified using thin-layer chromatography (TLC) and a Pearl Imager (LI-COR Biosciences, Lincoln, NE). The fluorescent imaging probes were added to the culture medium of HER2-overexpressing breast carcinoma cells (SK-BR3, ATCC) and low HER2-expressing breast carcinoma cells (MDA-MB231, ATCC) and then incubated for 4 hours. The cells were observed using a Zeiss optical microscope equipped with a near-infrared filter and a digital camera. Frozen sections of metastatic lymph node specimens were used to investigate the ability of the Affibody probes to image HER2-positive cells. The tissue was frozen in isopentane cooled with liquid nitrogen, after which ten-micrometer cryostat sections were prepared for staining with the Affibody probes. Immunohistochemistry was also performed to detect HER2 expression in the same tissue specimens. Female athymic nude mice were used for *in vivo* analysis of the probes. SK-BR3 and MDA-MB231 xenografts were generated by injecting the tongues of nude mice with cells. After the xenograft was established, Affibody probes were injected into the right side of the tongue, and then a dose of 9.3 MBq of ^{99m}Tc phytate suspended in a total volume of 0.1 mL was also injected into the tongue. Then, ^{99m}Tc phytate lymphoscintigraphy of the entire body of the mice was performed. The radioactivity in the sentinel lymph nodes was observed clearly. SK-BR3 cells presented with stronger NIR fluorescent signal when compared with MDA-MB231 cells. Our data suggest that a two-stage combined imaging method using ^{99m}Tc phytate and Affibody fluorescence offers a direct visualization technique for HER2-overexpressing cancer cells that have spread to the sentinel lymph nodes. Additional animal studies are needed to determine the value of this approach in sentinel lymph node biopsy.

AUTHORS (LAST NAME, FIRST NAME): Tsuchimochi, Makoto[2, 3]; Yamaguchi, Haruka[3]; Hayama, Kazuhide[2]; Yasuo, Okada[4]; Kawase, Tomoyuki[1]; Fujii, Hirofumi[5]

INSTITUTIONS (ALL):

1. Division of Oral Bioengineering, Institute of Medicine and Dentistry, Niigata University, Niigata, Niigata, Japan.
2. Department of Oral and Maxillofacial Radiology, The Nippon Dental University School of Life Dentistry at Niigata, Niigata, Japan.
3. Quantitative Diagnostic Imaging Program, The Nippon Dental University Graduate School of Life Dentistry at Niigata, Niigata, Niigata, Japan.
4. Department of Pathology, The Nippon Dental University School of Life Dentistry at Niigata, Niigata, Niigata, Japan.
5. Functional Imaging Division, Research Center for Innovative Oncology,, National Cancer Center Hospital East, Kashiwa, Chiba, Japan.

(No Image Selected)

CONTROL ID: 2233802

TITLE: Photoacoustic imaging of the endogenous molecular contrast of haemoglobin in preclinical models of colorectal cancer in response to vascular disruption with OXi4503

PRESENTER: Sean Johnson

ABSTRACT BODY:

Abstract Body: Introduction: Photoacoustic (PA) imaging provides high resolution (μm) 3D images based on the contrast provided endogenous chromophores in a completely non-invasive manner. In biological tissue the main tissue chromophore is haemoglobin (1). PA can therefore image blood within vessels in biological tissue to a depth of ≈1cm. For preclinical models of cancer this is sufficient to encompass entire subcutaneous tumours, and can be used to evaluate pharmacological intervention aimed at the vasculature.

Materials and method: The PA system used has been previously described (2). In this subcutaneous xenograft study OXi4503, a tumour specific vascular disrupting agent, was used to target the vasculature of two human colorectal carcinoma tumour types known to possess differing vascular pathophysiologies (SW1222, LS174T) at a range of concentrations (40mg/kg, 10mg/kg, 1mg/kg and sham dose control). Response to therapy was assessed by non-invasive PA imaging and via caliper volumetric measurements. A total of n=48 mice were imaged (n=6 per group), with n=2 from each group culled for histological assessment at 48hr and the remaining n=4 allowed to progress until vessel regrowth, as observed by PA imaging, occurred.

Results: The characteristic destruction of tumour-specific vasculature caused by OXi4503 was observed in vivo by PA and confirmed through histological H&E staining. Qualitative differences were observed between the two tumour types in terms of vascular response, demonstrating the importance of tumour microenvironment and pathophysiology on response to therapy. Qualitative difference in response to different doses of OXi4503 was observed, although quantitative assessment of this to obtain a dose-response curve proved difficult due to variability in the PA conversion efficiency within biological tissue.

Discussion: Work on quantification is ongoing, however from a purely qualitative manner it can be seen that PA imaging can act as a biomarker of response, potentially improving the translation of novel anti-vascular compounds to the clinic. This study shows clearly that PA can accurately assess the pharmacodynamic effect of OXi4503 in preclinical models of cancer. Further work to interrogate the differences in vascular microenvironment, such as exogenous antibody targeted fluorophores for specific antigen expression within the microenvironment is considered, however it is hindered by the large endogenous contrast from haemoglobin already present within the tumours.

Summary: Photoacoustic imaging has been used to image response to the vascular targeted drug OXi4503 in two different mouse subcutaneous models of human colorectal tumours, with qualitative results showing differences in response between the two vascular pathophysiologies. Different doses also showed different qualitative results, with the time course of pharmacodynamic action accurately observed. PA has therefore been demonstrated as a potential biomarker of response for vascular targeted therapies.

1 Beard P. Interface Focus 2011;1:602-31

2 Zhang E, Laufer J, Beard P. Appl Opt 2008;47:561-77

AUTHORS (LAST NAME, FIRST NAME): Johnson, Sean P.[1]; Ogunlade, Olumide O.[2]; Zhang, Edward Z.[2]; Laufer, Jan[4]; Rajkumar, Vineeth[3]; Pedley, R B.[3]; Beard, Paul[2]

INSTITUTIONS (ALL):

1. University College London, London, United Kingdom.
2. Medical Physics and Biomedical Engineering, University College London, London, United Kingdom.
3. UCL Cancer Institute, University College London, London, United Kingdom.
4. Institut für Optik und Atomare Physik, Technische Universität Berlin, Berlin, Germany.

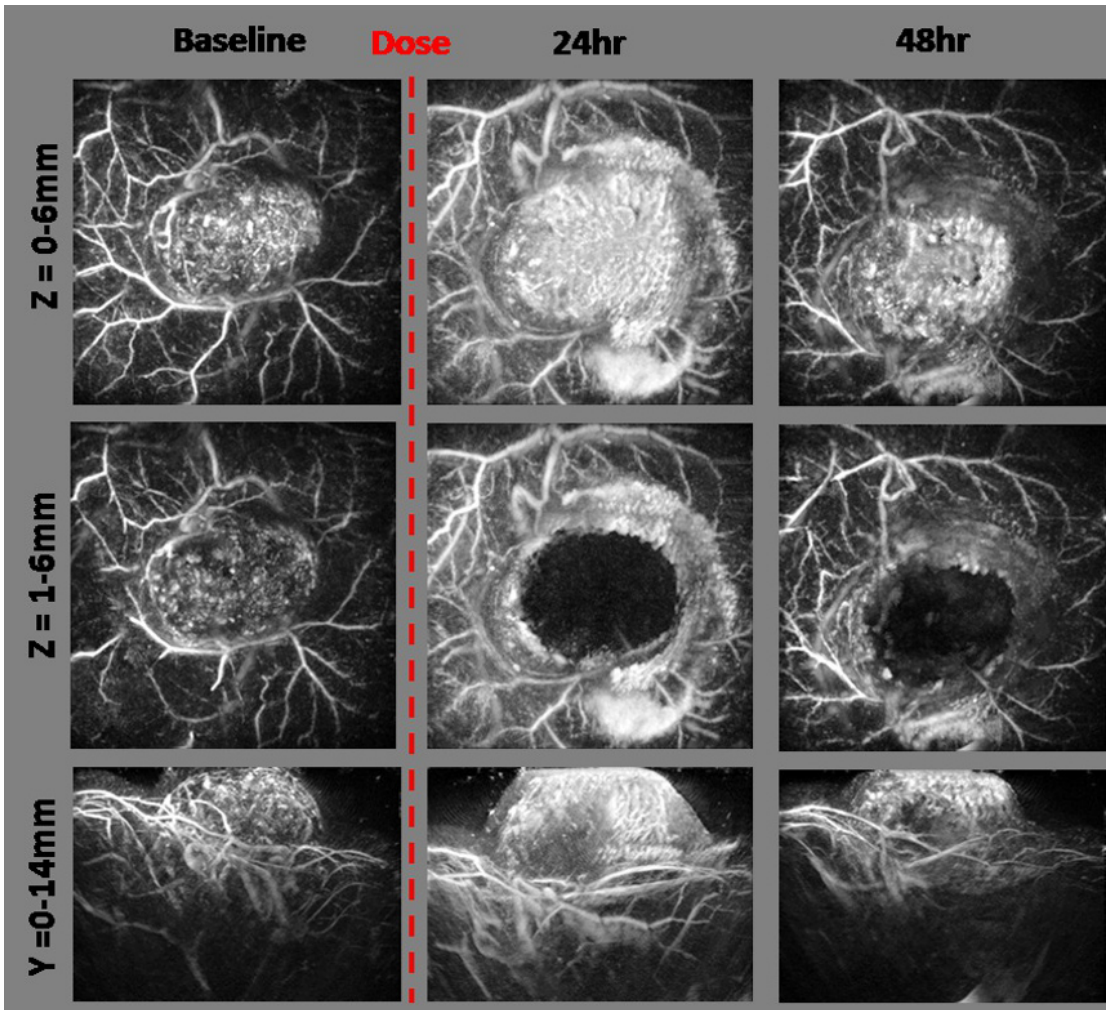

Figure 1 Photoacoustic response to vascular disruption with OXi4503 in SW1222 tumours

Representative photoacoustic images of SW1222 subcutaneous tumours following 40mg/kg of OXi4503 i.v. (n=6). The first and second rows are 14x14mm in the XY and 0-6mm and 1-6mm in the Y direction MIPs, whilst the third row is 14x6mm in the XZ with 14mm in the Y as an MIP. Each row shows baseline images followed by 24 and 48hr post dose.

CONTROL ID: 2232847

TITLE: New Albira PET generation based on SiPM, a comparison study using the NEMA standard

PRESENTER: Thomas Bruckbauer

ABSTRACT BODY:

Abstract Body: In this work we present the performance comparison of two generations of the Albira small animal PET detectors, based on PSPMT and Silicon Photomultiplier (SiPM). The SiPM based detector is aimed at improving the system performance in PET and PET/CT configurations and to enable hybrid PET-MR imaging in sequential or insert configurations.

The first generation of the Albira PET [1] uses detector modules made up by a trapezoidal monolithic LYSO crystal (entrance surface of 40x40 mm^2, exit face of 50x50 mm^2, with 10 mm thickness) coupled to a Hamamatsu H8500 PSPMT. It also features a resistive network based on the Anger logic to determine the 3D photon impact coordinates. The one ring configuration (up to 3 are possible) has axial and transaxial FOV of 40 and 80 mm, respectively. Similarly, the SiPM prototype ring features 8 detector modules, each with a 16x16 MPPC by Hamamatsu, covering an active area of roughly 51x51 mm^2. Coupled to the SiPM array is a LYSO monolithic scintillator crystal of 10 mm thickness. In contrast to the previous generation, the entrance surface of the scintillator is increased to about 48x48 mm^2. Given a higher number of photon detection elements when compared to previously used photomultiplier tubes (16x16 compared to 8x8) a better sampling of the light distribution is achieved. The axial FOV is increased to 47 mm and the transaxial FOV remains at 80 mm. Each MPPC array has been directly attached to a resistive readout circuit providing outputs for each row and column of the array.

The NEMA NU4-2008 protocol [2] has been used to evaluate the new SiPM based system performance in spatial resolution, sensitivity and noise equivalent count rate (NECR). The spatial resolution has been measured using FBP and MLEM algorithms. The results show a significant improvement when compared to the PSPMT version, reaching 1.1, 1.2 and 1.2 mm FWHM (radial, tangential and axial, respectively) compared to the previously measured values of 1.4, 1.5 and 1.5 mm FWHM.

The sensitivity of the SiPM prototype has been measured to be 2.9% at the FOV center, also increasing the value from the previous generation that was 2.5%. The crystal volume increase outweighs the fact of a slightly increased detector diameter. Finally, the NECR determined in the single ring PSPMT based system reached a peak of 16.9 kcps for an activity of 12.7 MBq using the mouse-like phantom. For the rat like phantom 12.8 kcps for 12.4MBq was measured. Using the new electronics and computer processing capabilities of the single ring SiPM prototype, the peak has been increased to about 60 kcps for 29 MBq for the mouse-like phantom and 35 kcps for 36 MBq for the rat-like phantom.

The new design for the Albira small animal PET featuring the emerging SiPM based detectors significantly outperforms its PSPMT based predecessor in all measured NEMA performance parameters. Moreover, the new system technology has the advantage of enabling future hybrid MRI possibilities.

[1] F. Sánchez *et al.,* Medical Physics 40, 051906-1, 2013.

[2] NEMA, *Performance Measurements of Small Animal Positron Emission*, NEMA Standard Publication NU 4-2008, 2008.

AUTHORS (LAST NAME, FIRST NAME): Moliner Martinez, Laura[1]; Gonzalez Martinez, Antonio J.[1]; Correcher Salvador, Carlos[2]; Aguilar Talens, Albert[1]; Barbera Ballester, Julio[2]; Hernádez Hernández, Liczanddro[1]; Molinos Solsona, Cesar[2]; Junge, Sven[3]; Lankes, Konrad[3]; Bruckbauer, Thomas[3]; Benlloch Baviera, Jose[1]

INSTITUTIONS (ALL):

1. Detectors, Institute for Instrumentation in Molecular Imaging, I3M, Valencia, Valencia, Spain.
2. Oncovision, Valencia, Valencia, Spain.
3. Bruker Isospin Corporation, Ettlingen, Germany.

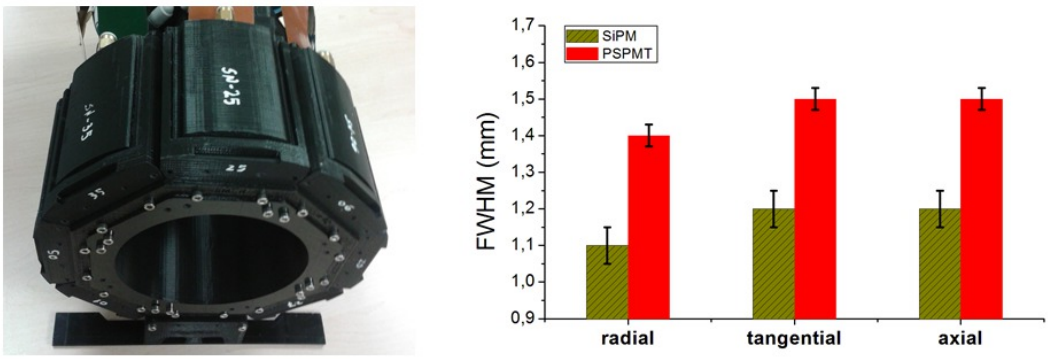

Figure. Left, photograph of the 1 ring prototype using SiPM arrays. Right, comparison of measured image spatial resolutions using MLEM at the CFOV with a Na source.

CONTROL ID: 2232852

TITLE: Physiology of breast parenchyma: Association of breast parenchymal uptake of ^{18}FDG with age, tissue composition and breast parenchymal enhancement on dynamic contrast-enhanced breast MRI

PRESENTER: Doris Leithner

ABSTRACT BODY:

Abstract Body: Introduction

^{18}FDG PET is an important tool in breast imaging, where not only malignant lesions show ^{18}FDG uptake, but tracer uptake can also be seen in normal breast tissue [1]. In dynamic contrast-enhanced (DCE) MRI of the breast, enhancement of the fibroglandular parenchyma of the normal breast is a known phenomenon, and regarded as a detrimental factor on diagnostic accuracy [2]. Our purpose was to correlate breast parenchymal uptake (BPU) in ^{18}FDG PET-CT with breast parenchymal enhancement (BPE) with DCE-MRI at 3T and to assess if BPU, BPE and FGT are influenced by age.

Material and Methods

129 patients undergoing ^{18}F-FDG PET-CT and 3T DCE-MRI of the breast due to a BIRADS 4/5 lesion were included in this IRB approved prospective study. Examinations were scheduled no longer than six days apart. In all patients, a prone PET-CT dataset over the breasts was acquired, allowing the same patient geometry as with MRI. Patients were injected with approximately 300 MBq ^{18}FDG. CT data was used for attenuation correction. The MRI protocol included a contrast-enhanced 3D-T1-weighted sequence before and after application of a standard dose of 0.1 mmol/kg Gd-DOTA (Dotarem®). In all patients BPU was assessed quantitatively by manually drawing ROIs for SUVmax calculation. BPU measurements were repeated by reader 1 to assess reproducibility. FGT and BPE of the normal contralateral breast were qualitatively assessed by two independent readers using the revised ACR BI-RADS® classification. BPE was graded as none, mild, moderate and marked. Reader 1 re-assessed all cases. Appropriate statistical tests were used to assess correlation of FGT, BPE and BPU, inter- and intra-reader agreement.

Results

There was no BPE in 58, mild in 54, moderate in 14 and marked in 3 patients. SUVmax for patients with no BPE was 1.57 (SD 0.6), for mild BPE 1.93 (SD 0.6), for moderate BPE 2.42 (SD 0.5), and for marked BPE 1.45 (SD 0.3). There were highly significant ($P<0.001$) correlations between age, BPU, BPE and FGT. The correlation coefficients ranged between moderate and strong. While BPE, BPU and FGT were positively correlated with each other, all of these parameters were negatively correlated with age (Figure 1). Inter-reader and intra-reader agreement for BPE was very good with a Kappa value of 0.860 and 0.822 respectively. The intraclass correlation coefficient for BPU measurements was excellent with 0.973.

Conclusion

BPU in ^{18}F-FDG breast PET-CT is positively correlated with BPE in DCE-MRI of the breast. BPU and BPE both show a positive correlation with FGT and a negative correlation with age.

Clinical Relevance

FGT and BPU decrease with age. In young patients with FGT grade 4 a possible masking effect of lesions by BPU/BPE is possible.

References

1. Vranjesevic D, Schiepers C, Silverman DH, Quon A, Villalpando J, Dahlbom M, Phelps ME, Czernin J (2003) Relationship between 18F-FDG uptake and breast density in women with normal breast tissue. J Nucl Med 44(8):1238-42

2. DeMartini WB, Liu F, Peacock S, Eby PR, Gutierrez RL, Lehman CD (2012) Background parenchymal enhancement on breast MRI: impact on diagnostic performance. AJR Am J Roentgenol 198(4):W373–380

AUTHORS (LAST NAME, FIRST NAME): Leithner, Doris[2]; Baltzer, Pascal A.[1]; Magometschnigg, Heinrich[1]; Wengert, Georg J.[1]; Helbich, Thomas H.[1]; Pinker-Domenig, Katja[1]

INSTITUTIONS (ALL):
1. Dept. of Biomedical Imaging and Image-guided Therapy, Division of Molecular and Gender Imaging, Medical University Vienna, Vienna, Austria.
2. Institute for Diagnostic and Interventional Radiology, University Hospital Frankfurt/Main, Mainz, Germany.

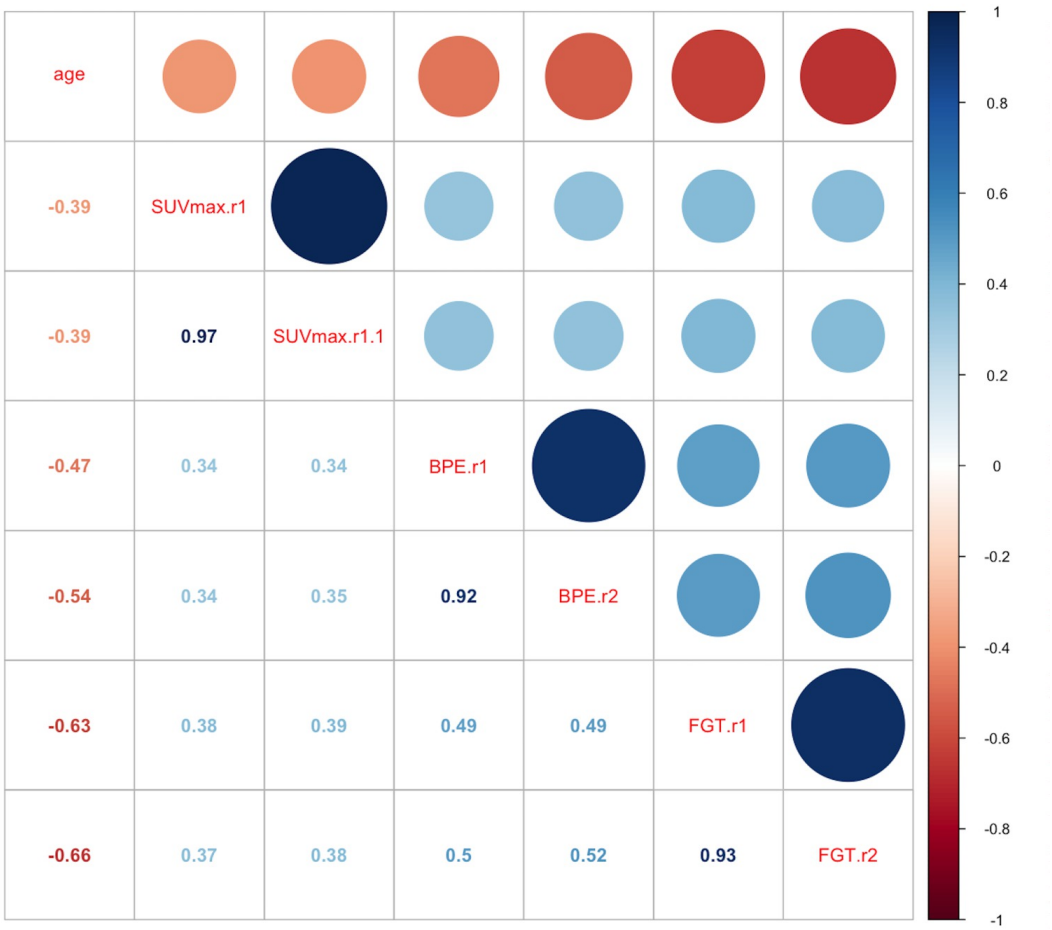
age
-0.39
SUVmax.r1
-0.39
0.97
SUVmax.r1.1
-0.47
0.34
0.34
BPE.r1
-0.54
0.34
0.35
0.92
BPE.r2
-0.63
0.38
0.39
0.49
0.49
FGT.r1
-0.66
0.37
0.38
0.5
0.52
0.93
FGT.r2
1
0.8
0.6
0.4
0.2
0
-0.2
-0.4
-0.6
-0.8
-1

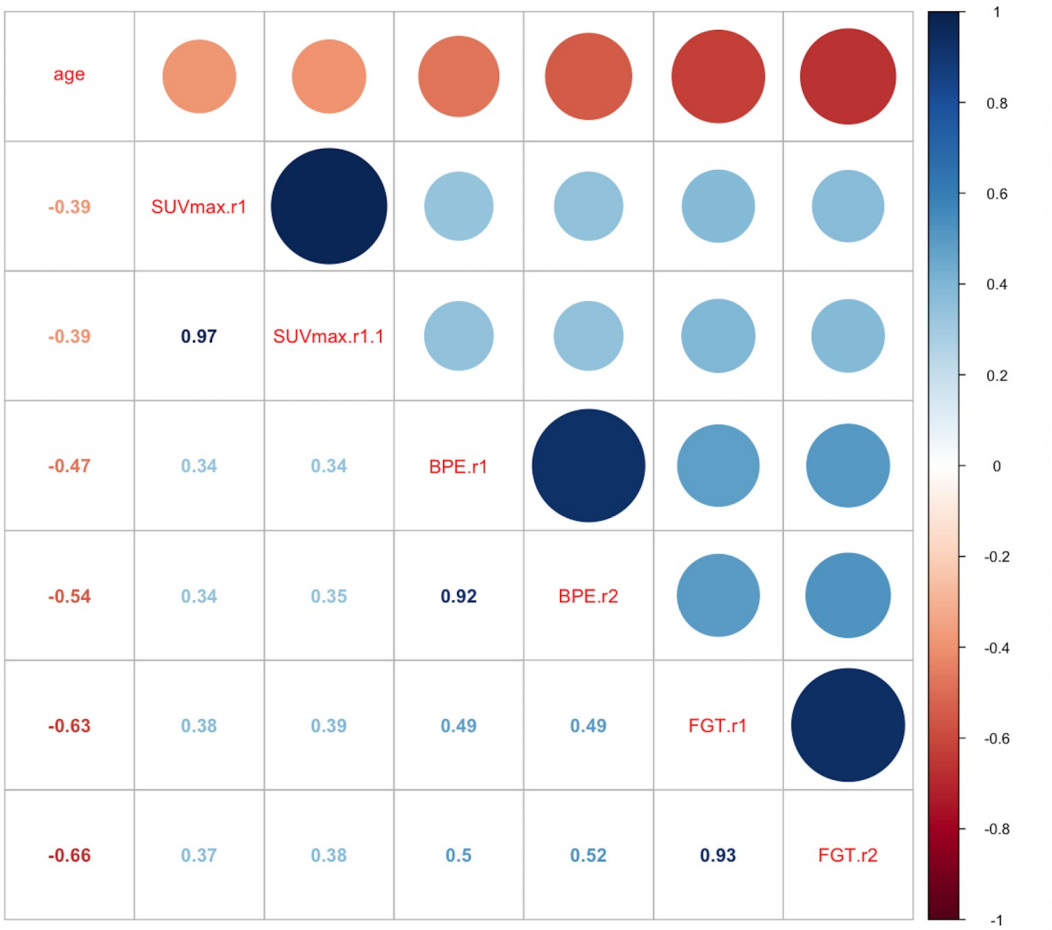

Correlation coefficient matrix: Pearson correlation coefficients for breast parenchymal uptake of ^{18}FDG, breast parenchymal enhancement in DCE-MRI, tissue composition and age.

CONTROL ID: 2232895

TITLE: Therapeutic Effect by High Intensity Focused Ultrasonic (HIFU)-Mediated Liposome Encapsulated Vascular Endothelial Growth Factor (VEGF)-Peptide in Hindlimb Ischemic Rodent Model

PRESENTER: MinJoo Kim

ABSTRACT BODY:

Abstract Body: Purpose

The aim of this study is increasing therapeutic effect of VEGF stimulated angiogenesis by HIFU treatment in low acoustic intensity. We evaluate therapeutic effect by HIFU-mediated liposome encapsulated VEGF on rodent model of hindlimb ischemia in vivo.

Method

Prepared the long circulating liposome (LCLP) with 1,2-distearoyl-sn-glycero-3-phosphoethanolamine-N-methoxy (polyethyleneglycol)-2000 (DSPE-PEG-$_{2000}$) and encapsulated VEGF peptide using the lipid thin-film hydration/extrusion method. The rodent model was prepared by tight ligation of right proximal femoral arteries with 3-0 silk ligature to block inflow of arterial blood. Rodent model of hihdlimb ischemia were divided into four groups (n=5): control group, injection of VEGF (VEGF group), injection of LCLP encapsulated (VEGF LCLP(VEGF)) group and HIFU treatment after injection of LCLP(VEGF) (LCLP/HIFU group). All samples were injected into the ligated artery with same volume after postoperative 1 day follow-up. The degree of the ischemia and the recovery of it was evaluated by blood perfusion ratio ischemic region to non-ischemic region at postoperative day 1, 7, 14, obtained using a gamma camera acquisition system after catheter injection of Tc-99m (1.9x108 Bq) through the tail vein. Statistical differences between groups were analyzed by one-way Analysis of Variance (ANOVA) test.

Result

The mean size of prepared liposomes was 123.5±45.0 nm when determined by dynamic light scattering (DLS). The loading efficiency of VEGF-peptide in LP-VEGF was about 62.0 % and the concentration of VEGF in LP-VEGF (200 ul) injected in this study was about 5.0 nM. The perfusion was increased with statistically significance in only LCLP/HIFU group after postoperative 1 week. The result was manifested in comparing with increasing ratio of perfusion after treatment. The HIFU exposure in low acoustic intensity caused increasing of VEGF-peptide released from liposome, having effective concentration followed uptake in ischemia region. It was showed rapid recovery of perfusion and consequently exhibited high efficacy of therapy.

Conclusion

The encapsulated VEGF-peptide in liposome could be released and uptake in hindlim ischemia region by HIFU treatment in low acoustic intensity. The HIFU treatment in low acoustic intensity combined with liposome encapsulated VEGF-peptide. It showed high therapeutic efficiency and probability of clinic use in peripheral arterial disease (PAD).

AUTHORS (LAST NAME, FIRST NAME): Kim, MinJoo[6]; Jeong, Hwan-Seok[5]; Hwang, Hyosook[3]; Kim, Eun-Mi[4]; Kim, Dong Hyun[7]; Lee, Tai Kyoung[2]; Oh, Philsun[8]; Kwon, Jeongil[1]; Kim, HyunSoo[9]; Kim, Eun ji[6]; Choi, Ji-Hae[6]; Lim, Seok Tae[10]; Sohn, Myung-Hee[11]; Jeong, Hwan-Jeong[12]

INSTITUTIONS (ALL):

1. Chonbuk National University Hospital, Jeonju-si, Korea (the Republic of).
2. Nuclear Medicine, Chonbuk National University Hospital, Jeonju, Korea (the Republic of).
3. Chonbuk National University Medical School and Hospital, Jeonju, Korea (the Republic of).
4. nuclear medicine, Chonbuk national university medical school, Jeonju-si, Korea (the Republic of).
5. Nuclear Medicine, chonbuk National University Medical School and Hospital, Jeonju, Korea (the Republic of).
6. Nuclear Medicine:Molecular Imaging & Therapeutic Medicine Research Center:Cyclotron Research Center:Institute for Medical Sciences:Biomedical Research Institute, chonbuk National University Medical School and Hospital, Jeonju, Jeonbuk, Korea (the Republic of).
7. Nuclear Medicine:Molecular Imaging & Therapeutic Medicine Research Center:Cyclotron Research Center:Institute for Medical Sciences:Biomedical Research Institute, chonbuk National University Medical School and Hospital, Jeonju, Jeonbuk, Korea (the Republic of).

8. Nuclear Medicine:Molecular Imaging & Therapeutic Medicine Research Center:Cyclotron Research Center:Institute for Medical Sciences:Biomedical Research Institute, chonbuk National University Medical School and Hospital, Jeonju, Jeonbuk, Korea (the Republic of).
9. Nuclear Medicine:Molecular Imaging & Therapeutic Medicine Research Center:Cyclotron Research Center:Institute for Medical Sciences:Biomedical Research Institute, chonbuk National University Medical School and Hospital, Jeonju, Jeonbuk, Korea (the Republic of).
10. Nuclear Medicine:Molecular Imaging & Therapeutic Medicine Research Center:Cyclotron Research Center:Institute for Medical Sciences:Biomedical Research Institute, chonbuk National University Medical School and Hospital, Jeonju, Jeonbuk, Korea (the Republic of).
11. Nuclear Medicine:Molecular Imaging & Therapeutic Medicine Research Center:Cyclotron Research Center:Institute for Medical Sciences:Biomedical Research Institute, chonbuk National University Medical School and Hospital, Jeonju, Jeonbuk, Korea (the Republic of).
12. Nuclear Medicine:Molecular Imaging & Therapeutic Medicine Research Center:Cyclotron Research Center:Institute for Medical Sciences:Biomedical Research Institute, chonbuk National University Medical School and Hospital, Jeonju, Jeonbuk, Korea (the Republic of).
(No Image Selected)

CONTROL ID: 2232855

TITLE: Advancing Bioluminescence Imaging and Tomography towards a true quantitative imaging modality for reliable pre-clinical studies

PRESENTER: Shelley Taylor

ABSTRACT BODY:

Abstract Body: Bioluminescence imaging (BLI) is a widely used imaging technique with applications in pre-clinical research in cancer research[1–3], and research involving stem cells[4], immune cells[5], bacteria[6] and viruses[7].

There are major limitations to BLI that prevent the true quantitative accuracy from being achieved. Assumptions about the origin of the BLI data are often inaccurate: on observation of a BLI image it is impossible to determine whether the signal arises from a deep but intense source, or a superficial but weaker and more diffuse source. Additionally the true number of sources present can be unclear due to the inherent scattering of biological tissue (Fig. 1). The system response of the imaging system is often not accounted for and the BLI images are assumed to give (often misleading) accurate intensity information about the source. These assumptions further prevent quantitative bioluminescence tomography (BLT). All of these problems will be addressed and solutions to overcome them will be presented.

Phantom studies have previously shown BLI to be dependent on the position and orientation of the imaging subject[9]. This dependence is demonstrated in multiple mouse models, showing that a small change in position (~13^{o}) affects the measured intensity by ~68%. To overcome this, a Free Space model[9] is applied to the data, removing the positional dependence, providing for the first time a repeatable, accurate and reliable means of performing same animal comparison studies.

The depth of the source within the animal is also shown to affect the measured BLI intensity. Data from multiple mice is presented which demonstrates that a 5 mm change in depth can produce an intensity variation of ~86%. To overcome this limitation, free space modelling followed by 3D tomography is used to demonstrate that the intensity, location and distribution of the source can be recovered regardless of source depth and animal orientation.

By using novel algorithms that consider system, animal and physical optics related variations, it is possible to use BLI accurately and reliably, with the further advancement of 3D spatial recovery using BLT. This will have a significant impact in pre-clinical research enabling true quantitatively accurate biological conclusions to be drawn from studies.

1. D. E. Jenkins et al., Clinical & Experimental Metastasis **20**(8), 733–744 (2003).
2. D. M. Barrett et al., Blood **118**(15), e112–7 (2011)
3. T. J. Sweeney et al., PNAS **96**(21), 12044–12049 (1999).
4. N. F. Huang et al., Theranostics **2**(4), 346–354 (2012)
5. J. Hardy et al., Experimental hematology **29**(12), 1353–1360 (2001).
6. T. C. Doyle et al., Cellular Microbiology **6**(4), 303–317 (2004)
7. K. E. Luker and G. D. Luker, Antiviral research **78**(3), 179–187 (2008)
8. J. A. Guggenheim et al., Measurement Science and Technology **24**(10), 105405 (2013)
9. J. A. Guggenheim et al., JOSA A, **30**(12), 2572–2584 (2013)

AUTHORS (LAST NAME, FIRST NAME): Taylor, Shelley L.[2, 1]; Perry, Tracey[3]; Styles, Iain[1, 2]; Cobbold, Mark[3]; Dehghani, Hamid[1, 2]

INSTITUTIONS (ALL):

1. School of Computer Science, University of Birmingham, Birmingham, United Kingdom.
2. PSIBS Centre for Doctoral Training, University of Birmingham, Birmingham, United Kingdom.
3. School of Immunity and Infection, University of Birmingham, Birmingham, United Kingdom.

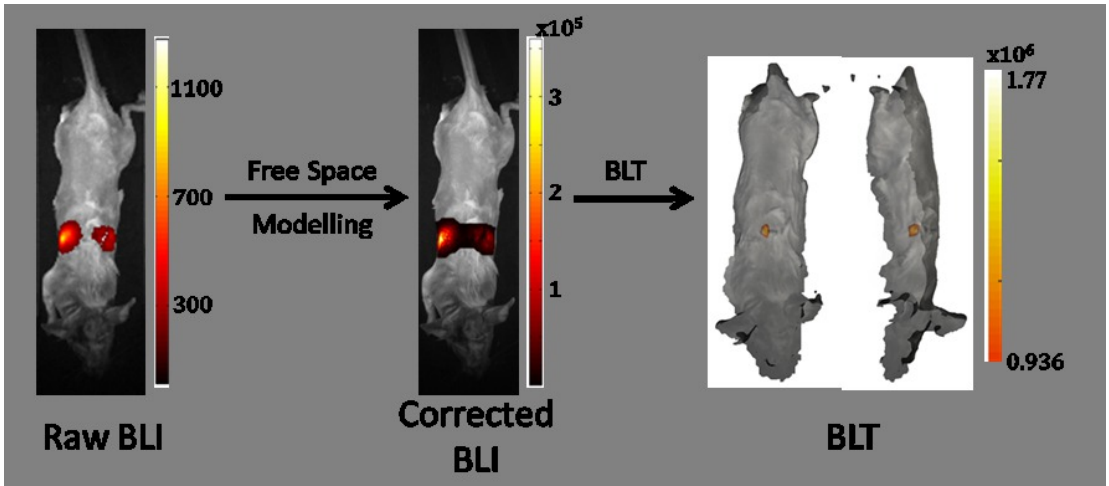

Figure 1 – Workflow demonstrating the novel algorithms used in this work. A single artificial light source is inserted into the chest of the animal, at a depth of ~10 mm. BLI images are taken using a recently developed imaging system with BLT, diffuse optical tomography (DOT) and surface capture capabilities (BLDOT)[8]. The animal was imaged at 600, 623 and 643 nm (bandpass filters, Semrock Inc.) to enable tomographic imaging. The raw BLI image shows two distinct areas of bioluminescence which could be assumed to be from two weaker sources. However, free space modelling, which removes the positional dependence on the measured intensity, followed by tomographic source recovery shows correctly that there is only a single source present.

CONTROL ID: 2232856

TITLE: Reporter gene imaging for exosome-mediated transfer of neurogenic miRNA during neuronal differentiation in neural precursor cells

PRESENTER: Hyun Jeong Oh

ABSTRACT BODY:

Abstract Body: Purpose: Neuronal cells release small vesicles known as secretory exosomes containing mRNAs, miRNAs and proteins to exchange signals as a form of intercommunication between cells. MicroRNAs (miRNAs) such as miR-124 or miR-9 play an important role in regulation of neuronal differentiation. The aim of this study is to monitor exosome-mediated transfer during neuronal differentiation using reporter imaging system in the microfluidic channels.

Methods: F11 cells, neural precursor cells, were stably transfected with reporter vector of pRV-effLuc/3xPT_miRNA which luciferase signal could be turned off by binding of the identified miRNA to the triplicates of miRNA binding site in the 3' UTR of effLuc. Exosomes were isolated from the conditioned media and characterized by western blot. Transwell chambers system and microfluidic device were used to examine exosome-mediated miRNA transfer.

Results: Target genes of identified miRNA considered as neurogenic miRNAs were related to cell proliferation, differentiation and axon guidance. Neurite outgrowth and neuronal marker expression such as βIII-tubulin, NeuroD and MAP2 were observed 3 days after identified miRNA treatment. *In vivo* bioluminescence signals were approximately 5 fold decreased after exogenous miRNA treatment until 2 days. Isolated exosomes were characterized for protein markers such as CD63, TSG101. Real-time PCR results showed that exosomes isolated from conditioned media in differentiated neuron highly increased identified miRNA level. Luciferase activity was significantly decreased 72 h after exogenous exosome treatment in F11 cells. In transwell chambers and microfluidic system, fluorescence signals of incorporated GFP-exosomes were detected within 2 days after co-culture with GFP-exosomes producing cells. Furthermore, exosomes secreted from F11 cells were transferred to other cells and induced progress of neuronal differentiation, showing increased neuronal marker expression.

Conclusions: In this study, we validated that neuronal differentiation was sufficiently induced by identified miRNA in neural precursor cells. We monitored that exosomes released from differentiated cells were transferred to other cells using fluorescence reporter gene system *in vitro*. Our imaging system can be useful for tracking the migration of exosomes during neuronal differentiation in microfluidic device.

AUTHORS (LAST NAME, FIRST NAME): Oh, Hyun Jeong[1, 2]; Shin, Yoojin[3]; Chung, Seok[3]; Youn, Hyewon[1, 4]; Hwang, Do Won[1, 2]; Lee, Dong Soo[1, 2]

INSTITUTIONS (ALL):

1. Department of Nuclear Medicine, Seoul National University, Seoul, Korea (the Republic of).
2. Department of Molecular Medicine and Biopharmaceutical Sciences, Graduate School of Convergence Science and Technology, and College of Medicine or College of Pharmacy, Seoul National University, Seoul, Korea (the Republic of).
3. Department of Mechanical Engineering, Korea University, Seoul, Korea (the Republic of).
4. Laboratory of Molecular Imaging and Therapy, Cancer Research Institute, Seoul, Korea (the Republic of).

(No Image Selected)

CONTROL ID: 2232924

TITLE: Biological Evaluation of RGD-EGF Fusion Protein as a Dual-targeting Theranostic Agent

PRESENTER: Jia-Je Li

ABSTRACT BODY:

Abstract Body: Objectives: RGD peptides could specifically bind to integrin $\alpha_v\beta_3$ which was highly expressed in tumor and angiogenic endothelial cells. EGFR has been validated as important tumor markers for developing anticancer drugs. This study developed a series of recombinant fusion protein as dual-targeting theranostic agents for the diagnosis and treatment of tumors with high EGFR/integrin expression.

Methods: EGF, RGD-EGF (contain a linear RGD) and RGD4C-EGF (contain a cyclic RGD) recombinant proteins were constructed and purified from *E.coli.*, and then labeled with I-123/131 to give their radioactive surrogates ($^{123/131}$I-EGF, $^{123/131}$I-RGD-EGF and $^{123/131}$I-RGD4C-EGF) with high radiochemical purity. The *in vitro* specific binding affinity, cellular uptake and competition binding assay of the three recombinant proteins toward tumor cells with different levels of EGFR-expression (MDA-MB-468, 1×10^6/cell; MDA-MB-231, 1×10^5/cell; and MCF-7, 1×10^4/cell) and with high integrin $\alpha_v\beta_3$ expression (U87MG) were studied. Animal SPECT/CT imaging of mice bearing subcutaneous U87MG tumor xenograft after intravenous injection of ^{123}I-labeled EGF, RGD-EGF and RGD4C-EGF, individually, are under investigating.

Result: The specific binding of RGD4C-EGF to EGFR (ELISA assay, K_d = 9.7±4.9 nM) was higher than that of EGF and RGD-EGF to EGFR (K_d = 18.6±4.2 and 29.7±7.5 nM, respectively). The binding affinity of RGD4C-EGF to integrin $\alpha_v\beta_3$ (K_d = 6.2±0.5 nM) was also higher than that of RGD-EGF (K_d = 22.1±5.3 nM). The cellular uptake of these three EGF-containing recombinant proteins correlated with the EGFR-expression of cells, highest in MDA-MB-468, followed by MDA-MB-231 and then MCF-7 after 1 h of incubation. The uptakes could be blocked by anti- EGFR antibody, cetuximab, but not by RGD peptide. As expected, the uptake of RGD4C-EGF in U87MG could be blocked both by cetuximab and RGD peptide.

Conclusion: Our study demonstrated that RGD4C-EGF fusion protein remained the biological specificity toward both EGF receptors and integrin $\alpha_v\beta_3$. This fusion protein is a good dual-targeting agent for the diagnosis and therapy of EGFR or integrin expressing cancers.

AUTHORS (LAST NAME, FIRST NAME): Li, Jia-Je[1]; Chang, Shun-Fu[3]; Chan, Pei-Chia[4]; Juan, Wei-Cheng[1]; Chen, Chao-Cheng[1]; Huang, Yi-Shuang[6]; Yen, Sang-Hue[5]; Liu, Ren-Shyan[2]; Chang, C. Allen[1]; Wang, Hsin-Ell[1]

INSTITUTIONS (ALL):

1. Department of Biomedical Imaging and Radiological Sciences, National Yang-Ming University, Taipei , Taiwan.
2. Dept of Nuclear Medicine, Faculty of Medicine, National Yang-Ming University, Taipei, Taiwan.
3. Department of Medical Research and Development Chiayi Branch, Chang Gung Memorial Hospital, Puzi, Taiwan.
4. Biophotonics & Molecular Imaging Research Center (BMIRC), National Yang-Ming University, Taipei, Taiwan.
5. Department of Oncology Medicine, Taipei Veterans General Hospital, Taipei, Taiwan.
6. Department of Biotechnology and Laboratory Science in Medicine, National Yang-Ming University, Taipei, No U.S. state/territory, Taiwan.

(No Image Selected)

CONTROL ID: 2232873

TITLE: MR-Optical dual-modality neuronal MHCI targeting peptide for early diagnosis of ischemic stroke *in vitro* and *in vivo*

PRESENTER: Jing Xia

ABSTRACT BODY:

Abstract Body: The major histocompatibility complex (MHC) gene family encodes molecules on the surface of cells that enable the immune system to recognize presented self- and foreign-derived peptides(Chemali, Radtke et al. 2011). Accumulating data have demonstrated MHCI expression by subsets of neurons in both adult and developing mammalian brain (Cullheim and Thams 2010). Many of these reports describe a role for neuronal MHC-I in synaptic plasticity, brain development and axonal regeneration (Cebrian, Loike et al. 2014). Previous works of our group showed that during development human and mouse cerebellar cortex share similar spatial-temporal expression pattern of MHCI molecules (Liu, Shen et al. 2013; Zhang, Yu et al. 2013; Lv, Shi et al. 2014). Recent studies suggest that neuronal MHCI was closely associated with ischemic stroke. It was founded that not only of H2-Kb and H2-Db, but also of PirB and downstream signaling were elevated in stroke, which exacerbate brain injury after ischemia(Adelson, Barreto et al. 2012). Cultured substantia nigra(SN) murine neurons found process and present foreign protein antigens with MHC-I; and MHC-I expressing SN murine neurons were destroyed in the presence of the appropriate antigen and CTLs.(Cebrian, Zucca et al. 2014).

we provide the first evident that cultured cortex neurons from C57/bl6j mice subject to Oxygen Glucose Deprivation (OGD) not only expressed MHCI but also present foreign protein antigen gp33(V3L) by MHCI. The MHC class I (MHCI) H2-Kb and H2-Db binding peptide named gp33(V3L) was identified as homing to ischemic stroke tissue. A series of experiments utilized *in vitro* stroke OGD model demonstrated that FITC-conjugated gp33(V3L) was specificly binding to neurons underwent ischemia. In the meanwhile, a FITC-conjugated scrambled control peptide showed no binding abilities. FITC-conjugated gp33(V3L) preferentially homed to ischemic stroke tissue after intravenous administration into the MCA occlusion C57/bl6j mice. The *in vivo* study of MCAO demonstrated that in the early acute phase of ischemia, gp33(V3L) showed neuronal MHCI binding ability, which depicted both CNS damage and recovery after ischemic stroke, as MHCI molecules are closely associated with CNS damage, inflammation and cell regeneration. Our study suggested such MHCI binding peptide could be used as a targeting moiety for molecular imaging and selective drug delivery to ischemic brain tissue.

AUTHORS (LAST NAME, FIRST NAME): Xia, Jing[1]; Zhang, Ying[1]; Wang, Jie[1]; Fu, Bo[1]; Lv, Dan[1]; Long, Wei[1]; Shen, Yuqing[1]; Liu, Jiane[1]; Zhang, Jianqiong[1]

INSTITUTIONS (ALL):

1. Medical School, Key Laboratory of Developmental Genes and Human Diseases, Nanjing, Jiangsu, China.

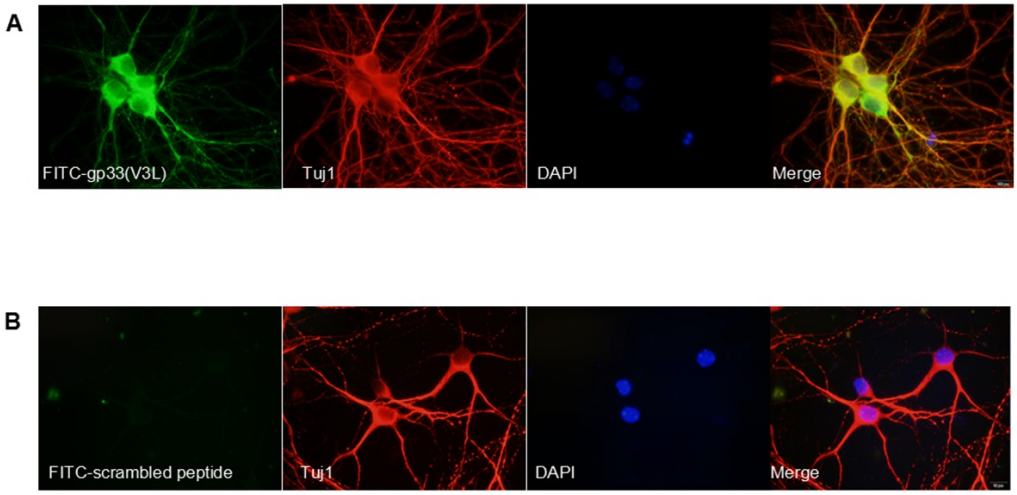

Figure 1 FITC-conjugated gp33(V3L) binding to neuronal MHCI. The upper row shows FITC-conjugated gp33(V3L) (green) binding with cultured mice cortex neurons underwent OGD imaged by fluorescence microscopy. Cultured C57/bl6j background neurons showed by Tuj1(red). The bottom row demonstrates control peptide (FITC-conjugated scrambled peptide) showed little binding ability with neurons. Scale bar, 100 μm.

CONTROL ID: 2232898

TITLE: Intestinal fatty acid utilization after bariatric surgery – cure for peripheral insulin resistance?

PRESENTER: Jukka Koffert

ABSTRACT BODY:

Abstract Body: *Background and aims* Pandemic rise of obesity and type 2 diabetes worldwide has increased our interest in energy balance - especially in intestinal fatty acid metabolism and lipid absorption. Gut senses dietary fat and regulates energy intake and utilization. While gastrointestinal tract is the first organ to encounter ingested food and nutrients, only few studies have addressed the role of small intestinal in fatty acid handling and metabolism. We hypothesized that intestinal fatty acid metabolism plays a role in the whole body fatty acid metabolism. The objective of this study was to investigate the effects of bariatric surgery on intestinal lipid metabolism, blood flow and glycemic control.

Materials and methods 27 morbidly obese and 15 healthy age-matched controls were recruited. Of the obese subjects, ten had type 2 diabetes. Intestinal, fatty acid (FA) uptake and blood flow were measured during fasting state using positron emission tomography (PET) coupled with a palmitate analogue [^{18}F]FTHA and radiowater [^{15}O]H_2O, respectively, as previously described (1). In morbidly obese subjects, these measurements were performed before and six months after bariatric surgery (either Roux-en-Y gastric bypass or sleeve gastrectomy).

Results Compared to lean subjects, morbidly obese ones had higher duodenal (3.1±12 *vs.* 1.8±10 mmol 100ml^{-1} min^{-1}, $P < 0.01$) and jejunal (3.1±1.2 *vs.* 1.6±1.0, $P < 0.001$) FA uptake, whereas intestinal blood flow was similar between obese and lean controls (0.61±0.23 *vs.* 0.56±0.28 for duodenum and 0.41±0.21 *vs. 0.44±0.33 for jejunum, NS for both). Intestinal FA uptake and blood flow were unrelated.*

Six months after bariatric surgery, patients had lost weight 26±8.3 kg and in 7 out of 10 patients' diabetes were in remission. Patients' FA levels remained still elevated (0.86±0.18mM vs. 0.76±0.17mM, post vs. pre) and higher than in lean subjects (0.56±0.17mM, p<0,03). Unlike expected, jejunal FA uptake was further increased (to 4.3±2.0, P<0.03), while FA uptake decreased in other organs, such as in the heart (p<0.03) and in the pancreas (p<0.05). In morbidly obese patients with diabetes before the operation, the increase in jejunal FA uptake was associated with favorable 2-h glucose in OGTT and fasting plasma glucose (r=-0.65, P=0.06 and r=-0.68; p<0,05, respectively). Conversely, bariatric surgery provoked a decrease in jejunal blood flow (0.25±0.14 vs. 0.41±0.33, P<0.05) while duodenal blood flow was preserved (NS).

Conclusions Bariatric surgery provokes marked changes in intestinal fatty acid uptake and blood flow. The former is associated with favorable glycemic status whereas fasting intestinal blood flow does not seem to regulate intestinal metabolism. Further studies are warranted to investigate whether the up regulation of intestinal FA fluxes play a role in the depletion of triacylglyserol storages leading to breakage of insulin resistance after bariatric surgery.

References (1) Honka H. et al. Diabetologia 2013; 56:893-900

AUTHORS (LAST NAME, FIRST NAME): Koffert, Jukka[1, 2]; Honka, Henri[2]; Hannukainen, Jarna[2]; Immonen, Heidi[2, 4]; Kauhanen, Saila[5, 2]; Iozzo, Patricia[6]; Nuutila, Pirjo[3, 4]

INSTITUTIONS (ALL):

1. Department of gastroenterology, Turku University Hospital, Turku, Finland.
2. Turku PET Centre, University of Turku, Turku, Finland.
3. Turku PET Centre, University of Turku, Turku, Finland.
4. Department of endocrinology, Turku university hospital, Turku, Finland.
5. Division of Digestive Surgery and Urology, Turku university hospital, Turku, Finland.
6. Institute of Clinical Physiology, National Research Council, Pisa, Finland.

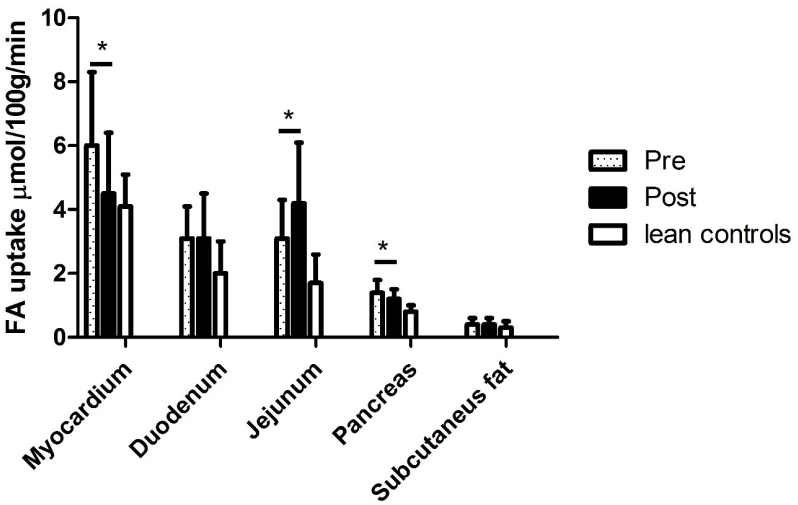

Fig1. Fatty acid uptake in morbidly obese and lean. *P<0,05

CONTROL ID: 2233014

TITLE: Optical Projection Tomography (OPT) with Polarized Light

PRESENTER: Mengjie Fang

ABSTRACT BODY:

Abstract Body: Traditional transmission OPT (tOPT) using non-polarized light can detect the distribution of light absorption coefficient of samples, but it is unable to present fiber-like structures such as the muscle fibers. Although emission OPT (eOPT) can display the muscle fibers by using fluorescent markers, it needs complicated transgenosis or staining which is inconvenient. To solve this problem, an optical projection tomography (OPT) system with polarized light was developed to detect the fiber-like structures in the samples. The proposed system could well detect the fiber-like structures by simply adding two polarizers in traditional tOPT system. We found that the fiber-like structures were specifically detected by using polarized light because their birefringence properties. The system was used to observe diaphragm and stomach of mouse. The experimental results showed that the diaphragm and smooth muscle were well detected by using our system. The contrast experiment presented that our system was more sensitive to the fiber-like structures than traditional OPT. Moreover, our method obtained three-dimensional contour and texture information of muscles.

AUTHORS (LAST NAME, FIRST NAME): Fang, Mengjie[1, 2]; Dong, Di[1]; Hui, Hui[1]; Tian, Jie[1]

INSTITUTIONS (ALL):

1. Key Laboratory of Molecular Imaging, Chinese Academy of Sciences, Beijing, China.
2. Department of Bio-medical Engineering, College of Life Science and Technology, Huazhong University of Science and Technology, Wuhan, Hubei, China.

(No Image Selected)

CONTROL ID: 2232961

TITLE: *In Vivo* Observation of Tumor with Triple-modality Imaging

PRESENTER: xiao liang

ABSTRACT BODY:

Abstract Body: Medical imaging is of great value in diagnosis of cancer, but single imaging modality cannot accurately locate the tumor. To solve this problem, we applied triple modality imaging to observe the breast cancer in vivo. In this work, computed tomography (CT), positron emission tomography (PET), and bioluminescence imaging (BLI) were used to locate subcutaneous 4T1 tumor. The tumor cells were stably transfected with firefly luciferase to enable serial BLI.The experimental results showed that BLI had the best signal noise ratio (SNR) of the tumor but it could not locate deep tumor. PET was very sensitive but it had poor SNR and low resolution. CT provided high resolution anatomical information of the whole mouse but it could not distinguish the tumor well. The combination of the three modalities presented the best location and accurate size of the tumor. Therefore, our work demonstrated that multimodality imaging were useful in tumor localization.

AUTHORS (LAST NAME, FIRST NAME): liang, xiao[1]; Dong, Di[1]; shi, liangliang[1]; zhang, shuaitong[1]; Hui, Hui[1]; Tian, Jie[1]

INSTITUTIONS (ALL):

1. Key Laboratory of Molecular Imaging, Chinese Academy of Sciences, Beijing, China.

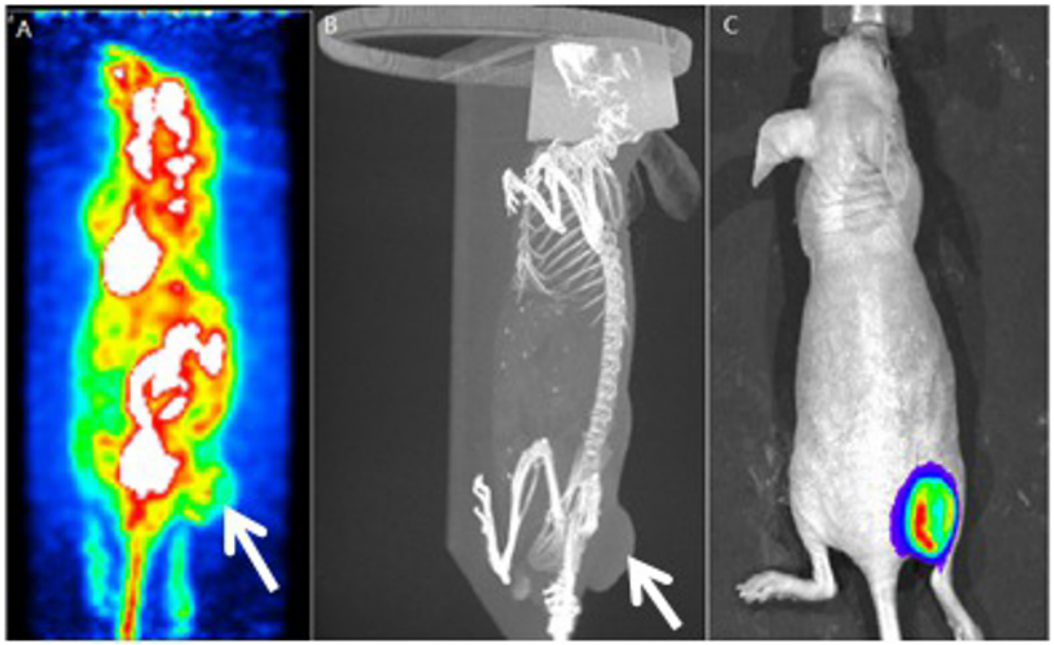
A
B
C

CONTROL ID: 2232892

TITLE: Identification of a novel phage display-derived peptide targeted to PirB as a promising moiety for molecular imaging of ischemic stroke tissue

PRESENTER: Jie Wang

ABSTRACT BODY:

Abstract Body: Mouse paired immunoglobulin-like receptor B (PirB) is a type I transmembrane glycoprotein with six extracellular immunoglobulin-like domain, a hydrophobic transmembrane segment and an intracellular polypeptide with four ITIM sequences (Takai T, 2005). PirB originally thought to function exclusively in the immune system, is now also known to be expressed by neurons. More and more observations imply that PirB plays an inhibitory role in neurite outgrowth and restricts neuronal plasticity (Syken J, et al. 2006;Atwal J K, et al. 2008; Djurisic M, et al. 2013). LILRB2 which has been identified as a human ortholog of PirB may execute these roles in humans (Kim T, et al. 2013).

In a stroke model, germline $PirB^{-/-}$ mice recover more rapidly than WT mice (Adelson J D, et al. 2012). Our results showed that PirB expression and its immediate downstream signaling were significantly increased at 6 hours and peaked at 24 hours in the ischemic hemisphere of the MCAO model, compared to the undamaged contralateral side (Fig. 1A and B). Majority of PirB immunostaining colocalized with neuronal marker NeuN post-MCAO (Fig. 1C). The oxygen glucose deprivation (OGD) model was used to test the expression of PirB in ischemic injury *in vitro*. At 24h after OGD injury, expression of PirB in cultured cortical neuron in the OGD group was remarkably higher than that in the control (Fig. 1D). Disregulation of PirB expression in neurons may play important roles in the pathogenesis of stoke, and selectively block PirB protein may not only be promising for treatment of stoke but also be as a targeting moiety for molecular imaging to stroke tissue.

We have successfully screened and obtained a novel phage display-derived peptide that targets both PirB and LILRB2 protein. Biopanning was performed using the Ph.D.-12 phage display peptide library (New England Biolabs). After three rounds of panning, the titer of phages recovered from recombinant LILRB2-Fc were significantly increased by approximately 856.4 fold, compared with its titers in the first round. The peptide whose appearance frequency ranking the top was named as LBP-1. The LBP-1 phage clone showed a significantly higher binding ability to the LILRB2 and PirB. There were almost no signals when insertless phage particles were added to each protein (Fig. 1E). These data demonstrated that LBP-1 peptide bound to the PirB and LILRB2 with very high affinity.

On the basis of LBP-1, we will consturct a new blood-brain-barrier (BBB) permeable MR-Optical dual-modality molecular probe for early diagnosis of stroke. The fifth generation (G5) PAMAM dendrimer will be chosen as a platform of the nanoprobes. PirB targeted peptides LBP-1 and BBB-permeable Angiopep-2 peptides (Yan H, et al. 2011) will be labeled on the dendrimer through a PEG linker. Near-infrared fluorophore Cy5.5 will be labeled and Gd^{3+}-DOTA will be chosen as the MR CAs functionalized on the nanoprobe (Fig.2). We believe that our future work will lay the foundation for early diagnosis, treatment and real-time monitoring of ischemic stroke.

AUTHORS (LAST NAME, FIRST NAME): Wang, Jie[1]; Shen, Yuqing[2]; Xia, Jing[1]; Zhang, Ying[2]; Fu, Bo[1]; Long, Wei[1]; Lv, Dan[1]; Zhang, Jianqiong[2, 1]

INSTITUTIONS (ALL):

1. Medical School, Key Laboratory of Developmental Genes and Human Diseases, Nanjing, Jiangsu, China.
2. Department of Microbiology and Immunology, Southeast University, Nanjing, China.

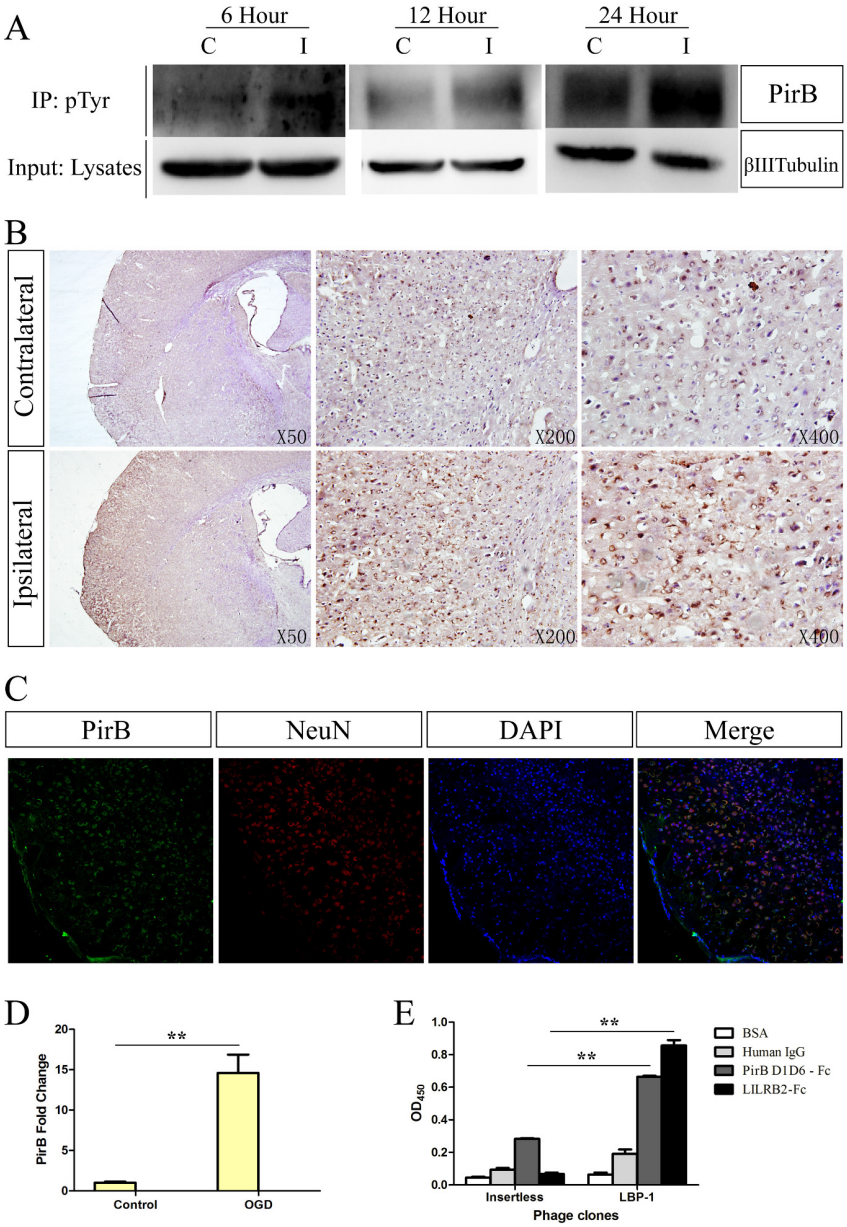

Fig.1 (A) Protein extracts from hemispheres of MCAO brains were subjected to immunoprecipitation for phosphotyrosine to assess levels of tyrosine phosphorylation of PirB. Expression of βIIItubulin was detected in input lysates. C, contralateral to ischemia; I, ipsilateral to ischemia. (B) Representative images of immunohistochemical staining showed that PirB protein levels were markedly increased in the damaged hemisphere 24 hours post-MCAO, compared to the contralateral side. (C) Majority of PirB immunostaining colocalized with neuronal marker NeuN 24 hours after ischemia. (D) Expression of PirB in cultured neurons was detected by real-time quantitative PCR. (E) Binding of LBP-1 phage clone to recombinant PirB and LILRB2 by monoclonal phage ELISA. Data were the mean±SEM of three independent experiments. Statistical significance was indicated by **P＜0.01.

CONTROL ID: 2232909

TITLE: Rapid esophageal cancer detection in fresh human specimens by topically applying aminopeptidase-activatable fluorescence probes

PRESENTER: Yasuteru Urano

ABSTRACT BODY:

Abstract Body: Early detection and complete resection of cancerous lesion are an important prognosticator for cancer treatment, however, the ability of the unaided human eye to detect small cancer foci during surgery or endoscopy is quite limited. Therefore, we tried to provide a new method for detecting human esophageal cancer by topically spraying activatable fluorescent probes.

We have prepared a library of activatable fluorescence probes composed of more than 300 probes for various aminopeptidases based on our molecular design strategy of intramolecular spirocyclization. We applied these probes on biopsy samples or resected specimens from esophageal cancer patients, and tried to find out tumor-specific aminopeptidase activities. As a result, we could find out the enzymatic activity of dipeptidyl peptidase-4 (DPPIV) were upregulated in tumor-positive biopsy samples, but not with tumor-negative biopsy samples. Further, we could also detect cancer region in the resected human fresh specimens by topically spraying DPPIV-activatable fluorescence probes within 10 min. The existence of tumor was confirmed by pathology and H&E staining, and immunohistochemical results indicated the elevated expression of DPPIV in the tumor site but not in the unaffected tissue.

These results clearly demonstrate that probes for DPPIV are practical for clinical application to detect human esophageal cancer during endoscopic or surgical procedures, because of its rapid and strong activation upon reaction with DPPIV on the surface of cancer cells.

AUTHORS (LAST NAME, FIRST NAME): Urano, Yasuteru[1, 2]; Onoyama, Haruna[3, 2]; Kuriki, Yugo[2]; Kamiya, Mako[1, 4]; Seto, Yasuyuki[3, 2]

INSTITUTIONS (ALL):

1. Graduate School of Medicine, The University of Tokyo, Tokyo, Japan.
2. CREST, JST, Tokyo, Japan.
3. The University of Tokyo Hospital, Tokyo, Japan.
4. PRESTO, JST, Tokyo, Japan.

(No Image Selected)

CONTROL ID: 2232912

TITLE: Intravital two-photon imaging of pulmonary invasive aspergillosis using fluorescent versions of the monoclonal antibody JF5 and its humanized variant

PRESENTER: Mike Hasenberg

ABSTRACT BODY:

Abstract Body: Among patients suffering from a profound suppression of their innate immune system, especially impaired neutrophil granulocyte responses, there is a high risk for the development of severe mold infections. *Aspergillus fumigatus* here plays the predominant role. As a ubiquitous airborne microorganism its spores (conidia) frequently reach deepest areas of the respiratory tract. Inside the alveoli the inhaled spore mass is generally eliminated by complex and in detail not well understood immune reactions. If this network of phagocytic and immune response modulating components is disturbed a high risk for the occurrence of invasive hyphal growth is given. At this stage, as soon as the fungus has generated mycelial structures inside an organ, the mold infection is hardly treatable. A standard therapy with a combination of cost-intensive antifungal drugs with severe side-effects is just able to cure a subset of patients. Mortality rates of up to 80 % after therapy are reported for specialized centers.

A key parameter for the therapeutic effect is the time frame of medication start after the onset of infection. The prognosis decreases dramatically with every day the fungal infection is not treated properly. Therefore fast and reliable diagnostic systems are indispensable for an efficient invasive aspergillosis therapy. At present there is a lack of such a diagnostic tool and clinicians have to rely on a combination of clinical symptoms, radiology, laboratory tests, microscopy and invasive biopsy. Together with colleagues from Tübingen, Germany (group of Bernd Pichler) we are evaluating the use of combined PET/MRI as novel diagnostic method for microbial infections. In this study we characterized the highly *A. fumigatus*-specific monoclonal antibody (mAB) JF5 and its humanized variant hJF5 as radioactively labelled PET tracer (see abstract of Anna-Maria Rolle *et al.*).

In parallel to the molecular imaging approach with a focus on specificity and signal strength we were interested in understanding the binding kinetics and target specificity of JF5 in infected lungs. For these characterizations we employed (intravital) microscopy in a murine, neutropenic infection model. Mice were rendered neutropenic by injection of an anti-Ly6G/Ly6C antibody, 24 h prior to intratracheal *A. fumigatus* infection. 24 h later fluorescently labelled versions of (h)JF5 were applied and after another 24 h infected lungs were screened for the appearance of fluorescent fungal elements. This screening was performed on lung slices as well as on whole lungs using a two-photon microscope. Both approaches clearly showed the specific binding of the mAB to galactomannan epitopes at the fungal cell wall surface. Control groups exactly behaved as in the molecular imaging study. Currently we combine our efforts to establish an intravital two-photon microscopy method for *A. fumigatus* infected mouse lungs. First results demonstrate the feasibility of stabilized image acquisition over time in the heavily moving organ during respiration. Soon this system will be used to investigate binding kinetics of (h)JF5 to the mycelial mass after systemic application of the mAB.

AUTHORS (LAST NAME, FIRST NAME): Hasenberg, Mike[2]; Solouk-Saran, Djamschid[2]; Weski, Juliane[2]; Thornton, Christopher R.[5]; Rolle, Anna-Maria[4]; Wiehr, Stefan[1]; Fischer, Eliane[6]; Schibli, Roger[6]; Krappmann, Sven[7]; Pichler, Bernd J.[4]; Gunzer, Matthias[3]

INSTITUTIONS (ALL):

1. Department of Preclinical Imaging and Radiopharmacy, Eberhard Karls University Tübingen, Tuebingen, Germany.
2. University of Duisburg/Essen, Essen, NRW, Germany.
3. Institute for Experimental Immunology and Imaging, University of Duisburg/Essen, University Hospital, Essen, Germany.
4. Department for Preclinical Imaging and Radiopharmacy, Werner Siemens Imaging Center, Tuebingen, Germany.
5. College of Life & Environmental Sciences, University of Exeter, Exeter, United Kingdom.
6. Paul Scherrer Institute, Research Department Biology and Chemistry, Center for Radiopharmaceutical Sciences, Villigen PSI, Switzerland.
7. Microbiology Institute, University Clinic of Erlangen, Erlangen, Germany.

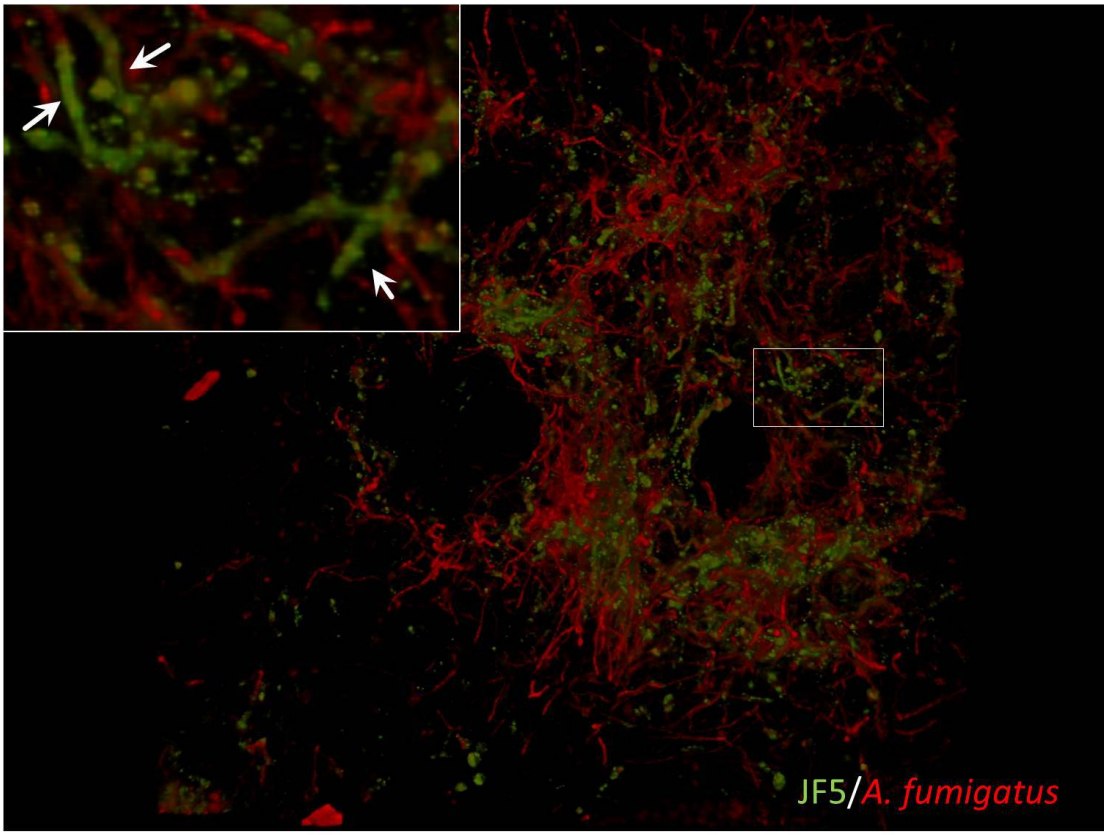
JF5/A. fumigatus

CONTROL ID: 2242651

TITLE: To evaluate the feasibility of F-18 FDG PET-CT in diagnosis of Infective Endocarditis

PRESENTER: Chetan Patel

ABSTRACT BODY:

Abstract Body: Introduction: Infective Endocarditis (IE) continues to pose a challenge due to high index of suspicion required for diagnosis, difficult diagnosis because of frequent non fulfillment of Duke's criteria & rapid downhill and sometimes unpredictable course despite best possible aggressive therapy.

Aim: We evaluated the feasibility of F-18 FDG PET-CT for diagnosing IE in Indian population and assessed its performance against Gold standard Duke's criteria.

Method This study was a prospective observational study. A total of 16 patients (11M: 5F, age range: 18-57 yrs, median age 30 yrs) with clinical diagnosis of IE were enrolled in the study. All patients were evaluated based on Modified Duke's Criteria. Patients having 2 major criteria or 1 major criterion and 3 minor criteria or 5 minor criteria were classified as Definite IE [n=10 (62.5%)]. Patients who fulfilled 1 major criterion and 1 minor criterion or minimum of 3 minor criteria were classified as Possible IE [n=6, (37.5%)]. Patients with proven endocarditis who have already received more than 7 days of optimal intravenous antibiotic therapy were excluded. All patients underwent F-18 FDG PET-CT cardiac study. In order to suppress normal myocardial uptake of FDG, patients were advised low carbohydrate, high fat diet for 48 hours followed by 12 hours overnight fasting before scheduled scan. The study was approved by Institutional Ethical committee.

Result: All patients underwent cardiac F-18 FDG PET-CT as per the study protocol. Focal increased uptake of FDG was noted in 6 (37.5%) patients and was classified as positive for IE. These correlated with anatomic localization on CT images. Out of remaining 10 (62.5%) patients, 3 patients with heterogeneous uptake and 7 patients with suppressed or 'no FDG uptake' were classified as negative on FDG PET-CT. In the definite IE group, 5/10 (50%) patients and in possible IE group 1/6 (16.67%) patient was positive on FDG PET-CT (p=0.307).

The sensitivity & specificity of FDG PET-CT for diagnosing IE was calculated against the definite IE diagnosed by the Gold standard Duke's criteria. The sensitivity, specificity, PPV, NPV was 50%, 83.3%, 83.3% & 50% respectively. Overall diagnostic accuracy of the FDG PET-CT for diagnosing IE in our study was 62.5 %. For overall study population of IE (both definite and possible), the yield of FDG PET-CT was 37.5%.

Conclusion: The results of this study suggest that Cardiac F-18 FDG PET-CT is feasible as an add-on investigation modality in diagnosis of IE. However the sample size in our study was small and a larger study is need for further validation.

AUTHORS (LAST NAME, FIRST NAME): Patel, Chetan D.[1]; Gupta, Abhinit[2]; Sharma, Gautam[2]; Bahl, Vinay K.[2]

INSTITUTIONS (ALL):

1. Nuclear Medicine, All India Institute of Medical Sciences, New Delhi, New Delhi, Delhi, India.
2. Cardiology, All India Institute of Medical Sciences, New Delhi, India, New Delhi, Delhi, India.

(No Image Selected)

CONTROL ID: 2232921

TITLE: Treatment response evaluation using ^{18}F-FDG PET-CT in patients with recurrent head and neck cancer.

PRESENTER: Rakesh Kumar

ABSTRACT BODY:

Abstract Body: BACKGROUND: Head and neck neoplasia (HNN) is a major form of cancer in India. The five-year survival varies from 20-90% depending upon the sub-site of origin and the clinical extent of disease in head & neck cancer. Clinical response evaluation after surgery/radiotherapy/chemotherapy is limited by the lack of standardised protocol, which would allow the differentiation between responders and nonresponders. The present study was aimed to evaluate the role of ^{18}F-FDG PET/CT in predicting tumor response to treatment of recurrent head and neck cancer (HNN).

PURPOSE: Evaluation of treatment response in patients with recurrent head and neck cancer using ^{18}F-FDG PET/CT.

METHODS: In the present study we retrospectively analysed 72 patients of head and neck cancer. The age range was 28 to 83 years with mean age of 49.16 years. All these patients had undergone a baseline ^{18}F-FDG PET/CT scan which showed active recurrent disease. All patients then underwent chemotherapy, radiotherapy or chemotherapy and radiotherapy/surgery. Follow-up ^{18}FDG PET/CT scan (post treatment) was done 4-6 weeks after last cycle of chemotherapy, radiotherapy, and surgery. Pre-treatment PET/CT was compared with follow-up post treatment PET/CT to evaluate treatment response. Decrease in SUV of more than 50% was considered as significant response (SR), decrease in SUV of more than 25% was considered as partial response (PR). Increase in SUV of more than 25% or appearance of new lesion (s) was considered as progression of disease (PD). No change in SUV or change of less than 25% was considered as stable disease (SD).

RESULTS: In this study of 72 patients, over all 33 had PD, 31 had SR (16 complete resolution and 15 patial response) and 8 SD. Of, 72 patients, 34 patients who underwent only chemotherapy 9 patients showed SR out of which 4 showed complete response (CR), while 4 patients showed SD and 21 patients were noted to have PD. There were 21 patients who underwent combined chemotherapy and radiotherapy in which 9 were found to have SR with 4 patients had CR, while PD was noted in 12 patients. In 12 patients, only radiotherapy was administered and of these 10 had SR with 5 patients with CR of disease, while 2 patients had SD. A combination of chemo-radiotherapy and surgery was given to 5 patients out of these 3 patients had SR and went into CR while stable disease was found in 2 patient.

CONCLUSION: ^{18}FDG PET-CT is a useful non-invasive modality in evaluating treatment response in recurrent head and neck cancer.

AUTHORS (LAST NAME, FIRST NAME): Kumar, Rakesh[1]

INSTITUTIONS (ALL):

1. Diagnostic Nuclear Medicine Division, Dept. of Nuclear Medicine, AIIMS, New Delhi, Delhi, India.

(No Image Selected)

CONTROL ID: 2243378

TITLE: CXCR4 chemokine receptor targeted probes: Radiopharmaeuticals, azamacrocycles and optimised chelators

PRESENTER: Benjamin Burke

ABSTRACT BODY:

Abstract Body: GPCRs are signal transduction proteins that span the cell membrane and form the target of around 30% of modern drugs. They include the sub-class chemokine receptors which are involved in cell signalling and implicated in diseases including atherosclerosis, asthma, rheumatoid arthritis, HIV infection and cancer. There is particular interest in imaging the CXCR4 chemokine receptor expression levels in cancers as a prognostic marker or to inform treatment selection. Metal containing drugs are ideal for disruption of the chemokine receptor signaling or use as imaging probes as the proteins have a high density of negatively charged surface residues including aspartates and glutamates that can form coordinate bonds with metal ions.

We have targeted the CXCR4 chemokine receptor using configurationally restricted metal complexes with either copper(II), zinc(II) or nickel(II), showing an improved binding profile with the protein (interaction strength and residence time) and enhanced blocking of intracellular signal transduction compared to purely organic antagonists [1-2]. This research demonstrates that an understanding and application of basic coordination chemistry principles to optimise protein binding can lead to an impressive increase in biological activity [3]. These compounds were combined with molecular imaging strategies to form optical and radiopharmaceutical probes.

Initial labeling studies were carried out with copper-64 to directly label the compounds without structural change. Further strategies have now been developed for two component system where an azamacrocycle targeting component was coupled to a separate chelator or prosthetic group for radiolabelling. The probe molecules have been validated using a series of in vitro analyses and preclinical PET/CT imaging.

Calcium signalling assays, residence time, receptor trafficking, structure activity relationships, radiolabelling protocols, cellular imaging (confocal) and in vivo PET/CT imaging will be presented.

1. Mewis R. E. and Archibald S. J., “Biomedical Applications of Macrocyclic Ligand Complexes.” *Coord. Chem. Rev.* **2010**, 1686-1712.

2. Smith, R.; Archibald S. J. Protein-Binding Metal Complexes: Noncovalent and Coordinative Interactions In *Comprehensive Inorganic Chemistry II*, Volume 3,Chapter 3.22, **2013**, 661-682.

3. Smith, R.; Mewis, R. E.; Huskens, D.; Dirk Daelemans, D.; Garcia, C. D.; Cain, A. N.; Carder Freeman, T. N.; Schols, D.; Pannecouque, C.; De Clercq, E.; Hubin, T. J.; Archibald, S. J. “Metal ion containing CXCR4 chemokine receptor antagonists: nickel(II) complexes of configurationally restricted macrocycles.” *Dalton Transactions* **2012**, *41*, 11369.

AUTHORS (LAST NAME, FIRST NAME): Burke, Benjamin P.[1]; Nigam, Shubhanchi[1]; Clemente, Gonçalo S.[2]; Lee, Rhiannon E.[1]; Miranda, Cecilia S.[3]; Cawthorne, Christopher[3]; Archibald, Steve[2]

INSTITUTIONS (ALL):

1. Chemistry, University of Hull, Hull, East Riding of Yorkshire, United Kingdom.
2. PET Research Centre, University of Hull, Hull, United Kingdom.
3. School of Biological, Biomedical and Environmental Sciences, University of Hull, Hull, United Kingdom.

(No Image Selected)

CONTROL ID: 2232929

TITLE: Optimising Gold Nanorods for Multispectral Optoacoustic (MSOT) Tracking of Stem Cells

PRESENTER: Joan Comenge

ABSTRACT BODY:

Abstract Body: Gold nanorods (GNRs) are perfect candidates to be used as contrast agents for photoacoustic imaging because of their high and tuneable absorption in the near infrared. However, their application for robust and reproducible biological imaging require a high degree of control over their physicochemical properties. The dimensions and capping agents influence colloidal stability, cell uptake and toxicity, which in turn determine the efficiency of cell labelling.Furthermore, since MSOT relies on the irradiation at different wavelengths, the preservation of the optical signature after uptake is crucial to achieve the expected results. This is not trivial because GNRs are plasmonic particles with spectra which are particularly sensitive to aggregation. Aggregation induced by cell medium or packing of nanoparticles within endosomes may both result in shift and broadening of the GNRs plasmon band.

Here, we demonstrate that covering the GNRs with a carboxylic ended short PEG or with a silica shell provide the best performance amongst all the ligands/coatings tested. Short PEG-COOH confers electrostatic stability to GNRs and promotes protein adsorption, which favours cell uptake and minimise coupling of surface plasmon inside the endosomes. Silica coating provides steric hindrance which results in a greater stability even inside endosomes. In addition, silica has been reported to be better thermal conductor than gold, which favours a faster dissipation of the heat after pulsed laser, which ultimately enhances the intensity of the generated ultrasounds.
After the optimisation, GNRs at concentrations as low as 6 pM were detected in a phantom. This very low limit of detection is needed to detect the few labelled cells that are in the plane of visualization with MSOT. Preliminary results in a kidney disease model show how the route of injection affects the biodistribution of mesenchymal stem cells, achieving a broader biodistribution (less stacking in the lungs) when intracardiac injection is used. Whilst IVIS gives a general overview of the distribution of luciferase-expressing cells, the specific localisation of cells inside target organs (in our model, kidneys) can only be imaged using high resolution techniques such as MSOT. Importantly, in addition to cell tracking, MSOT can be used to monitor organ function and therefore treatment efficacy, in the case of kidneys, by studying the renal clearance of an IR-Dye.

AUTHORS (LAST NAME, FIRST NAME): Comenge, Joan[1]; Fragueiro, Oihane[2]; Brust, Mathias[2]; Levy, Raphael[1]

INSTITUTIONS (ALL):

1. Institute of Integrative Biology, University of Liverpool, Liverpool, United Kingdom.
2. Chemistry department, University of Liverpool, Liverpool, United Kingdom.

(No Image Selected)

CONTROL ID: 2232937

TITLE: Introduction of an antibody based PET tracer for the imaging of Alveolar Echinococcosis compared to various standard clinical PET tracers

PRESENTER: Anna-Maria Rolle

ABSTRACT BODY:

Abstract Body: The rare and chronic zoonotic parasitic disease alveolar echinococcosis (AE) is caused by the larval form (metacestode) of *Echinococcus multilocularis*, known as the fox tapeworm. The parasite has a tumor-like, multi-vesicular structure and infiltrates surrounding tissues especially organs as the liver, kidney and central nervous system. Pathological changes of the host occur years or decades after the initial infection, which makes a diagnosis of the early infection essential for efficient management and treatment of the disease. Currently [^{18}F]FDG-PET, in particular delayed [^{18}F]FDG-PET combined with serological tests is used in the clinical setting for diagnosis and treatment monitoring. Our aim was to test and compare clinically used PET tracers with the highly specific antibody-based tracer [^{89}Zr]desferal-MAbG11 for the detection of AE in PET and MRI.

Mongolian gerbils (*Meriones unguiculatus*) were inoculated *i.p.* with *E. multilocularis* metacestodes. *In vivo* biodistribution studies were performed after injection of 13 MBq of [^{18}F]FDG, [^{18}F]FLT, [^{18}F]FAZA, [^{11}C]choline or the radiolabeled monoclonal *E. multilocularis* specific antibody [^{89}Zr]desferal-MAbG11 via the tail vein. Small animal PET images, including delayed [^{18}F]FDG-PET, were acquired in combination with MRI at early and late infection time points. *Ex vivo* biodistribution, autoradiography and histology were performed. To determine the binding specificity of MAbG11, confocal laser scanning microscopy was executed on parasite vesicles stained with Alexa Fluor 647-conjugated MAbG11. *In vitro* cell binding assays were performed in addition. Therefore control cells derived from naïve and infected gerbils as well as parasitic tissue were incubated with [^{64}Cu]DOTA-MAbG11 or a radiolabeled control antibody. Uptake was measured by gamma-counting.

In vitro binding asssays using [^{18}F]FDG, [^{18}F]FLT, [^{18}F]FAZA and [^{11}C]choline revealed elevated binding to *E. multilocularis* tissue and therefore great potential for further *in vivo* studies. Quantification of the PET images revealed focal accumulation of [^{18}F]FDG (%ID/g parasite tissue: 2.62±0.76) and [^{18}F]FLT ((%ID/g parasite tissue: 2.50±1.48) throughout the parasite tissue. [^{18}F]FAZA and [^{11}C]choline showed no accumulation in the parasitic tissue *in vivo*. In contrast, quantitative analysis of fused PET/MRI images showed a specific and enhanced uptake of [^{89}Zr]desferal-MAbG11 in parasite tissue (%ID/g parasite tissue: 9.23). Confocal microscopy showed the specific binding of the monoclonal antibody MAbG11 to the laminated layer of the parasite vesicle. *In vitro* cell assays supported the *in vivo* findings showing a 4-fold higher uptake of [^{64}Cu]DOTA-MAbG11 in *E. multilocularis* vesicles compared to the control antibody.

Whereas our *in vitro* binding assays displayed great potential of the various tracers to supplement current diagnostic and therapy monitoring strategies, the *in vivo* investigations confirmed that AE lesions are still difficult to discover and the determination between viable and non-active parasitic tissue remains a challenge. Therefore the monoclonal antibody MAbG11 represents an excellent candidate for a novel diagnostic tool.

AUTHORS (LAST NAME, FIRST NAME): Rolle, Anna-Maria[1]; Deplazes, Peter[2]; Soboslay, Peter[3]; Hoffmann, Wolfgang H.[3]; Maurer, Andreas[1]; Pichler, Bernd J.[1]; Wiehr, Stefan[1]

INSTITUTIONS (ALL):

1. Werner Siemens Imaging Center, Department of Preclinical Imaging and Radiopharmacy, Eberhard Karls University Tuebingen, Tuebingen, Germany.
2. Institute of Parasitology, University of Zürich, Zürich, Switzerland.
3. Institute of Parasitology, Eberhard Karls University Tuebingen, Tuebingen, Germany.

(No Image Selected)

CONTROL ID: 2232990

TITLE: Pathogen specific antibody-based molecular imaging of Invasive Aspergillosis with the newly developed PET tracer [^{64}Cu]DOTA-JF5 and its humanized variant [^{64}Cu]NODAGA-hJF5

PRESENTER: Anna-Maria Rolle

ABSTRACT BODY:

Abstract Body: Humans with impaired immunity, e.g. those with haematological malignancies or bone marrow transplant recipients are at an elevated risk of severe *Aspergillus fumigatus* infection known as invasive aspergillosis (IA). Currently IA is diagnosed based on clinical symptoms, radiology, laboratory tests and microscopy or relies on invasive biopsy, which is not always feasible in very sick patients. Most of these methods are unspecific and time consuming, which impedes an early and accurate diagnosis leading to fatalities of up to 80% in certain patient groups. Consequently, there is the potential to increase the survival rates of IA patients, if a definite diagnosis of IA could be obtained early and its response to treatment monitored and adjusted accordingly. The highly *A. fumigatus* specific monoclonal antibody (mAb) JF5 and its humanized variant hJF5 were radiolabeled with ^{64}Cu, tested in an experimental setup and compared to the standard PET tracer [^{18}F]FDG in various infection models.

In vivo biodistribution studies were performed with neutropenic *A. fumigatus* infected C57BL/6 mice after the injection of 13 MBq of [^{64}Cu]DOTA-JF5, the isotype control [^{64}Cu]DOTA-MG 3-35, [^{64}Cu]NODAGA-hJF5 or [^{18}F]FDG and compared to the distribution of the respective tracers in control infections (*S. pneumoniae* and *Y. enterocolitica*). The Gr-1 antibody RB6-8C5 was administered 24h prior to the intratracheal infection of the mice with *A. fumigatus* to mimic impaired immunity by the depletion of neutrophil granulocytes. 3, 24 and 48h after the injection of the ^{64}Cu labeled antibodies or [^{18}F]FDG, PET/MRI images of the respective infection groups were acquired and compared to PBS treated controls. Additionally, blocking studies, e*x vivo* biodistribution, autoradiography and plating of various organs for the detection of the pathogen were performed.

[^{18}F]FDG-PET showed similar results in *A. fumigatus* infected animals (%ID/cc lungs: 14.67±0.53), PBS treated control animals (%ID/cc lungs: 10.47±2.77) as well as in *S. pneumoniae* control infections with 13.05±2.80 and 12.37±1.19 %ID/cc in the respective PBS treated control group. Quantification of the PET images showed a significantly higher binding of the *A. fumigatus* specific JF5 mAb in neutropenic, *A. fumigatus* infected animals (%ID/cc lungs: 11.08±2.28) compared to PBS treated animals (%ID/cc lungs: 7.51±1.50). All control infections revealed a reduced uptake of JF5 in the lungs. Blocking experiments and studies with the unspecific isotype control antibody demonstrated the high specificity of JF5. Biodistribution studies with the newly developed humanized [^{64}Cu]NODAGA-hJF5 displayed similar uptake characteristics as the mouse mAb JF5 with 22.73±6.77 %ID/g in infected animals compared to 10.14±3.68 %ID/g in PBS treated animals.

[^{18}F]FDG-PET revealed to be highly unspecific and is therefore not suitable for monitoring disease progression and therapeutic success in IA. In contrast to that, [^{64}Cu]DOTA-JF5 and especially the humanized variant [^{64}Cu]NODAGA-JF5 have been developed and show great potential as novel timely and accurate diagnostic and therapeutic strategy for IA to improve the survival rates of patients.

AUTHORS (LAST NAME, FIRST NAME): Rolle, Anna-Maria[1]; Hasenberg, Mike[2]; Thornton, Christopher R.[3]; Maurer, Andreas[1]; Fischer, Eliane[4]; Spycher, Philipp R.[4]; Schibli, Roger[4]; Boschetti, Frederic[5]; Stegemann-Koniszewski, Sabine[6, 7]; Bruder, Dunja[6, 7]; Severin, Gregory W.[8, 9]; Elema, Dennis R.[11]; Autenrieth, Stella[10]; Pichler, Bernd J.[1]; Gunzer, Matthias[2]; Wiehr, Stefan[1]

INSTITUTIONS (ALL):

1. Werner Siemens Imaging Center, Department of Preclinical Imaging and Radiopharmacy, Eberhard Karls University Tuebingen, Tuebingen, Germany.
2. Institute for Experimental Immunology and Imaging, University Hospital and University of Duisburg/Essen, Essen, Germany.
3. School of Biosciences, College of Life & Environmental Sciences, University of Exeter, Exeter, United Kingdom.
4. Paul Scherrer Institute, Research Department Biology and Chemistry, Center for Radiopharmaceutical Sciences (CRS), Villigen PSI, Switzerland.

5. CheMatech, Faculté des Sciences Mirande, Dijon, France.
6. Immune Regulation Group, Helmholtz Centre for Infection Research, Braunschweig, Germany.
7. Infection Immunology Group, Institute of Medical Microbiology, Disease Control and Prevention, Otto-von-Guericke University Magdeburg, Magdeburg, Germany.
8. The Hevesy Laboratory, DTU Nutech, Technical University of Denmark, Roskilde, Denmark.
9. Center for Nanomedicine and Theranostics, Technical University of Denmark, Roskilde, Denmark.
10. Department of Hematology, Oncology, Rheumatology, Immunology and Pulmonology, University Hospital Tübingen, Tuebingen, Germany.
11. Center for Nuclear Technologies, Technical University of Denmark, Roskilde, Denmark.
(No Image Selected)

CONTROL ID: 2232943

TITLE: Site specific release of enzymatically sensitized liposomal-nanocarriers through remote activation by alternating magnetic field.

PRESENTER: Oula Penate-Medina

ABSTRACT BODY:

Abstract Body: Several small drug molecules have unfavorable pharmacokinetics like short circulation time in the blood. Liposomal delivery systems have been used to compensate this phenomenon in drug delivery and in imaging. At the moment liposomal delivery systems increase blood circulation time of the drugs but often substances remain entrapped inside the liposomes reducing efficacy. We have developed magnetoenzymatic sensitive liposome (MESL) carrier systems for imaging and targeted release of multifunctional nanotheranostic agents. The method utilizes alternating magnetic fields (AMF) and liposomal nanoparticles enzymatically sensitized to apoptosis, tumor and inflammation processes. We have used this phenomenon to develop more advanced image guided tumor and inflammation targeting and therapy methods utilizing upgraded phospholipase activation and secretion in the target tissues.

The liposomal construct was assembled as ICG-iron nanoparticle containing MESL nanocarrier. The construct was evaluated by using DLS and electron microscopy. Long term stability and in vitro activation assays were done using leakage assays. Preliminary in vivo imaging studies were performed at the Molecular Imaging North Competence Center (MOIN CC). Liposome payload accumulation was tested by using optical imaging (NightOwl and FMT 2500) and MRI. ROI analysis was used to assess tumor to background and tumor to organ ratios. In preliminary in vivo experiments 10-30 orthotopic xenograft mice were used per cell line for imaging, targeting and PK parameter assessment (Capan-2, Panc-89 pancreatic and SCC tongue carcinoma were used in from tumor models and , Arthtritis and Colitis models were used as models for inflammation targeting). All administrations were IV injections. The liposome accumulation was studied by using ICG fluorophores encapsulated in to the liposomes. The dye content in a target organ was assessed by using ICG fluorescence or absorbance. At the study endpoint a surgical microscope was used to examine the tumors of the mouse. After in vivo imaging the organs of the animals were harvested and optical microscopy, histology, operative microscopy was assessed. Imaging time points (pre treatment, injection, 30 min post AMF, 2h 24h 72h) were selected according to the previous liposomal imaging studies. Cisplatin was chosen as a model drug for further drug delivery function.

There were significant increase in the accumulation of available drug in the MESL treated mice versus control liposomes treated or free ICG. At post AMF 30 minutes time point there were significantly roughly twice as much signal in the tumor versus untreated control liposomes. The tumor to background ratio was steadily increased from around 8 to 12 in 24 hours in AMF release group contra 2 in control group. At 24h time point the MESL liposomes were able to give 10 times more signal than the free ICG.

There was clear synergy in using AMF and enzymatic activation in tandem. MRI and optical methods can be used to assess and develop this platform for further refinement. This method offers total new way to do imaging and drug delivery and has possible perspectives to be clinically translated

AUTHORS (LAST NAME, FIRST NAME): Peñate Medina, Tuula[1]; Purcz, Nicolai[3]; Damm, Jana[1]; Tower, Robert[2]; Will, Olga M.[1]; Gerle, Mirko[3]; Rohwedder, Arndt[1]; Kalthoff, Holger[4]; Glüer, Claus C.[1]; Penate-Medina, Oula[1]

INSTITUTIONS (ALL):

1. Radiology, Christian-Albrechts-Universität zu Kiel, Kiel, Germany.
2. University Hospital Schleswig-Holstein, Kiel, Germany.
3. University Hospital Schleswig-Holstein,, Campus Kiel, Germany, Kiel, Germany.
4. Division of Molecular Oncology, Institute for Experimental Cancer Research, University of Kiel, Kiel, Germany, Kiel, Germany.

Images of Orthotopic SCC bearing xenograft mice
six hours after tail vein injection of ICG containing liposomes together with alternating magnetic field treatment on the left and without treatment on the right

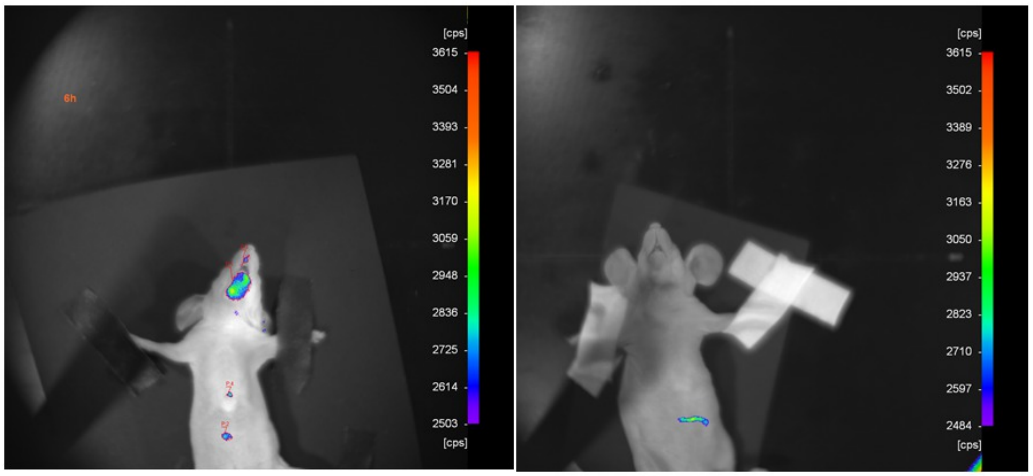

CONTROL ID: 2232939

TITLE: Application of texture analysis to SPECT images of ^{125}I-A5B7 anti-CEA antibody localisation in metastatic colorectal cancer models: Correlation with histological microarchitecture and response to antivascular therapy.

PRESENTER: Vineeth Rajkumar

ABSTRACT BODY:

Abstract Body: Background: There is growing evidence that the measurement of heterogeneity in medical images by textural analysis may allow better tissue characterisation, image segmentation, and prediction of therapy response and survival. One area in which this can be applied is to measure the heterogeneity of radiolabeled antibody distribution in solid tumours which is critical to the successful planning and monitoring of antibody-targeted radionuclide imaging and therapy. The aim of our current study was to compare the spatial heterogeneity of ^{125}I-A5B7 anti-carcinoembryonic antigen (CEA) antibody distribution using texture analysis of single photon emission computed tomography (SPECT) images in two pre-clinical models (LS174T and SW1222) of hepatic metastatic colorectal cancer before and after antivascular therapy with OXi4503 (combretastatin A1 di-phosphate / CA1P).

Methods: SPECT imaging of control tumours and tumours post-OXi4503 therapy in MF1 nude mice with liver metastases was performed following tail vein injection of 20MBq ^{125}I-A5B7. Second order, statistical-based texture analysis features, using grey-level co-occurrence matrices of ^{125}I-A5B7 distribution within metastases were measured on up to 3 liver metastases in each of the 14 mice.

Results & Discussion: Using second order textural features (uniformity, homogeneity, entropy and contrast), we showed that: Before treatment LS174T colorectal metastases (n=7) showed increased heterogeneity compared to SW1222 metastases (n=12) [0.6 x uniformity (p=0.028), 0.8 x homogeneity (p=0.01), 1.1 x entropy (p=NS), 1.9 x contrast (p=0.045)]. After OXi4503 treatment, the LS174T metastases (n=8) showed significantly less heterogeneity than the untreated LS174T controls (2.2 x uniformity (p=0.021), 1.2 x homogeneity (p=NS), 0.9 x entropy (p=0.006), 0.7 x contrast (p=NS)). However, OXi4503-treated SW1222 metastases (n=11) showed no difference in texture compared to controls [uniformity, homogeneity, entropy and contrast, (all p=NS)]. No significant difference in mean tumour size was observed between the groups.

Conclusions: For the first time we have demonstrated that texture analysis of ^{125}I-A5B7 SPECT images was able to confirm the expected differences in antibody distribution between SW1222 and poorly-differentiated LS174T liver metastases before treatment. Following antivascular treatment with OXi4503, LS174T metastases, but not the well-differentiated SW1222 metastases were texturally more homogeneous.

AUTHORS (LAST NAME, FIRST NAME): Rajkumar, Vineeth[1]; Goh, Vicky[2]; Siddique, Musib[2]; Vassileva, Vessela[1]; Robson, Mathew[1]; Boxer, Geoffrey[1]; Pedley, R B.[1]; Cook, Gary J.[2]

INSTITUTIONS (ALL):

1. UCL Cancer Institute, University College London, London, United Kingdom.
2. Division of Imaging Sciences and Biomedical Engineering, Kings College London, London, United Kingdom.

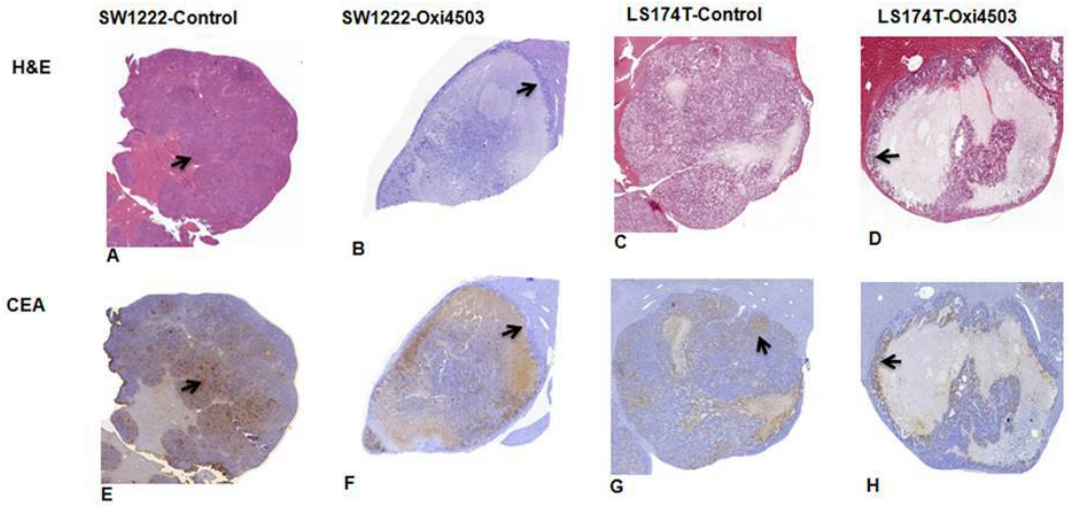

Figure 1. Representative haematoxilin and eosin (A-D) and anti-CEA immunohistochemical (E-H) micrographs demonstrating the effect of Oxi4503 on the distribution of viable cells and CEA in SW1222 (A,B,E,F) and LS174T (C,D,G,H) intrahepatic metastases.
Control SW1222 metastases are almost totally viable (arrow, A), with relatively uniform expression of CEA (arrow, E). After treatment with Oxi4503, viable CEA-expressing tumor cells are restricted to the peripheral rim (arrow, B and F). In control LS174T metastases (C), CEA expression (arrow, G) is more heterogeneous than in SW1222 metastases (E). After treatment with Oxi4503 (D), viable and CEA-expressing tumor cells are similarly restricted to the peripheral rim (arrows, D and H).

CONTROL ID: 2232940

TITLE: Radionuclide gene therapy combined with dendritic cell-based immunotherapy enhance antitumor effects in Lewis lung cancer model

PRESENTER: Hong Je Lee

ABSTRACT BODY:

Abstract Body: Objective

We investigated the combined-therapeutic effects using radioiodine gene therapy and dendritic cell (DC)-based immunotherapy in lung cancer model.

Methods

Recombinant retrovirus that expresses human sodium iodide symporter (hNIS), luciferase (Luc2) and wasabi gene under the control of a cytomegalovirus (CMV) promoter was transduced to Lewis lung cancer cell (LLC/NLW). Functional gene expression of hNIS, Luc2 and wasabi gene was confirmed using I-125 uptake, luciferase assay and flow cytometry. Bone marrow cells were isolated from femurs and tibias of C57BL/6 mice. GM-CSF and IL-4 induced dendritic cell differentiation. Nonadherent cells were harvested by a gentle pipetting and the surface molecules of these cells were analyzed with flow cytometry. For in vivo therapy, 5x106 LLC/NLW were transplanted into both thighs of C57BL/6 mice. In I-131 therapy group, the mice were treated with intraperitoneal injection of 1mCi of I-131. In DC-based immunotherapy group, 5x106 primary dendritic cells (pDCs) were injected intratumorally every 1 week. In dual therapy group, the mice were treated with intraperitoneal injection of 1mCi of I-131 and intratumoral injection of 5x106 of pDCs. Therapeutic effect of each group was serially monitored using in vivo PET/SPECT/CT and bioluminescence imaging systems.

Result

The hNIS, Luc2 and wasabi mRNA were identified in infected Lewis lung cancer cell (LLC) by RT-PCR. In fluorescence microscopy, wasabi protein was well expressed. The hNIS and luc2 transcription activity that were assessed using I-125 uptake and luciferase assay in LLC/NLW increased up to 50 and 100-fold than that in LLC, respectively. Potassium perchlorate blocked the iodine uptake completely in LLC/NLW. The survival rate of the LLC/NLW treated with I-131 decreased up to 50%. The surface molecules of MHCI, MHCII, CD86, ICAM-I and CCR7 that is phenotypic markers of pDCs were well expressed in pDCs. In small animal imaging study, LLC/NLW tumors showed higher I-124 uptake than LLC tumors. Bioluminescence imaging also demonstrated higher activity in LLC/NLW tumors than in LLC tumors. LLC/NLW tumor size was significantly decreased in dual therapy group.

Conclusion

This study supports combined-therapeutic effects using radioiodine gene therapy and dendritic cell (DC)-based immunotherapy in lung cancer model.

AUTHORS (LAST NAME, FIRST NAME): Lee, Hong Je[1]; Lee, You La[1]; Jeon, Yong Hyun[3]; Lee, Jaetae[2]; Ahn, Byeong-Cheol[3]

INSTITUTIONS (ALL):

1. Nuclear Medicine, Dongnam institution of Radiological & Medical Sciences (DIRAMS), Busan, Korea (the Republic of).
2. Daegu-Gyeongbuk Medical Innovation Foundation (DGMIF), Daegu, Korea (the Republic of).
3. Department of Nuclear Medicine, Kyungpook National University School of Medicine, Daegu, Korea (the Republic of).

(No Image Selected)

CONTROL ID: 2232949

TITLE: Small Animal PET Imaging of Striatal and Cortical Targets in the zQ175 Mouse Model of Huntingtons Disease

PRESENTER: Jenny Häggkvist

ABSTRACT BODY:

Abstract Body: Aim:

Huntington's disease is a neurodegenerative disorder, characterized by progressive loss of spiny neurons in the striatum. The loss of neurons leads to development of motor dysfunction, emotional disturbances, psychiatric symptoms and cognitive deficits. Huntington´s disease is caused by expansion of the CAG-repeat within the 5´end of the IT15 coding gene for the protein Huntingtin (Htt) [1]. Several animal models have been developed to study the progression of disease as well as to evaluate potential new therapeutics. The zQ175 knock-in mouse model is considered to show high face validity for the human condition [2, 3]. In the present study, we have used small animal positron emission tomography (PET) in order to examine the molecular phenotype of the zQ175 mouse model. We focused on subcortical and cortical markers, including the dopamine D2 and D1 receptors, the phosphodiesterase 10 A (PDE10A) enzyme and the serotonin $(5\text{-HT})_{2A}$ receptor.

Methods:

Male heterozygous zQ175 and wild-type (WT) animals were imaged with the dopamine D2-receptor radioligand [^{11}C]raclopride, the PDE10A radioligand [^{18}F]MNI-659, the dopamine D1-receptor radioligand [^{11}C]NNC 112 and the 5-HT_{2A} radioligand [^{11}C]MDL 100907 at 6 and 9 months of age using the nanoScan® PET/MRI scanner (Mediso Ltd, Hungary). The outcome measure was the binding potential (BP_{ND}), estimated using the cerebellum as reference region. Selected regions of interest were the striatum for all radioligands and the rostral cortex, dorsal cortex and hippocampus for [^{11}C]NNC 112 and [^{11}C]MDL 100907.

Results:

At 6 months of age, the BP_{ND} in the striatum was lower in zQ175 animals compared with WT animals by 40% in the case of [^{11}C]raclopride ($p<0.0001$), by 52% in the case of [^{18}F]MNI-659 ($p<0.001$), by 29% in the case of [^{11}C]NNC 112 ($p<0.001$) and 12% in the case of [^{11}C]MDL 100907 ($p<0.01$). In the rostral cortex, D1-receptor binding was 24% lower in zQ175 compared to WT. In the hippocampus, the BP_{ND} of [^{11}C]MDL 100907 in zQ175 was 12% lower compared to WT. At 9 months there was a slight reduction of D1, D2 and 5-HT2A in the striatum (with a 4-7 % further decrease in zQ175 compared to WT), whereas PDE10A reached a plateau. Cortical markers were also slightly further decreased at 9 months in zQ175 animals.

Conclusion:

These results from the present study show a marked loss of D1- and D2- receptors as well as loss of PDE10A enzyme in the striatum of Q175 mice, in agreement with data obtained in clinical PET studies. The 5-HT2A receptors seemed to be less affected. zQ175 mice represent a suitable model for understanding the pathophysiology of Huntington's disease and for evaluating new therapeutic strategies aimed to interfere with the progression of the disease.

1. The Huntington's Disease Collaborative Research Group. Cell, 1993. 72(6): p. 971-83.
2. Heikkinen, T., et al. PLoS One, 2012. 7(12): p. e50717.
3. Menalled, L.B., et al. PLoS One, 2012. 7(12): p. e49838.

AUTHORS (LAST NAME, FIRST NAME): Häggkvist, Jenny[1]; Tóth, Miklós[1]; Tari, Lenke[1]; Varnäs, Katarina[1]; Dominguez, Celia[2]; Munoz-Sanjuan, Ignacio[2]; Varrone, Andrea[1]; Halldin, Christer[1]; Mrzljak, Ladislav[3]

INSTITUTIONS (ALL):

1. Clinical Neuroscience , Karolinska Institutet, Stockholm, Sweden.
2. CHDI Management/CHDI Foundation Inc., Los Angeles, CA, United States.
3. CHDI Management/CHDI Foundation Inc., Princeton, NJ, United States.

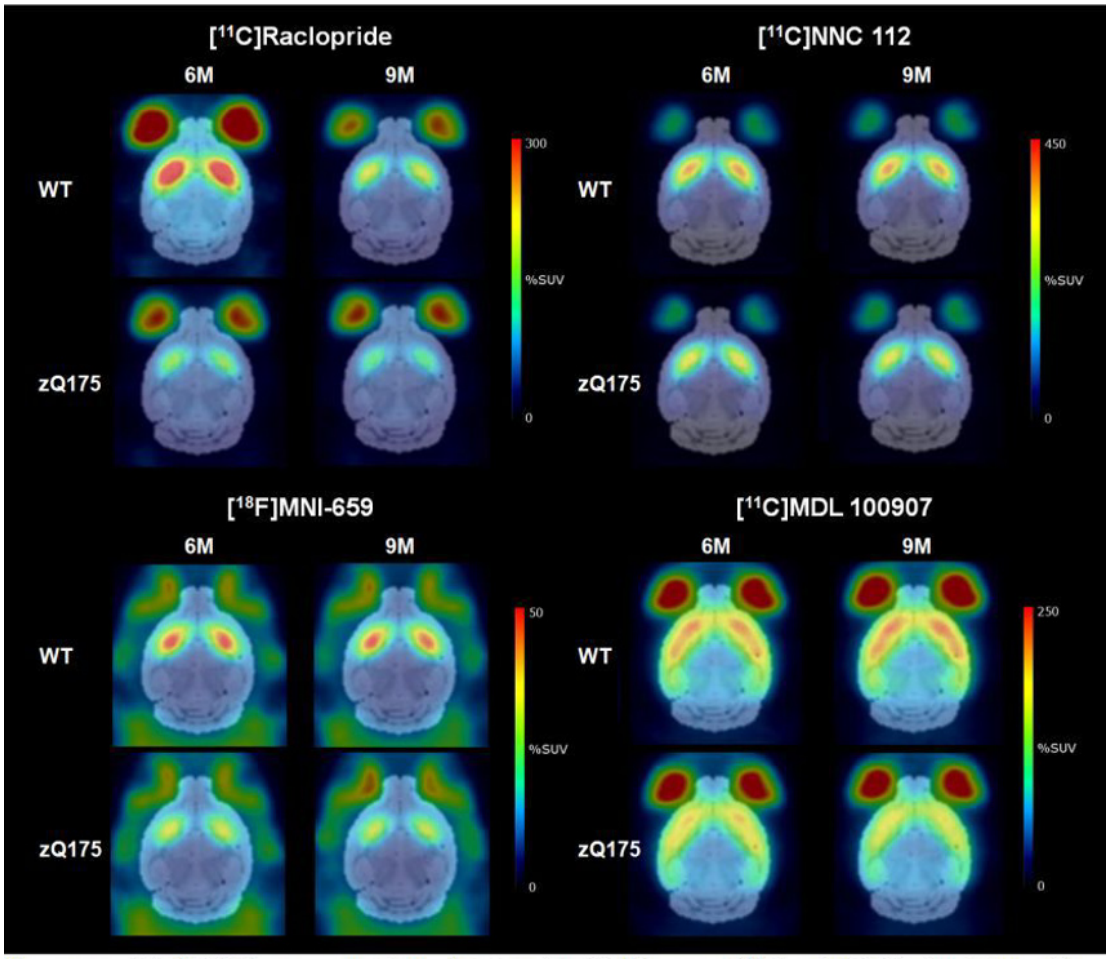

Average sagital %SUV images coregistrered to template MRI-images of WT and zQ175 animals imaged with [11C]raclopride [18F]MNI-659 [11C] NNC 112 and [11C]MDL 100907 at 6 and 9 months of age.

CONTROL ID: 2232962

TITLE: Detection of Amyloid-β Plaques in the Brain Using Dual-modality PET/NIR Fluorescent Probes

PRESENTER: Hualong Fu

ABSTRACT BODY:

Abstract Body:

Objectives: The accurate detection of amyloid-β (Aβ) plaques in the brain is important for the early diagnosis of Alzheimer's disease (AD) and several imaging modalities including PET, MRI and NIR imaging have been exploited for this purpose. Multi-modality imaging like PET-CT, PET-MRI and PET-optic combines information from more than one modality and provides more accurate molecular-level information of the target. In this study, we developed two dual-modality PET/NIR fluorescent probes for in vivo detection of Aβ plaques in the brain.

Procedures: The fluorescent properties including the excitation/emission wavelength and the intensity with/without Aβ aggregates in PBS and the quantum yields (QY) in dichloromethane were measured. Next, the selectively binding of the probes with Aβ plaques were determined by histological fluorescent staining. Furthermore, the binding affinities of the probes to Aβ aggregates was assessed by saturation binding assays. To validate the potential of the probes as PET/NIR imaging agents, the brain kinetics (the brain uptake and washout rate from the brain) of the probes were measured.

Results: The chemical structures of the two probes were presented in Figure 1A. In the detection of Aβ plaques, the two probes possess dual functions of being fluorescent probes and PET tracers when radiolabelled by fluorine-18. The spectroscopic measurement showed that the probes had proper emission maxima (> 650 nm) in PBS and high QYs (16.6% and 6.1% for **1** and **2**, respectively), which are prerequisites of NIR imaging. Furthermore, probe **2** showed great potential in NIR imaging with the emission maximum of 666 nm upon bound to Aβ aggregates in PBS; concurrently, remarkable increase in fluorescent intensity (560-fold) and a significant blue shift of 105 nm were observed. In the neuropathological staining, the probes could clearly stain the Aβ plaques in the brain sections of transgenic (Tg) mice and AD patients (Figure 1B). As shown in Figure 1A, the probes had high affinities to Aβ aggregates with the Kd values of 37.1 and 3.8 nM for **1** and **2**, respectively. The blood-brain barrier (BBB) penetration experiment demonstrated that probe **1** and **2** had efficient BBB penetration (10.97 and 6.88% ID/g at 2 min postinjection for **1** and **2**, respectively) and fast washout from the brain ($brain_{2\ min}/brain_{60\ min}$ = 15.5 and 6.7 for **1** and **2**, respectively).

Conclusions: Herein we reported on the design and assessment of two probes as dual-modality PET/NIR tracers for in vivo detection of Aβ plaques in the brain. Probe **2** basically fulfills all of the criteria (excellent fluorescent properties, high affinity and good brain kinetics) for an ideal PET/NIR probe targeting Aβ plaques. Furthermore, the ^{18}F-labeling of the probes and the PET/NIR imaging in Tg mice are currently underway.

Acknowledgements: Supported by NSFC (21201019)

Corresponding author: cmc@bnu.edu.cn

AUTHORS (LAST NAME, FIRST NAME): Fu, Hualong[1]; Cui, Mengchao[1]; Liu, Boli[1]

INSTITUTIONS (ALL):

1. College of Chemistry, Beijing Normal University, Beijing, China.

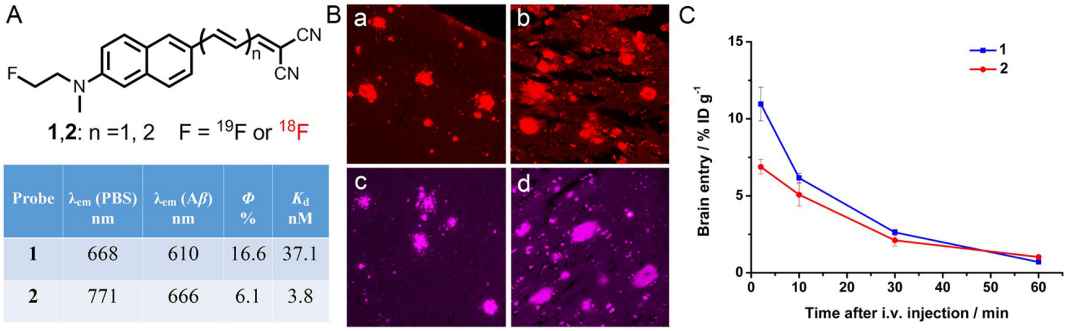

Probe	λ_{em} (PBS) nm	λ_{em} (Aβ) nm	Φ %	K_d nM
1	668	610	16.6	37.1
2	771	666	6.1	3.8

Figure 1. (A) The chemical structures and selected data of probe 1 and 2. (B) The histological fluorescent staining of 1 (a and b) and 2 (c and d) on the brain sections from Tg mice (a and c) and AD patients (b and d). (C) Brain kinetic curves of 1 (blue line) and 2 (red line).

CONTROL ID: 2232968

TITLE: Comprehensive characterization of tumor progression from precancer to invasive breast cancer using multiparametrical imaging

PRESENTER: Jennifer Schmitz

ABSTRACT BODY:

Abstract Body: Introduction: One of the challenges in oncology is the monitoring of heterogeneous tumor progression. In contrast to biopsy-based diagnosis, molecular imaging non-invasively provides whole-lesion information. In earlier work we investigated tumor herterogeneity by PET/MRI in the Tg(PyV-mT) model, which develops spontaneous tumors along the mammary glands (MG). We now further employed the Tg(PyV-mT)-MIN-O model which mimics multistep cancer progressing from hyperplasia to carcinoma in situ (CIS) and invasive carcinoma (IC). For a comprehensive characterization of tumor progression, including temporal *in vivo* detection of the angiogenic switch, we employed a variety of biomarkers combined with advanced image analysis. As pre- and lactating MGs represent a physiological situation of increased metabolism they represent an important control for this disease model.

Methods: 5 female FVB mice, transplanted with MIN-O tissue at 3w of age were measured longitudinally 3, 7, 10 and 13w post transplantation (p.t.) in a sequential PET/MRI setup. Anesthetized mice (1-2% isoflurane) were injected *i.v.* with 10±2 MBq of [68Ga]NODAGA-RGD, [11C]Meth, [11C]Chol or [18F]FDG. Anatomical MRI was subsequently fused with the PET data. Mean value and Gaussian Mixture Model (GMM) analysis was applied. Additional 2 mice per tracer were measured on day 16±1 of pregnancy and day 5±1 of lactation to assess the pre- and lactating MG.

Results: The uptake of the prelactating MG was lower than the uptake of all lesion stages for [18F]FDG, [11C]Chol and [11C]Meth. However, the uptake of the early neoplasia (3w) of [18F]FDG and [11C]Chol ([18F]FDG: 3.0±0.9 %ID; [11C]Chol: 2.1±0.8 %ID) was comparable to the lactating MG ([18F]FDG: 2.9±0.2 %ID and [11C]Chol: 1.7±0.2 %ID). [11C]Meth revealed initial increased uptake at 3w (3.3±1.7 %ID vs. lactating: 1.3±0.2 %ID) and a drop down at 7w (2.4±0.7 %ID). [18F]FDG and [11C]Meth then showed static increase from w7-w13, while [11C]Chol stayed stable. GMM confirmed these results, correlating the highest uptake population of [18F]FDG and [11C]Meth with the outgrowth of IC and the highest [11C]Chol uptake population with the CIS. [68Ga]NODAGA-RGD revealed very low angiogenesis from w3-w10 (0.6–0.8±0.2 %ID) in the range of the prelactating MG (0.7±0.2 %ID), but increased to 1.6±0.8 %ID at w13 (>lactating MG: 1.2±0.7 %ID). GMM analysis confirmed a single negative population from w3-w10 and the appearance of a positive population at w13, visualizing the angiogenic switch during tumor progression.

Conclusion: Lactating MGs could not be completely distinguished from the pathologic lesions. Especially since later lesions show mixtures of all stages the GMM analysis is crucial to distinguish these populations. The IC increase correlates with [18F]FDG and [11C]Meth, whereas the stable CIS proportion is represented by [11C]Chol. The *in vivo* detection of the angiogenic switch, as an important factor in multistep carcinogenesis, was feasible, applying advanced image analysis utilizing GMM. This preclinical set-up is an important platform to characterize multistep carcinogenesis and supports the establishment of clinical protocols for PET/MR breast imaging.

AUTHORS (LAST NAME, FIRST NAME): Schmitz, Jennifer[1]; Schwab, Julian[1]; Chen, Qian[2]; Hubbard, Neil E.[2]; Cardiff, Robert D.[2]; Borowsky, Alexander D.[2]; Pichler, Bernd J.[1]; Schmid, Andreas M.[1]

INSTITUTIONS (ALL):

1. Werner Siemens Imaging Center, Department of Preclinical Imaging and Radiopharmacy, Eberhard Karls University Tuebingen, Tuebingen, Germany.

2. Center for Comparative Medicine, University of California, Davis, Davis, CA, United States.

(No Image Selected)

CONTROL ID: 2232969

TITLE: Targeted Gold-Gallium Nanoparticles for Molecular Imaging of EGFR-overexpressing Tumors

PRESENTER: RAGHURAMAN KANNAN

ABSTRACT BODY:

Abstract Body: Introduction: The rapidly advancing field of cancer nanotechnology has generated several innovative radionuclide delivery systems to improve and enhance their targeted transport to the tumor sites. In particular, gold nanoparticles (AuNPs) have very attractive properties for biomedical application that include low immunogenicity, biocompatibility, good biological half-life, and easy functionalization with molecular vectors and with great potential for the development of (nano)radiopharmaceuticals. Herein, we will report on the synthesis, characterization and biological evaluation of AuNPs decorated with chelators for gallium complexation and with a bioactive peptide (GE11 derivative) for targeted radionuclide delivery to epidermal growth factor receptor (EGFR)-overexpressing cancer cells. EGFR is over expressed in many human tumors including colorectal tumor, non-small cell lung tumor, and breast tumor. In the present study, we have developed and optimized a Ga-67 labeled targeted gold nanoparticle for selective uptake in EGFR expressing tumor in mice. Upon substitution of Ga-67 to Ga-68 this construct can be used for PET imaging applications of EGF receptor expressing tumor. In addition, the same nanoconstruct can be used for selective drug delivery applications for cancer therapy.

Materials and Methods: AuNP-DTDTPA nanoparticles were synthesized by reduction of $HAuCl_4$ with $NaBH_4$ in the presence of a dithiolated DTPA derivative (DTDTPA) as stabilizer, followed by loading of the bioactive peptide, by reaction with a GE11 peptide derivative (TA-GE11-DOTA). Radiolabeling with ^{67}Ga was performed using two distinct routes: i) direct labeling of the GE11 peptide-containing AuNPs (Post-DTAu-GE11-DOTA); ii) pre-labeling approach, in which the GE11 peptide derivative was first labeled with 67Ga and then conjugated to AuNP-DTDTPA (Pre-DTAu-GE11-DOTA). Stability studies in physiological media and in the presence of apo-transferrin were performed for the 67Ga-labeled AuNPs as well as cell uptake in EGFR-overexpressing cancer cells (A431) and biodistribution studies in tumor-bearing mice. Further studies underway include the determination of binding affinity and evaluation of receptor activation.

Results and Discussion: Small core (2-3 nm) AuNPs stabilized with DTDTPA and decorated with TA-GE11-DOTA were successfully synthesized. Both direct and pre-labeling approaches provided 67Ga-labeled AuNPs decorated with a GE11 peptide derivative. Post-DTAu-GE11-DOTA displayed a lower capability to maintain suitable 67Ga coordination in physiological media and in the presence of apo-transferrin, compared with Pre-DTAu-GE11-DOTA. Both radiolabeled nanoconstructs display high internalization in A431 cells, with the highest internalization being observed for Post-DTAu-GE11-DOTA. However, blocking studies with EGF showed no significant difference in internalization for Post-DTAu-GE11-DOTA, while in the case of Pre-DTAu-GE11-DOTA about 30% decrease was observed. When administered in tumor-bearing mice, only Post-DTAu-GE11-DOTA showed significant tumor uptake, while in the case of Pre-DTAu-GE11-DOTA, no relevant uptake was observed.

AUTHORS (LAST NAME, FIRST NAME): Paulo, António[2]; Silva, Francisco F.[2]; Campello, M.P.C.[2]; Mendes, Filipa[2]; Belo, Maria M.[2]; Gano, L[2]; Singh, Amolak[1]; Zambre, Ajit[1]; Upendran, Anandhi[3]; KANNAN, RAGHURAMAN[1]

INSTITUTIONS (ALL):

1. RADIOLOGY, UNIVERSITY OF MISSOURI, Columbia, MO, United States.
2. Universidade de Lisboa, Centro de Ciências e Tecnologias e Nucleares (C2TN), Bobadela LRS, Portugal.
3. Institute of Clinical and Translational Science, University of Missouri, Columbia, MO, United States.

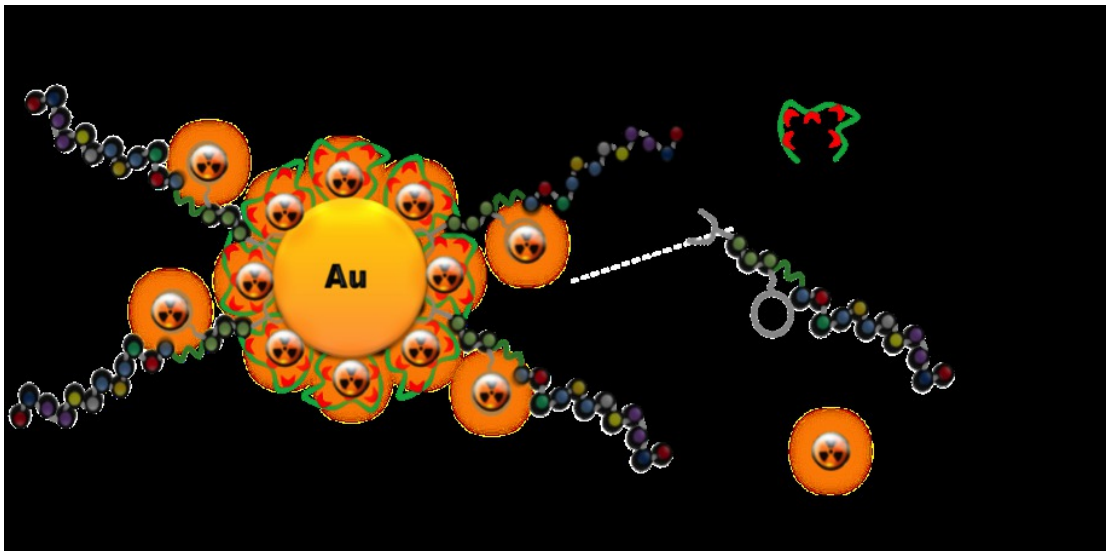
Au

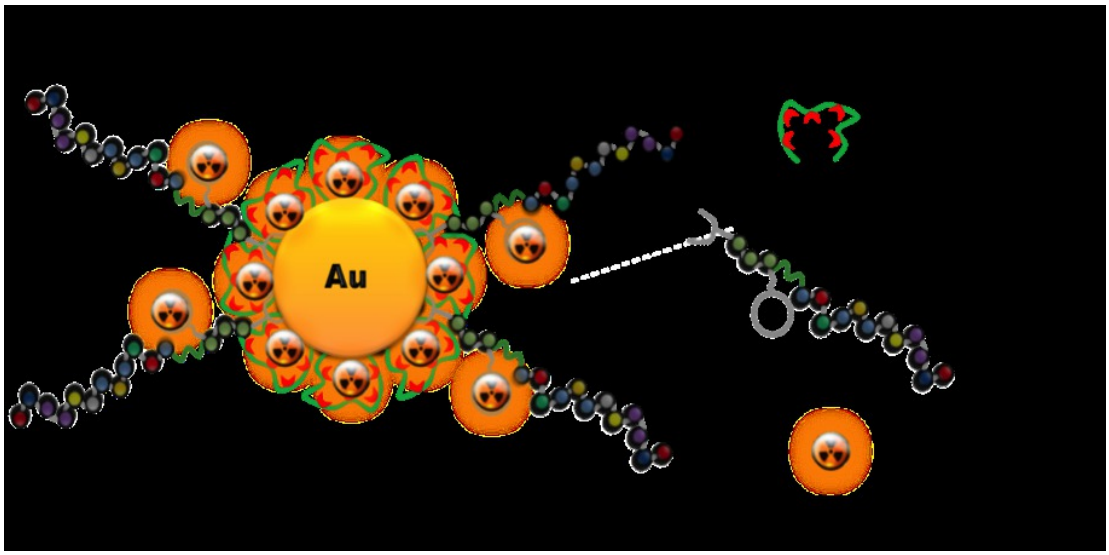

Schematic representation of EGFR targeted gold-gallium nanoparticles

CONTROL ID: 2233439

TITLE: SPECT Imaging in a mouse model of muscular dystrophy: MDX mice have higher uptake of ^{99m}Tc-MDP in muscle than healthy age-matched controls

PRESENTER: Jack Hoppin

ABSTRACT BODY:

Abstract Body: Objectives: ^{99m}Tc-MDP is an *in vivo* bone imaging agent that has been shown to highlight the inflammatory process and bone and muscle calcification in a wide range of osseous and non-osseous disorders[1]. Histological studies of muscle from C57BL/10ScSn-Dmd^{mdx} (MDX) mice have found degenerative lesions with calcification[2]. The objective of this study was to image calcified lesions with ^{99m}Tc-MDP in a mouse model of muscular dystrophy.

Methods: Subjects included male MDX mice (n=5) and controls (n=5). Mice were administered ^{99m}Tc-MDP intravenously (~700 µCi/animal) while awake and were allowed to be freely moving after tracer injection. Mice were anesthetized with isoflurane just prior to imaging and for the duration of each scan and were imaged on the nanoSPECT/CT (Mediso, Budapest, Hungary). A 1x20min static whole-body SPECT scan was acquired followed by CT at 2 hours after tracer injection. Mice were imaged at 6, 15, and 19 weeks of age. After the final *in vivo* imaging timepoint, animals were euthanized, perfused and imaged post-life at ~3 hours post injection. Following post-life imaging, the diaphragm was resected from each animal, fixed in a formalin gel, and imaged *ex vivo* with SPECT/CT. Regions of interest were defined for the scapular muscles, heart, kidneys, quadriceps, skeleton, and diaphragm. Concentration (in SUV) of ^{99m}Tc-MDP in these regions was compared between groups at different time points.

Results: At all imaging timepoints, ^{99m}Tc-MDP concentrations in the heart, left and right quadriceps were significantly ($p<0.05$) higher in MDX mice than controls. ^{99m}Tc-MDP concentrations in the left and right scapular muscles were also higher in MDX mice than control but only significantly higher in the right scapular at 6 weeks and left and right scapular at 15 weeks. Post-life imaging was consistent with *in vivo* imaging at the week 16 timepoint. In *ex vivo* diaphragm imaging, ^{99m}Tc-MDP signal was noticeably higher in the diaphragms from MDX mice.

Conclusions: The MDX mouse model of Duchenne Muscular Dystrophy shows greater uptake of ^{99m}Tc-MDP in muscle, particularly the quadriceps and diaphragm, as compared with controls. This agrees with histological reports of muscle calcification in MDX mice, and suggests that ^{99m}Tc-MDP could be a useful imaging assay in Muscular Dystrophy[2].

AUTHORS (LAST NAME, FIRST NAME): Gaut, Carolynn M.[1]; Sullivan, Jenna M.[1]; Woodson, Whitney[1]; Novicki, Andrew W.[1]; Leen, Molly J.[1]; Lane, Mark[2]; Kentala, Dustin R.[2]; Hoppin, Jack[1]; Verma, Ajay[3]

INSTITUTIONS (ALL):

1. inviCRO, LLC, Boston, MA, United States.
2. MPI Research, Mattawan, MI, United States.
3. Biogen Idec, Cambridge, MA, United States.

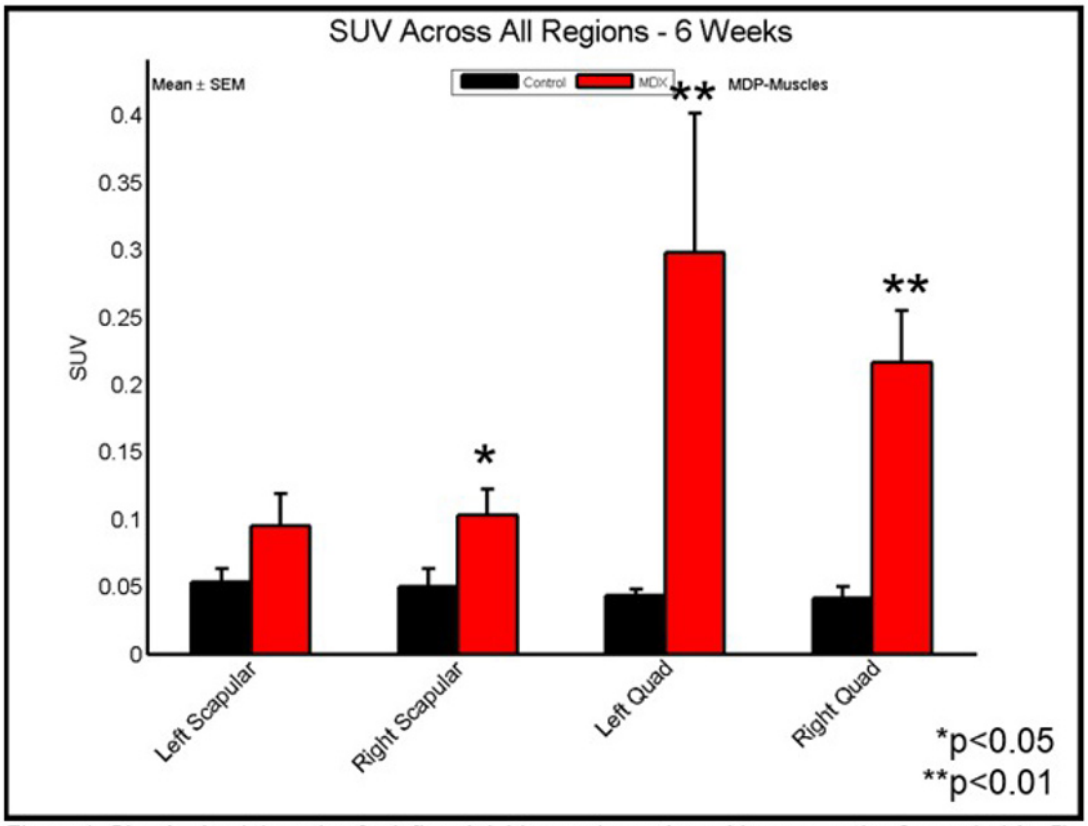

Figure 1: Standard uptake value for left and right scapular and quadriceps muscles for control (n=5) and MDX (n=5) mice at 6 weeks of age.

CONTROL ID: 2232999

TITLE: Photodynamic therapy inhibited tumor growth by targeting upregulated translocator protein in mitochondria

PRESENTER: Mingfeng Bai

ABSTRACT BODY:

Abstract Body: Objectives: Photodynamic therapy (PDT) is proposed a less invasive therapeutic approach for treating cancers. Mitochondrion is an attractive target for developing novel PDT agents, as it produces ATP and regulates apoptosis. Current mitochondrial targeting photosensitizers (PSs) are based on cationic molecules which aims the negatively charged mitochondria membrane. However, such PSs are not specific for cancerous cells, which may result in unwanted side effect. Herein, we report a novel tumor mitochondria-specific PDT approach by targeting translocator protein (TSPO), an 18kDa mitochondrial protein up-regulated in multiple types of cancers including breast, prostate, and brain cancer.

Methods: We developed a novel TSPO-targeted photosensitizer, IR700DX-C_6DAA1106, by conjugating a phthalocyanine dye IR700DX to a functional TSPO-targeted molecule C_6DAA1106. We evaluated the phototherapeutic effect of IR700DX-C_6DAA1106 both in vitro and in vivo.

Results: In vitro study indicated that IR700DX-C_6DAA1106 phototherapy induced photo damage in TSPO positive breast cancer cells (MDA-MB-231) but not TSPO negative breast cancer cells (MCF-7). The treatment resulted in an apoptosis-like cell death, typically seen in mitochondria mediated cell death. Remarkably, in vivo phototherapy study suggested that, IR700DX-C_6DAA1106-mediated phototherapy significantly inhibited the growth of MDA-MB-231 tumors.

Conclusions: In conclusion, we developed a novel mitochondria TSPO targeted photosensitizer IR700DX-C6DAA1106. This photosensitizer effectively induced apoptosis-like cell death in TSPO positive cancer cells. In addition, IR700DX-C6DAA1106 significantly inhibited tumor growth in TSPO positive tumor bearing mice. These combined data suggest that mitochondria TSPO-targeted photosensitizer appears to have great potential as a cancer phototherapeutic agent.

AUTHORS (LAST NAME, FIRST NAME): Bai, Mingfeng[1]; Zhang, Shaojuan[1]; Yang, Ling[1]; Ling, Xiaoxi[1]; Shao, Pin[1]

INSTITUTIONS (ALL):

1. Department of Radiology, University of Pittsburgh, Pittsburgh, PA, United States.

(No Image Selected)

CONTROL ID: 2233003

TITLE: Multiparametric longitudinal *in vivo* PET/MRI imaging of patient derived orthotope and subcutaneous colorectal cancer in rats

PRESENTER: Anna Kuhen

ABSTRACT BODY:

Abstract Body: Colorectal cancer (CRC) is one of the most common causes of cancer mortality worldwide. In preclinical studies, subcutaneous (*s.c.*) tumor models are commonly used. However, in most cases they do not resemble human tumors, since the surrounding tissue can have a high impact on tumor development. Orthotropic (*o.t.*) models have a better clinical relevance and give a better prediction in therapy studies. The aim of our study was to compare *in vivo* tumor development in rats bearing *ot* or *s.c.* CR-LRB-018P CRC in a longitudinal study using different PET tracers and MRI.

S.c. (n=4-6) and o.t. (n=5-7) xenograft tumors from a female patient with fairly differentiated CRC fragments (BRAF, p53 mutations) in rats were obtained from Oncodesign® and measured longitudinally using PET/MRI 2, 6 and 10 weeks (w) post implantation (p.i.). We performed *in vivo* PET scans using [^{18}F]FDG, [^{18}F]FLT and [^{18}F]FMISO as well as MRI to coregistrate PET images to anatomical information and diffusion weighted (DW)-MRI. Data was analyzed by calculating tumor to muscle (t/m) ratios. At w10 rats were sacrificed and tumors were removed for histological and autoradiographic analysis.

For the first imaging time point, w2 p.i., we observed a similar uptake in *o.t.* or *s.c.* tumors using [^{18}F]FDG, [^{18}F]FLT and [^{18}F]FMISO. At w6 p.i., no significant changes in *s.c.* or *o.t.* tumors could be observed for [^{18}F]FDG and [^{18}F]FLT compared to w2. In w10 p.i. we observed significant reduced t/m ratios in *s.c.* tumors compared to w2 using [^{18}F]FDG (w2 t/m=5.7; w10 t/m=4.4; p=0.01) and [^{18}F]FLT (w2 t/m=1.1; w10 t/m=0.9; p=0.006), indicating a reduced glucose metabolism and proliferation in the course of *s.c.* tumor progression over w10. Analyzing [^{18}F]FMISO, we observed a significant reduced tracer uptake in *s.c.* tumors starting in 6w p.i. which last until w10 (w6 t/m=0.8 p=0.004; w10 t/m=0.9, p=0.009) compared to w2 (t/m=1.3) indicating a change in tumor hypoxia due to tumor progression. DW-MRI correlated well with the *s.c.* tumor size. In contrast *o.t.* tumors showed no significant differences in t/m ratios at each time point using [^{18}F]FLT (w2 t/m=1.2; w10 t/m=1.2) and [^{18}F]FMISO (w2 t/m=1.4; w10 t/m=1.3). Only [^{18}F]FDG showed a significant increase in t/m ratios in *o.t.* tumors 10w p.i. versus w2 (w2 t/m=5.4, w10 t/m=7.4; p=0.007). Results indicate enhanced glucose metabolism, constant proliferation and hypoxia within *o.t.* tumors over 10w. Autoradiographic and histological investigations confirmed i*n vivo* PET results.

Our data showed clear differences of tumor metabolism over time between the same implanted fragments from one patient at different locations in rats. The increased glucose metabolism, proliferation and hypoxia detected by *in vivo* PET in *o.t.* tumors at late time points indicate that this model is closer to the clinical reality than the *s.c.* Therefore, it is important to take care of the right animal model in order to translate preclinical results into clinical applications and therapy approaches. As next steps, we will analyze tumor heterogeneity of these tumors over 10w to follow variations of tracer uptake and thus the spatial and temporal intratumoral molecular profile.

AUTHORS (LAST NAME, FIRST NAME): Kuhen, Anna[1]; Fuchs, Kerstin[1]; Harant, Maren[1]; Aidone, Sandro[1]; Pichler, Bernd J.[1]

INSTITUTIONS (ALL):

1. Werner Siemens Imaging Center, Department of Preclinical Imaging and Radiopharmacy, Eberhard Karls University of Tuebingen, Tuebingen, Germany.

(No Image Selected)

CONTROL ID: 2233010

TITLE: IRDye 700DX: Characterization of a 3rd generation photosensitizer for photodynamic therapy

PRESENTER: Joy Kovar

ABSTRACT BODY:

Abstract Body: IRDye 700DX is a near infrared phthalocyanine dye developed for optical imaging applications with structural attributes designed for photodynamic therapy (PDT) applications. The dye is a potential third generation PDT agent where the presence of a functional group (NHS ester or maleimide) allows for easy conjugation to a targeting moiety preserving normal tissues from subsequent damage. We measured IRDye 700DX singlet oxygen production and assessed the dye structural stability and integrity before and after light exposure at various levels of pH. IRDye 700DX NHS ester bound to cell walls induced cytotoxicity when irradiated with 690nm light (16 J/cm^2) confirming the dye to be the active moiety. Two reactions are possible when a photosensitizer is excited: 1) Type I reactions involving the production of a radical or 2) Type II reactions where excited energy is transferred directly to oxygen and generating a highly reactive singlet oxygen. Concentrations of methylene blue and IRDye 700DX (1μM) were irradiated and singlet oxygen production measured using a specific singlet oxygen sensor. IRDye 700DX and methylene blue exhibited a 4-fold increase in singlet oxygen production over non-dye controls. The addition of sodium azide, a singlet oxygen scavenger, at the time of irradiation significantly reduced measurable singlet oxygen production. IRDye 700DX fluorescence intensity was stable at pH levels >6. Photolytic cleavage of IRDye 700DX was assessed at pH 6, 7, and 8. Concentrations of dye (1mg/mL) were irradiated at levels up to 64 J/cm^2 and analyzed by HPLC. The data showed no significant increase in degradation products such as structural loss of either axial arm or decrease in the dye peak in any of the solutions. Percent increase in peaks associated with the axial arm loss from the t = 0 time point were 0.33, 0.07, 0.03, and 0.13% for pH 6, 7, 8, and DMEM control solutions, respectively. Taken together these data support IRDye 700DX as a Type II photosensitizer that remains structurally intact when undergoing PDT.

AUTHORS (LAST NAME, FIRST NAME): Kovar, Joy L.[1]; Cradduck, Mark D.[2]; Volcheck, Bill[2]; Wang, Han-Wei[3]; Draney, Daniel[4]; Urlacher, Teresa[5]

INSTITUTIONS (ALL):

1. Molecular Biology R&D, LI-COR Biosciences, Lincoln, NE, United States.
2. Chemistry R&D, LI-COR Biosciences, Lincoln, NE, United States.
3. Engineering, LI-COR Biosciences, Lincoln, NE, United States.
4. Chemistry, LI-COR Biosciences, Lincoln, NE, United States.
5. Molecular Biology R&D, LI-COR Biosciences, Lincoln, NE, United States.

(No Image Selected)

CONTROL ID: 2233573

TITLE: Challenges and Opportunities for the Development of Imaging Technologies for Global Health

PRESENTER: Tiffani Lash

ABSTRACT BODY:

Abstract Body: Advances in medical imaging technologies for early diagnosis of cancer have resulted in more effective treatments and increases in survival rates. However, in resource limited areas, such as lower and middle-income countries (LMICs) most cancers are diagnosed at a later stage when few treatment options are available resulting in higher mortality and low survival rates. The World Health Organization reports that LMIC's account for 70% of the world's cancer deaths. Most advances that allow early detection have not reached the majority of people around the globe due to their dependency on high cost infrastructure and specifically trained health care providers. Procedures such as PAP smears, considered routine in resource rich countries, are not available in large parts of the world due to lack of facilities and trained personal. Medical imaging technologies such as MRI, PET, CT developed and disseminated in high income countries, require highly trained medical personal to operate/interpret, are not necessarily portable (require appreciable infrastructure to operate) and/or are prohibitively expensive for LMICs. With the rapid rise in the cost of health care there is growing interest and a clear need in developing and translating advanced efficiebt and effective medical technologies for cancer detection, diagnosis and treatment for resource limited settings. Advances in consumer technologies, such as mobile phones with high resolution cameras and internet connectivity provide the perfect tool for expanding access to medical care with images sent to trained professionals at remote sites for analysis, reducing the need for "on site" professionals. Such devices can be used for telemedicine and guidance to health care workers in the field. Software tools can assist in the screening of large populations, enhanceing early detection, diagnosis, and treatment. In addition, emerging modalities for medical imaging, such as near-infra-red, spectroscopic imaging, etc, show great potential for use in LMICs. Such inherently lower cost, lower infrastructure technologies provide little financial incentive for industrial partners to invest developmental support, and governmental funding for research is constantly squeezed. A possible path forward may lie with collaborations among federal agencies, foundations and industry joining together to create funding opportunities and incentivize larger number of researchers to invest time and effort in developing and deploying low cost and efficient screening, diagnostic and treatment technologies. It is also important to point out that profits are also available from economies of scale and can be used to garner interest by industry to partner in the development of medical devices that can benefit LMICs.

This presentation will highlight challenges and opportunities to develop, adapt, integrate, optimize, validate and disseminate (the essence of translation) medical imaging technologies suitable for use in low resources settings. NCI and NIBIB's current efforts and promising results in addressing these issues will be discussed.

AUTHORS (LAST NAME, FIRST NAME): Tandon, Pushpa[3]; Ossandon, Miguel R.[1]; Baker, Houston[2]; Lash, Tiffani B.[4]

INSTITUTIONS (ALL):

1. Cancer Diagnosis Program, National Cancer Institute, Bethesda, MD, United States.
2. Cancer Imaging Program, National Cancer Institute, Bethesda, MD, United States.
3. Division of Cancer Treatment and Diagnosis, Cancer Imaging Program, National Cancer Institute, Rockville, MD, United States.
4. National Institute of Biomedical Imaging and Bioengineering, Bethesda, MD, United States.

(No Image Selected)

CONTROL ID: 2233035

TITLE: Molecular PET imaging of serotonin $5HT_{1A}$ receptor and brain metabolism after electrical stimulation of Medial Raphe Nucleus (MRN) in rats.

PRESENTER: Miguel Pozo

ABSTRACT BODY:

Abstract Body:

Introduction and aim

Brain stimulation is an alternative to drug therapy for the treatment of medically-intractable epilepsy (Ostergard & Miller, 2014). It is widely accepted that an imbalance between glutamatergic and GABAergic systems causes epileptic hyperexcitability. It has been reported that serotonin system through $5HT_{1A}$ receptor may modulate the epileptogenesis process (Bagdy et al., 2007). Therefore, we aimed to study the serotonergic projection to the forebrain in order to explore the eventual changes in $5HT_{1A}$ receptor functionality and brain metabolism induced by electrical stimulation of MRN.

Methods

All experiments involved male Sprague Dawley rats (300 ± 33 g) and were performed in accordance with guidelines of the European Union for the use of laboratory animals.

Stereotaxic electrode implantation was performed under isofluorane anaesthesia according to stereotaxic atlas. A bipolar-stimulating electrode was implanted in MRN. Electrical stimulation consisted of a 66 pulse-train (20Hz, 1 sec) of monophasic pulses (0.1 ms and 150 microA).

PET imaging studies were performed in Albira ARS scanner, Oncovision, Valencia (Spain). Dynamic acquisitions were performed for ^{18}F-MPPF. The length was 45 min and during the first 5 min, the rats were stimulated. On the other hand, for determination of the brain metabolism, 20 min static ^{18}F-FDG acquisitions were carried out.

Data analysis: ^{18}F-MPPF binding potential (BP) was obtained to evaluate the 5-HT_{1A} receptor functionality. Cerebellum normalized activity was calculated in different brain structures in order to determine the regional glucose brain metabolism.

Statistical analysis: Two-tailed Student-t test was carried out. Statistical differences was considered significant when $p<0.05$.

Results

This study shows that MRN stimulation decreased the BP of ^{18}F-MPPF in hippocampus ($p\leq\leqq0.03$), septum ($p\leqq0.05$) and cortex ($p\leq0.0001$). Furthermore, the brain metabolism was also significatly decreased ($p\leq0.05$) in the same brain areas.

Conclusions

Reduction in 18F-MPPF BP values could be due the release of the endogenous serotonin after MRN electric stimulation. In addition, the hypometabolism observed matches with regions in which the BP was declined. Overall, our results suggest that the putative antiepileptic effect by MRN stimulation it could be through the activating of 5-HT_{1A} receptors linked to inward-rectifying potassium current that hyperpolarized hippocampal and cortical neurons.

AUTHORS (LAST NAME, FIRST NAME): Bascuñana, Pablo[2]; El-Sayed, Ahmed A.[3]; Fernandez de la Rosa, Ruben[3]; Delgado, Mercedes[3]; Garcia-Garcia, Luis[3]; Pozo, Miguel A.[3, 1]

INSTITUTIONS (ALL):

1. Instituto Tecnológico PET, Madrid, Spain.
2. Preclinical Molecular Imaging, Nuclear Medicine Departmen, Medizinische Hochschule Hannover, Hannover, Germany.
3. Instituto Pluridisciplinar UCM, Madrid, Spain.

(No Image Selected)

CONTROL ID: 2233013

TITLE: High-resolution quantitative mapping of glucose metabolic disorders following mild traumatic brain injury using in vivo glucoCEST

PRESENTER: Tsang-Wei Tu

ABSTRACT BODY:

Abstract Body: INTRODUCTION

Tramatic brain injury (TBI) results in an instant perturbation to the cerebral glucose metabolism and longterm cognitive deficits. ^{18}F-FDG PET is the major molecular imaging modality to track the matabolic changes in brain [1-3]. The drawbacks of PET, including blurring images, low resolution, radiation dose limit and increased FDG accumulation, may cause false-positive results in a longitudinal study. Here we present an alternative MRI-based molecular imaging, named chemical exchange saturation transfer (CEST) MRI, to noninvasively detect the glucose metabolism without the need for a radioisotope. Our results indicate that the glucose CEST-MRI (glucoCEST) could be another sensitive molecular imaging technique for detecing glucose metabolism non-invasively in brain trauma.

MATERIALS AND METHODS

A phantom experiment was first conducted including five glucose concentrations close to that of the living tissues (2mM~10mM). For in vivo study, female 10-week-old SD rats (n=6) were scanned prior to injury, then undergone TBI via a 2m height/450g weight drop. CEST-MRI were acquired by a Doty coil in a Bruker 9.4T, 2D fast spin echo with magnetization transfer (MT) pulses (TR 3.5s, TE 11.5ms; resolution: 200μm, thickness: 0.8mm; MT pulse: 2μT, 2s). MT offset frequences (Δω) were -2kHz to +2kHz with 100Hz stepping (glucose at 1.2ppm, 2.1ppm, 2.9ppm) [4]. MTR asymmetry (MTR_{asym}) was derived by subtracting right (−Δω) and left (Δω) MT signal intensity in the unit of percentage. Animals were imaged at baseline, 1, 8, 16, 24 and 48 days-post-injury (DPI). One-way ANOVA with repeated measures was performed by Prism v6.

RESULTS

The CEST Z-spectrums and MTR_{asym} curves of the glucose phantom is showing in figure 1A, demonstrating the feasibility of measuring glucose concentration. MTR_{asym} delivered clear contrast by glucose concentraions and showed linearity (Fig. 1B, C). The MTR_{asym} maps exhibited temporospatial distributions of glucose in brain and clearly distinguished levels of metabolism between structures (Fig. 1D). The glucose metabolism was significantly decreased ($p<0.01$) in the injured cerebral cortex with progressive decreases from injury to 16 DPI, then slightly increased in 48 DPI (Fig. 1E).

DISCUSSION

In mild TBI, the energy substrate supply and consumption is crucial for the survival of traumatized brain tissue. The widespread hypometabolic changes, however, could affects the brain functions in learning and memory and results in progressive cerebral atrophy [3]. This study shows that glucose largely decreases after TBI, and persists chronically. glucoCEST could provide comparable results to previous PET studies [1-3], yet delivers better image quality, higher image resolution and sensitivity to the changes of glucose metabolism [5, 6]. glucoCEST is able to identify the potential window for effective treatments to increase the survival of traumatized tissue.

REFERENCES

1. Liu, J. Nuclear Medicine, 2010;
2. Li., J. Neurotrauma, 2012
3. Moore, JCBFM, 2000
4. W-Samuel, Nature Medicine, 2013
5. Kim. MRM, 2009.
6. Stancanello, NMR Biomed, 2008

AUTHORS (LAST NAME, FIRST NAME): Tu, Tsang-Wei[1]; Williams, Rashida[1]; Jikaria, Neekita[1]; Turtzo, Lisa[1]; Frank, Joseph[1]

INSTITUTIONS (ALL):

1. Radiology and Imaging Sciences, National Institute of Health, Bethesda, MD, United States.

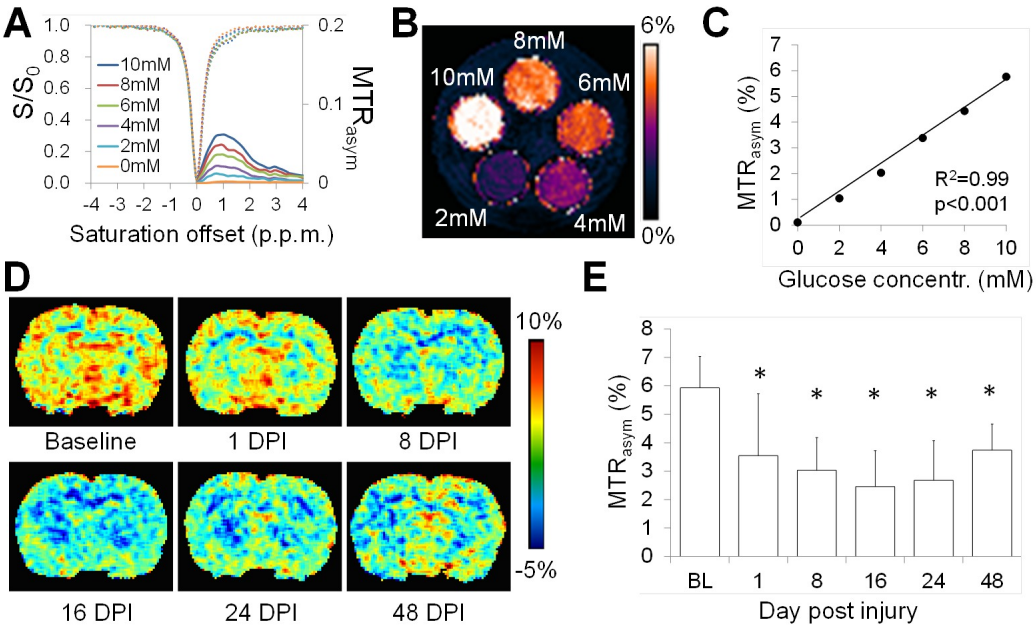

Fig. 1 CEST Z-spectrum (dotted lines) and the MT asymmetry curves (solid lines) of different glucose concentrations (A). The MTR_{asym} map of glucose phantom clearly differentiate the difference of glucose concentrations (B). The parameter of MTR_{asym} derived from glucoCEST generates a linear relation to the set glucose concentrations (C). A strong correlation is seen between the MTR_{asym} and the glucose concentrations. The in vivo glucoCEST imaging generated high quality glucose maps showing various level of glucose metabolism in different anatomical structure (D). The longitudinal glucose maps detected the changes of glucose metabolism in a rat brain following TBI. The glucose level significantly decreased in the cerebral cortex of the injured brain, suggesting the decrease of glucose metabolism after mild TBI. After trauma, compared to the baseline level, glucose metabolism progressively decreased down to 42% from day 1 to day 16. After reaching the lowest level at day 16, cerebral glucose metabolism slightly returned to 63% of the baseline at day 48. Data are reported as mean ± standard deviation. * $p<0.01$

CONTROL ID: 2233385

TITLE: ^{68}Ga-PSMA dynamic PET/CT in prostate cancer

PRESENTER: Antonia Dimitrakopoulou-Strauss

ABSTRACT BODY:

Abstract Body: Objectives: To date the contribution of imaging modalities in prostate cancer (PC) diagnostics and patient management is rather limited, and certainly smaller than in other common cancers. ^{68}Ga-PSMA PET/CT constitutes a promising step towards the improvement of PC diagnostics. Aim of our study is to assess the distribution patterns and pharmacokinetics of ^{68}Ga-PSMA in patients suffering from PC by means of dynamic and whole body PET/CT.

Methods: 47 patients with PC (18 primary PC, 29 pre-treated PC) were enrolled in the study. Their median PSA value was 3.6 ng/mL. All patients underwent dynamic PET/CT (dPET/CT) scanning (60 min) of the pelvis as well as whole body PET/CT studies with ^{68}Ga-PSMA. dPET/CT assessment was based on qualitative evaluation, SUV calculation, and quantitative analysis based on a 2-tissue compartment model and a non-compartmental approach.

Results: In 38 patients at least one lesion was detected, while 9 patients were ^{68}Ga-PSMA-negative. In total 205 lesions were detected (17 primary PCs, 6 recurrent PCs, 182 metastatic lesions in lymph nodes, soft tissue and bones). Semi-quantitative evaluations revealed the following values for the all PC-associated lesions: mean $SUV_{average}$ =12.8 (median =8.8) and mean SUV_{max} =20.6 (median =15.6). Dynamic PET/CT studies of the pelvis revealed the following absolute ^{68}Ga-PSMA quantitative values: K_1=0.25 (median=0.19), k_3=0.34 (median=0.27), influx=0.15 (median=0.10), FD=1.26 (median=1.29). Patients with no lesions on ^{68}Ga-PSMA PET/CT had a median PSA of 0.6 ng/mL, while patients positive on ^{68}Ga-PSMA PET/CT had a median PSA of 4.8 ng/mL. Spearman's correlation analysis demonstrated a weak positive but statistically significant ($p<0.05$) correlation between PSA and the following ^{68}Ga-PSMA PET parameters: $SUV_{average}$, SUV_{max}, influx and FD.

Conclusions: ^{68}Ga-PSMA PET/CT revealed at least one lesion in 38/47 patients. Patients positive on ^{68}Ga-PSMA PET/CT had higher PSA values than those who were ^{68}Ga-PSMA negative. Quantitative ^{68}Ga-PSMA parameters correlate weakly positive with PSA values.

AUTHORS (LAST NAME, FIRST NAME): Sachpekidis, Christos[1]; Kopka, Klaus[2]; Haberkorn, Uwe[3, 1]; Dimitrakopoulou-Strauss, Antonia[1]

INSTITUTIONS (ALL):

1. Clinical Cooperation Unit Nuclear Medicine, German Cancer Research Center, Heidelberg, Germany.
2. Division of Radiopharmaceutical Chemistry, German Cancer Research Center, Heidelberg, Germany.
3. Division of Nuclear Medicine, University of Heidelberg, Heidelberg, Germany.

(No Image Selected)

CONTROL ID: 2233038

TITLE: Near Infrared Imaging of Damaged and Dystrophic Muscle

PRESENTER: Glenn Walter

ABSTRACT BODY:

Abstract Body: Background: Though near infrared optical imaging (NIR-OI) has several current clinical uses [1]; its utilization to assess muscle damage is still developing. Through use of an FDA approved contrast agent (indocyanine green; ICG), we tested whether healthy and damaged muscle could be differentiated by NIR-OI in two animal models of muscle damage, an immobilization-reambulation model of acute damage and recovery [2] and in the *mdx* mouse model of Duchenne muscular dystrophy [3]. Muscle damage was confirmed noninvasively using Magnetic Resonance Imaging (MRI) and Spectroscopy (MRS) and by standard histology [3,4]. **Methods:** To assess acute muscle damage, single hindlimbs of C57/BL10 mice were cast immobilized in a plantar flexed position for two weeks [2]. Following cast removal, mice were allowed to freely ambulate and data (MRI, MRS, NIR-OI) were collected. To assess muscle damage and recovery in a model of chronic muscle damage, the limbs of *mdx* mice were compared to age-matched unaffected C57/BL10 mice. Next, MR and NIR-OI data were collected from older *mdx* mice that were subjected to a downhill treadmill running exercise. Prior to NIR-OI, mice were intravenously injected with preclinical grade ICG (Nirawave C). All mice were imaged on an Agilent 4.7T MR Scanner and an IVIS Spectrum In Vivo System to capture MRI/MRS and NIR-OI data, respectively. 2D fluorescence images were captured using excitation and emission wavelengths of 745 and 820 nm, respectively and tomographic data was acquired using a custom built FMT device. For MR, multiple slice spin echo scans were acquired to assess MRI-T_2 relaxation and ^1H_2O spectroscopic relaxometry was assessed using STEAM spectroscopy. Following imaging, mice were injected with Evan's blue dye and standard histological techniques were performed [4]. **Results:** In the immobilization-reambulation mouse model, damage was observed in the deep soleus muscle of the immobilized leg by MRI-T_2, ^1H_2O-T_2, and radiant efficiency (Fig.1) compared to the non-casted contralateral leg, peaking at the second day of reambulation ($p<0.05$) followed by a return to baseline. When comparing C57/BL10 to *mdx* limbs, MRI-T_2, ^1H_2O-T_2, and radiant efficiency were significantly elevated ($p<0.05$) in *mdx* muscles. Additionally, following downhill treadmill running, MRI-T_2, ^1H_2O-T_2, and radiant efficiency increased ($p<0.05$) in the post-treadmill cohort of *mdx* mice compared to their respective pre-running values measurements. **Conclusions:** NIR-OI demonstrated the ability to detect acute muscle damage after reambulation in control mice and downhill hill running in dystrophic mice, as well as chronic muscle damage in dystrophic muscle. To our knowledge, this study is the first to demonstrate the capability of NIR-OI to quantify muscle damage in pre-clinical models. This preliminary work supports NIR-OI as a feasible, cost effective, non-invasive, longitudinal means to quantify muscle damage.

References:

1. Frangioni J. *Curr Op in Chem Biol*, (2003). PMID: 14580568
2. Frimel T, et al. *Muscle & Nerve.* (2005). PMID: 16025524
3. Mathur S, et al. *Muscle & Nerve*. (2011). PMID: 21488051
4. Hamer P, et al. *J of Anat.* (2002). PMID: 11837252

AUTHORS (LAST NAME, FIRST NAME): Chrzanowski, Stephen M.[1]; Batra, Abhinandan[2]; Lee, Brittany[1]; Vohra, Ravneet[1]; Forbes, Sean[2]; Jiang, Huabei[3]; Vandenborne, Krista[2]; Walter, Glenn[1]

INSTITUTIONS (ALL):

1. Physiology and Functional Genomics, University of Florida, Gainesville, FL, United States.
2. Physical Therapy, University of Florida, Gainesville, FL, United States.
3. Biomedical Engineering, University of Florida, Gainesville, FL, United States.

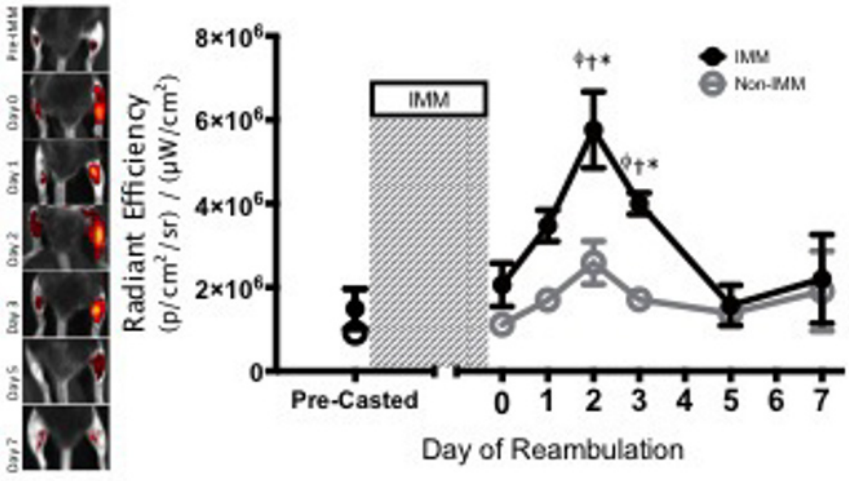

Two dimensional NIR optical imaging shows an increase and reocovery of muscle following immobilization. NIR optical images of immobilized (black) and non-immobilized (gray) mouse hindlimbs were acquired, and radiant efficiency was quantified during the week of reambulation following cast immobilization. Significant differences versus contralateral limb (Φ), pre-immobilized time point of the same limb (†) and Day 0 of the same limb (*) are indicated.

CONTROL ID: 2233048

TITLE: Commonly used ^{64}Cu chelating systems in direct comparison: Determination of complex stabilities using a combination of in vitro and in vivo methods

PRESENTER: Carmen Waengler

ABSTRACT BODY:

Abstract Body: A radionuclide of high potential for PET imaging is ^{64}Cu as it exhibits favorable physical decay characteristics. However, the stable complexation of $^{64}Cu^{2+}$ is intricate, resulting in elevated background radioactivity levels when the radioisotope gets liberated from the complex. Three chelating agents are commonly used for the introduction of ^{64}Cu: NODA-GA, CB-TE2A and CB-TE1A-GA. However, no studies are available directly comparing the stability of all three ^{64}Cu-complexes and some of the two-sided comparisons seem to give contradictory results. In general, the determination of complex stabilities in vivo by using the corresponding peptidic radiopharmaceuticals is of limited relevance as not only the complex stabilities influence the biodistribution of the radionuclide but also the ligand the nuclide is introduced in. However, the solely in vitro determination of the thermodynamic or kinetic stability of the complex is known not to be able to fully predict the complex stability in vivo.
Thus, we followed a combined in vitro and in vivo approach using different ^{64}Cu-radiolabeled peptide systems in order to clarify which is the most appropriate chelator system for Cu^{2+} radioisotopes with regard to complex stability.

The different peptidic labeling precursors were synthesized by solid phase peptide synthesis followed (in case of multimers) by liquid phase tetramerization. The ^{64}Cu-radiolabeled NODA-GA-, CB-TE2A- and CB-TE1A-GA-derivatized radiotracers could be obtained within 10 minutes reaction at ambient temperature or 99°C, yielding the products in high radiochemical yields and purities of ≥99% as well as non-optimized specific activities of 11 to 370 GBq/µmol using precursor amounts of 0.25 - 5 nmol.
For the determination of the in vivo complex stabilities, ^{64}Cu-c(RGDfC)-tetramers were synthesized as the use of such large peptidic systems should minimize the effect of the complex on the in vivo biodistribution of the radiotracer. Preceding evaluations showed absolutely comparably tracer lipophilicities of all tracers of -2.97 ± 0.06, -3.22 ± 0.09 and -3.12 ± 0.05 for ^{64}Cu-NODA-GA-RGD$_4$, ^{64}Cu-CB-TE2A-RGD$_4$ and ^{64}Cu-CB-TE1A-GA-RGD$_4$, meaning that the in vivo biodistribution experiments should not be influenced by the used chelating chemistry. The in vivo biodistribution properties of the ^{64}Cu-c(RGDfC)-tetramers are currently tested in mice.
For the in vitro stability determinations, challenge experiments of ^{64}Cu-PESIN derivatives with the respective other chelator systems were performed. The obtained results suggest a significantly higher complex stability of ^{64}Cu-CB-TE1A-GA compared to ^{64}Cu-NODA-GA and ^{64}Cu-CB-TE2A which is reflected in a considerably lower transchelation ratio, and also a considerable reduction of complex stability if one of the carboxylic functionalities of the chelator is converted into an amide upon conjugation.

The results of this study will answer the question which of the commonly applied chelator systems yields the most stable ^{64}Cu complexes producing the lowest background signals in in vivo PET imaging.

AUTHORS (LAST NAME, FIRST NAME): Litau, Shanna[1]; Seibold, Uwe[1]; Waengler, Bjoern[1]; Waengler, Carmen[1]

INSTITUTIONS (ALL):

1. Department of Clinical Radiology and Nuclear Medicine, Medical Faculty Mannheim of Heidelberg University, Mannheim, Germany.

(No Image Selected)

CONTROL ID: 2233065

TITLE: Intravoxel incoherent motion diffusion weighted imaging and dynamic contrast-enhanced MRI for *in vivo* monitoring the therapeutic efficacy of nanosecond pulsed electric field in cervical cancer xenograft model

PRESENTER: Jingjuan Liu

ABSTRACT BODY:

Abstract Body: Objective :

To monitor early and long-term therapeutic response and explore mechanism of nsPEF treating HeLa cervical cancer-bearing nude mice *in vivo* with multi b-value DWI and DCE-MRI.

Methods:

Nude mice bearing HeLa cervical cancer were randomly divided in the nsPEF-treated and control groups, the former one received 200 pulses nsPEF treatment with 100ns pulsed duration and 50kv/cm intensity. Multi b-values DWI and DCE-MRI were conducted separately using 3.0T MRI unit coupled with a 35mm diameter small animal coil. 10 nude mice (5 from nsPEF-treated and 5 from control group) got a continuous monitoring with DWI scan before, 24 hours and 14 days after nsPEF treatement or none; while the other 7 nude mice (4 from nsPEF-treated and 3 from control group) got the DCE-MRI scan before and 14 days after nsPEF treatement or none. D (pure molecular diffusion), D^* (perfusion related diffusion), and f (perfusion fraction) were obtained applying a bi-exponential IVIM model of multi b-values DWI, and a series of pharmacokinetic parameters such as CER, K^{trans}, K_{ep}, V_e ,fPV and AUC_{90} were obtained from a two-compartment model of DCE. All data were compared with

Immunohistochemical staining of CD31,CD34 and TUNEL test were performed in the excised tumors to evaluate the neovasculature and apoptosis/necrosis pathologically. Quantitative parameters as described above were acquired from the functional MRI and analyzed in student t test or repeated measures of multi-variance analysis in SPSS20.0, as well a less than 0.05 two-side p value is considered statistical significant.

Results :

Growth of tumor exposed to nsPEF has been inhibited by prominently than control group, whose tumor volume was decreased by 37% while the latter one was increased by 150%(p=0.025). In the multi b-value DWI team, D value showed significant rise in nsPEF group, particularly at 24h time point, which however decreased gradually in the control group along with tumor progression (p=0.022), indicating D can predict early response to nsPEF therapy. Pathological results verified necrosis and apoptosis induced by nsPEF in HE stain and TUNEL assay. In DCE-MRI team, quantitative neovasculature related parameters significantly decreased 14 days after nsPEF treatment ($\Delta K^{trans}=K^{trans}_{-14day}-K^{trans}_{pre}$, $\Delta K^{trans}_{control}=0.049\pm0.018 min^{-1}$ vs. $\Delta K^{trans}_{nsPEF}=-0.028\pm0.006\ min^{-1}$, p=0.005) and it correlated with lower vessel density of CD31 and CD34 in immunohistochemistrical stain.

Conclusion :

D value from the bi- exponential IVIM model of multi-b value DWI is a sensitive quantitative imaging biomarker for evaluating early response of nsPEF treatment in cervical cancer xenograft. DCE-MRI is a robust non-invasive tool to measure amounts and functions of tumor's angiogenesis and reaction to anti-angiogenic therapy in vivo. nsPEF can inhibit tumor growth by induce cellular apoptosis in early phase and suppress blood vessels in the long term.

AUTHORS (LAST NAME, FIRST NAME): Liu, Jingjuan[1]

INSTITUTIONS (ALL):

1. Radiology, Peking Union Medical College Hospital, Beijing, China.

(No Image Selected)

CONTROL ID: 2233146

TITLE: Phosphoramidon Improves the Theranostic Prospects of the GRPR-Antagonist SB3, Labeled with Different Radiometals

PRESENTER: Theodosia Maina

ABSTRACT BODY:

Abstract Body: Aim: Bombesin (BBN)-like peptides are well-known substrates for neutral endopeptidase (NEP), a cell-surface zinc-metalloproteinase abundantly expressed in mammal tissues [1]. In this study, we evaluated the impact of transient in vivo NEP inhibition on the theranostic potential of [^{68}Ga/^{111}In/^{177}Lu]SB3 for prostate cancer using the potent competitive NEP-inhibitor phosphoramidon (PA). SB3 is a new DOTA-functionalized analog of the potent and selective gastrin releasing peptide receptor (GRPR)-antagonist [DPhe^{6},Leu-NHEt^{13}]BBN(6-13), suitable for labeling with trivalent radiometals useful for SPECT or PET diagnostic imaging and radiotherapy [2,3].

Materials and Methods: The GRPR-affinities of SB3 and its metallated species were determined in PC-3 cell membranes against [^{125}I-Tyr^{4}]BBN. Radioligand internalization was assessed by 1 h incubation in PC-3 cells at 37°C in the absence or presence of 1 μM [Tyr^{4}]BBN. [^{67}Ga/^{111}In/^{177}Lu]SB3 were injected in mice without (control) or with PA (300 μg) and blood withdrawn 5 min post injection (pi) was analyzed by HPLC. Biodistribution studies were performed in SCID mice bearing PC-3 xenografts at 4 h and 24 h pi. [^{67}Ga/^{111}In/^{177}Lu]SB3 were injected without (control) or with PA (300 μg).

Results: SB3 and its Ga/In/Lu-metallated exhibited high GRPR-affinity with IC_{50} found in the lower nM-range. [^{67}Ga/^{111}In/^{177}Lu]SB3 specifically bound to the membrane of PC-3 cells without being internalized, as consistent with radioantagonists. While [^{67}Ga]SB3 was found >90% stable at 5 min pi in the mouse bloodstream, the observed degradation of [^{111}In/^{177}Lu]SB3 was suppressed by PA-treatment. [^{67}Ga]SB3 showed a very high uptake in the PC-3 tumors of 40.0±6.9%ID/g at 4 h pi independent of PA treatment. In contrast, tumor values for [^{111}In]SB3 and [^{177}Lu]SB3 were much lower in the 4 h pi control groups (8.8±3.0%ID/g and 8.2±1.6%ID/g, respectively). However, in the PA-treated mice these values impressively increased to 38.3±7.9%ID/g ([^{111}In]SB3) and 39.2±6.2%ID/g ([^{177}Lu]SB3). This effect was still evident at 24 h pi, as reflected for [^{177}Lu]SB3 in the tumor uptake increase from 2.22±0.15%ID/g (control) to 8.35±0.72%ID/g (PA-treated).

Conclusions: [^{67}Ga]SB3 is in vivo robust and effectively targets prostate cancer in a mouse model, but [^{111}In/^{177}Lu]SB3 can achieve similar profile only during NEP-inhibition. This strategy emerges as powerful new tool to strengthen the theranostic potential of GRPR-antagonist radioligand pairs and warrants further investigation for translation into the clinic.

Literature

1. Roques BP. Zinc metallopeptidases: active site structure and design of selective and mixed inhibitors: new approaches in the search for analgesics and anti-hypertensives. Biochem Soc Trans 21 (Pt 3) (3):678-685;1993.

2. Cescato R, Maina T, Nock B, et al. Bombesin receptor antagonists may be preferable to agonists for tumor targeting. J Nucl Med. 2008;49:318-326.

3. Nock BA, Maina T, Krenning EP, de Jong M. “To Serve and Protect” – Enzyme Inhibitors as Radiopeptide Escorts Promote Tumor Targeting. J. Nucl. Med. 55(1): 121-127; 2014.

AUTHORS (LAST NAME, FIRST NAME): Nock, Berthold[1]; Lymperis, Emmanouil[1]; Kaloudi, Aikaterini[1]; Krenning, Eric[2]; de Jong, Marion[2, 3]; Maina, Theodosia[1]

INSTITUTIONS (ALL):

1. Molecular Radiopharmacy, INRASTES, NCSR "Demokritos", Athens, Greece.
2. Department of Nuclear Medicine, Erasmus MC, Rotterdam, Netherlands.
3. Department of Radiology, Erasmus MC, Rotterdam, Netherlands.

(No Image Selected)

CONTROL ID: 2233632

TITLE: In Vivo Stabilized Theranostic Agent for PET Imaging and Radionuclide Therapy of Prostate Cancer

PRESENTER: Marion de Jong

ABSTRACT BODY:

Abstract Body: Significance: Prostate cancer represents a major burden for men in the western world, and survival rates decrease tremendously when the cancer has spread beyond the prostate. A single tool that would allow early detection, accurate staging, and treatment of prostate cancer (PCa) would be a major breakthrough in the field of PCa. Theranostics agents include molecules that can be used both for diagnosis and therapy. Theranostic agents can be targeted to specific biomarkers on PCa lesions. Such is the gastrin-releasing peptide receptor (GRPR), which is overexpressed in the majority of PCa, but not in healthy prostate. GRPR-directed antagonists are promising vectors for theranostic agents, offering rapid target access and fast washout from non-target tissues. However, safe delivery to the target is threatened by in vivo degradation by proteolytic enzymes. In this study, we show that co-injection of a single neutral endopeptidase (NEP) inhibitor, phosphoramidon (PA), can contribute to an impressive enhancement in diagnostic sensitivity and therapeutic efficacy of a GRPR-targeted theranostic agent. Methods: The GRPR-antagonist JMV4168 was radiolabeled with the positron-emitter ^{68}Ga for PET imaging and the β-emitter ^{177}Lu for radionuclide therapy and evaluated in mice bearing subcutaneous human GRPR-positive PC-3 xenografts. For blood stability studies, blood was drawn 15 min after injection of ^{177}Lu-JMV4168 (25 MBq, 200 pmol) with or without PA (300 µg) and analyzed by high-liquid performance chromatography. Biodistribution studies were performed at several time points after injection of ^{68}Ga-JMV4168 or ^{177}Lu-JMV4168, with or without PA (300 µg). PET/CT imaging was performed 2 h after injection of ^{68}Ga-JMV4168 (2-7 MBq, 200 pmol) with or without PA (300 µg). Radionuclide therapy studies were conducted in mice with ^{177}Lu-JMV4168 (4 cycles of 200 pmol, 50 MBq) with or without PA (300 µg). Tumor size was followed by caliper measurements. Immunofluorescence staining (53BP1, γH2AX, geminin) and TUNEL detection were performed on tumors taken out 8 days after the last injection of ^{177}Lu-JMV4168. Results: Co-injection of PA led to stabilization of ^{177}Lu-JMV4168 in mice blood, as shown by an increase from 48% to 84% intact radiopeptide after 15 min. In mice bearing PC-3 xenografts, tumor uptake increased from 9.86 % to 19.08 % and 8.97 % to 17.23 % with co-injection of PA, 1 h after injection, for ^{68}Ga-JMV4168 and ^{177}Lu-JMV4168, respectively. Visualization of PC-3 tumors in mice by PET imaging with ^{68}Ga-JMV4168 was substantially improved by co-injection of PA. Radionuclide therapy with ^{177}Lu-JMV4168 (4 cycles of 200 pmol, 50 MBq) in the PC-3 xenograft model showed regression of tumor size, enhanced DNA double strand break repair, decreased cell division and increased apoptosis. Increased survival and enhanced DNA damage were observed in the group treated with ^{177}Lu-JMV4168 + PA, as compared to the control group. This data shows that co-injection of a single peptidase inhibitor can greatly enhance the potential of GRPR-targeted peptide-based theranostic agents for PCa.

AUTHORS (LAST NAME, FIRST NAME): Chatalic, Kristell L.[1, 5]; Konijnenberg, Mark[3]; Nonnekens, Julie[6]; de Blois, Erik[3]; Hoeben, Sander[5]; de Ridder, Corrina[5]; Nock, Berthold[2]; Maina, Theodosia[2, 3]; van Weerden, Wytske[5]; de Jong, Marion[3, 4]

INSTITUTIONS (ALL):

1. Nuclear Medicine, Erasmus MC, Rotterdam, Netherlands.
2. Molecular Radiopharmacy, INRASTES, NCSR "Demokritos", Athens, Greece.
3. Department of Nuclear Medicine, Erasmus MC, Rotterdam, Netherlands.
4. Department of Radiology, Erasmus MC, Rotterdam, Netherlands.
5. Department of Urology, Erasmus MC, Rotterdam, Netherlands.
6. Department of Human Genetics, Erasmus MC, Rotterdam, Netherlands.

(No Image Selected)

CONTROL ID: 2233084

TITLE: Gold silver alloy nanoparticles (GSAN): a contrast agent for both dual energy x-ray mammography and computed tomography

PRESENTER: Pratap Naha

ABSTRACT BODY:

Abstract Body: Introduction

Early detection of breast cancer with mammography screening reduces mortality however, mammography has significantly reduced sensitivity in women with dense tissue. Therefore, additional methods are needed to effectively screen women with dense breasts. Contrast-enhanced dual energy (DE) mammography is a novel x-ray based imaging technique used to screen for breast cancer. Nanoparticle based imaging probes possess several advantages over clinically available small molecule contrast agents, such as higher payloads of contrast producing material, longer circulation half-lives and consequently improved tumor accumulation. Silver provides excellent contrast in DE mammography (Fig S1), but there is a safety concern as silver ions can leach from silver nanoparticles. We hypothesized that the inclusion of gold in the formulation could improve biocompatibility, while maintaining DE mammography contrast. We therefore synthesized gold-silver alloy nanoparticles (GSAN) with a range of silver:gold ratios. In this study we present ˂ 5 nm m-PEG capped GSAN (A) that are biocompatible, produce strong DE mammography and CT contrast, are expected to have long circulation half-lives and to perform well for tumor identification.

Methods and Results

A range of m-PEG capped GSAN formulations (termed Ag-100, Ag-90, Ag-80, Ag-70, Ag-60 and Ag-50) were synthesized by substituting several different percentages of silver nitrate with gold chloride. 0.01 M sodium citrate and 0.1 M sodium borohydride were used as reducing agents, and m-PEG (2 kDa) was used as a capping ligand. The resultant nanoparticles were purified using 10 kDa molecular weight cut off ultrafiltration tubes. GSAN were characterized using TEM (B), DLS (Table S1), UV-visible spectroscopy (Fig S2) and ICP-OES. The ICP-OES results showed both gold and silver to be present, suggesting that gold-silver alloys were formed. A phantom was scanned at two different x-ray energies, i.e. 46 keV and 26 keV, using a DE mammography system. DE subtraction images showed that GSAN produce strong DE mammography contrast (C), while suppressing background signal from tissue. A phantom was also scanned using a clinical CT scanner. The results show that GSAN produce strong CT contrast (D, Fig S3). The biocompatibility of GSAN was evaluated in HepG2 and J774A.1 cell lines at a dose of 200 µg/ml. GSAN were incubated with cells for 2 and 24 hours, after which cell viability was evaluated using MTS assay. The results suggested that formulations Ag-80 to Ag-50 are cytocompatible to HepG2 and J774A.1 (E). As the Ag-80 formulation was found to be biocompatible, contains the least gold and produces strong DE mammography and CT contrast, we will use this formulation to perform subsequent *in vivo* imaging, tumor accumulation and pharmacokinetic studies.

Conclusion

We were able to synthesize GSAN with a range of silver:gold ratios and demonstrated that inclusion of gold improves nanoparticle biocompatibility. GSAN produces strong DE mammography and CT contrast in phantoms. *In vivo* imaging with DE mammography and CT, tumor accumulation, circulation half-life and biodistribution of GSAN will be presented.

AUTHORS (LAST NAME, FIRST NAME): Naha, Pratap C.[1]; Uppuluri, Lahari[1]; Lau, Kristen [1]; Mian, Shaameen [2]; Cheheltani, Rabe'e[1]; Chhour, Peter[2]; McDonald, Elizabeth[1]; Maidment, Andrew D.[1]; Cormode, David[1, 2]

INSTITUTIONS (ALL):

1. Radiology, University of Pennsylvania, Philadelphia, PA, United States.
2. Bioengineering, University of Pennsylvania, Philadelphia, PA, United States.

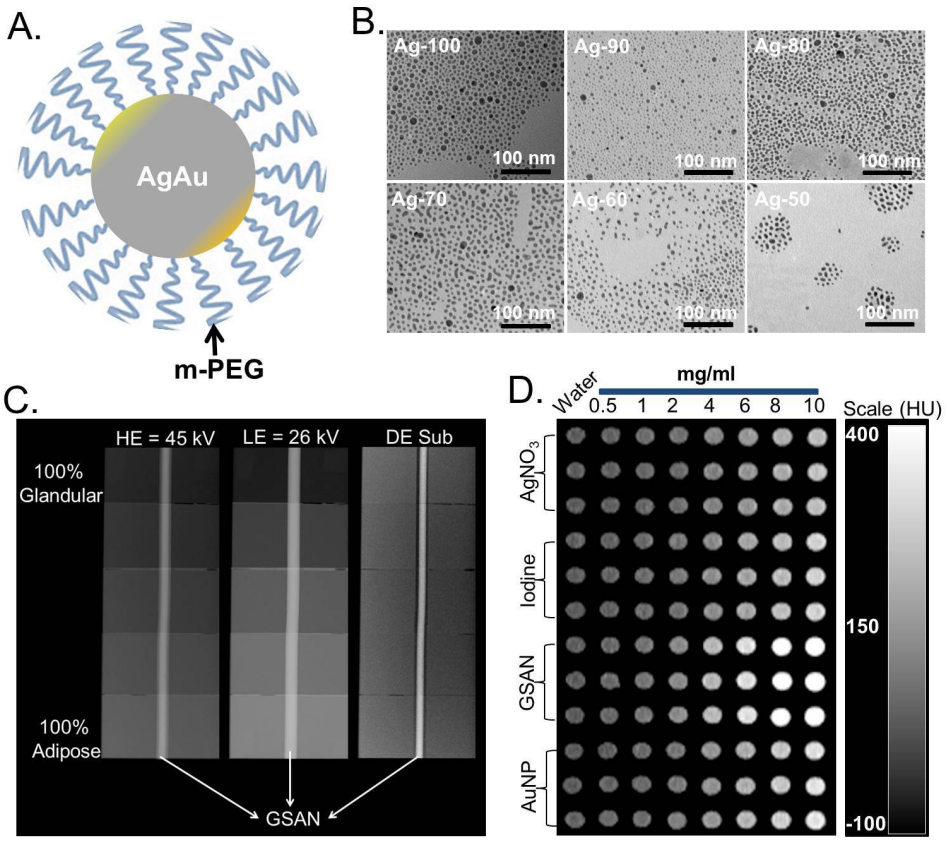

A) Schematic of m-PEG capped GSAN; B) TEM images of GSAN; C) DE mammography phantom images of GSAN; D) CT phantom images of GSAN; E) J774A.1 and HepG2 cell viability after incubation with different GSAN formulations.

CONTROL ID: 2233086

TITLE: Evaluation of ^{11}C-Acetate and ^{18}F-FDG PET/CT in Mouse Multidrug Resistance Gene-2 Deficient Mouse Model of Hepatocellular Carcinoma

PRESENTER: Paul Territo

ABSTRACT BODY:

Abstract Body: Hepatocellular carcinoma (HCC) remains a global health problem with unique diagnostic and therapeutic challenges, including difficulties in identifying the highest risk patients. Previous work from our lab has established the murine multidrug resistance-2 mouse (MDR2) model of HCC as a reasonable preclinical model that parallels the changes seen in human inflammatory associated HCC. The purpose of this study is to evaluate modalities of PET/CT in MDR2$^{-/-}$ mice in order to facilitate therapeutic translational studies from bench to bedside. **Methods**: ^{18}F-FDG and ^{11}C-acetate PET/CT was performed on 12m MDR2$^{-/-}$ mice (n=3/tracer) with HCC and 12m MDR2$^{-/+}$ control mice (n=3/tracer) without HCC. To compare PET/CT to biological markers of HCC and cellular function, serum alpha-fetoprotein (AFP), lysophosphatidic acid (LPA), cAMP and hepatic tumor necrosis factor α (TNFa) were quantified in 3-12m MDR2$^{-/-}$ (n=10) mice using commercially available ELISA analysis. To translate results in mice to patients ^{11}C acetate PET/CT was also performed in 8 patents suspected of HCC recurrence following treatment and currently on the liver transplant wait list. **Results:** Hepatic ^{18}F-FDG metabolism was not significantly increased in MDR2$^{-/-}$ mice. In contrast, hepatic ^{11}C-acetate metabolism was significantly elevated in MDR2$^{-/-}$ mice when compared to MDR2$^{-/+}$ controls. Serum AFP and LPA levels increased in MDR2$^{-/-}$ mice contemporaneous with the emergence of HCC. This was accompanied by a significant decrease in serum cAMP levels and an increase in hepatic TNFa. In patients suspected of HCC recurrence there were 5 true positives, 2 true negatives and 1 suspected false ^{11}C-acetate negative. **Conclusion:** HCC imaging by ^{11}C-acetate PET/CT in MDR2$^{-/-}$ mouse model tracks well with the clinical characteristics of human HCC, where the development of HCC is associated with chronic inflammation. Future studies are required to determine if 11C-acetate PET/CT is well suited to the study of new chemotherapeutics in murine models of HCC.

AUTHORS (LAST NAME, FIRST NAME): Territo, Paul R.[1]; Maluccio, Mary[2]; Riley, Amanda[1]; McCarthy, Brian[1]; Fletcher, James[1, 4]; Tann, Mark [1, 4]; Saxena, Romil[3]; Skill, Nicholas J.[2]

INSTITUTIONS (ALL):

1. Radiology and Imaging Sciences, Indiana University School of Medicine, Indianapolis, IN, United States.
2. Surgery , Indiana University School of Medicine, Indianapolis, IN, United States.
3. Pathology Laboratory, IU Health , Indianapolis, IN, United States.
4. Radiology, IU Health, Indianapolis, IN, United States.

(No Image Selected)

CONTROL ID: 2233101

TITLE: An Omics Approach to Traumatic Brain Injury in Human Patients

PRESENTER: Zhifeng Kou

ABSTRACT BODY:

Abstract Body: Traumatic brain injury (TBI) is a leading cause of death and disability and causes the nation billions of dollars each year in the United States alone. All previous clinical trials failed due to the heterogeneity and complexity of the disorder. Among TBI pathology spectrum, axonal injury and cerebral hemodynamic and metabolic disturbances are still under investigated. By using advanced magnetic resonance imaging (MRI) techniques, along with other novel tools, we took a systematic investigation of TBI in human patients, or called the "**omics approach**." This approach includes proteomics, metabolomics and connectomics investigation of mild traumatic brain injury (mTBI) at the acute stage.

We have successfully recruited 60 mTBI patients at the acute stage from the emergency department of Detroit Medical Center, a Level-1 trauma center, and 60 healthy controls from our local community and patients' friends and relatives. Our initial proteomics investigation demonstrated elevated level of GFAP and UCH-L1 proteins in mTBI patients at the acute stage ($p<0.001$) and patients' GFAP level is associated with patients' intracranial hemorrhage in even CT negative patients. Our metabolomics study showed that mTBI patients have increased cerebral blood flow ($p<0.03$) and venous blood oxygenation ($p<0.05$) at the acute stage, which suggests a compensatory effect at the acute stage that has never been reported before. For the first time, our connectomic analysis revealed that mTBI patients have large scale, or connectome-scale, brain network alterations in both structural connectivity (reported by DTI fiber tractography data) and functional connectivity (reported by resting state fMRI data). The connectomic features in our data resulted in 100% sensitivity and 98% specificity in mTBI detection. In summary, our data represent the first effort of an omics approach to investigating TBI. Our work further demonstrates the complexity of TBI pathology in a global manner.

AUTHORS (LAST NAME, FIRST NAME): Kou, Zhifeng[1]; Iraji, Armin[1]; Wiseman, Natalie[1]; Chen, Hanbo[2]; Welch, Robert D.[3]; O'Neil, Brian[3]; Liu, Tianming[2]; Haacke, E M.[1]

INSTITUTIONS (ALL):

1. Biomedical Engineering and Radiology, Wayne State University, Detroit, MI, United States.
2. Computer Science, University of Georgia, Athens, GA, United States.
3. Emergency Department, Wayne State University, Detroit, MI, United States.

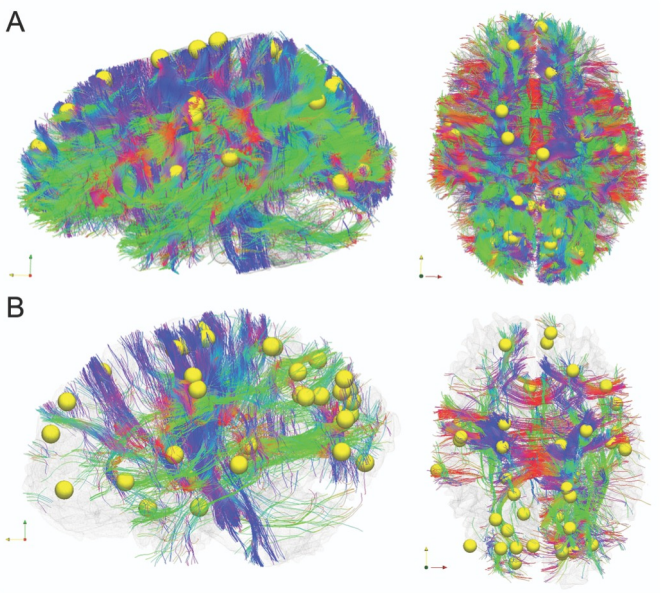

Figure 1. White matter fiber tractography of a randomly chosen control subject (A) and a randomly chosen mTBI patient (B) by using the identified discrepant network nodes as seed points. Despite the negative findings on the mTBI patient's structural MRI, the patient's white matter structure shows significant differences in the 41 discrepant networks in comparison with controls. Yellow bubbles are seed regions for fiber tractography. This demonstrates that mTBI results in connecome-scale brain network changes.

CONTROL ID: 2233106

TITLE: Rational Design of Surface-Enhanced Resonance Raman Scattering Nanoprobes with Attomolar Sensitivity

PRESENTER: Stefan Harmsen

ABSTRACT BODY:

Abstract Body: Objective: Surface-enhanced Raman scattering (SERS)-based Raman imaging has surfaced as a highly sensitive and specific imaging modality for the detection of cancer[1,2]. By adsorbing a 'reporter' molecule on a noble metal nanoparticle surface, the weak Raman effect ($1/10^7$ photons is Raman shifted) is massively amplified (10^7-10^{10}×) producing nanoprobes with low picomolar sensitivity. Orders-of-magnitude-higher sensitivities can be achieved when reporters are adsorbed that are in resonance with the 785-nm detection laser producing surface-enhanced resonance Raman scattering (SERRS) nanoprobes[2]. We hypothesized that the sensitivity of SERRS nanoprobes could be further increased by rationally designing resonant Raman reporters with increased affinity for the gold nanoparticles' surface.

Methods: We designed a novel class of resonant Raman reporters that are based on a chalcogenopyrylium (CP)-scaffold. Since the CP-scaffold is cationic, we first explored the effect of the counterion on the SERRS-spectrum, intensity, and colloidal stability of CP-based SERRS nanoprobes. Then, we introduced 2-thienyl substituents to enhance affinity for the gold surface. The benefit of this substituent is that it is stable, part of the chromophore, and it is rigorously co-planar with the rest of the CP-scaffold allowing the dye molecules to be within close proximity of the particle surface. We determined the effect of the increased dye affinity on the SERRS intensity and colloidal stability. Lastly, we compared the detection limit and in vivo signal of our rationally designed CP-SERRS nanoprobe to SERRS nanoprobes that were generated with a widely used cyanine dye IR792.

Results: Of the 4 counterions (Br^-,Cl^-,ClO_4^-,and PF_6^-) that were evaluated, chaotropic counterions produced high SERRS signal and colloidal stability. In contrast, Cl^-, a kosmotropic counterion, decreased colloidal stability and induced aggregation. The strongest chaotrope, PF_6^-, was used as a counterion in this study. Next, we determined the effect of the CP dyes' affinity for the gold nanoparticle surface by introducing 2-thienyl substituents. We show that the SERRS signal increased significantly with the number of 2-thienyl groups. The CP dye 3 that had the maximal amount of four 2-thienyl substituents produced the highest SERRS signal. The limit of detection of the CP-3-SERRS nanoprobe was 100 attomolar (10^{-18} M) – 10-fold lower than that of the IR792-SERRS nanoprobe (1.0 fM). In vivo comparison showed that the signal of an EGFR-targeted CP3-SERRS nanoprobe was higher than an EGFR-targeted IR792-SERRS nanoprobe in a A431-xenograft tumor (Fig.1)[3].

Conclusion: CP dyes represent a new class of resonant Raman reporters. The low limit of detection (*i.e.* close to single nanoparticle detection) in combination with the high resolution of Raman imaging, enables highly sensitive and specific, near-real-time tumor delineation and, as a result of the fingerprint-like spectra of the different SERRS nanoprobes, offers highly sensitive multiplexed disease marker detection in vivo.

References

1. Kircher *et al.* Nat. Med. (2012); 2. Harmsen *et al.* Sci. Transl. Med. (2015); 3. Harmsen *et al.* Nat. Commun., in press

AUTHORS (LAST NAME, FIRST NAME): Harmsen, Stefan[1]; Bedics, Matthew A.[2]; Wall, Matthew[1, 3]; Huang, Ruimin[1]; Detty, Michael R.[4]; Kircher, Moritz F.[5]

INSTITUTIONS (ALL):

1. Radiology, Memorial Sloan Kettering Cancer Center, New York, NY, United States.
2. Chemistry, University at Buffalo, Buffalo, NY, United States.
3. Chemistry, Hunter College of the City University of New York, New York , NY, United States.
4. Chemistry, University at Buffalo, Buffalo, NY, United States.
5. Radiology, Memorial Sloan Kettering Cancer Center, New York, NY, United States.

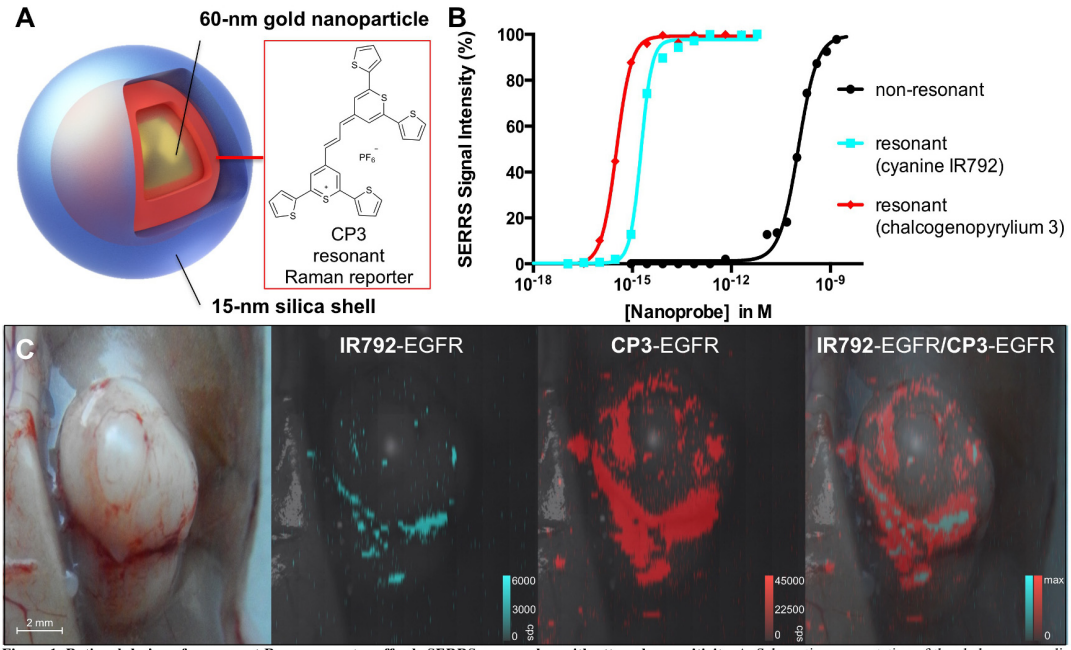

Figure 1. Rational design of a resonant Raman reporter affords SERRS nanoprobes with attomolar sensitivity. A. Schematic representation of the chalcogenopyrylium (CP) dye 3-based SERRS nanoprobe. The optimized CP dye 3 is adsorbed on a 60-nm gold nanoparticle and encapsulated in a 15-nm thick silica shell. **B.** The limit of detection of a non-resonant SERS nanoprobe[1] was compared to a resonant cyanine (IR792)-based SERRS nanoprobe and to the rationally designed CP-**3**-based SERRS nanoprobe. The limits of detection of the resonant SERRS nanoprobes were 1,000-10,000-fold lower than that of the non-resonant SERS nanoprobe. Between the resonant SERRS nanoprobes, the SERRS nanoprobe that used the chalcogenopyrylium-based dye 3 afforded a limit of detection (LOD) of 100 attomolar, which was 10-fold lower than the LOD of the cyanine (IR792)-based SERRS nanoprobe (100-mW laser power, 1.5-s acquisition time, 5× objective). **C.** The SERRS nanoprobes were compared in vivo. Equimolar doses (15 fmol/g) of EGFR-targeted CP-3-based and IR792-based SERRS nanoprobes were injected intravenously via tail vein in A431 tumor xenograft bearing nude mice (n=5). The next day, Raman imaging was performed (10-mW laser power, 1.5-s acquisition time, 5× objective). Raman maps were generated by a direct classical least-square (DCLS) algorithm with Wire 3.4 (Renishaw) software. (Figure adapted and expanded from Harmsen S, Bedics MA, Wall MA, Huang R, Detty MR, Kircher MF: Rational Design of a Chalcogenopyrylium-Based Surface-Enhanced Resonance Raman Scattering-Nanoprobe with Attomolar Sensitivity. *Nature Communications*, in press.)

CONTROL ID: 2233152

TITLE: Surface-Enhanced Resonance Raman Scattering Nanoprobes for Early Detection of Upper Gastrointestinal Lesions

PRESENTER: Stefan Harmsen

ABSTRACT BODY:

Abstract Body: Objective: Currently, endoscopic examination for the assessment of lesions of the esophagus and stomach is largely a subjective process. While the diagnosis of premalignant lesions is often impaired as a result of inter-observer variability in the interpretation of dysplasia, advanced lesions can also be missed or misinterpreted due to their subtle appearance. Moreover, lesions are often missed due to sampling errors inherent to a random-biopsy surveillance paradigm. Furthermore, surveillance for gastric lesions can be challenging due to the large surface area that needs to be examined. Although several chromophore-/fluorophore-assisted or image-guided endoscopic approaches have been developed, these approaches suffer from limited sensitivity and specificity. There is therefore a clear unmet need for endoscopic imaging approaches that enable highly sensitive and specific detection of premalignant and malignant lesions of the upper gastrointestinal tract (UGIT) with the ultimate goal of improved standardization and diagnostic accuracy.

Methods: Surface-enhanced resonant Raman scattering (SERRS)-based Raman imaging has shown great potential as a highly sensitive and specific imaging modality for the detection of cancer[1,2,3]. We developed a SERRS nanoprobe with attomolar sensitivity. The ability of the SERRS nanoprobe to enable detection of lesions of the UGIT was evaluated in clinically relevant animal models of Barrett's esophagus and gastric cancer. All animals were injected intravenously with the SERRS nanoprobes (30 fmol/g) via tail vein. The next day, the animals were sacrificed and Raman imaging was performed on the UGITs ex vivo. The scanned tissues were processed for histology and examined by an independent veterinary pathologist.

Results: In the L2-IL1β mouse model, which closely recapitulates the development of esophageal adenocarcinoma in humans[4], the SERRS nanoprobes enabled early detection of dysplastic lesions at the gastroesophageal junction, the site with the highest probability of esophageal adenocarcinoma development in humans (Fig.1). Furthermore, in *H.felis* infected genetically engineered insulin-gastrin (INS-GAS) mice co-treated with the carcinogen MNU[5] − a model that recapitulates human *H.pylori*-induced gastric cancer development − SERRS-positive lesions were detected in the gastric antrum. Histopathological examination identified the SERRS-positive antral lesions as hyperplasia and dysplasia.

Conclusion: We demonstrate the potential of SERRS-nanoprobe-based Raman imaging for the early detection and accurate delineation of (pre-)malignant lesions of the UGIT. Furthermore, the fact that nanoparticles of similar size and composition are already in clinic trials, and Raman endoscopic imaging devices are being developed, there is a viable path towards the clinical translation of this strategy to enable highly sensitive and accurate Raman-guided endoscopic detection and delineation of (pre-)malignant lesions of the UGIT.

References: 1. Kircher et al. Nat. Med. (2012); 2. Harmsen et al. Sci.Transl.Med. (2015); 3. Harmsen et al. Nat Commun.,in press; 4. Quante et al. Cancer Cell (2012); 5. Hayakawa et al. (2012) Cancers

AUTHORS (LAST NAME, FIRST NAME): Harmsen, Stefan[1]; Huang, Ruimin[3]; Spaliviero, Massimiliano[2]; Hayakwawa, Yoku[4]; Lee, Yoomi[4]; Tailor, Yagnesh[4]; Wall, Matthew[5, 6]; White, Julie R.[7]; Wang, Timothy C.[4]; Kircher, Moritz F.[8]

INSTITUTIONS (ALL):

1. Memorial Sloan Kettering Cancer Center, New York, NY, United States.
2. Urology, Memorial Sloan Kettering Cancer Center, New York, NY, United States.
3. Radiology, Memorial Sloan Kettering Cancer Center, New York, NY, United States.
4. Medicine, Columbia University , New York, NY, United States.
5. Radiology, Memorial Sloan Kettering Cancer Center, New York, NY, United States.
6. Chemistry, Hunter College of the City University of New York, New York, NY, United States.

7. Tri-Institutional Laboratory of Comparative Pathology, Memorial Sloan Kettering Cancer Center, New York, NY, United States.
8. Radiology, Memorial Sloan Kettering Cancer Center, New York, NY, United States.

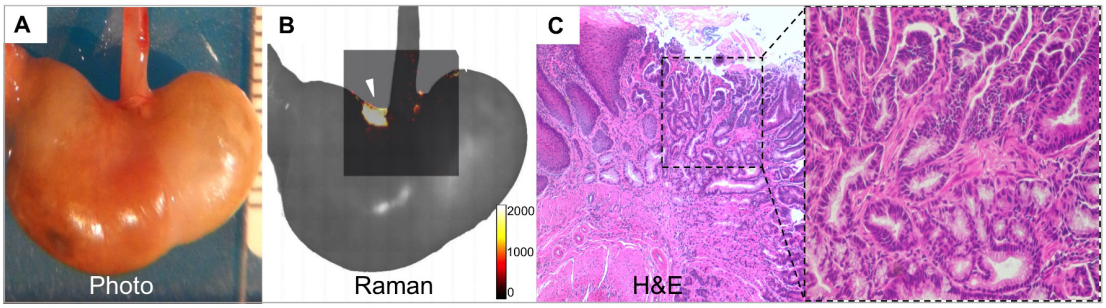

Figure 1. Visualization of lesions at the gastroesophageal (GE)-junction in L2-IL1β mouse model by SERRS-based Raman imaging. A. Photo of stomach and esophagus of an L2-IL1β mouse that was injected with SERRS nanoprobes (30fmol/g). **B.** Ex vivo Raman imaging identified a SERRS-positive lesion (arrow-head) at the gastroesophageal junction (Raman imaging conidtions: 10mW laser power, 1.5-s acquisition time, 5× objective). **C.** Histologic examination of the SERRS-positive region identified the lesion as dysplastic. SERRS nanoprobe-based Raman imaging was shown to enable the early detection of premalignant lesions at the GE-junction that have high propensity to eventually progress to adenocarcinoma.

CONTROL ID: 2233621

TITLE: Synthetic studies towards nitroreductase-activated fluorescent probes

PRESENTER: Elvira García de Jalón

ABSTRACT BODY:

Abstract Body: Cancer defines a range of diseases with high heterogeneity and challenging prognosis. Early detection by means of imaging remains the key to reduce mortality and morbidity. Optical imaging, particularly near-infrared (NIR) fluorescence, is a promising technique for detection of biological prosesses, such as metastasis.[1]

Squaraine dyes generally consist of a conjugated system composed of a cyclobutadiene core linking two nitrogen-containing heterocycles. Depending on the nature of the heterocycles and their substituents, these zwitterionic dyes may exhibit absorption and emission characteristics in the NIR region.[2,3] For *in vivo* applications, NIR fluorescence is key to minimize autofluorescence and light scattering in tissues.[1] We have recently demonstrated non-invasive NIR reporter gene imaging in preclinical metastatic cancers *in vivo* using the dinitrobenzyl containing dye CytoCy5S.[4] The introduction of a dinitrobenzyl group onto the squaraine dye efficiently quenches fluorescence. Upon reduction of the two nitro groups to hydroxylamines by the bacterial enzyme nitroreductase, which has been transfected into the cancer cells, fluorescence is restored and cancer cells can be detected.

In this work, we have investigated into improving the synthesis of CytoCy5S using either squaric acid or squaric acid dibutyl ester as starting materials. We have also investigated into the activation of the carboxylic acid of CytoCy5S in order to prepare derivatives that are suitable for labelling of monoclonal antibodies.

1. Condeelis, J.; Weissleder, R. *Cold Spring Harbor Perspectives in Biology* **2010,** *2*, 12.
2. Sreejith, S. *et al. J. Materials Chem.* **2008,** *18*, 264.
3. Hassan, M.; Klaunberg, B. A. *Comparative Medicine* **2004,** *54*, 635.
4. McCormack, E. *et al. Cancer Res.* **2013,** *73*, 1276.

AUTHORS (LAST NAME, FIRST NAME): García de Jalón, Elvira[1, 2]; Stigen, Endre[2]; Mayoral Safont, Mireia[2]; Popa, Mihaela[2]; Haug, Bengt Erik[1]; Mc Cormack, Emmet[2, 3]

INSTITUTIONS (ALL):
1. Department of Chemistry and Centre for Pharmacy, University of Bergen, Bergen, Norway.
2. Hematology Section, Department of Clinical Science, University of Bergen, Bergen, Norway.
3. Hematology Section, Department of Internal Medicine, Haukeland University Hospital, Bergen, Norway.

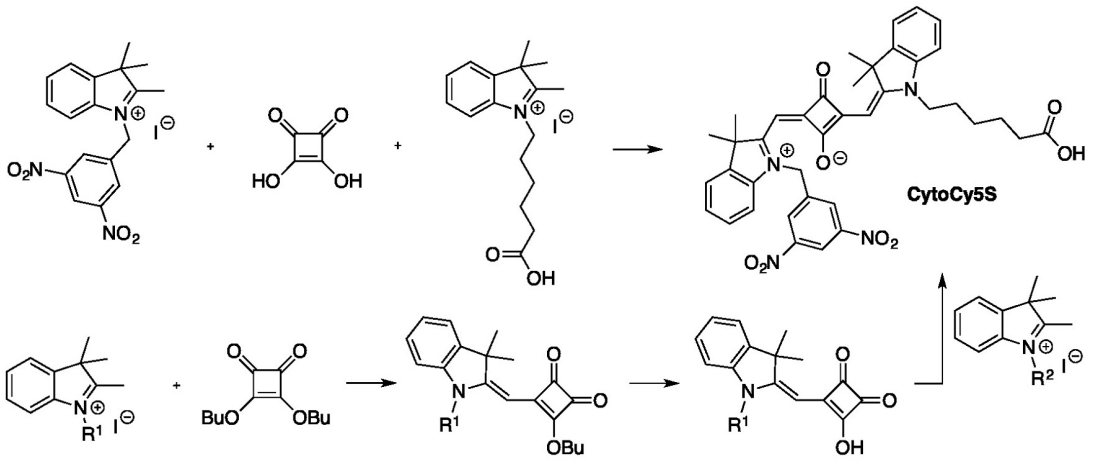
CytoCy5S

CONTROL ID: 2233113

TITLE: Non-invasive Bioluminescence Imaging of AKT Kinase Activity and Apoptosis Reveals Therapeutic Efficacy in Tumor Mouse Models of Human Lung and Brain Cancer

PRESENTER: Thomas Poeschinger

ABSTRACT BODY:

Abstract Body: Introduction:

In many types of human cancer, aberrant PI3K/AKT signaling plays a critical role in tumor growth, survival, resistance, and the evasion from apoptosis[1]. Thus, modulation of the key regulators in this signaling cascade provides a promising strategy for pharmaceutical intervention. Here, we studied the *in vivo* phosphorylation of the AKT serine/threonine kinase in response to targeted kinase inhibitors and compared its therapeutic impact on tumor growth and the induction of apoptosis in two tumor mouse models of lung and brain cancer.

Methods:

Two human cancer cell-lines, A549 (NSCLC) and D54 (glioblastoma), were stably transfected with the bioluminescence AKT reporter (BAR) providing a conditional luminescence light emission, when phosphorylation of AKT kinase is inhibited[2]. Similarly, a caspase-3/7-sensitive bioluminescence reporter cell line (D54-apoR) was used for imaging of apoptosis[3]. Tumor cells were either injected subcutaneously (A549-BAR, D54-BAR, D54-apoR) or intravenously (A549-BAR) into immunocompromised mice. Treatment was done using different doses of small molecule kinase inhibitors either targeting specifically AKT (perifosine) or the EGFR pathway (erlotinib). To evaluate the impact of AKT inhibition on the induction of apoptosis, D54-BAR cells and D54-apoR cells were separately injected into the left and right flank of the animals to permit side-by-side evaluation within the same mouse. Longitudinal tumor growth was monitored by caliper (s.c.) and *in vivo* micro-computed tomography (lung). *Ex vivo* validation was done by immunohistochemistry, western blotting, and ultramicroscopy.

Results:

Systematic *in vitro* bioluminescence imaging (BLI) experiments identified erlotinib and perifosine as potent AKT kinase inhibitors in A549-BAR and D54-BAR cells. *In vivo*, erlotinib showed a substantially higher BAR activitiy (10-fold increase) in s.c. A549-BAR tumor xenografts as compared to perifosine 3h after treatment, indicating a massive inhibition of AKT phosphorylation. After 6h, the inhibitory effect was almost diminished, but could be reinstated after re-dosing. Reduction of tumor volume was evident after 6 days treatment. *Ex vivo* analysis of phospho-AKT levels of explanted tumor tissue confirmed the imaging results. Similarly, in the orthotopic setting (i.v. injection of A549-BAR cells), repeated erlotinib treatment resulted in transient, but strong AKT kinase inhibition cycles that translated well to the reduction of tumor volume as observed longitudinally by *in vivo* micro-CT imaging of the lungs. Therapeutic challenge of double tumor xenografts (D54-BAR and D54-apoR) revealed a significant increase of apoptosis induction after inhibition of AKT phosphorylation.

Conclusion:

The BAR reporter technology was successfully applied to non-invasively assess the therapeutic activity of AKT kinase modulating drugs in preclinical tumor xenografts. Such reporter systems could help to optimize dosing and treatment schedules in preclinical drug development.

Reference:

1. Fumarola, C., *et al. Biochem Pharmacol* **90**, 197-207 (2014).

2. Zhang, L.*, et al. Nat Med* **13**, 1114-1119 (2007).

3. Weber, T.G.*, et al. Cancer Res* **74**, 1913-1923 (2014).

AUTHORS (LAST NAME, FIRST NAME): Suchowski, Karina[1]; Osl, Franz[1]; Galbán, Stefanie[2]; Rehemtulla, Alnawaz[2]; Scheuer, Werner[1]; Poeschinger, Thomas[1]

INSTITUTIONS (ALL):

1. Pharmaceutical Research & Early Development, Discovery Oncology, Roche Innovation Center Penzberg, Penzberg, Germany.

2. Department of Radiation Oncology and Radiology, University of Michigan, Ann Arbor, MI, United States.
(No Image Selected)

CONTROL ID: 2233126

TITLE: Radiosynthesis of [^{11}C]Ibrutinib as a PET tracer

PRESENTER: xia shao

ABSTRACT BODY:

Abstract Body: Objectives: Bruton's tyrosine kinase (BTK) is a mediator of the B-cell-receptor signaling pathway implicated in the pathogenesis of B-cell cancers. Early-stage clinical trials found ibrutinib, a BTK inhibitor, showed antitumor activity in several types of B cell lymphoma. The drug recently has been approved by the FDA for the treatment of mantle cell lymphoma and chronic lymphocytic leukemia[1]. Radiolabeled ibrutinib has the potential to function as a companion diagnostic for predicting response to ibrutinib therapy and also to support future drug discovery efforts around the BTK pathway. We report here a novel method for carbon-11 labeling ibrutinib.

Methods: The synthetic scheme was shown in Figure 1. Briefly, a solution of vinyl magnesium bromide in THF was sparged with [^{11}C]CO_2, followed by addition of HCl in dioxane to generate [^{11}C]acrylic acid. The precursor solution containing HATU and DIPEA was added. The product was purified by preparative HPLC and reconstituted into ethanolic saline using a C-18 Sep-Pak to provide [^{11}C]ibrutinib formulated for injection.

Results: [^{11}C]Ibrutinib was prepared in a multistep synthesis at room temperature. Total synthesis time was 50 minutes from end of beam. In non-optimized conditions, total radiochemical yield was 2-5% based on [^{11}C]CO_2 (non-decay corrected) with a radiochemical purity greater than 95% determined by HPLC analysis.

Conclusion: Cancer therapy agent, ibrutinib, has been radiolabeled with carbon-11 for the first time. This novel radiosynthetic method can be extensively used to label various amides from the required Grignard reagent and amine. Biological evaluation and preclinical studies of [^{11}C]ibrutinib are underway.

References: (1) Davids, Matthew S.; Brown, Jennifer R. *Future Oncology* (2014), 10(6), 957-967.

AUTHORS (LAST NAME, FIRST NAME): shao, xia[1]; Scott, Peter J.[2]

INSTITUTIONS (ALL):

1. Radiology, University of Michigan, Ann Arbor, MI, United States.
2. Radiology, University of Michigan, Ann Arbor, MI, United States.

(No Image Selected)

CONTROL ID: 2233132

TITLE: Molecular imaging of A431 tumor xenografts in mice to guide treatment regimen and obtain treatment response

PRESENTER: shun kishimoto

ABSTRACT BODY:

Abstract Body: Photoimmunotherapy (PIT) using the near infrared absorbing photosensitizer IR700 conjugated with tumor seeking antibody such as Panitumumab has shown efficacy in in vitro studies and several pre-clinical models in mice with promise for clinical translation (1). The efficacy of PIT is determined by the accumulation of the photoimmunoconjugate in the tumor, delivery of near infrared light to the tumor and the availability of molecular oxygen (2). In vitro and in vivo studies show that PIT using the photoimmunoconjugate proceeds predominantly by necrotic death (1,3). Rapid necrotic cell death in vitro and tumor shrinkage in vivo following PIT point to membrane damage induced by PIT. Therefore a priori information of tumor pO2 status is critical in planning PIT. Similarly assessment of necrosis in vivo after PIT will be useful in obtaining prognostic information.

Electron Paramagnetic Resonance (EPR) Imaging was used to determine pO2 in A431 tumor bearing mice. Tumors showed well oxygenated regions including hypoxic areas. Transient occlusion of tumors showed rapid onset of hypoxia in the tumors globally. Survival of tumor bearing mice was prolonged in PIT treated tumor bearing mice animals but mice whose tumors were made transiently hypoxic followed by PIT had no benefit of the treatment. The results from this study support a central role for molecular oxygen derived species in causing cell death. Hyperpolarized MRI studies using 13C-fumarate will be conducted to monitor the time course of necrosis in these tumors.

(1) Mitsunaga, M.; Ogawa, M.; Kosaka, N.; Rosenblum, L. T.; Choyke, P. L.;Kobayashi, H. Cancer cell-selective in vivo near infrared photoimmunotherapytargeting specific membrane molecules. *Nat. Med.* **17**: 1685–1691; 2011.

(2) Mitchell, J. B.; McPherson, S.; DeGraff, W.; Gamson, J.; Zabell, A.; Russo, A.Oxygen dependence of hematoporphyrin derivative-induced photoinactivation ofChinese hamster cells. *Cancer Res.* **45**: 2008–2011; 1985.

(3) Shirasu, N.; Yamada, H.; Shibaguchi, H.; Kuroki, M.; Kuroki, M. Potent andspecific antitumor effect of CEA-targeted photoimmunotherapy. *Int. J. Cancer***135**: 2697–2710; 2014.

AUTHORS (LAST NAME, FIRST NAME): kishimoto, shun[2]; Bernardo, Marcelino[1]; Saito, Keita[2]; Koyasu, Sho[1]; Mitchell, James B.[2]; Choyke, Peter L.[1]; Cherukuri, Murali K.[2]

INSTITUTIONS (ALL):

1. Molecular Imaging Program, NCI, Bethesda, MD, United States.
2. Radiation Biology Branch, NCI, Bethesda, MD, United States.

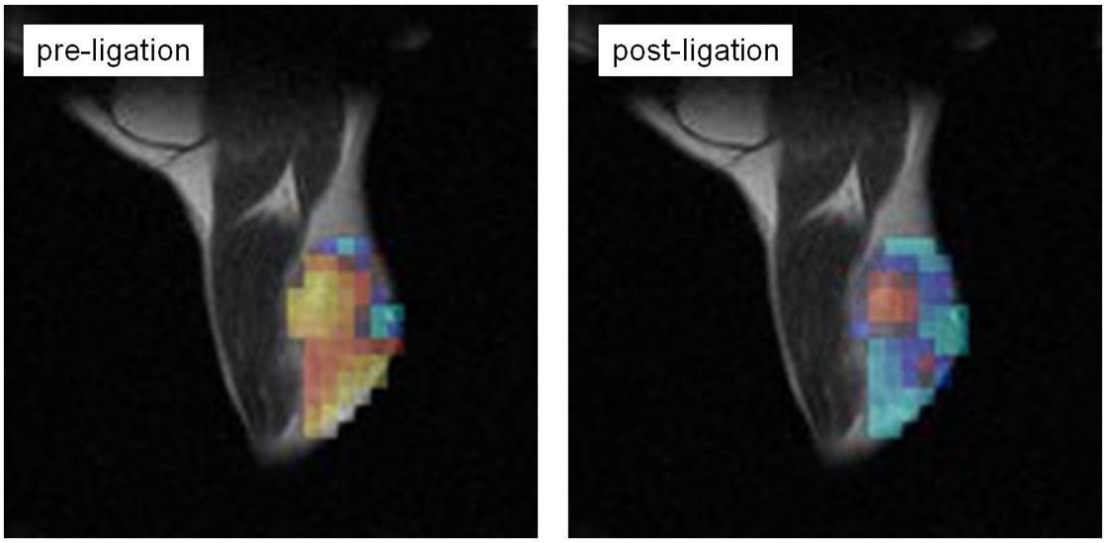
pre-ligation
post-ligation

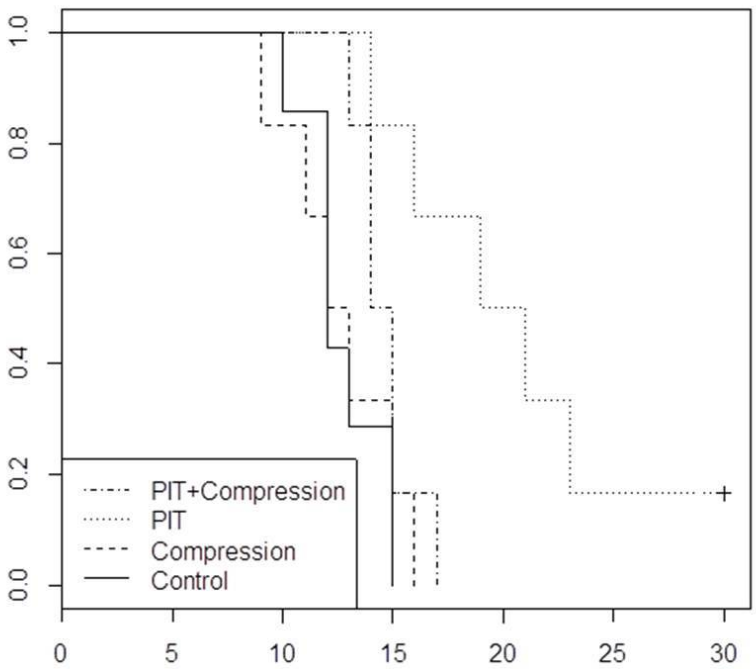
1.0
0.8
0.6
0.4
0.2
0.0
0
5
10
15
20
25
30
PIT+Compression
PIT
Compression
Control

CONTROL ID: 2233158

TITLE: Transcranial Manganese Delivery for Neuronal Tract Tracing using MEMRI

PRESENTER: Tatjana Atanasijevic

ABSTRACT BODY:

Abstract Body: Objective: There has been growing interest in using manganese (Mn) enhanced MRI (MEMRI) in rodents for neuronal tract tracing, in which Mn solutions are usually directly injected into specific brain regions[1-2]. Recently it was reported that Mn can diffuse through intact rat skull[3]. Here the local Mn quantities in the brain tissue after transcranial Mn application were quantified and the effectiveness of tracing from the area was determined.

Methods: Anesthetized adult rats were placed in a stereotaxic apparatus, a single midline incision with a scalpel was made through the skin of the skull, and the skull bone was exposed by scraping away the periosteum. Sterile saline solutions of $MnCl_2$ of concentrations ranging from 0 to 500 mM were placed directly on the skull bone, in various locations, for 2h. Images were acquired on an 11.7 T horizontal magnet immediately after Mn application as well as 24h later. Contrast enhancement by Mn was detected using a T_1-weighted spin echo pulse sequence whereas T_1 relaxation times were measured using a saturation recovery spin-echo sequence. Obtained T_1 relaxation maps were thresholded using the value of the background T_1 minus two standard deviations in order to obtain ROIs in which Mn had significantly shortened T_1 of the cortex tissue. The average T_1 relaxation times as well as total number of voxels in those ROIs were used to determine the local concentration and total amount of Mn in each slice, using $1/(T_1)_{obs} = 1/(T_1)_{backgr} + r_1 * c$. The previously reported value of 4.7 s^{-1} mM^{-1} was used for cortex T_1 relaxivity[4].

Results and Discussion: The effectiveness of the Mn diffusion through intact rat skull when applied on the bregma is demonstrated by the images in Fig. 1. Mn can diffuse to MRI detectable levels only through areas of the skull that contain or are near suture lines where the adjacent skull bone plates come together. To determine the effect of total osmolarity on Mn delivery, $CaCl_2$ was added to various concentrations of $MnCl_2$ while keeping the total salt concentration constant at 500 mM. The addition had a significant effect on applied Mn concentrations previously undetectable in the cortex, such as 100 mM, that became detectable. The total amount of Mn in an MRI slice with most efficient delivery was proportional to the Mn concentration applied on the skull (Fig. 1F). Mn introduced into S_1 cortex in this manner caused enhancement in the corticothalamic neuronal pathway 24h after application, analogously to Mn directly injected into S_1 area[5].

Conclusion: Intact rat skull is most permeable to Mn at the bone sutures and the permeability is dependent on the osmolarity. Transcranially applied Mn yields brain tissue enhancement patterns similar to those obtained when Mn is directly injected into desired brain area. This represents a new and much less invasive Mn delivery method for neuronal tract tracing using MEMRI and may open a whole new, less invasive path for brain delivery of various contrast agents and drugs.

References: 1. R.G.Pautler, Magn Reson Med, 1998; 2. R.G. Pautler, NMR Biomed, 2004, 3. T.L.Roth, Nature, 2014, 4.K.H.Chuang, Magn Reson Med, 2009, 5. T.B.Leergaard, NeuroImage, 2003.

AUTHORS (LAST NAME, FIRST NAME): Atanasijevic, Tatjana[1]; Bouraoud, Nadia[1]; McGavern, Dorian B.[2]; Koretsky, Alan P.[1]

INSTITUTIONS (ALL):

1. LFMI, NIH, NINDS, Bethesda, MD, United States.

2. NIH, NINDS, Bethesda, MD, United States.

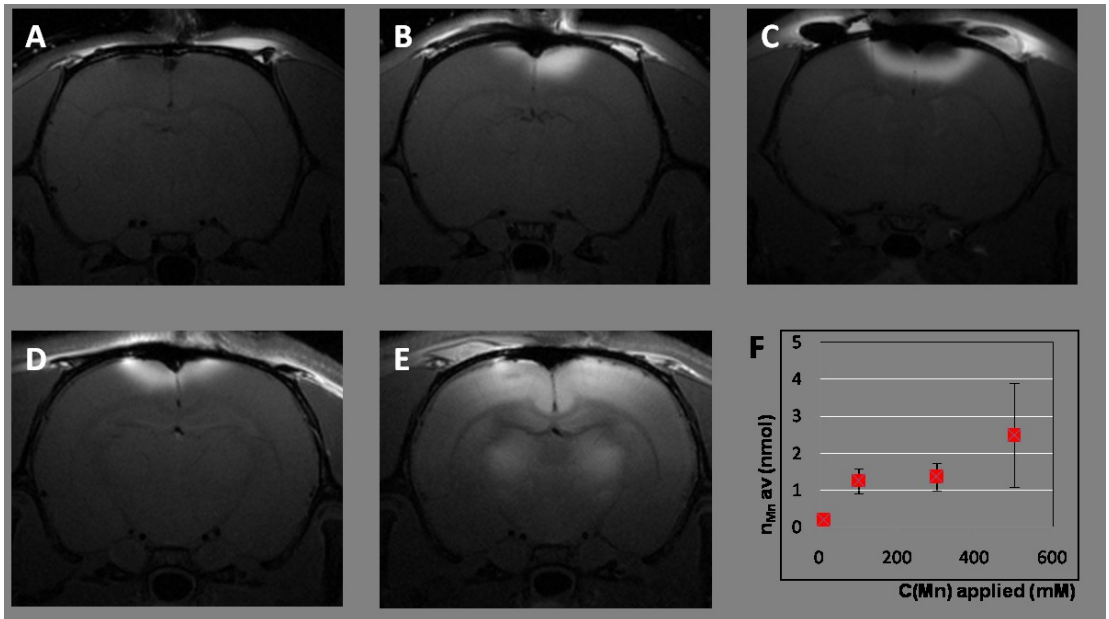

Figure 1: T_1-weighted images of rats receiving: 100 mM $MnCl_2$ solution without (A) and with (B) $CaCl_2$ addition, 500 mM $MnCl_2$ (C), 500 mM MnCl2 immediately after (D) and 24 h after application (D), as well as dependence of the total amount of cortex manganese on the concentration of $MnCl_2$ applied on the bregma (F). The applied solutions in (F) contained $CaCl_2$. The total concentration od $CaCl_2$ and $MnCl_2$ equaled 500 mM.

CONTROL ID: 2233170

TITLE: Preclinical evaluation of ^{68}Ga-DOTA-NT20.3 as a PET imaging agent for NTSR expression in a model of exocrine pancreatic adenocarcinoma.

PRESENTER: Aurélie Prignon

ABSTRACT BODY:

Abstract Body: Pancreatic ductal adenocarcinoma (PDA) grows extremely rapidly and early diagnosis is rarely possible.

Positron emission tomography computed tomography (PET-CT) imaging with ^{18}F- Fluorodeoxyglucose has several limitations and differentiating between PDA and focal mass-forming pancreatitis is still a major clinical problem. Recent studies suggest that increased expression of neurotensin receptor 1 (NTSR1) contributes to the progression and aggressiveness of PDA. In our previous study, new DOTA conjugated neurotensin analogue series that allowed PET imaging with gallium 68 of neurotensin receptor-positive colon carcinoma tumours was developed. The best analogue DOTA-NT20.3 was used as PET tracer for imaging over-expression of NTSR1 on human PDA model.

Methods

^{68}Ga-DOTA-NT20.3 dynamic PET imaging was performed in normal nude mice during 50 min to determine *in vivo* biodistribution. PET imaging was performed in human AsPC1 pancreatic adenocarcinoma model to evaluate biodistribution and tumour uptake of the tracer. SUVmax intensity was reported at each time point for tumour, kidneys and “non-tumour” which represents background close to the tumour area. The tumour-to-non tumour ratios were calculated. After imaging, 1h after injection of ^{68}Ga-DOTA-NT20.3, organs were gamma-counted. Tissue uptake was expressed as percentage injected dose per gram (%ID/g), corrected for decay.

Blocking experiment was performed with a 400-fold excess of non-labeled non-DOTA NT20.3 peptide. 10-min static PET images were acquired at 45min post injection (p.i.) and animals were sacrificed at 1 h p.i. Tumour uptake was compared to that obtained in the absence of non-DOTA NT20.3 peptide at the same time point.

Results

DOTA-NT20.3 peptide was radiolabelled in 30 min. The radiochemical yield was 76 to 85%. The radiochemical purity was ≥ 99% and a specific activity of 9.9 ± 0.9 MBq/nmol of peptide was achieved.

Normal mice and AsPC1 tumour–bearing mice were characterized by a rapid delivery of ^{68}Ga-DOTA-NT20.3 up to 2min p.i. into blood compartment, maximal renal excretion between 5 to 10 min p.i. and elimination by urinary bladder to reach 55 to 61% of injected dose (ID). No uptake was observed in pancreas, the organ of interest. High-contrast images were obtained and showed intense tracer uptake in tumours expressing NTRS1. Uptake by tumour is consistent over the PET acquisition representing 1.47 at 1.68 % of ID.

^{68}Ga-DOTA-NT20.3 *ex vivo* biodistribution, investigated 1h p.i., showed moderate kidneys retention with 5.38 ± 0.54 %ID/g, low activity in the pancreas with 0.22 ± 0.03 %ID/g and remaining organs, consistent with findings on PET imaging. Uptake in AsPC1 tumour was rapid and high, with 5.28 ± 0.93 %ID/g.

The NTSR1 specificity of ^{68}Ga-DOTA-NT20.3 tracer was verified. The tracer uptake in AsPC1 was reduced significantly from 3.7 ± 1.1 to 1 ± 0.1 on PET imaging and the ex vivo tumour uptake 1h p.i. from 5.8 ± 0.8 to 1.6 ± 0.3 % of ID/g.

Conclusion

^{68}Ga-DOTA-NT20.3 has a favorable pharmacokinetics and biodistribution profile, which would result in high quality PET images. ^{68}Ga-DOTA-NT20.3 seems to be a good PET tracer for imaging over-expression of NTSR1 on human PDA model.

AUTHORS (LAST NAME, FIRST NAME): Prignon, Aurélie[1]; Provost, Claire[1]; Talbot, Jean-Noël[1, 2]; Gruaz-Guyon, Anne[3]

INSTITUTIONS (ALL):

1. University Pierre and Marie Curie (Paris VI), Paris, Ile-de-France, France.
2. APHP, Paris, France.
3. Université Paris Diderot-Paris 7, Paris, France.

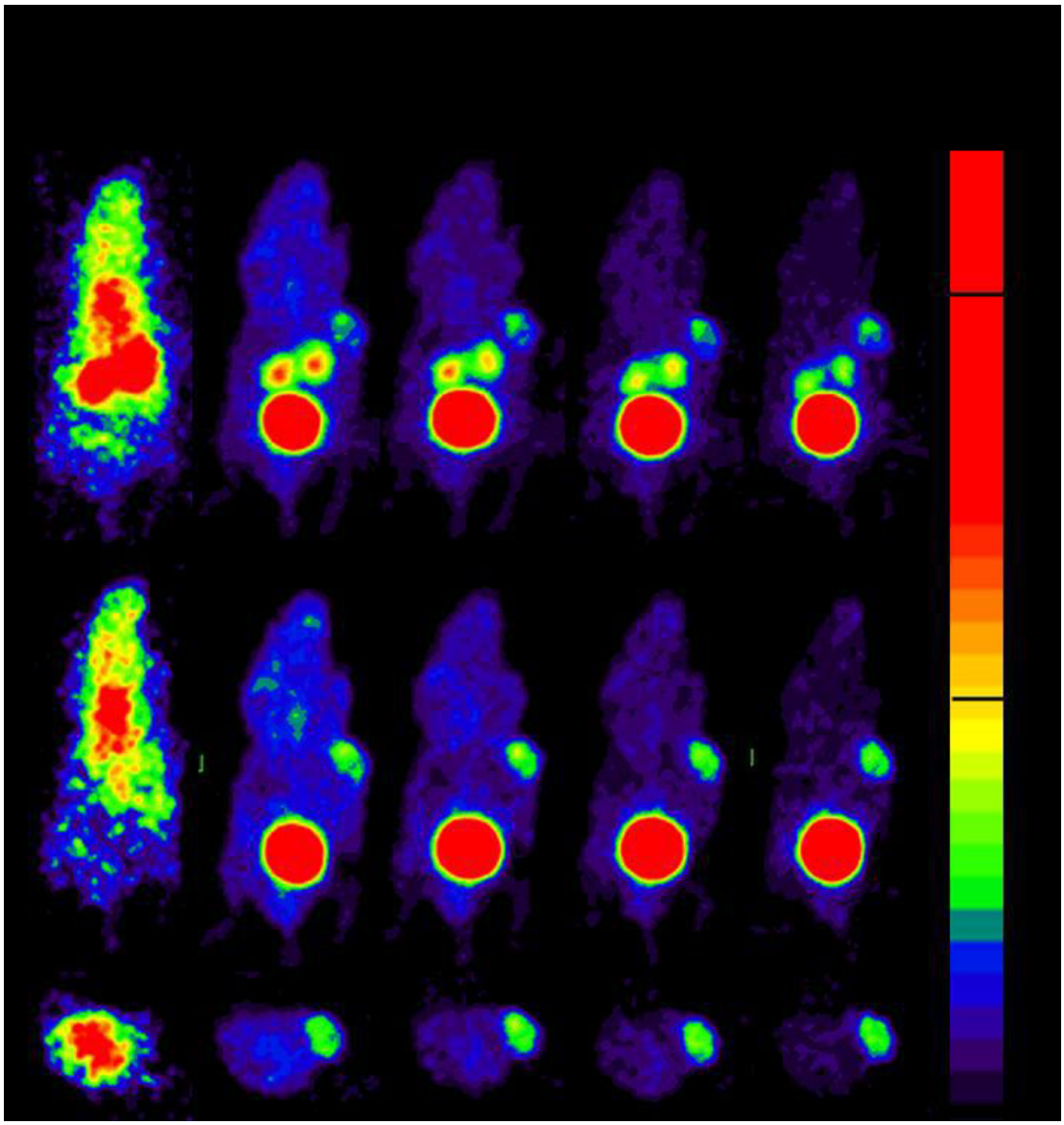

CONTROL ID: 2234122

TITLE: CXCR4 Targeted PAMAM Dendrimer Nanoparticles

PRESENTER: Wojciech Lesniak

ABSTRACT BODY:

Abstract Body: The G-protein coupled chemokine receptor 4 (CXCR4) is over-expressed in more than 23 tumor types. Interactions of CXCR4 with its natural ligand CXCL12 contributes to tumor growth, angiogenesis, and metastasis leading to poor prognosis.[1] Several CXCR4 targeted therapeutic and imaging agents are in clinical trials. Recently, POL3026 peptidomimetic was demonstrated as a promising template for the development of CXCR4 specific imaging agents.[2] Poly(amidoamine) (PAMAM) dendrimers are emerging as valuable building blocks for the development of multifunctional targeted nanoparticles for treatment and diagnosis of cancer.
Here, we report PAMAM dendrimers conjugated with POL3026 as CXCR4 binding nanoparticles (NPs) for imaging and drug delivery.

We have used generation 2 and 5 dendrimers, which were conjugated with -DOTA to enable radiolabeling, -POL3026 to enable CXCR4-specific targeting and -PEGs for modulation of pharmacokinetics (G2-X4 and G5-X4). Non-targeted NPs (G2-Ctrl and G5-Ctrl) were synthesized without POL3026 peptidomimetic. Competitive binding assays using fluorescent CXCL12 (CXCL12-red) were performed to determine binding affinity to CXCR4. Targeted and non-targeted NPs were labeled with [^{111}In] for *in vitro* and *in vivo* evaluation. Glioblastoma cell line U87 and an isogenic cell line stably transfected with CXCR4 (U87-stb-CXCR4) were used for *in vitro* binding experiments. NOD/SCID mice harboring U87 and U87-stb-CXCR4 subcutaneous xenografts were used for biodistribution and imaging studies.

Both targeted and non-targeted NPs were synthesized in good yields. Generation 2 and 5 targeted NPs contained 2 and 4 (average) POL3026 molecules, respectively. CXCL12-red binding to CXCR4 was inhibited by G2-X4 and G5-X4 NPs with IC_{50} values of 1.67 ±0.7 and 0.95 ±0.4 nM, respectively. Control NPs did not show appreciable inhibition. [^{111}In]-labeled targeted-NPs demonstrated 4 fold increase in uptake by U87-stb-CXCR4 cells compared to U87 cells. This uptake could be inhibited by 1μM POL3026 blocking dose, indicating CXCR4-specific uptake. Biodistribution studies with [^{111}In]G5-X4 NPs showed significantly higher accumulation (%ID/g) in U87-stb-CXCR4 tumors (8.42% ±0.49) compared to U87 tumors (4.39% ±0.31, p=0.01) at 3 h post injection (p.i.). [^{111}In-]G5-Ctrl NPs showed similar accumulation in U87-stb-CXCR4 (5.75% ±0.46) and U87 (4.79% ±0.67) tumors at 3 h p.i. In addition to the tumors, both NPs accumulated mainly liver, lungs, heart, and kidneys. Detailed biodistribution and imaging studies are ongoing to further characterize *in vivo* distribution properties of all the NPs.

Our studies demonstrate that POL3026 conjugated PAMAM-derived NPs show CXCR4 specific binding *in vitro* and *in vivo* and can be used for the development of CXCR4-targeted nanotherapeutics.

Teicher, B.A., Fricker, S.P. *Clin. Cancer Res.* 2010, *16*, (11), 2927-31.
Lesniak, W.G., Sikorska, E., Shallal, H., Azad, B.B., Liosk, A., Pullambhatla, M., Pomper, M.G., Nimmagadda, S. *Mol. Pharm.* 2015, DOI: 10.1021/mp500799

AUTHORS (LAST NAME, FIRST NAME): Lesniak, Wojciech[1]; Lisok, Ala[1]; Pullambhatla, Mrudula[1]; Pomper, Martin[1]; Nimmagadda, Sridhar[1]

INSTITUTIONS (ALL):
1. Johns Hopkins School of Medicine, Baltimore, MD, United States.

(No Image Selected)

CONTROL ID: 2235221

TITLE: Receptor Targeted Theranostic Nanoparticles for Targeted and Image-guided Therapy of Stromal-rich and Drug Resistant Human Cancer

PRESENTER: Lily Yang

ABSTRACT BODY:

Abstract Body: Drug resistance from highly heterogeneous cancer cells and tumor microenvironment represents a major challenge in clinical oncology. Early detection, efficient drug delivery, and precision surgical removal of tumors are essential components of successful cancer treatment. The development of multifunctional theranostic nanoparticles holds great promises for the effective treatment of drug-resistant cancers. We have developed an integrated image-therapy protocol that takes advantage of the multi-functionality of theranostic magnetic iron oxide nanoparticles (IONPs) and advanced imaging methods for targeted tumor imaging and drug delivery, monitoring of therapeutic responses, and optical image-guided surgery. Theranostic IONPs developed by our group are targeted to IGF-1R, and uPAR, which are cellular receptors highly expressed in drug resistant tumor cells as well as tumor stromal cells in human cancer tissues. The ability of uPAR and IGF1R targeted theranostic nanoparticles to penetrate tumor stromal barrier and enhance tumor cell killing has been demonstrated in human pancreatic cancer or triple negative breast cancer patient tissue derived (PDX) xenograft models. Repeated systemic administrations of those receptor-targeted theranostic IONP carrying a chemotherapy drug doxorubicin and/or cisplatin led to destroying tumor stromal barrier and delivering drugs into tumor cells for increased therapeutic responses (Figure). Near infrared (NIR) optical and MR imaging ability of the theranostic nanoparticles enabled noninvasive MRI for monitor drug delivery and responses. The presence of optical signals in drug resistant tumors should allow for image-guided surgery to remove drug resistant tumors. Furthermore, our results have shown the efficacy of targeted therapy and MRI-monitoring of drug delivery and treatment response after systemic delivery of the theranostic IONPs in the above animal models. The development of this novel integrated and image-guided cancer therapeutic protocol using targeted theranostic nanoparticles and new imaging approaches has great potential for translation into clinical applications for effective treatment of drug resistant cancer patients.

AUTHORS (LAST NAME, FIRST NAME): Zhou, Hongyu[1]; Qian, Weiping[1]; Guo, Xiangxue[1]; Wang, Liya[2]; Chen, Hongyu[3]; Wang, Andrew[3]; Kooby, David[1]; Lipowska, Malgorzata[2]; Staley, Charles A.[1]; O'Regan, Ruth M.[4]; Styblo, Toncred A.[1]; Mao, Hui[2]; Yang, Lily[1, 2]

INSTITUTIONS (ALL):

1. Surgery, Emory University School of Medicine, Atlanta, GA, United States.
2. Radiology and Imaging Sciences, Emory University, Atlanta, GA, United States.
3. Ocean nanotech LLC, San Diego, CA, United States.
4. Hematology and Oncology, Emory University, Atlanta, GA, United States.

A. Human pancretic cancer patient tissue derived orthotopic tumor xenograft model

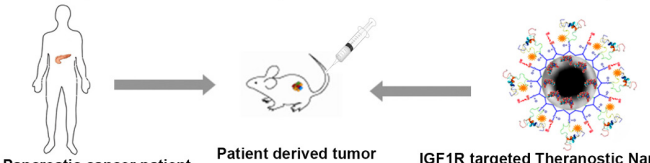

Pancreatic cancer patient

Patient derived tumor xenograft

IGF1R targeted Theranostic Nanoparticle

B. T2-weighted MRI monitor response

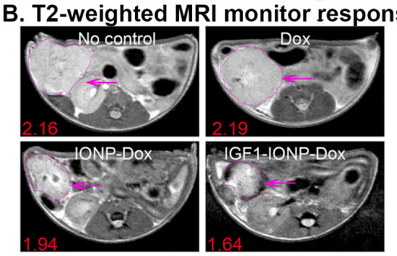

MRI of IONP-drug delivery and therapeutic response

C. Targeted cancer therapy

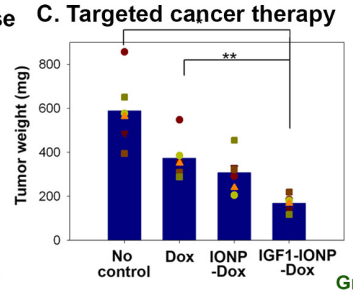

D. Breaking tumor stromal barrier for drug delivery into tumor cells to induce apoptotic cell death

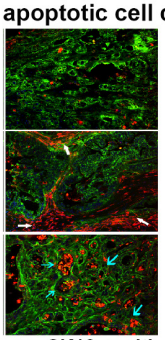

Dox

Non-targeted IONP-Dox

IGF1-IONP Dox

Green: CK19 positive tumor cells

Red: Active caspase 3 + cell death

CONTROL ID: 2233177

TITLE: Homomultivalent Fluorescent Imaging Agents Targeted to the Delta-Opioid Receptor for Cancer Imaging

PRESENTER: Amanda Shanks Huynh

ABSTRACT BODY:

Abstract Body: Multivalent targeting agents are being developed to improve binding avidity and tumor selectivity for delivery of image contrast and therapeutic payloads to cancer. Higher avidity targeting agents can theoretically be delivered at lower systemic dosages while maintaining high levels of agent retention in tumor. We have used a high affinity delta opioid receptor (δOR) antagonist ligand to develop homomultivalent versions (mono-, bi- and tri-valent) of a tumor targeted imaging agent using a novel cyclene scaffold conjugated to Cy5 near-infrared fluorescent dye (Figure 1A). We evaluated differences in binding, tumor selectivity, pharmacokinetics and biodistribution among these agents using in vitro and in vivo models of cancer. Target avidities were determined via a whole-cell lanthanide time-resolved fluorescence competition binding assay. A significant ($p<0.01$) increase in avidity was observed by increasing the number of binding moieties: monovalent (0.77 nM K_i), bivalent (0.34 nM K_i) and trivalent (0.24 nM K_i) (Supplemental Figure 1A). In vivo and ex vivo fluorescence signals of the agents were quantified from image acquisitions of a bilateral tumor xenograft mouse model. All three versions of agent demonstrated significant long lasting in vivo selectivity by exhibiting comparable levels of fluorescence signal in the δOR-expressing tumors relative to the δOR-negative tumors (Supplemental Figure 1B,C). However, only the monovalent version exhibited lower signal in the kidneys relative to the positive tumor and nearly complete kidney clearance by 24 h. The kidney fluorescence signal of the multivalent agents gradually decreased over time but was still at higher levels compared to the positive tumor until 120 h for the bivalent agent and greater than 144 h for the trivalent agent (Supplemental Figure 1C). To better understand the biology of kidney retention of the multivalent agents, mice were euthanized 24 h after agent injection, the kidneys removed and kept on ice and a 300 μm section immediately prepared from the kidney center using a vibratome. The fresh sections were treated with AlexaFluor 488 WGA to stain for glomeruli and tubules, and DAPI to stain the nucleus before high resolution macroscopic and microscopic fluorescence images were acquired. In vivo and ex vivo fluorescence imaging of non-tumor bearing mice showed that while the monovalent agent had mostly cleared the kidney by 24 h; the multivalent agents were retained at high levels in the proximal tubules in the cortex region of the kidney (Figure 1A,B,C). Figure 1D shows the accumulation of the bivalent agent's fluorescence signal within endosomes inside proximal tubule cells. Since similar kidney retention is not observed for monovalent versions, it is unlikely that the observed retention is related to δOR expression in proximal tubule cells, however, blocking studies will be conducted to rule this out. Ongoing studies are elucidating the agent properties (mass, charge, solubility/lipophilicity) associated with rapid kidney clearance. Understanding these properties will improve the future development of cancer targeting agents.

AUTHORS (LAST NAME, FIRST NAME): Huynh, Amanda Shanks[1]; Jeune-Smith, Yolaine[1]; Josan, Jatinder[5]; Wojtkowiak, Jonathan[1]; Lynch, Ronald M.[4]; Vagner, Josef[2]; Hruby, Victor[3]; Morse, David L.[1]

INSTITUTIONS (ALL):

1. Cancer Imaging & Metabolism, H. Lee Moffitt Cancer Center, Tampa, FL, United States.
2. BIO5 Institute, University of Arizona, Tucson, AZ, United States.
3. Chemistry and Biochemistry, University of Arizona, Tucson, AZ, United States.
4. Physiology, University of Arizona, Tucson, AZ, United States.
5. Center for Drug Discovery, Virginia Tech, Blacksburg, VA, United States.

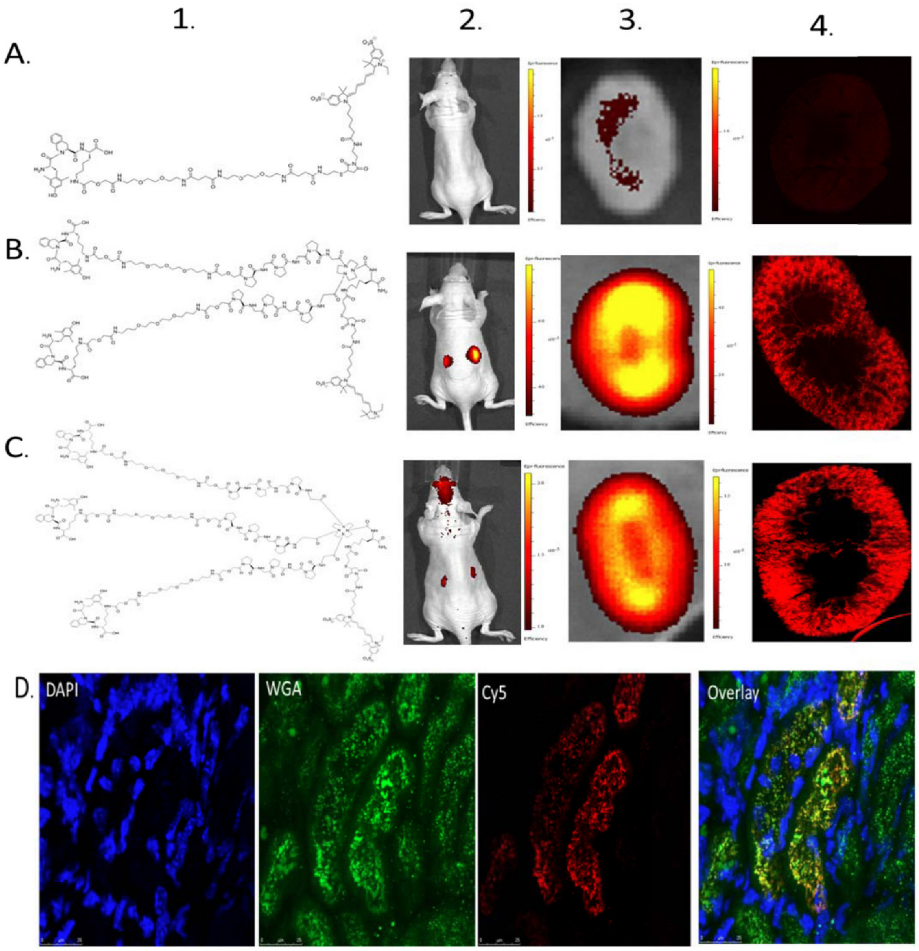

Figure 1. Kidney uptake of novel homomultivalent fluorescent imaging agents targeted to the delta opioid receptor (δOR) : A) monovalent agent, B) bivalent agent and C) trivalent agent. Each row shows the 1) structure of each Cy5 fluorescent dye conjugate, 2) in vivo fluorescence image acquired 24 h post-injection of 20 nmol/kg of agent in non-tumor bearing mice and corresponding ex vivo fluorescence signals in kidney center section acquired 3) macroscopically on the IVIS 200 and 4) microscopically on the LifeTech EVOS FL Auto. D) Confocal fluorescence microscopy images of the kidney cortex showing accumulation of the homobivalent agent in the proximal tubule cells within endosomes at 24 h post administration.

CONTROL ID: 2233193

TITLE: *In vivo* Imaging of Lung Apoptosis in an Emphysema Model

PRESENTER: Yared Tekabe

ABSTRACT BODY:

Abstract Body: INTRODUCTION:

Molecular imaging targeting cellular processes related to lung disease pathogenesis has the potential to assess disease activity over time to allow for clinical intervention prior to lung destruction seen on CT. Pulmonary epithelial and endothelial cell apoptosis is a cellular event unique to emphysema associated with cigarette smoking and is not seen at an increased rate in smokers without the disease. Development of *in vivo* imaging of this process may aid in the early identification and/or prognostication of patients at risk for emphysema.

METHODS:

Rabbits exposed to cigarette smoke for either 4 weeks (n=6) or 16 weeks (n=6) plus 6 room air controls for each time point were injected with 3.83 ± 1.17 mCi ^{99m}Tc-AnnexinV-128 (AxV-128) (Atreus Pharmaceuticals) and underwent SPECT imaging on Bioscan (Mediso) nanoSPECT fitted with 2 LEUHR collimators and high resolution spiral CT scanning on Siemens Biograph. SPECT data was reconstructed and merged with the CT using VivoQuant software (InVicro, Boston MA). ROIs were drawn on transverse 20 voxels thick slices from apex to base and counts summed for right lung (RL) and left lung (LL). Counts were converted to mCi (%ID) using camera efficiency, conversion factors and decay corrected ID. Tissue samples were taken from upper and lower lobes of both lungs for gamma well counting. Following imaging, animals were sacrificed, lungs lavaged and pressure perfused, formalin fixed, and sectioned for morphometry. TUNEL assay was performed for apoptosis.

RESULTS:

The low uptake of AxV-128 for both lungs in room air exposed rabbits at 4 and 16 weeks was not different and values were combined. AxV-128 SPECT imaging detected higher lung apoptosis (mean ± SD) with smoke exposure at 4 weeks (RL 2.37±0.73, LL 1.92±0.63 %ID) and at 16 weeks (RL 2.14±0.39, LL 1.56±0.16 %ID) compared to room air (RL 0.70±0.50, LL 0.56±0.38 %ID) ($p \leq 0.001$ for both lungs at 4 wk, $p < 0.001$ both lungs at 16 wk). There was no significant difference in uptake for either lungs between 4 and 16 wk ($P = 0.54$, $P = 0.25$). Gamma well counting data confirmed the imaging results. TUNEL staining confirmed increased lung apoptosis in smoke exposed lungs for both time points. CT lung volumes (mean ± SD) comparing smoke and room air exposed rabbits at 4 week were not different (RL=16.4cc, LL=15.7cc vs. RL=17.7cc, LL=14.4cc) while at 16 wk volumes were higher in smoke exposed (RL=28.2cc, LL=23.3cc vs. RL=18.3cc, LL=13.7cc) ($P = 0.05$, $P = 0.02$). The 16 wk smoked rabbits had at least one segment in both RL and LL with Hounsfield units below 2 SDs of the mean value for the lungs of room air rabbits while none of the 4 week smoked rabbits had values outside this range.

CONCLUSIONS:

AxV-128 SPECT/CT imaging identified ongoing lung apoptosis in cigarette smoke exposed rabbits from 4 to 16 wk compared to age and weight matched room air controls. At the later time point the CT scans showed increased lung volumes and lower segmental HUs. These data suggest that AxV-128 lung imaging may be a useful imaging marker to predict development of destructive lung changes leading to emphysema.

AUTHORS (LAST NAME, FIRST NAME): Tekabe, Yared[1]; Goldklang, Monica P.[2, 1]; D'Armiento, Jeanine M.[2, 1]; Zelonina, Tina[2]; Shiomi, Tomoe[2]; Trischler, Jordis[2]; Xiao, Rui[2]; Anthony, Tamykah[1]; Romanov, Alexander[3]; Shiomi, Takayuki[2]; Johnson, Lynne L.[1]

INSTITUTIONS (ALL):

1. Medicine, Columbia University, New York, NY, United States.
2. Anesthesiology, Columbia University, New York, NY, United States.
3. Institute of Comparative Medicine, Columbia University, New York, NY, United States.

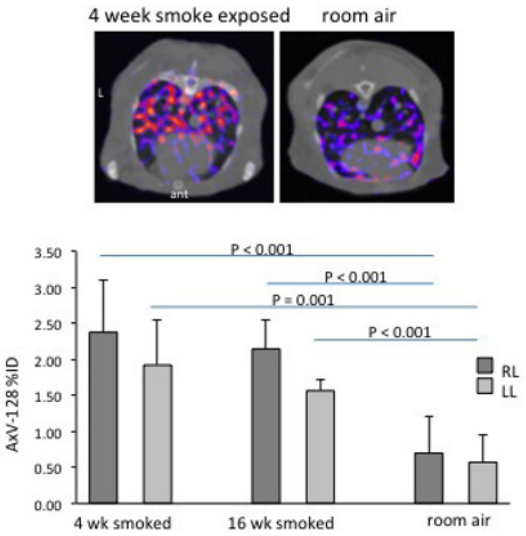
4 week smoke exposed
room air
L
ant
P < 0.001
P < 0.001
P = 0.001
P < 0.001
AxV-128 %ID
3.50
3.00
2.50
2.00
1.50
1.00
0.50
0.00
RL
LL
4 wk smoked
16 wk smoked
room air

CONTROL ID: 2233202

TITLE: Optimizing ^{99m}Tc-etarfolatide imaging of folate receptor-positive tumors: Effect of mass dose and post injection time

PRESENTER: Christopher Leamon

ABSTRACT BODY:

Abstract Body: Background: The folate receptor (FR) is overexpressed in many cancers and represents a potentially relevant target for biomarker and drug development. ^{99m}Tc-etarfolatide is a small-molecular-weight folate-targeted imaging agent that can be used for non-invasive, real-time assessment of functionally active and anatomically accessible FRs in tumor tissue. As seen in preclinical models and in the clinic, response to folate-targeted drugs, such as vintafolide, is dependent on FR expression. Therefore, the ability to screen patients for FR-positive disease in real time is of high value. The aim of these newly disclosed preclinical studies was to determine the effect of imaging time (post injection) and total mass dose on ^{99m}Tc-etarfolatide's biodistribution and imaging properties.

Methods: Etarfolatide kits were used for the preparation of ^{99m}Tc chelated radioactive drug substance. Radiochemical purity of ^{99m}Tc-etarfolatide was determined by HPLC attached to a radiodetector. ^{99m}Tc-etarfolatide was investigated *in vivo* using mice bearing FR positive human xenograft models. Test articles were administered intravenously in mice via the lateral tail vein. ^{99m}Tc biodistribution was determined by removing selected tissues and measuring their radioactivity content in an automatic gamma-counter. High resolution three dimensional images of the radiolabel were obtained using a dual microSPECT/CT system.

Results: Following intravenous administration, ^{99m}Tc-etarfolatide was rapidly captured and retained within FR-expressing tumor and kidney. Peak tissue levels occurred at 1 h post injection. Tumor retention remained near maximum for approximately 18 h, whereas ^{99m}Tc-etarfolatide levels in normal FR-negative tissues had quickly cleared to near baseline levels after 4-8 h. Time-based SPECT/CT imaging corroborated these tissue-based findings. While keeping the radiochemical dose constant, increasing the total etarfolatide mass dose was found to strikingly increase radiochemical uptake in tumor by more than 4-fold and reaching the "summit" at a mouse dose of ~100 nmol/kg. Tumor-to-nontumor ratios consequently increased thereby improving the quality of tumor imaging. Substituting the unlabelled etarfolatide mass with folic acid did not show these effects, likely because etarfolatide has distinct non-cognate binding sites in normal tissues. Importantly, tumor-to-nontumor ratios did decrease as the total etarfolatide mass dose was further escalated up to the point where complete, competitive tumor blockade was observed at 10,000 nmol/kg.

Conclusions: Our findings indicate that the biodistribution and SPECT/CT image quality of ^{99m}Tc-etarfolatide can be significantly improved by i) allowing sufficient time for non-cognate tissue uptake to clear, and/or ii) administering an appropriate mass dose of etarfolatide such that non-cognate binding sites on FR-negative tissues can be blocked or reduced to levels that enhance the tumor-to-nontumor contrast. Based on these findings, both of these experimental parameters (imaging time and mass dose) are currently being tested at the clinical level in cancer patients.

AUTHORS (LAST NAME, FIRST NAME): Leamon, Christopher P.[1]; Reddy, Joseph[1]; Vetzel, Marilynn[1]; Taylor, Christina[1]; Nelson, Melissa[1]

INSTITUTIONS (ALL):

1. Research, Endocyte, Inc., West Lafayette, IN, United States.

(No Image Selected)

CONTROL ID: 2233224

TITLE: Simultaneous in Vivo Monitoring Adipose Derived Mesenchymal Cells by Ffly-mcherry and Gaussia-GFP Reporter Genes

PRESENTER: Mengyu Wang

ABSTRACT BODY:

Abstract Body: Stromal vascular fraction (SVF) of adipose tissue is a rich source of preadipocytes, mesenchymal stem cells (MSC), endothelial progenitor cell, T cells, B cells, mast cells as well as adipose tissue macrophages. MSC were established from fresh SVF cells obtained from liposuction of excess adipose tissue. MSC bear promises in regeneration medicine. To study the mode of action of MSCs in tissue repair and the use of MSCs as carrier for gene therapy in vivo imaging must be considered. By using vector pCDH-EF1- MCS-T2A with Gaussia-GFP or pCDH-EF1-MCS-T2A with Ffly-mcherry we established an experimental tracking MSC model in vitro and vivo. Prior to inject the marked MSC they were cultured under normoxic and hypoxic conditions. To visualize the cells in vivo we used substrate D-Luciferin Firefly and RediJect Coelenterazine whis was injected separately i.p. into the mice. By the different time point the different type of MSCs can be detectable in the same mouse. As will be shown hypoxic treated MSCs had a significant longer survival than those MSCs that were grown under normoxic conditions during three months observation.

Recently we have started to study how MSCs migrate to the tumor. In this study we transfect MSC with Ffly-mcherry reporter gene and mouse breast cancer 4T1 cell line with Gaussia-GFP. Data from this study will be presented.

AUTHORS (LAST NAME, FIRST NAME): Wang, Mengyu[1]

INSTITUTIONS (ALL):

1. Cell Therapy, Oslo University Hospital, Oslo, Norway.

(No Image Selected)

CONTROL ID: 2233219

TITLE: ^{90}Y PET imaging: Optimization for Preclinical Settings

PRESENTER: Katerina Eigner Henke

ABSTRACT BODY:

Abstract Body: ^{90}Y (64.053 d) is commonly known as a 'pure' β^--emitter with end-point energy of 2.28 MeV. Its decay has a minor (≈ 10^{-4}) branch to the 0^+ first excited state of ^{90}Zr at 1.78 MeV. The ($0^+ \rightarrow 0^+$) de-excitation is constrained to follow 2-γ emission, internal conversion, or e^--e^+ pair creation (Ford 1955), which happens in 31.867 ± 0.47 out of million decays (Selwyn *et al* 2007, Langhoff and Hennies 1961).

For the last few years, ^{90}Y was only imaged using bremsstrahlung (continuous energy spectrum x-rays) (Mansberg *et al* 2007). Imaging utilizing bremsstrahlung suffers from low quality images resulting in difficulties for quantification and lack off spatial resolution. However, the occurring annihilation photons allow the possibility of using coincidence imaging via PET. For the purpose of lowering the count rate originating from the bremsstrahlung x-rays, and, therefore, improving the count rate performance, Elmbt et al 2011 suggested to insert a thin copper cylinder (~2.4 mm thickness) into the detector array. The aim of the presented work was to demonstrate the potential of ^{90}Y PET imaging while utilizing a copper insert as well as the resulting image quality and special resolution.

For validation of the proposed theorem ^{90}Y and ^{18}F filled NemaNu4 phantoms were imaged with and without a copper filter (9.98 cm outer diameter, 28 cm length, 2.4 mm walls) in a fully equipped ALBIRA PET/SPECT/CT multimodality small animal scanner (Bruker BioSpin, Ettlingen, Germany). Resulting images were reconstructed using standard reconstruction settings of the Albira Imaging Suite and analyzed using PMod software (PMod Technologies Ltd, Zürich, Switzerland). Phantoms were filled with a total of 150 MBq of ^{90}Y and ^{18}F (75 MBq mainbody, hotspheres: 50 MBq and 25 MBq) in saline solution.

Resulting images of the ^{18}F filled phantom without copper insert granted standard resolution and quantification of the measured data. Images of the same phantom with the copper filter placed inside the detector array, image quality was drastically improved due to a reduced background. However, quantification of the measured data resulted in approx. 20 – 25 % reduced yields, depending on the amount of activity within the measured ROI. The failure increased for lower activities. Imaging ^{90}Y filled phantoms resulted in grainy and not quantifiable images when not using the copper insert. Data acquisition for longer than 30 minutes resulted in no images. When using the copper insert while imaging the ^{90}Y phantom, within 60 minutes images of good special resolution could be obtained. Increased imaging times of up to 8 hours produced even higher image quality. Quantification of the obtained data remains problematic until now.

^{90}Y PET data acquisition utilizing a copper insert to lower the count rate of the bremsstrahlung x-rays and therefore improve the count rate for the 511keV photons seems to be a promising approach to ^{90}Y dosimetry. However, more detailed measurements and analysis of the effect of the copper insert need to be carried out to enable quantification of ^{90}Y PET images.

AUTHORS (LAST NAME, FIRST NAME): Eigner Henke, Katerina[1, 2]; Lebeda, Ondrej[1]; Waldeck, Jens[3]; Chapman, Sarah[4]; Leevy, W. M.[4]; Eigner, Sebastian[5, 2]

INSTITUTIONS (ALL):

1. Radiopharceuticals, NPI AS CR, Husinec-Rez, Czech Republic.
2. SKS Biotech, s.r.o., Litomerice, Czech Republic.
3. Bruker BioSpin MRI GmbH, Ettlingen, Germany.
4. Notre Dame Integrated Imaging Facility, Notre Dame, IN, United States.
5. Center for Advanced Preclinical Imaging, Institute of Pathological Physiology, First Faculty of Medicine, Charles University in Prague, Prague, Czech Republic.

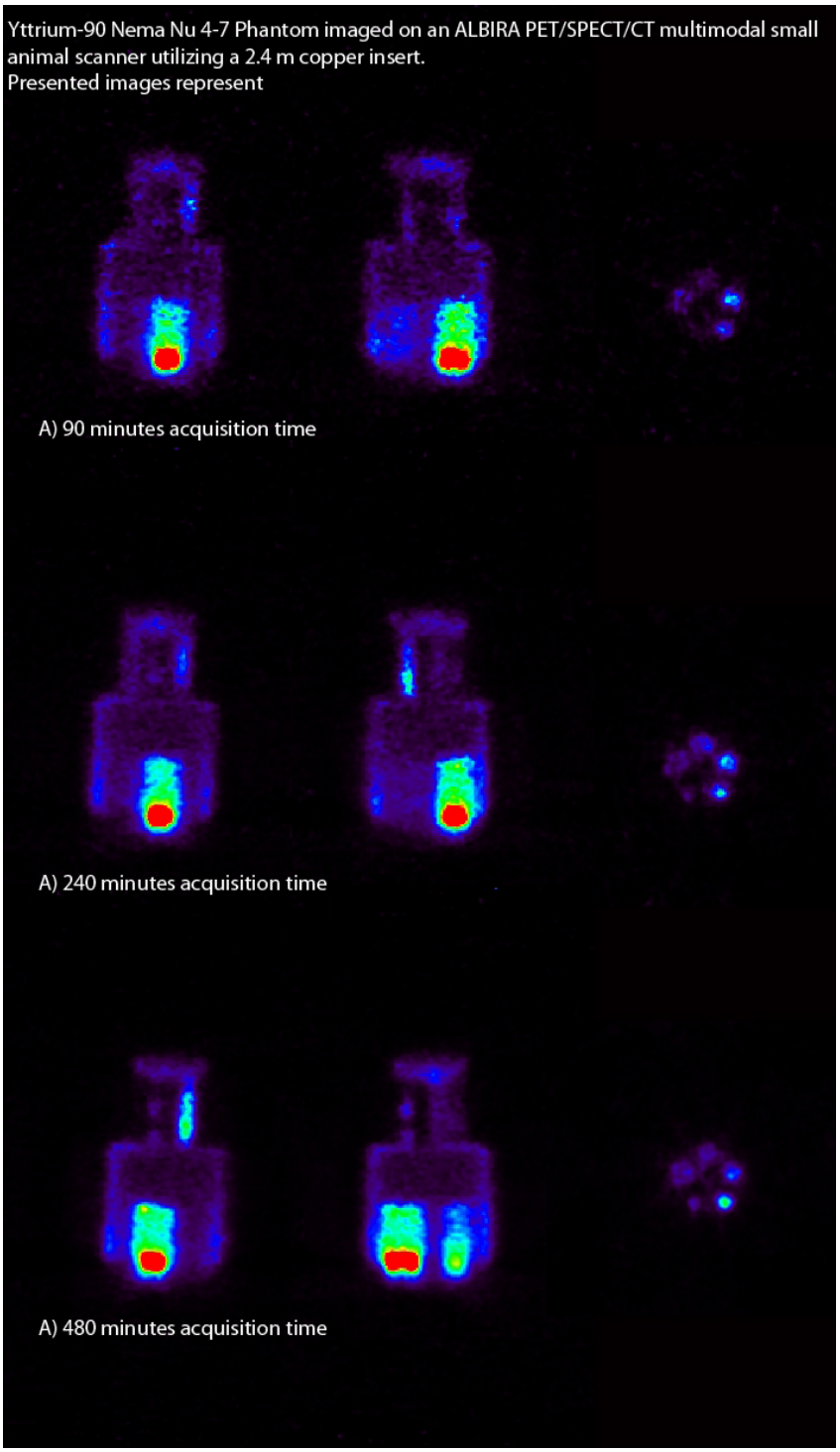
Yttrium-90 Nema Nu 4-7 Phantom imaged on an ALBIRA PET/SPECT/CT multimodal small animal scanner utilizing a 2.4 m copper insert.
Presented images represent
A) 90 minutes acquisition time
A) 240 minutes acquisition time
A) 480 minutes acquisition time

CONTROL ID: 2233229

TITLE: Single Injection of scVEGF/^{177}Lu Targeted to VEGF Receptors Inhibits Growth of 4T1luc Breast Bone Metastases in Syngeneic Mice

PRESENTER: Joseph Backer

ABSTRACT BODY:

Abstract Body: We have previously established that a single injection of novel radiopharmaceutic, recombinant single-chain VEGF (scVEGF), site-specifically derivatized with PEGylated chelator DOTA and radiolabeled with ^{177}Lu (scVEGF/^{177}Lu), induces a sustainable vascular regression in orthotopic breast cancer models and inhibits tumor growth (1).Here we report effects of scVEGF/^{177}Lu in clinically more relevant model, 4T1luc breast bone metastasis in immunocompetent syngeneic BALB/c mice.

Animals were inoculated with 5 x 10^4 luciferase-expressing mouse mammary carcinoma 4T1luc cells by intracardiac injection. At 8-9 days after cell inoculation animals were treated with scVEGF/^{177}Lu, 200 µCi per mouse, delivered via retro-orbital sinus. Growth of metastatic lesions in treated (n=10) and control (n=7) animals was followed with bioluminescent imaging (BLI) and CT, beginning on day 4 post cell inoculation and at 2-3 day intervals up to day 15 for controls and day 15-17 for treatment group. At sacrifice samples were prepared for immunohistochemical and H&E staining and flow cytometry on blood monocytes. Select animals were subject to high resolution microCT with 20.5 µm resolution.

Intracardiac injection of 4T1luc cells produced bone metastases detectable with BLI by day 4 after cell inoculation and developed throughout the animal, being most prominent in legs, shoulders and spine.The overall metastatic burden, as measured by whole body BLI, increased exponentially in all but one treated and one control mice. scVEGF/^{177}Lu treatment statistically significantly ($p=0.04$) increased doubling time for overall metastatic burden in individual mice from 0.97 ± 0.17 to 1.44 ± 0.48 days. In agreement with these findings, the survival for the scVEGF/^{177}Lu treated group was 80% on day15 and 50% on day 17, but only 14% for the control group at day 15. Immunostaining with anti-CD31 and anti-VEGFR-2 antibodies indicated angiogenesis in bone, and high resolution micro CT confirmed pronounced areas of osteolysis. Flow cytometry showed no change in monocyte population.

Judging by the inhibitory effect of a single injection of scVEGF/^{177}Lu on growth of primary tumors and bone metastasis in the 4T1luc metastatic breast tumor model, scVEGF/^{177}Lu can be further explored as a potential therapy agent for breast cancer.

(1) Blankenberg FG, Levashova Z, Goris MG, et al. Targeted systemic radiotherapy with scVEGF/177Lu leads to sustained disruption of the tumor vasculature and intratumoral apoptosis. J Nucl Med. 2011;52:1630-37.

AUTHORS (LAST NAME, FIRST NAME): Wang, Yuzhen[2]; Backer, Marina[1]; Rusckowski, Mary[3]; Backer, Joseph M.[1]

INSTITUTIONS (ALL):

1. SibTech, Inc., Brookfield, CT, United States.
2. Radiology, University of Massachusetts Medical School, Worcester, MA, United States.
3. Radiology, University of Massachusetts Medical School, Worcester, MA, United States.

(No Image Selected)

CONTROL ID: 2233232

TITLE: Tracer kinetic model selection of pre- and post-therapy cervical cancer DCE MRI data

PRESENTER: Joel Garbow

ABSTRACT BODY:

Abstract Body: INTRODUCTION. Dynamic Contrast Enhanced (DCE) MRI is being used increasingly in the assessment of cervical cancer, both pre- and post-radiotherapy. Predicting and assessing therapeutic outcome, and guiding radiation dose planning, will require extraction of quantitative physiological parameters from DCE-MRI data. Central to this challenge is selection of the "optimal" (most probable, given the data and prior information) DCE-MRI kinetic model. Bayesian probability theory, the optimal method of inference (1), provides an ideal mathematical formalism for performing model-selection calculations. Herein, Bayesian model selection (2) was employed to test four DCE models against high quality DCE-MRI data acquired prior to, and following, radiation therapy (RT) from a cohort (n = 10) of advanced-stage, cervical cancer patients.

METHODS. Data were acquired prospectively as part of EMBRACE, an international study of MRI-guided brachytherapy. Data were acquired on a 3-T Philips Achieva scanner *via* a 3D, saturation-recovery, spoiled gradient-echo technique. A T1 relaxation time-constant map was constructed before contrast-agent administration, allowing conversion of DCE-MRI signal intensity to contrast-agent concentration. Tumor tissue was identified on T2-weighted images by an experienced radiologist. Four Tracer Kinetic DCE models (3) were included in this model-selection study: (i) the two-parameter Tofts Model (TM), (ii) the three-parameter Extended Tofts Model (ETM), (iii) the three-parameter Compartmental Tissue Uptake Model (C-TU), and (iv) the four-parameter Two-Compartment Exchange Model (2CXM). Bayesian Probability Theory was used to compute the posterior probability for each of these models, using a Markov-chain Monte Carlo simulation with Thermodynamic Integration (4).

RESULTS. Figure 1A illustrates concentration *vs.* time curves for individual voxels within a single cervical tumor in which 2CXM (**Panel A1**), C-TU (**Panel A2**), ETM (**Panel A3**), or TM (**Panel A4**), respectively, are the Bayesian-preferred tracer kinetic models. **Figure 1B** shows Bayesian-derived model selection results, pre- and post-radiotherapy, from a cohort of ten patients.

DISCUSSION AND CONCLUSIONS. While any of the four tracer kinetic models may be favored in an individual voxel (**Figure 1A**), C-TU and TM are the highly dominant (most probable) models (**Figure 1B**). The increase in the percent of voxels best fit by the C-TU model following radiation treatment, with a concomitant decrease in those voxels best fit by TM, results from an increase in contrast-agent uptake (higher DCE signal-to-noise ratio). More complex 2CXM is unlikely to be supported at noise levels typical of clinical data. As signal-to-noise decreases, Bayesian model selection chooses simpler data representations, a manifestation of Occam's razor.

REFERENCES. 1) Jaynes ET. Probability Theory-The Logic of Science. Bretthorst GL, ed. Cambridge University Press; 2003. Press; 2003. **2)** Bretthorst GL. Maximum Entropy and Bayesian methods. Skilling J., ed. Kluwer Academic Publisher, pp.377-388. **3)** Sourbron SP and Buckley DL. NMR Biomed. 2013; 26: 1004-1027. **4)** Lartillot N and Philippe H. Syst. Biol. 2006; 55:195-207.

AUTHORS (LAST NAME, FIRST NAME): Duan, Chong[1]; Kallehauge, Jesper[2]; Tanderup, Kari[3]; Bretthorst, Larry[4]; Ackerman, Joseph J.[1, 4]; Garbow, Joel R.[4]

INSTITUTIONS (ALL):

1. Chemistry, Washington University, Saint Louis, MO, United States.
2. Medical Physics, Aarhus University, Aarhus , Denmark.
3. Oncology, Aarhus University, Aarhus , Denmark.
4. Radiology, Washington University, Saint Louis, MO, United States.

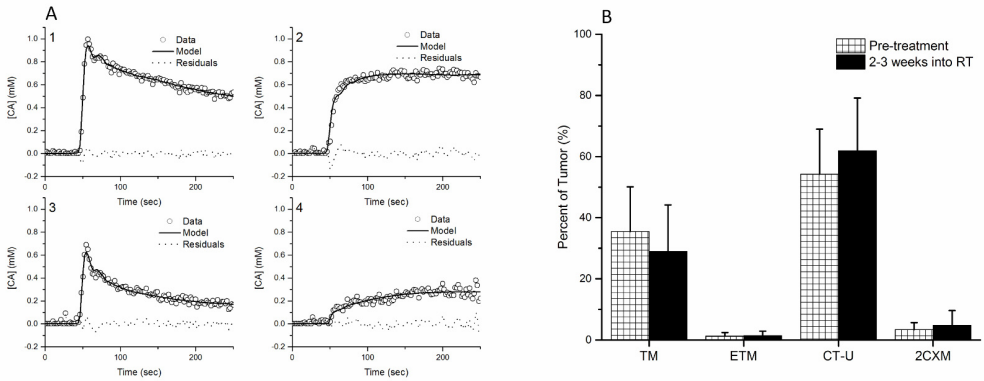

Figure 1. Panel A: Example DCE-MRI contrast-agent concentration *vs.* time curves (circles), along with optimal model fitting (solid lines). Residuals are shown as dotted lines. **Panel B:** Average percent distribution of the optimal kinetic model, pre- and post-therapy; DCE-MRI data are from a cohort of ten cervical cancer patients (39,365 total tumor voxels). Bar graphs represent mean ± SD. Following therapy, the percentage of voxels best fit by TM drops by 19% ($p = 0.16$) while the percentage of voxels best fit by C-TU increases by 14% ($p = 0.19$).

CONTROL ID: 2233234

TITLE: Targeting lysyl oxidase for molecular imaging in breast cancer – a preclinical study in mice with correlation to human tissue samples

PRESENTER: Melinda Wuest

ABSTRACT BODY:

Abstract Body: Lysyl oxidase (LOX) and LOX-like (LOXL)1-4 are copper-dependent extracellular matrix enzymes [1]. Compared to normal breast tissue, LOX expression is elevated in breast cancer (BC). Its expression correlates with level of tissue hypoxia, and it plays a key role during breast cancer metastasis [2]. The goal of the present study was to target LOX with a fluorescent and radiolabeled peptide to visualize LOX *in vivo* in three different preclinical models of BC.

Gene expression of all five members of the LOX family was analyzed at the transcript level via microarray analysis using tissue biopsy samples from 176 BC patients. Peptide GGGDPKGGGGG-NH_2 [3] was labeled with FITC for confocal microscopy in murine EMT6 BC cells. PET experiments using ^{18}F-labeled peptide were performed in three different BC models: EMT-6, MCF-7 and MDA-MB231. Specific interaction of the peptide with LOX *in vivo* was analyzed in the presence and absence of b-amino-propionitrile (BAPN), an irreversible LOX inhibitor.

Except LOXL4, all enzymes of the LOX family were up-regulated in human breast BC samples. In triple-negative BC LOX and LOXL4 mRNA transcript levels were even higher compared to estrogen receptor-positive BC. Elevated LOX expression correlated with increased HIF-1a expression in patient samples. All three preclinical BC models (EMT6, MCF-7 and MDA-MB231) were found to express LOX on protein level. Confocal microscopy using LOX-specific antibody revealed that selected compartments in EMT-6 cells expressed LOX under normoxia, while under hypoxia fluorescence became stronger and parts of the cell membrane also showed binding. Under the same conditions fluorescence staining with FITC-labeled peptide appeared to be more peri-nuclear, than membrane-localized. PET analysis revealed that in all three BC models initial high uptake of radioactivity after 5 min post injection (p.i.) of ^{18}F-labeled peptide was observed: SUV_{5min} 0.70±0.07 (n=3, EMT-6), 0.57±0.01 (n=3, MCF-7) and 0.68 (n=2, MDA-MB231). Following rapid initial uptake a continuous washout of radioactivity was observed over 60 min p.i.: SUV_{60min} 0.18±0.03 (n=3, EMT-6), 0.14±0.02 (n=3, MCF-7) and 0.13 (n=2, MDA-MB231). In EMT-6 tumor bearing mice presence of LOX inhibitor BAPN (100 mg/kg i.p.) 4 h prior i.v. injection of radiolabeled peptide reduced its maximum uptake levels into the tumor from SUV_{5min} 0.70±0.07 in the absence to 0.49±0.09 in the presence of BAPN (n=3, $p>0.05$).

The present study confirms hypoxia-dependent LOX expression in BC. Results demonstrate involvement of LOX as a specific molecular target in triple-negative BC. PET experiments with ^{18}F-labeled peptide GGGDPKGGGGG-NH_2 provide evidence of LOX-specific interactions *in vivo* and support further investigations aimed at the development of LOX-binding compounds for molecular targeting of LOX in BC *in vivo*.

[1] Mayorca-Guiliani A, Erler JT (2013) Onco Targets Ther 25:1729.

[2] Erler JT, Bennewith KL, Nicolau M, Dornhöfer N, Kong C, Le QT, Chi JT, Jeffrey SS, Giaccia AJ (2006) Nature 440:1222.

[3] Nagan N, Kagan HM (1994) J Biol Chem 269:22366.

AUTHORS (LAST NAME, FIRST NAME): Wuest, Melinda[1]; Kuchar, Manuela[3]; Sharma, Sai Kiran[2, 1]; Richter, Susan[1]; Hamann, Ingrit[1]; Vos, Larissa J.[1]; Mackey, John[1]; Wuest, Frank[1]; Loeser, Reik[3]

INSTITUTIONS (ALL):

1. Dept. of Oncology, University of Alberta, Edmonton, AB, Canada.
2. Memorial Slone Kettering Cancer Center, New York City, NY, United States.
3. Helmholtz Zentrum Dresden-Rossendorf, Dresden, Germany.

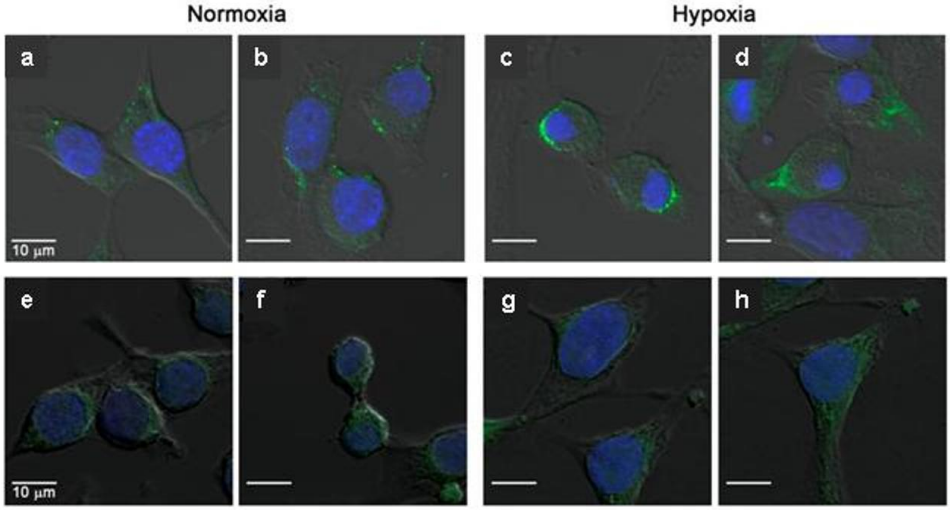

Figure 1a): Confocal microscopy images from EMT-6 cells cultured under normoxic (*left, a,b,e,f*) and hypoxic (*right,c,d,g,h*) conditions using primary anti-LOX mAb and a secondary Alexa fluor 488-mAb (*a-d*) and FITC-Ava-G_3DPKG_5-NH_2 (*e-h*). Cell nuclei stained with DAPI.

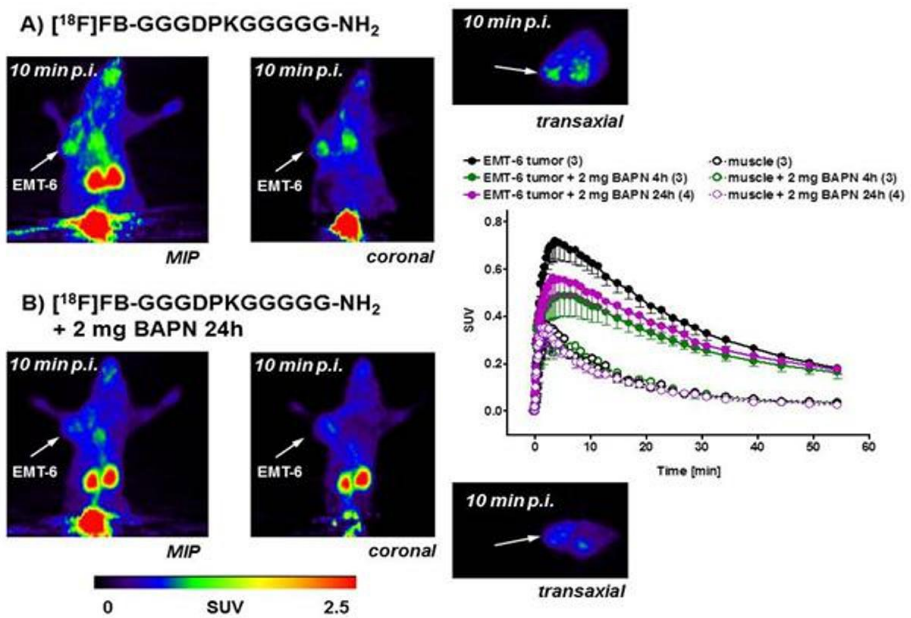

Figure 1b): Representative PET images after injection of [^{18}F]FB-GGGDPKGGGGG-NH_2 in the absence and presence of BAPN in EMT-6 tumor bearing mice at 10 min p.i.. Images are shown as maximum intensity projections (MIP), coronal, and transaxial slices from the tumor region. Right: Time-activity curves for the radioactivity uptake into EMT-6 tumors in comparison to muscle tissue in the absence and presence of BAPN.

CONTROL ID: 2234164

TITLE: Imaging glucose and fructose metabolism in breast cancer: A mouse study

PRESENTER: Melinda Wuest

ABSTRACT BODY:

Abstract Body: Aim: The role of [^{18}F]FDG-PET in clinical breast cancer (BC) imaging is still limited. Up to 50% of BCs do not express sufficiently high levels of hexose transporter GLUT1 which leads to a low sensitivity of [^{18}F]FDG-PET [1]. Fructose metabolism represents an alternative hexose metabolism in cancer cells. The main transporter for fructose is GLUT5. Elevated levels of GLUT5 were found in several types of cancer, including BC [2,3]. The goal of the present study was to evaluate the correlation between uptake characteristics of selected fructose and glucose-based PET tracers in a murine BC model *in vivo* and the mRNA expression of selected GLUTs.

Materials and Methods: The following fructose and glucose-based PET tracers were synthesized: 1-deoxy-1-[^{18}F]fluoro-D-fructose (1-[^{18}F]FDF), 6-deoxy-6-[^{18}F]fluoro-D-fructose (6-[^{18}F]FDF) and 6-deoxy-6-[^{18}F]fluoro-D-glucose (6-[^{18}F]FDG). Radiotracer uptake and PET imaging experiments were performed in EMT-6 cells and EMT-6 tumor-bearing mice, respectively. GLUT1, GLUT2 and GLUT5 mRNA expression levels were analyzed with RT-PCR using EMT-6 cell lysates and EMT-6 tumor tissue in comparison to muscle tissue.

Results: Fructose analogs 1-[^{18}F]FDF and 6-[^{18}F]FDF showed uptake into EMT-6 tumors. 1-[^{18}F]FDF revealed low uptake levels reaching a maximum after 20 min post injection (SUV 0.48±0.07) followed by a slow washout (SUV $_{120min}$ 0.31±0.06; n=3). Uptake of 6-[^{18}F]FDF was much higher (SUV$_{20min}$ 1.08±0.14) also followed by a slow washout (SUV$_{120min}$ 0.59±0.06; n=4). PET imaging studies confirmed radioactivity uptake but no trapping of fructose-based radiotracers. 6-[^{18}F]FDG also reached a maximum uptake level at 20 min (SUV$_{20min}$ 1.23±0.10) with no further accumulation over time (SUV$_{120min}$ 1.14±0.05; n=3). 2-[^{18}F]FDG showed continuous increase of radiotracer uptake: SUV$_{20min}$ 1.15±0.25 to SUV$_{120min}$ 1.97±0.24 (n=4). In EMT-6 cells, GLUT5 mRNA expression was ~10.000-fold lower compared to GLUT1, whereas GLUT2 was ~100.000-fold lower than GLUT1. mRNA expression for all three GLUTs were elevated in EMT-6 tumors (GLUT1 2-fold, GLUT2 10-fold and GLUT5 2.5-fold) compared to EMT-6 cells. Mouse muscle tissue also expressed high levels of GLUTs mRNA (tumor:muscle) (GLUT1 50:1; GLUT2 1:1.6; GLUT5 1:6).

Conclusion: The present study revealed that all fructose-based PET radiotracers showed tumor uptake but no trapping *in vivo*. Uptake of fructose-based PET tracers can not simply be explained by mRNA GLUT5 overexpression. We demonstrated that muscle tissue also expresses substantial levels of GLUT5 and GLUT2 mRNA. Further experiments focused on protein expression analysis will confirm whether mRNA expression levels of GLUT1, GLUT2 and GLUT5 correspond with protein expression levels of all GLUTs in tumor and muscle tissue, and how this correlates with radiotracer uptake profiles *in vivo*.

[1] Vermeulen JF et al. (2013) Cell Oncol (Dordr) 36:333.

[2] Zamora-León SP et al. (1996) Proc Natl Acad Sci U S A 93:1847.

[3] Godoy A et al. (2006) J Cell Physiol 207:614.

AUTHORS (LAST NAME, FIRST NAME): Wuest, Melinda[1]; Hamann, Ingrit[1]; Bouvet, Vincent[1]; Marshall, Alison[1]; Soueidan, Olivier M.[2, 3]; West, Frederick[2]; Cheeseman, Chris[3]; Wuest, Frank[1]

INSTITUTIONS (ALL):

1. Oncology, University of Alberta, Edmonton, AB, Canada.
2. Dept. of Chemistry, University of Alberta, Edmonton, AB, Canada.
3. Dept. of Physiology, University of Alberta, Edmonton, AB, Canada.

(No Image Selected)

CONTROL ID: 2234187

TITLE: Highly resolved fluorescence imaging using STED nanoscopy for visualizing conformational difference of mitochondria in skin cells and tissues

PRESENTER: Hyung Jun Kim

ABSTRACT BODY:

Abstract Body: Purpose: Mitochondria play an essential role in maintaining various cellular functions such as oxidative phosphorylation, respiration, and apoptosis. Since mitochondrial dysfunction is closely related with aging, we investigated the morphological dispersion of mitochondria both in sub-cultured primary skin fibroblasts and mouse tissues using stimulated emission depletion (STED) nanoscopy.

Methods: Skin primary fibroblasts from patient samples were isolated and sub-cultured for imaging. Sub-cultured fibroblasts were exposed to UVB irradiation to induce UV-mediated skin damage to change the structure of mitochondria. Tissues from skin of young (3 month) and old (1.5 year) SKH-1 hairless mice were also harvested. Fibroblasts were fixed with paraformaldehyde and stained. Skin tissues from mice were embedded with paraffin and cut with microtome to prepare 8 micron thick sections. Antibodies for Tom20 (translocase of mitochondrial outer membrane) and TFAM (mitochondrial transcription factor A) were used for labeling mitochondrial proteins. Alexa488 conjugated secondary antibodies were used for fluorescence detection. Prolong gold with DAPI was used for mounting media. Representative STED and corresponding confocal images were acquired for monitoring the structural changes of mitochondria.

Results: In sub-cultured fibroblasts, conventional confocal microscopy provides overall mitochondrial membrane structure and the location of TFAMs within diffraction limit. However, using super-resolution STED nanoscopy, we can resolve the localization of Tom20 and perform more accurate quantitative analysis of TFAM expression. In addition, it is possible to distinguish the distribution of Tom20 between young and old tissue sample.

Conclusions: Our results suggested that highly resolved fluorescence imaging can be useful for quantitative analysis of mitochondrial proteins and their distribution in cells

AUTHORS (LAST NAME, FIRST NAME): Kim, Hyung Jun[2, 3]; Jin, Seon-Pil[4]; Kang, Jooyoun[2]; Bae, So Hyeon[2]; Kim, Mi Jeong[3]; Youn, Hyewon[3, 1]; Kang, Keon Wook[6, 3]; Chung, Jin Ho[4]; Kim, Seong Keun[5, 2]

INSTITUTIONS (ALL):

1. Cancer Imaging Center, Seoul National University Hospitla, Seoul, Korea (the Republic of).
2. Department of Chemistry, Seoul National University, Seoul, Korea (the Republic of).
3. Department of Nuclear Medicine, Cancer Reaearch Institute, Seoul National University Hospital, Seoul, Korea (the Republic of).
4. Institute of Human-Environment Interface Biology, Seoul National University Hospital, Seoul, Korea (the Republic of).
5. Department of Biophysics and chemical biology, Seoul National University, Seoul, Korea (the Republic of).
6. Department of Biomedical Sciences, Seoul National University Hospital, Seoul, Korea (the Republic of).

Highly resolved fluorescence imaging using STED nanoscopy for visualizing conformational difference of mitochondria in skin cells and tissues

Advantage of super-resolution imaging

Individual translocase on mitochondrial membrane can be resolved

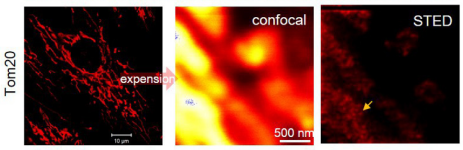

Distribution of TFAM on mitochondria can be analyzed quantitatively in cell level

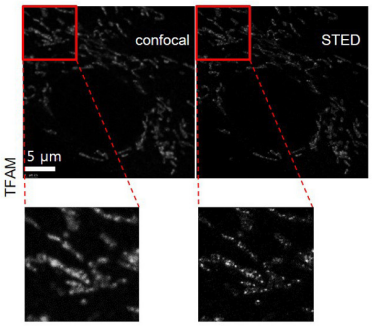

Ratio of the number of nucleoids detected by STED vs. confocal

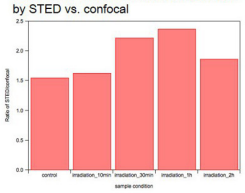

Quantitative analysis of the difference by UV irradiation

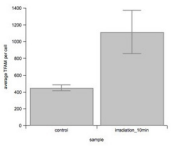

Structure of skin tissue by DIC

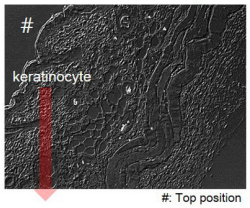

Distribution of Tom20 in mitochondria by STED

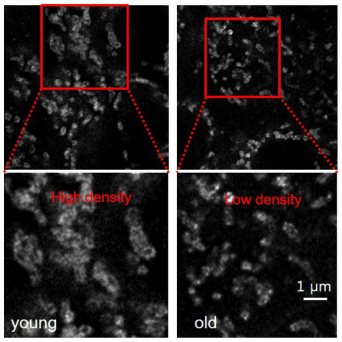

CONTROL ID: 2233980

TITLE: Double-targeted Gold Nanoparticles for PDT Drug Delivery in Brain Tumors

PRESENTER: Suraj Dixit

ABSTRACT BODY:

Abstract Body: Therapeutic drug delivery across the blood-brain barrier (BBB) is not only inefficient but also nonspecific, thereby posing a major shortcoming in effective treatment of brain cancer. Photodynamic therapy (PDT) is a localized treatment modality, relying on both a photosensitizer and drug activation using a specific wavelength. The widespread use of PDT in brain tumor therapy has been partially hampered by non-targeted phototoxicity towards healthy tissue. The development of nanoparticles selectively targeted to cell surface receptors that can act as drug delivery vehicles is critical for improving the treatment and therapeutic responsiveness in inaccessible tumors, such as glioblastomas. Gold nanoparticles (Au NPs) provide an excellent platform with a surface that can be tailored to attach biomolecules for targeted drug delivery and biocompatible coatings that can efficiently encapsulate the hydrophobic photosensitizer drug, Pc 4, thereby reducing off-site cytotoxicity. In this study, we demonstrate a novel double targeted, noncovalent Au NP drug delivery agent, which selectively delivers drugs to brain tumors for PDT. These double-targeted Au NPs loaded with Pc 4 have been compared with previously studied single targeted Au NPs. Hydrophobic AuNPs have been cap exchanged with mono- and bi-functional PEG linkers. Specific targeting of the PEGylatedAu NPs to glioma cells is achieved by coupling receptor-binding peptides to the carboxyl moiety of the bi-functional PEG linker. Subsequently, hydrophobic Pc 4 is adsorbed in the PEG corona (mono-functional linker) to form Pc 4 loaded and targeted Au NPs. Packaging of Pc 4 within the PEG core impedes leaching of the drug into the extracellular environment and improves circulation in vivo. UV-Vis absorption measurements indicate encapsulation of Pc 4 within the PEGylated Au NPs. Hydrodynamic diameter of these agents lies well within the limits needed to cross the BBB as determined by dynamic light scattering. In vitro cell uptake studies in glioma cell lines, LN229 and U87, which express differential patterns of the epidermal growth factor (EGF) and transferrin (Tf) receptor targets, show a significant increase in cellular uptake and intracellular localization for double targeted conjugates as compared to either single targeted Au NPs. Titration studies have been carried out in cells to optimize delivery; the optimal concentration for double targeted Au NPs is 500 nM, half of the current clinical standard observed for single targeted Au NPs over the same period of incubation. In vivo imaging utilizing real time, longitudinal fluorescence in mice shows notable accumulation of these agents in the tumor. Co-localization of the targeted Au NPs in regions overexpressing EGF and Tf receptors has been validated by immunohistochemistry. Upon activation of Pc 4 by PDT after delivery by the double-targeted Au NPs, increased cell death was observed as compared to free Pc 4.

AUTHORS (LAST NAME, FIRST NAME): Dixit, Suraj K.[1]; Zhu, Yun[1]; Moore, Alfred[1]; Kenney, Malcolm[2]; Broome, Ann-Marie[1]

INSTITUTIONS (ALL):

1. Radiology & Radiological Science, Medical University of South Carolina, Charleston, SC, United States.
2. Chemistry, Case Western Reserve University, Cleveland, OH, United States.

(No Image Selected)

CONTROL ID: 2233246

TITLE: Multi-modality imaging of invasive *Staphylococcus aureus* infections

PRESENTER: Jim Cassat

ABSTRACT BODY:

Abstract Body: *Staphylococcus aureus* is a Gram-positive bacterial pathogen capable of infecting nearly every organ in the vertebrate body to cause severe and life-threatening invasive infections. Central to staphylococcal virulence is the capacity to survive and adapt within diverse host environments. In order to study the mechanisms that underlie bacterial adaptation during invasive infection, as well as the host responses to infection and inflammation, two new preclinical multi-modality imaging models were created. In order to characterize bacterial responses during growth within tissue abscesses following septicemia, mice inoculated intravenously with *S. aureus* were subjected to three-dimensional, five modality imaging including MRI and blockface histological imaging for tissue delineation, bioluminescent imaging of bacterial promoter activity, imaging mass spectrometry for protein localization and identification, and inductively-coupled plasma mass spectrometry for elemental distribution within tissues. Subsequent co-registration of each modality allows an unparalleled view of the host-pathogen interface, and can be used to interrogate specific bacterial stresses *in vivo*, such as nutrient limitation. In order to characterize bacterial and host responses during osteomyelitis, one of the most common and recalcitrant manifestations of *S. aureus* infection, a second preclinical murine model was developed and utilizes high-resolution micro-computed tomographic imaging to quantify changes in bone remodeling induced by infection and inflammation. This murine osteomyelitis model allowed successful identification of bacterial toxins that directly incite bone destruction, as well as delineation of host inflammatory cells involved in the pathogenesis of osteomyelitis. Collectively these two preclinical murine models will substantially enhance our knowledge of host-pathogen interactions during invasive staphylococcal infection, and will serve as a platform for the development and evaluation of new antimicrobial therapies.

AUTHORS (LAST NAME, FIRST NAME): Cassat, Jim[2]; Wilson, Kevin[1]; Colvin, Daniel C.[1]; Virostko, John[1]; Hammer, Neal[1]; Caprioli, Richard[1]; Skaar, Eric[1]

INSTITUTIONS (ALL):

1. Vanderbilt University, Nashville, TN, United States.
2. Pediatric Infectious Diseases, Vanderbilt University Medical Center, Nashville, TN, United States.

(No Image Selected)

CONTROL ID: 2233250

TITLE: *In vivo* quantification of tissue engineered scaffold degradation using computed tomography

PRESENTER: Erik Shapiro

ABSTRACT BODY:

Abstract Body: Introduction:

Tissue engineered scaffolds (TES) are a promising tool for regenerative medicine. An important design parameter for TES is the *in vivo* degradation rate. The complex interaction between the biomaterials and the biological environment makes it difficult to model this *in vitro*. Various strategies for using MRI have been developed to monitor TES *in vivo*, accomplished either by directly labeling the TES or labeling cells which seed the TES. The label has most often been iron oxide nanoparticles, which afford very sensitive detection owing to the 'blooming' artifact in T_2 and T_2* weighted MRI. Yet while this enables the detection of the TES, the blooming artifact obscures many important facets of the material, especially if the material is porous. As such, we have developed TES doped with high Z metal nanoparticles, and this is the first report on the use of CT to analyze TES, *in vivo*.

Methods:

TES and bead construction: TES were constructed essentially as Lyman, et al, J Mater Sci: Mater Med (2011), beginning with a 2 x 2 x 2 mm template of polystyrene (PS) fibers surrounded by a poly(methyl methacrylate) (PMMA) matrix. Templates were etched in 80:20 Propylene Carbonate:Acetonitrile to remove the PMMA. Templates were backfilled with 3% w/w aqueous alginate containing 100mM Gd_2O_3 (<100nm nanocrystals) and cross-linked in 100mM $CaCl_2$. Fibers were etched with cyclohexane leaving channels. A similar process was used to produce 3% w/w aqueous agarose TES. Pore size is 200 μm and wall thickness is 67μm. Some agarose TES had pores drilled with pore size 300 μm. To form alginate beads, a solution containing 3% w/w aqueous alginate and 100mM Gd_2O_3 nanoparticles was pipetted into 100mM $CaCl_2$ to induce cross-linking.

μCT volume validation: TES and beads were imaged using μCT to verify fabrication and to validate repeatable volume measurements. μCT was performed *in vitro* and *in vivo* using a GE eXplore Locus RS μCT (parameters: 80 kVp, 450 μA, 800 ms exposure, 720 views, 46 μm resolution, 35 minutes long).

In vitro μCT:

To study Gd_2O_3-doped bead and TES degradation *in vitro*, beads were incubated at 37°C in PBS without Ca or Mg. μCT imaging was performed immediately and repeated every 24 h for 5 days. Following each scan PBS was exchanged. Gd_2O_3-doped TES - 1 agarose and 1 alginate - were similarly incubated in PBS and imaged at 2.5, 24, 29, and 36 h. PBS was exchanged once after 24 h.

In vivo μCT:

Gd_2O_3-doped agarose (n=4) and alginate (n=5) TES were implanted bilaterally into the hind limbs of male CD1 mice. Mice underwent *in vivo* μCT 4 times at 2 week intervals (2% isoflurane anesthesia in O_2).

Results and Discussion:

μCT volume measurement of TES using total variation filtering and automated minimum threshold differed by 4% of the calculated volume. Repeatability measurements and analysis produced standard deviations of 2% or less. *In vitro* degradation experiments revealed both decomposition (beads) as well as surface shearing (scaffolds). Serial *in vivo* imaging captured alginate scaffold decomposition while agarose remained intact. Due to its high image resolution and favorable acquisition times, CT is a promising tool for evaluating TES *in vivo*.

AUTHORS (LAST NAME, FIRST NAME): Forton, Stacey[1]; Latourette, Matthew T.[1]; Shahriari, Dena[2]; Sakamoto, Jeff S.[2]; Shapiro, Erik M.[1]

INSTITUTIONS (ALL):

1. Department of Radiology, Michigan State University, East Lansing, MI, United States.
2. Department of Mechanical Engineering, University of Michigan, Ann Arbor, MI, United States.

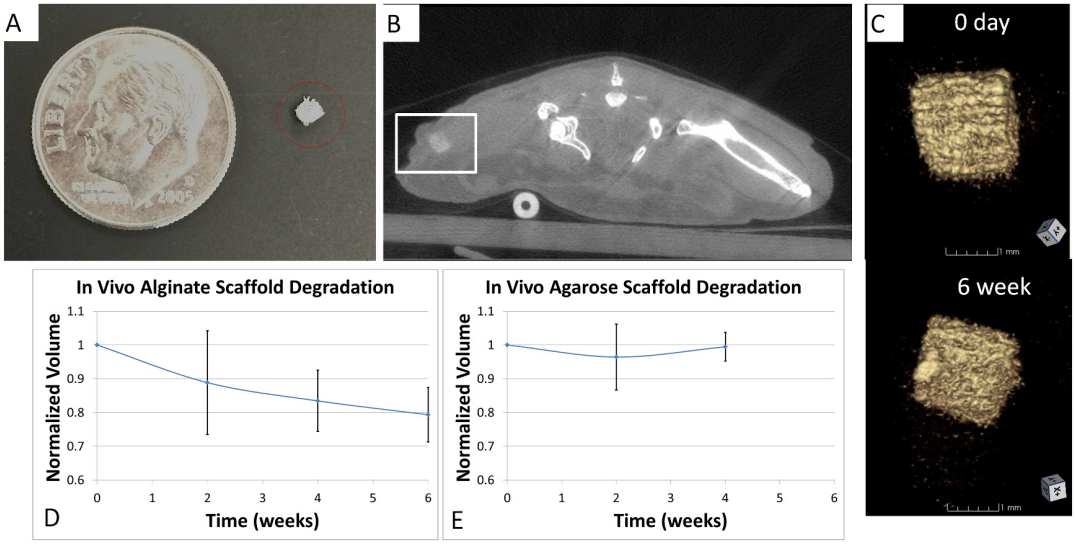

A) Scaffold size comparison B) In vivo µCT of alginate TES at Day 0. White box shows TES. C) Volume surface renderings of TES from B at Day 0 and Week 6. D,E) Plot of normalized *in vivo* volume changes for alginate (n=5) and agarose (n=4) TES.

CONTROL ID: 2233668

TITLE: Machine learning quantification of stem cell transplant into rodent brain using MRI-based single cell detection

PRESENTER: Erik Shapiro

ABSTRACT BODY:

Abstract Body: INTRODUCTION:

MRI detection of single cells is underutilized in MRI-based cell tracking. One reason has been a lack of methods for quantifying information in these images. To achieve single cell detection by MRI, cells are labeled with superparamagnetic iron oxide particles allowing their detection as punctate hypointensities (spots) in T_2^*-weighted MRI. Single cell detection and quantification would be useful for regenerative medicine and diagnostics, however, manual enumeration of cells is tedious and subjective. To solve this problem, we developed the first machine learning and computer vision based automatic approach for the generalizable detection and quantification of MRI-based single cell detection. We evaluated our approach *in vitro* using images of particle doped agarose phantoms, and *in vivo* on rat brain following stem cell delivery to the brain, and compared our results to published methodologies. Our approach detected spots/cells significantly better than the previous approaches, with accuracy of 98.9% *in vitro* and 89.14% *in vivo*.

METHODS:

MRI: Agarose phantoms were constructed with a dilute, known number of 4.5 micron diameter MPIOs from Dynal. Each bead has 10 pg of iron, simulating a labeled cell. We performed MRI of the agarose phantom at 7T using a 3D FLASH sequence with TR/TE=30/10ms, and 100 µm isotropic voxels. We further performed *in vivo* MRI of 5 rat brains. 3 rats were previously injected intracardiac with MPIO-labeled MSCs, delivering cells to the brain – 2 rats were naïve. MRI was identical to *in vitro*.

Machine learning based image quantification:

Machine learning is automatic programming by example. It first requires a training process. To create training examples, brain is first segmented from the MR images (A,B). Further segmentation is performed on brain at two scales using superpixels (C,D). Then, a 3D spot model is created for each small region by combining it with corresponding segments from neighboring slices (E,F). Feature values are extracted for each candidate spot model based on the average pixel intensity differences of the model and its surrounding segments. Features are then used by machine learning algorithms in their training and testing phase. During training, algorithms need ground truth definitions on what is a dark spot, to learn spot definitions in terms of features. Ground truth definitions - dark spots in an image - are manually defined. Once definitions are learned, algorithms can detect spots in any unseen MRI scan without manual assistance.

RESULTS and DISCUSSION:

In vivo MRI of rats injected with labeled MSCs had dark spots distributed throughout the brain whereas the control animal scans did not show spots. Single cell distribution in the brain was verified by histology. We used the area under the curve (AUC) as a standard measure to evaluate the performance of the trained model, taking the manual spot definitions as ground truth. Our approach can detect with an AUC of 98.9% on *in vitro* data and 89.14% *in vivo*. As shown (G,H), our performance is significantly superior to previously adopted approaches. Absolute quantification of cell transplant by MRI can be accomplished using this technique.

AUTHORS (LAST NAME, FIRST NAME): Afridi, Muhammed J.[1, 2]; Latourette, Matthew T.[1]; Bennewitz, Margaret F.[3]; Ross, Arun[2]; Liu, Xiaoming[2]; Shapiro, Erik M.[1]

INSTITUTIONS (ALL):

1. Department of Radiology, Michigan State University, East Lansing, MI, United States.
2. Department of Electrical and Computer Engineering, Michigan State University, East Lansing, MI, United States.
3. Vascular Medicine Institute, University of Pittsburgh, Pittsburgh, PA, United States.

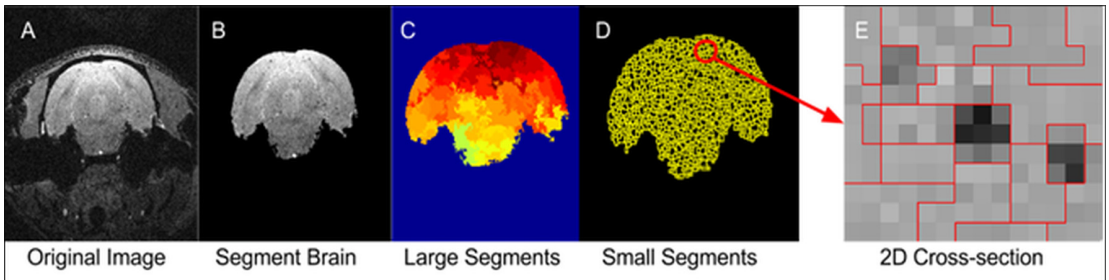

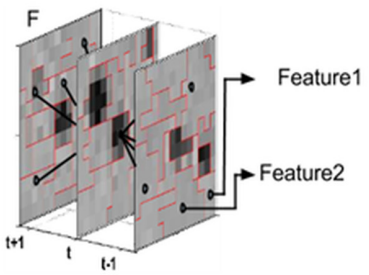

Feature extraction: mean intensity of every small region is compared with its 3D surrounding in different directions across consecutive slices. Here each feature represents the difference of intensities

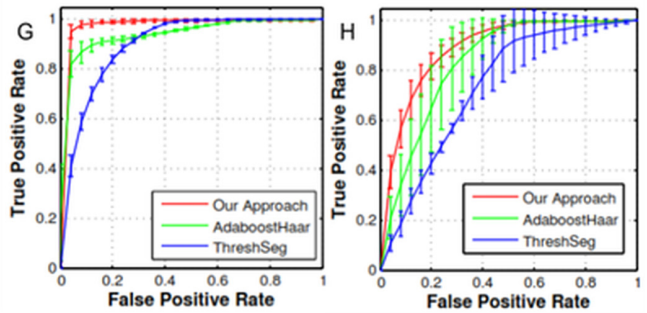

Results: In vitro Rat scans In vivo scans
Our Approach accuracy: 98.9%(in vitro) and 89.14% (in vivo)
AdaboostHaar accuracy: 95.0% (in vitro) and 82.64% (in vivo)
ThreshSeg accuracy: 89.97% (in vitro) and 73.72% (in vivo)

Refs: - **AdaboostHaar** (I. Smal et al. IEEE Medical Imaging, 2010)
- **ThreshSeg** (Y. Mori et al. Scientific Reports 4, 2014)

CONTROL ID: 2233272

TITLE: Illuminating the shadows of cervical disease using a mobile digital diffraction platform

PRESENTER: Cesar Castro

ABSTRACT BODY:

Abstract Body: Background: The global burden of cervical cancer and the disproportionate access to prompt pathology services and emerging cell profiling technologies increase the need for low-cost, portable, and rapid point-of-care (POC) approaches. Emerging genomic data for cervical cancers support the need for personalized profiling strategies more accessible to clinical providers and investigators. While conventional microscopy (e.g. fluorescence, confocal) retains diagnostic importance, their costs and complexity challenge reliable and feasible implementation within resource-challenged areas. **Methods**: We developed a digital diffraction diagnostic (D3) platform equipped with a portable smartphone module and: 1) optimized its protein and DNA readouts under preclinical conditions; and 2) conducted feasibility and pilot testing using human cervical biopsies from colposcopy. **Results**: Molecular analyses were achieved by labeling cells with polystyrene microbeads linked to antibodies targeting cervical cancer-related proteins. Diffraction patterns generated by the microbeads were detected with the smartphone camera using bright-field settings; digital processing reconstructed the images of bead-bound cells to retrieve molecular information (**Fig. 1A**). Optimizing the bead linking process and speeding up cell counting algorithms, led us to count thousands of beads and cells without washing steps (i.e. near *real time*). We enrolled 25 women with abnormal pap smears who were referred to the MGH Cancer Center for colposcopy and analyzed an extra biopsy specimen using our platform. Samples from higher risk patients showed increased numbers of microbeads per cell versus low risk and benign samples (**Fig. 1B**). The mean bead counts (n_{ad}) per targeted cell were significantly different among the clinical risk classifications ($p < 0.05$), indicating that n_{bead} could serve as a single diagnostic measure (**Fig. 1C**). The D3 assay generated readouts within 45 min and showed excellent agreement with gold-standard pathology (96%). We enhanced our platform's capabilities to enable DNA detection by developing a bead-dimer assay (**Fig. 1D**). A pair of oligonucleotides, whose sequences were complementary to that of HPV target DNA, were conjugated to silica and polystyrene microbeads, respectively. The target DNA was captured on polystyrene (PS) beads and sequentially labeled with silica (SI) beads. The hybridization yielded PS-SI bead dimers with unique diffraction signatures. The number of PS-SI hybrids correlated with the amount of target DNA. The observed detection sensitivity was in the atto-mole range for HPV DNA 16 and 18 (**Fig. 1D**), which account for >70% of cervical cancers worldwide. **Conclusion**: Our approach could have favorable global health applications where medical access is limited or when pathology bottlenecks challenge prompt cancer diagnostic readouts. Once validated prospectively, we anticipate that the D3 platform should enhance the breadth and depth of cervical cancer testing in a manner that is both sustainable and feasible for resource-limited settings.

AUTHORS (LAST NAME, FIRST NAME): Castro, Cesar M.[1, 2]; Im, Hyungsoon[1, 2]; Pathania, Divya[1, 2]; Weissleder, Ralph[1, 2]; Lee, Hakho[1, 2]

INSTITUTIONS (ALL):

1. Massachusetts General Hospital, Boston, MA, United States.
2. Harvard Medical School, Boston, MA, United States.

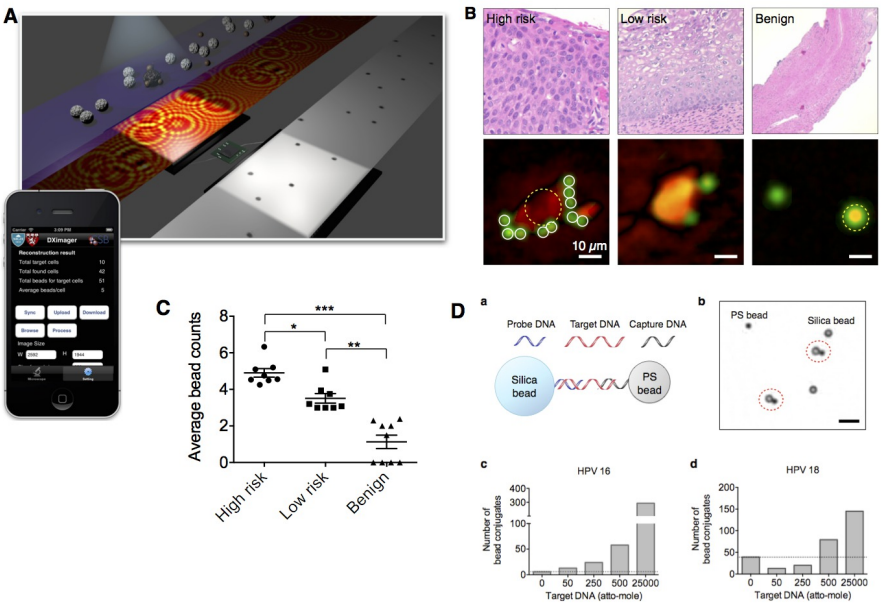

Figure 1: **A)** Digital diffraction diagnostic(D3) platform's assay schematic for cellular detection. Target cells in patient samples are immuno-labeled with microbeads, and their diffraction patterns are recorded. The diffraction images are then digitally reconstructed into object images wherein bead-labeled target cells are identified. **B)** Histology (top) and representative reconstructed image of cells (bottom) from high-risk (cervical intraepithelial neoplasia/CIN 2, 3), low-risk (CIN 1) and benign patient samples. Samples were targeted with a cocktail of EpCAM, CD44 and Trop-2 antibodies, followed by microbead labeling. **C)** The profiling result of patient samples (n = 25). **D)** Target DNA was captured by polystyrene (PS) beads conjugated with capture probes. Subsequently, silica beads with probe DNA were hybridized to form a bead dimer; the number of PS-silica dimers quantified the amount of target DNA. Measurements with using serial dilutions of DNA target (without PCR amplification) showed detection sensitivity in the atto-molar range for HPV.

CONTROL ID: 2233277

TITLE: Imaging of Retinal Vascular Disease Using Hypoxia-Sensitive Contrast Agents

PRESENTER: Md Imam Uddin

ABSTRACT BODY:

Abstract Body: Purpose: Retinal vascular diseases, including diabetic retinopathy and age related macular degeneration, are often associated with retinal hypoxia. Therefore, the ability to image hypoxic retinal tissue *in vivo* would be beneficial for improved clinical management of these diseases. For this purpose, a hypoxia-sensitive fluorescent contrast agent was developed and characterized for imaging of hypoxia in retinal tissue using established cell culture and animal models of retinal vascular disease.

Methods: Fluorescently-labeled, hypoxia-sensitive contrast agents were synthesized, purified chromatographically, and characterized using LCMS and NMR analysis. To evaluate the utility of this contrast agent for imaging hypoxia, in vitro assays using Human Retinal Microvascular Endothelial Cells (HRMEC), R28 cells, and primary Human Müller Cells and in vivo studies using mice with oxygen-induced retinopathy (OIR) or laser-induced choroidal neovascularization (LCNV) were performed to determine the hypoxia-associated sensitivity and specificity of this contrast agent. Fluorimetric assays were performed on normoxia- or hypoxia-conditioned HRMEC exposed to contrast agents to measure contrast agent binding and uptake. OIR and LCNV animal models were intravenously or intraocularly-injected with the contrast agents and analyzed by in vivo and ex vivo retinal fluorescence imaging to determine specificity and sensitivity of the contrast agent. Pimonidazole hydrochloride immunostaining was utilized to confirm specificity of the contrast agent for hypoxic tissue.

Results: HRMEC conditioned under hypoxia for varying durations of time up to 24 hours exhibited dose-dependent fluorescence enhancement due to hypoxia-selective uptake of the contrast agent. In animal models, regions of tissue hypoxia staining positive for pimonidazole hydrochloride were also colocalized with contrast agent uptake, as indicated by in vivo and ex vivo imaging. Contrast agent accumulation in hypoxic tissue was detectable within 2 hours post-injection.

Conclusions: These studies support the feasibility of imaging hypoxic tissue *in vivo* using targeted contrast agents in conjunction with readily available retinal fluorescence imaging equipment. Hypoxia-sensitive contrast agents, if clinically translated, may be useful for early detection of retinal vascular diseases and monitoring of therapeutic response in patients.

AUTHORS (LAST NAME, FIRST NAME): Uddin, Md Imam[1]

INSTITUTIONS (ALL):

1. Ophthalmology, Vanderbilt Eye Institute, Nashville, TN, United States.

(No Image Selected)

CONTROL ID: 2233286

TITLE: Multi Radioisotope Calibration Study of the Bioscan BioPET pre-clinical PET/CT Scanner

PRESENTER: Stephen Adler

ABSTRACT BODY:

Abstract Body: Introduction: A study of the Bioscan BioPET PET/CT was performed to gauge its accuracy and reproducibility in measuring a known quantity of activity in the FOV across several positron emitting isotopes.
Material and Methods: A Ge68 cylindrical phantom, 4cm in diameter and 6cm in length with approximately 16Mbq of activity was used to measure a 100% branching fraction calibration factor in nCi/mcps. Using this calibration factor, 15cc of F18 and Zr89 were filled in a 60cc syringe and imaged. Using the positron branching fractions as a correction factor for the 100% positron branching fraction calibration factor, the absolute activity concentration was measured for each isotope.
Results: The F18 and Zr89 samples were scanned and reconstructed using 2D and 3D iterative reconstruction algorithms. The samples were also collected using the three energy windows provided by the scanner acquisition interface of 100-700 KeV, 250-700 KeV and 400-700KeV. The activity as measured with the F18 sample was over estimated by 1-2% when doing a 2D iterative reconstruction and between 6-11% under estimated when doing a 3D iterative reconstruction. For Zr89, the 2D reconstruction generated images which under estimated the activity between 6-7% and 3D underestimated the activity between 9-15%. The samples were measured three times over the period of a week. The variation in absolute activity concentration variation varried on the order of 1% for the Ge68 phantom, 1% for the F18 and 3% for the Zr89.
Summary: Using a single isotope to calibrate the BioPET scanner works well for Ge68 and F18 when reconstructing the images using the 2D iterative reconstruction algorithm. Higher order corrections are needed beyond just the positron branching fraction for Zr89 and possibly other isotopes which have small positron branching fractions like Cu64 and Br76. There are other quantitation issues which are introduced by the 3D iterative reconstruction which make measuring absolute activity in the FOV less accurate by a few percent.

AUTHORS (LAST NAME, FIRST NAME): Adler, Stephen[2]; Seidel, Jurgen[1]; Griffiths, Gary[3]; Choyke, Peter L.[4]

INSTITUTIONS (ALL):

1. Molecular Imaging Program, NIH/NCI , Bethesda, MD, United States.
2. Molecular Imaging Program, National Cancer Institute, Bethesda, MD, United States.
3. Molecular Imaging Program, National Cancer Institute, Rockville, MD, United States.
4. Molecular Imaging Program, National Cancer Institute, Bethesda, MD, United States.

(No Image Selected)

CONTROL ID: 2233296

TITLE: Tracking Breast Cancer Tumor Growth and Angiogenesis *in vivo* with Perfluorocarbon Microbubbles

PRESENTER: Danny Robles

ABSTRACT BODY:

Abstract Body: Angiogenesis is the formation of new blood vessels in a tumor, which allows it to grow past its limit of nutrient diffusion (1-2 mm in diameter). Work by Folkman and others have alluded to the fact that angiogenesis must occur when the tumor size reached a diameter of 1 – 2 mm.[1,2] Furthermore, for the purposes of early detection, determination of enhanced permeability and retention (EPR) effects, and treatment paradigms, it is important to know the onset of angiogenesis as a function of tumor size, time, and growth. Hence, we hypothesized that if angiogenesis were to occur when tumor size reached 1-2 mm, the time to onset may differ from cell line to cell line. As such, it would be innovative to define the growth, extent, and time of onset for angiogenesis. In this study, we have tracked the progression of angiogenesis for three different types of breast cancer cell lines; MDA-MB-231, MCF-7, and MDA-MB-468. Each of these cell lines is known to overexpress different receptors, which can affect a tumor's growth rate and perhaps its ability to undergo angiogenesis. SCID mice models were used to profile each of the different breast cancer cells, and the growth of these tumors as a function of time was monitored and imaged using lipid-coated microbubbles and contrast-enhanced ultrasound (CEUS). On Day 0, mice were inoculated with $5x10^5$ cells in a Matrigel™ matrix. A Visualsonics™ Vevo 2100 pre-clinical ultrasound machine using a 50 MHz probe was used for the imaging experiments (Dynamic Range = 70 dB, Power Level= 5%, and frame rate = 10 fps). A custom image analysis program was developed in Matlab™ to eliminate breathing artifacts and track microbubble motion based on their high temporal frequency signature ("flicker"). To track development of angiogenesis, mice were injected with perfluorocarbon (perfluorobutane) gas microbubbles of 1-2 micron diameter. Bubble perfusion inside the tumor was suggestive of the presence of new blood vessel formation. Experiments not only demonstrated that different cell lines proliferate at different rates, but also microbubbles begin to penetrate the tumor when they reach approximately the same size (i.e., 3 mm in diameter or 7 mm^2 cross sectional area). Furthermore, the onset of angiogenic vessel imaging occurred at significantly different times (MCF-7 occurring first at an average of 9 days and MDA-MB-231 occurring over three times later at an average of 27 days post tumor cell inoculation).

The results suggest that microbubble perfusion closely correlates with the progression of tumor vascularization. This method may provide a means for early detection of tumor vasculature using CEUS, as well as monitoring delivery of cancer therapeutics that target angiogenic vessel development.

Folkman J., Merler E., Abernathy C., and Williams G., "Isolation of a tumor factor responsible for angiogenesis" *Journal of Experimental Medicine,* vol. 358, no. 19, pp. 275-288, 1971.

Schneider B. and Miller K. Angiogenesis and Breast Cancer. *American Society of Clinical Oncology*. 2005

AUTHORS (LAST NAME, FIRST NAME): Robles, Danny[1, 4]; Netherton, John[3]; Ingram, Pier[1]; Skovan, Bethany[2]; Witte, Russell[1, 3]; Matsunaga, Terry O.[1, 3]

INSTITUTIONS (ALL):

1. Medical Imaging, University of ARizona, Tucson, AZ, United States.
2. Experimental Mouse Shared Services, University of Arizona Cancer Center, Tucson, AZ, United States.
3. Biomedical Engineering, University of ARizona, Tucson, AZ, United States.
4. Chemistry and Biochemistry, University of Arizona, Tucson, AZ, United States.

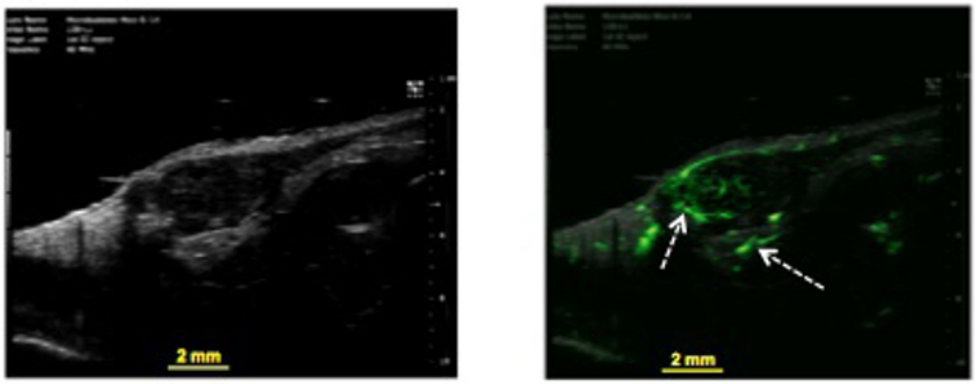

50 MHz ultrasound and microbubble-enhanced images of MCF-7 tumors in a SCID mouse. Left: B Mode image of a growing MCF-7 tumor before microbubble injection. Right: B Mode US image superimposed with cumulative microbubble intensity (green) following injection. Microbubble motion was enhanced and motion artifacts were eliminated using custom software developed in MATLAB™. Arrows reveal vascularization inside and near the tumor. It is noted that directional flow of the vessels could also be identified.

CONTROL ID: 2233290

TITLE: Determination of GD2 Expression in Osterosarcoma with PET

PRESENTER: Elizabeth Butch

ABSTRACT BODY:

Abstract Body: GD2 is a disialoganglioside that is widely expressed by pediatric solid tumors (*e.g.* >98% for NB) and minimally expressed in most other tissues, making it an excellent target for immunotherapy (Modak and Cheung, Cancer Invest (2007) 25:67-77). Anti-GD2 immunotherapy has shown significant clinical benefit in treating neuroblastoma (NB) with a 20% improvement in survival (Yu, et al. N Engl J Med (2010) 363:1324-34). However, anti-GD2 therapy has not yet been investigated in other pediatric malignancies due to a lack of information on the frequency of GD2 expression. Many osteosarcoma (OS) cell lines have higher GD2 expression than NB, and GD2 expression in recurrent OS is often higher than at initial biopsy (Roth et al. Cancer (2014) 120:548-54). However in contrast to NB, a significant fraction of OS tumors in our xenograft bank exhibit very low GD2 expression, and flow cytometry studies show that some OS are essentially GD2-negative. Thus, clinical trials would be facilitated by the availability of a PET radiotracer to determine GD2 expression and thus (potential) therapeutic efficacy, allowing screening protocols to be developed that maximize the clinical impact of anti-GD2 immunotherapy. We report here initial biodistribution studies using ^{64}Cu-NOTA-hu14.18K322A anti-GD2 antibody to detect GD2 expression in human OS xenografts and cell lines. Six primary OS xenografts, and two OS cell lines (U2OS (GD2+) and SoAS-2 (GD2-) as controls, were examined for GD2 expression by multi-parametric flow cytometry using the 14.G2a-PE anti-GD2 antibody conjugate (BD Biosciences). GD2 expression was determined as the percentage of viable GD2-positive human OS cells in the sample. These studies demonstrated a wide range of GD2 expression in the xenograft tissues (0-99.9% positive cells, mean fluorescence intensity of 300-32,000). PET-CT imaging (Siemens Inveon) was also performed on these six xenografts grown as flank tumors in athymic nude mice. Animals were injected r.o. with 75 μCi (100 μL) of ^{64}Cu-NOTA-hu14.18K322A and imaged 48 hours post-injection under isoflurane anesthesia (30 min static PET with CT attenuation correction). ROIs were drawn over the entire tumor volumes in the CT and transferred to the PET images. Mean radiotracer uptake values (% i.d./cc) for this series of xenografts strongly correlated with the *in vitro* flow cytometry data (R^2 = 0.91). Preliminary tumor uptake data (n = 3-6 per tumor type) from *ex vivo* counting of dissected tumors also correlated with both flow cytometry (R^2 = 0.88) and the PET data (R^2 = 0.62). These data demonstrate that a) GD2 expression in OS is highly variable and b) PET imaging with radiolabeled hu14.18K322A provides an index of GD2 expression in OS tumors and thus c) GD2 PET may have utility for directing anti-GD2 immunotherapy in our pediatric OS patients.

AUTHORS (LAST NAME, FIRST NAME): Butch, Elizabeth[1]; Mead, Paul E.[2]; Amador-Diaz, Victor[1]; Stewart, Elizabeth[3]; Snyder, Scott E.[1]

INSTITUTIONS (ALL):

1. Radiological Sciences, St. Jude Children's Research Hospital, Memphis, TN, United States.
2. Pathology, St. Jude Children's Research Hospital, Memphis, TN, United States.
3. Oncology, St. Jude Children's Research Hospital, Memphis, TN, United States.

(No Image Selected)

CONTROL ID: 2233297

TITLE: Development of Radiotherapeutic and Companion Imaging Agents to Target MC1R in Melanoma

PRESENTER: Narges Tafreshi

ABSTRACT BODY:

Abstract Body: Uveal melanoma is largely underserved by current therapies, the incidence of cutaneous melanoma is increasing and mortality from metastatic disease remains high. If discovered early, uveal and cutaneous melanomas can be cured by surgical resection, and/or radiation for uveal, but relapse is frequent for advanced disease and long-term survival of these patients has remained low at ~10%. Hence, new targeted therapies are needed for improved treatment options.

The melanocortin 1 receptor (MC1R) is expressed in 94% of uveal melanomas and 90% cutaneous melanoma metastases. However, it is not expressed in normal tissues of concern for toxicity. We have developed a MC1R specific ligand (MC1RL); have conjugated infrared imaging contrast agents to it, demonstrated high selectivity for MC1R expressing tumors in mice, and demonstrated rapid systemic clearance, without retention in tissues of concern for toxicity. The aim of this study is to use MC1RL as a targeting scaffold for development of a radiopharmaceutical by conjugation of ^{225}Ac chelate. ^{225}Ac is a therapeutic alpha emitting radionuclide. Using a targeted approach to deliver ^{225}Ac to melanoma without causing benign organ toxicity would provide clinicians with a powerful tool to treat this malignancy and its systemic metastases, which is currently unavailable to them. Additionally, a companion PET imaging tracer can be developed using the same conjugated chelator to deliver the positron emitting ^{68}Ga. The PET tracer could be used to identify patients that would benefit from treatment with the radiopharmaceutical and to non-invasively follow therapy response.

Here, we conjugated 1,4,7,10-tetraazacyclo-dodecane-1,4,7,10-tetraacetic acid (DOTA) to the MC1R specific scaffold (DOTA-MC1RL) and chelated the nonradioactive surrogates ^{139}La (substitute for ^{225}Ac) and $^{69/71}$Ga (substitute for ^{68}Ga positron emission tomography radionuclide) and demonstrated high binding affinity to MC1R (0.2 and 0.3 nM K$_i$, respectively). We anticipate that the radioactive conjugates will have comparable affinities. We also synthesized ^{225}Ac-DOTA-MC1RL and showed a radiochemical yield greater than 95% and in high radiochemical purity (≥99.8%) as determined by radio-TLC, radio-HPLC, and gamma-counter quantification. Moreover, ^{225}Ac -DOTA-MC1RL showed excellent *in vitro* stability even after 10 days in human serum at 37ºC. A maximum tolerated dosage (MTD) study was performed by administration of 0, 9, 18, 28, 37, 56, 74 and 148 kBq of ^{225}Ac-DOTA-MC1RL. Animals were followed for 120 days and there were no signs of altered behavior among the groups. The group that received the highest dosage had a slightly but significantly lower increase in body weight over the course of the study, suggesting that ^{225}Ac-DOTA-MC1RL is tolerated extremely well. Blood work and organ pathology are pending.

Studies to evaluate the in vivo tumor selectivity, pharmacokinetics (PK), biodistribution (BD), radiodosimetry and therapeutic efficacy of ^{225}Ac-DOTA-MC1RL in non-tumor bearing and melanoma xenograft tumor bearing mice are in process and include Cherenkov imaging to follow PK in longitudinal studies.

AUTHORS (LAST NAME, FIRST NAME): Tafreshi, Narges K.[1]; Doligalski, Michael L.[2]; Pandya, Darpan N.[3]; Huynh, Amanda Shanks[1]; Moberg, Valerie E.[4]; Wadas, Thaddeus[3]; McLaughlin, Mark L.[2, 5]; Morse, David L.[1]

INSTITUTIONS (ALL):

1. Cancer Imaging & Metabolism, H. Lee Moffitt Cancer Center, Tampa, FL, United States.
2. Dept. of Chemistry, USF, Tampa, FL, United States.
3. Dept. of Cancer Biology, Wake Forest University Health Sciences, Winston-Salem, NC, United States.
4. Cutaneous Data Management, H.Lee Moffitt Cancer Center and Institute, Tampa, FL, United States.
5. Dept. of Drug Discovery, H.Lee Moffitt Cancer Center and Institute, Tampa, FL, United States.

(No Image Selected)

CONTROL ID: 2233968

TITLE: Development of ^{68}Ga-labeled D-glucose analogue for studying virus-infected lung cancer cells

PRESENTER: Haixun Guo

ABSTRACT BODY:

Abstract Body: Objectives: Influenza A virus and its global pandemics have caused severe mortality in both history and recent years. In our previous study, we found that the pulmonary influenza A virus infection resulted in localized pulmonary accumulation of a D-glucose analogue, ^{18}F-FDG, in a ferret model [1]. We also know that ^{18}F-FDG was used in clinics to stage lung cancer patients. These results and fact inspired us to think about the situation of coexistence of virus infection and lung cancer, or what the glucose metabolism will behave for virus-infected lung cancer cells. To answer this question, we develop a new ^{68}Ga-labeled D-glucose analogue to test its uptake profiles in both lung cancer and influenza A virus-infected lung cancer cells.

Methods: Metal chelator NOTA(1,4,7-triazacyclononane-1,4,7-triacetic acid) was incorporated into the 1-thio-β-D-glucose molecule through cold chemistry for radiolabeling. The NOTA-thio-β-D-glucose was labeled with $^{68}GaCl_3$ using 0.5 M NH_4OAc (pH4.5) buffer according to our published procedure[2]. ^{68}Ga-NOTA-thio-β-D-glucose was purified by Radio-HPLC. The uptake characteristics of ^{68}Ga-NOTA-thio-β-D-glucose in both A549 and influenza A virus-infected A549 lung cancer cells were evaluated.

Results: NOTA-thio-β-D-glucose was successfully synthesized and characterized via LC-MS. ^{68}Ga-labeling showed more than 98% radiochemical yield for reaction at 25^{o}C for 10 min. The ^{68}Ga-NOTA-thio-β-D-glucose was successfully purified from the unlabeled compound and free $^{68}Ga^{3+}$ via Radio-RP-HPLC. The HPLC-purified ^{68}Ga-NOTA-thio-β-D-glucose showed quick and high uptake in both non-infected A549 and influenza A virus-infected A549 cells. For 30 min binding group, there was no uptake difference of ^{68}Ga-NOTA-thio-β-D-glucose between non-infected and infected A549 cells. But for 60 min binding group, the uptake of ^{68}Ga-NOTA-thio-β-D-glucose in infected A549 cells was significantly higher than that in non-infected A549 cells ($p << 0.05$). For infected-A549 cells, the uptake of ^{68}Ga-NOTA-thio-β-D-glucose in 60 min group was also significantly higher than the uptake in the 30 min group.

Conclusion: We successfully synthesized a D-glucose analogue ^{68}Ga-NOTA-thio-β-D-glucose and evaluated it in both lung cancer cells and influenza A virus-infected lung cancer cells. The significant uptake difference between non-infected and infected A549 cells suggests its potential for studying virus infected-lung cancer animal model via PET/CT.

Acknowledgements: The authors would like to thank the UofL startup funds.

References:

[1] Wu A, et al. ILAR J. 2012;53(1):E9-21

[2] Guo, H et al. Bioconjug Chem. 2012 Jun 20;23(6):1341-8.

AUTHORS (LAST NAME, FIRST NAME): Guo, Haixun[1, 2]; Camp, Jeremy V.[3]; Jonsson, Colleen B.[2, 3]

INSTITUTIONS (ALL):

1. Radiology, University of Louisville, Louisville, KY, United States.

2. Center for Predictive Medicine for Biodefense and Emerging Infectious Diseases, University of Louisville, Louisville, KY, United States.

3. Department of Microbiology and Immunolog, University of Louisville, Louisville, KY, United States.

(No Image Selected)

CONTROL ID: 2233304

TITLE: Orthotopic Human Hepatocellular Carcinoma Model in Rabbits for Combined Ultrasound-Guided and Transcatheter Hepatic Arterial Drug Delivery

PRESENTER: Sunitha Bachawal

ABSTRACT BODY:

Abstract Body: Background

Hepatocellular carcinoma (HCC) is the sixth most common cancer and the third most common cause of cancer-related deaths worldwide. New therapeutic strategies are critically needed as current treatment options are limited, particularly for those who are diagnosed late or cannot receive liver-directed therapies, such as chemoembolization. MicroRNAs (miRNAs) are potent gene expression regulators that when aberrantly expressed, play a profound role in cancer development and progression. Recent studies have shown successful administration of miRNA-loaded poly(lactic-co-glycolic acid)-nanoparticles (PLGA-NP) into subcutaneous tumors using ultrasound (US) and microbbuble (MB) mediated delivery in mice [1]. To work towards future clinical translation and to approximate liver-directed therapies, larger animal models of HCC are needed that allow insertion of a microcatheter into the hepatic artery. Such models currently do not exist. The goal of this study was to establish and test a larger (rabbit) model of human HCC for US and MB mediated delivery of miRNA in combination with a transcatheter hepatic arterial administration approach.

Methods

Rabbits were immunocompromised by administering cyclosporine (15 mg/kg b.w.; i.m.) once a day until blood levels reached 300ng/ml. After laparotomy, human HepG2 HCC cells were orthotopically injected ($20X10^6$) into the liver and US was performed twice a week to monitor tumor growth. Once tumors reached 0.5-1 cm, a microcatheter was placed into the proper hepatic artery via a common femoral artery approach and a hepatic arteriogram was performed with fluoroscopy followed by administration of miRNA-loaded PLGA-NP to the tumors through US and MB mediated delivery. A total of 2×10^9 microbubbles were mixed with 4.5×10^{12} PLGA-NP and intravenously injected into each animal. HCC tumor xenografts were then insonated with 5-cycle 1.8-MHz ultrasound pulses generated at a pulse repetition frequency of 100Hz. After 24h, the liver was perfused with PBS to remove excess circulating PLGA-NP in the blood pool, tumors were extracted, and tumor samples were processed for *ex vivo* histology and RT-PCR.

Results

All rabbits tolerated immunosuppression well, without any signs of renal or hepatic toxicity from cyclosporine. Tumors developed within 2 weeks after implantation as evidenced by US imaging. Histology confirmed successful tumor growth at the site of tumor implantation. US and MB mediated delivery combined with the transcatheter hepatic arterial administration approach resulted in a 10-17-fold increase of delivered miRNA in the human HCC xenografts compared to surrounding control hepatic tissue as analyzed by RT-PCR.

Conclusion

We describe a new human HCC xenograft model in rabbits which allows to combine locoregional and US and MB mediated delivery of miRNA-loaded PLGA-NP in HCC.

[1] Wang TY, Choe JW, Pu K, et al. Ultrasound-guided delivery of microRNA loaded nanoparticles into cancer. J Control Release 2015.

AUTHORS (LAST NAME, FIRST NAME): Bachawal, Sunitha[2]; Wang, David S.[2]; Wang, Tzu-Yin[2]; Mullick Chowdhury, Sayan[2]; Devulapally, Rammohan[2]; Felt, Stephen[1]; Paulmurugan, Ramasamy[2]; Willmann, Juergen K.[2]

INSTITUTIONS (ALL):

1. Comparative Medicine, Stanford University, Stanford, CA, United States.
2. Radiology/MIPS, Stanford University, School of medicine, Stanford, CA, United States.

Orthotopic Human Hepatocellular Carcinoma Model in Rabbits for Combined Ultrasound-Guided and Transcatheter Hepatic Arterial Drug Delivery

Sunitha V. Bachawal, David Wang, Tzu-Yin Wang, Sayan Mullick Chowdhury, Rammohan Devulapalli, Stephen Felt, Ramasamy Paulmurugan, Jürgen K. Willmann

Department of Radiology/MIPS, Stanford University, CA, USA

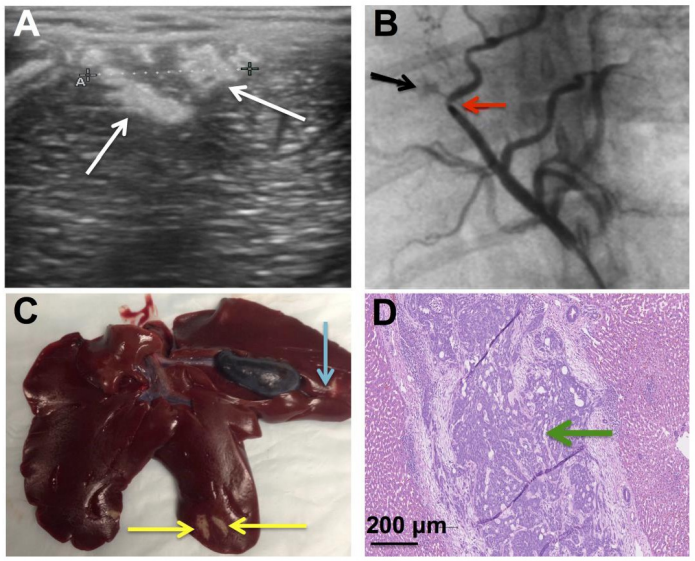

Figure 1. (A) Orthotopic human HCC in rabbit liver seen by US (white arrows). **(B)** Hepatic angiogram shows tip of microcatheter (red arrow) in proper hepatic artery and contrast flush in highly vascularized human HCC xenograft in rabbit (black arrow). **(C)** Macroscopic view of human HCC xenografts (arrows) implanted in right and left rabbit liver lobes. **(D)** Histology confirms xenografts (green arrow).

CONTROL ID: 2233450

TITLE: B7-H3, a Novel Target for Breast Cancer Detection Using Ultrasound Molecular Imaging

PRESENTER: Sunitha Bachawal

ABSTRACT BODY:

Abstract Body: Background

Ultrasound is a complimentary imaging modality to mammography in breast cancer detection in particular in patients with dense breast tissue, but is limited by its low diagnostic accuracy. Diagnostic accuracy of ultrasound can be significantly improved using contrast agents targeted at molecular signatures on tumor neovasculature. An ideal molecular imaging target for early cancer detection is differentially expressed in cancer compared to benign pathologies. B7-H3 (CD276) is a member of the B7 molecules involved in T-cell activation; and has been shown to be differentially expressed in human breast cancer tissues. However, it is not known whether B7-H3 is differentially expressed on the neovasculature of breast cancer compared to benign breast pathologies and normal breast tissue, which would make B7-H3 an attractive novel molecular imaging target for breast cancer detection using ultrasound. Here we assessed vascular B7-H3 expression in a large-scale immunohistochemical study, and evaluated feasibility of using novel B7-H3-targeted ultrasound contrast-microbubbles for cancer detection *in vivo* in transgenic mouse model of breast cancer.

Methods

Immunohistochemical analysis of B7-H3 expression was performed in 248 human breast samples including normal, 11 different benign and precancerous lesions, luminal A, luminal B, Her2 and triple negative cancer subtypes. Immunostaining of vessels was scored using a 4-point grading scale: 0 = no staining; 1 = weak; 2 = moderate; and 3 = strong vessel staining. Vessel staining was further analyzed for percentage positive vessels using a 5-point grading scale: 0 = no positive staining vessels; 1 = 1-10%; 2 = 10-33%; 3 = 33-66%; and 4 = 66-100% of positive staining vessels. The results obtained by these two scores were then multiplied together yielding a composite score. In addition, microvessel density (MVD) was calculated. The progression of breast tissue from normal to invasive cancer was examined using ultrasound molecular imaging (Vevo2100, Visualsonics) with $MB_{B7\text{-}H3}$ (n=183) in a transgenic breast tumor model (FVB/N-Tg(MMTV-PyMT634Mul). *Ex vivo* B7-H3 expression was quantified using fluorescence staining.

Results

B7-H3 expression was detected on both tumor epithelium and tumor associated vascular endothelium in human breast cancer samples. Expression in breast cancer was significantly higher (P<0.001) compared to normal, benign and precancerous breast pathologies. There was a significant (P <0.001) increase in B7-H3-targeted ultrasound imaging signal when breast tissue progressed from normal (5.0 ± 0.5 a.u.; n=37) to breast cancer (49.4 ± 5.3 a.u.; n=146) in mice. At a sensitivity of 85%, B7-H3-targeted ultrasound imaging can differentiate normal from cancer entities with specificity of 93% (AUC of 0.9) *Ex vivo* B7-H3 expression in mouse tissues highly correlated with imaging signal (R^2= 0.76, P<0.001).

Conclusions: Ultrasound imaging allowed the detection of breast cancer with high accuracies. Ultrasound molecular imaging of tumor angiogenesis using tumor specific endothelial markers in breast cancer may help improve accuracy of ultrasound in breast cancer detection in future clinical trials.

AUTHORS (LAST NAME, FIRST NAME): Bachawal, Sunitha[1, 5]; Jensen, Kristin C.[4, 5]; Wilson, Katheryne E.[1]; Tian, Lu[2]; Lutz, Amelie[1]; Willmann, Juergen K.[3]

INSTITUTIONS (ALL):

1. Radiology/MIPS, Stanford University, School of medicine, Stanford, CA, United States.
2. Health Research and Policy, Stanford University, Stanford, CA, United States.
3. Radiology/MIPS, Stanford University, School of medicine, Stanford, CA, United States.
4. Pathology, Stanford University, Stanford, CA, United States.
5. Veterans Affairs Palo Alto Health Care System, Stanford University, Palo Alto, CA, United States.

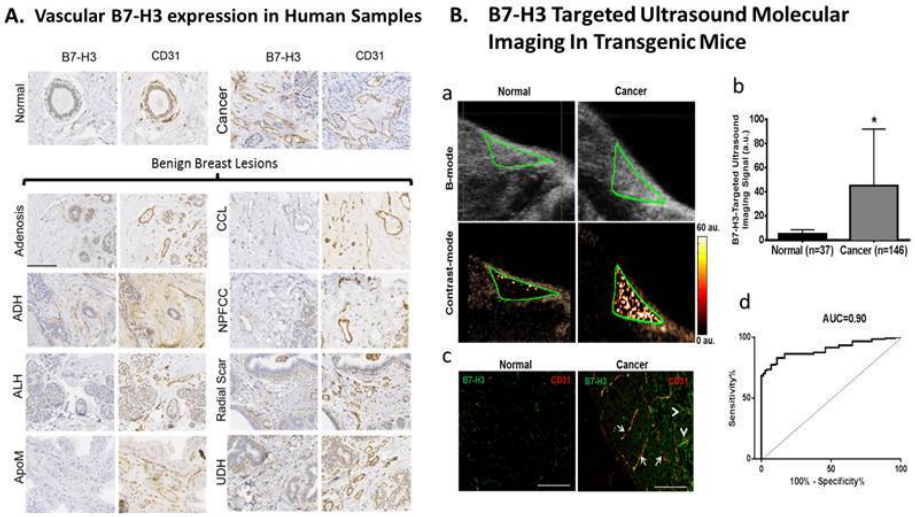

ADH=Atypical ductal hyperplasia; ALH=Atypical lobular hyperplasia; ApoM=Apocrine metaplasia; CCL=Columnar cell lesion; NPFCC=Non-proliferative fibrocystic changes; UDH=Usual ductal hyperplasia;

Figure 1. **(A)** Photomicrographs show representative staining results from normal, cancer and benign breast lesions obtained from women undergoing biopsy or surgical resection. **(B)** *In vivo* ultrasound molecular imaging in transgenic mice. **(a)** Representative transverse B-mode and contrast mode ultrasound images following injection of B7-H3-targeted contrast microbubbles show strong signal in breast cancer and only background signal in a mammary gland with normal breast tissue (both outlined by a green region of interest). **(b)** Photomicrographs of immunofluorescence images (double stained for both the vascular marker CD31 (red) and B7-H3 (green)) confirm expression of B7-H3 on tumor neovasculature (arrows, yellow signal on merged images) in breast cancer with little to no vascular expression in normal tissue. Note B7-H3 is also expressed on tumor epithelium (arrowheads; green). **(c)** Bar graph summarizes quantitative B7-H3-targeted ultrasound molecular imaging signal obtained in normal and breast cancer in a total of 183 mammary glands with significantly increased imaging signal in breast cancer versus normal tissue. *P<0.001; error bars = standard deviations. **(d)** Receiving operator characteristic (ROC) curve in distinguishing normal from breast cancer based on quantitative ultrasound molecular imaging signal.

CONTROL ID: 2233311

TITLE: Intraoperative fluorescence imaging of folate receptor alpha positive ovarian and breast cancer using the tumor specific agent EC17.

PRESENTER: Quirijn Tummers

ABSTRACT BODY:

Abstract Body: Introduction

Intraoperative fluorescence imaging of tumor tissue can improve surgical procedures in cancer care. The folate receptor alpha (FRa) is a promising tumor target expressed by various cancers.

Feasibility of intraoperative fluorescence tumor imaging with EC17, an FRa targeting agent that fluoresces at 500nm, was recently demonstrated in a limited series of ovarian cancer patients (1). Our objective was to evaluate the safety and efficacy of EC17 in a larger group of ovarian cancer patients and to assess feasibility of intraoperative fluorescence imaging with EC17 in patients with FRa positive breast cancer.

Material and methods

Two to three hours before surgery 0.1mg/kg EC17 was intravenously administered to 12 patients undergoing staging or debulking surgery for (high suspicion of) ovarian cancer and up to now to 3 patients with biopsy proven FRa positive breast cancer undergoing breast cancer surgery. The number of suspected lesions/positive margins detected with fluorescence and concordance between fluorescence and FRa-status on histopathology was assessed in addition to safety and pharmacokinetics (PK).

Results

Intraoperative fluorescence imaging in ovarian cancer patients allowed clear detection of ovarian cancer lesions. In total, 44 malignant lesions were resected, including 6 (14%) lesions that were not detected by inspection/palpation. Mean Tumor-to-Background ratio was 6.8 (range 1.7- 46.0). Histopathology demonstrated concordance between fluorescence and FRa- and tumor status. Fluorescence microscopy showed clear membranous and cytoplasmic accumulation of EC17 in tumor cells. Fluorescence signal was also identified in tumor negative lesions, in particular collagen-containing structures, this was related to autofluorescence of various human tissues at 500nm. Also in breast cancer, tumor-specific fluorescence signal was observed, however autofluorescence of healthy breast tissue was present in such extent that it interfered with tumor detection. In both ovarian and breast cancer patients infusion of EC17 was associated with mild, self-limiting hypersensitivity reactions. PK analyses are still ongoing.

Conclusions

Administration of EC17 was reasonably well tolerated and showed clear fluorescent signal in ovarian and breast cancer tissue. This even allowed detection of ovarian cancer lesions that were otherwise not detectable. Conversely, autofluorescence of benign, predominantly collagen-containing, tissues led to detection of false positive lesions and resulted in difficulty of detecting breast tumors. We conclude that FRa is a favourable target for fluorescence guided surgery. Replacing the 500nm fluorophore by a fluorophore in the near-infrared spectrum could further improve optical properties and thereby clinical relevance.

1. Van Dam GM et al. Intraoperative tumor-specific fluorescence imaging in ovarian cancer by folate receptor-α targeting: first in-human results. Nat. Med. 2011 Sep 18.

AUTHORS (LAST NAME, FIRST NAME): Tummers, Quirijn R.[1, 2]; Hoogstins, Charlotte E.[1, 2]; Cohen, Adam F.[2]; van de Velde, Cornelis J.[1]; Low, Philip S.[3]; Liefers, Gerrit-Jan[1]; Gaarenstroom, Katja N.[4]; Burggraaf, Jacobus[2]; Vahrmeijer, Alexander L.[1]

INSTITUTIONS (ALL):

1. Surgery, Leiden University Medical Center, Leiden, Netherlands.
2. Centre for Human Drug Research, Leiden, Netherlands.
3. Purdue University, West Lafayette, IN, United States.
4. Gynecology, Leiden University Medical Center, Leiden, Netherlands.

(No Image Selected)

CONTROL ID: 2233315

TITLE: EpCAM as multi-tumour target for fluorescence guided surgery in animal models

PRESENTER: Stijn Keereweer

ABSTRACT BODY:

Abstract Body: Evaluation of resection margins during cancer surgery can be challenging, often resulting in incomplete tumour removal. Fluorescence-guided surgery (FGS) aims to aid the surgeon to visualize tumours and resection margins during surgery. FGS relies on a clinically applicable imaging system in combination with a specific tumour-targeting contrast agent. In this study EpCAM (epithelial cell adhesion molecule) is evaluated as target for FGS using the novel Artemis imaging system.

The NIR fluorophore IRDye800CW was conjugated to the well established EpCAM specific monoclonal antibody 3T3/A3 and an isotype IgG1 as control. The anti-EpCAM/800CW conjugate showed preserved binding capacity as evaluated on EpCAM positive and negative cell lines using flow cytometry and cell-based plate assays. Four clinically relevant orthotopic tumour models, i.e. colorectal cancer, breast cancer, head and neck cancer, and peritonitis carcinomatosa, were used to evaluate the performance of the anti-EpCAM agent with the clinically validted Artemis imaging system. The Pearl Impulse small animal imaging system was used as reference. The specificity of the near-infrared fluorescence signal was confirmed using bio-luminescence imaging and green-fluorescent protein. All tumour types could clearly be delineated and resected 72 hours after injection of the agent. Millimetre sized tumour nodules were detected that were invisible for the naked eye. Fluorescence microscopy demonstrated the distribution and tumour specificity of the anti-EpCAM agent.

This study shows the potential of an EpCAM specific NIR-fluorescent agent to visualize various tumours using a clinically validated intraoperative imaging system. Clinical trials are currently being designed to establish clinical efficiency of this promising targeting agent.

AUTHORS (LAST NAME, FIRST NAME): Van Driel, Pieter[3]; Boonstra, Martin[2]; Prevoo, H.A.J.M.[2]; Van de Giessen, Martijn[2]; Snoeks, T.J.A.[3]; Tummers, Quirijn R.[2]; Keereweer, Stijn[1]; van de Velde, Cornelis J.[2]; Kuppen, P.J.K.[2]; Vahrmeijer, Alexander L.[2]; Iowik, Clemens W.[3]; Sier, Cornelis F.[2]

INSTITUTIONS (ALL):

1. Otorhinolaryngology Head and Neck Surgery, Erasmus Medical Center, Rotterdam, Netherlands.
2. Surgery, Leiden University Medical Center, Leiden, Netherlands.
3. Radiology & Molecular Imaging , Leiden University Medical Center, Leiden, Netherlands.

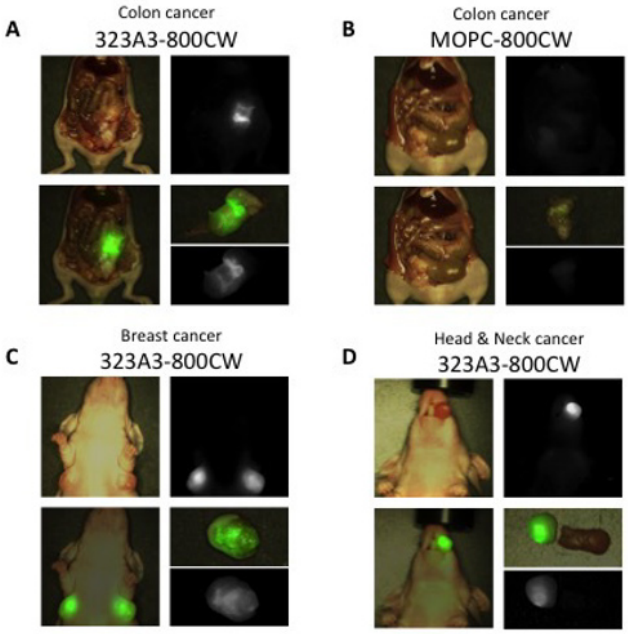

Figure 1 – Intra-operative NIR fluorescent delineation of colon, breast and head & neck cancer: Colon (A, B), breast (C) and head & neck tumors (D) could clearly be visualized during operation using EpCAM specific 323/A3-800CW (TBR colon 13.5, breast 6.7 and Head-and-neck 4.9) and the Artemis system. 323/A3-800CW (A, C, D, 1 nmol) and the non-specific antibody MOPC21-800CW (B, 1 nmol) were intravenously injected. After an incubation of 72 hours NIR fluorescence imaging was performed.

Figure 1 van Driel & Boonstra et al.

CONTROL ID: 2233316

TITLE: Automated detection, segmentation, axis extraction, and morphometric analysis of cortical and trabecular compartments of skeletal bones in small animal micro-CT imaging

PRESENTER: Ali Behrooz

ABSTRACT BODY:

Abstract Body: In vivo micro-computed tomography (micro-CT) imaging of small animals provides three dimensional anatomical maps of the subjects that can be used to study and analyze skeletal bone structures, formation, and diseases. Extracting the bones from raw micro-CT images is a key step in enabling such studies and analyses. While micro-CT images provide contrast between bone and soft tissue components, detecting the bone voxels in a micro-CT volume is challenging considering noise and partial volume effects which result in low voxel density in thin bones such as the pelvis. Furthermore, automated separation of individual bones contained fully or partially in the micro-CT image volume is necessary for performing analysis on different bones and the corresponding cortical and trabecular compartments when manual segmentation is impractical. In this work, a fully automated optimized framework is presented for robust detection, segmentation, and analysis of bones from raw micro-CT images. The imaging platforms used in this work consist of stand-alone Quantum® FX and Quantum® GX micro-CT systems (both by PerkinElmer, Inc.). Small animal data are acquired at different fields of view (5 mm, 10 mm, 24 mm, and 30 mm) and voxel resolutions of 10, 20, 46, and 58 microns for mice and rats *in vivo* and postmortem. The micro-CT data are converted to Hounsfield units prior to processing and analysis. For bone detection, a hybrid thresholding algorithm is presented which combines the benefits of fixed and histogram-based global thresholding as well as local thresholding (by Waarsing, et. al.) and offers significant improvements over existing auto-thresholding techniques. Once bone detection is performed, a watershed-based segmentation algorithm is used to split the binary bone mask into a labeled set of bones. Despite differences in shapes and structure of bones and partial volume effects (especially in low-resolution micro-CT images), the segmentation algorithm can robustly separate the individual bones. The robustness in the segmentation is obtained by applying splitting filters to the gray-scale masked dataset prior to performing marker-based watershed. For shape and structural analysis of the bone, a framework is presented for obtaining the principal and 3D medial axes of each bone. Additionally, a morphological algorithm is used to robustly separate the cortical and trabecular compartments of each individual bone. Finally, 3D morphometric ASBMR and structural parameters are computed separately for cortical and trabecular components of each bone. In this work we present results for a variety of ASBMR parameters including volume, thickness, porosity, density, anisotropy, and fragmentation, in addition to bone detection, segmentation, and axis extraction results for in vivo datasets with different voxel resolutions.

AUTHORS (LAST NAME, FIRST NAME): Behrooz, Ali[1]; Kask, Peet[1]; kempner, joshua[1]; Meganck, Jeffrey A.[1]; Yared, Wael[1]

INSTITUTIONS (ALL):

1. PerkinElmer, Hopkinton, MA, United States.

(No Image Selected)

CONTROL ID: 2233336

TITLE: An Improved Strategy for the Pretargeted PET Imaging of Colorectal Cancer

PRESENTER: Brian Zeglis

ABSTRACT BODY:

Abstract Body: *Rationale*: Pretargeted PET imaging is a potent strategy to combine the exquisitely sensitive tumor-targeting capabilities of antibodies with the rapid pharmacokinetics and favorable dosimetry of small molecule radioligands.[1] We have previously reported a methodology for the pretargeted PET imaging of colorectal cancer based on the inverse electron demand Diels-Alder reaction between a ^{64}Cu-NOTA-labeled tetrazine (^{64}Cu-NOTA-Tz) and a TCO-bearing huA33 immunoconjugate (huA33-TCO).[2] This method proved effective *in vivo*, selectively delineating SW1222 colorectal cancer xenografts with high tumor-to-background activity ratios. However, the clearance of the excess radioligand through the intestines understandably represented a critical obstacle to clinical translation. *The objective of this investigation was to improve this pretargeted PET imaging methodology by synthesizing and evaluating novel tetrazine radioligands with rapid renal pharmacokinetic profiles.*

Results: Two tetrazine constructs were synthesized and characterized: one with a PEG_7 spacer between the tetrazine and NOTA (Tz-PEG_7-NOTA) and one with a sarcophagine chelator in place of NOTA (Tz-SarAr).[3] These precursors were radiolabeled with ^{64}Cu to produce ^{64}Cu-Tz-PEG_7-NOTA and ^{64}Cu-Tz-SarAr in high yield (89.2 ± 4.7% and 91.1 ± 3.2%, respectively) and purity (>99%). PET imaging and biodistribution experiments in healthy mice revealed that while ^{64}Cu-Tz-PEG_7-NOTA is cleared via both the intestines *and* kidneys, ^{64}Cu-Tz-SarAr is rapidly excreted through the kidneys alone. On this basis, ^{64}Cu-Tz-SarAr was selected for further *in vivo* evaluation. To this end, huA33 was incubated with TCO-NHS and purified to yield huA33-TCO with an immunoreactivity of 0.96 ± 0.04 and 3.6 ± 0.5 TCO/mAb. Mice bearing SW1222 xenografts were first administered 100 μg huA33-TCO and subsequently, after 24 h, 350 mCi ^{64}Cu-Tz-SarAr. PET imaging and biodistribution experiments revealed the specific uptake of the radiotracer in the tumor at early time points (5.2 ± 0.6 %ID/g), high tumor-to-background activity ratios (e.g. tumor-to-muscle ratio = 44.2 ± 7.6 at 12 h p.i.), and, critically, the rapid excretion of excess radioligand via the kidneys. Notably, experiments with longer accumulation intervals (48 and 120 h) yielded slight decreases in tumor uptake but also concomitant increases in tumor-to-background activity ratios. Finally, this new system offers dosimetric benefits as well, with a total effective dose of 0.004 mSv/MBq compared to the 1st generation pretargeting strategy (0.012 mSv/MBq), as well as directly-labeled ^{64}Cu-NOTA-huA33 (0.036 mSv/MBq) and ^{89}Zr-DFO-huA33 (0.416 mSv/MBq).

Conclusions: The pretargeted PET imaging of colorectal cancer using the huA33-TCO/^{64}Cu-Tz-SarAr system marks a substantial improvement over the 1st generation pretargeting strategy primarily due to the altered pharmacokinetics of the radioligand. This methodology quickly and clearly delineates tumor tissue with high image contrast at only a fraction of the dose of directly-labeled radioimmunoconjugates.

[1] Goldenberg, *et al.* Theranostics 2012, 2, 523.
[2] Zeglis, *et al.* J. Nucl. Med. 2013, 54, 1389.
[3] Voss, *et al.* PNAS 2007, 104, 17489.

AUTHORS (LAST NAME, FIRST NAME): Zeglis, Brian M.[1, 2]; Brand, Christian[2]; Abdel-Atti, Dalya[2]; Carnazza, Kathryn E.[2]; Cook, Brendon[1, 2]; Carlin, Sean[2]; Reiner, Thomas[2]; Lewis, Jason S.[2]

INSTITUTIONS (ALL):

1. Department of Chemistry and Biochemistry, Hunter College, New York, NY, United States.
2. Department of Radiology, Memorial Sloan Kettering Cancer Center, New York, NY, United States.

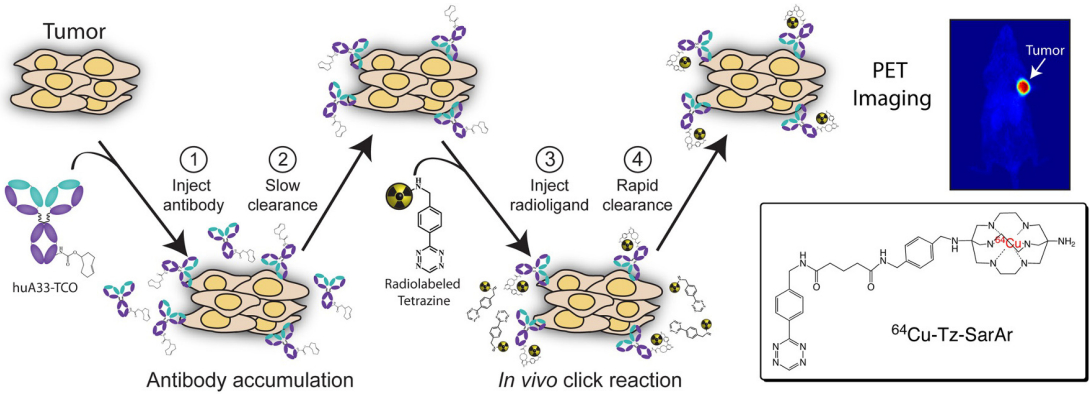
Tumor
1
Inject antibody
2
Slow clearance
huA33-TCO
Antibody accumulation
Radiolabeled Tetrazine
3
Inject radioligand
4
Rapid clearance
In vivo click reaction
PET Imaging
Tumor
64Cu-Tz-SarAr

CONTROL ID: 2233352

TITLE: Discrepant findings unrelated to the primary tumor on ^{68}Ga-DOTATATE PET/CT versus ^{18}F-FDG PET/CT and their potential significance.

PRESENTER: Corina Millo

ABSTRACT BODY:

Abstract Body: Introduction: The uptake mechanisms for ^{18}F-FDG and ^{68}Ga-DOTATATE are distinct. However, since activated macrophages seen in inflammatory processes show both enhanced glycolytic activity and upregulation of somatostatin receptor expression, it is reasonable to expect that both tracers would show increased uptake at sites of inflammation. This study compared concordant and discrepant findings unrelated to the primary tumor in patients who underwent PET/CT scans with both agents within an interval of less than 2 weeks, in order to explore the influence of inflammation on tracer uptake.

Patients and their characteristics: 22 patients were studied: 8 females, 14 males; age range: 21-75 y. Primary diagnoses leading to performance of ^{18}F-FDG and ^{68}Ga-DOTATATE scans were: pheochromocytoma (10); paraganglioma (4); VHL (4); TIO (1); NET (3).

Results: 15 patients had secondary findings, with 5 lesions that were concordant: increased uptake in Schmorl's nodule, adenopathy, myoma, post-radiation pneumonitis and the area surrounding a hematoma. There were 20 discrepant findings. 15 lesions showed positive ^{18}F-FDG/negative ^{68}Ga-DOTATATE uptake: adenopathy, postsurgical/postraumatic inflammation, bursitis, lung parenchymal infiltrates, adrenal and thyroid nodules, distal esophageal and gastric wall uptake, aortic wall associated with graft placement, talc pleurodesis-induced changes, and coccydiomycosis-induced lytic bone lesion. 5 secondary findings were negative ^{18}F-FDG/positive ^{68}Ga-DOTATATE: hemangioblastomas, prostatic focus, and adenopathy.

Conclusion: While both radiotracers target mechanisms within the inflammatory cascade, we identified many discrepant findings. The majority reflect an underlying inflammatory process; only a few of the discrepant lesions had a non-inflammatory etiology (myoma, hemangioblastoma). These discrepancies probably reflect either different stages of inflammation or different types of inflammatory processes, some related predominantly to macrophage activation and increased glycolytic activity, and others to upregulation of somatostatin receptors in macrophages or downregulation of these receptors in endothelial cells. Interestingly, in cases with known chronic inflammation, such as talc pleurodesis or skeletal coccydiomycosis, there was no ^{68}Ga-DOTATATE activity in spite of the presence of intense ^{18}F-FDG uptake, indicating lack of SSTR expression at sites of chronic inflammatory processes.

AUTHORS (LAST NAME, FIRST NAME): Millo, Corina[4]; Papadakis, Georgios Z.[3]; Lau, Chuen-Yen[5]; Janssen, Ingo[2]; Pacak, Karel[1]; Herscovitch, Peter[6]

INSTITUTIONS (ALL):

1. National Institute of Child Health and Human Developmnent (NICHD), National Institutes of Health (N.I.H.), Bethesda, MD, United States.
2. National Institute of Child Health and Human Developmnent (NICHD), National Institutes of Health (N.I.H.), Bethesda, MD, United States.
3. Radiology and Imaging Sciences, National Institutes of Health, Clinical Center, Bethesda, MD, Bethesda, MD, United States.
4. Positron Emission Tomography (PET) Department, National Institutes of Health, Clinical Center, Bethesda, MD, United States.
5. National Institute of Allergy and Infectious Diseases, National Institutes of Health , Bethesda, MD, United States.
6. Positron Emission Tomography (PET) Department, National Institutes of Health, Clinical Center, Bethesda, MD, United States.

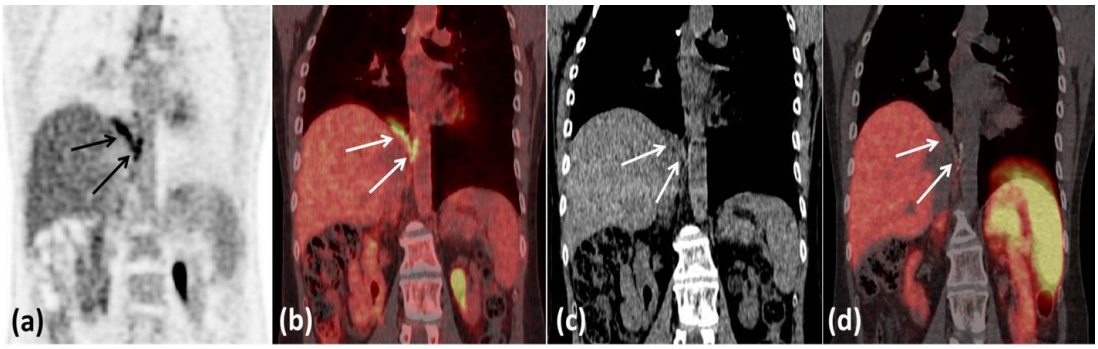

Image caption: Status post talc pleurodesis: ^{18}F-FDG-PET/CT showed increased hypermetabolic activity (SUVmax: 26.0) in the region of talc-placement (a, b, c), whereas PET/CT using ^{68}Ga-DOTA-TATE (d) showed no uptake

CONTROL ID: 2233364

TITLE: The value of intraoperative near-infrared fluorescence imaging based on enhanced permeability and retention of indocyanine green: feasibility and false-positives in ovarian cancer

PRESENTER: Leonora Boogerd

ABSTRACT BODY:

Abstract Body: Introduction

In ovarian cancer, 2 of the most important prognostic factors for survival are completeness of staging and completeness of cytoreductive surgery. Therefore, intraoperative visualization of tumor lesions is of great importance. Preclinical data already demonstrated tumor visualization in mice using near-infrared (NIR) fluorescence imaging and indocyanine green (ICG) as a result of enhanced permeability and retention (EPR)[(1)]. The aim of this study was to determine feasibility of intraoperative ovarian cancer metastases detection using NIR fluorescence imaging and ICG during surgery.

Materials and methods

Ten patients suspected of ovarian cancer scheduled for staging or cytoreductive surgery were included. Patients received 20 mg ICG intravenously after opening the abdominal cavity. The mini-FLARE™ NIR fluorescence imaging system was used to detect NIR fluorescent lesions. After resection, lesions were assessed for tumor status by the pathologist.

Results

Six out of 10 patients had malignant disease of the ovary or fallopian tube, of which 2 had metastatic disease outside the pelvis. Eight metastatic lesions were detected in these 2 patients, which were all NIR fluorescent (100% sensitivity). However, 13 non-malignant lesions were also NIR fluorescent, resulting in a false-positive rate of 62%. There was no significant difference in tumor-to-background ratio between malignant and benign lesions (2.0 vs 2.0; P=0.99).

Conclusions

This is the first clinical trial demonstrating intraoperative detection of ovarian cancer metastases using NIR fluorescence imaging and ICG. Despite detection of all malignant lesions, a high false-positive rate was observed. Therefore, NIR fluorescence imaging using ICG based on the EPR effect is not satisfactory for the detection of ovarian cancer metastases. The need for tumor-specific intraoperative agents remains.

1. Kosaka N et al. Near infrared fluorescence-guided real-time endoscopic detection of peritoneal ovarian cancer nodules using intravenously injected indocyanine green. Int J Cancer. 2011

AUTHORS (LAST NAME, FIRST NAME): Boogerd, Leonora S.[2]; Hoogstins, Charlotte E.[2]; Tummers, Quirijn R.[2]; de Kroon, Cor D.[3]; Iowik, Clemens W.[4]; van de Velde, Cornelis J.[2]; Gaarenstroom, Katja N.[3]; Frangioni, John V.[1]; Vahrmeijer, Alexander L.[2]

INSTITUTIONS (ALL):

1. Curadel, LLC, Worcester, MA, United States.
2. Surgery, Leiden University Medical Center, Leiden, Netherlands.
3. Gynaecology , Leiden University Medical Center, Leiden, Netherlands.
4. Radiology, Leiden University Medical Center, Leiden, Netherlands.

(No Image Selected)

CONTROL ID: 2233384

TITLE: In vivo vasculogenesis and fibrosis imaging defines the effect of PTH on calvarial bone allografts

PRESENTER: Wafa Tawackoli

ABSTRACT BODY:

Abstract Body: Craniofacial allografts may serve as useful grafts for bone repair- though often fail to integrate with host bone. We previously showed that intermittent PTH treatment enhances mesenchymal stem cell recruitment and differentiation, resulting in allograft osteo-integration in cranial membranous bones. In this study we hypothesize that PTH promotes scar-less bone healing by affecting blood vessel formation.

Calvarial bone defects were created in FVB/n mice. The mice were given implants of allografts, with or without daily PTH treatment. Neovascularization was evaluated using fluorescence imaging (FLI) and integrin $\alpha_v\beta_3$-targeted probe. Laser doppler imaging (LDI) was used to quantify blood perfusion. The mice were perfused with a radio-opaque agent that allowed micro-computed tomography (micro-CT) structural analysis of blood vessels. Infiltrating Mast cells to the graft-host suture were counted in histological samples. Scar tissue formation was measured using micro-Magnetic Resonance (micro-MRI).

Our results showed that a week after surgery, FLI signal was significantly lower and LDI showed less perfusion in the PTH-treated animals. Micro-CT analysis showed that by that time-point, mice given PTH had more small-diameter blood vessels and less large-diameter vessels. Interestingly, two weeks after surgery, the control animals had significantly more blood vessels of the smallest detectable diameter. Significantly less Mast cells were counted in the PTH-treated animals a week after the surgery. Micro-MRI demonstrated more organized collagen tissue and higher collagen content in animals given PTH.

In this work we showed that PTH induces the formation of narrower blood vessels, thus reducing mast cell infiltration to the allograft proximity. Eventually, PTH leads to less scar tissue formation allowing better integration of allografts in cranial bones.

AUTHORS (LAST NAME, FIRST NAME): Tawackoli, Wafa[1, 2]; Yakubovich, Doron C.[1]; Sheyn, Dmitriy[1, 3]; Da, Xiaoyu[2]; Pelled, Galit[1, 2]; Gazit, Dan[1, 3]; Gazit, Zulma[1, 3]

INSTITUTIONS (ALL):

1. Surgery, Cedars-Sinai Medical Center, Los Angeles, CA, United States.
2. Biomedical Imaging Research Institute, Cedars-Sinai Medical Center, Los Angeles, CA, United States.
3. Board of Governors Regenerative Medicine Institute, Cedars-Sinai Medical Center, Los Angeles, CA, United States.

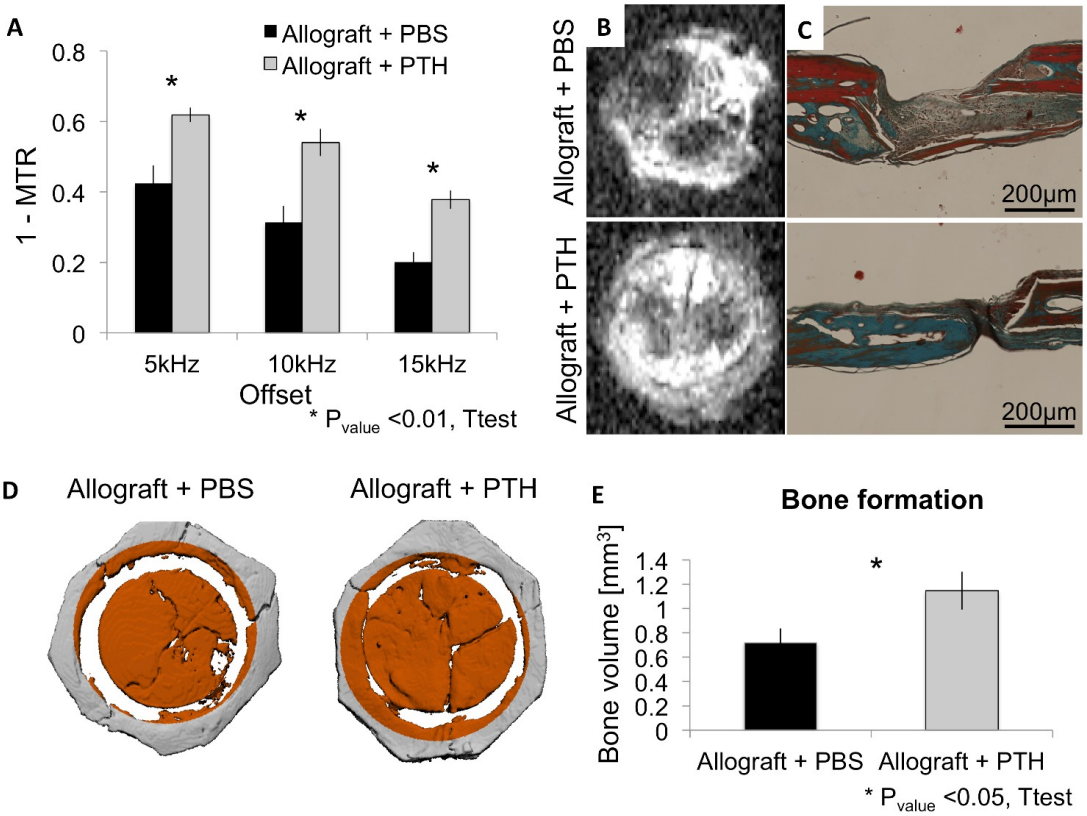

Calvarial defects were induced to mice, into which structural bone allograft were implanted. Half of the mice were given Parathyroid Hormone (PTH) therapy and half served as a control. Four weeks after surgery the animals were imaged using uMRI scanner and Magnetization Transfer Contrast parameters. MTC signal was significantly higher in the graft-host bone suture in PTH-treated animals, reflecting more rigid collagen fiber organization (A), which was supported by qualitative analysis (B). To validate the MTC-uMRI results we performed Masson Trichrome staining emphasizing collagen fibers (C), which demonstrated the prominent presence of collagen in the PTH-treated animals. These observations suggest that the PTH diverts the fibrosis that occurs in the graft-host gap to bone regeneration. uCT scan showed more bone formation in the PTH group, both qualitatively (D) and quantitatively (E).

CONTROL ID: 2233386

TITLE: Efficient Magnetic Resonance Imaging of lymph node using Hyaluronic Acid-conjugated Iron Oxide nanoparticles

PRESENTER: Ming-Chun Lin

ABSTRACT BODY:

Abstract Body: MRI lymphography is important to noninvasively determining whether a primary tumor has entered the stage of metastasis. Hyaluronic acid (HA) was known to be as a ligand for CD44 receptors over-expression on macrophages and was widely investigated for the anticancer drug conjugation as effective targeting ligand for CD44-overexpression tumor cells [1-2]. In the present study, a novel superparamagnetic iron oxide nanoparticles coated with hyaluronic acid (IOHA) were designed and prepared. The transverse relaxivity (R2) value of IOHA nanoparticles was measured as 350 $s^{-1}mM^{-1}$ by the 0.47T mini-spectrometer (MQ20, Bruker, Billerica, MA) and the particle size was observed in average of 197nm by Asymmetric-Flow Field Flow Fractionation. The mice MRI lymphography using IOHA as contrast agent was obtained with Gradient echo-T1, T2 and T2* images. The % signal intensity change in the sentinel lymph node was quantified before and after nanoparticle injection and compared to two other commercially available iron oxide nanoparticle contrast agents (MION, Feridex). The image data were illustrated in Fig1. The signal intensity decreased more than 90% after 24 hr in the present of IOHA, whether the signal change for MION was around 70% and around 15% for the Feridex. The stronger signal change indicated IOHA can label lymph node more efficiently and has the potential to be an effective MRI contrast agent for lymph node.

References

Yu, M. et al. *Nanoscale*, **2013**, *5*, 178–183.

Zhao, Q. et al. *ACS Appl. Mater. Interfaces*, **2014**, *6*, 20290–20299

AUTHORS (LAST NAME, FIRST NAME): Lin, Ming-Chun[1]; Chen, Yung-Chu[4]; Chen, Chiao-Chi[3]; Chang, Chen[3]; Hsieh, Wen-Yuan[2]

INSTITUTIONS (ALL):

1. Pharmaceutical Engineering Technology, Industry Technology Research Institute, Hsinchu, Taiwan.
2. Megapro Biomedical Co., Ltd., Hsinchu county, Taiwan.
3. Institute of Biomedical Sciences, Academia Sinica, Taipei, Taiwan.
4. Institute of Biomedical Engineering, College of Medicine and College of Engineering, National Taiwan University, Taipei, Taiwan.

(No Image Selected)

CONTROL ID: 2233395

TITLE: Photoacoustic Molecular Imaging Advancement by Unmixing and Non focoused Ultrasound Sonoporation Method as improvement in tumoral treatment

PRESENTER: Dieter Fuchs

ABSTRACT BODY:

Abstract Body: *Introduction*

Photoacoustic imaging (PAI) demonstrated a wide potential to obtain simultaneously structural, functional and molecular information. Liposomes are clinically used as nanocarriers for many drugs, including chemotherapeutics as theranostic agents. The aim of this work was to assess changes in tumor vascular dynamics with the use of PAI, followed by the systemic injection of theranostic liposomes, and to show the differences on nanosystem's flows with and without sonoporation treatments applied on tumoral masses and compare the behavior of tumoral necrotic zones. An important role in data analysis is the use of spectral unmixing tools. Unmixing techniques allow to separate the signals from different optical absorbers in a photo-acoustic image, thus providing estimates of their characteristic entropy behavior, optic flow, and distribution of the apparent velocities of the molecules in a time dependant manner.

Material and method

Ten Balb/C bearing a subcutaneous syngeneic breast cancer (TS/A) were enrolled in the study: five of them have been exposed to sonoporation treatment immediately after liposome injection (t=0). Sonoporation was carried out by using a custom system with a non-focused 1 MHz transducer and low acoustic intensity with an insonation time of 40 sec. The mice were injected i.v. with 200 µl of PEGylated liposomes (130 nm diameter). The liposomes were labeled with near-infrared cyanine dye in order to pick up the PAI signal. The image acquisition with VEVO LAZR system (Fujifilm VisualSonics Inc.), equipped with a highly sensitive photo-acoustic transducer at a frequency of 21 MHz, consisted in: 1) application of sequential laser pulses at 750 and 850 nm to obtain PAI of the tissue vasculature: this method allowed for quantification of Oxygen saturation (sO_2) and total hemoglobin (HbT) 2) scanning tumour in the range 680-970 nm to get a whole spectra profile. The maximum liposomes flow value, measured between 1 and 90 minutes after injection, was quantified using an Optical Flow Matlab code after using Unmixing Tool software onboard the VEVO-LARZ system.

Results

An increase in the values for Optical Flow in sonoporation presence can be observed in the graph shown in Fig.1. An obvious increment of the flow can be directly observed from the images obtained post Matlab code processing, applied in order to calculate the optical flow (Fig. B-B'). Moreover, thanks to the analysis of oxygen saturation and hemoglobin, we have been able to observe variations of these two parameters in the total tumor mass and in particular, in the necrotic areas. *(Tab.1)*

Conclusion

The results show a great improvement in oxygenation and flow only when sonoporation treatment was applied. Liposome flow has increased by 51.2% in the tumoral mass and increasing values sO_2, HbT in necrotic portion are observed. Each result is the average of five values. Non-invasive ultrasound sonoporation as tumor treatment method causing transient cell membranes permeabilization and PAI, as growing bioimaging modality, represent a powerful combination with great potential as clinical applications to improve effectiveness of cancer treatment.

AUTHORS (LAST NAME, FIRST NAME): Giustetto, Pierangela[1]; Rizzitelli, Silvia[2]; Fuchs, Dieter[3]

INSTITUTIONS (ALL):

1. Multi-Imaging Service Company, EPHORAN, Colleretto Giacosa, Torino, Italy.
2. Resonance Magnetique, Center de Resonance Magnetique des Systemes Biologiques, Bordeaux Cedex, France.
3. Fujifilm VisualSonics, Amsterdam, Netherlands.

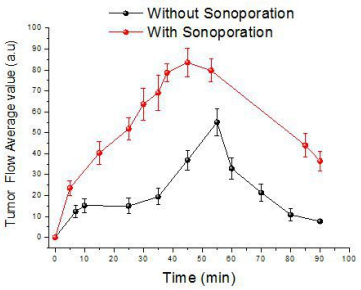

Fig. 1: Comparison of the Optical Flow average values in tumors treated with and without sonoporation

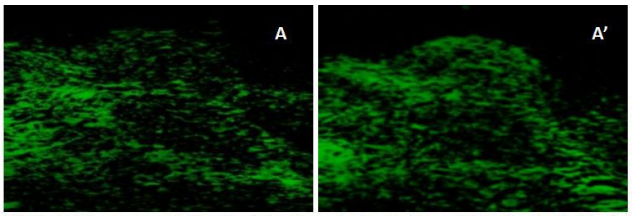

Fig.A: Cy 5.5 compound after Unmixing (time t=0) – Fig. A' : past 30 minutes (t=30 min)

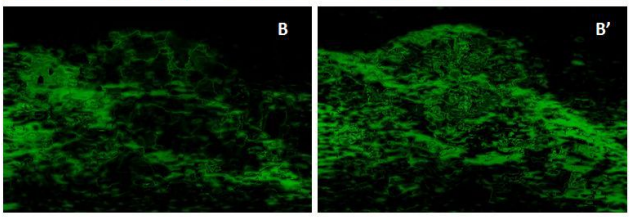

Fig.B: Cy 5.5 Unmixing image after Optical Flow elaboration at 1 min post liposomes bolus injection; FigB': after 30 min post liposomes bolus.

CONTROL ID: 2233393

TITLE: Towards Distinguishing Brain Tumor vs. Radiation Necrosis via O_2-Sensitive MRI

PRESENTER: Scott Beeman

ABSTRACT BODY:

Abstract Body: INTRODUCTION: Diatomic oxygen (O_2) is a critical determinant of cancer growth and radiation-based cancer therapies. O_2 is weakly paramagnetic and therefore influences the magnetic resonance imaging (MRI)-measured ^{1}H longitudinal relaxation rate constant (R_1) of tissue water. R_1 can thus be exploited as a marker of tissue oxygenation[1-5]. In principle, it is straightforward to create a map of tissue oxygen partial pressure (pO_2) from a map of R_1. In practice, however, blood flow contributes to R_1, masking the contribution of O_2 to the relaxation process. The goals of this work are two-fold: (i) establish a robust (flow insensitive) MRI technique to quantify the relationship (relaxivity, r_1) between R_1 and pO_2 in tissue and (ii) demonstrate that O_2-sensitive MRI can differentiate radiation necrosis from brain tumors – two commonly co-occurring pathologies that have proven extremely difficult to differentiate with standard radiological techniques.

METHODS: *In vivo* O_2 r_1: R_1 data were collected using a fast-spin-echo, inversion recovery imaging sequence (4.7 T, 30 inversion times) in healthy mice (n=4) during alternating free breathing of either 100% O_2, 12.5% O_2/87.5% N_2, or 95% O_2/5% CO_2 (carbogen). A non-slice-selective inversion pulse was employed to mitigate blood-flow contributions to R_1 measurements. From these data, R_1 was calculated using Bayesian probability theory-based methods (bayesiananalysis.wustl.edu). In a separate experiment, pO_2 was measured in the thalamus of healthy mice (n=4) using an optical probe (Oxford Optronix). O_2 r_1 was calculated via the relationship: $R_1 = R_{1,0} + r_1\ pO_2$ ($R_{1,0}$ is the inferred relaxation rate constant in the absence of O_2). *Animal models of pathology:* R_1 data were collected in control-state (n=4), DBT glioma model[6] (n=7), and radiation necrosis model[7] (n=6) mice during free breathing of the 12.5% O_2/87.5% N_2 and carbogen gas mixtures using the sequence described above.

RESULTS: *In vivo* O_2 r_1: Optically measured pO_2 values were 66±11 mmHg, 12±5 mmHg, and 88±7 mmHg during free breathing of 100% O_2, 12.5% O_2/87.5% N_2, and carbogen, respectively. R_1 values in the thalamus were 0.77±0.03 s^{-1}, 0.74±0.02 s^{-1}, and 0.81±0.02 s^{-1}, respectively. pO_2 and R_1 were strongly correlated (R^2=0.91, Fig. 1A). The relaxivity of O_2 in the brain was calculated to be 8.5×10^{-4} $mmHg^{-1}s^{-1}$. *Discernment of pathologies:* Lesion-specific changes in R_1 due to breathing-gas modulation distinguished the two pathologies ($p<0.01$): 0.01±0.02 s^{-1} in tumor, 0.05±0.01 s^{-1} in radiation necrosis lesions, and 0.07±0.01 s^{-1} in cortex from healthy control mice (Fig. 1B).

DISCUSSION AND CONCLUSIONS: The linear relationship between R_1 and optical (micro-) probe-determined brain tissue pO_2 was quantified (R^2=0.91). By monitoring the change in brain tissue R_1 (and thus oxygenation), we were able to differentiate tumor and radiation necrosis lesions.

Refs: [1]O'Conner, et al., Magn Reson Med. (2007); [2]Winter, et al., Acad Radiol. (2011), [3]Remmele, et al., Magn Reson Med. (2013), [4]Jordan, et al., Magn Reson Med. (2013), [5]Zhang, et al., Magn Reson Med. (2014), [6]Kumanishi, Jpn J Exp Med. (1967), [7]Jiang, et al., Clin Cancer Res. (2014).

AUTHORS (LAST NAME, FIRST NAME): Beeman, Scott C.[1]; Shui, Ying-Bo[4]; Perez-Torres, Carlos J.[1]; Engelbach, John A.[1]; Ackerman, Joseph J.[1, 2]; Garbow, Joel R.[1, 3]

INSTITUTIONS (ALL):

1. Department of Radiology, Washington University, Saint Louis, MO, United States.
2. Department of Chemistry, Washington University, Saint Louis, MO, United States.
3. Alvin J. Siteman Cancer Center, Washington University, Saint Louis, MO, United States.
4. Department of Ophthalmology, Washington University, Saint Louis, MO, United States.

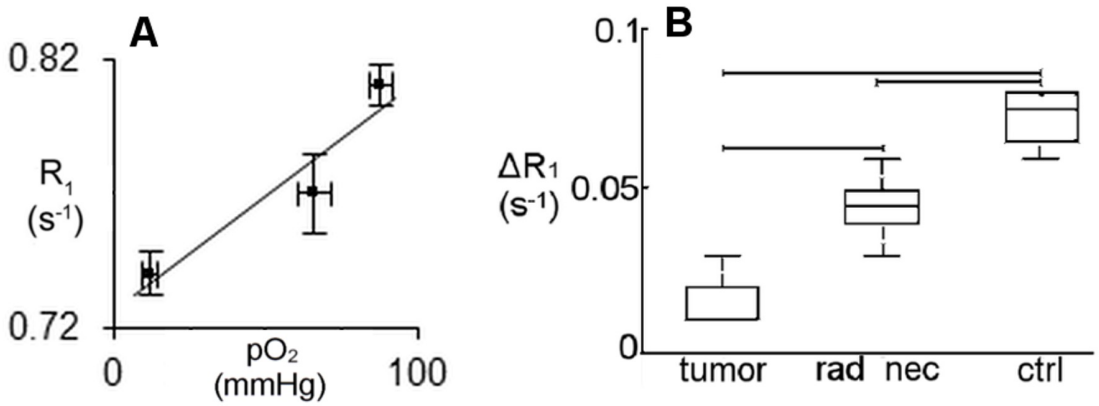

Figure 1 - (A) There is a linear relationship between pO_2 and R_1. The relaxivity of brain tissue O_2 is 8.5×10^{-4} $mmHg^{-1}s^{-1}$ ($R^2 = 0.91$). **(B)** Tumor lesions, radiation necrosis lesions, and healthy cortex showed small, moderate, and large changes is tissue R_1 (and thus oxygenation) during breathing-gas modulation. Lesion-specific change in R_1 due to breathing-gas modulation distinguished the two pathologies ($p<0.01$).

CONTROL ID: 2233398

TITLE: Mapping relative and absolute brain tissue pH using pixelwise, multipower SAFARI

PRESENTER: Kyle Jones

ABSTRACT BODY:

Abstract Body: Introduction: Tissue pH may be an outstanding biomarker for identifying brain ischemia and brain tumor recurrence vs. post-radiation pseudoprogression. Previous studies have interrogated brain tissue pH by exploiting CEST MRI between endogenous proteins and water, known as amide proton transfer (APT) MRI.[1] Saturation with Frequency Alternating RF Irradiation (SAFARI) MRI can measure APT without errors induced by direct water saturation and magnetization transfer.[2]

We have modified SAFARI MRI to obtain multi-slice APT MR images at multiple saturation powers. We have analyzed these results with a linear fitting method to rapidly generate pixelwise maps of chemical exchange rates.[4] We have used these exchange rate maps to create relative and absolute-value pH maps of the brain tissues of volunteers.

Methods: Clinical MRI studies were performed with a 3T Siemens Skyra MRI scanner and a head coil. SAFARI MRI requires the acquisition of four CEST MRI scans with different saturation schemes: +ω, -ω, alternating +ω and –ω, and alternating –ω and +ω where ω is the saturation offset. Our protocol used this saturation scheme over five different saturation offsets at 600, 550, 500, 450 and 400 Hz, four different powers at 0.7, 0.9, 1.0 and 1.2 mT. Ten axial image slices were acquired of a healthy volunteer's brain at 1.7x1.7 mm in-plane spatial resolution and 8 mm slice thickness in 17 minutes. The pixelwise chemical exchange rates were determined by fitting via the linear HW-QUESP method to the CEST amplitude vs. saturation power for each image pixel.[2] These chemical exchange rates were converted to relative and absolute pH values using a previously reported calibration.[1] In addition, pixelwise pH values were calculated from the SAFARI MRI signal acquired at 0.9 uT using a second previously reported calibration.[4]

Results and Discussion:

The saturation offset at 450 Hz was found to be most reliable for APT with SAFARI MRI (Fig. A,C in Persuasive Data). All saturation powers were acceptable for this clinical imaging study. Chemical exchange rates determined with linear HW-QUESP method were retained in the final map only if R^2 was greater than or equal to 0.9 (Fig. B,D). The pH-exchange rate calibration showed pixelwise pH values that were systematically too high relative to the known physiological pH range in the brain. We converted these absolute-value pH maps to maps that show a relative acidicty score, which represents the heterogeneity of pH in the brain (Fig. E). The pixelwise pH values determined from the SAFARI MRI signals showed results throughout the brain (Fig. F). This result suggested that a criterion is needed to ensure that these absolute pH values are reliable. Yet both pH maps showed that this methodology can be used to improve the relative pH values within brain tissue. Based on these results, we are starting clinical trials that apply this method to improve diagnoses of patients with cerebral ischemia or tumor recurrence vs. pseudoprogression after radiation therapy.

AUTHORS (LAST NAME, FIRST NAME): Jones, Kyle[2]; Randtke, Edward A.[2]; Yoshimaru, Eriko[1]; Li, Wen[3]; Kahn, Rihan[4]; Nael, Kambiz[4]; Pagel, Mark[2, 4]

INSTITUTIONS (ALL):

1. Cancer Biology GIDP, University of Arizona, Tucson, AZ, United States.
2. Department of Biomedical Engineering, University of Arizona, Tucson, AZ, United States.
3. Department of Radiation Oncology, University of Arizona, Tucson, AZ, United States.
4. Department of Medical Imaging, University of Arizona, Tucson, AZ, United States.

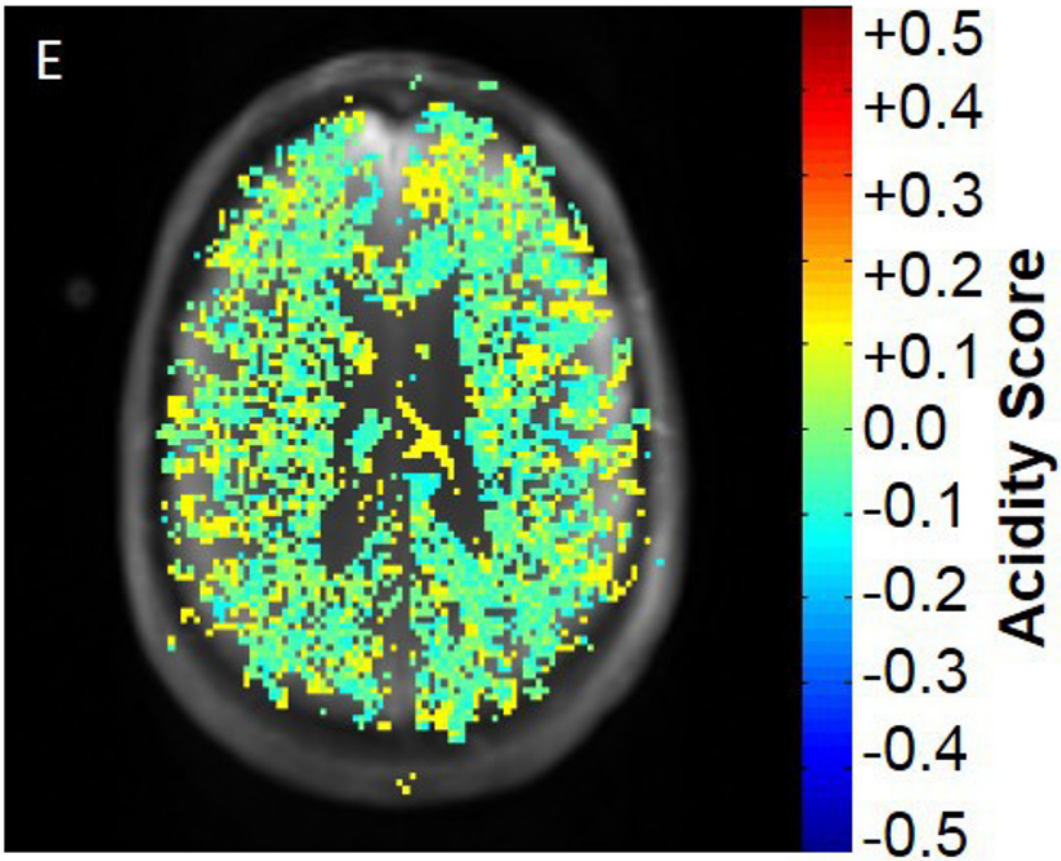
E
+0.5
+0.4
+0.3
+0.2
+0.1
0.0
-0.1
-0.2
-0.3
-0.4
-0.5
Acidity Score

CONTROL ID: 2233403

TITLE: Improved spatial resolution in “paired-agent” quantitative imaging of cancer cell-surface receptors using early photon fluorescence tomography

PRESENTER: Lagnojita Sinha

ABSTRACT BODY:

Abstract Body: Cancer is a very serious disease and its proper detection is a crucial factor for curing it. The success rates of cancer detection have failed to improve markedly, thereby severely limiting the growth of cancer therapy development[1]. Relationship between drug efficacy and tumor molecular heterogeneity is an important factor to understand drug resistance in the tumor. Therefore, proper detection of cancer at the molecular level is the ultimate goal of molecular imaging. Optical projection tomography is a fast and efficient method of visualizing complex structures inside tissue and enabling functional information to be obtained. Adaptating such imaging modalities to preclinical cancer imaging has the potential to significantly improve our understanding of intra-tumor molecular heterogeneity detection and its role in drug efficacy. However, conventional approaches are constrained by their spatial resolution, attributable to the high scattering nature of light in biological tissue. Spatial resolution can be increased manifold if only early-arriving photons from a narrow pulse light source (having undergone the least amount of scatter) can be adequately identified as inputs for tomographic reconstruction[2]. New single photon detection instrumentation coupled with time-tagging can be used as temporal thresholding to minimize detection of scattered photons. This paper describes the development and evaluation of a novel multi-imaging-agent early photon fluorescence emission tomography (EPFET) system, in which a 3ps detection window is achievable, and multiple-agent detection can be used to employ quantitative “paired-agent” receptor concentration imaging approaches[3].
The relationship between photon propagation path through the tissue and their arrival times at the detector was initially explored in two types of simulation: 1) an analytical model based on the solution of diffusion approximation of radiative transfer equation, and 2) Monte-Carlo photon tracking. Using the analytical model, it was demonstrated that a 3ps time detection window could limit the full width half maximum (FWHM) of the pathlength sensitivity function to 1.4mm in a 5mm diameter sample, compared to ~ 5mm FWHM results from no time-gating. This is a worst-case scenario as it assumes isotropic scattering of the photons (when in fact scattering is forward-weighted) and wide aperture of excitation and detection (which can be limited in the hardware of the imaging system). Monte-Carlo simulation, which accounted for forward scatter and small aperture of excitation and detection, estimated the FWHM to be considerable smaller, at approximately 300um.
In conclusion, this paper sums up the first step in the development of a novel EPFET system that can be used as a tool to analyze: drug delivery, drug-receptor binding and receptor density, on a spatial scale and at a quantitative level unachievable by any current *in vivo* imaging, allowing earlier identification of the most promising therapies to push into clinical trials.

1 DiMasi, J. A., et al., *Clin. pharmacol. and therapeutics*, 2013
2 Niedre, M. J. *et al. Proc. Natl. Acad. Sci. USA*, 2008
3 Tichauer, K. M. *et al., Mol. Imaging Biol.*, 2012

AUTHORS (LAST NAME, FIRST NAME): Sinha, Lagnojita[1, 2]; Wu, Sijia[2]; Brankov, Jovan G.[2]; Tichauer, Kenneth M.[1]

INSTITUTIONS (ALL):
1. Biomedical Engineering, Illinois Institute of Technology, Chicago, IL, United States.
2. Electrical Engineering, Illinois Institute of Technology, Chicago, IL, United States.

(No Image Selected)

CONTROL ID: 2233416

TITLE: Imaging of tumor-associated system x_C^- activity with 18F-fluoropropylglutamate (FSPG) PET/CT for intracranial malignancies.

PRESENTER: Erik Mittra

ABSTRACT BODY:

Abstract Body: Objective: The glutamate-cystine exchanger system x_C^- is an emerging target in oncology, mediating oxidative stress in cancer and providing an additional growth advantage for a variety of tumors, including those in the brain, and has been associated with higher-grade tumors. System x_C^- activity can be non-invasively visualized with 18F-FSPG. The aim of this study was to investigate the utility of 18F-FSPG PET/CT for intracranial malignancies.

Methods: Patients with primary brain tumors or brain metastases were recruited for this study. Eight mCi of 18F-FSPG were injected intravenously and a dynamic PET/CT brain scan from 0-30 min post-injection (p.i.) and a whole body scan at 60 min p.i. were acquired. Some patients also had a standard-of-care 18F-FDG PET/CT scan. The PET images were visually and quantitatively assessed and compared with other available imaging and pathology information.

Results: Eleven patients with primary brain tumors (6) or metastases (5) have been studied to date. Low uptake of FSPG in healthy brain parenchyma was observed (SUVmax 0.20±0.06). The dynamic images show increasing concentration of FSPG over the first 30 minutes in the brain lesions, and decreasing or minimal uptake in background tissues. At 60 minutes post-injection, FSPG uptake in suspected lesions had an SUVmax of 5.0±4.3, and SUVmean of 1.8±1.6. The average size of the lesions was 10.7 ± 7.4 mm. In most cases, the equivocal lesions seen on MRI showed prominent 18F-FSPG uptake. However, there were also some instances where non-specific MRI signals were not seen with 18F-FSPG or suspected malignancy is seen with 18F-FSPG but not MRI. Clinical follow-up and pathology evaluation as well as recruitment of patients with other pathologies (i.e., newly diagnosed or low-grade tumors) is ongoing. Updated data will be presented.

Conclusions: 18F-FSPG is a potentially useful PET imaging agent for the detection of residual/recurrent disease in the brain in settings where MRI alone is not definitive or discriminant, and can inform about system xC- levels and intracellular glutamate concentrations.

AUTHORS (LAST NAME, FIRST NAME): Mittra, Erik[1]; Minamimoto, Ryogo[1]; Barkhodari, Amir[1]; Jamali, Mehran[1]; Iagaru, Andrei[1]; Schneider, Bernadette[1]; Hoehne, Aileen[1]; Berndt, Mathias[2]; Koglin, Norman[2]; Stephens, Andrew W.[2]; Chin, Frederick T.[1]; Gambhir, Sanjiv S.[1]

INSTITUTIONS (ALL):

1. Radiology, Stanford University, Stanford, CA, United States.
2. Piramal Imaging GmbH, Berlin, Germany.

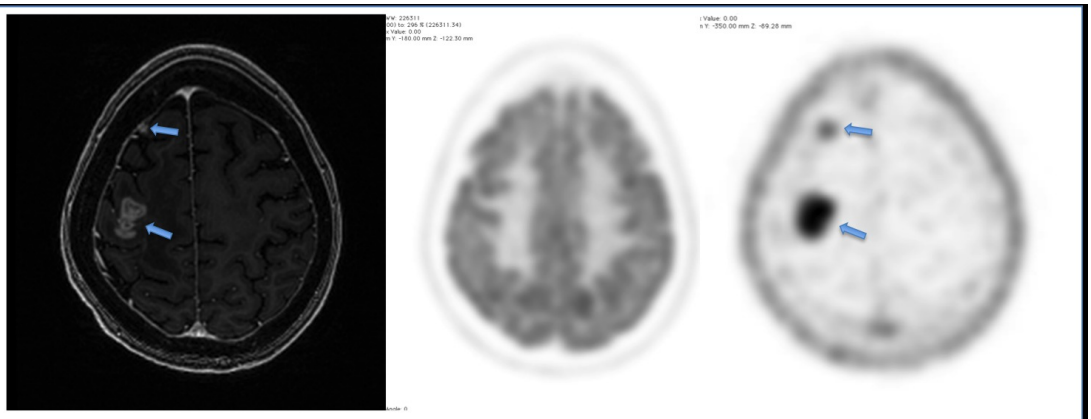

Supplementary Figure: Comparison of axial Gd-enhanced BRAVO MRI (left), 18F-FDG PET (center), and 18F-FSPG PET (right) images in a 65 year-old woman with metastatic Non-Small Cell Lung Cancer. The anterior lesion was stable (5 mm) and the posterior lesion was growing (15 mm) on MRI. The lesions were not seen with 18F-FDG. The lesions have an SUVmax of 1.4 and 7.5, respectively, with 18F-FSPG. Lack of background brain uptake of 18F-FSPG further enhances the image quality.

CONTROL ID: 2233441

TITLE: Experimental validation of proton-induced x-ray fluorescence imaging for visualization of gold nanoparticles

PRESENTER: Magdalena Bazalova-Carter

ABSTRACT BODY:

Abstract Body: X-ray fluorescence computed tomography (XFCT), conventionally performed with x-ray excitation beams, is an emerging modality for high-resolution molecular imaging of gold nanoparticles. A factor limiting the imaging sensitivity of conventional XFCT lies in the fact that x-ray fluorescence (XRF) signal is contaminated with background x-rays generated by Compton scatter. However, we noted that proton beam XRF material analysis is known for its high sensitivity due to its low x-ray background, which prompted us to investigate XFCT imaging performed with a proton beam. The goal of this work was to demonstrate the feasibility of proton-induced x-ray fluorescence CT (pXFCT) imaging of gold by means of experiments and Monte Carlo (MC) simulations.

The experimental pXFCT imaging system consisted of a 7-mm FWHM 220 MeV proton beam line, a 3×3 mm^2 photon-counting CdTe detector placed at 90° with respect to the incident proton beam at a distance of 45 cm from the imaging isocenter, which was defined by the center of a programmable in-house built translation/rotation stage, a solid water beam dump, and an imaging phantom. First, proton-induced gold x-ray fluorescence (pXRF) was measured as a function of gold concentration. Vials of 2.2 cm in diameter filled with 0-5% Au solutions (percent weight concentration) were irradiated with the 220 MeV proton beam and x-ray fluorescence induced by the interaction of protons and Au was detected with the CdTe detector. Second, a 7-cm diameter water phantom containing three 2.2-cm diameter vials with 3%-5% Au solutions was imaged with the proton beam in a 1^{st} generation CT scanning geometry. pXRF spectra were acquired at 21 translational steps spaced by 3 mm at each of the 36 projection angles spaced by 10° in 20-s intervals. pXFCT images of the phantom were reconstructed with filtered back projection. MC model of the actual pXRF data acquisition geometry was built in TOPAS, a MC code based on the GEANT4 MC simulation package. Additionally, a simplified geometry of the experimental pXFCT system, in which the 3×3 mm^2 CdTe detector was replaced with a 4π detector to significantly decrease the calculation time, was modeled. Simulated pXRF signal as well as pXFCT images were compared to the experimental data.

A linear relationship between gold pXRF signal and gold concentration was observed in both experimental and MC simulation data (R^2>0.99). All Au vials were apparent in the experimental and simulated pXFCT images. The 3% Au vial was detectable in the experimental (CNR=5.8) and simulated (CNR=11.5) pXFCT image. The detectability limit (CNR=4) of the presented pXFCT experimental setup was 1.7 % Au. MC simulations revealed that objects surrounding the phantom were the primary source of x-ray background in pXRF spectra.

Proton-induced x-ray fluorescence CT imaging of 3-5% gold solutions in a small animal sized water phantom has been demonstrated for the first time by means of experiments and MC simulations. In our future work, we will use MC simulations to design an optimized pXFCT with a higher imaging sensitivity, in which x-ray scatter is decreased by means of detector collimation.

AUTHORS (LAST NAME, FIRST NAME): Bazalova-Carter, Magdalena[1, 3]; Ahmad, Moiz[1]; Matsuura, Taeko[4, 3]; Takao, Seishin[4, 3]; Matsuo, Yuto[4]; Fahrig, Rebecca[2]; Shirato, Hiroki[4, 3]; Umegaki, Kikuo[4, 3]; Xing, Lei[1, 3]

INSTITUTIONS (ALL):

1. Radiation Oncology, Stanford University, Stanford, CA, United States.
2. Radiology, Stanford University, Stanford, CA, United States.
3. Global Institution for Collaborative Research and Education (GI-CoRE), Hokkaido University, Sapporo, Japan.
4. Medical Physics, Hokkaido University Hospital, Sapporo, Japan.

a) schematics of experimental setup for pXFCT imaging

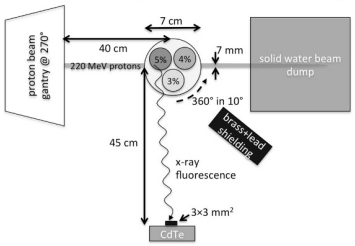

b) experimental setup

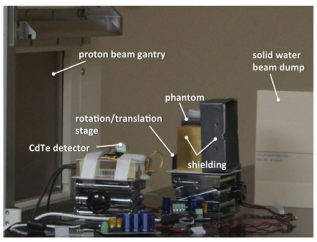

c) experimental pXFCT image

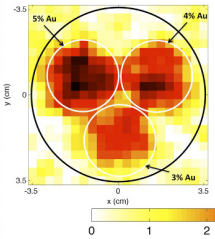

d) simulated pXFCT omage

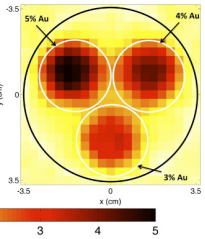

CONTROL ID: 2233440

TITLE: In vivo fluorescent imaging of tumor bombesin and transferrin receptor expression as early indicators of Sorafenib efficacy in small animal models

PRESENTER: Jeffrey Peterson

ABSTRACT BODY:

Abstract Body: Targeted cancer therapy aims to block key signaling pathways that are critical for tumor cell growth and survival. The blockage eventually results in cell death via apoptosis and eventual tumor growth suppression. This strategy has proven to be quite effective, and the FDA has approved several targeted therapeutics in the past decade. Encouraged by the success in clinical development, many academic and pharmaceutical researchers are in active pursuit of improved next generation targeted anti-cancer drugs. As a result, many new chemical and biological entities are emerging from initial screening of in vitro, in vitro and/or in silico selection processes. From the perspective of drug development, it poses a great challenge for the next stage of in vivo validation and demands a robust, accurate, and efficient method for assessment of these candidates in living animal models.

Cancer cells are known to have abnormally increased cellular metabolism, and in the early stages of effective drug treatment, cancer cells show decreased metabolism and proliferation. These events occur prior to overt signs of cell destruction, and often multiple days or weeks of treatment are required to see overt changes in tumor size. In some instances, bioluminescence imaging can be used to detect early changes in tumor viability in response to targeted therapy when using luciferase-expressing tumor cell lines, however, with many therapeutic treatments these early changes in tumor viability cannot be seen by bioluminescence imaging. To assess whether molecular imaging of biomarkers related to tumor metabolic state would be useful in early detection of treatment efficacy, the utility of non-invasive near infrared (NIR) fluorescence imaging, using NIR fluorescent imaging agents, was assessed. Highly metabolic cancer cells have accompanying elevations in receptors for bombesin and transferrin on their surface that can be readily imaged using targeted fluorescent agents (BombesinRSense 680 [BR680] and Transferrin-Vivo 750 [TV750]; PerkinElmer Inc.). In this report, we demonstrate the synergistic use of fluorescence (FLI) and bioluminescence imaging (BLI) to profile tumor metabolism and viability, respectively, in response to a targeted anti-cancer drug, sorafenib. Sorafenib is a clinically approved tyrosine kinase inhibitor that effectively blocks VEGFR, PDGFR and Raf signaling in cancer. At Sorafenib doses ranging from 40-150 mg/kg, there was a dose-dependent decrease in viability of HCT116-luc human colon xenograft tumors evident as early as 3 days at the higher doses but only after a week for low doses. Interestingly, even at a lower dose of 40 mg/kg, both BR680 and TV750 signal reduction can still be observed as early as 48 hours, a time/dose in which no significant reduction of tumor viability or size was observed. These results suggest the potential use of metabolic fluorescent imaging agents as sensitive and efficient and early biomarkers for pre-clinical assessment of targeted cancer drugs.

AUTHORS (LAST NAME, FIRST NAME): Peterson, Jeffrey D.[1]; Tseng, Jen-Chieh[1]

INSTITUTIONS (ALL):

1. PerkinElmer, Hopkinton, MA, United States.

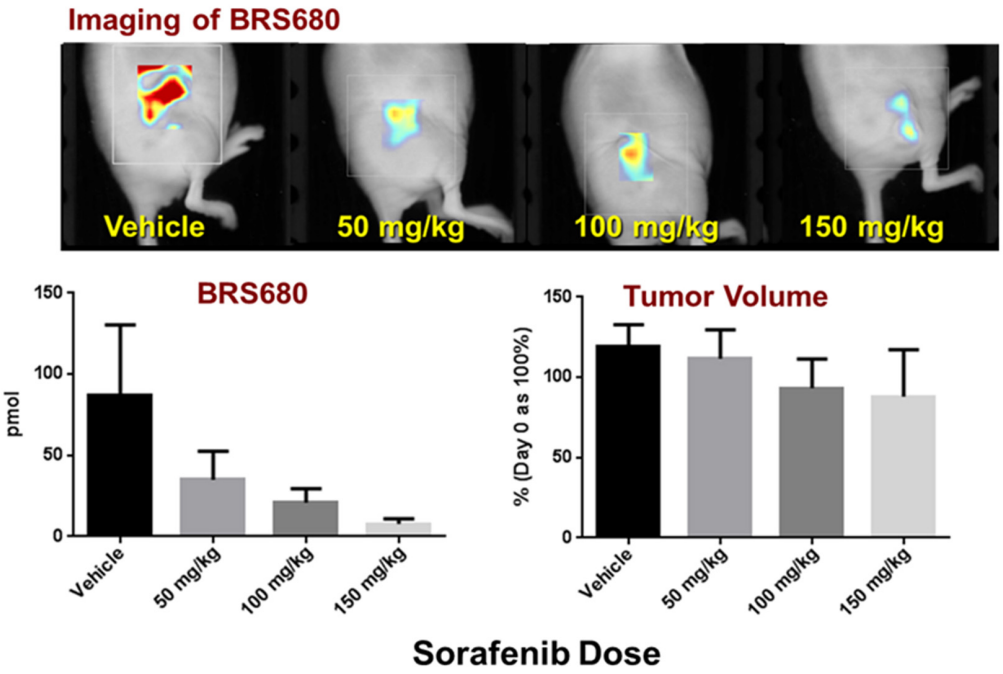

Nu/nu mice were injected SC with HCT-116-luc tumor cells and allowed to achieve a tumor volume of 150 mm3. Treatment with Sorafenib (at the indicated doses) was initiated, and mice were imaged 2 days later, after injection with BRS680 (2 nmol IV). Results show detection of changes in intratumoral bombesin receptor levels prior to overt changes in tumor size.

CONTROL ID: 2233452

TITLE: Identifying bacteria-specific positron emission tomography tracers using a three criteria *in silico* selection screen

PRESENTER: Allison Murawski

ABSTRACT BODY:

Abstract Body: Introduction. Identifying and localizing the source of disease is crucial for the appropriate treatment of patients ailing from a pathogenic bacterial infection. Current methods of biopsy and microbiologic culture are invasive, prone to contamination error, and may be inaccessible due to deep-seated infections. Rather, nuclear medicine techniques using positron emission tomography (PET) tracers, such as 2-[^{18}F]-fluorodeoxyglucose (^{18}F-FDG) and the newly discovered Enterobacteriaceae-specific 2-[^{18}F]-fluorodeoxysorbitol (^{18}F-FDS), could be useful for noninvasive localization and determination of the severity of bacterial infections. Additional PET tracers specific to certain bacterial classes would be useful in diagnosing the type of infection present in a patient, allowing for prompt and appropriate treatment.

Methods. Databases of compounds were screened in order to identify prokaryotic-specific candidates for PET tracers. Using information gathered from literature searches, compounds were scored based on three criteria: 1) prokaryotic-specific metabolism, 2) accumulation in prokaryotes, and 3) absence of known eukaryotic metabolism. For each criterion, a point was awarded to a compound if true or subtracted if false. Of the 750 compounds screened thus far, 38 scored +3, 22 scored +2, and 91 scored +1 (Figure 1a). Twenty were then selected and tested *in vitro* by incubating *Escherichia coli*, *Staphylococcus aureus*, and *Pseudomonas aeruginosa* with the radiolabeled compound. Radiation emitted by the bacteria, indicating uptake and accumulation of the compound, was measured after 120 minutes using a scintillation counter.

Results. Eight of the 20 compounds have been tested *in vitro* thus far. Four of the compounds tested showed positive uptake, validating our *in silico* screening with a 50% success rate. Compound JHU1 had a 66.7% uptake in *S. aureus* and an 18.5% uptake in *P. aeruginosa*, but did not accumulate in *E. coli*. JHU2, JHU3, and JHU4 were taken up by all three bacteria with JHU4 having the lowest percent uptake comparatively. *para*-Aminobenzoic acid (PABA), known to accumulate in all three bacteria, served as a positive control and heat-killed bacteria as a negative control (Figures 1b-e).

Discussion. This innovative screening technique, previously employed to discover ^{18}F-FDS, continues to accurately predict the uptake and accumulation of various compounds in prokaryotes. The ultimate goal will be to synthesize and develop a pipeline of radio-labeled bacteria-class specific PET imaging probes that would provide a platform to identify, localize, and monitor a wide range of pathogenic bacteria.

This work was funded by the NIH Director's NIH Director's Transformative Research Award R01-EB020539 (S.K.J.) and the NIH Director's New Innovator Award DP2-OD006492 (S.K.J.). E.A.W., A.A.O. and S.K.J. are inventors for an International patent PCT/US13/059897 filed by Johns Hopkins University.

AUTHORS (LAST NAME, FIRST NAME): Murawski, Allison M.[1]; Bambarger, Lauren E.[1]; Ordoñez, Alvaro A.[1]; Weinstein, Edward[1]; Jain, Sanjay K.[1]

INSTITUTIONS (ALL):

1. Johns Hopkins University, Baltimore, MD, United States.

(No Image Selected)

CONTROL ID: 2233463

TITLE: Breast Cancer Immuno-PET Imaging in Mice Using a Natural Nano-tracer

PRESENTER: Jun Tang

ABSTRACT BODY:

Abstract Body: Background: Immune cells, particularly myeloid-derived ones, play a pivotal role in the microenvironment of breast cancer. Because of the high diagnostic and therapeutic values of these immune cells, they have been extensively investigated, mostly invasively. Therefore, non-invasive breast cancer immune cell imaging methods can have great impact on diagnosis, disease management, and evaluation of therapy. Here, we describe the development of a high-density lipoprotein (HDL) -based positron emission tomography (PET) nano-tracer to non-invasively image immune cells in a breast cancer model.

Methods: Radiolabeled HDL-based nano-tracers were developed by using two different approaches that incorporated the long-lived positron-emitting nuclide ^{89}Zr into HDL. The nano-tracers are composed of the phospholipid DMPC and apolipoprotein A-I (apoA-I) in a 2.5 : 1 weight ratio. DFO chelators, conjugated to either phospholipids or apoA-I proteins, were used to complex with ^{89}Zr to generate ^{89}Zr-PL-HDL (phospholipid-labeled) or ^{89}Zr-AI-HDL (apoA-1-labeled). In vivo evaluation was carried out in an orthotropic mouse model of breast cancer and included pharmacokinetic analysis, biodistribution studies, and PET imaging. Ex vivo radioautography and histology analyses of tumor tissues were performed to assess regional distribution of the nano-tracers. Fluorescent analogs of the nano-tracers were used to determine cell-targeting specificity by using flow cytometry.

Results: ^{89}Zr-PL-HDL (phospholipid-labeled) was produced in 79 ± 13% (n = 6) radiochemical yield; ^{89}Zr-AI-HDL (apoA-I-labeled), 94 ± 6% (n = 6). Both nano-tracers had at least 99% radiochemical purity. Intravenous administration of both nano-tracers resulted in high tumor radioactivity accumulation (16.5 ± 2.8 %ID/g for ^{89}Zr-PL-HDL and 8.6 ± 1.3 %ID/g for ^{89}Zr-AI-HDL) at 24 hours post injection. Radioautography and histology analyses showed high co-localization of radioactivity with macrophage-rich areas in tumors. Flow cytometry revealed high accumulation of the nano-tracers in myeloid-derived immune cells (preferentially in tumor-associated macrophages and monocytes, followed by dendritic cells and neutrophils), whereas low uptake was observed in endothelial cells and tumor cells (n = 4).

Conclusions: Based on natural HDL particles, we have developed immune cell-targeting PET nano-tracers. In an orthotropic mouse model of breast cancer, we have demonstrated their specificity for myeloid-derived immune cells. Quantitative immune cell PET imaging with our ^{89}Zr-PET nano-tracers could be valuable for non-invasive diagnosis of breast cancer and evaluation of immunotherapy response.

AUTHORS (LAST NAME, FIRST NAME): Tang, Jun[2]; Perez Medina, Carlos[2]; Abdel-Atti, Dalya[5]; Fisher, Edward A.[7]; Merad, Miriam[8]; Fayad, Zahi A.[6]; Lewis, Jason S.[1]; Mulder, Willem J.[4]; Reiner, Thomas[3]

INSTITUTIONS (ALL):

1. MSKCC, New York, NY, United States.
2. Radiology, Memorial Sloan Kettering Cancer Center, New York City, NY, United States.
3. Radiology, Memorial Sloan Kettering Cancer Center, New York, NY, United States.
4. Radiology, Icahn School of Medicine at Mount Sinai, New York, NY, United States.
5. Radiology, Memorial Sloan Kettering Cancer Center, New York, NY, United States.
6. Radiology, Icahn School of Medicine at Mount Sinai, New York, NY, United States.
7. Cardiology, NYU School of Medicine, New York, NY, United States.
8. Tisch Cancer Institute, Icahn School of Medicine at Mount Sinai, New York, NY, United States.

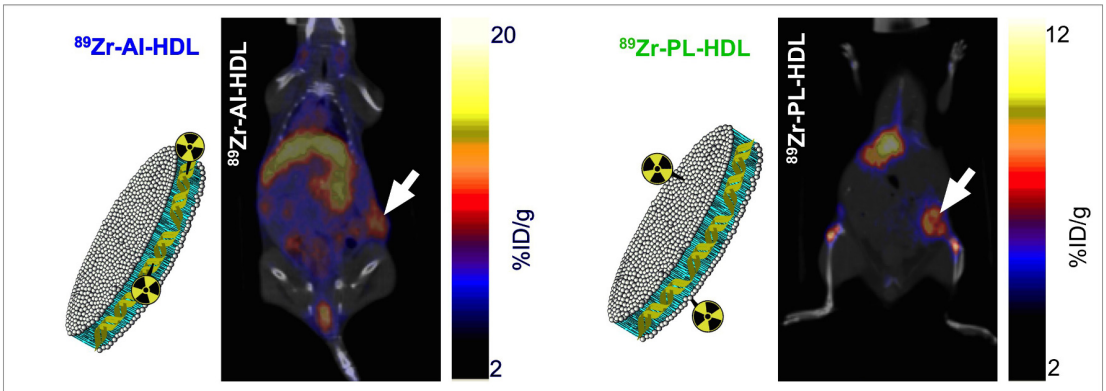

Schematic depiction of the nano-tracers and PET images of tumors in a mouse breast cancer model

CONTROL ID: 2244518

TITLE: High Throughput *in vitro* ^{18}F-FDG uptake assay in 2D and 3D format as an early screening tool for *in vivo* oncology studies

PRESENTER: Maria Borland

ABSTRACT BODY:

Abstract Body: FDG PET (2-[^{18}F]-2-Deoxy-D-Glucose Positron Emission Tomography) is increasingly part of the standard of care to monitor metabolic changes in response to cancer therapy that occur in advance of morphological changes. Though no consensus has been established in the literature on the relationship between glucose transporters and FDG uptake, earlier work suggests *in vitro* FDG uptake experiments could give insight into *in vivo* uptake. Previously, a 2D 96 well ^{18}F-FDG uptake assay was presented as a screening tool for basal FDG uptake during *in vivo* model development. While 2D cell culture formats are common, current research suggests such a format lacks physiologically relevant metabolism and nutrient gradients that may affect response to chemotherapeutic agents. In the present work, a 2D 96 well ^{18}F-FDG uptake assay has been adapted to 3D format to better reflect clinically relevant cancer models. As there are several levels of control in 18F-FDG uptake, kinase activity was also measured to investigate the relationship between FDG uptake and hexokinase activity. Future studies could involve using the 96 well 3D assay to screen other imaging agents and chemotherapeutic agents alone and in combination to evaluate their effect on glucose metabolism.

AUTHORS (LAST NAME, FIRST NAME): Borland, Maria[1]; Cvet, Donna[1]; Saylor, Melissa[1]; Robertson, Robbie[1]; Salem, Nicolas[1]; Yardibi, Ozlem N.[1]; Bradley, Daniel P.[1]

INSTITUTIONS (ALL):

1. Biomedical Imaging, Takeda Pharmaceuticals Inc., Cambridge, MA, United States.

(No Image Selected)

CONTROL ID: 2233491

TITLE: Positron Emission Tomography of Furin Activity in Living Subjects with a Smart-Activatable Self-assembling probe

PRESENTER: Niladri Chattopadhyay

ABSTRACT BODY:

Abstract Body: Purpose:

Furin is one of the central regulators of tumor progression and metastasis and is a proven drug target in vitro and in vivo. Consequently, the ability to non-invasively visualize furin activity in small animals is of high interest. Here, we report on the development of a ^{64}Cu PET small molecule probe that transforms into nanoparticles upon activation by furin. This self-assembly within tumor cells results in higher retention of the radiotracer in vivo as compared to an unactivatable control (which remains as a small molecule and is washed out from the tumor) in orthotopic breast cancer tumor bearing mice.

Methods:

The furin activatable probe was designed by employing a bioorthogonal intracellular condensation reaction that leads to formation of nanoparticles at the site of furin activity. The condensation reaction takes place in live cells between 2-cyano-6-aminobenzothiazole (CBT) and thiol and amino groups of a cysteine, which become accessible after proteolytic activity of furin. The probe carries the reactive groups and a reporter radiotracer (^{64}Cu) coupled to the furin substrate RVRR (where R is arginine and V is valine). The furin activated probe was validated by comparing to an unactivatable control probe consisting of a scrambled peptide (RRRV) which is not recognised by furin. The ability of the probe to be retained in tumors upon activation by furin was studied in two animal models representative of breast cancer (orthotopic MDA-MB-231 cells implanted in the mammary fat pad of SCID mice) and gliomas (U87-MG cells implanted subcutaneously in Nu/Nu nude mice). PET imaging results were correlated by ex-vivo autoradiography and assessment of furin activity in tumor sections.

Results:

The furin activated probe had significantly higher retention (2.4 ± 0.51 % ID/g) as compared to the control unactivatable probe (1.49 ± 0.19 % ID/g, p=0.016) in the orthotopic MDA-MB-231 breast cancer model in SCID mice starting at 60 mins post injection (p.i) until 24 h p.i. (Figures 1 and 2). However, in the subcutaneous (s.c.) U87MG glioma model in nude mice no significant difference in retention was observed between the Furin activatable probe (1.85 ± 0.55 % ID/g) or its unactivatable control (1.56 ± 0.78 % ID/g) over 24 h. Ex-vivo autoradiography of tumor sections demonstrated regions of hotspots for the activatable probe (Fig. 3C) in the orthotopic breast cancer model which was not observed in tumor sections obtained from animals s.c. bearing U87MG tumors (Fig. 3A). Further, immunofluorescence staining of the whole tumor sections for Furin activity using an anti-Furin monoclonal antibody (Abcam) demonstrated higher Furin activity in the orthotopic MDA-MB-231 breast cancer model (Fig 3D) as compared to the s.c U87MG tumors (Fig 3B) which could explain the differences in retention of the activatable probe versus control seen in these two animal models.

Conclusion: This study reports on the development and validation of the first activatable PET probe for visualizing furin activity in living subjects and has potential for highly specific early detection of cancer expressing furin.

AUTHORS (LAST NAME, FIRST NAME): Chattopadhyay, Niladri[5]; Lin, Jianguo[1]; Chen, Laura[5]; Palner, Mikael[3]; Shuhendler, Adam[4]; Rao, Jianghong[2]

INSTITUTIONS (ALL):

1. Jiangsu Institute of Nuclear Medicine, Wuxi, Jiangsu, China.
2. Stanford, Stanford, CA, United States.
3. Molecular Imaging Program at Stanford, Stanford, Stanford, CA, United States.
4. Radiology, Stanford University, Stanford, CA, United States.
5. School of Medicine, Stanford University, Stanford, CA, United States.

(No Image Selected)

CONTROL ID: 2233500

TITLE: A PEG-free Biomimetic Porphyrin Nanoplatform for Personalized Cancer Theranostics

PRESENTER: Juan Chen

ABSTRACT BODY:

Abstract Body: PEGylation is the most commonly adopted strategy to prolong nanoparticles' vascular circulation by mitigating the reticuloendothelial system uptake. However, there remain many concerns in regards to its immunogenicity, targeting efficiency, etc., which inspires pursuit of alternate, non-PEGylated systems. A novel PEG-free, porphyrin-based ultra-small nanostructure mimicking nature lipoproteins, termed PLP, is introduced here, which integrates multiple imaging and therapeutic functionalities, including positron emission tomography (PET) imaging, near-infrared (NIR) fluorescence imaging and photodynamic therapy (PDT). With an engineered lipoprotein-mimicking structure, PLP is highly stable in the blood circulation, resulting in favorable pharmacokinetics and biodistribution without the need of PEGylation. The prompt tumor intracellular trafficking of PLP allows for rapid nanostructure dissociation upon tumor accumulation to release monomeric porphyrins to generate efficiently fluorescence and photodynamic reactivity which are high-silenced in intact PLP, thus providing an activatable mechanism for low-background NIR fluorescence imaging and tumor-selective PDT. Its intrinsic copper-64 labeling feature allows for non-invasive PET imaging of PLP delivery and quantitative assessment of drug distribution. The general applicability of PLP for sensitive and accurate detection of primary and metastatic tumors, and for intraoperative imaging-guided surgery and tumor-selective PDT were demonstrated in various clinically-relevant animal models (Figure). Therefore, PLP offers a biomimetic theronostic nanoplatform for pre-treatment stratification using PET and NIR fluorescence imaging and for further customized cancer management via imaging-guided surgery, PDT, or/and potential chemotherapy.

AUTHORS (LAST NAME, FIRST NAME): Cui, Liyang[1, 2]; Chen, Juan[1, 2]; Zheng, Gang[1, 2]

INSTITUTIONS (ALL):

1. University Health Network, Toronto, ON, Canada.
2. Universtity of Toronto, Toronto, ON, Canada.

(No Image Selected)

CONTROL ID: 2233513

TITLE: ^{64}Cu labeled superparamagnetic iron oxide nanoparticles (SPIONs) as a PET/MR imaging agent.

PRESENTER: Renata Madru

ABSTRACT BODY:

Abstract Body: Hybrid PET/MRI systems are emerging as new clinical diagnostic tools including early detection and therapy planning of cancer [1]. In order to fully benefit from the strength of both modalities, dual-modality imaging agents are warranted. SPIONs have been introduced to detect liver and lymph-node metastases by MRI [2]. In addition they can act as a platform to carry other moieties for both targeting and therapy of cancer cells. Due to the low sensitivity, “negative contrast” and difficulties in quantifying SPIONs *in vivo*, here is reported on the development of a contrast agent based on ^{64}Cu-SPIONs.

The aim of this study was to demonstrate the feasibility of the agent in a mouse model using a hybrid preclinical system for simultaneous PET/MR imaging.

The one step ^{64}Cu labeling process of PEG coated SPIONs was optimized in HEPES pH 7 and ammonium acetate buffer solution at pH 5.5. ^{64}Cu-SPIONs were incubated in mice serum and ammonium acetate (pH 5.5) for 10 minutes and 24 h to determine the labeling efficiency and chemical stability. The ^{64}Cu-SPIONs were filtered using MACS columns, washed and eluted with ammonium acetate.

Six mice were anesthetized and subcutaneously injected in the right hind paw with ^{64}Cu-SPIONs (1.5-6 MBq, ~0.01 mL, ~0.1 mg Fe). The animals were imaged with a PET/MR system comprised of a Bruker Biospin 9.4T MRI scanner, and a custom-made, integrated MRI-compatible PET scanner with a custom built RF transceiver coil [3]. Both dynamic imaging technique (1-3 h) and short scans at 3, 6 and 24 h post-injection (p.i.) were performed using 3D FLASH and 2D RARE imaging sequences for MRI. The PET images were reconstructed with 3D maximum likelihood expectation maximization (ML-EM) iterative algorithm and coregistered with MRI using MATLAB and PMOD software. All animals were dissected and lymph nodes, liver, spleen, kidneys, intestine and injection site were dissected, weighed and assayed for radioactivity.

The labeling efficiency using ammonium acetate was found to be superior (97 %) compared to HEPES (88 %) after 10 minutes incubation time at room temperature. The in vitro stability of the agent was > 95 % in both buffer and mouse serum for 24 h. The accumulation of the agent in lymph nodes was highly evident in PET, MRI and fused images as soon as 30 minutes p.i. shown in the left and center image in **Figure 1**. ^{64}Cu-SPIONs introduce field inhomogeneity in the magnetic field; consequently there is a signal loss in MRI images (Figure 1, right), which is dose dependent. However, the PET imaging can compensate with highly sensitive images enabling to follow the tracer in almost real time. After 24 h p.i. the ^{64}Cu-SPIONs were still found to be retained in lymph nodes (4.8±1.73%IA) compared to spleen (1.3±0.3%IA), kidney (6.3±0.96%IA), liver (11±1.88%IA), small intestine (27±2.86%IA), large intestine (23±1.92%IA) and injection site (17.52±1.92%IA).

In this work, is presented a fast method to label SPIONs with ^{64}Cu at room temperature and demonstrated its feasibility for PET/MR imaging. Since ^{64}Cu has been used clinically and previous studies show low toxicity of SPIONs, this agent has the potential to be used in clinical applications.

AUTHORS (LAST NAME, FIRST NAME): Madru, Renata[1]; Budassi, Michael[2]; Benveniste, Helene[3]; Smith, David S.[4]; Schlyer, David J.[5]; Lee, Hedok[5]; Vaska, Paul[5, 6]; Knutsson, Linda[1]; Strand, Sven-Erik[7]

INSTITUTIONS (ALL):

1. Medical Radiation Physics Department, Lund University, Lund, Sweden.
2. Biomedical Engineering, Stony Brook University, Stony Brook, New York, NY, United States.
3. Anesthesiology in Stony Brook, Stony Brook University, Stony Brook, New York, NY, United States.
4. Physics Department, Brookhaven National Laboratory, Upton, New York, NY, United States.
5. Biosciences Department, Brookhaven National Laboratory, Upton, New York, NY, United States.
6. Stony Brook School of Medicine, Stony Brook, New York, NY, United States.
7. Medical Radiation Physics Department, Lund University, Lund, Sweden.

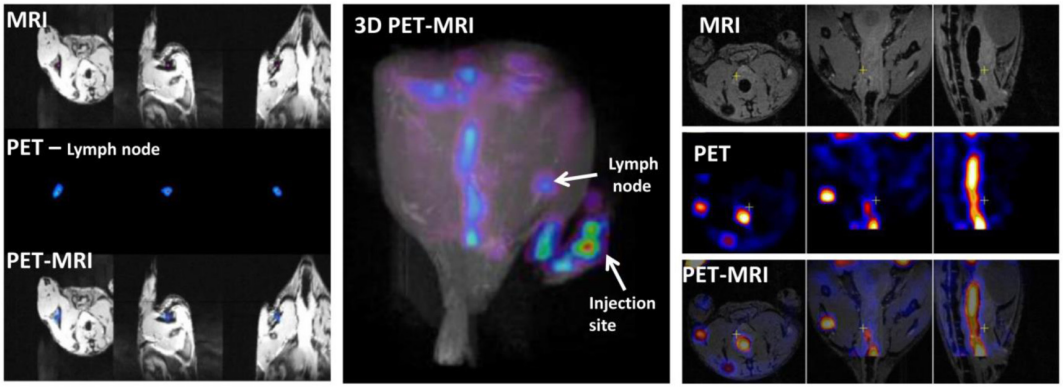

Figure 1. Example PET, MRI and fused PET-MRI images of mice injected with ^{64}Cu-SPIONs in the right hind paw. The agent rapidly accumulates in lymph nodes (left image, 30 min post injection). The signal loss in tissue containing ^{64}Cu-SPIONs in MRI is dose dependent (right image, 24 h post injection).

CONTROL ID: 2233531

TITLE: Engineering of Cephalosporin for Rapid Point-of-Care Detection of Mycobacterium Tuberculosis and Carbapenemase-Expressing Pathogen

PRESENTER: Yunfeng Cheng

ABSTRACT BODY:

Abstract Body: Antibiotic resistance, particularly, the resistance against broad-spectrum β-lactam antibiotics is emerging worldwide at an alarming rate due to the misuse and overuse of antibiotics. Among them, 1) Mycobacterium Tuberculosis (Mtb), infecting around one-third of the world's population and claiming the lives of 1.5 million each year, and 2) carbapenem-resistant pahtogen (CRE), which is resistant to "last reort" antibiotic cabapenem have become the major public health concerns. While with high mobidity and mortality, current detection methods are limited and are either time-consuming or require expensive instrument, which are not suitable for point-of-care diagnosis. Herein we present the design, synthesis and evaluation of two series of fluorogenic probes based on cephalosporin structure engineering, 1) One showed high specificity for BlaC, a biomarker expressed by Mtb, to enable rapid Mtb detection. The optimal fluorogenic probe CDG-3, demonstrating over 120,000-fold selectivity for BlaC over TEM-1 Bla, the most common β-lactamase. CDG-3 can detect 10 colony-forming units of BCG in human sputum in the presence of high levels of contaminating β-lactamases expressed by other prevalent clinical bacterial strains. In a trial with 50 clinical samples, CDG-3 detected tuberculosis clinical samples with 90% sensitivity and 73% specificity relative to Mtb culture within one hour; 2) another series of probes showed high specificity detection for carbapenemases including metallo-β-lactamases-active bacterial pathogens. Collectively, we, for the very first time, have demonstrated their great potential as a low-cost triage test at the point-of-care in resource-limited areas, where Mtb/CRE prevalence are the highest.

AUTHORS (LAST NAME, FIRST NAME): Cheng, Yunfeng[1]

INSTITUTIONS (ALL):

1. Radiology, Stanford, Stanford, CA, United States.

(No Image Selected)

CONTROL ID: 2233551

TITLE: Developing a Copper responsive MRI Contrast Agent

PRESENTER: Namini Paranawithana

ABSTRACT BODY:

Abstract Body: Copper is the third most abundant trace metal in the body. Normally bound to important biomolecules, copper is an essential redox cofactor in several enzymatic reactions. Disruption of copper homeostasis is associated with a number of diseases including Alzheimer's, Parkinson's, Menkes, and Wilson's disease.[1] Local concentrations of copper can vary from a few micromolar to several millimolar in these diseases.[2] Early versions of copper responsive MRI agents demonstrated that Zn^{2+} interferes with the Cu^{2+} response, limiting its use in MR diagnostic applications.[3] Here, we report the synthesis and MR properties of a new copper responsive contrast agent for magnetic resonance imaging (MRI). This MR sensor consists of a DO3A gadolinium-based contrast agent where a bis(benzoic-acid)methyl)amine copper-selective recognition motif (L_1), was introduced. The sensor shows high selectivity to copper ions. Also exhibits high relaxivity (r_1) with a 42% increase in relaxivity upon binding to 1 equivalent of Cu^{2+}. Interestingly, only when fully bound to Cu^{2+}, the sensor presents a 610% increase in r_1 (~35$mM^{-1}.s^{-1}$) in the presence of physiologic concentrations of human serum albumin (HSA), as uniquely reported for high affinity zinc sensors (Figure 1).[4] These results demonstrate that it is possible to design a functional MRI contrast agent responsive and selective to copper at low concentrations, paving the way for the possible translation to pre-clinical imaging.

References

(1) Gaggelli, E.; Kozlowski, H.; Valensin, D.; Valensin, G. *Chem. Rev.* **2006**, *106*, 1995.

(2) Que, E. L.; Gianolio, E.; Baker, S. L.; Wong, A. P.; Aime, S.; Chang, C. J. *J. Am. Chem. Soc.* **2009**, *131*, 8527.

(3) Que, E. L.; Chang, C. J. *J. Am. Chem. Soc.* **2006**, *128*, 15942.

(4) Esqueda, A. C.; López, J. A.; Andreu-de-Riquer, G.; Alvarado-Monzón, J. C.; Ratnakar, J.; Lubag, A. J. M.; Sherry, A. D.; De León- Rodŕiguez, L. M. *J. Am. Chem. Soc.* **2009**, *131*, 11387.

AUTHORS (LAST NAME, FIRST NAME): Paranawithana, Namini N.[1]; Martins, Andre F.[1]; Zhao, Piyu[1]; Sherry, A. D.[1, 2]

INSTITUTIONS (ALL):

1. Chemistry, UT Dallas, Richardson, TX, United States.

2. University of Texas Southwestern Medical Center, Dallas, TX, United States.

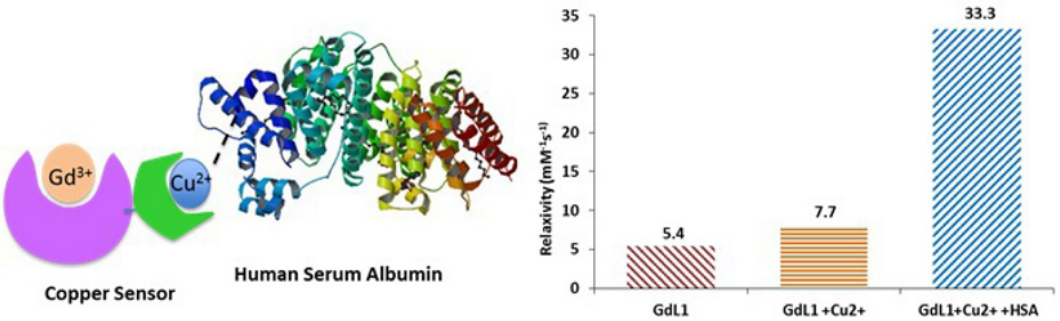

Figure 1. Longitudinal relaxivity (r_1) of the copper sensor in the presence of Cu^{2+} and Human Serum Albumin (HSA) at 0.6mM, 310K, pH=7.4 in TRIS buffer.

CONTROL ID: 2234412

TITLE: Radiation Effects of Non-uniform Dose Distribution to In-vitro Medulloblastoma on Bioluminescent Imaging

PRESENTER: Ji-Yeon Park

ABSTRACT BODY:

Abstract Body: To monitor radiation responses to non-uniform dose distributions optimized by intensity-modulated dose painting technique, the luciferase positive medulloblastoma cell line Daoy was irradiated in medical radiation treatment unit and cellular responses were evaluated using bioluminescent images.

Cultured cells were inserted into a dedicated acrylic phantom for obtaining the sophisticated calculation of predicted dose distributions and ensuring the accuracy of dose delivery. Planned doses using megavoltage photon beams were irradiated to the phantom including the cells. The irradiated cells were monitored using the bioluminescent images. The sub-volumes showing different cell responses were delineated and used to create optimized intensity-modulated fluences. After non-uniform dose distributions verified using EBT3 films were delivered, cell responses to dose painting technique were monitored on bioluminescent imaging. Irradiated cell responses were verified on a voxel-by-voxel basis using image registration of the bioluminescent image and dose distribution extracted from the corresponding coronal section where the cells were placed. Effects of non-uniform dose distribution for effective killing of cancer cells were compared with cancer responses to uniform dose distribution created from the initial treatment plan.

Dose painting technique provided non-uniform dose delivery with acceptable accuracy less than 5% and registered images facilitated monitoring of treatment responses of cancer cells. Cells irradiated to non-uniform dose distributions showed decreased cancer cell survival and viability than those irradiated to uniform dose distributions. Cellular responses to non-unniform dose distribution would be considered for dose re-optimization and in-vivo multi-modal molecular imaging for monitoring radiation effects can be integrated into the radiotherapy planning.

AUTHORS (LAST NAME, FIRST NAME): Park, Ji-Yeon[1, 3]; Lee, Do-Wan[3, 4]; Woo, Dong-Cheol[4]; Park, Hae-Jin[6]; Suh, Tae Suk[5, 3]; Contag, Christopher H.[2]

INSTITUTIONS (ALL):

1. Stanford University, Stanford, CA, United States.
2. Pediatrics, Stanford Universtiy, Stanford, CA, United States.
3. Research Institute of Biomedical Engineering, The Catholic University of Korea, Seoul, Korea (the Republic of).
4. ASAN Institute for Life Sciences, Asan Medical Center, Seoul, Korea (the Republic of).
5. Biomedical Engineering, The Catholic University of Korea, Seoul, Korea (the Republic of).
6. Radiation Oncology, Ajou University School of Medicine, Suwon, Korea (the Republic of).

(No Image Selected)

CONTROL ID: 2233572

TITLE: Quantitative In Vivo pO_2 Images with Electron Paramagnetic Resonance and Cancer

PRESENTER: Howard Halpern

ABSTRACT BODY:

Abstract Body: Images of low molecular oxygenation (pO_2), hypoxia, provide crucial guides to resistant tumor portions enhancing the delivery and monitoring of cancer therapy. Electron Paramagnetic Resonance oxygen images (**EPR O_2 images**) provides high spatial resolution, oxygen resolution, time resolution, and an absolute physically based (spin exchange) image of O_2 in the tissues and tumors of living animals. The images are created using novel pulse EPR in the presence of rapidly changing magnetic field gradients physically based for tomographic images derived from the spin lattice relaxation rates (R_1) of nontoxic spin probes that sample and report the tissue fluid pO_2. R_1 inversion recovery pulse sequences free images from confounding variations and, to within 1-2 torr uncertainties produce a near absolute pO_2 image (Fig.1).[1] Hypoxic fractions of image voxels less than 10 torr, HF10 predict radiation sensitivity and resistance in FSa tumors in the legs of C3H mice and provide the location within a tumor of the regions of resistant hypoxic tumor regions to which to guide additional radiation dose (Fig.2).[2,3] We have accelerated acquisition oxygen images to 1 minute intervals using navigator images. BACH1, a downstream kinase effector of RKIP, Ras Kinase Inhibitor Protein, is increased in triple negative breast cancer (TNBC) and correlates with more invasive, metastatic human cancer. EPR pO_2 images in BACH1 producing TNBC, compared with siRNA BACH1 knock tumors down are more hypoxic. (Fig. 3) This shows interaction between signaling and physiologic phenotype.

Fig. 1 Relaxation rate (R) depends on pO_2 and spin probe concentration (C). R_1 slope vs C is 1/5 that of R_2. ◊ Covers physiologic concentrations.

Fig. 2 Tumor control depends on O_2 image 10 torr hypoxic fraction HF10

Fig. 3 pO2 is less for BACH1 than BACH1 knock down tumors

AUTHORS (LAST NAME, FIRST NAME): Halpern, Howard J.[1]; Epel, Boris[1]; Krzykawska-Serda, Martyna[1]; Elas, Martyna[2]; Liang, Zhi-Pei[3]; Christodoulou, Anthony G.[3]; Tormyshev, Victor M.[4]; Rosner, Marsha[5]; Frankenberger, Casey A.[5]

INSTITUTIONS (ALL):

1. Radiation and Cellular Oncology, University of Chicago, Chicago, IL, United States.
2. Biophysics, Jagiellonian University, Krakow, Poland.
3. Electrical and Computer Engineering, University of Illinois, Urbana-Champagne, IL, United States.
4. Novosibirsk Institute of Organic Chemistry, Novosibirsk, Siberia, Russian Federation.
5. Ben May Dept. of Cancer Research, University of Chicago, Chicago, IL, United States.

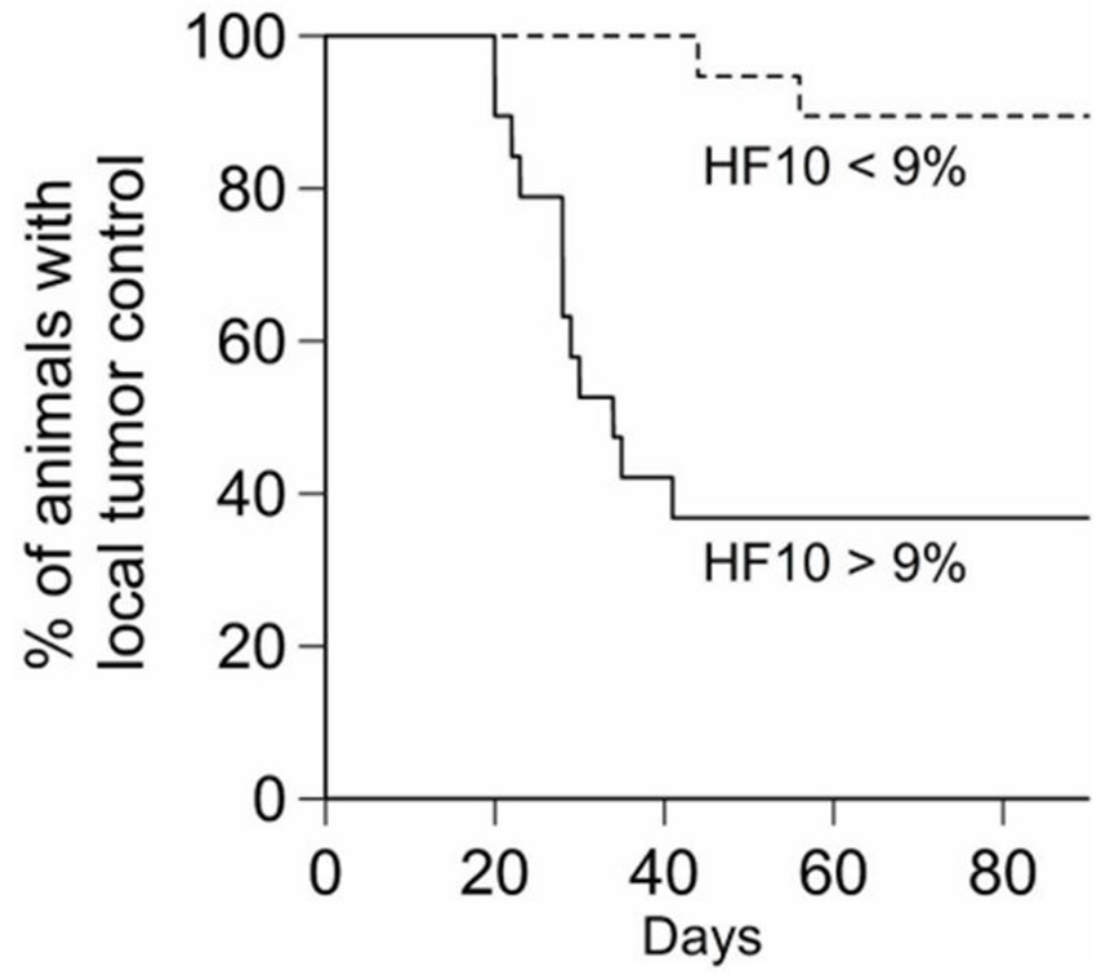
100
80
60
40
20
0
% of animals with local tumor control
HF10 < 9%
HF10 > 9%
0
20
40
60
80
Days

CONTROL ID: 2233567

TITLE: Intravital multi photon microscopy of intraarterial targeting of genetically engineered Glial Restricted Progenitors (GRPs) to stroke lesion.

PRESENTER: Anna Jablonska

ABSTRACT BODY:

Abstract Body: Stroke is one of the leading causes of death and severe disability, and, since thrombolysis - the only effective treatment is available to just a small fraction of patients, majority of stroke survivors are still without effective therapy. Stem cell transplantation is thought to be capable restoring brain function lost due to stroke. Restoration of damaged myelin in stroke is an attractive therapeutic target that in contrast to replacement of lost neurons is much more attainable. We have shown previously that Glial Restricted Progenitors (GRPs) transplanted into the brain of neonatal demyelinated mice restore myelin and significantly extend lifespan. Successful use of these cells in adult recipients is contingent upon access to efficient and safe method of cell delivery. With local, intraparenchymal injection non-suitable for targeting large lesions such as ischemic stroke we postulate that intraarterial route is most suitable for targeting cells to the entire stroke lesion. Our earlier studies with MRI-guided intraarterial injection of naïve GRPs showed poor homing to brain vasculature. The goal of this study was to improve homing of primary GRPs to stroke lesion via transient overexpression of adhesion molecule VLA4. The cells were co-transfected with DNA plasmids each encoding subunit of VLA4 (alpha4 and beta1). Transfected cells were cultured for 72 hours and used for in vitro functional assays and animal experiments. Prior to transplantation were labeled with cell CMFDA Green tracker and suspended in PBS at $2x10^5$cells/ 200ul. Recipient mice were subjected to 60 min MCAO filament occlusion and following placement of a cranial window over the cortex they were stabilized in the two photon microscope for imaging. To visualize brain vasculature mice were injected with 100ul of TexasRed conjugated dextran70kDa.

Transfection with two subunits of VLA4 resulted in successful expression in over 60% of the GRPs. In vitro functional assays with VCAM1-coated microfluidic devices showed slowed rolling of $VLA4^+$GRPs compared to naïve cells, indicating functionality of the transgene. Additionally, adhesion experiment with microfluidic devices coated with brain endothelial cells revealed higher number of $VLA4^+$GRPs binding to endothelial cells activated with TNFα. Intravital imaging with multi-photon microscopy show that $VLA4^+$GRPs transplanted intraarterially bind to blood vessels walls in the greater number than naïve cells. With longitudinal intravital imaging we have shown that the engineered GRPs extravasate to the brain parenchyma. These observations from in vivo imaging were confirmed by histopathology for brain tissue collected 3h after transplantation, and, quantitative analysis demonstrated significantly more VLA4+ GRPs present in the brains compared to naïve cells.

In summary, we were able to demonstrate that induction of VLA4 expression in GRPs increase their adhesion to blood vessels following stroke with the cells efficient extravasating to brain parenchyma.

AUTHORS (LAST NAME, FIRST NAME): Jablonska, Anna[1, 2]; Shea, Daniel J.[3]; Bulte, Jeff W.[1, 2]; Janowski, Miroslaw[1, 4]; Konstantopoulos, Konstantinos[3]; Walczak, Piotr[1, 5]

INSTITUTIONS (ALL):

1. Radiology and Radiological Science, Johns Hopkins University School of Medicine, Baltimore, MD, United States.
2. Cellular Imaging Section, Institute for Cell Engineering, Johns Hopkins University School of Medicine, Baltimore, MD, United States.
3. Department of Chemical and Biomolecular Engineering, Johns Hopkins University, Baltimore, MD, United States.
4. NeuroRepair, Mossakowski Medical Research Centre, Polish Academy of Sciences, Warsaw, Poland.
5. Pathophysiology, Faculty of Medical Sciences, University of Warmia and Mazury, Olsztyn, Poland.

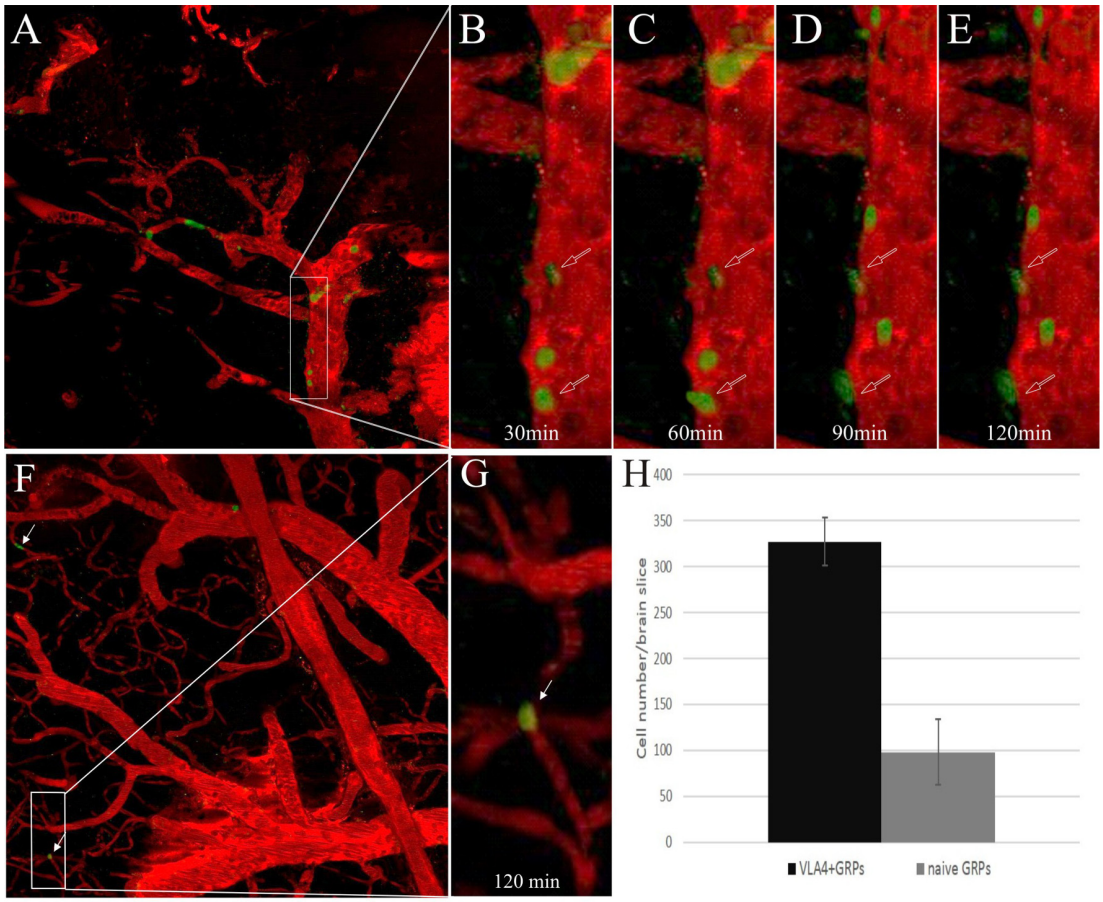

Fig.1. Intravital imaging of adhesion and extravasation of VLA4 transfected (A-E) and naïve (F-G) GRPs (green) transplanted intraarterially into mouse brain 24h after stroke. VLA4+GRPs adhere to blood vessels walls in the greater number in comparison to naïve GRPs, what was confirmed by *ex vivo* analysis of brains collected 3h after cell transplantation (H). Extravasation of VLA4+GRPs cells from blood vessels into brain parenchyma was visible in longitudinal intravital imaging (A-E).

CONTROL ID: 2233575

TITLE: Fluorescence-guided Resection of Glioma using Fluorescently-labeled Antibodies

PRESENTER: Jason Warram

ABSTRACT BODY:

Abstract Body: The standard treatment for Glioblastoma Multiforme (GBM) remains maximal safe surgical resection. Here, we evaluated the ability of a systemically administered antibody-dye probe conjugate (cetuximab-IRDye800CW) to provide sufficient fluorescent contrast for surgical resection of disease in both subcutaneous and orthotopic animal models of GBM (figure 1). Multiple luciferase positive GBM cell lines (D-54MG, U-87MG, U-251MG; n=5) were implanted in mouse flank and tumors fluorescently imaged daily using a closed-field NIR system after cetuximab-IRDye800CW (100ug/mouse) systemic administration. Orthotopic models were also generated (n=5) and tumor resection was performed under white-light and fluorescence guidance using an FDA-approved open-field NIR imaging system. Residual tumor was localized using luciferase imaging. Immunohistochemistry was performed to characterize tumor fluorescence, epidermal growth factor receptor (EGFR) expression, and vessel density. Daily imaging of tumors revealed an average tumor-to-background (TBR) of 4.5 for U-87MG, 4.1 for D-54MG, and 3.7 for U-251MG. Fluorescence intensity within the tumors peaked on day-1 post cetuximab-IRDye800CW administration, however the TBR increased over time in two of the three cell lines. For the orthotopic model, TBR on surgery day ranged from 19 to 23 during wide-field, intraoperative imaging. Surgical resection under white-light on day 3 post cetuximab-IRDye 800CW resulted in an average 41% reduction in luciferase signal while fluorescence-guided resection using wide-field NIR imaging resulted in a significantly (P=0.001) greater reduction in luciferase signal (87%). Reduction of luciferase signal was found to correlate (R^2=0.99) with reduction in fluorescence intensity. Fluorescence intensity was found to correlate (P<0.05) with EGFR expression in D-54MG and U-251MG tumor types but not U-87MG. However, tumor fluorescence was found to correlate with vessel density for the U-87MG tumors. Here we show systemic administration of cetuximab-IRDye800CW in combination with wide-field NIR imaging provided robust and specific fluorescence contrast for successful localization of disease in subcutaneous and orthotopic animal models of GBM.

AUTHORS (LAST NAME, FIRST NAME): Warram, Jason M.[1]; de Boer, Esther[1]; Moore, Lindsay S.[1]; Hartman, Yolanda [1]; Kovar, Joy L.[2]; Markert, James M.[4]; Gillespie, G. Yancey[4]; Rosenthal, Eben[3]

INSTITUTIONS (ALL):

1. Surgery, University of Alabama at Birmingham, Birmingham, AL, United States.
2. Molecular Biology R&D, LI-COR Biosciences, Lincoln, NE, United States.
3. Otolaryngology, Stanford University, Stanford, AL, United States.
4. Neurosurgery, University of Alabama at Birmingham, Birmingham, AL, United States.

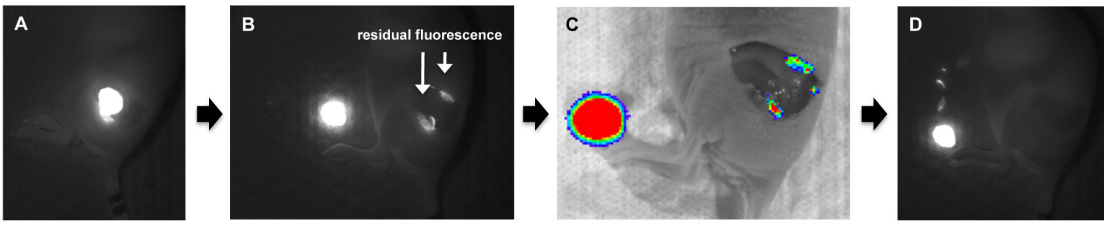

Figure 1: Cetuximab-IRdye800 in a subcutaneous xenograft model of malignant glioma. Fluorescent images of representative D54 tumor resection shows (A) skin removed, (B) tumor resection revealing positive fluorescence margins, (C) residual tumor confirmed using bioluminescence imaging, and (D) complete resection of positive margins as determined by fluorescent imaging.

CONTROL ID: 2234103

TITLE: Fluorescence-guided Surgical Navigation in Patients with Head and Neck Cancer

PRESENTER: Jason Warram

ABSTRACT BODY:

Abstract Body: The primary treatment for many solid cancers remains surgical resection, however surgical oncologists remain dependent on subtle tissue changes to identify cancer in real-time. Fluorescence-guided surgery is emerging as a viable intraoperative technique to guide surgeons in the complete resection of cancer. Based on extensive preclinical data establishing the feasibility of antibody-based imaging, we hypothesize that fluorescently labeled anti-epidermal growth factor receptor (EGFR) antibody (cetuximab) would be safe and enable intraoperative detection of squamous cell cancer in humans. We selected IRDye800 as the fluorescence reporter due to previous rodent studies demonstrated a lack of toxicity. Additionally, the dye is manufactured under conditions suitable for human use and preclinical studies in non-human primates comparing cetuximab-IRDye800 to cetuximab alone showed no clinically significant toxicities [Mol Imaging Biol. 2015 17:49-57]. A first-in-human dose escalation study of systemically administered cetuximab-IRDye800 (dose of 2.5mg/m^2, 25mg/m^2, 62.5mg/m^2) was performed in patients (n=12) undergoing surgical resection of squamous cell carcinoma arising in the head and neck. Fluorescence imaging was performed daily post cetuximab-IRDye800 infusion and in the operating room using a commercially available open-field near-infrared (NIR) imaging system. Resected specimens were imaged in pathology using a closed-field NIR imaging system prior to histological processing. Tissue fluorescence was correlated with histology. In patients receiving 25mg/m^2 and 62.5mg/m^2 cetuximab-IRDye800 doses, quantitative analysis of wide-field imaging revealed significantly (P<0.05) greater fluorescence detected in the tumor compared to surrounding normal tissue at each imaging time point. Intraoperative imaging (figure 1) could successfully differentiate tumor from normal tissue with an average tumor-to-background ratio of 4.8 for the 25mg/m^2 dose and 5.2 for the 62.5mg/m^2 dose. The fold-increase in tumor fluorescence over patient-matched muscle fluorescence for histologically confirmed tumor tissue (5.2, 11.2, 18.5) was significantly (P<0.02) greater than adjacent normal tissue (1.2, 2.2, 9.5) for the 2.5mg/m^2, 25mg/m^2, 62.5mg/m^2 doses, respectively. Additional analysis demonstrated that as little as 2.8mg of tumor tissue was found to contain 11–fold greater fluorescence than weight-matched muscle. Immunohistochemistry revealed a strong correlation (P<0.001) of tissue fluorescence with EGFR expression and tumor density (P<0.05) in all doses. There were no grade-2 or higher adverse events attributable to cetuximab-IRDye800 and four possibly related grade-1 adverse reactions occurred in the first cohort, seven in the second cohort, and two in the third cohort. Most common adverse events included tumor-site symptoms (n=4) and cardiovascular-related findings (n=4). Cetuximab-IRDye800 was well tolerated as a diagnostic agent and could detect microscopic fragments of tumor at a fraction of the therapeutic dose. Repurposing therapeutic antibodies for intraoperative navigation may be used to improve outcomes in surgical oncology.

AUTHORS (LAST NAME, FIRST NAME): Warram, Jason M.[2]; de Boer, Esther[2]; Moore, Lindsay S.[2]; Schmalbach, Cecelia E.[2]; Morlandt, Anthony[3]; Carroll, William R.[2]; Richman, Joshua S.[2]; Clemons, Lisa K.[2]; Zinn, Kurt R.[4]; Rosenthal, Eben[1]

INSTITUTIONS (ALL):

1. Otolaryngology, Stanford University, Stanford, AL, United States.
2. Surgery, University of Alabama at Birmingham, Birmingham, AL, United States.
3. Oral & Maxillofacial Surgery, University of Alabama at Birmingham, Birmingham, AL, United States.
4. Radiology, University of Alabama at Birmingham, Birmingham , AL, United States.

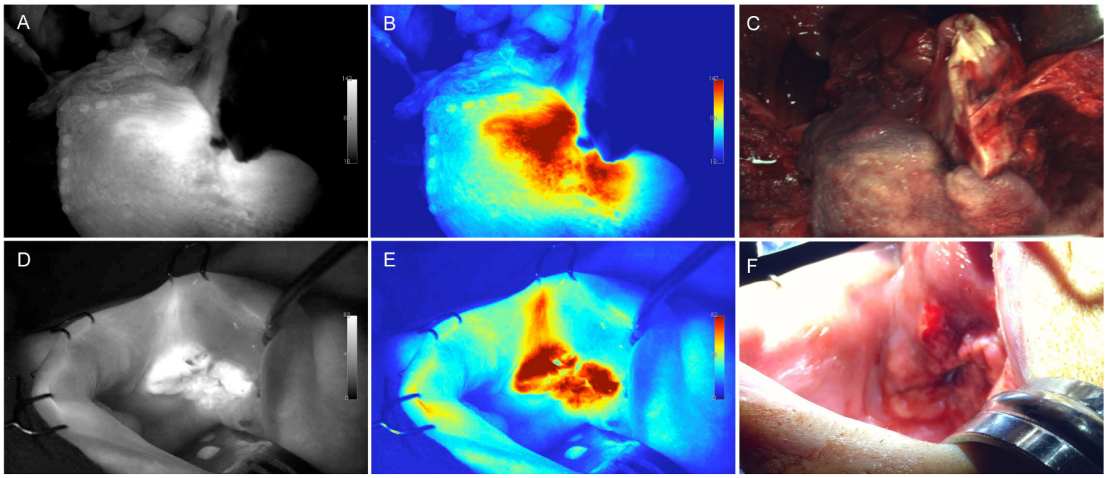

Figure 1. Intraoperative fluorescence imaging. Shown are **(A,D)** grayscale fluorescence, **(B,E)** color map fluorescence, and **(C,F)** corresponding brightfield acquired using the wide-field device prior to primary tumor resection from patients in the 25mg/m^2 dose group undergoing a total glossectomy **(A-C)** and a wide local excision of the buccal mucosa **(D-F)**.

CONTROL ID: 2233599

TITLE: Normal Tissue Irradiation Promotes Tumor and Immune Cell Infiltration

PRESENTER: Marjan Rafat

ABSTRACT BODY:

Abstract Body: Innovation/Impact: Breast cancer recurrence rates remain high for triple-negative cases despite aggressive surgical, radiological, and chemotherapeutic intervention [1]. Recent studies suggest that recurrence may be facilitated by circulating tumor cell re-seeding of primary tumors [2]. The role of the tumor microenvironment in recurrence, however, is not well established.

Hypothesis/Objectives: Radiation has been shown to promote tumor cell migration in a preclinical breast cancer model [3]. We hypothesize that the irradiated tumor microenvironment influences tumor and immune cell behavior. In this study, we characterize the effects of normal tissue irradiation on tumor and immune cell invasion and migration to evaluate how tumor-stromal interactions modulate recurrence after therapy. This work represents the first step toward elucidating the contribution of stromal tissues in tumor and immune cell recruitment following radiotherapy.

Materials/Methods: Mouse embryonic fibroblasts (MEF) were irradiated to 20 Gy. Supernatant was collected after 2 or 7 d incubation and used as a chemoattractant in an *in vitro* transwell assay to investigate 4T1 murine or MDA-MB-231 human mammary carcinoma cell invasion. An orthotopic breast cancer model was also used to evaluate the effect of radiation on tumor cell migration to normal tissues. Luciferase-labeled 4T1 cells were used for *in vivo* and *ex* vivo bioluminescence imaging (BLI). Nude mice were inoculated with 4T1 cells in the mammary fat pad (MFP) and injected with PBS in the contralateral MFP. The contralateral normal MFP was irradiated to a dose of 20 Gy, and cell migration was monitored with BLI 10 days after irradiation. Immunohistochemistry (IHC) was performed to stain irradiated and control tissues for F4/80 to determine the extent of macrophage infiltration. Flow cytometry was also performed on dissociated irradiated and control tissues to characterize immune cells. Of particular interest were CD11b+F4/80+ and CD11b+GR1+ cell populations representing macrophages and myeloid-derived suppressor cells (MDSCs), respectively.

Results: Tumor cell migration to normal tissues both *in vitro* and *in vivo* was stimulated by radiation. 4T1 and MDA-MB-231 cells exhibited an increase in invasion ($p<0.05$) *in vitro* when exposed to irradiated MEF media. *Ex vivo* BLI analysis demonstrated that normal tissue irradiation attracted tumor cells to the MFP and surrounding tissues, including the peritoneum and muscle ($p<0.01$). IHC staining revealed an increase in macrophage infiltration in irradiated tissue sections. Flow cytometric analysis confirmed enhanced macrophage and MDSC recruitment in irradiated tissues.

Conclusions: Our study establishes that normal tissue radiation response may play a role in modulating tumor cell migration after radiation. The radiation-induced increase in macrophage and MDSC infiltration indicates that the immune system may contribute to tumor cell migration. These results suggest that the tumor stroma may facilitate tumor cell invasion and tumor regrowth following radiotherapy.

References

[1] Kaplan HG et al. *The Breast J*. 2009. [2] Kim MY et al. *Cell*. 2009. [3] Vilalta M et al. *Cell Rep*. 2014.

AUTHORS (LAST NAME, FIRST NAME): Rafat, Marjan[1]; Vilalta, Marta[1]; Aguilera, Todd A.[1]; Giaccia, Amato[1]; Graves, Edward E.[1]

INSTITUTIONS (ALL):

1. Radiation Oncology, Stanford University, Stanford, CA, United States.

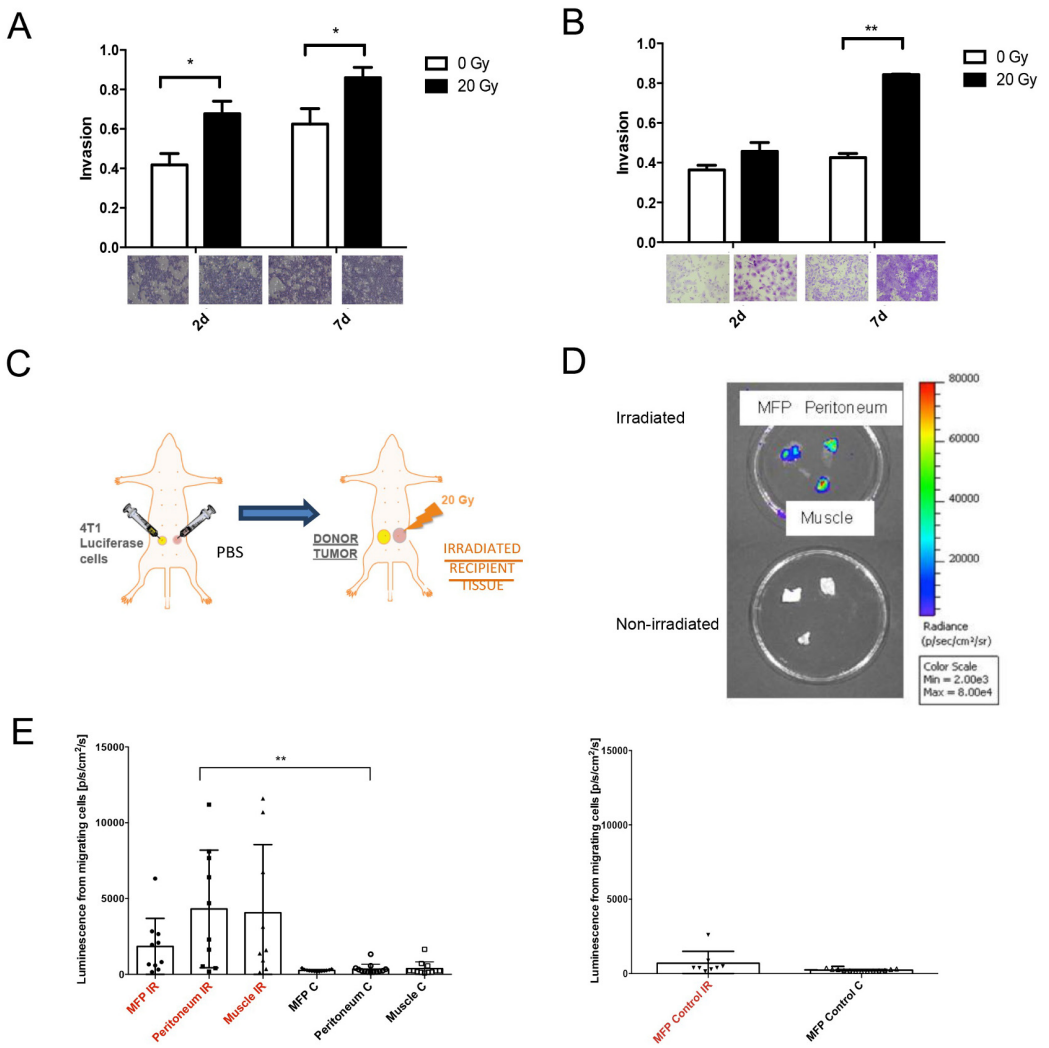

Irradiation of normal tissues promotes invasion and migration of cancer cells. Mouse embryonic fibroblasts (MEF) were irradiated to 20 Gy. Supernatant was collected after 2 or 7 d incubation, and an invasion assay was performed on (**A**) 4T1 mouse and (**B**) MDA-MB-231 human breast cancer cells. (**C**) Schematic of *in vivo* experiment. Mice were inoculated with 4T1 tumor cells in the mammary fat pad (MFP) and irradiated to 20 Gy in the contralateral normal MFP. (**D**) Tumor cell migration was monitored using BLI 10 days after radiation. Top dish: Irradiated contralateral tissues. Bottom dish: Non-irradiated control tissues. (**E**) Quantification of tumor cell migration after radiation with n = 10 irradiated (IR) and n= 13 control (C) mice per group. MFP Control indicates non-irradiated upper MFP tissues. Error bars show standard deviation with *p < 0.05 and **p < 0.01.

CONTROL ID: 2233597

TITLE: Ultrasound Microbubble Capture Using Bioorthogonal Coupling: An *In Vivo* Validation

PRESENTER: Melissa Yin

ABSTRACT BODY:

Abstract Body: Background, Motivation and Objective:

Contrast enhance ultrasound is currently used for various applications including but not limited to the detection of diseased tissue, the evaluation of tissue blood perfusion, and measurement of rate of blood flow. The availability of targeted ultrasound contrast agents further allows for the opportunity to visualize and track changes in molecular signalling pathways in relation to disease progression and response to therapy. To date, molecular ultrasound imaging using targeted microbubbles have demonstrated selective localization of MBs to sites of angiogenesis, inflammation, and intravascular thrombus formation [1]. However, the traditional approach has been to link biomolecules through strong noncovalent interactions such as biotin-streptavidin binding, which are not suitable for clinical use. Here we introduce a new strategy of microbubble targeting using a covalent, highly selective and rapid bioorthogonal coupling reaction: the inverse-electron-demand Diels-Alder reaction between tetrazine and *trans*–cyclooctene (TCO).

Statement of Contribution/Methods:

The ability of TCO-conjugated anti-VEGFR2 to capture tetrazine tagged microbubbles (MB_{TZ}) has been previously established, demonstrating target related localization of microbubbles *in vitro*, with flow chamber results comparable to conventional targeting strategies [2]. Here we report the results of an initial *in vivo* imaging study of microbubble capture through bioorthogonal coupling using a VisualSonics Vevo 2100 scanner. Ultrasound imaging was preformed at 18MHz on Lewis Lung Carcinoma tumour bearing SHO mice. Two groups of animals were used, one pre-administered with TCO-antiVEGFR2 (200μL, 0.5μg/μL) 24 hours prior to microbubble injection to allow antibodies to accumulate at the site of interest and clear out from non-targeted regions (n=4), and the other control (n=3). A disruption replenishment sequence was employed 4 minutes after MB_{TZ} injection (70μL, $6.9x10^6$ MBs/mL) and the differential targeted enhancement (dTE) signal was measured using the VevoCQ analysis software.

Results/Discussion:

Initial distribution of microbubbles after injection showed comparable vascularization in all of the LLC tumours, with relatively homogeneous distribution of contrast enhancement across each tumour. Region of interest selection therefore encompassed the whole tumour. Parametric maps generated for each tumour showed high retention of MB_{TZ} across all regions of the tumour in VEGFR2 targeted mice compared to control mice (see figure). Quantification of target specific contrast signal enhancement showed relatively consistent dTE values within each group, with the VEGFR2 targeted animals showing 2.5-fold higher dTE than the controls ($p = 0.03$, using student t-test). These initial *in vivo* results further validates previous *in vitro* observations to suggest that microbubble capture using bioorthogonal coupling reactions is a potential alternative for ultrasound molecular imaging, and establishes a path for their future development for specific applications.

1 Deshpande N, et al. *Clin. Radiol.* (2010)

2 Zlitni A, et al. *Angewandte Chemie int. Ed.* (2014)

AUTHORS (LAST NAME, FIRST NAME): Yin, Melissa[2]; Zlitni, Aimen[1]; Yan, Judy[2]; Valliant, John[1]; Foster, F. Stuart[2, 3]

INSTITUTIONS (ALL):

1. Chemistry and Chemical Biology, McMaster University, Hamilton, ON, Canada.
2. Physical Sciences, Sunnybrook Research Institute, Toronto, ON, Canada.
3. Medical Biophysics, University of Toronto, Toronto, ON, Canada.

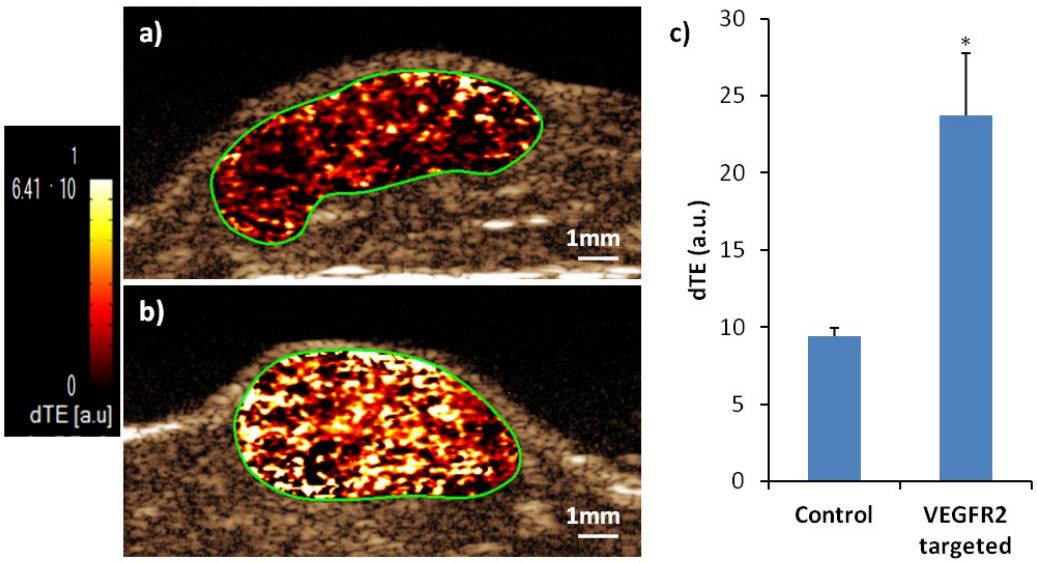

Representative parametric non-linear contrast mode ultrasound images of MB_{TZ} localization in a) control and b) VEGFR2 targeted tumours. dTE = differential targeted enhancement; regions of high dTE are represented by white and yellow, whereas low dTE are represented by orange and black. c) Averaged dTE for control (n=3) and targeted (n=4) tumours (mean±SEM, *p = 0.03).

CONTROL ID: 2233952

TITLE: In vivo Targeting of Silica-Coated Gold Nanorods for Photoacoustic Imaging

PRESENTER: Carolyn Bayer

ABSTRACT BODY:

Abstract Body: Photoacoustic imaging of molecularly-targeted contrast agents could offer a noninvasive method to provide a detailed profile of cancerous tumors, allowing for improved selection of cancer therapies. We have developed high contrast, spectrally resolvable and photothermally stable silica-coated gold nanorods, which are targeted to cell receptors for multiplex photoacoustic imaging of breast cancer. We are utilizing gold nanorods as photoacoustic contrast agents due to their high optical extinction coefficients; nanorods can produce photoacoustic signal an order of magnitude greater than gold spheres, and several orders of magnitude greater than conventional dyes. By encapsulating nanorods in a layer of amorphous silica, the photothermal stability of the gold nanorods (1) and the photoacoustic signal generated (2) are enhanced. To target the silica-coated nanorods to cell surface receptors of interest, we have developed a directional bioconjugation method. By incorporating an amine functional group, with a counter phosphate group for colloidal stability (3) , we are able to conjugate a monoclonal antibody to the surface of the nanoparticle (Figure 1). The amine functional groups on the silica surface are directionally conjugated to any oxidized glycosylated monoclonal antibody, enabling multiplex imaging. The specificity of the targeted nanorods has been verified in vitro by incubating the targeted nanorods with fixed cells overexpressing the targeted receptor, or with cells in an excess of free monoclonal antibody. The free monoclonal antibody effectively blocked the targeted silica-coated nanorod from binding to the cell surface, demonstrating targeting specificity. To test our contrast agents in vivo, we developed a nu/nu mouse model with two orthotopic xenografts in the mammary fat pad, one overexpressing HER2/neu, and the other overexpressing $\alpha_v\beta_3$ integrin. Next, we injected the tumor-bearing mice with a mixture of two types of nanorods. One nanorod, absorbing at 750 nm was targeted to HER2/neu, while the other, absorbing at 850 nm was targeted to $\alpha_v\beta_3$ integrin. The accumulation and retention of the nanorods in the tumors was imaged with spectral photoacoustic imaging. The spectral photoacoustic images were spectrally unmixed with linear least squares to assign image pixels to blood and nanoparticle spectra. In our in vivo experiments, we distinguished preferential retention of the HER2/neu targeted nanorods in the matching tumor, and $\alpha_v\beta_3$ integrin in its respective tumor. In summary, we have developed a directional bioconjugation method for silica-coated gold nanorods which are capable of producing a photoacoustic signal higher in magnitude than conventional gold nanoparticles and dyes. We have demonstrated targeting specificity in vitro and in vivo. Our experiments demonstrate the potential of multiplex spectral photoacoustic imaging to profile cancerous tumors in vivo.

References

1. Chen Y-S, et al. Opt Express. 2010;18(9):8867-78.

2. Chen YS, et al. Nano Letters. 2011;11(2):348-54.

3. Schroedter A, et al. Nano Letters. 2002;2(12):1363-7.

AUTHORS (LAST NAME, FIRST NAME): Bayer, Carolyn[1]; Tung, Andrea[1]; Emelianov, Stanislav Y.[2]

INSTITUTIONS (ALL):

1. Biomedical Engineering, The University of Texas at Austin, Austin, TX, United States.

2. The University of Texas at Austin, Austin, TX, United States.

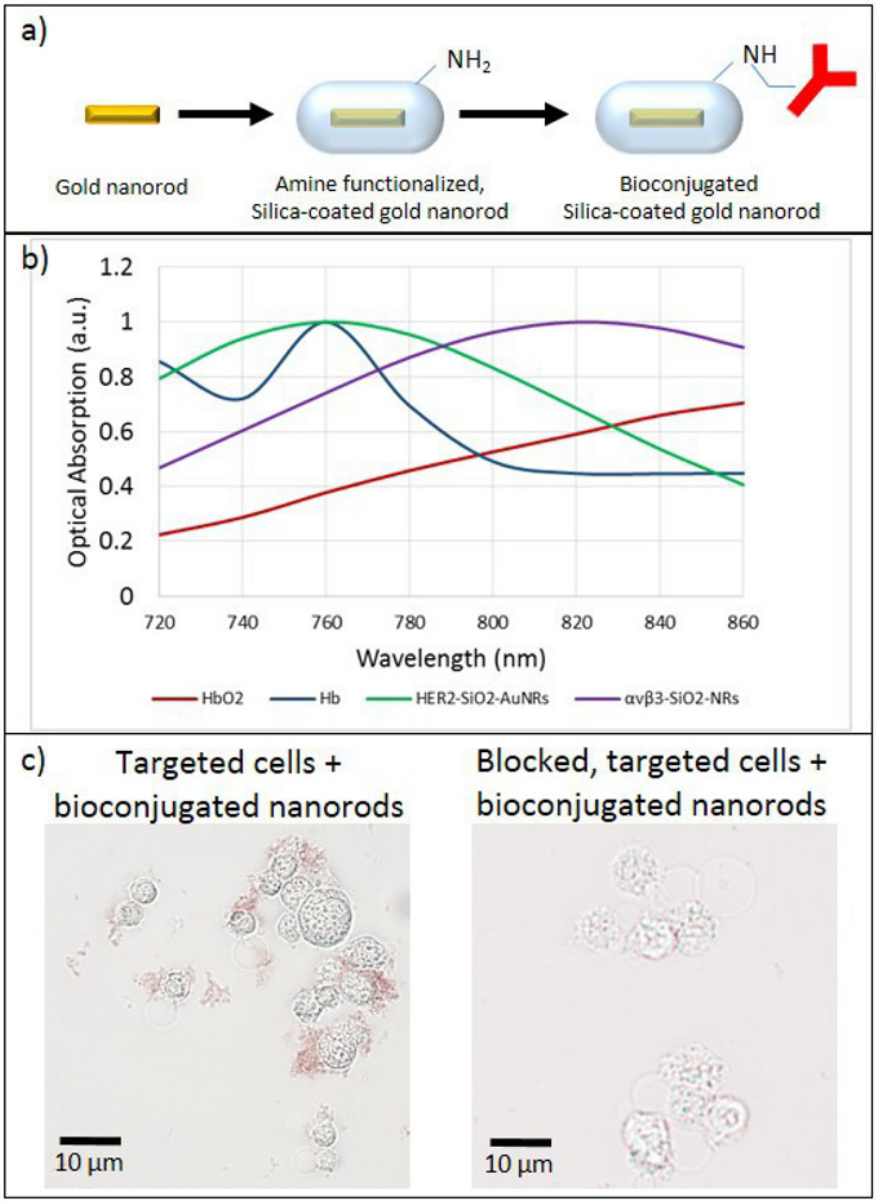

Figure 1: Development and specificity of directionally targeted, silica-coated gold nanorod contrast agent for multiplex photoacoustic imaging. A) Bioconjugation scheme. B) UV-Vis absorption spectra of targeted, silica-coated gold nanorods and endogenous hemoglobin. C) in vitro specificity of targeted, silica-coated gold nanorods.

CONTROL ID: 2233983

TITLE: IMPLICATIONS FOR UNDERSTANDING THE CELLULAR RESPONSE FOR PULSED FOCUSED ULTRASOUND ASSOCIATED WITH BLOOD-BRAIN BARRIER OPENING

PRESENTER: Zsofia Kovacs

ABSTRACT BODY:

Abstract Body: OBJECTIVE: Pulsed focused ultrasound (pFUS) in combination with ultrasound contrast agent (UCA) has been shown to facilitate drug delivery into the brain via the open blood-brain barrier (BBB). Graded cellular responses that may increase drug delivery are not well understood. We investigated the temporal expression of cytokines, chemokines and trophic factors (CCTF) following pFUS + UCA treatment to determine the possible cellular contributions associated with opening of the BBB.

METHODS: pFUS was performed in the rat brain: 0.3 MPa acoustic pressure was applied in 10 ms burst length and 10% duty cycle (2 x 4 focal points, 120 sec/4 focal points) using a single-element spherical FUS transducer (center frequency: 1.129 MHz; focal number: 0.8; active diameter: 7.5 cm; FUS Instruments). Sonications were accompanied by 200 µL Optison™ (GE Healthcare) infusion through the tail vein. Gd-enhanced T1-weighted images were obtained by 3.0 T MRI (Philips). Molecular changes in the brain upon pFUS treatment were analyzed with Bio-Plex Pro™ Assay (Bio-Rad Laboratories, Inc.) or immunofluorescent staining. Values were normalized to sham and statistical analysis was performed by one-way ANOVA corrected for multiple comparisons. Rats were injected with 8 mg/kg Rhodamine encapsulated magnetic polymers (Bangs Laboratories, Inc.) 3 days prior to pFUS to tag splenic macrophages. Histological evaluation of the brains revealed no evidence of damage.

RESULTS: Macrophages containing bead from the spleen were recruited to the sonication site. Molecular and immunofluorescent analysis of the pFUS-treated tissue revealed an increase in CCTF (Fig.1) such as macrophage colony-stimulating factor (MCSF), interleukin-1b (IL-1b), interleukin-6 (IL-6), stromal cell-derived factor-1a (SDF-1a), hepatocyte growth factor-2 (HGF-2) and RANTES. Overexpression of heat shock protein (HSP70), hypoxia-inducible factor-1a (HIF-1a) and tumor necrosis factor-a (TNF-a) are associated with mild ischemic trauma secondary to pFUS. Increased expression of vascular endothelial growth factor (VEGF) and glial fibrillary acidic protein (GFAP) was observed following pFUS.

CONCLUSIONS: The temporal changes in CCTF following pFUS are consistent with the increased expression of factors from the various cell components in the parenchyma. Endothelial cells, astrocytes and neurons produce VEGF, HSP70, HIF-1a in response to stress. Increased GFAP is a hallmark of reactive astrocytes. IL-1b, IL-6 and TNF-a are cytokines that are associated with activated microglia in response to inflammation or injury. RANTES and MCSF (trophic factors) along with IL-17 are also associated with microglial and neuronal activation in response to stress or injury and can trigger immunological response. The proteomic changes following pFUS + UCA underscores the contribution of CCTF to the mechanical effects in BBB opening and requires further evaluation to determine the long term effects on cell populations and drug interactions within the brain.

AUTHORS (LAST NAME, FIRST NAME): Kovacs, Zsofia I.[1]; Tracey, Joseph A.[1]; Bresler, Michele[1]; Williams, Rashida[1]; Jikaria, Neekita[1]; Burks, Scott R.[1]; Frank, Joseph[1, 2]

INSTITUTIONS (ALL):

1. Radiology and Imaging Sciences, National Institutes of Health, Bethesda, MD, United States.
2. National Institute of Biomedical Imaging and Bioengineering, Bethesda, MD, United States.

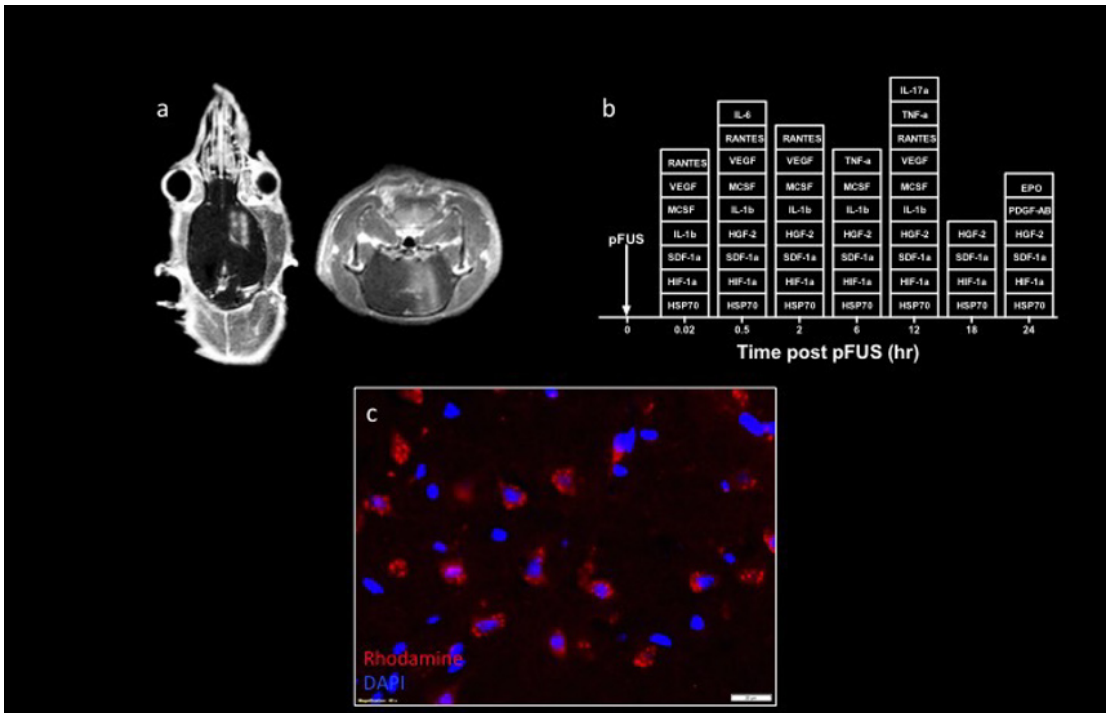

Fig.1. Molecular analysis of the pFUS treated brain.
Contrast-enhanced T1-weighted axial and coronal MR-images of a rat brain after pFUS (a).
The time course of molecular changes after pFUS showing the elevation of CCTF (b).
Recruited macrophages containing SPIO bead (red) in the area of Gd-enhancement (c).

CONTROL ID: 2233633

TITLE: Evaluation of high-intensity focused ultrasound ablation of prostate tumor with hyperpolarized C^{13} imaging biomarkers

PRESENTER: Jessie Lee

ABSTRACT BODY:

Abstract Body: Prostate cancer (PC) is the most frequently diagnosed noncutaneous cancer in men, and high-intensity focal ultrasound (HIFU) is being investigated as a technique for effective focal treatment for patients with low- or intermediate-risk PC.[1,2,3] Real-time hyperpolarized (HP) ^{13}C MR can be utilized during HIFU to improve treatment delivery strategies, provide treatment verification, and thus reduce the need for more radical therapies. The goal is to develop imaging biomarkers specific to thermal therapies of PC using HIFU, and to predict the success of thermal coagulation and identify tissues potentially sensitized to adjuvant treatment by sub-ablative hyperthermic heat doses. The results of this study will provide the basis for evaluation of these biomarkers in human clinical trials of HIFU therapy for low- to intermediate-risk PC.

The transgenic adenocarcinoma of the mouse prostate (TRAMP) model was used. Mice (n = 3) with solid prostate tumors received HIFU treatment (5.6 MHz, 160W/cm^2, 60 s), and the MR imaging was done on a wide-bore 14T microimaging system. Imaging time points included a baseline 1 day before the treatment and 1- and 5-day follow-ups post-treatment. ^{13}C-labeled pyruvate and urea were used to monitor tumor metabolism and perfusion accordingly. After the 5-day follow-up, tumors underwent histopathological analysis and were categorized into 3 regions: (1) the ablated region, (2) the sensitized region (tissues receiving sub-ablative heat dose), and (3) the untreated region (regions away from the treatment site and received nominally no heat dose).

After treatment, the untreated regions behaved as a normal untreated TRAMP prostate tumor would. The successfully ablated tumor tissue had a loss in metabolism and perfusion. The slight perfusion recovery (20%) observed in the ablated region was only shown by urea, not by DCE. A possible explanation is that urea molecules, smaller in size than gadolinium, extravasate more easily from the blood vessels. However, longer-term follow-ups are needed to understand the causes of the recovery and its effects on the tissues. In the sensitized regions, a time-dependent change in metabolism and perfusion was observed. The initial decrease by 1 day followed by recovery back to/beyond the baseline by 5 days in perfusion and metabolism can be a result of the tissues' wound healing response. Adjunct therapies (radiation/chemo) may be applied to the sensitized region to ensure treatment efficacy. The physiological and metabolic responses to HIFU therapy can be utilized to maximize the effects of the therapies. Immediate time points on the treatment day can not only help identify the metabolism and perfusion behavior caused by the applied heat dose but also act as an early evaluation of the treatment outcome. This promising preliminary study shows the potential of using ^{13}C MR imaging as biomarkers of HIFU/thermal therapies. The ultimate goal is to perform the HP ^{13}C studies during HIFU treatment in clinical systems for real-time feedback of treatment effectiveness in patients.

[1] ACS. *Cancer Facts & Figures 2012* [2] NCI: PDQ® Prostate Cancer Treatment [3] Cline, H.E. et al. *Rad.* **194**: 731-737 (1995)

AUTHORS (LAST NAME, FIRST NAME): Lee, Jessie[1]; Diederich, Chris J.[1]; Salgaonkar, Vasant A.[1]; Bok, Robert[1]; Taylor, Andrew G.[1]; Kurhanewicz, John[1]

INSTITUTIONS (ALL):

1. UCSF, San Francisco, CA, United States.

(No Image Selected)

CONTROL ID: 2233651

TITLE: Evaluation and comparison of Cu-64 and Ga-68 labeled DOTA-, NOTA- and NODAGA-AMBA in vitro and in vivo in a GRPR expressing prostate cancer model

PRESENTER: Ralf Bergmann

ABSTRACT BODY:

Abstract Body: Radiolabeled bombesin analogue AMBA shows great potential for the diagnosis and treatment of human cancers overexpressing gastrin-releasing peptide receptors (GRPR). The present study includes comprehensive assessment of the radiopharmacological profile of Cu-64 and Ga-68 labeled DOTA-, NOTA- and NODAGA-AMBA analogues using biodistribution, metabolite analysis and PET imaging.

The DOTA-, NOTA- and NODAGA-AMBA derivatives were radiolabeled with Cu-64 and Ga-68. Cell uptake and externalization, binding affinity and receptor activation was studied in GRPR-expressing prostate carcinoma PC3 cells. Biodistribution, metabolism and kinetics were studied in rats and in subcutaneous PC3 xenografted NMRI nu/nun mice.

All three peptides were labeled with Cu-64 and Ga-68 in high radiochemical purity and specific activity. Cell binding studies confirmed GRPR-specific uptake. Inhibitory binding potential of all peptides was in the low nanomolar range (0.9 and 3.0 nM), and peptides exhibited an agonistic profile upon binding to the GRPR. Peptides were rapidly internalized in vitro. Biodistribution and PET studies showed GRPR-mediated radioactivity uptake in PC3 tumors (average SUV(60 min) control 1.3, blocked 0.7) and in pancreas (average SUV(60 min) control 9.9, blocked 3.1), with high tumor to muscle ratios (T/M(5 min) 16.0, T/M(60 min) 13.6). Radioactivity uptake in rat pancreas was higher for the Cu-64 radiotracers (SUV(60 min) ± SD, n=8; Cu-64-DOTA 13.8 ± 3.3; Cu-64-NOTA 15.5 ± 2.3; Cu-64-NODAGA 14.1 ± 4.2; Ga-68-DOTA 3.8 ± 0.5; Ga-68-NOTA 4.3 ± 0.8; Ga-68-NODAGA 5.8 ± 0.9). Radioactivity accumulation in the kidneys as critical organ was relatively low and ranged between 1.9 to 4.7 SUV(60 min). The lowest activity retention in the kidneys was observed for Ga-68-NOTA and -NODAGA analogues. The radiometabolite fraction of the peptides in the arterial blood plasma was between 50% and 65% after 10 min p.i. and increased to 92% after one hour without significant differences between the radiotracers.

Cu-64 and Ga-68 labeled DOTA-, NOTA-, and NODAGA-AMBA analogues showed excellent specific tumor uptake characteristics with high target to background ratios. NODAGA-AMBA displayed most superior uptake characteristics. All radiolabeled peptides showed comparable metabolic profiles in vivo. Radioactivity accumulation in target tissues increased with increasing specific activity and was higher for Cu-64 labeled peptides. This comprehensive preclinical study showed the great potential of DOTA-, NOTA- and NODAGA-AMBA analogues for applications according to the theranostics concept.

AUTHORS (LAST NAME, FIRST NAME): Bergmann, Ralf[1]; Asti, Mattia[2]; Martin, Rene[4]; Richter, Susan[3]; Mueller, Marco [4]; Brennauer, Albert[4]; Pietzsch, Jens[1]; Rogers, Buck E.[5]; Wuest, Frank[3]; Steinbach, Joerg[1]

INSTITUTIONS (ALL):

1. Institute of Radipharmaceutical Cancer Research, Helmholtz - Zentrum Dresden - Rossendorf, Dresden, Saxony, Germany.
2. Advanced Technology Department , Santa Maria Nuova Hospital - IRCCS, Reggio Emilia, Italy.
3. Cross Cancer Institute, University of Alberta, , Edmonton, AB, Canada.
4. ABX advanced biochemical compounds, Radeberg, Saxony, Germany.
5. Department of Radiation Oncology, Washington University School of Medicine, St. Louis, MO, United States.

(No Image Selected)

CONTROL ID: 2233653

TITLE: Smart viral nanoparticles targeting angiogenic vasculature for tumor imaging and treatment

PRESENTER: John Lewis

ABSTRACT BODY:

Abstract Body: Recent advances in nanotechnology have driven the clinical and preclinical development of novel therapeutics with the potential to address the shortcomings of conventional drugs and imaging agents. The inherent multi-functionality of nanomedicines offers compelling advantages for improved drug delivery in cancer, allowing the development of sophisticated delivery systems that can incorporate unstable (e.g., siRNA) and/or highly toxic drugs, improve intracellular delivery, and precisely target cancer cells to reduce side effects. Viral nanoparticles (VNPs) are a novel class of bionanomaterials that harness the natural biocompatibility of viruses for the development of therapeutics, vaccines and imaging tools. We have utilized plant virus such as the *cowpea mosaic virus* (CPMV) to engineer novel “smart” cancer-targeted imaging and theranostic agents by incorporating fluorescent dyes, radioactive isotopes, polyethylene glycol (PEG) polymers and targeting ligands.

Angiogenesis is a key hallmark of cancer and required for sustained growth of solid tumors, as well as being a poor prognostic factor for many cancers. Here, I will discuss the development of viral nanoparticle platforms targeting key angiogenic factors such as VEGFR1, avb3 integrin, and epidermal growth factor-like domain 7 (EGFL7) for the purpose of highlighting and destroying aggressive primary tumors and occult metastatic disease. I will detail the development of a bead-based peptide library screening approach that has allowed us to identify novel high affinity peptide ligands for these molecular targets. I will highlight our use of intravital, or live imaging, in xenograft human tumor models, to visualize the accumulation of targeted nanoparticles in real time *in vivo*. Finally, I will detail efforts to accelerate the clinical translation of VNP-based imaging agents.

AUTHORS (LAST NAME, FIRST NAME): Lewis, John D.[1]

INSTITUTIONS (ALL):

1. University of Alberta, Edmonton, AB, Canada.

(No Image Selected)

CONTROL ID: 2233656

TITLE: Detection of human brown adipose tissue activity during cold exposure by magnetic resonance with hyperpolarized 129Xe gas.

PRESENTER: Rosa Tamara Branca

ABSTRACT BODY:

Abstract Body: Brown Adipose Tissue is a tissue present in all mammals and is specialized for non-shivering thermogenesis (NST)(1). Recent studies showed that BAT plays a regulatory role in human energy balance and glucose homeostasis and may have a protective role against obesity and diabetes as it does in mice. As the biochemical mechanisms that trigger the differentiation and the activity of BAT are being discovered, and as new therapeutic treatments that specifically target this tissue are being developed, non-invasive detection of BAT tissue and thermogenic activity remains challenging(2), especially in obese and overweight subjects(3).

Recently we demonstrated that magnetic resonance with HyperPolarized 129Xe gas (HP 129Xe) can be used in rodents to detect BAT mass with better sensitivity than FDG-PET for the lipid rich and thermogenically inactive BAT of obese phenotypes(4). This is because stimulation of thermogenic activity leads to a specific increase in blood flow to BAT and to a selective downstream accumulation of inhaled HP 129Xe gas into BAT, whether or not stimulation of NST is followed by BAT activation. At the same time, when xenon dissolves in BAT, the temperature dependence of its chemical shift can be used to directly measure BAT temperature and thermogenic activity in real time with high accuracy. This allows us to unveil differences in BAT thermogenic capacity between lean and obese mouse phenotypes(4).

Here we present our first preliminary human data, which mirror the results obtained in mice in that they show a specific and strong increase in the uptake of HP 129Xe by BAT during stimulation of thermogenesis by cold exposure in all subjects analyzed. We also present validation of this technique by MRI/FDG-PET scanning. As the detection of BAT by magnetic resonance with HP 129Xe is independent of blood glucose level, feeding, or exercise status, we anticipate its use as a tool to study diabetes or to directly assess the stimulatory effect of diet or exercise on BAT. The high sensitivity of HP129Xe MRI to the lipid rich BAT of obese phenotypes, coupled with direct measurement of its thermogenic activity, will allow us to correctly assess, in a larger number of human subjects, normal and abnormal BAT function, and to determine the efficacy of new anti-obesity and anti-diabetes therapies that specifically target this tissue.

References

1. Cannon B & Nedergaard J (2004) Brown Adipose Tissue: Function and Physiological Significance. *Physiological Reviews* 84(1):277-359.

2. Cypess Aaron M, Haft Carol R, Laughlin Maren R, & Hu Houchun H (2014) Brown Fat in Humans: Consensus Points and Experimental Guidelines. *Cell Metabolism* 20(3):408-415.

3. Vijgen GHEJ*, et al.* (2011) Brown Adipose Tissue in Morbidly Obese Subjects. *PLoS ONE* 6(2):e17247.

4. Branca RT*, et al.* (2014) Detection of brown adipose tissue and thermogenic activity in mice by hyperpolarized xenon MRI. *Proceedings of the National Academy of Sciences* 111(50):6.

AUTHORS (LAST NAME, FIRST NAME): Branca, Rosa Tamara[1, 2]; Zhang, Le[3, 2]; Burant, Alex B.[1, 2]; McCallister, Andrew[1, 2]

INSTITUTIONS (ALL):

1. Physics and Astronomy, University of North Carolina at Chapel Hill, Chapel Hill, NC, United States.
2. Biomedical Research Imaging Center, University of North Carolina at Chapel Hill, Chapel Hill, NC, United States.
3. Applied Physical Sciences, University of North Carolina at Chapel Hill, Chapel Hill, NC, United States.

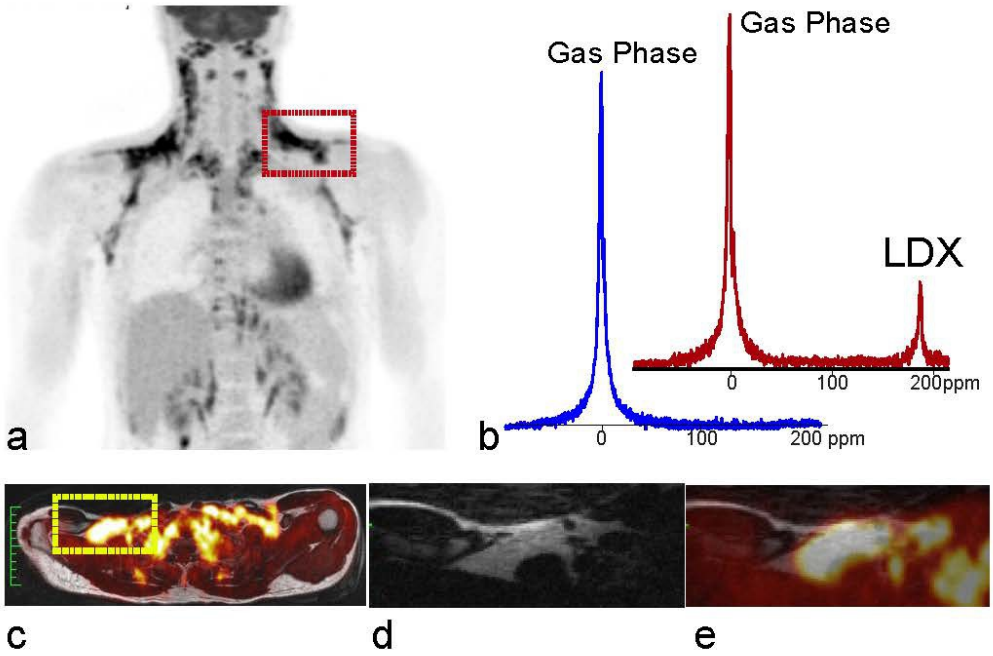
a
Gas Phase
Gas Phase
LDX
0
100
200ppm
b
0
100
200 ppm
c
d
e

CONTROL ID: 2233725

TITLE: Fluorine vs iron oxide labeling of mesenchymal stem cells (MSCs) for image-guided therapy of acid burns

PRESENTER: GHULAM MUHAMMAD

ABSTRACT BODY:

Abstract Body: Introduction: Acid attacks continue to be a social problem worldwide, with women being the predominant victims. Acid burns are profound, healing-resistant, and disfiguring for life. Available treatment options are insufficient; thus, there is an urgent need to search for effective solutions. There is growing interest in stem cell-based regenerative medicine, which is perfectly suited to the problem of skin regeneration after chemical injury. Stem cell imaging is instrumental in understanding the therapeutic mechanism, to identify unwanted distribution, which may lead to complications, as well as to ensure proof-of-procedure quality. There are various cell labeling systems, but only a few of these have been used clinically. Among them are superparamagnetic iron oxide nanoparticles (SPIO), which have been used most extensively due to their high sensitivity, and fluorine nanoemulsions with “hot spot” imaging capabilities, and these have become even more attractive after a clinical-grade product was introduced. Here, we investigated the utility SPIO-enhanced and fluorine MR imaging for tracking cells injected to treat acid burns in mice using bioluminescence as a reference standard.

Methods: Luc+ MSCs were derived from FVB-Tg(CAG-luc,-GFP) mice. Cells were labeled with contrast agents by overnight incubation with CS-ATM Green (Celsense) for 19F MRI imaging and with MIRB (BioPAL) for 1H MRI imaging. To evaluate the impact of labeling on cell function, we tested viability, size, migration, doubling time, and colony formation of various MSCs populations (age of donor: young vs. old; tissue origin: fat vs bone marrow; preconditioning: ascorbic acid vs hypoxia vs normal; and acidic conditions: yes or no). Labeled MSCs were transplanted into the wound of mice (n=42) one day after acid skin burn in a syngeneic and an allogeneic paradigm, and followed with BLI, F19, or 1H MRI. Skin was burned with 0.5 cm^2 filter paper soaked with 10N HCl for 1 minute. Healing was assessed by % wound size reduction and measurement of epithelialization.

Results: Multivariate regression analysis showed no influence of labeling on the investigated parameters, *in vitro,* in any MSC population. BLI revealed a stepwise drop in signal, with a complete loss of signal within two weeks in both types of recipients. A similar pattern was observed for fluorine imaging, while proton imaging was rather inconclusive due to background signal related to the high magnetic susceptibility artifacts in wounded area and signal persistence, despite cell death. Although short-lived, the transplanted cells accelerated healing compared to controls, with no difference between labeled and non-labeled cells.

Conclusions: We hypothesize that transplanted cells, although short lived, trigger a cascade of positive events upon cell death. Fluorine imaging is the most promising, an clinically applicable strategy to track cells transplanted into acid burns, and also allows for conclusions about cell survival. The knowledge about the lifespan of transplanted cells in patients may contribute to better treatment planning, including the choice of timing for potential additional cell injections.

AUTHORS (LAST NAME, FIRST NAME): MUHAMMAD, GHULAM[1, 2]; Xu, Jiadi[3]; Jablonska, Anna[1, 4]; Rose, Laura[1, 4]; Bulte, Jeff W.[1, 4]; Walczak, Piotr[1, 5]; Janowski, Miroslaw[1, 6]

INSTITUTIONS (ALL):

1. Radiology, Johns Hopkins University, Baltimore, MD, United States.
2. Stem Cell Laboratory, University of the Punjab, Lahore, Punjab, Pakistan.
3. F.M. Kirby Research Center, Kennedy Krieger Institute, Baltimore, MD, United States.
4. Institute for Cell Engineering, Johns Hopkins University, Baltimore, MD, United States.
5. Radiology, University of Warmia and Mazury, Olsztyn, Warmia and Mazury, Poland.
6. NeuroRepair Department, Mossakowski Medical Research Centre, Warsaw, Mazowsze, Poland.

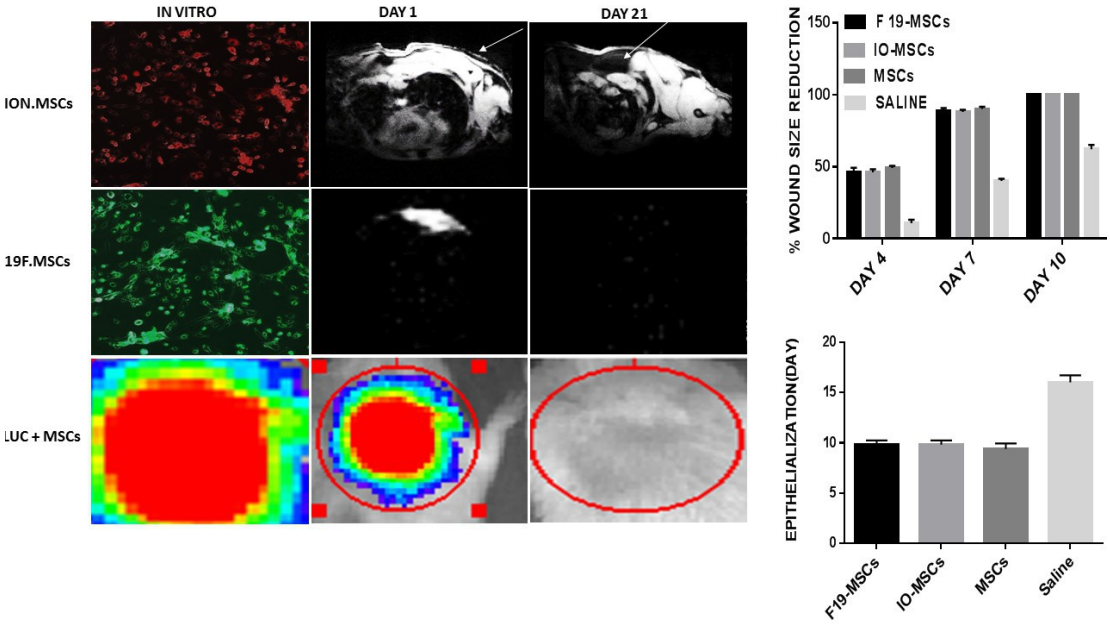

Fig 1. Image-monitored healing of acid burns (separate group of animals for iron oxide, fluorine, and control). The upper panel of pictures presents iron oxide labeling (in vitro) and in vivo proton MRI images. The corresponding 19F MRI images are presented in the middle row. BLI as a reference is presented in the lower panel. The graphs present wound size reduction and period of re-epithelialization in animals treated with iron oxide, 19F and non-labeled cells, versus control injection of saline.

CONTROL ID: 2233676

TITLE: Hyperpolarized ^{15}N-labeled Imidazoles: New pH MR Imaging Agents with Long Relaxation Times

PRESENTER: Charlie Khemtong

ABSTRACT BODY:

Abstract Body: BACKGROUND: Recently, we have reported a series of hyperpolarized (HP) ^{15}N-pyridine derivatives as potential pH MR imaging agents (1). The improved NMR sensitivity obtained by dynamic nuclear polarization (DNP) coupled with the highly pH-sensitive ^{15}N chemical shifts make ^{15}N-enriched pyridine derivatives attractive agents for pH imaging applications. In this study, we investigated imidazole derivatives as a new class of pH-sensitive HP ^{15}N agents with much longer HP ^{15}N life-times.

METHODS: A solution of imidazole derivatives (1.0 M) and trityl OX063 radical (15 mM) in 8 μL glycerol-water (1:1) was polarized in a HyperSense polarizer. The polarization was carried out at ~1.05 K with 94.096 GHz microwave irradiation for 2 hr. ^{15}N NMR spectra were acquired at room temperature (~23ºC) on a 400-MHz spectrometer using a 10-degree flip angle with a TR of 5 s. ^{15}N chemical shift imaging (CSI) was acquired on an Agilent 9.4T vertical bore microimager. All ^{15}N peaks were externally referenced to ^{15}N-nitrobenzen (372 ppm). ^{15}N CSI parameters: CSI2d sequence, field of view (FOV) = 30 x 30 mm^2; TR = 200 ms; TE = 1.26 ms; flip angle = 45°; number of average (NA) = 1. ^{1}H reference image was acquired at the same slice position using a GEMS sequence. ^{1}H imaging parameters: FOV = 30 x 30 mm^2; TR = 200 ms; TE = 2.6 ms; flip angle = 45°; NA = 2. Matrix = 8 x 8. The CSI data were processed to 128x128 matrix.

RESULTS: By fitting time-dependent ^{15}N signal decay curves, average T_1 values of HP imidazole derivatives **1**-**4** were calculated to be 125 s, 89 s, 138 s and 108 s, respectively (**Figure 1**). These T_1 values are much longer than previously reported HP ^{13}C- and ^{15}N-enriched metabolic imaging agents. pH titration experiments showed that the ^{15}N chemical shifts of HP-imidazoles are strongly pH-dependent. Chemical shift images of a phantom containing a HP ^{15}N-enriched ethyl imidazole (compound **3**) solution is shown in **Figure 1**. The results show that magnetic resonance spectroscopic imaging (MRSI) of ^{15}N ethyl imidazole is achievable due to the long-lived HP ^{15}N signal with significant signal enhancement by DNP. The HP ^{15}N signal has a very good signal-to-noise ratio (SNR) and appears localized within the inner tube of the phantom. Accurate pH measurements of phantoms containing HP ^{15}N ethyl imidazole at different pH were also obtained using HP ^{15}N MRSI as confirmed by a gold standard pH electrode.

CONCLUSIONS: We have synthesized and demonstrated the potential of using HP ^{15}N-imidazole derivatives as pH-sensitive probes for MRI. These molecules display long relaxation time and high signal enhancement by DNP. The combination of hyperpolarization and pH-sensitive ^{15}N imidazole derivatives offers new opportunities to develop highly sensitive imaging agents with long relaxation time.

REF.: (1) Jiang *et al*, *Sci. Reports*, *in press*

AUTHORS (LAST NAME, FIRST NAME): jiang, weina[1]; Moore, Christopher L.[1]; Sherry, A. D.[2]; Khemtong, Charlie[1]

INSTITUTIONS (ALL):

1. UT Southwestern medical center, Dallas, TX, United States.
2. UT southwestern medical center, Dallas, TX, United States.

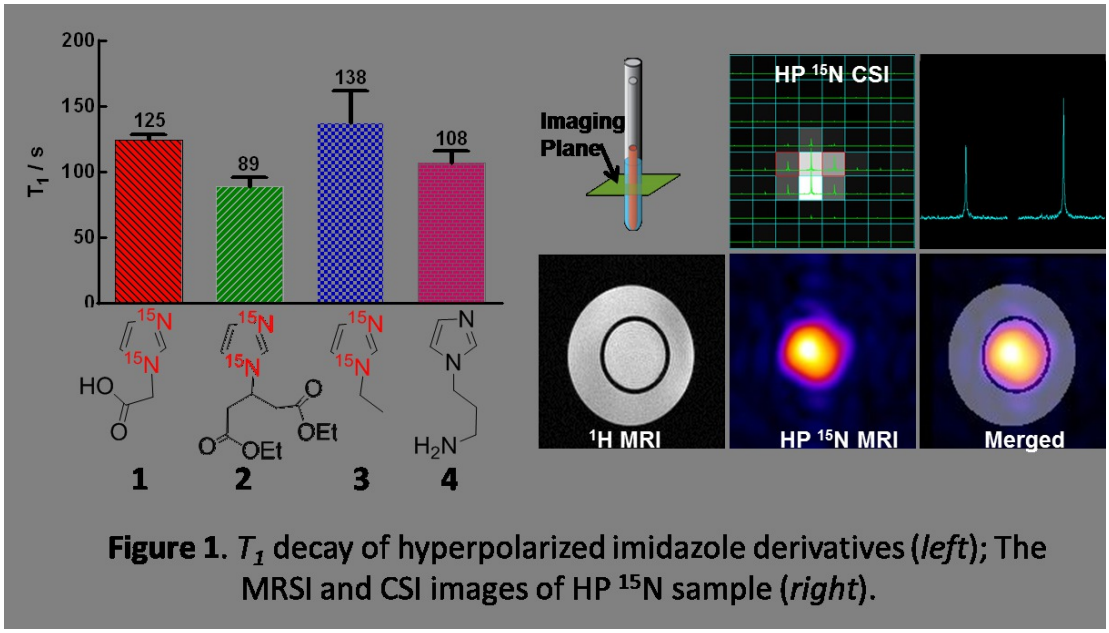

Figure 1. T_1 decay of hyperpolarized imidazole derivatives (*left*); The MRSI and CSI images of HP ^{15}N sample (*right*).

CONTROL ID: 2233678

TITLE: Assessment of low dose PET imaging of Non-Hodgkins lymphoma in a humanized transgenic mouse model using novel immunoPET tracer

PRESENTER: Frezghi Habte

ABSTRACT BODY:

Abstract Body: Purpose: Immuno–positron emission tomography (immunoPET) is an exciting novel option to improve diagnostic imaging and to guide mAb-based therapy. Compared to conventional FDG-PET, immunoPET can characterize and quantify antigen expression specific to a tumor type, which makes immunoPET a powerful molecular strategy for tracking, visualizing and measuring the tumor gene expression. ImmunoPET might play an important future role in cancer staging, in the improvement and tailoring of therapy response with existing mAbs, and in the efficient development of novel mAbs. We recently developed a new immunoPET tracer with an intact mAb labeled with ^{64}Cu to image human CD20, a marker for NHL, in a transgenic mouse model. This new tracer showed high specific spleen uptake over 9:1 contrast ratio of signals due to the accumulation of more of the CD20 expressing B-cells on the target organ relative the background. High sensitivity of PET/CT combined with high specific low dose PET tracer may allow injection of significantly dose reduction to the mouse model without compromising the image quality and quantitative accuracy.

Procedure: In this study, we evaluated the minimum dose capability of the immunoPET imaging using phantom and live mouse model. To assess the PET system limitations for low dose a phantom with a 1 mL fillable sphere inserted in a 20 ml syringe filled with diluted F-18 tracer of 5:1 sphere to background activity ratio (total ~10μCi) was used. Four of these phantoms were imaged simultaneously at several time points while decaying. For animal study, we injected 10, 25, 50 and 75 μCi of 64-Cu-rituximab (~25-35μCi/μg; >98% purity) in a group of four mice and imaged for 1, 5, 15, and 25 hrs.

Results: Phantom study showed imaging with very low total dose (< 6 μCi) is possible without significantly affecting signal variability of the system. Animal study showed improvement in signal contrast for low injected dose with similar inter-subject variability. An average spleen to liver ratio of 13.7, 9.2, 8.5 and 6.4 was obtained for 10, 20, 50 and 75 μCi-injected doses respectively.

Conclusion: The result clearly indicates that immunoPET imaging is possible with very low dose tracer. In addition, the study showed improved image contrast, which indicates there are other biological factors that govern the optimum dose other than the sensitivity of the microPET scanner.

AUTHORS (LAST NAME, FIRST NAME): Habte, Frezghi[1]; Natarajan, Arutselvan[1]; Gambhir, Sanjiv S.[1]

INSTITUTIONS (ALL):

1. Radiology, Stanford University, Stanford , CA, United States.

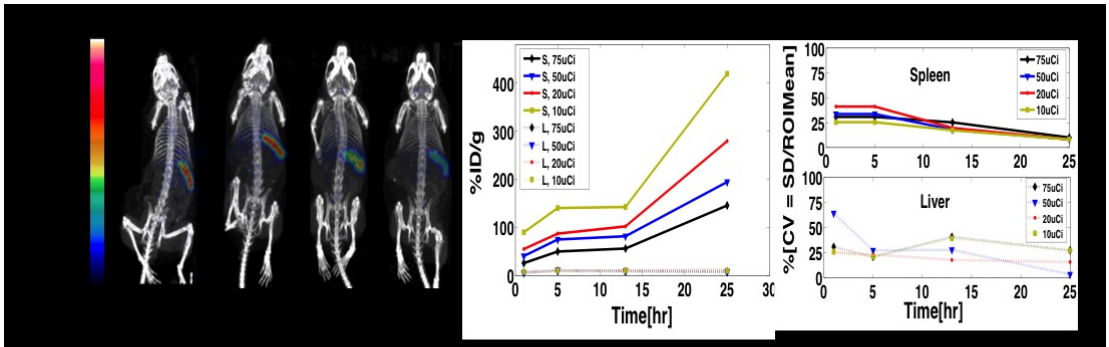

Figure 1: Animal study showing comparison of signal uptakes of different low injected does (10, 20, 50 and 75 µCi). Left shows sample of PET/CT images scaled to the highest %ID/g computed on the spleen. Middle shows comparison of ROI signals measured for Spleen (S) and Liver (L) for each of the injected doses as function on function of scan time. %ID/g was calculated with the decay corrected does at each time point. Right shows the percentage of coefficient of variability computed for both Spleen (top) and Liver (bottom).

CONTROL ID: 2232263

TITLE: Multi-scale Cryo-imaging Platform for Analysis of Molecular MR imaging of Micro-metastases

PRESENTER: David Wilson

ABSTRACT BODY:

Abstract Body: We created a quantitative metastasis imaging, analysis platform consisting of software and multi-spectral cryo-imaging hardware suitable for evaluating emerging imaging agents targeting micro-metastatic cancer. As an example, we used the system to analyze imaging agents with CREKA peptide targeting clotted plasmas proteins (fibrin-fibronectin complexes) expressed in the tumor micro-environment. We injected CREKA-Gd, visible in MR, and CREKA-Cy5, visible in red fluorescence, into a GFP metastasis mouse model. MRI was followed by cryo-imaging with CryoViz^{TM}, which re-peatedly sections and tiles microscope images of the tissue block face, providing ana-tomical brightfield and molecular fluorescence, enabling 3D mi-croscopic imaging of the entire mouse with single metastatic cell sensitivity. Selected histology sections were obtained using a tape system. To register MRI volumes to the cryo-brightfield reference, we developed mutual information non-rigid registration with proceeded rigid à affine à B-spline, non-rigid 3D registration. Histology images were also registered to the cryo-image brightfield reference. The result was GFP tumor, color brightfield anatomy, red fluorescence CREKA-Cy5, MRI CREKA-Gd, and optional histology, all within a high resolution, 3D digital visualization and analysis framework. Interactive, multi-scale visualization allowed us to identify a metastasis in GFP, determine the presence of CREKA-Cy5, determine if there is MR signal, and optionally examine histology for target molecules. Using a 3D extension of the Rose detection model, we determined those metastases with sufficient MR signal for detection.

As an example, we analyzed CREKA-Cy5 and CREKA-Gd in a 4T1 metastatic breast cancer model. Cryo-imaging found >100 tumor metastases in mice, primarily in lungs, liver, bone marrow, and adrenal gland with sizes ranging 0.001- 60 mm^3 (Fig A). Even single GFP labeled cells were found in the brain. In some organs, whole mouse 3D registration accuracy was within 0.2 mm, and in all organs, registration was sufficient to visually map single micro-metastases (<125 mm^3) reliably from cryo imaging to MRI without confusion. The 3D Rose criterion with a conservative detection threshold (SNR>4) predicted that 100% and 36% of metastases >0.16 mm^3 and >0.09 mm^3 were detectable, respectively (Fig B). At the conference, visualization software will be demonstrated which allowed us to probe 3D volumes for specific instances of labeling success and failure. Because we obtained a cryo-image and then acquired the corresponding histological section on tape, registration of histological images was very accurate (<25mm). Histology allowed us to assess tumor heterogeneity and availability of molecular targets.

In summary, we developed a new methodology which allows one to evaluate qualitatively and quantitatively metastatic cancer imaging with accuracy and precision heretofore unavailable. With optimization of software, this could become a methodology for routine analysis.

AUTHORS (LAST NAME, FIRST NAME): Qutaish, Mohammed Q.[1]; Zhou, Zhuxian[1]; Liu, Yiqiao[1]; Prabhu, David[1]; Lu, Zhengrong[2]; Wilson, David[3]

INSTITUTIONS (ALL):

1. Biomedical Engineering, Case Western Reserve University, Cleveland, OH, United States.
2. Biomedical Engineering, Case Western Reserve University, Cleveland, OH, United States.
3. Biomedical Engineering & Radiology, Case Western Reserve University, Cleveland, OH, United States.

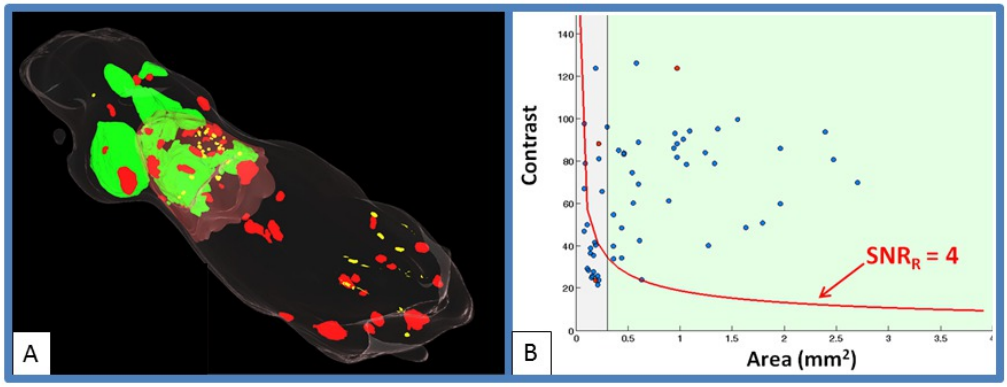

Analysis of molecular imaging of metastases with the cryo-imaging platform. A) Metastatic tumors labeled with GFP were segmented and rendered in different colors according to size. Colors were yellow (diameter <0.5 mm), red (0.5-2 mm), and green (>2 mm). In this mouse, there were 166 metastases with 92 (yellow), 63 (red), and 11 (green). B) Scatter plot of area and contrast of metasteses in lungs. The 3D Rose SNR for each metastasis was computed. All data points lying above the red curve corresponding to a Rose SNR of 4, should have detected signal.

CONTROL ID: 2234199

TITLE: Graft-versus-host Disease Suppression by Mesenchymal Stem Cells as Determined by Cryo-imaging

PRESENTER: David Wilson

ABSTRACT BODY:

Abstract Body: Introduction: Allogeneic bone marrow transplantation (alloBMT) is the only curative treatment for many types of leukemia and lymphomas. However, the development of GVHD limits the success of alloBMT. GVHD results from immunological attack on target recipient organs such as the lung, liver, skin and gut by donor allogeneic T-cells that are transferred along with the donor bone marrow {Nat Rev Immunol, 9:271-285}. Administration of mesenchymal stem cells (MSCs) has been shown to alleviate GVHD {Stem Cells, 33:601-14}. However, the biodistribution of the exogenous stem cells after injection and the immunologic mechanisms behind their protective effects remain to be fully elucidated {Regen Med, 5:121–143}. Our hypothesis is that allogeneic T-cells proliferate at high rates in secondary lymphoid organs (SLOs), that therapeutic MSCs home there, and that MSCs act to suppress T-cell proliferation.

Methods: In this study, we used multi-spectral cryo-imaging (CryoViz^{TM}) to quantitatively evaluate T-cell proliferation, MSC homing, and putative suppression of T-cells by MSCs. Cryo-imaging is a section-and-image method which allows one to image fluorescently-labeled cells anywhere in mouse with single cell sensitivity, allowing one to quantitatively evaluate cell densities far below detection limits of other imaging technologies.

There were four groups of mice: alloBMT (with GVHD), syngeneic BMT (synBME without GVHD), alloBMT + MSCs (GVHD with MSC treatment), and synBMT + MSCs, using methods described previously {Stem Cells: 33: 601-614}. T-cells were labeled with green-fluorescent CFSE dye, and MSCs were labeled with red-fluorescent quantum dots and tail vein injected. Cryo-imaging was performed on days 3, 4 and 5 post BMT.

Results: Using specialized 3D visualization {Comput Med Imaging Graph, 35:195-205}, we examined the bio-distribution of exogenous MSCs and T-cells (Fig A). We determined that MSCs homed to SLOs and localized in the marginal zone in spleen where they could come in contact with T-cells (Fig B). When cells divide, CFSE dye is distributed to daughter cells and the signal intensity of each cell decreases. Hence reduced CFSE signal intensity in the alloBMT group as compared to the synBMT group is consistent with a greater proliferation of T-cells in the alloBMT group as a precursor to GVHD (Figs C and D). However, in the presence of MSCs, the CFSE signal remained high, indicating a reduction in T-cell proliferation (Fig E). Similar results were obtained in lymph nodes. Quantitative assays showed homing of about 3,000-4,000 MSCs in alloBMT, significantly greater than that in synBMT. There was a significant reduction in T-cell proliferation and in SLO volumes when the alloBMT group was treated with MSCs. Treatment always gave results laying somewhere between those of alloBMT (with GVHD) and syngeneic BMT (without GVHD).

Conclusion: Multispectral cryo-imaging allowed us to determine that only a few thousand local MSCs could have significant effects on T-cell proliferation in SLOs. This appears to be at least one mechanism for MSC suppression of GVHD. Cryo-imaging is a useful tool for evaluating sites of action in stem cell regenerative medicine.

AUTHORS (LAST NAME, FIRST NAME): Wuttisarnwattana, Patiwet[1]; Cooke, Kenneth R.[2]; Wilson, David[3]

INSTITUTIONS (ALL):

1. Biomedical Engineering, Case Western Reserve University, Cleveland, OH, United States.
2. Division of Pediatric Oncology, Johns Hopkins University, Baltimore, MD, United States.
3. Biomedical Engineering & Radiology, Case Western Reserve University, Cleveland, OH, United States.

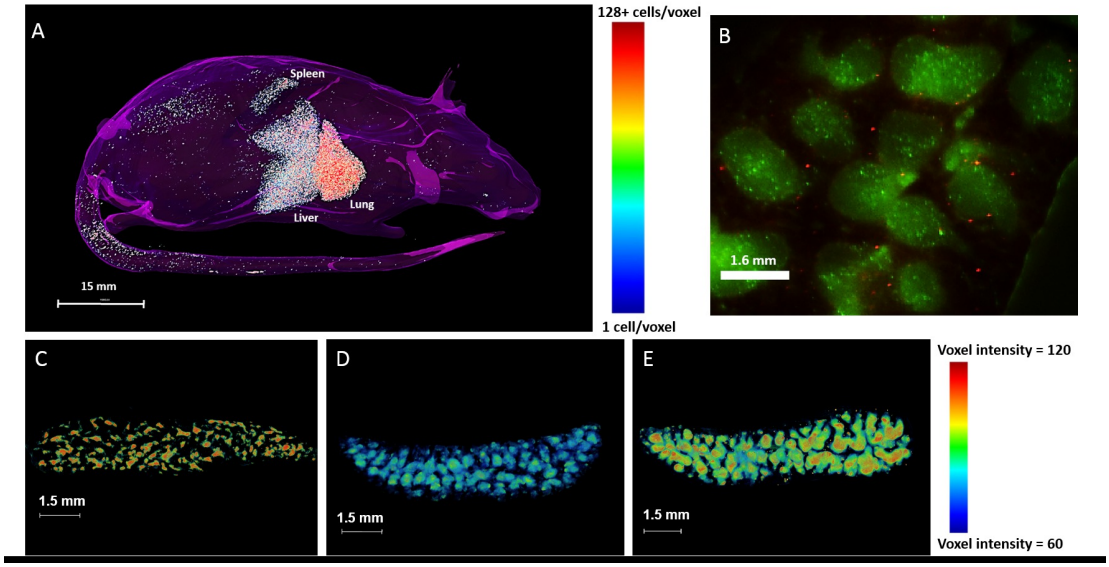
A
Spleen
Lung
Liver
15 mm
128+ cells/voxel
1 cell/voxel
B
1.6 mm
C
1.5 mm
D
1.5 mm
E
1.5 mm
Voxel intensity = 120
Voxel intensity = 60

CONTROL ID: 2234146

TITLE: Quantitative Whole Mouse Stem Cell Imaging with Single Cell Sensitivity using Cryo-imaging

PRESENTER: David Wilson

ABSTRACT BODY:

Abstract Body: Introduction: With its single cell sensitivity over volumes as large as or larger than a mouse, cryo-imaging enables imaging of stem cell biodistribution, homing, engraftment, and molecular mechanisms {Anat Rec (Hoboken); 292:342-51, Comput Med Imaging Graph; 35:195-205, Int J Biomed Imaging, 2012:698413}.

Methods: We developed and evaluated a highly automated software tool to detect fluorescently labeled stem cells within very large (~200GB) cryo-imaging datasets. Cell detection steps were: preprocess, remove immaterial regions, filter to create features, identify candidate pixels, classify pixels using bagging decision trees, segmentation of cell patches, and 3D labeling. To train the classifier, we created synthetic images by placing realistic digital cell models onto cryo-images of control mice devoid of cells.

Results: More than adequate cell detection results were (precision = 98.49%, recall = 99.97%) for synthetic cryo-images, (precision = 97.81%, recall = 97.71%) for manually evaluated, actual cryo-images, and <1% false positives in whole control mice. An α-multiplier on features enabled detection of dimmer stem cells as would be obtained in experiments with less efficient labeling. On dim cells (63% brightness reduction), we improved recall (49.26%→99.36%) without a significant drop in precision (99.99%→99.75%).

There were several options for analysis and visualization. Multi-scale volume visualization allowed one to visualize an entire mouse on the screen and zoom to higher and higher resolutions until single stem cells were seen. Organs could be interactively segmented in our software and organ counts determined. Cell spatial densities could be determined using an interactively defined volume of interest. Multi-cell clusters could be analyzed by generating histograms of size and intensity. With multi-spectral imaging, it was possible to examine colocalization of multiple cell types.

With tail vein injection, mesenchymal stem cells in a graft-versus-host-disease model {Stem Cells, 33:601-14} were predominantly found in lung, liver, spleen, and bone marrow. Distribution was not simply related to blood flow. The lung contained clusters of cells while other tissues contained single cells.

Conclusion: Our methods provided stem cell distribution anywhere in mouse with single cell sensitivity. Methods should provide a rational means of evaluating dosing, delivery methods, cell enhancements, and mechanisms for therapeutic cells.

AUTHORS (LAST NAME, FIRST NAME): Wuttisarnwattana, Patiwet[1]; Gargesha, Madhusudhana[2]; van't Hof, Wouter J.[3]; Cooke, Kenneth R.[4]; Wilson, David[5]

INSTITUTIONS (ALL):

1. Biomedical Engineering, Case Western Reserve University, Cleveland, OH, United States.
2. BioInVision, Inc., Mayfield Village, OH, United States.
3. Cell Processing Facility, Cleveland Cord Blood Center, Cleveland, OH, United States.
4. Division of Pediatric Oncology, Johns Hopkins University, Baltimore, MD, United States.
5. Biomedical Engineering & Radiology, Case Western Reserve University, Cleveland, OH, United States.

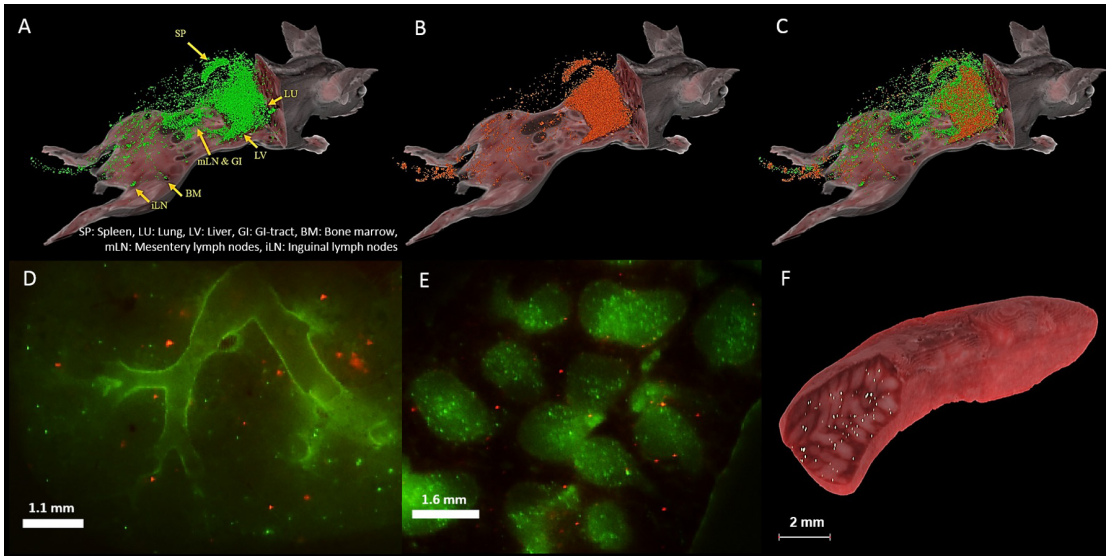
A
SP
LU
LV
mLN & GI
BM
iLN
SP: Spleen, LU: Lung, LV: Liver, GI: GI-tract, BM: Bone marrow,
mLN: Mesentery lymph nodes, iLN: Inguinal lymph nodes
B
C
D
1.1 mm
E
1.6 mm
F
2 mm

CONTROL ID: 2233689

TITLE: Antibody radiolabeling: Improving tumor contrast in vivo by blocking the neonatal Fc receptor.

PRESENTER: Gemma Dias

ABSTRACT BODY:

Abstract Body: Aim:

Monoclonal antibody (mAb) imaging can provide useful diagnostic information. The long circulation time of mAbs can result in high background and lower contrast for tumor imaging. Optimal uptake of radiolabeled mAbs is often seen after 3-7 days post-injection. The neonatal Fc receptor (FcRn) is an important regulatory mechanism that prolongs IgG circulation in the blood. Recently, high affinity mutant Fc fragments have been shown to accelerate the clearance rate of IgGs. We hypothesize that saturating FcRn with a high dose of rabbit IgG, which have high affinity for the mouse FcRn receptor, will enhance clearance rate of ^{111}In-labeled trastuzumab, and improve tumour contrast in HER2 positive tumour bearing mice.

Methods:

NODSCID-IL2RKO female mice were inoculated with SK-OV-3 breast cancer cells positive for HER2 receptor. Trastuzumab (1.0 mg) was conjugated with p-SCN-Bn-DTPA at a 5:1 molar ratio at room temperature and labeled with $^{111}InCl_3$. Samples were purified by ultracentrifugation, and radiolabeling was verified by size exclusion HPLC. Mice were injected with 53.9 ± 2.1 MBq ^{111}In -DTPA-Trastuzumab; 8 hours post-injection (p.i.) 4 mice were injected with 1 mg of rabbit IgG, while 4 mice served as control. Mice were imaged using SPECT/CT at 24 h p.i. followed by bio-distribution.

Results:

^{111}In- DTPA-Trastuzumab was obtained with > 95% radiochemical purity confirmed with SEC HPLC analysis. SPECT/CT imaging in both groups showed high uptake at 24 h p.i. in the tumour; however no significant differences were observed between the rabbit IgG cohort and the control group. Bio-distribution data showed higher tumour uptake in the rabbit IgG group (23.9 ± 4.5 %ID/g) compared to the control (18.8 ± 3.3 %ID/g). Blood uptake in the rabbit IgG group was higher (15.5 ± 1.3 %ID/g) compared to the control (4.6 ± 0.7 %ID/g). Muscle uptake was also higher in the rabbit IgG group (1.5 ± 0.1 %ID/g) compared to (0.9 ± 0.1 %ID/g). As a result, tumour-to-blood and tumour-to-muscle ratios were higher in the control group, (4.3 ± 1.5 and 22.2 ± 4.0 %ID/g respectively) compared to the rabbit IgG cohort (1.6 ± 0.3 and 15.8 ± 3.2 %ID/g respectively).

Conclusion:

Although successful radiolabeling and imaging of HER2 positive tumours was achieved, the use of rabbit IgG to enhance mAb clearance did not result in improved tumor contrast. To improve tumour contrast, the use of engineered Fc fragments or anti-FcRn antibodies might be preferable.

AUTHORS (LAST NAME, FIRST NAME): Dias, Gemma M.[1]; Lau, Joseph[1]; Jenni, Silvia[1]; Colpo, Nadine[1]; Lin, Kuo-Shyan[1]; Bénard, François[1]

INSTITUTIONS (ALL):

1. Molecular Oncology, BC Cancer Agency, Vancouver, BC, Canada.

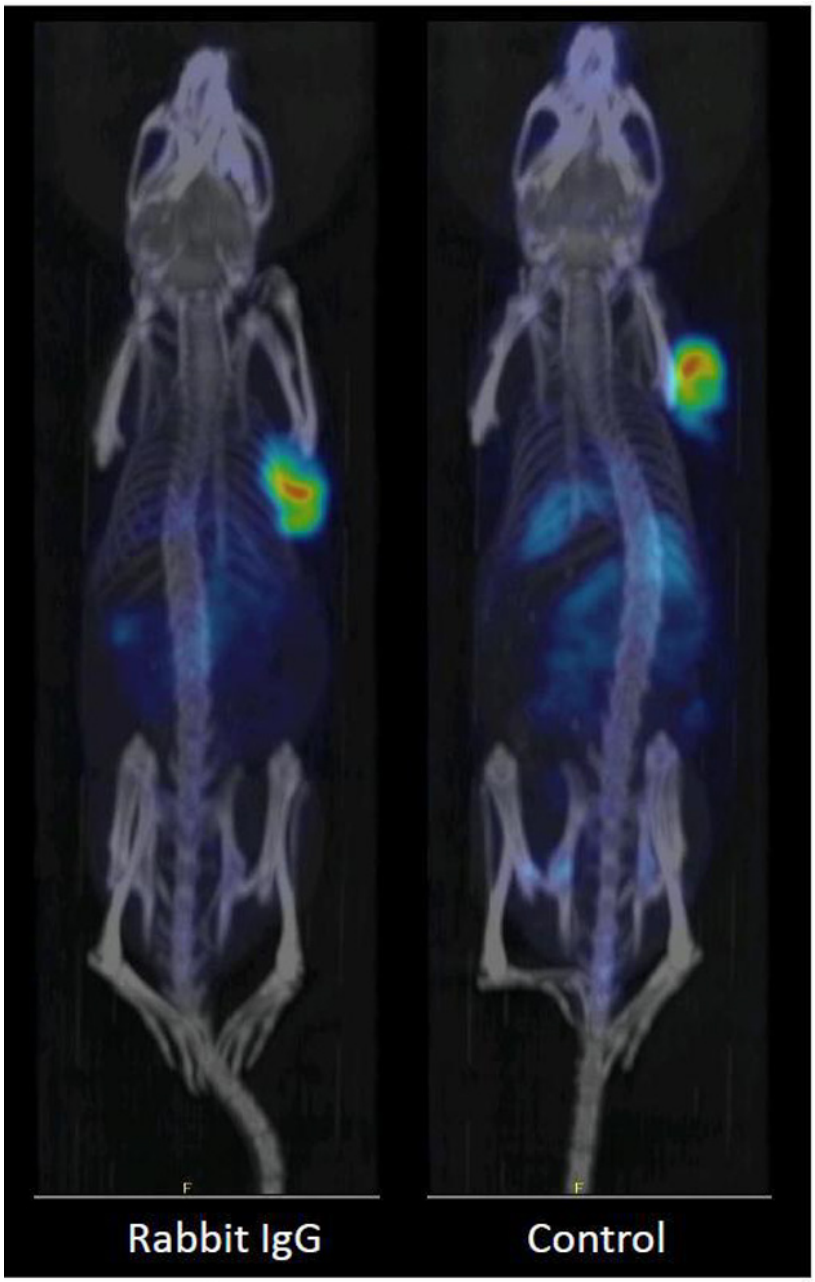

SPECT/CT images of ^{111}In-pSCN-Bn-DTPA-Trastuzumab in SK-OV-3 tumour bearing mice after rabbit IgG injection (left) and control (right) at 24h post injection.

CONTROL ID: 2234244

TITLE: E-cadherin as a potential target to image epithelial-to-mesenchymal transition *in vivo*.

PRESENTER: Gemma Dias

ABSTRACT BODY:

Abstract Body: Aim:

E-cadherin, a transmembrane glycoprotein is an epithelial marker that is expressed in tight adherent junction between normal epithelial cells. Many breast cancers anarchically overexpress E-cadherin, and loss of E-cadherin expression is linked to mesenchymal transition and propensity to metastasize. Interestingly, metastases have been reported to re-express E-cadherin at their homing site.

The goal of this study is to identify and image E-cadherin expression in tumour models of breast cancer using a radiolabeled E-cadherin antibody (anti-E-cad:) Cell Signaling Technology E-Cadherin 24E10, Rabbit mAb)..

Methods:

Western blot and flow cytometry analyses were performed to assess E-cadherin expression in Zr-75, MCF-7, T47D and MDA-MB-468 breast cancer cells. Female mice were inoculated with Zr-75 cells following the implantation of an estrogen pellet. Anti-E-cad (0.5mg;) reacting to both mouse and human E-cadherin) was conjugated with p-SCN-Bn-DTPA at a 5:1 molar and radiolabeled with $^{111}InCl_3$, purified with a 50 kDa filter and verified size exclusion HPLC. Mice were injected with 26MBq ^{111}In-DTPA-anti-E-cad. SPECT/CT imaging was performed at 1, 3 and5 days post injection (p.i.) followed by bio-distribution at day 5.

Results:

E-cadherin expression was confirmed with western blot and flow cytometry in Zr-75, MCF-7, T47D and MDA-MB-468 breast cancer cell lines with the anti-E-cad. ^{111}In- DTPA-anti-E-cad radiolabeling was confirmed with SEC HPLC analysis. SPECT/CT imaging following an injected dose (ID), i.v. of 26 MBq showed relatively high uptake at 24 h in the tumour but decreased over the course of the study, with low background activity in normal tissues. By day 5 bio-distribution data of tumour uptake was 8.88 ± 4.3 %ID/g; however, tumour-to-blood and tumour-to-muscle ratios were 6.28 ± 0.9, and 11.99 ± 4.7, respectively).

Conclusion:

Although this antibody showed promise *in vitro*, the uptake of ^{111}In-p-SCN-Bn-DTPA-anti-E-cad showed decreasing uptake over time in the Zr-75 breast cancer tumor model. Low background activity was noted, which suggests that E-cadherin remains a potential target for *in vivo* imaging. Further work is ongoing to evaluate other tumor models and alternate antibodies.

AUTHORS (LAST NAME, FIRST NAME): Dias, Gemma M.[2]; Zhang, Chengcheng[2]; Colpo, Nadine[2]; Hundal-Jabal, Navjit[1]; Lin, Kuo-Shyan[1]; Bénard, François[1]

INSTITUTIONS (ALL):

1. Molecular Oncology, BC Cancer Agency, Vancouver, BC, Canada.
2. Molecular Oncology, BC Cancer Research Centre, Vancouver, BC, Canada.

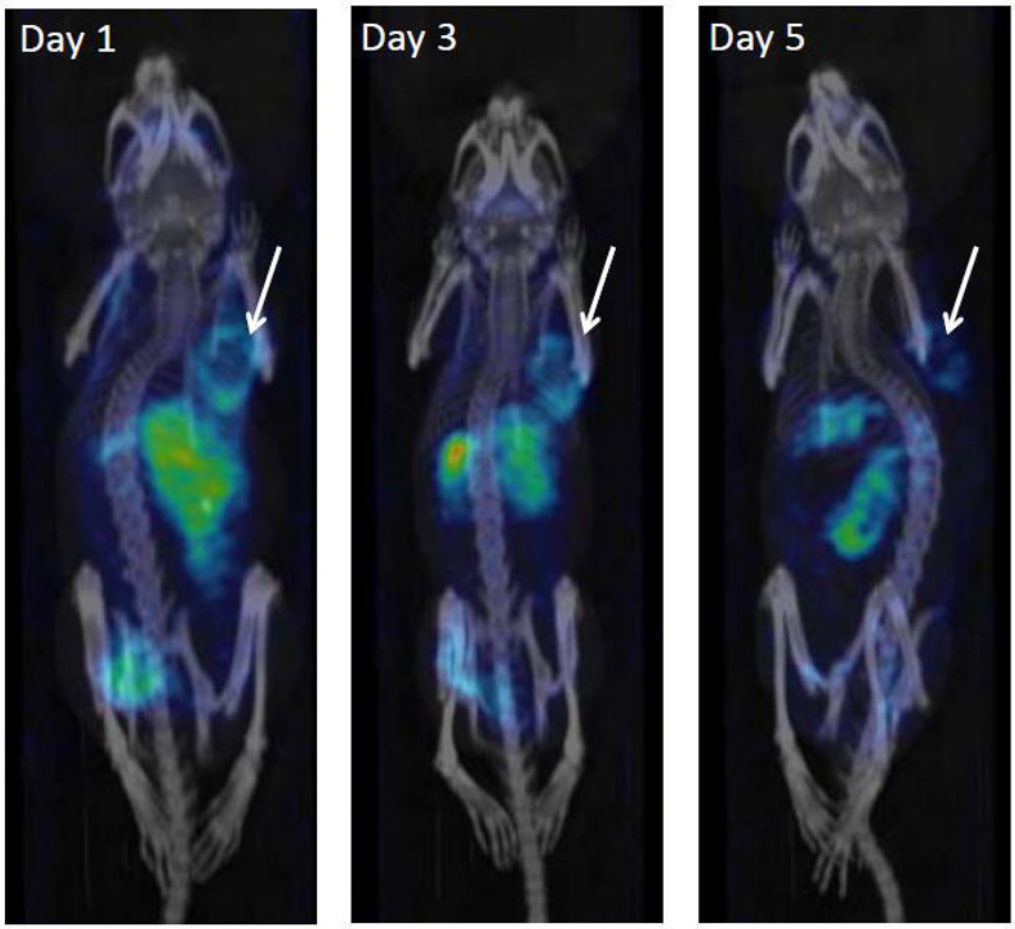

SPECT/CT images of ^{111}In-pSCN-Bn-DTPA-anti-E-cad in Zr-75 tumors (white arrow) at 1, 3 and 5 days post injection

CONTROL ID: 2233695

TITLE: Quantitative Optimization of the Targeting Ligand Density on Fluorescence Enhancing Gold Nanomatryushkas for maximal Target to Background and Tumor Accumulation.

PRESENTER: Amit Joshi

ABSTRACT BODY:

Abstract Body: Objective: Safe and biocompatible gold nanostructures designed to enhance NIR fluorescence and enable photo-thermal ablation can provide intra-operative guidance as well as thermal treatment options for non-resectable pancreatic cancer. Nanomatryushkas (gold-silica-gold multilayers) are a novel sub 100 nm nanostructure which can encapsulate and enhance the fluorescence quantum yield of NIR dyes, while simultaneously providing NIR photo-thermal ablation capabilities exceeding the conventional silica core gold nanoshells. [1,2] Herein, we optimize the tumor accumulation of Nanomatrushkas encapsulating Cy7 dye, which are further targeted to tumor associated inflamed vasculature via E-Selectin targeting thioaptamer (ESTA1) for image guided photo-ablation.

Methods: NIR resonant gold nanomatryushkas (NM) with overall size of ~95nm were synthesized with NIR dye Cyanine-7 covalently bound into the intermediate silica layer (Supporting Doc Fig S1). NM were surface functionalized with either thiol-PEG, thiol-PEG and thiol-PEG-ESTA1 or with only thiol-PEG-ESTA1. These NM variants had differing surface charges, and varying E-Selectin targeting efficacy, which was verified by a quantitative PCR assay developed to compute the number of targeting ligands on nanoparticle surface, and Surface Enhanced Raman Spectroscopy to further verify ESTA1 binding on NM. *In vitro* binding of NM-PEG-ESTA1 to HUVEC cells following TNF-alpha stimulation verified E-Selectin targeting. (Supporting Doc Fig S2). Nanoparticles were injected intravenously in the tail vein (200ul) in mice bearing flank xenografts of human pancreatic cancer created with mCherry labeled ASPC-1 cells. Mice were imaged for up to 72 hours with a home-built intensified CCD based NIR imaging system for tracking fluorescent NM distribution in mice. At 72 hours, tumors were harvested for ICP based analysis of gold content.

Results: Whole body NIR-images for representative mice as a function of time following injection of the three NM variants are depicted in Figure 1A. Highest tumor contrast was obtained with minimal no. of targeting ligands (~0.4 ESTA1 molecules per NM), vs non-targeted NM, or when maximal number of ESTA1 molecules were present on NM surface (84 ESTA1 per NM). Increasing targeting efficacy resulted in increasing negative surface charge, with corresponding decease in circulation time. ICP-MS analysis shows a significantly higher (2X) amount of gold detected from tumors injected with minimal ESTA1 per NM compared to when ESTA1 was maximized. These results highlight the sensitive interplay of molecular targeting and contrast loaded nanoparticle surface charge, and highlight the need for careful calibration of ligand distribution on nanoparticle surface for maximizing tumor accumulation.

[1] Ayala et. al., ACS Nano, 2014, 8 (6), pp 6372–6381

[2] Ayala et. al., Nano Lett., 2014, 14 (5), pp 2926–2933

AUTHORS (LAST NAME, FIRST NAME): Ayala-Orozco, Ciceron[2]; Charron, Heather M.[3]; Rao, Lokesh[4]; Volk, David E.[4]; Gorenstein, David G.[4]; Halas, Naomi[2]; Joshi, Amit[1]

INSTITUTIONS (ALL):

1. Radiology, Medical College of Wisconsin, Milwaukee, WI, United States.
2. Chemistry, Rice University, Houston, TX, United States.
3. Texas Heart Institute, Houston, TX, United States.
4. IMM, UT Health Sciences Center, Houston, TX, United States.

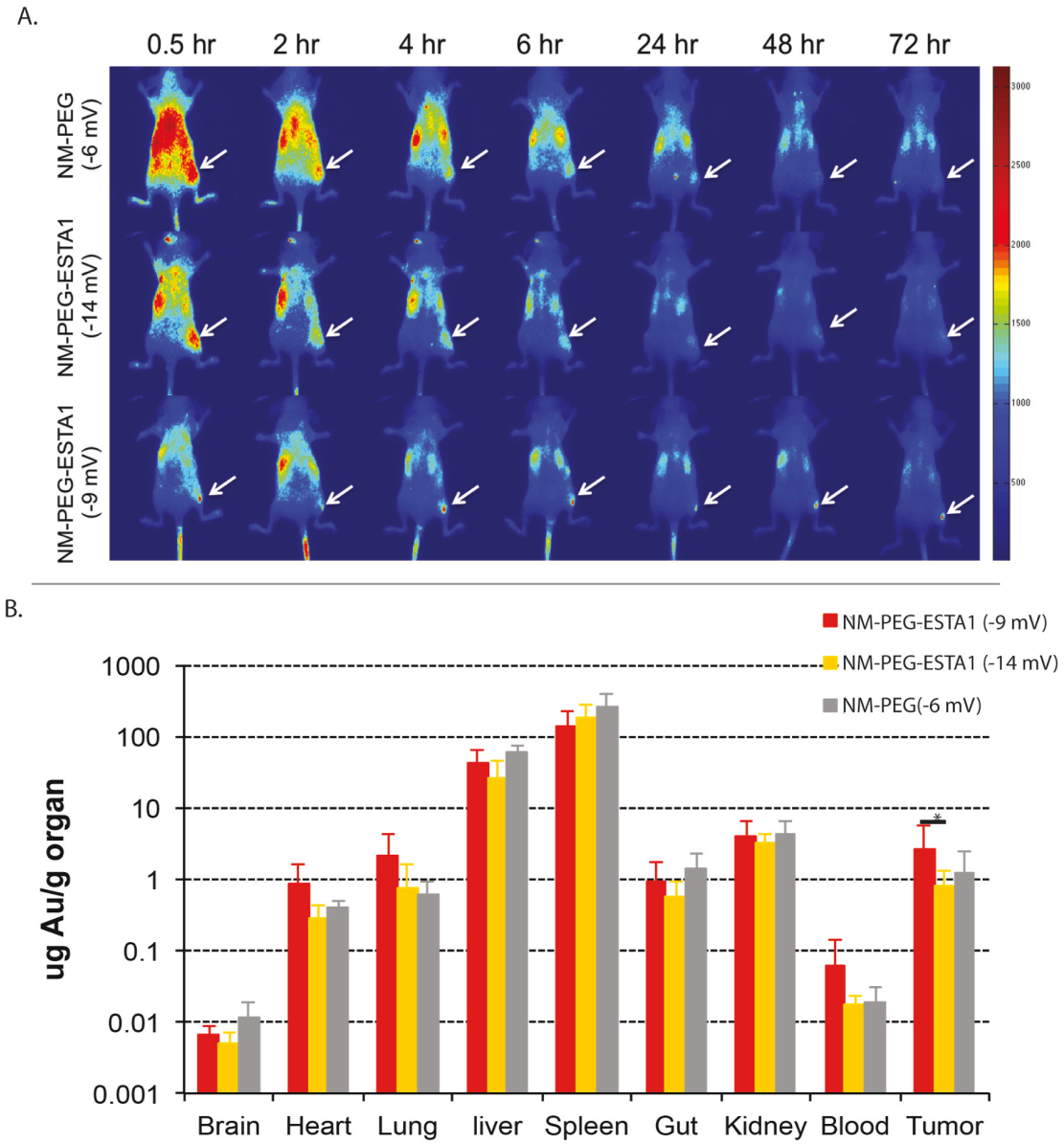

Figure A. Whole body NIR Fluorescence images at Cy7 emission for NM-PEG and NM-PEG-ESTA1 with varying concentrations of PEG-ESTA1 vs PEG on NM surface. B. ICP-MS based quantification of gold content in organs and tumor at 72 hours post injection.

CONTROL ID: 2233701

TITLE: Convertible MRI Contrast: Sensing the Delivery and Release of Anti-Glioma Nano-Drugs

PRESENTER: Dawen Zhao

ABSTRACT BODY:

Abstract Body: Glioblastoma multiforme (GBM) is the most lethal intracranial cancer. Despite the improvement in GBM survival when adding temozolomide (TMZ), recurrences are inevitable, suggesting the existence of endogenous TMZ-resistant cells or cancer stem-like cells in GBM[1, 2]. Several recent studies have shown that arsenic trioxide (ATO) is able to reverse GBM resistance by depleting the cancer stem-like cell population[2]. However, clinical efficacy of ATO on solid tumors has generally been limited due to its systemic cytotoxicity. We have developed a novel strategy of utilizing the MRI contrast agents, manganese (Mn) to enhance the nano-encapsulation of ATO. Moreover, formation of Arsenite (As)-Mn precipitates inside nanocarriers generated magnetic susceptibility effects, reflected as dark contrast on MRI. Intriguingly, the As-Mn complex decomposed in response to a low pH, releasing ionic As^{3+}, the active form of ATO, and Mn^{2+}, the T1 contrast agent that gave a bright signal. Thus, the convertible MRI contrast of Mn indicated not only the delivery but also the release of the active ATO. Building upon the previously established phosphatidylserine (PS)-targeted nanoplatform, we have further demonstrated the GBM cells-targeted delivery of nano-ATO (PS-L-AsMn). Our data showed that PS-L-AsMn was highly specific to PS-exposed GBM cells and thus effective against both TMZ-sensitive and TMZ-resistant GBM cells. Moreover, the binding and internalization of PS-L-AsMn and subsequent release of ionic Mn and As due to the low pH in endosome-lysosome system was successfully monitored by MRI, based on the conversion of MRI contrast from dark to bright. This study has built a foundation for in vivo application of PS-L-AsMn as a potential glioma-targeted theranostic agent.

Acknowledgments: Thanks to Peregrine Pharmaceuticals Inc., Tustin, CA, for the provision of PGN635 antibody. This work is supported in part by NIH R01 CA194578 and imaging was conducted by NIH P41 EB015908.

References:

1. Chen, J. et al. A restricted cell population propagates glioblastoma growth after chemotherapy. *Nature* **488**, 522-526 (2012).

2. Kim, J. et al. Itraconazole and arsenic trioxide inhibit Hedgehog pathway activation and tumor growth associated with acquired resistance to smoothened antagonists. *Cancer Cell* **23**, 23-34 (2013).

AUTHORS (LAST NAME, FIRST NAME): Zhang, Liang[1]; Zhang, Zhongwei[1]; Zhao, Dawen[1]

INSTITUTIONS (ALL):

1. Radiology, UT Southwestern Medical Center, Dallas, TX, United States.

(No Image Selected)

CONTROL ID: 2233705

TITLE: Dynamic Contrast Enhanced (DCE) MRI detects changes in vascular permeability following treatment with thermally-sensitive liposomal doxorubicin

PRESENTER: Brett Fite

ABSTRACT BODY:

Abstract Body: Introduction: Thermally sensitive liposomal formulations of chemotherapeutics promise reduced systemic toxicity while simultaneously achieving lethal concentrations at the tumor site via localized, often ultrasound, heating. The substantial local release of drug into the tumor vasculature can produce immediate changes in vascular permeability.

Objective: To examine the feasibility of dynamic contrast enhanced (DCE) MRI to assess chemotherapeutic agent release from temperature sensitive liposomes.

Methods: In female FVB mice bearing bilateral *neu* deletion (NDL) tumors, one tumor was insonified (1.5 MHz, 1.1 MPa, variable duty cycle) to 42 °C and maintained for 5 min before *i.v.* administration of doxorubicin (Dox, 543.5 MW) encapsulated in temperature-sensitive liposomes (TSL) at 6 mg-drug/kg-body weight. The tumor temperature was maintained at 42 °C for an additional 20 min[1]. Control groups consisted of hyperthermia only, drug only, and no treatment controls. Changes in permeability of the tumor vasculature following treatment were assessed with DCE-MRI. A T1w gradient echo (FLASH; TE/TR/FA: 2.7ms/100ms/30°; FOV = 4 x 2 cm, matrix = 160 x 80; 11 slices; 140-300 repetitions) was acquired with gadolinium contrast (Prohance, 559 MW; 0.3 μmol/g) injected as a bolus. An ROI was drawn over each tumor and intensity data were extracted as a function of time. Dox fluorescence was evaluated *in vivo* and *ex vivo* following treatment. The gradient echo signal intensity was converted to contrast agent concentration using the R1 of each tumor (measured prior to DCE-MRI) and the relaxivity of Prohance. The concentration versus time curve was used as input to a two-compartment pharmacokinetic model, and kinetic parameters were derived from the fit.

Results: We found that treatment with Dox+US hyperthermia resulted in a decrease of K^{trans} from 0.486 min^{-1} to 0.223 min^{-1} while tumors treated with hyperthermia exhibited an increased K^{trans} to 0.925 min^{-1} in the absence of drug. The apparent decrease in permeability into tumors receiving Dox+US hyperthermia was observed immediately following treatment but when examined over an extended period of time, we found the decreased permeability out of the tumor enhanced the area under the curve of the contrast agent and likely the drug. Dox fluorescence was increased in the treated tumors in proportion to the time of insonation. Histological sections revealed significant hemorrhage in tumors treated with Dox+US hyperthermia suggesting immediate gross changes in tumor vasculature resulting from intravascular release of Dox. H&E sections of tumors treated with hyperthermia alone were unchanged from tumors receiving no treatment. Changes in vascular permeabilty following treatment with TSLs correspond with increased drug accumulation. DCE MRI offers promise for evaluating the local release of Dox from liposomal carriers via the drug's ability to alter vascular permeability. Moreover, DCE MRI can potentially be utilized as a non-invasive technique to evaluate chemotherapeutic payload release *in vivo* of new liposomal drug formulations and insonation protocols.

[1] Journal of Controlled Release (2013); 172(1): 266-273.

AUTHORS (LAST NAME, FIRST NAME): Fite, Brett[1]; Foiret, Josquin[1]; Mahakian, Lisa M.[1]; Tam, Sarah M.[1]; Ferrara, Katherine[1]; Kheirolomoom, Azadeh[1]

INSTITUTIONS (ALL):

1. Biomedical Engineering, University of California Davis, Davis, CA, United States.

(No Image Selected)

CONTROL ID: 2233721

TITLE: Ultrasound-guided and mediated drug delivery combined with a TLR9 agonist accelerates the therapeutic response in a murine breast cancer model

PRESENTER: Azadeh Kheirolomoom

ABSTRACT BODY:

Abstract Body: Background: In the previous study[1] a complete therapeutic response was achieved upon repeated administration of low temperature-sensitive liposomes (LTSL) encapsulating copper-doxorubicin (CuDox-LTSL) two times per week for 4 weeks followed by mild hyperthermia mediated by ultrasound to trigger a rapid release of drug. Upon intravascular release of drug, induction of hemorrhage and the presence of hemosiderin-laden macrophages in histological sections of treated tumors suggested that a combination of chemotherapy and immune activation might be responsible for the complete response.

Objectives: Cytosine-phosphate guanosine oligodeoxynucleotides (CpG-ODN) are agonists of Toll-Like-Receptor 9 (TLR-9) and potent immune stimuli. It was hypothesized that administration of CpG following release of CuDox from LTSL by ultrasound would enhance immune response, accelerate tumor regression, achieve a complete response in a shorter time with fewer treatments, and provide immunity.

Methods: CuDox-LTSL were prepared from DPPC:MPPC:DSPE-PEG2k, 86:10:4 in the presence of copper (II) gluconate and triethanolamine at 0.2 mg-drug/mg-lipid. CuDox-LTSL were administrated *i.v.* to invasive *neu* deletion (NDL) tumor-bearing mice on days 0, 3, and 7 at 6 mg-drug/kg-body weight. The entire tumor was insonified with a peak ultrasound pressure of 1.1 MPa at a frequency of 1.5 MHz at 42°C for 5 min prior to and 20 min post drug injection with a variable duty cycle. Immediately upon completion of hyperthermia, 100 µg of CpG ODN 1826 was administered intratumorally with a single injection of 50 µl.

Results and Discussion: The formation of a complex between Dox and copper (CuDox) was created to enhance the circulation and stability of LTSL, and to reduce systemic toxicity. TSL were employed to release a rapid and large amount of the intact CuDox complex within tumor vasculature in respond to US-hyperthermia without dependence on particle extravasation. Using *in vivo* hyperspectral optical imaging, Dox fluorescence validated delivery in the insonified tumor **(Figure A)**. Hyperspectral optical imaging separated tissue and Dox fluorescence and confirmed enhanced drug accumulation. *Ex vivo* imaging demonstrated that Dox fluorescence in the insonified tumor was high and in the heart was low **(Figure B)**. All mice treated with the combination of CuDox-LTSL and whole-tumor US-hyperthermia followed by CpG showed a complete regression of tumor and extended survival, which was not achieved with individual treatments **(Figures C, D)**. Tumors treated with CpG alone and the contralateral tumors in treatment groups involving CpG suppressed tumor growth, indicating the development of a systemic immune response. Immunoanalysis of tumors treated with CuDox-LTSL+US+CpG ten days after treatment revealed a significant reduction in live tumor cells with an elevation in the leukocyte population. T cell recruitment with a shift toward a cytotoxic CD8+ phenotype indicated induction of adaptive immunity. Ultrasound has the potential to enhance local drug delivery and systemic anti-tumor immune response.

[1] Journal of Controlled Release (2013); 172(1): 266-273.

AUTHORS (LAST NAME, FIRST NAME): Kheirolomoom, Azadeh[1]; Ingham, Elizabeth S.[1]; Mahakian, Lisa M.[1]; Tam, Sarah M.[1]; Foiret, Josquin[2]; Ferrara, Katherine[1]

INSTITUTIONS (ALL):

1. Biomedical Engineering, University of California, Davis, Sacramento, CA, United States.
2. Department of Biomedical Engineering, University of California, Davis, Davis, CA, United States.

(No Image Selected)

CONTROL ID: 2233733

TITLE: Early Experience with Radium 223 Xofigo Therapy in Patients with Prostate Bony Metastases.

PRESENTER: Isis Gayed

ABSTRACT BODY:

Abstract Body: Introduction:

Radium-223 Dichloride (Xofigo) has recently been approved in the US for treatment of bony metastases from castrate refractory prostate cancer (CRPC).

Objective:

This study describes our initial experience in patients with different severity of bony metastases in attempt to identify patients that would best benefit from Ra 223 Xofigo therapy.

Methods:

All consecutive patients who were referred for treatment with Ra 223 Xofigo were prospectively followed up. Patients' demographics, functional status as per the Eastern Cooperative Oncology Group (ECOG) performance score, pain level as per the numeric rating score (NRS) score, PSA, creatinine and hematological values were compared before and at the end of therapy. Patients also had a bone scan (BS) prior to and at the end of therapy if they completed 5 or 6 injections of Ra 223 Xofigo. Patients were divided into favorable response (FR) group if their pain and/or functional status improved versus the unfavorable response (UR) group if they did not improve, deteriorated or deceased.

Results:

Twelve patients with average age 72.9 years were treated with Ra-223 Xofigo. One patient was lost to follow up after the first injection. The average time interval between the BS and the first dose of treatment was 62 days. Six patients had widespread bone metastases, 2 patients had superscans and 3 patients had 2-5 bony lesions. There were 6 patients in the UR and 5 in the FR group. Patients with UR had a mean ECOG and NRS pain scores of 1.8 and 5.2 versus 1.0 and 3.5 in the FR group. Mean PSA and creatinine levels in the UR group were 297.7 ng/mL and 1.4 mg/dL versus 25.0 ng/mL and 1.1 mg/dL in the FR group. The mean hemoglobin, platelets and absolute neutrophil values were 11.3 g/dL, 313.7 K/cmm, and 4.7 K/cmm in the UR group versus 11.7 g/dL, 178.8 K/cmm, and 3.8 K/cmm in the FR group. All patients with favorable response had a bone scan at the end of their therapy which showed improvement in their bony metastases. Only two of the patients with UR completed 5 or 6 injections and had bone scans which in one patient showed significant increase in bony metastases and in the other showed flare of a clavicular lesion with increasing arm pain but otherwise stable metastases.

Conclusion:

CRPC patients with good functional status, lower pain scores, PSA and creatinine levels in addition to stable hematological parameters respond favorably to Ra-223 Xofigo therapy of their bony metastases.

AUTHORS (LAST NAME, FIRST NAME): Gayed, Isis[1]; Amato, Robert[2]; Doshi, Gurjyot[3]; Fanous, Mina[1]; Wan, David[1]; Joseph, Usha[1]; Canfield, Steven[4]

INSTITUTIONS (ALL):

1. Department of Interventional and Diagnostic Imaging, University of Texas Health Science Center at Houston, Houston, TX, United States.
2. Depatment of Medical Oncology, University of Texas Health Science Center at Houston, Houston, TX, United States.
3. The US Oncology Network, The Woodlands, TX, United States.
4. Surgery Department, University of Texas Health Science Center, Houston, TX, United States.

(No Image Selected)

CONTROL ID: 2233744

TITLE: Therapy response monitoring of a highly efficient T cell and checkpoint inhibitor-based immunotherapy in mice with progressed pancreatic cancer with ^{18}F-FDG-PET/MRI

PRESENTER: Barbara Schörg

ABSTRACT BODY:

Abstract Body: Tumor antigen-specific interferon γ (IFN-γ)-secreting CD4^{+} T cells (Th1) mediate strong anti-tumoral effects in mice and in humans. Both malignant cells as well as immune cells express inhibitory receptor-ligand pairs inhibiting anti-tumoral T cells functions. Blockade of these inhibitory receptor-ligands such as lymphocyte activation gene 3 (LAG-3) and programmed death ligand 1 (PD-L1) with specific antibodies is applicable to restore T cell functions. Our aim was to establish a novel highly efficient Th1 cell and checkpoint inhibitor-based combined immunotherapy (CIT) in RIP1-Tag2 (RT2) mice with progressed endogenous pancreatic insular cell carcinomas. Second aim was to monitor tumor progression by 7 T MRI and glucose metabolism as an indicator of T cell activation in the spleen and lymph nodes (LNs) in RT2 mice with CIT using ^{18}F-FDG-PET/MRI.

CIT consists of Tag2-Th1 cells (TA-Th1; 1x10^{7} cells once weekly, *i.p.*), LAG-3 and PD-L1 antibodies (Abs; 1-2 x weekly *i.p.*) and an initial 2Gy whole body radiation (WBR). We started CIT in 10 weeks (wks) old RT2 mice (n = 5-6), which usually die at 14 wks of age due to low blood glucose levels (BGL). Mice were monitored twice weekly by detection of BGL (correlating with tumor burden) and by ^{18}F-FDG-PET/MRI to visualize carcinomas and to uncover the enhanced glucose metabolism of TA-Th1 in lymphatic organs at wk 11 and 14. Control mice underwent no WBR or 2Gy WBR and were treated with TA-Th1 cells and isotype control antibodies (Ctrl-Abs), with PBS (sham) and Abs or Ctrl-Abs. We sacrificed mice at wk 14 and conducted H&E histology and immunohistochemistry (CD3^{+}, B cells) of the pancreatic/tumor tissue and pancreatic LNs. Additionally we conducted FACS analysis focusing on the lymphocyte population.

In the CIT group the BGL increased from 88 ± 7 mg/dl (wk 10) to nearly normal values (100 ± 5 mg/dl, wk 13), ending with 80 ± 7 mg/dl (wk 14) while the BGL in the control group (PBS/Ctrl-Abs/WBR) dropped down to 40 ± 4 mg/dl (wk 14). MRI exhibited no carcinomas in the CIT group but large carcinomas in control group at wk 14. As a consequence of T cell activation, ^{18}F-FDG-PET/MRI uncovered an enhanced ^{18}F-FDG-uptake in the spleen of CIT mice (wk 14; %ID/cc: CIT: 6.1 ± 0.6; control: 3.0 ± 0.4, p=0.01). H&E histology and immunohistochemistry of the pancreas (wk 14) exhibited in the CIT group only very small insular cell carcinomas surrounded and infiltrated by CD3^{+} T cells and normal LNs. In sharp contrast, we found large strongly vascularized carcinomas with hardly any lymphocytic infiltrate and LN-metastasis in the control group. 7-9% of the CD4^{+} cells in the spleen and pancreatic LNs were TA-Th1 cells. To our knowledge this is the first report on combining a Th1 cell based immunotherapy with checkpoint-blockade. CIT is applicable to reinforce Th1-cell based immunotherapies and to induce insular cell carcinoma regression. Using ^{18}F-FDG-PET/MRI we were able to monitor enhanced T cell activity in the spleen of CIT treated RT2 mice. Thus, ^{18}F-FDG PET imaging of T cell activation might enable to distinguish checkpoint inhibitor therapy responders from non-responders in the clinical setting.

AUTHORS (LAST NAME, FIRST NAME): Schörg, Barbara F.[1]; Krüger, Dominik B.[1]; Griessinger, Christoph M.[1]; Eilenberger, Sabrina H.[1]; Reischl, Gerald[2]; Ehrlichmann, Walter[2]; Röcken, Martin[3]; Kneilling, Manfred[3]; Pichler, Bernd J.[1]

INSTITUTIONS (ALL):

1. Werner Siemens Imaging Center, Department of Preclinical Imaging and Radiopharmacy, Eberhard Karls University Tübingen, Tübingen, Germany.
2. Department of Preclinical Imaging and Radiopharmacy, Eberhard Karls University Tübingen, Tübingen, Baden-Württemberg, Germany.
3. Department of Dermatology, Eberhard Karls University Tübingen, Tübingen, Germany.

(No Image Selected)

CONTROL ID: 2233806

TITLE: The Role of Calprotectin (S100A8/A9) in Breast Cancer Malignancy

Yun Zhu and Ann-Marie Broome

Center of Biomedical Imaging, Department of Radiology, Medical University of South Carolina

PRESENTER: Yun Zhu

ABSTRACT BODY:

Abstract Body: Breast cancer in women is a malignant disease causing about 40,000 deaths in the United States every year. The molecular mechanism of malignancy in breast cancer is still unclear. Refractory relapse will occur inevitably by unknown mechanisms. The crosstalk between cancer cell and tumor microenvironment play imperative roles in promoting cancer progression. S100A8/A9 complex is a well known biomarker for inflammation and mediates important signaling networks in the tumor microenvironment. Interestingly, we screened several breast cancer cell lines with high, medium and no expression of S100A8/A9. In addition, TNFα, as a regulatory cytokine for normal mammary gland development and branch morphogenesis, can bind its receptors TNFR1 and TNFR2 to trigger transcriptional activation. This results in up-regulation and secretion of S100A8/A9 in breast cancer cells. Secretion of S100A8/A9 acts as a positive stimulator of EGFR activity. We also demonstrate that S100A8/A9 is able to activate downstream signal transduction cascade kinases, FAK, ERK, p38 and AKT, in S100A8/A9 positive breast cancer cells. S100A8/A9 can interplay with multiple oncogenic molecules to enhance the migration ability of breast cancer cells in the wound scratch assay. Meanwhile, we further show that there is a loss of S100A8/A9 expression at the migration front. By analyzing primary human breast tumor tissues, we reveal that S100A8/9 co-localizes with FAK in the invasive ductal carcinoma with high poorly differentiated lymph node metastasis. Our preliminary data indicate that S100A8/A9 heterodimers play an important role in breast cancer progression. The crosstalk between TNFα and S100A8/A9 signaling network establishes paracrine and autocrine regulation loops to facilitate the development of breast cancer malignancy. Our research goals aim to decipher the S100A8/A9 crosstalk between cancer cells and the tumor microenvironment, which leads to metastatic potential and drug resistance in breast cancer.

AUTHORS (LAST NAME, FIRST NAME): Zhu, Yun[1]

INSTITUTIONS (ALL):

1. RADIOLOGY, MUSC, Charleston, SC, United States.

(No Image Selected)

CONTROL ID: 2233736

TITLE: A HaloTag-Targeted AuDNA-Gd(III) Nanoparticle For Molecular Imaging and Detection of Gene Expression

PRESENTER: Luke Vistain

ABSTRACT BODY:

Abstract Body: Magnetic Resonance Imaging (MRI) provides among the best spatial and temporal resolutions for in vivo imaging [1]. These advantages could position MRI to be the modality of choice for in vivo research, however MRI has lagged behind other imaging modalities in its capacity for molecular imaging. It has been difficult to couple MR contrast to specific proteins, particularly surface receptors. This problem arises in part from the very high detection limit of MR contrast agents compared to the low cellular concentrations of proteins [2 3]. This problem was addressed by developing a targeted AuDNA nanoparticle capable of delivering several hundred Gd(III) chelates per binding event. These nanoparticles were targeted to the HaloTag protein, which serves as a quantifiable model system and lays the foundation for a T_1 MRI reporter gene. Cells that express HaloTag on the outer surface of their plasma membrane showed a significant increase in gadolinium uptake after nanoparticle incubation, resulting in an additional 1.2 fmol Gd(III)/cell compared to similarly treated cells that do no express HaloTag. This HaloTag-dependent uptake enabled clear identification of HaloTag expressing cells in cell pellet images with a 9.4 contrast-to-noise ratio compared to identical cells that did not express HaloTag. It is anticipated that the simple chemistry used to synthesize the targeted particle will be easily expanded to enable targeting to a wide range of cell surface receptors. Furthermore, the HaloTag reporter protein's functionality has been expanded beyond optical imaging to include an MR output.

1. Rudin, M.; Weissleder, R., Molecular imaging in drug discovery and development. *Nat. Rev. Drug Discov.* **2003,** *2* (2), 123-31.

2. Ahrens, E. T.; Rothbächer, U.; Jacobs, R. E.; Fraser, S. E., A model for MRI contrast enhancement using T1 agents. *Proc. Natl. Acad. Sci. USA* **1998,** *95* (15), 8443-8448.

3. Schwanhausser, B.; Busse, D.; Li, N.; Dittmar, G.; Schuchhardt, J.; Wolf, J.; Chen, W.; Selbach, M., Global quantification of mammalian gene expression control. *Nature* **2011,** *473* (7347), 337-342.

AUTHORS (LAST NAME, FIRST NAME): Vistain, Luke[2]; Rotz, Matthew[1]; Preslar, Adam[1]; Rathore, Richa[1]; Meade, Thomas J.[1]

INSTITUTIONS (ALL):

1. Chemistry, Northwestern University, Chicago, IL, United States.
2. Interdepartmental Biological Sciences, Northwestern University, Evanston, IL, United States.

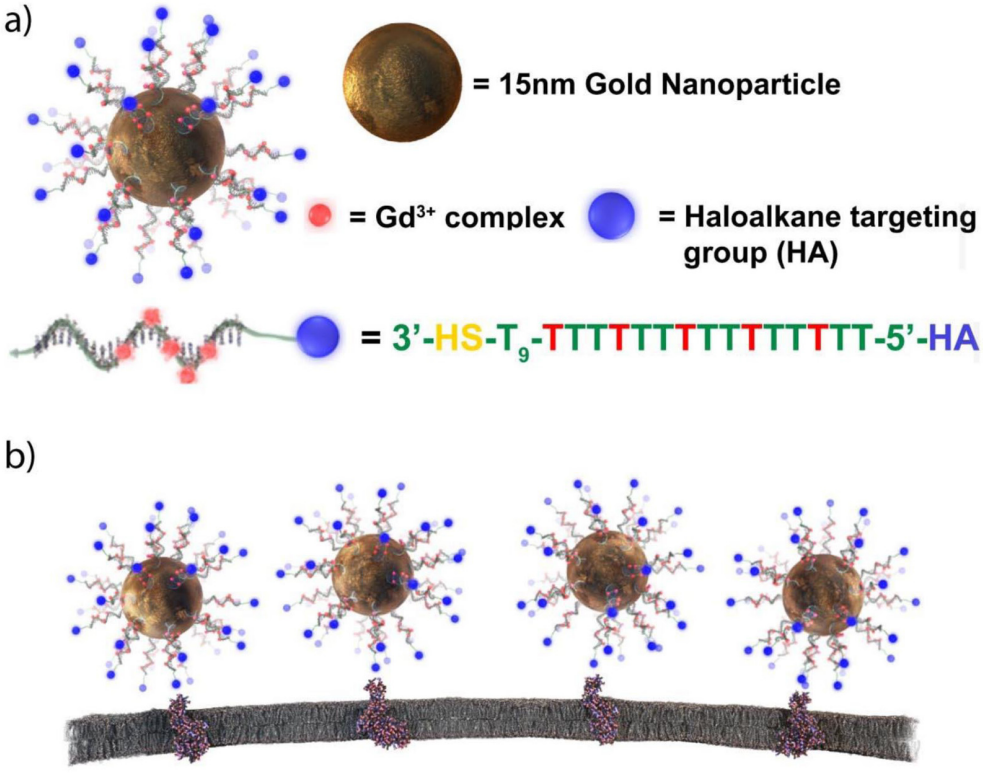

Figure 1: AuDNA-Gd(III)-HA. a) This HaloTag-targeted AuDNA nanoparticle is capable of delivering a large payload of Gd(III) to the HaloTag protein, enabling detection by magnetic resonance imaging. A 15nM gold nanoparticle is conjugated to poly-T ssDNA via thiol bond. Each strand of DNA includes 5 modified bases that can engage in "click" chemistry to attach a single Gd(III) chelate. In total, each particle contains 101 ± 11 strands per particle, yielding a Gd(III)-chelate payload of 508 ± 57 per particle. b) These particles bind readily to HaloTag when expressed on the outer surface of the plasma membrane.

CONTROL ID: 2233740

TITLE: Targeted near-infrared Imaging of Breast Cancer Xenografts in Mice using optimized CMKLR1-targeted Peptide Probes.

PRESENTER: Sarah Poenick

ABSTRACT BODY:

Abstract Body: With cancer being still one leading cause of death, there is an urgent need for personalized diagnostics and therapies. Knowledge about molecular properties as overexpression of certain receptors is thereby offering a promising tool for targeted imaging and tumor selective treatment of cancer cells. One of these challenging targets is the chemokine-like receptor 1 (CMKLR1), with its peptide ligand chemerin being an encouraging molecular entity for probe optimization.

Highly specific and affine peptide ligands for the G-protein coupled receptor CMKLR1 were obtained by substitution of wild type chemerin-9 and analysis of the structure-activity relationship. In consequence, a panel of peptide conjugates with different linkers and fluorophores was designed to gain novel probes for tumor targeting. The combination of near-infrared dye labeled peptides and an established target positive tumor model in immunodeficient nude mice enabled tumor-specific imaging in vivo.

The novel chemerin peptides demonstrated significantly improved properties compared to the wild type peptide concerning biological activity, affinity and metabolic stability. Their target is known to be over-expressed in different pathologies, including cancer. Beside other tumor entities like esophageal cancer, we could show chemerin receptor overexpression in the mamma carcinoma cell line Du4475. After establishment of the breast cancer model along with target negative tumors, near-infrared optical imaging revealed a strong target specific accumulation of the improved chemerin probes in mamma carcinoma tissue within twenty-four hours. As probe biodistribution strongly depended on hydrophilic properties as plasma protein binding, the ligand conjugates exhibited different in vivo tumor accumulation. Further expression analysis of the ex vivo tissue confirmed their target selectivity.

CMKLR1 was found to be overexpressed in the breast cancer cell line Du4475. With this, a model endogenously expressing the target was established to evaluate the optimized chemerin peptides as stable ligands with high affinity for potential imaging applications such as mammography and intraoperative imaging.

This study was supported by a grant from the German Federal Ministry of Education and Research (BMBF), Unternehmen Region 03IPT614A.

AUTHORS (LAST NAME, FIRST NAME): Poenick, Sarah[1]; Hallmann, Sandy[1]; Wagener, Asja[1]; Licha, Kai[2]; Bandholtz, Sebastian[1]; Grotzinger, Carsten[1]

INSTITUTIONS (ALL):

1. Department of Hepatology and Gastroenterology, Molecular Cancer Research Center , Charité - University medicine Berlin, Berlin, Berlin, Germany.
2. mivenion GmbH, Berlin, Berlin, Germany.

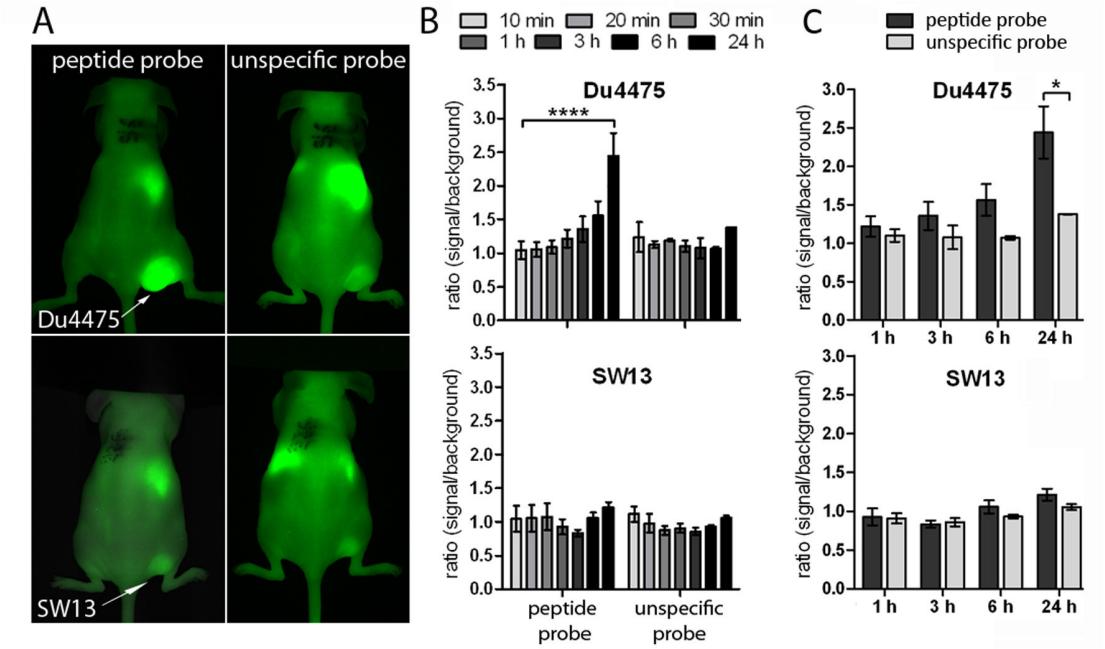

Figure 1: Near-infrared imaging and quantitative analysis of CMKLR1-targeted peptide probe. Optical imaging after 24 hours of fluorophore coupled peptide (left panel) and unspecific peptide probe (right panel) in CMKLR1 positive DU4475 and negative SW13 tumor bearing nude mice. Probe accumulation is indicated in green **(A)**. Quantitative and statistical analysis of tumor-to-background-ratios revealed significant accumulation of peptide probe within 24 hours in the Du4475 tumors, whereas SW13 tumors showed no significant effect **(B)**. Furthermore, imaging of the unspecific probe confirmed the target specific probe accumulation in Du4475 with significant difference after 24 hours **(C)**. (n = 2-6; mean ± SEM; * = $P < 0.05$; **** = $P < 0.0001$)

CONTROL ID: 2233742

TITLE: Matrix Metalloproteinase MMP-2 Detection by Photoacoustic Lifetime Contrast Imaging

PRESENTER: Ekaterina Morgounova

ABSTRACT BODY:

Abstract Body: Matrix metalloproteinases (MMPs) are a family of extracellular matrix degrading enzymes that play a critical role in several stages of cancer progression [1]. Their elevated expression and activity have been associated with a higher metastatic potential and poor disease outcome in patients, and they are a promising target for diagnosis and prognosis of cancer [2]. Here we describe an activatable photoacoustic lifetime probe that has the potential to image MMP-2 activity with high contrast and penetration depth. The probe can switch its excited-state lifetime from short (< 40 ns) to long (> 2,000 ns) upon cleavage by MMP-2. Photocoustic lifetime contrast imaging (PLCI), a new pump-probe photoacoustic technique that can measure the transient absorption of molecules, is used to measure the lifetime contrast between the inactive and active form of the probe [3]. The probe consists of two methylene blue (MB) molecules linked by a flexible linker and an electrostatic zipper that promotes the coupling of the two MB molecules into a dimer form, resulting in static quenching and shorter lifetime. The probe also comprises a recognition sequence specific to MMP-2 that can be cleaved off upon interaction with the enzyme. Upon cleavage, the MB molecules are released and recover their long intrinsic excited-state lifetime detectable with PLCI. A set of 9 peptide probes of varying length and structure were synthesized and compared according to their dimerization efficiency, their separation efficiency, the increase in lifetime upon activation, and their activation rate. Probes without a flexible linker present the highest degree of dimerization of all probes, and the dimerization efficiency is inversely related to the size of the flexible linker ($P < 0.005$). Furthermore, probes without a flexible linker present the highest degree of separation after cleavage. This suggests that probes without a flexible linker will potentially have a lower background noise and a higher contrast for in vivo applications. Interestingly, the presence of the flexible linker 6-aminohexanoic acid ([Ahx]) induces a decreasing linear relationship between the dimer-to-monomer ratio and the length of the electrostatic zipper ($r = 0.998$, $P < 0.05$). The transient photoacoustic amplitude increases 20-fold after activation by MMP-2. This increase was validated by measuring the transient absorption of the same probe using flash photolysis. Finally, the length of the zipper is inversely related to the activation rate of the probes without a flexible linker ($r = 0.999$, $P = 0.0559$), and among probes of the same length the probe without a flexible linker shows an activation rate 25 % higher than that of the probes with a flexible linker. Cell culture experiments are underway to assess the response of the probes to MMP-2 expressing cell lines of different metastatic potential. We believe that this work will provide a solid basis for translational research into early-stage cancer diagnosis, personalized treatment planning and monitoring of treatment efficacy.

[1] Gialeli *et al.*, *FEBS J.* 2011

[2] Morgia *et al.*, *Urol. Res.* 3005

[3] Morgounova *et al.*, *JBO* 2013

AUTHORS (LAST NAME, FIRST NAME): Morgounova, Ekaterina[1]; Johnson, Sadie[2]; Wilson, Michael J.[3, 4]; Hackel, Benjamin J.[2]; Ashkenazi, Shai[1]

INSTITUTIONS (ALL):

1. Biomedical Engineering, University of Minnesota - Twin Cities, Minneapolis, MN, United States.
2. Chemical Engineering and Materials Science, University of Minnesota - Twin Cities, Minneapolis, MN, United States.
3. Laboratory Medicine and Pathology, University of Minnesota - Twin Cities, Minneapolis, MN, United States.
4. Minneapolis VA Medical Center, Minneapolis, MN, United States.

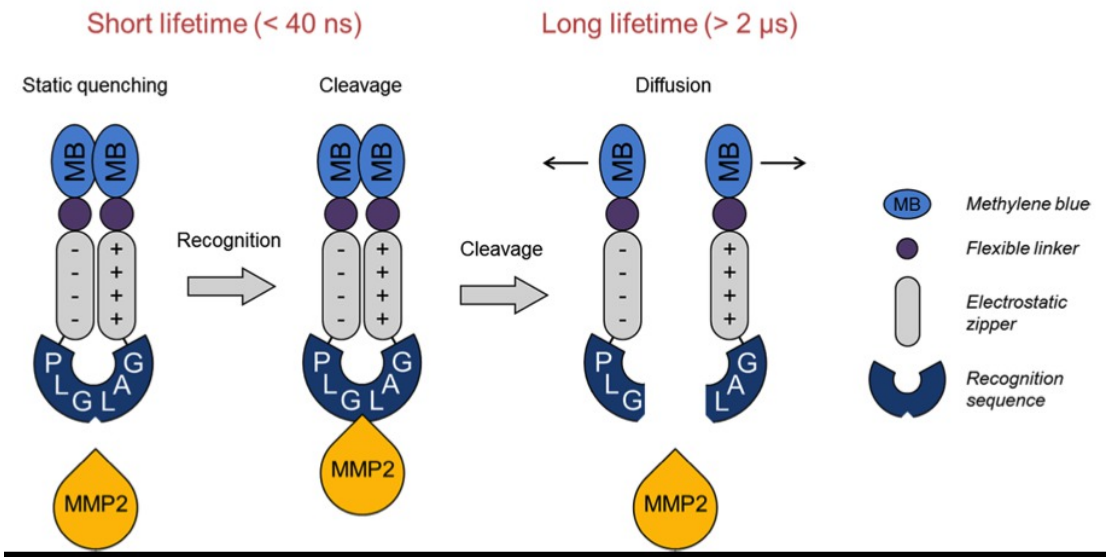

Figure 1. The activatable photoacoustic probe is composed of a MMP-2 recognition sequence, an electrostatic zipper comprising two side chains of opposite electronic charge, a flexible linker and a pair of MB molecules. The probe presents a short lifetime due to static quenching before activation, but recovers its long excited-state lifetime upon cleavage by MMP-2 and separation of its MB-bearing side chains.

CONTROL ID: 2234253

TITLE: Open air fluorescence imaging of tumors using the Solaris imaging system

PRESENTER: Jeffrey Meganck

ABSTRACT BODY:

Abstract Body: Intraoperative tumor resection relies on the ability of a surgeon to discriminate tumor from healthy tissue, either visually or by palpation. Small tumor nodules can be missed or tumor margins may be inadequately removed, resulting in the need for secondary treatment. Intraoperative fluorescence imaging can help improve the initial resection, both improving outcomes and reducing cost. First-in-human studies have examined this theorem using unconjugated fluorescent dyes.[1] However, dyes conjugated to a targeting moiety have better specificity for the tumor itself and provide improved guidance for the surgeon to locate the tumor and determine the margin of resection.[2]

The new Solaris system was recently introduced specifically for intraoperative imaging in research environments.[3] The system supports 4 different fluorescence channels to image common dyes (e.g. indocyanine green [ICG] and Fluorescein isothiocyanate [FITC]) and more unique functionalized targeted or activated near-infrared (NIR) fluorescent agents in an ambient light environment. Recent data illustrate sensitivities of 10 nM for static snapshots and 10-100 nM for real-time acquisition at video frame rates, all under ambient lighting conditions. Because the best sensitivity requires focused fluorescence images, an algorithmic autofocus approach has been implemented to find the best focal plane. In addition, snapshots acquired at different wavelengths can be overlaid to enable multiplexing and improve tumor identification; previously published studies have shown this to be useful for sentinel lymph node mapping.[4] For FITC, where the emission spectra overlaps with tissue autofluorescence, spectral unmixing software has been used to process narrow band images acquired through a liquid crystal tunable filter (LCTF).

Although this system is designed for larger animals, proof of concept intraoperative tumor resection has been performed in rodents. Dosing and timing effects for epi-fluorescence images of subcutaneous and intraoperative surgical imaging has been investigated with both targeted and activatable agents. Subcutaneous tumors have been resected with the aid of imaging in mice injected with either IntegriSense™ 680 or ProSense® 750. Tumor cell lines have also been implanted intrasplenically in rats; the subsequent deep tissue tumors were identified intraoperatively and removed after injection with either BombesinRSense™ 680 or MMPSense® 750. These results suggest that intraoperative resection of tumors identified with both targeted and activatable fluorescent agents is feasible using the new Solaris imaging system.

[1] SL Troyan et al., Ann. Surg. Onc. 2009
[2] GM van Dam et al., Nat. Med. 2011
[3] JA Meganck et al., WMIC 2014
[4] Y Ashitate et al., Theranostics 2014

AUTHORS (LAST NAME, FIRST NAME): Meganck, Jeffrey A.[1]; Vasquez, Kristine[1]; Peterson, Jeffrey D.[1]; Condron, Chris[1]; Behrooz, Ali[1]; kempner, joshua[1]; de Lille, Alexandra[1]; Tan, Yiyong[1]; Harvey, Peter[1]; Gu, Hongyan[1]; Kennedy, Paul[1]; Roxo, Mathew P.[1]; Faqir, Ilias[1]; Mirkin, Leo[1]; Miller, Peter[1]; Yared, Wael[2]

INSTITUTIONS (ALL):
1. PerkinElmer, Hopkinton, MA, United States.
2. PerkinElmer, Hopkinton, MA, United States.

(No Image Selected)

CONTROL ID: 2233974

TITLE: Imaging of tumor targeting by cytotoxic cells in mouse models with positron emission tomography

PRESENTER: Michael Weist

ABSTRACT BODY:

Abstract Body: Advances in cell-based therapies necessitate comprehensive imaging techniques for evaluating the distribution of cells in animals and most importantly patients. Early clinical studies indicate that treatments with chimeric antigen receptor (CAR) T cells and natural killer (NK) cells are effective in prolonging survival and reducing tumor progression in patients. To fully understand the *in vivo* dynamics and distribution of cell based therapies, methods for labeling cells for positron emission tomography (PET) will be developed that maximize radioactivity retention as well as minimize negative effects on cell viability and function. We have selected PET as an imaging modality due to its attractive sensitivity and quantification properties. The positron emitting radioisotopes, ^{64}Cu and ^{89}Zr, were chosen for cell imaging because their half-lives ($t_{1/2}$ = 12.7 and 78.4) approximate the *in vivo* lifespan of CAR T and NK cells. For the first time, we present methods for labeling cells with ^{64}Cu- and ^{89}Zr-oxine without the use of organic solvents. Both efficiently labeled cells with greater than 75% of the starting radioactivity in the cell pellet. Over 75% of ^{89}Zr remained cell associated after 24 hours of *in vitro* incubation; however, approximately 25% of ^{64}Cu was cell associated after 24 hours. Neither method significantly reduced viability as determined by trypan blue exclusion. Following ^{89}Zr-oxine labeling, the *in vitro* cytotoxicity of NK cells with or without cytokines was not affected. Likewise, *in vitro* antigen-dependent interferon gamma production by IL13Rα2-specific CAR T cells was unaffected by ^{89}Zr-oxine labeling. The tumor localization of CAR T and NK cells will be visualized in tumor-bearing mouse models with PET. Preparing cells labeled with ^{89}Zr-oxine is not specific for CAR T or NK cells and should be applicable to many other cell types. Future optimization of cell therapies will be greatly aided by the development of a cell labeling technique for PET imaging.

AUTHORS (LAST NAME, FIRST NAME): Weist, Michael R.[1]; Chea, Junie[1]; Li, Xiuli[1]; Starr, Renate L.[2]; Miles, Joshua[1]; Poku, Erasmus K.[1]; Brown, Christine E.[2]; Colcher, David [1]; Shively, John E.[1]

INSTITUTIONS (ALL):

1. Immunology, City of Hope, Duarte, CA, United States.

2. Cancer Immunotherapy & Tumor Immunology, City of Hope, Duarte, CA, United States.

(No Image Selected)

CONTROL ID: 2233762

TITLE: High Field In-Vivo MRI-Guided Development of Brain Edema Model

PRESENTER: Jeeva Munasinghe

ABSTRACT BODY:

Abstract Body: Introduction:

Peritumoral vasogenic edema (PTVE) of the brain causes major morbidity and mortality. PTVE also impacts treatment outcomes by altering drug delivery to tumors. The mechanisms and timeline of PTVE development remain poorly understood. Vascular endothelial growth factor (VEGF) secreted by tumors may cause blood brain barrier (BBB) breakdown and subsequent accumulation of excess fluid leading to PTVE. Causal relationship between VEGF exposure and BBB breakdown, and the timeline of edema formation in-vivo remains unknown. This study aims to create a reproducible preclinical model of pure vasogenic edema using MRI imaging to characterize PTVE and its relationship to VEGF.

Methods:

Thirty rat striata were infused (1µl/hr) with escalating doses of murine VEGF, or rat serum albumin (RSA - control), via stereotactic cannulae for 6 days. Using an 8-channel array rat head coil and high-field (9.4T) MRI, T1-weighted (T1W) with/without gadolinium contrast, dynamic contrast-enhanced images, T2-weighted (T2W), and diffusion weighted images (DWI) were obtained at 36 and 144 hours to evaluate edema and BBB breakdown. Histopathological characterization of inflammation, gliosis and necrosis was performed after final imaging.

Results:

Similar juxta-cannular and remote T2 signals were observed in VEGF and control rats at 36 hours. BBB breakdown on post-contrast T1W imaging became visible as early as 30 hours after beginning infusion with VEGF. At 144 hours, VEGF animals infused with 2-7µg/ml VEGF developed white matter tract edema on T2W images at least 2 times larger than BBB breakdown at cannula site. In controls, no BBB breakdown was observed, and edema remained constant throughout the study. FITC labeled albumin infusate showed a similar difference in distribution between the control and VEGF animals. Rats in both groups remained neurologically intact and showed no restricted diffusion on DWI images. Histopathology failed to detect signs of cytotoxic edema including inflammatory infiltrate, necrosis, or vessel disruption in either group.

Conclusions:

In this study, we used high-field MRI to confirm the development of a progressive vasogenic edema within 36 hours of exposure of brain tissue to VEGF. We have demonstrated a reproducible, pure vasogenic edema model with minimal cytotoxicity or inflammation. This model can enhance our understanding of the mechanisms and timeline of development of PTVE. Additionally, this model may be used to study the effects of PTVE on drug delivery in brain tumors and peritumoral regions. Future work will include in-vivo optical imaging to quantify and correlate MR imaging markers of BBB breakdown and brain edema.

AUTHORS (LAST NAME, FIRST NAME): Piazza, Martin[1]; Munasinghe, Jeeva P.[2]; Merrill, Marsha[1]; Chittiboina, Prashant[1]

INSTITUTIONS (ALL):

1. Surgical Neurology Branch, NIH/NINDS, Bethesda, MD, United States.
2. NIH/NINDS, Bethesda, MD, United States.

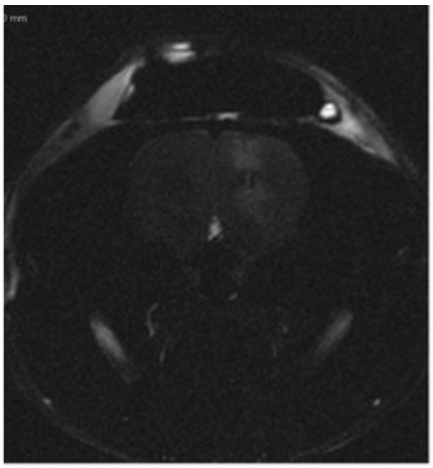

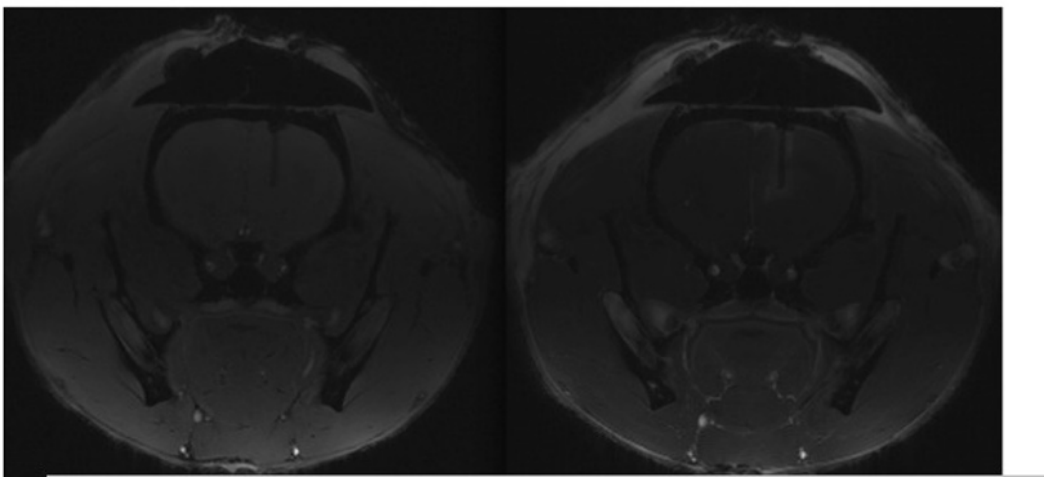

CONTROL ID: 2233771

TITLE: Biodistribution of Macrophage Internalized Gold Nanoshells in a 4T1 Murine Model

PRESENTER: Barry Edwards

ABSTRACT BODY:

Abstract Body: Introduction: Macrophages (MACs) can be loaded with gold nanoshells (AuNS) for efficient delivery of a therapeutic payload of AuNS for photothermal ablative therapy. MACs, recruited to the tumor site by chemoattractants, infiltrate the tumor in sites that are generally inaccessible to AuNS, such as regions of hypoxia. Therefore MACs could be a suitable delivery vehicle for AuNS in photothermal therapy. The goal of this research was to compare the tumoral uptakes of ^{64}Cu-AuNS alone or loaded into MACs in an experimental animal model of human cancer.

Methods: AuNS were synthesized as previously described by the addition of colloidal gold to amine functionalized silica nanoparticles and the subsequent reduction of excess $HAuCl_4$ onto the surface of silica nanoparticles to form a complete shell. The AuNS were functionalized with NODA-GA-PEG5000 and the remaining sites were blocked with PEG5000. After labeling with ^{64}Cu, the ^{64}Cu-AuNS were loaded into RAW264.7 mouse macrophages. Cytotoxicity of the ^{64}Cu-AuNS to the RAW264.7 mouse macrophages was determined with a two-color assay for live and dead cells. ^{64}Cu-labeled AuNS either loaded into MACs or alone were then administered to a 4T1 murine tumor model. After 24 hours, the animals were sacrificed and organs and tumors harvested for gamma counting.

Results: The AuNS had significant absorption in the NIR region and would be suitable for photothermal ablative therapy. After 18 hours of incubation of the ^{64}Cu-AuNS with the macrophages, approximately 500 AuNS/MAC were obtained and the viabilities were better than 80%. There was no significant difference observed in the uptake in the various organs between the ^{64}Cu-AuNS loaded in macrophages (experimental group) or alone (control group) other than the spleen uptake, which was statistically higher in the control group than the experimental group. Overall, the control group had higher uptake in the spleen than the liver, while the opposite was true for the experimental group. These results suggest filtration of the ^{64}Cu-labeled AuNS via the reticuloendothelial system. Mice tails were collected due to coloration of the tissue at the time of sacrifice, with the experimental mice displaying robust %ID/g values compared to the control group. This uptake varied highly between the four mice and uptake is hypothesized to be due to macrophage tracking to the injection site. While uptake of ^{64}Cu-labeled AuNS in the tumors of the control and experimental groups were not statistically significant, we will utilize confocal immunofluorescence microscopy and immunohistochemistry to identify the intratumoral location of the AuNS in each group.

Conclusions: In conclusion, the biodistribution data suggest that there is no difference in tumoral uptake of ^{64}Cu-AuNS in this 4T1 murine model when loaded within macrophage cells (active targeting) versus when delivered without delivery vehicle (passive targeting). Confocal immunofluorescence microscopy and immunohistochemistry will be crucial in validating differences in intratumoral location of ^{64}Cu-AuNS with different delivery platforms.

AUTHORS (LAST NAME, FIRST NAME): Edwards, Barry[1]

INSTITUTIONS (ALL):

1. Radiology, University of Pittsburgh, Pittsburgh, PA, United States.

(No Image Selected)

CONTROL ID: 2234399

TITLE: Dual-mode Prussian blue magnetic nanocubes for photoacoustic imaging and MRI

PRESENTER: Diego Dumani

ABSTRACT BODY:

Abstract Body: Molecular imaging promises to aid in early diagnosis of disease and treatment guidance. Numerous contrast agents have been developed for single modalities [1] [2]; however no single modality is ideal for all stages of patient care. To address this issue we developed Prussian blue nanocubes (PBNCs), which have high near-infrared absorption and are responsive to a magnetic field. These properties can be utilized with a myriad of optical and magnetic based imaging modalities for initial diagnosis, treatment guidance, and/or treatment monitoring.

We characterized the size (~43 nm) and shape using a combination of scanning and transmission electron microscopy. In addition, we characterized the optical absorbance spectra using a spectrophotometer and demonstrated the magnetic attraction of the PBNCs by observing the solution clearing and a pellet formation when exposed to a magnetic field.

To demonstrate the feasibility of PBNCs as a multimodality contrast agent, we used photoacoustic (PA) imaging and magnetic resonance imaging (MRI). We demonstrated the photostability of PBNCs using a 5 ns pulsed laser and exposed the PBNCs to 900 laser pulses across various fluences ranging from 5-28 mJ/cm^2. Unlike the more commonly used gold nanorods (~8.5 mJ/cm^2) or silica-coated gold nanorods (13 mJ/cm^2), no degradation in the PA signal was observed. A gelatin phantom with inclusions of superparamagnetic iron oxide nanoparticles (SPION), PBNCs and SiO2-AuNR was imaged to compare PA signal generation and to obtain optical absorption spectra. The mass of iron was matched on PBNCs and SPION inclusions, and the SiO2-AuNR were concentrated to match the absorbance of PBNCs. The PBNCs showed a brighter signal than that of SiO2-AuNR and SPION.

To demonstrate MRI contrast, a phantom of three plastic tubes containing water, SPION and PBNCs solutions was imaged using a 3T MRI scanner. First, a T1 weighted scan showed all tubes to identify their location. A T2 weighted scan was performed by keeping the repetition time (TR) constant at 3000 ms and varying the echo time (TE) from 50 ms to 1600 ms. SPION appear dark for all T2 weighted images, while PBNCs appeared bright for shortTE and dark for long TE. A difference image was taken from scans at TE = 1600 ms and TE = 50 ms to reveal only the tube containing PBNCs.

Our initial studies indicate that PBNCs are a promising multimodality contrast agent. Although we only demonstrate feasibility as a PA and MRI contrast agent, PBNCs can be utilized with other modalities, including magneto-motive imaging, and magneto-therapy. In the future we will better characterize the magnetization and potential fluorescent properties, and translate our findings for in-vivo imaging studies.

References:

[1] Luke, G. P., Yeager, D., & Emelianov, S. Y. (2012). Biomedical applications of photoacoustic imaging with exogenous contrast agents. *Annals of biomedical engineering*, *40*(2), 422-437.

[2] Na, H. B., Song, I. C. and Hyeon, T. (2009), Inorganic Nanoparticles for MRI Contrast Agents. Adv. Mater., 21: 2133–2148. doi: 10.1002/adma.200802366

AUTHORS (LAST NAME, FIRST NAME): Dumani, Diego S.[1]; Cook, Jason[2]; Luci, Jeffrey J.[4]; Emelianov, Stanislav Y.[3]

INSTITUTIONS (ALL):

1. Biomedical Engineering, The University of Texas at Austin, Austin, TX, United States.
2. Biomedical Engineering, The University of Texas at Austin, Austin, TX, United States.
3. Biomedical Engineering, University of Texas at Austin, Austin, TX, United States.
4. The University of Texas at Austin, Austin, TX, United States.

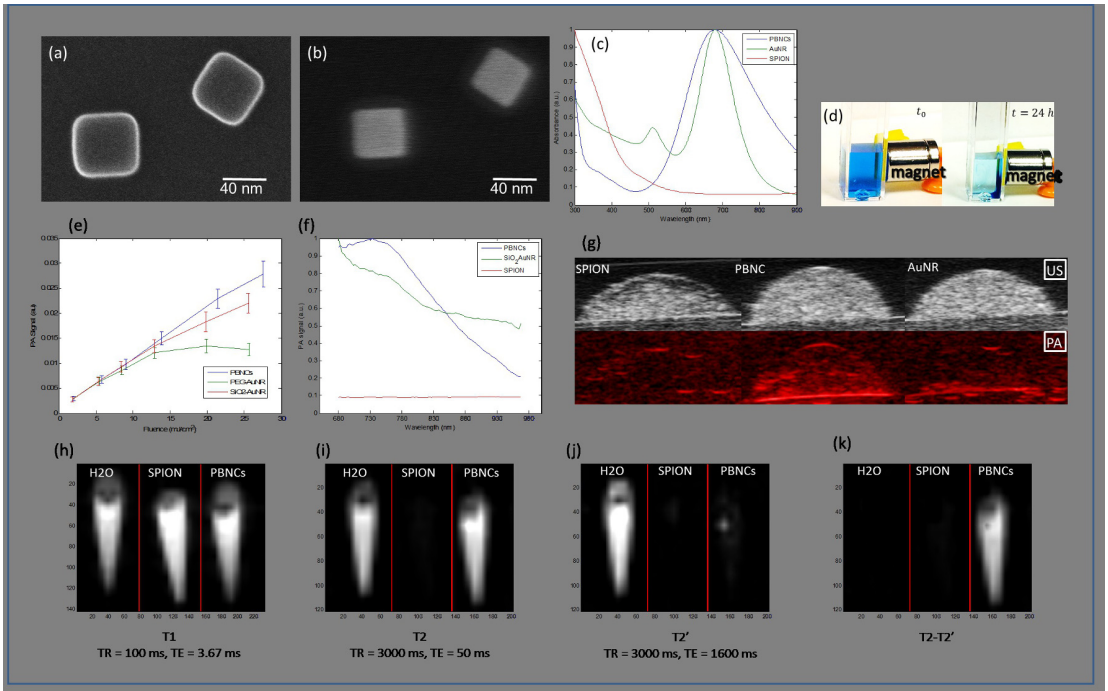

Figure 1. (a) Scanning and (b) transmission electron microscopy of PBNCs. (c) Optical absorbance spectra of the PBNCs. (d) A cuvette containing PBNCs was attached to a permanent magnet; the suspension turns clear after sitting overnight due to particle attraction towards the magnet. (e) Stability of the PBNC photoacoustic signal when exposed to 900 laser pulses at each given fluence. (f) Spectroscopic PA signal from PBNCs, SiO_2AuNR and SPION. (g) US and PA imaging of a gelatin phantom containing inclusions of SPION, PBNCs, SiO_2AuNR. (h) T1 weighted MRI of phantom containing H2O, SPION and PBNCs; (i) SPION show negative contrast in T2 weighted MRI; (j) PBNCs appear dark for long-TR long-TE MRI; (k) difference image shows PBNCs alone.

CONTROL ID: 2233982

TITLE: Bioluminescent Sensor to Image Drug Modulated Protein Sumoylation in Living Animals

PRESENTER: Thillai Sekar

ABSTRACT BODY:

Abstract Body: Sumoylation is a post-translational modification, involves covalent attachment of small ubiquitin-like modifier (Sumo) proteins to various target proteins. This process, in part, is responsible for protein stability, regulation of transcription, nuclear-cytoplasmic transport, cell-cycle control, and apoptosis. Failure of sumoylation in specific target protein and deformities in global sumoylation leads to many cellular diseases including cancer. Although sumoylation has been identified as a major player in many cellular diseases, the use of this process as a potential therapeutic target for drug development is in primitive stage owing to dearth of preclinical methods needed to evaluate the efficacy of small molecule drugs modulating sumoylation of specific target proteins. Developing imaging assay to study target proteins sumoylation would help understanding the biology of sumoylation mediated signaling that control cell growth and development, and also for screening and preclinical evaluation of small molecule drugs. In this study, we developed split-complementation reporter protein sensors to image sumoylation in 7 different target proteins, such as HDM2, ERα, p53, FKBP12, FRB, ID, and HDAC1. We examined all seven target proteins sumoylation by imaging in HepG2 cells, and the results showed significant level of sumoylation specific FLuc signals from 6 of 7 target proteins ($3.54 \times 10^4 \pm 4.9 \times 10^3$ to $3.46 \times 10^6 \pm 2.59 \times 10^5$ p/sec/cm^2/sr) **(Figure A)**. In order to enhance the sumoylation mediated FLuc signals, we constructed plasmid vectors expressing NFLuc with minimal length of sumo target proteins of 50 to 60 amino acids comprising ψKxD/E consensus motif of p53 and HDAC1. The cells co-transfected with CFLuc-Sumo1 with NFLuc-p53 (50aa) or NFLuc-HDAC1 (60aa) showed improved imaging signal of ~25 fold higher when compared to respective full-length target proteins. To confirm the specificity of sumoylation mediated FLuc signals, we constructed sumo1-mut (G96A, G97A) and Deletion mutant plasmids (Last 10 amino acids of C-terminal Sumo1 deleted) and co-transfected with NFLuc-p53, and NFLuc-HDAC1 constructs in HepG2 cells. The sumoylation mediated FLuc signals measured from mutant and Del-mut co-transfected cells were 25 to 30 fold lower when compared to FLuc signals measured from cells co-transfected with respective wild-type sensors **(Figure B)**. To further characterize the functional aspect of sumoylation, we used HepG2 stable cells expressing p53 imaging sensor. The sensitivity was confirmed by observing dose-dependent signal changes to sumo inhibitor, ginkgolic acid. Immunoblot analysis confirmed the dose-dependent signal changes **(Figure C&D)**. Further, to show the suitability of sumo imaging sensor for preclinical evaluation of drugs, we performed *in vivo* imaging in xenograft of HepG2 cells expressing p53 sensor in mice. Sumoylation mediated FLuc signal decreased in response to the treatment of increasing doses of ginkgolic acid **(Figure E&F)**. In summary the *in vitro* and *in vivo* imaging results of the developed sumoylation imaging sensor shows its suitability for pre-clinical evaluation of small molecules targets sumoylation of target proteins.

AUTHORS (LAST NAME, FIRST NAME): Sekar, Thillai V.[1]; Foygel, Kira[2]; Paulmurugan, Ramasamy[1]

INSTITUTIONS (ALL):

1. Radiology, Stanford University, Palo Alto, CA, United States.
2. Radiology, Stanford University School of Medicine, Palo Alto, CA, United States.

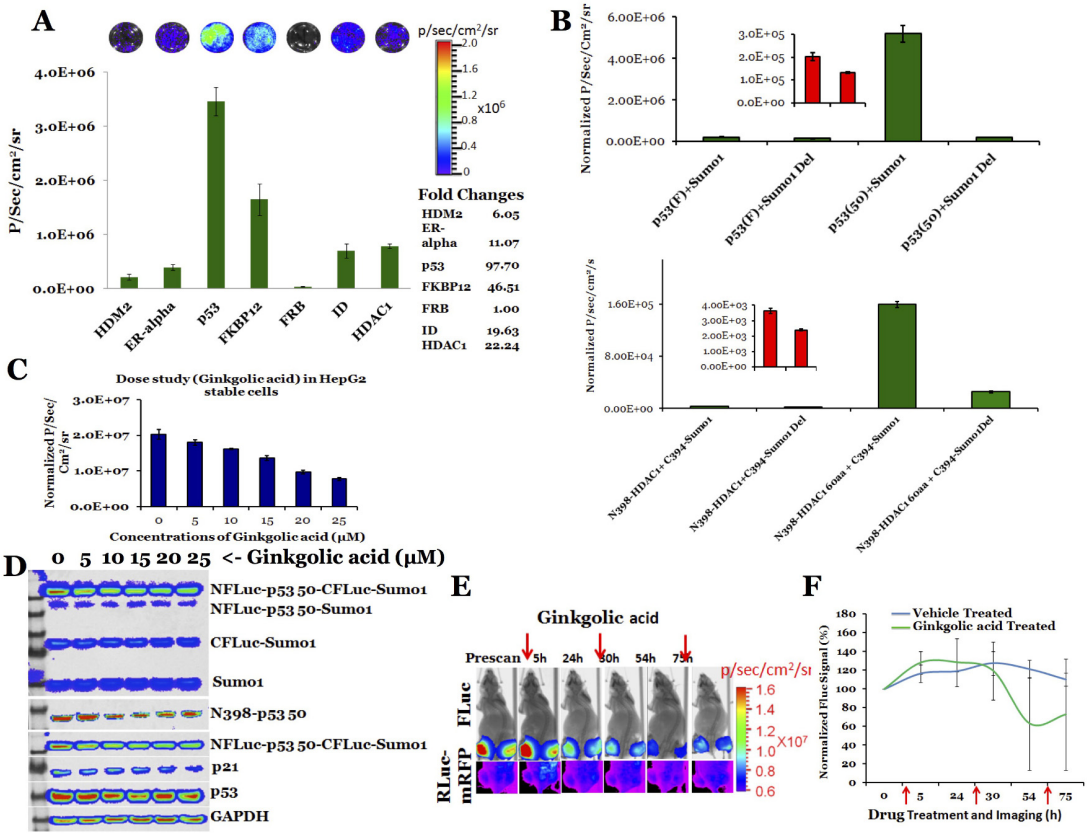

A, FLuc signals measured in HepG2 cells expressing sumo-imaging sensors for 7 different target proteins. Fold changes of target proteins relative to FRB is given in table. **B**, RLuc normalized FLuc signals measured in HepG2 cells expressing p53 and HDAC1 full length and minimal length [p53 (50aa) and HDAC1 (60aa)] sumo-imaging sensors. Inset graphs show the normalized FLuc signals of full length sensors. **C**, Normalized FLuc signals measured in HepG2 cells stably expressing p53 (50aa) sensor protein treated with various concentrations of ginkgolic acid. **D**, Immunoblot shows protein levels of sumo1 conjugated p53 (50aa) sensor, endogenous p53, sumo1 and p21 in stable HepG2 cells expressing p53 (50aa) sumo imaging sensor protein. **E**, Bioluminescence imaging of xenograft of stable HepG2 cells expressing p53 (50aa) sumo sensor protein in response to ginkgolic acid treatment in mice model. Panel at the bottom shows normalizing RFP signals. **F**, Graph shows the normalized FLuc signals measured in nude mice xenograft model expressing p53 (50aa) sumo sensor protein in response to ginkgolic acid at different time intervals.

CONTROL ID: 2234144

TITLE: Transgenic mice model expressing ERα-intramolecular folding reporter sensor for ER-ligand characterization–A special focus on environmental estrogen (Bisphenol-A) induced carcinogenesis

PRESENTER: Thillai Sekar

ABSTRACT BODY:

Abstract Body: Estrogen receptors alpha (ERα) is important mediator of estrogen (E2) signaling in cells, and control the growth of cells by regulating the expression of various cell cycle proteins. ERα has been implicated in many hormone responsive cancer types. A plethora of ligands were developed either as agonistic or antagonistic/selective estrogen receptor modulators specific to ERα, and many of them are in clinical practice. Tamoxifen is a selective estrogen receptor modulator (SERM) showing antagonistic effect in ER positive breast cancer, and agonistic effect in uterus and bone. However breast cancer response to tamoxifen treatment is very successful in the beginning, a significant percent of patients develop tamoxifen resistance. Therefore the need of alternate ligands which can control the growth of tamoxifen resistant breast cancer is inevitable. The *in vitro* competitive blocking assay is the only gold standard currently used to screen ligands, but it may not evaluate the potency of ligands in cell *in vivo* in its native environment where various co-factors are expressed at unique levels. Hence we developed a transgenic mouse harboring fusion genes of split-firefly luciferase (FLuc) and E2 non-responsive ERα ligand binding domain (NFLuc-ER LBD-CFLuc). The fusion protein leads to complementation signal upon a ligand binds to ER-LBD. We have confirmed the sensitivity of this transgenic mouse using a well-established ligand, Raloxifen (Ral) by imaging at different time interval after systemic and subcutaneous injection **(Figure A)**. Dynamic imaging of transgenic mouse exposed to Ral, 4-OHT and DES recorded peak signal intensity at 15min and 20sec, 21 min 2 sec, and 6 min 57sec respectively as a measure of ligands potency **(Figure B)**. After validating the transgenic mouse with known ligands, we studied the estrogen receptor activation of Bisphenol-A (BPA), an environmental estrogen, commonly used as a catalyst for making plastics and epoxy resins. BPA at concentrations of 2.8 and 5.8 nM (reported contaminant threshold in the environment) were given in drinking water for a period of 6 months and imaging was done fortnightly during the treatment period for tissue specific activation for luciferase complementation signal. Fluc signal was significantly high at 5.8 nM dose level of BPA ($3.09 \times 10^6 \pm 2.75 \times 10^4$ p/sec/cm^2/sr) when compared to vehicle treated transgenic mice group ($1.04 \times 10^6 \pm 1.12 \times 10^5$ p/sec/cm^2/sr) **(Figure C&D)**. *Ex vivo* imaging analysis of vital organs clearly showed high BPA induced FLuc signal in pancreas. Furthermore, BPA induced a tumor like outgrowth in flank region of 40% female matured transgenic mouse, and further histological and pathological analysis clearly showed the epithelial origin of the neoplastic outgrowth **(Figure E)**. We also isolated primary fibroplast and exposed to various concentrations of BPA **(Figure F&G)**. The immunoblot analysis confirmed the dose dependent increase of downstream pS2 gene expression with significant correlation with FLuc signal (R^2=0.9284). These results clearly showed that this transgenic mouse could be used to screen novel ligands for treating tamoxifen resistant hormone responsive breast cancers.

AUTHORS (LAST NAME, FIRST NAME): Sekar, Thillai V.[1]; Foygel, Kira[2]; Paulmurugan, Ramasamy[1]

INSTITUTIONS (ALL):

1. Radiology, Stanford University, Palo Alto, CA, United States.
2. Radiology, Stanford University School of Medicine, Palo Alto, CA, United States.

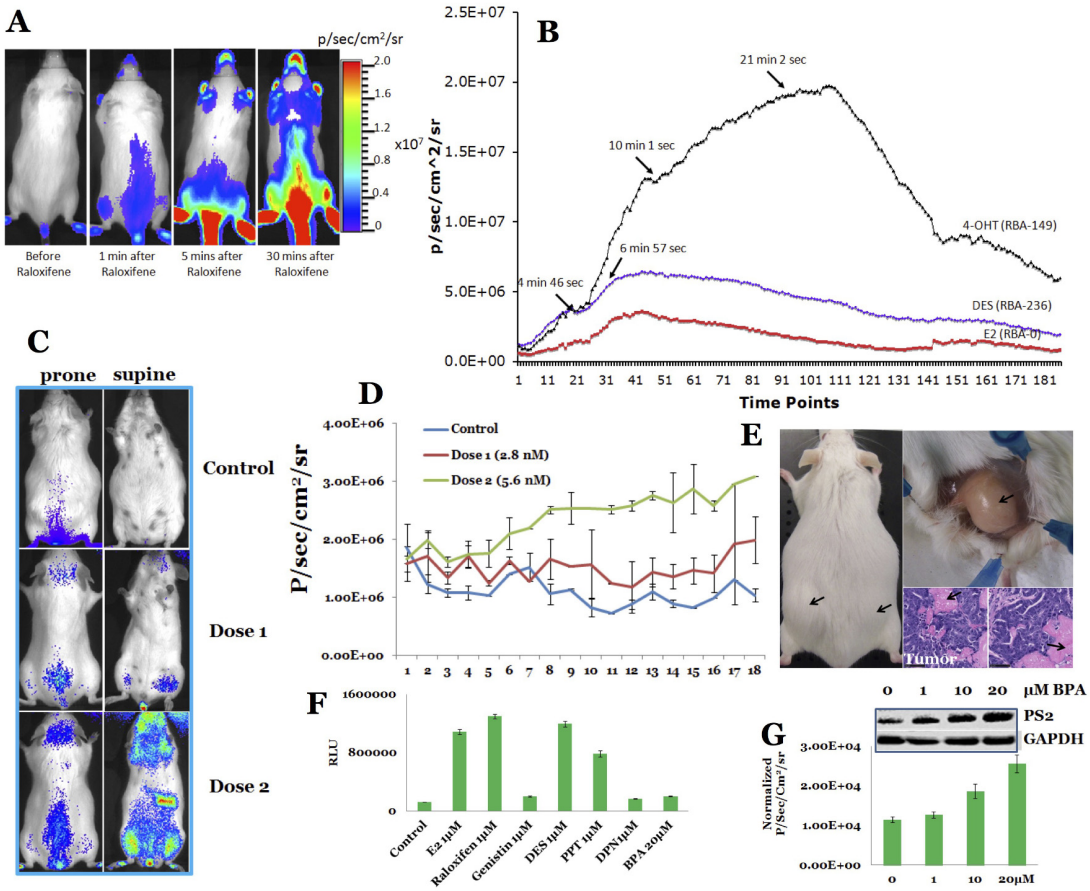

A, FLuc signals measured in ERα transgenic mice at 1, 5 and 30 min after Raloxifen injection. **B**, Graph shows the FLuc signals measured at different time points in transgenic mice injected with 1µM Ral, 4-OHT, DES and E2. **C,** Female transgenic mice show FLuc signals in response to two different doses (2.8 and 5.8nM) of BPA. **D**, Graph shows FLuc signals measured at different time intervals from female transgenic mice fed with water contain vehicle, 2.8 and 5.8nM BPA. **E**, Figure shows the neoplastic outgrowth observed in female transgenic mice exposed to 5.8nM BPA and respective H&E stained tissue. **F**, Fluc signals measured in primary fibroblast cells isolated from female transgenic mice treated with various ligands. **G**, Normalized Fluc signals measured in primary fibroblast exposed to different concentrations of BPA and the immunoblot shows pS2 protein level of primary fibroblast exposed to different concentrations of BPA.

CONTROL ID: 2233935

TITLE: Staff Exposure from Tc-99 Nuclear Medicine Department

PRESENTER: Khalid Alzimami

ABSTRACT BODY:

Abstract Body: Staff and patient are exposed to un avoidable radiation exposure to a wide range of radionuclides, as ^{99m}Tc, ^{67}Ga and ^{131}I during nuclear medicine procedures. Although the frequency of the nuclear medicine is increasing, few data are available regarding ambient and patient exposure worldwide. The The International Commission on Radiological Protection (ICRP) has lowered the annual dose limit for the eye lens from 150 mSv to 20 mSv (i.e., by a factor of 7.5) for occupational exposures, therefore it is crucial to evaluate its impact in the existing programs on radiation protection and safety. Therefore, measurement of staff doses and ambient doses are important. The objectives of this study are to measure the ambient radiation and patient dose during whole body bone scintigraphy, thyroid and renal scan procedures. The study was carried out at Alnilain Daignostic Center, Khartoum, Sudan. Staff radiation exposure personnel were calculated as a function of administered dose distance from the patient and at different times after the administration and workload. A calibrated survey meter and thermoluminescent dosimeters (TLDs- GR200A) were used to measure the ambient dose and staff dose, respectively. Prior to measurements, all TLD were calibrated in terms of air kerma free-in-air under reproducible reference condition using ^{99m} Tc with activity 10 mCi (370 MBq). Quality control performed before administration of the radiopharmaceutical and doses are carefully calculated. All scan procedures were performed using MiE single head gamma camera (Orbiter 37 Gamma camera) after administration of 20 mCi, 4 mCi and 5 mCi of ^{99m}Tc.

The average ambient dose equivalent rate equal to about 12, 25 and 10 μSv/h was obtained at distance of 1 m, at 1.3 m from patient during bone, renal and thyroid scan respectively. Injection room and hot lab has ambient dose equivalent rates of 1.0 and 30 μSv/h at the same order. The maximum dose were recorded at the reception area equal to 180 μSv/h. Staff may exposed to a dose range from 8.0 to 12.5 mSv annually. Knowledge of ambient dose values is crucial in order to determine exposure personnel who may limit the time spent at high dose areas. The dose values are within the safety limit in the light of the current practice. Although, the ambient dose is high compared to previous studies, the staff exposure was below the annual dose limits in the light of the current workload. Appropriate isolation of the patients, training of staff and a strict compliance with the established radiation safety standards are crucial in order to avoid unnecessary radiation exposure.

AUTHORS (LAST NAME, FIRST NAME): Alzimami, Khalid[1, 2]; Sulieman, Abdelmoneim[3]; Babikir, Esameldeen[4]; Alkhorayef, Mohammed[5]

INSTITUTIONS (ALL):

1. Radiology Sciences Department, King Saud University, Riyadh, Riyadh, Saudi Arabia.
2. King Saud University, Riyadh, Saudi Arabia.
3. Prince Sattam bun Abdulaziz University, Alkharj, Please select, Saudi Arabia.
4. King Saud University, Riyadh, Saudi Arabia.
5. King Saud University, Riyadh, Saudi Arabia.

(No Image Selected)

CONTROL ID: 2233787

TITLE: Early Glioblastoma Multiforme Detection through Imaging Deoxyhemoglobin Biomarkers by Active Feedback Magnetic Resonance Molecular Imaging

PRESENTER: Zhao Li

ABSTRACT BODY:

Abstract Body: **Purpose:** Early detection of high-grade malignancy, such as glioblastoma multiforme (GBM), using enhanced MR Molecular Imaging techniques significantly increases not only the treatment options available, but also the patients' survival rate. For this purpose, we have developed a new method, termed "Active-Feedback MR", to enhance the contrast originated from local magnetic-field gradient variations due to irregular water contents and deoxyhemoglobin concentration in early GBM [1].

Method: The general principles of the "Active-Feedback Controlled MR" can be found in our publications [2-6]. Here, its specific applications to image deoxyhemoglobin in early GBM were developed and demonstrated. (i) First, an active-feedback electronic device was home-built to generate feedback fields from the received FID current. The device is to filter, phase shift, and amplify the signal from the receiver coils and then retransmit the modified signal into the RF transmission coil, with adjustable and programmable feedback phases and gains. The MR console computer can execute the active-feedback pulse sequences to control the trigger signal, feedback phase/gain, and the duration of the feedback fields, allowing us to utilize the active feedback fields in novel ways. (ii) Next, an active-feedback pulse sequence was developed for early GBM detection and was statistically tested on *in vivo* orthotopic GBM mice models to enhance the contrast originated from local magnetic-field gradient variations due to irregular water contents and deoxyhemoglobin concentration in early GBM [5]. A quantum mechanical formulation for this approach, termed "Quantum Fixed-Point Spin Dynamics by Active Feedback Magnetic Resonance for Early Cancer Imaging", is attached as "Persuasive Data".

Result: Stage-1 orthotopic GBM mouse models infected with human U87MG cell line were imaged. Representative results from 5 mice were shown in Fig. 2. While T2 parameter images (3^{rd} column), T2-weighted images (4^{th} column), and T1-Gd-weighted images (5^{th} column) could not successfully locate the early GBM tumor, our active-feedback fixed-point images (2^{nd} column) and decay constant mapping (1^{st} column) successfully highlight the early GBM tumor with a close correlation with histopathology (6^{th} column). Statistical results (N>10) show that this new approach provides 5-6 times of improvements in GBM tumor contrast, as measured by "contrast-to-noise ratio" (CNR) or "Visibility".

Conclusion: *In vivo* orthotopic xenografts GBM mouse models validated the superior contrast/sensitivity and robustness of this approach towards early GBM detection. Statistical results (N>10) for GBM mouse models at various cancer stages, alternative active feedback pulse sequences with further improved performance will also be presented.

Reference: [1] Magn. Reson. Med. (in press) [2] Science 290, 118 (2001) [3] Magn. Reson. Med. 56, 776 (2006) [4] Magn. Reson. Med. 61, 925 (2009) [5] J. Phys. Chem. B 110, 22071 (2006) [6] Magn. Reson. Med. 73, 121 (2015)

AUTHORS (LAST NAME, FIRST NAME): Li, Zhao[1]; Hsu, Chao-Hsiung[1]; Lin, Yung-Ya[1]

INSTITUTIONS (ALL):

1. Chemistry and Biochemistry, UCLA, Los Angeles, CA, United States.

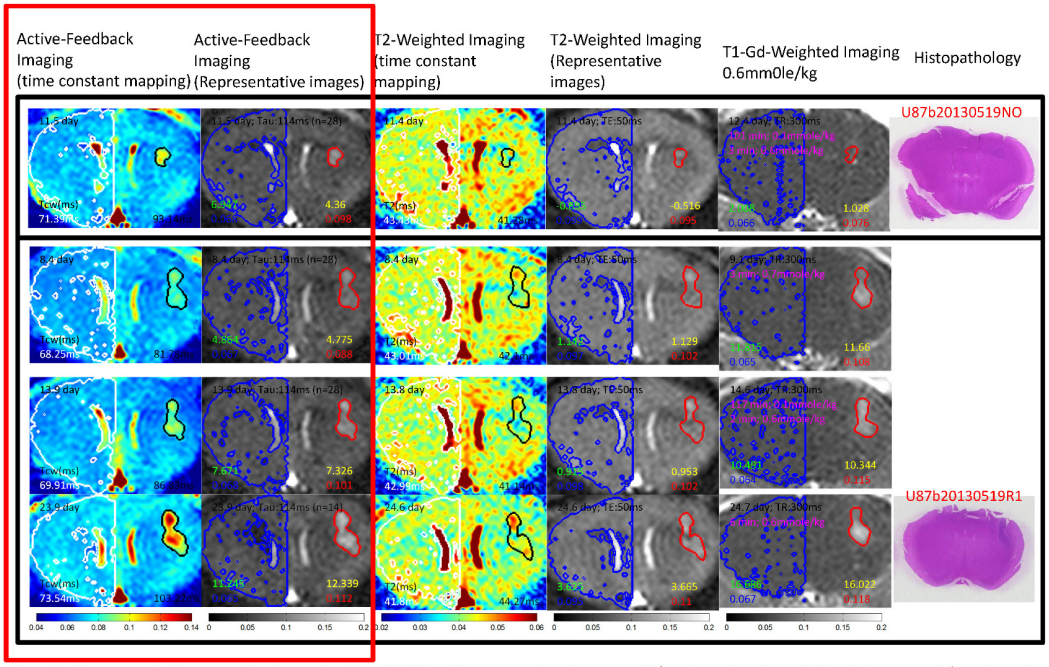

Fig. 1: Representative results from 5 mice. While T2 parameter images (3rd column), T2-weighted images (4th column), and T1-Gd-weighted images (5th column) could not successfully locate the early GBM tumor, the deoxyhemoglobin-based active-feedback fixed-point images (2nd column) and decay constant mapping (1st column) successfully highlight the early GBM tumor with a close correlation with histopathology (6th column).

CONTROL ID: 2234131

TITLE: 13C MR Molecular Imaging and Chemical Imaging by Indirect Detection and Spin Amplification

PRESENTER: Yung-Ya Lin

ABSTRACT BODY:

Abstract Body: **Purpose:** Low sensitivity is particularly problematic in heteronuclear (e.g., 13C) MR molecular imaging, where insensitive, dilute heteronuclear probe spins are detected. A general spin amplification scheme was developed to enhance the sensitivity of heteronuclear probe spins based on dynamic instability of the solvent 1H magnetization under collective feedback fields [1-5]. The heteronuclear probe spins are first detected by the solvent 1H spins through various magnetization transfer mechanisms and serve as small “input” signals to perturb the solvent 1H magnetization, which is prepared in an unstable state. The weakly detected signal is then amplified through subsequent nonlinear evolution of the solvent 1H magnetization. By manipulating bulk solvent 1H spins near the threshold of instability to detect dilute heteronuclear proble spins, sensitivity and signal-to-noise ratios (SNR) of the heteronuclear MR molecular imaging can be markedly improved.

Method & Result: This general spin amplification scheme is shown here to amplify indirectly detected heteronuclear probe signals. Low-gyromagnetic ratio and/or dilute nuclei (e.g., 13C) from the probe molecules can be detected through the large solvent 1H magnetization by the distant dipolar field (DDF) [6]. As shown in the "Persuasive Data", the modulated ^{1}H transverse magnetization precesses under the DDF created by the spatially modulated 13C longitudinal magnetization, generating an echo in the ^{1}H solvent magnetization that carries information about the 13C spins. Recently discovered self-refocusing of dephased solvent magnetization due to the joint action of radiation damping and the DDF is exploited to enhance the indirectly detected echo signal. The extreme sensitivity of the first and largest self-refocused echo's phase and amplitude to the phase and amplitude of the initial triggering magnetization (here, the indirectly detected signal) suggests that the nonlinear spin dynamics can serve as a high-gain spin amplifier to enhance the small initial magnetization transferred to the solvent from the dilute 13C probe spins. The amplification factor can be further improved by controlling the nonlinear spin evolution under the feedback fields. For example, if the 1H pulse flip angle > 90 degree, the instability of the inverted net 1H longitudinal magnetization under radiation damping aids in refocusing more ^{1}H transverse magnetization. Moreover, field inhomogeneity or weak continuous gradients may also be exploited to accelerate the self-refocusing process and increase SNR by more than 10x overall. Application of this approach to 13C MR molecular imaging is shown in the following figure for a phantom sample (top) and carrot stem (bottom), respectively.

Conclusion: Sensitivity enhancement by the dynamic instability of solvent 1H magnetization represents a new direction for surmounting a long-standing weakness of poor sensitivity in heteronuclear (e.g., 13C) MR molecular imaging.

Reference [1] *Science* 290, 118 (2000) [2] Magn. Reson. Med. 56, 776 (2006) [3] Magn. Reson. Med. 61, 925 (2009) [4] J. Phys. Chem. B 110, 22071 (2006) [5] Magn. Reson. Med. 73, 121 (2015) [6] J. Chem. Phys. 108, 1313 (1998)

AUTHORS (LAST NAME, FIRST NAME): Lin, Yung-Ya[1]; Li, Zhao[2]; Hsu, Chao-Hsiung[3]

INSTITUTIONS (ALL):

1. Chemistry and Biochemistry, UCLA, Los Angeles, CA, United States.
2. Chemistry and Biochemistry, UCLA, Los Angeles, CA, United States.
3. Chemistry and Biochemistry, UCLA, Los Angeles, CA, United States.

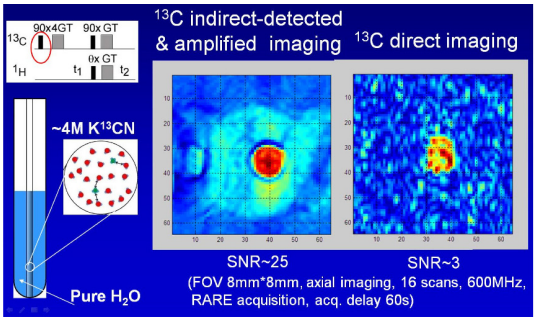

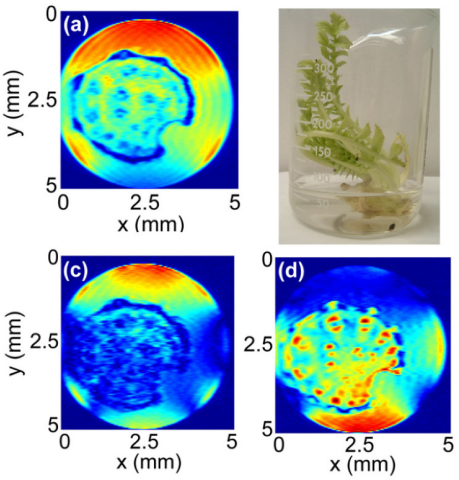

Left: 1H axial indirect-detected spin-amplified MR molecular images at 600 MHz of a capillary containing 4M K^{13}CN. Compared with direct detection of ^{13}C images (right), an enhancement of ~8 times in SNR is achieved for the difference image (left), where the 1st ^{13}C excitation pulse is on or off, respectively.

Right: ^{1}H axial MR molecular images of carrot stems at 600 MHz, acquired after being immersed in 1 M U-^{13}C glucose for 48 hours: (a) T_2-weighted, (b) the carrot, (c) T_1-weighted, and (d) the difference image acquired when the 1st ^{13}C excitation pulse is on or off, superimposed on the ^{1}H density image.

CONTROL ID: 2233796

TITLE: Immunosuppressive nanotherapeutic micelles downregulate endothelial cell inflammation and immunogenicity in models of transplantation

PRESENTER: Ann-Marie Broome

ABSTRACT BODY:

Abstract Body: We have developed a stable, nontoxic novel micelle nanoparticle to attenuate responses of endothelial cell (EC) inflammation when subjected to oxidative stress, such as observed in organ transplantation. Targeted Rapamycin Micelles (TRaM) were synthesized using PEG-PE-amine and N-palmitoyl homocysteine (PHC) with further tailoring of the micelle using targeting peptides (cRGD) and labeling with far-red fluorescent dye for tracking during cellular uptake studies. Our results revealed that the TRaM was approximately 10 nm in diameter and underwent successful internalization in Human Umbilical Vein EC (HUVEC) lines. Uptake efficiency of TRaM nanoparticles was improved with the addition of a targeting moiety. In addition, our TRaM therapy was able to downregulate both mouse cardiac endothelial cell (MCEC) and HUVEC production and release of the pro-inflammatory cytokines, IL-6 and IL-8 in normal oxygen tension and hypoxic conditions. We were also able to demonstrate a dose-dependent uptake of TRaM therapy into biologic tissues *ex vivo* (**Fig. 1**). Transplantation of aortic grafts into allogenic mice improved organ longevity after tranaplntation. Taken together, these data demonstrate the feasibility of targeted drug delivery in transplantation, which has the potential for conferring local immunosuppressive effects without systemic consequences while also dampening endothelial cell injury responses.

AUTHORS (LAST NAME, FIRST NAME): Nadig, Satish N.[2]; Dixit, Suraj K.[1, 4]; Esckilsen, Scott[2]; Miller, Kayla J.[1, 4]; Atkinson, Carl[3]; Broome, Ann-Marie[1, 4]

INSTITUTIONS (ALL):

1. Radiology & Radiological Science, Medical University of South Carolina, Charleston, SC, United States.
2. Surgery, Medical University of South Carolina, Charleston, SC, United States.
3. Microbiology and Immunology, Medical University of South Carolina, Charleston, SC, United States.
4. Center for Biomedical Imaging, Medical University of South Carolina, Charleston, SC, United States.

(No Image Selected)

CONTROL ID: 2233793

TITLE: Dynamic imaging of targeted versus passive diffusion of nanomedicines into tumours :A simultaneous PET-MR study

PRESENTER: Kristofer Thurecht

ABSTRACT BODY:

Abstract Body: Background. Nanomedicines are typically designed to have long residence times in the body as a result of the enhanced permeation and retention effect (EPR). Most nanomedicines in clinical use utilise the EPR effect to passively target tumours.[1] Despite the observation that active-targeting of nanoparticles with ligands such as antibodies enhances uptake and efficacy in pre-clinical models, nanomaterial formulations that have progressed to clinical use typically do not utilise active targeting.[2] Thus, there is a real need for new imaging models that provide a mechanism for assessing directly the advantages of active targeting.

Hypothesis. Simultaneous PET-MR and dynamic scanning in novel mouse models will provide a means to directly assess the kinetics of accumulation of nanomedicines in tumours. This will allow direct comparison of the two competing mechanisms of nanomedicine action and inform on new design of materials.

Aims. The aim of this study was to develop new nanomedicines that directly target prostate cancer cells by way of prostate specific membrane antigen (PSMA) and measure the relative uptake of Cu-64 labelled nanomedicine into two tumours (one that overexpressed PSMA (PC3-PIP) and one that didn't (PC3-FLU)[3]) using PET. A further aim was to measure the nanomedicine diffusion into the tumour tissue (beyond the vasculature) using simultaneous PET-MR and use this to inform on uptake kinetics.

Results. Pegylated nanoparticles were prepared and labelled with a reactive NOTA cage for Cu-64 binding. The small molecule inhibitor of PSMA (glutamate urea) was attached to the periphery of the nanomedicine for targeting the antigen.[4] This chemistry utilized well-established polymerization techniques for ensuring stoichiometric addition of targeting ligand to all PEG end-groups.
The mouse model utilised separate growth of two tumours per mouse, with PC3-PIP on the left flank and PC3-FLU on the right flank. Dynamic imaging of the animals following injection of ~10 MBq nanomedicine via catheter was achieved over the first hour (Bruker Clinscan simultaneous PET-MR), followed by longitudinal scanning over 2 days (Siemens Inveon PET-CT). The PC3-PIP tumour showed far higher uptake of the nanomedicine compared to the PC3-FLU during the first hour following injection (presumably due to enhanced accumulation due to receptor binding). This trend of enhanced uptake of targeted nanomedicine continued over the whole imaging period out to 24 hr (Fig. 1).

Summary. Targeted therapies not only provide a means of rapidly accumulating nanomedicines into tumours (compared to non-targeted materials), but they also show minimal wash-out during the lifetime of the imaging. Gd^{3+} contrast enhanced PET-MR offers a powerful methodology for investigating the distribution of nanomedicines throughout a tumour volume in vivo. This informs on depth of penetration away from primary blood vessels and can lead to development of more efficacious delivery vehicles.

References.

[1] Bertrand et al. Adv. Drug. Delv. Rev., 2014, 66, 2.
[2] Duncan. J. Control. Rel., 2014, 190, 371.
[3] Nakajima et al. Bioconj. Chem. 2011, 22, 1700.
[4] Pearce et al. Polym. Chem. 2014, 5, 6932.

AUTHORS (LAST NAME, FIRST NAME): Thurecht, Kristofer[1]; Blakey, Idriss[1]; Puttick, Simon[1]; Boase, Nathan[1]; Pearce, Amanda[1]; Fuchs, Adrian[1]; Whittaker, Andrew[1]

INSTITUTIONS (ALL):

1. Centre for Advanced Imaging and Australian Institute for Bioengineering and Nanotechnology, The University of Queensland, Brisbane, QLD, Australia.

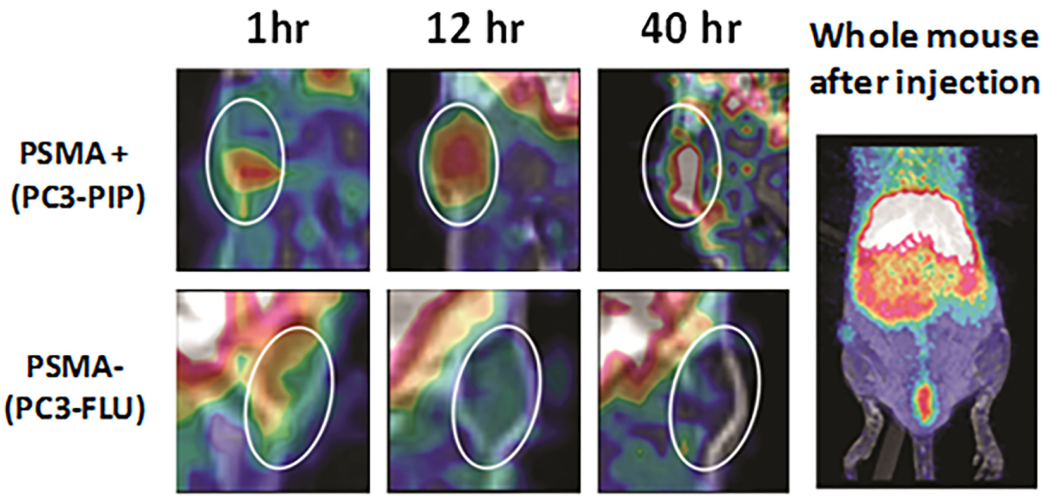

Figure 1. Simultaneous PET-MR images of targeted pegylated nanomedicines to PSMA in mouse model of PCa. PC3-pip cells are injected on left flank and PC3-flu on right flank. Nanomedicine is tracked by Cu-64 PET.

CONTROL ID: 2233791

TITLE: Targeted delivery of temozolomide to brain tumors using micelle-based theranostics

PRESENTER: Kayla Miller

ABSTRACT BODY:

Abstract Body: Diffuse intrinsic pontine glioma (DIPG) is the single most devastating pediatric brain tumor. Surgical excision of these tumors, due to the exquisite location of the pons, is dangerous and is not curative. No chemotherapy has been identified that can control these tumors. One theory for this failure is that the pons is a unique location into which delivery of medications at therapeutic concentrations is singularly challenging. Current standard of care utilizes temozolomide (TMZ), a pro-drug that releases a DNA alkylating agent that is used to kill glial cells. TMZ is very toxic when delivered systemically and therapeutic dosages are limited by severe side effects. These factors necessitate a selectively targeted carrier for TMZ to deliver the drug efficiently to malignant cells avoiding nonspecific interaction and reducing offsite toxicity. In order to design an efficient and effective drug carrier, we addressed several issues: a tailored surface on the carrier to attach biomolecules for targeted drug delivery; a biocompatible coating which can efficiently encapsulate the hydrophobic drug thereby reducing cytotoxicity; and stimuli-induced (pH) disruption of the carrier agent for slow and controlled drug release to the desired environment. Micelles are the preferred choice of carrier as they fulfill these requirements based on their composition. Micelles containing drug are synthesized using PEG-PE-Amine and N-palmitoyl homocysteine (pH sensitive lipid breaks in endosome pH 5.5). Specific targeting of the micelles to glioblastoma cells is achieved by coupling a short 12 a.a. PDGF (platelet derived growth factor) peptide to the amine moeity of the DSPE-PEG. In addition, these micelles have been labeled with a NIR fluorophore to track them for cellular uptake and can be used to image tumor internalization *in vivo*. These micelles have an advantage of small size (<80 nm, to cross blood brain barrier) and reduced toxicity due to robust packaging of TMZ drug inside the core as determined by dynamic light scattering and UV-vis spectroscopy. We have decreased the leaching of the drug in the circulation and in the extracellular microenvironment, resulting in reduced cytotoxicity. Cellular uptake studies via fluorescence imaging, flow cytometry, and spectroscopy of glioblastoma cells treated with either targeted or untargeted micellar nanoparticles demonstrate significant uptake of the PDGFR-targeted micelles, a 6-fold increase in delivered drug over untargeted micelle-TMZ. We show that uptake is mediated by receptor-mediated endocytosis using competition assays and is nontoxic to the cell until released as demonstrated by cytotoxicity assays. We can track the delivery of the micelle-encapsulated TMZ to tumors using NIR *in vivo* fluorescence imaging. Little drug escapes into the surrounding offsite organs. Future experiments involve pharmacokinetic and tissue distribution studies in *in vivo* orthotopic brain tumor models.

AUTHORS (LAST NAME, FIRST NAME): Miller, Kayla J.[1]; Dixit, Suraj K.[1]; Bredlau, Amy-Lee[3]; Broome, Ann-Marie[2]

INSTITUTIONS (ALL):

1. Radiology, Medical University of South Carolina, Charleston, SC, United States.
2. Radiology & Radiological Science, Medical University of South Carolina, Charleston, SC, United States.
3. Pediatrics, Medical University of South Carolina, Charleston, SC, United States.

(No Image Selected)

CONTROL ID: 2233794

TITLE: Feasibility of Dynamic Quantification of Knee Changes using 18F-FDG PET in an *In Vivo* Dog Model of Osteoarthritis

PRESENTER: Maria Menendez

ABSTRACT BODY:

Abstract Body: Background. Osteoarthritis (OA) is the most common form of arthritis. OA is most prevalent in the elderly, and about 50% of adults aged 65–75 years and almost 70% of those 75+ years suffer from this disease. Positron emission tomography (PET) using 2-deoxy-2-[^{18}F]-fluoro-D-glucose (FDG) reflects glucose metabolism and can detect inflammation. FDG PET can demonstrate the site of synovitis and bone marrow lesions associated with OA. Structural and metabolic changes in subchondral bone may play roles in the pathophysiology of osteoarthritis (OA) and even may precede cartilage degeneration in some models. OA osteoblasts have been shown to alter their expression of growth factors and signaling cytokines, modifying the phenotype of chondrocytes, and degrading OA cartilage matrix

Objective. The aim of this study was to quantitatively assess FDG dynamic uptake in the knee serially in an *in vivo* anterior cruciate ligament transection (ACLT) canine model.

Methods. Five skeletally mature Beagles underwent ACLT in one knee via arthroscopy, the contralateral knee served as control. Before, 3, 6 and 12 weeks after ACLT, under general anesthesia, the dogs underwent PET/CT. FDG was injected (3 mCi) and PET/CT was performed using a Philips Gemini TF 64 PET-CT system (Cleveland, Ohio). CT was acquired with 120KVp, 163mAs and 4 mm slice thickness, 90 seconds per bed position. For the dynamic, six frames of five minutes each were acquired. Philips IntelliSpace Portal were used to manually trace three dimensional regions of interest (ROIs) in the posterior cruciate ligament (PCL), medial femoral condyle (MFC), lateral femoral condyle (LFC), medial tibial plateau (MTP), lateral tibial plateau (LTP) and patella (PAT). Outcome measurements included: Area under the curve (AUC; SUV*min), Peak (SUV), time to peak (min) and slope (SUV/min) values (Fig 1).

Results. The ACLT femur, tibia, patella and PCL showed a greater AUC and slope than the controls, specifically at 3 weeks after surgery. Decreasing progressively at 6 weeks and 12 weeks. For the control femur, tibia, patella and PCL, all the timelines exhibit a similar AUC and slope pattern. The time to peak was 5 minutes for all the outcomes (Fig 2, 3, 4 and Table 1).

Conclusion. Quantitative dynamic FDG in a surgically induced OA model in a dog demonstrated feasibility to detect early OA changes in the different knee structures serially.

AUTHORS (LAST NAME, FIRST NAME): Menendez, Maria[1, 4]; Binzel, Katherine[2]; Hettlich, Bianca[4]; Zhang, Jun[3]; Knopp, Michael V.[2]

INSTITUTIONS (ALL):

1. Radiology, The Ohio State University, Columbus, OH, United States.
2. Wright Center of Innovation, The Ohio State University, Columbus, OH, United States.
3. Radiology, Wexner Medical Center at The Ohio State University, Columbus, OH, United States.
4. Veterinary Clinical Sciences, College of Veterinary Medicine. The Ohio State University, Columbus, OH, United States.

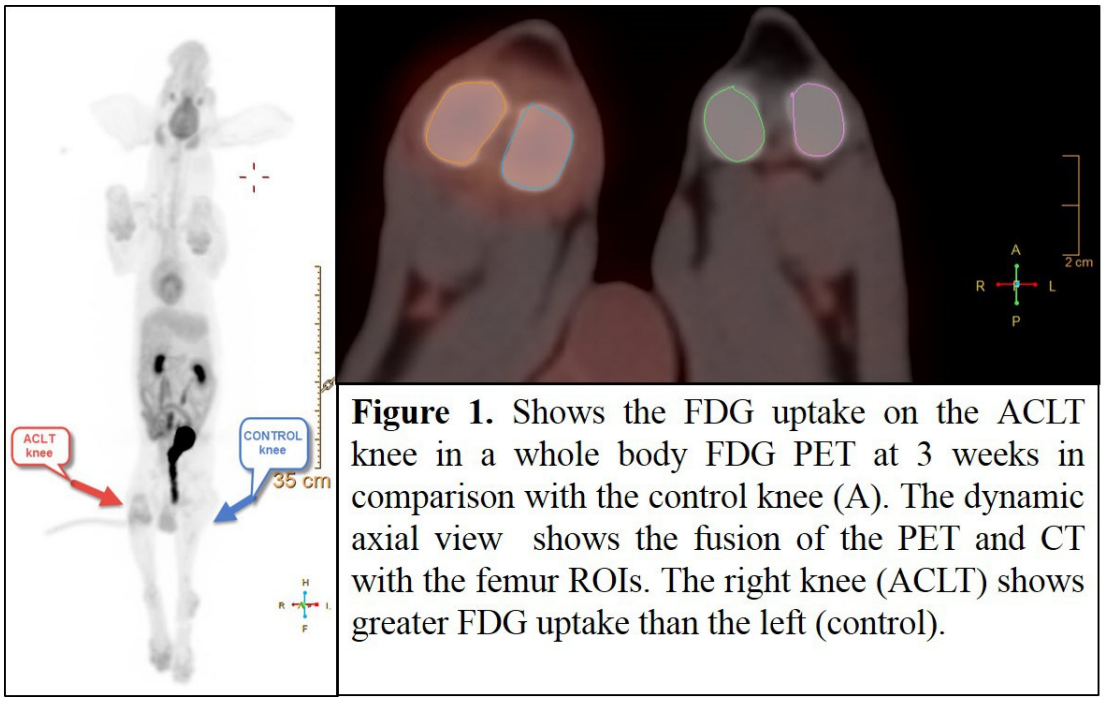

Figure 1. Shows the FDG uptake on the ACLT knee in a whole body FDG PET at 3 weeks in comparison with the control knee (A). The dynamic axial view shows the fusion of the PET and CT with the femur ROIs. The right knee (ACLT) shows greater FDG uptake than the left (control).

CONTROL ID: 2233817

TITLE: Novel multimodal embedded imaging platform dedicated to translational research in oncology: Ultrasound & Photoacoustic imaging associated with biophotonics.

PRESENTER: Florian RAES

ABSTRACT BODY:

Abstract Body: Introduction

The present work aims to develop an imaging platform combining Photoacoustic (PA), Ultrasound (US), Bioluminescence (BLI) and Near Infrared Fluorescence (NIRF) imaging, to improve characterization of tumor key biomarkers at the time of the exploration of a given animal. This assembly operates as true multimodality platform, PA and US being performed via a transducer while BLI and NIRF data were recorded with a camera.

Methods

For the study, bioluminescent HT-29 human colorectal adenocarcinoma was subcutaneously grafted in nude mice, and MDA-MB-231 human breast adenocarcinoma orthotopically implanted. Tumor proliferation was controlled by BLI and fluorescent probes were detected using an ORCA Cmos camera (Hamamatsu) filtered to receive 843±33nm. Fluorescence light source was a Xenon light filtered at 748±37nm (Solos Endoscopy ELS-2). Tumor volume was assessed by 3D Ultrasound (US) and PA signals from fluorescent probes were monitored using the VEVO LAZR system (FUJIFILM VisualSonics Inc.). The spectral unmixing tool was used to enhance the PA sensitivity. Electrocardiogram, breathing rate and body temperature were real time recorded using the VEVO mouse handling heated table. 24h prior imaging, IV injections of AlexaFluor or Indocyanine Green labeled monoclonal antibody towards human EGFR (cetuximab) were conducted. BLI was achieved following IP injection of firefly luciferase (2mg) according to usual protocols.

Results

Fig 1A presents the BLI and reflectance NIRF set up on the left and the PA/US imaging set up on the right. The use of CMOS camera allowed us to record BLI within only 10sec frames enabling dynamic acquisitions for kinetic studies in animal models with metastases. NIRF acquisitions were performed using 2sec frames leading to well delineated foci for superficial tumors. The explorations according to US and PA Modes allowed the confrontation of contrast, Doppler, oxygenation and PA data compared to biophonics.

Conclusions

The results confirmed the potential of this embedded multimodality imaging platform to collect PA and US data in a first step, NIRF and BLI being recorded immediately after, from the same animal. This development allows unique confrontation of data provided by PA/US (3D B-Mode, Doppler, Contrast, 3D PA-Mode, PA spectral unmixing) with a variety of already available NIRF biomarkers (integrins, carbonic anhydrase, proteases activatable probes…). This approach opens new perspectives for biological applications, more especially considering the connexions between hypoxia, neoangiogenesis and targeted drugs in preclinical cancer models in mice.

AUTHORS (LAST NAME, FIRST NAME): RAES, Florian[1]; Fuchs, Dieter[2]; Trochet, Philippe[2]; Needles, Andrew[2]; Lerondel, Stéphanie[1]; Le Pape, Alain[1, 3]

INSTITUTIONS (ALL):

1. Centre for Small Animal Imaging (CIPA), French National Centre for Scientific Research (CNRS), Orléans, Region Centre, France.
2. FUJIFILM Visualsonics Inc., Amsterdam, Netherlands.
3. Respiratory Pathology Study Center, INSERM U1100, Tours, France.

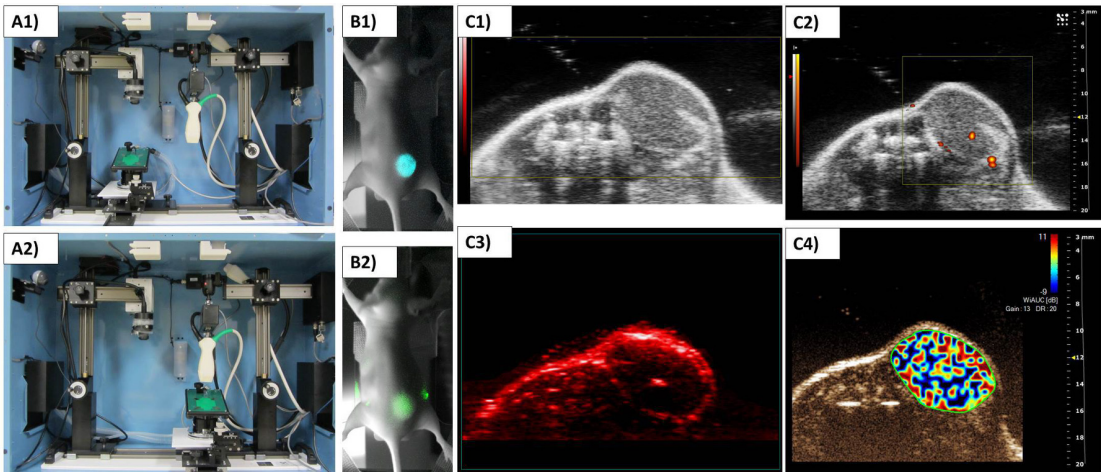

A1 & A2) Set up of the embedded multimodality imaging platform. B1) BLI acquisition. B2) NIRF acquisition. C1) B-Mode. C2) Doppler-Mode. C3) PA-Mode C4) Tumor perfusion in Contrast-Mode.

CONTROL ID: 2233946

TITLE: Investigation on a minimally invaded sentinel lymph node model by high resolution ultrasound coupled to PA imaging with spectral unmixing and NIRF imaging.

PRESENTER: Andrew Needles

ABSTRACT BODY:

Abstract Body: Introduction

The aim of this work was to develop new strategies for the exploration of the Sentinel Lymph Node (SLN) both on excised specimens & *in vivo* in order to improve the tumor micro-invasion detection. We considered an approach combining Photoacoustic (PA) & Near Infrared Fluorescence (NIRF) imaging coupled to high resolution echography. In a preclinical study, we needed to confirm in rats the absence of interaction between two dyes currently clinically used, the Indocyanine Green (ICG) and the Blue Patente V (BPV). Afterwards we combined NIRF imaging from ICG to PA imaging of the micro-biodistribution of BPV & ICG into Lymph Nodes (LN).

Methods

Protocol 1: BPV+ICG or ICG alone were injected in forepaws of healthy rats. NIRF was performed on their excised LN (IVIS-Lumina II system, Perkin Elmer). Protocol 2: BPV+ICG were injected in forepaws of rats. *In vivo* NIRF and PA imaging were done on LNs in order to detect specific signal of dyes (imaging was performed from 10 to 30 minutes after co-injection of dyes). This was achieved using an embedded multimodality platform with a new generation infrared Cmos camera (Hamamatsu Photonics) associated to a VEVO LAZR with spectral unmixing (SU) (FUJIFILM Visualsonics Inc.). Protocol 3: Development of a SLN invasion model in rats, consisting in forepaw injection of human breast adenocarcinoma MDA-MB-231-luc. Thanks to its sensitivity, Bioluminescence Imaging (BLI) allowed precise assessment of SLN minimal invasion.

Results

No fluorescence quenching was evidenced on ICG by BPV. Following a primary detection of LNs by NIRF & echography, results confirm the ability of the PA with SU to ascribe PA signals to each dye. It could be successfully achieved both *in vivo* & *ex vivo* on healthy and tumor associated LNs. *In vivo* BLI is reliable to estimate discreet invasion by cancer cells in the rats LN (about 2000 cells to be confirmed by histopathology).

Conclusions

We start our investigations on healthy LNs considering permeability disturbances associated to LN tumor invasion. PA-SU using true spectral deconvolution allows imaging micro-biodistribution of each specific dye on healthy LNs. Regarding the approach in SLN invasion model, BLI is a unique resource to estimate few tumor cells amount *in vivo* (almost 500 cells in a superficial area such as axillary LN). Targeting few tumor cells inside a micro-invaded SLN by molecular probe (MP) is not sensitive enough to enable direct *in vivo* NIRF. We plan to associate BPV and a PA dedicated MP (RGD mimetic peptide or monoclonal antibody labeled with ICG or Gold Nanorods) to target tumor cells inside the SLNs. With reference to future clinical applications, the co-injection of blue dye and MPs will allow to avoid any substantial modification of the standard surgical procedure. With the aim to detect tumor micro-invasion in LNs, only an *ex vivo* imaging of excised specimens appears to be realistic.

AUTHORS (LAST NAME, FIRST NAME): Badiane, Serigne Moussa[2]; RAES, Florian[1]; Natkunarajah, Sharuja[1]; Needles, Andrew[3]; Fuchs, Dieter[4]; Trochet, Philippe[5]; Lerondel, Stéphanie[1]; Le Pape, Alain[1, 6]

INSTITUTIONS (ALL):

1. Centre for Small Animal Imaging (CIPA), French National Center for Scientific Research (CNRS), Orléans, France.
2. Université Gaston Berger, UFR des Sciences de la Santé, Saint Louis, Senegal.
3. FUJIFILM Visualsonics Inc., Amsterdam, Netherlands.
4. FUJIFILM Visualsonics Inc., Amsterdam, Netherlands.
5. FUJIFILM Visualsonics Inc., Amsterdam, Netherlands.
6. Respiratory Pathology Study Center, INSERM U1100, Tours, France.

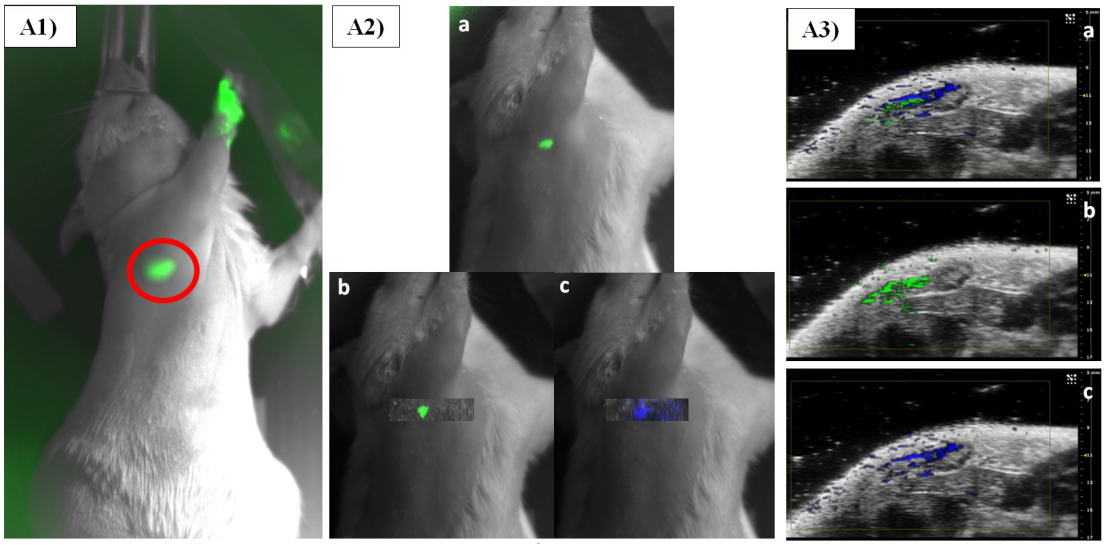

A1) NIRF imaging of the axillary LN in rats following a BPV and ICG forepaw injection. A2) a-NIRF signal; b-Render of the ICG PA signal seen from the top; c-Render of the BPV PA signal . A3) PA data for both ICG & BPV, ICG and BPV using the Spectral unmixing tool (respectively a,b,c).

CONTROL ID: 2233917

TITLE: Limits of bioluminescence imaging highlighted by High resolution Ultrasound and Photoacoustic imaging on orthotopic mice models of hypoxic cancers.

PRESENTER: Florian RAES

ABSTRACT BODY:

Abstract Body: Introduction

Photoacoustic imaging (PA), is an emerging modality increasingly used to perform the mapping of hemoglobin oxygen saturation (SO_2) as well in preclinical as in clinical imaging field. In solid tumors, the decrease in available oxygen because of the functional tumor vasculature deficiency leads to the apparition of a hypoxic micro-environment. This poorly oxygenated area results in alterations of cell metabolism, switching to an anaerobic proliferation, at the origin of chemo and radioresistances. It is thus crucial to document this phenomenon, which is elsewhere resulting in irrelevant data in Bioluminescence Imaging (BLI), this gene expression imaging being closely dependent upon aerobic metabolism. Some previous explorations on the Mia PaCa2-luc[1] (human pancreatic adenocarcinoma) and MDA-MB-231 (human breast adenocarcinoma) orthotopic models highlighted the relevance of these models for preclinical approach of hypoxic human tumors. This work was designed to characterize evolution of hypoxia in these tumor models, as it is essential for oncopharmacology studies to precisely document this hypoxic status.

Methods

Bioluminescent MIA PaCa-2 human pancreatic ductal adenocarcinoma and MDA-MB-231 human breast adenocarcinoma were orthotopically grafted in nude mice. Tumor proliferation was monitored by BLI using the IVIS-Lumina II imaging system (Perkin Elmer), whereas tumor volume was monitored by Ultrasound (US) using the VEVO LAZR system (FUJIFILM VisualSonics Inc.). Seven days after engraftments, tumors were explored both by BLI and US 3 times a week during 12 weeks. Moreover, tumors were investigated by PA imaging so that average values of SO_2 were assessed and hypoxic volumes documented.

Results

In these models, there was a correlation between US and BLI measurements but only during the first weeks of the tumor growth. Beyond this stage, we noticed a continuously increase in tumor volumes whereas a significant decrease in BLI signals occurred. Because of its O_2 and ATP dependency, BLI signals cannot be used as a relevant proliferation biomarker at the time a tumor becomes hypoxic. This phenomenon is clearly evidenced for pancreatic tumors that exhibit progressive decrease of BLI while tumors volumes are growing. For breast tumors, disturbances in BLI are more complex with a two phase process associated to a delayed peripheral tumor proliferation. So, BLI is only relevant in early tumor stages of hypoxic models to allow inclusion of animals into equivalent experimental groups. PA imaging enabled mapping hypoxic areas within the whole tumor volumes during tumor development.

Conclusions

This study confirms that BLI should be used very carefully as soon as hypoxia appears. The combination of these three methods (BLI, US, PA) should therefore allow to precisely characterize hypoxic status of tumor models, while pointing out the BLI limits as a relevant proliferation biomarker. Considering the substantial impact of hypoxia upon chemosensitivity towards antitumor drugs, the use of well characterized hypoxic tumor models should enable a better predictivity for translation to clinical research.

[1] Brulle et al. *PLoS ONE* 7(12): e52653.

AUTHORS (LAST NAME, FIRST NAME): RAES, Florian[1]; Sobilo, Julien[1]; Jose, Jithin[2]; Trochet, Philippe[3]; Lerondel, Stéphanie[1]; Le Pape, Alain[1, 4]

INSTITUTIONS (ALL):

1. Centre for Small Animal Imaging (CIPA), French National Centre for Scientific Research (CNRS), Orléans Cedex 02, France.
2. FUJIFILM Visualsonics Inc., Amsterdam, Netherlands.
3. FUJIFILM Visualsonics Inc., Amsterdam, Netherlands.

4. Respiratory Pathology Study Center, INSERM U1100, Tours, France.

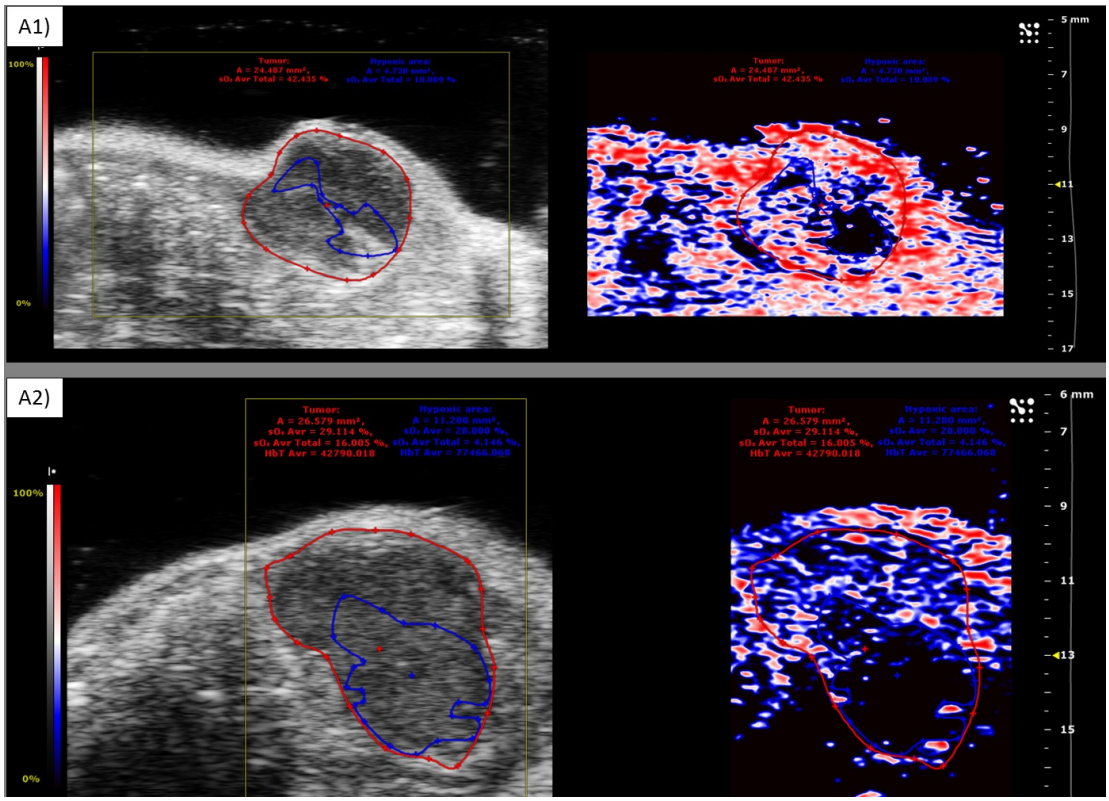

A1) PA oxygenation imaging of MDA-MB-231 breast adenocarcinoma model. A2) PA oxygenation imaging of MIA-PaCa2 pancreatic adenocarcinoma model.

CONTROL ID: 2233888

TITLE: Dual assessment of early tumor hypoxia: oxygen partial pressure measurement coupled to photoacoustic imaging in breast carcinoma models in mice.

PRESENTER: Florian RAES

ABSTRACT BODY:

Abstract Body: Introduction

A promising Photoacoustic Imaging (PA) field of application is the *in vivo* quantification of the hemoglobin oxygen saturation (SO_2). This modality allows to perform a true mapping of SO_2 distribution, thanks to the existing differences in optical absorption between oxygenated and deoxygenated hemoglobin. However, the reliability of data can be distorted by various factors including intensity and wavelength of exciting light. The quenching of ruthenium fluorescence by oxygen is a recognized and widely used technique to monitor the *in vivo* oxygen partial pressure (PO_2). Recent improvements in micro-fibered probes enable to perform minimally invasive measurements. In order to validate the PA data when assessing intratumoral oxygenation, the simultaneous use of these two modalities was employed comparing PO_2 and SO_2 in a 4T1 murine model of breast carcinoma becoming hypoxic in its core.

Methods

Regarding the experiments, the 4T1 murine model of breast tumor was orthotopically grafted in BALBc/by mice.Tumor volume was measured by ultrasound (US) using the VEVO LAZR system (Fujifilm Visualsonics Inc). Seven days after engraftments, tumors were explored both by PA and OxyLite (OL) (OxyLite, Oxford Optronix) once a week during 2 weeks. One OL probe was inserted into the hypoxic core of the tumor, while a second, as a reference, was located intramuscularly (IM). Confrontation of OL and PA measurements requires to perform an oxygenation challenge, changing the oxygen content of the gas mixture administered to mice (100% O_2, then 5% O_2, 2 min, then back to 100% O_2).

Results

To ensure a satisfactory matching between PA measurements and OL probes location, the control of the OL probe positioning was performed using the US transducer. Impacts of changes in gas mixture breathing mice were distinctly visible both on the OL probe and PA for the IM location (OL: 45 to 10 to 45 mmHg ; PA: 60 to 40 to 60% SO_2), whereas no fluctuations were detected into the hypoxic core of the tumor (OL: 1-2 mmHg ; PA: ~4% SO_2). Several regions were drawn in the area of interest and corresponding SO_2 values were obtained considering the heterogeneity of tumor.

Conclusions

Combination of PA with oxygen partial pressure measurements using OL fibered detector enables to validate the ability of the technique to highlight the tumor oxygenation variations. OL provides suitable support to the relevance of *in vivo* PA data and can be considered as a reference technique for PA quality management. PA is a unique resource to assess the entire tumor oxygenation.

AUTHORS (LAST NAME, FIRST NAME): RAES, Florian[1]; Collet, Guillaume[2]; Jose, Jithin[3]; Trochet, Philippe[4]; Kieda, Claudine[2]; Lerondel, Stéphanie[5]; Le Pape, Alain[6, 7]

INSTITUTIONS (ALL):

1. Centre for Small Animal Imaging (CIPA), French National Centre for Scientific Research (CNRS), Orléans, France.
2. Centre de Biophysique Moleculaire CBM, Orléans, France.
3. FUJIFILM Visualsonics Inc., Amsterdam, Netherlands.
4. FUJIFILM Visualsonics Inc., Amsterdam, Netherlands.
5. Centre for Small Animal Imaging (CIPA), French National Centre for Scientific Research (CNRS), Orléans Cedex 02, France.
6. Centre for Small Animal Imaging (CIPA), French National Centre for Scientific Research (CNRS), Orléans Cedex 02, France.
7. Respiratory Pathology Study Center, INSERM U1100, Tours, France.

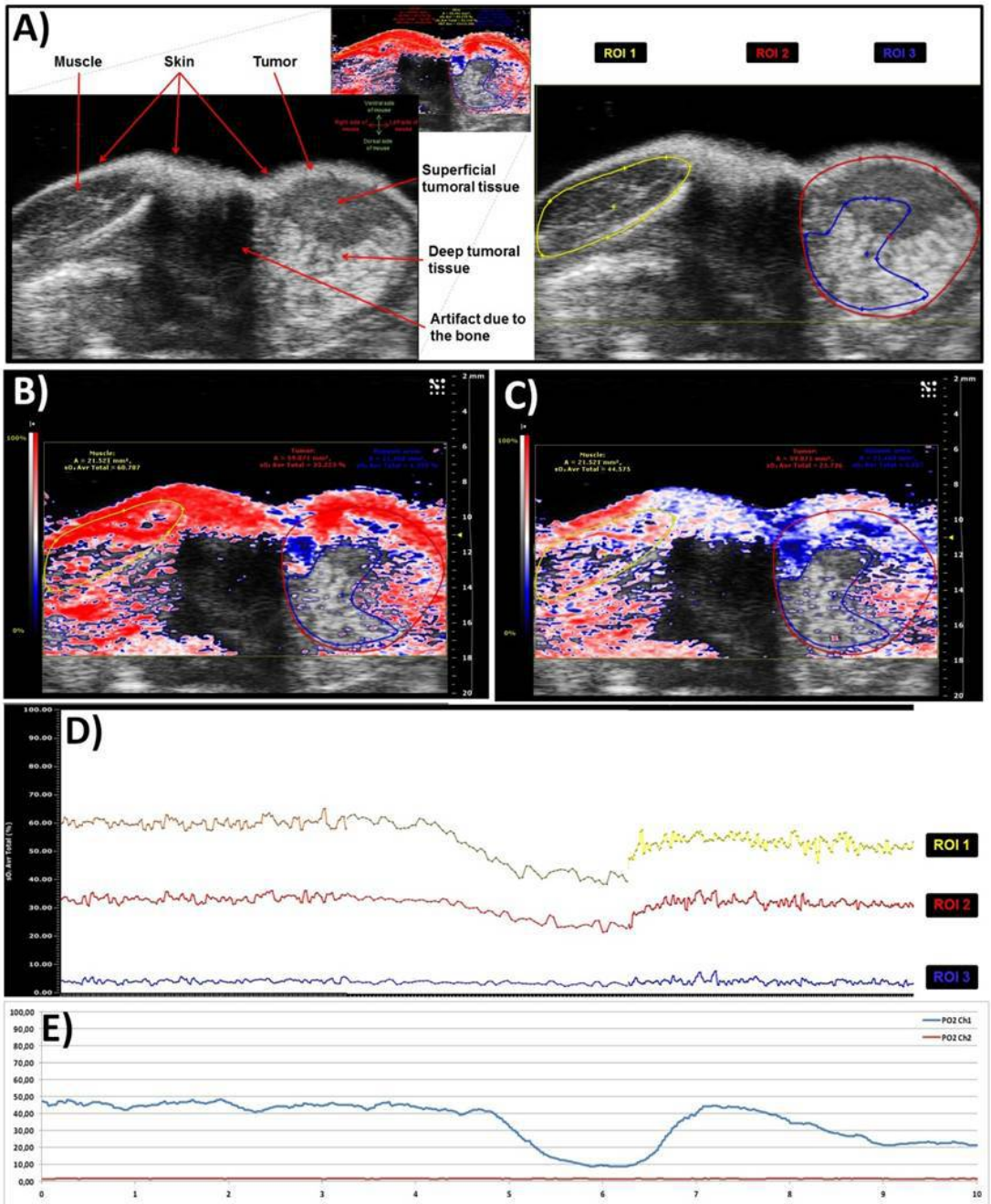

A), B) & C) Variation of hemoglobin saturation by PA after 100% O_2 (B), or 5% O_2 (C) breathing mice, into the muscle (ROI 1) and into the tumor (ROI 2 & 3). C) Graph representing SO_2 (%) in the 3 ROIs. E) OxyLite measurements with 2 different probes: intramuscularly (PO_2 Ch1) and into hypoxic area (PO_2 Ch2) (mmHg).

CONTROL ID: 2233832

TITLE: MicroPET/CT Imaging of Co-expressed EGFR and HER2 in Breast Cancer Tumour Xenografts in Mice using Bispecific Radioimmunoconjugates (bsRICs)

PRESENTER: Luke Yongkyu Kwon

ABSTRACT BODY:

Abstract Body: Background: HER2-EGFR heterodimerization is critical step in activation of cellular signaling pathways for growth of breast cancer (BC). Molecular imaging employs probes to detect biomarkers and could be a valuable tool in identifying BC patients with tumours that have high levels of HER2 and/or EGFR. The purpose of this study was to examine the imaging properties of bispecific radioimmunoconjugates (bsRICs) intended for imaging both EGFR and HER2 in human BC xenografts in mice using microPET/CT.

Methods: BsRICs (^{64}Cu-NOTA-Fab-PEG$_{24}$-EGF) were constructed by reacting maleimide derivatized trastuzumab Fab fragments which bind HER2 with thiolated Epidermal Growth Factor (EGF) through a 24-mer polyethylene glycol (PEG$_{24}$) spacer. Then, the bsRICs were conjugated with S-2-(4-Isothiocyanatobenzyl)-1,4,7-triazacyclononane-1,4,7-triacetic acid (p-SCN-bn-NOTA) before radiolabeling with ^{64}Cu. A one-point *in vitro* competition binding assay was performed to examine the binding specificity of ^{64}Cu-bsRICs to MDA-MB-231 (EGFR+/HER2-), 231-H2N (EGFR+/HER2+), and SKOV3 (EGFR-/HER2+). Pharmacokinetic studies were performed in healthy BALB/c mice to compare the elimination from the blood of bsRICs and monospecific RICs (^{64}Cu-NOTA-EGF and ^{64}Cu-NOTA-Fab) up to 42 hours post injection. MicroPET/CT was performed in NOD-SCID mice bearing subcutaneous 231-H2N (EGFR+/HER2+) human BC xenografts at 24 and 48 h post intravenous injection of ^{64}Cu-bsRICs (25-30 MBq; 10 µg). Tumour and normal tissue uptake were quantified by *ex vivo* biodistribution studies and compared to those for monospecific RICs.

Results: The binding of bsRICs to MDA-MB-231 cells was reduced to 24.5 ± 5.2% by excess EGF compared to no competition. The binding of bsRICs to SKOV3 cells was displaced to 38.6 ± 5.4 % by excess Fab. Calculated pharmacokinetic parameters (AUC_{total}, V_1, V_{dss}, CL_{total}) revealed that ^{64}Cu-bsRICs were eliminated more slowly from the blood than ^{64}Cu-bsRICs without PEG spacer, and much more slowly than both ^{64}Cu-NOTA-Fab and ^{64}Cu-NOTA-EGF. The AUC_{total} of ^{64}Cu-PEG-bsRICs (501 ± 37 %ID/mL * hr) was significantly higher than the AUC_{total} of ^{64}Cu-bsRICs with no PEG (189 ± 6.9%ID/mL * hr), ^{64}Cu-NOTA-Fab (57 ± 4.0 %ID/mL * hr) and ^{64}Cu-NOTA-EGF (70 ± 14 %ID/mL*hr). Tumour uptake of ^{64}Cu-bsRICs in 231-H2N xenografts was 5.1 ± 0.05 %ID/g at 48 hours post injection which was significantly greater than ^{64}Cu-NOTA-Fab (1.9 ± 0.3 %ID/g; p = 0.002) and ^{64}Cu-NOTA-EGF (0.68 ± 0.2 %ID/g; p = 0.0005).

Conclusions: New ^{64}Cu-labeled bsRICs were successfully constructed which exhibited specific binding to EGFR and HER2 *in vitro.* These bsRICs exhibited slower elimination from the blood and higher accumulation in tumours *in vivo* co-expressing EGFR and HER2 than monospecific RICs, permitting tumour visualization by microPET/CT.

Supported by grants from the Ontario Institute for Cancer Research (OICR Smarter Imaging Program) and the Canadian Institutes of Health Research .

AUTHORS (LAST NAME, FIRST NAME): Kwon, Luke Yongkyu[1]; Scollard, Deborah A.[2]; Reilly, Raymond M.[1]

INSTITUTIONS (ALL):

1. Pharmaceutical Science, University of Toronto, Toronto, ON, Canada.
2. STTARR Innovation Centre, Toronto, ON, Canada.

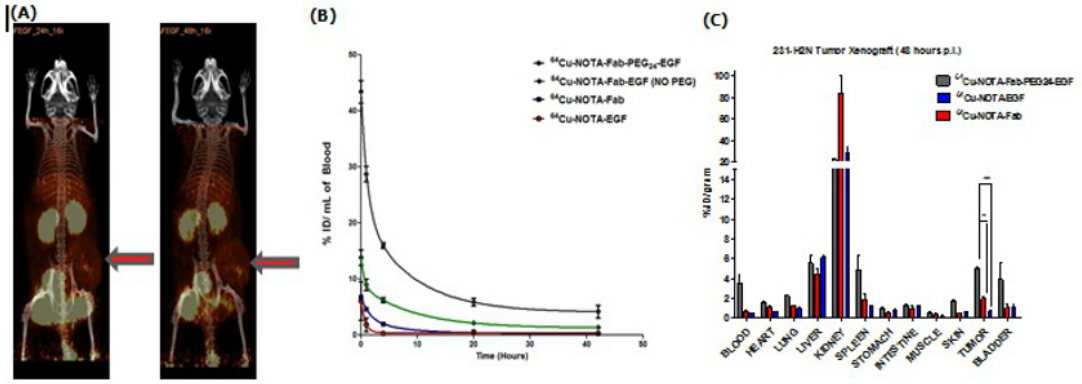

Figure 1. **(A)** MicroCT/PET imaging with ^{64}Cu-NOTA-Fab-PEG$_{24}$-EGF in NOD-SCID mice with 231-H2N (EGFR+/HER2+) xenograft (shown in red arrow) at 24 hours and 48 hours post injection. **(B)** Percent injected dose/mL of radioactivity remaining in the blood at various time points post injection (0-42 hours) of ^{64}Cu-labeled bsRICs and ^{64}Cu-labeled monospecific RICs. **(C)** Tumor and normal tissue uptake of ^{64}Cu-NOTA-Fab-PEG$_{24}$-EGF in NOD-SCID mice with 231-H2N xenograft at 48 h p.i. (* significantly different $p < 0.05$).

CONTROL ID: 2233836

TITLE: Multiparametric tumor characterization and therapy response evaluation by hyperpolarized ^{13}C magnetic resonance spectroscopic imaging

PRESENTER: Rickmer Braren

ABSTRACT BODY:

Abstract Body: Background & Aims: Individual tumor characterization and treatment response monitoring based on current medical imaging methods remains challenging. This work investigates hyperpolarized ^{13}C compounds in an orthotopic rat hepatocellular carcinoma (HCC) model system before and after transcatheter arterial embolization (TAE).

Methods: Measurements with hyperpolarized biomarkers were performed in tumor bearing rats before and after TAE. Hyperpolarized and selectively ^{13}C labelled urea, pyruvate and fumarate were used to study tumor perfusion, cell energy metabolism and necrosis. 2D slice selective metabolic imaging was used to obtain spatially resolved maps of tumor perfusion, conversion rate constants and necrosis. Immunohistochemistry was correlated with tumor necrosis.

Results: ^{13}C compounds (with respective metabolites) exhibited high structural similarity, yet inter-individual differences in metabolite ratios. Malate signal became detectable upon TAE only and systemic but not local malate to fumarate ratios showed a positive correlation with the amount of tumor necrosis, indicating distant enzyme activity or malate wash out. TAE induced a decrease of tumor to muscle and tumor to liver ratios of urea, pyruvate and its metabolites (alanine and lactate), whereas rate constants remained stable or increased upon TAE in all tissues.

Conclusions: This study presents ^{13}C metabolites as excellent candidate biomarkers for a comprehensive tumor characterization, enabling the simultaneous detection of individual differences in tumor perfusion, metabolism and necrosis.

AUTHORS (LAST NAME, FIRST NAME): Düwel, Stephan[1]; Durst, Markus[1]; Gringeri, Concetta[4]; Gross, Claudia[3]; Janich, Martin A.[4]; Haase, Axel[1]; Glaser, Steffen[5]; Schwaiger, Markus[2]; Schulte, Rolf F.[4]; Menzel, Marion I.[4]; Braren, Rickmer[3]

INSTITUTIONS (ALL):

1. IMETUM, Technical University of Munich, Garching, Bavaria, Germany.
2. Technische Universität München, München, Germany.
3. Institute of Radiology, Technische Universität München, Munich , Germany.
4. GE Global Research, Garching, Germany.
5. Department of Chemistry, Technische Universität München, Garching, Germany.

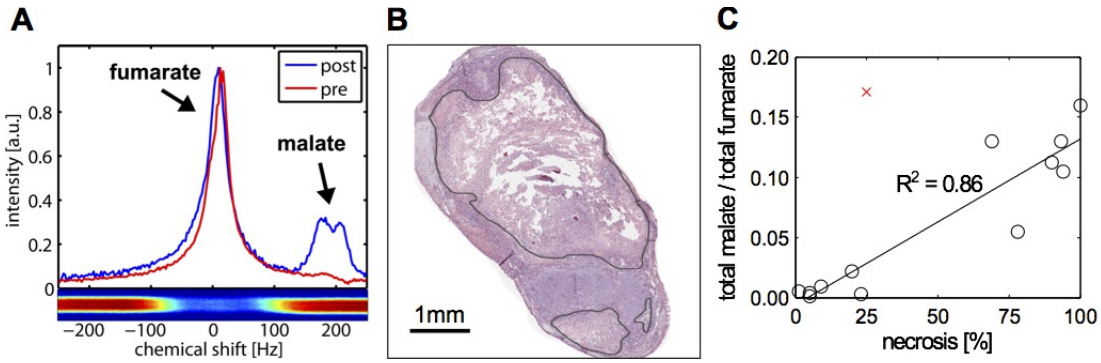
A
fumarate
malate
post
pre
intensity [a.u.]
chemical shift [Hz]
B
1mm
C
total malate / total fumarate
necrosis [%]
R2 = 0.86

CONTROL ID: 2233922

TITLE: Tumor cellularity is a negative prognostic factor of pancreatic cancer identified by diffusion weighted – magnetic resonance imaging

PRESENTER: Rickmer Braren

ABSTRACT BODY:

Abstract Body: Purpose Intra- and interindividual morphological heterogeneity including tumor cell abundance (cellularity) of pancreatic ductal adenocarcinoma (PDAC) is thought to be of key relevance for prognosis and therapy resistance. Purpose of this work was to identify morphological subtypes of PDAC that are of prognostic relevance and identifiable by clinical imaging parameters.

Patients, Materials and Methods Murine (mPDAC; N=141) and human (hPDAC; N=94 PDAC were histologically analyzed and subtyped based on tumor cellularity. Multimodal imaging by [^{18}F]-FDG PET, diffusion weighted- and dynamic contrast enhanced-MRI (DW-MRI, DCE-MRI) was evaluated for non-invasive characterization of mPDAC subtypes.

Results Three subtypes of mPDAC based on tumor cellularity could be defined (mPDAC^{high}, N=5; mPDAC^{med}, N=63; mPDAC^{low}, N=73). Regional ADC values revealed an excellent correlation with tumor cellularity (r=-0.86, CI=-0.92 – -0.78) and the highest discriminatory power of all tested imaging parameters (ROC: AUC=0.966, CI=0.898-1). Using the same morphological classification for a set of hPDAC (hPDAC^{high}, N=2; hPDAC^{med}, N=27, hPDAC^{low}, N=55) revealed a significantly better prognosis of hPDAC^{low} compared to hPDAC^{med} patients after partial pancreatectomy (19.8 versus 13.0 months, Log rank, $p<0.002$) and identified a subgroup of hPDAC G2 patients of poor prognosis (G2=22.8 versus G2/PDAC^{med}=19.3 months, Log rank, $p<0.019$). When ADC parameters were correlated with histologically defined subtypes in patients that received pre-operative MRI (hPDAC^{low}, N=14; hPDAC^{med}, N=9), a good correlation (r=0.45, CI=-0.73 – -0.05) and high discriminatory power (ROC: AUC=0.988, CI=0.9524-1) was identified.

Conclusion This study identifies the ADC parameter as an excellent candidate for the reliable distinction of cellularity based PDAC subtypes in mouse and human.

AUTHORS (LAST NAME, FIRST NAME): Heid, Irina[1]; Steiger, Katja[2]; Trajkovic-Arsic, Marija[3]; Schmid, Roland M.[3]; Rummeny, Ernst J.[1]; Schwaiger, Markus[4]; Esposito, Irene[5]; Siveke, Jens[3]; Braren, Rickmer[1]

INSTITUTIONS (ALL):

1. Institute of Radiology, Technische Universität München, Munich , Germany.
2. Institute of Pathology, Technische Universität München, Munich, Germany.
3. 2nd Medical Department, Technische Universität München, Munich, Germany.
4. Nuclear Medicine, Technische Universität München, Munich, Germany.
5. Institute of Pathology, Universität Insbruck, Insbruck, Austria.

(No Image Selected)

CONTROL ID: 2233842

TITLE: Novel ^{89}Zr based cell-labeling method for PET imaging of cell trafficking

PRESENTER: Mukesh Pandey

ABSTRACT BODY:

Abstract Body: Objectives: With the recent growth of interest in cell-based therapies and radiolabeled cell products, there is a need to develop more sensitive imaging methods for *in vivo* tracking of living cells. This study describes a novel cell labeling approach with ^{89}Zr ($T_{1/2}$ =78.4 h) for PET monitoring of stem cells in a myocardial ischemia model and in an arteriovenous fistula model.

Methods: A new cell labeling agent, ^{89}Zr-desferrioxamine-NCS (^{89}Zr-DBN), was synthesized. Human mesenchymal stem cells (hMSCs) were covalently labeled with ^{89}Zr-DBN via the reaction between the NCS group on ^{89}Zr-DBN and primary amine groups present on cell surface membrane protein. The stability of the label on the cell was tested by cell efflux studies for upto 7 days. The effect of labeling on cellular viability was tested by monitoring cell proliferation, trypan blue and cytotoxicity/apoptosis assays. The ^{89}Zr-labeled stem cells were tracked in a myocardial ischemia mouse model and an arteriovenous fistula mouse model by serial PET scans and *ex vivo* biodistribution following delivery of ^{89}Zr-hMSCs

Results: The labeling synthon, ^{89}Zr-DBN, was prepared in 55±5% decay-corrected radiochemical yield measured by iTLC. The cell labeling efficiency was ~30%. Radioactivity concentrations of labeled cells of up to 0.5MBq/1x10^{6} cells were achieved without a negative effect on cellular viability. No cellular efflux of ^{89}Zr was seen out to 7 d. Myocardially delivered ^{89}Zr-hMSCs showed major retention in the myocardium, as well as minor redistribution to lung and bone, whereas intravenous delivery of ^{89}Zr-hMSCs distributed primarily to lung and bone. Free $^{89}Zr^{4+}$ distributed to liver and bone. Thus, the stability of the radiolabel on hMSCs was evidenced. In the case of ^{89}Zr-hMSCs delivered to adventitia of arteriovenous fistula, it was possible to track the ^{89}Zr-hMSCs in the adventitia of arteriovenous fistula for up to 7 days.

Conclusions: The novel cell labeling strategy with ^{89}Zr-DBN is shown to be a general, mild and biostable ^{89}Zr labeling method with promise for wide applications of PET imaging studies of *in vivo* cell trafficking.

Research Support: The work was funded by the Mayo Clinic Department of Radiology.

AUTHORS (LAST NAME, FIRST NAME): Bansal, Aditya[1]; Pandey, Mukesh K.[3]; Demirhan, Yunus[1]; Nesbitt, Jonathan J.[2]; Yang, Binxia[4]; Crespo-Diaz, Ruben J.[2]; Terzic, Andre[2]; Misra, Sanjay[4]; Behfar, Atta[2]; DeGrado, Timothy R.[1]

INSTITUTIONS (ALL):

1. Radiology, Mayo Clinic, Rochester, MN, United States.
2. Cardiovascular Diseases , Mayo Clinic, Rochester, MN, United States.
3. Radiology, Mayo Clinic, Rochester, MN, United States.
4. Vascular & Interventional Rad , Mayo Clinic, Rochester, MN, United States.

Myocardial Infarction (MI) model

Arteriovenous (AV) fistula model

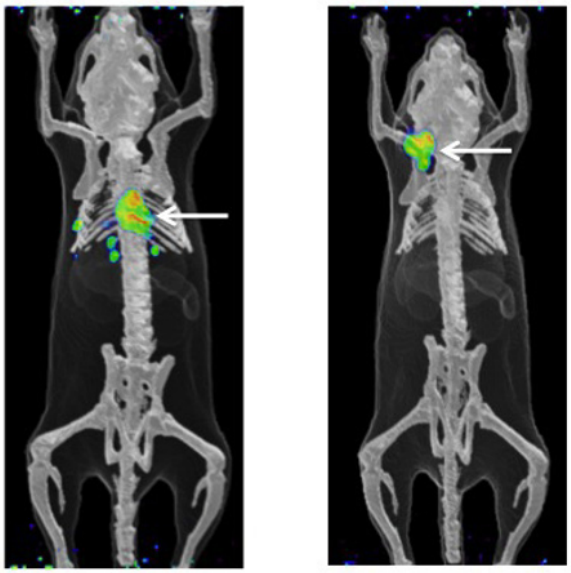

Maximum Intensity Projections (MIPS) of PET-X-Ray images showing localization of ^{89}Zr-labeled stem cells (white arrow) in infarcted heart in a MI mouse model after 7 days post-injection and in adventitia of AV fistula in AV fistula mouse model after 5 days post-injection.

CONTROL ID: 2234309

TITLE: Novel ^{89}Zr based virus-labeling method for PET imaging of viral trafficking

PRESENTER: Aditya Bansal

ABSTRACT BODY:

Abstract Body: Objectives: There is a growing interest in using viral based gene therapy for treating wide range of diseases. Viral based gene delivery agents for gene therapy hold tremendous promise but like drugs, a better understanding of their pharmacokinetics is critical to their advancement. This study describes a novel viral labeling approach with ^{89}Zr ($T_{1/2}$ =78.4 h) for potential PET imaging of viral biodistribution in the body.

Methods: A new viral labeling agent, ^{89}Zr-desferrioxamine-NCS (^{89}Zr-DBN), was synthesized. The adeno-associated serotype 2 viruses with GFP gene (AAV2-GFP) was covalently labeled with ^{89}Zr-DBN via the reaction between the NCS group on ^{89}Zr-DBN and primary amine groups present on capsid protein. Following labeling, the labeled viruses were purified using GE PD-10 desalting column (Sephadex G-25). The purified viral radiolabeling yield was quantified, following which cell binding and cell-infection assays were performed using 293T cells to evaluate the transfection potential of ^{89}Zr -AAV2-GFP.

Results: The adeno-associated serotype 2 virus like AAV2-GFP was labeled with ^{89}Zr with viral labeling yield of ~20mCi/10^{14} viral particles after 30 min of labeling and purification. A cell-binding assay was performed at 4°C with multiplicity of infection (MOI) = 10,000. Following 2 h of co-incubation of 2.5 X 10^{9} ^{89}Zr -AAV2-GFP particles and 2.5 X 10^{5} 293T cells at 4°C, 7% of the ^{89}Zr -AAV2-GFP were found to be bound to 293T cells as compared to 0.6% in control group including cells and ^{89}Zr-hydrogen phosphate. In the cell infection assay, ^{89}Zr -AAV2-GFP was incubated with 293T cells at 37°C for 5 days, at MOI = 2500 and 10,000. The fraction of 293T cells expressing GFP correlated with MOI of ^{89}Zr -AAV2-GFP.

Conclusion: The adeno-associated serotype 2 virus like AAV2-GFP was successfully labeled with ^{89}Zr-DBN. The ^{89}Zr -AAV2-GFP particles were able to bind to 293T cells. The transfection potential of ^{89}Zr -AAV2-GFP into 293T cells was retained which correlated changes in MOI. In principle, ^{89}Zr-DBN can be used to label a wide variety of viruses. The major advantages of this labeling method are that the viral labeling conditions are mild and there is no need for modification of the virus before labeling.

Research Support: The work was funded by the Mayo Clinic Department of Radiology.

AUTHORS (LAST NAME, FIRST NAME): Bansal, Aditya[1]; Pandey, Mukesh K.[1]; DeGrado, Timothy R.[1]

INSTITUTIONS (ALL):

1. Radiology, Mayo Clinic, Rochester, MN, United States.

Cell Infection assay using ^{89}Zr-labeled AAV2-GFP and 293T cells

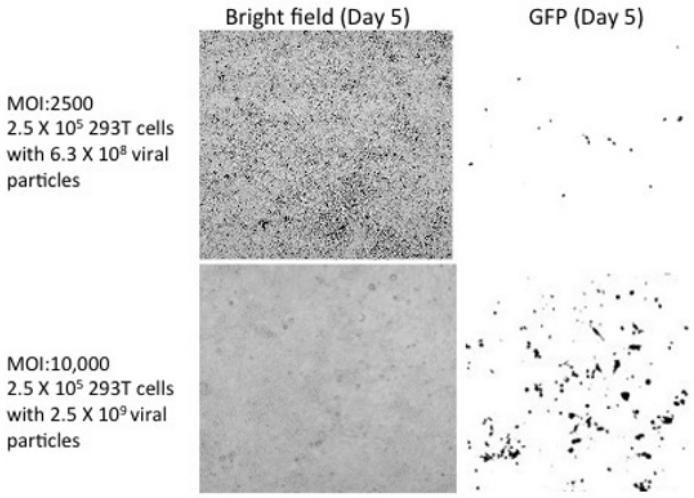

Representative data showing cell infection assay. Cell infection assay was performed with 2.5 X 10^5 293T cells with radiolabeled viral particles (~20mCi/10^{14} viral particles) at two multiplicity of infection (MOI) -2500 and 10,000 in DMEM culture medium + 1% FBS in CO_2 incubator. The GFP signal after 5 day incubation correlated with MOI

CONTROL ID: 2233854

TITLE: First in Human Study of PSMA-targeting small drug conjugates (SMDC) for SPECT Imaging (^{99m}Tc-EC0652) and Treatment (EC1169) of Men with Recurrent Metastatic Castrate-Resistant Prostate Cancer (MCRPC)

PRESENTER: Binh Nguyen

ABSTRACT BODY:

Abstract Body: Background

Prostate-specific membrane antigen (PSMA) is a plasma-membrane associated protein that is over-expressed on most prostate cancer (CaP) cells. Its expression increases with the grade and stage of prostate cancer as well as with castrate resistant CaP. PSMA expression is also observed in the neo-vasculature of many malignancies, while it is absent from the neo-vasculature of normal tissues. The differential expression of PSMA in cancerous and normal tissues makes it an ideal candidate for PSMA-based diagnostic imaging and targeted drug delivery in patients with MCRP.

^{99m}Tc-EC0652 is a SMDC of a DUPA (2-[3-(1, 3-dicarboxy propyl)-ureido] pentanedioic acid) moeity, which targets PSMA, and synthetic peptide moiety that chelates technetium-99 to facilitate SPECT imaging. EC0652 strongly (Kd=34 nM) and reversibly binds to the extracellular domain of PSMA. In tumor bearing mice, ^{99m}Tc-EC0652 rapidly accumulates in tumor and exits the blood compartment (<2% detectable at 30 minutes). A Phase 0 study of EC0652 in patients with CaP established the safety of EC0652. In addition, PSMA detected on pre-operative ^{99m}Tc-EC0652 SPECT scan in 2 patients was pathologically confirmed in surgical specimens.

EC1169 is a SMDC conjugate of a chemically modified DUPA moiety that targets PSMA and linked to the cytotoxic agent tubulysin B hydrazide (TubBH). Upon binding to PSMA, EC1169 undergoes endocytosis and intracellular cleavage of the TubBH moiety which then inhibit tubulin polymerization to cause metaphase arrest. In PSMA-positive LNCaP and MDA PCa 2b tumor-bearing mice, EC1169 has shown potent activity with both complete remissions and cures being observed.

Materials and Methods

The primary study objective is to determine the maximal tolerated dose (MTD) and recommended phase 2 dose of EC1169. Secondary objectives include EC1169 safety, pharmacokinetic profiles, antitumor activity, and correlation of anti-tumor activity with ^{99m}Tc-EC0652 uptake on SPECT scans. Key inclusion criteria are age ≥18 years, ECOG performance status 0–1, and adequate organ function. Patients must have failed prior or ongoing androgen-deprivation therapy, progressed on abiraterone or enzalutamide, and previously treated with a taxane unless contraindicated. All patients undergo a ^{99m}Tc-EC0652 SPECT scan at baseline. EC1169 is administered as an IV bolus three time weekly or once weekly during weeks 1, 2 of a 3-week cycle.

Results

To date, 7 pts have been enrolled and treated with EC1169 (3 pts on TIW schedule, 4 pt on QW schedule). There have been no DLTs and treatment was generally well tolerated. The number of cycles administered ranged from 1 to 4, with no omission due to toxicity. Stable disease was the best response in 4 pts. One pt had progressive disease as best response while two pts have not yet undergone response assessment. ^{99m}Tc-EC0652 SPECT scans showed good EC0652 uptake in both bone and soft tissue lesions.

Conclusions

Dose escalation is ongoing, currently at 0.45 mg/m^2 for both the TIW and QIW schedules. Updated clinical and ^{99m}Tc-EC0652 SPECT imaging data will be presented at the conference.

AUTHORS (LAST NAME, FIRST NAME): Ejadi, Samuel[1]; Tolcher, Anthony W.[2]; Sartor, Oliver[3]; Vogelzang, Nicholas J.[4]; Habbe, Andrew[5]; Nguyen, Binh[5]

INSTITUTIONS (ALL):

1. Virginia G. Piper Cancer Center, Scottsdale, AZ, United States.
2. South Texas Accelerated Research Therapeutics, LLC (START), San Antonio, TX, United States.
3. Tulane University, Tulane Cancer Center, New Orleans, LA, United States.
4. Comprehensive Cancer Centers of Nevada, Las Vegas, NV, United States.

5. Endocyte, Inc., Indianapolis, IN, United States.

(No Image Selected)

CONTROL ID: 2233858

TITLE: *Ex-vivo* detection of human oral cancer using an activatable fluorescence probe targeting γ-glutamyltransferase and the Artemis imaging system

PRESENTER: Maxime Slooter

ABSTRACT BODY:

Abstract Body: Introduction:

The membrane enzyme gamma-glutamyl transferase (GGT) is expressed on the cellular surface of several malignancies, including oral squamous cell carcinomas (OSCC). Currently, the treatment of OSCC consists of a multidisciplinary approach. However, during resection surgeons experience difficulty in determining the tumor margins. A promising substrate-based probe, gGlu-HMRG, can be of added value as it becomes fluorescent after activation by GGT and in that way labels the tumor, which can be visualized both *in vivo* and *ex vivo* using a specialised imaging system.

Materials and Methods:

The intraoperative Artemis imaging system was adapted to the 500nm spectrum and was used for the visualisation.[1] OSC-19, a well-differentiated human oral squamous cell carcinoma cell line of the tongue, was used for *in vitro*, *ex vivo and in vivo* experiments. For tumor induction, 60,000 cells were injected into the tip of the tongue of nude mice. Cyrosections were imaged up to 20 minutes after probe administration and tumor-to-background ratios (TBRs) were calculated. After protocol optimisation, resection specimens of *ex vivo* human oral cancers were sprayed with gGlu-HMRG and imaged up-to 10 minutes to identify possible tumor cells at the resections margin.

Results:

The expression of GGT in OSC19-cells was evaluated using flow cytometry and life cell imaging. The latter showed fast probe uptake and more intense signals over time. Using the Artemis imaging system a minimal number of 20,000 cells could be recognized. Cryosection analysis showed which imaging time point and concentration was most suitable to detect tumors. *Ex vivo* and *in vivo* imaging in mice showed clear tumor specific signals. The probe was internalized in a much lower extend in the *ex vivo* setting, so the signal could be washed away. The evaluation of human resection margins, a study that is currently ongoing, shows similarity with the verdict of the pathologist so far.

Conclusion:

We experience low autofluorescence in the head-and-neck region in the visual spectrum and the activated signal could be clearly seen using the Artemis imaging system. Fluorescent probes in the visible light spectrum show low tissue penetration, which provides the ability to solely visualize the surface. Substrate-based probes allow higher TBRs as it provides lower background signals regarding conventional fluorescent dyes and bypasses systemic administration as it can be sprayed onto the tissue of interest. This study assesses gGlu-HMRG, which can be sprayed on the resected specimen directly after surgery to help surgeons in recognizing irradical resected tumors and to adapt the surgical procedure in real time in order to improve patient outcome and survival.-

1. van Driel, P.B., M. van de Giessen, M.C. Boonstra, T.J. Snoeks, S. Keereweer, S. Oliveira, C.J. van de Velde, B.P. Lelieveldt, A.L. Vahrmeijer, C.W. Lowik, and J. Dijkstra, *Characterization and Evaluation of the Artemis Camera for Fluorescence-Guided Cancer Surgery.* Mol Imaging Biol, 2014.

AUTHORS (LAST NAME, FIRST NAME): Slooter, Maxime[1]; Boonstra, Martin[2]; Prevoo, H.A.J.M.[4]; Mooyaart, Antien[5]; Bierau, Katja[2]; Smit, Vincent[6]; van der Velden, Lilly-Ann[7]; Kobayashi, Hisataka[3]; Vahrmeijer, Alexander L.[8]; lowik, Clemens W.[9]

INSTITUTIONS (ALL):

1. Radiology, L.U.M.C., Amsterdam, Netherlands.
2. Surgery, Leiden University Medical Center, Leiden, Netherlands.
3. Molecular Imaging Program, NCI/NIH, Bethesda, MD, United States.
4. Surgery, L.U.M.C., Leiden, Netherlands.
5. Pathology, L.U.M.C., Leiden, Netherlands.

6. Pathology, L.U.M.C., Leiden, Netherlands.
7. Otorhinelaryngology, L.U.M.C., Leiden, Netherlands.
8. Surgery, L.U.M.C., Leiden, Netherlands.
9. Radiology, L.U.M.C., Leiden, Netherlands.
(No Image Selected)

CONTROL ID: 2233873

TITLE: IGF-1 Conjugated Theranostic Iron Oxide Nanoparticles for Targeting and Delivery of SN-38 to Pancreatic Cancer

PRESENTER: Yuancheng Li

ABSTRACT BODY:

Abstract Body: Iron oxide nanoparticles (IONPs) has been applied to targeted molecular imaging with magnetic resonance imaging (MRI) and the therapy delivery due to their superb MRI contrast enhancing effect and the capability of carrying therapeutic agents.[1] However, it is challenging to delivery theranostic nanoparticles to pancreatic cancer that has extensive tumor stroma and disordered tumor vasculatures. We have developed highly effective and tumor targeted IONPs using a recombinant human insulin-like growth factor 1 (IGF-1) to target insulin-like growth factor 1 receptor (IGF-1R) that is highly expressed in pancreatic cancer cells and stromal cells. Reported theranostic IONPs were coated with poly ethylene glycol (PEG)-*b*-allyl glycidyl ether (AGE) copolymer with capability of facile functionalization with the IGF-1 targeting ligand. IONPs (core size 10 nm) were functionalized with Sulfo-SMCC to introduce maleimide groups. Targeting ligands were thiolated (using Traut's reagent), and then installed to the IONPs through the reaction between thiols and maleimides.

7-Ethyl-10-hydroxycamptothecin (SN-38), a topoisomerase I inhibitor and an active metabolite of the FDA approved chemotherapy agent irinotecan (CPT-11) by carboxylesterases in liver and tumors, was selected for the nanoparticle delivery to pancreatic cancer, given its demonstrated efficacy against various malignancies but difficulty to apply clinically due to its extreme hydrophobicity and inability for conventional i.v. administration. Furthermore, SN-38 is 100- to 1000- fold more cytotoxic than CPT-11, thus requiring more targeted delivery to reduce the systemic toxicity.[2] In this work, SN-38 was mixed with PEG-*b*-AGE coated IONPs in organic phase before the organic solution was added to water dropwise. The SN-38 was stabilized in aqueous medium upon loading to the IONPs at the efficiency of 10% (w/w).

The *in vitro* investigation of IGF1 conjugated IONP loaded with SN-38 (IGF1-IONP-SN38) on MiaPaca2 pancreatic cancer cells showed similar efficacy to that of free SN-38. Moreover, IGF1-IONP-SN-38 exhibited greater cytotoxicity than non-targeted IONP, indicating targeted delivery of SN-38 intracellularly. The pancreatic cancer mouse model was prepared by injecting 5×10^6 MiaPaCa-2 cells into the pancreas of 7- to 8-week old nude mice. After 3 to 4 weeks, mice with orthotopically xenografted pancreatic tumors were treated with IGF1-IONP-SN-38 and non-targeted IONP. MR scan was performed on a 3-Tesla scanner (Tim/Trio, Siemens, Erlangen, Germany) using T_2-weighted fast SE sequence and multi-TE SE sequence for T_2 mapping. Image analysis using the region of interest (ROI) method showed that signal intensity of T_2-weighted images decreased 44% in the pancreatic tumors of mice injected with targeted IGF1-IONP comparing to 21% in tumors received non-targeted BSA-IONP. The higher accumulation of targeted IGF1-IONPs in the pancreatic tumor was confirmed by optical imaging using NIR dye labeled IGF1-IONP and BSA-IONP. The treatment of pancreatic cancer bearing mice with IGF1-IONP-SN38 was also investigated.

[1] Yang L. et al., *Gastroenterology* **2009**, *23*, 1514. [2] Gu Q. et al., *Nanotechnology* **2012,** *23*, 205101.

AUTHORS (LAST NAME, FIRST NAME): Li, Yuancheng[1]; Zhou, Hongyu[2]; Wang, Liya[1]; Yang, Lily[2]; Mao, Hui[1]

INSTITUTIONS (ALL):

1. Radiology and Imaging Sciences, Emory University, Atlanta, GA, United States.
2. Surgery, Emory University, Atlanta, GA, United States.

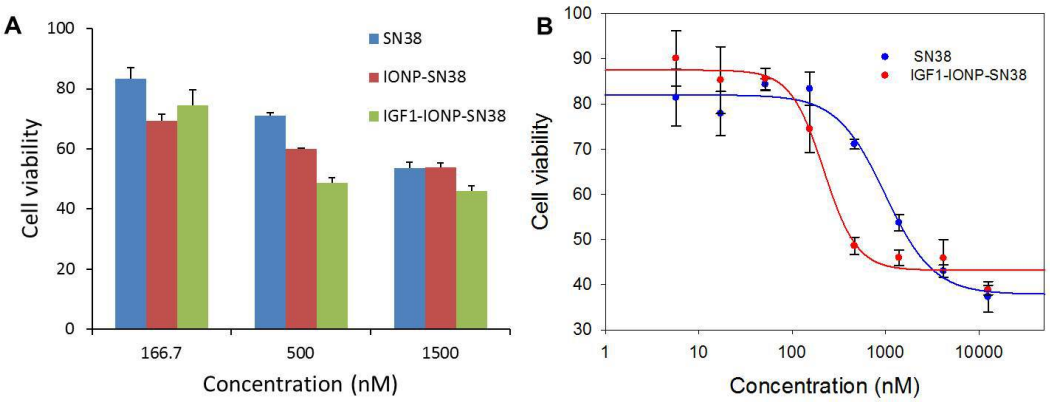

Viability of MiaPaca2 pancreatic cancer cells treated with (A) free SN-38, SN-38 loaded on PEG-*b*-AGE coated IONP (IONP-SN38), and SN-38 loaded on IGF-1 conjugated PEG-*b*-AGE coated IONP (IGF1-IONP-SN38) at three representative drug concentrations; and (B) free SN-38 and IGF1-IONP-SN38 at drug concentrations ranging from 8 to 11000 nM.

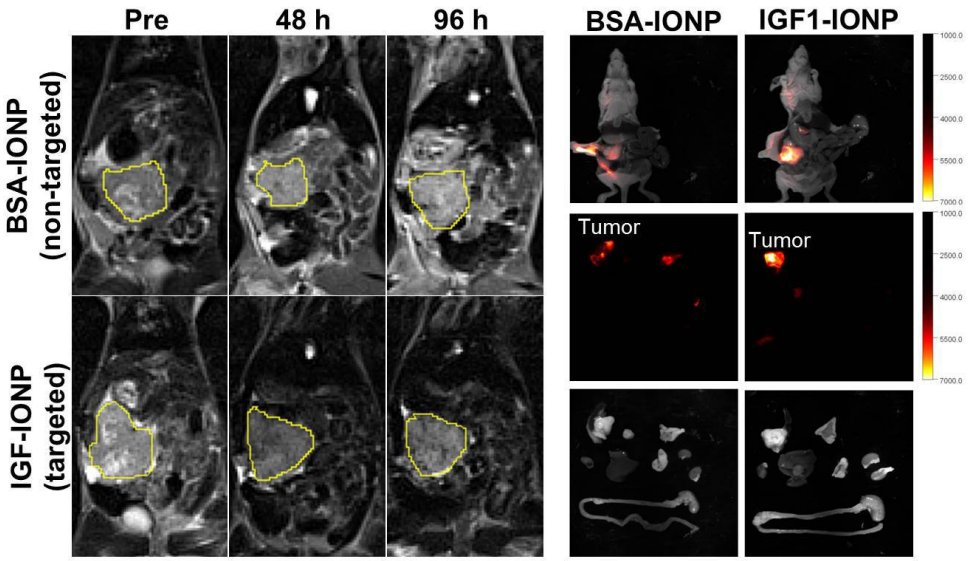

T_2-weighted MR images (left panel) and the NIR optical images (right panel) of tumor-bearing mice before (pre) and after injection of targeted IGF1-IONP and non-targeted BSA-IONP.

CONTROL ID: 2234236

TITLE: Facilitating Probe Delivery and Retention in Tumors with 3 nm Ultrasmall Iron Oxide Nanoparticle as Observed via Magnetic Resonance and Multiphoton Imaging

PRESENTER: Hui Mao

ABSTRACT BODY:

Abstract Body: Molecular imaging and image-assisted tumor therapy require delivery of a sufficient amount of nanoparticle probes/vehicles. For intravenously administered nanoparticles, however, only very small percentage can reach the targeted tumor due to the challenges in lack of proper pharmacokinetics, efficient penetration and optimal enhanced permeability and retention (EPR) effect, which is considered as one of the most important procedure for both passive and active targeting delivery. Generally, the EPR effect is affected by the particle size, shape, stiffness, and surface properties. Optimizing the physical/chemical properties of nanoparticles can improve the delivery efficiency and tumor accumulation. While earlier studies revealed larger sized nanoparticles (50-200 m) could enhance EPR by limiting nanoparticle intravasation back to circulation, here we report 3.5 nm core ultrasmall iron oxide nanoparticles (SIO-3) with T_1-T_2 switchable contrast that can easily extravasate into the tumor but with difficulty to re-enter the circulation after self-assembling to clusters in tumor interstitial at pH below 7, thus maximizing the passive targeting delivery via the EPR effect. Magnetic resonance and multiphoton imaging was used to investigate probe delivery using a 4T1 breast cancer mouse model, and to compare particles with different sizes (3.5, 10 and 20 nm). We observed greater MRI signal decrease in T_2-weighted MRI, indicating much higher tumor accumulation of SIO-3 compared to particles with larger sizes at 24 h after systemic i.v. administration (Figure 1 a). Switching T_1 contrast to T_2 contrast demonstrated that the highly single-dispersed SIO-3 in circulation self-assembled to clusters when entering the tumor interstitial. The higher accumulation of SIO-3 in tumor revealed by MRI was consistent with that measured with the colorimetric method (Figure 1b). To directly investigate the size effect, we used multiphoton imaging to follow/monitor particle extravasation out of tumor vessels and penetration into tumor tissue, by co-injecting dye labelled SIO3-TRITC (red fluorescence) and SIO20-FITC (green fluorescence) into mice bearing 4T1 tumors. At 3 h after administration, we observed extravasation of dye labelled nanoparticles from tumor vessels and accumulation of nanoprobes in tumor (Figure 1c). 3D reconstruction of z-stack images showed the enhanced passive targeting delivery of SIO-3 compared to SIO-20 (Figure 1d). Statistics analysis of nanoprobe accumulation in the tumor and distance away from the vessel further confirmed that SIO-3 exhibited higher accumulation and more efficient penetration into tumor. The improved tumor targeting and delivery of nanoprobes with 3 nm core size is ascribed to the enhanced extravasation into tumor and the reduced intravasation back into circulation by formation of clusters. In addition, the consequent MRI contrast switch from T_1 contrast to T_2 contrast can report the tissue environment where nanoparticles reside. Therefore, these ultrasmall multimodal nanoparticles are expected to be potent for tumor-targeted imaging and imaging-guided therapy.

AUTHORS (LAST NAME, FIRST NAME): Huang, Jing[1]; Wang, Liya[1]; Chen, Hongbo[1]; Wu, Hui[1]; Yang, Lily[2]; Mao, Hui[1]

INSTITUTIONS (ALL):

1. Radiology and Imaging Sciences, Emory University, Atlanta, GA, United States.
2. Surgery, Emory University, Atlanta, GA, United States.

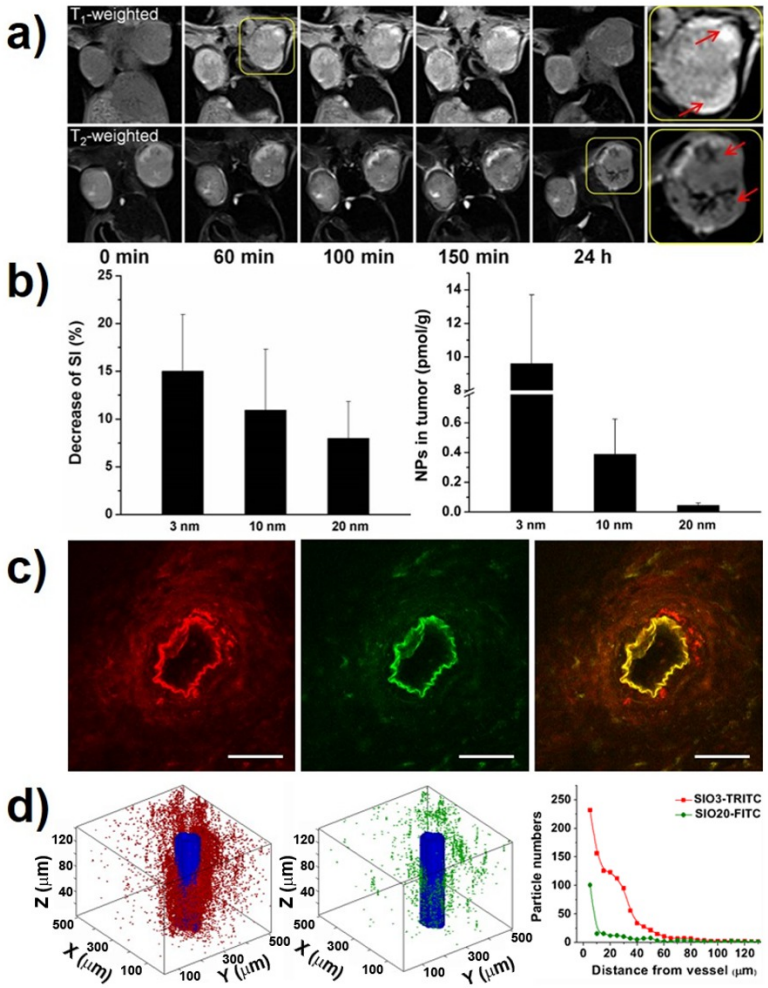

Figure 1. a) T_1- and T_2-weighted MRI of mice bearing orthotopic 4T1 tumors before and after i.v. administration of ultrasmall 3 nm iron oixde nanoparticles (SIO-3) at different time points. Bright signal in T1-weighted MR images was observed at early time points (i.e. 60-150 min) resulted from the single dispersed SIO-3, while darkened signal was observed at 24 h because of the self-assemble of SIO-3 into cluster forms. **b)** The comparison of T_2-weighted MRI signal changes in tumor at 24 h (left) and iron content measurement by the colorimetric method (right) (n=3). Although the clustered SIO-3 has lower r_2 value than larger counterparts (10 and 20 nm), it showed the greatest decrease of SI in tumor because of the largest accumulation amount. This result was further confirmed by the analysis of Fe concentration in tumor tissues. **c)** Multiphoton images of tumor section showing a tumor vessel at 3 h after i.v. co-injection of SIO3-TRITC (in red) and SIO20-FITC (in green). The extravasation of nanoparticles from tumor vessel can be observed, scale bar is 50 μm. **d)** 3D reconstruction of multiphoton Z stacks showing the distribution of nanoprobes in tumor after extravasating from the vessel (in blue), and corresponding statistics analysis of nanoprobe accumulation over the distance away from the vessel.

CONTROL ID: 2233878

TITLE: Biochemical and in vivo Diagnostic Characterization of Ratiometric Protease-activatable Fluorescent Imaging Agents in Preclinical Cancer Models: Supporting Clinical Translation

PRESENTER: Jesus Gonzalez

ABSTRACT BODY:

Abstract Body: Oncologic surgeons primarily rely on reflected light visualization and palpation for intraoperative identification of cancerous tissue. In the case of videoscopic procedures, it is even more limited as manual feel is not an option. We have developed intravenously administered fluorescent peptide dye conjugate agents with a design objective of providing surgeons improved intraoperative cancer visualization for detection of primary tumors and metastases to lymph nodes.

These agents employ protease-activatable cell-penetrating peptides that have been engineered for ratiometric fluorescence readout and have been optimized for in vivo applications. Increased proteolytic activity in tumors and the surrounding stromal microenvironment is known to be essential for cancer progression, invasion, and metastasis[1]. Matrix metalloproteinases (MMP) are one family of proteases that have increased activity in a variety of cancers. In human breast carcinomas, tumor tissue and microenvironment have elevated MMP activity[2]. The mechanistic basis for subject agent cancer visualization is the increased activity of pathological proteases. Protease substrate hydrolysis triggers tissue retention and fluorescence color change. Retention results from unmasking the cell-penetrating peptide and ratiometric visualization is achieved using two far-red or near-infrared (NIR) fluorescent dyes which undergo Förster's Resonance Energy Transfer[3]. Energy transfer between the two fluorophores is disrupted upon peptide hydrolysis, resulting in a large fluorescence ratio change generated from both dyes which can be visualized using a customized clinically-compatible imaging camera system capable of detecting two fluorescence channels and one reflected light channel simultaneously.

In vivo imaging studies in murine breast cancer models compared ratiometric fluorescence signal from tumor and lymph node tissue to H&E histopathological results independently assessed by pathologist blinded to imaging analysis. We determined fluorescence kinetics, correlation to histopathology, and Receiver Operating Characteristic curve analysis, which demonstrated high in vivo diagnostic sensitivity and specificity (both >95%). Protease:agent substrate hydrolysis kinetics were characterized and compared using recombinant enzymes. To understand the human translation potential, an in vitro diagnostic study was conducted to evaluate the ability of agent to differentiate human cancerous tissue from healthy adjacent tissue. Matched primary tumor tissue and healthy adjacent breast tissue from breast cancer patients were homogenized and incubated with agent and hydrolysis rates, determined from fluorogenic response, were compared. In every case, the tumor tissue had 2-3 fold faster hydrolysis than matched healthy adjacent breast tissue, similar to what was found using tissue from mouse models. These results provide efficacy support for human translation.

1. Mason SD, Joyce JA: *Trends in cell biology* 2011, **21**(4):228-237.
2. Jones JL, Glynn P, Walker RA: *The Journal of pathology* 1999, **189**(2):161-168.
3. Savariar EN et al.: *Cancer research* 2013, **73**(2):855-864.

AUTHORS (LAST NAME, FIRST NAME): Miampamba, Marcel[1]; Liu, Junjie[1]; Harootunian, Alec[1]; Gale, Andrew J.[1]; Gonzalez, Jesus[1]

INSTITUTIONS (ALL):

1. Avelas Biosciences, La Jolla, CA, United States.

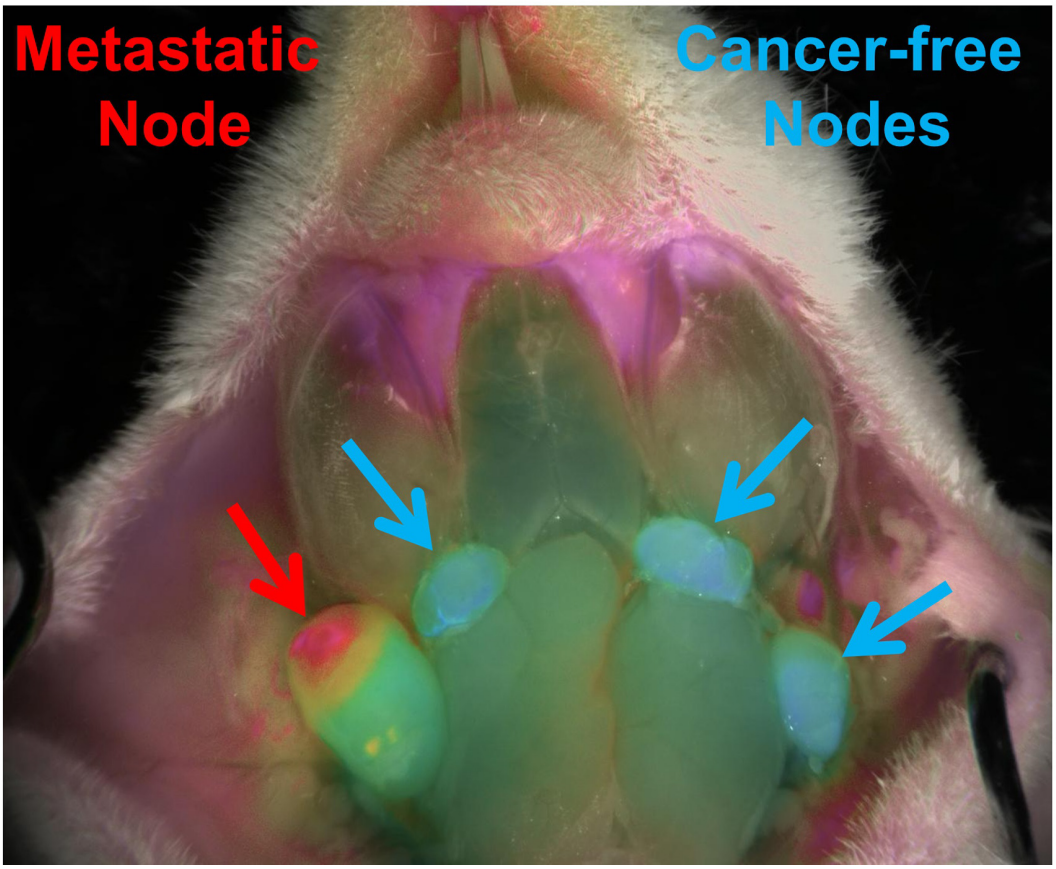
Metastatic
Node
Cancer-free
Nodes

CONTROL ID: 2233880

TITLE: New approach to hybrid light imaging technique using Cerenkov luminescence and liquid scintillation for beta- and gamma-ray emitted radionuclides

PRESENTER: Masako Shimamoto

ABSTRACT BODY:

Abstract Body: Cerenkov luminescence imaging (CLI) has recently been well known as one of molecular imaging modalities using radioactive tracers in both preclinical and clinical practices. For these radionuclides, the conventional CLI detects only Cerenkov radiation (CR) from beta-rays and still has a tissue penetration issue.

Here, we propose a new imaging technique “hybrid light imaging (HLI),” which uses the combination lights of Cerenkov emitted from beta-ray and liquid scintillation emitted from gamma-ray. In this study, the feasibility of HLI was investigated using a Cs-137 point source and tissue-like materials. The thicknesses of liquid scintillators and tissue-like materials were changed from 0-7mm and 0-14mm, respectively. All images were acquired using IVIS Spectrum. In the results, Cs-137 images of CLI showed very low and obscure signals for 12 mm thickness of the tissue-like material while the HLI could increase the signal intensity by up to 12 times compared to CLI alone. Moreover, HLI visualized the source shape more clearly in spite of the degraded spatial resolution. It was also found that the 3mm thickness was suitable for the further *in vivo* experiment.

NaI-131 and F-18-FDG were used to demonstrate the further application for in vivo experiment. In our *in vivo* experiments, thyroid grand uptake of NaI-131, and heart and bladder accumulation of F-18 FDG were observed with greater signal intensities by the HLI than CLI. In particular, the HLI could successfully visualize the deeper organs while CLI failed to detect. Although further investigation and the optimization of the liquid scintillator are still needed for the preclinical feasibility of the HLI, our results suggested that HLI can be a promising method to assist Cerenkov Luminescence imaging for radioisotopes that emit both beta-ray and gamma-ray, such as Cs-137, I-131 and F-18, leading to detect more enhanced light signal in deeper region of living animals as comparison with CLI alone.

AUTHORS (LAST NAME, FIRST NAME): Shimamoto, Masako[1]; Gotoh, Kumiko[1]; Hasegawa, Koki[1]; Kojima, Akihiro[1]

INSTITUTIONS (ALL):

1. Kumamoto University, Kumampto-city, Japan.

(No Image Selected)

CONTROL ID: 2233885

TITLE: In Vivo Molecular Contrast OCT imaging of Methylene Blue

PRESENTER: Brian Applegate

ABSTRACT BODY:

Abstract Body: Beyond the current clinical applications in ophthalmology and cardiology, Optical Coherence Tomography (OCT) is being widely investigated as a diagnostic and research tool for human disease and animal models of the same. It can provide non-invasive high-fidelity morphological images of highly scattering tissues at depths of 1-2 mm. The image contrast in OCT arises from variations in the tissue refractive index. Unfortunately in many cases there is very little change in the differential refractive index in morphologically distinct areas of soft tissues. One approach to engendering additional contrast is to use exogenous agents which are targeted either passively or actively to the morphological features of interest. Beyond simply highlighting a particular morphology this approach can target specific molecules or receptors to provide detailed information on the local biochemistry and yield enhanced visualization of pathological and physiological processes. This approach while common in microscopy is only slowly being adapted to OCT. A contributing factor is the lack of sensitivity to incoherent processes such as florescence emission.

In order to garner molecular contrast with OCT we have exploited a process know as transient absorption using Pump-Probe OCT (PPOCT). We have targeted methylene blue (MB) as a contrast agent where excitation at 660 nm leads to transient absorption at 830 nm, a common OCT wavelength. MB has a variety of clinical applications. It is a recommended treatment for methemoglobinemia and was one of the earliest antimalarial drugs. It is also a common stain used in chromoendoscopy of the gastrointestinal tract. MB has been shown to selectively stain specialized columnar epithelium in Barrett's esophagus. Monitoring of Barrett's esophagus is one of the emerging clinical applications of OCT.

Prior efforts at imaging MB with PPOCT have utilized nanosecond pulsed lasers at 532 nm as the pump and femtosecond pulsed lasers at 830 nm as the probe. These succeeded in imaging tissue phantoms, however there has never been a demonstration in a biological sample, either *in vivo* or *ex vivo*. A contributing factor is the fairly weak absorption of the 532 nm light which is far from the 660 nm peak. A second issue is the use of fairly atypical OCT light sources. Commercial instruments operating in the 800 nm band predominantly make use of superluminescent diodes (SLD) which are relativley cheap and robust. Our goal for the work described here was to develop an approach which would enable imaging of MB at powers below the ANSI limits using more common and robust light sources. We were motivated by the fact that such a development would facilitate clinical translation of the technology.

The approach we have developed does away with the expensive 532 and 800 nm pulsed lasers used previously in favor of a modulated 660 nm diode laser pump and an 830 nm SLD probe. Since the probe is the OCT light source, this paradigm shift enabled PPOCT imaging of MB with only minor modifications to a typical 830 nm band spectral-domain OCT system. The system was validated using tissue phantoms and in vivo imaging of MB unptake in the kidneys of a zebrafish.

AUTHORS (LAST NAME, FIRST NAME): Kim, Wihan[1]; Applegate, Brian E.[1]

INSTITUTIONS (ALL):

1. Biomedical Engineering, Texas A&M University, College Station, TX, United States.

(No Image Selected)

CONTROL ID: 2233909

TITLE: Arterial input graphical analysis for receptor concentration imaging with short acquisition times in glioma tumors

PRESENTER: Jonathan Elliott

ABSTRACT BODY:

Abstract Body: Recently developed receptor concentration imaging (RCI) techniques have opened up new possibilities for *in vivo* molecular imaging such as detecting 200 lymph node cancer cells *in situ* [1], providing a more realistic measurement of the affinity of available receptors than traditional *ex vivo* techniques [2] and quantifying binding potential (BP) with small animal tomography [3]. Emboldened by these developments, we explore the possibility of RCI for surgical guidance by hypothesizing that the molecular changes preceding enhanced permeability and retention (EPR) related vascular ones could provide a source of contrast differing from EPR-based fluorescein or MRI contrast enhancement. To perform RCI with shorter acquisition times (ATs) than the 60-120 min of current methods, an arterial-input approach is used to fit tissue uptake images and separate EPR and binding-specific effects. The innovation of using arterial-input graphical analysis (AIGA) enables rapid and accurate quantification of BP spatially when combined with targeted/untargeted tracer pairs and quantification of arterial input function (AIF) by direct imaging.

The AIGA approach is based on the Logan graphical analysis approach used in PET imaging [4], which is advantageous over PET models previously applied to fluorescence [5] because it uses the AIF to directly account for delivery. Additionally, rather than relying on a reference region to recover BP, the untargeted tracer provides an independent measure of the EPR-related properties in the tissue. Cumulative sum (CS) normalized uptake curves for the dye pair are plotted against the AIF normalized by the CS of the tissue uptake curves (Fig. 1D,E). The resulting slope is the apparent volume of distribution (V_d) and taking the ratio of V_d between the two dyes yields 1 + *BP*. Subcutaneous U251 tumor bearing mice (n = 11) were injected 2 nmol each of anti-EGFR affibody® molecules conjugated to IRDye® 800CW (ABY-029) and IRDye ®680RD neg. ctrl. affibody® molecules (Affibody AB and LI-COR). Emitted fluorescence was measured concomitantly with a planar imaging system every min for 1 h. The AIF was acquired by direct fluorescence imaging of a major blood vessel [6].

Group averages of BP (Fig. 1F) calculated with AIGA from tumor and muscle ROIs were 1.31 ± 0.26 and 0.16 ± 0.20, respectively, recovered from tissue uptake measured 15 to 25 min post injection (10 min AT), and AIF measured continuously from injection out to 25 min. These did not significantly differ from values recovered using the previously validated *in vivo* method [7]. Fig. 1C shows the intra-tumor variation captured by RCI, suggesting differential expression of EGFR across the tumor, as is well known from pathology analysis, but in this case is visualized *in vivo*. In particular, RCI of EGFR upregulation, specific to invasive tumor margins, could provide sensitive intraoperative contrast to improve extent of tumor resection.

1. Tichauer et al. Nat Med 20; 2014.
2. Samkoe et al. Canc Res 74; 2014.
3. Davis et al. PNAS 110; 2013.
4. Logan et al. JCBFM 10; 1990.
5. Tichauer et al. Mol Imag Biol 14; 2011.
6. Elliott et al. Mol Imag Biol 16; 2014.
7. Tichauer et al. Phys Med Biol 59; 2014.

AUTHORS (LAST NAME, FIRST NAME): Elliott, Jonathan T.[1]; Davis, Scott[1]; Samkoe, Kimberley S.[1, 2]; Gunn, Jason R.[1]; Pogue, Brian W.[1, 2]

INSTITUTIONS (ALL):
1. Thayer School of Engineering, Dartmouth College, Hanover, NH, United States.
2. Department of Surgery, Geisel School of Medicine at Dartmouth, Lebanon, NH, United States.

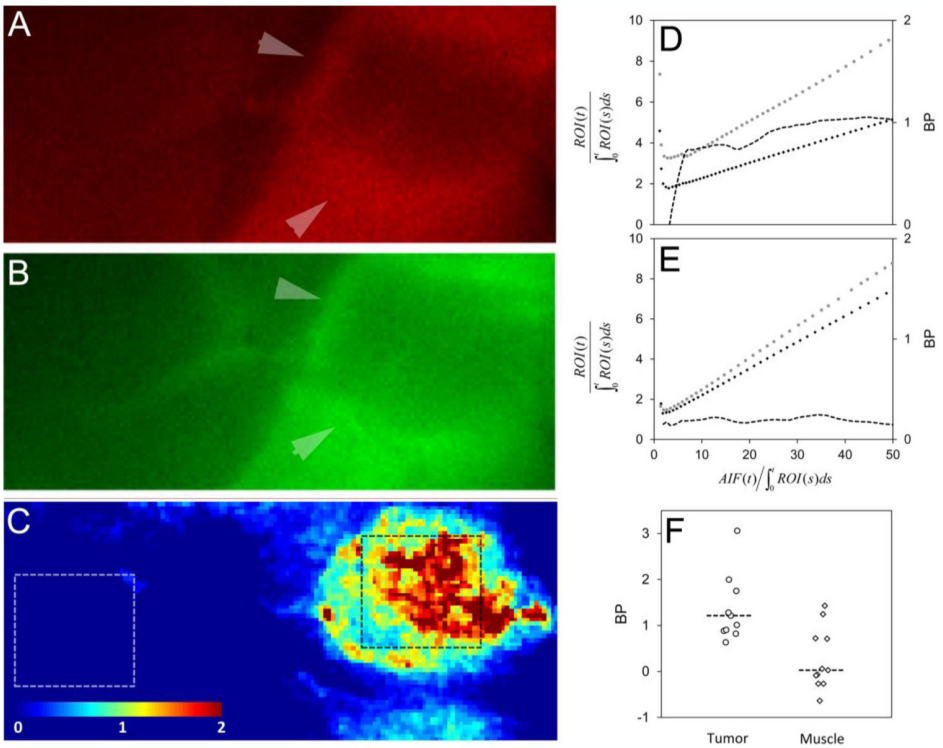

Figure 1 (A) Fluorescence intensity images of IRDye®60RD/negative control Affibody® and (B) ABY-029 acquired at 1 hour post injection in a U251 tumor-bearing mouse, showing some ring enhancement around tumor (white arrows). (C) Binding potential (BP) map of the same tumor showing marked improvement in contrast to background ratio. Region-of-interest graphic analysis plot showing relationship between cumulative-sum-normalized tissue uptake and AIF in tumor (D) and muscle (E) regions. Closed circles show untargeted tracer data, black solid diamonds show targeted tracer data, and dashed line shows the binding potential determined from a 10 data-point window centered at that spot. (F) Group averages (n = 11) of binding potential recovered for tumor and muscle regions-of-interest.

CONTROL ID: 2233911

TITLE: High-sensitivity x-ray fluorescence computed tomography using gold L-shell characteristic x-rays

PRESENTER: Moiz Ahmad

ABSTRACT BODY:

Abstract Body: Purpose/Objective(s): X-ray fluorescence CT (XFCT) imaging has been previously proposed for cancer imaging with high resolution and specificity; however, the sensitivity of this imaging modality has been insufficient for practical clinical applications. We demonstrate that x-ray fluorescence imaging with low-energy (9–11 keV) gold L-shell x-rays achieves high-sensitivity to small concentrations of contrast agent.

Methods: X-ray fluorescence (XRF) is the process of characteristic x-ray emission stimulated in contrast agents following x-ray absorption. Aqueous gold solution was chosen as the contrast agent which emitted L-shell XF at 9.72 and 11.42 keV. We built an experimental L-shell XFCT imaging system consisting of a portable x-ray source; two x-ray spectrometers: a high-energy resolution silicon drift detector (SDD, 220 eV energy resolution at 14.4 keV) and a cadmium telluride detector (CdTe, 660 eV energy resolution at 14.4 keV; typically used in XFCT experiments); and a programmable scanning motion stage. The x-ray source was operated at 50 kVp and 60 μA. First, we evaluated the linearity of the XRF signal over a range of gold concentrations. Second, we imaged a 28-mm diameter water phantom containing 4-mm diameter Eppendorf tubes containing gold solutions with concentrations of 0.06, 0.08, and 0.1% Au (percent weight concentration). The phantom was scanned with 1-mm x-ray beam using 36 1-mm translation steps across 30 mm and 36 rotation steps over 360°. XFCT images were reconstructed with maximum-likelihood expectation-maximization algorithm for both the SDD and CdTe data sets.

Results: The SDD XRF signal was approximately 13 times higher than the CdTe XF signal. The XF signal was linear with Au concentration for both detectors. While all 0.06−0.1% Au vials were detectable reconstructed XFCT image from the SDD data, none of the vials were visible when reconstructed from the CdTe detector data. The contrast-to-noise ratio of the 0.1% Au vial was 87.1 and 3.2 in the SDD and CdTe L-shell XFCT image, respectively. The detection limits of our imaging system were 0.007% and 0.126% Au when using the SDD and CdTe detector, respectively.

Conclusions: The SDD is an appropriate detector technology for gold L-shell XFCT imaging due to its high energy resolution, which produces high sensitivity. L-shell XFCT imaging may image small concentrations of targeted gold contrast agents in superficial malignancies such as melanomas and some breast tumors, and in small animal imaging. Further sensitivity improvement is expected with arrays of XF detectors. L-shell XFCT promises high resolution and sensitivity as a molecular imaging modality.

AUTHORS (LAST NAME, FIRST NAME): Ahmad, Moiz[1]; Bazalova-Carter, Magdalena[1]; Xing, Lei[1]; Fahrig, Rebecca[2]

INSTITUTIONS (ALL):

1. Radiation Oncology, Stanford University, Stanford, CA, United States.
2. Radiology, Stanford University, Stanford, CA, United States.

(No Image Selected)

CONTROL ID: 2233918

TITLE: Targeted imaging of GRP receptor-expressing prostate cancer with ^{68}Ga/IRDye-650 conjugated bombesin antagonist

PRESENTER: Hanwen Zhang

ABSTRACT BODY:

Abstract Body: Objectives: Gastrin releasing peptide receptors (GRPr) are frequently overexpressed by human prostate cancer cells, and radiolabeled GRPr-affinity ligands have shown significant promise for *in vivo* imaging of prostate cancer with PET. The goal of this study was to develop a dual-modality imaging probe that can be used for pre-operative PET imaging and intra-operative optical imaging of prostate cancer.

Methods: We designed and synthesized an IRDye-650 and DOTA conjugated GRPr antagonist, HZ220 (DOTA-Lys(IRDye650)-PEG_4-[D-Phe^6, Sta^{13}]-BN(6-14)NH_2), and studied its uptake at prostate cancer cells *in vitro* and *in vivo.* The control GRPr antagonists, DOTA-AR06 (DOTA-PEG_4-[D-Phe^6, Sta^{13}]-BN(6-14)NH_2) and HZ219 (DOTA-Lys-PEG_4-[D-Phe^6, Sta^{13}]-BN(6-14)NH_2) were also synthesized on solid phase by using Fmoc-strategy. ^{67}Ga/^{68}Ga/^{nat}Ga-labeled ligands were characterized with HPLC or LC-MS. Receptor specific binding of these ligands was compared for prostate cancer cells (PC-3) and tumor uptake in vivo was imaged with PET/CT (Inveon PET/CT) and fluorescence imaging (IVIS spectrum).

Results: HZ220, DOTA-AR06 and HZ219 were synthesized with yield of 20-40%. After HLB cartridge purification, the ^{68}Ga-labeling yields (decay-corrected) for HZ220 and DOTA-AR06 were 56±8% and 84±1%, respectively. Their radiochemical purities were greater than 95%. Ga-HZ220 displayed a lower affinity to GRPr (IC_{50} value: 21±8 nM) than Ga-DOTA-AR06 or Ga-HZ219 (0.48±0.18 or 0.69±0.18 nM). However, in vivo ^{68}Ga-HZ220 displayed a similar *in vivo* tumor accumulation as ^{68}Ga-DOTA-AR06 (4.5±0.8 vs 4.1±0.4 %ID/cc at 1 h p.i.); 2/3 of the tumor uptake could be blocked with an excess amount of HZ220 or Ga-DOTA-AR06. IVIS spectrum imaging also visualized PC-3 xenografts *in vivo* and *ex vivo.* In addition, both ^{68}Ga-HZ220 and ^{68}Ga-DOTA-AR06 displayed a similar accumulation in all other non-target organs, except for a significantly higher kidney uptake of ^{68}Ga-HZ220 (7.1±1.1 vs 2.3±0.6 %ID/g).

Conclusion: ^{68}Ga-HZ220 is a promising bimodal ligand for non-invasive preoperative PET imaging and intraoperative fluorescent imaging of GRPr-expressing malignancies. Thus, ^{68}Ga-HZ220 PET/fluorescent imaging may improve cancer staging and guide surgical resections.

Acknowledgements: Supported by NIH grant P50-CA84638. MSKCC Small Animal Imaging Core Facility was supported by NIH Small-Animal Imaging Research Program grant R24 CA83084 and NIH Center grant P30 CA08748).

AUTHORS (LAST NAME, FIRST NAME): Zhang, Hanwen[1]; Desai, Pooja[1]; Koike, Yusuke[1]; Carlin, Sean[1]; Tandon, Nidhi[1]; Touijer, Karim[2]; Weber, Wolfgang[1]

INSTITUTIONS (ALL):

1. Radiology, Memorial Sloan Kettering Cancer Center, New York, NY, United States.
2. Surgery, Memorial Sloan Kettering Cancer Center, New York, NY, United States.

MIP imaging of PC-3 xenografts with ^{68}Ga-HZ220 PET/CT & ^{68}Ga-HZ220 IVIS

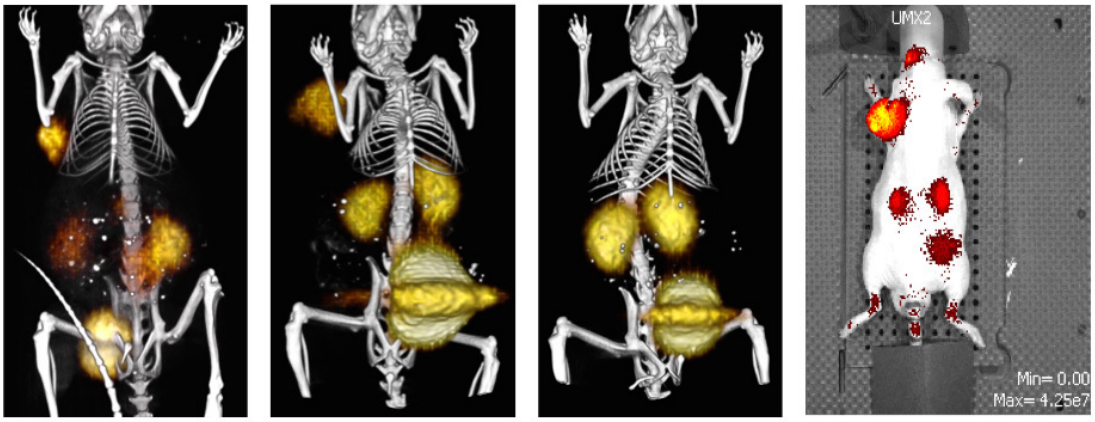

^{68}Ga-DOTA-AR06 ^{68}Ga-HZ220 ^{68}Ga-HZ220, blocked ^{68}Ga-HZ220

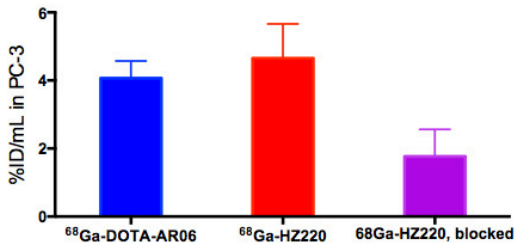

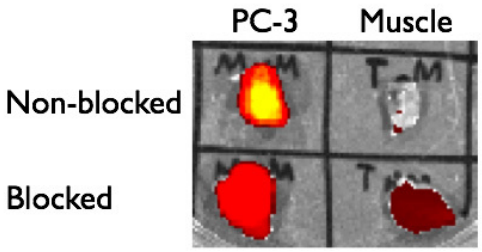

CONTROL ID: 2233993

TITLE: Evaluation of ^{68}Ga-labeled small molecules for targeted imaging of PSMA in prostate cancer xenografts

PRESENTER: Hanwen Zhang

ABSTRACT BODY:

Abstract Body: Objectives: PSMA (prostate specific membrane antigen) is highly expressed in prostate cancers, especially those with increased expression in poorly differentiated, metastatic, and hormone-refractory carcinomas, which makes PSMA as a promising target for noninvasive imaging. The goal of this study was to evaluate a urea-based PSMA inhibitor suitable for labeling with ^{68}Ga/^{18}F in-vitro and in mice bearing prostate cancer xenografts.

Methods: A NOTA-conjugated PSMA inhibitor was synthesized using a multi-step procedure and was labeled with ^{68}Ga. The in vitro validation of DUPA-NOTA-^{68}Ga was performed with PSMA-transduced PC-3 (PIP-PC-3), LNCaP, PC-3 cells and human prostate cancer tissue. The in vivo biodistribution and tumor uptake was assessed by small animal PET imaging of mice bearing LNCaP xenografts.

Results: DUPA-NOTA-^{68}Ga was obtained with a radiochemical purity of > 98%, and the specific activity was >22 MBq/nmol. DUPA-NOTA-$^{67/nat}$Ga had a nM-affinity to PSMA expressed in LNCaP, PIP-PC-3 and human prostate cancer tissues (Kd values: 22.9±3.6 vs 16 vs 20.6±4.3 nM). Cellular uptake of the tracer reflected the PSMA expression levels of the studied cell lines ((PIP-PC-3 > LNCaP >> PC-3); co-incubation with an excess of unlabeled PSMA inhibitor reduced the uptake in both PIP-PC-3 and LNCaP cells significantly. PET imaging showed that DUPA-NOTA-^{68}Ga had a rapid accumulation in PSMA-expressing LNCaP xenografts (5.1±0.7 %ID/mL at 1h p.i.). DUPA-NOTA-^{68}Ga showed a rapid renal clearance from all non-targeting organs resulting in high contrast PET images at 1 h p.i.

Conclusion: DUPA-NOTA is a promising ligand for PET imaging of PSMA-expressing tumors. The ligand has the potential for broad clinical use because it can be labeled with both ^{68}Ga and Al^{18}F.

Acknowledgements: Supported by NIH grant P50-CA84638. MSKCC Small Animal Imaging Core Facility was supported by NIH Small-Animal Imaging Research Program grant R24 CA83084 and NIH Center grant P30 CA08748).

AUTHORS (LAST NAME, FIRST NAME): Zhang, Hanwen[1]; Chen, Qingshou[2]; Desai, Pooja[1]; Carlin, Sean[1]; Tandon, Nidhi[1]; Koike, Yusuke[1]; Weber, Wolfgang[1]; Low, Philip S.[2]

INSTITUTIONS (ALL):

1. Radiology, Memorial Sloan Kettering Cancer Center, New York, NY, United States.
2. Chemistry, Purdue University, West Lafayette, IN, United States.

PET/CT imaging of LNCaP xenografts with DUPA-NOTA-^{68}Ga at 1 h p.i.

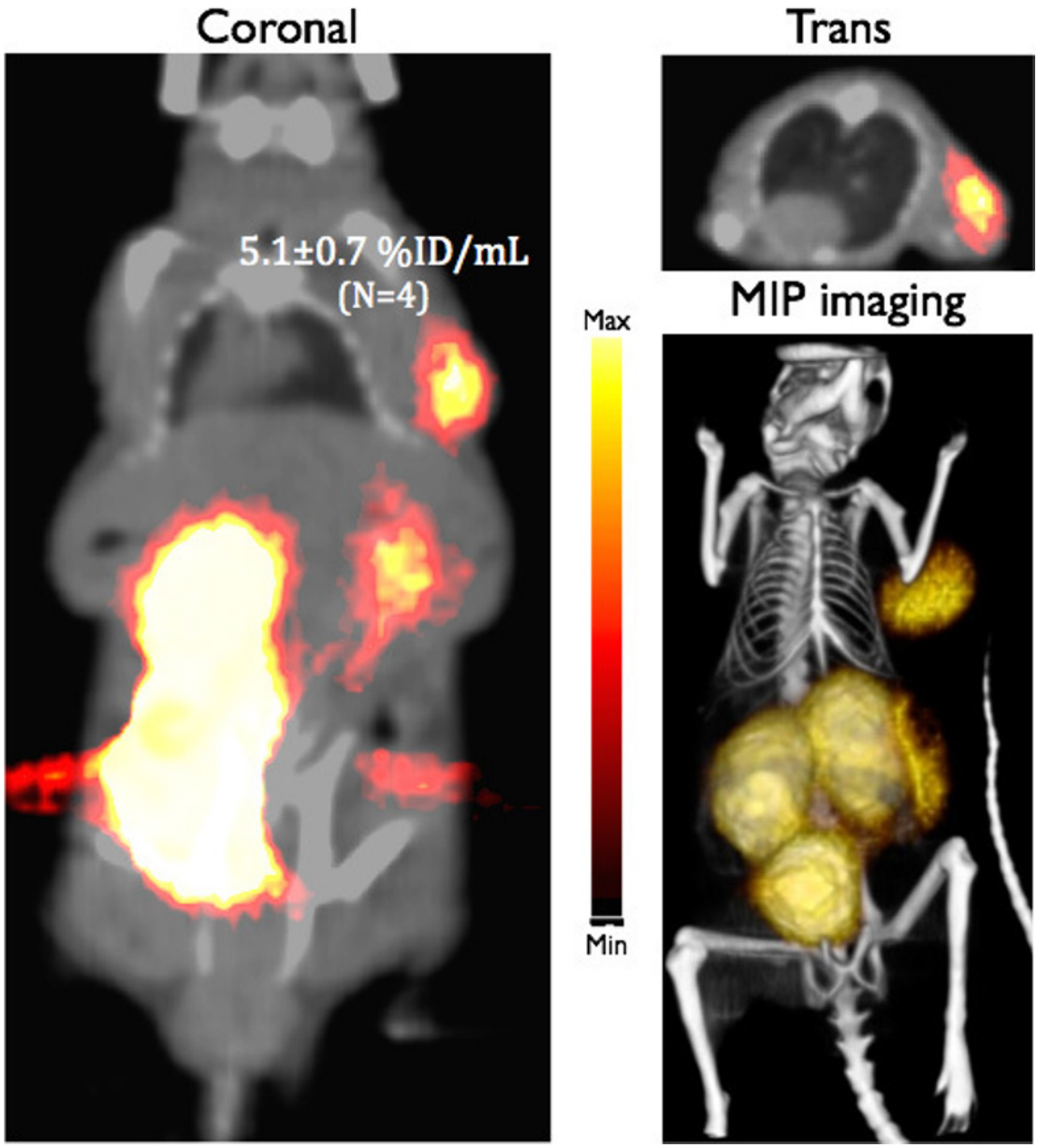

CONTROL ID: 2233931

TITLE: Segmental 360° Bioluminescent Imaging using the Mouse Imaging Spinner (MiSpinner) Shows Potential For Accurate Monitoring of Tumor Development

PRESENTER: Andrew Brannen

ABSTRACT BODY:

Abstract Body: Non-invasive monitoring of luciferase-expressing tumor cells over the span of weeks to months by bioluminescence imaging (BLI) serves as a useful tool to study tumor establishment, development, and ultimate metastasis. However, there exist inherent biases in the *in vivo* tracking of tumor development created during BLI sessions, with regard to positioning of the light source relative to the detector. To reach the detector, light must move through the tissue, which causes a scattering effect due to tissue acting as a non-homogenous medium for light propagation. The scattering of light diminishes the total signal intensity depending on the source depth as a direct result of the absorptive properties of the blood, fat, and muscle. Slight inconsistencies of subject positioning can increase variability in the small animal imaged over time, thereby reducing accurate measurement of bioluminescent tumor signal, and ultimately increasing animal usage as the researcher strives to reach statistical power. Our goal was to develop a consistent method for the collection of 360° data of a developing tumor in xenograft model to maximize the information collected from a single mouse at a single point in time. Furthermore, we sought to examine the signal-to-source orientation relationship in an *in vivo* cancer. Our prototype for collection of such images is a novel device developed to expand the capabilities of IVIS Lumina XRMS system (PerkinElmer Inc.), whereby we converted it into a full 360° imager through minimal effort and at low relative cost. Our invention is named the Mouse Imaging Spinner (MiSpinner; PROVISIONAL PATENT APPLICATION NO.: 62/020,056), which automates the actuated rotation of the animal during the imaging process. For our maiden study, progressive BLI of tumor growth in athymic NCR nude mice implanted subcutaneously in the flank with human prostate cancer cells expressing luciferase (PC-3-luc2) was performed with this device, in conjunction with the IVIS Lumina XRMS system, and the mouse was rotated precisely 7.5° per interval around a stringently maintained 360° central axis (Fig. 1). The rate of flux for each iteration around this 360° rotation was determined for regions of interest and plotted against the total rotated degrees for each weekly time point spanning the 9-week experiment. Our results demonstrate a distinctive peak of BLI flux at a specific angle, wherein BLI signal corresponds to a defined angle of rotation. The peak flux was used as a means of standardization for week-to-week comparisons of tumor development. Further, the integral area for each time point was determined, and correlated significantly with digital caliper measurements of tumor volume by Spearman Rank correlation analysis ($r = 0.93$; $P < 0.05$). Images acquired at each time point were compiled into video representations for visual demonstration of BLI signal change. This method of segmental 360° bioluminescent imaging provides powerful new tool for the collection non-invasive BLI data and reduces ambiguity of signal due to inconsistent animal positioning, particularly for longitudinal studies with tumor models.

AUTHORS (LAST NAME, FIRST NAME): Brannen, Andrew D.[1]; Eggert, Matthew W.[1]; Arnold, Robert D.[1]; Panizzi, Peter[1]

INSTITUTIONS (ALL):

1. Drug Discovery and Development, Auburn University, Auburn, AL, United States.

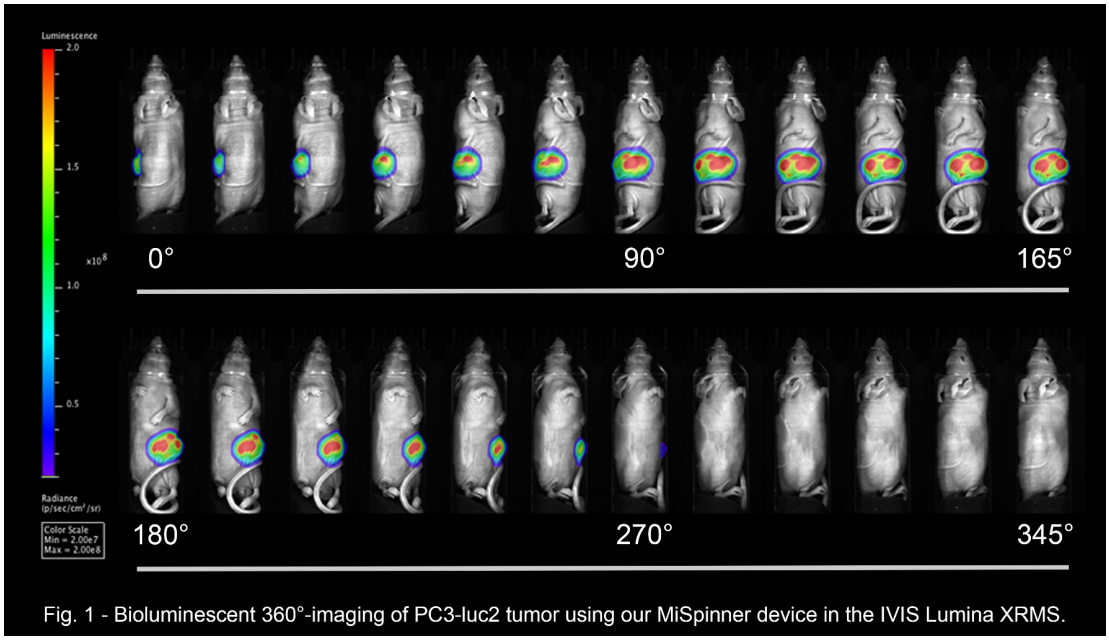

Fig. 1 - Bioluminescent 360°-imaging of PC3-luc2 tumor using our MiSpinner device in the IVIS Lumina XRMS.

CONTROL ID: 2233934

TITLE: QUESPOWR MRI of the human brain

PRESENTER: Edward Randtke

ABSTRACT BODY:

Abstract Body: Introduction: The Quantification of Exchange as a function of Saturation Power On the Water Resonance (QUESPOWR) MRI method can detect tissues that have fast exchanging labile protons with small chemical shifts. This method uses the OPARACHEE MRI pulse sequence[1] to measure water signal as a function of RF power, and uses QUESPOWER linear fitting methods that are similar to linear variations of QUESP fitting methods[2] to estimate the average chemical exchange rate for each pixel. This technique has been translated to a 3T clinical system.

Methods:

A phantom of glucose was prepared at 100 mM and pH 6.6, and a phantom of salicylic acid was prepared at 20 mM and pH 7.0. These samples were selected to model tissues dominated by hydroxyl groups at low pH and healthy tissues dominated by labile pools at high chemical shift at neutral pH. The QUESPOWR MRI method obtained a series of OPARACHEE MR images of the two phantoms with WALTZ16* RF pulse powers ranging from 0.5 to 6.0 mT in 0.1 mT increments; 6.2 to 8.0 mT in 0.2 mT increments; and at 8.5, 9.0, and 10 mT. To process the images on a pixelwise basis, the % water signal was normalized to the water signal acquired with 10 mT WALTZ16* RF power. The resulting profile was inverted and the high-power region of the signal profile was fit with the linear HW-QUESP method to obtain the weighted-average chemical exchange rate. A volunteer was imaged using the QUESPOWR technique at power levels of 3, 3.5, 4, 4.5 and 5 uT, and using the same image processing method.

Results: Figure 1 of Persuasive Data shows QUESPOWR MRI analysis of the two phantoms. The QUESPOWR results of the glucose phantom had a much stronger dynamic range as power was increased, and thus could be fit with outstanding precision. The fitted exchange rate was in good agreement with previously reported results for glucose at pH 6.6[5]. The QUESPOWR results of the salicylic acid peak had a much poorer dynamic range as power was increased, and thus had a less precise fit. Yet the fitted exchange rate for salicylic acid was in good agreement with previous results[4] and with alternative analysis with the HW-QUESP method.

The results from the volunteer are in agreement with the phantom results (Figure 1 of the Abstract). The poor dynamic range of QUESPOWR MRI signal in the brain tissues is likely a result of a pH-neutral brain tissue of the volunteer.

Discussion: The phantom results demonstrate that this technique is sensitive to the detection of chemical exchange from hydroxyl groups that have small chemical shifts and fast chemical exchange rates, which are difficult to analyze with standard CEST MRI methods. The clinical results demonstrate that pH-neutral tissues are difficult to analyze with this technique. We hypothesize that acidic tissues will be fit well with QUESPOWR MRI, such as tumors and ischemic tissues in the brain. Based on these initial results, we have initiated a clinical trial with QUESPOWR MRI.

References:

1. J Magn Reson 2005, 176:54-63.
2. Magn Reson Med 2014, 71:1603-1612.
3. Magn Reson Med 2006, 55:836–847.
4. Angew Chemie, 2013, 125(31), 8274-8277.
5. Magn Reson Med 2012, 68(6), 1764-1773.

AUTHORS (LAST NAME, FIRST NAME): Randtke, Edward A.[1]; Pagel, Mark[1]; Li, Wen[1]; Kahn, Rihan[1]; Nael, Kambiz[1]; Cárdenas-Rodríguez, Julio[2]

INSTITUTIONS (ALL):

1. Biomedical Engineering, University of Arizona, Tucson, AZ, United States.
2. Biomedical Engineering and Arizona Cancer Center, University of Arizona, Tucson, AZ, United States.

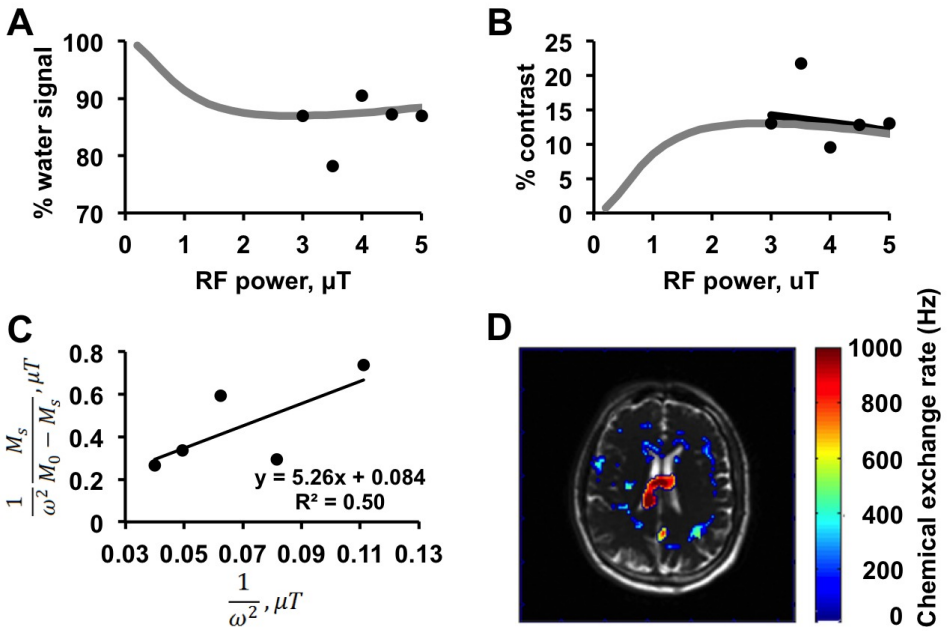

Figure 1: In vivo QUESPOWR MRI of human brain tissue. A) The experimental % water signal was dependent on the RF power of the WALTZ16* pulse (circles) which matched simulated QUESPOWR MRI results (gray line) B) The experimental results were normalized to the % water signal at 1.8 µT (circles), and analyzed with a linear fit (black line), which closely matched the simulated QUESPOWR MRI results (gray line). C) The HW-QUESP linear fitting method (line) was used to analyze the experimental results (circles). D) Brain tissue regions that were fit with the HW-QUESP method on a pixelwise basis are shown as a parametric map overlayed on an anatomical image. Because the brain tissue is healthy and not acidic, the dynamic range of the contrast response to power has a relatively low R^2 value. Acidic brain tissues (tumor, ischemia) is expected to have a higher correlation with a HW-QUESP plot.

CONTROL ID: 2244300

TITLE: Optimizing multislice acidoCEST MRI for assessments of extracellular pH in tumor and kidney tissues.

PRESENTER: Edward Randtke

ABSTRACT BODY:

Abstract Body: Introduction: Studies of extracellular pH (pHe) in solid tumor models can show spatial heterogeneity, necessitating multislice imaging of the entire tumor volume. Also, longitudinal studies of tumor pHe require consistent analysis of the same tumor regions, which is facilitated by multislice imaging. CEST MRI methods that use exogenous agents require fast imaging methods, which are typically limited to single-slice imaging. To address this problem, we have applied the Phase-Offset MultiPlanar (POMP) Simultaneous MultiSlice (SMS) technique (1) to acidoCEST MRI that uses an exogenous agent (2).

Methods: A MCF7 tumor model was imaged using a CEST-FISP MRI sequence with CW saturation applied at 3 mT for 2 sec; RF spoiling to suppress motion artifacts; 2.7 ms TE and a 5.8 ms TR; 0.5x0.5 mm in-plane resolution with 0.5 mm slice thickness. This pulse sequence was modified to include a 3.75° flip angle excitation pulse that consists of a sum of 4 Hermite pulses that simultaneously excites four non-contiguous slices. This pulse sequence was repeated 5 times to acquire 20 contiguous slices. Three CEST spectra were acquired prior to injection, then a 200mL bolusof 300 mg. of Iodine/mL iopamidol was administered i.v., followed by a 200mL/hr infusion of iopamidol for 54 minutes, while 3 sets of multislice CEST MR images were acquired. A fourth multislice image set was acquired after the infusion ended.

Images were filtered with a 3D Gaussian filter prior to fitting to mitigate noise. The Bloch-McConnell equations (3) were fit to pixelwise CEST spectra generated from subtracting the average pre-injection image from the average post-injection image. The k_{ex} values of iopamidol were calibrated with pH using phantoms, so that pHe could be fit directly in our model.

Results: The average tumor pHe was 7.00 pH units, with a decreasing pHe gradient from the core to the rim of the tumor in 3D. The average kidney pHe was 6.83 pH units, with an increasing pHe gradient from the medulla to cortex as expected. For comparison, we observed an average pHe of 7.3 units in muscle tissue. The median 95% confidence interval (CI) for voxelwise pHe measurements was 0.43 pH units in kidney and 0.55 pH units in the tumor, which shows that the average pHe should be analyzed for the tissue or sub-tissue regions (rim vs. core, medulla vs. cortex) to offset this voxelwise variance. Also, voxels with a lower pHe had higher variance, because base-catalyzed chemical exchange of iopamidol is weaker under acidic conditions.

Discussion: These results show that 3D acidoCEST MRI is feasible; Gaussian filtering is critical for improving CEST MRI for voxelwise analysis; the pHe in tumor, kidney, and muscle tissues can be measured using Bloch-McConnell fitting of CEST spectra; although voxelwise pHe measurements have some variance, pHe analyses of tissue and sub-tissue regions have excellent precision.

Glover, et al., J Magn Reson Imag 1991

Chen, et al., Magn Reson Med 2014

Woessner, et al. Magn Reson Med 2005

AUTHORS (LAST NAME, FIRST NAME): Randtke, Edward A.[2]; Howison, Christine M.[1]; Pagel, Mark[4]; Cárdenas-Rodríguez, Julio[3]

INSTITUTIONS (ALL):

1. University of Arizona, Tucson, AZ, United States.
2. Biomedical Engineering, University of Arizona, Tucson, AZ, United States.
3. Biomedical Engineering and Arizona Cancer Center, University of Arizona, Tucson, AZ, United States.
4. Medical Imaging, University of Arizona, Tucson, AZ, United States.

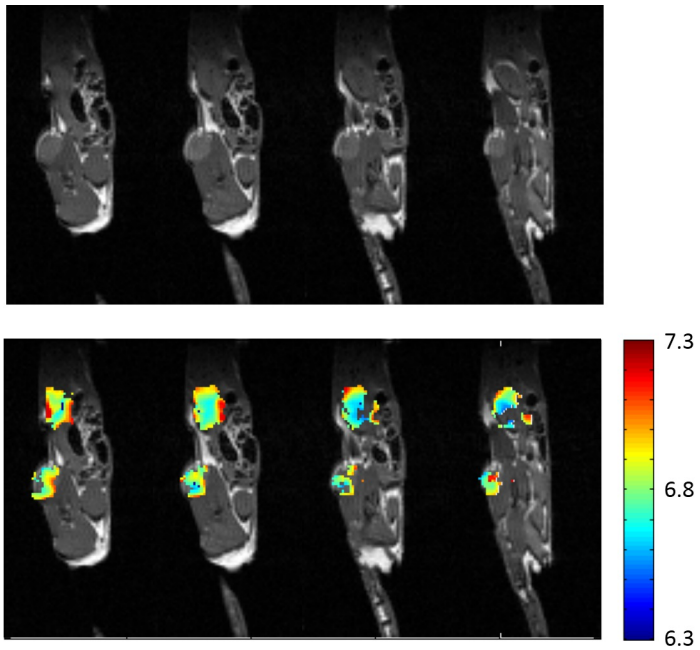

Figure 1: Pixel by pixel analysis of the tumor and kidney. Figure A) shows 4 T2 weighted RARE images. Figure B) shows the pH map overlayed onto the RARE images. Pixels with 95% confidence intervals greater than 0.5 pH units are pruned from the pH overlay. Pixels in empty space and in less vascular tissue are removed. A pH gradient across the kidney and through the tumor is apparent.

CONTROL ID: 2233944

TITLE: Imaging of Stem Cell in the Brain Using Integrated High-Performance SPECT/CT and SPECT/MR Systems

PRESENTER: Irina Balyasnikova

ABSTRACT BODY:

Abstract Body: There is a strong interest in utilizing neural stem cells (NSCs) as carriers for targeted delivery of therapeutics to brain tumors. Pre-clinical studies investigating tropism, distribution, safety and therapeutic efficacy of a clonal human NSC line, HB1.F3.CD, have led to approval of these cells in patients with recurrent high-grade glioma. Non-invasive imaging approaches for tracking of NSCs in the brain with a high sensitivity and spatial resolution can provide invaluable information necessary for tailored development of NSC-based therapies in various clinical settings. Innovative strategies of imaging NSCs in the brain have been developed in our laboratories. Novel approaches include the utilization of ^{111}In-labeled mesoporous silica nanoparticles (MSN-^{111}In) for NSC's tracing, as well as our own laboratory-built high-performance integrated SPECT/CT and SPECT/MRI systems[1]. The MSN-^{111}In complex showed low toxicity to NSCs, and robust *in vitro* and *in vivo* stability. The novel SPECT device employs energy-resolved, MR-compatible CdTe detectors with novel multi-pinhole collimators for high-resolution and high-sensitivity imaging. The specially designed 40-module "ring" device was constructed for stationery SPECT imaging without rotating the system or object, and can be integrated with a cone-beam CT imager for hybrid SPECT/CT imaging, or used as an insert for hybrid SPECT/MR imaging. We have used these two integrated dual-modality systems to conduct imaging of NSCs in the brain of mouse models. To evaluate the resulting imaging sensitivity and image quality in realistic experimental settings using the SPECT/CT and SPECT/MRI systems, two groups of MSN-^{111}In-NSCs with a 10-fold difference in NSCs concentrations, were injected into the left and right striatum of the mice. Hybrid SPECT/CT & SPECT/MR imaging sessions were performed with various time frames in both sequential SPECT and CT & MR imaging and simultaneous SPECT/CT & SPECT/MRI imaging. SPECT images were reconstructed with the use of different combinations of projection data employing OSEM-class reconstruction algorithms. Reconstructed SPECT images were also compared against those obtained in similar studies previously conducted using the commercial TriFoil pre-clinical imaging system. The resulting images show no detectable defects from simultaneous SPECT/MRI imaging, and the new SPECT scanner offers much higher imaging sensitivity and better spatial resolution than those produced by the TriFoil animal imager. Most importantly, our data demonstrate the capability of imaging of only hundreds of MSN-^{111}In loaded NSCs injected into the mouse brain using the SPECT/CT and SPECT/MRI systems, with both sequential and simultaneous imaging.

[1] Cai L, et al.. MRC-SPECT: A sub-500mm resolution MR-compatible SPECT system for simultaneous dual-modality study of small animals. *Nucl Instru & Methods A*. 2014; 734: 147–51.

[2] Balyasnikova, I.V., et al.: Intranasal delivery of mesenchymal stem cells significantly extends survival of irradiated mice with experimental brain tumors. *Mol Ther*, 2014. 22(1): 140-8.

AUTHORS (LAST NAME, FIRST NAME): Balyasnikova, Irina[1]; Lai, Xiaochun[2]; Cheng, Shih-Hsun[3]; Yu, Dou[1]; Leoni, Lara[3]; Lo, Leu-Wei[3, 4]; Lesniak, Maciej S.[1]; Meng, Ling-Jian[2]; Chen, Chin-Tu[3]

INSTITUTIONS (ALL):

1. Surgery, University of Chicago, Chicago, IL, United States.
2. University of Illinois at Urbana-Champaign, Urbana-Champaign, IL, United States.
3. Radiology, University of Chicago, Chicago, IL, United States.
4. Institute of Biomedical Engineering and Nanomedicine, National Health Research Institutes Nanomedicine, Zhunan, Miaoli, Taiwan.

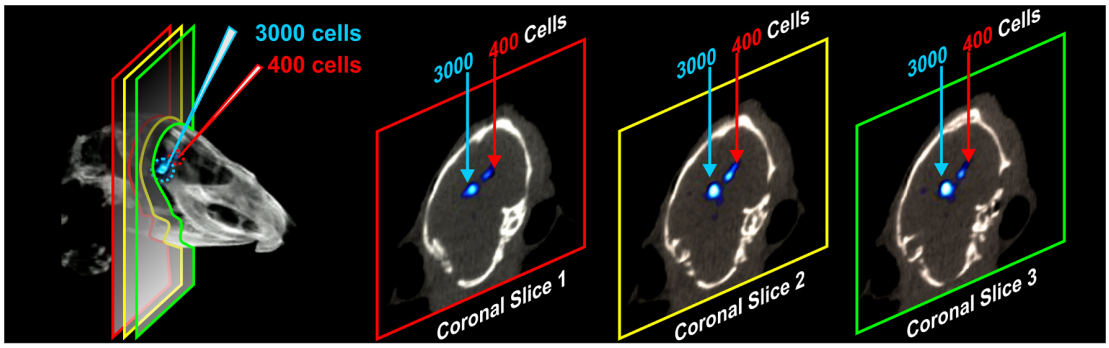

The CdTe-SPECT ring device was able to track as few as 400 NSCs loaded with MSN-^{111}In in a 2-hour imaging session.

CONTROL ID: 2233954

TITLE: X-ray Activated Nanoscintillators for Potential Radioluminescence-Guided Cancer Photodynamic Therapy

PRESENTER: Shih-Hsun Cheng

ABSTRACT BODY:

Abstract Body: We report the advance of X-ray activated nanoscintillators for potential imaging-guided cancer photodynamic therapy (PDT). The nanoscintillators composed of Eu(III) doped yttrium oxide nanocrystal core with biocompatible silica shell (Y_2O_3:Eu@SiO_2) have been developed. With this formulation, X-ray radiation absorbed by the yttrium oxide core of Y_2O_3:Eu@SiO_2 can subsequently introduce the downconversion to the Eu emitter in the proximity via intra-molecule energy transfer to induce near-infrared luminescence between 580 nm and 710 nm. We demonstrated, following X-ray irradiation, this nanoscintillator not only renders bright and stable radioluminescence but also generates cytotoxic reactive oxygen species including singlet oxygen and hydroxyl radical for potential cancer PDT, without the need of any photosensitizers. The X-ray induced deep-tissue cancer PDT studies have been conducted *in vitro* and *in vivo* using both radioresistant SKOV3 and radiosensitive CaOV3 ovarian cancer cell lines. The cytotoxicity resulted from X-ray induced photodynamic effect of Y_2O_3:Eu@SiO_2 nanoscintillators was successfully demonstrated with significantly enhanced inhibition of survival fractions of both radioresistant and radiosensitive ovarian cancel cell lines. By tuning the concentration of doped Eu(III) in Y_2O_3:Eu@SiO_2, we further demonstrated the radioluminescence intensity is independent from the induced ROS levels, thus providing the feasibility using this nanoscintillator as a theranostic platform for simultaneous X-ray activated optical tomography and PDT. With the progress of precision radiation therapy such as intensity modulated radiation therapy (IMRT) and volumetric modulated arc therapy (VMAT), our developed nanoscintillator should possess a great potential to be incorporated into these radiation systems as an adjuvant therapeutics to enhance the overall treatment efficacy, especially for the radioresistant cancers.

AUTHORS (LAST NAME, FIRST NAME): Cheng, Shih-Hsun[2]; Chen, Nai-Tzu[2]; Chu, Chia-Hui[1]; Souris, Jeffrey S.[2]; Chen, Chin-Tu[2]; Lo, Leu-Wei[1, 2]

INSTITUTIONS (ALL):

1. Institute of Biomedical Engineering and Nanomedicine, National Health Research Institutes, Zhunan, Taiwan.
2. Radiology, The University of Chicago, Chicago, IL, United States.

(No Image Selected)

CONTROL ID: 2234259

TITLE: Radiolabeled-Nanoparticles Facilitating *In Vivo* Tracking of Neural Stem Cells Migrating Towards Glioblastoma

PRESENTER: Shih-Hsun Cheng

ABSTRACT BODY:

Abstract Body: Glioblastoma (GBM), a grade IV astrocytoma, is the most aggressive primary brain tumor in adults. Patients with GBM have only 12-15 month median survival after standard treatments, including chemotherapy in conjunction with surgery or radiotherapy. One of the major obstacles for the treatment of GBM is the failure of targeted delivery of active anticancer drugs cross blood-brain barrier. There is strong interest in utilizing neural stem cells (NSCs) as carriers for targeted delivery of therapeutics to brain tumors due to their inherent tumor-tropic properties. Non-invasive imaging of NSCs is necessary for tailored development of NSC-based brain tumor therapies. A novel strategy has been developed in our laboratories to exploit NSC-encapsulated high-sensitivity radiolabeled nanoparticles to amplify the imaging signal of NSC and to dynamically profile the *in vivo* migration of NSC towards GBM via single-photon emission computed tomography (SPECT). ^{111}In was encapsulated in biocompatible mesoporous silica nanoparticles (MSNs) by using chelation chemistry with 1,4,7,10-tetraazacyclododecane-1,4,7,10-tetraacetic acid (DOTA). By taking advantage of high surface area of MSN, up to 95% of ^{111}In labeling efficacy was achieved at a molecular ratio of DOTA/MSN of 2,000. The average activity of ^{111}In-MSN was 574 μCi/mg. ^{111}In-MSN complexes showed low toxicity to NSCs and very robust stability both *in vitro* and *in vivo*. Phantom studies first demonstrated the feasibility of SPECT imaging of NSCs loaded with ^{111}In-MSN complexes. SPECT effectively distinguished NSC migration to glioma xenograft after local and systemic administration in a time dependent fashion from the non-migratory behaviors of NSCs in non-tumor bearing animals. NSCs with ^{111}In-MSN were implanted in the left cerebral hemisphere of the non-tumor-bearing control mouse. No further re-distribution of the signal at day 1 and at day 2 post-injection. By contrast, in the U87 xenograft-bearing mouse, the corresponding signal of NSCs loaded with ^{111}In-MSN was seen extending from the site of NSC injection (left cerebral hemisphere) toward the tumor graft site (right cerebral hemisphere) as early as 4 h post injection, within day 0 post-injection. The signal distribution shifted further at day 1 and day 2 post-injection with a more pronounced presence at the tumor side. The SPECT results were in agreement with data obtained via bioluminescent live animal imaging, *ex vivo* confocal microscopy and histology. Our data demonstrated potential broad application of these radiolabeled nanoparticles for tracking therapeutic NSCs in the brain in both preclinical and clinical protocols.

AUTHORS (LAST NAME, FIRST NAME): Cheng, Shih-Hsun[3]; Balyasnikova, Irina[2]; Tsai, Hsiu-Ming[3]; Morshed, Ramin[2]; Yu, Dou[2]; Leoni, Lara[3]; Kanojia, Deepak[2]; Zhang, Lingjiao[2]; Aboody, Karen[4]; Lesniak, Maciej S.[2]; Lo, Leu-Wei[1, 3]; Chen, Chin-Tu[3]

INSTITUTIONS (ALL):

1. Institute of Biomedical Engineering and Nanomedicine, National Health Research Institute, Zhunan, Miaoli, Taiwan.
2. Neurosurgery, The University of Chicago, Chicago, IL, United States.
3. Radiology, University of Chicago, Chicago, IL, United States.
4. City of Hope National Medical Center and Beckman Research Institute, Duarte, CA, United States.

(No Image Selected)

CONTROL ID: 2233958

TITLE: Near-Infrared Optical Imaging Agents with Dual Function: Probe for Necrotic Cells and Cell Fixation Agents for Assays in vitro

PRESENTER: Ivana Martinic

ABSTRACT BODY:

Abstract Body: Background: Cell necrosis, un-programmed cell death, is a crucial biological process and hallmark for numerous physiological and pathological conditions: sepsis, cancer, atherosclerosis, etc. Near-Infrared (NIR) optical imaging has a great clinical potential to significantly improve diagnosis of various human diseases in real time imaging experiments[1]. Currently used nucleic acid-binding NIR dyes are not optimal and fully reliable for optical in vivo imaging as they have drawbacks: low quantum yield, high energy excitation wavelengths, small Stocke shift and low photostability, thus limiting detection sensitivity, time and affecting image resolution[2]. The development of novel imaging technologies is *needed,* in order to unambiguously locate necrosis of cells and tissues in vitro and in vivo. Lanthanide-based probes have promising properties as NIR luminescence emitters and need to be sensitized with appropriate chromophoric groups[3].

Materials and methods: we have designed novel NIR-emitting metallacrown (MC) complexes the structure of which provide optimized sensitization of the lanthanide cation and protection against non-radiative deactivations. MCs are metal-rich macrocycles formed with organic backbones and a repeating [M-N-O] subunit[4]. Characteristic NIR emission of Yb (980 nm) or Nd (890 nm) ions in the $LnZn_{16}(pyzHA)_{16}$ MCs can be observed under excitation wavelengths ranging from the UV (377 band pass 40 nm filter) to the visible range (480 band pass 60 nm filter).

Results: we have shown that $LnZn_{16}(pyzHA)_{16}$ operate as NIR stains for nucleus as well as for cytoplasm of necrotic HeLa cancer cells and Mesenchymal Stem Cells (MSC). The necrosis of cells was confirmed with a commercially available marker, propidium iodide (PI)[5]. In addition, we identified a photochemical effect being a result of a short exposure to UVA light (377 band pass 40 nm filter) combined with the high concentration of $LnZn_{16}(pyzHA)_{16}$, causing a similar cell fixation effect to the one obtained classically with formaldehyde or methanol.

Conclusions: for both cell lines (HeLa and MSC), we observed a strong NIR luminescence signal for both Nd and Yb MCs. In addition, we were able for the first time to discriminate specific NIR emissions arising from Yb and Nd ions using band pass filters in a microscopy experiment opening the perspective for a multiplex detection system and simultaneous monitoring of independent biological entities, using the same excitation wavelength during the same experiment. The high brightness of MCs allows one to use standard CCD cameras usually installed on routine fluorescence microscopes. These MCs have a promising dual function as NIR imaging and fixation agents using a single molecule.

Bibliography:

[1] Hellebust A. and Richards-Kortum R., *Nanomedicine,* 2012. **7**: p. 429.

[2] Dasari M. et al., *Org. Lett.*, 2010. **12**: p. 3300.

[3] Eliseeva S. V. and Bunzli J.-C. G. *Chem. Soc. Rev.*, 2010. 39: p. 189.

[4] Trivedi, E.R., et al., *JACS*, 2014. **136**: p. 1526.

[5] Smith B.A. and Smith B.D., *Bioconjug. Chem.*, 2012. **23**: p. 1989.

AUTHORS (LAST NAME, FIRST NAME): Martinic, Ivana[1]; Eliseeva, Svetlana V.[1]; Nguyen, Tu N.[3]; Trivedi, Evan R.[3]; Chow, Chun Y.[2]; Pecoraro, Vincent .[3]; Petoud, Stephane[1]

INSTITUTIONS (ALL):

1. Center for Molecular Biophysics, CNRS, Orleans, France.
2. Chemistry, University of Michigan, Ann Arbor, MI, United States.
3. Department of Chemistry, University of Michigan, Ann Arbor, MI, United States.

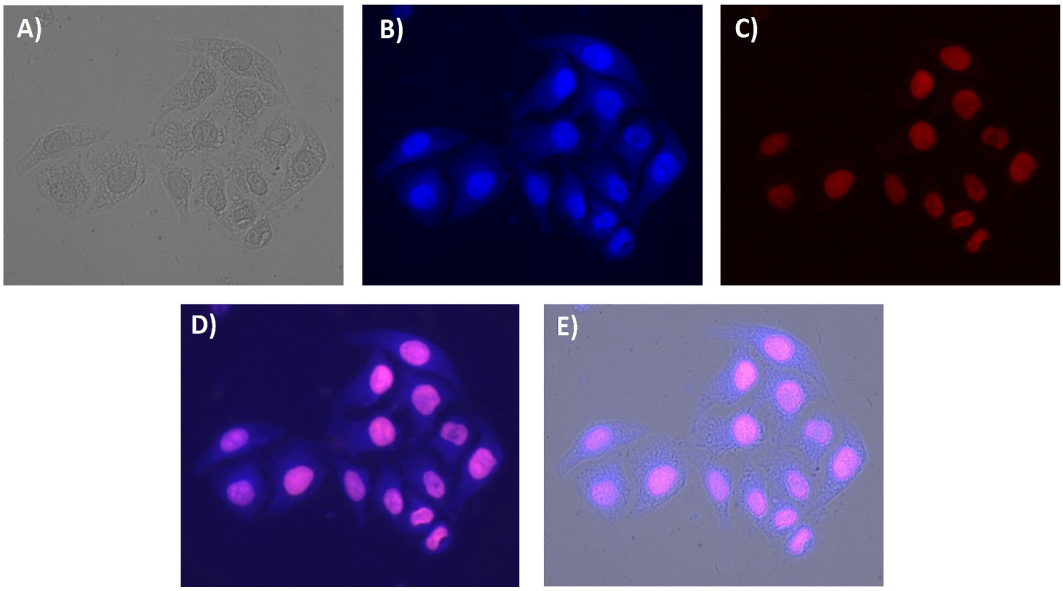

Figure 1. microscopy images of HeLa cancer cells: (A) Brightfield, after 15 min of incubation with 150 µM of $YbZn_{16}(pyzHA)_{16}$ + 5 min of illumination (at 377 nm), followed with incubation during 15 minutes (in order to allow the internalization of the complex) and washed with cell culture media (B) NIR signal arising from $YbZn_{16}(pyzHA)_{16}$, (λ_{ex}: 480 nm bp 50 , λ_{em}: long pass 805 nm, exposure time: 8s, 40x), (C) VIS signal arising from Propidium iodide (PI), after incubation with 3 µM PI during 5 min, (λ_{ex}: 535 nm bp 40 , λ_{em}: 617 nm bp, exposure time: 80 ms, 40x), (D) Merge (PI and $YbZn_{16}(pyzHA)_{16}$), (E) Merge (PI, $YbZn_{16}(pyzHA)_{16}$ and brightfield)

CONTROL ID: 2233962

TITLE: Theranostic pretargeting of HER2-expressing human carcinoma xenografts in immunocompromised mice with an anti-DOTA(metal) hapten IgG-scFv bispecific antibody

PRESENTER: Sarah Cheal

ABSTRACT BODY:

Abstract Body: *Purpose* Our aim was to develop a pretargeting approach to radionuclide diagnosis and therapy of HER2 overexpressing cancers using a novel bispecific antibody (BsAb) with high affinity for HER2 and DOTA(metal) chelate complex as the targeting vector.

Methods We cloned the sequences for the anti-HER2 antibody Trastuzumab and the anti-DOTA(metal) complex scFv C825 [1] into the expression vector for an IgG-scFv format [2] (MW ~ 210 kDa) named HER2-C825, and characterized the novel BsAb *in vitro* and *in vivo* for antigen binding and PK/PD properties. Next, we conducted pretargeting experiments using a three-step approach including: the HER2-C825, a dextran-based clearing agent, and a ^{177}Lu-radiolabeled DOTA hapten (PRIT) in immunocompromised mice bearing subcutaneous (s.c.) HER2-positive (HER2(+)) BT474 human breast carcinoma xenografts to determine optimum reagent doses as well as estimate absorbed doses for radionuclide therapy. Also, in BT474-tumored mice, single-cycle PRIT treatment with ^{177}Lu-radiolabeled DOTA hapten (as ^{177}Lu-radiolabeled aminobenzyl-DOTA, ^{177}Lu-DOTA-Bn) doses up to 56 MBq was carried out. Planar scintigraphy was used to verify tumor targeting and localization of the ^{177}Lu-DOTA-Bn therapeutic. In addition, non-invasive serial positron emission tomography (PET) was evaluated in mice bearing s.c. HER2(+) SKOV-3 human ovarian carcinoma xenografts that were given pretargeted ^{86}Y-DOTA-Bn (11-18 MBq).

Results Using optimized PRIT in BT474-tumor bearing mice, tumor-to-normal tissues ratios of 27:1 and 10:1 at 24 hours (h) post-injection (p.i.) were achieved for blood and kidney, respectively. Based on the biodistribution of ^{177}Lu-DOTA-Bn from 1-336 h p.i., estimated absorbed doses (cGy/MBq) to tumor, blood, liver, spleen, and kidney for PRIT were 43.2, 1.5 (therapeutic index (TI): 28), 3.6 (TI: 12), 0.3 (TI: 139), and 6.1 (TI: 7), respectively. A single cycle of PRIT treatment consisting of a ^{177}Lu-DOTA-Bn dose of 56 MBq produced 5/5 complete responses (starting tumor volume 10-25 mm^3) without recurrence up to 30 days post-treatment. In the absence of PRIT treatment, the tumor doubling time was approximately 10 days (average volume ~100 mm^3 30 days post-treatment). There were no clinical or histologic evidence of radiation induced toxicities during PRIT. When PRIT + ^{86}Y-DOTA-Bn was carried out in mice bearing HER2(+) SKOV-3, the s.c. tumor in the shoulder was visualized as early as 2 h and up to 48 h p.i., with minimal background activity evident in the gut, kidney, and bladder.

Conclusion Using a three-step pretargeting approach including HER2-C825 BsAb, we estimate that we can deliver sufficient doses of the β-emitting isotope ^{177}Lu to illicit tumor responses in HER2(+) BT474 tumor cells. In addition, we can also use PRIT + ^{86}Y-DOTA-Bn for non-invasive serial PET imaging up to 48 h p.i. for high-contrast imaging of s.c. HER2(+) human carcinoma xenografts, suggesting that pre-treatment imaging with ^{86}Y-DOTA-Bn could be used for individualized dosimetry for therapy with ^{90}Y-DOTA-Bn and/or ^{177}Lu-DOTA-Bn.

References

[1] Orcutt KD, et al. (2011) Nucl Med Biol, 38: 223-233

[2] Orcutt KD, et al. (2010) Protein Eng Des Sel, 23: 221-228

AUTHORS (LAST NAME, FIRST NAME): Cheal, Sarah M.[1]; Xu, Hong[1]; Guo, Hong-fen[1]; Punzalan, Blesida J.[1]; Singh, Manisha[1]; Lee, Sang-gyu[1]; Fung, Edward K.[1]; Kalidindi, Teja Muralidhar[1]; Zanzonico, Pat[1]; Cheung, Nai-Kong V.[1]; Larson, Steven M.[1]

INSTITUTIONS (ALL):

1. Memorial Sloan Kettering Cancer Center, New York, NY, United States.

(No Image Selected)

CONTROL ID: 2244384

TITLE: In vivo photoacoustic imaging of a non-fluorescent E2 crimson genetic reporter in mammalian tissues

PRESENTER: Olumide Ogunlade

ABSTRACT BODY:

Abstract Body: Introduction: Genetic reporters are valuable for providing insight into biological processes on a cellular level. Genetic reporters for photoacoustic (PA) imaging are broadly based on either the genetic expression of an enzyme, such as Tyrosinase[1], which catalyses to produce an absorbing chromophore or the genetic expression of an absorbing protein. Fluorescent proteins (eGFP and mCherry) have been demonstrated as PA genetic reporters[2], in the comparatively small and translucent zebra fish and fruitfly pupa. Fluorescent proteins (FP) can however exhibit low PA generation efficiency[3], due to the presence of radiative relaxation and ground state depopulation, limiting their use in deep mammalian tissues. To address this, a new non-fluorescent (NF) mutant of the FP E2crimson has been engineered, characterised in vitro and imaged in-vivo in mice, for the first time.

Materials and method: The absorption spectrum of the purified NF protein was measured using a spectrophotometer and compared to the PA absorption spectrum of human colorectal (LS174T) cells stably transduced to express the protein. 5 x 10^6 cells were injected subcutaneously into nude mice. 3D PA images of the cells and the surrounding vasculature was acquired at excitation wavelengths from 590 to 640 nm; using an all-optical, planar photoacoustic scanner based upon a Fabry-Perot ultrasound sensor. The imaging depth achievable with the scanner is on the order of 1 cm, with sub 100 μm resolution, which exceeds the depths/spatial resolution that can be interrogated by optical microscopy methods.

Results: In fig 1(a), the cells expressing E2crimson NF is seen from visual inspection be different compared to the transparent non-transduced (NT) cells. In fig. 1(b), the absorption and PA spectrum of E2crimson NF shows significant differential contrast, relative to haemoglobin, with a peak at around 582nm. After subcutaneous injection, the E2crimson NF cells are clearly visible in-vivo, at multiple wavelengths, as shown in fig 1c. From the in-vivo PA image at each wavelength, the mean PA signal intensity of a ROI, corresponding to the location of the E2crimson NF cells, was taken. A plot of the in-vivo signal intensity against wavelength (fig 1b) shows good qualitative agreement with the in-vitro absorption spectrum of the purified proteins and the in vitro PA spectra of the cells.

Conclusion: A new non-fluorescent mutant of E2crimson has been engineered. The suitability of this mutant as a genetic reporter for PA imaging has been demonstrated by stably expressing the protein in mammalian cells and imaging it in-vivo in mice. The differential contrast between the spectrum of E2crimson NF and that of haemoglobin allowed the cells to be visualised in-vivo.

1. Jathoul A et al., Deep *in vivo* photoacoustic imaging of mamalian tissues using a tyrosinase-based genetic reporter, Nature Photonics 2015;doi:10.1038/nphoton.2015.22

2. Razansky D et. al, Optoacoustic tomography of deep seated protein *in vivo*, Nature Photonics 2009; 3(7), 412 – 417

3. Laufer J et al., *In vitro* characterisation of genetically expressed absorbing proteins using photoacoustic spectroscopy, Biomed Opt Express 2013; 4(11) 2477-2490

AUTHORS (LAST NAME, FIRST NAME): Ogunlade, Olumide O.[2]; Jathoul, Amit P.[3]; Laufer, Jan[1]; Zhang, Edward Z.[2]; Pule, Martin [3]; Beard, Paul[4]

INSTITUTIONS (ALL):

1. Institut für Optik und Atomare Physik, Technische Universität Berlin, Berlin, Germany.
2. Medical Physics and Biomedical Engineering, University College London, London, United Kingdom.
3. Department of Heamatology, University College London, Gower Street, London, United Kingdom.
4. Department of Medical physics and Biomedical Engineering, University College London, London, United Kingdom.

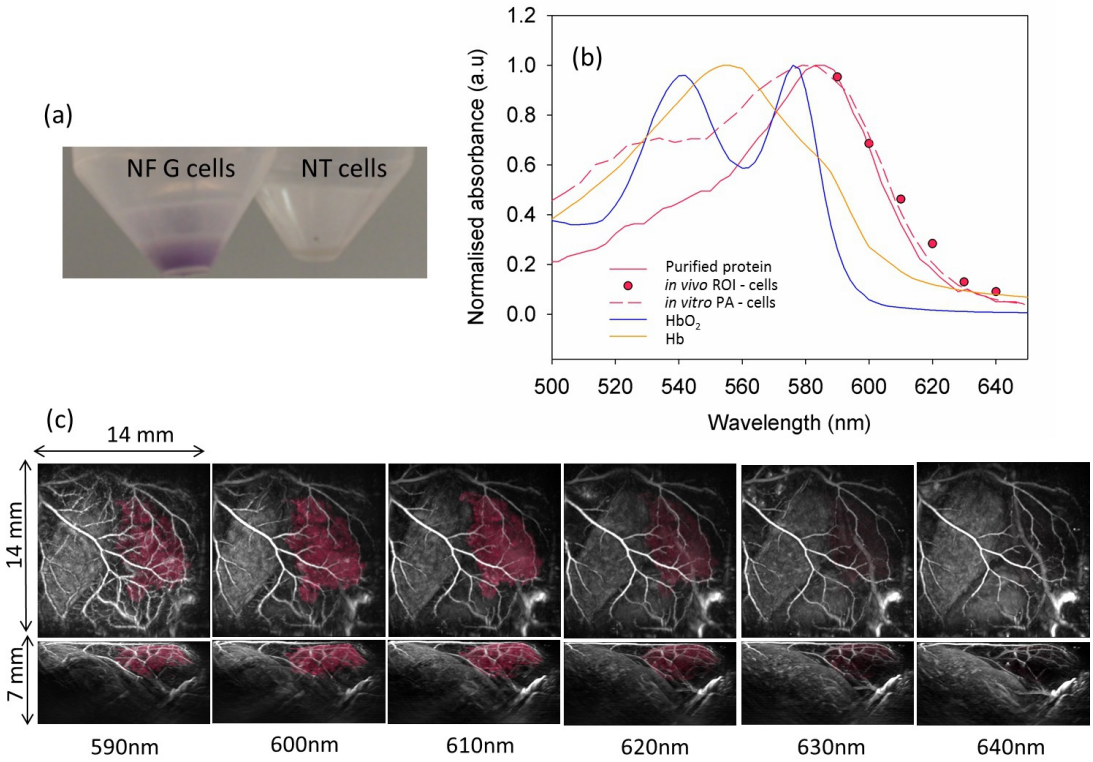

Figure 1 ***(a)*** Photograph showing LS174T cells expressing E2 crimson NF and non-transduced (NT) cells. **(b)** Spectrum of normalised absorbance of purified E2 crimson NF measured with spectrophotometer, normalised *in-vitro* PA signal amplitude from E2 crimson NF expressing cells in a cuvette, mean intensity of ROI from *in-vivo* PA images, plotted against wavelength. Also shown is the normalised absorbance of haemoglobin. **(c)** *in-vivo* photoacoustic images acquired at multiple wavelengths after subcutaneous injection of LS174T cells genetically expressing E2 crimson NF mutant. Images are *x-y* and *z-y* MIPs, manually segmented and false coloured.

CONTROL ID: 2233978

TITLE: In Vivo Early Detection of Oral Epithelial Cancer by Endogenous Fluorescence Lifetime Imaging (FLIM) Endoscopy

PRESENTER: Javier Jo

ABSTRACT BODY:

Abstract Body: This year alone, over 8,000 people in the US will die from oral or pharyngeal cancer, and over 42,000 new patients will be diagnosed. When oral cancer is diagnosed while the disease is still localized, the 5-year survival rate is ~80%. Unfortunately, only ~30% of patients are diagnosed at this early stage, while ~50% of patients are diagnosed when the cancer has already spread to nearby oral tissues or lymph nodes, at which the 5-year survival rate drops to ~50%. Once the cancer has spread further to distant organs, the 5-year survival rate falls below 30%. Moreover, while early stage treatment may only require minor surgery to remove the localized tumor, later stage treatment could include surgery to remove parts of the lip, tongue, cheek, jaw, or neck. In addition, ~30% of the patients who survive a first incidence, will develop a second cancer. Therefore, early detection of both new and recurrent oral cancer clearly holds great promise for improving both the survival rate and the quality of life of these patients.

Endogenous fluorescence lifetime imaging (FLIM) provides direct access to the concomitant functional and biochemical changes accompanying tissue transition from benign to precancerous and cancerous. Since FLIM can noninvasively measure different and complementary biomarkers of precancer and cancer, we hypothesize that it will aid in clinically detecting early oral epithelial cancer. Our group has recently demonstrated the detection of benign from premalignant and malignant lesions based on endogenous multispectral FLIM in the hamster cheek-pouch model. Encouraged by these positive preliminary results, we have developed a handheld endoscope capable of acquiring multispectral FLIM images in real time from the oral mucosa. This novel FLIM endoscope is being used for imaging clinically suspicious pre-malignant and malignant lesions from patients before undergoing tissue biopsy for histopathological diagnosis of oral epithelial cancer. Our preliminary results from 21 patients imaged thus far are already suggesting the potential of endogenous FLIM for distinguishing a variety of benign lesions from advanced dysplasia and squamous cell carcinoma (SCC). More interestingly, in some instances in which lesions were originally evaluated clinically as SCC, FLIM was able to discriminate true malignant from benign lesions as confirmed by histopathology.

To the best of out knowledge, this is the first in vivo study aiming to demonstrate the ability to predict the true malignancy of clinically suspicious lesions using endogenous FLIM. If successful, the resulting clinical tool will allow noninvasive real-time detection of epithelial precancerous and cancerous lesions in the oral mucosa and could potentially be used to assist at every step involved on the clinical management of oral cancer patients, from early screening and diagnosis, to treatment and monitoring of recurrence. Moreover, the demonstrated success of this clinical tool in oral epithelial cancer will herald future success with other cancers of the epithelium, which accounts for more than 80% of all cancers.

AUTHORS (LAST NAME, FIRST NAME): Jo, Javier A.[1]; Cheng, Shuna[1]; Cuenca, Rodrigo[1]; Olsovsky, Cory[1]; Hwang, Dae Yon[1]; Jabbour, Joey[1]; Malik, Bilal[1]; Cheng, Yi-Shing L.[2]; Wright, John[2]; Maitland, Kristen C.[1]

INSTITUTIONS (ALL):

1. Biomedical Engineering, Texas A&M Univ, College Station, TX, United States.
2. Baylor College of Dentistry, Texas A&M University, Dallas, TX, United States.

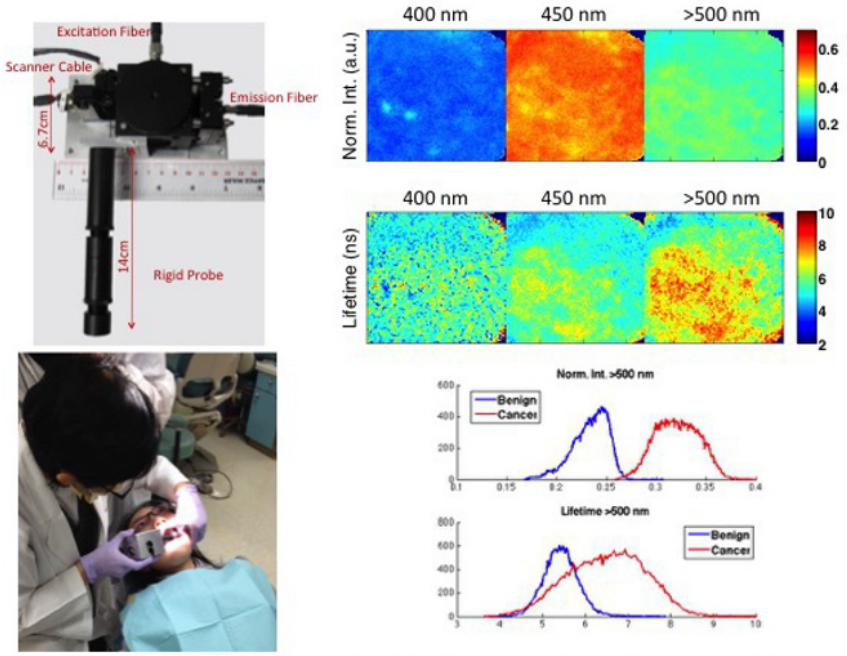

Left-Top: A rigid multispectral FLIM endoscope suitable for real-time endogenous fluorescence imaging of the oral mucosa has been developed. **Left-Bottom:** This novel FLIM endoscope is being used for imaging clinically suspicious pre-malignant and malignant lesions from patients before undergoing tissue biopsy for histopathological diagnosis of oral epithelial cancer. **Right-Top:** Multispectral FLIM maps of a malignant lesion: the normalized fluorescence intensity maps show significant emission at 450-nm and >500-nm; the fluorescence lifetime is relatively long (5-8 ns) at >500-nm. **Right-Bottom:** In some instances in which lesions were originally evaluated clinically as cancer, FLIM was able to discriminate true malignant from benign lesions as confirmed by histopathology.

CONTROL ID: 2234002

TITLE: A Precursor for Electrochemical radiosynthesis of [^{18}F]-*L*-DOPA

PRESENTER: Fan Yang

ABSTRACT BODY:

Abstract Body: Objective

[^{18}F]-*L*-DOPA (**1**, see **Scheme 1** in Persuasive Data for all the compounds and reactions) is a useful PET tracer for imaging of neuropsychiatric diseases, movement disorders, and brain malignancies. However, the widely used method to prepare [^{18}F]-*L*-DOPA depends on carrier-added introduction of ^{18}F, which leads to low radiochemical yield and specific activity[1]. To tackle this problem, we herein explore a method to synthesize [^{18}F]-*L*-DOPA via electrochemical fluorination.

Methods

A method was developed to introduce ^{18}F by electrochemical fluorination, in which *t*-Butyl group on aromatic ring can be activated and replaced by ^{18}F fluoride[2, 3]. The multistep synthesis of the *t*-Butyl containing precursor molecule for L-DOPA **2** is outlined here.

Result

We have explored two methods to attach *t*-Butyl group on the aromatic ring of *L*-Dopa. The most direct approach was to introduce *t*-Butyl onto L-DOPA **3**. Unfortunately this approach resulted in the 5-*t*-Butyl-isomer **4** as the only detected *t*-Butylated product. The electrofluorination of **5**, with *t*-Butyl as the leaving group, afforded F-labeled compound. The second method we are exploring is to start with the 5-*t*-Butyl containing synthesis block **6**, together with **7**, to construct the precursor **2**[4] via compound **8**.

Conclusion

The fluorination of precursor **5** by the electronchemical method provided a proof of concept for our strategy to synthesize **1** from **2**. It has also been demonstrated that *t*-Butyl in 4-*t*-Butyl-diBoc-catechol can be replaced by ^{18}F under carrier-free condition [3] with a radiochemical yield of 6.8±1.3%, and with a specific activity of 13 GBq/μmol. Therefore precursor **2** is expected to be converted to the desired **1** by no-carrier-added electrochemical radiofluorination[4], followed by deprotection.

AUTHORS (LAST NAME, FIRST NAME): Yang, Fan[1]; He, Qinggang[1]; Sadeghi, Sam[1]

INSTITUTIONS (ALL):

1. Department of Molecular and Medical Pharmacology, UCLA, Los Angeles, CA, United States.

(No Image Selected)

CONTROL ID: 2234016

TITLE: Development of Iodinated PARP Inhibitors for Glioblastoma Imaging

PRESENTER: Beatriz Salinas Rodriguez

ABSTRACT BODY:

Abstract Body: OBJECTIVE: Although the understanding of the genetic and molecular basis of cancer has advanced significantly over the last several decades, imaging and treatment options for glioblastoma patients have been more limited [1]. This is in part due to difficulties in diagnosing this disease early, combined with its diffuse, infiltrative growth. This study was therefore aimed at the development of a novel, early diagnostic tool for glioblastoma. Specifically, we have focused on the synthesis of novel radioiodinated, labeled poly(ADP-ribose)polymerase (PARP1) targeted small molecules. We have chosen this target, because in glioblastoma tissue, PARP1 is highly overexpressed [2-4].

METHODS: A small library of PARP1 inhibitors (Iodo-PARPi) was synthesized. For each library representative, we have established IC_{50} values using a commercially colorimetric assay (Trevigen), determined lipid solubility (logPs) and measured the plasma protein binding, as well as their ability to selectively bind nuclear PARP1 *in vitro* and *in vivo* , revealed by optical imaging with their fluorescent sister imaging agent, PARPi-FL [2]. Based on these results, the most successful candidate was radiolabeled with ^{131}I in presence of chloramine T, and biodistribution as well as imaging experiments performed.

RESULTS: The IC_{50} values of all the new compounds are between 9 ± 2 nM and 107 ± 4 nM, paired with suitable logPs and plasma protein binding (Fig. 1B). Fluorescence imaging *in vitro* assays confirmed selective accumulation of all our compounds in different glioblastoma cell lines, leading to a reduction in fluorescence signal between 76 ± 6% and 67 ± 13 % in the presence of the imaging agents. This is similar to the parent scaffold olaparib (73 ± 11 %). Similarly, *in vivo* injection of **I2-PARPi** can block the uptake of the fluorescent imaging agent, leading to a 78 ± 4 % reduction of fluorescence intensity. The radioiodinated PARP1 inhibitor **I2** was radiolabeled with ^{131}I with a radiochemical yield of 73%. *In vivo* application in xenograft and orthotopic mouse models confirmed the uptake in tumor tissue (tumor: 0.53 ± 0.11 ID/g, brain: 0.02 ± 0.01 ID/g, muscle: 0.24 ± 0.05 ID/g, liver: 3.57 ± 1.03 ID/g, thyroid: 0.38 ± 0.07 ID/g.), showing a specific accumulation in the tumor region in diseased brain.

CONCLUSION: We have synthetized a small library of iodinated PARP1 inhibitors, which have been tested *in vitro* and *in vivo*. The *in vivo* application of the ^{131}I-PARPi in xenograft and orthotopic models has showed the incorporation in tumor tissue in much higher concentration than in brain, showing a significant potential as tracer for imaging of glioblastoma.

REFERENCES: [1] Wen PY and Kesari S (2008). N Engl J Med 359:492–507. [2] Reiner T, et al. (2012). Neoplasia 14:169–177. [3] Thurber GM, et al. (2013). Nat Commun 4:1504. [4] Irwin et al. (2014) Neoplasia, 16(5):432-40.

AUTHORS (LAST NAME, FIRST NAME): Salinas Rodriguez, Beatriz[1]; Irwin, Christopher [1]; Kossatz, Susanne[1]; Weber, Wolfgang[1, 2]; Reiner, Thomas[1, 3]

INSTITUTIONS (ALL):

1. Radiology, Memorial Sloan Kettering Cancer Center, New York, NY, United States.

2. Molecular Pharmacology and Chemistry Program, Memorial Sloan Kettering Cancer Center, New York, NY, United States.

3. Center for Molecular Imaging and Nanotechnology, Memorial Sloan Kettering Cancer Center, New York, NY, United States.

A

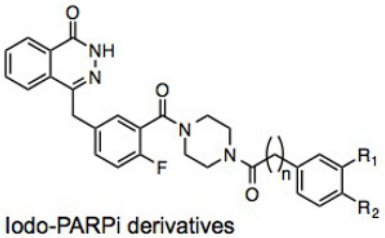

Iodo-PARPi derivatives

B

Compound	n	R_1	R_2	IC_{50} (nM)	$LogP_{CHI}$	Plasma free fraction
I1	0	I	H	11 ± 3	2.3	9.60 ± 1.47%
I2	0	H	I	9 ± 2	2.3	11.53 ± 0.11%
I3	1	I	H	34 ± 3	2.7	7.05 ± 0.13%
I4	1	H	I	74 ± 5	2.7	4.97 ± 0.26%
I5	2	I	H	107 ± 4	3.0	7.84 ± 1.41%
I6	2	H	I	47 ± 5	3.0	4.69 ± 0.45%

Figure 1. Properties of Iodo-PARPi. A) Structure of Iodo-PARP inhibitors. B) Basic pharmacologic properties of the different I-PARPi inhibitors.

CONTROL ID: 2234031

TITLE: Quantitative estimation of EGFR expression in orthotopic preclinical brain tumors with MRI-guided fluorescence tomography data: image reconstruction vs. projection analyses

PRESENTER: Negar Sadeghipour

ABSTRACT BODY:

Abstract Body: Epidermal growth factor receptor (EGFR) plays an important role in cell proliferation of different types of cancer (*e.g.*, breast, head and neck and brain). In order to have a personal treatment for patients with EGFR overexpression, it is necessary to have information about their receptor expression. For this, a non-invasive *in vivo* method to quantify the receptor density is of the utmost importance. “Paired-agent” kinetic modeling has emerged as a successful method to estimate the concentration of EGFR through the “binding potential” (BP) kinetic parameter[1]. The principle of the approach is relatively straightforward: in brief, an EGFR-targeted imaging agent is co-injected with a “control”, untargeted agent, wherein the kinetics of the control agent are used to account for nonspecific retention of the targeted agent. Prior work applied paired-agent kinetic modeling to MRI-guided fluorescence tomography data using fluorescently labeled anti-EGFR affibody paired with fluorescently labeled negative control affibody, demonstrating the feasibility of the approach[3]. This study compares these initial findings with this “projection” method of EGFR concentration estimation based MRI-guided fluorescence tomography data that does not require complicated image reconstruction. The aim of this work is to determine if full tomographic diffuse fluorescence tomography (DFT) data and image reconstruction was really necessary if one was only interested in the average EGFR concentration in a tumor.

Making the assumption that the EGFR concentration is negligible in all healthy tissues surrounding a tumor, we hypothesized that EGFR binding potentials extracted from the dynamic paired-agent fluorescence data from any source-detector pair in a MRI-DFT system would be proportional to the product of the EGFR concentration in an interrogated tumor and the fractional tumor sensitivity (*i.e.*, the proportion of light detected by a given source detector that passes through the tumor). Since the fractional tumor sensitivity can be determined by diffuse light propagation modeling based in the MRI anatomical information, these source-detector estimates of EGFR concentration can be directly converted to estimates of tumor EGFR concentration. The method was test by tail vein injection of a 0.2 nmol solution of both tracer in five athymic nude mice with U251 tumors. The mice were positioned in a 56 channel multispectral (DFT) system housed within an MRI. The targeted agent was Affibody anti-EGFR conjugated to Licor IRDye 800CW fluorescent dye. The untargeted agent was Affibody negative control, conjugated to the AlexaFluor 750 fluorescent dye. Their uptake was imaged for 40 min at roughly 2-min intervals.

For initial simulation results based on the collected data, the simple projection approach of estimating BP resulting in a value of 2.00 ± 0.03 for a simulated value, BP = 2 with 1% noise (similar to that measured in experimental data). By comparison, the more complex hard-priors image reconstruction approach, provided an estimate of 2.04 ± 0.23, demonstrating that the projection approach is much more robust to noise than the reconstruction approach.

AUTHORS (LAST NAME, FIRST NAME): Sadeghipour, Negar[2]; Samkoe, Kimberley S.[3]; Pogue, Brian W.[1]; Davis, Scott[4]; Tichauer, Kenneth M.[2]

INSTITUTIONS (ALL):

1. Engineering, Dartmouth College, Hanover, NH, United States.
2. Biomedical Engineering, Illinois Institute of Technology, Chicago, IL, United States.
3. Surgery, Dartmouth, Hanover, NH, United States.
4. Dartmouth, Hanover, NH, United States.

(No Image Selected)

CONTROL ID: 2234042

TITLE: *In Vivo* Verification of Efficient Radioisotope Energy Transfer (RET) by Gold Nanoclusters for Molecular Imaging and Therapy.

PRESENTER: Lei Xing

ABSTRACT BODY:

Abstract Body: Beta-emitting isotopes Fluorine-18 and Yttrium-90 were tested for their potential to stimulate gold nanoclusters conjugated with blood serum proteins (AuNCs). AuNCs were excited by both medical radioisotopes and were found to be highly effective ionizing radiation energy transfer mediators, suitable for *in vivo* optical imaging. AuNCs synthesized with protein templates converted beta-decaying radioisotope energy into tissue-penetrating optical signals in the 620-800nm range at physiological temperature. The detected signal was not due to gamma-radiation as no significant signal was detected from Technetium-99m, a pure gamma emitter that was used as a control. Optical emission from AuNCs was not proportional to Cerenkov radiation, indicating that the energy transfer between the radionuclide and AuNC is only partially mediated by Cerenkov photons. Direct Columbic interactions also appear to play a significant role in the transfer of energy from decaying radionuclides to AuNC. The studies were carried out *in vitro* and *in vivo*. The efficient conversion of radioisotope signal into optical signal was confirmed in tumor mice breast cancer model. The RET signal from AuNC was found to be correlated with a tumor size and dose. Development of RET probes may allow improved sensitivity and specificity for tumor imaging and detection.The results of this study also suggest the possibility to accurately determine the biodistributions of beta-emitting therapeutic radioimmunoconjugates such as (Iodine-131/Bexxar or Yttrium-90/Zevalin) that used to treat lymphomas.

AUTHORS (LAST NAME, FIRST NAME): Volotskova, Olga[1]; Stafford, Jason H.[1]; Sun, Conroy[3]; Koh, Ai Leen[4]; Pratx, Guillem[5]; Xing, Lei[2]

INSTITUTIONS (ALL):

1. Radiation Oncology, Stanford, Palo Alto, CA, United States.
2. Radiation Oncology, Stanford University, Stanford, CA, United States.
3. Department of Pharmaceutical Sciences, Oregon State University, Corvallis, OR, United States.
4. Stanford Nano Shared Facilities, Stanford, Stanford, CA, United States.
5. Radiation Oncology, Stanford, Palo Alto, CA, United States.

(No Image Selected)

CONTROL ID: 2234067

TITLE: A Potent and Selective C-11 Labeled PET Tracer for Imaging Sphingosine-1-phosphate Receptor 2 (S1PR2)

PRESENTER: Xuyi Yue

ABSTRACT BODY:

Abstract Body: Objectives: Multiple sclerosis (MS) is a neuroinflammatory disease with a much higher incidence in females. Experimental autoimmune encephalomyelitis (EAE) in the SJL mouse strain models this sexual dimporphism, and sphingosine-1-phosphate receptor 2 (S1PR2) has been identified as a sex- and strain-specific, disease-modifying molecule in these mice and in MS. To explore the important function of this receptor in the progression of MS, a new PET tracer that can specifically assess the expression of S1PR2 *in vivo* is urgently needed.

Methods: Five S1PR2 ligands were designed and synthesized. *In vitro* competitive cell membrane binding assays were conducted towards S1PR1, S1PR2, S1PR3. One of the promising ligands, **[^{11}C]TZ34125** was radiolabeled using [^{11}C]methyl iodide and further validated. The autoradiography, biodistribution, microPET studies were carried on autoimmune susceptible SJL mice. The expression level of S1PR2 in the cerebellum of both female and male SJL mice was assessed by **[^{11}C]TZ34125**.

Results: The syntheses of five S1PR2 ligands were successfully accomplished via nine steps. One of the compounds, **TZ34125** showed promising binding potency towards S1PR2 (IC_{50} = 9.52 ± 0.70 nM) and high selectivity over S1PR1 and S1PR3 (IC_{50} > 1000 nM). Furthermore, **TZ34125** showed seven-fold more potent than the well-known S1PR2 antagonist **JTE-013** (IC_{50}= 68.47 ± 7.45 nM). Radiolabeling conditions including reaction temperature, ^{11}C-methylating agents, base, HPLC mobile phase were optimized to improve the *O*-^{11}C-methylation ratio and radiochemical purity. **[^{11}C]TZ34125** was achieved with 20 ± 5% yield (decay corrected, n > 10) in 60 min, specific activity 2 – 5 Ci/μmol. Biodistribution studies revealed that the cerebellar uptake (% ID/g) of **[^{11}C]TZ34125** was significantly increased (1.59 ± 0.11 vs 0.84 ± 0.04, n = 4, p = 1.11×10^{-5}) when SJL mice were pretreated with a P-glycoprotein modulator, cyclosporine A (CsA) 30 min i.v. prior to the tracer injection. With CsA pretreatment the cerebellar uptake (% ID/g) in female SJL mice was significantly higher (1.59 ± 0.11 vs 1.27 ± 0.13, n = 4, p = 0.0073) than that in males. Autoradiography and microPET imaging consistently elucidated that female SJL mice had higher accumulation of **[^{11}C]TZ34125** in the cerebellum than males. The average cerebellar uptake (SUV) of **[^{11}C]TZ34125** from microPET scans (summarized 10 - 60 min images from dynamic scan) indicated female mice (0.58 ± 0.16) had statistically (n = 5, p = 0.021) higher accumulation than male mice (0.48 ± 0.12).

Conclusion: A C-1I labeled PET ligand **[^{11}C]TZ34125** for *in vivo* imaging S1PR2 was developed. The sexual dimorphism of S1PR2 expression in SJL mice was successfully demonstrated by **[^{11}C]TZ34125**: higher cerebellar uptake in females than in males following CsA pretreatment. The development of more promising radioligands for S1PR2 may greatly contribute to the diagnosis and treatment of neuroinflammatory diseases including MS.

Acknowledgment: This work was supported by the DOE-Training Grant: #DESC0008432 and the Washington University, Mallinckrodt Institute of Radiology (MIR) Pilot Grant: #14-017.

AUTHORS (LAST NAME, FIRST NAME): Yue, Xuyi[1]; Jin, Hongjun[1]; Liu, Hui[1]; Rosenberg, Adam J.[1]; Yang, Hao[1]; Klein, Robyn S.[2]; Tu, Zhude[1]

INSTITUTIONS (ALL):

1. Department of Radiology, Washington University School of Medicine, St. Louis, MO, United States.
2. Departments of Medicine, Anatomy & Neurobiology, Pathology & Immunology, Washington University School of Medicine, St. Louis, MO, United States.

(No Image Selected)

CONTROL ID: 2234085

TITLE: Pre-screening candidates for Optical Surgical Navigation by detecting GGT enzyme activity with catalyCEST MRI

PRESENTER: Sanhita Sinharay

ABSTRACT BODY:

Abstract Body: INTRODUCTION: Optical Surgical Navigation (OSN) uses fluorescent agents to detect tumors during surgery. For example, an enzyme-responsive fluorescent agent can detect g-glutamyl transpeptidase (GGT) that is overexpressed in the extracellular environment of ovarian tumors.[1] However, only ~60% of ovarian tumors show overexpression of this enzyme. Therefore, a method is needed to pre-screen patients before surgery to identify patients that have tumors with high GGT activity. To address this need, we have developed a CEST MRI contrast agent that detects GGT activity, and we have tested this agent during catalyCEST MRI studies of biochemical solutions and *in vivo* mouse models of ovarian cancer.

METHODS: Glutamic acid was coupled to 4-amino salicylic acid in four steps.[2] CEST MRI studies were performed with a 3 μT CW saturation pulse for 5 s, followed by a FISP MR acquisition.[3] The CEST signals of the agent were studied with respect to pH and temperature. The catalytic activity of GGT for the agent was monitored using catalyCEST MRI to determine Michaelis-Menten kinetics parameters.[4]

In vivo studies were performed with an OVCAR-8 orthotopic tumor model that expresses high levels of GGT, and an OVCAR-3 orthotopic model that expresses low levels of GGT.[1] CEST MR studies were performed after 150 μL of 500 mM of the agent was administered IV, and with 150 μL administered through IP infusion during the catalyCEST MRI scans.[5] Following in-vivo imaging experiments, the fluorescent agent gGLU-HMRG was injected IP, the peritoneal cavity was exposed and the location of the tumor confirmed with fluorescence imaging.[1]

RESULTS: The agent was synthesized in 15% overall yield. Chemical exchange from the agent was base-catalyzed as confirmed with pH studies. Temperature studies showed that chemical exchange of the salicylic acid ligand was non-Arrhenius.[6] The CEST signal of the agent at 5.4 ppm quickly disappeared after adding GGT, and the agent's CEST signal at 9.5 ppm slowly degraded. Michaelis-Menten studies confirmed that the disappearance of CEST was due to GGT activity.

Initial *in vivo* catalyCEST MRI studies showed that the agent could be detected in tumor tissues with statistical significance (Fig. **1**). However, the timing of the catalyCEST MRI protocol must be improved to quantify the differential disappearance of CEST effects at 5.4 ppm and 9.5 ppm within the tumor. *Ex vivo* fluorescence imaging showed that the OVCAR8 tumor could be detected during OSN, while the OVCAR3 tumor could not be detected.

DISCUSSION: The diamagnetic CEST agent can detect GGT activity in biochemical solutions. Initial *in vivo* catalyCEST MRI studies showed that the agent can be detected *in vivo*. *Ex* vivo fluorescence imaging confirmed that the OVCAR8 model had high GGT expression relative to the OVCAR3 model. Ongoing studies are optimizing the timing of catalyCEST MRI so that this MRI method can pre-screen for GGT-overexpressing ovarian tumors.

References:
1. *Sci Trans Med*, **2011**, *3*, 1-10
2. *Angew. Chem. Int. Ed. Engl.* 52, **2013**, 1-10
3. *Magn Reson Med*, 65, 2**011**, 432-437
4. *CMMI,* 2, **2007**, 189-198
5. *Magn Reson Med*,71, **2014**, 1221-1230
6. *J. Chem. Educ*, **2013**, 90, 1024-1027

AUTHORS (LAST NAME, FIRST NAME): Sinharay, Sanhita[4]; Jones, Kyle[3]; Randtke, Edward A.[3]; Howison, Christine[3]; Kobayashi, Hisataka[1]; Pagel, Mark[5]; Chambers, Setsuko K.[2]

INSTITUTIONS (ALL):

1. Molecular Imaging Program, NCI/NIH, Bethesda, MD, United States.
2. University of Arizona, Tucson, AZ, United States.
3. Biomedical Engineering, University of Arizona, Tucson, AZ, United States.
4. Chemistry and Biochemistry, University of Arizona, Tucson, AZ, United States.
5. University of Arizona, Tucson, AZ, United States.

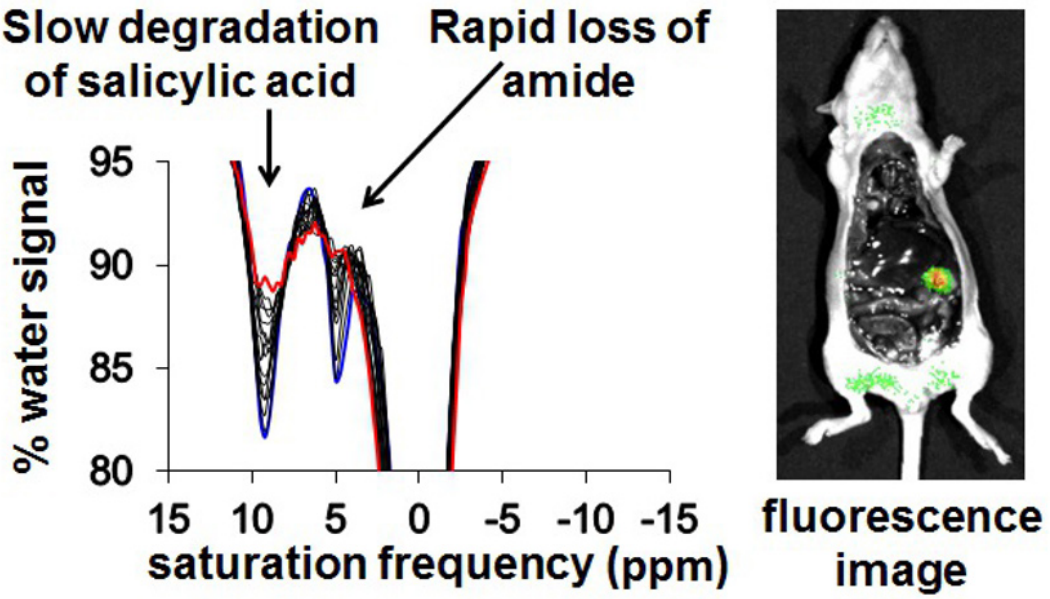
Slow degradation of salicylic acid
Rapid loss of amide
% water signal
95
90
85
80
15 10 5 0 -5 -10 -15
saturation frequency (ppm)
fluorescence image

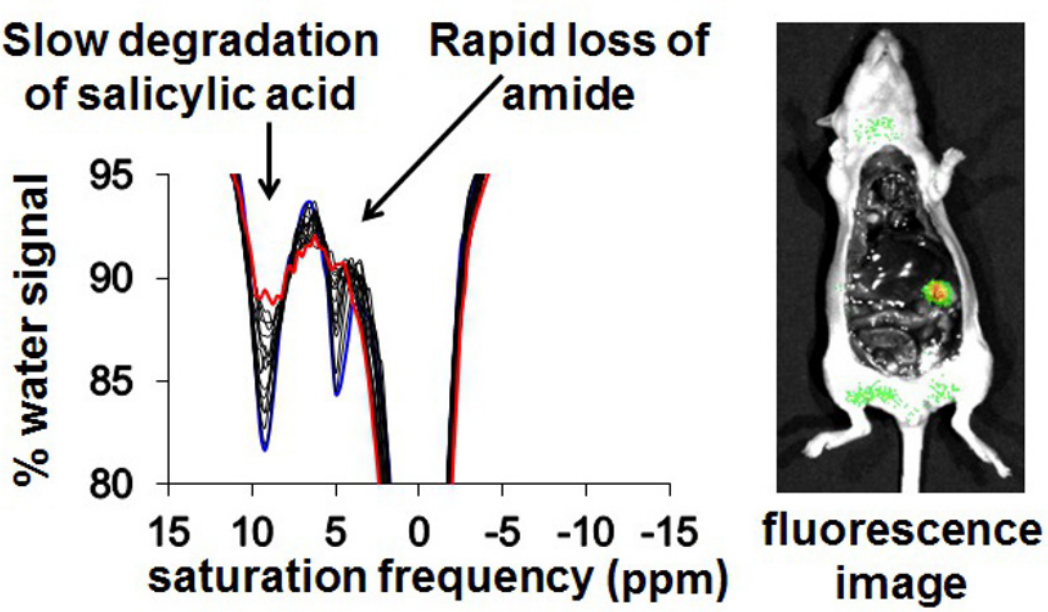

Left: The dynamic CEST spectra acquired for 8 hours after adding 0.4 units of GGT to 25 mM of the CEST contrast agent showed rapid catalysis of the amide and slower degradation of the salicylic acid moiety Right: Fluorescence imaging of OVCAR8 mouse model showed the location of the orthotopic tumor.

CONTROL ID: 2234089

TITLE: First experiences in triple modality characterization of brain connectivity in humans using simultaneous PET/MR/EEG

PRESENTER: André Thielcke

ABSTRACT BODY:

Abstract Body: The investigation of functional and metabolic brain connectivity is of utmost importance to gain a better understanding of brain organization and neuronal diseases. Here, for the first time, three modalities (PET, MR and EEG) were recorded simultaneously in order to investigate connectivity. fMRI and PET deliver higher spatial-resolution, but lower temporal-resolution – therefore the combination with higher temporal-resolution EEG offers a new dimension to study functional and metabolic networks in the brain. In this work we report our first experiences of simultaneously acquired BOLD-fMRI and [^{18}F]FDG-PET data as well as EEG in humans, measuring low frequency fluctuations on hemodynamic and glucose metabolism related levels as well as on electrical potential fluctuations.
Epilepsia patients (n=3, informed consent) were measured using a PET/MR system for humans installed in a 3 T MR scanner combined with simultaneous EEG-recording (256 channels, sampling rate 1000Hz). BOLD-fMRI imaging was performed in the resting state (EPI, TR=2500 ms, TE=32ms, Matrix Size: 64x64x36, Voxel Size: 3.5x3.5x3.5 m^3) with a simultaneous dynamic PET acquisition for 60 min using the tracer [^{18}F]FDG (injected dose: 180-200 MBq). PET-images were reconstructed (OSEM) into 60 s frames. fMRI and PET data were processed using SPM 12 and an independent component analysis (ICA, GIFT) was performed (20 components, ICASSO algorithm) on the group level. Preprocessing and analysis of EEG data was performed using the Fieldtrip toolbox, (Donders Institute for Brain, Cognition and Behavior). The influence of the EEG cap on the PET data was evaluated by comparison with scans without EEG cap. EEG quality was studied within the PET/MR system. PET and MR ICA data were compared in order to detect prominent brain networks.
Consecutive 5 min [^{18}F]FDG-PET scans of the same patient with and without EEG caps showed good agreement in the cortical areas with a relative difference in the range of ca. -5%. The quality of the recorded EEG-PET/MR data was on par with the quality obtained in EEG/fMRI settings. Some prominent brain networks were identified in both, PET and fMRI data such as the visual cortex. However, other networks e.g. in the area of the auditory cortex showed discrepancies between modalities.
The EEG cap showed, without being accounted for an effect on the PET data on the order of -5% in cortical regions. This effect can be further reduced by adding the EEG net to the attenuation correction. The results indicate that even low frequency neuronal activation can be measured by a triple modality approach with only minor mutual influence between PET, MR and EEG. Brain networks could be visualized using metabolic PET data as well as hemodynamic fMRI information. Statistical significance of the brain networks was smaller in the PET datasets partially caused by lower amount of images in PET compared to fMRI. This work shows that triple modality of simultaneous acquisition of combined PET/MR/EEG data is feasible and paves the way towards an integration of metabolic, hemodynamic and electric brain imaging data in research and clinics within the framework of cometomics

AUTHORS (LAST NAME, FIRST NAME): Thielcke, André[3]; Elshahabi, Adham[4, 5]; Bezrukov, Ilja[3]; Amend, Mario[3]; Schmidt, Holger[7]; Reimold, Matthias[1]; Bisdas, Sotirios[6]; Lerche, Holger[4, 5]; Biswal, Bharat[2]; Pichler, Bernd J.[3]; Focke, Niels[4, 5]; la Fougere, Christian[1]; Wehrl, Hans F.[3]

INSTITUTIONS (ALL):

1. Department of Nuclear Medicine, University of Tuebingen, Tübingen, Germany.
2. Biomedical Engineering, NJIT, Newark, NJ, United States.
3. Department of Preclinical Imaging and Radiopharmacy, University of Tuebingen, Tuebingen, Germany.
4. Department of Neurology and Epileptology, Hertie-Institute for Clinical Brain Research, Tuebingen, Germany.
5. Werner Reichardt Centre for Integrative Neurosciences, Tuebingen, Germany.
6. Department of Diagnostic and Interventional Neuroradiology, University Tuebingen, Tuebingen, Germany.
7. Department of Diagnostic and Interventional Radiology, University of Tuebingen, Tuebingen, Germany.

(No Image Selected)

CONTROL ID: 2234403

TITLE: The complementary nature of functional and metabolic connectivity assessed by simultaneous PET/MR in rats

PRESENTER: André Thielcke

ABSTRACT BODY:

Abstract Body:

Introduction

Revealing functional and metabolic networks in humans and small animals is important for basic neuroscience research as well as for the study of brain diseases. The majority of functional connectivity (fc) studies apply fMRI techniques to map these networks. Recent studies indicate that it is also possible to assess metabolic brain networks using PET [1]. In this work we compare networks derived from simultaneously acquired BOLD-fMRI and [^{18}F]FDG-PET in rats, measuring brain circuitry on hemodynamic and glucose metabolism related levels.

Methods

Lewis rats (male, ca. 350g ± 50) were measured using a PET/MR system for small animals installed in a 7 T MR scanner (isoflurane anesthesia). fMRI-BOLD imaging was performed in the resting state (EPI, TR=3000 ms, TE=18ms, Matrix Size: 64x64x16, Voxel Size: 0.5x0.5x1.0 m^3, 400 volumes) with a simultaneous dynamic PET acquisition for 60 min using the tracer [^{18}F]FDG (29.6 MBq). PET-images were reconstructed (OSEM) into 60 s frames. fMRI and PET data were processed using SPM 12 and an independent component analysis (ICA, GIFT) was performed (40 components, ICASSO algorithm) on the group level. MR and PET component images were compared. Prominent networks in the brain were assessed. The overlap between PET and fMRI networks was calculated (dice coefficient (dc) for the Z-score: 3, overlap (ov) in terms of percent of the PET component).

Results

Prominent brain networks and structures were identified with both modalities such as the cingulate cortex (Cg1,Cg2 dc: 0.47, ov: 68%), motor cortex (M1, dc: 0.20, ov: 22%), caudate putamen (CPu, dc: 0.40, ov: 48%), prelimbic cortex (PrL, dc: 0.63, ov: 0.77%). A network with some similarities to the default mode network (DMN) was identified in the MR data (8 components) and in the PET data (7 components), the left-right symmetry of the PET data was less pronounced when compared to MR. In general the MR data showed higher Z-scores compared to PET. There exists a disparity between PET and MR networks, with some components only found in the respective modality.

Discussion

We could successfully show, that it is possible to identify many brain networks using not only fMRI techniques, but also [^{18}F]FDG-PET. This indicates that important information about metabolic brain networks is coded in PET data. Overlaps between selected networks were in the range between 22%-77% (relative to the PET data). A DMN-like structure could be identified in both modalities, however its composition from single components is different. This, in addition to the disparity in components observed, that could not matched between modalities hints to a complementarity of hemodynamic and metabolic brain networks. Differences in statistical significance between MR and PET derived network components originate not only from the different physiological processes assessed with both modalities, but also from differences in SNR and acquired images. In conclusion, we showed that it is possible to derive functional and metabolic brain connectivity within one PET/MR scanning session, that delivers complementary information about brain circuits.

[1] Wehrl HF et al. Nature Medicine 2013

AUTHORS (LAST NAME, FIRST NAME): Thielcke, André[1]; Amend, Mario[1]; Biswal, Bharat[2]; Pichler, Bernd J.[1]; Wehrl, Hans F.[1]

INSTITUTIONS (ALL):
1. Department of Preclinical Imaging and Radiopharmacy, University of Tuebingen, Tuebingen, Germany.
2. Department of Biomedical Engineering, New Jersey Institute of Technology, Newark, NJ, United States.
(No Image Selected)

CONTROL ID: 2234095

TITLE: Radiation dosimetry of degradable polymer microspheres labeled with 99mTc and 68Ga intended for radiomicrosphere therapy planning

PRESENTER: Manuel Sztejnberg

ABSTRACT BODY:

Abstract Body: Liver cancer accounts for nearly 10% of all cancers in the US. Intrahepatic Arterial Radiomicrosphere Therapy (RMT) with 90Y microspheres is used to treat unresectable liver tumors. Successful outcomes require appropriate treatment planning prior to delivery of the therapy microspheres. For treatment planning 99mTc-MAA is infused into the hepatic artery and a perfusion scintigraphy is performed. A limitation of RMT is the difficulty of quantifying dosimetry during treatment planning because 99mTc-MAA scintigraphy is a SPECT technique, not optimal for obtaining proper attenuation correction as compared to PET. Therefore, RMT planning will benefit from the inclusion of a PET radioisotope, capable of absolute attenuation correction and better resolution. Also, the significant differences in size, shape, and other properties between the MAA and 90Y microspheres complicates the treatment planning because the MAA particles cannot be expected to distribute exactly like the 90Y spheres. Thus, the development of new biodegradable spheres for accurate RMT planning is desired. The objective of this study is to determine the radiation dosimetry of radiolabeled spheres developed for RMT planning.

Biodegradable chitosan (CHSg) microspheres (≤ 48 hours in vitro half-life) labeled with 68Ga or 99mTc suitable for the imaging component of RMT planning have been developed. Dosimetry evaluation of the particles was performed in rats following tail vein injection and deposition in lungs. This experimental model was used to avoid the surgery required for intrahepatic injection. Animals were euthanized at 2 or 4 hours. Several organ samples were collected for measuring radioactive content in a NaI(Tl) well counter. Monte Carlo particle transport code (MCNPX 2.7) simulating photon and electron transport and a rat whole body phantom (ROBY, kindly provided by Dr Paul Segars from Duke University) were used to calculate radiation dose distribution from experimental biodistribution measurements. The ROBY model geometry was voxelized with 0.5 mm resolution and 75 differentiated tissues/organs.

The simulations were performed using 99mTc and 68Ga as sources. Each radioisotope emission was simulated according to evaluated nuclear data and the emissions were distributed uniformly within each organ with the intensity derived from the biodistibution experiments. The experimental data was directly applied to the ROBY model in each of the measured organs. The figure shows the organ-by-organ emission distributions obtained from the simulations. For free 68Ga and 68GaCHSg, the organ with the maximum average dose per decay is bladder Marrow receives less than 10% of the maximum dose. Liver receives less than 12.5% of the maximum dose in all the cases. The dosimetry study carried out complements the study of the designed microspheres allocating specific radiation fields to specific organs. The study needs to be repeated following intrahepatic injection. In conclusion RMT planning agents for PET and SPECT imaging were designed and successfully evaluated.

AUTHORS (LAST NAME, FIRST NAME): McGoron, Anthony [1]; Gulec, Seza[2]; Amor-Coarasa, Alejandro[4]; Sztejnberg, Manuel[3]

INSTITUTIONS (ALL):

1. Biomedical Engineering , Florida International University, Miami, FL, United States.
2. Surgery, Radiology/Nuclear Medicine , Florida International University, Miami, FL, United States.
3. Lab. 123, Instrumentación, Centro Atómico Ezeiza, Ezeiza, Buenos Aires, Argentina.
4. Department of Radiology, Weill Cornell Medical College, New York, NY, United States.

^{99m}Tc-CHSg
^{99m}Tc-MAA
Free ^{99m}Tc
^{68}Ga-NOTA-CHSg
^{68}Ga-MAA
Free ^{68}Ga
2 hours
4 hours

CONTROL ID: 2234105

TITLE: Pre-clinical *In Vivo* Stem Cell Tracking using Magnetic Particle Imaging

PRESENTER: Bo Zheng

ABSTRACT BODY:

Abstract Body: Introduction: Magnetic Particle Imaging (MPI) is an imaging modality that maps the in vivo spatial distribution of magnetic nanoparticle contrast agents. The technique shows extraordinary promise as a molecular imaging technique since it sees only nanoparticles, and as a safe substitute for iodinated or gadolinium contrast angiograms in patients with poor kidney function who have difficulty excreting these standard contrast agents[1]. First introduced in 2005 by Gleich and Weizenecker[2], the technique exploits the nonlinear magnetization characteristics of superparamagnetic iron oxide (SPIO) nanoparticles to localize their spatial position.

The physics of MPI are well suited to molecular imaging. The MPI signal penetrates tissue with no attenuation, making signal strength independent of depth. The MPI signal is also linearly quantitative, allowing accurate estimation of nanoparticle concentration. Linear quantitation further enables counting small numbers of labeled cells over physiologically relevant time spans since the nanoparticle tracers slowly break down over days to weeks. Finally, MPI has incredible sensitivity for a non-ionizing imaging technique and already approaches 500 nanomolar in < 10 min, with the opportunity for more than an order of magnitude improvement as we optimize the main magnets and detection electronics. Indeed, we believe that MPI sensitivity already compares well with the radiation-dose limited sub-nanomolar sensitivity of SPECT.

Methods and Results: We have developed three generations of small animal MPI imagers and are now testing research applications of the technique such as cell tracking and blood pool imaging. Shown in Figure 1 is a comparison of MPI, Optical, and MRI, which shows the high contrast inherent to MPI. The technique is high contrast because MPI sees only the tracer and does not see tissue. This makes MPI near ideal tracking therapeutic stem cells, imaging immune cells migrating to sites of injury, and visualizing functionalized nanoparticles. In Figure 2 we demonstrate MPI tracking of therapeutic stem cells.

Conclusions: MPI offers extraordinary promise as an emerging molecular imaging modality. Moreover, MPI is perhaps the first imaging technique since MRI that can be scaled up easily to imaging deep within humans and we believe will one day be situated side-by-side with MRI, CT, and Nuclear Medicine.

[1] P. W. Goodwill, et. al. *Adv. Mater.*, vol 24, issue 28. July. 2012.

[2] B. Gleich and J. Weizenecker, *Nature*, vol. 435, no. 7046, pp. 1214–7, Jun. 2005.

AUTHORS (LAST NAME, FIRST NAME): Zheng, Bo[1]; von See, Marc Philip[1]; Yu, Elaine[1]; Lu, Kuan[1]; Goodwill, Patrick[1, 2]; Conolly, Steven[1]

INSTITUTIONS (ALL):

1. Bioengineering, University of California, Berkeley, Berkeley, CA, United States.
2. Magnetic Insight, Inc., Newark, CA, United States.

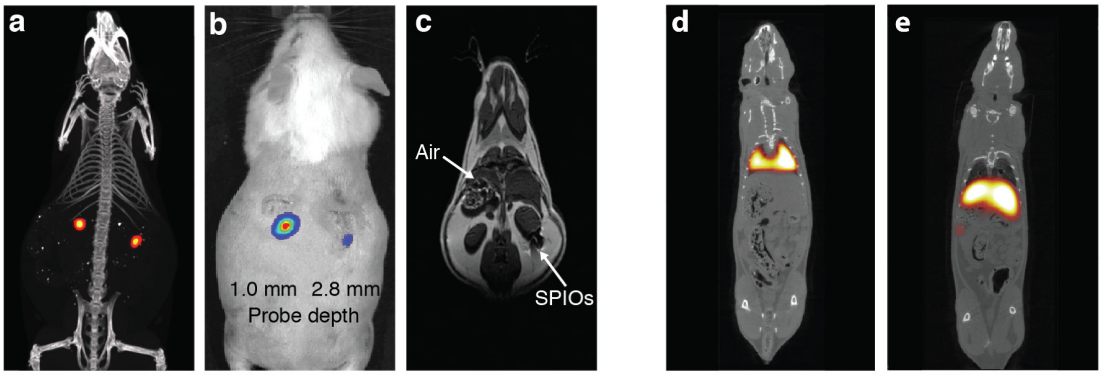

Figure 1: **[a-c]** Comparison of fluorescent imaging, MRI, and MPI/CT. (a) MPI / CT image shows no signal dependence on surrounding tissue. (b) Fluorescent imaging of two subcutaneous probes containing fluorescent and SPIO tracer showed signal dependence on probe depth. (c) SPIO- induced MR image dropout is challenging to distinguish from air artifacts. **[d,e]** MPI-CT imaging of intravascular injections of SPIO-labeled cells and SPIO tracer alone in rat. (d) 7-week old Fisher 344 rats were administered 8.4 million iron-labeled human mesenchymal stem cells via tail vein injection and immediately sacrificed for MPI and CT imaging. MPI images show the majority of administered cells lodged in the pulmonary vasculature of the animal. (e) MPI imaging shows liver and splenic uptake of SPIOs (Resovist, Bayer) administered via tail vein injection. MPI imaging: 4 x 3.75 x 9.5 cm field of view, 9 minute total scan time. CT imaging: 6 x 6 x 15 cm field of view, 25 minute total scan time.

CONTROL ID: 2234192

TITLE: *In Vivo* Perfusion Imaging using Magnetic Particle Imaging

PRESENTER: Patrick Goodwill

ABSTRACT BODY:

Abstract Body: Introduction: Myocardial perfusion imaging is the predominant nuclear medicine study [1]. A key enabler of perfusion imaging is the high contrast inherent to nuclear medicine, which sees only a tracer and does not see tissue. Magnetic Particle Imaging (MPI) is an emerging molecular imaging modality that, like nuclear medicine, sees only a tracer and does not see tissue [2-6]. Because of MPI's high contrast, high sensitivity, and signal linearity independent of depth, we believe MPI will excel at perfusion imaging.

As we push MPI towards quantitative perfusion imaging (blood volume, blood flow, mean transit time), we must first demonstrate high contrast imaging of the blood volume. Further technical development to reduce scan times will enable quantitative measurement of blood flow and mean transit time. Here we demonstrate this first step by performing in vivo blood pool imaging with a tailored MPI-specific nanoparticle tracer.

Methods: LodeSpin magnetic nanoparticle tracer (LS-7-2, 500 micro-liters, 1 mg total iron weight) injected into the tail vein of anesthetized Fischer 344 rats and imaged with respiratory gating or imaged following immediate sacrifice using carbon dioxide. Animals were imaged using a 7000 mT/m x 3500 mT/m x 3500 mT/m imager with a drive field of 15 mTpeak in the z axis (down the bore). Total field of view was 11 cm x 4 .5cm x 3.75 cm. Images were reconstructed using x-space reconstruction [6] and equalized or deconvolved using a theoretical point spread function. All experiments were conducted under an animal protocol approved by the university's animal care and use committee.

Results: Preliminary results for MPI blood pool imaging in a rat are shown in Figs 1. In Fig 1a, we see an MPI image of the thorax image of a live animal. In Fig 1b, we see the brain of the same animal following sacrifice two hours after injection. Fig 1c, we see brain vasculature, the jugular veins, the outline of the heart wall, and the lungs in an animal sacrificed immediately following injection. In Fig 1e we see the lungs, the liver, and the kidneys of the same animal.

Conclusion: We have used two improvements, larger magnetic field gradients and improved nanoparticle tracers, to enable higher quality MPI blood pool images. The images show the great potential of MPI for producing high contrast images of vasculature and organ perfusion.

Acknowledgments: The authors gratefully acknowledge support from: NIH 5R01EB013689-03, CIRM RT2-01893, Keck Foundation 034317, NIH 1R24MH106053-01, NIH 1R01EB019458-01, ACTG 037829, and NIH 2R42EB013520-02A1.

References:

[1] Mettler, F. et al.. Radiology, *253*(2), 520–531, 2009.
[2] Weizenecker, J., et. al.. PMB, 54(5), 2009.
[3] Rahmer, J., et. al.. PMB, 58(12), 3965–77, 2013.
[4] Saritas, E et. al.. JMR, 229, 116–26, 2013.
[5] Ferguson, et al. *MPI with Tailored Iron Oxide Nanoparticle Tracers*," IEEE-TMI, in press.
[6] Goodwill, PW and Conolly, SM. IEEE-TMI, 29(11), 1851–1859, 2010.

AUTHORS (LAST NAME, FIRST NAME): Goodwill, Patrick[1, 3]; Ferguson, R M.[2]; Yu, Elaine[1]; Zheng, Bo[1]; Lu, Kuan[1]; Khandhar, Amit[2]; Kemp, Scott[2]; Krishnan, Kannan[4]; Conolly, Steven[1]

INSTITUTIONS (ALL):

1. Bioengineering, University of California, Berkeley, Berkeley, CA, United States.
2. Lodespin Labs, Seattle, WA, United States.
3. Magnetic Insight, Inc., Newark, CA, United States.
4. University of Washington, Seattle, WA, United States.

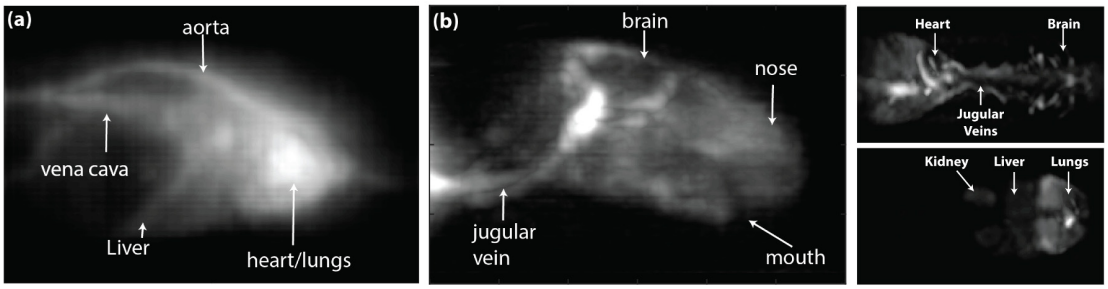

Figure 1: **(a,b)** Saggital images of a Fisher 344 rat. (a) Mid thorax Maximum Intensity Projection (MIP) of an anasthesized rat. (b) Anterior MIP following 2 hours tracer circulation time and sacrifice. Note signal blush showing blood pool. FOV: 6 cm x 4 cm. Scan time 20 Minutes. **(c,d)** Coronal MIP images of tracer in a sacrificed Fisher 344 rat. (c) Anterior image. (d) Mid and hind region of the rat. FOV: 11 cm x 4.5 cm x 3.75 cm, MIP: 11 cm x 4.5 cm. Scan time: 10 minutes. Scale Bar 1 cm.

CONTROL ID: 2234116

TITLE: Bioluminescence imaging reveals tissue specificity of extracellular vesicle-mediated biomolecule transfer in vivo

PRESENTER: Masamitsu Kanada

ABSTRACT BODY:

Abstract Body: Extracellular vesicles (EVs) are small, membrane-enclosed particles produced by all known cells. These entities play key roles in cell-cell communication via transfer of biomolecules between cells and tissues of the body. EVs have been shown to affect gene expression, cell function, and metastasis of tumors, and have been proposed for the controlled delivery of therapeutic agents and effector molecules. However, little is known about the mechanisms of EV function. Under physiological conditions EVs can be classified into two major forms, exosomes and microvesicles (MVs), distinguished by size, nucleic acid contents, marker proteins and lipid compositions. The biogenesis of the two types of EVs differs as they originate from either the endosomal (exosomes) or plasma (MVs) membranes. To elucidate the primary means, through which EVs mediate intercellular communication, their ability to encapsulate and deliver different types of macromolecules was characterized with fluorescence and bioluminescence imaging methods. Both EV types encapsulated reporter proteins and mRNA, but only MVs transferred the reporter function to recipient cells. De novo reporter protein expression in recipient cells resulted only from plasmid DNA (pDNA) delivery via MVs. Reporter mRNA was delivered to recipient cells by both EV types, but was rapidly degraded without being translated. To explore their differential biological functions in immune responses to tumors, macrophage J774 cells were cultured with fluorescently labeled exosomes and MVs derived from breast tumor 4T1 cells. Interestingly, within the 5 h culture period, macrophages preferentially took up the MVs, suggesting that MVs, but not exosomes, may play an important role in the communication between tumor cells and macrophages. MVs also mediated delivery of functional pDNA encoding Cre recombinase in vivo to specific tissues in transgenic Cre-lox reporter mice. In vivo bioluminescence imaging (BLI) revealed the localization of the MV-mediated biomolecule transfer. Within the parameters of this study, MVs delivered functional pDNA, but not RNA, whereas exosomes from the same source did not deliver functional nucleic acids. Our data thus show that exosomes and MVs are structurally and functionally distinct. These results have significant implications for our understanding of the role of EVs in cellular communication, and for the development of EVs as delivery vehicles. Live animal imaging by BLI provides a unique tool for the analysis of this process as interrogating the biological activity in entire bodies over time is currently not feasible with other methods.

AUTHORS (LAST NAME, FIRST NAME): Kanada, Masamitsu[1]; Bachmann, Michael H.[1]; Hardy, Jonathan W.[1]; Frimannson, Daniel O.[2]; Bronsart, Laura[1]; Wang, Andrew[1]; Sylvester, Matthew D.[2]; Schmidt, Tobi L.[1]; Kaspar, Roger L.[3]; Butte, Manish J.[1]; Matin, AC[2]; Contag, Christopher H.[1, 2]

INSTITUTIONS (ALL):

1. Pediatrics, Stanford University, Stanford, CA, United States.
2. Microbiology and Immunology, Stanford University, Stanford, CA, United States.
3. TransDerm Inc., Santa Cruz, CA, United States.

(No Image Selected)

CONTROL ID: 2234139

TITLE: Development of a Multimodality Imaging Dextran Microsphere-based Embolic Platform

PRESENTER: Bryan Hoang

ABSTRACT BODY:

Abstract Body: Introduction: Embolization using microparticles and microbeads has proven to be an effective treatment strategy for management of haemoptysis, arteriovenous malformations (AVMs) and tumors. However, there is an increasing need to visualize and localize the site of embolization during administration of adjuvant treatments such as radiation therapy. Recent advances in nano and micron-sized biomaterials engineering have enabled novel developments in embolic systems suitable for multimodality imaging. In the present work, an embolic platform that can be effectively visualized using CT, MR and near-infrared (NIR) fluorescence was developed by encapsulation of a liposomal nano-formulation with multimodality CT/MR/optical imaging capabilities within pegylated dextran microparticles. The unique feature of our embolic platform lies in its highly versatile multimodal visualization capability that allows for any combination among CT, MR and fluorescence imaging. **Methods/Results**: Dextran methyl-methacrylate was synthesized to allow crosslinking by free-radical initiated polymerization by reaction of dextran with glycidyl methacrylate in the presence of DMAP. The composition and degree of substitution (DS=10) was confirmed by ^{1}H NMR. Dextran microspheres encapsulating nano-liposomes were prepared in an all aqueous system. Briefly, a solution of PEG, dex-MA and CT/optical liposomes (co-encapsulating iohexol and indocyanine green) were flushed with nitrogen for 10 min. The two phase system was mixed for 30 s to create a water-in-water emulsion. The emulsion was stabilized at room temperature for 15 min, followed by the addition of N'N'N'N'-tetramethylethylenediamine and potassium persulfate. The resulting emulsion was incubated at 37^{o}C for 30 min. The size of the microparticles was 11.4 ± 2.7 μm as determined using a Beckman LS13 320 particle analyzer. Stability at 37^{o}C was measured for 4 weeks with no significant changes in particle size. Microparticles containing the CT/optical liposomes were injected subcutaneously into mice and imaged using the Perkin-Elmer Maestro optical imaging system and the GE Locus Ultra MicroCT to confirm fluorescence and CT imaging potential. The microparticles demonstrated high imaging contrast with respect to the surrounding tissues in both imaging modalities. **Conclusion:** A novel and stable embolic platform was developed and its multimodality imaging potential was validated in a subcutaneous mouse model. Ongoing investigation is focused on the evaluation of the embolization and post-embolization imaging performance of this microparticle platform.

AUTHORS (LAST NAME, FIRST NAME): Hoang, Bryan[1]; Murphy, Kieran[1, 2]; Jaffray, David A.[1, 3]; Zheng, Jinzi[1, 4]

INSTITUTIONS (ALL):

1. TECHNA Institute for the Advancement of Technology for Health, University Health Network, Toronto, ON, Canada.

2. Department of Interventional Radiology, Toronto Western Hospital , Toronto, ON, Canada.

3. Department of Radiation Physics, Radiation Medicine Program, University Health Network , Toronto, ON, Canada.

4. Institute of Biomaterials & Biomedical Engineering, University of Toronto, Toronto, ON, Canada.

(No Image Selected)

CONTROL ID: 2234120

TITLE: Targeted, osteolytic-responsive theranostics for cancer induced bone-metastasis

PRESENTER: Xuli Wang

ABSTRACT BODY:

Abstract Body:

Introduction

Metastatic cancers in bone are very difficult to treat and result in significant morbidity and mortality. Current therapeutic options for cancer induced bone-metastases are usually palliative, and planning an individual therapeutic strategy as early as possible to delay skeletal complications is the key to manage patients with bone metastases. Cancer induced bone metastasis directly or indirectly induce the formation of osteoclasts, which enhance bone resorption by increasing secretion of a key protease (cathepsin K) to degrade bone matrix, leading to osteolytic lesions and serious skeletal complications. Hence, bone-targeted, osteolytic-responsive systems with capacity to load therapeutics and imaging probes (i.e. theranostics) are greatly needed to improve clinical outcomes for this disease.

Methods and Results

A block copolymer of poly(ethylene glycol) and polypeptide (mPEG-*b*-P(Aspartic acid)-*b*-P(Ally-glycine)) has been synthesized as a nanocarrier to load therapeutics and imaging agents. The block copolymer was designed to possess a bone tropism peptide (i.e. poly(Aspartic acid)) to enable its bone seeking capacity. A short peptide with the sequence of CKGHPGGPQGK that includes a cathepsin K (CTSK)-cleavable substrate (HPGGPQ) was used to functionalize the block copolymer by using thiol-ene click chemistry. Near infrared fluorescence (NIRF) probe of Cy5.5 and a model anti-cancer agent of doxorubicin (DOX) were conjugated into CTSK peptide terminus for non-invasive optical imaging and anti-tumor studies, respectively. The block copolymer can spontaneously form nanosized construct with the size of approximately 100 nm in diameter. Over 90 % of polymeric micelles were able to bind to hydroxyl apatite, showing high bone binding capability. More importantly, a unique characteristic of a cathepsin K-triggered imaging enhancement was observed by confocal laser scanning microscopy. Improved tumor inhibition was further demonstrated in cultured cancer cells such as breast cancer cell line [i.e. MDA-MB-231] and prostate cancer cell line [e.g. PC-3 cells]. In the bone-metastatic animal model, the preferential tumor accumulation of Cy5.5 was clearly observed in the case of using nanocarrier. In sharp contrast, NIRF signal of free Cy5.5 without using nanocarrier quickly diminished from the animal body, suggesting the essential role of nanocarrier for tumor-tropic drug delivery. This improved delivery efficacy may be attributed to more selective delivery of imaging agents to bone metastatic tissues and/or responsiveness of the nanoparticles to cathepsin K, thus improving tumor uptake and enzymatic release of imaging probes, leading to imaging enhancement.

Conclusions

The promising results from this study may prompt the development of bone-targeted, enzyme-triggered drug delivery systems to improve their affinity to skeletal tissues, enhance selectivity for osteolytic regions and improve efficacy of anti-cancer agents and or imaging agents, thus facilitating the development of effective theranostics for bone metastasis.

AUTHORS (LAST NAME, FIRST NAME): Zhan, Le[1]; Liu, Tao[1, 2]; Feng, Jun[2]; Wang, Xuli[1]

INSTITUTIONS (ALL):

1. Department of Radiology, University of Utah, Salt Lake City, UT, United States.
2. Department of Chemistry, Wuhan University, Wuhan, Hubei, China.

(No Image Selected)

CONTROL ID: 2234126

TITLE: MetalloProbes: Structure–Activity Relationship Studies and Associated Geometrical Preferences for Identifying Second Generation Myocardial Perfusion PET/SPECT Imaging Agents

PRESENTER: Jothilingam Sivapackiam

ABSTRACT BODY:

Abstract Body: Myocardial perfusion imaging (MPI) plays an important role in the noninvasive assessment of the CAD. Herein, we postulate that multidrug resistance protein (*MDR1*, Pgp, ABCB1) recognized moderately hydrophobic cationic metalloprobes would undergo faster excretion from the liver to enable high contrast myocardium imaging via their localization within the mitochondria of the myocardium. To discover and develop second generation lead PET agents through Structure–Activity Relationship studies, we have synthesized new twenty-five metalloprobes, incorporated with gallium-67/68 and evaluated their uptake profiles in stably transfected MCF-7 Pgp cells and their empty vector control MCF-7 counterparts. $^{67/68}$Ga-metalloprobes and their unlabeled counterparts were synthesized by incubating corresponding Schiff base precursor ligands and trivalent gallium(III) chlorides using established procedures, and characterized through routine analytical methods. During crystallizations, these metalloprobes crystallized in two different geometric configurations (*cis* and *trans*) depending upon the length of the linear tetramine thus impacting their cavity formed by the chelator core and distribution of overall positive charge on their surface. The crystal structure data demonstrated an octahedral geometry, wherein *trans*-metalloprobe contained central metal symmetrically coordinated with four nitrogen atoms in the equatorial plane and two axial phenolate oxygen atoms. However, *cis*-metalloprobe indicated the central gallium(III) coordinated symmetrically with two amine nitrogen and two phenolate in the equatorial plane while two imine nitrogen atoms occupying the axial positions. For evaluation of cellular uptake profiles, ^{67}Ga-Metalloprobes were incubated in rat cardiomyoblasts (H9c2) and stably transfected MCF-7 and MCF-7/*MDR1* cells, either in presence or absence of LY-335979 (Pgp inhibitor). Lead agents demonstrated accumulation in rat cardiomyoblasts (H9c2), human breast cancer cells (MCF-7), and their uptake profiles were found to be inversely proportional to Pgp expression. Additionally, LY335979 (1μM), reversed efflux of radiotracers in Pgp expressing cells, equivalent to levels found in Pgp negative cells. Compared with metalloprobes having *cis* configuration of phenolates, those with *trans* configuration of phenolates showed the cellular uptake profiles mediated by Pgp expression thus indicating geometrical preferences in Pgp recognition profiles within this class of metalloprobes. MicroPET/CT imaging demonstrated initial penetration and sustained retention of second generation lead agents in rat myocardium accompanied by facile clearance from liver driven by transporter mediated excretion pathways. Overall, selected molecules provide template scaffolds for further validation and development of second generation myocardial perfusion PET imaging agents.

References: Sharma, V. et. al. PlosOne 2014, 9, e109361; Sivapackiam, J. et. al. Dalton Transactions, 2010, 39, 5842; Sharma, V. J. Nucl. Med. 2005, 46, 354; Bioconjugate Chem 2004, 15, 1464.

Funding: NIH RO1HL111163 (VS), R33AG033328 (VS), American Health A2007-383(VS)

AUTHORS (LAST NAME, FIRST NAME): Sivapackiam, Jothilingam[1]; Harpstrite, Scott E.[1]; Gu, Hannah [1]; Prior, Julie L.[1]; sharma, vijay[2]

INSTITUTIONS (ALL):

1. Department of Radiology, Washington University School of Medicine, Saint Louis, MO, United States.
2. Department of Radiology, Washington University School of Medicine, Saint Louis, MO, United States.

(No Image Selected)

CONTROL ID: 2234136

TITLE: Targeting RAGE expression in ovarian cancer for imaging and therapy

PRESENTER: Yared Tekabe

ABSTRACT BODY:

Abstract Body: BACKGROUND AND PURPOSE:
Receptor for Advanced Glycated Endproducts (RAGE) and its ligands are expressed and secreted by a variety of human tumors including ovarian and associated with metastases and poor outcome. We developed an anti-RAGE antibody against a unique peptide sequence on the V-domain of RAGE with immunoreactivity in mice, pigs, and humans. We have shown in imaging studies that the ^{99m}Tc labeled anti-RAGE F(ab')$_2$ bind vascular lesions and further demonstrated blocking properties in vascular and tumor cells. We hypothesized that this antibody may have potential for both imaging and treatment of RAGE expressing tumors.

IN-VITRO METHODS:
To determine growth suppressing property of our antibody, both human SKOV-3s (sensitive) and SKOV-3TR (multi drug resistant) cell lines were used in cell culture experiments. Cells were incubated with serial dilutions of anti-RAGE F(ab')$_2$ or control antibody for 24 hrs at 37^{0}C and 5% CO_2 then washed with respective media. CellTiter-Blue (50 µl of 1:5 dilutions) was added to plates and incubated at 37^{0}C and 5% CO_2 for 2 hrs. Fluorescence was recorded at (560 $_{Ex}$/590$_{Em}$) using BioTek fluorescence Plate reader.

IMAGING METHODS: Luciferase producing SKOV-3 cells (3 x 10^6 cells in 0.1 ml PBS) were injected into the right flank or peritoneal space of female nude mice aged 6 weeks (n=18). Tumor volumes were 1070±279 mm^3 at 4-5 wk when mice were injected with luciferin and with ^{111}In-anti-RAGE F(ab')$_2$ (n=10) or control nonspecific F(ab')$_2$ (n=8). Optical imaging was performed on BioSpace Lab scanner. Hybrid SPECT/CT imaging was performed on a micro-SPECT/CT (Bioscan/Mediso). After in-vivo imaging, tumors were explanted, ex-vivo images acquired, radioactivity counted, and sectioned for histological and immunohistochemical examination. To quantify tracer uptake, 5 voxel thick ROIs were drawn around activity in the tumor, summed for slices comprising the tumor and converted to mCi using calibration factor and expressed as %ID using Vivo Quant software (InVicro).

RESULTS: Incubation of both sensitive (SKOV-3s) and multidrug resistant (SKOV-3TR) cells with anti-RAGE F(ab')$_2$ for 24 h showed a dose-dependent reduction of viable cells, whereas no significant dose-dependent reduction of viable cells was observed with a control nonimmune IgG F(ab')$_2$. There was good co-localization of luciferase on the optical scan and tumor location at necropsy and with the focal uptake of the ^{111}In anti-RAGE F(ab')$_2$ on SPECT/CT. Quantitative tracer uptake in the tumor from scan showed that uptake of ^{111}In-anti-RAGE F(ab')$_2$ as %ID was 2.4 fold higher than ^{111}In-nonimmune IgG F(ab')$_2$ (P=0.008) confirmed by gamma well counting. Dual immunofluorescence staining for RAGE and PAX8 (ovarian specific antigen) in tumors showed high expression of RAGE and co-localization with PAX8 positive stained cells.

CONCLUSIONS: These results suggest potential for the anti-RAGE antibody for both diagnosis and treatment of ovarian cancer.

AUTHORS (LAST NAME, FIRST NAME): Tekabe, Yared[1]; Anthony, Tamykah[2]; Li, Qing[1]; Rodriguez, Krissy[1]; Khaw, Ban An[3]; Kokoshka, Jerry[1]; Johnson, Lynne L.[1]

INSTITUTIONS (ALL):
1. Columbia University, Yonkers, NY, United States.
2. Columbia University, New York, NY, United States.
3. Northeastern University, Boston, MA, United States.

(No Image Selected)

CONTROL ID: 2234141

TITLE: Nanoparticle-based translational MR Imaging for immune-therapy trials in glioblastoma

PRESENTER: Olga Lenkov

ABSTRACT BODY:

Abstract Body: TITLE

Nanoparticle-based translational MR Imaging for immune-therapy trials in glioblastoma

AUTHORS:

Olga Lenkov, Rogelio Esparza, Michael Iv, Nancy Fischbein, Kristen Yeom, Samuel Cheshier, Heike E. Daldrup-Link

PURPOSE:

To evaluate if ferumoxytol-enhanced MRI can detect response of tumor associated macrophages to anti-CD47 antibody treatment in mice implanted with human glioblastoma (GBM) tumors

MATERIALS AND METHODS

Brain tumor-initiating cells were isolated from primary human GBM samples, obtained from surgical resections, and transfected with a lentiviral construct allowing for constitutive expression of luciferase. 0.5-1 million tumor cells were stereotactically injected into the brains of 14 NOD-SCID x RAG g/d dko mice. Once tumor growth was confirmed by luciferase imaging (usually 5-6 weeks after implantation), treatment was initiated with either anti-CD47 mAb (n=8, 10 mg mAb/kg) or control IgG (n=6), administered every other day for 2 weeks. Mice then received a single intravenous injection of ferumoxytol (dose: 0.5mmol/kg). All mice underwent MRI before and 1 hour, 1 week and 2 weeks after ferumoxytol injection, using a 7T GE MR scanner and T2*-weighted FGRE sequences (flip angle:30, TE:2.36-7.62 ms, TR:300 ms, NEX:2). T2* maps were generated with Cinetool software (GE Global Research) and fused with original T2*-weighted MR images. Tumor size, tumor growth ($TG\%=((V_t-V_0)/V_0)*100$) and tumor T2* relaxation times, measured on these integrated images, were compared between treated and control tumors using Student T-test and a $p<0.05$.

RESULTS

MRI studies demonstrated marked and significant tumor growth inhibition by 50-60% after 1 week and 75-85% after 2 weeks of anti-CD47 mAb treatment compared to IgG-treated controls ($p<0.05$; Fig. 1A and 1B). Corresponding T2* maps demonstrated significant T2* shortening of both anti-CD47 mAb treated and control tumors ($p<0.05$). There was no significant difference in T2* values of anti-CD47 mAb treated and control tumors at 14 h post-injection ($p>0.05$). After 1 week of treatment, T2* values of anti-CD47 treated tumors were slightly but not significantly shorter. At 2 weeks, tumor T2*-enhancement was significantly shorter for anti-CD47 mAb treated tumors compared to controls ($p<0.05$). Corresponding histopathology demonstrated decreased size of tumor and increased quantities of macrophages in anti-CD47 treated tumors compared to controls.

CONCLUSION

Ferumoxytol-enhanced MRI can detect response of human glioblastoma tumor to anti-CD47 antibody therapy by significant tumor growth inhibition and significant T2* shortening.

Fig. 1) Growth rate and MRI enhancement of intraparenchymal tumors. (A) Representative MR images with superimposed T2* relaxation time maps of anti-CD47 mAb treated tumor and sham-treated control. (B) Corresponding growth rates and (C) T2* relaxation times of anti-CD47 mAb treated tumors (n=8) and sham-treated controls (n=6), displayed as means and SD. Please note that ferumoxytol-induced T2*-signal enhancement is quantified by shortened T2* relaxation times (shorter T2* time = stronger contrast enhancement). p.i.=post injection

AUTHORS (LAST NAME, FIRST NAME): Lenkov, Olga D.[1]; Esparza, Rogelio[2]; Iv, Michael[2]; Fischbein, Nancy[2]; Yeom, Kristen[2]; Cheshier, Samuel[2]; Daldrup-Link, Heike E.[3]

INSTITUTIONS (ALL):

1. Radiology, Stanford University, Stanford, CA, United States.
2. Stanford University, Stanford, CA, United States.
3. Radiology, Stanford University, Stanford, CA, United States.

Fig. 1) Growth rate and MRI enhancement of intraparenchymal tumors. (A) Representative MR images with superimposed T2* relaxation time maps of anti-CD47 mAb treated tumor and sham-treated control. (B) Corresponding growth rates and (C) T2* relaxation times of anti-CD47 mAb treated tumors (n=8) and sham-treated controls (n=6), displayed as means and SD. Please note that ferumoxytol-induced T2*-signal enhancement is quantified by shortened T2* relaxation times (shorter T2* time = stronger contrast enhancement). p.i.=post injection

CONTROL ID: 2245141

TITLE: *In vivo* visualization of murine KB tumors using folate-targeted photoacoustic nanoparticles

PRESENTER: Hoang Lu

ABSTRACT BODY:

Abstract Body: Photoacoustic imaging can be used to rapidly assess tumor physiology, and could help physicians visualize and remove cancerous lesions during surgery. However, there are limited cancer targeted photoacoustic absorbers available for use as contrast agents. We here present a series of new parylene-based photoacoustic nanoparticle absorbers, which target cancers and can be used to perform real-time *in vivo* molecular imaging with high resolution. The series of nanoparticles have a range of absorbance maxima ranging from 700 to 900 nm, and are ~50 nm in diameter. These nanoparticles are also coated with PEG chains that allow various targeting functional groups to be attached. Folic acid functionalized nanoparticles selectively accumulate within KB tumors in a murine KB-cancer model, and both the dynamics and microdistribution of nanoparticle accumulation can be assessed with photoacoustic imaging, using the Vevo LAZR combined ultrasound/photoacoustic imaging system. Targeted nanoparticles increasingly accumulate throughout the tumors over days, and can be visualized even at eight days after tail-vein injection. Non modified nanoparticles passively accumulate near the skin and surface of the tumor, and are tracked to study enhanced permeation and retention effects. Properties such as tumor morphology and hypoxia distribution are co-recorded during photoacoustic measurements, and can be overlaid with the nanoparticle localization data to provide dynamic relationships between tumor physiological properties and nanoparticle accumulation. In whole, these new photoacoustic agents represent a promising class of diagnostic materials for use in preclinical studies, or for use as contrast agents in imaging-guided surgery.

AUTHORS (LAST NAME, FIRST NAME): Lu, Hoang D.[3]; Heinmiller, Andrew[1]; Wilson, Brian K.[3]; Hejazi, Shahram[2]; Prud'homme, Robert K.[3]

INSTITUTIONS (ALL):

1. FUJIFILM VisualSonics, Toronto, ON, Canada.
2. Optimeos Life Sciences, Princeton, NJ, United States.
3. Chemical and Biological Engineering, Princeton University, Princeton, NJ, United States.

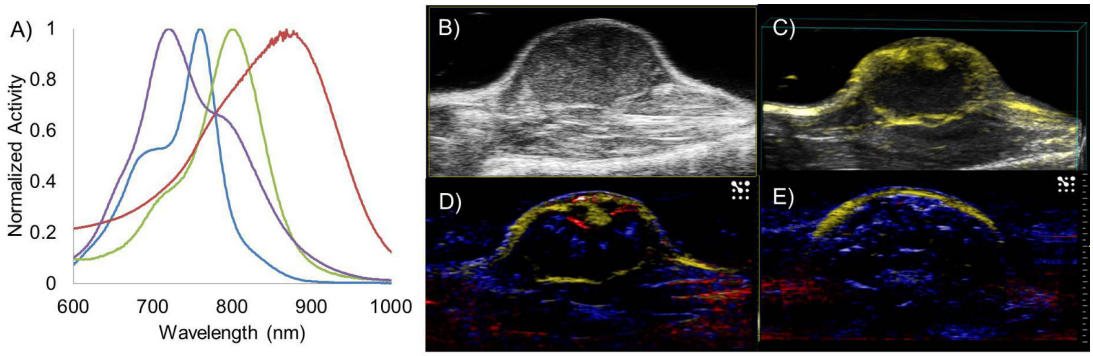

(A)Photoacoustic activities of nanoparticle variants which encapsulate different parylene-based absorbers
(B)High resolution ultrasound-based visualization of KB tumor anatomy
(C)3D coregistered ultrasound/photoacoustic-based visualization of tumor anatomy & targeted nanoparticle distribution
(D)Spectrally unmixed photoacoustic image showing targeted nanoparticle distribution and blood signals
(E)Spectrally unmixed photoacoustic image showing non-targeted nanoparticle distribution and blood signals

greyscale = ultrasound yellow = nanoparticle
red = oxyhemoglobin blue = deoxyhemoglobin

CONTROL ID: 2234150

TITLE: Thioredoxin Sensing MRI T1 Contrast Agent

PRESENTER: Jongeun Kang

ABSTRACT BODY:

Abstract Body: The protein thiol group is vulnerable to oxidation by reactive oxygen species and reactive nitrogen species, and plays principal role in maintaining an appropriate oxidation–reduction state of the protein, regulating signal pathways and responding to various diseases, such as cancer, diabetes, and neurodegeneration. As the reductive end of this redox buffer network, vicinal-dithiol-containing proteins (VDPs) are attracting more and more attention. VDPs are proteins that contain two thiol groups that are close to each other in space. Therefore, as one final end of the redox buffer network, protein vicinal dithiols show a higher tendency to cope with redox changes and are more sensitive and prone to free-radical oxidation. Thioredoxin is a class of small redox proteins known to be present in all organisms. It plays a role in many important biological processes, including redox signaling. To detect this vicinal thiol protein by magnetic resonance imaging (MRI) which is medically used noninvasive technique, new MR contrast agents were developed with two different chain lengths to utilize a receptor-induced magnetization enhancement (RIME) strategy which is a key method to restrict the motion of a contrast agent, and thereby increase the relaxivity. MRI T1 properties with/without thioredoxin (Trx) compared with human serum albumin (HSA) were elucidated, and in vitro cell study also was performed depending on Trx concentration. The contrast agent selectively binds with Trx, consequently resulting in enhanced (>40%) T1 relaxation effect.

AUTHORS (LAST NAME, FIRST NAME): Kang, Jongeun[3, 2]; Bhuniya, Sankarprasad[1]; Hong, Kwan Soo[3, 2]

INSTITUTIONS (ALL):

1. Amrita Centre for Industrial Research & Innovation, Amrita Vishwa Vidyapeetham, Coimbatore, Tamil Nadu, India.
2. Graduate School of Analytical Science and Technology, Chungnam National University, Daejeon, Korea (the Republic of).
3. Division of MR Research, Korea Basic Science Institute, Cheongju, Korea (the Republic of).

(No Image Selected)

CONTROL ID: 2234165

TITLE: L-Tyrosine Confers Greater Residualising Properties to a d-Amino Acid Rich Residualising Peptide for Radioiodination of Internalising Antibodies

PRESENTER: Fook Lee

ABSTRACT BODY:

Abstract Body: *Purpose* The targeting of tumors with antibodies is utilized for numerous therapeutic strategies, including immune effector function, signaling inhibition, and payload delivery. Noninvasive whole-body imaging techniques can aid in patient selection for antibody therapy by quantifying antibody binding in patients, including multiple and non-accessible lesions, or by determining the radiation dose in patients planned for radioimmunotherapy. The aims of the study were to develop and evaluate a novel residualising peptide for radioiodination with ^{124}I, thus improving diagnostic imaging with ^{124}I-labeled internalising antibodies to support clinical development. *Methods* The anti-EGFR antibody ch806 was radiolabeled using $^{124/131}$I-PEG$_4$-dThr-dPro-dThr-dAsp-dAsp-Tyr-dAsp-dAsp-dThr-dPro-dThr ($^{124/131}$I-PEG$_4$-tptddYddtpt), and for comparison ^{125}I-PEG$_4$-dThr-dPro-dThr-dAsp-dAsp-dTyr-dAsp-dAsp-dThr-dPro-dThr (^{125}I-PEG$_4$-tptddyddtpt), direct radioiodination using IODO-GEN (^{125}I-) and ^{111}In- N-[(R)-2-amino-3-(*p*-isothiocyanatophenyl)propyl]-*trans*-(S,S)-cyclohexane-1,2-diamine-N,N,N′,N",N"-pentaacetic acid (^{111}In-CHX-A″-DTPA). Radiolabeled azido-peptides were conjugated to dibenzylcyclooctyne (DBCO)-derivatized ch806 antibody via click chemistry. The radiochemical purities, EGFR-overexpressing U87MG.de2-7 human glioblastoma cell binding properties and targeting of U87MG.de2-7 human glioblastoma xenografts at 72 h after injection of all radioconjugates were compared. Biodistribution of ^{124}I-PEG$_4$-tptddYddtpt-ch806 at 2, 24, 48, 72, 120 and 168 h after injection and immunoPET imaging at 2, 72 and 168 h after injection were evaluated in U87MG.de2-7 tumor-bearing mice. *Results* In an initial biodistribution study using U87MG.de2-7 tumor-bearing mice at 72 h post injection, ^{131}I-PEG$_4$-tptddYddtpt-ch806 showed a percentage injected dose per gram tissue similar to ^{111}In-CHX-A″-DTPA-ch806 (^{125}I-PEG$_4$-tptddyddtpt-ch806, 22.79 ± 3.07 %ID/g; ^{111}In-CHX-A″-DTPA-ch806, 36.49 ± 5.33 %ID/g; ^{131}I-PEG$_4$-tptddYddtpt-ch806, 32.15 ± 3.52 %ID/g; ^{125}I-ch806, 12.74 ± 1.18 %ID/g). ^{124}I-PEG$_4$-tptddYddtpt-ch806 was produced at 23% labeling efficiency; 98% radiochemical purity, 25.9 MBq/mg specific activity, and 64% cell binding in the presence of antigen excess. Highest tumor uptake for ^{124}I-PEG$_4$-tptddYddtpt-ch806 was 36.03 ± 5.07 (mean ± SD) percentage injected dose per gram tissue at 72 h after injection and was similar to ^{111}In-CHX-A″-DTPA-ch806. High resolution
immunoPET/MRI imaging of tumors showed good correlation with biodistribution data. *Conclusions* The mixed d/l-enantiomeric peptide, dThr-dPro-dThr-dAsp-dAsp-Tyr-dAsp-dAsp-dThr-dPro-dThr, is suitable for radiolabeling antibodies with radiohalogens such as ^{124}I for high resolution immunoPET imaging of tumors, and for evaluating biodistribution and tumor targeting properties of internalising antibodies in early phase clinical trials.

AUTHORS (LAST NAME, FIRST NAME): Lee, Fook T.[1]; Burvenich, Ingrid J.[1]; Guo, Nancy Y.[1]; Tochon-Danguy, Henri[2]; Ackermann, Uwe[2]; O'Keefe, Graeme[2]; Gong, Sylvia J.[2]; Rigopoulos, Angela[1]; Liu, Zhanqi[2]; Gan, Hui[2]; Scott, Andrew M.[1, 2]

INSTITUTIONS (ALL):

1. Oliver Newton John Cancer Research Institute, Heidelberg, VIC, Australia.
2. Nuclear Medicine and PET, Austin Hospital, Heidelberg, VIC, Australia.

(No Image Selected)

CONTROL ID: 2234176

TITLE: Synthesis and evaluation of ^{18}F-AmBF$_3$-phosphonium cation for imaging enhanced negative mitochondrial membrane potential in cancers

PRESENTER: Zhengxing Zhang

ABSTRACT BODY:

Abstract Body: Objectives: Cancer cells have enhanced negative mitochondrial membrane potential compared to epithelial cells. Since this is a ubiquitous finding in cancer cells, the development of tracers targeting this aspect is of great benefit for molecular imaging of cancers. Due to potential difference, organic cations are electrophoretically driven through the plasma membrane into either mitochondrion-rich organs (such as the heart) or localize with energized mitochondria of cancer cells. Most of reported ^{18}F-labeled phosphonium cations for PET imaging were prepared in multiple steps or suffered from in vivo defluorination. Recently, a facile ^{18}F-labeling strategy via the ^{18}F-^{19}F isotope exchange reaction on an ammoniomethyl-trifluoroborate (AmBF$_3$) group was reported, and the resulting ^{18}F-AmBF$_3$ derivatives were stable in vivo. In this study, we investigated if this radiofluorination strategy could be exploited for the design of ^{18}F-labeled phosphonium cation for imaging enhanced negative mitochondrial membrane potential in cancers.

Methods: Z04026, an AmBF$_3$-conjugated phosphonium cation, was synthesized in 4 steps: coupling of tris(4-methylphenyl)phosphine and 1,3-dibromopropane, nucleophilic substitution using dimethylamine, reaction with 2-(iodomethyl)-4,4,5,5-tetramethyl-1,3,2-dioxaborolane, and the formation of BF$_3$ with potassium hydrogen difluoride. ^{18}F-labeling was performed via the one-step ^{18}F-^{19}F isotope exchange reaction on the AmBF$_3$ moiety in aqueous solution, and purified by solid-phase extraction. Lipophilicity was measured by the shake flask method and the tracer stability was assessed by incubation in mouse plasma at 37 degree. Biodistribution and imaging studies were performed in NSG mice bearing U87-MG glioblastoma xenograft.

Results: ^{18}F-labeled Z04026 was obtained in 12±4% radiochemical yield with >97% radiochemical purity. LogD$_{7.4}$ of ^{18}F-Z04026 was 0.1. The tracer was stable after 2-h incubation in mouse plasma without significant formation of metabolites. Imaging and biodistribution study showed rapid clearance of the tracer from blood, and the excretion was via both hepatobiliary and renal pathways. At 2 h p.i., the uptake values of tumour, heart, and bone were 0.21±0.03, 0.26±0.04, and 0.27±0.05 %ID/g, respectively. The heart-to-muscle and tumour-to-muscle ratios were 1.70±0.76 and 1.33±0.48, respectively.

Conclusion:

^{18}F-Z04026 could be facilely prepared in one-step, was stable in mouse plasma, and showed minimal in vivo defluorination in mice as expected. However, due to its low tumour and heart uptake ^{18}F-Z04026 is not suitable for imaging mitochondrial membrane potential.

AUTHORS (LAST NAME, FIRST NAME): Jenni, Silvia[1]; Zhang, Zhengxing[1]; Hundal-Jabal, Navjit[1]; Colpo, Nadine[1]; Liu, Zhibo (Zippo)[2]; Perrin, David M.[2]; Lin, Kuo-Shyan[1]; Bénard, François[1]

INSTITUTIONS (ALL):

1. Molecular Oncology, BC Cancer Agency, Vancouver, BC, Canada.

2. Chemistry Department, University of British Columbia, Vancouver, BC, Canada.

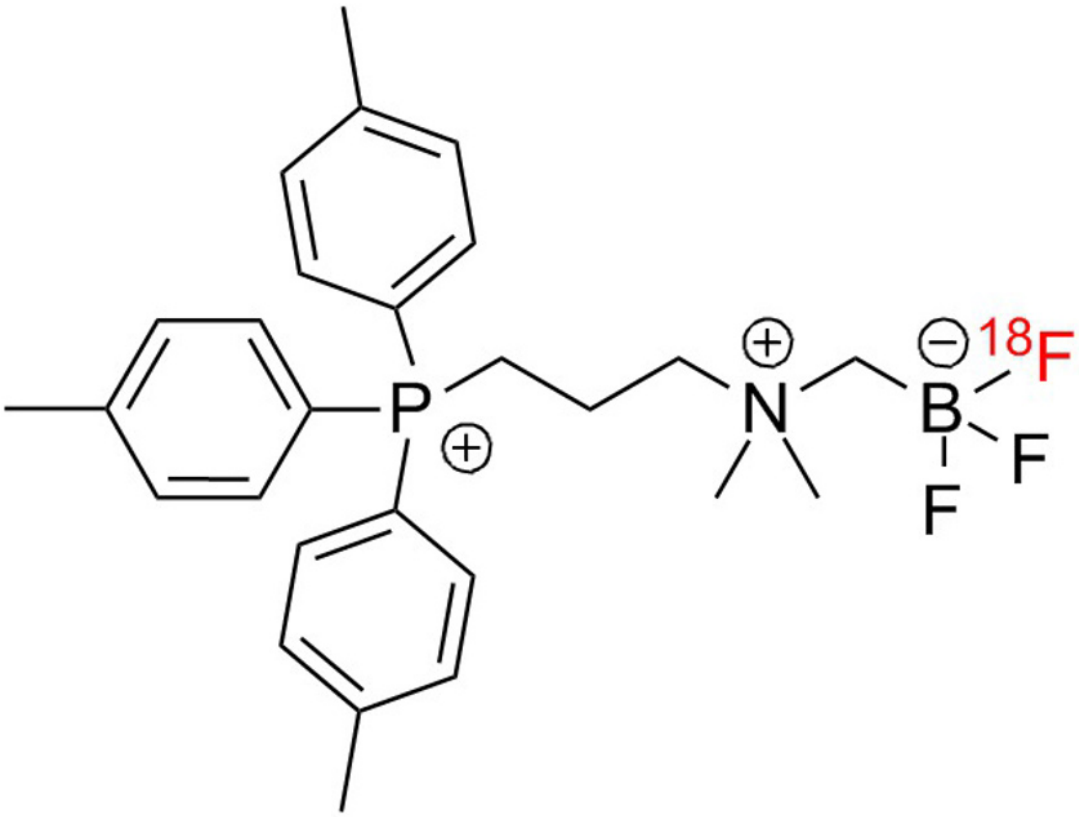

Z04026

CONTROL ID: 2234178

TITLE: Evaluation of Radioactivity Concentration Estimations with I-125 to Determine the Impact of Isotope Dependence on Accuracy between Dose Calibrator, Gamma Counter, and microSPECT

PRESENTER: Joshua Kentala

ABSTRACT BODY:

Abstract Body: Objective: Estimating radioactivity concentrations in tissues has been an essential part of nuclear medicine research. Preclinical imaging technologies such as PET and SPECT allow non-invasive quantitative evaluation of radiotracer *in vivo* within tissues in the same subject over time. Understanding the accuracy and operational range of these instruments is essential. Using traditional methods for assessing radioactive concentrations (i.e. dose calibrator, gamma counter), cross-calibration has been used to facilitate a correlation between the *in vivo* and *ex vivo* samples being assayed. While previous data suggests that over time these instruments could accurately estimate radioactivity concentrations spanning several orders of magnitude, there may be other factors that could lead to quantitative variance[1]. The purpose of this study was to determine if accuracy of these instruments could be isotope dependent. Methods: Identical tissue phantoms (0.6 mL Eppendorf) were prepared in triplicate starting with ~1000uCi of 125I. A series of ten-fold dilutions were performed down to approximately 0.001uCi. Activity for each phantom was first measured using a dose calibrator. The tissue phantoms were placed into a mouse phantom and remeasured using the dose calibrator. Following dose calibrator measurements, a 30 minute acquisition using nanoSPECT/CT Plus was performed. After SPECT acquisition, the tissue phantoms were removed and measured using a gamma counter. For the SPECT data, a fixed volume cylindrical ROI within the tissue phantom was used to estimate radioactivity. Results: Theoretical radioactivity was based off an average of the undiluted tissue phantom samples (~1003uCi). Estimated radioactivity measured by dose calibrator, SPECT and gamma counter were plotted against the theoretical values (Figure 1). Estimated values from measurements that failed, or produced a non-positive value were omitted. All instruments exhibited log-linear estimates of radioactivity. At the highest activity (~900-1000uCi), the average percent error from the theoretical estimates for the dose calibrator (measuring the mouse phantom) and microSPECT were 11.2% and 16.3%, respectively. At ~1uCi, percent error decreased to 5.6% and 12.9%, respectively. The average percent error at ~1uCi, the first passing measurement, for the gamma counter was 0.87%. At the next dilution (~0.1uCi), these numbers were 8.2%, 2.5%, and 1.0%, respectively. At the lowest dilution (~0.001uCi), percent error for the gamma counter increased to 37.2%. Conclusions: All three instruments are capable of accurately estimating radioactivity over seven orders of magnitude in varied combinations of each instrument. Taking into account which radioactivity level results in the most confidence in any one of these instruments, it may be possible to calibrate these systems to one another. Even when evaluating highly attenuated, low energy gamma emitters like 125I. Furthermore, these data are consistent with previous data collected looking at radioactivity estimations in 99mTc[1]. Albeit promising, further experimentation evaluating the effect of isotope dependence is required. References: [1]Kentala D, WMIC; 2011.

AUTHORS (LAST NAME, FIRST NAME): Kentala, Joshua L.[1]; Kentala, Dustin R.[1]; Williams, Stephen[1]; Zasadny, Ken[2]; Haller, Scott D.[1]

INSTITUTIONS (ALL):

1. Molecular Imaging, MPI Research, Mattawan, MI, United States.
2. inviCRO, LLC, Boston, MA, United States.

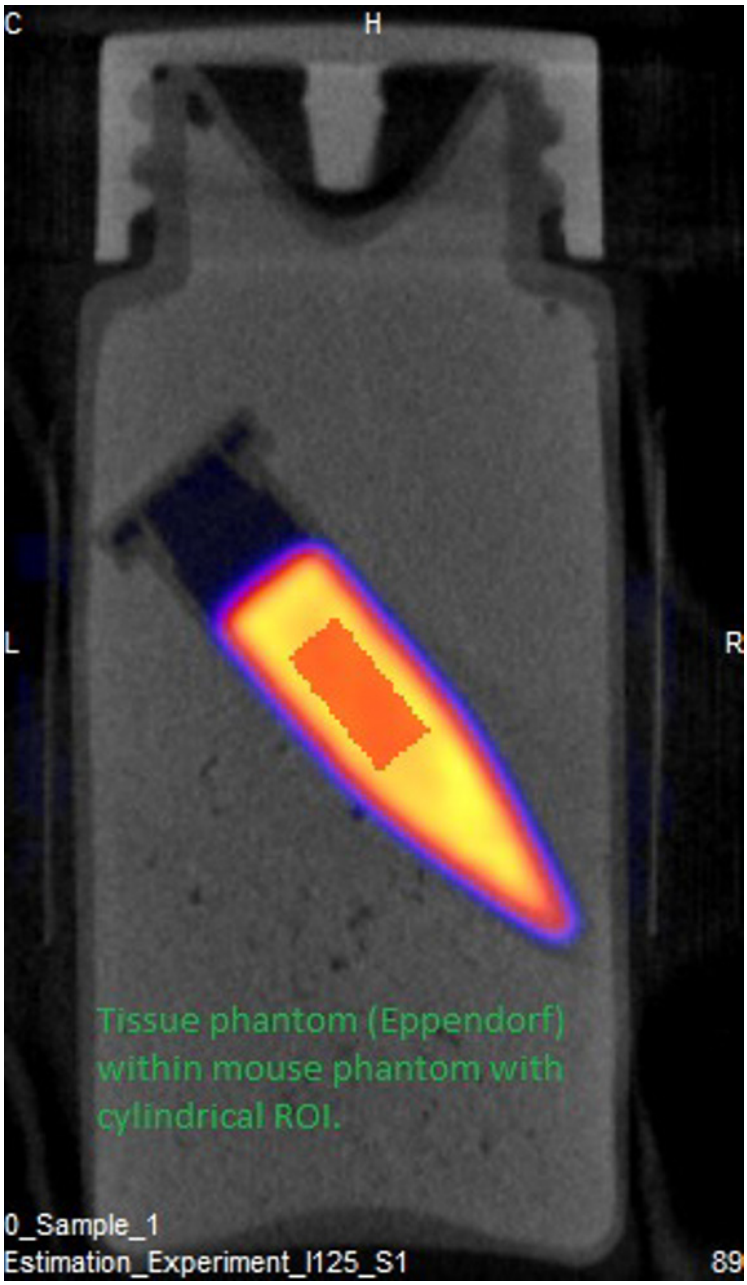
C
H
L
R
Tissue phantom (Eppendorf) within mouse phantom with cylindrical ROI.
0_Sample_1
Estimation_Experiment_I125_S1
89

CONTROL ID: 2234180

TITLE: Genetic engineering of recombinantly expressed gas vesicle contrast agents for ultrasound

PRESENTER: Raymond Bourdeau

ABSTRACT BODY:

Abstract Body: Gas vesicles (GVs) are hollow protein nanostructures originally found in cyanobacteria and haloarchea, where they serve as regulators of cellular buoyancy. It was recently demonstrated that GVs produce strong ultrasound contrast *in vitro* and *in vivo* (Shapiro 2014 Nat Nano), making them a promising candidate for the development of targeted and genetically encodable molecular imaging agents. Advantages of GVs compared to existing imaging agents are their small size (1-2 orders of magnitude smaller than microbubbles) and non-spherical shape. Nanoparticles are more likely to transit capillary beds and have enhanced permeability and retention in tumors (Maeda 2012 J Con Rel). Rod-shaped nanoparticles are beneficial as they resist elimination by the liver and spleen *in vivo* (Meyer 2012 Small).

Another unique aspect of GVs as ultrasound contrast agents is the prospect of modifying their size, shape, acoustic, and targeting properties at the genetic level. However, the initial work with these nanostructures was performed using wild-type GVs purified from their native organisms. Here we report the design of the first genetically modified gas vesicles expressed recombinantly in *E. coli*, and describe the use of genetic modifications to alter particle geometry, inter-particle interactions, and acoustic properties.

A segment of the GV gene cluster from *B. megaterium* (Li 1998 J Bacteriol) was expressed recombinantly in *E. coli* and modified using standard molecular biology techniques. The resulting GVs, which we call Mega GVs, were isolated by non-mechanical cell lysis and purified by buoyancy isolation. GVs were imaged with TEM and ultrasound in agarose gel phantoms *in vitro* and mouse tail-vein injection *in vivo*.

Mega GVs were found to be rod-shaped nanoparticles ~ 70 nm in width and up to 800 nm in length (Fig 1). Genetically unmodified Mega GVs are clustered together in higher order crystalline structures (Fig 1), mediated by protein-protein interactions that are disrupted by treatment with 6M Urea. Genetic modification of genes in the cluster alters GV properties. For example, deletion of the GvpT gene resulted in a complete loss of particle clustering (Fig 1). Clustered Mega GVs exhibit harmonic and fundamental ultrasound contrast both *in vitro* and *in vivo* (Fig 1). *In vivo* contrast is strongest in the circulatory system, where the GV signal persists for 10-15 seconds after injection. Unclustered Mega GVs also show contrast *in vitro* and *in vivo*, which is somewhat reduced compared to the clustered GVs.

These results provide the first evidence that recombinantly expressed Mega GVs can serve as ultrasound contrast agents and that genetic modification can alter their acoustic properties. Mega GVs are the smallest and highest-aspect ratio GV contrast agents developed to date, and their expression in *E. coli* enables rapid testing of genetic variants, which is currently underway. With genetic control, both rational designs and directed evolution screens can be used to search for new acoustic phenotypes. Also direct genetic linkages of targeting moieties may be possible for *in vivo* targeting to specific cells.

AUTHORS (LAST NAME, FIRST NAME): Bourdeau, Raymond W.[2]; Lakshmanan, Anupama[1]; Zhang, Xiaowei[2]; Shapiro, Mikhail G.[2]

INSTITUTIONS (ALL):

1. Bioengineeering, California Institute of Technology, Pasadena, CA, United States.
2. Chemistry and Chemical Engineering, California Institute of Technology, Pasadena, CA, United States.

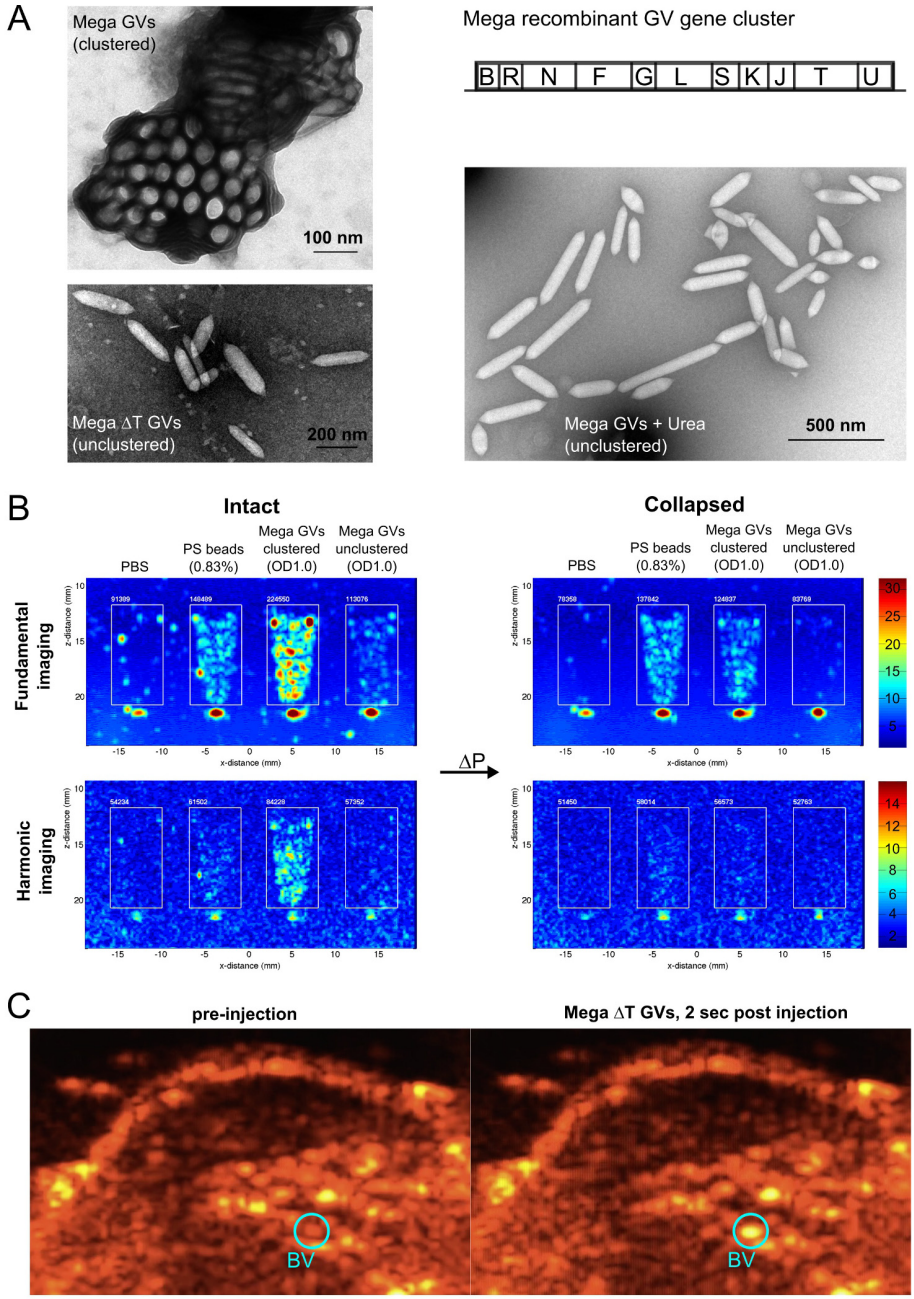

(A) B. megaterium gas vesicle genes B-U encode for recombinant Mega GVs. Purified Mega GVs are rod-shaped nanoparticles that exhibit tight packing. Urea treatment of Mega GVs or expression of GVs with the GvpT gene deleted (ΔT) causes the GVs to become unclustered. (B) Natively-clustered Mega GVs exhibit ultrasound contrast under both fundamental and harmonic imaging modes. Clustered Mega GVs exhibit a stronger response than unclustered GVs. Collapse of GVs by a high-pressure acoustic wave eliminates all harmonic contrast and reduces fundamental contrast. (C) Purified Mega ΔT GVs injected into the tail vain of nude mice show an increase in fundamental contrast in the circulatory system for 10-15 sec after injection.

CONTROL ID: 2234183

TITLE: Molecular Control of Harmonic Signals in Gas Vesicle Contrast Agents for Ultrasound

PRESENTER: Anupama Lakshmanan

ABSTRACT BODY:

Abstract Body: Ultrasound is among the most widely used medical imaging technologies in the world, but currently lags behind other modalities in terms of targeted molecular detection. Most existing ultrasound contrast agents are micron-sized synthetic bubbles that are typically confined to the vasculature and have limited residence times in the body. Recently, a new class of nanoscale imaging agents for ultrasound was introduced based on gas vesicles (GVs) - hollow protein nanostructures of 100-400 nm size isolated from haloarchea and cyanobacteria, in which they regulate cellular buoyancy (Shapiro, *Nat. Nano*. 2014). GVs are capable of producing powerful linear and harmonic ultrasound contrast *in vitro* and *in vivo*, and offer the possibility of engineering their acoustic properties at the protein level.

Here, we provide the first direct evidence that changes to the protein composition of gas vesicles can alter their acoustic properties. In particular, we show that removal or sequence modification of a key outer scaffolding protein in GVs derived from *Anabaena flos-aquae* (Ana GVs) results in gas vesicles with enhanced harmonic signals for non-linear imaging *in vitro* and *in vivo* as well as tunable collapse pressures for multiplexed imaging.

The most abundant proteins found in GVs are gas vesicle proteins A and C (gvpA and gvpC). GvpA assembles into the main structural backbone of the GV shell, while gvpC is the second most abundant protein forming an outer scaffold that confers enhanced structural and shape integrity (Pfeifer, *J. Bacteriol.* 1996) (Fig 1A). Removal of gvpC and truncations to its sequence were previously shown to result in a reduced pressure threshold for structural collapse of Ana GVs (Walsby, *Mol. Microbiol.* 1995). We hypothesized that changes in GV mechanical properties resulting from the removal, addition or modification of gvpC would alter the acoustic properties of Ana GVs, thereby allowing us to tune their ultrasound response. In particular, we aimed to increase the harmonic signals produced by Ana GVs to enable enhanced detection *in vivo*.

Ana GVs were purified, treated with 6M urea to remove their native gvpC protein, re-functionalized with recombinantly expressed and modified gvpC, followed by evaluation with ultrasound and pressurized absorbance spectroscopy. Consistent with previous data, the removal of gvpC reduced the critical collapse pressure of Ana GVs (Fig 1B). In addition, gvpC-stripped GVs showed a dramatic increase in harmonic ultrasound signals during *in vitro* imaging in agarose phantoms (Fig. 1C) and during *in vivo* imaging following intravenous injection into nude mice (Fig 1D). Re-addition of recombinant gvpC strengthened the GVs and eliminated their harmonic signal. Furthermore, engineered gvpC variants with truncated sequences allowed the tuning of the collapse pressure within a dynamic range of ~300 kPa.

These results provide the first demonstration of the engineering of gas vesicle acoustic properties at the level of their constitutive proteins, and describe harmonic Ana GVs – a new imaging agent that combines harmonic signals with smaller dimensions for potentially enhanced biodistribution and targeting.

AUTHORS (LAST NAME, FIRST NAME): Lakshmanan, Anupama[1]; Dykes, Jordan [3]; Nety, Suchita P.[3]; Bourdeau, Raymond W.[3]; Zhang, Xiaowei[2]; Shapiro, Mikhail G.[3]

INSTITUTIONS (ALL):

1. Bioengineeering, California Institute of Technology, Pasadena, CA, United States.
2. Caltech, Pasadena, CA, United States.
3. Chemistry and Chemical Engineering, California Institute of Technology, Pasadena, CA, United States.

Figure 1:

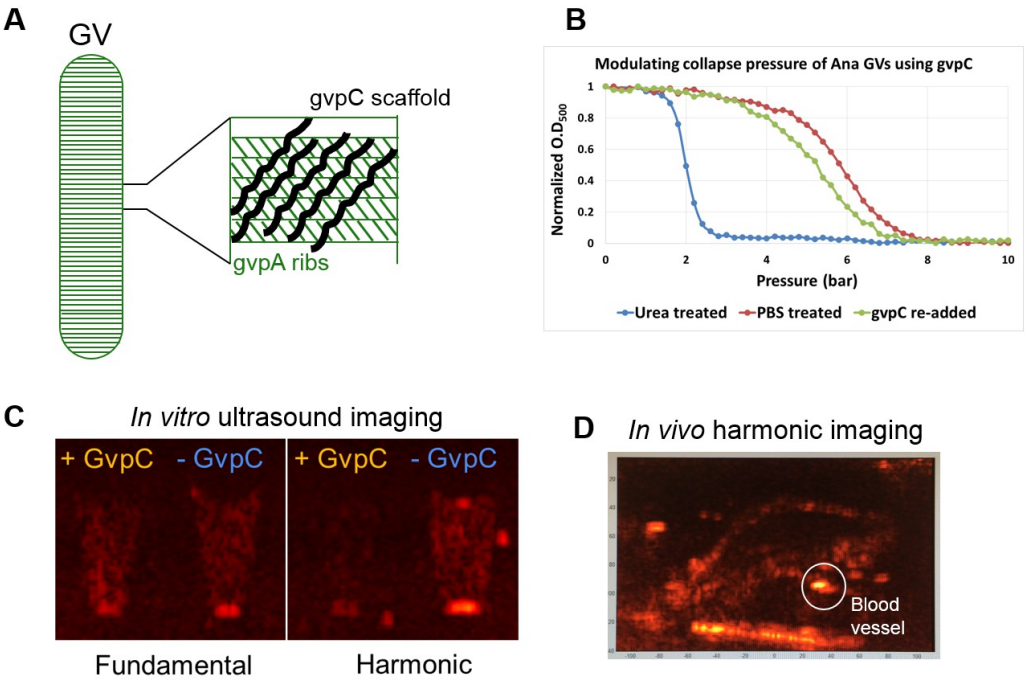

Figure 1 (A) Schematic showing the protein composition of gas vesicles made of gvpA ribs that form the shell backbone, with the outer scaffold protein gvpC conferring structural and shape integrity. (B) Reduction in critical collapse pressure of Ana GVs when native gvpC is removed by urea treatment. Re-addition of recombinantly expressed gvpC restores GV resistance to collapse. (C) *In vitro* ultrasound images taken at fundamental (4.46 MHz) and second harmonic (8.92 MHz) frequencies, showing a dramatic increase in harmonic signal for gvpC-stripped Ana GVs. (D) *In vivo* harmonic signals (encircled in white) were observed in the vasculature of nude mice following intravenous injection of gvpC-stripped Ana GVs. These signals persisted for 10-15 seconds post-injection.

CONTROL ID: 2234190

TITLE: Theranostic imaging of Yttrium-90 using new solid-state digital photon counting PET detectors

PRESENTER: Chadwick Wright

ABSTRACT BODY:

Abstract Body: **Objectives:** The selection of the Yttrium-90 (^{90}Y) and its use for targeted radiotherapy is complex and driven by the existing clinical need to deliver high doses of therapeutic radioactivity to specific targets within the body when standard external radiation therapy approaches are deemed impractical. Although the current imaging standard for ^{90}Y is bremsstrahlung scintigraphy, it has poor image quality and limited quantitative capability for post-therapy dosimetry. Conventional photomultiplier-based positron-emission tomography (cPET) systems are capable of imaging ^{90}Y internal pair production but it has not been clinically adopted due to its longer image acquisition times. Recently, a fundamental technology innovation has replaced these conventional photomultiplier tubes with next-generation solid-state digital photon counting detectors (i.e., digital PET or dPET). Manufacturers are already adopting this revolutionary PET technology for their next generation systems. Our objective is to assess the clinical capability of this new solid-state digital PET technology for image assessment of ^{90}Y radioactivity following microsphere radioembolization and compare to existing bremsstrahlung and conventional PET/CT approaches.

Methods: We are using a next-generation, solid-state dPET/CT system (Philips Vereos 64 ToF) to image post-^{90}Y microsphere radioembolization patients treated for malignant/metastatic liver lesions in an ongoing trial, and then assess its image characteristics, by matched pair comparison, with conventional photomultiplier detector time-of-flight cPET/CT (Philips Gemini ToF 64), standard bremsstrahlung SPECT/CT and bremsstrahlung scintigraphy (Siemens Symbia T16) to assess clinical value.

Results: When compared with standard bremsstrahlung imaging approaches, PET detection of ^{90}Y internal pair production provided image quality enabling improved qualitative assessment of ^{90}Y radioactivity in the liver. Digital PET detection of ^{90}Y is eminently practical for clinical management and moreover this new detector technology offers advantages over existing imaging approaches (e.g., faster scan times, smaller voxel volumes).

Conclusions: There is an unmet clinical need to improve non-invasive ^{90}Y imaging methodologies. At present, ^{90}Y imaging is arduous in terms of the standard low quality bremsstrahlung approaches versus the long image acquisition times necessary for cPET which can disrupt routine clinical workflows within nuclear medicine departments. The current results demonstrate that dPET technology can readily detect and image ^{90}Y *in vivo* and suggest new theranostic approaches for ^{90}Y image acquisition and reconstruction that will enable faster imaging with improved quality, dose quantification and predictive response assessment in ^{90}Y patients.

Research Support: This project was enabled by the Ohio Third Frontier Scholars, Wright Project and Innovation Platform project grants, the Wright Center of Innovation in Biomedical Imaging and Philips Healthcare providing the investigational pre-commercial release system.

AUTHORS (LAST NAME, FIRST NAME): Wright, Chadwick L.[1]; Zhang, Jun[1]; Binzel, Katherine[1]; Wuthrick, Evan J.[2]; Maniawski, Piotr[3]; Knopp, Michael V.[1]

INSTITUTIONS (ALL):

1. Wright Center of Innovation, The Ohio State University, Columbus, OH, United States.
2. Radiation Oncology, Wexner Medical Center at The Ohio State University, Columbus, OH, United States.
3. Clinical Science - Nuclear Medicine, Philips Healthcare, Cleveland, OH, United States.

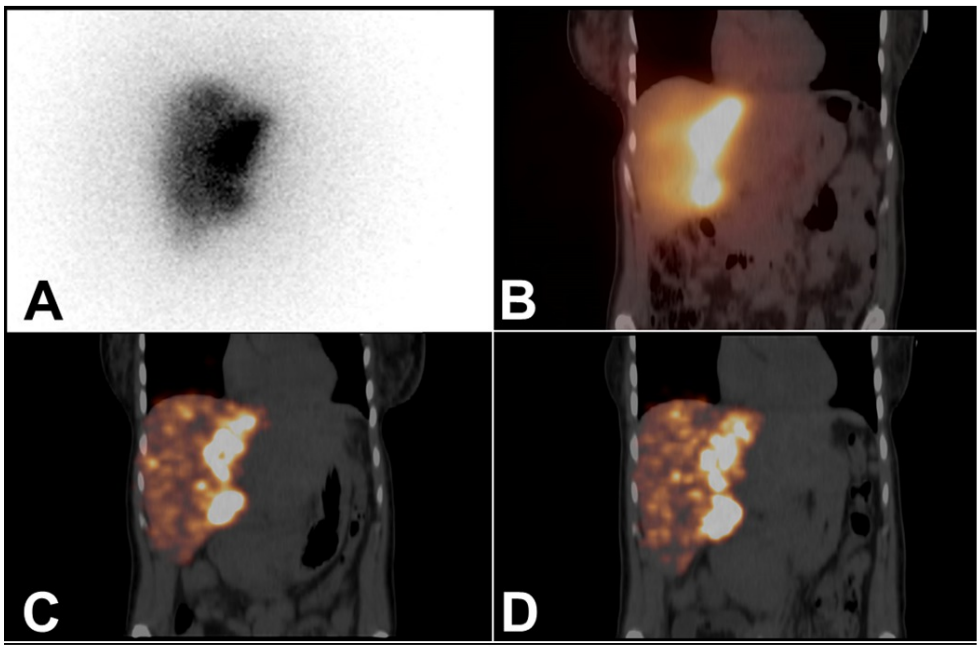

Figure 1. Yttrium-90 bremsstrahlung and internal pair production imaging following radioembolization with ^{90}Y glass microspheres. The patient was treated with intra-arterial administration of 3.26 GBq of ^{90}Y microspheres to the right hepatic lobe for neuroendocrine metastases. Post-therapy imaging included ^{90}Y bremsstrahlung planar and SPECT/CT imaging as well as ^{90}Y internal pair production PET/CT imaging. Standard bremsstrahlung planar and SPECT/CT imaging was obtained using the Symbia T16 system with medium-energy collimation (Siemens Healthcare). PET/CT imaging of internal pair production was obtained using conventional Gemini 64 ToF and digital Vereos 64 ToF systems (Philips Healthcare). **(A)** Planar bremsstrahlung image of the abdomen (anterior view) demonstrates intense bremsstrahlung activity corresponding to right hepatic lobe region as well as the presence of scatter photons in the field of view emanating from the treated right hepatic lobe. **(B)** Three-dimensional bremsstrahlung SPECT/CT image of the abdomen (fused SPECT/CT in the coronal plane) again demonstrates bremsstrahlung activity corresponding to the right hepatic lobe. Like the planar image, the fused SPECT/CT image demonstrates the presence of additional scatter photons and this additional scatter activity overlies several adjacent soft tissues and organs (e.g., heart, chest wall, left hepatic lobe, bowel). **(C)** Three-dimensional internal pair production cPET/CT image of the abdomen (fused PET/CT in the coronal plane) demonstrates ^{90}Y activity in the right hepatic lobe with better demarcation of ^{90}Y in the liver and improved ^{90}Y-to-background contrast in the adjacent soft tissues and organs. **(D)** Three-dimensional internal pair production dPET/CT image of the abdomen (fused PET/CT in the coronal plane) also demonstrates ^{90}Y activity with even more precise delineation within the liver parenchyma.

CONTROL ID: 2234195

TITLE: Meeting the Challenge of a one-step, late-stage, aqueous, HPLC-free method for labeling peptides with wet NCA 18F-fluoride

PRESENTER: David Perrin

ABSTRACT BODY:

Abstract Body: PET imaging is an emerging technique that can be used to visualize targets within deep tissue for preclinical lead development as well as personalized medicine. Given the relatively short half-life of F18 (~110 minutes), a rapid 1-step, reproducible, clean, and high yielding aqueous labelling of an intact biomolecule represents a long-standing challenge for PET imaging. We hypothesized that biomolecules could be labelled via a pendent aryltrifluoroborate. In doing this, we have set forth mulitple conditions that our objective must satisfy: 1) no azeotropic drying, 2) use of Curie-levels of NCA 18F-fluoride, 3) rapidity of labeling e.g. 15-20 min, 4) HPLC-free purification, 5) use of micrograms of precursor, 6) good-to-excellent tumor uptake, 7) very high T:NT ratios, 8) no bone uptake, 9) general applicability for labeling peptides.

In meeting all of these conditions, we have designed various organotrifluoroborate that can be "click" conjugated to various peptides. For labeling, we have identified QMA resins that enable direct elution of ~1Ci of NCA 18F-fluoride into <60 μL of PBS saline into a standard Eppendorf tube that contains 50-100 nmol of bioconjugate-RBF_3 precursor in buffered DMF. Following heating at 80° for 15-20 min, the tracer is purified by a C18-Sep-Pak push with ethanol-saline elution. Labeling is applied to analogs of bombesin, octreotate, bradykinin, trimeric-RGD, a trimeric CA-IX inhibitor, and a dual-mode fluorescent dimer of RBF_3-bisRGD; all of which are injected into mice with suitable xenograft tumors with blocking controls.

RCYs are routinely >25% (n>70). Standard curve analysis shows SA's are >3 Ci/μmol. QC radio/UV HPLC traces show purity >98%. Tumor:non-tumor ratios (T:M and T:Bone) are typically >20 and in some cases exceptionally high (>75). T:Blood ratios are >6. Interestingly, the specific activity of the dual-mode fluorescent tracer is so high that the associated injected mass was so low that even with 5%ID/g the associated mass in the tumor (<60 fmol) was below the limits of detection for florescence imaging.

In conclusion, complex peptidic bioconjugates linked to a novel organotrifluoroborates are eaily synthesized and stocked in aliquots of <100 ug for on-demand, one-step aqueous 18F-labeling using 1 Ci of NCA 18F-fluoride in fully shielded hot-cells. Labeling occurs in 15 min with good yields (e.g. 200-300 mCi) at very high SA and excellent purity. No HPLC purification is used. The exceptional radiosynthetic ease and high tumor uptake and T:NT ratios in various tumor models that are imaged with various peptides suggest broad utility of this method.

AUTHORS (LAST NAME, FIRST NAME): Perrin, David M.[4]; Liu, Zhibo (Zippo)[4]; Pourghiasian, Maral[1]; Pan, Jinhe[3]; Zhang, Zhengxing[1]; Jenni, Silvia[1]; Hundal-Jabal, Navjit[1]; Yapp, Donald[2]; Lin, Kuo-Shyan[1]; Bénard, François[2]

INSTITUTIONS (ALL):

1. Molecular Oncology, BC Cancer Agency, Vancouver, BC, Canada.
2. BC Cancer Agency and Research Centre, Vancouver, BC, Canada.
3. Molecular Oncology, BC Cancer Research Centre, Vancouver, BC, Canada.
4. Chemistry, UBC, Vancouver, BC, Canada.

(No Image Selected)

CONTROL ID: 2234197

TITLE: Defining the Priority of ^{18}F-FDG PET for Curative Intent Concurrent Chemoradiotherapy in Small Cell Lung Cancer

PRESENTER: Tzu-Chen Yen

ABSTRACT BODY:

Abstract Body: Objective:

The aim of this retrospective study was to define the priority of curative intent chemoradiotherapy with ^{18}F-FDG PET parameters in patients with limited disease small cell lung cancer (LD-SCLC).

Material and Methods:

A total of 27 LD-SCLC patients were included. All patients underwent ^{18}F-FDG PET for primary staging and had received curative intent concurrent chemoradiotherapy (CCRT). The clinical characteristics and the following ^{18}F-FDG PET derived variables were tested for their associations with 2-year OS: main tumor SUVmax, main tumor total lesion glycolysis (TLG_{MT}), total lesion glycolysis of all lesions (TLG_{all}) and textural features. The main outcome measure was overall survival (OS) at 2 years.

Results:

Among the parameters analyzed in this study, none of the clinical characteristics was significantly associated with 2-year OS. In contrast, the univariate analysis identified 18F-FDG PET derived parameters TLGall ≥ 210 g at main tumor and regional nodes and local entropy textural feature LV_Entropy_Kurtosis at main tumor as adverse prognostic factors for OS (p = 0.012 and 0.009, respectively). After adjustment for potential confounders in multivariate analysis, TLGall and LV_Entropy_Kurtosis were both independent predictors of OS in LD-SCLC patients. Based on these two parameters, we devised a prognostic stratification system by patients' tumor burden (TLGall) and tumor homogeneity (LV_Entropy_Kurtosis). A scoring system using these covariates defined 3 distinct prognostic groups: score 0 (HR = 1.00); score = 1 (HR = 2.12; 95% CI = 1.27 - 16.80); and score = 2 (HR = 6.21; 95% CI = 1.75 – 22.00) (P = 0.001).

Conclusions:

Using the risk score by ^{18}F-FDG PET derived parameters, TLG_{all} and LV_entropy_Kurtosis, ^{18}F-FDG PET parameters may help define priority in LD-SCLC patients before curative intent therapy.

Keywords: small cell lung cancer, limited disease, ^{18}F-FDG PET, total lesion glycolysis, texture analysis

AUTHORS (LAST NAME, FIRST NAME): Yen, Tzu-Chen[1]; Ho, Tsung-Ying[1]; Chung, Yi-Hsiu[2]

INSTITUTIONS (ALL):

1. Department of Nuclear Medicine and Molecular Imaging Center, Chang Gung Memorial Hospital, Taoyuan, Taiwan.

2. Nuclear Medicine , Chang Gung Memorial Hospital, Tao-yuan, Taiwan.

(No Image Selected)

CONTROL ID: 2234201

TITLE: Stripe artifact removal method for selective plane illumination microscopy

PRESENTER: Di Dong

ABSTRACT BODY:

Abstract Body: Selective Plane Illumination Microscopy (SPIM) is an emerging imaging technique for imaging 3-Dimensional distribution of fluorescence signal in fixed tissues. In SPIM the stripe artifacts caused by high absorption structures are very common, which greatly limits the application of SPIM in dense samples. To solve this problem, we proposed a stripe artifact removal method to remove the stripes. Our method included three steps. Firstly, we collected three SPIM image stacks which partially overlapped with each other. Secondly, we used an iterative filtering method to reduce the stripes in each SPIM image stacks. Finally, we averaged the three image stacks to smooth the final image. We tested our method on a mouse brain which was optically cleared with THF/DBE method. The experimental results showed that our method can effectively remove most of the stripes and restore the brain images. Moreover, our method could be applied to most SPIM system without any change of the setup.

AUTHORS (LAST NAME, FIRST NAME): Dong, Di[1]; Hui, Hui[1]; Fang, Mengjie[1]; liang, xiao[1]; Tian, Jie[1]

INSTITUTIONS (ALL):

1. Key Laboratory of Molecular Imaging, Chinese Academy of Sciences, Beijing, China.

(No Image Selected)

CONTROL ID: 2234200

TITLE: Pulmonary Nodule Detection during Fluorescence Image-guided Surgery with Indocyanine Green

PRESENTER: Hyun Koo Kim

ABSTRACT BODY:

Abstract Body: Objective

Recently, fluorescent imaging using indocyanine green (ICG) has been applied to cancer, not only to visualize the sentinel lymph node, but also to identify tumor during surgery. We hypothesized that this fluorescent imaging would be useful to identify and locate pulmonary nodules during surgery. We try to detect pulmonary nodules and measure fluorescence intensity by using reasonable dosage of ICG

Methods

We enrolled 11 patients who were diagnosed with a pulmonary nodule. ICG is administered intravenously at a dose of 1 mg/kg prior to operation. Surgical specimens were investigated using a near-infrared light camera system (SPY Elite) at 20 hours after injection. And we examined the histologic characteristics of the specimens

,

Results

ICG-fluorescent imaging was observed 10 out of the 11 patient. In 1 squamous cell carcinoma, fluorescent signal was not detected. 2 false positive nodules (necrotic inflammation) were identified among the 10 fluorescent specimens. Fluorescent signal of nodules (Signal to Background Ratio (SBR)) was 4.3 ± 2.5. There was no significant difference depending on histology, size and tumor grade. However, fluorescent signal of 2 false – positive nodules was 9.5 ± 0.7 which was higher than the other nodules.

Conclusions

This study demonstrated that fluorescent imaging using a low dosage of ICG can be useful to identify and locate pulmonary nodules during surgery. However, our results (2 false positive) also show limitation of present fluorescent imaging guided surgery which used only ICG for passive cancer targeting. Base on this result, we thought that for ideal fluorescence guided surgery, we will need a further study about active targeting by using biomarker as well as passive targeting.

AUTHORS (LAST NAME, FIRST NAME): Kim, Hyun Koo[2]; Quan, Yuhua[2]; Choi, Byeong Hyeon[2]; Kim, Minji[1]; Park, Ji Ho[5]; Choi, Yeonho[1]; Lee, Yun-Sang[3]; Lee, Kisung[1]; Kim, Beop-min[1]; Jeong, Jae Min[4]

INSTITUTIONS (ALL):

1. Biomedical Engineering, Korea University, Seoul, Korea (the Republic of).
2. Thoracic and Cardiovascular Surgery, Korea University Guro Hospital, Korea University College of Medicine, Seoul, Korea (the Republic of).
3. Department of Nuclear Medicine, Seoul National University College of Medicine, Seoul, Korea (the Republic of).
4. Department of Nuclear Medicine, Seoul National University College of Medicine, Seoul, Korea (the Republic of).
5. Korea Advanced Institute of Science and Technology, Daejeon, Korea (the Republic of).

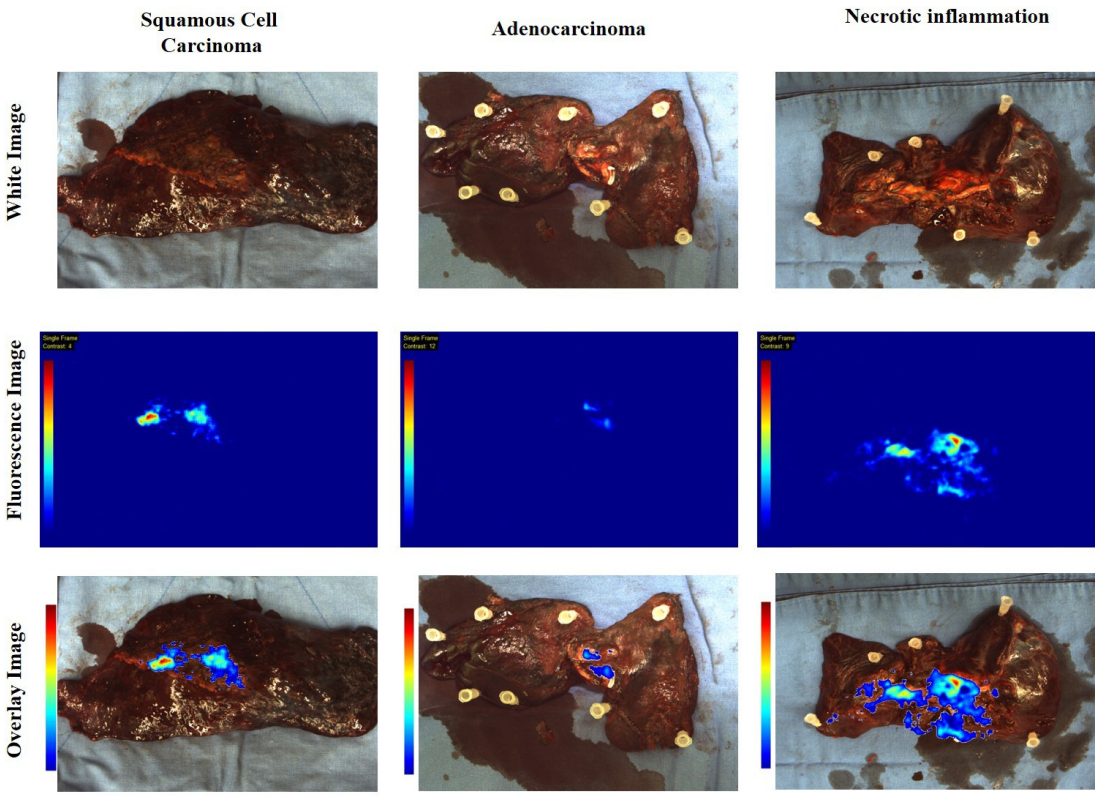

Flourescent images of lung cancer patients after systemic injection of indocyanine green

CONTROL ID: 2234225

TITLE: Comparisons in vitro and in vivo of biological behaviors of carbon-based nanomaterials for theranostic molecular imaging: potential relations with size and shape

PRESENTER: Ming-Wei Wang

ABSTRACT BODY:

Abstract Body: Biological behaviours of nanomaterials are critical to the potential applications as multifunctional in vivo nanocarriers for molecular imaging, drug delivery and nanomedicine. Carbon-based nanomaterials are the most widely-studied one, whose major members include carbon nanotube (CNT) and graphene oxide (GO). However, they have different shape and size, and the effects on the biological properties are the vital issues to consider. Herein, we aimed to investigate the effects of size and shape on biological behaviours of carbon-based nanomaterials by the comparative studies in vitro and in vivo. Three PEGylated carbon-based nanomaterials with the maximum size of < 100 nm , including CNT (> 50 nm), small GO (NGO, >50 nm), ultra-small GO (nGO, < 50 nm), were examined and fully characterized by AFM, Raman, dynamic light scattering, FT-IR, etc. Cell survival in vitro showed that there was no obvious cytotoxicity for PEGylated CNT and GOs with the concentration of up to 200 mg/mL within 48 hours. After conjugation with Cy5.5, confocal microscopy at different time points post incubation with cells revealed that nGO entered into cells rapidly with the highest rate, whereas NGO at the middle rate and CNT at the lowest rate. Furthermore, after radiolabeling via ^{125}I, in vivo small animal SPECT/CT imaging of tumor-bearing mice at different time post injection found that nGO presented higher tumor accumulation and lower liver uptake, whereas NGO and CNT showed obvious liver uptake and insignificant tumor accumulation. In conclusion, we found that biological behaviours of carbon-based nanomaterials have potential relations with the size and shape by the comparative studies in vitro and in vivo, and 2-D, ultra-small sized and PEGylated GO held more favourable properties for in vivo applications of cancer theranostics.

AUTHORS (LAST NAME, FIRST NAME): Wang, Ming-Wei[1, 2]; You, Peihong[1]; Cao, Tianye[1, 2]; Zhang, Yingjian[1, 2]

INSTITUTIONS (ALL):

1. PET Center, Department of Nuclear Medicine, Fudan University Shanghai Cancer Center, Shanghai, China.
2. Center for Biomedical Imaging, Fudan University, Shanghai, China.

(No Image Selected)

CONTROL ID: 2234264

TITLE: Folic acid-functionalized ultra-small nanographene oxide for molecular imaging of triple negative breast cancer by ^{125}I-radiolabeling and small animal SPECT/CT

PRESENTER: Ming-Wei Wang

ABSTRACT BODY:

Abstract Body: Graphene oxide (GO) is an emerging member of carbon-based nanomaterials and has exhibited a great application potentials as multifunctional in vivo nanocarriers for molecular imaging and theranostics against cancer. Triple negative breast cancer (TNBC), a kind of metastatic breast cancers with high risk to young women, is lack of effective therapies to battle with the related metastasis. There is an urgent need for non-invasive imaging strategies to follow the efficacy of newly-developed treatments against TNBC. Herein, we aimed to explore the feasibility of functionalized ultra-small nanographene oxide (nGO) as multi-purpose nanocarriers for nuclide/optical molecular imaging of TNBC. Ultra-small nGO was functionalized via PEGylation and conjugation with folic acid. nGO-FA with the size of < 50 nm was well characterized by AFM, Raman, DLS, FT-IR, etc. nGO-FA showed no obvious cytotoxicity with the concentration of up to 200 mg/mL within 48 hours according to cell survival assays in vitro. After conjugation with Cy5.5, confocal microscopy revealed that nGO-FA could selectively enter into cells overexpressed FA receptor according to the cell binding and blockage experiments. Optical imaging in vivo and ex vivo further proved that nGO-FA could highly accumulate into tumor tissue. Moreover, in vivo nuclide imaging via small animal SPECT/CT scanner of tumor-bearing mice at different time post injection of ^{125}I-radiolabeled nGO-FA demonstrated that nGO-FA selectively accumulate into FA-positive tumor, whose uptake could be blocked by the co-injection of FA. It was also found that nGO-FA showed low liver uptake with rapid clearance over time according to the imaging studies. In conclusion, FA-functionalized ultra-small nGO was proved to be a feasible multi-purpose nanocarrier for targeted multi-modal molecular imaging of TNBC, which would benefit the development of nGO-based theranostics and drug delivery against TNBC.

AUTHORS (LAST NAME, FIRST NAME): Wang, Ming-Wei[1, 2]; You, Peihong[1, 2]; Cao, Tianye[1, 2]; Zhang, Yingjian[1, 2]

INSTITUTIONS (ALL):

1. PET Center, Department of Nuclear Medicine, Fudan University Shanghai Cancer Center, Shanghai, China.
2. Center for Biomedical Imaging, Fudan University, Shanghai, China.

(No Image Selected)

CONTROL ID: 2234248

TITLE: Therapeutic evaluation of ^{188}Re-human serum albumin microsphere in hepatoma model by 3D ultrasound

PRESENTER: Liang-Cheng Chen

ABSTRACT BODY:

Abstract Body: Objectives: The aims of this study were to investigate the utility of three-dimensional (3D) high-frequency ultrasound in the therapeutic evaluation of ^{188}Re-human serum albumin microsphere (^{188}Re-HSAM) in GP7TB hepatoma model.

Methods: Male F344 rats were intrahepatic inoculation with GP7TB 1 mm^3 cubes. These studies were performed on rat at 26 d after tumor inoculation. The efficacy of ^{188}Re-HSAM was performed by a single-dose treatment in GP7TB hepatoma rat via intraarterial route. Rats were checked for survival every day until death. The body weight was measured once a week. Longitudinal and transverse-sectional ultrasound images of GP7TB hepatoma acquired once a week.

Results: To monitor the tumor growth, longitudinal tumor volumes were obtained from 3D segmentation of ultrasound imaging in the F344 rat with GP7TB hepatoma. The tumor volumes were inhibition with time after i.a. injection of ^{188}Re-HSA microsphere. In contrast to the mean tumor volume of 1803.2 ± 306.8 mm^3 in the treated normal saline group at 54 d, the mean tumor volumes of the treated groups at 54 d administration of 2.8 mCi and 6.5 mCi ^{188}Re-HSAM and were 381 ± 95.1 and 267.4 ± 54.7 mm^3, respectively. The mean growth inhibition rates achieved by 2.8 mCi and 6.5 mCi ^{188}Re-HSAM were 0.21 and 0.15, respectively.

Conclusions: The 3D high-frequency ultrasound with a high spatial resolution and contrast in soft tissue can become imaging modality for rat preclinical studies. The therapeutic evaluation of ^{188}Re-HSAM demonstrated better tumor growth inhibition for rat with increased dose in the GP7TB hepatoma model. These results suggested that intraarterial administration of ^{188}Re-HSAM could provide a benefit and promising strategy for delivery of radiotherapeutics in oncology applications.

AUTHORS (LAST NAME, FIRST NAME): Chen, Liang-Cheng[1]; Chang, Chih-Hsien[2]; Lee, Te-Wei[3]

INSTITUTIONS (ALL):

1. Institute of Nuclear Energy Research, Taoyuan County, Taiwan.
2. Institute of Nuclear Energy Research, Taoyuan, Taiwan.
3. Institute of Nuclear Energy Research, Taoyuan, Taiwan.

(No Image Selected)

CONTROL ID: 2234256

TITLE: Novel Sirt1-selective radiotracer substrate [^{18}F] 2FPhAHA for PET imaging of epigenetic regulation

PRESENTER: Robin Bonomi

ABSTRACT BODY:

Abstract Body: Histone Deacetylase Class III enzymes, sirtuins (SIRT 1-7), are a NAD-dependent class of enzymes that possess either mono-ADP-ribosytransferase, or deacetylase, desuccinylase, demalonylase, demyristoylase and depalmitoylase activity. SIRT1 is known to mediate cleavage of acetyl moiety from acetylated lysine residues of several proteins, most notable, enzymes of the p53 family, PPARg and NF-KB. The roles of SIRT1 in different diseases are wide-ranging, as it can activate or inhibit many cellular processes making it difficult to understand the implications of its activity for development of new treatments. Therefore, it is essential to develop selective substrates for imaging of SIRT1 expression-acitivity *in vivo.* The use of radiolabeled substrates for in vivo imaging allows for quantitative visualization of enzyme expression-activity in tissues rather than only the level of enzyme expression (i.e. using radiolabeled inhibitors).

We developed a novel radiotracer for PET imaging of SIRT1 expression-activity, based on *in silico* to create a rationally designed focused library of substrates that have been synthesized and screened for efficacy in a panel of SIRT 1-7 using *in vitro* fluorogenic assay. We demonstrated that SIRT1 could cleave and transfer the 2-fluorophenyl moiety to the adenine-dinucleotide (from NAD). The lead compound was optimized for blood-brain-barrier (BBB) permeability using "cap and linker" moieties from previously developed [^{18}F]-FAHA. The new compound 2-[^{18}F]fluorophenyl-aminohexanoicanilide ([^{18}F]2FPhAHA) has been synthesized noth in cold and radiolabeled versions. The one-pot radiosynthesis of [^{18}F]2PhAHA using a 2-nitro-substituted precursor is a high-yield reaction. The biochemically determined enzymatic cleavage metabolites: 2-[^{18}F]fluorobenzoate ethyl ester (2-[^{18}F]FBzOEt) and 2-[^{18}F]fluoro-benzaldehyde (2-[^{18}F]FBzAld), have also been radiosynthesized. Noteworthy, the radiolabeling in the 2-position (ortho) of a benzene ring with F-18 has not yet been reported previously; our radiolabeling approach can be used for other aromatic compounds such as [^{18}F]FDOPA.

The efficacy of non-radioactive cold analogue 2FPhAHA has been validated in vitro using isothermal calorimetry (ITC) to confirm its affinity to SIRT1 enzyme. Dynamic PET/CT imaging studies in rats demonstrated that [^{18}F]2FPhAHA crosses BBB and accumulates preferntially in the olfactory bulb and frontal cortex at higher levels than its radiolabeled metabolites (2-[^{18}F]FBzOEt) and (2-[^{18}F]FBzAld), which accumulate mostly in the olfactory bulb. These data confirm that SIRT1 mediates the retention of [^{18}F]2FPhAHA-derived radioactivity in the brain.

In conclusion, [^{18}F]2FPhAHA is the first selective and efficient radiotracer substrate of SIRT1 that allows for non-invasive, in vivo PET imaging of SIRT1 expression-activity in the brain. Additional studies using SIRT1 activators and inhibitors are on the way for the assessment of potential value of [^{18}F]2FPhAHA as a PET imaging agent for pharmacodynamic monitoring of novel SIRT1-targeted agents for treatment of different diseases.

AUTHORS (LAST NAME, FIRST NAME): Bonomi, Robin[1]; Turkman, Nashaat [1]; Shavrin, Aleksander[1]; Gelovani, Juri G.[2]

INSTITUTIONS (ALL):

1. Wayne State University, Livonia, MI, United States.
2. Biomedical Engineering, Wayne State University, Detroit, MI, United States.

(No Image Selected)

CONTROL ID: 2234255

TITLE: Early prediction of response to capecitabine with 3'-deoxy-3'-[^{18}F]Fluorothymidine positron emission tomography in mice bearing human colon cancer xenografts

PRESENTER: Seog-Young Kim

ABSTRACT BODY:

Abstract Body: *Purpose:* We investigated whether 3'-deoxy-3'-[^{18}F]fluorothymidine ([^{18}F]-FLT) positron emission tomography (PET) predicts therapeutic response to capecitabine in mice with human colon cancer xenografts.
Methods: We studied six xenograft models (HCT116, LOVO, COLO205, HCT8, HT29, and SW620) which have different sensitivity to capecitabine. Mice were orally treated with vehicle or capecitabine (2/3 maximum tolerated dose) for 3 weeks. [^{18}F]FLT PET images were acquired 110-120 minutes after intravenous injection of [^{18}F]FLT at baseline (day 0), day 1 and day 3 after administration of vehicle or capecitabine. SUVmean and ratios SUVmean values between day 0 and 1 (SUVmean 1/0) and day 1 and 3 (SUVmean 3/1) were measured. We measured tumor growth inhibition (TGI) to classify xenografts into sensitive and resistant groups.
Results: Capecitabine was sensitive in HCT116 (92.4%), LOVO (83.3%) and COLO205 (74.6%) xenografts (defined as >50%, TGI), but not in HCT8 (41.0%), HT29 (31.3%) and SW620 (4.5%). SUVmean was increased at day 1 compared with day 0 in capecitabine sensitive models (HCT116, LOVO and COLO205, $P < 0.05$) whereas resistant xenografts showed variable results. On the other hand, SUVmean at day 3 was variable depending on the tumor growth inhibition. All three xenografts with >50% TGI group showed decreasing SUVmean on day 3 (day 1 vs 3, HCT116: 2.59 ± 0.40 vs 0.98 ± 0.21, LOVO: 3.67 ± 0.57 vs 1.50 ± 0.44, and COLO205: 6.67 ± 0.93 vs 2.98 ± 0.26; $P < 0.05$, respectively), but those without growth inhibition had no significant change. SUVmean 3/1 in capecitabine sensitive group (0.61 ± 0.66) was significantly lower than that in the resistant group (2.49 ± 4.13, $P < 0.05$). Of SUVmean (day 0, 1, and 3), SUVmean 1/0 and SUVmean 3/1, only SUVmean 3/1 had significant correlation with % growth inhibition ($\rho = -0.943$, $P < 0.01$).
Conclusion: Increased [^{18}F]FLT uptake early after capcitabine ([^{18}F]FLT flare) is not predictive of response to capecitabine, but [^{18}F]FLT uptake following [^{18}F]FLT flare predicted the response. [^{18}F]FLT PET may be a potential imaging tool to predict response to capecitabine. Further works in human are needed.

Key words: [^{18}F]fluorothymidine, positron emission tomography, capecitabine, colon cancer

AUTHORS (LAST NAME, FIRST NAME): Kim, Seog-Young[1]; Chung, Jin Hwa[2]; Soh, Hyun Su[1]; Lee, Haeng Jeong[1]; Chae, Sun Young[3]; Lee, Sang Ju[3]; Oh, Seung Jun[3]; Moon, Dae Hyuk[3]

INSTITUTIONS (ALL):

1. Institute for Innovative Cancer Reserch, Seoul, Korea (the Republic of).
2. Asan Institute for life science, Seoul, Korea (the Republic of).
3. Nuclear Medicine, Asan Medical Center, Seoul, Korea (the Republic of).

(No Image Selected)

CONTROL ID: 2234274

TITLE: Stimulated Raman imaging of brain and breast cancer tissue for label-free surgical pathology

PRESENTER: Nathalie Agar

ABSTRACT BODY:

Abstract Body: Pathology consultation during cancer surgery relies heavily on microscopic examination of hematoxylin and eosin (H&E) stained crytosections. This procedure has been used for more than a century but its broader application toward the delineation of tumor margins for surgical guidance is limited by its time and labor intensive processes and in the case of gliomas by the difficulty in detecting rare infiltrating tumor cells. A tool that could rapidly identify cancer cells with comparable cellular resolution from freshly excised tissue could support surgical decision-making in near real time. Stimulated Raman imaging (SRI) is a novel, rapid, and sensitive microscopic technique for label-free chemical mapping based on the Raman signature of biomolecules. The usefulness of SRI has been demonstrated for brain tumor delineation based on the distribution of lipids and proteins in a xenograft mouse model. We report here SRI of both fresh and frozen human brain and breast cancer tissues from a large number of surgical cases, and validate our findings with standard histopathology evaluation. Our results show that multi-color SRI reveals significant pathological features for cancer diagnosis, such as tissue morphology, hypercellularity, necrosis, and nuclear atypia as well as lipid, protein and DNA distribution and quantification. Such information can provide comparable information to conventional H&E based histopathology without the need for freezing or staining. Once fully validated, the platform could provide a novel tool for surgical pathology to support intra-operative decision-making: ambient label-free section analysis.

AUTHORS (LAST NAME, FIRST NAME): Lu, Fa-Ke[1, 3]; Calligaris, David[1]; Norton, Isaiah[1]; Olubiyi, Olutayo I.[1]; Santagata, Sandro[2]; Xie, X. Sunney[3]; Golby, Alexandra[1, 4]; Agar, Nathalie Y.[1, 5]

INSTITUTIONS (ALL):

1. Neurosurgery, Brigham and Women's Hospital, Boston, MA, United States.
2. Pathology, Brigham and Women's Hospital, Boston, MA, United States.
3. Chemistry and Chemical Biology, Harvard University, Cambridge, MA, United States.
4. Radiology, Brigham and Women's Hospital, Boston, MA, United States.
5. Cancer Biology, Dana-Farber Cancer Institute, Boston, MA, United States.

(No Image Selected)

CONTROL ID: 2234282
TITLE: Clinical Trial: Safety of ^{68}Ga-DOTATATE PET/CT in Patients with Neuroendocrine Tumors
PRESENTER: Ronald Walker
ABSTRACT BODY:
Abstract Body: Introduction:

We report early results of a prospective, consecutively enrolled clinical trial (NCT01396382) of 97 patients comparing ^{68}Ga-DOTATATE PET/CT (**DOTATATE**) to US standard of care imaging neuroendocrine tumors (NETs) compared to standard of care imaging, conducted with local IRB approval, with informed consent obtained from all subjects. Patients were injected with 50 micrograms or less of the radiolabeled peptide similar to previously reported investigations.(1) Standard of care imaging included ^{111}In-DTPA-octreotide (**OCT**) imaging (n=87), diagnostic CT (n=91) and MRI of the liver (n=60). Safety and toxicity were also assessed with pre-injection and post-imaging vital signs, pulse oximetry on room air, 12 lead ECGs and blood tests, including tumor markers, liver and renal functions and blood counts. Co-morbidities included advanced metastatic disease in 44 patients.

Results:

No serious adverse events (**AEs**) occurred, even with frequent significant co-morbidities. Additional co-morbidities included various abnormal baseline ECGs (various conduction defects, one with a prior anteroseptal infarction with a left anterior fascicular block, 2 with T-wave inversions, 2 with nonspecific ST-T wave changes, 2 with first degree AV block, 2 with p-wave abnormities, one with a ventricular paced rhythm and one with a prior cardiac transplant). No dangerous arrhythmias, or other significant changes from baseline, were observed.

Various minor AEs one patient with minor itching the day after the DOTATATE injection at the injection site injection with spontaneous resolution, and one patient with an unexplained drop in post-scan oxygen saturation on room air (pre-injection 98%, post scan 90%), spontaneously resolving. Other patients had minor and transient changes in random blood work values, all asymptomatic. One patient with a baseline heart rate of 87 had a post-scan tachycardia (rate>100) of 112, asymptomatic, returning to <100 within an hour. There were no changes in Karnofsky scores or subjective changes in pre- and post-scan well-being, measured or reported by the patients.

Discussion: There were no observed serious AEs during this trial despite the presence of significant co-morbidities.

Conclusion: DOTATATE is safe in microdose (50 micrograms or less) amounts

1. Walker RC, Smith GT, Liu E, Moore B, Clanton J, Stabin M. Measured human dosimetry of 68Ga-DOTATATE. J Nucl Med. 2013;54(6):855-60.
AUTHORS (LAST NAME, FIRST NAME): Deppen, Stephen A.[2]; Bobbey, Adam[1]; Clanton, Jeff[3]; Sandler, Martin[5]; Delbeke, Dominique[4]; Walker, Ronald C.[1]
INSTITUTIONS (ALL):
1. Radiology & Radiological Sciences, Vanderbilt University Medical Center, Nashville, TN, United States.
2. Department of Surgery, Vanderbilt University Medical Center, Nashville, TN, United States.
3. Radiology & Radiological Sciences, Vanderbilt University Medical Center, Nashville, TN, United States.
4. Radiology & Radiological Sciences, Vanderbilt University Medical Center, Nashville, TN, United States.
5. Radiology & Radiological Sciences, Vanderbilt University Medical Center, Nashville, TN, United States.
(No Image Selected)

CONTROL ID: 2234335

TITLE: Clinical Trial: Efficacy of ^{68}Ga-DOTATATE PET/CT in Patients with Neuroendocrine Tumors

PRESENTER: Ronald Walker

ABSTRACT BODY:

Abstract Body: Introduction:

We report a prospective, consecutively enrolled clinical trial (NCT01396382) of 97 patients comparing ^{68}Ga-DOTATATE PET/CT (**DOTATATE**) to US standard of care imaging of neuroendocrine tumors (NETs) , with local IRB approval, with informed consent obtained from all subjects. Standard of care imaging included ^{111}In-DTPA-octreotide (n=87), diagnostic CT (n=91) and liver MRI (n=60). Impact on care was assessed by comparing the change in initial treatment plan formulated with all available clinical, pathologic and imaging to the treatment plan after reviewing DOTATATE scan. Impact was scored as none, minor (intramodality, e.g. a modification of planned surgery) or major (intermodality, e.g. cancel surgery).

Results: 100 scans were performed in 97 patients (**Figure 1**). Comparative DOTATATE and OCT scans were available in 80, with 17 excluded. Median days between scans was 182 (IQR: 105, 402). Mean DOTATATE activity was 5.3mCi (95%CI: 4.8, 5.8). In 61 (76.3%), DOTATATE and OCT were diagnostically concurrent (38, 47.5% tumor found, 23, 28.8% no tumor found). Of 17 patients with negative OCT scans but positive DOTATATE scans, 8 had no treatment impact, leaving 9 patients (9%) with negative OCT scans, of which 2/9 were false positive DOTATATE scans with no impact on care due to other imaging. There were 2 false positive OCT scans with true negative DOTATATE scans. Significant differences between DOTATATE and OCT in the finding of tumor (McNemar's chi-square, $p<0.001$) were observed. DOTATATE and OCT were concurrently false negative in 1 patient with tumor found on MRI. DOTATATE demonstrated 12 (15%) patients as nonsurgical candidates, with strong uptake to support peptide receptor radiotherapy (**PRRT**), of which 3/12 (25%) were misclassified by OCT as SSTR negative and not candidates for PRRT.

Discussion: In no case was DOTATATE false negative when OCT imaging was positive for NET. DOTATATE and OCT each had 2 false positive scans, in different patients.

Of 12 patients found by DOTATATE to have sufficient SSTR expression to support PRRT, 3 of these were misclassified by OCT, and would have been denied PRRT.

We found that correct clinical management could be made in all patients with imaging limited to DOTATATE plus diagnostic CT and/or contrast-enhanced liver MRI. No patient management decisions would have been adversely impacting by excluding the OCT scan, whereas 21 (26%) patients would have had negative impact with DOTATATE excluded.

Conclusion: DOTATATE changed management in 9 (11%) of patients with OCT plus CT and/or MRI. At no time did OCT add value when compared to DOTATATE. When diagnostic imaging was limited to whole body DOTATATE plus diagnostic CT and/or liver MRI, correct staging and treatment decisions would have been reached in all patients, compared to 59 (74%) patients with OCT plus CT and/or liver MRI. Given the superior imaging results for tumor (McNemar's chi-square, $p<0.001$), lower radiation dosimetry, 2 hour completion time, and estimated comparable cost, our results conclusively demonstrate in a large, prospectively enrolled trial, that DOTATATE should replace OCT imaging, where available.

AUTHORS (LAST NAME, FIRST NAME): Deppen, Stephen A.[2]; Bobbey, Adam[1]; Clanton, Jeff[1]; Sandler, Martin[1]; Delbeke, Dominique[1]; Walker, Ronald C.[1]

INSTITUTIONS (ALL):

1. Radiology & Radiological Sciences, Vanderbilt University Medical Center, Nashville, TN, United States.
2. Department of Surgery, Vanderbilt University Medical Center, Nashville, TN, United States.

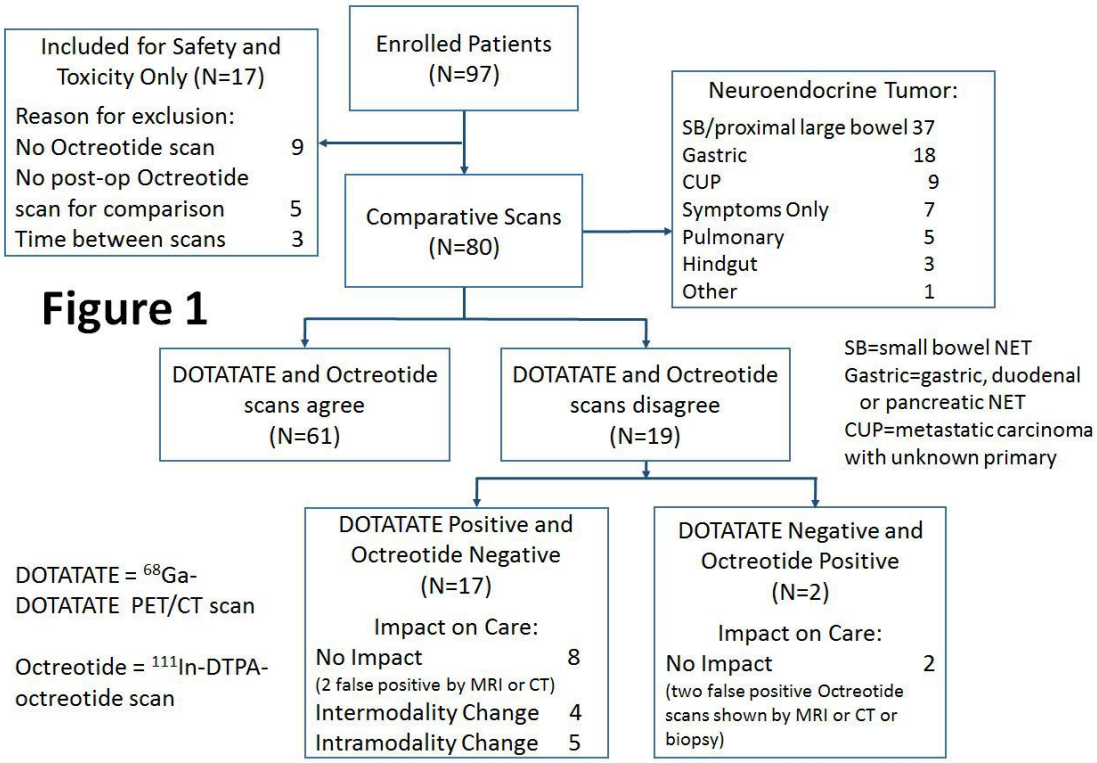
Included for Safety and Toxicity Only (N=17)
Reason for exclusion:
No Octreotide scan 9
No post-op Octreotide scan for comparison 5
Time between scans 3
Enrolled Patients (N=97)
Comparative Scans (N=80)
Neuroendocrine Tumor:
SB/proximal large bowel 37
Gastric 18
CUP 9
Symptoms Only 7
Pulmonary 5
Hindgut 3
Other 1
DOTATATE and Octreotide scans agree (N=61)
DOTATATE and Octreotide scans disagree (N=19)
SB=small bowel NET
Gastric=gastric, duodenal or pancreatic NET
CUP=metastatic carcinoma with unknown primary
DOTATATE = 68Ga-DOTATATE PET/CT scan
Octreotide = 111In-DTPA-octreotide scan
DOTATATE Positive and Octreotide Negative (N=17)
Impact on Care:
No Impact 8
(2 false positive by MRI or CT)
Intermodality Change 4
Intramodality Change 5
DOTATATE Negative and Octreotide Positive (N=2)
Impact on Care:
No Impact 2
(two false positive Octreotide scans shown by MRI or CT or biopsy)

Figure 1

CONTROL ID: 2234287

TITLE: Development of Benzyl [^{18}F]Fluoroacetate Radiosynthesis for PET Imaging of Ischemic Brain Injury

PRESENTER: Shinya Kagawa

ABSTRACT BODY:

Abstract Body: Recently, fully automated synthetic procedures of [^{18}F]Fluoroacetate ([^{18}F]FACE) for clinical use have been developed by not only a general on-column hydrolysis procedure, but also a two-pot distillation procedure. We developed a novel approach named as “one-pot distillation procedure” which was perfomed both hydrolysis of [^{18}F]Ethyl fluoroacetate ([^{18}F]EFA) and trap of [^{18}F]FACE on the same ion exchange resin column. Moreover, the relationship between [^{18}F]FACE uptake and the number of glial cells were investigated in rat ischemia/reperfusion injury. Benzyl acetate, among several aryl acetates, displayed much higher brain perfusion and retention than acetate (Momosaki et al., *NMB*, **34**: 939-44, 2007). Therefore, we developed a radiosynthesis of Benzyl [^{18}F]Fluoroacetate (Benzyl [^{18}F]FACE) for the purpose of early detection of the ischemic brain injury by PET.

The radiosynthesis of Benzyl [^{18}F]FACE was performed on a hybrid synthesizer, cassette-type multipurpose automatic synthesizer module (JFE Engineering Corporation). The fluorination of Benzyl Bromoacetate occurred in MeCN in presence of Krypofix 2.2.2 and potassium [^{18}F]fluoride. After purification of the crude product by HPLC, the isolated product fraction was formulated by solid phase extraction with a Sep-Pak C18 cartridge. As the result the final product reconstituted in 5% ethanol in distilled water. The quality control tests of final products were performed. Benzyl [^{18}F]FACE was produced in about 50 minutes with radioactivity of 16.6 ± 3.9 GBq, radiochemical yield (decay uncorrected) of 55.7 ± 5.5 %, radiochemical purity of 98.4 ± 1.4 % and specific activity of 191.0 ± 65.3 GBq/μmol. The analysis data about this drug were found to be the one that met the quality control such as Standards of Compounds Labeled with Positron Emitting Radionuclides Approved as Established Techniques for Medical Use (2009 revision). Based on these results, we have started the biodistribution and stability studies of Benzyl [^{18}F]FACE in vivo, in order to explore the future possibility of the Benzyl [^{18}F]FACE imaging using an animal model of ischemia/reperfusion injury.

AUTHORS (LAST NAME, FIRST NAME): Kagawa, Shinya[2, 4]; Mizuma, Hiroshi[3]; Nishii, Ryuichi[1]; Higashi, Tatsuya[2]; Yamauchi, Hiroshi[2]; Ono, Masahiro[3]; Tateishi, Hiroyuki[3]; Takahashi, Kazuhiro[3]; Onoe, Hirotaka[3]; Kawai, Keiichi[4]

INSTITUTIONS (ALL):

1. Radiology, University of Miyazaki, Miyazaki, Japan.
2. Division of PET imaging, Shiga Medical Center Research Instutute, Moriyama, Japan.
3. Division of Bio-Function Dynamics Imaging, RIKEN Center for Life Science Technologies, Kobe, Japan.
4. Graduate School of Medical Science, Kanazawa University, Kanazawa, Japan.

(No Image Selected)

CONTROL ID: 2234317

TITLE: Visualizing pathogenesis of Francisella tularensis (F. tularensis)

PRESENTER: Kee-Jong Hong

ABSTRACT BODY:

Abstract Body: Study on the pathogen-related disease requires the information of pathogen and host organism. However, variations of each experimental condition obstruct precise analysis of in vivo mechanism in many cases. For reliable study of pathogenesis and host immune-response, elaborate analyses which can provide spatio-temporal information are important. Here, we developed tracing method of bacteria, Francisella tularensis (F. tularensis), which can visualize its localization and population at the single cell level to whole animal level in vivo.

Four week old BALB/c mice were used for infection. For increasing sensitivity, putative bacterioferritin promoter from F. tularensis Live Vaccine Strain (LVS) was amplified and substituted with GroEL promoter of pKK214-GFP plasmid using PacI/PstI. Lux operon was amplified from pXen 13 plasmid and conjugated with pKK214-GFP. Then F. tularensis LVS (ATCC 29684) was transformed with pFtKK214-GFP-Lux. LPS of F. tularensis LVS was purified using LPS extraction kit, and mice were vaccinated with 500 ng of LPS purified from F. tularensis LVS by intra-peritoneal injection. Three weeks after vaccination, mice were infected with 105 CFU of FtLVS-GFP-Lux. Signals was measured with SpectraMax M2 and Fluoroskan. FACS analysis were performed with Cytomics FC500. Time lapse microscopy and animal imaging were performed with LSM710, In-Vivo Xtreme and IVIS Luminar.

We successfully traced the process of Francisella tularensis (F. tularensis) pathogenesis in mouse model and visualized the bacterial replication at the cellular level. We also confirm that vaccination with LPS purified from F. tularensis live vaccine strain (LVS) greatly reduce the bacterial replication of F. tularensis LVS in the mouse model. Our simple and integrated imaging analysis system would be useful for studying in vivo pathogenesis and immune-responses of infectious diseases.

AUTHORS (LAST NAME, FIRST NAME): Park, Pil-Gu[3]; Kim, Young-Hwa[3]; Youn, Hyewon[1]; Hong, Kee-Jong[2, 3]

INSTITUTIONS (ALL):

1. Cancer Imaging Center, Seoul National Univ, Seoul, Jongno-Gu, Korea (the Republic of).
2. Institut Pasteur Korea, Boondang, Korea (the Republic of).
3. Division of high-risk pathogen research, Center for Infectious Diseases and Prevention,, Korea National Institute of Health, Osong, Korea (the Republic of).

(No Image Selected)

CONTROL ID: 2234315

TITLE: Glycated chitosan retard the metastatic breast cancer cells properties through inhibition Twist that results in reversion of epithelial-to-mesenchymal transition.

PRESENTER: Wang Bo-Sheng

ABSTRACT BODY:

Abstract Body: Metastatic property is an inherent feature of breast cancer. One of the important regulators is Twist that driving tumor epithelial-to-mesenchymal transition (EMT). This study, we demonstrate that a novel, Non-toxic immunoadjuvant, glycated chitosan (GC), inhibits mobility and invasion of more metastatic breast cancer cells.

Here we used molecular imaging to track the progression of living cells in a metastatic tumor model, and ex vivo investigated the properties of this migration and invasion at late-stage tumor. The piggyBac transposon system was used to stably introduce the triple reporter genes, including firefly luciferase (luc2) gene, monomeric red fluorescent protein (mRFP) and herpes simplex virus type-1 thymidine kinase (HSV1-tk) genes for bioluminescent- and fluorescence-based imaging of tracking metastatic tumor in small animals, respectively.

The results indicated that GC enhanced the expression of p-Cofilin gradually implicated in EMT. Twist and epithelial-cadherin are down- and up-regulation by GC.

Taken together, our data suggest that GC can retard cancer cell motility and invasion.

AUTHORS (LAST NAME, FIRST NAME): Bo-Sheng, Wang[1]

INSTITUTIONS (ALL):

1. Biomedical Imaging and Radiological science, Taipei, Taiwan.

(No Image Selected)

CONTROL ID: 2234333

TITLE: Using Mortality Force to Illustrate Probable Onset Age of Spinocerebellar Ataxia Type 3 Based on Magnetic Resonance Spectroscopy Measurements

PRESENTER: Po-Shan Wang

ABSTRACT BODY:

Abstract Body: Objective: Magnetic Resonance Spectroscopy measurements could be correlated with onset age of disease, CAG repeat length, score of Scale for the Assessment and Rating of Ataxia (SARA) and disease duration of spinocerebellar ataxia type 3 (SCA3). We conducted a correlational study on those factors and used the disease-correlated factors and mortality force model to estimate probable onset age of SCA3.

Methods: From 2004 to 2010, a total of 47 SCA3 patients whom were examined by MRS were retrospectively recruited in this study. Another 42 healthy subjects were included and used as a control group. We obtained information of self-reported disease onset age and SARA score from each patient from patients. Polymerase chain reaction (PCR) was performed with the primers MJD25 and MJD52 to acquire CAG repeat number. Correlations between two MRS measurements, right and left cerebellar hemisphere N-acetyl aspartate (NAA)/creatine(Cr) ratios (denoted Rt-CB-NAA and Lt-CB-NAA respectively), and disease duration were checked. Adjusted Rt-CB-NAA and Lt-CB-NAA were derived through a linear regression model, which traced the original ratios back from the MRS examination date to the time of reported onset age. Patients were categorized into 3 different groups based on the CAG repeat length (CAG≤70, CAG 71~75, and CAG≥76) for subsequent investigation.

Results: Graphs of mortality force and cumulative probability were displayed to show the probable disease onset probability of the 3 different groups based on patients' age (see Figure 1). Rt-CB-NAA, Lt-CB-NAA and Vermis-NAA (V-NAA) of SCA3 patients were significantly different to those values compared to normal control (p-values < 0.001). Rt-CB-NAA, Rt-CB-NAA, Lt-CB-NAA and V-NAA were significantly different between SCA3 subgroups (p-values < 0.001). Also, Rt-CB-NAA, Rt-CB-NAA, Lt-CB-NAA and V-NAA of SCA3 patients were negatively correlated with disease duration (correlation coefficients were -0.411, -0.433 and -0.384, p-value < 0.01).

Conclusion: Rt-CB-NAA, Lt-CB-NAA and V-NAA are significantly different between normal controls and SCA3 patients. Also, these 3 ratios differ among categorized groups. Besides CAG repeat length, we show that adjusted Rt-CB-NAA and Lt-CB-NAA could also be potential indicators to estimate the onset age of SCA3. Because the onset of SCA3 is predestined and unavoidable, this study is helpful for SCA3 patients to assess disease onset age for a better future planning.

AUTHORS (LAST NAME, FIRST NAME): Wang, Po-Shan[2, 3]; Huang, Shang-Ran[4]; Soong, Bing-Wen[5]; Wu, Yu-Te[1, 4]

INSTITUTIONS (ALL):

1. Institute of Biophotonics, Taipei, ROC, Taiwan.
2. The Neurological Institute, Taipei Municipal Gan-Dau Hospital, Taipei, Taiwan, ROC, Taipei, ROC, Taiwan.
3. Institute of Biophotonics, National Yang-Ming University, Taipei, Taiwan.
4. Department of Biomedical Imaging and Radiological Sciences, National Yang-Ming University, Taipei, Taiwan.
5. Department of Neurology, Taipei Veterans General Hospital, Taipei, Taiwan.

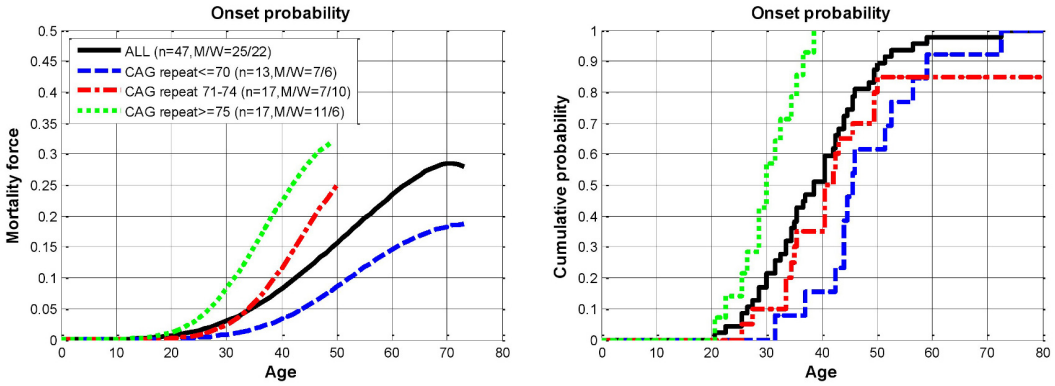

Figure 1. Graphs of mortality force and cumulative probability of SCA3 onset vs based on 3 different CAG repeat length groups (CAG ≤ 70, CAG 71~75, and CAG ≥ 76). (a) mortality force vs age (b) cumulative probability vs age. Black solid line stands for total patient group, Blue dashed line stands for the group with CAG ≤ 70, Red dash-dot line stands for the group with CAG between 71~75, and green dotted line stands for the group with CAG ≥ 76. Rt: right, CB: cerebellar hemisphere, NAA: ratio of N-acetyl aspartate/creatine.

CONTROL ID: 2234329

TITLE: [^{18}F]FDG PET/MRI Of Patients With Chronic Pain Alters Management: Early Experience.

PRESENTER: Deepak Behera

ABSTRACT BODY:

Abstract Body: Chronic pain sufferers currently face a lack of objective tools to identify the source of their pain. The overarching goal of this study is to develop clinical [^{18}F]FDG PET/MRI methods to more accurately localize sites of increased neuronal and muscular metabolism or inflammation as it relates to neurogenic sources of pain and to ultimately improve outcomes of chronic pain sufferers. The aims are to 1) correlate imaging findings with location of pain symptomology, 2) predict location of symptoms based on imaging findings alone, 3) compare PET/MR with MRI alone in their ability to detect pain related abnormalities and 4) to determine whether the PET/MR imaging results affect ongoing clinical management decisions.

METHOD: Seven patients suffering from chronic lower extremity neuropathic pain (4 complex regional pain syndrome, 2 chronic sciatica and 1 neuropathic pain) were imaged with a PET/MRI system (time-of-flight PET; 3.0T bore) from mid thorax through the feet. All patients underwent PET/MR imaging at approximately 4-8 min/bed position, one hour after an injection of 10mCi [^{18}F]FDG. MRI sequences obtained in each bed position include a coronal DESS, coronal PSIF (isotropic), axial LAVA FLEX (with water and fat separated). For chronic sciatica patients, additional axial T2 FSE with fat-saturation and sagittal T1 and STIR of the lumbar spine were performed. Two radiologists evaluated PET/MR images (one blinded and the other un-blinded to patient exam/history).

RESULTS:
1) PET/MRI findings correlated with pain symptomatology. ROI analysis showed focal increased [^{18}F]FDG uptake in affected nerves and muscles (approx 2-4 times more) over background tissue in 7 of 7 patients (100%) at the site of greatest pain symptoms and/or other areas of the body (SUVmax of Target 0.9-4.2 vs. Background 0.2-1.2).
2) It was possible to predict location of symptoms based on imaging findings. The radiologist blind to the patient history/exam was able to correctly identify side/location of the symptoms in 6 out of 7 patients (86%).
3) PET/MR was able to detect abnormal imaging findings in all chronic pain patients (100%) while MR alone was able to detect abnormalities in 3/7 patients (43%).
4) PET/MR imaging results changed management in majority of patients (in 6/7 or 86% of patients). Imaging results were reviewed with the referring physician, who then determined whether a modification in the management plan was needed: 1/7 needed no change, 2/7 needed mild modification (e.g., additional diagnostic test ordered) and 4/7 significant modification (e.g., new invasive procedure or new medical therapy ordered).

CONCLUSION: Early results suggest that [^{18}F]FDG PET/MRI can objectively identify inflammatory abnormalities in patients suffering from neuropathic pain and influence clinical management decisions. Therefore, it can potentially affect outcome. The ongoing study will confirm if PET/MRI is a more accurate predictor of pain generators over conventional methods, and will determine whether these interventions affect patient outcomes in terms of pain scores, disability indices and other outcome measures.

Reference:
Behera et al. (*J Nuc Med* (2011) 52(8):1308-12)

AUTHORS (LAST NAME, FIRST NAME): Behera, Deepak[1]; Yoon, DaeHyun[1]; Holley, Dawn[1]; Ith, Ma Agnes M.[2]; Carroll, Ian[3]; Smuck, Matthew[2]; Hargreaves, Brian[1]; Biswal, Sandip[1]

INSTITUTIONS (ALL):
1. Radiology, Stanford University School of Medicine, San Carlos, CA, United States.
2. Orthopaedic Surgery: Division of Spine, Stanford Medicine Outpatient Center (SMOC), Redwood City, CA, United States.
3. Anesthesia, Stanford University School of Medicine, Stanford, CA, United States.

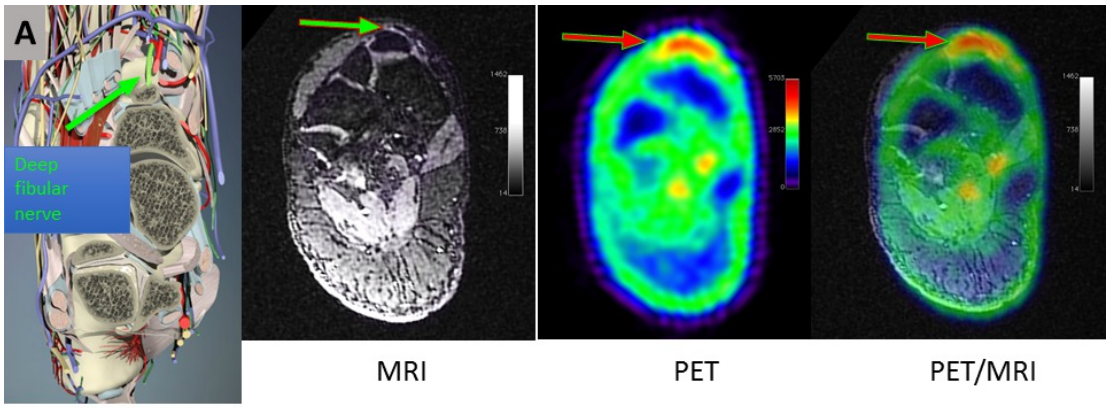

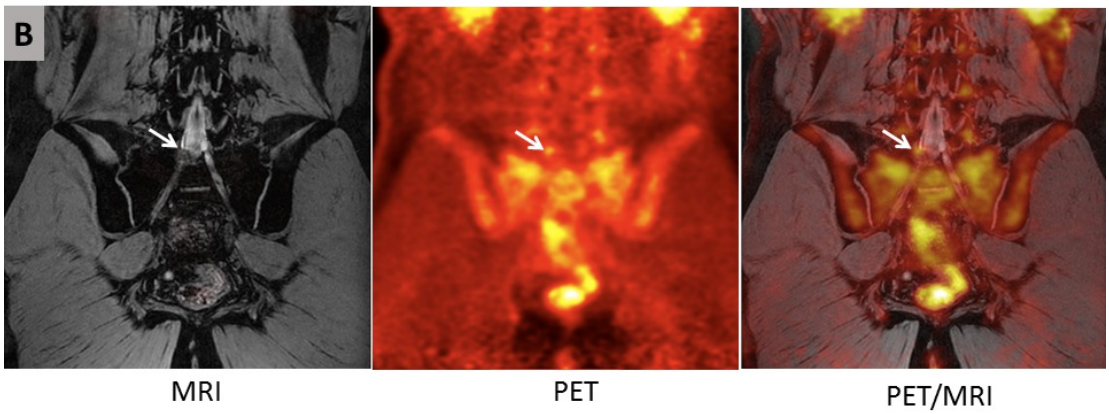

A: Axial [18F]FDG PET/MRI of a patient with complex regional pain syndrome of the right foot shows increased [18F]FDG uptake (red arrows) in the vicinity of the right deep fibular nerve (green arrows) and surrounding soft tissues in the dorsal part of the ankle/proximal foot.

B: Coronal MRI, PET and fused PET/MR image taken of a patient suffering from chronic right-sided chronic sciatica. The MR image is a coronal DESS through the lumbosacral spine through the neuroforamina of L5-S1 (white arrow). Coronal PET image shows increased FDG uptake at the lumbosacral junction in the right L5-S1 neuroforamina (white arrow) as confirmed by the fused PET/MR image. The patient's symptoms were confirmed to involve the right back and leg. Of note, this patient was treated prior to this scan with a transforaminal epidural injection at the right S1-S2 neuroforamina with little benefit.

CONTROL ID: 2245302

TITLE: PET/MRI Image-guided Therapy of Peripheral Neuropathic Pain using a Sigma-1 Receptor Antagonist

PRESENTER: Deepak Behera

ABSTRACT BODY:

Abstract Body: Neuropathic pain poses a tremendous health and financial burden for patients, physicians, and the healthcare system. Current therapeutic intervention is handicapped due to high non-specificity of current diagnostic methods. Molecular imaging, highlighting pathology in neural damage, has potential to identify and, thus, guide therapeutic intervention accurately to target sources of pain generation.

A potential neuropathic pain biomarker is the sigma-1 receptor (S1R), which is associated with peripheral nerve injury and inflammation. Additionally, S1R antagonists are well known to have analgesic properties. For example, BD1047, an S1R antagonist, has been used to treat pain. S1Rs are known to be abundantly expressed in rat sciatic nerves, especially in Schwann cells, which proliferate after nerve injury.

We have previously validated a new, highly selective radiotracer [^{18}F]FTC-146 for imaging S1Rs using PET/MRI in a neuropathic pain model. Therefore, our goal was to test the next logical step in diagnosing and treating chronic pain conditions, i.e., to evaluate efficacy of image-guided administration of non-radiolabeled FTC-146 (CM-304), an S1R antagonist, as a therapeutic agent.

Our aim was to evaluate the utility of S1R PET/MRI in image-guided therapy of peripheral neuropathic pain generators with the S1R antagonist FTC-146 by: 1) assessing if image-directed injection of FTC-146 produces analgesia as a potential therapeutic agent for neuropathic pain, and 2) quantifying the degree and duration of pain relief using FTC-146

METHODS:
FTC-146 was made in-house as previously described and prepared 10% ethanol in 0.9% saline for injection. A sciatic neuropathic pain model was generated using adult male rats, by transecting the left tibial and common peroneal branches. The animals were divided into 2 groups (n=6, each): 1) FTC-146 treated test group, 2) Saline (unmedicated) treated control group. A single rat was treated with bupivacaine as a positive control. Four weeks after surgery, allowing for pain development and wound healing, allodynia was measured using von-Frey's filaments. Under anesthesia and ultrasound guidance, 50 uL of drug was injected at the site of nerve injury (identifiable using [^{18}F]FTC-146 and PET/MRI in our prior experiments). Pain relief was measured using von-Frey's filaments (lower thresholds indicate greater pain). The right hindlimb (uninjured) served as a measurement for absence of pain.

RESULTS:
Local injection of FTC-146 and bupivacaine (positive control) via ultrasound guidance at the site of nerve injury reduces pain, while saline injection (control) does not reduce pain ($p<0.0003$). Degree of pain relief by FTC-146 appears to be lower than that produced by bupivacaine. However, pain relief by FTC-146 lasts longer (up to 7 days) than bupivacaine (1 day).

CONCLUSIONS:
FTC-146, which can be used to identify nerve injury associated neuropathic pain in its radiolabeled form, can also be used as an analgesic in its non-radioactive, cold form. The dual properties of a diagnostic and a therapeutic agent make this an attractive agent for accurate identification and image-guided treatment of chronic neuropathic pain.

AUTHORS (LAST NAME, FIRST NAME): Behera, Deepak[1]; Shen, Bin[1]; James, Michelle L.[1]; Zhou, Xiaoliang[1]; McCurdy, Christopher R.[2]; Chin, Frederick T.[1]; Biswal, Sandip[1]

INSTITUTIONS (ALL):
1. Radiology, Stanford University School of Medicine, Stanford, CA, United States.
2. Department of BioMolecular Sciences, University of Mississippi, School of Pharmacy, University, MS, United States.

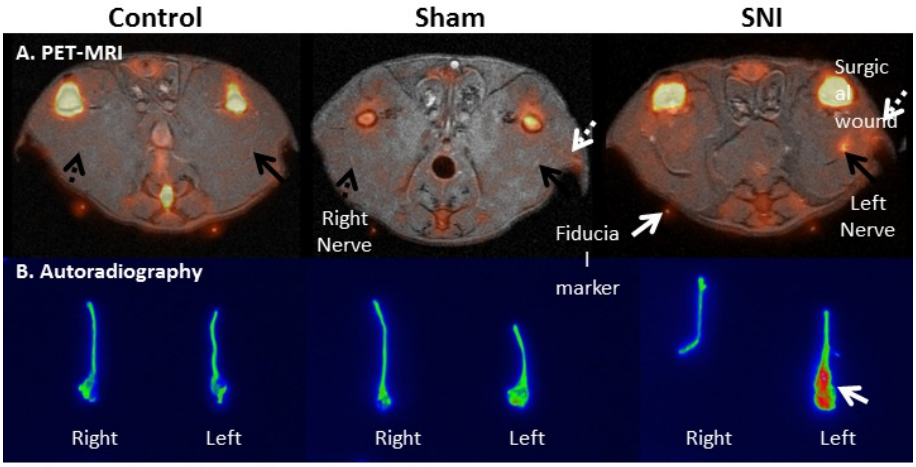

C. Nerve sections: Autoradiography and H&E

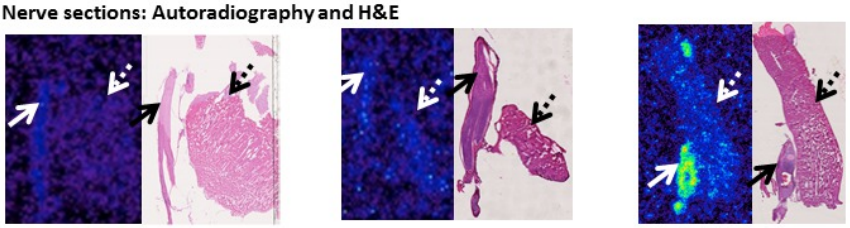

D. Treatment of neuroma with FTC-146

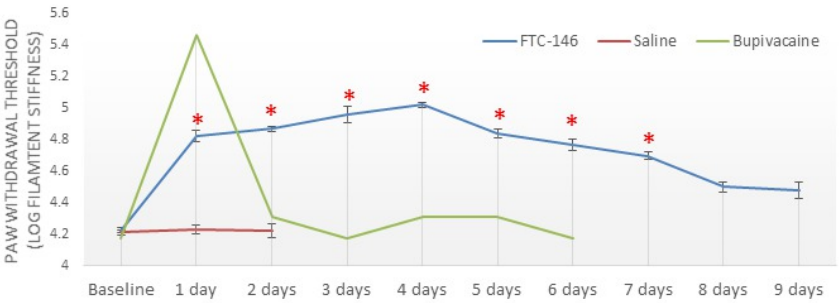

A. Transaxial fused PET-MRI images of representative Control, Sham and SNI animals showing increased 18F-FTC-146 uptake in the left sciatic nerve of SNI animal. (Solid black arrows: left sciatic nerve; dashed black arrow: right sciatic nerve; solid white arrow: fiducial marker; dashed white arrow: surgical wound.)

B. Autoradiography of excised sciatic nerves showing increased uptake in the neuroma in the injured left nerve from SNI animal. (Solid white arrow: neuroma)

C. Representative autoradiograms and corresponding H&E images of left sciatic nerve sections from Control, Sham and SNI animal showing increased 18F-FTC-146 uptake in the neuroma from the injured sciatic nerve from SNI animal, and increased inflammatory and regenerative cellularity in the neuroma. (Solid arrows (black or white): sciatic nerve; dashed arrow (black or white): adjacent muscle.)

D. Local injection of FTC-146 and bupivacaine reduce pain, while saline does not ($p<0.0003$). The pain relief by FTC-146 lasts 7 days.

CONTROL ID: 2234345

TITLE: A New Bottom-up Approach for the Synthesis of Self-assembled Nanostructures for Molecular Imaging

PRESENTER: Brenda Sanchez-Gaytan

ABSTRACT BODY:

Abstract Body: *Introduction*

As new and improved nanoparticle platforms are emerging, highly reproducible synthetic methods to generate homogenous nanoparticles at large scale become necessities. Typical methods for self-assembled nanoparticle systems involve ineffective and cumbersome procedures. Among the plethora of nanoparticles to be used as imaging agents, lipid-based nanoparticles such as nanoemulsions and the natural nanoparticles based on high-density lipoprotein (HDL) are of interest. Nanoemulsions (an oil nanodroplet core surrounded by a lipid corona) are typically synthesized through top-down approaches, which limits size modulation. Typical nanoemulsion synthetic procedures also limit the loading of various materials inside the oil core. HDL is structurally similar to an oil in water emulsion and can be modified with diagnostic molecules (e.g. paramagnetic, fluorescent) as well as hydrophobic payloads (e.g. nanocrystals).[1] Here, we present a single-step microfluidics-based method to synthesize nanoemulsions and HDL-like nanoparticles (μHDL) to be used for molecular imaging and therapeutic purposes.

Methods and Results

A new bottom-up microfluidics-based approach was used to synthesize the nanoparticles. μHDL of different phospholipid compositions (DMPC/MHPC and POPC/PHPC) were prepared. Briefly, a solution of phospholipids dissolved in ethanol was injected into the microfluidics module where it was instantaneously mixed with apolipoprotein AI (ApoA-I) in PBS. The impact of phospholipids ratio and flow rates of the components in the size and structure of the nanoparticles was studied as well as the incorporation efficiency of imaging and therapeutic components. μHDL had the same structural and biological properties (e.g. size, morphology, bioactivity) as native HDL. In addition, hydrophobic drugs and imaging agents could be easily incorporated. Nanoemulsions were generated by injecting an ethanolic solution containing oil, lipids and hydrophobic imaging agents (e.g. nanocrystals, dyes or functional lipids) into the microfluidics module where it was swiftly mixed with water. The ratios of oil/lipids as well as the flow rates were found to have a profound impact on the size and overall quality of the nanoparticle. Remarkably, the homogeneity of the batches and incorporation efficiency was also improved when compared with typical synthetic methods.

Conclusions

Synthetic lipid-based nanoparticles were produced using microfluidic-based technology. The ease of preparation allows the scaling-up of highly reproducible nanoparticle batches and allow for structure modulation not obtainable through other synthetic approaches.

1. Duivenvoorden et al. *Nat Commun*. **2014**. 5. 3065

AUTHORS (LAST NAME, FIRST NAME): Sanchez-Gaytan, Brenda[1]; fay, francois[2]; Zhao, Yiming[2]; Fayad, Zahi A.[3]; Mulder, Willem J.[1]

INSTITUTIONS (ALL):

1. Radiology, Icahn School of Medicine at Mount Sinai, New York City, NY, United States.
2. Translational and Molecular Imaging Institute, Icahn School of Medicine at Mount Sinai, New York City, NY, United States.
3. Radiology, Icahn School of Medicine at Mount Sinai, New York, NY, United States.

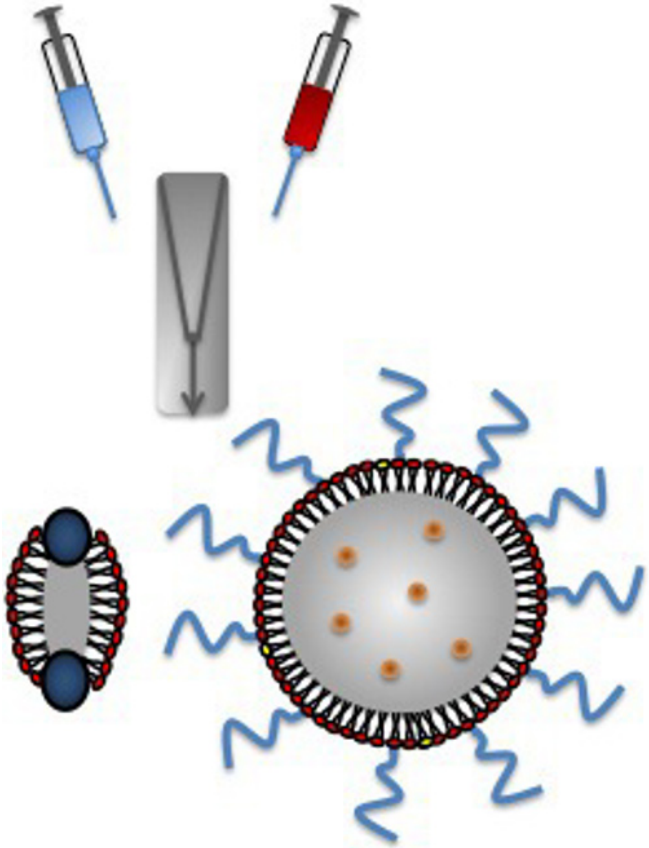

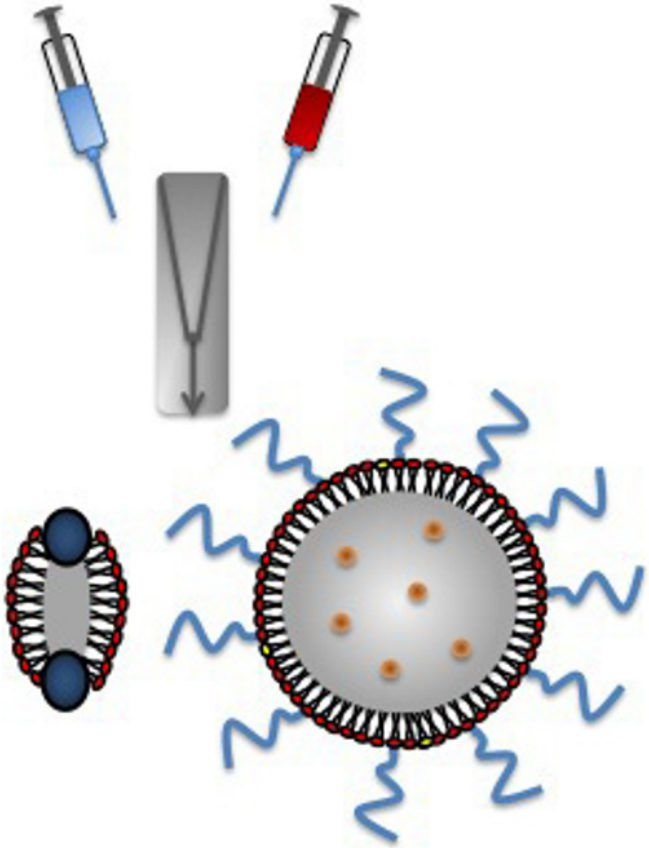

Synthesis of HDL-like nanoparticles and nanoemulsions through microfluidics

CONTROL ID: 2234351
TITLE: Electroporation mediated enhancement of Oregon green-488 Taxol uptake in Pancreatic cancer in vitro
PRESENTER: Derek West
ABSTRACT BODY:
Abstract Body: Introduction:

Pancreatic Ductal Adenocarcinoma (PDAC) is one of the most lethal forms of cancer and the high mortality rate is due, in part, to the advanced stage of the disease at the time of diagnosis, as well as lack of effective treatments. Desmoplasia is a significant contributor to chemoresistance in PDAC. Through elevated interstitial fluid pressures and intrinsic structural characteristics, desmoplasia decreases penetration of macromolecules, such as chemotherapeutic agents, through the tissue. Preclinical studies have demonstrated that electroporation increases the chemotherapeutic efficacy in pancreatic tumor models. Electroporation is the transient application of high electrical fields across the cells, creating nanoscale pores in the membrane and thereby increasing the cell permeability. The objective of the present study is to assess the potential of electroporation in enhancing the uptake of Oregon green-488 Taxol (OG-Taxol) in pancreatic cancer. OG-Taxol is a fluorescent (Alexa Fluor 488) conjugate of Paclitaxel, a mitotic inhibitor used as a cyotoxic agent in combination with other chemotherapy drugs in the treatment of pancreatic cancer.

Methods:

Human pancreatic cancer cells, MiaPaCa-2 were treated with different doses of OG-Taxol (0.5, 1, 1.5 and 2 mM) and electroporated at different field strengths; 500, 1000, 1500, 2000 and 2500 Vcm^{-1} using a Petri Pulser connected to ECM 830 Square Wave Electroporation System (BTX Harvard Apparatus, MA, USA) with a pulse length of 99 µs; 8 pulses; 100ms interval. After 24 hrs, cells were prepared for flow cytometry with DAPI. Alexa Fluor 488 and DAPI were detected using a BD FACSAriaII flow cytometer. Data analysis was done using BD FACSDiva software. Alexa Fluor 488 counts were normalized to DAPI.

Results:

For all the doses studied, increase in electroporation field strength increases the uptake of OG-Taxol, compared to control cells (treated with respective dose of OG-Taxol but not electroporated). At 500 Vcm^{-1}, the increase in uptake was not significant in all the doses studied. However, when cells were electroporated at field strengths 1000 Vcm^{-1} or more, the uptake of OG-Taxol was significantly higher compared to non-electroporated controls. At 0.5mM, the uptake of OG-Taxol increased by 53% when electroporated at 2500 Vcm^{-1}. At 1 mM, the maximum uptake of OG-Taxol was observed at 1500 & 2000 Vcm^{-1}. At 1.5 & 2 mM, the maximum uptake of OG-Taxol was observed at 2000 Vcm^{-1}. In cells treated with 2 mM OG-Taxol, the enhancement in uptake of OG-Taxol due to electroporation at 2000 Vcm^{-1} was less compared to that at 1.5 mM.

Conclusion:

Electroporation at field strengths above 500 Vcm^{-1} significantly increases the uptake of OG-Taxol in pancreatic cancer cells. Further, it should be noted that increasing the electroporation field strength beyond 2000 Vcm^{-1} (irreversible range) did not result in any significant enhancement in the uptake of OG-Taxol compared to the reversible range. This clearly demonstrates that reversible electroporation may be used as promising strategy to improve chemotherapeutic resistance of pancreatic tumors, by enhancing the membrane permeability.
AUTHORS (LAST NAME, FIRST NAME): West, Derek L.[1]; Sankaranarayanapillai, Madhuri[1]
INSTITUTIONS (ALL):
1. Radiology/ Bioengineering and nanomedicine, University of Texas HealthSciences Center at Houston, Houston, TX, United States.
(No Image Selected)

CONTROL ID: 2234371

TITLE: Imaging electroporation induced nanopores in Pancreatic cancer *in vitro* using Atomic Force Microscopy

PRESENTER: Derek West

ABSTRACT BODY:

Abstract Body: Introduction:

Electroporation is the application of strong electric pulses across a cell or tissue to create membrane nanopores which enhance the permeability of the cell membrane. Electroporation is reversible when the intensity and duration of the applied electric pulse is lower than the threshold value of the target cell/tissue. In this case, the created nanopores will not be permanent. Reversible electroporation has become an important technique in molecular medicine. It is used to introduce macromolecules such as genes or anti-cancer drugs, to which the cell membrane is normally not permeable, into the cytosol. Preclinical studies have demonstrated that electroporation enhances therapeutic efficacy of anticancer drugs in pancreatic tumor models. It has been further suggested that electroporation may enhance the intracellular nanoparticle uptake in tumors. With this perspective, the current project is aimed to study the electroporation induced nanopore formation in Pancreatic cancer *in vitro* using atomic force microscopy (AFM) in order to optimize the electroporation conditions for optimal drug delivery/nanoparticle uptake.

Methods:

Monolayers of human pancreatic cancer cells, Panc-1 were cultured in 35mm petri dishes. The cells were electroporated using a Petri Pulser connected to ECM 830 Square Wave Electroporation System (BTX Harvard Apparatus, MA, USA). The electroporation settings used were as follows: field strength of 500, 1000 and 1500 Vcm^{-1}; pulse length of 99 µs; eight pulses; interval 100ms. At different time points after electroporation (0min, 1hr, 2 hrs, 3 hrs and 4 hrs), the cells were fixed in 4% paraformaldehyde. The fixed cells were washed thoroughly with deionized water and dried. The AFM images of the nanopores formed by electroporation were acquired using a BioScope IITM Controller (Bruker Corporation; Santa Barbara, CA), integrated to a Nikon TE2000-E inverted optical microscope (Nikon Instruments Inc.; Lewisville, TX) to facilitate bright field imaging of the cells. AFM scanning was performed using RTESP cantilevers (fo=237-289 kHz, k=20-80 N/m, Bruker Corporation, Santa Barbara, CA). The nano-topography of the cell membrane was determined using tapping mode operated in air to a scan rate of 0.5 - 0.7 Hz. Images of the cell membrane were consecutively captured to a range of 25 to 5 μm^2 in air.

Results:

AFM images demonstrate that electroporated cells exhibit a relative increase in the number of cell membrane nanopores, compared to non-electroporated control cells (Fig.1). The increase in applied field strength increases both the number and size of the nanopores. The larger membrane pores observed at higher field strengths may be formed by combination of several single pores. Interestingly, Fig.1 also demonstrates that the nanopores remain open even after 4 hrs of electroporation.

Conclusion:

The current study clearly demonstrates the potential of electroporation to enhance membrane permeability in Panc-1 cells, by forming membrane nanopores which makes this a promising technique to improve chemotherapeutic efficacy of pancreatic tumors.

AUTHORS (LAST NAME, FIRST NAME): West, Derek L.[1]; Sankaranarayanapillai, Madhuri[1]; Moneva, Dessi[1]

INSTITUTIONS (ALL):

1. Radiology/ Bioengineering and nanomedicine, University of Texas HealthSciences Center at Houston, Houston, TX, United States.

(No Image Selected)

CONTROL ID: 2234356

TITLE: Imaging B cells in a mouse model of multiple sclerosis using [^{64}Cu]Rituximab-PET

PRESENTER: Michelle James

ABSTRACT BODY:

Abstract Body: Background: B cells are a key pathological feature of multiple sclerosis (MS), and are becoming an important therapeutic target for this condition. Molecular imaging of B cell infiltrates in MS could enable non-invasive tracking of disease progression and response to B cell-targeted therapies. We aim to evaluate [^{64}Cu]Rituximab, a radiolabeled antibody that specifically targets human CD20, for its ability to image B cells in a mouse model of MS using positron emission tomography (PET). **Methods:** Experimental autoimmune encephalomyelitis (EAE) was induced in transgenic mice that express human CD20 on B cells (huCD20tg) by subcutaneous injection of $MOG_{1–125}$ emulsified in complete Freund's adjuvant (CFA), followed by tail-vein injections of pertussis toxin (PT, 200 ng). Control mice received CFA emulsion without MOG, and the same amount of PT. PET/CT imaging of EAE and control mice was performed 1h, 4h, and 19h following [^{64}Cu]Rituximab administration (100-120 mCi). Mice were perfused and sacrificed after final PET scan, and radioactivity in dissected tissues was measured with a gamma-counter. Spinal cords and brain sections from these mice were further analyzed via digital autoradiography and subsequently stained to evaluate levels of B cells using a B220 antibody (marker of all B cells throughout development). **Results:** [^{64}Cu]Rituximab was synthesized with high specific activity of ≥35 mCi/mg and radiochemical purity >95%. Spinal cord and brain [^{64}Cu]Rituximab-PET signal was significantly higher in huCD20tg EAE mice compared to controls as early as 1h post-injection of radiotracer (lumbar: 5.44±0.37 vs. 3.33±0.20%ID/g, $p<0.01$; thoracic/cervical: 4.15±0.28 vs. 3.23±0.18%ID/g, $p<0.05$). Uptake in specific brain regions (see Fig. 1) ranged between 1.74±0.11 and 2.93±0.15%ID/g for EAE mice compared to 1.25±0.08 and 2.24±0.11%ID/g for controls, $p<0.05$ for all regions except pons (*n=4 per group*). Similarly, biodistribution results revealed significantly higher [^{64}Cu]Rituximab uptake in brain and spinal cord of huCD20tg EAE mice - whole brain: 0.23±0.04 vs. 0.11±0.02%ID/g, $p<0.05$; lumbar: 1.05±0.12 vs. 0.21±0.04%ID/g, $p<0.01$; thoracic/cervical: 0.69±0.10 vs. 0.20±0.04%ID/g, $p<0.01$ (*n=5 per group*). Furthermore, B220 immunostaining verified that increased [^{64}Cu]Rituximab uptake in specific brain/spinal-cord regions corresponded with elevated B cell levels in huCD20tg EAE mice. **Conclusion:** To our knowledge, this is the first report of imaging B cells in a mouse model of MS using PET. [^{64}Cu]Rituximab-PET shows great potential for visualizing B cells in the progression and treatment of MS, and also presents a possible translatable opportunity for stratifying patient sub-populations that could benefit from B cell targeted MS therapies. Imaging strategies like this could be game changing for MS precision medicine.

AUTHORS (LAST NAME, FIRST NAME): James, Michelle L.[1]; Hoehne, Aileen[1]; Natarajan, Arutselvan[1]; Gowrishankar, Gayatri[1]; Nguyen, Di-Son[1]; Chandra, Sudeep[2]; Gambhir, Sanjiv S.[1]

INSTITUTIONS (ALL):

1. Radiology, Stanford University, Stanford, CA, United States.
2. Clinical and Translational Imaging, Novartis Institute of Biomedical Research, Cambridge, MA, United States.

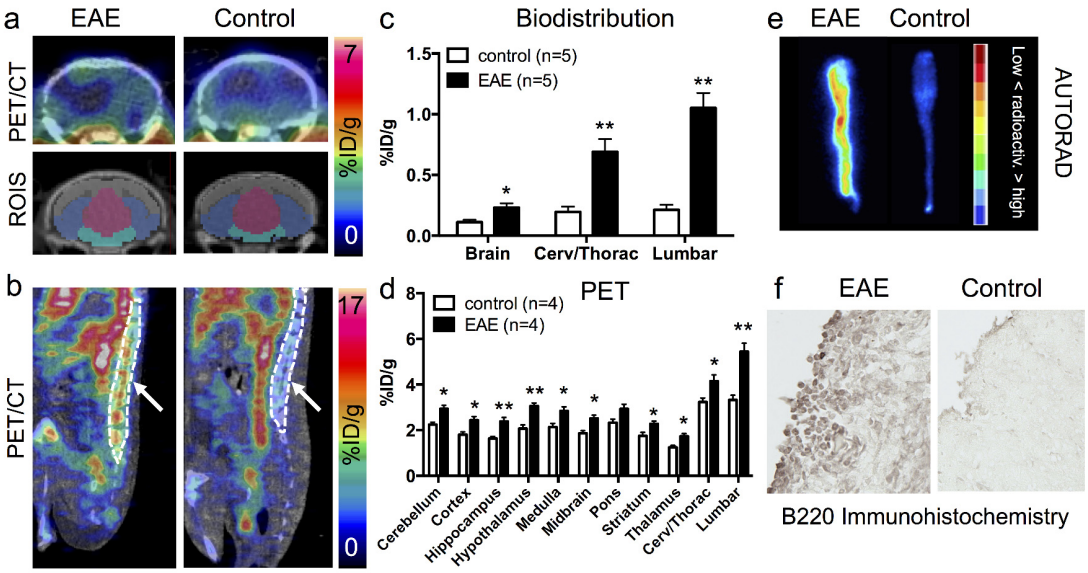

Figure 1. [^{64}Cu]Rituximab PET imaging enables visualization of B cells in a human CD20 mouse model of multiple sclerosis (huCD20tg-EAE). Representative fused PET/CT images of (a) coronal brain slices and (b) sagittal spinal cord slices visually depicts higher signal in brain and spinal cord of huCD20tg-EAE compared to control mice 1 hour after tail-vein injection with [^{64}Cu]Rituximab (100-120 mCi). Tracer uptake in specific brain regions of interest (ROIs) was calculated by coregistering a mouse brain atlas to PET/CT data, as shown below brain PET/CT images. Dashed lines and white arrows in (b) highlight lumbar spinal cord in sagittal PET/CT images. (c) Biodistribution of [^{64}Cu]Rituximab reveals higher levels of tracer uptake in whole brain, cervical/thoracic (cerv/thorac) spinal cord, and lumbar spinal cord of huCD20tg-EAE compared to control mice. Likewise, quantitation of PET imaging data in (d) shows that huCD20tg-EAE mice have significantly higher [^{64}Cu]Rituximab uptake in specific brain and spinal cord regions. (e) High resolution *ex vivo* autoradiography images of whole lumbar spinal cords (19 hours after [^{64}Cu]Rituximab administration) further confirm the higher uptake of [^{64}Cu]Rituximab in huCD20tg-EAE mice compared to controls in this tissue, which corresponds with (f) B220 (B cell) immunostaining results, using 10 µm-thick lumbar spinal cord sections, 40x magnification.

CONTROL ID: 2234360

TITLE: Accumulation of [^{18}F]FACE in cerebral ischemia

PRESENTER: Hiroshi Mizuma

ABSTRACT BODY:

Abstract Body: Fluoroacetate (FACE) has been known to be preferentially incorporated into astrocyte because of its high expression of monocarboxylic transporter (MCT) and acts as a metabolic toxin blocking the tricarboxylic acid (TCA) cycle. Therefore, [^{18}F]FACE is used to monitor the metabolism of astrocytes in brain. Recently, astrocyte has been reported to play a crucial role in neuronal cell death by ischemic injury in response to intracellular acidosis driven by its emergent lactate production (Beppu K, Neuron, 2014). In this study, to investigate changes in glial metabolism during ischemia, we performed PET imaging with [^{18}F]FACE in rat transient MCAO model. Imaging analysis has revealed that [^{18}F]FACE significantly accumulated in the ipsilateral region during ischemia in spite of low cerebral circulation. [^{18}F]FACE accumulation was also observed after the reperfusion but it was gradually decreased in a time dependent manner. [^{18}F]FACE remained mostly unchanged form even in ischemic region and distributed into cytosolic but not mitochondrial fraction in subcellular fraction analysis, indicating no metabolic trapping mechanism in its accumulation. In addition, histological analyses revealed that [^{18}F]FACE accumulation was not associated with appearance of reactive astrocyte and breakdown of blood brain barrier. Furthermore, FACE administration during cerebral ischemia with MCA occlusion in rats resulted in a significant reduction of the neurological and histological damages. Taken together, FACE itself, not fluorocitrate, may regulate the astrocyte energy metabolism, and [^{18}F]FACE can be a promising PET probe for early detection of cerebral ischemia.

AUTHORS (LAST NAME, FIRST NAME): Mizuma, Hiroshi[1]; Kagawa, Shinya[3]; Ono, Masahiro[1]; Kakumoto, Kyoko[1]; Matsumoto, Yoshino[1]; Higashi, Tatsuya[3]; Nishii, Ryuichi[2]; Onoe, Hirotaka[1]

INSTITUTIONS (ALL):

1. Division of Bio-Function Dynamics Imaging, RIKEN Center for Life Science Technologies, Kobe, Japan.
2. Radiology, University of Miyazaki, Miyazaki, Japan.
3. Division of PET imaging, Shiga Medical Center Research Institute, Moriyama, Japan.

(No Image Selected)

CONTROL ID: 2234368

TITLE: Targeting SLC1A5-mediated glutamine dependence in non-small cell lung cancer

PRESENTER: Pierre Massion

ABSTRACT BODY:

Abstract Body: We previously elucidated the pleotropic role of solute carrier family A1 member 5 (SLC1A5), as the primary transporter of glutamine (Gln), a modulator of cell growth and oxidative stress in non-small cell lung cancer (NSCLC). The aim of this study was to evaluate SLC1A5 as a potential new therapeutic target and candidate biomarker predictive of survival and response to therapy. SLC1A5 targeting was examined in a panel of NSCLC and human bronchial cell lines by RNA interference and by a small molecular inhibitor, gamma-l-Glutamyl-p-Nitroanilide (GPNA). The effects of targeting SLC1A5 on cell growth, Gln uptake, ATP level, autophagy, and cell death were examined. Inactivation of SLC1A5 genetically or pharmacologically decreased Gln consumption, inhibited cell growth, induced autophagy and apoptosis in a subgroup of NSCLC cell lines that overexpress SLC1A5. Targeting SLC1A5 function decreased tumour growth in NSCLC xenografts. A multivariate Cox proportional hazards analysis indicates that patients with increased SLC1A5 mRNA expression have significantly shorter overall survival (P= 0.01, HR=1.24, 95% CI,1.05-1.46), adjusted for age, gender smoking history and disease stage. In an immunohistochemistry study on 207 NSCLC patients, SLC1A5 protein expression remained highly significant prognostic value in both univariate (P <0.0001, HR=1.45, 95% CI, 1.15-1.50) and multivariate analyses (P=0.04, HR=1.22, 95% CI, 1.01-1.31). These results position SLC1A5 as a new candidate prognostic biomarker for selective targeting of Gln-dependent NSCLC.

AUTHORS (LAST NAME, FIRST NAME): Hassanein, Mohamed[1]; Qian, Jun[1]; Hoeksema, Megan[1]; Harris, Bradford K.[1]; Ji, Xiangming[1]; Chen, Heidi[1]; Eisenberg, Rosana[1]; Massion, Pierre P.[1]

INSTITUTIONS (ALL):

1. Vanderbilt University, Nashville, TN, United States.

(No Image Selected)

CONTROL ID: 2234376

TITLE: Copper-Free ‘Click’ Chemistry Mediated Directional Bioconjugation of Nanoparticle Contrast Agents

PRESENTER: Jason Cook

ABSTRACT BODY:

Abstract Body: Molecular imaging has the promise to enable cancer diagnosis at the very inception of disease. To help reveal disease, a vast library of contrast agents have been developed for all of the major imaging modalities. Although contrast-agents can be differentiate from tissues and cells throughout the body, in the scope of medical imaging they are only as good as their disease-specific targeting system. For nanoparticle-based contrast agents, which can extravasate form the vasculature, monoclonal antibodies are commonly selected to specifically label overexpressed antigens indicative of cancerous cells and tissues. However, simply attaching antibodies to the surface of nanoparticles can cause non-specific labeling of many immune cells in-vivo, in-vitro, or ex-vivo because of exposed fragment crystallizable regions (Fc).

To improve molecular-specificity, we have developed a directional bioconjugation strategy that functionalized the nanoparticle surface and the Fc portion of the antibody with high affinity copper-free ‘click’ chemistry agents. Specifically, dibenzocyclooctyne-amine is used to functionalize carboxylic acid coated nanoparticles via EDC/Sulfo-NHS chemistry. The antibody modification begins with the oxidation of glycosolates on the Fc region to aldehydes. The antibodies are then mixed with 4-azidobenzohydrazide, thus functionalizing the Fc region with azides. The modified nanoparticles and modified antibodies are combined forming the high affinity strain-promoted alkyne-azide cycloaddition. To enhance the nanoparticle stability, poly(ethylene glycol) methyl ether azide was used to react the remaining cyclootynes. The reaction diagram is shown in the upper part of the figure.

To test the specificity of the bioconjugated nanoparticles two cell lines were selected: epidermal growth factor receptor (EGFR) overexpressing A431 squamous cell carcinoma cells and Fc expressing J774A.1 macrophage cells. The cells were cultured, formalin fixed, and adhered to a glass microscope slide. After heat-induced epitope retrieval (to revive the antigens), cells were incubated with iron-oxide nanoparticles conjugated with clone 29.1 anti-EGFR antibody (specific for the A431 cells) and clone RG16 anti-rabbit immunoglobulins antibody (not specific for either cell line) for 60 minutes. To enhance optical image contrast, the samples were then stained using Prussian Blue stain. The cell samples were then rinsed, dehydrated, and mounted and coverslipped. As shown in the lower figure, the only sample that provided bright-field contrast was when the overexpression antigen was matched with the corresponding antibody conjugated nanoparticle.

In addition to excellent specificity, this and can minimize costly antibody waste with high affinity copper-free ‘click’ chemistry. Another benefit of using copper-free ‘click’ chemistry is that it is bioorthagonal. Overall, the directional bioconjugation of nanoparticle contrast agents using copper-free ‘click’ chemistry strategy can be used to enhance nanoparticle contrast agent specificity with current and developing molecular imaging modalities.

AUTHORS (LAST NAME, FIRST NAME): Cook, Jason[1]; Slaughter, Brandon V.[1]; Emelianov, Stanislav Y.[2]

INSTITUTIONS (ALL):

1. Biomedical Engineering, The University of Texas at Austin, Austin, TX, United States.
2. Biomedical Engineering, University of Texas at Austin, Austin, TX, United States.

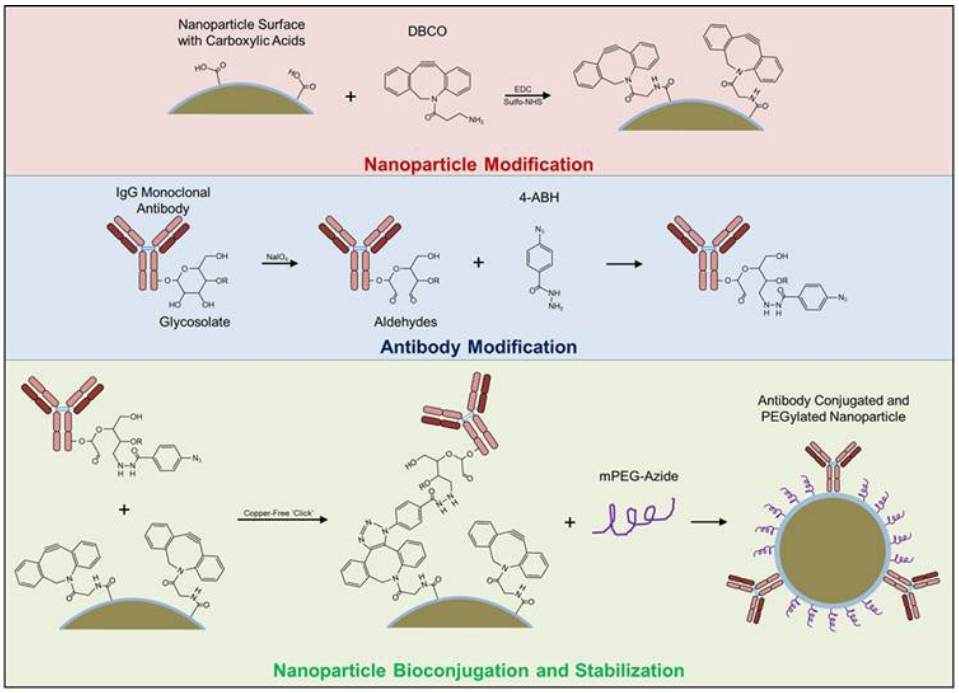

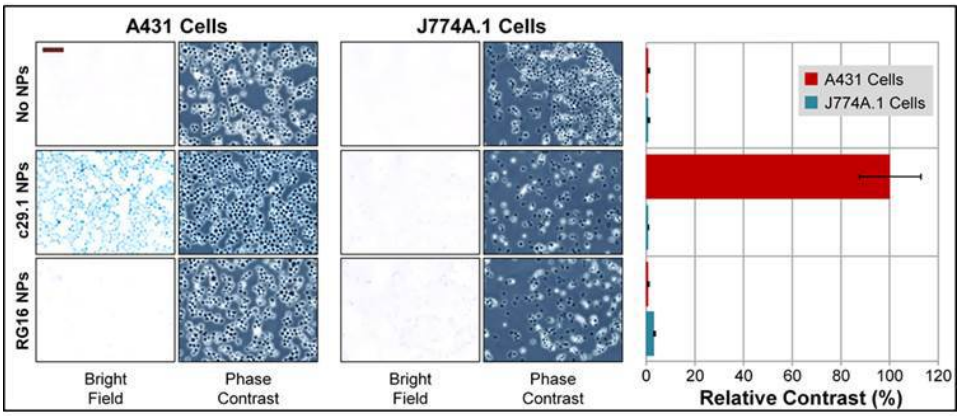

Figure 1: The upper portion of the figure is a diagram of the nanoparticle functionalization with cyclooctynes, the Fc portion of the antibody functionalization with azides, and the nanoparticle bioconjugation and PEGylation for stabilization. The lower portion of the figure demonstrates the antigen specificity of the bioconjugated nanoparticles. The only sample labeled was the EGFR-expressing A431 cells when incubated with nanoparticles conjugated with anti-EGFR antibodies. The phase-contrast images indicate the positions of the cells in the bright-field image. The graph on the right indicates the relative contrast, illustrating the specificity of the bioconjugated nanoparticles.

CONTROL ID: 2234389

TITLE: Radioluminescence Microscopy of FDG: Microenvironmental factors modulating FDG uptake

PRESENTER: Silvan Tuerkcan

ABSTRACT BODY:

Abstract Body: Fluorodeoxyglucose (FDG), a radiolabeled glucose analog, is widely used in medical imaging for staging, evaluation of treatment response, and detection of metastases. Yet, many factors influencing the uptake of FDG into tumor cells remain to be understood. *In-vivo* PET and autoradiography studies show that the tumor microenvironment influences FDG uptake in a tumor mass, but do not discriminate between tumor and non-tumor cells. *In-vitro* studies on cells highlight the importance of glucose transporter expression levels and hexokinase activity, but fail to capture more complex influences.

In the presented work, we aim at studying FDG uptake in single living cells to bridge the gap between *in-vivo* and *in-vitro* studies, and determine the driving microenvironmental factors that modulate FDG uptake. Using murine subcutaneous tumor graft models (4T1 and MDA-MB-231 cells), we surgically separated tumors into two components, namely the periphery and the core, before digesting the tissues into a single-cell suspension. We then applied a new technique, termed radioluminescence microscopy (RLM), to visualize FDG uptake in single living cells. This method allows us to study glycolysis, as represented by FDG uptake, in single cells that were exposed to radically different tumor microenvironments. Unlike *in vivo* approaches, we measure the intrinsic glycolysis of the cell, independently of the density of viable cells and the radiotracer delivery. At the same time, we can vary individual environmental factors in cell culture to test various hypotheses.

For tumors larger than 8 mm diameter (but not for smaller tumors), RLM revealed that FDG uptake was significantly larger in cells from the periphery of the tumor than from the core. Overall, uptake of FDG measured at the single-cell level was more heterogeneous in freshly excised tumors than in cultured cells, which lack the complex tissue microenvironment. The heterogeneity was also greater at the core of the tumor than at the edge. To better understand these variations, we investigated the effects of hypoxia, serum starvation, and lactic acid on FDG uptake in cultured cells. As expected, hypoxia increased FDG uptake in cell lines and therefore cannot explain the observed decrease of FDG uptake in the hypoxic core. We also found that cell quiescence (serum starvation) resulted in a decrease of 63% (4T1) and 37% (MDA) in FDG uptake in culture, but PI staining and flow cytometry indicated that cells from the tumor were not quiescent, ruling out quiescence as a driving force. Last, we found that lactic acid reduced FDG uptake by 70% in both cell lines. Given that this metabolite of glucose is concentrated at the center of the tumor, we conclude that it could be involved in modulating FDG uptake. Together, our results show that cells that have adapted to very different microenvironments metabolize glucose at different rate. While hypoxia and proliferation are well known for their effect on FDG uptake, lactic acid concentration is a novel modulator of FDG uptake. In conclusion, FDG uptake should be interpreted with caution as it depends both on the fraction of viable cells and on the microenvironment.

AUTHORS (LAST NAME, FIRST NAME): Tuerkcan, Silvan[2]; Sasportas, Laura S.[3]; Naczynski, Dominik J.[2]; Shen, Bin[1]; Chin, Frederick T.[3]; Pratx, Guillem[4]

INSTITUTIONS (ALL):

1. Stanford University, Stanford, CA, United States.
2. Radiation Oncology, Stanford University, Palo Alto, , CA, United States.
3. Radiology, Stanford University, Stanford, CA, United States.
4. Radiation Oncology, Stanford University, Palo Alto, CA, United States.

(No Image Selected)

CONTROL ID: 2234390

TITLE: Evaluation of Standard Performance of PET/MRI Systems for Imaging Small Animals, and Development of Protocol for Fused Images

PRESENTER: Jin Hwa Chung

ABSTRACT BODY:

Abstract Body: We evaluate the performance of NanoScan PET/MRI (NanoPM - Mediso, Hungary) systems for imaging small animals as first installation in Korea. We assessed physical features of boh PET/MR scanners using NEMA NU-1 2001 protocol, and developed a PET/MRI fused image protocol suitable for small animals imaging.

Method: We evaluate the PET performance of the NanoPM in terms of spatial resolution (SRES) and sensitivity (SENS) of the systems using the Na-22 point source (25uCi) at off-axial positons of at intervals of 1 mm, 10 mm, and 25 mm for SRES. Regarding SENS, we acquired 20-minute imaging at afforementioned positiones. We reconstructed PET images using the 2D OSEM(SSRB, ring difference 8, 400-600 keV). In addition, we evaluated FWHM, S_{tot} (kcps/kBq) and SA_{tot}(%) per NEMA protocol. To measure uniformity, recovery coefficient(RC), SOR_{water}, and SOR_{air}, image quality (IQ) phantom images filled with 3.2 MBq FDG were acquired and reconstructed using the 3D OSEM method. To measure the MRI performance, 35 mm and 60 mm coils' central frequency and SNR, and noise level and ghost level were measured, using cylinder phantoms filled with the 20 mM $NiCl_2$ solution. To establish a routine protocol for imaging the mouse whole body and brain, and rat brain, images were acquired using mice with Xenografted tumor, and rats with Parkinson disease. For whole body MR, 1mm slice thickness and 100 x 100 matrix (0.5mm pixel) were set up; for brain image the same slice thickness with 128 x 128 matrix (0.4mm pixel) were used. For brain, T2 FSE 3D sequence was also used. PET images were reconstructed using 3D OSEM algorithm and various energy windows, coincidence modes, voxel sizes, attenuation correction and iterations.

Results: PET image SRES (FWHM) was 0.77 mm(radius direction), 0.83 mm(tangential direction), and 0.92 mm(axial direction) at 1mm off-axial (1.13/0.89/1.02 mm at 10 mm; 1.14/1.14/1.4 mm at 25 mm). Regarding SENS, at the axial-direction center and at +/-25 mm, S_{tot}(kcps/kBq) and SA_{tot}(%) were measured as 0.02, 8.1%(center), 0.434, 4.3%(+25 mm), and 0.05,4.8%(-25 mm), respectively. The IQ phantom test revealed that the uniformity was an average of 115 and had a standard deviation of 3.8%. MR performance using 60mm coil in terms of central frequency, SNR, and noise level were 44.98, 5644, and 384, respectively; for 35 mm coil, 44.98, 11782, and 367, respectively. Ghost levels in axial/coronal/sagittal images with 60 mm coil were 1.1/0.9/1.5%; with 35 mm coil, 0.9/1.3/1.1%, respectively. The PET images were reconstructed using 250-750 keV Energy window, 0.5 mm voxel, iteration x subset: 4 x 6 for the body images, and 0.4mm voxel and 8 x4 for brain. When the slice thickness and the matrix thickness in body and brain images were changed, the time for acquiring total MR images was cut from 20 to 10 minutes with the image quality maintained, and the time for image reconstruction was cut from 20 to 7 minutes.

Conclusion: The NanoPM performance was suitable for imaging body/brain of small animals, and we optimized MR image proctrol in terms of clinically feasilbe scan time while image quality maintained using various MR acquisition parpamters.

AUTHORS (LAST NAME, FIRST NAME): Chung, Jin Hwa[1]; Oh, Jungsu S.[2]; Ryu, Jin-Sook[2]; Kim, Jae Seung[2, 1]

INSTITUTIONS (ALL):

1. Asan Institute for Life Sciences, Asan Medical Center, University of Ulsan College of Medicine, Seoul, Korea (the Republic of).

2. Dapartment of Nuclear Medicine, Asan Medical Center, University of Ulsan College of Medicine, Seoul, Korea (the Republic of).

(No Image Selected)

CONTROL ID: 2234382

TITLE: Targeted PET Imaging of Breast Cancer Using Bisphosphonates

PRESENTER: Brad Ahrens

ABSTRACT BODY:

Abstract Body: Early detection of breast cancer is paramount in improving chances of remission and survival by allowing treatment before the cancer can progress or metastasize. Currently, the most widely used form of breast cancer screening is mammography, which uses low energy radiography to visualize the micro-architecture of the breast in order to detect any masses or micro-calcifications which may indicate cancer. Microcalcifications in breast tissue are made up of a variety of calcium crystals, with the most common being hydroxyapatite – the major constituent of bone. In this study, we sought to exploit this observation by using a class of drugs known as bisphosphonates, which has a very high affinity for hydroxyapatite, as a targeting agent for these microcalcifications. We conjugated two bisphosphonates (Risedronate and Alendronate) to DOTA (1, 4, 7, 10-tetraazacyclododecane- 1, 4, 7, 10-tetraacetic acid) or desferoxamine then radiolabeled with copper (^{64}Cu) or zirconium (^{89}Zr), respectively for use as PET imaging agents. To assess the viability of these radiolabeled bisphosphonate compounds for imaging human breasts, we used aged, female, retired breeder rats. These animals have significantly developed mammary glands, which have undergone several cycles of pregnancy associated hypertrophy and atrophy, as in most human women and show similar age related histologic changes. Furthermore, aged rats develop spontaneous benign tumors, as well as reliable carcinomas, when induced with a specific carcinogen, NMU (*N*-Nitroso-*N*-methylurea). These tumors are both similar to those seen in humans. These rats provided us with an *in vivo* model for assessing neoplasic and normal age related changes of breast tissue using our bisphosphonate derived PET contrast agents. ^{64}Cu - Alendronate-DOTA has shown significant targeting to breast tissue in both normal and tumor bearing rats. In addition, we also conjugated bisphosphonates to FAM (carboxyfluorescein), and 1.4nm nanogold for use in confocal and electron microscopy to validate the targeting of the bisphosphonate derived PET imaging agents and to observe the histological and ultrastructural characteristics associated with microcalcifications. FAM and nanogold conjugated Alendronate both showed excellent specificity for breast microcalcifications in microscopy sections. We have found that bisphosphonates represent useful molecules for targeting microcalcifications in breast tissue and can be derivatized to create breast specific PET imaging agents.

AUTHORS (LAST NAME, FIRST NAME): Ahrens, Brad[1]; Weist, Michael R.[2]; Chea, Junie[2, 1]; Miles, Joshua[1]; Poku, Erasmus K.[1]; Colcher, David[1]; Shively, John E.[1]

INSTITUTIONS (ALL):

1. Immunology, Beckman Research Institute at City of Hope, Duarte, CA, United States.

2. Immunology, City of Hope, Duarte, CA, United States.

(No Image Selected)

CONTROL ID: 2234402

TITLE: Selective Imaging of Soluble Amyloid Beta Species Using Near Infrared Fluorescent Curcumin Analogues

PRESENTER: Chongzhao Ran

ABSTRACT BODY:

Abstract Body: Objective: Recent evidence shows that soluble Aβs are more neurotoxic than insoluble deposits, and thus could potentially serve as biomarkers for pre-symptomatic stages of Alzheimer's disease (AD). Originally, the burden of insoluble deposits was thought to cause neurodegeneration, but it correlates poorly with Alzheimer's disease severity. Previously, strategies using insoluble Aβ deposits as evaluation biomarkers in AD drug development have failed, and this failure has promoted a shift towards targeting soluble Aβs. In addition, the failure also has led to more clinical trials to be conducted at the early/pre-symptomatic stage. However, no imaging probe is available for detecting soluble Aβs either in preclinical animal research or clinical trial stages.

Method: The use of small molecules to differentiate soluble and insoluble Aβs is challenging, because they sharethe same amino acid sequence. To the best of our knowledge, no small-molecule probe has been reported for selective detection of soluble Aβs. We hypothesized that the different accessibility of the secondary/tertiary structures of Aβs can be harnessed to differentiate soluble and insoluble Aβs. Our preliminary SAR (structure activity relationship) studies suggest that a planar curcumin scaffold has access to both soluble and insoluble Aβs. We reason that sterically non-coplanar curcumin analogues have reduced accessibility to the insoluble Aβs, thus increasing their selectivity for soluble Aβs. A series of curcumin analogues with a bulky group at 4-position were designed and synthesized.

Results: In vivo two-photon imaging showed that CRANAD-75, a curcumin analogue with a bulky group at 4-poistion of the curcumin scaffold, could easily cross the BBB in mice. In addition, our data demonstrated that CRANAD-75 could selectively detect soluble Aβs in vitro, ex vivo and in vivo.

Conclusion: We believe that our imaging probes can be used to monitor the changes of soluble Aβs after treatment, and have tremendous potential for AD drug development.

AUTHORS (LAST NAME, FIRST NAME): Ran, Chongzhao[1]; Li, Yuyan[1]; Moore, Anna[1]

INSTITUTIONS (ALL):

1. Massachusetts General Hospital/Harvard Medical School, Charlestown, MA, United States.

(No Image Selected)

CONTROL ID: 2235383

TITLE: Influence of Disturbed Hemodynamics on Microbubble Targeting

PRESENTER: Sunil Unnikrishnan

ABSTRACT BODY:

Abstract Body: Objective: Atheroprone areas, like arterial bifurcations and curvatures, and vascular abnormalities, like stenoses and aneurysms, are sites of disturbed flow. At these locations, the flow separates from the wall and reattaches some distance downstream, establishing a recirculation zone. Additionally, the spatial distribution of wall shear rates (WSR) is non-uniform. These regions of the vasculature are important candidates for diagnostic imaging. Ultrasound molecular imaging using targeted microbubbles is a reliable technique for early detection of disease markers and monitoring disease progression. In this context, understanding the influence of disturbed flow on targeting is vital for the rational design of microbubbles. We hypothesized that disturbed flow would promote localized microbubble adhesion in the vasculature. This was tested in a model of disturbed flow implemented using a backward-step flow expansion chamber.

Methods: The flow studies were conducted with biotinylated microbubbles with dil dye incorporated in the lipid shell. A parallel-plate flow chamber was modified to create the disturbed flow environment. The step expansion was created by the layering of two gaskets. Step expansions of ratio 1:2 (inlet = 254 μm, outlet = 508 μm) and 1:3 (inlet = 127 μm, outlet = 381 μm) were generated by the arrangement of gaskets. For the 1:2 expansion, two shear rates were tested (350 s^{-1} and 700 s^{-1}). The binding study in the 1:3 expansion was conducted at 700 s^{-1}. Binding was also assessed with RBCs at 40% hematocrit and WSR 350 s^{-1} (1:2 expansion). Microbubble binding to streptavidin was quantified using fluorescent microscopy. Microbubbles were allowed to bind under flow for 2 min. After 2 min, images were sequentially collected, beginning at the step and up to a distance 2000 μm downstream. Image analysis was performed off-line. Each field-of-view was partitioned into sections 50 μm wide and the adherent microbubbles in each section were counted. Flow simulations using computational fluid dynamics (CFD) software COMSOL Multiphysics were conducted to compute the wall shear rates and the flow velocities in the vicinity of the flow reattachment zone.

Results: Microbubble adhesion was augmented in the vicinity of the reattachment zone relative to the region far downstream in all flow conditions. With 1:2 expansion ratio, the peak adhesion at the flow reattachment region relative to far downstream, was greater at higher WSR (4-fold at 700 s^{-1} vs 2-fold at 350 s^{-1}). With step expansion ratio of 1:3, the peak adhesion in the region was enhanced 8-fold at 700 s^{-1}. The enhancement in localized adhesion with RBCs was lower compared to that observed with plain buffer. Wall-directed normal velocity, computed from CFD simulations, correlated with the regions of elevated binding, suggesting that convective transport towards the wall enhances microbubble adhesion.

Conclusions: Disturbed flow enhanced localized microbubble targeting under flow (up to 8-fold). CFD simulation identified convective transport as an important determinant of adhesion. Overall, we demonstrate that locally disturbed hemodynamics play a critical role in microbubble targeting.

AUTHORS (LAST NAME, FIRST NAME): Unnikrishnan, Sunil[1, 2]; Klibanov, Alexander L.[2, 1]

INSTITUTIONS (ALL):

1. Biomedical Engineering, University of Virginia, Charlottesville, VA, United States.
2. Dept. of Medicine, Cardiovascular Div., University of Virginia, Charlottesville, VA, United States.

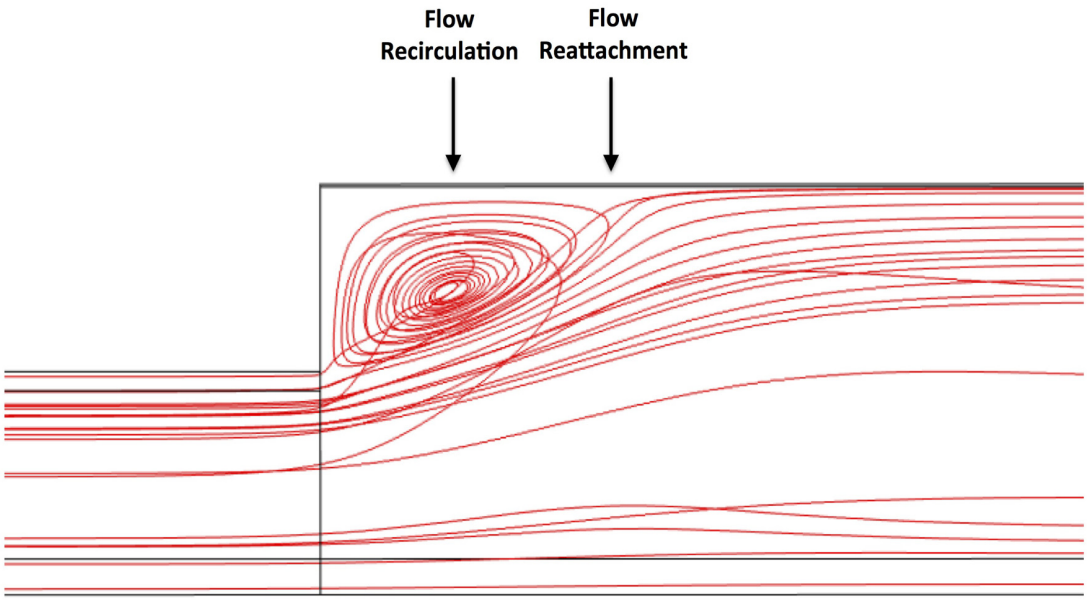
Flow
Recirculation
Flow
Reattachment

CONTROL ID: 2236352

TITLE: Planning lung radiotherapy incorporating motion freeze PET/CT imaging

PRESENTER: Kuei-Ting Chou

ABSTRACT BODY:

Abstract Body: **Objectives**: Motion freeze (MF) technology integrating 100% of the PET counts has the potential to eliminate the influences induced by respiratory motion in PET data. In this study, we investigated the impact of using PET/CT images obtained from motion freeze technology in intensity modulated radiation therapy planning in lung cancer radiotherapy.

Materials and Methods: Four patients with diagnosis of lung cancer confirmed by oncologists were recruited. 4D PET/CT with the Varian real-time position management for respiratory motion tracking was followed by a clinical 3D PET/CT scan procedure. Deformation matrices calculated by optical flow method was applied with MF technique to generate a single 3D effective PET image (PET_{MF}) using the data from all the 10 4D PET phases. PET_{MF}/CT images were registered with simulation CT for treatment planning. Two IMRT plans based on planning target volumes (PTV) delineated using PET and PET_{MF} were designed and compared in each patient. Dosimetric parameters of the two different plans were compared in terms of tumor coverage and avoidance of normal tissues and critical organs.

Results: Decreases of PTV were observed in the plans incorporated with PET_{MF} as compared of the plans using conventional PET. The median reductions of the mean doses to lung, heart, and spinal cord in the plan using PET_{MF} were 2.8, 1.6 and 1.2 Gy, respectively, compared with those in the plans using conventional PET. Plans using PET_{MF} demonstrated significant improvement in lung dose including V5, V20 and mean dose.

Conclusions: It is feasible to incorporate PET_{MF} on IMRT planning and, subsequently, to reduce dose to normal lung when target volumes are more accurately delineated by motion freeze correction.

AUTHORS (LAST NAME, FIRST NAME): Chou, Kuei-Ting[1]

INSTITUTIONS (ALL):

1. China Medical University, Taichung, Taiwan.

(No Image Selected)

CONTROL ID: 2238510

TITLE: ***FOXF1*** **Mediates Lung Cancer Cell Reprogramming to a Stem-like State Following Spontaneous Fusion with Mesenchymal Stem Cells**

PRESENTER: Win-Ping Deng

ABSTRACT BODY:

Abstract Body: Several reports suggest that tumor cells acquire a more aggressive, malignant phenotype through fusion with various types of bone-marrow derived cells (BMDCs) within tumor stroma. However, the role of mesenchymal stem cells (MSCs), a promising fusogenic candidate of BMDCs, in tumor progression via fusion has not been fully examined. Using a dual antibiotic/dual fluorescence marker strategy we found that MSCs fuse spontaneously with lung cancer cells. In vivo bioluminescence imaging was then used to demonstrate that fusion progeny are reprogrammed to a non-tumorigenic, stem-like state. We further show that FOXF1 regulates reprogramming toward stemness and to the p21-regulated growth suppression, and provide evidence using lung cancer specimens that FOXF1 is a tumor suppressor. Although MSC-lung cancer fusion progeny show reduced growth and are non-tumorigenic, they do promote growth of tumor xenografts indicating that via fusion MSCs can reprogram lung cancer cells to an atypical tissue-resident stem cell that itself is not malignant, but that promotes tumor growth via stromal effects.In summary, here we found that the intrinsic malignancy of lung cancer cells would not be promoted by MSC fusion. Such fusion process raises the therapeutic potential that MSC fusion can be utilized to reverse cellular phenotypes in cancer.

AUTHORS (LAST NAME, FIRST NAME): Deng, Win-Ping[1]; Wei, Hong-Jian[1]; Gelovani, Juri G.[2]

INSTITUTIONS (ALL):

1. Graduate Institute of Biomedical Materials and Engineering, College of Oral Medicine, Taipei Medical University, Taipei, Taiwan.
2. Biomedical Engineering, Wayne State University, Detroit, MI, United States.

(No Image Selected)

CONTROL ID: 2244314

TITLE: EGFR targeted nanobody-photosensitizer conjugates for imaging and photodynamic therapy in head and neck cancer – first preclinical studies

PRESENTER: Paul van Bergen en Henegouwen

ABSTRACT BODY:

Abstract Body: Introduction

Photodynamic therapy (PDT) induces cell death through local light activation of a photosensitizer (PS) (Agostinis et al. 2011). Targeted delivery of PS via monoclonal antibodies has improved tumor selectivity. However, these conjugates have poor tumor penetration and long half-lives, leading to relatively long photosensitivity in patients. To overcome these disadvantages, we have developed new conjugates consisting of nanobodies (NB) targeting the epidermal growth factor receptor (EGFR) and a traceable PS (IRDye 700DX) (Heukers et al. 2014). In this study we first evaluate the tumor specificity of NB-PS conjugates *in vivo* by imaging and fluorescence quantification. Thereafter, we investigated the phototoxicity induced by NB-PS *in vivo* and compared it to an antibody-PS conjugate.

Materials and Methods

The EGFR targeted nanobodies 7D12 and 7D12-9G8 were conjugated to the PS and NB-PS conjugates were characterized for their binding specificity and phototoxicity *in vitro* with EGFR overexpressing head and neck cancer cells (OSC-19). Fluorescence imaging and quantitative fluorescence spectroscopy (van Leeuwen-van Zaane et al. 2013) were performed in an orthotopic tongue tumor model (OSC-19-luc2-cGFP) to study the pharmacokinetics prior to PDT . For PDT, light was applied 1h p.i of the NB-PS or 24h p.i. of the antibody-PS (cetuximab-PS). The phototoxicity of NB-PS was evaluated and compared to that of cetuximab-PS and the nonspecific control R2-PS, by histological analysis of tongues collected 24h post PDT.

Results

NB-PS conjugates bind to EGFR expressing cells *in vitro* and induce cell death specifically on cells overexpressing EGFR. Already 1 hour after i.v. injection, fluorescence imaging showed tumor specificity and fluorescence spectroscopy showed tumor-to-background ratios (TBR) of 3.8 (±0.5) and 1.8 (±0.3) for 7D12-9G8-PS and 7D12-PS, respectively. The extent of tumor necrosis after PDT with 7D12-PS (80-90%) and 7D12-9G8-PS (60-90%) was substantially more than after R2-PS (20-60%) and cetuximab-PS (20-70%).

Conclusion

The smaller size of NB-PS enables earlier light application and leads to more evenly distributed and potent damage, compared to the antibody-PS conjugate. This study shows the potential of EGFR specific NB-PSs to specifically target head-and-neck cancers for fluorescence imaging and photodynamic therapy. This conjugate could in the future be used to first guide tumor resection and subsequently induce PDT to specifically treat residual tumor cells after resection.

AUTHORS (LAST NAME, FIRST NAME): Driel, Pieter V.[5]; Boonstra, Martin[3]; Slooter, Maxime[1]; Heukers, Raimond[7]; van Diest, Paul J.[9]; de Bruijn, Henriette[8]; Vahrmeijer, Alexander L.[6]; van Bergen en Henegouwen, Paul[7]; van de Velde, Cornelis J.[2]; Lowik, Clemens[4]; Robinson, Dominic[8]; Oliveira, Sabrina[7]

INSTITUTIONS (ALL):

1. Radiology, L.U.M.C., Amsterdam, Netherlands.
2. Leiden University Medical Center, Leiden, Netherlands.
3. Surgery, Leiden University Medical Center, Leiden, Netherlands.
4. radiology, leiden University Medical Center, Leiden, Netherlands.
5. Radiology, Leiden University Medical Center, Leiden, Netherlands.
6. Surgery, Leiden University Medical Center, Leiden, Netherlands.
7. Biology, Utrecht University, Utrecht, Netherlands.
8. Department of Otorhinolaryngology & Head and Neck Surgery, Erasmus Medical Center, Rotterdam, Netherlands.
9. Pathology, Utrecht University Medical Center, Utrecht, Netherlands.

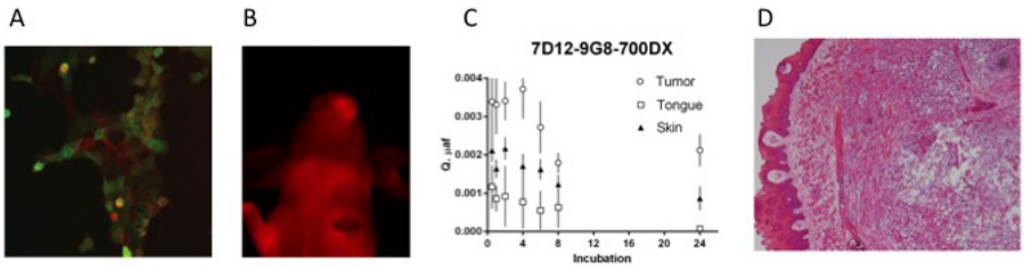

Fluorescence microscopy shows binding of 7D12-9G8-PS to EGFR expressing OSC cells (A). Tumor specific binding was confirmed *in vivo* one hour after intravenous injection of 7D12-9G8-PS (B). Spectroscopy shows a higher uptake in the tumor compared to that in normal tongue tissue and skin at every time point (C). Tumor specific cell death could be observed in histological analysis after PDT (D).

CONTROL ID: 2244081

TITLE: Development of a compact helmet-chin PET for high-sensitivity brain imaging

PRESENTER: Taiga Yamaya

ABSTRACT BODY:

Abstract Body: For a potential demand for brain molecular imaging, prototypes of brain dedicated PET scanners have been developed. However all previous developments are based on a cylindrical geometry, which is not the most efficient for brain imaging. Making the detector ring as small as possible is essential in PET, because sensitivity can be increased with a limited number of detectors. With appropriate depth-of-interaction (DOI) detectors, which reduce the parallax error caused by the thickness of the scintillators, spatial resolution can be maintained, or even improved by reducing the angular deviation effect. In this paper, therefore, we developed the world's first helmet-chin PET, in which detectors are arranged to form a hemisphere, for compact, high-sensitivity, high-resolution, and low-cost PET imaging.

Our basic idea relies on the evidence that the average sensitivity of a hemisphere PET is about 1.5-times higher than that of a cylinder PET of the same radius and height, while surface area is the same for both geometries. In addition, use of extra 12% detectors for "chin detectors", which are placed like a chin strap, improves sensitivity especially at the central area. In the prototype, 47 block detectors were used to form a hemisphere of 25cm inner diameter and 50cm outer diameter, and 7 block detectors were used for the chin strap. The total number of detectors was about only 1/5 of those to be used in whole body PET. Each detector block was a 4-layered DOI detector, which consisted of 1,024 Zr-doped GSO crystals (2.8 mm x 2.8 mm x 7.5 mm) and a high-sensitivity type of 64-channel flat-panel PMT. The data acquisition system was developed based on single events collection. An iterative reconstruction method with detector modeling was applied.

Measured sensitivity was 5% at the cerebellum region and 10% at the parietal region for a standard 400-600keV energy window. Averaged FWHM of point sources was 3.0 mm (FBP) and 1.4 mm (iterative).

In conclusion, the first prototype has provided a proof-of-concept of the helmet-chin PET.

AUTHORS (LAST NAME, FIRST NAME): Yamaya, Taiga[1]; Yoshida, Eiji[1]; Tashima, Hideaki[1]; Inadama, Naoko[1]; Shinaji, Tetsuya[1]; Wakizaka, Hidekatsu[1]; Nitta, Munetaka[1]; Tazawa, Shusaku[2]; Suhara, Tetsuya[1]; Fujibayashi, Yasuhisa[1]

INSTITUTIONS (ALL):

1. Molecular Imaging Center, National Institute of Radiological Sciences, Chiba, Japan.
2. ATOX Co. Ltd, Tokyo, Japan.

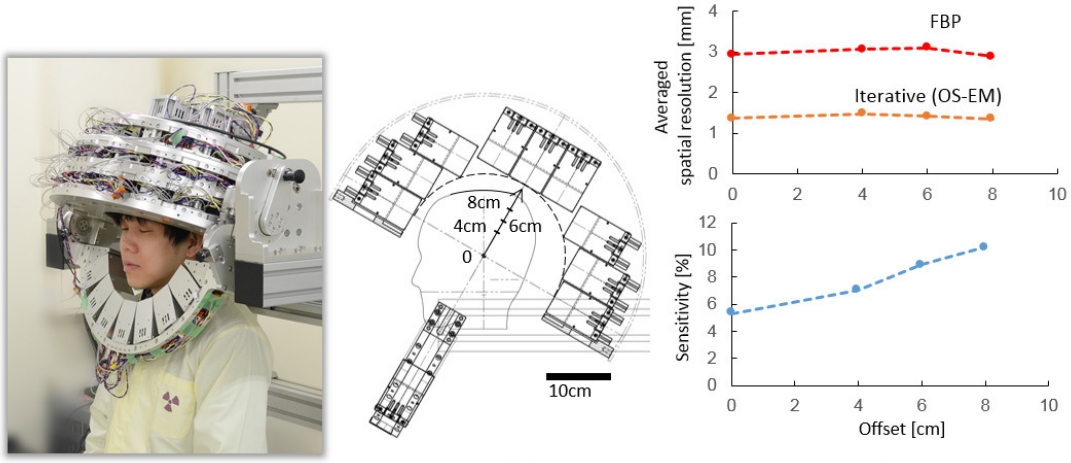

Developed prototype of the helmet-chin PET (a) and measured sensitivity and averaged spatial resolution (c) for 4 positions described in (b).

CONTROL ID: 2234384

TITLE: Comprehensive Approach to Localization of Sentinel Lymph Node and Detection of Micrometastases using Sound, Light and Molecular Contrast nanoAgents

PRESENTER: Geoffrey Luke

ABSTRACT BODY:

Abstract Body: In cancer patients, determination of whether a malignancy has spread is the single most important factor used to develop a therapeutic plan and to predict prognosis. In most cases, cancer cells initially spread through regional lymph nodes. Therefore, clinical evaluation for the presence of regional lymph node metastases is of paramount importance. Unfortunately, there are no real-time, non-invasive clinical methods that can reliably localize sentinel lymph node(s) and diagnose micrometastases in lymph nodes.

Previously, we introduced an ultrasound-guided spectroscopic photoacoustic imaging augmented with molecular plasmonic nanosensors for sensitive in vivo detection of lymph node micrometastases. Furthermore, using ultrasound-guided spectroscopic photoacoustic imaging, changes in blood oxygen saturation in lymph nodes were found to correlate with metastatic invasion. Here, we present an ultrasound contrast agent, ultrasound imaging protocol and image processing algorithm to identify location of sentinel lymph node thus completing the approach to identify the lymph nodes and to detect lymph node metastases.

An optically activated dual contrast nanoagent (Fig. 1A) for ultrasound imaging (Fig. 1B) consists of a liquid perfluorohexane nanodroplet encased in a surfactant shell and encapsulating a near infrared optical absorber. This droplet vaporizes in response to a pulsed laser irradiation, induces phase-change ultrasound contrast, and immediately recondenses due to its high boiling point relative to body temperature. By imaging the droplets using high frame rate ultrasound, we captured this rapid phase-change “blinking” behavior. Given the known pulse repetition rate of the laser and, therefore, nanodroplet vaporization, an autocorrelation applied to the differential ultrasound intensity was used to discern the nanodroplets from the surrounding tissue and provide a background-free map of the particles.

The experiments were performed using a metastatic murine model of oral squamous cell carcinoma. First, the ultrasound images of the known lymph nodes were acquired (Fig. 1C). Then the laser activated nanoagents were injected near the primary tumor and allowed to drain into lymph nodes. The lymph nodes were imaged using ultrasound transducer interfaced with the laser source (Vevo LAZR, Visualsonics, Inc.). The resulting set of high frame rate ultrasound images were used to discern the nanodroplets from the surrounding tissue and provide a background-free map of the particles within sentinel lymph node (Fig. 1D). Finally, the metastases within the lymph node of a mouse was confirmed by measuring blood oxygen saturation (Fig. 1E) using US-sPA imaging.

Overall, the developed molecular specific imaging contrast agents and advanced, in-vivo, noninvasive, integrated ultrasound and photoacoustic imaging form a foundation for a comprehensive approach capable of immediate localization of sentinel lymph node(s) and accurate assessment of sentinel lymph node micrometastases.

AUTHORS (LAST NAME, FIRST NAME): Luke, Geoffrey P.[1]; Hannah, Alexander[1]; Emelianov, Stanislav Y.[1]

INSTITUTIONS (ALL):

1. Biomedical Engineering, The University of Texas at Austin, Austin, TX, United States.

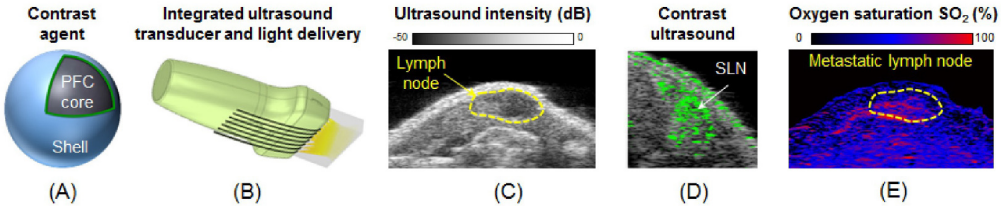

Figure 1: (A) Laser-triggered ultrasound contrast agent – PFC nanoDroplet; (B) Ultrasound imaging transducer integrated with light delivery system; (C) Ultrasound image of the lymph node; (D) Contrast-enhanced ultrasound localizes the sentinel lymph node (SLN); (E) Oxygen saturation map identifies the detected sentinel lymph node as metastatic.

CONTROL ID: 2240374

TITLE: Novel uPAR-targeted near-infrared fluorescent tracer for image-guided real-time en vivo detection of squamous cell carcinoma and cervical lymph node metastases in oral cancer in mice

PRESENTER: Anders Christensen

ABSTRACT BODY:

Abstract Body: Background: Fluorescence-guided surgery is a novel modality that enables intraoperative detection of tumor and assessment of resection margins. The urokinase-type plasminogen activator receptor (uPAR) is associated with tumor invasion and metastatic spread in oral cancer. The aim of this study was to investigate the feasibility of the optical probe ICG-Glu-Glu-AE105 targeting uPAR for detection of tumor and metastases by fluorescence-guided imaging in an orthotopic animal model of tongue cancer.

Methods: The human SCC cell line OSC-19-luc was injected into the tongue of nude mice. Tumor growth was monitored over time by bioluminescence imaging. On day 14 or day 19 10 nmol of ICG-Glu-Glu-AE105 was injected systemically and 15 hour post injection imaging in vivo and ex vivo was performed with a small-animal fluorescence scanner and with a clinically approved fluorescence camera. Injection of saline served as control. In adjacent tissue sections prepared from either fresh frozen or paraffin embedded tissue the microanatomical distribution of the fluorescent signal from ICG-Glu-Glu-AE105 was compared with H&E staining and immunohistochemical staining for uPAR and cytokeratin.

Results: Following the injection of ICG-Glu-Glu-AE105, fluorescence could successfully be detected in the primary tumor and cervical lymph node metastases. A mean tumor-to-background ratio of 3.0 (range 2.2-4.0) in the tongue tumors was observed. Real-time fluorescence-guided tumor resection was possible. Histological analysis showed microanatomical colocalization of the fluorescent signal, uPAR expression and tumor cell deposits demonstration the tumor-specific binding of ICG-Glu-Glu-AE105.

Conclusion: Specific real-time optical imaging of the primary tumor and cervical lymph node metastases with ICG-AE105 targeting uPAR proved feasible in a mouse model of tongue squamous cell carcinoma. Further study of this tumor-specific optical probe for surgical treatment of carcinomas is warranted.

AUTHORS (LAST NAME, FIRST NAME): Christensen, Anders[1, 2]; Juhl, Karina[2]; Persson, Morten[2]; Charabi, Birgitte[1]; Mortensen, Jann[2]; Kiss, Katalin[3]; buchwald, christian V.[1]; Kjaer, Andreas[2]

INSTITUTIONS (ALL):

1. Department of ORL-Head & Neck Surgery, Rigshospitalet, Copenhagen, Denmark.

2. Department of Clinical Physiology, Nuclear Medicine & PET and Cluster for Molecular Imaging, Rigshospitalet & University of Copenhagen, Copenhagen, Denmark.

3. Department of Pathology, Rigshospitalet, Copenhagen, Denmark.

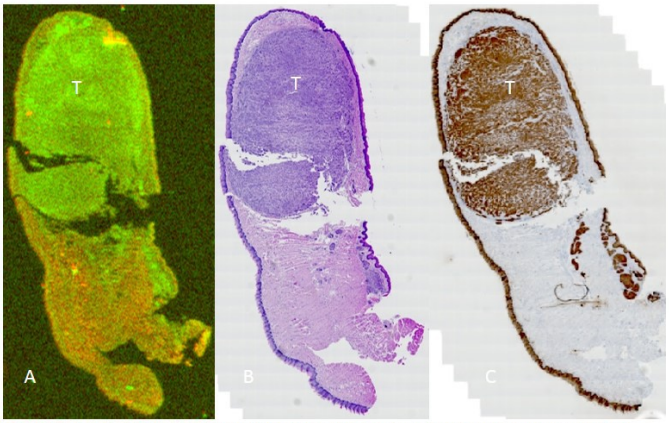

Sagittal histologial sections of a paraffin embedded mouse tongue with a squamous cell carcinoma (T) in the anterior part. The animal was systemically injected with ICG-Glu-Glu-AE105 targeting uPAR 15 hours prior to imaging. Near-Infrared flouresecence scanning of the unstained paraffin section (A), the same section after H&E staining (B) and the adjacent Cytokeratin staining. Colocalization of the fluorescent probe signal and tumor is observed while unaffected tissue is without probe signal.

CONTROL ID: 2236210

TITLE: Bioluminescence Imaging of Transplanted Human Endothelial Colony-Forming Cells in Ischemic Mice Model

PRESENTER: Jie Ding

ABSTRACT BODY:

Abstract Body: *Background and purpose*. Ischemic stroke is a devastating disorder lead to high mortality and morbidity worldwide every year. Endothelial colony-forming cells (ECFCs) therapy holds promise for treating such disease. It is necessary to safety monitor grafted ECFCs to understand the biological behavior in vivo for successful delivery. The objective of this study is to visualize the fate of infused human cord blood derived ECFCs via bioluminescence imaging (BLI) in ischemic stroke mice model and determine the therapeutic effects of ECFCs transplantation. *Methods.* ECFCs cultured from human umbilical cord blood was infected with lentivirus carrying double fusion reporter gene, enhanced green fluorescence protein (eGFP) and firefly luciferase (Luc2). Labeled ECFCs(1×10^6) was grafted into photothrombotic ischemic stroke mice model via intra-arterial injection though left cardiac ventricle. The homing of infused cells, functional recovery of stroke mice were evaluated with BLI, neurological score assay and immunohistochemistry, respectively. *Results.* Serial in vivo bioluminescence images were obtained at different time points after cell transplantation. BLI signals was observed highest in brain area on day 1 and decreased sequentially till day 14, GFP positive cells was found around the infarct border zones on brain slice in immunohistochemical staining, confirming the homing of ECFCs to the ischemia brain tissue. ECFCs migration and survival duration was monitored noninvasively by BLI for 2 weeks and confirmed histologically after infusion in animal model. Modified neurological severity score (mNSS) assay and histological analysis of brain section staining of CD31 and doublecortin (DCX) demonstrated the functional restoration possibly due to improved angiogenesis and neurogenesis in ischemic mice after ECFCs infusion. *Conclusions*. Our results show that ECFCs may serve as a promising therapeutic agent in stroke therapy. BLI is an ideal method for tracking the fate of transplanted cell and monitoring successful delivery.

AUTHORS (LAST NAME, FIRST NAME): Ding, Jie[2]; Zhao, Zhen[2]; Wang, Congxiao[2]; Qian, Cheng[2]; Cai, Yu[2]; Teng, Gao-jun[1]

INSTITUTIONS (ALL):

1. Radiology, Zhongda Hospital, Southeast Uni, Nanjing, China.
2. key laborary of molecular imaging and functional imaging , southeast university , Nanjing, China.

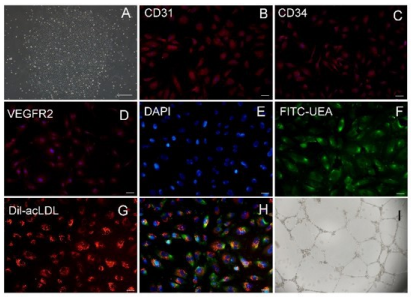

Figure 1. Morphology and characterization of ECFCs.

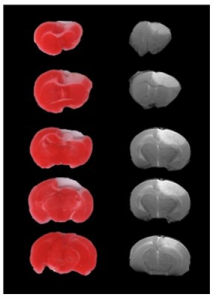

Figure 2. Establishment of focal cerebral ischemia mice model via TTC and MR staining.

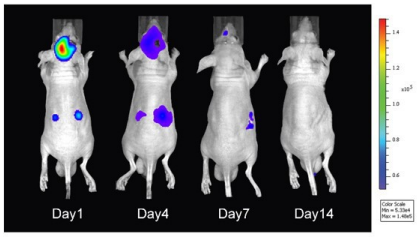

Figure 5. In vitro tracking of labeled ECFCs .

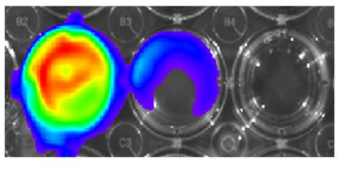

Figure 3. In vivo tracking of labeled ECFCs in ischemic mice.

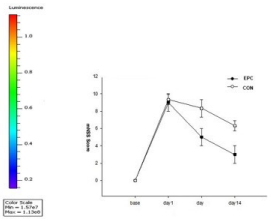

Figure 4. mNSS test between ECFCs and PBS treatment in stroke mice.

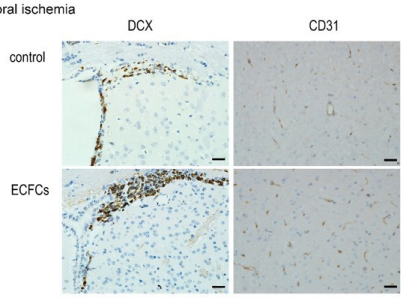

Figure 6. ECFCs transplantation promotes neuronal recovery via neurogenesis and angiogenesis.

CONTROL ID: 2236329

TITLE: Bioluminescent imaging and real time monitoring of hepatic apoptosis (caspase-3 activity) in mice.

PRESENTER: Michitaka Ozaki

ABSTRACT BODY:

Abstract Body: Apoptosis-mediated damage of cells and organs is a serious concern in various pathological situations and disease progression. Therefore, the *in vivo* and non-invasive visualization of capase-3 activity may lead to better understandings of damage mechanisms. Here, we demonstrate caspase-3 activity by the luciferase-based optical probe of live liver cells challenged by various stimuli, and also *in vivo* imaging of caspase-3 activity of the post-ischemic liver.

METHODS: We developed a novel probe (pcFluc-DEVD) of cyclic luciferase reflecting caspase-3 activity. Two fragments of DnaE inteins are fused to neighboring N- and C-terminal ends of firefly luciferase connected with a substrate sequence of caspase-3 (DEVD). After translation into a single polypeptide, the N- and C-terminal ends of luciferase are ligated by protein splicing, which produces a closed circular polypeptide chain. The structure of the cyclic luciferase is distorted. Therefore, the luciferase loses its bioluminescence activity (inactive form). Once caspase-3 is activated in cells (DEVD is cleaved), Fluc changes into an active form if the substrate sequence is digested using the protease, restoring luminescence activity. By transfecting an adenovirus cording for *pcFluc-DEVD* (Ad*pcFluc-DEVD*), we investigated whether this probe monitors apoptosis in live AML12 liver cells by staurosporine (STS), Fas-ligand (FasL) or hypoxia/reoxygenation (H/R), and in the post-ischemic liver in mice.

RESULTS: STS and FasL activate caspase-3 in caspase-8-independent and dependent manner, respectively. First, we measured caspase-3 activity in STS- or FasL (Jo2 antibody)-treated AML12 cells transiently transfected with Ad *pcFluc-DEVD*. In live AML12 cells, the signals from the probe started to increase immediately and peaked at 2-4 hr after 1 mM STS and 2 mg/ml Jo2 administration, respectively. In both stimuli, caspase-3 activity was paralleled with apoptotic cell death. Next, we measured caspase-3 activity in post-hypoxic AML12 cells by this probe. During hypoxia, caspase-3 activity dropped to the bottom level. However, it rapidly recovered to the pre-hypoxic level after reoxygenation and started to rise until 4 - 6 hr post-H/R.

Then, we tried to evaluate *in vivo* apoptosis by measuring caspase-3 activity in mouse hepatic ischemia/reperfusion (I/R). 60min of hepatic ischemia caused great increase of capase-3 activity at 6 - 9 hr post-I/R, whereas 30 min of liver ischemia caused small increase at 2 hr post-I/R (Figure). Prolonged ischemia (90 min), however, showed minimal increase of caspase-3 activity, reflecting extended necrotic cell death rather than apoptotic cell death.

CONCLUSIONS: The caspase3 probe successfully illustrated apoptotic damage in vitro and in vivo. Visualizing apoptotic damage of cells/organs may provide important insights into various physio-pathological conditions and diseases.

AUTHORS (LAST NAME, FIRST NAME): Ozaki, Michitaka[1]; Haga, Sanae[1]; Ozawa, Takeaki[2]

INSTITUTIONS (ALL):

1. Dept of Health Sciences, Hokkaido University School of Medicine, Sapporo, Hokkaido, Japan.
2. Department of Chemistry, School of Science, University of Tokyo, Tokyo, Japan.

Figure

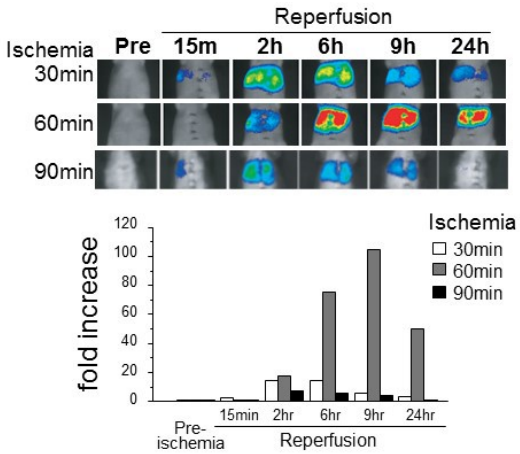

Bioimaging of casapase3 activity in the postischemic mouse liver

CONTROL ID: 2236333

TITLE: MRI measurements in the presence of a RF-penetrable PET insert for simultaneous PET/MRI

PRESENTER: Brian Lee

ABSTRACT BODY:

Abstract Body: I. Introduction

Simultaneous PET and MRI has shown promise to be a powerful tool in disease characterization as it acquires molecular and anatomical information of the subject [1, 2]. Despite the potential clinical benefits, the accessibility of integrated PET/MRI has been limited by its high cost. To address this issue, an RF penetrable PET insert that can be placed in any MR system has been developed [3]. This will allow the use of the built-in body coil as an RF transmitter, so existing MRI sites can achieve simultaneous PET/MR capability. In this study, the MR performance was evaluated with the RF penetrable PET insert system.

II. Methods

The PET insert can be RF penetrable if it is electrically floating relative to the MRI RF ground using electro-optical signal transmission technology [4]. In our prototype system (Figure), 16 PET detector modules are arranged in a 32 cm diameter ring pattern with small gaps. These gaps and the electro-optical coupling enable the RF fields from the built-in body coil to pass through the ring with some attenuation.

To evaluate the MR performance with the RF penetrable PET system, the following experiments were performed using the body coil as RF transmitter and receiver:

A. MR susceptibility was tested by calculating the resonant frequency shifts through ΔB_0 maps with a phase measurement method [5] to determine if the main magnetic field (B_0) is perturbed by the PET system.

B. RF transmit field penetrability was measured by calculating the flip angle distribution through B_1 mapping [6] and analyzing the B_1 amplitude and homogeneity.

C. The shielding effectiveness of the PET electronics noise emission was analyzed through RF noise spectra without applying any RF pulse and only receiving the background RF signals.

D. Receive penetrability of the RF signals was measured by calculating the SNR and homogeneity of the MR images taken with fast spin echo (FSE), gradient echo (GRE), and echo planar imaging (EPI).

III. Results & Discussion

Results figures can be found in the persuasive data.

A. There was no difference in ΔB_0 maps with and without the PET, showing that the PET system does not disturb the main magnetic field.

B. Compared to the case without the PET, the B_1 field amplitude and the homogeneity were reduced by -3.17 dB and 8.38%, respectively. The B_1 field amplitude drop can be compensated by increasing the transmit gain of the RF coil.

C. The RF receive noise spectra were compared with and without the PET and no noise emission was detected by the body coil.

D. The SNR reduction of the MR images in GRE and FSE were -2.55 and -4.55 dB respectively. Designing a custom RF receiver to be placed inside the PET ring can compensate for the SNR reduction. Ghosting artifacts were observed in the EPI image due to eddy currents induced in the shielding.

IV. Conclusion

We have shown that the RF penetrable PET system allows the RF field of the MR body coil to transmit through and successfully acquire MR images without significant degradation. If successful, this technology will enable lower cost and easier upgradability of an MR system to achieve simultaneous PET/MRI.

V. References

References are listed in the persuasive data.

AUTHORS (LAST NAME, FIRST NAME): Lee, Brian J.[2, 1]; Grant, Alexander M.[3, 1]; Chang, Chen-Ming[4, 1]; Levin, Craig S.[1]

INSTITUTIONS (ALL):

1. Radiology, Stanford University, Stanford, CA, United States.
2. Mechanical Engineering, Stanford University, Stanford, CA, United States.
3. Bioengineering, Stanford University, Stanford, CA, United States.
4. Applied Physics, Stanford University, Stanford, CA, United States.

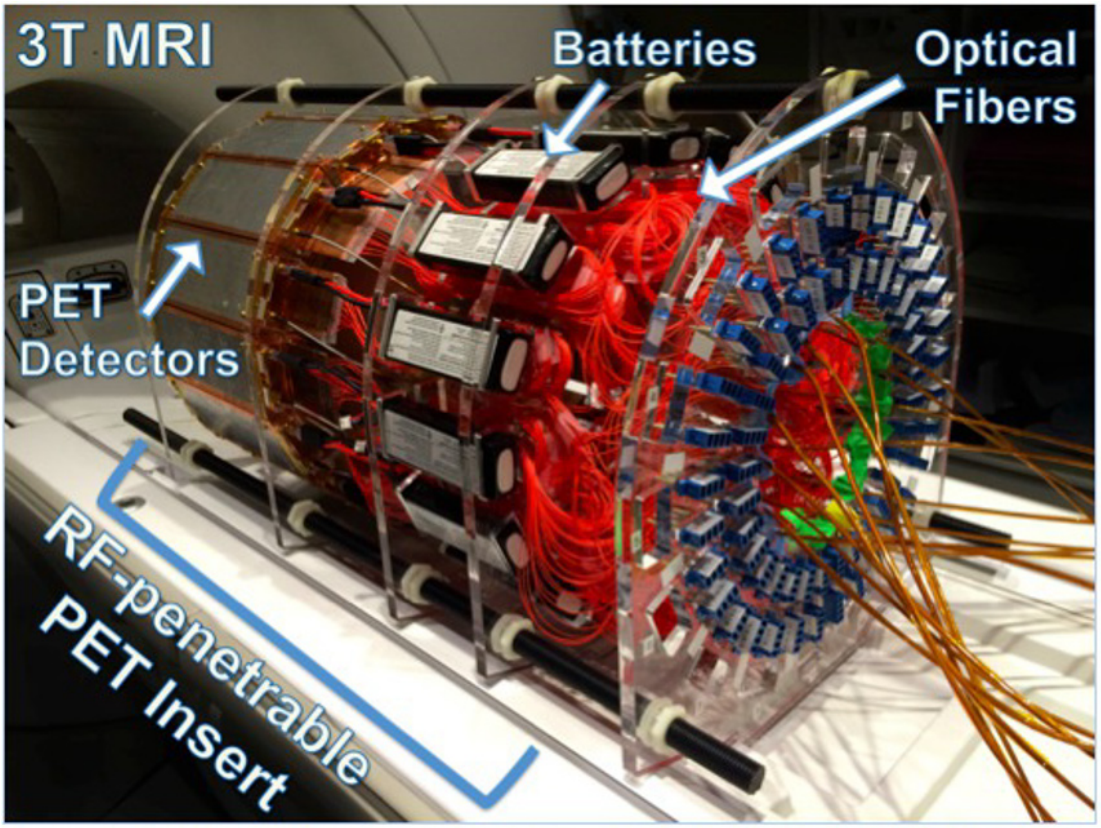

Figure. RF-penetrable PET insert shown on a 3T MRI patient bed. 16 PET detector modules encapsulated in copper Faraday cages are arranged in a 32 cm diameter ring-pattern with 1 mm inter-modular gaps. The electro-optical signal transmission technology converts the electrical scintillation detector signal into optical signal which is transmitted down 20 m optical fibers. The PET electronics are powered by electrically floating batteries, which isolate their ground with respect to the MRI RF ground. The electro-optical coupling, along with the inter-modular gaps, enables the RF-penetrability of the PET insert system.

CONTROL ID: 2236656

TITLE: ^{18}F-Sgc8 ssDNA aptamer for PET Imaging of Tumor PTK7 expression

PRESENTER: Orit Jacobson Weiss

ABSTRACT BODY:

Abstract Body: *Objectives*: Protein tyrosine kinase-7 (PTK7), also known as colon carcinoma kinase-4 (CCK-4), is a relatively new and less studied member of the receptor tyrosine kinase superfamily that is upregulated in many human malignancies including colon, lung, ovarian and gastric cancers. Its expression was found to correlate with aggressive biological behavior such as increased cell proliferation, invasiveness and migration. Currently there is no non-invasive method to determine tumoral PTK7 expression *in vivo*. This study aims to develop a specific, high affinity radioligand, labeled with F-18, for *in vivo* quantification of PTK7.

Methods: Sgc8, a 41-oligonucleotide single stranded DNA aptamer that binds to PTK7, was labeled with F-18 using a two-step radiochemical synthesis; specifically, direct one-step radiofluorination on the distinctive spirocyclic hypervalent iodine(III) precursor to give ^{18}F-fluorobenzylazide followed by “click” conjugation with alkyne-Sgc8. ^{18}F-Sgc8 was evaluated *in vitro* and *in vivo* in two cell lines, HCT116 and U87MG which express high and low amounts of PTK7, respectively.

Results & Discussion: Sgc8 was labeled with F-18 in radiochemical yield of 42 ± 2% based on F-18 activity and specific activity of 73 ± 8 mCi/μmol (2.7 ± 0.3 GBq/μmol). ^{18}F-Sgc8 was found to possess high affinity binding to both cell lines (IC_{50} 3 nM and 18 nM) for HCT116 and U87MG, respectively. *In vivo* PET imaging clearly visualized PTK7 expressing HCT116 xenograft tumors in mice with tumor uptake of 0.98 ± 0.12 %ID/g at 0.5 h and 0.81 ± 0.25 %ID/g at 1 h p.i. (Figure 1). U87MG xenograft tumors, which have significantly less expression of PTK7, were also visualized, but with significantly lower accumulation of the tracer (0.21 ± 0.10 %ID/g at 0.5 h and 0.18 ± 0.09 %ID/g at 1 h p.i.). The labeled aptamer showed rapid clearance from the blood through the kidneys and bladder to give high tumor-to-muscle and tumor-to-blood ratios of (10.25±2.08 and 7.29±1.51) at 0.5 and 1 h pi (Figure 1).

Conclusions: Our F-18 radiolabeling methodology is a very robust procedure for the synthesis of aptamers and similar chemical moieties, and can be applied to many different targets. ^{18}F-Sgc8 can be used to determine tumor PTK7 expression with good tumor to background contrast and rapid clearance. Quantification of PTK7 using ^{18}F-Sgc8 is suitable for clinical translation and might help in the future to select and monitor appropriate therapies.

AUTHORS (LAST NAME, FIRST NAME): Jacobson Weiss, Orit[1]; Weiss, Ido D.[2]; Wang, Lu[3]; Niu, Gang[1]; Kiesewetter, Dale O.[1]; Vasdev, Neil[3]; Liang, Steven H.[3]; Chen, Xiaoyuan[1]

INSTITUTIONS (ALL):

1. NIBIB/NIH, Bethesda, MD, United States.
2. NIAID/NIH, Bethesda, MD, United States.
3. Harvard Medical School, Boston, MA, United States.

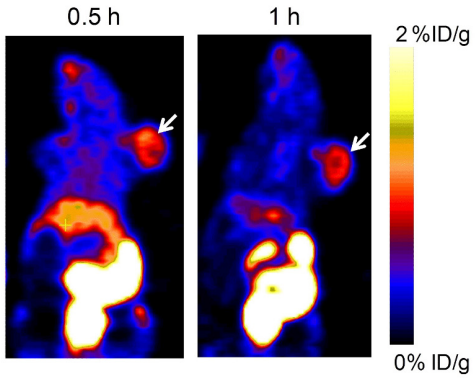

Figure 1. Representative coronal PET images of ^{18}F-Sgc8 at 0.5 and 1 h post-injection in HCT116-xenografted mice. White arrows represent tumor location.

CONTROL ID: 2243261

TITLE: A Novel Method for Dimerizing RGD peptides at Room Temperature Using ^{18}F-Hexafluorobenzene as a Prosthetic Group

PRESENTER: Orit Jacobson Weiss

ABSTRACT BODY:

Abstract Body: Objectives: Hexafluorobenzene (HFB) has been shown to react with free thiols to produce a unique and selective perfluoroaromatic linkage between the sulfurs (1). We set out to evaluate ^{18}F-HFB as a prosthetic group for dimerizing molecules and biomolecules and its usage in positron emission tomography (PET) imaging.
Methods: ^{18}F-HFB was prepared by a fluorine exchange reaction by an adaptation of the method previously published (2) using K_2CO_3 and $K_{2.2.2}$ at room temperature. The fluorination reactions were automated and optimized to use minimum amount of HFB. The product was isolated by distillation at room temperature into a collector of dimethylformamide (DMF) at dry ice/acetonitrile bath temperature. For dimerization reactions, 1 equivalent of ^{18}F-HFB was reacted with two equivalents of thiolated RGD peptide with excess amount of base (TRIS) and TCEP as a reducing agent at room temperature. Cell binding assay and PET imaging studies in αvß3 expressing cells and xenografted mice (U87MG) were conducted.
Results: ^{18}F-HFB was obtained in an isolated radiochemical yield of about 25 % in a reaction time of 50 min using only 500 µg of HFB. The specific activity (SA) was measured by quantitative HPLC and was found to be about 50 mCi/µmol. Aliquots of this solution were used for dimerization reactions such that the stoichiometry was controlled. The dimeric version of c(RGDfK), ^{18}F-RGD-HFB-RGD (Figure 1) was obtained in an optimized yield of 40% (isolated, ndc, based on ^{18}F-HFB) with a final specific activity (SA) of 15 mCi/µmol. PET imaging showed good tumor uptake (4%ID/g at 1 h post-injection) and good tumor-to-background contrast (Figure 1). IC_{50} values of RGD-HFB-RGD *vs* E[c(RGDfK)]$_2$ dimer were comparable (81nM vs. 62 nM).
Conclusions: ^{18}F-HFB can be incorporated into thiol-containing peptides at room temperature, with good efficiency to provide novel imaging agents.

1) A.M. Spokoyny, Y. Zou, J.J. Ling, H Yu, Y.S. Lin, B.L. Pentelute. J. Am. Chem. Soc. 2013, 135, 5946-5949. 2) E. Blom, F. Karimi, B. Langstrom J. Label Compd. Radiopharm, 2009, 52, 504-511

AUTHORS (LAST NAME, FIRST NAME): Jacobson Weiss, Orit[1]; Yan, Xuefeng[1]; Niu, Gang[1]; Kiesewetter, Dale O.[1]; Chen, Xiaoyuan[2]

INSTITUTIONS (ALL):

1. LOMIN, NIBIB/NIH, Bethesda, MD, United States.
2. National Institute of Biomedical Imaging and Bioengineering, National Institutes of Health, Bethesda, MD, United States.

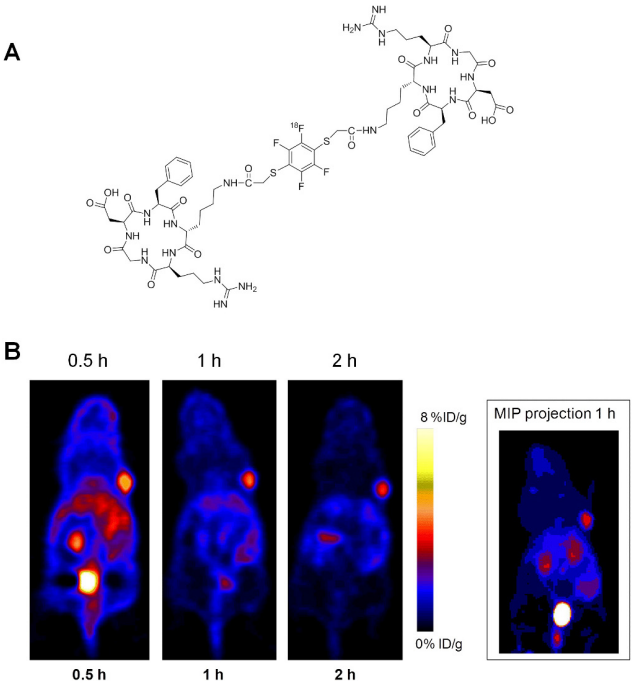

Figure 1. (A) Chemical structure of ^{18}F-RGD-HFB-RGD . (B) Representative coronal PET imaging at different time points of U87MG-xenograft injected with ^{18}F-RGD-HFB-RGD.

CONTROL ID: 2237059

TITLE: Combining radioimmunotherapy with cetuximab significantly enhances therapeutic efficacy in localized and metastatic models of colorectal cancer

PRESENTER: Vessela Vassileva

ABSTRACT BODY:

Abstract Body: We evaluated the pre-clinical efficacy of combining radioimmunotherapy (RIT), using a humanized ^{131}I-labelled anti-CEA antibody (^{131}I-huA5B7), with cetuximab in colorectal cancer (CRC).

Three human CRC cell lines, SW1222, LoVo and LS174T were used to generate subcutaneous xenografts and stably luciferase-transfected SW1222 cells were used to establish a model of hepatic metastasis in nude mice.

Imaging and biodistribution studies were conducted to confirm the selective tumor localization of ^{131}I-huA5B7.

Efficacy was evaluated based on tumor growth delay and survival, along with markers of DNA damage response, cell cycle, proliferation and apoptosis.

Selective tumor targeting was achieved with ^{131}I-huA5B7 alone or in combination with cetuximab without observable toxicity. Compared with monotherapy, combining cetuximab with RIT significantly and synergistically reduced tumor growth and prolonged survival of mice in two of the subcutaneous and in the metastatic tumor model. Evidence of DNA damage, G2/M arrest, significantly decreased proliferation and increased apoptosis were observed with RIT and the combination therapy. However, a significant decrease in DNA-PK expression with the combination regimen suggests that the addition of cetuximab suppressed DNA repair.

Our results demonstrate enhanced therapeutic efficacy with the combination of cetuximab and RIT in CRC, which could potentially translate into successful clinical outcomes. This strategy could improve the treatment of residual disease post-operatively and ultimately prevent or delay recurrence. Furthermore, other CEA-expressing malignancies could also benefit from this approach.

AUTHORS (LAST NAME, FIRST NAME): Vassileva, Vessela[2]; Rajkumar, Vineeth[3]; Badar, Adam[4]; Lythgoe, Mark F.[5]; Boxer, Geoffrey[6]; Pedley, R B.[1]

INSTITUTIONS (ALL):

1. oncology, UCL, London, United Kingdom.
2. Oncology, UCL Cancer Institute, London, United Kingdom.
3. UCL Cancer Institute, University College London, London, United Kingdom.
4. university college london, London, United Kingdom.
5. UCL, London, United Kingdom.
6. UCL Cancer Institute, London, United Kingdom.

(No Image Selected)

CONTROL ID: 2237285

TITLE: Histological characterisation of tumour-inhabiting bacteria and host cells

PRESENTER: Kevin Francis

ABSTRACT BODY:

Abstract Body: For decades, bacteria of different types have been isolated from patient tumours of various histological types [1]. In parallel to this, we and others have shown that deliberate systemic administration of bacteria to animals or human patients results in selective replication within solid tumours [2]. Recently, we have characterised the bacterial populations naturally present within patient tumours, reporting a multitude of different bacterial taxa living naturally within breast tumours and in the surrounding healthy tissue [3]. While bacterial presence in certain tumours is associated with tumourigenesis, in many cases bacterial presence may reflect local infections of existing malignant tissue [1]. Little is known about the patterns of intratumoural growth and local host responses to the bacteria. We have developed a novel histological procedure for examining bacteria in tissue, and describe histological analyses, qualitatively characterising tumour microbial content and relationships to tissue characteristics in terms of pattern of growth, location, and host cell associations. Using formalin fixed paraffin embedded or flash-frozen tissue from patients or mice, simultaneous cell-specific labelling of multiple bacterial and host cells, permitted characterisation of bacterial growth patterns, quantity, intra-tumoural location and the nature of immune responses. The relationship between the various cell types was examined on PerkinElmers Vectra and Mantra pathology imaging platforms. This strategy improves our understanding of factors relevant to the phenomenon of intratumoural bacterial growth, and the nature of the ‘tumour microbiome’.

References

1. Cummins J, Tangney M. Bacteria and tumours: causative agents or opportunistic inhabitants? Infect Agent Cancer 2013; 8: 11.
2. Cronin M, Akin AR, Collins SA, Meganck J, Kim JB, Baban CK, Joyce SA, van Dam GM, Zhang N, van Sinderen D, O'Sullivan GC, Kasahara N, Gahan CG, Francis KP, Tangney M. High resolution in vivo bioluminescent imaging for the study of bacterial tumour targeting. PLoS One 2012; 7: e30940.
3. Urbaniak C, Cummins J, Brackstone M, Macklaim JM, Gloor GB, Baban CK, Scott L, O'Hanlon DM, Burton JP, Francis KP, Tangney M, Reid G. Microbiota of human breast tissue. Appl Environ Microbiol 2014; 80: 3007-3014.

AUTHORS (LAST NAME, FIRST NAME): Murphy , Carola[2]; Cronin, Michelle[2]; Mansfield, James R.[1]; Francis, Kevin P.[1]; Tangney, Mark[2]

INSTITUTIONS (ALL):

1. Life Sciences, PerkinElmer, Hopkinton, MA, United States.
2. BioSciences Institute, Cork Cancer Research Centre, Cork, Ireland.

(No Image Selected)

CONTROL ID: 2237700

TITLE: Visualizing in vivo retinal pigment epithelium cell death using a caspase-targeted fluorescent probe

PRESENTER: Kabhilan Mohan

ABSTRACT BODY:

Abstract Body: Purpose: To detect real time retinal pigment epithelium (RPE) cell death in vivo using a fluorophore conjugated peptidomimetic in mouse models of retinal degeneration.

Innovation: The eye is an excellent model organ for imaging applications due to its transparent components that enable us to visualize the retina and even deeper choroid. However, thus far, no reliable method exists to detect in vivo caspase activation. In this study, we have developed a fluorescent probe which we have validated in different models of retinal degeneration.

Methods: *Wild type* C57BL/6J mice received subretinal injections of Alu RNA (300ng, n=5-6 eyes per group) or PBS as a negative control. At 24 and 72 hours after treatment, intravitreous injections of a near-infrared fluorophore (NIRF, Ex: 780 Em: 800) conjugated pan-caspase probe (VAD-aomk) were conducted. Fundus photos and near-infrared fluorescent imaging were acquired (Topcon 50-IX) at 8 and 24 hours. Similarly, intravitreous injections of the pancaspase probe was conducted in transgenic mice with mutant PRPH2 (Jackson Laboratories) at 2 weeks of age and near infrared fluorescent imaging was conducted at 8 hours. Eyes were then harvested and either prepared as frozen sections or RPE/choroid flatmounts.

Results: Treatment of *Wild-type* mouse eyes with Alu-derived dsRNAs caused RPE cell death whereas PBS did not. On frozen sections, a strong NIRF signal from the pancaspase probe was observed in the degenerating regions of RPE and retina. The flat-mounted tissues also revealed an intense and focal signal in the degenerating area where subretinal Alu RNA injections were performed. Eyes treated with vehicle PBS did not reveal probe signal on frozen sections or flat-mounts. A similar signal from the degenerating region of RPE was observed in the *prph2* transgenic mice.

Conclusion: We have previously developed a NIRF probe with a fluoromethyl ketone group that targeted caspases. In this study, we have utilized an acyloxymethylketone (AOMK) “warhead” instead, to circumvent potential toxicity due to the fmk moiety. Here, we have shown that an in vivo imaging strategy to visualize caspase activation is feasible in different mouse models of RPE cell death with probe signal co-localizing to cells in the outer retina and RPE. Future studies include evaluating different delivery routes and toxicity screening of the probe.

AUTHORS (LAST NAME, FIRST NAME): Mohan, Kabhilan[2]; Sanman, Laura[3]; Jung, Kyung-sik[2]; Lou, Dingyuan[2]; Abney, Jennifer[2]; Bogyo, Matthew[1]; Ambati, Jayakrishna[2]; Kleinman, Mark E.[2]

INSTITUTIONS (ALL):

1. Pathology, Stanford University, Stanford, CA, United States.
2. Ophthalmology & Visual Sci, Univ of Kentucky , Lexington, KY, United States.
3. Stanford University, Stanford, CA, United States.

(No Image Selected)

CONTROL ID: 2237890

TITLE: Radiofluorinated PET Imaging based on the PARP1 inhibitor Olaparib

Brandon Carney[1,2], Giuseppe Carlucci[2], Christian Brand[2], Christopher P. Irwin[2], Wolfgang A. Weber[2], Thomas Reiner[2,3]

[1] Ph.D. Program in Chemistry, The Graduate Center of the City University of New York, New York, NY 10016, [2] Memorial Sloan Kettering Cancer Center, New York, New York 10065, United States, [3] Weill Cornell Medical College, New York, New York 10065, United States

PRESENTER: Brandon Carney

ABSTRACT BODY:

Abstract Body: Objectives: AstraZeneca's Olaparib is a small molecule inhibitor that has recently won FDA approval, and targets PARP1, a DNA repair enzyme that is overexpressed a variety of different malignancies. This is particularly apparent for glioblastoma, where PARP1 is highly expressed, which is in stark contrast to healthy surrounding brain tissue. Previous studies have reported fluorescent imaging agents[1,2] based on the Olaparib scaffold. This study now introduces a new PET ^{18}F-conjugated PARP1 imaging agent, which could ultimately allow the non-invasive imaging of PARP1 on a whole-body level.

Methods: The cold version of the tracer was synthesized in a fashion similar to previously published methods[3]. Specifically, BDC003 was obtained by combining the a piperazine precursor with 4-fluorobenzoic acid in the presence of HBTU in acetonitrile at room temperature for 5 min. The product was then purified by HPLC and confirmed by LCMS. IC_{50} values were calculated by using a commercial PARP1 Assay Kit (Trevigen, MD). Blocking studies with PARPi-FL were performed by incubating 5×10^3 U251 or U353 glioblastoma cells per well seeded in a 96-well plate. The plate was then incubated at 37 °C and 24 hours later the media was aspirated and replaced with either 250nM PARPi-FL, or 250nM PARPi-FL spiked with 20-fold excess of either BDC003 or Olaparib (n=3 for each U251 or U353). The plate was then imaged by confocal fluorescence microscopy using a Zeiss LSM 5Live Line-scanning confocal microscope and the subsequent images were quantified using ImageJ image analysis software.

Results: So far, the cold molecule has been synthesized and has exhibited good enzyme inhibition (IC_{50} = 2.8nM compared to Olaparib's 5nm). Cell uptake by PARPi-FL, a PARP1 fluorescent reporter, was efficiently blocked by the cold molecule (80% blocked in U251 and 79% in U373 versus 70% and 71% respectively with Olaparib). Attempts at producing the hot PET tracer by an ^{18}F for NO_2 substitution via microwave synthesis are still ongoing.

Conclusion: A PARP1 targeted PET tracer exhibiting high in-vivo stability is an imaging agent worth pursuing due to its potential utility in quantifying PARP1 inhibition in-vivo. It's potential includes both preclinical and clinical applications.

Acknowledgments: Supported by the Brain Tumor Center of MSKCC (TR), the Imaging and Radiation Sciences Program of MSKCC (TR), the Weill Cornell Medical College Clinical and Translational Science Center (BC, NIH/NCATS Grant # TL1TR000459).

References:

1. Irwin, C. P. et al. *Neoplasia* **16**, 442-440 (2014).
2. Thurber, G. M. et al. *Nat Commun* **4**, 1504 (2013).
3. Menear, K. A. et al. *J Med Chem* **51**, 6581-6591 (2008).

AUTHORS (LAST NAME, FIRST NAME): Carney, Brandon[3]; Carlucci, Giuseppe[3]; Brand, Christian[4]; Irwin, Christopher[4]; Weber, Wolfgang[2]; Reiner, Thomas[1]

INSTITUTIONS (ALL):

1. MSKCC, New York, NY, United States.
2. Radiology, MSKCC, New York, NY, United States.
3. Memorial Sloan Kettering Cancer Center, New York, NY, United States.
4. Radiology, Memorial Sloan Kettering Cancer Center, New York, NY, United States.

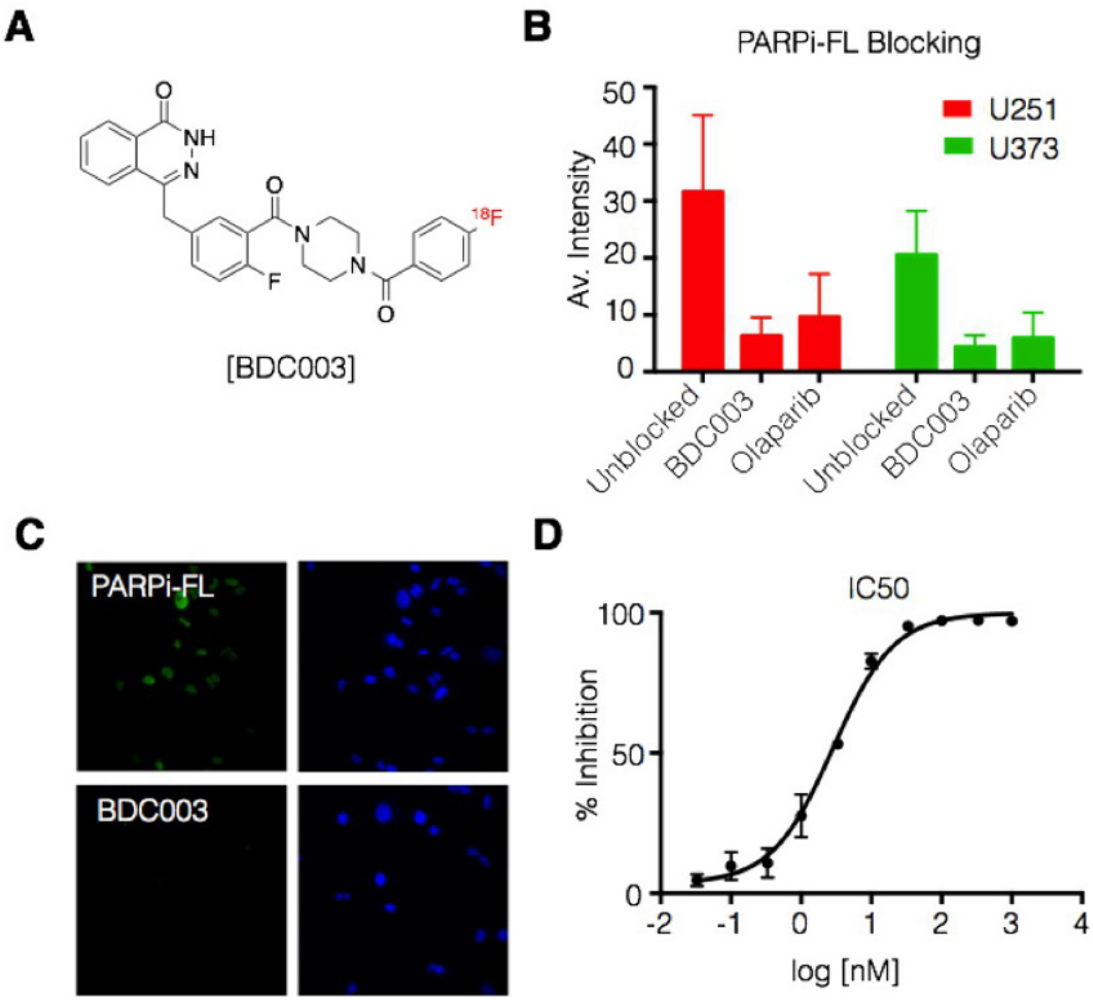

FIGURE 1. [BDC003]; (A) Structure of Molecule (B) PARPi-FL Blocking Study using U251 and U373 glioblastoma cell lines; (C) Fluorescence Microscopy showing PARPi-FL staining (top) and blocking by BDC003 (bottom); (D) IC_{50} Assay using Trevigen PARP1 Assay Kit

CONTROL ID: 2237795

TITLE: PET Imaging of β Cell Endoplasmic Reticulum Stress using 5-(2-^{18}F-Fluoroethoxy)-L-Tryptophan.

PRESENTER: Savita Dhanvantari

ABSTRACT BODY:

Abstract Body: Background: Diabetes develops as a result of death and/or dysfunction of the insulin-secreting β cells of the pancreatic islets of Langerhans. One mechanism of cell death (apoptosis) is mediated through prolonged endoplasmic reticulum (ER) stress. Activation of ER stress pathways significantly contributes to β-cell apoptosis and the eventual development of diabetes. Recently, Krokowski et al (JBC 288:17202, 2014) demonstrated that expression of a network of amino acid transporters is dramatically increased in islets in a mouse model of diabetes, leading to increased protein synthesis and ER stress. In particular, the System L transporter LAT1 was increased, suggesting that it could be a biomarker for diabetes onset. 5-(2-^{18}F-Fluoroethoxy)-L-Tryptophan (^{18}F-L-FEHTP), a Positron Emission Tomography (PET) radiotracer, has been used to image LAT1 expression in cancer. We hypothesize that ^{18}F-L-FEHTP can be used to non-invasively image changes in LAT1 in islets during the development of diabetes.

Methods and Results: ^{18}F-L-FEHTP was generated using a two-step procedure. We used the *Akita* mouse as a model for Type 1 diabetes, as it harbours a misfolded variant of proinsulin that induces ER stress and subsequent β-cell apoptosis. Adult *Akita* mice and age-matched controls (n=6) were injected i.v. with 9 MBq ^{18}F-L-FEHTP and dynamic PET images were acquired in list mode over 1h. Static PET scans were then acquired for 30 min. Immediately after scanning, mice were sacrificed, and organs collected for *ex-vivo* biodistribution analysis. Images were reconstructed using GE Healthcare Explore Vista software. Regions of interests (ROIs) comprising the pancreas were delineated in 3 slices and averaged, and standardized uptake values (SUVs) were calculated for both dynamic and static images. Data analyses for biodistribution and static SUVs were performed with an unpaired t-Test with significance set at $p<0.05$. For comparisons between multiple time points, a repeated measures ANOVA followed by paired comparisons using t-tests with Bonferonni correction was used.

Results: Biodistribution showed a 2-fold ($p<0.01$) greater normalized uptake of ^{18}F-L-FEHTP in the *Akita* pancreas compared to control, and significantly ($p<0.05$) greater uptake in the pancreas compared to other organs (except heart and liver). PET images showed signal only in the pancreas. For static images, SUVs were not significantly different between *Akita* and control (1.3±0.1 vs. 1.5±0.1, $p=0.06$). Dynamic imaging showed washout of the tracer in the kidney and gradual accumulation over time in the pancreas; accumulation in the pancreas of control mice was significantly ($p<0.01$) greater than in *Akita* mice.

Conclusion: Accumulation of ^{18}F-L-FEHTP appeared to be decreased in Akita mice compared to controls, although expression of the LAT1 transporter is increased. This may indicate an increased rate of flux through the islets, which will be revealed by tracer kinetic analysis. These results suggest that changes in pancreatic LAT1 expression in diabetes may be detected by ^{18}F-L-FEHTP PET, potentially leading to the development of a diagnostic tool for the non-invasive detection of β cell apoptosis.

AUTHORS (LAST NAME, FIRST NAME): Dhanvantari, Savita[1, 2]; Abbas, Ahmed[2]; McGirr, Rebecca[1]; Cockburn, Neil[1]; Krokowski, Dawid[3]; Kovacs, Michael[1]; Lee, Ting-Yim[1]; Hatzoglou, Maria[3]

INSTITUTIONS (ALL):

1. Imaging, Lawson Health Research Institute, London, ON, Canada.
2. Medical Biophysics, Western University, London, ON, Canada.
3. Pharmacology, Case Western Reserve University, Cleveland, OH, United States.

(No Image Selected)

CONTROL ID: 2243934

TITLE: Clinical translation of a novel dual integrin $\alpha_v\beta_3$ and GRPR targeting PET radiotracer ^{68}Ga-NOTA-BBN-RGD

PRESENTER: Jingjing Zhang

ABSTRACT BODY:

Abstract Body: OBJECTIVE: This study aims to document the first-in-human application of a ^{68}Ga-labeled-heterodimeric peptide BBN-RGD that targets both integrin αvβ3 and gastrin releasing peptide receptor (GRPR). We evaluated the safety, calculated the radiation dose, and assessed the clinical diagnostic value in tumors.

METHODS: A macrocyclic chelator, 1,4,7-triazacyclononane-N,N',N"-triacetic acid (NOTA) conjugated BBN-RGD was synthesized and labeled with ^{68}Ga. The quality control was performed with analytical HPLC and TLC. After the clinical protocol was approved by the institute review board, five healthy volunteers (M 4, F 1, 28–53 y) were enrolled to validate the safety of ^{68}Ga-NOTA-BBN-RGD. A total of 27 cancer patients including 15 prostate cancer, 5 glioma, 3 gastrointestinal tumor, 2 lung cancer and 2 pancreatic cancer patients with written informed consent were recruited. All the recruited patients underwent PET/CT scans 30–45 min after intravenous injection of 92.5-129.5 MBq (2.5–3.5 mCi) of ^{68}Ga-NOTA-BBN-RGD, and also accepted ^{68}Ga-NOTA-BBN and/or ^{68}Ga-NOTA-PRGD2 PET/CT within 2 weeks for comparison.

RESULTS: The whole labeling process of ^{68}Ga-NOTA-BBN-RGD took about 30 min with a radiochemical purity of greater than 95%. For this first-in-human study in healthy volunteers with a mean injected dose of 2.9 ± 0.4 mCi, no side effect was found during the whole procedure and 2 weeks follow-up, demonstrating the safety of ^{68}Ga-NOTA-BBN-RGD. A patient would be exposed to a radiation dose of 2.21 mSv with an injected dose of 2.5-3.5 mCi (92.5-129.5 MBq), which is much lower than the dose limit as set by the FDA. ^{68}Ga-NOTA-BBN-RGD PET/CT detected both the primary prostate cancer in 2 newly diagnosed by the biopsy and bone metastasis in 13 post-treatment patients, the average and maximum standard uptake values (SUVs) of all the 31 bone metastasis lesions were 2.87 ± 0.93 and 4.79 ± 1.57 at 30 min after injection respectively. The SUV_{avg} and SUV_{max} in glioma patients (n = 5) at 30 min after injection of ^{68}Ga-NOTA-BBN-RGD were 1.8 ± 1.1 and 3.2 ± 1.5 respectively, with low background and much lower choroid plexus uptake compared with ^{68}Ga-NOTA-PRGD2. Moderate uptake of ^{68}Ga-NOTA-BBN-RGD were demonstrated in 2 lung adenocarcinoma. For the gastrointestinal tumor, ^{68}Ga-NOTA-BBN-RGD PET/CT detected primary, recurrent and metastasis lesions in 3 gastric and 1 colon cancer, which may be more specific than ^{18}F-FDG PET/CT in assessing gastrointestinal tumor.

Conclusion: This study indicates the safety and the efficiency of a new PET radiotracer ^{68}Ga-NOTA-BBN-RGD. This novel dual integrin $\alpha_v\beta_3$ and GRPR targeting PET radiotracer showed significant value in prostate cancer, glioma, lung cancer and gastrointestinal tumor diagnosis.

Keywords: BBN-RGD; PET; first-in-human; integrin αvβ3; GRPR

AUTHORS (LAST NAME, FIRST NAME): Zhang, Jingjing[1, 2]; Niu, Gang J.[2]; Lang, Lixin[2]; Yan, Xuefeng[2]; Yao, Shaobo[1]; Zhu, Zhaohui[1]; Li, Fang[1]; Chen, Xiaoyuan[2]

INSTITUTIONS (ALL):

1. Department of Nuclear Medicine, Peking Union Medical College Hospital (PUMCH), Beijing, China.

2. National Institute of Biomedical Imaging and Bioengineering, National Institutes of Health, Bethesda, MD, United States.

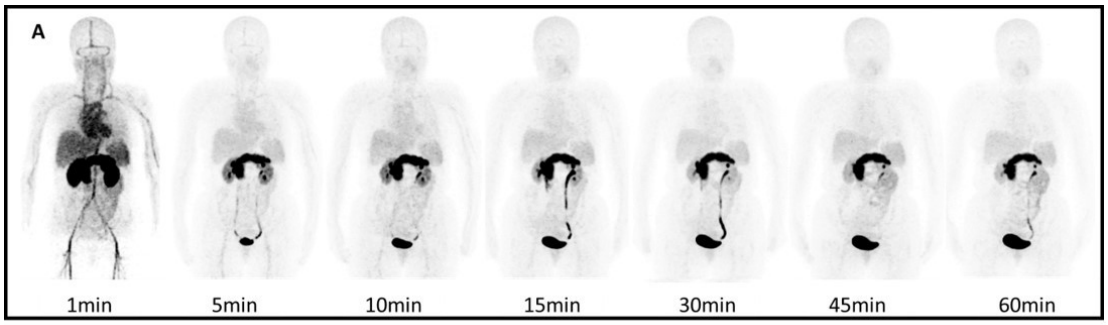

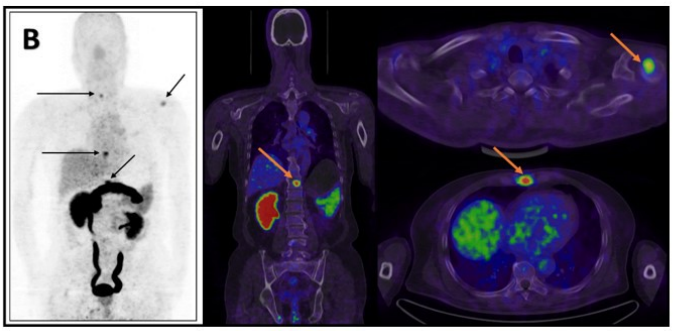

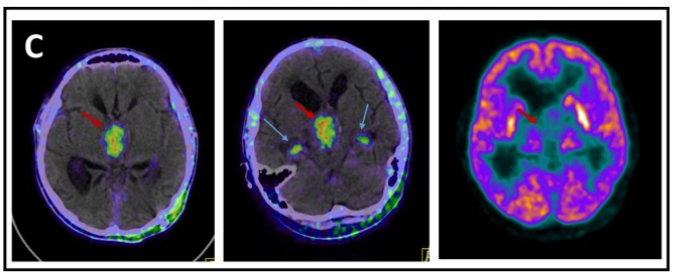

(A) Whole-body maximum intensity projection PET images: a 52-year-old woman volunteer at 1, 5, 10, 15, 30, 45, 60min after intravenous administration of ^{68}Ga-NOTA-BBN-RGD. (B) A 64-year-old man newly diagnosed as prostate cancer by biopsy. Coronal and axial slices of ^{68}Ga-NOTA-BBN-RGD PET/CT showed multiple intense uptake metastasis lesions (arrow). (C) Axial slices of ^{68}Ga-NOTA-BBN-RGD, ^{68}Ga-NOTA-PRGD2 and ^{18}F-FDG PET/CT imaging of a 12-year-old glioma patient. (D) Comparison of ^{68}Ga-NOTA-BBN-RGD PET/CT (D1) and ^{68}Ga-NOTA-BBN (D2) PET/CT in a 69-year-old man diagnosed as prostate cancer with multiple bone metastasis.

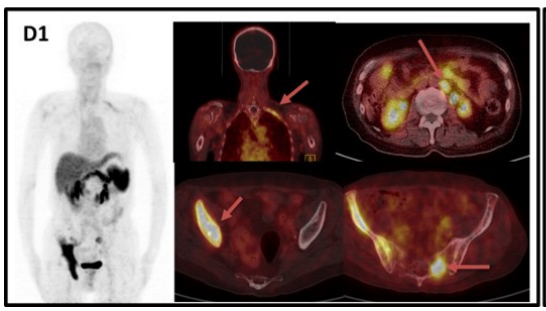

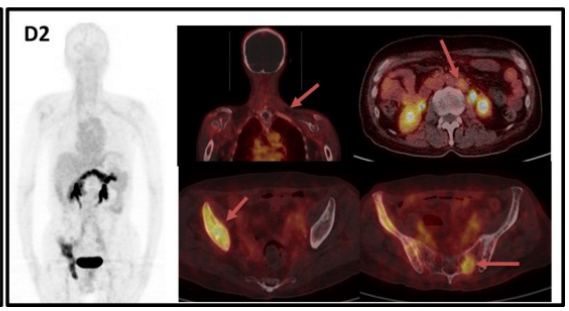

CONTROL ID: 2238318

TITLE: Spatially-precise brain-specific genetic reporter expression enabled by magnetic resonance-guided focused ultrasound and nonviral nanoparticle carriers

PRESENTER: Raag Airan

ABSTRACT BODY:

Abstract Body: Introduction:

Targeted delivery of agents to the brain, with spatial precision, is a long-standing unmet need of molecular imaging. Here, we demonstrate that spatially precise delivery of genetic reporters to the central nervous system (CNS) can be accomplished minimally invasively by combining magnetic resonance-guided focused ultrasound (MRgFUS) mediated blood brain barrier (BBB) permeabilization[1] with a nonviral nanoparticle carrier system that has specificity for neural tissue[2].

Methods:

Mice were anesthetized with isoflurane and placed supine on the bed of a small animal focused ultrasound system (RK300, FUS Instruments, Toronto, Canada) that was integrated with a horizontal bore 9.4T MRI (BioSpin, Bruker, Billerica, MA). With MRI guidance, three sonication foci were selected in the right cerebral hemisphere. Definity microbubbles (Lantheus Medical Imaging, N. Billerica, MA) were activated according to the product instructions. Definity ($6x10^3$ bubbles/gm) was administered via a tail vein catheter. Simultaneously, focused ultrasound at 1MHz was applied to each target (10 ms pulses/1 s x120 s, 0.45-0.5 MPa estimated *in situ* pressure). Following sonication, Gadopentetate contrast (0.2 µL/gm; Magnevist, Bayer, Whippany, NJ) was administered intravenously. Following contrast administration, nanoparticles were administered intravenously that consisted of a CMV::Luciferase plasmid (CMV promoter inserted into pGL3 from Promega, Madison, WI) complexed to either in vivo-jetPEI ('PEI', Polyplus transfection, Illkirch, France) or an in-house synthesized neural-specific poly(β-aminoester) polymer formulation 447 ('PBAE')[2]. A total of 40-50 µg of DNA was administered per mouse. Post contrast MRI was completed to ensure BBB permeabilization. After 6, 24, and 48 hours post nanoparticle administration, bioluminescence imaging was completed (IVIS Xenogen 200, PerkinElmer, Waltham, MA) after D-Luciferin (2.5 mg in PBS; Gold Biotechnology, St. Louis, MO) was administered intraperitoneally.

Results:

Hyperintensity in the brain on post-contrast MRI at the sonication targets indicated adequate BBB permeabilization. Bioluminescence signal localizing to the sonication targets was visualized at 24 and 48 hours for the PBAE nanoparticles, indicating target gene expression in the brain. Notably, no similar bioluminescence signal was visualized elsewhere in the body for PBAE. For PEI nanoparticles, strong off-target bioluminescence signal was visualized in the lungs, with no convincing specific bioluminescence signal corresponding to gene expression at the sonication target at 24 hours; a faint focus of bioluminescence was visualized near the sonication target at 48 hours.

Conclusion:

Specific and effective targeting of a genetic reporter to the CNS following intravenous administration was accomplished by combining MRgFUS BBB permeabilization with tissue-specific nonviral carrier nanoparticles. Future work will extend this functionality to targeting CNS tumors with tumor-specific genetic reporter systems, with improved delivery efficacy and efficiency.

References:

[1] Hynynen et al. *Radiology.* **2001.** 220(4):640.

[2] Mangraviti et al. *ACS Nano*. **2015**. 9(2):1236.

AUTHORS (LAST NAME, FIRST NAME): Airan, Raag D.[1]; Minn, Il[1]; Kozielski, Kristen[2]; Ellens, Nicholas P.[1]; Lee, Young M.[3]; Guerrero-Cazares, Hugo[3]; Quiñones-Hinojosa, Alfredo[3]; Pomper, Martin[1]; Green, Jordan J.[2, 3]; Farahani, Keyvan[1, 4]

INSTITUTIONS (ALL):

1. Radiology, Johns Hopkins Medical Institutions, Baltimore, MD, United States.

2. Biomedical Engineering, Johns Hopkins Medical Institutions, Baltimore, MD, United States.
3. Neurosurgery, Johns Hopkins Medical Institutions, Baltimore, MD, United States.
4. Cancer Imaging Program, National Cancer Institute, National Institutes of Health, Bethesda, MD, United States.
(No Image Selected)

CONTROL ID: 2243301

TITLE: Targeted delivery of GCPII/PSMA molecular imaging probes to the brain

PRESENTER: Raag Airan

ABSTRACT BODY:

Abstract Body: Introduction:

Many molecular imaging probes of interest are excluded from the central nervous system (CNS) by the blood-brain barrier (BBB). Here, we demonstrate that spatially precise delivery of molecular imaging probes of Glutamate Carboxypeptidase II (GCPII, also known as Prostate Specific Membrane Antigen, PSMA)[1,2] to the central nervous system can be accomplished minimally invasively via MR-guided focused ultrasound (MRgFUS) mediated blood brain barrier (BBB) permeabilization[3].

Methods:

Rats were anesthetized with isoflurane and placed supine on the bed of a small animal focused ultrasound system (RK300, FUS Instruments, Toronto, Canada) that was integrated with a horizontal bore 9.4T MRI (BioSpin, Bruker, Billerica, MA). With MRI guidance, three sonication foci were selected in the left cerebral hemisphere. Definity microbubbles (Lantheus Medical Imaging, N. Billerica, MA) were activated according to the product instructions. Definity ($6x10^3$ bubbles/gm) was administered via a tail vein catheter. Simultaneously, focused ultrasound at 1MHz was applied to each target (10 ms pulses/1 s x120 s, 0.45-0.5 MPa estimated *in situ* pressure). Following sonication, Gadopentetate contrast (0.2 µL/gm; Magnevist, Bayer, Whippany, NJ) was administered intravenously. T1-weighted post contrast MRI was then completed to ensure BBB permeabilization. For nuclear imaging experiments, rats were then transported to a small animal PET/CT system (SuperArgus, Sedecal, Madrid, Spain) and administered 9.1 MBq of the PET GCPII probe [^{18}F]-DCFPyL[1] intravenously as a bolus. Dynamic PET images were acquired over the course of two hours. For optical imaging experiments, rats were instead administered the fluorescent GCPII probe YC27[2] (1 nmol). After 24 hours, rats were imaged under small animal fluorescence (800 nm emission; Pearl Trilogy, Li-Cor, Lincoln, NE) with skin intact and then euthanized and imaged again with skin and cranium removed. The brains were then harvested and kept on dry ice prior to cryotome sectioning and imaging under fluorescence microscopy (800 nm emission; Odyssey CLx, Li-Cor, Lincoln, NE).

Results:

PET signal was visualized within the brain, localizing to the regions of BBB permeabilization noted on the contrast enhanced MRI. Over the course of two hours, there was progressive washout of the background blood pool activity. Target to background PET signal was maximal at 100-120 min, with more delayed acquisitions likely to yield reduced background, with a higher net target to background ratio. Fluorescence imaging at 24 hours confirmed successful binding of probe to these receptors in the CNS following BBB permeabilization, with low background activity.

Conclusion:

Specific and effective targeting of molecular probes of GCPII/PSMA to the CNS following intravenous administration was accomplished via MRgFUS BBB permeabilization. Future work will extend this functionality to targeting CNS tumors, such as gliomas that may variably express GCPII/PSMA.

References:

[1] Chen et al. *Clin Cancer Res*. **2011**. 17(24):7645.

[2] Chen et al. *Biochem Biophys Res Commun*. **2009**. 390(3):624.

[3] Hynynen et al. *Radiology*. **2001.** 220(4):640

AUTHORS (LAST NAME, FIRST NAME): Airan, Raag D.[1]; Foss, Catherine A.[1]; Ellens, Nicholas P.[1]; Minn, Il[1]; Mease, Ronnie C.[1]; Farahani, Keyvan[1, 2]; Pomper, Martin[1]

INSTITUTIONS (ALL):

1. Radiology, Johns Hopkins Medical Institutions, Baltimore, MD, United States.
2. Cancer Imaging Program, National Cancer Institute, National Institutes of Health, Bethesda, MD, United States.

(No Image Selected)

CONTROL ID: 2238417

TITLE: Three-dimensional bioluminescence imaging of gene expression during pupal stages of *Drosophila melanogaster* by using UAS-*P. matsumurai* Luc reporter line

PRESENTER: Ryutaro Akiyoshi

ABSTRACT BODY:

Abstract Body: Bioluminescence created by luciferin-luciferase reaction is widely used for promoter/reporter assay of gene activity in live cells and tissues. Despite advantages of bioluminescence such as non-invasive, non-autofluorescence and high quantification accuracy over fluorescence, fluorescence imaging has been used for gene expression analysis of *Drosophila melanogaster* because weak emission intensity of bioluminescence made it difficult to visualize gene expression pattern as image. Thus, we cloned novel luciferase gene from *Pyrocoelia matsumurai* that produces >3-fold increased bioluminescence signal compared with the luciferase originated from *Photinus pyralis* . To generate transgenic flies, we adopted the GAL4-UAS system, in which the transcription factor GAL4 binds to UAS to activate the downstream gene expression. We constructed a vector containing UAS fused to *P. matsumurai* luciferase gene as reporter. This vector was injected into fertilized eggs of *D. melanogaster* by microinjection. Undergoing processes of crossing the flies with another strain, we created UAS-*P. matsumurai* Luc reporter line. This reporter line was crossed with engrailed-GAL4 driver line to generate flies carrying engrailed-GAL4/UAS-*P. matsumurai* Luc. Gene expression pattern of the pupa of this strain was observed by the luminescence microscope (LV200, Olympus) attached with motorized Z-focus system to capture bioluminescence images at different Z-planes. As a result, we succeeded to make three-dimensional reconstruction images from a series of 51 images captured every 10μm of focal plane. Whereas it is difficult to capture fluorescent images of the deep part of the pupa because the penetration depth of the excitation light is limited to a shallow layer, bioluminescence imaging allowed detecting the bioluminescent signal over 500μm deep. Furthermore, these 3D images made it possible to analyze the spatiotemporal expression patterns of engrailed gene from white pupa to adult emergence in the same single pupa, which takes ~93 h.

We demonstrated that UAS-*P. matsumurai* Luc reporter line allows three-dimensional and real-time tracking of gene expression throughout the pupal stage continuously by bioluminescence imaging. This method would be an effective and versatile tool for gene expression analysis during *Drosophila* development when combined with various GAL4 driver lines.

AUTHORS (LAST NAME, FIRST NAME): Akiyoshi, Ryutaro[1]; Suzuki, Hirobumi[1]

INSTITUTIONS (ALL):

1. Advanced Analysis Technology R&D, Olympus corporation, Tokyo, Japan.

(No Image Selected)

CONTROL ID: 2238468

TITLE: STUDY ON TARGET EFFICIENCY OF FITC-NGR-GD TO HEPG2 CELLS IN VITRO

PRESENTER: xiaoguang you

ABSTRACT BODY:

Abstract Body: Objective: To construct FITC-NGR-Gd targeted contrast agents and observe its targeting efficiency to HEPG2 cells in vitro. **Methods**: To use amide linkage to chemically synthesize the stable connector of FITC-NGR-Gd. To establish HEPG2 experimental group and HT-29 control group for cell fluorescence assay and observe the targeting efficiency of contrast agent to HEPG2 in vitro. To establish HEPG2 experimental group and HT-29 control group for cell in vitro MRI test, change the gadolinium concentration and observe the targeting efficiency of contrast agent to HEPG2 in vitro by measuring changes in T1 values. **Results**: FITC-NGR-Gd has a higher T1 relaxivity; immunofluorescence assay shows that in the cell test, HEPG2 experimental group has more CY3 targeted red fluorescence on the surface of cell membrane and the HT-29 control group has no marked red fluorescent substance on the cell membrane; FITC-NGR-Gd cell fluorescence assay shows that HEPG2 experimental group has more green FITC targeted fluorescence on the surface of cell membrane and HT-29 control group has no marked green fluorescent substance on the cell membrane. In vitro the cell MRI test shows T1 values of HEPG2 experimental group are significantly higher than that of HT-29 control group, $P < 0.05$. There is statistically significant difference between two groups. With the increasing concentrations of gadolinium, T1 values of experimental groups increase progressively and the intensity enhances. **Conclusion**: FITC-NGR-Gd can take HEPG2 cells as target in vitro and realize targeted fluorescence imaging and MRI imaging.

AUTHORS (LAST NAME, FIRST NAME): you, xiaoguang[1]; To, Rong[1]

INSTITUTIONS (ALL):

1. Radiology, The Affiliated Hospital of Hainan Medical University , Haikou, Hainan Province, China.

(No Image Selected)

CONTROL ID: 2238760

TITLE: The Performance of Thresholding Image Segmentation Algorithms on Tc-99m Dimercaptosuccinic Acid (Tc-99m DMSA) Images.

PRESENTER: Hairil Rashmizal Abdul Razak

ABSTRACT BODY:

Abstract Body: Introduction:

Differential Renal Function is an operator-dependent qualitative assessment process that requires input to determine renal tissue from image background. An automated renal region delineation using thresholding image segmentation algorithms has been believed to reduce the quantitative study time and provide consistence region of interest depiction. This study aimed to assess the performance of thresholding image segmentation algorithms on Tc-99m dimercaptosuccinic acid (Tc-99m DMSA) images of varying severity of renal tissue deteriorations. It is essential to know the capability of studied algorithms compared to human drawn region.

Methods:

30 Tc-99m DMSA images were selected and equally grouped into normal renal tissue, mild renal tissue deterioration (acute infection) and severe renal tissue deterioration (chronic cases). Thresholding image segmentation algorithms; threshold multi otsu, maximum entropy threshold, seeded region growing and fuzzy k-mean had been applied to human drawn images successively. The total pixel counts of depicted renal region for all segmentation algorithms had been compared with the total pixel counts of human drawn region.

Results:

The results showed that the total pixel counts produced by fuzzy k-mean and seeded region growing algorithms had no significant differences with the total pixel counts of human drawn technique ($p > 0.05$).

Conclusion:

As a conclusion, we may postulate that both fuzzy k-mean and seeded region growing thresholding algorithms have shown a promising potential for automated renal region delineation. However, this preliminary outcome warrants for further investigations.

AUTHORS (LAST NAME, FIRST NAME): Ahmad, Mohd Solahuddin[2]; Abdul Razak, Hairil Rashmizal[1]

INSTITUTIONS (ALL):

1. Department of Medical Imaging, Universiti Teknologi MARA, Puncak Alam, Selangor, Malaysia.
2. Department of Biomedical Imaging, University Malaya Medical Centre, Kuala Lumpur, Malaysia.

(No Image Selected)

CONTROL ID: 2238904

TITLE: TbiLuc mouse: in vivo imaging of T cell localization and activation using multicolor bioluminescence.

PRESENTER: Laura Mezzanotte

ABSTRACT BODY:

Abstract Body: Introduction:

Imaging T cells in vivo provides useful information for immunological studies, in particular the spatio-temporal visualization of T cells and their activation status in animal models. Among different imaging technologies, optical imaging of luciferase-expressing T cells in small animals has used viral transduction of T cells and/or used a single luciferase that provides information on the location but not the function of T cells (1-3). Here, we describe the design and development of a transgenic mouse TbiLuc whose T cells constitutively express a green luciferase and an activation-dependent red luciferase.

Methods: a bicistronic vector containing hCD2 promoter controlling the expression of the click beetle green luciferase (CBG99) sequence and NFAT (nuclear factor of activated T cells) inducible minimal promoter controlling the expression of the red-emitting firefly luciferase (PpyRE9) sequence was used to generate the TbiLuc transgenic mouse on a B/CBA background. Founders were selected based on high light emission in blood and further back-crossed towards B6 background. Subsequently, the mouse was crossed to T cell receptor-transgenic OT-1 mice and OT-2 mouse whose CD8+ T cells and CD4+ T cells, respectively, recognize an epitope of ovalbumin (OVA). Finally, we assessed the functionality of the dual-luciferase construct in T cells both *in vitro* and *in vivo*.

Results: Analysis of isolated CD8+ T cells from the TbiLuc mouse confirmed the constitutive expression of CBG99 luciferase and the expression of PpyRE9 luciferase after activation. CD4+ T cells and B cells showed a lower light emission than CD8+ T cells. BLI of mice showed the localization of T cells in the lymphoid organs, both in the TbiLuc mice itself and after adoptive transfer of TbiLuc T cells into naïve mice. Moreover, analysis of isolated CD8+ T cells from OT-1*TbiLuc mice confirmed the expression of PpyRE9 luciferase after presentation of their cognate antigen by dendritic cells (DCs). Using MBLI of as few as $1x10^6$ OT-1 TbiLuc CD8+ T cells transferred into tumor-bearing mice, efficient T cell activation was obtained. Spectral unmixing algorithms showed PpyRE9-expressing activated T cells in MC38-OVA tumors, but not in MC38 control tumors not expressing the OVA antigen. This accumulation of activated CD8+ T cells coincided in time with a reduced tumor growth.

Conclusion: To our knowledge, development of TbiLuc and its crossing with OT-1 and OT-2 mice allowed in vivo imaging of naïve T cells and their activation for the first time in tumor bearing mice. These new mice will help in the assessment of T cell immunotherapies of cancer and the efficacy of cancer vaccines.

References:

1]Patel MR et al. Cancer Res. 2010 Dec 15;70(24):10141-9.

2] Rabinovich BA et al.Proc Natl Acad Sci U S A. 2008 Sep 23;105(38):14342-6. doi: 10.1073/pnas.0804105105.

3] Dobrenkov K et al.J Nucl Med. 2008 Jul;49(7):1162-70.

AUTHORS (LAST NAME, FIRST NAME): Mezzanotte, Laura[1]; Kleinovink, Jan Willem[1]; Stammes, Marieke[1, 2]; Fransen, Marieke F.[1]; Chan, Alan[2]; Ossendorp, Ferry[1]; Iowik, Clemens W.[1]

INSTITUTIONS (ALL):

1. Leiden University Medical Center, Leiden, Netherlands.
2. Percuros, Enschede, Netherlands.

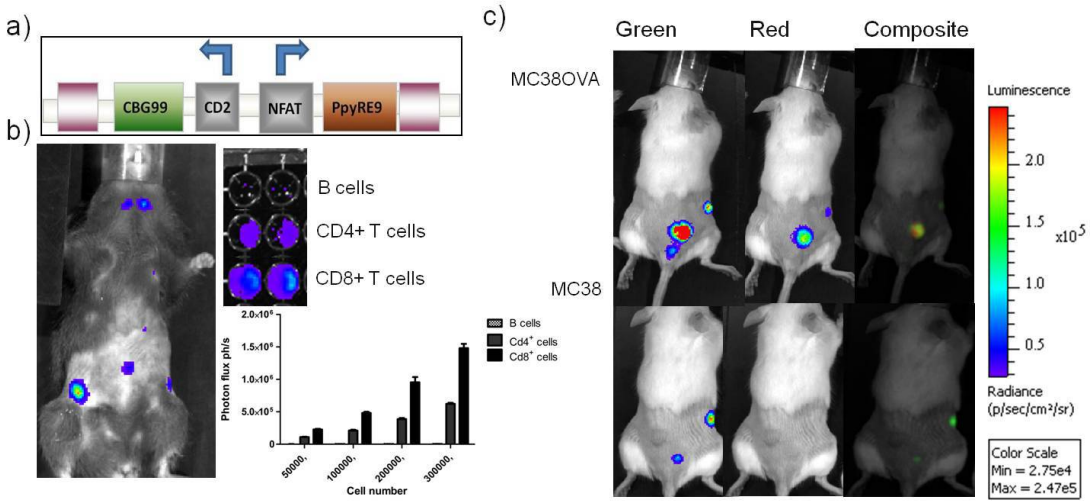

Figure 1.a) bicistronic construct generated for thedevelopment of TbiLuc transgenic mouse. b) bioluminescent images of TbiLuc mouse and isolated cells . Graph showing light emission from isolated CD8+ T cells, CD4+ T cells and B cells. c) Representative images of a MC38 OVA (upper images) and MC38 (lower images) bearing mice treated with luminescent OT-1 CD8+ T cells and vaccination. OT-1 CD8+ T cells accumulate and are active (red images) in MC38OVA tumors and not in MC38 tumors.

CONTROL ID: 2240312

TITLE: Ultrasound-bioluminescence hybrid modality imaging in a rodent model of breast cancer

PRESENTER: Ryan Gessner

ABSTRACT BODY:

Abstract Body: Background: In vivo bioluminescence imaging (BLI) plays an important role in the disease research and drug development pipeline. BLI has a limited depth of penetration and thus lack of anatomic information and context for where signals originate. Additionally, in situ morphological changes cannot be measured. With the addition of an anatomical modality, however, this paradigm shifts. Previous studies have shown BLI images co-registered with CT[1], and MRI[2] images of the same animal, though to our knowledge no in vivo studies have yet demonstrated alignment between high frequency 3D tomographic ultrasound (structural) and BLI (functional) images. Multimodality fusion yields many benefits, including more accurate region of interest definitions, more holistic understanding of anatomical context of in situ pathology, tomographic reconstruction of the BLI signal, and improvements in BLI spatial resolution. Contained herein is a proof of feasibility of a tomographic anatomical image acquisition with ultrasound (US) aligned with BLI images. Additionally, MR images were acquired of the same animals and compared to the 3D US data to confirm ROI accuracy.

Approach: A xenograft model for breast cancer (MDA-MB-231) was generated in a small cohort of female nude mice (N=8). 1.5x106 cells were injected in a lower lateral inguinal mammary pad. US imaging was performed on a prototype whole body imaging device (SonoVol). Briefly, animals were positioned in the supine position and imaged at 30 MHz from several different angles (±20 deg) over a field of view of 6x3x1.6 cm. The position of the US transducer was precisely controlled via the system's robotic stage apparatus. The 2D US images were reconstructed into tomographic volumes offline. MRI images were acquired of each animal on the same day as the US images. Data taken with a T2 weighted protocol on a 9.4T system (Bruker), with isotropic scan resolution of 0.2 mm, and field of view of 4x4x4 cm. Acquisition time was 1 hour. A standard 2D BLI protocol was acquired for all tumors on an IVIS Lumina. Four different readers defined ROIs within US and MRI datasets, from which 3D masks were generated. The volumes of the masks were then compared between the two modalities for each tumor. Images were aligned between 3D tomographic datasets and 2D BLI images via fiducial based registration.

Results: 3D tomographic US scans were acquired and reconstructed in <10 min. None of the tumor volumes were statistically different between MRI and SonoVol datasets ($p>0.05$ for all tumors). Average tumor diameter was 10.7±7.0 mm. On average there was an inter-modality deviation (MRI vs. SonoVol) of 5.3% in reported volumes for the same tumors, and an average deviation between readers of 11.3%.

Conclusion: Feasibility for whole-body tomographic anatomical imaging with US and registration with BLI has been established, with tumor ROI definition accuracy similar to MRI and a 6x decrease in image acquisition time.

References:[1] Beattie BJ, et al. J Biomed Opt. 2009 Mar-Apr;14(2):024045. [2] Allard M, et al. J Biomed Opt. 2007 May-Jun;12(3):034018.

AUTHORS (LAST NAME, FIRST NAME): Van Horne, Loic[1]; Saelens, Jeffrey M.[1]; Johnson, Kennita A.[1]; Rao, Sneha[1]; Dayton, Paul[1]; Gessner, Ryan C.[2]

INSTITUTIONS (ALL):

1. Joint Department of Biomedical Engineering, University of North Carolina-North Carolina State, Chapel Hill, NC, United States.

2. SonoVol, Chapel Hill, NC, United States.

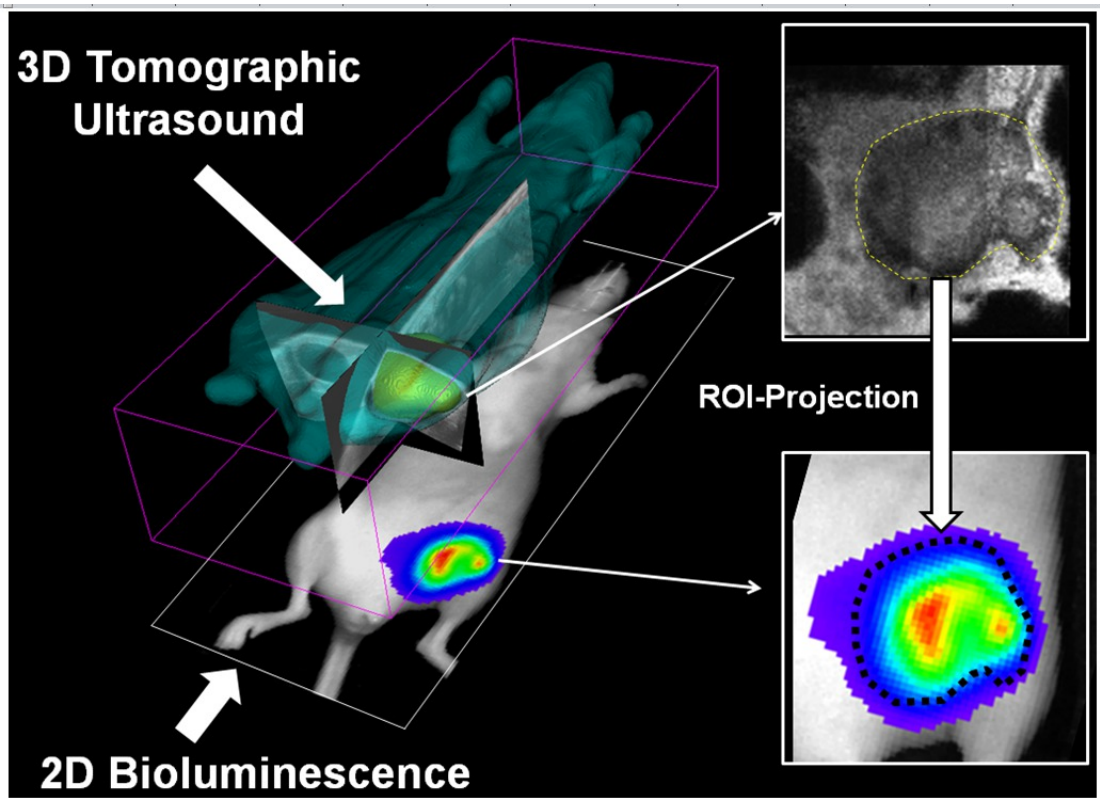

Figure caption: (Left) A 3D composite image showing the alignment between the whole-body ultrasound anatomical image (top) and 2D BLI functional image (bottom).Tumor ROI appears in yellow within the tomographic ultrasound dataset. (Right) The two foci of BLI signal can be mapped directly to the two distinct lobes in the high resolution ultrasound frame.

CONTROL ID: 2243596

TITLE: Nanoscaled Metal-Organic Frameworks Working as a Novel Multimodality Imaging Probe

PRESENTER: Wenting Shang

ABSTRACT BODY:

Abstract Body: Aim: Nanoscaled Metal-Organic Frameworks (NMOFs) as a class of novel crystalline materials have attracted much attention recently. They self-assemble from organic linkers and metal ion cluster, which lead to an infinite array of new materials with interesting properties for many applications, such as catalysis, gas separation and storage, nonlinear optics and drug delivery. We discuss the design and applications of MOFs and develope a kind of novel nanoparticles Au@Fe-BDC for chemical sensing and biological multimodality imaging, including optical imaging, the photoacoustic imaging(OAI) and the magnetic resonance imaging (MRI)for the in vivo tumor research. Although the research still in its infancy, we believe that the compositional easy controled and mild synthetic conditions of NMOF can greatly facilitate their further applications in clinical.

Methods: Human 4T1-luciferase breast tumor bearing nude mice were used, and Au@Fe-BDC probes were synthesis (as is shown in Figure 1) and injected intravenously. Small animal optical molecular imaging system (IVIS Imaging System, Caliper, USA) was used for animal fluorescence imaging acquisition.

Fig. 1 The mechanism of systhsis probes Au@Fe-BDC

AUTHORS (LAST NAME, FIRST NAME): Shang, Wenting[1]; Du, Yang[1]; jia, xiaohua[1]; Tian, Jie[1]

INSTITUTIONS (ALL):

1. Key Laboratory of Molecular Imaging, , Institute of Automation, Chinese Academy of Sciences, Beijing, China.

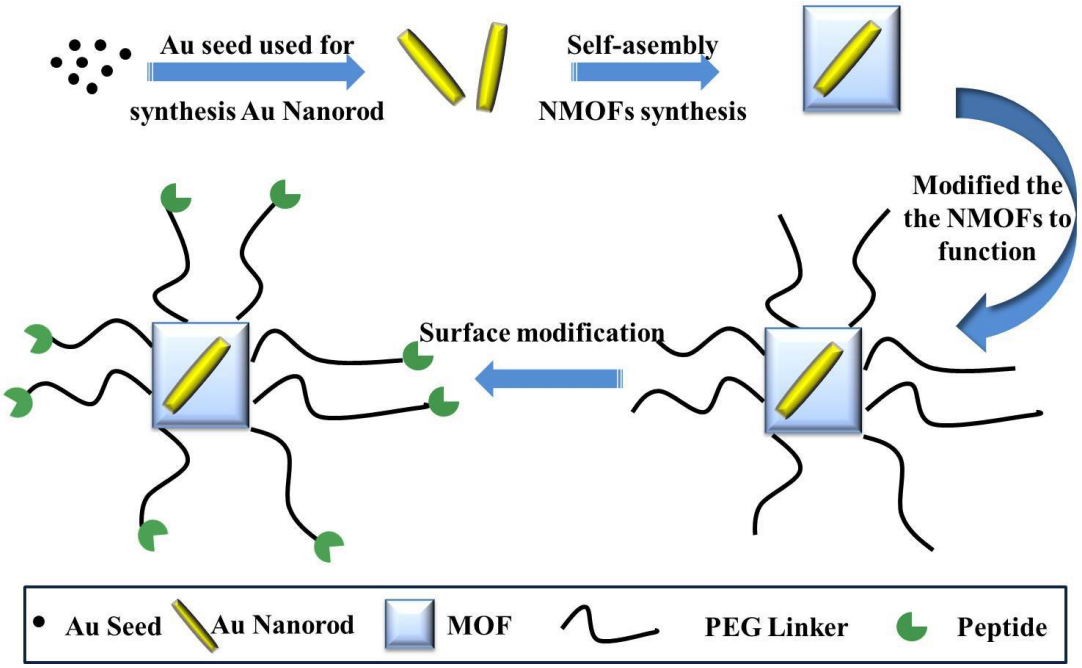
Au seed used for
synthesis Au Nanorod
Self-asembly
NMOFs synthesis
Modified the
the NMOFs to
function
Surface modification
Au Seed
Au Nanorod
MOF
PEG Linker
Peptide

CONTROL ID: 2244745

TITLE: An integrated approach to modeling targeted agent penetration into pancreatic tumors using intravital fluorescence microscopy.

PRESENTER: Veronica Estrella

ABSTRACT BODY:

Abstract Body: Pancreatic cancer is one of the most deadly forms of cancer with a 6% overall 5 year-survival rate. A major goal for increasing the low survival rates is to develop new methods that will improve the efficacy of treatment. Standard chemotherapeutic treatments are often not effective, thus novel therapies targeted specifically to pancreatic cancer cells are needed. We have reported Toll-like receptor 2 (TLR2) as a bona fide cell-surface marker for targeting pancreatic cancer (2). We developed an integrated approach by combining computational and experimental models to predict the clinical efficacy of targeted therapies in a pancreatic cancer. In order to achieve this goal, we used computational simulations (microPD-biomarker tool) and intravital fluorescence microscopy imaging to assess penetration of the TLR2L agent conjugated to near-infrared fluorescent dye, Cy5. Our previous reports have established the specificity of the TLR2L agent for targeting TLR2 and imaging pancreatic cancer in vitro and in vivo (1,2). We developed an intravital fluorescence microscopy method which allows for real time in vivo imaging of the agent using the mouse dorsal window chamber model of human pancreatic tumor xenografts. After the establishment of a growing tumor and patent vasculature, the targeted agent was intravenously injected and a series of confocal fluorescence images are acquired. In this current study, we monitored the uptake of the TLR2L-Cy5 agent into pancreatic cancer tumor xenografts with endogenous TLR2 expression and into non-TLR2 expressing tumors for up to 48 hours post injection. In the non-expressing tumors, we observed TLR2L-Cy5 agent perfusion and extravasation from GFP microvessels and clearance from the vasculature by 3 hours with no cellular uptake of the agent (Figure 1A&B). In contrast, once TLR2-expressing tumors were well established with a network of perfused vasculature, TLR2L-Cy5 perfusion was visible immediately and TLR2-expressing tumor cell uptake was seen 20 minutes following agent injection with peak uptake occurring at some point between 3 and 24 hours (Figure 1C). Extravasation and penetration rates determined from these experiments were used to calibrate the microPD mathematical model that allowed us to calculate how efficiently this targeted ligand extravasates and penetrates into tumor and binds to the receptor of interest. We have shown previously [3] that tumor cellular structure influences drug distribution within the tissue. Here, we present a novel methodology for predicting the extent and timing of intravascular transport of targeted drug or diagnostic imaging agents into tumor tissue. This method provides a means to optimize administration schedules in order to improve treatment efficacy, detection and prediction of patient outcomes. Besides assisting in the clinical translation of the current imaging agent, these methods will aid in the development of additional targeted imaging and therapeutic agents. In the long-term, this integrated model will be validated in human specimens to assist clinicians in making decisions about therapeutic treatments and treatment scheduling.

AUTHORS (LAST NAME, FIRST NAME): Estrella, Veronica C.[2]; Chen, Tingan[4]; Huynh, Amanda Shanks[1]; Morse, David L.[3]; Rejniak, Katarzyna A.[5]

INSTITUTIONS (ALL):

1. Cancer Imaging & Metabolism, H. Lee Moffitt Cancer Center, Tampa, FL, United States.
2. Cancer Imaging and Metabolism, H. Lee Moffitt Cancer Center, Tampa, FL, United States.
3. Cancer Imaging and Metabolism, H. Lee Moffitt Cancer Center and Research Institute, Tampa, FL, United States.
4. Moffitt Cancer Center, Tampa, FL, United States.
5. Integrated Mathematical Oncology, H. Lee Moffitt Cancer Center, Tampa, FL, United States.

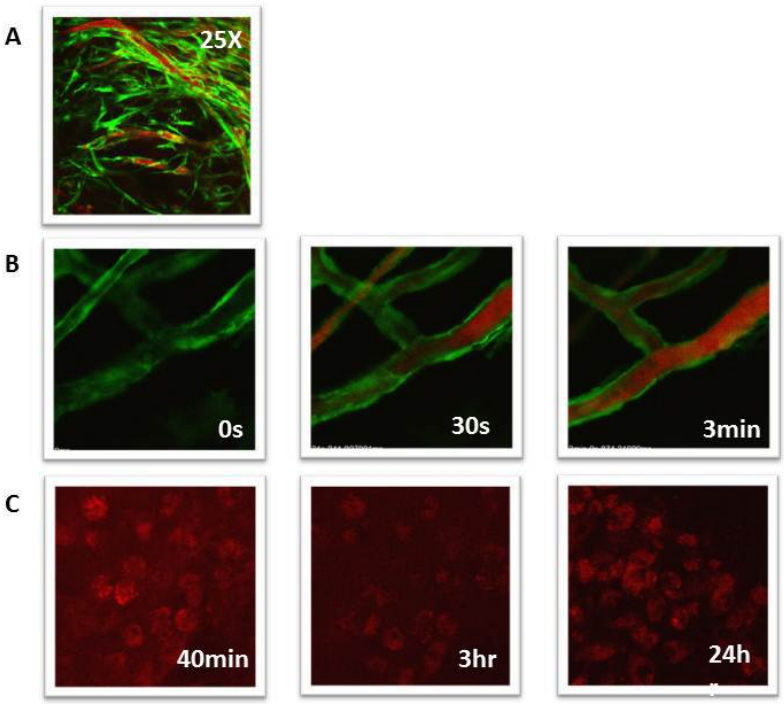

Figure 1. A) Intravital confocal flourescence image of patent GFP(Green) vessels following injection of TLR2L-Cy5 (red).
B) Timeline of TLR2L-Cy5 perfusion in GFP microvessels, images are at 100X magnification. C). Intravital fluorescence image s of TLR 2 positive tumor cells with bound Cy5 labeled agent.

CONTROL ID: 2242184

TITLE: Spatiotemporal opening of brain blood barrier by MRI-guided HIFU activation of transgene expression of stem cells

PRESENTER: Xiaobing Xiong

ABSTRACT BODY:

Abstract Body: Introduction: The blood-brain barrier (BBB), comprised of brain endothelial cells with tight junctions (TJ) between them, regulates the extravasation of molecules and cells into and out of the central nervous system (CNS). The BBB functions to hinder the delivery of many potentially important diagnostic and therapeutic agents to the brain. Overcoming the difficulty of delivering therapeutic agents to specific regions of the brain presents a major challenge to treatment of a broad range of brain disorders. Current strategies for BBB opening are invasive, not specific, and lack precise control over the site and duration of timing of BBB opening, which may limit their clinical translation. Purpose: The purpose of this study is to develop a translatable method, which allows precise spatiotemporal control over BBB opening to facilitate the entry of drugs for treatment of neurological diseases. Methods: A lentiviral expression plasmid, pLenti-Hsp70(F-Luc-2A-TNFα)-RSV(RFP-BSD), which contains the heat-inducible HSP70 promoter driving expression of firefly luciferase (F-Luc) and tumor necrosis factor alpha (TNFα), and RSV promoter driving expression of red fluorescent protein (RFP) and blasticidin selection marker (BSD), was constructed. Mesenchymal stem cells (MSCs) were engineered by transduction with this plasmid constructed by lentiviral vector. Engineeered MSCs were stereotactically implanted into the brains of athymic nude rats. The area of injection site was heated to 43°C by high-intensity focused ultrasound (HIFU) under guidance of MRI for 20 minutes to induce TNFα expression. Luciferase activity was monitored by bioluminescence after injection of F-luciferin. Opening of the BBB was confirmed on T1-weighted image after intravenous injection of Magnevist (Gd-DTPA, 0.125mmol/kg) via tail veil. A mixture of fluorescent nanoparticles of different sizes was intravenously injected to the rat. The brain was removed and frozen sections of 10 μm thickness were prepared. The sections were immediately examined under the fluorescence microscope. Results: HIFU treatment at 43°C for 20 minutes (**Fig. 1A**) demonstrated significantly stronger bioluminescence signal in the brain compared to control (**Fig. 1B**). T-weighted MR imaging demonstrated obvious contrast enhancement in the targeted regions of the rat brain implanted with MSCs transduced with pLenti-HSP70(TNFα-Luc) construct and treated with HIFU; Rats implanted with MSCs-HSP70(Luc-2A-TNFα) without HIFU treatment and rats implanted with MSCs-HSP70(Luc-2A-GFP) with HIFU treatment didn't show enhanced T1 contrast (**Fig. 1C**). Analysis of the T1-weighted images revealed a 3-fold contrast-enhancement in the target regions compared to the controls (**Fig 1D**). Both strong green (300 nm) and red fluorescence (100 nm) were observed in the frozen section, suggesting BBB permeability to the nanoparticles (**Fig. 1E**). Conclusion: MRI-guided HIFU activation of TNFα expression by stem cells can be used to remotely control BBB opening in space and time. This remote controlled cell-based therapeutic platform can have great impact in treatment of brain tumor and other disease processes in the central nervous system.

AUTHORS (LAST NAME, FIRST NAME): Xiong, Xiaobing[1]; Sun, Yao [1]; Jung, Youngkyoo [1]; Mintz, Akiva[1]; Li, King[1]

INSTITUTIONS (ALL):

1. Radiology, Wake Forest University Baptist Health, Winston-Salem, NC, United States.

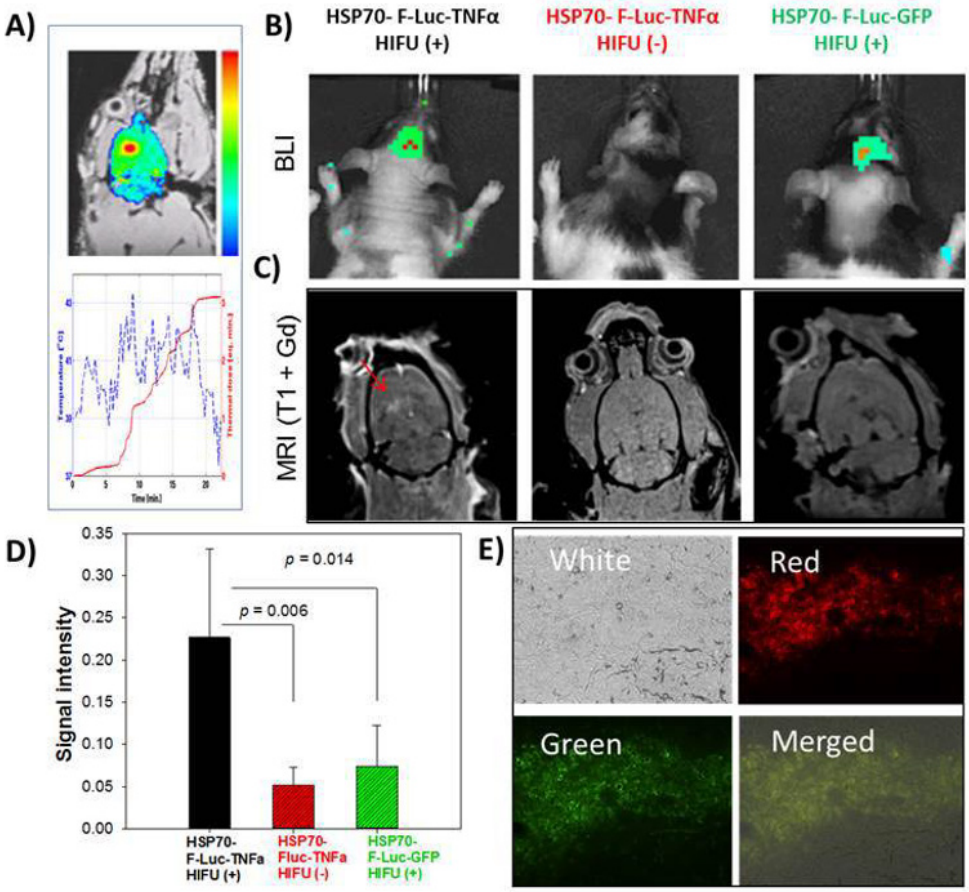

Figure 1. MRI-guided HIFU activation of TNFα production by MSCs to open BBB. MSCs transduced with HSP70(F-Luc-2A-TNFα)-RSV(RFP-BSD) or HSP70(F-Luc-2A-GFP)-RSV(RFP-BSD) were stereotactically implanted into the brains of athymic nude rats (1×106 cells per rat). 2 days after cell implantation, the area of injection site was heated to 43°C for 20 minutes by HIFU under guidance of MRI to induce TNFα expression (A). After 16 h, the luciferase expression was monitored by bioluminescence after luciferin injection (B), and BBB opening was confirmed with T1-weighted image after intravenous injection of the MRI contrast agent (Magnevist, 0.125 mmol/kg) by tail veil (C). The signal intensity of T1-enhanced contrast in the region of interest in the brains of rats was quantified after systemic injection of MR contrast agent (D). A mixture of fluorescent PLGA nanoparticles (Phosphorex, Inc., MA) with different sizes was injected via the tail vein. 24 hours after systemic nanoparticle injection, rats were euthanized and perfused with saline. The brain was removed and frozen in OCT embedding medium (Sakura, Torrance, CA, USA) at -80°C. Frozen sections of 10 μm thickness were prepared with a cryotome. The sections were immediately examined under the fluorescence microscope (E). Red: PLGA nanoparticles (mean size: 100 nm); Green: PLGA nanoparticles (300 nm).

CONTROL ID: 2242255

TITLE: Development of a FASTlab Cassette for the Synthesis of [^{18}F]-6-fluoro-L-DOPA Using Diaryliodonium Salts

PRESENTER: David Dick

ABSTRACT BODY:

Abstract Body: Objectives: Previous reports have shown the promise of efficient fluorination of diaryliodonium salt precursors to provide [^{18}F]-6-fluoro-L-DOPA via nucleophilic substitution[1]. To date, all of these methods have been performed by hand or on general-purpose nucleophilic substitution synthesis modules. The goal of this work was to develop a cassette based synthesis of [^{18}F]-6-fluoro-L-DOPA using the GE FASTlab radiosynthesis platform, which would provide an avenue for facile production of [^{18}F]-6-fluoro-L-DOPA by radiopharmaceutical manufacturers around the world.

Methods: The GE FASTlab Developer platform was used to generate the synthesis procedure. Stock GE FASTlab Developer parts were used to assemble the cassettes, with the exception being that the stock cyclic olefin copolymer (COC) reaction vessel was replaced with a reusable PEEK reaction vessel so that non-polar solvents could be used in the synthesis process. The FASTlab cassette performed the fluorine-18 drying, labeling, intermediate purification and hydrolysis. Final product purification was performed on a separate semi-preparative HPLC, as the FASTlab does not have an built-in HPLC. After azeotropic drying of the F-18 fluoride, the diaryliodonium precursor ALPDOPA was dissolved in anisole and added to the reaction vessel. The reaction vessel was heated at 160 degrees C for 13 minutes at 800 mbar overpressure. Radioactivity incorporation was determined by TLC methods (1:1 hexanes:ethyl acetate on Analtech uniplate silica gel GHLF 250 micron). After fluorination, the crude reaction mixture was diluted with heptane and passed through diol and silica sep paks, respectively. The reaction vessel and sep paks were washed with heptane, after which the crude product was eluted from the silica sep pak to the reaction vessel using ethyl acetate. Deprotection was performed using 1 M HCl and the mixture was neutralized with ammonium buffer prior to transfer to semi-prep HPLC for final purification.

Results: The azeotropic drying and reaction conditions (temperature and pressure) were optimized for the PEEK reaction vessel and synthesis runs were performed. Good incorporation of fluorine-18 was observed. Total synthesis time was 90 minutes.

Conclusions: The GE FASTlab Developer platform is amenable to the synthesis of [^{18}F]-6-fluoro-L-DOPA using diaryliodonium salts, with the minor modification of replacing the COC reaction vessel with a PEEK reaction vessel. Ongoing work is focusing on developing a solid phase extraction method for final product purification that could be incorporated onto the FASTlab cassette, allowing the entire synthesis and purification to be performed in an automated environment.

1. Willem-Jan Kuik, Ido P. Kema, Adrienne H. Brouwers, Rolf Zijlma, Kiel D. Neumann, Rudi A.J.O. Dierckx, Stephen G. DiMagno, and Philip H. Elsinga *J. Nucl. Med.* **2015**, *56*, 106-112. (DOI: 10.2967/jnumed.114.145730)

AUTHORS (LAST NAME, FIRST NAME): Dick, David W.[1]; Neumann, Kiel D.[2]; Stratton, Garrett[1]; DiMagno, Stephen G.[2]

INSTITUTIONS (ALL):

1. Radiology, University of Iowa, Iowa City, IA, United States.
2. Ground Fluor Pharmaceuticals, Lincoln, NE, United States.

(No Image Selected)

CONTROL ID: 2242271

TITLE: CEST and FLEX MRI for the detection of CNS graft rejection

PRESENTER: Sujith Sajja

ABSTRACT BODY:

Abstract Body: Introduction: Cell therapies for CNS disorders are of tremendous interest, but methods for the evaluation of graft survival are clinically inadequate (including MRI T1 with/without contrast, T2 and T2* imaging modalities). Because stem cells require several months to differentiate and become functional, it is critical to know the fate of cells during that time to avoid the necessity to administer strong immunosuppression. The aim of this study was to develop a novel, clinically applicable approach for the non-invasive detection of cellular graft infiltration by immune cells, which could be used as a proxy for graft rejection. The current study investigates novel indications for molecular MRI-based techniques: chemical exchange saturation transfer (CEST) and frequency-labeled exchange transfer (FLEX), to detect the exchange of protons between water and pools of mobile macromolecules and small metabolites.

Methods: Luciferase+ (luc+) glial-restricted progenitor cells (GRPs) were stereotactically transplanted into age-matched immunocompetent Balb/c and immunodeficient rag-/- mice. Bioluminescence was used on alternative days, for up to two weeks, as a reference standard for the survival of GRPs. T1, T2, T2*, CEST, and FLEX MRI were obtained at days 1, 7, and 14 post-transplantation, followed by animal sacrifice for IHC to identify immune infiltration of the graft using CD4, CD8, CD68, and CD45 in addition to luc+ staining for GRPs identification.

Results: BLI showed a ~92% drop for Luc+ cells two weeks after transplantation (Fig. 1A). Immunohistochemistry revealed immune cell infiltration with CD45+ and CD68+ cells at the transplantation site in Balb/c mice, but not in rag-/- mice. T1, T2, and T2* showed no imaging contrast; however, CEST showed higher asymmetry at the transplantation site compared to the contralateral side of the brain. In addition, CEST magnetization transfer ratio (MTR) asymmetry changed from day 1 to day 14 at the transplantation site. Longitudinal CEST assessment (1 to 14 days post engraftment) at 0.5 ppm showed a decrease in MTRasym on TS, but an increase in CTS in WT and rag-/- mice. Longitudinal assessment (1 to 14 days post engraftment) showed a significant decrease in FLEX contrast in rag-/- mice at 7 days and 14 days after transplantation, but not in WT animals (Fig. 1B).

Conclusions: CEST MRI can potentially be employed to detect immune response following cell transplantation, as evidenced by the changes in CEST contrast at the transplantation site (day 1 to day 14). This may be attributable to immune rejection of the graft, since the bioluminescence showed a dramatic decline in transplanted cells (day 1 to day 14). The evidence of high immune cell infiltration (CD45+ and CD68+) at the transplantation site further supports graft rejection, which would also contribute to a change in CEST contrast from day 1 to day 14. Changes in FLEX could reflect the differences in the inflammatory process between WT and rag-/- mice.

Thus, CEST MRI, in combination with FLEX, could potentially be used to detect CNS graft rejection that could be addressed clinically.

AUTHORS (LAST NAME, FIRST NAME): Sajja, Sujith[1, 3]; Liu, Guanshu[1, 4]; Yadav, Nirbhay N.[1, 4]; Xu, Jiadi[2]; McMahon, Michael[1, 4]; Van Jijl, Peter[1, 4]; Bulte, Jeff W.[1, 3]; Walczak, Piotr[1, 3]; Janowski, Miroslaw[1, 2]

INSTITUTIONS (ALL):

1. Dept. of Radiology and Radiological Science, Johns Hopkins School of Medicine, Baltimore, MD, United States.
2. NeuroRepair Department, Mossakowski Medical Research Centre, Polish Academy of Sciences, Warsaw, Poland.
3. Institute for Cell Engineering, Johns Hopkins University, Baltimore, MD, United States.
4. 3F.M. Kirby Research Center for Functional Brain Imaging, Kennedy Krieger Institute, Baltimore, MD, United States.

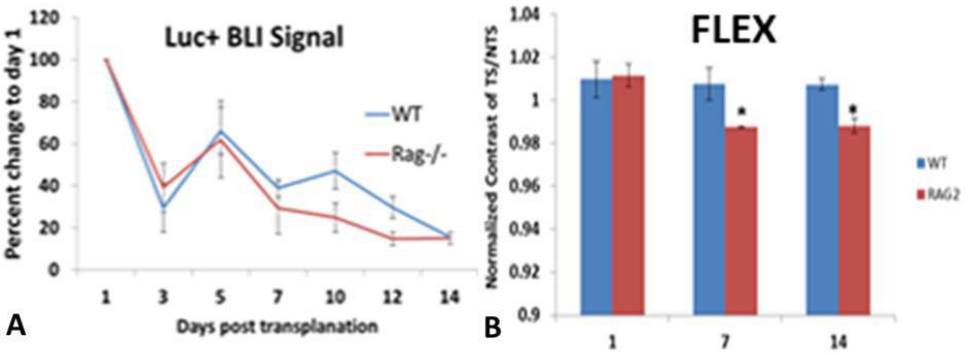

Figure 1: (A) Bioluminescence signal from the IVIS imaging system showed an ~92% drop for Luc+ cells two weeks after transplantation. (B) Longitudinal assessment showed a significant decrease in FLEX contrast in rag-/- mice at 7 days and 14 days after transplantation, but not in WT animals.

CONTROL ID: 2242722

TITLE: Photoacoustic tomography for pre-operative assessment of cutaneous melanoma and other pigmented cutaneous lesions

PRESENTER: Elizabeth Concannon

ABSTRACT BODY:

Abstract Body: Introduction:

Photoacoustic tomography is a novel, non-invasive diagnostic imaging modality. Experimental in-vitro and in-vivo studies have demonstrated promising clinical applications for photoacoustic tomography, including diagnosis, treatment planning and prognostication of cutaneous melanoma and metastatic melanoma[1-4]. Potential benefits include increasing the accuracy of clinical diagnosis of melanoma and reducing potential risks for mortality or morbidity from undue or excessive surgical resections, in addition to controlling costs by avoiding unnecessary procedures. However the role of photoacoustic tomography in a clinical setting has not yet been established.

Aim:

We designed a prospective observational study, aiming to investigate the potential role of photoacoustic tomography in pre-operative assessment of pigmented skin lesions, including lesions suspicious for melanoma.

Methods:

All patients attending the Plastic Surgery service with pigmented lesions warranting excision or suspicious for melanoma underwent pre-operative photoacoustic imaging using Vevo® 2100 LAZR Photoacoustic Tomography System (VISUALSONICS). 3D photoacoustic scanning was performed at multiple wavelengths and spectral unmixing allowed separation of melanin from other biologic tissue components. A comparison of pre-operative information obtained from in-vivo photoacoustic imaging with the gold standard of histological examination of resected surgical specimens using Mel-A staining was carried out.

Results:

We report the accuracy of pre-operative information obtained from photoacoustic imaging when correlated with histological findings from resected cutaneous specimens including histological diagnosis, tumour thickness and level of invasion. Correlation of photoacoustic imaging measurement of tumour thickness with histology was 90.0% (Mean Error 21.7%). Level of invasion was predicted accurately in all cases.

Conclusion:

Our result show that photoacoustic tomography has potential as a non-invasive imaging modality in accurate pre-operative assessment of pigmented cutaneous lesions. Information obtained using this imaging modality, in conjunction with clinical judgement, may guide clinicians in differentiating between benign and malignant pigmented cutaneous lesions in the future.

References:

1. 3D imaging of skin melanoma in vivo by dual wavelength photoacoustic microscopy. Oh J, Li M, Zhanga. J Biomed Opt 2006

2. First experiences of photoacoustic imaging for detection of melanoma metastases in resected human lymph nodes. Grootendorst D, Jose J, Wouters M et al. Lasers in Surg and Med 2012

3. Hu H. Wang L. Photoacoustic imaging and characterisation of microvasculature. JB Optic 2010

4. Zhou Y, Xing W, Konstantin I. Handheld photoacoustic microscopy to detect melanoma depth in vivo. Opt Lett 2014

AUTHORS (LAST NAME, FIRST NAME): Concannon, Elizabeth S.[1]; Breathnach, Aedan[2]; Aalto, Laura[3]; Leahy, Martin [2]; Kelly, Jack L.[1]

INSTITUTIONS (ALL):

1. Department of Plastic Surgery, Galway University Hospital, Galway, Ireland.

2. Tissue optics and microcirculation imaging Facility, National Biophotonics and Imaging Platform, National University of Ireland, Galway, Ireland., Galway, Ireland.

3. Department of Histopathology, Galway University Hosptial, Galway, Ireland.

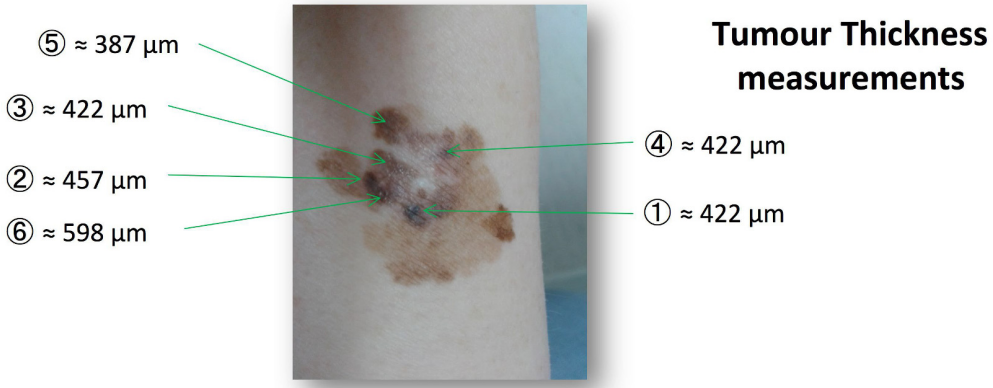

Fig. PA Thickness measurements.

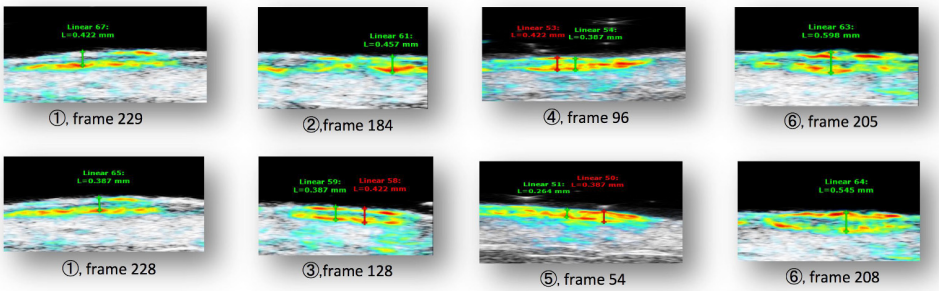

CONTROL ID: 2244195

TITLE: PET-based cell tracking with a Cre-switchable sr39tk PET reporter mouse line

PRESENTER: Martin Thunemann

ABSTRACT BODY:

Abstract Body: Tracking single cells or cell populations *in vivo* under healthy or diseased conditions is a central approach in biomedical research. Stable integration of reporter transgenes into the target genome is a powerful strategy to label cells, especially for longitudinal imaging studies. In this context, site-specific recombinases (e.g., Cre or ligand-inducible CreER^{T2}) are key tools to induce reporter gene expression in a given cell type, also in a time-dependent manner. However, this approach has not yet been realized for reporter genes detectable through positron emission tomography (PET). Such a reporter gene is sr39tk, an engineered thymidine kinase from *Herpes simplex* virus that is used with PET tracers like [^{18}F]FHBG. The aim of the present study was to generate and characterize a transgenic mouse line that allows flexible labeling of different cell types for PET-based cell tracking by activating sr39tk expression in a Cre-dependent manner.

We generated the R26-mT/sr39tk PET reporter mouse line via targeted integration of a construct for Cre-dependent sr39tk expression into the Rosa26 (R26) gene locus. Transgenic mice expressing Cre under control of different cell-type-specific promoters were bred to the new R26-mT/sr39tk PET reporter line. In respective Cre;R26-mT/sr39tk mice, sr39tk-expressing cell populations were detected after [^{18}F]FHBG injection *in vivo* by PET imaging with dedicated small-animal PET scanners and subsequently in selected organs via autoradiography and γ-counting. MR imaging was used to complement PET data with anatomical information. Cre-transgenic mice were also bred to R26-lacZ reporter mice that express β-galactosidase in a Cre-dependent manner, which allows *ex vivo* detection of Cre recombinase activity using X-Gal staining for β-galactosidase. X-Gal-staining of selected organs isolated from Cre;R26-lacZ mice was correlated with *in-vivo*- and *ex-vivo*-results obtained with Cre;R26-mT/sr39tk mice.

Expression of sr39tk was induced in pancreatic β cells, cardiomyocytes, platelets, smooth muscle cells, and T cells. [^{18}F]FHBG uptake quantified via PET imaging and/or by autoradiography and γ-counting was ten-to-hundred-fold higher in sr39tk-positive tissues as compared to Cre-negative controls. With some Cre mice, off-target recombination was detected *in vivo* by PET imaging and was then confirmed *ex vivo* in Cre;R26-lacZ mice via X-Gal staining. Proof-of-principle studies performed (1) to track T cells in a model of contact hypersensitivity and (2) to access cardiomyocyte viability in myocardial infarction show the usability of our approach to study disease models non-invasively through PET imaging.

Our experiments show the *in-vivo*-functionality of our new R26-mT/sr39tk PET reporter mouse line for non-invasive cell tracking in living animals under healthy and diseased conditions. Studies are ongoing to evaluate its potency to characterize Cre activity in an unbiased/holistic manner and to track diverse cell types under physiological and pathophysiological conditions.

AUTHORS (LAST NAME, FIRST NAME): Thunemann, Martin[1]; Schörg, Barbara F.[2]; Voelkl, Jakob[3]; Lin, Yun[2]; Golla, Matthias[1]; Feil, Susanne [1]; Griessinger, Christoph M.[2]; Kneilling, Manfred[2, 4]; Lang, Florian[3]; Pichler, Bernd J.[2]; Feil, Robert[1]

INSTITUTIONS (ALL):

1. Interfakultäres Institut für Biochemie, Eberhard Karls Universität Tübingen, Tübingen, Germany.
2. Department of Preclinical Imaging and Radiopharmacy, Werner Siemens Imaging Center, Tübingen, Germany.
3. Physiologisches Institut I, Eberhard Karls Universität Tübingen, Tübingen, Germany.
4. Department of Dermatology, Eberhard Karls Universität Tübingen, Tübingen, Germany.

(No Image Selected)

CONTROL ID: 2243080

TITLE: Evans Blue Conjugates: A General Platform Leverages the Blood Circulation of Peptide Probes

PRESENTER: Zhibo (Zippo) Liu

ABSTRACT BODY:

Abstract Body: Objectives: The fast clearance of peptide conjugates from the blood circulation is usually considered as a unique advantage compared with other targeting strategies (e.g. antibody). However, it is precisely this pharmacokinetics that is responsible for the relatively low tumor uptake and sometimes extremely high accumulation in the radioactivity-sensitive organs (e.g. kidneys). To improve this dissatisfying situation, here we present an albumin-binder (Evans blue, EB) based platform, which is designed to be generally applicable and able to prolong the blood circulation of otherwise rapidly cleared peptide probes.

Methods:

NOTA-alkyne was synthesized according to the previously published procedure, and subsequently conjugated to EB-azide and RGD-azide to afford NOTA-EB-RGD via copper-catalyzed “click” reaction (CuAAC). ^{68}Ga-labeling was performed at room temperature with 20 nmol of precursor followed by SPE purification using a C18 Sep-Pak cartridge. PET imaging and biodistribution studies were performed in healthy nude mice to evaluate the pharmacokinetics of the EB-conjugated peptide.

Results:

NOTA-EB-RGD was modularly synthesized in three steps from the readily available starting materials. The ^{68}Ga-labeled NOTA-EB-RGD was prepared in 20 min, and isolated in ~75% (n=3) radiochemical yield with >99% radiochemical purity and >30 GBq/μmol specific activity. ^{68}Ga-NOTA-EB-RGD was stable in plasma with <1% decomposition after 2 h incubation at room temperature. Based on the PET imaging, ventricles of the heart and major arteries were clearly visualized with EB-conjugated peptide. In addition, compared with original ^{68}Ga-NOTA-RGD, significantly higher level of the radioactivity was retained in the circulation system even at 90 min after injection.

Conclusions: Installation of an albumin-binding entity (EB) into the structure of a RGD-based radio-conjugate has increased the blood circulation significantly. Because of its modular construction, this EB-based platform can be a promising strategy to improve the pharmacokinetics of many other peptide probes.

AUTHORS (LAST NAME, FIRST NAME): Liu, Zhibo (Zippo)[2]; Kiesewetter, Dale O.[1]; Niu, Gang[3]; Chen, Xiaoyuan[4]

INSTITUTIONS (ALL):

1. NIBIB/LOMIN, NIH, Bethesda, MD, United States.
2. NIBIB, National Institute of Health, Bethesda, MD, United States.
3. National Institutes of Health, Bethesda, MD, United States.
4. National Institute of Biomedical Imaging and Bioengineering, National Institutes of Health, Bethesda, MD, United States.

(No Image Selected)

CONTROL ID: 2244848

TITLE: ^{18}F-Boramino Acid: the Traceable Amino Acid Mimicks for Cancer Imaging

PRESENTER: Zhibo (Zippo) Liu

ABSTRACT BODY:

Abstract Body: Objectives: Amino acid is the basis of life, and the transportation of amino acid has been found to be up-regulated in many types of cancers. Thus, radiolabeling amino acids for mapping amino acid transporter is of paramount importance but has been a long-standing challenge due to the extremely limited versatility of natural amino acid. In general, amino acid is radiolabeled with ^{18}F and ^{11}C. During the past three decades, even though enormous efforts have been devoted, only a few ^{18}F-labeled amino acids have been successfully developed and almost none of the ^{18}F-labeling strategies can keep the natural side chain of amino acids. Modification of the side chain of amino acid often results in poor *in vivo* performance as the original biological property of the parent amino acid has been inevitably changed. In addition, the ^{11}C-labeled amino acid, though shares the identical structure with the native amino acid, suffers from the poor radiochemistry and short half-life ($t_{1/2}$=20 min). To meet all these challenges, a series of ^{18}F-labeled “boramino acids” (boron + amino acids), that are based on “kit-like” radiolabeling and share the identical side chain with amino acids, have been developed to be the traceable bioisosteres of amino acids.

Methods: ^{18}F-Leu-BF_3 was synthesized as a representative boramino acid to mimic L-leucine. The transportation was blocked by 2-amino-2-norbornanecarboxylic acid (BCH), an inhibitor of system L amino acid transporters. To validate the equivalence between boramino acid and amino acid, ^{18}F-Leu-BF_3 was evaluated *in vitro* by the standard amino acid uptake assay and *in vivo* by PET imaging in tumor-bearing mice.

Results: ^{18}F-Leu-BF_3 was produced *via* ^{18}F-^{19}F isotope exchange reaction (**Figure 1.a**) within 25 min without the need of HPLC purification to give 60 ± 15% (n=5, non-decay corrected) radiochemical yield with >98% radiochemical purity and >37 GBq/μmol specific activity. The cell uptake of ^{18}F-Leu-BF_3 was time-dependent and increased to ~7.5%AD (added dose) at 60 min after incubation. Moreover, this uptake was specifically blocked by BCH under sodium-free environment (**Figure 1.b**) in a concentration dependent manner that fits well with Michaelis-Menten kinetics, giving the K_M of ^{18}F-Leu-BF_3 to be 25.1 ±2.3 μM (**Figure 1.c**, $K_{M,\ Leu}$= 19.7 ± 2.3 μM), further confirming the transporter-mediated uptake mechanism. In addition, a comprehensive animal study showed that the radiotracer was specifically accumulated in the tumor to give high tumor-to-background contrast at 120 min post injection (**Figure 1.d**), whereas the remainder gradually cleared *via* kidneys to the bladder.

Conclusions: In this work, we designed, synthesized and biologically evaluated ^{18}F-labeled ^{18}F-Leu-BF_3 as the traceable mimics of L-leucine. This novel strategy can be generalized to label other boramino acids as PET tracers to image amino acid transporters.

AUTHORS (LAST NAME, FIRST NAME): Liu, Zhibo (Zippo)[2]; Kiesewetter, Dale O.[1]; Niu, Gang[3]; Chen, Xiaoyuan[4]

INSTITUTIONS (ALL):

1. NIBIB/LOMIN, NIH, Bethesda, MD, United States.
2. NIBIB, National Institute of Health, Bethesda, MD, United States.
3. National Institutes of Health, Bethesda, MD, United States.
4. National Institute of Biomedical Imaging and Bioengineering, National Institutes of Health, Bethesda, MD, United States.

(No Image Selected)

CONTROL ID: 2243142

TITLE: Development about 19F chemical shift imaging of DNA conformation change

PRESENTER: Shigetaka Nakamura

ABSTRACT BODY:

Abstract Body: In addition to canonical right handed B-form structure, DNA has been demonstrated to adopt left handed Z-form DNA, bent DNA, triplex DNA, parallel stranded DNA and quadruplex DNA. Such polymorphism of structure has been suggested to play an important role in a number of transcriptional and replicative processes. Therefore, the analysis of the DNA structure in cells has the wide potentials for understanding the life and pathology. To analyze a modality of the DNA conformation, we focused on nuclear magnetic resonance imaging (MRI). It can provide noninvasive high-resolution images and expected as molecules imaging method using molecular probes of deep part of the living body because its living body background is low and detection sensitivity is relatively high. Here, we focused on conformational dynamics of DNA, such as the structural change from B-DNA to Z-DNA, and developed ^{19}F chemical shift imaging of DNA conformational transition using trifluorothymidine (^{TF}T). We observed a change of surrounding environment of nucleic acid base by the difference in DNA structure as a change of the fluorine nuclear magnetic resonance (NMR) signal by introducing trifluoromethyl group into pyrimidine base.

The CG- alternative DNA is known to form a stable Z-DNA at high salt concentration. We synthesized CG-alternative ODN containing ^{TF}T, and examined their ^{19}F NMR spectra. The ^{19}F NMR signal of ^{TF}T in B-DNA was appeared at -62.1 ppm. Then, by addition of $MgCl_2$ the chemical shift of the ^{19}F NMR signal clearly shifted toward the low magnetic field at -62.9 ppm dependent on the concentration of $MgCl_2$. The CD spectrum of ODNs in 0 M magnesium chloride indicated typical B-DNA CD signals, which a positive band around 280 nm and a negative band around 250 nm; at high salt concentration, the CD signals indicated a positive band around 270 nm and a negative band around 295 nm, which suggested that ODNs formed Z-DNA. Therefore, B-Z conformational change of ODNs adding salt concentration is easily distinguishable by monitoring the change in the ^{19}F NMR signal.

AUTHORS (LAST NAME, FIRST NAME): Nakamura, Shigetaka[1]; Hirata, Chihiro[1]; Fujimoto, Kenzo[1]

INSTITUTIONS (ALL):

1. materials science, Fujimoto-lab, Japan advanced institute of science and technology, Nomi, Ishikawa, Japan.

(No Image Selected)

CONTROL ID: 2243146

TITLE: Cell penetrating peptides improve tumor delivery of imaging probes through Neuropilin-1-dependent extravasation

PRESENTER: Tetsuya Kadonosono

ABSTRACT BODY:

Abstract Body: Efficient delivery from the blood vessels into tumor tissue is desired for improving specific imaging and targeting of cancers. It is well known that macromolecules can exude from blood vessels and accumulate within the tumor by enhanced vascular permeability and retention (EPR) effect. In addition to the EPR effect, recent studies have demonstrated that some synthetic peptides can increase vascular permeability by stimulating the permeability-regulating receptor, neuropilin-1 (NRP1).

Cell penetrating peptides (CPPs), also called protein transduction domains (PTDs) enable to facilitate the transport of fused proteins across cellular membranes. Recently, we developed CPP/PTD-fused optical imaging probe POH-N, with which we were able to achieve tumor-specific imaging shortly after its intravenous injection in several cancer mouse models. In a Transwell assay, we found that POH-N actively penetrated endothelial cell layer, suggesting that the tumor-specific delivery of POH-N is not only dependent on EPR effect but mediated by an unknown extravasation mechanism through endothelial cells.

To investigate the extravasation mechanism, we firstly evaluated the binding efficiency of a CPP/PTD-fused protein to NRP1; fluorescent dye-conjugating CPP/PTD peptides and CPP/PTD-fused green fluorescent proteins effectively bound to a human breast cancer MDA-MB-231 cells, which highly express NPR1, and the binding was abrogated by the addition of an anti-human NRP1 antibody or knockdown of NRP1 from MDA-MB-231 cells. These results suggest that NRP1 may be involved in the extravasation mechanism of CPP/PTDs. Next, *in vivo* optical imaging was applied for examining the function of NRP1 in delivery efficiency of a CPP/PTD-fused protein to tumors; POH-N probe was injected to tumor-bearing mice with or without an anti-mouse NRP1 antibody. A significant reduction of tumor-specific delivery of POH-N was observed after co-injection with NPR1 antibody compared to POH-N alone. Then, to further elucidate the contribution of NRP1 on the extravasation of CPP/PTD-fused proteins, we utilized iRGD peptide, a tumor-penetrating peptide, which enhances blood vessel permeability via binding to NRP1 [Science, 328(5981), 1031-1035 (2010)]. Contrary to expectations, when iRGD peptide was co-injected with POH-N into tumor-bearing mice, the delivery of POH-N to the tumors was suppressed. This result may suggest that POH-N and iRGD compete for binding at the same site on NRP1. Finally, to examine whether CPP/PTDs affect blood vessel permeability as iRGD peptide, we analyzed vascular permeability by Evans blue dye leakage to tumors after CPP/PTD-fused protein injection. CPP/PTD-fused protein did not increase the dye leakage, rather showed suppressive effect, strongly suggesting that CPP/PTDs can enhance extravasation through NRP1-binding by a totally different mechanism from iRGD. Further understanding of the molecular mechanism of the NRP1-mediated extravasation of CPP/PTDs would improve delivery of anti-cancer drugs and imaging probes.

AUTHORS (LAST NAME, FIRST NAME): Kadonosono, Tetsuya[1]; Tsubaki, Takuya[1]; Kuchimaru, Takahiro[1]; Kizaka-Kondoh, Shinae[1]

INSTITUTIONS (ALL):

1. Tokyo Institute of Technology, Yokohama, Japan.

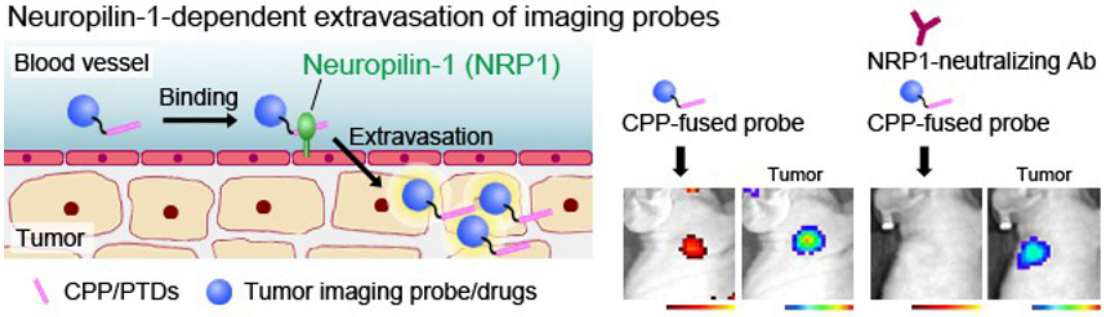
Neuropilin-1-dependent extravasation of imaging probes
Blood vessel
Binding
Neuropilin-1 (NRP1)
Extravasation
Tumor
CPP/PTDs
Tumor imaging probe/drugs
NRP1-neutralizing Ab
CPP-fused probe
CPP-fused probe
Tumor
Tumor

CONTROL ID: 2243175

TITLE: Development of Multifunctional Nanoparticles for Multimodal Imaging

PRESENTER: Chang Kyu Sung

ABSTRACT BODY:

Abstract Body: Our lab has developed multifunctional magnetic nanoparticles that possess well-ordered porous structures, excellent aqueous dispersion, and sufficient loading of visual contrast agents. This technology has both diagnostic and therapeutic applications, enabling simultaneous multimodal imaging and efficient drug delivery to targeted cells. The nanoparticles are composed of cobalt ferrite magnetic nanoparticles (MNP, $CoFe_2O_4$) coated with a silica shell (SiO_2) of stable and biocompatible material to avoid the potential toxic effects on cells. To acquire additional fluorescent properties, an organic fluorescent dye (rhodamine B isothiocyanate, RITC) was incorporated into the silica shell. Thus, the compound has a bifunctional property which enables dual modality detection by MRI and optical imaging. The surface of the dual-functionalized silica-coated nanoparticles was modified with biocompatible polyethylene glycol (PEG) groups to render them biocompatible by preventing the nonspecific adsorption of proteins to the nanoparticles. Attachment of the PEG did not significantly change the size of the nanoparticles. The average diameter of the nanoparticles was about 50nm. This small size permits greater delivery to target tissue, overcoming current challenges of aggregation and susceptibility to immune clearance. The r1 and r2 relaxivity values of the nanoparticles were 0.33 and 398 $mM^{-1} s^{-1}$ at 1.5T, respectively, and 0.29 and 453 $mM^{-1} s^{-1}$ at 3T, respectively. The absorption (λmax) and emission maxima (λem) were observed at 540 and 625 nm, respectively. The nanoparticles enabling simultaneous multimodal imaging were observed in vitro and in vivo with optical and MR imaging. The porous structure of these small nanoparticles allow sufficient volume loading of superparamagnetic and fluorescent contrast agents for imaging purposes. This new type of contrast agent can be a promising tool for multimodal imaging in medical application.

AUTHORS (LAST NAME, FIRST NAME): Sung, Chang Kyu[1]

INSTITUTIONS (ALL):

1. Departments of Radiology, SNU-SMG Boramae Medical Center, Seoul, Korea (the Republic of).

(No Image Selected)

CONTROL ID: 2243187

TITLE: “Turn-on” Optical Probes for Imaging Mn^{2+} in Live Cells.

PRESENTER: Anindita Sarkar

ABSTRACT BODY:

Abstract Body: Manganese (Mn) is an enzymatic cofactor essential for brain function. Intracellular Mn mostly exists as Mn^{2+} and weakly bound Mn^{2+} also acts as an anti-oxidant.[1] However, occupational and environmental overexposure to Mn results in a neurological disorder, Manganism which has symptoms similar to Parkinson’s disease. For a broader understanding of the molecular mechanisms underlying Mn regulation under physiological and pathological conditions, we need to quantify Mn^{2+} pools, live, *in vivo*. Conventional techniques for Mn^{2+} detection are often destructive and lack information on Mn^{2+} dynamics within live cells making fluorescence imaging the technique of choice that can offer in cellulo detection with unparalleled sensitivity.

Despite the requirement, there are limited reports of fluorescent sensors for Mn^{2+}. The reasons being low binding affinity of Mn^{2+} towards different ligands and the fluorescence quenching of dyes due to the paramagnetic nature of Mn^{2+}.

A ‘turn-on’ fluorescent sensor was designed by overcoming the above challenges.[2] The binding pockets of Mn^{2+} binding proteins and MnSOD synthetic mimics were carefully scrutinized to design and synthesize an Mn^{2+} selective penta-aza macrocyclic ligand with pendent oxygen arms. A dimethylaniline was strategically fused into the penta-aza macrocycle to which was attached a BODIPY reporter unit. The N-donors of the ligand quench the fluorescence of the covalently attached BODIPY via a photo-induced electron transfer mechanism in the absence of Mn^{2+}. Upon Mn^{2+} binding, the sensor affords a 52-fold fluorescence enhancement in a lipid mimetic solvent, acetonitrile. The probe elicits a maximum ‘turn-on’ response in presence of Mn^{2+} and offers excellent selectivity over biologically abundant metal ions like Ca^{2+}, which is also a major competitor for Mn^{2+} binding ligands. The sensors were successfully tested for Mn^{2+} detection in live cells. Co-localization studies of the probes with a lipophilic stain like Nile Red showed that the probes could detect Mn^{2+} within lipid rich entities.

The biochemistry of Mn^{2+} remains more elusive than other transition metal ions like Fe^{2+} or Cu^{2+}. Different cell types elicit different responses upon Mn exposure which is reflected in a differential subcellular distribution of Mn. The Mn^{2+} sensors can be employed to identify the cell types vulnerable to accumulate Mn^{2+} in overload conditions and image pools of labile Mn^{2+}.

The sensors are currently being explored in conjunction with other known metal ion sensors to study the effect of metal ion stress conditions on internal Mn^{2+} distributions. The next generation of sensors is being synthetically modified to target Golgi bodies which are implicated in Mn^{2+} efflux via lipid vesicles.[3] Studies are underway to employ the sensors for investigating Mn induced neuronal defects in vertebrate animal models.

1. K. Barnese, E. B. Gralla, J. S. Valentine, D. E. Cabelli, *PNAS*, **2012**, 109, 6892-6897.
2. Subha Bakthavatsalam,‡ Anindita Sarkar,‡ Ananya Rakshit, Shubhi Jain, Amit Kumar and Ankona Datta, *Chem. Commun.*, **2015**, 51, 2605–2608.
3. A. Carmona, S. Roudeau, L. Perrin, G. Veronesi and R. Ortega, *Metallomics*, **2014**, 6, 822–832.

AUTHORS (LAST NAME, FIRST NAME): Sarkar, Anindita[1]; Bakthavatsalam, Subha[1]; Rakshit, Ananya[1]; Datta, Ankona[1]

INSTITUTIONS (ALL):
1. Department of Chemical sciences, Tata Institute of Fundamental Research , Mumbai, Maharashtra, India.

(No Image Selected)

CONTROL ID: 2243368

TITLE: Preparation of ^{11}C-Labeled scFv Antibody by Cell Free Protein Synthesis System

PRESENTER: Kae Higuchi

ABSTRACT BODY:

Abstract Body: Aim: Immuno-PET is a promising approach for improving the characterization, diagnosis, and immunotherapy of tumors by taking advantage of the high specificity of antibodies. Therefore, many studies have been performed to prepare and evaluate positron-emitter labeled antibodies. This study shows a novel approach for synthesis of a ^{11}C-labeled single chain variable fragment antibody (scFv) against EGFRvIII (^{11}C-MR1-1) by cell free protein synthesis with ^{11}C-methionine.

Methods: Reaction solution of cell free protein synthesis (CFPS) system was prepared from the Escherichia coli S30 extract according to our standard protocol (Kigawa, T., et al. (2004), J. Struct. Func. Genom. 5, 63–68). Plasmid DNA encoding MR1-1 was added to the CFPS for MR1-1 synthesis. The product MR1-1 was isolated by affinity purification using an epitope peptide. The binding kinetics of cold MR1-1 to the EGFRvIII peptide was measured by a BIAcore 3000. Cell binding assay was also performed by using a fluorescently labeled MR1-1 and F98EGFRvIII rat glioma cells. Radiosynthesis of ^{11}C-MR1-1 was carried out by addition of ^{11}C-metionine in saline and plasmid DNA to the CFPS system. Production of ^{11}C-MR1-1 was monitored by SDS-PAGE autoradiography (ARG). ^{11}C-MR1-1 was also purified by affinity chromatography. In vivo distribution of ^{11}C-MR1-1 was evaluated small-animal PET and ex vivo biodistribution studies in mice bearing A431-tumors.

Results: MR1-1 prepared by CFPS system showed high affinity for the wild type peptide, with a Kd value of 1.06×10^{-8} M, while its affinity was significantly decreased for the mutant peptides, suggesting that the cell-free synthesized MR1-1 was able to strictly discriminate the antigen peptide. Cell binding assay confirmed the specific binding of MR1-1 to human EGFRvIII. The decay-corrected (DC) radiochemical yield of ^{11}C-MR1-1 at 5 min was 36.2 %, and the value was nearly constant (38%) after 10 min. The ^{11}C-MR1-1 was isolated in the yield of 8.3% with >95% radiochemical purity. The tumor was visualized by PET at 55-60 min post-injection and the tumoer-to-muscle ratio was determined to be 4.3 at 70 min post-injection by biodistribution study.

Conclusions: We have succeeded in the biochemical preparation of a ^{11}C-labeled scFv, ^{11}C-MR1-1, by CFPS-method. Although further optimization of the method is necessary, this novel approach would be a potential option for the preparation of immuno-PET radiotracers

AUTHORS (LAST NAME, FIRST NAME): Furumoto, Shozo[1]; Matsuda, Takayoshi[2]; Higuchi, Kae[2]; Ishikawa, Yoichi[1]; Yanai, Kazuhiko[1, 3]; Iwata, Ren[1]; Yokoyama, Jun[2]; Kigawa, Takanori[2]

INSTITUTIONS (ALL):

1. Cyclotron and Radioisotope Center, Tohoku University, Sendai, Japan.
2. RIKEN Systems and Structural Biology Center, Yokohama, Japan.
3. Tohoku University School of Medicine, Sendai, Japan.

(No Image Selected)

CONTROL ID: 2243510

TITLE: Wavelength shifting Zn^{2+} probe based on pyridine–pyridone core structure

PRESENTER: Masayori Hagimori

ABSTRACT BODY:

Abstract Body: Zinc is known to play important roles in biological processes including gene expression, apoptosis, etc. To understand the role of Zn^{2+} in physiology and particularly in the field of neurochemistry, a variety of fluorescent Zn^{2+} probes have been developed, and some have provided useful information regarding zinc biology. Most of the fluorescent Zn^{2+} probes presented so far possess a fluorescent core and a separate part for binding to Zn^{2+} within the molecule. Therefore, these probes usually have high molecular weights and hydrophobic properties, resulting in limited cell permeability and poor aqueous solubility. We previously reported water-soluble and low-molecular-weight fluorescent Zn^{2+} probes based on a pyridine–pyridone core structure, which acted as the chelating functionality for Zn^{2+}, and simultaneously provides the fluorescent part within this single molecule [1]. Here, we developed novel fluorescent probes with methylene spacers of varying lengths between the aryl ring and the pyridine–pyridone core. The spacer length greatly affected the fluorescence, as some led to a Zn^{2+} dependent bathochromic shift of the emission spectrum in addition to enhancements in the fluorescence.

We prepared compounds **1–3** with methylene spacers (between the phenyl ring and the 3-position of the pyridone ring of the pyridine/pyridone core) of different lengths (**1**: n = 0, **2**: n = 1, **3**: n =2). All spectroscopic measurements were carried out in HEPES buffer (100 mM, 5% DMSO, pH 7.4). The wavelength of emission maximum of **1–3** were 451 nm, 419 nm, and 415 nm, and the fluorescence quantum yields (Φ) were 0.035, 0.029, and 0.031, respectively. Upon addition of Zn^{2+}, **1** exhibited strong fluorescence at 451 nm, while **2** and **3** exhibited 30 nm and 34 nm bathochromic shifts of their emission wavelengths, respectively. The Φ values with Zn^{2+} were 0.671, 0.336, and 0.275 for compounds **1–3**, respectively. In compounds **2** and **3**, electron transfer from the phenyl ring was inhibited by the methylene spacer, resulting in lower Φ values. On the other hand, the emission intensity ratios in the presence/absence of Zn^{2+} of **2** and **3** were higher than that of **1**. After we confirmed the 1:1 complex formations with Zn^{2+}, the dissociation constants (K_d) of **1–3** were calculated as 4 - 8 × 10^{-5} M. Since **2** showed preferable properties, we performed further evaluation. When the solution pH decreased from pH 9.0 to pH 2.0, the fluorescence intensity remained constant >6. In the selectivity toward cations, the chelation enhanced fluorescence effects was not affected by alkali-metal ions and alkaline-earth metal ions. Then, to demonstrate potential biological applications, we evaluated cell permeability in mouse macrophage-like cells; RAW264, and hepatocellular carcinoma cells; HepG2. When the cells were supplemented with Zn^{2+} after being incubated with **2**, strong fluorescence was observed.

In conclusion, the pyridine–pyridone based low-molecular-weight fluorescent probe **2** would be useful for studying the biological functions of Zn^{2+}.

[1] Hagimori M., Mizuyama N., Mukai T., Saji H., et al., Sens. Act. B 2015; 213, 45-52.

AUTHORS (LAST NAME, FIRST NAME): Hagimori, Masayori[1]; Mizuyama, Naoko[2]; Saji, Hideo[3]; Mukai, Takahiro[1]

INSTITUTIONS (ALL):

1. Kobe Pharmaceutical University, Kobe, Japan.
2. Foundation for Biomedical Research and Innovation, Kobe, Japan.
3. Graduate School of Pharmaceutical Sciences, Kyoto University, Kyoto, Japan.

(No Image Selected)

CONTROL ID: 2243630

TITLE: A radiolabeled fluorescent nanoprobe electrostatically assembled with hyaluronic acid for tumor-targeted nuclear and optical imaging

PRESENTER: Masayori Hagimori

ABSTRACT BODY:

Abstract Body: Hyaluronic acid (HA), a naturally occurring polysaccharide, is widely used as cosmetic and pharmaceutical materials due to its biocompatibility, biodegradability, non-toxicity, and non-immunogenicity. HA binds with high affinity to CD44 which is over-expressed in various tumor cells and serves as a marker of cancer stem-like cells resistant to chemotherapy and radiotherapy. Therefore, HA is also a very attractive material for tumor-targeted delivery. In the previous study, we developed indium-111-labeled ternary complex composed of generation 4 PAMAM dendrimer conjugated with p-SCN-Bn-DTPA (G4-DTPA), polyethyleneimine (PEI), and anionic γ-polyglutamic acid (γ-PGA) by electrostatic interaction. The ^{111}In-labeled γ-PGA complex clearly visualized rat popliteal lymph node with SPECT/CT [1]. For in vivo fluorescence imaging of sentinel lymph node, we also prepared fluorophore-quencher conjugated γ-PGA complex based on fluorescence resonance energy transfer (FRET) quenching. Here, for tumor-targeted nuclear and optical imaging, ^{111}In- and Cy5 dye-labeled ternary complex was prepared using HA as an anionic polymer in place of γ-PGA.

G4-Cy5-DTPA was prepared by the reaction of G4 dendrimer and Cy5 NHS ester followed by conjugation with DTPA in 5% glucose. For the preparation of ternary complex, G4-Cy5-DTPA/PEI/HA, G4-Cy5-DTPA solution and PEI solution were mixed and left for 15 min, and then HA solution were mixed with G4-Cy5-DTPA/PEI complex and left for another 15 min. ^{111}In-labeled G4-Cy5-DTPA/PEI/HA complex was obtained by reacting G4-Cy5-DTPA-^{111}In with PEI and HA in turn. Formation of the complex was examined by Zetasizer Nano ZS at various molar ratios of HA to G4-Cy5-DTPA/PEI or ^{111}In-labeled G4-Cy5-DTPA/PEI. At a molar ratio of 32, stable complexes were obtained (an average diameter of 35 nm and a ζ-potential of -50 mV). The fluorescence intensity of G4-Cy5-DTPA/PEI/HA was lower than that of G4-Cy5-DTPA indicating aggregation-caused quenching. Next, we examined the specific uptake and dequenching of G4-Cy5-DTPA/PEI/HA complex in tumor cells. Upon incubation of G4-Cy5-DTPA/PEI/HA complex in CD44 positive cells (Panc-1 human pancreatic cancer cells and T24 human bladder carcinoma cells), time-dependent increases in intracellular fluorescence intensity of Cy5 were observed by fluorescence microscopy. The intracellular localization was confirmed by colocalization with the lysosomal marker LysoTracker after incubation of G4-Cy5-DTPA/PEI/HA complex in Panc-1 cells for 6 h, indicating the dissociation and dequenching of G4-Cy5-DTPA/PEI/HA complex in the lysosome. On the other hand, intracellular fluorescence was hardly observed in CD44-low-expressing cells (MCF7 human breast cancer).

In summary, ^{111}In- and Cy5-labeled ternary complex G4-Cy5-DTPA-^{111}In/PEI/HA was successfully synthesized by electrostatic interaction. In in vitro studies, the HA complex demonstrated aggregation-caused quenching effect and specific accumulation in CD44 positive cells. These results suggested that G4-Cy5-DTPA-^{111}In/PEI/HA would be useful as a nanoprobe for tumor-targeted nuclear and optical imaging.

[1] Sano K., Mukai T., et al., J. Control. Release 2014, 194, 310–315.

AUTHORS (LAST NAME, FIRST NAME): Hagimori, Masayori[1]; Sengoku, Azusa[1]; Mukai, Takahiro[1]

INSTITUTIONS (ALL):

1. Kobe Pharmaceutical University, Kobe, Japan.

(No Image Selected)

CONTROL ID: 2243525

TITLE: Melanin-coated magnetic nanoparticles for multi-modality imaging guided photothermal therapy

PRESENTER: Hao Hu

ABSTRACT BODY:

Abstract Body: Background: Cancer theranostics that combine both imaging and therapeutic functions is of great interest to cancer imaging and therapy community. Here, we report a melanin-coated magnetic nanoparticles (MCMPs) for multi-modality molecular imaging guided photothermal therapy (PTT). **Methods:** MCMPs were synthesized by biomimetic synthesis method using bioploymer melanin as the biotemplate. The radionuclide ^{64}Cu is labeled with MCMPs by the high affinity of metal ions for melanin. PET, MRI, and photoacoustic (PA) imaging were carried out on U87MG tumor-bearing mice. PTT was conducted both *in vitro* and *in vivo*. **Results:** the MCMPs were successfully synthesized by biomimetic synthesis method. The size of MCMPs is ~15 nm. The r_2 value is 163 $mM^{-1}s^{-1}$, which is much higher than spherical magnetic nanoparticles (16 nm, r_2=125.86 ± 9 $mM^{-1}s^{-1}$; and 10 nm, r_2=59.91 ± 6 $mM^{-1}s^{-1}$). The MCMPs were then labeled with PET radionuclide ^{64}Cu. PET showed high tumor uptake of MCMPs after intravenous injection (150 μCi, 9.5%ID/g, 24 h). MRI and PA imaging also showed high tumor uptake of MCMPs. Meanwhile, under 808 nm laser excitation (0.5 W/cm^2, 5 min), 100% tumor elimination was achieved by MCMP treatment group (10 mg/kg of MCMPs). **Conclusion:** MCMPs showed great potential as cancer theranostics with PET/MRI/PA multi-modality molecular imaging capability and potent PTT effects.

AUTHORS (LAST NAME, FIRST NAME): Hu, Hao[1]; Huang, Peng[2]; Wu, Kaichun[1]; Chen, Xiaoyuan[2]

INSTITUTIONS (ALL):

1. Xijing Hospital of Digestive Disease, Fourth Military Medical University, Xi'an, Shaanxi, China.
2. National Institute of Biomedical Imaging and Bioengineering, National Institutes of Health, Bethesda, MD, United States.

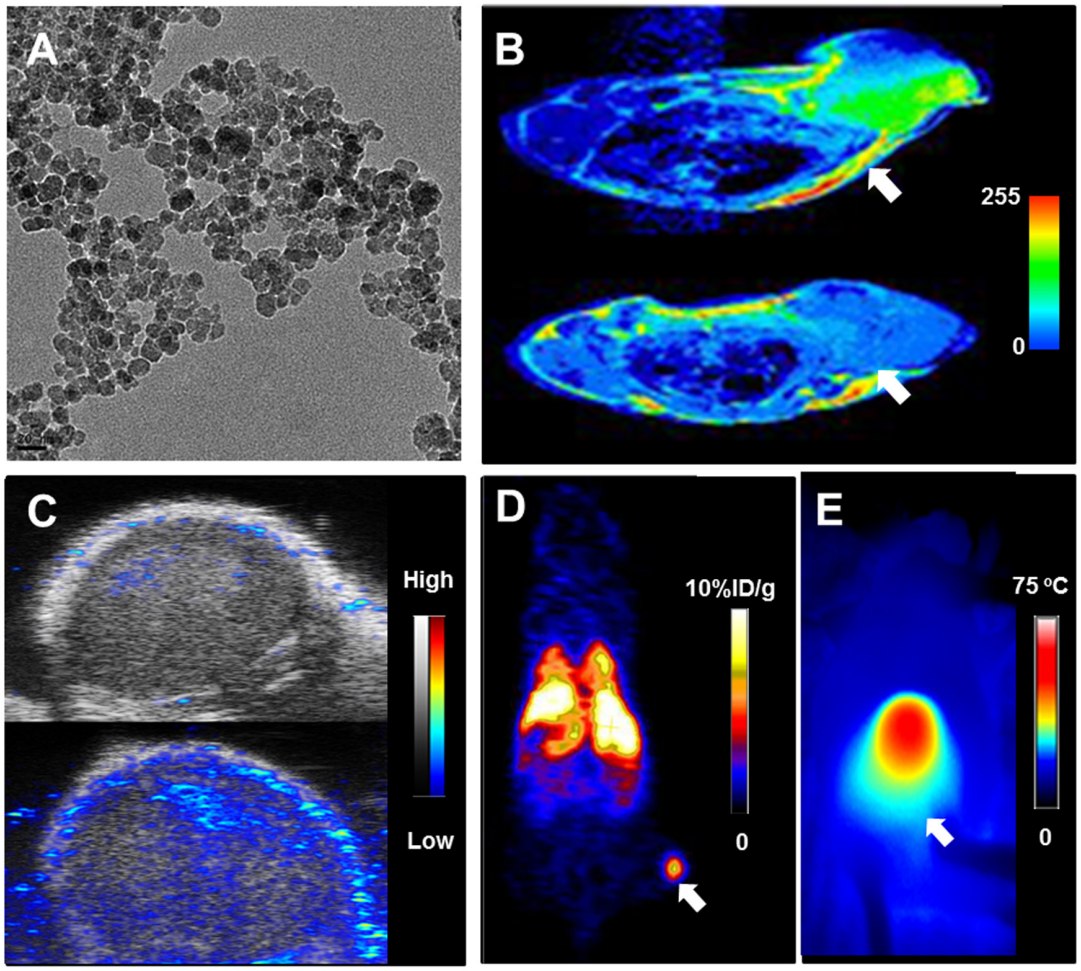

Figure (A) TEM image of melanin-coated magnetic nanoparticles (MCMPs); (B, C, D) MRI, PA, and PET images of MCMPs treated mice (intravenous injection, 10 mg/Kg of MCMPs); (E) Thermal image of mice upon laser irradiation (0.5 W/cm2, 5 min).

CONTROL ID: 2243626

TITLE: Understanding blood brain barrier breakdown in a metastatic tumor mouse model, using bioluminescence with ABCG2 inhibition

PRESENTER: Jeyan Kumar

ABSTRACT BODY:

Abstract Body: Introduction:

It has been reported that 20-40% of patients with cancer will experience brain metastases, which severely limit their survival and quality of life. As cancer patients experience increasing therapeutic benefits of their primary malignancies, the role of metastatic lesions will be increasingly relevant. Despite recent advancements in imaging technologies, the changes in the blood brain barrier (BBB) caused by the invading metastatic cells have not been adequately characterized. In addition, MRI, the gold standard of clinical brain tumor imaging often misses micrometastatic lesions presumably due to intact BBB. In the present study, we aim to use minimally invasive serial bioluminescence imaging (BLI) with inhibition of ABCG2, MRI, and histology in a mouse metastatic tumor model to compare the early time-dependent changes of the brain vascular permeability and tumor invasion.

Methods:

We inoculated athymic nude mice with a brain trophic prostate cancer cell line transfected with firefly luciferase. Bioluminescence imaging (BLI) and MRI (T1, T2, Diffusion, Gd, Gd-albumin) were performed at intervals up to three weeks serially to gather data from the earlier time points of tumor invasion. Imaging data were supplemented with immunohistochemistry, western blotting, as well as dye extravasation histology to correlate vascular leakage.

Results:

Metastatic lesions were seen in approximately 90% of mice with lesions detected between days 5-7 by BLI with inhibition of ABCG2, whereas lesions were undetectable without inhibition. MRI at early time points was unable to detect micrometastatic lesions with all the tested sequences, when compared to BLI. Metastatic lesions showed heterogeneous growth in regards to morphology and location.

Conclusions:

We found that molecular imaging using different BLI techniques (ABCG2 inhibition) can detect early metastases prior to a variety of MRI sequences. The ability to detect metastatic disease at an earlier stage and characterize the early changes to the BBB from metastases may allow for timely administration of effective chemotherapy that can improve patient outcome.

AUTHORS (LAST NAME, FIRST NAME): Kumar, Jeyan S.[1]; Yin, Juan[1]; Munasinghe, Jeeva P.[2]; Hall, Matthew[1]; Gottesman, Michael [1]

INSTITUTIONS (ALL):

1. NCI, National Institute of Health, Arcadia, CA, United States.
2. National Institute of Health, Bethesda, MD, United States.

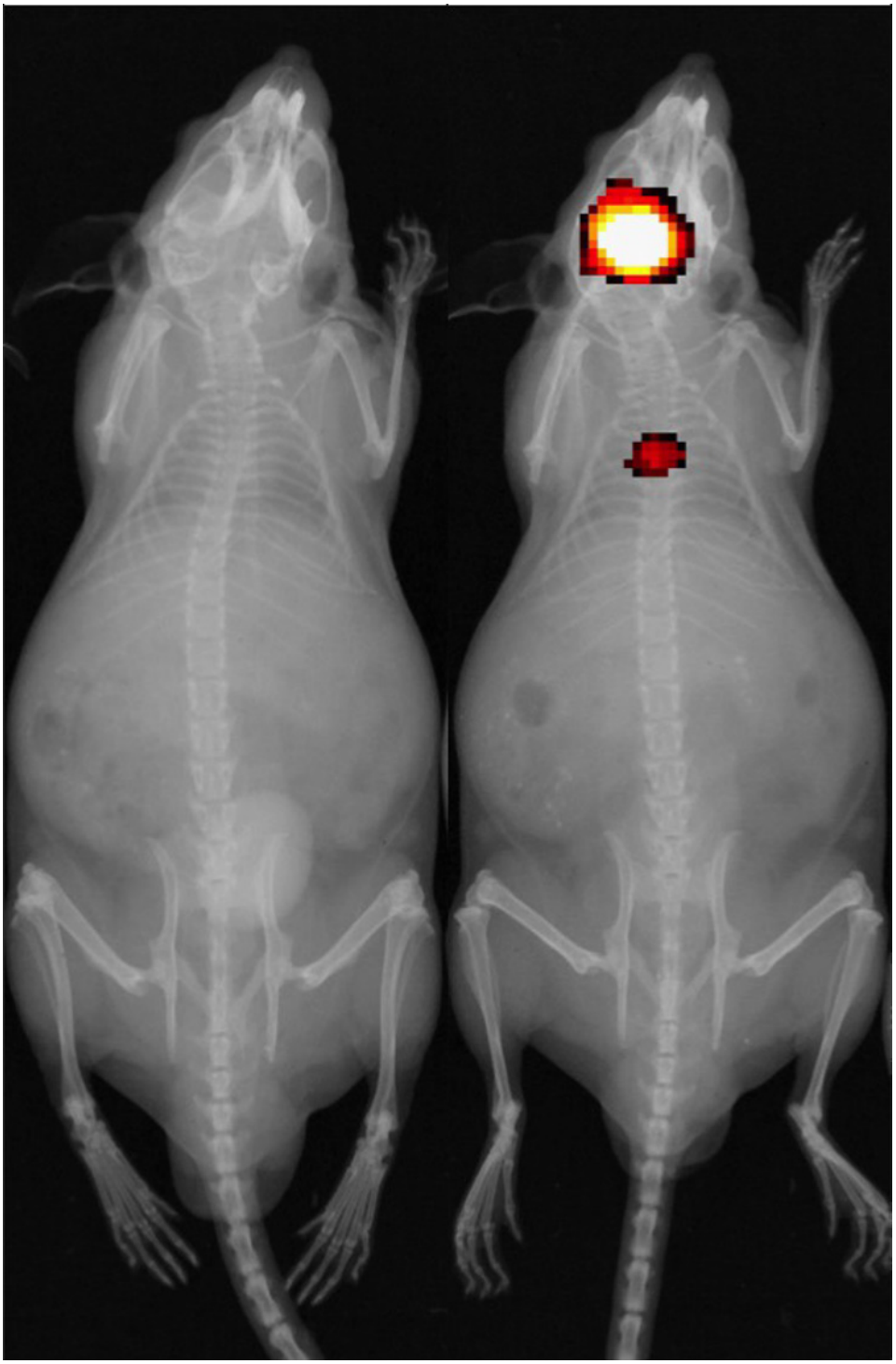

Figure 1: Metastatic tumor by BLI on day 7 without ABCG2 inhibition (left) and day 8 after ABCG2 inhibition with Ko143 (ABCG2 inhibitor) on the same mouse (right). Luciferin dosage was maintained at 150 mg/kg during both imaging sessions.

CONTROL ID: 2245157

TITLE: Assessing the utility of gadolinium-based contrast agents administered by the intravenous and the intraperitoneal route

PRESENTER: Jeyan Kumar

ABSTRACT BODY:

Abstract Body: Intravenous (IV) cannulation of the tail veins is a commonly used method to administer gadolinium-based contrast agents for magnetic resonance imaging (MRI) studies in mice. However, serial imaging in longitudinal studies is difficult due to problems with access and increased exposure to anesthesia with longer preparation times. Repeat probing of the tail vein can cause sclerosis and necrosis, which imposes the main limitation on the ability to serially obtain MR images of mice. This problem is compounded in studies when repeat administration of other drugs are required. In comparison to IV, intraperitoneal (IP) injections are a relatively facile approach to administering compounds to mice. We sought to establish an IP dose schedule for gadolinium based contrast agents in mice, and compare it to IV dosages.

We proposed to study contrast enhancement of the pituitary as a method to establish efficacy of the different dosages and routes of contrast enhancement. Since the vasculature of the pituitary is not comprised of the blood-brain barrier it is more permeable, allowing gadolinium based compounds to accumulate within the gland.

Methods:

In order to determine optimal IP dosages for MR imaging the efficacy, measured by pituitary enhancement, was gathered for commonly used IV dosages of 0.1 mmol/kg and 0.6 mmol/kg Gd-DTPA. IP dosages of 0.1, 0.6, 1.0, 2.5, 5.0, and 10.0 mmol/kg were chosen to ensure an appropriate dosage window. A group of 15 mice were randomized to both route of administration and dosage over the study period. MR images were gathered in a 9.4 Tesla Scanner (Bruker, Billerica, MA). T1 weighted images (Echo time/ Repetition time= 3.8/250 ms, slice thickness = 750 m, in-plane resolution= 79x76 m, total scan time 4 min15 sec) with five mid-saggital slices, centered about the pituitary gland, were acquired using a 4 channel mouse head array coil. T1 scan times were obtained before and after contrast administration, and maintained to less than 5 min to allow multiple measurements over a 60 min period to establish time-course measurements. The T1 enhancement due to Gd was evaluated as percentage intensity difference between post and pre contrast images.

To further validate IP administration of Gd-based contrast agents, mice bearing metastatic brain tumors were imaged to study contrast extravasation. Mice were inoculated by intra-cardiac injection with a brain trophic prostate cancer cell line and serially imaged over four weeks.

Results:

IP gadolinium contrast agent administration can provide similar pituitary signal enhancement when compared with IV administration. Enhancement of the pituitary with IP administration is delayed and requires a significantly larger dose of Gd-DTPA. No obvious adverse effects were noted in the study mice. In the tumor-bearing mice contrast extravasation was seen, further validating the utility of IP administration of Gd based contrast agents.

Conclusion:

IP administration of Gd-based contrast agents is a reasonable alternative to the intravenous approach. Comparable levels of pituitary enhancement are achieved with IV, however with increased dosages, and longer incubation period.

AUTHORS (LAST NAME, FIRST NAME): Kumar, Jeyan S.[1]; Diaz, Vivian[2]; Munasinghe, Jeeva P.[2]; Hall, Matthew[1]; Gottesman, Michael [1]

INSTITUTIONS (ALL):

1. NCI, National Institute of Health, Arcadia, CA, United States.
2. Neurological Disorders and Stroke, National Institutes of Health, Bethesda, MD, United States.

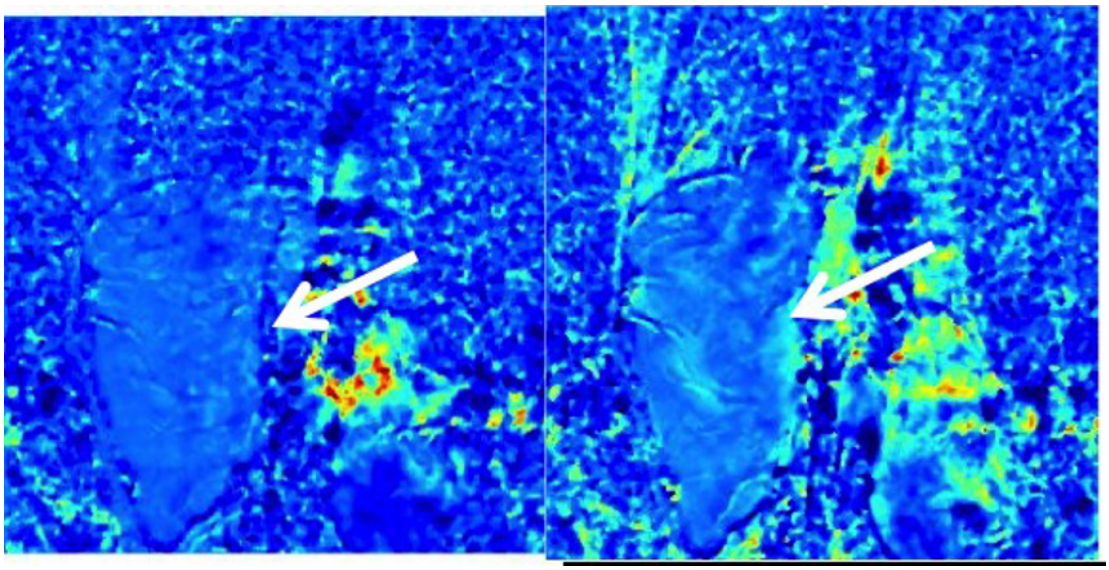

Midsaggital T1 section denoting pituitary (white arrows) with pre-contrast image (left) and 25 minute post contrast (right) administered by IV

CONTROL ID: 2243640

TITLE: REAL-TIME MOLECULAR IMAGING FOR DETECTING ONCOGENIC ACTIVITY IN MELANOMA USING THE MELANOMA DETECTION SYSTEM (MDS)

PRESENTER: Catherine Shachaf

ABSTRACT BODY:

Abstract Body: Melanoma is the fifth most common invasive cancer in men, and sixth in women. If identified late melanoma can be life threatening, yet it is curable if identified early.

Currently, the optimal method for detecting melanoma is a full-body visual skin examination by a health care professional using the visual ABCDE (Asymmetry, Border, Color, Diameter and Evolving) criteria for shape, color, size and change. The accuracy of visual diagnosis is limited, and since the risk of melanoma is great physicians tend to remove moles with a low suspicion of being melanoma to decrease the risk of missing a melanoma. More than 30 lesions are removed for each melanoma detected. As such, there is a true need for a more accurate, real-time test that will reduce the need for unnecessary biopsies of normal tissues and focus biopsies on lesions with a high level of suspicion for malignancy.

We have developed a real time molecular imaging method to identify oncogenic activity in melanoma skin lesions called the MDS (Melanoma Detection System). In a pilot study, we used MDS to differentiate between benign and melanoma lesions. MDS images were compared to the histopathology diagnosis of the moles. In this study we imaged 78 moles using the MDS. We identified all the melanomas diagnosed by pathology and recommended excising additional moles. With the MDS we could reduce the biopsy rate from 30 to 2 moles for each melanoma detected.

MDS provides biological information that is complementary to the visual evaluation of a mole. MDS has the potential to change how melanoma is currently detected.

AUTHORS (LAST NAME, FIRST NAME): Shachaf, Amit[1]; Manbeck, Kevin[1]; Shachaf, Catherine[1]

INSTITUTIONS (ALL):

1. Orlucent, Los Gatos, CA, United States.

(No Image Selected)

CONTROL ID: 2243864

TITLE: PET imaging for evaluation of neurogenesis in adult mammalian brain

PRESENTER: Yasuhisa Tamura

ABSTRACT BODY:

Abstract Body: In the adult mammalian brain, neurogenesis occurs only in two regions: the subventricular zone (SVZ) adjacent to the lateral ventricles and the subgranular zone (SGZ) of the dentate gyrus in hippocampus. Decreased activity of neurogenesis in SGZ is known to be a good indicator for evaluation of mood disorders. To date, however, proliferative activity involved in the neurogenesis in human brain has been detected only by histological methods applied to the postmortem brain, and there is no technique to observe adult neurogenesis in living condition. Using positron emission tomography (PET) with 3-deoxy-3-[^{18}F]fluoro-L-thymidine ([^{18}F]FLT), a PET tracer for cell proliferation, we succeeded to visualize the activity of neurogenesis non-invasively in adult rodents. We performed PET studies with [^{18}F]FLT in a corticosterone-induced depression model of rats, which has been known to show the decreased activity of hippocampal neurogenesis. Those studies showed that [^{18}F]FLT accumulation in SGZ of hippocampus decreased, but that in SVZ did not change compared with normal rats. The imaging data were well correlated with the number of newborn cells evaluated by histological observation in each neurogenic region. Moreover, we are now performing PET studies using anti-depressant drugs (SSRI, Selective Serotonin Reuptake Inhibitors)-administered rats since it has been reported that the number of newborn neurons increased in SGZ of hippocampus by the treatment with SSRI. This PET technique will realize non-invasive quantification of neurogenesis in the adult human brain and provide us a new way for objective diagnosis of mood disorders including depression.

AUTHORS (LAST NAME, FIRST NAME): Tamura, Yasuhisa[1]; Eguchi, Asami[1]; Takata, Kumi[1]; Yamato, Masanori[1]; Kume, Satoshi[1]; Nakano, Masayuki[1]; Kataoka, Yosky[1]

INSTITUTIONS (ALL):

1. Center for Life Science Technologies, RIKEN, Kobe, Japan.

(No Image Selected)

CONTROL ID: 2243892

TITLE: Correlation of ^{68}Ga-DOTATATE accumulation in adrenal gland with hormone levels in the patients with Cushing's syndrome

PRESENTER: Zhen Qiao

ABSTRACT BODY:

Abstract Body: Purpose: to correlate the ^{68}Ga-DOTATATE and ^{18}F-FDG accumulation with the corresponding hormone levels in the patients with Cushing's syndrome.

Patients and Methods: Twenty-five patients with Cushing's syndrome (Female 18, Male 7, aged 15–68 years) who underwent PET/CT between July 2013 and September 2014 were included in our study. All the patients were ACTH dependent (pituitary adenoma 12 and clinical suspected with ectopic ACTH syndrome 13). The mean SUV and the volume of the pituitary tumors were measured and the active tumor volume (ATV) was calculated by volume×SUV $_{mean}$. The maximum SUV of adrenal gland and the mean SUV of liver were measured. The SUVA/L (the ratio of the maximum SUV of adrenal gland and the mean SUV of liver) were calculated. The 24-h urinary cortisol levels at the same period were collected for correlation.

Results: ^{68}Ga-DOTATATE whole body scan were performed in 14 patients(12 patients clinical suspected with ectopic ACTH syndrome and 2 patients with pituitary adenoma), Significant correlations were found between the SUVA/L of arenal gland in ^{68}GA-DOTATATE PET/CT with the 24-h urinary cortisol levels(r=0.69，p=0.02). While there was no significant correlations between the SUVA/L of arenal gland in ^{18}F-FDG PET/CT with the 24-h urinary cortisol levels(n=16, r=0.4，p=0.15). There was no significant correlation between the ^{68}GA-DOTATATE and the ^{18}F-FDG uptake in the arenal gland (n=14, r=0.143, p=0.67). All adenomas were found with both ^{68}GA-DOTATATE accumulation and ^{18}F-FDG uptake except for one patient who was also negative MRI but confirmed with a very small ACTH-secreting adenoma by surgery and pathology finally. Significant correlations were not found between the ATV in ^{68}GA-DOTATATE PET/CT with the 24-h urinary cortisol levels in patients with ACTH tumor (n=12, P=0.45).

Conclusion: The ^{68}GA-DOTATATE accumulation of arenal gland have a correlation with the hormone levels in patients with Cushing's syndrome.

AUTHORS (LAST NAME, FIRST NAME): Qiao, Zhen[1]; Li, Fang[1]

INSTITUTIONS (ALL):

1. Department of Nuclear Medicine, Peking Union Medical College Hospital, Beijing, China.

(No Image Selected)

CONTROL ID: 2243945

TITLE: Effect of Cx-mimetic peptide administration on breast cancer brain metastasis development: a preclinical serial MRI study

PRESENTER: Valerie De Meulenaere

ABSTRACT BODY:

Abstract Body: Introduction

Brain metastasis occurs in 10-15% of the breast cancer patients and is a major problem in oncology. Brain metastasis entails a strong component of tumor-host interactions. Recent evidence suggests a crucial role for transmembrane connexin (Cx) proteins, primarily Cx43, in the tumor-host interactions by forming intercellular communication pathways. GAP27 is a Cx-mimetic peptide that inhibits Cx-based intercellular communication.

We aimed to examine the effect of GAP27 on the initial seeding and subsequent colonization of the brain by using a xenograftmodel for rat brain metastasis that allows follow-up by molecular magnetic resonance imaging (MRI) (1).

Materials & Methods

MDA-MB-231br/EGFP breast cancer cells were labeled with micron-sized particles of iron oxide (MPIO; 1µm, Dynabeads MyOne, Invitrogen). 2 groups of female nude rats (n=4 each; treatment group and control group) were inoculated with 10^5 MDA-MB-231br/EGFP labeled cells (2). In the treatment group GAP27 (25 mg/kg) was co-injected intracardially with the cancer cells, followed by daily IV injections of GAP27 for 2 days.

MRI was performed on a 7T system (PharmaScan 70/16, Bruker) at day 1, and then weekly until six weeks post-injection. T2*W (GRE FLASH, 120µm isotropic resolution, TR/TE 50/14ms), T2W (SE RARE, 109µm in plane-resolution, TR/TE 6346/37ms), and contrast-enhanced T1W (SE RARE, 117µm in plane-resolution, TR/TE 1382/9.7ms; 2 mmol/kg, Dotarem, Guerbet) sequences were run with a total acquisition time less than 90 minutes. MPIO-induced hypointensities were counted on the T2*W images; T2-visible lesions were coregistered with T2*W images.

Results & Discussion

Injection of GAP27 had no significant influence on the number of MPIO-induced hypointensities visible on T2*W images.

At week 3 to 4 the first signs of metastatic colonization were visible as hyperintensities on T2W images. All metastases visible on T2W images at week 6 could be correlated to their corresponding hypointensities on T2*W images. Although there was no significant difference between the control group and the treatment group with regard to the number of metastases the total brain metastasis volume in the GAP27 treated group was significant lower compared to the control group.

Conclusion

Serial MRI imaging allows evaluation of the growth of brain metastases without the need of sacrificing the animals. Early administration of GAP27 has no impact on metastatic seeding but reduces metastatic colonization of the brain.

References

(1) V. De Meulenaere, B. Descamps, S. Neyt, O. De Wever, E. Decrock, F. De Vos, et al., Six-weeks follow-up of developing metastases in the rat brain: preliminary results of a multi-modal imaging approach., Abstracts World Molecular Imaging Conference Seoul (2014).

(2) T. Yoneda, P.J. Williams, T. Hiraga, M. Niewolna, R. Nishimura, A bone-seeking clone exhibits different biological properties from the MDA-MB-231 parental human breast cancer cells and a brain-seeking clone in vivo and in vitro, J Bone Miner Res 16 (2001) 1486-1495.

AUTHORS (LAST NAME, FIRST NAME): De Meulenaere, Valerie[1]; Decrock, Elke[2]; Neyt, Sara[3]; De Wever, Olivier[4]; De Vos, Filip J.[3]; Vanhove, Christian[5]; Denys, Hannelore[6]; Descamps, Benedicte[5]; Deblaere, Karel[1]

INSTITUTIONS (ALL):

1. Radiology and Nuclear Medicine, Ghent University, Ghent, Belgium.
2. Basic Medical Sciences, Ghent University, Ghent, Belgium.
3. Laboratory of Radiopharmacy, Ghent University, Ghent, Belgium.
4. Experimental Cancer Research, Ghent University, Ghent, Belgium.
5. iMinds Medical IT - IBiTech - MEDISIP, Ghent University, Ghent, Oost-Vlaanderen, Belgium.

6. Medical oncology, UZGent, Ghent, Belgium.

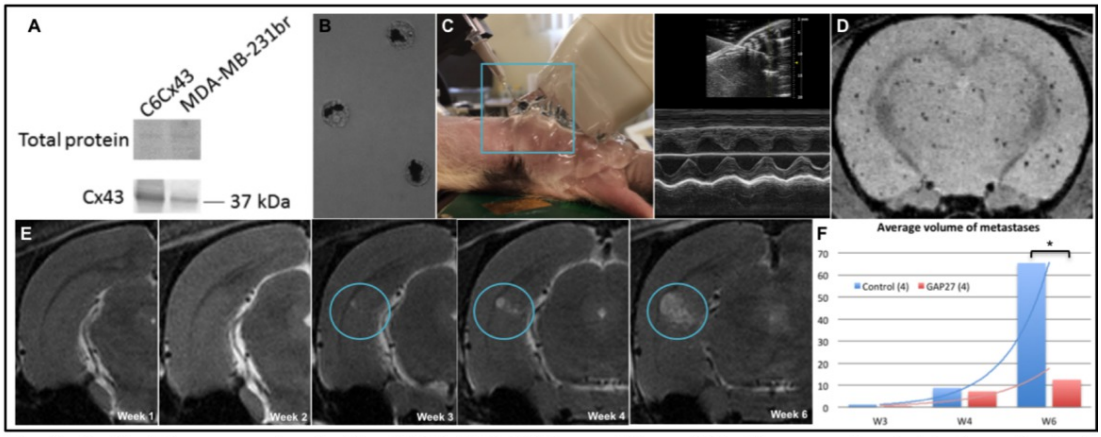

Fig 1: A. Cx43 expression in the MDA-MB-231br cell line. C6 glioma cells stably transfected with Cx43 were used as positive controls. B. MPIO (1µm)-labeled MDA-MB-231 cells. C. Ultrasound-guided intracardial injection of MPIO-labeled MDA-MB-231br cells. D. In vivo T2* MRI scan 1 day post-injection demonstrating multiple signal voids caused by labeled MDA-MB-231br cells. E. In vivo serial T2 MRI scans in the same animal showing metastasis as soon as three weeks post-injection. F. Comparison of the average metastatic volume between the control and the treatment group.

CONTROL ID: 2245101

TITLE: Visualization of CD44 expression and CD44^{+} cancer stem like cell in Breast cancer by Gamma irradiation

PRESENTER: Yong Jin Lee

ABSTRACT BODY:

Abstract Body: Objectives: This study aimed on noninvasive *in vivo* monitoring of CD44 positive breast cancer cells, using molecular image by fusing the bioluminescence reporter gene fLuc with the CD44 promoter.

Methods: Breast cancer cell line (MCF7) was transfected with recombinant lentivirus to express luciferase by CD44 promoter. We generated to stably express luciferase gene controlled by CD44 promoter (MCF7-CL). After induction of CSCs by sphere-formation or gamma irradiation, or both, luciferase activities of CD44 promoter were monitored by bioluminescence assay. For cell survival ratio with clonogenic assay by radiation in CD44 expression, we treated CD44 with siRNA. MCF7-CL or CD44+ MCF7-CL cells subsets were injected into the mice and irradiated by using a cobalt-60 source. Then, *in vivo* monitoring of CD44 expression in breast tumor by bioluminescence imaging (BLI) were performed to observe the tumor growth.

Results: After irradiation, sphere-formation, or irradiated sphere-formation, luciferase activity in MCF7-CL cells had increased by 1.1, 1.2, or 2.6 times of bioluminescence activity than those of control cells, respectively. Survived irradiated MCF7-CL cells had increased sphere-forming capacity, compared with non-treated cells. Irradiated sphere-formed cells showed up-regulated expression of CD44 and CD133, by immunofluorescence and flow-cytometry. Also, gene expression of various cancer stem cell markers in irradiated sphere-formed cells was relatively increased than non-treated cells. *In vivo* bioluminescence images of irradiated mice group showed stronger signal ($2.39x10^{4}$ counts/s) than the control group ($1.82\ x10^{4}$ counts/s) for four days. CD44+ CSCs increased radio-resistance and tumor growth *in vivo* and *in vitro*. When MCF7-CL was treated with siCD44 and irradiated, CD44 expression was inhibited and cell survival ratio was decreased. When breast cancer was irradiated with 6 Gy, relative BLI signal was increased than non-irradiated tumor, after 6 days, but tumor volume was decreased than non-irradiated tumor after 6 days.

Conclusions: These results indicate that increased CD44 expression, caused by general feature of CSCs by irradiation and sphere formation, can be monitored by using bioluminescence imaging. This system could be useful in evaluating CD44 expressed breast cancer by serial optical imaging *in vivo* as well as *in vitro.*

AUTHORS (LAST NAME, FIRST NAME): Kim, Mi Hyun [2, 3]; Kim, Min Hwan[2]; Kim, Kwang Il [2]; Lee, Tae Sup [2]; Ryu, Phyl Youl[3]; Kang, Joo Hyun[1]; Lee, Yong Jin[2]

INSTITUTIONS (ALL):

1. Molecular Imaging Research Center, Korea Institute of Radiological Medical Sciences, Seoul, Korea (the Republic of).

2. Molecular Imaging Research Center, Korea Institute of Radiological and Medical Sciences, Seoul, Korea (the Republic of).

3. Department of Microbiology, Chonnam National University College of Medicine, Gwangju, Korea (the Republic of).

(No Image Selected)

CONTROL ID: 2243961

TITLE: PET Imaging of copper delivery to brain by intravenous ^{64}Cu Acetate and ^{64}Cu-GTSM

PRESENTER: Erica Andreozzi

ABSTRACT BODY:

Abstract Body: Copper (Cu) is an essential nutrient required for healthy neurological function, and many neurodegenerative diseases involve Cu dyshomeostasis in brain.[1-3] To better understand the possible transport mechanisms contributing to Cu dysregulation, we intravenously administered radiocopper as both a lipophilic complex, ^{64}Cu(II)-GTSM, and a free Cu salt, ^{64}Cu(II)-Acetate, into normal mice (C57BL6, n=6) and evaluated the resulting whole body and brain biodistribution at 30 min and 24 h with PET/CT. We then complemented this *in vivo* PET data with *ex vivo* gamma counting and with digital autoradiography of brain tissue. Region-of-interest (ROI) analysis of PET and gamma counting of explanted organs showed that the ^{64}Cu uptake in most organs (kidneys, lungs, heart, and brain) is significantly higher ($p<0.001$) for ^{64}Cu-GTSM than ^{64}Cu-Acetate at both 30 min and 24 h. ^{64}Cu-GTSM uptake and retention in brain at 30 min (5.53 ± 0.68 %ID/g) and 24 h (5.41 ± 0.66 %ID/g) was nearly 10-fold higher than that observed for ^{64}Cu-acetate (0.73 ± 0.03 %ID/g and 0.76 ± 0.02 %ID/g).

PET and digital autoradiography showed that brain uptake of ^{64}Cu-GTSM was global and diffuse, whereas brain uptake of ^{64}Cu-Acetate was much more focal, with prominent signal in the hippocampal fimbria and the ventricles (lined by choroid plexus). Activity present in brain was largely retained at 24 h for the ^{64}Cu-GTSM mice but not the ^{64}Cu-Acetate mice, suggesting difference clearance mechanisms of ^{64}Cu depending on cellular uptake via passive or active transport. We conclude that acute trafficking of ^{64}Cu is both consistent with earlier literature of long-term Cu distribution in brain by X-ray fluorescence (XRF), which demonstrate elevated Cu levels in choroid plexus (CP).[5] It also agrees with literature reports indicating a high expression of metal transporters (Ctr1, DMT1, ATP1A and ATP7B) and metallothionein on the CP.

We have followed this up with our own XRF studies to further investigate how endogenous Cu distribution in brain relates to exogenous uptake of ^{64}Cu. Quantification of elemental Cu maps generated from XRF indicated statistically higher ($p<0.001$) Cu concentrations in the caudate putamen of Wildtype (C57BL6) compared to AD (TASTPM) mice, but higher Cu in the cerebellum of TASTPM. These endogenous Cu trends match some of the exogenous ^{64}Cu trends observed between TASTPM and Wildtype mice following administration of radiocopper.

The mechanism by which Cu is transported into the brain still remains unclear, and very little is known about the specific molecular mechanisms and the key transport proteins that regulate brain Cu homeostasis. Our investigation of ^{64}Cu-Acetate suggests a role for the CP in active transport of ^{64}Cu into brain. PET imaging of Cu radionuclides offers a valuable tool for assessing routes of Cu transport into and out of the brain over time *in vivo*, and can thus help elucidate deficiencies of Cu transport associated with many neurodegenerative diseases.

1. *Metallomics* 2010, 2, 596-608; 2. *Metallomics* 2013, 5, 43-51; 3.*Prog Neurobiol* 2014, 116, 33-57; 4. *Aging Cell* 2013, 12, 823-832; 5. *Journal of Clinical Investigation* 1996, 98, 207-215.

AUTHORS (LAST NAME, FIRST NAME): Andreozzi, Erica[2]; Baguña Torres, Julia[2]; Dunn, Joel T.[2]; Walker-Samuel, Simon[3]; So, Po-Wah[2]; Blower, Philip J.[1]

INSTITUTIONS (ALL):

1. Imaging Sciences and Biomedical Engineering, King's College London, London, United Kingdom.
2. Imaging Sciences, Kings College London, London, United Kingdom.
3. Centre for Advanced Biomedical Imaging, University College London, London, United Kingdom.

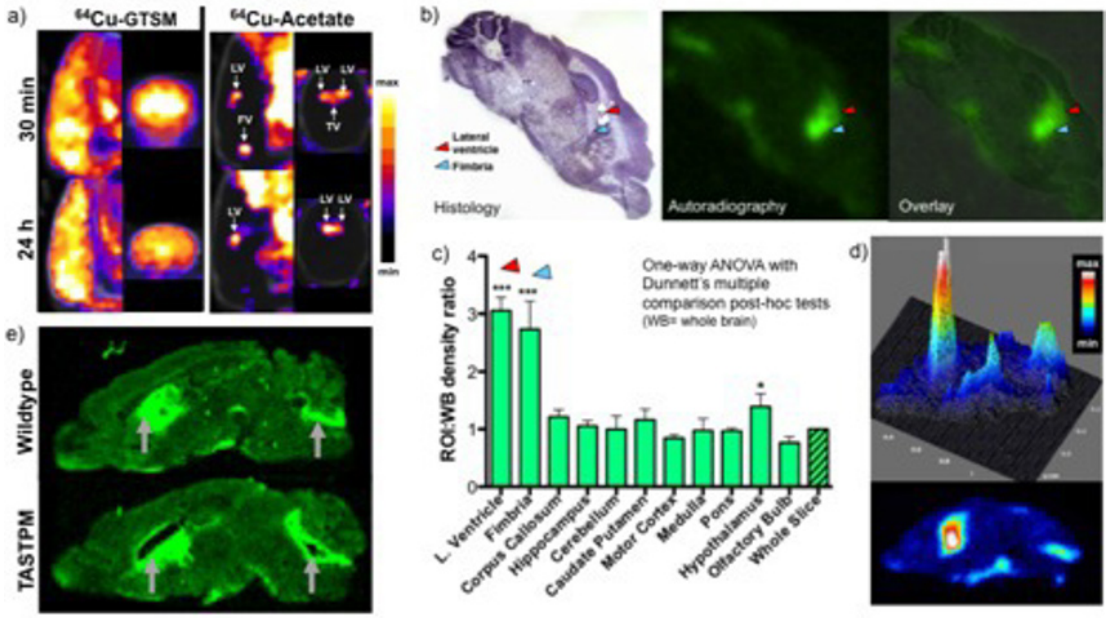

a) Representative coronal and sagittal slices through PET/CT images illustrate ^{64}Cu distribution in the brain of 6-8-month-old C57BL6J mice at 30 min (top) and 24 h (bottom) post-injection of both ^{64}Cu-GTSM and ^{64}Cu-Acetate. The ^{64}Cu brain uptake of ^{64}Cu-GTSM appears to be relatively global, whereas, the ^{64}Cu brain uptake of ^{64}Cu-Acetate is distinct to the lateral ventricles (LV), third ventricle (TV), and fourth ventricle (FV) at 30 min, with the signal in the FV almost gone by 24 h. b) Manual co-registration (overlay) of histology and autoradiography images corresponding to the same tissue slice shows high signal intensity in the lateral ventricle (red arrow) and hippocampal fimbria (blue arrow). c) Quantification of this overlay image (confirmed objectively with automated co-registration software) demonstrated significant differences of ROI:WB phosphor density ratio in the lateral (L) ventricles (p-value <0.0001, F=65) and fimbria (p-value <0.0001, F=65) vs. WB, as well as hypothalamus (p-value <0.05, F=65) vs. WB. d) Autoradiograph (top) and corresponding surface plot (bottom) of a brain tissue slice at 24 h post IV injection ^{64}Cu-Acetate shows distinct focal accumulations in and around the LV, confirming the prominent uptake of these regions in (c). e) XRF Cu maps show different Cu levels in the caudate putamen and cerebellum of Wildtype vs. TASTPM mice (8 months old).

CONTROL ID: 2243964

TITLE: Preparation and Biological Evaluation of ^{188}Re-labeled Lactam Cyclized α-MSH Analog for Melanoma Targeting

PRESENTER: Young-Don HONG

ABSTRACT BODY:

Abstract Body: Introduction: Melanocortin-1 receptor (MC1-R) is an attractive melanoma specific target for peptide radionuclide therapy and diagnosis because the receptor was expressed over 80% of human metastatic melanoma. Since the α-melanocyte stimulating hormone (α-MSH) had high affinity for MC1-R, several α-MSH analogues were evaluated as a vehicle for noninvasive imaging and therapy of melanoma.

Method: The α-MSH analogue was synthesized by applying standard peptide synthesis, in which Mercaptoacetyl-Gly-Cys was attached as a N_2S_2-type bifunctional chelating agent (BFCA) for the radiolabeling with ^{188}Re. The analogue radiolabeled by employing the transchelation method using a glucoheptonate (GH) kit as a ligand exchange partner. Stability was examined in human serum to assess the resistance of the radiopeptide to proteolytic degradation and biodistribution study was performed in B16/F1 xenograft mice.

Results: In an attempt to develop a novel targeting molecule for melanoma therapy using ^{188}Re, a diamidedithiol (N_2S_2) chelator conjugated lactam-bridge cyclized α-MSH analogue was synthesized. The amino acid sequences of cyclic(α-MSH) analogue was Mercaptoacetyl-Gly-Cys-Gly-Dap-Gln-His-$_D$-Phe-Arg-Trp-Asp-Lys-Pro-Val-NH_2 (Cyclized Dap-Asp) [Mercaptoacetyl-Gly-Cys-Gly-(Dap^4,Gln^5,$_D$-Phe^7,Asp^{10}-(α-MSH)$_{4-13}$, N_2S_2-cyclic(α-MSH)], in which Mercaptoacetyl-Gly-Cys was introduced as a N_2S_2-type bifunctional chelating agent (BFCA) for the radiolabeling with ^{188}Re. The ^{188}Re-N_2S_2-cyclic(α-MSH) was prepared with a high radiolabeling yield (>98%) even at the concentration of 1 nmol by applying the ligand exchange reaction using a lyophilized glucoheptonate (GH) kit and maintained a high radiochemical purity (>98%) in human serum for 72 h. Biodistribution studies in B16/F1-bearing mice demonstrated a rapid clearance from the blood stream and major non-target organs except the organs related to its excretion pathway as well as a high tumor uptake and extended retention by the receptor mediated targeting mechanism. Tumor uptake value was 8.42±1.48 at 2 h and 4.80±0.55 %ID/g at 24 h after injection, respectively. The tumor-to-blood (T/B) ratios were 6.98 at 2h and 6.04 at 24 h, whereas the T/B ratio in a blockage group was significantly decreased to 1.71 at 2 h post-injection. The radiopeptide was rapidly cleared from the blood stream and major non-target organs except the organ related to its excretion pathway such as liver and intestine.

Conclusion: The ^{188}Re-N_2S_2-cyclic(α-MSH) is a promising radiopharmaceutical for melanoma treatment because of its receptor-mediated uptake with a high tumor accumulation and retention. Furthermore, since the ^{188}Re-N_2S_2-cyclic(α-MSH) demonstrated its great potential for MC1-R positive tumor targeting, the prepared peptide, N_2S_2-cyclic(α-MSH), can be a good candidate for further investigations for both noninvasive diagnosis and therapy of melanoma.

AUTHORS (LAST NAME, FIRST NAME): HONG, Young-Don[1]

INSTITUTIONS (ALL):

1. Radioisotope research Division, Korea Atomic Energy Research Institute, Daejeon, Korea (the Republic of).

(No Image Selected)

CONTROL ID: 2243970

TITLE: Contrast agent for hybrid in-vivo fluorescence/micro-CT imaging system

PRESENTER: Ashwinkumar N

ABSTRACT BODY:

Abstract Body: Aim: The study aims to develop a contrast agent for a dual modality imaging system comprising of micro-CT and in-vivo fluorescence set-up.

Rationale: Hybrid imaging systems are being increasingly used in pre-clinical research. We are working to develop a dual modality contrast agent targeted towards a hybrid imaging modality comprising of micro-CT system and in-vivo fluorescence imaging system. A dual modality contrast agent presents many advantages. The contrast agent can be spatially localized using the reconstructed micro-CT images, thus providing a priori information for solving the ill-posed problem of 3D in-vivo fluorophore localization and concentration estimation. We propose to use a combination of tantalum oxide (for CT) [1] and gold nano-particles (for optical imaging) [2]. Gold and tantalum elements are high atomic number and inert materials can be used for imaging. Both gold and tantalum are used for CT imaging but in terms of contrast concentration of gold is much higher than tantalum [3]. This unique combination not only provides diagnostic information but can also be used for photo thermal therapy.

Methods: Synthesis of gold nanoparticles using LASER Ablation: Gold nanoparticles (GNP) were prepared using 99.9% gold metal target. GNPs in the size range of 20-50nm were synthesized by laser ablation (NdYAG,1064nm, 40mJ, 10Hz) in 2 mM Citric acid solution **(stabilizing agent)**. The absorption peak at 518 nm by UV absorption spectrometry confirms the presence of gold nanoparticles. Color change between 1 mM citric acid and 2 mM citric acid showed the difference in particle size.

Synthesis of tantalum oxide nanoparticles: Micro-emulsion technique is a simple technique used to prepare the tantalum oxide nanoparticles with a size range of 2-10nm. The mixture of cyclohexane, ethanol, Sodium hydroxide (NaOH) and igepal-Co520 added to the tantalum (V) ethoxide resulting in the formation of tantalum oxide nanoparticles. Digital X-ray radiographs of the resulting solution were obtained using a micro-CT scanner. Formation of TaOx and GNPs would form a core-shell nanoparticles by simple ionic interaction.

References:

1. Myoung et.al., J. Am. Chem. Soc. 2011, 133, 5508–5515
2. Hua he et.al., Anal. Chem. 2008, 80, 5951–5957
3. Danielle et.al., Nano Lett. 2011, 11, 2678–2683

AUTHORS (LAST NAME, FIRST NAME): N, Ashwinkumar[1]; Rao, M.S. Ramachandra; Krishnamurthi, Ganapathy

INSTITUTIONS (ALL):

1. Department of Engineering design, Indian Institute of Technology, Chennai, India.

Synthesis of gold nanoparticles using LASER Ablation

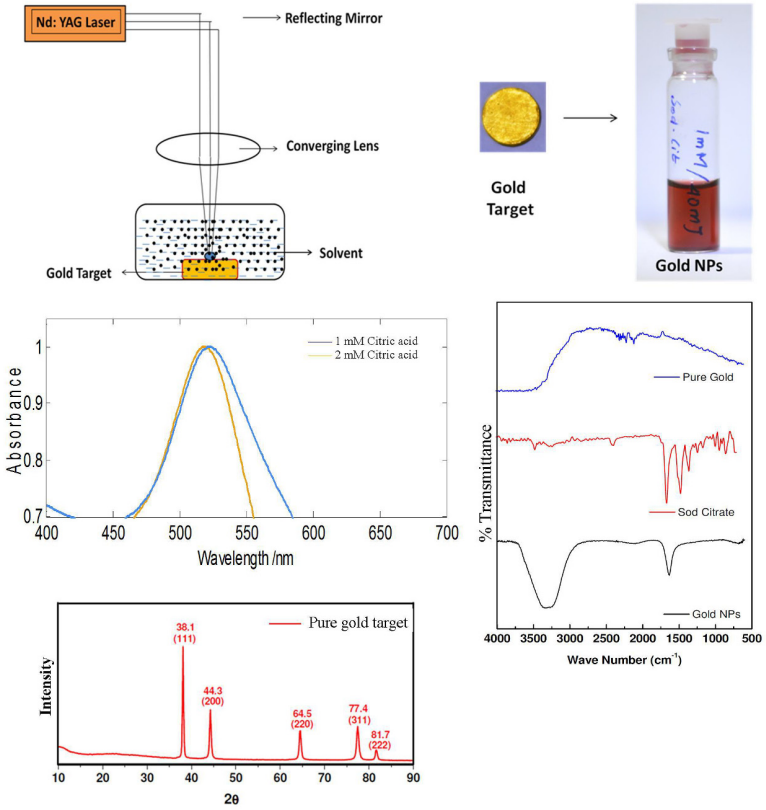

Synthesis of Tantalum Oxide nanoparticles by Micro emulsion method

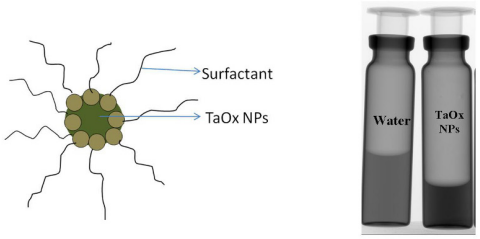

CONTROL ID: 2244070

TITLE: A 3D mouse atlas from in vivo micro-CT and its applications for preclinical evaluation

PRESENTER: Liqin Xie

ABSTRACT BODY:

Abstract Body: Changes in the vascular network and organ morphology have been associated with the emergence and progression of many diseases, such as bone fracture, inflammation and cancer. In vivo quantification of vascular changes and macrophage accumulation in small animals is critical to the development and evaluation of new therapies for inflammation and tumor growth. However, there are few published papers for the in vivo imaging of vasculature in small animals, due to technical challenges, such as low image resolution and low vessel contrast in surrounding tissues. We have developed an in vivo CT imaging technique to visualize and quantify vasculature, organ structure and macrophage accumulation in disease models.

With 1-4 minutes scanning by a high speed in vivo micro-CT scanner (Quantum CT), and injection of a high efficient contrast agent (Exitron nano), vasculature and organ structure (Fig 1. A-B) were semi-automatically segmented and quantified via image analysis software (Analyze). Exitron Nano is taken up by, and remains in, the reticuloendothelial system of macrophages, and allows macrophages to be traced in vivo one day after injection. The image quality, voxel size down to 20 μm, is higher than currently published mouse vasculature images. With this technique, in vivo vasculature imaging becomes feasible for preclinical evaluation in small animals.

Non-bone CT imaging has many potential applications for preclinical evaluation at Regeneron. To date, it has been used to visualize angiogenesis in bone metastasis model (Fig 1. C-D) and rheumatoid arthritis model (Fig 1. E), and to monitor macrophage accumulation in a rheumatoid arthritis model, liver fibrosis model, and lung metastasis model (Fig 1. F). It has also been used to quantify lung volume, inflammation region, and peribronchial density in an asthma model.

AUTHORS (LAST NAME, FIRST NAME): Xie, Liqin[1]

INSTITUTIONS (ALL):

1. Regeneron, Ossining, NY, United States.

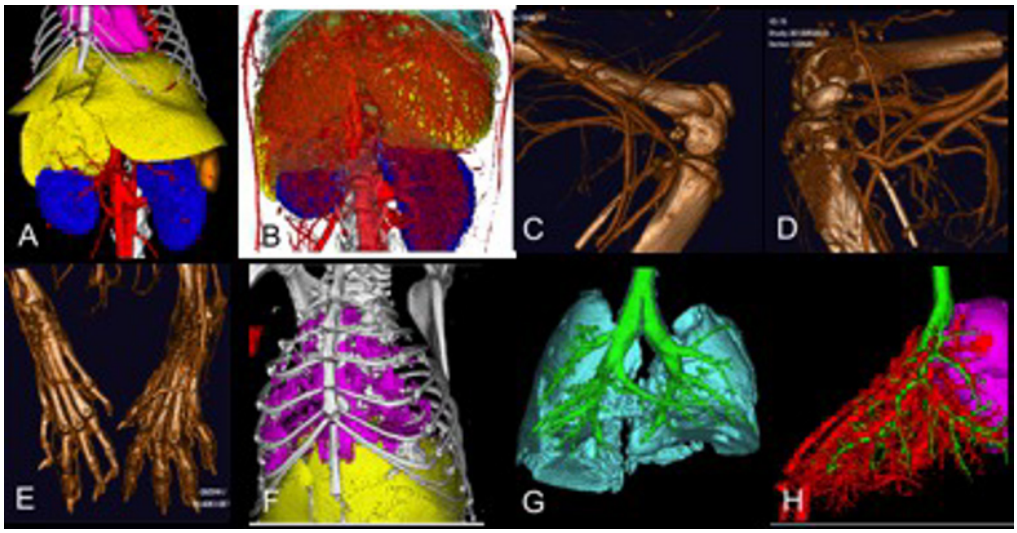

Figure 1: 3D micro-CT for vasculature, organ structure and macrophage accumulation. Organs and vasculature (A-B), vasculature in control (C) and in bone metastasis model (D), vasculature in arthritic paw (E), macrophage accumulation (pink) in lung metastases mode (F), airway in lung (G), and vasculature and airway in lung (H).

CONTROL ID: 2244093

TITLE: Thyroid Absorbed Dose Estimate Using I-123 MIBG Imaging

PRESENTER: Jianqiao Luo

ABSTRACT BODY:

Abstract Body: Purpose: To evaluate the use of thyroid blockade prior to AdreView Iobenguane I-123 (GE HealthCare) injection by estimating radiation absorbed dose to patients with I-123 Metaiodobenzylguanidine (MIBG) gamma camera imaging.

Methods: A hundred and five patients were administrated with I-123 MIBG, 370 MBq each for adults and adjusted per weight for pediatric patients, through intravenous injection. No thyroid blockade (Potassium Iodide Oral Solution) was used prior to the I-123 injection. Some of the patients had contrast from CT scans before the gamma camera imaging. Whole body planar imaging was performed 24 hours following administration of the radiopharmaceutical. Dual head gamma cameras with LEHR collimators were used to obtain anterior and posterior scans simultaneously. 15% energy window centered at 159 keV was set and scan speed was 9 cm/min. Region of interest (RoI) was defined manually for thyroid and for whole body as well. Geometric mean of the RoI counts from anterior and posterior views was used to calculate absorbed dose. Calibration factor was obtained using total body counts and injected activity. This was done in two ways: using each patient or average of twenty patients. Using the averaged total body counts to generate a single calibration factor would reduce statistical uncertainty. Internal dosimetry software (Olinda/EXM 1.1) was also used to compare the doses. Numbers of disintegrations per unit activity (hr) entered to the Olinda was 17.6 hours based on 25% thyroid uptake. **Results:** Average effective dose was 490 uSv for whole body and 23.4 uSv for thyroid with the single calibration factor. If individual calibration factors were used, the average effective dose was 2.07 mSv for whole body and 27.2 uSv for thyroid. The Olinda dosimetry program yielded an effective dose 480 nSv.

Conclusions: Gamma camera imaging of I-123 MIBG provided an estimate to thyroid absorbed dose. Accuracy of the dosimetry depends on quantification of the images and calibration factor. The thyroid blockade may not be necessary.

AUTHORS (LAST NAME, FIRST NAME): Luo, Jianqiao[1]

INSTITUTIONS (ALL):

1. Radiology, Virginia Commonwealth University, Richmond, VA, United States.

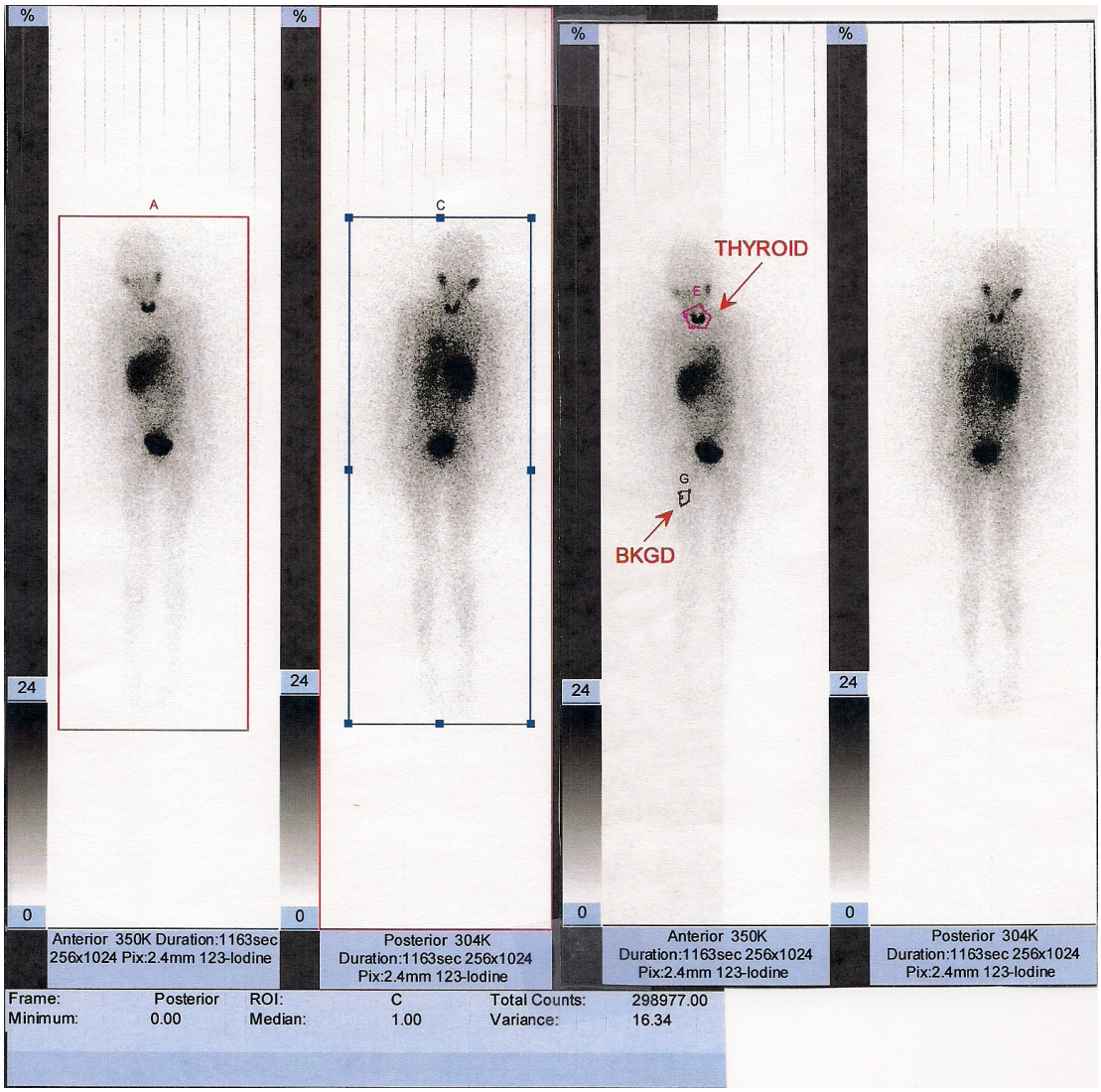
%
A
24
0
Anterior 350K Duration:1163sec
256x1024 Pix:2.4mm 123-Iodine
%
C
24
0
Posterior 304K
Duration:1163sec 256x1024
Pix:2.4mm 123-Iodine
%
THYROID
E
G
BKGD
24
0
Anterior 350K
Duration:1163sec 256x1024
Pix:2.4mm 123-Iodine
%
24
0
Posterior 304K
Duration:1163sec 256x1024
Pix:2.4mm 123-Iodine
Frame: Posterior ROI: C Total Counts: 298977.00
Minimum: 0.00 Median: 1.00 Variance: 16.34

CONTROL ID: 2244139

TITLE: Design and Development of a Novel Bombesin Peptide analog for the targeting of bombesin-receptor-positive tumors.

PRESENTER: Subhi Okarvi

ABSTRACT BODY:

Abstract Body: *Objectives*: In recent years bombesin (BN) receptors have attracted great clinical interest as molecular targets for diagnosis and therapy due to the fact that all three BN receptor subtypes are overexpressed in various human cancers. Despite significant developments, the limitations imposed by peptide pharmacokinetics in terms of binding and clearance kinetics suggest that significant improvements of these radiolabeled BN peptides are still required. This study was undertaken to develop a BN peptide having a wide receptor affinity and favorable biokinetics and able to be labeled both with diagnostic and therapeutic radionuclides to produce a potential theranostic agent for targeting BN receptor-positive tumors.

Methods: We have designed a unique BN peptide composition containing a GGC chelating sequence for ^{99m}Tc and DOTA chelating moiety for labeling with ^{68}Ga/^{177}Lu. Also a hippurate-type spacer (aminobenzoyl-Gly) was introduced between the receptor-binding and chelating-site in order to enhance excretion through the renal pathway. DOTA-Abz-Gly-Gly-Cys-Gln-Trp-Ala-Val-Cha-His-Nle-Met-NH_2 was synthesized on solid phase using standard Fmoc strategy. Labeling with ^{99m}Tc was achieved by ligand exchange method and with ^{68}Ga in the presence of NaOAc buffer. In vitro cell-binding was conducted on BN receptor-positive MDA-MB-231 and T47-D breast cancer cell lines and pharmacokinetic characteristics were studied on balb/c mice at 1 and 4 h p.i.

Results and Discussion: The structural composition of the DOTA-BN peptide was confirmed by mass spectrometry and MALDI and its purity by HPLC. Radio-HPLC analysis revealed that the BN analog radiolabeled efficiently with ^{99m}Tc/^{68}Ga under mild conditions and with high labeling efficiency (~90%). In vitro cell-binding assay indicated the high affinity and specificity of ^{99m}Tc/^{68}Ga-labeled peptide towards human breast cancer cell lines, with binding affinity below 25 nM; a significant internalization (~20%) into the breast cancer cells was also observed. In mice, ^{99m}Tc/^{68}Ga-labeled BN peptide displayed a fast clearance from the blood and excreted by the renal route (67% ID) possibly because of the presence of a hippurate-like spacer in the peptide molecule. Furthermore, a low uptake/retention by the kidneys was observed (<4% ID/g) indicating a significant influence of hippurate-like spacer on the biokinetics. The uptake in other major organs (i.e., lungs, stomach, liver, intestines, etc.) was low (<5% ID/g) both at 1 and 4 h p.i.

Conclusions: This initial study towards the development of a potent and broad affinity BN-like peptide suggest that the peptide under investigation possesses certain favorable in vitro/in vivo properties and seems potential candidate for further evaluation. Studies are in progress to determine the real usefulness of this theranostic agent for tumor targeting.

AUTHORS (LAST NAME, FIRST NAME): Okarvi, Subhi M.[1]; AlJammaz, Ibrahim[1]

INSTITUTIONS (ALL):

1. King Faisal Specialist Hospital, Riyadh, Saudi Arabia.

(No Image Selected)

CONTROL ID: 2244488

TITLE: Preparation and initial evaluation of a rhodamine-angiotensin conjugate as a breast cancer targeting agent

PRESENTER: Subhi Okarvi

ABSTRACT BODY:

Abstract Body: Objectives: Rhodamine (Rh) is a lipophilic cationic dye that accumulates in the mitochondria of the living cells. Rh dyes are known to accumulate in the heart and share several properties with clinically-useful cardiac imaging agent, ^{99m}Tc-MIBI. Additionally, mitochondrial-specific Rh fluorescent dye has been evaluated as a potential anticancer agent because of its long retention in various human cancer cells and rapid release from normal cells. Change in mitochondrial potential is an important feature in tumor cells. It is believed that cancer cells as compared to normal epithelial cells may have higher mitochondrial or plasma trans membrane potential and Rh crosses these barriers because of net positive charge on the molecule. The high specificity for mitochondria and low toxicity to the healthy cells coupled with selective accumulation in carcinoma cells suggest that ^{99m}Tc-Rh-AngII conjugate may prove to be a new and effective tumor targeting agent.

Methods: Rh-angiotensin (Rh-AngII) Rh-Lys-Gly-Gly-Cys-βAla-Asp-Arg-Val-Tyr-Ile-His-Pro-Phe-NH_2 was synthesized by solid-phase peptide synthesis according to Fmoc/HBTU chemistry. Carboxytetramethyl-rhodamine (TAMRA) was added to the AngII peptide via the free amino group of Lys residue by manual conjugation. The identity of the structure was confirmed by mass spectrometry. Rh-AngII was radiolabeled with ^{99m}Tc via Gly-Gly-Cys chelating sequence by ligand exchange method. *In vitro* cell binding was performed on ER-ve MDA-MB-231 and ER+ve MCF-7 breast cancer cell lines and *in vivo* clearance kinetics was determined in balb/c female mice.

Results and Discussion: Rh-AngII hybrid conjugate was prepared conveniently on solid-phase and radiolabeled efficiently with ^{99m}Tc under mild labeling conditions. In vitro tumor cell-binding demonstrated high affinity and specificity of ^{99m}Tc-Rh-AngII towards human breast cancer cells (binding affinities below 20 nM). The binding characteristic of ^{99m}Tc-Rh-AngII was found to be comparable with ^{99m}Tc-MIBI. In vivo biodistribution pattern in mice showed that the ^{99m}Tc-Rh-AngII conjugate cleared rapidly from the blood and other major organs and tissues after 1 h post-injection. The radioconjugate exhibited rapid clearance kinetics with major route of excretion was found to be the urinary, with some elimination via the hepatobiliary system.

Conclusion: To conclude, this preliminary study for the development of a SPECT-based breast cancer imaging agent demonstrates some similarities of ^{99m}Tc-Rh-AngII with ^{99m}Tc-MIBI, highlighting the potential of using hybrid conjugate for targeting of breast cancer. The use of hybrid molecule appears to hold a great promise as a new and attractive approach for tumor targeting.

AUTHORS (LAST NAME, FIRST NAME): Okarvi, Subhi M.[1]

INSTITUTIONS (ALL):

1. King Faisal Specialist Hospital, Riyadh, Saudi Arabia.

(No Image Selected)

CONTROL ID: 2244483

TITLE: Iterative CT Image Reconstruction with non-local Prior Image Integration

PRESENTER: Maik Stille

ABSTRACT BODY:

Abstract Body:

Computed tomography (CT) remains one of the key methods in medical imaging [1]. The image quality of reconstructed CT slices is reduced by the occurrence of different artifacts, which are caused by physical phenomena such as scatter, beam hardening, noise, or total absorption. Since the publishing of the PICCS algorithm by Chen et al. the integration of prior images in the reconstruction of CT images has become a fast developing topic in the field [2]. In the following we propose a CT reconstruction with a regularization term that penalizes intensity variations between the image to be reconstructed and a prior image. The prior should hold information from an image that looks similar to the image that is to be reconstructed. However, the goal of the regularization term is to keep anatomical information of the original image while reducing artifacts that may occur due to the presence of high density objects within the field of view or due to a limited data problem [3].

Given a set of intensity measurements $\{n_i\}_{i=1}^{M}$, the negative log-likelihood function for transmission tomography is defined as

$$l(f) = \Sigma_{i=1}^{M} \left(-n_i \ln(n_0) + n_i \Sigma_{j=1}^{N} a_{ij} f_j + \ln(n_i!) + n_0 \exp(-\Sigma_{j=1}^{N} a_{ij} f_j)\right) \quad (1)$$

where $f \in R^N$ is a vector that consists of the expected attenuation coefficients [1]. Therefore, let

$$f^* = \operatorname{argmin}_f \left(l(f) + \delta R(f, \Gamma(g,\gamma))\right) \quad (2)$$

be the optimization problem that is to be solved in order to reconstruct an image of the tomographed object, where $R(f, \Gamma(g, \gamma))$ is a regularization term that is added to the objective function and δ a regularization parameter that controls the influence of the regularization. Similar to [4] we propose a non-local regularization defined as

$$R(f, \Gamma(g, \gamma)) = \operatorname{sqrt}\left(\Sigma_{j=1}^{N} \left(f(x) - 1/w_x \Sigma_{y \in Nx} \Gamma(g, \gamma) \exp\left((-\|f(\eta_x) - \Gamma(g(\eta_y), \gamma)\|_p) / h^2\right)\right)^2\right) \quad (3)$$

where $\Gamma(g, \gamma)$ is the transformed prior image g with the transformation parameter γ. Furthermore, denotes ηx a patch window around pixel x, Nx denotes a search window around pixel x, and $\| \cdot \|_p$ denotes the Minkowski distance of order p. The optimization problem (2) is solved by the l-BFGS-b algorithm [5], while in every iteration step k the registration problem $D(f^{(k)}, \Gamma(g,\gamma)) = \min$, where D denoting a distance measure, is solved in order to gain the transformation parameter γ. Therefore the similarity of the prior image g and the image f increases for every interim result of the optimization problem (2). While the transformation Γ is general, in practice it is advisable to use a non-rigid registration, e.g. a demon's algorithm [6]. In Fig. 1 first results of the proposed algorithm are presented.

AUTHORS (LAST NAME, FIRST NAME): Stille, Maik[1]; Buzug, Thorsten M.[1]

INSTITUTIONS (ALL):

1. Institute of Medical Engineering, University of Luebeck, Lübeck, Schleswig-Holstein, Germany.

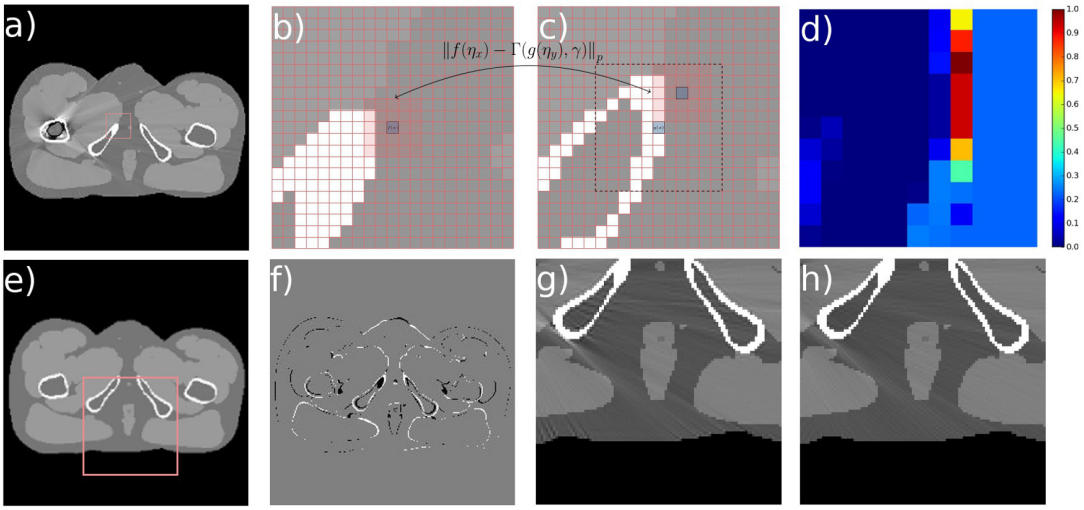
a)
b)
c)
d)
e)
f)
g)
h)
$\|f(\eta_x) - \Gamma(g(\eta_y), \gamma)\|_p$
1.0
0.9
0.8
0.7
0.6
0.5
0.4
0.3
0.2
0.1
0.0

CONTROL ID: 2244272

TITLE: Why is it challenging to develop a gastro-oesophageal reflux disease by using rat as animal model? A new discovery: duodenum-gastric reflux in rat is a physiologic phenomenon.

PRESENTER: Luca Basso

ABSTRACT BODY:

Abstract Body: *Objectives*

Demonstration of physiological presence of duodeno-gastric reflux can explain failure of previous studies about induction of esophago-gastric carcinoma. To investigate this event and to visualize it we used Manganese-Enhanced Magnetic Resonance Imaging (MEMRI) as hepatobiliary imaging tecniques by using a wrist coil applied to a clinical 3T MR scanner.

Material and methods

In vivo experiments were approved by the Institutional Review Committee of the National Cancer Institute (IST), and were performed in accordance to the National Regulation on Animal Research Resources (D.L. 116/92). Male Sprague-Dawley rat was anaesthetised by intraperitoneal injection of xylazine (30 mg/kg) and ketamine (100 mg/kg) and was successively inoculated i.v. with 250 mmol solution of $MnCl_2$. Rat was positioned in a wrist coil, applied to a clinical 3T MR scanner. T1-3D-SPGR-weighted sequence with a slices thickness of 230 micron, before $MnCl_2$ i.v. inoculation and 20 minutes after, was performed. Both qualitative and quantitative analysis by using a clinical functool software 9.4.05a were performed.

Results

Twenty-one minutes after $MnCl_2$ i.v. injection duodenalgastric reflux and marked contrast enhancement of ectopic pancreatic tissue in the gastric were visualized on T1-Wghted Images.

Conclusion

In vivo MEMRI was able to provide the demonstration of the presence of physiological duodeno-gastric reflux (DGR). Here, for the first time, we demonstrate by Manganese enhanced Magnetic Resonance Imaging (MEMRI), how DGR is a physiological phenomenon which occurs in rats. The impact of this finding could help the scientific community to better understand the mechanism behind DGR, its relationship with GRE, its complications and possible new treatments. Moreover, visualization of ectopic pancreas confirms MEMRI as an excellent tool for anatomical and functional imaging of the exocrine glands.

AUTHORS (LAST NAME, FIRST NAME): Basso, Luca[3]; Rosa, Francesca[2]; Pace, Daniele[1]; Boccardo, Simona[5]; Migone, Stefania[3]; Neumaier, Carlo Emanuele[3]; Baio, Gabriella[4]

INSTITUTIONS (ALL):

1. Radiology, IRCCS AZIENDA OSPEDALIERA UNIVERSITARIA SAN MARTINO IST - ISTITUTO NAZIONALE PER LA RICERCA SUL CANCRO, Genoa, Italy.
2. radiology, IRCCS IST- San Martino, Genova, Genova, Italy.
3. Radiology, IRCCS San Martino IST Hospital, Genova, Italia, Italy.
4. Aberdeen Biomedical Imaging Centre, University of Aberdeen, Aberdeen, United Kingdom.
5. Anatomical Pathology, IRCCS San Martino IST, Genova, Genova, Italy.

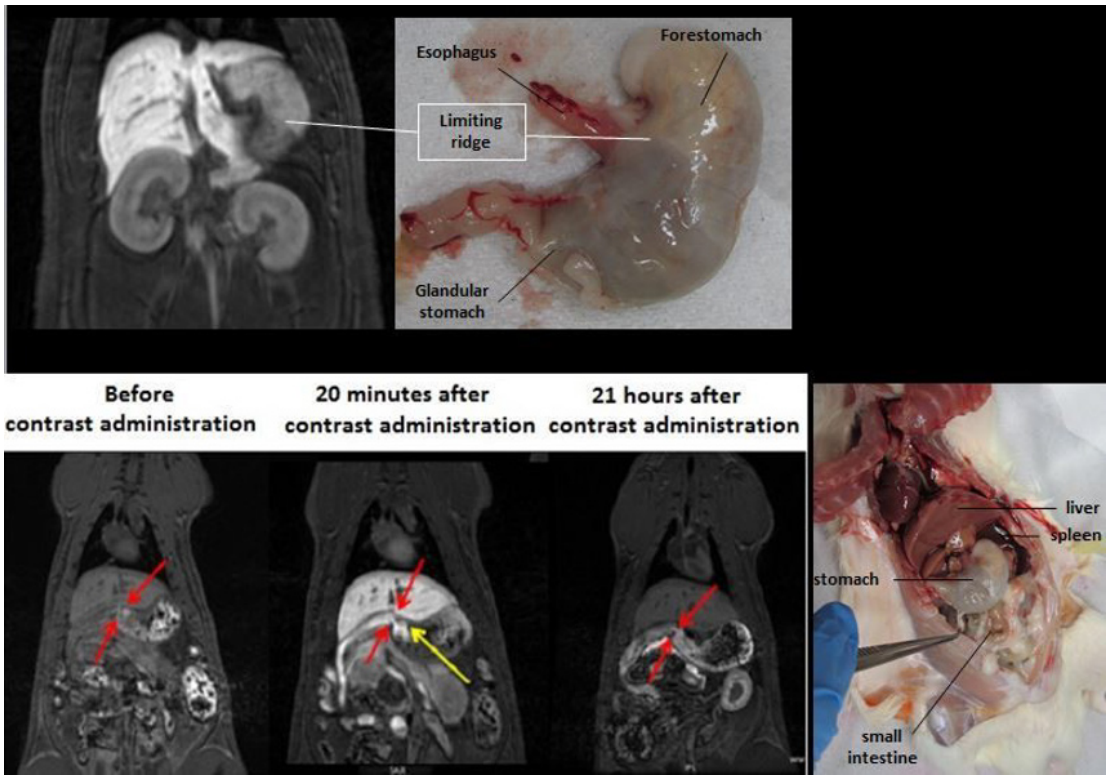

In the upper images is possible to appreciate morphological details, which can be precisely visualized at MRI after contrast administration. Below, MEMRI provides functional information, showing physiological Duodeno-Gastric Reflux.

CONTROL ID: 2244931

TITLE: Magnetic Exchange Coupling as a Tool for Reducing T_{1e} of Gd(III)

PRESENTER: Laura Lilley

ABSTRACT BODY:

Abstract Body: The inherent lack of sensitivity of Gd(III) contrast agents is a significant barrier to the widespread implementation of magnetic resonance imaging (MRI) in molecular imaging applications. All bioactivated Gd(III) agents possess high background signal (up to 40%) due to second- and outer-sphere water relaxation in the “off” state. To overcome this limitation we are employing bi- and trimetallic complexes to shorten the electron relaxation time (T_{1e}) of Gd(III), consequently reducing the background signal of the agent prior to activation. These preliminary studies investigate magnetic coupling of Gd(III) to a first-row transition metal with a short T_{1e} . Magnetic exchange coupling results in an agent with a shortened $T_{1e,}$ and thus low relaxivity (r_1 $mM^{-1}s^{-1}$). Ultimately, we will employ this methodology towards zero-background Gd(III) molecular imaging MR probes.

AUTHORS (LAST NAME, FIRST NAME): Lilley, Laura[1]; Du, Kang[1]; Harris, Dave[1]; Meade, Thomas J.[1]

INSTITUTIONS (ALL):

1. Chemistry, Northwestern University, Chicago, IL, United States.

(No Image Selected)

CONTROL ID: 2244290

TITLE: An operator independent method for lesion segmentation to evaluate metabolic response in MET-PET studies

PRESENTER: Alessandro Stefano

ABSTRACT BODY:

Abstract Body: Background: Lesion volume delineation of PET images is challenging because of the low spatial resolution and high noise level. Aim of this work is the development of an operator independent (OI) segmentation method of Metabolic Tumor Volume (MTV) to evaluate the functional follow-up in patients with cervical cancer.

Methods: An algorithm based on random walks (RW) on graphs has been adapted for PET image delineation (A. Stefano, et al. A Graph-Based Method for PET Image Segmentation in Radiotherapy Planning: A Pilot Study, in A. Petrosino, ed., Image Analysis and Processing – ICIAP 2013: Lecture Notes in Computer Science, v. 8157, Springer Berlin Heidelberg, p. 711-720.). This method represent an image as a graph in which the voxels are its nodes and the edges are defined by a cost function which maps a change in image intensity to edge weights. Then, RW partitions the nodes into two disjoint subsets (lesion and background). To create an OI method starting from previous work, we propose an automated seed localization framework to identify RW seeds in PET images. The user select the lesion of interest using a basic interactive procedure to exclude false positives. The algorithm automatically identifies the PET slice with the highest SUVmax and the seeds for each volume slice. The voxels with a SUV>95% of SUVmax are marked as target seeds. Then, the method explores the hottest voxel neighborhood to identify the voxels with a SUV<30% of SUVmax (background seeds). Once the target and background seeds are localized, RW performs a 3D delineation. Our framework was used in 3 patients with cervical metastases. Patients underwent a 11C-labeled Methionine PET/CT examinations before and 2 months after the radiotherapy treatment. Lesions were segmented to evaluate therapeutic response using SUVmax, MTV, and Total Lesion Glycolysis (TLG) variations in sequential scans.

Result: The MTV delineation was not subject to both intra and inter-operator variability. The first patient showed a decrease of 30.21%, 64.13%, 74.96% of SUVmax, MTV and TLG, respectively. The second patient showed a decrease of 26.27%, 31.53%, 49.52% of SUVmax, MTV and TLG, respectively. The last patient showed a decrease of 0.95%, 62.09%, 62.45% of SUVmax, MTV and TLG, respectively.

Conclusions: Results show that our algorithm is an OI method, satisfying a critical requirement in clinical environment. In addition, MTV and TLG reflect metabolic changes throughout the entire tumor mass, and, should be more accurate methods of detecting global changes than a single-pixel value measurement such as SUVmax. The third case study could be a demonstration of this theory (minimal change in SUVmax and great variation in the metabolic tumor mass). On the other hand, in the literature cut-offs for SUV are reported, instead there are no data for TLG or MTV evaluations. ROC analyses to estimate these cut-offs will be the topic of future studies.

AUTHORS (LAST NAME, FIRST NAME): Stefano, Alessandro[1]; Vitabile, Salvatore [4]; Mocciaro, Vanessa[1]; Russo, Giorgio[1]; Sabini, Maria Gabriella[3]; Gambino, Orazio[2]; Pirrone, Roberto[2]; Ardizzone, Edoardo[2]; Gilardi, Maria Carla[1]; Ippolito, Massimo[5]

INSTITUTIONS (ALL):

1. CNR-IBFM, Cefalù, Palermo, Italy.
2. DICGIM, University of Palermo, Palermo, Italy.
3. Medical Physics Unit, Cannizzaro Hospital, Catania, Italy.
4. DIBIMEF, University of Palermo, Palermo, Italy.
5. Nuclear Medicine Department, Cannizzaro Hospital, Catania, Italy.

(No Image Selected)

CONTROL ID: 2244365

TITLE: CXCR4 targeted imaging and therapy in cancer patients

PRESENTER: Hans-Juergen Wester

ABSTRACT BODY:

Abstract Body: The C-X-C chemokine receptor type 4 (CXCR4) is a G-protein coupled receptor that mediates recruitment of cells towards its ligand SDF-1alpha (SDF-1). Engagement of CXCR4 triggers various intracellular signal transduction pathways, including AKT and MAPK/ERK activity, ultimately resulting in chemotaxis, proliferation, and cell survival. The SDF-1/CXCR4 axis is a major determinant for retaining and recruiting hematopoietic stem cells into the bone marrow niche. In cancer, high CXCR4 expression is frequently associated with tumor dissemination and poor prognosis. Furthermore, there is experimental evidence that cancer cells are recruited to putative protective niches, from where relapse is thought to occur. We evaluated the novel CXCR4 probe [^{68}Ga]Pentixafor for in vivo mapping of CXCR4 expression density in mice xenografted with human CXCR4-positive aggressive B-cell lymphoma and multiple myeloma (MM) cell lines, and in patients with advanced hematologic malignancies, including B- and T-cell Non-Hodgkin lymphoma, MM, and various solid tumors by means of Positron Emission Tomography (PET). [^{68}Ga]Pentixafor-PET provided images with excellent specificity and contrast in several lymphoproliferative cancer entities and selected solid tumors. In a cohort of 14 patients with advanced MM, [^{68}Ga]Pentixafor-PET/CT/MRI scans revealed MM manifestations in 10 of 14 patients, whereas only 9 of 14 standard [^{18}F]fluorodeoxyglucose-PET/CT scans were rated visually positive. Assessment of blood counts and standard CD34+ flow cytometry did not reveal significant blood count changes associated with tracer application. [^{68}Ga]Pentixafor-PET/CT showed also high-medium uptake in patients with SCLC, adrenal carcinoma, mammary cancer and CUPs. In addition to these imaging marker, a therapeutic probe capable for labeling with Lu/Y/Bi and other (radio)metal has been developed. First studies in patients with MM demonstrated high uptake and long retention of these probes over a period of 2 weeks with a metabolic response of 34-50% within two weeks after application of e.g. 15 GBq ^{177}Lu-pentixather (optimized dose by individual dosimetry). Our findings identify the CXCR4 PET tracer Pentixafor as a novel tool for *in vivo* imaging of hematologic neoplasms. In addition, Pentixafor not only seems to be a biomarker suitable for identifying patients who could be treated with CXCR4-directed drugs, but also represents a valuable lead structure for targeted therapy by means of Pentixather and radionuclide therapy of the cancer cell and its protecting niche.

AUTHORS (LAST NAME, FIRST NAME): Herrmann, Ken[4, 7]; Schottelius, Margret[2]; Philipp-Abbrederis, Katrin[3]; Osl, Theresa[2]; Poschenrieder, Andreas[2]; Buck, Andreas K.[4]; Kessler, Horst[5]; Schwaiger, Markus[1]; Lassmann, Michael[4]; Einsele, Herrmann[6]; Knop, Stefan[6]; Keller, Ulrich[3]; Wester, Hans-Juergen P.[2]

INSTITUTIONS (ALL):

1. Nuklearmedizinische Klinik und Poliklinik, Klinikum rechts der Isar, Technische Universität München , München, Germany.
2. Chair for Pharmaceutical Radiochemistry, Technische Un iversitaet Muenchen, Garching , Bavaria, Germany.
3. III. Medical Department of Hematology and Medical Oncology, Technische Universität München, Munich, Germany, Munich, Germany.
4. Department of Nuclear Medicine, Universitätsklinikum Würzburg, Germany, Würzburg, Germany.
5. Institute for Advanced Study and Center of Integrated Protein Science, Technische Universitaet Munich, Garching, Germany.
6. Department of Internal Medicine II, Division of Hematology and Medical Oncology, Universitätsklinikum Würzburg, Würzburg, Germany.
7. Department of Molecular and Medical Pharmacology, David Geffen School of Medicine at UCLA, Los Angeles, CA, United States.

(No Image Selected)

CONTROL ID: 2244376

TITLE: Using anatomic and metabolic imaging in Gamma Knife treatments

PRESENTER: Massimo Ippolito

ABSTRACT BODY:

Abstract Body: Background: *Gamma Knife* is a mini-invasive technique for stereotactic neuro-radiosurgery to deal with inaccessible or insufficiently treated lesions with traditional surgery or radiotherapy. Nowadays, in the planning phase of the Gamma Knife treatment, the target volume is identified with slice-by-slice manual segmentation on MR datasets, acquired while the patient is already wearing the stereotactic helmet just before the execution of the treatment. This procedure is time expensive: dozens of slices to be manually segmented in a brief time. Although MRI is characterized by a high spatial resolution and is able to discern the various cerebral soft tissues, it contains just anatomical information. These pictorial data are used for the definition of the morphological volume, the *Gross Tumour Volume (GTV)*. This volume often will not match with the “living” part of the lesion, and therefore metabolic imaging must be integrated during treatment planning. For this reason, the definition of a volume-based on PET images is mandatory.

Manual segmentation is also an operator-dependent procedure: an objective evaluation of the Gamma Knife treatment effectiveness must be performed through (semi)automatic segmentation methods to support the clinicians in the planning phase and to improve the assessment of the treatment response.

Methods: It is known that FDG-PET is not able to detect metabolic active regions, because the whole brain has a high uptake of glucose appearing as a hyper-intense area. Consequently, another radiotracer must be used in order to have functional information about brain lesions. ^{11}C-labeled Methionine is an amino acid that shows a greater transport within the active cancer cells. In this way, the *Biological Target Volume (BTV)* can be well defined through MET-PET and used as a complementary information to the *GTV*. The *Clinical Target Volume (CTV)*, is thus defined from PET/MR registration and fusion. Two novel semi-automatic and operator-independent methods to segment brain lesions from PET and MR images of 7 patients have been implemented: the former based on clustering for MR and the latter based on graphs for PET.

PET-MR image acquisitions and Gamma Knife treatment were performed at Cannizzaro Hospital (Catania), whereas the segmentation methods were developed at IBFM CNR - LATO (Cefalù).

Result: The physician was assisted during the treatment planning phase with fused PET/MR images, in which the lesions have been previously segmented using the two above indicated semi-automatic approaches. The workflow was optimized by minimizing execution times. The treatment evaluation was executed with RECIST and PERCIST criteria for MR and PET, respectively.

Conclusions: A clinical protocol for Gamma Knife treatment, including patient follow-up, must be defined by using operator-independent procedures through semi-automatic segmentation methods to support the treatment planning and to accurately assess the therapy response.

AUTHORS (LAST NAME, FIRST NAME): Ippolito, Massimo[2]; Cosentino, Sebastiano [2]; Militello, Carmelo[1]; Stefano, Alessandro[1]; Rundo, Leonardo[1]; Russo, Giorgio[1]; D'Urso, Davide[1]; Pisciotta, Pietro[1]; Vitabile, Salvatore [3]; Sabini, Maria Gabriella[4]; Valastro, Lucia Maria[4]; Pittera, Salvatore [4]; Patti, Valeria[4]; D'Arrigo, Corrado[6]; Marletta, Francesco [5]; Gilardi, Maria Carla[1]

INSTITUTIONS (ALL):

1. CNR-IBFM, Cefalù, Palermo, Italy.
2. Nuclear Medicine Department, Cannizzaro Hospital, Catania, Italy.
3. DIBIMEF, University of Palermo, Palermo, Italy.
4. Medical Physics Unit, Cannizzaro Hospital, Catania, Italy.
5. Radiotherapy Department, Cannizzaro Hospital, Catania, Italy.
6. Neuroradiology Unit, Cannizzaro Hospital, Catania, Italy.

(No Image Selected)

CONTROL ID: 2244419

TITLE: Convenient One-Step Nucleophilic [^{124}I]-Iodinations of Diaryliodonium Salts

PRESENTER: Stephen DiMagno

ABSTRACT BODY:

Abstract Body: Objectives: Diaryliodonium salts are commonly used precursors for the preparation of ^{18}F-labeled radiopharmaceuticals, however, radioiodination of these compounds remains largely unexplored. Our objectives were to ascertain the selectivity of radioiodination of diaryliodonium salts, to develop a facile nucleophilic route to ^{124}I-labeled compounds using these precursors, and to describe the origins of the different functional group tolerance in radiofluorination and radioiodination reactions. The goal of these studies was to demonstrate that radioiodination of diaryliodonium salts is a simple, and widely applicable method to prepare high specific activity tracers.

Methods: Diaryliodonium triflate precursors to m-[^{124}I]Iodobenzylguanidine (MIBG), aryl succinimidyl esters and maleimides were afforded by conventional diaryliodonium salt coupling chemistry. Nucleophilic halogenation (with chloride, bromide, and iodide) was studied to gauge the effects of solvents and reaction conditions on halogenation rate and selectivity. Optimized conditions for ^{127}I-iodination (90 °C, 30 min, CH_3CN/toluene) were used for ^{124}I-radiolabeling of these substrates. One microliter of aqueous sodium [^{124}I] iodide (approximately 1 mCi) in 0.1M NaOH was added to a reaction vial along with 1 uL of 1.0 M AcOH to prepare an acidic, slightly buffered solution. The diaryliodonium triflate precursor, dissolved in 400 uL of CH_3CN was added and the solution was evaporated with a stream of dry argon at 90 °C. CH_3CN (250 ul) and toluene (250 ul) were added and the mixture was heated at 90 °C for 30 minutes. The final products were concentrated and separated from the precursor salts by silica sep pak (for the maleimides and succinimidyl esters) or HPLC purification (MIBG). Radiochemical yields and chemical and radiochemical purity were assessed by HPLC.

Results: All diaryliodonium salt precursors were radioiodinated in good to excellent yield (65-90%) in 60-90 minute syntheses. Regioselectivity of radioiodination was excellent (>90%), and it was found that the regioselectivity of radioiodination mirrored that of bromination under identical conditions.

Conclusions: Nucleophilic radioiodination of diaryliodonium salts is an efficient, one-step route to radioiodinated compounds. It is much simpler than fluorination of these same precursors, it is highly tolerant of reactive functional groups, and complex protection schemes are not required.

AUTHORS (LAST NAME, FIRST NAME): DiMagno, Stephen G.[3]; Hu, Bao[3]; Apana, Scott M.[1]; Dostzada, Khaled[4]; Blecha, Joseph E.[2]; Lusinger, Destiny L.[1]; VanBrocklin, Henry[4]; Berridge, Marc S.[1]

INSTITUTIONS (ALL):

1. 3D Imaging, Little Rock, AR, United States.
2. Radiology and Biomedical Imaging, University of California San Francisco, San Francisco, CA, United States.
3. Chemistry, University of Nebraska-Lincoln, Lincoln, NE, United States.
4. Radiology, UCSF School of Medicine, San Francisco, CA, United States.

(No Image Selected)

CONTROL ID: 2244517

TITLE: Imaging Bacterial Infection Induced Inflammation in a Mouse Model using ^{68}Ga-transferrin

PRESENTER: Delphine Chen

ABSTRACT BODY:

Abstract Body: Introduction: Postoperative bacterial infections greatly contribute to the morbidity and mortality. However, current methods lack sensitivity and/or specificity for detecting infections[1,2]. Positron emitting tomography (PET)/CT is a highly sensitive and quantitative imaging approach that could be used for diagnosing infections. Transferrin can be labeled with ^{68}Ga and may be useful in imaging bacterial infections because holo-transferrin is one of the major iron sources for invading bacteria[3,4]. In our study, we tested whether PET imaging with ^{68}Ga-transferrin could detect bacterial infections specifically by assessing uptake in bacteria and activated neutrophils and macrophages in vitro and in the lungs of mice infected with Pseudomonas aeruginosa (PA01).

Methods: Apo-transferrin was labeled with ^{68}Ga eluted from a ^{68}Ge/^{68}Ga generator in carbonate buffer. PA01 was cultured in standard lysogeny broth (LB). Neutrophil and monocytes were isolated from human peripheral blood and activated in vitro using phorbol myristate acetate (PMA) and lipopolysaccharide (LPS), respectively. In vitro tracer cell uptake in PA01 and in resting and activated neutrophil and macrophages was assessed by incubating the tracer with cells at 37°C for one hour and quantified by the % injected dose (%ID) per 10^7 cells. C57BL/6J mice were inoculated with PA01, LPS or PBS control intratracheally and imaged by small animal PET (Inveon PET/CT or Focus 220 PET scanners, Siemens/CTI) at 6 hour or 24 hour post inoculation. The tracer uptakes in the lungs were quantified by %ID/ml and assessed across different groups. Mouse bronchoalveolar lavage (BAL) and lungs were harvested for the validation of bacteria counts by colony forming unit (CFU) assay and inflammation response by IHC and flow cytometry using neutrophil and macrophage specific markers.

Results: PA01 ^{68}Ga-transferrin uptake in vitro was 0.14±0.02 %ID per 10^7 cells compared to activated neutrophil or macrophage uptake of 1.2±0.5 and 2.6±0.5 %ID per 10^7 cells, respectively. MicroPET imaging demonstrated 5.7±0.8 and 7.2±0.9 %ID/ml at 6 and 24 hour post-infection, respectively, which correlates positively with inflammation (an average of 0.97×10^6 versus 2.75×10^6 neutrophils in BAL) but negatively with bacterial counts. In addition, bacteria infected mice and LPS installed mice that were imaged at the same time point post infection and developed comparable inflammation respond showed similar uptake indicating the insignificance of bacterial uptake of the tracer.

Conclusion: The above results suggest that the uptake of ^{68}Ga-transferrin is likely targeting the host response rather than bacterial proliferation in vivo.

(1) Signore, A.; Glaudemans, A. W. *Annals of nuclear medicine* **2011**, *25*, 681.

(2) Palestro, C. J.; Glaudemans, A. W.; Dierckx, R. A. *Clinical and Translational Imaging* **2013**, *1*, 385.

(3) Ratledge, C.; Dover, L. G. *Annual Reviews in Microbiology* **2000**, *54*, 881.

(4) Kumar, V.; Boddeti, D. K.; Evans, S. G.; Roesch, F.; Howman-Giles, R. *Nuclear medicine and biology* **2011**, *38*, 393.

AUTHORS (LAST NAME, FIRST NAME): Wang, Ruqi[1]; Bandara, Nilantha[2]; Lapi, Suzanne[1]; Chen, Delphine[1]

INSTITUTIONS (ALL):

1. Radiology, Washington University, Saint Louis, MO, United States.
2. Radiation Oncology, Washington University School of Medicine, Saint louis, MO, United States.

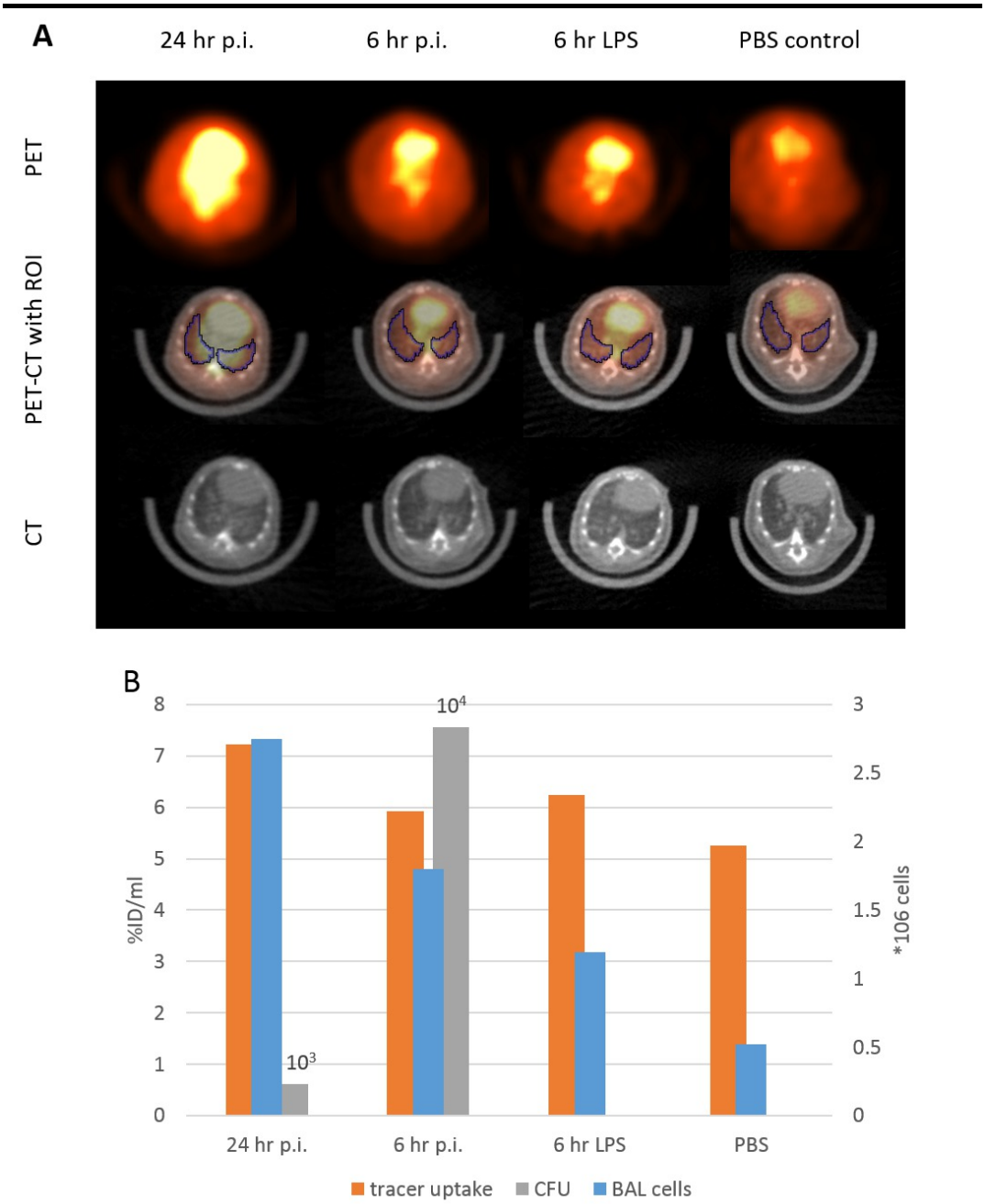

Figure 1 A) PET/CT images from 60 min acquisition of bacterial infected, LPS installed and PBS control mice. B) Average tracer uptake (orange), BAL cell counts (blue) and CFU counts (grey) of the same groups of the mice. P.i. = post bacterial inoculation, %ID/ml = percent injected dose per ml lung.

CONTROL ID: 2244527

TITLE: Folate receptor beta is a target for macrophage imaging in acute lung inflammation

PRESENTER: Timothy Blackwell

ABSTRACT BODY:

Abstract Body: Introduction: Activated macrophages are crucial in initiation and progression of inflammatory diseases. Identification of activated macrophage markers could facilitate development of novel methodologies for monitoring disease activity. Prior studies have shown that folate receptor-β (FRβ) is overexpressed on activated macrophages compared with resting macrophages. We investigated whether SPECT imaging with a technetium-labeled folate probe could be used to identify activated macrophages in the setting of acute lung inflammation.

Methods: Mice treated with LPS (3ug/g body weight) by intratracheal (n = 7) injection were anesthetized and injected with ~37 MBq/0.2 mL ^{99m}Tc-folate retro-orbitally. At 60 minutes following radiotracer administration, mice were positioned in a NanosSPECT/CT for imaging. For blocking studies, mice received folic acid (10 mg/kg) mixed in 10% tween approximately 5 min prior to radiotracer administration. All SPECT acquisitions were reconstructed using HiSPECT software and the Ordered Subsets Expectation Maximization (OSEM) iterative reconstruction algorithm with 9 iterations and 4 subsets. The SPECT images were reconstructed into 128 x 128 x 140 slices with a voxel size of 0.3 x 0.3 x 0.3 mm^3. CT images were conducted at an x-ray beam intensity of 90 mAs with x-ray energy of 45 kVp. Regions-of-interest (ROIs) were manually drawn around the lungs in the CT images for each mouse using the medical imaging analysis tool AMIDE and superimposed on the SPECT images. The mean radiotracer concentration within the ROI was measured, normalized to the injected dose and displayed as percent injected dose per unit volume (%ID/cc).

Results: In control mice at 60-80 min post ^{99m}Tc-folate administration, radiotracer uptake was predominantly observed in the choroid plexus, salivary glands, liver, and kidneys while minimal radiotracer was detected in the heart and lungs. Radiotracer uptake in the lungs was significantly higher in mice imaged at 48 hours after LPS treatment compared to untreated control mice. Radiotracer concentration in the LPS-treated lungs was 1.24 ± 0.31 %ID/cc (mean ± SD) compared with 0.63 ± 0.26 %ID/cc in the lungs of control mice. In blocking studies, the radiotracer concentration in lungs of LPS-treated mice was significantly decreased following delivery of excess folate (0.76 ± 0.04 %ID/cc versus 1.24 ± 0.31 %ID/cc), indicating specific binding of the radiotracer to folate receptors.

Conclusions: We found that radiolabeled folate uptake was increased in the inflamed lungs of LPS-treated mice. Based on these data and prior studies, it appears that folate-targeted molecular imaging is useful for quantifying and sequentially monitoring lung inflammation through detection of activated macrophages. Development of folate-based radiopharmaceuticals could represent novel precision imaging diagnostics for inflammatory lung diseases in humans.

AUTHORS (LAST NAME, FIRST NAME): Blackwell, Timothy S.[2]; Han, Wei[2]; Nickels, Michael L.[1]; Peterson, Todd[4]; Manning, H. Charles[3]

INSTITUTIONS (ALL):

1. VUIIS, Vanderbilt Medical Center, Nashville, TN, United States.
2. Medicine, Vanderbilt Univeristy, Nashville, TN, United States.
3. Radiology and VUIIS, Vanderbilt University, Nashville, TN, United States.
4. Radiology & Radiological Sciences, Vanderbilt University Medical Center, Nashville, TN, United States.

(No Image Selected)

CONTROL ID: 2244685

TITLE: Chemotherapy driven by evolutionary principles informed by MRI shows improved outcome in preclinical models of triple-negative breast cancer

PRESENTER: Pedro Enriquez Navas

ABSTRACT BODY:

Abstract Body: Introduction: Disseminated cancers are typically treated with the highest possible dose of drug (i.e. maximum tolerated dose) to achieve the goal of killing as many tumor cells as possible. However, these therapies eventually fail due to emergence of resistant clones. Using mathematical models of Darwinian dynamics, we have predicted that adapting the chemotherapeutic dosing schedule to the tumor spatial variability and tumor microenvironment can retard the emergence of chemoresistance. Here, we present an evolutionary-guided treatment strategy (Adaptive Therapy, AT) designed to maintain stable chemosensitive populations while limiting the proliferation of chemoresistant clones by exploiting the fitness cost of the resistant phenotype.

Methods: Four cohorts (composed by 12, 11, 13, and 10 mice, respectively) of nude mice were injected with $10x10^6$ MDA-MB-231 (triple-negative breast cancer) cells in the mammary fat pad. Control animals didn't receive any treatment. Mice under standard therapy received 20mg/kg of Paclitaxel twice per week for a total of 5 times. We defined two different Paclitaxel AT algorithms (Table 1), under which AT mice were treated depending on the tumor volume calculated by means of MRI. When the tumors achieve the volume of, approximately 300 mm^3, MRI T_2 and Diffusion Weighted acquisitions were performed on a horizontal Agilent ASR 310 7T scanner, with 205/120/HDS gradients and 310 mm bore to determine volume and cellularity, respectively. Thereafter, dynamic contrast enhanced (DCE-) MRI was preformed following bolus of 0.1mmol/kg Magnevist to assess distribution of blood flow. Images were processed with different in-house developed MATLAB scripts to obtain reliable information from these images. At the end of the monitoring time, tumors were collected and processed for H&E and CD31 immunohistochemistry staining to study the viable and necrotic tissue, and vessel presence, respectively. The slides were examined using the Aperio ScanScope XT microscope. Using different selected slides, an algorithm was built in order to analyze all tissue samples with a pixel-wise resolution.

Results and Discussion: Tumor growth was monitored during the treatment period using the MRI techniques previously described. The AT treatment algorithm has been modified to fine tune the dose and scheduling based on tumor volume. Among these three protocols (2 AT and one ST), AT-1 resulted in the most significant cancer control. As shown in figure 1, treatment of mice with the AT-1 protocol was able to maintain tumors at a small size for >120 days. Also, AT-1 treated tumors had a lower percent tumor necrosis, and an increased vascular density (figure 2).

Conclusion: In summary, these results indicate that AT schema, guided by MRI measurement of tumor volume, can maintain a stable small tumor burden with prolonged progression-free survival compared to standard high dose therapy. Also, AT is able to maintain the lower necrotic volume and a higher vessel density, which was correlated with tumor stabilization.

AUTHORS (LAST NAME, FIRST NAME): Enriquez Navas, Pedro M.[1]; Wojtkowiak, Jonathan[1]; Ruiz, Epi [1]; Hassan, Sabrina[1]; Gillies, Robert[1]; Gatenby, Robert[1]

INSTITUTIONS (ALL):

1. Dept. Cancer Imaging and Metabolism, Moffitt Cancer Center, Tampa, FL, United States.

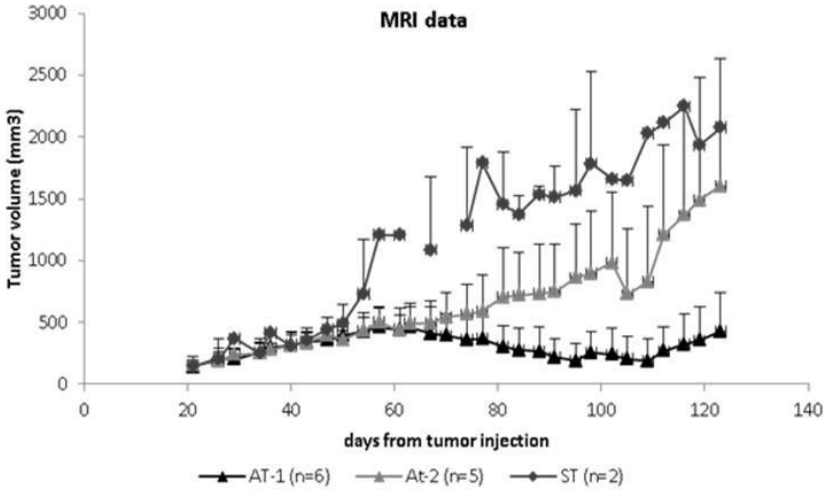

Figure 1: MRI data showing the evolution of tumor volume under different treatment algorithms. *n* corresponds to the number of animals in each treatment. Error bars correspond to the standard deviation.

CONTROL ID: 2244763

TITLE: Brain tumor cellularity maps trained with co-registered histology predict tumor presence in pathologically confirmed regions sampled ex-vivo

PRESENTER: Peter LaViolette

ABSTRACT BODY:

Abstract Body: **Purpose** Recent advances in the voxel-wise co-registration of histology obtained from ex-vivo whole brain samples and in-vivo imaging have been used to determine the level of diffusion restriction necessary for defining regions of brain tumor hypercellularity and diffusion restricted necrosis[1]. The methodology presented in this recent study has opened up the possibility of training algorithms to predict histological features based on the MR voxel values and the co-registered histological features of interest.

Methods *Patient Population* Seven patients with high-grade gliomas were included in this IRB approved study. Patients donated their brains following death. *Ex-vivo Histology Processing* Large tissue samples (approximately 4cm^2) were taken from regions suspicious of tumor and free from MR acquisition artifacts in each of the 7 patients. Histological samples were hematoxylin and eosin (H&E) stained. Each slide was then digitized and individually segmented to locate cells using k-means clustering algorithm. A representative segmentation is shown in the center of Figure 1A.

Precise Histology to MRI Correlation Co-registration of histology to MRI was performed using a manually defined linear rotational and translational transformation applied to align each histology slide to the MRI. The location of each sample was matched visually to the MRI slice that best represented the sample's location[1]. Histology from within each region of interest drawn using the HISTtoMRI toolbox was then down-sampled to the MRI resolution for a direct 1 to 1 comparison (method shown in Figure 1). Histological segmentation values, along with the MRI values within each voxel were then extracted and combined across all samples. Partial least squares (PLS) regression was applied to the MRI values using cellularity as the independent variable to train a model. The PLS trained model was then applied to the patient's entire stack of whole brain MR images to generate imaging based histology trained maps (IBHTMs) of cellularity (Figure 1B). Voxels outside the brain were excluded. The resulting maps were thresholded based on a 95% confidence interval determined from cellularity calculated within a normal histology sample for each patient (Figure 1C, Top). To validate the algorithm's accuracy, additional histology samples were gathered from regions indicated as hypercellular by the IBHTM. These samples were scanned and the predicted values were compared to the actual cellularity values using a Pearson correlation.

Results Figure 1C shows the IBHTMs of cellularity for each of the seven patients. Samples gathered in regions implicated, all demonstrated viable tumor. Pearson correlation coefficients ranged from 0.31 to 0.69 and all were significantly positively correlated, $p<0.00001$. We found viable tumor in regions that appeared normal on conventional imaging in 5 of 7 patients.

Discussion We present a novel method for mapping brain cancer cellularity with imaging based histological trained maps. This new method will potentially improve surgical planning, radiation guidance, and tumor progression detection.

References 1. LaViolette, P.S.*, et al. Neuro-Oncology.* 2014.

AUTHORS (LAST NAME, FIRST NAME): LaViolette, Peter S.[1]; Mickevicius, Nikolai J.[2]; Cochran, Elizabeth J.[3]; Schmainda, Kathleen M.[1, 2]; Connelly, Jennifer[4]; Rand, Scott D.[1]

INSTITUTIONS (ALL):

1. Radiology, Medical College of Wisconsin, Milwaukee, WI, United States.
2. Biophysics, Medical College of Wisconsin, Milwaukee, WI, United States.
3. Pathology, Medical College of Wisconsin, Milwaukee, WI, United States.
4. Neurology, Medical College of Wisconsin, Milwaukee, WI, United States.

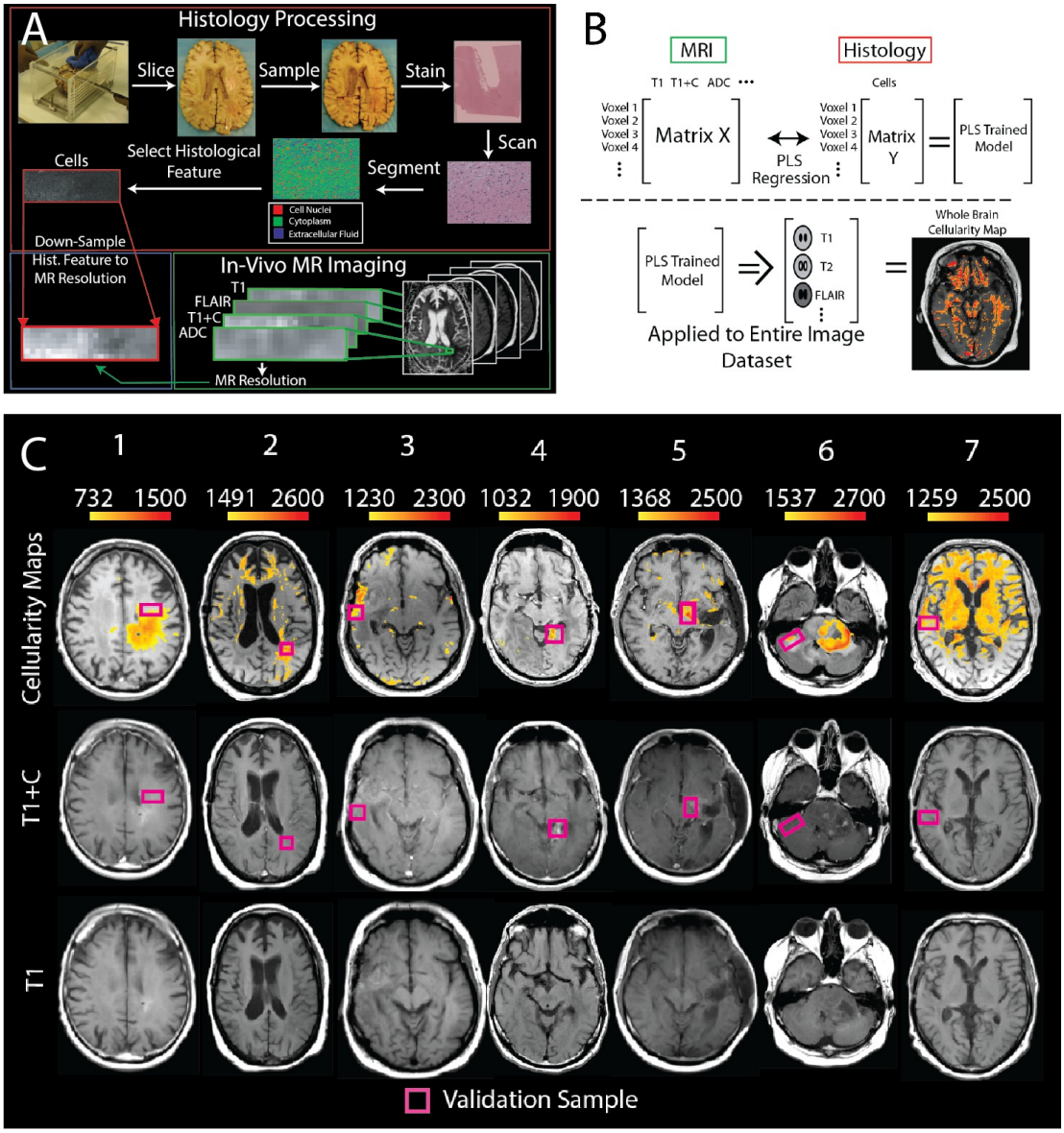

Figure 1. (A) Demonstration of down-sampling histology to clinical MRI resolution for a voxel-wise comparison1. (B) Diagram of PLS regression trained model applied to entire image dataset for generation of an IBHT map of cell count (i.e. cellularity). (C) Resulting IBHTMs of cellularity (Top) for each patient along with the region sampled to validate the maps. (Middle) T1+contrast (Bottom) T1 images in the same slice.

CONTROL ID: 2244826

TITLE: Phosphorescent probes for *in vivo* two-photon microscopy of oxygen

PRESENTER: Tatiana Esipova

ABSTRACT BODY:

Abstract Body: The ability to quantify oxygen in vivo in 3D with high spatial and temporal resolution is invaluable for understanding of oxygen metabolism, delivery and consumption in normal and diseased tissues. An optical method based on oxygen-dependent quenching of phosphorescence is being developed, that allows quantitative minimally invasive real-time imaging of partial pressure of oxygen (pO2) in tissue.

In the past, dendritically protected phosphorescent oxygen probes with controllable quenching parameters and defined bio-distributions have been developed [1], and more recently our probe design strategy has been expanded on two-photon excitable oxygen probes [2]. These latter molecules comprise FRET-based antenna-core constructs, which brought about first demonstrations of two-photon phosphorescence lifetime microscopy (2PLM) of oxygen *in vivo*, providing new valuable information for neuroscience [3-6] and stem cell biology [7]. However, current two-photon oxygen probes suffer from a number of limitations, such as low brightness and high cost of synthesis, which dramatically reduce imaging performance and limit usability of the method.

Here we present an approach to new bright phosphorescent chromophores with internally enhanced two-photon absorption cross-sections, which allow construction of antenna-free probes for 2PLM. In addition to substantial increase in performance, the new probes can be synthesized by much more efficient methods, thereby greatly reducing the cost of synthesis.

References:

1. Vinogradov, S. A., and Wilson, D. F. Porphyrin-dendrimers as biological oxygen sensors, In Designing Dendrimers (Capagna, S., and Ceroni, P., Eds.), Wiley, New York (2012)
2. Finikova, O. S. et al. Oxygen microscopy by two-photon-excited phosphorescence. ChemPhysChem 9, 1673 (2008).
3. Sakadzic, S. et al. Two-photon high-resolution measurement of partial pressure of oxygen in cerebral vasculature and tissue. Nature Methods 7, 755 (2010).
4. Lecoq, J. et al. Simultaneous two-photon imaging of oxygen and blood flow in deep cerebral vessels. Nature Medicine 17, 893 (2011).
5. Devor, A. et al. "Overshoot" of O2 is required to maintain baseline tissue oxygenation at locations distal to blood vessels. J. Neuroscience 31, 13676 (2011).
6. Parpaleix, A., Houssen, Y. G. & Charpak, S. Imaging local neuronal activity by monitoring pO2 transients in capillaries. Nature Medicine 19, 241 (2013).
7. Spencer, J. A. et al. Direct measurement of local oxygen concentration in the bone marrow of live animals. Nature 508, 269 (2014).

AUTHORS (LAST NAME, FIRST NAME): Esipova, Tatiana V.[1]; Vinogradov, Sergei A.[1]

INSTITUTIONS (ALL):

1. Biochemistry and Biophysics, University of Pennsylvania, Philadelphia, PA, United States.

(No Image Selected)

CONTROL ID: 2244877

TITLE: Real-Time Magnetic Particle Imaging with a Field Free Line

PRESENTER: Matthias Weber

ABSTRACT BODY:

Abstract Body: The emerging imaging modality Magnetic Particle Imaging (MPI) [1] is capable of determining distributions of superparamagnetic particles in real-time and high spatial resolution by utilizing time-variable magnetic fields without introducing any harmful ionizing radiation. This suits MPI especially for medical applications as angiographies and stem cell tracking. Imaging is realized by moving a gradient field that features a field free point (FFP) over the region of interest (ROI). A characteristic signal can be detected if this point crosses a particle distribution. By utilizing FFP trajectories, the whole particle concentration in the ROI can be detected. A new promising spatial encoding scheme is based on a field free line (FFL) and is ten times more sensitive than the conventional imaging with a FFP [2]. Particle signals are generated by translating the FFL over the region of interest while receiving a characteristic projection signal for every FFL angle. The acquired data can be represented in a sinogram. Well-known algorithms from computed tomography allow one to reconstruct the actual particle concentration. So far, imaging could only be realized for discrete FFL angles or by rotating the particle sample and time scales in the minute range [3], [4]. Within this paper, we present the worlds first realization of a real-time FFL-MPI scanner that features a FFL rotation with 100 Hz and a translation of 25 kHz. Furthermore, the image reconstruction is calculated in real-time allowing for two-dimensional MPI with 100 frames per second at a gradient of 1.08 T m^{-1} μ_0^{-1} and a field of view with a diameter of 25 mm. As a preliminary test, a phantom was built and filled with three delta samples of undiluted Resovist . During an imaging time of 2 s the phantom was moved through the imaging slice twice and 200 images were acquired. The reconstructed images can be seen in Fig. 1. These first real-time results confirm the potential of FFL-MPI and promise great application scenarios for angiographies. Further work will focus on sensitivity limits and a detailed evaluation of flow measurements.

AUTHORS (LAST NAME, FIRST NAME): Weber, Matthias[1]; Bente, Klaas[1]; von Gladiss, Anselm[1]; Buzug, Thorsten M.[1]

INSTITUTIONS (ALL):

1. Institute of Medical Engineering, Universität zu Lübeck, Lübeck, Germany.

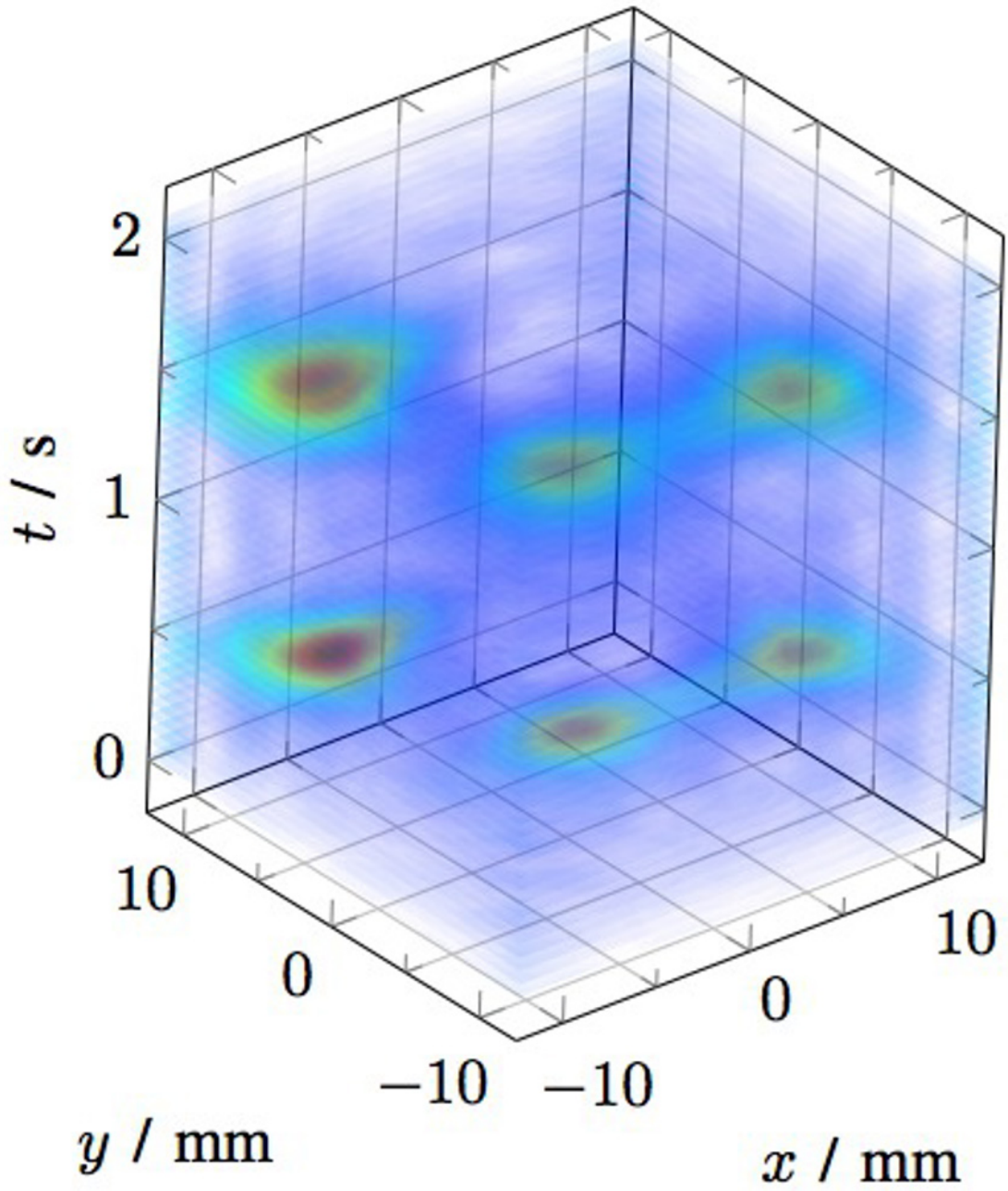
2
1
0
t / s
10
0
−10
y / mm
−10
0
10
x / mm

CONTROL ID: 2244950

TITLE: Rapid Screening of the Biodistribution of Adeno-associated Vectors Using NIS Reporter Gene Imaging

PRESENTER: Kah-Whye Peng

ABSTRACT BODY:

Abstract Body: Biodistribution (BD) studies of viral vectors can be labor intensive as it requires harvest of multiple animals at multiple time points, performing necropsies, extraction of the nucleic acid from tissues, and analysis of tissue samples for viral transcripts. Bioluminescent imaging has greatly facilitated high throughput BD studies. However, optical imaging is not easily performed in larger animals, lacks resolution, and because bioluminescent imaging is so sensitive, it is difficult to differentiate between low and high expressing tissues. Here we evaluated the use of the sodium iodide symporter (NIS) as a reporter gene to track the biodistribution of adeno-associated viral (AAV) vectors. AAV are small non-integrating vectors that are being developed for a number of gene therapy applications. Different AAV serotypes, armed with constitutive or tissue specific promoters, capable of infecting various tissue types have been engineered to enable preferential transduction of the target tissues. In order to rapidly screen and evaluate the best AAV serotype and promoter for high levels of transgene expression in a specific organ, we engineered NIS into the AAV2 vector. In this study, we have generated a panel of AAV vectors of serotype 1, 2, 5, 8, and 9 and administered the vectors via various routes of delivery. The mice and rats were imaged using SPECT (I-125 or Tc99m pertechnetate) isotopes on a high resolution microSPECT/CT scanner. Results indicate robust AAV gene expression by 2 weeks post vector administration. For example, AAV9-CMV-NIS gave high levels of cardiac gene expression and interestingly, of subcutaneous brown fat (scapular region). In contrast AAV1-CMV-NIS resulted in highest gene expression in the subcutaneous brown fat only whereas AAV-LST-NIS (liver specific promoter) gave only NIS expression in the liver. When the regions of interests were quantitated, we found that AAV-NIS gene expression was stable over 90 days (end of study) in immunocompetent rats and over 200 days in immunocompromised mice. Using NIS as the reporter gene, we are able to use the same vector construct and perform similar noninvasive NIS imaging studies in large animal models using the same SPECT isotopes in combination with clinical SPECT/CT scanners.

AUTHORS (LAST NAME, FIRST NAME): Peng, Kah-Whye[1]; Pham, Linh[1]; Suksanpaisan, Lukkana[2]; Russell, Stephen[1]

INSTITUTIONS (ALL):

1. Molecular Medicine, Mayo Clinic, Rochester, MN, United States.
2. Imanis Life Sciences, Rochester, MN, United States.

(No Image Selected)

CONTROL ID: 2245226

TITLE: NIS-guided drug development: the contribution of reporter gene imaging

PRESENTER: Stephen Russell

ABSTRACT BODY:

Abstract Body: NIS, the sodium iodide symporter, is expressed endogenously in the thyroid, salivary glands, gastric mucosa and mammary glands of mammals, from mice to humans. For more than 70 years, NIS has been exploited in the nuclear medicine to provide diagnosis of thyroid disorders. MV-NIS is an oncolytic measles virus engineered to express the human NIS. The virus is selectively destructive to a variety of human tumor cell types including myeloma plasma cells, and its in vivo spread can be monitored by noninvasive imaging of NIS gene expression. MV-NIS potency can be boosted by appropriately timed administration of high dose radioiodine (radiovirotherapy). The virus is currently in phase 2 clinical testing as an experimental therapy for multiple myeloma, and NIS imaging studies were critical at a number of key go/no-go decision points in its preclinical and early clinical development. FDA responded favorably to the inclusion of a NIS reporter gene in the MV-NIS virus. No significant safety concerns were raised and the NIS imaging approach was immediately accepted as a viable way to obtain otherwise unobtainable pharmacokinetic data in the early phase clinical testing of a biological therapy. After FDA approved the IND, a phase I clinical trial was initiated to determine the maximum tolerated dose of intravenously administered MV-NIS in patients with advanced, refractory multiple myeloma. A standard cohort of three design was employed with a first dose level of 10^6 $TCID_{50}$ (~2 $x10^4$ per kg) MV-NIS, increasing by 10-fold dose increments to a maximum feasible dose of 10^9 $TCID_{50}$ (~2 x 10^7 per kg). Clinical responses were not seen at any dose level and the approach might have been abandoned, but the NIS imaging studies gave positive post-therapy intratumoral signals in a small number of patients, thereby definitively confirming its tumor targeting ability in human subjects with myeloma. Because of the positive NIS imaging data at subtherapeutic virus doses, which showed that that the virus could selectively infect myeloma deposits in human subjects, the decision was made to further escalate the dose of MV-NIS. A revised virus manufacturing process was developed to generate (much) higher quantities of MV-NIS and FDA approval was obtained to extend the trial. The first responses to intravenous MV-NIS therapy were seen in two of six patients treated at the new maximum feasible dose of 10^{11} $TCID_{50}$ (~2 x 10^9 per kg). Both responding patients had multiple glucose-avid plasmacytomas and tumor targeting was clearly documented by NIS-mediated radioiodine uptake in virus infected tumor deposits day 8 and 15 post MV-NIS administration. One patient had a complete remission at all disease sites which lasted for 9 months. Based on these encouraging findings in the phase I trial, the decision was made to proceed with a phase 2 clinical trial of MV-NIS therapy in myeloma patients. NIS imaging remains an integral part of the trial design and is expected to further elucidate the variability in tumor uptake and intratumoral spread of the virus in different myeloma patients depending on the stage, grade and distribution pattern of their myeloma. This trial is currently ongoing.

AUTHORS (LAST NAME, FIRST NAME): Russell, Stephen[1]; Peng, Kah-Whye[1]; Zhou, Yumei[1]; Dispenzieri, Angela[2]

INSTITUTIONS (ALL):

1. Molecular Medicine, Mayo Clinic, Rochester, MN, United States.
2. Internal Medicine, Mayo Clinic, Rochester, MN, United States.

(No Image Selected)

CONTROL ID: 2245051

TITLE: MUSE (Microscopy with UV Surface Excitation): full-color, high-resolution slide-free tissue imaging

PRESENTER: Richard Levenson

ABSTRACT BODY:

Abstract Body: A new microscopy system is described that provides a unique slide-free approach to diagnostic-quality images obtained directly from the cut surfaces of fresh or fixed tissues. **MUSE** (microscopy with UV surface excitation) is **non-destructive**, and eliminates any requirement for conventional histology processing, formalin fixation, paraffin embedding, or thin-sectioning. MUSE is easy to implement and use, requires no lasers, confocal, multiphoton or OCT optics, and can cost a few thousands of dollars or even less. The samples are stained within seconds using familiar histology stains, such as eosin and DAPI, and the resulting high-resolution images are as easy to interpret as those from conventional hematoxylin- and eosin- (H&E) stained glass slides.

MUSE relies on two principles:

1) rejection of out-of-focus light from thick specimens due to micron-scale tissue penetration of ultraviolet light at wavelengths below 300 nm;

2) efficient excitation of many visible-range fluorescent stains by UV illumination in 250-300 nm range.

The resulting signals are bright enough to be detected with sub-second exposure times using conventional color cameras, allowing rapid imaging of large fields of view. Images can be converted from fluorescence to H&E-like brightfield appearance on the fly (i.e., essentially live) via high-speed customizable color conversion. Due to the oblique illumination geometry, **no special optics are required** beyond appropriate UV LED sources, which can currently be purchased at prices around 100 dollars each.

AUTHORS (LAST NAME, FIRST NAME): Levenson, Richard[1]; Fereidouni, Farzad[1]

INSTITUTIONS (ALL):

1. Pathology and Laboratory Medicine, University of California, Davis, Sacramento, CA, United States.

(No Image Selected)

CONTROL ID: 2245148

TITLE: Mitophagy: What happens *in vivo*?

PRESENTER: Nuo Sun

ABSTRACT BODY:

Abstract Body: Alterations in mitophagy, the selective removal of dysfunctional and damaged mitochondria, are increasingly linked to neurodegenerative conditions, tumor suppression, immunity, as well as aging itself. To date, however, there are no convenient or robust methods to analyze mitophagy in vivo. Here, we describe a transgenic mouse model in which we have used site-specific integration to express a mitochondrial-targeted form of a fluorescent reporter, which is resistant to lysosomal proteases, and whose excitation is pH dependent. These properties allow cells and tissues that express the reporter to provide a quantitative assessment of mitophagic flux, by Confocal, Two-Photon and Stimulated Emission Depletion (*STED*) microscopy. Comparison of primary cells and tissues from the transgenic mice reveals significant variations in basal mitophagic flux. Moreover, we observed significant spatial heterogeneity in mitophagy within a given tissues. In the mouse brain, mitophagic flux appears markedly enhanced in regions known to contain neural stem cells. In those regions of the brain containing high basal mitophagy, the magnitude of this observed flux markedly diminishes with age. We further use the mice to analyze how mitophagy is affected by changes in diet, oxygen availability, expression of the Huntington transgene, the absence of macroautophagy, mitochondrial mutations and the presence of metastatic tumors. The ability to quantify mitophagic flux under a host of varying environmental and genetic perturbations provide a valuable reagent to understand the in vivo role of mitophagy in a range of physiological and pathological conditions.

AUTHORS (LAST NAME, FIRST NAME): Sun, Nuo[1]; Finkel, Toren[1]

INSTITUTIONS (ALL):

1. NIH/NHLBI, Bethesda, MD, United States.

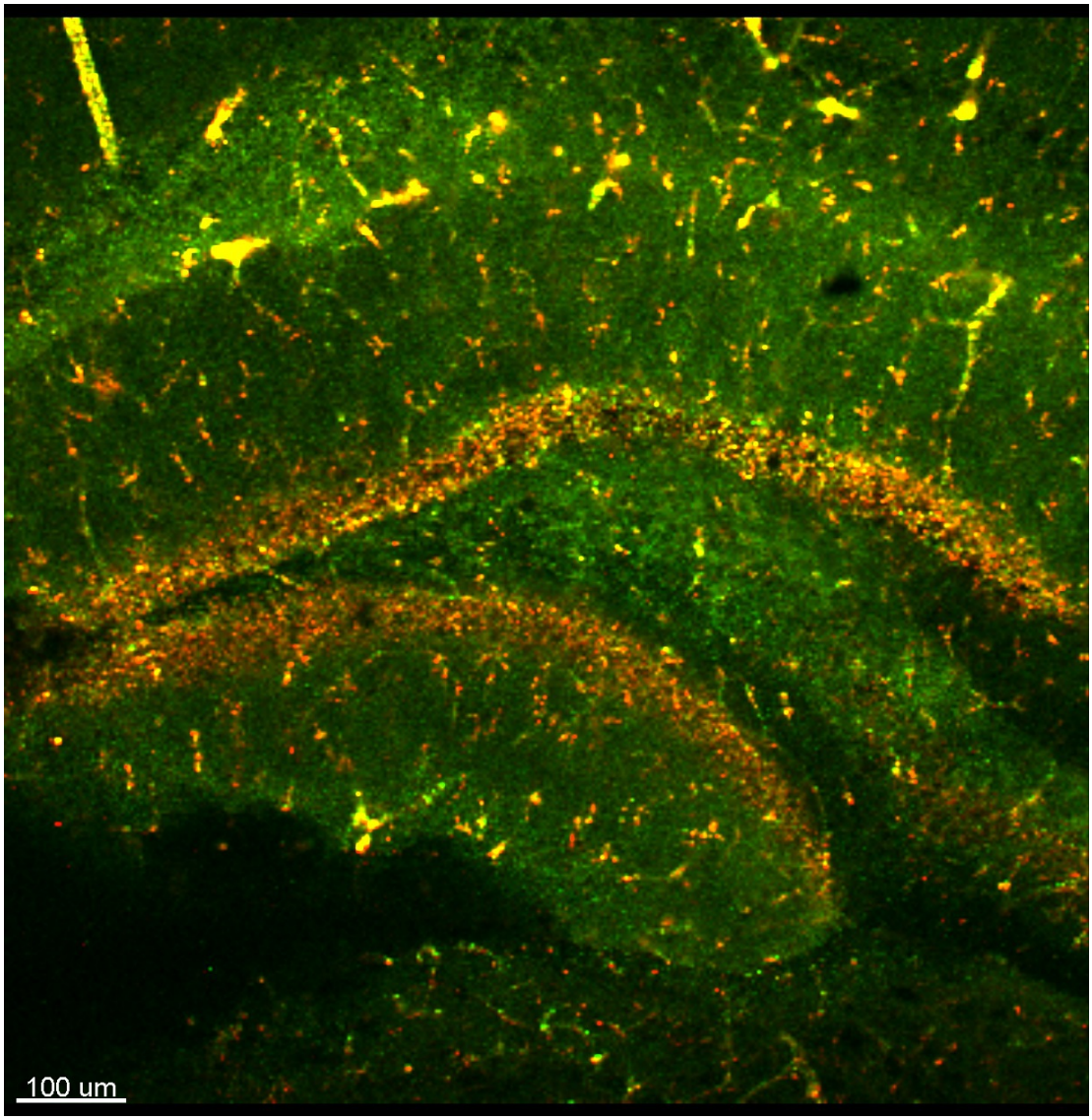
100 um

CONTROL ID: 2245206

TITLE: Measuring HER2-receptor expression in metastatic breast cancer using [^{68}Ga]ABY-025 PET/CT

PRESENTER: Jens Sorensen

ABSTRACT BODY:

Abstract Body: Purpose: Accurate PET imaging of HER2 could select patients with metastastic breast cancer for HER2-targed therapy, predict response based on uptake and be used for monitoring. In this pivotal phase I study the HER2-binding Affibody molecule ABY025 was labeled with ^{68}Ga for PET to study correlation of quantified uptake in tumors to histopathology, test-retest variability and volumetric assessments of total tumor-receptor burden.

Methods: Sixteen women with known metastatic breast cancer and on-going treatment were included and underwent FDG PET/CT to identify viable metastases. Eleven had HER2-positive primary tumors and five HER2-negative primary tumors. Four were included as HER2-negative controls. After iv injection of 212±46 MBq ^{68}Ga-ABY025 whole-body PET was performed at 2h. In five patients repeated ^{68}Ga-ABY025 PET were done as a test-retest of uptake in individual lesions. Biopsies from metastases were collected for verification of HER2 expression. SUVmax and tumor volumes were defined from each metastases and the summed product was used to index total lesional glycolysis (TLG) for FDG and total lesional receptor expression (TLR) for ABY025.

Results: Sixteen metastases in 12 patients were biopsied and evaluated by immunohistochemistry and in-situ hybridization. ^{68}Ga-ABY025 SUVmax in biopsied metastases ranged from 0.8 to 19 and were three times higher in HER2-positive than in HER2-negative lesions (n=8 in both groups, p=0.003). A cut-off of SUVmax 6 had an accuracy of 88% in discriminating HER2-status. Twelve biopsied metastases in eight patients were also imaged at 4h, at which time point groups differed by a factor of 5 with no overlap. Half of the patients had heterogeneous disease according to PET, confirmed by biopsies in two. TLR ranged from 9 to 1377 and TLG from 54 to 1251. The test-retest intra-class correlation was r=0.996 (p<0.001). ^{68}Ga-ABY025 PET led to change in HER2-targeting treatment in 3 of the 16 patients due to documented receptor up- or down-regulation.

Conclusion: ^{68}Ga-ABY025 PET accurately quantifies whole-body HER2-receptor status in metastatic breast cancer. The total receptor burden varies by a factor of >100 in HER2-positive patients. ^{68}Ga-ABY025 PET might facilitate a non-invasive approach to personalized HER2-targeting treatments.

AUTHORS (LAST NAME, FIRST NAME): Sorensen, Jens[2]; Feldwisch, Joachim[1]; Wennborg, Anders[1]; Olofsson, Helena[3]; Tolmachev, Vladimir[3]; Lubberink, Mark[2]; Sandberg, Dan[2]; Carlsson, Jörgen[3]; Lindman, Henrik[3]

INSTITUTIONS (ALL):

1. Affibody AB, Solna, Sweden.
2. Nuclear medicine and PET, Uppsala University, Uppsala, Sweden.
3. Uppsala University, Uppsala, Sweden.

(No Image Selected)

CONTROL ID: 2245305

TITLE: Integration of Craniocaudal Rotation System in Molecular Image Guided Radiation Therapy.

PRESENTER: Rao Papineni

ABSTRACT BODY:

Abstract Body: Accurate dose delivery to malignant tissue in radiotherapy is essential for enhancing the treatment efficacy while minimizing morbidity of surrounding normal tissues. The confluence of molecular imaging and nanotechnology fields are bridging physics and medicine opening new avenues and therapeutic strategies complementing radiation therapy. We recently demonstrated radiation induced endogenous bioluminescence, and coined it as radiobioluminescence. With the growing needs in radiation research, for integrating optical imaging module directly with radiation therapy, the design, construction, and validation of Molecular Image Guided Radiation Therapy (MIGRT) instrumentation is carried out. The MI module was designed to immobilize and position either small animals or tissue culture plates. Phosphor screens between the animal chamber and the detector facilitated both the optical and radiographic images to be captured at the same focal plane. Radiation therapy is achieved using x-ray tube with a homogenic beam powered by 320 kV stable X-ray generators using fixed and/or adjustable collimators. As a proof of concept, here, tools including X-ray excitable luminescent nanoparticles (100 KeV) are used to image sentinel lymph nodes in swiss albino mice. Further, the capability to assess the physical attributes of the radiation beam and dose using the phosphor integrated optical imaging is described. To allow irradiation at multiple angles, we integrated the animal rotation system capable of Multiple Angle Dosing (MAD), wherein the instrument allows craniocaudal rotation of the animal for focal irradiation. Non-invasive imaging at multiple angles allows positioning the target tissue for collimated dose delivery. Functional and molecular imaging PRIOR or DURING or POST radiation therapy, together with the findings on radiation induced radiobioluminescence opens novel opportunities to determine and explore the molecular mechanisms in radiation biology.

AUTHORS (LAST NAME, FIRST NAME): Papineni, Rao V.[1, 2]

INSTITUTIONS (ALL):

1. Precision X-Ray Inc, North Branford, CT, United States.
2. Physiology, University of Kansas Medical Center , Kansas, KS, United States.

(No Image Selected)

CONTROL ID: 2245384

TITLE: Theranostic silver coated gold nanorods for *in vivo* molecular photoacousic angiography of tumor

PRESENTER: Shouhui Chen

ABSTRACT BODY:

Abstract Body: We reported novel silver coated gold nanorods Au/Ag core/shell nanorods (Au/Ag NRs) for photoacoustic tumor angiography. Au/Ag NRs with different shell thickness of < 80 nm in dimension have been synthesized using chemically depositing silver on gold nanorods surface. in an aqueous solution. Au/Ag NRs signal and hemodynamic were quantitatively decoupled by using two-wavelength measurements. Compared with rare gold nanorods, the Au/Ag NRs increases the imaging sensitivity and specificity in tumor. In the PA images, the microvascular network was significantly enhanced by the contrast agents. Neovascularization in tumor angiogenesis at multiple scales was clearly imaged in the tumor. Our results showed that the novel nanopariticles were found to have a long retention time in vascular and high accumulation in tumor. Our results suggested their potential use as a new class of contrast agents for optical imaging and photothermal therapy.

AUTHORS (LAST NAME, FIRST NAME): Chen, Shouhui[1]

INSTITUTIONS (ALL):

1. Shanghai Jiaotong University, Shanghai, China.

(No Image Selected)